EAC2011 Manchester

European Aerosol Conference Handbook

4-9 Sept 2011

Handbook sponsored by:

Biral
The Aerosol Company

Organised by:

THE AEROSOL SOCIETY
the science of airborne particles

European Aerosol Conference 2011,

Manchester, United Kingdom, September 4 to 9, 2011
Conference co-chairs: Ian Ford and Hugh Coe
Hosting Aerosol Association:
The Aerosol Society – United Kingdom and Ireland

Contents:

Abstracts:

Monday, September 5, 2011

Tuesday, September 6, 2011

Wednesday, 7 September 7, 2011

Thursday, September 8, 2011

Friday, September 9, 2011

Welcome

The Aerosol Society of the UK and Ireland welcomes participants to the 2011 European Aerosol Conference in Manchester, held under the auspices of the European Aerosol Assembly. Aerosol scientists make up a diverse community and meetings such as EAC serve to demonstrate this richness, whilst underlining the connectivity between different branches of the field. This Handbook describes the programme of events, and together with the conference website it should provide most of the information you need. We hope you find the meeting stimulating and valuable.

Ian Ford and Hugh Coe, co-chairs of EAC2011

Front cover: Photo by Nicholas J. Higham, School of Mathematics, University of Manchester. *www.maths.manchester.ac.uk/~higham/*

NOTES:

Table of Contents

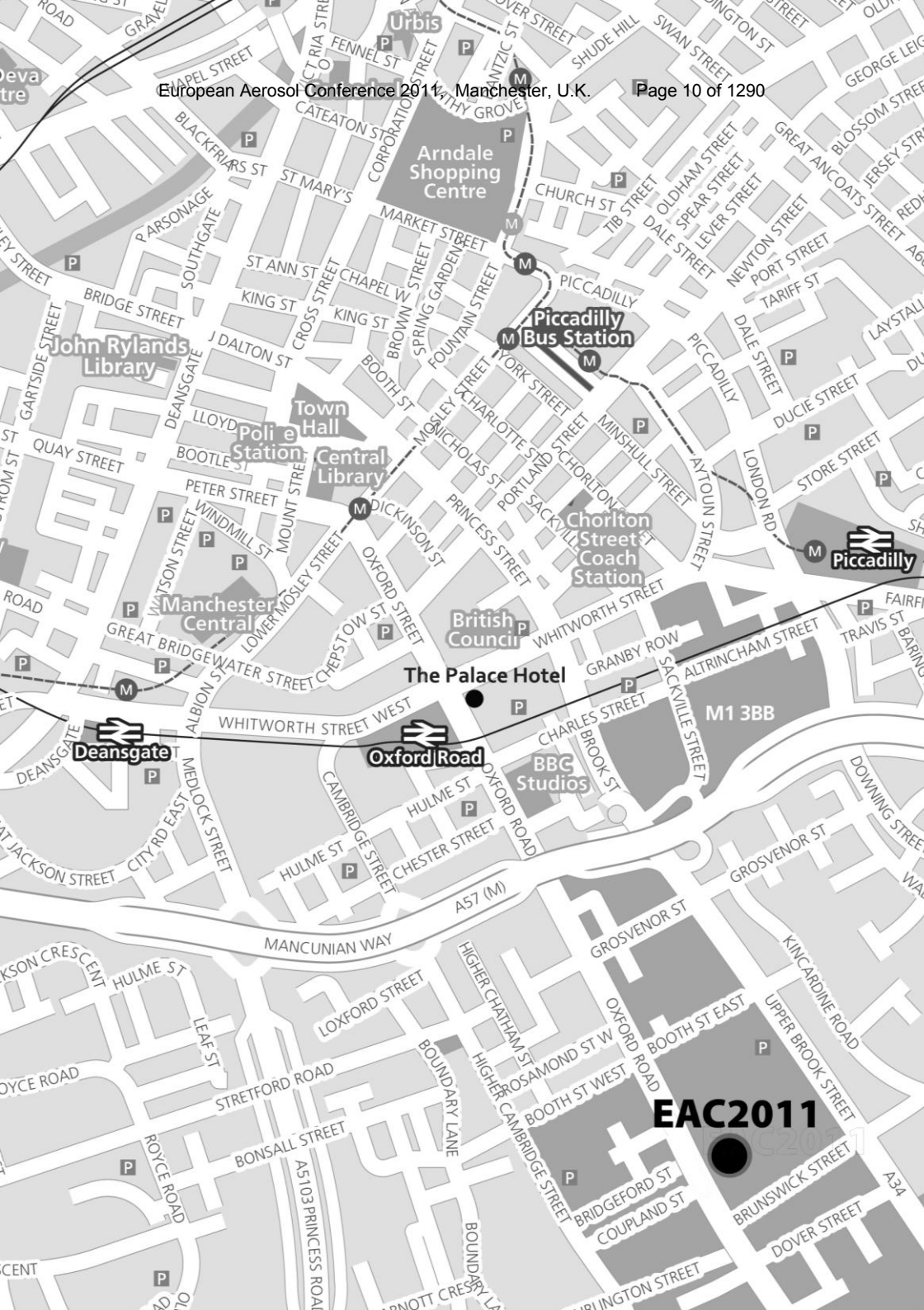
Urbis
Arndale Shopping Centre
Piccadilly Bus Station
John Rylands Library
Town Hall
Police Station
Central Library
Chorlton Street Coach Station
Piccadilly
Manchester Central
British Council
The Palace Hotel
M1 3BB
Deansgate
Oxford Road
BBC Studios
EAC2011
MARKET STREET
PICCADILLY
CHURCH ST
ST ANN ST
KING ST
CROSS STREET
BRIDGE STREET
DEANSGATE
QUAY STREET
PETER STREET
OXFORD STREET
WHITWORTH STREET
GREAT BRIDGEWATER STREET
WHITWORTH STREET WEST
CHARLES STREET
GRANBY ROW
ALTRINCHAM STREET
GROSVENOR ST
MANCUNIAN WAY
A57 (M)
HULME ST
CHESTER STREET
OXFORD ROAD
STRETFORD ROAD
BONSALL STREET
BOUNDARY LANE
HIGHER CAMBRIDGE STREET
BOOTH ST WEST
BOOTH ST EAST
ROSAMOND ST W
BRUNSWICK STREET
DOVER STREET
COUPLAND ST
BRIDGEFORD ST
KINCARDINE ROAD
UPPER BROOK STREET
A5103 PRINCESS ROAD
A34

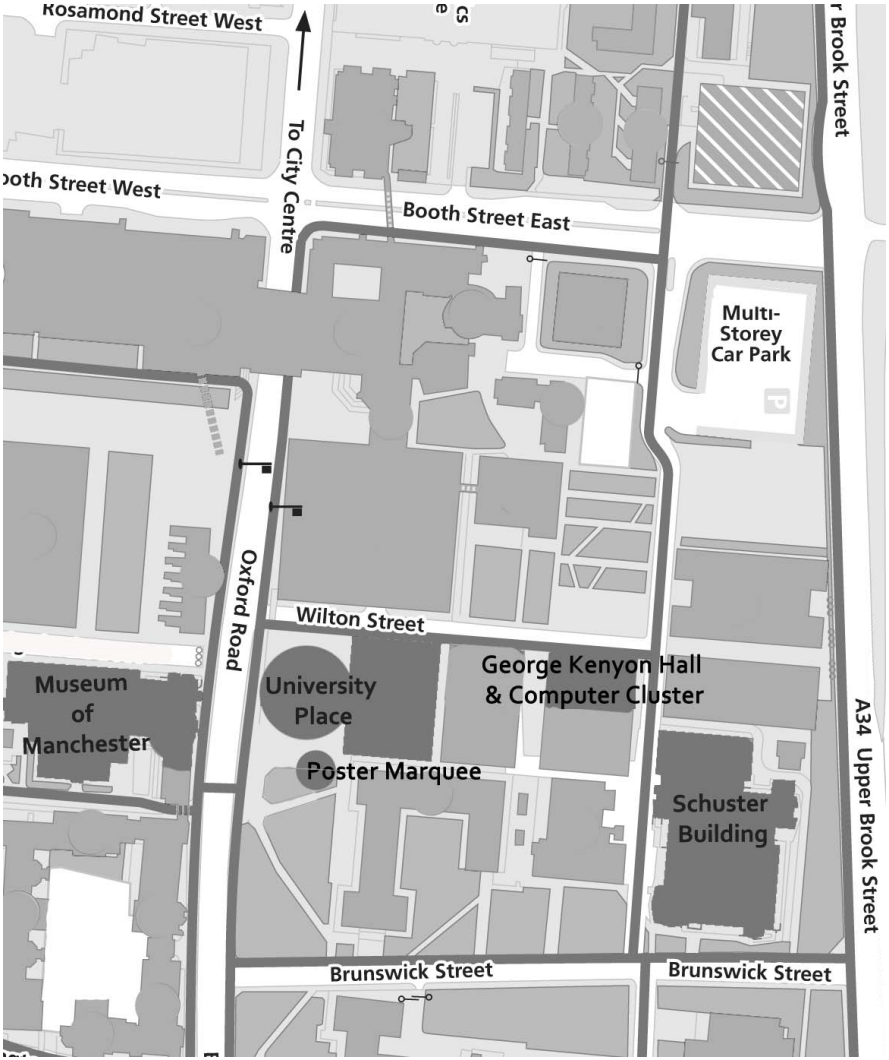
Rosamond Street West
To City Centre
Booth Street West
Booth Street East
Multi-
Storey
Car Park
Oxford Road
Wilton Street
Museum
of
Manchester
University
Place
George Kenyon Hall
& Computer Cluster
Poster Marquee
Schuster
Building
A34 Upper Brook Street
Brunswick Street
Brunswick Street

1	Ecotech
2	Airmonitors
3	Cambustion
4-5-6	TSI
7	Topas
8	URG Corp
9	AirModus
10	Palas
11	Particle Measuring Systems
12	PMT
13	Grimm
14-15	Dekati
16-17	Biral
18-19	Comde
20	Meritics
21	Copley Scientific
22	Droplet Measurement Technologies
23	Biotest
24	NPL
25	Enviro Technology Services & Digitel
26	Surface Measurement System & Sunset Laboratory
27	Matter Aerosol

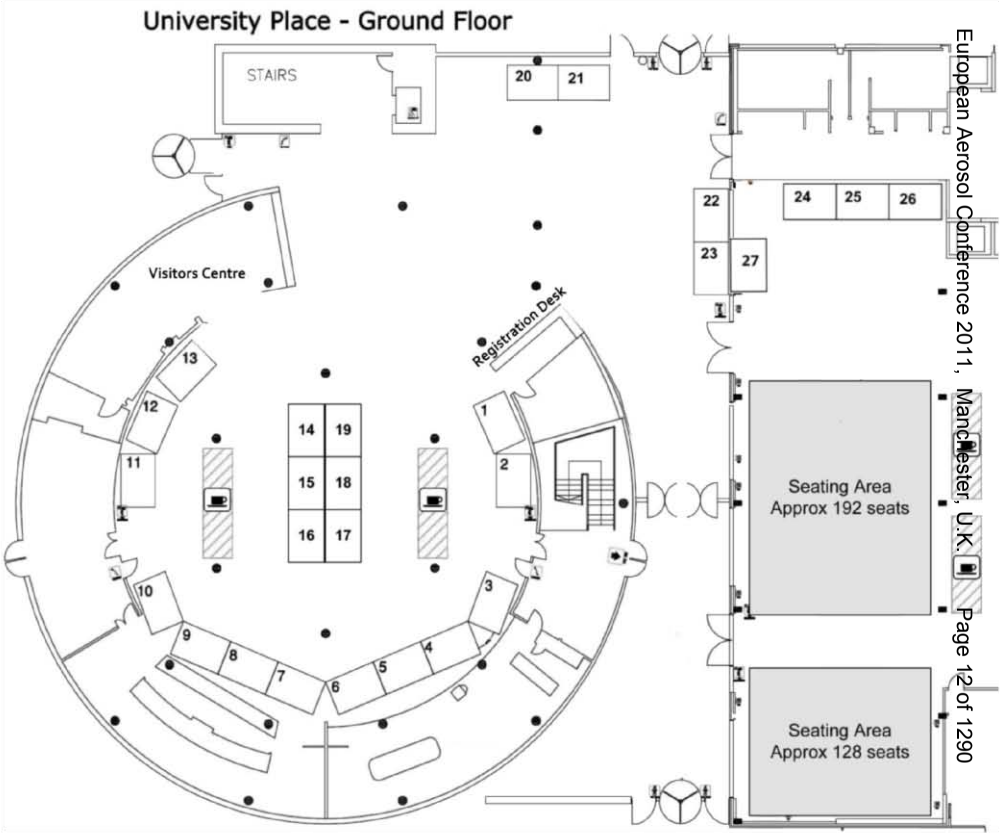

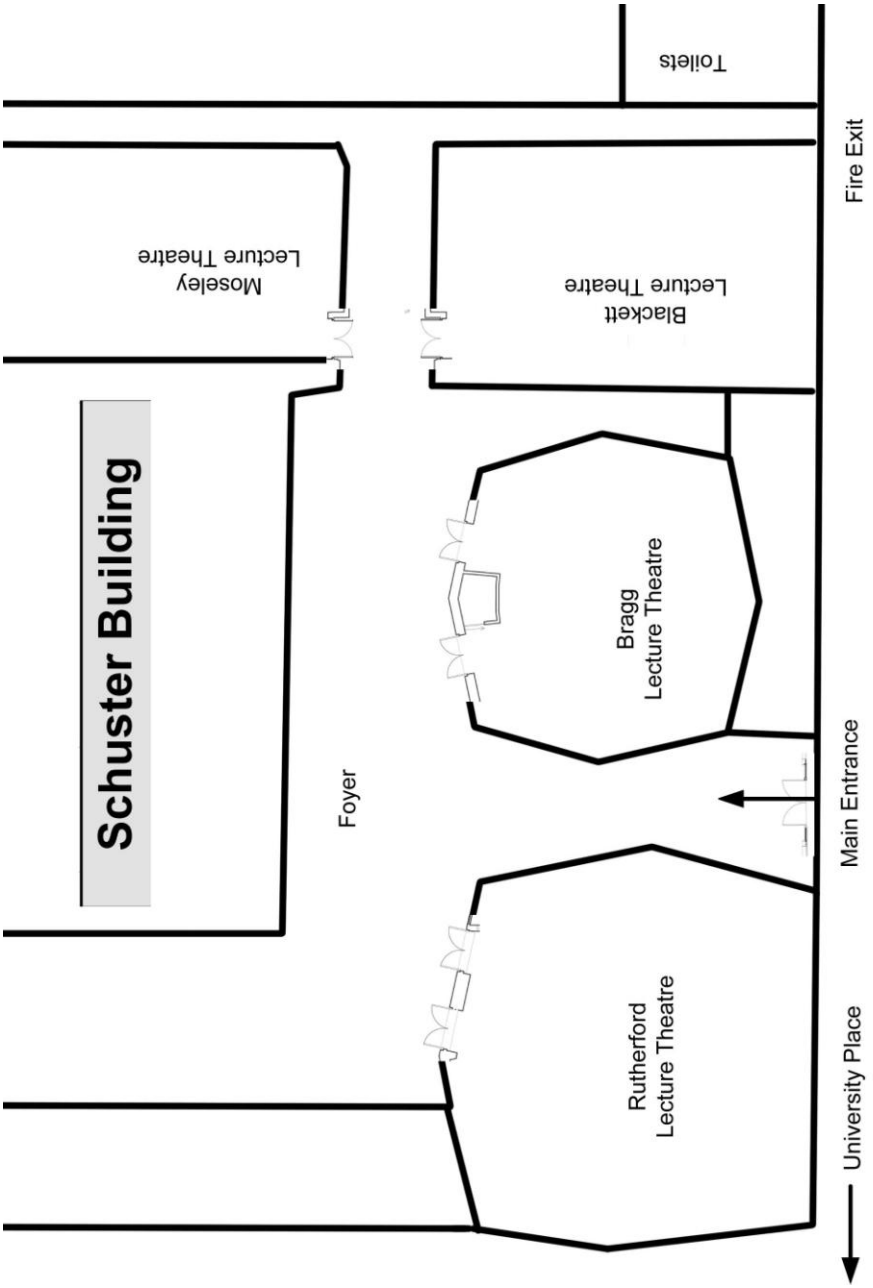
Toilets
Fire Exit
Moseley
Lecture Theatre
Blackett
Lecture Theatre
Schuster Building
Bragg
Lecture Theatre
Foyer
Main Entrance
Rutherford
Lecture Theatre
University Place

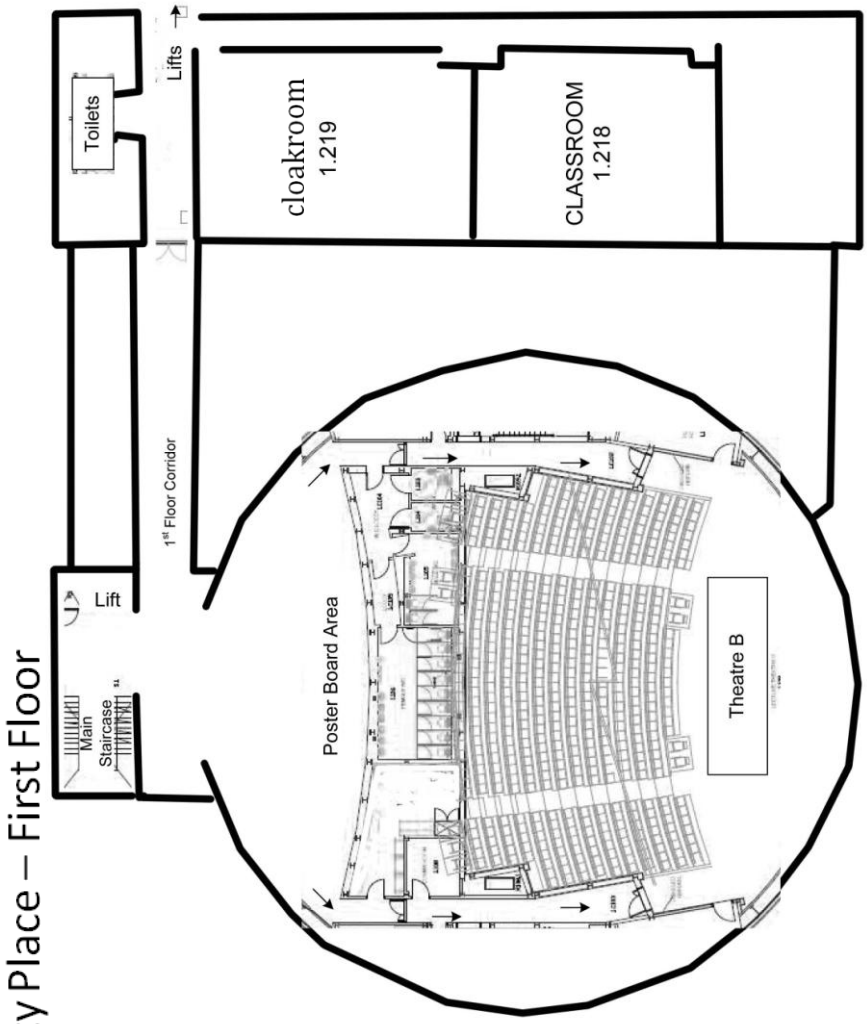
University Place – First Floor
Toilets
Lifts
cloakroom
1.219
CLASSROOM
1.218
Lift
Main
Staircase
1st Floor Corridor
Poster Board Area
Theatre B

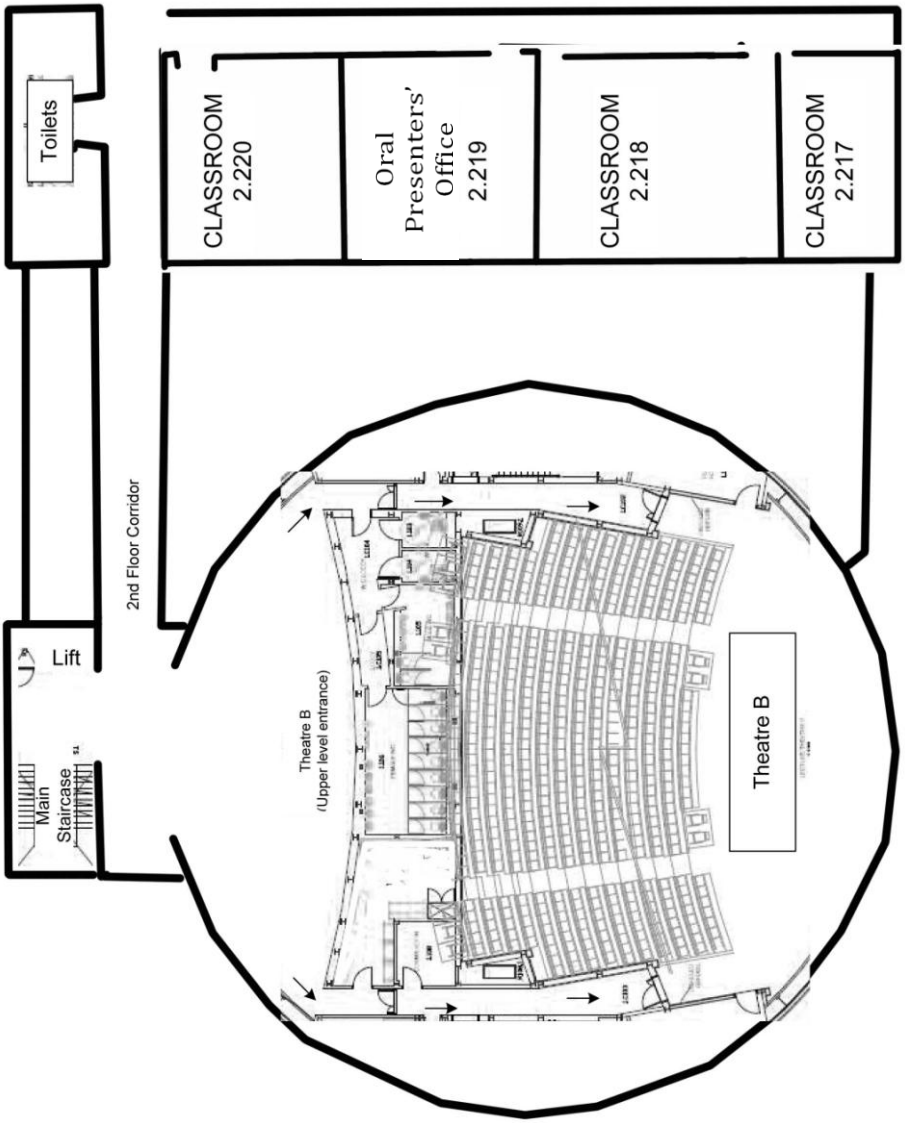

University Place – Second Floor

University Place First Floor: Additional Poster Space

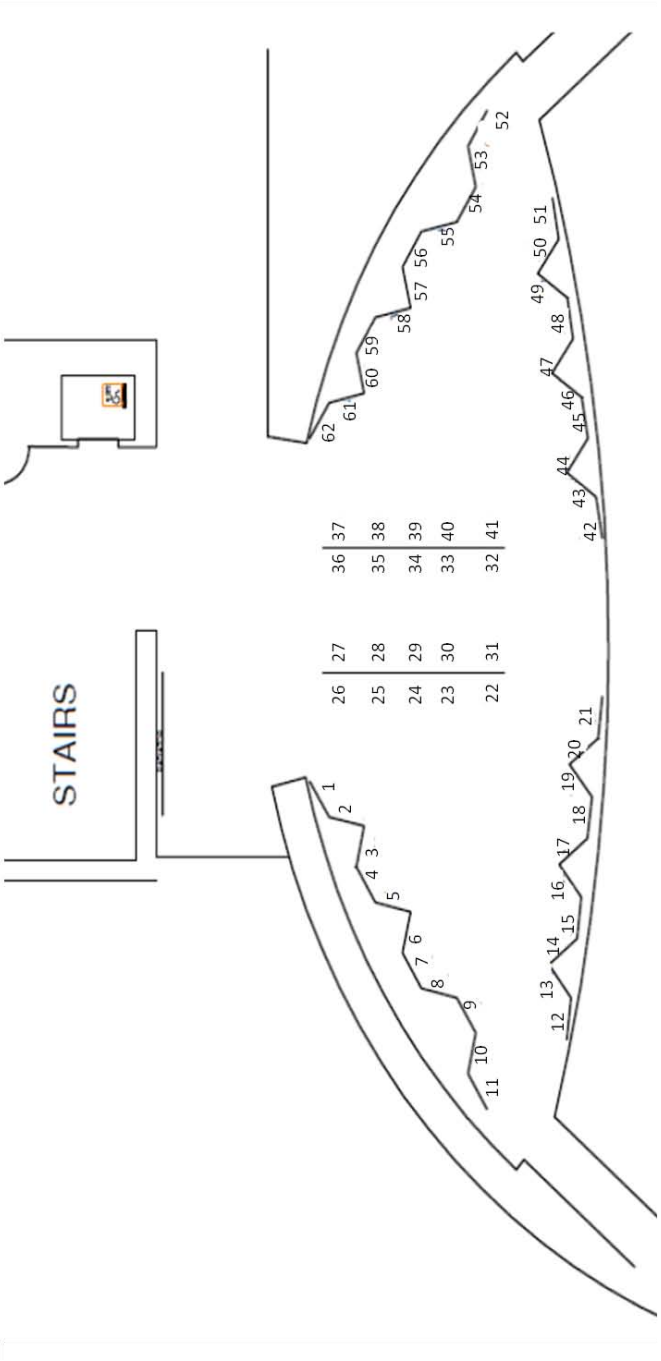

University Place Marquee – Main Poster Hall

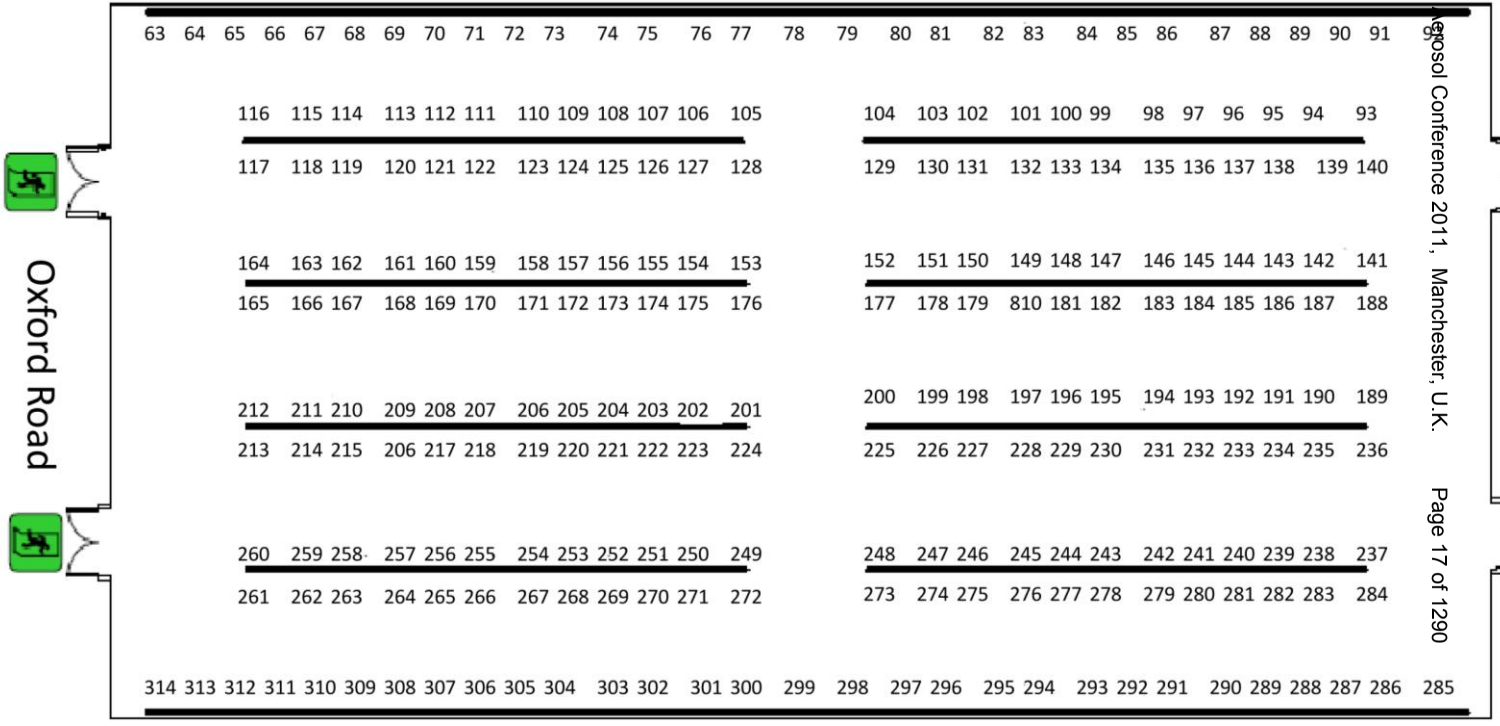

Committees

Programme committee:

- Ian Ford (chair)
- Charles Clement
- Sophie Cross
- Alan Jones
- John McAughey
- Conor McGrath
- Darragh Murnane
- Simon Parker

Organising committee:

- Hugh Coe (chair)
- Miriam Byrne
- Don Clark
- Sheila Coates
- Ian Colbeck
- Mark Crooks
- Virginia Foot
- Rebecca Hopkins
- Julie Hipperson
- Jessica Perkins
- Steve Preston
- Julie Samson

The international advisory committee, responsible for much of the reviewing of abstracts, consists of the following chairs and co-chairs of the EAA working groups:

- Lucas Alados-Arboledas
- Christof Asbach
- Ari Asmi
- Andrei Bologa
- David Broday
- Jose Castillo
- Charles Clement
- Aladar Czitrovszky
- Johanna Gietl
- Martin Gysel
- Regina Hitzenberger
- Yoshi Inuma
- Martina Krämer
- Francois-Xavier Ouf
- Hanns-Rudolf Paur
- Otmar Schmid
- Olli Sippula
- Wendelin Stark
- Roberta Vecchi
- Elisabetta Vignati
- Birgit Wehner
- Sabine Wurzler
- Caner Yurteri

The European Aerosol Assembly

The European Aerosol Assembly (EAA) consists of 12 national or regional societies across Europe, though membership of these societies is not limited to European nationals. The major activity of the EAA and its working groups takes place at the European Aerosol Conference, held in three out of every four years.

The Aerosol Society

The Aerosol Society held its inaugural meeting in 1986 as a forum for the then embryonic community of aerosol scientists in the UK and Ireland. Hence 2011 is our silver jubilee and the hosting of the European Aerosol Conference is a suitable way to celebrate this 25 year history.

General Information

Venue

The European Aerosol Conference 2011 is being held at the Oxford Road campus, University of Manchester. The major sessions (in particular plenaries and exhibition) take place in the University Place Conference Centre, with parallel oral sessions also in the Schuster Building. The poster sessions will be in the marquee adjacent to the conference centre and in an area adjacent to plenary lecture theatre B.

Transport to the Conference Centre

By taxi

Mantax Taxis 0161 230 3333
Union Cars 0161 225 5566
Black Cabs 0161 227 1888

A typical taxi fare from the Conference Centre to Manchester city centre in a black cab is £4-£6.

By bus

From Piccadilly Railway Station catch the 147 bus (80p per single trip or £1.50 for day ticket) and ask for the University.

From Piccadilly Bus Station catch any of the following buses:
14, 16, 41, 42, 43, 44, 48, 111, 140, 142, 157 and 250
A bus fare costs approx 80p-£1.20 for a single journey.

From Victoria Railway Station, catch the Metro tram to Piccadilly Bus Station and catch one of above services.

From Manchester Airport take bus 43, or a train to Piccadilly or Oxford Road Railway Stations and proceed from there.

Name badges

Upon registration you will receive a name badge which should be worn at all conference events including the social functions. The double sided badge is designed for maximum visibility.

Lunch, coffee/tea and snacks

Coffee/tea points

Refreshments will be available at coffee and tea points in the University Place Conference Centre during the designated morning and afternoon breaks in proceedings. Water will also be available from coolers and from the Eats restaurant.

Lunch boxes

Sandwich lunches will be provided in boxes from the Eats restaurant area during the designated lunch breaks. A vegetarian option will be available. This will be inclusive in the registration fee.

Vending machine/Snacks

Vending machines for crisps/chocolate/drinks can be found in the Williamson Building, to the right of University Place when viewed from Oxford Road. The machines are located on the ground floor facing the

first set of double doors, and on the second floor to the right of the stairwell.
There is a Spar shop which sells snacks, baked goods, groceries, etc, located about 100 metres north along Oxford Road in the University Precinct, which also contains various other food outlets.

Cafeterias/Restaurants

Couture at the Manchester Museum (opposite University Place), from 8am-2.30pm, breakfast and lunch.

Christies Bistro (opposite University Place) from 9am-5pm, breakfast and lunch.

Potters Bar (cafe) Simon Building, Brunswick Street, from 8am-4pm, snacks, breakfast, lunch.

Kro2, 325 Oxford Road Manchester (opposite Student Union), from 8am – 10pm, breakfast, lunch, dinner.

Tai Pan, Cantonese Restaurant 81 Upper Brook Street (top of Brunswick St, turn right).

Internet

A Wi-Fi internet connection is available throughout the conference buildings. Please contact the registration and information desk for a username and password. Desktop connections will be available in George Kenyon Computer Cluster, 9-5pm Monday to Friday (see map page 5).

The conference website www.eac2011.com will carry up to date information about programme changes etc.

Sponsors and Exhibitors

The organisers wish to acknowledge the support of the many exhibitors present at EAC2011. Please visit their stands on the ground floor in the University Place Conference Centre, and consult their entries at the back of this handbook. The exhibitors are listed below:

Air Monitors Ltd	Droplet Measurement Technologies	Particle Measuring Systems
AirModus Oy	Ecotech Pty Ltd	PMT GB
Biotest UK	Enviro Technology Services plc	Surface Measurement Systems Ltd
Biral	Grimm Aerosol Technik	Sunset Laboratory Inc
Cambustion	Matter Aerosol	Topas GmbH
Comde	Meritics	TSI
Copley Scientific Ltd	NPL	URG Corporation
Dekati Ltd	Palas GmbH	Wiley
Digitel		

We are grateful for the financial and administrative support provided by Visit Manchester, the University of Manchester and University College London.

Conference Information

Registration and information desk (during the conference):
+44 (0)161 306 4098
info@eac2011.com

General information (outside the conference period)
Sheila Coates
The Aerosol Society
Tel: 01275 849019
Fax: 01275 844877
admin@aerosol-soc.org.uk

Main presentation sessions

The conference will open at 9:00 on Monday 5th September and close at 16:00 on Friday 9th September according to the schedule shown later in this Handbook.

Exhibition

The exhibition is situated in the University Place Conference Centre and is available 8:30 – 18:00 Monday to Thursday and 8:30 – 13:45 on Friday.

Registration and information desk

The registration and information desk will be open at the University Place Conference Centre as follows:
Sunday 4th September: 14:00 – 18:00
Monday 5th September: 08:00 – 18:00
Tuesday 6th September: 08:30 – 18:00
Wednesday 7th September: 08:30 – 13:30
Thursday 8th September: 08:30 –18:00
Friday 9th September: 08:30 –13:30

Certificate of attendance

Certificates will be available by request at the registration and information desk.

Social Programme

Sunday 4th September

Drinks Reception – The Manchester Museum & Whitworth Hall
Address: Oxford Road, Manchester M13 9PL (opposite the University Place Conference Centre)
Time: 18:00 – 20:00.
Delegates are invited to wander through the museum where drinks and canapés will be served. The museum features collections and galleries of animal life, plants, rocks and minerals, prehistoric life, an aquarium and a vivarium. This icebreaker event is included in the registration fee.

Wednesday 7th September

The afternoon is left free for you to explore Manchester. Much tourist information is to be found online, but from a science perspective, the Museum of Science and Industry is well worth a visit. Lab tours at the University of Manchester are also planned.

Thursday 8th September

Conference dinner – Palace Hotel
Address: Oxford Street, Manchester M60 7HA (next to the Oxford Road Railway Station)
Time: 19:00

Menu:

Oyster Bar

*****

Goats cheese crotin with slow roasted roma tomatoes, marinated vegetables and homemade roquette pesto

*****

Breast of chicken, sautéed spring cabbage, smoked bacon, crushed jersey royals, chanteney carrots, thyme & white wine sauce

Vegetarian Option:

Cepe, shallot & grilled asparagus tartlet, baby spinach, sautéed potatoes & salsa verde

*****

Vanilla bourbon pannacotta with peach and champagne syrup, biscotti and berries

English cheeses and oat cakes

Coffee and petit fours

Awards

Smoluchowski Prize

The award will be given by GAeF to a young researcher (as a rule under 40 years of age) who has achieved and published significant new results in aerosol science in the preceding 3 years.

Alan Cussens Memorial Award

Alan Cussens played an important role in setting up the Aerosol Society and served for many years on its committee. He also founded Biral plc, the well known distributor and developer of aerosol instrumentation based in the UK. His untimely death in 2010 is to be marked by the Aerosol Society at EAC2011 through the Alan Cussens Memorial Award, consisting of a prize of £500 and a certificate.

Best Poster Prizes

To recognise excellence in poster presentation, the EAA will award a number of Best Poster Prizes at the conference. The criteria for selection are effective design, clarity of communication and scientific quality. The Prize Committee is chaired by Dr François-Xavier Ouf.

Board meetings

- Journal of Aerosol Science Editorial Board. Monday 5th September 18:00-19:00. Room 2.217 University Place.

- GAeF Board meeting. Tuesday 6th September, 12:00-13:00. Room 2.217 University Place.

- EAA Board meeting. Wednesday 7th September, 12:45:13:45. Room 2.217 University Place.

- Workplace and Indoor Aerosols 2012, Scientific Board meeting. Wednesday 7th September, 13:00-15:00. Blackett Theatre.

- EAA Working Group chairs meeting. Friday 9th September, 12:45-13:45. Room 2.217 University Place.

- Atmospheric Environment Editorial Board. Friday 9th September, 12:00-14:00. Room 3.205 University Place.

Assemblies

GAeF General Assembly. Theatre B, Tuesday 6th September, 18:00-19:00

Aerosol Society AGM. Theatre A, Tuesday 6th September, 18:00-19:00

EAA Working Group meetings

The purpose of these meetings is to discuss general matters within the various topic areas and to help plan future events, particularly the next EAC. All delegates are welcome.

Tuesday 6th September, 17:10-18:00. The following groups meet:

Aerosol Modelling	Theatre A
Aerosol Chemistry	Rutherford Theatre
Aerosol-based Nanotechnology	Blackett Theatre
Atmospheric Aerosols	Theatre B
PMx	Moseley Theatre

Thursday 8th September, 17:10-18:00. The following groups meet:

Fundamentals	Blackett Theatre
Combustion	Rutherford Theatre
Instrumentation	Bragg Theatre
Particle-Lung Interactions	Moseley Theatre
Electrical Effects	Theatre A

Presentation Information

Abstracts

All abstracts will be published in electronic form and distributed to participants on a USB memory stick. Abstracts are arranged in folders by working group and scientific topic and are most easily located by searching for the abstract number. Identifying the slot occupied by a presentation is possible by cross-referencing against the list on the stick and the website ordered by abstract number.

Instructions for oral presentations

Please report to the Oral Presenters' Office 2.219 as far in advance of your presentation as possible to hand in your presentation on a USB memory stick. For organisational reasons, personal laptops cannot be used for presentations. A copy of your presentation will be made available on the PC installed in the appropriate conference room. Speakers are requested to come to their oral session at least 10 minutes prior to its beginning and identify themselves to the chairs.
The time available for oral presentations is 20 minutes (15 minutes for the talk and 5 minutes for discussion).

Instructions for oral reserve presentations

Oral reserve presentations are poster presentations that will also be offered a slot for oral presentation should a vacancy become available. Presenters should check the situation with chairs at the start of the relevant oral session.

Instructions for poster presentations

Posters are displayed in the Poster Marquee in front of the conference centre, and in the space outside Theatre B on the first floor of the University Place building. The poster designation 4P*xyz* or 8P*xyz* indicates board *xyz* in session 4 (Tuesday) or session 8 (Thursday). The location of board *xyz* is indicated on the poster hall plans in this handbook.
– **Poster session A** (4P) on Tuesday 6th September, 10:30 – 12:00.
Posters for this session can be mounted from Monday lunchtime, and left on display until the Wednesday morning coffee break.
– **Poster Session B** (8P) on Thursday 8th September, 10:30 – 12:00.
Posters for this session can be mounted from Wednesday lunchtime and left on display until Friday lunchtime.

Presenting authors are kindly asked to be available to present their posters during the poster sessions. The poster board space is 120 cm high and 100 cm wide. Velcro pads for fixing will be available.

Late-breaking posters

Late breaking posters will be on display on the first floor of University Place, next to the poster area.

Next Aerosol Society Event

Annual Aerosol Science Conference
3rd & 4th April 2012

School of Chemistry, University of Bristol.

The scientific programme will include a broad range of aerosol science topics, including: nucleation, aerosol instrumentation, atmospheric aerosols, aerosol inhalation, etc.

Plenary Speakers:
Professor Gary Martin, Kings College London
Professor Jonathan Reid, University of Bristol

Contact: Sheila Coates, admin@aerosol-soc.org.uk
For a full programme of other meetings, please visit:
www.aerosol-soc.org.uk/

Programme overview

Extra Event

The EAC2011 Satellite Workshop: Aerosols from domestic biomass heating, characterisation and toxicity - Critical pathways towards sustainability of biomass based heating will be held 3-4 September 2011, University Place, Manchester, UK. Organised by the European Aerosol Association and Deutsches Biomasse Forschungs Zentrum gemeinnützige GmbH (DBFZ, German Biomass Research Centre).

Sunday 4th September	14:00-18:00	Registration in the foyer of University Place Conference Centre
	18:00-20:00	Drinks Reception – The Manchester Museum and Whitworth Hall

		THEATRE A	THEATRE B	RUTHERFORD	MOSELEY	BRAGG	BLACKETT
Monday 5th September	09:00-10:00	Opening Ceremony and Plenary 1. Jasper Kirkby: Atmospheric nucleation in the CERN CLOUD experiment - THEATRE B					
		Break					
	10:30-12:30	1A: Ultrafine particles in Urban Areas	1B: Aerosol-Cloud Interactions 1	1C: Molecular Characterisation of Aerosol Constituents	1D: Physico-chemical PM properties	1E: Engineered Nanoparticle Release from Nanostructured Materials into the Air	1F: Aerosol Nucleation
		Lunch					
	13:30-15:30	2A: Bioaerosols	2B: New Particle Formation 1: Chamber Studies	2C: Instrumentation for Chemical Characterisation of Aerosol	2D: Source Apportionment Studies	2E: Gas-phase Synthesis of Nanoparticles	2F: Aerosol Mobility and Capture
		Break					
	16:00-18:00	3A: Bioaerosols / Specific Aerosol Types	3B: New Particle Formation 2: Experimental Studies	3C: Chemical Mechanisms and Transformation Processes in Aerosol	3D: PMx Data Interpretation	3E: Aerosol-based Nanotechnology Fundamentals	3F: Thermal and Optical Effects
Tuesday 6th September	09:00-10:00	Plenary 2. Wendelin Stark: Aerosols for materials: medical and industrial applications and the role of nanotoxicology - THEATRE B					
		Break					
	10:30-12:00	4P: Poster session A					
		Lunch	GAeF Board meeting (2.217)				
	13:00-15:00	5A: PM Sources	5B: Aerosol-Cloud Interactions 2	5C: Smog Chamber Experiments and SOA 1	5D: Aerosols in Disease and Therapy	5E: Health Effects of Nanoparticles	5F: Aerosols in Turbulent Flows 1
		Break					
	15:30-17:10	6A: New Particle Formation 3: Theory and Modelling	6B: Climate Effects of Aerosols / Transport and Transformation	6C: Smog Chamber Experiments and SOA 2	6D: Direct Impacts of Aerosol on Climate (ADIENT Project)	6E: Enhanced Aerosol Measurement Technology	6F: Aerosols in Turbulent Flows 2
	17:10-18:00	Aerosol Modelling Working Group meeting	Atmospheric Aerosols Working Group meeting	Aerosol Chemistry Working Group meeting	PMx Working Group meeting		Aerosol-based Nanotechnology Working Group meeting
	18:00-19:00	Aerosol Society AGM	GAeF General Assembly				
Wednesday 7th September	09:00-10:00	Plenary 3. Uta Griesenbach: UK Cystic Fibrosis Gene Therapy Consortium - Developing and Delivering a Complex Respiratory Therapy - THEATRE B					
	10:00-10:15	Awards Ceremony - THEATRE B					
		Break					
	10:45-12:45	7A: Carbonaceous Aerosol and Meteorology	7B: Aerosol-Cloud Interactions 3	7C: High Temperature Systems: Sampling and Quenching before Detection	7D: Particle-Lung Deposition and Pharmacological Aerosol	7E: New Developments in Aerosol Instrumentation	7F: Modelling Nuclear Particles and Health Effects
		Lunch	EAA Board meeting (2.217)				
	13:45	Alan Cussens Award (Bragg Theatre)					
	14:00	Free Afternoon					

		THEATRE A	THEATRE B	RUTHERFORD	MOSELEY	BRAGG	BLACKETT
Thursday 8th September	09:00-10:00	Plenary 4. Phil Rasch: The scientific challenges involved in using aerosols as a strategy for geoengineering climate - THEATRE B					
		Break					
	10:30-12:00	8P: Poster session B					
		Lunch					
	13:00-15:00	9A: Aerosols in Geoengineering	9B: Field Observations from Global Hot Spots	9C: Biomass and Biofuels	9D: In-vitro Toxicity and Health Effects of PM	9E: Aerosol-based Nanotechnology: Methods and Applications	9F: Charged Aerosols
		Break					
	15:30-17:10	10A: Aerosols in Geoengineering / Aerosols in Global Climate Models	10B: Remote Sensing of Aerosol Properties	10C: Control Technologies for Combustion Emissions	10D: Turbulent Aerosol Transport and Exchange / Transport and Transformation	10E: Spark Generators for Nanoparticle Generation	10F: Modelling Aerosol Formation
	17:10-18:00	Electrical Effects Working Group meeting		Combustion Working Group meeting	Particle-Lung Interactions Working Group meeting	Instrumentation Working Group meeting	Fundamentals Working Group meeting
	19:00-21:30	Conference Dinner - Palace Hotel					

Friday 9th September	09:00-10:00	Plenary 5. Andreas Petzold: Global aviation and particulate matter: from climate impact to volcanic ash and back - THEATRE B					
	10:00-10:15	Awards Ceremony - THEATRE B					
		Break					
	10:45-12:45	11A: Biomass Burning	11B: Chemical and Physical Properties of SOA	11C: Combustion Aerosol Measurements and Analysis	11D: From PM exposure to Health Effects 1	11E: Comparison of Different Measurement Methods	11F: Atmospheric Applications of Aerosol Modelling 1
		Lunch	EAA Working Group Chairs' meeting (2.217)				
	13:45-15:45	12A: Marine Aerosols / Mineral Dust	12B: Optical Properties	12C: Engine-related Aerosols	12D: From PM exposure to Health Effects 2	12E: Application of New Instrumentation for Study of New Processes and Phenomena	12F: Atmospheric Applications of Aerosol Modelling 2
	15:45-16:00	Closing Ceremony Theatre B					

Working Group

Atmospheric Aerosols: Aerosol Processes and Properties	Aerosol-based Nanotechnology
Atmospheric Aerosols: Specific Aerosol Types	Instrumentation
Aerosol Chemistry	Aerosol Modelling
Combustion Aerosols	Fundamentals
PMx	Electrical effects
Particle Lung Interactions	Special Sessions

NOTES:

Monday 5th September

09:00-10:00 Opening Ceremony and Plenary 1
Jasper Kirkby: *Atmospheric nucleation in the CERN CLOUD experiment*
Room: Theatre B
Chairs: Ian Ford / Hugh Coe

10:30-12:30 **Session 1A: Ultrafine particles in Urban Areas**
Room: Theatre A
Chairs: Thomas Kuhlbusch / Gary Fuller

10:30	1A1	1075	**Martine Van Poppel**, Vinit Mishra, Patrick Berghmans *Concentrations of UFP in a tunnel in Belgium*
10:50	1A2	85	**Khan Alam**, Majid Hussain, Ahmad Mukhtar, Pierre Madl, Said Rehman, Thomas Trautmann, Thomas Blaschke *Measurement of Atmospheric aerosol size distribution, mass concentration and lung deposition in four cities of Pakistan*
11:10	1A3	657	**Tibor Borsos**, Imre Salma, Tamás Weidinger, Pasi Aalto, Markku Kulmala *Ultrafine particles in various urban microenvironments in Budapest*
11:30	1A4	162	**Noor Yahaya**, Noor Zaitun *Analysing roadside Particle Number Concentrations using Boosted Regression Trees (BRT)*
11:50	1A5	633	**Guy Coulson**, Ian Longley, Woodroe Pattinson, Simon Kingham, Lou Reddish, Gustavo Olivares *Street-to-street variations in PM, PNC and BC in a motorway-dominated urban neighbourhood*
12:10	1A6	560	**Rayk Rinke**, Andreas Wieser, Bernhard Vogel, Ulrich Corsmeier, Christoph Kottmeier *Determination of the spatial variability of particle number concentration, particle size distribution and*

			the concentrations of NO and NO2 in an urban region and the surrounding using one year mobile measurements with the AERO-TRAM
Reserve	1AR	1100	**Holger Gerwig**, Werner Pecher, Klaus Wirtz *Local sources of UFP at an urban BG station*

10:30-12:30 **Session 1B: Aerosol-Cloud Interactions 1**
Room: Theatre B
Chairs: Martina Krämer / David Topping

10:30	1B1	76	**Heike Wex** *Ground-based and airborne examination of particle hygroscopicity at Barbados*
10:50	1B2	212	**Karin Ardon-Dryer**, Zev Levin, Heinz G. Bingemer, Holger Klein *Atmospheric ice nuclei in the Eyjafjallajökull volcanic ash plume over Germany and Israel*
11:10	1B3	619	**Darrel Baumgardner**, Neda Boyouk, Martial Haeffelin *Single particle depolarization studies: Unraveling the mysteries of Paris Fog*
11:30	1B4	686	**Jonathan Reid**, Rachael E.H. Miles, Taina Yli-Juuti, Ilona Riipinen *Factors affecting the molecular flux during evaporation and condensation of water on an aqueous droplet surface*
11:50	1B5	566	**Martin Gysel**, Marie Laborde, Nicolas Bukowiecki, Zsofia Juranyi, Emanuel Hammer, Paul Zieger, Urs Baltensperger, Ernest Weingartner *In situ measurement of cloud droplet activation behaviour of black carbon particles*
12:10	1B6	960	**Paul Connolly**, Tom Choularton, Chris Dearden *Aerosol Cloud Interactions in a deep tropical convective storm, Hector*
Reserve	1BR	462	**Gary Lloyd**, Thomas Choularton and Paul Connolly *Anthropogenic Snowfall Events from Urban Fogs*

10:30-12:30 **Session 1C: Molecular Characterisation of Aerosol Constituents**

Room: Rutherford Lecture Theatre

Chairs: Markus Kalberer / Manabu Shiraiwa

10:30	1C1	488	**Scot Martin**, Qi Chen, Yingjun Liu, Neil Donahue, John Shilling *Measured O:C and H:C Elemental Ratios Constrain the Production Mechanisms of Biogenic Secondary Organic Material*
10:50	1C2	157	**Barbara Noziere** *Reaction products of glyoxal in atmospheric aerosols*
11:10	1C3	748	**Markus Kalberer**, Angela Rincon, Stephen Fuller, Peng Lin, Jianzhen Yu, Celia Alves, Catia Goncalves, Ana Calvo, Heidi Bauer, Anne Kasper-Giebl *Influence of biomass burning on organic aerosol composition - an ultra-high resolution mass spectrometry study*
11:30	1C4	943	**Angela-Guiovana Rincon**, Ana Isabel Calvo, Mathias Dietzel, Christine Braban, Markus Kalberer *S-containing organic components from water soluble fraction of Atmospheric Aerosol Collected in Cambridge and Auchencorth Moss EMP supersite*
11:50	1C5	499	**Johany Ringuet**, Eva Leoz-Garziandia, Helene Budzinski, Eric Villenave *Particulate PAHs and nitro/oxy-PAHs: on sampling degradation and size distribution in the south-west of Paris.*
12:10	1C6	959	**Paul Winkler**, John Ortega, Jun Zhao, Hans Friedli, James Smith *Size resolved nanoparticle composition from SOA formation events*
Reserve	1CR	370	**Lili Tang**, Shengjie Niu, Dantong Liu, Xuwen Li, Xiangzhi Zhang, Shuxian Fan,Hong Nie, Hugh Coe *Size Distribution and Source Analysis of Polycyclic*

			Aromatic Hydrocarbons (PAHs) contained in PM10 in Waliguan and Xining of China

10:30-12:30 **Session 1D: Physico-chemical PM properties**
Room: Moseley Lecture Theatre
Chair: Jordy Vercauteren / Maria Chiara Pietrogrande

10:30	1D1	471	**Maria Chiara Pietrogrande**, Dimitri Bacco, Sara Chiereghin *Simultaneous determination of water-soluble organic tracers in atmospheric aerosol using silyl-derivatization and GC-MS analysis*
10:50	1D2	461	**Marsailidh Twigg**, Chiara Di Marco, Ian Leith, Sara Leeson, Netty van Dijk, Ivan Simmons, Matt Jones, Eiko Nemitz, Neil Cape *Four years of high resolution monitoring of inorganic water soluble aerosol components over a semi-natural ecosystem in South East Scotland*
11:10	1D3	931	**Jose Bothorel-Nicolas** *Aerosol chemical mass closure in Corsica Island: towards a better understanding of the seasonal variation of aerosol sources in the Western Mediterranean*
11:30	1D4	1102	**Mats Gustafsson**, Göran Blomqvist, Eva Brorström-Lundén *PAH in PM10 from tyre and pavement wear*
11:50	1D5	302	**Beatrix Turóczi**, András Hoffer, Nóra Kováts, András Ács, András Gelencsér *Characterization of resuspended and respirable urban particulate matter*
12:10	1D6	353	**Anna Verena Broich**, Lydia Elisabeth Gerharz, Otto Klemm *Personal Monitoring of Exposure to Particulate Matter with a High Temporal Resolution*

10:30-12:30 **Session 1E: Engineered Nanoparticle Release from Nanostructured Materials into the Air**

Room: Bragg Lecture Theatre

Chairs: Heinz Fissan / Keld Alstrup Jensen

10:30	1E1	1135	**Keld Alstrup Jensen**, Ismo K. Koponen *Exposure to nanostructured particles during powder handling and mixing, sanding nanoparticle-doped paints and grinding windmill blades*
10:50	1E2	545	**Burkhard Stahlmecke**, Juri Romazanov, Christof Asbach, Heinz Fissan, Thomas Kuhlbusch *Investigations on (Nano-) Particle Release during Mechanical Treatment of Different Composite Materials*
11:10	1E3	227	**Daniel Göhler**, Lars Hillemann, Michael Stintz *Sanding induced nanoparticle release into air from artificially aged/weathered surface coatings*
11:30	1E4	1137	**Matthias Meier**, M. Mertler, W, Wohlleben *Release of nanoparticles from composite materials under abrasive stress*
11:50	1E5	284	**Albert Hellmann**, Siegfried Ripperger, Markus Berges, Stefan Sticher, Thomas Burkhart *Characterisation of Particles produced by Abrasion of Nanocomposites with a Grinding Machine*
12:10	1E6	490	**Heinz Fissan,** Burkhard Stahlmecke, Christof Asbach, Thomas Kuhlbusch, Karsten Wegner *Strategies for Nanoparticle Release Assessment from Powders, Liquid and Solid Materials into the Environment*

10:30-12:30 **Session 1F: Aerosol Nucleation**
Room: Blackett Lecture Theatre
Chairs: Charles Clement / Yannis Drossinos

10:30	1F1	58	**Hanna Vehkamäki**, Matthew J. McGrath, Theo Kurten, Kari Lehtinen, Markku Kulmala *Rethinking the first nucleation theorem in atmospheric nucleation*
10:50	1F2	693	**Jens Olaf Pepke Pedersen**, Martin Enghoff, Ulrik Uggerhøj, Sean Paling, Henrik Svensmark *Aerosol nucleation induced by a high energy particle beam*
11:10	1F3	674	**Jonathan Duplissy** *Binary sulfuric acid–water nucleation, including ion-induced nucleation mechanism*
11:30	1F4	913	**Brian Steer**, Vinay Ranganathan, Harald Gnewuch, Boris Gorbunov, Fiona Larner *Formation of Zn and ZnO nanoparticles by homogeneous nucleation*
11:50	1F5	1118	**Christopher Hogan**, Ranganathan Gopalakrishnan, Thaseem Thajudeen *A Shape Independent Collision Kernel Valid for All Knudsen Numbers*
12:10	1F6	948	**Joao Almeida-Simoes**, Curtius, Joachim, Kirkby, Jasper and the CLOUD collaboration *Nucleation rates and parametrisation in the CLOUD experiment*
Reserve	1FR	804	**Kimmo Neitola**, David Brus, Mikko Sipilä, Tuija Jokinen, Pauli Paasonen, Heikki Lihavainen *Influence of trimethylamine to sulphuric acid-water homogeneous nucleation*

13:30-15:30 **Session 2A: Bioaerosols**

Room: Theatre A

Chairs: Uli Pöschl / Janine Fröhlich

13:30	2A1	132	**Christoph Haisch**, Kathrin R. Schwarzmeier, Maria Knauer, Reinhard Niessner, Natalia P. Ivleva *Bioaerosol analysis by a combined microarray / SERS (surface-enhanced Raman scattering) approach*
13:50	2A2	454	**Ian Colbeck**, Viswanath Mula, Zaheer Ahmad Nasir, Mark Loeffler *Assessment of bacterial and fungal aerosol in hospital air*
14:10	2A3	1088	**Ulrich Poeschl** *Bioaerosols in the Earth System: Sources, Interactions and Effects*
14:30	2A4	445	**Francis Pope**, Jon-Selous Borlace, Paul Griffiths, Pete Gallimore, Markus Kalberer *Pollen are efficient cloud condensation nuclei*
14:50	2A5	335	**Maosheng Yao** *Development of a Lightweight, Simple and Efficient Exhaled Breath Condensate Collection Device and Method*
15:10	2A6	845	**Jeroen Buters**, M. Thibaudon, M. Smith, C. Galan, R. Brandao, C. Antunes, L. Grewling, A. Uruska, G. Reese, B. Weber, A. Rantio-Lehtimäki, M. Sofiev, S. Jäger, U. Berger, I. Sauliene, Albertini, L. Cecchi *Allergens from Birch, Grass and Olive in ambient air deviate from pollen counts across Europe: the EU-HIALINE project*
Reserve	2AR	330	**Maosheng Yao** *Development of a Lightweight, Simple and Efficient Exhaled Breath Condensate Collection Device and Method*

13:30-15:30 **Session 2B: New Particle Formation 1: Chamber Studies**
Room: Theatre B
Chairs: Jasper Kirkby / Joachim Curtius

13:30	2B1	853	**Siegfried Schobesberger**, Alessandro Franchin, Heikki Junninen, Mikael Ehn, Katrianne Lehtipalo, Stephanie Gagne, Tuomo Nieminen, Markku Kulmala, Douglas R. Worsnop *Measurements of ions and ion clusters in the CLOUD chamber nucleation events by mass spectrometry*
13:50	2B2	1025	**Francesco Riccobono**, Ernest Weingartner, Urs Baltensperger, CLOUD collaboration *Early stage particle growth rates during the CLOUD experiment*
14:10	2B3	701	**Sebastian Ehrhart**, Luisa Ickes, Jan Kazil, Karl D. Froyd, Edward R. Lovejoy, Joachim Curtius *Modelling of ion-induced binary nucleation in the CERN CLOUD experiment*
14:30	2B4	434	**Jens Voigtländer**, Frank Stratmann *Numerical simulation of H2SO4 cycle and new particle formation in the Cern CLOUD chamber*
14:50	2B5	716	**Linda Rondo** *Sulphuric acid measurements by CIMS at the CLOUD chamber and cross-check with independent methods to derive [H2SO4]*
15:10	2B6	767	**Alessandro Franchin** *Physical characterization of ions in the CLOUD chamber*
Reserve	2BR	517	**Einhard Kleist**, Thomas Mentel, Astrid Kiendler-Scharr, Sebastian Broch, Monika Springer, Katja Behnke, Jörg-Peter Schnitzler, Ralf Tillmann, Stefanie Andres, Florian Rubach, Bettina Steitz, Jürgen Wildt *SOA formation from stress induced biogenic VOC emissions and the contribution of isoprene to particle formation and growth – lessons learned from grey poplar trees*

13:30-15:30 **Session 2C: Instrumentation for Chemical Characterisation of Aerosol**

Room: Rutherford Lecture Theatre

Chairs: Jonathan Reid / Ari Leskinen

13:30	2C1	34	**Stefan Georg Gonser**, Andreas Held *Development of a novel aerosol mass spectrometer for nucleation mode particles*
13:50	2C2	324	**Alexander Laskin** *Molecular Characterization of Organic Compounds in Atmospheric Aerosols*
14:10	2C3	673	**Stephen Fuller**, Jenny Nutter, Stephen Platt, Lisa Pfaffenberger, Peter Barmet, Josef Dommen, Urs Baltensperger, Andre Prevot, Markus Kalberer *On-line measurements of particle bound ROS in ambient and combustion aerosols*
14:30	2C4	892	**Scott Noblitt**, Charles Henry, Jeffrey Collett, Susanne Hering, Gregory Roberts *Microchip Electrophoresis Interfaced to a Cloud Condensation Nuclei Collector for Online Monitoring of CCN Chemistry*
14:50	2C5	709	**Jose Ruiz-Jimenez** *Comprehensive GCxGC, a valuable technique for the screening and semiquantitation of different chemical compounds in ultrafine aerosol particles*
15:10	2C6	855	**Peter Mertes**, Josef Dommen, Markus Kalberer, Urs Baltensperger *A new sensitive long-path absorption spectrometer for peroxide measurements in secondary organic aerosol*
Reserve	2CR	537	**Alexander Vogel**, Aline Bayerle, Martin Beck, Mikko Äijälä, Mikael Ehn, Heikki Junninen, Tuukka Petäjä, Douglas Worsnop, Markku Kulmala, Jonathan Williams, Thorsten Hoffmann *Field measurement of secondary organic aerosol in a boreal forest site in southern Finland using on-line soft ionization ion trap mass spectrometry*

13:30-15:30 **Session 2D: Source Apportionment Studies**
Room: Moseley Lecture Theatre
Chairs: Juergen Schnelle-Kreis / Regina Hitzenberger

13:30	2D1	981	**Cozic Julie**, Piot Christine, Jean-Luc Besombes, Jean-Luc Jaffrezo and the Particulair Team *Source apportionments in a multi rural sites experiment in France (Particulair): Seasonality and regional specificities*
13:50	2D2	806	**Michael Bressi**, Jean Sciare, Veronique Ghersi, Nicolas Bonnaire, Sophie Moukhtar, Jose Nicolas, Amandine Rosso, Jean-Eudes Petit, Philippe Lameloise, Anais Feron, Malvina Artufel, Mikael Reynaud *A comprehensive study of the major sources of fine aerosols (PM2.5) in the region of Paris (France): contribution of local versus imported emissions*
14:10	2D3		**Godwin Ayoko** *Multi-criteria ranking and source apportionment of air pollutants*
14:30	2D4	501	**Matthias F.D. Gianini**, Robert Gehrig, Andrea Fischer, Adrian Wichser, Andrea Ulrich, Julie Cozic, Jean-Luc Jaffrezo, Christoph Hueglin *Chemical composition and source apportionment of PM10 at different Swiss locations 2008/2009 compared to 1998/1999.*
14:50	2D5	205	**Jürgen Schnelle-Kreis**, Jianwei Gu, Gülcin Abbaszade, Jürgen Diemer, Ralf Zimmermann *Spatial distribution of ambient particulate matter and source contributions in Augsburg, Germany*
15:10	2D6	392	**Ravindra Khaiwal**, Samantha Lawrence, Ranjeet Sokhi *Source apportionment modelling to quantify atmospheric particle emissions using tunnel measurements*

13:30-15:30 **Session 2E: Gas-phase Synthesis of Nanoparticles**
Room: Bragg Lecture Theatre
Chairs: Robert Grass / Einar Kruis

13:30	2E1	793	**Alexander Stepuk** *Flame-spray derived complex fluoride upconversion nanoparticles*
13:50	2E2	138	**Christian Mehringer**, Benjamin Butz, Erdmann Spiecker, Wolfgang Peukert *Aerosol synthesis of silicon-germanium nanostructures*
14:10	2E3	760	**Henning Förster**, Christian Wolfrum, Wolfgang Peukert *Copper nanoparticle synthesis by an arc evaporation / condensation process*
14:30	2E4	479	**Russell Saunders**, John Plane *Photochemical synthesis of olivine (Mg2xFe2-2xSiO4; 0 <x < 1) nanoparticles*
14:50	2E5	1131	**Adam Boies**, Steven Calder, Pingyan Lei, Steven Girshick *Chemical Kinetic Model of the In-Flight Silica Coating of Nanoparticles by Photo-Induced Chemical Vapour Deposition*
15:10	2E6	830	**Jan Frederik Quaatz**, Marcus Giglmaier, Nikolaus Andreas Adams *Assessment of Size Distribution Models in Coupled 3D CFD Simulations for the Prediction of Nanoparticle Coagulation in Transonic Flows*
Reserve	2ER	151	**Andrei Onischuk**, Anatoly Baklanov, Olga Borovkova, Vladimir Karasev, Stefano di Stasio, Sergey Vosel *Formation of metal nanoparticles from supersaturated vapor (Zn, Bi).*

13:30-15:30 **Session 2F: Aerosol Mobility and Capture**
Room: Blackett Lecture Theatre
Chairs: J. L. Castillo / F-X. Ouf

13:30	2F1	754	**Anastasios Melas**, Athanasios G. Konstandopoulos, Yannis Drossinos *Calculation of the mobility radius of fractal aggregates*
13:50	2F2	442	**Anne Maißer**, Vinay Premnath, Abhimanyu Gosh, Michel Attoui, Chris Hogan *Mobility measurements of electrosprayed protein ions in the sub 10 nm size range*
14:10	2F3	275	**Sarah Dunnett**, Charles Clement *Deposition on fibrous filters in the interception region*
14:30	2F4	685	**Mika Ihalainen**, Terttaliisa Lind, Salih Güntay, Jorma Jokiniemi *Break-up of agglomerated TiO2 particles due to impaction*
14:50	2F5	206	**François-Xavier OUF**, Sun Wenxin, Mourad Kessoum, Dominique Thomas, François Gensdarmes, Pierre Rolland *Characterization of nanoparticles aggregates deposits produced by filtration: influence of aggregates morphology and filtration velocity*
15:10	2F6	308	**Dagmar Koch**, Alfred P. Weber *Transfer of gas-borne carbon nanoparticles onto liquid surfaces*
Reserve	2FR	149	**Virginia Gómez**, C.H. Huang, F. Alguacil and M. Alonso, *Deposition of Nanoparticles on Wire Screens by Diffusion and Image Force*

16:00-18:00 **Session 3A: Bioaerosols / Specific Aerosol Types**
Room: Theatre A
Chairs: J. Schneider / M.R. Alfarra

16:00	3A1	612	**Noa Burshtein**, Naama Lang-Yona, Yinon Rudich *Ergosterol, arabitol and mannitol as tracers for biogenic aerosols in the eastern Mediterranean*
16:20	3A2	1126	**Michael Gatari**, Samuel Gaita, Keith Shepherd, Johan Boman, Sofia Thorsson, Annamarie Wagner *Long range transported mineral dust to the Equatorial Global Atmosphere Watch (GAW) Station on Mt Kenya*
16:40	3A3	329	**Maosheng Yao** *Real-time Detection of Airborne Influenza A Viruses Using Silicon Nanowire Field Effect Transistor*
17:00	3A4	564	**Silvia Becagli**, Rita Traversi, Costanza Ghedini, Silvia Nava, Massimo Chiari, Franco Lucarelli, Giulia Calzolai, Alcide di Sarra, Giandomenico Pace, Daniela Meloni, Damiano Massimiliano Sferlazzo, Carlo Bommarito, Francesco Monteleone, Roberto Udisti *Characterization of aerosol from ship emissions in the Central Mediterranean Sea (Lampedusa island)*
17:20	3A5	437	**Johan Friberg**, Bengt G. Martinsson, Sandra M. Andersson, Carl A. M. Brenninkmeijer, Markus Hermann, Peter P.F. van Velthoven, Andreas Zahn *Particulate Carbon and Sulfur in the Lower Stratosphere*
17:40	3A6	909	**Darius Ceburnis**, Jurgita Ovadnevaite, Russell Greaney, Cinzia Perrino, Jakub Bialek, Baerbel Langmann, Martin Hensch, Harald Berresheim, Colin O'Dowd *New insights into physical and chemical properties of volcanic ash from Eyjafjallajokull eruption during long-range transport*

16:00-18:00 **Session 3B: New Particle Formation 2: Experimental Studies**

Room: Theatre B

Chairs: Birgit Wehner / Michael Boy

16:00	3B1	498	**Imre Salma**, T. Borsos, T. Weidinger, P. Aalto, M. Dal Maso, M. Kulmala *Relationship between new particle formation and pollutant gases in an urban environment*
16:20	3B2	375	**Jovana-Maria Diesch**, Frank Drewnick, Vinayak Sinha, Jonathan Williams, Stephan Borrmann *Influence of key aerosol, trace gas and meteorological parameters on new particle formation in Southern Spain*
16:40	3B3	918	**Michael Pikridas**, I. Riipinen, L. Hildebrandt, E. Kostenidou, H. Manninen, N. Mihalopoulos, N. Kalivitis, J. F. Bukhart, A. Stohl, M. Kulmala, S. Pandis *New particle formation at a remote marine site in the Eastern Mediterranean*
17:00	3B4	455	**Karine Sellegri** *First observations of nucleation of new particles in a volcanic plume*
17:20	3B5	967	**Miikka Dal Maso**, Thomas Mentel, Astrid Kiendler-Scharr, Einhard Kleist, Ralf Tillmann, Mikko Sipilä, Tuukka Petäjä, Jani Hakala, Li Liao, Katrianne Lehtipalo, Heikki Junninen, Mikael Ehn, Joonas Vanhanen, Jyri Mikkilä, Markku Kulmala, Jurgen Wildt, Douglas Worsnop *Nanoparticle formation from sulphuric acid and BVOC oxidation at atmospheric concentrations*
17:40	3B6	280	**Boris Bonn**, Stratos Bourtsoukidis, Boris Bonn, Werner Haunold, Evan Palmer-Young, Jonathan Gershenzon *New particle formation by tobacco plants stressed by ozone: The potential role of mono- and sesquiterpenes*
Reserve	3BR	517	**Einhard Kleist**, Thomas Mentel, Astrid Kiendler-Scharr, Sebastian Broch, Monika Springer, Katja

			Behnke, Jörg-Peter Schnitzler, Ralf Tillmann, Stefanie Andres, Florian Rubach, Bettina Steitz, Jürgen Wildt *SOA formation from stress induced biogenic VOC emissions and the contribution of isoprene to particle formation and growth – lessons learned from grey poplar trees*

16:00-18:00 **Session 3C: Chemical Mechanisms and Transformation Processes in Aerosol**
Room: Rutherford Lecture Theatre
Chairs: Barbara Noziere / Andreas Tilgner

16:00	3C1	692	**Jonathan Reid**, Ben J. Dennis-Smither, Rachael E.H. Miles, Nana-O.A. Kwamena *Evolving morphology, hygroscopicity and volatility of mixed oleic acid/sodium chloride/aqueous aerosol during oxidative aging*
16:20	3C2	858	**Christian Pfrang**, Manabu Shiraiwa, Uli Pöschl *Ozonolysis of oleic acid: mixed systems, oligomerisation and phase changes.*
16:40	3C3	982	**Slowik Jay** *Real-time, controlled OH-initiated oxidation of biogenic secondary organic aerosol*
17:00	3C4	209	**Manabu Shiraiwa**, Yulia Sosedova, Aurélie Rouvière, Hong Yang, Yingyi Zhang, Jonathan P. D. Abbatt, Markus Ammann, Ulrich Pöschl *Long-lived reactive oxygen intermediates in the reaction of ozone with aerosol particles and aerosol health effects*
17:20	3C5	319	**Will Morgan**, James Allan, Michael Le Breton, Jennifer Muller, Carl Percival, Hugh Coe *The power of the dark side: Night-time measurements of aerosol chemical composition in North-Western Europe*
17:40	3C6	135	**Douglas Lowe**, Steven Utembe, David Topping, Gordon McFiggans

			Predictions of Night-time Atmospheric Processes using a Coupled Model of Multi-phase Chemistry and Aerosol Microphysics
Reserve	3CR	185	**Asit Ray**, Venkat Rajagopalan, Eric A. Grulke *Phase transformation of evaporating solution droplets of immiscible polymers*

16:00-18:00 **Session 3D: PMx Data Interpretation**
Room: Moseley Lecture Theatre
Chair: Andre Prevot

16:00	3D1	953	**Robert Wolf**, Claudia Mohr, Monica Crippa, Jay Slowik, André S.H. Prévôt, Urs Baltensperger *Mobile measurements of submicron particulate matter in Central Europe during wintertime inversions*
16:20	3D2	388	**Dominik van Pinxteren** *A GIS based approach to combine back trajectory statistics and land cover analysis for the source apportionment of aerosol constituents*
16:40	3D3	730	**Alessandro Di Menno di Bucchianico**, Giorgio Cattani, Alessandra Gaeta, Giuseppe Gandolfo, Anna Maria Caricchia *To exceed, or not to exceed: are the air quality standards adequate to describe the particulate matter pollution?*
17:00	3D4	601	**Francesco Canonaco**, Jay Slowik, Andre Prévôt, Urs Baltensperger *Long-term on-line measurement of non-refractory submicron aerosol in the city of Zurich*
17:20	3D5	833	**Ernie Weijers**, Martijn Schaap, Lan Nguyen, Jan Matthijsen, Hugo Denier van der Gon, Harry ten Brink, Ronald Hoogerbrugge *Anthropogenic and natural constituents in particulate matter in the Netherlands*

17:40	3D6	463	**Andre Prevot**, Iakovos Barmpadimos, Miriam Nufer, Daniel Oderbolz, Johannes Keller, Sebnem Aksoyoglu-Sloan, Christoph Hueglin *The weekly cycle of ambient concentrations and traffic emissions of coarse (PM10-PM2.5) atmospheric particles*
Reserve	3DR	606	**Tareq Hussein**, Rasha Abu Al-Ruz, Tuukka Petäjä, Heikki Junninen, Dia-Eddin Arafah, Kaarle Hämeri, Markku Kulmala *Local air pollution versus short–range transported dust episodes: a comparative study for submicron particle number concentration*

16:00-18:00 **Session 3E: Aerosol-based Nanotechnology Fundamentals**

Room: Bragg Lecture Theatre

Chairs: Heinz Fissan / Alfred Weber

16:00	3E1	298	**Anna Lähde**, Noora Kokkonen, Antti Karttunen, Sirpa Jääskeläinen, Unto Tapper, Tapani Pakkanen, Jorma Jokiniemi *Chemical vapor synthesis of Cu-Si/SiO2 nanoparticles*
16:20	3E2	220	**Albert Nasibulin**, Marina Timmermans, Antti O. Kaskela, Kimmo Mustonen, Toma Susi, Virginia Ruiz, Simas Rackauskas, Ying Tian, Ilya V. Anoshkin, Sergey D. Shandakov, Esko I. Kauppinen *Applications of single-walled carbon nanotubes synthesised by aerosol CVD method*
16:40	3E3	470	**Scot Martin**, Mikinori Kuwata, Qi Chen *Cloud condensation nuclei (CCN) activity and oxygen-to-carbon elemental ratios following thermodenuder treatment of organic particles grown by α-pinene ozonolysis*
17:00	3E4	101	**Andrei Onischuk**, Sergey Vosel, Peter Purtov *Surface tension of nanosized drops of mono- and bivalent metals*

17:20	3E5	407	**Michel ATTOUI**, M. Chen , P. H. McMurry *Study of Heterogeneous Nucleation upon Nanoparticles in Condensation Particle Counters (CPCs): Effects of Particle and Vapor Composition*
17:40	3E6	354	**Silvan Schmid**, Tom Larsen, Anja Boisen *Particle mass spectrometry based on micro string resonators for the application in portable aerosol monitors*
Reserve	3ER	159	**Bon Ki Ku**, Gregory Deye and Leonid A. Turkevich *Characterizing lengths and aerodynamic diameters of airborne glass fibers*

16:00-18:00 **Session 3F: Thermal and Optical Effects**
Room: Blackett Lecture Theatre
Chairs: P. L. Garcia-Ybarra / David Bones

16:00	3F1	430	**Rory Power**, Jim Walker, Antonia Carruthers, Jonathan Reid *Using holographic optical landscapes to manipulate aerosol arrays, compare particle hygroscopicity and study aerosol coagulation*
16:20	3F2	935	**Manuel Arias-Zugasti**, Daniel E. Rosner *Impact of Temperature Gradients on Brownian Coagulation*
16:40	3F3	975	**Alexander Cheremisin**, Kushnarenko Andrei *Photophoretic interaction of aerosol particles in rarefied gas medium*
17:00	3F4	83	**Konstantin Volkov**, Vladislav Emelyanov *Optical breakdown and detonation in aerosol systems*
17:20	3F5	231	**Edouard Brugiere**, François Gensdarmes, François-Xavier Ouf, Jérôme Yon, Alexis Coppalle *Thermophoresis of non-spherical particle: experimental prospect on soot particles*
17:40	3F6	250	**Yi-Hung Liu**, Graham Calvert, Colin Hare, Mojtaba Ghadiri, Shuji Matsusaka

			Size measurement of dry ice particles in a jet flow using laser diffraction method

Notes:

Tuesday 6th September

09:00-10:00 Plenary 2

Wendelin Stark: *Aerosols for materials: medical and industrial applications and the role of nanotoxicology.*

Room: Theatre B

Chair: John McAughey

10:30-12:00 Session 4P: Poster Session A

Room: Poster Marquee and adjacent to Theatre B

Aerosol Chemistry			
4P1	148	Smog chamber experiments	**Pavel Mikuska**, Martin Vojtesek, Zbynek Vecera, Kamil Krumal, *Semi-continuous system for analysis of water-soluble fraction of metals in atmospheric aerosols*
4P2	358	Smog chamber experiments	**Urmas Hõrrak**, Aare Luts, Tiia-Ene Parts, *Gaseous iodine as a substantial cause of new specific air ions*
4P3	373	Smog chamber experiments	**Zhijun Wu**, L. Poulain, O. Böge, R. Gräfe, H. Herrmann, A. Wiedensohler, Helbig, T. Schröder, J. von Sonntag, I. Hartmann, *Modifications in hygroscopicity and volatility of wood combustion aerosols after chemical aging*.
4P4	421	Smog chamber experiments	**Mijung Song**, Claudia Marcolli, Ulrich K. Krieger, Thomas Peter *Morphology and phase transitions of internally mixed dicarboxylic acids/ammonium sulfate/water particles during hygroscopic cycles*
4P5	487	Smog chamber experiments	**Mukesh Sharma**, Sailesh N. Behera, *Influence of Existing Particle Surfaces on Formation of Secondary Inorganic Aerosols in Fine Mode*
4P7	706	Smog chamber experiments	**Jose Ruiz-Jimenez,** *Influence of the sampling site, the season of the year, the particle size and the number of nucleation events on the chemical composition of atmospheric ultrafine particles*.

4P8	713	Smog chamber experiments	**Jose Ruiz-Jimenez**, *Elucidation of organic volatile compounds in Antarctic aerosol particles. Influence of the nucleation events on the chemical composition of the particles*.
4P9	747	Smog chamber experiments	**Mikael Ehn,** *Ion studies of organic precursor molecules for secondary particle formation*.
4P10	847	Smog chamber experiments	**Mathias Barthel**, S. Seeger, O. Hahn, O. Wilke, W. Horn and O. Jann, *Quantitative and qualitative characterisation of ultrafine particles emitted by laser printing devices*.
4P11	952	Smog chamber experiments	**Ravi Kant Pathak**, K. Salo, T. F. Mentel, R. Tillmann, E.U. Emanuelsson, A. Lutz,M. Hallquist, *Effect of reaction temperature on the volatility of limonene ozonolysis products*.
4P12	1130	Secondary Organic Aerosol - SOA	**Ioan Hoare**, David Stewart, Gemma Brittan, Andrew Russell, Sami Al Mabrok, Marianna Ghosh, Christian Pfrang, George Marston, *The Formation of Secondary Organic Aerosol from Intermediates in the Ozonolysis of α-pinene*.
4P13	1002	Secondary Organic Aerosol - SOA	**Eleni Athanasopoulou**, Heike Vogel, Max Bangert, Christoph Knote, Bernhard Vogel, Ben Murphy, Alexandra Tsimpidi, Spyros Pandis, *Simulating secondary organic aerosol (SOA) formation over Europe using the volatility basis-set approach (VBS) in the online coupled model COSMO-ART*.
4P14	946	Secondary Organic Aerosol - SOA	**Teresa Raventos-Duran**, Marie Camredon, Richard Valorso, Camille Mouchel-Vallon, Sasha Madronich, Julia Lee-Taylor, Bernard Aumont, *Modelling SOA formation from Anthropogenic VOCs using an explicit chemical mechanism*.
4P15	894	Secondary Organic Aerosol - SOA	**Harald Saathoff**, Karl-Heinz Naumann, Ottmar Möhler, Neil Donahue, Thomas Mentel, Ralf Tillmann, Thomas Leisner, *Reaction of OH radicals with secondary organic aerosol from the ozonolysis of alpha-pinene*.

4P16	746	Secondary Organic Aerosol - SOA	**Sergei Dubtsov**, Galina Dultseva, *Gas-to-particle conversion in biogenic aromatic aldehydes and their complexes with heavy metals: a contribution into the biogeochemical cycles of elements*.
4P17	745	Secondary Organic Aerosol - SOA	**Tatyana Maksimova**, Sergei Dubtsov, Galina Dultseva, *Evaluation of the atmospheric aerosol-forming potential of aliphatic and aromatic aldehydes in the presence of nitrogen oxides and/or ozone: modelling and experiment*.
4P18	672	Secondary Organic Aerosol - SOA	**Claudia Keunecke**, Thomas Zeuch, *Observation of decreased final product volatility in the gas ozonolysis of unsaturated carboxylic acids in the absence of oxygen*.
4P19	537	Secondary Organic Aerosol - SOA	**Alexander Vogel**, Aline Bayerle, Martin Beck, Mikko Äijälä, Mikael Ehn, Heikki Junninen, Tuukka Petäjä, Douglas Worsnop, Markku Kulmala, Jonathan Williams, Thorsten Hoffmann, *Field measurement of secondary organic aerosol in a boreal forest site in southern Finland using on-line soft ionization ion trap mass spectrometry*.
4P20	282	Secondary Organic Aerosol - SOA	**Boris Bonn**, Friedemann Ebach, Matthias Hummel, Stratos Bourtsoukidis, Boris Bonn, Werner Haunold, Robert Sitals, *Understanding particle formation by alkene-ozone reactions: Experimental studies and theoretical simulations*.
4P21	359	Monoterpene and isoprene SOA chemistry	**Anke Mutzel**, Yoshiteru Iinuma, Olaf Böge, Ariane Kahnt, Hartmut Herrmann, *Oxidation of nopinone - Influence of relative humidity and particle acidity on particulate products*.
4P22	277	Secondary Organic Aerosol - SOA	**Marco Paglione**, Emanuela Finessi, Stefano Decesari, Astrid Kiendler-scharr, Amewu Mensah, Matteo Stocchero, MariaCristina Facchini, *NMR spectroscopic characterization and factor analysis of the oxidized organic*

			aerosol components in Cabauw, Netherlands, during the May 2008 EUCAARI IOP.
4P23	1015	Molecular characterization of aerosol constituents	**Silvia De Pieri**, Joan Coppola, Elisa Morabito, Carlo Barbante, Andrea Gambaro, *Determination of organic compounds in ultrafine particles*.
4P24	803	Molecular characterization of aerosol constituents	**Ehgere Abidi**, Nicolas Marchand, Anne Monod, Julie Cozic, Jean-Luc Jaffrezo, *Wintertime and summertime source apportionment of PM2.5, using organic compounds as tracers, in a European megacity : Paris*.
4P25	761	Molecular characterization of aerosol constituents	**Roberta Zangrando**, Elena Barbaro, Elisa Scalabrin, Valentina Fellin, Carlo Barbante and Andrea Gambaro, *Microcystins and Bisphenol A in the urban aerosol of the Venice Lagoon*.
4P26	57	Molecular characterization of aerosol constituents	**Celia Alves**, Cátia Gonçalves, Ana Patrícia Fernandes, Luís Tarelho, Casimiro Pio, *PM2.5 emissions from wood combustion in a fireplace and a woodstove: carbon content and inorganic speciation*.
Fundamentals			
4P27	159	General physical properties of aerosols	**Bon Ki Ku**, Gregory Deye, Leonid A. Turkevich, *Characterizing lengths and aerodynamic diameters of airborne glass fibers*
4P28	341	General physical properties of aerosols	**Delphine Lottin**, Daniel Ferry, Jean-Marc Gay, David Delhaye, Jérôme Yon, François-Xavier Ouf, *On methods determining the fractal dimension of combustion aerosols and particle clusters*.
4P30	589	General physical properties of aerosols	**Thaseem Thajudeen**, Christopher J Hogan Jr, *Computationally efficient methods for computing the free molecular and continuum friction factors of non spherical aerosol particles*.

4P31	640	General physical properties of aerosols	**Gerhard Steiner**, Tuija Jokinen, Heikki Junninen, Mikko Sipilä, Georg P. Reischl, Doug R. Worsnop, Markku Kulmala, *Simultaneous Mobility and Mass Determination of Ionic Molecular Clusters produced in a bipolar 241Am Charger*.
4P32	605	Optical properties	**Vladimir Maksimenko**, Vladimir Ignatov, *Optical cloaking and agglomerated fractal clusters*.
4P33	90	Aerosol interaction with surfaces	**Russell Lyons**, *Non conventional indoor model for submicron particulates*.
4P34	33	Heat and mass transfer theory and experiments	**Leonie Brachert**, Sokratis Sinanis, Karlheinz Schaber, *Characterization of sulphuric acid aerosols in industrial processes*.
4P35	323	Heat and mass transfer theory and experiments	**Jarmo Kalilainen**, Terttaliisa Lind, Pekka Rantanen, Ari Auvinen, Abdel Dehbi, Salih Guntay, Jorma Jokiniemi, *Experimental work on particle motion inside a differentially heated cavity*.
4P36	122	Aerosol dynamics	**Peter Vainshtein**, Michael Shapiro, *Agglomerate drag in continuum and rarefied flow regimes*.
4P37	127	Aerosol dynamics	**Damir Gubaidullin**, Rinat Zaripov, Aleksey Tukmakov, Ludmila Tkachenko, *Nonlinear oscillations and deposition of aerosol in tubes*.
4P38	250	Aerosol dynamics	**Yi-Hung Liu**, Graham Calvert, Colin Hare, Mojtaba Ghadiri, Shuji Matsusaka, *Size measurement of dry ice particles in a jet flow using laser diffraction method*.
4P39	381	Aerosol dynamics	**Alexander Girin**, *Dynamic structure of two-phase polydisperse spray in wake of a shattering drop*.
4P40	382	Aerosol dynamics	**Alexander Girin**, *Equations of kinetic of drop shattering in a speedy uniform flow*.
4P41	668	Aerosol dynamics	**Max Eggersdorfer**, Dirk Kadau, Hans J. Herrmann, Sotiris E. Pratsinis, *Multi-Particle Sintering Dynamics: From Fractal-like*

			Aggregates to Compact Structures.
Aerosol Chemistry			
4P42	546	Monoterpene and isoprene SOA chemistry	**Yoshiteru Iinuma**, Ariane Kahnt, Anke Mutzel, Olaf Boege, Hartmut Herrmann, *SOA formation from campholenic aldehyde ozonolysis*.
4P43	620	Monoterpene and isoprene SOA chemistry	**Anna van Eijck**, Domenico Taraborrelli, Rolf Sander, Thorsten Hoffmann, *Atmospheric degradation of β-caryophyllene: laboratory and field studies*.
Fundamentals			
4P44	149	Aerosol filtration	**Virginia Gómez**, C.H. Huang, F.J.Alguacil and M. Alonso, *Deposition of Nanoparticles on Wire Screens by Diffusion and Image Force*.
4P45	198	Aerosol filtration	**Young-Ok Park**, Naim Hasolli, *Depth filtration performance characteristics in accordance with the filter layer structure*.
4P46	274	Aerosol filtration	**Franco Belosi**, Gianni Santachiara, Franco Prodi, Kristin Syverud, *Nanofibril filters for environmental nanoparticles*.
4P47	299	Aerosol filtration	**Sascha Schiller**, Hans-Joachim Schmid, *Development of a fine particle filter for domestic wood-fired heaters*.
4P48	483	Aerosol filtration	**Andrey Grishin**, Ivan Yagodkin, Petr Martynov, Andrey Posagennikov, Valerii Melnikov, *Development of the Electro-physical Method of Aero-ion Cleaning of Gaseous Atmosphere*.
4P49	539	Aerosol filtration	**Tomasz Jankowski**, *Filtration of oil mists and dust - machining and grinding operations*.
4P50	563	Aerosol filtration	**Nikolaus Koch**, Anne Maißer, Ania Jackiewicz, Albert Podgorski, Wladek Szymanski, Leon Gradon, *Penetration of sub 30 nm particles through mechanical and electret fibrous filters*.
4P51	753	Aerosol filtration	**Seyoung Kim**, *Collection efficiency of axial-flow cyclone for air handling unit of subway station*.

4P52	60	Nucleation theory and experiments	**Stefano di Stasio**, Andrey Onischuk, Anatoly Baklanov, Vladimir Karasev, *Experimental Study on Transition from Bismuth Saturated Vapors to Liquid Nuclei*.
4P53	93	Nucleation theory and experiments	**Sergey Vosel**, Andrei Onischuk, Peter Purtov, *Translation-Rotation Correction Factor in the Theory of Homogeneous Nucleation*.
4P54	456	Nucleation theory and experiments	**David Brus**, Kimmo Neitola, Tuukka Petäjä, Heikki Lihavainen, *Diffusion coefficient measurements of sulphuric acid in air*.
4P55	562	Nucleation theory and experiments	**Valeri Levdansky**, Jiri Smolik, Vladimir Zdimal, Pavel Moravec, *Size effect in homogeneous nucleation in nanoscale particles*.
4P56	671	Nucleation theory and experiments	**Ville Loukonen**, Hanna Vehkamäki, *Contact angle, seed particle radius and the onset of heterogeneous nucleation*.
4P57	728	Nucleation theory and experiments	**Agnieszka Kupc**, Aron Vrtala, Paul E. Wagner, Paul M. Winkler, CLOUD Collaboration, *Heterogeneous nucleation of water vapor on nanoparticles and ions, and its temperature dependence*.
4P58	804	Nucleation theory and experiments	**Kimmo Neitola**, David Brus, Mikko Sipilä, Tuija Jokinen, Pauli Paasonen, Heikki Lihavainen, *Influence of trimethylamine to sulphuric acid-water homogeneous nucleation*.
4P59	921	Nucleation theory and experiments	**Jussi Malila**, Kari Lehtinen, Ismo Napari, Robert McGraw, Ari Laaksonen, *Coagulation scavenging of precritical clusters and the first nucleation theorem*.
4P60	1014	Nucleation theory and experiments	**Vladimir Chernyak**, *Light-induced drift of aerosol particle*.
4P61	1054	Nucleation theory and experiments	**Athanasios Mamakos**, Yannis Drossinos, *Particle activation via heterogeneous nucleation in n-butanol condensation particle counters*.
4P62	1154	Nucleation theory and experiments	**Jake Stinson**, Ian Ford, *Is quantum nuclear dynamics significant in the study of the structure of sulphuric acid hydrates?*

Bioaerosols			
4P63	616	Bioaerosols	**Jaehee Jung** *Real-time Detection of Bacterial Bioaerosols Using the Aerosol Fluorescence Sensor with Dual Channels of UV- and Vis-band*
PMx			
4P64	953	Source apportionment	**Robert Wolf**, Claudia Mohr, Monica Crippa, Jay Slowik, André S.H. Prévôt, Urs Baltensperger, *Mobile measurements of submicron particulate matter in Central Europe during wintertime inversions*.
4P65	735	Source apportionment	**Aki Kortelainen**, *Exploring aerosol chemical composition in the Finnish boreal forest in late-spring by Aerosol Mass Spectrometry.*
4P66	164	Source apportionment	**Daniela Cesari**, Fulvio Amato, Marco Pandolfi, Daniele Contini, Andres Alastuey, Xavier Querol, *Comparison of PM10 source apportionment using PMF and PCA: an analysis of accuracy and robustness of results*.
4P68	53	Other	**Milan Vana**, Jaroslava Svobodova, Tomas Fory, Marek Hladik, Zdenek Roubal, Jan Hadinger, *Aircraft measurement of PM vertical profile above the Czech EMEP stations during EMEP-EUSAAR-EUCAARI intensive campaign.*
4P69	1101	Other	**Goeran Blomqvist**, Mats Gustafsson, Cecilia Bennet, Tomas Halldin, *PM10 suspension of road dust is depending on the road surface macro texture*.
4P70	1038	Legislation and policy	**Konstantinos Eleftheriadis**, Evangelia Diapouli, Constantini Samara, Athanassios Kungolos, Athina Proyou, Mihalis Lazaridis, *Development of a Cost Efficient Policy Tool for reduction of Particulate Matter in Air*.
4P71	161	Physico-chemical analysis	**Giorgia Sangiorgi**, Luca Ferrero, Maria Grazia Perrone, Ezio Bolzacchini, *PM2.5, PM1 and PM0.4 acidity during spring and summer at*

			one Po Valley site.
4P72	186	Physico-chemical analysis	**Maria Rita Perrone**, Adelaide Dinoi, Silvia Becagli, Roberto Udisti, *PM2.5 and PM1 particles over south-eastern Italy: seasonal trend of levels and composition*.
4P73	290	Physico-chemical analysis	**Bohumil Kotlik**, Radek Zboril, Ales Kapicka, Miroslav Roxer, *Magnetic properties of PM10 collected at industrial and urban sites during heating and non-heating seasons*.
4P74	777	Physico-chemical analysis	**Wen-Yinn Lin**, Y.L. Yan, C.C. Chen, C.T. Chang, C.Y. Lai, Y.L. Wu, C.Y. Young, *Evaluating the Effects of Aeolian Dust from Jhuoshuei River on the Air Quality*.
4P75	819	Physico-chemical analysis	**Pietrogrande Maria Chiara**, G. Abbaszade, J. Schnelle-Kreis, D. Bacco, R. Zimmermann, *Seasonal variation and source estimation of organic compounds in urban aerosol of Augsburg, Germany.*
4P76	963	Physico-chemical analysis	**Alexandre Caseiro**, Fátima Mirante, Célia Alves, Casimiro Pio, Begoña Artíñano, *Size-segregated chemical characterization of PM at two sites in the city of Madrid*.
4P77	1049	Physico-chemical analysis	**Doerthe Mueller-Ebert**, Martin Ebert, Stephan Weinbruch, *Characterization of Aerosol Particles around an Open pit coal mine in Germany by electronmicroscopic individual particle analysis*.
4P78	1077	Physico-chemical analysis	**Silvia Canepari**, Cinzia Perrino, Stefano Materazzi, Elisabetta Marconi, Carmela Farao, Luca Tofful, Simonetta De Angelis Curtis, *Thermal behaviour of water and inorganic ions in particulate matter*.
4P79	1084	Physico-chemical analysis	**Eduardo Yubero**, Jose Nicolás, Javier Crespo, Milagros Santacatalina, Adoración Carratalá, Massimo Chiari, Silvia Nava, Franco Lucarelli, *Identification and characterization of fine and coarse particulate matter by means of an hourly sampler*.

4P80	1108	Physico-chemical analysis	**Maria Catrambone**, *Determination of Cr(III) and Cr(VI) in atmospheric particulate samples*.
4P81	242	Interpretation of data	**Chien-Lung Chen**, Chien-Hua Chen, Feng-Chao Chung, Su-Ching Kuo, Li-Ying Hsieh and Ying I. Tsai, *Characteristics of fine and coarse aerosol compositions in central Taiwan*.
4P82	317	Interpretation of data	**Alessia Di Gilio**, Martino Amodio, Eleonora Andriani, Paolo Rosario Dambruoso, Gianluigi De Gennaro, Miriam Intini, Jolanda Palmisani, Maria Tutino, *Fugitive Emissions*.
4P83	320	Interpretation of data	**Eduardo Yubero**, Nuria Galindo, Juan Gil-Moltó, Carolina Chofre, *Size distribution of atmospheric aerosols and associated ion species on the western Mediterranean*.
4P84	385	Interpretation of data	**Libor Hejkrlik**, Helena Placha, *Routine monitoring of coronene in the Czech Republic*.
4P85	425	Interpretation of data	**Stefania Squizzato**, Mauro Masiol, Elena Innocente, Eliana Pecorari, Flavia Visin, Giancarlo Rampazzo, Bruno Pavoni, *PM 2.5 and Water Soluble Inorganic Ions in the Venice area*.
4P86	496	Interpretation of data	**Mauro Masiol**, Angelika Hofer, Elena Centanni, Federico Fiorotto, Stefania Squizzato, Eliana Pecorari, Giancarlo Rampazzo, Bruno Pavoni, *Impacts of local atmospheric circulation on PM2.5-bound Polycyclic Aromatic Hydrocarbons in three different emission scenarios in Venice-Mestre (Italy)*.
4P87	497	Interpretation of data	**Mauro Masiol**, Stefania Squizzato, Eliana Pecorari, Elena Centanni, Elena Innocente, Giancarlo Rampazzo, Bruno Pavoni, *Characterization of PM2.5 chemical composition in Venice (Italy) and their relation with the regional-scale movement of the air masses*.
4P88	726	Interpretation of data	**Edvinas Krugly**, Tadas Prasauskas, Linas Kliucininkas, Dainius Martuzevicius,

			Qualitative Source Identification of PAHs Using Diagnostic Compounds.
4P89	766	Interpretation of data	**Janusz Jaroslawski**, Aleksander Pietruczuk, Izabela Pawlak, *Variability of PM10 concentrations at different types of locations in central Poland, 2007-2010*.
4P90	908	Interpretation of data	**Roland O'Donoghue**, Roy Harrison, *Source apportionment of trace metals in atmospheric aerosols in the United Kingdom*.
4P91	934	Interpretation of data	**Miguel A. Barrero**, Berasaluce A., Cantón L., *Estimation of PM10 local sources contribution to background levels in an area of the Basque Country*.
4P93	65	Sampling	**Quitterie Brossard**, *Bioaerosols & air quality testing with an innovative microbial air sampler*.
4P94	123	Sampling	**Mihalis Lazaridis**, *Variability of physico-chemical aerosol properties in the Eastern Mediterranean*.
4P95	146	Sampling	**Jordy Vercauteren**, Christine Matheeussen, Edward Roekens, Reinhilde Vermeylen, Willy Maenhaut, Magda Claeys, *CHEMKAR PM10 'wood burning' A year-long chemical characterization of PM10 in Flanders (Belgium) with a focus on the contribution of wood burning*.
4P96	328	Sampling	**Theodoros Tzamkiozis**, Leon Ntziachristos, Erkki Lamminen, Ville Niemelä, Zissis Samaras, *A new integrated device for on-board particle measurements: Sampling system*.
4P97	397	Sampling	**Minkyun Kim**, *Chemical composition of PM1.0, PM2.5 and PM10 in the industrial city in Korea*.
4P98	468	Sampling	**Benjamin Fahlbusch**, Gerald Spindler, Achim Grüner, Markus Wallasch, Hartmut Herrmann, *Chemical characterization of PM10 and trace gas measurements with the online-system MARGA at the research station Melpitz in Germany*.

4P99	519	Sampling	**David Walters**, Y.A Sevcenco, R. Marsh, A.P. Crayford, P. Bowen, *Evaluation of Paticulate Matter Line Losses From Simulated Aircraft Exhaust for Different Residence Times and Dilution Conditions*.
4P100	606	Sampling	**Tareq Hussein**, Rasha Abu Al-Ruz, Tuukka Petäjä, Heikki Junninen, Dia-Eddin Arafah, Kaarle Hämeri, Markku Kulmala, *Local air pollution versus short–range transported dust episodes: a comparative study for submicron particle number concentration*.
4P101	721	Sampling	**Maria Gini**, S. Vratolis, E. Diapouli, V. Vasilatou, S. Zero, C. Potiriadis, L. Samek,J. Huremovic, V. Vuletic, K. Sega, M.C. Freitas, R. Radic, A. Misurovic, N. Civici, A. Adamopoulos, A. Chaloulakou,H. Papaefthymiou, T. Maggos, A. Rodriguez, A. Markowicz, K. Elefthe, *Intercomparison exercise for ambient mass concentration measurement of atmospheric particulate matter by gravimetric samplers*.
4P102	884	Sampling	**Francesca Pieri**, Alessandra Cincinelli, Martina Giannoni, Tania Martellini, Silvia Becagli, Robeto Udisti, Massimo Chiari, Franco Lucarelli, Silvia Nava, Luciano Lepri, *The organic fraction of PM2.5: results from 1-year sampling campaign in Tuscany (Italy)*.
4P103	997	Sampling	**Godwin Ayoko**, *Sources of particulate matter and gaseous pollutants at some suburban sites in South East Queensland, Australia*.
4P104	1062	Sampling	**Cinzia Perrino**, Silvia Canepari, Maria Catrambone, Stefano DallaTorre, Elena Rantica, Tiziana Sargolini, *Different performance of Teflon and quartz fibre filters in collecting atmospheric PM*.
4P106	264	Health effects	**Barbara Elisabetta Daresta**, Gianluigi de Gennaro, Massimo Trotta, *Atmospheric PM10. Effects of Polycyclic Aromatic Hydrocarbons and organic extracts on Rhodobacter sphaeroids*.

4P107	645	Health effects	**SungChul Seo**, Mina Kim, Seungil Lee, Youngmin Cho, Kyonghee Kim, and Jaewook Choi, *Characterization of Hazardous Materials Released from a Laser Printer with a New and a Refilled Toner Cartridge*.
4P108	704	Health effects	**Freidhelm Schneider**, Markus Pesch, *New Software for simultaneous real time determination of particle number distribution and mass fractions with laser aerosol spectrometer*.
4P109	786	Health effects	**Maria Grazia Perrone**, Luca Ferrero, Marzo Moscatelli, Alessandro Orro, Giorgia Sangiorgi, Pasqualina D'Ursi, Luciano Milanesi, Ezio Bolzacchini, *A methodological approach to quantify health hazard from PM2.5 pollution levels in the Northern Italy*.
4P110	1139	Health effects	**Yu-Feng Kuo**, *Cytotoxicity of fly ashes with various inorganic components emitted from a municipal solid waste incinerator*.
Aerosol-based Nanotechnology			
4P111	110	Health effects and environmental impact of engineered nanoparticles	**Andrea Tiwari**, Erin Davis, Yafen Zhang, John Morris, Linsey Marr, *Oxidation of C60 aerosol by ozone*.
4P112	152	Health effects and environmental impact of engineered nanoparticles	**Virginia Gómez**, Silvia Irusta, Francisco Balas and Jesús Santamaría, *Rare earth labelling of TiO2 engineered nanoparticles for identification of aerosols in occupational environments*.
4P113	218	Health effects and environmental impact of engineered nanoparticles	**Jussi Lyyränen**, Merja Järvelä, Timo Tuomi, Joe Pimenoff, Ari Auvinen, Jorma Jokiniemi, *Characterisation of CeO2 engineered nanoparticles from a liquid flame spray process – exposure of workers*.

4P114	679	Structuring of engineered nanoparticles	**Naoki Nishida**, Akira Miyashita, Hideki Tanaka, *Synthesis of copper nanoparticles by photochemical process*.
4P117	831	Application of engineered nanoparticles	**Igor Agranovski**, *Multiplex real time bioaerosol detection*.
4P118	800	Application of engineered nanoparticles	**Valery Zagaynov**, D.V.Vodyanek, Yu.G.Biryukov, A.A. Lushnikov, I.E. Agranovski, S.F.Timashev, *Development of atmospheric aerosol data by flicker noise spectroscopy method*.
4P119	193	Application of engineered nanoparticles	**Shui-Jen Chen**, Jen-Hsiung Tsai, Kuo-Lin Huang, Chun-Li Chou, Wu-Jou Yu, *Size distributions of particle-bound polycyclic aromatic hydrocarbons emitted from a diesel generator fueled with waste-edible-oil biodiesel blends*.
4P120	142	Application of engineered nanoparticles	**Chang-Mao Hung**, *Platinum-based nanoparticles supported on cordierite as high active materials for catalytic ammonia decomposition*.
4P121	273	Engineered nanoparticle release from nanostructured materials into the air	**Ulrika Backman**, Jussi Lyyränen, Jouni Hokkinen, Ari Auvinen, Jorma Jokiniemi, *Aerosol emissions from nanotechnology-based products at end-of-life*.
4P122	150	Charged nanoparticles and deposition	**Virginia Gómez**, C.H. Huang, J.P. Borra, F.J. Alguacil and M. Alonso, *Effect of Image Force on Penetration of Nanoparticles through a Laminar Flow Tube*.
4P123	785	Charged nanoparticles and deposition	**Jose L Castillo**, Santiago Martin, Pedro L Garcia-Ybarra, *Morphology of catalyst layers deposited by electrospray*.
4P124	372	Fundamentals and measurement of	**Fedor Dultsev**, *Measurement of particle size distribution in the gas phase. QCM-based procedure*.

		nanoparticles	
4P125	470	Fundamentals and measurement of nanoparticles	**Scot Martin**, Mikinori Kuwata, Qi Chen, *Cloud condensation nuclei (CCN) activity and oxygen-to-carbon elemental ratios following thermodenuder treatment of organic particles grown by α-pinene ozonolysis*.
4P126	493	Fundamentals and measurement of nanoparticles	**Fissan Heinz**, Kaminski Heinz; Pui David; Liu Zhun; Wang Jing, *Characterization of Agglomerates and Aggregates in Gases along the Exposure Pathway*.
4P127	614	Fundamentals and measurement of nanoparticles	**Michel Attoui**, *Performance evaluation of the Airmodus PSM (nano CPC) in the sub 3 nm range.*
4P128	715	Fundamentals and measurement of nanoparticles	**Daisuke Sugiura**, Naoki Nishida, Hideki Tanaka, *Heating process of silver nanoparticles diameter-selected by DMA*.
4P129	111	Gas phase synthesis of nanoparticles	**Georgios Sotiriou**, *Color tunable nanophosphors made by flame aerosol synthesis*.
4P130	151	Gas phase synthesis of nanoparticles	**Andrei Onischuk**, Anatoly Baklanov, Olga Borovkova, Vladimir Karasev, Stefano di Stasio, Sergey Vosel, *Formation of metal nanoparticles from supersaturated vapor (Zn, Bi).*
4P131	252	Gas phase synthesis of nanoparticles	**Olga Borovkova**, Anna Goryunova, Anatoliy Baklanov, Andrey Onischuk, Sergey Vosel, *Antimony nanopaticles formation from supersaturated vapor*.
4P132	253	Gas phase synthesis of nanoparticles	**Lin-Chi Wang**, *Single-step thermal synthesis of nano N-modified titanium dioxide powders for visible light photocatalysis using atmospheric-pressure microwave plasma*.
4P133	300	Gas phase synthesis of	**Mirella Miettinen**, *Characterization of silicon-carbon nanoceramics synthesized from*

		nanoparticles	*hexamethyldisilane in high temperature aerosol reactor at atmospheric pressure*.
4P134	457	Gas phase synthesis of nanoparticles	**Alexander Samodurov**, Anatoly Baklanov, Andrey Onishchuk, Sergey Vosel, *Ibuprofen nanoparticle formation from supersaturated vapor in the flow chamber*.
4P135	458	Gas phase synthesis of nanoparticles	**Sergey Valiulin**, V. Karasev, A. Onishchuk, S. Vosel, A. Baklanov, S. di Stasio, A. Komarovskikh, *Sulfur vapor homogeneous nucleation from a supersaturated vapor in a flow chamber*.
4P136	779	Gas phase synthesis of nanoparticles	**Unto Tapper**, Pirjo Koskela, Jouni Hokkinen, Minna Murto, Unto Tapper, Ari Auvinen, Jorma Jokiniemi, *Copper caoting of silicon, nickel and cobalt nanoparticles*.
4P137	781	Gas phase synthesis of nanoparticles	**Anatoliy Baklanov**, S. Valiulin, A. Onishchuk, V. Karasev, A. Komarovskikh, S. Vosel, S. di Stasio, *Method for measurement of diameter of critical nucleus in vapor-to-liquid nucleation*.
4P138	828	Gas phase synthesis of nanoparticles	**Marcus Giglmaier**, Frederik Quaatz, Jan Matheis, Nikolaus Andreas Adams, *in Numerical Analysis of particle growtha microwave-driven plasma reactor and comparison with experimental data*.
4P139	964	Gas phase synthesis of nanoparticles	**Kun Gao**, Martin Seipenbusch, Gerhard Kasper, *Synthesis of the Pt/Al2O3 catalyst particles by MOCVS/MOCVD process at atmospheric pressure*.
Atmospheric Aerosols - Specific Aerosol Types			
4P140	59	Other	**Alexandra Ioannidou**, Jussi Paatero, *Activity Size Distribution and Residence Times of Radioactive Aerosols in the Arctic Atmosphere*.
4P141	118	Other	**Yuri Samsonov**, *Chemical composition and dispersal property of smoke emission from forest fires in Siberia*.
4P142	162	Other	**Noor Yahaya**, Noor Zaitun, *Analysing roadside*

			Particle Number Concentrations using Boosted Regression Trees (BRT).
4P143	400	Other	**Antonella Malaguti**, C. Telloli, M. Berico, C. Vaccaro, M. Mircea, *Chemical and mineralogical composition of particulate matter released from agricultural operations*.
4P146	707	Other	**Natalia Ivleva**, Susanne Huckele, Bernadett Weinzierl, Reinhard Niessner, Christoph Haisch, Thomas Baumann, *Identification of Eyjafjallajökull volcanic ash particles collected in Munich in spring 2010 by Raman microspectroscopy*.
4P147	712	Other	**Farah Halek**, Ali Kavousirahim, *Characterization of particulate trace elements in Tehran air*.
4P148	734	Other	**Tadas Prasauskas**, Dainius Martuzevicius, Edvinas Krugly, Linas Kliucininkas, *Characterization of particle size distributions of powdery building materials aerosol*.
4P149	915	Other	**Gregor Jereb**, Boris Marzi, Franka Cepak, Goran Dražic, Borut Poljšak, *Monitoring of the Particulate Matter Deposition Around Port of Koper*.
4P150	966	Other	**Cecilia Bennet**, Mats Gustafsson, Göran Blomqvist, *Efficiency of CMA as a dust binding agent*.
4P151	1058	Other	**Eduardo Yubero**, Javier Crespo, Franco Lucarelli, Silvia Nava, Nuria Galindo, Jose Nicolas, Massimo Chiari, Giulia Calzolai, *Influence of fireworks on the atmospheric levels of trace metals*.
4P152	1098	Other	**Holger Gerwig**, Werner Pecher, Klaus Wirtz, *New Year´s Day Fireworks: Elevated particle area and number concentrations at an urban background station in Germany 2009 - 2011*.
Aerosol-based Nanotechnology			
4P153	740	Fundamentals and	**Taiki Shinohara**, Naoki Nishida, Hideki Tanaka, *Size-selected Ag nanoparticle clusters*

		measurement of nanoparticles	*deposited on carbon nanotubes*.
4P154	752	Fundamentals and measurement of nanoparticles	**Yasuhiro Kojima**, Naoki Nishida, Hideki Tanaka, *Chiroptical property of Ag triangular nanoplate protected by chiral molcules*.
4P155	824	Fundamentals and measurement of nanoparticles	**Yeon Kyoung Bahk**, J. Buha, Z. Liu, D.Y.H. Pui and J. Wang, *Relationship between the geometrical length and mobility diameter of airborne carbon nanotubes*.
4P156	854	Fundamentals and measurement of nanoparticles	**Vidmantas Ulevicius**, Vadimas Dudoitis, Gediminas Raciukaitis, Narciza Spirkauskaite, *Peculiarities of particle generation by laser ablation of nickel*.
4P157	972	Fundamentals and measurement of nanoparticles	**Pavel Moravec**, Jiri Smolik, Snejana Bakardjieva, Valeri V. Levdansky, *Binary CoOx/SiO2 nanoparticle synthesis*.
4P158	384	Process monitoring in nanoparticle technology	**Sascha Engel**, Yi Gao, Andreas F. Koegler, Daniel Kilian, Thomas Seeger, Wolfgang Peukert, Alfred Leipertz, *Laser diagnostics based flame characterization of a flame spray pyrolysis process*.
4P159	630	Process monitoring in nanoparticle technology	**Jing Wang**, Drew Thompson, Lin Li, David Pui, *Exposure Measurement in an Industrial Production Facility for CNT-imbedded Nanocomposites*.
4P160	832	Process monitoring in nanoparticle technology	**Martin Schmidt**, Sven Schuetz, *Optical online particle measurement in hot gases up to 450°C and in chemically aggressive gas components*.
4P161	881	Process monitoring in nanoparticle	**Hans-Georg Horn**, Christof Asbach, Heinz.Fissan, Melissa.Grose, Tim Hülser, Rolf.Jacob, Jason Johnson, Jorma Jokiniemi,

		technology	Michael Mertler, Jarno Ruusunen, *Near Real Time Characterization of Si-Nanoparticles from a Hot Wall Reactor with the Universal Nanoparticle Analyzer UNPA*.
Combustion Aerosols			
4P162	965	High temperature aerosols	**Senem Ozgen**, Stefano Cernuschi, Michele Giugliano, Giovanna Ripamonti, *Ultrafine particles in flue gas from waste-to-energy (WTE) plants*.
4P163	383	High temperature aerosols	**Jérôme Yon**, Chloé Caumont-Prim, Alexis Coppalle, Kuan Fang Ren, *Measurement of soot size distribution in flames by inversion of angular light scattering*.
4P165	70	High temperature aerosols	**Maria Rita Perrone**, Andrea Piazzalung, Marco Prato, *Methodology to determine carbonate carbon from Thermal Optical Transmittance measurements*.
4P166	104	High temperature aerosols	**Torben Seidel**, Hans Ruppert, *Fluxes of volatile and non-volatile elements in small-scale biomass combustion systems*.
4P167	119	High temperature aerosols	**Svetlana Popova**, Valerii Makarov, *Chemical composition of smoldering combustion products of some forest materials and cellulose*.
4P168	199	High temperature aerosols	**Young-Ok Park**, Jei-Pil Wang, Yong-Ha Kim, *Effect of various operating conditions to remove SO2 in sorbent inter-circulating desulfurization unit*.
4P169	243	High temperature aerosols	**Elena Kireeva**, Olga Popovicheva, Michal Vojtisek-Lom, *Infrared spectroscopy of diesel and biofuel combustion particles*.
4P170	276	High temperature aerosols	**Patrik Nilsson**, Azhar Malik, Magnus Lindskog, Joakim Pagels, Jenny Rissler, Anders Gudmundsson, Mats Bohgard, Mehri Sanati, *Evaluation of a high temperature particle sampling setup for separation of inorganic and organic phase using laboratory model compounds*.

4P171	352	High temperature aerosols	**Shun-I Shih**, Wen-Jhy Lee, Wei-Yu Huang, Lin-Chi Wang, Guo-Ping Chang-Chien, *Characteristics of Polychlorinated Dibenzo-p-dioxins and Dibenzofurans in the atmosphere in northern Taiwan*.
4P173	542	High temperature aerosols	**Hanns-Rudolf Paur**, Baumann, W., Gehrmann, H.-J., Mätzing, H., Paur, H.-R., Seifert, H., *Carbon burnout of a multi-fuel dust-burner in co-combustion situations*.
4P174	662	High temperature aerosols	**Nickolas Meyer**, Thomas Heck, *Wood combustion emissions in Switzerland and associated impact assessments*.
4P175	810	High temperature aerosols	**Khageshwar Singh Patel**, R. Baghel, N.K. Jaiswal, H. Saathoff, T. Leisner, *Carbonaceous particulate concentration in Indian kitchens*.
4P176	1119	High temperature aerosols	**Ying Fang Wang**, Perng Jy Tsai, *Characterization of welding fume and application of exposure model to predict concentrations in the ship-building industry*.
4P177	288	Other	**Bellivier Axel**, Delorme Robert, Dupont Sylvie, Benhaiem Philippe, Chen Yuansi, Le Bars Patrick and Bazin Hervé, *Study of local aerosol combustion concentration with a differential white light opacimeter*.
4P178	340	Other	**Delphine Lottin**, David Delhaye, Daniel Ferry, Andreas Petzold, Heidi Bauer, Yura Sevcenco, Richard Marsh, Mark Johnson, *Influence of aircraft combustion chamber conditions on physical and chemical properties of soot aggregates*.
4P179	491	Other	**Annika Hukkanen**, Heikki Lamberg, Terhi Penttilä, Olli Sippula, Jarkko Tissari, Jorma Jokiniemi, *Comparison of emissions with pellet fuel and wood logs from a hybrid masonry heater*.
4P180	554	Other	**Tiina Torvela**, Jani Leskinen, Annika Hukkanen, Terhi Penttilä, Heikki Lamberg, Tapio Kettunen, Ilpo Nuutinen, Olli Sippula, Jarkko Tissari, Jorma Jokiniemi, *Physico-*

			chemical properties of particles formed in efficient, intermediate and smouldering wood chip combustion.
4P181	555	Other	**Tapio Kettunen**, Miika Kortelainen, Olli Sippula, Ilpo Nuutinen, Heikki Lamberg, Jorma Jokiniemi, *Novel laboratory-scale biomass combustion reactor for studies on emission formation and ash behaviour*.
4P182	642	Other	**Paul Williams**, Mark Johnson, Richard Marsh, Hugh Coe, *Comparison of organic aerosol from different aircraft combustion sources using an Aerodyne Aerosol Mass Spectrometer (AMS)*.
4P183	661	Other	**David Delhaye**, François-Xavier Ouf, Delphine Lottin, Daniel Ferry, Olivier Penanhoat, Philippe Novelli, *Characterisation behind a modern civil engine: investigation on new particulate certification*.
4P184	54	Other	**Charles Motzkus**, Carine Chivas-Joly, Eric Guillaume, Sébastien Ducourtieux, Laurent Saragoza, Damien Lesenechal, Tatiana Macé, François Xavier Ouf, François Gensdarmes, *Count Size distribution of the aerosol emitted by the combustion of nanocomposites*.
4P185	166	Other	**Natalia P. Ivleva**, Henrike Bladt, Johannes Schmid, Elena Kireeva, Olga Popovicheva, Reinhard Niessner, *Structure and reactivity of laboratory-produced soot containing iron*.
4P186	194	Other	**Tzi-yi Wu**, Yan-Min Chen, *Analysis of carbonyl compounds emissions from a heavy-duty diesel engine fueled with paraffinic/biodiesel blends*.
4P187	249	Other	**Kuo-Lin Huang**, Kuo-Lin Huang, Shui-Jen Chen, Mao-Sung Wang, Chih-Chung Lin, Chun-Li Chou, *Persistent organic pollutants emitted from a municipal solid waste incinerator*.
4P188	267	Other	**Jesús Rodríguez-Maroto**, J.L. Dorronsoro-Arenal, D. Sanz-Rivera, E. Rojas-García, M. Fernández-Díaz, P. Galán-Valera and E. Conde

			Vilda, *Enrichment of trace metal by particle size. Emissions from steel foundries.*
Atmospheric Aerosols - Aerosol Processes and Properties			
4P189	105	New particle formation	**Hannele Korhonen**, Sanna-Liisa Sihto, Veli-Matti Kerminen, Kari E.J. Lehtinen, *How accurate are the nucleation event analysis tools?*
4P190	313	New particle formation	**Anne Hirsikko**, Ville Vakkari, Hanna Elina Manninen, Heikki Laakso, Markku Kulmala, Aadu Mirme, Sander Mirme, D. Dabaso, Lauri Laakso, *Small ion concentrations and particle formation in a polluted environmnet in South-Africa*.
4P191	368	New particle formation	**Dimitrios Siakavaras**, Constantini Smara, Christodoulos Pilinis, Maximos Petrakakis, Apostolos Kelesis, George Biskos, *Classification of Nucleation Events during the Summer Period in Thessaloniki, Greece: Kerbside versus urban background measurements*.
4P192	380	New particle formation	**Ari Asmi**, *Time-frequency analysis of aerosol number concentrations in Europe -- \\ 28 day period in nucleation and the (lack of) weekly cycle in CCN-sized particles*.
4P193	413	New particle formation	**Niku Kivekas**, Eija Asmi, Heikki Lihavainen, Mika Komppula, Antti-Pekka Hyvärinen, Yrjö Viisanen, Pasi Aalto, Tuomo Nieminen, Birgitta Svenningsson, Almut Arneth, *Regional extent of new particle formation*.
4P194	446	New particle formation	**Eija Asmi**, Niku Kivekäs, Mika Komppula, Antti-Pekka Hyvärinen, Juha Hatakka, Yrjö Viisanen, Heikki Lihavainen, *Over 10-years of new particle formation and growth in sub-Arctic Pallas station*.
4P195	482	New particle formation	**Amar Hamed**, Harri Portin,Ari Leskinen, Mika Komppula,Kari Lehtinen,Sami Romakkaniemi, James Smith, Jorma Joutsensaari, Ari

			Laaksonen, *Characterization of New Particle Formation Events in Kuopio, Finland*.
4P196	517	New particle formation	**Einhard Kleist**, Thomas Mentel, Astrid Kiendler-Scharr, Sebastian Broch, Monika Springer, Katja Behnke, Jörg-Peter Schnitzler, Ralf Tillmann, Stefanie Andres, Florian Rubach, Bettina Steitz, Jürgen Wildt, *SOA formation from stress induced biogenic VOC emissions and the contribution of isoprene to particle formation and growth – lessons learned from grey poplar trees*.
4P197	651	New particle formation	**Tuija Jokinen**, Mikko Sipilä, Tuukka Petäjä, Markku Kulmala, Douglas Worsnop, Heikki Junninen, *Sulfuric acid measurements with CI-TOF-MS*.
4P198	695	New particle formation	**Zsuzsanna Becsi**, Ágnes Molnár, Kornélia Imre,Tuomo Nieminen, Jani Hakala, Tuukka Petäjä, Markku Kulmala, *New aerosol particle formation and event classification in Hungarian background air at K-puszta*.
4P199	697	New particle formation	**Daniela Wimmer**, *Performance of an Ultrafine Diethylene Glycol (DEG) based Condensation Particle Counter*.
4P200	767	New particle formation	**Alessandro Franchin**, *Physical characterization of ions in the CLOUD chamber*.
4P201	923	New particle formation	**Federico Bianchi**, Josef Dommen, Urs Baltensperger, Serge Mathot, *Ammonia measurements in the gas phase at ppt levels by long-path absorption spectroscopy*.
4P202	1065	New particle formation	**Ravi Kumar**, Samantha MacDonald, Russell Saunders, Benjamin Murray, and John Plane, *Reduction of Iodate (IO3-) to Iodide (I-) in seawater and recycling of Iodine (I2) to the atmosphere by the uptake of Ozone (O3): Links to new particles formation*.
4P203	1094	New particle formation	**Mar Sorribas**, Anoop Mahajan, Juan Carlos Gomez Martin, Samantha M MacDonald, Manuel Gil, John M C Plane, Alfonso Saiz

			Lopez, *Coastal nucleation events: relation to atomic and molecular iodine concentration*.
4P204	1095	New particle formation	**Mar Sorribas**, Juan Francisco Lopez, Mercedes Fernandez Leon, Benito Arturo de la Morena, *Sub-arctic nucleation events: Observation at ALOMAR Station, Norway*.
4P205	1111	New particle formation	**Ondrej Vlcek**, Tove Svendby, Linton Corbet, *New parametrization of SOA formation from anthropogenic VOCs for the CAMx model*.
Atmospheric Aerosols – Specific Aerosol Types			
4P206	256	Specific Aerosol Types - remote continental upper troposphere	**Chin-Hsiang Luo**, C.-Y. Wen, K.-H. Lin and S.-H. Chiu, *Digital visibility quantification for atmospheric environment with a Harris corner detector*.
4P207	283	Specific Aerosol Types - remote continental upper troposphere	**Boris Bonn**, Stratos Bourtsoukidis, Hannele Hakola, Jann Schrod, Claudia Fuchs, Friedemann Ebach, Werner Haunold and Stefan Jacobi, *New particle formation by biogenic emissions: Potential organic nucleation pathway and implications on climate feedbacks*.
4P208	725	Specific Aerosol Types - remote continental upper troposphere	**Sandra Andersson**, Bengt Martinsson, Johan Friberg, Carl Brenninkmeijer,Markus Hermann, Peter van Velthoven , Andreas Zahn, *Composition and evolution of volcanic aerosol following three eruptions 2008 - 2010*.
4P209	796	Specific Aerosol Types - remote continental upper troposphere	**Silvia Becagli**, G. Calzolai, C. Ghedini, F. Lucarelli, A. di Sarra, M. Mazzola , C. Di Biagio, R. Traversi, V. Vitale, and R. Udisti, *Chemical size distributions and bulk composition of Arctic aerosol sampled at Ny Ålesund (Svalbard Islands) and Thule (Greenland) during the 2010 campaign*.
4P210	799	Specific Aerosol Types	**Silvia Becagli**, Roberto Udisti, Silvia Becagli, Maurizio Busetto, Massimo Chiari, Uri Dayan,

		- remote continental upper troposphere	Daniele Frosini, Silvia Nava, Francesco Rugi, Mirko Severi, Rita Traversi, *Transport processes affecting chemical composition of Antarctic plateau aerosol from size segregated sampling at Station Concordia (Dome C, East Antarctica)*.
4P211	1126	Specific Aerosol Types - remote continental upper troposphere	**Michael Gatari**, Samuel Gaita, Keith Shepherd, Johan Boman, Sofia Thorsson, Annamarie Wagner, *Long range transported mineral dust to the Equatorial Global Atmosphere Watch (GAW) Station on Mt Kenya*.
Atmospheric Aerosols - Aerosol Processes and Properties			
4P212	103	Physical and chemical properties	**Wenjie Zhang**, Zhipeng Bai, Jianzhong Ma, Jianhua Chen, Wen Yang, Baohui Yin, *n-situ aircraft observations on gases and particulate pollutants around Beijing area: distributions and influencing factors*.
4P213	129	Physical and chemical properties	**Nadezda Zikova**, Vladimir Zdimal, Jiri Smolik, *SMPS spectra under various meteorological conditions*.
4P214	136	Physical and chemical properties	**Mark Barley**, David Topping, Gordon McFiggans, Douglas Lowe, *Development of chemical informatics tools for calculating fundamental properties of atmospheric aerosol components*.
4P215	200	Physical and chemical properties	**Marina Chichaeva**, Anton Syroeshkin, *D-elements and peptides in aerosols above water: interdependence between size and chemical composition.*
4P216	222	Physical and chemical properties	**Eugene Mikhailov**, Vlidimir Merkulov, Sergey Vlasenko, Ulrich Poeschl, *Mass-based aerosol water uptake measurements, hygroscopicity parameters and solute interaction parameters*.
4P217	254	Physical and	**Young Joon Kim**, Batmunkh T., Cayetano

		chemical properties	M.B.G., Kim SungYong, Shin Ju S., Kim KwanChul, *Optical, physical and chemical characteristics of sub-urban atmospheric aerosols during very clean and local biomass burning events*.
4P218	270	Physical and chemical properties	**Andreas Held**, Josefine Walz, Douglas Orsini, Caroline Leck, *The volatile fraction of Arctic aerosol particles derived from thermodenuder/mobility spectrometer measurements during ASCOS*.
4P219	420	Physical and chemical properties	**Antti-Pekka Hyvärinen**, Kimmo Neitola, Eija Asmi, Heikki Lihavainen, *Hygroscopic properties of sub-Arctic aerosols: continuous HTDMA measurements from Pallastunturi, Finnish Lapland*.
4P220	447	Physical and chemical properties	**Eija Asmi**, Heikki Lihavainen, Antti-Pekka Hyvärinen, David Brus, Mika Aurela, Juha Hatakka, Taneil Uttal, Victor Ivakhov, Alexander Reshetnikov, Alex Zinchenko, Alexander Makshtas, Yrjö Viisanen, Petteri Taalas, Ari Laaksonen, Tuomas Laurila, *Measurements of Siberian Arctic aerosols in Tiksi, Russia*.
4P221	522	Physical and chemical properties	**Jose Francisco Nicolas**, Carlos Pastor, Joaquin Giménez, Ramon Castañer, Eduardo Yubero, Javier Crespo, *Particle number variation due to the disappearance of a thermal inversion*.
4P222	524	Physical and chemical properties	**David Bones**, Haijie Tong, Jonathan Reid, *Inhibited water diffusion and inhomogeneities in glassy atmospheric aerosol proxies*.
4P223	592	Physical and chemical properties	**Jianhua Chen**, *Field observation of the hygroscopic properties of the ambient aerosols in Beijing*.
4P224	654	Physical and chemical properties	**Santtu Mikkonen**, Sami Romakkaniemi, James Smith, Tuukka Petäjä, Christian Plass-Duelmer, Michael Boy, Peter McMurry, Hannele Korhonen, Kari E.J. Lehtinen, Jorma Joutsensaari, Amar Hamed, Tuomo Nieminen,

			Lee Mauldin, Wolfram Birmili, Markku Kulmala and Ari Laaksonen, *Approximating sulphuric acid concentration in the atmosphere. A multilocational statistical study*.
4P225	664	Physical and chemical properties	**Katrianne Lehtipalo**, Joonas Vanhanen, Jyri Mikkilä, Juha Kangasluoma, Hanna Manninen, Tuukka Petäjä, Markku Kulmala, *Field measurements of atmospheric sub-2nm particles with Particle Size Magnifier*.
4P226	676	Physical and chemical properties	**Liqing Hao**, *Aerosol mass spectrometer measurements at the SMEAR IV semi-urban station*.
4P227	738	Physical and chemical properties	**Katharina Kamilli**, Laurent Poulain, Andreas Nowak, Andreas Held, Wolfram Birmili, Alfred Wiedensohler, *Hygroscopic properties of the urban aerosol in Paris in relation to its chemical compositions*.
4P228	807	Physical and chemical properties	**Luca Ferrero**, D. Cappelletti, M. Petitta, F. Scardazza, M. Castelli, M.G. Perrone, G. Sangiorgi, E. Bolzacchini, *Vertical profiles of aerosol physico-chemical and optical properties measured along Italy over basin valleys*.
4P229	811	Physical and chemical properties	**Luca Ferrero**, G. Sangiorgi, M.G. Perrone, E. Bolzacchini, *PM2.5, PM1 and PM0.4 hygroscopicity during spring and summer at one Po Valley site.*
4P230	816	Physical and chemical properties	**Jani Hakala**, *Measurements with a VH-TDMA in CalNex 2010 campaign*.
4P231	848	Physical and chemical properties	**Annele Virtanen**, Jonna Kannosto, Jorma Joutsensaari, Erkka Saukko, Heino Kuuluvainen, Li-Ping Hao, Pasi Yli-Pirilä, Petri Tiitta, Jarmo Holopainen, Douglas R. Worsnop, James N. Smith, Ari Laaksonen, *Bounce behavior of freshly nucleated biogenic secondary organic aerosol particles*.

4P232	879	Physical and chemical properties	**Andréa Arana**, Paulo Artaxo, *Elemental Composition of the Atmospheric Aerosol in the Central Amazon Basin.*
4P233	893	Physical and chemical properties	**Gaurav Singh**, Tarachand Lohia, Gazala Habib, Tarun Gupta, *Chemical characterization and source identification of roadside aerosol*.
4P234	916	Physical and chemical properties	**Gloria Titos**, Inmaculada Foyo-Moreno, Hassan Lyamani, Xavier Querol, Andres Alastuey and Lucas Alados-Arboledas, *Optical and chemical properties of aerosol particles over an urban location. Estimating mass scattering and absorption efficiencies.*
4P235	933	Physical and chemical properties	**Jakub Ondracek**, Petr Vodicka, Vladimir Zdimal, Jaroslav Schwarz, Jiri Smolik, *Hygroscopicity of aerosol particles at Kosetice background station (Czech Republic) using the HTDMA system*.
4P237	984	Physical and chemical properties	**Tuukka Petaja**, Heikki Junninen, Mikko Aijala, Alessandro Franchin, Siegfried Schobesberger, Hanna Manninen, Anne Hirsikko, Joonas Vanhanen, Jyri Mikkila, Katrianne Lehtipalo, Joshua McGrath, Darius Ceburnis, Harald Berresheim, Douglas Worsnop, Markku Kulmala, Colin O'Dowd, *Air ion chemical and physical characterization during MaCLOUD Inc at Mace Head*.
4P238	1066	Physical and chemical properties	**Suzanne Visser**, M. Furger, A. Richard, U. Flechsig, K. Appel, A.S.H. Prevot, U. Baltensperger, *Elemental composition of PM10, PM2.5 and PM1.0 aerosols in Paris*.
4P239	1078	Physical and chemical properties	**Paulo Artaxo**, L.V. Rizzo, K.T. Wiedemann, E. Swietlicki, A. Wiedensohler, *Long term aerosol optical properties in pristine and biomass burning areas in the Amazon Basin*.
4P240	1079	Physical and chemical properties	**Paulo Artaxo**, Glauber G. Cirino, Rodrigo Souza, *Strong effect of aerosols on the CO2 flux in the central Amazon*.
4P241	1110	Physical and chemical	**Paulo Artaxo**, Paulo Artaxo, Luciene Lara, Maria Lucia Antunes, *Aerosol and*

		properties	*precipitation chemistry in a remote site in Central Amazonia: the role of biogenic contribution*.
Atmospheric Aerosols – Specific Aerosol Types			
4P242	45	Bioaerosols	**Janine Froehlich**, Viviane Despres, Ulrich Poeschl, *Fungal Diversity and Biogeography in the Air*.
4P243	82	Bioaerosols	**Cristina Ruzene Nespoli**, Janine Fröhlich-Nowoisky, Viviane R. Després, Ulrich Pöschl, *Determination of airborne plant pathogens by DNA analysis: fungus-like microorganisms*.
4P244	89	Bioaerosols	**Christopher Pöhlker**, J. Alex Huffman, Janine Fröhlich-Nowoisky, Ulrich Pöschl, *Autofluorescence of Bioaerosol Standards – Characterization by Fluorescence Spectroscopy and Microscopy*.
4P245	96	Bioaerosols	**Isabell Müller-Germann**, Janine Fröhlich-Nowoisky , U. Pöschl, V. R. Després, *Allergenic Asteraceae in urban air: DNA analysis and relevance for human health*.
4P246	126	Bioaerosols	**Eleftheria Katsivela**, Louiza Raisi, Mihail Lazaridis, *Size distribution of viable airborne microbes in a Mediterranean suburban site*.
4P247	130	Bioaerosols	**Reinhard Niessner**, Michael Seidel, Georg Hartmann, Veronika Langer, *Production, sampling and microarray-based detection of bioaerosols containing E. coli and L. pneumophila*.
4P248	172	Bioaerosols	**Janine Jordan**, Tom Hawkyard, Richard Thomas, *Techniques to investigate bacterial survival within the airborne state*.
4P249	176	Bioaerosols	**Aleksandr Safatov**, Vladimir Ternovoi, Vladimir Generalov, Galina Buryak, Yurii Marchenko, Sergei Olkin, Boris Antipkin, Natalya Lapteva, Aleksandr Sergeev, *The comparison of diversity of microorganisms in aerosol and seawater surface microlayer*.

4P250	177	Bioaerosols	**Aleksandr Safatov**, Galina Buryak, Ksenia Grishkina, *The effect of meteorological factors on bioaerosol concentration in Southwestern Siberia*.
4P251	262	Bioaerosols	**Chane-Yu Lai**, Chun-Wei Chen, Shin-Ran Wun, Po-Chen Hung, Cheng-Ping Chang, *The Study of Surviving of Bacteria on Charcoal Filters under Nutrient, Moisture Regain and Water Content Conditions*.
4P252	330	Bioaerosols	**Maosheng Yao**, *Differences in Positively and Negatively Charged Bacterial Aerosol Diversity in Indoor and Outdoor Environments*.
4P253	331	Bioaerosols	**Maosheng Yao**, *Use of Electrostatic Sampling and ELISA method in Studying Charge Distributions of Airborne Allergens*.
4P254	332	Bioaerosols	**Maosheng Yao**, *Effects of Microwave Irradiation on Culturability and Diversity of Biological Aerosols of Different Sizes in Different Environments*.
4P255	333	Bioaerosols	**Maosheng Yao**, *Use of six-stage Andersen Sampler in Investigating Bioaerosol Inhalation Risks in Different Environments*.
4P256	334	Bioaerosols	**Maosheng Yao**, *Performance of a Button Inhalable Sampler with Modified MCE Filter Method in Enumerating Culturable Bacterial and Fungal Aerosol Concentration and Diversity*.
4P257	336	Bioaerosols	**Maosheng Yao**, *Effects of single-walled carbon nanotube filter on culturability and diversity of environmental bioaerosols*.
4P258	337	Bioaerosols	**Maosheng Yao**, *Influences of Air Volume, DNA Template, and Dilution Factor on the Performance of qPCR Coupled with a Modified BioStage Sampling Method in Quantifying Bioaerosols*.
4P259	351	Bioaerosols	**Andrew Gabey**, *Fluorescence and bioaerosol measurements at a high-altitude site (Puy de Dôme)*.
4P260	379	Bioaerosols	**Bertrand Dupont**, Pascale Ehouarn, Ludovic

			Tatoulian, Jerome Jusseaume, *Pharmaceutical deposition of peanut proteins on skin patches by EHDA in cone-jet mode*.
4P261	610	Bioaerosols	**Ranjit Kumar**, K. Maharaj Kumari, J.N. Srivastava, *Biochemical characteristics of aerosol*.
4P262	759	Bioaerosols	**Elena Innocente**, Isabella Gandolfi, Andrea Franzetti, Valentina Bertolini, Giuseppina Bestetti, Stefania Squizzato, Giancarlo Rampazzo, *Assessment of temporal variability in microbial communities associated to atmosheric particulate matter in a urban area through Illumina sequencing*.
4P263	808	Bioaerosols	**Gi Byoung Hwang**, *Effect of relative humidity on antimicrobial filter using Sophora flavescens natural product nanoparticles*.
4P264	924	Bioaerosols	**Douglas Nilsson**, Camilla, Fahlgren, Ulla-Li, Zweifel, *One year seasonal cycle of airborne bacteria and fungus in southern Sweden: implications on sinks, sources and turn-over time*.
Atmospheric Aerosols - Aerosol Processes and Properties			
4P265	95	Aerosol Cloud Interaction	**Stelios Kazadzis**, Vassilis Amiridis, Evangelos Gerasopoulos, Antti Arola, *Aerosol absorption retrieval at ultraviolet wavelengths in a complex environment*.
4P266	128	Aerosol Cloud Interaction	**Ying Duan**, Yan Yin, *The study on distribution characteristics of atmospheric aerosols over*.
4P267	134	Aerosol Cloud Interaction	**David Topping**, Mark Barley , Gordon McFiggans, *Aerosol particle property sensitivities to choice of predictive technique in SOA partitioning calculations*.
4P268	145	Aerosol Cloud Interaction	**Evangelos Gerasopoulos**, Nikolaos Mihalopoulos, Stelios Kazadzis, Michalis Vrekoussis, George Kouvarakis, Natalia Kouremeti, *Influence of aerosol optical properties on NO2 and O1D photolysis rates measured at Eastern Mediterranean*.

4P269	180	Aerosol Cloud Interaction	**Juan Luis Guerrero-Rascado**, M.J. Costa, A.M. Silva, J. Preißler, *Towards an assessment of the cloud-aerosol interaction determined by Raman lidar*.
4P270	204	Aerosol Cloud Interaction	**Mihalis Lazaridis**, *Analysis of the ambient particle number size distributions characteristics during nucleation events in the Eastern Mediterranean*.
4P271	239	Aerosol Cloud Interaction	**Elena Fuentes**, *Evaluation of uncertainties in determining particle volatility properties from experiments with standard thermal-denuder techniques*.
4P272	255	Aerosol Cloud Interaction	**Daya Kaul**, S.N.Tripathi, Tarun Gupta, *Enhanced Secondary Organic Aerosols during Fog Episodes*.
4P273	265	Aerosol Cloud Interaction	**Florian Ditas**, Birgit Wehner, Holger Siebert, Heike Wex, Gregory C. Roberts, Katrin Mildenberger, Tina Schmeißner, Frank Stratmann, Alfred Wiedensohler, *Aerosol number size distributions in the vicinity of trade wind cumuli*.
4P274	350	Aerosol Cloud Interaction	**Anja Roth**, Stephan Mertes, Dominik van Pinxteren, Thomas Klimach, Johannes Schneider, Stephan Borrmann, *Analysis of cloud and aerosol particles by single particle mass spectrometry during a hill-cloud-field experiment in Central Europe*.
4P275	357	Aerosol Cloud Interaction	**Hazel Jones**, Dantong Liu, Keith Bower, Jonathan Crosier, Piers Forster, Martin Gallagher, Jim Haywood, *Preliminary investigation of contrails sampled during the COntrails Spreading Into Cirrus (COSIC) campaign in June 2009*.
4P276	363	Aerosol Cloud Interaction	**Silvia Leise**, Andreas Hoy, Frank Zimmermann, Jörg Matschullat, *Weather condition – air quality relationships in Eastern Germany (1999 – 2009)*.
4P277	414	Aerosol Cloud Interaction	**Vanes Poluzzi**, Isabella Ricciardelli, Silvia Ferrari, Claudio Maccone, Arianna Trentini,

			Fabiana Scotto, Linda Passoni, *Spatial and seasonal variation of number concentration and size distribution of aerosol (5.6 – 560 nm) in urban and rural areas of Bologna (Italy)*.
4P278	449	Aerosol Cloud Interaction	**Gerard Capes**, Paul Williams, Michael Flynn, Keith Bower, Thomas Choularton, *Composition and hygroscopic properties of background aerosols at a rural U.K. site*.
4P279	462	Aerosol Cloud Interaction	**Gary Lloyd**, Thomas Choularton, Paul Connolly, *Anthropogenic Snowfall Events from Urban Fogs*.
4P280	466	Aerosol Cloud Interaction	**Martin Bødker Enghoff**, Jacob Svensmark, Henrik Svensmark, *The effect of coronal mass ejections on cloud microphysics*.
4P281	472	Aerosol Cloud Interaction	**Laurent Poulain**, Zhijun Wu, Andreas Tilgner, Dominik van Pinxteren, Markus Müller, Barbara D'Anna, Christian George, Johannes Schneider, Alfred Wiedensohler, Hartmut Herrmann, *Comparison of three AMS measurements during the Hill Cap Cloud Thuringia 2010 (HCCT 2010) campaign*.
4P282	502	Aerosol Cloud Interaction	**Francisco J. Gomez-Moreno**, Mariano Sastre, Manuel Pujadas, Javier Plaza, Jesús J. Rodríguez-Maroto, Pablo Martínez-Lozano and Begoña Artíñano, *Atmospheric particle number concentrations and nucleation events in an urban background site*.
4P283	506	Aerosol Cloud Interaction	**Moa Sporre**, Erik Swietlicki, Paul Glantz, Markku Kulmala, *A Long-Term Study of the Aerosol Effects on Convective Clouds over Southern Sweden and Finland*.
4P284	507	Aerosol Cloud Interaction	**Georgios Tsagkogeorgas**, Heike Wex, Frank Stratmann, *Hygroscopicity parameter measurements of cloud condensation nuclei from nucleation experiments at the CLOUD chamber*.
4P285	597	Aerosol Cloud Interaction	**Francisco Jose Olmo Reyes**, A.Valenzuela, F.J. Olmo, H. Lyamani, A.Quirantes, D. Perez, L. Alados-Arboledas, *Aerosol properties during*

			long-range transport of African dust air masses over Granada (Spain).
4P286	598	Aerosol Cloud Interaction	**Francisco Jose Olmo Reyes**, A. Quirantes, F.J. Olmo, A. Valenzuela, H. Lyamani, L. Alados-Arboledas, *Shape dependence of atmospheric aerosol light scattering parameters:ALFA simulation and comparison to AERONET data*.
4P287	629	Aerosol Cloud Interaction	**Hossein Saghafifar**, *Number concentration measurement of nanometer-sized particles and its correlation with wind velocity*.
4P288	641	Aerosol Cloud Interaction	**Neda Boyouk**, *Evolution of aerosol size distributions related to air masses origins in Paris Fog*.
4P289	644	Aerosol Cloud Interaction	**Liudmila Uvarova**, Yurii Birykov, Valerii Zagainov, Vladimir Kostin, Dmitrii Kiselev, Irina Krivenko, Tatiana Kazarova, Liudmila Vasil'eva, Kiril Goryunov, *Aerosol particles transport on areas of water: experiments and modelling*.
4P290	647	Aerosol Cloud Interaction	**Rosemary Fedele**, Melita Keywood, Paul Selleck, John Gras, Nichola Porter, *Australian aerosol and cloud condensation nuclei (CCN)*.
4P291	681	Aerosol Cloud Interaction	**Francisco J. Gomez-Moreno**, M. Sastre, B. Artíñano, V. Juncal Bello, M. Piñeiro Iglesias, P. López Mahía, J. Pey, A. Ripoll, A. Alastuey, M. Sorribas, M. Fernández, B. A. de la Morena, J. L. Trujillo de Cabo and S. Rodríguez, *Main activities of the Spanish network on environmental DMAs*.
4P292	689	Aerosol Cloud Interaction	**Stephanie Gagne**, Tuomo Nieminen, Johannes Leppä, Hanna E. Manninen, Tuukka Petäjä, Veli-Matti Kerminen, Lauri Laakso, Markku Kulmala, *Charging states and ion-induced nucleation fractions in an urban and forested area, Finland*.
4P293	719	Aerosol Cloud Interaction	**Hugh Coe**, Grant Allen, Geraint Vaughan, Pat Minnis, Thomas Toniazzo, *Gravity waves observed as a causal mechanism for transition from closed to open cellular convection in the*

			remote South East Pacific.
4P294	729	Aerosol Cloud Interaction	**Otto Hanninen**, Riikka Sorjamaa, Josef Cyrys, Mike Pitz, Juha Pekkanen, Timo Lanki, *Apparent particle density in Helsinki during the ULTRA II campaign*.
4P295	736	Aerosol Cloud Interaction	**Antti Jaatinen**, Antti Jaatinen, Sami Romakkaniemi, Liqing Hao, Aki Kortelainen, Pasi Miettinen, David Brus, Harri Portin, Mika Komppula, Ari Leskinen, James Smith, Ari Laaksonen, *Cloud droplet activation during the PuCE 2010 campaign*.
4P296	741	Aerosol Cloud Interaction	**Sami Romakkaniemi**, Helmi Keskinen, Antti Jaatinen, James Smith, Ari Laaksonen, *Water adsorption and CCN properties of silica particles*.
4P297	743	Aerosol Cloud Interaction	**Julia Burkart**, Regina Hitzenberger, Georg Reischl, Gerhard Steiner, Heidi Bauer, Klaus Leder, Maria Rzaca, Hans Puxbaum, *Activation of "synthetic atmospheric aerosols" – relation to chemical composition of particles <100nm*.
4P298	764	Aerosol Cloud Interaction	**Katrin Mildenberger**, Michael Schäfer, Silvia Henning, Andreas Nowak, Eike Sommerhage, Eva Hallbauer, Tina Göbel, Bettina Nekat, Dominik van Pinxteren, Zhaoze Deng, Pengfei Liu, Chunsheng Zhao, Stephan Henne, Alfred Wiedensohler, Frank Stratmann, *Seasonal and Sourece Depending Activation Behaviour of Aerosol Particles in the North China Plain*.
4P299	768	Aerosol Cloud Interaction	**Katrin Mildenberger**, Silvia Henning, Jens Voigtländer, Heike Wex, Frank Stratmann, *A Sensitivity Study: The Influence of Scrit on kappa*.
4P300	769	Aerosol Cloud Interaction	**Aleksander Pietruczuk**, Janusz Jaroslawski, *Correlation between aerosol parameters measured in-situ and by means of Sun-photometer technique*.
4P301	788	Aerosol Cloud Interaction	**Aditya Vaishya**, D. Ceburnis, J. Ovadnevaite, C. Monahan, J. Bialek, S.G. Jennings, C.D.

			O'Dowd, *Hygroscopic properties of aerosols associated with different air masses arriving at Mace Head, Ireland.*
4P302	797	Aerosol Cloud Interaction	**Christina Mitsakou**, George Kallos, Stavros Solomos, Jonilda Kushta, *An improved description of cloud droplets development in climate studies over the Mediterranean region*.
4P303	836	Aerosol Cloud Interaction	**Tuomo Nieminen**, Hanna Manninen, Jenni Kontkanen, Pauli Paasonen, Anne Hirsikko, Veli-Matti Kerminen, Markku Kulmala, *Charged and neutral clusters and their connection to new particle formation in Europe*.
4P304	852	Aerosol Cloud Interaction	**Nicolas Bukowiecki**, *In-situ investigation of cloud microphysics and aerosol optical properties during the CLACE 2010 campaign at Jungfraujoch, Switzerland (3580 m asl): An Overview*.
4P305	882	Aerosol Cloud Interaction	**Staffan Sjogren**, M. Berghof, G.P. Frank, S. Sjogren, B.G. Martinsson, K. Acker, W. Wieprecht, D. Kalass, *Aerosol-cloud interaction measurements with the Droplet Aerosol Analyser*.
4P306	899	Aerosol Cloud Interaction	**Jaroslav Schwarz**, Jindrich Karban, Eva Chalupnícková, Radek Pokorný, Jirí Novák, Jirí Smolík, *The influence of biomass burning on PM2.5 at urban and rural background sites in the Czech Republic*.
4P307	900	Aerosol Cloud Interaction	**Jaroslav Schwarz**, *The ionic composition of PM2.5 at a rural background site in Central Europe on daily basis*.
4P308	955	Aerosol Cloud Interaction	**Bettina Nekat**, Dominik van Pinxteren, Thomas Gnauk, Konrad Müller, Hartmut Herrmann, *The Size- and Time-Resolved Determination of the Water-Soluble Organic Fraction of Submicron Aerosol Particles from the Beijing Area*.
4P310	989	Aerosol Cloud	**Ilona Riipinen**, Jeffrey R. Pierce, Taina Yli-

		Interaction	Juuti, Silja Häkkinen, Christos Fountoukis, Markku Kulmala, Douglas R. Worsnop, Merete Bilde, Spyros N. Pandis, Neil M. Donahue, *On ultrafine aerosol growth and the condensation/evaporation properties of atmospheric organics*.
4P311	993	Aerosol Cloud Interaction	**Su Hang**, Diana Rose, Yafang Cheng, Sachin S. Gunthe, Alfred Wiedensohler and Ulrich Pöschl, *Aerosol hygroscopicity distribution in size-resolved CCN measurements: the concept, validation and applications*.
4P312	1022	Aerosol Cloud Interaction	**Ondrej Vlcek**, L Corbet, J Licki, K Zemankova, *Effect of the biogenic emissions of isoprene and monoterpene on the CAMx model results in Central and South Europe*.
4P314	1117	Aerosol Cloud Interaction	**Ying I. Tsai**, Su-Ching Kuo, Chien-Lung Chen, Li-Ying Hsieh, Pei-Ling Wu, Yi-Hui Lee, *Chemical contribution of dicarboxylic acids to wet deposition and acidity of wet deposition in southern Taiwan*.

13:00-15:00 **Session 5A: PM Sources**

Room: Theatre A

Chairs: Sabine Wurzler / Oliver Bischof

13:00	5A1	1127	**Michael Gatari**, Johan Boman, Sofia Thorsson, Anna Mooe *Particle size distribution, number concentration, CO and sources of aerosol particles in Nairobi, Kenya*
13:20	5A2	838	**Carmen Nickel**, Heinz Kaminski, Bryan Hellack, Thomas A.J. Kuhlbusch *Source apportionment, surface area and particle number concentration analysis of ultra fine particles at an urban background station in the Ruhr area, Germany*
13:40	5A3	973	**Liisa Pirjola**, Aki Pajunoja, Aleksi Malinen, Jari Walden, Jukka-Pekka Jalkanen, Topi Rönkkö *Mobile measurements of ship emissions in two*

			harbour areas in Finland
14:00	5A4	586	**Gary Fuller**, Anja Tremper, Timothy Baker, Karl Espen Yritt, David Butterfield, Ian Mudway, Rosamund Dove, Frank Kelly *Contribution of biomass burning to London's PM10*
14:20	5A5	880	**Barbara D'Anna**, Nicolas Marchand, Jean-Luc Jaffrezo, Chrstian Georgem Olivier Favez, Antoinette Boreave, Melanie Nicolas, Imad El Haddad, Henry Wortham, A. Armengaud, C. Piot, J-L Desombes *Source apportionment of fine aerosol in Marseille and Grenoble*
14:40	5A6	922	**Andreas Massling**, Matthias Ketzel, Thomas Ellermann, Jacob K. Nøjgaard, Bjarne Jensen, Claus Nordstrøm, Peter Wåhlin *Measurements of the urban Copenhagen aerosol from 2002 – 2010: physical properties and their trends*
Reserve	5AR	1100	**Holger Gerwig**, Werner Pecher, Klaus Wirtz *Local sources of UFP at an urban BG station*

13:00-15:00 **Session 5B: Aerosol-Cloud Interactions 2**
Room: Theatre B
Chairs: Martin Gysel / Heike Wex

13:00	5B1	481	**Keith Bower**, Jonathan Crosier, Thomas Choularton, Paul Connolly, Chris Dearden, Martin Gallagher, James Dorsey, Gerard Capes, Chris Westbrook. Zhiqiang Cui, Alan Blyth *Observations and Modelling of Cloud-Aerosol Interaction in Mixed Phase Frontal Layer Cloud*
13:20	5B2	1011	**Di Chang**, Hang Su, Philipp Reutter, Jörg Trentmann, Meinrat O. Andreae, Ulrich Pöschl *The effects of biomass burning aerosols on the formation of convective mixed-phase clouds and precipitation*

13:40	5B3	844	**Martina Krämer**, J. Meyer , A. Afchine, D. Baumgardner, R. Newton, A. Abdelmonem, S. Benz, O. Möhler, M. Schnaiter *Partitioning of drops & ice in mixed phase clouds: laboratory and field observations*
14:00	5B4	857	**Nicolas Bukowiecki** *On the activation and ambient peak supersaturation of CCNs at Jungfraujoch, Switzerland (3580 m asl): Results from the CLACE 2010 campaign*
14:20	5B5	660	**Erik Fors** *Indirect measurement of water vapour supersaturation ratios in continental boundary layer clouds using H-TDMA and DMPS data*
14:40	5B6	980	**Greg Roberts**, S.D. Noblitt, J.M. Creamean, J.L. Collett, C.S. Henry, S.V. Hering, K.A. Prather *Linking CCN chemistry and supersaturation spectra: characterizing cloud-active aerosol in California's Sierra Nevada Mountains*
Reserve	5BR	350	**Anja Roth**, Stephan Mertes, Dominik van Pinxteren, Thomas Klimach, Johannes Schneider, Stephan Borrmann *Analysis of cloud and aerosol particles by single particle mass spectrometry during a hill-cloud-field experiment in Central Europe*

13:00-15:00 **Session 5C: Smog Chamber Experiments and SOA 1**
Room: Rutherford Lecture Theatre
Chairs: Yoshi Inuma / Rami Alfarra

13:00	5C1	802	**Josef Dommen**, Torsten Tritscher, Peter DeCarlo, Peter Barmet, Arnaud Praplan, Ernest Weingartner, Martin Gysel, Andre Prevot, Neil Donahue, Urs Baltensperger *Aging of secondary organic aerosol in a smog chamber*

13:20	5C2	771	**Ari Leskinen**, Kari Kuuspalo, Olli Sippula, Pasi Jalava, Maija-Riitta Hirvonen, Jorma Jokiniemi, Kari Lehtinen *Transformation of diesel exhaust in a new smog chamber*
13:40	5C3	599	**Erik Nordin**, Axel Eriksson, Jonatan Carlsson, Patrik Nilsson, Maija Kajos, Pontus Roldin, Jenny Rissler, Erik Swietlicki, Birgitta Svenningsson, Mats Bohgard, Markku Kulmala, Mattias Hallquist, Joakim Pagels *Smog Chamber Studies on SOA Formation from Gasoline Exhaust and Pure Precursors*
14:00	5C4	988	**Stephen Platt** *Investigations of primary and secondary organic aerosol emissions from mopeds*
14:20	5C5	163	**Eszter Horváth**, András Gelencsér, András Hoffer, Csaba Dobolyi, Flóra Sebok, Sándor Szoboszlay, Balázs Kriszt *Microscopic fungi as significant sesquiterpene emission sources*
14:40	5C6	440	**Stephanie Rossignol**, Laura Chiappini, Emilie Perraudin, Jean-François Doussin *Study of SOA formation from limonene ozonolysis in indoor environments: a new approach involving simultaneous investigation of gas and particulate phases molecular composition*
Reserve	5CR	373	**Zhijun Wu**, L. Poulain, O. Böge, R. Gräfe , H. Herrmann, A. Wiedensohler, Helbig, T. Schröder, J. von Sonntag, I. Hartmann *Modifications in hygroscopicity and volatility of wood combustion aerosols after chemical aging*

13:00-14:40 **Session 5D: Aerosols in Disease and Therapy**
Room: Moseley Lecture Theatre
Chair: Darragh Murnane

13:00	5D1	171	**Richard Thomas** *Large particle aerosols within high level microbiological containment*
13:20	5D2	1142	**Tom Pottage**, Allan Bennett, Simon Parks *Anthrax, aerosols and drums*
13:40	5D3		**Lea Ann Dailey**, *From deposition to molecular action – studies from the interface*
14:00	5D4		**Sean J Cheng,** *Controlling dry powder inhaler performance by using computational fluid dynamics to tune miniature cyclone separators*
14:20	5D5		**Darragh Murnane,** *Understanding fine particle interactions in powder delivery systems*

13:00-15:00 **Session 5E: Health Effects of Nanoparticles**
Room: Bragg Lecture Theatre
Chairs: Hanns-Rudolf Paur / Wendelin Stark

13:00	5E1	112	**Georgios Sotiriou** *Antibacterial activity by nanosilver ions and particles*
13:20	5E2	504	**Helmi Keskinen**, Romakkaniemi, Sami, Jaatinen, Antti, Miettinen, Pasi, Saukko, Erkka, Joutsensaari, Jorma, Mäkelä, Jyrki, Virtanen, Annele, Smith, James, and Laaksonen, Ari *Water uptake on silica nanoparticles*
13:40	5E3	682	**Christian Svensson**, Maria Messing, Alexander Schollin, Knut Deppert, Bengt Meuller, Joakim Pagels, Jenny Rissler, Mats Bohgard, Sara Linse, Tommy Cedervall *Direct deposition of aerosol generated AuNPs into biological buffers produce specific protein corona in*

			lung-fluid and blood serum
14:00	5E4	349	**Joonas Koivisto**, Mikko Aromaa, Jussi Lyyranen, Ari Auvinen, Jorma Jokiniemi, Kaarle Hämeri *Assessing inhalation exposure to nanoparticles during nanoparticle synthesis and packing*
14:20	5E5	260	**Luana Golanski** *Release-ability of nano fillers from different nanomaterials*
14:40	5E6	829	**Robert N. Grass**, K. Birbaum, L.K. Limbach, E. Martinoia, D. Gunther, W.J. Stark *No evidence of cerium oxide nanoparticle translocation in maize plants*
Reserve	5ER	218	**Jussi Lyyränen**, Merja Järvelä, Timo Tuomi, Joe Pimenoff, Ari Auvinen, Jorma Jokiniemi *Characterisation of CeO2 engineered nanoparticles from a liquid flame spray process – exposure of workers*

13:00-15:00 **Session 5F: Aerosols in Turbulent Flows 1**
Room: Blackett Lecture Theatre
Chair: Alain Pumir

13:00	5F1	917	**Bernhard Mehlig**, Kristian Gustavsson *Distribution of relative velocities in turbulent aerosols*
13:20	5F2	977	**Michael Reeks**, Elena Meneguz *Statistical properties of particle segregation in homogeneous isotropic turbulence*
13:40	5F3	315	**Roar Skartlien** *Particle and droplet transport in turbulence and inertial effects*
14:00	5F4	1070	**Mathieu Gibert**, Simon Klein, Eberhard Bodenschatz *Full motion measurement of finite-size neutrally buoyant particles together with the turbulent flow field carrying them*

14:20	5F5	140	**Max Eggersdorfer**, Dirk Kadau, Hans J. Herrmann, Sotiris E. Pratsinis *Aerosol Coagulation & Break-up in Homogeneous Isotropic Turbulent Flows*
14:40	5F6	669	**Fan Zhang**, Mike Reeks, Martin Kissane *Particle Resuspension Modeling in Turbulent Flows*

15:30-17:10 **Session 6A: New Particle Formation 3: Theory and Modelling**
Room: Theatre A
Chairs: Boris Bonn / Amar Hamed

15:30	6A1	910	**Christos Fountoukis** *Simulating Ultrafine Particle Formation in Europe using the 3-D Chemical Transport Model PMCAMx-UF*
15:50	6A2	75	**Theo Kurten**, Joseph Lane, Solvejg Jørgensen, Camilla Jensen, Henrik Kjaergaard *Computational studies of atmospheric sulfur oxidation mechanisms*
16:10	6A3	911	**Adam Kristensson**, Erik Swietlicki, Birgitta Svenningsson, Tareq Hussein, Tuomo Nieminen, Mikka Dal Maso, Heikki Junninen, Hanna Manninen, Vidmantas Ulevicius, Markus Fiebig, Peter Tunved, Johan Ström, Andreas Massling, Markku Kulmala *Geographical mapping of new particle formation events over Northern Europe*
16:30	6A4	549	**Ismael Kenneth Ortega Colomer**, Oona Kupiainen, Theo Kurten, Hanna Vehkamaki *Formation of neutral sulphuric acid clusters containing base molecules*
16:50	6A5	628	**Neil Donahue**, Erica Trump, Ilona Riipinen, Jeffrey Pierce *Growth of Particles via Organic Condensation: Is Gas-Phase Chemistry Enough?*

Reserve	6AR	105	**Hannele Korhonen**, Sanna-Liisa Sihto, Veli-Matti Kerminen, Kari E.J. Lehtinen *How accurate are the nucleation event analysis tools?*

15:30-17:10 **Session 6B: Climate Effects of Aerosols / Transport and Transformation**

Room: Theatre B

Chairs: Andreas Held / Eiko Nemitz

15:30	6B1	930	**Jonatan Carlsson**, Jenny Rissler, Erik Nordin, Axel Eriksson, Patrik Nilsson, Cerina Wittbom, Maija Kajos, Pontus Roldin, Erik Swietlicki, Birgitta Svenningsson, Mats Bohgard, Markku Kulmala, Joakim Pagels *Atmospheric processing of diesel soot aerosols studied in a smog chamber*
15:50	6B2	813	**Thomas Bjerring Kristensen**, Heike Wex, Bettina Nekat, Dominik van Pinxteren, Katrin Mildenberger, Frank Stratmann, Jacob K. Nøjgaard, Christian B. Koch, Anna G. Hallar, Thomas F. Mentel, Merete Bilde *Hygroscopic properties of HULIS from different environments*
16:10	6B3	820	**Wolfgang Junkermann**, Bernhard Vogel, Mark Sutton *On the regional effects of clean fossil fuel combustion aerosols*
16:30	6B4	683	**Rafaella - Eleni Sotiropoulou**, Nicholas Meskhidze, Jules Kouatchou, Lazaros Oreopoulos, Jose M. Rodriguez, and Athanasios Nenes *Sensitivity of cloud radiative forcing to cloud formation parameterization under three different meteorological fields*
16:50	6B5	289	**Helmuth Horvath**, Alexander Cheremisin, I. Shnipkov

			The global picture of aerosol layers formation in the stratosphere and in the mesosphere under the influence of gravito- and magneto-photophoretic forces.

15:30-16:50 **Session 6C: Smog Chamber Experiments and SOA 2**
Room: Rutherford Lecture Theatre
Chairs: Josef Dommen / Harald Saathoff

15:30	6C1	1002	**Eleni Athanasopoulou**, Heike Vogel, Max Bangert, Christoph Knote, Bernhard Vogel, Ben Murphy, Alexandra Tsimpidi, Spyros Pandis, *Simulating secondary organic aerosol (SOA) formation over Europe using the volatility basis-set approach (VBS) in the online coupled model COSMO-ART*.
15:50	6C2	583	**M. Rami Alfarra**, Jacqui Hamilton, Kevin Wyche, Timo Carr, Annette Ryan, Rogelio Ayala, Paul Monks, Robert MacKenzie, Alastair Lewis, Nick Hewitt, Gordon McFiggans *Chemical composition, Hygroscopicity and CCN properties of biogenic secondary organic aerosols*
16:10	6C3	801	**Eva Emanuelsson**, B. Bohn, A. Buchholz, B. Kammer, A. Kiendler-Scharr, B. Kortner, Th. F. Mentel, S. Nehr, R. Tillmann, E. Kleist, K. Kristensen, M. Fenger-Lauridsen, M. Glasius, M. Hallquist *Physical and chemical characterisation of mixed anthropogenic and biogenic secondary organic aerosol*
16:30	6C4	279	**Marco Paglione**, Stefano Decesari, Emanuela Finessi, Risto Hillamo, Samara Carbone, Sanna Saarikoski, Tomi Raatikainen, Manuel Dall'Osto, Colin O'Dowd, Astrid Kiendler-scharr, Amewu Mensah, Urs Baltensperger, Andre Prevot, Douglas Worsnop, MariaCristina Facchini *Source apportionment of atmospheric organic aerosols by nuclear magnetic resonance (NMR)*

			spectroscopy during the EUCAARI project
16:50	6C5	1145	**Urs Baltensperger**, Maarten Heringa, Roberto Chirico, Stephen Platt, Lisa Pfaffenberger, Peter Barmet, Jay Slowik, Peter DeCarlo, Josef Dommen, Andre Prevot *Discrimination of secondary organic aerosol from different sources*
Reserve	6CR	282	**Boris Bonn**, Friedemann Ebach, Matthias Hummel, Stratos Bourtsoukidis, Boris Bonn, Werner Haunold, Robert Sitals, *Understanding particle formation by alkene-ozone reactions: Experimental studies and theoretical simulations*.

15:30-17:10 **Session 6D: Direct Impacts of Aerosol on Climate (ADIENT Project)**
Room: Moseley Lecture Theatre
Chairs: Don Grainger / Gareth Thomas

15:30	6D1	318	**Will Morgan**, James Allan, Michael Bane, Keith Bower, Bethan Harris, Bas Henzing, Eleanor Highwood, Astrid Kiendler-Scharr, Gordon McFiggans, Gavin McMeeking, Amewu Mensah, Simon Osborne, Megan Northway, Paul Williams, Radovan Krejci, Hugh Coe *Measurement and modelling of ammonium nitrate aerosol and its impacts in North-Western Europe*
15:50	6D2	234	**Eleanor Highwood**, Megan Northway, Gavin McMeeking, Hugh Coe, William Morgan, Dantong Liu, Claire Ryder, Paul Williams, Keith Bower, Simon Osborne *Optical and Radiative Properties of Aerosol as Determined During the ADIENT Project*
16:10	6D3	291	**Gareth Thomas**, Nicky Chalmers, Bethan Harris, Ellie Highwood, Don Grainger *ADIENT satellite based aerosol direct radiative forcing*

16:30	6D4	278	**Helen Brindley**, Alexandros Georgiadis, Jacqueline Russell *Testing methods to derive top of the atmosphere reflected shortwave fluxes in the presence of aerosol during the ADIENT campaign: application to GERB and SEVIRI*

15:30-17:30 **Session 6E: Enhanced Aerosol Measurement Technology**
Room: Bragg Lecture Theatre
Chairs: Jim Davis / Martin Fierz

15:30	6E1	856	**Peter Jani**, Lenard Vamos, Attila Nagy, Attila Kerekes *Nanoparticle measurements with photon correlation LDA*
15:50	6E2	864	**Axel Eriksson**, A.C. Eriksson, E. Z. Nordin, P. T. Nilsson, J. E. Carlsson, C. Wittbom P. Roldin, M.K. Kajos, J. Rissler , F. Abdisa, M. Hallquist, M. Kulmala, B. Svenningssson, J. Pagels and E. Swietlicki *Soot Particle AMS measurement in smog chamber experiments*
16:10	6E3	787	**Erkka Saukko**, Heino Kuuluvainen, Annele Virtanen *Aerosol particle phase state measurement technique using a low pressure impactor*
16:30	6E4	527	**James Davies**, Allen Haddrell, Jon Wills, Jonathan Reid *Rapid measurements of single aerosol droplets in conditions far from equilibrium using an electrodynamic balance*
16:50	6E5	732	**Regina Hitzenberger**, Elisabeth Traxler, Bernadette Rosati *Interferences in thermo-optical measurements of elemental and organic carbon caused by other aerosol constituents*

17:10	6E6	88	**Constantinos Sioutas**, Nancy Daher, Zhi Ning, Arthur K. Cho, Martin Shafer, James J. Schauer *Comparison of the chemical and toxicological characteristics of particulate matter (PM) collected by different methods: filters, impactors and BioSamplers*
Reserve	6ER	902	**Harald Bresch**, Falk Reinhardt, Ulrich Waldschlaeger, Beatrix Pollakowski, Burkhard Beckhoff, Stefan Seeger *Size selected nanoparticle quantification of deposited aerosol by GIXRF*

15:30-17:10 **Session 6F: Aerosols in Turbulent Flows 2**
Room: Blackett Lecture Theatre
Chair: Mike Reeks

15:30	6F1	587	**Charles Clement** *Turbulence and Condensation*
15:50	6F2	867	**Juergen Vollmer** *Rain in the test tube?*
16:10	6F3	1128	**Andrew Bragg**, David C Swailes *Non-local closure model for particle dispersion tensors in a turbulent boundary layer*
16:30	6F4	826	**Michael Wilkinson**, Alain Pumir *Tumbling in turbulence and irrational quantisation*
16:50	6F5	1124	**Alain Pumir** *Motion of large particles in turbulent flow: rotational motion and lift*
17:10	6F6	669	**Fan Zhang**, Mike Reeks, Martin Kissane *Particle Resuspension Modeling in Turbulent Flows*

17:10-18:00 EAA Working Group meetings

Aerosol Modelling	Theatre A
Aerosol Chemistry	Rutherford Theatre
Aerosol-based Nanotechnology	Blackett Theatre
Atmospheric Aerosols	Theatre B
PMx	Moseley Theatre

NOTES:

Wednesday 7th September

09:00-10:00 Plenary 3
Uta Griesenbach: UK Cystic Fibrosis Gene Therapy Consortium: Developing and Delivering a Complex Respiratory Therapy
Room: Theatre B
Chair: Darragh Murnane

10:00-10:15 Awards Ceremony Theatre B

10:45-12:45 **Session 7A: Carbonaceous Aerosol and Meteorology**
Room: Theatre A
Chairs: Regina Hitzenberger / Andre Prevot

10:45	7A1	588	**Jonathan Taylor** *Changes in black carbon undergoing SOA coating measured with SP2, SP-AMS and optical instruments.*
11:05	7A2	950	**Sandra Wagener**, Marcel Langner, Ute Hansen, Heinz-Joern Moriske, Wilfried Endlicher *Spatial and seasonal variations of biogenic organic compounds in ambient PM10 and PM1 samples in Berlin*
11:25	7A3	225	**James Allan**, Jonathan Taylor, Michael Flynn, Hugh Coe, Tim Onasch, Paola Massoli, John Jayne, Douglas Worsnop, Greg Kok, Xiaolu Zhang and Rodney Weber *Composition and Optical Properties of Black Carbon and its Coatings in the Los Angeles Area During CalNex*
11:45	7A4	611	**Godwin Ayoko**, Leigh Crilley, Mandana Mazaheri, Graham Johnson, Lidia Morawska, Eduard Stelcer and David Cohen *Effect of vehicle emissions on the chemical composition of airborne particulates in urban schools*

12:05	7A5	990	**Hang Su**, Y. Cheng, A. Wiedensohler, M. Berghof, B. Wehner, P. Achtert, A. Nowak, D. Rose, S. Gunthe, Y. Gong, N. Takegawa, Y. Kondo, M. Shao, M. Hu, T. Zhu, L. M. Zeng, U. Pöschl, Y. H. Zhang *Size-resolved mixing state of soot (black carbon) particles in the Beijing Megacity, China: aging rates, the condensable vapor pressure and parameterizations*
12:25	7A6	584	**Claire Ryder**, Ralf Toumi *Does aerosol in London create an urban solar flux island?*
Reserve	7AR	1043	**Kornélia Imre**, András Gelencsér, Ágnes Molnár, Viktor Dézsi *Role of the hysteresis and water content in PM10 measurements*

10:45-12:45 **Session 7B: Aerosol-Cloud Interactions 3**
Room: Theatre B
Chairs: Paul Connolly / Katrin Mildenberger

10:45	7B1	386	**Dominik van Pinxteren** *Hill Cap Cloud Thuringia 2010 (HCCT-2010) – Overview and first results*
11:05	7B2	577	**Johannes Schneider**, Anja Roth, Stephan Mertes, Dominik van Pinxteren, Stephan Borrmann *Microphysical and chemical characterization of cloud droplets, cloud droplet residuals, and interstitial aerosol particles during a hill-cloud field experiment in Central Europe*
11:25	7B3	202	**Ming Chee Yeung**, Chak K. Chan *Understanding phase transition and hygroscopic behavior of organic acid particles and their mixtures with ammonium sulfate by micro-Raman spectroscopy*

11:45	7B4	1031	**Staffan Sjogren**, E. Fors, E. Swietlicki, M. Martin, B. Sierau *Cloud Condensation Nuclei Closure Study on Summer Arctic Aerosol*
12:05	7B5	937	**Noenne Prisle**, D. Topping, S. Romakkaniemi, G. McFiggans, M. Dal Maso, H. Kokkola *Importance of different surfactant representations for cloud droplet numbers predicted with the ECHAM5.5-HAM2 aerosol-climate model*
12:25	7B6	947	**Max Bangert**, Athanasios Nenes, Bernhard Vogel, Heike Vogel, Donifan Barahona, Prashant Kumar *The impact of mineral dust particles on cloud properties and the state of the atmosphere during an intense Saharan dust event over Western Europe*
Reserve	7BR	265	**Florian Ditas**, Birgit Wehner, Holger Siebert, Heike Wex, Gregory C. Roberts, Katrin Mildenberger, Tina Schmeißner, Frank Stratmann, Alfred Wiedensohler *Aerosol number size distributions in the vicinity of trade wind cumuli*

10:45-12:45 **Session 7C: High Temperature Systems: Sampling and Quenching before Detection**

Room: Rutherford Lecture Theatre

Chairs: Jorma Jokiniemi / Ralf Zimmermann

10:45	7C1	292	**Santiago Jiménez**, Javier Ballester *Experimental study of aerosols and vapours at high temperatures: past and recent application of aerodynamic quenching*
11:05	7C2	322	**Jarmo Kalilainen**, Teemu Kärkelä, Ari Auvinen, Pekka Rantanen, Johanna Forsman, Leif Kåll, Jorma Jokiniemi *Automated sampling system for studying iodine chemistry at high temperature*

11:25	7C3	690	**Ralf Zimmermann**, T.Streibel, M.Sklorz, C. Busch, M.Elsasser, J.Schnelle-Kreis, C. Deuerling, J.Orasche, T. Adam, M.C. Astorga-Llorens, H.Hartmann *On-line measurement of chemical composition and size distribution of high-temperature combustion aerosols*
11:45	7C4	702	**Michael Strand**, Eva Gustafsson, Leteng Lin, Jingjing Yang *High-Temperature extraction of aerosol particles from biomass combustion and gasification*
12:05	7C5	723	**Olli Sippula**, Jarno Ruusunen, Tarmo Koponen, Mika Ihalainen, Jorma Jokiniemi *Porous tube diluting probe for high temperature sampling of aerosols*
12:25	7C6	874	**Miren Larrion**, Cristina Gutierrez-Canas, Luisa Marroquin, Gaizka Aragon, Inaki Mugica, Egoitz Pena and Juan Andres Legarreta *The effect of dilution and cooling on the chemistry and structure of samples from stainless steel and Al welding fumes*

10:45-12:45 **Session 7D: Particle-Lung deposition and Pharmacological Aerosol**

Room: Moseley Lecture Theatre

Chair: Jan Marijnissen / David Broday

10:45	7D1	687	**Caner Yurteri**, J.C.M. Marijnissen *Producing Drug particles for Inhalation via Electrospray*
11:05	7D2	518	**Ross Cabot** *Development of an anatomically correct segmented model of the human mouth for deposition studies of the particle and vapour phase of tobacco smoke during inhalation*

11:25	7D3	393	**Winfried Möller**, Uwe Schuschnig, Gülnaz Khadem Saba, Gabriele Meyer, Manfred Keller, Karl Häussinger and Wolfgang G. Kreyling *Pulsating Aerosols for Topical Treatment of Upper Airway Diseases*
11:45	7D4	79	**Andrei Onischuk**, Tatiana Tolstikova, Irina Sorokina, Anatoly Baklanov,Vladimir Karasev, Vladimir Boldyrev,Vasilyi Fomin *Anti-inflammatory and analgesic effect from nanoparticlate non-steroid anti-inflammatory drugs inhaled by male mice*
12:05	7D5	158	**Alison Buckley**, Rachel Smith, Robert Maynard *Carbon Nanotubes – too "big" AND too "small" to deposit efficiently in the lungs?*
12:25	7D6	1061	**Lukas Pichelstorfer**, Werner Hofmann *Modelling coagulation of liquid particles within the human respiratory system*
Reserve	7DR	837	**John McAughey**, Colin Dickens *Regional lung deposition of tobacco smoke constituents*

10:45-12:45 **Session 7E: New Developments in Aerosol Instrumentation**

Room: Bragg Lecture Theatre

Chairs: Oliver Bischof / Martin Pesch

10:45	7E1	257	**Chuen-Jinn Tsai** *A Novel IOSH-NCTU Personal Nanoparticle Sampler*
11:05	7E2	233	**Chris Stopford**, Paul Kaye, Edwin Hirst, Richard Greenaway, Warren Stanley *Portable real-time detection of airborne asbestos fibres for tradespersons*
11:25	7E3	191	**Maria Giamarelou**, Giorgos Biskos *The Transfer Function and the Resolution of a DMA with Multiple Monodisperse Outlets: Sensitivity Analysis for the Case with the Two Monodisperse*

			Particle Outlets
11:45	7E4	369	**Francisco Romay**, Aaron M. Collins, William D. Dick, Benjamin Y.H. Liu *Development and Characterization of a Novel Approach for Water-Based Condensation Growth of Aerosols*
12:05	7E5	919	**Markus Gaelli**, Kathleen Erickson, Fred Quant, Rob Caldow, Sean Morell, Jeremy Kolb, Brian Osmondson, Edwin Pickens *Comparison Testing of Model 3783 Environmental Particle Counters*
12:25	7E6	750	**Soohyun Ha**, Chirag K. Vyas, Atul Kulkarni, Vijay K. Manchanda, Taesung Kim *A Novel Optical Real Time Sensor for Radioactive Aerosol*
Reserve	7ER	365	**Martin Fierz**, Peter Steigmeier, Michael Glettig, Benjamin Wyrsch, Heinz Burtscher *Direct integration of a GPS-GPRS unit into a miniature diffusion size classifer*

10:45-12:45 **Session 7F: Modelling Nuclear Particles and Health Effects**

Room: Blackett Lecture Theatre

Chairs: A. Jones / E. Nemitz

10:45	7F1	534	**Alan Jones**, Roland Zeyen *Nuclear aerosols in primary circuit and containment: a review of the Phebus experiments*
11:05	7F2	772	**Claudia Lopez del Pra**, Luis E. Herranz *Uncertainty Analysis of Aerosol Retention in the Break Stage of a Vertical Steam Generator under SGTR Accident Conditions*
11:25	7F3	925	**Martin Lustfeld**, Thomas Barth, Manuel Banowski *Multilayer deposition and resuspension studies of aerosol particles between periodic steps in turbulent channel flows*

11:45	7F4	366	**David Broday**, Rob Levy, Ayala Cohen *Classification of Dust Days over Israel by Integration of Satellite Remote Sensing Products*
12:05	7F5	585	**Jakob Löndahl**, Erik Swietlicki, Elisabet Lindgren, Steffen Loft *Aerosol exposure in combination with aerosol impacts on climate: What is the total health outcome?*
12:25	7F6	439	**Mingzhou Yu** *Modeling and Measurement of ENP Dynamics in a Ventilated Two-Zone Chamber*
Reserve	7FR	399	**Eiko Nemitz**, Massimo Vieno, Ulrike Dragosits, Chiara F. Di Marco, Marsailidh Twigg, Mark A. Sutton *The response of PM concentrations in the UK to changes in industrial and agricultural emissions: implications for the exceedance of Air Quality Standards*

13:45-14:30 Alan Cussens Award, Bragg Theatre

NOTES:

Thursday 8th September

09:00-10:00 Plenary 4
Phil Rasch: The scientific challenges involved in using aerosols as a strategy for geoengineering climate.
Room: Theatre B
Chair:Charles Clement

10:30-12:00 Session 8P: Poster session B
Location: Poster Marquee and adjacent to Theatre B

Combustion Aerosols			
8P1	72	Industrial aerosols	**Rainer Jonas**, Gerfried Lindenthal, *Determination of loss factors of aerosol particles in the sampling systems of nuclear power plants*.
8P2	141	Industrial aerosols	**Chang-Mao Hung**, *Development of high-performance Cu-La nanomaterials as efficient catalyst for ammonia removal*.
8P3	182	Industrial aerosols	**Lin-Chi Wang**, *Global control strategies for polybrominated diphenyl ethers require significant changes*.
8P4	238	Industrial aerosols	**Ting-Yu Hsieh**, W.J. Lee, L.P. Changand L.C. Wang, *Polybrominated diphenyl ethers (PBDEs) in the stack flue gases*.
8P5	248	Industrial aerosols	**Chih-Chung Lin**, Shui-Jen Chen, Jen-Hsiung Tsai, Kuo-Lin Huang, Wu-Jou Yu, Chun-Li Chou, *Particle size distributions of ambient aerosol in the vicinity of semiconductor plants*.
8P6	268	Industrial aerosols	**Jose Luis Dorronsoro Arenal**, J.Rodriguez Maroto, D. Sanz Rivera, E. Rojas García, M. Fernández Díaz, P. Galán Valera and E. Conde Vilda, *Distributions of heavy metal traces by particle size (PM10, PM2.5 y PM1). Emissions from non ferrous smelters* .
8P7	396	Industrial aerosols	**Elzbieta Jankowska**, *Workplace exposure to fine particles from welding fumes*.
8P8	515	Industrial aerosols	**Andrei Bologa**, Hanns.-Rudolf Paur, Helmut Seifert, Friedhelm Weirich, Klaus Woletz, *Study of*

			particle chemical composition and size distribution in the pyrolysis gas flow.
8P9	541	Industrial aerosols	**Tomasz Jankowski**, *Evaluation of the efficiency of the fume cupboards in the laboratory*.
8P10	615	Industrial aerosols	**Shun-I Shih**, W.J. Lee, Y.C. Hsu, Z.S. Wu, L.C. Wang, G.P. Chang-Chien, *Removal of Polychlorinated Dibenzo-p-dioxins and Dibenzofurans for physico-chemical pre-treatment and thermal treatment of Electric Arc Furnace fly ashes*.
8P11	107	Automotive combustion aerosols	**Gabriele Hörnig**, Reinhard Niessner, *The role of diffusiophoresis in fouling of exhaust gas recirculation heat exchangers*.
8P12	184	Automotive combustion aerosols	**Jen-Hsiung Tsai**, Shui-Jen Chen, Kuo-Lin Huang, Shiunn-Cheng Chuang, Lin-Chi Wang, Chih-Chung Lin, *Characterizations of PCDD/Fs emitted from gasoline and diesel fueled vehicles*.
8P13	203	Automotive combustion aerosols	**Lothar Keck**, Markus Pesch, Matthias Richter, Georg Reischl, *Performance of a new condensation particle counter for engine exhaust gas (PMP-CPC)*.
8P14	215	Automotive combustion aerosols	**Johannes Schmid**, Benedikt Grob, Reinhard Niessner and Natalia P. Ivleva, *Characterization of soot structure and reactivity based on Raman microspectroscopy*.
8P15	294	Automotive combustion aerosols	**Wen-Yinn Lin**, Shui-Jen Chen, Shiunn-Cheng Chuang, Kuo-Lin Huang, Lin-Chi Wang, Juei-Yu Chiu, Chuen-Huey Chiu, Chih-Chung Lin, *Characterization of PCDD/Fs emitted from motorcycles*.
8P16	489	Automotive combustion aerosols	**Svetlana Stevanovic**, Branka Miljevic, Nicholas Surawski, Steven Bottle, Richard Brown, Zoran Ristovski, *Reactive oxygen species (ROS) emissions from diesel engines running on various biofuels*.
8P17	516	Automotive combustion aerosols	**Reinhard Niessner**, *Electrical conductivity as sensor principle for a sensor to measure soot aerosols*.
8P18	540	Automotive combustion aerosols	**Jan-Christoph Wolf**, Reinhard Niessner, *Laboratory investigation of post-combustion nitro-PAH formation*.

8P20	658	Automotive combustion aerosols	**Anssi Arffman**, Topi Rönkkö, Panu Karjalainen, Tero Lähde, Juha Heikkilä, Liisa Pirjola, Dieter Rothe, Jorma Keskinen, *Thermodenuder with low nanoparticle losses: design, simulations, laboratory tests and diesel exhaust particle studies*.
8P21	758	Automotive combustion aerosols	**Souzana Lorentzou**, Margaritis Kostoglou, Athanasios Konstandopoulos, *Microstructural Aspects of Catalytic Soot Oxidation in Diesel Particulate Filters*.
8P22	762	Automotive combustion aerosols	**Ken-Hui Chang**, W.Y. Lin, J.Y. Syu, Y.Y. Chang, C.C. Chen, *Effects of Emulsion Fuels on the Characterization of Exhaust from a Diesel Engine Generator*.
8P23	805	Automotive combustion aerosols	**Souzana Lorentzou**, Dimitrios Zarvalis, Ioannis Dolios, Christodoulos Lekkos, Christos Agrafiotis, Athanasios Konstandopoulos, *Pilot-Scale Aerosol Infiltration Synthesis and Deposition of Catalyst Particles on Diesel Particulate Filters*.
8P24	987	Automotive combustion aerosols	**Michal Vojtisek-Lom**, Martin Mazac, Rafael Lozano Espasandin, *Particulate matter emissions from a winter operation of a modern on-road diesel engine powered by heated rapeseed oil*.
8P25	1138	Automotive combustion aerosols	**Markus Pesch**, Georg Reischl, Lothar Keck, *A new device for high speed measurements of nano particles*.
Particle-Lung Interactions			
8P26	175	Dosimetry and detection of particles in organisms tissues and cells	**Der-Jen Hsu**, Ming-Hsiu Chuang, *Deposition efficiency of micro-size particles in the upper airway of Taiwanese adults*.
8P27	312	Biological response of organisms cells and proteins to particle exposure	**Takako Oyabu**, T. Myojo, Y. Morimoto, A. Ogami, M. Hirohashi, Y. Mizuguchi, M. Hashiba, T. Kambara, BW. Lee, I. Tanaka, *Biopersistence and pulmonary effects of intratracheally instilled titanium dioxide nanoparticles at four different doses to rat lungs*.
8P28	355	Biological	**Dirk Broßell**, Sabine Plitzko, Nico Dziurowitz,

		response of organisms cells and proteins to particle exposure	Erhardt Gierke, Volker Bachmann, Gunter Linsel, Nkwenti Azong-Wara, Christof Asbach, Heinz Fissan, Andreas Schmidt-Ott, *A Thermal Precipitator for Nanoparticle Cytotoxicity Screening*.
8P29	415	Biological response of organisms cells and proteins to particle exposure	**Marco Sala**, *A 3-year-follow-up Study of Traffic Related Respiratory Alterations in Schoolchildren in Milan, Italy*.
8P30	416	Biological response of organisms cells and proteins to particle exposure	**Francesco Cetta**, *Alteration of respiratory function in asymptomatic subjects living in Milan (Italy) and in Aprica (Italy), an Alpine site with different levels of environmental pollution. Spirometric and laboratory evaluation.*
8P31	417	Biological response of organisms cells and proteins to particle exposure	**Luigi Allegra**, *A plea for a more "doubtful" and "skeptic" approach to the role of intrinsic toxicity of airborn pollutants as the main responsible for observed cardiovascular, respiratory and cancerous diseases or deaths in humans.*
8P32	374	Aerosol-based medical diagnostics and drug delivery	**Lukasz Zywczyk**, *Deposition of aerosol particles in dosing tubes (endotracheal tubes) used in aerosol drugs therapy for infants*.
8P33	426	Aerosol-based medical diagnostics and drug delivery	**Laura Moltoni**, *"Perinatal susceptible window" as a main responsible for cardiovascular and respiratory diseases occurring later in life because of PM exposure*.
8P34	428	Aerosol-based medical diagnostics and drug delivery	**Jacopo Martellucci**, *The "harmful potential" of PM, evaluated "in vitro" must be used with a great causation as a surrogate for risk assessment in humans*.
8P35	399	Modelling aerosol impact on human	**Eiko Nemitz**, Massimo Vieno, Ulrike Dragosits, Chiara F. Di Marco, Marsailidh Twigg, Mark A. Sutton, *The response of PM concentrations in the*

		health	*UK to changes in industrial and agricultural emissions: implications for the exceedance of Air Quality Standards*.
8P36	840	Modelling aerosol impact on human health	**James McGrath**, Miriam Byrne, Mike Ashmore, Andrew Terry, Sani Dimitroulopoulou, *Modelling the effect of variable air exchange rates on indoor aerosol concentrations*.
8P37	301	Particle lung deposition clearance and translocation to other organs	**Agata Penconek**, Arkadiusz Moskal, *Artificial lung as an alternative for measurement pulmonary deposition in vivo.*
8P38	325	Particle lung deposition clearance and translocation to other organs	**Jakub Elcner**, Frantisek Lizal, Matej Forman, Jan Jedelsky, Miroslav Jicha, *Respiratory airflow in human upper airways*.
8P39	460	Particle lung deposition clearance and translocation to other organs	**Mathias Forjan**, Katharina Stiglbrunner, Andreas Drauschke, *Development of a Setup for the Purpose of Respiratory Research and Aerosol Deposition in the Lung Using a Novel Active Lung Simulator*.
8P40	677	Particle lung deposition clearance and translocation to other organs	**Attila Nagy**, Arpad Farkas, Imre Balashazy, *Numerical simulation of aerosol deposition and clearance in the large bronchial airways*.
8P41	837	Particle lung deposition clearance and translocation to other organs	**John McAughey**, Colin Dickens, *Regional lung deposition of tobacco smoke constituents*.
8P42	1051	Particle lung deposition clearance and translocation to other organs	**Pierre Madl**, Renate WInkler-Heil, Werner Hofmann, *Implementation of morphometric mouse lung data into a stochastic deposition model*.
8P43	1107	Particle lung deposition clearance and translocation to other organs	**Majid Hussain**, Werner Hofmann, *Comparison of stochastic particle lung deposition predictions with experimental data*.

8P44	326	Particle-induced health effects - toxicology and epidemiology	**Yasuo Morimoto**, Y. Morimoto, M. Hirohashi, A. Ogami, T. Oyabu, T. Myojo, M. Hashiba, Y. Mizuguchi, T. Kambara, B-W. Lee K. Mizuno, N. Kobayashi, and I. Tanaka, *Pulmonary toxicity of well-dispersed single-wall carbon nanotube following 4 week inhalation*.
8P45	418	Particle-induced health effects - toxicology and epidemiology	**Rosalia Zangari**, *Comparison between in vitro results of PM incubation with cell-lines and health effects in children.*.
8P46	423	Particle-induced health effects - toxicology and epidemiology	**Paolo Paladini**, *Mesothelioma incidence is likely not going to decline, despite asbestos ban in Western countries*.
8P47	427	Particle-induced health effects - toxicology and epidemiology	**Simona Benoni**, *Measurement of damages to exposed populations during concomitant evaluation of PM concentration and health effects usually doesn't consider damage to newborns.*
8P48	717	Particle-induced health effects - toxicology and epidemiology	**Mikko Happo**, Oskari Uski, Pasi Jalava, Joachim Kelz, Thomas Brunner, Jorma Jokiniemi, Ingwald Obernberger, Maija-Riitta Hirvonen, *Comparison of toxicological responses in mice lung induced by PM1 emissions from heating appliances of old and new technologies*.
8P49	722	Particle-induced health effects - toxicology and epidemiology	**Niklas Moehle**, *Prevalidation of the CULTEX method: In vitro analysis of the acute toxicity of inhalable fine dusts and nanoparticles after direct exposure of cultivated human cells from the respiratory tract.*
8P50	1083	Particle-induced health effects - toxicology and epidemiology	**Paulo Artaxo**, Valdir S. Andrade Filho, Melina Paixao, Sandra Hacon and C.N. Carmo, *Particulate matter emitted in biomass burning and respiratory diseases hospitalizations in children of Manaus, central Brazilian Amazon region*.
8P51	495	Other	**Sonja Muelhopt**, Christoph Schlager, Hanns-Rudolf Paur, *A novel exposure system for testing the lung toxicity of domestic wood combustion aerosols*.
8P52	958	Other	**Riikka Sorjamaa**, Timo Lanki, Josef Cyrys, Otto Hänninen, *From Outdoor Particle Concentration to*

			the Health Impact of Aerosol Particles – a Multidisciplinary Modelling Study, Part I.
8P53	102	Indoor aerosols	**Ludmila Maskova**, Jiri Smolik, Jakub Ondracek, Lucie Ondrackova, Susana Lopez-Aparicio, *Relationship of Indoor and Outdoor PM and Gaseous Pollutants in the National Library in Prague*.
8P54	173	Indoor aerosols	**Teresa Nunes**, Joana Silva, Alexandre Caseiro, Priscilla Pegas, Célia Alves, Casimiro Pio, *Chemical characterisation of PM10 in primary schools, Portugal*.
8P55	197	Indoor aerosols	**Peter Molnár**, Sandra Johannesson, *Smoking neighbours – a possible source to ETS exposure in homes*.
8P56	791	Indoor aerosols	**Maria Grazia Perrone**, Zelda Lazzati, Roberta Zangrando, Luca Ferrero, Giorgia Sangiorgi, Andrea Gambaro, Ezio Bolzacchini, *Bispehnol A concentrations in indoor and outdoor PM2.5 samples*.
8P57	1089	Indoor aerosols	**Shinhao Yang**, *Inactivation efficiency of avian influenza H6N1 bioaerosol using the aptamer-filter*.
8P58	1044	Indoor air quality and associated health effects	**Christina Isaxon**, Andreas Dahl, Erik Nordin, Gunilla Wieslander, Dan Norback, Anders Gudmundsson, Aneta Wierzbicka, Mats Bohgard, *Particles in Indoor Air – measurements in residential dwellings*.
8P59	422	Lung morphology and patho-physiology	**Gianfranco Schiraldi**, *Environmental pollution in Metropolitan Areas and alterations of respiratory function*.
8P60	590	Lung morphology and patho-physiology	**Donald Hagen**, Elizabeth Black, Philip Whitefield, Prem Lobo, *Surface Area Deposition Index for Jet Engine PM Exhaust*.
8P61	387	Bioaerosols and allergens	**Kathrin Selzle**, Yingyi Zhang, Hong Yang, Ulrich Pöschl, *Protein Nitration and Health Effects*.
8P62	643	Bioaerosols and allergens	**Gregor Jereb**, Štefan Pintaric, Uroš Krapež, Alenka Dovc, *Pigeons as Source of Airborne Circoviruses*.

Aerosol Chemistry			
8P63	927	Structuring of engineered nanoparticles	**Georgia Kastrinaki**, Athanasios G Konstandopoulos, *Synthesis and Surface Area evaluation of Solid Core Porous Shell Particles*.
8P64	99	Chemical mechanisms and transformation processes in aerosol	**Yuri Samsonov**, *Physicochemical transformations and photochemical reactions of high-disperse pesticide chemicals*.
8P65	185	Chemical mechanisms and transformation processes in aerosol	**Asit Ray**, Venkat Rajagopalan, Eric A. Grulke, *Phase transformation of evaporating solution droplets of immiscible polymers*.
8P66	360	Chemical mechanisms and transformation processes in aerosol	**Tiia-Ene Parts**, Aare Luts, Urmas Hõrrak, *Diethylamine and new charged particles formation*.
8P67	441	Chemical mechanisms and transformation processes in aerosol	**Andrey Sorokin**, *To some mechanisms of UV-light induced SO2 Oxidation to H2SO4 and Aerosol Formation*.
8P68	897	Chemical mechanisms and transformation processes in aerosol	**Peter Gallimore**, Francis Pope, Pattanun Achakulwisut, Markus Kalberer, *Importance of aerosol phase and water uptake for understanding organic aerosol oxidation*.
8P70	210	Multiphase chemical processes and interactions involving aerosol	**Manabu Shiraiwa**, Markus Ammann, Thomas Koop, Ulrich Pöschl, *Gas uptake and chemical aging of amorphous semi-solid aerosol particles*.
8P71	343	Multiphase	**Ingrid George**, Barbara Brooks, Lisa Whalley,

		chemical processes and interactions involving aerosol	Andrew Goddard, Pascale Matthews, Neil Howes, Maria-Theresa Baeza-Romero, Dwayne Heard, *Heterogeneous uptake of HO2 onto submicron aerosol particles*.
8P72	394	Multiphase chemical processes and interactions involving aerosol	**Andreas Tilgner**, Peter Bräuer, Ralf Wolke, Hartmut Herrmann, *SPACCIM model studies of tropospheric aerosol-cloud interactions with the extended multiphase chemistry mechanism MCM-CAPRAM*.
8P73	410	Multiphase chemical processes and interactions involving aerosol	**Ingrid George**, Lisa Whalley, Daniel Stone, Dwayne Heard, *The impact of clouds on radical concentrations: Observations of OH and HO2 during HCCT-2010*.
8P74	486	Multiphase chemical processes and interactions involving aerosol	**Scot Martin**, Mackenzie Smith, Allan Bertram, *Phase Transitions and Separation of Mixed Organic-Inorganic Particles*.
8P75	505	Multiphase chemical processes and interactions involving aerosol	**Raluca Ciuraru**, Michael Ward, Nicolas Visez, Sylvie Gosselin, Denis Petitprez, *Experimental study of heterogeneous reactivity between*.
Aerosols in Geoengineering			
8P76	438	Aerosols in geoengineering	**Anton Laakso**, *Injection of sulfur compounds into the stratosphere by using modified commercial aircrafts*.
8P77	581	Aerosols in geoengineering	**Annabel Jenkins**, Piers Forster, *Geoengineering the Earth's Climate – An assessment of potential effectiveness and side-effects*.
8P78	733	Aerosols in geoengineering	**Francois Benduhn**, Mark G. Lawrence, *Sensitivity Studies on the Role of Particle Sedimentation and*

			Subscale Microphysics within a Geoengineered Stratosphere.
Atmospheric aerosols - Aerosol Processes and Properties			
8P79	259	Climate effects of aerosols	**Anna Esteve**, Víctor Estellés, Pilar Utrillas, José Antonio Martínez-Lozano, *Radiative forcing from aerosols measured at a coastal site in the Mediterranean*.
8P80	348	Climate effects of aerosols	**Tzi-yi Wu**, Yan-Min Chen, *Atmospheric transport characteristics of dust storm arrive at Taiwan*.
8P81	809	Climate effects of aerosols	**Roberto Pedros**, J.L. Gómez-Amo, C. Marcos, M.P. Utrillas, J.A. Martínez-Lozano, M. Sicard, *Preliminary results on the influence of the vertical distribution of aerosols in the direct radiative forcing*.
8P82	954	Climate effects of aerosols	**Rafaella - Eleni Sotiropoulou**, Donifan Barahona and Athanasios Nenes, *Global distribution of cloud droplet number concentration, autoconversion rate and first aerosol indirect effect under diabatic droplet activation*.
8P83	1116	Climate effects of aerosols	**Paulo Artaxo**, *Spatial variability of the direct radiative forcing of biomass burning aerosols in the Amazon Basin and the influence of surface reflectance*.
Atmospheric aerosols – Specific Aerosol Types			
8P84	346	Carbonaceous aerosol	**Patricia Krecl**, Admir C. Targino, Christer Johansson, *Spatiotemporal distribution of light-absorbing carbon in Stockholm*.
8P85	770	Carbonaceous aerosol	**Jaiprakash Jaiprakash**, Saood Manzer, Tarun Gupta, Gazala Habib, Papiya Mandal, J. K. Basin4, *Carbonaceous aerosol in Delhi: Link with regional meteorology and long range transport*.
8P86	949	Carbonaceous aerosol	**Darius Ceburnis**, Andrius Garbaras, Soenke Szidat, Karl Espen Yttri, Vidmantas Remeikis, Colin O'Dowd, *Source apportionment of ambient particulate carbonaceous matter at Mace Head during the joint EMEP/EUCAARI intensive measurement periods in fall 2008 and spring 2009*.
8P87	956	Carbonaceous	**Ágnes Filep**, Tibor Ajtai, Noémi Utry, András

		aerosol	Gelencsér, András Hoffer, Zoltán Bozóki, Gábor Szabó, *In-situ spectral characterisation of atmospheric aerosols after the red sludge disaster in Hungary during the autumn of 2010 based on our novel multi-wavelength photoacoustic instrument*.
8P91	1004	Carbonaceous aerosol	**Robert Bergstrom**, David Simpson, *Carbonaceous aerosol in Europe – Multi-year study with the EMEP PCM model including validation using source-apportionment data*.
8P92	1041	Carbonaceous aerosol	**Andrius Garbaras**, R. Bariseviciute, K. Kvietkus, J. Sakalys, J. Didzbalis, R. Skipityte, V. Remeikis, *Chemical composition and δ13C values of OC and EC in the size-segregated aerosol particles*.
8P93	1105	Carbonaceous aerosol	**Peter Zotter**, A.S.H. Prévôt, Y. Zhang, S. Szidat, X. Zhang, Y.-H. Lin, P. Hayes, J. D. Surratt, J.L. Jimenez, R. Weber, J. Slowik, U. Baltensperger, *Diurnal cycle of fossil and non-fossil total carbon using 14C analyses during CalNex*.
8P94	71	Biomass burning	**Jennifer Brooke**, Jim McQuaid, Barbara Brooks, Simon Osborne and Jackie Wilson, *Transformation by aging processes of soot particles from laboratory combustion experiments*.
8P96	266	Biomass burning	**Vijay Kumar Verma**, *Gaseous and fine particle emissions from the combustion of agro-forestry pellets in a residential boiler*.
8P97	297	Biomass burning	**Haryono Huboyo**, Puji Lestari, Susumu Tohno, *The basic performance of Jatropha curcas seed stove and its indoor air pollution over traditional wood stoves*.
8P98	304	Biomass burning	**Celia Alves**, A.I. Calvo, A.P. Fernandes, L.A.C. Tarelho, J.R. Pinho, M.C. Duarte, J.F. Silva, *Characterization of trace gases and PM2.5 emitted during the combustion of shrub biomass in a Portuguese stove*.
8P99	310	Biomass burning	**Ana Vicente**, *Gases and aerosols emitted from wildfires in summer 2009 (central Portugal)*.
8P101	1045	Biomass burning	**Su-Ching Kuo**, Ying I. Tsai, Li-Ying Hsieh, Chien-Lung Chen, Yu-Ting Hsu, *Organic markers and*

			anhydrosugars in particulate matter from incense burning.
Atmospheric aerosols - Aerosol Processes and Properties			
8P102	208	Turbulent aerosol transport and exchange	**Pierre Roupsard**, Muriel Amielh, Alexis Coppalle, Hubert Branger, Philippe Laguionie, Olivier Connan, Didier Hébert, Denis Maro, Martine Talbaut, *Submicronic aerosols dry deposition on urban surfaces: a wind tunnel study to improve the lack of knowledge*.
8P103	523	Turbulent aerosol transport and exchange	**James Whitehead**, James Dorsey, Martin Gallagher, Michael Flynn, Gordon McFiggans, *Particle fluxes over arctic sea ice during COBRA*.
8P104	680	Turbulent aerosol transport and exchange	**Matteo Carpentieri**, Prashant Kumar, Alan Robins, *Dispersion of nanoparticles in vehicle wake – Part II: analysis of wind tunnel work*.
8P105	939	Turbulent aerosol transport and exchange	**Philippe Laguionie**, Denis Maro, Basile Letellier, Serge Le Cavelier, *Rain scavenging of below-cloud aerosol particles: field measurements using Electrical Low Pressure Impactor and Scanning Mobility Particle Sizer coupled with Aerodynamic Particle Sizer*.
Aerosol Chemistry			
8P106	56	Identification of tracers	**Celia Alves**, *Organic composition of size-distributed particles emitted from field burning of garden and agriculture residues*.
8P107	64	Instrumentation for chemical characterization of aerosol	**Pushpa Raju Made**, P.D.Safai, P.S.P.Rao, P.C.S.Devara and K.B.Budhavant, *Aerosol Characteristics over the Tropical Urban Station Pune, India*.
8P108	224	Instrumentation for chemical characterization of aerosol	**Friederike Freutel**, Thomas Klimach, Johannes Schneider, Frank Drewnick, Stephan Borrmann, *Cluster analysis of single particle data acquired with a Light Scattering Probe AMS during the MEGAPOLI campaigns in Paris, France*.
8P109	402	Instrumentation for chemical	**Christopher Pöhlker**, Meinrat O. Andreae, Paulo Artaxo, Mary K. Gilles, Arthur L. D. Kilcoyne, Scot

		characterization of aerosol	T. Martin, Ryan C. Moffet, Ulrich Pöschl, Bärbel Sinha, Mackenzie Smith, Kenia Wiedemann, *STXM-NEXAFS Investigations of Laboratory Secondary Organic Aerosols and Amazonian Background Aerosols*.
8P110	503	Instrumentation for chemical characterization of aerosol	**Murray Booth**, David Topping, Gordon McFiggans, Carl Percival, *Physico-chemical property measurements for aerosols at Manchester*.
8P111	553	Instrumentation for chemical characterization of aerosol	**Klaus-Peter Hinz**, Elmar Gelhausen, Karl-Christian Schäfer, Zoltan Takats, Bernhard Spengler, *Instrumental improvements and applications of the compact laser mass spectrometer LAMPAS 3 for on-line single particle characterization*.
8P112	98	Other	**Dhananjay Deshmukh**, M.K. Deb, *Chemical characterization of fine aerosols over eastern central India*.
8P113	370	Other	**Lili Tang**, Shengjie Niu, Dantong Liu, Xuwen Li, Xiangzhi Zhang, Shuxian Fan,Hong Nie and Hugh Coe, *Size Distribution and Source Analysis of Polycyclic Aromatic Hydrocarbons (PAHs) contained in PM10 in Waliguan and Xining of China*.
8P114	666	Other	**Ditte Mogensen**, Sampo Smolander, Anke Nölscher, Jonathan Williams, Vinayak Sinha, Tuomo Nieminen, Markku Kulmala, Luxi Zhou, Andrey Sogachev, Alex Guenther, Michael Boy, *Modelling atmospheric OH-reactivity over boreal forest*.
8P115	835	Other	**Ana María Sánchez de la Campa**, A. Gracía, J.L. Ramos and J. de la Rosa, *Characterization chemical and microbiological of atmospheric particulate matter during an intense African Dust Event on Sourth Spain*.
8P116	839	Other	**Jesús D. de la Rosa**, Sánchez de la Campa, Ana M.; Fernández-Camacho, Rocío; González-Castanedo, Yolanda, *Levels and composition of atmospheric particulate matter deposited in the Doñana Natural Park, southwest of Spain*.

8P118	872	Other	**Milagros Santacatalina**, Eduardo Yubero, Adoración Carratalá, *Rainfall composition evolution in an urban industrial area: Comparison with PM10 wet chemistry.*
Spark generators for nanoparticle generation			
8P117	667	Spark generators for nanoparticle generation	**Shubhra Kala**, Frank Einar Kruis, Marcel Rouenhoff, Christian Blumberg, *Scaling up the production rate of Ge nanoparticles by spark discharge*.
Aerosol Modelling			
8P119	229	Modelling new particle formation	**Christoph Winkelmann**, Arkadiusz K. Kuczaj, Steffen Stolz, Bernard J. Geurts, *Multi-scale modeling of aerosol formation in pipe flow*.
8P120	377	Modelling new particle formation	**Alexander Girin**, *Distribution of stripped droplets by sizes at drop shattering in a uniform flow*.
8P121	404	Modelling new particle formation	**Henri Vuollekoski**, Hannele Korhonen, Luxi Zhou, Kari E. J. Lehtinen, Veli-Matti Kerminen, Michael Boy, Markku Kulmala, *UHMAEMO – University of Helsinki Multicomponent Aerosol Module*.
8P122	509	Modelling new particle formation	**Luxi Zhou**, Michael Boy, Henri Vuollekoski, Chatriya Wathcarapaskorn, Ditte Mogensen, Sampo Smolander, Andrea Sogachev, Markku Kulmala, *The first long-term model study of particle formation and growth with detailed chemistry and aerosol dynamics in a boreal forest environment*.
8P123	561	Modelling new particle formation	**Rosa Gierens**, Lauri Laakso, Johanna Lauros, Risto Makkonen, Ville Vakkari, Luxi Shou, Ditte Mogensen, Henri Vuollekoski, Michael Boy, *Modelled new particle formation and growth in Southern African savannah environment*.
8P124			**Ari Laaksonen**, *Representation of new particle formation in large scale models: Selection criteria for activation and kinetic coefficients*
8P125	631	Modelling new particle	**Xinze Zhen**, Hans-Joachim Schmid, *Simulation of binary aerosol droplet formation*.

		formation	
8P126	650	Modelling new particle formation	**Johannes Leppa**, Stéphanie Gagné, Lauri Laakso, Markku Kulmala, Veli-Matti Kerminen, *Behaviour of the aerosol charging state under asymmetric concentrations of small ions*.
8P127	714	Modelling new particle formation	**Matthias Karl**, Allan Gross, Caroline Leck, Liisa Pirjola, *Can dimethyl sulphide cause new particle formation over the central Arctic Ocean?*
8P128	751	Modelling new particle formation	**Emmi Laukkanen**, Hannele Korhonen, Hao Liquing, Jorma Joutsensaari, James Smith, Kari Lehtinen, Harri Korhonen, *Adsorption in biogenic SOA formation*.
Atmospheric aerosols - Specific Aerosol Types			
8P129	251	Mineral dust	**Ikuko Mori**, Masataka Nishikawa, *Relationship between water soluble calcium and anions in a kosa (Asian dust) aerosol*.
8P130	552	Mineral dust	**Konrad Kandler**, Kirsten Lieke, Nathalie Benker, Martin Ebert, Lothar Schütz, Dirk Scheuvens, Simon Jäckel, Alexander Schladitz, Branimir Šegvic, Stephan Weinbruch, *Mineral dust chemistry, mineralogy, shape, mixing state, complex refractive index and microphysics determined by electron/optical microscopy and by X-ray diffraction at Praia, Cape Verde, in winter 2008*.
8P131	778	Mineral dust	**Vasiliki Vasilatou**, Diapouli, Karanasiou, Skoullos, Eleftheriadis, *Investigation of potential Sahara dust transport event indicators by means of aerosol trace metal concentration ratios in the Eastern Mediterranean.*
8P132	782	Mineral dust	**Matt Woodhouse**, Ken Carslaw, Micheal Krom, Ivan Savov, Alex Baker, Barb Brooks, Tim Jickells, Liane G Benning1, *Small increase in dust fractional iron solubility due to physical sorting of large particles during trans-Atlantic transport*.
8P133	1042	Mineral dust	**Jose A. G. Orza**, Maria Cabello, Asuncion Romero-Diaz, Francisco Belmonte-Serrato, Aitor Berasaluce, Miguel Angel Barrero, Lourdes Canton, *Characterization of Severe Wind Erosion Episodes*

			in a Western Mediterranean Location.
8P134	1125	Mineral dust	**Maria Cabello**, Jose A.G. Orza, Aitor Berasaluce, Miguel Angel Barrero, Lourdes Canton, Asuncion Romero-Diaz, Francisco Belmonte-Serrato, *Wind Erosion and Suspended Particle Concentration in an area of Ephemeral Lakes*.
Atmospheric aerosols - Aerosol Processes and Properties			
8P135	622	Other	**Valentina Yakovleva**, Artem Vukolov, Ivan Ippolitov, Vladimir Karataev, Petr Nagorsky, Sergey Smirnov, *Futures of atmospheric radioactive aerosol monitoring by β- and γ-radiation*.
8P136	756	Other	**Jonathan Dredge**, *Aerosol contributions to speleothem chemistry*.
8P137	901	Other	**Svetlana Samoilova**, *Investigations of the vertical distribution of tropospheric aerosol layers using the data of multi-wavelength lidar sensing*.
8P138	338	Remote sensing of aerosol properties	**Franco Marenco**, Ben Johnson, Robin Hogan, *Quantifying the concentration of volcanic ash aerosol in ground-based lidar returns*.
8P139	395	Remote sensing of aerosol properties	**Monica Campanelli**, Victor Estelles, Tim Smyth, Teruyuki Nakajima, Makiko Hashimoto, Angelo Lupi, Claudio Tomasi, *Retrieval of aerosol radiative properties from sun-sky radiometers measurements of ESR network: comparison between the inversion codes Skyrad4.2.pack and the new Skyrad5.pack*.
8P140	444	Remote sensing of aerosol properties	**Svetlana Terpugova**, Mikhail Panchenko, Victor Polkin, Valerii Kozlov, *Modelling of aerosol scattering and absorption parameters in the troposphere of West Siberia*.
8P141	511	Remote sensing of aerosol properties	**Vassiliki Kotroni**, Stelios Kazadzis, Kostas Lagouvardos, Vasilis Amiridis, Evangelos Gerassopoulos, *Influence of wind field patterns on aerosol optical depth over Athens and the Aegean sea*.
8P142	550	Remote sensing of	**Eleni Marinou**, Vasilis Amiridis, Stelios Kazadzis, Alexandros Papayiannis, *Aerosol Optical Depth in*

		aerosol properties	*East Mediterranean using MODIS and CALIPSO satellite retrievals*.
8P143	572	Remote sensing of aerosol properties	**Carmen Cordoba-Jabonero**, Mar Sorribas, Juan-Luis Guerrero-Rascado, Jose-Antonio Adame, Yballa Hernandez, Hassam Lyamani, Victoria Cachorro, Manuel Gil, Lucas Alados-Arboledas, Emilio Cuevas and Benito de la Morena, *Synergetic monitoring of Saharan dust plumes: A case study of dust transport from Canary Islands to Iberian Peninsula. Part 2: Evaluation of potential dust impact on surface*.
8P144	710	Remote sensing of aerosol properties	**Francisco Molero**, F. J. Andrey, J. Preißler, F. Navas-Guzmán, A. Giunta, M. Sicard, A. J. Fernandez, M. C. Parrondo, F. Wagner, M.J. Granados, G. D'Amico, S. Tomas, M. Pujadas, C. Córdoba-Jabonero, J.L. Guerrero-Rascado, L. Alados-Arboledas, A. Amodeo, A. Comeron, J.A. Bra, *Aerosol size distribution study by airborne and ground-level in-situ measurements and remote sensing during EARLINET lidar intercomparison campaign: SPALI10*.
8P145	926	Remote sensing of aerosol properties	**Francisco Navas-Guzman**, *Three years of Raman lidar measurements in correspondence with CALIPSO overpasses over the South of the Iberian Peninsula*.
8P146	951	Remote sensing of aerosol properties	**Mika Komppula**, Tero Mielonen, Kimmo Korhonen, Antti Arola, Heikki Lihavainen, Lauri Laakso, Ville Vakkari, Heikki Laakso, Paul Beukes, Pieter Van Zyl, Kobus Pienaar, Petri Tiitta, Rikus le Roux, Kgaugelo Chiloane, Holger Baars, Ronny Engelmann, Dietrich Althausen, Kari, *One year of Raman lidar measurements at the South African EUCAARI site*.
8P147	1146	Remote sensing of aerosol properties	**Rahul Reddy**, *An Aerosol Dipole - A new found mode*.
Atmospheric aerosols - Specific Aerosol Types			

8P148	261	Marine aerosols	**Anne Gry Hemmersam**, Torben Nørgaard Jensen, Keld Grønne Nielsen, Henrik Tarp, Morten Køcks Lykkegaard, Mikael Poulsen, *Shipboard characterization of particle and gas emission from a Danish inland ferry*.
8P149	521	Marine aerosols	**Jurgita Ovadnevaite**, Darius Ceburnis, Jakub Bialek, Colin O'Dowd, Harald Berresheim, *Quantitative real time sea salt measurements by HR-ToF AMS*.
8P150	646	Marine aerosols	**Petri Vaattovaara**, Luke Cravigan, Nick Talbot, Gustavo Olivares, Cliff Law, Mike Harvey, Zoran Ristovski, Ari Laaksonen, *Secondary organic aerosol on southern Pacific Ocean*.
8P151	817	Marine aerosols	**Andrew Butcher**, Stephanie King,Thomas Rosenoern, Douglas Nilsson, Merete Bilde, *Characterization of a bubble tank for Sea Spray Aerosol Studies*.
8P152	843	Marine aerosols	**Stephanie King**, Thomas Rosenoern, Andrew Butcher, Douglas Nilsson, Merete Bilde, *Investigating the morphology and organic fraction of particles from bubble-bursting*.
Aerosol Modelling			
8P153	131	Atmospheric applications	**David Topping**, Douglas Lowe, *A new reduced complexity thermodynamic methodology (PF-FiTE) to calculate equilibrium vapour pressures of organic compounds above a multi-component solution*.
8P154	170	Atmospheric applications	**Efthimios Tagaris**, Rafaella-Eleni Sotiropoulou, Nikos Gounaris, Spyros Andronopoulos, *Modelling PM2.5 concentrations over Europe*.
8P155	183	Atmospheric applications	**Qingyang He**, *A new model for estimation emissions of biogenic volatile organic compounds (BVOCs) from Hyytiälä in the southern Finland*.
8P156	305	Atmospheric applications	**Joni-Pekka Pietikäinen**, Declan O'Donnell, Markku Kulmala, Daniela Jacob, Ari Laaksonen, *Model comparison between global and regional climate-*

			aerosol models ECHAM5-HAM and REMO-HAM: European aerosols.
8P157	401	Atmospheric applications	**Mihaela Mircea**, M. Mircea, G. Briganti, A. Cappelletti, L.Vitali, G. Pace, M. D'Isidoro, I. Cionni,G. Righini, A. Piersanti, G. Cremona, C. Silibello, S. Finardi, G. Calori, L. Ciancarella, G. Zanini, *Modelling the buildup of aerosol loading over Italy during high-pressure conditions*.
8P158	450	Atmospheric applications	**Stephanie Fiedler**, Joni Pietikäinen and Daniela Jacob, *Validation of the regional aerosol climate model REMO-HAM under East Asian conditions*.
8P159	600	Atmospheric applications	**Gopalkrishnan Kokkatil**, M. Boy, H. Vuollekoski, S. Smolander, A. Sogachev and T. Vesala, *New 3-Dimensional Model to Study atmospheric processes in Planetary Boundary Layer*.
8P160	609	Atmospheric applications	**Shamil Zaripov**, Wolfgang Koch, *Numerical study of performances of RespiCon sampler in calm air*.
8P161	635	Atmospheric applications	**Sat Ghosh**, Sathish Kumar, Kshitiz Sethia, Jason Picardo, *Bio-particle emission and distribution over slums in a tropical Indian metropolis*.
8P162	705	Atmospheric applications	**Sabine Wurzler**, Peter Bruckmann, Volker Diegmann, Florian Pfäfflin, Andreas Brandt, *Further experience with low emission zones in Germany: will the next stage do the job?*
8P163	708	Atmospheric applications	**Sergey Beresnev**, Victor Gryazin, *Stabilizing action of the vertical wind on spatial distribution of stratospheric aerosol*.
8P164	744	Atmospheric applications	**Bjarke Moelgaard**, Tareq Hussein, Jukka Corander, Kaarle Hämeri, *Bayesian forecast of urban particle number concentrations*.
8P165	851	Atmospheric applications	**Scott Archer-Nicholls**, Steven Utembe, Douglas Lowe, Gordon McFiggans, *Regional chemical weather modelling of the UK using WRF-Chem as part of the RONOCO project*.
8P166	896	Atmospheric applications	**Timur Zaripov**, Andrey Egorov, Denis Demidov, *Motion of charged aerosol particles in a cylinder array*.
8P168	945	Atmospheric applications	**Matthew Woodhouse**, Graham Mann, Ken Carslaw, Jean-Jacques Morcrette, Olivier Boucher,

			Implementation and evaluation of a microphysical aerosol module in the ECMWF Integrated Forecasting System.
8P169	968	Atmospheric applications	**Risto Makkonen**, Ari Asmi, Veli-Matti Kerminen, Michael Boy, Almut Arneth, Alex Guenther, Pertti Hari, Markku Kulmala, *Role of biogenic organics on aerosol forcing in 2100*.
8P170	190	Transport and transformation for modelling applications	**Steven Utembe**, *Using the Common Representative Intermediates Mechanism (CRIv2-R5) coupled to an aerosol microphysics model to simulate formation and transformation of atmospheric aerosols*.
8P171	236	Transport and transformation for modelling applications	**Mihaela Mircea**, Sandro Finardi, *Estimate of the Saharan dust contribution to PM10 concentrations over Italy: a modelling approach*.
8P172	295	Transport and transformation for modelling applications	**Shubha Verma**, S Bhanja, *Source evaluation of aerosols measured over the Indian subcontinent and ocean from combined measurement and modeling platforms*.
8P173	378	Transport and transformation for modelling applications	**Alexander Girin**, *Distribution function for daughter droplets at theoretical law of parent drop motion*.
8P174	473	Transport and transformation for modelling applications	**Roland Schrödner**, Andreas Tilgner, Ralf Wolke, *Regional modelling of the tropospheric multiphase system using COSMO-MUSCAT*.
8P175	508	Transport and transformation for modelling applications	**Stefania Squizzato**, *A modelling approach to study PM2.5 dispersion and transformation in Venice area*.
8P176	625	Transport and transformation for modelling applications	**Valentina Yakovleva**, Artem Vukolov, Petr Nagorsky, Yaroslav Luzhanchuk, Irina Gvai, Fedor Sannikov, *Radioactive disequilibrium between radon and its decay products in surface atmosphere*.
Atmospheric Aerosols - Aerosol Processes and Properties			
8P177	80	Transport and transformation	**Afrim Syla**, *Pollution from tailings and mass transport of deposited aerosol in Mitrovica*.

8P178	230	Transport and transformation	**Pouyan Joodatnia**, Prashant Kumar, *Passenger exposure to nanoparticles inside a transport microenvironment*.
8P179	544	Transport and transformation	**Styliani Pateraki**, *Atmospheric circulation role on PM fractions*.
8P180	749	Transport and transformation	**Matteo Carpentieri**, Prashant Kumar, Alan Robins, *Dispersion of nanoparticles in vehicle wake – Part II: analysis of wind tunnel work*.
8P181	765	Transport and transformation	**Hugo Ricketts**, Geraint Vaughan, Hugh Coe, *Aerosol entrainment footprints over the South East Pacific as observed during VOCALS*.
8P182			**Konradin Weber,** *Investigation of re-suspended volcanic ash around the region of the Eyjafjallajökull volcano with mobile measurements*
8P183	812	Transport and transformation	**Seung-Bok Lee**, Dong-Hun Lee, Seung-Jae Lee, Hyoun Cher Jin, Jae Hyun Choi, Seung-Ho Park, Nguyen Tri Quang Hung, Gwi-Nam Bae, *Exposure level of traffic-related air pollutants near a busy road in Seoul, Korea*.
Atmospheric Aerosols – Specific Aerosol Types			
8P184	97	Urban aerosols	**Mihalis Lazaridis**, Victoria Aleksandropoulou, Kostas Eleftheriadis, *Assessing PM10 source reduction in urban agglomerations for air quality compliance*.
8P185	214	Urban aerosols	**Martin Branis**, Tomas Cajthaml, Pavla Stehlikova, Jiri Safranek, *Particle-associated polycyclic aromatic hydrocarbons in Prague schools*.
8P186	217	Urban aerosols	**Yongwon Jung**, Sehyun Han, Woojoong Kim, Yoonho Seo, Minsang Yoo, *PM2.5 Source Profiles for Resuspended Road Dust in Seoul and Incheon, Korea.*
8P187	287	Urban aerosols	**Kamil Krumal**, Pavel Mikuska, Martin Vojtesek, Zbynek Vecera, *Comparison of organic compounds in atmospheric aerosols in urban areas in the Czech Republic*.
8P188	303	Urban aerosols	**Beatrix Turóczi**, András Hoffer, Ádám Tóth, Nóra Kováts, András Ács, András Gelencsér, *Source*

			apportionment and health effects of winter urban atmospheric aerosol.
8P189	356	Urban aerosols	**Angeliki Karanasiou**, *Road dust resuspension and chemical composition with regards to street washing activities*.
8P190	391	Urban aerosols	**George Proias**, *Meteorological impacts in the modification of PM10 concentration levels in the urban area of Volos, Greece*.
8P191	452	Urban aerosols	**Ian Colbeck**, Zaheer Ahmad Nasir, *Mass and number concentration of particulate matter in Lahore, Pakistan.*
8P192	477	Urban aerosols	**Nina Schleicher**, *Spatio-temporal variations of particulate air pollution in Beijing, China*.
8P193	556	Urban aerosols	**M. Aránzazu Revuelta**, Francisco Javier Gómez-Moreno, Lourdes Núñez, Begoña Artíñano, *Analysis of a time series of particulate sulfate in a suburban site*.
8P194	594	Urban aerosols	**Farah Halek**, Ali Kavousirahim, *Atmospheric nano-sized particle counting in Tehran air*.
8P195	595	Urban aerosols	**Rocio Fernandez-Camacho**, Ana M. Sanchez de la Campa, Javier Aroba, Jesus D. de la Rosa, Fernando Gomez-Bravo, Sergio Rodriguez, *Ultrafine particles ambient air pollution in an industrial area in Southwest Europe: A fuzzy logic qualitative model*.
8P196	617	Urban aerosols	**Mario Federico Meier**, Telma Castro, Maria Isabel Saavedra, Bernard Grobety, *PM characterization of Mexico City aerosols by automated single particle analysis*.
8P197	618	Urban aerosols	**Stephane Percot**, Veronique Ruban, Pierre Roupsard, Denis Maro, Maurice Millet, *An original device for the measure of aerosol deposition. First results on the Pin Sec catchment in Nantes, France*.
8P198	634	Urban aerosols	**Ian Longley**, Kreepa Shrestha, Simon Kingham, Jennifer Salmond, Woodroe Pattinson, *Statistical distributions of particle number concentrations observed in urban transport microenvironments during commuting*.
8P199	637	Urban	**Arthur Zaripov**, Andrew Jouravlev, *Urban aerosol*

		aerosols	*variability from meteoparameters on various time scales*.
8P200	659	Urban aerosols	**Markus Pesch**, Wolfgang Brunnhuber, Hans Grimm, Thomas Külz, Matthias Richter, Friedhelm Schneider, *Continuous Measurement with High Tim Resolution of Semi-Volatile Components in the Atmospheric Aerosol*.
Aerosol Modelling			
8P201	77	Other	**Matthew McGrath**, Kenty Ortega, Pauli Paasonen, Tinja Olenius, Kari Lehtinen, Markku Kulmala, Hanna Vehkamäki, *Simulation of Small Ion Aerosol Dynamics*.
8P202	81	Other	**Lindsay Collins**, Ken Carslaw, Kirsty Pringle, Graham Mann, Dominick Spracklen, *Emulation of a global aerosol model to quantify model sensitivity to uncertain parameters*.
8P203	652	Other	**Rohit Srivastava**, S. Ramachandran, *Measured and modelled aerosol radiative forcing over an urban location*.
8P204	905	Other	**Carly Reddington**, Maria Grazia Frontoso, Ken S. Carslaw, Gavin R. McMeeking, Hugh Coe, *Model evaluation of the physical properties of black carbon in the boundary layer over Europe during the EUCAARI Intensive Observation Period*.
8P205	1020	Other	**Renate Winkler-Heil**, Werner Hofmann, *Implementation of coagulation into a Lagrangian deposition model*.
8P206	269	Industrial applications	**Mourad Ben Othmane**, Michel HAVET, Evelyne GEHIN,Camille SOLLIEC, Gorges ARROYO, *Particle mass flux deposition in ventilation ducts of food factories*.
8P208	1090	Industrial applications	**Hsin I Hsu**, P.J. Tsai, J.C. Soo, *Assessing Long-term Oil Mist Exposures to Workers in a Fastener Manufacturing Industry by Using the Bayesian Decision Analysis Technique*.
8P209	986	Atmospheric applications	**Miikka Dal Maso**, Hannele Korhonen, Kari Lehtinen, Hanna Vehkamäki, *Studying the effect of*

			coagulation and condensation on the perceived nucleation rate vapour dependence using a molecular-resolution aerosol dynamics model.
8P210	1023	Atmospheric applications	**Silvia Verrilli**, Gabriele Curci; Marino Mazzini, Iliano Ciucci; Leonardo Tognotti, *Air Quality Modelling with CAMx: a case study of PM distribution in Tuscany (Italy)*.
8P211	1073	Atmospheric applications	**Constantini Samara**, K. Eleftheriadis, E. Diapouli, M.I. Gini, V. Vasilatou, G. Argyropoulos, *Source apportionment of airborne particulate matter for three urban centres in Greece*.
8P212	1132	Atmospheric applications	**Marta G. Vivanco**, Manuel Santiago, Ariel Stein, *Modelling SOA formed in a chamber from a mixture of organic gases*.
Electrical Effects			
8P213	63	Charged aerosol generation and applications	**Rohan Jayaratne**, Xuan Ling, Congrong He, Lidia Morawska, *Charged Particles From Laser Printers*.
8P214	189	Charged aerosol generation and applications	**Kuang-Nan Chang**, Yu-Kang Chen, Sheng-Hsiu Huang, Yu-Mei Kuo and Chih-Chieh Chen, *Penetration of charged particle through metallic tubes*.
8P215	529	Charged aerosol generation and applications	**Inyong Park**, Woojin Kim, Sang Soo Kim, *High-throughput multi-jet mode electrospray for two fluids using a coaxial grooved nozzle*.
8P216	558	Charged aerosol generation and applications	**Peter Kallinger**, Gerhard Steiner, Wladyslaw W. Szymanski, *Investigation of charge conditioning of aerosols by means of soft X-ray and AC corona discharge devices*.
8P218	192	Electrostatic discharges non-thermal plasma and related phenomena	**Kye Soon Hwang**, D.N. Shin, *Optimum conditions of two-stage ESP system for oil mist control*.
8P219	624	Electrostatic discharges non-thermal plasma and related phenomena	**Bangwoo Han**, Hak-Joon Kim, Dong-Keun Song, Won-Seok Hong, Wan-Ho Shin, Yong-Jin Kim, *Comparison of charging characteristics between particle chargers using different discharging materials*.

8P220	684	Electrostatic discharges non-thermal plasma and related phenomena	**Chih-Wei Lin**, Sheng-Hsiu Huang, Chih-Chieh Chen, *Factors affecting ESP aerosol generation*.
8P221	696	Electrostatic discharges non-thermal plasma and related phenomena	**Maida Domat**, M Angeles Rodriguez-Braña, Einar Kruis, Julio Manuel Fernandez-Diaz, *Calculation of the electrical field and charge density in a corona unipolar charger with a complex geometry*.
8P222	907	Electrostatic discharges non-thermal plasma and related phenomena	**Nicolas Jidenko**, Manuel Alonso, J-P Borra, *Comparison of measured and calculated charge distributions in post negative corona discharge*.
8P223	623	Electrohydro-dynamics effects and applications	**Valentina Yakovleva**, Ivan Ippolitov, Michail Kabanov, Vladimir Karataev, Natalia Multcina, Petr Nagorsky, Sergey Smirnov, Artem Vukolov, *Monitoring of atmospheric electrical, meteorological and radioactive parameters of surface layer of the storm atmosphere. Preliminary results*.
Atmospheric aerosols – Specific Aerosol Types			
8P224	636	Other	**Jason Picardo**, Atanu Mukherjee, Sat Ghosh, *Dispersion and deposition pathways of combustion aerosols over tropical evergreens*.
8P225	737	Urban aerosols	**Angela Stortini**, R. Zangrando, E. Barbaro, F. Bonetto, N. Kerward, C. Barbante and A. Gambaro, *Source emission studies and biomass burning assessments in Venice Lagoon area*.
8P226	784	Urban aerosols	**Angela Stortini**, Laura Cadamuro, Silvia De Pieri, Dragana Dordevic, Alexandra Mihajlidi-Zelic, Ljubinko Ignjatovic, Dubravka Relic, Jasna Huremovic , Tatjana Milovanovic and Andrea Gambaro, *Trace elements on particulate matter (PM) in the urban areas of Belgrade and Sarajevo*.
8P227	889	Urban aerosols	**Maximilian Weiss**, Juergen Spielvogel, *Continuous time resolved measurements of environmental aerosols especially during New Year 2011 with a*

			new fine dust monitoring system.
8P228	932	Urban aerosols	**Jakub Ondracek**, Vladimir Zdimal, Jaroslav Schwarz, Vladislav Bizek, Jiri Smolik, *Influence of the road traffic intensity on air pollution in the Prague*.
8P229	992	Urban aerosols	**Chien-Lung Chen**, Chien-Hua Chen, Feng-Chao Chung, Su-Ching Kuo, Li-Ying Hsieh and Ying I. Tsai, *Characteristics of compositions in fine and coarse aerosols in central Taiwan*.
8P230	999	Urban aerosols	**Ganesh Pawar**, Gajanan Aher and P. C. S Devara, *Estimation of direct aerosol radiative forcing at Pune*.
8P231	1000	Urban aerosols	**Gajanan Aher**, Sanjay More and P. Pradeep Kumar, *Seasonal and statistical features of aerosol optical properties over different Indian sites*.
8P232	1032	Urban aerosols	**Martine Van Poppel**, Nico Bleux, Ann Meeusen, Bart Elen, Luc Int Panis, *Mobile mapping of BC, PNC and PM2.5 in an urban environment using the Aeroflex bike*.
8P233	1043	Urban aerosols	**Kornélia Imre**, András Gelencsér, Ágnes Molnár, Viktor Dézsi, *Role of the hysteresis and water content in PM10 measurements*.
8P234	1072	Urban aerosols	**Stephan Weber**, Jan Gauweiler, Klaus Kordowski, Stephan Weber, *Personal exposure to urban aerosol in terms of mobile particle number and surface area concentrations measurements*.
8P235	1091	Urban aerosols	**John Backman**, Luciana Rizzo, Tuukka Petäjä, Hanna Manninen, Tuomo Nieminen, Jani Hakala, Pasi Aalto, Fernando Morais, Risto Hillamo, Paulo Artaxo, Markku Kulmala, *FIRST NEW PARTICLE FORMATION EVENTS MEASURED DURING THE BIOFUSE CAMPAING MEASURING OPTICAL PROPERTIES AND SIZE DISTRIBUTIONS AT SÃO PAULO, BRAZIL*.
8P236	1096	Urban aerosols	**Axel Zerrath**, Oliver Bischof, Hans-Georg Horn, Thomas Krinke, Tim Johnson, Kathleen Erickson, *Comparison of a New Optical Particle Sizer to Reference Sizing Instruments for Urban Aerosol Monitoring*.

8P237	1100	Urban aerosols	**Holger Gerwig**, Werner Pecher, Klaus Wirtz, *Local sources of UFP at an urban BG station*.
8P238	1104	Urban aerosols	**Giovanni Lonati**, Senem, Ozgen, Giovanna Ripamonti, *Personal exposure to fine PM in Milan: a comparison of different travel modes*.
Atmospheric aerosols - Aerosol Processes and Properties			
8P239	91	Optical properties	**Thomas Trautmann**, Khan Alam, Thomas Trautmann, Thomas Blaschke, *Ground-based Aerosol Optical Properties and radiative forcing over Karachi Pakistan*.
8P240	113	Optical properties	**Sihye Lee**, S.-C. Yoon, Y.-P. Kim, S.-W. Kim, *Carbonaceous particles and their influence on spectral optical properties and humidification response*.
8P241	179	Optical properties	**Xuguang Chi**, Jens-Christopher Mayer, Niklas Jürgens, Alexey Panov, Meinrat O. Andreae, *Long-Term Measurements of aerosols light absorption coefficient, scattering coefficient and Carbon Monoxide at the ZOTTO tall tower, Siberia*.
8P242	237	Optical properties	**David McCall**, Evelyn Hesse, Joseph Ulanowski, *Light Scattering by airborne Saharan Dust Particles*.
8P243	263	Optical properties	**Victor Estelles**, Monica Campanelli, Tim Smyth, Pilar Utrillas, Francisco Exposito, *Comparison of SKYRAD4.2 and AERONET inversions on a CIMEL CE318 radiometer*.
8P244	293	Optical properties	**Shubha Verma**, Soumendra Bhanja, Shantanu Pani, *Wintertime aerosol properties and their implications to radiative forcing over Eastern India*.
8P245	316	Optical properties	**Eleonora Andriani**, *Particle concentrations in Apulia Region PM natural excedancees*.
8P247	435	Optical properties	**Chul Han Song**, R. S. Park, K.M. Han, M.E. Park, *Aerosol optical properties over East Asia: An integrating CMAQ-simulated and satellite-retrieved aerosol data using a data assimilation technique*.
Electrical Effects			
8P249	94	Fundamentals	**Celine Durniak**, Dmitry Samsonov, *Molecular*

		of electrostatics	*simulation of dynamic phenomena in complex plasmas*.
8P250	285	Fundamentals of electrostatics	**Kilian Schmidt**, Albert Hellmann, Siegfried Ripperger, Markus Berges, Stefan Sticher, *Measurement and Simulation of Nanoparticle Deposition at Microfibres*.
8P251	484	Fundamentals of electrostatics	**Asit Ray**, Mark Warren, *Electrostatic charging of spray droplets by addition of ionic compounds*.
8P252	73	Other	**James Matthews**, Alison Buckley, Matthew Wright, Denis Henshaw, *Corona ion production and aerosol charging downwind of high voltage power lines*.
8P253	627	Other	**Kuo-Pin Yu**, S.-C. Yang and W.-M. G. Lee, *Effect on relative humidity on the electric field strength established, negative air ion concentration produced and aerosol removal by an air ionizer*.
8P254	626	Measuring techniques	**Valentina Yakovleva**, Petr Nagorsky, Elena Baranchikova, *Variations in electrical and meteorological parameters of the atmosphere in conditions of fog*.
8P255	929	Measuring techniques	**Markus Wild**, Joerg Meyer, Gerhard Kasper, *A simplified procedure for particle charge distribution measurements and its application to the characterization of the annual DBD aerosol neutralizer*.
Instrumentation			
8P256	178	Other	**Aleksandr Safatov**, Sergei Kiselev, Yurii Marchenko, Aleksandr N. Sergeev, Artem. Sergeev, Aleksandr A. Sergeev, Elena Emelyanova, Vasilii Marchenko, Galina Buryak, *The comparison of bioaerosol disinfection efficiencies of several new commercial air purifiers manufactured in Russia*.
8P257	405	Other	**Chris Stopford**, Paul Kaye, Edwin Hirst, Joseph Ulanowski, Richard Greenaway, Warren Stanley, *A miniaturised Airborne Particle Classifier (APC)*.
8P258	494	Other	**Hiroshi Kume**, Mizuno Yusuke, Masahiko Fujiwara,

			A new analyser for continuous measurement of the concentration and composition of aerosols.
8P259	500	Other	**Lenka Skrabalova**, Vladimír Ždímal, *The calibration of an aerosol dilution system*.
8P260	821	Other	**Valery Zagaynov**, Yu.G.Biryukov, I.E.Agranovski, O.V.Karpov, D.M.Balakhanov, E.V.Lesnikov, A.A. Lushnikov, *Aerosol measurements of nanometer particles, obtained by spark generator*.
8P261	850	Other	**Thomas Mueller**, Marie Laborde, Grant Kassel, Alfred Wiedensohler, *Intercomparison of scatter and backscatter integrating nephelometers: Characteristics and angular sensitivity correction*.
8P262	914	Other	**Estibaliz Garcia**, Francisco Romay, J. Cambra, J. Legarreta and David Pui, *Jet interaction in multi-nozzle inertial impactors*
8P263	1046	Other	**Jeonghoon Lee**, *Level of light absorption coefficient at an engineering classroom*.
8P265	492	Aerosol standards	**Janek Uin**, Eduard Tamm, *Determining the transfer function of a Very Long DMA using polymer size standards*.
8P266	902	Aerosol standards	**Harald Bresch**, Falk Reinhardt, Ulrich Waldschlaeger, Beatrix Pollakowski, Burkhard Beckhoff, Stefan Seeger, *Size selected nanoparticle quantification of deposited aerosol by GIXRF*.
8P267	327	Comparison of different measurement methods	**Paul Quincey**, Tom Gardiner, Fabrizio Innocenti, Marc Coleman, Jordan Tompkins, *A chamber for aerosol instrument comparisons*.
8P268	551	Comparison of different measurement methods	**Guillaume Bacon**, Antonio Donateo, Daniele Contini, Denis Maro, Franco Belosi, *Measurement of sub-micron aerosols dry deposition velocity on a heterogeneous field by eddy correlation using an Electrical Low Pressure Impactor and a Condensation Particle Counter*.
8P269	842	Comparison of different measurement methods	**Javier Andrey**, Yasmine Bennouna, Maria Jose Granados, Jose Luis Gomez-Amo, Bruno Piguet, Andreas Minikin, Jorgen Jensen, Radovan Krejci, *Intercomparison of airborne aerosols size distribution measurements*.

8P270	868	Comparison of different measurement methods	**Axel Eriksson**, E. Z. Nordin, P.T. Nilsson, J. E. Carlsson, J. Rissler, M. Kulmala, B. Svenningssson, J. Pagels and E. Swietlicki, *AMS Collection Efficiencies of dry smog chamber aerosols, dependence on (NH4)2SO4, NH4NO3 and SOA fractions*.
8P271	985	Comparison of different measurement methods	**Kingsley Reavell**, Jonathan Symonds, Mark Rushton, *Simplified approximations to Centrifugal Particle Mass Analyser performance*.
8P272	1048	Comparison of different measurement methods	**Franco Lucarelli**, Massimo Chiari, Martina Giannoni, Giulia Calzolai, Alessandra Cincinelli, Silvia Nava, *EC/OC Measurements on Aerosol Samples by Thermal-Optical Methods: Benchmarking Different Protocols*.
Atmospheric aerosols - Aerosol Processes and Properties			
8P274	530	Optical properties	**Sascha Pfeifer**, Thomas Müller, Andreas Weigelt, Alfred Wiedensohler, *The influence of particle shape on optical particle sizers*.
8P275	538	Optical properties	**Martine Collaud Coen**, E. Weingartner, C. Ketterer, O. Maier, S. Frey, P. Zieger, N. Bukowiecki, U. Baltensperger, *Planetary boundary layer influence at the Jungfraujoch: in-situ and remote sensing measurements.*
8P276	548	Optical properties	**Veerle De Bock**, Hugo De Backer, Alexander Mangold, *Improved cloud screening for aerosol optical depth measurements with a Brewer spectrophotometer*.
8P277	559	Optical properties	**Ben Johnson**, Kate Turnbull, James Dorsey, Jim Haywood, *Aircraft measurements of volcanic ash properties*.
8P278	565	Optical properties	**Frank Wagner**, Jana Preißler, *One Year Aerosol Measurements with LIDAR in Portugal*.
8P279	579	Optical properties	**Kate Turnbull**, Ben Johnson, Franco Marenco, James Dorsey, Jim Haywood, *In situ volcanic aerosol measurements made using the FAAM research aircraft: a case study*.
8P280	775	Optical	**Agnes Molnar**, Diana Benko, Zsuzsanna Becsi,

		properties	Andras Hoffer, *Optical properties of rural aerosol as the function of mass concentration in Central Europe*.
8P281	795	Optical properties	**Aditya Vaishya**, S.G. Jennings, C.D. O'Dowd, *Seasonal characteristics of the radiative properties of aerosols at Mace Head, Ireland*.
8P282	890	Optical properties	**Johannes Ofner**, Natalia Balzer, Hinrich, Grothe, Heinz-Ulrich Krueger, Philippe Schmitt-Kopplin, Cornelius Zetzsch, *Aerosol-halogen interaction: Change of aerosol optical properties*.
8P283	891	Optical properties	**Paulo Artaxo**, Kenia Teodoro Wiedemann, Fernando Morais, Paulo Artaxo, Thomas Muller, Alfred Wiedensohler, *Seasonality of aerosol optical properties in the Amazon Basin*.
8P284	969	Optical properties	**Antonis Gkikas**, Hatzianastassiou, Nikos, Korras-Carraca, Marios, *Comparison of MODIS Deep Blue aerosol single scattering albedo and asymmetry parameter with AERONET for northern Africa, Middle East and Europe*.
8P285	1074	Optical properties	**Kenia Wiedemann**, Paulo Artaxo1 Alexandre Correia, Steven C. Wofsy, Meinrat O. Andreae, Christoph Gerbig, *Aerosol optical properties in Amazonia - Spatial and seasonal variability*.
Instrumentation			
8P286	66	Application of new instrumentation for study of new processes and phenomena	**Mirvatte Francis**, Jean-Baptiste Renard, *Evaluation of the influence of the primary particle diameter of soot on their optical properties*.
8P287	144	Application of new instrumentation for study of new processes and phenomena	**Y.-Ping Hsieh**, Kevin Robertson, Glynnis Bugna, *Characterizing organic matter in aerosols of biomass burnings and the ambient air by a multi-element scanning thermal analysis (MESTA) technique*.
8P288	211	Application of new instrumentation	**Sylvia Bach**, Eberhard Schmidt, *Correlating the opacity-based dustiness behaviour to material specific properties*.

		for study of new processes and phenomena	
8P289	216	Application of new instrumentation for study of new processes and phenomena	**Vladimir Mitrochenko**, Anatoly. M. Baklanov, Petr.P. Moiseenko, Tamara.A. Ovchinnikova, Sergei.I. Eremenko, Sergei.N. Dubtsov, *New aerosol spectrometer for 3 – 1000 nm size range.*
8P291	342	Application of new instrumentation for study of new processes and phenomena	**Hee-Siew Han**, *Performance of a High Resolution Optical Particle Spectrometer*.
8P292	403	Application of new instrumentation for study of new processes and phenomena	**Leonidas Ntziachristos**, Pavlos Fragkiadoulakis, Zissis Samaras, Kauko Janka, Juha Tikkanen, *Sensor for vehicle on-board particle measurements*.
8P293	520	Application of new instrumentation for study of new processes and phenomena	**Paul Warrington**, *Development of an instrument to simulate puffing, inhaling and exhaling cigarette smoke*.
8P294	543	Application of new instrumentation for study of new processes and phenomena	**Burkhard Stahlmecke**, Margit Hildebrandt, Nico Dziurowitz, Sabine Plitzko, Heinz-Juergen Kiesling, Matthias Voetz, Thomas Kuhlbusch, *Effect of Different Sampling Methods on the Collection Efficiency of CNF- and CNT-Fibres*.
8P295	638	Application of new instrumentation for study of new processes and phenomena	**Tamara Pinterich**, Paul M. Winkler, Paul E. Wagner, Aron Vrtala, *Development of a Versatile Size Analyzing Nuclei Counter (vSANC)*.
8P296	656	Application of new instrumentation for study of new	**Anssi Arffman**, Marko Marjamäki, Jorma Keskinen, *Impaction velocities of particles in low pressure impactor*.

		processes and phenomena	
8P297	703	Application of new instrumentation for study of new processes and phenomena	**Sanchita Roy**, *Simulation of light scattering from air borne tea dust particles: possible carriers of pathogen*.
8P298	742	Application of new instrumentation for study of new processes and phenomena	**Achim Trimborn**, Urs Rohner, Marc Gonin, John Jayne, Douglas Worsnop, *New and Compact Single Particle Laser Ablation Mass Spectrometer (LAAPTOF)*.
8P299	757	Application of new instrumentation for study of new processes and phenomena	**Birgit Wehner**, Markus Hermann, Holger Siebert, Florian Ditas, Alfred Wiedensohler, *Setup and characterization of a new fast mixing type CPC*.
8P300	876	Application of new instrumentation for study of new processes and phenomena	**Dean Venables**, Jun Chen, John C. Wenger, *Extinction of aerosols in an atmosphere simulation chamber: broadband cavity spectrometer measurements extending from 320 to 450 nm*.
8P301	886	Application of new instrumentation for study of new processes and phenomena	**Jacob Swanson**, D.B. Kittelson, A. Bergmann, B. Giechaskiel, M. Twigg, *Design and Evaluation of a Mini Catalytic Stripper*.
8P302	68	Implementation of existing measurement methods and instruments for novel studies	**Amina Akachat**, Hakima Rebbah, *Diisocyanate aerosols in polyurethane manufacture*.
8P304	345	Implementation of existing measurement methods and instruments for	**Martin Hollertz**, John T. Elliott, Jacob Lewis, Eric R. Mansfield, Wynchester D. Whetten, Thomas A. Knotts IV, Michael J. Tarlov, Michael R. Zachariah, Leonard F. Pease III, *Hormone structural differentiation using a high resolution DMA*.

		novel studies	
8P305	365	Implementation of existing measurement methods and instruments for novel studies	**Martin Fierz**, Peter Steigmeier, Michael Glettig, Benjamin Wyrsch, Heinz Burtscher, *Direct integration of a GPS-GPRS unit into a miniature diffusion size classifer*.
8P306	573	Implementation of existing measurement methods and instruments for novel studies	**Thomas Barth**, Martin Lustfeld, *Influence of probe nozzle diameter on aerosol particle size distribution for isokinetic sampling in gas streams*.
8P307	596	Implementation of existing measurement methods and instruments for novel studies	**Konrad Kandler,** Eckart Schultz, *Recent enhancements and new applications of passive sampling of ambient particles*.
8P308	613	Implementation of existing measurement methods and instruments for novel studies	**Jeonghoon Lee**, Seung Cheol Han, *Using nigrosin as a surrogate for black carbon to study aerosol light absorption*.
8P309	718	Implementation of existing measurement methods and instruments for novel studies	**Jaan Salm**, Urmas Hõrrak, *Diffusion of charged particles in a DMA with inclined electric field and with a particle collector in gas outlet*.
8P310	861	Implementation of existing measurement methods and instruments for novel studies	**Florian Rubach**, Achim Trimborn, Thomas Mentel, Andreas Wahner, *Adapting the Aerodyne Aerosol Mass Spectrometer for Zeppelin-based measurements*.
8P311	865	Implementation of existing measurement methods and instruments for novel studies	**Juha Kangasluoma**, Heikki Junninen, Katrianne Lehtipalo, Tero Toivola, Tuukka Petäjä, Markku Kulmala, *Calibration of Condensation Particle Counters – analysis of sub-3nm calibration ions using mass spectrometry*.

8P312	906	Implementation of existing measurement methods and instruments for novel studies	**Caner Yurteri**, M. Stowers, W.A. Kleefsman, J.C.M. Marijnissen., *Mobilization of Aerosol MALDI Mass Spectrometry for Bioaerosol Analysis*.
8P313	1003	Implementation of existing measurement methods and instruments for novel studies	**Michelle Barker**, Cameron McLeod, Diane Ciaparra, Kevin Jackson, *Development and validation of a novel experimental system to investigate particulate matter emitted from a steelworks*.
8P314	1115	Implementation of existing measurement methods and instruments for novel studies	**Attila Nagy**, Attila Kerekes, Attila Nagy, Daniel Oszetzky, Aladar Czitrovszky, *Development of a pulmonary waveform generator for study the aerosol propagation and deposition in transparent hollow airway models*.

13:00-15:00 **Session 9A: Aerosols in Geoengineering**
Room: Theatre A
Chairs: Thomas Leisner / Francis Pope

13:00	9A1	823	**Hauke Schmidt** (Invited talk) *Implications of geoengineering assessed in simulations with complex climate models*
13:20	9A2	774	**Francis Pope**, Tony Cox, Markus Kalberer, Peter Braesicke, Andy Ward, Matt Watson *Impact of Geoengineered Aerosols on Stratospheric Ozone Chemistry*
13:40	9A3	567	**Thomas Leisner** (Invited talk), Stefan Müller-Klieser, Ulrich Platt *Near vessel dynamics of sea salt sprays: How efficient can maritime clouds be seeded?*
14:00	9A4	862	**Kristina Lundgren**, Max Bangert, Heike Vogel, Bernhard Vogel *The impact of controlled sea salt emissions on cloud features based on comprehensive regional model studies*

14:20	9A5	451	**Antti-Ilari Partanen**, Harri Kokkola, Sami Romakkaniemi, Veli-Matti Kerminen, Kari E.J. Lehtinen, Hannele Korhonen *Effects of sea spray geoengineering on clouds and Earth's radiative balance*
14:40	9A6	223	**Kirsty Pringle**, Ken Carslaw, Tingting Fan *Exploring efficiency of sea spray geo-engineering*

13:00-15:00 **Session 9B: Field Observations from Global Hot Spots**
Room: Theatre B
Chairs: Andreas Minikin / M. Krämer

13:00	9B1	116	**Petri Tiitta**, Lauri Laakso, Ville Vakkari, Philip Croteau, Miroslav Josipovic, Paul Beukes, Pieter Van Zyl, Andreas Venter, Kerneels Jaars, Heikki Laakso, John Jayne, Kobus Pienaar, Markku Kulmala, Ari Laaksonen, Douglas Worsnop *First on-line aerosol chemical composition measurements in South African grassland region*
13:20	9B2	453	**Ville Vakkari**, Heikki Laakso, Markku Kulmala, Desmond Mabaso, Lauri Laakso *Aerosol particle size distributions in clean and polluted environments in South Africa*
13:40	9B3	898	**Paulo Artaxo**, L.V. Rizzo, K.T. Wiedemann, E. Swietlicki, A. Wiedensohler *Long term aerosol optical properties in pristine and biomass burning areas in the Amazon Basin*
14:00	9B4	235	**Niall Robinson**, J. D. Allan, G. Allen, H. Coe *Inflow and outflow of Borneo: the regional setting of aerosol compositional measurements in and above a maritime tropical rainforest*
14:20	9B5	241	**Jai Devi Jeyaraman**, Priya Choudhry, Marykutty Michael, S.N. Tripathi, Tarun Gupta *Direct Evidence of Elevated Absorbing Layer Associated with Coarse Mode Particles over CTCZ Region from Aircraft Experiment 2009*

14:40	9B6	174	**Wenjie Zhang**, Zhipeng Bai, Jianzhong Ma, Jianhua Chen, Wen Yang, Baohui Yin *In-situ aircraft observations on gases and particulate pollutants around Beijing area: distributions and influencing factors*
Reserve	9BR	807	**Luca Ferrero**, D. Cappelletti, M. Petitta, F. Scardazza, M. Castelli, M.G. Perrone, G. Sangiorgi, E. Bolzacchini *Vertical profiles of aerosol physico-chemical and optical properties measured along Italy over basin valleys*

13:00-15:00 **Session 9C: Biomass and Biofuels**
Room: Rutherford Lecture Theatre
Chair: Olli Sippula

13:00	9C1	571	**Alejandro Keller**, Heinz Burtscher *Micro Smog Chamber: a Candidate Tool for Evaluating Wood Burning Emissions*
13:20	9C2	464	**Terhi Penttilä**, Heikki Lamberg, Annika Hukkanen, Olli Sippula, Jarkko Tissari, Jorma Jokiniemi. *Comparison of emissions from wood and oil boilers in small (20–25 kW) and medium (5–10 MW) scale*
13:40	9C3	815	**Heikki Lamberg**, Olli Sippula, Jarkko Tissari, Jorma Jokiniemi *The effects of air-staging and fuel characteristics on PM1 emissions from small-scale pellet combustion*
14:00	9C4	860	**Joakim Pagels**, Joakim Pagels, Axel Eriksson, Erik Z. Nordin, Robin Nyström, Esbjörn Pettersson, Erik Swietlicki and Christoffer Boman *Time resolved PAH-emissions from residential wood combustion investigated with aerosol mass spectrometry*
14:20	9C5	621	**Heinz Burtscher**, Alejandro Keller, Martin Fierz *Electrostatic precipitators for domestic wood stoves*
14:40	9C6	512	**Andrei Bologa**, Hanns-Rudolf Paur, Klaus Woletz *High temperature electrostatic precipitation for small*

			scale biomass combustion
Reserve	9CR	662	**Nickolas Meyer**, Thomas Heck *Wood combustion emissions in Switzerland and associated impact assessments*

13:00-15:00 **Session 9D: In-vitro toxicity and health effects of PM**
Room: Moseley Lecture Theatre
Chairs: Francesca Cetta / Otmar Schmid

13:00	9D1	424	**Marcello Galeazzi** *The inflammatory response elicited in vitro by air pollutants is greater in synoviocytes from patients with Rheumatoid Arthritis than in those with osteoarthrosis*
13:20	9D2	306	**Iris Raquel Gutiérrez** *Microbial test battery for risk assessment of fine particles originating from the combustion of wood*
13:40	9D3	724	**Pasi Jalava**, Joachim Kelz, Thomas Brunner, Mikko Happo, Jorma Mäki-Paakkanen, Pasi Hakulinen, Terhi Penttilä, Annika Hukkanen, Jorma Jokiniemi, Ingwald Obernberger, Maija-Riitta Hirvonen *Residential wood combustion technology affects the toxicological responses of particulate emissions*
14:00	9D4	321	**Lisa Künzi**, Sarah Schneider, Peter Mertes, Josef Dommen, Urs Baltensperger, Andre Prevot, Markus Kalberer, Marianne Geiser *Responses of lung cell cultures after realistic exposure to primary and secondary carbonaceous aerosols*
14:20	9D5	443	**Susanne Gauggel**, Joachim Wiese, Bart Pieterse, Daniel R. Dietrich *General and PAH-mediated cytotoxicity in particulate matter from wood combustion*
14:40	9D6	307	**Birte Hegemann** *Health risk assessment of wood combustion fine dust particles with Caenorhabditis elegans*
Reserve	9DR	355	**Dirk Broßell**, Sabine Plitzko, Nico Dziurowitz, Erhardt Gierke, Volker Bachmann, Gunter Linsel, Nkwenti

			Azong-Wara, Christof Asbach, Heinz Fissan, Andreas Schmidt-Ott *A Thermal Precipitator for Nanoparticle Cytotoxicity Screening*

13:00-15:00 **Session 9E: Aerosol-based Nanotechnology: Methods and Applications**

Room: Bragg Lecture Theatre

Chairs: Andreas Schmidt-Ott / Michael Mertler

13:00	9E1	226	**Stephanie Bubenhofer**, Wendelin Stark, Robert Grauss *From Embedded to Supported Metal/Oxide Nanomaterials: Thermal Behavior and Structural Evolution at Elevated Temperatures*
13:20	9E2	1047	**Dennis Kiesler**, Thomas Bastuck, Frank Einar Kruis, Markus Kennedy *Scaling of an aerodynamic lens for use in coating technology*
13:40	9E3	167	**Christoph Kellenberger** *Use of aerosol-derived nanoparticles for the fabrication of polymer ultrafiltration membranes*
14:00	9E4	120	**Nicole Neubauer**, Martin Seipenbusch, Gerhard Kasper *A new measurement technique for the process monitoring of the catalytic activity of nanoparticles during their production process*
14:20	9E5	168	**Sotiris Pratsinis** *Hybrid Plasmonic-Magnetic Biomarkers*
14:40	9E6	436	**Peter Pikhitsa**, Daegyu Kim, Hongjoo Yang, Mansoo Choi *Room temperature gas sensor based on carbon nanoparticles*

13:00-15:00 **Session 9F: Charged Aerosols**
Room: Blackett Lecture Theatre
Chairs: A. Bologa / C. Yurteri

13:00	9F1	962	**Stephanie Sigmund**, Mingzhou Yu, Joerg Meyer, Martin Seipenbusch, Markus Wild, Gerhard Kasper *Electrostatic controlled coating of particle surfaces with nanoparticles*
13:20	9F2	834	**Luewton Agostinho**, E.C. Fuchs, J. Wartena, C. U. Yurteri, J. C. M. Marijnissen *Characterization of EHDA in the simple-jet mode*
13:40	9F3	514	**Andrei Bologa**, Hanns.-Rudolf Paur, Helmut Seifert, Klaus Woletz *Study of corona discharge ionizer for high temperature/high pressure electrostatic precipitator*
14:00	9F4	106	**Dmitry Samsonov**, Celine Durniak, Paul Harvey, Neil Oxtoby, Jason F. Ralph, Sergey Zhdanov, Grogor Morfill *Particle diagnostics and wave phenomena in complex plasmas*
14:20	9F5	878	**Stephan Rennecke**, Alfred P. Weber *Contact charging of metal nanoparticles*
14:40	9F6	1071	**Lena Knobel**, Hans-Joachim Schmid *Comparison of methods to achieve a stationary charge distribution*
Reserve	9FR	929	**Markus Wild**, Joerg Meyer, Gerhard Kasper *A simplified procedure for particle charge distribution measurements and its application to the characterization of the annual DBD aerosol neutralizer*

15:30-17:10 **Session 10A: Aerosols in Geoengineering / Aerosols in Global Climate Models**
Room: Theatre A
Chairs: Hannele Korhonen / James Haywood

15:30	10A1	938	**Francois Benduhn**, Kenneth Carslaw *A New Hybrid Solver of Dissolution of Inorganics into*

			the Particle Liquid Phase: Evaluation and Global Scale Implications on Aerosol Properties.
15:50	10A2	409	**Zhiqiang Cui**, Kenneth Carslaw, Alan Blyth *More precipitation from melting ice particles in deep convective clouds in a warm and moist environment*
16:10	10A3	936	**Matthew Woodhouse**, Graham Mann, Ken Carslaw, Olivier Boucher *Weak response of CCN to changes in DMS flux: implications for the CLAW feedback in current climate assessments*
16:30	10A4	818	**Catherine Scott**, Piers Forster, Kenneth Carslaw, Dominick Spracklen *Estimating the radiative impacts of biogenic secondary organic aerosol, their variation with location and climate, and the implications for climate geoengineering*
16:50	10A5	389	**Jim Haywood**, Andy Jones, Lieven Clarisse, Adam Bourassa, John Barnes, Paul Telford, Nicolas Bellouin, Olivier Boucher, Paul Agnew, Cathy Clerbaux, Pierre Coheur, Doug Degenstein, Peter Braesicke *Modelling the volcanic eruption of Sarychev*

15:30-17:10 **Session 10B: Remote Sensing of Aerosol Properties**
Room: Theatre B
Chairs: Lucas Alado-Arboledas / Paul Zieger

15:30	10B1	339	**Franco Marenco**, Ben Johnson, Kate Turnbull, Jim Haywood, Stuart Newman, Alan Vance, James Dorsey, Martin Gallagher, Hugo Ricketts *The FAAM volcanic ash flights in May 2010: results from the lidar, the CAS, and ARIES*
15:50	10B2	469	**Alain Miffre**, Grégory David, Benjamin Thomas, Patrick Rairoux *Volcanic ash optical properties with an UV-depolarization Lidar*

16:10	10B3	570	**Carmen Cordoba-Jabonero**, Mar Sorribas, Juan-Luis Guerrero-Rascado, Jose-Antonio Adame, Yballa Hernandez, Hassam Lyamani, Victoria Cachorro, Manuel Gil, Lucas Alados-Arboledas, Emilio Cuevas, Benito de la Morena *Synergetic monitoring of Saharan dust plumes: A case study of dust transport from Canary Islands to Iberian Peninsula. Part 1: Dust detection, identification and vertical structure analysis*
16:30	10B4	825	**Lucas Alados-Arboledas**, F. Navas-Guzmán, J.A. Bravo-Aranda, H.Lyamani, J D. Pérez-Ramírez, J. L. Guerrero-Rascado , I. Foyo, I. Alados, M.J. Granados, G. Titos, J. Fernández Gálvez, A. Valenzuela, M. Antón, A. Quirantes, X. Querol, A. Alastue, F. J. Olmo *Multi-instrumental characterization of the mixing of Eyjafjallajökull volcanic aerosols and boundary layer aerosols at Granada, Spain*
16:50	10B5	875	**Paul Zieger** *Closure study of aerosol optical properties using in-situ and remote sensing techniques*
Reserve	10BR	951	**Mika Komppula**, Tero Mielonen, Kimmo Korhonen, Antti Arola, Heikki Lihavainen, Lauri Laakso, Ville Vakkari, Heikki Laakso, Paul Beukes, Pieter Van Zyl, Kobus Pienaar, Petri Tiitta, Rikus le Roux, Kgaugelo Chiloane, Holger Baars, Ronny Engelmann, Dietrich Althausen, Kari Lehtinen *One year of Raman lidar measurements at the South African EUCAARI site*

15:30-17:10 **Session 10C: Control Technologies for Combustion Emissions**

Room: Rutherford Lecture Theatre

Chairs: A.G. Konstandopoulos / C. Gutierrez-Canas

15:30	10C1	513	**Cristina Gutierrez-Canas**, Miren Larrion, Alfredo Perez, Egoitz Pena, Sergio Fernandez, and Juan Andres

			Legarreta *Nanostructure of fine and ultrafine particles from start-ups and shutdowns of a 250MW natural gas power plant*
15:50	10C2	1082	**Johannes Ebert**, Gernot Pranghofer, Ole Petzoldt *Optimization of Dust Collectors in Incineration Plants to control Fine Particulate, Dioxins and NOx by using ePTFE Membranes and Catalytic Filtration Technologies*
16:10	10C3	314	**David Sanz**, Jesús J. Rodríguez-Maroto, Jose L. Dorronsoro, Enrique Rojas, Alberto Bahillo, Raquel Ramos, Esperanza Ruiz, Pilar Galán, María A. Martínez, Cristina Gutierrez-Cañas, Miren Larrion, Egoitz Peña, Wilhelm Hagemann, Saioa Astarloa *Hybrid filtration and catalytic control of toxic pollutants from a 1.2MW waste biomass cofiring boiler*
16:30	10C4	789	**Dimitrios Zarvalis**, Suzana Lorentzou, Alexantra Zygogianni, Athanasios Konstandopoulos, Christopher Severin, Markus Shönen, Raimund Vedder, Michel Fiebig, Stephane Zinola, Jacques Lavy *Diesel Engine Exhaust Emission Control: Performance Assessment of a Multi-Functional Reactor under Conventional and Advanced Combustion Conditions*

15:30-17:10 **Session 10D: Turbulent Aerosol Transport and Exchange / Transport and Transformation**

Room: Moseley Lecture Theatre

Chairs: Birgit Wehner / Thomas Kristensen

15:30	10D1	763	**Birgit Wehner**, Florian Ditas, Alfred Wiedensohler, Holger Siebert *Vertical transport of aerosol particles in the marine boundary layer near Barbados*
15:50	10D2	412	**Daniele Contini**, Antonio Donateo, Cosimo Elefante, Fabio Grasso *Analysis of particles and CO2 fluxes in an urban area: correlation with traffic rate and micrometeorology*

16:10	10D3	364	**Malte Julian Deventer**, Frank Griessbaum, Otto Klemm *Highly size resolved particle fluxes over an urban area*
16:30	10D4	870	**Mark Gordon**, Ralf Staebler, John Liggio, Jeff Brook, Shao-Meng Li, Jeremy Wentzell, Cris Mihele, Gang Lu, Patrick Lee *Transport and mixing of aerosols due to highway-generated turbulence*
16:50	10D5	137	**Prashant Kumar**, Matteo Carpentieri *Dispersion of nanoparticles in vehicle wake – Part I: analysis of field measurements*
Reserve	10DR	208	**Pierre Roupsard**, Muriel Amielh, Alexis Coppalle, Hubert Branger, Philippe Laguionie, Olivier Connan, Didier Hébert, Denis Maro, Martine Talbaut *Submicronic aerosols dry deposition on urban surfaces: a wind tunnel study to improve the lack of knowledge*

15:30-17:10 **Session 10E: Spark Generators for Nanoparticle Generation**

Room: Bragg Lecture Theatre

Chairs: Knut Deppert / Einar Kruis

15:30	10E1	649	**Shubhra Kala**, Frank Einar Kruis, Ralf Theissmann *Generation of Au-Ge nanocomposites by spark discharge*
15:50	10E2	970	**Maria E Messing**, S. Blomberg, N.M. Martin, J. Gustafson, J.N. Andersen, L.E. Walle, A. Borg, H. Grönbeck, M.E. Grass, Z. Liu, E. Lundgren and K. Deppert *In situ high pressure XPS investigations of PdAg alloy nanoparticles: Towards cheaper catalysts*
16:10	10E3	877	**Tobias Pfeiffer**, Anca Anastasopol, Vincent Vons, Walter Legerstee, Stephan Eijt, Fokko Mulder, Andreas Schmidt-Ott *Direct Synthesis of Magnesum Hydride using Spark*

			Discharge
16:30	10E4	1076	**Konstantinos Barmpounis**, Tobias Pfeiffer, Vincent Vons, George Biskos, Andreas Schmidt-Ott *Self-charge Distribution of Nanoparticles Generated by Spark Discharge*
16:50	10E5	971	**Maria E Messing**, C.R. Svensson, B.O. Meuller, M. Bohgard, K. Deppert, J. Pagels and J. Rissler *Spark generated particles for nanotoxicology studies*

15:30-17:10 **Session 10F: Modelling Aerosol Formation**
Room: Blackett Lecture Theatre
Chairs: K. Carslaw / H. Junninen

15:30	10F1	419	**Florian Couvidat**, Youngseob Kim, Karine Sartelet, Christian Seigneur *H2O: A new model to predict secondary organic aerosol formation*
15:50	10F2	871	**Carolina Rojo**, Xavier Vancassel, Jean-Luc Ponche *Environmental impact of aviation-produced aerosols: Towards alternative fuels*
16:10	10F3	863	**Heikki Junninen**, Mikhail Paramonov, Anne Hirsikko, Miikka Dal Maso, Markku Kulmala *Automatic classification of new particle formation events*
16:30	10F4	883	**Carly Reddington**, Ken S. Carslaw, Dominick V. Spracklen, Maria Grazia Frontoso, Lindsay Collins, Joonas Merikanto, Andreas Minikin, Thomas Hamburger, Hugh Coe, Markku Kulmala, Pasi Aalto, Harald Flentje, Christian Plass-Duelmer, Wolfram Birmili, Alfred Wiedensohler, Thomas *Primary versus secondary contributions to particle number concentrations in the European boundary layer during the EUCAARI campaign*
16:50	10F5	920	**Christos Fountoukis** *Organic Aerosol over Europe: Model Evaluation and Response to Increasing Temperature*

Reserve	10FR	229	**Christoph Winkelmann**, Arkadiusz K. Kuczaj, Steffen Stolz, Bernard J. Geurts *Multi-scale modeling of aerosol formation in pipe flow*

17:10-18:00 EAA Working group meetings

Fundamentals	Blackett Theatre
Combustion	Rutherford Theatre
Instrumentation	Bragg Theatre
Particle-Lung Interactions	Moseley Theatre
Electrical Effects	Theatre A

Friday 9th September

09:00-10:00 Plenary 5
Andreas Petzold: Global aviation and particulate matter: from climate impact to volcanic ash and back
Room: Theatre B
Chair: Martina Krämer

10:00-10:15 Awards Ceremony – Theatre B

10:45-12:45 **Session 11A: Biomass Burning**
Room: Theatre A
Chairs: M.R. Alfarra / J. Schneider

10:45	11A1	912	**Christine Piot**, Matthias Gianini, Julie Cozic, Lucie Polo, Jean-Luc Besombes, Aurélie Charron, Jean-Luc Jaffrezo, Christoph Hueglin *Comparison of qualitative and quantitative approaches for source apportionment of PM at urban and rural alpine sites*
11:05	11A2	459	**Xuefang Sang** *Stable carbon isotope ratio analysis of anhydrosugars in biomass burning aerosol*
11:25	11A3	311	**Cátia Gonçalves** *Organic compounds in PM2.5 emitted from fireplace and wood stove combustion of typical Portuguese wood species*
11:45	11A4	607	**Jürgen Orasche**, Jürgen Schnelle-Kreis, Gülcin Abbaszade, Hans Ruppert, Ralf Zimmermann *Diurnal concentrations of organic tracers originated from wood combustion*
12:05	11A5	398	**Harri Portin**, Tero Mielonen, Mika Komppula, Ari Leskinen, Antti Arola, Ari Laaksonen, Kari Lehtinen *Biomass burning aerosols measured with in-situ and remote sensing instruments in Eastern Finland during the forest fires in Russia 2010*

12:25	11A6	465	**Mikhail Sviridenkov**, Gennady Gorchakov, Natalia Chubarova, Yevgenia Semutnikova, Alexander Emilenko *Optical and microphysical characteristics of smoke aerosol during fire events in Moscow region in summer 2010*
Reserve	11AR	547	**Chung-Te Lee** *Carbonaceous aerosols in the Asian Brown Clouds transported from Southeast Asia: downstream observations at Mt. Lulin in Taiwan*

10:45-12:45 **Session 11B: Chemical and Physical Properties of SOA**
Room: Theatre B
Chairs: Gordon McFiggans / Neil Donahue

10:45	11B1	187	**Mark Barley**, David Topping, Gordon McFiggans, Douglas Lowe *Modelling the sensitivity of aerosol properties to variations in key inputs:- 1) vapour pressures; 2) non-ideality; 3) hydrolysis of acid-anhydrides*
11:05	11B2	866	**Neil Donahue**, Lea Hildebrandt, Kaytlin Henry, Jesse Kroll, Douglas Worsnop, Spyros Pandis, Neil Donahue *Evaluating the mixing of organic aerosol components using high-resolution aerosol mass spectrometry*
11:25	11B3	1008	**Angela Buchholz**, TH. F. Mentel, F. Rubach, C. Spindler, R. Tillmann, E. Kleist, J. Wildt *Towards a better understanding of hygroscopic growth and cloud droplet activation of biogenic secondary aerosols*
11:45	11B4	608	**Taina Yli-Juuti**, Alessandro Zardini, Markku Kulmala, Merete Bilde, Joakim Pagels, Axel Eriksson, Erik Swietlicki, Douglas Worsnop, Ilona Riipinen *Study on equilibrium vapour pressure of succinic acid in binary aqueous solution and ternary inorganic - organic aqueous solutions using flow tube*

			experiments
12:05	11B5	361	**Lorena Miñambres**, Estíbaliz Méndez, María N. Sánchez, Fernando Castaño and Francisco J. Basterretxea *Water Uptake Properties of internally mixed sodium halide and succinic acid particles*
12:25	11B6	885	**Johannes Ofner**, Natalia Balzer, Joelle Buxmann, Hinrich, Grothe, Heinz-Ulrich Krueger, Ulrich Platt, Philippe Schmitt-Kopplin, Cornelius Zetzsch *Aerosol-halogen interaction: Halogenation processes of secondary organic aerosols*
Reserve	11BR	989	**Ilona Riipinen**, Jeffrey R. Pierce, Taina Yli-Juuti, Silja Häkkinen, Christos Fountoukis, Markku Kulmala, Douglas R. Worsnop, Merete Bilde, Spyros N. Pandis, Neil M. Donahue *On ultrafine aerosol growth and the condensation/ evaporation properties of atmospheric organics*

10:45-12:45 **Session 11C: Combustion Aerosol Measurements and Analysis**

Room: Rutherford Lecture Theatre

Chair: Stefano di Stasio

10:45	11C1	658	**Anssi Arffman**, Topi Rönkkö, Panu Karjalainen, Tero Lähde, Juha Heikkilä, Liisa Pirjola, Dieter Rothe, Jorma Keskinen *Thermodenuder with low nanoparticle losses: design, simulations, laboratory tests and diesel exhaust particle studies*
11:05	11C2	888	**Jonathan Johnsson**, Anders Karlsson, Nils-Erik Olofsson, Henrik Bladh, Per-Erik Bengtsson *Soot particle aggregates: numerical construction and analysis of influence on laser-induced incandescence and elastic light scattering signals*
11:25	11C3	207	**François-Xavier Ouf**, Jérôme Yon, Ghislaine Frebourg, Sébastien Pontreau

			Electronic tomography of nanoparticles aggregates: from 2D to 3D
11:45	11C4	61	**Stefano di Stasio**, J.Brian A. Mitchell, Jean-Luc LeGarrec *Effect of Alkali Metal Salt Addition on Hierarchic Assembly of Flame Aerosol Nanoparticles detected by Synchrotron Small-Angle X-ray Scattering*
12:05	11C5	474	**Alexis Coppalle**, J. Yon, C. Caumon, K. F. Ren, G. Martel *Determination of the refractive index of soot particles in the visble spectrum by extinction spectra*
12:25	11C6	213	**Reinhard Niessner**, Johannes Schmid, Benedikt Grob and Natalia P. Ivleva *Prediction of soot oxidation reactivity by Raman microspectroscopy*
Reserve	11CR	383	**Jérôme Yon**, Chloé Caumont-Prim, Alexis Coppalle, Kuan Fang Ren, *Measurement of soot size distribution in flames by inversion of angular light scattering*.

10:45-12:45 **Session 11D: From PM exposure to health effects 1**
Room: Moseley Lecture Theatre
Chairs: Jeroen Buters / Otto Hanninen

10:45	11D1	429	**Valentina Guercio** *Selection of proper markers for a better knowledge of health effects of air pollution. Difficulty in the choice of markers or in the recognition of causative mechanisms?*
11:05	11D2	699	**Sebastian Oeder**, Rudolf Jörres, Wolfgang Schober, Ingrid Weichenmeier, Rudolf Schierl, Silvio Dietrich, Hermann Fromme, Jutta Lintelmann, Heidrun Behrendt, Jeroen Buters *Effects of elementary school indoor/outdoor PM10 on gene expression and blood coagulation*
11:25	11D3	347	**Rohan Jayaratne**, Megat Mokhtar, Lidia Morawska, Mandana Mazaheri *Personal Exposure Assessment of School Children to*

			Airborne Nanoparticles
11:45	11D4	720	**Evangelia Diapouli**, Maria I. Gini, Vasiliki Vasilatou, Thomas Maggos, Stella Pateraki, Antigoni Katsanaki, Dikaia Saraga, Konstantinos Eleftheriadis *Workers exposure to particulate and gaseous pollutants in a photocopy / printing center*
12:05	11D5	1021	**Aneta Wierzbicka**, Aneta Wierzbicka, Patrik T. Nilsson, Erik Z. Nordin, Joakim Pagels, Andreas Dahl, Jakob Löndahl, Anders Gudmundsson, Mats Bohgard *Can Storage of Cleaning Products be a Source of Ultrafine Particles in a Supermarket?*
12:25	11D6	755	**Kaarle Hameri**, Eija Asmi, Bjarke Molgaard *Particle exposure in public transport – seasonal dependence*
Reserve	11DR	1044	**Christina Isaxon**, Andreas Dahl, Erik Nordin, Gunilla Wieslander, Dan Norback, Anders Gudmundsson, Aneta Wierzbicka, Mats Bohgard *Particles in Indoor Air – measurements in residential dwellings*

10:45-12:45 **Session 11E: Comparison of Different Measurement Methods**

Room: Bragg Lecture Theatre

Chairs: Rob Caldow / Wladyslaw Szymanski

10:45	11E1	211	**Sylvia Bach**, Eberhard Schmidt, *Correlating the opacity-based dustiness behaviour to material specific properties*.
11:05	11E2	431	**Marie Laborde**, M. Gysel, M. Schnaiter, C. Linke, H. Saathoff, K.-H. Naumann, O. Möhler, J. Taylor, M. Flynn, J. Allan, H. Coe, K. Heimerl, F. Dahlkötter, B. Weinzierl, A. Wollny, L. Polo, J. Cozic, P.Laj, J.M. Flores, Y. Rudich, S. Berlenz,U. Wagner *Single Particle Soot Photometer (SP2) intercomparison: Results from 6 instruments*
11:25	11E3	533	**Christof Asbach**, Thomas A.J. Kuhlbusch, Heinz Fissan, Burkhard Stahlmecke, Hans-Georg Horn,

			Heinz Kaminski *Evaluation of an improved unipolar diffusion charger for size distribution measurements*
11:45	11E4	675	**Federico Karagulian**, Claudio A. Belis, Fritz Lagler, Maurizio Barbiere, Michel Gerboles *Evaluation of the performances of SidePak AM510 nephelometer compared to the Tapered Element Oscillating Microbalance (TEOM) method for PM2.5 mass measurement*
12:05	11E5	846	**Jonathan Symonds**, Mark Rushton, Kingsley Reavell, Charlie Lowndes, Andrew Ellison, Jason Olfert *Evaluation of the High Resolution Centrifugal Particle Mass Analyser*
12:25	11E6	869	**Paul Zieger** *Comparison of ambient aerosol extinction coefficients obtained from in-situ, MAX-DOAS and LIDAR measurements in Cabauw*

10:45-12:45 **Session 11F: Atmospheric Applications of Aerosol Modelling**

Room: Blackett Lecture Theatre

Chairs: S. Wurzler / Heike Vogel

10:45	11F1	478	**David Topping**, Gordon McFiggans *A 19th Century model for secondary organic aerosol*
11:05	11F2	557	**Wanmin Gong**, Craig Stroud, Sun-Ling Gong, Paul Makar, Mike Moran, Junhua Zhang, Nicole Shantz, Richard Leaitch *Impact of aerosol activation on modelled regional particulate matter*
11:25	11F3	648	**Nicole Riemer**, Matthew West, Richard Easter, Rahul Zaveri *Particle-resolved modelling of the aging process of atmospheric soot particles*
11:45	11F4	698	**Sabine Wurzler**, Heike Hebbinghaus, Michael Memmesheimer, Georg Piekorz, Elmar Friese,

			Herman Jakobs, Christoph Kessler, Adolf Ebel, Peter Bruckmann *Time evolution of the concentration of PM10, PM2.5, and NO2 in Central Europe until 2015: will we meet the limit values set by the European Commission in time?*
12:05	11F5	976	**Heike Vogel**, Max Bangert, Bernhard Vogel, Terry L. Lathem, Athanasios Nenes, Jochen Förstner *Simulation of the impact of Eyjafjallajökull plume on cloud formation and precipitation over Europe with COSMO-ART*
12:25	11F6	940	**Eimear Dunne**, Kenneth Carslaw, Carly Reddington, Joao Almeida, the CLOUD collaboration *The influence of ion-induced nucleation on atmospheric aerosols based on data from the CERN CLOUD experiment*

13:45-15:45 **Session 12A: Marine Aerosols / Mineral Dust**
Room: Theatre A
Chairs: D. Baumgardner / A.C. Butcher

13:45	12A1	240	**Matteo Rinaldi**, Stefano Decesari, Emanuela Finessi, Marco Paglione, Sandro Fuzzi, Euripides G. Stephanou, Thrasivoulos Tziaras, Apostolos Spyros, Darius Ceburnis, Colin D. O'Dowd, Maria Cristina Facchini *Primary and secondary marine organic aerosols over the North Atlantic ocean during the MAP experiment*
14:05	12A2	798	**Hamish Struthers**, Annica Ekman, Paul Glantz, Monica Mårtensson, Douglas Nilsson *Predicted change in emissions of sea salt aerosols for the years 1870-2100*
14:25	12A3	817	**Andrew Butcher**, Stephanie King,Thomas Rosenoern, Douglas Nilsson, Merete Bilde *Characterization of a bubble tank for Sea Spray Aerosol Studies*

14:45	12A4	569	**Claas H. Koehler**, Thomas Trautmann, Erwin Lindermeir *Radiative properties of mixed biomass-mineral dust aerosol in the thermal infrared during SAMUM-2*
15:05	12A5	983	**Bernard Grobety**, Cedric Botter, Mario Meier *Volcanic sulfate aerosols*
15:25	12A6	996	**Adriana Pietrodangelo**, Roberto Salzano, Salvatore Pareti, Elena Rantica, Cinzia Perrino *Source profile of the local wind-blown soil contribution to respirable airborne particulate matter in the southern area of Rome (Italy)*

13:45-15:45 **Session 12B: Optical Properties**
Room: Theatre B
Chairs: Helmuth Horvath / Francisco José Olmo Reyes

13:45	12B1	582	**Claire Ryder**, Ellie Highwood, Paola Formenti, Helen Brindley *Dust optical, chemical and radiative properties from the DODO and Fennec aircraft campaigns*
14:05	12B2	139	**Sachchida Nand Tripathi**, S.K. Mishra, S. G. Aggarwal, A. Arola *Optics of semi-externally mixed polluted mineral dust*
14:25	12B3	773	**Agnes Molnar**, Denes Parkany, Kornelia Imre, Vera Gacser *Reconstruction of aerosol extinction from visibility and aerosol mass concentration in Budapest, Hungary*
14:45	12B4	904	**Tibor Ajtai**, Martin Schnaiter, Claudia Linke, Ágnes Filep, Noémi Utry, Zoltán Bozóki, Gábor Szabó *Wavelength dependent Angström exponent based source apportionment and its correlation with aerosol size distribution*
15:05	12B5	711	**Sumita Kedia**, S. Ramachansran *Retrieving aerosol size distribution using wavelength dependence of aerosol optical depths*

15:25	12B6	873	**Paul Zieger** *Effects of relative humidity on aerosol light scattering: Results from different European sites*
Reserve	12BR	1074	**Kenia Wiedemann**, Paulo Artaxo Alexandre Correia, Steven Wofsy, Meinrat Andreae, Christoph Gerbig *Aerosol optical properties in Amazonia - Spatial and seasonal variability*

13:45-15:45 **Session 12C: Engine-related Aerosols**
Room: Rutherford Lecture Theatre
Chairs: Andreas Petzold / Zoran Ristovski

13:45	12C1	1114	**Karsten Fuglsang**, Kai Dirscherl, Morten Lykkegaard, Jacob Markussen, Anne Hemmersam, Olga Popovicheva, Elena Kireeva, Mikael Poulsen, David Larsson *Characterization of particles emitted from a marine diesel engine: Influence of sampling temperature on measured particle number, size, and morphology*
14:05	12C2	663	**David Delhaye**, Delphine Lottin, Daniel Ferry, Jany Gouge, Olivier Penanhoat *Microphysical properties of carbonaceous particulate matter emitted by three different aircraft turbofan engines*
14:25	12C3	362	**Andreas Petzold**, Mattia Righi, Johannes Hendricks, Veronika Eyring, Peter Lauer, Fritz Fleischer, Uwe Fritsche *The potential of biofuels in shipping for mitigating the climate impact – Results from the integrated BIOCLEAN study*
14:45	12C4	1029	**Zoran Ristovski**, Nicholas Surawski, Branka Miljevic, Svetlana Stevanovic, Godwin Ayoko, Sohai Elbagir, Kathryn Fairfull-Smith, Steven Bottle *On the Influence of Biodiesel Feedstock on Diesel Particulate Emissions*

15:05	12C5	814	**Tero Lähde**, T. Rönkkö, M. Happonen, C. Söderström, A. Virtanen, A. Solla, M. Kytö, D. Rothe, L. Pirjola and J. Keskinen *Effect of fuel injection pressure on diesel engine exhaust non-volatile particle size distribution*
15:25	12C6	221	**Panu Karjalainen**, Matti Happonen, Topi Rönkkö, Toni Kinnunen, Piotr Bielaczyc, Rafal Sala, Jakub Dzida, Jorma Keskinen *Exhaust particles of a light duty diesel engine equipped with an oxidative aftertreatment operating with different sulfur level fuels*
Reserve	12CR	489	**Svetlana Stevanovic**, Branka Miljevic, Nicholas Surawski, Steven Bottle, Richard Brown, Zoran Ristovski *Reactive oxygen species (ROS) emissions from diesel engines running on various biofuels*

13:45-15:45 **Session 12D: From PM exposure to health effects 2**
Room: Moseley Lecture Theatre
Chair: Mats Bohgard

13:45	12D1	143	**Tobias Schripp**, Ina Kirsch, Sebastian Willenborg, Tunga Salthammer *Exposure Analysis for the Inhalation of Ultra-fine Particles Emitted from Household Devices*
14:05	12D2	974	**Anja Schmidt**, Ken Carslaw, Bart Ostro, Marge Wilson, Thor Thordarson, Graham Mann *Modelling excess mortality in Europe following a future Laki-style Icelandic eruption*
14:25	12D3	688	**Jenny Rissler**, Joakim Pagels, Christian Svensson, Jakob Löndahl, Maria Messing, Mats Bohgard *Novel methodology for estimation of mass and surface area of aggregated particles deposited in the human respiratory tract*
14:45	12D4	632	**Ian Longley**, Jennifer Gadd *Optical scattering observations in two occupied*

			residences with wood-burning stoves
15:05	12D5	727	**Alessandro Di Menno di Bucchianico**, Giorgio Cattani, Alessandra Gaeta, Giuseppe Gandolfo, Anna Maria Caricchia, Marco Inglessis, Gaetano Settimo, Biagio Bruni, Cinzia Perrino *Outdoor/indoor particle infiltration factor in Rome and its relation with urban air quality*
15:25	12D6	169	**Admir Targino**, Patricia Krecl, Christer Johansson *Simulated airway particle deposition in an urban environment impacted by biomass smoke*
Reserve	12DR	590	**Donald Hagen**, Elizabeth Black, Philip Whitefield, Prem Lobo *Surface Area Deposition Index for Jet Engine PM Exhaust*

13:45-15:45 **Session 12E: Application of New Instrumentation for Study of New Processes and Phenomena**
Room: Bragg Lecture Theatre
Chairs: Denis Boulaud / Igor Agranovski

13:45	12E1	244	**James Farnsworth**, Don Grant, Gary Van Schooneveld, Mark Litchy, Brian Osmondson, Robert Caldow *Ultrafine nebuliser for aerosolization of nanoparticles in colloidal suspensions*
14:05	12E2	272	**Mariana Ghosh**, S.Almabrok, D.J. Stewart, I.Hoare, G.Marston, C.Pfrang *A Study of Terpenes by Raman Acoustic Levitation*
14:25	12E3	531	**Christof Asbach**, Heinz Kaminski, Daniel von Barany, Christian Monz, Nico Dziurowitz, Johannes Pelzer, Knut Berlin, Silvio Dietrich, Uwe Götz, Heinz-Jürgen Kiesling, Rudolf Schierl *Handheld nanoparticle monitors – An intercomparison study*
14:45	12E4	841	**Gensdarmes Francois**, Roynette Audrey, Maro Denis, Laguionie Philippe, Boulaud Denis, Tikanen

			Juha *Evaluation of PEGASOR PPS response time for real time aerosol concentration measurements*
15:05	12E5	849	**Juergen Spielvogel**, Maximilian Weiss *A new versatile condensation particle counter for research and environmental monitoring*
15:25	12E6	887	**Kathy Erickson**, Fred Quant, Sean Morell, Susanne Hering, Robert Caldow *Two New Fast Response Laminar-Flow Water-based CPCs*

13:45-15:45 **Session 12F: Atmospheric Applications of Aerosol Modelling**

Room: Blackett Lecture Theatre

Chairs: A. Asmi / K. Barsanti

13:45	12F1	305	**Joni-Pekka Pietikäinen**, Declan O'Donnell, Markku Kulmala, Daniela Jacob, Ari Laaksonen *Model comparison between global and regional climate-aerosol models ECHAM5-HAM and REMO-HAM: European aerosols*
14:05	12F2	480	**Kelley Barsanti**, Annmarie Carlton, Serena Chung *Development and Application of Two-Product Secondary Organic Aerosol Model Parameters Based on Volatility Basis Set Fits*
14:25	12F3	1132	**Marta G. Vivanco**, Manuel Santiago, Ariel Stein, *Modelling SOA formed in a chamber from a mixture of organic gases*.
14:45	12F4	665	**Marion Devilliers**, Christian Seigneur, Edouard Debry, Karine Sartelet *A new algorithm to solve condensation/evaporation growth, coagulation and nucleation of nanoparticles*
15:05	12F5	578	**Craig Stroud**, Paul Makar, Mike Moran, Wanmin Gong, Junhua Zhang, Jeff Brook, Gang Lu, Jay Slowik, Jonathan Abbatt, Maygan McGuire, Greg Evans, David Sills, Q. Li

			Evaluation of Chemical-Transport-Model Predictions of Primary Organic Aerosol for Air Masses Classified using Back Trajectory and Particle-Component Factor Analysis
15:25	12F6	678	**Christoph Knote**, Dominik Brunner, Ulrike Lohmann *Aqueous-phase chemistry and its interactions with gases and aerosols in COSMO-ART*

15:45-16:00 Closing ceremony Theatre B

Sponsors and Exhibitors

Air Monitors Limited

Unit 2, Bredon Court
Brockeridge Park
Twyning - Tewkesbury
Gloucestershire GL20 6FF

Tel: +44 (0) 1684 857530
Fax: +44(0) 1242 292028
E-mail: enquire@airmonitors.co.uk
www.airmonitors.co.uk

Air Monitors Limited is a Sales and Service organisation representing market leading manufacturers. Specialising in the supply of instrumentation and systems for the monitoring of gaseous and particle/ aerosol parameters in ambient air, AML also has expertise in process and workplace applications.

Products include continuous particulate monitors using TEOM, Beta Attenuation and Light-Scattering technologies, Aethalometers and Nephelometers, together with Filter based Samplers, portable/ personal monitors and sampling equipment.

Our portfolio of products also features fixed and portable gas analysers, together with gas detection instrumentation, traffic monitoring and meteorological parameters, allowing AML to configure high performance, fully configured, cost effective AQM systems, with extensive diagnostic capability. AML also works with innovators to assist in the development of new technology, including web-based data acquisition (combining AQ, Traffic and Met. data), nanoparticle and mobile multi-gas monitoring.

AML are represented at EAC 2011 on Booth 2, further information is also available at www.airmonitors.co.uk

AirModus Oy
Katariina
Saksilaisen katu
14 A 11
00560 Helsinki
Finland

Tel: +358 44 3038 378
E-mail: joonas.vanhanen@airmodus.com
www.airmodus.com

Airmodus offers state of the art measurement solutions for nanosized aerosol particles. Airmodus is a group of aerosol physicists specialized in aerosol particle measurement technology, having long experience both in laboratory and field experiments. The company is based in Helsinki and as a spin-off company from the University of Helsinki it has straight contact to the leading research in the field of aerosol physics.
We specialize in providing tools for measuring the smallest sub - 2 nm aerosol particles.

The Airmodus Particle Size Magnifier A09 has been successfully used in nucleation laboratory experiments giving insight of the initial steps of atmospheric nucleation (Sipila et al. 2010, Science). It is also suitable for atmospheric measurements in field stations. It is capable of measuring aerosol particles down to 1.1 nm in diameter making it a powerful tool for filling the gap between conventional aerosol particle measurements and gas measurements.

Biotest UK Ltd

28 Monkspath Business Park
Highlands Road
Solihull
West Midlands
B90 4NZ

Tel: +44 121 733 3393
Fax: +44 121 733 3066
sales@biotestuk.com
www.biotestuk.com

Biotest with our sister company Heipha are a manufacturer and supplier of a full range of high quality room temperature storage, long shelf life Media for sterility testing. Equipment for particle monitoring, including the APC Smart touch which is the world's first dual flow rate machine for both validation and routine monitoring, and Microbial air sampling with the new RCS High Flow touch.

Biral

P O Box 2,
Portishead
Bristol,
BS20 7JB
United Kingdom

Tel: +44 (0)1275 847787
Fax: +44 (0)1275 847303
Email: aerosol@biral.com
www.biral.com

Biral specialises in the design and manufacture of aerosol size, shape and fluorescence instruments as well as forward scatter visibility and present weather sensors. Biral also represents Dekati and Met One in the UK and Ireland, further enhancing our particle measurement offering.

Biral's Aspect™ instrument measures the size and shape of particles using our unique ASAS (Aerosol Size and Shape) light scattering technology and when combined with the Biral AFS™, our dual waveband fluorescence chamber, this adds measurement of fluorescence for discrimination of many types of organic particles.

If you need accurate and detailed aerosol information for atmospheric and environmental studies such as cloud physics, ice crystal formation, particle populations, atmospheric pollutants, indoor pollution, source apportionment, fluorescence of organic aerosols (including ultrafines), or similar we may have just what you are looking for.

Please visit our booth to see sophisticated aerosol characterisation instrumentation or to discuss the design of a customised solution tailored to meet your research needs.

Cambustion Ltd

J6 The Paddocks
347 Cherry Hinton Road
Cambridge CB1 8DH
United Kingdom

Tel: +44 1223 210250
Email: cambustion@cambustion.com
www.cambustion.com

Cambustion instrumentation is already used in over 25 countries for both academic research and commercial R&D, with local representation in China, France, India, Japan and North America.

The new Centrifugal Particle Mass Analyzer (CPMA) allows classification of ultrafine aerosol according to mass: charge ratio. With a touch screen interface plus analog and digital connectivity to other aerosol instruments (e.g. CPCs) the CPMA facilitates a wide range of aerosol studies.

Our DMS series instruments offer the fastest (from 200 ms $T_{10\text{-}90\%}$ at 10 Hz) real-time electrical mobility size/number spectra available from 5nm – 2.5µm, with unrivalled sensitivity. Applications include ambient monitoring, combustion aerosol, workplace exposure and engineered nanoparticle research.

With fully integrated sampling and dilution options, DMS series instruments can be used for both ambient applications and straightforward direct sampling of high concentration aerosol sources through software selection of appropriate dilution.

Meet us at the Cambustion exhibit – booth No. 3

Copley Scientific Ltd

Colwick Quays Business Park
Private road no. 2
Colwick
Nottingham 234
United Kingdom

Tel: +44 (0)115 961 6229
E-mail: sales@copleyscientific.co.uk
www.copleyscientific.com

Copley Scientific is a major supplier of air sampling and aerosol characterisation equipment for academic research and industrial applications. In the pharmaceutical industry, the company is also recognised as the world's leading manufacturer and supplier of inhaler test equipment and is a major provider of testing systems for other pharmaceutical dosage forms.

Having offices in the UK and Switzerland, Copley Scientific works in partnership with US based aerosol particle science experts MSP Corporation, whose air sampling and aerosol characterisation products the company distributes throughout Europe. Such products include the market leading range of MOUDI cascade impactors, the real-time fibre monitor model 7400AD and the unique wide-range particle spectrometer (WPS) covering the particle size range: 5 nm to 10 microns.

Dekati Ltd.

Osuusmyllynkatu 13
33700 Tampere
Finland

Tel: +358 3357 8100
E-mail: sales@dekati.fi
www.dekati.com

Dekati Ltd. develops, manufactures and markets instrumentation needed in fine particle measurement and sampling. In 1995, Dekati introduced the world's first real-time fine particle concentration and size distribution measurement instrument. Since then, our R&D department has continually increased the range of products. Through the extensive global sales network, we are able to serve our customers around the world.
Dekati develops new products in close co-operation with the world's leading universities and companies. Our mission is to provide our customers with innovative fine particle measurement solutions that guarantee accurate results.

Dekati instruments are used for example in the following application areas:

- Combustion Processes (Diesel, Gasoline, Oil, Coal, Bio-fuels etc.)
- Environmental Ambient Aerosol Research and Monitoring
- Pharmaceutical Drug Screening and Inhalator R&D
- Nanotechnology
- Material Processing

Visit www.dekati.com for more details on our company and our products, or contact us at sales@dekati.fi for further information.

Derenda

Ingenieurbüro Norbert Derenda
Kieler Str. 9
D-14532 Stahnsdorf/Germany

Tel: +49 (0)3329-690 27 10
Email: info@derenda.de
www.derenda.de

In January 1972 Derenda Engineering Office was founded in Berlin by Norbert Derenda. Our current portfolio includes:

- Low- and High Volume Sampling devices and accessories
- Online Air Pollution Monitoring
- Automatic weighing systems for 47 and 150mm filters.

Our next generation of devices will be based on X-Ray diffraction with on-line analysis of the chemistry of the pollutants, as well as their size-distribution and shape.

Derenda is a pioneer in the field of fine-dust measuring, in cooperation with the Federal Health Office, Berlin the first fine dust measurement unit was developed to determine particulate concentrations in outdoor air. The resulting LVS was continuously refined over time and in 1999 adopted as reference unit in the European directives.

We listen to our customers carefully, to improve and service the existing material with our R&D department. Innovation is fueled by designing material that is based on the challenges our customers are or will be confronted with.

Digitel Elektronik AG

Regula Muther
DIGITEL Elektronik AG,
Alte Gasse 18, CH- 8604 Hegnau

Tel.: +41 44 908 20 30
Fax: +41 44 908 20 31
E-Mail: info@digitel-ag.com
www.digitel-ag.com

Since 1970 DIGITEL Elektronik AG has been a manufacturer of aerosol, gas and rain samplers in operation all over the world. Their experience and the state-of- the- art production processes stand for approved first-class quality products.

Digitel provide a full range of High and Low Volume sampler products for immission measurement such as PM10 according to the directives EN12341 and PM2,5 according to the
directives EN 14907 as well as for other measuring purposes with different flow rates and cut-off point characteristics. In addition to their standard products Digitel offer customer-specific solutions with specialised know-how and profound experience.

Droplet Measurement Technologies

2545 Central Avenue
Boulder
Colorado, 80301
United States

Tel: +1 303-440-5576
E-mail: info@dropletmeasurement.com
www.dropletmeasurement.com

Droplet Measurement Technologies offers accurate and sensitive instruments for real-time measurement of black carbon particles. The new Photoacoustic Extinctiometer (PAX) and Photoacoustic Soot Spectrometer (PASS) measure particulate light absorption and scattering at different wavelengths, producing BC mass and climate-relevant properties like single scattering albedo (SSA) from a single instrument. The Single Particle Soot Photometer (SP2) measures incandescence from BC-containing particles providing BC mass (independent of mixing state), number concentration and size distribution. Both techniques measure particles in-situ, eliminating filter artifacts.

DMT's extensive line of electro-optical particle analyzers are used by scientists worldwide for airborne and ground-based measurement applications in atmospheric and climate research, air quality monitoring, meteorology, aircraft certification, spray characterization, weather modification and cloud seeding,. In addition to black carbon, DMT instruments characterize aerosols, dust, volcano ash, sprays, cloud droplets, ice crystals, fog and precipitation, and cloud condensation nuclei.

For more information, please visit us in the exhibition hall, call +1 303-440-5576, visit our website www.dropletmeasurement.com, or email info@dropletmeasurement.

Ecotech Pty Ltd

1492 Ferntree Gully Road
Knoxfield
Victoria 3180
Australia

Tel: +61 3 9730 7800
E-mail: info@ecotech.com
www.ecotech.com.au

Specialising in EN and U.S. EPA approved ambient air quality monitoring instrumentation for gases, particulates and meteorological parameters, whilst also designing sophisticated data collection, validation and reporting software, Ecotech provides solutions that ensure air quality and climate data are accessible to everyone.

Our series of integrating nephelometers ranges from single to multiple wavelength versions and incorporates both polar and particle correlating options. Ecotech's Aurora range of integrating nephelometers are gaining a world-wide reputation for quality and reliability. Using an innovative LED light source, the Aurora 3000 nephelometer simultaneously measures at 525nm (green), 450nm (blue) and 635nm (red) to enable wide and in-depth analysis of particulate matter. The Aurora 3000 includes backscatter measurement in the standard unit.

Our MicroVol and HV3000 Air Particulate Samplers incorporate microprocessor technology to accurately measure and control the samplers flow rate and enable remote communication using conventional 3G modems. Our newest aerosol product is our MegaVol 3000 dust sampler. An ultra high volume sampler designed to sample dust, specifically heavy metals such as lead and radioactive particulates.

With more than 35 years designing and supplying air quality instrumentation Ecotech is regarded as one of the world's leading suppliers in air monitoring. Our network of distributors throughout the

world are highly trained and experienced in Ecotech's products and able to offer you the products you need at the price that you want.

Visit us at stand 1 to find out more or visit our website at www.ecotech.com

Enviro Techonology Services plc

Duncan Mounsor
Sales & Marketing Director
Enviro Technology Services Plc
Kingfisher Business Park
London Road
Stroud
Glos GL5 2BY
UK

Tel: +44 (0)1453 733200
Email: sales@et.co.uk
Web: www.et.co.uk

Enviro Technology Services Plc (ET) is a world leading supplier of continuous air quality monitoring instrumentation and systems.

Sectors served include Air Quality Monitoring (AQM), Continuous Emissions Monitoring (AQM) and gaseous and particulate monitors and samplers for Scientific & Research applications including, particulate chemical composition, atmospheric chemistry and stable isotopes. ET is proud to work with world leading instrument manufacturers including Teledyne API, Met One Instruments, Opsis, Digitel AG, URG Corp and Los Gatos Research.

ET specialises is "bespoke" air monitoring stations and networks.

GRIMM Aerosol Technik GmbH & Co. KG

Achim Edfelder
Dorfstrasse 9
83404 Ainring
Germany

Tel: +49 (0) 8654 578-33
E-mail: ae@Grimm-Aerosol.com
www.grimm-aerosol.com

GRIMM Aerosol Technik GmbH & Co.KG was founded over 25 years ago by Dr.-Ing. Hans-Jurgen Grimm in Bavaria/Germany. Today, GRIMM Aerosol Technik is one of the worldwide leading companies in the field of high-tech aerosol measurement instrumentation due to its innovations and quality manufacturing.

GRIMM Aerosol Technik offers a wide range of complete solutions for the continuous measurement of fine and ultrafine aerosols.
Instruments such as Environmental Dust Monitors, Aerosol Spectrometers, Particle Counters and Sizers, Filter Testers, and Aerosol Generators consistently meet the requirements of a world-wide increasing number of customers in research and industry. Specialists in-house will advise about the correct instruments for particular applications, e.g. for ambient air, emission, occupational health, filter efficiency and / or exhaust gas measurements, for quality control and for pharmaceutical, atmospheric or epidemiological studies.

Recently expanded production facilities are located in Pouch/Saxony-Anhalt/Germany. World-wide first-class customer service is offered through our U.S. subsidiary and our offices in Canada, UK, Middle East and Asia, and supplemented by a close network of international representatives.

Matter Aerosol

Andreas Knecht
Bremgarterstrasse 62
5610 Wohlen
Switzerland

Tel: +41 56 6186630
Fax: +41 56 6186639
E-mail: infot@matter-aerosol.ch
www.matter-aerosol.ch

Matter Aerosol (formally Matter engineering) specialises in the measurement and characterisation of nanoparticles from combustion processes and nanoparticles in ambient air. Matter Aerosol combines over 50 years of experience in instrument design and development with latest research results about nanoparticles, for application in laboratories to real-world problems.

Key Competencies:

- Equipment - design, development and production of equipment to sample, dilute, measure and characterise nanoparticles from combustion and ambient air.

- Services - nanoparticle emission measuring and testing programs for combustion engines, boilers, particle traps, fuels and additives at our partners' test benches or at the customer's site.

- Transfer - conferences and seminars on nanoparticle measurement.

Meritics

Tel: 01582 704807
E-mail: info@meritics.com
www.meritics.com

Meritics will be exhibiting the HCT range of aerosol and airborne particle counting and sizing instrumentation. From simple cleanroom particle sensors to the Scanning NanoParticle system the HCT range offers a solution for most measurement needs. The options available include PM sensors and a water based 1cfm CNC.

NPL

National Physical Laboratory
Hampton Rd , Teddington
Middlesex , TW11 0LW

Office: +44 (0) 208 943 6121
www.npl.co.uk/environment

The National Physical Laboratory (NPL) is the UK's national measurement institute and is a world-leading centre of excellence in developing and applying the most accurate measurement standards, science and technology available. Our research and measurement services are aimed at new ways of measuring the mass and number concentration and composition of aerosols and particles in ambient air and emissions from a variety of industrial sources. We can carry out sampling and analysis for particle mass, number, anion and cation composition, black carbon, elemental/organic carbon, heavy metals, PAHs and bioaerosols. We have unique facilities for the calibration and intercomparison of aerosol/particulate measurement equipment, which we are offering for joint research and bespoke measurement projects.

Palas® GmbH
Greschbachstr. 3b
76229 Karlsruhe
Germany

Tel: +49 (0)721 96213-0
Fax: +49 (0)721 96213-33
E-mail: mail@palas.de
www.palas.de

With more than 50 submitted patents, the Palas® GmbH has effectively set standards in aerosol technology since 1983. Today, Palas® offers a complete product range for the continuous aerosol measurement from 5 nm to 100 µm.

Our innovations result in superior quality and durability of the products that lead to unique technical and economic advantages for our customers. Our core competencies are:

- Particle generation
- Particle measurement systems (for high pressures, temperatures, processes, environment and workplace, inhalation)
- Nanoparticle measurement systems
- Filter test systems
- Fine dust monitor systems
- Dilution systems
- Cleanroom particle technology
- Calibration systems

Well-known industrial enterprises and research institutions worldwide have decided in favour of Palas® products and have thus established Palas® as a worldwide market leader.

Particle Measuring Systems

Bernard Billat
Particle Measuring Systems
5475 Airport Road,
Boulder, CO 80301
Telephone: +33 682 991 798
Mobile: +33 682 991 798
E-mail: info@pmeasuring.com
www.pmeasuring.com

Robert Muir
Naneum Limited
University Road
Canterbury, Kent, CT27FG
Telephone: +44 1227811705
Mobile: +44 7976617820
E-mail: info@naneum.com
www.naneum.com

As the global technology leader in the environmental monitoring industry, Particle Measuring Systems invests in research, engineering, manufacturing, and support of:

- particle counting and monitoring instrumentation
- microbial monitors
- molecular gas analyzers
- data management and automation software

Particle Measuring Systems also provides our customers value-added services including:

- risk analysis
- laboratory testing
- installation and commissioning
- project management
- validation and GMP compliance
- calibration and maintenance
- rentals and leases
- training

Our comprehensive instrumentation suite enables process-driven companies to monitor environmental quality and make fact-based decisions to improve process yield and meet regulatory requirements. Particle Measuring Systems equipment is used in monitoring applications across multiple by companies throughout the world. Our customers are concerned about the impact environmental contamination has on their products, processes, and equipment.

PMT (GB) Ltd

Particle Measuring Technique (GB) Ltd.
Willow End Park
Malvern
Worcestershire WR13 6NN

Phone: +44 16 84 31 29 50
Fax: +44 16 84 31 29 69
E-Mail: info@pmtgb.com
www.pmtgb.com

Surface Measurement Systems Ltd.

5 Wharfside
Rosemont Road
Alperton
London HA0 4PE
UNITED KINGDOM

Tel: + 44 (0) 208 795 9400
Fax:+ 44 (0) 208 795 9401
Direct +44 (0) 208 795 9405
Email: jgorgol@smsuk.co.uk
www.thesorptionsolution.com

Surface Measurement Systems (SMS) develops and engineers innovative experimental techniques and instrumentation for physico-chemical characterisation of complex solids. World leaders in sorption technology instrumentation solutions, providing professional world-class scientific and technical support for our international customers. By carefully controlling, measuring and analysing the physiochemical interactions of vapours with solid samples SMS can help solve your atmospheric problems. With this expertise we are releasing a Portable Humidity generator as an add-on to atmospheric studies techniques such as EDB.

Sunset Laboratory Inc

Main Office and Sales
10180 SW Nimbus Avenue
Suite J/5
Tigard, OR 97223-4338
Tel: 503 624 1100
E-mail: ben@sunlab.com
http://www.sunlab.com

Sunset Laboratory Inc. has specialized in the analysis of air pollution for carbon aerosols since 1984. As well as performing the OCEC analysis, Sunset Laboratory also provides instrumentation for carbon aerosol analysis. Our equipment is suitable for the laboratory or in the field, and ready for use with the NIOSH method 5040, IMPROVE, and EUSAAR 2 protocols.
Clients include researchers working for government regulatory agencies, private companies, commercial laboratories, and universities.

Topas GmbH
Tel: +49 (351) 21 66 43 - 0
Fax: +49 (351) 21 66 43 55
E-Mail: office@topas-gmbh.de
www.topas-gmbh.de

Topas GmbH Dresden is a specialist company in the field of particle technology and filter testing systems. Our standard product range comprises:

- aerosol generators (mono - and polydisperse, solid and liquid particles)
- particle size measuring instruments for aerosols and liquids
- aerosol dilution systems
- electrostatic aerosol neutralizers
- process aerosol monitors
- filter testing technology and instruments
- clean room measuring equipment
- pore size measuring instruments

Topas also provides solutions for special applications like the dispersion of complex powders, test stands for particle filters and for adsorptive filters, filter media testing, blow-by measuring etc. Our corporate philosophy allows us to meet of a variety of customer needs. Many years of experience, our know-how as well as close cooperation with universities, research centres and industrial partners is the ideal basis for the development of new and innovative solutions. Our reliable measuring and testing equipment has proven successful worldwide.

TSI

TSI Instruments Ltd.
Stirling Rd, Cressex Business Park
High Wycombe, Buckinghamshire
HP12 3ST - United Kingdom
Telephone: +44 (0) 149 4 459200
Fax: +44 (0) 149 4 459700
E-mail: tsiuk@tsi.com
http://particle.tsi.com

TSI GmbH
Neuköllner
Strasse 4
52068 Aachen - Germany
Telephone: +49 241-52303-0
Fax: +49 241-52303-49
E-mail: tsigmbh@tsi.com
http://www.tsiinc.de

For more than 50 years TSI Incorporated has been setting the standard for high performance measurement solutions. Our Particle Instrument product line is a comprehensive collection of precision instrumentation for counting, sizing and generating particles, from just two nanometers to a few hundred microns in diameter. TSI Particle Instruments are used the world over in such diverse applications as urban aerosol and fine dust measurements, climate studies, nanoparticle characterization, air filter testing, work place assessments and vehicle emissions testing.

A number of new TSI instruments will be highlighted at the EAC 2011. Our Nano Water-based CPC Model 3788 is the latest addition to TSI's CPC family and is designed for detecting nanoparticles down to 2.5 nm with a less than 100 milliseconds rise time response, making it the fastest CPC commercially available. Our new Advanced Aerosol Neutralizer Model 3087 offers a non-radioactive alternative to α- and β-neutralizers traditionally used for aerosol measurements and is drop-in compatible with TSI's 3936-series Scanning Mobility Particle Sizer™ (SMPS™) spectrometer. The new Aerosol Instrument Manager® software version 9.0 for the SMPS™ spectrometer enables computer flow control and records sheath flow temperature and absolute pressure before every sample. Our product line also features a new light and portable Optical Particle Sizer (OPS). The affordable OPS Model 3330 provides accurate measurements of particle concentration and size in the range from 0.3 to 10 microns, with superior resolution and adjustable size channels.
Please come and visit the TSI exhibition at booth No. 4-5-6!

URG Corporation

116 South Merritt Mill Rd.
Chapel Hill, North Carolina 27516 USA

Tel: 919-942-2753
E-mail: info@urgcorp.com
www.urgcorp.com

URG Corporation manufactures the **Ambient Ion Monitor (AIM) System** for the *continuous direct* measurement of particulate nitrate, sulfate, ammonium in PM2.5 plus gas measurements of nitric acid, SO_2 and ammonia. The **AIM System** analyzes particles, gases and organics. The **AIM System** incorporates a **Dionex Reagent-Free Ion Chromatograph**. The **AIM System** has detection limits of 0.1µg/m^3 for each of the required analytes and 0.081µg/m^3 for ammonia. The multi-pollutant data is instantly available on an hourly basis.

URG provides a wide variety of instruments for indoor and outdoor air sampling. Our **Annular Denuder System (ADS)** collects both acidic and basic gases and is designed to meet USEPA's Compendium Method IO-4.2. URG's complete collection of **aluminium cyclone inlets** are Teflon© coated, a patented process that minimizes the losses of reactive gases such as HNO_3 and NH_3 to the internal surfaces of the cyclone. URG provides **stainless steel cyclones** and **filter holders** for diesel emissions.

URG air sampling instrumentation is used in Europe, Asia, North America, Australia, Antarctica, Africa and South America.

Wiley-Blackwell

John Wiley & Sons
The Atrium
Southern Gate
Chichester
West Sussex
PO19 8SQ
UK

Wiley-Blackwell is the world's leading society publisher, publishing more than 1400 scholarly peer-reviewed journals including a vast selection of Earth and Environmental Sciences publications and a prestigious books collection, written and edited by the best international scholars and instructors.

To browse our extensive range of journals and books and to sign up to receive our e-newsletters and email Table of Content alerts go to: wileyonlinelibrary.com/subject/earthscience.

Monday, September 5, 2011

Plenary: Atmospheric nucleation in the CERN CLOUD experiment

by Jasper Kirkby

Atmospheric nucleation in the CERN CLOUD experiment

Jasper Kirkby
On behalf of the CLOUD Collaboration
Physics Department, CERN, CH1211, Geneva, Switzerland
Keywords: atmospheric aerosols, particle formation, ion-induced nucleation, molecular clusters, CLOUD experiment.
jasper.kirkby@cern.ch

The possible influence of cosmic rays on aerosols and clouds is of considerable interest (Carslaw *et al.*, 2002). The CLOUD experiment at CERN is designed to study the effects of cosmic rays on aerosols, cloud droplets and ice particles under precisely controlled laboratory conditions.

The CLOUD chamber and gas system have been built to the highest technical standards of cleanliness and performance. Owing to its large volume (26 m^3), highly-stable operating conditions and advanced instrumentation, the chamber allows nucleation rates to be reliably measured over a wide range from 0.001 to above 100 $cm^{-3}s^{-1}$ and at aerosol growth rates down to a few $\times$ 0.1 nm h^{-1}.

The experiment has several unique aspects, including precise control of the "cosmic ray" beam intensity from the CERN Proton Synchrotron (PS), the capability to create an ion-free atmosphere inside the stainless-steel chamber with an electric field, precise and uniform adjustment of the sulphuric acid concentration by means of ultraviolet illumination from a fibre-optic system, and highly-stable operation at any temperature between 185K and 310K. The contents of the chamber are continuously analysed by a suite of state-of-art instruments connected to sampling probes that project into the chamber.

The measurements obtained by CLOUD at the CERN PS in 2010 and 2011 represent the most rigorous laboratory evaluation yet accomplished of binary, ternary and ion-induced nucleation of sulphuric acid particles under atmospheric conditions between the boundary layer and mid-troposphere. The results include first measurements of ion-induced versus neutral nucleation, and of the molecular composition of the critical clusters. The ternary vapours that have been studied include ammonia, amines and oxidised biogenic organic compounds. The measurements provide new insights into the nucleation mechanism and into the contributions of binary and ternary nucleation to particle formation in the atmosphere.

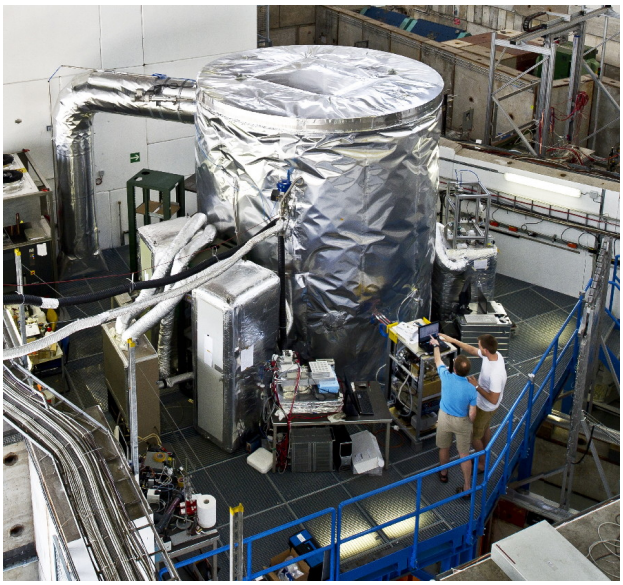

Figure 1: The CLOUD experiment in the CERN PS experimental zone, July 2010. The 3 m stainless-steel CLOUD chamber is enclosed inside the thermal housing visible in the photograph.

We would like to thank CERN for supporting CLOUD with important technical resources, and for providing a particle beam from the CERN Proton Synchrotron. This research has received funding from the EC's Seventh Framework Programme under the grant agreement no. 215072 (Marie Curie Initial Training Network "CLOUD-ITN"), the German Federal Ministry of Education and Research (project no. 01LK0902A), the Swiss National Science Foundation, and the Academy of Finland Center of Excellence Program (project no. 1118615).

Carslaw, K.S., Harrison, R.G., and Kirkby, J. (2002). Cosmic rays, clouds, and climate, Science **298**, 1732–1737.

Monday, September 5, 2011

Session 1A: Ultrafine particles in Urban Areas

Concentrations of UFP in a tunnel in Belgium

M. Van Poppel, V. Mishra, P., Berghmans
[1]VITO – Flemish Institute for Technological Research, 2400 Mol, Belgium

Keywords: ultrafine particles, traffic emissions, elemental carbon, $PM_{2.5}$, NOx

Presenting author email: martine.vanpoppel@vito.be

Epidemiological studies have suggested associations between traffic emissions and adverse health effects. In roadway tunnels, people can be exposed to higher concentrations, due to poor ventilation. In addition, a tunnel environment is an ideal case to study UFP dynamics to support UFP model development.
In this study, UFP concentrations have been measured together with nitrogen oxides, EC (elemental carbon) and PM mass fractions (PM_{10}, $PM_{2.5}$, PM_1) in the Craeybeckx tunnel in Antwerp (Belgium).

Measurements were performed in the Craeybeckx tunnel in June 2010. The tunnel is about 1600 meters long and is divided in two separate tubes, with four driving lanes per tube. Measurements were performed in the east bore of the tunnel, which carries the highway traffic towards Antwerp.
Size distribution of (ultrafine) particles was measured, with a Scanning Mobility Particle Sizer (SMPS, model 3936, TSI). $PM_{2.5}$ mass concentration measurements were performed using a low volume filter sampler (Partisol, Thermo). Filters were subsequently analyzed for EC/OC using TOT (Thermo Optical Transmission, Sunset) technique. In addition, the time profiles of PM fractions (PM_{10}, $PM_{2.5}$, PM_1) were measured using a Grimm optical counter (model 1.108). Nitric oxides were measured using a mobile platform (Airpointer, Recordum) comprising a Chemiluminescent technique for measuring NO and NO_2.
All pollutants were measured at 800 m from the tunnel entrance. Nitrogen oxides and PM fractions were measured at the tunnel entrance (at 100 m) and at 800m.
In addition, mobile measurements were performed during one day using DMS 50 (Cambustion) to measure the size distribution when driving through the tunnel. PNC were additionally measured using a handheld CPC (P-track, TSI), simultaneously inside and outside the car.

UFP number concentrations (PNC) and size distribution were measured as function of time in the middle of the tunnel. A good correlation of PNC with traffic intensities was observed. (Figure 1). Also size distributions showed a clear temporal trend, related to traffic intensities. When concentrations are higher, only one broad peak is observed (at 50 – 60 nm), whereas at lower concentrations a bimodal size distribution can be observed with an additional peak at 20 nm.

A temporal variation and correlation with traffic intensities was also observed for EC and NOx.
The average EC concentrations was 15.4 µg/m^3. The lowest value was observed on a Sundays (9.5 µg/m^3) and the highest on one of the weekdays (21.8 µg/m^3). The fraction of EC in total $PM_{2.5}$ mass ranges from 18.7 - 33.8% whereas TC (total carbon) accounts for 54.7 – 76.0 %. The average NOx concentration increased from 198 ppb (at 100 m) to 620ppb (at 800 m); 83 % of increased NOx concentration was NO, which is the major compound of NOx emitted by vehicles.
Correlations of number concentrations with NOx, EC and $PM_{2.5}$ will be discussed.

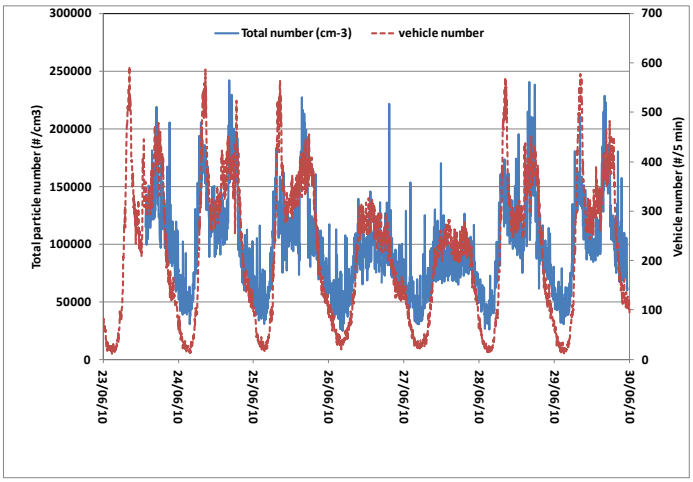

Figure 1: Total number concentrations and vehicle numbers as a function of time

Mobile measurements showed a change in size distribution when driving through the tunnel. A bimodal size distribution was observed with one peak below 10 nm and one around 55-65 nm. An increase of the largest peak was observed when driving through the tunnel, however the smallest peak decreased again in the middle of the tunnel and shifted to larger sizes. Total number concentrations in the car were about 70% compared to tunnel concentrations, in the size range (20 nm – 1 µm).

In this study increased concentrations of traffic-related pollutants (EC, NOx, PNC) were observed in a tunnel. A clear temporal trend of different particle characteristics and NOx was found. UFP size distribution showed highly transient dynamics (temporal

and spatial). These results can be used for UFP model optimization.

Measurement of Atmospheric aerosol size distribution, mass concentration and lung deposition in four cities of Pakistan

K. Alam[1*], M. Hussain[2], A. Mukhtar[3], P. Madl[2], S. Rehman[4], T. Trautmann[5], T. Blaschke[1]

[1]Department of Geography and Geology, University of Salzburg, Hellbrunnerstrasse 34, Salzburg 5020, Austria
[2]Department of Materials Research and Physics, Division of Physics and Biophysics, University of Salzburg, Hellbrunnerstrasse 34, Salzburg 5020, Austria
[3]Institute of Chemical Technologies and Analytics, Vienna University of Technology, A-1060 Vienna, Austria
[4]Pakistan Space and Upper Atmosphere Research Commission (SUPARCO), P.O.Box 8402, Off University Road, Karachi-75270, Pakistan
[5]German Aerospace Center, Remote Sensing Technology Institute, Oberpfaffenhofen, 82234 Wessling, Germany
Key words: Aerosols, Volume size distribution, PM_{10}, $PM_{2.5}$, Pakistan, lung deposition
Khanalamso@gmail.com

During March and April 2010 aerosol inventories of four big cities in Pakistan have been assessed in terms of size distribution, mass concentration (M), particle mass concentrations (PM), and aerosol lung deposition. For *Karachi*, *Lahore*, *Rawalpindi* and *Peshawar* mass concentration (M) and particulate matter (PM) concentrations were obtained from volume concentrations (V) using a native algorithm based on the Grimm model 1.109. The resulting V, M and PM concentrations confirm high levels for all four cities. The results reveal the following major contributions to the aerosol concentrations: resuspension of road dust, sea salt aerosols, and vehicular as well as industrial emission.

During the study period, the 24h average PM_{10} concentrations for three sites in *Karachi* were found to be 461 $\mu g/m^3$, 270 $\mu g/m^3$, and 88 $\mu g/m^3$, whereas the average values of 198 $\mu g/m^3$,448 $\mu g/m^3$ and 540 $\mu g/m^3$ were observed in *Lahore, Rawalpindi* and *Peshawar*, respectively (Figure 1). Likewise, the 24h $PM_{2.5}$ for the three sites in *Karachi* and *Lahore, Ralwalpindi* and *Peshawar* were found to be 185 $\mu g/m^3$, 151 $\mu g/m^3$, 60 $\mu g/m^3$, 91 $\mu g/m^3$, 140 $\mu g/m^3$, and 160 $\mu g/m^3$, respectively. The low $PM_{2.5}/PM_{10}$ ratios reveal a high share of coarser particles which originate from a) traffic, b) other combustion sources, and c) resuspension of dust.

Our calculated 24h averaged PM_{10} and $PM_{2.5}$ concentrations at all sampling points are 2-10 times higher than the WHO PM guideline values. The collected aerosol samples were analyzed for crustal elements (Al, Fe, Si, Mg, Ca) and trace elements (B, Ba, Cr, Cu, K, Na, Mn, Ni, P, Pb, S, Sr, Cd, Ti, Zn and Zr). The averaged concentrations for crustal and trace elements ranged from 1.02±0.76 $\mu g/m^3$ for Si (Sea view location in *Karachi*) to 74.96±7.39 $\mu g/m^3$ for Ca in *Rawalpindi* and from 7.0±0.75 ng/m^3 (B, SUPARCO, *Karachi*) to 17.84± 0.30 $\mu g/m^3$ (Na, M. A. Jinnah, *Karachi*) respectively. Furthermore, the deposition fractions upon inhalation in the human lung were calculated using the latest version of the IDEAL code, which is based on the stochastic airway generation model. The results derived from the model disclose that extrathoracic (ET) deposition is in the range of 20 to 25 % and total deposition in the lungs varies from almost 40 to 44 % for the measured particle size range.

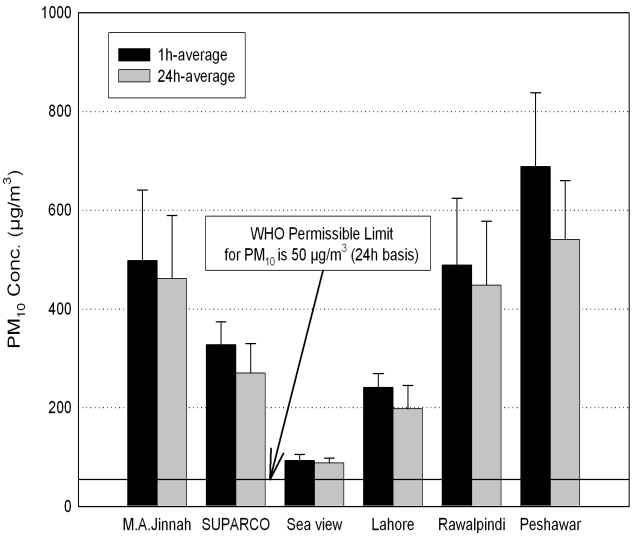

Figure 1. PM_{10} 1-h and 24-h average concentrations along with their corresponding standard deviations over six sampling sites in Pakistan. All the sampled sites reveal a 2-10 fold exceedance with respect to WHO PM_{10} value.

We would like to acknowledge the Higher Education Commission (HEC), Pakistan and the Austrian Exchange Service (ÖAD) for providing a three year Ph.D. scholarship 2008-2012 to Khan Alam.

Ultrafine particles in various urban microenvironments in Budapest

T. Borsós[1], I. Salma[1], T. Weidinger[2], P. Aalto[3] and M. Kulmala[3]

[1] Institute of Chemistry, Eötvös University, H-1525 Budapest, P.O. Box 32, Hungary
[2] Department of Meteorology, Eötvös University, H-1525 Budapest, P.O. Box 32, Hungary
[3] Department of Physical Sciences, University of Helsinki, FIN-00014 Helsinki, P.O. Box 64, Finland
Keywords: DMPS, number size distribution, urban aerosols.
Presenting author email: bteebi@gmail.com

Ultrafine aerosol has an important role in urban environments as far as its health and environmental effects are concerned. Our research was initiated to study formation and growth processes, and other properties such as health effects of ultrafine aerosol particles at various places in Budapest including different central urban sites, a tunnel and an urban background site.

On-line measurements have been performed using a differential mobility particle sizer (DMPS) for determining particle number concentrations in 30 bins in the mobility diameter range of 6–1000 nm. A meteorological station was also used for recording basic parameters such as air temperature, wind speed and direction, global radiation, etc. Time resolution of all measurements is ca. 10 min. The instruments were first set up near central Budapest, and later in the Castle District Tunnel.

Number size distributions were inverted from the DMPS data. These data were fitted by lognormal distribution functions to determine modal concentrations and number median mobility diameters (NMMDs). At the same time, concentrations in selected size ranges were also calculated, to allocate their contributions to the total number concentration, and to identify their time series. Temporal evolution of and changes in the nucleation mode, Aitken mode and accumulation mode were utilised for classifying the days and for the identification of new particle formation events.

Diurnal variation of concentrations was compared for different microenvironments. During this evaluation, several aspects were taken into consideration including workdays and weekends, as well as days with and without new particle formation. There were significant differences between the sites and distributions.

Daily median number concentration of particles in the measured size range varied from 3.8×10^3 to 29×10^3 cm^{-3} with a median value of 11.8×10^3 cm^{-3} near the city centre. For the tunnel site, it ranged from 5.1×10^3 to 465×10^3 cm^{-3} with a median of 143×10^3 cm^{-3}. Variability is related to micrometeorological conditions, traffic flow, vehicular emission as well as formation (source) and sink (coagulation and condensation) processes.

For the central site, contribution of ultrafine particles to the total particle number varied from 58 to 92% with a mean ratio and standard deviation of (79±6)%, while in the tunnel site, these values ranged from 61% to 98% with a mean and standard deviation of (85±1)%, which is slightly larger than for the urban ambient air.

Overall mean for the NMMD of the Aitken and accumulation modes were 26 and 93 nm, and 33 and 86 nm for the central and the tunnel site, respectively. All these values are substantially smaller than for rural or background environments. The reason is that the smallest particles are affected by coagulation and wall losses more extensively than the larger ones, and these effects can shift the modes to larger median diameters. Semi-volatile compounds that are present in larger concentrations in the Tunnel can condense on the surface of the particles, which also contributes to the shift.

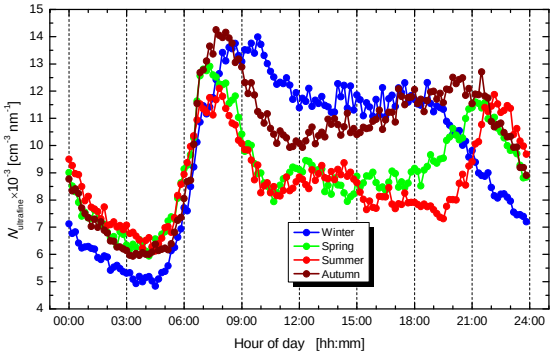

Figure 1. Diurnal variation of ultrafine particle concentrations for the four seasons in central Budapest.

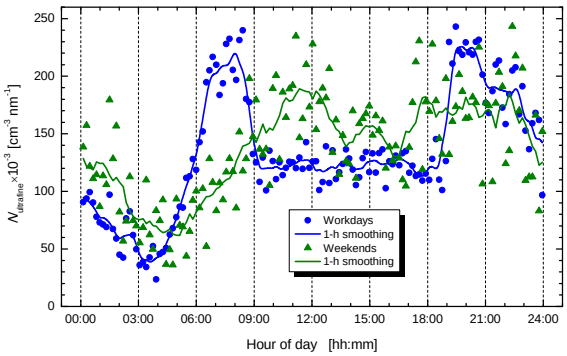

Figure 2. Diurnal variation of ultrafine particle number concentration for workdays and weekends in the Castle District Tunnel.

This work was supported by the Hungarian Scientific Research Fund under grant K84091.

Salma, I., Borsós, T., Aalto, P. & Kulmala, M. (2011) Boreal Env. Res., accepted for publication.

Analysing roadside Particle Number Concentrations using Boosted Regression Trees (BRT).

N.Z.Yahaya, J.E. Tate and M.R.Tight

[1]Institute for Transport Studies, University of Leeds, UNITED KINGDOM
Keywords: particle number concentration, street canyon, stochastic boosted regression trees, wind factors
Presenting author email: tsnzy@leeds.ac.uk

The influence of traffic flow and wind factors on roadside Particle Number Concentration [PNC] have been continuously surveyed for a 12 month period around a congested urban traffic signal controlled junction intersection in the suburb of Headingley, City of Leeds, UK. The experimental work was conducted at the semi-permanent 'Instrumented Junction' research site. Instrumentation includes: traffic flow and speed sensors, above roof-top and in-street sonic anemometers and four air quality stations measuring ultra-fine PNC.

Analysis has demonstrated significant variations in PNC between the stations, largely influenced by the prevailing and in-street winds, building geometries, background concentrations and tidal traffic flows. There is strong evidence of along canyon flow channelling at the sites located in irregular street canyon environments, with air-flows commonly parallel to the street axis. Across-canyon air-flows were also observed, which led to elevated concentrations on the leeward side of the street canyon at two of the monitoring stations as shown in Figure 1.

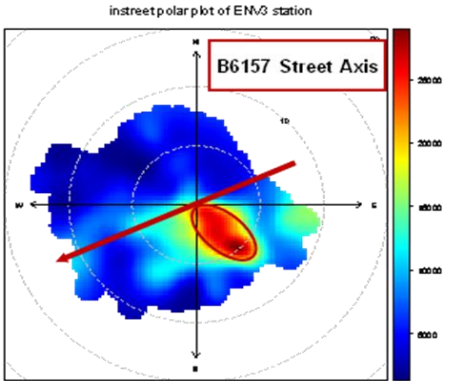

Figure 1. Bivariate polar-plot of [PNC] at ENV3

An new approach methodology to analyse PNC, Stochastic Gradient Boosting, or Boosted Regression Trees (BRTs) (Friedman, 2001, Friedman, 2002) is used to explore the relative influence of a variety of source and meteorological variables on PNC at the urban roadside locations. BRTs differ substantially from traditional regression-based approaches. Simple regression models only provide a single relationship between response and predictor variables BRTs are constructed of multiple regressions models. The BRTs were fitted using the 'gbm' package (R Development Core Team, 2008 and Ridgeway, 2007). Sensitivity testing of model parameters has been carried out (e.g. learning rates (0.005-0.5), number of trees (1000-10000) and interaction depth (1-10)) to identify the optimal parameterisation.

The BRT analysis has provided an importance rank of predictor (relative influence) variables expressed as a percentage. Figure 2 illustrates the relative influence results for site ENV1. It was found that the most important variable was the roof-top wind direction, followed by the traffic flow and vehicle speed. The roof-top wind speed was also found to be a significant influence on PNC concentration. These phenomena are in line with expectations as wind direction and speed are known to strongly influence dispersing air-flows and concentrations in street canyons.

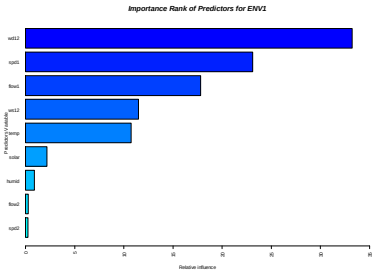

Figure 2. Relative importance of the PNC predictors at ENV1.

A clear benefit of BRTs for air pollution applications in particular PNC study, is their ability to model complex variable interactions and non-linear effects, which are the norm in air pollution research and can be difficult to determine using traditional statistical approaches.

References

Friedman, J. H. (2001). Greedy Function Approximation: A Gradient Boosting machine. *Ann. od Statistic*, 29**,** 367-378.

Friedman, J. H. (2002). Stochastic gradient boosting. *Computational Statistics & Data Analysis*, 38**,** 367-378.

R Development Core team (2008). R: a language and environment for statistical computing. R foundation for statistical computing, Vienna, Austria,URL. http://www.R-project.org

Ridgeway, G. (2007). GBM: Generalizes Boosted Regression Models. *In:* 1.6-3., R. Package. Version 1.6-3.1.

Street-to-street variations in PM, PNC and BC in a motorway-dominated urban neighbourhood

I.D. Longley[1], W. Pattinson[2], S.Kingham[2], L. Reddish[1], G.Olivares[1], G.Coulson[1]

[1] National Institute of Water & Atmospheric Research Ltd, Auckland 1010, New Zealand
[2]Department of Geography, University of Canterbury, Christchurch 8041, New Zealand
Keywords: Traffic, Field Measurements, Urban pollution, Number concentrations.
Presenting author email: i.longley@niwa.co.nz

Introduction

Recent international research shows that the air quality impact of major roads is significant up to a 250 m distance and possibly further (Zhou & Levy, 2007). Negative health outcomes are increasingly being related to a traffic emission source. In New Zealand, as elsewhere, exceedence of National Environmental Standards for air quality (and WHO guidelines) based on short-term concentration peaks may occur alongside major roads. However, many observed health impacts are associated with chronic long-term exposure at times when standards are not breached (e.g. Brugge *et al.*, 2007). Ignoring this burden, as is currently the norm, leads to an undervaluation of the resulting health-care costs attributable to traffic (Künzli *et al*., 2008). Management is complicated by the multi-source nature of urban air pollution and whether road traffic sources are a major or significant source at any given location. A rational judgment of the cost-benefit of mitigation of traffic emission exposure requires that its full impact be quantified.

Methods

An observational campaign (lasting 5 months in total) has been conducted in Auckland (New Zealand) within an urban residential neighbourhood, of a scale of approximately 1 km^2, which is strongly affected by a major road. Three modes of monitoring have been employed. As well as three conventional fixed-site monitoring sites (including measurements of PM_{10} using beta-attenuation monitors, and one site equipped with an SMPS), mobile measurements of PM, black carbon and particle number concentrations have been made by cycle and car.

The fixed sites were deployed to represent 'background', 'kerbside' and 'setback' locations with respect to the motorway in the prevailing wind direction. The data generated is designed to be used to train a range of models aimed at capturing the spatio-temporal variation in concentrations across the study area.

The mobile monitoring was conducted to provide temporally limited but spatially detailed information on the finer-scale variation across the study area, as well as investigate the location and impact of emission sources other than the motorway (local roads, motorway intersection, woodsmoke from domestic heating, etc). Spatially dense passive monitoring of NO_2 was also conducted across the Study Area to further inform an understanding of long-term (persistent) fine-scale variation in the impacts of traffic emissions.

Results

Although analysis is still ongoing, early results indicate that the motorway (which carries 6 lanes of traffic and approximately 100,000 vehicles per day) contributes relatively little to PM_{10} concentrations across the Study Area compared to other (background) sources (which may include other, non-local traffic sources). However, the contribution of the motorway to concentrations of NO_x and NO_2 (and, by implication, long-term variations in all other traffic-related pollutants) within 0 – 200 m of the motorway is substantial. Data captured by mobile survey is strongly influenced by close encounters with vehicle plumes. However, when these encounters are filtered from the data significant fine-scale variations in particle and black carbon concentrations are revealed.

This work was supported by the Foundation for Research, Science & Technology and the New Zealand Transport Agency.

Brugge, D., Durant, JL., Rioux, C., 2007. Near-highway pollutants in motor vehicle exhaust: A review of epidemiologic evidence of cardiac and pulmonary health risks. *Environ. Health* 2007, doi:10.1186/1476-069X-6-23

Künzli, N., Perez, L., Lurmann, F., Hricko, A., Penfold, B., McConnell, R., 2008. An attributable risk model for exposures assumed to cause both chronic disease and its exacerbations. *Epidemiology* 19, 179–85.

Zhou, Y., Levy, J.I., 2007. Factors influencing the spatial extent of mobile source air pollution impacts: a meta-analysis. *BMC Public Health* 7, 89 doi:10.1186/1471-2458/7/89.

Determination of the spatial variability of particle number concentration, particle size distribution and the concentrations of NO and NO_2 in an urban region and the surrounding using one year mobile measurements with the AERO-TRAM

R. Rinke, A. Wieser, B. Vogel, U. Corsmeier, Ch. Kottmeier

Institute for Meteorology and Climate Research, Karlsruhe Institute for Technology,
Hermann-von-Helmholtz-Platz 1, 76344 Eggenstein-Leopoldshafen, Germany
Keywords: urban aerosols, mobile measurements, air quality
Presenting author email: rayk.rinke@kit.edu

The spatial and temporal variation of selected aerosol and gas phase parameters is assessed in longterm measurements for the Karlsruhe (Germany) area with an automated self calibrating mobile laboratory. As measurement platform a tramway (AERO-TRAM) operating in the public transport is used. For the year 2010 measurements on more then 2300 runs are obtained resulting in an extraordinary dataset for ground based mobile applications. The AERO-TRAM operates on two selected lines. Both lines connecting the rural and suburban hinterland of Karlsruhe with the city centre. They are crossing areas with high concentrations of particles and trace gases and areas where only background concentrations are expected. Therefore, the obtained comprehensive dataset is useful for determining regional variation of particles and trace gases as well as for the identification of source areas. The differences in regional particle number concentrations, particle size distribution and also in the NO and NO_2 concentrations, which are important precursors for particles, will be presented for the year 2010 (figure 1 shows concentration differences for selected regions in May 2010). The obtained concentration distributions will be discussed focussing on different surrounding parameters, which are characterising rural, suburban and urban regions and also under consideration of meteorological conditions. An interesting feature of the mobile system is the use of analysers with high response times leading in a high spatial resolution of the measurements. This gives the possibility to study the impact of emission hot spots (e.g. crossroads with high traffic amount) on the closed surrounding based on a high resolved dataset. In figure 2 the particle number and the NO and NO_2 concentrations as a mean for May 2010 along an inner city street canyon are shown. Two emission hot spots exist along the street canyon (fig. 2, A and D) influencing the shown concentration profiles. Profiles along the AERO-TRAM track at different hot spots will be discussed in detail.

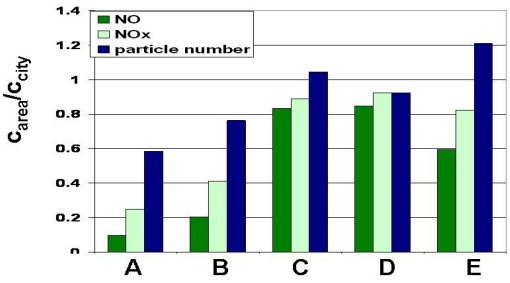

Figure 1. Regional particle number and NO, NO_x concentrations relative to the inner city region (mean values over all drives for May 2010 for A rural area, B suburban area C pedestrian area, D main station, E motorway).

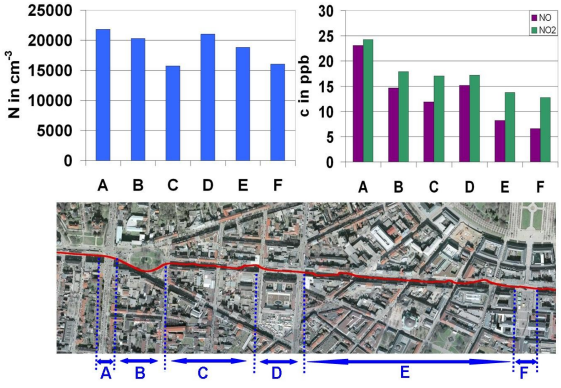

Figure 2. Particle number (left) and NO, NO_2 concentrations (right) for an inner city street canyon as mean over all drives for May 2010 and over the areas A crossroad with high traffic amount, B place next a crossroad, C road with low traffic amount, D crossroad, E pedestrian area and F market place.

Particle area and number concentrations influenced by local sources at an urban background station in Germany

H. Gerwig[1], W. Pecher[1] and K. Wirtz[1]

[1]Section Air Quality Standards and Monitoring Methods, UBA – Federal Environmental Agency, 63225 Langen, Germany.

Keywords: particle area, car traffic, asphalt grinding, gas-fired CHP, airport

The European Union defined a daily average PM_{10}-limit of 50 µg · m^{-3} for the protection of human health (2008/50/EC). Epidemiological and toxicological studies give evidence that ultrafine particles (< 100 nm, UFP) show negative health effects (Knol *et al.*, 2009).

Reduction limits for diesel cars are fixed (EURO VI). To control the results of reducing emitted particle numbers from cars and especially trucks, governmental agencies in Germany started to measure ultrafine particles on a routine base (Birmili *et al.* 2009 and Löschau *et al.* 2010).

Table 1 1-h av. tracheobronchial particle area and particle conc. 09-09-2009 – 14-06-2010

	NSAM	UCPC	SMPS
	µm²/cm³	p / cm³	p / cm³
nm	10 - 1000	3 - 1000	10 - 500
Median	5.0	9 900	8 600
Std	3.1	6 100	6 000
5 Perc	1.9	4 600	3 700
95 Perc	11.7	22 500	21 000

The urban background station was situated in Langen, Germany: 15 km south of Frankfurt a. M. and 5 km south east of the airport in the Rhine-Main-Area. Three different particle measuring instruments (TSI Inc.) were running continuously (09-09 – 06-11, 1 min av. and SMPS 6 min av.) on a rooftop at 14 m above ground with cut of at 1 µm. NSAM measures the deposited tracheobronchial (= tb) particle area within particle diameter of 10 - 1000 nm. With UCPC 3776 particle number concentration from 3 - 1000 nm was measured. With SMPS 3936 and CPC 3010 particle number size distributions between 10 – 500 nm were detected. 6 size classes were calculated from SPMS data (10 |30 |50 |70 |100 |200 |500). The difference of UCPC and total SMPS was expected to be size class 3 – 10 nm Offsets between both instruments cannot be excluded.

Temperature, humidity, wind speed, wind direction, precipitation was collected by WS600 (LUFFT GmbH). Only complete datasets of 1 h av. were used for evaluation (85 % of time period). For diurnal Mo-Fr variations data from official holidays and from 23-12-09 until 03-01-10 were excluded.

During the measuring period the median of the tb particle area concentration was 5 µm²/cm³, particle number concentration from 10 to 500 nm was about 8 600 p · cm^{-3}. 1 300 p · cm^{-3} more particles were found from 3 to 1 000 nm range (s. Tab. 1). The temperature was between -15 and +30°C, wind speed up to 14 m · s^{-1}.

For diurnal variations from Monday to Friday 2 different shapes were detected (Fig 1). Shape A: Tb particle area and particles 30 – 500 nm showed a 1st min. around 4:00, max. at 9:00 and 2nd min. at 15:00, similar to previous observations at an urban background during UFIPOLNET (Wehner *et al.*, 2008). Shape B: Particles 3 – 10 nm showed 1st max between 13 – 15:00 probably caused by particle nucleation events and a 2nd max at 7:00. Particles 10 – 30 nm show almost the same diurnal variation as shape A except for afternoon, were the second min. looks as if overlayed by effects responsible for shape B.

Grinding up asphalt and other road construction work in 10 to 100 m distance caused raised particle area and number concentrations. Elevated particle concentration occurred with winds from a nearby combined heat and power gas-fired power plant (CHP). The influence of the airport will be evaluated. The influence of fireworks is described elsewhere (Gerwig *et al.*, 2011).

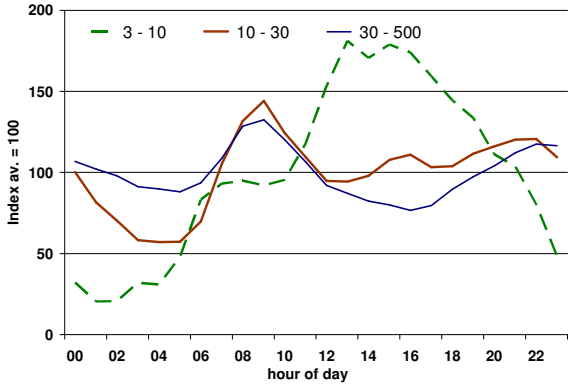

Figure 1. Diurnal variations of 1 h av. Mo – Fr; particle classes 3 – 10, 10 – 30 and 30 - 500 nm

Birmili, W. *et al.* (2009), *Gef .Reinh. Luft*, **69**, 31–35.
Gerwig, H. *et al.* (2010), *IAC 2010, Helsinki.*
Gerwig, H. *et al.* (2011), *EAC 2011, Manchester.*
Knol, A. B. *et al.* (2009), *Part. Fibre Tox.*, **6**, 19.
Löschau, G. *et al.* (2010), *Gef. Reinh.Luft,***70**,183–187.
Wehner, B. *et al.* (2008), *EAC 2008, Thessaloniki.*

Monday, September 5, 2011

Session 1B: Aerosol-Cloud Interactions

Ground-based and airborne examination of particle hygroscopicity at Barbados

H. Wex[1], G. Roberts[2,3], K. Mildenberger[1], B. Wehner[1], F. Ditas[1], M. A. Izaguirre[4], F. Stratmann[1] and H. Siebert[1]

[1] Leibniz Institute for Tropospheric Research, Physics department, Leipzig, Germany
[2] Centre National de Recherche Scientifique, Météo France, Toulouse, France
[3] Scripps Institution of Oceanography, Center for Atmospheric Sciences, La Jolla, United States
[4] Meteorology and Physical Oceanography, University of Miami RSMAS, Miami, USA
Keywords: Atmospheric aerosols, Aerosol cloud interaction.
Presenting author email: wex@tropos.de

In November 2010, the measurement campaign CARRIBA2010 (Clouds, Aerosol, Radiation, and tuRbulence in the tRade wInd regime over BArbados) took place in the Caribbean (Barbados), during which ground-based and airborne measurements were done.

Measurement that we want to report about here aimed at the examination of aerosol cloud interactions for the cumulus clouds typical for the trade wind regions. For that, on the ground, particle number size distributions and the activation of particles to cloud droplets were measured. The latter was done using two different CCNc (Cloud Condensation Nucleus counters), the one available from DMT (Droplet Measurement Technologies), which was used for size segregated measurements, and a miniaturized CCNc (mini-CCNc, designed following Roberts and Nenes (2005)), used to measure the number concentration of CCN (N_{CCN}) while scanning the supersaturation. The measurement platform ACTOS (Airborne Cloud Turbulence Observation System, Siebert *et al.* (2006)) was flown at altitudes up to 2500m, being carried by a helicopter. ACTOS carried instrumentation for the characterization of meteorological parameters, turbulence, cloud droplets and aerosol particles. The airborne aerosol characterization consisted of instruments measuring particle number concentration (N_{CN}), number size distribution and particle activation, where for the latter a mini-CCNc was used.

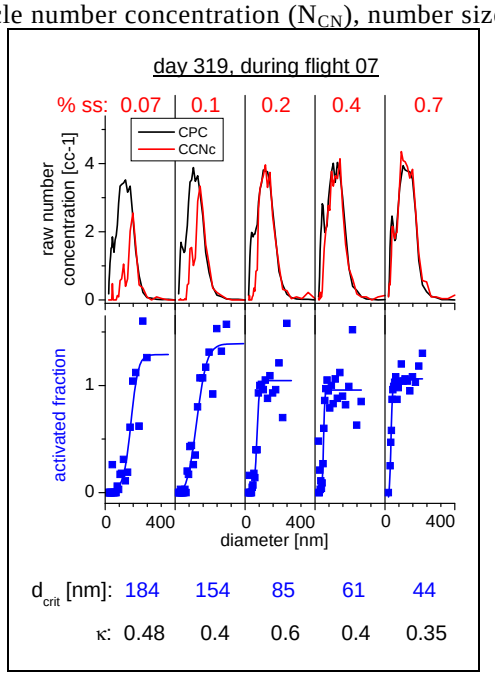

Figure 1. Ground based measurements taken during one of the ACTOS-flights.

On ground, measurements were performed continuously for 22 days. Cumulus clouds were almost always present, short rain showers (lasting for some minutes only) occurred on some days. N_{CN} measured on ground ranged from around 200 to 800 cc^{-1}, while N_{CCN} at a supersaturation of 0.3% was measured to be about 50 to 400 cc^{-1}. From the size segregated CCNc measurements done on ground, a particle hygroscopicity parameter κ (Petters and Kreidenweis, 2007) can be derived – as shown exemplarily in Figure 1. κ varied with time but also with dry particle size, however was consistently larger than generally found for continental aerosol, with κ of about 0.5 to 0.6 on average, a value similar to the one modelled as an annual mean by Pringle *et al.* (2010) for the Caribbean region.

During the campaign, 17 research flights were done. N_{CCN} was always measured at a supersaturation of 0.3%, at least during one profile. Additionally, during some flights the supersaturation was scanned during level flight legs. A first comparison of N_{CCN} measured on ground with those measured on ACTOS within the boundary layer (below 500m) showed good agreement, besides for times with increased rainfall intensity, when N_{CCN} measured on ground was lower than that derived from the airborne measurements. Besides for lofted aerosol layers that were observed seldom, a decrease in N_{CCN} was seen above the boundary layer.

With our study we aim at a thorough characterization of the marine aerosol as it occurs in the Caribbean, with respect to N_{CN}, particle size distributions and particle hygroscopicity, at the variation of these parameters both, with time and height, and at the link between these aerosol parameters with the cloud properties.

We thank Joe Prospero for providing the infrastructure at his monitoring station on Barbados, the CIMH for help prior to and during the campaign, and the people at the Concord Center for providing us the office space. This project was funded by DFG-grant SI 1534/3-1 and the IfT.

Petters, M. D., and S. M. Kreidenweis (2007) *Atmos. Chem. Phys.*, **7**, 1961-1971.
Pringle, K. J. et al. (2010), *Atmos. Chem. Phys.*, **10**, 5241-5255.
Roberts, G., and A. Nenes (2005) *Aerosol Sci. Technol.*, **39**, 206-221.
Siebert, H. et al. (2006) *Bull. Am. Meteor. Soc.*, **87**, 1727 - 1738.

Atmospheric ice nuclei in the Eyjafjallajökull volcanic ash plume over Germany and Israel.

K. Ardon-Dryer[1], Z. Levin[1], H.G. Bingemer[2] and H.Klein[2]

[1] Department of Geophysics and Planetary Science, Tel Aviv University, Tel Aviv, Israel
[2] Institute for Atmospheric and Environmental Sciences, Goethe-University, Frankfurt/M, Germany

Keywords: Heterogeneous ice nucleation, Ice nuclei, volcanic particles
Presenting author email: karinard@tau.ac.il

The effectiveness of volcanic ash as ice nuclei has been debated in the past. Some reported that volcanic ash particles are very effective as ice nuclei, while others reported just the opposite. In this work we show that the volcanic ash particles from Eyjafjallajökull are very effective ice nuclei (IN). We observe that in some cases these particles are as effective as or even more so than mineral dust particles.

Measurements of IN concentrations have been carried out at Tel Aviv University (TAU) in Israel and at the Taunus Observatory (TO) in central Germany on a daily basis using the same methods and identical instruments.

The aerosols were collected on 47mm diameter silicon substrates using a specially designed electrostatic precipitator (Klein et al., 2010). All the samples were collected at a flow rate of 2 liters min^{-1} with 10 liters and 5 liters sampled at TO and TAU, respectively. Substrates were analyzed in the isothermal static vapor diffusion chamber FRIDGE (Klein et al., 2010). Ice nuclei concentrations were measured at three different temperatures between −8ºC to −18ºC and RH_{ICE} between 103% and 119%. The ice crystals were observed by a CCD camera and were counted automatically.

In this research we show that the plume of the volcanic ash from Iceland passed over Germany and even more interesting, it reached Israel, which is located about 5000 km away from the source (Fig 1).

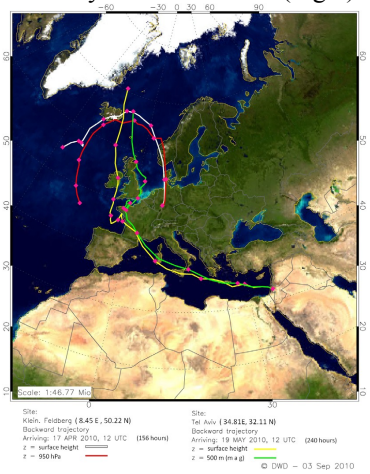

Figure 1.Backward trajectories from Eyjafjallajökull volcano arriving at Germany in April 2010 and at Israel in May 2010. Trajectories were calculated by the German Weather Service DWD.

High concentration of IN were found as the plume passed over Germany and over Israel. The concentrations of IN were higher than those measured during a dust storm that passed over Germany (Bingemer et al., 2011). They were of similar to those measured during dust storms passing over Israel (see Fig. 2)

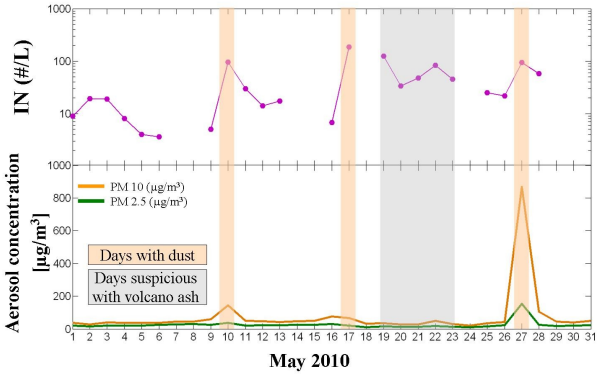

Figure 2.Number concentration of ice nuclei (at −18°C and water saturation) and concentration of PM_{10} and $PM_{2.5}$ at TAU during May 2010. A dust storm is defined when PM_{10} increases above 100 µg/m^3.

Such high concentrations of ice nuclei and high activation temperatures (forming ice at warmer temperatures) point to the potential impact of volcanic ash on microphysical and radiative properties of tropospheric clouds.

This work was supported by Deutsche Forschungsgemeinschaft (DFG) under the Collaborative Research Centre 641, the German Israeli Foundation for Scientific Research and Development (GIF), and the Virtual Institute “Aerosol-Cloud-Interactions” of the Helmholtz-Gemeinschaft. We thank the German Weather Service DWD for providing the trajectory analysis.

Bingemer, H., et al.: Atmospheric ice nuclei in the Eyjafjallajökull volcanic ash plume, Atmos. Chem. Phys. Discuss., 11, 2733-2748, 2011

Klein, H., Haunold, W., Bundke, U., Nillius, B., Wetter, T., Schallenberg, S., and Bingemer, H.: A new method for sampling of atmospheric ice nuclei with subsequent analysis in a static diffusion chamber, Atmos. Res., 96, 218–224, 2010.

Single particle depolarization studies: Unraveling the mysteries of Paris Fog

Darrel Baumgardner[1], Neda Boyouk[2], and Martial Haeffelin[2]

1 Universidad Nacional Autonoma de Mexico, Ciudad Universitaria, Mexico City, DF, 04510

2 Labratoire Meteorologie dynamique (LMD), SIRTA - Ecole Polytechnique, Palaiseau, France

Presenting author Contact: Darrel Baumgardner , darrel.baumgardner@gmail.com.

As part of the Paris Fog campaign, conducted from October, 2010 to March 15, 2011, measurements were made with the Aerosol Particle Spectrometer with Depolarization (APSD), an optical particle counter that measures single particle light scattering. Side scattered light collected at an angle of 90° ± 53° is used to derive particle diameter between 0.5 and 10μm. Back scattered light collected at 160° ± 13° gives information on composition when compared with the side scattering and depolarized light collected at 160° ± 13° is proportional to shape and surface roughness.

The measurements were evaluated to study the evolution of aerosol from the period before fog formation, then during the fog events, and following the dissipation of fog. We create maps of the relationship between size, backscattering and depolarization to derive unique "fingerprints" related to the aerosol properties and the air mass origins.

Figure 1 illustrates one set of fingerprints that relate the ratio of backscattering to side scattering to the depolarization to side scattering. The three maps are for the three hour period before fog, then the period in fog, followed by the three hour post fog period. These three were created for all fog events when the air was in the 180-270° quadrant three hours previously. The fingerprints are distinctly different showing the result of fog processing of the particles. Additional fingerprints have been created for those fog events when the air mass came from the other three quadrants.

This presentation will describe the fingerprints in the context of their physical significance as they relate to the optical, chemical and morphological characteristics of the particles and how these are modified when fog forms.

In the example shown in Fig. 1, the most frequent events, denoted by the red color, occur at a relative backscatter ratio (arbitrary units) around 15 with no clear correlation with depolarization ratio. In the cloud this pattern changes to a clear positive correlation between the two ratios followed by another pattern, also correlated but with a different slope after the fog.

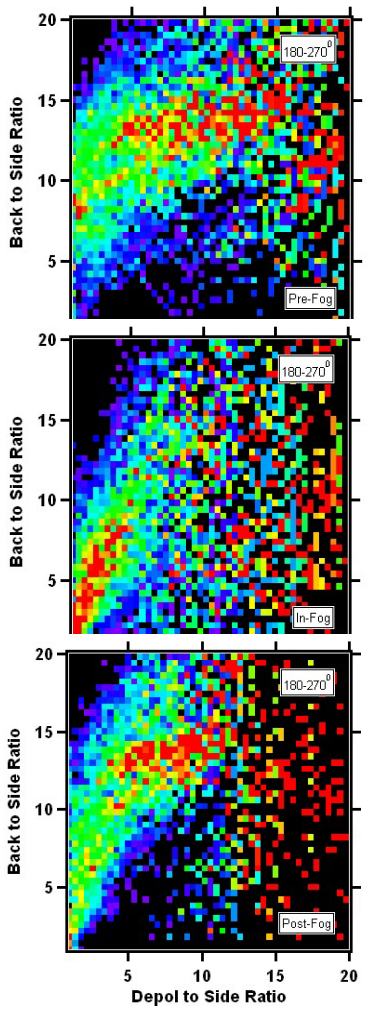

Figure 1

Keywords: aerosol fingerprints, aerosol/cloud interaction

Factors affecting the molecular flux during evaporation and condensation of water on an aqueous droplet surface

R. E. H. Miles[1], T. Yli-Juuti[2], I. Riipinen[2,3] and J. P. Reid[1]

[1] School of Chemistry, University of Bristol, Cantocks Close, Bristol, BS8 1TS, United Kingdom
[2] Department of Physics, University of Helsinki, P.O. Box 64, FI-00014 Helsinki, Finland
[3] Department of Chemical Engineering, Carnegie Mellon University, 5000 Forbes Avenue, Pittsburgh, PA 15213-3890, USA

Keywords: mass accommodation, heat and mass transfer, Raman spectroscopy.
Presenting author email: j.p.reid@bristol.ac.uk

The rate at which the equilibrium state of an aerosol is achieved depends on both the kinetics of mass transfer between the droplet surface and surrounding gas phase, and the coupling between heat and mass transfer. An understanding of mass transfer to and from particles is important for determining the number of activated cloud condensation nuclei (CCN) in cloud physics models. Treating particles as existing at equilibrium when their size is kinetically controlled could give uncertainties in the number of activated CCN, compromising the accuracy of aerosol indirect effect predictions (Chuang *et al*., 1997; Davidovits *et al*., 2004). Here we present direct measurements of the molecular flux of water at the surface of aqueous aerosol particles as a function of pressure, particle size, solute concentration and solute type.

In this work, an optically tweezed aqueous droplet several micrometers in diameter is periodically illuminated with a second laser beam of the same wavelength, 532 nm. When exposed to the secondary heating beam the droplet temperature rises, increasing its vapour pressure and leading to droplet evaporation as the solute effect seeks to re-establish equilibrium with the surrounding relative humidity. Upon removal of the heating beam, the droplet temperature falls, decreasing the droplet vapour pressure and initiating droplet growth. Changes in particle size caused by the droplet temperature fluctuations can be monitored using Cavity Enhanced Raman Scattering, with time resolution down to 0.06 s and a sizing accuracy of < 1 nm in radius (Figure 1).

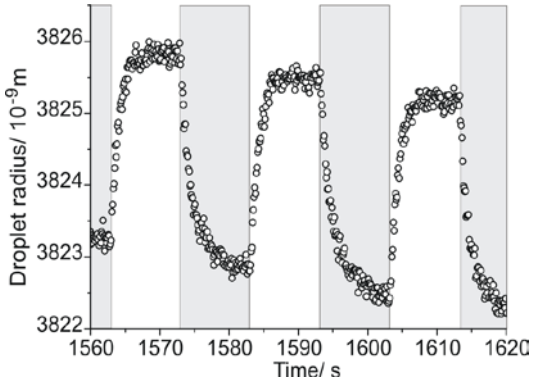

Figure 1. Change in droplet radius with time. Grey shaded regions show when the heating beam is on.

By fitting a first order exponential to the condensation and evaporation events an experimental time constant can be determined, providing information on the rates of the two processes. Measurements can be taken at pressures down to ~ 3 kPa by partially evacuating the sealed trapping cell, allowing the effect of gas phase diffusion on the mass flux to be investigated. Preliminary results (Miles *et al.*, 2010) show a clear pressure dependence of the measured molecular flux during condensation events at the droplet surface. Representative data for water condensing on a ~ 0.36 M aqueous sodium chloride droplet is shown in Figure 2.

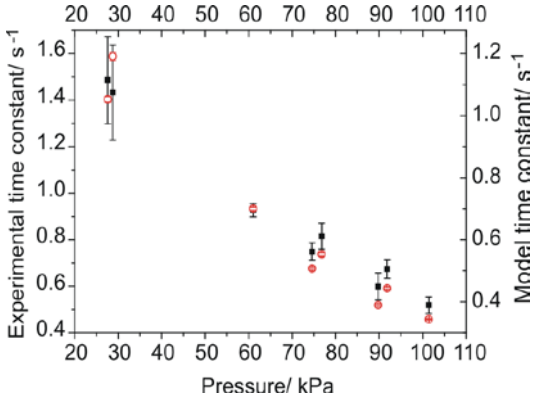

Figure 2. Experimentally measured pressure dependence of the condensational growth time constant (squares) compared with model predictions (circles) for $\alpha_m = \alpha_t = 1$ using the model of Kulmala *et al.* (1993). Proportional change on each axis is the same.

Measurements have been performed on aqueous sodium chloride particles with radii in the range 3000 nm to 4400 nm and concentrations varying between 0.36 M and 0.91 M. When pressure, temperature and latent heat effects are taken into account, striking agreement is seen between rate data collected from different droplets. Measurements are currently underway to investigate the effect of the inorganic solute type on the molecular flux. Future work will look at the effect of organic thin films on the rate of condensation and evaporation.

This work was supported by the EPSRC.

Chuang, P. Y., Charlson, R. J., and Seinfeld, J. H. (1997), Nature, 390, 594
Davidovits, P., Worsnop, D. R. *et al*. (2004), Geophysical Research Letters, 31, L22111
Miles, R. E. H., Knox, K. J. *et al.* (2010), Physical Review Letters, 105, 116101.
Kulmala, M., Vesala, T. and Wagner, P. E. (1993), Proc. Roy. Soc. London, Series A 441, 589.

In situ measurement of cloud droplet activation behaviour of black carbon particles

M. Gysel, M. Laborde, N. Bukowiecki, Z. Jurányi, E. Hammer, P. Zieger, U. Baltensperger and E. Weingartner

Laboratory of Atmospheric Chemistry, Paul Scherrer Institut, 5232 Villigen PSI, Switzerland
Keywords: black carbon, aerosol cloud interaction, mixing state, CCN.
Presenting author email: martin.gysel@psi.ch

Black carbon (BC) emitted from combustion sources is the major absorbing component of atmospheric aerosols. The Earth's climate can be influenced by BC particles in several ways, for example by absorption of solar radiation or by decreased surface albedo of glaciers through deposition of BC particles. Cloud droplets only form on cloud condensation nuclei (CCN). The CCN properties of BC particles are important for their atmospheric life cycle as wet removal is an important sink. Several laboratory and field studies have shown that BC particles are less hygroscopic and less CCN active than inorganic or water-soluble organic aerosol components. The aim of this study is to compare the activation behaviour of BC particles in real clouds with the activation behaviour of non-BC particles.

In-situ measurements of the cloud droplet activation behaviour of aerosol particles were done at the high alpine research station Jungfraujoch (3580 m asl), Switzerland. Two different inlets were employed to selectively collect the interstitial aerosol (all particles that did not form cloud droplets) as well as the total aerosol (interstitial aerosol plus cloud droplet residuals) during cloud episodes. Both aerosol samples were characterized using a Single Particle Soot Photometer (SP2), which provides quantitative detection of BC mass in individual particles as well as optical sizing, and a Scanning Particle Mobility Sizer (SMPS), which measures the particle number size distribution. Comparison of the aerosol samples from the two inlets makes it possible the characterize both CCN active and inactive particles.

Results from a cloud event on the 29/07/2010 with a condensed water content of ~0.2 g/m^3 are discussed here. The SMPS measurement reveals a 50% activation diameter of 95 nm, and the activated fraction reaches a plateau value of 80% at diameters >200 nm (Fig. 1). A plateau value of less than 100% up to a diameter of 550 nm (not shown) in this particular example is likely due to the Bergeron-Findeisen mechanism or entrainment. The SP2 makes it possible to distinguish between BC containing (BC core mass >0.3 fg BC) and "purely scattering" particles (BC core mass <0.3 fg BC). The activation behaviour measured by the SP2 for both purely scattering particles (red line) and BC containing particles (black circles) is equal to that of the whole particle ensemble as measured by the SMPS.

The BC mass in single particles is reliably detected down to ~0.3 fg BC, corresponding to a mass equivalent BC core diameter of D_{core}≈70 nm. The black line in Fig. 2 shows the fraction of activated BC particles as a function of D_{core}. The activated fraction of BC particles is ~80% for D_{core}>200 nm and drops down to 50% at D_{core}≈90 nm. Most BC particles with a core diameter of 90 nm must have a total diameter larger than 95 nm, which is the 50% activation cut-off of the whole aerosol ensemble, since the SP2 indicated that the BC particles generally had substantial coatings of variable thickness. This provides evidence that BC particles require a larger diameter for cloud droplet activation than the reminder of the aerosol. The drop of the activation curve of all BC particles with small BC core diameters (Fig. 2, black line, D_{core}<180 nm) is not seen in the activation curve of optically sized BC particles (Fig. 1, black circles) due to different lower detection limits.

The orange line in Fig. 2 shows the activation curve of the subset representing the most thickly coated BC particles. The orange line is above the black line, thus indicating preferential activation of the most thickly coated BC particles in the range of small core diameters (D_{core}<180 nm). This provides evidence that the mixing state of BC particles matters for their CCN activation.

The results from further cloud events indicate considerable variability. Sometimes BC activation was insensitive to mixing state down to BC core diameters D_{core}<100 nm. In other cases an influence of coating thickness on CCN activation of BC particles was still observed at overall diameters as large as D_{opt}>180 nm.

A more comprehensive analysis of numerous cloud events and a discussion of results in the context of previous literature will be presented.

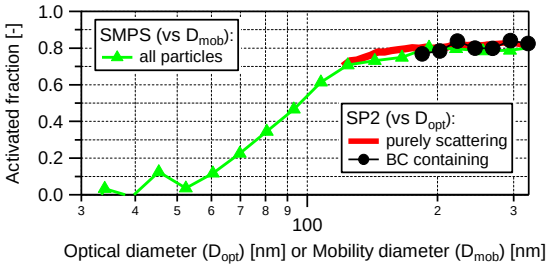

Figure 1. Activation as measured by SMPS and SP2.

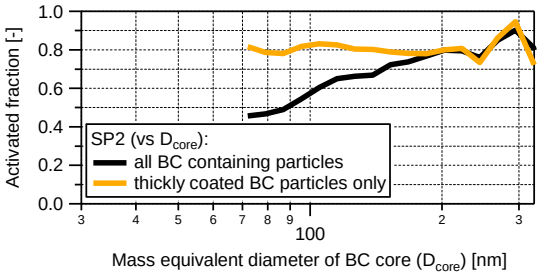

Figure 2. Activation as measured by the SP2.

This work was supported by the Swiss National Science Foundation and by MeteoSwiss.

Aerosol Cloud Interactions in a deep tropical convective storm, Hector

P.J. Connolly[1], C. Dearden[2] and T. Choularton[2]
[1]School of Earth, Atmospheric and Environmental Science, University of Manchester, Manchester, M13 9PL, United Kingdom
Keywords: ice, storm, aerosol, intensity
Presenting author email: p.connolly@manchester.ac.uk

Model studies have shown that convective clouds are sensitive to the amount of aerosol entrained into them (Connolly et al., 2007; Khain et al., 2005). The study by Connolly et al. (2007) simulated a deep tropical storm known as Hector, which occurs daily during the transition to and the break period from the Australian monsoon over a group of islands known as the Tiwi Islands. The findings of their study was that aerosols in the form of Cloud Condensation Nuclei (CCN) were able to affect the amount of precipitation from the storm due to the effect they had on both the liquid and ice microphysics within the storm.

In summary:

- When CCN concentrations were relatively low (below 200 cm^{-3}) the warm rain process (i.e. Collision and coalescence of drops) was very efficient and resulted in removal of condensate from the cloud.
- When CCN values were relatively high (above 400 cm^{-3}) liquid water did not precipitate initially, but this created regions of high supercooled liquid water content (LWC) in the upper regions of the cloud, following which hail generation was quite efficient.
- In between these two values the warm rain process was relatively inefficient and neither was hail generation. This resulted in effective transport of supercooled liquid water to temperatures lower that -35°C where the water froze homogeneously. This resulted is less precipitation and maximal anvil coverage.

During the Aerosol and Chemical Transport in Tropical Convection (ACTIVE) field campaign, radar observations were made with the C-POL radar at Gunn Point. This enabled quantification of the Hector storm during the transition from the dry to wet season in November and December 2005 and the break from the monsoon in February 2006. Aerosols were also measured using a suite of instruments: the Ultra High Sensitivity Aerosol Spectrometer (UHSAS), Condensation Particle Counter (CPC), Forward Scattering Spectrometer Probe (FSSP) and aerodyne Aerosol Mass Spectrometer (AMS) on board a Donier 228 aircraft. The composition and meteorology were sufficiently different to warrant classification into four distinct periods: a biomass burning period; a pre-monsoon period; the monsoon and the monsoon break as described by Allen et al. (2008). So the natural question that arose was *can observed differences in storm intensity be attributed to the differences in aerosol loading?*

In order to summarise the effects that the aerosols had on the number of cloud drops we applied the Aerosol-Cloud-Precipitation Interaction Model (ACPIM) in the configuration of a cloud parcel model. We then fitted curves to the relation of updraught speed against number of activated cloud drops, which unsurprisingly showed that clouds forming in the burning period had the most cloud drops and those in the break the least, having been cleaned by the effects of the monsoon (see Figure 1). These data were fitted to the model of Twomey and yielded curves of the form $N = Cs^k$ where N is the number of cloud drops, s the supersaturation and C and k are constants.

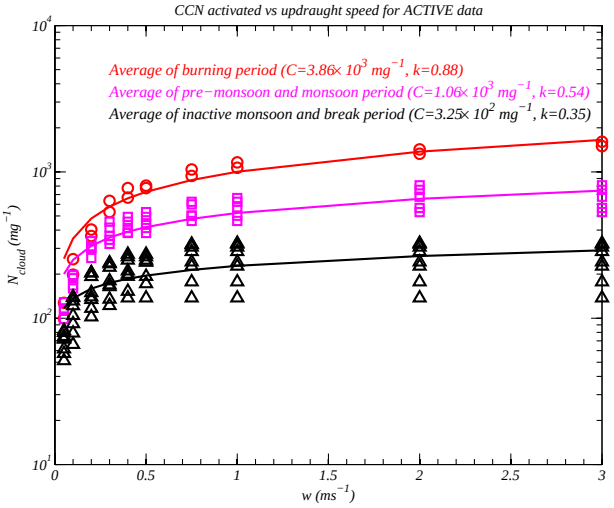

Figure 1: Model runs deriving the number of CCN vs the updraught speed.

In the presentation we will present an analysis that attempts to attribute the differences in observed storm intensity to the changes in aerosol throughout the period. Further results from Weather Research and Forecast Model (WRF) and the campaign data supporting it will be presented at the conference.

References

Allen, G., et al., 2008: Aerosol and trace-gas measurements in the darwin area during the wet season. *J. Geophys. Res.*, **113**(D06306).

Connolly, P. J., T. W. Choularton, M. W. Gallagher, K. N. Bower, M. J. Flynn, and J. Whiteway, 2007: Cloud resolving simulations of intense tropical, hector thunderstorms: Implications for aerosol cloud interactions. *Quart. J. Roy. Meteor. Soc.*, **132**, 3079–3106.

Khain, A., D. Rosenfeld, and A. Pokrovsky, 2005: Aerosol impact on the dynamics and microphysics of deep convective clouds. *Quart. J. Roy. Meteor. Soc.*, **131**, 2639–2663.

Anthropogenic Snowfall Events from Urban Fogs

G.J. Lloyd[1], T.W. Choularton [1]and P.Connolly[1]

[1]School of Earth Atmospheric and Environmental Sciences, University of Manchester, Manchester, M13 9PL,
Keywords: urban fog, snow, anthropogenic aerosols, ice nuclei
Presenting author email: Gary.Lloyd@student.manchester.ac.uk

During periods of anticyclonic weather, increasing numbers of Anthropogenic Snowfall Events (ASEs) from slightly supercooled fogs are being reported in the UK. The phenomenon was first recognised in the 1970s in America after work by Agee (1971) and Farn et al. (1978) noted a connection between industrial sources of aerosols created through combustion and inadvertent seeding of snowfall from fog. More recently work by Wood and Harrison (2009) described several events in the UK and striking satellite imagery provided by Van Den Berg (2008) revealed many patches of snow situated downwind of industrial areas after a period of freezing fog in the Netherlands.

In this paper we explain how the introduction of aerosol able to act as ice nuclei slightly below 0°C influences the microphysical processes that lead to these events. This is done through examination of reported ASEs, results from ice nucleation experiments using fly ash and other anthropogenic aerosol, together with analysis of meteorological data collected from the Whitworth Observatory during several events in Manchester, which for the first time provides valuable information obtained during the evolution of a number of ASEs.

A review of all reported ASEs reveals that these events occur in anticyclonic conditions in industrialised areas, close to potential sources of ice nuclei, when slightly supercooled fog is present at temperatures around -5°C. It is likely to be significant that these events occur within a temperature range where a known mechanism of secondary ice particle production occurs, as a few primary nucleated crystals fall through the supercooled fog (The Hallett-Mossop Process). Just one ASE at temperatures between -10°C to -14°C was reported by Farn et al. (1978) and in this temperature zone there is no known method of producing secondary ice particles hence it is very likely that all the snow crystals observed were produced through primary nucleation by aerosol.

The hypothesis, therefore, is that man made aerosol, is responsible for initiating the ice in these slightly supercooled fogs with, in many cases, secondary ice particle production enhancing the number of ice crystals leading to a detectable snowfall.

In order to investigate this, ice nucleation experiments using a cold stage and drops of deionised water polluted with fly ash confirmed the effective nature of this particular combustion product in triggering ice formation at higher temperatures, the average onset of ice nucleation being -3.4°C. Future ice nucleation experiments with man-made aerosol will be conducted to further investigate these preliminary findings and the results will be presented. This will identify whether an anthropogenic source of ice nuclei is able to cause ice formation in a temperature range where natural ice nuclei are very few.

Analysis of data obtained from the Whitworth Observatory Disdrometer reveals the precipitation types as an ASE on the 20th December in Manchester took place. Initially freezing drizzle is recorded before a transition to snow grains and eventually snowfall. Temperatures recorded at the beginning of this event were -2°C falling to -2.7°C. It is likely that further ASEs will be recorded by the observatory, providing the opportunity for detailed comparison of events, which will be crucial in the understanding of snowfall from urban fogs.

This sequence of precipitation provides one possible answer as to how an ASE may triggered. The introduction of efficient ice nuclei from a source of combustion, close to Manchester City Centre, will cause some of the fog droplets to freeze and as these fall they begin to sweep up other supercooled drops, growing by riming as they do so with the precipitation type making a transition to snow grains. As this riming takes place the Hallet-Mossop Process provides a powerful secondary ice production mechanism that is sufficient enough to cause the subsequent snowfall.

The significance of these results extends beyond that of the local importance of snowfall from radiation fog. The ability of certain man made aerosol to initiate snowfall from slightly supercooled layer cloud will substantially influence the water balance, water content and microphysics of these clouds. This will in turn shorten the lifetime of the clouds and their radiative properties. Hence this is potentially an important man made aerosol indirect effect in the atmosphere.

Agee, E.M. (1971) *Bull. Amer. Meteorology Society*. **52,** 557–560.

Farn, P., Parungo., Paul, A., Alee., Helmut, K. and Weickmann HK. **(**1978) *Geophysical Research Letters.* **5,** 515–517

Van den Berg W. (2008) *Weather.* **63,** 248

Wood, Curtis R and Harrison, R. Giles. (2009) *Weather.* **64,** 227-280

Monday, September 5, 2011

Session 1C: Molecular Characterisation of Aerosol Constituents

Measured O:C and H:C Elemental Ratios Constrain the Production Mechanisms of Biogenic Secondary Organic Material

Q. Chen[1], Y. Liu[1], N. M. Donahue[2], J. E. Shilling[3], and S. T. Martin[1, 4]

[1]School of Engineering and Applied Sciences, Harvard University, Cambridge, MA, 02138, USA
[2]Center for Atmospheric Particle Studies, Carnegie Mellon University, Pittsburgh, PA, 15213, USA
[3]Atmospheric Sciences and Global Change Division, PNNL, Richland, WA, 99352, USA
[4]Department of Earth and Planetary Sciences, Harvard University, Cambridge, MA, 02138, USA

Keywords: MCM, elemental ratio, SOA, peroxide.
Presenting author email: scot_martin@harvard.edu

In the atmospheric sciences, chemical mechanisms for the production of secondary organic material are derived in the context of environmental chambers and extrapolated to the more complex and dynamic context of the atmosphere. A stringent testing of mechanisms is therefore particularly important. A paradigm for doing so is presented herein for a C_5-C_{10}-C_{15} terpenoid sequence important in the atmosphere, derived from the photooxidation of isoprene, the dark ozonolysis of the α-pinene, and the dark ozonolysis of the β-caryophyllene.

The analysis paradigm compares measurements and model predictions in a multidimensional framework, including (1) particle mass yields, which depend on the thermodynamics of organic phase partitioning, and (2) particle composition, expressed as O:C and H:C elemental ratios. Secondary organic material (SOM) was produced in the Harvard Environmental Chamber over a range of organic particle mass concentrations. Elemental ratios of particle-phase SOM were measured by a high resolution time-of-flight aerosol mass spectrometer (HR-ToF-AMS). A chemically detailed model was applied, which couples the gas-phase oxidation scheme from the Master Chemical Mechanism (MCM v3.1) to an on-line gas-to-particle absorptive partitioning model using a group contribution method (SIMPOL) for the prediction of vapour pressure of organic compounds.

This study shows the importance of calibration of H_2O^+ peaks for accurate elemental analysis of AMS data, suggesting that the O:C and H:C ratios published in the last two years are systematically too low for laboratory-generated SOM. The measured ratios of SOM by using these calibrations are 0.75-0.97 (O:C) and 1.80-1.88 (H:C) for isoprene photooxidation, 0.33-0.52 and 1.47-1.56 for α-pinene ozonolysis, and 0.33-0.53 and 1.47-1.51 for β-caryophyllene ozonolysis.

With just information on particle mass yields, measurement and model were in good agreement, yet a higher dimensional comparison between the in situ O:C and H:C measurements and the values calculated from known products and their yields revealed important disagreement, in part because of unspeciated organic peroxides. In qualitative support, the MCM-SIMPOL model overpredicted the organic peroxides in the particle phase. While retaining the production of organic peroxides to an extent, the model had to be evolved by including pathways that moved the SOM composition in the direction of $\Delta(H:C) < 0$ and $\Delta(O:C) < 0$. In this light, the present study concludes that the model-measurement gap can be significantly reduced by a newly proposed reaction pathway: the particle-phase homolytic decomposition of organic peroxides and subsequent radical-promoted oligomerization (Fig. 1).

The presented paradigm of a stringent test and evolution of mechanism is important because climate-relevant chemical transport models use these mechanisms under the full domain of atmospheric conditions. The accuracy of the SOM production mechanisms, as a key component of biosphere-atmosphere-climate feedbacks, significantly affects the predictions of climate-related endpoints, both in today's world and in scenarios of future climate change.

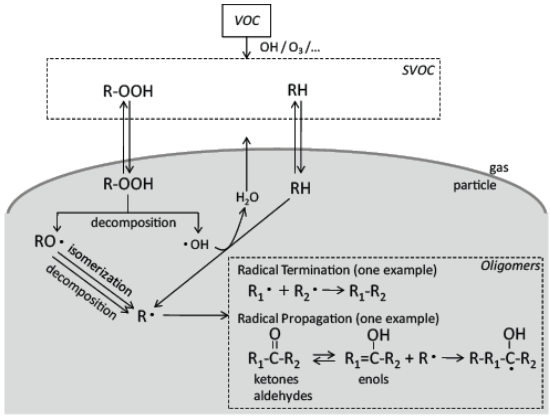

Figure 1. Proposed dehydration and oligomerization reaction sequence.

This work was supported by U.S. DOE Grant DE-FG02-08ER64529 (STM), U.S. EPA STAR Grant R833746 (NMD), PNNL Aerosol Climate Initiative (JES), and NASA ESS Fellowship (QC).

Chen, Q., Liu Y., Donahue N.M., Shilling J.E., and Martin S.T. (2010) submitted.

Reaction products of glyoxal in atmospheric aerosols

B. Noziére[1,2], T. Alsberg[1], J. L. Jaffrezo[3], R. Volkamer[4], E. Waxman,[4] P. DeCarlo[5,6], A. Praplan,[5] A.S.H. Prevot[5], J. Dommen[5], and U. Baltensperger[5]

[1]Department of Applied Environmental Science, Stockholm University, 106 91, Stockholm, Sweden
[2]Now at the Institute for Catalysis and Environment of Lyon (IRCELYON), 69626 Villeurbanne, France
[3]Laboratoire de Glaciologie et Geophysique de l'Environnement, 38402 Saint Martin d'Hères, France
[4]Department of Chemistry & Biochemistry, University of Colorado, Boulder, CO 80309, USA
[5]Laboratory of Atmospheric Chemistry, Paul Scherrer Institut, Villigen, Switzerland
[6]Now an AAAS Science and Technology Policy Fellow hosted at the US EPA, Washington DC, USA
Keywords: glyoxal, Secondary Organic Aerosols (SOA)
Presenting author email: barbara.noziere@ircelyon.univ-lyon1.fr

In recent years, atmospheric observations (Volkamer *et al*., 2007) and laboratory experiments (Kroll *et al*., 2005; Volkamer *et al*., 2009) have shown that glyoxal and its reactions in the aqueous phase of atmospheric particles (Carlton *et al*., 2007; Nozière *et al*., 2009; Galloway *et al*., 2009; Shapiro *et al*., 2009; Lim *et al*., 2010) are likely to contribute significantly to the mass of Secondary Organic Aerosols (SOA) in the atmosphere, at least in some regions. But while these reactions have been studied in laboratory, no evidence for their occurrence in atmospheric aerosols has been reported until now. In this work, we report the identification of reaction products of glyoxal in aerosols from different origins (Aspvreten, Sweden; Paris France…), confirming the contribution of glyoxal chemistry to these aerosols.

Prior to analyzing atmospheric aerosol samples the products from different reactions of glyoxal were studied in laboratory and in smog chamber. The laboratory experiments focused on the liquid-phase reactions of glyoxal in differentes solutions, corresponding to different reaction mechanisms: water exposed to UV light (OH-radical mechanisms), ammonium sulfate solutions in the dark (ionic mechanisms), persulfate solutions in the dark (sulfate-radical mechanisms) and ammonium sulfate exposed to UV light. The smog chamber experiments were performed at the Paul Scherrer Institut (PSI), Switzerland, and focused on the gas-phase photooxidation of acetylene, producing mostly gas-phase glyoxal. The secondary particles produced in the chamber were collected on Quartz filters for chemical analysis. Both the laboratory reaction mixtures and the secondary particles from the smog chamber were analyzed by the same method, using liquid chromatography/Q-tof tandem mass spectrometry (LC/MSMS). In all cases, the mass spectra obtained displayed a large number of products, among which where identified glyoxal oligomers and products specific to some reactions, such as imidazoles (reactions with NH_4^+ in the dark, cf. Galloway *et al*., 2009) or organosulfates.

Fine aerosols ($PM_{2.5}$) collected on Quartz filters in Aspvreten, Sweden, and in Paris, France during the MEGAPOLI campaign, were analyzed by the same method. A number of compounds were identified in the spectra obtained, which had been previously identified as glyoxal products in laboratory or the smog chamber (Figure 1).

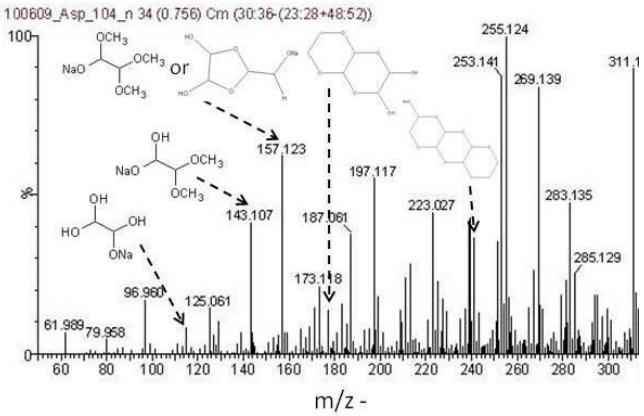

Figure 1. Examples of mass spectrum evidencing some products of glyoxal in aerosols from Aspvreten, Sweden.

So far, most of the products identified correspond to reactions involving ammonium sulfate salts (imidazoles, organosulfates…).

Carlton, A. G, Turpin, B. J., Altieri, K. E., Seitzinger, S., Reff, A., Lim, H.-J., and Ervens, B. (2007) *Atmos. Environ.* **41**, 7588–7602.

Galloway M. M. Chhabra, P. S., Chan, A. W. H., Surratt, J. D., Flagan, R. C., Seinfeld, J. H., and Keutsch, F. N. (2009) *Atmos. Chem. Phys.* **9**, 3331–3345.

Kroll J. H., Ng, N. L., Murphy, S. M., Varutbangkul, V., Flagan, R. C., Seinfeld, J. H. (2005) *J. Geophys. Res.* **110**, D23207, doi:10.1029/2005JD006004.

Lim Y. B., Tan, Y., Perri, M. J., Seitzinger, S. P., and Turpin B. J. (2010) *Atmos. Chem. Phys.* **10**, 10521–10539.

Nozière B., Dziedzic, P., and Cordova, A. (2009) *J. Phys. Chem. A* **113**, 231-237.

Shapiro, E. L., Szprengiel, J., Sareen, N., Jen, C. N., Giordano, M. R., and McNeill V. F. (2009) *Atmos. Chem. Phys*. **9**, 2289-2300.

Volkamer, R., San Martini, F., Molina, L. T., Salcedo, D., Jimenez, J. L., and Molina M. J. (2007) *Geophys. Res. Lett*. **34**, doi:10.1029/2007GL030752.

Volkamer, R., Ziemann, P. J., and Molina, M. J. (2009) *Atmos. Chem. Phys*. **9**, 1907-1928.

Influence of biomass burning on organic aerosol composition - an ultra-high resolution mass spectrometry study

M. Kalberer[1], A.G. Rincon[1], S. Fuller[1], P. Lin[2], JZ. Yu[2], C. Alves[3], C. Gonçalves[3], A.I. Calvo[3], H. Bauer[4], A. Kasper-Giebl[4]

[1] *Department of Chemistry, Univerity of Cambridge, Cambridge, UK*
[2] *Department of Chemistry, Hong Kong University of Science & Technology, Clear Water Bay, Kowloon, Hong Kong*
[3] *Centre for Environmental and Marine Studies, Department of Environment, University of Aveiro, Aveiro, Portugal*
[4] *Institute for Chemical Technologies and Analytics, Vienna University of Technology, Vienna, Austria*
Keywords: Atmospheric aerosols, Biomass burning, Chemical composition, Organic compounds
Presenting author email: markus.kalberer@atm.ch.cam.ac.uk

A significant fraction of the organic aerosols mass in the atmosphere originates from biomass burning sources such as wild fires, agricultural activities or residential heating and cooking. The fraction of biomass burning particle mass is not easily identified with conventional analytical techniques due to the highly complex compound mixtures in organic aerosols.
Here we will present results of ultra-high resolution mass spectrometry (UHR-MS) analyses, a technique, which has unique capabilities to characterize complex samples. UHR-MS allows identifying unambiguously the elemental composition of thousands of compounds in a single analysis and gaining information about the structure and formation mechanisms of organic compounds in aerosols (Reinhardt et al., 2007).

The unprecedented, very detailed picture of UHR-MS analyses of the thousands of organic compounds present in atmospheric aerosols reveals that the sample work up process is of critical importance to avoid artifacts introduced, e.g., by the reactions of aerosol components with solvents such as methanol. Such solvent-induced artifacts can change significantly the distribution of oxygenated functional groups, e.g., through formation of methyl esters when using methanol as solvent (Bateman et al., 2008) and can shift overall O/C atomic ratios, an indicator of atmospheric age often applied in aerosol field studies.
Different liquid extraction and separation conditions (methanol vs. acetonitrile) are compared in this study and we show that most of the reported artifacts in the literature can be avoided by carefully choosing ionization conditions during the MS measurement.
These solvent-extraction methods will be compared with direct measurement techniques from the filter surface, i.e., desorption electrospray ionization (DESI) and liquid extraction surface analysis (LESA).

Applying the improved sample work up conditions, several important types of biomass burning source samples from Central and Southern Europe and from South China will be compared. Using van Krevelen (i.e., distributions of elemental ratios) and Kedrick mass defect analysis (i.e., identification of homologous series) common pattern and source specific tracers are identified in the biomass burning samples. Mass spectral pattern of these source samples are also compared to ambient samples to identify the biomass burning signatures in the ambient samples. More highly oxidized compounds, including organo sulfates and organo nitrates are more abundant in ambient samples compared to source samples. Whereas in source samples the O:C ratio does mostly not exceed 1.2, in ambient samples the O:C ratio extends to 3 and possibly higher, which is consistent with organic aerosols aged in laboratory experiment.

Acknowledgement: part of this study was supported by BIOEMI (PTDC/AMB/65706/2006, Portuguese Science Foundation).

Reinhardt et al., Ultra-high mass resolution and accurate mass measurements as new tools to characterize oligomers in secondary organic aerosol (2007) Anal. Chem., 79, 4074-4082.
Bateman et al., The Effect of Solvent on the Analysis of Secondary Organic Aerosol Using Electrospray Ionization Mass Spectrometry (2008) Environ. Sci. Technol., 42, 7341–7346.

S-containing organic components from water soluble fraction of Atmospheric Aerosol Collected in Cambridge and Auchencorth Moss EMP supersite

A.G. Rincón[1], A.I. Calvo[2], M. Dietzel[3], C. Braban[4], M. Kalberer[1]

[1]Department of Chemistry, University of Cambridge, Cambridge, CB2 1EW, UK
[2]Centre for Environmental and Marine Studies, Department of Environment, University of Aveiro, Aveiro, Portugal
[3]Institute of Nano and Microfluidics Center of Smart Interfaces, Technical University Darmstadt, Darmstadt, Germany
[4]Centre for Ecology and Hydrology, Bush Estate Penicuik, Midlothian, UK
Keywords: Water-soluble organic fraction, SOA, Ultra-high resolution mass spectrometry
Presenting author email: agr36@cam.ac.uk

Organic compounds are major constituents of fine continental aerosols. The understanding of their chemical composition, their properties and reactivity are important for assessing aerosol effects upon both global climate change and human health. Among organic aerosols, secondary organic aerosols (SOA) are predominant especially in summer due to the intense photochemical activity.
Here we compare the chemical composition of aerosols with particle diameters <1µm collected at an urban and rural site in the UK, Cambridge and Auchencorth Moss (EMP supersite), during summer 2009. We focus here in the organic components which contain sulfur as heteroatom in their elemental composition.

The water-soluble organic fraction of the filters was separated from inorganic ions (e.g., sulfate, nitrate) by a solid phase extraction step and re-dissolved in acetonitrile-water prior to the analysis. Ultra-high resolution mass spectrometry analyses were performed using an LTQ Orbitrap Velos, with an accuracy bellow 2ppm, using an electrospray ion source. Mass spectra were measured by direct infusion, in negative and positive polarities and recorded within the range of 50-1000m/z. Molecular formulas were assigned to the exact masses of the more than 5000 compounds in a single sample using the Xcalibur™ software. After subtraction of peaks present in blank samples, a series of criteria were used to determine the molecular formula of the compounds such as chemically reasonable atomic ratios. Visualization schemes, such as van Krevelen diagrams and Kendrick mass defect plots were used for data exploration. The main molecular signatures of products were established, by analysis of the functional group relationships among compounds and their relative intensity.

Summer samples from Cambridge generally have more components than samples from Auchencorth; however van Krevelen diagrams containing the entire data matrix exhibit qualitatively the same shape. Molecular series containing C_cH_h, $C_cH_hO_o$, $C_cH_hO_oS_s$, $C_cH_hO_oN_n$ and $C_cH_hO_oN_nS_s$ were observed. 90% of the data from Cambridge contains organic compounds with OSN heteroatoms; only 10% of the data contains compounds with C_cH_h and/or O_o. This value slightly decreases to 6% for Auchencorth samples. About 60% of components in both samples contain sulfur atoms.

Figure 1a and b shows the ratios O/C vs H/C for a subset of components containing $C_cH_hO_oS_s$. The data for Auchencorth sample is more scattered and contains more oxidized components with lower H/C. The average value for O/C and H/C ratio for Cambridge samples is 0.41 and 1.6 while for Auchencorth O/C increased to 0.52 and H/C decreased to 1.4. That is consistent with the evolution of the O/S ratio vs molecular mass, (not shown), where the Auchencorth samples exhibit higher values (average 3.3) than the Cambridge samples (average 2.7). In addition, only 9% of the components in Fig 1 have the same elemental composition. Based on our study, we infer that the samples collected in Auchencorth are the result of more aged organic aerosols while samples in Cambridge, collected in the city center, are the result of a mixture of fresh and aged aerosol.

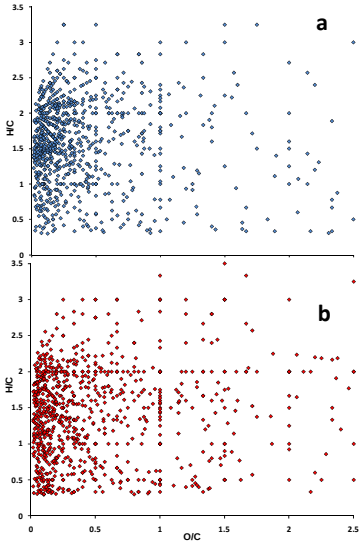

Fig 1. Van Krevelen diagram of S_sO_o-containing organics for a sample collected in Cambridge (a) and Auchencorth (b) in Summer 2009. $(M-H)^-$ ions were detected in a range of 70-1000Da.

Size resolved nanoparticle composition from SOA formation events

P.M. Winkler[1], J. Ortega[1], J. Zhao[1], H.R. Friedli[1] and J.N. Smith[1,2]

[1]NCAR's Earth System Laboratory, National Center for Atmospheric Research, Boulder, CO, 80301, USA.
[2]Department of Physics and Mathematics, University of Eastern Finland, Kuopio, FIN-70211, Finland.
Keywords: Nanoparticle, secondary organic aerosol (SOA), TDCIMS, chemical composition.
Presenting author email: pwinkler@ucar.edu

The chemical composition of secondary organic nanoparticles is among the key issues to understand processes responsible for nucleation and subsequent growth. While aerosol mass spectrometry has typically been restricted to particle sizes above 100 nm due to the small amount of substance carried by the nanoparticles, only few techniques exist to investigate particle composition in a size range close to where nucleation and growth by organic vapours takes place. We employed the thermal desorption chemical ionization mass spectrometer (TDCIMS, Voisin *et al*., 2003) to investigate the chemical composition of particles in the size range from 10 nm to 80 nm. Ambient aerosol as well as aerosol formed in a biogenic aerosol chamber was used as source of particles.

TDCIMS comprises of a particle collection unit, an electrostatic precipitator, a ^{241}Am ion source and a triple quadrupole mass spectrometer. At the inlet, the aerosol is charged and size classified by three DMAs (McMurry *et al*., 2009) and subsequently collected on a platinum wire. After collection (typically in the order of ~10 minutes, depending on particle size) the wire is translated into the ion source where the collected material gets thermally desorbed and ionized. Positive and negative ion mass-to-charge ratio is alternatingly analysed in the mass spectrometer. It is notable that by ramping the temperature of the wire valuable information on the volatility of the substances is obtained (Smith and Rathbone, 2008).

SOA formation was studied at the NCAR biogenic aerosol chamber consisting of a 10 m^3 teflon FEP bag. Different kinds of monoterpenes of varying concentration as well as live tree emissions were oxidized by ozone under dark conditions. Running the chamber as a continuous flow system, we initiate particle formation after a steady state concentration of the organic vapour has been reached by subsequently adding ozone. Gas-phase and particles were analysed using gas chromatographs, scanning mobility particle spectrometers (SMPS), Cluster-CIMS and TDCIMS. For comparison, ambient measurements were taken at Manitou Forest Observatory operated by NCAR, BEACHON*, in the southern Rocky Mountains, Colorado. This site is located in a ponderosa pine dominated forest with expectedly high monoterpene emissions. Oxidation products of monoterpenes can thus be expected to play a crucial role in new particle formation and growth.

The system studied most intensely in the chamber was related to the ozonolysis of α-pinene. Typical concentrations were ~ 5ppb of α-pinene and ~ 50 ppb of ozone. In Figure 1, a corresponding mass spectrum of positive ions after collection of particles exhibiting 80 nm mean mobility diameter is illustrated. As can be seen, a distinct grouped pattern is observed up to ion masses of 200 amu. A similar behaviour was also found for negative ions. For high mass loadings on the wire (~200pg) this grouped pattern was observed even up to 250 amu suggesting high molecular weight compounds in the particles. Similar conclusions have been drawn recently by Hall and Johnston (2010) showing that oligomers account for 50% of the SOA mass. Preliminary results for 10 nm particles suggest, however, that these particles exhibit substantially different composition, indicating different vapours being responsible for particle growth at different sizes.

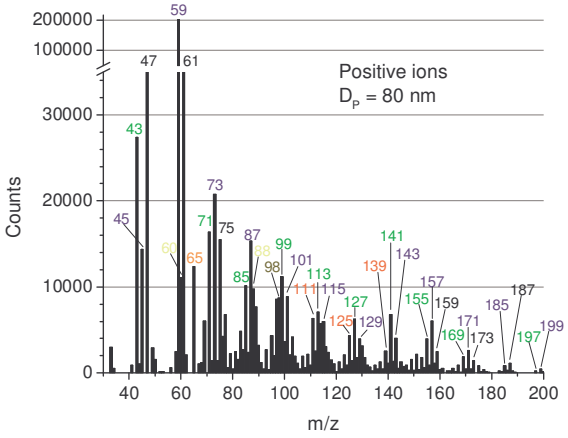

Figure 1. Positive ions measured from 80 nm particles formed from the dark ozonolysis of α-pinene.

The National Center for Atmospheric Research is supported by the National Science Foundation. JS acknowledges the financial support of the Saastamoinen Foundation.

*Bio-hydro-atmosphere interactions of Energy, Aerosols, Carbon, H_2O, Organics and Nitrogen

Voisin, D. *et al*. (2003) *Aerosol Sci. Technol*. **37**, 471-475.

McMurry, P. H., *et al*. (2009) *Environ. Sci. Technol.* **43**, 4653-4658.

Smith, J. N. and Rathbone, G. J. (2008) *Int. J. Mass. Spectrom.* **274**, 8-13.

Hall, W. A. and Johnston, M. V. (2010) *Aerosol Sci. Technol.* ***45****, 37-45.*

Size Distribution and Source Analysis of Polycyclic Aromatic Hydrocarbons (PAHs) contained in PM_{10} in Waliguan and Xining of China

L.L Tang[1,2], S.J. Niu[1], D.T. Liu[2], X.W. Li[3], X.Z. Zhang[3], S.X. Fan[1],H. Nie[4] and H. Coe[2]

[1]Jiangsu Key Laboratory of Atmospheric Environment Monitoring and Pollution Control, Nanjing University of Information Science & Technology, Nanjing, 210044, China
[2] School of Earth, Atmospheric and Environmental Sciences, the University of Manchester, Manchester, M13 9NL, United Kingdom
[3] The Center of Jiangsu Environmental Monitoring, Nanjing, 210016, China
[4] China Global Atmospheric Watch Baseline Observatory, Xining, 810001, China
author email: lili.tang@nuist.edu.cn; lili.tang@manchester.ac.uk

Abstract:

To explore the properties and sources of polycyclic aromatic hydrocarbons (PAHs) contained in PM10 in Waliguan and Xining of Qinhai Province, China during summer, 10-group aerosol samples were installed at the Waliguan Atmospheric Background Observatory and Qinghai Station of Meteorology. Waliguan station (36° 17'N, 100° 54'E) is the highest GAW (Global Atmospheric Watch) station, and is located in a remote region on the northeastern boundary of the Qinghai-Tibetan plateau at a height of 3810 meters. Qinghai Station（36° 34'N, 101° 45'E）is located in the center of Xining city at a height of 2275 meters. Size-segregated particles were sampled using cascade impactors (Thermo) from May 24 to June 4, 2007. Size resolved chemical compositions of aerosol were investigated in order to characterize regional aerosol pollution. The meteorological conditions during the measurements maintained high temperatures and high RH. The mass concentration and size distribution of PM_{10}, and the spectral distributions of PAHs were analyzed. The daily mean concentration of PM_{10} was 24.85μg·m^{-3} and the particle size distribution exhibited three-modes in Waliguan; whereas the daily mean concentration of PM_{10} was 65.25μg·m^{-3} in Xining where the particle size distribution showed dual-modes.

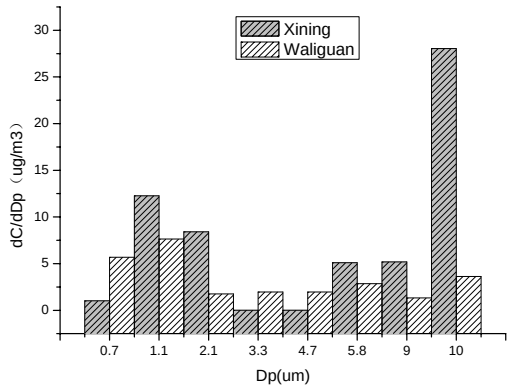

Figure 1. Mass size distribution of average PM_{10} mass concentration in sampling periods.

The percentage of accumulated particle mass in Waliguan was greater than in Xining. The concentration of PAHs in PM_{10} was 8.38ng·m-3 in Waliguan, much lower than Xining .

Due to the different photochemical pathways, the properties of PAHs and long-range transport of particles, PAHs with high molecular weight were mainly distributed in the fine particles and PAHs with lower molecular weight are relatively richer in the coarse particles at Waliguan. High molecular weight polycyclic aromatic hydrocarbons in the two sample sites were monodispersed in size. It is concluded that the PAHs pollution in Waliguan was associated with the seasonal transitions with the Asian monsoon system and transport from eastern/central China industrial emissions.

Keywords: Waliguan；Xining； Polycyclic aromatic hydrocarbons； Size distribution；PM_{10}

This work was supported by the Scientific Research Foundation of Jiangsu Environmental Monitoring (NO.1016) and the Research Foundation of Nanjing University of Information Science & Technology.

Reference

1. Wania F, Shen L, Lei Y D, *et al.* (2003) *Environ. Sci. Technol.*, 37, 1352-1359.
2. Fernandez P, Grimalt J O, Vilanova R M. (2002) *Environ. Sci. Technol.*, 36, 1162-1168.
3.Venkataraman C, Thomas S, Kulkarni P. (1999) *J. Aerosol Science*,30,759-770.
4. Bin Zhu, Hajime Akimoto, Zifa Wang, *et al.*（2004） *J.Geophysical Research Letters*, 31, 7104-7108

Monday, September 5, 2011

Session 1D: Physico-chemical PM properties

Simultaneous determination of water-soluble organic tracers in atmospheric aerosol using silyl-derivatization and GC-MS analysis

M.C. Pietrogrande, D. Bacco, S. Chiereghin

Department of Chemistry, University Ferrara, Ferrara, I44121, Italy

Keywords: water soluble organic compounds, dicarboxylic acids, sugars, chemical analysis.
Presenting author email: mpc@unife.it

This paper describes the development and application of a GC-MS method for the simultaneous analysis of a wide range of water-soluble molecular tracers in atmospheric aerosol, including short-chain dicarboxylic acids and sugars/sugar alcohols. Short-chain dicarboxylic acids are emitted directly into the atmosphere by a multiplicity of sources including power plants, vehicular circulation, meat cooking operations and biomass burning. They are also produced through the secondary organic aerosol (SOA) formation initiated by photochemical reactions with volatile hydrocarbons of both anthropogenic and biogenic nature [1].
Among the sugars, glucose and fructose may originate from plant pollens, microorganisms, and fragments of plants and animals, while arabitol and mannitol have been established as suitable markers for fungal spores [1]. Some sugars may also be produced by hydrolysis of the corresponding anhydrosugars when biomass is burned or emitted directly by thermal stripping during wildfires. This is the case of the anhydrosugars levoglucosan, mannosan and galactosan that are highly specific molecular tracers for biomass burning [2].

GC-MS analysis of carboxylic acids and saccharides requires a preliminary chemical derivatization to convert these polar compounds into volatilizable and stable derivatives.

With the aim of developing a multi-residue analytical method, that achieves simultaneous analysis of several molecular tracers in atmospheric PM samples, the silylation procedure using BSTFA (N,O-bis(trimethylsilyl)-trifluoroacetamide) as silylation reagent was investigated [3,4]. The response surface methodology (RSM) including central composite design (CCD) was applied to optimize the reaction operating conditions in order to achieve the highest response for a large number of dicarboxylic acids and sugars. The operative factors considered were: (i) reaction temperature (50°C-90°C), (ii) reaction duration (60 min-120 min), (iii) reagent concentrations (10%-100% of the total solution volume) and (iv) pyridine concentration (0%-50% of the derivatization reagent).

The CCD model makes it possible to investigate the interacting effect of the different operative parameters on the reaction yield. The highest BSTFA concentration maximizes the derivative yield with a pyridine concentration level close to the center value for acids (Fig. 1) and close to upper boundary for sugars. On the basis of the RSM model and experimental evidence, the optimum derivatization conditions were defined as reaction temperature of 75°C, reaction duration of 70 min, BSTFA reagent concentration of 55% and pyridine concentration of 35%.

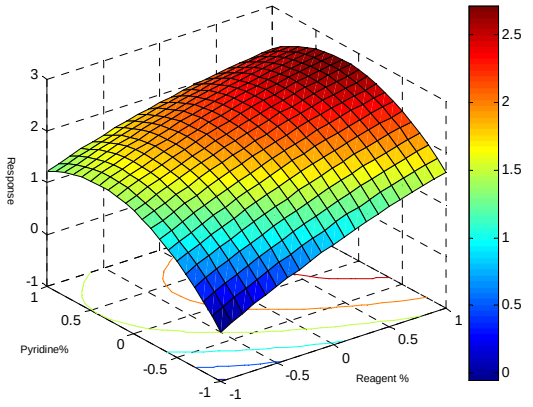

Figure 1: 3D plots of reaction yield of acids as a function of BSTFA and pyridine concentrations.

The optimized protocol was applied to 22 target analytes that are relevant chemical markers, i.e., 15 carboxylic acids and 7 sugars. The optimized procedure provides low detection limits ($\leq 2\ ngm^{-3}$) and satisfactory reproducibility (RSD%≤13%) suitable for environmental analysis.
The optimized procedure was applied to PM filters collected in a regional area close to Bologna, Northen Italy, under different conditions, i.e., different seasons (summer vs. winter), different sampling sites (urban vs. rural), different particle size dimensions ($PM_{2.5}$ vs. PM_1). The obtained results show that the developed method allows quantification of several molecular tracers suitable for source apportionment studies for evaluating contribution of specific primary emission sources and atmospheric photochemical reactions.

This work was in part financially supported by the Moniter project of the Environment Agency of Emilia Romagna region (ARPAER).

Bi, X., Simoneit, B.R.T., Sheng, G., Ma, S., Fu, J. (2008) *Atmos. Res.* **88** 256-265.
Mochida, M., Kawamura, K., Fu, P.Q., Takemura, T. (2010) *Atmos. Environ.* **44** 3511-3518.
Pietrogrande, M.C., Bacco, D., Mercuriali, M. *Anal. Bioanal. Chem.* (2010) **396** 877-885.
Pietrogrande, M.C., Bacco, D. *Anal. Chem. Acta* (2011) doi:10.1016/j.aca.2011.01.047 |

Four years of high resolution monitoring of inorganic water soluble aerosol components over a semi-natural ecosystem in South East Scotland

M. Twigg[1,2], C.F. Di Marco[1], I. Leith,[1], S. Leeson, [1], N. van Dijk[1], I. Simmons[1], M. Jones[1], E. Nemitz[1] and J.N. Cape[1]

[1]Centre for Ecology and Hydrology, Penicuik, EH26 0QB, UK
[2]School of Geosciences, University of Edinburgh, Edinburgh, EH9 3JF, UK
Now at NCAS, University of Leeds, Leeds, LS2 9JT, UK

Keywords: Measurements, ammonium nitrate, sulphate, PM_{10}, $PM_{2.5}$, long range transport.
Presenting author email: sail@ceh.ac.uk

Traditionally, bulk mass methods have been used to monitor the long-term trends of PM_{10} and $PM_{2.5}$ aerosol mass. Bulk mass methods, however, provide limited information on the chemical speciation of aerosol. Recent epidemiological research has suggested that health effects of aerosol may be less closely linked to the total mass of PM_{10} or $PM_{2.5}$ aerosol than to the physicochemical characteristic of the aerosol. Long-term, high resolution monitoring of speciated aerosol is therefore required to further understand aerosol metrics on human health. In addition, secondary aerosols and their precursor gases are required to be monitored to understand atmospheric processes and to validate chemical transport models, which are used to inform policy, such as the UNECE Convention for Long-range Transboundary Air Pollution (CLRTAP) and the revised European Air Quality Framework Directive (Directive 2008/50/EC).

Long term monitoring of water soluble inorganic aerosols have been taking place in South East Scotland at a 'supersite' within the European Monitoring and Evaluation Program (EMEP). Hourly PM_{10} and $PM_{2.5}$ measurements of NO_3^-, Cl^-, SO_4^{2-}, Na^+, NH_4^+, K^+, Mg^{2+} and Ca^{2+} have been made since June 2006 using a Measurement of Aerosols and Reactive Gases Analyser (MARGA, Applikon, NL). The MARGA instrument is a wet chemistry technique which utilises a rotating wet denuder and steam jet aerosol collector (Khlystov *et al.* 1995) to capture water soluble gases and aerosol compounds, respectively. Analysis is then carried out by use of online ion chromatography. As a dual system this particular MARGA measures the aerosol chemical composition of both $PM_{2.5}$ and PM_{10}.

The data presented will be an overview of 4 years of measurements made by the MARGA at the Northern UK EMEP 'Supersite'.

Results

Long term monitoring at Auchencorth Moss has shown the site to be a relatively clean site, with a median PM_{10} SO_4^{2-} concentration of 0.75 µg m^{-3} from the years 2007 to 2009. Seasonal trends have been observed in aerosol, with both Cl^- and Na^+ having lower median concentrations during the months of May – July.

A large proportion of the aerosol measured by bulk mass methods can be explained by the MARGA. It was observed 67% of the PM_{10} aerosol measured by a TEOM FDMS could be explained by the chemical components resolved by the MARGA alone on average in 2008. The remaining unexplained mass is likely to be from organic and black carbon as well as unresolved crustal components.

Due to the high resolution of the MARGA it has been possible to investigate periods where air quality limits are exceeded. In March 2007, for example, a PM_{10} mass of 82 µg m^{-2} was measured by TEOM. The increase in concentration coincided with an increase in NH_4^+, SO_4^{2-}, NO_3^- and K^+ measured by the MARGA. Three day back trajectory analysis revealed that the origins were from Eastern Europe, where biomass burning had been observed.

Carrying out cluster back trajectory analysis has shown air masses from the Atlantic and Artic are associated to large contributions of Na^+ and Cl^- (Fig. 1) to the measured mass. The UK, Western Europe and Eastern Europe, on the otherhand, were associated to larger contributions of NH_4^+, NO_3^- and SO_4^{2-} to measured mass.

To summarise, the application of the MARGA system at the EMEP 'supersite' has furthered the understanding of atmospheric composition, large pollution events and long range transport in the South East Scotland.

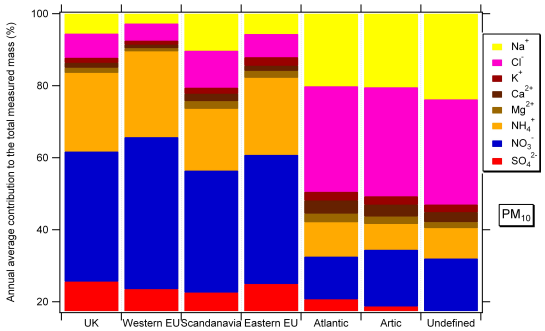

Figure 1. Average contribution of different aerosols species to different air masses from the years 2007-2009, based on 6 hourly values.

British Atmospheric Data Centre (BADC), 2010. BADC Trajectory Service. Accessed at http://badc.nerc.ac.uk/community/trajectory/ on 28/09/10.

Khlystov, A. Wyers, G. P. Slanina, J. 1995. The steam-jet aerosol collector. *Atmospheric Environment* 29 (17), 2229–2234.

Aerosol chemical mass closure in Corsica Island: towards a better understanding of the seasonal variation of aerosol sources in the Western Mediterranean

J. B. Nicolas[1], M.-D. Loÿe-Pilot[2], H. Cachier[1], J.Sciare[1], K. Oikonomou[1], N. Mihalopoulos[3], and F. Dulac[1]

[1]Laboratoire des Sciences du Climat et de l'Environnement (LSCE), CNRS-CEA, Gif-sur-Yvette, 91191, France
[2]Environmental Research and Teaching Institute (CERES/ERTI), Ecole Normale Supérieure, Paris, France
[3]Environmental Chemical Processing Laboratory (ECPL), Uni. of Crete, Heraklion Voutes, Greece

Keywords: Western Mediterranean, aerosol chemical mass closure, $PM_{2.5}$, black carbon.
Presenting author email: jose.nicolas@lsce.ipsl.fr

The Mediterranean population is expected to reach 550 million inhabitants within the next 30 years. This increasing anthropogenic pressure will be associated with higher emissions of atmospheric pollutants in a region holding already the highest PM (Particulate Matter) loadings in Europe. This increasing particulate pollution will induce climate changes at a regional scale that is still hardly predictable. In this context a better characterization of aerosols in this area is crucial and will comprise a better understanding of their sources, chemical composition, (trans)formation processes and impacts.

A 20-month field experiment (Aug 2001- Apr 2003) was performed in Corsica Island (France) within the EU-FP5 ADIOS project* (Atmospheric Deposition and Impact on the Mediterranean Sea) in order to better characterize the chemical composition of West Mediterranean aerosols. These results are presented here and compared (for Black Carbon (BC)) with recent measurements (2010-2011) performed in Corsica within ChArMEx (the Chemistry-Aerosol Mediterranean Experiment).

Methodology

Weekly aerosol sampling was performed at Ile Rousse in Corsica (2001-2003) for 2 size fractions having aerodynamic diameter below 2.5µm (Fine mode) and upper than 2.5µm (Coarse mode), respectively. Pre-fired quartz filters were used for carbon analyses (EC, OC) and pre-weighed nuclepore AOX filters for mass determination (PM) and major ion analyses (Cl, SO_4, NO_3, Na, NH_4, K, Mg, Ca). Weekly aerosol chemical mass closure was performed based on these chemical analyses. Co-located BC measurements were performed with an Aethalometer (Magee Scientific) and are compared with similar measurements performed 10 years after (2010-2011) at another site however.

Results

On a yearly basis, contrasted chemical compositions have been found in the two aerosol modes. In the Fine mode (Fig.1), Particulate Organic Matter (POM) contributed to almost half of the PM and ammonium sulfate about 40%. By contrast, the major part in the Coarse mode (75%) was composed from sea salts, dust and nitrate (Fig.2).

The seasonal variations of the major chemical components of Western Mediterranean aerosols will be presented here, providing new insights on the major aerosol sources in this region. Comparison will also be performed with similar measurements performed in Eastern Mediterranean (Crete Island, Finokalia) during the same period (Sciare *et al*, 2008) providing a unique characterization of the major aerosol sources in the whole Mediterranean.

Comparison of sectorized BC (seasonal) variations performed 10 years apart (2001 - 2011) will also be presented here providing insights of recent BC emission trends in the Western Mediterranean.

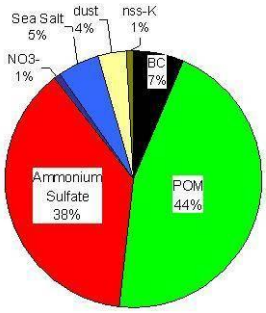

Figure 1. Mass closure in the Fine mode (< 2.5 µm), 2001-2003

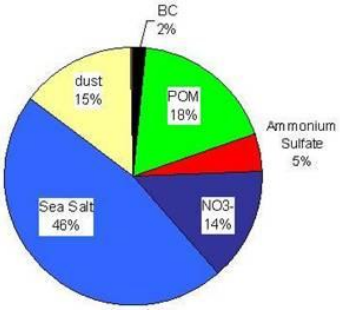

Figure 2. Mass closure in the Coarse mode (> 2.5 µm), 2001-2003

This research was funded by EU* (EVK3-2000-00604C), CNRS, CEA and ADEME. The Ersa semaphore French Navy staff is thanked here for hosting the Aethalometer since May 2010.

Cachier H. et al. (2003), in: ADIOS final report.
Sciare, J., et al. (2008) Long-term measurements of carbonaceous aerosols in the Eastern Mediterranean: Evidence of long-range transport of biomass burning, *Atmos. Chem. Phys.*, 8, 1–13.

PAH in PM_{10} from tyre and pavement wear

M. Gustafsson[1], G. Blomqvist[1], and E. Brorström-Lundén[2]

[1]Swedish National Road and Transport Research Institute (VTI), Linköping, 581 95, Sweden
[2]Swedish Environmental Institute (IVL), Göteborg, 400 14, Sweden
Keywords: tyre, pavement, PM_{10}, PAH, road dust
Presenting author email: mats.gustafsson@vti.se

The interaction between pavement and tyre is an important traffic source to inhalable particles (PM_{10}). Especially in Nordic countries, where studded tyres are used, pavement wear contributes to high concentrations of PM_{10} during winter and spring. Except for minerals emanating in pavement stone material, the binder of the pavement and the tyres themselves contribute to inhalable PM. Both these particle sources contain polyaromatic hydrocarbons (PAH), some of which are classified as carcinogenic (Brorström-Lundén, 1995). The use of high aromatic (HA) oils in tyres is regulated by an EG directive (2005/69/EG).

At VTI, a road simulator (Figure 1) is used to study physical and chemical properties of particles formed from wear of pavements and tyres. Any desired pavement and wheels can be tested in different combinations in speeds up to 70 km/h.

Figure 1. The VTI Road Simulator

To study if tyres and bitumen contribute to PAH in PM_{10}, three studded winter tyres and three summer tyres were tested on one pavement in the road simulator. PM_{10} samples were taken using IVL low volume samplers (Ferm et al., 2001). PAH content of tyre rubber, bitumen and PM_{10} was analysed using soxhlet extraction and an HPLC (High Performance Liquid Chromatograph) fitted with a fluorescence detector (Varian Prostar363). The PAH analysed were the ones listed by the US Environmental Protection Agency as prioritised PAH.

The results show that for studded winter tyres, PAH in PM_{10} produced from pavement and tyre wear has a stronger correlation to PAH content in tyres than to that in bitumen (Figure 2). The tests with summer tyres show the same pattern but much lower correlation (R^2 = 0.17 and 0.01 for tyres and bitumen respectively).

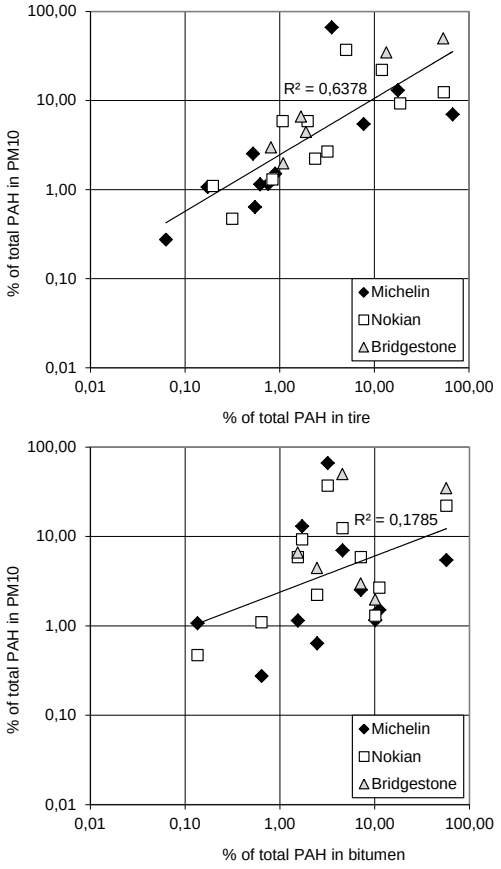

Figure 2. Percentage of total PAH in PM_{10} as related to percentage of total PAH in three studded winter tyres (makes in legend) and bitumen.

The results indicate that the winter tyres, although low in HA oils and following the EU directive on PAH, contribute to PAH content in PM_{10} from tyre and pavement wear, while bitumen is of less importance. Summer tyres seem to contribute in much lower degree to PAH in PM_{10}. It is hypothesised that the softer rubber in winter tyres are more prone to wear than summer tyres and therefore contribute more to PAH in PM_{10}.

This work was supported by the Emission Research Program EMFO.

Brorström-Lundén, E., 1995: Measurements of Semivolatile Organic Compounds in Air and Deposition. Thesis. Göteborgs Universitet.

EG directive 2005/69/EG

Ferm, M., A. Gudmundsson, and K. Persson, (2001) *NOSA Aerosol Symposium* Lund, Sweden.

Characterization of resuspended and respirable urban particulate matter

B. Turóczi[1], A. Hoffer[2], N. Kováts[1], A. Ács[1], A. Gelencsér[1]

[1]Institute of Environmental Sciences, University of Pannonia, Veszprém, Hungary
[2]Air Chemistry Group of the Hungarian Academy of Science, Veszprém, Hungary
Keywords: PM, resuspension, respirable aerosols, source apportionment, health effects of aerosols
Presenting author email: turoczi.beatrix@indamail.hu

Urban air quality has becoming increasingly affected by traffic related particulate matter, including direct emissions from exhaust, brake pad, tire wear and resuspended road dust. Road dust can be resuspended easily by passing vehicles and wind in urban street canyons. Resuspended dust may contribute up to about 30% to urban PM10 mass concentrations. Fugitive dust from paved and unpaved roads and bare grounds as well as construction and demolition works can also be important contributors to PM10 in urban aerosol. Prolonged exposure to emissions from road traffic has been associated with adverse health effects and linked to an increased risk of respiratory illnesses.

In previous studies resuspension of urban particulate matter was usually performed by sieving of collected road dust followed by separation through size selective inlets in the laboratory (Han *et al*, 2007, Zhao *et al*, 2006). These off-line procedures and sample handling may result in the loss of fine particles and distortion of particle size distribution.

A mobile resuspended road dust PM10 sampler was developed and constructed which collects PM10 samples directly from road surfaces. A PARTISOL-FRM MODEL 2000 sampler is fixed on the mobile sampling cart which collects the PM(10-1) fraction in a cyclone separator without filters. The collection of bulk PM(10-1) samples makes it possible to deploy analytical methods which are not suited for the analysis of filter samples. The lack of a filter substrate significantly reduces the analytical background. The Partisol sampler collects the PM1 fraction on a backup filter.

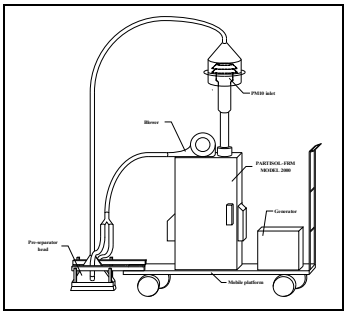

Figure 1. The mobile resuspended PM10 sampling unit

The sampler was tested by collecting resuspended particulate matter at kerbside locations in Veszprém, Hungary for 2 hours. The collected PM(10-1) fractions were weighted with a microbalance and PM10 mass concentrations in the duct were established. This simulates potential resuspension of particles under gusting wind conditions. The mean mass concentration of the resuspended and respirable particulate matter was 17.714 mg m^{-3} (standard deviation 2.147 mg m^{-3}).

The collected PM(10-1) fractions were analyzed by various analytical methods to establish mass balance and get insight into the contribution of possible sources to deposited dust. The main constituents of the resuspended urban particulate matter are the crustal elements. It was also possible to determine mineral phase composition of PM(10-1) dust which is generally not possible from samples collected on filter substrate. The major mineral phases were dolomite, calcite, clinochlore, muscovite, quartz, albite, orthoclase and gypsum. The major water-soluble inorganic ions in the resuspended road dust were Ca^{2+}, K^{+}, Na^{+}, Mg^{2+}, Cl^{-}, NO_3^{-} and SO_4^{2-}. PAHs were analyzed which are key tracers in different combustion processes.

The results indicate that the major components of the resuspended PM10 are crustal minerals, but with the help of quantitative phase composition the contribution of individual primary sources can be assessed. A unique feature of bulk elemental analysis by X-ray fluorescence spectrometry is the capability of direct quantitative measurement of oxygen. This, together with the analysis of trace metals and soluble ions complements source apportionment and mass balance calculations. (Han *et al*, 2007).

The ecotoxicity of resuspended and respirable particulate matter was directly determined by *Vibrio fischeri* bioluminescence inhibition bioassay in a special instrument developed for the analysis of solid sediment samples (Lappalainen *et al*, 1999). The specific toxicity of the resuspended bulk PM(10-1) and PM1 filter samples were compared with those obtained for urban PM10 and special emission samples.

The authors are grateful for the financial support of the grant TAMOP-4.2.1/B-09/1/KONV-2010-0003: Mobility and Environment: Researches in the fields of motor vehicle industry, energetics and environment in the Middle- and West-Transdanubian Regions of Hungary. The Project is supported by the European Union and co-financed by the European Regional Development Fund.

Han, L., Zhuang, G., Cheng, S., Wang, Y. and Li, J. (2007) Atmospheric Environment 41, 7485-7499.

Zhao, P., Feng, Y., Zhu, T., Wu, J. (2006) Atmospheric Environment 40, 5807-5814.

Lappalainen, J., Juvonen, R., Vaajasaari, K., Karp, M. (1999) Chemosphere 38 (5), 1069-1083.

Personal Monitoring of Exposure to Particulate Matter with a High Temporal Resolution

A.V. Broich[1], L.E. Gerharz[2] and O.Klemm[1]

[1]Climatology Working Group, Westfälische-Wilhelms-Universität, Münster, 48149, Germany
[2]Institute for Geoinformatics, Westfälische-Wilhelms-Universität, Münster, 48151, Germany
Keywords: particulate matter, individual behaviour, GPS, personal exposure, mobile measurements, indoor air
Anna.Broich@gmail.com

Air pollution with particulate matter is one of the key environmental health problems today. Several studies reported that long-term exposure to aerosol particles potentially leads to a number of cardiovascular diseases and premature deaths every year (Pope et al. 2002, Hoek et al. 2002). Continuous monitoring of air quality is implemented by governmental institutions at ambient fixed sites. These measurements only represent distinct outdoor locations in a city. However, humans in industrialized countries spent approximately 90 % of their time indoors (Klepeis et al. 2001).

In the present study we measured the personal exposure to particulate matter of sixteen individual persons during their daily routine. This was realized by an equipped measurement backpack, containing the Grimm Aerosol Spectrometer model 1.109, a GPS tracker, and a video camera.

Table 1: Comparison between 24-hour-mean concentrations of ambient fixed site measurements and personal monitoring of PM_{10}

Profiles	Ambient fixed site measurement ($\mu g\ m^{-3}$)	Personal monitoring ($\mu g\ m^{-3}$)
P1	41.5	41.0
P2	31.8	65.7
P3	31.6	28.5
P4	26.0	83.9
P5	23.8	117
P6	16.6	322
P7	13.0	114
P8	28.2	70.6
P9	24.2	28.7
P10	33.8	42.0
P11	22.2	36.6
P12	33.8	42.8
P13	28.5	27.0
P14	33.9	122
P15	30.0	33.5
P16	18.4	27.6

Novel in this study was the set-up allowing portable measurements indoors and outdoors with a high temporal resolution. The test persons carried the backpack for a time period of 24 hours. The time resolution was set to six seconds to identify variability in short-term exposure related to the persons' activities, as tracked and logged by camera and GPS.

Table 1 shows the comparison between ambient fixed site measurements and personal monitoring. It becomes evident that fixed site measurements alone do not describe the real concentration of PM an individual is exposed to over the day. Furthermore, the individual exposure is highly dependent on personal activity and lifestyle, leading to large differences between individuals.

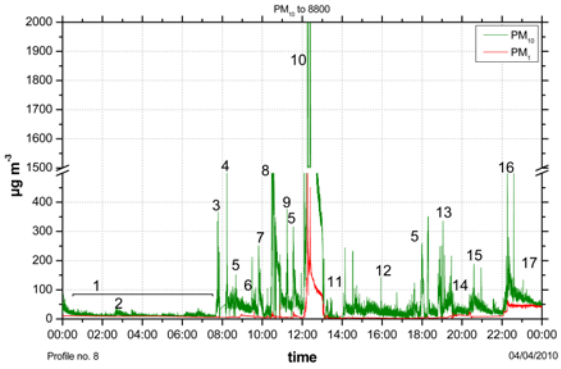

Figure 1: Diurnal course of 6-sec-measurements of PM_1 and PM_{10} during 24 hours from profile of a single test person; with: 1 sleeping ; 2 bathroom visit; 3 dressing; 4 take down laundry; 5 cellar room, 6 breakfast, 7 vacuuming, 8 changing bedcover, 9 changing clothes, 10 frying cutlets, 11 go for a walk outside; 12 coffee and cake time with guests; 13 relight wood stove; 14 dinner; 15 sweeping (open windows); 16 closing bedroom door; 17 sleeping with windows open (Easter Fire outside).

Figure 1 shows the course of PM_{10} and PM_1 of one single profile (P8) of a test person. The variability of PM_{10} was mostly related to indoor activities such as food preparing or just dressing or vacuuming. Night concentrations and concentration while going for a walk outside were distinctly lower.

We suggest that studies of this nature should be conducted in larger dimension and include biometric parameters as well. In this way, the exposure of individual persons, age groups, professional groups, and lifestyles towards PM can be quantified more representatively. Eventually, exposure models (Gerharz et al., 2009) can be parameterized more realistically.

Gerharz, L.E., Krüger, A. & Klemm, O. (2009) *Sci. Total Environ.* **407**, 5184-5193.

Hoek G., Brunekreef B., Goldbohm S., Fischer P., van den Brandt P. A. (2002) *The Lancet* **360**: 9341:1203-1209.

Klepeis N. E., Nelson W. C., Ott W. R., Robinson J. P., Tsang A. M., Switzer P., Behar J.V., Hern S. C., Engelmann W. H. (2001) *J. Expo. Anal. Environ. Epidem.* 11: 231-252.

Pope C. A., Burnett R., Thun M., Calle E., Krewski D., Ito K., Thurston G. D. (2002) *J. of the Am. Med. Association* **287**:1132–1141.

Suglia S. F., Gryparis A., Wright R. O., Schwartz J., Wright R. J. (2007) *Am. J. Epidem.*. **167**, 280-286.

Thanks to Grimm Aerosol Technik GmbH & Co. KG for providing the Aerosol Spectrometer Model 1.109.

Monday, September 5, 2011

Session 1E: Engineered Nanoparticle Release from Nanostructured Materials into the Air

Exposure to nanostructured particles during powder handling and mixing, sanding nanoparticle-doped paints and grinding windmill blades

K.A. Jensen and I.K. Koponen

National Research Centre for the Working Environment, Copenhagen, DK-2100, Denmark
Keywords: engineered nanoparticles, workplace, exposure, risk.
email: kaj@nrcwe.dk

Currently there is intensive focus on the potential health risk of exposure to engineered nanoparticles. The risk may be ascribed to small particle size, higher chemical reactivity per mass and/or even special nano-scale properties. However, very little is currently known about the actual or potential exposure levels as well as the characteristics of this exposure. Airborne engineered nanoparticles may occur as free single particles as well as in aggregates and agglomerates. The different types of nanostructured particulates may have formed already in the source material (eg, powders, slurries and composites), as a consequence of work-processes or due to aerosol dynamic processes (coagulation and scavenging). Consequently it is often difficult to determine the fraction of engineered nanoparticles from on-line monitoring in workplace measurements. Such data are crucial to enable a proper risk assessment. Improved assessments can be obtained by more detailed of-line analysis using e.g., electron microscopy and chemical analysis.

In this paper, we present the characteristics of real and potential workplace exposures to engineered nanoparticles based on a number of case studies. The investigations comprise both workplace measurements and measurements during simulated work-processes in the laboratory.

Workplace measurements were done using a TSI Fast Mobility Particle Sizer (FMPS; 5.6-560 nm) and a GRIMM Dust Monitor Model 1.109 (0.28-30ɛm) in the activity zone (< 2 m from the source). Background measurements were done in the workplace areas using a CPC Model 2022 (TSI) and a GRIMM Dust Monitor. PM_1 and Total Suspended Particulates (TSP) was collected on cellulose and Teflon filters filters at the activity and background measurement positions as well as on the operator using Conical Inhalable Samplers (CIS) and Millipore TSP samplers. In laboratory studies, an FMPS was used for nanoparticle measurements. Coarser particles were measured using TSI Aerodynamic Particle Sizer Model 3321 (0.523-20 μm). Dust particles were characterized by analytical Scanning (Quanta 200 FEG MKII) and Transmission Electron Microscopy (Tecnai G20) both from FEI Company, Hillsboro, Oregon, USA.

The case-studies are briefly summarized below emphasizing some of the major general conclusions.

Laboratory handling of nanoparticle powders: There is a potential risk of exposure to nanoparticles even when working in fume hoods. The level of exposure risk is related to type of fume hood and worker behaviour. Here we investigated the exposure during handling of very low-mass powder and during simulated accidental loss of up to 100 g nanoparticulate powder in a fume hood. The result showed that no particle release could be measured to the air outside of the fume-hood at 1 sec. time-resolution in either of the cases. Short-term bursts were detected inside the fume-hood and visual observations showed that powder jets may be released from the fume hood during accidents.

Industrial scale pouring and mixing of nanoparticles powders: Pouring and mixing was found to be the most typical activity in the workplaces visited. Our current examples include companies compounding nanoparticles and pigments into plastic and companies producing paints and lacquers. Workplace exposure during nanoparticle mixing and dosing for twin-screw extrusion was studied in a research and development company and at a large-scale industrial plant. All exposures related to the paint and lacquer factories were studied at industrial workplaces. These studies strongly suggest that the airborne nanoparticles are dominated by aggregates and agglomerates. Moreover, exposure levels are not necessarily linked to the amount of material used. The work procedure, the design of the workplace and use of local exhaust ventilation plays a major role in reducing the risk of exposure.

Sanding and grinding surfaces with and without nanoparticles-based coatings: Finishing and repair is another potential source of exposure to nanostructured dust particles. Our cases include a laboratory study of the emission characteristics of dust particles generated during sanding of paint and lacquer products with and without engineered nanoparticles and a workplace study of particle exposures during grinding a glasfiber-based windmill wing for repair. Carbon nanotube re-enforced epoxy-paints for windmill wings are currently in the R&D phase. Both studies revealed high concentrations of small nm-size particles in the air. Some of these are ascribed to the electrical motors in the power-tools. However, at least in some cases, a fraction of the dust particles consists of free engineered nanoparticles and larger pigments or agglomerates and aggregates thereof. We conclude that mechanical reworking may be associated with very high exposure concentrations in particle numbers.

This work was supported by the Occupational Safety and Health Advisory Boards for the Industry, Teaching and Research, and the Ministry of Science, Technology and Innovation in Denmark as well as the The Danish Working Environment Research Fund (Nanokem, Grant #20060068816).

Investigations on (Nano-) Particle Release during Mechanical Treatment of Different Composite Materials

B. Stahlmecke[1], J. Romazanov[1], C. Asbach[1], H. Fissan[1,2], T.A.J. Kuhlbusch[1,2]

Air Quality & Sustainable Nanotechnology Division, Institute of Energy and Environmental Technology, Bliersheimer Strasse 60, 47229 Duisburg, Germany
[2]CeNIDE, Center for Nanointegration Duisburg-Essen, 47229 Duisburg, Germany
Keywords: Nanoparticles, Nanotubes, Release Scenarios, Measurements, Size Distribution
Presenting author email: stahlmecke@iuta.de

Due to the increasing use of nanomaterials and especially nanoparticles in different composite materials there is an enhanced likelihood of unwanted particle release, which may cause adverse health effects. Besides the unknown amount of released particles during different treatments the origin (release from composite, machinery or other sources) and composition of the released particles is also often unknown.

In order to characterize possible releases from a composite material, the emission of particles during different treatments of the composite has to be investigated in a first step. In a second step a further analysis is required to investigate the degree of separation of the original particles from the surrounding matrix material. This step requires particle sampling and consecutive analysis, e.g. by using electron-microscopy. In many cases the released particles consist of a mixture of nanoparticle and matrix material (e.g. Vorbau et al., 2009).

We will present results from two different studies. The first study aimed at the investigation of a possible particle release from composite building materials made of matrix material and aerogel particles under realistic conditions. The term realistic condition indicates conditions for handling of the composites which are present in the DIY sector. Handling includes e.g. drilling into the composite materials or polishing of the surface of the material. The number size distribution of released particles was measured using a fast mobility particle sizer (FMPS, TSI model 3091) and an aerodynamic particle sizer (APS, TSI model 3321). Furthermore, particles were sampled on glassy carbon substrates by applying a nanometer aerosol sampler (NAS, TSI model 3089).

Different types of composite materials (with and without aerogel particles) were examined by applying several handling procedures ranging from simple dropping to grinding of the materials. Using this approach the energy input, and thus the likeliness of particle release from the material, was increased. Special emphasis was laid on the distinction of particles stemming from the actual working process and particles stemming from other activities.

The main advantage of this approach is the assessment of particles emitted under realistic conditions, thus providing at least information on possible particle emissions in the private sector, where usually no or little measures are taken to inhibit a particle release. The main drawback is the complicated calculation of the different particle fractions: Particle release from the composites has to be quantified versus a background of particles from other sources (e.g. from outside, originating from the process or from the machines used).

The second study was conducted on composite materials containing multiwalled carbon nanotubes. These experiments were conducted in a clean enclosure, where the material was disintegrated by a shredder. No background particles where present during the experiments, so that any measured particles could only stem from the shredding process, which may also include motor emission from the shredder. This study aimed on the simulation of a typical recycling process to assess the number and size distribution of the released particles, especially in view of a possible release of carbon nanotubes.

We will present the rationale of data analysis and the results of the abovementioned experiments conducted for a realistic appraisement of the released particles. Furthermore, we will discuss the advantages and drawbacks of the two different applied approaches. Special emphasis will be given to the comparability of such studies, including the minimum data set that should be presented along with additional information on experimental conditions which may affect the measurements.

This work is partly funded by the German Federal Ministry of Education and Research (BMBF) within the CarboSafe project as part of the Inno.CNT initiative by Grant No. 03X0043D.

M. Vorbau, L. Hillemann, M. Stintz (2009), J. Aerosol. Sci. **40**, 209-217

Sanding induced nanoparticle release into air from artificially aged/weathered surface coatings

D. Göhler, L. Hillemann and M. Stintz

Institute of Process Engineering and Environmental Technology - Research Group Mechanical Process Engineering, Technische Universität Dresden, 01062 Dresden
Keywords: nanoparticle release, aged surface coatings, sanding process, engineered nanoparticle additives
Presenting author email: daniel.goehler@tu-dresden.de

Nanoparticle additives (NPA) and nanoscaled pigments (NSP) are increasingly used in surface coatings and composite materials to achieve customized product properties. After appropriate processing, the NPAs and NSPs should be firmly embedded in the matrix material. However, since their possible risks to health, safety and environment are still under discussion, it is necessary to investigate their (possible) release from coatings and composites.

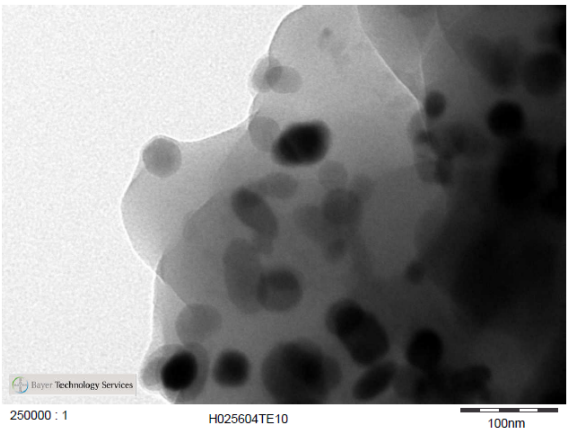

Figure 1: TEM-image of a electrostatic-precipitated polyurethan swarf particle with firmly embedded ZnO NPAs

The release of NPAs and NSPs into air, has already been analyzed in several studies. Weak, but long-term abrasion processes on surface coatings containing and not containing NPAs were simulated by Vorbau et al. (2009) and Guiot et al. (2009). Both studies showed only a slight release of particles. Even more, thorough analyzes of the wear particles with electron microscopy could not confirm the existence of free NPAs. Similar results are given by Hsu & Chein (2007), who investigated the abrasive effect of sunlight, wind and human contact. Koponen et al. (2009 & 2010) and Göhler et al. (2010) characterized the nanoparticle release due to the sanding of coatings with and without NPAs, while cutting and drill processes on CNT-composite materials were simulated by Bello et al. (2009 & 2010). The last mentioned studies based on a relatively high energy input which leads in each case to a considerable generation of nanoparticles, whether NPAs or NSPs were added to the matrix material or not. Nearly all studies have shown, that no free NPA were observed.

External impacts like sunlight, moisture or temperature fluctuations can destruct the matrix material of coatings and composites. This can lead to a denudation of the NPAs and NSPs, which is probably associated with a higher release risk. To our knowledge, no study has been reported the possible nanoparticle release of samples with partially or completely degenerated matrix material.

Based on the sanding test apparatus presented by Göhler et al. (2010) artificially aged/weathered samples of surface coatings and composites were exposed to a defined sanding process. A fast mobility particle sizer (FMPS) and an optical particle size spectrometer (OPS) were employed for the determination of the particle size distribution in a size range of 5.6 nm - 20 µm, while a condensation particle counter (CPC) was chosen to measure the total particle number concentration. Additionally, samples of the swarf aerosol were electrostatic precipitated for subsequent scanning electron microscopy (SEM), transmission electron microscopy (TEM) and energy dispersive X-ray spectroscopy (EDX).

First results on artificially UV-light aged surface coatings show an increase of the nanoparticle release, possibly caused by embrittlement of the matrix material, since no free NPAs were observed during TEM analyses. In addition to the results of this study, the presentation will discuss the experimental apparatus, setup and procedure in detail. Furthermore, measurement results in terms of particle size distributions and numbers of released particles will be presented.

Bello, D.; Wardle, B.L.; Yamamoto, N.; deVilloria, R.G.; Garcia, E.J.; Hart, A.J.; Ahn, K.; Ellenbecker, M.J. and Hallock, M. (2009) *J. Nanopart. Res.,* **11**, 231-249.

Bello, D.; Wardle, B.L.; Zhang, J.; Yamamoto, N.; Santeufemio, C.; Hallock, M. and Virji, M.A. (2010) *Int. J. Occup. Environ. Health*, **16**, 434-450.

Göhler, D.; Stintz, M.; Hillemann, L. and Vorbau, M. (2010) *Ann. Occup. Hyg.*, **54**, 615-624.

Guiot, A.; Golanski, L. and Tardif, F. (2009) *J. Phys.: Conf. Ser.*, **170**, 012014.

Hsu, L. Y. and Chein, H. M. (2007*) J. Nanopart. Res.*, **9**, 157-163.

Koponen, I.K.; Jensen, K. and Schneider, T. (2009) *J. Phys.: Conf. Ser.*, **151**, 012048.

Koponen, I.K.; Jensen, K.A. and Schneider, T. (2010) *J. Expo. Sci. Env. Epid.*, 1-11.

Vorbau, M.; Hillemann, L. and Stintz, M. (2009) *J. Aerosol Sci.*, **40**, 209-217.

Release of nanoparticles from composite materials under abrasive stress

M.W. Meier[1], M. Mertler[1] and W. Wohlleben[2]

[1]Dust Separation and Aerosol Technology GCP/TP, BASF SE, 67056 Ludwigshafen, Germany
[2]Experimental Toxicology GV/T, BASF SE, 67056 Ludwigshafen, Germany
Presenting author email: matthias.w.meier@basf.com

1. Introduction

Nanocomposites are internally nanostructured materials [1], generated spontaneously or by nanofillers (nano-particles, -platelets, -fibers) dispersed in a continuous matrix material. Consumer contact with nanocomposites has generally been considered as low risk, but substantiation is missing.

In this study, the release of selected nanocomposite materials upon abrasive stressing is characterized. The amount and particle size distribution of released particles is measured, and the released particles were collected for further (toxicological) investigations.

2. Experiments

For the abrasion test rig, a setup similar to that of Vorbau et al (2009) has been used (see Fig. 1). The entire test rig is standing in a housing that is supplied with filtered air, in order to reduce the background particle concentration from the ambient air. A stamp equipped with a sanding paper is pressed with a defined force onto a sample of the studied composite material rotating on a plate. Via a suction cap located above the stamp, an air flow containing released particles is drawn from the housing. The concentration and size distribution of the aerosol is measured by a Scanning Mobility Particle Sizer (SMPS). Particles are collected on a membrane filter for further investigations (SEM, particle size, surface chemistry by XPS and SIMS).

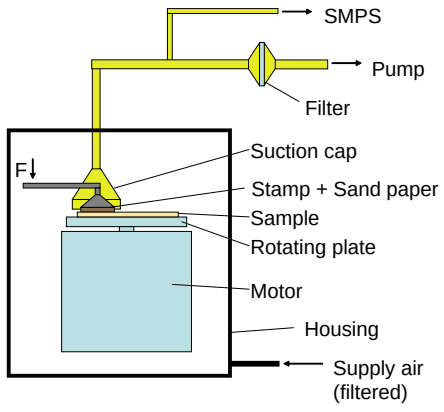

Figure 1: Test rig for abrasion experiments

Studied materials were two polymers and two cementitious materials, with and without nanofillers added.

3. Results

From the abrasion tests it was found that the major fraction of abraded material consists of relatively coarse particles between 10 µm and 80 µm. Only around 5% of the abraded polymeric material and 20% of the abraded cementitious material was found to be smaller than 2 µm. The surface chemistry of the abraded particles was assessed by XPS and SIMS, in order to check whether free nanofillers might adhere to the surfaces of larger particles. For the materials studied here, no release of free nanofillers could be detected.

A closer look is taken at the finest particle fraction in the gas phase by using an SMPS. Particle number concentrations between 500 and 100 000 #/cm³ were found, depending on the material. It was also material-dependent whether an addition of nanofillers led to a higher concentration of released submicron particles or not. For example, an increase was found for SiO_2 particles in polyamide, while no increase in concentration was found for carbon nanotubes in polyoxymethylene. A strong scatter of the data is found especially when higher particle concentrations were measured, which is mainly due to an unsteady dispersion process of abraded material from the stamp surface into the surroundings. Similar observations regarding this scatter were made by Göhler et al. (2010) and Vorbau et al. (2009).

4. Conclusions

Upon abrasion experiments on composite materials containing nanofillers, the release of nanoparticles was investigated. In some cases, an increase of particle release was found in the presence of nanofillers, in others not. No indications were found that free nanofillers were released during the abrasive stressing.

References

[1] ISO TC229. ISO/AWI TS 80004-4 2010.
[2] M. Vorbau, L. Hillemann, M. Stintz. J. Aerosol Sci. 2009, 40, 209-217
[3] D. Göhler, M. Stintz, L. Hillemann, M. Vorbau. Ann. Occup. Hyg. 2010, 1-10

Characterisation of Particles produced by Abrasion of Nanocomposites with a Grinding Machine

A. Hellmann[1], S. Ripperger[1], M. Berges[2], S. Sticher[2], T. Burkhart[3]

[1]Chair of Particle Process Engineering, Kaiserslautern University of Technology, Kaiserslautern, Rhineland-Palatinate, 67663, Germany
[2]Institute for Occupational Safety and Health of the German Social Accident Insurance (IFA), Sankt Augustin, North Rhine-Westphalia, 53757, Germany
[3]Institut für Verbundwerkstoffe GmbH (IVW), Kaiserslautern University of Technology, Kaiserslautern, Rhineland-Palatinate, 67663, Germany
Keywords: Composite nanoparticles, Nanoparticles, Characterization, Occupational health
Presenting author email: albert.hellmann@mv.uni-kl.de

The interest in nanocomposites including nanoparticles with a scale below 100 nm is still of rising interest in industry. The physical and chemical properties of the respective nanocomposites can be adjusted very nicely via using the right nanoparticles as well as the right matrix (polymer, metal, ceramic).

A still open question of those nanocomposites is the potential toxicity during industrial use, because harmful nanoparticles might be released by thermal and mechanical stresses.

The focus of our work is on the mechanical treatment, like drilling, cutting and grinding. Therefore it is essential to know which and how many nanoparticles will be generated in view of the occupational health. An experimental setup was designed to characterize the released particles. The setup for the experiments is shown in figure 1.

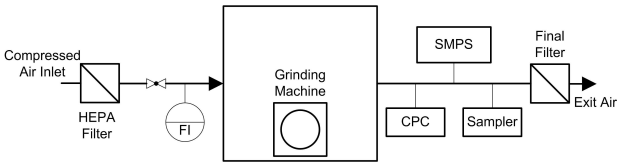

Figure 1. Scheme of the experimental setup with a grinding machine.

The test rig is equipped with a common grinding machine in which a nanocomposite can be handled under realistic conditions. Measurements will be performed with a Condensation Particle Counter (CPC), Scanning Mobility Particle Sizer (SMPS) and Electrical Low Pressure Impactor (ELPI).

Common polymeric materials, nanocomposites, have been chosen with and without nanoparticles. All materials were produced specially for this purpose. An example for an epoxy resin is shown in figure 2 with a volume percentage of 0.5 % of MWCNTs.

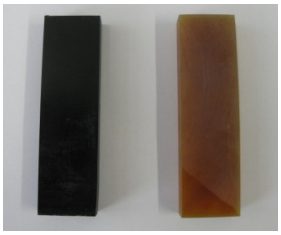

Figure 2. Example of a composite including (left) and excluding (right) Carbon Nano Tubes (CNT).

The results of measurements and the collected particles will be presented and compared. One of the first results is shown in figure 3.

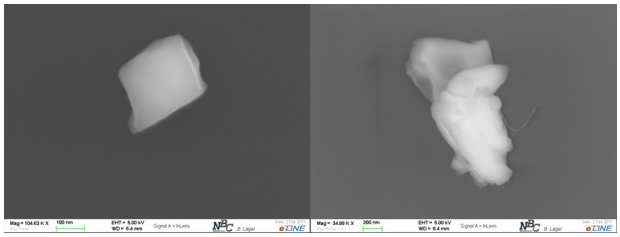

Figure 3. Generated particles of a composite including (right) and excluding (left) Carbon Nano Tubes (CNT).

This work is supported by the Institute for Occupational Safety and Health of the German Social Accident Insurance (IFA)

Vorbau M., Hillemann L. and Stintz M., *Method for the characterization of abrasion induced nanoparticle release into air from surface*, Journal of Aerosol Science 40, 209 - 217, 2008

Guiot A., Golanski L. and Tardif F., *Measurment of Nanoparticles removal by abrasion,* Journal of Physics, Conference Series 170, 2009

Strategies for Nanoparticle Release Assessment from Powders, Liquid and Solid Materials into the Environment

Fissan, Heinz[1,2]; Stahlmecke, Burkhard[1]; Asbach, Christof[1];Kuhlbusch, Thomas A.J. [1,2] and Wegner, Karsten[3]
[1]Air Quality & Sustainable Nanotechnology Division, Institute of Energy and Environmental Technology e.V. (IUTA), Bliersheimer Strasse 60, 47229 Duisburg, Germany
[2] CENIDE, Center for Nanointegration, Duisburg-Essen, Duisburg, Germany
[3]Particle Technology Laboratory, ETH-Zürich, Sonneggstr. 3, 8092 Zürich, Switzerland

Keywords: nanostructured materials, handling processes, nanoparticle release testing standardisation

There is an increasing interest in making use of nanoobjects to take advantage of their properties to improve the functionality of powders and composite materials. Those nanoobjects can occur in form of nanoparticles and fibers (e.g. CNT) (NP) as well as their agglomerates and are used either as powders or dispersed in liquids or solids. A discussion about the possibility of negative health effects of NPs and their agglomerates/ aggregates in air has started. However, negative effects in human beings and nature can only occur, if NPs and their agglomerates/aggregates are emitted, e.g. during synthesis, from products during their lifetime and recycling or after littering in the environment. The latter case is not considered here. To reduce the chances for NP emission, the following topic areas have to be addressed: control of emission and exposure including adequate measurement techniques, abatement strategies and standardized procedures to assess the probability of nanoparticle-release from nanomaterials into the environment.

To form nanostructured materials, NPs are produced in form of powders and suspended into liquid and most often in solid materials. Different methods under different conditions trying to simulate the real world activities like in case of handling of composite material, sawing and drilling have been used thus far.The approach thus far taken to investigate the NP-release from all kinds of materials containing NPs and the different handling processes, however, is extremely time consuming. An understanding of the underlying basic processes and their representation by a limited number of test methods is needed. It should be based on determining the release probabilities of NPs for different materials. This is depending in a first step on the easiness to separate the matrix material from the NPs, which may become airborne in a second step.

Besides the complex environmental stress, two types of stress can be differentiated for the NP containing materials: mechanical and thermal stress. Almost all treatment processes (like drilling, sawing and so on) start with mechanical stress forming chunks of matrix materials containing NPs. Except in cases where the particles are loosely bound to surfaces with direct access to the environment – actually they are already matrix material free – there is no real chance to liberate the NPs, because the achievable smallest chunk size is still too big. To get to smaller and smaller dimensions of these blocks, one has to locally introduce more and more mechanical energy into the material, which becomes increasingly difficult. In case of powders existing dustiness tests may be modified to especially concentrate on NP-release. For liquids very small droplets are produced with electrospray containing just one particle each.
In case of composites the mechanical energy input causes a (local) heating of the material.
The thermal energy input leads to evaporation and oxidation processes, which transfer material into the gas phase. In cases where the needed evaporation and /or oxidation energy for the matrix material is lower than for the NPs, there will be free NPs without matrix material. The knowledge of the basic physics and chemistry already allows for setting up a list of separation probabilities for different nanostructured materials, based on the thermal properties of the matrix material.

Since thermal energy input is the most likely relevant process to separate matrix material and NPs in case of composites, which is the first, but needed step to release NPs into air, the determination of the separation probability should be based on a thermal process, which finally can be standardized. The Thermo-Gravimetric Analysis (TGA) is a well defined and representative process, which allows the determination of the release of the matrix material into the air in comparison to nanoparticle combustion or sintering as a function of temperature.
Starting with a matrix containing a systematic order of the different forms of nanostructured materials and the list of different handling procedures, the handling procedures will be sorted according to different stress situations. Possible standard processes for different stress situations will be identified and described. Available first results for different stress situations will be discussed. It will be demonstrated how the tremendous work needed for investigating all possible handling procedures for all existing and expected nanostructured materials can be reduced by concentrating on representative processes for different stress situations, which may become standards in the future.

Monday, September 5, 2011

Session 1F: Aerosol Nucleation

Rethinking the first nucleation theorem in atmospheric nucleation

H. Vehkamäki[1], M. J. McGrath[1], T. Kurten[1,2], K. Lehtinen[3], and M. Kulmala[1]
[1]Department of Physics, P. O. Box. 64, University of Helsinki, Helsinki, FI-00014, Finland
[2]Copenhagen Centre for Atmospheric Research, Department of Chemistry, University of Copenhagen, Copenhagen, Denmark
[3]Department of Physics and Mathematics, P. O. Box 1627, University of Eastern Finland, Kuopio, FI-70211, Finland
Keywords: cluster ions, fundamental aerosol physics, numerical simulation.
Presenting author email: hanna.vehkamaki@helsinki.fi

The first nucleation theorem is a very useful tool in experimental studies of vapor–liquid nucleation, as it relates the derivative of the nucleation rate with respect to saturation ratio to the critical cluster size of the system. In other words, one can measure the nucleation rate of a system at various saturation ratios (holding all other variables, e.g temperature, constant), and learn information concerning the structure of the critical nucleus. This is an invaluable tool, as it is quite difficult to probe the structure of the critical nucleus directly. It has been well-established that the theorem is accurate for systems with a single maximum in the free energy profile. In the case of systems which have a local minimum on the free energy surface in addition to the maximum, the situation is not as clear. This is the case in ion-induced nucleation under moderate saturation ratios, where the addition of multiple neutral molecules (such as water) serve to stabilize the ion before the free energy barrier to nucleation. In addition, quantum chemical calculations indicate that such a local minima also exists for the case of sulfuric acid-base molecule nucleation, e.g. the amine-containing SA dimer evaporates much more slowly than the amine-containing SA trimer. It has been argued that the first nucleation theorem can still be used in this case, either without modification or with a minor systematic modification, although in-depth exploration is lacking in the literature.

Through the use of the Atmospheric Cluster Dynamics Code (ACDC), a collection of Perl and MATLAB scripts, we have solved the birth-death equations (the system of differential equations describing the cluster interactions) for various fictitious free energy profiles displaying a free energy maximum and one (or zero) free energy minimums, including one directly applicable for ion-induced nucleation. Here, "fictitious" means that all of the physical properties of the system are taken to be that of water (mass, vapor pressure, etc.), but the free energy profile has been arbitrarily changed to display a local minimum at small cluster sizes. The ion-induced case uses the free energy curves computed by classical theory for the quasi-one-component water + ion nucleation system. In addition to the first nucleation theorem, a generalization of the first nucleation theorem derived by McGraw and Wu was also used. Given that these versions of the nucleation theorem were both derived under the assumption that only monomers can collide and evaporate from clusters, and given that this same restriction is not present in explicit solution of the differential equations governing the system, both cases (allowing only monomer collisions/evaporations, and allowing all collisions/evaporations) were tested by ACDC.

In order to compare to the experimental case, we explored the possibility of holding various concentrations constant while computing the derivative of the nucleation rate with respect to the saturation ratio: the monomer concentration, the concentration of the cluster at the free energy minimum, and the total concentration of molecules in the system. We have found that the first nucleation theorem holds true for the case where there is no free energy minimum (as expected). For the fictitious free energy profile with one free energy minimum, the first nucleation theorem predicts incorrect results, regardless of the quantity held constant. For a curve produced by considering the ion-induced nucleation of water, the first nucleation theorem was found to give decent results when the concentration of the cluster located at the free energy minimum or the total number of ions was held constant, but not in the case of holding the naked ion concentration constant. These results have a significant impact on the determination of critical cluster composition from field studies and laboratory experiments related to atmospheric nucleation.

This work was supported by the Academy of Finland and the National Council for Aerosol Research under grant JB/005.

Aerosol nucleation induced by a high energy particle beam

M.B. Enghoff[1], J.O.P. Pedersen[1], U.I. Uggerhøj[2], S:M: Paling[3], and H. Svensmark[1]

[1]National Space Institute, Technical University of Denmark, Copenhagen, Denmark
[2]Department of Physics and Astronomy, University of Aarhus, Aarhus, Denmark
[2]Department of Physics and Astronomy, University of Sheffield, Sheffield S10 2TN, U.K.
Keywords: ion-induced nucleation
Presenting author email: jopp@space.dtu.dk

The importance of ion-induced nucleation for the Earth' atmosphere is a subject of intense discussions which is being studied both in field measurements and in modeling work. Previous laboratory studies using gamma rays have found a positive correlation between ionizing radiation intensity and aerosol concentration in air (Raes and Janssens (1985), Svensmark *et al.* (2007), Enghoff *et al.* (2008)), but systematic laboratory experiments on aerosol nucleation with ionizing particle radiation have so far only been performed with very high radiation doses far above natural atmospheric levels using radioactive sources or high intensity electron and proton beams. Preliminary measurements with a more realistic 3.5 GeV/c pion beam have been reported to show indications of ion-induced nucleation, but suffered from unstable conditions in the reaction chamber (Duplissy *et al.* (2010)). A new experimental facility dedicated to these studies is under commissioning at the CERN Proton Synchrotron (PS) and is likely to resolve these problems.

The present experiments took place in a 50 L cylindrical, elec-tropolished stainless steel reactor, previously used by Enghoff *et al.* (2008). A mixture of pure humidified synthetic air is continuously flowed through the vessel at a rate of 3.1 L/min together with trace amounts of (typically 2 ppb) sulfur dioxide and approximately 55 ppb ozone with the relative humidity held at about 50\%. UV light was used to initiate the photochemistry in the chamber leading to an in situ production of sulfuric acid. The temperature was kept at 21.2^{o}C and the pressure at 1-2 mbar above room pressure.

A low-intensity beam of 580 MeV electrons from the Aarhus Storage Ring ASTRID at the University of Aarhus was used as the ionizing source. The energy of the electron beam falls within the main part of the natural cosmic ray spectrum and the induced ion concentrations cover the full range of atmospheric values.

Production of aerosols was measured using a condensation particle counter (CPC) with a nominal 50 % cutoff diameter of 4 nm. The chamber volume could be ionized using the 580 MeV electrons going coaxially through the chamber. The ionization level from the beam was adjustable by changing the amount of beam extracted and the electrons pass through the volume of air almost undisturbed. Alternatively a 33.5 MBq Na-22 gamma source could be used.

The procedure for each experiment involved turning the UV lamps on for 10 minutes giving a burst of sulfuric acid and then recording the resulting particle number. The time between UV bursts was 60 minutes, in order to allow the aerosol concentration (as measured by the CPC) to reach zero by the end of each burst, with the aerosols being lost to walls and by dilution.

We found a clear and significant contribution from ion-induced nucleation and consider this to be the first unambiguous observation of the ion-effect on aerosol nucleation using a particle beam under conditions that resemble the Earth's atmosphere. By comparison with ionization using a gamma source we further found that the nature of the ionizing particles is not important for the ion-induced component of the nucleation (Enghoff *et al.* (2011)).

This work was supported by the Carlsberg Foundation.

Duplissy, J. *et al* (2010) *Atmos. Chem. Phys.***10**, 1635-1647.
Enghoff, M.E. *et al* (2008) *J. Phys. Chem. A* **112**, 10,305-10,309.
Enghoff, M.E. *et al* (2011) *preprint.*
Raes, F. and A. Janssens (1985) *J. Aerosol Sci.***16**, 217-227.
Svensmark, H. *et al.*(2007) *Proc. Roy. Soc. A*, **463**, 385-396.

Binary sulfuric acid–water nucleation, including ion-induced nucleation mechanism

J. Duplissy[1,2], A. Franchin[1], S. Schobesberger[1], K. Lehtipalo[1], D.R. Worsnop[1,3], H. Vehkamäki[1], M. Kulmala[1] and the CLOUD collaboration

[1]Department of Physics, University of Helsinki, FI-00014, Helsinki, Finland
[2]Physics Department, CERN, CH1211, Geneva, Switzerland
[3]Aerodyne Research Inc., Billerica, MA 01821, USA

Keywords: CLOUD experiment, ion-induced nucleation, ions, sulfuric acid, smog chamber.

The possible influence of cosmic rays on aerosols and clouds is of considerable interest (Carslaw, 2009). The CLOUD experiment at CERN aims to study under controlled conditions the effects of cosmic rays on nucleation. CLOUD was installed at CERN in 2009 and three successful campaigns were carried out in 2009 and 2010 to study ion-induced and neutral binary nucleation of H_2SO_4 and H_2O, for tropospheric and stratospheric conditions. Here we present the nucleation data obtain in the CLOUD chamber together with the result of the new model including ion-induced nucleation mechanism.

Methods

Technical input for the CLOUD design was obtained in a pilot experiment in 2006 (Duplissy *et al.*, 2010). The chamber is a 3m-diameter electro-polished stainless-steel cylinder (26.1 m^3). A field cage is installed inside the chamber to allow the removal of ions, when required. The contents of the chamber are irradiated by UV light in the range 250-400 nm. Experimental runs can be performed at stable temperatures between 40°C and -90°C.

The chamber is exposed to a 3.5 GeV/c secondary pion beam from the CERN PS, corresponding to the characteristic energies and ionization densities of cosmic ray muons in the lower troposphere. The beam intensity can be adjusted to cover the natural range from ground level to the stratosphere. Ultra-pure air is obtained from the evaporation of cryogenic liquid N_2 and liquid O_2. The air is humidified with a Nafion humidifier. Ozone is added to the air by UV irradiation. Trace gases such as SO_2 are added from gas cylinders containing pressurised N_2 as the carrier.

The chamber instrumentation includes PTRMS, CIMS, Nano-SMPS, CPC battery, PSM, API-ToF, NAIS, Gerdien, LOPAP, dew point sensor, SO_2 and O_3 analyser, as well as T, P and UV sensors.

Model

The classical nucleation theory including the hydrate interaction model and the ion-induced nucleation will be merged into one model. From this improved model an extension of the parameterisation from Kulmala et al., (1998) and Vehkamäki et al. (2002) will be developed, and compared with the CLOUD data.

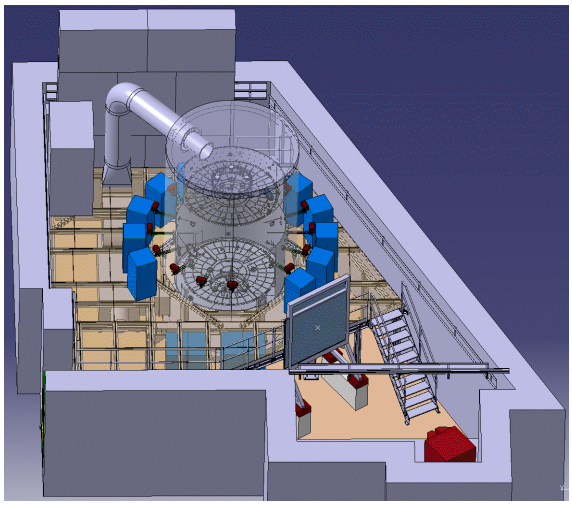

Figure 1. An illustration of CLOUD in the experimental zone at the CERN PS. The de-focused particle beam exits a dipole magnet (bottom right), crosses the hodoscope counter (middle) and then traverses the 3m-diameter CLOUD chamber. The instruments (blue boxes) analyse the contents of the chamber via sampling probes fitted with valves.

We would like to thank CERN for supporting CLOUD with important technical resources, and for providing a particle beam from the CERN Proton Synchrotron. This research has received funding from the EC's Seventh Framework Programme under grant agreement no. 215072 (Marie Curie Initial Training Network "CLOUD-ITN"), from the German Federal Ministry of Education and Research (project no. 01LK0902A), from the Swiss National Science Foundation, and from the Academy of Finland Center of Excellence program (project no. 1118615).

Carslaw, K. (2009). *Cosmic rays, cloud and climate*. Nature, 460, 332-333.

Duplissy, J. *et al.* (2010). *Results from the CERN CLOUD experiment*, Atm. Chem. and Phys., 10, 1635-1647.

Kulmala, M. et al. (1998), *Parametrizations for sulphuric acid/water nucleation rates*, J. Geophys. Res., 103, 8301–8308*et al.* (2010).

Vehkamäki, H *et al.* (2002), *An improved parameterization for sulfuric acid–water nucleation rates for tropospheric and stratospheric conditions*, J. Geophys. Res., 107, 4622

Formation of Zn and ZnO nanoparticles by homogeneous nucleation

B. Steer[1], V. Ranganathan[2], H. Gnewuch[2], B. Gorbunov[2] and F. Larner[3]

[1]University of Kent at Canterbury, University Road, Canterbury CT2 7NJ, UK
[2]Naneum Ltd., CIC, University Road, Canterbury CT2 7FG, UK
[3]Department of Earth Science and Engineering, Imperial College London, London SW7 2AZ, UK
Keywords: homogeneous nucleation, Zn nanoparticles, engineered nanoparticles.
Presenting author email: brian.steer@naneum.com

Zn and ZnO nanoparticles are widely used for many applications in nanotechnology. Mechanisms of Zn and ZnO nanoparticles formation are not fully understood. A novel system for the generation of engineered nanoparticles (ENPs) was developed. This system was based on vapour to particle conversion technique and it was used to generate Zn nanoparticles over the size range from 5 nm to 500 nm (diameter). These particles can subsequently be oxidized to ZnO. Freshly produced Zn nanoparticles generated in the gas phase were characterised using a range of state-of-the-art-techniques.

Homogeneous nucleation of Zn ENPs was observed in clean nitrogen and argon at atmospheric pressure at flow rate from 0.3 to 3 l/min and oven temperatures 300 to 700°C. Nanoparticles number size distributions obtained with an NPS500 SMPS were influenced by the oven temperature and by the flow rate of the carrier gas. Two distinct modes were observed at about 6nm and 75nm in size distributions recorded with an NPS500. Variation of the oven temperature slightly affects the median diameter of the modes. Temperature variation changes relative heights of the modes in the size distributions. TEM images of the nanoparticles collected with a thermal precipitator show two distinct particle shapes that indicates two mechanisms of nanoparticle formation. The first mechanism of Zn formation takes place at the lower temperatures of the oven when rectangular shaped particles of about 50nm were observed. Therefore, these particles were formed directly by vapour to solid phase mechanism (similar to sublimation).

At higher temperatures spherical particles were the dominant morphology in TEM photographs. This indicates the formation of Zn particles via a stage where liquid droplets were formed. Therefore, Zn ENPs might be generated in two stages: first formation of liquid droplets from the vapour, and second crystallisation of these droplets.

Theoretical modelling of homogeneous nucleation was performed using self-consistent classical nucleation theory modified by Gorbunov (1999). The free energy of embryo formation was calculated for spherical embryos in the case of liquid particle formation from vapour (Abraham, 1974). The Zeldovich factor was introduced according to Pruppacher and Klett (1997).

In the case of vapour to solid Zn particle formation it was assumed that embryos were of equilibrium crystalline shape. Supersaturation in the Zn generator was calculated using the commercially available finite element software COMSOL. The modelling confirmed that at lower temperatures, vapour to solid ENPs formation is the dominant process. At higher temperatures, solid Zn particles are formed via an intermediate stage of liquid particles: vapour – liquid-solid. Thus modelling confirms observed formation of spherical particles at higher temperatures.

The generator was modified by adding another oven with an air inlet of 0.5 to 2 l/min flow rate where Zn aerosol particles were oxidised to ZnO. Regimes were found to generate ZnO particles in the size range from 10 to 300 nm.

This enables the morphology of Zn and ZnO ENPs as well as the size of particles to be controlled in a flow system. The findings in this work can be used for production of ENPs with predetermined sizes and shapes for various nanotechnology applications.

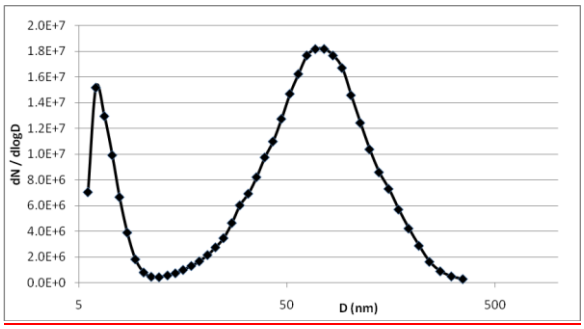

Figure 1. Example Zn distribution.

This work was supported by the DEFRA and TSB under grant “Prospect”.

Abraham F. F. (1974) *Homogeneous nucleation theory* (Academic Press, NY)

Gorbunov B. (1999) Free energy of embryo formation for heterogeneous multicomponent nucleation *J. Chem. Phys.* 110, N20, pp. 10035-45.

Pruppacher, H. R. and Klett, J. D. (1997) *Microphysics of Clouds and Precipitation*, Kluwer Acad., Norwell, Mass.

A Shape Independent Collision Kernel Valid for All Knudsen Numbers

Ranganathan Gopalakrishnan[1], Thaseem Thajudeen[1], Christopher J. Hogan Jr.[1]

[1]Department of Mechanical Engineering, University of Minnesota, Minneapolis, MN, USA
Keywords: condensation, coagulation, brownian dynamics
Presenting author email: Hogan@me.umn.edu

Aerosol particle growth is invariably driven by either particle-gas molecule collisions (condensation) or particle-particle collisions (coagulation/agglomeration). Aerosol systems are typically dilute, thus collisional growth can be modelled by only considering the motion of the two colliding entities. Therefore, the collision rate between two entities in the gas phase can be calculated as the product of the number concentrations of the entities in question multiplied by the collision kernel. For neutral aerosol particles, collision kernel determination is simplified by the fact that the force between colliding entities in this situation is often negligibly small. However, as characteristic aerosol particle sizes are typically similar in magnitude to the mean persistence distance of colliding entities (particles or gas molecules), thus neither a continuum approach (Smoluchowski's analysis) nor a free molecular approach (from gas dynamics) to collision kernel calculation is appropriate for aerosol particles.

While a number of "transition regime" collision kernels have been developed for both condensation and coagulation processes, there a several pending issues with modelling transition regime collisions. First, while condensation and coagulation have typically been modelled using distinctly different equations, the collision of a fast moving vapor molecule with a particle is simply a limiting case of more general particle-particle collisions. Therefore, there should be a single collision kernel valid for both condensation and coagulation. Second, all previously developed transition regime collision kernels apply for spherical particles only. In this presentation, we show that through Langevin equation (Ermak & Buckholz 1980) modelling and mean hitting calculations, a collision kernel which accurately describes both condensation and coagulation can be constructed. Through dimensionless analysis of the collision process and further mean hitting time calculations we show that this collision kernel is valid for aerosol particles of arbitrary shape across the transition regime (the entire Knudsen number range).

Theoretical Approach

Dimensionless analysis of the collision process reveals that for colliding entities at thermal energy kT, with radii a_1 and a_2, masses m_1 and m_2, and friction factors f_1 and f_2, the collision kernel, β, can be written is dimensionless form as:

$$H = \phi(Kn_D) \qquad (1)$$

where $H = (\beta\mu)/(f_{red}[a_1+a_2]^3)$ (dimensionless collision kernel), $Kn_D = (kT\mu)^{1/2}/((f_{red}[a_1+a_2]^3)$ (diffusive Knudsen number), $f_{red} = (f_1 f_2)/(f_1+f_2)$ (the reduced friction factor), and $\mu = (m_1 m_2)/(m_1+m_2)$ (the reduced mass). Regardless of whether the collision is between particle and vapour molecule or particle with particle, the relation $H(Kn_D)$ should describe the collision process in the transition regime.

Results

Langevin based mean hitting time calculations are used to determine $H(Kn_D)$ for both condensation (where a gas molecule moves around a stationary aerosol particle) and coagulation (where two particles move relative to each other. In addition, we redefine H and Kn_D for non-spherical by appropriately replacing the particle radius (the collision size parameters) in H and Kn_D with appropriate functions of their continuum radius and orientationally averaged projected surface area. We then use mean hitting time calculations to also determine $H(Kn_D)$ for condensation onto nonspherical particles. Results of all computations are shown in Figure 1.

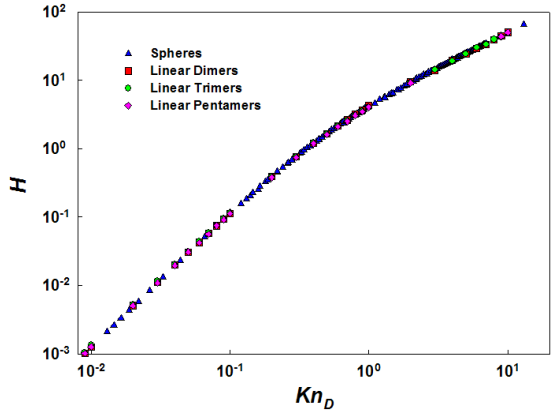

Figure 1. $H(Kn_D)$ relation from mean hitting time calculations. Particles of all shape collapse to a single curve.

The single $H(Kn_D)$ relationship found for both condensation and coagulation, and for non-spherical particles suggest that the combined approach of dimensionless analysis and mean hitting calculations can be employed to construct a universal collision kernel across the entire Knudsen number range.

Ermak, D. L. & H. Buckholz (1980). "Numerical-Integration of the Langevin Equation - Monte-Carlo Simulation." *Journal of Computational Physics* 35(2): 169-182.

Nucleation rates and parametrisation in the CLOUD experiment

Almeida-Simões, João[1,2], Curtius, Joachim[1], Kirkby, Jasper[2], and the CLOUD collaboration

[1] Goethe-University of Frankfurt am Main, 60438 Frankfurt am Main, Germany
[2] Physics Department, CERN, CH1211, Geneva, Switzerland

Keywords: CLOUD experiment, cosmic rays, atmospheric nucleation, nucleation rate, parametrisation.

The possible influence of cosmic rays on aerosols and clouds is of considerable interest (Carslaw, 2009). The CLOUD experiment at CERN aims to study under controlled conditions the effects of cosmic rays on nucleation, cloud droplets and ice particles.

The CLOUD experiment involves a 3m stainless steel aerosol chamber exposed to a pion beam from the CERN Proton Synchrotron. A suite of instruments continuously analyse the contents of the chamber via sampling probes. Each instrument has its own data acquisition system which delivers data in real-time to the CLOUD server. The CLOUD chamber is able to reproduce a wide range of well-controlled atmospheric conditions, including temperatures -90°C to 100°C, ion-pair concentrations 1-4000 cm^{-3} and relative humidities, RH, 0-100%. The nucleation and growth of new particles has been studied in the presence of various trace gases, including H_2SO_4 (10^6-10^9 cm^{-3}), NH_3 (35pptv to 1ppbv), amines and organics.

One of the primary goals of CLOUD is a quantitative evaluation of the dependency of the nucleation rate, J, on variables such as [H_2SO_4], [NH_3], [IONS], RH, T, etc. We have developed an accurate, automated method to determine the nucleation rate of critical clusters from the time evolution of the particle number concentration measured by each of the particle counters attached to the CLOUD chamber (CPC, DEG-CPC or PSM). Each particle counter is characterised by certain detection size threshold, d_{50}. To obtain the nucleation rates at the critical size, a correction is required to account for losses before the particles are eventually detected at size d_{50}. The losses occur due to wall-losses, coagulation and chamber air dilution. A Monte-Carlo model (AeroCLOUD) was developed to calculate these corrections numerically (Fig.1). The output of the model has been verified by comparison with experimental measurements made near to the critical size using the Particle Size Magnifier (PSM).

Since 2009, CLOUD has measured the nucleation rate of new particles over a broad range of conditions relevant for the atmosphere. Using measurements from multiple instruments that analyse the CLOUD chamber, we have derived an empirical J parametrisation that combines the measured J values with current theoretical understanding. The parametrisation is tuned using a nonlinear numerical Levenberg-Marquardt algorithm. The parametrisation successfully predicts all nucleation rates measured so far by CLOUD and is designed to be well-behaved when extrapolating outside the experimentally-explored region.

The CLOUD parametrisation is based on the most rigorous laboratory measurements of ion-induced and neutral atmospheric nucleation achieved so far, and so constitutes an important new tool for evaluating the global contributions of nucleation in atmospheric models such as GLOMAP (Dunne, E.M., et al., this conference).

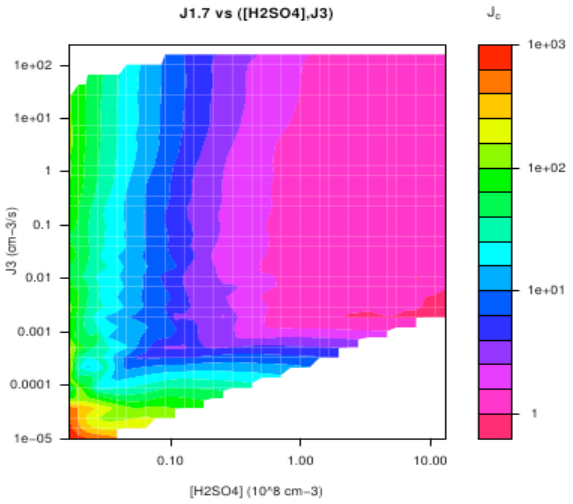

Figure 1. Example AeroCLOUD-calculated corrections for $J_{2.5}$ values (ie. detection with a 2.5nm-threshold CPC). The colour contours relate sulphuric acid concentration (x axis) and $J_{2.5}$ (y axis) with a correction factor that ranges from 1 (plotted in blue-magenta) for high [H_2SO_4] up to 1000 (plotted in orange-red) for low [H_2SO_4] and low $J_{2.5}$ values.

We would like to thank CERN for supporting CLOUD with important technical resources, and for providing a particle beam from the CERN Proton Synchrotron. This research has received funding from the EC's Seventh Framework Programme under the grant agreement no. 215072 (Marie Curie Initial Training Network "CLOUD-ITN"), from the German Federal Ministry of Education and Research (project no. 01LK0902A), and from the Swiss National Science Foundation, and from the Academy of Finland Center of Excellence Program (project no. 1118615).

Carslaw, K. (2009). Cosmic rays, clouds and climate. Nature, 460, 332-333.
Dunne, E.M., et al. (2011). The influence of ion-induced nucleation on atmospheric aerosols, this conference.

Influence of trimethylamine to sulphuric acid-water homogeneous nucleation

K. Neitola[1], D. Brus[1,3], M. Sipilä[2], T. Jokinen[2], P. Paasonen[2] and H. Lihavainen[1]

[1]Finnish Meteorological Institute, Erik Palménin aukio, P.O. Box 503, FI-00101 Helsinki, Finland
[2]Department of Physical Sciences, University of Helsinki, P.O.Box 64, FI-00101 Helsinki, Finland
[3]Laboratory of Aerosol Chemistry and Physics, Institute of Chemical Process Fundamentals Academy of Sciences of the Czech Republic, Rozvojová 135, CZ-165 02 Prague 6, Czech Republic
Keywords: homogeneous nucleation, sulphuric acid, amine, flow tube.
kimmo.neitola@fmi.fi

Sulphuric acid is known to play a key role in atmospheric nucleation (gas to particle conversion). The attention has shifted lately towards a third nucleating species (ammonia, amines) in addition to sulphuric acid and water. This is due to recent quantum chemical calculations that suggest a third species to thermodynamically stabilize sulphuric acid-water molecular clusters.

Flow tube technique was used to study homogeneous nucleation of sulphuric acid and water with and without the presence of trimethylamine (TMA) in 2 different relative humidities (30% and 50%). Sulphuric acid was produced using a thermally controlled cylinder which is half filled with pure (97%) sulphuric acid. Dry, particle free compressed air is flown through the saturator with constant flow rate (0.1 lpm) to saturate the flow with sulphuric acid vapour. The concentration is controlled by the temperature of the saturator. The sulphuric acid concentration was measured with CIMS (Petäjä et al., 2009) or APi-TOF (Junninen et al., 2010).

The concentration of nucleated particles was monitored with Particle Size Magnifier (PSM, Vanhanen et al., 2009). The size of the particles was measured with DMPS system (HAUKE DMA, UCPC, TSI model 3025A) in the range of 3 to 200 nm.

Five different concentration levels of TMA was used (170, 480, 800, 1700 and 3600 ppt) with sulphuric acid concentration range between 10^5 and $5 \cdot 10^7$ mol./cm^3. The flow tube was operated is several hours in same conditions to ensure stable state. TMA concentration was changed only after a full cycle of saturator temperatures (0-45^{o}C) was done for both RH's separately.

Figure 1 shows DMPS size distribution (upper panel) and total count (lower panel) data without TMA for one saturator temperature cycle at RH 30%. Figure 2 shows data from DMPS (upper panel) and PSM (lower panel) for exactly similar conditions as in figure 1, except the addition of TMA. The sizes of the particles are similar in both figures before adding TMA. After the addition of TMA the size decreases out of the DMPS size range and concentration of particles decreases to 1/3 of the original concentration. Increasing the RH to 50% increases the concentration temporarily but after stable state is achieved concentration is decreased to about 800 cm^{-3}.

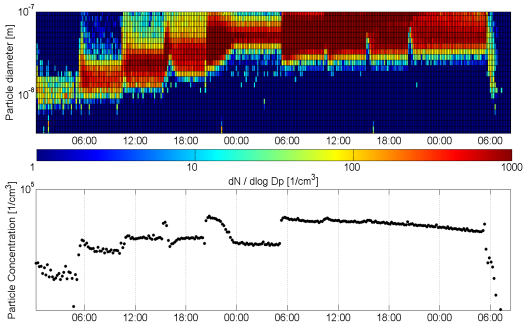

Figure 1. DMPS data for size distribution (upper panel) and total concentration (lower panel) for one saturator temperature cycle without TMA.

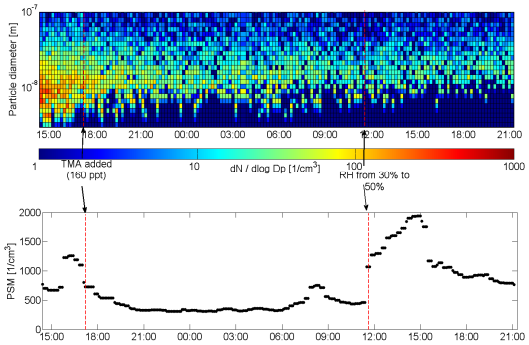

Figure 2. DMPS and PSM data over one cycle of saturator temperatures at RH 30% with lines when TMA (160ppt) was added and RH changed to 50%.

Results imply that TMA forms thermodynamically stable clusters with sulphuric acid with sizes below the detection limit of the PSM (~1.5 nm) suppressing the condensation of sulphuric acid to the surface of the particles and preventing the growth to detectable sizes. This was predicted by Anttila et al., (2005).

This work was supported by the Maj & Torr Nessling and KONE foundations.

Anttila T., et al., (2005), *Boreal Env. Res.*, **10**, 511-523.
Junninen, H., et al., (2010), *Atmos. Meas. Tech.*, **3**, 1039–1053.
Petäjä, T., et al., (2009), *Atmos. Chem. Phys.*, **9**, 7435-7448.
Vanhanen, J., et al., *18th International conference on Nucleation and Atmospheric Aerosols (ICNAA)*, Prague, Czech Republic (2009).

Monday, September 5, 2011

Session 2A: Bioaerosols

Bioaerosol analysis by a combined microarray / SERS (surface-enhanced Raman scattering) approach

K. R. Schwarzmeier, M. Knauer, R. Niessner, N. P. Ivleva and C. Haisch

Chair for Analytical Chemistry, Technische Universität München, Munich, D-81377, Germany
Keywords: Bioaerosols, Raman spectroscopy, SERS, microarray
Presenting author email: Christoph.Haisch@ch.tum.de

Bacterial contamination of indoor air is a serious threat to human health. Pathogenic germs can be transferred from the liquid to the aerosol phase for instance when the water is sprayed in air like in showers, air conditioners, or fountains. Existing analytical instruments for the of indoor air quality assessment and contamination monitoring are mostly time consuming as they generally require for a cultivation step. The need for a rapid, sensitive and selective detection method of bioaerosols is evident. We developed a new method, which allows for a direct measurement of the microorganisms.

Our approach is based on the combination of a commercial wet particle sampler (Coriolis µ, Bertin Technology, France), an immunologic capture of the specific microorganisms in the detection liquid and a consecutive detection, characterization, and quantification by surface-enhanced Raman scattering (SERS). The bacteria are impinged and collected into PBS buffer by the Coriolis µ sampler. The sampling liquid is pumped in a closed flow system over a microarray chip. Antibodies against the targeted microorganisms are bound to the surface of the chip (Fig. 1). They selectively collect the microorganisms from the liquid and immobilize them on the surface.

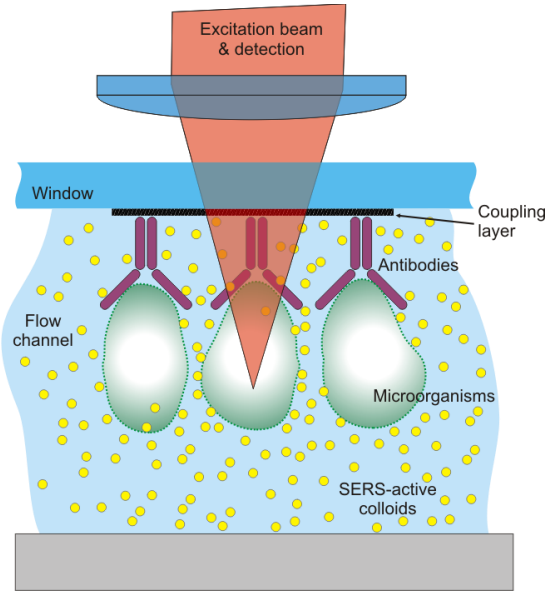

Figure 1. Principle of the SERS detection and characterization.

Quantification of the collected samples is carried out by SERS. The flow cell is installed underneath a Raman microscope, which stepwise scans over the chip surface. Quantification is not based on the signal intensity, but on the number of surface positions, where microorganisms are bound This approach was already demonstrated successfully for the detection of bacteria in water (Knauer *et al.* 2010a). The SERS effect is achieved by adding silver colloids into the flow system. It amplifies the signals by several orders of magnitude. Additionally, the information content of the spectra is increased by the chemical and electromagnetic interaction between the microorganism and the silver colloids (Knauer *et al.* 2010b).

The first tests of the system were carried out by placing the sampler onto, or alternatively into an aerosol chamber with a volume of 1 m^3. These first experiments we carried out with heat-inactivated E. coli and legionella bacteria. The bacteria were dispersed by a cross-flow nebulizer and depending on the experimental conditions, directly or after drying and discharging, lead into the chamber. Knowing the bacteria concentration in the dispersed liquid and its volume, the particle number concentration in the chamber could be calculated. Additionally, an Aerodynamic Particle Sizer (APS, model 3310a, TSI Inc., USA) was employed for reference analysis. Measurements in the chamber were carried out primarily in particle-free air, for later experiments, room air with a typical particle number concentration of about $6 \cdot 10^4$ cm^{-3} was in the chamber to simulate natural background contamination.

From these preliminary results we can deduce that a minimum number concentration of about 10^4 particles/m^3 can be detected by our system. Furthermore, we did not observe a significant influence of the natural background by ambient air in the lab on our measurements.

We believe that this combined approach has several advantages. The wet sampling by Coriolis effect is a rather efficient sampling approach for bioaerosols. Selective binding of the specific target microorganisms by the antibody reduced the analysis time significantly, particularly in case of high-load samples, as the SERS measurement of non-targeted particles is avoided. The SERS analysis, finally, reveals highly specific information on the collected organisms, which may even surpass the specificity of the antibody collection. Compared to conventional immunological microarray readout, SERS does not require for laborious labelling steps, and the SERS amplification allows for short measuring times.

(a) Knauer, M., Ivleva, N. P., Liu, X., Niessner, R. and Haisch, C. (2010) *Anal. Chem.* **82** 2766-2772.
(b) Knauer, M., Ivleva, P. N., Niessner, R. and Haisch, C. (2010) *Anal. Sci.* **26,** 761-766.

Assessment of bacterial and fungal aerosol in hospital air

Viswanath Mula[1], Zaheer Ahmad Nasir[2], Ian Colbeck[2], Mark Loeffler[1]

[1]NHS Colchester Hospital University
[2]Department of Biological Sciences, University of Essex, Colchester, CO4 3SQ, U K

Keywords: bioaerosols, size distribution, hospitals

Airborne nosocomial infections in health care settings are often related to aerobiological sources. In order to reduce the dispersion of airborne biological particles in hospitals various air control measures are in practice and monitoring of airborne microorganism is generally carried out during epidemic outbreaks. However the regular assessment of microbial load in hospital air, especially in operation theatres, is of great importance to assess, not only, the air control efficiency but also to identify any introduction of airborne pathogens. This study aims to assess the levels of airborne bacteria and fungi in two different types of orthopaedic theatres (with and without laminar flow), a general ward and outdoors. The sampling was carried out with an Anderson 6 stage viable impactor over a period of 8 weeks. In both the theatres samples were collected in the morning and evening, while the samples in the ward and outdoors were taken at noon. The sampler was loaded with six Petri dishes containing either malt extract agar (Oxoid, UK), Nutrient agar (Oxoid, UK), or MacConkey Agar (Oxoid, UK), prior to sampling and the sampling interval was 5 minutes.

The highest mean concentration of total bacteria was found outdoors (1375 CFU/m^3) followed by the general ward (1265 CFU/m^3), an orthopaedic operation theatre without laminar flow (141 CFU/m^3) and an orthopaedic operation theatre with laminar flow (82 CFU/m^3). In general, higher concentrations were found in the operation theatre without laminar flow than the operation theatre with laminar flow. With reference to gram negative bacteria, the general ward had the highest mean concentration (130 CFU/m^3) followed by outdoors (91 CFU/m^3 at 20°C) and the operation theatre without laminar flow (2 CFU/m^3). No gram negative bacteria were detected in operation theatre with laminar flow. Similar to bacteria, the higher concentration of fungi was present outdoors and in the general ward as compared to the operation theatres. The mean concentration of fungi outdoors and in the general ward was 1318 CFU/m^3 and 1062 CFU/m^3, respectively. In the operation theatres the concentrations were higher in the evening than the morning. The mean concentration of fungi in operation theatres without laminar flow and with laminar flow, during morning and evening, was 22 CFU/m^3 and 38 CFU/m^3, 5 CFU/m^3 and 80 CFU/m^3, respectively (Table 1).

Table. 1 Mean, standard deviation, and % of less than 4.7μm of total culturable bacteria, gram –ve bacteria and fungal aerosol in different settings in a hospital.

OOT(M)	Bacteria (20°C)	Bacteria (30°C)	Gram -ve Bacteria	Fungi
Mean	141	49	2	22
St Dev.	119	31	6	27
% < 4.7μm	27	39	0	58
OOT(E)				
Mean	82	77	0	38
St Dev.	33	52	0	46
% < 4.7μm	44	58	0	54
LFOOT(M)				
Mean	25	110	0	5
St Dev.	38	227	0	9
% < 4.7μm	69	71	0	65
LFOOT(E)				
Mean	82	11	0	80
St Dev.	91	16	0	179
% < 4.7μm	53	46	0	12
Gen. Ward				
Mean	1265	1197	130	1062
St Dev.	836	775	92	1386
% < 4.7μm	76	73	83	72
Outdoor				
Mean	1375	1190	91	1318
St Dev.	1405	1400	59	1858
% < 4.7μm	66	72	81	77

OOT(M) Orthopaedic Operation Theatre without laminar flow (Morning), OOT(E) Orthopaedic Operation Theatre without laminar flow (Evening), LFOOT(M) Laminar Flow Orthopaedic Operation Theatre (Morning), LFOOT(E) Laminar Flow Orthopaedic Operation Theatre (Evening), Gen. Ward (General Ward).

Overall, lower concentrations of airborne microorganisms were found in the laminar flow theatre than non laminar flow theatre. However these levels were higher than suggested levels by The Department of Health. The concentrations in the ward were slightly lower than outdoors. This study not only provides an insight to microbial load of hospital air but also draws attention to the need of regular air sampling in heath care facilities in order to check that various systems and procedures to reduce microbial load are working effectively. Appropriate heating and ventilation systems, effective infection-control procedures and surveillance systems hold the key to limit airborne microbial load in hospitals.

Bioaerosols in the Earth System: Sources, Interactions and Effects

U. Pöschl

Max Planck Institute for Chemistry, Biogeochemistry Department, Mainz 55128, Germany

Keywords: PBAP, bioprecipitation, diversity, emission and transport, measurement and modeling
Presenting author email: u.poschl@mpic.de

Bioaerosols consisting of primary biological particles such as bacteria, spores and pollen are essential for the spread of organisms in the biosphere, and numerous studies have suggested that they may be important for atmospheric processes, including the formation of clouds and precipitation.

However, the sources and diversity, atmospheric abundance and transport, physicochemical properties and transformation of bioaerosols, including their activity as cloud condensation and ice nuclei (CCN, IN), are not well characterized. Thus, their actual influence on the evolution, present state and future development of the Earth system, the hydrological cycle and other biogeochemical cycles is poorly constrained.

Figure 1 illustrates the cycling of aerosols and water over pristine rainforest (bioprecipitation cycle) as observed during the wet season in the Amazon basin. Secondary organic aerosols (SOA) formed by photo-oxidation of volatile organic compounds (VOC) and primary biological aerosols (PBA) emitted from biota in the rainforest (plants and microorganisms) serve as CCN and IN, which induce warm or cold rain formation, precipitation, and wet deposition of gases and particles.

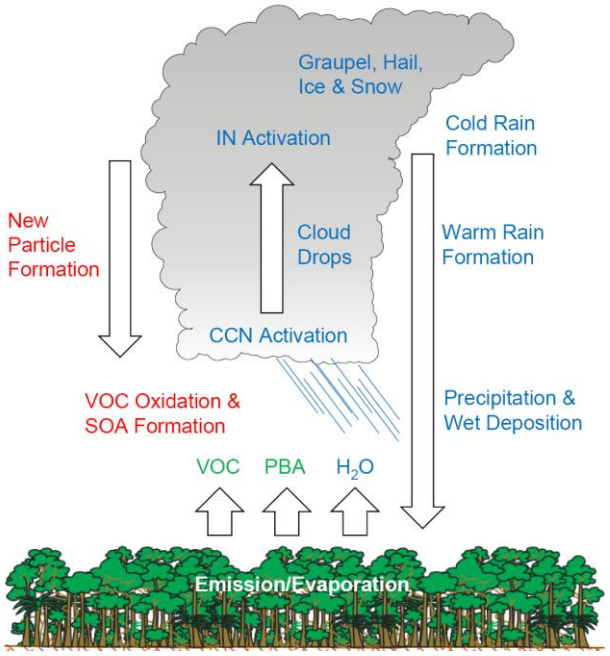

Figure 1. Aerosol and water cycle over pristine rainforest (Pöschl et al., 2010).

Clearly, bioaerosols are an important element of the Earth system. Their abundance and diversity, regional and temporal variability, and responses and feedbacks to climate change, however, are hardly quantified and not yet well understood.

The current state of knowledge of bioaerosol sources, interactions and effects will be outlined, recent advances will be presented and discussed, and major challenges and perspectives of future research will be explored.

Bowers, R. M., Lauber, C. L., Wiedinmyer, C., Hamady, M., Hallar, A. G., et al. (2009) Appl. Environ. Microbiol. 75, 5121-5130.

Burrows, S. M., Elbert, W., Lawrence, M. G., and Pöschl, U. (2009) Atmos. Chem. Phys., 9, 9263-9280.

Burrows, S. M., Butler, T., Jöckel, et al. (2009) Atmos. Chem. Phys., 9, 9281-9297.

Christner, B.C., Morris, C. E., Foreman, C.M., Cai, R.M., Sands, D.C. (2008) Science, 319, 1214-1214.

Deguillaume, L., Leriche, M., Amato, P., et al. (2008) Biogeosciences, 5, 1073-1084, 2008.

Elbert, W., Taylor, P. E., Andreae, M. O., Pöschl, U. (2007) Atmos. Chem. Phys., 7, 4569–4588.

Fröhlich-Nowoisky, J., Pickersgill, D. A., Despés, R. V., Pöschl, U. (2009) Proc. Natl. Acad. Sci., 106, 12814-12819.

Gabey, A. M., Gallagher, M. W., Whitehead, J., Dorsey, J. R., et al. (2010) Atmos. Chem. Phys., 10, 4453-4466.

Heald, C. and Spracklen, D. (2009) Geophys. Res. Lett., 36, doi:10.1029/2009GL037493.

Huffman, J. A., Treutlein B. and Pöschl, U. (2010) Atmos. Chem. Phys., 10, 3215-3233, 2010.

Möhler, O., DeMott, P. J., Vali, G., and Levin, Z. (2007) Biogeosciences, 4, 1059-1071.

Pöschl, U. (2005) Angew. Chem. Int. Ed., 44, 7520-7540.

Pöschl, U., Martin, S. T., Sinha, B., et al. (2010) Science, 429, 1513-1516, 2010.

Pratt, K. A., DeMott, P. J., French, J. R., Wang, Z., Westphal, D. L., et al. (2009) Nature Geosci., 2, 398-401.

Prenni, A. J., Petters, M. D., Kreidenweis, S. M., et al. (2009) Nature Geosci., 2, 6, 401-404.

Sesartic, A., Lohmann, U., and Storelvmo, T. (2011) Atmos. Chem. Phys. Discuss., 11, 1457–1488.

Womack, A. M., Bohannan, B.J.M., Green, J.L. (2010) Phil. Trans. R. Soc. B 365, 3645–3653.

Pollen are efficient cloud condensation nuclei

F.D. Pope[1], J.-S. Borlace[1], P.T. Griffiths[2], P.J. Gallimore[1] and M. Kalberer[1]

[1]Department of Chemistry, University of Cambridge, Cambridge, CB2 1EW, UK
[2]Department of Geography, University of Cambridge, Cambridge, CB2 3EN, UK
Keywords: bioaerosols, CCN, single particle analysis, ESEM.
Presenting author email: fdp21@cam.ac.uk

The hygroscopicity of various pollen species of different phylogenies has been studied. Species investigated include the following genera: Artemisia, Betula, Cryptomeria, Iva, Juglans, Kochia, Narcissus, Salix, and Secale (Pope, 2010). The single pollen grains were investigated using both the electrodynamic balance (EDB) and environmental scanning electron microscope (ESEM) methodologies.

This is the first study to fully characterise the response of pollen mass, size and morphology to increases in environmental relative humidity. It was previously known that pollen grains swell internally at high humidity. The use of the EDB, in this study, quantified the mass growth of the pollen with respect to the environmental relative humidity. All investigated pollen grains exhibited remarkably similar hygroscopicities, with a mass increase of ~16% at 75% relative humidity when compared to dry conditions.

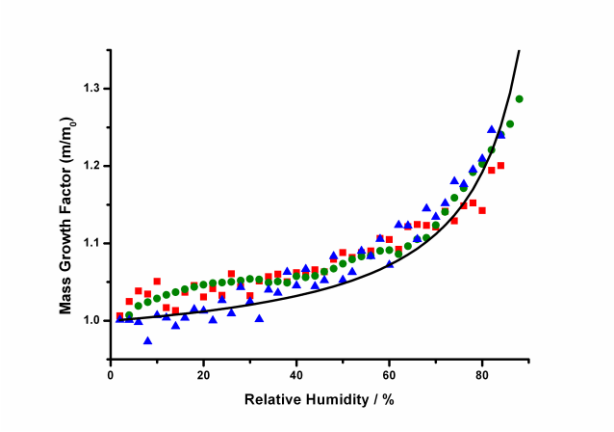

Figure 1. Humidograms of three pollen types measured in the EDB apparatus. Symbols: Red square – Narcissus, Green circle – Salix, Blue triangle – Betula. Line – modelled average humidogram of the three pollen species using κ-Köhler theory.

Studies using the ESEM indicate that the surface of the pollen grain is wettable, and so at least in part, some of the water uptake by the pollen grain is taken up externally. Low temperature studies in the ESEM investigated the ice nucleation ability of pollen via depositional freezing.

The hygroscopic response of the pollen to subsaturated relative humidities is parameterised using kappa-Köhler theory (Petters and Kreidenweis, 2007). It is found that whilst the pollen grains are only moderately hygroscopic, with kappa parameters = 0.05 – 0.1, their large size can allow activation at critical supersaturations of 0.001% and lower, and thus pollen will readily act as cloud condensation nuclei.

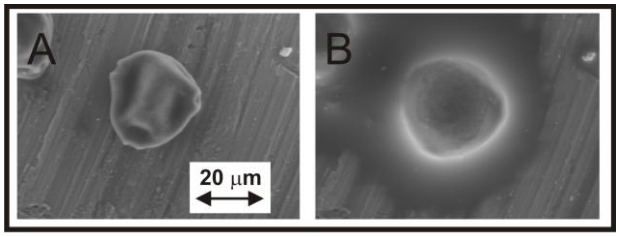

Figure 2. ESEM images of Betula occidentalis pollen at 68% (A) and 96% (B) relative humidity. Notice the internal swelling and external wetting of the particle in the high humidity environment.

The number density of pollen is too low to represent a significant global source of cloud condensation nuclei. However, the large sizes of pollen suggest that they will be an important source of giant cloud condensation nuclei (Johnson, 1982). By quantifying their size in a supersaturated environment, this study allows the effect of pollen, either as activated or as interstitial particles, on the autoconversion processes to be quantified. Current work is involved in incorporating the laboratory determined range of pollen critical supersaturations and hygroscopicities into a cloud resolving model. This will allow for the global and regional significance of this biospheric/atmospheric interaction to be assessed.

Pope, F.D. (2010) Environmental Research Letters, 5(4), 044015.
Petters, M.D. and Kreidenweiss, S.M. (2007) Atmospheric Chemistry and Physics. 7, 1961.
Johnson, D.B. (1982) Journal of Atmospheric Science, 39, 448.

Development of a Lightweight, Simple and Efficient Exhaled Breath Condensate Collection Device and Method

Zhenqiang Xu and Maosheng Yao*

Principal Contact: Maosheng Yao, Professor, State Key Joint Laboratory for Environmental Simulation and Pollution Control, College of Environmental Sciences and Engineering, Peking University, Beijing 100871, China, Ph: +86 010 6276 7282, Email: yao@pku.edu.cn,

Abstract

Exhaled breath condensate (EBC) is increasingly being used as a non-invasive method for disease diagnosis in clinical settings. However, current available collectors often appear to be heavy, complex and to take longer time to get adequate amount of EBC. Here, a portable EBC collection device and method were developed and tested. The device consists four major parts: a trapezoidal cover with a round air inlet, a cuboid box, ultra-low temperature treated hydrophobic parafilm, and a layer of ice. During the EBC collection, the layer of ice was first placed onto the bottom of the cuboid box, followed by the hydrophobic parafilm, then tightly covered with the trapezoidal cover. In this study, seven volunteers were selected to exhale toward the device using a sterilized straw inserted into the air inlet of the trapezoidal cover for 5 min. The collected EBC appeared to be small water droplets formed on the surface of hydrophobic parafilm. When collecting the EBC, the trapezoidal cover was removed, and 10 μl of deionized water was pipetted onto the parafilm surface. Using a pipette tip, the deionized water drop was dragged over entire parafilm surface.

Due to the hydrophobic nature of the surface, the collected EBC on the surface was scavenged into the deionized water droplet, finally forming a droplet of 40-80 μl. The collected EBC was then analyzed using both culturing method and polymerase chain reaction (PCR) for culturable and total bacterial concentrations, respectively. Results indicated that the culturable bacterial concentrations ranged from 400 to 4000 CFU/ml with an average of 1452 CFU/ml of the EBC collected. Preliminary PCR tests showed that the EBC collected from some volunteers appeared to be bacteria positive with cycle threshold values of 20-26 with a bacterial DNA concentration of 0.5 to 1.5 ng/μl. While, for some volunteers the EBC was tested not positive, which was likely due to the inhibition problems. In this study, a simple and fast EBC collection device and method were developed and demonstrated. However, sample purification method needs to be developed for post-sample analysis using a variety of techniques for different bio-markers in diverse clinical settings. The developed EBC collection device and method would have great application potentials in early disease screening and diagnosis.

Keywords : Exhaled Breath Condensate, Hydrophobic Parafilm, Bacteria, Cultuirng, PCR

Allergens from Birch, Grass and Olive in ambient air deviate from pollen counts across Europe: the EU-HIALINE project

J.T.M. Buters[1] and the HIALINE working group[2]

[1] Division of Environmental Dermatology and Allergology, Helmholtz Zentrum München/TUM, ZAUM - Center for Allergy and Environment, Technische Universität München, Munich, Germany

[2] M. Thibaudon, France, M. Smith, United Kingdom, C. Galan, Spain, R. Brandao and C. Antunes, Portugal, L. Grewling and A. Uruska, Poland, G. Reese and B. Weber, Germany, A. Rantio-Lehtimäki and M. Sofiev, Finland, S. Jäger and U. Berger, Austria, I. Sauliene, Lithuania, R. Albertini and L. Cecchi, Italy

Keywords: biogenic particles, health effects of aerosols, outdoor aerosols, PM10, PM2.5, allergens.

Background The developed world is confronted with an epidemic of allergic diseases. Allergic disease is now affecting 20% of the European population, up from 3% in the 1950`s. Exposure to allergens is one of several factors determining allergic disease and symptoms in individuals. The major aeroallergens in Europe originate from house dust mite, grass, cat, birch and olive (in this sequence). Of these, all outdoor allergens stem from pollen. Exposure to aeroallergens from pollen is assessed by counting pollen in ambient air. However, several publications show that pollen count is not representative for allergen exposure[1], and allergen from pollen could be influenced by climate change independently from pollen numbers. We therefore monitored simultaneously pollen count and the major allergens from pollen in different size fractions of ambient air in 10 countries in the EU-HIALINE (Health Impacts of Airborne Allergen Information Network).

Methods Ambient air was sampled at 800l/min with a Chemvol high-volume cascade impactor equipped with stages PM>10µm, 10 µm>PM>2.5µm, and in Munich also 2.5 µm>PM>0.12µm. The polyurethane impacting substrate was extracted with 0.1M NH_4HCO_3, pH8.1. The major pollen allergens from birch Bet v 1, grass Phl p 5 and olive Ole e 1 were determined with allergen specific ELISA´s. Pollen counts were assessed with Burkard pollen traps.

Results We measured that we collected >99% of the airborne allergen in PM larger than 2.5µm. Our quality control showed that using antibodies as a detection method (ELISA) a 20-25% interassay-variation across Europe was observed. Pollen from birch correlated acceptable with allergen release for birch pollen (r^2 about 0.7). In contrast, pollen from grass released >100-200% more Phl p 5 in France and the UK than in other countries in Europe. In detail we could show that allergen release form all pollen depended strongly on the day, with days with very potent pollen being flanked by days with a weak allergen release. For olive, large amounts of allergen we detected at the end of the season when few pollen were airborne.

The effect of climate on allergen release is currently being evaluated by a computer simulation program SILAM of the Finnish Meteorological Institute. Aim is to determine which climatic factor influences allergen release.

Conclusions Aeroallergens were only found in PM>2.5µm, the fraction containing pollen. Pollen from different years, different trees, even different days and different countries could release up to 10-fold different amounts of allergen from the same amount of pollen. Thus exposure to allergen is poorly monitored by only monitoring pollen count. We think that monitoring the allergens itself in ambient air might be an improvement in allergen exposure assessment. In addition, airborne allergens could be a better indicator of climate change than pollen flight.

The research leading to these results has received funding from the EU public health project from the Executive Agency for Health and Consumers under grant agreement No 2008 11 07 and funding from Christine Kühne - Center of Allergy Research and Education-Munich (CK-CARE A).

[1.] Buters JTM, Weichenmeier I, Ochs S, Pusch G, Kreyling W, Boere AJ, W. Schober and H.

Behrendt. The allergen Bet v 1 in fractions of ambient air deviates from birch pollen counts. Allergy 65:850-8, 2010 .

Development of a Lightweight, Simple and Efficient Exhaled Breath Condensate Collection Device and Method

Zhenqiang Xu and Maosheng Yao*

Principal Contact: Maosheng Yao, Professor, State Key Joint Laboratory for Environmental Simulation and Pollution Control, College of Environmental Sciences and Engineering, Peking University, Beijing 100871, China, Ph: +86 010 6276 7282, Email: yao@pku.edu.cn,

Abstract

Exhaled breath condensate (EBC) is increasingly being used as a non-invasive method for disease diagnosis in clinical settings. However, current available collectors often appear to be heavy, complex and to take longer time to get adequate amount of EBC. Here, a portable EBC collection device and method were developed and tested. The device consists four major parts: a trapezoidal cover with a round air inlet, a cuboid box, ultra-low temperature treated hydrophobic parafilm, and a layer of ice. During the EBC collection, the layer of ice was first placed onto the bottom of the cuboid box, followed by the hydrophobic parafilm, then tightly covered with the trapezoidal cover. In this study, seven volunteers were selected to exhale toward the device using a sterilized straw inserted into the air inlet of the trapezoidal cover for 5 min. The collected EBC appeared to be small water droplets formed on the surface of hydrophobic parafilm. When collecting the EBC, the trapezoidal cover was removed, and 10 μl of deionized water was pipetted onto the parafilm surface. Using a pipette tip, the deionized water drop was dragged over entire parafilm surface.

Due to the hydrophobic nature of the surface, the collected EBC on the surface was scavenged into the deionized water droplet, finally forming a droplet of 40-80 μl. The collected EBC was then analyzed using both culturing method and polymerase chain reaction (PCR) for culturable and total bacterial concentrations, respectively. Results indicated that the culturable bacterial concentrations ranged from 400 to 4000 CFU/ml with an average of 1452 CFU/ml of the EBC collected. Preliminary PCR tests showed that the EBC collected from some volunteers appeared to be bacteria positive with cycle threshold values of 20-26 with a bacterial DNA concentration of 0.5 to 1.5 ng/μl. While, for some volunteers the EBC was tested not positive, which was likely due to the inhibition problems. In this study, a simple and fast EBC collection device and method were developed and demonstrated. However, sample purification method needs to be developed for post-sample analysis using a variety of techniques for different bio-markers in diverse clinical settings. The developed EBC collection device and method would have great application potentials in early disease screening and diagnosis.

Keywords : Exhaled Breath Condensate, Hydrophobic Parafilm, Bacteria, Cultuirng, PCR

Monday, September 5, 2011

Session 2B: New Particle Formation 1: *Chamber Studies*

Measurements of ions and ion clusters in the CLOUD chamber nucleation events by mass spectrometry

S. Schobesberger[1], A. Franchin[1], H. Junninen[1], M. Ehn[1,2], K. Lehtipalo[1], S. Gagné[1], T. Nieminen[1], the CLOUD collaboration, M. Kulmala[1], and D.R. Worsnop[1,3]

[1]Department of Physics, University of Helsinki, Helsinki, FI-00014, Finland
[2]Forschungszentrum Jülich GmbH, Jülich, 52425, Germany
[3]Aerodyne Research, Inc., Billerica, MA 01821-3976, USA
Keywords: nucleation, sulfuric acid, cluster ions, mass spectrometry.
Presenting author email: siegfried.schobesberger@helsinki.fi

Several proposed mechanisms link solar variability with changes in the climate through effects of cosmic rays on weather, aerosols and clouds (Carslaw *et al.*, 2002). However, the details, as well as the significance, of those mechanisms remain unclear.

The CLOUD (Cosmics Leaving OUtdoor Droplets) experiment aims at understanding the possible influence of cosmic rays on aerosol particles and clouds. It provides exceptionally clean and well-defined experimental conditions in an aerosol chamber of 26.1 m^3, together with the possibility of simulating cosmic rays "on demand" by making use of the CERN Proton Synchrotron's particle beam.

It has been well established that nucleation from gaseous precursors form an important source of particles in the atmosphere, and that sulfuric acid (H_2SO_4) plays a crucial role in atmospheric nucleation (e.g. Kulmala *et al.*, 2004, and Riipinen *et al.*, 2007). Hence, the focus was on the investigation of sulfuric acid nucleation under different conditions (e.g. varying beam intensity, concentrations of ammonia (NH_3), relative humidity, etc.).

The APi-TOF (Atmospheric Pressure interface Time-Of-Flight Mass Spectrometer) is a high-resolution mass spectrometer produced by Tofwerk AG, and Aerodyne Research, Inc. It is described in detail by Junninen *et al.* (2010). Sampling occurs from atmospheric pressure through a critical orifice. While passing through differentially pumped chambers, the sampled ions are focused and guided to the mass spectrometer. Note that no ionization of the sampled aerosol was performed, and only naturally charged ions are detected by this setup.

In the course of the experiments, sulfuric acid nucleation events were produced in the chamber. Depending on conditions, nucleation occurred either mainly by negative ions, or mainly by ions of both polarities. During those nucleation events, the ion species registered by the APi-TOF were almost exclusively sulfur-containing compounds or molecular clusters in both polarities. Their composition could be determined based on their exact masses and isotopic patterns, facilitated by the cleanliness of the chamber. Growing clusters of negative and positive polarity could be observed at a time resolution of less than 1 minute, starting at the single ion, up to 3300 Da (corresponding to mobility equivalent diameters of around 2 nm). The identified cluster ions were found to always contain H_2SO_4. Depending on the exact experimental conditions, they also contained NH_3, organic compounds (mainly amines), or both. A part of a typical spectrum during one experiment is shown in Figure 1. The appearance of the larger clusters coincides with the onset of particle formation as detected by other instruments. Clear correlations can be found between features of the steady-state cluster distributions and experimental variables, giving detailed insights into the early steps of new (charged) particle formation driven by sulfuric acid.

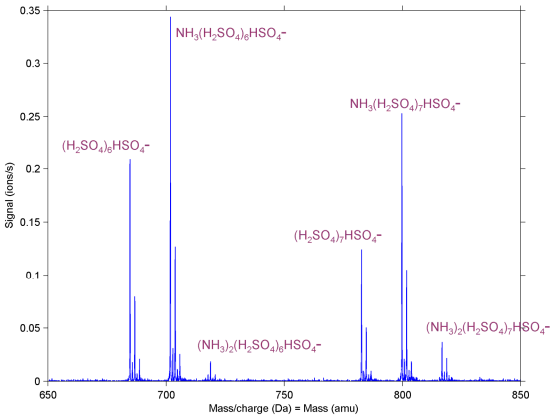

Figure 1. Part of a typical negative ion spectrum, and interpretations for the largest signals in this section.

We thank CERN for supporting CLOUD with important technical resources, and for providing a particle beam from the PS. This research was funded by the EC's 7th Framework Programme (grant agreement number 215072: Marie Curie Initial Training Network "CLOUD-ITN"), the German Federal Ministry of Education and Research (project number 01LK0902A), the Swiss National Science Foundation, and the Academy of Finland Center of Excellence program (project number 1118615).

Carslaw, K. S., *et al.* (2002). *Science*, 298, 1732
Junninen, H., *et al.* (2010). *Atmos. Meas. Tech.*, 3, 1039–1053.
Kulmala, M., *et al.* (2004). *J. Aerosol Sci.*, 35, 143-176.
Riipinen, I., *et al.* (2007). *Atmos. Chem. Phys.*, 7, 1899–1914.

Early stage particle growth rates during the CLOUD experiment

Riccobono, Francesco[1], Weingartner, Ernest[1], Baltensperger, Urs[1], and the CLOUD collaboration

[1]Laboratory of Atmospheric Chemistry, Paul Scherrer Institut, CH-5232 Villigen PSI, Switzerland

Keywords: ion-induced nucleation, growth, CLOUD

Formation of atmospheric aerosol has been observed in a wide range of atmospheric conditions in many different locations and altitudes all over the globe (Kulmala *et al.*, 2004). Nucleation and subsequent condensational growth increase the total number of particles and modify the aerosol size distribution in the atmosphere, affecting the global radiation balance through both direct and indirect effects. Among the various nucleation mechanisms that occur in the atmosphere the ion induced nucleation mechanism is still poorly understood. One of the goals of the CLOUD experiments at CERN is to investigate to what extent the presence of ions in the atmosphere affects the formation of new particles (Kirkby, 2007).

Almost 200 experiments have been performed in the CLOUD aerosol chamber at CERN during the fall 2010 campaign. The CERN Proton Synchrotron provided an adjustable and precisely measurable beam of artificial cosmic rays, spanning the atmospheric ionization range from the upper troposphere to ground level (Kirkby *et al.*, 2011, submitted). Several particle formation events were observed following both neutral and charged pathways with a wide range of nucleation rates and growth rates at sulfuric acid concentrations comprised between 10^6 and 10^9 molecules per cm^3.

The early growth rates of the freshly nucleated particles determine which fraction of these particles can grow to CCN sizes and which fraction is lost by coagulation with larger pre-existing aerosol. In order to study the growth rate in different size ranges as function of the gas and ion concentrations we optimized different instruments. The Scanning Mobility Particle Sizer (SMPS) provides an accurate mean diameter measurement down to ~7 nm, but for particles smaller than this size the SMPS suffers from a poor size resolution due to the extremely low charging probability and to the high particle diffusion losses in the charger and in the DMA column. To retrieve the size information in the 2-10 nm size range we developed the Laminar Diffusion Tube (LDT). This instrument uses the 1.2 meter long sampling line of the CLOUD chamber as a diffusion tube, in which the particles are lost to the walls by diffusion as a function of the sample flowrate and of the particle diameter. Downstream of the LDT the particle concentration is determined with a Condensation Particle Counter (CPC, TSI 3786). By varying the flow rate through the sampling line (by changing the make-up air) the losses are controlled according to laminar diffusion theory.

In a next step, the mean diameter of the particle size distribution of particles with ~2 < *D* < ~10 nm is retrieved by a comparison of the diffusion losses at different make-up flow rates. This calculation does not require any assumption on the shape of the particle size distribution. Another advantage is that it does not depend on the specific detection efficiency curve of the CPC, it only assumes that the diffusion losses in the LDT do not depend on the particle composition.

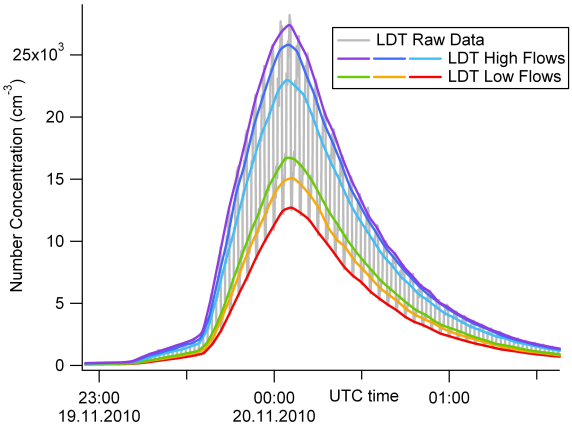

Figure 1. Laminar Diffusion Tube output during CLOUD run 318. The color curves correspond to different make-up flow rates and thereby different effective detection thresholds.

Growth rates enhancement factors obtained with the Laminar Diffusion Tube will be presented for various sets of gases (H2SO4, NH3) and ion concentrations.

Acknowledgments: We would like to thank CERN for supporting CLOUD with important technical resources, and for providing a particle beam from the CERN Proton Synchrotron. This research has received funding from the EC's Seventh Framework Programme under grant agreement number 215072 (Marie Curie Initial Training Network "CLOUD-ITN"), from the German Federal Ministry of Education and Research (project number 01LK0902A), from the Swiss National Science Foundation, and from the Academy of Finland Center of Excellence program (project no. 1118615).

Kulmala, M. et al. (2004). *J. Aerosol Sci.*, 35, 143-176.
Kirkby, J. (2007). *Surv. Geophys.*, 28, 333-375.
Kirkby, J. et al. (2011), submitted.

Modelling of ion-induced binary nucleation in the CERN CLOUD experiment

S. Ehrhart[1], L. Ickes[1], J. Kazil[2,3], K. D. Froyd[3], E. R. Lovejoy[3], J. Curtius[1] and the CLOUD collaboration
[1] Institute for Atmospheric and Environmental Sciences, Goethe University, Frankfurt am Main, Hessen, Germany
[2] CIRES, University of Colorado, Boulder, Colorado, USA
[3] NOAA Earth System Research Laboratory, Boulder, Colorado, USA
Keywords: nucleation modelling, ion induced nucleation, CLOUD experiment.
Presenting author email: ehrhart@iau.uni-frankfurt.de

A potential connection between cosmic ray intensity, low cloud cover and climate has been postulated (Marsh and Svensmark, 2000; Carslaw *et al*, 2002; Kirkby, 2007). Ion-induced nucleation could be the mechanism to explain such a connection due to the increased ion-production by galactic cosmic rays. Therefore a better understanding of nucleation mechanisms in general and ion induced nucleation as special case is of crucial importance.

To improve the scientific knowledge about ion-induced nucleation, the CLOUD-project (Cosmics Leaving OUtdoor Droplets) was established at CERN (European Organization for Nuclear Research). The experimental setup consists of an aerosol chamber into which a beam of particles is sent from a Proton Synchrotron to investigate the effects of ions on the aerosol production under controlled laboratory conditions. The chamber itself provides a nearly perfectly clean environment. Concentrations of possible third nucleation agents are almost negligible or are controlled in order to study these.

We modelled the binary sulphuric acid/water nucleation processes in the CLOUD-chamber based on earlier work (Lovejoy *et al*, 2004; Kazil, J., and Lovejoy, E. R., 2007). The models are based on uptake and loss of single sulphuric acid molecules and therefore span a range from a single molecule to particles with a few nanometer size. The special conditions of a chamber experiment makes certain adjustments to the model necessary for instance the main source of losses is the chamber wall. We present results for both steady state conditions and time evolution of nucleation processes. For the time evolution of nucleation we integrate the rate laws numerically using a similar approach to that of Lovejoy *et al*. The steady state solution is calculated with a direct iteration method, which is designed to be suitable to be extended to ternary systems.

The rate constants for charged nucleation are based on laboratory measurements, ab initio results and a smooth parameterisation to bulk phase properties as the particle size increases (Lovejoy te al, 2004). Neutral rate constants are currently based on the liquid drop model with corrections terms. These terms can be optimized with pure binary nucleation experiments. With appropriate parameterisation of neutral nucleation rates we expect to extend the current understanding of transitions from gas to condensed matter.

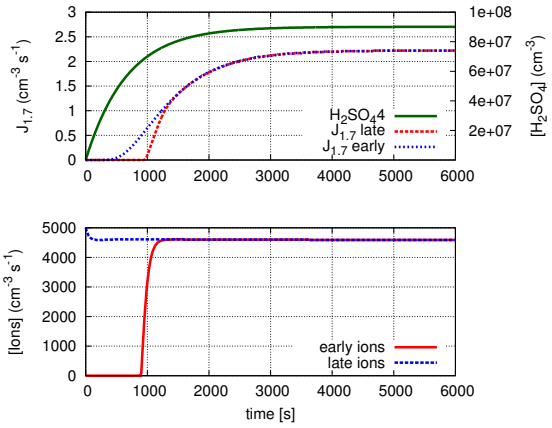

Figure 1: An example model result showing $J_{1.7nm}$ vs time (upper plot) with different starting concentrations of ions (lower plot). The sulphuric acid is shown as function of time (upper plot).

We would like to thank CERN for supporting CLOUD with important technical resources, and for providing a particle beam from the CERN Proton Synchrotron. This research has received funding from the EC's Seventh Framework Programme under grant agreement no. 215072 (Marie Curie Initial Training Network "CLOUD-ITN"), from the German Federal Ministry of Education and Research (project no. 01LK0902A), from the Swiss National Science Foundation, and from the Academy of Finland Center of Excellence program (project no. 1118615).

Marsh, N. D., and Svensmark, H. (2000) Physical Review Letters, **85**, 5004-5007.

Carslaw, K. S. et al (2002) Science, **298**, 1732-1737.

Kirkby, J. (2007) Surveys in Geophysics, **28**, 333-375.

Lovejoy, E. R., Curtius, J. and Froyd K. D. (2004) J. Geophys. Res. - Atmospheres, **109**, D08204.

Kazil, J., and Lovejoy, E. R. (2007) Atmos. Chem. Phys., **7**, 3447-3459.

Numerical simulation of H2SO4 cycle and new particle formation in the Cern CLOUD chamber

J. Voigtländer[1], F. Stratmann[1], and the CLOUD collaboration

[1]Leibniz Institute for Tropospheric Research, Leipzig, Germany
Keywords: CLOUD-ITN, cloud chamber, modelling, mixing state, sulphuric acid, particle formation
Presenting author email: jensv@tropos.de

To study the effect of galactic cosmic rays on aerosols and clouds, the Cosmic Leaving OUtdoor Droplets (CLOUD) project was established. Within this project, experiments are carried out at a large volume cloud chamber (26m^2), located at Cern (Switzerland). In the chamber, aerosol particles, cloud droplets and ice crystals can be exposed to simulated atmospheric conditions and a particle beam provided by the Cern particle accelerator.

A big issue in large volume chambers like the CLOUD chamber at Cern is to achieve spatial homogeneity of thermodynamic conditions, gas composition and particle properties. Homogeneity in the tank becomes more complicated, if several parameters are changed during the experiments (e.g., UV-illumination system, particle nucleation, trace gas input, wall cooling). To achieve homogeneity, mixing fans are usually applied in such experiments. To check the mixing state, measurements are made at several selected points. However, it is not possible to check all relevant parameters continuously. Therefore, numerical simulations are carried out to evaluate the experimental configuration. For this study, the model was the commercially available fluid dynamics (CFD) model FLUENT (Ansys Inc., Canonsburg, PA, USA), fully coupled with the particle model FPM (Fine Particle Model, Particle Dynamics GmbH, Leipzig, Germany). The model provides the spatial and temporal distributions of all fluid (e.g., velocity, temperature) and particle dynamical (e.g., number, size, composition) properties resulting from the coupled processes of mass and heat transfer, flow and phase transition.

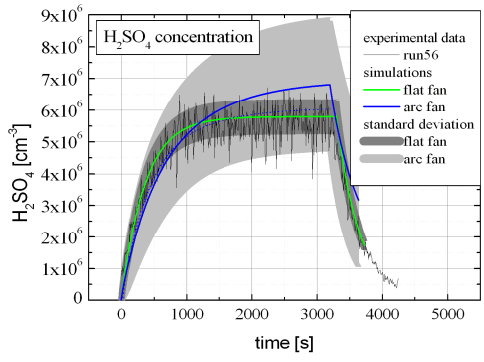

Figure 1: Simulated temporal evolution of the H_2SO_4 concentration in the CLOUD chamber compared to H_2SO_4 lifetime experiments. Simulations shown here were carried out for different fan shapes, but for equal H_2SO_4 production rates (4e5 cm^{-3}s^{-1}).

Due to the cylindrical shape of the CLOUD chamber, simulations were done on a 2-D grid. The mixing fans were described by zero thickness pressure jump layers. The actual parameters used to parameterize the mixing fans were derived by a comparison of calculated with measured H_2SO_4 concentrations of so-called H_2SO_4 lifetime experiments. In these experiments the temporal evolution of the H_2SO_4 concentration in the chamber, influenced by photolytic formation and wall loss of H2SO4, was investigated. A measured internal velocity profile was additionally included into the fitting procedure. Based on these results, the model was also applied to investigate 1/e mixing times of the tank to an instantaneous change of wall temperature and water mass fraction, and to study particle nucleation and growth.

Simulation results show that the mixing state of the tank's contents largely depends on the characteristics of the mixing fans. Simulations with a fan adjusted only to measured H_2SO_4 concentrations suggest that the tank's contents can be considered as homogeneously mixed (small standard deviations, Fig.1). In contrast, simulation results with boundary conditions giving results fitting both, a) temporal evolution of the H_2SO_4 concentration and b) measured internal velocity profile, indicate that a 1-fan configuration, as used in first experiments, is not sufficient to provide a homogeneously mixed chamber (large standard deviation, Fig.1). In particular, the mixing fan of such a configuration is only able to mix one half of the tank.

The 1/e response times for instantaneous changes of wall temperature and saturation ratio inside the chamber were found to be in the order of few minutes. A second fan reduces the time, dependent on fan shape, by a factor up to about 3. Particle number size distribution properties of the fresh nucleated particles (particle number, size, standard deviation of the assumed log-normal distribution) were found to be mixed over the tank's volume very similar to the gas species.

The investigations contribute to evaluate the experimental configuration of a tank like the CLOUD chamber and show that only 2 mixing fans, as already installed for actual and future experiments, can guarantee well mixed conditions inside the tank.

Acknowledgement: We would like to thank for financing through the BMBF CLOUD-09 and the EU Marie-Curie CLOUD-ITN projects.

Sulphuric acid measurements by CIMS at the CLOUD chamber and cross-check with independent methods to derive [H_2SO_4]

Rondo, Linda[1] , Kürten, Andreas[1], Ehrhart, Sebastian[1], Curtius, Joachim[1] and the CLOUD collaboration
[1]Institute for Atmospheric and Environmental Sciences, University of Frankfurt am Main, Altenhöferallee 1, 60438, Frankfurt am Main, Germany
Keywords: CIMS, sulphuric acid, H_2SO_4 calibration system, CLOUD Experiment

Laboratory studies indicate that sulphuric acid vapor is the most important precursor gas responsible for the nucleation of aerosol particles (Kuang et al., 2008). However, huge discrepancies still exist between different studies trying to determine at what sulphuric acid concentrations the onset of atmospherically relevant nucleation rates occurs.

The CLOUD (Cosmics Leaving Outdoor Droplets) experiment (Duplissy et al., 2009) at the CERN Proton Synchrotron aims to resolve this discrepancy. Additionally, it is designed to investigate the possible link between galactic cosmic rays and aerosol formation.

An instrument based on CIMS (Chemical Ionization Mass Spectrometry) is used for the measurement of gaseous sulphuric acid produced in the CLOUD chamber. The principle of this measurement is based on the reaction between H_2SO_4 and NO_3^- primary ions and the subsequent detection of HSO_4^- ions by a mass spectrometer (Tanner and Eisele, 1993). Mainly due to uncertainties in the reaction rate coefficient and the reaction time in the ion drift region, it is necessary to calibrate the H_2SO_4-CIMS. This is crucial in order to provide the most accurate numbers for the sulfuric acid concentration and to reliably interpret the CLOUD data. Here we present different methods allowing to cross-check the measured concentrations which are based on the calibrated H_2SO_4-CIMS.

The calibration method is based on the production of H_2SO_4 through the reaction of known concentrations of OH and SO_2. OH is formed by the photo-dissociation of water vapor inside a quartz tube, which is illuminated by bandpass-filtered 185 nm light from a mercury lamp (Edwards, 2003). Independently to the calibration, the validity of the measured H_2SO_4 concentrations at CLOUD was cross-checked with two other methods. The first method is based on the measured depletion of SO_2 during the experimental runs when the UV light in the chamber was turned on and the photo chemistry lead to the conversion of SO_2 to H_2SO_4. The concentration of H_2SO_4 is related to the consumption rate of the SO_2 according to the following relation (when a steady-state between the production and the wall loss of H_2SO_4 is reached) : $[H_2SO_4] = d[SO_2] / (dt \cdot k_{wall\ loss})$.
This method, however, allows only a crude estimation of the H_2SO_4 concentrations due to the relatively small changes in $[SO_2]$.

The second method is based on the measurement of the aerosol growth rates which can be used to estimate the H_2SO_4 concentration. The dependence of the particle growth rate on vapour concentrations and its molecular composition is known from theory (Nieminen et al., 2010). Following this theory, the condensational growth rates of aerosol particles smaller than 10 nm are used to determine the concentrations of sulphuric acid.

Such analyses provide very useful indirect information on the concentration of sulphuric acid even in the absence of a direct measurement. It is also an excellent method to cross-check the validity of the measured values with a calibrated H_2SO_4-CIMS. For the experiments during 2009 and 2010, the data evaluation studies showed good agreement between the measured values and the values derived from the independent methods described above (see Fig. 1).

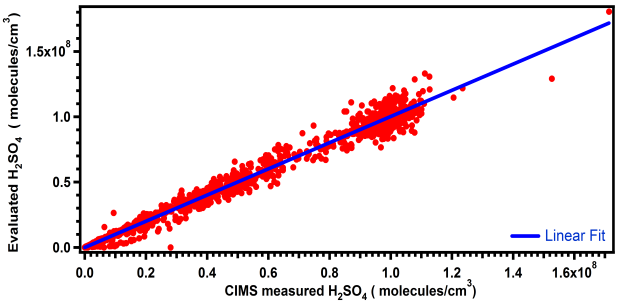

Figure 1. Example of the correlation between the evaluated [H_2SO_4] from the growth rate and the [H_2SO_4] measured by CIMS.

We would like to thank CERN for supporting CLOUD with important technical resources, and for providing a particle beam from the CERN Proton Synchrotron. This research has received funding from the EC's Seventh Framework Programme under grant agreement number 215072 (Marie Curie Initial Training Network "CLOUD-ITN"), from the German Federal Ministry of Education and Research (project number 01LK0902A), from the Swiss National Science Foundation, and from the Academy of Finland Center of Excellence program (project number 1118615).

Kuang, C., et al., J. Geophys. Res., 113, D10209 (2008).
Duplissy, J., et al., Atmos. Chem. Phys., 10, 1635-1647 (2010).
Edwards, G., et al., Anal. Chemistry, 75, 5317 – 5327 (2003).
Tanner and Eisele, J. Phys. Chem. 104, 830-836, (1993).
Nieminen et al., Atmos. Chem. Phys. Discuss., 10, 9773-9779 (2010).

Physical characterization of ions in the CLOUD chamber

A. Franchin,[1], S. Schobesberger[1], K. Lehtipalo[1], V. Makhmutov[2], Y. Stozhkov[2], S. Gagné[1], T. Nieminen[1], H. E. Manninen[1], T. Petäjä[1], M. Kulmala[1] and the CLOUD collaboration.

[1]Department of Physics, University of Helsinki, P.O. Box 64, FI-00014, Helsinki, Finland
[2]Lebedev Physical Institute RAS, 119991, Moscow, Russia.
Keywords: atmospheric ions, ion-induced nucleation, sulfuric acid, CLOUD experiment.
Presenting author email: alessandro.franchin@helsinki.fi

Nanoparticle formation in the boundary layer is a frequent phenomenon (Kulmala *et al.*, 2004). Sulfuric acid has been identified as a plausible candidate to participate in the nucleation (Weber et al. 1996). Ion-induced nucleation is one of the possible pathways for new particle formation in the atmosphere, but it is still unclear how important the contribution of ions is with respect to neutral pathways. Ion concentration and their size distribution are key quantities to understand ion-induced nucleation processes and dynamics.

During the CLOUD (Cosmics Leaving OUtdoor Droplets) 2010 fall campaign, several experiments of sulfuric acid-water neutral and ion-induced nucleation were performed in an aerosol chamber. In this experiment, Galactic Cosmic Rays (GCR) and the Proton Syncrotron (PS) accelerator at CERN were used as sources to generate ions in the 26.1 m^3 CLOUD aerosol chamber under precisely controlled conditions. Both GCR and the PS pion beam were constantly monitored by a GCR counter and by a hodoscope, respectively.

The ion concentration in the CLOUD chamber was measured with a Neutral cluster and Air Ion Spectrometer, (NAIS, Kulmala *et al.*, 2007). The NAIS is able to measure air ion number size distributions in the mobility equivalent diameter range of 0.8 to 40 nm and correspondingly neutral particle number size distributions from ~2 to 40 nm mobility diameter.

It was also possible to use a PSM (Particle Size Magnifier; Vanhanen e*t al. 2011*), a scanning CPC with a cut off varying from 1 to 2 nm, to retrieve the size distribution of the atmospheric ions created in the chamber and compare it to the NAIS in absence of neutral particles in the chamber (Figure 1).

Based on the measured GCR and beam intensities we were able to calculate the expected ion concentrations in the chamber as a function of beam intensity. The calculated ion concentrations were then compared with the measured values in the NAIS, therefore we retrieved the ion-ion recombination coefficient, performing a dedicated set of experiments at different conditions: in sulfuric acid free ($[H_2SO_4]$<5e5 cm^{-3}) and in sulfuric acid rich environment ($[H_2SO_4]$~3e6 cm^{-3}).

The ratio of formation rates of charged and total particles give information about the contribution of ion-induced nucleation. Charged nucleation rates were retrieved from the NAIS ion mode and from two CPCs one of which was equipped with a switchable ion trap both results will be compared.

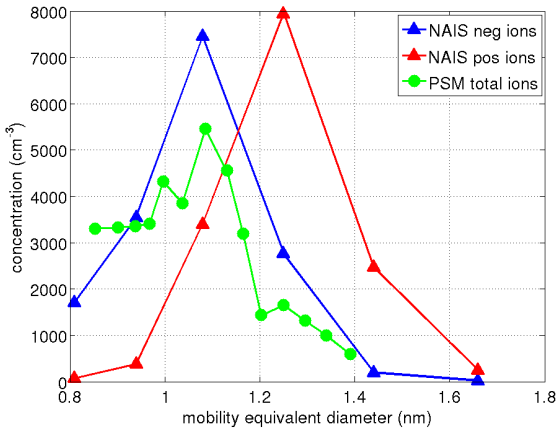

Figure 1. Comparison of number size distribution of ions from NAIS (blue for negative ions red for positive) and from PSM (green).

We would like to thank CERN for supporting CLOUD with important technical resources, and for providing a particle beam from the CERN Proton Synchrotron. This research has received funding from the EC's Seventh Framework Programme under grant agreement number 215072 (Marie Curie Initial Training Network "CLOUD-ITN"), from the German Federal Ministry of Education and Research (project number 01LK0902A), from the Swiss National Science Foundation and from the Academy of Finland Centre of Excellence program (project number 1118615).

Kulmala, M. *et al.* (2004). *J. Aerosol Sci.*, 35, 143 – 176.
Kulmala, M. *et al.* (2007). *Science*, 318: 89-92, 2007.
Vanhanen, J. e*t al.* (2011). *Aerosol Sci. Tech.,* 45, 4, 533-42
Weber, R. J., *et al.* (1996). *Chem. Eng. Commun.,* 151, 53–64.

SOA formation from stress induced biogenic VOC emissions and the contribution of isoprene to particle formation and growth – lessons learned from grey poplar trees

E. Kleist [1], T. Mentel [2], A. Kiendler-Scharr [2], S. Broch [2], M. Springer [2], K. Behnke [3], J.-P. Schnitzler [3], R. Tillmann [2], S. Andres [2], F. Rubach [2], B. Steitz [2], J. Wildt [1]

[1] Institute Plant Sciences, IBG-2, Research Centre Jülich GmbH, 52428 Jülich, Germany
[2] Institute Troposphere, IEK-8, Research Centre Jülich GmbH, 52428 Jülich, Germany
[3] Institute of Biochemical Plant Pathology, Department Environmental Engineering, German Research Center for Environmental Health (GmbH), 85764 Neuherberg, Germany

Keywords: particle formation and growth, SOA formation potential, Biogenic VOCs.
Presenting author email: e.kleist@fz-juelich.de

Vegetation is the major source of biogenic volatile organic compounds (BVOC) in the troposphere. These BVOC impact atmospheric oxidation capacity and serve as precursors for secondary organic aerosols (SOA). In regions with low pre-existing particulate matter, BVOC oxidation by OH, ozone, and NO_3 can produce low volatile products which are involved in SOA formation.

Isoprene and monoterpene emissions from vegetation are well known. However, during and after stress situations plants emit many other BVOC. Sesquiterpenes (SQT) such as α- and β-farnesene, C_6-aldehydes and -alcohols produced within the octa-decanoid pathway (green leaf volatiles, GLV), or many different aromatic compounds originating from the phenylpropanoid pathway are typical BVOC emitted during biotic and abiotic stress.

In this study we measured the formation of secondary organic aerosols (SOA) from stress-induced BVOC emissions emitted from grey poplar seedlings (*Populus x canescens*). The experiments were conducted in the Jülich Plant Atmosphere Chamber (JPAC, Mentel *et al*., 2009). This system consists of two temperature controlled chambers, one housing the plants (plant chamber) and the second one was used for photochemical SOA production (reaction chamber). BVOC emitted from the poplar plants in the plant chamber were transferred into the reaction chamber where they were oxidized by ozone and by OH radicals. OH was produced by photolysis of ozone in presence of H_2O. OH concentrations were typically in the range of 3-8×10^7 cm^{-3}. Ambient conditions such as temperature, relative humidity, photosynthetic active radiation (PAR), CO_2, O_3, and NO_x levels were controlled.

We used 4-month-old wild type (WT) poplar plants that emit high amounts of isoprene and transgenic poplar lines down-regulated in isoprene emission (R-lines, Behnke *et al.*, 2007). Comparing particle formation from BVOC emitted from these plants enabled the characterization of the impact of isoprene on the SOA formation from plant emissions. Unstressed poplar plants emitted nearly exclusively isoprene whereby the emissions from the down regulated R-lines were more than an order of magnitude lower than those from the wild type. Using unstressed plants as BVOC sources for particle formation we found inefficient SOA formation with nucleation rates far below 1 cm^{-3} s^{-1}.

All lines showed strong additional emissions of sesquiterpenes and aromatic compounds after stressing the plants by short ozone pulses. Their emission rates and therefore the BVOC emission pattern changed on a time scale of several days after stress application, allowing to study SOA formation under nearly steady state conditions. Feeding BVOC mixes into the reaction chamber resulted in very strong SOA formation events with nucleation rates exceeding 3000 cm^{-3} s^{-1}. Normalized to the BVOC turnover the nucleation rates were generally lower for the isoprene emitting WT poplars compared to non-emitting mutants. This observation confirmed former findings of suppression of nucleation by isoprene (Kindler-Scharr *et al*., 2009).

Rapid variations of PAR in the plant chamber resulted in fast changes of isoprene emissions whereas the emissions of the other BVOC responded on a much longer time scale. Hence, switching off the lamps in the plant chamber allowed removing isoprene very fast while keeping the level of other BVOC concentrations high. Conducting this procedure during a particle formation event caused a fast decrease of isoprene concentration and a strong increase of OH concentrations in the reaction chamber followed by increases in particle number and mass. This also shows that suppression of OH concentrations by isoprene is the major reason for suppression of nucleation from non-isoprene BVOC.

Using a low isoprene emitting poplar plant as BVOC source and adding deuterated isoprene from a diffusion source we estimated isoprenes' contribution to the SOA mass formed from the BVOC emitted from poplar. While isoprene contributed to about 7% [C/C] to the BVOC in the gas phase the contribution to the particulate phase was only 1 %. Thus isoprene oxidation products partitioning into the SOA can not compete with that of oxidation products from the other BVOCs. However the SOA mass produced by isoprene oxidation products does not compensate the decrease of other BVOC particle precursors caused by the decrease of OH concentrations in the presence of isoprene.

Behnke *et al.* (2007) Plant J., **51**, 485–499,
Kiendler-Scharr, A. *et al.* (2009), *Nature*, **461**, 381-384,
Mentel, T. F. *et al.* (2009), *ACP*, **9**, 4387-4406

Monday, September 5, 2011

Session 2C: Instrumentation for Chemical Characterisation of Aerosol

Development of a novel aerosol mass spectrometer for nucleation mode particles

S. G. Gonser[1] and A. Held[1]

[1]Bayreuth Centre of Ecology and Environmental Research (BayCEER), University of Bayreuth, 95448 Bayreuth, Germany

Keywords: Aerosol mass spectrometry, Nucleation mode, Secondary aerosol, Chemical composition.

Presenting author email: stefan.gonser@uni-bayreuth.de

Formation mechanisms and chemistry of secondary aerosol in the atmosphere are not fully understood today. This is due to the small number of instruments being able to analyze freshly nucleated particles with diameters smaller than 30 nm. In order to improve the fundamental understanding of the atmospheric aerosol, its formation mechanisms and chemistry we are developing a field portable aerosol mass spectrometer for particles smaller than 30 nm in diameter – CAChUP (Chemical Analyzer for Charged Ultrafine Particles).

CAChUP consists of an aerosol sizing and collection unit (similar to Voisin *et al* (2003)) coupled to a time of flight mass spectrometer (ToF-MS). The aerosol sizing and collection unit is composed of three major parts: (1) a unipolar corona discharge aerosol charger, (2) a radial differential mobility analyzer (rDMA) for the size separation of the particles, and (3) the actual collection unit. In the collection unit, the charged and sized aerosol particles are deposited on a filament. Once enough particles have been collected, the filament is heated gradually in order to evaporate the sample. The resulting gas phase is subsequently analyzed for its molecular composition in the ToF-MS.

A crucial part of CAChUP is the unipolar aerosol charger, since its charging efficiency determines the number of particles collected and eventually analyzed by the ToF-MS. For practical reasons regarding its transportability the charger design is based on corona discharge instead of using a radioactive source. The corona discharge is generated on bundles of carbon fibres, enabling the charger to be operated with voltages below 3 kV. These relatively low voltages minimize the production of ozone (Han *et al*, 2008), and consequently, the oxidation of the particles.

For the size separation of the particles, an rDMA was constructed (adapted from Zhang *et al* (1995)). The compact radial design allows to separate particles with diameters far below 10 nm, though our design limits the upper threshold to about 100 nm (Fig. 1). During preliminary tests our rDMA was able to separate nearly monodisperse aerosol distributions (geometric standard deviations of about 1.09) from broad distributions produced in a smog chamber.

To evaluate the performance of the collection unit in combination with the ToF-MS, molecular analysis of artificially produced secondary organic aerosol (SOA, with limonene as precursor) will be presented. After successful laboratory tests CAChUP will be ready for field experiments.

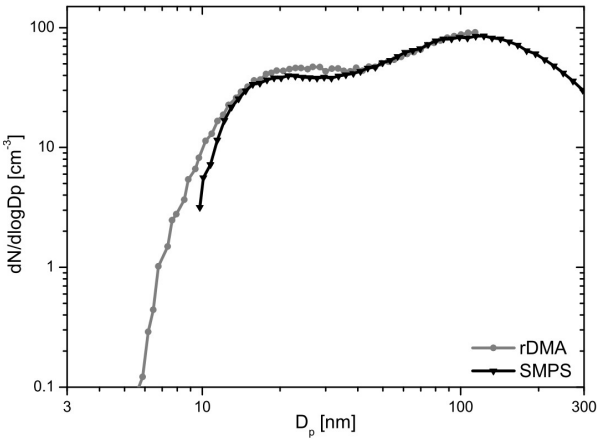

Figure 1. Preliminary intercomparison between our rDMA and a scanning mobility particle sizer (SMPS) at ambient air.

This work is funded by the Deutsche Forschungsgemeinschaft (DFG) under grant DFG HE 5214/3-1.

Han, B., Kim, H. J., Kim, Y. J. and Sioutas, C. (2008) *Aerosol Sci. Technol.* **42**, 793-800.

Voisin, D., Smith, J. N., Sakurai, H., McMurry, P. H. and Eisele, F. L. (2003) *Aerosol Sci. Technol.* **37**, 471-475.

Zhang, S. H., Akutsu, Y., Russell, L. M., Flagan, R. C. and Seinfeld, J. H. (1995) *Aerosol Sci. Technol.* **23**, 357-372.

Molecular Characterization of Organic Compounds in Atmospheric Aerosols

A.Laskin,[1] J. Laskin,[2] S.A. Nizkorodov[3]

[1]Chemical and Materials Sciences Division, and [2]Environmental Molecular Sciences Laboratory, Pacific Northwest National Laboratory, Richland, Washington 99352, USA.
[3]Department of Chemistry, University of California, Irvine, California 92617, USA.

Keywords: Aerosol chemistry, Organic Aerosol, High-Resolution Mass Spectrometry.
Presenting author email: Alexander.Laskin@pnl.gov

Understanding the molecular composition and fundamental chemical transformations of organic constituents of atmospheric aerosols during their formation and aging is both a major challenge and the area of great uncertainty in atmospheric and environmental research. Particularly, little is known about fundamental relationship between the chemical composition and physicochemical properties of organic aerosol (OA), their atmospheric history, evolution, and the impact on the environment.

Analysis of OA samples using soft-ionization methods combined with high-resolution mass spectrometry (HR-MS) analysis provide detailed information on the molecular content of OA that is pivotal for improving the understanding of their complex composition, multi-phase aging chemistry, direct (light absorption and scattering) and indirect (aerosol-cloud interactions) effects on atmospheric radiation and climate, health effects. The HR-MS methods can detect thousands of individual OA constituents at once, provide their elemental formulae from accurate mass measurements and structural information based on tandem mass spectrometry. Integration with additional analytical tools, such as chromatography and UV/Vis absorption spectroscopy, makes it possible to further separate OA compounds by their polarity and ability to absorb solar radiation.

This presentation will feature a summary of recent research projects focused on the detailed chemical characterization of OA, conducted in the groups of the co-authors. We will describe contemporary HR-MS methods (*Laskin, J. et al*, 2010; *Roach et al*, 2010), review recent applications in field and laboratory studies of OA (*Nizkorodov, Laskin, J., Laskin, A.*, 2011), and explain how the information obtained from HR-MS methods can be translated into an improved understanding of OA chemistry

Acknowledgment. The work at *UCI* was supported by the National Science Foundation. The work at *PNNL* was supported by the offices of Basic Energy Sciences (BES) and Biological and Environmental Research (OBER) of the U.S. Department of Energy (DOE). HR-MS analysis has been performed at the W. R. Wiley Environmental Molecular Sciences Laboratory (EMSL) located at PNNL.

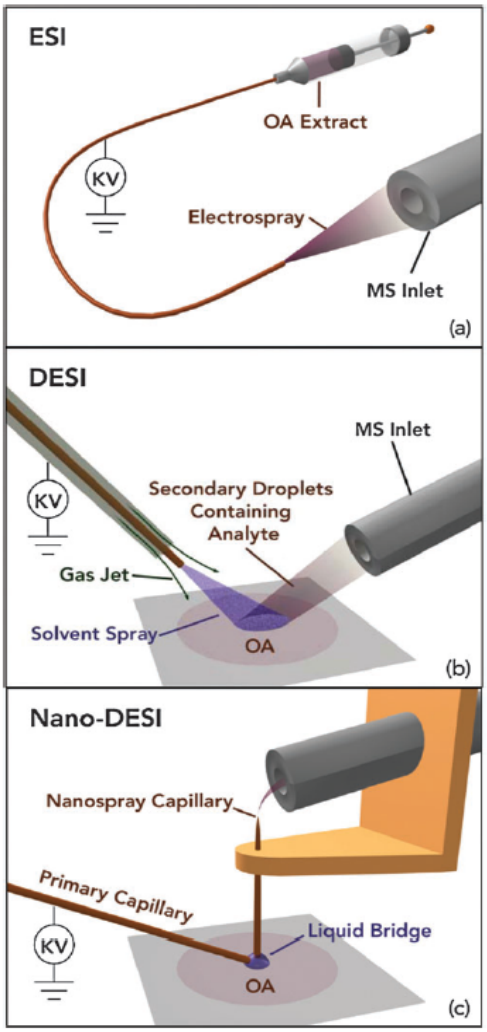

Figure 1. Schematics of the sample introduction and ionization setups used for the analysis of OA: (a) direct infusion electrospray ionization (ESI); (b) desorption electrospray ionization (DESI) (c) nanospray DESI. Reproduced from ref. *Nizkorodov et al*, 2011.

References

Laskin, J., Laskin, A., Roach, P., Slysz, G., Anderson, G., Nizkorodov, S., Bones, D., Nguen, L. (2010) *Analytical Chemistry*, **82,** 2048–2058.

Nizkorodov, S., Laskin, J., Laskin, A. (2011). ” *Phys. Chem. Chem. Phys.*, **13,** 3612–3629

Roach, P., Laskin, J., Laskin, A. (2010) *Analytical Chemistry*, **82,** 7979–7986.

On-line measurements of particle bound ROS in ambient and combustion aerosols

S. J. Fuller[1], J. S. Nutter[1], S. Platt[2], L. Pfaffenberger[2], P. Barmet[2], J. Dommen[2], U. Baltensperger[2], A. Prevot[2], M. Kalberer[1]

[1]Department of Chemistry, University of Cambridge, Cambridge, CB2 1EW, UK
[2]Paul Scherrer Institut, 5232 Villigen, Switzerland
Keywords: reactive oxygen species, on-line measurements, SOA, combustion particles.
Presenting author email: sjf53@cam.ac.uk

Adverse health effects associated with aerosol particles in ambient air are well documented by epidemiological studies (e.g., increase in respiratory and cardiovascular diseases) and are supported by biological mechanistic animal and cell culture studies. On a cellular level, inflammation and oxidative stress reactions have been observed in cell culture experiments after exposure of aerosol particles to lung cells. However, due to the large variability in ambient particulate matter it is still unknown what physical or chemical properties are responsible for these negative health effects. Previous studies have highlighted reactive oxygen species (ROS) in components of organic particulate matter, as being potentially a major cause.

Most previous aerosol ROS studies have used off-line techniques to determine the concentration of these compounds, i.e., particles were collected on filters, extracted into a solvent and then analyzed for their ROS content. ROS are known to have often very short life times and time delay between particle sampling and ROS quantification using such offline techniques could allow for loss of reactive species, leading to a significant underestimation of ROS. Online ROS analysis has been developed to reduce this and also allows for more detailed time resolved analysis (Venkatachari *et al*, 2008).

An online measurement system was developed in the study presented here that collects water-soluble aerosol components and determined the ROS concentration by reaction with the fluorescent probe 2-7 dichlorofluorescein (DCFH). Particles were collected and continuously extracted on a wetted hydrophilic filter (Takeuchi *et al*, 2005). The particle collector samples air at up to 5 litres per minute (lpm) and collects particles larger than an aerodynamic diameter of 50 nm with greater than 95% efficiency. The particles are collected and extracted in a solution of horseradish peroxidase (HRP) (0.5 units per ml) that allows immediate reaction of ROS on collection. The concentration of ROS is characterised following subsequent reaction of the oxidised HRP with DCFH (5 µM) for 10 minutes at 37^{o}C, yielding the fluorescent product DCF in the continuous flow set-up. The concentration of DCF is measured using fluorescence spectroscopy in a flow-through cell and calibrated to ROS concentration with hydrogen peroxide. With a sampling rate of 5 lpm the detection limit of the system is approximately 10 nMoles of hydrogen peroxides per cubic meter of air.

This system was used to measure particle bound ROS concentrations during the ageing of primary moped combustion emissions in the presence of UV light and NOx in smog chamber experiments carried out at the Paul Scherrer Institut, Switzerland. During collection a charcoal denuder was used to remove oxidising gaseous species and the sensitivity aerosol free baseline was measured using an inline HEPA filter.

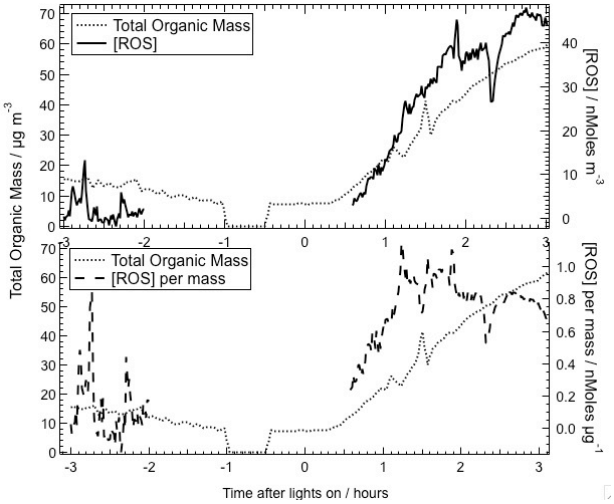

Figure 1 shows increasing ROS concentrations with increasing mass concentrations of SOA.

Primary moped emissions showed very low ROS concentrations per µg of aerosol. When the UV lights were turned on, at time zero in figure 1, the ROS concentrations increased with the concentration of SOA. ROS concentrations of up to 1 nMoles per µg of SOA were measured during the experiment. Un-aged primary emissions with mass concentrations of up to 200 µg/m^3 showed undetectable levels of ROS that were independent of mass concentration. This demonstrated that the reactivity seen during the ageing experiments was purely due to SOA.

This work was supported by the Natural Environment Research Council, UK.

Venkatachari *et al* (2008): Development and Laboratory Testing of an Automated Monitor for the Measurement of Atmospheric Particle-Bound Reactive Oxygen Species (ROS), *Aerosol Science and Technology*. **42**, *629-35*.

Takeuchi *et al* (2005): Continuous collection of soluble atmospheric particles with a wetted hydrophilic filter, *Analytical Chemistry*. **77**, *8031-40*.

Microchip Electrophoresis Interfaced to a Cloud Condensation Nuclei Collector for Online Monitoring of CCN Chemistry

S.D. Noblitt[1,2], C.S. Henry[2], J.L. Collett[3], S.V. Hering[4], and G.C. Roberts[1,5]

[1]Center for Atmos. Sciences and Phys. Oceanography, Scripps Inst. of Oceanography, La Jolla, CA, 92093, USA
[2]Department of Chemistry, Colorado State University, Fort Collins, CO, 80523, USA
[3]Department of Atmospheric Science, Colorado State University, Fort Collins, CO, 80523, USA
[4]Aerosol Dynamics, Inc., Berkeley, CA, 94710, USA
[5]Centre National de Recherche Scientifique – Météo France, Toulouse, 31057, France

Keywords: aerosol chemistry, CCN, instrumentation/chemical char., aerosol measurement
Presenting author email: noblitts@lamar.colostate.edu

Cloud condensation nuclei (CCN) are atmospheric aerosols that play critical roles in climate, specifically from their effects on the radiative budget and the hydrological cycle. Aerosols act as CCN when atmospheric water vapor spontaneously condenses on them, rapidly increasing their size. Each particle requires a specific water vapor supersaturation to activate, termed the critical supersaturation. Not all aerosols are CCN active, and the critical supersaturation depends on the size, morphology, and chemistry of the aerosol. Currently, direct measurement of CCN chemistry and its effect on CCN spectra has not been well characterized. This shortcoming is, in part, due to the difficulty in collecting a well-defined population of CCN with sufficient mass for conventional chemical analysis. Thus, improved methods for chemical analysis of aerosol are needed to understand the impact of chemistry and their origins on CCN activity.

Microchip electrophoresis (MCE) offers a promising new method for online monitoring of the chemical composition of CCN particles and possesses advantages over conventional monitoring equipment, including smaller instrumentation, shorter analysis times, increased portability, lower energy consumption, and the ability to make measurements from small liquid volumes. These attributes make MCE an attractive option for monitoring the chemistry of aerosol particles. MCE is particularly enticing for monitoring the chemistry of particles activated by CCN collectors because flow rates are very low (less than 1 L min^{-1}), resulting in the deposition of very low aerosol masses that cannot be adequately measured by ion chromatography (IC). Here, we present the coupling of MCE to a miniature CCN collector (Roberts and Nenes, 2005) for online monitoring of CCN chemistry at a single supersaturation. The outlet stream of the CCN system inertially impacts wetted CCN particles into a buffer-filled sample reservoir on a microchip for immediate electrophoretic analysis, which requires < 1 min per run. The instrument can operate unattended for at least two days. This approach is based upon an earlier instrument developed using a growth tube operating at very high supersaturation values to analyze the bulk composition of aerosols above a 10-nm diameter cutoff (Noblitt *et al.*, 2009). The integrated CCN-MCE system collects aerosols at ~50 mL min^{-1} and deposits them into ~20 µL of solution to provide detection limits of ~0.1 µg m^{-3} with 10 min of sampling. Concentrations are measured via differential analysis, and detection limits are inversely proportional to collection time, which can extend over an hour, further lowering detection limits. Currently, the system can monitor the anionic species chloride, sulfate, nitrate, and oxalate using existing separation chemistry (Noblitt *et al.*, 2009b). An example separation is shown in Figure 1. Inorganic cation species can also be analyzed with the instrument using chemistry that is currently in development. Here, we show the technical aspects of the instrument as well as anion data from preliminary ambient sampling.

This work was supported by the California Energy Commission (CEC 500-08-046) and the United States National Science Foundation (ATM-0737201).

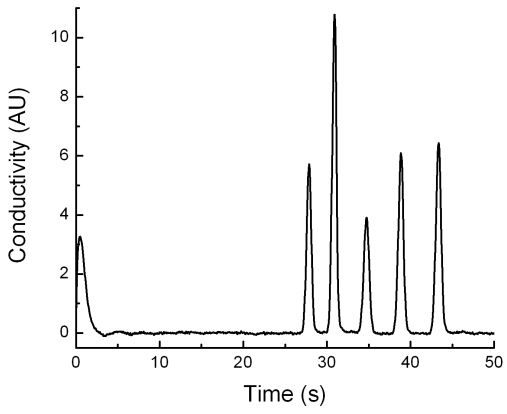

Figure 1. Example separation of anions found in aerosols. Peak order is chloride, sulfate, nitrate, oxalate, and the internal standard. Concentration = 5 µM.

Noblitt, S.D.; Lewis, G.S.; Liu, Y.; Hering, S.V.; Collett, J.L.; and Henry, C.S. (2009) *Anal. Chem.* **81.** 10029-10037.

Noblitt, S.D.; Schwandner, F.M.; Hering, S.V.; Collett, J.L.; and Henry, C.S. (2009) *J. Chromatogr. A* **1216.** 1503-1510.

Roberts, G.C. and Nenes, A. (2005) *Aerosol Sci. Technol.* **36.** 206-221.

Comprehensive GCxGC, a valuable technique for the screening and semiquantitation of different chemical compounds in ultrafine aerosol particles

J. Ruiz-Jimenez[1], J. Parshintsev[1], T. Laitinen[1,2], K. Hartonen[1], M.–L. Riekkola[1],T. Petäjä[2], M. Kulmala[2]
[1]Laboratory of Analytical Chemistry, Department of Chemistry, University of Helsinki, P.O. Box 55, FI-00014 Finland, [2]Division of Atmospheric Sciences, Department of Physics, University of Helsinki, P.O. Box 64, FI-00014, Finland

Keywords: Comprehensive gas chromatography, mass spectrometry, time-of-flight, ultrafine aerosol particles
Presenting author email: jose.ruiz-jimenez@helsinki.fi

Comprehensive two dimensional gas chromatography – time-of-flight mass spectrometry (GCxGC-TOF-MS) has been used for the screening and semi-quantitation of volatile organic compounds in aerosol particles. Because volatility was required, some compounds were transformed via derivatization such as silylation into volatile ones. The identification of the analytes was made by comparing the GC retention indices and the TOF mass spectra ,with the NIST and the Golm metabolome database reference libraries. The data treatment was simplified by exploiting a double classification of the identified compounds, namely the main functional group and the specific elements chemical groups present in the molecule (Table 1).

Table 1. Classification of the identified compounds was based on the main functional group or specific element present in the molecule

Hydroc	Alkanes, alkenes, cyclic, aromatic
Halogen	Fluorinated, chlorinated, brominated , iodinated
Nitrogen	Amino acids, nitro, amines, amides, nitriles, imides, urea deriv, amino acids-N-deriv, amino-sugars, heterocyclic
Sulphur	Suphonamides, mercapto, sulphonic, thio
Carboxyl	Free acids, hydroxyl-a, keto-a, esters, anhyd
Hydroxyl	Alcohols, polyols, ethers
Carbonyl	Aldehydes, ketones

This methodology was applied to the identification of compounds in 30 nm, 50 nm and total suspended particles (TSP) collected during spring and autumn 2009 and summer 2010 at the Station for Measuring Forest Ecosystem Atmosphere Relations (SMEAR II) at Hyytiälä (Finland).

Table 2. Number of identified compounds and relative peak areas in SMEAR II samples

	Number		Relative peak area (m^{-3})	
	Mean	Range	Mean	Range
TSP	444	380-560	2.110^{7}	$7.9\ 10^{6}$-$5.0\ 10^{7}$
50-nm	429	385-476	3.510^{7}	$1.2\ 10^{7}$-$8.3\ 10^{7}$
30-nm	441	395-511	1.210^{8}	$5.1\ 10^{7}$-$2.7\ 10^{8}$

The number of identified compounds was higher than 400 (Table 2), resulting in the concentrations of the most relevant compounds present in the samples.
Significant differences were found in the compound profiles of TS, 50-nm and 30-nm particles. The highest values in terms of the number of compounds and the relative peak area were found for 30-nm particles, collected in a different season of the year. It is clear that alkenes, thio compounds, amino acids, esters, simple alcohols and ketones were the most abundant compounds in the aerosol particles under study in terms of the number of compounds but it was not possible to find any clear correlation for halogenated compounds that together with sulphur containing compounds and acids existed as relatively high peak areas (concentrations).
The analysis of different sized, simultaneously collected aerosol particles, revealed that the number of compounds increased with the enhanced particle size but the concentrations decreased in the most of the cases, except aldehydes (Figure 1). The decrease is presumable linked to the formation of new low-volatile compounds.

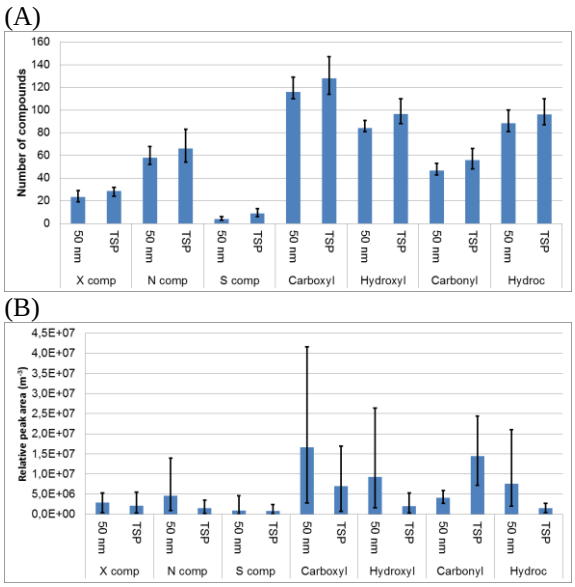

Figure 1. Chemical groups in different sized and TS particles as a function of A) number of compounds, B) relative peak areas

This work was supported by the Academy of Finland Centre of Excellence program (project no 1118615).

A new sensitive long-path absorption spectrometer for peroxide measurements in secondary organic aerosol

P. Mertes[1], J. Dommen[1], M. Kalberer[2], and U. Baltensperger[1]

[1]Laboratory of Atmospheric Chemistry, Paul Scherrer Institute, 5232, Villigen, Switzerland
[2]Centre for Atmospheric Science, Cambridge University, Cambridge, CB2 1EW, United Kingdom

Keywords: peroxides, smog chamber, SOA, spectrophotometry.
Presenting author email: peter.mertes@psi.ch

Beside their decisive role in atmospheric processes ambient fine and ultrafine particles have also an important impact on human health, predominantly on respiratory and cardiovascular systems (Pope and Dockery, 2006). Up to about 70% of these ambient particles are composed of organic material. However, the highly complex organic mixture is chemically still poorly characterized. The reaction of volatile organic compounds with ozone and OH radicals in the polluted troposphere mainly generates aldehydes, carboxylic acids and organic peroxides. The contribution of these peroxides to health risk is assumed to be especially important because of their high reactivity and oxidation potential (Morio *et al.*, 2001).

This project aims at developing an analytical method to determine the total amount of peroxides in secondary organic aerosol (SOA). Former studies indicate that the total amount of peroxides is considerably high in SOA (Ziemann, 2005). Using iodometry, quantification of peroxides in SOA was performed, and interesting time trends were observed (Gaschen *et al.*, 2008). However, due to insensitive spectrophotometry with 1-cm cuvettes, these experiments had to be performed at very high aerosol concentrations, and time resolution was rather low (2 hours).

In this study we describe a more sensitive method for peroxide quantification using a liquid core waveguide (LCW) in long pathlength absorbance spectroscopy (LPAS). According to Lambert-Beer's law, the sensitivity of spectrophotometry can be enhanced by increasing the optical path length. Absorbance is measured by a spectrophotometer (Ocean Optics, SD 2000). As detection cell we use a 50-cm Teflon AF 2400 LCW tube (DuPont, 0.6 mm i.d.). White light is supplied via a 200-μm glass fiber from a deuterium lamp (Avantes, AvaLight-DH-S). Solutions of hydrogen peroxide in 0.1 M $HCl_{(aq)}$/ethanol (1/1 by volume) were used for calibration. The reaction time was reduced to 40 min at an elevated temperature of 40°C. The detection limit was about 0.15 μM at 420 nm which is 80 times lower than reported by Gaschen *et al.* (2008).

We tested this instrument with aerosols produced in the PSI smog chamber. This is a 27-m^3 flexible teflon bag suspended in a temperature controlled wooden enclosure. Four xenon arc lamps combined with 80 black light lamps (SUN POWER Performance 100W) are used to simulate the solar light spectrum for photochemical aging. SOA was produced from α-pinene (biogenic precursor) or 1,3,5-trimethylbenzene (anthropogenic precursor). Aerosol particles were collected by impaction on stainless steel (A4) plates. The amount of peroxide functional groups was measured and normalized to the aerosol mass collected. Finally peroxide concentrations in SOA as a function of photochemical age and precursor were determined.

First measurements showed that SOA from the photooxidation of 1,3,5-trimethylbenzene contained between 30 and 250 pmol of peroxy-groups per μg collected aerosol. Assuming an average molecular weight of 150 Da for the peroxides this corresponds to 0.4 to 3.6 wt%. The peroxide content was highest within the first hour after experiment start and decreased during the experiment. In SOA from α-pinene we measured comparable amounts.

With our new setup using long pathlength absorbance spectroscopy to quantify peroxides in aerosol particles we find considerably lower amounts of peroxides than hitherto published studies have shown.

This work was supported by the Swiss National Science Foundation.

Gaschen, A., Kalberer, M., Dommen, J., Duplissy, J. and Baltensperger, U. (2008) *Geophysical Research Abstracts, EGU General Assembly* **10**, EGU2008-A-09959.

Morio, L. A., Hooper, K. A., Brittingham, J., Li, T-H., Gordon, R. E., Turpin, B. J. and Laskin, D. L. (2001) *Toxicol. Appl. Pharmacol*. **177**, 3, 188-199.

Pope III, C. A. and Dockery, D. W. (2006) *J. Air Waste Manage. Assoc.* **56**, 709-742.

Ziemann, P. J. (2005) *Faraday Discuss.* **130**, 469-490.

Field measurement of secondary organic aerosol in a boreal forest site in southern Finland using on-line soft ionization ion trap mass spectrometry

A. L. Vogel[1], A. Bayerle[1], M. Beck[1], M. Äijälä[2], M. Ehn[2], H. Junninen[2], T. Petäjä[2], D. R. Worsnop[2], M. Kulmala[2], J. Williams[3], T. Hoffmann[1]

[1]Institute for Inorganic and Analytical Chemistry, Johannes Gutenberg-University of Mainz, 55128 Mainz, Germany
[2]Department of Physical Sciences, University of Helsinki, 00014 Helsinki, Finland
[3]Max Planck Institute for Chemistry, Department of Atmospheric Chemistry, 55128 Mainz, Germany
Keywords: field measurement, instrumentation/chemical characterization, SOA, gas-particle distribution
Presenting author email: vogelal@uni-mainz.de

Emission of biogenic volatile organic compounds (BVOCs) by vegetation in the boreal forest and subsequently atmospheric oxidation leads to the formation of secondary organic aerosol (SOA). Oxidation of the BVOCs produces a variety of mostly unidentified organic species. Dependent on the volatility of the products, they partition between gas and particle phase. Seen from this perspective, organic acids are of particular importance for the particle phase, since the higher oxidation state and molecular mass, compared to the corresponding terpenes or aldehydes, is accompanied by a much lower volatility. However, very little is known about intermediate volatility organic compounds (IVOCs) which are residing almost entirely in the gas phase and generate efficiently lower volatility products by further reaction with atmospheric oxidants or by oligomerization (Donahue et al., 2006).

Here we show the high potential for gaining new insights into gas-to-particle-partitioning of individual organic acids by measuring them in both phases with the same instrument. This was achieved by coupling a miniature Versatile Aerosol Concentration Enrichment System (mVACES) as described by Geller et al. (2005) with an Atmospheric Pressure Chemical Ionization Ion Trap Mass Spectrometer (APCI-IT-MS; Hoffmann et al., 2002). The benefits of the on-line APCI-IT-MS are soft ionization with nearly no fragmentation, high time resolution and less sampling artifacts than in the common procedure of taking filter samples, extraction and detection with LC-MS. Furthermore the ion trap allows to perform MS/MS-experiments by isolation of single m/z ratios of particular ions. By subsequent addition of energy, the trapped ions form characteristic fragments which enable structural insight on the molecular level.

The sophisticated aerosol concentrator mVACES is a necessary unit for operation of the APCI-IT-MS in the field. It improves the limit of detection by concentrating particles without lowering the time resolution. Physical and chemical alteration of the particles, especially the change of gas-particle partitioning, was evaluated.

Field measurement during HUMPPA-COPEC10 campaign

The setup mVACES coupled to APCI-IT-MS was tested successfully in the laboratory and afterwards used during the large HUMPPA-COPEC field campaign at the SMEAR station in Hyytiälä, Finland in summer 2010. The comprehensive instrumental equipment of gas and particle phase measuring instruments during the campaign made it possible to compare the APCI-MS-data with a variety of different techniques. Especially the comparison between APCI-MS and the c-ToF-AMS (compact Time of Flight Aerosol Mass Spectrometer) of the University of Helsinki is predestinated, since these two instruments were connected to the same aerosol inlet line. Very good correlation coefficients between APCI-MS and AMS for sulfate (R^2=0.93) and for total organics (R^2=0.94) in particle phase have been determined. Furthermore organic acids were measured by filter sampling and subsequent analysis with LC-MS in order to resolve possible isobaric interference of the APCI-MS technique. For the first time in a field measurement in situ MS/MS-experiments for chemical characterization of the major abundant organic acids have been carried out. Results show similar pattern to those MS/MS-experiments in laboratory generated secondary organic aerosol.

However, not only comparison to different instruments and techniques revealed interesting results, but also the temporal behavior of specific compounds allows interpretation possibilities. For example fast mixing processes in the atmosphere (e.g. boundary layer processes) show a strong influence on the concentration levels of IVOCs. These short-term processes can only be monitored by an on-line technique. In addition we could show that gas-particle-partitioning of single organic compounds is not only driven by the molecular mass but most notably by the oxidation state of the regarded species. This means there exist highly oxidized organic acids with a relative small molecular mass which contribute more to particle mass than other organic acids with higher molecular masses.

Donahue, N. M., Robinson, A. L., Stanier, C. O., Pandis, S. N. (2006) *Environ. Sci. Technol.* **40**, 2635-2643.

Geller, M. D., Biswas, S., Fine, P. M., Sioutas, C. (2005) *J. Aerosol Sci.* **36**, 1006-1022.

Hoffmann, T., Bandur, R., Hoffmann, S., Warscheid B. (2002) *Spectrochimica Acta B* **57**, 1635-1647.

Monday, September 5, 2011

Session 2D: Source Apportionment Studies

Source apportionments in a multi rural sites experiment in France (Particulair): Seasonality and regional specificities

Cozic J.[1], Piot C[2,1], Besombes JL[2], and Jaffrezo JL[1] and the Particul'air Team

[1] UJF-CNRS, LGGE, Rue Molière, BP 96, 38402 St Martin d'Hères Cedex, France.
[2] Université de Savoie - Polytech, LCME, Campus Scientifique, 73376 Le Bourget du Lac Cedex, France.

Keywords: aerosol chemistry, biomass emission, large scale characterization, rural environments, France.

There is an increasing concern all over Europe about a worsening of Air Quality due to domestic biomass combustion. Many studies showed over the last years that this source is responsible for a large share of particulate matter (PM) loading in very different types of environments (eg., large cities, alpine valleys, ..). However, there are still very few data available in order to evaluate the impact of this source in rural environments, particularly in France.

The program Particul'Air was design to investigate this aspect together with the impact of other sources (vehicle emission, marine emission...) simultaneously over a large portion of France. Nine sampling sites (cf figure 1) were selected in small rural villages (pop below 2500 inhabitants), spreading from the West (Brittany) to the East (Franche Comté) of the country.

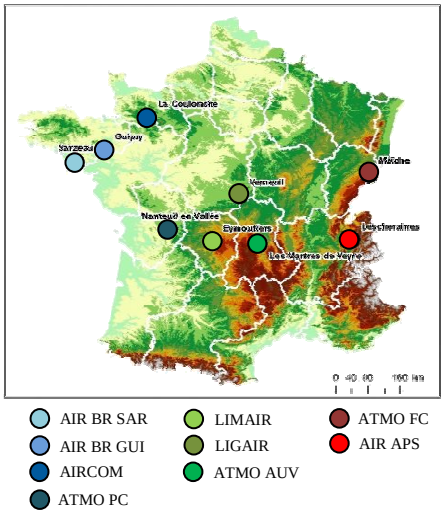

Figure 1. The 9 sampling sites.

Nine sampling periods of one week each (C1 to C9) were conducted simultaneously at the 9 sites, from March 2009 to February 2010, with daily sampling of PM10 at high flow rate. Additional measurements including PM mass (PM2.5 and PM10) and meteorological data were monitored. All filter samples were analyzed for EC/OC, major ionic species and LMW organic acids, levoglucosan, PAH, and trace metals. In addition, molecular speciation of organic matter (for about eighty compounds from different chemical families: hydrocarbons, PAH, organic acids…) was conducted on all samples of 5 of the campaigns.

The influence of the different sources can be estimated from different approaches, for instance by mono-tracer method using organic carbon (OC), levoglucosan and elemental carbon (EC) concentrations. Figure 2 presents the contribution of the different OM sources to OM for winter and summer depending of the region and shows that biomass combustion can indeed represent a very large share of the OM, with large variations according to the period and the site. Sites in mountainous areas (East) are more subjected to high concentrations and large impacts due to this source. However, sites close the Atlantic are far from being immune (West).

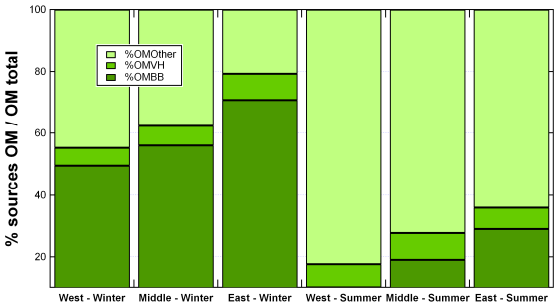

Figure 2. Contribution of the different OM sources to OM for Winter and Summer depending of the region.

This approach will be compared to the results obtained when using Molecular Marker - Chemical Mass Balance modeling (chemical aerosol composition and multiple tracers).

This work was supported by ADEME, CNRS, UJF and AASQA (AIRAPS, ATMO Poitou-Charentes, ATMO Auvergne, ATMO Franche-Comté, LIMAIR, LIGAIR, AIRBREIZH, AIRCOM).

A comprehensive study of the major sources of fine aerosols ($PM_{2.5}$) in the region of Paris (France): contribution of local versus imported emissions

M. Bressi[1], J. Sciare[1], V. Ghersi[2], N. Bonnaire[1], S. Moukhtar[2], J. Nicolas[1], A. Rosso[2], J.E. Petit[1], P. Lameloise[2], A. Féron[1], M. Artufel[1], and M. Reynaud[2]

[1]Laboratoire des Sciences du Climat et de l'Environnement, LSCE (CNRS-CEA), Gif sur Yvette, 91191, France
[2]AIRPARIF, Surveillance de la Qualité de l'Air en Ile-de-France, Paris, 75004, France
Keywords: $PM_{2.5}$, Aerosol component composition, Chemical Mass closure, Source Apportionment, PMF
Presenting author email: michael.bressi@lsce.ipsl.fr

Paris is amongst the most populated urban zone in Europe with approximately 11 millions inhabitants (ca. 20% of the French population). With its specific meteorological conditions (oceanic versus continental air masses), this modern urbanized area represents a location of high interest for the investigation of Particulate Matter (PM).

Since 2007, the local air quality network AIRPARIF is monitoring particulate mass of fine aerosol with aerodynamic diameters below 2.5µm ($PM_{2.5}$) using a conventional on-line automatic system (R&P TEOM-FDMS). Since then, yearly averaged $PM_{2.5}$ levels have constantly been around 20µg/m^3 for urban background, which is the annual E.U. limit value of 2020. There is therefore a need to reduce $PM_{2.5}$ concentrations by applying efficient abatement strategies, which requires a comprehensive knowledge of this PM pollution. In particular, one needs to address the geographical origins of fine particles (local, regional or trans-frontier) as well as its main aerosol sources. These are the two main objectives of the AIRPARIF-AEROSOL project that will be discussed here.

Methodology

A large aerosol filter sampling network has been deployed in the region of Paris (ca. 120*100 km), composed by three rural, one suburban, one urban and one traffic stations. Daily (24h) sampling of $PM_{2.5}$ have been conducted at each station for a period of one year (11/09/2009–11/09/2010), using two Leckel low volume filter samplers (one for QMA, the other for PTFE filters) running at 2.3 m^3/h. After having determined their masses by gravimetry, the sampled filters have been thoroughly chemically characterized, by determining their content in carbon (EC, BC, OC, WSOC), major ions (NH_4^+, NO_3^-, SO_4^{2-}…), metals (Pb, Ti, Fe…) and specific tracers (levoglucosan, arabitol…).

Results

We will present here the $PM_{2.5}$ chemical characterization obtained at our 6 stations for the entire duration of the project (one year). We will first present the methodology developed to achieve the chemical mass closure on each station all along the year (See Figure 1.a). The temporal variability of $PM_{2.5}$ mass and its specific chemical components will be discussed, with an emphasis on pollution events.

Insights on the geographical origin of fine particles will be addressed by the "Lenshow" methodology (Lenshow et. al, 2001). It allows estimating the PM contribution of different geographical areas (long-range transport, rural, urban…) for each of the chemical constituent in $PM_{2.5}$.

Insights on the major aerosol sources of fine particles will be addressed from the results obtained by a source apportionment technique (PMF 3.0 model from EPA). Six major sources are likely to be at the origin of $PM_{2.5}$ over the Paris region (see Figure 1.b). A detailed chemical profile of each source, as well as their contributions (temporally resolved) to PM will be showed. These results will be compared with other European source apportionment studies (Viana et. al, 2008). Back-trajectory analyses (HYSPLIT trajectory model) will be used here to support our PMF factors identification. These different techniques are illustrated in Figure 1.

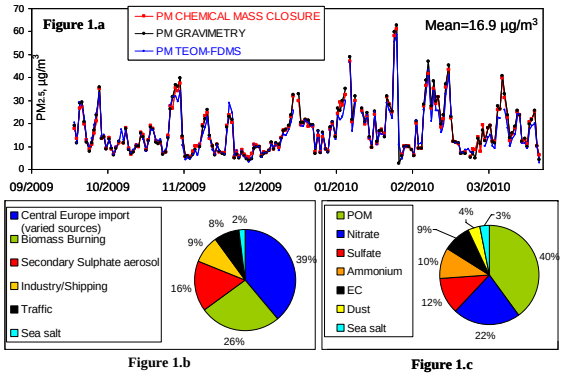

Figure 1. A comprehensive study of fine aerosols ($PM_{2.5}$) of the urban background of Paris (11/09/2009-27/03/2010).
Figure 1.a: Temporal evolution of $PM_{2.5}$ mass using three independent methods
Figure 1.b: Average contribution of the major sources of $PM_{2.5}$
Figure 1.c: Average chemical composition of $PM_{2.5}$

This work is supported by the Région Ile de France, Ville de Paris, ADEME, CEA, AIRPARIF and CNRS.

Lenshow, P., Abraham, H.J., Kutzner, K., Lutz, M., Preuss, J.D., Reichenbächer, W. (2001) *Atmospheric Environment* **1**, S22-S33.

Viana, M., Kuhlbusch, T.A.J., Querol, X., Alastuey, A., Harrison, R.M., Hopke, P.K., Winiwarter, W., Vallius, M., Szidat, S., Prévôt, A.S.H., Hueglin, C., Bloemen, H., Wahlin, P., Vecchi, R., Miranda, A.I., Kasper-Giebl, A., Maenhaut, W., Hitzenberger, R. (2008) *Aerosol Science* **39**, 827-849.

Sources of particulate matter and gaseous pollutants at some suburban sites in South East Queensland, Australia

A. Morrison[1], S.Law[1], G. A. Ayoko[1]* and H. Guo[2]

[1]Discipline of Chemistry, Queensland University of Technology, Brisbane, QLD 4001, Australia
[2]Department of Civil and Structural Engineering, Hong Kong Polytechnic University, Hong Kong

Keywords: Source apportionment, PMF, PM10, gaseous pollutants.
Presenting author email: g.ayoko@qut.edu.au

Given the growing links between air quality and adverse environmental and human health effects (see, e.g., Chow, 2006; Teller and Levin, 2005), there has been an upsurge of interest in the spatial and temporal variations in the concentrations of airborne pollutants and use of receptor models for source identification and source apportionment.

In this paper we describe trends in air quality data obtained at two air monitoring stations in South East Queensland, and preliminary results on their source identification and apportionment. The goal of the work is to generate information that could aid the understanding of the source, transport and accumulation of pollutants in the region, and facilitate the formulation of mitigating measures.

The two sites examined in the paper are the Eagle Farm (EF) and Flinders View (FV) air monitoring stations, which were part of Queensland Environmental Protection Agency network of air monitoring sites within South-East Queensland. Their role was to monitor $PM_{10,}$ meteorological conditions and the concentrations of ozone, nitrogen oxides, sulphur dioxide, and visibility reducing particles. The Eagle Farm (EF) monitoring site was located in a light industrial area on Curtin Avenue (latitude -27.4383 and longitude 153.0798) the between 1998 and 2005 while FV monitoring site is located at Ipswich which is approximately 35 km south west of Brisbane. The site is located at latitude – 27.6528 and longitude 152.7741. It is bordered on the south by rural acreage blocks and located approximately 500 meters east of a highway and four kilometres east of the a power station, a landfill and a company that produces organic compounds..

The data collected between 2000 - 2004 at these site were pre-treated before Positive Matrix Factorisation (PMF) and other statistical analyses. Preliminary analysis of the data showed that the concentrations of the pollutants were generally below the Australian National Standards for each pollutant. However, there are a few days when the National Standards were exceeded by some pollutants. Further analysis of the data by advanced factor analytic methods revealed instructive details about the temporal and spatial variation, as well as the possible sources of the pollutants. Thus the main sources of the pollutants were identified as traffic and industrial emissions.

Conditional probability function (CPF) analysis identified the most likely sources of the pollutants measured at EF as the M1 motorway, Kingsford Smith drive, local traffic and the local industrial area, while the Cunningham highway, Swanbank power station and aircrafts operated by the Royal Australian Air Force were identified as the main sources at FV.

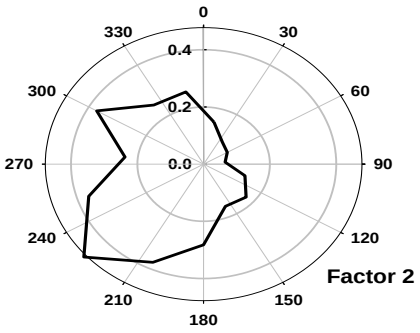

Fig 1: CPF plot for the highest 25% of the mass contribution for the PM factor.

The development of air quality management strategies and prioritisation of remedial action could greatly be enhanced by considering the resolved sources and the contributions of each source to the species measured at each of the sites.

We thank the former Queensland Environmental Protection agency for the data used for this work.

Chow, J.C., (2006). Health effects of fine particulate air pollution: lines that connect, Journal of the Air & Waste Management Association, 56, 6-7.

Teller, A., Levin, Z., 2005.The effects of aerosols on precipitation and dimensions of subtropical clouds; a sensitivity study using a numerical cloud model, Atmospheric Chemistry and Physics Discussion., 5, 7211-7245.

Kim, E., Larson, V. T., Hopke, P.K., Slaughter, C., Sheppard, L.E., Claiborn, C., (2003) . Source identification of PM2.5 in an arid Northwest U.S City by positive matrix factorization. Atmospheric Research, 66, 291 – 305

Chemical composition and source apportionment of PM10 at different Swiss locations 2008/2009 compared to 1998/1999.

M.F.D. Gianini[1], R. Gehrig[1], A. Fischer[1], A. Wichser[1], A. Ulrich[1], J. Cozic[2], J.-L. Jaffrezo[2], and C. Hueglin[1]

[1]Empa, Swiss Federal Laboratories for Materials Science and Technology, CH-8600, Switzerland.
[2]Université Joseph Fourier-CNRS, LGGE, St-Martin d'Hères, F-38400, France

Keywords: PM10, chemical composition, source apportionment.
Presenting author email: matthias.gianini@empa.ch

During a one year period (from August 2008 to July 2009) PM10 samples from different locations in Switzerland (urban kerbside, urban background, suburban and rural) were collected and analysed for inorganic ions, trace elements and the carbonaceous fraction. In addition, a detailed speciation of organic compounds was performed for selected PM10 samples. The data provide a detailed picture of the variation of the PM10 chemical composition between different site types, regions and seasons.

Ten years earlier, from January 1998 to March 1999, a similar study has been performed. As in the recent study, the data provided a detailed picture of the PM10 chemical composition at different Swiss sites (Hueglin et al. 2005) and allowed the identification and characterisation of the main emission sources.

During the last decades the concentrations of atmospheric PM10 slightly but steadily decreased in Switzerland (Barmpadimos *et al.*, 2010). PM10 concentrations measured in 1998/1999 and 2008/2009 reflect this trend (Fig. 1).

Between the two studies the most noticeable change in major PM10 constituents was observed for sulphate: at all sites average annual concentrations decreased between 1.1 and 1.5µg/m^3 (Fig, 1). Decreasing concentrations were also observed for elemental carbon (EC), ammonium and the sum of trace elements. Decreasing trace element concentrations were especially pronounced at the urban kerbside site, indicating declining trace element emissions from road traffic. Organic matter (OM) showed only decreasing concentrations at the urban kerbside site, the nitrate concentrations were slightly increasing at all sites. The average concentration of natural mineral dust as calculated from the concentrations of Al and Mg as well as from estimates of the crustal fractions of total measured Fe, K and Ca slightly decreased at the urban kerbside site, while at the other sites remained constant.

Both data sets were analysed (respectively re-analysed) by Positive Matrix Factorization (PMF). The main PM10 sources and components were identified as: road traffic, wood combustion, mineral dust, sulphate rich secondary aerosols, nitrate rich secondary aerosols, and a Na and Mg rich factor. It was found that wood combustion is an important source of PM10 at all sites. The estimated contribution of wood combustion related aerosols was highly correlated to the concentrations of levoglucosan. The results also revealed clear differences in properties of wood combustion emissions at the rural sites north and south of the Alps. The contribution of mineral dust as determined by PMF was in good agreement to the mineral dust concentration as calculated from the element concentrations. This gives us additional confidence in the reliability of the PMF results.

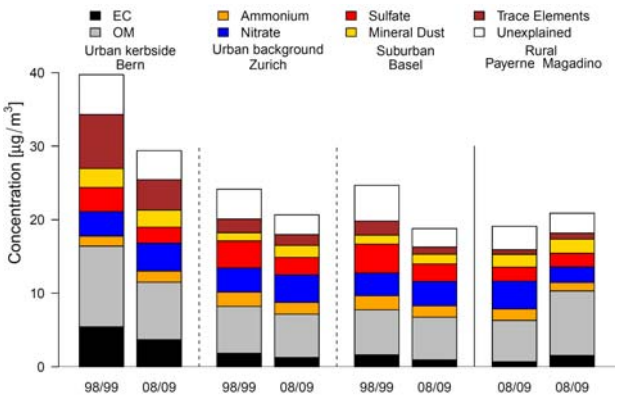

Figure 1: Chemical composition of atmospheric PM10 at urban kerbside, urban background ad suburban sites in 1998/1999 and 2008/2009 and at two rural sites in 2008/2009.

This work was supported by the Competence Center Environment and Sustainability of the ETH Domain (CCES- IMBALANCE) and by the Swiss Federal Office for the Environment (FOEN).

Hueglin, C., R. Gehrig, M. Gysel, U. Baltensperger, C. Monn and H. Vonmont (2005). Chemical characterisation of PM10 and PM2.5 at urban, near-city and rural sites in Switzerland. *Atmos. Environ.* **39**: 637-651.

Barmpadimos, I., Hüglin, C., Keller, J., Henne, S., and Prévôt, A. S. H.: Influence of meteorology on PM_{10} trends and variability in Switzerland from 1991 to 2008, Atmos. Chem. Phys. Discuss., 10, 26961-27014, 2010.

Spatial distribution of ambient particulate matter and source contributions in Augsburg, Germany

J. Schnelle-Kreis[1], J. Gu, G. Abbaszade[1], J. Diemer[2], R. Zimmermann[1,3]

[1]ICooperation Group Analysis of Complex Molecular Systems, Helmholtz Zentrum München, D-85764 Neuherberg, Germany
[2]Bavarian Environment Agency, 86179 Augsburg, Germany
[3]Analytical Chemistry, University Rostock, Dr.-Lorenz-Weg 1, D-18051 Rostock, Germany
Keywords: PM_{10}, PMF, source apportionment, spatial variability
Presenting author email: juergen.schnelle@helmholtz-muenchen.de

Ambient particulate matter (PM) has long been found to be associated with adverse health effect. In order to better understand and clarify the health impacts of different air pollution sources, there is a growing interest on the relationship between source-specific PM, spatial variability of PM and adverse health effects.

The aim of the study is to identify sources of urban PM_{10} in a winter season and to provide information on the temporal and spatial variability of PM composition and source contributions. The study location is Augsburg, a median sized city in southern Germany. In a previous study five sources of organic compounds have been identified using PMF based on concentrations of semi-volatile organic compounds (SVOC) in $PM_{2.5}$ (Schnelle-Kreis et al. 2007).

In the present study daily PM_{10} samples have been collected from November 14th 2007 to March 31st 2008 at a central, mainly traffic influenced site (Tr). In an intensified campaign from February 13th to March 12th parallel samples have been collected at 7 further sites. These sites are characterised as follows: industry (In), residential area with one-family dwellings (Re), urban background (Ub), tower in city centre with sampling site 100 m above ground (To), and three suburban sites (Su 1 to Su 3). Meteorological data including temperature, humidity, wind direction and speed as well as mixing layer height have been determined at a central site.

A total of 330 PM_{10} samples have been analysed for inorganic ions, elements, EC/OC and particulate organic compounds.

In the intensified campaign with 8 parallel sampling sites in operation the temporal variation of PM composition was determined by the Pearson correlation coefficients (r) of individual PM constituents. The spatial variation was characterised by means of coefficients of divergence (COD) (Wongphatarakul et al. 1998).

High correlations and medium to low COD values were found for most inorganic compounds including $NH4^+$, SO_4^{2-} and NO_3^-, EC and OC, and some organic compounds like PAH or levoglucosan. Some elements such as Ca, Mg, Na, Ti and Zn and most organic compounds including hopanes showed medium or weak correlations and higher COD values. These compounds are most probably influenced by local sources at the respective sites.

Positive matrix factorisation (PMF (Paatero 1997)) has been used for source apportionment analysis. Seven factors, associated with traffic emissions, biomass combustion, re-suspended dust, sodium chloride, Nitrate, and sulphate have been separated.

The PMF analysis strengthened the evidence of temporal and spatial variations of the PM composition. Factors with strong local impact like traffic and NaCl showed greatest differences between the different sites. Factors dominated by regional background or long distance transport like Nitrate or sulphate showed only very little spatial variation (Figure 1).

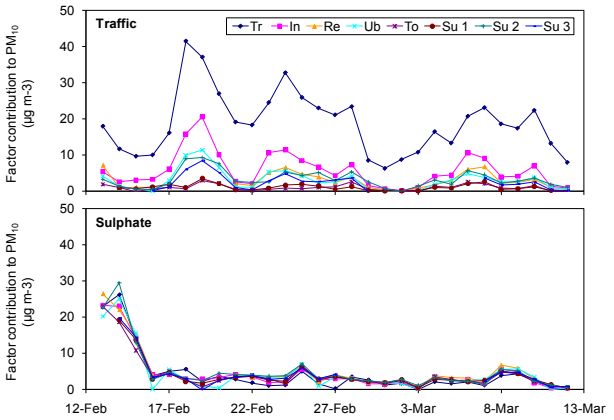

Figure 1: Contributions of source factors "Traffic" and "Sulphate" to ambient PM_{10} at the sampling 8 Sites in Augsburg.

This work was supported by the Bavarian State Ministry of the Environment, Public Health and Consumer Protection und Research Grant U47.

Paatero, P. (1997). "Least squares formulation of robust non-negative factor analysis." Chemometrics and Intelligent Laboratory Systems **37**(1): 23-35.

Schnelle-Kreis, J., M. Sklorz, J. Orasche, M. Stolzel, A. Peters and R. Zimmermann (2007). "Semi volatile organic compounds in ambient PM2.5. Seasonal trends and daily resolved source contributions." Environmental Science & Technology **41**(11): 3821-3828.

Wongphatarakul, V., S. K. Friedlander and J. P. Pinto (1998). "A comparative study of PM2.5 ambient aerosol chemical databases." Environmental Science & Technology **32**(24): 3926-3934.

Source apportionment modelling to quantify atmospheric particle emissions using tunnel measurements

Samantha Lawrence, Khaiwal Ravindra* and Ranjeet Sokhi

Centre for Atmospheric and Instrumentation Research (CAIR), University of Hertfordshire, Hatfield, Hertfordshire, AL10 9AB, United Kingdom
Keywords: PMx, metals, PAHs, non-exhaust emissions, emission factors.
Presenting author email: r.khaiwal@herts.ac.uk

Introduction: The link between increased particle pollution and health issues has prompted the introduction of strict exhaust emission standards. However, research has shown that non-exhaust emissions also contribute significantly to atmospheric particle concentrations. This highlights the need to chemically identify the non-exhaust emissions and their sources. Considering this, we quantified the exhaust / non-exhaust emissions by combining innovative motorway tunnel sampling and source apportionment receptor modelling.

Hatfield tunnel: The Hatfield Tunnel is located in Hatfield, Hertfordshire forming part of the A1(M) motorway between junctions 3 and 4; 0.8 km west of Hatfield town centre. The tunnel is 1115m in length, which provides sufficient distance for satisfactory gap between sampling sites. Furthermore, the dispersion is limited, providing an ideal location for sampling low concentration analytes.

Source apportionment: Analytical techniques ICP-AES and GC-MS were used to identify the metallic and organic composition of PM_{10}. Good correlation was observed between Fe, Cu, Mn, Ni, Pb and Sb and change in traffic volume. The concentration of polycyclic aromatic hydrocarbon and other organics varies significantly at the entrance and exit site of tunnel. Fluoranthene, pyrene, benzo[a]pyrene, chrysene and benzothiazole shows the highest incremented concentrations.

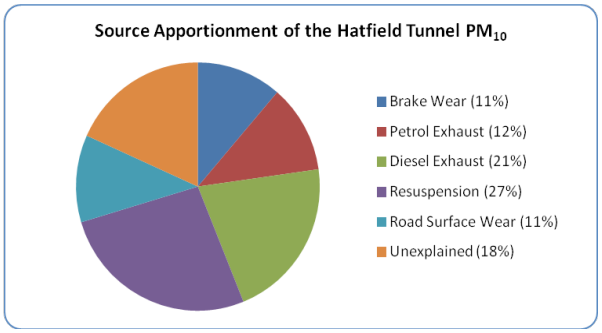

Figure 1. Source apportionment of PM_{10} using combined dataset.

The application of Principal Component Analysis and Multiple Linear Regression Analysis helped to identify the emission sources for 82% of the total PM_{10} mass inside the tunnel (Figure 1). These sources includes resuspension (27%), diesel exhaust emissions (21%), petrol exhaust emissions (12%), brake wear emissions (11%) and road surface wear (11%).

Atmospheric particle emissions: Road Tunnels are like large laboratories with known boundary conditions. The current work compares the High Volume, Dichotomous Stacked Filter Unit and Partisol Air Sampler for coarse, PM_{10} and $PM_{2.5}$ particle concentration measurement and found that they do not differ significantly (p= 95%). $PM_{2.5}$ fraction contributes 66% of PM_{10} proportions and significantly influenced by traffic (turbulence).The mean PM_{10} emission factors varies from 21.3±1.9 – 28.8±3.4 mg/vkm and composed of motorcycle, cars, LDVs, HDVs and buses as shown below:

Table 1. Comparison of mean PM_{10} mass emission factors (mg/km)

Fleet Type	Current Study	NAEI
Motorcycles	0.0003 - 0.001	0.002
Cars	26.1 - 33.4	33.0
LDVs	2.5 - 3.0	10.3
HDV	2.4 - 2.8	22.3
Buses	0.1 - 0.1	0.7

The source apportionment modelling identifies break wear (3.8-4.4 mg/vkm), petrol exhaust (3.9-4.5 mg/vkm), diesel exhaust (7.2-8.3 mg/vkm), resuspension (9-10.4 mg/vkm), road surface wear (3.9-4.5 mg/vkm), and unexplained (7.2 mg/vkm) as major sources of PM_{10} emissions. The current study shows that combined non-exhaust fleet PM_{10} emission factor (16.7-19.3 mg/vkm) is higher than the combined exhaust emission factor (11.1-12.8 mg/vkm).

This study shows that chemical components of PM_{10} linked to a number of health issues originate from exhaust and non-exhaust sources; signifying the need to mitigate not only exhaust but also non-exhaust emissions, as they will become major source of PM_{10}.

This work was supported by NERC (Studentship NER/S/A/2004/13004) and the BOC Foundation who

provided financial assistance. We acknowledge Ian Bull, Hongjun Mao, Douglas Prain, Lakhumal Luahana, Emma Tomlinson and sampling assistants for their help during sampling and/or analysis.

Monday, September 5, 2011

Session 2E: Gas-phase Synthesis of Nanoparticles

Flame-spray derived complex fluoride upconversion nanoparticles

A. Stepuk, D. Mohn and W.J. Stark

Institute for Chemical and Bioengineering, ETH Zurich, Zurich, 8093, Switzerland
Keywords: flame spray pyrolysis, upconversion nanoparticles, complex fluorides, luminescence.
Presenting author email alex.stepuk@chem.ethz.ch

Nowadays, various applications, such as bioimaging, solar cells (Shalav *et al*, 2005) and luminescent displays use upconversion phosphors. These materials consist of a host matrix filled with rare earth elements which are responsible for the visible emissions. The rare earth based upconversion phosphors are usually represented by oxysulfide, fluoride, gallate, and silicate types hosts, doped with Yb-Er and Yb-Tm couples (Auzel, 2004). One of the most efficient host matrices for the near-infrared (NIR) to visible upconversion phosphors is hexagonal sodium yttrium fluoride (Sommerdijk, 1973). Mass-produced upconversion phosphors $NaYF_4$: Yb, Tm are fabricated in bulk microcrystalline form by high-temperature solid-state synthesis. Recent reports demonstrated several novel approaches in mass-production of nanocrystalline UC phosphor materials: decomposition of multi-precursors, co-precipitation, hydrothermal and solvothermal methods (Martin *et al*, 1999). Nonetheless, those methods in the UC nanoparticles synthesis are limited to the predictable crystallites morphology, low production rate and complicated synthesis schemes.

In this study, flame spray technique (Grass and Stark, 2005) was applied to synthesize hexagonal $NaYF_4$ nanoparticles, doped with Yb^{3+} and Tm^{3+} ions. The prepared powders consisted of nanoparticles sized 20-40 nm. TEM analysis (Fig. 1a) of powders shows the presence of hexagonal particles in nanometric scale. The SEM micrographs of flame sprayed $NaYF_4$: Yb, Tm displayed the agglomerated uniformly sized nanoparticles (Fig. 1b).

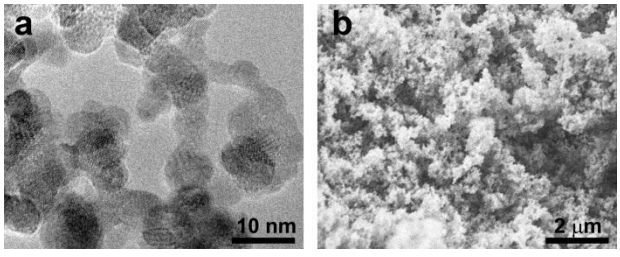

Figure 1. (a) TEM and (b) SEM images of $NaYF_4$:Yb,Tm nanoparticles.

Thermal treatment of the powders changed the phase composition, morphology and size of the particles (Fig. 2).

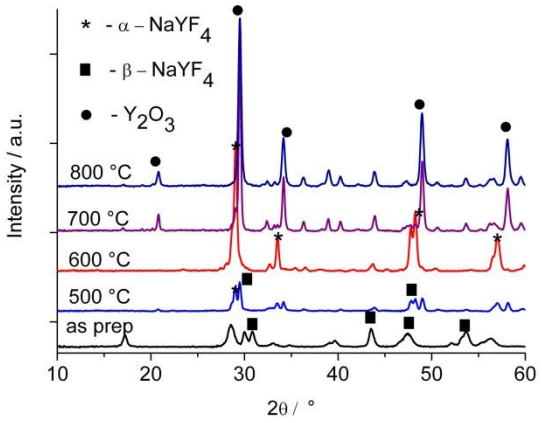

Figure 2. XRD patterns of the $NaYF_4$: Yb, Tm powders sintered at different temperatures.

Excitation by near-infrared (980 nm) laser revealed visible emissions formed by the particles, proving their upconversion properties. Upconversion luminescence of the materials strongly depends on the synthesis and sintering conditions.

Various flame regimes, doping by different rare-earth elements, variation of dopant concentration influenced the formation of cubic and hexagonal phases. Kinetics and thermodynamics, as critical factors of phase type, are to be discussed within the presentation. During this talk we will show, that aerosol processing is also applicable for non-oxidic nanoparticles, such as highly potential complex fluoride phosphors.

Auzel, F. (2004) *Chem. Rev.*, **104**, 139-173.

Grass, R. N. and Stark, W. J. (2005) *Chemical Communications*, 1767-1769.

Martin, N., Boutinaud, P., Mahiou, R., Cousseins, J. C. and Bouderbala, M. (1999) *Journal of Materials Chemistry*, **9**, 125-128.

Shalav, A., Richards, B. S., Trupke, T., Kramer, K. W. and Gudel, H. U. (2005) *Appl. Phys. Lett.*, **86**.

Sommerdijk, J. L. (1973) *Journal of Luminescence*, **8**, 126-130.

Aerosol synthesis of silicon-germanium nanostructures

R. Körmer[1], C. Mehringer[1], B. Butz[2], E. Spiecker[2] and W. Peukert[1]

[1]Institute of Particle Technology, Friedrich-Alexander-University Erlangen-Nuremberg, Cauerstr. 4, 91058 Erlangen, Germany
[2]Center for Nanoanalysis and Electron Microscopy (CENEM), Friedrich-Alexander-University Erlangen-Nuremberg, Cauerstr. 6, 91058 Erlangen, Germany
Keywords: material synthesis, core-shell nanoparticles, silicon, germanium.
Presenting author email: c_meh@web.de

Nanocrystalline silicon is a promising material for the application in printable electronics (Holman et al, 2010). Silicon nanoparticles (SiNP) are typically synthesized via gas phase route by pyrolysis of diluted silane (SiH_4). These particles can be dispersed in organic liquids and deposited as thin functional films. As a prerequisite for the functionality of the film, good contacts between individual particles are necessary. It is difficult to sinter Si films due to the high melting point. A thin germanium layer around a silicon core might be a suitable composite material for improvement. Si and Ge are familiar from the electronic properties but Ge has a much lower melting point.

A reactor system with two consecutive hot-wall reactors was used in the experiments. The first reactor stage is operated at temperatures between 900°C and 1200°C for the synthesis of the SiNP with defined properties (Körmer et al, 2010). Silane, diluted in argon, is used as precursor mixture. After the first reactor the aerosol is quenched by additional argon. Prior to the second reactor stage, GeH_4 is fed into the system. In the second reactor stage Ge films are deposited on the SiNP aerosol at temperatures between 500°C and 700°C. At the reactor exit the aerosol is quenched by nitrogen. The particles are collected with a membrane filter or sampled with a low pressure impactor by deposition on TEM grids or silicon wafers.

The spherical silicon particles from the first reactor are characterized by a specific surface area of 90 m^2/g, which is equal to a mean diameter of about 29 nm. The average crystal size was determined from XRD analysis to 25 nm. The composite materials exhibit crystalline domains for Si as well as for Ge, which can be seen in the X-ray diffraction pattern in figure 1. The Ge shell thickness can be influenced by the temperature or the amount of GeH_4 added to SiNP aerosol.

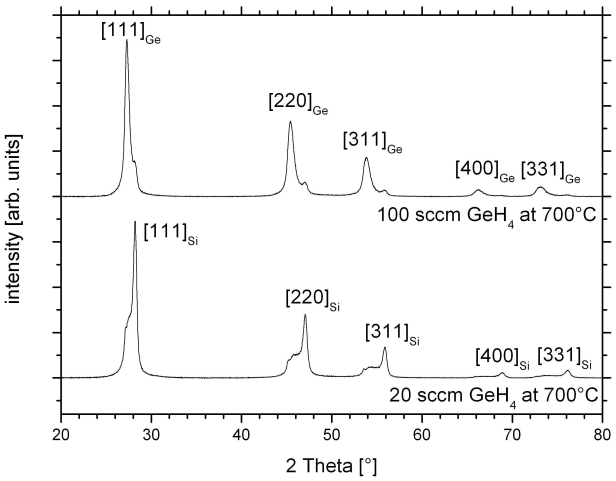

Figure 1. XRD data for Si-Ge composite material.

The core-shell structure was proven by STEM analysis. In figure 2 the z-contrast due to the different atomic weight of Si and Ge is visible. It shows representative particles synthesized at reaction conditions where thick Ge layers are formed. The deposition of Ge leads to varying shell thicknesses around the Si core and patchy particles are formed. This can be explained by energetically favoured sites for the initial island growth. Due to the slight misfit between the crystal lattices the Ge grows preferentially on itself and only partially around the Si core. The influence of the reaction conditions on the morphology of the hybrid particles will be discussed.

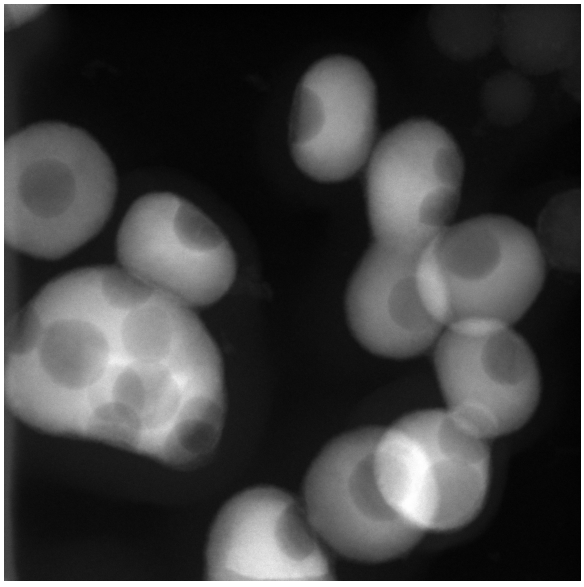
Figure 2. STEM picture of Si-Ge core-shell structures (dark: Si, bright: Ge).

This work was supported by the German Research Council (DFG) and the Cluster of Excellence "Engineering of Advanced Materials" (EAM).

Holman, Z. C., Liu, C.-Y. & Kortshagen, U. R. (2010) *Nano Lett.* **10**, 2661-2666.
Körmer, R., Jank, M.P.M., Ryssel, H., Schmid, H.-J. & Peukert, W. (2010*) J. Aerosol Sci.* **41**, 998-1007.

Copper nanoparticle synthesis by an arc evaporation / condensation process

H. Förster[1] , C. Wolfrum[2] and W. Peukert[1]

[1]Institute of Particle Technology, Friedrich-Alexander-University Erlangen-Nürnberg, Cauerstr. 4, 91058 Erlangen, Germany
[2]ECKART GmbH, Werk Güntersthal, 91235 Velden, Germany

Keywords: metal nanoparticles, synthesis, arc evaporation/condensation.
Presenting author email: H.Foerster@lfg.uni-erlangen.de

Metal nanoparticles exhibit special properties which make them favourable for numerous applications in different fields, such as electronics, sensor technology, catalysis and optics. In this work the synthesis of copper nanoparticles in an arc aerosol furnace by the evaporation/condensation method is systematically investigated. Apart from the usual advantages of gas phase processes (e.g. high purity, scalability) the evaporation/condensation process allows direct synthesis using pure metals as starting materials and thus avoiding routes including reactions of expensive and potentially poisonous precursors.

In the system used for this study a d.c. arc provides the energy for evaporation of the metal target which is contained in a graphite crucible and has anodic polarity to avoid micro droplet formation (Mahoney, 1995). The cathode consists of a sharpened tungsten needle protected by a sheath gas flow (Ar). The arc length is adjustable by vertical movement of the anode setup. For transportation of the metal vapour out of the plasma zone and subsequent aerosol dilution a carrier (Ar) and quench gas flow (N_2) are applied respectively. To prevent any oxidation in the system, gases with purity grade 5.0 are used. Additionally the sheath gas stream is enriched with small amounts of hydrogen as getter material.

The arc stability and its effect on particle size are investigated (see Fig. 1).

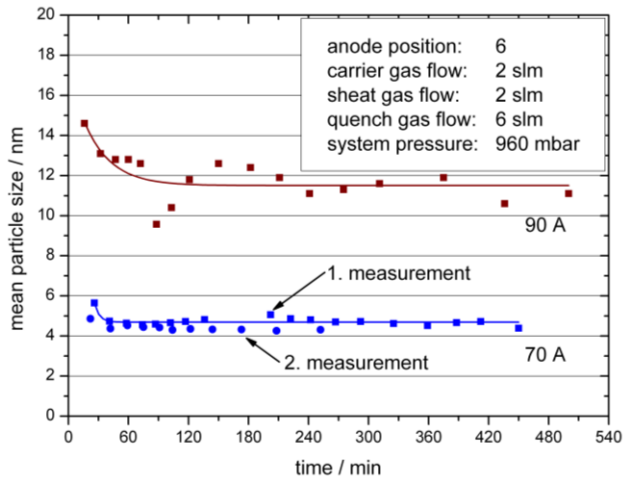

Figure 1. Long term stability and reproducibility of mean particles sizes (SMPS-measurement)

After a warm-up time of 1 h for an arc current of 70 A respectively 2 h for an arc current of 90 A the experiments reveal excellent long term arc stability for at least 6 h continuous operation delivering aerosols with high reproducibility (± 10 % of average mean particle size). The electric characteristics of the arc are studied for various operating conditions. The influence of the arc current and length (exemplarily shown in Fig. 2), the flow rates of the applied gases, the system pressure and the addition of hydrogen to the sheath gas on the average particle size and the agglomerate structure are analysed by scanning mobility particle sizing (SMPS), scanning electron microscopy (SEM) and transmission electron microscopy (TEM). The average particle size could be well controlled in a size range from 4 to 50 nm by selecting appropriate operating parameters. The standard deviation exceeded not more than 5.5 % of the average particle size (minimum of 3 measurements per parameter set).

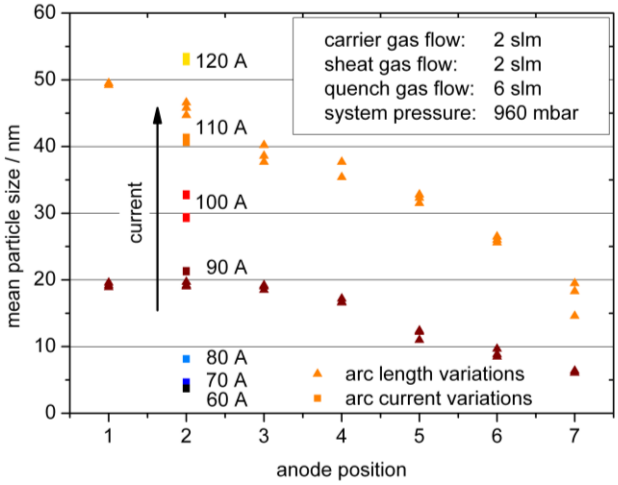

Figure 2. Influence of arc length and arc current on mean particle sizes (SMPS-measurement).

The material properties are analyzed by X-ray diffraction (XRD), energy dispersive X-ray spectroscopy (EDX) and thermo gravimetric analysis.

This work was supported by the Bavarian Science Foundation (BFS).

Mahoney, W., & Andres, R. P. (1995). *Materials Science and Engineering*, A204, 160-164.

Photochemical synthesis of olivine ($Mg_{2x}Fe_{2-2x}SiO_4$; $0 \leq x \leq 1$) nanoparticles

R.W. Saunders and J.M.C. Plane

School of Chemistry, University of Leeds, Leeds, LS2 9JT, UK
Keywords: Photochemical reaction, Generation of nanoparticles, Electron microscopy
Presenting author email: r.w.saunders@leeds.ac.uk

The *olivine* family of minerals (end members: *forsterite* - - Mg_2SiO_4 and *fayalite* - Fe_2SiO_4) are a significant component of the Earth's crust/mantle in crystalline form, and are also considered to be the dominant composition, in both crystalline and amorphous structures, for nano-size meteoric smoke particles formed in planetary atmospheres and cosmic dust grains in the interstellar medium (Henning, 2010).

The laboratory synthesis of such mixed-metal silicates for crucial fundamental studies of their optical and physico-chemical properties has to date been restricted to a 'top down' bulk, sol-gel approach, whereby generated powders can be dried and ground down to micron-size particles. However, the properties of such particles at the nano-scale are likely to be significantly different, primarily as a consequence of the increasingly high surface area to volume ratios below sizes of ~ 100 nm (Hochella *et al.*, 2008).

In order to generate nano-sized olivine particles with variable Fe-Mg content (x) for further study, we have developed a novel photochemical technique (described in Saunders and Plane, 2011), whereby gas-phase Fe, Mg and Si oxide species are produced from the photo-oxidation of suitable precursor vapours ($Fe(CO)_5$ – iron pentacarbonyl, $Mg(OC_2H_5)_2$ – magnesium ethoxide and $Si(OC_2H_5)_4$ – tetraethyl orthosilicate) in a flow cell. Particles nucleate and grow from this oxide vapour 'mix', and are captured for electron microscope (TEM) imaging and compositional analysis (energy dispersive x-ray or EDX spectroscopy and electron energy loss spectroscopy or EELS).

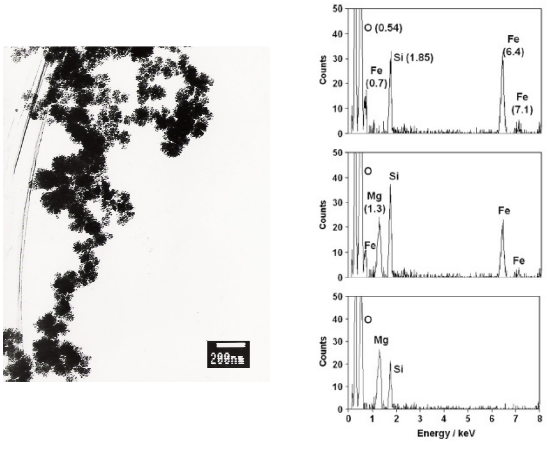

Figure 1. *Left* – TEM image of a particle aggregate formed in the tertiary vapour experiments described. *Right* – EDX spectra of olivine particles of varying Fe-Mg composition

Figure 1 (left panel) shows a typical 'fractal-like' particle aggregate (composed of primary particles of ~ 10 nm diameter), captured and analysed for composition. The right panel of this figure gives examples of EDX spectra (with characteristic elemental peaks indicated) acquired from particles formed in experiments with the absence of Mg-precursor (top) and of Fe-precursor (bottom) – leading to Fe_2SiO_4 and Mg_2SiO_4 particle compositions respectively. The middle panel is a spectrum of a mixed-metal olivine particle (x ~ 0.5) formed with all three precursor vapours generated in the reaction cell.

Control over the stoichiometry (value of x) of the end particle composition was found to be possible from the tertiary vapour photochemical system simply through careful variation of the initial flow ratio (R_p) of Mg and Fe precursor vapours i.e. R_p = $Mg(OC_2H_5)_2$ / $Mg(OC_2H_5)_2$+$Fe(CO)_5$, with quantitative EDX and EELS analysis indicating atomic Mg/Fe in particles α R_p – see Figure 2 below.

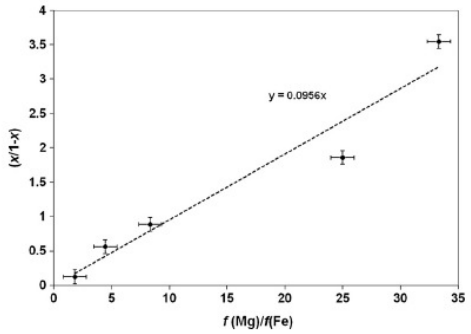

Figure 2. Correlation plot of the ratio of x/1-x (equivalent to measured Mg/Fe in particles) to the ratio of precursor flows used for particle generation.

In conclusion, we have shown that it is possible to efficiently and controllably generate mixed-composition olivine nanoparticles using a photochemical system (at atmospheric pressure and room temperature) and appropriate precursors for the formation and reaction of initial gas-phase metal oxide and Si oxide vapours, leading to particle nucleation.

This work was supported by funding from the UK Natural Environment Research Council (NERC).

Henning, T. (2010) *Annu. Rev. Astron. Astrophys.* **48**, 21-46.

Hochella, M.F., et al. (2008) *Science* **319**, 1631-1635.

Saunders, R.W. and Plane, J.M.C. (2011) *Icarus* doi:10.1016/j.icarus.2010.12.019.

Chemical Kinetic Model of the In-Flight Silica Coating of Nanoparticles by Photo-Induced Chemical Vapour Deposition

Adam M. Boies*[1], Steven Calder[2], Pingyan Lei[3] and Steven L. Girshick[3]

[1]Current Address: Department of Engineering, University of Cambridge, Cambridge CB2 1PZ, UK
Department of Chemistry[2] and Mechanical Engineering[3], University of Minnesota, Minneapolis, MN 55455
*Corresponding Author, Email: a.boies@eng.cam.ac.uk, Phone: +44 1223 746972

Key Words: core-shell, nanoparticle synthesis, chemical kinetics, photochemistry

The synthesis of silica-encapsulated nanoparticles has received much interest in recent years as the production of such structures can enhance particle properties such as thermal stability and surface functionality. The production of composite nanoparticles by gas-phase methods allows for particles to be produced at high throughputs in inert or non-reacting environments with little or no surface impurities. Photochemical vapor deposition (photo-CVD) is a gas-phase approach that allows for the production of a variety of core-shell compositions, including organic (Zhang *et al.* 2008) and inorganic coatings (Boies *et al.* 2009) on nanoparticles. While the approach has been shown to work experimentally, a fundamental understanding of the chemical mechanisms involved in the coating process has not been presented.

This study presents a chemical mechanism of the photo-CVD process to describe the production of silica coatings from the decomposition of tetraethyl orthosilicate (TEOS). The chemical mechanism builds on the work of previous thermal TEOS decomposition mechanisms, but is the first to include photochemical reactions and nanoparticle surface growth. The mechanism is modeled within a plug-flow reactor with conditions that mimic those of previous experimental results. As shown in Figure 1, the particles and precursor enter near the vacuum ultraviolet (VUV, λ=172 nm) radiation source and are transported down the chamber by the bulk fluid motion as a series of gas-phase and surface reactions result in a silica coating.

The photochemical model is validated by examining the photodecomposition of O_2, a reaction that can be solved analytically. Results from the comparison confirm that photodecomposition can be adequately determined within the modeling environment, CHEMKIN-PRO. Modeled results of the entire photo-CVD mechanism indicate that the dominant reactions for the production of silica coatings are the photodecomposition of TEOS and the removal of surface ethyl groups from adsorbed TEOS species. Analysis of the effect of oxygen within the system indicated that it participates in both the gas-phase decomposition of TEOS and surface formation of silica, but is not the primary reaction pathway for most modeled conditions.

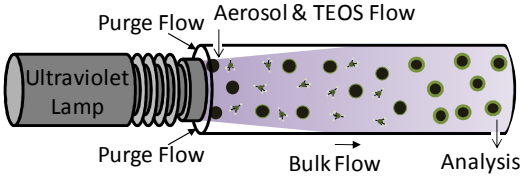

Figure 1: Experimental schematic of nanoparticle silica coating by photo-CVD with TEOS as a precursor.

Particle growth due to surface coating was modeled for a variety of precursor concentrations, radiation intensities and system residence times corresponding to previous experimental studies. Results from the modeled findings were compared to experimental studies published previously (Boies *et al.* 2009). As shown in Figure 2, the model is in agreement with experimental results, showing an increase in coating thickness with respect to increased TEOS flow and decreased nitrogen flow. The modeled growth trends of coating thickness as a function of TEOS flow rates most closely match experimental results in the case of greater TEOS absorption cross sections (an unknown parameter within the system) and diffuse radiation. These modeled results show a similar trend and are within an order of magnitude of the experimental results, which represents good agreement given uncertainties of many parameters including absorption cross sections and reaction rates.

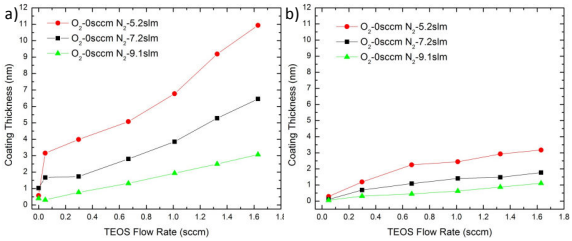

Figure 2: a) Experimental coating thickness, and b) modeled coating thickness as a function of TEOS and nitrogen flow rates.

This research was primarily supported by NSF CBET-0730184, by the MRSEC Program of the NSF DMR-0819885, and by the Minnesota Futures Grant Program. This work was carried out in part using computing resources at the University of Minnesota Supercomputing Institute.

Boies, A. M., Roberts, J. T., Girshick, S. L., Zhang, B., Nakamura, T. and Mochizuki, A. (2009). *Nanotechnology*: 295604.

Zhang, B., Liao, Y. C., Girshick, S. and Roberts, J. (2008). *Journal of Nanoparticle Research* 10:173-178.

Assessment of Size Distribution Models in Coupled 3D CFD Simulations for the Prediction of Nanoparticle Coagulation in Transonic Flows

J.F. Quaatz, M. Giglmaier and N.A. Adams

Lehrstuhl für Aerodynamik und Strömungsmechanik, Technische Universität München
D-85748 Garching b. München, Germany
Keywords: Nanoparticles, Aerosol modelling, CFD, Number size distribution
Presenting author email: frederik.quaatz@aer.mw.tum.de

The presented research is part of the joint project DFG PAK 75 that has the objective to design a gas dynamic process and a facility for the production of high-quality nanoparticles. The motivation is the coupling of 3D CFD simulations with particle-growth models to predict the size distribution and the number density. The focus of this report is the evaluation of combinations of 3D flow simulations with three different established coagulation models using experimental data obtained from the novel facility.

Main component of the facility (Figure 1) is a double-chocked flow channel. A precursor (TEOS – tetraethyl orthosilicate) is injected into the subsonic flow upstream of the first critical cross section A_1^*. Within the first nozzle the flow accelerates to supersonic speed of up to $M \approx 1.8$. A shock in the divergent part of the first Laval nozzle causes an instantaneous temperature increase above the ignition temperature of the precursor. Consequently, the flow is decelerated to subsonic conditions. Particle growth occurs within the subsequent reaction zone with constant cross section. A particular property of the novel facility is that in the reaction zone quasi constant thermodynamic conditions are maintained ($T = 1300K$, $p = 6bar$) that lead to a homogeneous coagulation. Particle growth is terminated by re-accelerating the flow to supersonic speed within the second Laval nozzle. This gas dynamic quenching process enables a cooling rate of $O(10^7)$ K/s. Furthermore, the total temperature of the gaseous flow is sufficiently reduced by water injection. Due to homogeneous and controllable thermodynamic operating conditions this gas dynamic process promises high-quality nanoparticles with well defined properties, such as narrow size distributions.

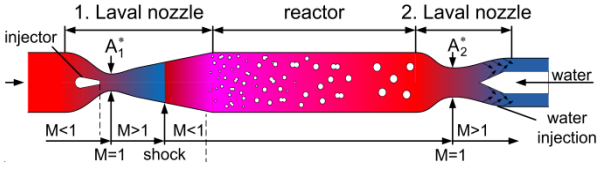

Figure 1. 1D sketch of the simplified gas dynamic process – M is the Mach Number of the flow, A_1^*, A_2^* are the chocked cross sections of both Laval nozzles, cool regions are indicated with blue color, hot regions are highlighted in red

We perform 3D CFD simulations of the full facility including both Laval nozzles and taking into account the heat release by the precursor combustion. For a proper consideration of secondary flows, e.g. corner vortices, an Explicit Algebraic Reynolds Stress Model (EARSM) is applied. In order to take turbulent mixing effects into account the particle-growth model is coupled with the CFD simulation. The characteristic quantities of the particle -size distribution are modeled as transported passive scalars. The coagulation terms of the General Dynamic Equation (GDE) are implemented as sources. Due to high super-saturation, nucleation processes are negligible. We compare three different approaches for approximating the particle size distribution (Figure 2): An efficient bimodal monodisperse model, a bimodal polydisperse model using the method of moments (Jeong, 2004) and a computationally rather expensive sectional model (Hounslow, 1988). We relate the model-specific underlying assumptions to the operating conditions within the given facility. Also, feasibility is assessed by comparing the numerical results with experimental data.

Since our numerical method couples CFD with the particle models, the size distribution of the nanoparticles is predicted at an arbitrary location within the 3D flow field. In order to highlight this advantage, we compare our results with a common post-processing-type method where the particle growth is only computed along isolated streamlines.

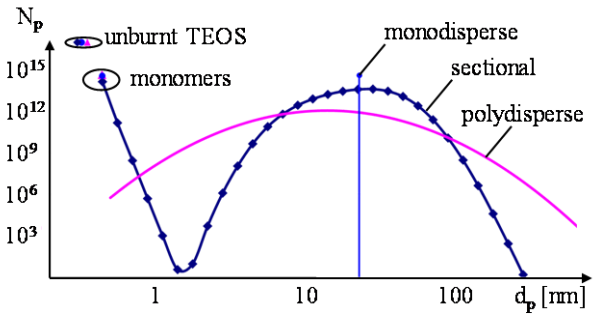

Figure 2. Particle size distribution at the symmetry axis of the facility (Fig. 1) performed with the monodisperse, the poldydisperse and the sectional model (Giglmaier, 2010)

Giglmaier, M., Al-Hasan, N.S., Quaatz, J.F., Adams, N.A. (2010) Numerical prediction of average size and size distribution of gasdynamically generated nano-particles by coupled reactive 3-D CFD simulations and comparison to experimental data, *IAC 2010*, Helsinki

Hounslow, M.J., Ryall, R.L., Marshall, V.R. (1988) A Discretized Population Balance for Nucleation, Growth, and Aggregation *AIChE Journal* **34**:11

Jeong, J.I., Choi, M. (2004) A bimodal moment model for the simulation of particle growth, *JoAS* **35**

Formation of metal nanoparticles from supersaturated vapor (Zn, Bi).

A. A. Onischuk[1], A. M. Baklanov[1], O. V. Borovkova[1], V. V. Karasev[1], S. di Stasio[2], S. V. Vosel[1]

[1]Institute of Chemical Kinetics and Combustion, Novosibirsk 630090, Russia
[2]Istituto Motori CNR-IM Aerosol and Nanostructures Lab, Via Marconi 8, Napoli, 80125, Italy
Keywords: metal nanoparticles, homogeneous nucleation, nucleation rate.
Presenting author email: onischuk@kinetics.nsc.ru

Nucleation of metals differ essentially from other systems nucleation and needs a detailed investigation. This work compares experimental routes of measurement of the nucleation rate from Zn and Bi vapor in a laminar flow chamber. The flow chamber consisted of a quartz tube (of i.d. = 0.7 - 1.0 cm) with an outer heater. A flow of Ar was supplied to the inlet with the rate 8 - 17 cm^3/c. A piece of metal (Zn, Bi) was put inside the heated zone, and that resulted in saturated vapor generation. At the outlet of the heated zone the temperature dropped down resulting in the nucleation onset. The concentration, size and shape of particles at the outlet of the tube was analyzed by TEM and automatic diffusion battery. The analysis of thermophoretic depletion of particle concentration in the region of temperature decrease, and the numerical simulation of nucleation coupled with the experimental axial and radial profiles of temperature have shown that the nucleation onset occurs within the layer of 1 mm near the wall of tube. Therefore, the axial profile and morphology of the wall deposit can give the information on the location of the region of maximum nucleation rate and the nucleation volume. However, there can be two different situations: the nucleation temperature T is less than the melting point (as it was in the case of Zn) and higher (Bi). In the first case it is easy to determine the nucleation rate, because the nucleation zone is easy to distinguish by the transition from smooth to powder-like deposit (Fig. 1a), the nucleation time may be estimated from the length of the initial increase in the wall mass deposit profile (Fig. 1b) and as the outlet particles are not aggregated (Fig. 1c) the nucleation rate can be estimated from the outlet particle concentration and the nucleation time. Thus, for example, for T = 660 K and supersaturation S = 15 the nucleation rate was found to be 10^{10} $cm^{-3}s^{-1}$.

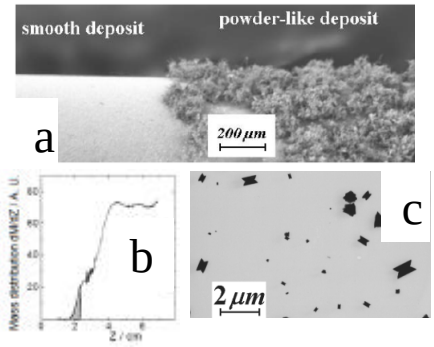

Fig. 1. Zn nucleation data :a) SEM image of wall deposit, b) wall deposit axial profile, c) TEM images of the outlet particles. Nucleation temperature T =660 K.

The situation is quite different in the case of Bi. At the outlet of the tube we observed the aggregates of small primary particles. Thus, to estimate the nucleation rate one should account the mean number of primary particles in aggregates. As the nucleation temperature is higher than the melting point, it is not possible to determine the nucleation zone just by the wall deposit SEM images. Additional methods are to be involved. One of them is light scattering. The light beam passes in the axial direction and the beginning of light scattering gives some information on the location of zone of maximum nucleation rate. Besides, the method of the "supersaturation cut-off" gives an additional information about the nucleation rate. The last experimental technique is as follows. A metal grid is inserted to the quartz tube perpendicularly to the flux. The outlet aerosol concentration is measured continuously. When the grid is downflow essentially after the nucleation onset point the outlet concentration is not disturbed by the presence of grid due to the low particle-to-grid diffusion deposition efficiency (because of the large size of particles). When moving the grid upflow the outlet concentration is decreasing (due to the vapor-to-grid deposition as well as the increase the particle-to-grid deposition efficiency) and the maximum rate of decrease of concentration corresponds to the region of maximum nucleation rate. The numerical simulation of vapor-to-particle transformation coupled with the experimentally measured axial and radial temperature profiles was also made. The simulation included wall vapor deposition, nucleation, particle growth due to vapor deposition and coagulation, particle wall deposition (diffusion + thermophoresis). An example of comparison of simulation results with the experimental measurements is shown in Fig. 3.

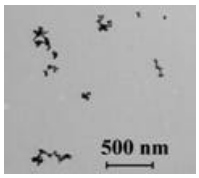

Fig. 2. TEM image of Bi aggregates. T = 710 K

Fig. 3. Bi concentration (as a constituent of both vapor and aerosol particles), light scattering intensity, nucleation rate vs. axial coordinate. Symbols and noisy line - experiment, smooth lines - simulation. T = 710 K.

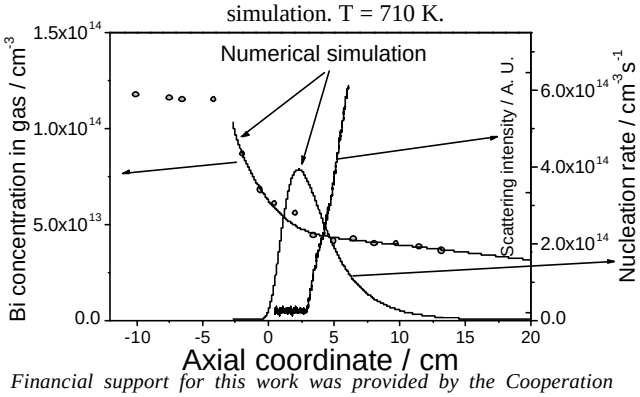

Financial support for this work was provided by the Cooperation Agreement between CNR (Italian National Research Council) and RAS (Russian Academy of Science) years 2008-2010 and Siberian Branch of RAS (Interdisciplinary Integration Project No. 3).

Monday, September 5, 2011

Session 2F: Aerosol Mobility and Capture

Calculation of the mobility radius of fractal aggregates

A.D. Melas[1,2], A.G. Konstandopoulos[1,3] and Y. Drossinos[2]
[1]Department of Chemical Engineering, Aristotle University, P.O. Box 1517, 54006 Thessaloniki, Greece
[2]European Commission, Joint Research Centre, 21027 Ispra (VA), Italy
[3]Aerosol & Particle Technology Laboratory, CERTH/CPERI, P.O. Box 60361, 57001 Thessaloniki, Greece
Keywords: fractal aggregates, friction, mobility radius, radius of gyration.
A.D. Melas: Anastasios.Melas@jrc.ec.europa.eu

Aerosol particles are of great importance because they influence the climate via direct and indirect processes and they may also induce adverse human health effects. Many aerosol particles are fractal-like objects composed of primary spherical monomers, e.g., combustion-generated nanoparticles. Their transport properties are characterized by the mobility radius R_k which is the radius of a spherical particle with the same friction coefficient under similar dynamic condition. The aggregate diffusion coefficient becomes $D_k = k_B T/6\pi\mu R_k$, where μ is the fluid viscosity, T the fluid temperature, and k_B Boltzmann's constant.

In this study we use a numerical method to calculate the mobility radius of fractal aggregates composed of k identical, spherical primarily particles (monomers of radius R_1) in the continuum regime, and to correlate it to their radius of gyration R_g. The aggregates are generated via a tunable cluster-cluster algorithm (Thouy and Jullien, 1996) as a function of a prescribed fractal dimension d_f to satisfy the scaling law $k = k_f(R_g/R_1)^{d_f}$, with k_f the fractal prefactor.

Experimental studies on the transport properties of nanoparticles have shown that the total mass transfer coefficient times the aggregate mobility is constant (Keller *et al.*, 2001). This approximate relationship holds for a large range of mobilities, and it is independent of the particle shape and chemical nature. Consequently, the molecule-aggregate collision rate K_k, which is proportional to the mass transfer coefficient, is proportional to the friction coefficient. The collision rate is calculated from the steady-state molecular diffusion equation via integrating the molecular diffusive flux over the aggregate surface. The appropriate boundary conditions are total absorption on the aggregate surface, fluid density $\rho = 0$ on the surface, and $\rho = \rho_\infty$ far from it. The k-aggregate friction coefficient, and its mobility radius, is obtained from the ratio of two molecular collision rates: the molecular collision rate with the k-aggregate and the molecular collision rate with a monomer K_1. Specifically,

$$\frac{\beta_k}{\beta_1} = \frac{K_k}{kK_1} = \frac{R_k}{kR_1} \quad ,$$

where the aggregate friction coeffient is $f_k = km_1\beta_k$, with β_k its average friction coefficient per unit monomer mass, and m_1 the primary-particle mass.

Isella and Drossinos (2011) validated this method for straight chains (d_f=1, $k_f = \sqrt{3}$) by solving the diffusion equation in cylindrical coordinates. We reproduced their calculations in 3d. Furthermore, we calculated the average friction coefficient of two three-dimensional, symmetric shapes composed of eight particles: a cube and a rectangle. The simulations were performed with the commercial finite-element code COMSOL. A comparison of our results with average friction coefficients calculated from a multipole expansion of the Stokes velocity (Filippov, 2000) is presented in Table 1. The good agreement suggests that the method is reliable to determine the friction coefficient of aggregates with $d_f \neq 1$.

Structure	Filippov (2000)	Collision rate
Cube ($2\times2\times2$)	0.293	0.290
Rectangle ($2\times4\times1$)	0.361	0.366

Table 1: Friction coefficient of two symmetric objects.

According to the tunable cluster-cluster algorithm the computer-generated fractal aggregates (composed of uniform spherical primary particles) can have prescribed fractal dimensions between 1 and 2.5. A typical 256-monomer cluster is presented below.

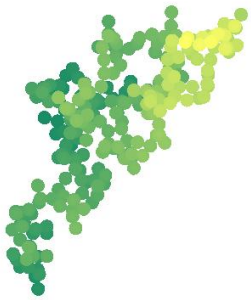

Figure 1: A random 256-monomer aggregate of $d_f = 2$.

A.D.M. acknowledges a Joint Research Centre doctoral Fellowship.

Keller, A., Siegmann, K., Siegmann, A.C., Filippov, A. (2001), J. Vacuum Sci. Technol. A **19**, 1.

Isella, L., Drossinos, Y. (2011), J. Colloid Interface Sci. (in press).

Filippov A.V. (2000), J. Colloid Interface Sci. **229**, 184.

Thouy, R., Jullien, R. (1996), J. Phys. I France **6** 1365-1376.

Mobility measurements of electrosprayed protein ions in the sub 10 nm size range

A. Maißer[1], V. Premnath[2], A. Ghosh[2], M.B. Attoui[3], and C.J. Hogan[2]

[1]Faculty of Physics, University of Vienna, Vienna, 1090, Austria
[2]Department of Mechanical Engineering, University of Minnesota, Minneapolis, Minnesota, 55455, USA
[3]Faculty of Science and Technology, University of Paris XII, Paris, 94010, France

Keywords: DMA, Mass spectrometry, mobility, proteins
Presenting author email: anne.maisser@univie.ac.at

Differential mobility analysis (DMA) has been widely applied for mobility measurements of electrosprayed, charge reduced globular proteins. In conjunction with mass spectrometric measurement (MS), DMA permits examination of the density and structure of proteins in the gas phase. In previous studies by Bacher *et al.* (2001), and Kaddis *et al.* (2007) a gas-phase electrophoretic mobility molecular analyzer (GEMMA, TSI Inc.) has been used. This device consists of a modest resolution DMA (the TSI nano-DMA) in combination with an electrospray aerosol generator (EAG) and a condensation particle counter (CPC). A linear relation between particle diameter and the 1/3rd power of the protein ion mass has been found in these studies. However, the density calculated from those measurements is ~0.6 g cm^{-3}, which, when compared to density of peptides (~1.35 g cm^{-3}), is anomalously low. While mobility measurement of charge reduced protein ions is no doubt a promising analytical technique for protein structural analysis, the questionable protein density inferred from these measurements casts doubt on the conclusions drawn in prior work. In an effort to better understand the structure of gas-phase protein ions, we have performed systematic measurements of the mobility diameters of various protein ions in air with a higher resolving power DMA (the Nanoengineering ½ mini DMA, which has a resolving power of ~25, Fernandez de la Mora, and Attoui, 2008) than has been used in prior work.

Experimental Results

Five different proteins in the sub 10 nm size range were examined: Lysozyme, Cytochrome C, Myoglobin, Ovalbumin, and Bovine Serum Albumin.

Gas-phase protein ions were produced using the TSI electrospray aerosol generator, in which a Po-210 radioactive alpha source is used for charge reduction of the highly charged droplets generated during the electrospray process. The electrospray was operated in Cone-jet mode, which was verified by both measurement of the electrospray current as well as visual observation of the electrospray cone. To produce protein ions, solutions were made in two different buffer solutions: a 20 mM ammonium acetate aqueous buffer thought to prevent the denaturation of proteins during the electrospray process, and a strongly denaturing formic acid in 50:50 methanol to water buffer solution. For each electrosprayed protein, the mobility spectra was determined by stepping the DMA voltage with a constant step size. The measured mobilities were inverted to mobility diameters using the Stokes-Millikan equation. In addition to the mobility measurements the same proteins were investigated for their molecular mass using a TOF-MS (QSTAR Pulsar I, Applied Biosystems). In that case a home made electrospray source, without charge reduction is used.

The relation between measured mobility diameters and protein ion masses is shown in Fig. 1. The data points were fitted with a power function $y=cx^3$ were c is a constant.

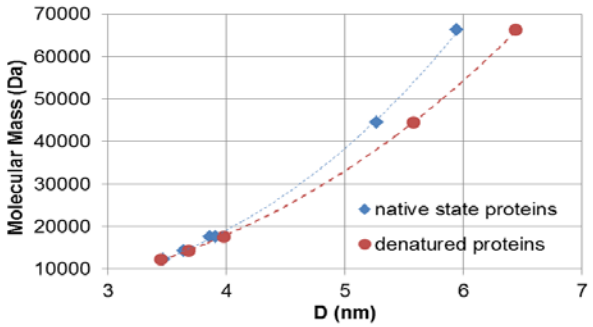

Figure 1. Mobility diameters of singly charged monomers of native state proteins and denatured proteins

The mean density found from measured mobility diameters of proteins electrosprayed from non-denaturing buffer solutions is 0.970 ± 0.043 g cm^{-3}. For denaturing buffer solutions the density is slightly less with a mean value of 0.863 ± 0.06 g cm^{-3}. These values are significantly higher than what has been found with standard DMA instruments before, but are in good agreement with recent DMA-MS measurements of non-charge reduced protein ions (Hogan & Fernandez de la Mora, 2011) as well as measurements made in N_2 with a drift tube mobility spectrometer (Bush et al., 2010).

Bacher, G., Szymanski, W.W., Kaufman, S.L, Zöllner, P., Blaas, D., and Allmaier, G. (2001) *J. Mass Spectrom.* **36,** 1038-1052.

Kaddis, C.S, Lomeli, S.H., Yin, S., Berhane, B., Apostol, M.I., Kickhoefer, V.A., Rome, L.H., Loo, J.A. (2007) *J. Am. Soc. Mass Spectrom.* **18,** 1206-1216**.**

Fernandez de la Mora, J., and, Attoui, M., (2008) *Annual meeting of the Spanish Aerosol Association (RECTA)*

Hogan, C., and Fernandez de la Mora, J., (2011) J. Am Soc. Mass Spectrom.

Bush, M.F, Hall, Z., Giles, K., Hoyes, J., Robinson, C.V., and Ruotolo, B.T., (2010) *Analyt. Chem.* **82,** 9557-9565.

Deposition on fibrous filters in the interception region

Sarah J. Dunnett[1], Charles F. Clement[2]

[1]Department of Aeronautical and Automotive Engineering, Loughborough University, Loughborough, Leics. LE11 3TU, U.K.
[2]15 Witan Way, Wantage, Oxon, OX12 9EU, U.K.

Keywords: fibrous filter, filtration, numerical simulation, particle deposition

INTRODUCTION

When deposit accumulates inside a fibrous filter the fluid flow through the filter, and hence the filters collection efficiency, is altered. Although this is well known, it is difficult to model the particle build up within a filter. However it is crucial that a full understanding of the process of particle deposition and its effects upon further deposition is obtained in order to understand the performances of fibrous filters. We have been developing a numerical model of fibrous filtration aimed at investigating deposition due to various mechanisms and the effect filter properties and particle characteristics have upon it (Dunnett and Clement 2006, 2009). We have shown that, for small particles where the dominant mechanism by which particles deposit is diffusion, the porosity of the deposit formed does not significantly influence further deposition. For larger particles the porosity of the deposit has been seen to have a greater influence upon the flow field, and hence upon particle behaviour. In this paper we consider particles for which interception is the main mechanism of deposition.

NUMERICAL MODEL

In earlier work, Dunnett and Clement (2009), a numerical model has been developed which determines the flow field, and particle motion, around a single fibre which has a porous deposit made up of collected particles on its surface. Flow through the porous material is described by the Darcy equation in the model. Neighbouring fibres are taken into account by the application of boundary conditions. Further deposition of particles onto the porous surface has then been determined. It was found that the parameter $s = \kappa/\delta$ was the main factor determining the deposition mechanism. In this expression κ is the ratio of the particle to fibre diameters also known as the interception parameter, and δ is the non-dimensional thickness of the diffusion layer. For $s<1$ diffusion is the dominant mechanism of deposition, for $s=O(10^0)$ interception dominates and for large values of s impaction becomes important. For small particles for $s<<1$ where diffusion is dominant, deposition remains mainly spherically symmetric around the fibre as the deposit builds up and the porosity does not significantly affect further deposition. However as particle size increases and $s>1$ then the porosity has a more significant affect. In this work deposition by interception has been considered and we will report the results obtained from our model as the deposit builds up. Initial results have shown that the shape of the deposit formed is dependent upon the flow through the initial porous deposit. As an example, the particle build up is shown in Figure 1a for the case when $\kappa=0.05$ and $\varphi=0.9$ when the numerical model has been used to build the deposit up in layers starting with a clean fibre. Here φ is the fraction of the porous media that is occupied by void space. In Figure 1b the particle build up is shown also for $\kappa=0.05$ and $\varphi=0.9$ but in this case it has been assumed that the fibre initially has a layer of deposit on it, shown by the line in the Figure flattened at the front

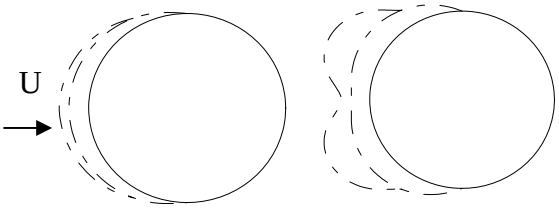

Figure 1a. Figure 1b

As can be seen the shape of the initial deposit has a significant effect upon the subsequent deposit. The deposit shown in Figure 1b resembles that observed by Kanaoka et al (1986) and indicates that the assumptions made in the numerical model may lead to inaccuracies for the initial particle build up.

The validity of the assumptions made is being investigated. We find that Darcy's equation should ideally be replaced by the Brinkmann equation for the porous flow when the deposited layer is thin. We also investigate the effect of various parameters as the deposit builds up.

REFERENCES

Dunnett, S.J. and Clement, C.F. (2006) J. Aerosol Sci., 37, 1116-1139.

Dunnett, S.J. and Clement, C.F. (2009) Eng. Anal. Boundary Elem. 33, 601-610.

Kanaoka, C.,Emi,H.Hirage,S.,Myojo,T.(1986) Aerosols,formation and reactivity 2nd Int. Con. Berlin

Break-up of agglomerated TiO_2 particles due to impaction

Ihalainen M.[1,2], Lind T.[1], Güntay S.[1], and Jokiniemi J.[2,3]

[1]PSI Paul Scherrer Institut, The Laboratory for Thermal-Hydraulics, CH-5232 Villigen PSI, Switzerland
[2]Fine Particle and Aerosol Technology Laboratory, Department of Environmental Science, University of Eastern Finland, P.O. Box 1627, FI-70211 Kuopio, Finland
[3]VTT Technical Research Centre of Finland, Fine Particles, P.O. Box 1602, 02044 VTT, Espoo, Finland

Keywords: de-agglomeration, impactor.

The interparticle forces in an agglomerate significantly affect how that agglomerate behaves when it is stressed with external forces, i.e. whether the agglomerate breaks up, bounces or sticks to the surface during impaction onto a surface. During a postulated pressurized water reactor (PWR) steam generator tube rupture accidents involving core melt, agglomerate behaviour during impaction at high velocity on tube surfaces adjacent to the breach needs to be characterized (Güntay *et al*., 2004). Possible deagglomeration during impaction might modify the physical properties of the particle, e.g., the particle size which is one of the key parameters affecting further deposition/transport behaviour in the secondary side of the steam generator.

In this study the agglomerates are impacted onto a surface at controlled conditions and the bond energies are estimated from several measured quantities. Similar approach to study agglomerate break up has been used in earlier empirical studies (Froeschke *et al*., 2003; Seipenbusch *et al*., 2007), however in this study, in addition to the break-up, the study of the bounced particles due to the impaction is also emphasised. The conditions leading to particle bouncing and the characteristics of the bounced particles will be studied.

A chemical vapour synthesis was used to generate TiO_2 agglomerates and a differential mobility analyzer (DMA) was used for size classification of the agglomerates. In these measurements electrical mobility of 250nm for the agglomerates was used.

The agglomerates were impacted onto an impaction plate located in a single stage Micro-Orifice Uniform Deposit Impactor (MOUDI). There was also a Transmission Electron Microscope (TEM) grid on the impaction plate for the TEM analysis of the impacted particles. The agglomerate impaction velocity was adjusted by changing the pressure difference over the impactor. The impaction velocities were estimated by calculating the particle trajectories with Euler method. The gas properties, e.g. gas velocities, needed to calculate the particle trajectories were evaluated with the Computational Fluid Dynamics (CFD) modeling. Similar method was previously used by e.g. Arffman *et al*, 2011.

The bounced particles were measured with a Scanning Mobility Particle Sizer (SMPS), an Electrical Low Pressure Impactor (ELPI) and a TEM-grid sample. For these measurements the air stream after the impactor, which is at low pressure, was collected to a sampling chamber, which was designed and built for this purpose (Ihalainen *et al*. 2010). After the collection of the sample the chamber was pressurized to the normal pressure and the measurements from the chamber were carried out. The measurements were also conducted without the impaction plate. This way the intact agglomerates could be sampled and studied from the chamber, as the agglomerates flow through the same measurement set-up but without impaction.

TiO_2 agglomerates were impacted onto an impaction plate at different velocities. In Figure 1. the size distributions of the bounced particles, measured with the SMPS, are shown. As the impaction velocity increases the size of the particles decreases, i.e. agglomerate fragments into smaller pieces. The number concentration of the bounced particles increased as the velocity increased. Further analysis of the break-up process will be presented, as well as particle shape characterization. In addition, impacted particles will be characterized.

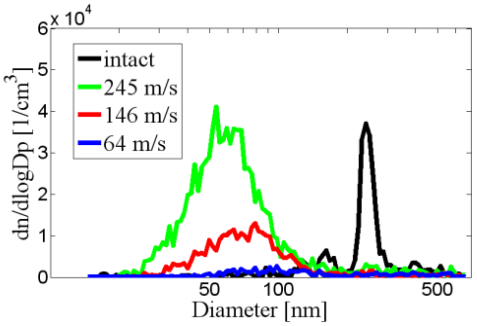

Figure 1. Size distributions of the TiO_2 agglomerates before impaction (intact) and the bounced particles

Arffman, A., Marjamäki, M., & Keskinen, J., Accepted in *J. of Aerosol Sci.* on Feb 11, 2011

Froeschke S., Kohler S., Weber, A.P. & Kasper G., *Aerosol Science*, 34 (2003), 275-287.

Güntay, S., Suckow, D., Dehbi, A. & Kapulla, R. (2004). *Nuclear Engineering and Design*, 231, 109-120.

Ihalainen, M., Lind, T., Güntay, S., & Jokiniemi., J. (2010). *International Aerosol Conference* 2010,

Seipenbusch M., Toneva P., Peukert W. & Weber A.P., (2007). *Particle & Particle System Characterization*, 24, 193-200.

Characterization of nanoparticles aggregates deposits produced by filtration: influence of aggregates morphology and filtration velocity

Ouf, F.X.[1], Wenxin, S.[1,2], Kessoum M.[1], Thomas, D.[2], Gensdarmes, F.[1] and Rolland P.[3]

[1]Aerosol Physics and Metrology Laboratory, IRSN, BP 68, 91192, Gif-sur-Yvette Cedex, France.
[2] LRGP , Nancy Université, 1 rue Grandville, BP 20451, 54001 Nancy cedex, France.
[3]Alicona SARL, 11 rue de Savoie, 91940 Les Ulis, France.

Keywords: filtration, nanoparticle, fractal aggregates, porosity.
Presenting author email: francois-xavier.ouf@irsn.fr

The manufacturing of nanoparticles is increasing and opens new applications and economical developments. According to a recent report of the National Science Foundation, the nanomaterials marketplace will represent in 2010-2015 more than 300 billions $. Nevertheless, these economical concerns should not occult the social impact of nanoparticles and investigations dealing with toxicity of such products must be carried out. As a consequence of this social concern, the containment of nanoparticles during production processes is a key issue to reduce as much as possible workers exposure. In this field, dynamic containment devices like glove boxes associated to High Efficiency Particulate Air filters are a widely used solution and the question of penetration of nanoparticles through media and clogging (Kim et al., 2009a and b) of such filters must be investigated.

The aim of this study is to measure experimentally the porosity of cake deposits formed during filtration of nanoparticles aggregates and to propose a theoretical description of the clogging of filters by such particles. The experimental device presented in figure 1 is composed of two different sources of nanoparticles aggregates; a spark discharge generator (PALAS GFG 1000) with carbon electrodes and a combustion aerosol generator using propane as fuel (miniCAST 5201 Jing.).

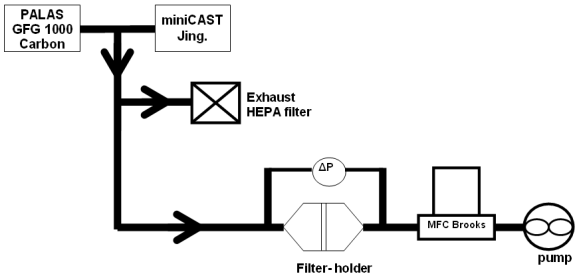

Figure 1. Experimental device of clogging of media by nanoparticles aggregates

A filter holder is implemented at the outlet of these aerosol generators, the filtration flow-rate is controlled by a mass flow rate controller (MFC Brooks 5850) and the pressure drop is measured with a differential pressure transducer (Wöhler DC2000 Pro). In order to reduce the in-depth filtration regime, PTFE membranes (Millipore FSLW04700 with 3.0 µm pore size) have been used and the deposited mass of nanoparticles has been measured with a METTLER AE 240 weighing cell with a resolution of 0.01 mg. The filtration surface area has been measured with an optical microscope and the height of the cake with a focus-variation surface metrology system (InfiniteFocus ALICONA). The porosity of the cake ε is computed according to the following relationship:

$$\varepsilon = 1 - \frac{M_c / \rho_{pp}}{H.A_f},$$

where M_c is the mass of the cake, ρ_{pp} is the density of nanoparticles (kg/m^3), H the height of the cake (m) and A_f is the filtration surface area (m²). Table 1 presents mean porosity obtained for the following experimental conditions.

Table 1. Experimental conditions and mean porosity

Aerosol generator	GFG 1000		CAST	
Monomer diameter (nm)	7		19	
Fractal dimension	2		1.6	
Density (kg/m^3)	2000		1800	
Filtration velocity (cm/s)	1.1	8.8	1.1	8.8
Mean porosity	**0.987**	**0.985**	T.b.m.	

T.b.m.: to be measured

According to our results for the GFG 1000, one must noticed that the porosity is not significantly modified by the filtration velocity. A mean value close to 0.986 can be proposed to be typical of our nanoparticles deposits on membrane in the range 1.1 – 8.8 cm/s. Further investigations are actually conducted on the CAST generator in order to underline the influence of the size of primary particles/aggregates and the fractal dimension. Finally, a theoretical description of the clogging of filter by nanoparticles aggregates, including the fractal morphology of such particles, will be presented and compared to experimental results.

Kim, S.C., Wang, J., Emery, M.S., Shin, W.G., Mulholland, G.W. & Pui, D.Y.H. (2009). *Aerosol Sci. Technol.,* 43, 344 – 355.

Kim, S.C., Wang, J., Shin, W.G., Scheckman, J.H. & Pui, D.Y.H. (2009). *Aerosol Sci. Technol.,* 43, 1033 – 1041.

Transfer of gas-borne carbon nanoparticles onto liquid surfaces

D. Koch and A.P. Weber
Institute of Particle Technology, Clausthal University of Technology, 38678 Clausthal-Zellerfeld, Germany
Keywords: nanoscale carbon particles, surfactants, deposition, bubble column.
Presenting author email: koch@mvt.tu-clausthal.de

The transfer of gas-borne nanoparticles into a liquid consists of a diffusional transport step onto the liquid surface, the wetting of the adsorbed nanoparticles and the incorporation into the liquid. Such processes are relevant for gas cleaning in wet electrostatic precipitators and wet scrubbers, but also for the recovery of nanoparticles. Basis for the present study was the synthesis of organic nanoparticles from pharmaceutical substances by Rapid Expansion of Supercritical Solutions (RESS) which are discharged into aqueous solution to prevent further growth by coagulation (Türk and Lietzow, 2004 and 2008). To stabilize the small particle size and, therefore, to preserve the high bioavailability, surfactant molecules have been added to the solution. Thus, the nanoparticles arriving at the interface encounter a surfactant-loaded liquid surface.

In order to study the deposition behaviour of nanoparticles in different suspensions, nitrogen-borne carbon nanoparticles are generated in a spark generator. The aerosol is injected via a nozzle (diameter: 150 μm) into a bubble column, in which the different suspensions are filled. The internal aerosol flow is expected to depend on the properties of the gas-liquid interface. To vary the interface properties, different surfactants (e.g. polyvinylpyrrolidone (PVP) of the types K25 and K90) with varying concentrations are used.

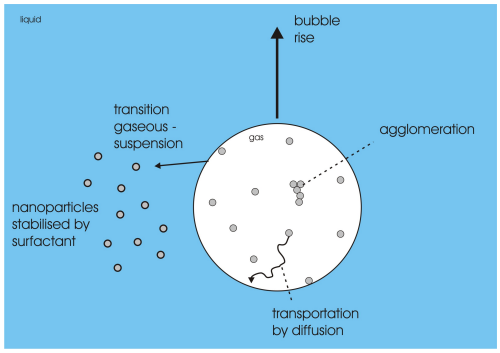

Figure 1: Transfer steps of gas-borne nanoparticles.

During the experiment, the mass transfer of the carbon particles (see fig. 1) is measured twice by an extinction device, from which the precipitated mass in the liquid can be calculated, and furthermore by a “Scanning Mobility Particle Sizer (SMPS)”. According to these measurement results, the deposition efficiency of the liquid phase can be calculated by the quotient of the number concentration before and after the bubble column. Table 1 shows the experimental results for the deposition efficiency of carbon nanoparticles (mean mobility equivalent diameter: $60-70$ nm , number concentration: $1.6\cdot10^{7}$ cm^{-3}).

Solution	Concentration (% (weight))	Deposition efficiency (-)
Water	-	0.71
PVP K25	0.4	0.18
PVP K25	1.0	0.16
PVP K90	0.4	0.24
PVP K90	1.0	0.25

Table 1: Deposition efficiency of pure water and different PVP solutions.

In order to proof the experimental results, existing models for the transfer of aerosol particles to the interface in rising bubbles (Fuchs, 1964; Pich and Schütz, 1991) can be used. Fuchs introduced the model for larger bubble sizes (0.3 to 0.6 cm), bigger particles ($1\cdot10^{-7}$ m) and pure water as liquid. For the particle sized used here, the diffusional deposition is the major process, which takes mainly place in the equatorial region of a gas bubble and depends on the internal circulation inside it (fig. 2).

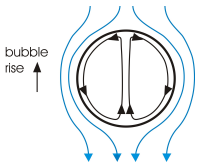

Figure 2: Internal circulation (Hill’s vortex) inside a gas rising bubble.

In this contribution further separation efficiencies of different systems (combination of surfactant and concentration) depending on the relative bubble velocity will be presented, which are the profit of additional experiments. Additionally the Fuchs model will be discussed and possible extensions for the description for the deposition of nanoparticles in surfactant-containing liquids will be proposed.

This work was supported by the Deutsche Forschungsgemeinschaft (DFG) under grant DFG-We 2331/5-2.

N.A. Fuchs (1964) *The Mechanics of Aerosols*, Pergamon Press, Oxford.

Pich, J. and Schütz, W. (1991) *J. Aerosol Science, 22, 267-272*.

M. Türk, R. Lietzow (2004) *AAPS PharmSciTech, 5 (4), Article 56*.

M. Türk, R. Lietzow (2008) *J. of Supercritical Fluids, 45, 346-355*.

Deposition of Nanoparticles on Wire Screens by Diffusion and Image Force

V. Gómez[1], C.H. Huang[2], F.J.Alguacil[3] and M. Alonso[3]

[1]Instituto de Nanociencia de Aragón (INA), Edificio I+D, c/ Mariano Esquillor s/n, 50018 Zaragoza,Spain.
2Department of Environmental Engineering and Health, Yuanpei University, 30015 Hsinchu, Taiwan
[3]National Center for Metallurgical Research (CSIC), Avenida Gregorio del Amo, 8. 28040 Madrid, Spain.
Keywords: Nanoparticles; Aerosol filtration; Charged particles.
Presenting author email: virgomez@unizar.es

This abstract presents the results of an experimental investigation on the deposition of charged and neutral nanoparticles on wire screens by the combined mechanisms of diffusion and image force. Experiments were performed with particles having diameters below 10 nm and using four different flow rates and three kinds of wire screens.

As the experimental results have shown, the single fiber efficiencies for the mechanisms of image force, $\eta_{IM,}$ and diffusion, η_D, are of the same order of magnitude and, furthermore, they are both much smaller than one. Under these conditions, the total capture efficiency can be approximated as the sum of the efficiencies by diffusion and image force deposition, $\eta = \eta_D + \eta_{IM}$. The efficiency for the image force mechanism will be obtained from fitting of experimental results to an expression of the form $\eta_{IM} = AK_{IM}^B$, where

$$K_{IM} = \left(\frac{\varepsilon_f - 1}{\varepsilon_f + 2}\right)\frac{Cp^2e^2}{12\pi^2\mu\varepsilon_0 u d_p d_f^2} \qquad (1)$$

is the image forcé number (ε_f : dielectric constant of the fiber; ε_o: vacuum permittivity; C: slip correction factor; p: number of charges per particle, e: elementary charge; μ: air viscosity; u: air flow velocity; d_p:: particle diameter; d_f: fiber diameter).

For the experiments, an evaporation-condensation NaCl aerosol was charged in a ^{241}Am neutralizer. Positively charged particles of known size were withdrawn from a differential mobility analiyzer (DMA, TSI short column, L=11.11 cm) operated at an aerosol-to-sheath flow rate ratio of 2/20. Since our study has been restricted to particle size below 10 nm, all the particles classified by DMA were singly charged. These positively singly-charged monodisperse particles can follow two alternative routes: one, containing a ^{241}Am neutralizer and an electrostatic precipitator, and the second one, a bypass route to transport the +1 particles into the filter unit.

The filtration unit consists essentially in a grounded cylinder made of brass having a length of 186 mm and inner diameter of 8 mm. A series of five rings, 4 mm in width and made of brass, were placed inside the main cylinder. The wire screens were placed in between any two consecutive rings, so that the screen fibers are in contact with the grounded cylinder.

Three types of screen were used in the experiments; their characteristics are listed in Table 1. The “sandwich” wire screen consisted of a gold wire screen between a pair of aluminum wire screens; it has been experimentally assessed and its characteristics are also showed in Table 1**.** Penetrations were determined for varying values of: (i) aerosol flow rate through the filter; (ii) particle size; and (iii) number of charges on the particles (0, +1).

Material	Aluminium	Stainless steel	Sandwich
Fibre diameter, d_f (μm)	100	66	55
Opening (μm)	110	103	
Thickness (μm)	260	120	524
Density (g cm^{-3})	2.70	7.96	
Surface density (g cm^{-2})	0.02	0.03	
Open area fraction (-)	0.27	0.37	
Solid volume fraction (-)	0.30	0.32	0.32
Screen parameter , S	1.44	1.08	5.77

Table 1. Characteristics of the wire screens employed

From the experimental results, the following correlation has been obtained:

$$\eta_{IM} = 36.06K_{IM}^{0.55} \qquad (2)$$

The total penetration can then be calculated as

$$P = \exp\left[-nS\left(2.7Pe^{-2/3} + 36.06K_{IM}^{0.55}\right)\right] \qquad (3)$$

where n is the number of screens, and is compared in Figure 1 with typical experimental results obtained in the course of this work.

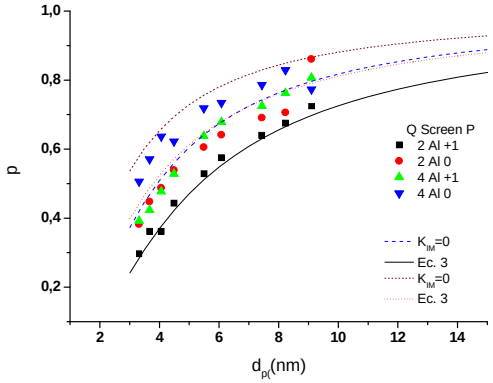

Figure 1. Comparison between experimental penetrations and those calculated with Ec. (3) for 2 and 4 aluminium screens and aerosol flow rates of 2 lmin^{-1} and 4 lmin^{-1}.

This work was supported by grants DPI2008-06199, CSIC 2009TW0017 and NSC 99-2923-E-264-001-MY2.

Monday, September 5, 2011

Session 3A: Bioaerosols / Specific Aerosol Types

Ergosterol, arabitol and mannitol as tracers for biogenic aerosols in the eastern Mediterranean

N. Burshtein, N. Lang-Yona, and Y. Rudich

Department of Environmental Sciences, Weizmann Institute of Science, Rehovot 76100, Israel

Keywords: bioaerosols, fungi, ergosterol, arabitol, mannitol.
Presenting author email: noa.burshtein@weizmann.ac.il

Aerosols containing biological components can have a significant effect on human health by causing primarily irritation, infections and allergies. Specifically, airborne fungi can cause a wide array of adverse responses in humans depending on the type and quantity present.

In this study we used chemical biomarkers for analyzing fungi-containing aerosols in the eastern Mediterranean region during the year 2009 in order to quantify annual fungal abundances. The prime marker for fungi used in this study was ergosterol, and its concentrations were compared with those of mannitol and arabitol which were recently suggested to also correlate with fungal spores concentrations (Bauer et al., 2008a).

	Arabitol vs. mannitol	Mannitol vs. ergosterol	Arabitol vs. ergosterol
Winter	−0.18	−0.06	−0.03
Spring	**0.78**	**0.60**	**0.81**
Summer	**0.83**	−0.11	−0.24
Autumn	**0.66**	***0.41***	**0.66**

±0.70–1.00 – high correlation
±0.50–0.70 – moderate correlation
±0.30–0.50 – low correlation.

Table 1: Pearson coefficient (r) was used in order to determine the correlation between the markers during each season.

Back trajectory analysis, inorganic ions abundance, humidity and temperature were used in an attempt to identify sources as well as the dependence on seasonal and environmental conditions.

We found that the ambient concentrations of ergosterol, arabitol and mannitol range between 0 and 2.73 ng m−3, 1.85 and 58.27 ng m−3, 5.57 and 138.03 ng m−3, respectively. The highest levels for all biomarkers were during the autumn, probably from local terrestrial sources, as deduced from the inorganic ions and back trajectory analysis. Significant correlations were observed between arabitol and mannitol during the entire year except for the winter months. Both sugars correlated with ergosterol only during the spring and autumn.

We conclude that mannitol and arabitol might not be specific biomarkers for fungi and that the observed correlations during spring and autumn may be attributed to high levels of vegetation during spring blossoms and autumn decomposing. (Burshtein *et al. ACP, **11**, 829–839 (2011)).*

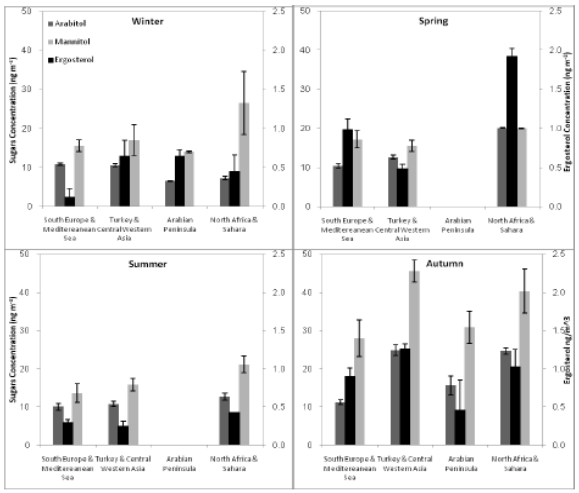

Figure 1: Average concentrations of the biomarkers divided to the typical air mass sectors, according to seasons.

Acknowledgements

This research was partially funded by a grant from the Angel Faivovich Foundation. The authors acknowledge the help given by Ilan Levy and Noam Levin. We also gratefully acknowledge the NOAA Air Resources Laboratory (ARL) for the provision of the HYSPLIT transport and dispersion model used in this publication. Y. R. acknowledges support by the Helen and Martin Kimmel Award for Innovative Investigation.

References:

Bauer, H., Claeys, M., Vermeylen, R., Schueller, E., Weinke, G., Berger, A., and Puxbaum, H, (2008a) Arabitol and mannitol as tracers for the quantification of airborne fungal spores, Atmos. Environ., 3(42), 588–593.

Lau, A. P. S., Lee, A. K. Y., Chan, C. K., and Fang, M, (2006) Ergosterol as a biomarker for the quantification of the fungal biomass in atmospheric aerosols, Atmos. Environ., 40(2), 249–259.

Long range transported mineral dust to the Equatorial Global Atmosphere Watch (GAW) Station on Mt Kenya

M. J. Gatari[1], S. M. Gaita[1], K. Shepherd[2], J. Boman[3], S. Thorsson[4], A. Wagner[5]

[1]Institute of Nuclear Science and Technology, University of Nairobi, P. O. Box 30197-00100, Nairobi, Kenya
[2]World Agroforestry Centre (ICRAF), P. O. Box 30677-00100, Nairobi, Kenya
[3]Chemistry Department, University of Gothenburg, Gothenburg, SE-412 96, Sweden
[4]Deapartment of Earth Sciences, University of Gothenburg, Gothenburg, SE-405 30, Sweden
[5]Department of Applied Physics, Chalmers University of Technology, Gothenburg, SE-412 96, Sweden
Keywords: tropospheric aerosol, PM10/PM2.5, EDXRF, laser particle analyzer.
Presenting author email: mgatari@uonbi.ac.ke

Understanding of the free tropospheric aerosol is important in the investigation of transboundary and interhemispherical contribution to local air pollution. The Global Atmosphere Watch (GAW) station is located on the northern western slopes of Mt Kenya (Fig. 1). It is on the equator at 37^0 E at altitude 3700 m and has free view in all directions thus offering a good site for free troposheric aerosol characterization (Henne et al 2008). Gatari et al (2009) reported high elemental concentrations of Ca, Fe and K in all analyzed $PM_{2.5}$ and PM_{10} samples implying high mineral dust in the aerosol. However the local soil dust influence due to the mountain winds was not assessed. This study was therefore designed to assess the contribution of long-range transported mineral dust and local contribution through mountain winds.

In August 2009 two cyclone samplers (BGI 400 personal samplers) and an Andersen dichotomous impactor were used to sample $PM_{2.5}$ and size segregated PM_{10} respectively. In August 2010 the measurements were repeated and an aerosol monitor (TSI model 8530 DUST TRAK II) fitted with a $PM_{2.5}$ sampling head was included. The measurement reported here were from 10 day field campaign at the GAW station which included random collection of top soil samples from the area.

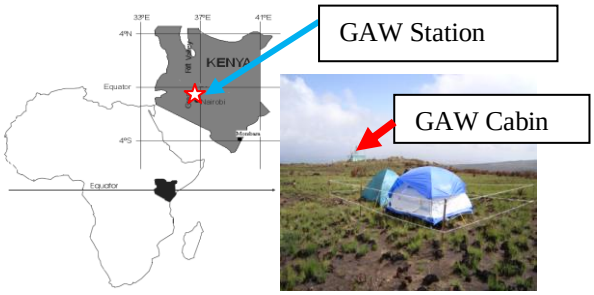

Figure 1. The location of Mt Kenya in Kenya in Africa

Teflon filters (Pall R2PJ037) were used in all the samplers. The monitor gave real time readings and particles on its internal filter. All the filter samples from all the instruments were analyzed for elemental content using EDXRF. The soil samples were analyzed for particle size distribution using a Laser particle diffraction analyzer (LPDA) (Horiba model LA-950V2), and for soluble and insoluble elemental content by TXRF (Bruker model AXS S2 PICOFOX). A digital microbalance (Mettler model MT5) was used for gravimetric determination of the filter collected PM. The LPDA uses Mie theory and its measurements are in equivalent spherical particle diameter (Eshel et al 2004).

The mean $PM_{2.5}$ concentration was 10 µg m^{-3} out of which 22 % was nighttime contribution on average. The elemental concentrations of Ca, Fe, K and Ti were 50 ± 29, 50 ± 12, 31 ± 2, 4 ± 1 g kg^{-1} in the particulate aerosol, respectively and 5 ± 0.005, 42 ± 0.01, 5 ± 0.006, 8 ± 0.005 g kg^{-1} in the top soil. These results and in addition the small available percentage of $PM_{2.5}$ particles in the top soil implied negligible contribution of Ca and K bearing particles to the aerosol while Fe and Ti was substantial. The study also showed high daytime contribution of mineral dust and that which is from long range transport as a major component that needs further investigation besides other aerosol components.

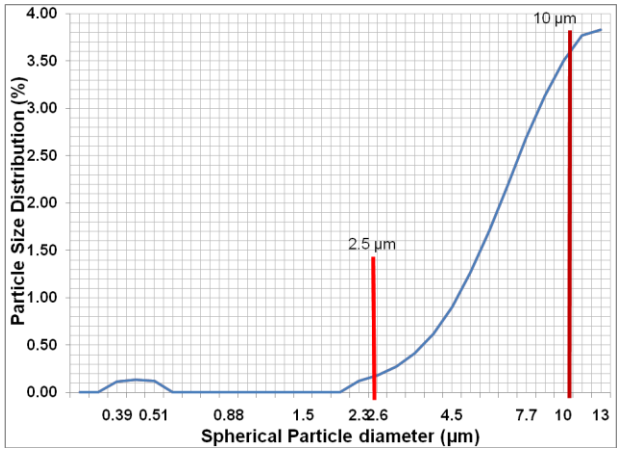

Figure 2. Particle size distribution in the top soil within the area of the GAW site on Mt Kenya.

This work was supported by International Science Program, Uppsala University Sweden and World Agroforestry Centre (ICRAF), Nairobi, Kenya.

Henne, S., Junkermann, W., Kariuki, J. M. and Aseyo, J. (2008) J. Appl. Meteor. 47, 2946–2962.
Gatari M. J., Pettersson J. B. C., Kimani W. and Boman J. (2009) X-Ray Spectrom. 38, 26-36.
Eshel, G., Levy, G. J., Mingelgrin, U. and Singer, M. J. (2004) Soil Sci. Soc. Am. J. 68, 736-743.

Real-time Detection of Airborne Influenza A Viruses Using Silicon Nanowire Field Effect Transistor

Fangxia Shen[1], Miaomiao Tan[1], Zhenxing Wang[2], Maosheng Yao[1,*], Zhenqiang Xu[1], Yan Wu[1], Jindong Wang[2], Xuefeng Guo[2,*], and Tong Zhu[1]

***Principal Contact:** Maosheng Yao, Professor, [1]State Key Joint Laboratory for Environmental Simulation and Pollution Control, College of Environmental Sciences and Engineering, Peking University, Beijing 100871, China, Ph: +86 010 6276 7282, Email: yao@pku.edu.cn,

[2]College of Chemistry and Molecular Engineering, Peking University, Beijing 100871, China

Abstract

Numerous threats from biological aerosol exposures, such as H1N1 influenza, SARS, bird flu, and bio-terrorism necessitate the development of a real-time bioaerosol sensing system, which however is a long standing challenge in the field. Here, we reported real-time detection of airborne influenza H3N2 viruses by integrating electrically addressable silicon nanowire (SiNW) sensor devices with microfluidics and a bioaerosol-to-hydrosol air sampling system. Influenza A viruses were aerosolized into exposure chamber, and collected by an automated electrostatic sampler (AES) at a sampling flow rate of 5 L/min and transported onto the SiNW sensor device via microfludic channel via a peristaltic pump at a flow rate of 0.4 L/min in a real-time manner. The electrical conductance of the SiNW device was monitored using a pre-amplifier and a lock-in amplifier.

Results show that when airborne influenza H3N2 virus samples were collected and delivered to antibody-modified SiNW devices, discrete nanowire conductance changes were observed within seconds. However, the conductance levels remained relatively unchanged when indoor air or clean air samples were delivered. Quantitative polymerase chain reaction (qPCR) tests indicated that higher virus concentrations in the air samples corresponded to higher conductance levels in the SiNW devices. The sensing system here has been demonstrated to have the capability to monitor the airborne presence of influenza A viruses in a real-time manner, typically from 1 to 2 minutes. This response time scale exceeds many of those available bioaerosol sensing systems. The work here opens a new arena for real-time monitoring of biological aerosols by integrating the technologies in different disciplines, holding great promise in the combat of fighting both infectious diseases and bio-terrorism.

Keywords : Influenza A H3N2 virus, bioaerosol, Silicon Nanowire, aerosol-to-hydrosol, qPCR, real-time detection

Characterization of aerosol from ship emissions in the Central Mediterranean Sea (Lampedusa island)

S. Becagli[1], R. Traversi[1], C. Ghedini[1], S. Nava[2], M. Chiari[2], F. Lucarelli[2], G. Calzolai[2], A. di Sarra[3], G. Pace[3], D. Meloni[3], D. M. Sferlazzo[4], C. Bommarito[4], F. Monteleone[4] and R. Udisti[1]

[1] Department of Chemistry, University of Florence, Sesto Fiorentino, Florence, I-50019, Italy
[2]INFN, Sez. Firenze, Sesto Fiorentino, Florence, I-50019, Italy
[3]ENEA CR Casaccia, S. Maria di Galeria, Roma, I-00123, Italy
[4]ENEA, Climate Laboratory, , Palermo, I-90141, Italy
Keywords: ship aerosol, Central Mediterranean Sea, PM10, chemical characterization.
Presenting author email: silvia.becagli@unifi.it

One of the most important task for atmospheric research, air pollution and climate policy is the evaluation of ship emissions and their impacts on environment.
Studies on ship aerosol contribution are so far based on inventories and modellistic approach (e.g. Marmer et al., 2009 and references therein) and show that the simulated contributions of ships to air pollutant levels in the Mediterranean atmosphere are significant, although strongly dependent on the inventory applied. The validation of the consistency of ship emissions inventories with observations is a difficult task due to lack of continuous observations over the open sea.
We present here the estimate of ship emissions to PM10 in Central Mediterranean Sea by chemical characterization of PM10 sampled at Lampledusa Island (35.5°N, 12.6° E).
Ship emissions events are identified using the soluble fraction of V and Ni in HNO_3 at pH1.5 (V_{sol} and Ni_{sol}). Events of ship aerosol presents V_{sol} higher than 6 ng m^{-3}; this threshold was established on the basis of V/Si enrichment factor with respect to the upper continental crust. The V_{sol} and Ni_{sol} are as average 80% of the total V and Ni content determined by PIXE during the identified events of ship aerosol. On the contrary the soluble fraction results less than 50% in events characterized by high crustal content (Saharan dust events).

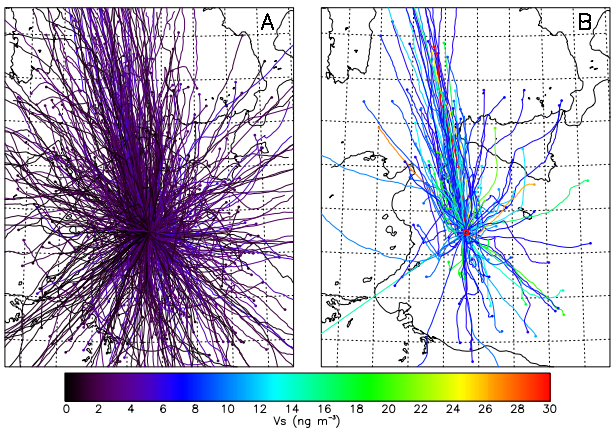

Figure 1. 18-hours back trajectories corresponding to the measurements of V_{sol} less than (plot on the left) or greater/equal to (plot on the right) 6 ng m^{-3}.

Back trajectory analysis (Fig.1) confirms that the selected events are affected by sea-going ships and not by local pollution (i.e. Lampedusa harbour), establishing their origin from the ship tracks crossing the Strait of Sicily. The longer and more relevant events are related to episodes lasting more than one day, confirming that the ship contribution to aerosol load in central Mediterranean can be regarded as a "continuous" emission corresponding to the main ship track that increases the aerosol load and whose contribution at Lampedusa is modulated by the atmospheric dispersion and transport.
Seasonal behaviour with summer maxima is observed for all the ship aerosol markers and in particular for the V_{sol}. Such a pattern can be explained by several factors: (i) increased photochemical activity of atmosphere in summer, leading to an increased production of secondary aerosol, mainly $nssSO_4^{2-}$, but also metals from heavy oil combustion related to particles containing sulphur, (ii) lower rain fall that increases the atmospheric life-time of aerosol species, (iii) higher marine boundary layer stability in summer.
A very intense event in spring 2008 was chemically and size characterised showing that elements arising from heavy oil combustion (V, Ni, Al, Fe) are distributed in the sub-micrometric fraction of aerosol and the metals are present as carbonates, idroxides or metallorganic compounds, so that they are dissolved in mild condition (HNO_3, pH1.5).
Taking into account the source emission profile obtained from exhaust samplings at sea-going ships (Agrawal et al., 2008) it was possible to estimate the ship aerosol contribution to the total PM10 sampled at Lampedusa island. In the selected events we found that aerosol from this source contributes as average for about 0.9 μg m^{-3} and represents as average the 3% of the PM10 mass.

Agrawal, H., W. A. Welch, J. W. Miller, and D. R. Cocker (2008) *Environ. Sci. Technol.* **42**, 7098–7103, doi:10.1021/es703102y.

Marmer E., F. Dentener, J. v. Aardenne, F. Cavalli, E. Vignati, K. Velchev, J. Hjorth, F. Boersma, G. Vinken, N. Mihalopoulos, and F. Raes (2009) *Atmos. Chem. Phys.* **9**, 6815–6831, www.atmos-chem-phys.net/9/6815/2009/.

Particulate Carbon and Sulfur in the Lower Stratosphere

Johan Friberg[1], Bengt G. Martinsson[1], Sandra M. Andersson[1], Carl A. M. Brenninkmeijer[2], Markus Hermann[3], Peter P.F. van Velthoven[4] and Andreas Zahn[5]

[1]Division of Nuclear Physics, Lund University, Lund, Sweden
[2]Max-Planck-Institut für Chemie, Mainz, Germany; [3]Leibniz-Institut für Troposphärenforschung, Leipzig, Germany; [4]Royal Netherlands Meteorological Institute, de Bilt, the Netherlands; [5]Institut für Meteorologie und Klimaforschung, Karlsruhe, Germany

Keywords: carbonaceous aerosol, elemental composition, lowermost stratosphere, upper troposphere

Introduction

Previous measurements in the upper troposphere (UT) and the lowermost stratosphere (LS) have indicated the presence of a carbonaceous component in the aerosol (Murphy et al.,1998, Nguyen et al. 2008, Martinsson et al. 2009). Here the occurrence of carbonaceous and sulfurous particles around the tropopause is investigated. The data were taken from the CARIBIC (Civil Aircraft for Regular Investigation of the atmosphere Based on an Instrument Container) platform, where instruments onboard a Lufthansa passenger aircraft on inter-continental flights are implemented for examination of the atmospheric composition in the UT/LS at 8-12 km altitude (Brenninkmeijer et al. 2007). CARIBIC undertakes aerosol sampling for chemical characterization, as well as measurements of particle number concentrations and mixing ratios of a large number of trace gases including O_3, CO, NO/NO_y, Hg, water (gaseous and condensed), acetonitrile, greenhouse gases and halogenated hydrocarbons. The CARIBIC dataset also contains data on meteorological conditions.

Methods

900 aerosol samples were collected during 200 flights with a typical sampling time of 100 minutes by an impaction technique (Nguyen et al., 2006). Specimen are then analyzed by quantitative multi-elemental analysis by PIXE (Particle-Induced X-ray Emission) and PESA (Particle Elastic Scattering Analysis) to obtain elemental concentrations for sulfur, iron, titanium, potassium, hydrogen, carbon, nitrogen and oxygen among others (Nguyen and Martinsson, 2007).

Results and Conclusions

The concentrations of particulate carbon and sulfur shows an increase from the tropopause into the LS, with a strong dependence on potential vorticity (PV). A seasonal cycle in the concentration to PV ratios is observed in the LS for ozone, carbon and sulfur (Fig.1).

The peak of the oscillations is found in the end of April to the beginning of May for carbon and ozone. The sulfur peak is shifted more than a month in respect to ozone and carbon, indicating different formation patterns for carbonaceous and sulfurous aerosol in the stratospheric circulation.

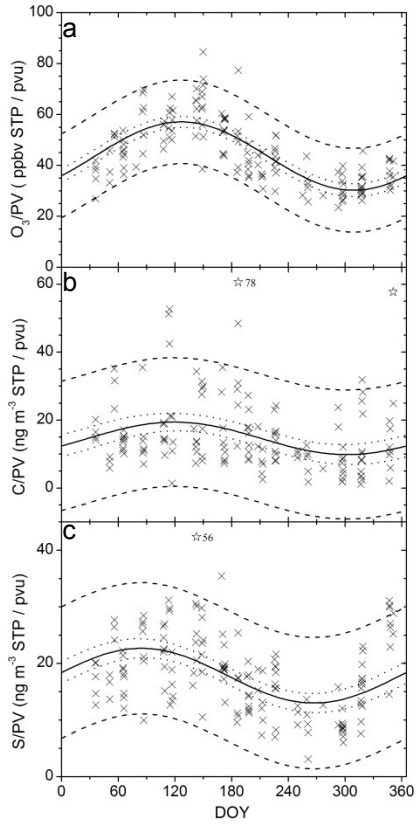

Figure 1. Concentration to potential vorticity ratios vs. day-of-year for a) ozone, b) particulate carbon and c) particulate sulfur, from stratospheric measurements. Solid lines shows regressions. Dotted lines shows 95% confidence interval for model. Dashed lines 95% prediction interval for data. Stars represents outliers not included in the model.

Brenninkmeijer C.A.M. et al. (2007). Atmos. Chem. Phys., 7, 4953-4976.
Martinsson B.G. et al. (2009). Geophys. Res. Lett., 36, L1281.
Murphy D.M. et al. (1998). Science, 282, 1664-1669.
Nguyen H.N. and Martinsson B.G. (2007). Nucl. Instr. and Meth. B264, 96-102.
Nguyen H.N. et al. (2006). Aerosol Sci. and Technol., 40, 649-655.
Nguyen H.N. et al. (2008). J. Geophys. Res., 113, D23209.

New insights into physical and chemical properties of volcanic ash from Eyjafjallajokull eruption during long-range transport

D. Ceburnis[1], J. Ovadnevaite[1], R. Greaney[1], C. Perrino[2], J. Bialek[1], B. Langmann[3], M. Hensch[4], H. Berresheim[1] and C.D. O'Dowd[1]

[1] School of Physics and Centre for Climate and Air Pollution Studies, Ryan Institute, National University of Ireland Galway, Galway, Ireland
[2]Institute for Atmospheric Pollution, National Research Council, I-00015 Montelibretti (Rome), Italy
[3]Institute of Geophysics, University of Hamburg, D-20146 Hamburg, Germany
[4]Nordic Volcanological Centre, University of Iceland, 101 Reykjavik, Iceland
Keywords: volcano, ash, aerosol, composition, long-range transport
Presenting author email: darius.ceburnis@nuigalway.ie

Volcanoes represent a major source of natural aerosol, including ejected rock, ash, $nssSO_4$ and are contributing to the whole array of secondary processes either directly or by catalysing chemical reactions. Even passive (non-eruptive) volcanic emissions contribute significantly to natural sulphur cycle along with regional impacts as demonstrated by Ovadnevaite *et al* (2009).

Eyjafjallajokull volcano explosively erupted on April 14, 2010 and while it was a moderate eruption has caused havoc in European air space. Due to the dominated south-south-easterly flow from Iceland it had an impact on air quality as well with over 30 plumes of nss sulphate detected at Mace Head station on the west coast of Ireland (O'Dowd et al, 2011).

Volcanic ash was observed in aerosol samples at Mace Head station, about 1000km downwind from volcano, when several major ash plumes were encountered as demonstrated by increased sulphate concentrations (Figure 1). A combination of on-line (AMS) and off-line chemical analysis (IC and XRF) revealed significant chemical processing of ash during long-range transport including gypsum formation and mineralization of metal oxides. Major compound classes present in particulate mass during two major plumes are summarised in Table 1 exhibiting similar share of ash, $nssSO_4$ and sea salt in PM_{10} mass. More importantly, volcanic ash elemental composition was well preserved after 1000km long-range transport and dominated by silicon and aluminium oxides as they were in volcanic lava and ash fall-out.

In-situ volcanic ash was obtained from ash fall-out samples at various distances from volcano and different times during eruption period and was examined by physical and chemical methods. Ash samples were dissolved in water and atomised for size distribution measurements by SMPS and APS which spectra revealed not only the presence of super-micron particles, but significant amount of sub-micron ones. SEM images confirmed the abundant presence of sub-micron particles with the aforementioned elemental composition. The result confirmed that sub-micron particles associated with volcanic ash plumes in the atmosphere are made of not just by secondary formation of $nssSO_4$, but indigenous ash as well. These results should help to better constrain regional atmospheric models used to predict volcanic ash advections.

Table 1. Percentage contribution of major compound classes to particulate mass concentrations (24h) at Mace Head derived from XRF analysis.

Date	PM_x*, $\mu g/m^3$	Nss SO_4, %	Ash, %	Sea salt, %
	PM_{10}			
04/05/10	9.23	35	24	40
17/05/10	11.45	33	39	28
	$PM_{2.5}$			
04/05/10	3.53	76	22	1
17/05/10	5.03	64	30	7
	$PM_{2.5-10}$			
04/05/10	5.70	10	26	64
17/05/10	6.42	10	46	44

*PM_x concentrations exclude nitrate, ammonium, organic matter (all in negligible amount) and compound bound water (as in gypsum, sulphuric acid, etc.).

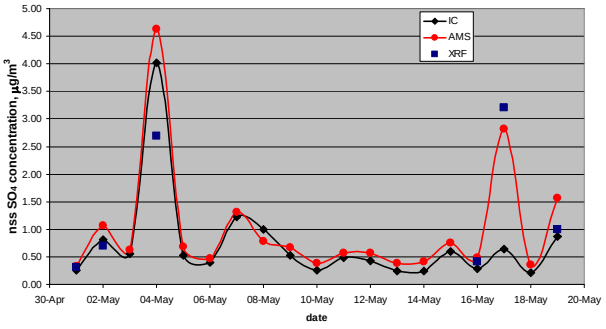

Figure 1. Time trend of 24h $PM_{2.5}$ $nssSO_4$ concentrations during May 2010 by IC, AMS and XRF. Significant volcanic plumes were detected on May 2, 4, 17 and 19.

This study presents new insights into volcanic ash formation and transformation in the atmosphere which should have significant climatic implications.

This work was supported by EPA Ireland, SFI (08/RFP/GEO1233) and HEA-PRTLI4.

Ovadnevaite, J. et al. (2009) *Atmos. Eviron.* **43,** 4968–4974.
O'Dowd, C.D. et al. (2011) *Atmos. Eviron.*, submitted.

Monday, September 5, 2011

Session 3B: New Particle Formation 2: *Experimental Studies*

Relationship between new particle formation and pollutant gases in an urban environment

I. Salma[1], T. Borsós[1], T. Weidinger[2], P. Aalto[3], M. Dal Maso[3] and M. Kulmala[3]

[1] Institute of Chemistry, Eötvös University, H-1525 Budapest, P.O. Box 32, Hungary
[2]Department of Meteorology, Eötvös University, H-1525 Budapest, P.O. Box 32, Hungary
[3]Department of Physical Sciences, University of Helsinki, Fi-00560 Helsinki, P.O. Box 64, Finland
Keywords: new particle formation, particle growth, condensation sink, gas-phase sulphuric acid
Presenting author email: salma@chem.elte.hu

Number concentrations of atmospheric aerosol particles were measured by a flow-switching type differential mobility particle sizer (DMPS) in an electrical mobility diameter range of 6–1000 nm in 30 channels at the campus of the Eötvös University near central Budapest with a time resolution of 10 min continuously from 3 November 2008 to 2 November 2009. Air temperature, ambient relative humidity, solar radiation and wind speed were also recorded with a time resolution of 10 min at the campus. Concentration of criteria air pollutants including SO_2, O_3, NO_x, CO and PM_{10} aerosol mass were obtained from municipal authorities at a site near our measurements.

New particle formation and growth obviously occurred on 83 days, which represent 27% of all relevant days. The frequency is comparable to that for rural and background locations. Hence, new particle formation is not a rare phenomenon in Budapest. Its frequency showed an apparent seasonal variation with a minimum of 7.3% in winter and a maximum of 44% in spring.

New particle formation events are usually linked to increased gas-phase H_2SO_4 concentrations, which could not be unfortunately obtained for our measurement site, and, therefore, a simple but reasonable proxy containing both source and sink terms for H_2SO_4 was calculated from SO_2 concentration ($[SO_2]$), solar radiation (Rad) and condensation sink (CS) as:

$$[H_2SO_4] \propto \frac{[SO_2] \times Rad}{CS}.$$

The results are summarized in Table 1. It is seen that concentration of SO_2 did not change substantially for the event and non-event days. The larger value for the non-event days in winter is related to temperature inversions. Solar radiation was larger by a factor of ca. 2 for the event days than for non-event days over the whole year. The difference is, however, biased by the seasonal cycle of solar radiation via the seasonal variation of new particle formation frequency. Condensation sink was smaller for the event days than for the non-event days by approximately 30% over the year. In winter, daily average CS for the event days was smaller by 64% than for the non-event days. This can be explained by generally higher level of air pollutants – including pre-existing aerosol particles – in winter due to temperature inversions that often occur in Budapest in winter.

Table 1. Median SO_2 concentration, solar radiation (Rad), condensation sink (CS) and gas-phase H_2SO_4 proxy (Proxy) averaged separately for the days with (NPF yes) and without new particle formation event (NPF no) over the seasons and year.

Period	NPF	SO_2	Rad	CS $\times 10^3$	Proxy $\times 10^{-3}$
		[μg m^{-3}]	[W m^{-2}]	[s^{-1}]	[μg m^{-5} Ws]
Winter	yes	6.7	60	6.8	50
	no	8.6	37	18.7	18
Spring	yes	6.1	228	12.6	93
	no	6.1	182	14.4	63
Summer	yes	5.8	239	9.4	150
	no	5.8	244	13.7	114
Autumn	yes	7.5	183	15.4	90
	no	7.1	78	17.5	43
Year	yes	6.6	215	12.3	96
	no	6.8	104	15.6	47

The combination of these three effects caused that the median H_2SO_4 proxy was larger by a factor of about 2 for the event days than for the non-event days over the year, and similar tendency is observed for the seasons. This clearly indicates the relationship between new particle formation and gas-phase H_2SO_4. In summer, the proxy for the event days was larger by a factor of 1.32 than for the non-event days with almost identical solar radiation for the event and non-event days. In the studied area, new particle formation is favoured by low pre-existing aerosol concentration level, low condensation sink, and high solar radiation. At the same time, the formation process seems to be not sensitive to SO_2. This suggests that this precursor gas is always available in excess.

This work was supported by the Hungarian Scientific Research Fund (contract K84091).

Salma, I., Borsós, T., Weidinger, T., Aalto, P., Hussein, T., Dal Maso, M. & Kulmala, M. (2011) *Atmos. Chem. Phys.* **11**, 1339–1353.

Influence of key aerosol, trace gas and meteorological parameters on new particle formation in Southern Spain

J.-M. Diesch[1], F. Drewnick[1], V. Sinha[2,3], J. Williams[2] and S. Borrmann[1,4]

[1]Particle Chemistry Department, Max Planck Institute for Chemistry, Mainz, 55128, Germany
[2]Air Chemistry Department, Max Planck Institute for Chemistry, Mainz, 55128, Germany
[3] now at: Indian Institute of Science Education and Research, Mohali, 160019, India
[4]Institute for Atmospheric Physics, University of Mainz, Mainz, 55128, Germany
Keywords: particle nucleation, source regions, aerosol mass spectrometry, coastal location.
Presenting author email: j.diesch@mpic.de

Atmospheric particle formation and subsequent growth have been observed in different locations including coastal, rural and urban areas (Zhang *et al.*, 2004). Regardless of the environment, nucleation events are one of the major sources of ultrafine particles which are potentially hazardous to human health (Jeong *et al.*, 2010). Both sulfuric acid and organic precursors are believed to play a key role in particle formation and growth (Kulmala *et al.*, 2005).

Measurements of the ambient aerosol, various trace gases and meteorological parameters were performed at the Southern coast of Spain within the framework of the DOMINO (*Diel Oxidant Mechanisms In relation to Nitrogen Oxides*) project. The field campaign took place from November 20 to December 9, 2008 at the atmospheric research station "El Arenosillo". The station is located at the interface between a natural park, industrial cities (Huelva, Seville) and the Atlantic Ocean. Number and mass concentrations as well as PAH and black carbon concentrations were measured in PM_1 and size distribution instruments (OPC, FMPS, APS, ELPI) covered the size range from 5.6 nm to 32 µm. The chemical composition of the non-refractory aerosol in the submicron range was measured by means of an Aerosol Mass Spectrometer (Aerodyne HR-ToF-AMS). Gas phase species analyzers monitored various trace gas concentrations in the air and a weather station provided meteorological parameters.

The variability of the air composition associated with advection from different source regions affects the emergence and temporal evolution of nucleation events. Nucleation events occurring in continental air masses and the so-called "pollution events" measured when trajectories pass urban source regions exhibit different characteristics. For the fine particle aerosol fraction, a sharp transition to a predominant mode at 10 nm with subsequent growth of the diameter was typically observed for nucleation events (Figure 1a). Pollution events are characterized by clearly bimodal size distributions during the growth period indicating the additional occurrence of freshly formed particles of industrial origin (Figure 1b). This additional particle surface results in smaller growth rates (~2 nm/h) during pollution events compared to nucleation events in "cleaner" air masses (~3 nm/h). During nucleation events the number concentration of particles increased abruptly from $6*10^3$ to $7.5*10^4$ # cm^{-3} (formation rate: 14 cm^{-3} s^{-1}) however, maximum particle number concentrations were reached during pollution events (~$1.2*10^5$ # cm^{-3}). At the beginning of the nucleation events low PM_1 mass (0.9 µg m^{-3}) and gas phase concentrations (SO_2: 0.2 ppb) were measured. In contrast, pollution events were characterized by enhanced gas and aerosol mass concentrations, with sulfur dioxide and sulfate concentrations originating from industrial sources in particular, being substantially higher. Hence, different influences of anthropogenic and biogenic emissions onto particle formation and growth in urban and continental source regions can be identified. Generally, ultrafine mode particles were found to be more acidic during the particle growth period compared to the nucleation period in both cases.

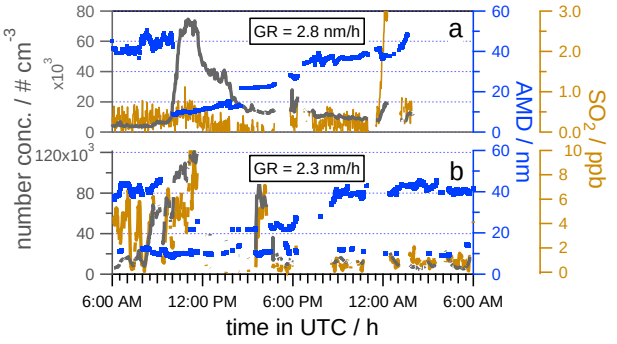

Figure 1. Variation of the number concentration (PM_1), arithmetic mean diameter (AMD, 5.6-560 nm) and sulphur dioxide concentration during a particle nucleation (a) and a pollution event (b) .

In addition to a detailed investigation of the characteristics of particle nucleation and pollution events, we will discuss differences of the measured parameters during nucleation, coagulation and growth periods. We will also focus on precursor gases, OH reactivity and meteorological conditions which favor the occurrence of new particle formation.

J.-M. Diesch thanks the German Research Foundation (DFG) for financing her work through the Research Training School GRK 826.

Zhang, Q. et al. (2004) *Environ. Sci. Technol.* **38**, 4797-4809.
Jeong, C.-H. et al. (2010) *Atmos. Chem. Phys.* **10**, 7979-7995.
Kulmala, M. et al. (2005) *Atmos. Chem. Phys.* **5**, 409-416.

New particle formation at a remote marine site in the Eastern Mediterranean

M. Pikridas[1,2], I. Riipinen[1,3], L. Hildebrandt[3], E. Kostenidou[1,2], H. Manninen[4], N. Mihalopoulos[5], N. Kalivitis, J. F. Bukhart[6], A. Stohl[6], M. Kulmala[4], S. N. Pandis[1,2,3]

[1] Dept. of Chemical Engineering, University of Patras, Greece
[2] Institute of Chemical Engineering and High Temperatures (ICE-HT), FORTH,Greece
[3] Dept. of Chemical Engineering, Carnegie Mellon University, Pittsburgh, USA
[4] Dept. of Physics, University of Helsinki, Helsinki, Finland
[5] Dept. of Chemistry, University of Crete, Greece
[6] Norwegian Institute for Air Research, Kjeller, Norway

Presenting Author: Michael Pikridas (mpikridas@chemeng.upatras.gr)

Keywords: Nucleation, Trajectory analysis, Ultrafine aerosols.

A year (6-April-2008 to 14-April-2009) of particulate monitoring was conducted at the remote coastal station of Finokalia (35°24′ N 25°60′ E) on the island of Crete, Greece in the Eastern Mediterranean. Ambient size distributions ranging between 0.8 – 40 nm were measured by an Air Ion Spectrometer (AIS) and between 10 – 600 nm by a Differential Mobility Particle Sizer (DMPS). 58 regional particle formation events were identified half of which occurred during the coldest months of the year (December-March).

A back trajectory analysis was conducted, using 20-day retroplume calculations with the particle dispersion model FLEXPART in backward mode and five (5) source regions were identified (West Crete, Greece, Turkey, East Crete, Marine). Particle formation was favored by air masses arriving from the west that crossed Crete or southern Greece prior to reaching the site (Table 1). This is consistent with the hypothesis of a missing reactant which has sources over land. When the air mass does not pass over Crete, it is conceivable that this reactant is exhausted and nucleation does not take place.

Table 1. Back-trajectory analysis of events.

	Airmass Origin				
	West Crete	Greece	Turkey	East Crete	Marine
Retroplumes investigated	216	161	298	185	186
Events	21	19	6	5	7
Normalized Frequency ($year^{-1}$)	102	123	21	28	39

Aerosol composition data, which were acquired during month-long campaigns in the summer and winter (named FAME-08 and FAME-09 respectively), suggest that nucleation events occurred only when particles were neutral (Fig. 1). This is consistent with the hypothesis that a lack of NH_3 which is not present in the gas phase during periods when the particles are acidic may limit nucleation in sulfur-rich environments (Jung *et al.*, 2008).

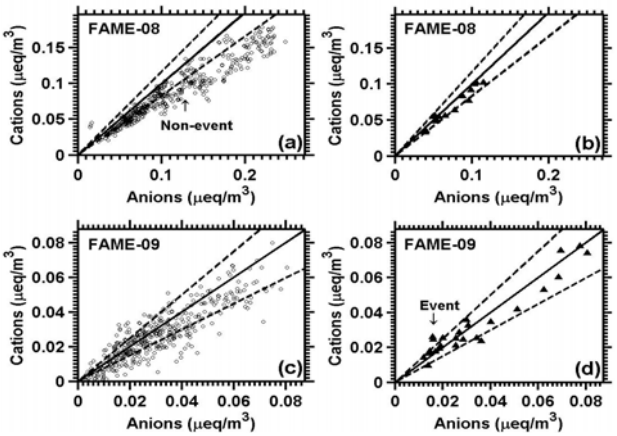

Figure 1. Cations versus anions during summer 2008 (FAME-08) and winter 2009 (FAME-09). (a) summer period without nucleation, (b) summer period during nucleation events, (c) winter period without nucleation and (d) winter period during nucleation events. Dashed lines correspond to one and two standard deviations from unity in the cases of FAME-09 and FAME-08, respectively. Solid line corresponds to neutral aerosol.

Nucleation was not limited by the availability of SO_2 alone, as nucleation events often did not take place during periods with high SO_2 or H_2SO_4 concentrations. The above results support the hypothesis that an additional reactant (other than H_2SO_4) plays an important role in the formation and/or growth of new particles (Berndt *et al.*, 2010). Our results are consistent with NH_3 or compounds which covary with it, being this missing reactant.

Berndt, T., Stratmann, F., Sipilä, M., Vanhanen, J., Petäjä, T., Mikkilä, J., Grüner, A., Spindler, G., Lee Mauldin III, R., Curtius, J., Kulmala, M., and Heintzenberg, J. (2010) *Atmos. Chem. Phys.*, **10**, 7101-7116.

Jung, J. G., Pandis, S. N. and Adams, P. J. (2008) *Aerosol Sci. Technol*. **42**, 495-504, 2008.

First observations of nucleation of new particles in a volcanic plume

J. Boulon[1], K. Sellegri[1], M. Hervo[1] and P. Laj[2]

[1]Laboratoire de Météorologie Physique, Observatoired e Physique du Globe, Université Blaise Pascal, Clermont-Ferrand, 63170 France
[2] Laboratoire de Glaciologie et G´eophysique de l'Environnement, CNRS UMR5183, Saint Martin d'H´eres, France
Keywords: Aerosol formation, nucleation, volcanic particles
Presenting author email: K.Sellegri@opgc.univ-bpclermont.fr

Introduction

Volcanic eruptions caused major weather and climatic changes on timescales ranging from hours to centuries in the past. Particles emitted during these eruptions absorb the incoming solar radiation, thus cooling the Earth (Zielinski et al. 1994). The volcanic particles that are injected in the atmosphere as primary particles (supermicronic ashes) are responsible for a cooling effect in the vicinity of the volcano, but these particles are rapidly deposited due to their large sizes. On another hand, sulphur dioxide is also substantially enhanced (Self et al. 2006) in volcanic ash plumes and subsequently many authors (Highwood et al. 2003) suspect that sulphuric acid may be formed by photochemical processes within the stratosphere, thus giving rise to new secondary particle formation (Kulmala et al. 2000) which are implicated in a more long-term effect. However, large condensational sinks due to pre-existing particles within the plume, and unknown nucleation mechanisms under these circumstances make the hypothesis uncertain. In this work, we report the first observation of a nucleation and new secondary particle formation events in a volcanic plume.

Methods

These measurements were performed at the puy de Dôme atmopsheric research station in central France during the Eyjafjallajokull volcano eruption in Spring 2010. The puy de Dôme research station is located at 1465 m above sea level in central France (45°46' N, 2°57 'E). The station is surrounded mainly by a protected area where fields and forests are predominant;the city of Clermont-Ferrand islocated 16 km East of the station. Meteorological parameters and radiation, atmospheric trace gases (O_3, NO_x, SO_2, CO_2) and particulate black carbon (BC) are monitored continuously throughout the year. Particle measurements were performed using a Neutral cluster and Air Ion Spectrometers (NAIS, 0.5- 42 nm), a Scanning Mobility Particle Sizer (SMPS, 10-450 nm) and an optical particle counter (Grimm spectrometer, 0.3-20 microns). Atmospheric dynamics and stratification are monitored using a Rayleigh-Mie LIDAR (355 nm), with parallel and perpendicular polarization channels.

Results

A strong depolarization signal indicative of volcanic ahses[19] was detected using LIDAR measurements from the 18th to the 20th of May 2010 in the boundary layer (Fig. 1) where it could be characterized by ground-based in situ instrumentation. During this period, condensation nuclei (CN) concentrations follow a clear diurnal variation, both on the 19th and on the 20th of May, with number concentrations that are multiplied by 5 in the size range 0.5 – 42 nm. The size distribution measured with the NAIS unambiguously shows that these particles are formed from the nanometric scale, i.e. by nucleation and subsequently growth process. Simultaneously, SO_2 concentrations peaked until reaching a maximum value of 2.25 ppt exceeding the 99th-percentil over the 2005-present period. We show that nucleation is linked to exceptionally high concentrations of sulphuric acid and unusually high particle formation rates. In addition, we demonstrate that the binary H_2SO_4-H_2O nucleation scheme, as it is usually considered in modeling studies (Zhao et al. 1995), underestimates by 7 orders of magnitude the observed particle formation rate and, therefore, cannot be applied at least under tropospheric conditions.

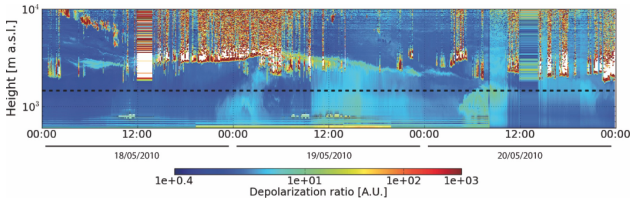

Figure 1. Depolarization ratio from the LIDAR showing non-spherical particles linked to the volcano plume entering the BL. The dahs line is for the puy de Dôme altitude

This work was supported by EUSAAR, EUCAARI, OPGC.

Highwood, E. J. & Stevenson, D. S. (2003) *Atmos. Chem. Phys.* **3**, 1177-1189, doi: 10.519/acp-3-1177-2003

Kulmala, M., Pirjola, L. & Mäkelä, J. M. (2000) *Nature* **404**, 66-69.

Self, S., Widdowson, M., Thordarson, T. & Jay, A. E. (2006) *Earth Planet. Sci. Lett.* **248**, 518-532.

Zhao, J., Turco, R. & Toon, O. *J.* (1995) *Geophys. Res.* **100**, D4, 7315-7328.

Zielinski, G. A. et al. (1994) *Science* **264**, 5161, 948-952

Nanoparticle formation from sulphuric acid and BVOC oxdidation at atmospheric concentrations

Dal Maso, Miikka[1,2], Mentel, Thomas F.[2], Kiendler-Scharr, Astrid[2], Kleist, Einhard[2], Tillmann, Ralf[2], Sipilä, Mikko[1], Petäjä, Tuukka[1], Hakala, Jani[1], Liao, Li[1], Lehtipalo, Katrianne[1], Junninen, Heikki[1], Ehn, Mikael[1], Vanhanen, Joonas[1], Mikkilä Jyri[1], Kulmala, Markku[1], Wildt, Jürgen[2], Worsnop, Douglas[1]

[1]Department of Physics, University of Helsinki, PO Box 48, 00014, Helsinki, Finland
[2]Institut für Chemie und Dynamik der Geosphäre (ICG), Forschungszentrum Jülich, 52425 Jülich, Germany
Keywords: particle formation, VOCs, sulphuric acid, nucleation
Presenting author email: miikka.dal@helsinki.fi

The controlling mechanism of tropospheric nanopartile formation is still being debated. Field and laboratory measurements have clearly indicated a strong correlation between observed sulphuric acid – a product of oxidation of SO_2 by the OH radical – and nanoparticle concentrations and formation rates. On the other hand, observed seasonality and comparisons with plant-emitted volatile organic compound (VOC) emission strengths show that aerosol formation is also correlated with biogenic organic compound oxidation products. Laboratory studies with real plant emissions have shown a clear dependence of aerosol formation on the VOC emission strength and also the chemical mixture, thereby ruling out the possibility that aerosol formation would be completely independent of organic compounds.

As it is likely that atmospheric particle formation is caused by several different processes, each of which dominate in different precursor concentration domains, reconciling the sulphuric acid and VOC-dependent explanations for aerosol formation is key to understanding the production of aerosol number in the lower atmosphere. We investigated the formation of nanosized condensation nuclei (nano-CN) from sulphuric acid and plant emissions in the Jülich Plant atmosphere Chamber setup (JPAC, see eg. Mentel et al., 2009). The extensive measurement setup consisted of several condensation nuclei counters (CPCs) including a pulse-height CPC and a Particle Size Magnifier for detection of sub-3 nm CN. Particle size distributions were monitored using an SMPS. Sulphuric acid levels were measured using chemical ionization mass spectrometry, while VOC concentrations were monitored with proton transfer reaction mass spectrometers and a gas chromatograph – mass spectrometer. We also deployed an Atmospheric Pressure Interface TOF spectrometer (API-TOF) to monitor the concentrations and distribution of charged clusters and molecules in the chamber.

We performed a series of experiments using boreal forest tree emissions at levels commonly found in the boreal boundary layer. The sulphuric acid concentration in the chamber was varied by changing the intensity of hydroxyl radical production and addition of SO_2 to the chamber; sulphuric acid levels were on par with atmospheric observations. The reaction chamber was flushed with ozone to achieve a steady-state concentration of 60 ppb when no OH was produced. During the experiment series we varied the emissions of BVOC, the OH production intensity, the O_3 concentration and performed experiments with addition of specific organics, e.g. isoprene.

We found that while the variation of the VOC concentration had a strong impact on the gas phase chemistry and also the hydroxyl radical and sulphuric acid levels, the changes in particle formation rates were not explainable by sulphuric acid concentration variations alone, but the particle formation process is directly influenced by the organic compounds. Also, the effects of different organics via their OH reactivity could be observed, for example the suppression of particle formation by isoprene as observed earlier (Kiendler-Scharr et al., 2009).

We present a detailed description of the evolution of the early nano-CN distribution and the influence of both sulphuric acid and biogenic organic oxidation products on it. The connections to the dynamics of the charged cluster and large molecule distribution as a function of ongoing oxidation by both ozone and the hydroxyl radical will also be discussed. We will discuss the implications of our findings regarding atmospheric nucleation by presenting a comparison of our results to findings from atmospheric field observations of natural nano-CN formation.

We thank Academy of Finland for financial support of this project (No. 128731) as well as the Maj and Tor Nessling foundation.

Mentel, Th. *et al.*, *Atmos. Chem. Phys.*, **9**, 4387–4406 (2009)

Kiendler-Scharr, A., *et al.*, *Nature*, 461, (7262): 381-384, 2009. DOI: 10.1038/nature08292

New particle formation by tobacco plants stressed by ozone: The potential role of mono- and sesquiterpenes

S. Bourtsoukidis[1], B. Bonn[1], W. Haunold[1], E. Palmer-Young[2] and J. Gershenzon[2]

[1]Institute for Atmospheric and Environmental Sciences, J.W. Goethe University, D-60438 Frankfurt/Main, Germany
[2]Max-Planck-Institute for Chemical Ecology, Beutenberg Campus, D-07745 Jena, Germany
Keywords: nucleation, ultrafine aerosols, VOC(s), activation.
Presenting author email: bonn@iau.uni-frankfurt.de

Abstract

Based on the studies of Haagen-Smit and Went, new aerosol particle formation by biogenic terpene oxidation products has been proposed. This certainly has remarkable atmospheric effects, since vegetated areas are extensive in space but diverse in composition and emission of reactive volatile organic compounds (VOCs). So far independent pathways from sulphuric acid derived nucleation have not been formulated and accepted. Here we aim to explain the observed nucleation process by a purely organic algorithm obtained from laboratory investigations, which we could perform successfully. The important role of organic radical (RO_2) formation by monoterpenes was elucidated, which activated the sesquiterpene derived nucleation core. Therefore both terpene groups and their reactivity with respect to ozone and OH are important for new aerosol particle formation in a non-linear system.

Methods

We focus on two controlled greenhouse experiments a) at Frankfurt University in June 2010 and b) at Max-Planck Institute for Chemical Ecology in Jena, in December 2010. While the first measurements were done in a greenhouse with changing light and temperature conditions, the second set of measurements were run at a constant temperature T of 24°C and constant illumination. The used three different tobacco plant types provided three different emission patterns with respect to sesquiterpenes, i.e. (i) one wild type and two genetically modified ones emitting (ii) a mixture of two sesquiterpenes (α-farnesene and α-bergamotene) or (iii) α-farnesene only.

In Frankfurt plant incubation was done using a Teflon bag while in Jena each plant was incubated in a single plant cuvette and was treated with different ozone stress intensities between 400 and 833 ppb_v.

Total particle concentration was measured by a condensation particle counter (UCPC 3776, TSI) with a lower cut-off size of 2.7 nm. All measurements have been conducted on the 13th-18th of December 2010 at the Max-Planck Institute in Jena.

Nucleation mechanism assumed

Based on the laboratory investigation on new particle formation by alkenes and ozone (see other presentation), the following mechanism was assumed:

1. Formation of stabilised Criegee intermediates (sCI) by sesquiterpenes and ozone
2. Formation of reactive secondary ozonides (SOZ) from sCI and available carbonyl compounds.
3. Activation (reaction) by monoterpene and OH derived large organic peroxy radicals (RO_2).

Taking into account the inhomogeneity of the cuvettes and the uncertainty of the radicals, a reasonable match between observation and calculation was obtained. As a conclusion it can be stated: The reaction rate constants of sesquiterpenes and of monoterpenes with O_3 and OH affect the entire nucleation process and the system is non-linear.

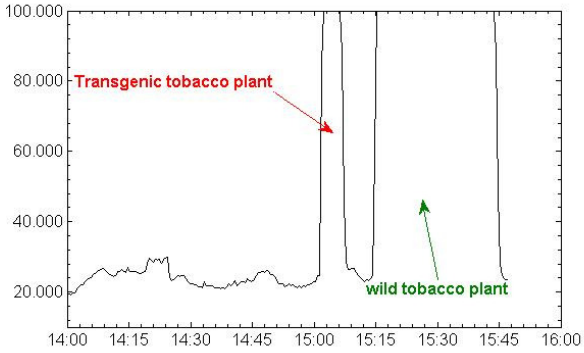

Figure 1. Effect of sudden rise in provided ozone. Particle number and sesquiterpenes concentrations rapidly increased in Frankfurt.

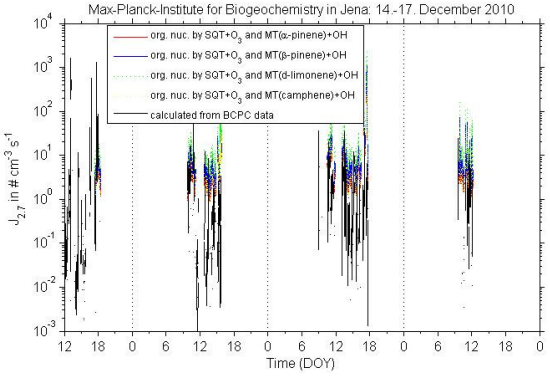

Figure 2. Simulated and measured nucleation rates for experiments performed at Jena.

This work was supported by Max-Planck and the biochemistry department of Goethe University Frankfurt.

SOA formation from stress induced biogenic VOC emissions and the contribution of isoprene to particle formation and growth – lessons learned from grey poplar trees

E. Kleist [1], T. Mentel [2], A. Kiendler-Scharr [2], S. Broch [2], M. Springer [2], K. Behnke [3], J.-P. Schnitzler [3], R. Tillmann [2], S. Andres [2], F. Rubach [2], B. Steitz [2], J. Wildt [1]

[1] Institute Plant Sciences, IBG-2, Research Centre Jülich GmbH, 52428 Jülich, Germany
[2] Institute Troposphere, IEK-8, Research Centre Jülich GmbH, 52428 Jülich, Germany
[3] Institute of Biochemical Plant Pathology, Department Environmental Engineering, German Research Center for Environmental Health (GmbH), 85764 Neuherberg, Germany

Keywords: particle formation and growth, SOA formation potential, Biogenic VOCs.
Presenting author email: e.kleist@fz-juelich.de

Vegetation is the major source of biogenic volatile organic compounds (BVOC) in the troposphere. These BVOC impact atmospheric oxidation capacity and serve as precursors for secondary organic aerosols (SOA). In regions with low pre-existing particulate matter, BVOC oxidation by OH, ozone, and NO_3 can produce low volatile products which are involved in SOA formation.

Isoprene and monoterpene emissions from vegetation are well known. However, during and after stress situations plants emit many other BVOC. Sesquiterpenes (SQT) such as α- and β-farnesene, C_6-aldehydes and -alcohols produced within the octa-decanoid pathway (green leaf volatiles, GLV), or many different aromatic compounds originating from the phenylpropanoid pathway are typical BVOC emitted during biotic and abiotic stress.

In this study we measured the formation of secondary organic aerosols (SOA) from stress-induced BVOC emissions emitted from grey poplar seedlings (*Populus x canescens*). The experiments were conducted in the Jülich Plant Atmosphere Chamber (JPAC, Mentel *et al*., 2009). This system consists of two temperature controlled chambers, one housing the plants (plant chamber) and the second one was used for photochemical SOA production (reaction chamber). BVOC emitted from the poplar plants in the plant chamber were transferred into the reaction chamber where they were oxidized by ozone and by OH radicals. OH was produced by photolysis of ozone in presence of H_2O. OH concentrations were typically in the range of 3-8×10^7 cm^{-3}. Ambient conditions such as temperature, relative humidity, photosynthetic active radiation (PAR), CO_2, O_3, and NO_x levels were controlled.

We used 4-month-old wild type (WT) poplar plants that emit high amounts of isoprene and transgenic poplar lines down-regulated in isoprene emission (R-lines, Behnke *et al.*, 2007). Comparing particle formation from BVOC emitted from these plants enabled the characterization of the impact of isoprene on the SOA formation from plant emissions. Unstressed poplar plants emitted nearly exclusively isoprene whereby the emissions from the down regulated R-lines were more than an order of magnitude lower than those from the wild type. Using unstressed plants as BVOC sources for particle formation we found inefficient SOA formation with nucleation rates far below 1 cm^{-3} s^{-1}.

All lines showed strong additional emissions of sesquiterpenes and aromatic compounds after stressing the plants by short ozone pulses. Their emission rates and therefore the BVOC emission pattern changed on a time scale of several days after stress application, allowing to study SOA formation under nearly steady state conditions. Feeding BVOC mixes into the reaction chamber resulted in very strong SOA formation events with nucleation rates exceeding 3000 cm^{-3} s^{-1}. Normalized to the BVOC turnover the nucleation rates were generally lower for the isoprene emitting WT poplars compared to non-emitting mutants. This observation confirmed former findings of suppression of nucleation by isoprene (Kindler-Scharr *et al*., 2009).

Rapid variations of PAR in the plant chamber resulted in fast changes of isoprene emissions whereas the emissions of the other BVOC responded on a much longer time scale. Hence, switching off the lamps in the plant chamber allowed removing isoprene very fast while keeping the level of other BVOC concentrations high. Conducting this procedure during a particle formation event caused a fast decrease of isoprene concentration and a strong increase of OH concentrations in the reaction chamber followed by increases in particle number and mass. This also shows that suppression of OH concentrations by isoprene is the major reason for suppression of nucleation from non-isoprene BVOC.

Using a low isoprene emitting poplar plant as BVOC source and adding deuterated isoprene from a diffusion source we estimated isoprenes' contribution to the SOA mass formed from the BVOC emitted from poplar. While isoprene contributed to about 7% [C/C] to the BVOC in the gas phase the contribution to the particulate phase was only 1 %. Thus isoprene oxidation products partitioning into the SOA can not compete with that of oxidation products from the other BVOCs. However the SOA mass produced by isoprene oxidation products does not compensate the decrease of other BVOC particle precursors caused by the decrease of OH concentrations in the presence of isoprene.

Behnke *et al.* (2007) Plant J., **51**, 485–499,
Kiendler-Scharr, A. *et al.* (2009), *Nature*, **461**, 381-384,
Mentel, T. F. *et al.* (2009), *ACP*, **9**, 4387-4406

Monday, September 5, 2011

Session 3C: Chemical Mechanisms and Transformation Processes in Aerosol

Evolving morphology, hygroscopicity and volatility of mixed oleic acid/sodium chloride/aqueous aerosol during oxidative aging

B.J. Dennis-Smither, R.E.H. Miles, N.-O.A. Kwamena and J.P. Reid

School of Chemistry, University of Bristol, Bristol, BS8 1TS, United Kingdom
Keywords: oxidative aging, organic aerosol, hygroscopicity, volatility.
Presenting author email: j.p.reid@bristol.ac.uk

We present measurements of the oxidative aging of mixed component aerosol trapped using optical tweezers. Single particles containing an effloresced sodium chloride phase and a liquid organic phase are exposed to gas phase ozone and the particle composition and size are monitored during the heterogeneous reaction. Partitioning of organic products between the gas and condensed phases is observed along with an increase in the hygroscopicity of the condensed organic phase. The impact of relative humidity (RH) on the oxidation kinetics/mechanism is explored.

Atmospheric aerosol is formed from variety of inorganic and organic components and this can lead to complex particle morphology. Organic components can modify aerosol properties including hygroscopicity, optical properties and toxicity. The chemical processing of organic compounds through the heterogeneous reaction with gas phase oxidants such as OH, O_3 and NO_3 forms aged organic aerosol and is of key importance when considering the composition and physical properties atmospheric aerosol.

The oleic acid – ozone reaction system has emerged as a benchmark system for the study of heterogeneous oxidation of organic compounds (Zahardis & Petrucci, 2007). Oleic acid (OL) is a C_{18} mono-unsaturated fatty acid and acts as a proxy for unsaturated organic matter in atmospheric aerosol and a model compound for the study of aerosol reactivity. OL reacts with ozone via cleavage of the C=C double bond to form initial C_9 products. Complex secondary chemistry involving the initial products leads to a variety of oxygenated final products, including C_9 compounds and oligomeric structures (Zahardis *et al.*, 2006).

We have used optical tweezers to isolate a single aqueous sodium chloride particle which is then coagulated with OL aerosol. The trapping of a single particle at the focal point of a tightly focused laser beam allows the mixed component particle to be suspended in an environment with controlled RH and ozone mixing ratio over several days. The composition and structure of the trapped droplet is probed using Raman spectroscopy.

The mixed component aerosol has 2 distinct liquid phases at RHs above the efflorescence point of the sodium chloride. The OL and aqueous phases have very low mutual solubilities and the particle phase separates to forms a partially engulfing OL lens on the aqueous droplet as predicted by a recent equilibrium morphology study (Kwamena *et al.*, 2010). The organic phase is observed to have negligible impact on the phase transitions of the sodium chloride. In particles containing effloresced sodium chloride, a spherical structure is adopted which we propose consists of a crystalline sodium chloride core coated in an organic shell.

Raman spectroscopy is used to probe the core-shell particles during the oxidative aging by ozone. The spontaneous Raman scattering allows the composition of the droplet to be investigated and the relative OL content to be monitored. The occurrence of sharp stimulated Raman peaks provides insight into the structure of the core-shell particles and allows determination of the particle radius, allowing the kinetics of oxidation to be monitored with considerable accuracy. The products of the reaction have a range of volatilities and the formation of highly volatile species leads to rapid decrease in organic volume on the timescale of the OL oxidation. Semi-volatile products are observed to evaporate on much longer timescales. The formation of a significant volume of involatile organic that remains in the condensed phase even over long timescales (days) is observed and we propose this as evidence for the formation of very low volatility oligomeric species. The measurement of particle radius as the RH is varied allows the hygroscopicity of the organic phase to be measured before and after oxidation and a significant increase in the hygroscopicity of the condensed organic phase is determined. The oxidative aging of the single aerosol particles has been investigated at RHs from less than 2 % to 70 % and ozone mixing ratio from less than 1 ppm up to 20 ppm.

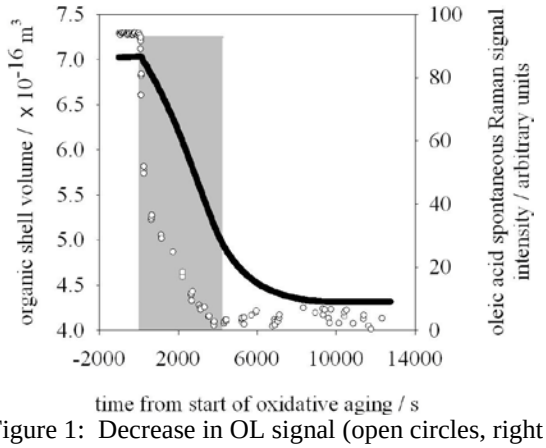

Figure 1: Decrease in OL signal (open circles, right axis) and decrease in size (black squares, left axis) revealing the reaction kinetics and particle-vapor partitioning

This work was supported by EPSRC.

Kwamena, N.-O. A., Buajarern, J. and Reid, J. P. (2010) *J. Phys. Chem. A* **114**, 5787–5795.

Zahardis, J. and Petrucci, G. A. (2007) *Atmos. Chem. Phys.* **7**, 1237–1274.

Zahardis, J., LaFranchi, B. W. and Petrucci, G. A. (2006) *Atmos. Environ.* **40**, 1661–1670.

Ozonolysis of oleic acid: mixed systems, oligomerisation and phase changes.

C. Pfrang,[1,2] M. Shiraiwa[2] and U. Pöschl.[2]

[1]Department of Chemistry, University of Reading, P.O. Box 224, RG6 6AD Reading, UK
[2]Max Planck Institute for Chemistry, Biogeochemistry Department, P. O. Box 3060, 55128 Mainz, Germany
Keywords: aerosol chemistry, ozone, organic aerosols, kinetic modelling, solidification
Corresponding author's email: c.pfrang@reading.ac.uk
Session: Multiphase chemical processes and interactions involving aerosol

Cooking aerosols have recently been recognised to contribute substantially to the urban aerosol burden.[1] One of its most prominent reactive components is oleic acid. The importance of the amorphous solid state in aerosols has been illustrated by Virtanen *et al.*[2] Synthesising previous work in a detailed model analysis we explored if variations in the aerosol diffusivity may explain long lasting controversies. We extend recently developed models[3,4] for description of a 12-component mixture representative of atmospheric cooking aerosols. We show how this model may be used to resolve surface and bulk processes in varying phases considering diffusivities altered by oligomerisation of reaction products. This new model allows consideration of aerosol ageing over much extended lifetimes since properties of product species may be described in detail.

Ozonolysis of oleic acid is a model system for ageing of organic aerosols in the atmosphere. Recent experimental evidence underlines the importance of changes in diffusivity inside atmospheric aerosols. We review recent studies that investigate the importance of phase transitions on the ageing of oleic acid in the atmosphere and model a 12-component aerosol mixture by applying and extending the KM-SUB model (see Fig. 1).[3]

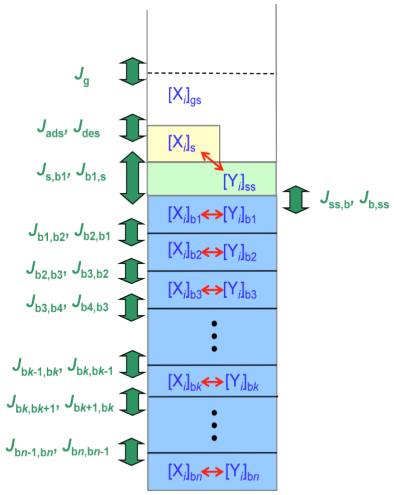

Figure 1. Model description of a 12-component mixed aerosol system and its chemical and physical transformations: model layers, chemical species (X and Y) and fluxes (*J*) between these layers based on KM-SUB.[3] Gas-phase species X is O_3 and 12 liquid-phase Y components are described here in 250 bulk layers. Product formation and oxidation-induced viscosity changes are also described (not shown for visual clarity).

Fig. 1 illustrates the structure of the model used for the present study. The model was validated by comparison with experimental data from Huff Hartz *et al.*[5] We explored if changes in the diffusivity may explain the observed evolution of loss rates in ageing aerosols.

Fig. 2 (a) illustrates matching time decays of oleic acid molecules in model and experiment. Fig. 2 (b) shows the evolution of the concentration of oleic acid resolved in depth (layer 250: aerosol core) and time. We observe crust formation on the aerosol surface with diffusion being reduced due to formation of viscous products.

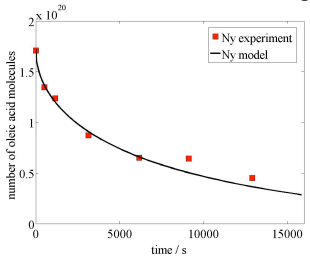

(a)

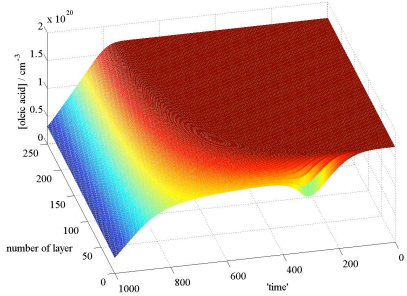

(b)

Figure 2. Selected modelling results and comparison with experimental data from Huff Hartz *et al.*[5]

The work presented is the first application of recently developed kinetic models[3,4] to multi-component atmospheric aerosols. We successfully describe the time evolution of multiple reactive species on the surface and in the bulk. Our model description is consistent with retardation of the reactive loss of the organic species caused by increased viscosity in aged aerosols. Viscosity and phase changes of atmospheric aerosols could reconcile discrepancies between lifetimes derived from laboratory and field observations.

1. Allan *et al.*, *Atmos Chem Phys*, 10, 647 (2010)
2. Virtanen *et al.*, *Nature*, 467, 824 (2010)
3. Shiraiwa *et al.*, *Atmos Chem Phys*, 10, 3673 (2010)
4. Pfrang *et al.*, *Atmos Chem Phys*, 10, 4537 (2010)
5. Huff Hartz *et al.*, *J Geophys Res*, 112, D04204, doi:10.1029/2006JD007526, (2007)

Real-time, controlled OH-initiated oxidation of biogenic secondary organic aerosol

J.G. Slowik[1,2], J.P.S. Wong[1] and J.P.D. Abbatt[1]

[1]Department of Chemistry, University of Toronto, Toronto, ON, M5S 3H6, Canada
[2]Laboratory of Atmospheric Chemistry, Paul Scherrer Institut, 5232 Villigen PSI, Switzerland
Keywords: biogenic particles, OH-induced oxidation, aerosol mass spectrometry, boreal forest
Presenting author email: jay.slowik@psi.ch

Atmospheric aerosol particles have important effects on human health, visibility, and climate. Quantification of these effects requires a detailed understanding of particle sources and atmospheric transformations. The wide array of sources and processes contributing to ambient aerosol composition makes it difficult to quantitatively resolve the effects of specific factors via ambient measurements. Laboratory studies enable controlled studies of simple systems, but may not adequately capture the complexity of the atmosphere, contributing to discrepancies with atmospheric measurements. Controlled investigation of atmospheric processes via oxidation of real-world particle/gas mixtures provides a promising approach to addressing this challenge. Here we present results from the initial field deployment of the Toronto Photo-Oxidation Tube (TPOT), a system for real-time analysis of OH-initiated oxidation of ambient gas/particle mixtures.

Ambient aerosol are continuously sampled by the TPOT and mixed with N_2, O_2, O_3, and H_2O. This flow is then split into reaction and bypass tubes. Both tubes are constructed from Silco Steel and contain a glass tube on the center axis, which in the reaction tube houses a 254 nm Hg lamp. Photolysis of O_3 in the presence of H_2O vapors produce OH radicals, which control experiments indicate are the dominant oxidants in the system. OH concentrations are controlled by varying the input O_3 concentration. Flows are pulled continuously in both tubes, while measurement of aerosol composition alternates between the tubes with a period of ~12 min. The composition is measured by an Aerodyne time-of-flight aerosol mass spectrometer (AMS) (Drewnick *et al.*, 2005).

The TPOT was deployed in Whistler, BC, Canada, during the WCAS 2010 (Whistler Cloud and Aerosol Study) field campaign, from 8 to 27 July, 2010). Sampling was conducted in the boreal forest on Whistler Mountain at 1300 m asl. The site is strongly influenced by biogenic secondary organic aerosol (SOA) from terpene emissions. Periods of influence by anthropogenic emissions and biomass burning plumes were also observed.

Under the conditions present during WCAS 2010, oxidative processing in the TPOT was dominated by heterogeneous oxidation and/or gas-phase reaction of semivolatile organics, rather than SOA formation. However, this is likely due in part to the low SOA yields of current flow tube systems (Lambe *et al.*, 2010). Figure 1 shows the effects of heterogeneous OH processing on the total organic mass, as well as the signal at *m/z* 43, 44, and 91. After ~10 days of oxidation, the figure shows a 20% decrease in total organic mass. Larger decreases are evident in the signals at *m/z* 43 (~40%) and 91 (~70%), which are characteristic of fresher, less-oxidized SOA. In contrast, a mass increase of up to ~30% is observed at *m/z* 44 (CO_2^+, characteristic of carboxylic acids). These trends are also evident at shorter time periods, with increased *m/z* 44 (~10%) and decreased *m/z* 91 (~20%) after less than a day of oxidation. OH oxidation of the ambient aerosol causes spectra to approach the low-volatility oxygenated organic aerosol (LV-OOA) spectra that have been widely extracted from factor analysis of AMS datasets and are thought to represent aged organics (e.g. Ng *et al.*, 2010).

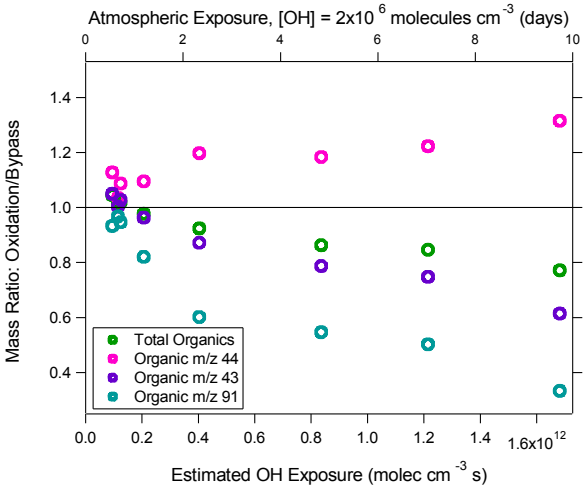

Figure 1. Evolution of the organic aerosol mass spectrum with OH oxidation.

Support for this work was provided by Environment Canada and by the Canadian Foundation for Climate and Atmospheric Sciences through the Cloud-Aerosol Feedbacks and Climate Network.

Drewnick, F., *et al.* (2005) *Aerosol Sci. Technol.* **39**, 637-658.

Lambe, A.T., *et al.* (2010) *Atmos. Meas. Tech. Discuss.* **3**, 5211-5251.

Ng , N.L., *et al.* (2010) *Atmos. Chem. Phys.*, **10**, 4625-4641.

Long-lived reactive oxygen intermediates in the reaction of ozone with aerosol particles and aerosol health effects

Manabu Shiraiwa[1], Yulia Sosedova[2], Aurélie Rouvière[2], Hong Yang[1], Yingyi Zhang[1], Jonathan P. D. Abbatt[3], Markus Ammann[2], Ulrich Pöschl[1]

[1]Max Planck Institute for Chemistry, Department of Biogeochemistry, Mainz, Germany
[2] Paul Scherrer Institute, Villigen, CH-5232, Switzerland
[3] University of Toronto, Department of Chemistry, Toronto, Canada
Keywords: ozone, heterogeneous reaction, health effects, PAH, soot, protein
Presenting author email: m.shiraiwa@mpic.de

Heterogeneous reactions of ozone with aerosol particles have been studied extensively, but the molecular mechanism and kinetics remained unresolved. Among the organic aerosol components readily reacting with ozone, polycyclic aromatic hydrocarbons (PAHs) are one of the most prominent groups related to health effects. Chemical transformation can change the toxicity of PAHs and modify the hygroscopic properties and climate effects of combustion aerosol particles. Several studies have shown that ozone can also promote the nitration of protein molecules contained in primary biological aerosol particles like pollen and fungal spores (Franze et al. 2005). This posttranslational modification can enhance the allergenic potential of proteins. It provides a molecular rationale for the enhancement of allergic diseases by traffic-related air pollution in urban and rural environments, which has been observed in epidemiological studies but remains to be elucidated on a molecular level (Gruijthuijsen et al. 2006).

Based on new experimental data and model calculations, here we show that long-lived reactive oxygen intermediates (ROIs) are formed upon oxidation of PAH and nitration of protein (Shiraiwa et al. 2011). The chemical lifetime of these intermediates exceeds 10^2 s, which is much longer than the surface residence time of molecular O_3 (~10^{-9} s). The ROIs explain and resolve apparent discrepancies between earlier quantum mechanical calculations and kinetic experiments. They play a key role in the chemical transformation and adverse health effects of toxic and allergenic air particulate matter, such as soot, polycyclic aromatic hydrocarbons and proteins. Moreover, ROIs may contribute to the coupling of atmospheric and biospheric multiphase processes.

Apart from chemical aging of air particulate matter, long-lived ROIs might also participate in the formation and growth of secondary organic aerosols. In particular, surface interactions of long-lived ROIs may lead to the formation of multifunctional organic substances (acids, nitrates, sulfates, dimers/oligomers, etc.) with high molecular mass and low vapor pressure that are required for the nucleation and growth of new particles and may also influence their phase state (Virtanen et al. 2010). The experimental and theoretical information currently available suggests that long-lived ozone-generated ROIs play a central role in the multiphase chemistry of atmospheric aerosols.

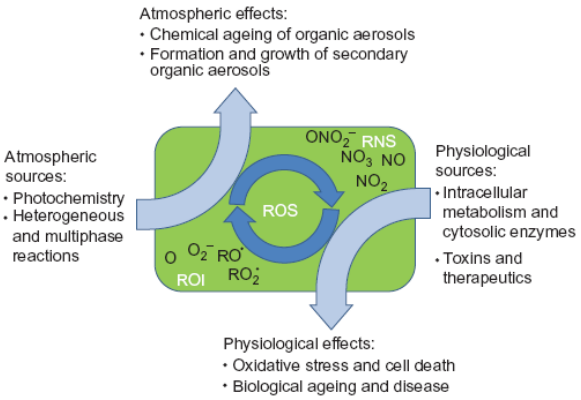

Figure 1. Illustration of the atmospheric and physiological sources, coupling and effects of reactive oxygen species(ROS), reactive oxygen intermediates (ROI), and reactive nitrogen species (RNS).

Acknowledgements.
This work was funded by the Max Planck Society (MPG), the Swiss National Science Foundation (grant no. 130175), and the European Integrated Project on Aerosol, Cloud, Climate and Air Quality Interactions (No 036833-2 EUCAARI). We thank M. Birrer, T. Bartels-Rausch and M. Kerbrat for support. The staffs of the PSI accelerator facilities are acknowledged for providing stable proton beams used to produce ^{13}N.

References.

Franze, T., et al,, Protein nitration by polluted air. *Environ. Sci. Technol.*, **39**(6): p. 1673-1678, 2005.

Gruijthuijsen, Y.K., et al., Nitration enhances the allergenic potential of proteins. *Int. Arch. Allergy Immunol*, **141**(3): p. 265-275, 2006.

Shiraiwa, M., et al., The role of long-lived reactive oxygen intermediates in the reaction of ozone with aerosol particles, *Nature Chemistry*, doi: 10.1038/NCHEM.988, 2011.

Virtanen, A., et al., An amorphous solid state of biogenic secondary organic aerosol particles. *Nature*, **467**: p. 824-827, 2010.

Measurement and modelling of ammonium nitrate aerosol and its impacts in North-Western Europe

W. T. Morgan[1], J. D. Allan[1,2], M. K. Bane[1*], K. N. Bower[1], B. Harris[3], J. S. Henzing[4], E.J. Highwood[3], A. Kiendler-Scharr[5], G. McFiggans[1], G. R. McMeeking[1], A. A. Mensah[5], S. Osborne[6+], M. J. Northway[3], P. I. Williams[1,2], R. Krejci[7], and H. Coe[1]

[1]Centre for Atmospheric Science, University of Manchester, Manchester, UK
[2]National Centre for Atmospheric Science, The University of Manchester, Manchester, UK
[3]Department of Meteorology, University of Reading, Reading, UK
[4]TNO, Utrecht, Netherlands
[5]Institute for Chemistry and Dynamics of the Geosphere, Institute 2: Troposphere, Jülich, Germany
[6]Met Office, Exeter, UK
[7]Department of Applied Environmental Science, Atmospheric Science Unit, Stockholm University, Stockholm, Sweden
*Now at Research Computing Services, University of Manchester, Manchester, UK
[+]Now at Met Office, Cardington, UK

Keywords: ammonium nitrate, AMS, Aerosol Optical Depth (AOD), European Pollution.

Ammonium nitrate aerosol exhibits highly scattering properties across the solar spectrum. Further to this, it displays hygroscopic tendencies (Tang, 1996), allowing enhanced water uptake for a given relative humidity. Consequently, its ability to scatter incident solar radiation is increased leading to an enhancement of the aerosol direct radiative forcing. Anticipated reductions in sulphur dioxide in polluted regions will result in an increase in the availability of ammonia to form ammonium nitrate as opposed to ammonium sulphate. Consequently, the relative importance of ammonium nitrate to the aerosol burden is likely to increase.

This paper presents an assessment of the contribution, properties and impact of ammonium nitrate upon the European aerosol burden. In-situ measurements of aerosol properties made onboard the UK Facility for Airborne Atmospheric Measurements (FAAM) BAe-146 aircraft will be presented. The aircraft employs a suite of aerosol instruments, which resolve the chemical composition, number size distribution, optical and hygroscopic properties of the in-situ aerosol population. This includes an Aerodyne Aerosol Mass Spectrometer (AMS) which measures the size resolved chemical composition of both volatile and semi-volatile particulate matter (Canagaratna *et al.*, 2007). The measurements were conducted as part of the EUCAARI-LONGREX (European Integrated Project on Aerosol Cloud Climate Air Quality Interactions–LONG Range EXperiment) and APPRAISE-ADIENT (Aerosol Properties, Processes and influences on the Earth's climate – Appraising the aerosol direct impact on climate) campaigns. Science flights were conducted across Europe, during predominantly clear sky conditions during 2008.

Ammonium nitrate was found to dominate in North-Western Europe during episodes of high pollution, reflecting the enhanced NO_x and ammonia sources in this region. Ammonium nitrate and organic matter were often observed to increase with altitude in the atmospheric boundary layer. This was attributed to partitioning of semi-volatile gas phase species to the particle phase at reduced temperature and enhanced relative humidity. Increased ammonium nitrate concentrations in particular were found to strongly increase the ambient scattering potential of the aerosol burden. During particularly polluted conditions, increases in boundary layer aerosol optical depth of 50-100% were estimated to occur due to the observed increase in secondary aerosol mass with altitude and associated water uptake. These enhancements significantly increase the direct aerosol radiative forcing. Such increases have major ramifications for regional climate predictions as semi-volatile components are often not included in aerosol models.

Our observations over North-Western Europe indicate that failure to include the semi-volatile behaviour of ammonium nitrate will result in significant errors in predicted aerosol direct forcing.

The ability of a sophisticated regional aerosol transport model to represent the complex spatial distribution of ammonium nitrate will be explored. This will include the observed horizontal spatial gradients in North-Western Europe and in particular the vertical distribution of the aerosol.

This work was supported by the Natural Environment Research Council ADIENT project NE/E011101/1 and EUCAARI project 036833-2. We would like to acknowledge the efforts of FAAM, DirectFlight, Avalon, DLR, the Met Office and IMPACT teams.

Tang, I. N. (1996), *J. Geophys. Res.*, **101 (D14)**, 19245-19250.

M. R. Canagaratna, *et al*, (2007), *Mass Spectrometry Reviews*, **26 (2)**, 185-222.

Predictions of Night-time Atmospheric Processes using a Coupled Model of Multi-phase Chemistry and Aerosol Microphysics

D. Lowe[1], S. Utembe[1], D. Topping[1,2], and G. McFiggans[1]

[1]Centre for Atmospheric Science, SEAES, University of Manchester, Manchester, UK, M13 9PL
[2]National Centre for Atmospheric Science, University of Manchester, Manchester, UK, M13 9PL
Keywords: aerosol modelling; multiphase chemistry; NOx

Aerosol particles play an integral part in the chemistry of the atmosphere – by acting as reaction surfaces for heterogeneous chemistry, as chemical sources, and by removing components through scavenging and dry deposition. They have an important influence on the lifetime of the nitrate radical (NO_3), which can be an important oxidant in polluted nocturnal atmospheres. NO_3 and NO_2 are in thermal equilibrium with N_2O_5, which acts as a reservoir species for NO_3. However N_2O_5 also provides an important loss pathway for NOx by conversion to HNO_3 via heterogeneous reactions on aerosol particles, the rates of which are dependent on aerosol composition, RH and T (Allan *et al.*, 1999, Davis *et al.*, 2008; Evans & Jacob, 2004). In order to properly predict the oxidative capacity of the nocturnal atmosphere we must understand the influence of aerosols on gas-phase chemistry.

This study uses a one-dimensional column model, built upon the sectional Microphysical Aerosol Numerical box-model Including Chemistry (MANIC) (Lowe *et al.*, 2009). Constructed using the Kinetic Pre-Processor (KPP, Damian *et al.*, 2002); all gas and condensed phase reactions, as well as gas-aerosol mass transfer, and gas and aerosol source and loss terms, within a single level of the column model are included into one system of ODE's, solved using a third-order Rosenbrock solver. In the condensed-phase we use the PD-FiTE (Partial Derivative Fitted Taylor Expansion) method for calculating the non-ideal activity coefficients for components of the H^+-NH_4^+-Na^+-SO_4^{2-}-HSO_4^--NO_3^--Cl^- system (Topping et al, 2009) and for a reduced complexity condensed organic phase consisting of 13 semi-volatile and 2 involatile species (Topping and Lowe, 2011). Other chemical species in the condensed-phase are treated as being in ideal conditions. Gas-phase chemistry is simulated using the CRI v2R5 scheme (Watson *et al*., 2008).

Here we present an investigation into the influence of size-resolved condensed-phase chemistry on the oxidant capacity of the troposphere with a range of pollutant loadings. The aerosol-phase for all studies consists of two externally mixed modes: one seasalt, the other non-seasalt. Each aerosol mode has been split into 8 size-bins. A vertical column model will be run along lagrangian trajectories through a range of different conditions (from clean marine, to polluted continental) – to investigate component variability within a parameter space which will be suitable for comparisons with FAAM 146 measurements.

We will present analysis of the evolution of the night-time nitrogen budget. This will consist of vertically-, temporally-, and size-resolved (for the condensed-phase) nitrogen species concentrations and trends. We will further identify the major production and loss channels for nitrogen processing, comparing the relative importance of the condensed- and gas-phase oxidised nitrogen reservoirs, formulating testable hypotheses for evaluation of the airborne measurements of reactive gaseous nitrogen and aerosol nitrate.

This work was conducted as part of the RONOCO (ROle of Nighttime chemistry in controlling the Oxidising Capacity of the atmOsphere) and RHaMBLe (Reactive Halogens in the Marine Boundary Layer) projects.

Allan, B. J., Carslaw, N., Coe, H., Burgess, R. A., and Plane, J. M. C. (1999). *J. Atmos. Chem.*, 33, 129–154

Davis, J. M., Bhave, P. V. & Foley, K. M. (2008), Parameterization of N_2O_5 reaction probabilities on the surface of particles containing ammonium, sulfate, and nitrate, *Atmos. Chem. Phys.*, 8, 5295–5311

Damian, V., Sandu, A., Damian, M., Potra, F., & Carmichael, G.R. (2002). *Computers and Chemical Engineering*, 26, 1567-1579

Evans, M. J. & Jacob, D. J. (2005) Impact of new laboratory studies of N_2O_5 hydrolysis on global model budgets of tropospheric nitrogen oxides, ozone and OH, *Geophys. Res. Lett.*, 32, L09813, doi:10.1029/2005GL022469.

Lowe, D., Ryder, J., Leigh, R., Dorsey, J. R., & McFiggans, G. (2011). *Atmos. Chem. Phys.*, 11, 979-994, doi:10.5194/acp-11-979-2011

Topping, D., Lowe, D., & McFiggans, G. (2009). *J. Geophys. Res.*, 114, doi:10.1029/2008JD010099

Topping, D., & Lowe, D. (2011), *in preparation*

Watson, L., Shallcross, D. E., Utembe, S. R., & Jenkin, M. E. (2008), *Atmos. Environ.*, 42, 7196-7204

Phase transformation of evaporating solution droplets of immiscible polymers

V. Rajagopalan, E. A. Grulke and A. K. Ray

Department of Chemical Engineering, University of Kentucky, Lexington, KY 40506, USA
Keywords: polymer blend particle, multicomponent droplet evaporation, VOAG.
Presenting author email: akray@engr.uky.edu

Polymer blends have wide range of applications (e.g., opto-electronic devices, organic solar cells) that often require microparticles with uniform properties. In many cases, the polymers are incompatible with one another and thus separate into distinct phases. Conventional methods based on melt blending and miniemulsions can reduce the extent of phase separation in many polymer blends, but are limited to polymer pairs in certain property ranges. There is a need for a synthesis method that can blend immiscible arbitrarily polymer pairs. Blended microparticles produced by evaporating solution microdroplets, containing two immiscible polymers dissolved in a common solvent, are expected to exhibit a high degree of phase uniformity under conditions where the timescale of solvent evaporation is lower than that of polymer diffusion and self-organization. In such a situation, the phase separation is inhibited within the atto- to femto-liter volume of the droplet, and homogeneous blends of immiscible polymers can be produced.

We have examined multicomponent polymer particles produced from highly monodisperse micrordroplets that were generated using a Vibrating Orifice Aerosol Generator (Devarakonda et al. 1998; Gao et al. 2007). Equal proportions of two highly incompatible polymers, polystyrene (PS, Mw=280,000) and polyvinyl chloride (PVC, Mw=75,000), were dissolved in a common solvent, tetrahydrofuran (THF), to get a desired total polymer concentration in the solution in the range of 2 to 4 wt%. Droplets were generated from the homogeneous solution; in addition to THF, ethanol was added in varying amounts to reduce evaporation rates of the solution droplets. The morphology of the polymer blend particles produced from the droplets of various composition was studied by an SEM (Hitachi SEM-3200N). To obtain the distribution of each component inside the particle, samples were placed in Beem capsules, embedded in Spurr's resin, and kept under vacuum for 48 hours. They were then polymerized at 60^0C for 48 hrs, and finally, sliced thinly on a Reichert-Jung Ultracut E microtome. The thickness of the slices was about 60 nm. The slices were placed on copper grids and examined in the FEI Tecnai Biotwin 12 transmission electron microscope (TEM). An Energy Dispersive X-ray Analysis (EDS) (coupled with SEM) was performed for the presence of chlorine. All the samples were coated with a thin layer of Gold and Palladium before using them under the SEM.

The SEM micrographs of polymer particles show that the particles are of spheroidal shape and often have indentations. Even though the initial droplets generated by the VOAG have the same size, the final solid particles have varied morphologies. This is due to nonuniform drying conditions inside the experimental chamber. Surface hollows and indentations observed in the particles can be attributed to the rapid drying of the droplets. Even though the physical characteristics of the particles were not uniform, the objective was to study the extent of phase separation or the lack of it thereof. The elemental difference between PS and PVC is the presence of chlorine in PVC. This prompted us to do EDS on the thin slices of the blend particles that were prepared using the microtome. The slices were about 60 nm thick with diameter of about 12 μm. Each analysis was done over an area of 3x3 μm^2. The EDS spectra from various locations of a particle clearly show primary and secondary peaks of chlorine. For particles produced from solutions with THF as the sole solvent, chlorine peaks were observed to have approximately the same intensity. This suggests that the distribution of chlorine is more or less uniform throughout the cross-section. Thus, qualitatively, PVC and PS are dispersed uniformly in the particle.

The results of this study show that uniform polymer blend microparticles can be produced by rapid evaporation of microdroplets. The morphology of the final particles that form after the solvent evaporation depends on the initial droplet size, polymer concentration, solvent volatility, and temperature. Future studies would involve more quantitative measurements. The mapping of chlorine in the samples are needed to fully ensure that the particles produced are indeed uniformly blended microparticles.

This work was supported by the National Science Foundation (grant # ATM-0634789), and National Institute for Occupational Safety and Health (grant # 1R01OH009802-01).

Devarakonda V., Ray, A. K., Kaiser, T., and Schweiger G. (1998) *Aerosol Sci. Technol.* **28**, 531-547.

Gao Z., Grulke E. A., and Ray A. K. (2007) *Colloid and Polymer Sci.* **285**, 847-854

Monday, September 5, 2011

Session 3D: PMx Data Interpretation

Mobile measurements of submicron particulate matter in Central Europe during wintertime inversions

R. Wolf, C. Mohr, M. Crippa, J. Slowik, A.S.H. Prévôt and U. Baltensperger
Laboratory of Atmospheric Chemistry, Paul Scherrer Institute, CH-5232, Villigen PSI, Switzerland
Keywords: Organic aerosols, Wood burning, Aerosol mass spectrometry, Source apportionment.
Presenting author email: robert.wolf@psi.ch

Wintertime inversions lead to an increase in concentrations of particulate matter. This phenomenon is of special interest because of the adverse effects of particles on health and visibility. During such episodes, aerosol mass concentrations are strongly influenced by local sources and topography. Recent studies (Weimer *et al.*, 2009, Alfarra *et al.*, 2007) indicate that both traffic and wood burning significantly contribute to particulate mass which accumulates in narrow Alpine valleys.

A mobile laboratory was deployed to determine the spatial distribution and the chemical composition of atmospheric aerosols during atmospheric inversion. The mobile unit contains a series of instruments including an Aerodyne quadrupole aerosol mass spectrometer (Q-AMS), a multi-angle absorption spectrometer (MAAP) and a fast mobility particle sizer (FMPS). The sampling was performed in both rural and urban areas along the Rhine Valley in Switzerland, Austria and Liechtenstein.

The main components of particulate matter and its sources were identified using Positive Matrix Factorization (PMF) (Paatero *et al.*, 1994). The organic fraction can be classified as primary (POA) or secondary organic aerosol (SOA). The primary organic aerosol classification includes contributions from wood burning and traffic. Local emissions of individual species were estimated by subtraction of SO_4-normalized background concentrations (Mohr *et al.*, 2011).

The results for the total mass concentration and the mean chemical composition are shown in Figure 1. It indicates a substantial difference in mass concentrations between the Austrian section (A) of the route ($\approx 53\ \mu g/m^3$) and the urban area of Chur in the southern Rhine Valley ($\approx 15\ \mu g/m^3$). According to Figure 2, the carbonaceous aerosol dominates the local contribution.

It can be concluded that the high amount of heavy-duty traffic and emissions from diesel powered cars in the Austrian part of the Rhine Valley lead to an increased concentration of organic aerosol and elevated emissions of black carbon (BC). In contrast, the local contribution of organic mass from wood burning, which can be attributed to domestic heating in this region, is lower (9 – 13 %).

We will present for this campaign and in addition the Mesolcina Valley with a higher ratio of wood burning the local and regional contributions to PM_1 and compare these with measurements in downtown Zurich.

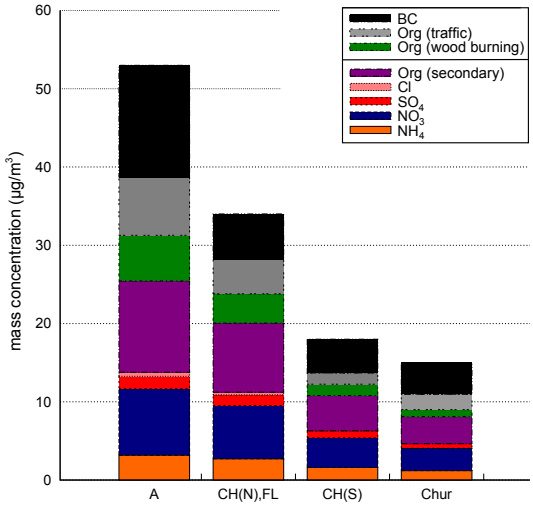

Figure 1: Mean chemical composition of PM_1 in the Rhine Valley at four different sections of the route (A Austria, CH(N) northern Switzerland, CH(S) southern Switzerland, FL Principality of Liechtenstein).

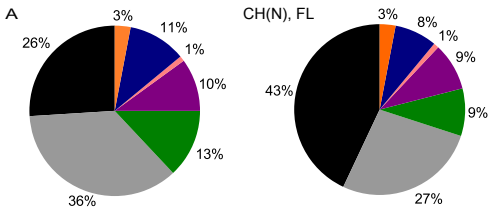

Figure 2: Relative local contributions after subtraction of the SO_4-normalized background concentrations of different species to PM_1 in the northern part of the Swiss Rhine Valley.

References:
Weimer, S., Mohr, C., Richter, R., Keller, J., Mohr, M., Prévôt, A.S.H., Baltensperger, U. (2009) *Atmos. Environ.* **43** 624-630.
Alfarra, M.R., Prévôt, A.S.H., Szidat S., Sandradewi, J., Weimer, S., Lanz, V.A., Schreiber, S., Mohr, M., Baltensperger, U. (2007) *Environ. Sci. Technol.* **41**, 5770-5777.
Paatero, P., Tapper, U. (1994) *Environmetrics* **5**, 111-126.
Mohr, C., Richter, R., DeCarlo, P.F., Prévôt, A.S.H., Baltensperger, U. (2011) *Atmos. Chem. Phys.* to be submitted.

A GIS based approach to combine back trajectory statistics and land cover analysis for the source apportionment of aerosol constituents

D. van Pinxteren[1], E. Brüggemann[1], T. Gnauk[1], K. Müller[1], C. Thiel[2], H. Herrmann[1,*]
[1]Leibniz-Institute for Tropospheric Research, 04318 Leipzig, Germany
[2]University of Jena, Institute for Geography, Department of Earth Observation, 07743 Jena, Germany

Keywords: Source apportionment, Trajectory statistics, Size distribution, Chemical composition
Presenting author email: dominik@tropos.de

Source apportionment models have since long been used to elucidate the impacts of specific emissions on observed pollutant concentrations. Principal component analysis (PCA) and positive matrix factorisation (PMF) are popular examples of such receptor models.

Another common approach in source apportionment studies are trajectory statistical methods (TSMs, Stohl, 1998). The results of these methods are usually presented in the form of maps where possible geographic locations of source areas can be identified.

An alternative approach to back trajectory analysis was presented by Lammel et al., 2003. Rather than pinpointing geographic locations, the authors aimed at identifying ground surface types which determine the abundance of pollutants at a receptor site.

The present work aimed at further developing this approach. The proposed method based on the calculation of hourly back trajectories using the HYSPLIT model (Draxler, 2003) in the ensemble mode. In this mode, the air mass history of a 24 h aerosol sample is described by an ensemble of 648 trajectories, leading to a much better representation of possible air mass pathways as compared to the calculation of a few single trajectories.

The trajectories were intersected with freely available satellite-derived land cover data (GLC2000), by calculating an index $L_{ik}(P)$ for each back trajectory i within a sampling period P and for each land cover class k as follows:

(1)

where $j = 0,1,2,...,J$ corresponds to the hourly endpoints of trajectory i ($j=0$ is starting location and $J=96$ for 96 hours back trajectories as used here), F_{mnkj} corresponds to the area fraction F of land cover class k within grid cell (m,n) that is hit by the trajectory endpoint j and $w_j=1–j/J$ corresponds to a linear weighting function. Next, the index $L_k(P)$ is derived as the arithmetic mean of all $L_{ik}(P)$, i.e. the indices of all back trajectories that fall into the sampling period P. $L_k(P)$ thereby serves as a proxy for the age-weighted residence time above land cover class k within the sampling period P. Land cover classes under consideration in this work are: Marine areas, natural vegetation, agricultural lands, urban areas, and bare areas. In Figure 1 the cumulative residence times are shown for a dataset of 29 samples (see below).

The method has been implemented within a GIS-enabled database system to allow for an efficient processing of large datasets with low computational demands. To validate the modelled residence times and further calculated parameters (mean trajectory length, solar radiation along trajectory, and local height of the boundary mixing layer), a PCA was performed on a dataset including the modelled parameters and the concentrations of 10 particle constituents (inorganic ions and organic and elemental carbon) in 5 particle size ranges for 29 winter- and summertime samples, sampled during 2003 to 2005 at an urban background site in Leipzig, Germany.

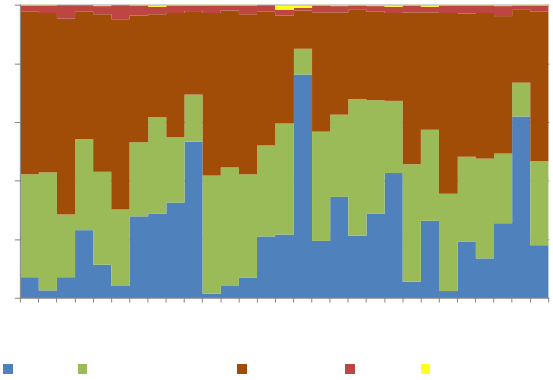

Figure 1: Cumulative residence times above the different land cover classes for all samples of the dataset

Six principal components could be extracted which together explained about 80 % of the total variance in the dataset. The factors could be attributed to the influence of meteorology on continental background pollution, secondary formation processes in polluted air masses, wood burning, aged sea-salt, local traffic, and long-range transported crustal material. Most of these factors have been frequently observed in previous European source apportionment studies (Viana et al., 2008), indicating the validity of the results. The modelled residence times and calculated meteorological parameters generally facilitated the interpretation of the extracted factors. The results proved that the intersection of trajectory data with land cover data by the presented method yields consistent and valuable additional information on the history of sampled air masses in the form of numeric indices which can readily be included into further data analysis.

Lammel, G., Brüggemann, E., Gnauk, T. et al. (2003) *J. Aerosol Sci.* **34**, 1.
Stohl, A (1998) *Atmos. Environ.* **32**, 947.
Viana, M., Kuhlbusch, T.A.J., Querol, X. et al. *J. Aerosol. Sci.* **39**, 827.

To exceed, or not to exceed: are the air quality standards adequate to describe the particulate matter pollution?

A. Di Menno di Bucchianico, G. Cattani, A. Gaeta, G. Gandolfo and A.M. Caricchia.

ISPRA – Italian National Institute for Environmental Protection and Research, Via Brancati 48, 00144, Rome, Italy

Keywords: legislation and policy, air quality, urban pollution.

Presenting author email: alessandro.dimenno@isprambiente.it

Information to the public on air quality in urban areas and on the effects of atmospheric pollutants on human health is a common demand.

Some usual queries made by policy-makers or by the so-called stakeholders are if the compliance with limit values was ensured, or if air pollution levels were decreasing in a specific area. Besides, according to the European legislation (Directive 2008/50/EC) air quality plans should be developed for zones and agglomerations within which concentrations of pollutants in ambient air exceed the relevant air quality target values or limit values.

Nevertheless, it is not easy to describe air quality status of a macro-area only on the basis of the exceedances of fixed limit values registered by the urban monitoring networks. On the contrary, the simple reading of these data can lead misleading evaluations for a series of reasons. Limit values can be contradictory: it is well known, as an example, that European daily PM_{10} standard is considered more stringent than the annual average limit value (this ambiguity, introduced in the past Directive 99/30/EC, has been maintained in the new one), but it is less known that a similar discrepancy has been set up for the brand new $PM_{2.5}$ European standard. In few words, it is practically impossible to respect at the same time the three limit values for PM_{10} and $PM_{2.5}$. It must be remarked that a different, and more coherent, definition of particulate matter standards was not impossible, this can be clearly demonstrated looking at the US-EPA particulate matter standards. On the other hand $PM_{2.5}$ US-EPA, based on more complex application conditions (3-year and different sites average) can lead to opposite evaluations using the same data only with a simple variation in the averaging criterion (see case A vs. B in table 1).

Table 1. Example of attainment for US-EPA $PM_{2.5}$ annual standard (LV: 15µg/m^3; 3-year average).

	Year	Site 1	Site 2	Site 3	Site 4	Mean (Y)
	I	12.7	-	-	-	12.7
A	II	13.3	17.4	14.7	-	15.1
	III	12.9	16.7	12.3	20.1	15.5
[µg/m^3]				***limit not exceeded***		**14.4**
	I	12.7	-	-	-	
B	II	13.3	17.4	14.7	-	
	III	12.9	16.7	12.3	20.1	
mean (s) [µg/m^3]		13.0	17.1	13.5	20.1	**15.9** ***limit exceeded***

Nevertheless, analysing air quality data from different geographical areas in Italy, it clearly appears that PM_{10} levels identified different seasonal patterns in northern, central and southern regions and, consequently, an interesting incongruity emerges: two stations with the same annual mean and almost the same daily exceedances (see Fig. 1) can be characterized by a completely different distribution of daily concentrations and dissimilar 90.4 percentile values (the parameter that should be evaluated instead of the number of exceedances according to the Directive 08/50/EC). This is clearly shown by the cumulative frequency in Fig. 2.

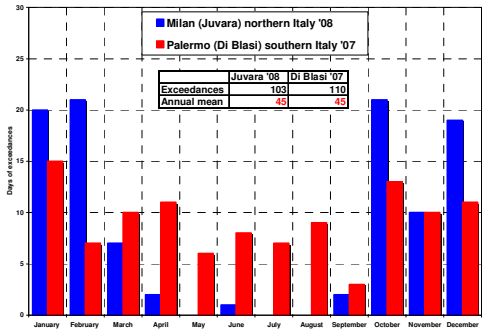

Figure 1. Northern and southern monthly distribution of PM_{10} daily exceedances in Italy.

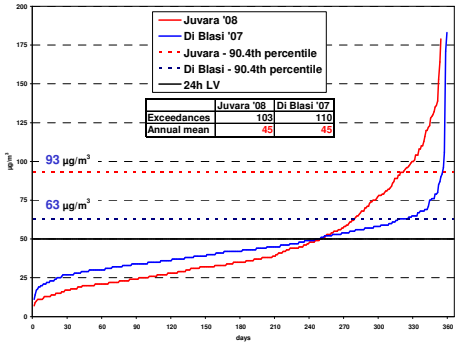

Figure 2. PM_{10} limit value and 90.4th percentile.

These evidences, if undervalued, can bring unexpected consequences: for example the fact that if the 24h PM_{10} European limit value were lower than 50 µg/m^3, on the basis of the same concentration data southern Italian cites could appear sometimes more polluted than northern cities; if limit were higher (just like in some non-European countries) southern cites never exceed the target so the PM_{10} pollution question could be easily and inexpensively solved for that area.

Long-term on-line measurement of non-refractory submicron aerosol in the city of Zurich

F. Canonaco[a], J. Slowik[a], A.S.H. Prévôt[a], U. Baltensperger[a]

[a]Laboratory of Atmospheric Chemistry, Paul Scherrer Institut, 5232 Villigen PSI, Switzerland
Keywords: AMS, PMF, ACSM
Presenting author email: francesco.canonaco@psi.ch

The role of aerosols in the atmosphere is of pivotal importance, because they affect climate (Forster *et al.,* 2007), human health (Peng *et al.,* 2005), ecosystems, e.g., acidification (Matson *et al.,* 2002), and visibility (Watson, 2002). These effects are controlled by particle concentration, composition, and size, which are in turn governed by sources and formation processes. Thus, the identification and quantification of formation mechanisms and sources is of high priority. However, this task is complicated due to the complexity of particle composition.

Long-term monitoring of aerosol composition provides a powerful tool for the analysis of the effects described above. This approach enables elucidation of the seasonal variability of different aerosol constituents, which is not possible with shorter-term campaigns. Long-term measurement records also allow for evaluation of emissions control strategies. Further, these measurements enhance epidemiological studies, permitting them to be carried out not only on the total aerosol concentration (Peng *et al.,* 2002) but on its components. Long-range, mesoscale, and local air quality models are improved through comparison with long-term datasets. Finally, the existence of long-term sampling records at a given site provides a framework for the interpretation of datasets from short-term intensive measurement campaigns.

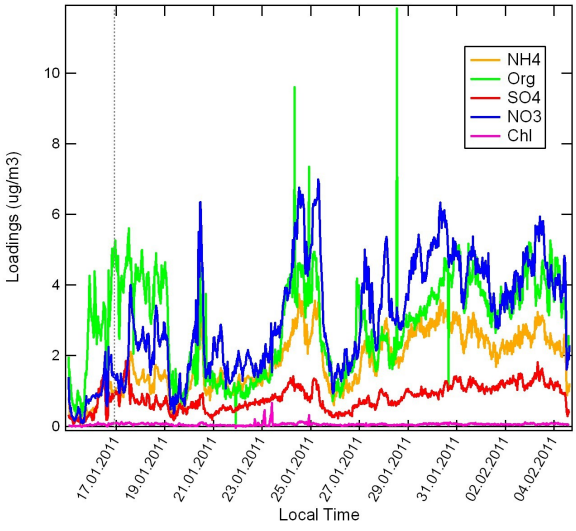

Figure 1. Preliminary results of the ACSM. The aerosol, SO_4, NO_3, NH_4, Cl and organics were measured.

We present measurements of submicron aerosol composition from an aerosol chemical speciation monitor (ACSM, Aerodyne Research, Inc.) deployed in downtown Zurich. The ACSM yields quantitative mass spectra of the non-refractory aerosol component with an averaging period of 30 minutes. As shown in Fig. 1, the ACSM is capable of resolving inorganic species such as NH_4, SO_4, NO_3, Cl, and the organic fraction. The mass spectra can be further analyzed by positive matrix factorization algorithm (PMF) or related techniques, which allow for identification and apportionment of the inorganic and organic fraction to important sources and processes.

Data from downtown Zurich collected during two weeks in January 2011 is shown in Fig. 1. PMF analysis of the organic component resolves the following factors: oxygenated organic aerosol (OOA), hydrocarbon-like organic aerosol (HOA) and biomass burning organic aerosol (BBOA). Mean concentrations for these components are shown in Table 1.

Table 1. Preliminary results of PMF applied to the organic portion. The algorithm allowed to deconvolve the organic data into three factors, i.e., OOA, HOA and BBOA.

factors	Loadings ($\mu g \cdot m^{-3}$)	Loadings (%)
OOA	2.40	52
HOA	1.40	26
BBOA	1.22	22

We will discuss identification and source apportionment of AMS and PMF data at an urban site over a six-month period (January to July 2011). Aerosol composition and source apportionment will be used to investigate the seasonal variability in the relative importance of specific emission sources and processes in the city of Zurich.

This work was supported by the Swiss Federal Office for the Environment (FOEN).

Forster, P. et al. (2007) *Changes in Atmospheric Constituents and in Radiative Forcing, in: Climate Change 2007,* Cambridge University Press,

Cambridge, United Kingdom and New York, NY, USA.
Matson, P. et al. (2002) *Ambio* **31**, 113-119.
Peng, R. et al. (2005) *Am. J. Epidem.* **161**, 585-594.
Watson, J.G. (2002) *J. Waste Air Manage.* **52**, 628-713.

Anthropogenic and natural constituents in particulate matter in the Netherlands

E.P. Weijers[1], M. Schaap[2], L. Nguyen[3], J. Matthijsen[4], H.A.C. Denier van der Gon[2], H.M. ten Brink[1], R. Hoogerbrugge[3]

[1] Department of Air Quality and Climate Change, Energy research Centre of the Netherlands (ECN), 1755ZG Petten, the Netherlands
[2] TNO, Business unit Environment, Health and Safety, Utrecht, the Netherlands
[3]National Institute for Public Health and the Environment (RIVM), Bilthoven, the Netherlands
[4] Netherlands Environmental Assessment Agency (PBL), Bilthoven, the Netherlands
Presenting autor email: weijers@ecn.nl

An intensive, one-year measurement campaign from August 2007 to August 2008 was carried out to determine the composition of PM_{10} and $PM_{2.5}$ at five locations in the Netherlands. The major goal of this study was to reduce uncertainties concerning composition, distribution and origin of particulate matter in the Netherlands. The work presented here was done within the framework of the Netherlands Research program on Particulate matter (BOP).

In the case of $PM_{2.5}$ the sum of all components measured in the collected filter samples explained 75-80%. Existing knowledge was used to partially close the remaining gap. After this procedure, 85-90% of the mass could be accounted for.

Generally, a considerable conformity in the chemical composition of $PM_{2.5}$ (and PM_{10}) is observed. In the case of $PM_{2.5}$, the secondary inorganic aerosol – the sum of sulphate, nitrate and ammonium - is the most dominant (42-48%). Higher contributions are measured at the rural locations. The second dominant contribution to PM2.5 comes from total carbonaceous matter and ranged between 22 and 32%. Sea salt, mineral dust and metals each comprises about 5% of total $PM_{2.5}$.

A detailed overview of the composition of the coarse fraction in the Netherlands could be presented. The chemical distribution shows a more even distribution among the components present in PM. Compared to the fine fraction, the presence of secondary inorganic aerosol and total carbonaceous matter become less dominant with contributions lower than 30%. Contributions of sea salt, mineral dust and metals are larger.

On days with high PM concentrations, all components except sea salt show higher concentrations. Relatively, the nitrate and unexplained contributions increase most on these types of days, while the relative contribution of the remaining components is mostly stable as function of PM level (figure 1). Sea salt maximises in marine air masses with clean air conditions.

From a literature study, the potential contribution from natural sources to the main components is estimated. The most important natural contributions came from sea salt and organic material. Although the analysis was rather pragmatic, it illustrates that the majority of PM in the Netherlands is of anthropogenic origin (Figure 2) being much higher than than originally assumed.

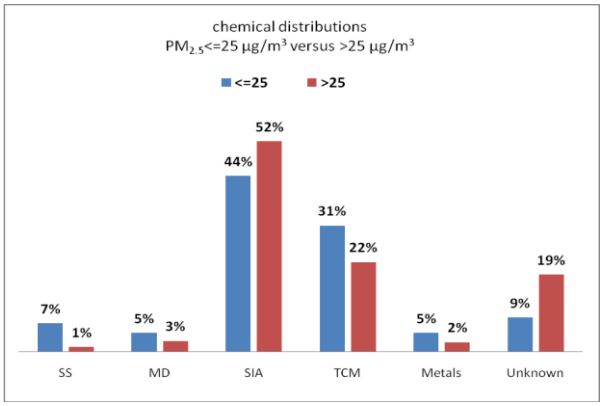

Figure 1. Change in chemical distribution in data substes for PM2.5 V<= 25 and PM2.5>2.5 µg/m^3.

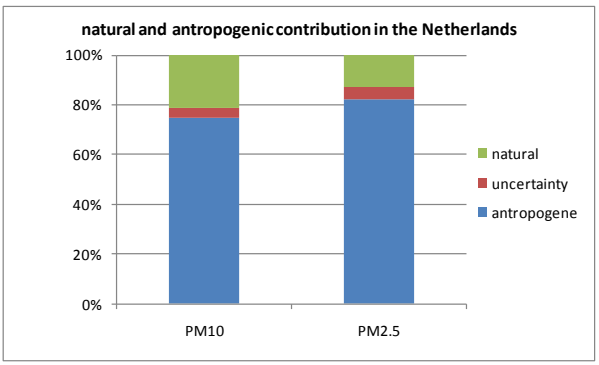

Figure 2. Natural and anthropogenic contributions to PM_{10} and $PM_{2.5}$ as estimated from the BOP data set.

The weekly cycle of ambient concentrations and traffic emissions of coarse (PM10-PM2.5) atmospheric particles

I. Barmpadimos[1], M. Nufer[2], D.C. Oderbolz[1], J. Keller[1], S. Aksoyoglu-Sloan[1], C. Hueglin[3], and A.S.H. Prevot[1]

[1]Laboratory of Atmospheric Chemistry, Paul Scherrer Institut, Villigen, 5232, Switzerland
[2]A Swiss Federal Institute of Technology (ETH), 8092 Zürich, Switzerland
[3]Swiss Federal Laboratories for Material Testing and Research (EMPA), 8600 Dübendorf, Switzerland
Presenting author email: andre.prevot@psi.ch

The aim of the study is to investigate the existence of a weekly cycle of coarse mode (PM10 – PM2.5) atmospheric particles, to compare this weekly cycle to the weekly cycle of PM2.5 and to compare the strength of the coarse mode weekly cycle in different seasons and different wind speed and precipitation conditions. In addition, an estimate of the contribution of traffic to the total ambient coarse mode particulate matter in urban areas is provided by estimating the weekly cycle of coarse mode emissions and by comparing it to the weekly cycle of ambient concentrations. The coarse mode data used in the study are the result of simultaneous daily measurements of PM10 and PM2.5 at seven sites located in Switzerland. The measurements cover a period of 7-12 years for six stations and 3 years for one station (Figure 1). It is found that a coarse mode weekly cycle is present in various types of urban and rural stations. Two examples are shown in Figure 2.
Ambient concentrations on weekdays are higher than on Sundays by a factor of 1.53 on average over all urban and suburban sites and by a factor of 1.32 on average over all rural sites. Moreover, the relative increase of coarse mode ambient concentrations on weekdays compared to Sundays was larger than the relative increase of PM2.5 concentrations by a factor of 2.7 on average over all urban and suburban sites whereas no considerable difference was found at the rural sites. A calculation of coarse mode traffic emissions for an urban scenario was carried out using traffic-induced dust resuspension and brake wear emission factors for light and heavy duty vehicles and traffic counts from urban areas in Switzerland. It is shown that coarse mode emissions on weekdays are greater than on Sundays by a factor of 1.73.

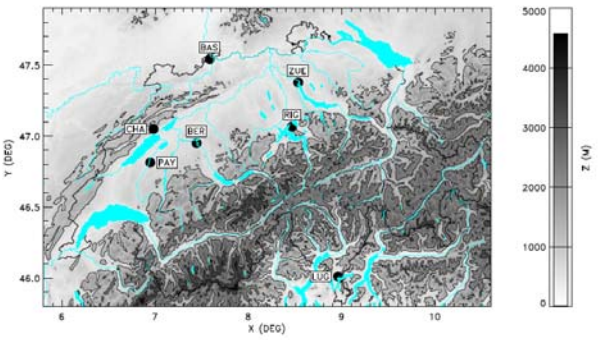

Figure 1: Locations of stations in this study. From West to East: Payerne, Chaumont, Bern, Basel, Rigi Zurich, Lugano

The contribution of traffic to coarse mode urban ambient concentrations was estimated to be 0.7 (0.52-0.9) on weekends and 0.8 (0.68-0.93) on weekdays.

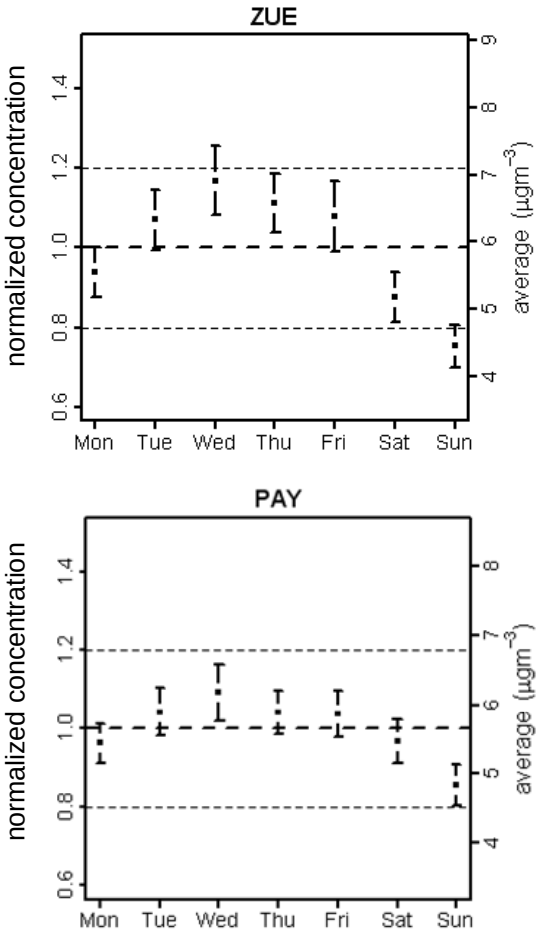

Figure 2: Weekly cycle of coarse particulate matter (PM10-PM2.5) for the urban background site Zurich and the rural site Payerne.

Acknowledgments

This work was financially supported by the Federal Office for the Environment and the COST fund of the Swiss State Secretariat for Education and Research (SER-Nr. C05.0128).

Local air pollution versus short–range transported dust episodes: a comparative study for submicron particle number concentration

T. Hussein[1], R. Abu Al-Ruz[1], T. Petäjä[2], H. Junninen[2], D.-E. Arafah[1], K. Hämeri[2,3], M. Kulmala[2]

[1] The University of Jordan, Department of Physics, Amman 11942, Jordan
[2] University of Helsinki, Department of Physics, P. O. Box 48, FI-00014 UHEL, Helsinki, Finland
[3] Finnish Institute of Occupational Health, Topeliuksenkatu 41 a A, FI-00250, Helsinki, Finland
Keywords: Urban; Suburban; Back-trajectory; Dispersion; Daily-pattern.
Presenting author email: t.hussein@ju.edu.jo

Jordan is a country under continuous development that faces a rapid increase in air pollution due to rapid increase in population density and industrial activities. Research on aerosols is rather sparse in Jordan. Very few studies have only focused on atmospheric aerosols because of the lack of air quality data as well as the absence of routine monitoring of ambient air pollution. However, previous research activities and studies have not focused on the capital city, Amman, neither they included measurements of particle number concentrations. Therefore, the purpose of this study was to investigate the number concentration of submicron particles in urban and suburban atmosphere of Amman during the spring season of year 2009. We specifically focused on the following aspects: (1) characteristics dispersion of submicron particle number concentrations at urban/suburban areas in the absence of dust episodes and (2) the influence of short-range transported dust episodes on the characteristics of submicron particle number concentrations.

We performed a measurement campaign at two sites (Hussein et al. 2011): suburban (University of Jordan campus) and urban (Al-Hashmi Al-Shamali). The aerosol measurements were performed with a portable Condensation Particle Counter (CPC, TSI model 3007).

Our findings confirmed that the particle number concentration of submicron aerosol particles is characterized by a daily pattern (Figure 1). This suggests that traffic emissions can be one of the main sources in Amman. Our speculations from both the measurement setup and with comparison with previous studies indicate that most of the submicron particles at the urban site were mainly in the Aitken and accumulation modes. The number concentration of submicron aerosol particles, which originated from the nearby highway, at the urban site decreased exponentially with the wind speed.

The dust loading in the atmosphere took several hours to build up and wash out before and after the air masses crossing over Amman region. In general, the total number concentration of submicron particles during a dust episode can be about 1/5 of what is typically observed during workdays without dust episodes. The low concentrations during dust episodes suggests that dust particles act as a coagulation sink for the submicron particles where their concentrations are reduces significantly, and thus, the total number concentration is also reduced. In addition, the wind speed during the observed dust episode was high enough to dilute the locally produced urban particles and disperse them efficiently. On the following days of a dust episode the number concentration gradually builds up in the urban atmosphere indicating the loading of aerosols from local sources within the city.

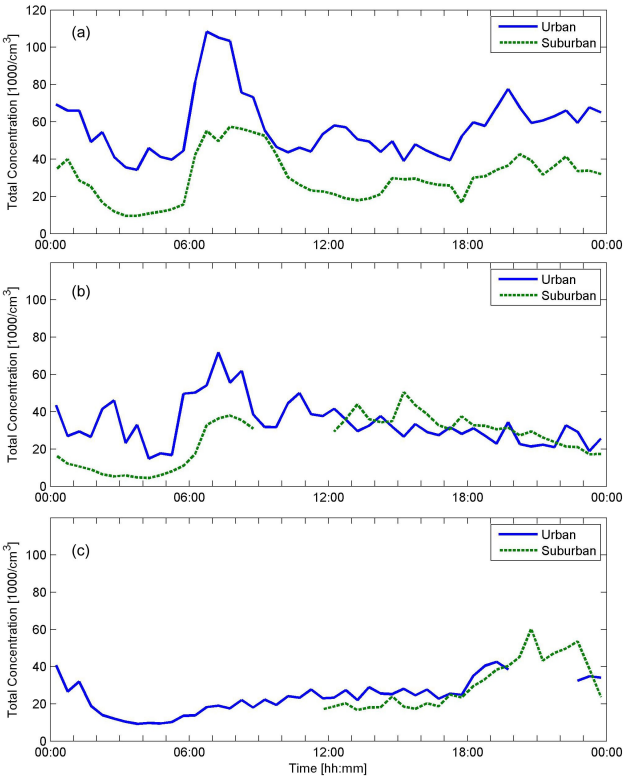

Figure 1. Daily patterns of the particle number concentrations (30-minutes means) at urban and suburban sites: (a) Saturdays–Wednesdays, (b) Thursdays, and (c) Fridays.

Hussein, T., Abu Al-Ruz, R., Petäjä, T., Junninen, H., Arafah, D.-E., Hämeri, K. and Kulmala, M. (2011) *Aerosol Air Quality Res.* (in press)

Monday, September 5, 2011

Session 3E: Aerosol-based Nanotechnology
Fundamentals

ChemChemical vapour synthesis of Cu-Si/SiO_2 Nanoparticles

A. Lähde[1], N. Kokkonen[2], A.J. Karttunen[2], S. Jääskeläinen[2], U. Tapper[3], T.A. Pakkanen[2] and J. Jokiniemi[1,3]

[1]Department of Environmental Science, University of Eastern Finland, 70211 Kuopio, Finland
[2]Department of Chemistry, University of Eastern Finland, 80101 Joensuu, Finland
VTT Fine Particles, 02044 VTT, Finland
Keywords: Coated nanoparticles,, copper, silicon gas phase synthesis.
Presenting author email: anna.lahde@uef.fi

The copper nanoparticles and nanocomposites hold great promise for electronics, ceramics, optical (Takeda et al. 2002) and thin film applications (Baxter et al. 1995), and high surface catalyst (Karakhanov et al. 2010). However, metals such as copper are very susceptile to oxidation forming nonconductive oxides. In order to prevent the oxidation, a protective coating layer (e.g. SiO_2) is typically applied on the particle surface (Fotou et al. 2000).

In this paper, we present an atmospheric pressure chemical vapour synthesis method (APCVS) for the prepration of nanocomposite particles composed of Si/SiO_2 with Cu nanometer size core. Metal-organic Cu(I) complex, $[CuN(Si(Me_3)_2]_4$, was synthesized and used as a precursor in APCVS that enable continuous production of highly pure materials in one-stage. The particle formation is based on the decomposition of the precursor that leads to homogeneous nucleation of released Cu and Si species and subsequent formation of nanoparticles with narrow size distribution. Since the Si coated Cu particles are prepared in one-stage under inert atmosphere, the oxidation of ultrafine Cu particles can be avoided.

Figure 1 shows the number size distributions of particle prepared at the vaporization temperature of 200 ºC in inert (N_2) and reductive (H_2/N_2 10 v-%) atmospheres.

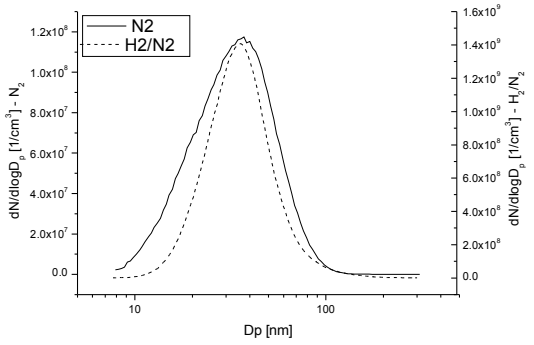

Figure 1. The number size distribution of Cu/Si particles prepared from non-purified precursor and vaporized at the heat bath temperature between 234-239 ºC. (Size distribution not dilution corrected, dilution ratio 1:19).

The geometric mean diameter of the particles was around 30 nm and the geometric standard deviation 1.3 in both cases. However, the total number of particles was baout nune times lower at N_2 ($N=6.2\times10^7$ 1/cm^3) compared at H_2/N_2 ($N=5.6\times10^8$ 1/cm^3) atmosphere. This is due to the enhanced decomposition of Cu(I) complex.The rapid decomposition lead also to a fast depletation of the precursor vapour and formation of copper film on the walls of the vaporisation flask.

The produced particles collected on the filter had reddish brown colour typical for metallic copper. Figure 2 shows the TEM images of the composite particles in inert (A) and reductive (B) atmosphere. The spherical coated primary nanoparticles were obtained when prepared under N_2. Since the components originated from the one precursor and not from the mixture of compounds, they were uniformly distributed in the gas phase resulting a uniform coating layer around the particles. Based on TEM/EDS analysis, the metallic copper was protected against oxidation with the shell consisting of Si/SiO_2. Under H_2/N_2 atmosphere, matrix type particles with ultrafine Cu particles embedded in SiO_2 were formed, see Figure 2B.

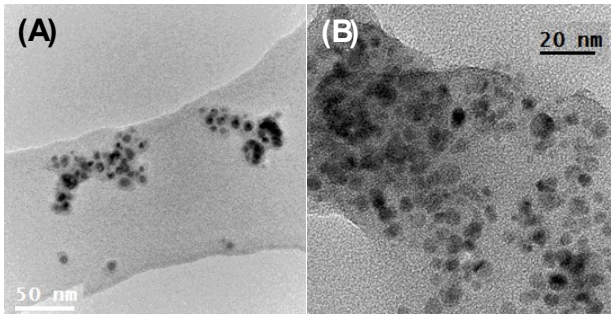

Figure 2. TEM images of Si/SiO_2 coated copper core particles formed at 800 (A) in nitrogen and (B) H_2/N_2 atmosphere.

We thank the Finnish Funding Agency for Technology and Innovation, TEKES, for financial support via "Active Nanocomposite Materials" (40072/08) project.

Takeda, Y., Lee, C.-G., Bandourko, V.V., Kishimoto, N. (2002) *Mater. Trans.* **43**, 1057-1060.

Baxter, D.V., Chisholm, M.H., Gama, G.J., Hector, A.L. Parkin, I.P.. (1995) *Chem. Vap. Deposition* **1**, 49-51.

Karakhanov, E.A., Maximov, A.L., Kardasheva, Y.S., Skorkin, V.A., Kadrashev, S.V., Predeina, V.V., Talanova, M.Y., Lurie-Luke, E., Seeley, J.A., Cron, S.L. (2010) *Appl. Catal. A.***385**, 62-72.

Fotou, G.P., Kodas, T.T., Anderson, B. (2000) *Aerosol Sci. Tech.* **33**, 557-571.

Applications of single-walled carbon nanotubes synthesised by aerosol CVD method

Albert G. Nasibulin[1], Marina Timmermans[1], Antti O. Kaskela[1], Kimmo Mustonen[1], Toma Susi[1], Virginia Ruiz[1], Simas Rackauskas[1], Ying Tian[1], Ilya V. Anoshkin[1], Sergey D. Shandakov[2], Esko I. Kauppinen[1]

[1] NanoMaterials Group, Center for New Materials and Laboratory of Physics, Aalto University, Finland;
[2] Laboratory of Carbon NanoMaterials, Kemerovo State University, 650043, Kemerovo, Russia;
Keywords: Nanotubes, Growth, Material synthesis, Applications
Presenting author email: albert.nasibulin@hut.fi

Carbon nanotubes (CNTs) are a unique family of materials exhibiting diverse useful chemical and physical properties. The CNTs and especially single-walled CNTs (SWCNTs) were found to have exceptional mechanical, thermal and electronic properties. Among different routes to synthesize SWCNTs, an aerosol CVD method is one of the most promising. This method allows to grow high quality and clean SWCNTs with certain diameters and lengths. CNTs can be easily deposited onto practically any substrate, including temperature nontolerant polymers, so that time-consuming steps of CNT purification from the catalyst and support, dispersion and deposition processes are avoided. Supplementary advantages of the aerosol method are possibilities to on-line control of the CNT quality and separate individual and bundled CNTs. This continuous aerosol CVD process is one of the most promising and powerful methods for the high-yield synthesis at controlled conditions. (Nasibulin & Shandakov, 2010)

This paper reviews the latest results obtained by two different aerosol synthesis methods elaborated in our group. In the first method, catalyst particles were produced by evaporating catalyst material from resistively heated Fe wire (a hot wire generator, HWG method) (Nasibulin *et al.*, 2005). The second method is based on ferrocene vapor decomposition in carbon monoxide atmosphere (Moisala *et al.*, 2006).

We report the investigations of the mechanism of single-walled carbon nanotube formation (Anisimov *et al.*, 2010; Nasibulin *et al.*, 2006) and charging of CNTs in the gas phase due to the bundling process (Nasibulin *et al.*, 2008). The paper also discusses the discovery and growth mechanism of a novel hybrid material, NanoBuds (Nasibulin *et al.*, 2007), SWCNTs with covalently attached fullerenes.

Direct integration of the CNTs produced by the aerosol methods into different applications, especially for high-performance flexible electronics, is discussed. (Kaskela *et al.*, 2010; Sun *et al.*, 2011). Produced SWCNT/polyethylene composite films have exhibited excellent optical and electrical properties as well as high mechanical flexibility. It was found that the electrical conductivity of the SWCNT films could be significantly improved by ethanol densification and chemical doping. SWCNT/polyethylene thin films demonstrated excellent cold electron field emission properties. We have fabricated state-of-the-art key components from the same single component multifunctional SWNT material for several high-impact application areas: high efficiency nanoparticle filters with a figure of merit of 147 Pa^{-1}, transparent and conductive electrodes with a sheet resistance of 84 Ω/□ and a transmittance of 90%, electrochemical sensors with extremely low detection limits below 100 nM, and polymer-free saturable absorbers for ultrafast femtosecond lasers. Furthermore, the films are demonstrated as the main components in gas flowmeters, gas heaters and transparent thermoacoustic loudspeakers.

This work was supported by the Academy of Finland (Pr. No. 128445), ’08 NEDO Grant, by Aalto University MIDE program via CNB-E project, and by Russian Federal Agency for Science and Innovation.

Anisimov, A.S., Nasibulin, A.G., Jiang, H., Launois, P., Cambedouzou, J., Shandakov, S.D., & Kauppinen, E.I. (2010). *Carbon*, **48**, 380-388.

Kaskela, A., Nasibulin, A.G., Zavodchikova, M.Y., Aitchison, B., Papadimitratos, A., Tian, Y., Zhu, Z., Jiang, H., Brown, D.P., Zakhidov, A., & Kauppinen, E.I. (2010). *Nano Lett.*, **10**, 4349–4355.

Moisala, A., Nasibulin, A.G., Brown, D.P., Jiang, H., Khriachtchev, L., & Kauppinen, E.I. (2006). *Chem. Eng. Sci.*, **61**, 4393-4402.

Nasibulin, A.G., Moisala, A., Brown, D.P., Jiang, H., & Kauppinen, E.I. (2005). *Chem. Phys. Lett.*, **402**, 227-232.

Nasibulin, A.G., Pikhitsa, P.V., Jiang, H., Brown, D.P., Krasheninnikov, A.V., Anisimov, A.S., Queipo, P., Moisala, A., Gonzalez, D., Lientschnig, G., Hassanien, A., Shandakov, S.D., Lolli, G., Resasco, D.E., Choi, M., Tomanek, D., & Kauppinen, E.I. (2007). *Nat. Nanotechnol.*, **2**, 156-161.

Nasibulin, A.G., Queipo, P., Shandakov, S.D., Brown, D.P., Jiang, H., Pikhitsa, P.V., Tolochko, O.V., & Kauppinen, E.I. (2006). *J. Nanosci. Nanotech.*, **6**, 1233-1246.

Nasibulin, A.G., & Shandakov, S.D. (2010). In *Aerosols: Science and Technology* (Edited by Agranovski, I.), *Aerosols: Science and Technology* pp. 65-89). Wiley-VCH, Weinheim.

Nasibulin, A.G., Shandakov, S.D., Anisimov, A.S., Gonzalez, D., Jiang, H., Pudas, M., Queipo, P., & Kauppinen, E.I. (2008). *J. Phys. Chem. C*, **112**, 5762-5769.

Sun, D.-M., Timmermans, M.Y., Nasibulin, A.G., Kauppinen, E.I., Kishimoto, S., Mizutani, T., & Ohno, Y. (2011). *Nat. Nanotechnol.*, **6**, DOI: 10.1038/NNANO.2011.1031.

Cloud condensation nuclei (CCN) activity and oxygen-to-carbon elemental ratios following thermodenuder treatment of organic particles grown by α-pinene ozonolysis

M. Kuwata, Q. Chen and S. T. Martin

School of Engineering and Applied Sciences & Department of Earth and Planetary Sciences,
Harvard University, Cambridge, Massachusetts, 02138 USA
Keywords: CCN, secondary organic material, elemental ratio, volatility
Presenting author email: scot_martin@harvard.edu

Introduction CCN activity of aerosol particles is important as a regulator of cloud properties, including their brightness, lifetime, and precipitation. Although CCN activity of pure compounds is predictable from their chemical characters, CCN activity of secondary organic material (SOM) is not understood for quantitative prediction due to their complexity in chemical composition.

In the present study, we systematically controlled SOM chemical composition generated using the Harvard Environmental chamber (HEC) by (1) altering SOM concentration (M_{org}) in the HEC, and (2) increasing the thermodenuder (TD) temperature (T) connected to the HEC. SOM chemical composition was measured simultaneously with CCN activity. This experimental design allows us to relate CCN activity and chemical composition, as both M_{org} and T controls SOM chemical composition based on volatility.

Experiment The HEC is consisted of a 4.7 m^3 Teflon bag housed in a temperature controlled (25 °C) room. It was operated as a continuous stirred tank reactor, providing sufficient time to measure SOM. SOM was produced by dark ozonolysis of α-pinene (8 – 80 ppb) with the presence of 2-butanol as an OH scavenger. SOM concentration in the chamber ranged from 1.4 to 37μg m^{-3}, depending on α-pinene concentration. 30-nm $(NH_4)_2SO_4$ seed particles, those were provided from a differential mobility analyzer (DMA), were also continuously injected into the chamber. Ozone concentration and relative humidity were feedback controlled as 50 ppb and 40%, respectively.

SOM particles generated in the HEC were injected into a thermodenuder (TSI 3065), which was operated at bypass, 25, 60, 80, and 100 °C. The flow passed through the TD was split to three flows to measure size-resolved CCN activity (DMA-CCN counter(CCNC)), chemical composition (high-resolution time-of-flight aerosol mass spectrometer (HR-ToF-AMS), and number size-distribution (scanning mobility particle sizer (SMPS).

CCN activation curve measured by the DMA-CCNC was fitted by a sigmoid function to obtain dry activation diameter (d_{dry}) κ values, which is defined as $\kappa = i\, MW_{water}\rho_{org}/MW_{org}\rho_{water}$, were employed to represent CCN activity [i: van't Hoff factor, MW_x: molecular weight of x, ρ_x: density of x]. κ was iteratively calculated to reproduce d_{dry} obtained from size-resolved CCN spectra.

Results and discussion

We observed ~50% of decrease in M_{org} following TD treatment at 100 °C regardless of M_{org} in the HEC. This demonstrates that evaporation is the main process occurring in the TD. Elemental composition of SOM measured by the HR-ToF-AMS revealed that both M_{org} and T dependences are consistent in terms of volatility: oxygen-to-carbon (O:C) ratio increased for lower volatility compounds (lower M_{org}/higher T), while H:C ratio decreased for these conditions. This trend was further confirmed using a Van Krevelen diagram. All data points aligned on a straight line ([H:C] = -0.8 [O:C] + 1.8), including both M_{org} and T dependences. These results demonstrate that the main process occurring in the thermodenuder is evaporation of relatively volatile compounds.

κ did not depend on M_{org} at 25 °C, which may lead to predict that T also does not alter κ, considering the consistent dependences of elemental ratios on M_{org} and T. However, κ decreased at higher T. The magnitude of the decrease was significant (~20 % at 100 °C) at higher M_{org} (> 10μg m^{-3}), while the decrease was not significant at the low M_{org} (1.4μg m^{-3}).

These apparently contradicting results can be consistently interpreted as follows. TD evaporates relatively volatile materials, which cause decrease in M_{org} and changes in elemental ratios. At the same time, it enhances oligomer concentration in particles due to (1) evaporation of relatively volatile monomers, and (2) thermally induced oligomer formation reactions. These processes decrease κ, as oligomers have higher MW_{org} than original monomers. A variety of functional groups such as carbonyl groups is required for oligomerization reactions. Decrease in κ was significant at higher M_{org}, as relatively volatile carbonyl compounds could partition to particle phase due to higher concentration. This interpretation was supported by a model calculation employing master chemical mechanism coupled with SIMPOL vapour pressure prediction method, which predicted that carbonyl groups are depleted at lower M_{org}, while a variety of functional groups exist at higher M_{org}.

Acknowledgements: This material is based upon work supported by the Office of Science (BES), U.S. Department of Energy, Grant No. DE-FG02-08ER64529.

References:

Kuwata, M., Chen, Q., and Martin, S. T. (submitted)

Surface tension of nanosized drops of mono- and bivalent metals

A. A. Onischuk, S. V. Vosel, P. A. Purtov

Institute of Chemical Kinetics and Combustion, Novosibirsk 630090, Russia
Keywords: surface tension, nanoparticles, homogeneous nucleation, nucleation rate.
Presenting author email: onischuk@kinetics.nsc.ru

The surface tension of nanosized drops is a rather sharp function of radius [1]. It is not possible to measure this quantity experimentally for radius of about 1 nm and numerical calculations are possible only for simple systems, like Lennard-Jones(LJ) fluids [2]. In this work we demonstrate the way to determine the small drop surface tension from the experimental nucleation rate.

The nucleation theory gives the rate of nucleation I (the number of critical nuclei formed per unit time per unit volume) as [3, 4]:

$$I = KSn_1^{sat}\beta Z \exp\left(-\frac{4\pi R_S^2 \sigma_S(R_S)}{k_B T}\right) \quad (1)$$

where S is the supersaturation, n_1^{sat} is the saturated vapor concentration, K is the translation-rotation free energy correction factor (arising due to the so-called replacement free energy [3]), R_S is the radius of the surface of tension, β is the collision frequency of the vapor molecules with the critical nucleus, Z is the so-called Zeldovich factor, $\sigma_S(R_S)$ is the surface tension of the critical nucleus referred to the surface of tension, k_B is the Boltzmann constant, T is the absolute temperature. The Classical Nucleation Theory (CNT) assumes that the drop surface tension is equal to that of a flat surface (σ_∞). This simplification results sometimes in an error in the nucleation rate of tens to hundreds orders of magnitude. Besides, it was put $K \approx 1$ in CNT, however, the direct numerical calculation have shown that $K \approx 10^9$ - 10^{13} (for the LJ systems) [3]. To obtain the rigorous analytical formula for the nucleation rate one should derive the formula for Zeldovitch factor Z accounting the dependence of drop surface tension on radius and an analytical expression for the correction factor K. Quite recently we obtained the analytical formula for the correction factor in the framework of the Frenkel's theory of liquids, Reiss theory accounting the fluctuations of the drop center of mass, and Kusaka theory of replacement free energy [4]. In the present work we derived the analytical formula for Zeldovitch factor in the framework of the Nishioka thermodynamic theory of non-critical drop [5]. Thus, the rigorous formula for the nucleation rate is

$$I = K\left(Sn_1^{sat}\right)^2 \sqrt{\frac{2m\sigma_S(R_S)}{\pi}} \frac{\varphi(x)}{\rho} \exp\left(-\frac{4\pi R_S^2 \sigma(R_S)}{k_B T}\right), \quad (2)$$

where ρ is the density of the liquid macroscopic reference phase (having the same chemical potential as the critical nucleus), m is the mass of molecule, $x=\delta/R_S$, δ is the Tolman length which is equal to $\delta = R_e - R_S$, R_e is the equimolar radius, $\varphi(x)$ is some function of x [6]. In this work we have analysed the nucleation rate from the supersaturated vapor of mono- and bivalent metals as measured in our laboratory (Zn Ag) and elsewhere (Li, Na, Cs, Ag, Hg, Mg) [7-11]. It was found from this analysis that the $\varphi(x)$ can be set as equal to unity with the accuracy of 10%. Then, accounting the analytical formula for the correction factor [4] the final formula for the nucleation rate can be written as:

$$I \approx 6 \times 10^2 \pi^{7/2} Sn_1^{sat} \frac{(u\rho)^3 R_S^9}{m^2 (k_B T)^{3/2}} \sqrt{\sigma_S(R_S)} \exp\left(-\frac{4\pi R_S^2 \sigma_S(R_S)}{3k_B T}\right) \quad (3)$$

where u is the sound velocity in the reference phase. If the nucleation rate is measured at some T and S, the surface tension and the radius R_S can be found by solving Eq. (3) together with the Kelvin equation. The surface tension thus found is shown in Fig. 1 for mono and bivalent metals. The plotted points are not dependences σ_S/σ_∞ vs. R_S, but there are three independent values σ_S/σ_∞ for each metal corresponding to three different temperatures and three values of R_S. All the metals considered can be divided into two groups Li, Na, Cs, Ag (monovalent metals) $\sigma_S/\sigma_\infty > 1$ and Mg, Zn, Hg (bivalent metals) $\sigma_S/\sigma_\infty < 1$. In all the cases the surface tension for drops of radius about 1 nm differs essentially from that of the flat surface, i.e. the surface tension is a strong function of size.

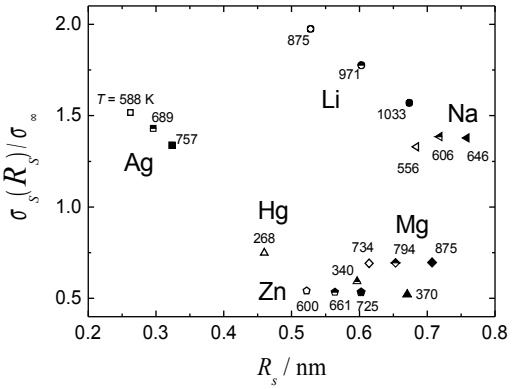

Fig. 1. $\sigma_S(R_S)/\sigma_\infty$ and R_S (T is shown in the plot).

Financial support for this work was provided by the Cooperation Agreement between CNR (Italian National Research Council) and RAS (Russian Academy of Science) years 2008-2010 and Siberian Branch of RAS (Interdisciplinary Integration Project No. 3).

1. L. S. Bartell, *J. Phys. Chem*. B 2001, 105, 11615.
2. P. R. ten Wolde, D. Frenkel, *J. Chem. Phys*., 1998, **109,** 9901.
3. I. Kusaka, *Physical Review* E 2006, 73, 031607.
4. S. V. Vosel, et al., *J. Chem. Phys*. 2009, **131**, 204508.
5. K. Nishioka and I. Kusaka, *J. Chem. Phys*. 1992, 96, 5370.
6. S. V. Vosel et. al. *J. Chem. Phys*. 2010, **133**, 047102.
7. J. Martens et. al., *J. Phys. Chem*. 1987, *91,* 2489.
8. F. T. Ferguson et. al., *J. Chem. Phys*. 1996, **104**, 3205.
9. F. T. Ferguson and J. A. Nuth III, *J. Chem. Phys*. 2000, **113**, 4093.
10. D. M. Martinez et. al., *J. Chem. Phys*. 2005, 123, 054323.
11. J. A. Nuth et al., *J. Chem. Phys*. 1986, **85**, 1116.

Study of Heterogeneous Nucleation upon Nanoparticles in Condensation Particle Counters (CPCs): Effects of Particle and Vapor Composition

M. Chen [1] , M. Attoui[2] , and P. H. McMurry [1]

1 University of Minnesota, 111 Church ST. SE., Minneapolis, MN, 55455

2 Faculté des Sciences, Université XII-Val des Marne, Paris, France

Keywords: heterogeneous nucleation, CPC, counting efficiency, chemical composition, electrical charges

Presenting author email: attoui@univ-paris12.fr

Recent developments have led to significant reductions in the minimum size that can be detected with condensation particle counters (CPCs), allowing the detection of individual particles as small as 1 nm (Gamero and Fernandez de la Mora 2000, Jiang et al. 2011, Vanhanen et al. 2011)

While CPCs are widely used as particle detectors due to their high sensitivity and high signal-to-noise ratio, previous laboratory work shows that the activation efficiencies for particles smaller than 3nm are influenced by the chemical composition of particles and the condensing vapor, which lead to measurement uncertainties that are difficult to quantify.

On the other hand, in spite of the work on heterogeneous nucleation in the past decades, discrepancies between measurements and theory still exist.

In this study, we carry out experiments to explore the effects of nanoparticle chemical composition, electrical polarity (+1, 0, -1), and charge (+1, +2, +3, +4) on heterogeneous nucleation of several supersaturated vapors.

Particle materials studied include (NaCl, W, Ag, and polyethylene glycol). Several condensing vapors (water, n-butanol, and diethylene glycol) were investigated.

The comparison between the experimental result and the existing theories is discussed. This study not only enriches our knowledge of activation efficiencies of different CPCs, which are essential for aerosol scientists who work with them, but also serves as an attempt to explore the fundamental scientific mystery of heterogeneous nucleation.

Gamero-Castano, M., and Fern´andez de laMora, J. (2000). J. Aerosol Sci. 31:757–772.

Jiang,J., , Zhao, J., Chen,Fred L. Eisele,F.L., Jacob Scheckman, J., Williams,B.J., Kuang,C. and McMurry,P.H. 2011. AS&T 45 p ii-v

Vanhanen, J., Mikkilä, J., Lehtipalo, K., Sipilä, M. Manninen, H.E. Siivola, E., Petäjä, T., Kulmala, M. 2011 AS&T 45 p 533-543

Particle mass spectrometry based on micro string resonators for the application in portable aerosol monitors

S. Schmid, T. Larsen and A. Boisen

Department of Micro- and Nanotechnology, Technical University of Denmark, DTU Nanotech, DK-2800 Kgs. Lyngby, Denmark

Keywords: MEMS, aerosol sensor, mass spectrometry, string resonator.

Presenting author email: silvan.schmid@nanotech.dtu.dk

The use of engineered nanoparticles in commercial applications has increased and personal monitoring devices for the assessment of nanoparticle exposure doses are highly demanded (Nel, 2006). We present a micro sensor for the real-time measurement of the mass spectrum of airborne micro and nanoparticles for the implementation in a portable aerosol nanoparticle monitor.

The micro sensor is based on resonant strings, as shown in Fig. 1, and measures the particle mass spectrum of airborne particles with a mass range of up to 5 orders of magnitude. Every time a particle lands on the string it causes a resonant frequency shift. The frequency shift depends on the mass and landing position of a particle on the string. Based on an analytical mechanical model, both, the mass and position of individual particles can be calculated by measuring the shifts of the first two bending modes (Schmid, 2010). This method is fast and requires low computing power which is important for a the implementation in a portable device.

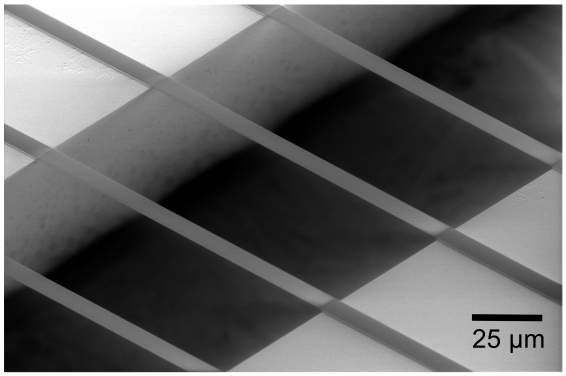

Figure 1. Scanning electron microscopy image of silicon nitride string resonators.

The sensor has been tested by distinctively measuring 3 different particles with weights Δm of 4.8±0.18 pg, 14.9±5.4 pg and 111.8±14.4 pg, respectively, with a 216 µm long and 340 nm thick silicon nitride string with a weight of m_0 = 0.6 ng. From the resulting particle-number versus particle-mass histogram, shown in Fig. 2, mean particle masses of 4.5±0.8 pg, 17.6±1.8 pg and 125.2±1.0 pg were obtained. The measured values are precise and correspond to the expected masses (see Fig. 3). The 4.8 pg particles caused an average relative frequency shift of 0.6%. At atmospheric pressure, the typical frequency resolution of micro beam resonators is approximately 4e-4% (Li, 2007) which gives a mass resolution in the femtogram range.

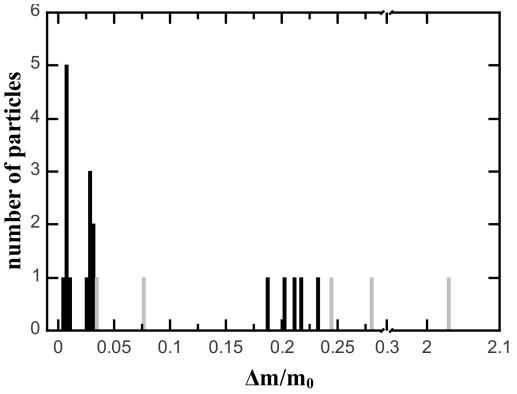

Figure 2. Histogram of number of particles versus mass ratio

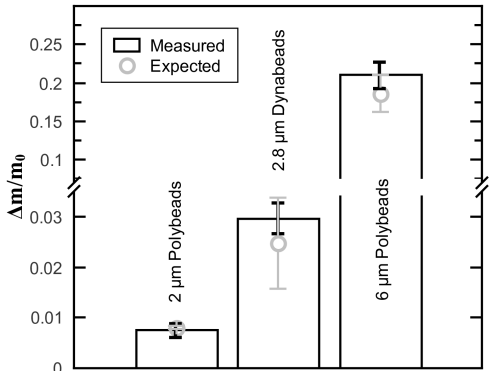

Figure 3. The average measured mass ratios for the three different types of micro particles compared to the expected values.

The sensitivity of the sensor can be increased by decreasing the string mass. With a string of one picogram, nanoparticles in the attogram range can be detected. In order to increase the sensor efficiency, beforehand unipolarly charged nanoparticles can be focused onto the string by an electrostatic lens. The presented micro sensor enables real-time mass spectrometry for portable personal aerosol monitoring devices.

This project has received funding from the European Community's Seventh Framework Programme (FP7/2007-2013) under grant agreement no. 211464-2.

Nel, A., Xia, T., Mädler, L., Li, N. (2006) *Science* **311**, 622-627.

Schmid, S., Dohn, S., Boisen, A. (2010) *Sensors* **10**, 8092-8100.

Li, M., Tang, H. X., Roukes, M. L. (2007) *Nat. Nanotech.* **7**, 114–120.

Characterizing lengths and aerodynamic diameters of airborne glass fibers

Bon Ki Ku[1], Gregory Deye[1] and Leonid A. Turkevich[1]

[1]Centers for Disease Control and Prevention (CDC), National Institute for Occupational Safety and Health (NIOSH), Cincinnati, Ohio 45226, USA
Keywords: Glass fiber, length, diameter, screen.
Presenting author email: BKu@cdc.gov

Introduction

Historically, fiber-related research primarily grew out of health and manufacturing issues regarding asbestos. Current fiber measurement techniques also arose primarily due to health concerns over asbestos exposure. Fiber toxicity appears to be mostly a function of fiber concentration, dimensions (diameter and length) and durability in the lungs. During the past decade, airborne fibrous particles such as carbon nanotubes and carbon nanofibers have come under scrutiny owing to their asbestos-like appearance (Poland et al. 2008). This suspicion hinges on thin fiber-like structure of these particles and their presumed insolubility in the lungs, both attributes of harmful asbestos fibers. To better understand the toxicity of fibers, it is essential to classify fibers by length for toxicology studies. In this study we investigated how feasible it would be to use screens combined with asbestos sampling cassettes for length classification of fibers.

Methods

Glass fiber powder (GW1) supplied by the Japan Fibrous Material Research Association (JFMRA) was used as a surrogate of asbestos to generate airborne glass fibers by a vortex shaking method (Ku et al., 2006). The glass fiber sample had a geometric mean length 20.0 μm with geometric standard deviation (GSD) of 2.58 and geometric mean diameter 0.88 μm with geometric standard deviation (GSD) of 3.10 (Kohyama et al., 1997). Size distributions of the airborne glass fibers from the vortex shaker were measured by an Aerodynamic Particle Sizer (3321, TSI Inc.), and the airborne fibers were collected on a mixed cellulose ester filter (SKC Inc) in a 25 mm conductive cassette to measure length distribution of the fibers by a phase contrast microscope (PCM) with 40X and 10X magnifications. Nylon net screens with different screen mesh sizes (60, 20, and 10 μm) were used to examine the effect of screen size on length distribution.

Results and Conclusion

Figure 1 shows cumulative number concentration of glass fibers as a function of fiber length for different screen sizes. The red and blue lines in Fig. 1 represent mesh sizes of screen 20 and 60 μm. With no screen, the length distribution of the fibers is similar to the one reported in a previous paper. As screen mesh size decreases from screen 60 to 20, 50% cut-off length decreases from about 10 μm to about 7.5 μm. Compared to no screen case, using screens could give reduced lengths of fibers. It is worth noting that the 50% cut-off length for screen 10 is similar to the one for screen 60, but the slope of the cumulative curve for screen 10 becomes steeper, which means that the length distribution for screen 10 is narrower than the one for screen 60. The percentage of fibers longer than 20 and 60 μm for screen 20 and 60 is about 17 % and 3 %, respectively while the percentage of fibers longer than 10 μm for screen 10 is about 50 %,

APS measurements showed that fibers with no screen have bimodal distributions, with a primary aerodynamic diameter 1.5-2 μm and secondary aerodynamic diameter 7 μm. Using screen 60 and 20 slightly decreased primary modal diameters and significantly reduced the secondary mode. Screen 10 removed almost completely the second mode. The loading of fibers on the filter was also investigated. Using screens resulted in relatively uniform loading along the diameter of the filter.

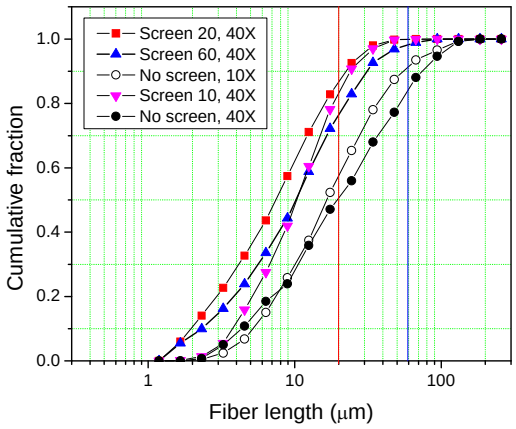

Figure 1. Cumulative fraction of fiber number concentration as a function of fiber length for different screen sizes. 10X and 40X mean magnifications used.

Acknowledgments

We would like to thank Dr. Ono-Ogasawara for sending us samples of glass fibers through the JFMRA in Japan, and Elizabeth Ashley for taking images of fibers and analyzing length distributions using the PCM. This work was supported by the National Institute for Occupational Safety and Health under the NORA project 927ZJFB.

Kohyama, N et al. (1997) *Ind. Health.* **35**, 415-432.
Poland, C. A. et al. (2008). *Nat. Nanotechnol.* **3**, 423-428
Ku, B. K., et al. (2006). *Nanotechnol.* **17**, 3613-3621.

Monday, September 5, 2011

Session 3F: Thermal and Optical Effects

Using holographic optical landscapes to manipulate aerosol arrays, compare particle hygroscopicity and study aerosol coagulation.

R.M. Power,[1] J.S.Walker,[1] A.E. Carruthers[1] and J.P. Reid[1]

[1]School of Chemistry, University of Bristol, Bristol, BS8 1TS, United Kingdom

Keywords: Optical trapping & guiding, holographic optical tweezers, aerosol sampling & analysis, aerosol coalescence

Presenting author email: Rory.Power@bristol.ac.uk

Optical forces can be used to manipulate arrays of aerosol particles[1] in order to study their dynamics.[2] We demonstrate the use of multiple gradient force optical traps in studying the hygroscopic growth and coalescence of aerosol particles. These are two of the most fundamental processes that govern size distribution of aerosols a critical parameter for characterizing the role of aerosols in atmospheric science and drug delivery.

Aerosol particles can be confined in three dimensions by a tightly focused Gaussian laser beam. At the focus an optically induced gradient force several orders of magnitude larger than gravity acts to restore particles to the point of highest light intensity. This technique is referred to as 'optical tweezing'. Recently we have demonstrated the use of a spatial light modulator (SLM) in creating complex intensity patterns [2] in the optical trapping plane for the aerosol. By displaying a hologram onto the SLM the phase and intensity of light across the wavefront of the incident laser beam can be modified to produce the desired optical landscapes referred to as holographic optical tweezers (HOTs). A sequence of these holograms can be animated to produce a dynamically evolving optical landscape allowing complex manipulation of arrays of aerosol particles in three dimensions. [3]

Figure 1. An array of droplets trapped within an SLM generated holographic 'optical landscape'

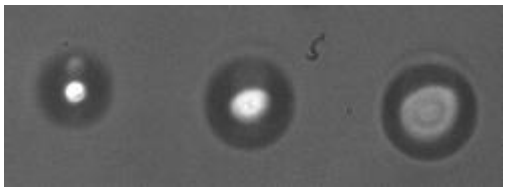

HOTs can be used to manipulate particles of different size and composition independently in three dimensions. Optical barriers formed by the SLM can shield trapped droplets from the flow of free aerosol allowing additional droplets of chemically distinct composition to be added to the ensemble.[3] This can for example, allow an isolated droplet of known composition can be used as a probe of the gas phase conditions in an aerosol ensemble.

We will report two examples of the application of HOT aerosol arrays. The first application will examine the use of HOTs to perform comparative hygroscopicity measurements allowing validation of the aerosol diameter dependent equilibrium model (ADDEM) at high relative humidity (RHs approaching 100%). Such conditions are very difficult to replicate in the laboratory but are essential for understanding the activation of cloud condensation nuclei and the radiative forcing of atmospheric aerosol.

Cavity enhanced Raman scattering (CERS) allows droplet size to be determined with nanometre accuracy. [4] Using CERS in tandem with HOTs, we will show how the size of two chemically distinct droplets can be simultaneously measured, providing thermodynamic data on various aerosol species

In the second application we will show how aerosol HOTs can be used to study the factors governing particle interactions and coalescence. Tracking the position of a trapped particle from the brightfield image with millisecond resolution can be used to measure positional correlation of nearby particles and the interactions between them, providing information on droplet surface charge and the trapping forces. Further, measurements of elastic light scattering can provide information on the processes which occur over microsecond timescales during the coagulation event.

In conclusion, using novel HOT techniques we can gain considerable insight into the fundamental processes of aerosol coagulation and hygroscopic growth, processes that are responsible for controlling the evolution of aerosol size distributions in many complex environments.

This work was supported by the Engineering and Physical Sciences Research Council, UK

[1] Burnham, D.R, & McGloin, D. (2006), Opt. Express, 14, 4175-4181
[2] Butler, J.R, Wills, J.B, Reid, J.P. (2008), Lab On A Chip, 9, 521-528
[3] Butler, J.R, Wills, J.B, Reid, J.P. (2009), Phys. Chem. Chem. Phys, 11, 8015-8020
[4] Hopkins, R.J, Mitchem, L, Reid, J.P. (2004), Phys. Chem. Chem. Phys, 6, 4924-4927

Impact of Temperature Gradients on Brownian Coagulation

M. Arias-Zugasti[1] and D.E. Rosner[2]
[1] Dept. de Física Matemática y de Fluidos, UNED, Apdo: 60141, 28080 Madrid, Spain
[2] Chemical & Environmental Engineering Dept., Yale University, New Haven, CT 06520-8286, USA
Keywords: Coagulation; Fundamental aerosol physics; Aerosol modelling.
Presenting author email: maz@dfmf.uned.es

It has been recently shown that size-dependent particle thermophoresis, i.e. the movement of particles induced by a temperature gradient, provides a new coagulation mechanism [Rosner and Arias-Zugasti (2011)], which can either induce the coagulation of non-Brownian particles, or alter the coagulation frequency in the case of Brownian particles.

In the present work we consider this second scenario, in which an aerosol of Brownian particles evolves under the influence of both coagulation mechanisms: the well-known Brownian coagulation studied by Smoluchowski and the thermophoresis-induced coagulation. Rather than considering the addition of both coagulation frequencies, we derive a combined coagulation frequency based on a thermophoresis-modified formulation of the derivation of the coagulation frequency in the continuum limit by Smoluchowski. Hence, the Brownian-thermophoresis combined coagulation frequency is modeled in a way similar to the Brownian-sedimentation coagulation frequency [Simons (1986)], but with the gravitational sedimentation velocity replaced by the size-dependent thermophoresis velocity.

We show that the relative intensity of each coagulation process is given by a Peclet number, defined as the ratio of the characteristic coagulation frequencies: $\beta_{\mathrm{TP,ref}}/\beta_{\mathrm{B,ref}}$. Then, introducing the combined coagulation frequency as a kernel into a Smoluchowski-type population-balance integro-PDE, we perform a systematic parametric study of the time evolution of a coagulation aged, initially log-normal population, as a function of the control parameters of the problem: i.e. the aforementioned Peclet number (Pe) and the particle/gas Fourier thermal conductivity ratio k_p/k_g.

Our results show that in the long-time limit a quasi-self-preserving population is reached. The dependence of this quasi-self-preserving distribution function on Pe and on the particle/gas Fourier thermal conductivity ratio is analyzed. In this respect, we find that when the reference Peclet number is much smaller than, say 0.1, we recover the previously well-studied/characterized Brownian self-preserving populations. However, for intermediate Peclet-values characteristic distortions set in, corresponding to increased spread and skewness, and slightly smaller departures from log-normality. Ultimately (for Peclet-values larger than about 10 our quasi-self-preserving droplet size distributions become indistinguishable from our previously reported TP-dominated results [Rosner and Arias-Zugasti (2011)]. Remarkably, it has been observed that the dependence on the particle/gas Fourier thermal conductivity ratio reduces to a slight modification of the characteristic time and size scales (for $k_p/k_g > 10$), and hence the results for the self-similar normalized distribution function reached in the long-time limit are almost independent of the particle/gas Fourier thermal conductivity ratio in the whole range of values of the Peclet number. At the same time, our numerical results also show a non-trivial behavior of the quasi-self preserving particle size distribution for intermediate values of the Peclet number, which shows a non-monotonic behavior for some of its moments for values of the Peclet number of order unity (for instance the asymmetry-related skewness).

This work was supported by NSF under Grant: CBET-1037733 to Yale University. MAZ also gratefully acknowledges grants by Ministerio de Ciencia e Innovación (#ENE2008-06515-C04-03) and Comunidad de Madrid (#S2009/ENE-1597) at UNED.

Rosner D.E. and Arias-Zugasti M. (2011) Phys. Rev. Lett. **106** 015502

Arias-Zugasti M. and Rosner D.E. (2011) Phys. Rev. E submitted

Rosner D.E. and Arias-Zugasti M. (2011) Industrial & Engineering Chemistry Research submitted (Invited Paper for Churchill 90)

Simons S., M. M. R. Williams, and J. S. Cassell (1986) Journal of Aerosol Science **17** 789

Photophoretic interaction of aerosol particles in rarefied gas medium

A.A. Cheremisin[1], A.V. Kushnarenko[2]

[1] Institute of Engineering Physics and Radio Electronics, Siberian Federal University, Krasnoyarsk, 660036, Russia

[2] Institute of Space and Information Technology, Siberian Federal University, Krasnoyarsk, 660036, Russia

Keywords: photophoresis, coagulation, heat and mass transfer

Presenting author email: aacheremisin@gmail.com, avkushnarenko@gmail.com

The main concepts underlying contemporary coagulation models have been known for a long time. This is Brownian motion of particles and interparticle interaction which occurs due to Van der Waalce forces and Coulomb electrostatic forces, if coagulating particles are charged.

The particles interaction that takes place as a result of gas-kinetic phenomenon – photophoresis has been investigated in this paper. The calculations are based on approximation of free molecular gas-kinetic regime and earlier developed Monte-Carlo algorithms (Cheremisin, 2010). In our previous work we have investigated the influence of gravito-photophoresis on aerosol stratification in the middle atmosphere (Cheremisin *et al*, 2005).

Photophoretic interaction forces of two spherical particles depending on particles sizes and distance between them under different ranges of gas medium pressure have been calculated. The example is shown on Figure1.

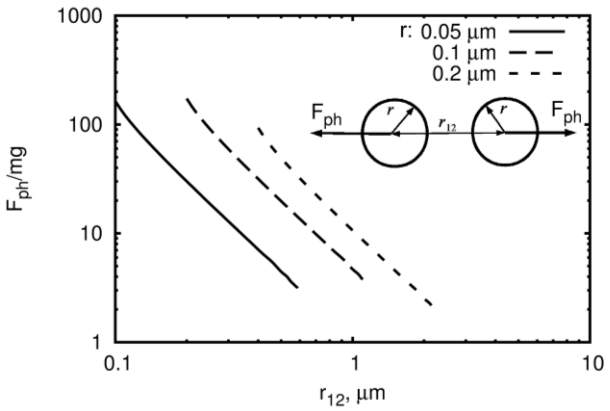

Figure 1. Relative photophoretic interaction force between two identical spherical particles of various sizes versus distance.

Here F_{ph} is photophoretic force and mg is gravity. The density of particles material is equal to 1000 kg per cubic meter. Accommodation coefficient for surface of each particle is equal to 0.5. Particles strongly absorb solar radiation, the optical properties are determined by the complex index of refraction, the value of which doesn't depend on wavelength and is equal to $1.95 - 0.66 \cdot i$, corresponding to soot optical properties. Absorption cross-sections have been calculated using Mie theory. Temperature of surrounding gas (air) is equal to 293K and pressure is 1220 Pa. The temperature of particles surfaces was calculated on the basis of requirement for thermal balance with flux of the solar and IR energy absorbed by particles, the flux of IR radiation emitted by particles, and the flux of molecular heat exchange taken into account.

We can see that repulsion photophoretic force occurs in condition of solar radiation with the pressure of about 0.1 atmosphere or less. These force is tens or hundreds times larger than gravity. Dependence of this interaction on distance between particles is similar to Coulomb type. The photophoretic force is important when the size of system of particles is smaller than the mean free path of the gas molecule, at distance where the value of Knudsen number is larger than 1.

Gas molecules continuously impact on the surface of aerosol particles and are reflected, the reflection can be specular and diffuse, with and without accomodation. For photophoresis accomodation is important. If the reflection is asymmetric a net force on each particle may result due to presence of the other particle. During reflection the molecules may pick up some energy and leave the surface with a higher thermal energy compared with the temperature of gas medium and then molecules may reach the surface of the other particle. Thus the particles with hot surfaces repulse due to gas molecule momentum exchange.

A higher radiation flux leads to increase in the particles temperature and, consequently, in interaction force value.

Photophoretic interaction forces have been calculated for laboratory vacuum chambers and for atmospheric conditions.

We estimated an impact of photoporetic interaction on coagulation constants. Photophoretic forces are capable of influencing aerosol particles coagulation depending on their size, optical properties, radiation and gas medium conditions.

This investigation is supported under grant 10-05-00907a by the Russian Fund of Basic Research and Ministry of Science and Education of Russian Federation (project 2.1.1/ 6996).

Cheremisin A.A. (2010) *Transfer matrices and solution of the heat-mass transfer problem for aerosol clasters in a rarefied gas medium by the Monte Carlo method,* Russ. J. Numer. Anal. Math. Modelling (RJNAMM) **25,** 209-233.

Cheremisin A.A., Vassilyev Yu.V., Horvath H. (2005). *Gravito-photophoresis and aerosol stratification in the atmosphere,* J. Aerosol Sci 36, 1277-1299.

Optical breakdown and detonation in aerosol systems

K.N. Volkov[1] and V.N. Emelyanov[2]
[1]Faculty of Engineering, Kingston University, London, SW15 3DW, United Kingdom
[2]Faculty of Physical and Mechanical Sciences, Baltic State Technical University, Saint Petersburg, 190005, Russia
Keywords: combustion aerosols, droplets, multiphase processes, aerosol fundamentals, CFD.
Presenting author email: k.volkov@kingston.ac.uk

The subject of the study stems from the increasing role of aerosol systems appearing in industry, technology and environment. Interaction of laser pulse with aerosols plays an important role in different areas (e.g., environmental monitoring of high-risk industrial objects and enclosed spaces, measurements of flammability and explosibility limits, propagation of laser radiation through explosive mixtures, laser ignition of volumetric explosion for application to fire mitigation). The role of particles and droplets in these applications is two-fold: particles and droplets may pose potential hazard for human activity (e.g., deposition of particles in human lungs) or can be successfully used in engineering solutions (e.g., to suppress acoustic instabilities of thermal processes). Processes that control transport and combustion of particles and droplets remain unresolved, and introduce significant uncertainties into modeling and simulation.

When a laser radiation interacts with a gas, the gas breaks down and becomes highly ionized. This process is accompanied by a light flash and generation of sound. The development of electron cascade requires the existence of initial free electrons in a gas. For every particle size of any material there is threshold intensity at which the particle material converts into the meta-stable condition and its intense evaporation leads to heat destruction of the particle. The injection of metal particles with low evaporation temperature and low ionization potential (e.g., aluminium) or liquid droplets decreases threshold value of optical breakdown on individual particle or droplet, and leads to drop of detonation minimum pulse energy (MPE). Vapour aureole around particle or droplet is a source of free electrons and optical breakdown in the gas-particle or gas-droplet mixture comes for lower energy of laser pulse than in pure gas (Emelyanov, 2007).

In this study, physical and mathematical models and up-to-date numerical methodology for computer modeling of optical breakdown are developed and validated. Laser-induced detonation in aerosol systems is studied, and advantages of the new methodology are demonstrated.

The mathematical formulation of the problem is divided into low-level models and high-level models. Low-level models correspond to the processes in the volume occupied by an individual particle or droplet induced by its interaction with a laser pulse. The high-level models correspond to the processes in the volume occupied by multiphase mixture due to energy supply to it. The data obtained from solution of low-level problem are used to calculate source terms in the governing equations describing high-level problem based on multi-velocity and multi-temperature continuum. It is assumed that particles and droplets are uniformly distributed in the domain. Some volume of the mixture depending on particle volume fraction is associated with each particle (individual reactor of a particle). The model of unsteady well-stirred reactor is used to calculate physical quantities in this volume. The solution of high-level problem provides volume fraction of particles and volume occupied by an individual particle or droplet. The numerical solution is based on finite volume method and splitting scheme on physical factors. Pseudo-gas of particles does not have internal pressure, so artificial pressure is introduced (Emelyanov, 2004).

The threshold value of optical breakdown and MPE of laser-induced detonation depending on total power and spot of laser pulse, mass fraction of particles and volume fraction of oxidant are computed. Some results are presented in the Figure 1 for fish-plate aluminium particles with size $50 \times 50 \times 5\ \mu m$ in the oxygen–acetylene mixture. Mass fraction of particles is 0.5 g/m^3. Wave-length of laser beam is 4.2 μm, radius of laser spot is 1.5 cm, and time of pulse is 2.6 μs. The results obtained are in a good agreement with the experimental data.

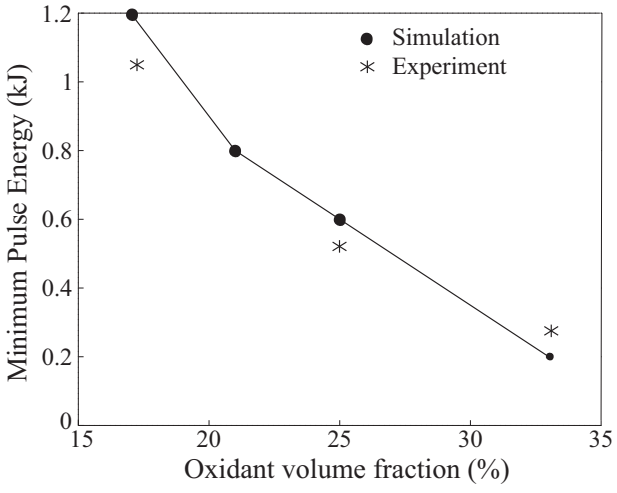

Figure 1. MPE of laser-induced detonation depending on oxidant volume fraction.

Emelyanov, V. and Volkov, K. (2007) Proc. 6th Int. Conf. on Multiphase Flow, Leipzig, Germany.

Emelyanov, V. and Volkov, K. (2004) Proc. 3rd Int. Symp. on Two-Phase Flow Modelling and Experimentation, Pisa, Italy, **3**, 1655–1665.

Thermophoresis of non-spherical particle: experimental prospect on soot particles

E. Brugière [1,2], F. Gensdarmes [1], F.-X. Ouf [1], J. Yon [2] and A. Coppalle [2]

[1] Aerosol Physics and Metrology Laboratory, IRSN, BP 68, 91192, Gif-sur-Yvette Cedex, France.
[2]UMR 6614 CORIA, Avenue de l'université, BP 8, 76801 Saint Etienne du Rouvray, France.
Keywords: thermophoresis, fractal aggregate, deposition.
Presenting author email: edouard.brugiere@irsn.fr

Thermophoresis is an important mechanism of micro-particle transport due to a temperature gradient in the surrounding medium. Extensive studies, both theoretical and experimental, have been carried out to understand the nature of this phenomenon which is well known for spherical particles contrary to non-spherical particles like soot particles. In fact, the soot particles are characterized by a complex morphology called "fractal" and, currently, the real impact of this morphology on deposition due to thermophoresis is not well known.

Thermophoresis of non spherical particles is more complex than the case of spheres. The theoretical solutions are more difficult and other parameters are needed, such as the diameter or the number of primary particles, the particle shape or orientation in the temperature gradient. The existing theory of the thermophoresis for non-spherical particles is limited and there are few solutions to formulate thermophoresis velocity in the continuum and the free molecule limits for several simple particle shapes. The reader is referred to a comprehensive review on thermophoresis of the two major categories, spherical and non-spherical particles, by Zheng (2002).

Mackowski (1990) analysed the thermophoresis of aggregates made of two-spheres in the near continuum regime. He shown that the aggregate thermophoretic velocity is not collinear to the temperature gradient. Moreover, Mackowski (1990) found that the thermophoretic force tends to rotate and aligns the aggregate along the temperature gradient.

Mackowski (2006) and Suzuki *et al.* (2009) demonstrated the influence of the number and the diameter of primary particles on the thermophoresis velocity of aggregates. On the one hand, Mackowski (2006) found in the free molecular regime that the thermophoretic velocity of an aggregate increases with the number of primary particles. On the other hand, Suzuki *et al*. (2009) found that thermophoretic velocity of an aggregate in the continuum regime is governed by the primary particle size and is much larger than those expected based on the size of aggregates and rather close to the velocity for particles in the free molecular regime. However, there is few reliable data to test the validity of these theories. Therefore, the influence of the particle shape and its orientation in a temperature gradient on the thermophoresis velocity are not mastered.

In order to show the particle orientation in the temperature gradient and the primary particle influence on the thermophoretic behavior, a new experimental device designed for the proposed experimental study is presented. This device called *SpectroMètre Thermique Circulaire* (SMTC) is based on the concept of a simplified version of the radial flow differential mobility analyser (DMA): the *Spectromètre de Mobilité Electrique Circulaire* (SMEC) developed by Pourprix (1989). The SMTC consists of a parallel arrangement of two circular plates (hot and cold). A schematic diagram is given in Figure 1; a sheath air flow (Qf) and an aerosol air flow (Qa) are passed between those two plates and for different flow rates and temperature gradients this new device will enable to determine with low uncertainties the mean thermophoresis velocity of spherical and non-spherical particles. In this presentation, the theoretical thermal study and the transfer functions of the SMTC will be presented. A comparaison between mean thermophoretic velocity of spherical and agregates particules having same mobility diameters will be proposed.

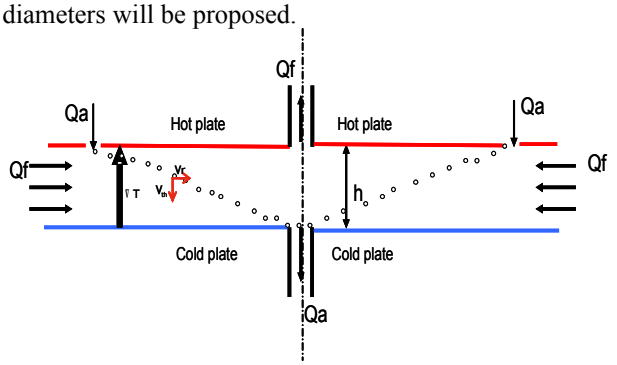

Figure 1. Schematic diagram of the SMTC.

Mackowski, D.W. (1990). Phoretic behavior of asymmetric particles in thermal nonequilibrium with the gas: two-sphere aggregates. *J. Colloid Interface Sci.* **140**: 139-157.

Mackowski, D.W. (2006). Monte Carlo simulation of Hydrodynamic drag and thermophoresis of fractal aggregates of spheres in the free-molecule flow regime. *J. Aerosol Sci*. **37**: 242-259.

Pourprix, M. (1989). Capteur électrostatique de particules d'aérosols. Brevet Français n° 89 08400.

Suzuki, S., Kuwana, K., and Dobashi, R. (2009). Effect of particle morphology on thermophoretic velocity of aggregated soot particles. *Int. J. Heat Mass Transfer* **52**: 4695-4700.

Zheng, F. (2002). Thermophoresis of spherical and non-spherical particles: a review of theories and experiments. *Advances in Colloid and Interface Science* **97**: 255-278.

Size measurement of dry ice particles in a jet flow using laser diffraction method

Yi-Hung Liu[1], Graham Calvert[2], Colin Hare[2],
Mojtaba Ghadiri[2], Shuji Matsusaka[1]

[1]Department of Chemical Engineering, Kyoto University, Nishikyo-ku, Kyoto 615-8510, Japan
[2]Institute of Particle Science and Engineering, University of Leeds LS2 9JT, UK
Keywords: dry ice, jet flow, size distribution, agglomeration.
Presenting author email: liu@cheme.kyoto-u.ac.jp

Dry ice blasting has been utilized as a dry cleaning method, which can be applied in many industrial fields, such as semiconductor, plastics, food, and pharmaceuticals, etc. The properties of dry ice particles, including size, shape, density, and hardness are thought to be important factors affecting the cleaning process (Spur *et al*., 1999). The agglomeration process of dry ice particles in the jet flow has been investigated (Liu *et al.*, 2010). It was shown that a chamber was effective for the generation of agglomerated dry ice particles. However, a precise measurement of the size of dry ice particles in the jet flow proved to be difficult due to the sublimation process. In the present study, the state of dry ice particles in the jet flow has been analyzed by an on-line laser diffraction method.

Dry ice particles were produced by rapid expansion of liquid carbon dioxide, based on Joule-Thomson effect. In this process, the temperature rapidly decreased by adiabatic expansion from the pressure of 5.5 ± 0.1 MPa to atmospheric pressure. The inner diameters of the nozzles used for expansion were 0.1, 0.2, and 0.5 mm. As an agglomeration chamber, ABS tubes, 50 mm in length and 2, 4, 6 mm in inner diameter, were attached to the nozzle outlet. The size of dry ice particles ejected from the nozzle or the ABS tube were measured by an aerosol analyzer (Spray-Tech, Malvern Instruments Inc.) based on the technique of laser diffraction. The laser beam and dry ice jet were both horizontal and oriented perpendicular to each other.

Figure 1 shows an example of the cumulative size distribution of dry ice particles in a steady state. For the distance from the nozzle $d \leq 40$ mm the median diameter was in the range from 1 to 2 μm and increased with the distance. As for $d = 50$ mm, the dry ice particles shrank to submicron size. A normal-like distribution can be ascertained at a short distance, i.e. $d \leq 40$ mm, while the distribution deviated as the distance increased ($d = 50$ mm). In the size distribution, two size regions were observed, i.e. a smaller diameter region of submicron and a larger diameter region around ten microns. It is found that the primary dry ice particles ejected from the nozzle still grew up and/or agglomerated up to a certain distance. When the distance was sufficiently large, two opposite phenomena, i.e. sublimation and agglomeration occurred. As a result, a bimodal distribution was obtained.

Figure 2 shows the cumulative size distribution of dry ice particles exhausted from the tube in a steady state. Comparing with Fig. 1, the particle size is remarkably larger, indicating that dry ice particles exhausted from the nozzle have already agglomerated in the tube. In addition, the median diameter decreased with increasing nozzle diameter.

Nucleation, condensation, agglomeration and sublimation processes all compete to yield the size distribution as measured. Among them, agglomeration is the most important in the tube (Liu *et al.*, 2010); i.e. dry ice particles of several micrometers are deposited on the tube wall and form a deposition layer; then, agglomerates are reentrained from the layer into the jet flow. The size of the reentrained agglomerates decreases with increasing flow velocity. In these experiments, the flow velocity increases with the nozzle diameter. This is considered as a reason for the trend of the results observed here.

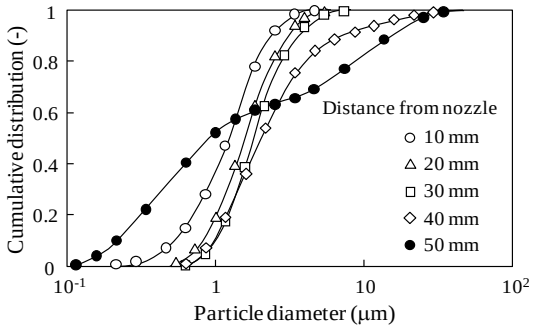

Figure 1. Cumulative size distribution of dry ice particles exhausted from nozzle (nozzle diameter = 0.2 mm).

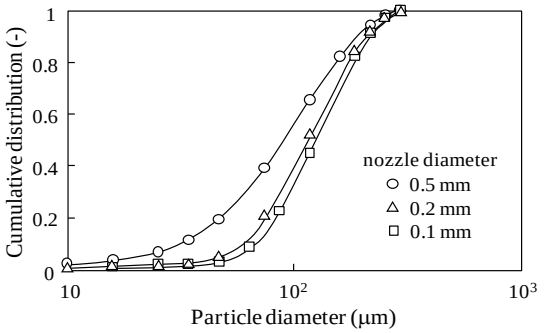

Figure 2. Cumulative size distribution of dry ice particles exhausted from tube (tube diameter = 6 mm, distance from the tube = 40 mm).

This research was supported by Core-to-Core Program for Advanced Particle Handling Science, JSPS, the Global COE Program (No. B-09) and a Grant no. S0901039 from MEXT, Japan.

Liu, Y. H., Maruyama, H. and Matsusaka, S. (2010). *Adv. Powder Technol.*, **21**, 652-657.
Spur, G., Uhlmann, E. and Elbing, F. (1999). *Wear*, 233-235, 402-411.

Tuesday, September 6, 2011

Plenary:

Aerosols for materials: medical and industrial applications and the role of nanotoxicology.

By Wendelin Stark

Aerosols for Materials: Medical and Industrial Applications and the Role of Nanotoxicology

Wendelin J. Stark

Department of Chemistry and Applied Biosciences, ETH Zurich, 8093 Zurich
Keywords: Chemical Aerosol Engineering, Metal Nanoparticles, Nanomedicine
Presenting author email: wstark@ethz.ch

This presentation will highlight how chemical and biological insight into aerosols opens above avenues as emerging scientific disciplines. Aerosol science has recently strongly contributed to the following large, emerging areas of research:

A) Materials Fabrication

Industrial aerosol processing has been chemically developed to extend traditional products (titania, silica and soot) to novel nanomaterials (Athanassiou et al., 2010). Reducing aerosol synthesis has taken flame synthesis from oxides to pure metal nanoparticle preparation and thereby opens access to technical use of metal nanoparticle aerosols. Using chemical understanding, we can design reactions inside aerosol producing reactors as to prepare salt and glass nanoparticles of complex composition in a single step process.

B) Aerosol Derived Nanomaterials

Whilst most aerosol research proceeds at low concentrations (mass and number conc.), the basics physics stays the same at high concentrations. Aerosols containing milligram to gram amounts of nanoparticles per cubic meter allow a technically attractive access to the production of advanced materials. Why are dry processes of particular attraction?

The alternative nanomaterial fabrication in the wet phase (precipitation reactions) always proceeds at moderate temperature and therefore cannot yield high temperature phases, complex glasses, and sintered, single nanoparticles. Latter are of particular interest for high performance applications like heterogeneous catalysts and ceramics and have become available easily by flame spray synthesis.

Reactive nanoparticles can be obtained from high temperature phases (e.g. amorphous particles) that allow preparation of nano-construction cements or injectable bone cements and dental materials (Hild et al., 2011).

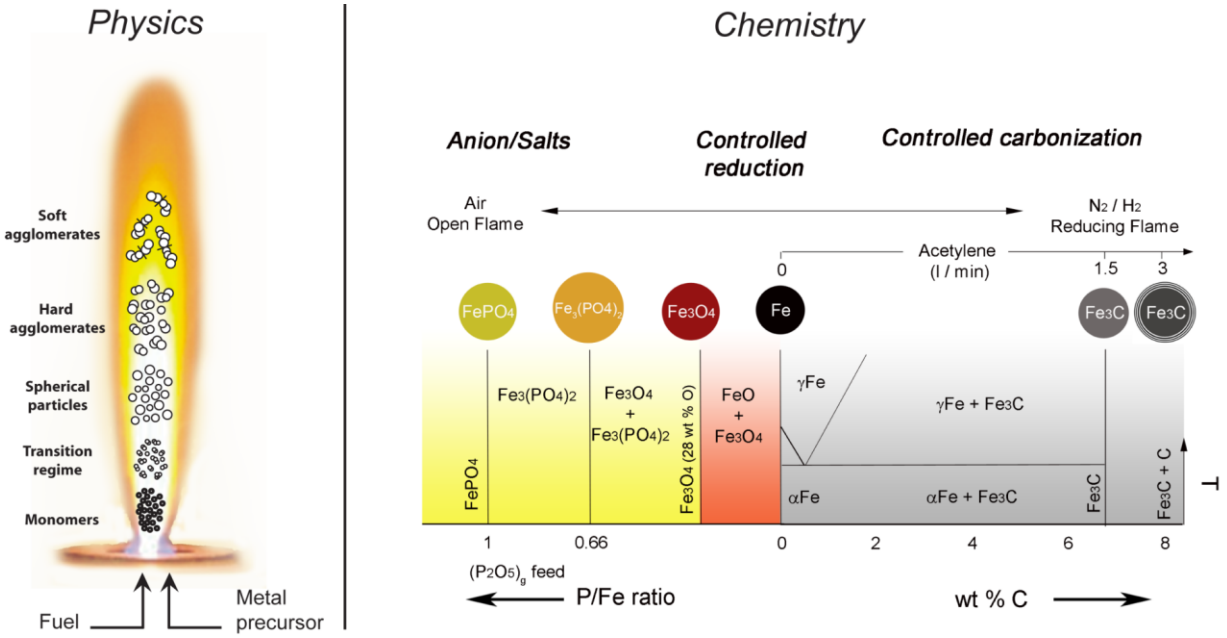

Figure 1: Physical understanding of particle formation in a gas stream (left) and the variety of chemical compositions (right) of nanoparticles (present example: iron) prepared by flame spray synthesis are shown.

C) Metal Aerosols for Nanometals

Classical flame aerosol synthesis uses combustion of a (limited) fuel in air. The aerosol reactor is then limited by the area of fuel combustion and the aerosol travels from the inside of the reactor (precursor) to the outside where gases are cooled down by mixing. As a result, only air-compatible materials are available.

Metal aerosols of non-air stable materials (e.g. iron, copper, cobalt…) can be obtained by inversing the flame reactor: If a limited amount of oxygen is injected together with fuel into a reducing atmosphere (e.g. nitrogen with 1% hydrogen), a special flame is obtained where the growing aerosol particle travels from the inside (precursor) through the combustion zone to the outside, where combustion gases cannot get enough oxygen for full combustion and the gas stays highly reducing (e.g. $CH_4 + O_2 => CO + H_2O + H_2$). As a result, aerosol reactors can also make reduced phases and metals.

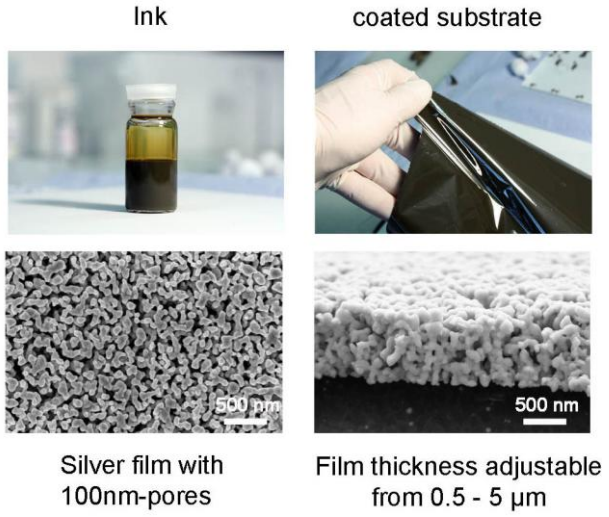

Figure 2: An ink consisting of aerosol derived metallic silver and calcium carbonate to produce a porous film that can be used for membrane filtration.

D) Biomaterials from Aerosols

Calcium phosphates and bioglasses are the prominent materials used in bone and dental medicine. Aerosol synthesis has enabled preparation of reactive particles which are not accessible otherwise, as a high temperature is needed to provide glasses (amorphous mixtures of silicate and phosphates) or non-crystalline phosphates. These aerosol derived materials are now used as parts of a number of preclinical medical devices, both for repair of broken bone, or infected teeth (Schneider et al., 2010; Mohn et al., 2010).

E) Nanoparticles and Organisms

The rapidly increasing use of nanoparticles in consumer products demands in depth understanding on the environmental and health effect of nanoparticles to numerous disciplines. The major route for nanoparticle uptake into an organism has been identified as over the lung. The intrinsic differences between a classical, molecular toxine ("classical chemicals") and a nanoparticle sample in terms of mobility (different diffusion coefficients), time dependent behaviour (agglomeration), chemical behaviour (surface related effects, catalysis) makes the design of relevant nanotoxicological experiments rather challenging (Stark, 2011). Particularly the concept of dose is changed (classical toxins are discussed in terms of a time and mass dose) and needs a clear definition of the relevant parameters (size, colloid stability, chemical activity etc.).

Nanomedicine and nanotoxicology can therefore be regarded as two viewpoints concerning the interaction between (aerosol-derived) particles and living organisms.

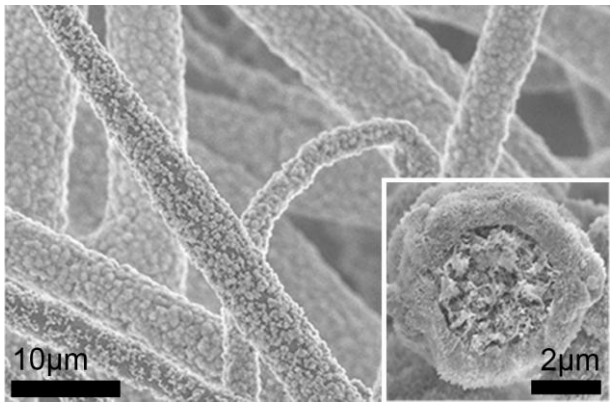

Figure 3: Aerosol derived calcium phosphates are smoothly incorporated in polymer fibres and showing a highly reactive phase.

This work was supported by ETH Zurich, the Swiss National Science Foundation, Gebert Rüf Foundation, numerous industrial partners and the Bundesamt für Gesundheit BAG, Switzerland.

W. J. Stark (2011), ***Angew. Chem. Int. Ed.***, 50, 1242-58.
I.K. Herrmann, et al. (2010), ***Small***, 6, 1388-92; ***Nature Nanotechn.***, 5, 628 (research highlight).
E. K. Athanassiou, R. N. Grass, W. J. Stark (2010), ***Aerosol Sci. Tech.***, 44, 161-72.
R. N. Grass et al. (2010), ***J. Aerosol Sci.***, 41, 1123-1142.
N. Hild et al. (2011), ***Nanoscale***, 3, 401 – 409.
A. Studer et al, (2010), ***Toxicol. Lett.***, 197, 169-174.
A. Schätz, R. N. Grass, W. J. Stark (2010), ***Chem. Eur. J.***, 16, 8950-67.
Lüchinger et al. (2010), ***Chem. Mater.***, 22, 4980 – 4986.
Rossier et al (2010), ***Ind. Eng. Chem. Res.***, 49, 9355 – 9362.
Schneider et al. (2010), ***Acta Biomater.***, 6, 2704 – 2712.
Mohn et al. (2010), ***Polym. Eng. Sci.***, 50, 952 – 960.
Misra et al. (2010), ***Biomaterials***, 31, 2806 – 2816.

Tuesday, September 6, 2011

Session 4P: Poster Session A: *Aerosol Chemistry*

Semi-continuous system for analysis of water-soluble fraction of metals in atmospheric aerosols

P. Mikuška, M. Vojtěšek, Z. Večeřa and K. Křůmal

Institute of Analytical Chemistry of the ASCR, v.v.i., Veveří 97, Brno, CZ-60200, Czech Republic
Keywords: atmospheric aerosols, metal, in-situ measurements, on-line measurements.
Presenting author email: mikuska@iach.cz

Metals released into air from both natural and anthropogenic sources are associated with particulate matter. Recent studies indicate that particulate metals are correlated with the pulmonary toxicity and for a lot of metals, their carcinogenic effects and/or their potential to attack the nervous system, are now well established.

The routine methods for the determination of metals in atmospheric aerosols involve aerosol sampling on filters with off-line analysis of filters in laboratory, which provides time averaged results. To obtain high time-resolved particle composition, the real-time methods have been developed such as mass spectrometry (Wood and Prather, 1998). Simple and cheap way of real-time measurement of chemical composition of aerosols can be obtained alternatively by application of aerosol collectors operating mostly on the principle of steam condensation (Khlystov et al, 1995; Poruthoor et al, 1998) or a Venturi scrubber (Belostotsky et al, 2001; Mikuška and Večeřa, 2005).

The new system for the in-situ determination of water-soluble metallic components of atmospheric aerosols based on the combination of continuous collection of aerosols and on-line analysis is described. Aerosol particles are collected in an Aerosol Counterflow Two-Jets Unit (ACTJU) (Mikuška and Večeřa, 2005) continuously from air (5 L/min) into a deionised water (1 mL/min) and the ACTJU concentrate is on-line analysed for the content of water-soluble fraction of selected particulate metals at collected aerosols. Metal analysis using a continuous flow system includes preconcentration, HPLC separation and chemiluminescent detection by the reaction with luminol (Fletcher et al, 2001).

Co^{2+}, Cu^{2+} and Fe^{3+} were selected as model metals to show a potential of the method for the analysis of water-soluble fraction of metals in atmospheric aerosols with high sensitivity and high time resolution. The system allows the determination of concentration of water-soluble fraction of particulate metals in real time with time resolution of 30 min. The detection limit of particulate Co^{2+}, Cu^{2+} and Fe^{3+} (S/N=3) is 0.3 ng m^{-3}, 37 ng m^{-3} and 65 ng m^{-3}, respectively. The whole system is sufficiently robust for the field application. The system was applied to the measurement of selected metals in urban aerosols in Brno in the Czech Republic (Figure 1).

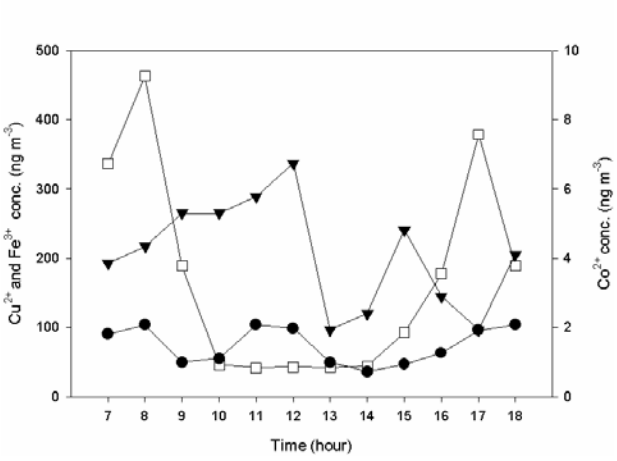

Figure 1. The measurement of metals in urban aerosol in Brno, Kotlářská street, 28th June 2010; (●) Fe^{3+}, (□) Cu^{2+}, (▼) Co^{2+}.

This work was supported by Institute of Analytical Chemistry of ASCR under an Institutional research plan No. AV0Z40310501, by Grant Agency of the CR under grant No. P503/11/2315 and by Ministry of the Environment of the Czech Republic under grants No. SP/1b7/189/07, SP/1a3/148/08 and SP/1a3/55/08.

Belostotsky, I., Gridin, V.V., Schechter, I. and Yarnitzky, N.C. (2001) *Anal. Chim. Acta* **429**, 215–226.

Fletcher, P., Andrew, K.N., Calokerinos, A.C., Forbes, S. and Worsfold, P.J. (2001) *Luminescence* **16**, 1-23.

Khlystov, A., Wyers, G.P. and Slanina, J. (1995) *Atmos. Environ.* **29**, 2229-2234.

Mikuška, P. and Večeřa, Z. (2005) *Anal. Chem.* **77**, 5534-5541.

Poruthoor, K.S. and Dasgupta, K.P. (1998) *Anal. Chim. Acta* **361**, 151-159.

Wood, S.H. and Prather, K.A. (1998) *TRAC-Trends in Anal. Chem.* **17**, 346-356.

Gaseous iodine as a substantial cause of new specific air ions

A. Luts, T.-E. Parts and U. Hõrrak

Institute of Physics, University of Tartu, Ülikooli 18, 50090 Tartu, Estonia
Keywords: aerosol chemistry, aerosol spectrometry, mass spectrometry, ion-induced nucleation.
Presenting author email: urmas.horrak@ut.ee

The observations have shown that new particle formation (NPF) depends on many factors, including the air gas-phase composition. Several studies concluded that iodine vapour is one, which can be responsible for the NPF. To study of the effect of iodine on negative air ions, we combined two simultaneous measurement methods: mass and mobility spectrometry (Sciex API-300 and AIS). We observed the noticeable MS peaks up to *m/z* 836. We modified the concentration of iodine vapour (by sublimation of I_2) and humidity. Iodine leads to enhanced concentration of the charged aerosol particles above 4 nm, which, in turn, decrease substantially the concentration of cluster ions due to ion-aerosol attachment. The concentration of 20 s old cluster ions decreases by about 90%. Work by Kärkelä *et al* (2009) demonstrated the results, which resemble our iodine effect: UV-radiation, ozone and gaseous iodine together induced almost instant burst of new particles.

After addition of iodine, major MS peaks were at *m/z* 381 $I^-(I_2)$ and 635 $I^-(I_2)_2$ (Fig. 1). Humid air favours the formation of pentaiodide $I^-(I_2)_2$. The gas-phase chemistry of iodides is not well known to explain such a result. More is known about the iodine reactions in aqueous solutions. In the present study no iodine solution was used, we recorded gaseous (complex) ions, which arouse due to sublimated iodine (I_2). We assume formation of iodine and iodide complexes surrounded by large number of water molecules. The assumption is supported by the AIS mobility spectra with numerous ions with the size above 4 nm, which could be just iodides and their agglomerates plus water molecules. The MS inlet could remove the water molecules and only iodide ions could be recorded by the MS. Numerous water molecules around iodide could make possible the reactions, known in aqueous solutions, where rapidly the equilibrium $I^- <> I_3^- <> I_5^-$ develops (Clough and Starke, 1985). Increased concentration of water vapour causes a larger number of iodine molecules to dissolve, which can shift the equilibrium of the process to the right, resulting in the increased formation of I_5^-. Also, it is known that pentaiodide molecules need H^+ to stabilize itself (Svensson and Kloo, 2003). The ionization of water molecules by radioactive source produces OH^- and the wanted H^+, which also favours the formation of I_5^-. We speculate that such reactions could result in the observed change in the balance of the peaks at *m/z* 381 and 635.

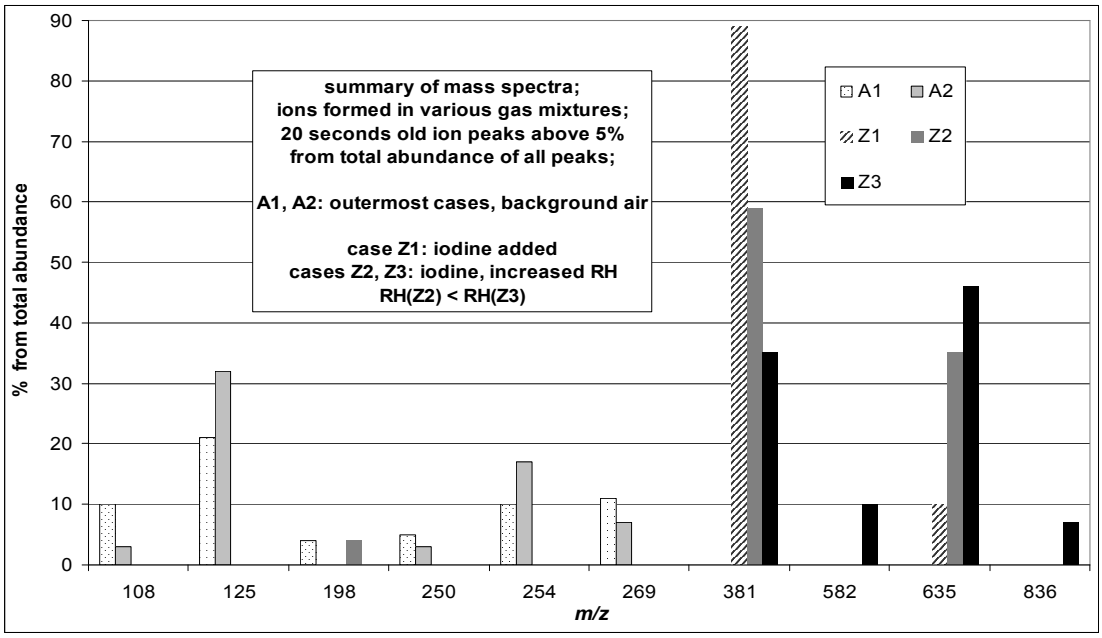

Figure 1. Main peaks, observed in the old ion mass spectrum evolved in the background air, and the effect of addition of iodine at the different humidities.

This research was supported by the Estonian Science Foundation through grant 8342. We thank Tapio Kotiaho and Alexey Adamov and Timo Maurila from the Helsinki University for help in MS experiments.

Clough, P.N. and Starke, H.C. (1985) *European Applied Research Reports: Nuclear Science and Technology* 6, 631–776.

Kärkelä, T., Holm, J., Auvinen, A., Ekberg, C. and Glänneskog, H. (2009) ISBN 978-87-7893-273-0.

Svensson, P.H. and Kloo, L. (2003) *Chemical Reviews*, **103**, 1649–1684.

Modifications in hygroscopicity and volatility of wood combustion aerosols after chemical aging

Z. J. Wu[1], L. Poulain[1], O. Böge[1], R. Gräfe[1], , H. Herrmann[1], A. Wiedensohler[1]
K. Helbig[2], T. Schröder[2], J. von Sonntag[2], I. Hartmann[2]
[1] Leibniz Institute for Tropospheric Research, Permoserstr. 15, 04318 Leipzig, Germany
[2] German Biomass Research Centre, Torgauer Str. 116, D - 04347 Leipzig
Presenting author email: wuzhijun@tropos.de

Combustion of biomass is known to be a major source of gas- and particle- phase air pollution in the atmosphere and to be mainly made of a complex mixture of organics. To date, however, the atmospheric behaviours of these mixtures and their health effects are still largely unknown.

In this study, aging processes of different types of wood burning aerosols (see Table 1) are investigated. The wood burning aerosols are introduced into the IfT LEAK chamber (19 m^3, Iinuma et al. 2004) with and without ozone and /or UV lights simulating day- and night- times. Several online instruments including a Hygroscopic Tandem Differential Mobility Analyzer (H-TDMA), a Volatility Tandem Differential Mobility Analyzer (V-TDMA), a Multi-Angle Absorption Photometer (MAAP), a Scanning Mobility Particle Sizer (SMPS), and an Aerosol Mass Spectrometer (AMS) were used to measure the changes of physical and chemical properties of aerosols. In parallel to the physico-chemical study, modifications of the aerosols toxicity during the aging process were also investigated.

Table 1: Wood species and stoves

Wood	Stove
Spruce log	downdraught stove
Beech log	downdraught stove
WoodPellet	Pellet oven firing

In this abstract, the modifications in volatility and hygroscopicity of spruce burning aerosols via photochemical aging are presented as an example. Fig. 1 shows the comparisons of particle number size distributions before and after turning on the UV-lights. Fig. 2 and 3 display the temporal evolution of growth factor and shrink factor for different size particles, respectively. The growth factor is defined as the ratio of the wet particle mobility diameter D at RH=90% to dry diameter D0. The shrink factor is defined as the ratio of the particle diameter at a certain temperature (here, 120 and 300 °C) to the diameter at room temperature (25 °C).

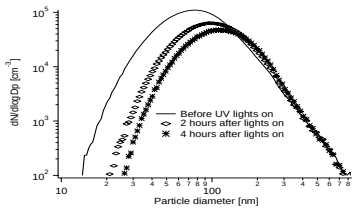

Fig. 1: Particle number size distribution

Before the UV-lights on, the growth factors for 50, 75, and 100 nm particles are within 1.3-1.4, and only 1.1 for 200 nm particles. This indicates that smaller particles are dominated by hydrophilic components, such as inorganic salts, while, larger particles are dominated by hydrophobic fraction, such as soot. After lights on, the growth factors of smaller particles decrease with time consuming. This means that more low hygroscopic organic species produced or condensed on the particles during aging process. But, no any changes in 200 nm particles were observed.

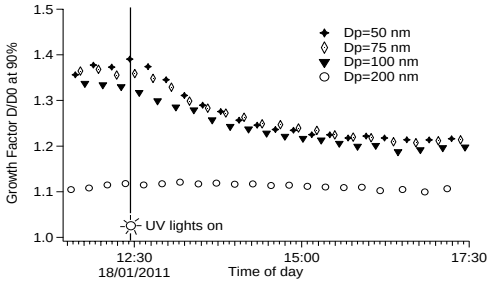

Fig. 2: Temporal evolution of hygroscopic growth

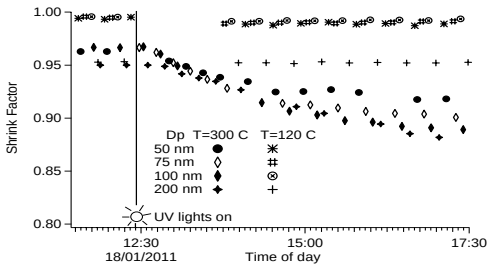

Fig. 3: Temporal evolution of volatility

At 120 °C, there is no any difference in shrink factor before and after UV-lights on, indicating that no high-volatile components, such as low carbon-number carboxylic acids, produced during chemical aging. At 300 °C, the particles freshly emitted with diameter of 50, 75, and 100 nm are non-volatile. After lights on, the aerosols are more volatile in contrast to primary particles. A detail study on the modifications in hygroscopicity and volatility of wood burning aerosols will be performed by combining the AMS data and filter measurements in the future work.

Acknowledgements:
This work was founding by Federal Ministry for the Environment, Nature Conservation and Nuclear Safety

Reference:

Y. Iinuma, O. Böge, T. Gnauk and H. Herrmann. Atmospheric Environment 38 (5) (2004), pp. 761–773.

Morphology and phase transitions of internally mixed dicarboxylic acids/ammonium sulfate/water particles during hygroscopic cycles

Mijung Song, Claudia Marcolli, Ulrich K. Krieger, Thomas Peter

Institute for Atmospheric and Climate Sciences, ETH Zurich, Zurich, 8092, Switzerland.

Keywords: morphology, phase transition, hygroscopicity, dicarboxylic acids.
Presenting author email: mijung.song@env.ethz.ch

Tropospheric aerosols are complex mixtures of inorganic and organic substances. The phases and morphology of the aerosol particles are influenced by their chemical composition, hygroscopicity and size (Ciobanu *et al*., 2009). In particular, interactions between organic and inorganic compounds in aerosol particles may lead to liquid-liquid phase separations (LLPS) depending on relative humidity (RH) (Marcolli and Krieger, 2006). During hygroscopic cycles, particle morphology may also change (Kwamena *et al*., 2010). However, the physical state and morphology of atmospheric aerosol particles are difficult to derive from field measurements. Laboratory experiments are, thus, needed to gain insight into the possible morphologies and phase transitions of internally mixed organic/inorganic aerosol particles of atmospheric relevance and to further our understanding of aerosols.

Table 1. Investigated dicarboxylic acid mixtures, their measured solubility in dry weight percent and oxygen-to-carbon ratios.

Organic substances	Measured solubility (wt %)	O:C
C5		
Glutaric acid	58.8	
Methylsuccinic acid	32.0	0.8
Dimethylmalonic acid	10.5	
C6		
2-methylglutaric acid	52.7	
3-methylglutaric acid	45.3	0.7
2,2-dimethylsuccinic acid	8.3	
C7		
3-methyladipic acid	17.1	
3,3-dimethylglutaric acid	14.2	0.6
Diethylmalonic acid	19.5	

We investigated three representative model systems with ammonium sulfate (AS) as salt, namely C5/AS/H_2O, C6/AS/H_2O and C7/AS/H_2O using optical microscopy and micro-Raman spectroscopy in order to determine phase transitions and morphologies for mixtures with different organic-to-inorganic ratios (OIR) during a hygroscopic cycle. Table 1 presents the dicarboxylic acids that are mixed in equal weight ratios to yield the C5, C6 and C7 mixtures containing five, six and seven carbon (C) atoms leading to O:C ratios of 0.8, 0.7 and 0.6, respectively. These mixtures are increasingly hydrophobic with increasing carbon chain lengths.

Micrometer sized internally mixed particles of C5/AS/H_2O, C6/AS/H_2O and C7/AS/H_2O systems showed significantly different behaviors during RH cycles. In particles of C5/AS/H_2O, AS effloresced at 37.9 % RH and deliquesced at 77.5 % RH without LLPS. On the other hand, LLPS of C6/AS/H_2O particles appeared for an AS dry mass fraction of 0.1 to 0.8 at RHs between 70 % and 90 % (depending on OIR) when water was released. Depending on the OIR, it was induced by fundamentally different mechanisms like nucleation-and-growth, spinodal decomposition and growth of a second phase at the surface of the particle. Interestingly, after LLPS had occurred, the inner phase, confirmed to consist of aqueous AS by Raman spectroscopy, tended to move from the core toward the edge of the particle (Figure 1 (a)). Such partial engulfing structures have also been observed by Kwamena *et al.* (2010). LLPS in C7/AS/H_2O particles took place at RH as high as 90 % over a wider range of OIR both upon drying and moistening. Core-shell structure was the main configuration in these systems (Figure 1 (b)). Overall, the RH range of coexistence of two liquid phases and the processes resulting in LLPS depend on the chemical compositions leading to different O:C ratios and hydrophilicity of the particles. The observed morphologies of the investigated particles might very likely be present in the troposphere.

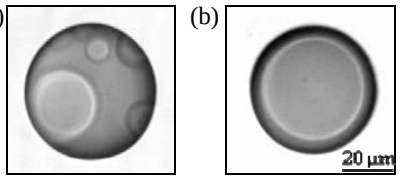

Figure 1. Optical images of morphologies of single particles of (a) C6/AS/H_2O and (b) C7/AS/H_2O for OIR =1:1 at 66 % and 89 % RH, respectively.

This work was supported by the Swiss National Foundation Project No. 200020-125151.

Ciobanu, V.G., Marcolli, C., Krieger, U., Weers U., and Peter, T. (2009) *J. Phys. Chem. A.* **113**, 10966-10978.

Marcolli, C. and Krieger, U. K. (2006) *J. Phys. Chem. A* **110**, 1881–1893.

Kwamena, N. -O. A., Buajarern, J., and Reid, J. P. (2010) *J. Phys. Chem. A*, **114**, 5787-5795.

Influence of Existing Particle Surfaces on Formation of Secondary Inorganic Aerosols in Fine Mode

Mukesh Sharma[1, 2]*, and Sailesh N. Behera[1]

Centre for Environmental Science and Engineering, Indian Institute of Technology Kanpur, Kanpur 208016
Department of Civil Engineering, Indian Institute of Technology Kanpur, Kanpur 208016, India
Keywords: gas-to-particle conversion, rate constants, acid gases, existing particle surface, and ammonia
*Presenting author email: mukesh@iitk.ac.in

Reduction of ambient levels of particulate matter of diameter less than 2.5 µm ($PM_{2.5}$) is a common challenge to all air pollution control engineers because of the fact that 20–40% to $PM_{2.5}$ mass is formed in the atmosphere involving ammonia and acid gases (Baek et al., 2004 and Sharma et al., 2007). Specifically, ammonia produces secondary inorganic aerosols (SIA) in fine mode, which comprise ions of ammonium salts (i.e., NH_4^+, SO_4^{2-}, NO_3^- and Cl^-).

While the gas to particle conversion is now a common knowledge, role of surface provided by existing particles in formation of SIA needs investigations. This research attempts to examine the kinetics of formation of ammonium salts through interactions of precursor gases (NO_2, SO_2 and NH_3), primary aerosols and meteorology that can produce secondary aerosols. An outdoor environmental chamber facility (volume 12.5 m^3 made of FEP Teflon-film) was used for simulating multiple reactions concurrently. The chamber was checked for wall losses, leaks, solar transparency and ability to simulate photochemical reactions. Total 29 no of experimental runs were performed at elevated levels of precursor gases (concentration > 200 µg/m^3) with varying levels of existing $PM_{2.5}$ levels.

Reaction rate constants k_S, k_N and k_{Cl} for reactions R1, R2, and R3 (see below) have been estimated to address the issue of formation of SIA.

$$2NH_3(g) + H_2SO_4(aq) \xrightarrow{k_s} (NH_4)_2SO_4(aq) \quad (R1)$$

$$NH_3(g) + HNO_3(g) \xleftrightarrow{k_N} NH_4NO_3(s) \text{ or } (aq) \quad (R2)$$

$$NH_3(g) + HCl(g) \xleftrightarrow{k_{cl}} NH_4Cl(s) \text{ or } (aq) \quad (R3)$$

The estimated rate constants are: k_S = 2.68×10^{-4} (±1.38×10^{-4}) m^3/µmol/s, k_N = 1.59×10^{-4} (±8.97×10^{-5}) m^3/µmol/s, and k_{Cl} = 5.16×10^{-5} (±3.50×10^{-5}) m^3/µmol/s. It has been observed that the rate of formation of $(NH_4)_2SO_4$ was enhanced during daytime, while the rate of formation of NH_4NO_3 has been favored during nighttime.

Figure 1 illustrates the association between initial $PM_{2.5}$ concentration and rate constants for formation of $(NH_4)_2SO_4$, NH_4NO_3 and NH_4Cl (both for day and nighttime). The order of correlation coefficient (Figure 1) between initial $PM_{2.5}$ concentration and rate constants was: 0.71 for k_S; 0.59 for k_N and 0.42 for k_{Cl}. The significant positive correlations suggest that surface provided by initial aerosols augments condensation and adsorption of precursor gases that could facilitate enhanced formation of $(NH_4)_2SO_4$, NH_4NO_3 and NH_4Cl. In the cases of NH_4NO_3 and NH_4Cl, once formed on aerosols, backward reactions (in R2 and R3) are unlikely to occur and thus results in enhanced rates of formation of NH_4NO_3 and NH_4Cl.

It was an important conclusion of this study that in the urban environments having high background aerosol concentration, conditions become conducive for formation of SIA. A better control of primary aerosols is helpful in preventing formation of secondary fine particles.

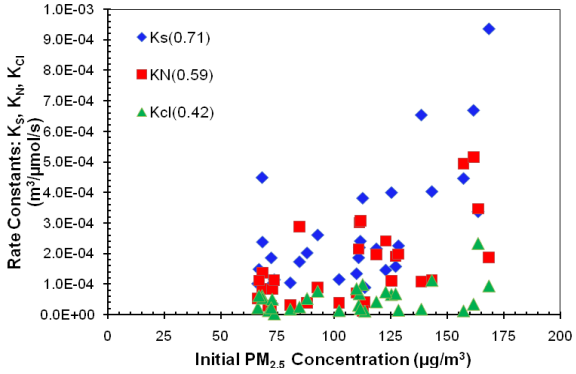

Figure 1: Relationship between reaction rate constants (k_S, k_N, k_{Cl}) and existing $PM_{2.5}$ concentration. Correlation coefficients are indicated in parentheses.

Behera, S.N., Sharma, M. (2010). Reconstructing primary and secondary components of $PM_{2.5}$ aerosol composition for an urban atmosphere. *Aerosol Sci. Technol.* **44**,983–992.

Baek, B.H., Aneja, V. P., Tong, Q. (2004). Chemical coupling between ammonia, acid gases, and fine particles. *Environ. Pollut.* **129**, 89-98.

Sharma, M., Kishore, S., Tripathi, S.N., Behera, S.N. (2007). Role of atmospheric ammonia in the formation of inorganic secondary particulate matter: a study at Kanpur, *India. J. Atmos. Chem.* **58**, 1-17.

Lin, Y-C., Cheng, M-T. (2007). Evaluation of formation rates of NO_2 to gaseous and particulate nitrate in the urban atmosphere. *Atmos. Environ.* **41**, 1903–1910.

Influence of the sampling site, the season of the year, the particle size and the number of nucleation events on the chemical composition of atmospheric ultrafine particles

J. Ruiz-Jimenez[1], J. Parshintsev[1], T. Laitinen[1,2], K. Hartonen[1], M.–L. Riekkola[1],T. Petäjä[2], M. Kulmala[2]
[1]Laboratory of Analytical Chemistry, Department of Chemistry, University of Helsinki, P.O. Box 55, FI-00014 Finland, [2]Division of Atmospheric Sciences, Department of Physics, University of Helsinki, P.O. Box 64, FI-00014, Finland
Keywords: ultrafine particles, biogenic organic compounds, statistical analysis
Presenting author email: jose.ruiz-jimenez@helsinki.fi

Twenty one biogenic organic compounds, 9 dicarboxylic acids, 4 monocarboxylic, 3 polyols, 1 amine and 4 aldehydes, were determined in 61 atmospheric aerosol particle samples of different particle sizes (30 nm, 40 nm, 50 nm and TSP). The samples were collected in two different sampling sites (SMEAR II and SMEAR III) during different seasons of the year (Table 1). The validated methodology used for the collection, sample preparation, individual separation and determination of biogenic organic compounds has been recently described (Ruiz-Jimenez, 2011).

Table 1. Mean concentrations (ng m^{-3}) obtained for the target analytes

	All	SMEAR II	SMEAR III
N	61	39	22
Di acids	8.2	5.1	13.1
Mono acid	47.4	48.1	45.9
Polyols	18.7	6.7	39.8
Amines	2.0	1.8	3.4
Aldehydes	10.1	4.6	20.1
NNEV/NCD	0.5	0.6	0.3

Non-supervised pattern recognition techniques, such as Hierarchical Cluster Analysis and Principal Component Analysis, were used for the clarification of the influence of the collection place, the season of the year and the particle size on the concentration and behavior of the target compounds.

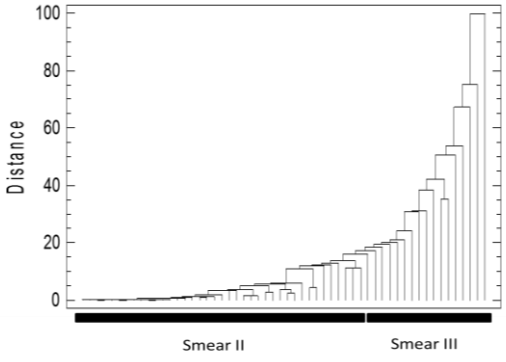

Figure 1. Influence of the sampling site on the composition of the aerosol particles.

The results achieved demonstrate the clear correlation of the sampling site, the season of the year and the particle size on the composition of the atmospheric aerosol particles. The explained data variation was over 88% in all the cases.

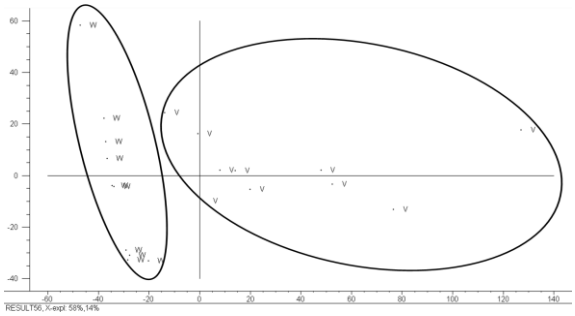

Figure 2. Effect of the season of the year on the composition of the aerosol particles. PCA models for samples collected at SMEAR III station.

Quantitative analysis methodologies, such as Partial Least Squares Regression and Principal Component Regression models, were used for the elucidation of the influence of the number of nucleation events on the chemical composition of the particles (Table 2).

Table 2. Statistical models developed for the study of the influence of the number nucleation event days in the composition of the atmospheric aerosol particles. (S, spring; A, autumn; V, summer; W, winter)

	GM	SMEAR II			SMEAR III		
	All	All	S	A	All	V	W
N	52	36	12	18	19	10	10
Model	PLSR	PLSR	PCR	PLSR	PLSR	PCR	PCR
R^2 pred.	0.71	0.65	0.80	0.71	0.77	0.69	0.82

Correlations were found between analyte profiles and the number of nucleation events during collection of the sample. Although the model was generated on the basis of the total profile of analytes, it was possible to clarify the influence of each individual analyte on the model.

This work was supported by the Academy of Finland Centre of Excellence program (project no 1118615).

Ruiz-Jiménez, J., Parshintsev, J., Laitinen, T., Hartonen, K., Riekkola, M.-L., Petäjä, T., Virkkula, A. and Kulmala. M. (2011) Determination of Biogenic Organic Compounds in Atmospheric Ultrafine Particles. submitted to *Environ. Sci. Technol. (2011).*

Elucidation of organic volatile compounds in Antarctic aerosol particles. Influence of the nucleation events on the chemical composition of the particles

J. Ruiz-Jimenez[1], J. Parshintsev[1], T. Laitinen[1,2], E.–M Kyrö[2], A. Virkkula K. Hartonen[1], M.–L. Riekkola[1],T. Petäjä[2], M. Kulmala[2]

[1]Laboratory of Analytical Chemistry, Department of Chemistry, University of Helsinki, P.O. Box 55, FI-00014 Finland, [2]Division of Atmospheric Sciences, Department of Physics, University of Helsinki, P.O. Box 64, FI-00014, Finland

Keywords: Comprehensive gas chromatography, nucleation, total suspended particles, ABOA station
Presenting author email: jose.ruiz-jimenez@helsinki.fi

Comprehensive two dimensional gas chromatography – time-of-flight mass spectrometry (GCxGC-TOF-MS) was used for the screening and semi-quantitation of volatile organic compounds, such as volatile and low-volatile compounds in total suspended aerosol particles (TSP). The samples were collected during the summer 2009 at the Finnish Antarctic Research Station (ABOA), and during the summer 2010 at the Station for Measuring Forest Ecosystem Atmosphere Relations (SMEAR II) at Hyytiälä (Finland).

The classification of the identified compounds was based on the main functional group or specific element present in the molecule (Figure 1).

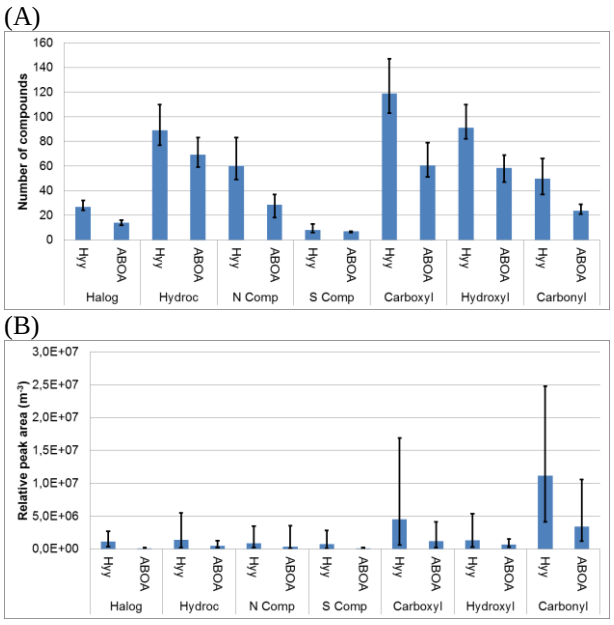

Figure 1. Chemical groups in different sized and TS particles as a function of A) number of compounds, B) relative peak areas.

The number of identified compounds and the relative peak areas were smaller in ABOA than in SMEAR II samples. The differences were clear especially in the case of acids and aldehydes. Totally different sampling site locations with different surroundings can explain these results.

The samples collected at the ABOA station can be divided into three groups as a function of the intensity of the nucleation events during the sampling —no-nucleation days (13 samples), normal nucleation days (4 samples) or very strong nucleation days (2 samples). Non- supervised pattern recognition techniques, such as Hierarchical Cluster Analysis and Principal Component Analysis were exploited for the clarification of the influence of the nucleation event on the particle composition.

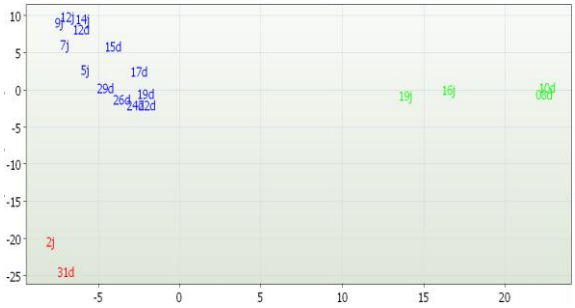

Figure 2. PCA models for samples collected in the ABOA station.

The clear differences revealed by the chemometrical analysis were confirmed by the use of time-series for the individual compounds leading to the classification of the compounds into six different trends, according to their concentrations in the different samples that can explain the differences in the particle composition associated to the nucleation events (Figure 3).

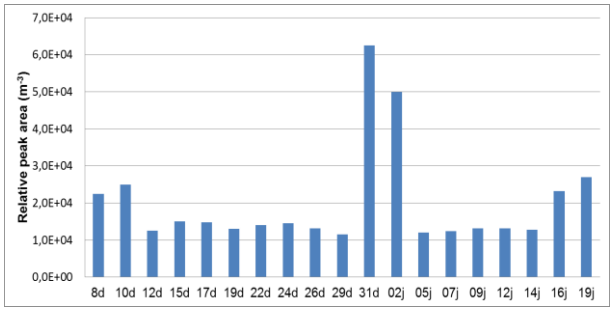

Figure 3. Time-series profile obtained for mevalonic acid, dithioerythriol, adipic acid and 1-hexanol.

This work was supported by the Academy of Finland Centre of Excellence program (project no 1118615).

Ion studies of organic precursor molecules for secondary particle formation

M. Ehn[1], J. Wildt[2], E. Kleist[2], M. Dal Maso[3], H. Junninen[3], A. Trimborn[1], and T. Mentel[1]

[1]Institue for Energy and Climate research, Forschungszentrum Jülich, Jülich, Germany
[2]Institute Plant Sciences, Forschungszentrum Jülich, Jülich, Germany
[3]Department of Physics, University of Helsinki, Helsinki, Finland
Keywords: Aerosol formation, mass spectrometry, secondary organic aerosol (SOA)
Presenting author email: m.ehn@fz-juelich.de

Secondary aerosol formation is believed to account for the majority of particles in the atmosphere (Merikanto et al., 2009). Other studies have shown that the dominant mass fraction of organic aerosol has been produced secondarily (e.g. Hallquist et al., 2009). Volatile organic compounds (VOCs) are oxidized in several steps whereby the vapor pressure of the oxidation products can be reduced. This reduction in vapor pressure increases the ability of the product to either condense on to existing particles, or take part in the formation of completely new particles.

To better understand early steps of particle formation from VOCs it is therefore of importance to measure such vapors. The most volatile vapors are typically measured by e.g. PTR-MS or GC-MS techniques. The VOCs themselves and many of their high volatile oxidation products are available at high concentrations and do not easily stick to surfaces. However, as the oxidation of these compounds progresses, the concentrations and stability in the gas phase decrease, and neither of the above-mentioned techniques are capable of detecting such compounds. Chemical ionization mass spectrometry (CIMS) has evolved a lot during the recent decade, and is able to measure both inorganic and organic acids in the gas phase down to sub-ppt levels.

The study of naturally charged ions with the atmospheric pressure interface time-of-flight mass spectrometer (APi-TOF; Junninen et al, 2010) has been shown to be very sensitive to acidic, highly oxidized atmospheric molecules (Ehn et al, 2010). Though the instrument cannot directly give quantitative estimates of the neutral compound concentrations, it is to our knowledge the most sensitive instrument available to detect many acidic trace compounds. With the addition of a chemical ionization source in front, the instrument can also be converted into a CIMS, sacrificing some of the high sensitivity and selectivity for quantitative measurements.

The APi-TOF has been deployed at a boreal forest site in Hyytiälä, southern Finland, where several typical ions were identified. During nucleation events, H_2SO_4 dominated the negative ion spectra, but during evening and night when the particles continued growing, the H_2SO_4 signal decreased significantly, and other organic peaks became visible.

To get a better understanding of the processes forming these organic species, and their role in new particle formation and growth, plant chamber measurements were conducted with both real tree emissions and single compound precursors.

Many features of the ion spectra were reproduced in the chamber experiments, both with real plant emissions from a mix of boreal species, and by using pure alpha-pinene as a precursor. Several ions typically found in Hyytiälä, lacking a conclusive identification (Ehn et al, 2010) were also detected in the chamber studies during experiments with alpha-pinene and ozone, i. e. at low OH concentrations (Fig. 1). The peaks are believed to be nitrate-containing, highly oxidized organic molecules with an O:C:H ratio close to 1:1:1. The plotted mass/charge region shows the dominant peaks in the Hyytiälä spectra, however, in the chamber also larger ions, not visible in ambient air, were detected. Additionally, observations of sulfuric acid and its clusters up to the trimer were detected during new particle formation events both in the chamber, and in the field. However, much stronger nucleation events could be produced in the chamber with only small H_2SO_4 signals, indicating the importance of organic precursors in the formation process.

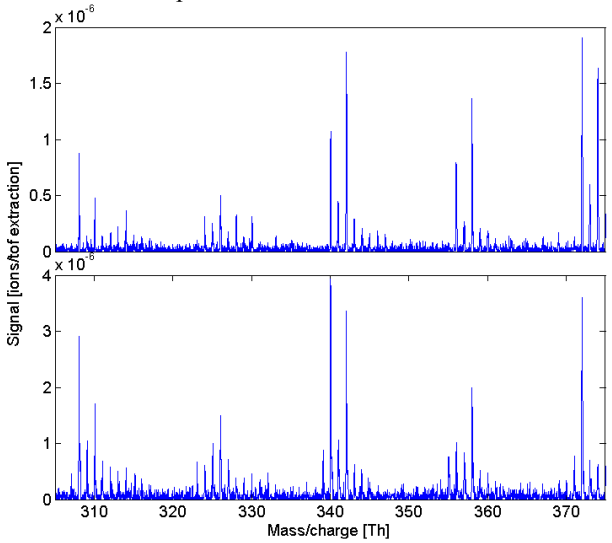

Figure 1. Ion spectra of alpha-pinene oxidation products in the JPAC plant chamber (top), and night-time ion spectrum in Hyytiälä, Finland (bottom).

J. Merikanto et al., *Atmos. Chem. Phys.,* 9(21), 8601-8616, 2009.
M. Hallquist et al., *Atmos. Chem. Phys.* 9, 5155, 2009.
H. Junninen et al., *Atmos. Meas. Tech.*, 3, 1039–1053, 2010.
M. Ehn et al., *Atmos Chem. Phys*., 10, 8513–8530, 2010

Quantitative and qualitative characterisation of ultrafine particles emitted by laser printing devices

M. Barthel, S. Seeger, O. Hahn, O. Wilke, W. Horn and O. Jann

BAM Federal Institute of Materials Research and Testing, Division 4.2 Environmental Material and Product Properties, Unter den Eichen 87, 12205 Berlin, Germany
Keywords: Aerosol measurement, indoor aerosols, chemical composition, XRF, GC-MS.
Presenting author email: mathias.barthel@bam.de

Among the main sources for indoor ultrafine particle aerosols are electronic devices with laser printing function (LPDs) (Seeger *et al.*, 2006; Destaillats *et al.*, 2008, Schripp *et al.*, 2008). The characterisation of particles emitted by LPDs and the investigation of formation processes involved has been the subject of recent research (Morawska *et al.*, 2009; He *et al.*, 2010). In this work the quantitative and qualitative characterisation of ultrafine particles originating from 10 different laser printers is presented.

The experiments were carried out in stainless steel emission test chambers to ensure constant and reproducible conditions. In order to study the effect of chamber volume on particle agglomeration two chambers with different volumes (1 and 5 m^3) were used. The particle number concentration was measured using an Engine Exhaust Particle Sizer (*TSI*) and different types of condensation particle counters (*Grimm, TSI*) with subsequent calculation of the emission rate PER(t) and total number of emitted particles TP.

For qualitative analysis the particles were sampled with a 13 stage low pressure cascade impactor (*Dekati DLPI 10*). The samples were examined by the use of both µXRF and thermal desorption GC-MS. Depending on the method different substrates (Al or Polycarbonate foils) were used in order to minimize background signals.

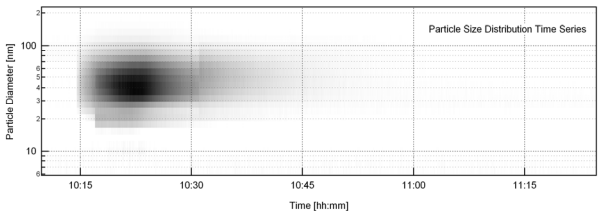

Figure 1. Particle Size distribution time series of particles emitted from a laser printer into an environmental test chamber during and after printing.

It could be shown that the variation in chamber volume (1 and 5 m^3) has no effect on particle emission rates and total particle numbers provided that particle loss factors are considered properly in the calculations. Furthermore data from different particle counting devices (CPC, EEPS) are in good agreement. To ensure working order of the instruments as well as repeatability and comparability of the measurements a standard operational procedure (ECMA, 2010) was worked out.

The results from the µXRF- and GC/MS-analysis of sampled particles reveal their chemical composition. Comparison of particle spectra with those from materials involved in the printing process, such as paper, toner and printer assemblies (e.g. fuser unit) are used to identify the sources of the particles.

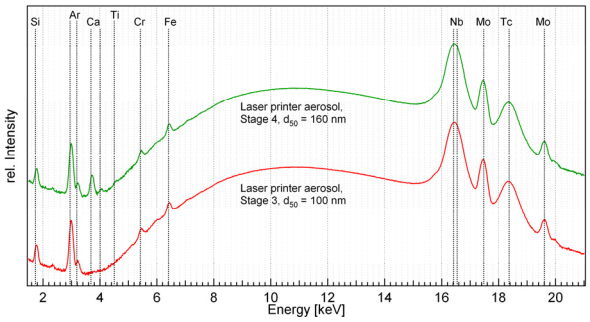

Figure 2. Qualitative analysis of size-resolved printer aerosol deposited on polycarbonate substrate using µXRF.

Among other results the presence of a Si-peak in the µXRF spectrum in combination with the absence of siloxanes in the GC-MS spectra indicates that non-volatile Si-compounds, such as SiO_2 play a role in particle formation. This thesis is supported by the results of evaporation experiments carried out using a thermo diluter.

The above findings allow for conclusions being drawn considering particle formation mechanisms relevant to the generation of indoor aerosols. Furthermore the chemical identification of some components of the emitted particles will contribute to an evaluation of potential health risks related to indoor aerosols.

This work was supported by The Federal Environment Agency UBA under grant UFOPLAN 3708 95 301.

Destaillats, H. *et al.* (2008) *Atmos. Environ.* **42**, 1317 – 1388.

He, C. *et al.* (2010) *J. Aero. Sci.* **41**, 523 – 530.

Morawska, L. *et al.* (2009) *Environ. Sci. Technol.* **43**, 1015 – 1022.

Schripp, T. *et al.* (2008) *Environ. Sci. Technol.* **42**, 4338 – 4343.

Seeger, S. *et al. Healthy Buildings*, Lisbon, Portugal, June 4-8, 2006; de Oliveira Fernandes, E., Ganeiro da Silva, M., Rosado Pinto, J.: Portugal; Vol. 2, pp 447 – 450.

Standard ECMA-328, 5th edition (2010): http://www.ecma-international.org/publications/files/ECMA-ST/ECMA-328.pdf

Effect of reaction temperature on the volatility of limonene ozonolysis products

R.K. Pathak[1], K. Salo[1], T. F. Mentel[2], R. Tillmann[2], E.U. Emanuelsson[1], A. Lutz[1] and M. Hallquist[1]

[1]Department of Chemistry, University of Gothenburg, Gothenburg, SE-412 96, Sweden
[2]Institut fur Chemie und Dynamik der Geosphare, ICG, Forschungszentrum Jülich, 52425 Jülich, Germany
Keywords: SOA, volatility, temperature dependence, partitioning
Presenting author email: ravikantpathak@gmail.com

A significant portion (up to 60%-70%) of atmospheric fine particles can be comprised of secondary organic aerosol (SOA). Therefore, a detailed understanding on the formation, properties and transformation of SOA is essentially needed to evaluate its impact on atmospheric processes, climate and human health. However, a significant progress in SOA research in recent years, the formation and properties of SOA are not fully understood, which poses a major research challenge in atmospheric science (Hallquist *et al.*, 2009). Biogenic volatile organic compounds (BVOC) are major SOA precursors. Among the BVOCs limonene can potentially yield high SOA depending upon the atmospheric conditions (Griffin *et al.*, 1999). One key feature not yet explored in details for the limonene oxidation is the thermodynamic property, e.g. volatility. In this study, the effect of reaction temperature on the volatility behaviour of SOA from limonene ozonolysis was investigated. The results from these flow tube reactor experiments were compared to previous smog chamber studies.

Experiments were carried in a flow-reactor named G-FROST (**G**öteborg- **F**low **R**eactor for **O**xidation **S**tudies at low **T**emperatures; Jonsson *et al.*, 2008). The average reaction time was kept constant (238 s). Generally system was maintained at 30-50% RH. SOA was created using limonene and ozone. Cyclohexane (CH) was used an OH scavenger (OHS). Some experiments were also conducted in presence of aldehyde/ketone (Pinonaldehyde (PA); Nopinone (NP)). The experimental scheme is presented in Table 1.

Table 1: Experimental conditions

Reaction Temp (K)	SOA	SOA +OHS	SOA+ Aldehyde	SOA+ Aldehyde +OHS
298	Lim+O_3 +CH	Lim+O_3 +CH	Lim+O_3+ NP/PA	Lim+O_3+ CH+ NP/PA
273	Lim+O_3 +CH	Lim+O_3 +CH	Lim+O_3+ NP/PA	Lim+O_3+ CH+ NP/PA
253	Lim+O_3 +CH	Lim+O_3 +CH	Lim+O_3+ NP	Lim+O_3+ CH+NP

SOA volatility was measured using the Volatility Tandem Differential Mobility Analyzer (VTDMA), which consists of two differential mobility analyzers (DMA1 & DMA2) in tandem with a set of 8 controlled heating ovens. Size selected monodisperse aerosol (75nm) using DMA1 were fed to the heated ovens (298K-525K). The volume fraction remaining (VFR) of the aerosol feed was subsequently measured by DMA2 and the VFR normalized to that at 298K was estimated.

Results

Figure 1 shows the change in SOA volatility curves corresponding to different reaction temperatures in the experimental system in comparison to data from the AIDA chamber (Saathoff *et al.*, 2009 and Salo *et al.*, 2011). Any change in volatility may signify the variation in the distribution of reaction products at different temperature due to change in reaction kinetics etc. In general, the SOA volatility increased with decrease in reaction temperature in the two systems except for the 253K in the G-FROST system, which was lower than that for 273K. The two experimental systems showed difference in SOA volatility at the same reaction temperature e.g. the volatility at 273K in the G-FROST was higher than that in the AIDA chamber. A number of factors are addressed including fresh-aerosol in the G-FROST vs few hours aged in the AIDA chamber, chamber wall effect etc. Detailed results and analysis on the effect of OHS and impact of aldehydes/ketones on the partitioning and volatility of SOA at different reaction temperature will be presented.

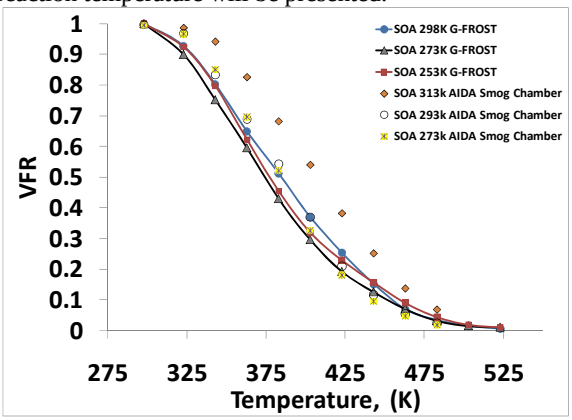

Figure 1: Volatility of SOA formed at different reaction temperatures in the two experimental set-ups

This work was supported by Formas (214-2010-1756), The Swedish Research Council (80475101). The research presented is a contribution to the Swedish strategic research area ModElling the Regional and Global Earth system, MERGE.

Griffin, R.J., Cocker III, D.R., Flagan, R.C. and Seinfeld, J.H. (1999) *J. Geophys. Res.*, **104**, 3555–3567.
Jonsson, A.M., Hallquist, M. and Ljungstrom, E. (2008) *Atmos. Chem. Phys.*, **8**, 6541–6549.
Hallquist, M. *et al.* (2009), *Atmos. Chem. Phys.*, **9**, 5155–5236.
Saathoff, H. *et al.* (2009) *Atmos. Chem. Phys.*, **9**, 1551–1577.
Salo, K. *et al.* (2011) Volatility of SOA during OH induced aging, *Manuscript in preparation.*

The Formation of Secondary Organic Aerosol from Intermediates in the Ozonolysis of α-pinene.

I.D. Hoare, D.J. Stewart, G. Brittan, A.T. Russell, S. Almabrok, M.V. Ghosh, C. Pfrang and G. Marston.
Department of Chemistry, University of Reading, Whiteknights, PO Box 217 Reading, RG6 6HA
Presenting Author email: i.d.hoare@reading.ac.uk

The oxidation of volatile organic compounds (of which α-pinene is an important species) in the atmosphere is important for a number of reasons. Oxidation products, both closed shell (carbonyl species) and radicals (OH, HO_2 and RO_2) have a major importance in the chemistry of the troposphere (Johnson and Marston, 2008). Modelling studies have shown that the reaction of ozone with alkenes could be the dominant source of HO_x in polluted urban environments as well as being a significant contributor in less polluted rural locations (Paulson and Orlando, 1996). The oxidation of VOCs can also contribute significantly to the nucleation and production of aerosol particles in the atmosphere (Went, 1960; Marti *et al.* 1997), which has a significant effect on air quality, global climate (Twomey *et al.* 1984; Charlson *et al.* 1992), cloud formation (Novakov and Penner, 1993) and also has important impacts on visibility and human health (Donaldson *et al.* 1998).

The oxidation of α-pinene by ozone is known to proceed *via* the initial production of two reactive Criegee Intermediates (CIs), it is now well established which final chemical products of the reaction are produced from which CI (Ma *et al.* 2007a, 2007b, 2008); however, it is still uncertain which of the chemical species resulting from which CI are responsible for the formation of secondary organic aerosol. In order to elucidate which CI produces the products responsible for SOA formation "enal" and "enone" compounds structurally related to α-pinene but which on ozonolysis will give only one of the Criegee Intermediates have been synthesized using the procedures below.

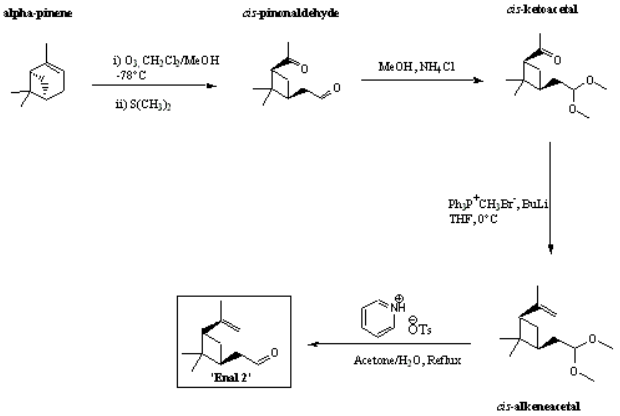

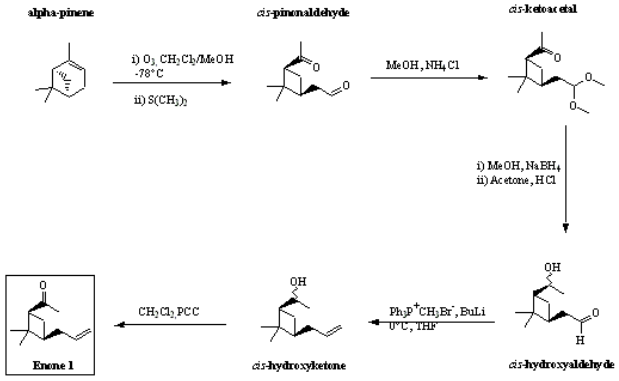

In static chamber experiments the aerosol yields from the "enal" and the "enone" will be compared to the aerosol yield from α-pinene to ascertain which reaction pathway is dominant in SOA production. This is the first attempt to elucidate the mechanism of SOA formation from α-pinene oxidation in this way.

R.J. Charlson, S.E. Schwartz, J.M. Hales, R.D. Cess, J.A. Coakley Jr, J.E. Hansen, D.J. Hoffmann, *Science* 1992, **255**, 423

K. Donaldson, X.Y. Li, W.J. MacNee, *J. Aersol Sci.* 1998, **29,** 553

D. Johnson and G. Marston, *Chem. Soc. Rev.*, 2008, **37,** 699

Y. Ma, T. Luciani, R.A. Porter, A.T. Russell, D. Johnson, G. Marston, *PCCP* 2007 **9** 5084-87

Y. Ma, R. Willcox, A.T. Russell, G. Marston, *ChemComm* 2007, 1328-1330

Y. Ma, A.T. Russell, G. Marston *PCCP* 2008 **10** 4294-4312

J.J. Marti, R.J. Weber, P.H. McMurry, F. T. Novakov J.E. Penner, *Nature* 1993, **365**, 823

Eisele, D.Tanner, A. Jefferson, *J. Geophys. Res.*1997, **102(D5)**, 6331

S.E. Paulson and J.J. Orlando, *Geophys. Res. Lett.* 1996, **23**, 3727

S.A. Twomey, M. Piepgrass, T.L. Wolfe, *Tellus* 1984, **36B,** 3

F.W. Went, *Nature*, 1960, **187,** 641

Simulating secondary organic aerosol (SOA) formation over Europe using the volatility basis-set approach (VBS) in the online coupled model COSMO-ART

Eleni Athanasopoulou[1], Heike Vogel[1], Max Bangert[1], Christoph Knote[2], Bernhard Vogel[1], Ben Murphy[3], Alexandra Tsimpidi[4], Spyros Pandis[3,4]

[1]Institute for Meteorology and Climate Research, Karlsruhe Institute of Technology (KIT), Eggenstein-Leopoldshafen, Germany
[2]Empa, Dübendorf, Switzerland
[3]Department of Chemical Engineering, Carnegie Mellon University, Pittsburgh, USA
[4]Department of Chemical Engineering, University of Patras, Patra, Greece
Keywords: SOA (Second. Organic Aerosols), aerosol modeling, volatility basis-set.
Presenting author email: eleni.athanasopoulou@kit.edu

COSMO-ART is a recently developed regional model that couples meteorological and air quality processes online (Vogel et al., 2009). Comparisons of aerosol predictions against measurements suggested an underestimation of the total aerosol mass, which was attributed mainly to low organic aerosol (OA) predictions (Knote et al., 2010). This finding became the stimulation for revising SOA treatment within COSMO-ART, presented in the current study.

Previous research suggests that the models' inability to reach OA observations is strongly related to gas-particle partitioning of all (thousands) organics emitted and formed into the atmosphere, but not in simulations. An efficient way to incorporate this chemical evolution of organics into modelling (aging), is their group treatment by saturation concentrations (VBS) (Donahue et al., 2006).

Recent model applications using VBS confirm model's improved efficiency in predicting OA mass (Murphy and Pandis, 2009; Tsimpidi et al., 2010 etc). According to their results, SOA can represent more than 50% of total OA mass, while their absolute values can reach more than 5μgm^{-3}, which seems promising for improving COSMO-ART performance (Fig. 1).

In the framework of this study, COSMO-ART is modified to include the VBS treatment of SOA. Nine biogenic and anthropogenic SOA precursors (higher alkanes and alkenes, terpenes, isoprene) are grouped into 4 surrogate species with effective saturation concentrations of 1, 10, 100, 1000 μgm^{-3}, modified according to the spatial-temporal variation of temperature (Clausius-Clapeyron eq.). Aerosol yields after each precursor's oxidation to OH, O_3 and NO_3^- alter with its condensation effectiveness and are a combination of the low and high NOx mass yields used in Murphy and Pandis (2009). Further oxidation of surrogate species decreases their saturation concentration by 1 order of magnitude (aging) and increases their mass by 7.5% (to account the oxygen added).

The VBS approach is then coupled with the existing gas-particle partitioning module and with the chemical mechanism RADMKA (Regional Acid Deposition Model Version Karlsruhe). The simulation domain covers Europe with an horizontal grid size of 14km and 40 vertical layers up to a height of 20km. The meteorological initial and boundary conditions are achieved from the IFS model of ECMWF for May 2008. COSMO-ART results by applying the prior (SORGAM) and the current (VBS) SOA module are inter-compared and evaluated against field measurements of OA collected during the EUCAARI campaign for selected stations.

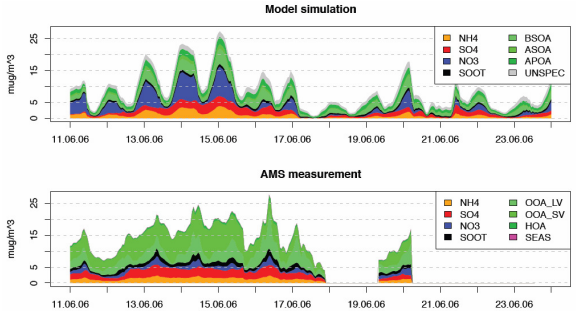

Figure 1. Evaluation of COSMO-ART aerosol composition AMS campaign measurement (PSI) in Payerne (CH) (Knote et al., 2010)

A similar grouping and aging approach used in global applications, showed an effect on CCN concentrations, due to the enhanced condensation and particle growth (Yu, 2011). The fully coupled approach used by COSMO-ART, gives to this study the opportunity to investigate the feedback of the VBS approach on cloud formation. Results will be presented during the conference.

Vogel, B., Vogel, H., Baumer, D., Bangert, M., Lundgren, K., Rinke, R. And Stanelle T. (2009) *Atmos. Chem. Phys.* **9**, 8661–8680.

Knote, C., Brunner, D., Vogel, H., Vogel, B., and Lohmann U. (2010) *Proc.Int. Aerosol Conference.*

Donahue, N.M., Robinson A.L., Stanier C.O. and Pandis S.N. (2006) *Environ. Sci. Technol.* **40**, 2635-2643.

Tsimpidi, A.P, Karydis, V.A., Zavala, M., Lei, W., Molina, L., Ulbrich, I.M., Jimenez, J.L. and Pandis S.N. (2010) *Atmos. Chem. Phys.* **10**, 525–546

Murphy, B.N and Pandis, S.N. (2009) *Environ. Sci. Technol.* **43**, 4722-4728.

Yu (2011) *Atmos. Chem. Phys.* **11**, 1083-1099.

Modelling SOA formation from Anthropogenic VOCs using an explicit chemical mechanism

T. Raventos-Duran[1], M. Camredon[1], R. Valorso[1], C. Mouchel-Vallon[1], S. Madronich[2], J. Lee-Taylor[2], and B. Aumont[1]

[1]LISA, UMR CNRS/INSU 7583, Universite Paris Est Creteil et Universite Paris Diderot, Institut Pierre Simon Laplace 94010 Creteil Cedex, France.
[2]Atmospheric Chemistry Division, NCAR, Boulder, Colorado
Keywords: SOA (Second. Organic Aerosols), aerosol modelling, carbon oxidation, thermodynamic equilibrium.
Presenting author email: teresa.raventos@lisa.u-pec.fr

An explicit chemical mechanism model (GECKO-A, detailed in Aumont *et al.* 2005) was applied to over 150 gas-phase anthropogenic species with up to C22 (taken from the emissions inventories AIRPARIF and CITEPA), to describe the formation of SOA in the city of Paris and the chemical composition evolution during several days of reactivity. Some biogenic compounds (i.e. isoprene and α-pinene) were also included to account for nearby rural emissions.

The resulted chemical mechanism was coupled to a two-layer box-model which includes anthropogenic and biogenic emissions of VOCs and NOx and dry deposition. Variations of emissions were considered throughout day and night with temperature and light following parameterisations described in Aumont *et al.* (2003). Compounds are exchanged between the two layers during the growth and the decay of the continental boundary layer.

To our knowledge, this is the first time that such a detailed chemical scheme including hundreds of thousands of secondary VOCs is evaluated for its potential to form SOA.

First modelling results are presented with the assessment of SOA concentrations and chemical speciation, identification of major SOA contributors and analysis of Van Krevelen diagrams (H:C vs. O:C) at different time sets, recently acknowledged as a valuable tool to graphically interpret the mass spectrometric measurements (Heald *et al.* 2010).

Results from the model are evaluated with typical observed concentrations from the MEGAPOLI project with special focus on the representation of SOA formation.

References:

Aumont B., S. Szopa, and S. Madronich. Modelling the evolution of organic carbon during its gas-phase tropospheric oxidation: development of an explicit model based on a self generating approach. *Atmos. Chem. Phys.*, 5: p. 2497-2517, 2005.

Inventaire des Emissions en Ile-De-France, Ed. 2010, Methodologie et resultats – annee 2005. By AIRPARIF, Surveillance de la qualite de l'air en Ile-de-France. (http://www.airparif.asso.fr/airparif/pdf/Rinventaire_2005_201004.pdf)

Inventaire Deepartementalise des Emissions de Polluants Atmospheriques en France en 2000. Mise a jour de fevrier 2005. Centre Interprofessioneel Technique d'Etudes de la Pollution Atmospherique. (http://www.citepa.org/publications/Rapport_departement_2000_v2005-web.pdf)

Aumont B., F. Chervier and S. Laval. Contribution of HONO sources to the NOx/HOx/O3 chemistry in the polluted boundary layer. *Atmos. Environ.* 37: p. 487-498, 2003.

Heald C. L., J. H. Kroll, J. L. Jimenez, K. S. Docherty, P. F. DeCarlo, A. C. Aiken, Q. Chen, S. T. Martin, D. K. Farmer, and P. Artaxo. A simplified description of the evolution of organic aerosol composition in the atmosphere. *Geophys. Res. Lett.*, 37, L08803, doi:10.1029/2010GL042737, 2010

Reaction of OH radicals with secondary organic aerosol from the ozonolysis of alpha-pinene

H. Saathoff[1], K.-H. Naumann[1], O. Möhler[1], N. Donahue[2], T. Mentel[3], R. Tillmann[3], and T. Leisner[1]

[1]Institute for Meteorology and Climate Research, Karlsruhe Institute of Technology, Hermann-von-Helmholtz-Platz 1, 76344 Eggenstein-Leopoldshafen, Germany
[2]Carnegie Mellon University, Centre Atmospheric Particle Studies, Pittsburgh, PA 15213 USA
[3] Institute für Energie- und Klimaforschung IEK-8 Troposphäre, Forschungszentrum Jülich, Leo-Brandt-Str. 52428 Jülich, Germany

Keywords: aerosol chamber, aerosol chemistry, aerosol modelling, OH radicals, SOA

OH radicals are the most important agents for oxidation of atmospheric constituents and they play an important role in formation and aging of atmospheric aerosols e.g. secondary organic aerosols (SOA). Since the influence of temperature on aerosol formation and aging is one of the major uncertainties for understanding aerosol transformations (Tsigaridis et al., 2005) we investigated SOA aging by OH radicals in the large temperature controlled simulation chamber AIDA (Saathoff et al., 2009).

As a dark source of OH radicals we employed controlled ozonolysis of 2,3-dimethyl-2-butene (TME). The OH radical concentrations generated in the AIDA simulation chamber were calculated by comparing the results of master chemical mechanism (MCM 3.1) with the measured evolutions of all trace gases measured. SOA was generated by ozonolysis of alpha-pinene with an excess of ozone under simulated tropospheric conditions in the AIDA chamber on time scales of up to 30 hours and at temperatures between 253 and 313 K. Various instruments were used to measure the time evolutions of hydrocarbons (PTR-MS, FTIR), ozone (UV-Absorption), aerosol particle mass & size (TOF-AMS, SMPS) and number concentrations (CPC). The experimentally determined values were analysed using the aerosol behaviour code COSIMA (Naumann, 2003), supplemented by a SOA module.

The model calculations can reproduce the observations based on known rate coefficients and the measured trace gas concentrations. Generating the OH radicals in the order of 10^6 to 10^7 molecules cm^{-3} in the presence of SOA from ozonolysis of alpha-pinene resulted in additional formation of SOA mass in the order of 10-35% within two hours or less. The additional mass formed is smaller for lower temperatures. The model analysis takes into account the wall losses of semi volatile SOA compounds and also the impact of the OH radicals formed already during the terpene ozonolysis.

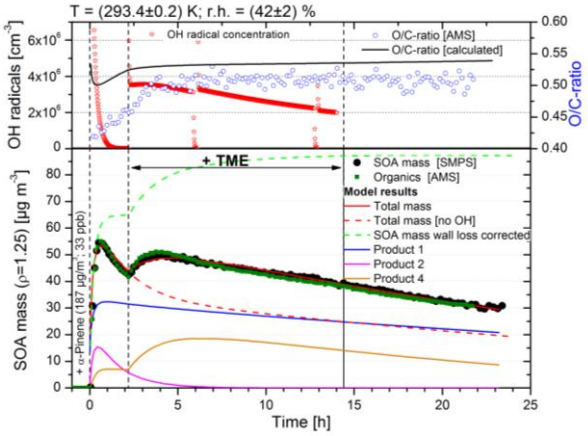

Figure 1. Evolution of SOA mass and composition during ozonolysis of α-pinene and aging with OH radicals from TME oxidation at 293.4 K.

Figure 1 shows the evolution of the measured SOA mass and O/C-ratio compared to model results including SOA composition (4 different products assumed) and OH radical levels. Please note that already during ozonolysis of the terpene OH radicals are formed which strongly influence yield and properties of the SOA particles.

This paper will present quantitative results on the OH radical induced aging of alpha-pinene SOA for simulated tropospheric conditions.

Naumann, K.-H. (2003) J. Aerosol Science, 34, 1371-1397.

Saathoff, H., Naumann, K.-H., Möhler, O., Jonsson, Å. M., Hallquist, M., Kiendler-Scharr, A., Mentel, Th. F., Tillmann, R., Schurath, U. (2009) Atmos. Chem. Phys. 9 (5), 1551-1577.

Tsigaridis, K., Lathiere, J., Kanakidou, M., Hauglustaine, D. A. (2005) Atmos. Chem.Phys. 5, 1891-1904.

Gas-to-particle conversion in biogenic aromatic aldehydes and their complexes with heavy metals: a contribution into the biogeochemical cycles of elements

S.N. Dubtsov[1], G.G. Dultseva[1,2],
[1]Institute of Chemical Kinetics and Combustion, SB RAS, Novosibirsk, 630090, Russia
[2]Department of Natural Sciences, Novosibirsk State University, Novosibirsk, 630090, Russia
Keywords: organic aerosols, particle formation, photochemical properties
Email: dubtsov@kinetics.nsc.ru

Biogenic aldehydes emitted into the atmosphere by vegetation often contain aromatic fragments and/or double bonds, which makes these compounds potential participants of nucleation both under the action of sunlight and through chemical reactions with such atmospheric minor gases as ozone or nitrogen oxides. The contribution from biogenic aldehydes into atmospheric aerosol of the nanometer size scale remains poorly investigated due to the experimental difficulties connected with identification of trace amounts of very reactive species. The occurrence of metals in the form of complex compounds with aldehydes in the emissions of vegetation, though reliably detected in field observations, remains a subject to be studied more thoroughly under laboratory conditions to exclude the effect of numerous uncontrollable factors existing in natural atmosphere.

The present work deals with the investigation into the mechanisms of photonucleation, atmospheric oxidation and gas-to-particle conversion of biogenic aromatic aldehydes and their volatile complexes with heavy metals (of soil origin). Many green plant species when growing on soil with increased heavy metal content, either of natural or anthropogenic origin, are able to release such complexes; this is a kind of detoxication for plants but brings about the danger of atmospheric pollution with the breathable nanometer-sized metal-containing aerosol. We studied the kinetics and mechanism of photonucleation of aromatic aldehydes alone and in complexes with heavy metals under laboratory conditions in a flow photochemical reactor under UV irradiation. Analysis of major and minor intermediate and final products was carried out using UV, IR, NMR, EPR spectroscopy, GC-MS, chemical analysis for functional groups, and HPLC. Both the gas-phase products and the particulate matter formed under irradiation were analysed. The concentration and size distribution of the particulate matter formed under UV irradiation were studied using the diffusion spectrometer of aerosol (DSA) designed and built at the Institute of Chemical Kinetics and Combustion, Novosibirsk.

Special attention was paid to the part played by water vapour, ozone and nitrogen oxides as the participants of the general gas-to-particle conversion process. The initial stages of cluster formation preceding nucleation were modelled using the previously developed approach (Dultseva *et al.*, 2008) based on semiempirical estimations. It was demonstrated that the presence of additional functional groups, for example OH (in salicylic aldehyde) creates additional possibilities for clustering and thus routes the process to quite different products. Benzaldehyde and salicylic aldehyde exhibited quite opposite dependences of photolysis and photonucleation kinetics on water vapour concentration Figure 1 shows the dependences of photolysis constants for both aldehydes on water vapour concentration.

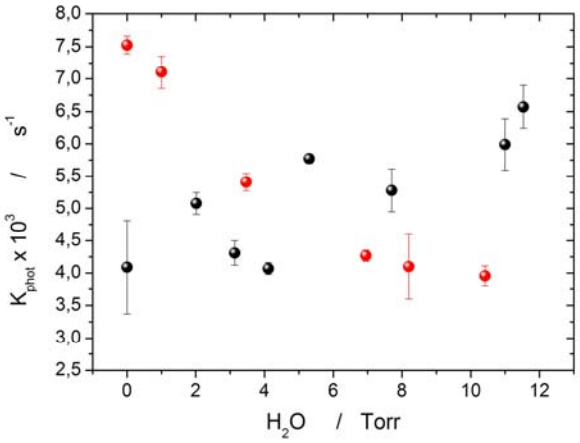

Fig. 1. Dependence of photolysis rate on water vapour concentration: black dots – benzaldehyde, red dots – salicylic aldehyde.

Investigation of the participation of short-lived free radicals was carried out using the spin trapping procedure and showed that no free radicals appear during the photolysis of salicylic aldehyde, though benzaldehyde under photolysis gives rise to phenyl radicals that take part in further transformations. Complexes of aldehydes with metals under photolysis did not give rise to the formation of spin adducts, so it may be supposed that no free radicals are formed in this case and intramolecular processes are prevailing.

The yields of particulate matter measured under laboratory conditions allow us to suppose that gas-to-particle conversion may be an efficient process forming a link in the biogeochemical cycles of heavy metals by bringing them from soil into plants and then into the atmosphere, where photonucleation turns these compounds into solid particles. The results obtained in the investigation prove the significance of plant-mediated flux of elements into the atmosphere.

This work was supported by the Russian Foundation for Basic Research under Project No 08-05-00727-a.

Dultseva, G.G., Dubtsov, S.N. and Dultsev, F.N. (2008). *J. Phys. Chem. A*, **112**, No. 23, 5264–5268

Ankilov, A. N. et al. (2002). *Atmospheric Research* **62**, 177–207.

Evaluation of the atmospheric aerosol-forming potential of aliphatic and aromatic aldehydes in the presence of nitrogen oxides and/or ozone: modelling and experiment

T.A. Maksimova[1], S.N. Dubtsov[1], G.G. Dultseva[1,2],
[1]Institute of Chemical Kinetics and Combustion, SB RAS, Novosibirsk, 630090, Russia
[2]Department of Natural Sciences, Novosibirsk State University, Novosibirsk, 630090, Russia
Keywords: photochemical processes, particle formation, organics
Email: dubtsov@kinetics.nsc.ru

Aldehydes are important minor components of urban air that possess the aerosol-forming potential. The mechanisms of gas-to-particle conversion in the atmosphere include a large number of elementary stages starting from the photochemical decomposition under the action of sunlight and finishing with the formation of nanometer-sized particles. We studied the processes of this kind in detail under laboratory conditions, with noble gases or air as carrier gases, and discovered that even the simplest aliphatic aldehydes (formaldehyde, acetaldehyde) are able to form particulate matter under UV irradiation (Dultseva et al., 2001). Results obtained under laboratory conditions suggested that the presence of oxygen has a crucial effect on the process mechanism. So does the presence of some other minor atmospheric gases such as nitrogen oxides and ozone. In the present work we studied the kinetics and mechanisms of photonucleation of aldehyde vapour in the presence of nitrogen oxide, nitrogen dioxide, and ozone.

Among the important products of aldehyde photolysis in the presence of nitrogen oxides, peroxyacylnitrates are of special ecological significance. We studied the mechanisms of gas-to-particle conversion in the system {aldehyde + nitrogen oxides} both experimentally in the photochemical reactor and theoretically by means of kinetic modelling at the level of elementary stages. The effect of ozone was also evaluated. Analysis of the intermediate and final products, both gaseous and particulate ones, was performed using HPLC, NMR, GC-MS, short-lived free radicals were identified by means of EPR spectroscopy using the spin trapping procedure. The concentrations and size distribution of the particulate matter formed in the process were determined with the help of the diffusion spectrometer of aerosol (DSA) designed and built at the Institute of Chemical Kinetics and Combustion, Novosibirsk.

The role of ozone was evaluated with special focus on its gas-phase reactions with organic species participating in the process. Ozone is known to be formed in polluted air through the addition process $O_2 + O \rightarrow O_3$; where O is generated by the photolysis of NO_2 under sunlight. Atmospheric organic compounds play an essential part in $NO \rightarrow NO_2$ conversion ($RH + OH + O_2 \rightarrow RO_2$; then $RO_2 + NO \rightarrow RO + NO_2$) thus making their contribution into the formation of NO_2 and therefore ozone in polluted atmosphere. Thus formed ozone interacting with organic species gives rise to peroxy radicals, peracids, hydroperacids, organic peroxides and many other oxygenated species that are able to undergo gas-to-particle conversion. Moreover, ozone itself can be consumed in the reactions taking place at the active surface of freshly formed particles. This very complicated mechanism can hardly be understood in detail without the kinetic simulation. Simulation results were tested with kinetic measurements. An example is shown in Fig. 1.

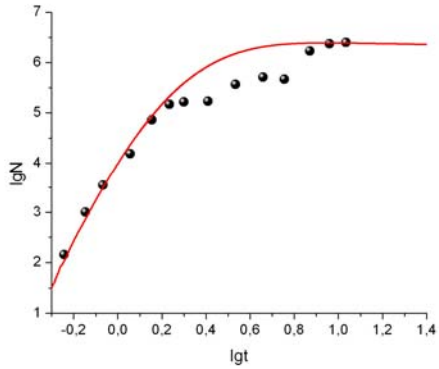

Fig. 1. Time dependence of particle concentration formed in benzaldehyde photolysis. Points – experiment, line – simulation.

It was demonstrated that the concentration of peroxybenzoyl nitrate can reach 10^9-10^{11} cm^{-3}, which generally agrees with the values obtained by measurements in urban atmosphere. Simulation suggests and experiment proves that among the aldehydes present in urban atmosphere (formaldehyde, acetaldehyde, acrolein, benzaldehyde etc.) the major contribution into the formation of organic particulate matter is made by acetaldehyde and benzaldehyde (Dubtsov et al., 2006). So, the aerosol-forming potential of organic compounds, even so reactive ones as aliphatic and aromatic aldehydes, in the presence of oxygenated species can be evaluated by means of experimental measurements and kinetic simulations of the process mechanism at the level of elementary stages with permanent intercomparison of theoretical results with the experimental ones.

This work was supported by the Russian Foundation for Basic Research under Project No 08-05-00727-a.

Dultseva, G.G., Dubtsov, S.N., Skubnevskaya, G.I..(2001). Aldehydes as initiators of photonucleation. Chemical composition of aldehyde photolysis products. *J.Aerosol Sci.*, 32, 645.

Dubtsov, S.N., Dultseva, G.I., Dultsev, E.N., and Skubnevskaya, G.I. (2006) Investigation of aerosol formation during benzaldehyde photolysis *Phys. Chem. B*, 110, 645-649.

Observation of decreased final product volatility in the gas ozonolysis of unsaturated carboxylic acids in the absence of oxygen

C. Keunecke, T. Zeuch

Institut für Physikalische Chemie, Georg-August-Universität, Göttingen, 37077, Germany
Keywords: SOA, Ozone, Carbon oxidation, Organic acids.
Presenting author email: ckeunec@gwdg.de

In the past decades large efforts have been made in laboratory studies to elucidate the secondary organic aerosol (SOA) formation mechanism. Critical issues have been studied such as reaction product formation and the influence of relative humidity, temperature, presence of additional organic matter and seed aerosol. However, the mechanism of organic nucleation is still controversial. Consequently significant uncertainty remains in closing the gap between laboratory experiments, theoretical predictions and nucleation rates observed in field studies. In a recent study we could show that (besides volatility considerations of detected reaction products) SOA formation during alkene ozonolysis experiments depends also on kinetic parameters and is linked to intermediate species like peroxy radicals (Wolf *et al*., 2009, 2011).

To obtain an acceptable compromise between controlled reaction chamber filling and minimized aerosol wall losses during laboratory SOA experiments (e.g. a large reaction volume to surface ratio), we constructed a 64 L stationary reaction cell with ozone / alkene premixing chambers, FTIR spectroscopy for gas phase species analysis and a SMPS system for measuring particle size distributions in the submicron size range. With the new reactor we achieve a well controlled mixing within a few seconds allowing a controlled variation of process parameters including reaction pressure (Wolf et al. 2011).

Due to atmospheric relevance we use unsaturated acids, as possible oxidation products of biogenic emitted terpenes, as well as unsaturated alcohols, which are released by plants after leaf damage (Kesselmeier *et al*., 1999) as reactants.

With our comparative studies we can show the influence of reaction parameters, such as reaction pressure and presence or absence of O_2, on the ability to produce low-volatile oxidation products or condensation nuclei during the ozonolysis of different functionalized respectively oxidized alkenes.

As Fig. 1 shows, the presence of various amounts of oxygen in the reactive mixture influences the observed aerosol yield of organic acids.

Our approach is to illuminate the dependency of aerosol formation, both on oxidation state of the alkene and on the relative distance between the double bond and the oxygenated carbon atom in the backbone. The influence of arborisation can be of interest as well, due to different (kinetic) behaviour of substances with otherwise identical atomic composition.

Whereas the aerosol yields during the ozonolysis of unsaturated acids are considerably reduced in the presence of oxygen, they are enhanced in case of alcohols (not shown).

The influence of molecular oxygen can be interpreted as follows:

During the ozonolysis alkyl radicals are formed either by external H atom abstraction by OH radicals or by internal H atom abstraction in the hydroperoxid channel of Criegee intermediates. In synthetic air O_2 is added immediately to the radicals forming peroxy radicals. Our results suggest that in case of the acids the fate of the peroxy radicals is to a significant degree C-C bond fission increasing the volatility of products and reducing the observed aerosol yields.

The same reaction regarding unsaturated hydrocarbons and alcohols leads to a reduction of volatility and a noticeably growing aerosol yield with the amount of oxygen enclosed in the reactive mixture.

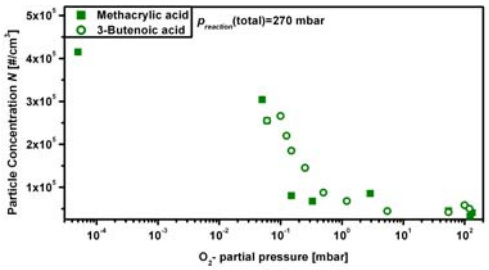

Figure 1. This figure illustrates the dependence of the total particle concentration on the amount of oxygen in the reactive mixture. Constant quantities of reactants were converted: $p_{0,\,acid}$=5 Pa, $p_{0,\,ozone}$=0.1 Pa for 3-Butenoic acid, $p_{0,\,ozone}$=0.2 Pa for Methacrylic acid.

J. L. Wolf, M. A. Suhm, and T. Zeuch, *Ang. Chem. Int. Ed.*, **48** (2009), 2231.

J. L. Wolf, S. Richters, J. Pecher, and T. Zeuch, *Phys. Chem. Chem. Phys.*, DOI:10.1039/C0CP02499F.

J. Kesselmeier, M. Staudt, *J. Atmos. Chem.*, **33** (1999), 23.

Field measurement of secondary organic aerosol in a boreal forest site in southern Finland using on-line soft ionization ion trap mass spectrometry

A. L. Vogel[1], A. Bayerle[1], M. Beck[1], M. Äijälä[2], M. Ehn[2], H. Junninen[2], T. Petäjä[2], D. R. Worsnop[2], M. Kulmala[2], J. Williams[3], T. Hoffmann[1]

[1]Institute for Inorganic and Analytical Chemistry, Johannes Gutenberg-University of Mainz, 55128 Mainz, Germany
[2]Department of Physical Sciences, University of Helsinki, 00014 Helsinki, Finland
[3]Max Planck Institute for Chemistry, Department of Atmospheric Chemistry, 55128 Mainz, Germany
Keywords: field measurement, instrumentation/chemical characterization, SOA, gas-particle distribution
Presenting author email: vogelal@uni-mainz.de

Emission of biogenic volatile organic compounds (BVOCs) by vegetation in the boreal forest and subsequently atmospheric oxidation leads to the formation of secondary organic aerosol (SOA). Oxidation of the BVOCs produces a variety of mostly unidentified organic species. Dependent on the volatility of the products, they partition between gas and particle phase. Seen from this perspective, organic acids are of particular importance for the particle phase, since the higher oxidation state and molecular mass, compared to the corresponding terpenes or aldehydes, is accompanied by a much lower volatility. However, very little is known about intermediate volatility organic compounds (IVOCs) which are residing almost entirely in the gas phase and generate efficiently lower volatility products by further reaction with atmospheric oxidants or by oligomerization (Donahue et al., 2006).

Here we show the high potential for gaining new insights into gas-to-particle-partitioning of individual organic acids by measuring them in both phases with the same instrument. This was achieved by coupling a miniature Versatile Aerosol Concentration Enrichment System (mVACES) as described by Geller et al. (2005) with an Atmospheric Pressure Chemical Ionization Ion Trap Mass Spectrometer (APCI-IT-MS; Hoffmann et al., 2002). The benefits of the on-line APCI-IT-MS are soft ionization with nearly no fragmentation, high time resolution and less sampling artifacts than in the common procedure of taking filter samples, extraction and detection with LC-MS. Furthermore the ion trap allows to perform MS/MS-experiments by isolation of single m/z ratios of particular ions. By subsequent addition of energy, the trapped ions form characteristic fragments which enable structural insight on the molecular level.

The sophisticated aerosol concentrator mVACES is a necessary unit for operation of the APCI-IT-MS in the field. It improves the limit of detection by concentrating particles without lowering the time resolution. Physical and chemical alteration of the particles, especially the change of gas-particle partitioning, was evaluated.

Field measurement during HUMPPA-COPEC10 campaign

The setup mVACES coupled to APCI-IT-MS was tested successfully in the laboratory and afterwards used during the large HUMPPA-COPEC field campaign at the SMEAR station in Hyytiälä, Finland in summer 2010. The comprehensive instrumental equipment of gas and particle phase measuring instruments during the campaign made it possible to compare the APCI-MS-data with a variety of different techniques. Especially the comparison between APCI-MS and the c-ToF-AMS (compact Time of Flight Aerosol Mass Spectrometer) of the University of Helsinki is predestinated, since these two instruments were connected to the same aerosol inlet line. Very good correlation coefficients between APCI-MS and AMS for sulfate (R^2=0.93) and for total organics (R^2=0.94) in particle phase have been determined. Furthermore organic acids were measured by filter sampling and subsequent analysis with LC-MS in order to resolve possible isobaric interference of the APCI-MS technique. For the first time in a field measurement in situ MS/MS-experiments for chemical characterization of the major abundant organic acids have been carried out. Results show similar pattern to those MS/MS-experiments in laboratory generated secondary organic aerosol.

However, not only comparison to different instruments and techniques revealed interesting results, but also the temporal behavior of specific compounds allows interpretation possibilities. For example fast mixing processes in the atmosphere (e.g. boundary layer processes) show a strong influence on the concentration levels of IVOCs. These short-term processes can only be monitored by an on-line technique. In addition we could show that gas-particle-partitioning of single organic compounds is not only driven by the molecular mass but most notably by the oxidation state of the regarded species. This means there exist highly oxidized organic acids with a relative small molecular mass which contribute more to particle mass than other organic acids with higher molecular masses.

Donahue, N. M., Robinson, A. L., Stanier, C. O., Pandis, S. N. (2006) *Environ. Sci. Technol.* **40**, 2635-2643.

Geller, M. D., Biswas, S., Fine, P. M., Sioutas, C. (2005) *J. Aerosol Sci.* **36**, 1006-1022.

Hoffmann, T., Bandur, R., Hoffmann, S., Warscheid B. (2002) *Spectrochimica Acta B* **57**, 1635-1647.

New particle formation by tobacco plants stressed by ozone: The potential role of mono- and sesquiterpenes

S. Bourtsoukidis[1], B. Bonn[1], W. Haunold[1], E. Palmer-Young[2] and J. Gershenzon[2]

[1]Institute for Atmospheric and Environmental Sciences, J.W. Goethe University, D-60438 Frankfurt/Main, Germany
[2]Max-Planck-Institute for Chemical Ecology, Beutenberg Campus, D-07745 Jena, Germany
Keywords: nucleation, ultrafine aerosols, VOC(s), activation.
Presenting author email: bonn@iau.uni-frankfurt.de

Abstract

Based on the studies of Haagen-Smit and Went, new aerosol particle formation by biogenic terpene oxidation products has been proposed. This certainly has remarkable atmospheric effects, since vegetated areas are extensive in space but diverse in composition and emission of reactive volatile organic compounds (VOCs). So far independent pathways from sulphuric acid derived nucleation have not been formulated and accepted. Here we aim to explain the observed nucleation process by a purely organic algorithm obtained from laboratory investigations, which we could perform successfully. The important role of organic radical (RO_2) formation by monoterpenes was elucidated, which activated the sesquiterpene derived nucleation core. Therefore both terpene groups and their reactivity with respect to ozone and OH are important for new aerosol particle formation in a non-linear system.

Methods

We focus on two controlled greenhouse experiments a) at Frankfurt University in June 2010 and b) at Max-Planck Institute for Chemical Ecology in Jena, in December 2010. While the first measurements were done in a greenhouse with changing light and temperature conditions, the second set of measurements were run at a constant temperature T of 24°C and constant illumination. The used three different tobacco plant types provided three different emission patterns with respect to sesquiterpenes, i.e. (i) one wild type and two genetically modified ones emitting (ii) a mixture of two sesquiterpenes (α-farnesene and α-bergamotene) or (iii) α-farnesene only.

In Frankfurt plant incubation was done using a Teflon bag while in Jena each plant was incubated in a single plant cuvette and was treated with different ozone stress intensities between 400 and 833 ppb_v.

Total particle concentration was measured by a condensation particle counter (UCPC 3776, TSI) with a lower cut-off size of 2.7 nm. All measurements have been conducted on the 13th-18th of December 2010 at the Max-Planck Institute in Jena.

Nucleation mechanism assumed

Based on the laboratory investigation on new particle formation by alkenes and ozone (see other presentation), the following mechanism was assumed:

1. Formation of stabilised Criegee intermediates (sCI) by sesquiterpenes and ozone
2. Formation of reactive secondary ozonides (SOZ) from sCI and available carbonyl compounds.
3. Activation (reaction) by monoterpene and OH derived large organic peroxy radicals (RO_2).

Taking into account the inhomogeneity of the cuvettes and the uncertainty of the radicals, a reasonable match between observation and calculation was obtained. As a conclusion it can be stated: The reaction rate constants of sesquiterpenes and of monoterpenes with O_3 and OH affect the entire nucleation process and the system is non-linear.

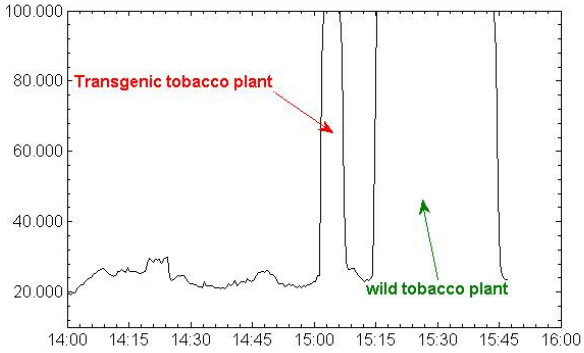

Figure 1. Effect of sudden rise in provided ozone. Particle number and sesquiterpenes concentrations rapidly increased in Frankfurt.

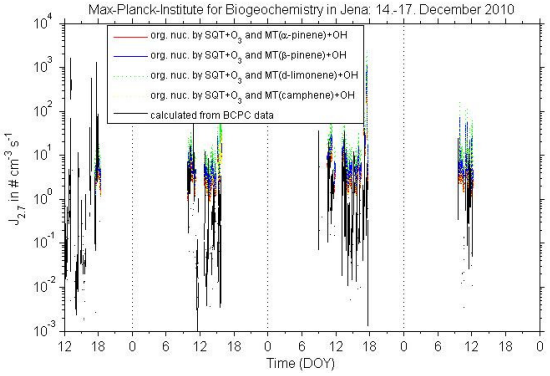

Figure 2. Simulated and measured nucleation rates for experiments performed at Jena.

This work was supported by Max-Planck and the biochemistry department of Goethe University Frankfurt.

Oxidation of nopinone - Influence of relative humidity and particle acidity on particulate products

A.Mutzel, Y. Iinuma, O. Böge, A. Kahnt and H. Herrmann

Leibniz-Institut für Troposphärenforschung, Permoserstr. 15, Leipzig D-04318, Germany
Keywords: VOCs, SOA, Aerosol characterization
heinolda@tropos.de

The oxidation of biogenic volatile organic compounds (BVOCs) leads to the formation of low volatile compounds. Especially, the formation of secondary organic aerosol (SOA) from the oxidation of monoterpenes has been investigated extensively in the past years (see a review paper by Hallquist *et al*., 2009). The first generation oxidation products of monoterpenes are still volatile and are further oxidized in the gas phase to form a wide range of products that contribute to SOA formation. Although, a spate of studies report SOA products from monoterpene oxidation, little is known about the influence of relative humidity and seed particle acidity on the formation of monomeric and oligomeric compounds from the first generation oxidation products.

In the present study, we conducted a series of chamber experiments to study the influence of the reaction conditions on the formation and composition of SOA in the OH radical reaction of nopinone (Table 1). Nopinone is one of the first generation products that orginates from β-pinene oxidation. Three different reaction parameters were examined: seed particle acidity, relative humidity and NO_x mixing ratio. Each set of experiment was performed using two different OH sources: the ozonolysis of tetramethylethylene and the photolysis of methylnitrite in the presence of nitrogen oxide.

Table 1. Conditions for the oxidation of nopinone. (Initial mixing ratio 50 ppb, temperature 20±1°C)

Relative humidity [%]	Set 1 (0.07M)	Set 2 (0.076M/0.003M)	Set 3 (0.04M)
0	Na_2SO_4	$(NH_4)_2SO_4/H_2SO_4$	NH_4HSO_4
50	Na_2SO_4	$(NH_4)_2SO_4/H_2SO_4$	NH_4HSO_4
75	Na_2SO_4	$(NH_4)_2SO_4/H_2SO_4$	NH_4HSO_4

The formed particulate products were collected using a denuder/PTFE filter sampling device. The filter were extracted and analyzed using HPLC/(-)ESI-TOFMS. The analysis of the particle-phase revealed a number of monomeric and oligomeric compounds.

The major monomeric products were detected at the mass to charge ratios (*m*/*z*) 157, 171, 185, 203 and 231 corresponding to terebic acid, terpenylic acid (Claeys *et al*., 2009), pinic acid, 3-methyl-1,2,3-butanetricarboxylic acid (Szmigielski *et al*., 2007) and diaterpenylic acid acetate (Iinuma *et al*., 2009). These compounds are not influenced by relative humidity or particle acidity but their yields decreased in the presence of NO_x.

A decrease in the yield of monomeric compounds and the associated decrease in SOA mass in the presence of NO_x can be explained by the favoured production of more volatile compounds such as aldehyds over low volatile acidic compounds due to the reaction of the alkylperoxyradical (RO_2) with NO (Kroll and Seinfeld, 2008).

The analysis of the higher molecular weight compounds indicates two major oligomeric products with *m*/*z* 357 and 371, corresponding to $C_{17}H_{25}O_8$ and $C_{18}H_{27}O_8$, respectively. Both compounds showed an influence of NO_x levels and particle phase acidity though only *m*/*z* 371 compound was influenced by relative humidity. In the presence of NO_x the formation of both compounds was reduced. The highest amount of the *m*/*z* 371 compound was observed under higher relative humidity and in the presence of strongly acidic particles, indicating that this compound is likely formed through acid catalysed accretion reaction. Surprisingly, an opposite behaviour was observed for the *m/z* 357 compound, which decreased in the presence of acidic particles. This observation gives a hint that the formation of this compound is either not related to acid catalysed accretion reaction or decomposed in the presence of strong acidity.

This work was supported by the Deutsche Forschungsgemeinschaft DFG under grant HE-3086/14-1 and code name FuProTer.

Claeys, M. *et al*., (2009), *Environ. Sci. Technol*. **53**, 6976-6982

Hallquist, M. *et al*., (2009) Atmos. Chem. Phys. 9, 5155-5236

Iinuma, Y. *et al*., (2009), *Environ. Sci. Technol* **43**, 280-285

Kroll, J.H. and Seinfeld, J.H. (2008) *Atmos. Environ*. **42**, 3593-3624

Szmigielski *et al.,* (2007) *Geophys. Res. Lett.* **34**, L24811, DOI: 10.1029./2007GL031338

NMR spectroscopic characterization and factor analysis of the oxidized organic aerosol components in Cabauw, Netherlands, during the May 2008 EUCAARI IOP

M. Paglione[1], E. Finessi[1], S. Decesari[1], A. Kiendler-scharr[2], A. Mensah[2], M. Stocchero [3], and M.C. Facchini[1]

[1]Institute of Atmospheric Sciences and Climate, National Research Council, Bologna, I-40129, Italy.
[2] Forschungszentrum Juelich, Germany.
[3] S-IN Soluzioni Informatiche, Vicenza, Italy.

Keywords: HNMR spectroscopy, Source apportionment, Statistical analysis, PMF, AMS.
Presenting author email: m.paglione@isac.cnr.it

Outside urban areas, oxidized organic aerosols (OOA) dominate the composition of the organic atmospheric particulate matter. In the frame of the EUCAARI (European integrated project on Aerosol Cloud Climate Air Quality Interactions) project, the submicron aerosol chemical composition in Cabauw, Netherlands, was characterized by means of proton-Nuclear Magnetic Resonance (^{1}H-NMR) spectroscopy with aim of organic aerosol characterization and source apportionment. The analysis was applied to water-soluble organic aerosols (WSOA),which is a proxy for OOA.

The experiment was conducted throughout May 2008 during a period of prolonged stable anticyclonic conditions, which favoured the accumulation of pollutants over western/central Europe, interrupted by an outbreak of Atlantic air masses between 17th and 20th May. A set of 25 PM1 filter samples were analysed by ^{1}H-NMR spectroscopy and the resulting collection of spectra was processed using a suite of chemometric techniques, including PCA, cluster analysis and factor analysis (Positive Matrix Factorization or PMF, Non-negative Matrix Factorization or NMF, Multivariate Curve Resolution-Alternating Least Squares or MCR-ALS) aiming to identify recurrent spectral profiles. The contributions of the identified factors to total NMR-detected organics were used to trace the temporal variations of the various organic aerosol types at the sampling location and to identify different prevalent sources.

Factor analysis identified three factors with characteristic spectral profile: (a) OOA associated to metanesulphonic acid (MSA), (b) humic-like substances (HULIS) and (c) other complex OOA enriched in aliphatic acids. The analysis of metadata (meteorological variables, concentrations of nitrate, sulfate, ammonium, potassium, black carbon, and air masses origin), shows that the MSA-containing OOA factor is associated to northerly marine air masses, the HULIS are carried by polluted continental air masses, whereas the aliphatic-rich OOA have no clear dependence on wind direction.

The comparison of these results with those of Positive Matrix Factorization (PMF) applied to a parallel AMS dataset showed a good agreement between NMR "HULIS"-factor and one type of AMS "LV-OOA" (a-type).

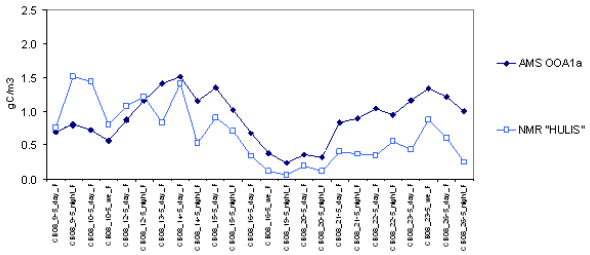

Fig. 1: Comparison between contributions (μgC/m^3) of NMR "HULIS"-Factor and AMS "LV-OOA" a-type at Cabauw during May 2008 EUCAARI IOP

Additional measurements performed at other European EUCAARI stations during May 2008 shows that the HULIS factor characterized the OOA composition in the polluted boundary layer air at the regional scale. Nevertheless, the aliphatic-rich OOA of Cabauw were not found in the central European stations and it can be related to different sources of oxidized organic aerosols active at that time in the North Sea area with respect to continental Europe.

This work has been supported by European Commission 6th Framework program project EUCAARI, contract no 036833-2 (EUCAARI).

Determination of organic compounds in ultrafine particles

S. De Pieri[1], J. Coppola[2], E. Morabito[1], C. Barbante[1,2] and A. Gambaro[1,2]

[1] Department of Environmental Sciences, Informatics, and Statistics, University Ca' Foscari, 30123 Venice, Italy
[2] Institute for the Dynamics of Environmental Processes, National Research Council (IDPA-CNR), 30123 Venice, Italy

Keywords: nanoparticles, PAH, organic compounds, pollution.
Presenting author email: depierisilvia@unive.it

Nanoparticle emissions are associated with cardiopulmonary health impacts and increased mortality. The emission and, evolution, and exposure-uptake of particles with diameters equal to or less than of these particles, 100 nanometers and smaller in diameter, are fundamentally quantified by their by the number concentration as a function of particle size. Nanoparticle number distributions are widely variable and rapidly change fast changing as their concentrations are strongly influenced by local environmental conditions .

In this work four sampling campaigns were conducted under differing meteorological conditions. We collected ultrafine particles on the roof of the university in Venice using a low-pressure impactor (DLPI DEKATI). The impactor classifies 13 size fractions from 0.03 to 10 μm.

The literature, many authors (Di Filippo et al., 2009) suggests that the fraction of particles collected on impactor-stages 1–3 (Dp < 0.1 μm) is defined referred to as the ultrafine fraction, while the portions on impactor-stages 4–8 (0.17 μm < Dp < 1.0 μm) and on impactor-stages 9–13 (Dp > 1.0 μm) are respectively referred to as the fine and the coarse fractions.

The samples were analyzed for PAHs, PBDEs, PCNs and PCBs. Ultrafine particles were recovered from aluminum filters. The filter were extracted by ultrasonic bath in a mix Dichloromethane:Hexane 1:1 (v:v) for ten minutes, and their volumes were reduced to 500 μL under a gentle nitrogen flow.

The concentrations of organics compounds were determined by high-resolution GC-High Resolutions MS. PAH identification were as performed by comparison of the sample chromatograms with PAH certified mixtures. Before the extraction the samples were spiked with 13C-labeled standard.

Quality control of the analytical procedure was conducted carried out by controlling blanks control, and by evaluating detection limits, recoveries, accuracy. The LOD was quantified as the mean concentration in the blank plus three times the standards deviation (IUPAC, 1978). The LOD for PAHs ranged from 1.17ng for Naphtalene to 0.02ng for Acenaphtalene. The recovery of nanoparticles-PAH determination was tested by spiking the filters with known amounts of PAH and subsequent extraction and analysis using the procedures reported above. The accuracy of "nanoparticles-PAH" determinations were estimated by analyzing five different filters. The means of accuracy are approximately estimated around to 90% for Naphtalene and Acenaphtalene. The accuracy ranges between to 2% for Phenantrene, to 20% for Benzo(a)Antracene.

The preliminary results demonstrated that the main contributors to the total concentration in the ultrafine fractions are Pyrene and Anhthracene. In the fine fraction the main contributor are represented Anthracene and Fluorene while in the coarse fraction is dominated by congeners with m/z 178.1. These preliminary results represent the first effort to estimation of the concentrations of organic contaminants in the Venice lagoon nanoparticles; and will be compared with the measurements which are still in progress.

Di Filippo, P., Riccardi, C., Pomata, D., Buiarelli, F. (2009) *Atmospheric Environment, in press*.

IUPAC. Nomenclature, symbols, units and their usage in spectrochemical analysis II. (1978) *Spectrochim Acta*, **33B**:242

Wintertime and summertime source apportionment of PM2.5, using organic compounds as tracers, in a European megacity : Paris

E. Abidi[1], N. Marchand[1], A. Monod[1], J. Cozic[2] and J.-L. Jaffrezo[2]

[1]Laboratoire de Chimie Provence, Universités d'Aix-Marseille I, II et III-CNRS, 3 place Victor Hugo, 13331 Marseille Cedex 3, France.
[2]Laboratoire de Glaciologie et Géophysique de l'Environnement, CNRS-UJF, 38400 Saint Martin d'Hères cedex, France
Keywords: Megacity, organic tracer, PM and source apportionment.
Email : ehgere.abidi@etu.univ-provence.fr

The project MEGAPOLI-PARIS, elaborated in a European regulation context, aims at gaining an increasing comprehension of major processes affecting the abundance of particulate matter in a polluted atmosphere so as to better assess primary sources of carbonaceous aerosols, secondary sources of organic aerosols through gas-to-particle conversion and to evaluate and improve process and air quality models. To reach these objectives, an experimental campaign in the Paris agglomeration, a major anthropogenic emission source surrounded by rural areas, has been conducted during summer (from 01 to 31 July 2009) and winter (from 15 January to 15 February 2010).

The project MEGAPOLI-PARIS, elaborated in a European regulation context, aims at gaining an increasing comprehension of major processes affecting the abundance of particulate matter in a polluted atmosphere so as to better assess primary sources of carbonaceous aerosols, secondary sources of organic aerosols through gas-to-particle conversion and to evaluate and improve process and air quality models. To reach these objectives, an experimental campaign in the Paris agglomeration, a major anthropogenic emission source surrounded by rural areas, has been conducted during summer (from 01 to 31 July 2009) and winter (from 15 January to 15 February 2010).

In order to develop effective control strategies for fine particulate air pollution abatement, knowledge of the relative importance of the various sources that contribute to the particulate matter concentrations at the ambient air monitoring sites is required.

Chemical analyses have been carried out for major anions, trace metals, OC/EC, and for individual organic marker species including n-alkanes, hopanes, PAHs, levoglucosan, organic acids, sterols, phtalates, tetrols and other secondary organic markers. Source apportionment has been performed using the US EPA chemical mass balance (CMB) model.

This study was conduced in two sampling sites in Paris : one urban supersite (LHVP) and one suburban supersite (SIRTA). The contributions of up to 5 primary fine particles source types can be separately identified in ambient samples based on this method. In summer, the organic aerosol is mainly from secondary origin and the largest primary source contributors to fine particle mass concentrations in Paris are found to include mainly diesel engine exhaust, with smaller contribution from vegetative detritus as combustion aerosol. In winter, the main primary source emission is wood combustion.

Acknowledgement

The research leading to these results has received funding from the European Union's Seventh Framework Programme FP/2007-2011 within the project MEGAPOLI, grant agreement n°212520.

Microcystins and Bisphenol A in the urban aerosol of the Venice Lagoon

R. Zangrando[1], E. Barbaro[2], E. Scalabrin[2], V. Fellin[2], C. Barbante[1,2] and A. Gambaro[1,2].

[1]Institute for the Dynamics of Environmental Processes CNR, Dorsoduro 2137, 30123, Venice, Italy.
[2] Department of Environmental Sciences, University of Venice, Ca' Foscari, Calle Larga Santa Marta 2137, 30123, Venice, Italy
Keywords: microcystins, bisphenol A, LC/MS, urban aerosol.
Presenting author email: roberta.zangrando@idpa.cnr.it

Cyanobacteria are a small group of photosynthetic-planktonic bacteria, which produce a large group of potent hepatotoxin, microcystins.
Past research was conducted to determine the microcystins' concentration in drinking waters, marine waters and foods but few studies were focus on identification and quantification of microcystins in marine and urban aerosol.

Algae cells, bacteria, and waterborne toxins can be aerosolized by a bubble-bursting process. It is demonstrated that respiratory symptoms are associated with exposure to higher levels of cyanobacteria during recreational activities (Paddle, 2003). Aerosolized toxins may be absorbed through the skin, inhaled into the lungs or enter the gastrointestinal system after being deposited in the major airways or following ingestion of food and water.

Bisphenol A is an industrial chemical used as an intermediate compound in the production of epoxy resins and carbonate plastics. Many studies have demonstrated that bisphenol A is an ubiquitous pollutant (Staples et al. , 1998; Fromme et al., 2002; Wilson et al., 2001; Matsumoto et al., 2005) and has toxic proprieties, including estrogenic endocrine disruption and promotion of tumorigenic progression (Keri et al., 2007).

The aim of this work is the development of a comprehensive analitical procedure for the determination of six microcystins (LA, LR, LW, LF, LY, YR), the toxin nodularin and bisphenol A in the aerosol of the Venice Lagoon. Instrumental analysis employed an Agilent 1100 series HPLC system (Agilent, Waldbronn, Germany) coupled to an API 4000 triple quadrupole mass spectrometer (Applied Biosystems/MDS SCIEX, Toronto, Ontario, Canada). In this work leucine enkephalin acetate and bisphenol A $^{13}C_{12}$ are used as internal standard for the quantification of toxins and bisphenol A, respectively. The analytical procedure was validated: the accuracy, precision and recovery have been evaluated.

In order to apply this method, 8 samples collected in Venice on the Sacca San Biagio Island near Venice harbor from June to July 2007, were analysed. Three toxins (LA, LW and LF) were observed; LA: average concentration 275 fg/m^3 (with a range between 90 and 706 fg/m^3), LW average concentration 230 fg/m^3 (177 - 250 fg/m^3) and LF average concentration 221 fg/m^3 (130 - 369 fg/m^3)
To our knowledge this is the first time the presence of microcystins is observed in the Venice Lagoon.

Research demonstrates the presence of bisphenol A in Venice Lagoon waters (Pojana et al., 2004) but this is the first research to investigate the presence of bisphenol A in the urban aerosol of Venice Lagoon. We demonstrate that bisphenol A was present in the urban aerosol of Venice Lagoon with an average concentration 0.65 pg/m^3 (with a range between 0.16 and 1.92 pg/m^3).
The preliminary results of our study suggest that further research should be conducted to better define the temporal trend of microcystins and bisphenol A , in the aerosol of the Venice Lagoon.

Paddle, B. M. (2003) *Journal of Applied Toxicology* **23**, 139–170.

Staples, C.A., Dorn, P.B., Klecka, G.M., O'Block, S.T., Harris, L.R. (1998) *Chemosphere* **36**, 2149-2173.

Fromme, H., Küchler, T., Otto, T., Pilz, K.J.M., Wenzel, A. (2002) *Water Res*. **36**, 1429-1438.

Wilson, N.K., Chuang, J.C., Lyu, C. (2001) *J. Exposure Anal. Environ. Epidemiol.* **11**, 449-458.

Matsumoto, H., Adachi, S., Suzuki, Y. (2005) *Arch. Environ. Contam. Toxicol.* **48**, 459-466

Keri, R.A., Ho, S.M., Hunt, P.A., Knudsen, K.E., Soto, A.M., Prins, G.S., (2007) *Reprod. Toxicol.* **24**, 240–252.

Poiana, G., Bonfà, A., Busetti, F., Collarin, A., Marcomini, A., (2004) *Environmental Toxicology and Chemistry*, **23**, 1874–1880.

$PM_{2.5}$ emissions from wood combustion in a fireplace and a woodstove: carbon content and inorganic speciation

Célia Alves, Cátia Gonçalves, Ana Patrícia Fernandes, Luís Tarelho, Casimiro Pio
Centre for Environmental and Marine Studies (CESAM), Department of Environment, University of Aveiro, 3810-193 Aveiro, Portugal
Keywords: woodstove, fireplace, $PM_{2.5}$, biomass burning, water-soluble ions, metals
Presenting author e-mail: celia.alves@ua.pt

Residential wood burning is known to be a significant source of particulate matter in many regions worldwide. Several studies have been carried out to characterise the organic composition of wood smoke particles (e.g. Fine *et al*., 2004; Schmidl *et al*., 2008). However, only limited information exists on the combustion-related trace elements and water-soluble ions, which are biogeochemically active species and may represent a substantial portion of the toxicity of particles.

Wood from seven species of trees grown in the Portuguese forest and briquettes produced from forest biomass waste were burned in a fireplace and in a woodstove to determine the chemical composition of fine particle ($PM_{2.5}$) emissions. Samples were analysed for organic and elemental carbon (OC/EC), water soluble ions (Na^+, NH_4^+, K^+, Mg^{2+}, Ca^{2+}, Cl^-, NO_3^- and SO_4^{2-}) and 67 elements, using a thermo-optical transmission technique, ion chromatography and ICP-MS, respectively.

The fireplace was the combustion appliance with the highest $PM_{2.5}$ emissions. Organic carbon contributed to about 50% of the fine particle mass in the emissions from every wood species studied (Table 1). The water-soluble ions accounted for about 1 to 14% of the $PM_{2.5}$ mass. The Golden wattle wood smoke showed a much higher ionic content than the emissions from the other wood types. Trace elements represented 0.4 to 2.5% of the $PM_{2.5}$ mass with an average total emission of 110±64 mg kg^{-1} wood burned. Among these, K, Pb, Al, Mn and Sr were present in all samples.

The water soluble potassium (K^+) comprised 77±20% and 71±30% of the analysed inorganic ions in particles emitted from the fireplace and the woodstove, respectively. The water soluble potassium (K^+) comprised 77±20% and 71±30% of the analysed inorganic ions in particles emitted from the fireplace and the woodstove, respectively. A good correlation between the potassium levels determined by ICP-MS and the water-soluble form of the element was found ($K_{water\ soluble}=0.73\times K_{ICP\text{-}MS}+0.06$; $r^2=0.89$). Thus, most of the potassium observed in the wood smoke emissions of this study is water-soluble, as indicated by the high K^+/K ratios: 0.80±0.19. Watson *et al.* (2001) reported K^+/K ratios ranging from 0.1 in geological material profiles to 0.9 in vegetative burning emissions. The elemental potassium accounted for 0.87±0.52 wt % of $PM_{2.5}$, representing 0.092±0.058 g kg^{-1} wood burned.

Table 1. Fine particulate emission factors and chemical composition of selected Portuguese biomass fuel types.

Appliance	Biomass type	$PM_{2.5}$ emission factor (g kg^{-1} fuel burned, dry basis)	OC (wt % of $PM_{2.5}$ mass)	EC (wt % of $PM_{2.5}$ mass)	Water soluble ions (wt % of $PM_{2.5}$ mass)	Metals (wt % of $PM_{2.5}$ mass)	Σ of chemical components (wt % of $PM_{2.5}$ mass)
Fireplace	Maritime pine	14.2	43.2	7.5	1.8	0.392	91.8
	Eucalyptus	20.2	43.2	2.2	2.9	0.835	82.8
	Cork oak	13.4	51.8	2.6	0.64	0.510	98.5
	Golden wattle	10.0	38.7	6.6	11.3	2.48	84.6
	Olive	9.9	48.5	4.2	0.98	0.981	95.9
	Portuguese oak	19.1	48.0	2.5	1.87	1.27	92.2
	Holm oak	16.0	53.0	2.2	0.75	0.540	99.9
	Briquettes	15.3	47.7	5.4	2.7	0.596	96.4
Woodstove	Maritime pine	16.3	49.2	3.9	1.7	0.179	95.6
	Eucalyptus	6.7	48.0	3.7	3.2	1.35	94.6
	Cork oak	15.1	53.6	1.9	0.53	0.394	100
	Golden wattle	11.7	45.0	2.0	13.6	1.97	87.6
	Olive	6.2	45.6	7.7	1.4	1.49	97.5
	Portuguese oak	9.8	49.4	3.9	1.6	1.26	97.3
	Holm oak	10.2	53.4	2.2	1.82	0.610	101
	Briquettes	4.2	47.1	3.9	9.1	2.17	94.7

Σ chemical components = $OC\times1.8 + EC + NH_4^+ + Cl^- +$ Metals

The application of cluster analysis to the individual smoke composition indicated that emissions from the cork and Holm oak combustion, whether in the fireplace or in the woodstove, can be grouped into the same composite source profile, while those from the Portuguese oak should be separated into another profile, which also may include the emissions from eucalyptus. Emissions from the combustion of maritime pine in both appliances may also be averaged to obtain a single profile. The comparison of emissions from this study with literature data showed dissimilarities, confirming the need of obtaining specific values for the combustion of Mediterranean biomass fuels in order to appropriately use these profiles in source attribution studies.

This work was funded by the Portuguese Science Foundation through the PTDC/AMB/65706/2006 (BIOEMI) project. C. Gonçalves acknowledges the PhD grant SFRH/BD/36540/2007.

Fine *et al*. (2004) *Environ. Eng. Sci.* 21, 705-721.
Schmidl *et al*. (2008) *Atmos. Environ*. 42, 126-141.
Watson *et al.* (2001) *Chemosphere* 43, 1141–1151.

Tuesday, September 6, 2011

Session 4P: Poster Session A: *Fundamentals*

Characterizing lengths and aerodynamic diameters of airborne glass fibers

Bon Ki Ku[1], Gregory Deye[1] and Leonid A. Turkevich[1]

[1]Centers for Disease Control and Prevention (CDC), National Institute for Occupational Safety and Health (NIOSH), Cincinnati, Ohio 45226, USA
Keywords: Glass fiber, length, diameter, screen.
Presenting author email: BKu@cdc.gov

Introduction

Historically, fiber-related research primarily grew out of health and manufacturing issues regarding asbestos. Current fiber measurement techniques also arose primarily due to health concerns over asbestos exposure. Fiber toxicity appears to be mostly a function of fiber concentration, dimensions (diameter and length) and durability in the lungs. During the past decade, airborne fibrous particles such as carbon nanotubes and carbon nanofibers have come under scrutiny owing to their asbestos-like appearance (Poland et al. 2008). This suspicion hinges on thin fiber-like structure of these particles and their presumed insolubility in the lungs, both attributes of harmful asbestos fibers. To better understand the toxicity of fibers, it is essential to classify fibers by length for toxicology studies. In this study we investigated how feasible it would be to use screens combined with asbestos sampling cassettes for length classification of fibers.

Methods

Glass fiber powder (GW1) supplied by the Japan Fibrous Material Research Association (JFMRA) was used as a surrogate of asbestos to generate airborne glass fibers by a vortex shaking method (Ku et al., 2006). The glass fiber sample had a geometric mean length 20.0 μm with geometric standard deviation (GSD) of 2.58 and geometric mean diameter 0.88 μm with geometric standard deviation (GSD) of 3.10 (Kohyama et al., 1997). Size distributions of the airborne glass fibers from the vortex shaker were measured by an Aerodynamic Particle Sizer (3321, TSI Inc.), and the airborne fibers were collected on a mixed cellulose ester filter (SKC Inc) in a 25 mm conductive cassette to measure length distribution of the fibers by a phase contrast microscope (PCM) with 40X and 10X magnifications. Nylon net screens with different screen mesh sizes (60, 20, and 10 μm) were used to examine the effect of screen size on length distribution.

Results and Conclusion

Figure 1 shows cumulative number concentration of glass fibers as a function of fiber length for different screen sizes. The red and blue lines in Fig. 1 represent mesh sizes of screen 20 and 60 μm. With no screen, the length distribution of the fibers is similar to the one reported in a previous paper. As screen mesh size decreases from screen 60 to 20, 50% cut-off length decreases from about 10 μm to about 7.5 μm. Compared to no screen case, using screens could give reduced lengths of fibers. It is worth noting that the 50% cut-off length for screen 10 is similar to the one for screen 60, but the slope of the cumulative curve for screen 10 becomes steeper, which means that the length distribution for screen 10 is narrower than the one for screen 60. The percentage of fibers longer than 20 and 60 μm for screen 20 and 60 is about 17 % and 3 %, respectively while the percentage of fibers longer than 10 μm for screen 10 is about 50 %,

APS measurements showed that fibers with no screen have bimodal distributions, with a primary aerodynamic diameter 1.5-2 μm and secondary aerodynamic diameter 7 μm. Using screen 60 and 20 slightly decreased primary modal diameters and significantly reduced the secondary mode. Screen 10 removed almost completely the second mode. The loading of fibers on the filter was also investigated. Using screens resulted in relatively uniform loading along the diameter of the filter.

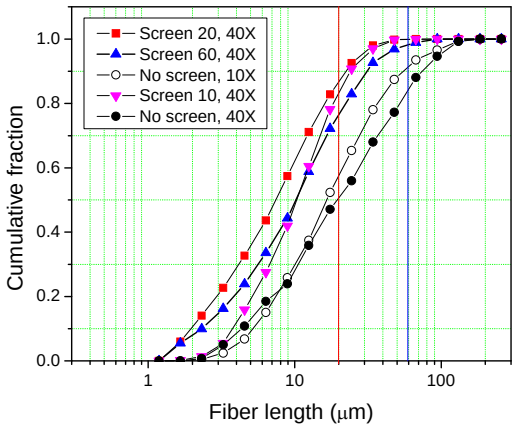

Figure 1. Cumulative fraction of fiber number concentration as a function of fiber length for different screen sizes. 10X and 40X mean magnifications used.

Acknowledgments

We would like to thank Dr. Ono-Ogasawara for sending us samples of glass fibers through the JFMRA in Japan, and Elizabeth Ashley for taking images of fibers and analyzing length distributions using the PCM. This work was supported by the National Institute for Occupational Safety and Health under the NORA project 927ZJFB.

Kohyama, N et al. (1997) *Ind. Health.* **35**, 415-432.
Poland, C. A. et al. (2008). *Nat. Nanotechnol.* **3**, 423-428
Ku, B. K., et al. (2006). *Nanotechnol.* **17**, 3613-3621.

On methods determining the fractal dimension of combustion aerosols and particle clusters

D.Lottin[1], D. Ferry[2], J.M. Gay[2], D. Delhaye[1], J. Yon[3], F.X. Ouf[4]

[1]Department of Physics and Instrumentation, ONERA, Châtillon, 92322, France
[2]CINaM-CNRS UPR 3118, Marseille, 13288, France
[3]CORIA-CNRS UMR 6614, Université et INSA de Rouen, Saint-Etienne de Rouvray, 76801, France
[4]Aerosol Physics and Metrology Laboratory, IRSN, BP 68, Gif-sur-Yvette Cedex, 91192, France.
Keywords: carbonaceous particles, TEM, fractals.
Presenting author email: delphine.lottin@onera.fr

Atmospheric aerosol particles meet a growing interest in today's environmental concerns because of their potential impact on the global radiative budget. In the context of the global warming assessment, combustion aerosols are extensively studied as they originate from industrial and transport activities for a large part. They usually are in the form of more or less compact aggregates made of primary particles. The compactness of these clusters is commonly quantified in terms of fractal dimension (Samson, 1987).

The aim of this study is to compare different methods reported in the literature for determining the fractal dimension (D_f) of aggregates from Transmission Electron Micrographies. Two classes of methods may be identified. The first one is based on the statistical study of an assembly of aggregates and the power law dependence of characteristic quantities of each aggregate like N_{pp} the number of primary particles, L_{2D} the maximal projected length, A_{2D} the projected area and P the perimeter. The fractal dimension is determined for the whole set of investigated aggregates. The second class of method focuses on the scale law of each individual aggregate with the nested squares method or the covering set method (Cleary, 1990) providing the fractal dimension of each of them.

The reported work is based on bidimensional projection images of soot aggregates generated by a CAST burner (soot generator mini CAST 5201^{TM}) and emitted by an aircraft combustion chamber (Figure 1). Three major issues are addressed. First, similar fractal dimensions come out from the various statistical approaches based on parameters sensitive to the inner content of the aggregates (e.g. N_{pp}, A_{2D}, see Table 1) whereas deviations are observed when using parameters related to the contour of the object (e.g. P). Then the relationship between the fractal dimension of an assembly of aggregates of various sizes and the averaged fractal dimension of single aggregates studied at different scale sizes is investigated as a second issue. This work is discussed with the previous study of the fractal dimensions of quartz grains by Takahashi and Nagahama (2003) where they showed that the fractal dimensions of individual quartz grains converge to the fractal dimension of the population composed by these objects when the size of these latter increases. This characteristic has never been studied for soot aggregates. The last issue investigated concerns the bandwidth limits to consider (smallest and largest sizes of the aggregates) in the fractal dimension determination. These limits have to respect the sizes of primary particles and of the considered aggregates to bring an analysis that is consistent with the physical structure of the objects.

The three issues investigated in this study should bring clues on the understanding of the methods developed to determine the fractal characteristic of environmental objects that are not fractals (in the mathematical sense) and their uses.

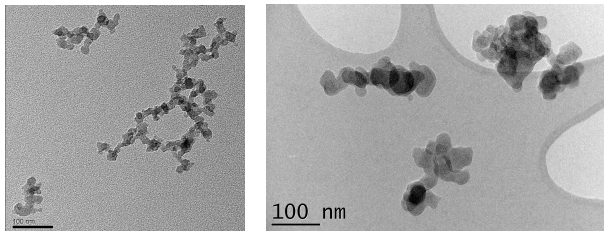

Figure 1. TEM pictures of soot aggregates emitted by a CAST burner (left) and an aircraft combustion chamber (right).

	$A_{2D} \propto P^{\frac{2}{D_f}}$	$A_{2D} \propto L_{2D}^{D_f}$	$N_{pp} \propto \left(\frac{L_{2D}}{d_p}\right)^{D_f}$
D_f	1.4	1.8	1.8

Table 1. Fractal dimensions of soot aggregates emitted by an aircraft combustion chamber using statistical approaches.

Cleary, T., Samson, R., Gentry, J.W. (1990) Aerosol Science and Technology **12**, 518-525.

Samson, R.J., Mulholland, G.W., Gentry, J.W. (1987) Langmuir **3**, 272-281.

Takahashi, M., Nagahama, H. (2003) The Arabian Journal for Science and Engineering **28**, 1C, 213-221.

Computationally efficient methods for computing the free molecular and continuum friction factors of non spherical aerosol particles.

Thaseem Thajudeen, Christopher J Hogan Jr
University of Minnesota, Twin cities
thaju001@umn.edu
Keywords: Monte Carlo Simulations, Agglomerates, Aerosol Fundamentals

Without appropriate drag models, non-spherical aerosol particle mobility/friction factor measurements allow for little inference of particle size and shape. Efficient computational models are therefore necessary to calculate the drag on aerosol particles in both the continuum and free molecular regimes, from which more relevant physical descriptors of non-spherical particles can be inferred from drag measurements. In this work we modify two previously developed methods to calculate the friction factors of non spherical aerosol particles in continuum and free molecular regimes, respectively.

Computational Methods

We first adopt algorithm of Zhou et al. (1993) to determine the drag on non-spherical particles in the continuum regime. This algorithm was originally developed to determine the diffusion controlled reaction rate on an arbitrarily shaped particles in liquid solvent. Specifically, Brownian dynamics simulations are utilized to compute the capacitance of nonspherical objects, which is found, to an excellent approximation, to be well correlated the hydrodynamic radius of the particles. Calculated hydrodynamic radii (R_h, the relevant size parameter in the continuum regime) are shown for fractal agglomerates with a varying number of primary particles per agglomerate and fractal dimension in Figure 1. These fractals were generated randomly using a sequential algorithm, which can produce effective mimics of agglomerates generated by a diffusion limited aggregation (DLA) process for ~50 primary particles or less. Although the larger agglomerates are less representative of those produced by DLA, they nonetheless serve as suitable test particles for our continuum drag/friction factor calculation method.

In the free molecular regime we modify the method developed by Nakamura & Hidaka (1998), which was utilized for drag calculation on non-spherical extraterrestrial particles (e.g. asteroids). In the modified approach we employ, trajectory simulations of the diffuse scattering (in angle, while kinetic energy conserved, mimicking a rough specular molecule surface) of point mass gas molecules with a non-spherical aerosol particle in a low velocity flow are used to determine the momentum transfer to the aerosol particle. This momentum transfer rate is compared to the momentum transfer rate to a sphere of known diameter colliding with the same gas molecules, but with perfectly specular scattering between the sphere and point masses. As the collision cross section (Ω) of the sphere is known, the ratio of the net momentum transfer to the non-spherical agglomerate to the net momentum transfer rate to the sphere gives Ω of the agglomerate.

Results

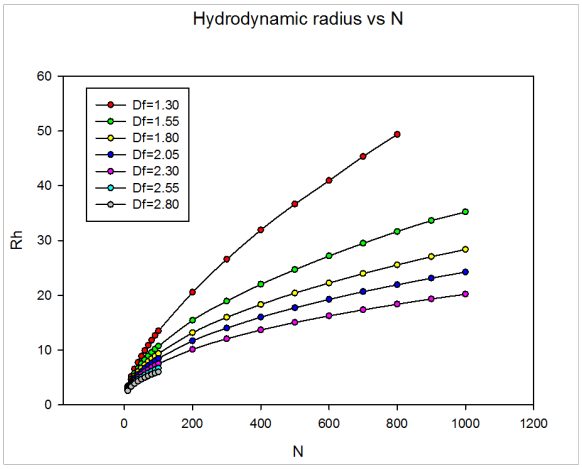

Fig 1. Variation of hydrodynamic radius, R_h, with fractal dimension and number of primary particles.

Overall, these new computational methods allow for calculation of R_h and Ω for any non-spherical particle. These two parameters are the revelant descriptors of any particle with regards to momentum transfer in the continuum and free molecular regimes respectively. Future work will involve determination of how these parameters influence transition regime momentum transfer, which would allow for inference of R_h and Ω from mobility measurements.

Zhou et al.*1993 J.Chem.Physics* Vol. 100 pp.3821-3826
Nakamura R, Hidaka Y 1998 Astronomy and Astrophysics Vol. 340 pp.329-334

Simultaneous Mobility and Mass Determination of Ionic Molecular Clusters produced in a bipolar ^{241}Am Charger

G. Steiner[1], T. Jokinen[2], H. Junninen[2], M. Sipilä[2], G.P. Reischl[1], D.R. Worsnop[2] and M. Kulmala[2]

[1]Faculty of Physics, Aerosol Physics and Environmental Physics, University of Vienna, 1090 Wien, Austria
[2]Faculty of Physics, Department of Atmospheric Sciences, University of Helsinki, P.O. Box 64, 00014, Finland

Keywords: Ion clusters, Ion mobility, chemical properties, electrical mobility, DMA.
Presenting author email: g.steiner@univie.ac.at

In this work, ionic molecular clusters that were generated in a commonly used ^{241}Am neutralizer are characterized with respect to mass and electrical mobility at the same time. The ions are produced by the ionizing radiation occurring during the alpha decay of ^{241}Am. The measurements were performed using a Vienna type high resolution DMA (UDMA, Steiner et al. 2010), running in a closed loop arrangement for the mobility classification and with a novel high resolution atmospheric pressure interface time-of-flight mass spectrometer (APi-TOF, Junninen et al. 2010) for the mass determination in terms of m/q ratios.

The detailed processes governing the generation of the molecular ions within a charger are still somehow uncertain, but the general idea is that the ionizing radiation forms primary ions that will subsequently combine with polar molecules present in the carrier gas to form larger clusters. Therefore, special attention was paid to the purification of the carrier gas led through the ^{241}Am charger, as already very small amounts of trace gases and/or contaminants will strongly alter the species of the generated ions (Steiner et al. 2009).
For the experiments, high purity nitrogen, (N_2 5.0) was used as carrier gas which was additionally purified by means of two silica gel diffusion dryers, two active carbon filters and a hepa filter. The tubing from the purifying equipment to the DMA and APi-TOF was chosen to be either of PTFE or stainless steel to avoid any contaminations.

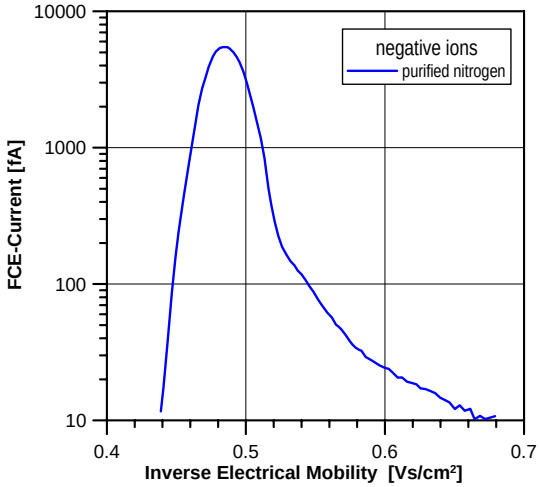

Fig.1 Mobility distribution of negative ions

The resulting mobility distribution of negatively charged ions is shown in Fig.1. For very clean and dry conditions, the ion mobility spectrum is reduced from several to one single peak with a small shoulder facing towards lower mobility/larger size.

The UDMA is continuously classifying the molecular clusters and feeding them to the APi-TOF which allows the identification of the chemical composition of the investigated ion clusters. The mass spectrum of negatively charged ion clusters is dominated by approximate m/q ratios of 46 (NO_2^-), 62 (NO_3^-, nitric acid) 80 $(H_2O{\cdot}HNO_3)^-$ and 125 $(HNO_3{\cdot}NO_3^-$, nitric acid dimer); (Fig.2). Similar experiments were performed for positive ion polarity.

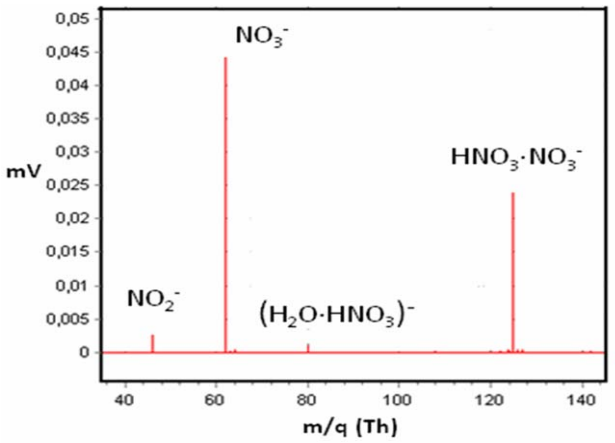

Fig.2 Mass spectrum of negative ions with dominant m/q (Th) peaks

This work was supported by the Austrian Science Fund FWF, Project P20837-N20 and the University of Helsinki.

Steiner, G. et al. (2010) A medium flow, high-resolution Vienna DMA Running in Recirculating Mode. *Aerosol Sci Technol 2010, 44, 308-315*

Junninen, H. et al. (2010) A high-resolution mass spectrometer to measure atmospheric ion composition. *Atmos. Meas. Tech., 3, 1039-1053, 2010.*

Steiner, G. et al. (2009) Formation of ionic molecular clusters in the presence of spurious gases in a bipolar charger. *Proc.18th International Conference on Nucleation and Atmospheric Aerosols, Prague, pp. 456-459*

Optical cloaking and agglomerated fractal clusters

V.V. Maksimenko [1] and V.N. Ignatov [2]

Karpov Institute of Physical Chemistry, Moscow, 10, ul. Vorontsovo Pole, 105064, Russia.
Moscow Engineering Physics Institute, 31, Kashirskoe shosse, Russia.

Keywords: fractals, cluster, nanoparticles, agglomerates
Presenting author email: wmaksim@mail.ru

An idea to make a macroscopic object invisible for external observer is now one of the most exciting problems of modern optics. Recent interest to this problem is related to the discovery of so-called meta-materials with negative dielectric and magnetic permeability at certain frequency range (Sarychev & Shalaev, 2007). In this case, light can circulate around an object just as a laminar fluid flux circulates around a cylinder (see Fig. 1)

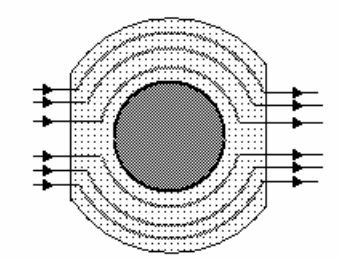

These ideas were successfully realised in experiments performed in centimetric range of the wave lengths. Typical covering meta-material used were solid matrixes containing a large number of ordered thin metal wires and rings with size comparable with wave-length of the incident radiation. In principle, such systems can also be created in optical spectrum, but sizes of these heterogeneities inside the matrix must be submicron. The latter is extremely hard to do. Moreover, the problem of reflection from boundary of these materials also exists. One should remember about considerable weight of such covering.

It is desirable to create a covering which entirely absorbs any radiation without any reflection. But this is impossible as we know. Absorbed irradiation heats the object and it re-emits on any wave-length. Nobody could violate the heat radiation rules.

However, the possibility to create a system capable to trap incident radiation without its dissipation and re-emission exists. In this case, the trapped photons move along closed trajectories inside the system on nonabsorbing scatterrers without heating the system. This phenomenon is called the light localization. The most appropriate object for the realization of this aim is a covering consisting of agglomerated fractal clusters containing nonabsorbing nanoparticles.

The localization of light is concerned with closed loops on a photon trajectory. If a photon moves along a closed loop, the phase shift of the wave function of the photon is equal to zero. The probability amplitudes corresponding to both possible ways of the loop passing (clockwise and counterclockwise) interfere constructively. Each loop means indispensable return to the starting point. Due to the increase of the probability of the loop generation (because of above mentioned interference) the flux of light scattered into the back hemisphere also increases. This, in turn, stimulates production of new loops on the photon trajectory, and so on. The photon localization in a finite space region results from such self-sustaining process.

Localization is a purely interference phenomenon, but it can be easily interpreted as the appearance of a bound state of pair of virtual photons passing the closed loop on the photon trajectory by two alternative ways. This phenomenon is analogous of the effective interaction of electron-hole pair due to its scattering on the same impurities in lattice. The latter, as is known, is the reason for the Anderson localization.

The cross section of the photon elastic scattering by an agglomerate of fractal clusters containing nonabsorbing nanoparticles is calculated. It is shown that a photon scattered in the forward direction is not localized, i.e. its life time inside the system is equal to zero. At the same time, every photon scattered at a non-zero angle is trapped by the system. Its life time in the system is of the order of $N^2 \exp(N^2)T$, where T is the period of the incident electromagnetic wave and N is the number of correlated particles inside a separate fractal cluster inside the agglomerate.

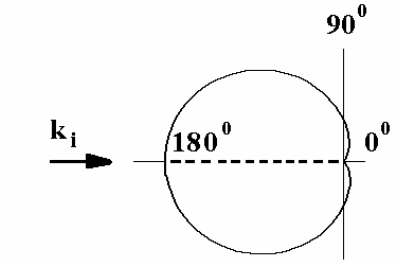

In Fig. 2 angular distribution of the intensity of p-polarized light scattered by fractal a cluster is presented. The enhanced scattering to the back hemisphere, in comparison with Rayleigh's indicatrix of an isolated particle is just the physical reason for photon cycling in a cluster (Maksimenko et. al., 2009)

This work was supported by the RPFI under grant 10-03-00511.

Sarychev A. K. & Shalaev V. M. (2007), *Electrodynamics of Metamaterials*, World Scientific, Singapore.
Maksimenko V. V., Kupriyanov L.Yu., Zagaynov V. A. (2009), Nanotechnologies in Russia, 4, 795-801.

Non conventional indoor model for submicron particulates

Lyons Russell

Radiation Health Unit, Environmental Health Branch, Queensland Health, Brisbane, 4000, Australia

Keywords: submicron, particulates, deposition, indoor, aerosol, modelling.

Abstract

This paper describes the mechanisms of deposition and particle exchange. The term particle exchange in this paper refers to the movement of particle into and out of an enclosure due to the movement of air into and out of an enclosure. At low concentration coagulation is expected to be small in comparison to deposition and particle exchange.

This model seems to have the ability to produce quick and accurate predictions for particle deposition loss and the gain or loss of particles due to particle exchange. Thus this model has the potential to be a powerful tool to aid in further understanding of the phenomenon of coagulation.

Introduction

The deposition component of the model was derived from a non conventional theoretical modelling of the probability of a collision of particles with the walls of the enclosure. Since the particle concentration of the aerosol in the enclosure changes with time, due to the deposition and particle exchange, the model needs to predict these changes and looped the predictions back into the model for the next calculation. This process is repeated for each second.

The model was used to predict the size distribution after ~106 minutes for tobacco smoke. The model appears to give a very accurate prediction as shown in figure 1. Figure 1 graphically compares the actual measured data after 106 minutes and model's prediction after 6360 iterations.

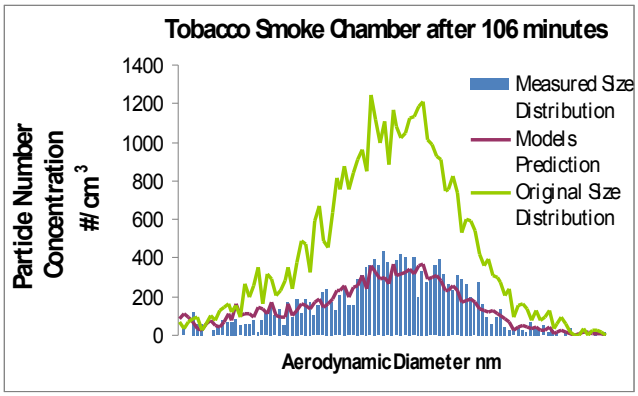

Figure 1. This figure illustrates good agreement between theories and experiment data after 106 minutes (International Lab. For Air Quality and Health, QUT)

The original aerosols distribution in the enclosure is also shown in Figure 1 to give perspective of the particle changes.

The indoor particle model for deposition and particle exchange used is Figure 1 is given below

$$N_x^t = N_x^{t-1} - \frac{AreaN_x^{t-1}}{4\times Volume}\times\left\{\sqrt{\frac{4kTC_{cx}}{3\pi\eta d_x\times 10^{-9}}}\right\} + \frac{f\times\left(N_x^{Outside} - N_x^{t-1}\right)}{Volume\times 10^6}$$

Nomenclature

Area	internal surface area	m2
Volume	internal volume	m^3
f	flow rate	cm^3
k	Boltzmann Constant	
T	Temperature	K
Cc	Cunningham Slip correction factor	
η	dynamic viscosity of air	kg.m-1 s-1
N	Particle concentration	$\#/cm^3$

This paper describes the theoretical development of this indoor particle model used for predicting the changes of total particle number concentration of a decaying aerosol and its changing size distribution over extended time period, for an indoor environment under natural ventilation conditions.

The model used only the following input data for predicting the changes in number concentration; the original size distributions, which is the aerosol size distribution concentration, in the enclosure (after the source has been extinguished) and outside the enclosure, the flow rate into the enclosure, the surface area and volume of the enclosure.

References

Einstein, Albert; R. Fürth, transl. by A. D. Cowper (1926, reprinted in 1956). "On the Movement of Small Particles Suspended in a Stationary Liquid Demanded by the Molecular-Kinetic Theory of Heat". Investigations on the theory of the Brownian motion. Dover Publications. ISBN 0486603040

Characterization of sulphuric acid aerosols in industrial processes

L. Brachert[1], S. Sinanis[1] and K. Schaber[1]

[1]Institute of Technical Thermodynamics and Refrigeration, Karlsruhe Institute of Technology, Karlsruhe, 76131, Germany

Keywords: Absorption, Homogeneous nucleation, Industrial aerosols.

Presenting author email: leonie.brachert@kit.edu

The formation of volatile sulphuric acid aerosols is a phenomenon which emerges frequently in industrial processes such as absorption, mixing and cooling. An important domain is the absorption-based flue gas cleaning in power plants using fossil fuels. The formation of aerosols during absorption and quenching of acids in general and its possible harm to downstream equipment have been exposed by Schaber (1995). The formation of aerosols contributes to an increased emission of the pollutant as the droplets are carried with the gas stream. As a consequence, expensive facilities for aerosol precipitation have to be installed. For this reason, it is very important to have an instrument to investigate the formation of aerosols and subsequently to provide conditions which prevent their formation.

The absorption of several acids such as HBr and HCl has already been examined in a pilot plant for flue gas cleaning at the institute (Wix, 2008).

A simulation tool (AerCoDe) has been developed which used a monodisperse model for heterogeneous nucleation in the beginning (Ehrig et al, 2002) and recently has been extended for homogeneous nucleation, based on a polydisperse model (Wix *et al*, 2010). The latter is needed when the nucleation of sulphuric acid aerosols is investigated. The reason for this is the occurrence of high supersaturations during the absorption of sulphuric acid as a result of the extreme phase equilibrium of the binary system "sulphuric acid – water.

The results of the simulation yield small aerosols (<200 nm) and high number concentrations up to 10^{16} m^{-3}. The dependence of the number concentrations on the H_2SO_4 inlet concentration of the flue gas is illustrated in Figure 1, which shows lower number concentration at high inlet concentrations of H_2SO_4 in the flue gas. This can be explained by the two competing mechanisms for the depletion of supersaturation: nucleation and growth. At low inlet concentrations, the binary system H_2SO_4-H_2O reveals a steep descent of the saturation pressure with increasing concentration of H_2SO_4 (and subsequently high supersaturations). Hence, at low inlet concentrations the driving force for nucleation is high, whereas there is not much substance in the gas phase which would enforce growth. The higher the inlet concentration, the higher is the driving force for growth and the number concentration of aerosol decreases.

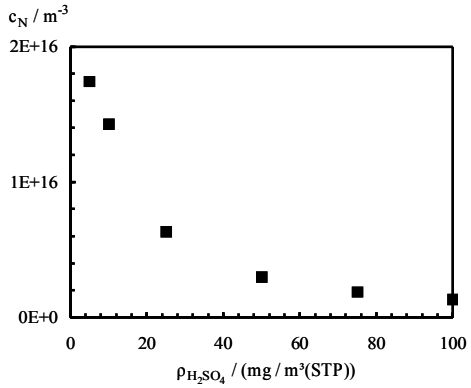

Figure 1. Total number concentration of all droplet classes in the quench column outlet as a function of the H_2SO_4 inlet concentration (Wix 2008)

Because of the expected small diameters, there is currently no in-situ measuring method known which could be used to verify the simulation by experiments. Therefore, a condensation particle counter (CPC) combined with a dilution cascade is used in experiments in order to investigate this correlation in ongoing experiments. As a result of the measuring method, the information about the size distribution of the aerosol is lost.

The combination of simulation and experiments could provide a possibility to fully characterize the aerosols formed during the absorption process in terms of number concentrations, size distribution and contents of acid of the droplets. This could serve as a base for the improvement of absorption processes in industrial applications.

Ehrig, R., Ofenloch, O., Schaber, K. and Deuflhard, P. (2002) *Chemical Engineering Science* **57**, 1151-1163

Schaber, K. (1995) *Chemical Engineering Science* **50**, 1347-1360

Wix, A., Brachert, L., Sinanis, S. and Schaber, K. (2010) *Journal of Aerosol Science* **41**, 1066-1079

Wix, A. (2008) *Fortschritt-Berichte VDI*, Reihe 3, Nr. **894**, VDI-Verlag

Experimental work on particle motion inside a differentially heated cavity

J. Kalilainen[1,2], T. Lind[2], A. Auvinen[1], P. Rantanen[1], A. Dehbi[2], S. Güntay[2] and J. Jokiniemi[1,3]

[1] VTT Technical Research Centre of Finland, P.O.box 1000, BI7, FI02044 VTT Espoo, Finland
[2]Paul Scherrer Institut, CH-5232 Villigen PSI, Switzerland
[3]Univ. of Eastern Finland, Department of Environmental Science, P.O. Box 1627, FI-70211 Kuopio, Finland
Keywords: particle image velocimetry, deposition, fission product, severe accident.
Presenting author email: jarmo.kalilainen@vtt.fi

In the case of nuclear reactor severe accident, fission products can be released from the core into the containment. In the presence of temperature gradients inside the containment, natural turbulent convective flows will occur, inducing turbulent flow which can affect aerosol particle deposition rates on containment walls.

The phenomenon of particle deposition in differentially heated cavity (DHC) was investigated in a PhD work with direct numerical simulation (DNS) (Puragliesi, 2010). Also, ongoing PhD work at Paul Scherrer Institut (PSI) uses large eddy simulation (LES) to study the same process. DNS work provided information, such as flow field and temperature profile (shown in Fig. 1), for three-dimensional closed cubic cavity with turbulent Rayleigh number of 10^9. The objective of the LES work is to be able to simulate turbulent conditions with Rayleigh number 10^{10}.

The main aim of this investigation is to experimentally determine the fluid motion, temperature fields, and particle motion inside a differentially heated cavity. Special emphasis is to enable validation of models used in LES, as well as enable comparison with earlier computational work using DNS..

First part of the experimental work is the design and manufacture of the DHC facility. The DHC facility will be a cube with side length no more than 0.8 m. Rayleigh number inside the facility will be varied between 10^9 and 10^{10} by altering the gas composition in the cavity atmosphere. The facility has a heated and a cooled wall for thermal gradient between the walls, and four adiabatic walls. In order for the Oberbeck-Boussinesq approximation, used in the simulation work (Puragliesi, 2010), to be valid the heat difference between the walls must remain below 50 K. Also, the facility must allow optical access for different laser-based measurement devices used to determine the flow properties. This means that besides the heated / cooled walls, all other walls must be at least partly made of transparent material, such as quartz glass.

The facility will be designed to allow geometrical modifications after the first set of tests. For example, the ratio of the cavity height to its width will be varied to better simulate aspect ratios of real containment geometries.

Particle Image Velocimetry (PIV) will be used for measuring the fluid flow velocities. Especially, fluid motion in the boundary layer close to heated / cooled wall must be measured with high resolution.

Particle concentration inside the facility will be measured using Laser-Induced Incandescence (LII). In addition, aerosol instrumentation, such as Condensation Particle Counter (CPC) and Tapered Element Oscillating Microbalance (TEOM) can be used to measure particle number and mass concentrations, respectively. Particle depletion inside the facility due to different mechanisms is investigated by using different particle sizes. In the DNS work, the particle diameters used were 15, 25 and 35 µm. In the experimental work, also smaller particles with diameter close to 1 µm are used in order to investigate the effect on particle depletion of different forces such as turbophoresis. Monodisperse particles will be used in all experiments.

As a result of this work, improved models for fluid and particle motion may be developed and implemented to analytical tools. Based on the experimental results, correlations for particle depletion within DHC will be determined using the validated DNS-LES simulations. These correlations are to be transferred to a CFD code, e.g., Fluent. Particle concentration within DHC will be then modeled with CFD applying the new and improved correlations for turbulent convective flow.

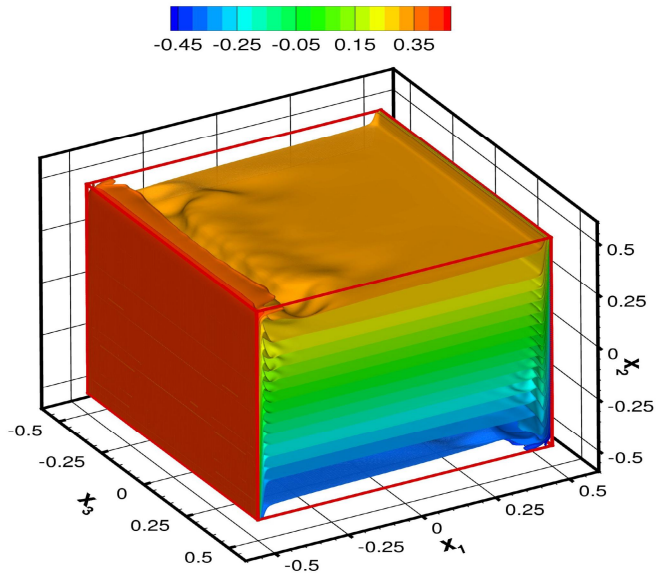

Figure 1. Time-averaged dimensionless temperature profile of DHC, acquired with DNS (Puragliesi, 2010).

Puragliesi, R. (2010) *Numerical Investigation of Particle-Laden Thermally Driven Turbulent Flows in Enclosure*, Ph.D. thesis. no:4600, École Polytechnique Fédérale de Lausanne. Lausanne.

Agglomerate drag in continuum and rarefied flow regimes

P. Vainshtein and M. Shapiro

Faculty of Mechanical Engineering, Technion-Israel Institute of Technology, Haifa, 32000, Israel
Keywords: agglomerate, fractal, mobility, rarefied.
Presenting author email: merpeva@tx.technion.ac.il

Submicron particulates emitted from automotive engines oftentimes have a fractal agglomerates structure. The fractal relationships have one of the following forms $N_p = k_f (d / d_p)^{D_f}$ or $N_p = k_g (d_g / d_p)^{D_f}$, where N_p is the number of primary particles per aggregate, d_p is the diameter of the primary particles, D_f is the fractal dimension, k_f, k_g are the prefactors; d, d_g are the outer and gyration diameters.

Drag acting on moving agglomerates can be specified by the Knudsen number, which is a mean free path of the medium molecules, λ, divided by a characteristic sizes of the agglomerate; for instance the outer diameter d and the size of the primary particles d_p (Vainshtein and Shapiro, 2005).

The developed model for calculation of hydrodynamic drag and mobility of fractal aggregates in the transition flow regime employs an adjusted sphere diameter (Dahneke, 1973) and is based on the knowledge of the continuum and vacuum mobility diameters. In the continuum regime the model accounts for internal flow rarefaction and porous fractal structure and their effects on the apparent viscosity and effective permeability of agglomerates. It employs the Stokes equations outside the agglomerate, the Brinkman equations inside the agglomerate and continuity of momentum and stress on the interface. In the free-molecular regime the model uses a semi-empirical relationship for the vacuum mobility diameter of Koylu et al. (1995). The spherically symmetrical model also includes the effects of agglomerate non-sphericity on the drag by assuming agglomerate spheroidal shape (Vainshtein et al., 2004).

We compare our results with those obtainable by Rogak et al. (1993), who used a similar interpolation assuming in addition that the mobility diameter in the continuum regime equals the gyration diameter. Their model thus does not account for internal flow rarefaction and agglomerate porous structure. These phenomena, however, are of importance for determining agglomerate drags especially for large-number agglomerates.

The obtained results on the continuum and transition mobility diameters are compared with the existing experimental and theoretical data. Figure 1 provides an example of such a comparison. The model predicts the ratio between the mobility diameter and gyration diameter about 20% lower than the experimental points. The non-sphericity factor when introduced in the model leads to increasing of the diameters' ratio thereby allowing rationalization of the experimental data.

The large-number colloid RLCA and DLCA aggregates in the continuum regime (Wiltzius, !987; Wang and Sorensen, 1999) behave as oblate spheroids, whereas small-number aerosol DLCA aggregates in the transition regime (Schmidt-Ott, 1988; Cai and Sorensen, 1994; Park et al., 2004; Katzel et al., 2008) behave as prolate spheroids.

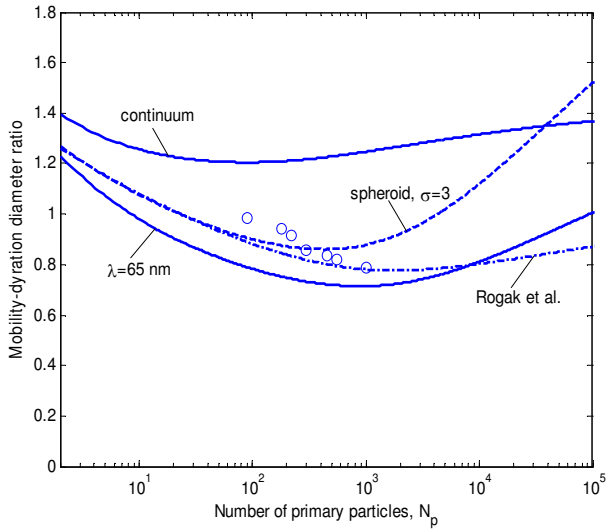

Figure 1. $D_f = 1.8$, $d_p = 10$ nm, $k_f = 1.0$. The solid lines correspond to the spherical model; dashed line to the prolate spheroid with aspect ratio $\sigma = 3$; dashdot line shows the ratio calculated using Rogak et al. (1993). Circles – experimental data of Katzel et al. (2008).

Vainshtein, P.. and Shapiro, M. (2005) *Colloid Interface. Sci.*. **284**, 501-509.

Dahneke, B. J. (1973) *J. Aerosol Sci*. **4**, 139-145.

Koylu, U.O., Faeth, G.M., Farias, T.L., and Carvalno, M.G. (1995) *Combust. Flame* **100**, 621-633.

Vainshtein, P., Shapiro, M. and Gutfinger C. (2004) *J. Aerosol Sci*. **35** 383-404.

Rogak, S.N., Flagan, R.C., and Nguyen, H.V. (1993) *Aerosol Sci Techn*. **18**, 25-47.

Wiltzius, P. (1987) *Phys. Rev. Let*. **58**, 710-713.

Wang, G.M. and Sorensen, C.M. (1999) *Phys. Rev. E* **60**, 3036-3044.

Schmidt-Ott, A. (1988) *Appl. Phys. Lett*. **52**, 964-956.

Cai, J. and Sorensen, C.M. (1994) *Phys. Rev. E* **50**, 3397-3400.

Park, K., Kittelson, D.B., McMurry, P.H. (2004) *Aerosol Sci. Techn.* **38**, 1-9.

Katzel, U., Vorbau, M., Stintz, M., Gottschalk-Gaiding, T., and Bartel, H. (2008) *Part. Part. Syst. Charact*. **25**, 19-30.

Nonlinear oscillations and deposition of aerosol in tubes

D.A. Gubaidullin, R.G. Zaripov, A.L. Tukmakov and L.A. Tkachenko

Institute of Mechanics and Engineering, Kazan Science Center, Russian Academy of Sciences, Kazan, 2/31, Lobachevsky str., 420111, Russia

Keywords: aerosol, coagulation, deposition, particles, oscillations.

Presenting author email: damirgubaidullin@gmail.com

In the present work, longitudinal oscillations of an aerosol of different initial number concentration and dynamics of particles is considered in tubes of different length with various geometry on the end near to resonant frequencies.

Experimental investigations oscillations of an aerosol were carried out for different length of tubes in a shock-wave and no shock-wave modes near to subharmonic and natural resonances. Di-ethyl-hexyl-sebacate $C_{26}H_{50}O_4$ was used as the working fluid to generate aerosol. The majority of droplets have the geometric diameter 0.863 μm. Number concentration of drops for all experiments monotonously decreases with time and with growth of the excitation frequency. In the case of a closed tube, this process is defined by the coagulation of aerosol and deposition of droplets on the tube walls. In an open tube, the discharge of aerosol to the environment is observed in addition to the coagulation of aerosol and deposition of droplets on the tube walls. The dependence of the time of coagulation of aerosol on the excitation frequency likewise exhibits a nonmonotonic pattern with a maximum and a minimum when passing the resonance. It is established, that presence of a flange slows down process of a coagulation of an aerosol. Reduction of internal diameter of a flange results in increase in the time of coagulation. In so doing, the time of coagulation of aerosol in the case of an open tube is reduced by a factor of two and more compared to the time of coagulation in a closed tube. Nonlinear dependence of the time of coagulation of droplets is established at nonlinear oscillations of an aerosol in a tube from initial number concentration of an aerosol. It has been found that a decrease in the tube length and increase oscillation intensity results in a decrease in the time of coagulation of aerosol. It is shown, that with increase of intensity of the oscillations, the caused increase of amplitude, time of coagulation and deposition of an aerosol decreases. Time of a coagulation and deposition of drops of an aerosol in no shock-wave mode in 2-4 times is lower, than at a natural deposition. Ordered space-time structures of different densities have been revealed in the visible region in the vicinity of the middle of a closed tube.

The numerical modeling of a drift of the solid spherical particles were in a suspension in a nonlinear wave field of the closed tube and open flat channel at excitation of oscillations of a gas column on three first fundamental frequencies is executed. These researches have been carried out about use of model of a single particle and with application of model of interpenetrating continuums. It is obtained, that easy particles drift under an operation of acoustical current, and heavy are displaced under an action of wave pressure. In result easy and heavy particles concentrate in different areas of the resonator: easy are displaced to antinodes of a standing wave of velocity, heavy – to nodes. Depending on a steepness of a wave front of compression, the same particles can behave as easy at small nonlinearity, or as heavy at steep enough fast-head wave front. Drift of heavy particles in the open channel proceeds in two stages. The first quickly proceeding stage is connected to the mechanism of drift due to asymmetry of a wave, and the second with drift under action of developed acoustic stream. Influence of radius of particles on distribution of temperature and average density of a disperse phase along an axis of the channel is revealed.

Dynamics of a single particle with various physical and geometrical parameters is experimentally investigated at the longitudinal oscillations gas in tubes. Along an axis of a tube the particle moves from the closed (open) end to the piston, near to a wall – to the return side, making longitudinal oscillations with increase in the oscillations swing that is caused by acoustic streaming. In a radial direction, the oscillating particle moves from an axis to a wall of the tube up to a boundary point. Outside of a tube, the particle moves from the open end to an exterior wave field practically without oscillations with nonlinear increase of coordinate from time. It is revealed, that the increase in lengths of a tube and excitation frequency of gas in up to - resonant modes gives in growth of an oscillations swing of a particle and increase of its average velocity. Nonmonotonic character for dependence of oscillations swing and average velocity of a spherical particle from excitation frequency of gas is detected. At approach to a resonance oscillations swing and average velocity are incremented, attain the maximum value on a resonance frequency and decrease behind a resonance. Effect of a weight and diameter of a particle on its oscillations swing and average velocity is investigated. Shift of a curve maximum for dependence of a particle average velocity from oscillation frequency aside magnifications of frequency is shown at increase of a weight or diameter of a particle.

This work was supported by the Russian Fund of Foundation Investigation under grant 10-01-00098 and within the framework of the Federal target program "Scientific and scientific and pedagogical shots of innovative Russia for 2009-2013" (state contract №14.740.11.0351).

Size measurement of dry ice particles in a jet flow using laser diffraction method

Yi-Hung Liu[1], Graham Calvert[2], Colin Hare[2],
Mojtaba Ghadiri[2], Shuji Matsusaka[1]

[1]Department of Chemical Engineering, Kyoto University, Nishikyo-ku, Kyoto 615-8510, Japan
[2]Institute of Particle Science and Engineering, University of Leeds LS2 9JT, UK
Keywords: dry ice, jet flow, size distribution, agglomeration.
Presenting author email: liu@cheme.kyoto-u.ac.jp

Dry ice blasting has been utilized as a dry cleaning method, which can be applied in many industrial fields, such as semiconductor, plastics, food, and pharmaceuticals, etc. The properties of dry ice particles, including size, shape, density, and hardness are thought to be important factors affecting the cleaning process (Spur *et al*., 1999). The agglomeration process of dry ice particles in the jet flow has been investigated (Liu *et al.*, 2010). It was shown that a chamber was effective for the generation of agglomerated dry ice particles. However, a precise measurement of the size of dry ice particles in the jet flow proved to be difficult due to the sublimation process. In the present study, the state of dry ice particles in the jet flow has been analyzed by an on-line laser diffraction method.

Dry ice particles were produced by rapid expansion of liquid carbon dioxide, based on Joule-Thomson effect. In this process, the temperature rapidly decreased by adiabatic expansion from the pressure of 5.5 ± 0.1 MPa to atmospheric pressure. The inner diameters of the nozzles used for expansion were 0.1, 0.2, and 0.5 mm. As an agglomeration chamber, ABS tubes, 50 mm in length and 2, 4, 6 mm in inner diameter, were attached to the nozzle outlet. The size of dry ice particles ejected from the nozzle or the ABS tube were measured by an aerosol analyzer (Spray-Tech, Malvern Instruments Inc.) based on the technique of laser diffraction. The laser beam and dry ice jet were both horizontal and oriented perpendicular to each other.

Figure 1 shows an example of the cumulative size distribution of dry ice particles in a steady state. For the distance from the nozzle $d \leq 40$ mm the median diameter was in the range from 1 to 2 μm and increased with the distance. As for $d = 50$ mm, the dry ice particles shrank to submicron size. A normal-like distribution can be ascertained at a short distance, i.e. $d \leq 40$ mm, while the distribution deviated as the distance increased ($d = 50$ mm). In the size distribution, two size regions were observed, i.e. a smaller diameter region of submicron and a larger diameter region around ten microns. It is found that the primary dry ice particles ejected from the nozzle still grew up and/or agglomerated up to a certain distance. When the distance was sufficiently large, two opposite phenomena, i.e. sublimation and agglomeration occurred. As a result, a bimodal distribution was obtained.

Figure 2 shows the cumulative size distribution of dry ice particles exhausted from the tube in a steady state. Comparing with Fig. 1, the particle size is remarkably larger, indicating that dry ice particles exhausted from the nozzle have already agglomerated in the tube. In addition, the median diameter decreased with increasing nozzle diameter.

Nucleation, condensation, agglomeration and sublimation processes all compete to yield the size distribution as measured. Among them, agglomeration is the most important in the tube (Liu *et al.*, 2010); i.e. dry ice particles of several micrometers are deposited on the tube wall and form a deposition layer; then, agglomerates are reentrained from the layer into the jet flow. The size of the reentrained agglomerates decreases with increasing flow velocity. In these experiments, the flow velocity increases with the nozzle diameter. This is considered as a reason for the trend of the results observed here.

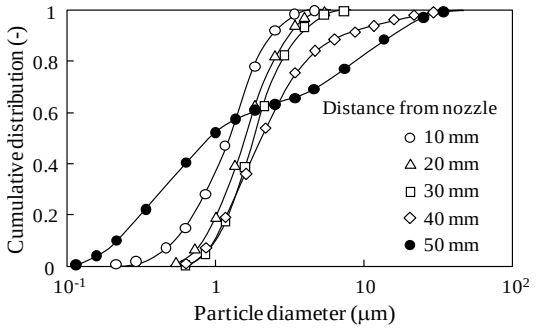

Figure 1. Cumulative size distribution of dry ice particles exhausted from nozzle (nozzle diameter = 0.2 mm).

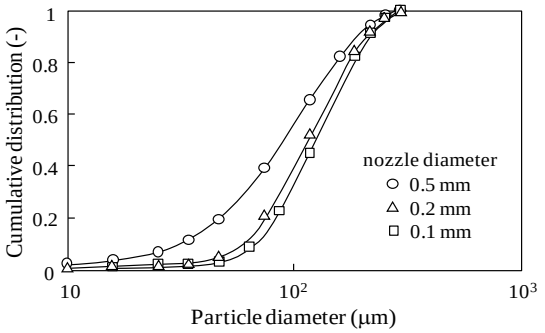

Figure 2. Cumulative size distribution of dry ice particles exhausted from tube (tube diameter = 6 mm, distance from the tube = 40 mm).

This research was supported by Core-to-Core Program for Advanced Particle Handling Science, JSPS, the Global COE Program (No. B-09) and a Grant no. S0901039 from MEXT, Japan.

Liu, Y. H., Maruyama, H. and Matsusaka, S. (2010). *Adv. Powder Technol.*, **21**, 652-657.
Spur, G., Uhlmann, E. and Elbing, F. (1999). *Wear*, 233-235, 402-411.

Dynamic structure of two-phase polydisperse spray in wake of a shattering drop

A.G. Girin[1]

[1] Odessa National Maritime University, Odessa, 65029, Ukraine
Keywords: spray, evaporation, generation of combustion aerosol, aerosol dynamics.
Presenting author email: club21@ukr.net

Mathematical model for dynamic processes in wake of a drop, shattering in uniform gas stream, is elaborated. It allows to describe quantitatively evaporation and acceleration of stripped mass of daughter droplets and thereby – formation of liquid-phase jet and vapor cloud in a wake. Parent drop is regarded as a source of daughter droplets with distribution function $f_{\rm n}(r,\tau)$ and in turn, each daughter droplet is regarded as moving point source of vapor; their totality forms the distribution of vapor mass. Evolution of distribution function $f_{\rm n}(r,x,\tau)$ in space and time is governed by equation of dispersed fuel (Williams, 1964), which must be added to equations of motion of daughter droplets and of vapor influx. The dependencies of droplet's drag coefficient on velocities and variable sizes as well as intensification of their evaporation due to streamlining were taken into account. The distribution function was taken for the case $h=1$ of equality of rates of torn mass efflux and of relaxational decreasing of relative velocity of gas flow and parent drop (Girin, 2011).

Formulated non-stationary two-dimensional problem for system of differential equations of dynamics of two-phase polydisperse spray was solved numerically with a help of Lax – Vendroff finite-difference scheme for kerosene drop in air stream. Calculations showed, that times of living of finest and largest droplets are the characteristics of liquid jet formation in a spray. Soon after time moment $\tau_{\min}$ of vanishing (entire evaporation) of droplets of minimum in spray radius $r_{\min}$, that were stripped at $\tau=0$, evaporation mass rate $\dot{M}_{\rm v}$ and current value of liquid-phase mass M_l in spray exceed their maximum values because of beginning of droplets vanishing. After moment $\tau_{\max}$ of vanishing of droplets of maximum radius $r_{\max}$ the vanishing of droplets of new radii doesn't occur, and this is the necessary condition for stabilization of length of liquid-phase jet in considered case $h=1$, which is confirmed by analysis of dispersive parameters.

For conditions behind shock waves and in rocket engines the intensification of evaporation by streamlining flow is substantial, so, the fuel is presented in spray generally in vapor phase.

In considering non-stationary process the proposed model allows to calculate all mean diameters d_{ij} of liquid-phase jet and to analyze evolution of its dispersive properties in space and time. Parameters of two kinds were considered: $\Omega_{ij}(x)=d_{ij}(x,\tau_{\rm c})$ are defined at every cross section x of jet and characterize its spatial structure at fixed moment $\tau_{\rm c}$, while $D_{ij}(\tau)=\int d_{ij}(x,\tau)dx$ are calculated at any τ for whole set of droplets and describe temporal changing of dispersity of jet in total. At the beginning the bunch of curves $\Omega_{ij}(x)$ is narrow, that testifies to weak polydispersity of jet, but after droplets vanishing starts, the polydispersity increases. Each curve and bunch as a whole tend to their limit positions at $\tau\to\tau_{\max}$. The stabilization proceeds gradually along jet from astern part to the tip. Soon after $\tau_{\max}$ all the parts of $\Omega_{ij}(x)$ are stabilized and remain still. The dependencies $D_{ij}(\tau)$ confirm the conclusions. In final state jet polydispersity is much greater than that produced by source.

The process of vapor cloud formation was studied. At the beginning of shattering the capacity of source is highest, therefore the intensification of evaporation due to rapid growth of surface of liquid is so large, that vapor wave appears which has sharp front similar to blast wave. After losing contact with liquid jet this wave has convectional drift, keeping its form invariable. Gradual weakening of capacity of source of daughter droplets leads to generating of rarefied wave in distribution of vapor mass, so at distances $x_{\rm f}>100R_0$ from wave front to source distribution tends to "triangle" form, which is also characteristic of blast waves.

Evaluations show that fuel – air mixture in a wake of shattering drop is substantially overreached in average, as vapor density several times exceeds the stoichiometric value, except of regions near spray borders. Vapor oversaturation leads to overcooling of the combustible mixture. Equation of heat balance for process of vapor – air mixing for considered conditions yields the temperature dropping in about 300°K, which means that delay of combustible mixture ignition may jump several orders high.

The elaborated model, which is grounded on obtained earlier distribution function, permits to obtain all the main characteristics of developing two-phase polydispersed spray in a wake of shattering drop and to investigate its internal structure. Development of the model will allow to reflect correctly the kinetics of further processes of mixing, heat transfer and chemical reactions of fuel burning.

Williams, F. (1964) *Combustion theory*, Addison – Wesley Publ. Comp.

Girin, A. (2011) *Inzhen.-fiz. zhurnal.* **84**, No 2, 248-254.

Equations of kinetic of drop shattering in a speedy uniform flow

A.G. Girin[1]

[1] Odessa National Maritime University, Odessa, 65029, Ukraine
Keywords: dispersion, size distribution, aerosol dynamics, modelling.
Presenting author email: club21@ukr.net

An investigation of local surface instability with due regard to changing of velocity profile across the boundary layers, as well as to changing of boundary layers thickness and velocity along drop surface (Aslanov, Girin, 1981) revealed for weak-viscosity liquids a new type of hydrodynamic instability – "gradient instability". Mechanism of this type is caused by sufficiently large velocity gradient inside liquid boundary layer. The theory explains the "stripping" mode of breakup as quasi-continuous dispersing from unstable part of drop surface. At some simplifications it permits below to derive differential equations of drop mass efflux and of quantity of stripped droplets.

Using regularities of boundary layer theory and dependencies of wavenumber Δ_m and increment $\mathrm{Im}(z_m)$ of dominant unstable disturbance from "surface" Webber number (Girin, 1985), we obtain condition for gradient instability to exist on surface of shattering drop:

$$\frac{2.475\,\alpha}{(1+\alpha^{\xi})^2}\sqrt{R(\tau)\left(1-W(\tau)\right)^3}\,\sin^2\varphi\;\Psi(\varphi)\;\mathrm{GI} > 0.004\,, \quad (1)$$

where R, W are dimensionless radius and velocity of shattering drop, $\alpha=\rho_g/\rho_l$, $\mu=\mu_g/\mu_l$, $\xi=\log_{\alpha}(\alpha\mu)^{1/3}$ is parameter of mutual viscous engagement of media in boundary layers, $\mathrm{GI}=\mathrm{We_d}/\mathrm{Re_d^{0.5}}$ is criterion of gradient instability, $\Psi(\varphi)=((6\varphi-4\sin 2\varphi+0.5\sin 4\varphi)\sin^{-5}\varphi)^{0.5}$. Equality in (1) defines position of a critical point $\varphi_{cr}(\tau)$ on drop surface, which divides it on stable $\varphi<\varphi_{cr}$ and unstable $\varphi>\varphi_{cr}$ parts (φ is polar angle of ground on drop surface). At $\alpha\,\mathrm{GI}>(\alpha\,\mathrm{GI})_{cr}\approx 4\cdot 10^{-4}$ we have $\varphi_{cr}<\pi/2$, so, the part of drop surface, adjacent to edge, is unstable, providing a possibility of dispersing. Values of φ_{cr} are small enough in speedy flows: $\varphi_{cr}\ll\pi$, so, most part of drop surface generates a mist of droplets.

The quantity of unstable waves on any ground of surface equals to quantity of torus, that are torn from corresponding spherical belt. Assuming that radius of torn droplet is proportional to the length of dominant wave $r=k_r\lambda_m$, and relating volume of torus to volume of droplet, we obtain the equation for quantity Δn of droplets, torn from the ground, and their radius r:

$$\Delta n(\varphi,\tau)=B_2\sqrt{R(\tau)(1-W(\tau))^5}\,\Psi^{-3}(\varphi)\sin^2\varphi\,\Delta\varphi\,\Delta\tau\,, \quad (2)$$

$$r(\varphi,\tau)=B_1\left(R(\tau)/(1-W(\tau))\right)^{0.5}\Psi(\varphi)\,, \quad (3)$$

where $B_1=\dfrac{3.1\pi k_r\alpha^{1-2\xi}}{\Delta_m\,\mathrm{Re_d^{0.5}}}$, $B_2=\dfrac{0.3\Delta_m^2\,\mathrm{Im}(z_m)\,\mathrm{Re_d^{1.5}}}{\pi k_r k_t\alpha^{3.5-7\xi}(1+\alpha^{\xi})}$.

Relating now the stripped mass to the period $t_i=k_t\,\mathrm{Im}^{-1}(z_m)$ of its stripping, we obtain the rate of mass efflux from the ground, and by integrating along windward surface from φ_{cr} to $\pi/2$, obtain the differential equation for rate of mass efflux from drop:

$$\frac{dM}{d\tau}=-AR^2(\tau)(1-W(\tau))\left(1-\frac{2\varphi_{cr}(\tau)}{\pi}+\frac{\sin 2\varphi_{cr}(\tau)}{\pi}\right), \quad (4)$$

where $A=0.46(1+\alpha^{\xi})^{-1}(\mu^2/\alpha)^{1/6}$ is characteristic rate of mass efflux, $M=m/m_0$. It demands simultaneous solution of equation of drop motion in order to determine $W(\tau)$, and equation (1) to determine $\varphi_{cr}(\tau)$. For speedy flows, when $\mathrm{GI}>>\mathrm{GI_{cr}}\simeq 0.3$ and $\varphi_{cr}\ll\pi$, we obtain, assuming spherical shape of drop: $M(\tau)=$ $=\left(1-A\left(\tau-\alpha^{0.5}X_d(\tau)\right)/3\right)^3$, that indicates the direct influence of law of drop motion $X_d(\tau)$ on its ablation law. Using empirical data of Reinecke, Waldman (1975), we can write down law of drop motion in the form $\sqrt{\alpha}X_d(\tau)=\tau-(1-\exp(-H\tau))/H$, $H=2\sqrt{\alpha}$ whence

$$W=1-\exp(-H\tau)\,,\quad M=\left(1-h(1-\exp(-H\tau))\right)^3\,. \quad (5)$$

Parameter $h=A/3H$ is rate ratio of two governing factors of shattering: mass efflux ($\sim A$) and relaxational decreasing of relative velocity of gas and drop ($\sim H$). When $h>1$, the whole drop is dispersed to moment $\tau_b=H^{-1}\ln(h/(h-1))$. When $h<1$, dispersing terminates before the drop is shattered, because latter factor leads to quick reducing of main reason of dispersing – relative velocity $1-W$ (see (4)). Remnant may be shattered by another mechanism, for example, by Rayleigh – Taylor instability (Girin, 1985). Comparison of ablation law (5) with experimental data (Reinecke, Waldman, 1975) indicates their agreement.

System (2)–(4) allows mutual integration together with equation of drop motion without any empirical data. In both cases distribution of droplets by sizes is obtained.

Aslanov, S., Girin, A. (1981) *Dokl. AN Ukr. SSR. Ser. A*, No 12, 25-28.
Girin A. (1985) *Inzhen.-fizich. zhurn*. **48**, 771-775.
Reinecke, W, Waldman, G. (1975) *AIAA Paper*. **152,** 22.

Multi-Particle Sintering Dynamics: From Fractal-like Aggregates to Compact Structures

M.L. Eggersdorfer[1], D. Kadau[2], H.J. Herrmann[2] and S.E. Pratsinis[1]

[1]Particle Technology Laboratory, Institute of Process Engineering, Department of Mechanical and Process Engineering, ETH Zurich, Sonneggstrasse 3, CH-8092 Zürich, Switzerland.
[2]Computational Physics of Engineering Materials, Institute of Building Materials, Department of Civil, Environmental and Geomatic Engineering, ETH Zurich, Schafmattstrasse 6, CH-8093 Zürich, Switzerland.
Keywords: Aerosol dynamics, Sintering, Morphology, Nanoparticles.
Presenting author email: meggers@ptl.mavt.ethz.ch

Multi-particle sintering of fractal-like aggregates occurs in systems where initially coagulation dominates and aggregates are formed before sintering becomes significant. This is controlled by the temperature profile and particles residence time. Multi-particle sintering is typically encountered in many natural and industrial applications like aerosol production of nanoparticles (SiO_2) in flame, hot-wall and spray pyrolysis reactors (Tsantilis & Pratsinis, 2004). Detailed aerosol reactor models were developed combining particle and fluid dynamics (Johannessen et al., 2000) including particle sintering rates with the theoretically predicted fractal dimension D_f = 1.8 of diffusion limited cluster-cluster aggregation (DLCA). Sintering rates are commonly based on two-particle models and do not consider a change in aggregate structure. On account of this, limited information of particle morphology is available. The challenge lies in understanding the change in aggregate morphology and properties during sintering.

Now it is reasonably well understood that such aggregates form by gas and surface reaction, coagulation and partial coalescence (or sintering). As chemical reactions in high temperature aerosol processes are completed much faster than particle dynamics, the detailed structure of these aggregates is largely determined by the interplay of particle collision and coalescence. In the absence of such sintering between primary particles, agglomerates (rather than aggregates) are formed by collision and mere cohesion with well-defined structure and fractal-dimension, D_f, depending only on the particle collision mechanism. Once coalescence or sintering starts between constituent primary particles, sinter necks are formed between them converting the agglomerates to aggregates. During sintering, the latter progressively densify until complete compact (e.g. D_f = 3) structures are formed at sufficiently long process times at high temperatures. This has been experimentally demonstrated during silica formation in hot-wall (Seto et al., 1997)

Several models have been proposed for viscous sintering of mainly equally sized pairs of particles (Frenkel, 1945; Koch & Friedlander, 1990). Particles produced in flame reactors have typically a size distribution and complex morphology. In this work a simple model is introduced, which can describe the sintering of differently sized pairs of particles and multi-particle sintering. The sintering of amorphous spherical particles like fumed silica (SiO_2) is investigated with a new geometric sintering model, based on the conservation of volume and the energy balance proposed by Frenkel (1945). The change in surface energy equals the energy dissipated by the viscous flow. The advantage of the new model is its simple applicability and efficiency compared to more elaborate simulations (Kirchhof et al. 2009). Nevertheless the new model is able to reproduce the neck growth and evolution of surface area for equally and differently sized pairs of particles compared to the existing sintering models. Additionally it is applied for viscous sintering of irregular particle morphologies to study the evolution of surface area, radius of gyration and effective fractal dimension (Fig. 1).

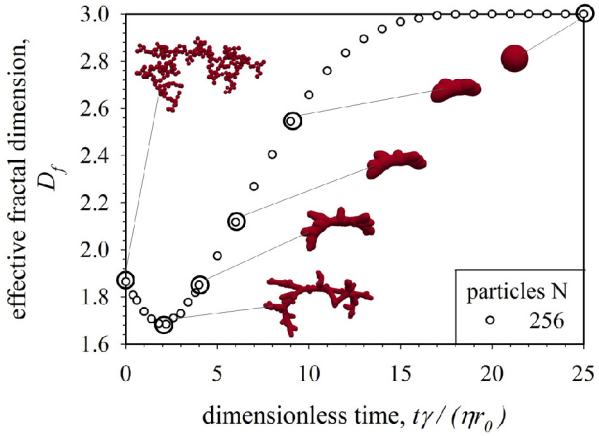

Figure 1. Evolution of D_f of a DLCA aggregate with initially 256 primary particles.

Financial support by ETH Research Grant (ETHIIRA) ETH-11 09-1 and the European Research Council is gratefully acknowledged.

Frenkel, J. (1945) *J. Phys.* **9**, 385-391.
Kirchhof, M.J., Schmid, H.J., and Peukert, W. (2009) *Phys. Rev. E* **80**, 026319.
Koch, W. and Friedlander, S.K. (1990) *J. Colloid Interface Sci.* **140**, 419-427.
Johannessen, T., Pratsinis, S.E. and Livbjerg, H. (2000) *Chem. Eng. Sci.* **55**, 177-191.
Seto, T., Hirota, A., Fujimoto, T., Shimada, M., and Okuyama, K. (1997) *Aerosol Sci. Technol.* **27**, 422-438.
Tsantilis, S. and Pratsinis, S.E. (2004) *Langmuir.* **20**, 5933-5939.

Tuesday, September 6, 2011

Session 4P: Poster Session A: *Aerosol Chemistry*

SOA formation from campholenic aldehyde ozonolysis

Y. Iinuma, A. Kahnt, A. Mutzel, O. Böge and H. Herrmann

[1]Leibniz-Institut für Troposphärenforschung, Leipzig, 04318, Germany
Keywords: BVOC, LC/MS, Aerosol Chemistry
Presenting author email: yoshi@tropos.de

Atmospheric degradation of biogenic terpenes has a significant impact on the tropospheric ozone and SOA formation. Among various naturally occurring terpenes, the oxidation of monoterpenes such as α-pinene and β-pinene has been intensively investigated due to their relatively high emissions and SOA formation potentials. Although these studies have improved our knowledge about SOA formation from monoterpenes, little is known about SOA formation from other classes of terpenes such as oxygenated monoterpenes. Campholenic aldehyde ($C_{10}H_{16}O$) is an oxygenated monoterpene that can be readily formed in the oxidation of α-pinene (Jaoui and Kamens, 2003) or from α-pinene oxide in the presence of Lewis acid (Iinuma *et al.*, 2009). Jaoui and Kamens (2003) suggested that the formation and oxidation of campholenic aldehyde may explain some of SOA compounds in the α-pinene oxidation systems though the exact products and the SOA formation from campholenic aldehyde oxidation remain unclear. In the present study, a series of aerosol chamber experiments were conducted to provide information on the SOA products and yields for the reaction of campholenic aldehyde with ozone. The resulting SOA products were analysed using ultra-performance liquid chromatography coupled to electrospray ionisation ion mobility spectrometer quadrupole time of flight mass spectrometer (UPLC/ESI-IMS-QTOFMS).

Table 1 summarises the experimental conditions used in this study. The experiments were performed in the presence and absence of an OH scavenger to investigate its influence on SOA yields and products.

Table 1. Experimental conditions

Campholenic aldehyde (ppb)	RH (%)	Ozone (ppb)	CO (ppm)	Seed particle $(NH_4)_2SO_4/H_2SO_4$
100	50	60	-	pH 2
100	50	60	105	pH 2

Figure 1 shows time dependent SOA yield curves as a function of the mass concentration of formed SOA. SOA yields were very high for both sets of experiments, reaching plateau around 0.75 to 0.8. These values are much higher than SOA yields typically observed from the ozonolysis of non-oxygenated monoterpenes such as α-pinene, β-pinene and limonene (e.g. Hoffmann et al., 1997), suggesting that the formation and subsequent oxidation of campholenic aldehyde is important in the SOA formation of α-pinene oxidation.

Figure 2 shows typical chromatograms obtained from the analysis of campholenic aldehyde SOA samples. The SOA samples contained a number of highly oxygenated compounds such as detected at *m/z* 215 ($C_{10}H_{15}O_5^-$) and *m/z* 229 ($C_{10}H_{13}O_6^-$), indicating low volatile nature of campholenic aldehyde oxidation products.

In summary, highly oxygenated nature of campholenic aldehyde SOA compounds is consistent with very high SOA yields and the oxidation of oxygenated monoterpenes may be an important source of atmospheric SOA.

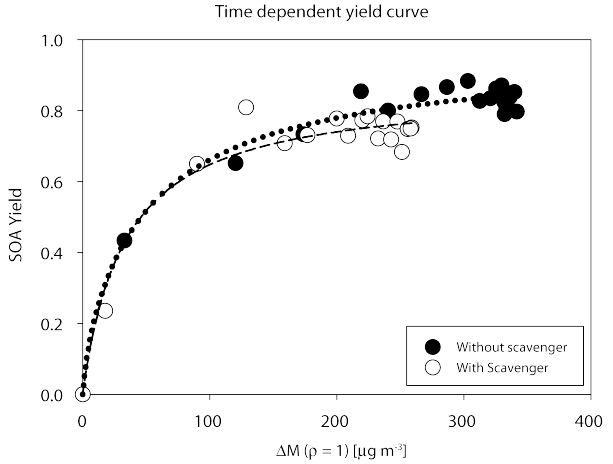

Figure 1. Time dependent SOA yields as a function of the mass concentration of formed SOA.

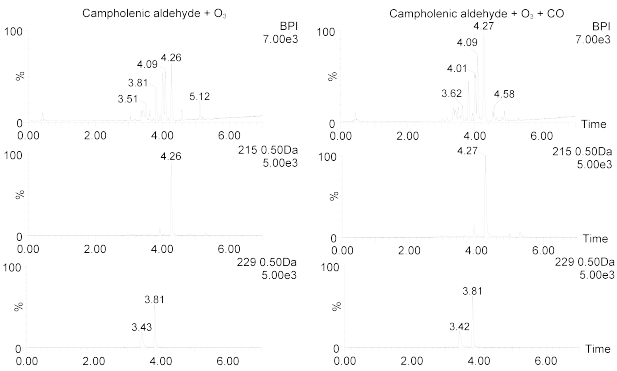

Figure 2. Base Peak Chromatograms (BPC) and extracted ion chromatograms (EIC) obtained from UPLC/(-)ESI-IMS-QTOFMS analysis of campholenic aldehyde SOA samples.

Hoffmann, T., Odum, J.R., Bowman, F., Collins, D., Klockow, D., Flagan, R.C., Seinfeld, J.H. (1997) J. Atmos. Chem., **26**, 189-222.

Iinuma, Y., Boge, O., Kahnt, A. and Herrmann, H. (2009) Phys. Chem. Chem. Phys., **11**, 7985-7997.

Jaoui, M., and Kamens R. M. (2003) J. Atmos. Chem., **44**, 259-297.

Atmospheric degradation of β-caryophyllene: laboratory and field studies

A. van Eijck[1], Taraborrelli, D.[2], Sander, R.[2], T. Hoffmann[1]

[1]Institute for Inorganic and Analytical Chemistry, Johannes Gutenberg-University, Duesbergweg 10-14, 55128 Mainz, Germany
[2]Atmospheric Chemistry Department, Max Planck Institute for Chemistry, P.O. Box 3060, 55020 Mainz, Germany
Keywords: Aerosol component composition, Degradation, Field measurements, GC-MS, HPLC-MS, Organic tracer, Reaction chamber, SOA
Presenting author email: van.Eijck@uni-mainz.de

Secondary organic aerosol (SOA) has a huge impact on air quality and climate change. It influences the Earth radiative budget through absorbing, scattering and reflecting radiation as well as the formation of clouds because the particulates can act as cloud condensation nuclei (CCN). Furthermore, it plays an important role for human health; through inhaling it can reach the alveoli and deposit. SOA is formed from gaseous precursors which get oxidized by ozone, OH- and NO_3-radicals in the atmosphere. Due to their low vapor pressure these degradation products can nucleate to form new particles or they can condense on existing aerosol particles. Despite the major progress in research during the last few years the actual chemical composition as well as the contribution of various volatile organic compounds (VOCs) to the formation of secondary organic aerosol is still partially unknown.

Recent studies indicate that sesquiterpenes play an important role in the formation of secondary organic aerosol because of the low volatility of their oxygenated products (Lee *et al*., 2006). Their emission is estimated to be about 14,8 Tg per year (Henze *et al*., 2008), however, these emission rates remain highly uncertain due to the lack of quantitative emission rate measurements. In addition, the knowledge about the actual atmospheric degradation mechanism and the main oxidation products of sesquiterpenes is quite limited. β-caryophyllene is found to be one of the most abundant sesquiterpenes in the atmosphere (Helmig *et al*., 2007). Because of its high reactivity and the low volatility of the oxygenated products it produces high aerosol yields in photooxidation chamber experiments (Lee *et al.*, 2006). Furthermore, the oxidation products of β-caryophyllene were found to play an important role in the formation of SOA over boreal forest (Parshintsev *et al*., 2008).

To determine the major oxygenated products of the atmospheric degradation of β-caryophyllene a new method was developed to synthesize the acidic compounds through ozonolysis in the liquid phase followed by further oxidation of specific eliminated products. The synthesized compounds were separated by preparative HPLC and identified by ^{1}H-NMR.

Atmospheric simulation experiments were performed in a 100 L reaction chamber to determine the influence of different ozone and OH-radical concentrations on the distribution of the β-caryophyllene oxidation products. To measure the time dependent formation of initial oxidation products, an APCI-IT-MS was directly connected to the reaction chamber. After 2 hours the APCI-IT-MS was replaced by a filter holder and the generated aerosol was collected for 5 hours. The results show that in the presence of OH-radical producers (e.g. 2,3-dimethyl-2-butene) the concentration of the acidic products which still contain double bonds decreases, whereas in the presence of OH-radical scavengers (e.g. cyclohexane) the concentration of these acids increases. In addition, the atmospheric chemistry box model CAABA/MECCA (Sander *et al*., 2011) was extended to calculate the influence of different ozone and OH-radical concentrations on the distribution of the different oxidation products of β-caryophyllene. The box model was adjusted to reaction chamber conditions. Reaction equations and rate coefficients of the oxidation reactions of β-caryophyllene with ozone and OH-radicals as well as the consecutive reactions were added to the model. The results of the atmospheric chemistry box model were compared with the results of the atmospheric simulation experiments.

Finally several atmospheric air samples taken during the HUMPPA campaign summer 2010 in Finland were analyzed for β-caryophyllene oxygenated products.

This work was supported by the Max Planck Graduate Center, Mainz, Germany.

Helmig, D., Ortega, J., Duhl, T., Tanner, D., Guenther, A., Harley, P., Wiedinmyer, C., Milford, J. and Sakulyanontvittaya, T. (2007) *Environmental Science & Technology* **41**, 1545-1553.

Henze, D.K., Seinfeld, J.H., Ng, N.L., Kroll, J.H., Fu, T.M., Jacob, D.J. and Heald, C.L. (2008) *Atmospheric Chemistry and Physics* **8**, 2405-2421.

Lee, A., Goldstein, A.H., Kroll, J.H., Ng, N.L., Varutbangkul, V., Flagan, R.C. and Seinfeld, J.H. (2006) *Journal of Geophysical Research* **111**, D17305.

Parshintsev, J., Nurmi, J., Kilpeläinen, I., Hartonen, K., Kulmala, M. and Riekkola, M.J. (2008) *Analytical and Bioanalytical Chemistry* **390**, 913-919.

Sander, R., Baumgaertner, A., Gromov, S., Harder, H., Jöckel, P., Kerkweg, A., Kubistin, D., Regelin, E., Riede, H., Sandu, A., Taraborrelli, D., Tost, H. and Xie, Z.-Q. (2011) *Geoscientific Model Development Discussions* **4**, 197-217.

Tuesday, September 6, 2011

Session 4P: Poster Session A: *Fundmentals*

Deposition of Nanoparticles on Wire Screens by Diffusion and Image Force

V. Gómez[1], C.H. Huang[2], F.J.Alguacil[3] and M. Alonso[3]

[1]Instituto de Nanociencia de Aragón (INA), Edificio I+D, c/ Mariano Esquillor s/n, 50018 Zaragoza,Spain.
2Department of Environmental Engineering and Health, Yuanpei University, 30015 Hsinchu, Taiwan
[3]National Center for Metallurgical Research (CSIC), Avenida Gregorio del Amo, 8. 28040 Madrid, Spain.
Keywords: Nanoparticles; Aerosol filtration; Charged particles.
Presenting author email: virgomez@unizar.es

This abstract presents the results of an experimental investigation on the deposition of charged and neutral nanoparticles on wire screens by the combined mechanisms of diffusion and image force. Experiments were performed with particles having diameters below 10 nm and using four different flow rates and three kinds of wire screens.

As the experimental results have shown, the single fiber efficiencies for the mechanisms of image force, $\eta_{IM,}$ and diffusion, η_D, are of the same order of magnitude and, furthermore, they are both much smaller than one. Under these conditions, the total capture efficiency can be approximated as the sum of the efficiencies by diffusion and image force deposition, $\eta = \eta_D + \eta_{IM}$. The efficiency for the image force mechanism will be obtained from fitting of experimental results to an expression of the form $\eta_{IM} = AK_{IM}^B$, where

$$K_{IM} = \left(\frac{\varepsilon_f - 1}{\varepsilon_f + 2}\right)\frac{Cp^2e^2}{12\pi^2\mu\varepsilon_0 u d_p d_f^2} \qquad (1)$$

is the image forcé number (ε_f : dielectric constant of the fiber; ε_o: vacuum permittivity; C: slip correction factor; p: number of charges per particle, e: elementary charge; μ: air viscosity; u: air flow velocity; d_p:: particle diameter; d_f: fiber diameter).

For the experiments, an evaporation-condensation NaCl aerosol was charged in a ^{241}Am neutralizer. Positively charged particles of known size were withdrawn from a differential mobility analiyzer (DMA, TSI short column, L=11.11 cm) operated at an aerosol-to-sheath flow rate ratio of 2/20. Since our study has been restricted to particle size below 10 nm, all the particles classified by DMA were singly charged. These positively singly-charged monodisperse particles can follow two alternative routes: one, containing a ^{241}Am neutralizer and an electrostatic precipitator, and the second one, a bypass route to transport the +1 particles into the filter unit.

The filtration unit consists essentially in a grounded cylinder made of brass having a length of 186 mm and inner diameter of 8 mm. A series of five rings, 4 mm in width and made of brass, were placed inside the main cylinder. The wire screens were placed in between any two consecutive rings, so that the screen fibers are in contact with the grounded cylinder.

Three types of screen were used in the experiments; their characteristics are listed in Table 1. The “sandwich” wire screen consisted of a gold wire screen between a pair of aluminum wire screens; it has been experimentally assessed and its characteristics are also showed in Table 1**.** Penetrations were determined for varying values of: (i) aerosol flow rate through the filter; (ii) particle size; and (iii) number of charges on the particles (0, +1).

Material	Aluminium	Stainless steel	Sandwich
Fibre diameter, d_f (μm)	100	66	55
Opening (μm)	110	103	
Thickness (μm)	260	120	524
Density (g cm^{-3})	2.70	7.96	
Surface density (g cm^{-2})	0.02	0.03	
Open area fraction (-)	0.27	0.37	
Solid volume fraction (-)	0.30	0.32	0.32
Screen parameter , S	1.44	1.08	5.77

Table 1. Characteristics of the wire screens employed

From the experimental results, the following correlation has been obtained:

$$\eta_{IM} = 36.06K_{IM}^{0.55} \qquad (2)$$

The total penetration can then be calculated as

$$P = \exp\left[-nS\left(2.7Pe^{-2/3} + 36.06K_{IM}^{0.55}\right)\right] \qquad (3)$$

where n is the number of screens, and is compared in Figure 1 with typical experimental results obtained in the course of this work.

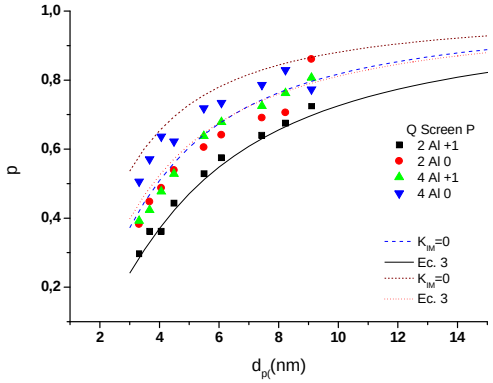

Figure 1. Comparison between experimental penetrations and those calculated with Ec. (3) for 2 and 4 aluminium screens and aerosol flow rates of 2 lmin^{-1} and 4 lmin^{-1}.

This work was supported by grants DPI2008-06199, CSIC 2009TW0017 and NSC 99-2923-E-264-001-MY2.

Depth filtration performance characteristics in accordance with the filter layer structure

Y.O. Park[1] and N. Hasolli[1,2]

[1]Clean Fossil Energy Research Center, Korea Institute of Energy Research, Daejeon, Korea
[2]Department of Chemical Engineering, Chungnam University, Daejeon, Korea
Keywords: Depth filter media, filtration, particle size distribution, particle collection efficiency, clogging.
Presenting author email: yopark@kier.re.kr

Introduction

Until recently the cartridges used for the gas turbine intake air filtration were made mainly of surface filter media which are periodically cleaned using air pulsing. Some of these systems have been modified by installing the depth filter media cartridges instead of conventional surface media cartridge filters. Depth filter media are usually composed by a number layers which build the filter media sheet. During the development process, the aim is to reach the optimum of the main filtration parameters which are: filter pressure drop (DP), dust holding capacity (DHC) and the particle collection efficiency (PCE). Depth filter media layers should be arranged so that the gross particles are collected by the first upstream layer. The fine particles are captured by the final layer made of meltblown fibres. The arrangement of layers in a depth filter media should form a gradient as explained in Purchas and Sutherland (2002). The effect is noticeable in the patterns of the pressure drop as function of dust loading where is possible to spot the clogging of depth filter media as shown in Brown (1993).

The aim of this study is to analyse the effect of various layer structure on the filtration performance of the depth filter media samples.

Experimental method and material

All the sample cartridges are made of the depth filter media with the pleat count 90 and the filtration area of 5.5 m^2. Dimensions of the cartridges are: Outer diameter (OD) 328 mm, inner diameter (ID) 210 mm and the height (H) 660 mm. In the Table 1 there are some of the specifications of the flat sheet depth filter media samples which were tested using standard testing units. The testing procedures are explained in detail in our previous work Park et al (2009).

Table 1. Depth filter media sample specifications.

Specification	***A***	***B***	***C***	***D***
Thickness, mm	1.55	1.95	1.5	1.95
Permeability, cfm	140	130	165	220
NaCl PCE, %	91.5	93.7	81.5	83.1
Initial DP, mmH_2O	1.3	1.4	0.9	0.7
Spec. weight, g/m^2	204	254	190	240

The loading particles are of standard test dust A2 Fine (ISO Standard 12130-1). The inlet concentration was set 500 mg/m^3. The particle concentration is measured at the inlet and outlet sampling ports. The particle size analysis and size distribution is measured using the Portable Aerosol Spectrometer (GRIMM, model 1.108). The cartridge samples were tested using the gas turbine filter test unit with the nominal flow rate of 1000 m^3/min. Pressure drop tests are conducted by varying the flow rate. The dust holding capacity resulted from gravimetric measurements of the cartridges before and after the loading test. Overall and fractional collection efficiency is evaluated by comparing the mass particle concentration at the inlet and the outlet duct.

Results and Discussion

The patterns of the DP are different according to the difference in the upstream layer which is 0.4 mm thicker than the other two samples A and C are clearly visible. The meltblown layer of the sample C and D has a lower DP and lower PCE than the other two A and B samples as shown in the Table 1. Accordingly the particle collection efficiency is lower for sample cartridges C and D (97.69% and 97.38% respectively) than that of the samples A and B (99.67% and 99.65% respectively) at the initial stage of the dust loading. Right below the Dp = 80 mmH_2O all four samples exhibit an overall collection efficiency of over 99.9%.

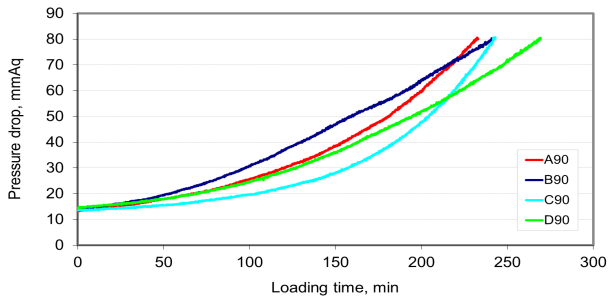

Figure 1. Pressure drop increase vs. loading time for samples A,B,C and D

This work was supported in part by the Eco-Technopia 21 Projects of the Korea Ministry of Environment through the Korea Environmental Industry & Technology Institute.

Purchas, D.B. and Sutherland, K (2002) *Handbook of filter media*, Elsevier.

Brown, R.C. (1993) *Air filtration – An integrated approach to the theory and application of fibrous filters*, Pergamon Press.

Park, Y.O., Hasolli, N., Choi, H.K., Rhee, Y.W. (2009) *Characterization of depth filter media for gas turbine intake air filtration,* PAAR, Vol.5, No.4, 159-170.

Nanofibril filters for environmental nanoparticles

F.Belosi[1], G.Santachiara[1], F. Prodi[1] and K. Syverud [2]

[1]ISAC-CNR, Clouds and Precipitations Group, Bologna, 40129 - Italy
[2]PFI Paper and Fibre Research Institute, Trondheim, 7491-Norway
Keywords: Nanofibre, filtration efficiency, nanoparticles.
Presenting author email: f.belosi@isac.cnr.it

The development of nanofibrillar cellulose filters are very promising to enhance aerosol filtration at the most penetrating aerosol particles and could help in the prevention of nanoparticles connected pathologies (nanopathologies). Cellulose nanofibrils are the building blocks of the fibres, just like the fibers are the building blocks of the trees. The raw material for production of cellulose nanofibrils is cellulose fibres, produced from wood by chemical pulping. The fibrils are composed of bundles of cellulose molecules, arranged in crystalline and amorphous areas, giving a tread-like material with fibril diameters of typically 20 nm and with high aspect ratio and high specific surface area. The material retains many of the advantageous properties of cellulose fibers, such as the high strength and the ability to adhere to each other and make strong inter-fibril bonds. In addition, the small dimensions and the large specific surface area open up for applications that may not yet be foreseen (Syverud and Stenius, 2009).

Filtration tests have been carried out on filter samples made of glass fibers mixed with nanofibrills produced from pinus radiata using five passes through a homogenizer at 1000 bar pressure. Solvent was used to blend the various components before the filter was formed in a cylindrical arrangement.

The challenge particles for the filter transmission assessment was NaCl obtained through a Collison nebulization (1 bar pressure) of a water solution. The filter face velocity was set at 5.5 cms^{-1}. Particle number concentration upstream and downstream the filter was measured by means of an SMPS+C system (CPC model 5.4 with DMA model 5.5, Grimm GmbH). Pressure drop across the filter was measured using an electronic manometer (Testo mod. 511 AG, Germany). The filter Figure Of Merit (FOM), given by the ratio between the logarithim of the particle penetration and the pressure drop, was measured. Table 1 shows the integrated filter efficiency (Eninger et al., 2008) between 20 nm and 500 nm and between 100 nm and 500 nm for two different samples (A and B).

Table 1. Integrated filter efficiency for two filters.

Size interval (nm)	Filter A (%)	Filter B (%)
20 -500	72 ± 2	67 ± 4
100-500	62 ± 1	52 ± 6

Figure 1 and 2 show respectively the filter efficiencies and the FOM for both filters.

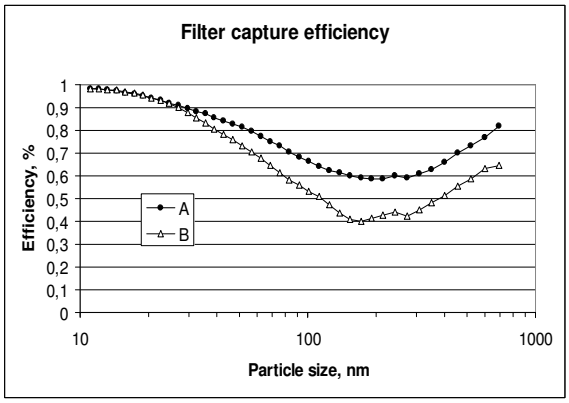

Figure 1. Filter capture efficiency for filters A and B.

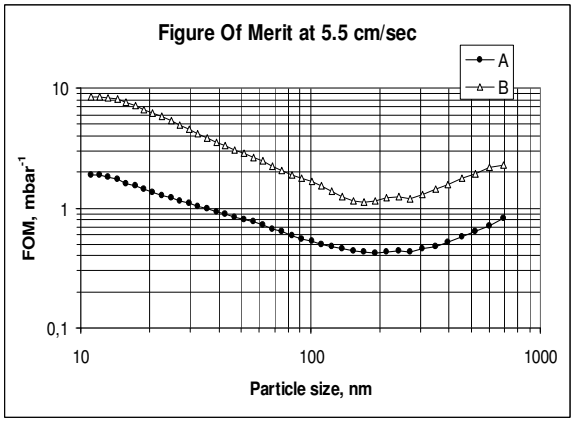

Figure 2. FOM for filters A and B.

Results show that filter A, 5% nanofibrills with a debonding agent containing a quaternary ammonium salt (berocell) has the better capture efficiency respect to the filter B (0% nanofibrills). However nanofibrills increase the pressure drop through the filter as shown in Figure 2. Pressure drop for filter A is 0.8 mbar while for filter B is 0.2 mbar at 5.5 cm s^{-1} face velocity.

This work was supported by PFI project 196119/V30 – Nanofilter: Nanofibril filter for environmental nanoparticles, financed through the Research Council of Norway.

Eninger R.M., Honda T., Adhikari A., Heinonen-Tanski H., Reponen T., Grinshpun S. A. (2008) A*nn. Occup. Hyg*., 52, 385-396.

Syverud, K. and Stenius P. (2009). *Cellulose* 16: 75-85.

Development of a fine particle filter for domestic wood-fired heaters

Dipl.-Ing. Sascha Schiller[1], Prof. Dr.-Ing. Hans-Joachim Schmid[1]

[1]Department of Mechanical and Environmental Process Engineering, University of Paderborn, Paderborn, 33098, Germany
Keywords: fine dust, baghouse filter, wood-fired heaters
Presenting author email: Sascha.Schiller@upb.de

In the recent decades wood combustion has become increasingly popular for private households. In our atmosphere the concentration of fine particles emitted by private wood-fired heaters has exceeded the emission concentration of the total road traffic. To control and reduce these emissions the German government decided in 2010 to renew emission regulations (1st BImSchV). The new limit contained therein was fixed in order to reduce the concentration of fine particles in the atmosphere. To comply with legal requirements a fine particle filter has to be developed, which combines good separation efficiency with convenience in operation for wood-fired heaters (e.g. pellet heaters or woodchip heaters).
For the first time a prototype of a baghouse filter (Fig. 1) has been designed with the aim to reduce the fine dust emissions to values substantially smaller compared to legislative limits. A special engineered test rig allows for analysis and optimization of the prototype and the required filter materials. CFD simulations are used to optimize temperature distribution and fluid flows through the filter.

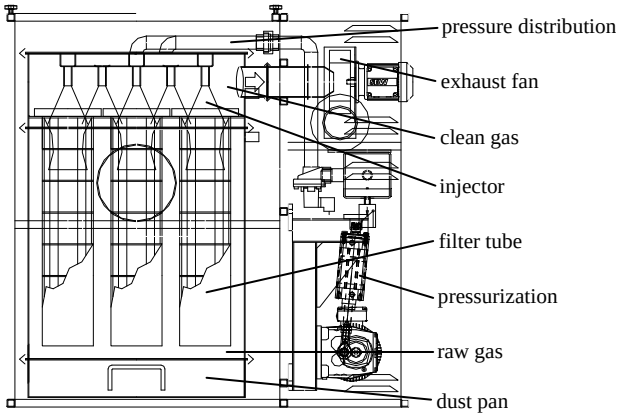

Figure 1. Prototype of the baghouse filter.

The development of a competitive filter system for private households makes it necessary to keep down acquisition costs and operating costs (electricity costs for the de-dusting process, costs for precoat material and costs for maintenance and repair). What are also inalienable are the process reliability (e.g. only annual checkup by the chimney sweeper) and the safety of the whole working process (flying sparks or kickback while de-dusting).

Results

First gravimetric analysis of the baghouse filter coupled with a pellet heater shows a mean fine dust concentration below 1 mg/m³ behind the filter, so the collection efficiency (compared to the fine dust concentration in front of the filter) amounts over 99.5%.
In order to prevent clogging of the filter cloth by sticky small particles, it is necessary to use a precoat. For this purpose different precoat materials were analysed (e.g. lime powder). In a test run that took over 48 hours the pressure drop of the filter has been determinated (Fig. 2) under real conditions.

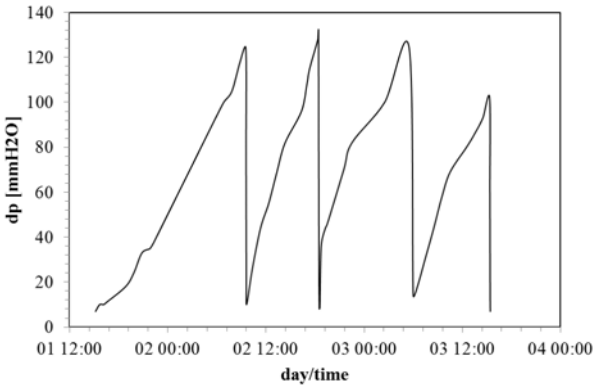

Figure 2. Pressure curve of a 48 h test run.

The pressure curve in Fig. 2 shows a nearly constant increase in pressure and a low level of remanent pressure drop after de-dusting (about 8 mmH2O). It is comparable to a typical pressure curve of a stable operated and online regenerated filter.
Some fluctuations are caused by variations of raw gas emissions due to internal ash removal cycles of the pellet heater.

These results are based upon a co-operation with the PEK GmbH in Konstanz, Germany. The project is supported by the AIF Berlin, Germany (support code: KF 2363802OH9).

Development of the Electro-physical Method of Aero-ion Cleaning of Gaseous Atmosphere

A.G Grishin, P.N. Martynov, I.V. Yagodkin, A.M. Posagennikov, V.P. Melnikov

FGUP State Scientific Center of the Russian Federation – Institute for Physics and Power Engineering (FGUP SSC RF IPPE), Obninisk, Kaluga Region, 249033, Russia
Keywords: Aero-ion cleaning, electro-physical method, high-efficient aerosol filters, air cleaning.
Presenting author email: grishin.andrew@gmail.com

Cleaning of gas-air flows in different branches of industry remains one of the most important directions in the field of technologies of environmental protection from aerosols of the different origin, including radioactive and toxic ones.

High-efficient aerosol filters being used today at NPP are the source of large volumes of radioactive waste subject to burial. They have a limited lifetime, and their fabrication and operation are costly.

The situation arisen with gas cleaning from radioactive and toxic aerosol particles at NPP requires, on the one hand, updating of traditional approaches and, on the other hand, development of fundamentally new methods and aids of air cleaning, namely, the principle of combined cleaning based on the fact that particles take up specific properties in ionized gas and then are to be caught on filters.

The problems of experimental investigation of the effect of intensive aeronization on catching of aerosol particles from the air flow using combined filtering systems is the subject of this paper.

Filtration of oil mists and dust - machining and grinding operations

T. Jankowski
Department of Chemical and Aerosol Hazards, Central Institute for Labour Protection – National Research Institute, 00-701 Warsaw, Poland
Keywords: nonwovens, oil mist, dust, filtration efficiency, machining

Air pollution in industrial workplaces in the form of liquid aerosols (mineral oil mist) and solid (dust) is the dispersed phase side effects of the processes with the use of coolant oil. The actual conditions of industrial processes, particularly with the use of coolant oil, the primary goal is to provide users with the work premises protection against the risks associated with simultaneous exposure to solid and liquid aerosols.

Numerous scientific studies conducted around the world, mainly focused on the mechanisms of dust filtration. We have conducted several studies on the harmful effects of aerosol particles of liquid in man. The available information suggests that the mechanism of aerosol filtration with a liquid phase is distributed differently from dust filtration mechanism. Hence it is important to conduct research leading to the knowledge of relationships and phenomena occurring during the simultaneous emission and deposition of aerosol particles from the liquid and solid dispersed phase.

To protect against the risks associated with exposure to dust and liquid aerosols particles are used in various purification systems, the basic structural element is nonwoven filter. Nonwovens are characterized by extensive spatial structure, so that dust and liquid aerosol particles can deposit inside the structure of the individual fibers.

The CIOP-PIB conducted the study are unknown filtering process for protecting workers from harmful solid and liquid aerosols by using filtration systems. The test method is to study the efficiency of filtration through systems consisting of nonwovens made of synthetic fibers of different morphology, which are used in ventilation, capture and separation systems during machining and grinding using oil coolant. Investigations are performed synthetic dust (ASHRAE 52/76) and aerosol ester bis (2-ethylhexyl) sebacic acid (DEHS) test using an optical particle counter OPC and scanning mobility particle sizer SMPS.

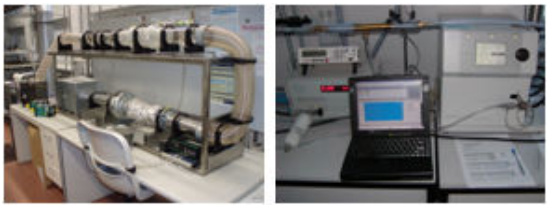

Figure 1. Experimental set-up.

Figure 1 illustrates the experimental set-up involving units generating, sampling and counting of dust and liquid aerosol particles.

Total and fractional filtration efficiency and inlet particle size distributions of solid and liquid aerosol for different values of aerosol velocity are presented in Figure 2, 3 and 4.

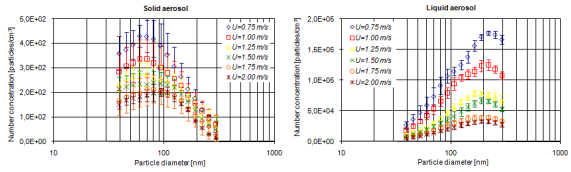

Figure 2. Inlet particle size distributions of solid and liquid aerosol.

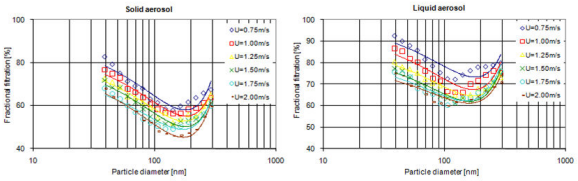

Figure 3. Fractional efficiency of solid and liquid aerosol at different aerosol velocities.

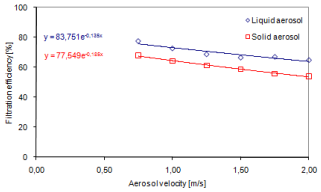

Figure 4. Total filtration efficiency of solid and liquid aerosol.

Based on the studies will be possible to define rules for assessing the efficiency of filtration systems for reducing or eliminating the risks associated with simultaneous exposure to aerosol particles of liquids and solids. This will allow the establishment of guidelines supporting their use to predict the deposition of solid and liquid aerosol particles, while maintaining the most favorable conditions for filtration.

This paper has been prepared on the basis of the results of research task carried out within the National Programme “Improvement of safety and working conditions” partly supported in 2011-2013 within the scope of research and development by the Ministry of Science and Higher Education. CIOP-PIB has been the Programme main coordinator.

Podgórski A., Bałazy A. (2003) *Journal of Aerosol Science, vol. II, 1197-1198*.
Mullins B. J., Kasper G. (2006) *Proc. Int. Aerosol Conf., Minneapolis, USA.*

Penetration of sub 30 nm particles through mechanical and electret fibrous filters

Maißer, A.[1], Jackiewicz, A.[2], Podgórski, A.[2†], Koch, N.[1], Szymanski, W.W.[1] and Gradoń, L.[2]

[1]Faculty of Physics, University of Vienna, Boltzmanngasse 5, 1090 Vienna, Austria
[2]Faculty of Chemical and Process Engineering, Warsaw University of Technology, Waryńskiego 1, 00-645 Warsaw, Poland
[†]recently deceased

Keywords: aerosol filtration, electret filter, fibrous filter, nanoparticles
Presenting author email: nikolaus.koch@univie.ac.at

In this study the penetration of neutral and singly charged particles in the sub 30 nm size range through polydisperse fibrous filter media has been investigated. The particles used for these measurements are proteins and silica particles. All particles are aerosolized from appropriate suspensions using a commercial electrospray aerosol generator (EAG Mod. 3480, TSI, Inc.).

To analyze and classify generated aerosol a home-made parallel DMA (PDMA) that uses two identical Vienna type nano-DMAs (nDMA1 and nDMA2) in parallel (Allmaier et al., 2008) is used. The first DMA scans for size distribution over the entire size range and the second one is used to classify the peak of the size distribution to generate highly monodisperse aerosol particles for filtration experiments.

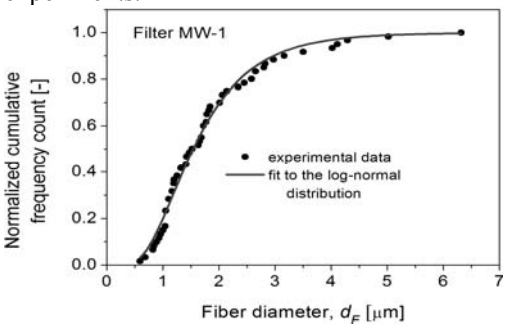

Filter symbol	D_{fg} [μm]	ε [%]	L [mm]	Q_s [kg/m2]	σ [-]
○	1.54	97.50	2.05	0.039	1.67
Δ	1.45	97.40	1.94	0.041	1.72

Fig. 1. Fiber size distribution and filter characteristics

To determine the penetration through filter media two identical branches are used. Both consist of a steel Millipore™ filter holder and a 2-way valve to select between the two branches. In the first branch the filter holder is empty and used to determine upstream concentration and correct for particle losses. In the second branch the filter to investigate is placed inside. As a detection instrument a TSI CPC (CPC Mod. 3025, TSI, Inc.) is used in high flow mode (1.5 lpm) which leads to a face velocity of 8.8cm/s.

The melt-blown polypropylene filters consist of polydisperse filter fiber diameters. Their structural characteristics (porosity, ε, thickness, L, basis weight, q_S, geometric mean fiber diameter, d_{Fg}, and the geometric standard deviation, σ) are shown in the table within Fig. 1.

As shown in Fig. 2. measured penetration values indicate that the classical filtration theory, using a fiber mean diameter, significantly underestimates the penetration through polydisperse fibrous filters.

In addition it can be seen that for neutral particles there is no significant difference of penetration through electrical neutral or electret filter media. This indicates that the electrostatic effects such as polarization effects play a minor role in the investigated nm size range.

A theoretical approach to determine penetration of charged particles through mechanical filter media has been developed. The so called Partially Segregated Flow Model (PSFM) for fibrous filters uses a log-normal distribution (shown in Fig.1) of fiber diameters for calculations of penetration through the filter material. This theoretical approach has been experimentally, successfully validated (Podgórski et al., 2010).

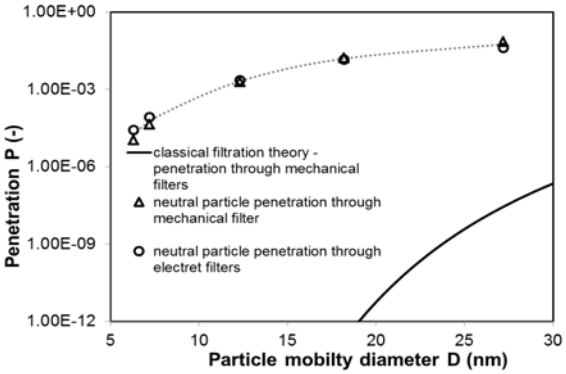

Fig. 2. Experimental penetration through the filters

This work was supported in part by the ÖAD-WTZ, Project No. PL-06/2007.

Allmaier, G., Laschober, G., and Szymanski, W.W., (2008). *J. Amer. Soc. Mass Spectrom.* **19,** 1062-1068

Podgórski A., Maißer, A., Szymanski, W.W., Jackiewicz, and Gradon, L., (2010). *Aerosol Sci. and Technol.* **45,** 196-214

Collection efficiency of axial-flow cyclone for air handling unit of subway station

Seyoung Kim[1], Soon-Bark Kwon[2], Myungjoon Kim[1], Joong-Goo Kang[3], Chang-Heon Shin[4] and Taesung Kim[1]

[1] Department of Mechanical Engineering, SungKyunKwan University, Suwon, 440-746, Korea
[2]Railroad Environment Research Department, Korea Railroad Research Institute, Uiwang, 437-757, Korea
[3]RITCO, Seoul, 120-700, Korea
[4]Seoul Metro, Seoul, 156-080, Korea
Keywords: Axial-flow cyclone, Air handling unit(AHU), subway
Presenting author email: syspace@krri.re.kr

In Korea, particulate matter (PM) is one of the major indoor air pollutants especially in the subway. In order to remove PM in the subway station, several kinds of PM removal system such as medium filter, auto suction filter, auto washing filter and electrostatic precipitator are used in the air handling unit (AHU) of subway stations. However, those systems are prone to operation and maintenance problems since the filter-regeneration unit consisting of electrical or water jet parts might malfunction due to the high load of particulates unless the filter medium is periodically replaced. In this study, we suggested axial-flow cyclone system with minimized maintenance requirement comparing to above mentioned method.

Cyclone is widely used for dust or droplet removing from the main flow. This device has some advantages such as, constant pressure drop, high throughput with moderate efficiency and low maintenance cost (Slack *et al*., 2000). The axial-flow cyclone was developed based on previous numerical study (Kim et al., 2009). The mock-up system was evaluated by particle collection efficiency and pressure drop experimentally. The results obtained from particle number concentration showed that the collection efficiency of 41.2 ~ 85.9% for the particles of 1.5 ~ 5.8 μm with the pressure drop of less than 20 mmH_2O (fig. 2). The collection efficiency estimated by total mass collection also showed 65.7% which was higher than that of current filter system by 2 times.

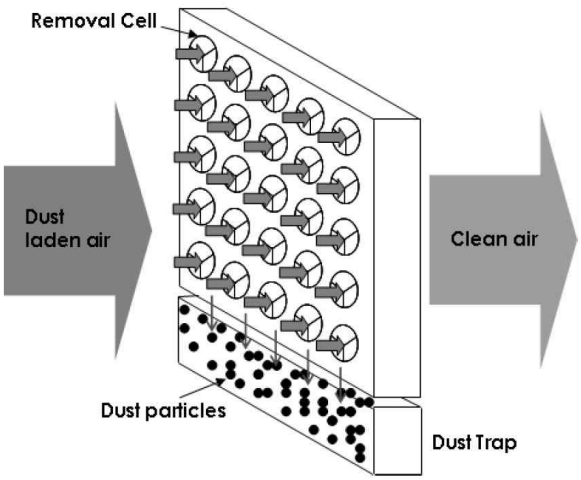

Figure 1. Schematic of air filter system of axial-flow cyclone.

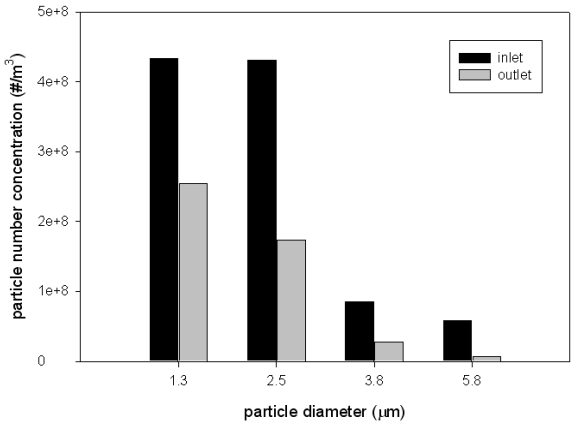

Figure 2. Particle number concentration of axial-flow cyclone inlet and outlet.

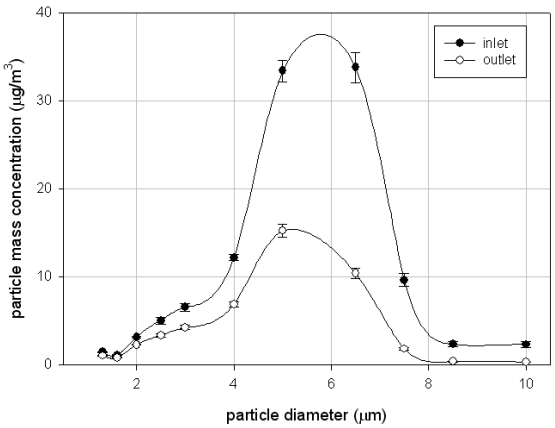

Figure 3. Particle mass concentration of axial-flow cyclone inlet and outlet.

ACKNOWLEDGEMENT

This work was supported by a grant(Urban Transit Standardization A01) from "The 4rd phase of R&D on the urban transit standardization." funded by Ministry of Land, Transport and Maritime Affairs of Korean government

Slack, M. D., Prasad, R. O., Bkker, A., et al. (2000). Chem. Eng. Res. Des., 78, 241-242.

Kim, M., Kim, H., Kwon, S. B., et al. (2009). International Journal of Air-Conditioning and Refringeration, 17(3), 94-99.

Experimental Study on Transition from Bismuth Saturated Vapors to Liquid Nuclei

S. di Stasio[1], A.A. Onischuk[2] , A.M. Baklanov[2], V.V. Karasev[2]

[1]Istituto Motori CNR-IM Aerosol and Nanostructures Lab, Via Marconi 8, Napoli, 80125, Italy
[2]Institute of Chemical Kinetics and Combustion RAS, Institutskaya, 3, Novosibirsk, Russia
Keywords: Metal nanoparticles, Nanoparticles generation, Nucleation, Vapour Pressure
Presenting author email: stefano.distasio1600@gmail.com

Bismuth is a very interesting material. In the bulk state it is a metal with a very small overlap (38 meV at 0 K) between valence and conduction band but, if it is synthesized as nanomaterial below certain dimensions, it becomes semiconductor. Synthesis of differently shaped Bi nanostructures has been proposed (Wang et al, 2006). Bismuth is also widely used as material for Hall effect -nanosensors (Koseva et al, 2010) and scanning Hall probe microscopy (Sandhu et al, 2004).

In this study we present the results of our experiments on the process of transition from Bi saturated vapors to liquid nuclei in a classical evaporation-condensation generator. We performed measurements by Authomatic Diffusion Batteries (ADB), TEM, SEM and HR-TEM. Thin filaments (about 1 mm diameter) of quartz have been used to probe Bi deposits occurring during the stages of nucleation at different abscissas/residence times. An example of nucleation process with evaporation temperature 600 °C is discussed in the following. The analysis at SEM (LEO 1430 VP) of filament portion inside the furnace shows a deposition of a uniform layer of saturated vapors formed by islands (Fig. 1a, 1b, X=-26 mm, X=0 outlet section of furnace). At larger abscissas in proximity of furnace outlet section (X>0), some pillars and elongated structures are observed to form, first sporadically and after organized in skein (Fig. 1c, X=+4 mm). Later on, the first nanoparticles which deposit on the underlying island substrate are observed on the sample (Fig. 1d, X=+19 mm). This latter stage correspond to the start of homogeneous nucleation.

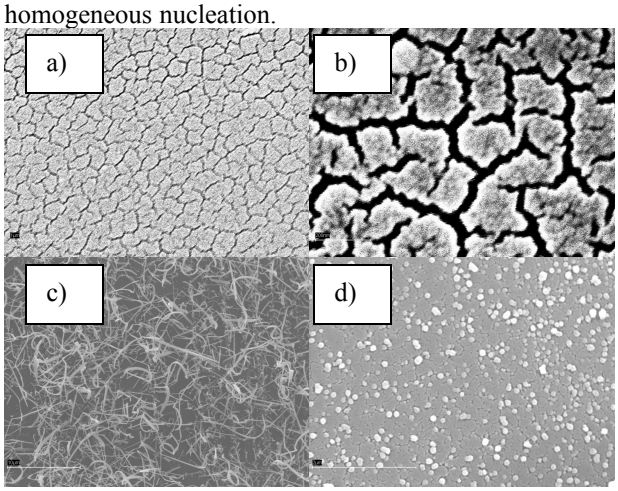

Fig. 1. SEM images of Bi deposit on quartz filament.

The measurements of Bi nanoparticles by ADB are reported in Fig. 2a, 2b. One inconvenient of the experiments is that at exit from furnace (X=0) the temperature is still above the melting point of Bismuth (T_{melt}=208.98 °C) and therefore liquid particles undergo a continuous coagulation and partial re-evaporation. In order to find out the placement of nucleation zone, we sample with metal grids (dia 8 mm, mesh ~ 0.7 mm) inside the reactor. At nucleation start a depletion of Bi vapor gas molecules does occur very quickly and the very small nuclei diffuse rapidly and deposit onto the grids. The fast growth of Bi nanoparticles produces soon a much smaller diffusion effect. Therefore with ADB we measure out of reactor a minimum of particle concentration just when the grid is positioned at the nucleation burst abscissa (Fig. 3).

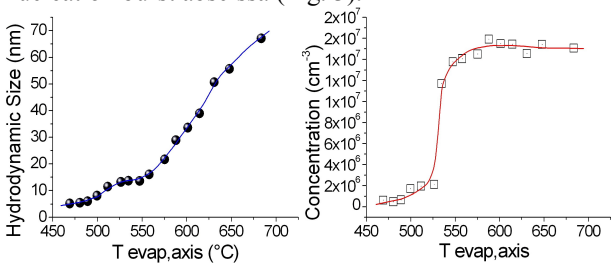

Fig. 2a, 2b. Size (left) and concentration (right) of Bi nanoparticles as measured by ADB.

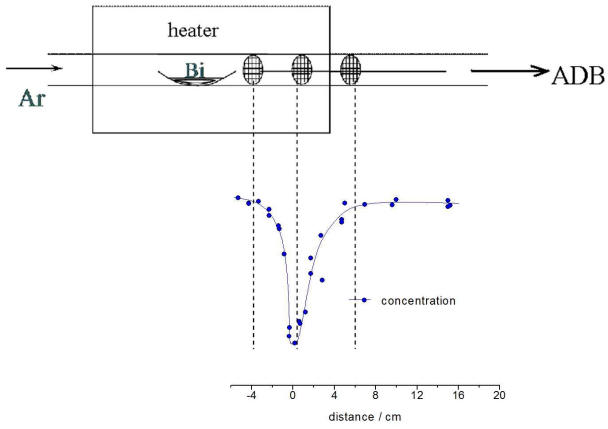

Fig. 3. Experimental determination of nucleation position inside the flow reactor.

Support by Cooperation Agreement between CNR (Italian National Research Council) and RAS (Russian Academy of Science) years 2008-2010 is sincerely thanked.

References

Wang WZ et al (2006) *J. Phys. Chem. B* **110**, 25702-25706.
Sandhu A et al (2004) *Japanese J. Appl. Phys.* **43**, 777-778.
Koseva R et al. (2010). *Thin Solid Films* **518**, 4847-4851.

Translation-Rotation Correction Factor in the Theory of Homogeneous Nucleation

S. V. Vosel, A. A. Onischuk, P. A. Purtov

Institute of Chemical Kinetics and Combustion, Novosibirsk 630090, Russia
Keywords: translation-rotation correction factor, homogeneous nucleation.
Presenting author email: onischuk@kinetics.nsc.ru

In the theory of nucleation from the vapor phase the contribution to the free energy of the critical nucleus from the translational and rotational degrees of freedom should be accounted. Due to this contribution the so-called free energy correction factor arises in the formula for the nucleation rate. Lothe and Pound [1] have estimated (within the framework of the Gibbs imaginary process of drop formation) the correction factor for water of about 10^{17}. Reiss and co-workers [2] have argued that the Lothe and Pound correction factor was exaggerated too much due to the neglect of the fluctuation of the center of mass of the nucleus and a new correction was proposed to be a factor of 10^3 - 10^6. Recently Kusaka [3] has derived a rigorous formula for the correction factor within the framework of the Gibbs process of drop formation and calculated numerically this factor for the Lennard-Jones system which was 10^9 to 10^{13}. The formula of Kusaka is applicable only for numerical calculations. However, the calculations of this kind are only possible for simple systems and, therefore, an analytical expression for the correction factor applicable to a wide range of real systems is necessary. In this work we give the derivation of the analytical formula for the translation-rotation correction factor. This formula is based on the Reiss approach considering the contribution from the clusters translational degrees of freedom, the Frenkel's kinetic theory of liquids, and Kusaka theory.

Accordung to the Lothe-Pound and Kusaka theory the free energy correction factor K can be determined within the framework of the Gibbs imaginary process of the drop extrusion from the homogeneous macroscopic liquid phase (reference phase) having the same chemical potential as the critical nucleus: $K = \frac{Q_{tr}Q_{rot}}{q_{rep}}$, where Q_{tr} and Q_{rot} are the partition functions for free translations and free rotations of the critical drops, respectively, $q_{rep} = Q_{tr}^{l}Q_{rot}^{l}$, is the partition function for the six degrees of freedom of the drop embedded into the reference phase (Q_{tr}^{l} and Q_{rot}^{l} are the translational and rotational partition functions, respectively) which are to be deactivated in the Gibbs extrusion process. We have shown that Q_{tr}^{l} and Q_{rot}^{l} can be determined as the partition functions for translational fluctuations of the center of mass of embedded drop and rotational vibrations of the embedded drop, respectively. The resulted analytical formula for the correction factor is:

$$K = \frac{\pi^{7/2}}{Sn_1^{sat}\sigma^3} \times \left(\frac{32R_S^5\rho k_B T}{15h^2}\right)^{3/2} \exp\left(\frac{3h\nu_{\max}}{2k_B T}\right)\left\{1 - \exp\left(-\frac{h\nu_{\max}}{k_B T}\right)\right\}^3 \quad (1)$$

where k_B is the Boltzmann constant, T is the absolute temperature, S is the supersaturation ratio, n_1^{sat} is the saturated vapor number density, R_S is the radius of the surface of tension of the critical nucleus, ρ is the density of the reference bulk liquid, h is Planck's constant, $\nu_{\max}$ is the Debye frequency for the reference phase $\sigma \approx \frac{0.2}{(4\pi/3)^{1/6}}\left(\frac{m}{\rho R_S}\right)^{1/2}$ is the standard deviation in any of the three Cartesian coordinates for the fluctuations of the center of mass of the embedded drop [2], m is the molecule mass. Fig. 1 compares the correction factor estimated analytically vis Eq. (1) and that calculated numerically by Kusaka [3]. One can see that these two factors are in a good agreement with each other. The temperature dependences are in an excellent agreement.

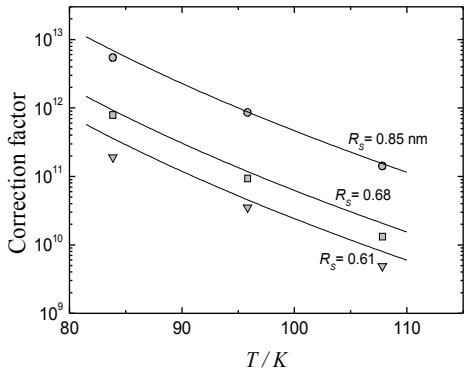

Fig. 1. Translation-rotation correction factor as estimated for Ar analytically via Eq. (1) (lines) and numerically [3] (symbols).

Financial support for this work was provided by the Cooperation Agreement between CNR (Italian National Research Council) and RAS (Russian Academy of Science) years 2008-2010 and Siberian Branch of Russian Academy of Sciences (Interdisciplinary Integration Project No. 3).

References

1. J. Lothe, G. M. Pound, *J. Chem. Phys.* 1962, 36**,** 2080
2. H. Reiss, J. L. Katz, E. R. Cohen, *J. Chem. Phys*. 1968, 48, 5553.
3. I. Kusaka, *Physical Review* E 2006, 73, 031607.

Diffusion coefficient measurements of sulphuric acid in air

D. Brus[1,2], K. Neitola[1], T. Petäjä[3] and H. Lihavainen[1]

[1]Finnish Meteorological Institute, Erik Palménin aukio, P.O. Box 503, FI-00101 Helsinki, Finland
[2]Laboratory of Aerosol Chemistry and Physics, Institute of Chemical Process Fundamentals Academy of Sciences of the Czech Republic, Rozvojová 135, CZ-165 02 Prague 6, Czech Republic
[3]Department of Physics, University of Helsinki, P.O.Box 64, FI-00101 Helsinki, Finland

Keywords: diffusion coefficient, sulphuric acid, flow tube, CIMS.
Presenting author email: david.brus@fmi.fi

Sulphate aerosols play an important role in atmospheric chemistry. They have indispensable impact on climate, radiation balance, and human health. In the atmosphere sulphate aerosols are formed due to secondary particle production (gas to particle conversion) from sulphuric acid and water, and probable participation of other trace specie like ammonia or amines. The sulphuric acid diffusion coefficient data has wide application in atmospheric and aerosol mass transfer models.

The diffusion coefficient was estimated from the first-order rate coefficients for the wall loss of H_2SO_4. The wall loses were measured as a function of relative humidity (RH) in the range from 2 to 70 % in a laminar flow tube. The chemical ionization mass spectrometer (CIMS) was used to detect the H_2SO_4 concentration (Petäjä et al. 2009).

The H_2SO_4 loss measurements were carried out at three temperatures 5, 15 and 25°C and atmospheric pressure in a vertically positioned thermostated cylindrical tube with I.D.= 6 cm and length of 200 cm. The sulphuric acid vapour was generated by passing purified dry particle free air through a temperature controlled saturator filled with 95-97 % pure H_2SO_4 and subsequently mixed with humidified air in a mixer. The vapour gas mixture was then introduced to a laminar flow tube made of stainless steel where the H_2SO_4 concentration was measured with CIMS at six different positions along the reactor. The wall losses were determined from the slopes of the fits to experimental data in the plot H_2SO_4 concentration as a function of position in the tube. To ensure the independence of wall losses on H_2SO_4 concentration, the measurements were carried out at different H_2SO_4 concentrations (~10^5-10^8 molecules cm^{-3}) and different total flow rates (8-11 l/min).

Figure 1 shows the measured diffusion coefficients of H_2SO_4 in air as a function of RH and at three temperatures 5, 15 and 25 °C. The measured points are accompanied with the fit to H_2SO_4-N_2 data published by Hanson and Eisele, 2000. The diffusion coefficient values decreased as the RH was increased. The diffusion coefficient dependency on RH flattens in the range of RH = 20-50 %, where the difference is less than 5%. These results show lower wall losses and slower diffusion to the wall due to strong hydration of H_2SO_4 molecules (Jaecker-Voirol and Mirabel, 1988).

The temperature dependency was found to be the power of 6 to measured diffusion coefficient when data for the whole range of RH are considered. This discrepancy is possibly due to higher order losses of H_2SO_4 to bigger clusters at lower temperatures.

The calculated value of diffusion coefficient of H_2SO_4 in dry air using the Fuller method (Reid et al, 1987) is 0.11 cm^2s^{-1}, which is in close agreement with measured data at 25 °C.

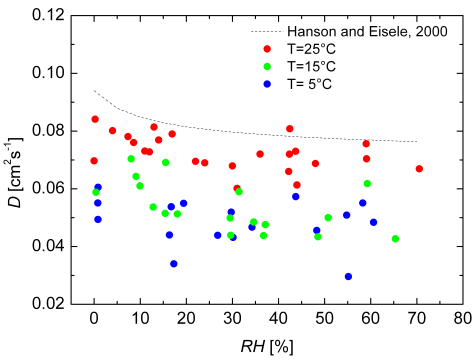

Figure 1. Diffusion coefficient data of H_2SO_4 in air as a function of relative humidity (RH) at three temperatures 5, 15 and 25 °C compared to fit to H_2SO_4-N_2 data of Hanson and Eisele, 2000.

This work was supported by KONE foundation and Academy of Finland Centre of Excellence program.

Petäjä, T., Mauldin, R. L.,Kosciuch, E., McGrath, J., Nieminen, T., Paasonen, P., Boy, M., Adamov, A., Kotiaho, T.. and Kulmala, M. (2009), *Atmos. Chem. Phys.*, 9, 7435-7448.

Hanson, D. R. and Eisele, F. (2000). *J.Phys.Chem A 104*, 1715-1719.

Jaecker-Voirol A., and Mirabel, P., (1988) *J. Phys. Chem*., 92, 12.

Reid, R. C., Prausnitz, J. M, Poling , B. E. (1987). *The Properties of Gases and Liquids*. fourth edition, Mc Graw-Hill Inc., New York.

Size effect in homogeneous nucleation in nanoscale particles

V.V. Levdansky[1], J. Smolik[2], V. Zdimal[2] and P. Moravec[2]

[1]Heat and Mass Transfer Institute NASB, 15 P. Brovka Str., Minsk 220072, Belarus
[2]Institute of Chemical Process Fundamentals AS CR, v.v.i., Rozvojova 135, 165 02 Prague, Czech Republic
Keywords: nanoparticles, nucleation, size effect.
Presenting author email: vlev5@yahoo.com

The nucleation process in nanoscale particles is of interest both for the new technology and atmospheric physics. It is known that many physicochemical processes in the systems with nanoscale objects are characterized by some specific features. In particular, the physicochemical processes in the aerosol systems with nanoscale particles and in aerosol particles themselves can depend on the particle size. Some questions related to the influence of the size effect on the critical size of aerosol particles and on homogeneous gas-phase nucleation were considered in (Levdansky *et al*., 2010). Here we study the influence of the size effect on homogeneous nucleation inside nanoparticles.

Let us consider the situation when supersaturation of one component in the two-component nanoparticle takes place that can lead to nucleation of this component. The rate of nucleation J_n by analogy with (Ring, 2001) can be written as

$$J_n = k_Z k_r n N_c = k_Z k_r n^2 \exp\left(-\frac{\Delta G_c}{kT}\right), \qquad (1)$$

where k is the Boltzmann constant, T is the temperature, k_r is the effective rate constant for the attachment of monomers (molecules or atoms) to the critical cluster allowing for both diffusion of monomers to the critical cluster and their incorporation into the cluster, k_Z is the Zeldovich factor, n is the number concentration of monomers, N_c is the number concentration of the critical clusters, ΔG_c is the free energy of critical cluster formation.

The value of k_r in the case under consideration can be estimated as

$$k_r = \frac{2\pi d_c v a^2 \exp\left(-\frac{Q_p}{kT}\right)}{1+\frac{2a}{d_c}\exp\left(\frac{Q_c - Q_p}{kT}\right)}, \qquad (2)$$

where d_c is the diameter of the critical cluster, Q_c is the activation energy for the incorporation of monomers into the critical cluster, Q_p is the activation energy for the diffusion of monomers in the particle, v and a are respectively the values characterizing the vibration frequency and the jump length of monomers.

Taking into account (Vanithakumari and Nanda, 2008; Rekhviashvili and Kishtikova, 2006), the values of Q_c and Q_p can be written as

$$Q_c = Q_{c\infty}\exp\left(-\frac{4}{1+d_{c0}}\right), \qquad (3)$$

$$Q_p = Q_{p\infty}\exp\left(-\frac{4}{1+d_{p0}}\right), \qquad (4)$$

where $d_{c0} = d_c/\delta_c$, $d_{p0} = d_p/\delta_p$, d_p is the particle diameter, δ_c is the Tolman length for the critical cluster, δ_p is the Tolman length for the particle, $Q_{c\infty}$ and $Q_{p\infty}$ are the values of Q_c and Q_p without considering the size effect.

From the foregoing it follows that the size dependence of the activation energies Q_c and Q_p can affect the nucleation rate in nanoscale particles. Let us consider for simplicity the case when the second term in the denominator of Eq. 2 is much more than unity. Figure 1 shows for this case the dependence of $k_{r0} = k_r/k_{r\infty}$, where $k_{r\infty}$ is the value of k_r for $Q_c = Q_{c\infty}$, on d_{c0}. It is seen that k_{r0} increases with a decrease in d_{c0}.

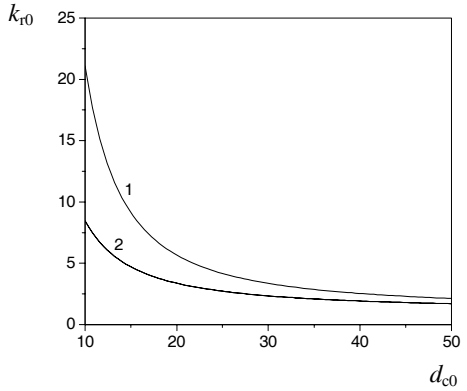

Figure 1. Dependence of k_{r0} on d_{c0}; 1: $Q_{c\infty}/kT = 10$, 2: $Q_{c\infty}/kT = 7$.

This work was supported by GAAVCR projects IAA400720804, IAA200760905 and GACR project 101/09/1633.

Levdansky, V.V., Smolik, J. and Moravec, P. (2010) *Int. Commun. Heat Mass Transfer* **37**, 593-595.

Rekhviashvili, S.Sh. and Kishtikova, E.V. (2006) *Tech. Phys. Lett.* **32**, 439-441.

Ring, T.A. (2001) *Adv. Colloid Interface Sci.* **91**, 473-499.

Vanithakumari, S.C. and Nanda, K.K. (2008) *Phys. Lett. A* **372**, 6930-6934.

Contact angle, seed particle radius and the onset of heterogeneous nucleation

V. Loukonen[1] and H. Vehkamäki[1]
[1]Department of Physics, University of Helsinki, P.O. Box 64, FI-00014 Helsinki, Finland
Keywords: Heterogeneous nucleation, Classical nucleation theory
ville.loukonen@helsinki.fi

Perhaps the most common framework in both experimental and theoretical nucleation studies is the classical nucleation theory (CNT). Based on thermodynamics, it can be used as soon as a few macrosopic parameters are known, and as a computationally efficient method, it is the standard choice for large systems.

Regardless of its popularity, some details in CNT are still unclear. In the present work we study how the size of the condensation seed particle and the contact angle formed between the seed particle and the nucleating droplet affect the onset of heterogeneous nucleation.

Definitions

In one-component homogeneous nucleation, the onset is typically taken to be a nucleation rate of $J_{\mathrm{hom}} = 1/\mathrm{cm}^3\,\mathrm{s}$ or the corresponding value of saturation ratio S. In the heterogeneous case the existence of condensation seed particles introduces some complications, as now also the concentration and size distribution of the seed particles matters. To circumvent these problems, often an auxiliary quantity of nucleation probability is used. It is defined as

$$P \equiv 1 - \exp\left(-4\pi R^2 J_{\mathrm{het}}\tau\right),$$

where R is the radius of the condensation seed particle, J_{het} is the heterogeneous nucleation rate and τ is nucleation time interval. The onset of heterogeneous nucleation is often chosen to be the saturation ratio corresponding to the nucleation probability of $P = 1/2$.

Even though the both definitions of onset are somewhat arbitrary, they are frequently used in the literature. However, as it turns out, the definitions are inconsistent with each other.

Discrepancies

In Figure 1, heterogeneous onset curves for several contact angles are shown as a function of the condensation seed particle radius for water and non-soluble, electrically neutral seed particles at the temperature of 285 K.

It can be seen that with large enough contact angle, the saturation ratio required for the onset of heterogeneous nucleation is always larger than what is required for the onset of homogeneous nucleation. Although heterogeneous nucleation is energetically more favourable than homogeneous, it does not necessarily begin at the lower values of saturation ratio. The radius of the condensation seed particle and the contact angle have a strong effect on the onset of heterogeneous nucleation. From Figure 1 it is also evident that the homogeneous nucleation is not restored from the heterogeneous nucleation as the contact angle approaches the value of 180°, i.e. when the contact disappears.

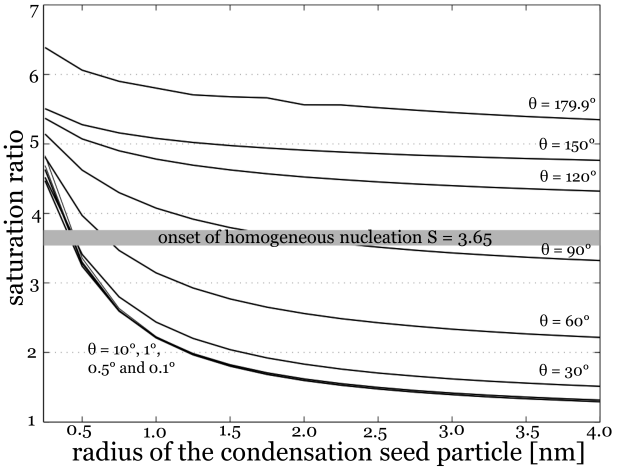

Figure 1: Heterogeneous onset curves for water at $T = 285$ K. Each point on the curves corresponds to a nucleation probability of $P = 1/2$ with an indicated contact angle in the (R,S)-plane. The onset of homogeneous nucleation, $S = 3.65$, is marked with a grey bar.

Furthermore, while interpreting experimental data, the seed particles are often assumed to be fully "wettable", that is, the contact angle is assumed to be zero. However, within CNT this assumption is geometrically possible only when the seed particle is smaller than the critical cluster. Close attention should be paid to the assumptions regarding the contact angle and radius of the condensation particle.

These issues bear some significance, as it is often important to know the conditions where nucleation begins. Thus consistent definitions for the onsets are called for, or perhaps altogether a novel way of comparing homogeneous and heterogeneous nucleation.

This research has been supported by the Maj and Tor Nessling Foundation and the Academy of Finland.

Heterogeneous nucleation of water vapor on nanoparticles and ions, and its temperature dependence

A. Kupc[1], A. Vrtala[1], P.E. Wagner[1], P. M. Winkler[2] and CLOUD Collaboration

[1]Faculty of Physics, University of Vienna, Vienna, A-1090, Austria
[2]Advanced Study Program, National Center for Atmospheric Research, Boulder, Colorado, 80305, USA

Keywords: heterogeneous nucleation, water vapour, aerosols
Presenting author email: agnieszka.kupc@univie.ac.at

Although particle formation processes have been the subject of investigation by many scientists, further research and detailed description of nucleation mechanisms are essential to better understand atmospheric aerosols, their interactions and influence on global climate.

In the present study we focus on the activation of molecular ions, as well as charged and neutral aerosol particles with diameters down to about 1nm in supersaturated water vapor. Seed particles of different composition (e.g. Ag, NaCl, WO_x) are investigated. The aim is to clarify the dependence of the heterogeneous nucleation of water vapor on seed particle size and charging state, with particular focus on nucleation behavior at different nucleation temperatures. Heterogeneous nucleation probabilities are determined using an expansion chamber, the Size Analyzing Nuclei Counter (SANC; Wagner et al., 2003), for measuring droplet number concentration. Besides the SANC, the experimental system consists mainly of aerosol-, and vapor generation units. Particles inducing heterogeneous nucleation in the SANC system at the vapor supersaturations considered, lead to the formation and growth of liquid droplets, which then are optically detected by means of the Constant-Angle Mie Scattering (CAMS, Wagner, 1985) method. Figure 1 presents an example of the growing droplets. Experimental findings on the activation of seed particles by heterogeneous nucleation of water vapour are compared with theoretical calculations (Kelvin and Fletcher theory, Fletcher, 1958), and other results from similar experiments for n-propanol, n-nonane vapour where inorganic insoluble seed aerosol (WO_x, Ag, $(NH_4)_2SO_4$), and soluble NaCl particles were used (Winkler et al. (2008a, b), Schobesberger S. et al., 2010). Currently, a mobile and more versatile version of the SANC is being developed and planned to be integrated in the experiments set up of the CLOUD (Cosmics Leaving Outdoor Droplets) project at CERN. At CLOUD various aspects of the interaction of cosmic rays with aerosols and clouds are investigated, bearing on the possibility of a 'solar indirect' influence on climate. The goal is to contribute to the understanding of mechanisms leading to new particle formation by studying ion induced and binary and ternary nucleation.

Experimental investigations on the activation of nanoparticles and ions by heterogeneous nucleation of water vapour at defined vapour saturation ratios and various temperatures will be presented.

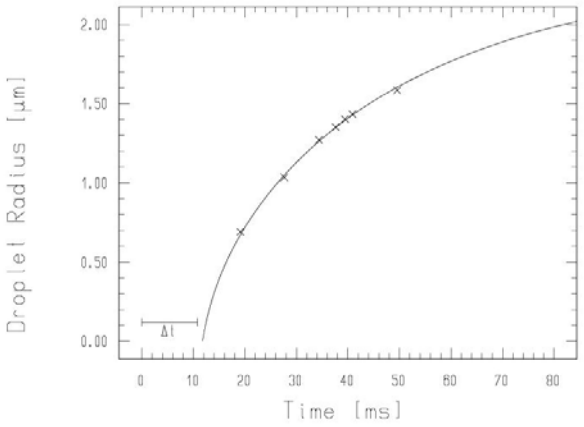

Figure 1. Radii of the growing water droplets measured versus time after expansion for one sample experiment. Oxidised Ag particles at 8nm size are used here. Markers present experimental values, while line presents theoretical calculations.

We would like to thank CERN for supporting CLOUD with important technical resources, and for providing a particle beam from the CERN Proton Synchrotron. This research has received funding from the EC's Seventh Framework Programme under the grant agreement no. 215072 (Marie Curie Initial Training Network "CLOUD-ITN"), from the German Federal Ministry of Education and Research (project no. 01LK0902A), and from the Swiss National Science Foundation, and from the Academy of Finland Center of Excellence Program (project no. 1118615).

Fletcher, N. (1958) J. Chem. Phys. 29, 572
Schobesberger S. *et al.*, (2010) *Atmos. Chem. Phys*. 11, 3874-3882
Wagner, P.E. (1985) *Journal of Colloid and Interface Science*, 105: 456-467
Wagner, P.E. *et al.* (2003) Phys. Rev. E 67, 021605
Winkler, P.M., *et al.*, (2008a) *Science* 319, 1374
Winkler, P.M. et al., (2008b) *Atmos. Res.* 90, 187-194

Influence of trimethylamine to sulphuric acid-water homogeneous nucleation

K. Neitola[1], D. Brus[1,3], M. Sipilä[2], T. Jokinen[2], P. Paasonen[2] and H. Lihavainen[1]

[1]Finnish Meteorological Institute, Erik Palménin aukio, P.O. Box 503, FI-00101 Helsinki, Finland
[2]Department of Physical Sciences, University of Helsinki, P.O.Box 64, FI-00101 Helsinki, Finland
[3]Laboratory of Aerosol Chemistry and Physics, Institute of Chemical Process Fundamentals Academy of Sciences of the Czech Republic, Rozvojová 135, CZ-165 02 Prague 6, Czech Republic
Keywords: homogeneous nucleation, sulphuric acid, amine, flow tube.
kimmo.neitola@fmi.fi

Sulphuric acid is known to play a key role in atmospheric nucleation (gas to particle conversion). The attention has shifted lately towards a third nucleating species (ammonia, amines) in addition to sulphuric acid and water. This is due to recent quantum chemical calculations that suggest a third species to thermodynamically stabilize sulphuric acid-water molecular clusters.

Flow tube technique was used to study homogeneous nucleation of sulphuric acid and water with and without the presence of trimethylamine (TMA) in 2 different relative humidities (30% and 50%). Sulphuric acid was produced using a thermally controlled cylinder which is half filled with pure (97%) sulphuric acid. Dry, particle free compressed air is flown through the saturator with constant flow rate (0.1 lpm) to saturate the flow with sulphuric acid vapour. The concentration is controlled by the temperature of the saturator. The sulphuric acid concentration was measured with CIMS (Petäjä et al., 2009) or APi-TOF (Junninen et al., 2010).

The concentration of nucleated particles was monitored with Particle Size Magnifier (PSM, Vanhanen et al., 2009). The size of the particles was measured with DMPS system (HAUKE DMA, UCPC, TSI model 3025A) in the range of 3 to 200 nm.

Five different concentration levels of TMA was used (170, 480, 800, 1700 and 3600 ppt) with sulphuric acid concentration range between 10^5 and $5 \cdot 10^7$ mol./cm^3. The flow tube was operated is several hours in same conditions to ensure stable state. TMA concentration was changed only after a full cycle of saturator temperatures (0-45^{o}C) was done for both RH's separately.

Figure 1 shows DMPS size distribution (upper panel) and total count (lower panel) data without TMA for one saturator temperature cycle at RH 30%. Figure 2 shows data from DMPS (upper panel) and PSM (lower panel) for exactly similar conditions as in figure 1, except the addition of TMA. The sizes of the particles are similar in both figures before adding TMA. After the addition of TMA the size decreases out of the DMPS size range and concentration of particles decreases to 1/3 of the original concentration. Increasing the RH to 50% increases the concentration temporarily but after stable state is achieved concentration is decreased to about 800 cm^{-3}.

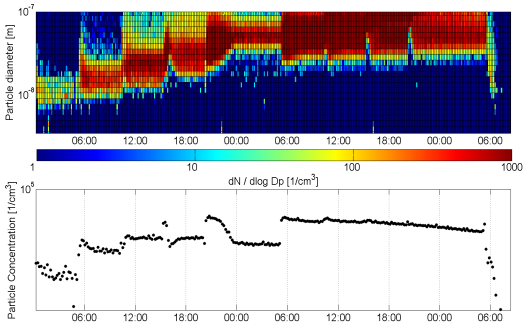

Figure 1. DMPS data for size distribution (upper panel) and total concentration (lower panel) for one saturator temperature cycle without TMA.

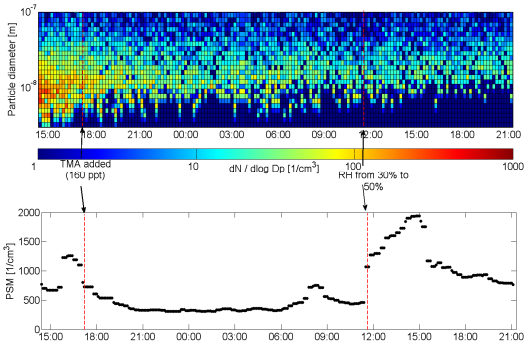

Figure 2. DMPS and PSM data over one cycle of saturator temperatures at RH 30% with lines when TMA (160ppt) was added and RH changed to 50%.

Results imply that TMA forms thermodynamically stable clusters with sulphuric acid with sizes below the detection limit of the PSM (~1.5 nm) suppressing the condensation of sulphuric acid to the surface of the particles and preventing the growth to detectable sizes. This was predicted by Anttila et al., (2005).

This work was supported by the Maj & Torr Nessling and KONE foundations.

Anttila T., et al., (2005), *Boreal Env. Res.*, **10**, 511-523.
Junninen, H., et al., (2010), *Atmos. Meas. Tech.*, **3**, 1039–1053.
Petäjä, T., et al., (2009), *Atmos. Chem. Phys.*, **9**, 7435-7448.
Vanhanen, J., et al., *18th International conference on Nucleation and Atmospheric Aerosols (ICNAA)*, Prague, Czech Republic (2009).

Coagulation scavenging of precritical clusters and the first nucleation theorem

J. Malila[1], K.E.J. Lehtinen[1,2], I. Napari[3], R. McGraw[4], and A. Laaksonen[1,5]
[1]Department of Applied Physics, University of Eastern Finland, P. O. Box 1627, 70211 Kuopio, Finland
[2]Finnish Meteorological Institute, Kuopio Unit, P. O. Box 1627, 70211 Kuopio, Finland
[3]Department of Physics, University of Helsinki, P. O. Box 64, 00014 Helsinki, Finland
[4]Environmental Sciences Department, Brookhaven National Laboratory, Upton, N.Y. 11973, U.S.A.
[5]Finnish Meteorological Institute, Climate Change, P. O. Box 503, 00101 Helsinki, Finland
Keywords: nucleation, coagulation, scavenging, nucleation theorem.
Presenting author email: jussi.malila@uef.fi

During recent years, the first nucleation theorem has become a standard tool to estimate the number of constituents forming the critical cluster in nucleation kinetics, and consequently to compare to measurements, simulations and nucleation theories at molecular level. Although it is nowadays generally considered as a model-free result, it is typically used in form

$$\left(\frac{\partial \ln J}{\partial \ln S}\right)_T = g^* + 1 \qquad (1)$$

that can be obtained only if homogeneous nucleation of ideal vapour is taking place isothermally in particle-free, inert carrier gas, conditions that might be feasible in the laboratory, but rarely met in real world phenomena, such as combustion aerosol or atmospheric new particle formation. In Eq. (1), J is the nucleation rate, S the saturation ratio and g^* the (excess) number of particles in critical cluster. With the aforementioned assumptions, Eq. (1) can be derived directly from the kinetic Becker–Döring theory (Ford, 1997; McGraw and Wu, 2003).

The extended kinetic treatment for the effect of foreign aerosol in the nucleating vapour can be found from the literature (Friedlander, 1978; McGraw and Marlow, 1983). For continuously reinforced vapour and i-mer scavenging rate Q_i depending linearly on i-mer concentration, this extended Szilard model yields

$$\left(\frac{\partial \ln J}{\partial \ln S}\right)_{T,\{q_i\}} = \tilde{g} + 1 = \frac{J + \sum_{i=2}^{g^*} Q_i}{J} g^* + 1. \qquad (2)$$

Here J is now the rate of formation of new stable clusters of size $g^* + 1$ and q_i the i-mer scavenging coefficient.

Results of model calculations are given in Fig. 1, where the ratio of apparent and true excess numbers of molecules in the critical cluster, $\tilde{g}/g^*$, is given as a function of S. Model values presenting homogeneous nucleation of water vapour in nitrogen at 260 K and 1 atm with different background aerosol distributions are given. For simplicity, classical nucleation theory expressions and Fuchs' form for the coagulation kernel are used, but the results do not depend qualitatively on these choices. As obvious from Eq. (2), $\tilde{g} > g^*$ with $\tilde{g}/g^* \to 1$ at high S or low total scavenging rate $\sum_i Q_i$, and $\tilde{g}/g^* \to \infty$ as $J \to 0$: these results imply that application of Eq. (1) to nucleation measurements in presence of background aerosol overestimate g^*.

As coagulation scavenging is not restricted into precritical clusters, suitable transformation (*e.g.* Anttila *et al.*, 2010) should be applied on measured data before using Eq. (2). Furthermore, to calculate $\sum_i Q_i$ one has to resort on theoretical schemes like the one described above. On the other hand, if nucleation rate measurements on same system with and without background aerosol are available, these can be used to confirm different molecular schemes for coagulation scavenging of nanosized clusters. However, for most practical applications, extensions of Eq. (2) into multicomponent systems are required.

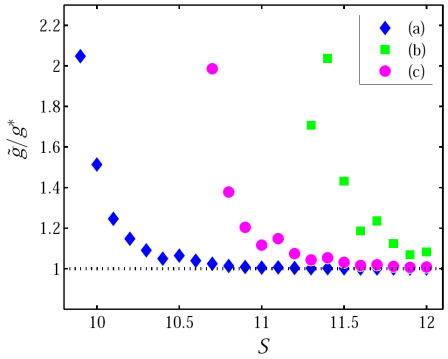

Figure 1: Ratio of apparent and true critical sizes for water at 260 K with three monodisperse background aerosol distributions: (a) diameter d_p = 100 nm and number concentration N = 10000 m^{-3}, (b) d_p = 10 μm and N = 10000 m^{-3}, and (c) d_p = 10 μm and N = 1000 m^{-3}.

J. M. acknowledges support from the graduate school "Atmospheric Composition and Climate Change: From Molecular Processes to Global Observations and Models." This work was also supported by the Academy of Finland through the Centre-of-Excellence Programme.

Anttila, T., Kerminen, V.-M. and Lehtinen, K.E.J. (2010) *J. Aerosol Sci.* **41**, 621-636.
Friedlander, S.K. (1978) *J. Colloid Interface Sci.* **67**, 387-388.
Ford, I.J. (1997) *Phys. Rev.* E **56**, 5615-5629.
McGraw, R. and Marlow, W.H. (1983) *J. Chem. Phys.* **78**, 2542-2548.
McGraw, R. and Wu, D.T. (2003) *J. Chem. Phys.* **118**, 9337-9347.

Light-induced drift of aerosol particle

V.G. Chernyak

Department of Physics, Ural State University, Yekaterinburg, 620083
Keywords: particle, gas, molecule, optical radiation.
Presenting author email: vladimir.chernyak@usu.ru

In the present work we study the photophoresis of a particle that does not absorb light or absorbs it homogeneously. The particle is suspended in a binary gas mixture in which the molecules of the absorbing gas are excited selectively as to velocity by resonant optical radiation. We examine the dependence of the force and velocity of photophoresis on the detuning of the radiation frequency from the center of the absorption line and on the concentration and mass ratios of the molecules of absorbing and buffer gases.

Let the radiation is a traveling light wave whose frequency is close to that of an electronic or vibrational-rotational transition of molecules of a gas. In this case the light is absorbed by one of components of gaseous mixture. Because of the Doppler effect, the radiation is absorbed selectively as to molecular velocity. This gives rise to light-induced fluxes of matter and energy (Gel'mukhanov and Shalagin, 1979). The difference in the scattering of excited and unexcited molecules by the particle surface and the difference in the transport cross sections of their interaction lead to the emergence of a resonant photophoresis force on the particle. If the aerosol particle is suspended in a mixture of a light-absorbing gas and a buffer gas, the total momentum transferred to the aerosol particle also proves to be unbalanced because of the difference in the masses of the molecules.

We consider a spherical aerosol particle suspended in a binary gas mixture. We irradiate the system with a monochromatic traveling light wave. Let the radiation be absorbed by the molecules of one of the components in an electronic or vibrational-rotational transition from the ground state *n* to the first excited state *m*. Due to the Doppler effect, only the molecules whose velocity projection on the radiation direction lines within a certain velocity range can be excited.

The velocity distribution functions for the excited, unexcited and buffer gas molecules satisfy the linearized Boltzmann equations, considering the stimulated transitions and radiative decay of the excited level for absorbing molecules.

We analyze the Knudsen regime, in which the mean free path of molecules is much greater than the particle radius. We can then neglect the perturbation of the distribution functions for the molecules incident upon the particle due to collisions with emitted molecules.

In respect of the distribution functions for molecules emitted from the particle surface we assumed that the fraction ε_i of molecules of species *i* is reflected by the particle surface diffusely with a Maxwellian distribution, while the fraction $(1 - \varepsilon_i)$ is specularly reflected. The accommodation coefficients for excited ε_m and unexcited ε_n molecules are different. The unknown number densities of the molecules reflected from the surface of the aerosol particle are founded from the nonpercolation conditions.

The light-induced particle velocity is

$$U_f = \mu_\varepsilon \Delta\varepsilon + \mu_d \frac{\Delta d}{d_n},$$

$$\Delta\varepsilon = \varepsilon_n - \varepsilon_m, \quad \Delta d = d_n - d_m.$$

Here d_m and d_n are respectively effective diameters of excited and unexcited molecules of absorbing gas. The kinetic coefficient μ_S characterizes the surface mechanism of photophoresis, which is related to the difference in the accommodation coefficients for excited and unexcited molecules of the absorbing gas. The kinetic coefficient μ_d characterizes the contribution related to the differing effective diameters of excited and unexcited molecules.

The kinetic coefficients are proportional to the radiative intensity, and depend on the ratio of the rate of radiative decay of the excited level to the intermolecular collision rate, the detuning of the radiation frequency from the center of the absorption line of absorbing molecules, the component concentrations, and the molecular mass ratio.

The directions of the surface component of the force and velocity of photophoresis are determined by the signs of the difference of the accommodation coefficients $\Delta\varepsilon$ of the unexcited and excited molecules and the frequency detuning Ω. If $\Delta\varepsilon > 0$, the direction of the surface component coincides with the direction of light propagation when $\Omega < 0$, and is opposite the direction of light propagation when $\Omega > 0$.

The directions of the bulk component of the force and velocity of photophoresis are determined by the signs of the difference Δd of the effective diameters of the unexcited and excited molecules and the frequency detuning Ω. If $\Delta d > 0$, the direction of the bulk component coincides with the direction of light propagation when $\Omega < 0$ and is opposite that direction when $\Omega > 0$.

The numerical estimates give for an aluminum particle of radius 1μm suspended in a mixture of sodium vapor and argon, that the velocity of the particle is $U_f \approx 20\ \mathrm{m/s}$.

This work was supported by the Russian Foundation for Basic Researches (Grant No. 09–01–00052).

Gel'mukhanov, F.Kh. and A.M. Shalagin (1979) *JETP Lett.* **29**, 711.

Particle activation via heterogeneous nucleation in *n*-butanol condensation particle counters

A. Mamakos and Y. Drossinos
European Commission, Joint Research Centre, 21027 Ispra (VA), Italy
Keywords: activation, heterogeneous nucleation, condensation particle counter (CPC), contact angle.
A. Mamakos: thanasis.mamakos@jrc.ec.europa.eu

Interest in particle activation in Condensation Particle Counters (CPCs) has recently resurged due to the introduction of Euro 5/6 legislation for particulate emissions from light-duty diesel vehicles. The legislation introduces a non-volatile particle number emission limit: the particle concentration is to be measured by a full-flow CPC.

We performed experimental and theoretical studies on the effect of particle chemical composition on particle activation in *n*-butanol CPCs. The detection efficiencies at various electical mobility diameters of graphite particles and Emery oil droplets (PAO, polyalpha olefin, is a component of synthetic oil) were measured by a TSI 3790 CPC. The CPC was operated at different saturator wall temperatures to study the effect of the bulk-to-wall temperature difference; the saturator inlet bulk temperature was kept constant at 38.3°C.

Particle activation at particle diameter d was studied theoretically via the activation probability $P_d(t)$, defined as the ratio of the concentration of activated particles to their saturator-inlet concentration. In terms of the activation rate constant per seed particle k the activation probability is

$$P_d(t) = 1 - \exp(-kt) \quad .$$

Particles are considered to be activated once their activation probability is greater or equal to 0.5. The activation rate constant was chosen to be the heterogeneous nucleation rate as is appropriate for activation of particles insoluble in *n*-butanol. The heterogeneous nucleation rate was calculated as described in Giechaskiel *et al.* (2011). In addition, we considered the effect of curvature on the surface tension of the heterogenous nucleating droplet via Tolman's length δ_T, namely $\gamma(R) = \gamma_\infty/(1+2\delta_T/R)$ with R the nucleating droplet radius and γ_∞ the planar surface tension. The effect of line tension was also investigated.

An essential ingredient of heterogeneous nucleation theories is the contact angle between the critical cluster and the curved particle surface. The contact angle determines a multiplicative geometric factor that lowers the free energy of formation of the critical cluster on the surface, and hence it enhances the nucleation rate (particle activation occurs at lower saturation ratios). The contact angle depends on the condensing species and on the chemical nature of the particle to be activated.

Calculated *n*-butanol contact angles as a function of CPC detection efficiencies for the two different species are shown in Figs. 1 (graphite particles) and 2 (PAO droplets). The curvature dependence of the surface tension was neglected, $\delta_T = 0$. Different colors correspond to different saturator-wall temperatures.

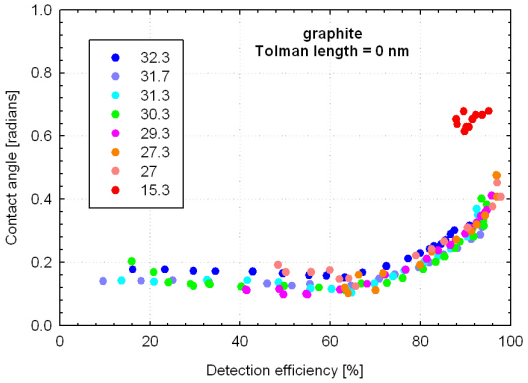

Figure 1: Calculated *n*-butanol contact angles on graphite particles.

Inspection of the Figures shows that for counting efficiencies less than approximately 70% a well defined contact angle, independent of the saturator-wall temperature, reproduces the experimental detection efficiencies. Furthermore, the contact angle depends on the chemical nature of the activated species: it is approximately zero for PAO and approximately 10° for graphite.

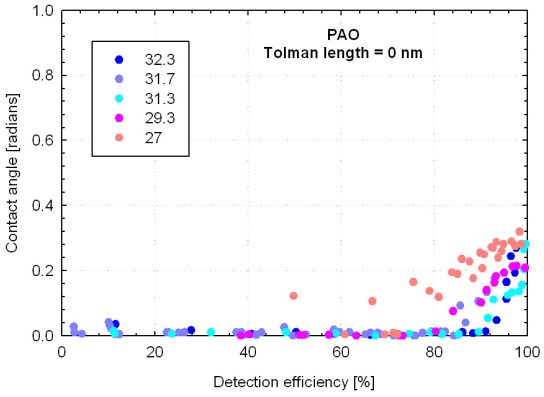

Figure 2: Caption as in Fig. 1, PAO droplets.

Thus, for a range of bulk-to-saturator wall temperature differences, a constant contact angles that depends on the chemical composition of the activated particle maybe identified to reproduce experimental CPC detection efficiencies (up to approximately 70%) .

Giechaskiel, B., Wang, X., Gilliland, D., Drossinos, Y. (2011), J. Aerosol Sci. **42**, 20-37.

Particle activation via heterogeneous nucleation in *n*-butanol condensation particle counters

A. Mamakos and Y. Drossinos
European Commission, Joint Research Centre, 21027 Ispra (VA), Italy
Keywords: activation, heterogeneous nucleation, condensation particle counter (CPC), contact angle.
A. Mamakos: thanasis.mamakos@jrc.ec.europa.eu

Interest in particle activation in Condensation Particle Counters (CPCs) has recently resurged due to the introduction of Euro 5/6 legislation for particulate emissions from light-duty diesel vehicles. The legislation introduces a non-volatile particle number emission limit: the particle concentration is to be measured by a full-flow CPC.

We performed experimental and theoretical studies on the effect of particle chemical composition on particle activation in *n*-butanol CPCs. The detection efficiencies at various electical mobility diameters of graphite particles and Emery oil droplets (PAO, polyalpha olefin, is a component of synthetic oil) were measured by a TSI 3790 CPC. The CPC was operated at different saturator wall temperatures to study the effect of the bulk-to-wall temperature difference; the saturator inlet bulk temperature was kept constant at 38.3°C.

Particle activation at particle diameter d was studied theoretically via the activation probability $P_d(t)$, defined as the ratio of the concentration of activated particles to their saturator-inlet concentration. In terms of the activation rate constant per seed particle k the activation probability is

$$P_d(t) = 1 - \exp(-kt) \quad .$$

Particles are considered to be activated once their activation probability is greater or equal to 0.5. The activation rate constant was chosen to be the heterogeneous nucleation rate as is appropriate for activation of particles insoluble in *n*-butanol. The heterogeneous nucleation rate was calculated as described in Giechaskiel *et al.* (2011). In addition, we considered the effect of curvature on the surface tension of the heterogenous nucleating droplet via Tolman's length δ_T, namely $\gamma(R) = \gamma_\infty/(1+2\delta_T/R)$ with R the nucleating droplet radius and γ_∞ the planar surface tension. The effect of line tension was also investigated.

An essential ingredient of heterogeneous nucleation theories is the contact angle between the critical cluster and the curved particle surface. The contact angle determines a multiplicative geometric factor that lowers the free energy of formation of the critical cluster on the surface, and hence it enhances the nucleation rate (particle activation occurs at lower saturation ratios). The contact angle depends on the condensing species and on the chemical nature of the particle to be activated.

Calculated *n*-butanol contact angles as a function of CPC detection efficiencies for the two different species are shown in Figs. 1 (graphite particles) and 2 (PAO droplets). The curvature dependence of the surface tension was neglected, $\delta_T = 0$. Different colors correspond to different saturator-wall temperatures.

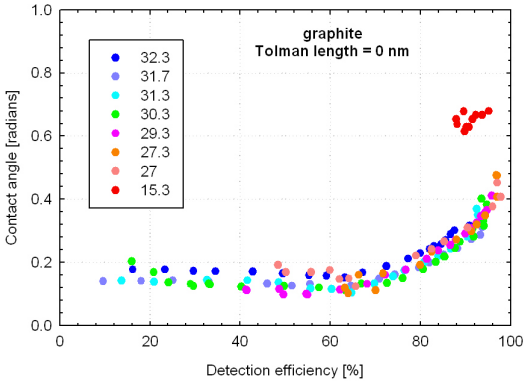

Figure 1: Calculated *n*-butanol contact angles on graphite particles.

Inspection of the Figures shows that for counting efficiencies less than approximately 70% a well defined contact angle, independent of the saturator-wall temperature, reproduces the experimental detection efficiencies. Furthermore, the contact angle depends on the chemical nature of the activated species: it is approximately zero for PAO and approximately 10° for graphite.

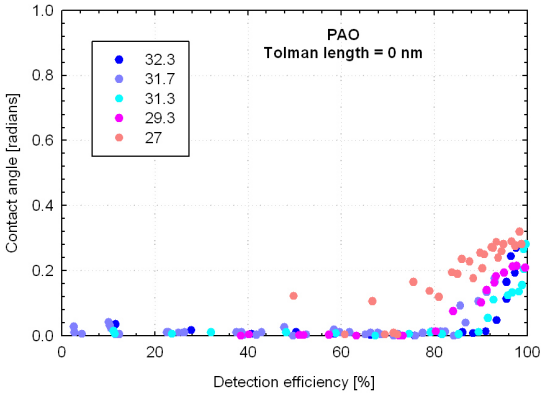

Figure 2: Caption as in Fig. 1, PAO droplets.

Thus, for a range of bulk-to-saturator wall temperature differences, a constant contact angles that depends on the chemical composition of the activated particle maybe identified to reproduce experimental CPC detection efficiencies (up to approximately 70%) .

Giechaskiel, B., Wang, X., Gilliland, D., Drossinos, Y. (2011), J. Aerosol Sci. **42**, 20-37.

Is Quantum Nuclear Dynamics significant in the study of the structure of sulphuric acid hydrates?

J.L. Stinson[1], I.J. Ford[1] and S. Kathmann[2]
[1]Department of Physics and Astronomy, University College London, Gower Street, London, WC1E 6BT, UK
[2]Fundamental and Computational Sciences Directorate, Pacific Northwest National Laboratory, Richland, Washington, U.S.A.
Presenting author email: j.stinson@ucl.ac.uk

Sulphuric acid has been identified as an important molecule influencing the formation of aerosols in the atmosphere and as such is seen as a promising player in the field of geoengineering. The nucleation of clusters including this species has been studied using a variety of methods including Classical Nucleation Theory (CNT), Dynamical Nucleation Theory (DNT), Density Functional Theory (DFT), Quantum Monte Carlo (QMC), Quantum Chemistry (QC) and classical Force Field methods (FF). The various methods employed can address short and long timescale phenomena relevant to the nucleation event, and promise varying levels of accuracy, appropriate to the questions posed. Classical theory can be set aside since the small critical sizes relevant to atmospheric conditions makes the capillary approximation inadequate. Furthermore, typical atmospheric vapour supersaturations means that event time scales are difficult to achieve in brute-force simulation. Single molecular modelling schemes seem most appropriate, but those that neglect electronic detail make proton transfer events in hydrated clusters difficult to describe, and this is believed to affect the cohesion of such clusters. The most appropriate modelling method at present seems to be based on DFT.

B3LYP and PW91 are popular implementations of DFT but it has been some years since they were introduced in the DFT community and the field is highly active. Most noticeable is the progress made for non-covalent interactions such as hydrogen bonds (Burns *et al* (2011)). Interesting extensions that attempt to capture the quantum mechanics of nuclear motion have also been proposed. It is very plausible that such effects might influence the clustering, particularly where hydrogen bonding and proton transfer are important. Recent developments such as Centroid Molecular Dynamics (CMD) can accurately describe the quantum nuclear dynamics associated with proton transfer (Pavese *et al* (2000)). We have therefore undertaken a set of studies to determine whether the outcomes of this approach will differ significantly from treatments that neglect such quantum effects. An illustration of the difference in approach is provided in the images in Figure 1. Proton positional uncertainty is represented by replacing each atom by a collection of coupled beads, four in this case, and evolving the structure by classical molecular dynamics.

Centroid molecular dynamics promises to provide greater accuracy than standard DFT in determining structural properties of molecular clusters containing sulphuric acid. Our aim is to use such methods to parametrise a reactive force field (FF) that will be efficient for simulations at size and length scales where DFT is inappropriate. Such parametrisation will involve a force-fitting procedure applied to DFT-driven molecular dynamics of a few sulphuric acid and water molecules, and we aim to achieve a suitable compromise between accuracy and efficiency.

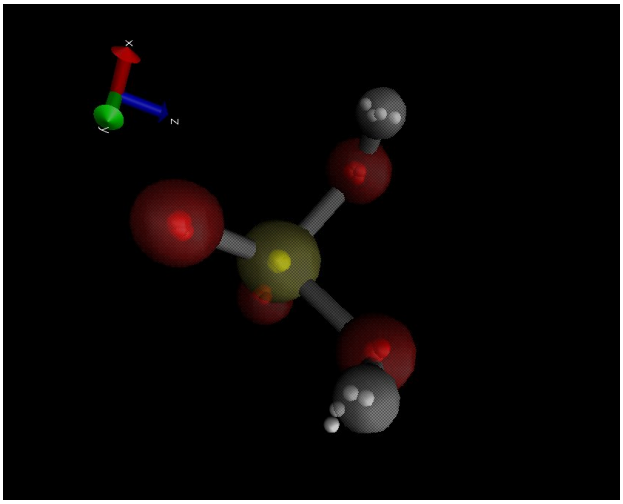

Figure 1: The image shows overlaid configurations of a single sulphuric acid molecule equilibrated at 300K using DFT with the PBE exchange-correlation functional. The centres of the large transparent spheres represent atomic positions determined with the neglect of quantum uncertainty. The four smaller beads are a representation of the quantum uncertainty in atomic position in the CMD model. The difference in sphere size is for clarity of image only. Quantum uncertainty is obviously larger for the hydrogens than for the heavier sulphur and oxygens.

Ideally the FF should be able to represent every event possible so as to fully capture the dynamics of the system. However it is quite apparent that accounting for bond breaking events is a particularly difficult task for classical FF. To this end ReaxFF (van Duin *et al* (2001)) has been developed, and is a candidate for our future work.

A.C.T. van Duin, S. Dasgupta, F. Lorant and W.A. Goddard III, J. Phys. Chem. **A105**, 9396-9409 (2001).

M. Pavese, S. Jang and G.A. Voth, Parallel Computing **26**, 1025-1041 (2000).

L.A. Burns, A.Vazquez-Mayagoitia, B.G. Sumpter and C.D. Sherrill, J. Chem. Phys. **134**, 084107 (2011).

Tuesday, September 6, 2011

Session 4P: Poster Session A: *Bioaerosols*

Real-time Detection of Bacterial Bioaerosols Using the Aerosol Fluorescence Sensor with Dual Channels of UV- and Vis-band

Jae Hee Jung[1], Jung Eun Lee[2], Gwi Byoung Hwang[1], and Gwi Nam Bae[1]

[1]Environment Center, Korea Institute of Science and Technology (KIST), Hawolgok-dong, Seongbuk-gu, Seoul 136-791, Republic of Korea
[2]Public Health Microbiology Laboratory, Graduate School of Public Health, Seoul National University, Gwanak-ro, Gwanak-gu, Seoul 151-742, Republic of Korea
Keywords: Bioaerosols-monitoring, Fluorescence, Measurement (Characterization).
Presenting author email: jaehee@kist.re.kr

In the search for methods by which an ambient environment can be continuously monitored for potentially harmful biological aerosols, particle fluorescence methods have received considerable attention over the past decade. The aerosol fluorescence sensor (AFS; Biral, Bristol, UK) is a promising monitoring device for the continuous real-time detection of airborne microorganisms, which is based upon the principle of Ultra-violet light induced fluorescence (UV-LIF) targeting the intrinsic fluorescence response from common amino acids found in living matter. The sensor uses an UV optical excitation source of 280 (+20/-40) nm to illuminate an airstream flowing drawn continuously through the sensor detection volume. Fluorescence from all particles instantaneously present within a sensing volume is measured using two photomultiplier detectors optically filtered to detect radiation in the bands 305-385 nm (UV) and 415-550 nm (Vis), enabling a generic discrimination between different aerosol populations.

In this study, we demonstrate the fluorescence characteristics of bacterial bioaerosols using aerosol fluorescence sensor to distinguish between microorganism particles and environmental particles. Using AFS and aerodynamic particle sizer (APS), the aerosol and fluorescence characteristics of various particles, including bacterial (e.g., *Escherichia coli* and *Bacillus subtilis*) and non-bacterial aerosols (e.g., polystyrene latex) can be determined.

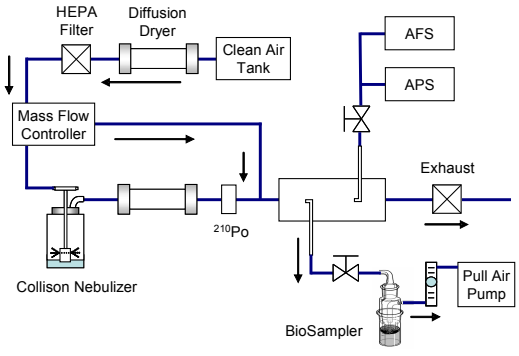

Figure 1. Experimental setup.

The experimental setup, illustrated schematically in Figure 1, included three major components: (i) a system for generating aerosols, (ii) AFS and APS aerosol measurement system, and (iii) a sampling system for culturability analyses of the bacterial bioaerosols.

In results, the UV-fluorescence intensity of both bacterial bioaerosols was higher than that of PSL at same total particle surface area concentration. In particular, the ratio of UV- to Vis-fluorescence intensity of bacterial bioaerosols showed sufficiently higher values than that of PSL particles, which is able to differentiate between bacterial bioaerosols and PSL particles. This minimum aerosol concentration to which AFS can respond were approximately 100 $\mu m^2/cm^3$ (c.f. 30 particles/cm^3) at UV fluorescence range and 330 $\mu m^2/cm^3$ (c.f. 200 particles/cm^3) at Vis fluorescence range in all test particles. In a view point of AFS operation, the variation in characteristics of fluorescence intensity was evaluated under various the sensor gain settings (Low and High) for the two fluorescence channels and the frequency (1-10 Hz) of the flash excitation light operation. The amplitude of the measured fluorescence offset and dynamic measurement range are dependent on the gain of the system. The coefficient of variance of reading values is increased with decreasing frequency of the flash light.

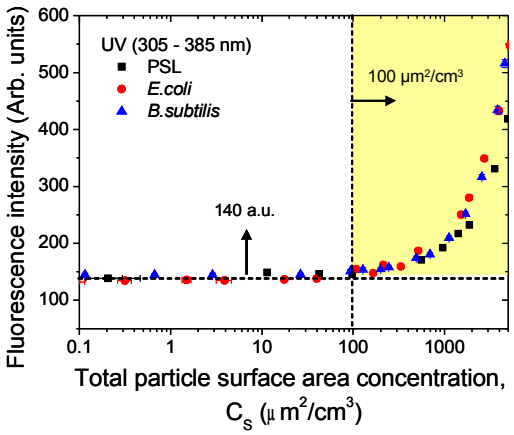

Figure 2. UV-fluorescence intensity (Arb. units) vs. particle concentration.

This research was supported by the Converging Research Center Program through the National Research Foundation of Korea (NRF), funded by the Ministry of Education, Science and Technology (2009-0081928).

Kaye, P. H., Hirst, E., Foot, V., Clark, and Baxter, K. (2004) *Proc. SPIE* 5617, 388-398.

Tuesday, September 6, 2011

Session 4P: Poster Session A: *PMx*

Mobile measurements of submicron particulate matter in Central Europe during wintertime inversions

R. Wolf, C. Mohr, M. Crippa, J. Slowik, A.S.H. Prévôt and U. Baltensperger
Laboratory of Atmospheric Chemistry, Paul Scherrer Institute, CH-5232, Villigen PSI, Switzerland
Keywords: Organic aerosols, Wood burning, Aerosol mass spectrometry, Source apportionment.
Presenting author email: robert.wolf@psi.ch

Wintertime inversions lead to an increase in concentrations of particulate matter. This phenomenon is of special interest because of the adverse effects of particles on health and visibility. During such episodes, aerosol mass concentrations are strongly influenced by local sources and topography. Recent studies (Weimer *et al.*, 2009, Alfarra *et al.*, 2007) indicate that both traffic and wood burning significantly contribute to particulate mass which accumulates in narrow Alpine valleys.

A mobile laboratory was deployed to determine the spatial distribution and the chemical composition of atmospheric aerosols during atmospheric inversion. The mobile unit contains a series of instruments including an Aerodyne quadrupole aerosol mass spectrometer (Q-AMS), a multi-angle absorption spectrometer (MAAP) and a fast mobility particle sizer (FMPS). The sampling was performed in both rural and urban areas along the Rhine Valley in Switzerland, Austria and Liechtenstein.

The main components of particulate matter and its sources were identified using Positive Matrix Factorization (PMF) (Paatero *et al.*, 1994). The organic fraction can be classified as primary (POA) or secondary organic aerosol (SOA). The primary organic aerosol classification includes contributions from wood burning and traffic. Local emissions of individual species were estimated by subtraction of SO_4-normalized background concentrations (Mohr *et al.*, 2011).

The results for the total mass concentration and the mean chemical composition are shown in Figure 1. It indicates a substantial difference in mass concentrations between the Austrian section (A) of the route ($\approx 53\ \mu g/m^3$) and the urban area of Chur in the southern Rhine Valley ($\approx 15\ \mu g/m^3$). According to Figure 2, the carbonaceous aerosol dominates the local contribution.

It can be concluded that the high amount of heavy-duty traffic and emissions from diesel powered cars in the Austrian part of the Rhine Valley lead to an increased concentration of organic aerosol and elevated emissions of black carbon (BC). In contrast, the local contribution of organic mass from wood burning, which can be attributed to domestic heating in this region, is lower (9 – 13 %).

We will present for this campaign and in addition the Mesolcina Valley with a higher ratio of wood burning the local and regional contributions to PM_1 and compare these with measurements in downtown Zurich.

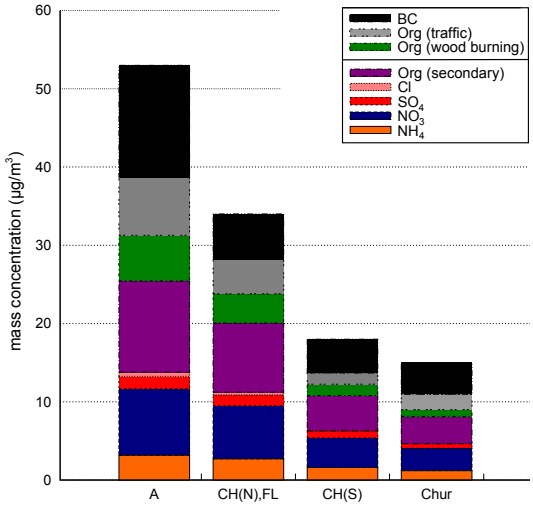

Figure 1: Mean chemical composition of PM_1 in the Rhine Valley at four different sections of the route (A Austria, CH(N) northern Switzerland, CH(S) southern Switzerland, FL Principality of Liechtenstein).

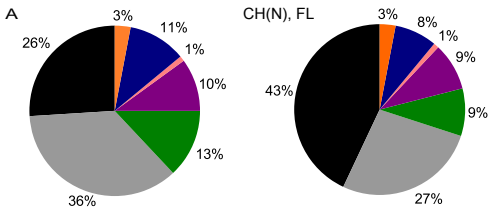

Figure 2: Relative local contributions after subtraction of the SO_4-normalized background concentrations of different species to PM_1 in the northern part of the Swiss Rhine Valley.

References:
Weimer, S., Mohr, C., Richter, R., Keller, J., Mohr, M., Prévôt, A.S.H., Baltensperger, U. (2009) *Atmos. Environ.* **43** 624-630.
Alfarra, M.R., Prévôt, A.S.H., Szidat S., Sandradewi, J., Weimer, S., Lanz, V.A., Schreiber, S., Mohr, M., Baltensperger, U. (2007) *Environ. Sci. Technol.* **41**, 5770-5777.
Paatero, P., Tapper, U. (1994) *Environmetrics* **5**, 111-126.
Mohr, C., Richter, R., DeCarlo, P.F., Prévôt, A.S.H., Baltensperger, U. (2011) *Atmos. Chem. Phys.* to be submitted.

Exploring aerosol chemical composition in the Finnish boreal forest in late-spring by Aerosol Mass Spectrometry.

A. Kortelainen[1], L. Hao[1], P. Miettinen[1], A. Jaatinen[1], J. Joutsensaari[1], J. N. Smith[1,4], D. R. Worsnop[1,2,3,5] and A. Laaksonen[1,2]

[1]Department of Applied Physics, University of Eastern Finland, Kuopio, 70211, Finland
[2]Finnish Meteorological Institute, Climate Change Research Unit, Helsinki, 00101, Finland
[3]Department of Physics, Division of Atmospheric Sciences, University of Helsinki, Helsinki, 00014, Finland
[4]National Center for Atmospheric Research, Boulder, Colorado, 80305, USA
[5]Aerodyne Research Inc., Billerica, MA, 01821, USA
Keywords: chemical composition, organics, AMS, PMF.
Presenting author email: Aki-Matti.Kortelainen@uef.fi

Atmospheric aerosol formation and aging are widely researched areas, however there are still many uncertainties related to both. Secondary organic aerosols (SOA) form through the oxidation of gaseous organic emissions; as SOA age their oxidation ratio increases. In a remote forest setting, urban aerosol are long-range transported and are thus more oxidized, often correlating with particulate sulphate. Markers of combustion come out in long-range transported air mass plumes and correlate with substances like black carbon, levoglucosan and CO_2.

This work focuses on characterizing organic sources in the clean northern boreal forest area using Positive Matrix Factorization (PMF) applied to Aerosol Mass Spectrometer measurements of particulate-phase organics (Paatero, 1994; Ulbrich 2009). PMF analysis was done for unit mass resolution (UMR) and time-of-flight mass spectrometer V-mode-based high resolution (HR) organics spectra. The factors found in the UMR and HR data sets were defined by correlation with trace gases, particle data, volatility, organic growth and meteorology. An example of PMF solution for 5 factors, their proportions of organics mass loading and organics average mass loadings are listed in Table 1.

The measurements were performed at the Station for Measuring Forest Ecosystem-Aerosol Relations (SMEARII) station, at Hyytiälä (61° 51'N, 24° 17'E, 180m ASL) between 10.5-13.6.2009. The study was performed during IS4FIRES (Integrated Monitoring and Modelling System for Wildland Fires) project and included measurements of aerosol chemical composition by Aerodyne High Resolution Time-Of-Flight Aerosol Mass Spectrometry and aerosol properties such as volatility by Volatility Tandem Differential Mobility Analyzer and organic growth by Ultra-Fine Organic Tandem Differential Analyzer (Vaattovaara, 2005). Other particle information (e.g., particle size distributions) and key trace gases such were measured during the study.

In Hyytiälä, organics consist mainly of LV- and SV-OOA (Low Volatile- and Semi Volatile-Oxidized Organics Aerosol respectively), whereas the mix of BBOA (Biomass Burning Organic Aerosol) and HOA (Hydrocarbon-like organic aerosol) cover roughly quarter of the organics mass loading. It was found that less oxidized, locally produced, organic aerosol constituents correspond to more volatile aerosol, whereas long-range transported SOA correspond to lower volatilities. The semi-volatile less oxidized organics aerosol, whose fraction increases during the daytime from new particle formation, correlate with the more organophilic aerosol fraction. In addition SV-OOA correlate with nitrate and normally increase during the night. The low volatile more oxidized organic aerosol was long-range transported, exhibited low volatility, correlated with sulphate, nitrate and ammonium and increased during the daytime. Hydrocarbon-like organic aerosol seem to be related to local traffic at the measurement site with correlation to black carbon, CO, NO_x and nitrate. Biomass burning came out in air mass plumes originated from urban areas and correlated with black carbon, CO, CO_2, NO_x and nitrate. HOA and BBOA showed distinct time trends, mainly low mass loadings and higher during the separate air mass plumes. BBOA correlated with masses of levoglucosan in HR PMF. The HOA factor was separated in HR PMF with unique time trend and the mass spectrum was characterized by hydrocarbon peaks.

Table 1. 5-factor-solution, factors proportions of organics and organics average mass loadings.

factor	*UMR (%)*	*HR(V)(%)*
LV-OOA	33.9 and 21.3	31.8 and 9.2
SV-OOA	21.1	29.3
BBOA	16.3 and 7.3	23.7
HOA		6.0
organics average mass (ug/m^3)	2.1	1.8

The financial support by the Academy of Finland Centre of Excellence program (project no 1118615) is gratefully acknowledged.

Paatero, P. and Tapper, U.:, *Environmetrics*, 5, 111-126, 1994.

Ulbrich, I.M. ,et. al., *Atmospheric Chemistry and Physics* , 9(9), 2891-2918, 2009.

Vaattovaara, P., et. al., , *Atmospheric Chemistry and Physics*, 5, 3277-3287, 2005.

Comparison of PM10 source apportionment using PMF and PCA: an analysis of accuracy and robustness of results

D. Cesari [1], F. Amato [2], M. Pandolfi [2], D. Contini [1], A. Alastuey [2], X. Querol [2]

[1] Institute of Atmospheric Science and Climate (ISAC-CNR), 73100, Lecce, Italy
[2] Institute of Environmental Assessment and Water Research (IDÆA-CSIC), Barcelona 08034, Spain
Keywords: Source Apportionment, PCA, PMF, Apportionment Accuracy, PM10
Presenting author email: d.cesari@isac.cnr.it

A general overview of atmospheric aerosol Source Apportionment (SA) results shows a lack of uniformity in the analysis proposed in terms of "working variables", such as the number of samples present in the data-set and the number of chemical species included. Moreover, the comparison of different methods of SA, applied to the same data-set, shows that the number or the types of sources can be different (Amato et al., 2009). There are also difficulties in the characterization of sources with similar chemical profiles, if a sufficient number of specific markers are not analysed. This variability of SA output appears to be related to the specific characteristics of the measurement site and to the meteorological characteristics of the site analysis.

This work aims to analyze the performance of two SA models: EPA-PMF 3.0 and PCA through an inter-comparison of results obtained at three measurements sites: one Italian urban background site (Lecce, Contini et al., 2010), one Spanish urban background site (Barcelona, Amato et al., 2009) and one Spanish industrial site (Algeciras, Pandolfi et al., 2011). A second target of the analysis was to study the accuracy and robustness of the results proposed by the models and how these parameters are influenced by the typology of the measurement site and the chemical species available in the data-sets. For this purpose the data-sets were used with full inorganic chemical characterisation and Total Carbon of PM10 (complete data-sets), and with reduced data-sets, obtained from the complete ones removing specific chemical species (Total Carbon, Ti, P, Rb, Sr, As, Cd, Sn, Sb, Li, Se and La).

The results show that both techniques provide similar solutions in the identification of sources: "Crustal", "Traffic", "Industrial", "Marine", "Secondary Inorganic Aerosol (SIA)" and "Fossil Fuel Combustion" (this last one limited to the Spanish sites). However, the number of factors identified by PMF is different from the number of components of PCA. The differences are mainly related to SIA and marine contributions. In the Lecce site PCA finds an industrial contribution separated from SIA but PMF finds a single contribution that include both sources. In both Spanish sites the source "SIA" is disentangled by the PMF into two factors (secondary sulphate and secondary nitrate), while the PCA analysis identifies one unique SIA component. This trend, already observed in literature (Callen et al., 2009, Viana et al., 2008) is related, presumably, to the different operating method of the mathematical model and/or to the different role of measurements uncertainties in the two receptor models. Further, the source profiles, provide by PCA and PMF, are sometimes different. In the data-set of Algeciras, the PCA component "Marine" is loaded with nitrate, suggesting that this source identified is an "aged" marine aerosol, including a portion of sodium nitrate that the PMF model associate to secondary nitrate, identifying a "fresh" marine that does not include a significant contribution of nitrate.

The comparison of complete and reduced data-sets shows that the PCA solutions are more sensitive to changes in the chemical species available with respect to PMF that appears more stable. However, for both models, the elimination of the TC causes a difficulty in identifying the "Traffic" source, mainly characterised by TC, that could be confused with an industrial emission. In Figure 1 the "Traffic" PCA component derived from Barcelona site is reported for the complete and reduced data-set as an example. However, for PMF, the elimination of the TC does not influence relevantly the calculated contribution of the traffic source to PM10. Instead significant differences are observed with PCA.

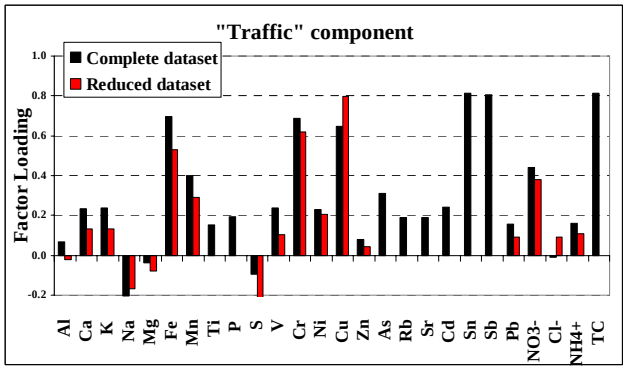

Figure 1. PCA loads for "Traffic" component in Barcelona. Complete dataset (black bar) and reduced dataset (red bar).

Amato, F., Pandolfi, M., Escrig, A., Querol, X., Alastuey A., Pey J., Pérez N., Hopke P.K. (2009) *Atmos. Environ.* **43**, 2770-2780.

Contini, D., Genga, A, Cesari D., Siciliano M., Donateo A., Bove M.C., Guascito M.R. (2010) *Atmos. Res.* **95**, 40-54.

Pandolfi M., Gonzalez-Castanedo Y., Alastuey, A., D. de la Rosa J., Mantilla, E., Sanchez de la Campa, A., Querol, X., Pey, J., Amato F. and Moreno T. (2011) *Environ. Sci. Poll. Res.* **18**, 2, 260-269.

Callén, M.S., de la Cruz, M.T., López, J.M., Navarro M.V. and Mastral, A.M. (2009) *Chemosp*. **76**, 1120-1129.

Aircraft measurement of PM vertical profile above the Czech EMEP stations during EMEP-EUSAAR-EUCAARI intensive campaign.

M. Vana[1], J. Svobodova[1] ,T. Fory[2] M.Hladík[2], Z.Roubal[2], J. Hadinger[2]

[1] Czech Hydrometeorological Institute, Kosetice Observatory, 394 22 Kosetice, Czech Republic
[2] Czech Hydrometeorological Institute, Plzeň regional office, 323 00 Plzeň, Czech Republic
Keywords: PM measurements, vertical distribution, EMEP, regional background.
Presenting author email: milan.vana@chmi.cz

Aircraft measurement of PM vertical profile was implemented within the EMEP-EUSAAR-EUCAARI intensive monitoring campaign. The campaign was organized in the period from February 25th to March 26th 2009 (winter part). General aim of the campaign was to improve our knowledge about the behaviour of atmospheric aerosols in the CLRTAP region.

The measurement was carried out on March 21st 2009 by one-motor aircraft Cessna 172 Skyhawk. Fractions PM_{10}, $PM_{2,5}$ and PM_1 were measured according to the US EPA guidelines; automatic analyzer GRIMM Model 1.109 was used. The main task was to measure PM vertical profile above the Czech EMEP stations Košetice (49° 35' N; 15° 05' E; 534 m a.s.l.) and Svratouch (49° 73' N; 16° 03' E; 737 m a.s.l.). Moreover, the experiment was extended of measurement above the Ostrava region in the north-eastern part of the Czech Republic, which belongs to the most polluted areas by PM in Europe.

Meteorological situation in Central Europe was controlled by an anticyclone above north-western Europe and low pressure area above Baltic region in the period 18th-22nd March. Mean daily temperatures varied round freezing point, the majority of the territory was covered by snow. Meteorological conditions were favourable for long-range transport. According to the transport trajectories (NILU, 2011), air masses from far north areas came to the Central Europe on 21st March.

The aircraft ascended to the cloudiness level above Kosetice Observatory (1460 m a.s.l.). The vertical profile was characterized by homogeneous ratios between fine and course fractions; $PM_{2,5}$ / PM_{10} ratio was 85% in average and the PM_1 a $PM_{2,5}$ concentrations were almost identical during the ascend. Concentration levels ranged from 17 to 20 $\mu g.m^{-3}$ by PM_{10} and from 14,5 to 17 $\mu g.m^{-3}$ by $PM_{2,5}$ and PM_1.

The climb above Svratouch station reached the height 2038 m a.s.l. Concentrations were slightly higher than above Kosetice (5 $\mu g.m^{-3}$ averagely). The vertical profile and ratios between individual fractions below cloud layer showed similar patterns as above Kosetice. Concentrations of all fractions decreased very rapidly above cloudiness (1 600 m a.s.l.) to one third of those measured below the cloud layer. Ratios between fractions were not constant as below the level. Mean $PM_{2,5}/PM_{10}$ ratio above the cloud layer was 75% and dropped from 80% closely above the layer to 70% on the top of the flight. $PM_1/PM_{2,5}$ ratio declined from almost 100% to 94% on the top point.

After descend from Svratouch, the flight continued to the north-east. Concentrations above the north-eastern part of the Czech-Moravian Highland ranged between 17 - 20 $\mu g.m^{-3}$ by coarse fraction and 13 - 17 $\mu g.m^{-3}$ by fine fractions respectively. Approaching Ostrava, concentrations increased significantly to the limit value of 24-hour PM_{10} concentrations (50 $\mu g.m^{-3}$).

PM concentrations above main emission sources and locations with chronic target value exceedances of Ostrava-Karviná region were measured at the flight level 200-300 m above terrain. PM_{10} concentrations oscillated round the limit value of 24-hour PM_{10} level. The values were slightly higher than the target limit above industrial parts, while above urban background localities ranged between 40 – 50 $\mu g.m^{-3}$.

Aircraft measurement of PM vertical profile was the first attempt in this field in the Czech Republic. It is not possible to generalize the results of presented experiment. They represent the PM vertical profiles in the wintertime by specified meteorological conditions.

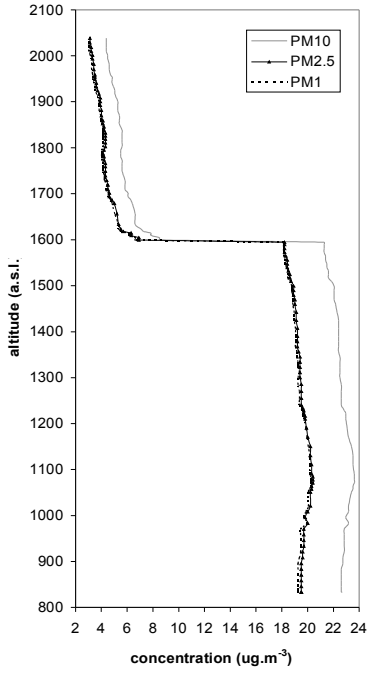

Figure1: Vertical profile of PM concentrations above Svratouch station.

3D trajectories, www.emep.int. Kjeller, NILU (2011).

PM_{10} suspension of road dust is depending on the road surface macro texture

G. Blomqvist, M. Gustafsson, C. Bennet, and T. Halldin

Swedish National Road and Transport Research Institute, SE-581 95 Linköping, Sweden
Keywords: road dust, resuspension, modelling, road surface texture.
Presenting author email: goran.blomqvist@vti.se

Emissions of road dust particles are influenced by both direct generation in the tyre/road interface and by suspension of particles deposited on the road surface. Suspension will be a result both from the action of the tires on the road surface and the turbulence occurring under passing vehicles. This abstract is aiming to find whether there is a relationship between the road surface characteristic 'macro texture' and the dust emission potential.

Road surface macro texture has been measured on five different asphalt surfaces (Table 1), all worn by studded tyres in a road simulator (Gustafsson *et al* 2009). The emission potential was established by measuring the PM_{10} (TSI, DustTrak) in a confined chamber placed on the road surface where 2 g filler material (crushed stone <200 µm) with 20% PM_{10} was distributed manually using a brush. Suspension of the particulate material was achieved by the method presented by Etyemezian *et al* (2007) at 1000 rpm. Each measurement was replicated five times.

Table 1. Pavement type, stone mineral and road surface macro texture on the tested pavement surfaces.

No	Pavement type	Stone mineral	Road surface texture (mm)
1	SMA 16	Porphyry	2.1
2	SMA 11	Quartzite	1.6
3	AC 11	Limestone	1.4
4	SMA 8	Porphyry	2.1
5	SMA 16	Quartzite	1.3

SMA = Stone Mastic Asphalt
AC = Asphalt Concrete
8, 11, 16 = maximum stone size (mm) in pavement

The PM10 concentration in the chamber during each test is described by an increase until a peak is reached and thereafter an exponential decrease (Figure 1). The mean peak value is used in this test as a measure of the dust emission potential for each pavement.

The results (Figure 2) show that there is a strong linear relationship (R^2=0.97) between the road surface texture and the emission potential of the five pavement surfaces. This implies that road surface texture is an important property for road dust emission through suspension and thus should be a parameter in emission modelling.

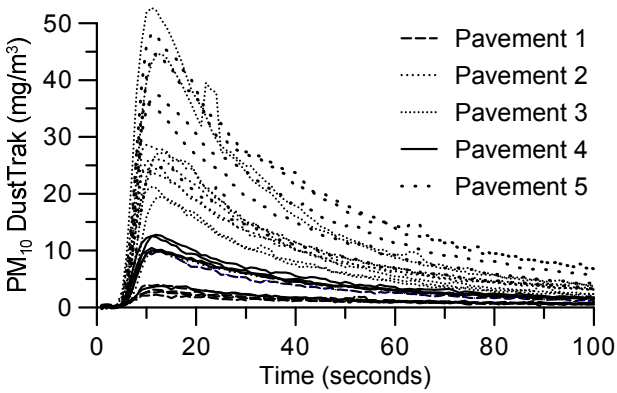

Figure 1. PM10 concentration in the measuring chamber during the test cycle.

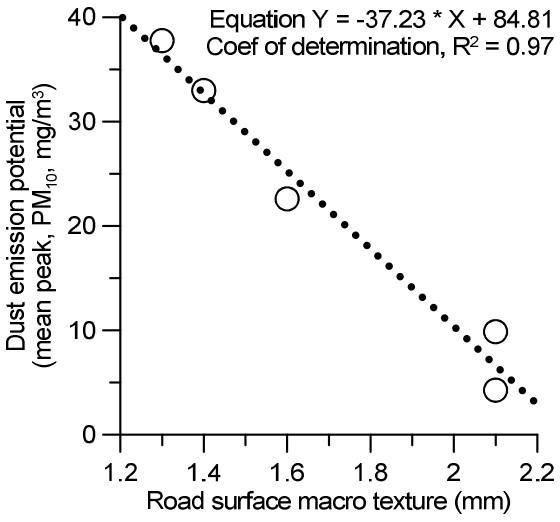

Figure 2. The relation between road surface macro texture and dust emission potential.

Etyemezian, V., G. Nikolich, S. Ahonen, M. Pitchford, M. Sweeney, R. Purcell, J. Gillies, and H. Kuhns. (2007) *Atmospheric Environment* **41**(18), pp. 3789-3796.

Gustafsson, M., Blomqvist, G., Gudmundsson, A., Dahl, A., Jonsson, P. & Swietlicki, E. (2009) *Atmospheric Environment*, **43**(31), pp. 4699–4702.

Sand patch, macro texture CEN-standard, EN 13036-1 (equivalent to ASTM E965)

Development of a Cost Efficient Policy Tool for reduction of Particulate Matter in Air

K. Eleftheriadis[1], E. Diapouli[1], C. Samara[2], A. Kungolos[3], A. Proyou[4], M. Lazaridis[5]

[1]Institute of Nuclear Technology and Radiation Protection, Environmental Radioactivity Laboratory, National Centre of Scientific Research "Demokritos", 15310 Ag. Paraskevi, Attiki, Greece
[2]Department of Chemistry, Environmental Pollution Control Laboratory, Aristotle University of Thessaloniki, University Campus, 54124 Thessaloniki, Greece
[3]Department of Planning & Regional Development, University of Thessaly, Volos 38334, Greece.
[4]AXON Enviro Group Ltd, Athens 11257, Greece,
[5]Department of Environmental Engineering, Technical University of Crete, Chania, Greece

Keywords: environmental policy, emission inventories, Source apportionment.
Presenting author email: elefther@ipta.demokritos.gr

$PM_{2.5}$ and PM_{10} ambient concentration levels are still a major environmental problem in several urban areas in the E.U., while new evidence of its long term impacts on human health continues to emerge. The Commission of E.C. is moving towards the implementation of the thematic strategy on air Pollution and requirements of lower limit values for PM in air will come in effect. National Authorities will have to re-evaluate the present environmental policies and measures and develop new ones.

The Development of a Cost Efficient Policy Tool for reduction of Particulate Matter in Air (ACEPT-AIR) is an effort materializing through a dedicated LIFE+ project in order to enable Authorities (both at central regional and local level) to assess the reduction of key environmental pollutants, as well as their interdependencies, thus responding in a competent way to environmental issues, specific to particulate matter atmospheric concentrations.

The work is targeting, firstly, to unravel the relative contribution of the multiple anthropogenic and other sources to the observed PM air concentrations, Secondly it will document the relative contribution of secondary aerosol particles to those from primary emissions, by taking into account the atmospheric processes which contribute secondary and primary PM at any given receptor site. State of the art data and models will be incorporated in a versatile tool which will combine comparative analysis of source contributions calculated from air concentrations and emission inventories. The tool will create a historical record of control measures, changes in emissions, targeted or economy driven, and provide results in measured concentration reductions apportioned to changes in every accounted source. This can allow the policy makers to evaluate the effects of control measures applied on specific emission sources as well as plan new ones.

Three urban areas have been selected for study: Athens Metropolitan Area, Thessaloniki Metropolitan Area and Greater Volos Area. Historical data from previous studies including results on PM_{10} and $PM_{2.5}$ concentration levels at these three urban centres, covering a period of approximately two decades, as well as source apportionment results (identification of main PM sources and quantification of their relative contribution to the observed concentration levels will be reviewed. New data sets will be constructed by carrying out aerosol campaigns at the same sites that the previous samples were collected. Special attention will be given at three regions Athens Metropolitan Area (AMA), Thessaloniki Metropolitan Area (TMA) and Greater Volos Area (GVA). Aerosol samples PM_{10} and $PM_{2.5}$ at a daily basis will be collected at these 3 sites covering the warm and the cold period of the year. These sites (receptor sites for the source apportionment) will be selected as representatives of traffic-impacted and urban background areas, respectively. In addition, data collected at the "Demokritos" urban background station, which is already in operation, will be utilized.

Source apportionment techniques such as PMF (Karanasiou et al., 2009) and CMB modelling (Samara et al., 2003) will be employed for the sources contribution strength to be determined. The design of the policy tool requires at least two reference periods for performing calculations, trend analysis and construction of scenarios of the emission strength for the different sources. The historical and new databases will be used as the two reference periods. A comprehensive emission inventory will be constructed for the three areas of interest (AMA, TMA and the Greater Area of Volos). The operational platform will allow evaluation of both emission and source strength data. Historical trends and forecasted projections will be produced in order to associate emission sources and the respective air quality data and provide the optimum emission reductions and measures assisting with effective air pollution abatement and sustainability.

This work was supported by the European Community LIFE + Environment Policy and Governance programme

Karanasiou A.A., Siskos P.A, Eleftheriadis K., 2009, *Atmos. Environ*, Vol 43, pp 3385-3395

Samara C, Kouimtzis T, Tsitouridou R, Kanias G, Simeonov V., 2003, *Atmos. Environ*, Vol 37, pp 41-54

$PM_{2.5}$, PM_1 and $PM_{0.4}$ acidity during spring and summer at one Po Valley site.

G. Sangiorgi[1], L. Ferrero[1], M.G. Perrone[1] and E. Bolzacchini[1]

[1]POLARIS Research Centre, Department of Environmental Sciences, University of Milan - Bicocca, Milan, I-20126, Italy

Keywords: water soluble compounds, acidity, water content, PM2.5/PM1/PM0.4.

Presenting author email: giorgia.sangiorgi1@unimib.it

Nitrate, sulphate and ammonium are the three main important water-soluble inorganic ions of PM. Typically, they account for 30-60% of the total PM mass (Seinfled and Pandis, 2006; Lonati *et al*, 2005). In the Po Valley, they show a typical seasonal trend: during the summer sulphate is the dominant inorganic ion (13% of PM_1 and $PM_{2.5}$; Perrone *et al*, 2010) because of the strong atmospheric photochemistry, while during the winter nitrate becomes the most abundant inorganic ion (23-29% of PM_1 and $PM_{2.5}$; Perrone *et al*, 2010). This seasonal pattern affects the characteristics of aerosol acidity, because sulphuric and nitric acids are two of the most important aerosol precursors. Typically, ammonia is the main neutralizing species. The goal of this study is to expand the knowledge about aerosol acidity characteristics.

PM_x samples (Table 1) were collected at Sannazaro de' Burgondi (Pavia, Italy), a rural site located in the middle of the Po Valley (North of Italy). Three dimensional sizes of PM were sampled: $PM_{2.5}$ (4-h filters), PM_1 (8-h filters) and $PM_{0.4}$ (24-h filters). The sampling period was 24 March – 19 April (spring) and 10 June – 2 July 2010 (summer). All the collected filters were extracted in ultra-pure water and analyzed by IC to determine the concentration of water soluble inorganic ions (Na^+, NH_4^+, K^+, Mg^{2+}, Ca^{2+}; F^-, Cl^-, NO_3^-, PO_4^{3-}, SO_4^{2-}) and mono-/dicarboxylic acids (acetic, propionic, formic, glutarric, succinic, malonic, maleic, oxalic acids).

Table 1. Mean ± standard deviation of PM_x concentration ($\mu g/m^3$).

	$PM_{2.5}$	PM_1	$PM_{0.4}$	$PM_1/PM_{2.5}$	$PM_{0.4}/PM_1$
SPRING	21±14	12±8	3±1	0.61±0.12	0.23±0.05
SUMMER	13±8	12±7	5±1	0.64±0.13	0.35±0.08

While the ammonium concentration was at the same level during spring (e.g., PM_1=1.2±1.1 μg m^{-3}) and summer (e.g., PM_1=1.4±1.0 μg m^{-3}), nitrate and sulphate showed the typical seasonal pattern described above. For example in PM_1, NO_3^- was three times higher during spring (spring: 2.9±3.2 μg m^{-3}; summer: 0.8±1.0 μg m^{-3}); on the contrary, SO_4^{2-} was three times higher during summer (spring: 1.0±0.8 μg m^{-3}; summer: 2.9±2.3 μg m^{-3}).

All the samples (regardless of season, time of the day, and PM size) were ammonium-rich, i.d. $[NH_4^+]/[SO_4^{2-}]$ molar ratio was always >1.5. Moreover, it was clearly visible that the ammonium concentration increased at the increasing of the nitrate concentration, suggesting that nitrate formation was a consequence of the gas-phase reaction between ammonia and nitric acid.

However, the spring strong correlation between excess of NH_4^+ (excess $NH_4^+=[NH_4^+]-[SO_4^{2-}]$) and NO_3^- ($R^2 \geq 0.98$) was lost during the summer ($R^2 \geq 0.46$) (Figure 1), suggesting that the presence of ammonium in PM samples could not be attributed to this inorganic ion.

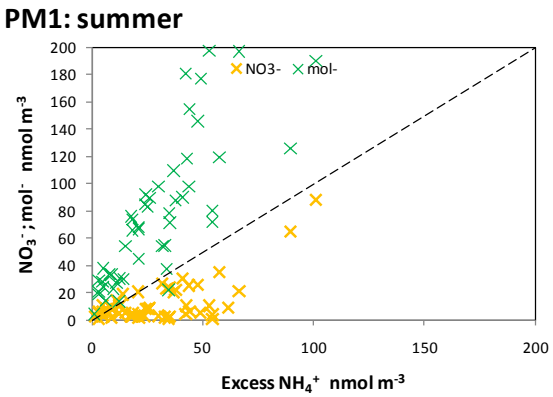

Figure 1. Relationship between excess of NH_4^+ and NO_3^- concentration.

The summer higher level of ammonium in PM_x could be explained by the increased concentration of mono- and dicarboxylic acids, due to stronger photochemical processes than in spring. In fact, the concentration of these acids was double in summer (e.g., PM_1=0.20±0.19 μg m^{-3}) than in spring (e.g., PM_1=.011±0.10 μg m^{-3}).

In addition to strong acidity (i.e., H^+ derived from strong acids in an aqueous extract of PM samples; Pathak *et al*, 2004), also free acidity (i.e., the actual concentration of free H^+; Pathak *et al*, 2004) is an important parameter to describe the aerosol acidity characteristics. Then, a thermodynamic model (*E-AIM*) will be used to determine free acidity for the collected samples.

Lonati, G., Giugliano, M., Butelli, P., Romele, L. and Tardivo, R. (2005) *Atmos. Environ.* **39**, 1925-1934.

Pathak, R.K., Louie, P.K.K., Chan, C.K. (2004) *Atmos. Environ.* **38**, 2965-2974.

Perrone, M.G., Gualtieri, M., Ferrero, L., Lo Porto, C., Udisti, R., Bolzacchini, E., Camatini, M. (2010) *Chemosphere* **78**, 1368-1377.

Seinfeld, J.H. and Pandis, S.N. (2006) *Atmospheric Chemistry and Physics: From Air Pollution to Climate Change*, John Wiley & Sons: New York, USA.

PM2.5 and PM1 particles over south-eastern Italy: seasonal trend of levels and composition

M.R.Perrone[1], A. Dinoi[1], S. Becagli[2], R. Udisti[2]

[1]CNISM, Department of Physics, University of Salento, Via per Arnesano, 73100, Lecce, Italy
[2]Department of Chemical, University of Firenze, via della Lastruccia 3, I-50019 Sesto F.no, Italy
Keywords: aerosol component composition, PM2.5/PM1, carbonaceous particles, air pollution
perrone@le.infn.it

Epidemiological studies on particulate matter (PM) healt effects have highlighted a strong relationship between fine particles and increased cardio respiratory morbidity and mortality. These effects are stronger for particles with aerodynamic diameter d ≤ 2.5 μm, since they can penetrate deeper into the airways of the respiratory system and can reach the alveoli at the lung. It is therefore, important to investigate the dependence of concentration and composition on particle size and study the relationship between particle size and toxicity. 24-hour PM2.5 and PM1 samples have simultaneously been collected in a suburban site of south-east Italy (40.34° N, 18.01° E) from July 2008 to April 2009 to contribute to the characterization of fine fraction particle properties. The PM sampling has been carried out by means of a low-volume (2.3 m^3 h^{-1}) dual-sampler (HYDRA, FAI Instruments, Italy) located on the roof of the Physics Department building of University of Salento, at about 10 m from ground. Atmospheric particles have been collected on 47 cm-diameter pre-fired quartz-fiber filters. Mass concentrations of main water-soluble ions, metals and of organic carbon (OC) and elemental carbon (EC) have been measured in 29 randomly selected PM2.5 and PM1 samples, respectively, to characterize the particle composition. The ion chromatography (IC) technique has been used to determine the mass concentration of the major inorganic anions (Cl^-, F^-, NO_3^-, NO_2^-, SO_4^{2-}) and cations (Na^+, NH_4^+, K^+, Mg^{2+}, Ca^{2+}), and of methanesulfonate (MSA). Mass concentration of metals (Al, Cd, Cr, Cu, Fe, Pb, Mn, Ni, Ba, Mo, V, Zn) has been determined by the ICP-AES technique. OC and EC mass concentrations have been quantified by the thermal-optical transmission (TOT) method using the Sunset Labortatory Carbon Analyzer and the NIOSH 5040 protocol.

Mean mass concentrations (± 1SD) of the 29 PM2.5 and PM1 analyzed samples are 25±11 μg/m³ and 15±7 μg/m³, respectively. Hence, on average 60% of the PM2.5 mass is due to PM1 particles. Standard deviations provide a measure of the mass concentration variability. Non-sea-salt-sulfate (nss-SO_4^{2-}), ammonium (NH_4^+), nitrate (NO_3^-), OC and EC have been identified in both fractions as the main components of the particulate mass concentration, accounting on average for almost 50% of the total sampled mass. The mass concentration of tested ions accounts on average for 17% and 22% of the PM1 and PM2.5 sampled mass, respectively. The seasonal variation of ions concentrations is significant, with the highest concentrations observed in spring-summer and the lowest in autumn-winter. Figure 1 shows as an example, the MSA mass concentration evolution. Methanesulfonate is an oxidation product due to the marine biological activity. Hence, it is exclusively of biogenic origin (Mihalopoulos, 1997) and can significantly contribute to the Mediterranean PM. A clear seasonal trend is revealed by Fig. 1. MSA levels range from 0.003 to 0.06 μg/m³ in PM1 (full dots) and from 0.006 to 0.085 μg/m³ in PM2.5 (open boxes). MSA presents in both fractions significantly higher concentrations from May to September and a dramatic decrease from November to April. The observed seasonal trend of MSA reflects the higher phytoplankton activity during summer. Hence, MSA can be a good marker to evaluate the contribution of the biogenic source to the sulfur budget.

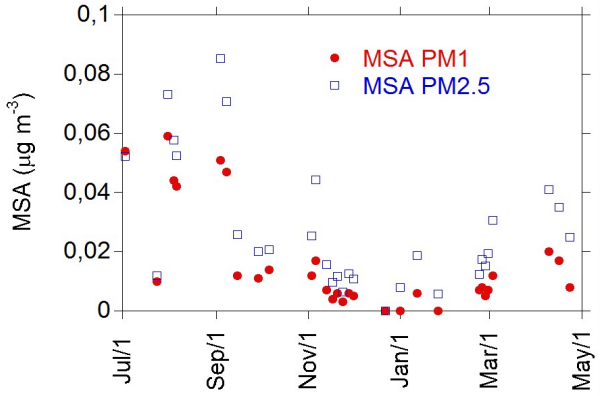

Figure 1. Seasonal evolution of MSA mass concentrations in PM1 and PM2.5 samples.

OC and EC mass concentrations also show a seasonal dependence: OC and EC mean levels are 7±4 μg/m³ and 3±2 μg/m³, respectively in PM2.5 samples and 4±2 μg/m³ and 2±1 μg/m³ in PM1 samples, respectively in autumn-winter. In spring-summer, OC and EC mean levels are 5±2 μg/m³ and 2±0.5 μg/m³, respectively in PM2.5 samples and 3.5±1 μg/m³ and 1.5±0.5 μg/m³ in PM1 samples, respectively. The higher concentrations of carbonaceous particles in autumn-winter are probably due to enhanced emissions coupled with unfavorable meteorological conditions. The mass concentration of tested TC accounts for 39% and 36% of the PM1 and PM2.5 sampled mass, respectively. These last results highlight the significant contribution of carbonaceous particles to PM1 and PM2.5 particles.

Work supported by "Progetto Strategico SIMPA", Puglia Region, Italy.
Mihalopoulos, N. , Tellus, Ser. B, 314–326, 1997.

Magnetic properties of PM10 collected at industrial and urban sites during heating and non-heating seasons

E. Petrovsky[1], B. Kotlik[2], A. Kapicka[1], R. Zboril[3] and M. Roxer[1]

[1]Institute of Geophysics ASCR, Bocni II/1401, Prague 4, 14131, Czech Republic
[2]National Institute of Public Health, Srobarova 48, Prague 10, 10042, Czech Republic
[3]Center for Nanomaterial Sciences, Palacky University, Slechtitelu 11, Olomouc, 78371, Czech Republic
Keywords: PM10, magnetite, concentration, coercivity.
Presenting author email: b.kotlik@szu.cz

Atmospheric particulate matter contains significant portion of magnetite-like iron oxides with concentrations and properties depending upon the source and environmental stress at the deposition/collection site. In many cases, they may reflect such effects as differences between heating and non-heating season, source-specific information (e.g. in proximity to steel works), etc. In our contribution, we present concentration and grain-size dependent magnetic data of PM10, collected at industrial (close to steel works) and urban (city of Prague) sites, collected over period including heating and non-heating season. Magnetic phases were determined using thermomagnetic analyses. Further magnetic characteristics were determined using measurements of hysteresis loops and IRM acquisition and remagnetization curves. In addition, SEM observations and Mossbauer spectroscopy were employed to characterize the anthropogenic contribution to atmospheric dust. Concentration of iron oxides present in the samples is compared with the PM10 concentration. Interpretation of the data is based on comparison with meteorological data, namely wind direction and speed. Our data suggest that magnetic properties may be used for the assessment of source-specific PM. Moreover, in the case of industrial site, specific meteorological conditions – wind direction and speed – seem to affect significantly the contribution of the steel works to generally high air pollution by particulate matter at the nearby site.

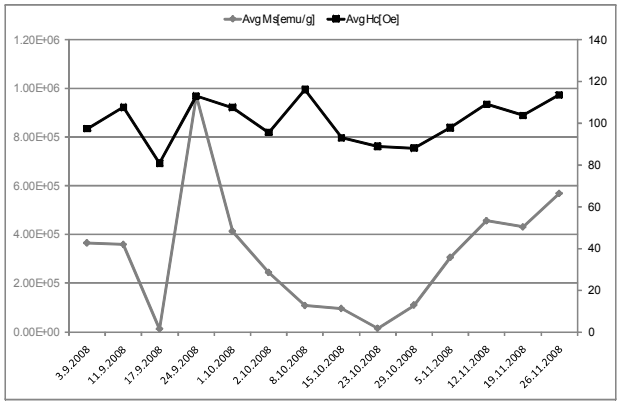

Figure 1. Concentration of magnetite (Ms, left axis) and grain-size sensitive coercivity (Hc, right axis).

This work was supported by the Czech Science Foundation under grant P210/10/0554.

Evaluating the Effects of Aeolian Dust from Jhuoshuei River on the Air Quality

W.Y. Lin[1*], Y.L. Yan[2], C.C. Chen[3], C.T. Chang[4], C.Y. Lai[5], Y.L. Wu[6] C.Y. Young[7], and S.J. Chen[8]

[1]Institute of Environmental Engineering and Management, National Taipei University of Technology, Taipei, Taiwan
[2]Department of Safety, Health and Environmental Engineering, National United University, Miaoli, Taiwan
[3]Occupational Medicine and Industrial Hygiene, National Taiwan University, Taipei, Taiwan
[4]Department of Environmental Engineering, National I-Lan University, No. 1, Sheen-Long Road, I-Lan City, Taiwan
[5]Department of Occupational Safety & Health, College of Health Care & Management, Chung Shan Medical University, Taichung, Taiwan
[6]Department of Environmental Engineering, National Cheng-Kung University, Tainan, Taiwan
[7]Department of Natural Resource, Chinese Culture University, Taipei, Taiwan
[8]Department of Environmental Science and Engineering, National Pingtung University of Science and Technology, Pingtung, Taiwan

Keywords: aeolian dust, PM mass concentration, Jhuoshuei River
Presenting author email:wylin@ntut.edu.tw

Abstract

Due to the extreme steepness of the upstream of the rivers in Taiwan, the sediment yields in the downstream of the rivers are extremely huge. Furthermore, the dams obstruct most of the water thus leading to the formation of large areas of bare-soil downstream during the drought season. Dust emissions from the dry riverbed surface are an environmental concern in the west part of Taiwan (Kuo et al., 2010). These pollutants may pose adverse effects to human health and the environment.

In order to understand current status of the Jhuoshuei riverbed, dust sampling was conducted in this study. PM mass concentration and wind speed samplers from Jhuoshuei River bed near Hsin-Hsing Community, Yunlin, Taiwan were collected from 14 o'clock to 17 o'clock on November 25, 2010. $PM_{10\text{-}2.5}/PM_{2.5}$ mass concentrations were measured by Dichotomous Sampler on the upwind, riverbed, and downwind at the same time (Fig 1).

The result showed that the coarse particle ($PM_{10\text{-}2.5}$) of aeolian dust was about 4600 μg/m^3, and the fine particle ($PM_{2.5}$) was about 1200 μg/m^3 on the riverbed. However the PM mass concentrations of upwind and downwind were lower than 100 μg/m^3 (Fig 2). Moreover, the wind speed was above 12 m/s on the riverbed, and below 10 m/s on the upwind and downwind. The dominant wind direction was from North. Although very high PM concentration found on the riverbed (sampling at 1.5m high), however, not significant impact on the selected downwind site, It might be because of the sampling height (10m) and the relative location.

Figure 1.Sampling sites of Jhuoshuei River, Taiwan.

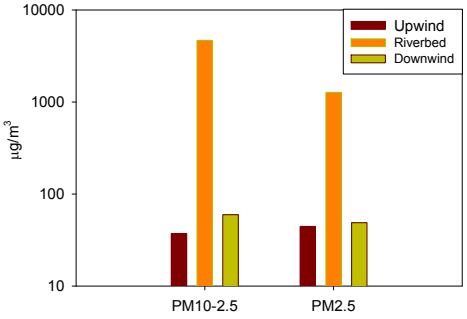

Figure 2.The $PM_{10\text{-}2.5}/PM_{2.5}$ mass concentrations were measured by Dichotomous Sampler on the upwind, riverbed, and downwind.

Kuo, C.Y., Lin, C.Y., Huang, L.M., Wang, S., Shieh, P.F., Lin, Y.R., and Wang, J.Y. (2010) *Journal of Hazardous Materials*, 179:1-3, 1022-1030.

Seasonal variation and source estimation of organic compounds in urban aerosol of Augsburg, Germany.

M.C. Pietrogrande[1], G. Abbaszade[2], J. Schnelle-Kreis[2], D. Bacco[1], R. Zimmermann[2,3]

[1]Department of Chemistry, University Ferrara, Ferrara, I44121, Italy
[2]Cooperation Group Analysis of Complex Molecular Systems, Helmholtz Zentrum München, D-85764 Neuherberg, Germany
[3]Analytical Chemistry, University Rostock, Dr.-Lorenz-Weg 1, D-18051 Rostock, Germany

Keywords: chemical composition, organic tracers, source identification
Presenting author email: mpc@unife.it

This study reports a general assessment of the organic composition of the $PM_{2.5}$ samples collected in the city of Augsburg, Germany in a summer (August-September 2007) and a winter (February-March 2008) campaign of 36 and 30 days, respectively.

The collected PM filters were directly submitted to in situ derivatisation thermal desorption gas chromatography coupled with time of flight mass spectrometry (IDTD-GC-TOFMS) to simultaneously determine the concentrations of many classes of molecular markers: C_{20}-C_{35} n-alkanes, anteiso- and iso-C_{29}-C_{33} n-alkanes, 10 PAHs and 7 oxidized PAHs, and more polar compounds, including long chain n-alkanoic acids, levoglucosan and cholesterol.

The concentrations of the homologous series of n-alkanes were determined and the summer and winter concentrations were compared (Fig. 1). The summer profile is dominated by the heavier n-alkanes ($C \geq C_{27}$) mainly emitted from plant waxes, introduced into the atmosphere from plant abrasion or as products of incomplete biomass combustion: the C_{29}-C_{33} level is nearly 1.5 times higher in the warmer period. N-alkanes from these sources are characterized by a strong odd/even prevalence (CPI≥2) with maximum for the C_{29} and C_{31}terms.

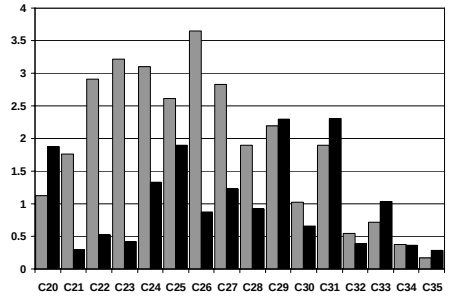

Figure 1: Winter (grey bars) and summer (black bars) distribution of C_{20}-C_{32} n-alkane concentrations

On average, the PAHs showed 8.8-fold higher mean values whereas the O-PAH mean concentrations increased 6.2-fold in the colder period. The higher winter abundance is mainly the result of increased emissions from primary sources, i.e. motor vehicle traffic and domestic heating, and the concomitant effect of atmospheric conditions, with consequent reduction of atmospheric transport and mixing. A comparison between winter and summer distribution of PAH and O-PAH concentrations (Fig. 2) shows an increased influence of non-traffic sources in the colder period characterized by an increased relative abundance of BaP, BaA, BbkF, CRY, IND, and BdA-O — related to domestic heating — vs. compounds prominent in emissions from gasoline and diesel vehicles, i.e., BeP, BghiP, COR, BaF-O.

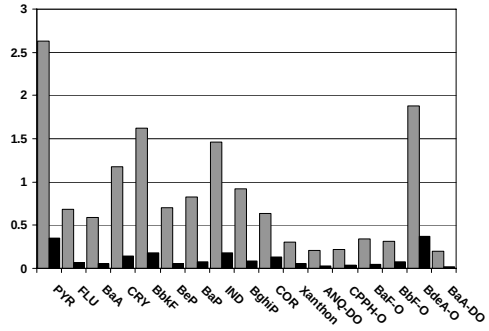

Figure 2: Winter (grey bars) and summer (black bars) distribution of PAH and O-PAH concentrations

Finally, some polar organic species were investigated as valuable markers in tracking the sources of atmospheric aerosols: in particular fatty acids, dehydroabietic acid, levoglucosan and cholesterol were quantified to estimate the contribution from specific biomass/biofuel burning and fossil fuel combustion.

The PCA analysis of the data identified the contributions of three emission sources, i.e., combustion sources, including fossil fuel emissions and biomass burning, vegetative detritus, and oxidized PAHs. These factors make it possible to discriminate PM samples according to seasonality. Winter is characterized by high emissions from petroleum/wood combustion while the contributions from higher plant waxes and atmospheric photochemical reactions are dominant in summer.

The results obtained confirm that IDTD–GC-MS is an effective technique applicable to atmosphere monitoring since it provides a large data set for simultaneous characterization of many chemical markers in particulate samples.

1. Schnelle-Kreis, J., Sklorz, M., Peters, A., Cyrys, J., Zimmermann, R. (2005) *Atmos. Environ.* ***39*** 7702–7714.

Size-segregated chemical characterization of PM at two sites in the city of Madrid

A. Caseiro[1], F. Mirante[1], C. Alves[1], C. Pio[1], B. Artiñano[2]

[1]CESAM and Department of Environment and Planning, University of Aveiro, 3810-193 Aveiro, Portugal
[2]Centro de Investigaciones Energéticas, Medioambientales y Tecnológicas (CIEMAT), Ministerio de Ciencia y Innovación, 28040 Madrid, Spain

Keywords: Aerosol chemistry, size-segregator analysis, summer/winter concentrations

Presenting author email: alexandrecaseiro@ua.pt

The growing awareness of the impact of atmospheric particulate matter (PM) on climate, and the incompletely recognised but serious effects of anthropogenic aerosols on air quality and human health, have led to diverse studies involving almost exclusively the coarse or the fine PM fractions. However, these environmental effects, the PM formation processes and the source assignment depend greatly on the particle size distribution. The purpose of this work was to study the size-resolved particulate carbonaceous and ionic vehicular emissions in Madrid.

The Madrid Metropolitan Area is bordered to the north-northwest by a high mountain range 40 km from the city, and to the northeast and east by lower mountainous terrain. The metropolitan area has nearly 6 million inhabitants, involving a car fleet of almost 3 million vehicles with very intense traffic on weekdays on the two existing ring roads and the roads connecting Madrid with the surrounding towns, where more than 2.5 million residents live. Since its industrial activity consists essentially of light factories, the Madrid plume is typically urban, fed by traffic emissions.

Size-segregated (<0.5µm, 0.5-1µm, 1-2.5 µm, 2.5-10 µm) PM was collected with hi-vol samplers simultaneously at two sites (kerbside and urban-background) in the city of Madrid during two one-month long campaigns (winter and summer). After collection, the organic and elemental carbon fractions were determined by a thermo-optical method, while soluble ionic species were measured by ion chromatography.

Total PM_{10} mass was higher at the kerbside than at urban-background. The main species that contributed to this difference were organic and elemental carbon. Ionic species contribution to overall mass showed little spatial variations.

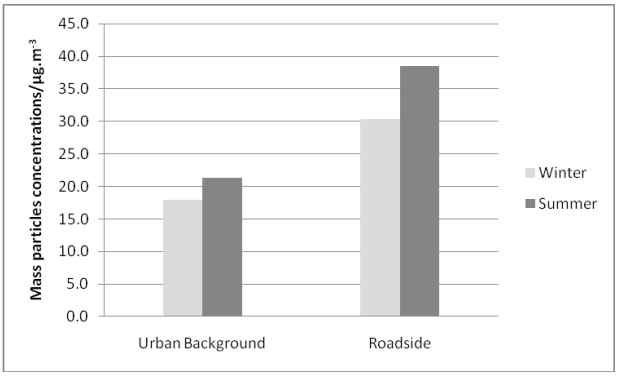

Figure 1. Total mass concentrations in PM_{10} at the urban background and roadside in both seasons.

Soluble calcium concentrations showed a significant spatial variation, mainly in the coarser modes and in winter, with higher concentrations at Roadside than at urban-background, due to the soil particles suspended by traffic.

In the coarser modes, organic carbonaceous species and nitrate were preponderant.

Elemental carbon and the secondary species gain importance towards the finer modes, but organic carbon generally remained the main contributor to the particulate mass.

The main seasonal differences were mainly found for sodium and chloride ions in the coarser modes, due to the use of thawing salt. On the other hand, potassium seasonal variations in the finer modes showed low amplitudes both at kerbside and urban-background, possibly indicating that residential wood burning is not a main source of PM in Madrid.

Table 1. Mean mass concentrations of measured ions at the urban background and roadside.

		WINTER							
		Cl- (µg/m3)	NO3- (µg/m3)	SO42- (µg/m3)	Na+ (µg/m3)	NH4+ (µg/m3)	K+ (µg/m3)	Mg2+ (µg/m3)	Ca2+ (µg/m3)
Urban Background	$PM_{2.5-10}$	0.269	0.117	0.071	0.195	0.002	0.008	0.013	0.052
	$PM_{1-2.5}$	0.094	0.290	0.135	0.091	0.075	0.011	0.009	0.035
	$PM_{0.5-1}$	0.027	0.303	0.174	0.033	0.106	0.023	0.003	0.026
	$PM_{0.5}$	0.024	0.534	0.284	0.034	0.245	0.024	0.001	0.032
Roadside	$PM_{2.5-10}$	0.508	0.165	0.163	0.376	0.003	0.015	0.017	0.145
	$PM_{1-2.5}$	0.200	0.360	0.193	0.145	0.086	0.018	0.011	0.096
	$PM_{0.5-1}$	0.064	0.345	0.188	0.054	0.141	0.017	0.004	0.039
	$PM_{0.5}$	0.097	0.720	0.414	0.087	0.364	0.034	0.005	0.088

		SUMMER							
		Cl- (µg/m3)	NO3- (µg/m3)	SO42- (µg/m3)	Na+ (µg/m3)	NH4+ (µg/m3)	K+ (µg/m3)	Mg2+ (µg/m3)	Ca2+ (µg/m3)
Urban Background	$PM_{2.5-10}$	0.020	0.201	0.125	0.078	0.011	0.011	0.011	0.057
	$PM_{1-2.5}$	0.011	0.078	0.219	0.025	0.058	0.012	0.006	0.059
	$PM_{0.5-1}$	0.029	0.270	0.098	0.112	0.003	0.011	0.014	0.068
	$PM_{0.5}$	0.129	0.425	0.672	0.106	0.150	0.032	0.008	0.105
Roadside	$PM_{2.5-10}$	0.082	0.313	0.155	0.094	0.003	0.019	0.014	0.098
	$PM_{1-2.5}$	0.028	0.213	0.178	0.069	0.013	0.013	0.012	0.080
	$PM_{0.5-1}$	0.019	0.098	0.283	0.042	0.056	0.015	0.008	0.075
	$PM_{0.5}$	0.103	0.376	0.721	0.032	0.175	0.032	0.009	0.179

This work was supported by Portuguese Science Foundation under PhD grant SFRH/BD/45473/2008. And partially carried out under the framework of the *Acción Integrada* PT2009-0151 funded by the Spanish Ministry of Science and Innovation or Action nº E-130/10 funded by CRUP.

Characterization of Aerosol Particles around an Open pit coal mine in Germany by electronmicroscopic individual particle analysis

D. Müller-Ebert[1], M. Ebert[1] and S. Weinbruch[1]

[1]Environmental Mineralogy, Institute of Applied Geosciences, Technical University Darmstadt, 64287 Darmstadt, Germany
Keywords: individual particle analysis, carbonaceous aerosol, open pit coal mine, PM10.
Presenting author email: doe@geo.tu-darmstadt.de

PM_{10} around open pit coal mines in Germany frequently exceeds the 24 hours limit value of 50 µg/m^3. To comply with current EU regulations appropriate mitigation strategies have to be developed. For this goal accurate source apportionment is an indispensable prerequisite. In this study electronmicroscopic individual particle analysis was performed for the characterization of the dust immission around an open pit coal mine.

Particles were collected at two places in the direct vicinity of the open pit mine. One sampling site was chosen in the northeast and one in the southwest. At both sampling sites optical particle counters were operated for the determination of PM_1, $PM_{2.5}$ and PM_{10}. From March until August 2010 particle samples for electronmicroscopic analysis were collected with a two stage cascade impactor (aerodynamic particle diameter: 0.1 – 1 µm and 1 – 10 µm). In order to deduce the PM_{10} contribution of the open pit mine, sampling was only performed for situations with local winds coming from northeast (45 – 75°). During these situations a "luv/lee-situation" is received at the two sampling sites in respect to the open pit coal mine.

The size, shape, and chemical composition of more than 30,000 particles within twelve samples were determined by individual particle analysis performed by automated scanning electron microscopy (SEM) and energy-dispersive X-ray microanalysis (EDX).
The most abundant particle groups encountered are secondary aerosol particles, soot, silicates, silicate/coal mixtures, coal, calcium sulfates, carbonates, Fe-rich particles and (aged) sea salt.

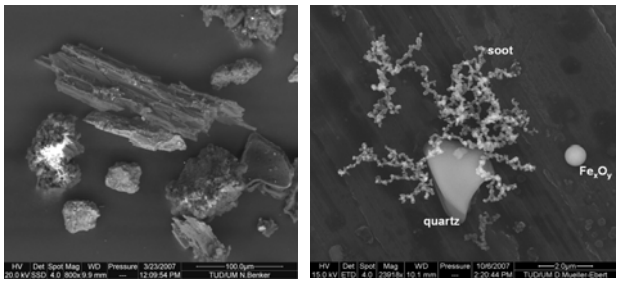

Figure 1. a) Backscatter electron image of a lignite particle; b) Secondary electron image of a soot, quartz and iron oxide particle.

Within the $PM_{10-2.5}$ fraction a high abundance of silicates and silicate/coal mixtures were observed, which can mainly be assigned to the open pit mine activity. Only a low number of pure coal particles were observed. In this way the main particle source from the open pit coal mine seems to be the excavated material and not the coal itself.
At two days also a high abundance of aged sea-salt was observed in this size-fraction.

In contrast the PM_1 fraction is completely dominated by a typical urban/rural background aerosol, characterized by a high abundance of soot and secondary aerosols (sulphate/nitrate/organics) and mixtures of these groups.

Following these results, significant reduction potentials for PM_{10} only exist for the contribution of the excavated material of the open pit mine (silicates and silicate/coal mixed particles) and for urban background aerosols (secondary aerosol particles and soot).
As the contribution of the open pit mine is mainly apparent in the $PM_{10-2.5}$ fraction, but adverse health effects are more likely associated to the PM_1 fraction (respectively particle number concentrations or surface area) a possible conflict of goals in the reduction strategies may arise depending if the focus is set at permissible value of PM_{10} or the relevance for adverse health effects.

Thermal behaviour of water and inorganic ions in particulate matter

S. Canepari[1], C. Perrino[2], S. Materazzi[1], E. Marconi[1], C. Farao[1], L. Tofful[1], S. De Angelis Curtis[1]

[1]Department of Chemistry, Sapienza University of Rome, Rome, 00185, Italy
[2] CNR Institute of Atmospheric Pollution Research, Monterotondo St. (Rome), 00015, Italy
Keywords: water soluble compounds, chemical analysis, thermal desorption, salt aerosol.
Presenting author email: silvia.canepari@uniroma1.it

Thermal analysis have widely been used for the characterization of various materials, but only few studies concern its application to atmospheric particulate matter (Matuschek et al., 2004; Duarte and Duarte, 2008). All these studies are focused on the identification or quantification of desorbed organic species.

Among inorganics, the species that are expected to thermally desorb from PM are ammonium salts and water. Ammonium salts are subjected to solid/vapour equilibria that are responsible for one of the main artefacts in PM determination. The extent of these artefacts has been proved to be influenced by water vapour, which may be absorbed on particles. In the scientific literature, however, only a few and contrasting results have been reported about the analytical determination of water in PM samples, and they have been mostly obtained by the Karl Fischer method (Otha et al., 1998; Tsai and Kuo, 2005).

In this work, the thermal behaviour of water and ammonium salts has been examined under controlled conditions, with the purpose of exploring the potential of thermogravimetry and thermal desorbtion techniques with respect to both the analytical determination of water and the study of sampling artifacts mechanisms.

The themogravimetric curves of reference materials NIST 1648 and NIST 1649a (figure 1) show, as expected, different steps of mass loss. In the range from 25°C to 180°C a loss of ca. 6% (6.3% for NIST 1648 and 4.9 % for NIST 1649a) in two steps has been evidenced. These losses have been assigned, respectively, to weakly and strongly bounded water by using hyphenated TG-MS and TG-FTIR and by carrying out the chemical analysis of the residual obtained after heating at different temperatures. Although the method needs further validation, the thermo-gravimetric determination of PM water content seems to be a convenient alternative to the use of Karl Fischer method.

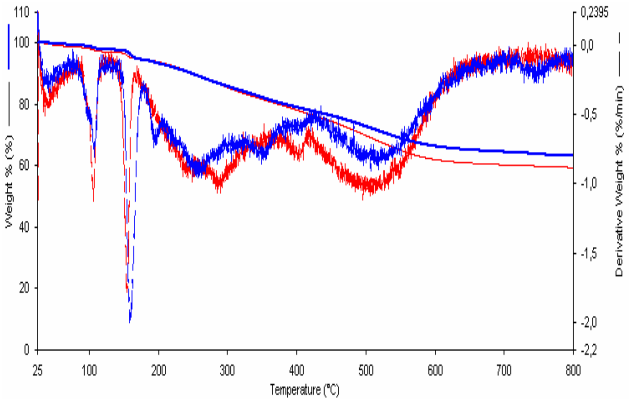

Figure 1. TG curve of NIST 1648 (blue) and NIST 1649a (red) in nitrogen, heating rate 10 °C/min.

Despite the evidence of ammonium salts evolution during the sampling at ambient temperature, the loss of ammonium salts from reference materials starts above 180°C and the residual concentrations of nitrate, chloride and ammonium become negligible at about 310°C. Mass loss registered by the TG analysis in the 180-310 °C range is 7.2% for NIST 1648 and 7.9 % for NIST 1649a. This loss is partially due to inorganic salts (i.e. for NIST 1648: ammonium 1.8%, nitrate ca. 1,1%, chloride 0.3% and sulfate, that partially decomposes to SO_2, ca. 1.1%) and partially to organic matter. The latter has been estimated to be about 2.5% by EC/OC thermoanalysis carried out in the same temperature range.

Similar results have been obtained also on real PM_{10} samples collected on Teflon membranes at an urban site in Rome, Italy. Even though the presence of the filter causes a worsening of signal to background ratio, also in this case water loss at T<120 °C may be measured with sufficient repeatability (about 10% on pairs of equivalent samples).

In the case of real PM samples, all the other release processes occur at lower temperatures than in the case of NIST (about 60°C less). The reasons for this behavior are not clear, but it is reasonable to hypothesize that the aging of dust plays a significant role. Anyway, no significant losses of inorganic ions and OC can be detected below 120°C, in contrast with the usual behaviour observed during the sampling phase (negative artifact due to the release of ammonium salts).

About 80% of the mass losses in the range 120-250°C were due to inorganic ions and OC. After heating up to 250°C ammonium concentration was always below 15% of the initial value, while nitrate and chloride residual amounts strongly depended on the nature of collected PM and were much higher in case of high contribution of natural dust (sea-salt and soil contributions). This residual nitrate and chloride concentrations remain constant also after further heating and are probably associated with sodium salts.

This work was supported by private fundings

Duarte, R.M.B.O. and Duarte A.C. (2008) *Atmos. Environ.* **42,** 6670–6678.

Matuschek, G., Saritas, Y., Karg, E., Schroeppel, A. (2004) *J. Therm. Anal. Cal.* ***78,*** *575–586.*

Ohta, S., Hori, M., Yamagata, S., Murao, N. (1998) *Atmos. Environ.* **32**, 1021-1025.

Tsai, Y.I., Kuo, S.C. (2005) *Atmos. Environ.* **39**, 4827–4839.

Identification and characterization of fine and coarse particulate matter by means of an hourly sampler

E. Yubero[1], J. Nicolás[1], J. Crespo[1], M. Santacatalina[4], A. Carratalá[3]; M. Chiari[2], S. Nava[2], F. Lucarelli[2]

[1]Atmospheric Pollution Laboratory, Miguel Hernández University, 03202 Elche, Spain
[2] Physics Department, University of Florence and INFN, Via Sansone 1, I-50019 Sesto Fiorentino, Italy
[3] Department of Chemical Engineering, University of Alicante, P. O. Box 99, 03080 Alicante, Spain
[4]University of Alicante's General Foundation, 03690, Alicante, Spain
Keywords: Atmospheric Aerosol, PIXE, PMF, cement plant.
Presenting author email: eyubero@umh.es

The aim of the present study is to characterize and identify possible PM sources in an industrial zone in southeastern Spain. This zone has an important presence of cement plants and ceramic industries. Unlike other studies already published in the same zone, in this one, the hourly evolution of the concentration of different elements is studied. In this way, it is possible to get a clearer identification of the sources responsible for the emission of these elements. To accomplish this objective, a 2-stage sequential streaker manufactured by PIXE International was used. This sampling device continuously collects the coarse (PM2.5-10) and fine (PM2.5) fractions separately along a circle. A pre-impactor stage is used to remove particles having aerodynamic diameters larger than 10 µm. The coarse fraction was collected on a Kapton foil and the fine fraction on a Nucleopore filter with 0.3 µm pore diameter. The elemental composition of the samples was determined by the particle induced X-ray emission (PIXE) analytical method. The measurements were carried out using the PIXE facility at the LABEC Lab. of the INFN in Florence, Italy. An SO_2 monitor was also used.

Element	Fine fraction (ng/m^3)	Coarse Fraction (ng/m^3)
S	427	343
Ca	418	2773
V	10.2	18.5
Fe	51.4	222
Ni	2.4	2.1
Cu	2.3	7.4
Zn	3.8	5.7
Pb	4.2	2.7

Table 1. Mean concentrations of some elements during the study period.

Although several campaigns were carried out during the entire year, one sampled week was selected in which there was neither the influence of long-range transport of particulate matter (African intrusions) nor a rain period that could interfere with the measurements of locally emitted contaminants. The sampling period was between 5 and 11 April 2006.

The average concentration of some elements during the measurement week is shown in table 1. High sulphate concentrations are found in both the coarse and fine fractions. Ca appears mainly in the coarse fraction with an average value close to 3 $\mu g/m^3$. Fe has a similar behaviour. V, Ni, Cu, Zn are distributed in both fractions although with higher concentrations in the coarse one.

Pb, an industrial source tracer, appears mainly in the fine fraction, although a significant amount is found in the coarse fraction.

A PMF study was performed in order to characterize the possible sources affecting the PM; in the coarse fraction, six sources were found: Aged sea salt, sea salt, traffic, industrial, and two crustal sources, one more characterized by Ca and the other for the other crustal elements (Al, Si, Ti and Fe). Several sources were found in the fine fraction: Traffic, aged sea salt, secondary sulphate, an industrial source characterized by K, Zn, and Pb, another characterized by V and Ni, and the two crustal sources found in the coarse fraction.

Temporal evolution of the sources related with industrial sources and traffic showed very marked concentration peaks. For instance, the source characterized by V displays peaks that reach values close to 90 ng/m^3 in both fractions. One of these peaks, shown in Figure 1, coincides with the SO_2 peak, pointing out that the plume coming from the cement plant chimney affects the sampling point. Both SO_2 and V could be a product of the petroleum coke combustion that takes place in the cement plant kiln. The traffic source displays different peaks that coincide with the traffic rush hours.

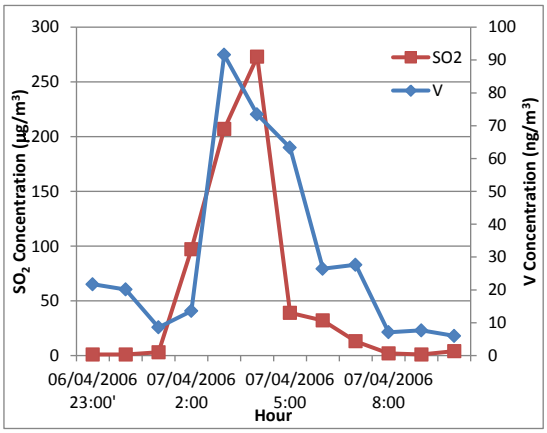

Figure 1. Coinciding evolution of the SO_2 and V concentrations

All these results are confirmed by means of CPF plots.

Work partially supported by CGL2009-08036 (PASSE) project.

Determination of Cr(III) and Cr(VI) in atmospheric particulate samples

M. Catrambone [1], S.Canepari[2], C. Perrino[1]

[1]CNR Institute of Atmospheric Pollution Research, Monterotondo St. (Rome), 00015, Italy
[2]Department of Chemistry, Sapienza University of Rome, 00185, Italy
Keywords: aerosol sampling, filters, chemical analysis, soluble fraction.
Presenting author email: catrambone@iia.cnr.it

Chromium is released to the atmosphere in the form of particulate matter (PM) and may be originated by both natural sources (volcanic eruptions, erosion of soils and rocks) and industrial sources (metallurgic industries, refractory brick production, electroplating, fuel combustion) (Kotas and Stasicka, 2000). However, the relative impact of the several sources of chromium is still largely unknown and the source apportionment of this element requires further investigations.

As well known, the effect of chromium on human health may be influenced by its oxidation state: Cr(III) is essential for the metabolism of lipid, glucose and protein and is generally present as insoluble species, while Cr(VI) is carcinogenic, toxic for humans and animals, absent in nature and its species are characterized by higher solubility.

It is widely recognized that chemical speciation may be a valid instrument for improving studies on both emission sources identification and health and environmental impact. However, most of the studies about the distribution of Cr(III) and Cr(VI) forms in environmental matrices concern natural waters and soils and, to our knowledge, only a few research groups have attempted Cr speciation in airborne particulate matter (Domiınguez and Arcos, 2002; Grabarczyk, 2008).

This study addresses the optimization of an analytic method based on the ultrasound-assisted extraction of water soluble Cr from PM and the determination of Cr(III) and Cr(VI) by catalytic adsorptive stripping voltammetry (CAdSV) using diethylenetriammino pentaacetic acid (DTPA) as complex agent.

The influence of various filter materials and of extracting conditions has been evaluated. The method has been validated on both reference material and real PM_{10} samples and the accuracy of total extractable Cr determination was checked by parallel ICP-OES measurements.

In order to assess the relevance of the two soluble Cr species with respect to total Cr amount in atmospheric PM, the method has been applied to PM_{10} and size-segregated real PM samples. These samples were collected in the industrial areas of Ferrara (Italy) and Tunis, and at a peri-urban site near Rome (Italy).

At the peri-urban site, the total Cr concentrations in the analysed samples ranged from 2 to 5 ng/m^3, with a soluble fraction of 5-13% and Cr(VI) concentrations always below the detection limit (1 pg/m^3). In the industrial area of Ferrara, total Cr concentrations were between 4 and 8 ng/m^3, the soluble fraction was higher (10-12%) and detectable amounts of Cr(VI) were found, with a Cr(VI)/Cr(III) ratio ranging from 0.5 to 1. A further increase of Cr(VI) relevance was evidenced at the industrial site of Tunis, where Cr(VI)/Cr(III) ranged from 1.8 to 3.4 (see figure 1).

The results of the analysis of size-segregated samples, collected at the Ferrara site by a 10-stage cascade impactor, indicate a relevant fine fraction of Cr(VI), with Cr(III)/Cr(VI) ratios increasing with the decrease of particle size.

The proposed method will be in the next future applied to further intensive monitoring campaigns in order to verify the selectivity of Cr(VI) as source tracer. However, these preliminary results clearly indicate that Cr(VI) concentration in PM is strongly dependent on the presence of industrial emission in the area under study.

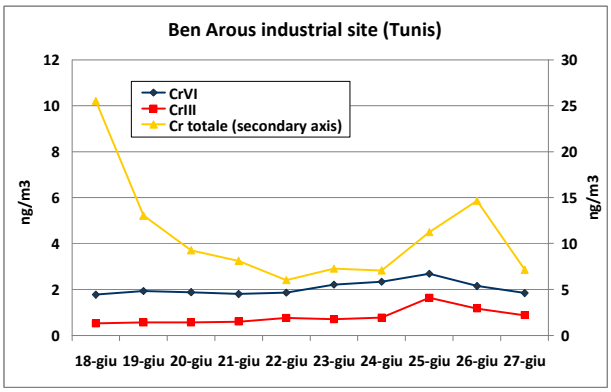

Figure 1. Total Cr (XRF determination), Cr(III) and Cr(VI) during a short monitoring campaign at the industrial site of Tunis

Kotas, J., Stasicka, Z. (2000) *Environ. Poll.* **107**, 263-283.

Domiınguez, O., Arcos, M. J. (2002) *Anal. Chim. Acta,* **470**, 241–252.

Grabarczyk, M. (2008) *J. Hazard. Mater.* **158**, 491–498.

Characteristics of fine and coarse aerosol compositions in central Taiwan

Chien-Lung Chen[1], Chien-Hua Chen[2], Feng-Chao Chung[3], Su-Ching Kuo[4], Li-Ying Hsieh[5] and Ying I. Tsai[6]

[1] Dept of Industrial Engineering and Management, Fortune Institute of Technology, Kaohsiung 831, Taiwan
[2] Dept of Finance, Fortune Institute of Technology, Kaohsiung 831, Taiwan
[3] Dept of General Education Center, Fortune Institute of Technology, Kaohsiung 831, Taiwan
[4] Dept of Medicinal Chemistry, Chia Nan University of Pharmacy and Science, Tainan 717, Taiwan
[5] Dept of Chemistry, National Cheng Kung University, Tainan 701, Taiwan
[6] Dept of Environmental Engineering and Science, Chia Nan University of Pharmacy and Science, Tainan 717, Taiwan
Keywords: particulate matter, chemical composition, urban aerosols.
Presenting author email: clchen@center.fotech.edu.tw

Airborne particulate matters (PM) have been studied intensively for their environmental effects on the public health, the reducing visibility and solar radiation balance (Yatkin and Bayram, 2008). The aim of this study is to characterize and compare the PM and their composition fractions at urban of central Taiwan and provide the input data for air quality model. The sampling site is located in National Chung Hsing University campus, influenced by local sources. Thirty-six of 24-hour daily samples were collected at Taichung from April to December 2009 using Dichotomous Sampler (Andersen Instruments, Model 241, USA). Water-soluble ions (Na^+, Mg^{2+}, K^+, Ca^{2+}, NH_4^+, Cl^-, NO_3^-, SO_4^{2-}) collected with quartz-fibers filters were determined using ion chromatography (DX-100, Dionex Ltd., USA). Total carbon (TC) and element carbon (EC) were measured using an element analyzer (W.C. Heraeus elemental analyzer CHN-O-Rapid, EA).

The mass concentrations and the fractions of $PM_{2.5}$ and $PM_{2.5-10}$ chemical compositions sampling in diurnal and night time are presented in Figure 1 and Table 1, respectively. The average concentration of diurnal $PM_{2.5}$ is 31.1μg m^{-3} including SO_4^{2-} (25.3%), Organics (13.8%), EC (10.9%), NH_4^+ (10.6%), NO_3^- (6.0%), Mg^{2+} (3.5 %) and sea salt (1.9%). The percentage of other compositions is 26.6%. In the other hand, the average concentration of diurnal $PM_{2.5-10}$ is 23.4μg m^{-3}. The percentage of other compositions in coarse particle is up to 47.1%. The major fractions of $PM_{2.5-10}$ compositions are EC (16.7%), Organics (12.4%), NO_3^- (10.3%) and then sea salt (4.8%) in daytime. The results of daytime particle composition in $PM_{2.5}$ and $PM_{2.5-10}$ are shown that the hygroscopic aerosols including sulphate, nitrate, Organics and EC mainly exist in the fine particle (Tsai and Chen, 2006; Pope et al., 2010).

The average concentration of nighttime $PM_{2.5}$ is 35.7μg m^{-3}. Like the main $PM_{2.5}$ compositions sequence in daytime, that of main $PM_{2.5}$ compositions in nighttime is SO_4^{2-} (23.4%), Organics (14.1%), EC (10.5%), NH_4^+ (9.8%), NO_3^- (7.4%), Mg^{2+} (3.6 %) and sea salt (1.3%). The average concentration of nighttime $PM_{2.5-10}$ is 20.8μg m^{-3}. The fraction of other compositions in fine and coarse particle at nighttime is 28.4% and 39.7%, respectively. The major fractions of $PM_{2.5-10}$ compositions in nighttime are EC (18.0%), NO_3^- (13.9%), Organics (13.8%) and then sea salt (5.5%). Comparing the particle compositions at night between the fine and coarse particulate matters, the hygroscopic particles grow up in $PM_{2.5}$ mainly in theory and can be observed from Figure 1. Basically, there is no obvious difference for the composition proportions among the $PM_{2.5}$ and $PM_{2.5-10}$ aerosols sampling in daytime and night time.

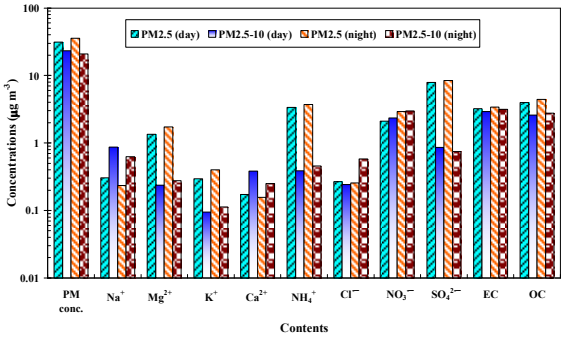

Figure 1. Mass concentrations of fine and coarse particulate matter compositions at Taichung, Taiwan in April – December 2009.

Table 1. Fractions of fine and coarse particulate matter at Taichung, Taiwan in April – December 2009.

Category	Fractions (%)										
	Na^+	Mg^{2+}	K^+	Ca^{2+}	NH_4^+	Cl^-	NO_3^-	SO_4^{2-}	EC	OC	others
$PM_{2.5}$ (day)	1.0	3.5	0.9	0.6	10.6	0.9	6.0	25.3	10.9	13.8	26.6
$PM_{2.5-10}$ (day)	3.6	0.9	0.4	1.8	.7	1.2	10.3	4.0	16.7	12.4	47.1
$PM_{2.5}$ (night)	0.6	3.6	1.0	0.5	9.8	0.6	7.4	23.4	10.5	14.1	28.4
$PM_{2.5-10}$ (night)	3.0	1.2	0.6	1.3	2.3	2.4	13.9	3.9	18.0	13.8	39.7

This work was supported by the Environmental Protection Bureau, Taichung City, Taiwan.

Pope, F.D., Harper, L., Dennis-Smither, B.J., Griffiths, P.T., Clegg, S.L. and Cox, R.A. (2010) *Journal of Aerosol Science* **41**(5), 457-467.

Tsai, Y. I. and Chen, C.-L. (2006) *Atmospheric Environment* **40**(25), 4734-4750.

Yatkin, S. and Bayram, A. (2008) *Science of the Total Environment* **390**, 109-123.

Fugitive Emissions

M. Amodio, E. Andriani, P. R. Dambruoso, G. de Gennaro, A. Di Gilio, M. Intini, J. Palmisani, M. Tutino

Department of Chemistry, University of Bari, Bari, Puglia, via Orabona, 4, 70126, Italy
Aerosol characterization, Industrial aerosols, metals, PAHs
alessia.digilio@uniba.it

Industrialization, urbanization, economic growth and the associated increase in energy demands have resulted in a profound deterioration of air quality. In particular, in recent years, the growing interest about particulate matter (PM) is due to its dangerous consequences on human health. The particles, in fact, may be the carriers of acidic or toxic species such as heavy metals, acids and carcinogenic organic compounds in the human.

Heavy metals and polycyclic aromatic hydrocarbons (PAHs) are important and well known pollutants that have been identified in several environmental matrices world-wide. In particular PAHs are carcinogenic with mutagenic potential and they are derived mainly from incomplete combustion processes. Metals and metalloids are potentially toxic, even at low exposure levels and they're mainly emitted by anthropogenic sources (Bosco et al., 2005). This pollutants locally emitted, undergo dilution with ambient air and various types of transformations during the transport process. The particles number concentration, the information about the vertical diffusive properties of the low layers of the atmosphere and the weather data could be a useful tool to identify the transport and dispersion of pollutants locally emitted. For this reason, plans to suggest right policy controls for human health protection have to taken into account the most relevant emission sources for the area under investigation and how PM concentrations at receptors can be influenced by transport, mixing and transformation processes. Fugitive emission campaign was performed from 15th April to 6th May 2010 in three different sites around the iron and steel pole of Taranto (Apulia Region, South of Italy). The main interest on Taranto is due to the presence of several activities of high impact as very wide industrial area close to the town and the numerous maritime and military activities in the harbor area (Amodio et al., 2008). The aim of the campaign was to triangulate in the neighbourhood of the examined site on the basis of the direction of the wind in order to determine the impact of the local emissive source on the surrounding areas. A prototype for the determination of the contributions of a single source ('fugitive emission') to the PM concentrations has been used: it consists of a Swam dual-channel sampler, an OPC Monitor, a sonic anemometer and a PBL Mixing monitor. The PM concentrations with the data on the advective trends of the air masses provided by the sonic anemometer, allowed to evaluate the pollutant concentrations according to the wind direction. Moreover, thanks to the PBL monitor, it was is possible to determine the dynamic and mixing characteristics of the low layers of the atmosphere and the pollutants dispersion. Finally, the chemical characterization of PM2.5 and PM10 samples was performed to determine PAHs and metals. The preliminary analysis of collected data for all three sites, showed that when the wind direction (reported as wind direction probability between 0 and 1, in Fig.1) allowed the transport from the plant to one of the considered receptor site, iron (Fe-Fg.1), manganese (Mn), zinc (Zn) and PAHs concentration greater than those observed in other two sites can be obtained. Moreover, in these days the Mn concentration exceeded the EPA threshold limit (50 ng m^{-3}), Benzo(a)Pyrene concentration exceeded the limit set by Directive 2008/50/EC (1 ng m^{-3}) and Arsenic concentration exceeded the limit set by Directive 2004/107/CE (6 ng m^{-3}). The statistical analysis, performed by Principal Component Analysis (PCA), was used for a detailed study of the impact of the local emissive source on the neighboring areas. The PCA analysis provided four components, in particular it allowed to identify the coke contribution (PC1), characterized by PAHs high loadings, and the mineral park component with Zn, Fe, Mn and As high loadings (PC2). PC3 was characterized by Si, Ti and Ca high loadings and it was identified as crustal contribution, while PC4 was characterized by high Vanadium loadings and it can be identified as traffic or harbour contribution.

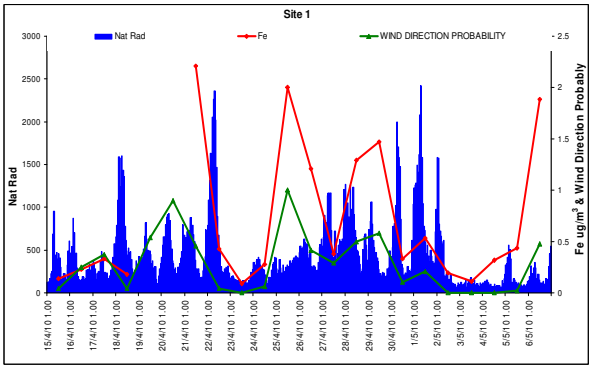

Fig. 1: Natural radiation, Fe concentration and wind direction probability (between 0-1)

This work was supported by the Strategic Project PS_122 founded by Apulia Region.

Amodio, M., Caselli, M., Daresta, B.E., de Gennaro, G.,Ielpo, P., Placentino, C.M., Tutino, M. (2008). *Chemical Engineering Transactions 16, 193-199.*

Bosco, M.L., Varrica, D., Dongarra, G., (2005). *Environmental Research 99, 18– 30.*

Size distribution of atmospheric aerosols and associated ion species on the western Mediterranean

M. Varea, N. Galindo, J. Gil-Moltó, C. Chofre and E. Yubero

Department of Physics, Miguel Hernández University, Avda. de la Universidad s/n, 03202, Elche, Spain
Keywords: ambient PM, ions, size distribution, urban aerosols.
Presenting author email: eyubero@umh.es

Between October 2008 and June 2010 PM10, PM2.5 and PM1 samples were simultaneously collected by means of Derenda low volume samplers (2.3 m^3/h) at an urban background site located in Elche, approximately 12 km from the Spanish Mediterranean coast. Gravimetric and ion chromatography analyses were performed in order to determine PM and water-soluble ions mass concentrations.

Table 1 shows average concentrations of PM1, PM2.5, PM10, and associated ions during the whole study period. PM levels were considerably lower than those measured by Pérez *et al.* (2008) at Barcelona, a much more populated and industrialized city. The differences were more significant for PM2.5 and PM1 because these fractions are more influenced by anthropogenic emissions than PM10. If the levels of PM and ionic species shown in Table 1 are compared with those previously registered at the same city (Nicolás *et al.* 2009), a visible reduction can be observed. This could be partially attributed to meteorological conditions (Galindo *et al.* 2010) and to a decrease in pollutants emissions' caused by the economic crisis.

Table 1. Mean levels of PM and associated inorganic ions between October 2008 and June 2010.

	PM1 (μg/m^3)	PM2.5 (μg/m^3)	PM10 (μg/m^3)
PM	9.2	13.5	24.9
SO_4^{2-}	1.79	2.21	2.56
NO_3^-	0.76	1.34	2.80
Cl^-	0.22	0.29	0.65
NH_4^+	0.63	0.78	0.52
Na^+	0.28	0.38	0.84
Mg^{2+}	0.02	0.03	0.13
Ca^{2+}	0.32	0.35	1.51
K^+	0.20	0.22	0.25

Nitrate, sulfate and calcium were the most abundant ions in PM10, accounting for 11, 10 and 6% respectively, while in PM1 and PM2.5 secondary inorganic ions (SO_4^{2-}, NO_3^- and NH_4^+) were the major contributors, representing more than 40% of the PM mass. Although the percentage contribution of nitrate was very similar for the three size fractions, around 20% of the PM1 mass was made up of sulfate, which doubles SO_4^{2-} contribution in PM10. Ammonium concentration in PM10 was lower than in PM2.5 and PM1, indicating a substantial loss of NH_4Cl by reaction of NH_4NO_3 with NaCl in the PM10 filter (Nicolás *et al.* 2009). Ca^{2+} was reduced in PM2.5 and PM1 with respect to PM10 due to its crustal origin.

Figure 1 shows the distribution of PM and water-soluble ions between PM1, PM2.5–1 and PM10–2.5. For chloride, only the relative distribution between the fine (PM2.5) and coarse (PM10–2.5) fractions could be determined since a large number of PM1 samples were under the detection limit. Approximately 35% of PM10 particles were below 1 μm, indicating lower emission rates of fine anthropogenic particles compared with other urban areas in Europe. Crustal (Ca^{2+}) and marine (Na^+, Mg^{2+}, Cl^-) ions were mainly associated with particles larger than 1 μm. Almost 60% of K^+ was distributed in PM1, revealing the prevalence of anthropogenic over natural sources. Nitrate was almost evenly distributed between the fine and coarse fractions, although important seasonal variations in its size distribution were observed. Around 70% of SO_4^{2-} and NH_4^+ were associated with particles smaller than 1 μm.

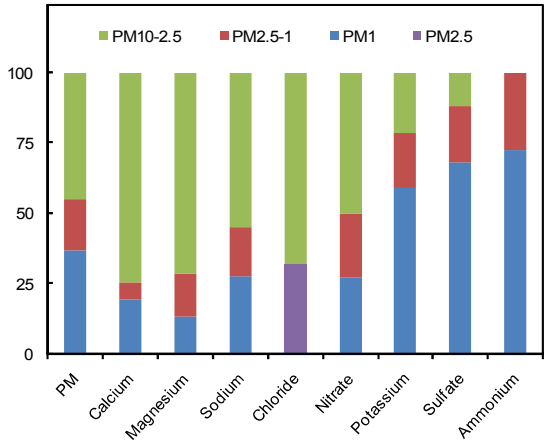

Figure 1. Relative distribution of PM and inorganic ions between different size fractions.

This work was supported by the Ministerio de Educación y Ciencia and the Generalitat Valencia under the CGL2007-63326 (DAPASE) and ACOMP/2010/110 projects, respectively.

Galindo, N., Varea, M., Gil-Moltó, J., Yubero, E., Nicolás, J. (2011). *Water Air Soil Pollut.* **215**, 365-372.

Nicolás, J.F., Galindo, N., Yubero, E., Pastor, C., Esclapez, R. and Crespo, J. (2009). *Water Air Soil Pollut.* **201**, 149-159.

Pérez N., Pey, J., Querol, X., Alastuey, A., López, J.M. and Viana, M. (2008). *Atmos. Environ.* **42**, 1677-1691.

Routine monitoring of coronene in the Czech Republic

L. Hejkrlík, H. Plachá

Czech Hydrometeorological Institute, Branch office in Ústí nad Labem, Czech Republic
Keywords: PM, PAH(s), coronene
Presenting author email: hejkrlik@chmi.cz

Air pollution caused by suspended particles and by PAHs is a particular problem in industrial areas and at places with heavy traffic loads, but also in small communities.

In the Czech Republic exists an extensive programme for automated monitoring of the PM_{10} and $PM_{2.5}$ by radiometry - beta ray absorption, mainly for the sake of smog warning system, low volume sequential sampling of both fractions of PM in a manual network, providing the possibility of monitoring the heavy metals and also the non-sequential manual measurement of PAHs.

Monitoring of PAHs is based on notorious U.S. EPA TO-13A (1999) method of collection of chemicals from ambient air onto a quartz filter and a polyurethane foam (PUF) cartridge using a high volume sampler. The sampler is operated at a low flow rate of 38.5 l/min for up to 24 hours. The 19 target compounds are extracted and analyzed by gas chromatography-mass spectrometry (GC/MS). The GC/MS method is applicable to the determination of PAHs compounds involving three member rings or higher. Naphthalene, acenaphthylene, and acenaphthene have only ~35 percent recovery when using PUF as the sorbent; therefore, they are not included in this study. With optimization to reagent purity and analytical conditions, the detection limits for the GC/MS method range from 1 ng to 10 pg based on field experience.

The Branch office of Czech Hydrometeorological Institute (CHMI) in Ústí nad Labem is responsible for organizing the measuring system of PAHs in the Czech Republic. The laboratory was established in 2002, first measurements began in 2004 and since October 2008 there has been routine monitoring of PAHs at more than 20 stations over the whole Czech Republic.

One of the monitored substances is coronene that is recommended in literature (Leníček *et al*, 2011) as possible traffic pollution indicator. In Table 1. are given some examples of annual concentrations of coronene at various types of measuring stations in the network of CHMI.

Table 1. Select stations of ambient air pollution control measuring coronene in 2009

Station	Classification	Annual conc. ng/m^3
Sokolov	Suburban	0.2
O. Přívoz	Industrial	1.7
Zlín	Suburban	0.5
Košetice	Rural	0.2
H. Králové	Traffic	0.6

It is evident from Figures 1. and 2. that the concentrations of coronene (and also of benzo(a)pyrene and benzo(g,h,i)perylene) exhibit significant seasonality. It is known (Dvorska *et al*, 2009) that coronene as a marker for traffic should be used with care, so we plan to carefully evaluate by means of diagnostic ratios of various PAHs, similar to examples from Figures 1. and 2., the possibility to identify the sources of PAHs at a great number of localities at the end of the campaign of 2010.

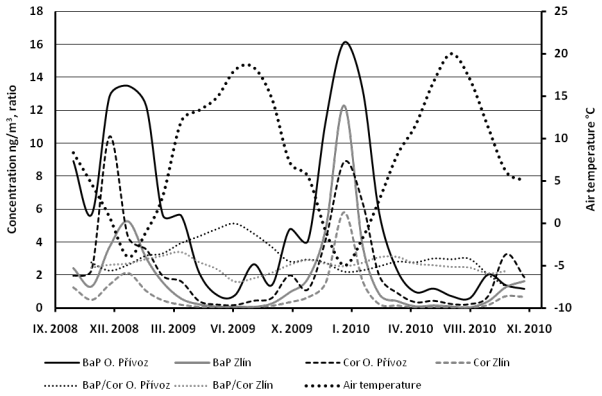

Figure 1. Monthly concentrations of benzo(a)pyrene, coronene and the ratio benzo(a)pyrene/coronene at O. Přívoz and Zlín

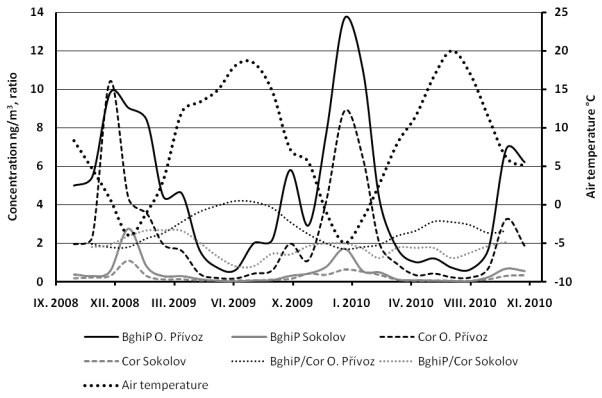

Figure 2. Monthly concentrations of benzo(g,h,i)perylene, coronene and the ratio benzo(g,h,i)perylene/coronene at O. Přívoz and Sokolov

Dvorska A., Jarkovsky J., Lammel G., Klanova J. (2009) *Geophysical Research Abstracts*, **11**, EGU2009-9469, EGU General Assembly 2009

Leníček, J., Kováč, M., Sekyra M., Synek V., Plachá H., Richterová D. (2011) *Ochrana ovzduší* **22**, 3-9.

$PM_{2.5}$ and Water Soluble Inorganic Ions in the Venice area

S. Squizzato[1], M. Masiol[1], E. Innocente[1], E. Pecorari[1], F. Visin[1], G. Rampazzo[1], B. Pavoni[1]

[1] Dipartimento di Scienze Ambientali, Informatica e Statistica, Università Ca' Foscari Venezia, Venice, 30123, Italy

Keywords: $PM_{2.5}$, Aerosol characterization, Inorganic Ions

Presenting author email: stefania.squizzato@unive.it

Pollution from fine particles is an important environmental risk factor for both human health and the possible effects on climate and ecosystems. In polluted urban environments, it affects human health and deteriorates visibility. On a global and regional scale aerosol particles and trace gases have the potential to change weather patterns and the hydrological cycle. Venice area is affected by several emission sources: (i) the medium size urban area of Mestre; (ii) the industrial zone of Porto Marghera; (iii) a crowded road-network; (iv) the artistic glass-making area of Murano; (v) the shipping traffic and (vi) the Marco Polo airport. To better and deeper understand air pollution in the study area, in particular $PM_{2.5}$ and the secondary inorganic aerosol fraction, a collaboration between Università Ca' Foscari Venezia and Ente della Zona Industriale di Porto Marghera started in 2008.

This study is focused on the detailed characterization of Water Soluble Inorganic Ions (WSII) and Secondary Inorganic Aerosol (SIA) on $PM_{2.5}$ in the Venice area. Three sampling sites in different environmental conditions were chosen to evaluate spatial variations: (i) Punta Sabbioni (PS, semi-rural-background costal site); (ii) Mestre-Via Lissa (VL, urban background site); (iii) Malcontenta (MC, industrial site) (fig. 1).

Twenty four hours samples were collected onto quartz fiber filters in all the sampling locations simultaneously, with a flow of 2.3 m^3 h^{-1} according to EN 14907. The experimental campaign has been developed in 2009 and then four periods have been selected to evaluate seasonal differences: (i) spring, 26th February - 3rd April; (ii) summer, 11th June - 16th July; (iii) autumn, 20th September -31st October; (iv) winter, 22nd December - 31st January.

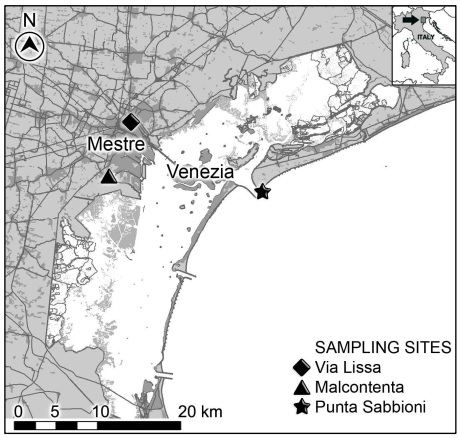

Figure 1. Sampling sites location.

Ultrasonic method was used to extract all filters for determination of inorganic ions by ion chromatography (Na^+, NH_4^+, K^+ Mg^{2+}, Ca^{2+}, F^-, Cl^-, NO_3^-, SO_4^{2-}).

Monthly average concentrations show a typical pattern with maximum values in cold season and minimum in warm season. Ammonium, nitrate and sulfate result to be major ions in $PM_{2.5}$ in all periods. Nitrate highest values have been detected in spring and winter. Sulfate presents maximum concentration in summer and autumn. On annual basis, results of the linear regression between NO_3^-+$nssSO_4^{2-}$ and NH_4^+ (expressed as neq m^{-3}) show a strong correlation (fig. 2). These results indicate that ammonium neutralizes almost completely sulfates and nitrates. Consequently, SIA fraction can be estimated as sum of NH_4^+, NO_3^- and $nssSO_4^{2-}$ masses. SIA mass shows similar values in the three sites but Punta Sabbioni presents the highest SIA% on $PM_{2.5}$ mass (36%).

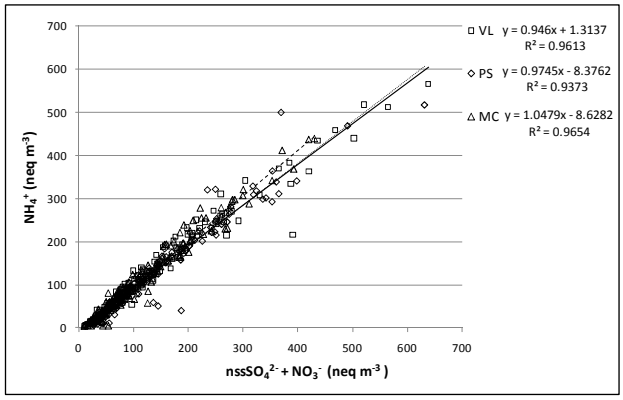

Figure 2. Regression between NO_3^-+$nssSO_4^{2-}$ and NH_4^+.

A Q-mode Hierarchical Cluster Analysis (qHCA, using Ward's method and the squared Euclidean distance measure) was performed to select groups of samples on the basis of their similar chemical composition. Then, each cluster has been interpreted according to local wind data. Preliminary results indicate that heavy pollution events were usually observed in days characterized by low wind speed and high % of wind calm hours.

This work was supported by Ente della Zona Industriale di Porto Marghera. The authors also express thanks to Environmental Protection Agency of Veneto Region (ARPAV) for the valuable support and logistics.

Impacts of local atmospheric circulation on $PM_{2.5}$-bound Polycyclic Aromatic Hydrocarbons in three different emission scenarios in Venice-Mestre (Italy)

M. Masiol[1], A. Hofer[1], E. Centanni[1], F. Fiorotto[1], S. Squizzato[1], E. Pecorari[1], G. Rampazzo[1] and B. Pavoni[1]

[1]Dipartimento di Scienze Ambientali, Informatica e Statistica, Università Ca' Foscari Venezia, 30123, Venice, Italy

Keywords: GC-MS, Meteorology, PAH(s), PM2.5.

Presenting author email: masiol@unive.it

The occurrence of Polycyclic Aromatic Hydrocarbons (PAHs) in the urban atmosphere is demonstrated being a result of anthropogenic emissions from transportation, domestic heating, oil refining, waste incineration, industrial activities, asphalt production, burning of biomass, etc. Particulate-phase PAHs have recently received particular attention because of their diffused presence in the atmosphere and their potentially toxic, carcinogenic and mutagenic effects on humans (Ravindra *et al.*, 2008). Hence, most studies include these compounds in the analyses of priority pollutants for air quality management.

The whole Po Valley is recognized having the highest levels of airborne pollutants in Europe. Venice-Mestre is a large city located in the Eastern part of Po Valley with a population of more than 270,000 inhabitants. It hosts one of the most important industrial zones of Italy, including several chemical factories, waste incinerators and thermoelectric power plants.

This study presents some preliminary results of a one-year sampling campaign focused on the determination of 11 $PM_{2.5}$-bound PAHs collected in three different sites of Venice-Mestre area. These were selected to represent different emission scenarios and were categorized as urban background, industrial- and semi-rural-coastal site. The main aims of this study are: (i) to determine the level of selected congeners; (ii) highlight the most probable emission sources; (iii) investigate on the effects on PAHs levels of local meteorological conditions including air circulation; (iv) assess the human exposure to PAHs and the associated health risk.

About 180 daily samples were collected simultaneously at the sampling sites during Autumn (October, 2009) and Winter (December, 2009-January, 2010 according to EN 14907 standards. $PM_{2.5}$ masses were measured by gravimetric determination. 9 PAHs mainly associated to particle-phase, Benz(a)anthracene (BaA), Chrysene (Chr), Benzo(b)fluoranthene (BbF), Benzo(k)fluoranthene (BkF), Benzo(e)pyrene (BeP), Benzo(a)pyrene (BaP), Indeno(1,2,3-cd)pyrene (IP), Dibenzo(a,h)anthracene (DBahA), Benzo(ghi)perylene (BghiP), and 2 PAH congeners in particle-gas-phase, Fluoranthene (Fla), Pyrene (Pyr), were quantitatively determined using Gas Chromatography-Mass Spectroscopy after solvent extraction and clean-up on silica gel.

Results show for both $PM_{2.5}$ and PAHs significantly higher concentrations in the winter campaign. From PAHs profiles (percent contribution of each congener to $\sum_{11}$PAHs), it is evident that average molecular weight PAHs (Chr, BbF, BkF, BeP and BaP) largely prevail. Profiles for the Autumnal sampling campaign are presented in Figure 1.

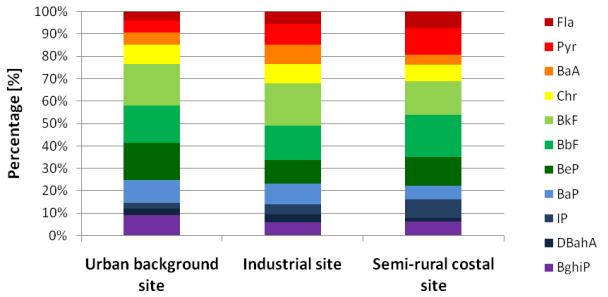

Figure 1. Representative PAHs profiles for each sampling site.

On the basis of diagnostic ratios and statistical analyses vehicular emission are the probable major source for PAHs. The analyses of seasonal variations and spatial distribution provide some interesting information on air quality in this highly polluted part of Southern Europe. A study of experimental data in combination with micro-meteorological conditions and atmospheric circulation patterns was conducted to evaluate the impact and the location of local sources. Results show that the levels of pollutants are strongly affected by local atmospheric circulation. In particular, the increasing of pollutants during winter is associated to air mass stagnation (low wind velocities) in the study area.

An estimation of BaP equivalent toxic and mutagenic factors highlighted a possible risk for humans due to PAH exposure. Results can also be useful to verify changes in air quality and probable source emissions in the Venetian region.

This work was supported by Ente della Zona Industriale di Porto Marghera. The authors also express thanks to Environmental Protection Agency of Veneto Region (ARPAV) for the valuable support and logistics.

Ravindra, K., Sokhi, R. and Van Grieken, R. (2008) *Atmos. Environ.* **42**, 2895–2921.

Characterization of $PM_{2.5}$ chemical composition in Venice (Italy) and their relation with the regional-scale movement of the air masses

M. Masiol[1], S. Squizzato[1], E. Pecorari[1], E. Centanni[1], E. Innocente[1], G. Rampazzo[1]., B.Pavoni[1]

[1]Dipartimento di Scienze Ambientali, Informatica e Statistica, Università Ca' Foscari Venezia, 30123, Venice, Italy

Keywords: PM2.5, Source apportionment, Back trajectories.

Presenting author email: masiol@unive.it

The Po Valley expands over a great part of Northern Italy and is recognized as the most industrialized and populated region of Italy, hosting large cities, such as Turin, Milan, Verona, Boulogne and Venice-Mestre. Air quality is strongly affected by anthropogenic emissions and unfavourable weather conditions frequently trap pollutants. Air quality in Venice is influenced by local complex multi-emission sources, regional long-range transport of pollutants and a peculiar micro-meteorology due to the sea/land breezes (Masiol *et al.*, 2010). Target values for the fine particulate matter ($PM_{2.5}$) fixed by the directive 2008/50/CE are frequently exceeded. The urgent implementation of strategies to reduce the $PM_{2.5}$ levels is therefore mandatory. The identification of the various emission sources is one of the main goals of atmospheric research and plays a key role in formulating and applying $PM_{2.5}$ abatement strategies.

This study is a part of an extended project to characterize the $PM_{2.5}$ in the Venice area by coupling chemical analyses and modelling approaches. The main goal is to detect and quantify the contribution of local emission, aerosol generation processes and regional-scale transport episodes that may contribute to atmospheric pollution.

A one year-long sampling campaign was carried out in three sites characterized by different emission scenarios: urban background, industrial and semi-rural-coastal environments. This study presents the preliminary results for the Spring (March, 2009) and Summer (June-July, 2009) seasons. About 180 daily samples were collected simultaneously in all the sampling sites according to EN 14907 standards. $PM_{2.5}$ masses were measured by gravimetric determination. 9 inorganic ions (F^-, Cl^-, NO_3^-, SO_4^{2-}, Na^+, NH_4^+, K^+, Mg^{2+}, Ca^{2+}), 18 elements (Al, Ca, Mg, Fe, K, Na, S, As, Ni, Cu, Cd, Pb, Mn, V, Zn, Ba, Ti, Sr) and 11 Polycyclic Aromatic Hydrocarbons (Fluoranthene, Pyrene, Benz(*a*)anthracene, Chrysene, Benzo(*b*)fluoranthene, Benzo(*k*)fluoranthene, Benzo(*e*)pyrene, Benzo(*a*)pyrene, Indeno(1,2,3-*cd*)pyrene, Dibenzo(*a*,*h*)anthracene and Benzo(*ghi*)perylene) were quantitatively determined using Ion Chromatography, ICP-OES, ICP-MS and GC-MS, respectively.

A preliminary source apportionment study was performed by using the principal component coupled with the multi-linear regression analyses, using absolute score factors as source tracers. Some independent $PM_{2.5}$ sources were identified and interpreted basing on the presence of tracers and the results of previous studies (Rampazzo *et al.*, 2008a;b; Masiol *et al.*, 2010): combustions, road dust resuspension, glass factories, secondary inorganic aerosol, marine aerosol. In a second step, the daily contribution of each source on the $PM_{2.5}$ mass was quantitatively assessed.

A cluster analysis on air mass backward trajectories was then performed to evaluate the influence of long-range transport on $PM_{2.5}$ mass and chemistry. Four main cluster of trajectories were extracted. Significant differences in air quality and air mass histories were found, showing that the levels of $PM_{2.5}$ increase when air masses move from Northern to Central and Northwestern Europe and a drop when the trajectories originate from the Mediterranean area. Heavy polluted episodes were found when air masses spend most time over the Po Valley.

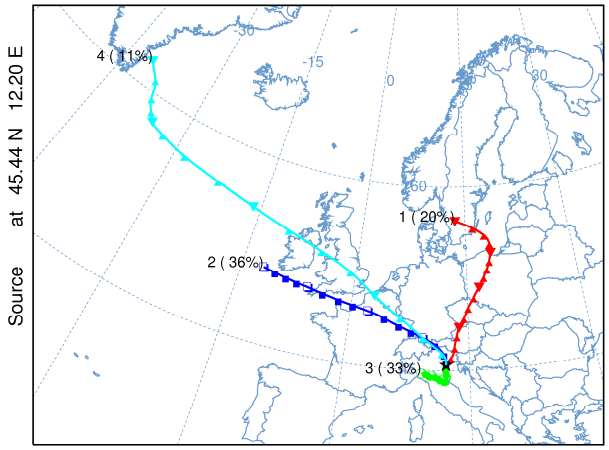

Masiol, M., Rampazzo, G., Ceccato, D., Squizzato, S., Pavoni, B. (2010) *Chemosphere* **80,** 771–778.

Rampazzo., G., Masiol, M., Visin, F., Rampado, E., Pavoni, B. (2008a) *Chemosphere* **71**, 2068–2075.

Rampazzo, G., Masiol, M., Visin, F., Pavoni, B. (2008b) *Water Air Soil Poll.* **195**, 161–176.

Qualitative Source Identification of PAHs Using Diagnostic Compounds

E. Krugly[1], L. Kliucininkas[1], T. Prasauskas[1] and D. Martuzevicius[1]

[1]Department of Environmental Engineering, Kaunas University of Technology, Kaunas, LT-50254, Lithuania
Keywords: PM, PAHs, indoor, outdoor.
Presenting author email: edvinas.krugly@ktu.lt

Experiment

The sources of particulate-phase polycyclic aromatic hydrocarbons (PAHs) in ambient and indoor air in Kaunas, Lithuania were analyzed. The ambient and indoor particulate matter (PM) were sampled at two locations: Vydunas alley (Site 1, representing residential area) and Kestutis street (Site 2, representing city centre). Both sampling sites were located within 10 m from busy streets. PAH concentrations of outdoor (PM_4, $PM_{2.5}$, and PM_{10}) and indoor (PM_4) PM fractions were investigated during analysis period.

PM was collected on glass microfiber filters (GF/A, Whatman International Ltd., Maidstone, UK; diameter 25 mm, pore size 1.6 mm) over a sampling period of 8 hours. PM_4 fraction was sampled using a flow rate of 2.2 l min^{-1} (0.13 m^3 h^{-1}) by SKC Conductive Plastic Cyclones for respirable dust sampling with personal sampling pumps, as well as PM2.5 and PM10 cyclones (URG). PM mass concentrations (μg m^{-3}) were determined from the gravimetric analysis of samples, using a MXA5 microbalance (Radwag, Poland). Deposited particles were extracted from the filters by means of a Sonica ultrasonic extractor (Soltec Srl, Italy) in 3 mL of dichloromethane for 10 min. The extract solutions were filtered through Pasteur pipettes filled with Na_2SO_4, then concentrated by purging with ultra-pure nitrogen gas to 200–300 mL. The MS instrument (a 5973 model connected to a 6890N GC, both made by Agilent Technologies, Inc., Santa Clara, CA, USA) was operated in electron impact (EI) ionization, selected ion monitoring (SIM) mode. The GC column was a non-polar capillary column (60 m _ 0.32 mm id and 0.25 mm film thickness; J&W DB-5, Folsom, USA). 36 PAH compounds were determined.

Several methods for determining sources of PAHs by specific compounds have been published. In our study, diagnostic ratios method was used to analyze collected data on PAH concentrations on purpose to identify the sources of PAH formation (Ravindra et al, 2008). Diagnostic ratios of IdP/(IdP+BghiP) and Fla/(Fla+Pyr) demonstrates the prevailing sources of PAHs (Yunker et al, 2002). Retene has been suggested as an indicator of biomass burning and has a unique formation mechanism or environmental pathway (Li et al, 2009).

Results

The relationships of diagnostic ratios IdP/(IdP+BghiP) and Fla/(Fla+Pyr) are presented in Figure 1. Both sampling sites have revealed a clear urban transport-related source of PAHs emissions. This was actually expected, since both sampling locations were situated near busy streets. At the same time, in Site 1, which was situated in residential area with single family houses, the IdP/(IdP+BghiP) in $PM_{2.5}$ and PM_{10} fractions indicated PAH particles generated in individual heating boilers. This was also confirmed by peaking concentrations of Retene. Wood and coal are very commonly used fuels for heating individual houses in Kaunas. At the same time, in indoor environment, only petroleum-combustion compounds were identified.

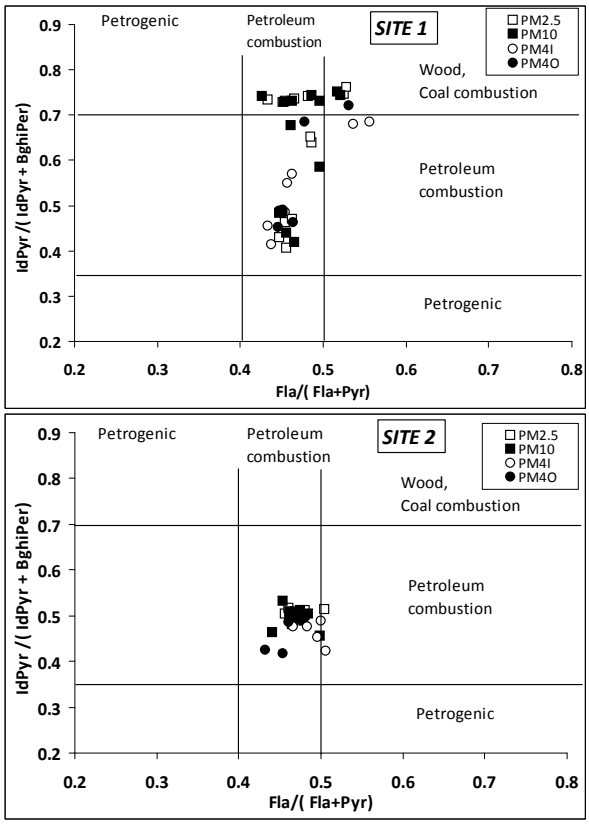

Figure 1. Interdependence of different phase praticles diagnostic ratios IdP/(IdP+BghiP) and Fla/(Fla+Pyr) in different sites .

Yunker, M., Backus, S., Pannatier, E., Jeffries, D., Macdonald, R. (2002). *Estuarine, Coastal and Shelf Science 55, 1– 31.*

Ravindra, K., Sokhia, R., Griekenb, A. (2008). *Atmospheric Environment 42 2895–2921.*

Li, Z., Porter, E. N., Sjodin, A., Needham, L. L., Lee, S., Russell A. G., and Mulholland. J. A. (2009) *Atmospheric Environment 43, 4187–4193.*

Variability of PM10 concentrations at different types of locations in central Poland, 2007-2010

Janusz Jarosławski, Aleksander Pietruczuk and Izabela Pawlak

Institute of Geophysics Polish Academy of Sciences, ul. Księcia Janusza 64, 01-452, Warsaw, Poland

Keywords: PM10, air pollution.

Atmospheric PM10 is one of the air pollution components which concentration is difficult to control in respect of the fulfillment of air quality standards specified in the EU air quality Directives. This problem was noticed in Poland, where, after joining the EU, air pollution monitoring networks have been significantly expanded. This made possible to obtain more detailed information about the levels of main air pollutants such as PM10. After several years of measurements it was found, that air pollutants such as ozone, nitrogen oxides, carbon monoxide do not pose a risk from the standpoint of EU air quality standards. A different situation occurs in the case of particulate matter PM10. The concentration limits are exceeded for most analyzed stations especially in the winter season.

In this paper we present the results of measurements of concentrations of PM10 in the central region of Poland (Mazowieckie voivodship). The measurement data were collected in the period 2007-2010. Different types of stations (hot spot, urban, suburban, rural) appear in the analyzed area. Four of them are located in Warsaw, three in small or medium size cities up to 100 km from Warsaw and one is located in a rural area about 50 km southwest of Warsaw. All stations are equipped with TEOM ambient particulate monitor model 1400 expanded by FDMS module. Measurements were performed continuously. The daily means that are calculated from hourly means are used for data analysis.

Selected results of the measurements are shown in Tables 1 and 2 and Figure 1. Table 1 shows yearly means of PM10 concentrations for all stations in the analyzed area. It may be noted that similar levels of PM10 occur at all stations regardless of the type of station except one station with higher levels in Warsaw which is located on the road with heavy traffic (Wa2). The limit for annual average (40 μg/m3) is exceeded systematically at Wa2 station. Another air quality parameter which is not fulfilled, is the number of days with PM10 concentrations exceeding 50 μg/m3 per year (35). At all stations in the region, this limit is almost always exceeded (Table 2).

Figure 1 shows the monthly average concentrations of PM10 for the year 2009, which is typical when it comes to seasonal variations of PM10. One station (Wa2) has distinctly higher levels of PM10 due to position directly with a heavy traffic road, while for the other stations the concentrations of PM10 are very similar. This may indicate that PM10 concentrations are more the result of larger-scale phenomena such as the presence of long range transport than local sources of PM10.

Table 1. Annual mean concentrations of particulate matter PM10 in Mazowieckie voivodship (μg/m^3).

	Bel	Pło	Rad	Wa1	Wa2	Wa3	Wa4	Żyr
2007	-	30	36	38	47	32	27	32
2008	28	32	37	-	47	32	28	34
2009	32	33	37	-	50	36	34	39
2010	35	35	38	38	52	41	35	46

Table 2. Number of days exceeding the daily concentration limits (50 (μg/m^3)/

	Bel	Pło	Rad	Wa1	Wa2	Wa3	Wa4	Żyr
2007	-	37	66	71	138	53	22	40
2008	24	38	66	-	134	38	24	45
2009	42	49	70	-	148	64	56	83
2010	59	60	87	52	157	97	51	90

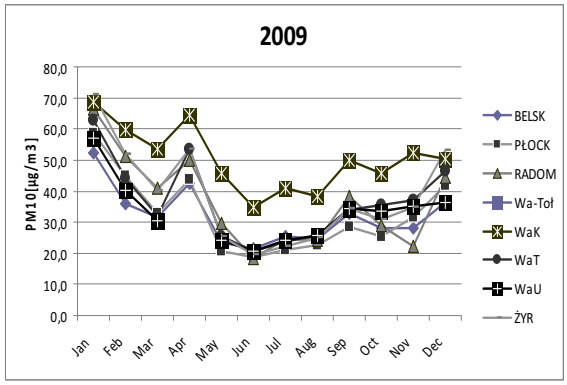

Figure 1. Monthly means of PM10 concentration in 2009

This work was supported by the Polish Ministry of Science under grant 0281/B/P01/2009/36.

Source apportionment of trace metals in atmospheric aerosols in the United Kingdom

R. T. O'Donoghue[1], R.M. Harrison[1]

[1]Division of Environmental Health and Risk Management, University of Birmingham, B15 2TT, UK
Keywords: Source apportionment, PMF, long range transport.
Presenting author email: r.odonoghue@bham.ac.uk

Coarse ($PM_{2.5-10}$) and fine ($PM_{2.5}$) particulate matter (PM) was sampled and analysed for trace metals and SO_4^{2-} at an urban background site in Birmingham, United Kingdom. Daily 24 hour bulk samples were obtained and analysed for Al, Ti, V, Cr, Mn, Fe, Co, Ni, Cu, Zn, As, Cd, Sb, Ba and SO_4^{2-}. The sampling period ran for approximately 4 months, from 15/02/2010 to 10/05/2010. This time period coincided with the Eyjafjallajökull volcano eruption in Iceland.

To assess the data in relation to source apportionment, we applied positive matrix factorisation (PMF) using USEPA PMF 3.0. The uncertainty matrix applied to the PMF analysis was calculated based on literature guidelines (Tauler et al, 2009).

From the PMF analysis carried out on coarse PM, we identified 3 factors associated with dominant sources at the receptor site.

The first factor identified is associated with emissions from the nearby rail line. As the vast majority of traffic on this line is in the form of electric trains, any associated emissions are likely to be linked to steel and copper abrasion i.e. from tracks, wheels, brakes and the overhead traction line. Under such conditions the predominant emissions are Fe / Cu / Cr and Mn, all of which are present in considerable proportions in this factor.

The second factor determined in the coarse mode relates to road traffic non-exhaust emissions. The large contributions for Cu, Fe, Ba and Sb confirm this as the main source. These elements are typically associated with brake and tyre wear. To further corroborate that this factor is locally sourced and primarily associated with road traffic, we examined the plot of locally measured NOx against the daily factor contributions. From the results we deduced that the factor is indeed traffic related, the large scatter (R=0.46) observed is due to the emissions of NOx associated with hot exhaust compared to the brake and tyre wear emissions for the metals (in addition to re-suspension).

In relation to the third factor, it was determined that these concentrations are associated with regional transport of mainly naturally sourced species. The high concentrations of elements Mn, Fe, Al, Ti in this fraction seem to confirm the mainly crustal associations with this grouping. For the regional factor it is readily apparent from Figure 1, the increased relative contributions associated with the time period post 16/04/2010. The peaks observed in Figure 1 relate to the 16/04, 18/04, 21/04 and 22/04, a time associated with the volcano eruption of Eyjafjallajökull. Additional evidence was obtained associating this factor with the Eyjafjallajökull incident through the assessment of species ratios and correlations of daily factor contributions with regional wind directions. In addition, air mass backtrajectory analysis confirmed the air mass movements associated with the Icelandic volcano for these time periods. Finally, comparison between the regional factor concentrations and the Eyjafjallajökul plume composition suggested similar sources. From our analysis we estimated that if such an event occurred on a yearly basis, we could expect an approximate contribution of 2%, 4%, 4% and 3% to ambient coarse concentrations for the metals Al, Ti, Mn and Fe respectively.

Lastly, to compare behaviour across PM modes, we applied similar receptor modelling techniques to the fine PM fraction. The PMF analysis led us to positively identify 2 factors; a regional factor and a traffic and resuspension factor. The regional factor was associated with mainly SO_4^{2-} and primarily of anthropogenic origin. Most notably, compared to the coarse mode, we did not obtain any clear sources for the fine mode relating to the Eyjafjallajökul volcanic plume. This is perhaps not surprising bearing in mind the nature of the eruptive incident, which would likely emit any smaller particles higher into the atmosphere inhibiting their deposition over the UK due to the longer time period required for deposition.

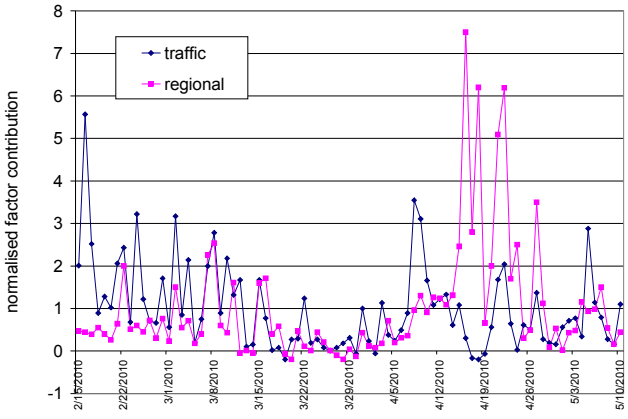

Figure 1. Normalised daily factor contributions for the traffic and regional coarse PM factors

Tauler, R., Viana, M., Querol, X., Alastuey, R.M., Flight, R.M., Wentzell, P.M. and Hopke, P.K. (2009). *Comparison of the results obtained by four receptor modelling methods in aerosol source apportionment studies.* Atmos. Env. 43, 3989-3997.

Estimation of PM_{10} local sources contribution to background levels in an area of the Basque Country

Barrero M.A., Berasaluce A., Cantón L.

Department of Applied Chemistry, University of the Basque Country, 20018, San Sebastián, Spain

Keywords: PM10, spatial variation, major pollutants

Pollutant concentrations in a certain site are dependent mainly on the incidence of emission sources and meteorology and their relative strengths. Therefore, the evaluation of their concentrations simultaneously in several points in a region can yield relevant information about which are the main processes having influence on pollutant levels. This work focuses on the variations of PM_{10} and other major pollutants in six urban locations with different anthropogenic inputs placed in the surroundings of Donostia - San Sebastián, in the Basque Country.

A wintertime measurement campaign (from November to March) was carried out with mobile units of the Basque Government's Air Quality Monitoring Network that measured PM_{10} and major pollutants concentrations (CO, NO, NO_2, O_3, SO_2) and meteorological variables.

Time series of the daily PM_{10} concentrations were evaluated, showing a very similar evolution in the majority of sites. One of the sampling points exhibited high values of PM_{10} comparing with the other ones. Therefore, daily PM_{10} values showed significant, high correlations between sites (Fig.1), the lowest coefficients corresponding to that with high values of PM_{10} (about 0.80). This pointed to a common behaviour of PM_{10} concentrations which could be attributed to similar pollutant sources affecting the area and/or to the effect of meteorological phenomena, with little variations between sites.

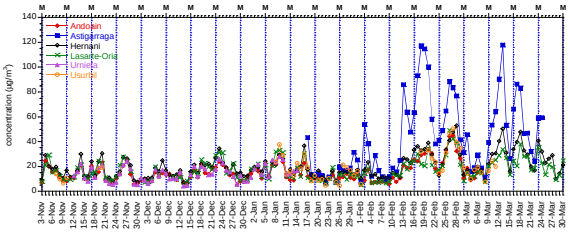

Figure 1. PM_{10} concentration time series in the different sampling locations. M = Monday.

An "area background" daily PM_{10} level was defined, and local contributions were identified using the concentrations of the other major pollutants as some of the "local" PM_{10} peaks were coincident with maxima of other primary pollutants such as carbon monoxide or nitric oxide.

The "area background" contribution to regional background PM_{10} concentration was 8.27, 5.77 and 2.89 $\mu g/m^3$ for working days, Saturdays and Sundays respectively.

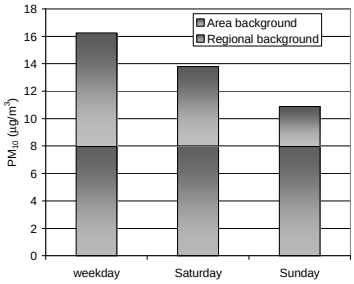

Figure 2. Average levels of PM_{10} regional and "area" background in the study area on weekdays and weekend days.

As well as the "area background" daily levels, the diurnal patterns of the pollutants clearly reflected the incidence of anthropogenic (weekdays-weekend differences).

Bioaerosols & air quality testing with an innovative microbial air sampler

Brossard-Desjonqueres Q

[1]Bertin technologies – CNIM Group, 10 avenue Ampère, Parc d'activité du Pas du Lac, 78180 Montigny le Bretonneux, France

Keywords: Air sampling, aerobiocontamination, cleanroom, indoor air quality, *Stachybotrys*, *Aspergillus*

Presenting author email: brossard@bertin.fr

In the context of indoor air quality and environmental bio-contamination control, Bertin Technologies (France) has developed a technology dedicated to the monitoring of airborne bio-particles. The goal is to propose a sampling method compatible with Rapid Microbiological Methods to get reliable and specific data about the airborne biocontamination (bacteria, molds, pollen, viruses, endotoxins…) in any environment. With this cyclonic technology, airborne particles are separated from the air and collected into a sterile liquid media which is compatible with Rapid Microbiological Methods (RMM) such as immunoassay, PCR assay, Cytometry. This tackles the drawbacks of the traditional impaction method by significantly reducing the time-to-result, providing more information than only cultivable flora (VNC, viruses, allergens…) and avoiding the saturation of the collection media.This sampler is validated according to ISO14698-1 (Health Protection Agency HPA, Porton Down, UK). With the Coriolis® technology, many studies have been carried out to detect bacteria, viruses, pollens, allergens or non-cultivable pathogens. Different applications using Coriolis can be presented.

In one study, an audit on the air quality at workplace was carried out following to employees' complaints headaches and respiratory troubles. Suspicious contamination of *Stachybotrys chartarum,* notorious producer of mycotoxin which is often associated with the "sick building syndrome" was found out to be the cause. Sampling with the Coriolis® revealed the presence of *Stachybotrys chartarum* which is hardly detected by traditional method.

As for air contamination control in pharmaceutical cleanrooms, RNSA Laboratory (France) carried out an investigation in which pollen were identified in the culture supernatant of a pharmaceutical laboratory. Yet these contaminants were not detected by traditional impaction methods. The implementation of an active air sampler and RMM methods were shown to be essential in this case to avoid contamination incidents.

Monitoring of bioaerosol emissions and related risk assessments are indispensable for waste treatment facilities where microorganisms are highly concentrated. Agar plates get quickly saturated and often results in the underestimation of the level of microorganisms. UK's National Physical Laboratory (NPL) developed a new method dedicated to the study of the presence of *Aspergillus* released from composting process. This method combines Coriolis® with subsequent qPCR determination, which produces reliable results within a few hours.

RMM and cyclonic air sampling open up a new horizon for bio-contamination control, and lead a way to a most efficient microbiological monitoring for the well-being of human and the safety of products.

O. Le Goff, V. Bru-Adan, H. Bacheley, J.-J. Godon and N. Wery «*The microbial signature of aerosols produced during the thermophilic phase of composting*» Journal of Applied Microbiology 108 (2010) 325–340 doi:10.1111/j.1365 2672.2009.04427.x

P. Gadal, Q. Desjonquères «*Active air sampling with Coriolis µ air sampler and ScanRDI*»,Environmental Monitoring, a comprehensive Handbook, Vol 3 – Jeanne Moldenhauer Editor, November 2009

A. Brown, A. Knight, N. Kumarswami, B. Lamarre, B. Lipscombe, R.Robinson, M. Williams «*Rapid and Responsive Monitoring Network for Bioaerosol Emissions»* NPL REPORT AS 33, October 2009 www.npl.co.uk/biotechnology/productsservices/aspergillusfumigatus-bioaerosol-monitoring-service

L.Chen, W; Snapp, S.Fennell, M.Boquet, C. Seeger, J.Reyes, and C. Denoya, Pfizer,«*Evaluation of rapid microbiological methods in environmental monitoring : the use of adevice that collects air samples into liquid media*», Scientific poster for 2009 PDA's 4th Annual Global Conference on Pharmaceutical Microbiology, October 2009

Q. Desjonqueres, S. Hamdi. «*Air Sampler Qualification According to ISO14698 Norm*», Controlled environments, p19-23, July/August 2009

Albertini R., Ugolotti M., Ridolo E., Usberti I., Campaniello G., Vitali P., Dall'Aglio P., Brossard Q. «*Il campionamento del lattice ambientale: due metodi a confronto*» Poster for the Congresso Nazionale Associazionie Italiana di Aerobiologia, May 2009

Variability of physico-chemical aerosol properties in the Eastern Mediterranean

I. Kopanakis[1], K. Eleftheriadis[2], N. Mihalopoulos[3], N. Lydakis – Simantiris[4], E. Katsivela[4], D. Pentari[5], P. Zarmpas[3], and M. Lazaridis[1]

[1] Department of Environmental Engineering, Technical University of Crete, Chania, Greece
[2] Institute of Nuclear Technology and Radiation Protection N.C.S.R. Demokritos, Ag. Paraskevi, Attiki, Greece
[3] Department of Chemistry, University of Crete, Heraklion, Greece
[4] Department of Natural Resources and the Environment, Technological Educational Institute of Crete, Chania, Greece
[5] Department of Mineral Resources Engineering, Technical University of Crete, Chania, Greece

Keywords: PM_{10}, $PM_{2.5}$, mass concentration, Saharan dust events.

Particulate matter (PM) measurements were performed during the period 2003 – 2009 at the Akrotiri monitoring station on the island of Crete, Greece. The objective of the study was to determine the ambient mass levels of PM on continuous basis and their chemical composition at selected time intervals. Emphasis was given to the analysis of pollution events due to transportation of particulate matter form Northern Africa (Sahara dust events), since they have an influential impact on the atmospheric composition and dynamics on the Mediterranean area.

The measurements were performed at Akrotiri, a suburban area of the city of Chania, Crete (Lazaridis et al., 2008). It is a coastal site at an elevation of 137 m from sea level.

The PM mass concentration was continuously measured using an automatic beta radiation attenuation monitor. The head of the instrument was changed at selected time intervals and measurements of PM_{10} and $PM_{2.5}$ particles were performed. Meteorological data were collected on continuous basis as well. The path that the air masses travelled before arriving at the station was estimated using back trajectories provided by the HYSPLIT model. In addition, the PM mass size distribution of metals, ions and organic carbon / elemental carbon (OC/EC) was characterized using an 8-stages cascade impactor and a gravimetric sequential particulate sampler during two selected periods.

The mean PM_{10} mass concentration during the measuring period (01.01.2003 – 31.12.2009) was equal to 36.1 ± 9.5 μg/m^3, whereas the $PM_{2.5}$ mass concentration was equal to 23.6 ± 5.8 μg/m^3. Figure 1 shows the monthly averaged PM_{10} and $PM_{2.5}$ concentrations and the corresponding standard deviations. As it is depicted in Figure 1, throughout the winter period (mainly during the months January and December) both PM_{10} and $PM_{2.5}$ mass concentrations were lower than the corresponding mass concentrations in other seasons.

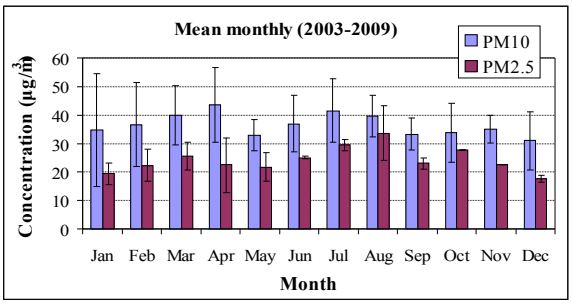

Figure 1: Mean monthly PM_{10} and $PM_{2.5}$ concentrations (in period 2003-2009).

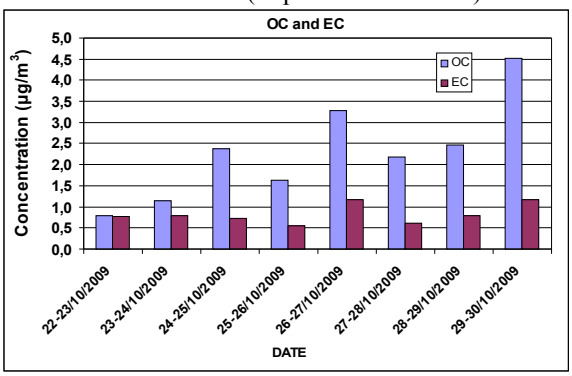

Figure 2: Mean PM_{10} concentrations for EC and OC.

An example of the chemical composition measurements is shown in Figure 2 which depicts the mean 24-h PM_{10} concentration for EC and OC for a selective measurement period (October 2009). During this measurement period (except at 22-23/10/2009), OC had a mean 3 times higher concentration than EC (OC/EC = 2.8 ± 1.0).

Furthermore, several major Saharan dust events were identified in the region of west Crete. The 24-h limit value of PM_{10} mass concentration (50 μg m^{-3}) was exceeded approximately by 14 % throughout the whole measurement period. On the other hand, the lowest daily PM concentrations were measured during intense storm events.

Lazaridis et al. (2008). *Water Air & Soil Pollution* **189**, 85-101.

CHEMKAR PM10 'wood burning'
A year-long chemical characterization of PM_{10} in Flanders (Belgium) with a focus on the contribution of wood burning

J. Vercauteren[1], C. Matheeussen[1], E. Roekens[1], R. Vermeylen[2], W. Maenhaut[2] and M. Claeys[2]

[1] Flemish Environment Agency (VMM), Kronenburgstraat 45, 2000 Antwerpen, Belgium
[2]University of Antwerp (UA), Dept. of Pharmaceutical Sciences, Universiteitsplein 1, 2610 Antwerpen, Belgium

Keywords: PM_{10}, wood burning, levoglucosan, EC/OC

Presenting author email: j.vercauteren@vmm.be

From February 2010 to February 2011 the Flemish Environment Agency (VMM) carried out its third "*Chemkar PM10*" project. Just like the two previous projects this was a large scale chemical characterization project of PM_{10} in Flanders (Belgium). The focus of the current project was mostly on the contribution of wood burning. Although the two previous Chemkar projects[1] had shown that organic matter (OM) is the second most important fraction of PM_{10} (approx. 20%), little is known about the average contribution of wood burning to this fraction in Belgium.

Setup:

During one full year PM_{10} was sampled simultaneously on every 4th day at 7 monitoring sites with different characteristics resulting in **about 700 samples** (including field blanks). The sites are listed below with a short description:

- **Houtem** (rural background near coast)
- **Gent** (urban background)
- **Hamme** (rural background)
- **Borgerhout** (urban background)
- **Mechelen** (suburban background)
- **Lier** (rural background in horticulture area)
- **Retie** (rural background)

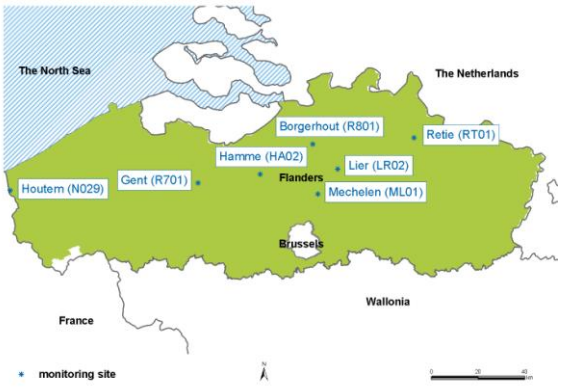

Fig 1: Location of the project sampling sites

Sampling was done for 24h with one Leckel SEQ 47/50 low volume sampler at 2.3 m^3/h on 47mm Pallflex® Tissuquartz™ 2500 QAT-UP filters. After sampling the PM_{10} mass concentration was determined by dual weighing of the filters according to the European reference method EN14907. Next, the filters were punched for chemical analysis and stored at -18°C until analysis. One punch (1.5 cm^2) was used for the determination of **elemental and organic carbon** (thermal/optical transmittance) with the NIOSH protocol. Another punch (1 cm^2) was used for determination of **levoglucosan** by means of GC/MS after derivatisation with *N,O*-bis(trimethylsilyl)trifluoroacetamide (BSTFA) containing 1% trimethylchlorosilane (TMCS).

Preliminary results:

Results for the first four months of the project (Feb-May) show average levoglucosan concentrations between 0.08 en 0.30 µg/m^3 and daily maxima up to 1.6 µg/m^3.

[Wood burning OM] = [levoglucosan] x 7.35 x 1.4

The common conversion factors[2] above were used to calculate wood burning OC and OM. The **average 'wood burning OM'** concentrations were in the range of **0.8 - 3.0 µg/m^3** and maximum daily values for the various sites were between 4 and 16 µg/m^3. The highest concentrations were measured in Hamme, where there are some known sources of domestic wood burning.

Based on these preliminary results, estimates suggest that the average relative contribution of wood burning to total organic matter is in the range of 15-40%, and that the average contribution of wood burning to total PM_{10} is in the range of 3-8%. The latter value is comparable to the contribution of diesel soot in Flanders.

Results of the full project and additional analysis of the data will be presented at the conference.

[1] www.vmm.be/pub

[2] Puxbaum et al. 2007, doi:10.1029/2006JD00811

A new integrated device for on-board particle measurements: Sampling system

T. Tzamkiozis[1], L. Ntziachristos[1], E. Lamminen[2], V. Niemelä[2] and Z. Samaras[1]

[1]Laboratory of Applied Thermodynamics, Aristotle University of Thessalonica, Greece
[2]Dekati Ltd., Tampere, Finland
Keywords: PEMS, PFSS, sampling, on-board, EPONIMOS.
Presenting author email: thtzam@auth.gr

The European Commission introduced the Particle Measurement Programme (PMP) to develop a rigorous sampling and measuring system that would be suitable to regulate the number of particles emitted by vehicles. In addition to type approval testing, advanced sampling and real-time measuring systems will also be employed in portable emission measurement systems (PEMS) for testing the in-use-compliance of heavy duty vehicles. Currently available aerosol instrumentation has not been developed to be exposed in the hostile, real-word environments of vehicle or engine testing. In addition, the constant-flow sampling systems, which are usually employed for this kind of applications, suffer from sensitivity in exhaust pressure fluctuations, being unable to retain a constant dilution ratio (DR).

This work presents a new, simple concept of an on-Board Sampling System (BOSS), which leads to constant DR sampling, independently of exhaust gas pressure and pressure variations. BOSS is consisted of two cascaded stages (primary and secondary), each involving a capillary and a stabilization chamber. The sample is drawn by the primary capillary, due to the under-pressure maintained in the stabilization chamber by means of a pump. Pressure difference between ambient and the primary stabilization chamber forces air to enter the latter. The dilution air has been purified before entering the chamber, while a throttling valve can be used for the regulation of its flow-rate. The capillary diameter is 550 um (prototype), hence, BOSS samples only a very small fraction of the exhaust gas (in the order of 1 lpm), according to Ntziachristos *et al* (2008).

Due to the very small exhaust gas quantity sampled, no tight fixation between the capillary and the exhaust line is required. The capillary is fully surrounded by the exhaust gas, which freely exhausts to ambient pressure, through an opening in the exhaust line. In this way, the capillary inlet is always exposed to exhaust gas of ambient pressure, regardless of the gas pressure inside the exhaust line. Since the inlet and outlet of the capillary are exposed to constant pressure conditions, the sample flow-rate and, therefore, the DR remain constant during the measurement.

The prototype BOSS has been tested regarding the stability and absolute level of the DR against a commonly used sampling system, i.e. an FPS-4000 (Dekati Ltd., Tampere, Finland) cascaded with an ejector diluter (ED) of the same company. To this aim, a turbocharged Euro 3 common rail unit of 2.2 l capacity was employed, also equipped with exhaust gas recirculation. The DR of both systems was determined by measuring the CO_2 concentration at raw exhaust and at their outlets. The engine operated at various steady-state modes.

Figure 1 shows that the DR of the BOSS remains quite constant (CV=1%) and unaffected by the pressure variations in the exhaust line. This characteristic combined with key features like low power consumption (less than 0.5 kW) and small size, make it the ideal candidate for PEMS.

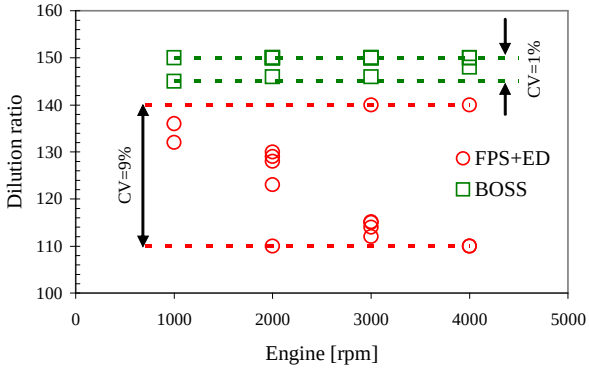

Figure 1. BOSS is compared to a commonly used sampling system, available in the market.

To this direction, the Laboratory of Applied Thermodynamics launched a co-operation with Dekati Ltd. in the framework of a Marie Curie action, in order to develop a PEMS candidate, employing this technique. The system is intended to be used for aerosol sampling on-board the vehicles. The results of this co-operation are demonstrated in Figure 2, where some initial designs of the parts, which will be used for the attachment of the BOSS to the exhaust line, are depicted.

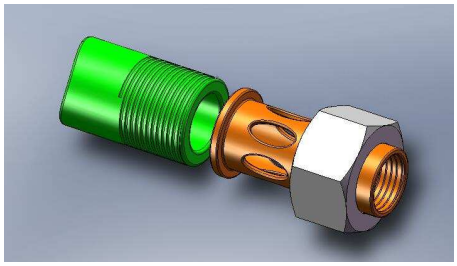

Figure 2. 3D depiction of BOSS parts

This work is supported by the Seventh Framework Programme under Grant Agreement no. 218149.

Ntziachristos, L., Tzamkiozis, T., Mamakos, A. and Samaras, Z. (2008). SAE, doi: 10.4271/2008-01-0762.

Chemical composition of $PM_{1.0}$, $PM_{2.5}$ and PM_{10} in the industrial city in Korea

M.K. Kim[1], and J.Y. Lee[2], S.K. Park[3]

[1]Environment Research Department, Research Institute of Industrial Science & Technology, Pohang, Gyeongbuk, 790-330, Korea
[2]Environment & Health Department, POSCO, Pohang, Gyeongbuk, 790-300, Korea
[3]POSCO-Europe Office, POSCO, Duesseldorf, Nordrhein-Westfalen, 40474, Germany
Keywords: particle size distribution, PM_1, $PM_{2.5}$, PM_{10}, chemical composition
Presenting author email: kimmk@rist.re.kr

The twenty two inorganic elements such as iron, manganese, nickel, lead, carbon, nitrate, sulfate were determined from selected $PM_{1.0}$, $PM_{2.5}$ and PM_{10} samples collected at three monitoring sites near iron and steel complex of Pohang city during different seasons from March 2009 to February 2010. Pohang is the largest industrial city producing iron and steel in Korea and has distinguishing chemical composition in the airborne particular matter. The aim of this study is to detect the seasonal and diurnal variations of the size distribution and chemical compositions of PM related to iron and steel industry. The sample collections of daily $PM_{1.0}$, $PM_{2.5}$ and PM_{10} were carried out every fifteen days for each season.

Table 1. Summary of mean concentration at three monitoring sites in four seasons.

unit : ug/m3

Season	Site	$PM_{1.0}$	$PM_{2.5}$	PM_{10}
Spring (Apr.)	S1	25.1	41.3	67.5
	S2	22.6	35.2	52.2
	S3	27.3	39.4	55.6
	Mean	25.0	38.6	58.4
Summer (Jul.)	S1	23.7	36.7	58.9
	S2	17.9	25.6	40.1
	S3	22.4	34.7	45.4
	Mean	21.3	32.3	48.1
Fall (Oct.)	S1	21.8	38.5	60.6
	S2	20.4	30.9	47.2
	S3	26.7	37.1	51.1
	Mean	23.0	35.5	53.0
Winter (Jan.)	S1	27.9	43.2	62.9
	S2	19.4	27.6	48.4
	S3	22.2	34.7	50.7
	Mean	23.2	35.2	54.0
Annual mean	S1	24.6	39.7	62.5
	S2	20.1	29.8	47.0
	S3	24.7	36.5	50.7
	Mean	23.1	35.4	53.4

The average mass concentrations of $PM_{1.0}$, $PM_{2.5}$ and PM_{10} at three monitoring sites were 23.1 ug/m^3, 35.4 ug/m^3 and 53.4 ug/m^3, respectively. $PM_{2.5}$/ PM_{10} and $PM_{1.0}$/ PM_{10} of three monitoring sites ranged from 0.63 to 0.72 (average 0.66) and $PM_{1.0}$/ PM_{10} ranged from 0.39 to 0.49 (average 0.43). S1, S2 and S3 monitoring sites is located at industrial area, residential area and traffic area, respectively.

Table 2 shows the average concentration of major components in $PM_{1.0}$, $PM_{2.5}$ and PM_{10} at S1 monitoring site. The concentration of components such as arsenic, lead, cadmium, chromium, nickel and nitrate in $PM_{2.5}$ were above 70% of PM_{10}. In contrast, the concentration of aluminum, iron, sodium and calcium in $PM_{2.5}$ were below 30% of PM_{10}. The concentrations of most components in PM1.0 were above 70% of $PM_{2.5}$ except sodium, nitrate and sulfate.

Table 2. The average concentration of major components in PM at S1(industrial area) monitoring site.

unit : ng/m3

Component	$PM_{1.0}$	$PM_{2.5}$	PM_{10}
Al	326.7	459.1	2019.2
Fe	256.4	373.6	1276.3
Mn	135.1	166.8	485.9
Zn	128.3	169.5	372.8
As	4.6	5.1	5.3
Pb	34.2	45.8	62.7
Cd	0.8	0.9	1.1
Cu	16.7	23.1	30.9
Cr	9.4	12.6	18.3
Ni	6.1	8.3	10.1
Na	55.7	114.1	461.5
Ca	133.5	153.7	924.3
C	NA	NA	9209.8
NO_3	1423.8	3106.5	3816.5
SO_4	1329.7	2294.3	4492.6
NH_4	1033.5	1503.7	2716.4

Yin, J. and Harrison, M. (2008) *Atmospheric Environment,* **42**, 980-988.
Wang, S., Feng, X., Zeng, X., Ma, Y. and Shang, K. (2009) *Atmospheric Environment,* **43**, 2823-2828.
Makkonen, U., Hellen, H., Anttila, P. and Ferm, M. (2010) *Sci Total Environ,* **408**, 644-651.
Hieu, N. T. and Lee, B. K. (2010) *Atmospheric Research,* **98**, 526-537.

Chemical characterization of PM_{10} and trace gas measurements with the online-system MARGA at the research station Melpitz in Germany

B. Fahlbusch[1], G. Spindler[1], A. Grüner[1], M. Wallasch[2] and H. Herrmann[1]

[1]Leibniz-Institut für Troposphärenforschung e. V., Permoserstr. 15, 04318 Leipzig, Germany
[2]Umweltbundesamt, Wörlitzer Platz 1, 06844 Dessau-Roßlau, Germany

Keywords: PM_{10}, Instrumentation, Long-range transport, Tropospheric aerosols, Chemical composition

Presenting author email: fahlbusch@tropos.de

In this study the new sampling system MARGA (***M***onitor for **Aer**osols & **G**ases in ambient **A**ir, Applikon Analytical, NL, *ten Brink et al., 2007*) was connected to a PM_{10} inlet to measure the mass concentrations of the water-soluble ions Cl^-, NO_3^-, SO_4^{2-}, Na^+, NH_4^+, K^+, Mg^{2+}, Ca^{2+} and their corresponding trace gases HCl, HNO_2, SO_2, HNO_3 and NH_3 at a time resolution of one hour. Measurements were carried out for more than one year (October 2009 – January 2011) at the research station of the Leibniz Institute for Tropospheric Research in Melpitz, Germany (12°56'E, 51°32'N, 86 m a.s.l.). The station is located 50 km north-east of the city of Leipzig near the river Elbe in a flat terrain surrounded by agriculture land without wind obstacles. Melpitz is an urban background site in Europe. Two main wind directions are influencing the station: Wind from the south-west transports maritime air after crossing a large area of Germany. The second main wind direction is east with anthropogenic polluted air masses from eastern Europe (long-range transport, *Spindler et al., 2010*).

The hourly PM_{10} MARGA measurements were analyzed with consideration of the meteorological conditions (relative humidity, temperature and wind direction).

The data set obtained by the MARGA was compared with results of gas monitors (UV-fluorescence for SO_2 and cavity-ring-down spectroscopy for NH_3) and with daily filter samples (HV-DIGITEL DHA-80 sampler with a PM_{10}-inlet and quartz-fibre filter by Munktell, Sweden) to evaluate the new measuring system.

The SO_2 concentration of the MARGA and the gas monitor are in very good agreement. The comparison between the MARGA and a NH_3 gas monitor (Picarro G1103), however, shows significant differences due to a particle filter inside the Picarro system. The filter is needed to guard the measuring cell against particles. But NH_3 can evaporate from the particles collected on this filter due to the volatility of NH_4NO_3 and generate positive artefacts.

A good agreement was observed for the concentrations of NH_4^+ and SO_4^{2-} between filter and MARGA measurements. Discrepancies occurred during the summer month for the nitrate concentration. NO_3^- measured by the MARGA was on average two times higher than the concentration determined by the filter-based method in July 2010. Again this artefact of the filter measurements can be explained with the volatility of NH_4NO_3. During months with high mean temperatures the corresponding trace gases HNO_3 and NH_3 evaporate from the particle phase collected with the filter. During the winter this artefact is not detected (figure 1).

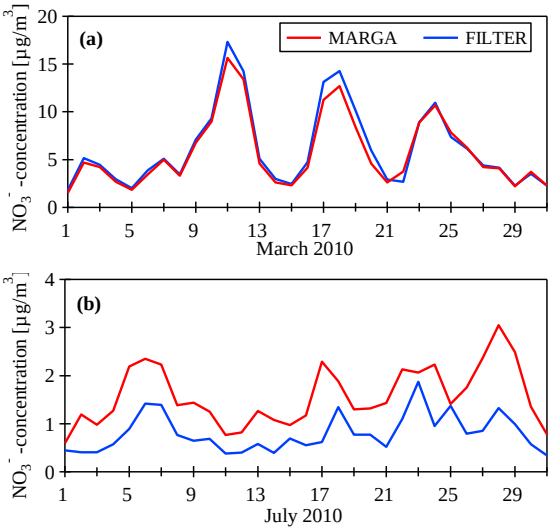

Figure 1. Nitrate measurements in PM_{10}. Comparison of daily High-Volume filter measurements (quartz-fibre filter, DIGITEL DHA-80, blue line) with MARGA measurements (red line) in (a) March 2010 and (b) July 2010.

The authors gratefully acknowledge financial support by the Umweltbundesamt in Dessau-Roßlau, Germany (grant no. 351 01 070).

ten Brink, H., Otjes, R., Jongejan, P., Slanina, Sjaak (2007) *An instrument for semi-continuous monitoring of the size-distribution of nitrate, ammonium, sulphate and chloride in aerosol*. *Atmos. Environ.* **41**, 2768-2779.

Spindler, G., Brüggemann, E., Gnauk, T., Grüner, A., Müller, K., Herrmann, H. (2010) *A four-year size segregated characterization study of particle s PM10, PM2.5 and PM1 depending on air mass origin at Melpitz, Atmos. Environmen*., **44**, 164-173.

Tuesday, September 6, 2011

Session 4P: Poster Session A:
Aerosol-based Nanotechnology

Oxidation of C_{60} aerosol by ozone

A. J. Tiwari[1] , E. D. Davis[2], Y. Zhang[2], J. R. Morris[2], and L. C. Marr[1]

[1]Department of Civil & Environmental Engineering, Virginia Tech, Blacksburg, Virginia, United States
[2]Department of Chemistry, Virginia Tech, Blacksburg, Virginia, United States
Keywords: nanoparticles-characterization, carbon oxidation, ultrafine aerosols, nano-DMA
Presenting author email: ajtiwari@vt.edu

In studies that have explored the potential environmental impacts of manufactured nanomaterials, the atmosphere has largely been viewed as an inert setting that acts merely as a route for inhalation exposure. Carbonaceous nanoparticles, such as C_{60} fullerenes, will enter the atmosphere during production, use, and disposal (Yeganeh *et al.*, 2008). Rather than simply being transported, they will be subject to physical and chemical transformations which could modify their cross-media transport from the atmosphere to terrestrial and aqueous ecosystems, as well as their fate, transport, bioavailability, and toxicity within those ecosystems. In one such transformation, it is likely that C_{60} fullerenes will become oxidized in the presence of ozone (O_3).

The objective of this research is to determine the products and rates of reaction of aerosolized C_{60} with atmospherically relevant concentrations of ozone. Batch reactions are carried out in a $6m^3$ Teflon chamber using ozone concentrations from 40 – 120 ppb. C_{60} aerosol is introduced into the chamber through atomization of an aqueous suspension prepared by stirring C_{60} in water without surfactants or transfer solvents, a method that is believed to produce more environmentally relevant form of C_{60}. Aerosol samples are collected from the chamber onto filters, gold slides, and TEM grids for offline analyses.

Analytical techniques employed include infrared spectroscopy (RAIRS), liquid chromatography (HPLC), UV-Visible absorbance spectroscopy (UV-Vis), and transmission electron microscopy (TEM). Additionally, online techniques include a scanning mobility particle sizer (SMPS) to monitor the evolution of the particle size distribution and an ozone analyzer to monitor ozone consumption during the reaction.

Results

X-ray photoelectron spectroscopy (XPS) analysis indicates that the aqueous C_{60} suspension resulting from stirring in water contains less than 10% oxygen, as shown in Table 1. This oxygen is primarily attributable to hydroxyl groups on the surface of C_{60} aggregates, affording them enough hydrophilicity to exist stably in aqueous suspension (Labille *et al.*, 2009).

Figure 1 shows an infrared spectra of C_{60} aerosols exposed to ozone. In addition to two of C_{60}'s characteristics peaks (1182 cm^{-1} and 1429 cm^{-1}), the formation of the $C_{60}O$ epoxide and various carbonyl groups is suggested by peaks at 1461 cm^{-1} and in the 1700 cm^{-1} range (Cataldo 2008).

Table 1. Oxygen content of C_{60} sample before and after preparation of aqueous suspension.

C_{60} Processing Stage	% C	% O
As received	94	6
After stirring	91	9

Results from complementary analytical methods are expected to verify the identities of epoxides and carbonyls, to allow calculation of reaction rates, and to describe C_{60} aerosol size and morphology before and after ozonation.

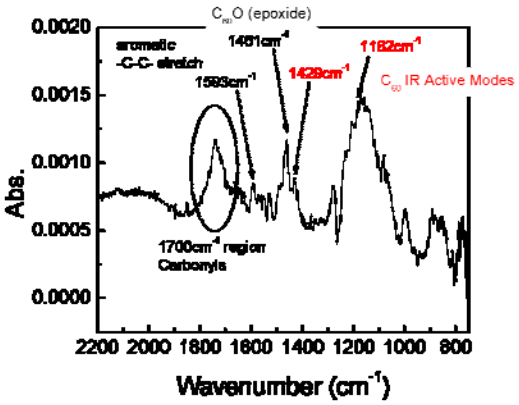

Figure 1. A Reflection-Absorption Infrared spectra (RAIR spectra) of C_{60} aerosol exposed to ozone.

This work was supported by the (US) National Science Foundation under award CBET-0537117, an NSF IGERT fellowship for A. Tiwari, and by the Institute for Critical Technology and Applied Science (ICTAS) at Virginia Tech.

Cataldo, F. (2008) *J. Nanoscience and Nanotechnol.* **74,** 1439-1445.

Labille, J. Masion, A., Ziarelli, F., Rose, J., Brant, J. Villieras, F., Pelletier, M. Borschneck, D., Wiesner, M., Bottero, J-Y. (2009) *Langmuir* **25**, 11232-11235.

Yeganeh, B., Kull, C., Hull, M., and Marr, L. (2008) *Environmental Science & Technology* **42**, 4600-4606.

Rare earth labelling of TiO_2 engineered nanoparticles for identification of aerosols in occupational environments

V. Gómez[1], Silvia Irusta, Francisco Balas and Jesús Santamaría
Instituto de Nanociencia de Aragón (INA), Edificio I+D, c/ Mariano Esquillor s/n, 50018 Zaragoza (Spain)
Keywords: Nanoparticles, Occupational exposures.
virgomez@unizar.es

There is a growing interest in the impact of engineered nanoparticles (ENPs) on the human health and environment. Because of their reduced size (less than 100 nm), ENPs pose hazards that cannot be tackled with the conventional industrial safety and hygiene methods without further considerations [1].

Among the most common ENPs used for technological applications, the TiO_2 ENPs were chosen as test nanoparticles. This increases the interest on discriminating the TiO_2 ENPs from the naturally occurring TiO_2 in the environment. An effective way to distinguish this contribution to the total concentration of nanoparticles in air streams is labeling the TiO_2 ENPs with trace amounts of lanthanides that could be easily identified using online and offline analysis techniques.

Microwave radiation has been applied to synthesize different nanomaterials. The synthesis procedure of Ce-TiO_2 ENPs combines a sol-gel processing followed by microwave treatment. This procedure leads to anatase ENPs avoiding the aggregation due to high temperature treatments. Monodisperse Ce-doped anatase ENPs were prepared from titanium tetraisopropoxide. Several Ce(III) amounts were added using $Ce(NO_3)_3$ as precursor up to 0,5, 1, 3, 6 and 9% Ce/Ti atomic ratio. The synthesized Ce-TiO_2 ENPs were analyzed by XRD, TEM, SEM, EDX, N_2 adsorption, UV-VIS and DLS. XRD patterns show the characteristic anatase diffraction peaks. Regardless the amount of Ce doping, no signals of Ce (III) or Ce(IV) oxide were observed. The morphology of Ce-TiO_2 samples can be seen in the TEM images of Figure 1, which show homogenous particle shapes together with an average particle size about 15 nm. Ce 4d XPS spectra of nanoparticles with 0.5, 1 and 3 % Ce/Ti atomic ratio are also shown in Figure 1.

In a set of experiments, a certain mass of 3% Ce TiO_2 ENPs powder is added for ten consecutive portions of similar mass with a spatula to a glass flask. During the experiment, the nanoparticle aerosol formation is alternatively monitored with a Condensation Particle Counter (CPC, Grimm) and an Optical Particle Counter (OPC, Grimm). As the CPC and OPC take the aerosol from the chamber at 0.3 and 1.2 l/min, the same flow of HEPA-filtered clean air is added during the experiment.

In Figure 2 is showed the real time aerosol evolution using the OPC in the closed environment. Every added portion of the test can be seen in the time evolution as peaks in the ENP number concentration in the experiment chamber. It is also worth noticing that the highest ENPs increase corresponds to those between 300 to 400 nm of aerodynamic particle size. Larger size ENPs show a moderate increase up to the end of the test. The almost total elimination of ENPs from the chamber is achieved in 3 h.[3] rise during nanopowder additions. The fraction of small-size ENPs, between 5 to 10^3 nm detected with the CPC is about thousand of millions of particles.

The TiO_2 ENPs from laboratory aerosols can be therefore identified using this labeling procedure. This procedure could be used as an adequate method to detect, analyze and identify ENPs in occupational enviroments, which are needed in the risk assessment schemes in nanotechnology.

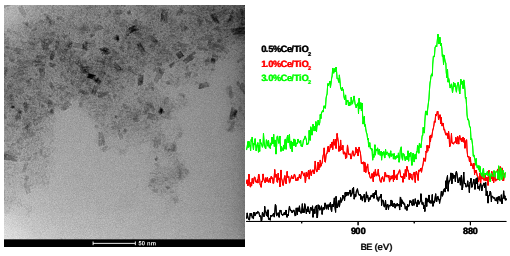

1. (a) TEM image 3 % at Ce TiO_2 nanoparticles. (b) Cerium 4d core level for nanoparticles with different amounts of cerium.

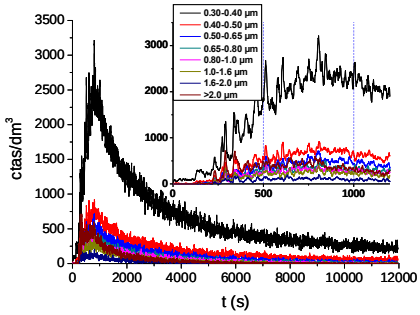

2. Time evolution of Aerosol particle size measured with OPC

This work was supported by MICINN through research projects MAT2008-01319/NAN and PSE-2008-420000-3. V.G. acknowledges the FPU scholarship AP2008-02067

[1] F. Balas, M. Arruebo, J. Urrutia, J. Santamaria (2010) *Nat. Nanotechnol.* 5 93-96.

Characterisation of CeO_2 engineered nanoparticles from a liquid flame spray process – exposure of workers

J. Lyyränen[1], M. Järvelä[2], T. Tuomi[2], J. Pimenoff[3], A. Auvinen[1] and J. Jokiniemi[1,4]

[1]VTT Technical Research Centre of Finland, P.O. Box 1000, 02044 VTT, Espoo, Finland
[2] Finnish Institute of Occupational Health, Topeliuksenkatu 41 a A, FI-00250 Helsinki, Finland
[3]Beneq Oy, P.O. Box 262, FI-01511 Vantaa, Finland
[4]Univ. of Eastern Finland, Department of Environmental Science, P.O. Box 1627, FI-70211 Kuopio, Finland
Keywords: Nanoparticle, characterisation, flame spray, exposure
Presenting author email: jussi.lyyranen@vtt.fi

In this work a liquid flame spray process called nHALO® (hot aerosol layering operation) producing engineered nanoparticles (ENPs) used for coating and surface modification of materials was studied. The process reagents, which are usually nitrate salts and water or alcohol as carrier, are vaporised in a hydrogen-oxygen flame. In the flame, particles nucleate and grow via condensation and coagulation into nanosized particulate matter. The produced particles may be metal, metal oxide or multicomponent. The process was installed inside an enclosure to minimise particle emissions into the surroundings. The focus of the research was to characterise the particles inside the enclosure, in the surroundings and at the exit points of the enclosure where the workers may be exposed to the engineered particles.

Particle number concentration was measured with a TSI 3022 CPC and number size distribution with a TSI 3080 electrostatic classifier with a TSI 3085 Nano-DMA connected with a TSI 3775 CPC and controlled by the SMPS software and with an ELPI. Mass concentration was measured with a TEOM 1400a. Individual particle samples for electron microscopy (EM) analyses were collected with an aspiration EM sampler.

Average particle number concentration inside the enclosure varied from $1.0 \cdot 10^4$ to $2.1 \cdot 10^5$ 1/cm^3 and average mass concentration from 1.2 to 2.6 mg/m^3 during process operation. The highest particle concentration was observed when the furnace was heated and when the flame was on. The high peaks in the number concentration levelled out rapidly indicating a batch-type process and efficient ventilation inside the process enclosure (Fig. 1a). It should be noted that the process enclosure was not occupied by the workers.

Particle number concentration in the surroundings was typically $6.0\text{-}8.0 \cdot 10^3$ 1/cm^3, and average mass concentration 66 µg/m^3. It is noteworthy, that after the door opening at around 14:40 (scaled time), the particle number concentration stayed at higher level than before the door opening (white line in Fig. 1a). This was probably caused by the opening of the door to the enclosure at 14:56, 15:05 and 15:55 (Leppänen, et al.).

Comparing the number and mass concentration in the surroundings to the enclosure concentrations during the nHALO® process it was evident that the ventilated enclosure worked well in isolating the particle source from the surroundings.

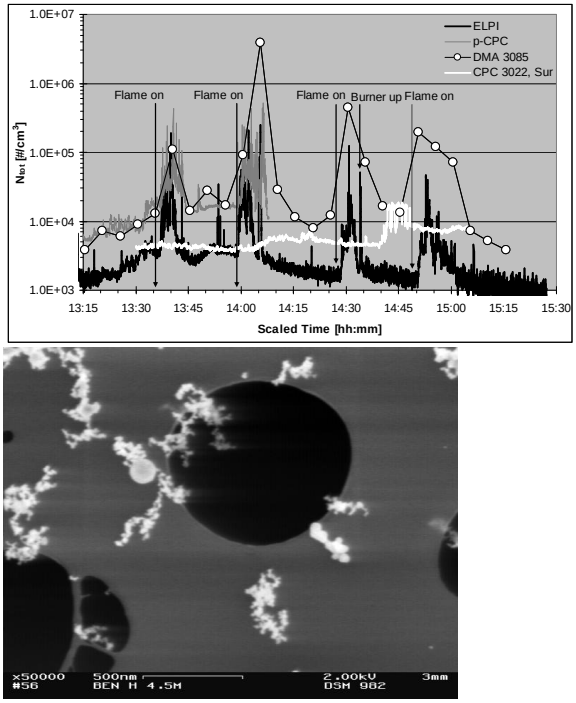

Figure 1: a) Particle number concentration for nHALO® inside the process enclosure and in the surroundings (white curve, scaled time) b) A scanning electron microscope (SEM) micrograph of the collected nanoscale particles from inside the enclosure. Particles were mainly aggregates, primary particle size approximately 20-30 nm.

This work was supported by the Finnish Funding Agency for Technology and Innovation, Beneq Oy and The Federation of Finnish Technology Industries.

M. Leppänen, J. Lyyränen, M. Järvelä, A. Auvinen, J. Jokiniemi, J. Pimenoff and T. Tuomi. Exposure to CeO_2 Nanoparticles during Flame Spray Process. Submitted to *Nano Research.*

Synthesis of copper nanoparticles by photochemical process

N. Nishida, A. Miyashita, and H. Tanaka

Department of Applied Chemistry, Faculty of Science and Engineering, Chuo University,
1-13-27 Kasuga, Bunkyo-ku, 112-8551, Tokyo, Japan
Keywords: Copper nanoparticle, optical property, photochemical process, STEM
Presenting author email: nnishida@kc.chuo-u.ac.jp

Since atmospheric nanoparticles are well known to be usually generated by sunshine, investigations of the generation of nanoparticles by photochemical process are regarded to be important in the basic nanoscience and applied nanotechnology. In addition, copper nanoparticles are also regarded to be important because of their high electrical, thermal conductivities and low cost. In this study, we have investigated synthesis of copper nanoparticles with single nanometer sizes by photoreduction of copper acetate at room temperature.

A detailed description of the experimental setup for nanoparticle production has been given elsewhere [1]. Copper acetate powder and PVP powder (polyvinylpyrrolidone, K = 15, Mw = 10000) were dissolved in ethanol. The mixed solution was photoirradiated using a high-pressure Hg lamp at room temperature.

When the solution was photoirradiated, blue color of the copper acetate changed to yellow. The more photoirradiation led the color deeper, and the color had finally turned deep red.

Figure 1 shows absorption spectra with photoirradiation at 0, 1, 5, and 18 h. In the spectrum at 0 h, a broad peak is observed at ~700 nm. This peak is ascribed to the Cu^{2+} ions. On the other hand, in the spectrum at 1 h, the broad peak at ~700 nm disappears. This disappearance indicates that the Cu^{2+} ions were reduced to Cu metal by photoirradiation.

In the spectrum at 5 h, a broad peak is observed at ~570 nm. This broad peak is ascribed to surface plasmon band for copper nanoparticles. Furthermore, in the spectrum at 18 h, this peak is prominently observed. These facts indicate that the nanoparticles were formed and grown by photoreduction. Additionally, the STEM observation supports that most of the nanoparticles were smaller than 10 nm indicator. Furthermore, the observed diameter for the nanoparticles depends on the concentration of copper acetate, implying that the observed nanoparticles are composed of copper atoms photoreduced from the copper acetate.

In summary, we have synthesized copper nanoparticles through the photoreduction of copper acetate at room temperature.

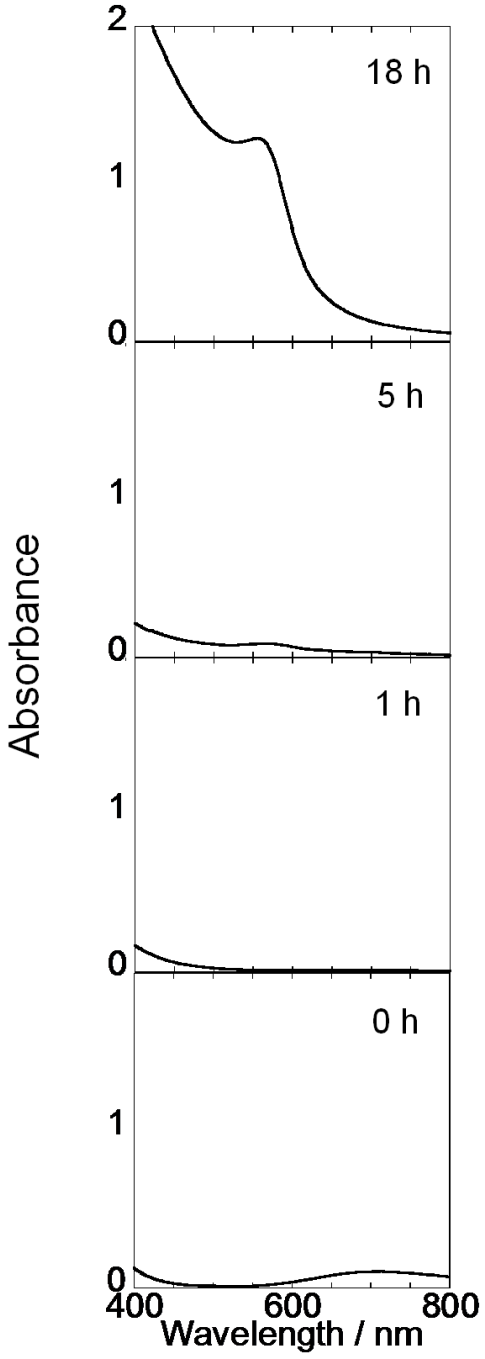

Figure 1. Absorption spectra with photoirradiation at 0, 1, 5, and 18 h.

[1] N. Nishida, A. Miyashita, N. Hashimoto, H. Murayama, H. Tanaka, *Eur. Phys. J. D*, in press.

Multiplex real time bioaerosol detection

Evgeny V. Usachev[1], Anna V. Pankova[2], Elina A. Rafailova[2], Oleg V. Pyankov[1] and Igor E. Agranovski[1]

[1]Griffith School of Engineering, Griffith University, Brisbane, 4111 QLD, Australia
[2]Department of Biochemistry, Kazan Federal University, Kazan, 420008, Tatarstan, Russia

Keywords: Bioaerosol detection, personal sampler, multiplex real-time PCR.
Presenting author email: i.agranovski@griffith.edu.au

Bioaerosols could cause various severe human and animal diseases and their opportune and qualitative precise detection and control is becoming a significant scientific and technological topic for consideration. In addition, over the last decades bioaerosol detection has become an important bio-defense related issue. Many types of portable and stationary bioaerosol samplers have been developed and, in some cases, integrated into automated detection systems utilizing various microbiological techniques for analysis of collected microbes.

In this project we used our recently developed personal bioaerosol sampler in conjunction with a real-time PCR technique. The main idea of the project was to investigate some possibility of using single fluorescent dye in multiplex format for qualitative detection of numerous targeted bioaerosols in one PCR tube making the suggested technology a reliable "first alert" device.

To prove the concept, we used the following experimental protocol. Two microorganisms, MS2 and T4 bacteriophages, were simultaneously aerosolized in the aerosol chamber (see details in Agranovski et al., 2005) and sampled by three personal samplers installed in parallel. On completion of sampling, the collecting liquid was mixed with PCR reagents and amplified to detect various

Firstly, it was found that the personal sampler has a collection efficiency higher than 90% even for small-sized viruses (>20 nm) and stable performance over extended operating periods for all combinations of microorganisms involved.

Figure 1 shows results of PCR amplification of MS2 and T4 in single format (one microorganism per reaction tube). As is seen, the results are perfectly correlated with the tenfold dilutions of the collecting liquid.

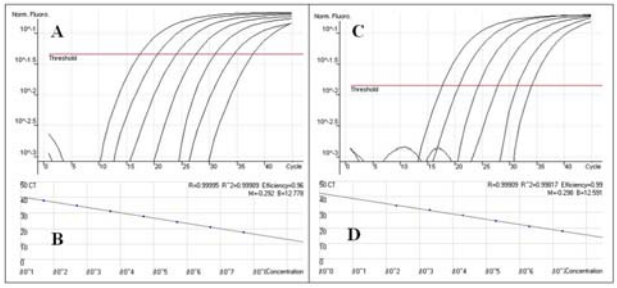

Figure 1. PCR amplification of ten-fold dilutions of MS2 and T4 phages in single format. A (results) and B (calibration curve) – for MS2; C (results) and D (calibration curve) – for T4 phage. Concentrations are presented in PFU/ml.

For the multiplex format, we used a mixture of primers and probes for both microorganisms trying to detect one out two targeted species. The results of these experiments are shown in Figure 2. As is seen, both targets were reliably detected in multiplex format and look very promising for development of hardware capable to identify a range of substances by compact portable devices.

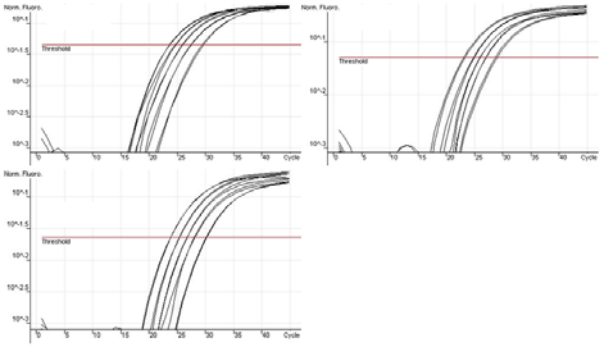

Figure 2. PCR amplification of phages MS2 (A), T4 (B) and their mixture (C) collected from the aerosol stream. PCR assays were performed in duplex format.

In addition, we used some experimentation to evaluate possibility to use PCR protocol for unpurified nucleic acids. It was found that for microorganisms used in this project (bacteriophages MS2 and T4) elimination of nucleic acids isolation and purification step during sample preparation does not lead to the system sensitivity reduction. This finding is extremely important allowing development of miniature bioaerosol monitoring instrumentation running PCR protocols directly on collected microorganisms and eliminating time consuming and cumbersome RNA/DNA purification step.

Agranovski, I., Safatov, A., Borodulin, A., Pyankov, O., Petrishchenko, V., Sergeev, A.A., Sergeev, A.N., Agranovski, V. and Grinshpun, S. (2005). *J. Aerosol Sci.* 36, 609 – 617.

Development of atmospheric aerosol data by flicker noise spectroscopy method

V.A.Zagaynov, D.V.Vodyanik, Yu.G.Biryukov, A.A. Lushnikov, I.E. Agranovski, S.F.Timashev

[1]Karpov Institute of Chemical Physics, Vorontsovo Pole, 10, 105064 Moscow, Russia
Keywords: flicker noise spectroscopy, atmospheric aerosols.
Presenting author email: zagaynov@cc.nifhi.ac.ru

There are many various gas subsystems in the atmosphere and their parameters are mutually interrelated. This fact has to be taken into account during atmospheric aerosol monitoring to achieve the most accurate and representative results. The main goal of this study is to distinguish factors that determine the state of the atmosphere. To consider such problems, a phenomenological analysis of the primary experimental data $V(t)$ has to be performed. This analysis considers dynamics of measured aerosol characteristics and their correlations are obtained to be used for following mathematical modeling. The main preference of this method is its capability of quantitative characterization of correlated data.

At this stage, the relation between various parameters of the ambient air (particle concentrations, particle size distributions, SO_2 concentrations, strength of electric field) has been established enabling one to evaluate a nature of aerosol generation and age of the aerosol system. The chaotic time related dynamics of these systems is represented by the measured dynamic variable $V(t)$ over the time interval T. The carriers of information contained in the measured chaotic series, including time series $V(t)$, are sets of distinguishable irregularities, such as bursts, jumps, and discontinuities of derivatives of various orders that occur at each space-time level of the hierarchy of the system (it is assumed that $<V(t)>= 0$). Because of the distinguish ability of the irregularities introduced, the parameters characterizing the combined properties of types of parameters are distinguishably extracted in an analysis of incomplete cosine spectra.
To get quantitative criteria on autocorrelation and correlation between different values:

$$\sigma_i(\tau) = (< (V_i(t) - V_i(t+\tau))^2 >)^{\frac{1}{2}}$$

and

$$q_{ij}(\tau;\vartheta) = < \frac{(V_i(t) - V(t+\tau))(V_j(t+\vartheta_{ij}) - V(t+\vartheta_{ij}+\tau))}{\sqrt{2}\sigma_i \sqrt{2}\sigma_j} >$$

here τ – is time delay for autocorrelation, ϑ - time delay for correlation between two measured values. These calculated correlations present information on measured connection between two values. The nature of this connection is twofold: firstly, one process may be consequence of the previous process, which is resulted by the fact that these values are related by some definite equations. On the other hand these values may be related randomly. The values σ and q in the above equations could be used to analyze the nature of the process and evaluate is it random or consequential. For example, it was found during our atmospheric monitoring of Baikal lake region, that measured particle concentration in the atmosphere was changed due to some presence of anthropogenic pollutions, air transport and photochemical reactions $SO_2 \rightarrow$ aerosol particles. These values, including SO_2 concentration and aerosol particle concentration and size distribution were continuously measured and then analyzed. The calculated values of q, obtained for the atmosphere of Baikal Lake are presented in Fig 1.

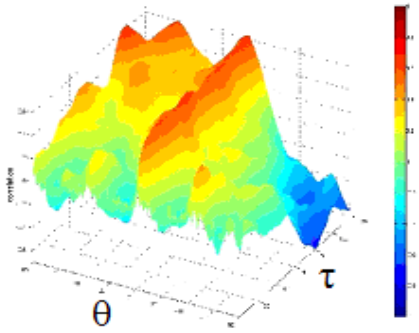

Figure 1. Correlation between SO_2 concentrations and total aerosol particle concentrations. ϑ - time shift between two values, τ – time shift for autocorrelation

This figure shows that for time shift ϑ =0 correlation is positive and has crucial meaning. At the same time for $\vartheta \approx 2$ hours this correlation again is positive. For both time intervals, $q \geq 0.7$ showing that the processes occurring at high gas and particle concentration are related by the some chemical and kinetics equations. The form of the relation may be obtained by mathematical modeling of these processes, by using calculated correlations, as shown in Fig.1.
This work was supported by the State Contract № 02.518.11.7079 (RF).

Timashev, S.F., Polyakov, Yu.S. (2007) *Review of flicker noise spectroscopy in electrochemistry*. Fluctuation and Noise Letters. V. 7. N. 2. P. R15-R47.

Timashev, S.F., Zagaynov, VA., . Lushnikov, A.A., Biryukov, Yu. G., Agranovskii, I.E., Lamukhin, E.M. (2008) Flicker Noise Spectroscopy in an Analysis of the Dynamics of Atmospheric Aerosol *Russian*

Journal of Physical Chemistry A, Vol. 82, No. 10, pp.1756-1768

Size distributions of particle-bound polycyclic aromatic hydrocarbons emitted from a diesel generator fueled with waste-edible-oil biodiesel blends

S.J. Chen[1,*], J.H. Tsai[1], K.L. Huang[1], C.L. Chou[2] and W.J. Yu[1]

[1]Department of Environmental Science and Engineering, National Pingtung University of Science and Technology, Pingtung County, Nei Pu, 91201, Taiwan
[2]Content Engineering Consulting Services, Ltd., New Taipei City, Zhonghe Dist., 23553, Taiwan
Keywords: Biodiesel, waste-edible-oil, polycyclic aromatic hydrocarbons, size distribution, generator.
Presenting author email: chensj@mail.npust.edu.tw

Diesel engines usually emit particulate matter (PM). Diesel exhaust particles (DEPs) mainly comprise fine and ultrafine particles (dia. <2.5 μm – 0.1 μm) such as carbonaceous matter, fats, polycyclic aromatic hydrocarbons (PAHs), and miscellaneous organic compounds, etc. (Kittelson, 1998; Reynold et al., 2000). Some studies have demonstrated that DEP exposure significantly affects human or animal bodies, and such exposure gives rise to cardiovascular and respiratory tract diseases (Yoshino et al., 1999; Sagai et al., 1996; Schwartz et al., 1996; Seaton et al., 1995). Although the use of biodiesel may significantly reduce PM emission from diesel engines (Lin et al., 2008; Tsai et al., 2010), it is necessary to evaluate the potential impact of DEP size distribution on health when using biodiesel.

In this study, the size distributions of particle-bound PAHs emitted from a biodiesel-fueled generator operated at stable energy output (110 V/60 Hz, 1800 rpm) loads (unload (0 kW) and 3 kW) were investigated. We tested two types of fuels: D100 (pure petroleum diesel) and W20 (v/v = 20% waste-edible-oil based/converted biodiesel/80% D100). The size distributions of particle-bound PAHs emitted from the generator using different fuels were measured with a micro-orifice uniform deposit impactor (MOUDI) and a Nano-MOUDI (with 0.01–18 μm aerodynamic diameters). Each sample was extracted in a *Soxhlet* extractor with a mixed solvent (n-hexane and dichloromethane 1:1 vol/vol) for 24 hr. The extracts were then concentrated, cleaned up, and re-concentrated by purging with ultra-pure nitrogen to exactly 1.0 mL for GC/MS analysis.

When operating at 0 kW (unload), the particle-bound Total-PAHs and Total-BaP_{eq} emitted from the diesel generator using D100 and W20 all exhibited single-peak distributions (both major peaks in 0.32–0.18 μm) (Fig. 1). Similar phenomenon was also observed at a heavier load (3 kW); the major peaks of Total-PAHs and Total-BaP_{eq} were in 0.032–0.010 μm and 0.32–0.18 μm for D100 and W20, respectively. Dissimilarly, Lin *et al.* (2008) found that the average particulate total-PAHs in five samplings displayed a trimodal distribution with a major peak in the Aitken mode (0.032–0.056 μm). Lower emission concentrations of Total-PAHs and Total-BaP_{eq} were observed for W20 than for D100 despite the loads; the reductions of Total-PAHs and Total-BaP_{eq} were ~50% and ~80%, respectively. Therefore, using waste-edible-oil biodiesel (W20) is helpful to reduce particle-bound PAHs emission from the diesel engine generator, especially for particles in ultrafine size range.

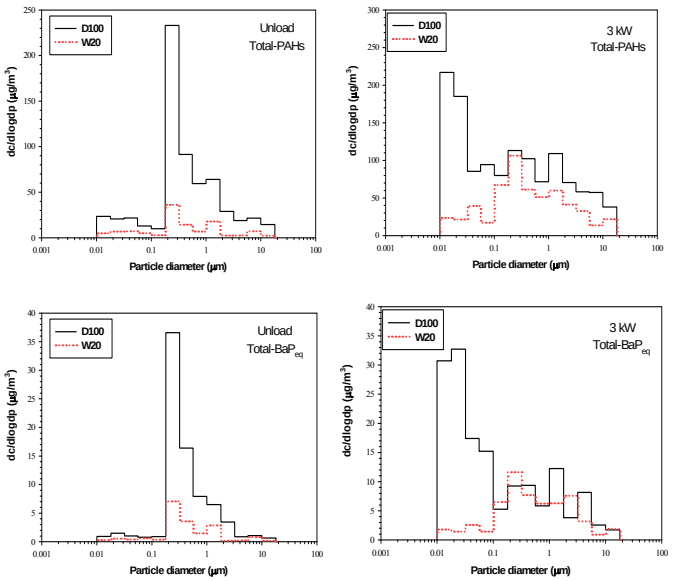

Figure 1. Size distributions of particle-bound total-PAHs and total-BaP_{eq} emitted from the biodiesel generator.

Kittelson, D.B. (1998) *J. Aeros. Sci.* **29**, 575–588

Lin, Y.C., Lee, W.J., Chao, H.R., Wang, S.L., Tsou, T.C., Chang-Chien, G.P. and Tsai, P.J. (2008) *Environ. Sci. Technol.* **42**, 3849–3855.

Reynolds, L.J., Murphy, S.A. and Richards, R.J. (2000) *In Vitro Mol. Toxicol.* **13**, 173–179.

Sagai, M., Furuyama, A. and Ichinose, T. (1996) *Free Radical Biol. Med.* **21**, 199–209.

Schwartz, J., Dockery, D.W. and Neas, L.M. (1996) *J. Air. Waste. Manag. Assoc.* **46**, 927–939

Seaton, A., MacNee, W., Donaldson, K. and Godden, D. (1995) *Lancet.* **345**, 176–178.

Tsai, J.H., Chen, S.J., Huang, K.L., Lin, Y.C., Lee, W.J., Lin, C.C. and Lin, W.Y. (2010) *J. Hazard. Mater.* **179**, 237–243.

Yoshino, S., and Sagai, M. (1999) *J. Pharmacol. Exp. Ther.* **290**, 524–529.

Platinum-based nanoparticles supported on cordierite as high active materials for catalytic ammonia decomposition

Chang-Mao Hung

Department of Vehicle Engineering, Yung-Ta Institute of Technology and Commerce, 316 Chung-shan Rd, Linlo, Pingtung 909, Taiwan, R.O.C.
Keywords: ammonia, selective catalytic oxidation, Pt-Pd-Rh nanoparticles cordierite substrate catalyst.
Presenting author email: hungcm1031@gmail.com

Ammonia (NH_3) is an extremely important component contributing to acidification and eutrophication of terrestrial ecosystems had attracted much attention in Taiwan. Typically, NH_3 is emitted during ammonium nitrate, nitric acid and urea production is present in livestock waste and vehicle exhaust, and is a byproduct of fossil fuel combustion, petroleum refineries and the refrigeration industry. Therefore, removal and control of NH_3 emissions in gas and waste streams are necessary due to increasingly stringent emission standards.

Till now, catalytic oxidation using dedicated catalysts increases the effectiveness of advanced oxidation technology potentially reducing oxidation reaction times and allowing oxidation to proceed under relatively mild operating conditions. The selective catalytic oxidation approach of ammonia (NH_3-SCO) in a stream to N_2 and H_2O can reduce NH_3 pollution. Cordierite, a crystalline magnesium aluminosilicate ($2MgO\text{-}2Al_2O_3\text{-}5SiO_2$) with a hexagonal structure, combines a relatively low thermal expansion coefficient with thermal shock resistance and sufficient refractoriness has been reported (Hung, 2009; Hung, 2010; Hung, 2010; Hung, 2011).This study elucidates NH_3 oxidation by selective catalytic oxidation (SCO) over a Pt-Pd-Rh nanoparticles cordierite substrate catalyst in a tubular fixed-bed flow quartz reactor (TFBR) at temperatures of 423-623 K. The overall selectivity of N_2 production was 12-68%, and that of NO production was 0-8% over the range of 11-98% NH_3 conversion at NH_3 concentrations of 800 ppm (Fig. 1). It is noteworthy that nitrogen gas was formed primarily by direct dissociation of the NO produced by oxidation of adsorbed NH_3. Therefore, the hypothesize that NH_3 and oxygen were adsorbed onto specific sites on the Pt-Pd-Rh nanoparticles cordierite substrate catalyst, promoting rapid conversion of NH_3 to nitrogen and water. Consequently, nitrogen was the dominant gas, and a small amount of NO was detected in the resultant stream. Fig. 2a shows that the catalyst surface is more aggregated and crystalline than observed in Fig. 2b. Rather, disaggregated and dispersed phases formed when the catalyst surface aged or when poisoning occurred due to plugging, implying that particle porosity changed (Fig. 2b). Generally, these crystal phases may be responsible for the marked activity of catalysts. These experimental results also confirm that the dispersion phenomena of the catalyst increase the efficiency of NH_3 removal.

This work was supported by the National Science Council of the Republic of China, Taiwan, for financially supporting this research under Contract No. NSC98-2221-E-132-003-MY3.

Hung, C. M. (2009). *Envir. Eng. Sci.*, **26**, 351-358.
Hung, C. M. (2010). *Powder Tech.*, **200**, 78-83.
Hung, C. M. (2010). *J. Hazard. Mater.*, **180**, 561-565.
Hung, C. M. (2011). *J. Hazard. Toxic Radio. Waste*, **15**, 37-41.

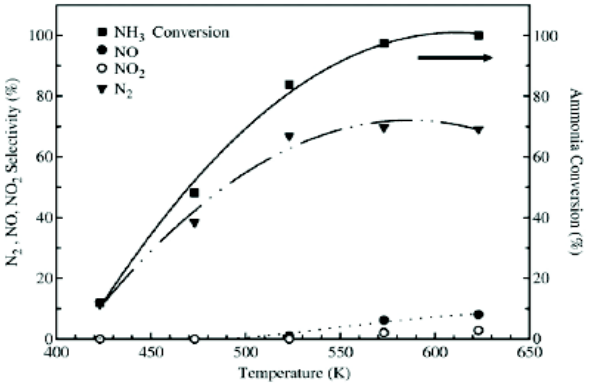

Figure 1. Relationship of the ammonia conversion, N_2, NO and NO_2 yield at various temperatures over the Pt-Pd-Rh nanoparticles cordierite substrate catalyst. Test conditions: 800 ppm NH_3 in He, O_2 = 4%, RH=12%, Temperature = 423-623 K, GHSV = 92000 hr^{-1}.

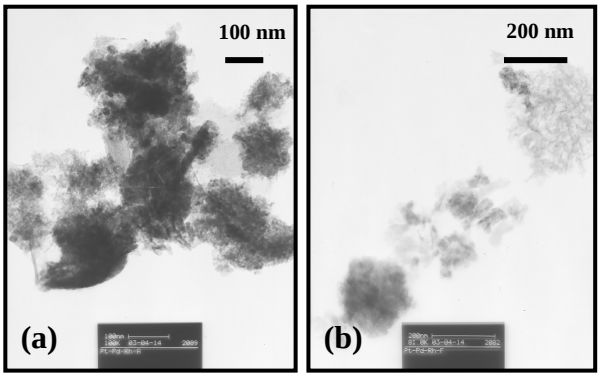

Figure 2. TEM photograph of (a) fresh and (b) after activity test Pt-Pd-Rh nanoparticles cordierite substrate catalyst. Test conditions: 800 ppm NH_3 in He, O_2 = 4%, GHSV = 92000 hr^{-1}.

Aerosol emissions from nanotechnology-based products at end-of-life

U. Backman[1], J. Lyyränen[1], J. Hokkinen[1], A. Auvinen[1] and J.K. Jokiniemi[1,2]

[1]VTT Technical Research Centre of Finland, Fine Particles, P.O. Box 1000, 02044 VTT, Espoo, Finland
[2]University of Eastern Finland, Department of Environmental Science, Fine Particle and Aerosol Technology Laboratory, P.O. Box 1627, FI-70211 Kuopio, Finland

Keywords: recycling, final treatment, incineration.
Presenting author email: Ulrika.Backman@vtt.fi

Nanomaterials are already used in many consumer products today and the number of products available to consumers is expected to increase. As the exposure of people to nanomaterials is becoming more common, there is an increasing concern that the beneficial properties of nanoscale particles might have negative impact on human health and the environment. For example, it is expected that the increased surface to volume ratio will make particular chemicals more toxic because these particles will be more absorbable and capable to cross cell membrane or the blood-brain barrier. Today we lack knowledge on the hazards of nanomaterials and nanotechnology-based products as there is only limited data available on toxicology of and exposure to nanoparticles.

Since production of nanotechnology-based industrial and consumer products is dramatically increasing, the amount of products reaching the end of their life-cycle is also increasing. We do not yet know if and to what extent, toxic nanomaterials may be released or may leach from products to the environment during use or after use, i.e. during final treatment and/or disposal in land fills. In this presentation the focus will be on possible aerosol emissions during recycling and final treatment, i.e. incineration. Incineration was chosen because the number of incinerators has increased in Europe due to the ban on landfilling untreated municipal waste. The example cases studied are the recycling of coated glass panels and the incineration of CNT-containing composites.

Glass panels are coated for a number of reasons. For example, glass panels coated with nano-ZnO can be used as filter screens for lamps. The nano-ZnO coating protects the products in showrooms against bleaching. The biggest advantage, however, is the lifetime of the effect, which is in principle as long as the substrate exists. As these materials are chemically fixed to the glass panels, the recycling of the composite (glass with treatment) is not well understood. In this presentation an experimental setup for the mimicking of the established glass recycling process (by melting) will be presented. The results for aerosol emissions during recycling process of nano-ZnO containing glass are presented. These results include measuring of the nanoparticle emissions to air by means of aerosol instrumentation for ultra-fine particles. Elemental analysis of the emitted particles is also carried out.

Carbon nanotubes (CNT) containing epoxy composites have increased impact resistance, elongation to break and fatigue compared to traditional epoxies. These composite materials are suitable for filament winding, laminating, pultrusion, infusion and many other applications. These composites are for instance applied in the manufacture of sporting equipments, yachts and windmill blades. As they cannot be melted to another shape, they cannot be recycled as epoxy unlike many other plastic materials, but are disposed of at the end of their lifecycle. An important but still open question is the behaviour of CNT in incineration plants. Although there are reasons to expect that they will be totally oxidised, very little data or information exists so far on their final fate.

Results on emissions to air from waste incineration of CNT-containing composites will be presented, including the particle number concentration as well as the particle size, chemical composition and mass size distributions. The aerosol particles are collected and analysed for size, shape and chemical composition using electron microscopy. The composition of the ash is also analyzed.

This work was supported by the European Commission under grant number 247989 (NanoSustain – Development of sustainable solutions for nanotechnology-based products based on hazard characterisation and LCA).

Effect of Image Force on Penetration of Nanoparticles through a Laminar Flow Tube

V. Gómez[1], C.H. Huang[2], J.P. Borra[3], F.J. Alguacil[4] and M. Alonso[4]

[1]Instituto de Nanociencia de Aragón (INA), Edificio I+D, c/ Mariano Esquillor s/n, 50018 Zaragoza,Spain
[2]Department of Environmental Engineering and Health, Yuanpei University, 30015 Hsinchu, Taiwan
3Laboratoire de Physique des Gaz et Plasmas (UMR 8578 CNRS – Univ. Paris-Sud XI) Gif sur Yvette, France
[4]National Center for Metallurgical Research (CSIC), 28034 Madrid, Spain
Keywords: nanoparticles, diffusion, penetration.
Presenting author email: virgomez@unizar.es

An experimental study has been carried out to examine the effect of image force on the diffusional penetration of sub-10 nm particles through a laminar flow tube.

The experimental setup is shown in Figure 1. An evaporation-condensation NaCl aerosol was size-classified with a TSI short column DMA operated in open mode at a aerosol-to-sheath flow rate ratio of 2/20. Three different test monodisperse aerosols were used for the penetration experiments: (1) the singly charged particles as drawn from the DMA; (2) uncharged particles produced by passing the DMA-classified aerosol through a ^{241}Am neutralizer and an electrostatic precipitator (ESP) operated at a voltage sufficient to remove the charged fraction; and (3) a "globally" neutral aerosol, consisting of a mixture of uncharged, positive and negative particles, obtained by switching off the ESP voltage. Penetration of each of the test aerosols through a 100 cm long, 4 mm ID tube was determined form comparison of concentrations measured at the outlet of two tubes of lengths 20 and 120 cm. The use of a 20 cm tube as reference ensures the attainment of fully developed parabolic flow at the aerosol flow rate used in the experiments (2 lpm). Equal lengths of conducting Tygon tubes were employed for the connections AB and AC. Before the condensation particle counter (CPC), an additional ^{241}Am neutralizer was inserted to eliminate the possibility of counting errors due to the effect of charges on the condensation of the CPC working fluid onto the particles; with this arrangement, the three test aerosols were brought to the same charge equilibrium state before entering the CPC.

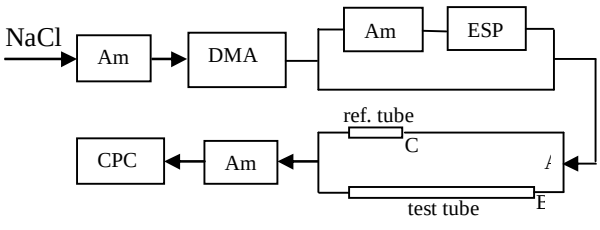

Figure 1. Experimental setup

The experimental results are shown in Figure 2. Penetration of uncharged particles (0) is fairly well predicted by the Gormley-Kennedy equation (full line). Each experimental value is the average of ten measurements. Penetration of the mixture of uncharged and charged particles (0,+,-) is slightly smaller than that of uncharged particles, and this may be attributed to the electrostatic attraction between the charged particles and the image charges induced on the tube wall (for particles under 10 nm the fraction of charged ones is very small, and this explains why the penetration differs little from that of the uncharged particles).

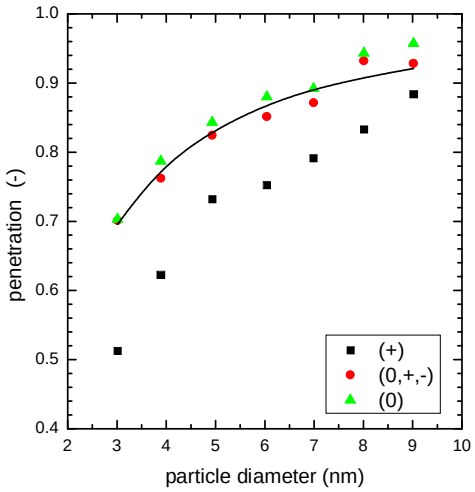

Figure 2. Experimental results

On the contrary, the penetration of the charged particles (+) is notably smaller than that of the other two test aerosols. However, according to the currently accepted theory this strong image force effect should not be observed for singly-charged nanoparticles. Indeed, the transport equation $\mathbf{u}\cdot\nabla n+\nabla\cdot\left(-D\nabla n+nZ\mathbf{E}\right)=0$ has been solved numerically using the expression given by Yu (1977) for the electric field, and the numerical results show that the effect of image force on penetration should be less than 0.1% for the particle size range below 10 nm. Electrostatic repulsion effects (space-charge) are absent in our experiments because the aerosol concentration was kept below 10^4 cm^{-3}. Clearly, the theoretical explanation of the above results needs further elaboration; we also intend to perform additional experiments, changing the aerosol flow rate and the tube radius.

This work was supported by grants DPI2008-06199, CSIC 2009TW0017, NSC 99-2923-E-264-001-MY2 and FPU AP2008-02067.

Yu, C.P. (1977) *J. Aerosol Sci.* **8**, 237-241.

Morphology of catalyst layers deposited by electrospray

S. Martin, P.L. Garcia-Ybarra and J.L. Castillo

Dept. Fisica Matematica y de Fluidos, Facultad de Ciencias, UNED, Madrid 28040, Spain
Keywords: Electrospray, Particle deposition, Deposit morphology, Fuel cell.
Presenting author email: jcastillo@ccia.uned.es

The morphology of granular deposits growth from aerosol particles depends on the aerosol particle dynamics over the collecting surface. Theoretical simulations of deposit formation (Rodriguez-Perez *et al*, 2005 & 2007) have shown that an increase in the particle arrival velocity leads to denser deposits whereas nanostructured deposits with open tree-like dendritic structures can be formed for weak particle velocities.

Based on these theoretical simulations, an experimental investigation is being carried out to grow platinum catalyst layers (for use as electrodes in Proton Exchange Membrane Fuel Cells, PEMFC) starting from the electrohydrodynamic atomization of a liquid suspension containing the catalyst Pt/C nanoparticles. This technique has demonstrated to be an efficient method of depositing catalyst layers especially in the range of ultra-low platinum loadings even below 0.1 $mg_{Pt}cm^{-2}$ (Martin *et al*, 2010 a&b). The advantages of the electrospray deposition method are numerous. Since the droplet size in the electrospray is controlled by the flow rate, the size of the deposited particle may be selected. As the spray is charged, it may be focused by an electric field in a particular position with any shape. Moreover, coalescence phenomena in the spray droplets are reduced due to the electrostatic repulsion between the charged droplets. Other remarkable benefits are the feasibility of the scaling up to bulk production and the inexpensive and simple experimental set up.

The range of the parameters governing the electrospray deposition has been studied under the scope of the preparation of optimum catalyst layers for PEMFC use. Thus, the domain for stable electrospraying was determined (Martin *et al*, 2011) showing that the range of liquid flow rates with a stable cone-jet electrospray can be substantially enlarged with a proper control of the voltages applied to the needle and to the collecting plate.

Furthermore, a classification of the different types of deposits according to the morphology (fractal-like, based on spheroids or compact deposits) has been carried out. The enclosed figure depicts the two first types of deposit structures for the same platinum loading of 0.1 $mg_{Pt}cm^{-2}$.

Nanostructured deposits with very high porosity (97%) and a large active area due to their dendritic growth were obtained for specific setting of the experimental parameters (*i.e*. needle-substrate distance, liquid flow rate, voltages applied to the needle and to the substrate and concentration of the catalyst ink).

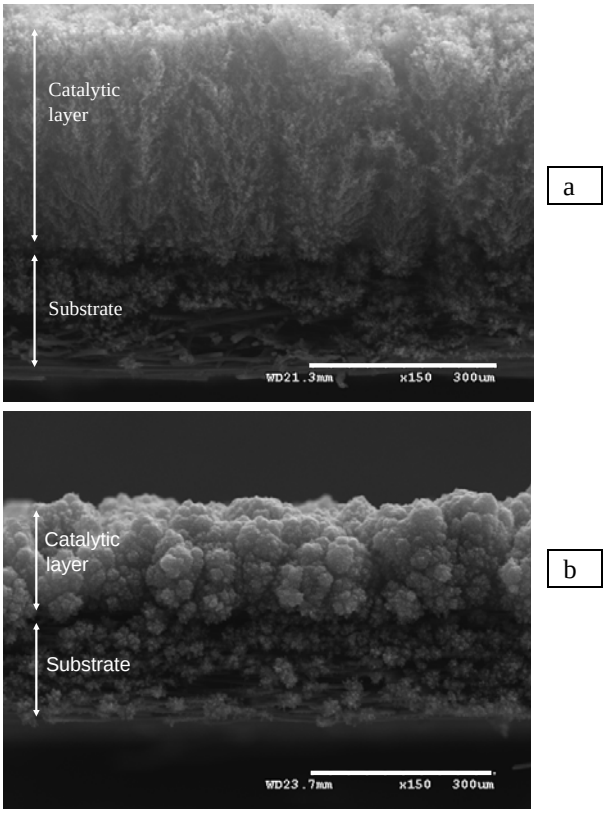

Figure. Cross-sectional SEM micrographs of the profiles of electrosprayed Pt/C catalytic layers over a carbon paper substrate (for the same catalyst loading). (a) fractal-like structures for a flow rate of 0.2 ml h^{-1}, and (b) Deposits based on spheroids for 0.5 ml h^{-1}. In both images the micron bar corresponds to 300 μm.

This work was supported by the Ministerio de Ciencia e Innovación (Spain) under grants ENE2008-06683-C03-01, and program Consolider-Ingenio 2010 (CSD2010-00011), and also by Comunidad de Madrid (project HYSYCOMB, S2009ENE-1597).

Rodriguez-Perez, D., Castillo, J.L. and Antoranz, J.C. (2005) *Phys. Rev. E* **72**. Paper number 021403.

Rodriguez-Perez, D., Castillo, J.L. and Antoranz, J.C. (2007) *Phys. Rev. E* **76**. Paper number 011407.

Martin, S., Garcia-Ybarra, P.L. and Castillo, J.L. (2010a) *J. Power Sources* **195**, 2443-2449.

Martin, S., Garcia-Ybarra, P.L. and Castillo, J.L. (2010b) *Int. J. Hydrogen Energy* **35**, 10446-10451.

Martin, S., Garcia-Ybarra, P.L. and Castillo, J.L. (2011) *J. Electrost.*, submitted.

Measurement of particle size distribution in the gas phase. QCM- based procedure

F.N. Dultsev

Institute of Semiconductor Physics, Siberian Branch of the Russian Academy of Sciences, Novosibirsk, 630090, Russia
Keywords: Aerosol size distribution
Presenting author email: fdultsev@thermo.isp.nsc.ru

QCM-based procedure for the determination of particle size within the nanometer-range is proposed. The essence of the procedure is the rupture of adsorbed aerosol particles from the surface of the quartz resonator during oscillations of the quartz resonator surface under dynamically increasing oscillation amplitude. It was established experimentally that the achievement of threshold values of the QCM surface oscillation amplitude (with an increase in voltage U_0 at the resonator plates) causes breakage of the bonds holding a body on the surface; the rupture event is accompanied by a sharp acoustic signal (click) at the high harmonics of the resonator.

Recording the intensity of the acoustic signal and the voltage at which it appears, one may extract the information about the properties of the detached body. The same quartz substrate acts as an integrated device playing several parts at a time: an active resonator and a sensitive microphone.

If the measurements are performed not at a fixed frequency of the chosen harmonics as described in (Dultsev *et al.*, 2000) but scanning within a frequency band around that value, this excludes the necessity of precise adjustment (tuning) of frequency, eliminates signal misalignment during measurements and allows one to achieve well reproducible results without any dependence on temperature, time or any random factors. .

Test measurements were carried out using the standard nanospheres Nano Glass Beads with the declared glass bead diameter 20-30 nm (Microspheres-Nanospheres a Corpuscular company, catalogue No. 149015-05). Deposition onto the surface was carried out from water suspension.

Measurements were carried out at the third harmonic; voltage U_0 at the resonator plates was linearly increasing during the sweep up to 5 volts. One can see in the plot that there are some threshold voltage values U_0 corresponding to quite specific values of surface oscillation amplitude, when the signal inside the band gives a sharp overshoot, which corresponds to particle rupture. This points to the presence of the particles of several types, with different binding strength values. It should be noted that the band of signal scanning over frequency was chosen with a small excess in order to exclude the loss of information. The integral plot shown in Fig. 1 represents the signal *versus* voltage $U0$ at the resonator plates, averaged over the band (200 points over scanning frequency). According to the plot, there are six types of particles in the test system; the six sharp peaks are marked with asterisks.

The use of the proposed procedure for measuring particle size distribution is shown in Fig. 3. Aerosol particles 20-30 nm in size were generated with a device described in (Ankilov *et al.,*2002). The generator was calibrated with the help of diffusion battery (Ankilov *et al.*, 2002). Varying the rate of flow through the generator we can vary particle size as one can clearly see in Fig. 2.

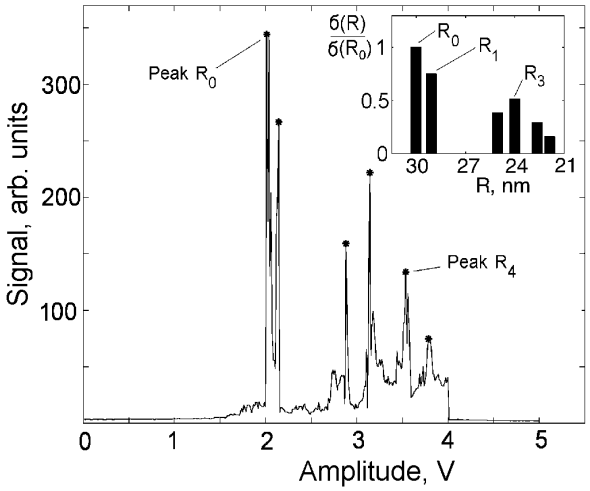

Figure. 1. Resulting rupture signal versus voltage supplied to the quartz resonator. The resulting particle size distribution is shown in the insert.

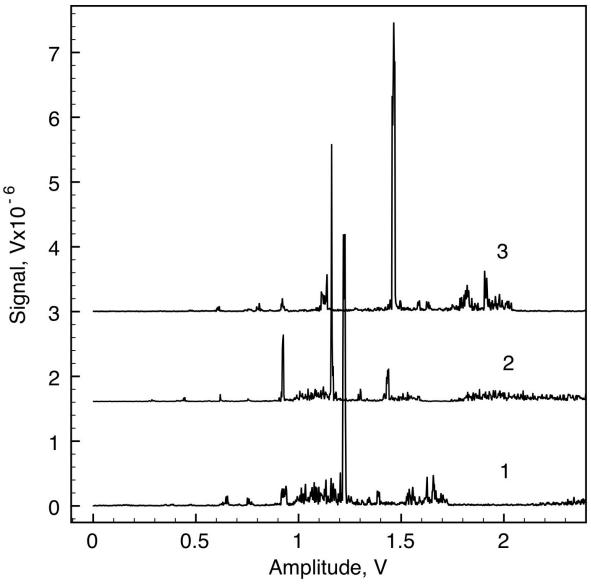

Figure 2. QCM measurements with different rates of gas flow through the generator for constant W filament temperature, curve 1 – chosen conditions, curve 2 - air flow decreased by10%, and curve 3 - air flow increased by 10%.

Dultsev, F.N., Ostanin, V.P., and Klenerman, D. (2000) *Langmuir* **16,** 5036–5040.

Ankilov, A., Baklanov, A., Colhoun, M. et al., Atmos. Res. (2002) ***62,*** *177–207.*

Cloud condensation nuclei (CCN) activity and oxygen-to-carbon elemental ratios following thermodenuder treatment of organic particles grown by α-pinene ozonolysis

M. Kuwata, Q. Chen and S. T. Martin

School of Engineering and Applied Sciences & Department of Earth and Planetary Sciences,
Harvard University, Cambridge, Massachusetts, 02138 USA
Keywords: CCN, secondary organic material, elemental ratio, volatility
Presenting author email: scot_martin@harvard.edu

Introduction CCN activity of aerosol particles is important as a regulator of cloud properties, including their brightness, lifetime, and precipitation. Although CCN activity of pure compounds is predictable from their chemical characters, CCN activity of secondary organic material (SOM) is not understood for quantitative prediction due to their complexity in chemical composition.

In the present study, we systematically controlled SOM chemical composition generated using the Harvard Environmental chamber (HEC) by (1) altering SOM concentration (M_{org}) in the HEC, and (2) increasing the thermodenuder (TD) temperature (T) connected to the HEC. SOM chemical composition was measured simultaneously with CCN activity. This experimental design allows us to relate CCN activity and chemical composition, as both M_{org} and T controls SOM chemical composition based on volatility.

Experiment The HEC is consisted of a 4.7 m^3 Teflon bag housed in a temperature controlled (25 °C) room. It was operated as a continuous stirred tank reactor, providing sufficient time to measure SOM. SOM was produced by dark ozonolysis of α-pinene (8 – 80 ppb) with the presence of 2-butanol as an OH scavenger. SOM concentration in the chamber ranged from 1.4 to 37μg m^{-3}, depending on α-pinene concentration. 30-nm $(NH_4)_2SO_4$ seed particles, those were provided from a differential mobility analyzer (DMA), were also continuously injected into the chamber. Ozone concentration and relative humidity were feedback controlled as 50 ppb and 40%, respectively.

SOM particles generated in the HEC were injected into a thermodenuder (TSI 3065), which was operated at bypass, 25, 60, 80, and 100 °C. The flow passed through the TD was split to three flows to measure size-resolved CCN activity (DMA-CCN counter(CCNC)), chemical composition (high-resolution time-of-flight aerosol mass spectrometer (HR-ToF-AMS), and number size-distribution (scanning mobility particle sizer (SMPS).

CCN activation curve measured by the DMA-CCNC was fitted by a sigmoid function to obtain dry activation diameter (d_{dry}) κ values, which is defined as $\kappa = i\, MW_{water}\rho_{org}/MW_{org}\rho_{water}$, were employed to represent CCN activity [i: van't Hoff factor, MW_x: molecular weight of x, ρ_x: density of x]. κ was iteratively calculated to reproduce d_{dry} obtained from size-resolved CCN spectra.

Results and discussion

We observed ~50% of decrease in M_{org} following TD treatment at 100 °C regardless of M_{org} in the HEC. This demonstrates that evaporation is the main process occurring in the TD. Elemental composition of SOM measured by the HR-ToF-AMS revealed that both M_{org} and T dependences are consistent in terms of volatility: oxygen-to-carbon (O:C) ratio increased for lower volatility compounds (lower M_{org}/higher T), while H:C ratio decreased for these conditions. This trend was further confirmed using a Van Krevelen diagram. All data points aligned on a straight line ([H:C] = -0.8 [O:C] + 1.8), including both M_{org} and T dependences. These results demonstrate that the main process occurring in the thermodenuder is evaporation of relatively volatile compounds.

κ did not depend on M_{org} at 25 °C, which may lead to predict that T also does not alter κ, considering the consistent dependences of elemental ratios on M_{org} and T. However, κ decreased at higher T. The magnitude of the decrease was significant (~20 % at 100 °C) at higher M_{org} (> 10μg m^{-3}), while the decrease was not significant at the low M_{org} (1.4μg m^{-3}).

These apparently contradicting results can be consistently interpreted as follows. TD evaporates relatively volatile materials, which cause decrease in M_{org} and changes in elemental ratios. At the same time, it enhances oligomer concentration in particles due to (1) evaporation of relatively volatile monomers, and (2) thermally induced oligomer formation reactions. These processes decrease κ, as oligomers have higher MW_{org} than original monomers. A variety of functional groups such as carbonyl groups is required for oligomerization reactions. Decrease in κ was significant at higher M_{org}, as relatively volatile carbonyl compounds could partition to particle phase due to higher concentration. This interpretation was supported by a model calculation employing master chemical mechanism coupled with SIMPOL vapour pressure prediction method, which predicted that carbonyl groups are depleted at lower M_{org}, while a variety of functional groups exist at higher M_{org}.

Acknowledgements: This material is based upon work supported by the Office of Science (BES), U.S. Department of Energy, Grant No. DE-FG02-08ER64529.

References:

Kuwata, M., Chen, Q., and Martin, S. T. (submitted)

Characterization of Agglomerates and Aggregates in Gases along the Exposure Pathway

Heinz Fissan[*1], Heinz Kaminski[1], Dave Pui[2], Zhun Liu[2], Jing Wang[3,4]
[1*] Institute of Energy and Environmental Technology (IUTA) e.V., Bliersheimer Str. 60, 47229 Duisburg, Germany, Tel.: + 49-2833-4689; Fax: +49-2833-572775.
[2] Particle Technology Laboratory, University of Minnesota, Minneapolis, 55455 USA
[3] Institute of Environmental Engineering, ETH Zürich, 8093 Zürich, Switzerland
[4] Empa, Analytical Chemistry, 8600 Dübendorf, Switzerland
*Corresponding author e-mail:heinz.fissan@uni-due.de

Keywords: nanoparticle agglomerates and aggregates, exposure, size distribution, UNPA

There are increasing interests in using nanostructured materials, because of their specific properties. The starting point is engineered nanoparticles (ENP), which are mass produced f. i. in the gas phase. Because of their high concentration they form agglomerates and the stronger bonded aggregates already during synthesis. The agglomerate/aggregate structures and sizes dictate the powder and material properties after dispersion in matrix material. Agglomerates/aggregates besides single nanoparticles from the matrix material may be unintentionally released into the workplace and environment during synthesis, further processing and handling. For risk assessment the exposure to agglomerates and aggregates has to be determined especially if there is a chance for them to break apart during transport in the environment. To discuss the impact of agglomerates/aggregates it is important to characterize the agglomerates/aggregates along their exposure pathway. Number-size distributions are therefore of the greatest value.

The most important tool for size distribution measurements thus far is the Scanning Mobility Particle Sizer (SMPS), which is based on the assumption that the particles are spherical. In case of agglomerates it delivers only equivalent values with respect to size (electrical mobility diameter) and also the concentration values are affected through different charging efficiencies.

In addition the agglomerate/aggregate size cannot be described by just one parameter. In case of loose agglomerates besides the agglomerate size the primary particle size is needed.

The recently developed Universal NanoParticle Analyzer (UNPA) [1] allows measurement of loose agglomerates, enabling determination of the primary particle size and the agglomerate distribution based on a model for loose agglomerates derived by Lall and Friedlander [2]. The largest difference between using a sphere and an agglomerate model in the data evaluation procedure occurs in the volume distribution calculation, which therefore has been used to check the agglomerate approach for data evaluation [3].

There does not exist a model for aggregates. The UNPA determines the number distribution as a function of the mobility diameter and with a second sensor the charges per particle as a function of the mobility diameter. We observed that this particle property changes, when the agglomerate becomes an aggregate and finally a sphere in a sintering process. This information can be used to determine the number concentration for aggregates. With the relationship between the mobility diameter and volume diameter, which may be determined by sintering experiments with monodisperse agglomerates or aggregates, number distributions of aggregates as a function of the aggregate volume can be derived.

The change can also be related to the difference in surface area per particle between aggregate and sphere derived from a model or from calibration with other techniques. In the presentation we will describe the data evaluation procedures and show examples of agglomerate and aggregate analysis.

The work was partially supported by the NSF grant (Award ID: 1056479) on "Real Time Measurement of Agglomerated or Aggregated Airborne Nanoparticles Released from a Manufacturing Process and Their Transport Characteristics".

[1] Wang, J., Shin, W. G., Mertler, M., Sachweh, B., Fissan, H., Pui, D. Y. H. Measurement of Nanoparticle Agglomerates by Combined Measurement of Electrical Mobility and Unipolar Charging Properties, *Aerosol Science and Technology*, 44: 2, 97-108, 2010

[2] Lall, A.A. and Friedlander, S.K. On-line Measurement of Ultrafine Aggregate Surface Area and Volume Distributions by Electrical Mobility Analysis: I. Theoretical Analysis, Journal *of Aerosol Science*: 37, 260–271, 2006

[3] Liu, Z., Kim, S. C., Wang, J., Fissan, H. and Pui, D. Y. H. (2011) Measurement for Metal Nanoparticle Agglomerates Generated from

Spark-discharge using the Universal NanoParticle Analyzer (UNPA), submitted to *Aerosol Science and Technology.*

Performance evaluation of the Airmodus PSM (nano CPC) in the sub 3 nm range.

M. B. ATTOUI
Paris East University, France

Keywords : nanoparticle CNC, mobility, growth, sizing,
Presenting author email: attoui@univ-paris12.fr

Detection and sizing of sub 3 nm particles in air is more and more growing interest in the atmosphere (Sipila et al 2010), in nanostructed material field (Peineke et al. 2010) and biochemistry nanoparticles such viruses and virus fragments, bacteriophages, DNA , proteins and protein complexes (Laschober et al 2007). Aerosol Faraday Cage is used as a detector in the sub 3 nm range charged particles since the detection efficiency of the best commercial version CPC –the TSI ultrafine CPC based on the well known work of Mark Stolzenburg and Peter McMurry (1991)- is 2.7 nm. Airmodus (Helsinki Finland) has introduced a commercial version - robust and transportable- CPC sensitive to sub 3 nm with 'high' detection efficiency (40% at 1 nm positive particles). This nano CPC-called PSM- is tested and characterized in this paper in the sub 3 nm range.

Detection efficiency of the PSM is measured – against and aerosol electrometer as a reference- for particles, ions and clusters. Particles of different composition including Sodium Chloride, Silver, Tungsten oxide, polyethylene glycol, proteins and sucrose), clusters of sucrose, nickel chrome and silver, standard positive ions of tetra-alkyl ammonium halides and sub 2 nm positive and negative droplets of ionic liquids are used in this study.

Experiments on the effect of the charge (polarity and number) are done with proteins and polyethylene glycol.

The figure 1 gives the measured detection efficiciency for hydrophilic positive and negative particles of sodium chloride while the figure 2 gives the results for hydrophobic positive and negative particles of silver. The particles are produced by evaporation condensation with an oven following the Sheibel and Porsthndorfer method. A high flow and high resolution DMA (Hermann and or Attoui type) is used to classify the particles generated by the oven.

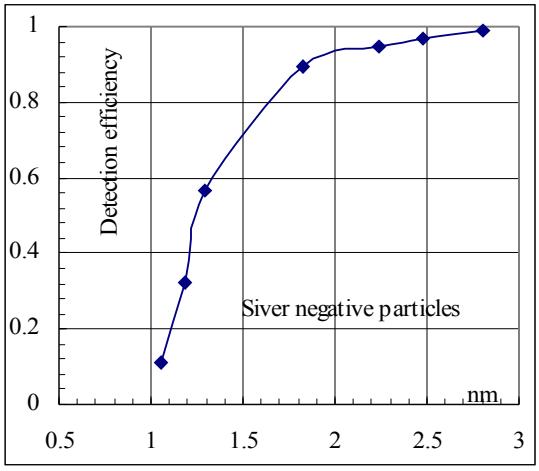

Peineke C., Attoui,M., Robles,A.R., A.C. Reber,A.C., Khanna, S.N., and Schmidt-Ott, A., (2009). J. Aerosol Sci . 423-430.
Laschober et al. (2007). J. Experimental Nanoscience, Vol.2 p. 291-301
Sipila et al 2010: Science Vol. 327 no. 5970 pp. 1243-1246.
Stolzenburg MR and PH McMurry (1991) *Aerosol Science and Technology* 14:48-65.

Heating process of silver nanoparticles diameter-selected by DMA

D. Sugiura, N. Nishida, and H. Tanaka

Institute of Science and Engineering, Chuo University, 1-13-27 Kasuga, Bunkyo-ku, Tokyo, 112-8551, Japan.

Keywords: Ag nanoparticles, DMA, melting point, heating process.
bonganeko@gmail.com

It is well known that the physical properties of metal nanoparticles significantly depend on the particle diameter. Therefore it is essentially important to measure the physical properties with diameter-selected nanoparticles. Especially, heating behavior of the nanoparticles is fascinating because surface of the nanoparticles which depends strongly on their diameter is considered to be affected by heating. In this study, we have investigated heating process of diameter-selected Ag nanoparticles. The Ag nanoparticles prepared by a gas aggregation technique were diameter selected by a differental mobility analyzer (DMA). The heating process was monitored by ion intensity change passed through a heating furnace.

Ag nanoparticles were generated to heat Ag grains up to 1100 °C with N_2 gas flow under atmospheric condition. The Ag nanoparticles were then passed through ^{241}Am for ionization. Ionized Ag nanoparticles were diameter-selected by a DMA. The diameter-selected Ag nanoparticles were admitted into a heating furnace, and were counted by a condensation particle counter (CPC). In this measurement, the particle number was measured as a function of the heating temperature of the furnace. Particle number ratio was estimated from the particle number normalized by that value at 700 °C.

Figure 1 shows reciprocal-diameter dependence of temperature at half particle-number ratio. The temperature was found to decrease linerly with increasing the reciprocal diameter. When the dependence was fitted by a liner function, the intercept was estimate to be 966 °C. Because this temperature is quite close to that for melting temeperature of bulk silver (961 °C) , the measured temperature at half ratio indecates the melting temperature for the diameter–selected Ag nanoparticles. In addition, decrease of the detected particle-number can be explained by the melting because liquified nanoparticles evaporate Ag atoms from their surface and are vanished.

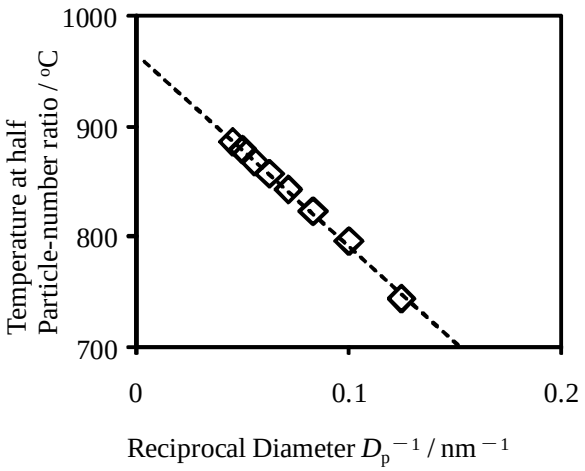

Figure 1. Diameter dependence of temperature at half particle-number ratio. Dotted line exhibits fitting line.

Color tunable nanophosphors made by flame aerosol synthesis

G. A. Sotiriou, M. Schneider, S. E. Pratsinis

Particle Technology Laboratory, Institute of Process Engineering, Department of Mechanical and Process Engineering, ETH Zurich, Sonneggstrasse 3, CH-8092, Zurich, Switzerland
Keywords: yttrium oxide, terbium, europium, codoping.
Presenting author email: sotiriou@ptl.mavt.ethz.ch

Biological labels are used in bio-imaging and the ability to tag cells and biomolecules facilitates diagnosis and therapy. Even though organic dyes are used for such applications, their photobleaching inhibits their further employment. Quantum dots do not exhibit photobleaching and their emission color can be tuned by their size, however, their optical blinking and the high toxicity of their components restrict their use in bio-applications. An alternative strategy for such biolabeling applications are inorganic nanoparticles consisting of a host crystal matrix doped with lanthanide ions, the so-called nanophosphors. The color of these particles depends on the doping ion and not on their size, while their optical properties are superior to organic dyes and quantum dots.

One of the most studied ceramics as host matrix for phosphors is yttrium oxide (Y_2O_3). Several studies investigate the synthesis of nanosized Y_2O_3 based phosphors, and most often doped with Eu^{3+} ions because of its bright red emission. Such phosphor nanoparticles are made either by wet[1-3] or dry[4-6] synthetic routes, while it is not unusual that further annealing process steps are required to obtain the desired crystallinity.[7,8] Nanosized Y_2O_3:Eu particles have enhanced photoluminescence than their bulk counterparts, because of lattice distortions.[1] When Y_2O_3 is doped with another rare-earth element (e.g. Tb) the emission wavelength changes. In fact, this is exploited already by combining three different colored phosphors (blue, green, red) for white-light lamps.[9] For all rare-earth phosphors, there is an optimum concentration of the doping material.[10] This concentration, however, depends on several parameters, such as synthetic route or even the size of the phosphors.[11] The target of this project is the flame synthesis of Y_2O_3 nanoparticles doped with Tb^{3+} and Eu^{3+}. The co-doping of these ions in the Y_2O_3 matrix allows for the fine color tuning of the emission bandwidth.[12]

Figure 1 shows the control of the emitted color of the as-prepared nanophosphors by flame-spray pyrolysis [1]. Clearly, a color change from green to red can be observed. This shows that the emission spectra of the nanophosphors can be tuned by controlling the ratio of the doping atoms in the crystal Y_2O_3 matrix.

Financial support by the Swiss National Science Foundation (No. 200020-126694) is kindly acknowledged.

References

1 T. Igarashi, M. Ihara, T. Kusunoki, K. Ohno, T. Isobe and M. Senna, *Appl. Phys. Lett.* **76**, 1549 (2000).
2 J. Dhanaraj, R. Jagannathan, T. R. N. Kutty and C. H. Lu, *J. Phys. Chem. B* **105**, (2001).
3 G. K. Das and T. T. Y. Tan, *J. Phys. Chem. C* **112**, 11211 (2008).
4 A. Camenzind, R. Strobel and S. E. Pratsinis, *Chem. Phys. Lett.* **415**, 193 (2005).
5 H. Chang, I. W. Lenggoro, K. Okuyama and T. O. Kim, *Jpn. J. Appl. Phys.* **43**, (2004).
6 R. Kubrin and W. Bauhofer, *J. Lumin.* **129**, (2009).
7 A. Camenzind, R. Strobel, F. Krumeich and S. E. Pratsinis, *Adv. Powd. Technol.* **18**, 5 (2007).
8 S. Mukherjee, V. Sudarsan, R. K. Vatsa, S. V. Godbole, R. M. Kadam, U. M. Bhatta and A. K. Tyagi, *Nanotechnology* **19**, 325704 (2008).
9 T. Justel, H. Nikol and C. Ronda, *Angew. Chem.-Int. Edit.* **37**, 3085 (1998).
10 G. Blasse and B. C. Grabmaier, *Luminescent Materials*. Springer: Berlin, 1994.
11 R. E. Muenchausen, L. G. Jacobsohn, B. L. Bennett, E. A. McKigney, J. F. Smith, J. A. Valdez and D. W. Cooke, *J. Lumin.* **126**, (2007).
12 G. A. Sotiriou, M. Schneider and S. E. Pratsinis, *J. Phys. Chem. C* **115**, 1084 (2011).

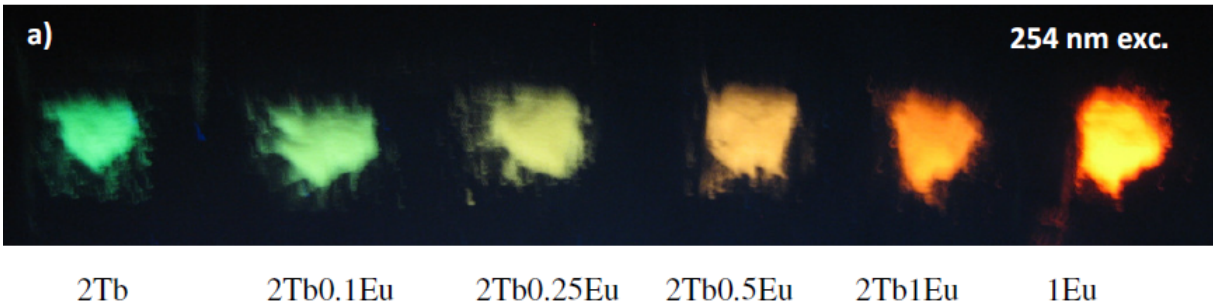

Figure 1. Images of the as-prepared powders under 254 nm irradiation

Formation of metal nanoparticles from supersaturated vapor (Zn, Bi).

A. A. Onischuk[1], A. M. Baklanov[1], O. V. Borovkova[1], V. V. Karasev[1], S. di Stasio[2], S. V. Vosel[1]

[1]Institute of Chemical Kinetics and Combustion, Novosibirsk 630090, Russia
[2]Istituto Motori CNR-IM Aerosol and Nanostructures Lab, Via Marconi 8, Napoli, 80125, Italy
Keywords: metal nanoparticles, homogeneous nucleation, nucleation rate.
Presenting author email: onischuk@kinetics.nsc.ru

Nucleation of metals differ essentially from other systems nucleation and needs a detailed investigation. This work compares experimental routes of measurement of the nucleation rate from Zn and Bi vapor in a laminar flow chamber. The flow chamber consisted of a quartz tube (of i.d. = 0.7 - 1.0 cm) with an outer heater. A flow of Ar was supplied to the inlet with the rate 8 - 17 cm^3/c. A piece of metal (Zn, Bi) was put inside the heated zone, and that resulted in saturated vapor generation. At the outlet of the heated zone the temperature dropped down resulting in the nucleation onset. The concentration, size and shape of particles at the outlet of the tube was analyzed by TEM and automatic diffusion battery. The analysis of thermophoretic depletion of particle concentration in the region of temperature decrease, and the numerical simulation of nucleation coupled with the experimental axial and radial profiles of temperature have shown that the nucleation onset occurs within the layer of 1 mm near the wall of tube. Therefore, the axial profile and morphology of the wall deposit can give the information on the location of the region of maximum nucleation rate and the nucleation volume. However, there can be two different situations: the nucleation temperature T is less than the melting point (as it was in the case of Zn) and higher (Bi). In the first case it is easy to determine the nucleation rate, because the nucleation zone is easy to distinguish by the transition from smooth to powder-like deposit (Fig. 1a), the nucleation time may be estimated from the length of the initial increase in the wall mass deposit profile (Fig. 1b) and as the outlet particles are not aggregated (Fig. 1c) the nucleation rate can be estimated from the outlet particle concentration and the nucleation time. Thus, for example, for T = 660 K and supersaturation S = 15 the nucleation rate was found to be 10^{10} $cm^{-3}s^{-1}$.

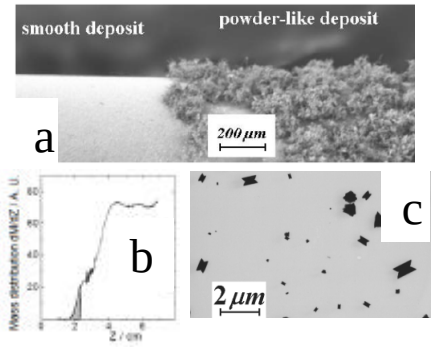

Fig. 1. Zn nucleation data :a) SEM image of wall deposit, b) wall deposit axial profile, c) TEM images of the outlet particles. Nucleation temperature T =660 K.

The situation is quite different in the case of Bi. At the outlet of the tube we observed the aggregates of small primary particles. Thus, to estimate the nucleation rate one should account the mean number of primary particles in aggregates. As the nucleation temperature is higher than the melting point, it is not possible to determine the nucleation zone just by the wall deposit SEM images. Additional methods are to be involved. One of them is light scattering. The light beam passes in the axial direction and the beginning of light scattering gives some information on the location of zone of maximum nucleation rate. Besides, the method of the "supersaturation cut-off" gives an additional information about the nucleation rate. The last experimental technique is as follows. A metal grid is inserted to the quartz tube perpendicularly to the flux. The outlet aerosol concentration is measured continuously. When the grid is downflow essentially after the nucleation onset point the outlet concentration is not disturbed by the presence of grid due to the low particle-to-grid diffusion deposition efficiency (because of the large size of particles). When moving the grid upflow the outlet concentration is decreasing (due to the vapor-to-grid deposition as well as the increase the particle-to-grid deposition efficiency) and the maximum rate of decrease of concentration corresponds to the region of maximum nucleation rate. The numerical simulation of vapor-to-particle transformation coupled with the experimentally measured axial and radial temperature profiles was also made. The simulation included wall vapor deposition, nucleation, particle growth due to vapor deposition and coagulation, particle wall deposition (diffusion + thermophoresis). An example of comparison of simulation results with the experimental measurements is shown in Fig. 3.

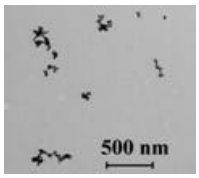

Fig. 2. TEM image of Bi aggregates. T = 710 K

Fig. 3. Bi concentration (as a constituent of both vapor and aerosol particles), light scattering intensity, nucleation rate vs. axial coordinate. Symbols and noisy line - experiment, smooth lines - simulation. T = 710 K.

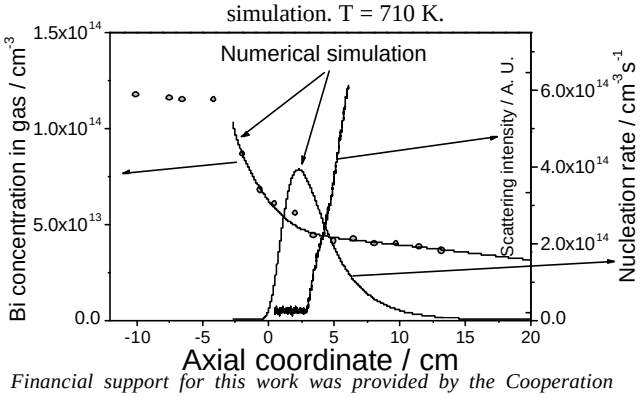

Financial support for this work was provided by the Cooperation Agreement between CNR (Italian National Research Council) and RAS (Russian Academy of Science) years 2008-2010 and Siberian Branch of RAS (Interdisciplinary Integration Project No. 3).

Antimony nanopaticles formation from supersaturated vapor

O.V. Borovkova, A.V. Goryunova, A.M. Baklanov, A.A. Onischuk, S.V. Vosel

Institute of Chemical Kinetics and Combustion, SB RAS, 3 Institutskaja Ave., 630090 Novosibirsk, Russia
Keywords: homogeneous nucleation, metal nanoparticles, nucleation rate, supersaturation.
Presenting author email: borovkova@kinetics.nsc.ru

Formation of metal nanoparticles from supersaturated vapor is of interest due to both fundamental aspects and applications in nanotechnology. This paper is devoted to the experimental study of nucleation from Sb vapor in a laminar flow diffusion chamber (Fig.1a). The flow diffusion chamber consists of a quartz tube with a heater outside. Some amount of Sb was put inside the heated zone to generate the saturated vapor. At the outlet of the heated zone the temperature came down resulting in the vapor supersaturation and nucleation. The particle size and number concentration at the outlet of chamber was measured using diffusion aerosol spectrometer (Ankilov *et al*, 2002). The morphology of the outlet particles was thoroughly studied using JEOL-JEM 100SX TEM (Fig. 1b). At temperatures of the heater above 650 K the aggregates consisting of small primary particles were observed. The aggregate size, concentration (Fig. 2) and fractal dimension were studied as a function of heating temperature as well as size and number of primary particles per aggregate.

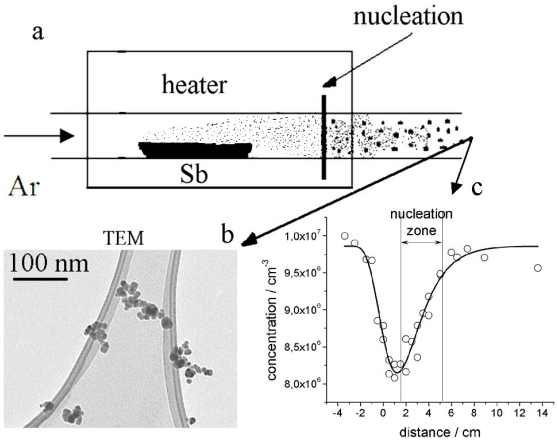

Figure 1. a) Experimental setup b) TEM image of aggregates c) Illustration of the "supersaturation cut-off" method.

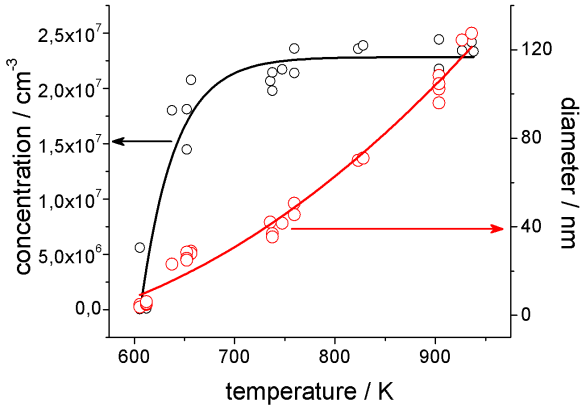

Figure 2. Aerosol concentration and aggregate size vs heating temperature.

"The supersaturation cut-off" method was used to find the approximate location of the nucleation zone (Rybin *et al*, 1975). The probe (metal grid with the diameter equal to inner diameter of the tube) was put inside the quartz tube perpendicularly to the flow. While changing the position of the probe we observed the changes in the concentration of the outlet particles (Fig. 1c). The method is based on the partially condensation of the vapor because of its diffusion on the grid. Thus, the homogeneous nucleation is reduced after the grid. Therefore, the approximate nucleation zone position can be found by the outlet particle concentration decrease. The vapor distribution inside of the generator was calculated from the diffusion mass transfer equation to estimate the supersaturation. The temperature field was determined experimentally using the chromel-alumel thermocouple.

The nucleation volume was estimated from the concentration and temperature profiles using the classical nucleation theory equation for nucleation rate. The number of particles formed in the nucleation zone can be determined using the outlet aerosol concentration and mean number of primary particles per aggregate. The coagulation rate estimations have shown that the coagulation + coalescence of liquid particles (before crystallization and aggregation) make a negligible contribution (<1%) to the decrease of aerosol concentration.

At nucleation temperature 456 K the supersaturation ratio was found to be 14.8 and the nucleation rate $3 \cdot 10^{10} cm^{-3} s^{-1}$.

Ankilov A., Baklanov A., Colhoun M. et al./ – *Atmos. Res.* – 2002. – V. 62. – №3/4. – p. 177-207

E.N. Rybin, M.E. Pankratova, Ya.I. Kogan / *Phys. Chem. J. (*in Russian) – 1975. – №3. – pp. 769-771.

Antimony nanopaticles formation from supersaturated vapor

O.V. Borovkova, A.V. Goryunova, A.M. Baklanov, A.A. Onischuk, S.V. Vosel

Institute of Chemical Kinetics and Combustion, SB RAS, 3 Institutskaja Ave., 630090 Novosibirsk, Russia
Keywords: homogeneous nucleation, metal nanoparticles, nucleation rate, supersaturation.
Presenting author email: borovkova@kinetics.nsc.ru

Formation of metal nanoparticles from supersaturated vapor is of interest due to both fundamental aspects and applications in nanotechnology. This paper is devoted to the experimental study of nucleation from Sb vapor in a laminar flow diffusion chamber (Fig.1a). The flow diffusion chamber consists of a quartz tube with a heater outside. Some amount of Sb was put inside the heated zone to generate the saturated vapor. At the outlet of the heated zone the temperature came down resulting in the vapor supersaturation and nucleation. The particle size and number concentration at the outlet of chamber was measured using diffusion aerosol spectrometer (Ankilov *et al*, 2002). The morphology of the outlet particles was thoroughly studied using JEOL-JEM 100SX TEM (Fig. 1b). At temperatures of the heater above 650 K the aggregates consisting of small primary particles were observed. The aggregate size, concentration (Fig. 2) and fractal dimension were studied as a function of heating temperature as well as size and number of primary particles per aggregate.

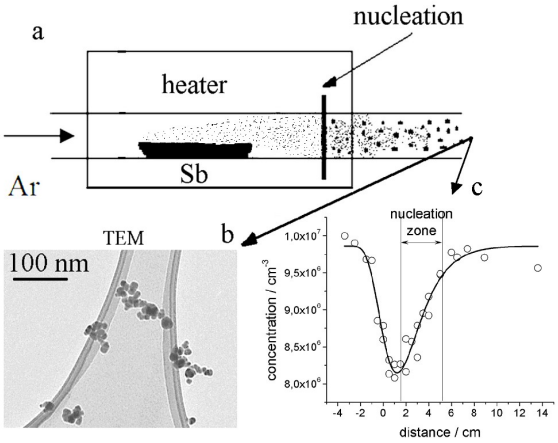

Figure 1. a) Experimental setup b) TEM image of aggregates c) Illustration of the "supersaturation cut-off" method.

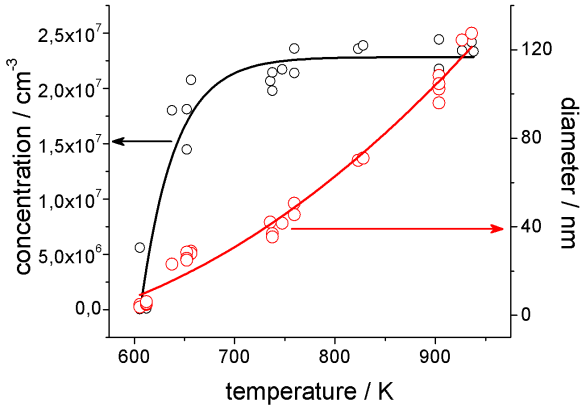

Figure 2. Aerosol concentration and aggregate size vs heating temperature.

"The supersaturation cut-off" method was used to find the approximate location of the nucleation zone (Rybin *et al*, 1975). The probe (metal grid with the diameter equal to inner diameter of the tube) was put inside the quartz tube perpendicularly to the flow. While changing the position of the probe we observed the changes in the concentration of the outlet particles (Fig. 1c). The method is based on the partially condensation of the vapor because of its diffusion on the grid. Thus, the homogeneous nucleation is reduced after the grid. Therefore, the approximate nucleation zone position can be found by the outlet particle concentration decrease. The vapor distribution inside of the generator was calculated from the diffusion mass transfer equation to estimate the supersaturation. The temperature field was determined experimentally using the chromel-alumel thermocouple.

The nucleation volume was estimated from the concentration and temperature profiles using the classical nucleation theory equation for nucleation rate. The number of particles formed in the nucleation zone can be determined using the outlet aerosol concentration and mean number of primary particles per aggregate. The coagulation rate estimations have shown that the coagulation + coalescence of liquid particles (before crystallization and aggregation) make a negligible contribution (<1%) to the decrease of aerosol concentration.

At nucleation temperature 456 K the supersaturation ratio was found to be 14.8 and the nucleation rate $3 \cdot 10^{10} cm^{-3} s^{-1}$.

Ankilov A., Baklanov A., Colhoun M. et al./ – *Atmos. Res.* – 2002. – V. 62. – №3/4. – p. 177-207

E.N. Rybin, M.E. Pankratova, Ya.I. Kogan / *Phys. Chem. J.* (in Russian) – 1975. – №3. – pp. 769-771.

Single-step thermal synthesis of nano N-modified titanium dioxide powders for visible light photocatalysis using atmospheric-pressure microwave plasma

Y.F. Wang[1], L.C. Wang[2], Y. M. Kuo[3], H.M. Chen[4] and C.H. Tsai[4,*]

[1]Department of Bioenvironmental Engineering, Chung Yuan Christian University, Taiwan
[2]Department of Chemical and Materials Engineering, Cheng Shiu University, Taiwan
[3]Department of Environmental and Safety Engineering, Chung Hwa College of Medical Technology, Taiwan
[4]Department of Chemical and Materials Engineering, National Kaohsiung University of Applied Sciences, Taiwan
Keywords: Synthesis, Discharge, Titania, Modification, Nano Particles, Size Distribution.
Presenting author email: lcwang@csu.edu.tw

Nano particles of N-modified TiO_2 photocatalyst for visible light catalysis have great potential application on the environmental and energy industry. The preparation for the titania-based visible light photocatalyst usually are carried out by liquid phase synthesis, while with the drawbacks, including long reaction time (1-24 hr), residual carbon matter, and high cost of precursors. Rapid gas phase synthesis of titania is not easily for control of operating condition and size distribution. Moreover, the modification of titania need be performed via multiple stages.

In this study, N-modified (or N-doping) TiO_2 particles are rapid synthesized in 0.14 seconds by an atmospheric-pressure microwave plasma torch. The continue microwave plasma system was assembled by a commercially available magnetron (National Electronics YJ-1600, 2.45 GHz) with maximum stationary power of 5 kW. A quartz tube are intersected the waveguide (ASTEX WR340) and the resonator perpendicularly. The powders were collected by 14-stage impactors (MOUDI) and were analyzed by XRD, TEM, UV-Vis spectrum, and XPS.

The experimental conditions are as follows: titanium tetrachloride solution with a $H_2O/TiCl_4$ inlet molar ratio = 8 was sprayed as aerosols into the reactor at 900 W, total flow rate of $NH_3/N_2/O_2$ mixtures (0.5/13.5/1.5) = 15.5 slm, and 550-600 for producing $TiO_{2-x}N_x$ powders.

The mass-fractionated particle samples were collected by 14-stage impactors (MOUDI), and then the size distributions were calculated. The results showed that the most of particles (in number) were in 5-10 nm stage impactor, reaching 97.8% of total particle number with the normalized particle number percentage ($dn'/d\log Dp$) reaching 324.8 (Table 1).

The photographs of powders by SEM and TEM show that the spherical TiO_2 with a primary particle of about 10 nm was found, and the secondary particles were aggregated by the primary particles. In addition, the XRD patterns show that the structural characteristics of powders for before and after sintering were mainly anatase crystallization with the average grain size being consistent with the primary particle size.

Elemental analysis by EDS shows that N atoms were about 0.17 at.%. Chemical bonding analysis by XPS confirms the N-doping. The N_{1S} peak could be fitted to three line shapes with binding energies at 395.8, 399.1, and 401.5 eV. These different binding energy peaks are fitted to N^{1+} at 395.8 eV, N^{2+} at 399.1 eV and N^{3+} at 401.5 eV, respectively. In this case, the total area of the N_{1S} peak was 21.2% of N^{1+}, 65.5% of N^{2+}, and 13.3% of N^{3+}. The N^{1+} is assigned to the TiN or $TiN_{X>1}$ bond. The most intense N^{2+} peak is attributed to the Ti-N-O or molecularly chemisorbed γ-N_2 bond. The other weak N^{3+} peak corresponding to higher energy bond was probably the O-Ti-N bond.

UV-Visible absorption spectrum was used to confirm the red shift of band gap to 510 nm (P25 at 396 nm) for N-modified TiO_2. The photocatalytic efficiency of unmodified and N-doped TiO_2 is consistent with commercial P25 powders for the duration of UV-light degradation. By visible light degradation, the conversion of methylene blue is about 2.5 times for N-doped TiO_2 than P25, indicating that by using MW plasma torch for producing N-modified, nano TiO_2 powders is an excellent approach.

Table 1. Size distribution of N-modified TiO_2 powders prepared by $NH_3/N_2/O_2$ MW plasma

Size distribution (μm)	Medium size Dp, (μm)	TiO_2 particles no. percentage n', %	$dn'/d\log Dp$, %
0.005~0.01	**0.008**	**97.77**	**324.8**
0.01~0.018	**0.014**	**1.812**	**7.100**
0.018~0.032	0.025	0.32286	1.292
0.032~0.056	0.044	0.050894	0.209
0.056~0.1	0.078	0.039655	0.157
0.1~0.19	0.145	0.000287	0.0010
0.19~0.32	0.255	0.004587	0.0202
0.32~0.54	0.430	0.000228	0.0010
0.54~1	0.770	0.000463	0.0017
1~1.8	1.400	0.000115	0.00045
1.8~2.5	2.150	0.000009	0.00006
2.5~6.2	4.350	0.000003	0.00001
6.2~10	8.100	0.000000	0.000001
10~18	14.00	0.000000	0.0000004
18~50	34.00	0.000000	0.0000001

Characterization of silicon-carbon nanoceramics synthesized from hexamethyldisilane in high temperature aerosol reactor at atmospheric pressure

M. Miettinen[1], A. Lähde[1], U. Tapper[2] and J. Jokiniemi[1,2]

[1]Fine Particle and Aerosol Technology Laboratory, Department of Environmental Science, University of Eastern Finland, P.O. Box 1627, FI-70211 Kuopio, Finland
[2]Fine Particles, Technical Research Centre of Finland, P.O. Box 1000, FI-02044 VTT, Espoo, Finland

Keywords: nanoparticle production, nanocrystalline material, chemical composition.
Presenting author email: mirella.miettinen@uef.fi

Amorphous alloys of silicon and carbon are of interest because they have a great potential in number of applications in the electronic, chemical and mechanical industries; including e.g. transparent or doped thin films, catalysts, sensors, magnetic materials and high efficient solar cells. However, the characteristics of the particles such as composition (e.g. SiC, $Si_xC_yH_z$, $Si_xC_yO_z$), size, shape and degree of crystallinity have a high impact on their performance in various applications (Carter et al. 2005).

We have synthesized silicon-carbon nanoceramics from metalorganic liquid precursor hexamethyldisilane (HMDS, $C_6H_{18}Si_2$) in high temperature aerosol reactor at atmospheric pressure. The particle formation is based on the decomposition and subsequent reaction of a precursor in the reactor. Low-vapor-pressure decomposition or reaction products nucleate to form molecules or clusters and immediately grow to larger particles that agglomerate further.

The colour of the produced powder changed when the reactor temperature was increased and was yellow, red-brown, brown, brown-black and black at the temperatures of 800, 900, 1000, 1200 and 1400°C, respectively. TEM analysis showed that particles were agglomerated and amorphous at 800 °C, but that crystallinity of the particles clearly increased at higher reactor temperatures (Fig. 1). A cubic 3C-SiC crystal structure d(111)=2.52 Å (2.54 Å), d(220)=1.54 Å (1.54 Å), d(311)=1.31 Å (1.32 Å) (measured values in parenthesis) was observed at synthesis temperature of 1400 °C.

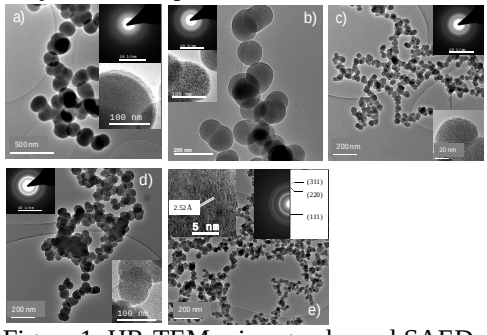

Figure 1. HR-TEM micrographs and SAED diffraction patterns of the produced particles at different temperatures: a) T = 800 °C, b) T = 900 °C, c) T = 1000 °C, d) T = 1200 °C and e) 1400 °C

The XRD pattern of the powders produced at 1200 and 1400 °C showed peaks of the cubic 3C-SiC crystal structure (35° d(111), 60° d(220), 72° d(311)). Based on the TEM and XRD analyses, the crystallite size of the powders was under 5 nm.

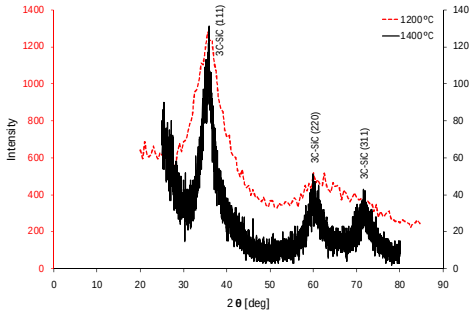

Figure 2. XRD patterns of the powders produced at temperatures of 1200 and 1400 °C

FTIR and NMR analyses showed that the composition of the powder evolved from the structure that contains SiC_4, H-Si and Si-CH_2-Si units at synthesis temperature of 800 °C towards inorganic, nanocrystalline 3C-SiC when the reaction temperature was increased to 1400 °C.

The preceramic produced at the synthesis temperature of 800 °C belongs to amorphous silicon-carbon alloys that are among the most promising nanomaterials today for technologies such as high efficiency solar cells and transparent or doped thin films. On the other hand, the cubic 3C-SiC nanocrystalline silicon carbide that was produced at higher reaction temperatures is an attractive semiconductor and high temperature structural material e.g. in nanocomposites and electroceramics. Thus our synthesis method opens up a possibility for continuous, highly adjustable production of silicon-carbon nanoceramics with desired composition.

This work was funded by the Finnish Funding Agency for Technology and Innovation (TEKES) in the Active Nanocomposite Materials project (40072/08).

Carter, R.S., Harley, S.J., Power, P.P. and Augustine, M.P. (2005) *Chem. Mater.* **17**, 2932-2939.

Ibuprofen nanoparticle formation from supersaturated vapor in the flow chamber

A.V. Samodurov[1,2], A.M. Baklanov[1], A.A. Onishchuk[1] and S.V. Vosel[1]

[1] Institute of Chemical Kinetics and Combustion, SB RAS, Novosibirsk, 630090, Russia
[2] Novosibirsk State University, Novosibirsk, 630090, Russia
Keywords: homogeneous nucleation, nanoparticles, ibuprofen
Presenting author email: samodurovav@gmail.com

Ibuprofen is a popular nonsteroidal anti-inflammatory drug. However health effects occur when using it as tablets or injections. Nanoparticle administration of ibuprofen via lungs can reduce therapeutic dose of this drug and diminish side effects.

The ibuprofen nanoparticles formation has been investigated in this work. The flow chamber was made of quartz tube (inner diameter 0.5 cm) with an outer heater. Argon was used as a carrier gas. Gas flow entered the inlet of the chamber (Fig. 1). Racemic ibuprofen (Ratiofarm, Germany) was put in the hot zone inside the tube. A saturated vapor was formed inside the chamber. The temperature dropped down at the outlet of heater resulting in vapor supersaturation and nucleation. The aerosol concentration at the outlet of the chamber was measured with the Automatic Diffusion Battery.

The supersaturation "cut-off" method was used to determine experimentally the approximate position of homogeneous nucleation zone. A metal grid was inserted into the tube perpendicular to the gas flow and number aerosol concentration at the outlet of the chamber was measured as a function of the grid coordinate (Fig. 2). This method is based on the fact that homogeneous nucleation is inhibited due to the vapor condensation on the grid. As can be seen from Fig. 2 the outlet number aerosol concentration changes sharply when grid is moved from 2 to 5 cm. This means that nucleation proceeds more intensively in this region.

Mean vapor concentration was found from the difference between the mass of a vaporized substance and the mass of the substance condensed on the inner wall of the chamber. The latter mass was found by cutting the tube with condensed substance, dissolving ibuprofen in isopropanol and measuring optical density at the 272.5 nm (ε = 243.4 $mol^{-1} \cdot l \cdot cm^{-1}$). It allowed us to determine radial and axial ibuprofen vapor concentration profiles using the numerical solution of mass-transfer equation in the chamber from 2 to 5 cm. Also radial temperature profiles were measured at the temperature drop zone. Then radial profiles of supersaturation ratio were calculated. Maxima of these profiles as function of axial coordinate are shown in Fig. 2. Axial profile of nucleation rate J_{cl} was calculated from supersaturation ratio maxima profile. Classical nucleation formula was used to calculate J_{cl}. Properties of bulk liquid ibuprofen (density, surface tension) were additionally measured as there were no literature data concerning this substance.

A specified position of homogeneous nucleation zone was found as the position of maximum of J_{cl} curve (Fig. 2). Experimental nucleation rate J_{exp} was determined from the volume of homogeneous nucleation zone and the outlet number concentration of aerosol particles. A width at the half of the height of nucleation rate J_{cl} curve was used as nucleation zone length. Analogous procedure was performed to find the zone radial thickness. The calculated nucleation zone volume had a value of $3 \cdot 10^{-8}$ m^3 and experimental nucleation rate had a value $J_{exp} = 2 \cdot 10^{13}$ $m^{-3}s^{-1}$. The supersaturation ratio in the homogeneous nucleation zone was equal to 10 (see Fig. 2); the temperature of nucleation was equal to 311K.

Basing on experimental data a model of homogeneous nucleation of ibuprofen vapor was developed. It included homogeneous nucleation of supersaturated vapor, particle growth and diffusion of ibuprofen molecules to the wall of the chamber. Coagulation of particles has been shown to give negligible effect.

Financial support for this work was provided by the Siberian Branch of Russian Academy of Sciences (SBRAS): Interdisciplinary Integration Project No. 3 and SBRAS-Taiwan Collaboration Project No. 151.

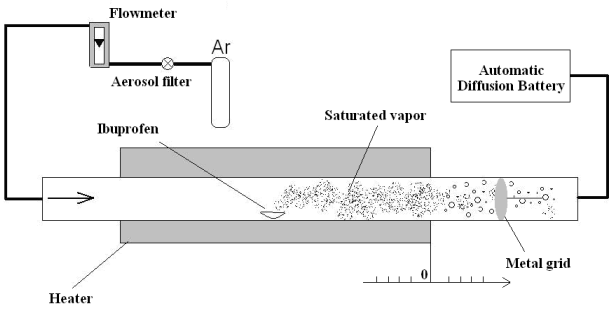

Fig. 1 The scheme of the flow chamber.

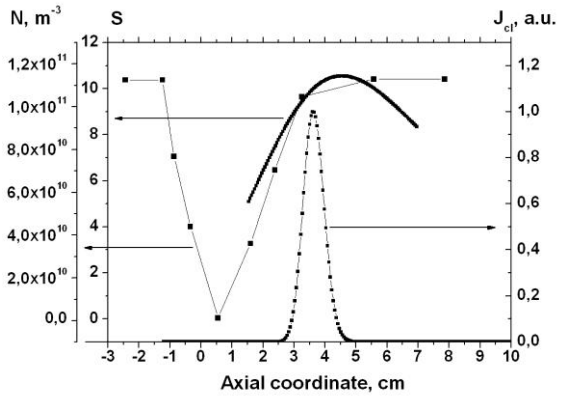

Fig. 2 The axial profiles of supersaturation ratio (S), homogeneous nucleation rate (J_{cl}) and schematic function of the outlet number concentration of aerosol during "cut-off" experiments. The "0" position corresponds to the geometric end of the heater.

Sulfur vapor homogeneous nucleation from a supersaturated vapor in a flow chamber

S.V. Valiulin[1], V.V. Karasev[1], A.A. Onishchuk[1], S.V. Vosel [1], A.M. Baklanov[1], S. di Stasio[2], A.Yu. Komarovskikh[1]

[1]Institute of Chemical Kinetics and Combustion, Novosibirsk 630090, Russia
[2]Istituto Motori CNR-IM Aerosol and Nanostructures Lab, Via Marconi 8, Napoli, 80125, Italy
Key words: homogeneous nucleation, nanoparticles, sulfur
Presenting author email: valiulin@kinetics.nsc.ru

Sulfur, as fine powder, can be used for polymer production, for agriculture and medicine. The application of sulfur nanoparticles for storage batteries can double their capacity as compared with standard lithium-ion storage systems. Sulfur nanoparticles synthesis from the vapor phase is the most convenient way since it produces high purity material in one step. The sulfur nanoparticle formation mechanism via homogeneous nucleation from a supersaturated vapor in a flow diffusion chamber (Fig. 1) was investigated in this work. The flow chamber consisted of a glass tube (of i.d. = 1.2 cm) with an outer heater. A flow of Ar was supplied to the inlet with the rate 15 cm^3/c. A spoon with sulfur was inserted inside the heated zone (saturation zone), and that resulted in saturated vapor generation. At the outlet of the heated zone the temperature dropped down resulting in the nucleation onset. Number concentration and size distribution of aerosol particles at the outlet of reactor were measured by a diffusion spectrometer of aerosol (DSA) and a photoelectric counter AZ-10. Morphology of nanoparticles (Fig. 2) was observed using a transmission electron microscope (TEM). The crystal structure of nanoparticles of sulfur was studied by the X-ray analysis.

The approximate location of the homogeneous nucleation region was determined experimentally using the "supersaturation cut-off" method. Round metallic grid with diameter equal to the inner diameter of the tube was inserted into the tube perpendicularly to the flow (Fig. 1). Due to the vapor-to-grid condensation the homogeneous nucleation was suppressed downstream and the outlet concentration was decreased. The concentration of particles at the reactor outlet was changing is most essentially when moving the grid in the range of axial coordinate 15 to 25 cm (Fig. 3), which means that the nucleation rate is the highest in this location.

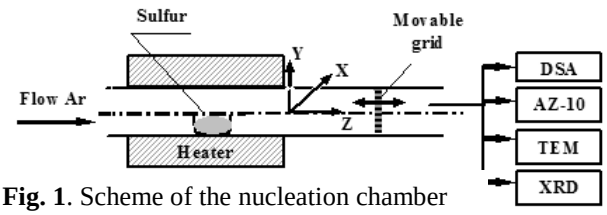

Fig. 1. Scheme of the nucleation chamber

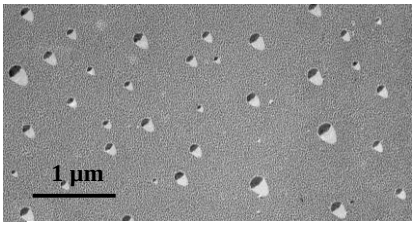

Fig. 2. TEM image of particles.

The rate of sulfur evaporation in the saturation zone and the axial profile of wall vapor deposition rate were measured experimentally. The difference between these two quantities gave the vapor concentration n averaged over the tube cross section vs. the axial coordinate Z. Then using the experimental function n(Z) the radial profiles of sulfur vapor concentration were determined solving the mass transfer equation for 15< Z <25 cm. The temperature radial and axial profiles were measured by a chromel-alumel thermocouple. The supersaturation radial profiles as calculated from the concentration and temperature profiles have demonstrated a maximum for the radial coordinate 0 to 0.1 cm. The maximum supersaturation vs. axial coordinate is shown in Fig. 3. To evaluate the nucleation volume the rate of nucleation J_{cl} was estimated by the classical formula (Fig. 3). The nucleation zone was considered as that within the half maximum of J_{cl} which gave nucleation volume of about V_n=0.202 cm^3. It was found that thermophoresis and coagulation give no contribution to aerosol outlet concentration. Finally, using the estimated value of V_n and the outlet particle concentration 9.5×10^3 cm^{-3} the nucleation rate was estimated $J_{exp} \approx 7\cdot10^5$ $cm^{-3}\cdot s^{-1}$. The supersaturation and temperature were estimated as S = 1200 and T = 308 K, corresponding to this value of nucleation rate.

Financial support for this work was provided by the Siberian Branch of Russian Academy of Sciences (SBRAS): Interdisciplinary Integration Project No. 3 and SBRAS-Taiwan Collaboration Project No. 151;RFBR project no. 09-01-12028-ofi_m and the cooperation Agreement between CNR (Italian National Research Council) and RAS (Russian Academy of Science) years 2008-2010.

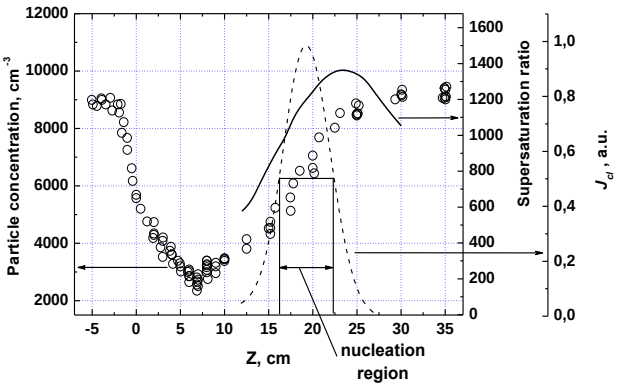

Fig. 3. Outlet concentration of aerosol particles (circles) as a function of the grid coordinate Z, the axial profiles of supersaturation (solid line) and reference nucleation rate J_{cl}, evaluated via the classical formula (dashed line).

Copper coating of silicon, nickel and cobalt nanoparticles

P. Koskela[1], J. Hokkinen[1], M. Murto[1], U. Tapper[1], A. Auvinen[1] and J.K. Jokiniemi[1,2]

[1]VTT Technical Research Centre of Finland, P.O. Box 1000, 02044 VTT, Espoo, Finland
[2]Univ. of Eastern Finland, Department of Environmental Science, P.O. Box 1627, FI-70211 Kuopio, Finland
Keywords: nanoparticles, copper coating, core-shell nanoparticles, magnetic nanoparticles.
Presenting author email: unto.tapper@vtt.fi

Production and coating of functional nanocomposite materials are studied for industrial applications. The capacity of anode materials for Li-ion cells could be increased for anode materials by using copper coated silicon particles, and the permeability and the permittivity of polymer composites could be enhanced with magnetic nanoparticles for GHz frequency range EM wave absorbers.

In this work we used previously developed gas phase hydrogen reduction method (Forsman et al. 2008) that uses metal chlorides as precursors. The experimental setup was utilised for in-situ copper coating of cobalt particles to produce magnetic core-shell copper-cobalt nanoparticles. The apparatus used was further modified to allow copper coating of micron sized silicon and nickel particles. Commercial Ni (OM Group, Inc., NiHP No. 68, Nickel Fine Powder) and Si (NOAH silicon elemental powder 99% ≤10 µm) powders were used in these studies. The nickel and silicon core particles were conducted to the reduction part of the reactor using a fluidised bed aerosol generator (TSI 3400A). N_2 gas was used as carrier in all experiments. The produced powders were characterized for crystal structure, purity as well as magnetic properties.

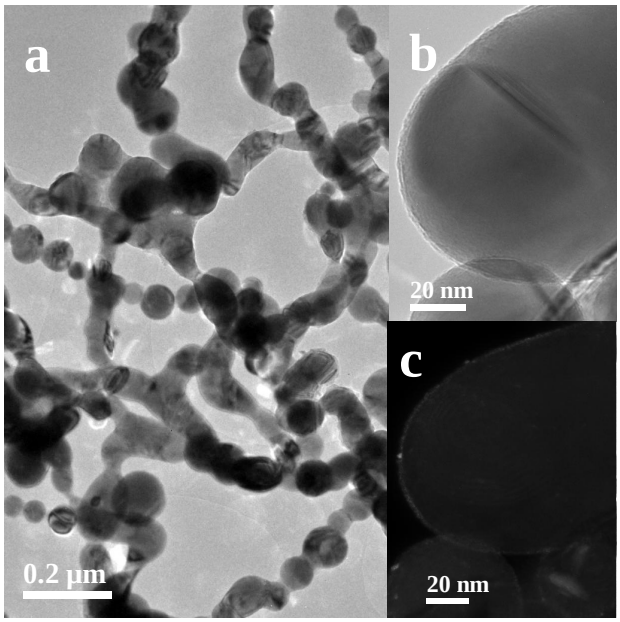

Figure 1. TEM micrograph of copper coated cobalt particles (a). Insert b) shows a coated Co particle at higher magnification. In c) the corresponding dark field image indicates the copper coating on the particle surface.

Tapered Element Oscillating Microbalance (TEOM) and filter samples were used for mass concentration measurements. Fourier Transformation Infrared Spectroscopy was used to monitor the HCl reaction product.

The produced powders were characterised using electron microscopy (SEM and TEM). Image analysis of TEM micrographs gave particle mean diameter of 56 nm and standard deviation of 12 nm for Co+Cu particles. According to X-ray fluorescence analysis the mass concentration of copper and cobalt were 31 m-% and 68 m-%, respectively.

Ni and Si core particle sizes were <100 nm. Based on TEOM measurements, the mass ratio of the produced Ni/Cu and Si/Cu powders was estimated to be 7:12 and 2:1, respectively.

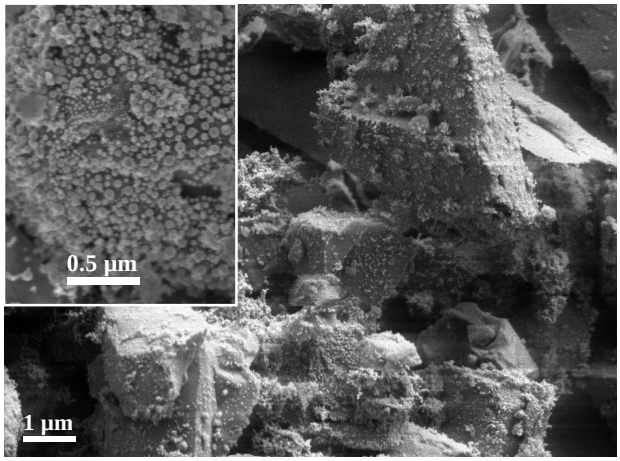

Figure 2. SEM micrograph of copper coated silicon particles. The insert shows the coating particles in more detail.

This work was partly supported by ActKom project (no. 40072/08) funded by the Finnish Funding Agency for Technology and Innovation (Tekes), SAFT, OMG Kokkola Chemicals Oy and Nokia Oyj.

Forsman, J., Tapper, U., Auvinen, A., & Jokiniemi, J. (2008). *J. Nanopart. Res.*, 10, 745-759.

Method for measurement of diameter of critical nucleus in vapor-to-liquid nucleation

A.M. Baklanov[1], S.V. Valiulin[1], A.A. Onishchuk[1], V.V. Karasev[1], A.Yu. Komarovskikh[1], S. V. Vosel[1], S. di Stasio[2]

[1]Institute of Chemical Kinetics and Combustion, Novosibirsk 630090, Russia
[2]Istituto Motori CNR-IM Aerosol and Nanostructures Lab, Via Marconi 8, Napoli, 80125, Italy
Key words: nucleation, nanoparticles, sulphur, critical diameter
Presenting author email: anatoli@kinetics.nsc.ru

The properties of critical nucleus are important to know in studying the thermodynamics of phase transition. There is a deficit of approaches for the experimental measurement of critical nucleus size, because the living time of critical cluster is very low (often in gas-to-liquid nucleation it is 0.1 - 10 μs) and its concentration is also very small. In our laboratory the experimental method for measurements of the critical nucleus diameter was developed. In this article we demonstrate this method for sulphur vapor nucleation. The experimental set-up consists of a horizontal flow nucleation chamber (Fig. 1). The sulphur vapor is generated inside the chamber with the concentration just below the homogeneous nucleation limit. Air was used as a carrier gas. The idea of the method is in sending seed particles to the nucleation chamber. Tungsten oxide particles are used as seeding ones generated by a hot wire generator with the average size being varied in the range 4 to 15 nm. Fig. 2 compares the inlet seeding particles spectra (upper pictures) with the spectra of particles measured at the outlet of chamber. It is possible to see that when the seeding particles diameter d is less than about 7 nm no vapor-to-seeding particle deposition occurs and the outlet spectrum is almost identical to the inlet one (Fig. 2a). When the inlet diameter is larger than about 8 nm the original spectrum transfers to a single mode outlet spectrum with the mean diameter of about 70 nm, i.e. all the original particles were increased in diameter due to the heterogeneous nucleation (Fig. 2c). When the inlet mean diameter is about 7 nm the single peak in the original size spectrum is transformed into two peaks at the outlet (Fig. 2b). One of these two peaks is referred to the original particles with the diameter less then the critical one (small size part of the original spectrum), the other peak is referred to the seeding particles with the diameter larger then critical one (large size part of the original spectrum). The comparison of the outlet and inlet spectra gives the critical diameter $d_{crit} \approx 7.0$ nm.

To determine the nucleation temperature and supersaturation the metal grid was inserted to the nucleation chamber perpendicularly to the flux and the outlet particle concentration was measured as a function of the grid axial position (Fig. 3). For comparison the outlet concentration of particles as measured in the grid experiment without the vapor of sulphur is shown (which demonstrates the seeding particle-to-grid deposition efficiency) and the axial temperature profile is given as well. As seen from Fig. 3 the seed particles + sulphur vapor curve for outlet concentration have a minimum at the axial coordinate $Z \approx 1$ cm (the outlet edge of the oven is taken as zero). The reason for the outlet concentration increase for $Z > 1$ cm is in the particle size growth due to the sulphur vapor-to-particle deposition. Therefore, $Z \approx 1$ is assumed to be the nucleation onset coordinate. The nucleation temperature and supersaturation were estimated to be 330 K and 7.5 respectively.

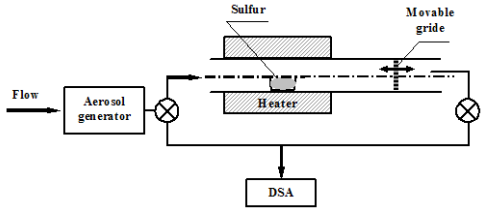

Fig. 1. Scheme of the experimental set-up

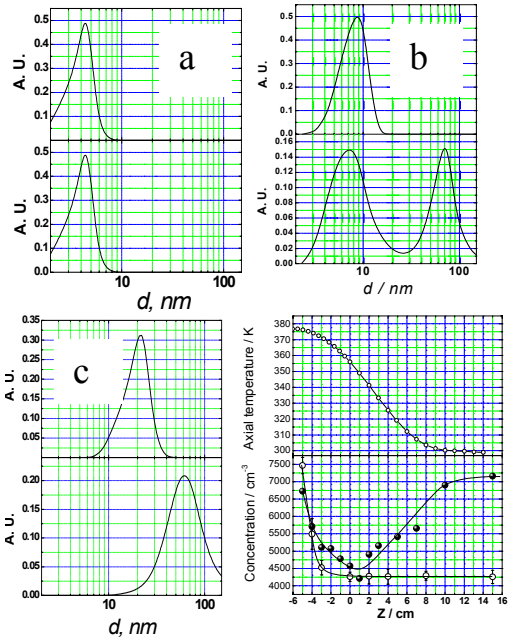

Fig. 2. Inlet (upper) and outlet (lower) particle size spectra;
Fig. 3. Axial temperature profile (upper); outlet particle concentration as a function of grid coordinate, solid - seeding partilces + sulphur vapor, open symbols - just seeding particles without sulphur vapor.

Siberian Branch of Russian Academy of Sciences (SBRAS): Interdisciplinary Integration Project No. 3 and SBRAS-Taiwan Collaboration Project No. 151; RFBR project no. 09-01-12028-ofi_m and the cooperation Agreement between CNR (Italian National Research Council) and RAS (Russian Academy of Science) years 2008-2011

Numerical Analysis of particle growth in a microwave-driven plasma reactor and comparison with experimental data

M. Giglmaier, J.F. Quaatz, J. Matheis and N.A. Adams

Lehrstuhl für Aerodynamik und Strömungsmechanik
Technische Universität München, D-85748 Garching b. München, Germany
Keywords: Nanoparticles, aerosol modelling, CFD, number size distribution.
Presenting author email: marcus.giglmaier@aer.mw.tum.de

With this work we present a numerical analysis of particle growth within a micro-wave driven plasma reactor. The commercial solver Ansys CFX is used to analyze flow field and heat fluxes in the facility. The mixing of the injected gaseous precursor is modeled by scalar transport. A bimodal monodisperse model, a moment model (Jeong 2004), and a sectional model (Hounslow 1988) are implemented and modified to describe the decomposition of the precursor tetraethyl orthosilicate (TEOS), and the subsequent particle growth. Numerical results are compared with experimental data (Abdali 2010).

To investigate the particle growth of silica particles a microwave-driven plasma reactor connected to a hot-wall reactor was constructed at the University of Duisburg-Essen. A parameter study was carried out to gain a better understanding of factors affecting particle size, size distribution, and particle morphology. Samples were analyzed by transmission electron microscopy (TEM). A sketch of the reactor is shown in fig 1.

Our contributions to this development are detailed 3D CFD simulations that provide a detailed insight into flow physics and particle- growth processes. First, a simplified geometry was considered, and the bimodal monodisperse model was applied (Giglmaier 2010). The governing equations for the flow are the 3D time dependent Favre-averaged Navier-Stokes equations for compressible mixtures of gases. For an accurate prediction of the fully turbulent flow and dominant mixing mechanisms an explicit algebraic Reynolds stress turbulence model (EARSM) is applied. Heating by the micro-wave antenna is efficiently modelled by adding a source term to the energy equation. Due to the short residence time of the flow within the microwave antenna the phase change to plasma can be neglected, and the flow is modelled as an ideal gas. The decomposition rate of the precursor is prescribed by an Arrhenius-equation. Because of the high super-saturation in the wall furnace nucleation is neglected. A consideration of sintering effects is not necessary as the experiment delivers spherical particles. We demonstrate that the particle size in each finite volume of the CFD-calculation can be predicted. A comparison of experimentally observed sizes with the calculated particle sizes is shown in fig. 2-3. Upon varying the reactor pressure the numerical prediction follows the expected behaviour, and the resulting particle size fits the measured one. However, the experimentally observed maximum of the particle diameter at a precursor mass concentration of 2.2% was not reproduced by the current numerical model. Abdali et al. suggested that at low precursor concentrations nucleation might be important for the prediction of the correct particle size. We will evaluate this assumption by taking nucleation into account. Furthermore, we present a detailed numerical analysis of the flow within the plasma reactor including the assessment of the implemented particle models. In particular we will demonstrate the ability of the sectional model (Hounslow 1988) to correctly predict the particle-size inhomogeneity due to multidimensional flow, especially due to local recirculation regions.

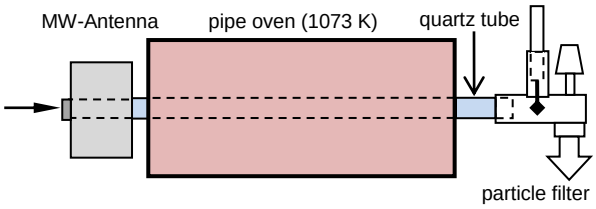

Figure 1: Schematic of the reactor (Abdali 2010)

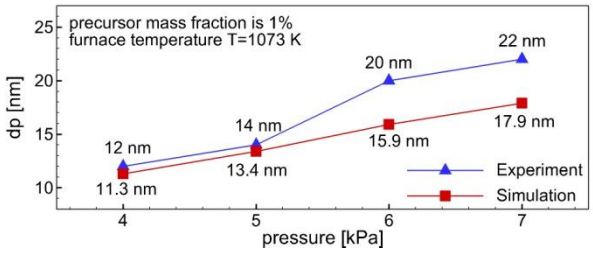

Figure 2: Variation of the reactor pressure

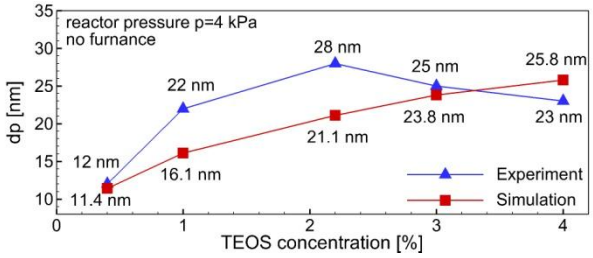

Figure 3: Variation of the precursor concentration

Abdali, A., Moritz, B., Gupta, A., Wiggers, H. and Schulz, C. (2010) *J. Optoelectron. Adv. M.* **12** 3

Giglmaier, M., Al-Hasan, N.S. and Adams, N.A. (2010) *Proc. 7th Int. Conf. on Multiphase Flow*

Hounslow, M.J., Ryall, R.L., Marshall, V.R. (1988) *AIChE Journal* **34** 11

Jeong, J.I., Choi, M. (2004) *J. Aerosol Sci.* **35**

Synthesis of the Pt/Al_2O_3 catalyst particles by MOCVS/MOCVD process at atmospheric pressure

Kun Gao[1], Martin Seipenbusch[1] and Gerhard Kasper[1]

[1]Institute for Mechanical Process Engineering and Mechanics, Karlsruhe Institute of Technology, Karlsruhe, 76131, Germany
Keywords: CVD, catalyst, particle sizes, catalytic activity.
Presenting author email: kun.gao@kit.edu

Catalysts have been used in over 90% of the chemical industry since the first catalyst revolution: the Haber – Bosch process. Because of its significant impact on the chemical industry, the catalyst industry becomes the largest single economic activity today [1]. There are still lots of work to do, such as development of new catalysts and synthesis methods, increasing catalytic activity, selectivity and also lifetime of catalysts.

Usually, noble metal catalysts like Pt or Pd are supported by a thermally stable material, on which the active species form highly dispersed spots. First of all, the present work deals with the synthesis of supported catalysts (Pt/Al_2O_3) by a MOCVS/MOCVD process at atmospheric pressure. Pt/Al_2O_3 is an important catalyst for catalytic reforming (petrol reforming) and can also be used as exhaust catalyst. Nanostructured Al_2O_3, due to its high surface area (100 – 600 m^2/g), like SiO_2 and TiO_2, is used today as an important support substance for supported catalysts.

In this work, Al_2O_3 was prepared with precursor $(C_4H_9O)_3Al$ (Aluminium tri-sec-butoxide) by a MOCVS (metal-organic Chemical Vapour Synthesis) process at 1000 ℃ and atmospheric pressure.

$$(C_4H_9O)_3Al + O_2 \rightarrow Al_2O_3 + H_2O + CO_2$$

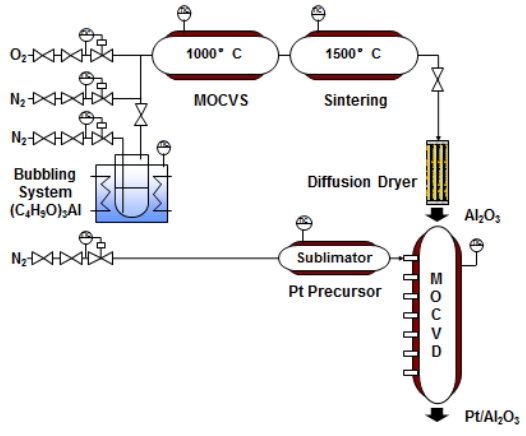

Figure 1. Experimental set up for the synthesis of the Pt/Al_2O_3 catalyst particles by MOCVS/MOCVD process

After the CVS reactor the aerosol (Al_2O_3 nuclear with N_2) was sintered in a sintering furnace at 1500 ℃. The Al_2O_3 particles were coated with Pt in the next step MOCVD (metal-organic Chemical Vapour Deposition) and two different Pt precursors for the MOCVD were used here: $MeCpPtMe_3$ and $isoPrCpPtMe_3$.

Table 1. Properties of the two Pt precursors [2]

Precursor	Properties
$MeCpPtMe_3$	vapour pressure: 6.93 Pa at 23 ℃ decomposition temperature: 120 ℃ melting point: 23 ℃
$isoPrCpPtMe_3$	vapour pressure: unknown decomposition temperature: 122 ℃ melting point: -38 ℃

The experimental set up is shown in the Figure 1. The Pt precursor molecules from the sublimator decomposed on the surface of the Al_2O_3 carrier particles at different decomposition temperatures in the MOCVD reactor. The Pt particle sizes were determined by TEM (Transmission Electron Microscopy) image analysis (Figure 2.), comparing with the catalytic activity.

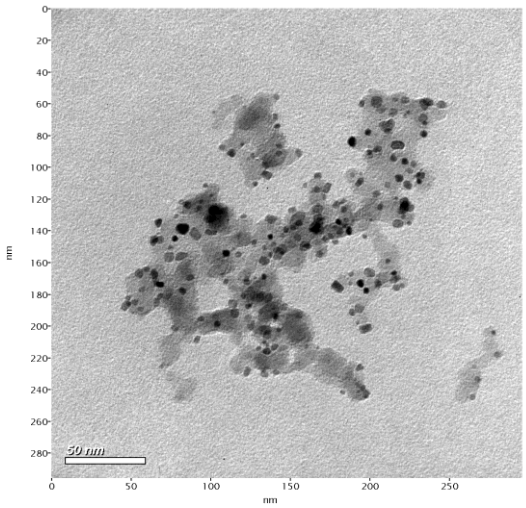

Figure 2. TEM images of Pt/Al_2O_3 particles by MOCVS/MOCVD process

This work was supported by Land Baden-Württemberg, Germany and Joint-Lab IP[3], BASF SE.

[1] K.P. de Jong, Cat. Tech.3 (1998), 87
[2] Kumar, Chem. Mater. 3 (1991), 677-685

Tuesday, September 6, 2011

Session 4P: Poster Session A:
Atmospheric Aerosols - Specific Aerosol Types

Activity Size Distribution and Residence Times of Radioactive Aerosols in the Arctic Atmosphere

Alexandra Ioannidou[1]*, and Jussi Paatero[2]

[1] Department of Physics, Aristotle University of Thessaloniki, 54124, Thessaloniki, Greece
[2] Finnish Meteorological Institute (FMI), Observation Services, P.O.Box 503, FI-00101 Helsinki, Finland

Keywords: AMAD, radioactive aerosols, size distribution, arctic aerosols
*Presenting author email: anta@auth.gr

The objective of this work is to define the aerodynamic size distribution of naturally occurring radioactive aerosols of ^{7}Be in the boreal atmosphere. The Arctic Research Centre of the Finnish Meteorological Institute (FMI) at Sodankylä, Finland (67°22' N, 26°38' E, 180m asl) offers unique possibilities for carrying out research on atmospheric radioactivity in the northernmost continental Europe.

Beryllium-7 is a cosmogenic radionuclide ($t_{1/2}$ = 53.3 d) with an important fraction of its production taking place in the upper troposphere. Soon after its formation ^{7}Be is attached to atmospheric aerosol particles (Porstendörfer et al., 1991; Papastefanou & Ioannidou, 1995; Eleftheriadis et al., 2007).

Aerosol samplings were carried out in the open air (2 m above the ground), at Sodankylä. The aerodynamic size distribution of ^{7}Be aerosols was obtained by using a high volume 6-stage cascade impactor with a regulated air flow rate of about 0.57 m^3 min^{-1} (20 cfm) and Efficient Cutoff Diameters of 0.39, 0.69, 1.4, 2.1, 4.2 and 10.2 μm.

Two collection periods were chosen. One during 26-Mar-2010 – 10-Apr-2010. And the secont one from 27-Jul – 9-Sept-2010. The length of each collection period was 48 h. Glass fiber filters were used as impaction substrates. The filters were measured for ^{7}Be with HPGe gamma spectrometry

The activity median aerodynamic diameter (AMAD) ranged from 0.54 μm to 1.05 μm (avg 0.83 μm) (Table 1). More than 75% of the ^{7}Be activity was found to be associated with particles smaller than 1.3 μm (Fig. 1). Finally, the age of aerosol particles was defined in the order of week.

During the first three samplings it was snowing and the temperature was below zero degrees. Only in these cases the AMAD values were strongly anticorrelated with ^{7}Be activities (R=-0.96, p<0.17522), while they are strongly correlated with RH% (R=0.99, p<0.09207). A weak anticorrelation (R=0.34, p<0.44869) was observed between the AMAD values and ^{7}Be activities during the summer period. During high RH% conditions condensation processes become more intense, resulting in increased particle sizes. But this associated with possibly higher scavenging rates of aerosols does not necessarily alone explain the anticorrelation between the AMAD and the ^{7}Be activities. The air mass origin associated with synoptic scale weather phenomena may contribute to that. Air masses coming from the North Atlantic Ocean usually have a low ^{7}Be activity concentration (Paatero & Hatakka 2000). On the other hand these air masses are usually moist thus enhancing the particle growth by condensation.

Table 1. Experimental Data

Start of sampling	^{7}Be (mBq m^{-3})	AMAD (μm)	σ_s
26-Mar-10	5.01	0.92	2.00
29-Mar-10	2.57	1.05	1.87
1-Apr-10	3.91	1.01	2.09
4-Apr-10	0.70	0.54	1.81
7-Apr-10	2.37	0.73	1.94
20-Jul-10	3.72	0.87	2.86
27-Jul-10	6.88	0.90	2.19
3-Aug-10	2.93	1.05	2.95
10-Aug-10	1.20	0.82	3.06
17-Aug-10	3.89	0.63	2.48
24-Aug-10	3.69	0.86	2.35
7-Sep-10	7.46	0.63	2.43

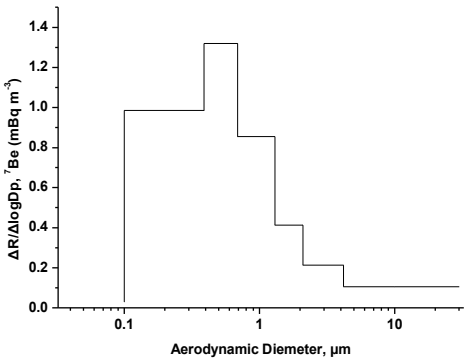

Fig. 1.Activity size distribution of ^{7}Be aerosols

We acknowledge the support of the European Community - Research Infrastructure Action under the FP6 "Structuring the European Research Area" Programme, LAPBIAT (RITA-CT-2006-025969).

Eleftheriadis, K., Karanasiou, A.A., Siskos, P.A., & Psomiadou,C. (2007). *EAC*2007, Salzburg, Austria

Paatero, J. & Hatakka, J. (2000). *Health Phys.* 79, 691-696.

Papastefanou, C., & Ioannidou, A. (1995). *J. Environ. Radioactivity 26*, 273-282.

Porstendörfer, J., Butterweck, G., & Reineking, A. (1991). *Atmos. Environment* 25A (3/4), 709-713.

Chemical composition and dispersal property of smoke emission from forest fires in Siberia

Yuri N. Samsonov

Institute of Chemical Kinetics and Combustion, 630090, Novosibirsk. Russia,
Keywords: forest fire, emissions, chemical composition, elemental carbon, carbonaceous particles
samsonov@kinetics.nsc.ru

The fires in boreal forests of Siberia (about 550 mil. ha) burn 10-14 million hectares annually. The burning of forest biomass results in emission into the atmosphere of large quantities, 300–500 million tons annually, of the gaseous combustion products and the solid/liquid smoke particulates. Our study of smoke emissions from more than 30 modeling fires conducted over two forest territories of Siberia in 2000-2010 (in collaboration with researchers from the USDA Forest Service and Canadian Forest Service), show that the total amount of particulate matter emitted during a typical fire is 0.2- 1 t/ha. These values represent 1-7% of the total biomass, 15-30 t/ha, consumed during a fire depending on the pre-fire weather conditions, the biomass qualities, and the combustion rates. The above share of particulate matter seems to be small, but just the fine particles, particularly those containing a great amount of elemental carbon (soot, char, black carbon), can disturb the heat transfer in the air through the effects on the scattering and the absorption of solar radiation. The emission of large quantities of smokes can, possibly, affect climatic processes (presumably atmospheric cooling?). The potential climatic impacts from the gaseous products (hypothetically atmospheric warming?) and from the particulate emission act contrary to each other, but they depend strongly on the chemical, dispersal and morphological properties of smoke particulates. Thus, we are in need of quantitative data on the smoke emission from the large-scale forest fires to predict the possible changes in chemical and optical conditions of the atmoshere, to create and verify the computational models for global climate or regional weather, and to control the respiratory quality of the near-ground air.

The mentioned above modeling fires, including those conducted at the forest plots of 200 x 200 m, mimic properly the gas-and-aerosol emissions from the wildland fires. The advantage of the modeling fires is that they are carried out under prescribed conditions. In this case, it is possible to record the kinds and the pyrological properties of forest fuels, to register the weather conditions before and during fires, to measure the amounts of burned biomass, the rates of fire spread and the energies released. The smokes were sampled by pumping through the polymeric fine-fiber and the glass-fiber filters. The Synchrotron Radiation X-Ray Fluorescence is used to determine the trace element composition (K, Ca, Fe and other 15-17 elements). The quantities of organic matter and elemental carbon are measured by gas chromatography. Fig.1 shows a typical composition of particulate emissions. Fig.2 shows the typical distribution functions measured *in situ* with an optical counter/analyzer depending on the combustion conditions. One can see that 90-95% of the particulate matter consist of fine particles which can strongly influence the optical and chemical conditions of the atmosphere.

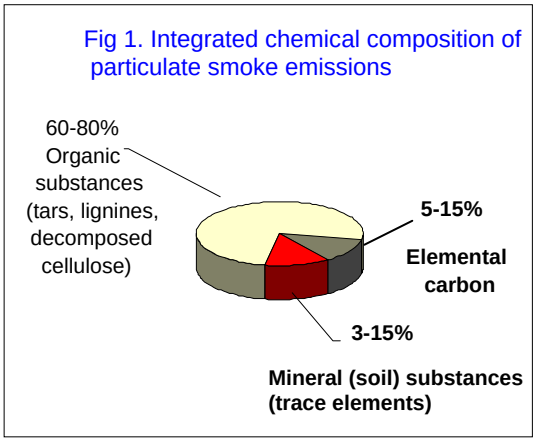

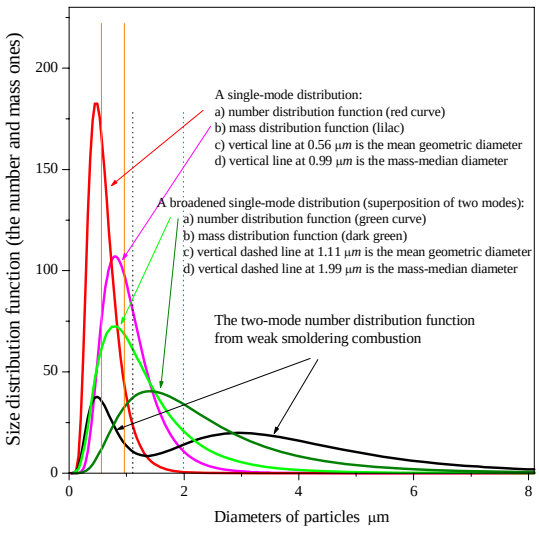

Fig. 2. Size distribution functions of fine fractions of smoke emissions upon different combustion conditions:
the number function: a percentage of particles per a one micron size range, % of particles μm^{-1}
the mass function: a percentage of emission mass per a one micron size range, % of mass μm^{-1}

The work was supported by the International Science and Technology Center (Project 3695) and the Russian Based Research Foundation (08-05-00083, 11-05-01025).

Analysing roadside Particle Number Concentrations using Boosted Regression Trees (BRT).

N.Z.Yahaya, J.E. Tate and M.R.Tight

[1]Institute for Transport Studies, University of Leeds, UNITED KINGDOM
Keywords: particle number concentration, street canyon, stochastic boosted regression trees, wind factors
Presenting author email: tsnzy@leeds.ac.uk

The influence of traffic flow and wind factors on roadside Particle Number Concentration [PNC] have been continuously surveyed for a 12 month period around a congested urban traffic signal controlled junction intersection in the suburb of Headingley, City of Leeds, UK. The experimental work was conducted at the semi-permanent 'Instrumented Junction' research site. Instrumentation includes: traffic flow and speed sensors, above roof-top and in-street sonic anemometers and four air quality stations measuring ultra-fine PNC.

Analysis has demonstrated significant variations in PNC between the stations, largely influenced by the prevailing and in-street winds, building geometries, background concentrations and tidal traffic flows. There is strong evidence of along canyon flow channelling at the sites located in irregular street canyon environments, with air-flows commonly parallel to the street axis. Across-canyon air-flows were also observed, which led to elevated concentrations on the leeward side of the street canyon at two of the monitoring stations as shown in Figure 1.

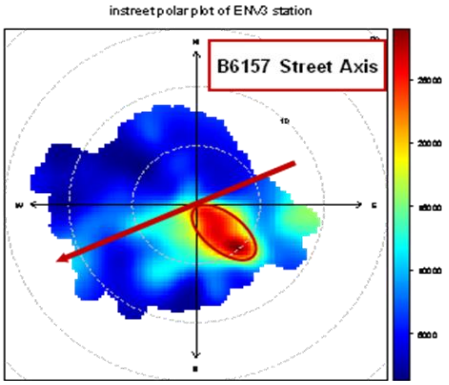

Figure 1. Bivariate polar-plot of [PNC] at ENV3

An new approach methodology to analyse PNC, Stochastic Gradient Boosting, or Boosted Regression Trees (BRTs) (Friedman, 2001, Friedman, 2002) is used to explore the relative influence of a variety of source and meteorological variables on PNC at the urban roadside locations. BRTs differ substantially from traditional regression-based approaches. Simple regression models only provide a single relationship between response and predictor variables BRTs are constructed of multiple regressions models. The BRTs were fitted using the 'gbm' package (R Development Core Team, 2008 and Ridgeway, 2007). Sensitivity testing of model parameters has been carried out (e.g. learning rates (0.005-0.5), number of trees (1000-10000) and interaction depth (1-10)) to identify the optimal parameterisation.

The BRT analysis has provided an importance rank of predictor (relative influence) variables expressed as a percentage. Figure 2 illustrates the relative influence results for site ENV1. It was found that the most important variable was the roof-top wind direction, followed by the traffic flow and vehicle speed. The roof-top wind speed was also found to be a significant influence on PNC concentration. These phenomena are in line with expectations as wind direction and speed are known to strongly influence dispersing air-flows and concentrations in street canyons.

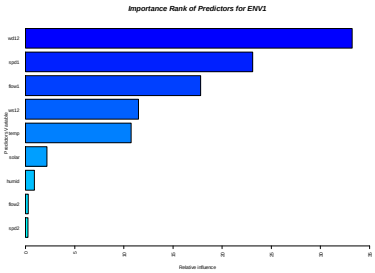

Figure 2. Relative importance of the PNC predictors at ENV1.

A clear benefit of BRTs for air pollution applications in particular PNC study, is their ability to model complex variable interactions and non-linear effects, which are the norm in air pollution research and can be difficult to determine using traditional statistical approaches.

References

Friedman, J. H. (2001). Greedy Function Approximation: A Gradient Boosting machine. *Ann. od Statistic*, 29**,** 367-378.

Friedman, J. H. (2002). Stochastic gradient boosting. *Computational Statistics & Data Analysis*, 38**,** 367-378.

R Development Core team (2008). R: a language and environment for statistical computing. R foundation for statistical computing, Vienna, Austria,URL. http://www.R-project.org

Ridgeway, G. (2007). GBM: Generalizes Boosted Regression Models. *In:* 1.6-3., R. Package. Version 1.6-3.1.

Chemical and mineralogical composition of particulate matter released from agricultural operations

A. Malaguti[1], C. Telloli[2], M. Berico[1], C. Vaccaro[2], M. Mircea[1]

[1]ENEA, National Agency for New Technologies, Energy and Sustainable Economic Development, via Martiri di Monte Sole 4, 40129, Bologna, Italy
[2]Department of Earth Science, Ferrara University, Ferrara, Italy

Keywords: agricultural aerosols, chemical composition, mineralogical composition
Presenting author email: mihaela.mircea@enea.it

The aerosol produced by agricultural operations has significant contribution to the atmospheric aerosol loadings and, therefore, its impacts on visibility, climate forcing and human health should be considered.

This work shows the chemical and mineralogical composition of agricultural aerosols produced during wheat harvest threshing, ploughing and wheat seeding as a function of size. The sampling was carried out on 25 June 2009 for wheat harvest threshing, on 7 and 8 October 2009 for ploughing and on 17 November 2009 for wheat seeding, near Comacchio Valleys (44 ° 36' 40.79" N - 12° 04' 10:52" E,-1m), in Po valley in the north east of Italy, close to the sea.

The aerosol was sampled with an 9-stage Andersen-Marple impactor with a quartz fiber filter SKC 225-1826 1.2µm R-100, and with a modified Millipore Swinnex 47 Polypropylene holder with a quartz fiber filter Pallflex® Air Monitoring Filters Tissuquartz™ 2500 QAT-UP, within the dust plume generated by the agricultural machines.

The chemical composition of sampled aerosol was extracted from the filter and analyzed by Inductively Coupled Plasma Mass Spectrometry (ICP-MS) (X Series spectrometer from Thermo Electron Corporation collision/reaction cell CCT^{ED}) (Heal, 2005; Pekney, 2005). The analyses show that the aerosol chemical composition released during wheat harvest threshing, ploughing and wheat seeding operations is similar with soil composition (Fig. 1).

The surface morphology of sampled aerosol particles studied by Scanning Electron Microscopy (SEM) (CARL-ZEISS EVO 40) shows the presence of fungal spores, bacteria, pollens, fragments of plants, etc.

This work is part of the MINNI (Integrated National Model in support to the International Negotiation on Air Pollution) project, funded by the Italian Ministry for Environment and Territory and Sea and carried out by ENEA.

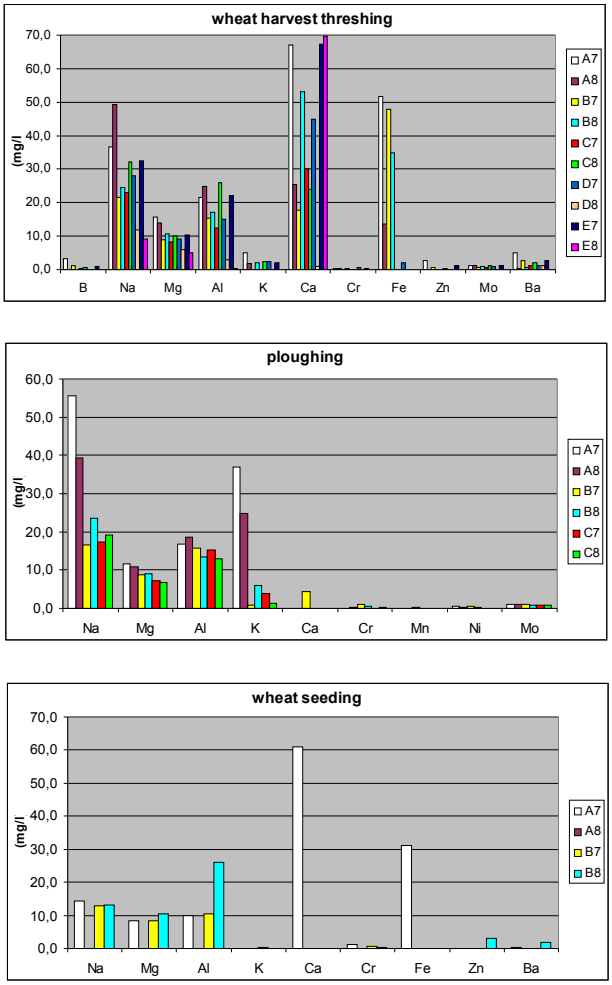

Figure 1. Chemical composition of aerosol sampled during wheat harvest threshing (top graph), ploughing (middle graph) and wheat seeding (both graph).

Heal, M.R., Hibbs, L.R., Agius, R.M. and Beyerland, L.J. (2005) Total and water-soluble trace metal content *of urban background PM_{10}, $PM_{2.5}$ and black smoke in Edinburgh, U.K.* Atmospheric Environment, 39: 1417–1430.

Pekney, N.J. and Davidson, C.I. (2005) *Determination of trace elements in ambient aerosol samples*. Analytica Chimica Acta, 540(13): 269–277.

Identification of Eyjafjallajökull volcanic ash particles collected in Munich in spring 2010 by Raman microspectroscopy

S. Huckele[1], B., Weinzierl[2], R., Niessner[1], C., Haisch[1], T., Baumann[1], N. P. Ivleva[1]

[1]Technische Universität München, Institute of Hydrochemistry, Chair for Analytical Chemistry, Marchioninistr. 17, Munich, D-81377, Germany
[2]Deutsches Zentrum für Luft- und Raumfahrt (DLR), Institut für Physik der Atmosphäre, Oberpfaffenhofen, D-82234, Germany
Keywords: Eyjafjallajökull, particle characterization, fingerprint, Raman microspectroscopy (RM)
Presenting author email: Natalia.Ivleva@ch.tum.de

During the eruption of the volcano Eyjafjallajökull in Iceland in April/May 2010, about 140 million m³ of ash were belched into the atmosphere to over 8000 m height. This ash cloud was dispersed all over Europe and reached the Munich area on April 16, 2010. Due to the amount of ash in the atmosphere, air traffic was grounded in 23 European countries for several weeks.

In 17 flights, operated by Deutsches Zentrum für Luft- und Raumfahrt (DLR), particle samples in the airspace near the eruption and over Europe (April/May 2010) were collected. It was found that the volcanic particles mainly consist of silica grains mixed with various minerals indicating their basaltic origin. Analyses of the ash collected near the eruption zone (DLR, May 2, 2010) showed a varying chemical composition in the different particle size fractions. The Si/Al-ratio was about 3.6±2.8 and the Fe/Si-ratio was about 0.33 (Schumann *et al*, 2010; Pskarsson, 2010).

In parallel, aerosol samples were collected at ground level in an urban setting at the Intitute of Hydrochemistry of Munich using an electrical low pressure impactor (ELPI) and in precipitation using a wet-only/dry-only sampler. As the ash particles could serve as a tracer for airborne particles, the seeping waters in the vadose zone were collected and analyzed. All samples were studied using Raman microspectroscopy (RM). Based on the effect of an inelastic light scattering by molecules, RM provides fingerprint spectra and allows the distinction of a wide range of chemical substances in air particulate matter with the spatial resolution of an optical microscope (Ivleva *et al*, 2007).

Figure 1 shows representative volcanic particles collected in the DLR flights near the eruption zone (a, May 2, 2010), from the air space over Munich (b, April 16, 2010), and particles collected with the ELPI at ground level in Munich (c, April 16-19, 2010). The Raman spectrum of the particle from the air space near the volcano (a) shows characteristic, broad peaks near 140, 315, 380, 420, 540, 720 and 850 cm^{-1}. The spectra of the volcanic particles collected in the airspace over Munich (b) and at ground level (c) demonstrate similarities with the particles close to the volcano. The differences between spectra suggest aging of the particles during the transport with the ash plume and during precipitation. Additionally soot, sodium nitrate and titanium dioxide particles were identified in particular matter sampled on ground level, indicating anthropogenic influence.

In order to interpret the Raman spectra of volcano particles and to characterize their chemical composition a wide range of reference materials: iron(III) oxide (α-Fe_2O_3, hematite), aluminium oxide, quartz, basaltic rock minerals as well as volcanic ash from the ground near Eyjafjallakökull was analyzed. Although the Raman spectra of hematite and quartz are characterized by very narrow peaks we found the similarities in their positions compared to the broad bands in spectra of volcanic particles collected by DLR flights near the eruption (a). This suggests that the ash particles contain iron(III) and silicon oxides. Thus RM is an effective method which enables for the identification and chemical characterization of individual volcanic particles.

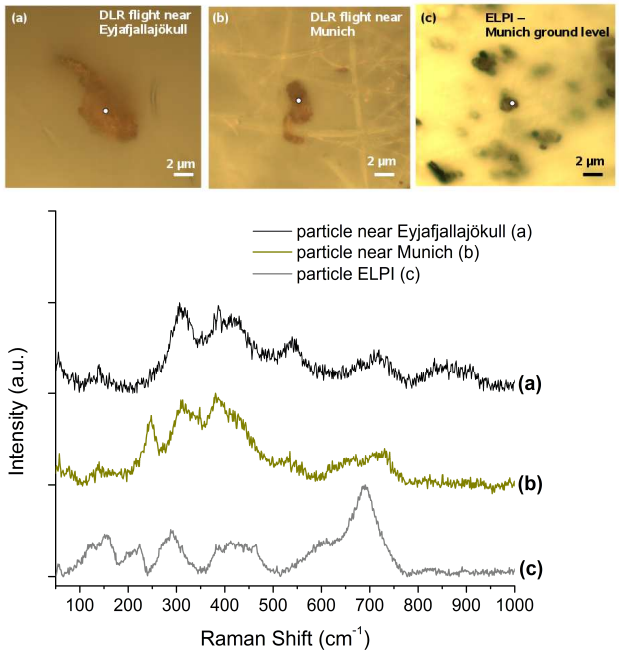

Figure 1. Optical images and corresponding Raman spectra of particles collected in the air space close to the volcano (a), over Munich (b), and particles sampled at ground level in Munich (c).

Ivleva, N. P., McKeon, U., Niessner, R. and Pöschl, U. (2006) *Aerosol Sci. Technol.* **41**, 655-671.

Pskarsson, N. (2010) http://www.earthice.hi.is/page/IES-EY-CEMCOM.

Schumann, U., Weinzierl, B., Reitebuch, O., Schlager, H., Minikin, A., Forster, C. et al. (2010) *Atmos.Chem.Phys.Discuss.* **10**, 22131-22218.

Characterization of particulate trace elements in Tehran air

F. Halek and A. Kavousirahim

Department of Energy & Environment, Materials & Energy Research Centre, Tehran, P.O.Box 14155-4777, Iran
Keywords: particulate matter, PM_{10}, $PM_{2.5}$, trace elements, Tehran air pollution.
Presenting author email: f-halek@merc.ac.ir

Tehran, the capital city of Iran with over 10 million populations, is facing great risk from various pollutants, especially suspended particulate matters (Madanipour, 2006; Atash, 2007). It is well established that inhalable particles carry higher concentrations of many potentially toxic trace elements such as Pb, Cd, V, Fe, Zn, Cr, Ni and Mn (Liu et al, 2000; Harrison and Yin, 2000). Trace elements are released into the atmosphere by human activities, such as combustion of fossil fuels and industrial activities; and natural sources such as forest fires, oceans and volcanoes (Querol et al, 2007; Rajsic et al, 2008; Yatkin and Bairam, 2008). The concentration of particulate matter in Tehran increases drastically in the winter time and as the result, Tehran experiences such days quite often, forcing schools to close and people with heart and lung problems to stay home.

Experimental

In this study, the experiments were carried out during winter (Jan., Feb. and March) 2009 to determine the concentration of PM trace elements, as well as elements characterization of PM and source assessment. Four different sites including: Vanak Square (VS), Arjantin Square (AS), Sadeghieh Square (SS) and North Karegar Avenue (NK) all located in the north-western parts of Tehran were selected for samplings. This part of Tehran is highly populated and jammed with traffic and also many schools, universities, commercial areas, terminals, and hospitals are involved in their daily activities. Daily 24 hrs sampling started at 8:00 A.M. Sampling height was chosen according to average height of Iranian people which is 1.65 m (Haghdoost et al, 2008). Studied 11 trace elements and their limit of detection (LOD) are listed in Table 1 were investigated

PM_{10} and $PM_{2.5}$ collections were done using cascade impactors (Sierra Ins., USA) on Wathman glass fiber filters (type GF/A). All the samples were acid digested according to the method EPA-3051, using microwave oven (Mile Stone - ATC - FO 300 - Italy). The filtrates were analyzed for the elements, according to EPA-6010 method, using Inductive Coupling Plasma instrument (ICP-ARL 3410, Switzerland).

Table 1. Studied elements and attributed LOD (mg/l).

Element	Zn	Fe	Pb	Mg	Al	Cu
LOD	0.001	0.0005	0.01	0.00002	0.02	0.0003
Element	**S**	**Ti**	**Mn**	**Cr**	**As**	
LOD	1	0.1	0.0001	0.002	0.05	

Results & Discussion

Table 2 lists the average concentrations of different elements on PM_{10} and $PM_{2.5}$. The total concentration of these elements in PM_{10} and $PM_{2.5}$ is more or less the same to the concentration of Fe alone in the particulates. Among these elements, As and Mn have more health risk in human.

Table 2. Average concentrations of different elements on PM_{10} and $PM_{2.5}$ (μg/m^3).

	Zn	Fe	Pb	Mg	Al	Cu
PM_{10}	26.60	7.87	0.94	20.15	0.12	1.92
$PM_{2.5}$	24.26	3.73	0.58	12.08	0.08	1.37
	S	**Ti**	**Mn**	**Cr**	**As**	
PM_{10}	3.00	1.56	0.42	0.33	0.27	**SUM: 63.17**
$PM_{2.5}$	1.11	0.96	0.32	0.30	0.20	**SUM: 44.98**

The list suggests that the tendency of PM_{10} and $PM_{2.5}$ in combining with the elements is different. For example, trace elements such as Cr and Zn are more combined with $PM_{2.5}$, while PM_{10} contained more S and Fe. The total concentrations of all the trace elements attributed with PM_{10} averaged to be 63.17 μg/m^3, while for $PM_{2.5}$ was 44.98 μg/m^3. This lead to the ratio of $C(PM_{2.5})$ / $C(PM_{10})$ = 0.71, which suggests that more trace elements in Tehran atmosphere are combined with smaller particulate matter. Since the smaller particles can accumulate deeper in lungs, therefore the smaller the size of the particles the more dangerous they become for human health.

It is noticed that the concentrations of the Zn, Mg and Fe are much higher than the other elements. In addition, iron could be found as one of the constituents of soil in the various forms of its salts. The concentrations of the other elements compared to these 3 elements, are low and could be considered as anthropoid sources emitted mostly from the industrial activities. The order of PM elemental concentration in different sites was: NK > VS > SS > AS.

Atash, F. (2007) *Cities* **24**, 399-409.
EPA 3051 Method: Available via. *www.epa.gov*.
EPA 6010 Method: Available via. *www.epa.gov*.
Haghdoost A.A., Mirzazadeh A. and Alikhani, S. (2008) *Iran. J. Pub. Health* **37**, 1-7.
Harrison, R.M. and Yin, J. (2000) *Sci. Total Env.* **249**, 85-101.
Liu, D.Y., Prather, K.A. and Hering, S.V. (2000) *Aerosol Sci. Technol.* **33**, 31-86.
Madanipour, A. (2006) *Cities* **23**, 433-438.
Querol, X. et al. (2007) *Atmos. Environ.* **41**, 7219-7231.
Rajsic, S., Mijic, Z., Tasic, M., Radenkovic, M. and Joksic, J. (2008) *Environ. Chem. Lett.* **6**, 95-100.
Yatkin, S. and Bayram, A. (2008) *Chemosphere* **71**, 685-696.

Characterization of particle size distributions of powdery building materials aerosol

T. Prasauskas[1], D. Martuzevicius[1], E. Krugly[1] and L. Kliucininkas[1]

[1]Department of Environmental Engineering, Kaunas University of Technology, Radvilenu pl. 19, LT50254, Kaunas, Lithuania

Keywords: Air pollution, powdery building materials, particulate matter, resuspension, particle size distribution

Presenting author email: tadas.prasauskas@ktu.lt

Introduction

There have been numerous studies assessing the potential aerosolization of various contaminants from building materials and its relation to respiratory problems. These emissions are most often the cause of respiratory problems, whilst many may increase susceptibility to asthma and allergies, and in some cases they include highly toxic and carcinogenic substances. Polluting particles can also be a problem during the demolition phase. A wide range of common building materials emit particles and gases that carry a variety of health risks (Berge, 2009). Thus, particle size distribution is an important physical property of solids with respect to potential health impacts.

Methods

We have aimed to identify particle size distributions of various powdery building materials by two aerosol generation methods: fluidization and gravitation (Gill et al., 2006). These two methods represent actual industrial activities, such as pneumo transportation and unloading, and are easily modelled in laboratory conditions. Various powdery building materials aerosols was generated in laboratory by fluidization (dust is resuspended by direct entrainment into airflow in a tube) and gravitation (a source sample fell as a discrete slug through the air into an enclosed chamber, from which dust is evacuated) methods. Particle size distribution was determined for 11 materials: cement, chalk, clay, coarse sawdust, fine sawdust, gypsum, hydrated lime, masonry grout, quartz sand, sand, structural lime.

Using the fluidization method, 0.1 g of powdery building material was inserted into the injection tube. The material sample was dispersed into the experimental chamber by the short-term gust of compressed air. The air was withdrawn from the chamber via sampling tubes together with sampled particles. In case of gravitation method, 1.0 g of powdery building material was dropped from 40 cm height into an enclosed chamber, from which dust was evacuated. In both cases, particle size distribution was determined by the Aerodynamic particle sizer (APS) (3321, TSI Incorporated) and optical particle counter (OPC) (3016, Lighthouse worldwide solutions). Aerosol was sampled by separate Tygon tubes at the same height (20 cm from the chamber bottom).

Results

The PSDs of resuspended particulate matter from powdery building materials were rather similar by both fluidization and gravitation methods, with exception of coarse sawdust and sand, which varied substantially comparing to other materials. According to APS data (number concentration (dN) the highest mode by fluidization method was assessed for fine sawdust and equal to 3.278 μm, and the lowest for gypsum - 1.981 μm (Table 1.). In case of gravitation method highest mode also was assessed for fine sawdust - 3.523 μm and the lowest for coarse sawdust 0.542 μm.

With respect to mass concentration (dM), the highest modes by the fluidization method were determined 19.810 μm and 15.960 μm for coarse sawdust and sand, respectively. The lowest mode was determined for the gypsum - 2.839 μm. In case of gravitation, the highest modes were assessed for coarse sawdust and chalk (19.810 and 13.820, respectively) and the lowest one for gypsum (3.051 μm).

Table 1. Value of modes (dN and dM) of building materials.

Building material	Fluidization		Gravitation	
	Mode, μm		Mode, μm	
	dN	dM	dN	dM
Cement	2.288	3.278	2.642	3.523
Chalk	2.288	3.051	2.642	13.820
Clay	2.642	3.523	3.051	4.068
Coarse sawdust	2.642	19.810	0.542	19.810
Fine sawdust	3.278	5.048	3.523	5.829
Gypsum	1.981	2.839	2.288	3.051
Hydrated lime	2.288	4.371	3.051	4.698
Masonry grout	2.458	3.523	3.278	4.371
Quartz sand	2.642	4.371	2.642	3.786
Sand	2.288	15.960	3.278	4.698
Structural lime	2.129	4.371	2.642	5.048

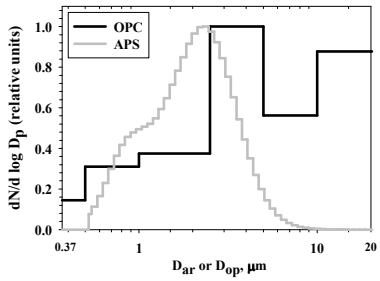

Figure 1. Particle size distribution (dN) of cement during fluidization by APS and OPC.

The comparative analysis of highest aerosol modes generated by fluidization and gravitation methods revealed general trend that slightly higher modes of number (dN) and mass (dM) concentrations were observed for aerosols generated by gravitation method.

Berge, B. (2009) *The ecology of building materials. Second edition,* Elsevier Ltd.

Gill, T.E., Zobeck, T.M., Stout, J.E. (2006) *Technologies for laboratory generation of dust from geological materials*, J. Hazard. Mater. **132**, 1-13.

Monitoring of the Particulate Matter Deposition Around Port of Koper

G. Jereb[1], B. Marzi[2], F. Cepak[2], G. Dražič[3] and B. Poljšak[1]

[1] University of Ljubljana, College of Health Studies, Poljanska 26 a, 1000 Ljubljana, Slovenia
[2] Port of Koper, Vojkovo Nabrežje 38, 6000 Koper, Slovenia
[3]Department for Nanostructured Materials, Jožef Stefan Institute, Jamova 39, 1000 Ljubljana, Slovenia

Keywords: particulate matter, deposition, monitoring, coal and iron ore

Port of Koper already introduced several dust control measures in order to reduce dusting in the environment from the EET terminal (coal and iron ore manipulation and storage place). Dust control measures include construction of an 11 m high anti-dust emission wall, spraying the body of the landfill with water and wet cleaning of the transportation roads around the landfill at least twice per day. For assessment the effectiveness of such preventive measures long-term monitoring of particulate matter deposition is rather reasonable approach. Therefore three one year measurement campaign were adopted. During time interval 2009/10 it was the third year of monitoring of the particulate matter deposition in the observed area. First campaign started in October 2005 and lasted until October 2006; the second measurement campaign was conducted in 2007/08 and the last one in the period 2009/10.

The amount of particulate matter deposition was determined gravimetrically, samples were qualitative and quantitative analyzed using SEM EDXS. Chemical analysis on annual samples was also carried out in order to determine the amount of selected (Fe, Al, Cu, Zn, Cd, Pb, Cr, Ni, As) metals.

The study was designed to assess the dustiness in the region and determine the difference between vertical and horizontal (contribution of wind) deposition. Additionally the impact of background and correlation between dust deposition, the weather (especially extreme) and the activity at the Port of Koper was evaluated.

During the preliminary study, which was carried out during 2005/06 (Figure 1) extreme values of particulate matter deposition in Port's surroundings were detected. Values exceeded the monthly limiting value by a factor of 12. Also yearly limiting value was exceeded. In time period 2007/08 (Figure 2) and 2009/10 (Figure 3) elevated levels of suspended particles were not detected. The reason for relatively lower values of dust deposition might be in weather conditions (low wind in the observed directions), but also in precautionary measures taken by the Port of Koper. These anti dust measures are obviously an effective approach to reducing or limiting emissions of dust particles to the surroundings.

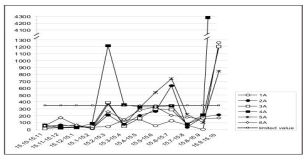

Figure 1: Particulate matter deposition - 2005/06

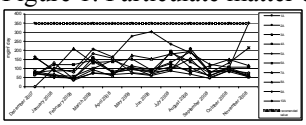

Figure 2: Particulate matter deposition - 2007/08

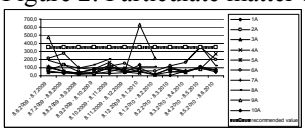

Figure 3: Particulate matter deposition - 2009/10

Based on the results of measurements of particulate matter deposition on other locations (results were obtained in annual reports of the Environment Agency of Republic of Slovenia - ARSO, 2005 - 2009) in Slovenia, where particulate matter deposition is also measured (most sampling sites are located in the vicinity of major power plants), a comparison with particulate matter deposition around Port of Koper was performed. The results indicate that the area around the Port of Koper, despite the fact that the levels decline during last years, is still burdened with high dust deposition (higher than in comparable locations in Slovenia - Figure 4).

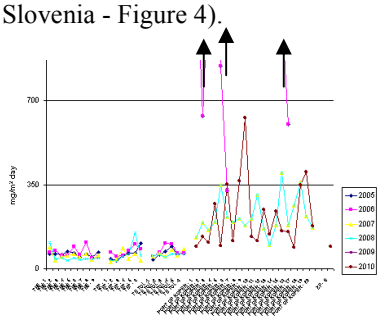

Figure 4: Particulate matter deposition - comparison of different locations around Slovenia

Literature

ARSO, Annual reports, 2005 - 2009. http://www.arso.gov.si/zrak/kakovost%20zraka/poro%C4%8Dila%20in%20publikacije/kakovost_letna.html <1.2.2011>

Efficiency of CMA as a dust binding agent

C. Bennet[1], M. Gustafsson[1] and G. Blomqvist[1]

[1]Environment, Swedish National Road and Transport Research Institute, Linköping, SE-581 95, Sweden
Keywords: road dust, dust binding, emission factor, measurements.
Presenting author email: Cecilia.Bennet@vti.se

Calcium Magnesium Acetate, CMA, is used for dust binding in the Austrian and Italian cities Klagenfurt, Bruneck and Lienz in order to reduce the contribution of road dust to PM_{10}. The effect of this method is evaluated within the EU Life project CMA+.

One method is to make controlled experiments where the tyre-pavement emission is investigated (Gustafsson et al., 2009). In the laboratory four studded tyres are spinning on an orbital pavement and the emitted particles are measured by SMPS, APS and TEOM instruments. The CMA is applied and the resulting changes in the aerosol are analysed.

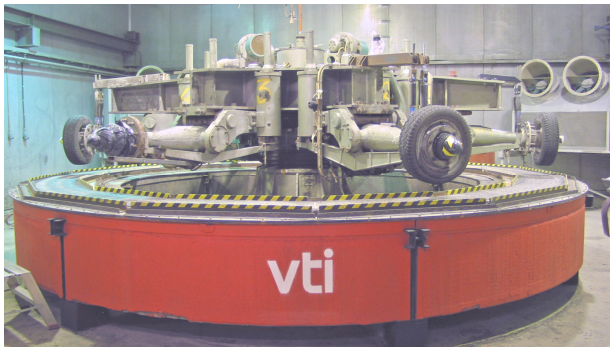

Figure 1. Experimental setup for emissions of the interaction between tyre and pavement.

Two parameters are characterising the effect of the dust binding agent. The maximum decrease in the concentration and the duration of the effect (Figure 2)

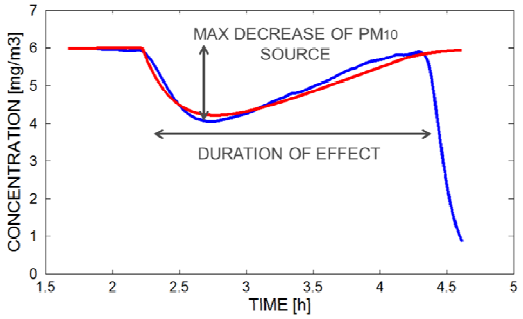

Figure 2. Definitions of the two parameters that characterise the effect of the dust binding agent.

The results can be translated to emission factor and show an effect that is increasing with dose (Figure 3).

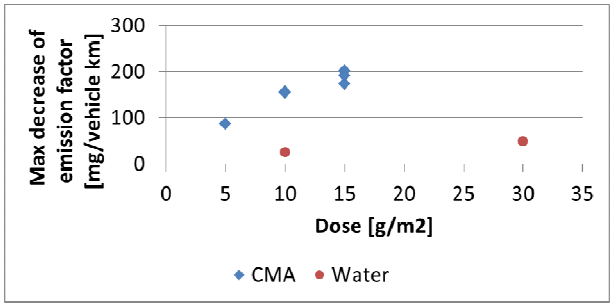

Figure 3. The absolute maximum decrease of the emission factor assuming a constant deposition velocity in the room. A normal emission factor for the studded tyre setup is between 290 and 570 mg/vehicle km.

The measurements also indicate that the number of particles is *increasing* when the PM10 is decreasing as an effect of the application of CMA (Figure 4). This result is interesting as the health effect might be more sensitive to number of particles than to PM_{10} or $PM_{2.5}$. The reason might be a change in the emission itself, a change in the deposition to surfaces in the room or the change of larger particles that act as a sink to the smaller more numerous particles.

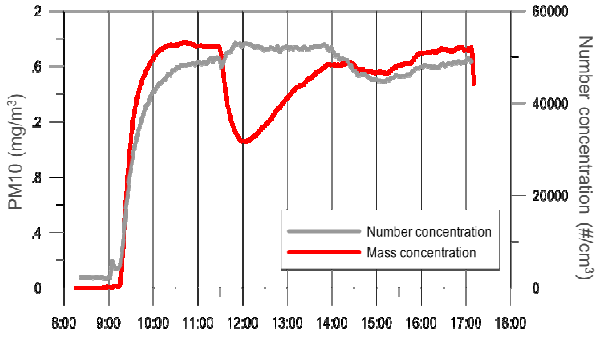

Figure 4. Concentration of particulate mass (PM10) and number concentration when CMA is applied in the road emission experimental setup.

This work was supported by the EU Life project CMA+.

Gustafsson, M., Blomqvist, G., Gudmundsson, A., Dahl, A., Jonsson, P & Swietlicki, E. (2009). *Factors influencing PM10 emissions from road pavement wear*. Atmospheric Environment, 43, 4699-4702.

Influence of fireworks on the atmospheric levels of trace metals

E. Yubero[1], J. Crespo[1], F. Lucarelli[2], S. Nava[2], N. Galindo[1], J. Nicolás[1], M. Chiari[2] and G. Calzolai[2]

[1]Department of Physics, Miguel Hernández University, Avda. de la Universidad s/n, 03202, Elche, Spain
[2]Department of Physics, University of Florence and INFN, via Sansone 1, I-50019, Sesto Fiorentino, Italy

Keywords: Elemental composition, PIXE, Number size distribution, Size-segregated aerosols
Presenting author email: eyubero@umh.es

Las Hogueras de San Juan is the biggest festival of the city of Alicante (southeaster Spain) celebrated every June. Throughout this festival, huge quantities of firecrakers and sparkles are burnt everyday in the city centre during a few minutes. This event represents an unusual but important source of atmospheric particles, especially metals. To evaluate "in situ" the impact of craker and sparkle burning on the levels and composition of atmospheric particles, both the fine and coarse fractions of the aerosol were collected by a streaker sampler with 1-h time resolution; a multistage cascade impactor (SDI, Dekati) was also used. PIXE analysis of these samples allows the assessment of hourly resolution elemental time trends and elemental size distributions, respectively. The temporal evolution of the number of particles was determined by an optical particle counter (GRIMM). Results obtained by the whole campaign will be presented; here, some examples concerning the 1-hour time resolution concentration data are shown.

Figs. 1-2 show the concentrations (ng/m^3) of Cl and K (fine fraction), Ba and Sr (fine fraction). All these elements have very sharp peaks, every day, in correspondence of the time of mascletas burning (3.00 p.m.) and lasting only few hours (the quick decrease after the events can be explained by sea breeze). A similar time pattern is also shown by Mg, Si, V, Cr, Mn, Co, Cu, Zn, Br, Rb, Sr, Ba, Pb. All these elements clearly represents the firework-related elements.

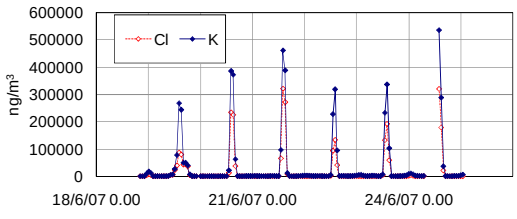

Fig. 1. Fine mode Cl and K concentrations (ng/m^3)

K and Cl reach very high concentrations of about 500 μg/m^3 and 300 μg/m^3 in the fine fraction, with an increase of a factor more than 1500 respect to background levels. Other elements related to firework colors like Sr, Al, Mg, Ba, Cu, Co, Zn, Pb also present a large increase, reaching concentrations of about many μg/m^3 (while their normal values are around some ng/m^3) with increase factors of more than 100 (more than 1000 for Sr) for the fine fraction respect to background levels.

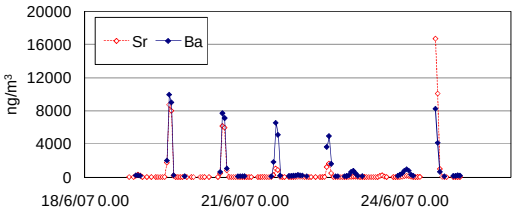

Fig. 2. Fine mode Sr and Ba concentrations (ng/m^3)

For all these elements, an increase of their concentrations is also present in the coarse fraction, but less pronounced.

Also most of the elements of crustal origin like Fe, Ca, Si, Ti, etc. show a temporal pattern similar to that reported in fig 1 and 2, but with a higher increase in the coarse fraction than in the fine one. In sharp contrast to what seen for the elements reported in fig 1 and 2, the ratio between the concentration of these elements during the mascletà and during the background period is constant, pointing out, hence, that the concentration increase is not due to the combustion products but to the resuspension of crustal origin material deposited in the ground where the explosions take place. This hypothesis is confirmed by the calculation of the Enrichment Factors (EF) using Si as reference element. All these elements show EF close to 1. The resuspended soil dust concentration varies from 44 to 130 μg/m^3, while the background concentration is normally less than 10μg/m^3.

This work was supported by the Spanish Ministerio de Educación y Ciencia under the GRACCIE project. (Consolider-Ingenio 2010, program 22422).

New Year´s Day Fireworks: Elevated particle area and number concentrations at an urban background station in Germany 2009 - 2011

H. Gerwig[1], W. Pecher[1] and K. Wirtz[1]

[1]Section Air Quality Standards and Monitoring Methods, UBA – Federal Environmental Agency, 63225 Langen, Germany.

Keywords: tracheobronchial particle area, particle number, fireworks, New Year´s Day

For the protection of human health the European Union defined PM_{10}- and $PM_{2.5}$ limit values. But particle number and particle area become more important because of epidemiological studies and toxicological studies giving evidence of its negative health effects (Knol *et al.*, 2009).

Traffic is supposed to be one of the largest sources of particle number concentrations (Birmili *et. al.*, 2009, Löschau *et al.*, 2010). Also fireworks are known sources for elevated particle mass concentrations (Ponten *et al.* 2003) but result only in combination with low wind speed and bad air exchange to an exceedance of the daily PM_{10} limit value (Branis, 2003).

During New Year's Eve and New Year´s Day (NYD) in Germany in almost all parts of the country fireworks are ignited in large quantities. Most of these activities take place before and after midnight. The same day is often characterised by low number of vehicles during the whole year. Only 50 % of the average number of vehicles was observed during NYD compared to the average of other days of a year in Dresden, Germany (Gerwig, 2005).

Table 1 average, max. particle number and tb area conc. in 2009 and 2010; max minute conc. during New Year's Day 2009 - 2011.

1-h av.	NSAM $\mu m^2 \cdot cm^{-3}$	UCPC $p \cdot cm^{-3}$
av. 2009	6.1	10 600
av. 2010	5.8	11 200
max. 2009	33	65 000
max. 2010	26	65 000
max 1 min av.		
NYD 2009	89	57 000
NYD 2010	17	22 000
NYD 2011	49	35 000

The urban background station was situated in Langen, Germany: 15 km south of Frankfurt a. M. with residential areas to the south and west. Two different particle measuring instruments (TSI Inc.) were running continuously (12-08 – 01-11, 1 min av.) on a rooftop at 14 m above ground with cut of at 1 µm. Meteorological data was collected by WS600 (LUFFT GmbH).

- Deposited tracheobronchial (tb) particle area 0 - 1000 nm: NSAM.
- Particle number concentration 3 - 1000 nm: UCPC 3776.

From 2008 to 2009 the average concentration (s. Tab. 1) of tb particle area was about 6 $\mu m^2 \cdot cm^{-3}$ and particle concentration 11 000 $p \cdot cm^{-3}$.

During NYD 2009 max. 1 min av. of 89 $\mu m^2 \cdot cm^{-3}$ tb particle area concentration was detected accompanied with lowest wind speed (< 1 m s^{-1}) and wind from a nearby residential area. Temperature was between -7 to -1 °C.

During NYD 2011 the tb particle area concentration rose by a factor of ten compared to time periods before and after fireworks. In NYD 2011 wind came also from residential area but higher wind speed of 2 $m \cdot s^{-1}$ occurred.

During NYD 2010 the lowest max. tb particle area was observed while wind came not from residential areas at wind speed of 2 $m \cdot s^{-1}$.

We found, that NYD fireworks from a residential area is a source for elevated particle area and particle number concentration at an urban background station.

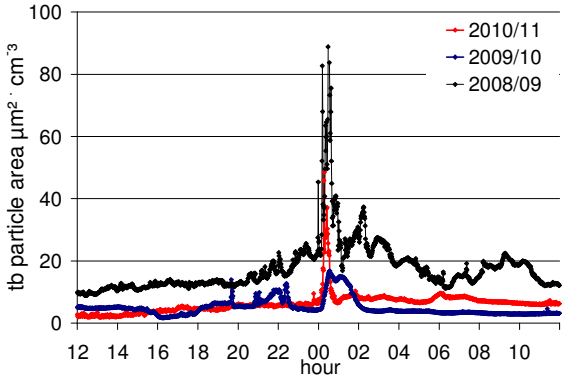

Figure 1 Tracheobronchial particle area in $\mu m^2 \cdot cm^{-3}$, 31-12-XX – 01-01-YY.

Birmili, W. *et al.* (2009), *Gef .Reinh. Luft*, **69**, 31–35.
Branis, M. (2003*), J. Aerosol Sci.,* **34**, S697-698.
Gerwig, H. (2005), Korngrößendifferenzierte Feinstaubbelastung in Straßennähe in Ballungsgebieten Sachsens, report from LfULG.
Knol, A. B. *et al.* (2009), *Part. Fibre Tox.*, **6**, 19.
Löschau, G. *et al.* (2010), *Gef. Reinh. Luft,* **70**, 183 – 187.
Ponten, D. *et al.* (2003), J. Aerosol Sci. **34**, S709-710.

Tuesday, September 6, 2011

Session 4P: Poster Session A:
Aerosol-based Nanotechnology

Size-selected Ag nanoparticle clusters deposited on carbon nanotubes

T. Shinohara, N. Nishida, H. Tanaka

Institute of Science and Engineering, Chuo Univ. 1-13-27 Kasuga, Bunkyo-ku, Tokyo, 112-8551, Japan

Keywords: Ag nanoparticle cluster, carbon nanotube, cluster number, fission.

Presenting author email: hnznshubiduba1354@yahoo.co.jp

Nanoparticle clusters which are composed of nanoparticles are expected to open a new world of the nanomaterials because of their characteristic structures. For example, we have synthesized Ag nanoparticle clusters which can be regarded as a combination of surface-active Ag nanoparticles and surface-inactive C_{60} nanoparticles [1]. In this study, we have investigated the deposition of the Ag nanoparticle clusters onto carbon nanotubes. Cluster number of the Ag nanoparticle clusters was selected by a differential mobility analyzer (DMA). Their structures were analyzed by scanning transmission electron microscope (STEM).

Ag nanoparticles were produced by a gas aggregation method and were passed through C_{60} vapor. The nanoparticles thus produced were admitted into an ionizer equipped with radioactive ^{241}Am and were size-selected by a DMA. The selected nanoparticles were electrically collected onto CNT deposited on a Mo grid, and were analyzed by STEM. Number of the constituent Ag nanoparticles was estimated from the STEM images. In addition, number for the intact nanoparticle clusters themselves was also estimated for the clusters collected directly onto a collodion-coated Cu grid.

As shown in fig 1 (a) , the number for the isolated cluster on CNTs is observed to be smaller than that for the intact nanoparticle clusters. This indicates that the gas-born nanoparticle clusters dissociate some nanoparticles when they were deposited onto the CNTs.

On the other hand, the number for the two clusters located at nearest neighbor is good agreement with that for the intacts. This agreement indicates that fission of the nanoparticle clusters proceeds in the deposition process.

In addition, the number for the three clusters located at nearest neighbor is found to be larger than that for the intacts. This indicates that the nanoparticle clusters are not fragmented into three or more.

[1] Tanaka, H. and Maeda, F. (2009) *Chem. Phys. Lett.* **484**, 37-40.

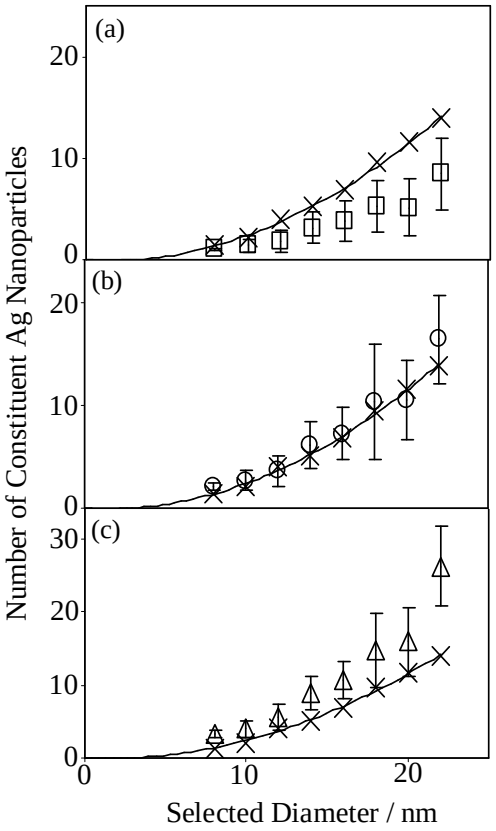

Figure 1. Diameter dependence of number of the constituent Ag nanoparticles for (a) isolated clusters, (b) two clusters located at nearest neighbor , and (c) three clusters located at nearest neighbor. The plots (×) and solid lines exhibit number for the intact nanoparticle clusters themselves.

Chiroptical property of Ag triangular nanoplate protected by chiral molcules

Y. Kojima, N. Nishida and H. Tanaka

Institute of Science and Engineering Chuo University, 1-13-27 Kasuga Bunkyo-ku, Tokyo, 112-8551, Japan

Keywords: chirality, Ag-triangular nanoplate, circular dichroism spectra, surface plasmon resonance.

Presenting author email: yacchi.kojima@gmail.com

Ag triangular nanoplates have attracted much attention because their specific structure induces the novel optical properties such as surface plasmon resonance (SPR) which is different from Ag nanoparticles. On the other hand, metal nanoparticles protected by chial molecules have also attracted much attention because their chiroptical property is specifically different from the chiral molecules themselves. In this study, we have synthesized Ag triangular nanoplates protected by chiral molecules. Produced nanoplates were analysed by scanning transmission electron microscope (STEM), optical absorption spectroscopy and circular dichroism (CD) spectroscopy.

Ag triangular nanoplates were synthesized under irradiation of ultraviolet lights for $AgNO_3$ ethanol solution in the presence of PVP at room temperature as described previously [1]. The Ag nanoplate solution was mixed with methanol solution of enantiopure D-form penicillamine (D-Pen). After the mixed solution was stirring, precipitation with dark blue was formed. This precipitation was further washed with ethanol. The structure of the products thus obtained was analyzed by STEM. In addition, water solution of the products was measured using UV-Vis spectrometer and CD spectrometer. In addition, the products using L-Pen instead of D-Pen were also examined in the same procedure.

Figure 1 shows typical STEM image of the products. The triangular nanoplates with 130 nm are observed in the STEM image. Because this shape is the almost same as that for the Ag triangular nanoplates before the addition of D-Pen, the addition process of D-Pen does not affect on the structure of the nanoplates.

Since the nanoplates added with D-Pen were well dispersed with water, the products are found to have hydrophilic property. Taking into consideration that the nanoplates before the addition of D-Pen were decomposed by water [1], this hydrophilic property indicates that the produced nanoplates were protected by D-Pen molecules which are known as hydrophilic molecules.

When absorption spectrum for the nanoplates added with D-Pen was measured, characteristic absorption was observed. Because this can be ascribed to the SPR for the Ag triangular nanoplates, shape of the nanoplates does not be affected by the water dispersion.

When CD spectrum for the nanaplates addition with D-Pen was measured, two major cotton effects differs from that for the D-Pen molecules themselves, these effects are considered to be induced by protection of D-Pen molecules. In fact, CD spectrum for the nanoplates added with L-Pen, was measured as almost mirror-image one for that with D-Pen. This observation supports that the observed Cotton effects are induced by the protection.

In summary, Ag triangular nanoplates protected by the D-/L-penicillamine were successfully synthesized by the present method. Their chiroptical property is induced by the protention of D-/L-penicillamine.

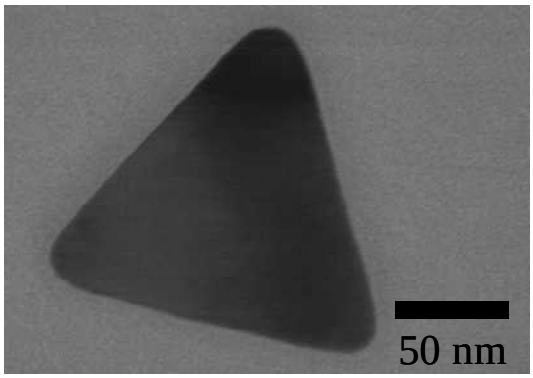

Figure 1. STEM image of precipitates obtained by addition of D-Penicillamine.

[1] H. Murayama, N. Hashimoto, H. Tanaka, *Chem. Phys. Lett.*, 482 (2009) 291.

Relationship between the geometrical length and mobility diameter of airborne carbon nanotubes

Y.K. Bahk[1, 2], J. Buha[1, 2], Z. Liu[3], D.Y.H. Pui[3] and J. Wang[1, 2]

[1]Institute of Environmental Engineering, ETH Zurich, Zurich, ZH, CH-8093, Switzerland
[2]EMPA, Dubendorf, ZH, CH-8600, Switzerland
[3]Department of Mechanical Engineering, University of Minnesota, Minneapolis, Minnesota, MN55455, USA
Keywords: airborne CNTs, geometrical length, mobility diameter, CNTs dispersion.
Presenting author email: ykbahk@ifu.baug.ethz.ch

In recent years, various kinds of engineered nanoparticles are used in a large number of applications such as sports equipments, semiconductor devices, etc. Carbon nanotubes (CNTs) are well known as the structual material for industrial composites. Due to its geometrical similarity with asbestos, airborne CNTs are important in inhalation exposure studies, air pollution and atmospheric sciences (Wang et al, 2011). This paper presents results of dipersion of carbon nanotubes (CNTs) and relation between the geometrical length and electrical mobility size of airborne CNTs. The relationship between the length and mobility size of CNTs is significant for a real-time measurement of airborne nanoparticles.

Experimental results of different types of CNTs, including multi-walled CNTs (MWCNTs) with diameters of 40 – 45 nm and 80 – 90 nm, and single-walled CNTs (SWCNTs) with diameters of 5 -10 nm, are reported in the study. These CNTs were aerosolized from suspensions with either atomizer or electrospray. For example, MWCNTs Baytubes, BMS, Germany with diameters about 40 – 45 nm were dispersed in different solvents using the nitric acid refluxing method. An atomizer was used to generate airborne MWCNTs with solvents such as DI water, ethanol and isopropyl alcohol (IPA).

In order to classify the generated airborne CNTs, differential mobility analysers (DMAs) are used. The mobility size distribution of airborne CNTs was also measured with the scanning mobility particle sizer (SMPS). Classified CNTs are collected on Nuclepore track-etched membranes (Pore size 400nm, whatman, UK) and analysed with scanning electron microscopy (SEM). Collected CNTs are also measured with transmission electron microscopy (TEM).

Experimental results show that MWCNTs suspensions in IPA provided better and longer dispersion condition than in other solvents. The mode of the mobility size distribution was 60-65 nm as shown in Fig. 1. Classified CNTs were collected at several points in the mobility size range from 65nm to 300 nm. Fig.2 shows SEM image of collected MWCNTs with 75 nm mobility size. Length of the CNTs was obtained by SEM and TEM analysis. For each mobility size, the average length of a large number of collected CNTs was estimated.

These results were compared with theoretical model. Kim et al. (2007) developed a model for the mobility size of nanowires. Vainshtein and Shapiro (2005), Lall and Friedlander (2006) developed models for the mobility size of agglomerates. The results of these models for straight chain type of agglomerates are used to approximate CNTs. Comparison with our experimental results show that the models give satisfactory results with proper choices of parameters.

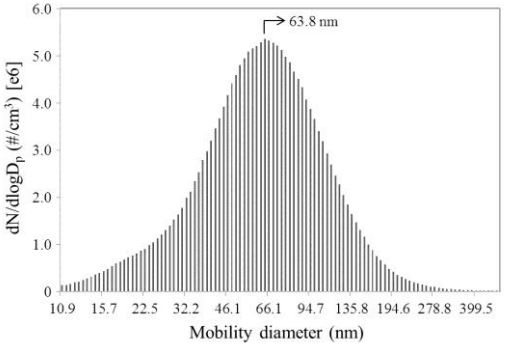

Figure 1. The mobility size distribution of airborne MWCNTs in IPA solvent.

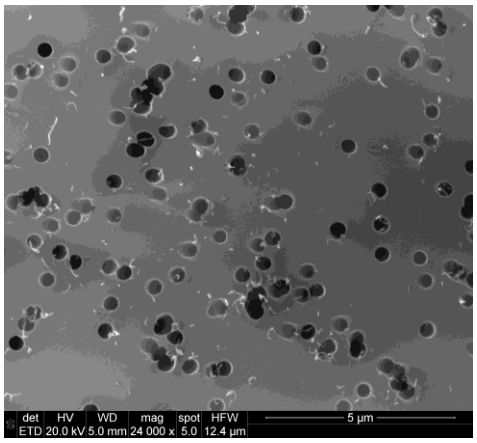

Figure 2. The SEM image of collected airborne MWCNTs with 75 nm mobility size.

Kim, S. H., Mulholland, G. W., and Zachariah, M. R. (2007) *J. Aerosol Sci*. **38**, 823-842.

Lall AA, Friedlander SK (2006) *J. Aerosol Sci*. **37**, 260-271.

Liu, J., Rinzler, A. G., Dai, H., Hafner, J. H., Bradley, R. K., Boul, P. J., Lu, A., Iverson, T., Shelimov, K., Huffman, C. B., Rodriguez-Macias, F., Shon, Y. S., Lee, T. R., Colbert, D. T. and Smalley, R. E. (1998) *Science* **280**, 1253-1256.

Vainshtein, P., and Shapiro, M. (2005) *J. Colloid Interface Sci.* **284**, 501-509.

Wang, J., Kim, S. C. and Pui, D.Y. H. (2011) *Aerosol Science and Technology* **45:3**, 443 – 452.

Peculiarities of particle generation by laser ablation of nickel

V. Dudoitis, V. Ulevicius, G.Raciukaitis and N. Spirkauskaite

Center for Physical Sciences and Technology
Vilnius, LT-02300 Lithuania
Keywords: laser ablation, nanoparticles, formation, size distribution.
email: ulevicv@ktl.mii.lt

Laser ablation is attracting even an increasing attention as a new technique to prepare nanoparticles from the metals, which has been widely used for a variety of applications in the science and technology, for example, nickel particles as magnetic materials for information storage Liu *et al* (2007), Gonzalez *et al* (2007), Lee and Chang (2004). However, a series of characteristics of the generated particles by laser ablation are not fully known. The investigation of the particle formation kinetics in the ambient air during the laser processing are essential to understand the mechanism of their formation. The aim of this study was to characterize the difference of particle formation by laser ablation of nickel due to the laser irradiation type (ns, ps) in varied media.

Particle-free ambient air or the argon gas were delivered to a closed dynamic chamber. Two different types of lasers were used: one with the nanosecond (NL640, λ=1064 nm, τ=15 ns), another with the picosecond (PL10100 λ=532 nm, τ=10 ps) pulse duration (both from Ekspla Ltd.). The lasers were working at a high pulse repetition rate (from 10 kHz to 100 kHz). Laser beam was steered at a scanning speed: 10 - 1000 mm/s.

The particle number concentration was measured with a condensation particle counter (UF-02) (cut-size at 4.5 nm) and their size distribution with the differential mobility particle sizer (ELAS-5MC) (working range: 10 – 200 nm). The average air temperature in the chamber was 25^{o}C (for argon 18^{o}C), the relative humidity of claen air 25 - 30%.

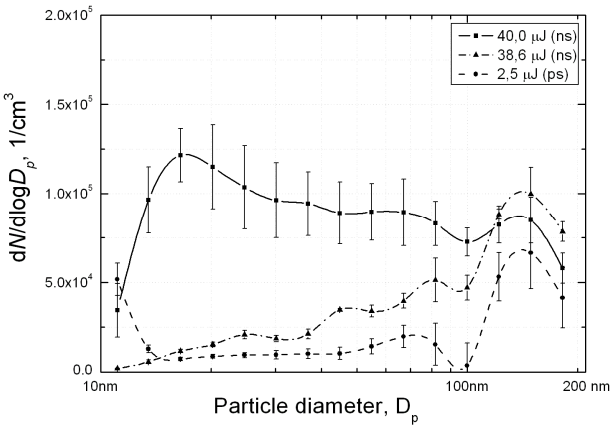

Figure 1. Dependence of generated particle size distribution on the laser pulse energy during the ns and ps laser ablation of nickel **in the ambient clean air**.

Nanosecond and picosecond lasers' ablation data gave different aerosol formation results. It was observed in experiments with picosecond laser ablation that applied pulse energy, repetition rate and beam scanning speed had influence on particle formation (Figs. 1,2).

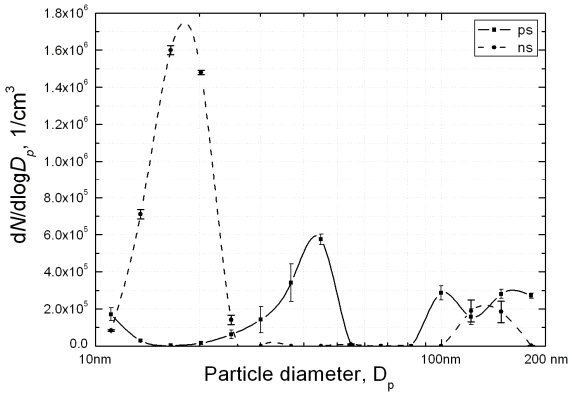

Figure 2. Dependence of generated particle size distribution on laser pulse energy during the ns and ps laser ablation of nickel **in the argon gas**.

The particle size distribution of generated particle varied in shape and concentration due to the applied laser parameters: pulse duration, energy and repetition rate, and beams scanning speed. Wide size particle distribution (Fig. 1) during the ns laser ablation in the ambient clean air can be related with the influence to the particle formation processes from gas phase and futher condensation and coagulation. The most intensive nickel particle generation in ambient air was observed with these nanosecond laser parameters: 10 kHz, 200mm/s (Fig.1). Very different particle size distribution of the nickel was observed in the argon gas. Increase pulse energy led to the formation of a narrow size distribution of the nanoparticles in the argon gas (Fig.2).

This research has shown that the aerosol particle size distribution and concentration depend on laser characteristics, laser operating parameters and the target material. The methods of aerosol measurement were able to monitor variations in particle size distribution, depending on the processing parameters and varied media.

Liu, B., Hu, Z., Che, Y., Chen, Y. and Pan, X. (2007) *App. Phys. Lett.* **90**, 044103.

Gonzalez, J.J., Liu, C., Wen, S.-B., Mao, X. and Russo, R.E. (2007) *Talanta* **73**, 567-576.

Lee, D.-W. and Cheng, M.-D. (2007) *J. Aerosol Sci.*, 35, 1513-1526.

Binary CoO_x/SiO_2 nanoparticle synthesis

P. Moravec[1], J. Smolík[1], S. Bakardjieva[2] and V.V. Levdansky[3]

[1]Institute of Chemical Process Fundamentals AS CR, v.v.i., Prague, 16502, Czech Republic
[2]Institute of Inorganic Chemistry AS CR, v.v.i., Husinec Řež, 25068, Czech Republic
[3]Heat and Mass Institute NASB, Minsk, 220072, Belarus

Keywords: binary nanoparticle generation, metal organics CVD, hot wall tube reactor.
Presenting author email: moravec@icpf.cas.cz

Cobalt and cobalt oxide nanoparticles have attracted substantial research effort in recent years because of their potential applications such as protective materials, catalysts, magnetic data recorders, batteries and gas sensors (Jang *et al.*, 2004). Nanoparticles are frequently coated with SiO_2 to improve their functionality and biocompatibility (Teleki *et al.*, 2008). In this work, we studied CoO_x-SiO_2 binary nanoparticle synthesis by metal organics chemical vapor deposition (MOCVD) using organo-compound precursors cobalt acetyl acetonate (CoAA) and tetraethyl orthosilicate (TEOS).

Particles were synthesized in an externally heated tube flow reactor with i. d. 25 mm and the length of heated zone 1 m. Experiments were performed in an inert atmosphere using nitrogen as a carrier gas (pyrolysis) as well as in oxidizing atmosphere at 10 vol. % of oxygen in the reaction mixture (oxidation). Particle production and their characteristics were studied in dependence on reactor temperature (T_R), concentrations of precursors (P_{CoAA}, P_{TEOS}), oxygen concentration (c_O), and reactor flow rate (Q_R). Precursor concentrations were controlled by the variation of the saturator temperature (P_{CoAA}) or by carrier gas flow rate through the saturator (P_{TEOS}). The particle production was monitored by scanning mobility particle sizer (SMPS, TSI model 3936) and samples for particle characterization were deposited onto TEM grids using nanometer aerosol sampler (NAS, TSI model 3089) and on Sterlitech Ag filters. Particle characteristics were studied by HRTEM, SAED, EDS, XRD and XPS.

The particle production was affected by all investigated parameters, in particular by concentrations of precursors (P_{CoAA}, P_{TEOS}). Particle characteristics were predominantly a function of the chemistry of precursor decomposition, but they were also affected by reactor temperature and concentration of precursors. At lower T_R, particles had broader size distribution, typically from 5 to 25 nm, at T_R 900 °C, the typical particle size varied between 5 and 10 nm.

Particles produced by pyrolysis were XRD amorphous and selected area electron diffraction (SAED) patterns were usually rather week. HRTEM images revealed lattice fringes in the cores of particles, which were typically indexed as hexagonal Co or, in some cases, cubic Co_3O_4. Samples prepared by oxidation showed much better developed SAED patterns and also XRD confirmed cubic CoO and cubic Co_3O_4 crystalline structures. XPS analysis showed Si in the oxide state in the surface layer of particles prepared both in an inert and oxidizing atmosphere. Co-O bonds were identified in the samples prepared by oxidation and mixture of Co-Co and Co-O as well as C-CH_x, C-O and C=O bonds were detected in particles prepared by pyrolysis.

From the above mentioned we can conclude that Co nanoparticles encapsulated in SiO_2 and partially decomposed CoAA were synthesized in an inert carrier gas, and mixture of CoO and Co_3O_4 covered by SiO_2 were prepared in an oxidizing atmosphere.

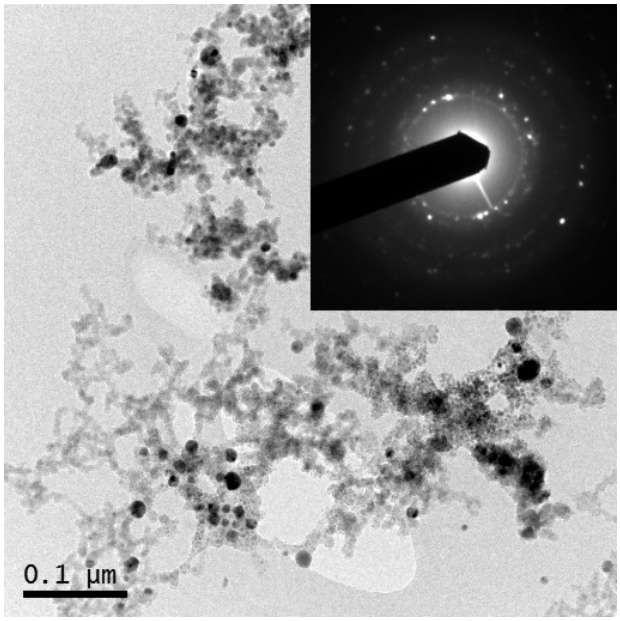

Figure 1. HRTEM image and SAED pattern of particles prepared at T_R=700°C, c_O=10 vol. %, P_{CoAA}=0.32 Pa, P_{TEOS}=1.89 Pa, Q_R=800 cm^3/min.

This work was supported by the Grant Agency of the Czech Republic under grants 104/07/1093 and P503/11/2315. XPS analyses were performed by Dr. Josef Zemek, Institute of Physics AS CR, v.v.i. and XRD analyses by Dr. Petr Bezdička, Institute of Inorganic Chemistry AS CR, v.v.i.

Jang, H. D., Hwang, D.W., Kim, D.P., Kim, H.C., Lee, B.Y. and Jeong, I.B. (2004). *Mater. Res. Bull.*, **39**, 63-70.

Teleki, A., Heine, M.C., Krumeich, F., Akhtar, M.K. and Pratsinis, S.E. (2008), *Langmuir*, **24**, 12553-12558.

Laser diagnostics based flame characterization of a flame spray pyrolysis process

Sascha R. Engel[1,2], Yi Gao[1,2], Andreas F. Koegler[1], Daniel Kilian[3], Thomas Seeger[2,4], Wolfgang Peukert[3] and Alfred Leipertz[1,2]

[1]Institute of Engineering Thermodynamics, University of Erlangen-Nuremberg, Erlangen, Bavaria, 91058, Germany
[2]Erlangen Graduate School in Advanced Optical Technologies, University of Erlangen-Nuremberg, Erlangen, Bavaria, 91052, Germany
[3]Institute of Particle Technology, University of Erlangen-Nuremberg, Erlangen, Bavaria, 91058, Germany
[4]Institute of Engineering Thermodynamics, University of Siegen, Siegen, North Rhine-Westphalia, 57072, Germany
Presenting author email: sascha.engel@ltt.uni-erlangen.de

For the production of nanoparticles at a commercial scale flame processes are most frequently used [Kammler, 2001]. Despite the simplicity of the set-up, the process control is rather complex. Consequently, a profound knowledge of the particle formation mechanism during combustion in dependence of process conditions is required. As minor changes of the process parameters may have a huge impact on the product, there is a huge demand for non-invasive advanced optical measurement tools.

We have studied the formation of silica from a Hexamethydisiloxane (HMDSO) precursor dissolved in ethanol [Mädler, 2002]. Figure 1 shows the burner and the schematic diagram of the process.

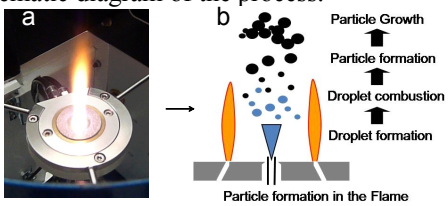

Figure 1. a) burner (Tethis NPS 10); b) particle formation in the flame

As a first step the flame shape was characterized by chemiluminescence imaging under various conditions. Therefore the integral OH chemiluminescence signal was imaged on an ICCD camera for different flame conditions. Furthermore the distribution of the liquid ethanol regime was studied. Figure 2 shows OH chemiluminscence images on the left and an averaged Mie scattering image on the right.

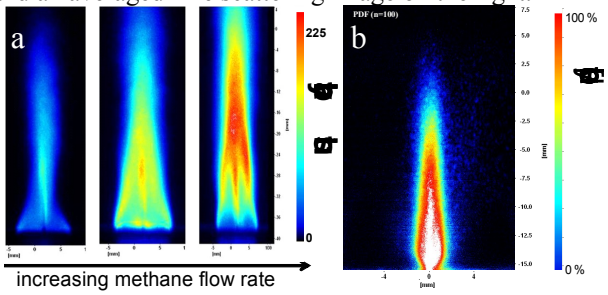

Figure 2. a) OH chemiluminescence images of the flame with increasing methane flow rate (from left to right); b) probability density function of 100 Mie scattering images

Averaged Mie scattering and chemiluminescence images provide complementary information about gas and the liquid phase distribution. These results allow the allocation of pointwise measured scalar quantities within the flame. Pointwise temperature information was achieved by using dual-broadband rotational CARS for oxygen. The CARS system used is based on a multimode frequency-doubled 30 Hz Nd:YAG laser system (Spectra Physics, PRO 250-30) with a pulse energy of 500 mJ at 532 nm. 90 % of the energy was split off to pump a broadband dye laser (DCM). The dual-broadband rotational CARS signal was generated by two broadband dye laser beams and one frequency-doubled Nd:YAG laser beam. The DCM dye, centered around 630 nm with a width of 500 cm^{-1}, produced approximately 25 mJ per pulse. In order to obtain high spatial resolution in the point measurements, a three-dimensional BOXCARS configuration with a focusing lens of f = 300 mm was used. The probe volume was measured to 2 mm. A sanity-check proved that the probe volume is sufficiently small to resolve the dimension of the flame. The CARS signal was dispersed by a 0.5-m spectrograph (Triax 550) equipped with a 2400 g/mm grating and recorded by a CCD camera (PCO 2000). Beside gas temperature results by using the RCARS spectra of oxygen also diffusion of nitrogen at some flame positions could be observed and quantified. Temperature and composition evaluation from CARS spectra has been done with a computer code which compares the experimental spectra with a spectrum out of a pre-calculated library.

The obtained data reveals the location where nitrogen of the surrounding air penetrates the flame, respectively the liquid ethanol regime. Furthermore, the influence of evaporative cooling of the ethanol on the flame temperature could be observed. In a nutshell the results show that the CARS technique is a strong tool to to gather relevant temperature and composition information within the spray combustion. Accordingly, significant improvements in the understanding of the flame spray pyrolysis could be achieved.

The authors gratefully acknowledge the funding of the German Research Council (DFG), which, within the framework of its 'Excellence Initiative' supports the Cluster of Excellence 'Engineering of Advanced Materials' at the University of Erlangen-Nuremberg.

Kammler H. K., Mädler L. and Pratsinis S. E. (2001), *Chemical Engineering & Technology* **24**, 583-596.
Mädler L., Kammler H. K., Mueller R. and Pratsinis S. E., *J. Aerosol Sci*. **33**, 369-389 (2002).

Exposure Measurement in an Industrial Production Facility for CNT-imbedded Nanocomposites

Wang, Jing[1,2], Thompson, Drew[3], Li, Lin[3] and Pui, David Y.H.[3]

[1]ETH Zurich, Institute of Environmental Engineering, 8093 Zurich, Switzerland
[2]Empa, Analytical Chemistry, 8600 Dübendorf, Switzerland
[3]Particle Technology Laboratory, University of Minnesota, Minneapolis, 55414, USA

Keywords: exposure, CNT, composite, dispersion.

The unique properties of carbon nanotubes (CNTs) have led to their increased usage in advanced materials. CNTs are used in structural composites for sporting equipment, conductive plastics, electron field emitters, semiconductor devices, etc. As more industries incorporate CNTs into consumer products the opportunities for worker exposure will rise. The National Institute of Occupational Safety and Health (NIOSH, US) plans to develop recommended exposure limits (RELs) for ultrafine titanium dioxide and CNTs for the period of 2009–2012 (NIOSH 2009).

We measured exposure in an industrial production facility for CNT-imbedded nanocomposites (Wang et al. 2011). In the extrusion operation, CNTs were mixed with melted polymer and other compounds to produce nanocomposite pellets. First polymer was melted and mixed with CNTs. The mixture was extruded from a die into a water bath. Cooled strands passed through a dryer before entering a cutter. The pieces were fed into a second extruder with CNT dispersing agent. At the exit of the second extruder the strands were pelletized. The pellets passed through a shaker and a cyclone for size selection.

A suite of instruments was used to obtain air-borne particle number concentration, surface area concentration, and size distribution data. The instruments were placed in the closed room near the extrusion system. The measurement results are shown in Fig. 1. Very high airborne concentrations were observed during full production of the CNT-embedded pellets. The particle number concentration increased to about 90,000 – 100,000 #/cm^3 and the particles were mainly in the range of 30 – 90 nm. We believe that volatile polymer fumes were a major particle source. This is corroborated by the observation that the particle concentrations were highest near the extrusion barrel and vapor was visible at the extrusion barrels.

We also used a filter to collect samples for electron microscopic analysis. We found a number of CNT agglomerates on the filter. The sizes of the CNT agglomerates are in the range of 1 µm to 20 µm. The individual CNTs are much smaller, with the diameter of about 40 nm. Further research is needed to find out the fraction of CNTs in the total particle concentration.

Dispersion plays a significant role in CNT studies as CNTs often form large agglomerates of the order of microns when provided by manufacturers. We developed an electrospray system to disperse and aerosolize CNT colloidal suspensions with controlled degree of agglomeration. The droplet size produced by electrospray can be monodisperse in the range of 20 to 500 nm and controllable by varying the electrical properties of the liquid and the liquid feed rate. The aerosolized CNTs were used in toxicity studies (Kim et al. 2010, Wang et al 2011).

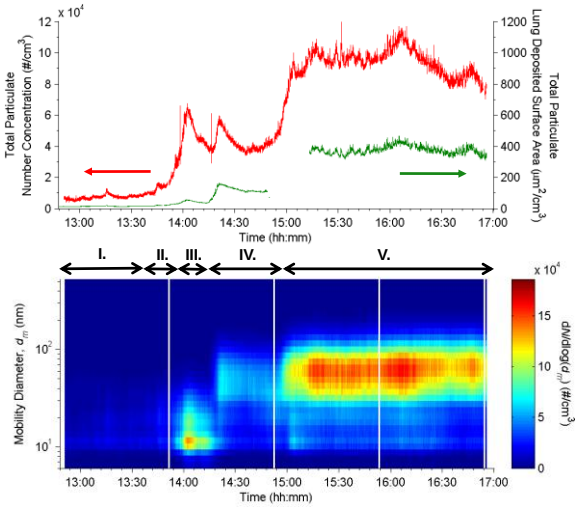

Figure 1. Measurement for air-borne particles during the extrusion operation for CNT-imbedded nanocomposites. Upper panel shows the total number concentration and lung-deposited surface area concentration; lower panel shows the evolution of the particle number-size distribution.

This work was supported by the US National Institute of Environmental Health Sciences under grant 1RC2ES018741-01 (sub-grant 100029-D) and US NSF grant (Award ID: 1056479).

Kim, et al. (2010) *Nanotoxicology*, 4(1), 42-51.

NIOSH (2009) Strategic Plan for NIOSH Nanotechnology Research and Guidance - Filling the Knowledge Gaps, DHHS (NIOSH) Publication No. 2010–105.

Wang, et al. (2011) *J. Nanoparticle Research*, DOI 10.1007/s11051-011-0236-z.

Optical online particle measurement in hot gases up to 450°C and in chemically aggressive gas components

M. Schmidt, S. Schütz

Palas® GmbH, Greschbachstr. 3b, 76229 Karlsruhe, Germany
Keywords: high temperature aerosols, combustion aerosols, particle size distribution, number concentration
Presenting author email: schmidt@palas.de

Currently the combustion and gasification fuels from biomass and the corresponding limitations concerning particle emissions are a point of scientific as well as public discussions. The quantity of particle emissions is depending on the process parameters and the particle separators used in the process. Their effect on the clean gas emissions is an example for the need of optical particle measurement systems in hot gases, which additionally may be contaminated with chemically aggressive gas components.

To avoid the condensation of tar which is produced in the gasification of biomass, the optical particle size and concentration measurement must be carried out in gas temperatures above 450°C. Otherwise the particle measurement may be falsified by condensation of tars or other gas components or by the aggregation of particles during or prior to the measurement.

The particle size and concentration measurement at these high temperatures is performed with the Promo® aerosol spectrometer system in combination with a newly developed welas® 2070 T470 aerosol sensor.

A further special advantage of this system is that the velocity of the particles carried by the gas flow is being measured simultaneously with the single particle measurement. Thus the values of measured concentrations can easily be calibrated with regard to the operating conditions.

The selection of appropriate materials for the sampling tubes and the gas flow inside the optical sensor can minimize corrosion effected by gas components as e.g. sulfuric acid or hydrochloric acid.

The problems occurring during particle measurement in hot gas flows as well as advantages and limitations of this measurement method are discussed. The measurement data is evaluated and presented in this paper.

Setup of the aerosol sensor:

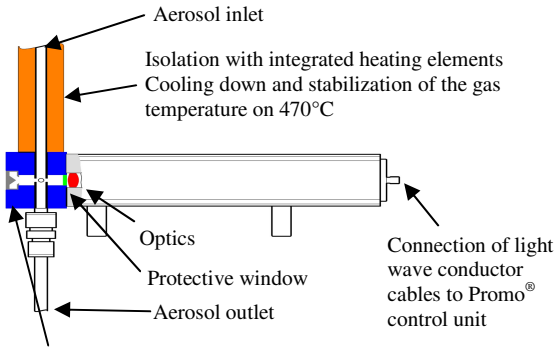

Ceramic application for aerosol guiding
+ Temperature resistant
+ Further down cooling of the aerosol temperature on approx. 450°C
+ Easy exchangeable integrated protection window
+ Easy detachable ceramic application for cleaning

Complete setup:

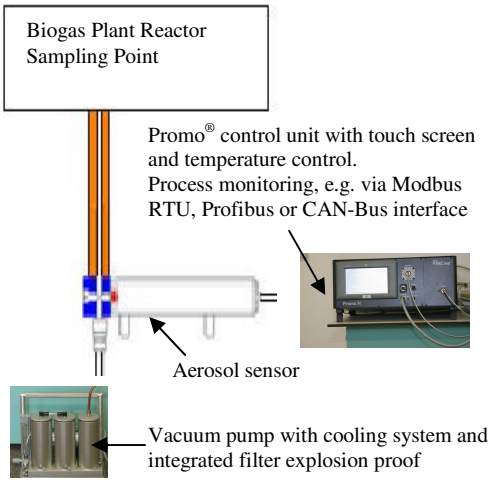

Leonie Brachert, Sokratis Sinanis, Karlsruhe Institute of Technology (2010);*Charakterisierung von Schwefelsäureaerosolen in technischen Prozessen*; 24th Palas® Aerosol Technology Seminar

Martin Schmidt, Palas® GmbH (2010); *Online control of production processes regarding particle size and concentration with optical aerosol spectrometers*; poster presentation at WCPT 2010

Near Real Time Characterization of Si-Nanoparticles from a Hot Wall Reactor with the Universal Nanoparticle Analyzer UNPA

H.G. Horn[1], C. Asbach[2], H. Fißan[2], M. Grose[3], T. Hülser[2], R. Jacob[4], J. Johnson[3], J. Jokiniemi[5], M. Mertler[4], J. Ruusunen[5]

[1]TSI GmbH, Aachen, 52068, Germany
[2]IUTA Institut für Energie- und Umwelttechnik e.V., Duisburg, 47229, Germany
[3]TSI Inc., Shoreview, Minnesota, 55126, USA
[4]BASF SE, Ludwigshafen, 67056, Germany
[5]University of Eastern Finland, Kuopio, 70211, Finland
Keywords: Nanoparticles, Aggregates, Agglomerates, Particle Characterization, Dilution.
Presenting author email: Hans-Georg.Horn@tsi.com

The Universal Nanoparticle Analyzer (UNPA) facilitates a new, on-line and near real time method to characterize airborne nanoparticles. Based on the parallel measurement of particle number concentration and particle charge concentration of DMA-classified nanoparticles, UNPA measurements and data analysis derive the agglomerate or aggregate number size distribution, information about the degree of agglomeration as well as the mean primary particle size of lose agglomerates (Wang et al., 2010).

First UNPA prototypes were built and evaluated by the University of Minnesota and by BASF Company. This lead to the development of a commercial version of UNPA by TSI Inc. In order to compare both instrument versions and to test the applicability of different sampling and dilution systems, measurements were made at the hot wall reactor at IUTA, Duisburg. During the tests, the hot wall reactor produced Si nanoparticles. For all selected conditions (C.1 to C.5, see Table 1), the temperature in the hot wall reactor was controlled at 1000 °C. The silane feed flowrate was either 1 l/min (C.1 to C.3) or 0.7 l/min (C.4 and C.5). Temperature after quench (~ 150 °C), pressure (~ 60 kPa) and process safety (high hydrogen content in the process gas) had to be considered for sampling and dilution: UNPA requires near ambient inlet conditions and optimum particle number concentration is 10^5 to some 10^6 cm^{-3}.

Table 1. Sampling and dilution configurations, silane feed flow rate, diluted aggregate particle number concentration and number mean aggregate diameter.

Condition	Sampling Configuration	SiH_4 Flowrate [l/min]	Total UNPA Concentration [cm^{-3}]	Mean Diameter [nm]
C.1	ED+DP	1.0	2.7e5 ± 1.1e4	208 ± 0.7
C.2	PRD+ED	1.0	2.7e6 ± 3.3e5	236 ± 0.5
C.3	PRD+ED	1.0	1.3e6 ± 7.0e4	239 ± 1.1
C.4	PRD+ED	0.7	1.4e6 ± 9.6e4	228 ± 1.1
C.5	CP+ED	0.7	8.8e5 ± 9.4e4	220 ± 2.1

For all 5 conditions, an ejector diluter (ED) was used to draw the sample from the process. Upstream of the ED, two different probes were tested: A porous tube diluter (PRD) provided by University of Eastern Finland and a coolable probe (CP) with integrated dilution provided by Karlsruhe Institute of Technology. Also tested (C.1) was a combination of the ED followed by a probe built by the University of Duisburg Essen with dilution right at the sampling probe tip and secondary dilution by a built-in ejector (DP). This probe had to be placed downstream of the ED because the built-in ejector was limited to an inlet pressure of approximately 85 kPa. Size distributions measured with UNPA operated in SMPS mode demonstrate that - at least from 50 to 300 nm - no significant differences in size-dependent transfer through the probes were observed. Dilution ratios were 510:1 (C.1), 190:1 (C.2, C.3 and C.4) and 300:1 (C.5).

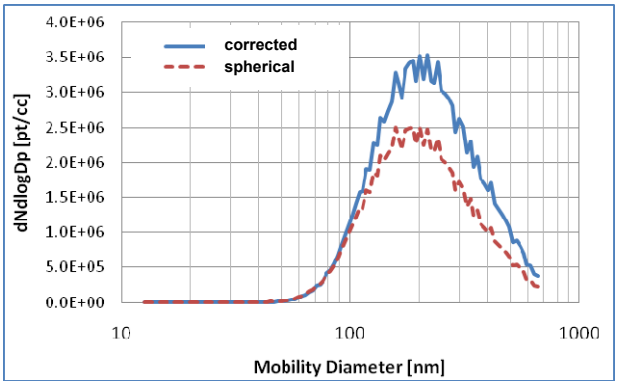

Figure 1. Spherical and corrected aggregate number size distribution, example taken from condition C.4

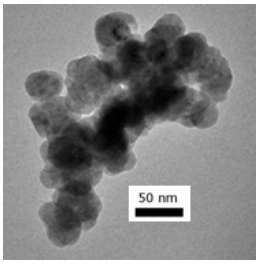

Figure 2. TEM example from Condition C.2

Figure 1 shows an example for UNPA size distribution correction due to particle structure. UNPA measurements also indicate that the analyzed Si-particles have a relatively open structure, as confirmed by TEM images (see Figure 2). Mean *primary* particle sizes reported by UNPA were around 25 nm (C.2 to C.5) and 34 nm (C.1). These diameters were in good agreement with TEM analysis (e.g. 26±7 nm for C.2). Results from both UNPA instruments compared very well.

Wang, J., Shin, W-G, Mertler, M., Sachweh, B., Fissan, H., Pui, D.Y.H. (2010) *Measurement of Nanoparticle Agglomerates by Combined Measurement of Electrical Mobility and Unipolar Charging Properties*, Aerosol Sci. & Technology, 44, 97 – 108

Tuesday, September 6, 2011

Session 4P: Poster Session A:
Combustion Aerosols

Ultrafine particles in flue gas from waste-to-energy (WTE) plants

S. Cernuschi[1], M. Giugliano[1], S. Ozgen[1] and G. Ripamonti[1]

[1]DIIAR Environmental Section, Politecnico di Milano, Milano, 20133, Italy
Keywords: ultrafine particles, waste to energy plants, bag filter, condensable particulate matter.
Presenting author email: senem.ozgen@polimi.it

The research on the emission levels of particulate matter is recently focused on ultrafine (UFP) and nanoparticle size fractions, with dimensions included in the range from 0.1 µm down to few nm. Particular attention in this field has been paid to combustion activities, with most of the available investigations focused on vehicle sources and very few limited studies for stationary energy production systems.

Present work reports the main findings of extensive field investigations at four municipal waste-to-energy (WTE) plants, equipped with flue gas treatment configurations included in most recent Best Available Techniques reference options, and addressed to the evaluation of UFP stack emissions (EC, 2006).

Measurements were conducted with a specifically designed sampling line, assembled for evaluating UFP of primary as well as condensable origin and equipped with a dilution system and a particle counting device for measuring total particle number and size distributions at different dilution ratios (Figure 1) and for raw undiluted flue gases. Particle number concentrations and size distributions were measured with an electrical low pressure impactor (ELPI™), capable of giving values for 12 different size intervals in the range 7 nm - 10 µm.

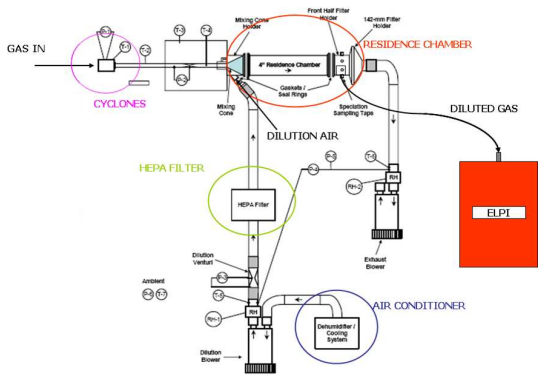

Figure 1. Scheme of dilution sampling and PM measurement system.

Mean number concentrations of UFP resulting from cold sampling tests are included between $5 \cdot 10^3$ and $3 \cdot 10^5$ particles cm^{-3}, with the ultrafine fraction largely prevailing in size distributions. Table 1 shows the average, minimum and maximum values of UFP concentration and the relative contribution of UFP to the total particle number emitted from the four WTE plants.

Results, as a whole, address also some differences arising from the flue gas treatment process design (FTPD), with the utilization of wet scrubbing that seems to affect the presence of primary UFP as well as their formation from condensable origin with respect to dry treatment systems.

Table 1. UFP number concentration (cm^{-3}).

Plant ID	FTPD	UFP concentration (cm^{-3})		%UFP
		average	min-max	
WTE1	dry	1.3E+04	$1.8 \cdot 10^3$ - $5.6 \cdot 10^4$	95%
WTE2	dry	5.3E+03	$3.7 \cdot 10^2$ - $4.2E \cdot 10^4$	93%
WTE3	dry+wet	5.8E+04	$1.2 \cdot 10^4$ - $1.3 \cdot 10^5$	95%
WTE4	dry+wet	2.7E+05	$1.0 \cdot 10^4$ - $5.0 \cdot 10^6$	97%

FTPD: Flue Gas Treatment Process Design

Finally, measurements across a pilot scale fabric filter demonstrate very efficient removal in the UFP size ranges of interest, with extended capabilities for reducing the emitted particles from condensable origin (Figure 2).

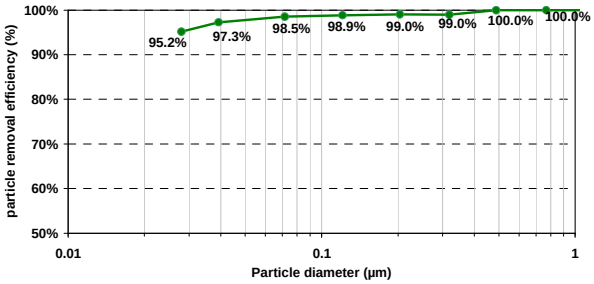

Figure 2. Bag filter submicron particles removal efficiency.

The research program was conducted by LEAP (Laboratorio Energia e Ambiente Piacenza) and Politecnico di Milano with the financial support of FederAmbiente, Italian Federation of Public Environmental Services.

EC (2006). European Commission Integrated Pollution Prevention and Control Reference Document on the Best Available Techniques for Waste Incineration, August 2006.

Measurement of soot size distribution in flames by inversion of angular light scattering

Caumont-Prim C., Yon J., Coppalle A. and K.-F. Ren

UMR 6614 CORIA, Avenue de l'université, BP 8, 76801 Saint Etienne du Rouvray, France.

Keywords: soot particles, fractals, aggregates, light scattering
Presenting author email: yon@coria.fr

Soot particles are produced by combustion processes. Since a long time, these particles give rise to numerous investigations for their modelling and due to their important implications in human health, flame radiative transfer and climatic impact. Among other information, the determination of soot size distributions at different Height Above the Burner (HAB) in flames is essential. The soot size distribution is determined often by using ex-situ granulometers, after sampling of the particles. But the quenching of aggregation process in the sampling is difficult and raises the question of representativeness of the results (Ouf *et al.* 2010). For this reason, optical measurements are more adapted. By knowing the temperature of the flame, Dynamic Light Scattering technique permits to determine a mobility diameter. But without any more information, soot size distribution can't be derived by this technique. Moreover, soot particles are not spherical and their specific fractal morphology has to be taken into account. Thanks to a simple theory called Rayleigh – Debye – Gans for Fractal Aggregates (RDG-FA theory - Dobbins *et al.*, 1991), measurement of static light scattering can be interpreted in order to determine another size parameter called gyration radius. The inversion by this theory to infer the gyration radius of monodisperse aggregates has been recently validated (Caumont et al. 2010).

Some authors (Dobbins & Megaridis 1991, Köylü 1994) have proposed to determine a representative gyration radius of the polydisperse population with this optical technique. But two distinct radii can be calculated if particles are suspected to scatter only in Guinier or in Power Law regime and that assumption cannot be done without knowing the researched size distribution. Koylu & Faeth (1996) and Iyer *et al.* (2007) proposed an inversion method to calculate the characteristics of the soot size distributions by coupling scattering and extinction measurements. But this method relies on the knowledge of the soot optical index which is unfortunately not accurately known. That's why it is necessary to develop a new approach which doesn't need any primary knowledge.

The present work presents a new inversion method for the determination of the soot size distribution in flames by measuring the scattered light at different angles. It consists in determining for each studied angle, by using the RDG-FA theory, a gyration radius $Rg^*(\theta)$ of a monodispersed population of the same optical behaviour as that of the real polydisperse population.

The $Rg^*(\theta)$ function thus determined informs us polydispersity of the soot. For example, in monodisperse case, $Rg^*(\theta)$ must be constant. In contrary, the variation of this function informs us of the range of polydispersity. So, by supposing the nature of the size distributions (lognormal or self-preserving), it is possible to determine, by this technique, governing parameters of these distributions.

In the present study, that inversion method is proposed to determine the soot size distributions at different HAB in a laminar diffusion ethylene flame.

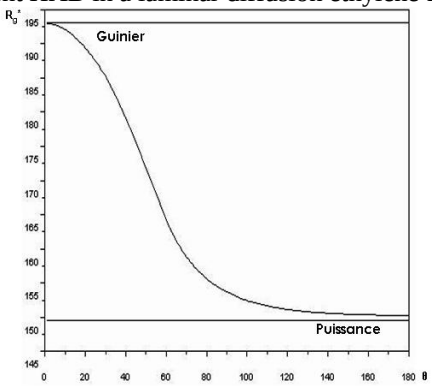

Figure 1. Theoretical dependence of Rg* to the scattering angle for a polydisperse population of soot.

Brasil, A.M., Farias, T.L. & Carvalho, M.G. (1999). *J. Aerosol Sci.*, 30 (10), 1379-1389

Caumont, C., Yon, J., Ren, K.-F., Coppalle, A. (2011). *Proc. 26ième Congrès Français sur les Aérosols*, Paris, France.

Dobbins, R.A., Megaridis, CM, *Applied Optics* (1991), 30 (33), 4747-4754.

Iyer S. S., Litzinger, T. A., Lee, S-Y, Santoro R. J (2007), *Combustion and flame*, 149 (1-2), 206-216.

Köylü, Ü, Ö, *Combustion and flame*, (1997), 109, 488-500.

Ouf, F.X., Yon, J., Ausset, P., Coppalle, A. Maillé, M. (2010). *Aerosol Sci. Technol.*, 44, (11), 1005-1017.

Methodology to determine carbonate carbon from Thermal Optical Transmittance measurements

M. R. Perrone[1], A. Piazzalunga[2] and M. Prato[3]

[1] CNISM, Physics Department, University of Salento, Via Arnesano, 73100 Lecce, Italy
[2] Department of Environmental Science, University of Milano Bicocca, 20126 Milano, Italy
[3] Department of Pure and Applied Mathematics, University of Modena and Reggio Emilia, Modena, Italy
Keywords: carbonaceous particles, aerosol chemistry, air pollution, TSP/PM2.5
Presenting author email:perrone@le.infn.it

Carbonate carbon (CC) is often not considered in atmospheric aerosol chemistry studies which comprise the measurement of elemental carbon (EC) and organic carbon (OC). The reason for this may be its low contribution to fine particle mass in most area along with the difficulties in its analytical determination in atmospheric aerosol collected on filter matrices. Carbonate particles are expected to significantly contribute to the Mediterranean PM mainly during the intrusion of air masses from North Africa. However, the CC fraction in particulate matter may not be negligible if high concentrations of mineral dust, either natural (natural erosion, sand storms) or originating from street abrasion or construction sites are present. Some thermal–optical methods have recently been used to determine carbonate carbon, along with different organic fractions and EC and it has been shown that the interference of CC with the signal of EC or OC may lead to overestimations of either of these two carbon fractions during thermal-optical analysis (Karanasiou et al., 2010). The use of a sample pretreatment with HCl fumes to eliminate CC prior to the thermal analysis is suggested to avoid the interference by carbonate particles. We have used the sample pretreatment to identify the CC contribution to the flame ionization detector (FID) signal from TOT measurements and implement a numerical procedure to determine CC, EC, and OC levels. The time evolution analysis of the FID signal before and after the treatment with HCl fumes of TSP and PM2.5 samples, has revealed that the CC peak may occurs within the 220-250 s time interval and that it is characterized by a full-with-at-half-maximum (FWHM) $\Delta t^* = 25\pm3$ s, in accordance with previous studies. We have assumed that the CC volatilization contributes to the FID signal with a pulse which can be fitted by a Gaussian function with the peak at the time t_i (within the 220-250 s time interval) and the FWHM width $\Delta t_i = 25\pm3$ s, to determine CC levels. In particular, we have calculated the Gaussian function area ascribed to the CC volatilization and the area of the calibration signal, to quantify CC levels in the analyzed PM samples. This calculation has been carried out through a fitting procedure, in which the FID signal is represented as a weighted sum of Gaussian functions, $S(t)$, through an algorithm implemented by ourselves in Matlab®. In fact, we have assumed that $S(t)$ can be represented by the following relationship:

$$S(t) = \sum_{i=1}^{N} a_i \, e^{-(t-t_i)^2/2\sigma_i^2} \qquad (1)$$

where a_i, t_i and σ_i represent amplitude, peak-time and standard deviation of the Gaussian function i and N represents the total number of Gaussian functions. The FID signal has at first been interpolated with cubic splines to obtain a straightforward calculation of its first and second derivatives. Then, through the analysis of the second derivative minima we have automatically identified the number N of Gaussian functions composing $S(t)$. A FWHM $\Delta t_i = 25\pm3$ s has been imposed to the Gaussian function ascribed to CC, in accordance with experimental results. We have assumed that CC level uncertainties are mainly due to the uncertainties of the parameters defining the Gaussian function fitting the CC volatilization signal. The implemented technique has been tested by determining CC, OC, and EC levels in 26 TSP and PM2.5 samples which have simultaneously collected over south-eastern Italy, in the Central Mediterranean. We have found that uncertainties on CC levels vary from 0.1% up to 9% and from 0.2% up to 20% in TSP and PM2.5 samples, respectively. It has also been shown that OC levels may be quite overestimated mainly in the coarse fraction, if the CC contribution is not accounted for. Figure 1 shows as an example Ca^{2+} and CO_3^{2-} levels (calculated from CC concentrations) in the 26 analyzed TSP samples. The good correlation between Ca^{2+} and CO_3^{2-} levels support the reliability of the implemented technique: carbonate-containing mineral dust is often associated with calcium. The anion deficit defined as an excess of positive charge, which is often found in Mediterranean PM samples, has been used in some Mediterranean studies to infer and estimate carbonate mass concentrations.

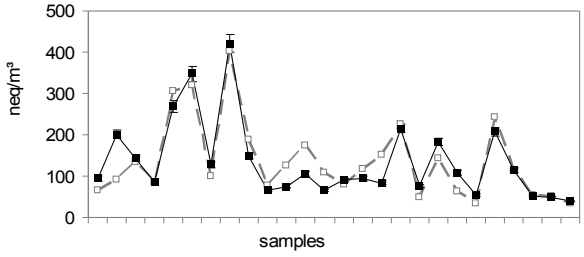

Fig. 1 Ca^{2+} (full boxes) and CO_3^{2-} (open boxes) levels (neq/m^3) in the 26 analyzed TSP samples

Work supported by “Progetto Strategico SIMPA”

Karanasiou et al., Atmos. Meas. Tech. Discuss., 3, 5375-5409, 2010.

Fluxes of volatile and non-volatile elements in small-scale biomass combustion systems

Torben Seidel & Hans Ruppert

Dept. of Sedimentology and Environmental Geology, Geoscience Center, Goettingen University, Goldschmidtstrasse 3, D-37077 Goettingen, Germany
Keywords: biomass burning, concentration, fluxes, heavy metals
Presenting author email: tseidel1@gwdg.de

The application of biomass as an energy supplier may play an essential future role due to the greenhouse effect, the shortage of fossil energy sources and the striving autonomy from fossil fuels. Biomass combustion in Europe is widely applied e.g. for residential heating in stoves and boilers and combined heat and power plants on an industrial basis. The growing contribution of biomass burning may have an adverse influence on its acceptance due to the arising emissions of harmful inorganic and organic substances inducing health problems.

Especially for in house burning facilities reliable measurements of concentrations and fluxes of heavy metals in the flue gas are lacking.

For a reliable reconstruction of element fluxes and for input/output balances, the originating ashes e.g. grate ash, heat exchanger ash and fly ash are collected. The manually fueled furnaces tend to have recovery rates way higher than 100% whereas automatically fuelled furnaces have recovery rates slightly lower than 100% of the theoretically ash content determined at 550°C.

To collect the hazardous fly ash, an innovative filter holder with a 150mm diameter consisting of PTFE was applied in our study. It guarantees sufficient material for the inorganic analysis and assures a low contamination background.

In the ideal case the amount of elements contained in the unburnt biomass should be identical with the combined element amounts in the different ash fractions. Especially the recovery rates of the environmentally or health relevant elements such as Cd, Zn, Sn, Tl, and Pb of burnt wood or straw in automatically fuelled furnaces are fairly low (Figure 1) suggesting that they leave the chimney as molecules or ultrafine particles. Other elements such as Co, Mo, Cr and Ni features likewise recovery rates lower than 100% attributed to a contamination of the fuel e.g. by an abrasion of the cutting mill at the preparation. Elements like Ca, Ti, Mn, Ba, Fe, REE (represented by La) and Zr have recovery rates higher than 100% indicating a contamination e.g. due to the refractory lining materials of the furnaces.

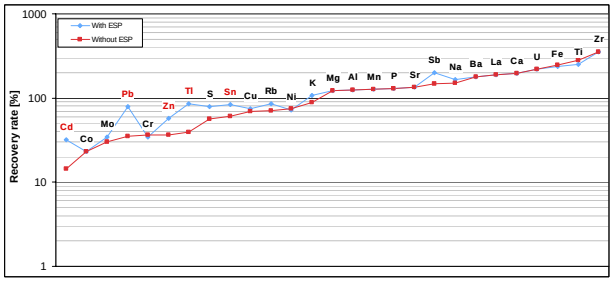

Figure 1. Recovery rate (%) of elements by burning wood-chips in a 30 kW boiler (combined element amounts in grate ash, internal heat exchanger ash, ESP ash and fly ash divided by the element amounts contained in the wood chips)

Electrostatic precipitators (ESP) in the exhaust gas stream can diminish the dust load e.g. from 55mg/Nm^3 to 18mg/Nm^3 at 13% O_2 respectively for a 30kW boiler fuelled by spruce wood-chips. Therefore the amount of risky elements can be diminished if the elements are bound on particles but not if they are in a gaseous state. Figure 2 shows the fluxes of a number of elements in a 30kW boiler with downstream ESP fuelled by spruce wood-chips. The application of an ESP decreases the dust load and lowers the emission of associated elements such us Cd, Zn, Pb, and Tl. Nevertheless, some fractions of the most volatile elements are not retained.

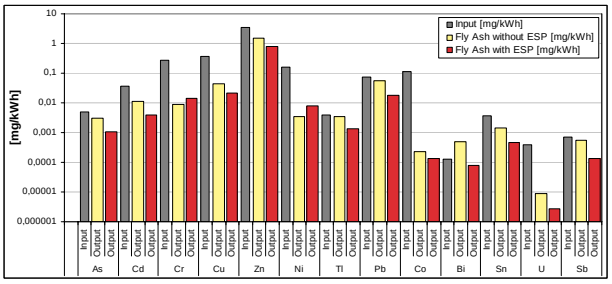

Figure 2. Input and fluxes [mg/kWh] of elements in a 30kW boiler fuelled by spruce wood-chips without and with ESP

A flue gas condenser (FGC) can diminish the dust load in the exhaust gas e.g. from 13mg/Nm^3 to 11mg/Nm^3 at 13% O_2 respectively for the same boiler fuelled by straw-pellets. The retention potential of a FGC for total suspended particulate matter is extremely slight. By enhancing the heat efficiency, however, it can slightly diminish the emission of dust and associated elements per energy unit (Figure 3).

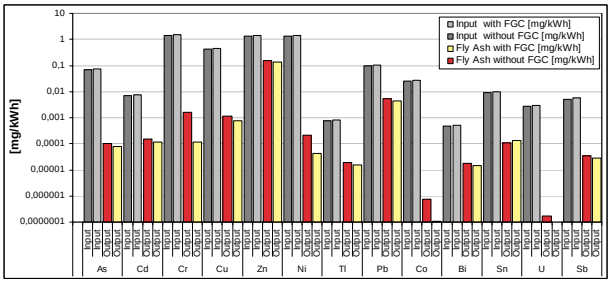

Figure 3. Input and fluxes [mg/kWh] of elements in a 30kW boiler fuelled by straw-pellets without and with FGC

A reduction of the dust load in the exhaust gas by applying secondary steps is connected with a decreased flux for most of the risky elements.

To assess the environmental impact of a furnace, fluxes of elements are much more relevant than simple concentration data. In addition, only element fluxes enable the comparison of emissions from different furnaces and fuels under different burning conditions, etc.

Chemical composition of smoldering combustion products of some forest materials and cellulose

S.A. Popova and V.I. Makarov

Institute of Chemical Kinetics and Combustion, Novosibirsk, 630090, Russia
Keywords: biomass burning, laboratory experiments, wood smoke, cellulose
Presenting author email: popova@kinetics.nsc.ru

Wild forest fires and prescribed burning are known as a powerful source of environmental pollution. Smoke emission, evolved by biomass burning, can produce effect on the chemical, optical, and radioactive properties of atmosphere, forest ecosystems, and various biological media (soil, water, plants, etc.). It is difficult to determine a reliable relation between the initial composition of forest combustible materials and the chemical composition of the resulting emission upon biomass burning when herbage, vegetative and soil cover burn. Since the capacity and composition of burning products depend on the type of combustible material, burning phase (flaming or smoldering), weather conditions, etc., of necessity are the laboratory experiments on the combustion of individual plant materials.

In the present work, the quantitative data on the chemical composition of gaseous products and particulate matter emitted by smoldering combustion of the dominating vegetation of the Siberian boreal forests (pine tree (Pinus sylvestris), Siberian larch (Larix sibirica), marsh tea (Ledum palustre), and lichen (Cladonia sp.)), are presented. Experiments were conducted using a modernized laboratory setup described by Edye and Richards (1991). However, as compared to (Edye and Richards, 1991), the smoke emitted was first deposited on a glass-fiber filter (particulate matter) and then frozen out by cooling at -50ºC (gaseous products). It is worth noting the gaseous products are the low-molecular organic substances condensed at low temperatures. The chemical composition of the smoldering combustion products of forest materials was determined by gas chromatography/mass spectrometry. Emission of carbon dioxide, carbon monoxide, methane and other gases was not measured.

It is experimentally demonstrated that during the smoldering combustion of the various types of forest material, 1-2% of the burnt plant biomass transform into particulate matter and almost the same is the amount of combustion products resulting from freezing.

Essential distinctions are observed in the composition of the smoldering combustion products of various materials. For example, guaiacol (2-methoxyphenol) and its substitutes, resin acids and other compounds are emitted by the smoldering combustion of pine tree and Siberian larch. Syringol (2,6-dimethoxyphenol) and its substitutes are emitted by marsh tea burning. The data obtained confirm conclusions (Simoneit *et al*, 1993) about the distribution of methoxyphenols with respect to the wood type, i.e., that the syringol derivatives are dominant in deciduous wood, and the guaiacol derivatives prevail in the coniferous one.

The absence of aromatic compounds in the lichen combustion products is assigned to the fact that there is no lignin in the cellular walls of mushrooms and algae. The content of levoglucosan in lichen smoke emission is shown to be much higher than that of other burnt materials.

In addition, we have studied the cellulose thermal degrade products. Note that furfural, produced by the freezing of combustion products, is one of the dominant components of forest materials and cellulose smoke emission (fig. 1.).

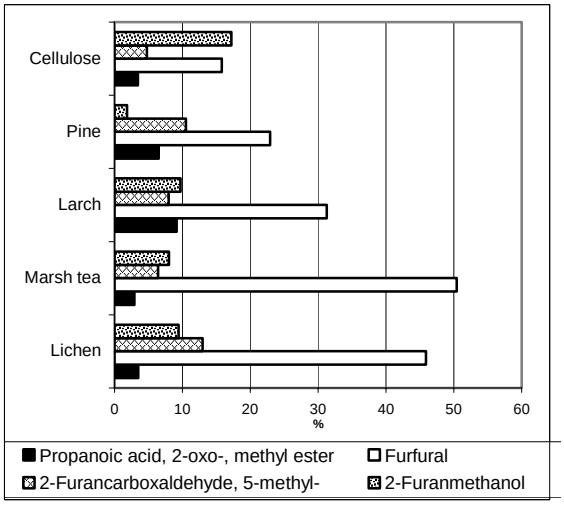

Figure 1. Distribution of organic substances in gaseous fraction.

The work was supported by the International Science and Technology Center (Project 3695) and the Russian Foundation for Basic Research (08-05-00083, 11-05-01025).

Edye, L. and Richards, G. (1991) *Environ. Sci. Technol.* **25**, 1133-1137.

Simoneit, B., Rogge, W., Mazurek, M., Standley, L., Hildemann, L. and Cass, G. (1993) *Environ. Sci. Technol.* **27**, 2533-2541.

Ti-Mn-Cu tri-metallic oxides for selective catalytic reduction of NO with NH_3 at low temperature.

Y.O. Park[2], K.H. Park[1], S.W. Kim[3], K.H. Baek[4] and W.S. Cha[4*]

[1]Department of Environmental Energy Systems Engineering, Kyonggi University, Suwon, Gyeonggi, 442-760, Korea
[2] Clean Fossil Energy Research Center , Korea Institute of Energy Research, Daejeon, 305-343, Korea
[3]Leadgenex, Co.
[4] Department of Environmental Engineering, Kusan National University, Kusan, Chunbuk, 573-701, Korea
Keywords: NOx, Low-temperature SCR, Ti-Cu-Mn, NH_3 oxidation
Presenting author email: wscha@kunsan.ac.kr

Selective catalytic reduction (SCR) of nitrogen oxides (NOx) with ammonia is one of the prospective process for cleaning the flue gas for stationary source. In this process, NOx contained in flue gases is reduced to N_2 and H_2O by ammonia:

$$4NO + 4NH_3 + O_2 \rightarrow 4N_2 + 6H_2O$$

It is well established commercial technology, which employing V_2O_5/TiO_2(anatase) promoted with WO_3 or MoO_3. The optimum operating temperature window of this catalyst is in the range of 300~400□, which makes necessary to reheat the flue gas after the electrostatic precipitator and de-sulfurizer(150~250□).

For the reasons above, there have been strong interests to develop high active SCR catalysts for low temperature(<250□). Success in developing such a catalyst would significantly improve the economics of SCR.

To increase the catalyst activity of manganese oxides, various transition-metal oxides were incorporated as a promoter, such as MnOx-CeOx, Cr-MnOx, Mn-Cu, Fe-Mn catalysts. Among the these catalyst, mixed oxides containing Cu and Mn as main metal element have been reported to be very active for complete oxidation reaction at low temperature. This can help the facile formation of NO_2 and promoted the NO reduction with ammonia at low temperature.

In our study, Mn-Cu bimetallic oxides and Ti mixed Ti- Mn-Cu tri-metallic oxides compared SCR activity for low temperature.

Table 1. Textual property and surface atomic concentrations determined by XPS of Mn-Cu and Ti-Mn-Cu catalysts.

Sample	SBET (m^2/g)	XPS atom(%)				
		Mn	Cu	O	Ti	Mn/Cu
Mn-Cu	195.4	18.8	8.4	72.8	-	2.24
Ti-Mn-Cu	141.1	21.9	9.5	66.1	2.4	2.31

Water vapour is one of the main components in the flow gas and frequently leads to catalysts deactivation. NOx conversions of Mn-Cu bimetallic oxides catalyst were decreased by water vapour. But Ti-Mn-Cu tri-metallic oxides catalyst which made by TiO_2 powder mixing is more resistant to water vapour.

On wet condition, adsorption O-H on surface of Mn-Cu bimetallic oxides promotes NH_3 oxidation. Beside, NH_3 is competitive adsorption with water vapour on Ti-Mn-Cu tri-metallic oxides.

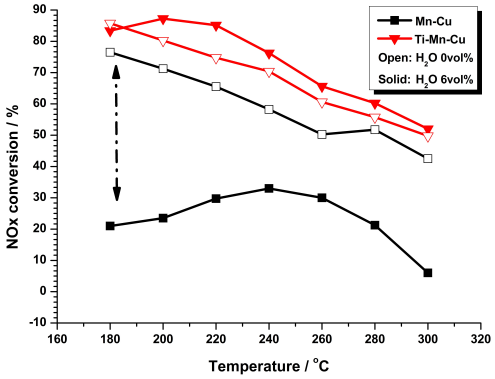

Figure 1. NOx conversion over Mn-Cu and Ti-Mn-Cu catalysts. Reactants: 800ppm NO, 800ppm NH_3, 3 vol.% O_2 and 0, 6 vol.% H_2O. GHSV was 60,000 hr^{-1}.

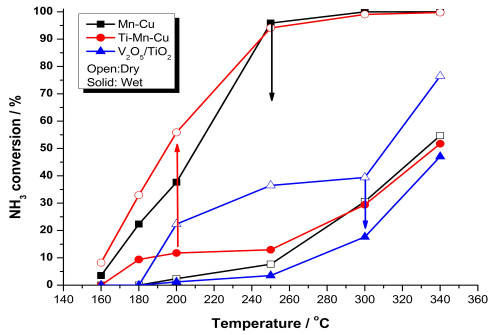

Figure 2. NH_3 oxidation over Mn-Cu, Ti-Mn-Cu and V_2O_5/TiO_2 catalysts. Reactants: 800ppm NH_3, 3 vol.% O_2 and 0, 6 vol.% H_2O. GHSV was 60,000 hr^{-1}.

This work was supported by the Power Generation & Electricity Delivery of the Korea Institute of Energy Technology Evaluation and Panning grant funded by the Korea Ministry of Knowledge Economy.

Yuejin, L. and John, N., A. (1997) *Appl. Catal. B: Environ.* **13**, 131-139

Maria, C., Oliver, K., and Martin, E.(2009) *Appl. Catal. B: Environ.* **88,** 413–419

M., Kang, E., D., Park, J., M., Kim, and J., E., Yie. (2006) *Catal. Today.* **111**, 236-241

Pavani, M., S., Donovan, A., P., and Panagiotis G., S., (2006) *Ind. Eng. Chem. Res.* **45**, 6444-6449

Infrared spectroscopy of diesel and biofuel combustion particles

E.D. Kireeva[1], O.B. Popovicheva[1], and M. Vojtisek-Lom[2]

[1]Institute of Nuclear Physics, Moscow State University, 119991, Moscow, Russia
[2]Department of Vehicles and Engines, Technical University of Liberec, Liberec, Czech Republic
Keywords: combustion particles, biofuels, surface chemistry, hygroscopicity.
Presenting author email: elenakireeva2@gmail.com

The growing anxieties about the environmental impacts of fossil fuels and their future availability have resulted in the intensive development of alternative energy sources. Vegetable oil based biofuels – oils in their pure, non-esterified form and their methylesters (FAME - fatty acids methylesters, also called biodiesel)– are commonly used as alternative fuels in existing engines. Compared to diesel fuel, they have similar energy density, lower sulphur and aromatic contents, lower greenhouse gas emissions. Rapeseed, soybean, sunflower, palm and other oils can be produced from local renewable resources. However in spite of spreading of vegetable oils as biofuels the climate impact of their emission into the atmosphere is poor understood. The main reason of this situation is limited information concerning the composition, surface chemistry, and hygroscopicity of combustion particles produced by burning vegetable oils. This work is devoted to investigation of surface chemistry of diesel and biofuel combustion particles using the Infrared (IR) spectroscopy.

Particles produced by burning diesel fuel EN 590 (DF) and vegetable oils, namely heated rapeseed oil (HRO), HRO with ethylhexylnitrate, and heated palm oil (HPO) were sampled from the exhaust of a diesel-electric locomotive and a Zetor 1505 tractor engine at different engine operation conditions (fast idle, full load, ISO 8178C-1, ISO 8178C-2) (Vojtisek-Lom *et al* 2009). PallFlex filter samples are measured by Fourier Transform IR (FTIR) spectroscopy using Shimadzu IRPrestige-21 spectrometer in a transmission mode. The spectra of loaded filters and blank filter are obtained with respect to the atmosphere, then the scaled subtraction is performed and the baseline correction is applied. Identification of IR absorption bands for each particles type is carried out according organics and ions database (Coates, 2000). The relationship between IR bands of polar carbonyl C=O and non-polar aliphatic C-H functional groups allows an estimate of the extent of the particle oxidation (Cain *et al* 2010). The comparative analysis of surface chemistry of combustion particles produced by diesel and biofuels is carried out as well as the impact of different engine load on the surface properties.

The IR spectra of combustion particles from Zetor tractor engine produced by burning DF and HPO at ISO 8178C-1 load are presented in Figure 1. The main characteristic band of black carbons, including DF particles is one at 1590 cm^{-1} which is assigned to aromatic C=C stretching vibrations, which can be augmented by adsorbed oxygen. The absence of this band on the spectra of HPO particles, as well as on other biofuel-produced particles, may have a relation to their amorphous structure, quite different from the ordered morphology of soot microcrystallines, formed when insufficient polyaromatic hydrocarbons are available during the soot inception. The prominent feature of all biofuel-produced particles is the significant bands of oxygenated functional groups. Vibrations of carbonyl C=O groups are found at 1701-1790 cm^{-1}, together with a wide band of hydroxyl O-H group in a range 3300-2500 cm^{-1} they may be assigned to carboxylic acids. The high hygroscopicity of the particle surface is proved by hydroxyl O-H vibrations at 2100-2190 cm^{-1}. The bands of vibrations in the range 1550-1475 cm^{-1} and 1650-1580 cm^{-1} could be assigned to N-O nitrogroups and N-H groups in amines and nitro compounds which can be formed as a result of biofuel burning.

This work allows decreasing the uncertainties in chemical identity of original combustion particles produced by burning diesel and vegetables oils and in comparisons of their environmental effects.

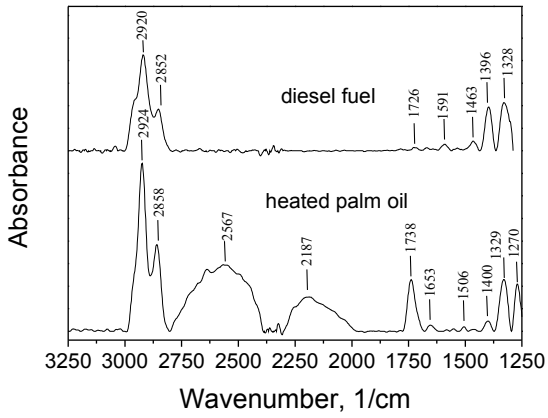

Figure 1. IR spectra of particles produced by burning diesel fuel and heated palm oil by a Zetor tractor engine.

Coates, J. (2000). Encyclopedia of analytical chemistry. 10815-10837.

Cain, J.P., Gassman, P.L., Wang, H., Laskin, A. (2010). PCCP. **12**. 5173-5488.

Vojtisek–Lom, M., Pechout, M., Blazek, J., Moc, L., Hlavenka,T. (2009). SAE Technical Paper Series, 2009-01-1913.

Evaluation of a high temperature particle sampling setup for separation of inorganic and organic phase using laboratory model compounds

Keywords: High temperature, aerosol sampling, biomass

P. Nilsson*, A. Malik, M. Lindskog, J. Pagels, J. Rissler, A. Gudmundsson, M. Bohgard and M. Sanati
Ergonomics and Aerosol Technology, Lund University, P.O. Box 118, SE-22100, Lund, Sweden
*Presenting author email: patrik.nilsson@design.lth.se

The particulate matter formed in gasification processes are dominated by carbonaceous compounds (Gustafsson, 2007). Volatile material such as tars may pass high-temperature cleaning devices in the gas-phase and condense at lower temperatures downstream the cleaning system. In order to achieve efficient removal of particles it is therefore crucial to investigate the mechanisms of fine particle formation in thermochemical conversion of biomass and also fully characterize the particulate matter present in the product gas.

The aim with this work was to design a dilution setup with which the solid fraction could be separated from the volatile fraction, preventing it from contributing to the particle phase as the temperature was reduced for subsequent particle characterization. Model aerosols, for combustion and gasification processes, consisting of inorganic compounds (KCl) or soot internally mixed with a tar model compound (Dioctylsebacete, DOS) were generated. The dilution setup consisted of a high temperature dilution probe (Lindskog, 2009) followed by either a denuder (length 400 mm, diameter center net-tube: 10 mm, diameter outer tube 31 mm) or a packed bed of activated carbon (length: 100 mm, diameter: 25 mm). The model aerosol was heated to 200 ^{o}C, which was sufficient to keep the DOS in vapor phase, and diluted in the probe at the same temperature. By allowing the temperature to slowly decrease in the denuder/packed bed the volatile material could be captured by the activated carbon.

The performance of the setup was evaluated by comparing particle size distributions (Figure 1), obtained with a Scanning Mobility Particle Sizer (SMPS), after the dilution setup. In addition to the SMPS, an Aerosol particle mass analyzer (APM), coupled with a DMA and a heater (DMA-heater-APM), was used during soot measurements. Two particle sizes where selected with the DMA, 87 and 150 nm. By measuring with and without the heater the fraction of volatile material, condensed on the soot particles, could be determined.

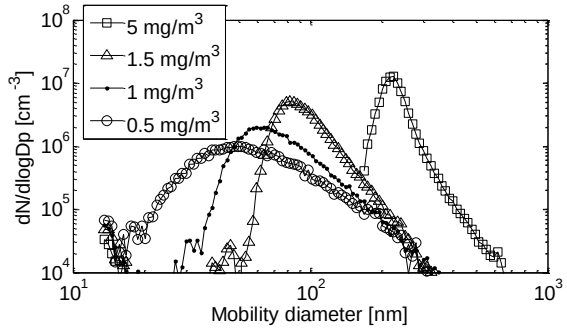

Figure 1. Effect on particle size distribution by allowing different amounts of DOS and constant amount of KCl (0.5 mg/m^3) enter the denuder at 1 lpm.

When a denuder flow rate of 3 lpm was used measurements with KCl showed that the denuder was able to handle 6 mg/m^3 of DOS, compared to 0.5 mg/m^3 when using a flow rate of 1 lpm. Concentrations below 6 mg/m^3 did not render changed particle size distributions compared to the distribution for pure salt.

Despite that the soot particle size distributions did not indicate any condensation, due to the agglomerated structure of the soot particles, mass measurements with the DMA-heater-APM revealed that at a DOS level of 12 mg/m^3 the denuder was unable to prevent obvious condensation on the soot (Figure 2). In order to enhance the removal efficiency of organics, a packed bed of activated carbon was used as a replacement to the denuder. DOS concentrations as high as 17 mgm^{-3} could enter the packed bed without any significant condensation on the soot particles.

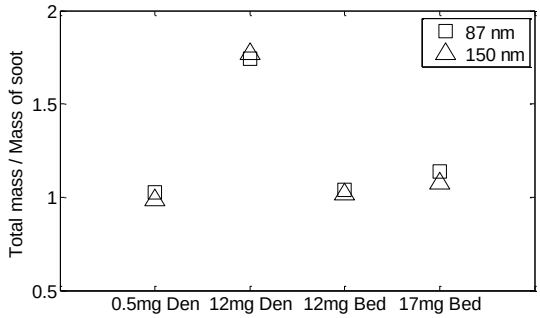

Figure 2. Ratio between obtained total mass and mass of soot core using different inlet DOS concentration for denuder (Den) and packed bed (Bed)

A sampling probe was designed and optimized to collect fine particles in flue gas model aerosols at laboratory conditions. In future measurements it will also be used in field to evaluate cleaning devices operating at the slipstream from a biomass gasifier.

This work was supported by European Commission (EC) 7th framework programme (GREENSYNGAS Project contact number 213628)

Gustafsson, E., Strand, M., and Sanati, M. (2007) Energy & Fuels 21, 3660-3667

Lindskog, M., Malik A., Pagels J., Rissler, J., Wierzbicka, A. and Sanati M. (2009) NOSA, Conference proceeding, p51

Characteristics of Polychlorinated Dibenzo-*p*-dioxins and Dibenzofurans in the atmosphere in northern Taiwan

S.I. Shih[1], W.J. Lee[2], W.Y. Huang[2], L.C. Wang[3] and G.P. Chang-Chien[3]

[1]Department of Environmental Engineering, Kun Shan University, Tainan City, Yung Kang, 710, Taiwan
[2]Department of Environmental Engineering, National Cheng Kung University, Tainan City, 701, Taiwan
[3]Department of Chemical and Materials Engineering, Cheng Shiu University, Kaohsiung City, 833, Taiwan
Keywords: PCDD/Fs, Dry deposition, Polyurethane foam, Concentration.
Presenting author email: ssi10@mail.ksu.edu.tw

Polychlorinated Dibenzo-*p*-dioxins and Dibenzofurans (PCDD/Fs) have drawn much attention in Taiwan, not only for their adverse health effects, but also for their wide distribution in the atmosphere (Kao *et al*., 2006; Lee *et al*., 2008). Municipal Solid Waste Incinerators (MSWIs) had been identified as the largest contributors to the environmental levels of PCDD/Fs, particularly in Europe.

The objectives of the present study were to develop the concentrations of PCDD/Fs, the gas-particle partitioning of PCDD/Fs and dry deposition fluxes of PCDD/Fs in the ambient air of three MSWIs in northern Taiwan. The results of this study will provide important database to assist the decision makers for formulating policies to alleviate dioxin concern.

In the ambient air of three MSWIs (A, B and C), sampling was conducted at 7 different sites for two seasons. Each ambient air sample was collected using a polyurethane foam (PUF) sampler according to the revised U.S. EPA Compendium Method TO-9A. Each sample was collected continuously on three consecutive days yielding a sampling volume of 972 m^3. The PUF sampler was equipped with quartz-fiber filter for sampling particle-phase PCDD/Fs, and followed by a glass cartridge containing PUF for sampling gas-phase PCDD/Fs, respectively. A known amount of surrogate standard was spiked to the PUF in the laboratory before the field sampling was conducted.

Table 1. PCDD/F concentrations in the ambient air of three MSWIs in northern Taiwan.

	MSWI-A	MSWI-B	MSWI-C
Total PCDD/Fs (pg/Nm^3)	0.360	0.449	0.575
Total TEQ (pg I-TEQ/Nm^3)	0.0207	0.0272	0.0297

Analyses of PCDD/Fs were performed according to the US EPA Reference Method TO9A. Each sample was extracted for 24 h, the extract was then concentrated, treated with concentrated sulphuric acid, and followed by a series of cleanup and fractionation procedures. The elute was concentrated to approximately 1 mL and transferred to a vial. The concentrate was further concentrated to near dryness, using a stream of nitrogen. A high-resolution gas chromatograph/high-resolution mass spectrometer (HRGC/HGMS) was used for PCDD/F analyses. Helium was used as the carrier gas. The analyzer mode of the selected ion monitoring with a resolving power at 10,000 was used.

As Table 1 listed, the mean PCDD/F I-TEQ concentrations in the ambient air at the vicinity of three MSWIs in northern Taiwan were 0.0207, 0.0272 and 0.0297 pg I-TEQ/Nm^3, respectively. They were all much lower than the air quality standard in Japan (0.6pg I-TEQ/Nm^3). The comparisons of PCDD/F congener profiles indicated that, they closely resemble each other and OCDD, 1,2,3,4,6,7,8-HpCDD, 1,2,3,4,6,7,8-HpCDF and OCDF are the top four dominant species in all cases (Figure 1).

According to the percentage of gas-particle partitioning in the ambient air, the PCDD/Fs in the atmosphere were mainly in particle phase. For dry depositions, the dominant mechanism of the dry deposition was the particle-phase deposition. The PCDD/F dry deposition fluxes in the vicinity of three MSWIs in the atmosphere were 131, 196 and 217 pg/m^2-day, respectively.

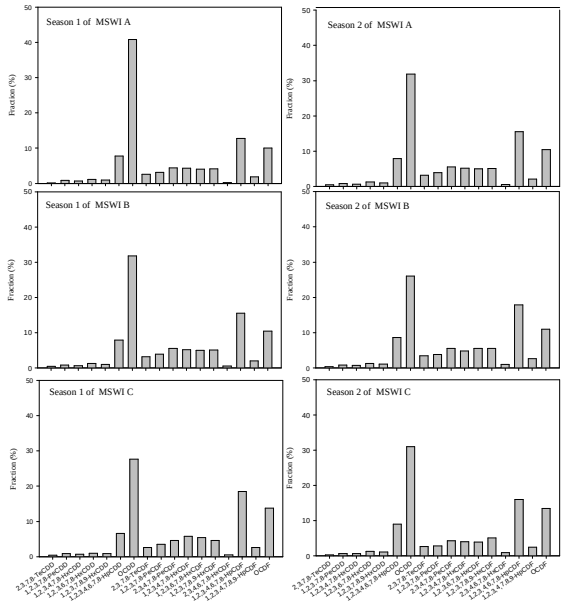

Figure 1. PCDD/F congener profiles in the ambient air of three MSWIs

Kao, J.H., Chen, K.S., Chang-Chien, G.P. and Chou, I.C. (2006) *Aerosol Air Qual. Res.* **6**, 170–179.

Lee, S.J., Ale, D., Chang, Y.S., Oh, J.E. and Shin, S.K. (2008) *Environ. Pollut.* **153**, 215–222.

Carbon burnout of a multi-fuel dust-burner in co-combustion situations

W. Baumann, H.-J. Gehrmann, H. Mätzing, H.-R. Paur and H. Seifert

Karlsruher Institut für Technologie,
Institut für Technische Chemie, Bereich Thermische Abfallbehandlung,
Postfach 3640, D-76021 Karlsruhe, Germany

Keywords: co-combustion, low rank fuels, camera-based process control, load flexibility, fuel flexibility

The growth of the world population is associated with an increase of the specific energy consumption per person, particularly in developing countries. This poses the challenging task to a sustainable management of fossil fuel ressources at increasing energy demand. In Germany, 80 % of the primary energy is provided by use of fossil fuels today. Modern power plants, operated with hard coal, have efficiencies up to 46 % (electric). Very high conversion efficiencies can be achieved with low rank fuels (LRF), e.g. rice husk and wood char, also by the co-combustion technology, which is already applied in some European countries. Together with a carbon capture and storage technology (CCS), co-combustion supports the reduction of CO_2 emissions and favours reduced investment and operation costs.

At the Karlsruhe Institute for Technology (KIT), a load-flexible multi-fuel burner is under development. The multi-fuel burner is tested at a 2 MW combustion chamber (BRENDA). Fig. 1 gives an overview of the experimental arrangement. The flame stability is controlled and improved by an optical camera system (Keller et al., 2007). Measurements of temperature, gas composition and dust properties are performed at several locations upstream and downstream of the burner, as indicated in Fig. 1. Here we report dust measurements performed at the first location downstream of the burner, which corresponds to a residence time around 1.5 sec. The dust samples were taken from the center of the combustion chamber with a non-cooled heat resistant nozzle using isokinetic conditions. The particles were collected on quartz fiber filters free of organic binder. Probe sampling intervals of only 15 minutes could be used, so multiple samples were obtained with high time resolution. The particle mass concentration was determined gravimetrically. Some filters were used for elemental analysis, performed by ICP-OES, and others for carbon analysis to determine the carbon burnout and hence the combustion behaviour.

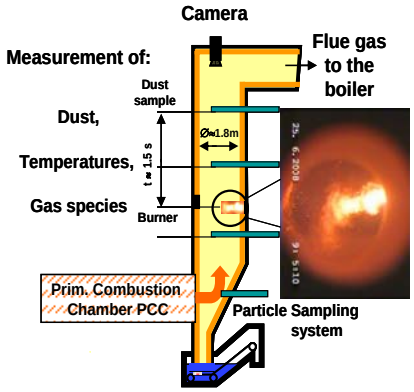

Figure 1. Experimental arrangement at the BRENDA combustion chamber.

Fig. 2 shows the final carbon concentrations measured in the dust samples which are in the range 0.5 – 3.4 wt.-%. The operation conditions of the different co-combustion experiments were similar. The rice husk particles burnt out worse than the hard coal because of bad mixing with the main flow, while the wood char had a very high initial carbon content. In future experiments, it will be investigated, how the carbon burnout of different co-combustion materials depends on specific operation conditions at various sampling points.

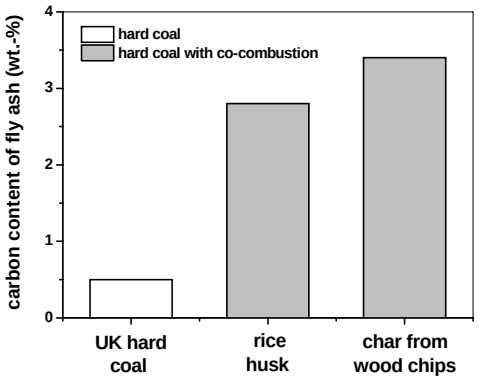

Figure 2. Final particulate carbon concentrations for different fuel mixtures.

Keller, H. B.; Matthes, J.; Zipser, S.; Schreiner, R.; Gohlke, O.; Horn, J., & Schönecker, H. , *VGB PowerTech*, 3, 85-92, 2007.

Wood combustion emissions in Switzerland and associated impact assessments

Meyer, Nickolas K.[1], Heck, Thomas[1]
[1]Laboratory for Energy Systems Analysis, Paul Scherrer Institute, Switzerland
Keywords: wood combustion emissions, life cycle analysis, sustainability, external costs

Woody biomass combustion produces 5% of Swiss heating energy and 20 - 50 % of airborne, organic and particulate emissions during winter. Further, future energy scenarios suggest that wood consumption could sustainably increase by a factor of two [1], likely leading to increased emissions. On this basis, an inventory describing combustion emissions produced by 25 in-use residential, commercial, and industrial biomass combustion appliance classes was developed for Switzerland. This inventory is used to assess current and historical emissions, to identify those appliance classes contributing most to emissions, to assess future emissions based on sustainable scenarios and finally, to quantify external costs associated with wood combustion in Switzerland.

The inventory incorporates over 200 direct and indirect (life cycle) emission species. Of these species, particulate matter (PM), carbon monoxide (CO), particle bound black carbon (BC), particle bound organic matter (POM) and total organic carbon (TOC), nitrogen oxides (NO_x) and greenhouse gases form a set of core species [2,3]. PM data utilised in this inventory was size classified to represent, total particulate emissions (TPE), and particulate matter having diameters less than 10, 2.5 and 1 μm respectively (PM_{10}, $PM_{2.5}$ and PM_1).

Direct emission factors for core species were collected for average, high and low emission scenarios (based on appliance operating characteristics). Non-core species have so far been considered only for average operating cases. Using these emission factors, annual emissions were determined for each species (for the period 1990 – 2009, with a base year of 2009), and in some cases used to determine future emission scenarios. For the average current emission scenario, annual TPE was calculated to be 6520 tonnes. Analysis of the size dependency of TPE was made (Fig. 1), as was the size dependent contribution of BC and POM to PM (not shown).

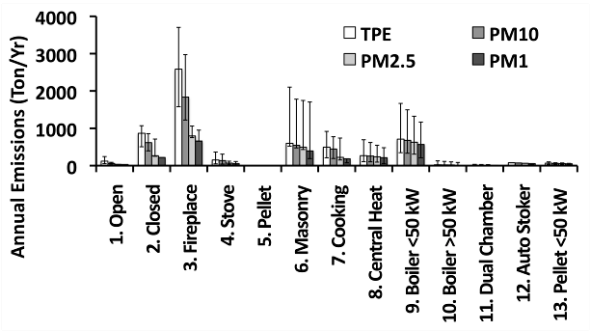

Fig. 1. Annual particulate matter emissions for 13 residential wood combustion appliances in Switzerland, 2009.

In addition to the emission inventory, direct and indirect global warming potentials (GWPs) were calculated for representative systems (Fig. 2). These preliminary GWP calculations highlight variances in potential climate impacts between biomass and fossil systems (particulates are excluded from prelim. GWP)

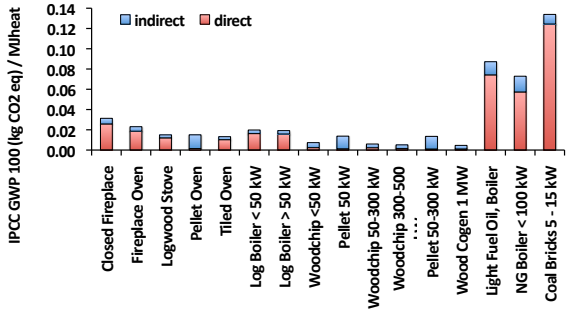

Fig. 2. Direct and indirect global warming potentials for selected combustion systems

As a method of valuing impacts associated with the combustion of wood, external costs methods were employed [3]. Using both direct and indirect emissions, estimates of external costs attributable to wood combustion in Switzerland were made. Further comparison with fossil fuel systems and wood combustion systems incorporating emission reduction devices were also made. Currently, cost estimates exclude aerosol induced climate effects - these should be included within the coming year. Estimates presented here show costs per MJ of useful heat for selected combustion systems (Fig. 3) [3]. Life cycle impact assessment results will be included as well.

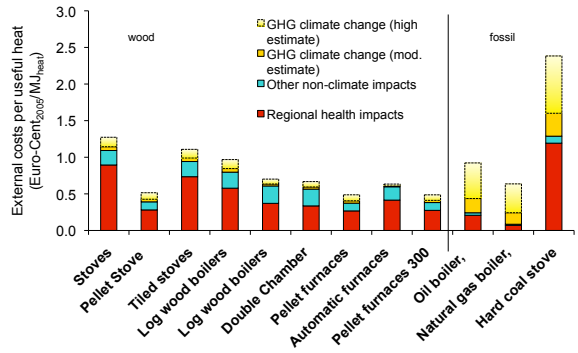

Fig 3. External costs per MJ useful heat for wood and fossil fuel systems in Switzerland.[3]

This work was conducted as part of the research project IMBALANCE and funded by the Competence Center Environment and Sustainability of the ETH Domain (CCES).

[1].Grünenfelder T, Rutschmann C. Holzenergie x 2. Zürich: Swiss Federal Office of Energy; 2004.
[2]. Meyer, N.K., ETH Nanoparticle Conference, Zürich 2010
[3]. Heck, T., Meyer, N.K., CCES-Latsis Symposium, Zürich 2010,

Carbonaceous particulate concentration in Indian kitchens

K.S. Patel[1], R. Baghel[1], N.K. Jaiswal[1], H. Saathoff[2] and T. Leisner[2]

[1]School of Studies in Chemistry, Pt. Ravishankar Shukla University, Raipur, India
[2]Institute for Meteorology and Climate Research (IMK), KIT, Karlsruhe, Germany
Keywords: BC, OC, BC/OC ratio, India.
Presenting author email: patelks_55@hotmail.com

Biomass (i.e. wood, crop waste and animal dung) is primary cooking fuel for a large majority of households in developing countries. There are an estimated 1.6 million deaths per year due to toxic indoor air pollution (*Smith & Mehta, 2003*). Exposure to these smokes has also been linked to several health effects (i.e. increased prevalence rate of chronic bronchitis in women and acute respiratory infections in children) especially for women who cook with these fuels and in young children. The smoke is a complex mixture of particulate matters (PM) including organic carbon (OC), black carbon (BC), silica, elements, various salts, etc. The OC represent a large variety of organic compounds which can be classified into general compounds such as aliphatic, aromatic compounds, acids and numerous unidentified compounds. Black Carbon is one of the unique pollutants that have a large direct negative impact on human health, indoor and outdoor air quality, temperature, cloudiness, precipitation, mountain glaciers, sea ice, and snow packs (*Ramanathan & Carmichael, 2008*). Black-carbon particulate matter is also damaging to human health (*Rich et al. 2005*). The BC concentration in the indoor environment of some countries was reported (*Fromme et al. 2005; Kwangsam & Crocker 2005; Moloi et al.2002*). The commercial cooking is a surprisingly large source of a range of air pollutants that could pose risks to human health and the environment in India. Therefore, in the present work, the concentration of BC and OC, BC/OC ratio and their fraction in the PM in the Kitchen environment are described.

Thirty five kitchens cooking with fuels i.e. LPG, kerosene, coal, cow dung, biomass and agricultural residue were selected for the present investigation in November, 2008. The Partisol Model 2300 (Thermo Sci. USA) samplers were used for collection of the fine ($PM_{2.5}$) and coarse particulate material (PM_{10}) in the microenvironment. The PM was collected by using Partisol sampler on 47-mm quartz fiber filters (Whatmann, QMA) housed in the molded filter cassettes. The loaded filters were dismounted, brought to laboratory, and heated up to 50 ^{o}C for 6 hrs to remove the moisture contents. The filters were transferred into the desicator, and finally weighted to measure the particulate mass load. A standard thermal method was used for analysis of OC and BC.

The ratio of the $PM_{2.5}/PM_{10}$ is found to be > 95%. It means all PM during the burning processes lie in fine and ultrafine modes. The BC and OC concentration ranged from 31 – 3068 and 121 – 17786 μg m^{-3} with mean value of 1535 and 6648 μg m^{-3}, respectively. The OC/EC ratio is ranged from 0.2 – 11.3 with mean value 4.3±0.7. The mean value of BC, OC and OC/BC ratio for the various fuels are summarized in Table 1. The highest and lowest OC/BC ratio is observed when agricultural residue and kerosene are burnt.

Table 1. Mean BC and OC concentration (μg m^{-3}) in the indoor air with OC/BC ratio

Fuel	BC	OC	OC/BC
LPG(2)	41	126	3.3
Kerosene(2)	1614	312	0.2
Cow dung(2)	734	3139	4.3
Coal(2)	644	2588	4.1
BM(19)	1935	8488	4.3
AR(8)	1362	7387	5.4

BM = Biomass, AR = Agricultural residue

The OC and BC fraction in the PM_{10} is ranged from 8.1 – 72.3% and 2.4 – 53.0% with mean value of 50.1±5.5% and 14.3±3.6%, respectively. Among them, the highest and lowest BC fraction is observed in the kerosene (52.8%) and LPG (3.8%) PM, respectively. The elevated levels of OC and EC are emitted during burning of the fuel. Among these fuels, the kerosene is seemed to be most dirty fuel due to association of high BC fluxes. The fluxes of the PM, BC and OC emitted during burning are described.

Fromme, H., Lahrz, T., Hainsch, A., Oddoy, A., Piloty, M. and Ruden, H. (2005) *Indoor Air* **15**, 335 – 341

Kwangsam, N. and Cocker, D.R. (2005) *Atmos. Environ*. 39, 3325-3333.

Moloi K, Chimidza, S, Lindgren, E. S. Viksna, A. and Standzenieks P. (2002) *Atmos. Environ*. **36**, 2447–2457.

Ramanathan, V. & Carmichael, G. (2008) *Nature Geosci*. **1,** 221–227.

Rich, D.Q., Schwartz, J., Mittleman, M.A., Link, M., Luttmann-Gibson, H., Catalano, P.J., et al. (2005) *Am. J. Epidemiol.* **161**,1123–1132.

Smith, K R and Mehta, S. (2003) *Inter. J. Hyg. Environ. Health*, **206**, 279-289.

Characterization of welding fume and application of exposure model to predict concentrations in the ship-building industry

Y.F. Wang[1], P.J. Tsai[1,2]

[1] Department of Environmental and Occupational Health, Medical College, National Cheng Kung University, 138, Sheng-Li Rd., Tainan 70428, Taiwan
[2] Sustainable Environment Research Center, National Cheng Kung University, 1, University Road, Tainan 70101, Taiwan

Keywords: welding fume, exposure, three-zone model, ship-building industry.
Presenting author email: sakuray66@gmail.com

The whole study was conducted at welding workplaces in a ship-building industry. Samplings were conducted to welders, and the results were compared with model predictive models in order to assess the feasibility of the currently available predictive models.

Results show that the predicted values obtained from the Three-Zone Model has a better prediction to the corresponding measured values than that of Two-Zone Model based on the laboratory data. To measure fume particle sized distributions for the Near field, Lower room zone, and Upper room zone were consistently in a unimode form, and the smallest MMAD were found in that of the Near field. For measured total fume concentrations, we found that big block area> assembly area> small assembly area. The concentrations found in the Near field were much higher that of Lower and Upper room zone, but no significant difference could be found between that of Lower and Upper zones. The main metal contents in welding fumes were Fe and Mn. Using the Three-zone Model to predict welder's exposures, in real workplaces indicates that a systemic bias might exist in the predicted Near field concentrations. The above results might because of the variations of Q and β among different zones. In addition, the stratification of the emitted fume in different zone might not be uniformly distributed and result in different β for the same zone in the practical situation. It is suggested that the use of Three-Zone Model in the field is still required further investigations, particularly in determination of Q and β for the predicative model.

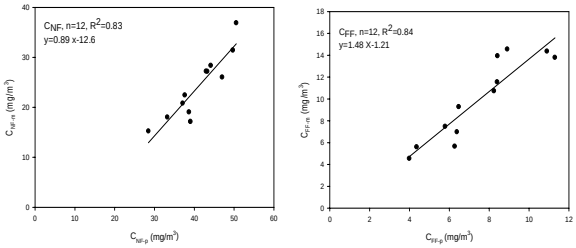

Figure 1. The relationship between predicted value (C_{NF-p} v.s C_{FF-p}) and measured value (C_{NF-m} v.s C_{FF-m}) were obtained by using Two-Zone model in the near and far field.

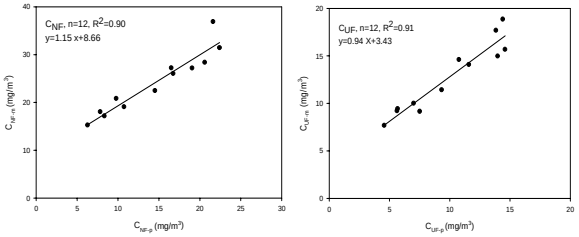

Figure 2. The relationship between predicted value (C_{NF-p} v.s C_{UF-p}) and measured value (C_{NF-m} v.s C_{UF-m}) were obtained by using Three-Zone model in the near field and upper room zone.

Table 1. Mass-based size distributions(μm） obtained from the selected work area.

	small assembly area		assembly area		big block area	
	MMAD	GSD	MMAD	GSD	MMAD	GSD
Near Field	0.69	3.77	0.80	2.98	0.82	3.06
Lower Zone	1.47	2.69	1.64	2.63	0.93	2.97
Upper Zone	1.40	2.66	1.27	2.79	0.91	2.97

Table 2. The relationship between predicted value (C_p、C_p) and measurement value (C_m) ($\mu g/m^3$) obtained from different exposure zone and different work area.

	emission ratio	small assembly	assembly area	big block area	relationship between predicted(p,p') and
C_{NF-p}	f_1=0.2	1.78	1.79	4.82	y=0.97x+3.68 , R^2=0.95
C_{LR-p}	—	3.66	5.47	11.3	y=0.35x-0.73, R^2=0.99
C_{UR-p}	f_2=0.27	0.07	0.47	1.15	y=2.96x+0.07, R^2=0.98
$C_{NF-p'}$	f_1=0.2	10.7	10.7	14.2	y=0.86x-3.8 , R^2=0.96
$C_{LR-p'}$	—	3.66	5.47	11.3	y=0.35x-0.73, R^2=0.99
$C_{UR-p'}$	f_2=0.27	3.49	3.87	4.51	y=3.13x-10, R^2=0.98
C_{NF-m}	—	5.83	5.09	8.49	—
C_{LR-m}	—	0.58	1.13	3.21	—
C_{UR-m}	—	0.42	1.24	3.56	—

Fred, W.B., Catherine, E.S., Laurel, B., Peter, S., 2009; Two-Zone model application to breathing zone and area welding fume concentration data. Journal of Occupational and Environmental Hygiene 6:298–306.

Nicas, M., 2009; A three-zone model for welding fume concentrations. Journal of Occupational and Environmental Hygiene. 6:D69–D71.

Study of local aerosol combustion concentration with a differential white light opacimeter.

A. Bellivier, R. Delorme, S. Dupont, P. Benhaiem, Y. Chen, P. Le Bars and H. Bazin
Department of Physical Measure and Fire Sciences , Laboratoire Central de la Préfecture de Police
39bis rue de Dantzig, 75015 Paris, France
Keywords: soot particules, concentration, light-extinction, measurements.
Presenting author email: axel.bellivier@interieur.gouv.fr

A differential white light opacimeter is been developing in order to measure smoke concentration directly into the flow over the time. It will allows local measures simultaneously in different parts of the area studied. It is tested in a smoke chamber equipped with a photometer. Concentrations are calculated from the measure of light-extinction, such as Mulholland and al (2000). Six samples of wood are burned : 10; 20; 30; 40; 50 and 60 mm width (respectively 1.49; 3.17; 4.73; 6.07; 8.81 and 10.53 g). The sample is exposed to a heat flux of $2.5W.cm^{-2}$.

Theorical

Following the Beer-Lambert law, the concentration of soot is obtained from measuring the output voltage and maximum voltage of the prototype :

$$C_s = \alpha \frac{-ln(1-\frac{U_{out}}{U_{max}})}{\sigma_s L_{prototype}}$$

with C_s soot concentration $[g.m^{-3}]$; α the calibration coefficient [-]; U_{out} the output voltage [V]; U_{max} value of the max (= 5) $[V]$; σ_s specific extinction coefficient (= 4.4) $[m^2.g^{-1}]$; $L_{prototype}$ opacimeter the optical path of the device (= 0.05) $[m]$.

As above, the concentration of soot is obtained from the Optical Density (OD) measured by the smoke box's photometer (French norme NF X 10-702-1) :

$$C_s = \frac{ln(10^{\frac{OD}{132}})}{\sigma_s L_{photometer}}$$

with C_s soot concentration $[g.m^{-3}]$; 132 chamber's constant; OD optical density provided by the smoke chamber [-]; σ_s specific extinction coefficient (= 4.4) $[m^2.g^{-1}]$; $L_{photometer}$ the optical path of the device (= 0.914) $[m]$.

The prototype is calibrated using Wratten Gelatin Filters. The Fig. 1 present the reference optical density of filters versus optical density obtained with the smoke box's photometer (thin line) and the prototype (bold line). A calibration correction is necessary (dashed bold), $\alpha = 1.4$.

Results

The measurements are presented in Fig. 2. The prototypes measurements are consistent with the photometrics ones. For a given sample, prototype concentrations are lower then the photometers one in case of the difference

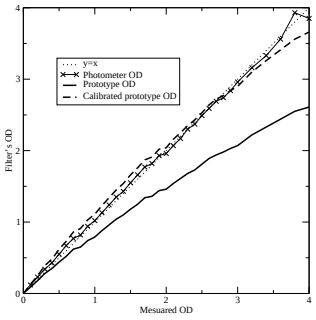

Figure 1: Filter's OD vs Measured's OD.

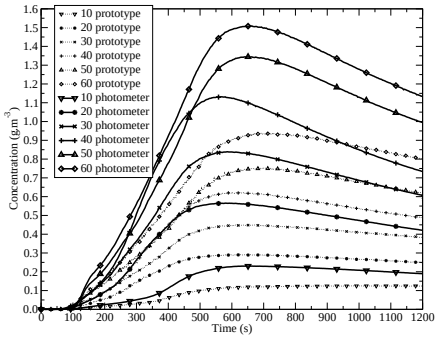

Figure 2: Results for tests with the photometer.

of optical path length. Other position of prototype would be explored to characterize the whole concentration field of the chamber.

Conclusion

A prototype of differential white light opacimeter is been developing. A light-extinction measurement based on the Beer-Lambert' law is made in a smoke chamber. The first measures done with the prototype are very satisfactory. Future works will mainly consist in the comparison of our measurements with non light-extinction devices and look at the fouling problem following Putorti (1999).

Mulholland, G. W.; Johnsson, E. L.; Fernandez, M. G.; Shear, D. A. (2000), Design and Testing of New Smoke Concentration Meter, Fire and Materials, Vol. 24, No. 5, 231-243.

Putorti, A. D., Jr. (1999) Design Parameters for Stack-Mounted Light Extinction Measurement Devices, NISTIR 6215; 34 p.

Influence of aircraft combustion chamber conditions on physical and chemical properties of soot aggregates

D. Lottin[1], D. Delhaye[1], D. Ferry[2], A. Petzold[3], H. Bauer[4], Y. Sevcenco[5], R. Marsh[5] and M. Johnson[6]

[1]Department of Physics and Instrumentation, ONERA, Châtillon, 92322, France
[2]CINaM-CNRS UPR 3118, Marseille, 13288, France
[3]Institut für Physik der Atmosphäre, DLR, Oberpfaffenhofen, 82234, Germany
[4]Vienna University of Technology, 1060 Vienna, Austria
[5]Gas Turbine Research Centre, Cardiff School of Engineering, Cardiff, CF24, UK
[6]Rolls-Royce plc, Derby, DE24, UK
Keywords: combustion particles, soot agglomerates, TEM, size distribution.
Presenting author email: delphine.lottin@onera.fr

Aircraft engine emissions are regulated by two international committees of experts: CAEP (Committee on Aviation Environmental Protection): regulatory, and SAE (Society of Automotive Engineers): measurement methodology. The existing visibility metric for certification of an aircraft engine is based on the Smoke Number filter method. New measurement metrics are required because the quantity and characteristics of emitted particulate matter, mainly consisting of soot, need to be considered due to the affect of soot on the global radiative budget (Lee *et al.*, 2010) and the impact on local air quality and thus on the human health (Ferry *et al.*, 2011).

Real-time particulate measurements are starting to be used to investigate engine emissions but the interpretation of the signals often requires assumptions about the physical particle properties, which are still poorly known. This work aims to enlarge the knowledge of soot particles by determining their physical and chemical characteristics according to aircraft combustor chamber conditions to improve the accuracy of their description.

The experimental setup used in SAMPLE (Petzold *et al.*, 2009) allowed the investigation of three combustion settings representing low smoke/low organic (LS/LO), low smoke/high organic (LS/HO) and high smoke/low organic (HS/LO) conditions. SAMPLE II (Marsh *et al.*, 2010) allowed a more accurate investigation with five different combustion settings. For each condition, the soot morphology, structure and size are determined by Transmission Electron Microscopy (TEM) and size distribution measurements obtained by a Differential Mobility Spectrometer (DMS). In addition, measurements are obtained on the relative carbon composition using a thermal method.

Results show that the geometric mean diameter d_p of soot primary particles which constitute the aggregates, and the geometric mean gyration diameter d_g of these latter vary between the combustion conditions (Table 1). The evolution of these characteristics is more precisely defined with the analysis of aggregates sampled during this work.

The measurements allow comparisons to be made between two equivalent diameters (gyration and electric mobility, d_m) at various combustion conditions. This is performed by combining results from both DMS and TEM analysis. The β parameter that links the two sizes usually ranges between 0.77 and 1.4 (Gwaze *et al.*, 2006) and is evaluated in this study.

Soot acts in the atmosphere as the most efficient absorber of visible radiation. As the light-absorbing and light-scattering properties of soot aggregates change with the size of primary spheres and fractal characteristics, our results can be used to model these properties according to combustor conditions and be applied within atmospheric radiation modelling.

	d_p (nm) (TEM)		d_g (nm) (TEM)		d_m (nm) (DMS)	
	GMD	*GSD*	GMD	*GSD*	GMD	*GSD*
LS/HO	3.6	*1.88*	58	*1.34*	45.5	*1.31*
LS/LO	3.7	*1.93*	39	*1.92*	53.1	*1.39*
HS/LO	3.2	*1.73*	38	*1.97*	58.1	*1.46*

Table 1. Comparison of soot size characteristics between three combustion conditions (GMD: geometric mean diameter; GSD: geometric standard deviation).

This work has been undertaken within EASA (European Aviation Safety Agency) SAMPLE programs and the European Network of Excellence ECATS.

Ferry, D., Rolland, C., Delhaye, D., Barlesi, F., Robert, P., Bongrand, P., Vitte, J. (2011) Inflammatory Research **60**, 255-263.

Gwaze, P., Schmid, O., Annegarn, H.J., Andreae, M.O., Huth, J., Helas, G. (2006) Aerosol Science **37**, 820-838.

Lee, D.S., Pitari, G., Grewe, V., Gierens, K., Penner, J.E., Petzold, A., Prather, M.J., Schumann, U., Bais, A., Berntsen, T., Iachetti, D., Lim, L.L., Sausen, R. (2010) Atmospheric Environment **44**, 4678-4734.

Marsh, R., Crayford, A., Petzold, A., Johnson, M., Williams, P., Ibrahim, A., Kay, P., Morris, S., Delhaye, D., Lottin, D., Vancassel, X., Raper, D., Christie, S., Bennet, M., Miller, M., Sevcenco, Y., Rojo, C., Bowen, P. (2010) EASA report.

Petzold, A., Marsh, R. Johnson, M., Miller, M., Sevcenco, Y., Delhaye, D., Vancassel, X., Ibrahim, A., Veira, A., Williams, P., Bauer, H., Crayford, A., Morris, S., Kay, P., Bowen, P.,Bachalo, W., Raper, D. (2009) EASA report. http://www.easa.eu.int/ws_prod/r/doc/research/SAMPLE_Report_Final.pdf

Comparison of emissions with pellet fuel and wood logs from a hybrid masonry heater

A. Hukkanen[1], H. Lamberg[1], T. Penttilä[1], O. Sippula[1], J. Tissari[1], J. Jokiniemi[1,2]

[1] University of Eastern Finland, Department of environmental science, Fine Particle and Aerosol Technology Laboratory, P.O. Box 1627, FI-70211 Kuopio, Finland
[2]VTT Technical Research Centre of Finland, P.O. Box 1000, 02044 VTT, Finland
Keywords: Wood combustion, combustion aerosols, emissions, abatement strategies, PM
Presenting author email: annika.hukkanen@uef.fi

In order to avoid further increase of CO_2 in the atmosphere from the use of fossil fuels the use of renewable energy should be increased. This includes the use of biomass in residential heat production. However, the increase of other harmful compounds, such as fine particles, soot, CO and organic gaseous compounds (OGC) including PAH, should be minimized. The batch wise operated residential scale combustion appliances are troublesome with their high emissions of the incompletely oxidized compounds. Therefore, there is a need to investigate the options to reduce the emissions from biomass combustion.

Batch-wise fired appliances using pellets as fuel may provide an option to significantly decrease emissions. In these appliances a single batch of pellets in burned for heating the stove. In this study a hybrid masonry heater was used where the grate used for combustion of wood logs could be replaced with a specially designed pellet burner. Primary and secondary airs were applied to the fuel bed and additional tertiary air above the fuel bed.

Comprehensive measurement equipment was used. Gaseous compounds CO, CO_2 and O_2 were measured straight from the stack with FTIR, and OGC with FID. A sample of total suspended particles (TSP) was also collected from the hot undiluted flue gas. The sample gas was diluted with porous tube diluter and ejector diluter for the collection of PM_1 and particle mass size distribution (DLPI) samples. PM_1 samples were collected separately from ignition, steady firing and burn out phases and the mass size distribution sample from the total combustion. The organic (OC) and elemental carbon (EC) contents were analyzed from PM_1. Time-weighted average values $PM_{1,ave}$, OC_{ave} and EC_{ave} were calculated for total combustion from the samples of different combustion phases. The flue gas was further diluted with another ejector diluter for online measurement of particle number size distribution (ELPI and FMPS), total particle number (CPC) and mass (TEOM) concentrations. In addition, the combustion air flow rates were measured from air supply ducts separately for primary air and combined for secondary and tertiary air.

For comparison, the hybrid masonry heater was also operated with wood logs, and the same measurements were performed. When operated with logs, only primary combustion air was used.

Compared to the conventional technology of wood log combustion the pellet combustion resulted in clearly lower emissions. OGC and CO concentrations were 24-fold and 8-fold, respectively, lower in the pellet combustion. TSP was 1.7-fold and PM_{10} 2-fold lower in the pellet combustion, whereas $PM_{1,ave}$ was 3.4-fold lower in the pellet combustion. The difference of OC_{ave} was greater than of EC_{ave}, the OC_{ave} being 12.3-fold lower and EC_{ave} 2-fold lower in the pellet combustion. In the pellet combustion the OC_{ave}/EC_{ave} ratio was 1:7.2, whereas in wood log combustion the ratio was 1:1.15. In the different phases of pellet combustion, the PM_1 emission from the ignition phase was clearly higher than from the two other phases, especially EC was high, the PM_1 constituting 78% of EC and 9% of OC. During the steady firing PM_1 was the lowest, below 10 mg/MJ. No significant differences in total number concentrations were observed between the different fuels. The geometric mean diameter was 75 nm and 110 nm in pellet and wood log combustion, respectively. The mass mean diameters were 250 nm and 320 nm, respectively.

The emissions from the pellet combustion were clearly lower than from the wood log combustion, and well comparable to what has previously been measured from modern masonry heaters (Tissari et al., 2009).

The authors thank Warma-Uunit Ltd. This work was supported by the Finnish Funding Agency for Technology and Innovation.

Tissari J, Hytönen K, Sippula O & Jokiniemi J: *The effects of operating conditions on emissions from masonry heaters and sauna stoves*. Biomass and Bioenergy (2009) 33, pp 513-520.

Physico-chemical properties of particles formed in efficient, intermediate and smouldering wood chip combustion

T. Torvela[1], J. Leskinen[1], A. Hukkanen[1], T. Penttilä[1], H. Lamberg[1], T. Kettunen[1], I. Nuutinen[1], O. Sippula[1], J. Tissari[1], J. Jokiniemi[1,2]

[1]University of Eastern Finland, Department of Environmental Science, Fine Particle and Aerosol Technology Laboratory, P.O. Box 1627, FIN-70211, Finland
[2]VTT Technical Research Centre of Finland, Fine Particles, P.O. Box 1000, FIN-02044 VTT, Finland
Keywords: Aerosol component composition, Biomass burning, Combustion aerosols
Presenting author email: tiina.torvela@uef.fi

It is known that the physico-chemical properties of combustion emissions have effects on health and the environment. However, the formation mechanisms of fine particles and their relationships with toxicological properties and effects on climate are poorly understood. In this study the physico-chemical properties of wood chip originated fine particles from three different combustion conditions were characterized. Of specific interest were to 1) find out the effect of combustion conditions on the particle morphology and composition, 2) verify whether the elemental carbon (soot) is internally or externally mixed with the fine particle fly ash, and 3) investigate the appearance of volatile metals in the complex mixture of elements present in the fine particle fraction.

A novel grate combustion reactor with a nominal output of 40 kW as well as adjustable air flows and staging of the combustion air was used to produce efficient (low CO and organics), intermediate (elevated CO) and smoldering (high CO and organics) wood chip combustion conditions. The dilution for on and off-line measurements was done with dry pressurized air using a porous tube diluter and two ejector diluters in series.

The emissions were characterized using ELPI (Dekati), SMPS (TSI) and FMPS (TSI) for number size distributions, TEOM (Thermo Scientific) and CPC (TSI) for particle mass and number concentrations, NSAM (TSI) for particle surface area, APM (Kanomax) for single particle mass measurements, as well as FTIR (Gasmet) and single gas analyzers (ABB) for measurement of gaseous compounds. Samples for chemical characterization were collected using quartz filters for OC/EC, silver filters for XRD and polycarbonate DLPI impaction plates for SEM/EDX and PIXE analyses. PM1 filter samples were collected for analysis with ICP-MS, ion chromatography (IC) and with thermal-optical carbon analyser.

Two types of electron microscopy samples were collected on holey carbon Cu-grids. First, the diluted exhaust aerosol was sampled directly. Second, the aerosol was size classified with a DMA (TSI) before sampling. The mobility diameters of 37, 40, 80, 100, 150, 220 and 250 nm were selected on the basis of the *in-situ* measurements. The electron microscope analyses were done using TEM (JEM 2100F, JEOL Ltd.) and STEM/EDS (NS7, Thermo Scientific).

Figure 1 shows the particle number size distribution for the three different conditions. Two particle phases, containing mainly of elemental carbon (soot) agglomerates (150-2000 nm) and ash (10-200 nm), were observed using TEM. The separation of soot and ash phases agrees with the study of Tissari et al. (2008). The PM1 inorganic fraction analyzed with ICP-MS and IC contained mostly K, S and Cl but also PO_4, Zn, Pb, Na, Fe, Ca and Al. Preliminary results on STEM/EDS point analyses (spot 0.5 nm) for unclassified samples suggest that the large particle fraction contained mainly C, O, K and traces of Fe, Si, S and Cl. On the other hand, Zn, Ca, P and Cr were found only in the smaller particle fraction. The size classified samples will be analysed in the near future to clarify the actual locations of the ash-forming elements.

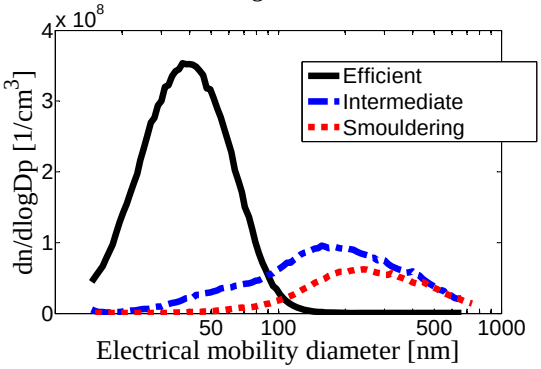

Figure 1. Averaged number size distributions from the different combustion conditions, measured with SMPS.

The combustion reactor was found to be suitable for generating different combustion conditions. Particles from efficient combustion were mainly formed of ash-forming elements and the particles had a closed structure, in agreement with Sippula et al. (2009). In contrast, in smouldering combustion large amount of chain-like agglomerates containing a large fraction of carbonaceous material was present. Furthermore, presence of trace metals was found to vary with the particle morphology.

Sippula, O., Hokkinen, J., Puustinen, H., Yli-Pirilä, P. and Jokiniemi, J. (2009) *Atmospheric Environment* **43**, 4855–4864.

Tissari, J., Lyyränen, J., Hytönen, K., Sippula, O., Tapper, U., Frey, A., Saarnio, K., Pennanen, A.S., Hillamo, R., Salonen, R.O., Hirvonen, M-R. and Jokiniemi, J. (2008) *Atmospheric Environment* **42**, 7862-7873.

Novel laboratory-scale biomass combustion reactor for studies on emission formation and ash behaviour

T. Kettunen[1], M. Kortelainen[1], O. Sippula[1], I. Nuutinen[1], H. Lamberg[1], J. Jokiniemi[1,2]

[1]Univ. of Eastern Finland, Dept. of Environmental Science, P.O. Box 1627 FIN-70211, Kuopio, Finland
[2]VTT Technical Research Centre of Finland, Fine Particles, P.O. Box 1000, FI-02044 VTT, Espoo, Finland
Keywords: Biomass burning, Combustion aerosols, drop tube furnace, boiler.
Presenting author email: Tapio.Kettunen@uef.fi

The research on combustion emissions and development of effective and low emission technologies requires a laboratory-scale biomass combustion device to model full scale combustion in large-scale plants. The aim of this work was to design and construct a laboratory setup for versatile combustion research. This includes different air staging and temperature controlling possibilities which allow wide-ranging combustion conditions. In addition, different additives can be supplied into the furnace to study ash-related problems.

The novel modular combustion setup includes a fully logic-controlled fuel feeding system, a solid-fuel burner (40 kW), a liquid fuel burner, a ceramic insulated combustion chamber, an electrically heated drop tube furnace, a boiler, a stack, and a cooling circuit. The drop tube furnace was equipped with high-temperature sampling ports for the studies on aerosol formation and ash deposition. The moving step-grate burner is designed for solid biomass e.g. wood chips, pellets, peat and is also suited to melt forming fuels. Ash melting on a grate usually causes air feed clogging and therefore the grate has three moving steps to remove melted ash layers and make fuel mixing more effective. The conditions in the reactor can be adjusted to simulate conditions in large-scale boilers, with similar temperatures (max. 1200 °C), residence times (2 s.) and turbulent flue gas flows (max. 14 m/s, Re=2000-8000). Primary and secondary air can be supplied through the burner air fans and the tertiary air through alternative points in the upper part of the chamber.

The influence of air staging on PM1 and gaseous emissions

The influences of different primary, secondary and tertiary air settings on combustion behavior and especially for PM1 and gaseous emissions were studied. The aim was also to find settings to produce different combustion conditions for a study on aerosol physico-chemical properties. Primary, secondary and tertiary air was supplied by the frequency controlled fans and the flows were measured by the air flow sensors (Schmidt). Based on the measured flow rates, lambda values (air-to-fuel ratios) for primary, secondary and tertiary combustion were determined.

The settings 1-4 were operated with total lambdas of 2.0-2.3 and primary lambdas of 0.7-1.6, respectively. The setting 5 was operated with total lambda of 1,5 leading to very low combustion efficiency and high emissions.

The flue gas composition was analyzed with a FTIR (Gasmet) and single gas analyzers (ABB). The sample for particle measurements was diluted by porous tube & ejector combination with a total dilution ratio of 36-45. The particle number concentration was measured using CPC (TSI, 3775) and particle size distributions using ELPI (Dekati) and DLPI (Dekati). PM1 samples were collected for gravimetrical and chemical analyses including thermal-optical carbon analysis (Sunset laboratories), ICP-MS and ion chromatography. The release of the fuel ash forming elements into the flue gas was evaluated on the basis of the bottom ash analysis and PM1 emissions.

PM1 emissions were between 11 mg/MJ and 22 mg/MJ and they were found to correlate with the primary lambda (Figure 1). This agrees with the study of Lamberg et al. (2009). CO emissions increased while the secondary lambda was higher, but similar correlation was not found with the primary lambda.

The new combustion reactor was found to be suitable for generating different combustion conditions. The experimental results show that air staging has a significant effect on emissions and temperature profiles on the fuel bed.

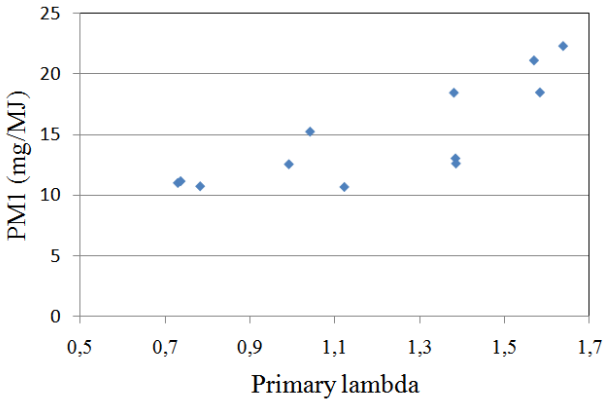

Figure 1. PM1 emission as a function of primary lambda.

The authors thank the Finnish Funding Agency for Technology and Innovation for financial support.

Lamberg, H., Sippula, O., Tissari, J., Jokiniemi, J., (2009*). 4th International Bioenergy Conference*. Book of Proceedings. Part II. 31.8-4.9.2009, Jyväskylä, Finland, 667-672.

Comparison of organic aerosol from different aircraft combustion sources using an Aerodyne Aerosol Mass Spectrometer (AMS)

P. I. Williams[1,4], M. Johnson[2], R. Marsh[3] and H. Coe[1]

[1]Centre for Atmospheric Science, University of Manchester, Manchester, M13 9PL, UK
[2] Rolls-Royce plc, PO Box 31, Derby DE24 8BJ, UK
[3] Mechanical, Manufacturing and Medical Engineering, University of Cardiff, Cardiff, CF24 3AA, UK
[4] Facility for Ground based Atmospheric Measurements, of Manchester, Manchester, M13 9PL, UK
Keywords: Aerosol, aircraft, organics.
Presenting author email: paul.i.williams@manchester.ac.uk

Emissions from aircraft engines impact both on local air quality at regional airports and climate change globally. All new engines manufactured have to pass certain emissions standards before they are certified to fly. Historically, the metric for particle emissions is the smoke number which is a measure of visibility. This metric was defined in the 1960's when inefficient combustion was causing significant air pollution around airports. As newer, more efficient engines are produced and as the concern of the impact of engine emissions shifts, a new metric is need. The main regulatory bodies in the Northern Hemisphere (CAA, EASA, FAA, EPA and FOCA) have all agreed that this new metric should be none volatile number and mass.

Work presented here is from the SAMPLE I + II studies (Study on sampling and measurement of aircraft particulate emissions) which is being used to help define the protocols and metrology of the new standard. Although none volatile particles were the focus of these studies, the volatile and semi volatile composition was also measured.

Particle measurements were made from an aircraft combustor attached to a Hot End Simulator (HES), which replicates the temperature and pressure changes of the turbines of a real engine, at the Gas Turbine Research Centre at Port Talbort. Being only the combustor section of the engine, there are no moving parts, therefore no lubrication oil. Measurements were also made on a current, modern engine at a test bed.

The chemical composition of the volatile and semi volatile particles (VP and SVP) was measured using the Aerodyne Aerosol Mass Spectrometer: for SAMPLE I the High Resolution AMS (Decarlo *et al.*, 2006); For SAMPLE II the HR and the Compact AMS.

Figure 1. Normalised organic MS for three different thrust settings from the modern engine.

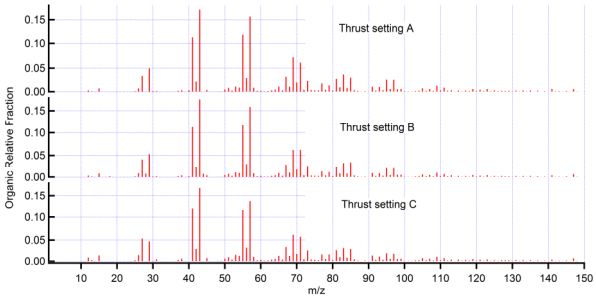

The composition of the VP and SVP was dominated by organic material with small amounts of sulphate. It was found that the organics varied between the two combustion sources. However, for the modern engine, the form of the organics did not change with changing engine conditions (thrust, see Figure 1)

The sulphate concentration was sensitive to the ambient conditions. When the inlet was switched between ambient and the combustor/HES with instances of high local loadings (>10 µg m-3), the sulphate mass remained unchanged, although the mean Dp decreased from ~450nm to ~100nm, presumably from the evaporation and re-condensation as the sulphate passed through the combustor/HES.

The results were compared with data from unprocessed engine lubrication oil. These clearly show that unprocessed lubrication oil is not the major component in the condensed organics for the modern engine (combustor/HES is lubrication oil free)

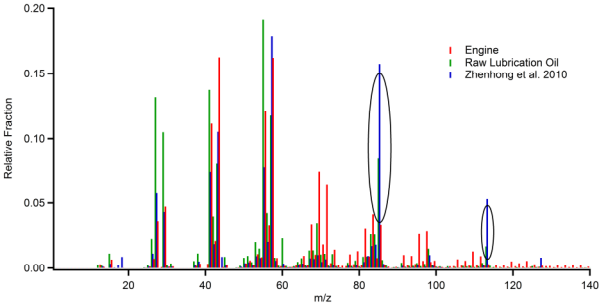

Figure 2. Comparison of organic MS for an engine, its lubrication oil and Zhenhong *et al.*, 2010.

This work was supported by EASA, grants EASA.2008.OP.13 and EASA.2009.OP.18

DeCarlo, P.F. *et al. Field-Deployable, High-Resolution, Time-of-Flight Aerosol Mass Spectrometer, Analytical Chemistry,* 78: 8281-8289, (2006)

Drewnick, F. *et al. A new Time-of-Flight Aerosol Mass Spectrometer (ToF-AMS) – Instrument Description and First Field Deployment*, AS&T, 39:637–658, (2005)

Characterisation behind a modern civil engine: investigation on new particulate certification

D. Delhaye[1], F. X. Ouf[2], D. Lottin[1], D. Ferry[3], O. Penanhoat[4] and P. Novelli[1]

[1]ONERA, Châtillon, 92322, France
[2]Aerosol Physics and Metrology Laboratory, IRSN, Gif-sur-Yvette, 91192, France
[3]CINaM-CNRS UPR 3118, Marseille, 13288, France
[4]Emissions & Regulation R&T, SNECMA / SAFRAN Group, Moissy Cramayel, 77550, France
Keywords: aircraft engine, emissions, nanoparticle, measurement (characterization).
Presenting author email: david.delhaye@onera.fr

The impact of the aviation commercial activities on the global warming and on the air quality is still a topic of needed investigations. Indeed, the actual official certification on particulate matter measurement called Smoke Number consists on the coloration of a filter. This way of the evaluation of the amount of particulate is not adapted to the new clean engine technology and to the nanoscale of the soot emitted because it does not measure mass and distinguish sizes. The French government funded a project lead by ONERA that includes a campaign of measurements behind a modern civil engine manufactured by Snecma in order to support the international effort on a better taking account of the particulate matter (SAE, 2002; SAE, 2004; SAE, 2009).

During this campaign, ICAO engine set-up test points are applied on the turboreactor. Sampling is performed through a mobile arm that allows sampling at few centimetres at a well defined location behind engine exit. Then aerosol is drive into a sampling line that follows the in place certification to measure the smoke number. From this line, a second line has been built in accordance within the Aerospace Recommended Practice (ARP) of the SAE E-31 to measure mass, number and size of the soot particles behind aircraft engine. Moreover, other properties are investigated by collection of sample on various supports like transmission Electron microscopy grids or filters. Table 1 recaps the set of instruments used.

Main results expected will be in one hand fine traverse measurements, radial and angular profiles, in term of CO2, NOx, Smoke Number, Emission Indices (number and mass) and size distribution profiles. In other hand, this campaign will contribute to the design of the final ARP with some sensibility investigation on the sampling line set-up.

Acronym	Equipment	measurements	
SN	Smoke Number	Certification reference	
LII	Laser Induced Incandescence	Mass concentration	mg/m^3
MAAP	Multi Angle Absorption Photometer	Mass concentration	$\mu g/m^3$
Pegasor®		Mass concentration	mg/m^3
CPC	Condensation Nuclei Counter	Particle number concentration	No/cm^3
SMPS+C	Scanning Mobility Particles Sizer + Condensation Nucléi Counter	Size/number distributions concentration	nm - dN/dln(dp) [$/cm^3$]
SMPS+E	Scanning Mobility Particles Sizer + Faraday Cup	Size/number distributions concentration	nm - dN/dln(dp) [$/cm^3$]
DMS 500	Differential Mobility Analyser	Size and number distributions concentration	nm - No/cm^3
MI	Mini-impactor	Physical properties (size…)	
NSAM	Nano-particle Surface Area Monitor	Specific Aera	m^2/g
EC/OC filter	Quartz filter	Elemental Carbon (EC)/ Organic Carbon (OC)	µg/m3

Table 1. Bench of instruments.

Delhaye, D. (2007) PhD Thesis, University of Aix-Marseille II.
SAE (2002) Position paper on particulate measurements, SAE E-31 committee, 3 April 2002
SAE (2004), AIR 5892: Nonvolatile Exhaust Particle Measurement Techniques, SAE
Aerospace Information Report.
SAE (2009), AIR 6037: Aircraft Exhaust Nonvolatile Particle Matter Measurement - Method Development, SAE Aerospace Information Report.

Count Size distribution of the aerosol emitted by the combustion of nanocomposites

C. Motzkus[1], C. Chivas-Joly[1], E. Guillaume[1], S. Ducourtieux[1], L. Saragoza[1], D. Lesenechal[1], T. Macé[1], F.X. Ouf[2], F. Gensdarmes[2]

[1]Air Quality and gas Flowmetering Departement, Laboratoire National de Métrologie et d'Essais, 1 rue Gaston Boissier, 75724 Paris Cedex 15, France
[2]Aerosol Physics and Metrology Laboratory, Institut de Radioprotection et de Sûreté Nucléaire, B.P 68, 91192 Gif-sur-Yvette Cedex, France

Keywords: nanocomposites, combustion, airborne nanoparticles, size-distribution.

Presenting author email: charles.motzkus@lne.fr

Day after day, new applications using nanoparticles appear in industry increasing the probability to find these particles in the workplace as well as in ambient air and thus their potential adverse effects on health of exposed workers and general population. Both assessments of these risks, preventive actions, and remediation, when needed, will rely on the measurements and characterization of nanoparticles. Consequently, it is necessary to improve our knowledge in this field to assess the potential toxicology risks; it is particularly important to characterize aerosols emitted by different sources of emission; like for example, during the combustion of composites filled with nanoparticles.

The present work is the continuation of the study led in the framework of the NANOFEU project supported by the French Research Agency (ANR). For this project, several partners (INERIS, LNE, Ecole des mines d'Alès, ISMANS and PlasticsEurope France) collaborated to characterize the fire behaviour of polymers filled with suitable nanoparticles (Chivas *et al.*, 2010).

An experimental setup has been developed to measure the count size distribution of the emitted aerosol produced during the combustion of different formulations of polymers containing nanocomposites. This setup is composed of a Differential Mobility Spectrometer (DMS500 / Cambustion) and a Scanning Mobility Particle Sizer (DMA 3080L + CNC 3022 / TSI) coupled with a cone calorimeter according to standard ISO 5660-1. The sampling flow rates of the DMS 500 and the CNC used are respectively equal to 8.0 l/min and 1.2 l/min. The cone calorimeter main duct is modified in order to minimize the deposition of soot on the 90° angle of the exhaust duct, and also to allow aerosol sampling at a point where the effluent can be considered as homogeneous. The heat flux is fixed at 50 kW/m², with the standard ventilation rate of 24 l/s. The sampling probe diameter has been selected to respect isokinetic conditions.

A Diluter FPS-4000 (DEKATI) coupled at the equipments has been used. This diluter is well adapted for fire effluent dilution because of its two-stages dilution setup. The first dilution stage is heated, and the second operates at ambient temperature. This system allows aerosol dilution, avoids condensation and particle perturbation compared to a simple cold dilution. The dilution ratio used is equal to 28:1. The samples of polymers containing nanocomposites are sized to 50x50x4 mm³ (corresponding to around 12 g of material, depending of the polymer matrix).

The evolution of the characteristics of the aerosol emitted during the combustion of the different polymers is very important. The advantage of the DMS 500 compared to SMPS is to provide real-time measurement (10Hz) on a large scale (5 to 1000 nm) which allows comparison between kinetics of aerosol production according to the kinds of polymers which are burned in different tests. First experiments were carried out with the DMS in a way to point out the mode diameters of the particles produced during the combustion. The Figure 1 presents the count size distribution of the aerosol obtained for Polyamide-6 filled with carbon nanotubes (CNT) measured by DMS 500.

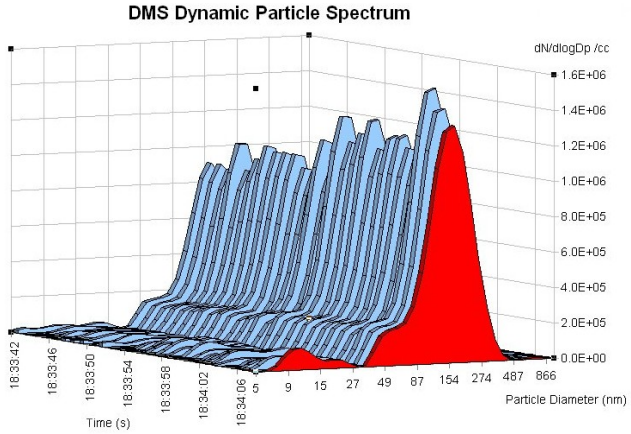

Figure 1. Count size distribution of the aerosol obtained in the case of combustion of PA-6 filled with CNT

Further measurements of kinetic of the particles concentration were performed with the CNC at the DMS 500 mode electrical mobility diameters observed fixed on the DMA (13.3, 23.7 and 200 nm). Several polymers (PMMA–, PA-6) containing another nanofillers (silica and alumina) were investigated.

Chivas-Joly C, Guillaume E, Ducourtieux S, Saragoza L, Lopez-Cuesta J M, Longuet C, Duplantier S, Bertrand J, Calogine D, Minisini B (2010) *Proc. Conf. INTERFLAM 2010*, Nottingham.

ISO 5660-1 2002 Reaction to fire tests - Heat release, smoke production and mass loss rate - Part 1: Heat release rate (cone calorimeter method).

Structure and reactivity of laboratory-produced soot containing iron

H. Bladt[1], J. Schmid[1], E. Kireeva[2], O. Popovicheva[2], R. Niessner[1] and N. P. Ivleva[1]

[1]Chair for Analytical Chemistry, Technical University Munich, Munich, 81377, Germany
[2]Institute of Nuclear Physics, Moscow State University, Moscow, 119991, Russia
Keywords: combustion aerosols, iron oxides, Raman spectroscopy.
Presenting author email: bladt@tum.de

It is widely accepted that Black carbon (BC), produced by incomplete combustion of fossil fuel, has a major influence on climate and human health (Dockery, 1994). Therefore, it is necessary to evaluate the effect of transport emission on the environment and to define the resultant limitations by determination of the specific characteristics of particle emission of different vehicles and different fuels. The objective is to develop methods for characterization of soot composition, structure and reactivity in accordance with the current requirements.

Among others, metal contaminations of multicomponent aerosols produced by diesel and gas turbine engines due to fuel additives, oil contaminations, or corrosion may be accumulated on the surface of the particles or inside them. Those impurities can cause significant changes in the physical and thermo-chemical properties of soot as they may catalyze the oxidation of soot particles in a thermite-analogue reaction. Especially heavy fuel used by large marine engines exhibits a high amount of inorganic impurities of transition, earth and alkaline metals (Popovicheva *et al*, 2009).

In-depth investigations of composition, structure and reactivity of soot aerosols internally mixed with metal compounds are performed. Therefore, Raman-Microspectroscopy (RM) is applied for structural characterization of the carbonaceous soot fraction as shown by Schmid *et al* (accepted 2011) as well as for identification of metal contaminations in soot. Further comprehensive characterization is performed by scanning electron microscopy (SEM), FTIR spectroscopy, Temperature-Programmed-Desorption (TPD) and -Oxidation (TPO) as well as by conventional thermal methods used for measuring elemental (EC), organic (OC) and total carbon (TC) contents in soot samples in order to evaluate the impact of elemental composition, surface chemistry, nanostructure, organic fraction (OC) and metal compound content on the soot oxidation behavior.

In present experiments emphasis is placed on soot internally mixed with iron compounds. Iron is a relevant metal component that can be found for example in soot emission of shipping. Two different laboratory approaches for the production of iron-containing soot are conducted. The first approach is a test-bench including a diffusion burner unit. Propane as fuel gas is burned in an oxygen stream. The flame is fed with a nitrogen stream charged with iron pentacarbonyl and soot is sampled on quartz fiber filters. RM at λ_0 of 633 nm reveales signals in the lower shift range from 200 to 800 cm^{-1} in addition to the characteristic disordered (D) and graphitic (G) bands of soot at 1350 and 1600 cm^{-1}, respectively (Figure 1). Burning of the filter samples in an oxygen stream revealed an orange residue. Two different iron oxide species could be characterized on the thermally treated filter by RM. Species 1 could be identified to be hematite due to significant Raman bands at 225, 292, 411, 498, 610, 657 and 1318 cm^{-1}. Species 2 to can be assigned to be a mixture of hematite and magnetite due to the observation of significant bands for hematite and additional bands for magnetite at 540 and 665 cm^{-1}.

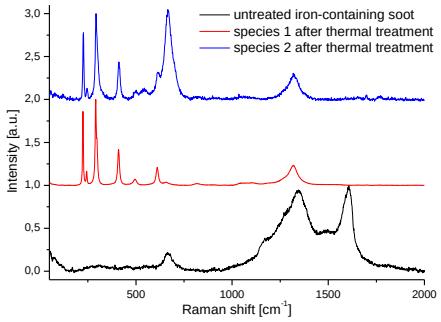

Figure 1. Raman spectrum of iron-containing soot untreated and thermally treated.

The other laboratory approach for the production of iron-containing soot was undertaken by burning diesel fuel mixed with ferrocene with an oil lamp. SEM images reveal the specific morphology of those soot particles containing 10 wt% of iron (Figure 2).

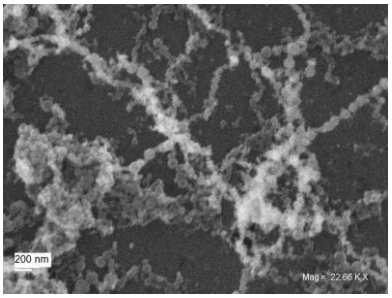

Figure 2. SEM image of soot produced by burning diesel fuel mixed with ferrocene.

This novel approach shall be applied to investigate different soot aerosols from different sources. In particular, the characterization of ship engine exhaust residuals by heavy fuel burning is planned.

Dockery, D. W. and Pope, C. A. III. (1994) *Annu. Rev. Public Health* **15**, 107-13.

Popovicheva, O., Kireeva, E., Shonija, N. et al (2009) *J. Env. Mon.* **11**, 2077-86.

Schmid, J., Grob, B., Niessner, R. and Ivleva, N. P. (accepted 2011) *Analytical Chemistry*.

Analysis of carbonyl compounds emissions from a heavy-duty diesel engine fueled with paraffinic/biodiesel blends

T.Y. Wu[1,2], Y.C. Lin[3,*], Y.M. Chen[4]

[1] Department of Materials Engineering, Kun Shan University, Tainan 71003, Taiwan
[2] Department of Chemistry, National Cheng Kung University, Tainan 70101, Taiwan
[3] Institute of Environmental Engineering, National Sun Yat-Sen University, Kaohsiung 804, Taiwan
[4] Sustainable Environment Research Center, National Cheng Kung University, Tainan 701, Taiwan
Keywords: Emission factor, Emissions, Diesel exhaust, Combustion aerosols.
Presenting author email: yuanchung.lin@gmail.com

Diesel engines have higher fuel efficiency, power output, fuel economy, and lower emissions of traditional pollutants such as hydrocarbons (HCs) and carbon monoxide (CO) than gasoline-powered engines. The alternative fuels such as biodiesels are being widely discussed in many countries because they used as alternative fuels in diesel engines can reduce HCs and CO emissions (Lin *et al.*, 2006; Yuan *et al.*, 2007). Carbonyl emissions are a part of the exhaust of diesel engines, the main goal of the present study is to analyze CBCs emission factor and emissions of CBCs from HDDEs (heavy-duty diesel engine), especially for formaldehyde and acetaldehyde.

The fuel specifications of the five test fuels are D100, P100, P20, PF80P20, and PF95P05. The total CBC emission factors of them in the exhaust of the HDDE are shown in Tables 1, the total CBC emission factors of D100, P100, P20, PF80P20, and PF95P05 were 1360, 1440, 1370, 1070, and 966 mg L^{-1}, respectively. Using P100 and P20 instead of D100 in the HDDE increased CBC emissions by 80.0 and 10.0 mg per liter-fuel, respectively. However, using PF80P20 and PF95P05 instead of D100 in HDDEs decreased CBC emissions by 290 and 394 mg per liter-fuel, respectively.

Table 1. CBC emission factor (mg L^{-1}) in the exhaust of the HDDE fueled with various biodiesel blends.

CBCs	D100	P100	P20	PF80 P20	PF95 P05
Formaldehyde	988	1086	1036	782	679
Acetaldehyde	32.6	52	42.8	31.6	25.4
Acrolein	47.3	59.2	51.3	38.2	44.9
Acetone	30.5	47	37.6	20.1	25.8
Propionaldehyde	41.2	49.1	43.9	26	33.2
Crotonaldehyde	38.3	41.6	39.6	30.7	34.3
Butyraldehyde	13.1	7.8	8.62	9.87	9.24
Benzaldehyde	14.7	8.4	10.8	11.5	10.5
Isovaleraldehyde	33	17	19.2	29.1	25.7
Valeraldehyde	2.54	3.32	3.09	1.3	1.64
o-Tolualdehyde	2.23	0.838	1.35	1.75	1.47
m-Tolualdehyde	56.7	34.8	40.2	44.8	38.5
p-Tolualdehyde	35.2	22.4	24.2	27	23.6
Hexaldehyde	15.7	9.77	11.4	13	10.1
2,5-Dimethyl-benzaldehyde	5.76	2.54	4.36	3.2	2.28
Sum	1360	1440	1370	1070	966

The emission factor and concentrations of regulated harmful matters (traditional pollutants) in the exhaust of the HDDE are shown in Table 2. The emissions of PM, THC, and CO for D100 were mostly higher than those for other test fuels, indicating palm-biodiesel is an oxygenated fuel that improves combustion efficiency. The added fraction of palm-biodiesel should be restricted to be less than 20 vol%. P20, PF80P20, and PF95P05 can reduce the emissions of THC, CO, CO_2, NO_x, and PM as compared to D100. From the results of emission factor, using P20 instead of D100 in the HDDE reduced THC by 22.9%, CO by 4.91%, CO_2 by 3.65%, NO_x by 6.00%, and PM by 9.64%. Using PF95P05 and PF80P20 instead of D100 in the HDDE reduced THC by 39.0–46.46%, CO by 34.0%, CO2 by 1.37–7.60%, NO_x by 12.2–24.3%, and PM by 11.1–11.8%. Similar results were found for emission concentrations.

Table 2. Emission factor (EF) and emission concentrations (EC) of regulated harmful matters (traditional pollutants) in the exhaust of the HDDE fueled with various biodiesel blends.

CBCs	Regulated harmful matters	D100	P100	P20	PF80 P20	PF95 P05
EF	CO (g BHP^{-1} h^{-1})	2.85	2.88	2.71	1.88	1.88
	CO_2 (g BHP^{-1} h^{-1})	658	654	634	649	608
	THC (g BHP^{-1} h^{-1})	0.608	0.515	0.469	0.326	0.371
	NO_x (g BHP^{-1} h^{-1})	6.5	6.13	6.11	5.71	4.92
	PM (g BHP^{-1} h^{-1})	0.289	0.35	0.261	0.255	0.257
EC	CO (ppm)	40.2	40	38.2	26.5	26.5
	CO_2 (ppm)	5880	5780	5690	5810	5450
	THC (ppm)	17.4	14.5	13.4	9.3	10.6
	NO_x (ppm)	55.9	51.8	52.4	48.9	42.2
	PM (mg m^{-3})	4.73	5.63	4.26	4.16	4.19

These analytical results indicate that PF95P05 and PF80P20 are feasible for traveling diesel vehicles (TDVs). Replacing D100 with PF95P05 significantly decreased total CBC (30.3%), PM (11.1%), THC (39.0%), CO (34.0%), NO_x (24.3%), and CO2 (7.60%) emissions. The wide usage of paraffinic–palmbiodiesel blends as alternative fuels could protect the environment.

This work was supported in part by the National Science Council under grant NSC-97-2218-E-110-009.

Lin, Y.C., Lee, W.J., Hou, H.C. (2006) *Atmospheric Environment* **40**, 3930–3940.
Yuan, C.S., Lin, H.Y., Lee, W.J., Lin, Y.C., Wu, T.S., Chen, K.F. (2007) *Journal of the Air &Waste Management Association* **57**, 465–471.

Persistent organic pollutants emitted from a municipal solid waste incinerator

K.L. Huang[1], S.J. Chen[1,*], M.S. Wang[2], C.C. Lin[1], and C.L. Chou[3]

[1]Department of Environmental Science and Engineering, National Pingtung University of Science and Technology, Pingtung County, Nei Pu, 91201, Taiwan
[2]Department of Chemical and Materials Engineering, and Super Micro Mass Research & Technology Center, Cheng Shiu University, Kaohsiung City, 83347, Taiwan
[3]Content Engineering Consulting Services, Ltd., New Taipei City, Zhonghe Dist., 23553, Taiwan
Keywords: Municipal solid waste incinerators, brominated flame retardants, persistent organic pollutants.
Presenting author email: huangkl@mail.npust.edu.tw

Persistent organic pollutants (POPs), such as chlorinated and brominated aromatics, have been of great concern because of their persistence in the global environment. POPs are lipophilic and may bioaccumulate in the food chain, posing a potential threat to human health (Jones and de Voogt, 1999). Many such compounds (such as polychlorinated dibenzo-*p*-dioxins and dibenzofurans [PCDD/Fs], polybrominated dibenzo-*p*-dioxins and dibenzofurans [PBDD/Fs], polybrominated diphenyl ethers [PBDEs], polychlorinated biphenyls [PCBs], and polybrominated biphenyls [PBBs]) are considered to act as environmental hormones, which disrupt the reproductive cycles of humans and wildlife (Lohmann et al., 2001; Kim et al., 2004; Mari et al., 2008). With the extensive usage of PBDEs as brominated flame retardants (BFRs), they have been found in the emission of municipal solid waste incinerators (MSWIs). However, little attention has been paid to the study of closely related brominated compounds emitted from MSWIs, partially due to the lack of standard methods for sampling and analyzing these compounds.

In this study, the characteristics of five target compounds (2,3,7,8-substituted PCDD/Fs and PBDD/Fs, PBDEs, PCBs, and PBBs) in the stack flue gases of a large-scale continuous MSWI (capacity: 1350 tons/day) were investigated. The stack flue gas sampling procedures were collected isokinetically following U.S. EPA Modified Method 23 using U.S. EPA Modified Method 5 samplings train (USEPA, 2001). ^{13}C-labeled internal standards (ISs) (PCDD/Fs, PBDD/Fs, PBDEs, and PCBs) were added to samples that were then extracted for 24 h in *Soxhlet* extractors with toluene. The extract was concentrated by rotary evaporation in an N_2 gas stream, and then transferred to a vial. The concentrated extract was then treated by a series of simultaneous sample cleanup and fraction procedures, including the use of silica gel, alumina, and active carbon columns. A higher solution gas chromatograph/high-resolution mass spectrometer (HRGC/HRMS) was used for PCDD/Fs, PBDD/Fs, PCBs, PBDEs, and PBBs analyses.

The mean PCDD/F, PBDD/F, PCB, PBDE, and PBB concentrations in stack gases of an MSWI were 0.0719 ng WHO-TEQ/Nm^3, 0.00169 ng WHO-TEQ/Nm^3, 0.00546 ng WHO-TEQ/Nm^3, 20.7 ng/Nm^3, and 0.958 ng/Nm^3, respectively (Fig. 1). Although the dioxin-like PCBs and PBDD/Fs represented only 6.9% and 2.1%, respectively, of the total WHO-TEQ (the sum of PCDD/Fs, PBDD/Fs, and dioxin-like PCBs), the MSWI is regarded as a potential source that may emit dioxin-like compounds.

The emission factors of PCDD/Fs, PBDD/Fs, PCBs, PBDEs, and PBBs were 0.300 µg WHO-TEQ/ton-waste, 0.00667 µg WHO-TEQ/ton-waste, 0.0207 µg WHO-TEQ/ton-waste, 84.5 µg/ton-waste, and 1.05 µg/ton-waste, respectively, in flue gases of the MSWI (Fig. 2). Therefore, in addition to PCDD/Fs, the emissions from MSWIs of other dioxin-like compounds (such as BFRs) should also be concerned.

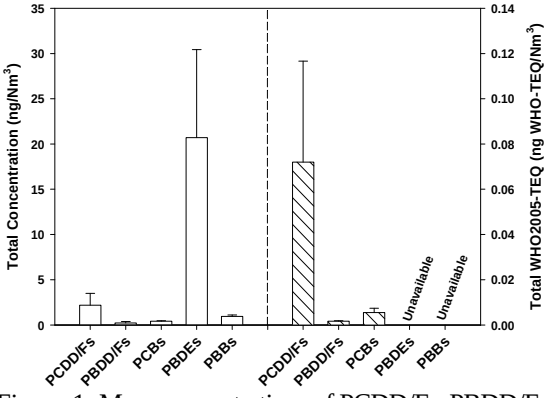

Figure 1. Mean concentrations of PCDD/Fs, PBDD/Fs, PCBs, PBDEs, and PBBs in stack flue gases of the MSWI.

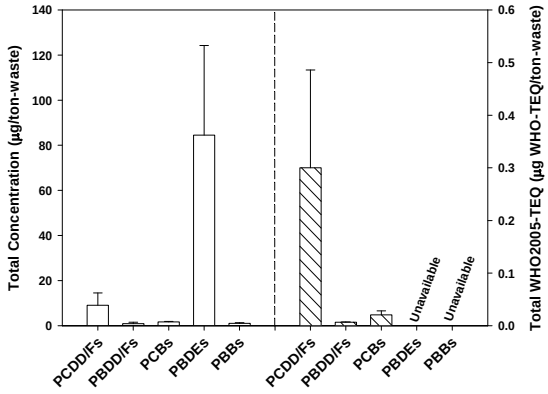

Figure 2. Mean emission factors of PCDD/Fs, PBDD/Fs, PCBs, PBDEs, and PBBs in stack flue gases of the MSWI.

Jones, K.C. and de Voogt, P. (1999) *Environ. Pollut.* **100**, 209–221.
Kim, K.S., Hirai, Y., Kato, M., Urano, K. and Masunaga, S. (2004) *Chemosphere* **55**, 539–553.
Lohmann, R., Ockenden, W.A., Shears, J. and Jones, K.C. (2001) *Environ. Sci. Technol.* **35**, 4046–4053.
Mari, M., Nadal, M., Schuhmacher, M. and Domingo, J.L. (2008) *Chemosphere* **73**, 990–998.
US EPA (2001). *Determination of particulate emission from stationary sources*, Method 5.

Enrichment of trace metal by particle size Emissions from steel foundries

J.J. Rodríguez-Maroto[1], J.L. Dorronsoro-Arena[1], D. Sanz-Rivera[1], E. Rojas-García[1], M. Fernández-Díaz[2], P. Galán-Valera[2] and E. Conde Vilda[2]

[1] Departamento de Medioambiente, CIEMAT, Avda. Complutense 22, 28040, Madrid, Spain
[2] Departamento de Tecnología, CIEMAT, Avda. Complutense 22, 28040, Madrid, Spain
Keywords: Aluminium smelter, emissions, heavy metal, PM10, PM2.5, PM1.
Presenting author email: jesus.maroto@ciemat.es

In the foundry industry, the emissions to air arise from the storage, handling, pre-treatment and pyro-metallurgical stages. With the purpose to obtain a data base of emissions from ferrous and non-ferrous metal foundries in Spain, a measurement program was planned and is being carried out. One of the data to be assessed is the size distribution of the particulate matter PM: PM10, PM2.5 and PM1, as well as the size distribution of metals that could accompany it in these emissions.

To carry out this aim, seven steel foundries have participated in the study. Cast steel is normally melted in electric arc furnaces (EAF) or in coreless induction furnaces (IF). Once melted, the liquid metal can be refined and deoxidised, depending on the base material and the quality requirement of the finished product. PM is emitted from metal melting, sand moulding, casting and finishing. A series of campaigns was made to sample, to evaluate the dust fractionation and to analyze the metallic traces in emissions coming from melting stage.

Sampling and measurement was carried out in accordance with US EPA 201A and VDI 2066/5 procedures using three types of cascade impactors: Mark III with eight collection stages and DEKATI 30LPM or KS207 Kalman System GMBH with three stages. The samples of collection substrates were chemically analyzed according to method EPA IO-3.1 as previous step to the determination by ICP-OES and/or ICP-MS and FAAS.

Four ranges of particle aerodynamic diameter have been analyzed, dp (in microns): dp>10, 10>dp>2.5; 2.5>dp>1; dp<1.

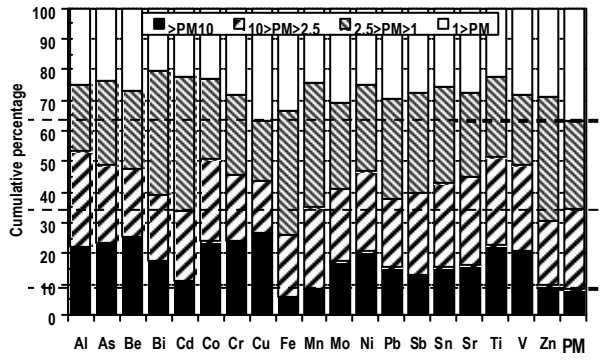

Figure 1. Distribution of metals and particulate matter, PM by size

The total concentrations of particles, PM and metals in the emissions varied in more than one order of magnitude. Also, it was observed significant dispersions in the metals distribution data by particle size.

The distribution of metallic traces by size not always agrees with the distribution of total mass of particles. This means that an enrichment of trace metal occurs for certain particle size ranges.

The predominant interval is the submicron range (36 % of the emitted total mass). Only eight percent of PM corresponds to particles bigger than ten micron. Al, Cu, Fe, Mn, Pb, Sb and Zn were found to be the main metals by mass in PM (higher than 102 $\mu g/Nm^3$). All of the metals except Fe and Mn enrich the fraction of particles larger than 10 microns.

Most of these effects have its origin in the heterogeneity into the furnace bed and the differences in the emission gas cleaning systems. The first one is mainly due to selection and pre-treatment of raw material used (scrap containing impurities and other secondary materials, also the addiction of fused salt and recovered from slag and other additives used to bind the sand) with diversity of shapes and chemical composition. The second one is due to the different cooling system technologies (air injection, heat exchanger, etc.) and separators (cyclone, sedimentation chamber, bag filter…) used in each foundry.

This work was supported by the Ministry of the Environment and Rural and Marine Environs. Special thanks to UNESID (Spanish Association of Companies Producing Steel and Primary Steel Processing Products.) and to each one of the staffs of facilities.

European Commission, (2005). *Integrated Pollution Prevention and Control BREFT on BAT in the Smitheries and Foundries Industry.*
Ehrlich C. et al. (2007). *Atmospheric Environment 41 (2007) 6236–6254.*
Su-Ching Kuoa et al. (2007). *Atmospheric Environment 41 (2007) 6884–6900.*

Tuesday, September 6, 2011

Session 4P: Poster Session A:
Atmospheric Aerosols - Aerosol Processes and Properties

How accurate are the nucleation event analysis tools?

H. Korhonen[1], S.-L. Sihto[2], V.-M. Kerminen[3] and K. E. J. Lehtinen[1,4]

[1]Kuopio Unit, Finnish Meteorological Institute, Kuopio, Finland
[2]Department of Physics, University of Helsinki, Helsinki, Finland
[3]Climate Change, Finnish Meteorological Institute, Helsinki, Finland
[2]Department of Applied Physics, University of Eastern Finland, Kuopio, Finland

Keywords: nucleation, growth, modelling
Presenting author email: hannele.korhonen@fmi.fi

According to current knowledge, atmospheric nucleation events initiate at a particle diameter of ~1.5 nm. However, until very recently, most field instruments measuring the aerosol size distribution have had a low-end cut-off at ~3 nm. Therefore, several mathematical approaches have been developed in order to quantify nucleation rates at the initial cluster size as well as nucleation mechanisms from the measured distribution data (e.g., Sihto et al., 2006; Kuang et al., 2008).

We have evaluated these analysis tools with over 1200 numerical nucleation events for which the nucleation mechanism and formation rates are known exactly. We have tested the performance of different formulations of the tools as well as the sensitivity of the results to the various assumptions that have to be made in the analysis. In order to resemble the atmospheric measurement data as closely as possible, the model output was regridded into typical size channels of a DMPS instrument with 10-minute time intervals.

We find that calculating the growth rate of sub-3 nm clusters from the time delay between the diurnal curves of H_2SO_4 and 3-6 nm particle concentration can overestimate the growth rate during strong nucleation events. This is because of coagulation scavenging of the clusters to the earlier formed nucleation mode, which can under some conditions lead to apparent negative time delays. However, the cases in which the time delay remains positive but is shortened compared to time delay corresponding to the actual growth rate are more problematic for the analysis.

In general, the particle formation rate at 3 nm (J_3) is captured reasonably well by the analysis tools with 43-97% of the events falling within a factor-of-two accuracy from the actual simulated value. However, the accuracy of the analysed values show clear sensitivity to the specific form of the analysis equations used and assumptions made about the initial size of nucleating clusters. On the other hand, the estimates of the actual nucleation rate at 1.5 nm were clearly less accurate with only 37-59% of the events within a factor-of-two accuracy. The main reason for the large errors is that the analysis methods do not take into account the size-dependence of particle growth rates below 3 nm. Moreover, the results are also sensitive to the assumption made about initial cluster size.

The poor estimates of $J_{1.5}$ can lead to fairly large uncertainties in the nucleation prefactors (i.e. constant P in nucleation equation $J_{1.5} = P \times [H_2SO_4]^k$). However, all the analysis set-ups tested in this study resulted to an order-of-magnitude accuracy for almost 90% of the simulated events. This can be considered reasonable since the coefficients derived from atmospheric data typically exhibit a variation of 1-3 orders of magnitude. This indicates that the high variation of observed nucleation prefactors is not a consequence of inaccuracies in the analysis methods, but a real phenomenon caused by (so far unknown) environmental factors.

Large uncertainties were found also when the analysis tools were used to determine the nucleation mechanism in terms of the number of H_2SO_4 molecules in a critical cluster (i.e. exponent k in previous equation). Although our results suggest that in general the analysis tools tend to overestimate the number of H_2SO_4 molecules in the critical cluster, also significant underestimation was found in up to 41% of the cases. This indicates that one cannot automatically rule out more than 2 sulphuric acid molecules in a critical cluster even if field data shows nucleation exponents in the range 1-2. Our analysis also suggests that combining data from several new particle formation events to scatter plots of H_2SO_4 vs formation rates ($J_{1.5}$ or J_3) and determining the slope of the regression line may not give reliable information about the nucleation mechanism.

This work has been supported by the Computational Science Research Programme of the Academy of Finland (decision: 135199) and EU's Sixth Framework Program (EUCAARI project).

Kuang, C., McMurry, P. H., McCormick, A. V., and Eisele, F. L. (2008) *J. Geophys. Res.*, 113, D10209, doi:10.1029/2007JD009253, 2008.

Sihto, S.-L., Kulmala, M., Kerminen, V.-M., Dal Maso, M., Petäjä, T., Riipinen, I., Korhonen, H., Arnold, F., Janson, R., Boy, M., Laaksonen, A., and Lehtinen, K. E. J. (2006) *Atmos. Chem. Phys.*, 6, 4079-4091.

Classification of Nucleation Events during the Summer Period in Thessaloniki, Greece: Kerbside versus urban background measurements

D. Siakavaras[1], C. Samara[2], C. Pilinis[1], M. Petrakakis[3], A. Kelesis[3], G. Biskos[1,4]

[1] Department of Environment, University of the Aegean, Mytilene 81100, Greece
[2]Department of Chemistry, Aristotle University of Thessaloniki, Thessaloniki 54124, Greece
[3]Environmental Department, Municipality of Thessaloniki, Paparigopoulou 7, Thessaloniki 54630, Greece
[4]Faculty of Applied Science, Delft University of Technology, Delft 2628-BL, The Netherlands

Keywords: nucleation events, number size distribution, SMPS, classification

Thessaloniki is one of the most densely populated urban centers of Greece suffering from high concentrations of atmospheric particulate matter (PM). The physical and chemical properties of PM as well as the size distributions of ultrafine aerosol particles (i.e., particles having diameter smaller than 1 μm) in the atmosphere over the city have been determined by a number of previous studies (e.g., Voutsa *et al*., 2002; Manoli *et al.,* 2002; Samara *et al*., 2003; Terzi *et al*., 2010; Siakavaras *et al*., 2008).

In the present study we report particle nucleation and growth events observed at a kerbside and an urban background monitoring station in Thessaloniki during the summer period. The two monitoring stations (Venizelou – kerbside site, and Eptapyrgio – urban background site) exhibit the maximum and minimum levels of PM_{10} and $PM_{2.5}$ in Thessaloniki (Petrakakis *et al*., 2007). Two identical Scanning Mobility Particle Sizers (TSI Model 3034) have been employed to measure simultaneously the size distributions of the particles having diameters in the range 10-487 nm at the two sites. Gaseous pollutants (CO, NO_x, SO_2 and O_3) and meteorological parameters (wind speed, wind direction, temperature and relative humidity) were also recorded during the measurements. The experiments were conducted during two summer periods (June to September 2007 and June to October 2009).

Nucleation events were observed at 27% of the days at Venizelou (kerbside site) and at 29% of the days at Eptapyrgio (urban background site). Regional growth events when the increase in particle number concentration having diameters less than 20 nm, N_{20}, lasted for several hours occurred at 20% and 23% of the nucleations at Venizelou and Eptapyrgiou, respectively. The rest of the events were short-lived and did not exhibit growth of the nucleation mode particles to larger sizes.

Depending on the net rate of increase in N_{20} during the first hour of the event (dN_{20}/dt) we further classified the events as weak and strong (Figure 1). In all cases the observed nucleation events started in the morning and were more frequent during July at Venizelou and during July and September at Eptapyrgio. The observations of the events correlated well with high concentrations of SO_2 and NO_x.

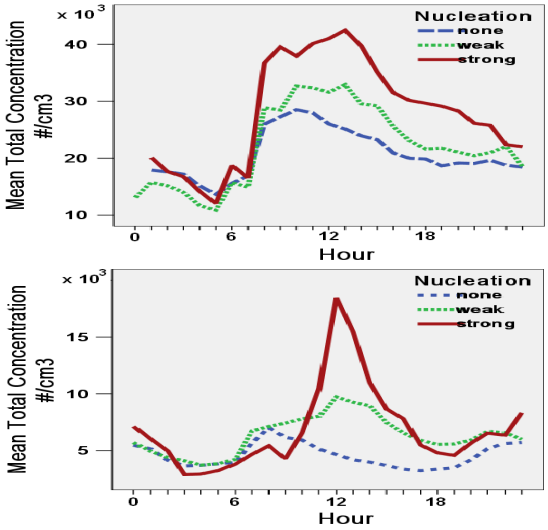

Figure 1. Diurnal particle number concentration vs time for days that exhibit no, weak and strong nucleation events at Venizelou (upper part) and Eptapyrgio (lower part)

References

Manoli, E., Voutsa, D., Samara, C. (2002). *Atmospheric Environment*, 36, 949-96.

Voutsa, D., Samara, C., Kouimtzis, Th., Ochsenkuehn, K. (2002). *Atmospheric Environment*, 36, 4453-4462.

Samara, C., Kouimtzis, Th., Tsitouridou, R., Kanias, G., Simeonov, V. (2003). *Atmospheric Environment,*37, 41-54.

Siakavaras, D., Samara, C., Pilinis, C., Kelesis, A. *EAC2008, Thessaloniki, Greece, August 24-29, 2008 (*Abstract T02A043P).

Terzi, E., Argyropoulos, G., Bougatioti, A., Mihalopoulos, N., Nikolaou, K., Samara, C. (2010). *Atmospheric Environment,* 44, 2231-2239.

Petrakakis, M.J., Kelessis, A.G., Samara, C., Tzoumaka, P., Zoumakis, N.M., Iosifidis, E. CEMEPE 07*, Skiathos, June 24-28, 2007* (Proceedings pp 2471-2477).

Acknowledgements
The SMPS used in this study was obtained through the AKMON 5 project, co-funded by the European Regional Development Fund (70%) and the Greek Ministry of Development (30%).

Time-frequency analysis of aerosol number concentrations in Europe – 28 day period in nucleation and the (lack of) weekly cycle in CCN-sized particles

A. Asmi
Department of Physiucs, University of Helsinki, Helsinki, FI-00014 UHEL, Finland
Keywords: wavelets, CCN, nucleation, field study.
Presenting author email: ari.asmi@helsinki.fi

Two aerosol-climate interactions are directly connected to cyclicity of aerosol particles. The potential of cosmic-ray or sun-mediated variation in new particle formation, has been under extensive scientific interest. Similarily, a correlation between potentially anthropogenic weekly cycle of particle concentrations and several meteorological parameters has been proposed.

We follow the work of Asmi *et al* (2011), where the EUSAAR measurements did not show any weekly cycle in the CCN-sized aerosol number concentrations. By using long-period measurements from 3 stations in Europe (SMEAR II and Pallas in Finland, Melpitz in Germany), we can extract the time-frequency variations of both nucleation and CCN-sized particles to detect any weekly or monthly cycles in the aerosol concentrations. We used all of the available data from the stations and thus have at longest almost 14 years of continuous dataset. The method used is discrete wavelet analysis, which provides us time-frequency spectra of the concentrations (Torrence and Compo, 1998).

We see no clear signal in weekly or weekly-type (e.g. 5 or 2 days) variation of CCN-sized aerosol in the stations (Fig 1A). This suggests that the number concentration of CCN-sized aerosols are not strongly varying with anthropogenic work week, at least in regional background. The low signal of weekly-type variations do not support indirect aerosol effect based weekday or weekend cycles in European boundary layer regional background.

The nucleation mode results show that the 28 days cycle can be seen in the nucleation mode aerosol concentrations in *almost every spring* at SMEAR II station and visible in all stations (Fig 1B). This period is the same as solar rotation period and related parameters, such as neutron counts on surface and hemispheric energetic particle deposition (Fig 1B bottom). More support on this potential hypothesis comes from the fact that the month-like periodicities of solar-related parameters also are strongest in spring and autumn. The mechanism how this periodicity would actually influence the nucleation rates is not, however, easily defined. To study this phenomena closer, we separated the times of opposite phases of the periodic oscillation in nucleation. By analysing re-analysis weather information during these periods, we noticed that the oscillation was connected to periodic oscillation between of high and low pressure systems around North sea and Barents sea, already discovered by Rinne and Järvenoja (1995). This suggests that the observed 28 day periodicity in nucleation is more likely of meteorological origin, and the underlying reason for the oscillation is periodic Arctic air outbreaks to Scandinavia.

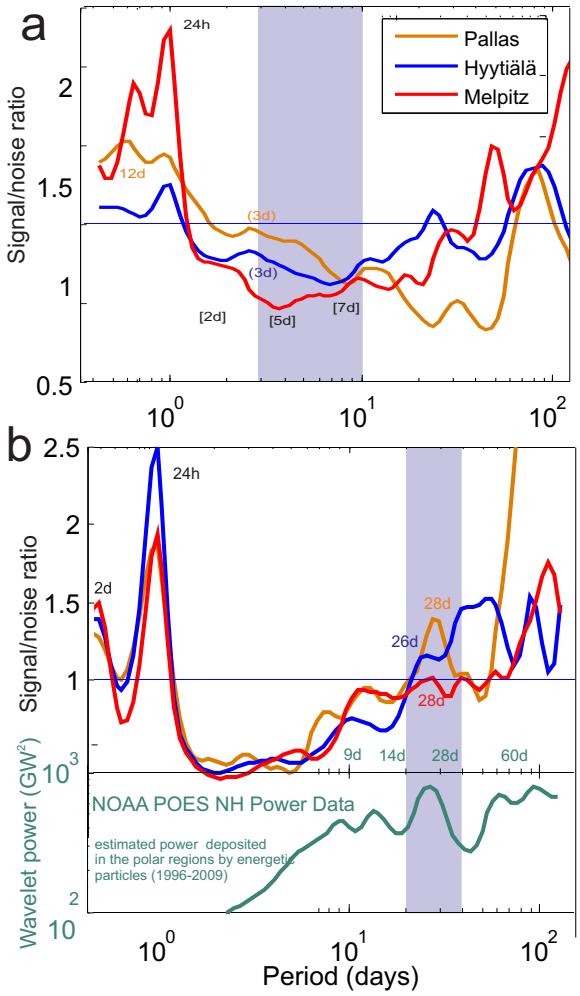

Figure 1: A) Global wavelet power compared to background red noise of $d_p > 100$ nm particles B) Same for of $d_p < 10$ nm, NOAA POES global wavelet power shown for comparison

This work was supported by the EUCAARI and EUSAAR projects and by the Finnish Academy.

Asmi, A. et al, (2011) Atmospheric Chemistry and Physics. (Submitted).

Rinne, J and Järvenoja S. (1995), Tellus, **47A**, 561–574

Torrence, C. and Compo, P.C. (1998) Bulletin of the American Meteorological Society, **79**, p 61–78

Regional extent of new particle formation

N. Kivekäs[1], E. Asmi[1], H. Lihavainen[1], M. Komppula[1], A-P. Hyvärinen[1], Y. Viisanen[1], P. Aalto[2], T. Nieminen[2], B. Svenningsson[3] and A. Arneth[4]

[1]Research and Developments, Finnish Meteorological Institute, Helsinki, PO. Box 503, Finland
[2]Department of Physics, University of Helsinki, Helsinki, 00101, Finland
[3]Department of Nuclear Physics, Lund University, Lund, 223 62, Sweden
[4]Department of Physical Geography and Ecosystems Analysis, Lund University, Lund, 223 62, Sweden
Keywords: Particle formation, Particle growth, Ambient aerosols, DMPS
Presenting author email: niku.kivekas@fmi.fi

Atmospheric new particle formation (NPF) has been observed all around the world, often by using continuous particle size distribution measurements at a fixed location. In Class I NPF event a new mode of particle is observed in small size classes, and the mode grows to larger sizes when time passes on (Dal Maso *et al*., 2005). As air mass passes over the measurement site, the measurements at different time points do not represent the same air parcel. The fact that the growth of the mode can be observed at a fixed location is usually explained by assuming that new particles are formed over a large area simultaneously.

The duration of a Class I event can be calculated from the time the new mode appears and the latest time the same mode can be observed (figure 1). This also tells us how long the last observed particles have been in the air. When air mass trajectories are available, this information can be used to determine where the new particles were formed. The last observed particles are the ones formed furthest (along the trajectory) from the station. Later in this abstract this point referred as the event-start-location of the NPF event.

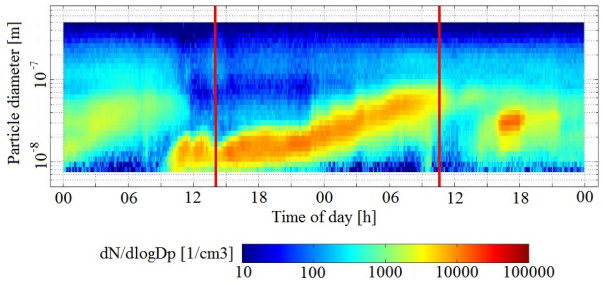

Figure 1. A Class I new particle formation event observed at Pallas April 22-23, 2002. The vertical red lines show the starting time and ending time of the event.

10 years of DPMS data from Pallas Global Atmosphere Watch (GAW) station in northern Finland was analysed (Asmi *et al*., 2011). FLEXTRA trajectories (Stohl *et al*, 1995) were used to calculate the arriving path and speed of the air mass. Total of 68 Class I NPF events were found. Most of these events were associated with air masses arriving to the site from North-Atlantic or Arctic Ocean, and very few Class I events were observed in air masses originating from south or south-east.

Some of the event-start-locations were traced to be far on the ocean while some were clearly inland. Yet 65% of the event-start-locations were within 150 km from the Atlantic- or Arctic Ocean coastline, and 52% within 100 km (figure 2). The 100 km distance from the shoreline is well within the uncertainty of the trajectories and the uncertainty caused by the estimation of the start- and end times of the events.

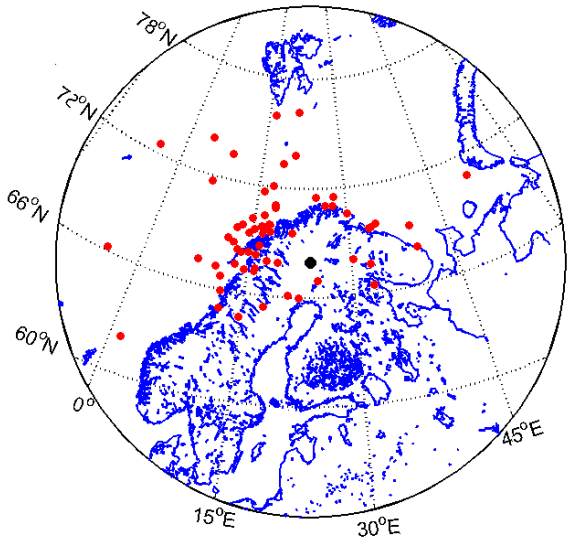

Figure 2. The event-start-locations of the 68 observed Class I new particle formation events (red). The black dot is the location of Pallas measurement site.

Future work will include more detailed analysis of the NPF events in order to separate those cases where the observed end of the growing mode is caused by clear air mass change or meteorological change. Also data from other stations in Northern Scandinavia will be analysed in order to see whether they give similar results on the regional extent of new particle formation. One of the main goals of this investigation is to resolve whether the commonly used assumption of the spatial homogeneity of the new particle formation events over the same air mass is well justified around the Pallas site.

Asmi, E., Kivekäs, N., Komppula, M., Hyvärinen, A-P., Hatakka, J., Viisanen, Y. and Lihavainen, H. *Abstract in the European Aerosol Conference 2011 proceedings*.

Dal Maso, M., Kulmala, M., Riipinen, I., Wagner, R., Hussein, T., Aalto, P. and Lehtinen, K. (2005) *Bor. Environ. Res*. 10, 323-336.

Stohl, A., Wotawa, G., Seibert, P. and Kromp-Kolb, H. (1995) *J. Appl. Meteor*. 34, 2149-2165.

Over 10-years of new particle formation and growth in sub-Arctic Pallas station

E. Asmi[1], N. Kivekäs[1], M. Komppula[1], A.-P. Hyvärinen[1], J. Hatakka[1], Y. Viisanen[1] and H. Lihavainen[1]

[1]Finnish Meteorological Institute, Erik Palménin aukio 1, 00560 Helsinki, Finland
Keywords: particle formation and growth, Arctic aerosols, long-term trend, DMPS.
Presenting author email: eija.asmi@fmi.fi

Secondary new particle formation (NPF) has been recognised as an important source of atmospheric aerosol particles worldwide (Kulmala *et al*. 2004). Yet, there are numerous open questions on how this process proceeds or what its climatic importance at different geographic regions is. These questions relate to e.g. particle formation mechanisms, compounds involved in the process, environmental boundaries required as well as the ability of freshly formed tiny particles to grow up to the sizes of climatic relevance. To contribute for answering these questions, we analysed nearly 11-years (April 2000 – December 2010) of continuous measurement data from Finnish sub-Arctic GAW (Global Atmospheric Watch) station Pallas with the focus on NPF events. We classified the days into NPF event, undefined and non-event days following Dal Maso *et al.* (2005), determined the particle formation and growth rates, examined which factors (air mass properties, local meteorology, condensation sink, sulphuric acid concentration, etc.) promote or hinder particle formation, analysed the long-term trends, and in addition, the probability of particles to grow up to the CCN (Cloud Condensation Nuclei) sizes.

The analysis of NPF relied on Differential Mobility Particle Sizer (DMPS) measurements on particle number size distributions (Komppula *et al*. 2003). From the measured distributions, we determined the particle formation and growth rates following the procedure presented in Komppula *et al.* (2003). Auxiliary data on local meteorological variables, as well as on air mass backward trajectories, calculated with FLEXTRA (Stohl *et al.* 1995), were used. Sulphuric acid has been suggested to be a key parameter in atmospheric NPF, and while lacking the direct measurement of H_2SO_4, we used a proxy based on global radiation, condensation sink (CS) and SO_2 (Petäjä *et al.* 2009).

Seasonal variation of NPF events was congruent with previous studies, showing a spring maximum and a winter minimum (Komppula et al 2003). Equally, NPF was found to be favoured by clean Arctic air masses and bright, sunny weather. The observed seasonal trend was by a large part explained by inter-annual changes in climatic and meteorological conditions. Monthly median growth rates varied within the limits of 1.9 and 4.6 nm h^{-1}, being highest in summer months, and as such providing evidence of the significance of organic vapours for the particle growth.

The inter-annual trend of NPF days versus non-event days suggests a decrease in the beginning of the decade and vice versa, increases in the end of the decade (Fig. 1). As the external climatic and meteorological quantities seemed to predict the NPF occurrence fairly well, we developed a proxy for NPF based on air mass origin, visibility and global radiation. It however turned out that this proxy was insufficient for predicting the inter-annual trend and thus other non-specified factors played a role in particle formation, our best guess of these being the quantity of nucleating or condensable vapours.

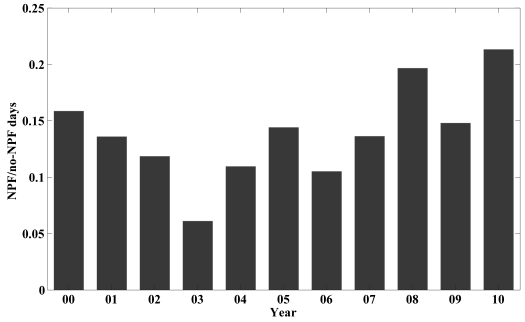

Figure 1. NPF days vs. non-event days – 11 year trend.

Finally, the climatic impact of NPF was examined by separating the events with the growing mode exceeding 80 nm size, previously found to be a good approximation of CCN size limit in Pallas (Komppula et al 2005). In 34% of the class I (for definition, see Dal Maso *et al.* 2005) events this limit was reached with the maximum probability of CCN_{80} formation in summer season. This is in agreement with the higher growth rates observed in summer. We may conclude on the climatic importance of NPF that while the observable CCN_{80} formation from NPF was infrequent, its impact on CCN number was large; the average increase in CCN_{80} number by NPF was 211 %.

Dal Maso, M., Kulmala, M., Riipinen, I., Wagner, R., Hussein, T., Aalto, P.P. and Lehtinen K.E.J. (2005) *Boreal Environ. Res*. **10**, 323-336.

Komppula, M., Lihavainen, H., Kerminen, V.-M., Kulmala, M. and Viisanen, Y. (2005) *J. Geophys. Res.* **110**(D06204), doi: 10.1029/2004JD005200.

Komppula, M., Lihavainen, H., Hatakka, J., Paatero, J., Aalto, P., Kulmala, M. and Viisanen, Y. (2003) *J. Geophys. Res.* **108**(D9), 4295.

Kulmala, M., Vehkamäki, H., Petäjä, T., Dal Maso, M., Lauri, A., Kerminen, V.-M., Birmili, W. and McMurry, P.H. (2004) *J. Aerosol Sci.* **35**, 143-176.

Petäjä, T., Mauldin III, R.L., Kosciuch, E., McGrath, J., Nieminen, T., Paasonen, P., Boy, M., Adamov, A., Kotiaho, T. and Kulmala M. (2009) *Atmos. Chem. Phys*. **9**, 7435-7448.

Stohl, A., Wotawa, G., Seibert, P. and Kromp-Kolb, H. (1995) *J. Appl. Meteor*. **34**, 2149-2165.

Characterization of New Particle Formation Events in Kuopio, Finland Based on a three-year analysis

A. Hamed[1], H. Portin[1,2], A. Leskinen[2], M. Komppula[2], K.E. J. Lehtinen[1,2], S. Romakkaniemi[1], J.N. Smith [1,3], J. Joutsensaari[1] and A. Laaksonen[1, 4]

[1] Department of Applied Physics, University of Eastern Finland, P. O. Box 70211 Kuopio, Finland
[2]Finnish Meteorological Institute, Kuopio Unit, P.O. Box 1627, FIN-70210 Kuopio, Finland
[3]National Center for Atmospheric Research, P.O. Box 3000, Boulder, CO 80307, USA
[4]Finnish Meteorological Institute, P.O. Box 503, 00101 Helsinki, Finland

Keywords: Nucleation, Aerosol formation, Emission sources, Particle formation and growth.

The new aerosol particles formed by atmospheric nucleation is a global phenomenon proven to take place in different atmospheric environments (Kulmala et al., 2004). A direct chemical analysis of particles < 5 nm in diameter is not technically feasible at the moment; therefore, knowledge on the atmospheric nucleation and particle growth mechanism and its governing circumstances has only been gathered indirectly, for instance by time series analysis of the number concentration of freshly formed particles, gas phase precursor, and meteorological variables. A comparison of sufficiently long atmospheric data sets in different environments is expected to reveal useful information on how different sources and transformation processes modify properties of aerosol particles.

Here, we study, for the first time, the new particle formation (NPF) at the Puijo tower research station. The station is on the top of the Puijo tower; 62° 54′ 32″ N, 27° 39′ 31″ E, and 306 m a.s.l and 224 m above the surrounding lake and located about 2 km northwest of the center of Kuopio city, Eastern Finland. Details of the station can be found in Leskinen et al. (2009).

The quantification of aerosol nucleation in the Puijo research station took place from June 2006 to November 2009. The Puijo data set is unique in the sense that the surroundings of the station are different in each side. There are distinct sectors for cleaner and more polluted air, which give us a good opportunity to investigate the effects of local emission sources on aerosol particle formation. Our analysis uses the measured particle number size distribution (measurements were carried out using a twin DMPS system (Differential Mobility Particle Sizers) at the Puijo site, with particle size ranges of 7-800 nm), trace gas concentrations (SO_2, NO_x, O_3) and basic meteorological variables (T, RH , P, wind speed and wind direction).

In the process of the NPF analysis from Puijo research station, the particle formation events were identified and classified into three different categories according to the local emission sources; Class 1 includes normal NPF days (similar to what has been observed in different environments) with very high number particle concentrations and clear growth of the newly formed particles that last for many hours; Class 2 includes clean NPF days (with relatively low growth rates and low amount of SO_2 concentrations); and Class 3 includes polluted NPF days caused by local sources (with high amount of SO_2 concentrations when the wind comes from N, NE directions, see Fig. 1).

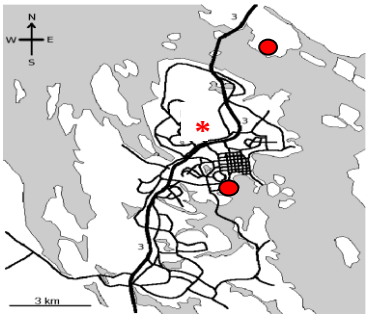

Figure1. The location of Puijo measurement station in Kuopio, Finland, marked by red star, red circles show the location of point sources nearby. The lake is in gray. The highway is marked by number 3.

The number of NPF days were the highest when the wind comes from north and northeast where there is a pulp mill located ~5km from the site (Fig.1). This facility is considered a potential source of high concentrations of SO_2, NO_x and particles, but not soot. We observed moderate numbers of NPF days in which the wind is from the clean biogenically dominated sector to the west. Emissions from a nearby freeway and also the city center of Kuopio, located southeast of Puijo, are associated with higher levels of SO_2, NO_x and particles (especially soot) and showed high number of NPF events. Fewer NPF days of were observed when the wind was from the east, another relatively clean sector.

This pre-study emphasizes the diversity of sources that exist in the Kuopio region, and the interplay between NPF events and local emissions motivates the ongoing comprehensive analysis.

This work is financially supported by the North Savo Regional Foundation.

Kulmala, M., *et al.* (2004). *J Aerosol Sci*, **35**,143-176
Leskinen, A., *et al.* (2009). *Boreal Env. Res.*, **14**, 576-590

SOA formation from stress induced biogenic VOC emissions and the contribution of isoprene to particle formation and growth – lessons learned from grey poplar trees

E. Kleist [1], T. Mentel [2], A. Kiendler-Scharr [2], S. Broch [2], M. Springer [2], K. Behnke [3], J.-P. Schnitzler [3], R. Tillmann [2], S. Andres [2], F. Rubach [2], B. Steitz [2], J. Wildt [1]

[1] Institute Plant Sciences, IBG-2, Research Centre Jülich GmbH, 52428 Jülich, Germany
[2] Institute Troposphere, IEK-8, Research Centre Jülich GmbH, 52428 Jülich, Germany
[3] Institute of Biochemical Plant Pathology, Department Environmental Engineering, German Research Center for Environmental Health (GmbH), 85764 Neuherberg, Germany

Keywords: particle formation and growth, SOA formation potential, Biogenic VOCs.
Presenting author email: e.kleist@fz-juelich.de

Vegetation is the major source of biogenic volatile organic compounds (BVOC) in the troposphere. These BVOC impact atmospheric oxidation capacity and serve as precursors for secondary organic aerosols (SOA). In regions with low pre-existing particulate matter, BVOC oxidation by OH, ozone, and NO_3 can produce low volatile products which are involved in SOA formation.

Isoprene and monoterpene emissions from vegetation are well known. However, during and after stress situations plants emit many other BVOC. Sesquiterpenes (SQT) such as α- and β-farnesene, C_6-aldehydes and -alcohols produced within the octa-decanoid pathway (green leaf volatiles, GLV), or many different aromatic compounds originating from the phenylpropanoid pathway are typical BVOC emitted during biotic and abiotic stress.

In this study we measured the formation of secondary organic aerosols (SOA) from stress-induced BVOC emissions emitted from grey poplar seedlings (*Populus x canescens*). The experiments were conducted in the Jülich Plant Atmosphere Chamber (JPAC, Mentel *et al*., 2009). This system consists of two temperature controlled chambers, one housing the plants (plant chamber) and the second one was used for photochemical SOA production (reaction chamber). BVOC emitted from the poplar plants in the plant chamber were transferred into the reaction chamber where they were oxidized by ozone and by OH radicals. OH was produced by photolysis of ozone in presence of H_2O. OH concentrations were typically in the range of 3-8×10^7 cm^{-3}. Ambient conditions such as temperature, relative humidity, photosynthetic active radiation (PAR), CO_2, O_3, and NO_x levels were controlled.

We used 4-month-old wild type (WT) poplar plants that emit high amounts of isoprene and transgenic poplar lines down-regulated in isoprene emission (R-lines, Behnke *et al.*, 2007). Comparing particle formation from BVOC emitted from these plants enabled the characterization of the impact of isoprene on the SOA formation from plant emissions. Unstressed poplar plants emitted nearly exclusively isoprene whereby the emissions from the down regulated R-lines were more than an order of magnitude lower than those from the wild type. Using unstressed plants as BVOC sources for particle formation we found inefficient SOA formation with nucleation rates far below 1 cm^{-3} s^{-1}.

All lines showed strong additional emissions of sesquiterpenes and aromatic compounds after stressing the plants by short ozone pulses. Their emission rates and therefore the BVOC emission pattern changed on a time scale of several days after stress application, allowing to study SOA formation under nearly steady state conditions. Feeding BVOC mixes into the reaction chamber resulted in very strong SOA formation events with nucleation rates exceeding 3000 cm^{-3} s^{-1}. Normalized to the BVOC turnover the nucleation rates were generally lower for the isoprene emitting WT poplars compared to non-emitting mutants. This observation confirmed former findings of suppression of nucleation by isoprene (Kindler-Scharr *et al*., 2009).

Rapid variations of PAR in the plant chamber resulted in fast changes of isoprene emissions whereas the emissions of the other BVOC responded on a much longer time scale. Hence, switching off the lamps in the plant chamber allowed removing isoprene very fast while keeping the level of other BVOC concentrations high. Conducting this procedure during a particle formation event caused a fast decrease of isoprene concentration and a strong increase of OH concentrations in the reaction chamber followed by increases in particle number and mass. This also shows that suppression of OH concentrations by isoprene is the major reason for suppression of nucleation from non-isoprene BVOC.

Using a low isoprene emitting poplar plant as BVOC source and adding deuterated isoprene from a diffusion source we estimated isoprenes' contribution to the SOA mass formed from the BVOC emitted from poplar. While isoprene contributed to about 7% [C/C] to the BVOC in the gas phase the contribution to the particulate phase was only 1 %. Thus isoprene oxidation products partitioning into the SOA can not compete with that of oxidation products from the other BVOCs. However the SOA mass produced by isoprene oxidation products does not compensate the decrease of other BVOC particle precursors caused by the decrease of OH concentrations in the presence of isoprene.

Behnke *et al.* (2007) Plant J., **51**, 485–499,
Kiendler-Scharr, A. *et al.* (2009), *Nature*, **461**, 381-384,
Mentel, T. F. *et al.* (2009), *ACP*, **9**, 4387-4406

Sulfuric acid measurements with CI-TOF-MS

T. B. A. Jokinen[1], M. Sipilä[1], T. Petäjä[1], M. Kulmala[1], D. R. Worsnop[1], and H. Junninen[1]

[1]Department of Physics, University of Helsinki, P.O.Box 64, Helsinki, Finland

Keywords: sulfuric acid, chemical ionization, mass spectrometry.
Presenting author email: tuija.jokinen@helsinki.fi

Sulfuric acid is a key compound in atmospheric nucleation (Sipilä et al., 2010). In atmosphere sulfuric acid is produced mainly photochemically via reaction of OH with SO_2. Concentration of sulfuric acid is typically very low, rarely exceeding 10^8 molecules cm^{-3} (e.g. Paasonen et al., 2010). The low concentrations set certain requirements for the detector to be used for quantitative measurements. Method for measuring gas phase sulphuric acid by means of chemical ionization mass spectrometer were developed by Eisele and Tanner (1993). They used nitrate ion, NO_3^-, and its clusters with nitric acid, HNO_3, for selective chemical ionization of H_2SO_4 via $NO_3^-\cdot(HNO_3)_n + H_2SO_4 \rightarrow n(HNO_3) + (HNO_3)\cdot HSO_4^-$. Resulting $(HNO_3)\cdot HSO_4^-$ clusters together with remaining $NO_3^-\cdot(HNO_3)_n$ were dissociated and HSO_4^- and NO_3^- were detected with a quadrupole mass spectrometer.

Here we present a measurement system in which the atmospheric pressure chemical ionization inlet, with geometry similar to Eisele and Tanner (1993), is combined with a high resolution atmospheric pressure interface time-of-flight mass spectrometer (Tofwerk Ag., Junninen et al., 2010). In the present setup, clusters are not broken on purpose, instead the high resolution and mass range of the TOF allows separation and summing of different clusters. Advantage of the method is that it allows one to seek for neutral sulphuric acid containing clusters formed by nucleation in the atmosphere (Kuang et al., 2008) or in laboratory systems (Sipilä et al., 2010).

In this laboratory experiment we generated reagent ions by mixing a small amount of nitric acid to nitrogen flow and exposed it to a radioactive source (^{241}Am). Sulfuric acid vapour is produced by leading synthetic air through a saturator containing pure 95-97% H_2SO_4. Sulfuric acid vapour was then introduced to the CI inlet with multiple different flow rates and diluted with laboratory air to create a constant sample flow of 10 lpm. The mixing with the reagent ions is done by applying voltage between a set of ion lenses.

The sample is guided to the TOF for mass per charge (m/Q) determination. Pressure is reduced to 10^{-6} mbar and by three separately pumped chambers. Ions are guided to TOF using two quadrupoles and an ion lens assembly. We operated TOF in negative ion mode to monitor sulfuric acid and its dimer, trimer and tetramer at m/Q 97, 195, 293, 391 and nitric acid monomer, dimer and trimer at m/Q 62, 125 and 188.

Figure 1 shows increase in deprotonated sulfuric acid concentration when flow rate trough the saturator is elevated from 0.1 lpm to 9,5 lpm. With flow rates under 1 lpm we only detect sulfuric acid monomer and dimer but at elevated flow rates, < 2 lpm, we can detect bigger clusters forming also. Nitric acid is been neutralized during ionization process which can be seen in descending signals of NO_3^-, its dimer and trimer.

The aim is to use CI-TOF-MS to measure aerosol clusters in ambient air and coupling CI with TOF-MS now offers an effective and selective way of ionizing and detecting ambient neutral sulfuric acid and its clusters.

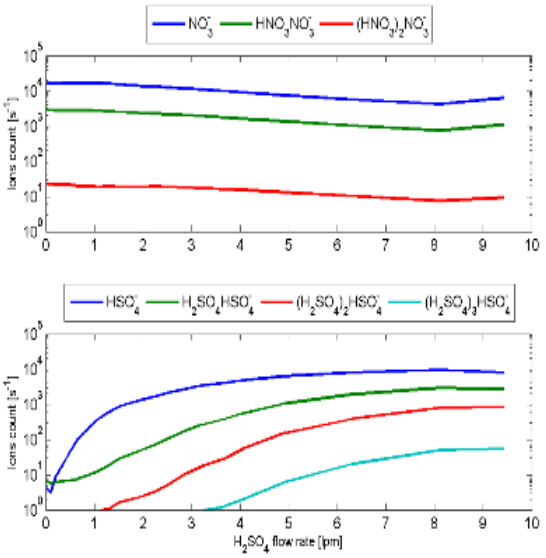

Figure 1. Sulfuric acid and reagent ion concentrations in CI-TOF-MS spectrum.

This work was supported by the Academy of Finland Centre of Excellence program and KONE foundation.

Sipilä, M., Berndt, T., Petäjä, T., Brus, D., Vanhanen, J., Stratmann, F., Patokoski, J., Mauldin III, R. L., Hyvärinen, A.-P.,Lihavainen, H., and Kulmala, M., *Science*, 327, 1243–1246, 2010.

Paasonen, P., Nieminen, T., Asmi, E., Manninen, H.E., Petäjä, T., Plass-Dülmer, C., Flentje, H., Birmili, W., Wiedensohler, A., Hõrrak, U., Metzger, A., Hamed, A., Laaksonen, A., Facchini, M.C., Kerminen, V.-M. and Kulmala, M., *Atmos. Chem. Phys. Discuss*. 10, pp. 1795–11850, 2010.

Eisele, F. and Tanner, D, *J. Geophys. Res*., 98, 9001–9010, 1993

Junninen, H., Ehn, M., Petäjä, T., Luosujärvi, L., Kotiaho, T., Kostiainen, R., Rohner, U., Gonin, M., Fuhrer, K., Kulmala, M. and Worsnop, D.R., *Atmos. Meas. Technol. Discuss.*, 3, pp. 599-636, 2010.

Kuang C., McMurry, P. H., McCormick, A. V., Eisele, F. L., *J. Geophys. Res.*, 113, 2008

New aerosol particle formation and event classification in Hungarian background air at K-puszta

Zs. Bécsi[1], Á. Molnár[2], K. Imre[1], T. Nieminen[3], J. Hakala[3], T. Petäjä[3] and M. Kulmala[3]

[1]Department of Earth and Environmental Sciences, University of Pannonia, Veszprém, P.O. Box 158, H-8201, Hungary
[2]Air Chemistry Group of the Hungarian Academy of Sciences, University of Pannonia, Veszprém, P.O. Box 158, H-8201, Hungary
[3]Department of Physics, University of Helsinki, Helsinki, P.O. Box 64, FI-00014, Finland
Keywords: fine and ultrafine fractions, nucleation, number size distribution, particle formation and growth, seasonal patterns.
Presenting author email: becsi.zsuzsanna@gmail.com

New particle formation events can be observed all over the world both in polluted and background air and have been studied for a long time because of the climatic and health effects of the fine particles. Data on new particle formation in Hungarian background air is rather sparse. However, a DMPS (Differential Mobility Particle Sizer) installed in 2007 operates at the Hungarian background air monitoring station and provides aerosol data in order to study the particle formation and growth. The study of the size distribution, the diurnal and seasonal variation in the occurrence of the maximum number concentrations helps to get more information on the parameters, reasons and processes which lead to new particle formation events.

In this work we summarize our results on the particle formation at K-puszta station between Nov. 2008 and Nov. 2009. The time resolution of the DMPS measurements makes the study of the particle formation and growth possible. The size distribution of the particles between 3-800 nm is evaluated. On the basis of DMPS spectra the classification of particle formation events was carried out according to the recommendations of Yli-Juuti *et al* (2009). The event classification was studied with respect to the seasonal variation and the frequency of the particle formation event types (event, non-event and unclassified) was also discussed.

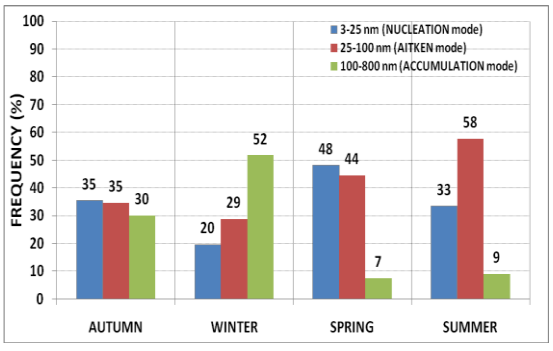

Figure 1. The seasonal frequency of the maximum concentrations in different particle modes.

In new particle formation (NPF) winter was the most inactive period. In winter the total number concentration and the number of NPF events were the lowest during the year due to the unfavourable ambient conditions (lowest solar radiation, weak or lack of photochemical processes and aerosol precursors). The number of NPF events was found to be the highest in spring while a second peak occurred in autumn.

On the basis of the data the frequency of the daily maximum concentrations with respect to the particle size mode was also calculated (Figure 1). The frequency of the nucleation mode (3-25 nm) was the highest during spring and autumn. On the other hand, in winter the accumulation mode (100-800 nm) showed the highest, while in spring and summer the lowest frequency. In autumn all the three modes were evenly distributed.

The growth rate of the freshly formed particles can also be calculated (Hirsikko *et al* (2005), Yli-Juuti *et al* (2009). Our preliminary results show that at K-puszta the particle growth rate is highly variable, it can reach even the 14 $nmhr^{-1}$.

It is well-known that meteorological parameters play an important role in new particle formation. In this work the relationship between new particle formation and meteorological parameters like temperature, wind speed and direction, relative humidity, precipitation, global radiation was also studied.

This work was supported by the FP6 projects: European Integrated project on Aerosol Cloud Climate and Air Quality Interactions (EUCAARI, contract No: 036833-2) and European Super-sites for Atmospheric Aerosol Research (EUSAAR, contract No: RII3-026140).

Yli-Juuti, T., Riipinen, I., Aalto, P.P., Nieminen, T., Maenhaut, W., Janssens, I.A., Claeys, M., Salma, I., Ocskay, R., Hoffer, A., Imre, K. and Kulmala, M. (2009) *Boreal Env. Res.* **14**, 683-698.

Hirsikko, A., Laakso, L., Hőrrak, U., Aalto, P., Kerminen, V.-M. and Kulmala, M. (2005) *Boreal Env. Res.* **10**, 357-369.

Performance of an Ultrafine Diethylene Glycol (DEG) based Condensation Particle Counter

Wimmer, Daniela[1], Fabian, Kreissl[1], Metzger, Axel[1], Kürten, Andreas[1], Curtius, Joachim[1], Riccobono, Francesco[2] Lehtipalo, Katrianne[3] and the CLOUD collaboration.

[1]Institute for Atmospheric and Environmental Sciences, Goethe University of Frankfurt, Frankfurt, Germany
[2]Paul Scherrer Insitute, Villigen, Switzerland
[3]Department of Physics, University of Helsinki, Helsinki, Finland

Keywords: nucleation, nano particles, DEG CPC, working fluid, CLOUD experiment

The physical as well as the chemical properties of nano particles are of special interest in various scientific fields, e.g. when atmospheric nucleation events are studied or within the wide field of nano-technology and its applications. Especially for nucleation studies it is crucial to achieve the lowest cut-off diameter possible in order to derive accurate numbers for the nucleation rates (Sipilä et al., 2010). Standard commercial condensation particle counters rely on the activation of aerosol particles using butanol as the condensation fluid and achieve lower cut-off diameters around 2.5 nm. However, using diethyleneglycol (DEG) as the condensation liquid cut-offs well below 2 nm have been realized (Iida et al., 2010). Due to the low vapour pressure of DEG, particles only grow to sizes ~100nm and are therefore too small to be directly detected with the optical systems usually used. This means, whenever using DEG as working liquid a second CPC (the so-called 'booster') is needed to grow the already activate particles further to count them optically.

For the work presented here we modified a standard TSI 3776 ultrafine butanol CPC. The modifications that were necessary are the following. (1) The wick which is used for the butanol version cannot be wetted by DEG therefore it was replaced by a cellulose filter. This filter was wrapped around a perforated stainless steel tube housed in the saturator part of the CPC. (2) Since the TSI software does not allow for controlling the saturator temperature to values larger than 50°C, an additional temperature control was established. It consists of a Pt1000 installed in a bore inside the saturator block and a Watlow PID heat control. (3) The optics part of the CPC was removed and instead an adapter piece was attached to the outlet of the condenser in order to connect it to the second booster CPC. Test measurements were performed to determine the highest saturatuor temperature where no homogeneous nucleation occurs while having the condenser at a fixed temperature of 10°C. This saturator temperature was found to be 52°C.

Detailed calibration measurements were carried out where the DEG CPC was compared to different TSI CPCs and a particle size magnifier (PSM, Vanhanen et al. 2011). The cut-off curves were determined for these CPCs using a high resolution DMA (Herrmann DMA, Hermann et al., 2000) for classifying the particles. Several different methods were used to generate test aerosol particles. These include an electrospray source providing different mobility standards, a Grimm WO_x generator (model nr.: 7.860), a tube furnace for NaCl particles and H_2SO_4 particle generator. Due to its special design the high resolution DMA cannot classify particles bigger than 4nm in mobility diameter. Therefore to provide bigger particles a Grimm nano-DMA (model nr.: 5.710) was used. The CPC concentrations were normalized by the concentrations obtained from two different electrometers (models 5.705 and 3068B). A cut-off curve for the DEG-CPC is shown in Figure 1.

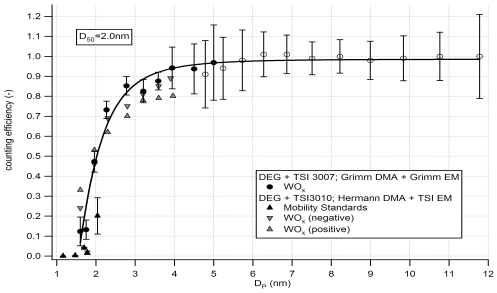

Figure 1 Cut-off curve of the DEG CPC using different types of particles.

During these measurements a TSI 3010 was used as the booster CPC. The cut-off diameter (the size where 50 % of the particles are being detected) of the DEG CPC is 2nm in mobility diameter for this measurement.

The instrument described in this work has also shown to work reliably during a long time period. It was operated during the CLOUD 2010 fall campaign at CERN.

Further tests with the CPC will be performed using a particle generator providing sulphuric acid particles. In addition we would like to test the performance of the CPC in a cool chamber where we can both set and control the temperature well below 0°C, since the temperatures in the CLOUD chamber should be decreased further (down to -90°C)

We would like to thank CERN for supporting CLOUD with important technical resources, and for providing a particle beam from the CERN Proton Synchrotron. This research has received funding from the EC's Seventh Framework Programme under grant agreement number 215072 (Marie Curie Initial Training Network "CLOUD - ITN"), from the German Federal Ministry of Education and Research (project number 01LK0902A), from the Swiss National Science Foundation and from the Academy of Finland Center of Excellence program (project number 1118615).
We would also like to thank TSI Inc., especially Oliver Bischof for providing us important equipment.

Iida, Kenjiro, Stolzenburg, Mark R. and McMurry, Peter H. (2009) *Effect of Working Fluid on Sub-2 nm Particle Detection with a Laminar Flow Ultrafine Condensation Particle Counter*, Aerosol Science and Technology, 43:1, 81 — 96

Herrmann, W., Eichler, T., Bernardo, N., and Fernandez de la Mora, J. (2000). Turbulent Transition Arises at Reynolds Number 35,000 in a Short Vienna Type DMA with a Large Laminarization Inlet. *Annual Conference of the AAAR, St. Louis, Mis souri.*

Vanhanen, J. et al, (2011) *Particle Size Magnifier for Nano-CN Detection*, Aerosol Science and Technology, 45: 4, 533 — 542

Sipilä, M. et al, 2010, *The Role of Sulphuric Acid in Atmospheric Nucleation,* Science

Physical characterization of ions in the CLOUD chamber

A. Franchin,[1], S. Schobesberger[1], K. Lehtipalo[1], V. Makhmutov[2], Y. Stozhkov[2], S. Gagné[1], T. Nieminen[1], H. E. Manninen[1], T. Petäjä[1], M. Kulmala[1] and the CLOUD collaboration.

[1]Department of Physics, University of Helsinki, P.O. Box 64, FI-00014, Helsinki, Finland
[2]Lebedev Physical Institute RAS, 119991, Moscow, Russia.
Keywords: atmospheric ions, ion-induced nucleation, sulfuric acid, CLOUD experiment.
Presenting author email: alessandro.franchin@helsinki.fi

Nanoparticle formation in the boundary layer is a frequent phenomenon (Kulmala *et al.*, 2004). Sulfuric acid has been identified as a plausible candidate to participate in the nucleation (Weber et al. 1996). Ion-induced nucleation is one of the possible pathways for new particle formation in the atmosphere, but it is still unclear how important the contribution of ions is with respect to neutral pathways. Ion concentration and their size distribution are key quantities to understand ion-induced nucleation processes and dynamics.

During the CLOUD (Cosmics Leaving OUtdoor Droplets) 2010 fall campaign, several experiments of sulfuric acid-water neutral and ion-induced nucleation were performed in an aerosol chamber. In this experiment, Galactic Cosmic Rays (GCR) and the Proton Syncrotron (PS) accelerator at CERN were used as sources to generate ions in the 26.1 m^3 CLOUD aerosol chamber under precisely controlled conditions. Both GCR and the PS pion beam were constantly monitored by a GCR counter and by a hodoscope, respectively.

The ion concentration in the CLOUD chamber was measured with a Neutral cluster and Air Ion Spectrometer, (NAIS, Kulmala *et al.*, 2007). The NAIS is able to measure air ion number size distributions in the mobility equivalent diameter range of 0.8 to 40 nm and correspondingly neutral particle number size distributions from ~2 to 40 nm mobility diameter.

It was also possible to use a PSM (Particle Size Magnifier; Vanhanen e*t al. 2011*), a scanning CPC with a cut off varying from 1 to 2 nm, to retrieve the size distribution of the atmospheric ions created in the chamber and compare it to the NAIS in absence of neutral particles in the chamber (Figure 1).

Based on the measured GCR and beam intensities we were able to calculate the expected ion concentrations in the chamber as a function of beam intensity. The calculated ion concentrations were then compared with the measured values in the NAIS, therefore we retrieved the ion-ion recombination coefficient, performing a dedicated set of experiments at different conditions: in sulfuric acid free ($[H_2SO_4]$<5e5 cm^{-3}) and in sulfuric acid rich environment ($[H_2SO_4]$~3e6 cm^{-3}).

The ratio of formation rates of charged and total particles give information about the contribution of ion-induced nucleation. Charged nucleation rates were retrieved from the NAIS ion mode and from two CPCs one of which was equipped with a switchable ion trap both results will be compared.

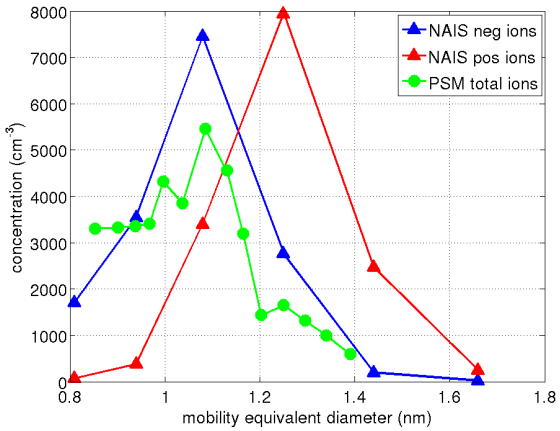

Figure 1. Comparison of number size distribution of ions from NAIS (blue for negative ions red for positive) and from PSM (green).

We would like to thank CERN for supporting CLOUD with important technical resources, and for providing a particle beam from the CERN Proton Synchrotron. This research has received funding from the EC's Seventh Framework Programme under grant agreement number 215072 (Marie Curie Initial Training Network "CLOUD-ITN"), from the German Federal Ministry of Education and Research (project number 01LK0902A), from the Swiss National Science Foundation and from the Academy of Finland Centre of Excellence program (project number 1118615).

Kulmala, M. *et al.* (2004). *J. Aerosol Sci.*, 35, 143 – 176.
Kulmala, M. *et al.* (2007). *Science*, 318: 89-92, 2007.
Vanhanen, J. e*t al.* (2011). *Aerosol Sci. Tech.,* 45, 4, 533-42
Weber, R. J., *et al.* (1996). *Chem. Eng. Commun.,* 151, 53–64.

Ammonia measurements in the gas phase at ppt levels by long-path absorption spectroscopy

Bianchi, F.[1,2], Dommen, J.[1], Baltensperger, U.[1], Mathot, S.[3], and the CLOUD collaboration

[1] Laboratory of Atmospheric Chemistry, Paul Scherrer Institut, Villigen, 5232, Switzerland
[2]University of Milan, Department of Inorganic, Metallorganic, and Analytical Chemistry, Milan, Italy
[3]CERN, Genève, 1211, Switzerland
Keywords: CLOUD experiment, ammonia, nucleation, spectrometer
Presenting author email: federico.bianchi@psi.ch

New particle formation from trace vapours may be responsible for up to one-half of global cloud condensation nuclei, CCN. Sulphuric acid, produced by the photooxidation of sulphur dioxide, is thought to be the primary vapour responsible for the nucleation of new particles in the atmosphere. A mechanism which has been proposed to enhance nucleation rates is ternary nucleation involving ammonia. This process is thought to be effective already at ppt levels of ammonia. In the framework of the EU-ITN project CLOUD (Cosmics Leaving OUtdoor Droplets) this mechanism was investigated in a large simulation chamber at CERN.

We describe here the development of an instrument to measure ammonia at low ppt levels (Figure 1). This is very challenging and hardly reached by any instrument. Furthermore, the inlet of the sampling line plays also a crucial role as ammonia is a rather sticky compound and may adsorb on the walls of the inlet. Therefore, our instrument consists of a specifically designed sampling system to minimize losses of ammonia. Ammonia is stripped from the gas phase into the water phase at the tip of the sampling line. This sample solution is then derivatised by the Berthelot reaction (Patton and Crouch, 1977), which is a reaction between ammonia, hypochlorite and phenol. A blue indophenol is formed which is detected by a long-path absorption spectrometer (Schwab *et al.,* 2007). The latter consists of a liquid core waveguide (LCW) with an effective path length of 5 m. The light source is a red power LED (Luxeon) coupled via a glass fiber to the LCW. Absorbance is measured by a spectrophotometer (Ocean Optics, SD 2000).

The instrument was calibrated with a solution of NH_4^+. We assumed a stripping efficiency of the sampling line of 100% due to the high solubility of ammonia and the very short inlet line of 5 mm without water. The detection limit reached was about 10 nM which corresponds to a gas phase mixing ratio of 40 ppt.

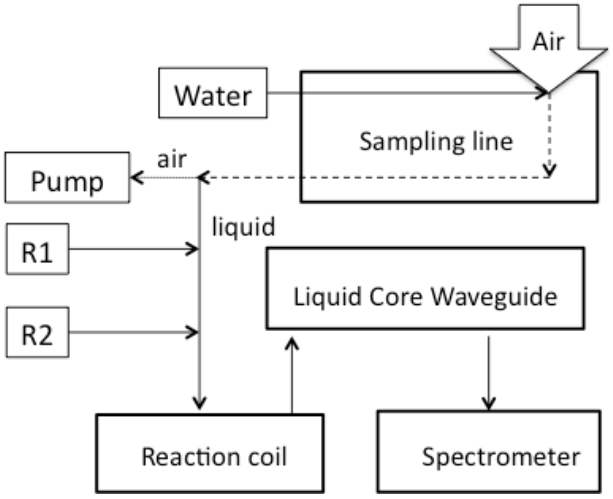

Figure 1. Scheme of the instrument. R1 and R2 denote the reagents phenol and hypochlorite.

We will present the ammonia measurements taken during two CLOUD campaigns. Based on these measurements it was possible to determine the nucleation rate of the system H_2SO_4, /H_2O/NH_3 as a function of different concentrations of ammonia inside the CLOUD chamber.

Acknowledgments: We would like to thank CERN for supporting CLOUD with important technical resources, and for providing a particle beam from the CERN Proton Synchrotron. This research has received funding from the European Commission (Marie Curie Initial Training Network CLOUD-ITN and the Research Infrastructures Programme EUROCHAMP-2), the German Federal Ministry of Education and Research, the Swiss National Science Foundation, and the Academy of Finland Center of Excellence program.

Patton, C.C., Crouch, S.R. (1977) Spectrophotometric and kinetics investigation of the Berthelot reaction for the determination of ammonia. *Anal. Chem.* **49**, 464-469.

Schwab *et al.* (2007) A laboratory intercomparison of real-time gaseous ammonia measurement methods. *Environ. Sci. Technol.* **41**, 8412-8419.

Reduction of Iodate (IO_3^-) to Iodide (I^-) in seawater and recycling of Iodine (I_2) to the atmosphere by the uptake of Ozone (O_3): Links to new particles formation

Ravi Kumar[1,2], Samantha MacDonald[1], Russell W. Saunders[1], Benjamin J. Murray[2], and John M.C. Plane[1]

[1]School of Chemistry, University of Leeds, Leeds, Woodhouse Lane, LS2 9JT, United Kingdom
[2]School of Earth and Environment, University of Leeds, Leeds, Woodhouse Lane, LS2 9JT, United Kingdom

Keywords: Laboratory experiments, MBL, Marine Aerosol, Particle formation,
Presenting author email: cmrk@leeds.ac.uk

Iodine exists in open seawaters mainly in the inorganic forms iodate (IO_3^-) and iodide (I^-) (Wong and Zhang, 2008). While the concentration of IO_3^- predominates in deep water, I^- concentrations increase toward the surface. The primary precursor for iodine oxide particle (IOP) formation in the coastal marine boundary layer (MBL) is iodine (I_2) (Saiz-Lopez and Plane, 2006) originating from algae, but recent field measurements suggest that such biogenic iodine emissions cannot account for the observed levels of gas-phase iodine species (Read *et al.*, 2008). Recently, it has also been reported that oxidation of iodide (I^-) at the sea surface resulting from uptake of ozone (O_3) could enhance the emission of I_2 into the MBL (Sakamoto *et al.*, 2009). Thus, these studies indicate additional, non-biogenic global sources of I_2 from oceans which may contribute to IOP formation in the remote MBL.

We have conducted a series of experiments to investigate three potentially important processes likely to participate in the recycling of I_2 from seawater in the presence of sunlight: (i) the role of dissolved organic materials (i.e. humic acid), (ii) the effect of salinity (Cl^- concentration) and (iii) deposition and uptake of O_3.

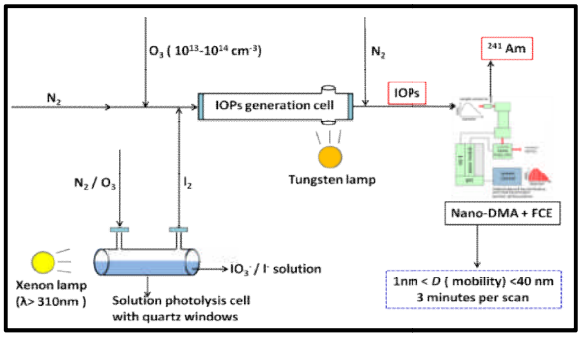

Figure 1. Schematic of experimental set-up used to study the reduction of IO_3^- to I^- and subsequent emission of I_2.

The experiments involved the initial photolysis of IO_3^- solutions with either humic acid or Cl^- added, or of an I^- solution with a flow of O_3 passing through the cell (see Fig. 1). The formation of I^- in solution (due to IO_3^- reduction) was detected using time-resolved UV-Vis spectroscopy. I_2 formation and release to the gas-phase was determined indirectly by its photo-oxidation in a second cell, leading to IOP formation and detection using a coupled differential mobility analyser (DMA) and Faraday cup electrometer (FCE) system.

Fig. 2 shows a series of UV-Vis spectra taken from a photolysed IO_3^- solution (photolysis time indicated in hours) to which humic acid had been added. The appearance of an absorption feature due to I^- at ~ 230 nm is evident.

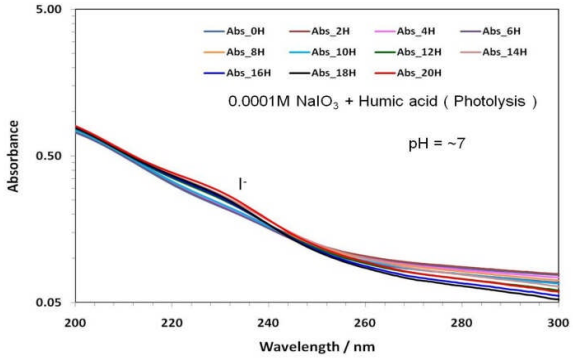

Figure 2.UV-visible spectra of a photolysed 10^{-4}M $NaIO_3$ solution (+ Humic acid).

The addition of Cl^- ions to the IO_3^- solution was found to enhance the formation of I_2 (deduced from increased IOP formation).

Finally, Fig. 3 shows the effect of O_3 uptake on a photolysed I^- solution, with increased I_2/IOP formation occurring as the O_3 concentration is increased.

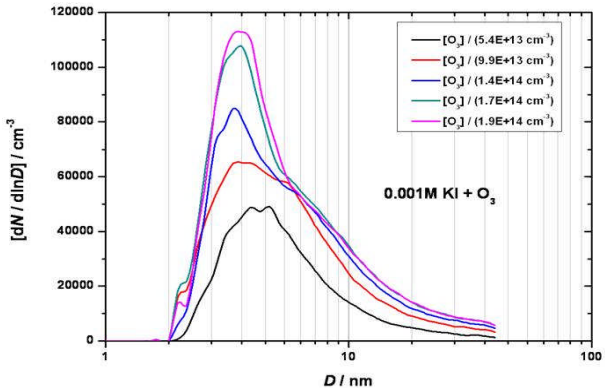

Figure 3. Iodine oxide particle (IOP) formation due to the uptake of O_3 by an I^- solution.

Wong, G.T.F., and Zhang, L.S. (2008) *Mar. Chem.*, **111**, 22-29.
Read, K.A., et al., (2008), *Nature*, **6**, 883-895.
Saiz-Lopez, A., and Plane, J.M.C. (2006) *Geophys. Res. Lett.*, **31**, L04112.
Sakamoto, Y., et al. (2009) *J. Phys. Chem. A.*, **113**, 7707-7713.

Coastal nucleation events: relation to atomic and molecular iodine concentration

Sorribas, M.[1], Mahajan, A.[2], Gómez-Martín, J.C.[2], MacDonald, S.M.[3], Gil, M.[1], Plane, J.M.C[3], Saiz-López, A.[2]

[1] Atmospheric Research and Instrumentation Branch, National Institute for Aerospace Technology (INTA), Mazagón, Huelva, 21130, Spain
[2] Laboratory for Atmospheric and Climate Science (CIAC), Toledo, 45007, Spain
[3] School of Chemistry, University of Leeds, Leeds, LS1 3HE, UK
Keywords: atmospheric aerosol, climate, homogeneous nucleation, coastal particles
Presenting author email: sorribasmm@inta.es

Bursts of ultrafine particles formed from gas-to-particle processes that grow to detectable sizes are called nucleation events. It has been observed at different environments (Kulmala et al., 2004), included the coastal areas around the world. When the new particles grow into CCN (cloud condensation nuclei) sizes by condensation and coagulation processes, they are able to influence over the direct and the indirect aerosol effects to the incoming solar radiation. Though many nucleation events have been observed, the key questions, such as what precursor gases form the particles and what produces the nucleation and the growth are unresolved.

Seaweeds, in particular the *Laminaria macroalgae*, have been directly related to new particle formation in coastal locations. When macroalgae is exposed to the solar radiation at low tide molecular iodine (I_2) is emitted to the atmosphere (Saiz-Lopez and Plane, 2004), subsequent photolysis and reaction of atmospheric ozone leads to the formation of iodine oxide (IO), which in turn reacts with itself to nucleate new particles (Saiz-Lopez et al., 2006).

In this work, we present the first observations of the ultrafine particles in the Northwest of Spain and the relationship of these observations with concurrent measurements of atomic iodine (I) and I_2.

Methods

Measurements were made at O' Grove, Galicia (42.50º N, 8.87ªW) on the Northwest coast of Spain as part of the "Laminariae Emissions in Galicia: Observation by fLuorescence and Absorption Spectroscopy" (LEGOLAS) field campaign, from 30th Abril to 7th May 2010 (Mahajan et al., 2010).

Continuous particle size measurements were simultaneously carried out by two subsystems monitoring different size ranges of dry particles. Particle number size distribution in the 9-407 nm range was measured using a Scanning Mobility Particle Sizer (SMPS) with 5 min time resolution. Total concentration for particles larger than 3 nm was measured by a second UCPC (TSI Model 3776). Although the lower size limits for the UCPC are not well defined, the difference in total particle number concentration between the UCPC and SMPS system is attributed to particles in the size range between 3 and 9 nm.

Concurrent measurements of I_2 and I were performed using a newly developed instrument based on the detection of molecular and atomic resonance and off-resonance ultraviolet fluorescence excited by lamp emission (Gómez Martín et al., 2011).

Conclusions

A correlation between I_2, I and ultrafine particles concentrations, and the tide was observed (see Figure 1) but the source of each one was not at the same location. Bursts in the number concentration between 3-9 nm were observed only during daytime and low tide on 5 days. The background concentration for ultrafine particles was 1700 cm^{-3} and the highest values were achieved with 18000 cm^{-3} on 2nd May during a nucleation event.

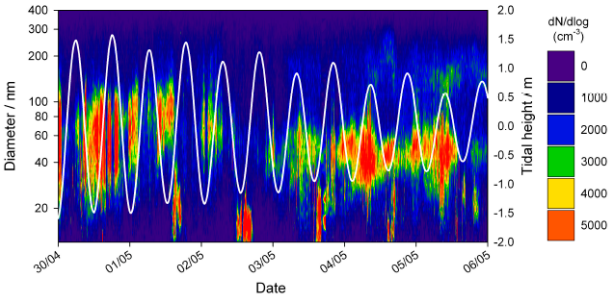

Figure 1. Particle number size distributions and tide cycle (white line), throughout LEGOLAS campaign.

This work was supported by a Research Project (CGL2008-05939-C03-03/CLI) of the Spanish Ministry of Science and Education.

Gómez Martín, J.C., Blahins, J., Gross, U., Ingham, T., Goddard, A., Mahajan, A.S., Ubelis, A. and Saiz-Lopez, A. (2011) *Atmos. Meas. Tech., 4, 29-45,*

Kulmala, M., Vehkamaki, H., Petäkä, T., Dal Maso, M., Lauri, A., Kerminen, V.-M., Birmili, W., McMurry, P.H. (2004) *Aerosol Sci., 35, 143-146.*

Mahajan, A.S., Sorribas, M., Gómez-Martín, J.C., MacDonald, S.M., Gil, M., Plane, J.M.C. and Saiz-Lopez, A. (2010) *Atmos. Chem. Phys. Discuss., 10, 27227-2725.*

Saiz-Lopez, A., Plane, J.M.C., McFiggans, G., Williams, P.I., Ball., S.M., Bitter, M., Jones, R.L., Hongwei, C., Hoffmann, T. (2006) *Atmos. Chem., Phys., 6, 883-895.*

Saiz-Lopez, A., Plane, J.M.C. (2004) *Geophys. Res. Lett., 31, L04112, doi:10.1029/2003GL019215.*

Sub-arctic nucleation events: Observation at ALOMAR Station, Norway

Sorribas, M.[1], López, J.F.[1] Fernández-Léon, M.[1], De la Morena, B.A.[1]

[1] 'El Arenosillo' Atmospheric Sounding Station, Atmospheric Research and Instrumentation Branch, National Institute for Aerospace Technology (INTA), Mazagón, Huelva, 21130, Spain
Keywords: atmospheric aerosol, climate, homogeneous nucleation, coastal particles
Presenting author email: sorribasmm@inta.es

Atmospheric particulates contribute to light absorption and scattering solar radiation, cloud formation and they are a key in the global climate system. Important contributions to atmospheric particle number concentration are made by homogeneous nucleation of supersaturated vapours. The feedback of this size range on global climate is highly uncertain, although potentially large and opposite of the warming effect of greenhouse gases.

Climate change is proceeding fastest at the high latitudes of the Arctic region because it is an extremely clean area. Its impact can be able to produce serious worldwide consequences and then, it is a region where a better understanding of the processes leading to climate change is the most urgently needed. POLARCAT (*Polar Study using Aircraft, Remote Sensing, Surface Measurements and Models, of Climate, Chemistry, Aerosol, and Transport*) is a coordinated international programme of measurements and modelling to quantify the impact of the diverse atmospheric components over the Arctic, to study the pollutant deposition and climate change in the region. In this framework, an intercomparison and an intensive measurement campaign for aerosol characterization were carried out during summer 2008. The aim of this work is to show the first results and conclusions about different aerosol parameters at ground level surface, during some nucleation events.

Methods

The ALOMAR Station is situated in And∅ya Island (69º16'N, 16º00', 380 m.a.s.l), on the North Atlantic coast of Norway. From June to July the sun is 24 hr above the horizon and the climate is very warm during the entire year because this area is influenced by the Gulf Stream.

Sampling aerosol system was designed by INTA following the general recommendations for the Reynolds Number and the system geometry. Thus, in-situ aerosol measurements were carried out 1 m above the top of the main building with a flow rate of 87 $lmin^{-1}$ and *Re* 6240, using a vertical stainless steel tube (19 cm inner diameter and 300 cm length). A splitter was situated in the end with three different outs which had different diameters to provide aerosol flow with laminar conditions to the different instruments. Sampling system efficiency was calculated, resulting in an efficiency of about 50% for 7.0 μm particle and 98% for 16 nm particle. Sampling effects were corrected for data processing. A heating around the principal tube was situated in order to control the relative humidity of the sample aerosol below 40%.

Dry ambient particle number size distributions within the size range (3 – 10000) nm were monitored with a UCPC (TSI – Model 3776), a SMPS spectrometer (TSI - Model 3936) and an APS spectrometer (TSI – Model 3321). Finally, an integrated nephelometer (TSI – 3563) with three wavelengths measured the scattering and backscattering aerosol coefficients.

Conclusions

Number concentration was calculated for (0.003-10) μm size range with 2340 cm^{-3} and mean modal concentration were 1400 cm^{-3}, 300 cm^{-3}, 670 cm^{-3} and 330 cm^{-3} for the nucleation 1, nucleation 2, Aitken and accumulation modes respectively. The concentration for nucleation modes presented high variability due to the very frequent nucleation mechanisms. There were 13 observations that show new particle formation over the Andøya Island which had a long life until 14 hours, increasing the concentration for Aitken mode as well as for accumulation mode during the last hours. Some new particle formation happened even when the previous event was not finished. Then, new particles became optically actives and its influence over the scattering mechanism will be presented.

Particle formation rates were evaluated by dividing an increase of the number concentration for nucleation mode, (size ranges: 3-14 nm and 3-30 nm) by the elapse time. They were mostly within the range (1-7) cm^{-3} s^{-1}. Particle growth rate was evaluated considering a closely linear fashion with time. Then, the range of growth rates spanned (3-10) nm h^{-1}. The maximum diameter was ranged from 26 nm to 107 nm.

Nucleation events have been investigated in terms of meteorological parameters, air-mass conditions, different metrics of the particle size distribution and the scattering coefficient.

This work was supported by a Complementary Action (CGL2007-29842-E/ANT) and Research Project (CGL2008-05939-C03-03/CLI) of the Spanish Ministry of Science and Education.

Sorribas et al., (2009). *Proc. III Spanish Meeting on aerosol science and technology (RECTA), Bilbao, Spain.*

New parametrization of SOA formation from anthropogenic VOCs for the CAMx model

O. Vlček[1], T. Svendby[2] and L. Corbet[1]

[1] Czech Hydrometeorological Institute, Na Šabatce 17, Praha 4 – Komořany, 143 06, Czech Republic
[2] Norwegian Institute for Air Research (NILU), P.O. Box 100, N-2027 Kjeller, Norway
Keywords: SOA (Second. Organic Aerosols), particle formation, m-xylene, CAMx, Europe.
Presenting author email: vlcek@chmi.cz

Formation of the secondary organic aerosols (SOA) from its volatile organic compound (VOC) precursors is a very complex process and different parametrizations are used for its description. The formation is often described in terms of the fractional mass yield, $Y = \Delta M_0 / \Delta VOC$, where ΔM_0 [$\mu g \cdot m^{-3}$] is the mass concentration of SOA produced from the reaction of ΔVOC [$\mu g \cdot m^{-3}$]. Yield Y is very sensitive to the outside temperature, PM concentration and also NOx concentration. Svendby *et al.* (2007) reviewed SOA formation experiments and proposed a new parametrization of the SOA formation among others from m-xylene and toluene, which should be more realistic for the low temperature conditions and which should also reflect high constant yield under the low NOx conditions according to Ng e*t al.* (2007). Parametrization of the anthropogenic SOA formation in the Eulerian photochemical dispersion model CAMx was changed according to the new one (Svendby and Bartonova, 2010). Experiments for the summer 2008 and winter 2008/2009 were performed to assess the effect of the new parametrization.

Model CAMx v5.2 was used for the experiment. Aerosols were modeled in the fine/coarse mode within the chemistry mechanism SAPRC-99. **Modeling domain** consisting of 309 x 277 cells was covering Central and South Europe and also parts of the West and East Europe with horizontal resolution of 9 km. Its vertical extent was 16 levels with the average hight of the first level 15 m AGL and of the last level 8 – 9 km AGL. Input data were supplied with 1 hr time step. **Meteorology** was provided by the NWP model ALADIN/CE (version CY35T1star). Its assimilation cycle consisted of the analysis followed by 6 hr forecast at 0, 6, 12 a 18 hr UTC. **Anthropocentric emissions** corresponding to the year 2006 were prepared by the emission model developed by B. Krüger from Universität für Bodenkultur Wien. They were based on the EMEP inventory with resolution of 50 km. For Austria, the Czech Republic, Hungary, and the Slovak Republic more detailed emissions of ozone precursors were used. EMEP emissions included a group of XYLA = ARO2 – which is a precursor of the anthropogenic SOA (Environ, 2010). Normalized **biogenic emissions** of isoprene and monotermene were based on the merged AFOLU and USGS databases with a resolution of 1km (Zemánková, 2010). They were further processed by the version 3.12 of SMOKE-BEIS3 model.

Increase in the average concentration of the anthropogenic and biogenic SOA was observed mainly during the summer. However for the biogenic SOA it was much more moderate. Modeled gas species remained without any significant change. The results will be compared against station measurements to see if the modified parametrization brought better agreement between the modeled and observed time series.

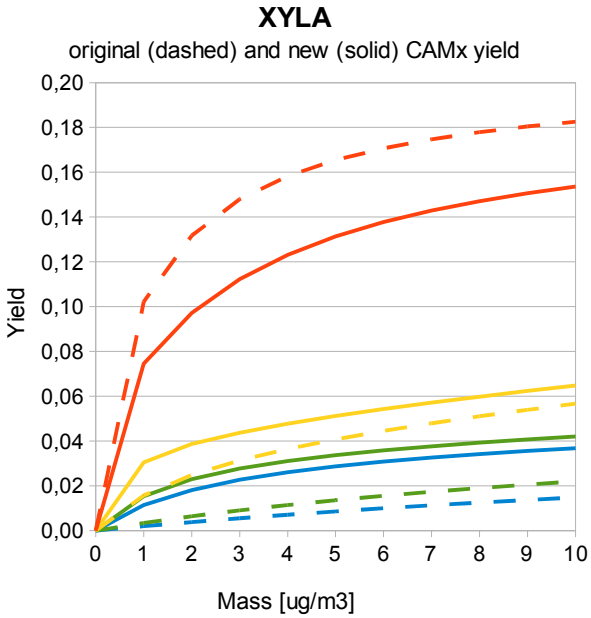

Figure 1. Comparison of the m-xylene yield functions currently used in CAMx 5.2 (dashed) and with a new parametrization (solid). The lowest curve is for 310 K then curves for 303, 283, and 250 K follow. The concentration of already formed aerosols is on the bottom axis.

This work was supported through the Norwegian Financial Mechanism under grant CZ0049 and by the Ministry of the Environment of the Czech republic under grant SP/1a4/107/07.

ENVIRON (2010) User's guide to the Comprehensive Air Quality model with extensions (CAMx) v5.20.

Harrison, R.M, Yin, J. (2000) *Sci. Total Environ.* **249**, 85-101

Ng, N.L., Kroll, J. H., Chan, A.W.H., Chhabra, P.S., Flagan, R.C., Seinfeld, J.H. (2007) *Atmos. Chem. Phys.* **7**, 3909–3922

Svendby, T.M., Bartonova, A. (2010) Implementation of a secondary aerosol module in the CAMx model. Project CZ0049 – Activity 2 Tech. Rep., NILU TR 4/2010, ISBN: 978-82-425-2210-8 (print)

Svendby, T.M., Lazaridis, M., Tørseth., K. (2008) *J. Atmos. Chem.* **59**, 25-46

Zemánková, K. (2010) Study of links between biogenic VOC emissions and concentration of tropospheric ozone. PhD. thesis. *Charles University in Prague*.

Tuesday, September 6, 2011

Session 4P: Poster Session A:
Atmospheric Aerosols – Specific Aerosol Types

Digital visibility quantification for atmospheric environment with a Harris corner detector

C.-H. Luo[1,*], C.-Y. Wen[2], K.-H. Lin[3] and S.-H. Chiu[3]

[1]Department of Safety, Health and Environmental Engineering, Hungkuang University, Taichung, 43302, Taiwan
[2]Department of Forensic Science, National Central Police University, Taoyuan, 33304, Taiwan
[3]Department of Materials Science and Engineering, National Taiwan University of Science and Technology, Taipei, 10607, Taiwan
Keywords: atmospheric visibility, image processing, visual environment, corner detection.
Presenting author email: andyluo@sunrise.hk.edu.tw

Atmospheric clarity presents the visual quality of the atmospheric environment and is detected by visual range or optical measurements. The regular visibility measurement in a meteorological station is to focus on whether selected targets in a concerned area can be identified by eyes of trained observers. Recently technological improvement in atmospheric visibility measurement is digital image processing applied to real time and on-line visibility detection and confirmed as a useful tool (Luo, et al., 2005; Luo, et al., 2011). The blurred image of a landscape is related with visibility impairment and implies that atmospheric degradation and visual contamination happen, because of adverse meteorological conditions and severe pollution events, such as anthropogenic exhaust, dust storms, and wildfires.

A digital image of atmospheric environment acquired in the field acquisition provides the data for space dimension and digitized brightness which are employed in the $M \times N$ matrix (Petrou and Bosdogianni, 1999). The value in the matrix function is a pixel that presents the digitized brightness at any location of (x, y). The details of the site and equipment setups for this investigation can refer to Luo, et al. (2005). The visibility targets were orientated with GPS. The distance between the targets and site ranges from 3.0 to 14.5 km.

In digital image processing and computer vision, corner can be used in the investigation of shape analysis, pattern recognition, picture matching, data compression, motion analysis and so on. For atmospheric environment, the corners contain important information about the visibility targets. The Harris corner detection algorithm (Harris and Stephens, 1988) is used to detect object corner through the autocorrelation matrix and differential operators which can reflect the gray change of every pixel in any direction. Given a sift (Δx, Δy) around the pixel (x, y), a auto-corelation function is first defined:

$$c(x,y) = \sum_{W} [I(x_i, y_i) - I(x_i + \Delta x, y_i + \Delta y)]^2 \quad (1)$$

The $I(x_i, y_i)$ denotes the intensity on pixel (x_i, y_i). $I(x_i+\Delta x, y_i+\Delta y)$ can be aprrximated using a Taylor expansion. Second, the gradients along x- and y-direction are presnted, respectively. Finally, a 2×2 matrix, **H**, and two eigenvalues of the matrix **H**, λ_1 and λ_2, are evalulated. According to an Harris emprical formula, the corner response (R) is used to solve the eigenvalues of **H**.

The Harris corner detection operator needs to apply a Gaussian smoothing window. A larger Gaussian smoothing window makes the location of the corner have a greater offset. A corner is defined as detectable while eigenvalues of related **H** are large enough. Corner points in an image are defined as the intersections between detected targets and surrounding background.

The corner detection results showed that the number (c) of detectable corners increased when visual range (v) enlarged. A good correspondence (R^2= 0.8129) between c and v is shown in Figure 1. A larger value of the digital index, c, appears for better atmospheric visibility. It was confirmed that the camera-computer system equipped with a Harris corner detecting programs has the potential to record a visibility investigation in real-time.

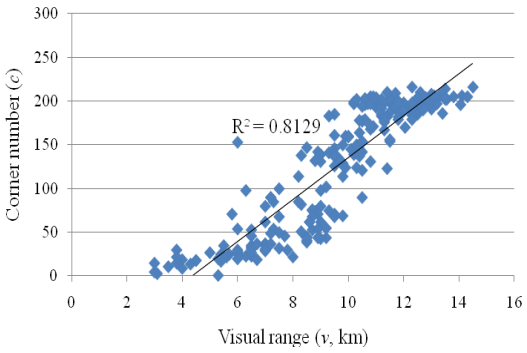

Figure 1. Relationship between the corner number and visual range measured by trained observers.

This work was financially supported by the National Science Council of Taiwan under Contract No. NSC 99-2628-E-241-001.

Harris, C. and Stephens, M. (1988) *Proceeding of the Fourth Alley Vision Conference*, 189-192.

Luo, C.-H., Liaw, J.-J., Wen, C.-Y., Yuan, C.-S. and Lo, C.-C. (2005) *Atmospheric Environment* **39**, 2545-2552.

Luo, C.-H., Lin, K.-H., Wen, C.-Y., Chiu, S.-H., Yuan, C.-S., Yang, S. (2011) accepted by *International Journal of Remote Sensing*.

Petrou, M. and Bosdogianni, P. (1999) *Image Processing: The Fundamentals*. John Wiley & Sons Ltd, England.

New particle formation by biogenic emissions: Potential organic nucleation pathway and implications on climate feedbacks

B. Bonn[1], S. Bourtsoukidis[1], H. Hakola[2], J. Schrod[1], C. Fuchs[1], F. Ebach[1], W. Haunold[1]and S. Jacobi[3]
[1]Institute for Atmospheric and Environmental Sciences, J.W. Goethe University, Frankfurt/Main, Germany
[2]Finnish Meteorological Institute, Helsinki, Finland
[3]Hessian Agency for the Environment and Geology (HLUG), Wiesbaden, Germany
Keywords: nucleation, climate effects, VOC(s), activation.
Presenting author email: bonn@iau.uni-frankfurt.de

Abstract
New atmospheric particle formation above coniferous forests has been observed for many years. Nucleation events have been detected predominantly at daytime with maxima during May and August, while night-time events occur less frequent with their maxima shifted towards winter, thus cooler and cleaner periods. A link to biogenically emitted terpenes has been reported at least for the growth process of ultrafine particles to cloud condensation nuclei sizes. However the origin of newly formed particles is intensively discussed, i.e. either sulphuric acid initiated or biogenically initiated. This presentation summarise the current findings at a Central German spruce forest site (Taunus Observatory, 810 m a.s.l.). A potential explanation by a new organic nucleation pathway and its implications for climate feedbacks will be explained and discussed.

Methods
(Experimental) Particle size distributions have been recorded at Taunus Observatory (50°13'25" N, 8°26'56" E) by an SMPS (TSI 3936) since spring 2008 (9.8 nm < D_p < 422 nm). Ambient and emission volatile organic compound (VOC) measurements were performed in October 2010 using a high sensitivity PTR-MS (Ionicon) accompanied by sample GC-MS analysis of individual mono- and sesquiterpene contributions. Meteorological parameters have been measured continuously by the HLUG in 30 min averaged intervals.
(Theoretical) Based on nucleation event classification criteria, non-event and event conditions have been intercompared and correlations with measured trace gases, meteorological parameters and sinks computed.

Findings – A. Nucleation events and correlations
As found earlier by Hyvönen *et al.* (2005) for Hyytiälä (Finland) daytime nucleation is positively correlated with temperature, solar radiation and ozone and negatively correlated with condensation sink, water vapour and sometimes pollution. During night-time the situation is mainly linked to dropping ozone and high NO_2 values and higher temperature.

Nucleation mechanism assumed
Based on laboratory investigations of new particle formation by alkenes and ozone, a new organic nucleation mechanism can be postulated: Sesquiterpenes react with ozone forming a nucleation inducing molecule that is activated by large RO_2 radicals produced by monoterpenes and OH. Subsequently, the partitioning of VOCs causes particles to grow to CCN sizes.

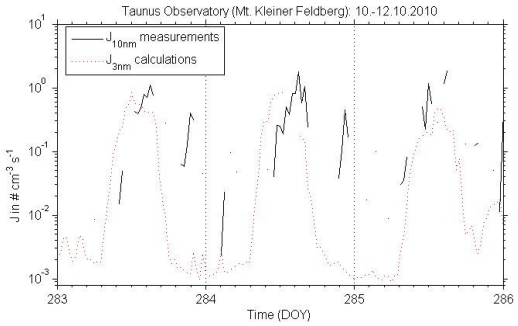

Figure 1. Nucleation rates calculated (dashed line) and measured (solid line) using OH only (day). The observed time shift is caused by different particle sizes and growth time in between.

B. Organic nucleation proposed
Applying the potential organic nucleation mechanism, new particle formation can be explained for October. However, chemical analysis of these particles is currently impossible. It is interesting to note that a change in sesqui- or monoterpene composition with different reactivities for ozone and OH, can remarkably affect the calculated nucleation rates. Moreover, the presence of isoprene can act as nucleation suppressive, since it scavenges OH.

C. Biosphere climate feedbacks
Apart from the changes in biomass, leaf area index and thus albedo and transpiration increase with increasing temperature making the air more humid. However the relative increase in water vapour per Kelvin is very similar to the rise in ozone. Consequently, the emission and the reactions of terpenes are potentially the key to understand particle formation under a future, warmer climate [Bonn *et al*., 2009]. Once particles are formed they partially grow by the uptake of semi-volatile vapours to CCN. Comparing the situation before and after a nucleation event an increase of CCN by a factor between 1.1 and 4 has been observed. This affects the radiation balance at the Earth's surface to compensate about 25% of the warming at maximum partially supporting the biosphere to survive.

References:
Bonn *et al., Atmos. Chem. Phys*., 9, 8079-8090., 2009.
Hyvönen *et al.*, *Atmos. Chem.. Phys*., 5, 3345-3356, 2005)

Composition and evolution of volcanic aerosol following three eruptions 2008 - 2010

Sandra M Andersson[1], Bengt G Martinsson[1], Johan Friberg[1], Carl A. M. Brenninkmeijer[2], Markus Hermann[3], Peter P.F. van Velthoven[4] and Andreas Zahn[5]

[1]Division of Nuclear Physics, Lund University, Lund, Sweden
[2]Max-Planck-Institut für Chemie, Mainz, Germany; [3]Leibniz-Institut für Troposphärenforschung, Leipzig, Germany; [4]Royal Netherlands Meteorological Institute, de Bilt, the Netherlands; [5]Institut für Meteorologie und Klimaforschung, Karlsruhe, Germany

Keywords: volcanic particles, elemental composition, aerosol evolution, stratospheric aerosol

Introduction

Major volcanic eruptions inject gases and particles deep into the atmosphere. Measurements of atmospheric aerosols by the CARIBIC (Civil Aircraft for Regular Investigation of the atmosphere Based on an Instrument Container) platform following the Kasatochi (Alaska), Sarychev (Russia) and Eyjafjallajökull (Iceland) eruptions in the period 2008-2010 (all with VEI4) are presented. After the eruption of Kasatochi, analyses of the stratospheric aerosol composition showed enhanced concentrations of sulfur and carbon for several months. On the other hand the ash component, which could clearly be seen in a sample seven days after the eruption, was not detected a month later (Martinsson et al., 2009). To further investigate the composition of the volcanic aerosol three flights trough the volcanic plume of the Eyjafjallajökull eruption were performed. The CARIBIC platform operates on a Lufthansa passenger aircraft usually on inter-continental flights, measuring the atmospheric composition in the UT/LS at 8-12 km altitude once per month (Brenninkmeijer et al., 2007). Instruments on the platform perform aerosol sampling for chemical characterization and particle number concentration measurements. The CARIBIC data set also includes meteorological information and measurements for mixing ratios of a large number of trace gases.

Methods

Specific flights bringing the CARIBIC platform through the volcanic ash cloud from the Eyjafjallajökull eruption were carried out on April 20, May 16 and May 19, 2010. Aerosol samples were collected by an impaction technique with a cut off diameter of 2 µm (Nguyen et al., 2006) and analyzed by quantitative multi-elemental analysis by PIXE (Particle-Induced X-ray Emission) to obtain concentrations of elements with atomic number larger than 13. Also PESA (Particle Elastic Scattering Analysis) was used to obtain elemental concentrations for hydrogen, carbon, nitrogen and oxygen (Nguyen and Martinsson, 2007).

Results and Conclusions

Three samples taken during the special flights to study the Eyjafjallajökull eruption contained unusually high concentrations of elements pointing to crustal origin. The composition of these samples was compared to ash from a fall out sample (Sigmundsson et al., 2010). The ratio of detected elements to iron in both sample types shows good agreement for most of the elements for all three aerosol samples (Fig.1). The deviation in content of potassium (K) and Zirconium (Zr) could be caused by fractioning in concentration between different sizes of aerosol due to degassing of these elements from the magma followed by condensation onto aerosol particles. The composition is compared to earlier stratospheric samples influenced by the Kasatochi and Sarychev eruptions, and the evolution in time of the volcanic influence on aerosol after eruptions is investigated.

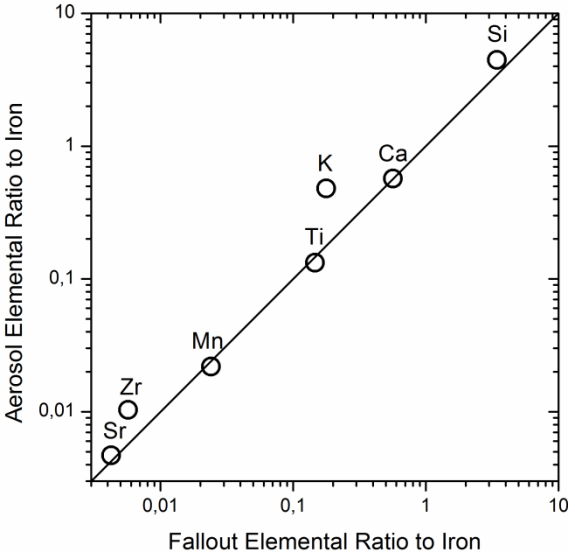

Figure 1. Geometric mean of elemental ratio to iron in aerosol samples collected by the CARIBIC platform vs. fall out sample (SRG 5a, Sigmundsson et al., 2010). The solid line indicates equal ratio.

Brenninkmeijer C.A.M. et al. (2007). Atmos. Chem. Phys., 7, 4953-4976.
Martinsson B. G. et al. (2009). Geophys. Res. Lett., 36, L12813, doi:10.1029/2009GL038735.
Nguyen H.N. et al. (2006). Aerosol Sci. and Technol., 40, 649-655.
Nguyen H.N. and Martinsson B.G. (2007). Nucl. Instr. and Meth. B264, 96-102.
Sigmundsson F. et al. (2010). Nature, 468, 426-430.

Chemical size distributions and bulk composition of Arctic aerosol sampled at Ny Ålesund (Svalbard Islands) and Thule (Greenland) during the 2010 campaign

S. Becagli [1], G. Calzolai [2], C. Ghedini [1], F. Lucarelli [2], A. di Sarra [3], M. Mazzola [4], C. Di Biagio [3], R. Traversi [1], V. Vitale [4], and R. Udisti [1]

[1] Department of Chemistry, University of Florence, Sesto Fiorentino, Florence, I-50019, Italy
[2]Dept. of Physics, University of Florence and INFN Sez. Firenze, Sesto Fiorentino, Florence, I-50019, Italy
[3]ENEA/UTMEA-TER, S. Maria di Galeria, Roma, I-00123, Italy
[4] ISAC CNR, Bologna, I-40129, Italy
Keywords: Arctic aerosol, size distribution, PM10, chemical characterization.
Presenting author email: silvia.becagli@unifi.it

One of the most important properties of the polar remote aerosols is their size distribution, giving valuable information on the source of these aerosols and on the atmospheric processes modifying their properties during atmospheric transportation. The size distribution and the chemical composition play also a crucial role in the interaction aerosol-solar radiation, in the properties of clouds and how they affect the long-range transport and deposition pattern of anthropogenic pollutants over the polar areas.

We report here the preliminary result on size distribution and bulk chemical composition of Arctic aerosol sampled at Ny Ålesund (Svalbard Islands, Norway) and Thule (North Greenland) in March – September 2010.

Svalbard Islands (Norway), located in the northernmost point yet influenced by the warm West Spitsbergen Current, are an ideal location to study the interaction between the climate changes and the atmosphere, ocean and land variations. In particular, Ny Ålesund (78.6°N, 11.6°E) is a site where international cooperation ensures the continuous study and monitoring of a large number of physical and chemical key-parameters characterizing the Arctic ecosystem. During the 2008-2010 period, two relevant scientific platforms were built in the framework of the CNR CCT-IP (Integrated Project Climate Change Tower) and PRIN07 "Dirigibile Italia" scientific projects: a 34-m high tower, with meteo probes and photometers (up-welling and down-welling radiation) distributed on 5 levels, and an observatory (Gruvebadet) for aerosol measurements and sampling.

During the 2010 campaign, the measurement of physical, optical and radiative properties of snow and aerosol in the PBL were coupled with an intensive sampling of size-segregated aerosol particles, by several kinds of impactors and at different time resolutions. The aerosol particles size distribution was carried out by using SMPS (Scanning Mobility Particle Sizer), working in the range 6 - 500 nm, and APS (Aerodynamic Particle Sizer), able to count the atmospheric particulate in the range 0.5 – 20 um. The two instruments were synchronized in order to obtain a unique spectrum of 106 size-classes in the range 6 nm – 20 um every 10 minutes.

Aerosol sampling was carried out by several collectors: a PM10 sampler (24 h resolution) with Teflon filters, for ions and metal determination; a 4-stage impactor (4-days resolution) with polycarbonate (>10, 10-2.5, 2.5-1 um fractions) and Teflon (< 1 um) filters, for ions and metal size-segregated analysis; a 12-stage impactors (4-days resolution) with polycarbonate filters, for elemental characterization by PIXE analysis; a TSP medium-volume collector with quartz filters, for EC and OC measurements.

Chemical composition have been compared with the high-resolution particle size-distribution, meteo conditions, back-trajectory reconstruction and statistical analysis (Positive Matrix Factorization and Absolute Principal Components Analysis) for source apportionment and to understand changes in source intensity and transport processes during the March-September 2010 period.

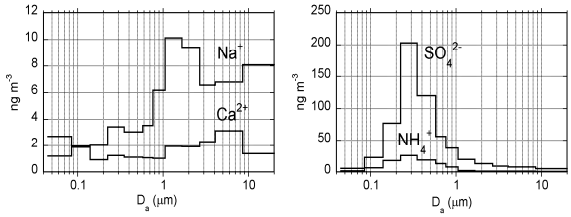

Figure 1. Size distribution of sea salt (Na^+), crustal (Ca^{2+}) and secondary (SO_4^{2-},NH_4^+) markers in an aerosol sample collected in march 2010 at Ny Ålesund.

In parallel with the scientific activity in Ny Ålesund, a PM10 sampling campaign was carried on at Thule (76.5°N 68.8°W), Greenland. In the same site, measurements of optical properties and vertical distribution of atmospheric aerosol (by LIDAR) have been also carried out.

This wide data set will help to clarify origin, transport and deposition of aerosol particles in the Arctic and their relationships with the optical atmospheric properties and the PBL dynamics.

This work was supported by MIUR-PRIN 2007.

Transport processes affecting chemical composition of Antarctic plateau aerosol from size segregated sampling at Station Concordia (Dome C, East Antarctica)

R. Udisti[1], S. Becagli[1], M. Busetto[2], M. Chiari[3], Uri Dayan [4], D. Frosini[1], S. Nava[3], F. Rugi [1], M. Severi[1], and R. Traversi[1]

[1]Department of Chemistry, University of Florence, Sesto Fiorentino, Florence, I-50019, Italy
[2] ISAC CNR, Bologna, I-40129, Italy
[3]Dept. of Physics, University of Florence and INFN Sez. Firenze, Sesto Fiorentino, Florence, I-50019, Italy
[4]Dept. of Geography, Hebrew University of Jerusalem, Jerusalem, 91905 Israel
Keywords: Antarctic aerosol, chemical composition, transport processes.
Presenting author email: silvia.becagli@unifi.it

Aerosol studies carried out at internal sites of Antarctica are focused in improving our knowledge on present-day source intensity, transport efficiency and atmospheric pathways (including stratosphere-troposphere interchanges) of atmospheric particles reaching these remotes sites. Understanding the properties and behaviours of Antarctic aerosol is essential in the study regarding the cycles of natural compounds as well as in the interpretation of past climate based on Antarctic ice core data. Chemical aerosol measurements in Antarctica are sparse and mainly confined to coastal areas (e.g. Minikin et al. 1998, Legrand et al. 2001, Jourdain and Legrand 2002), on the contrary very few aerosol data are related to central Antarctic regions.

Size-segregated aerosol and surface snow samples have been collected at Station Concordia (Dome C - East Antarctica, 75°06'S, 123°23'E, 3233 m a.s.l., about 1100 km far from the coastline), in the framework of an Italian PNRA-French IPEV joint program, by using different low- and medium-volume systems, including pre-selected cut-off samplers (PM10, PM2.5 and PM1) and multi-stage impactors.

All-year round aerosol collection for a long period (so far, covering the 2005-2009 period) allowed reconstructing the seasonal trends of the size-distribution and the chemical composition of aerosol particles, as well as investigating their main sources and transport processes. In particular, sea spray, crustal, biogenic and tropospheric (photochemistry) sources were identified by chemical markers. Besides, meteo conditions on synoptic scale and back-trajectory analysis were used in order to understand atmospheric processes leading to abrupt high concentration levels of specific aerosol components.

The chemical analysis of size-segregated aerosol and daily superficial snow samples can contribute to clarify some aspects yet under discussion. In particular: the possible seasonal pattern of sea spray aerosol could be related to sea ice formation timing and/or to changes in zonal wind intensity and atmospheric pathway; the mineralogical analysis of insoluble dust particles can allow the identification of continental sources, by comparison with soils collected in the potential source areas (PSAs); finally, the seasonal pattern of biogenic markers (such as methanesulphonic acid and non-sea-salt sulphate) can be linked to sea surface temperature, sea-ice cover and southern-hemisphere circulation modes (e.g., SOI, AAO or SAM and ACW). Indeed, oxidised sulphur compounds deserve a particular attention because they are assumed to affect the climate system by influencing the Earth's radiative budget, both directly (solar light scattering) and indirectly (acting as cloud condensation nuclei). Methanesulphonic acid (MSA) and H_2SO_4 (from DMS phytoplanktonic emission), are the best tracers of marine productivity. Their use as reliable markers of oceanic biogenic emissions is hindered by poorly known mechanisms (temperature and photochemistry induced) controlling the MSA-H_2SO_4 ratio from DMS. Since DMS in route toward central Antarctica is subjected to lower temperatures and lower humidity and, in summer, to larger atmospheric concentrations of OH (and/or BrO) radical, all conditions promoting the preferential H_2SO_4 formation, non-sea-salt sulphate is the most reliable biogenic marker at Dome C. Depositional and post-depositional processes, able to potentially modify in the time the snow composition, were also investigated. The analysis of chemical markers in aerosol, superficial snow and hoar crystals, sampled contemporaneously, allowed evaluating the contribution of some key-factors (snow acidity, solar irradiation) affecting the preservation of components reversibly fixed in the snow layers (such as, for instance, MSA, nitrate and chloride).

The study of the changes in source intensity, atmospheric processes and transport pathways of the present aerosol at Station Concordia will allow improving our understanding on past climatic and environmental changes, through ice core stratigraphies of aerosols components trapped in the snow layers by atmospheric scavenging processes. These studies will deserve particular relevance for the interpretation of the chemical records along the EDC ice core, drilled in the framework of the EPICA project.

This work is supported by PNRA and "Station Concordia" projects.

Jourdain B. and M. Legrand, (2002). *J. Geophys. Res.*, 107, 10.1029/2002JD002471

Legrand M.,J. Sciare, B. Jourdain, and C. Genthon, (2001) *J. Geophys. Res*., 106, 14,409-14,422.

Minikin A., M. Legrand, J. Hall, D. Wagenbach, C. Kleefeld, E. Wolff, E.C. Pasteur, and F. Ducroz, (1998). *J. Geophys. Res*., 103, 10,975-10,990.

Long range transported mineral dust to the Equatorial Global Atmosphere Watch (GAW) Station on Mt Kenya

M. J. Gatari[1], S. M. Gaita[1], K. Shepherd[2], J. Boman[3], S. Thorsson[4], A. Wagner[5]

[1]Institute of Nuclear Science and Technology, University of Nairobi, P. O. Box 30197-00100, Nairobi, Kenya
[2]World Agroforestry Centre (ICRAF), P. O. Box 30677-00100, Nairobi, Kenya
[3]Chemistry Department, University of Gothenburg, Gothenburg, SE-412 96, Sweden
[4]Deapartment of Earth Sciences, University of Gothenburg, Gothenburg, SE-405 30, Sweden
[5]Department of Applied Physics, Chalmers University of Technology, Gothenburg, SE-412 96, Sweden
Keywords: tropospheric aerosol, PM10/PM2.5, EDXRF, laser particle analyzer.
Presenting author email: mgatari@uonbi.ac.ke

Understanding of the free tropospheric aerosol is important in the investigation of transboundary and interhemispherical contribution to local air pollution. The Global Atmosphere Watch (GAW) station is located on the northern western slopes of Mt Kenya (Fig. 1). It is on the equator at 37^0 E at altitude 3700 m and has free view in all directions thus offering a good site for free troposheric aerosol characterization (Henne et al 2008). Gatari et al (2009) reported high elemental concentrations of Ca, Fe and K in all analyzed $PM_{2.5}$ and PM_{10} samples implying high mineral dust in the aerosol. However the local soil dust influence due to the mountain winds was not assessed. This study was therefore designed to assess the contribution of long-range transported mineral dust and local contribution through mountain winds.

In August 2009 two cyclone samplers (BGI 400 personal samplers) and an Andersen dichotomous impactor were used to sample $PM_{2.5}$ and size segregated PM_{10} respectively. In August 2010 the measurements were repeated and an aerosol monitor (TSI model 8530 DUST TRAK II) fitted with a $PM_{2.5}$ sampling head was included. The measurement reported here were from 10 day field campaign at the GAW station which included random collection of top soil samples from the area.

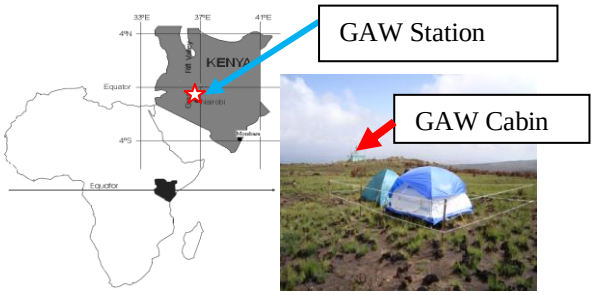

Figure 1. The location of Mt Kenya in Kenya in Africa

Teflon filters (Pall R2PJ037) were used in all the samplers. The monitor gave real time readings and particles on its internal filter. All the filter samples from all the instruments were analyzed for elemental content using EDXRF. The soil samples were analyzed for particle size distribution using a Laser particle diffraction analyzer (LPDA) (Horiba model LA-950V2), and for soluble and insoluble elemental content by TXRF (Bruker model AXS S2 PICOFOX). A digital microbalance (Mettler model MT5) was used for gravimetric determination of the filter collected PM. The LPDA uses Mie theory and its measurements are in equivalent spherical particle diameter (Eshel et al 2004).

The mean $PM_{2.5}$ concentration was 10 µg m^{-3} out of which 22 % was nighttime contribution on average. The elemental concentrations of Ca, Fe, K and Ti were 50 ± 29, 50 ± 12, 31 ± 2, 4 ± 1 g kg^{-1} in the particulate aerosol, respectively and 5 ± 0.005, 42 ± 0.01, 5 ± 0.006, 8 ± 0.005 g kg^{-1} in the top soil. These results and in addition the small available percentage of $PM_{2.5}$ particles in the top soil implied negligible contribution of Ca and K bearing particles to the aerosol while Fe and Ti was substantial. The study also showed high daytime contribution of mineral dust and that which is from long range transport as a major component that needs further investigation besides other aerosol components.

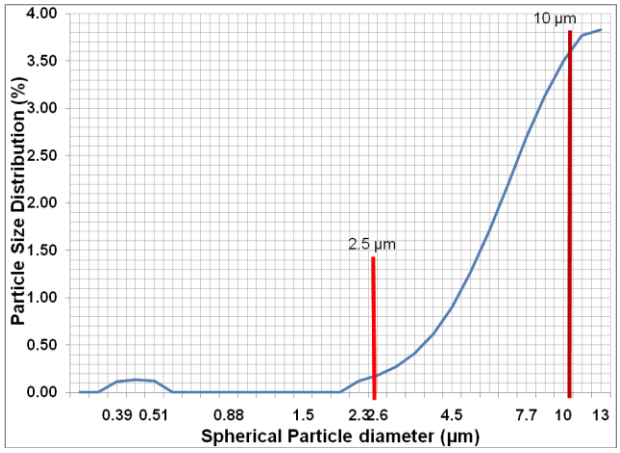

Figure 2. Particle size distribution in the top soil within the area of the GAW site on Mt Kenya.

This work was supported by International Science Program, Uppsala University Sweden and World Agroforestry Centre (ICRAF), Nairobi, Kenya.

Henne, S., Junkermann, W., Kariuki, J. M. and Aseyo, J. (2008) J. Appl. Meteor. 47, 2946–2962.
Gatari M. J., Pettersson J. B. C., Kimani W. and Boman J. (2009) X-Ray Spectrom. 38, 26-36.
Eshel, G., Levy, G. J., Mingelgrin, U. and Singer, M. J. (2004) Soil Sci. Soc. Am. J. 68, 736-743.

Tuesday, September 6, 2011

Session 4P: Poster Session A:
Atmospheric Aerosols - Aerosol Processes and Properties

In-situ aircraft observations on gases and particulate pollutants around Beijing area: distributions and influencing factors

W.J. Zhang[1*], Z.P Bai[1], J.Z. Ma[2], J.H. Chen[1], W. Yang[1], B.H. Yin[1]

[1]Chinese Research Academy of Environmental Sciences, Beijing, 100012, China
[2] Chinese Academy of Meteorological Sciences, Beijing, 100081, China
Keywords: Aircraft measurement, Gaseous pollutants, Particles, Back trajectory
Corresponding author email: zhangwj@craes.org.cn

At present, the air pollution around Beijing area has become a complex problem with a combination of different types of sources: coal smoke, traffic emission, dust re-suspension, and so on. Additionally, the transport of particulates seems to be a large-scale regional pollution. It is of great value to conduct aircraft measurements of pollutants at different altitudes (Wang et al., 2008).

In-situ measurements of gaseous pollutants, including ozone (O_3), sulfur dioxide (SO_2), nitrogen oxides (NO_X = NO + NO_2), carbon monoxide (CO), particle concentration (5.6-560 nm and 0.47-30 μm), and related meteorological information (T, RH, P) were conducted around Beijing area during Sep. 17-Oct. 7 in 2008. A two-engine light aero-transport YUN-12 (made in China) was used. The flight altitude ranged from ground to 4000m with the central point of Gucheng (N39°08′, E115°42′) in Hebei province around 5~15 km range, and the cruising velocity was generally kept at about 180 km h^{-1}. The total effective flight time was 23 h with 6 flights. This measurement was to characterize the regional variation of air pollution during and after the Olympics of 2008, the impacts of different transport direction and possible influencing factors.

Results suggested different characteristics of different gaseous pollutants and particles. (1) The meteorological factors showed significant influences for all the pollutants, as shown different pollutant levels at the ground level for different flights. (2) SO_2, NO_X, and CO showed highest concentration at the ground level, and decreased with the increasing of the height. It suggested the characteristics of major sources from ground emission for these gaseous pollutants. Figure 1 showed the variation of gaseous pollutants on flight Oct. 2 as an example. (3) Two different characterization of O_3 variation was obtained. It includes: ①similar variation with other gases, highest at the lowest altitudes, indicating the effects of ground emission sources; ② lowest concentration at the ground level, and increasing with the increase of altitudes until to 3000 m. For the O_3 variation above 3500 m, it showed similar range of 43~53 ppb at all flights, indicating the regional pollution level at high altitudes. (4) Backward trajectory analysis showed different transport direction of air masses, i.e. the pollutant transport of the southern direction with higher pollutants level; the cleaner long-range transport of the northern or northwestern direction with lower pollutants level; the transport from the eastern direction with characteristics of sea sources, i.e. middle level of gases pollutants and higher particle concentration; the transport of mixing directions, i.e. lower altitudes from the pollutant transport direction or local pollution but higher altitudes from the clean transport direction. (5) Coarser particles (0.47-30 μm) showed peaks of 0.6~0.8 μm, and highest in the ground level, and decreased abruptly with the increasing of heights, as Figure 2 showed. (6) For the ultrafine particles, the size distribution showed bimodal or multiple peaks variation, and concentrated on 10 nm and 20~100 nm. While, no obvious peaks were observed above 200 nm in the 5.6~560 nm range.

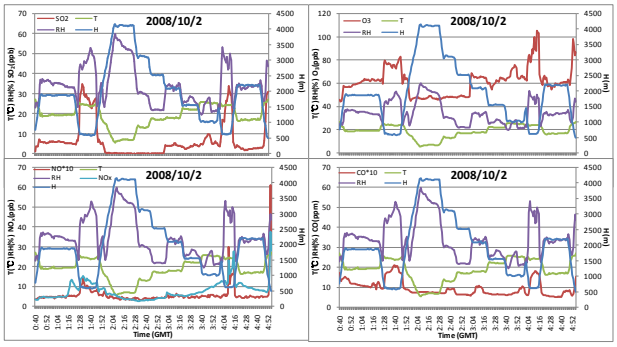

Figure 1. Variation of gaseous pollutants with meteorological factors and height on the flight of Oct. 2.

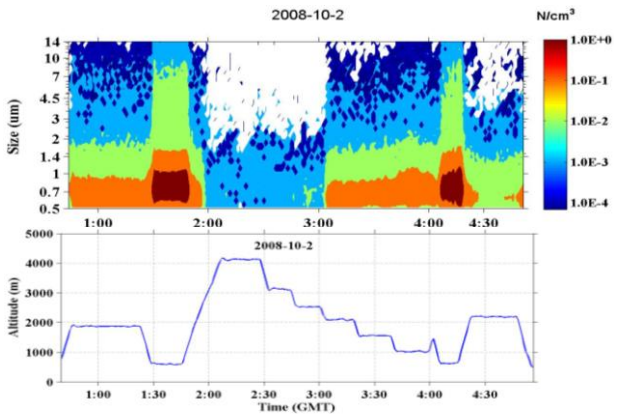

Figure 2. Variation of coarser particles with heights on the flight of Oct. 2.

This work was supported by COPES in China (GYHY200706005).

Wang, W., Ma, J., Hatakeyama, S., Liu, X., Chen, Y., Takami, A., Ren, L., Geng, C. (2008) *Atmos Environ*, **42**, 5715– 5720.

SMPS spectra under various meteorological conditions

N. Zikova[1.2], V. Zdimal[1], J. Smolik[1]

[1] Department of Aerosol and Laser Studies, Institute of Chemical Process Fundamentals of the AS CR, v.v.i, Prague, 16502, Czech Republic (ICPF)
[2]Department of Meteorology and Environment Protection, Charles University in Prague, Prague, 180 00, Czech Republic
Keywords: atmospheric aerosol, particle size distributions, meteorology
Presenting author email: zikova@icpf.cas.cz

Particle size distributions (PSD) of atmospheric aerosols have been studied extensively due to the confirmed influence of aerosols on global climate, aerosol – clouds interactions, atmospheric visibility, human health etc. (Kerminen *et al* 2005; IPCC, 2007; Wichmann *et al*, 2000). Strong feedback mechanisms of the atmosphere acting on PSD have been found as well (Mikkonen *et al*, 2011). To evaluate these feedbacks, it is necessary to describe a connection between individual meteorological phenomena and atmospheric aerosol.

The variety of measured meteorological variables able to alter or adapt aerosol PSD in its shape or amplitude is wide. But their contributions vary a lot. The most important characteristics, besides temperature, radiation and wind speed, are relative humidity (RH) and precipitation amount (Zikova *et al*, 2010). This work describes first results of categorization of aerosol PSD according to the various meteorological conditions connected to atmospheric humidity.

The data were collected during the first 22 months of measurements from 05/2008 to 02/2010 at Observatory Košetice located in the Czech Highlands (49°35'N, 15°05'E, altitude 534 m). This background station, operated by the Czech Hydrometeorological Institute, specializes on environmental quality monitoring but is also a part of the national professional meteorological measurement network. Recently, the observatory became a part of the EUSAAR network and was equipped by the IfT-SMPS run by ICPF.

SMPS was sampling every 5 minutes over mobility size range from 9 to 900 nm. Data were averaged according to the EUSAAR standards into one hour intervals. Cumulative concentrations up to 30, from 30 to 50 nm, from 50 to 100 and above 100 nm were computed along with total concentrations. Results were compared to the standard meteorological data (RH, precipitation amount and temperature) and professional observer's records taken simultaneously in one hour time resolution describing the character of weather at the station and types of precipitation. Then, typical SMPS spectra were derived.

Bimodal distributions are typical for very dry conditions (Fig. 1). With the growing RH, particles under 50 nm in diameter are most effectively removed or grown into the accumulation mode. Above 60% RH, the accumulation mode particles' concentrations increase, reach maxima around 80 % RH, and then start to drop again.

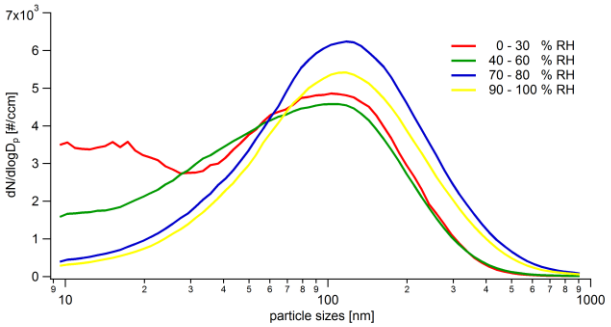

Figure 1. Averaged particle number size distribution for different amounts of atmospheric relative humidity. The fog or precipitation events were removed. (IfT SMPS, Košetice station).

During foggy days, no bimodal distributions had been recorded with concentrations being well below average (Fig. 2).

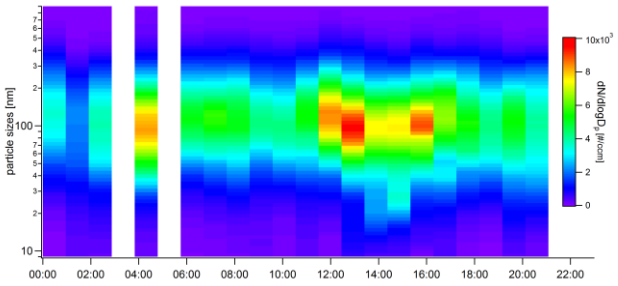

Figure 2. Typical particle number size distribution for a day with a fog recorded in every hour. Averaged from the real measured data in individual hours of the day. (IfT SMPS, Košetice station).

We thank to the projects EUSAAR (FP6-026140), CSF No. P209/11/1342 and SVV-2010-261308 for financial support, and Dr. Milan Váňa from the Czech Hydrometeorological Institute for providing meteo and air pollution data.

IPCC (2007) *Climate Change 2007: The Physical Science Basis*, Cambridge University Press.
Kerminen, V.-M. *et al* (2005), *Geophys. Res. Lett.*, **32**, L14803, doi:10.1029/2005GL023130.
Mikkonen, S. *et al* (2011) *Geosci. Model Dev.*, **4**, doi:10.5194/gmd-4-1-2011.
Wichmann H.-E. *et al* (2000) *Phil. Trans. R. Soc. Lond. A*, **358**, 2751-2769
Zikova N. *et al* (2010) *International Aerosol Conference 2010*, IAC 2010 Registration Handbook, P3LP12.

Development of chemical informatics tools for calculating fundamental properties of atmospheric aerosol components

M. H Barley[1] , D. Topping[1,2], G.McFiggans[1] and D. Lowe[1]

[1] Centre for Atmospheric Science, Manchester University, Manchester, M13 9PL
[2]National Centre for Atmospheric Science (NCAS), Manchester University, Manchester, M13 9PL
Keywords: modelling, organic aerosols, physical properties, molecular informatics
Presenting author email: mark.barley@manchester.ac.uk/david.topping@manchester.ac.uk

Introduction

Atmospheric aerosols have significant but highly uncertain impacts upon both the climate and human health. The quantification of these impacts requires the development of novel technological applications, owing to the complexity and diversity of atmospheric aerosol components. Both inorganic and organic material can transfer between the gas and particle phase. Inorganic material is restricted to a few well-understood compounds; but the organic component can comprise many thousands, as yet largely unidentified, compounds with a vast range of properties.

Predicting the evolution of aerosol requires calculation of the distribution of all components between the gas and aerosol phase according to equilibrium absorptive partitioning or disequilibrium mass transfer. Either treatment requires knowledge of all component vapour pressures and other thermodynamic properties. Furthermore, the physical properties of aerosol particles that determine their climatic impacts require detailed knowledge of fundamental properties of all components. The many thousands of individual organic aerosol components ensure that explicit manual calculation of these properties is impractical. The emergence of explicit automatic mechanism generation techniques (Aumont, et al., 2005**)** including up to many millions of individual gas phase products as aerosol precursors renders the process impossible and automation is necessary.

In this presentation we present development of a chemical informatics suite that will enable prediction of key properties of components in complex aerosol which can then be used to predict bulk aerosol properties for comparison with atmospheric analytical techniques.

The model system

The software is written in PYTHON. This high-level language is widely used as a scripting language for web applications. It supports both fixed-point and floating-point numeric calculations, string manipulation and facilities for structures and arrays. It is distributed under a permissive free software license and is available for all major operating systems, which will enable our software to be highly portable. Also, a PYTHON interface has been developed for our selected chemical parsing software (OpenBabel)(O'Boyle et al., 2008).

The Automated extraction of molecular substructure information is performed using the SMILES format (**S**implified **M**olecular **I**nput **L**ine **E**ntry **S**ystem) for the target molecule. SMILES is a simplified chemical notation that allows a user to represent a two dimensional chemical structure in linear textual form. The notation is commonly employed in commercial and public software for prediction of chemical properties. It can be imported by most molecule editors for conversion into 2D/3D models and has a wide base of software support and extensive theoretical backing (see www.daylight.com).

The 'OpenBabel' chemical toolbox has the ability to filter and search molecular files using the SMARTS format (created by Daylight Chemical Information Systems, Inc alongside the SMILES format) (figure 1). Prediction of specific properties such as pure component vapour pressures requires development of bespoke SMARTS libraries. For example, SMARTS libraries have been initially designed for a set of vapour pressure models using the 2742 compounds within the master chemical mechanism (MCM; Jenkin et al., 2003).

Example applications

Examples will be given to illustrate how this approach reduces problems associated with currently available parsing tools within the community. Extensions to a wider set of atmospherically relevant compounds will be discussed, as will novel links with commercially available software which enable direct model/measurement comparison for the first time. All of these tools will be made available via a web portal hosted at Manchester University.

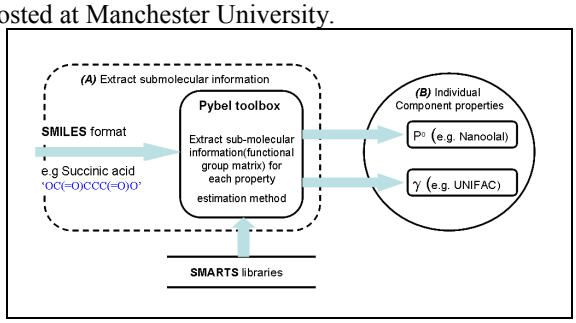

Figure 1. Dataflow diagram highlighting (A) the use of SMILES and SMARTS format with the Pybel toolbox to extract functional group matrices for input into (B) individual component property estimations

This work was supported by the National Centre for Atmospheric Science (NCAS) and the NERC grant NE/H002588/1

Aumont, B., Szopa, S., and Madronich, S. (2005) *Atmos. Chem. Phys*., **5**, 2497-2517.

O'Boyle, N. M., Morley, C., and Hutchison, G. R. (2008) *Chem. Cent. J.,* **2**, 1–7.

Jenkin, M et al., (2003) *Atmos. Chem. Phys,* **3**, 181-193.

D-elements and peptides in aerosols above water: interdependence between size and chemical composition.

M.A. Chichaeva[1], A.V. Syroeshkin[2]

[1]Analytical department, Institute of applied geophysics, Moscow, 129128, Russia
[2]Laboratory of applied hydrochemistry and analytical chemistry, State Oceanographic Institute, 119034, Moscow, Russia
Keywords: aerosol chemistry, biogenic particles, nanoparticles, primary marine aerosols.
Presenting author email: MAChichaeva@gmail.com

Transference and concentration of toxicants from ocean surface to the low atmosphere can cause significant contamination of air in coastal zones (Kolesnikov, 2005). Toxicity of marine aerosols in coastal cities is the main factor of pulmonary and allergic diseases growth (Fleming, 2008; Pierce, 2008).

In experiment White, Baltic, Barents, Kara, Azov seas, south Atlantic and Noth pole area were discovered. Time period of experiment is from 2002 to 2009. Concentrations of heavy metals and biotoxins in the article are averaged and characterize areas in whole.

One of the investigation goals was finding of correlations between concentrations of HM and physical parameters of aerosol, such as mean diametr; total, number and volume concentration. Sought – for correlations were found on all aquatories. In significant number of cases it was linear with correlation coefficient 0.99 – 0.85. Such physical characteristics as volume concentration of particles with diameters 1.5 ($V_{1.5}$); 4.3($V_{4.3}$); 5.5 ($V_{5.5}$) mkm had the most frequency of occurrence. Concerning heavy metals Ni, Zn, Cd, Pb have the most number of linear correlation (see tab.1). These elements have high toxicity and carcinogenicity. Due to association with submikrometer particles that heavy metalls becomes capable to freely enter the body, bypassing the larynx. These toxic particles during the ingalation prosess may caurse canser of nose and throat, lungs.

Table 1. The equations of interdependence between the physical and chemical characteristics of marine aerosol.

HM	Phys. param.	Formula	R	sea
Ni	$V_{4.3}$	Y=3925x-21	0.99	Black
Ni	$V_{1.4}$	Y=1610x-25	0.98	Black
Cu	$V_{1.5}$	Y=44.5+339x	0.97	White
Zn	$V_{1.5}/V_{3.7}$	Y=184=56x	0.99	Black
Cd	$V_{1.5}/V_{5.5}$	Y=49x-2	0.95	Black
Pb	$V_{5.5}$	Y=18.4x-0.3	0.99	White

In specific hydrometeorological conditions marine aerosol can bring a threat to the health of the inhabitants of the coast.

Another investigation goal was to compare mean concentration level of heavy metals within marine aerosols of the seas of Russian coastline, southern Atlantics. Aerosols of North Pole area were considered as the background (see fig.1).

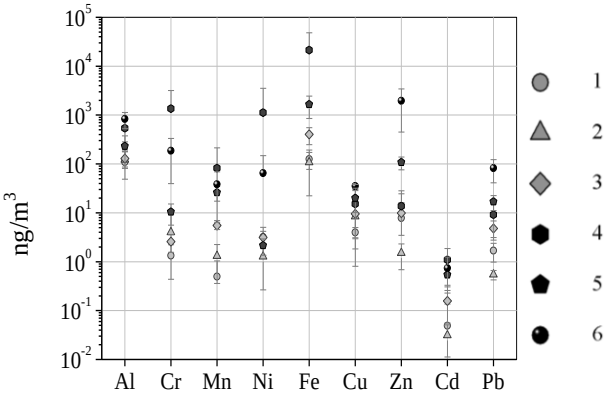

Figure 1. Comparison of concentrations of heavy metals within marine aerosols of southern and northern seas. 1 - South Atlantic Ocean, 2 - high-latitude regions of the Arctic Ocean, 3 - Kara Sea, 4 - Baltic Sea 5 – Azov sea, 6 - Mediterranean

Investigation showed that moving from northernmost seas to areas of southern seas concentrations of heavy metals in marine aerosols increases significantly.

Biogenic nanoparticles (less than 200 nm) were also in focus of the work. Nanoparticles are the basic form of transportation of biotoxins. It is well-known that marine biotoxins, forming during degradation of marine ecosystems, are the menace to human health. Viruses are also belongs to this type of nanoparticles. Sedimentation speed of nanoparticles is negligible. Concentration of biogenic nanoparticles in the lowest layer of atmosphere of southern Atlantics (in 2008) was established. Content was evaluated, using Fabry-Perot interferometer, methods for the quantitative determination of aerosoled DNA of marine heterotrophic bakterioplankton and peptide analysis. Concentration may rise to more 10^{15} m^{-3}. In areas with constraint turbulence diffusion it can reach contagious level.

Fleming L.E., Kirkpatrick B., et. all (2008) *Chest.* **131**, 187-194.

Kolesnikov M.V., Syroeshkin A.V., et. all (2005) *Oceanology.* **45,** 102-111.

Pierce RH, Henry MS. (2008) *Ecotoxicology.* **17**, 623 631.

Mass-based aerosol water uptake measurements, hygroscopicity parameters and solute interaction parameters

E. Mikhailov[1,2], V. Merkulov[2], S. Vlasenko[2] and U.Pöschl[1]

[1]Max Planck Institute for Chemistry, Biogeochemistry Department, 55128 Mainz, Germany
[2]St. Petersburg State University, Atmospheric Physics Department, Institute of Physics, 198904 St. Petersburg, Russia

Keywords: aerosol hygroscopicity, mass-based theory, interaction parameters.
Presenting author email: Eugene.Mikhailov@paloma.spbu.ru

In this study we have presented an expanded version of single hygroscopicity parameter model (Petters and Kreidenweis, 2007) based on mass water uptake by pure and mixed aerosol particles (Mikhailov et al.,2011a). The mass hygroscopicity parameter κ_m describes the particles hygroscopic behavior including early stage of particles growth where all solutes are in solid state and final stage where all solutes are completely dissolved. Non-ideal behavior of the concentrated particle solution is accounted for cross- and self – interaction terms in κ_m.

The hygroscopicity parameter when combined with the Kelvin term into κ_m-Köhler theory determines the equilibrium water vapor saturation ratio, as over partially dissolved particle and over fully dissolved aqueous droplet and can be used to predict the particle critical diameter for activation to a cloud droplet.

If the chemical composition, interaction parameters and solubilities of the multicomponent aerosol particles are known the hygroscopicity κ_m can be determined over the all water activity range. In the absence of information on these characteristics, experimental data for complex particles can be fitted to obtain the mass hygroscopicity parameter.

In this work the experimental mass growth factors, G_m directly obtained from a new filter-based differential hygroscopicity analyzer (FDHA) (Mikhailov et al. 2011b) were used to test the theory approach on example of pure and mixed particles. It was shown that two-parameter model including Rault mass hygrosocopicity and self- interaction term is well-suited to describe hygroscopic behavior of the pure inorganic (NaCl, $(NH_4)_2SO_4$) and organic (LG, OA) particles including highly concentrated droplets are in the metastable state.

For natural aerosols collected in Amazon Basin and in suburb of Saint-Petersburg it was disclosed that upon particle humidification the mixed particles exhibited the three pronounced sections on the κ_m-G_m dependence (Fig.1). The first linear section corresponds to beginning stage of particles growth when all solutes are in solid state (5-64%RH) and the concentration of any water soluble compound is equal to eutonic solubility, the second nonlinear section is responsible for gradual dissolution of the water soluble compounds with different solubility (64-96%RH), and the third section stands for completely dissolved mixed particles, where concentration dependence of κ_m disappears with particle growth (96-99% RH). The κ_m- theory model provides a good fit on the all stages of mixed particle evolution (Fig.1). We suggest that κ_m-model may be useful in describing particle hygroscopicity both in under- and in super-saturated water vapor. The experimental mass hygroscopicity can be converted into standard volume-based hygroscopicity κ throughout the all water activity range.

In the mass hygroscopicity model all components are weighted by their mass fraction. That substantially facilitates its validation and practical application since the commonly used aerosol analytical equipment determine the mass of chemical species in the particle.

The κ_m values can be derived from electrodynamic balance and other technique based on water mass uptake. The further research on quantification cross- and self-interaction hygroscopicity terms for pure and mixed particles is needed.

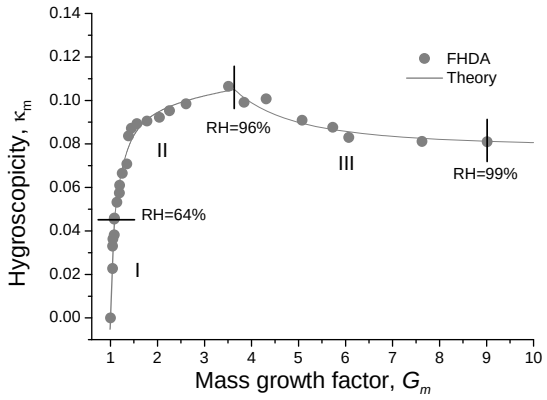

Figure 1. A comparison between theory predicted particle hygroscopicity and experimental data. Explanations are in the text.

This work was supported by the Russian foundation for basic research, under grant No. 09-05-00883-a, and European integrated project on aerosol cloud climate and air quality interactions (EUCAARI), No.036833-2.

Petters, M. D., and Kreidenweis, S. M. (2007) *Atm.Chem.Phys.*, **7**, 1961-1971.

Mikhailov, E., Merkulov, B., Vlasenko, S., and Pöschl, U., (2011a), *Atm. Chem. Phys*., (to be published)

Mikhailov, E., Merkulov, B., Vlasenko, S., and Pöschl, U., (2011b), *Izv. Atmos. Ocean. Phys. RAN* (Russia), to be published

Optical, physical and chemical characteristics of sub-urban atmospheric aerosols during very clean and local biomass burning events

Kwang Y. Lee[1], Young J. Kim[1*], T. Batmunkh[1], M.B.G. Cayetano[1], Sung Yong Kim[1], Ju S. Shin[1], and Kwan Chul Kim[1]

[1]Advanced Environmental Monitoring Research Center (ADEMRC), School of Environmental Science and Engineering, Gwangju Institute of Science and Technology (GIST), Gwangju 500-712, Republic of Korea
Keywords: Clean day, Biomass burning, Spectral absorption
yjkim@gist.ac.kr

In order to understand the characteristics of sub-urban aerosols under different atmospheric environmental conditions, chemical, physical and optical properties were continuously measured using PILS-IC, grimm OPC, semi-continuous EC/OC analyzer, 7-wavelength aethalometer and nephelometer (NGN-3) during spring (May. 24 ~ Jun. 10, Figure 1) and fall (Nov. 9 ~ Dec. 9, Figure 2) intensive measurement periods in Gwangju (126˚50'E, 35˚13'N), Korea.

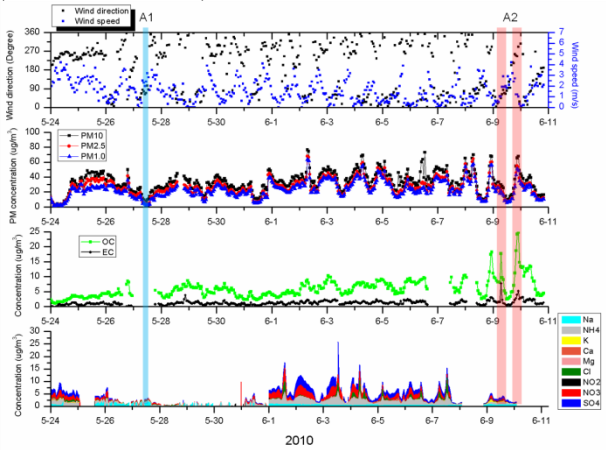

Figure 1. Temporal plots of wind speed, wind direction, PM, OC, EC and ion concentrations during the spring intensive measurement period

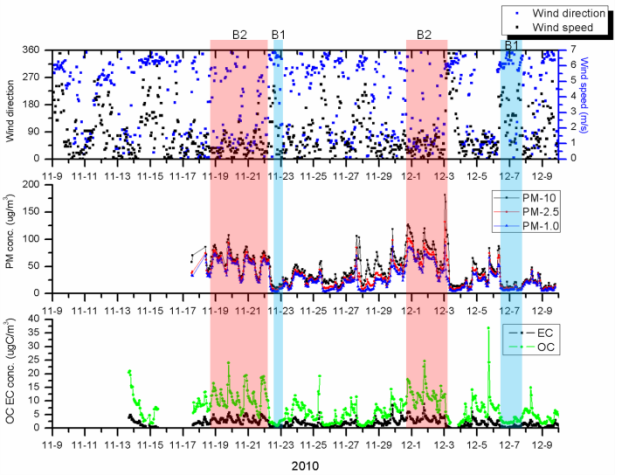

Figure 2. Temporal plots of wind speed, wind direction, PM, OC and EC concentrations during fall intensive measurement period

Average PM_{10} and $PM_{2.5}$ concentrations were measured to be 33.1±13.8㎍/m^3 and 26.1±12.0㎍/m^3 in spring and 44.4±28.4㎍/m^3 and 34.8±23.7㎍/m^3 in fall, respectively.

Several different events including very clean, long range transport of aerosols, and local biomass burnings cases were identified based on aerosol measurements and 4-day Hysplit air mass backward trajectory analyses (Table 1).

Table 1. Average concentrations of PM, OC, EC, σ_{abs} and σ_{scat} during different event periods

	Spring		Fall	
	Clean	BB	Clean	LTP+BB
PM_{10} (㎍/m^3)	8.7±1.5	57.5±14.4	12.4±3.4	83.5±17.4
$PM_{2.5}$ (㎍/m^3)	4.7±1.1	48.0±13.3	9.5±1.9	71.6±11.5
OC (㎍C/m^3)	-	19.4±3.7	2.5±0.5	14.0±4.0
EC (㎍C/m^3)	-	4.0±1.9	0.7±0.2	3.8±1.4
σ_{abs} (Mm^{-1})	5.7±2.2	49.9±15.4	4.4±2.2	78.2±35.6
σ_{scat} (Mm^{-1})	11.4±4.7	126.7±37.5	22.6±4.0	206.3±36.4

The most clean event (A1, excluding rainy days) was observed 9AM ~ 1PM (UTC+9) on May 27. $PM_{2.5}$ was observed as low as 6.6㎍/m^3 when the air mass originated from East Sea. The highest OMC (OMC =1.7[OC]) concentration of 42.2㎍/m^3, consisting of 78.7% of total $PM_{2.5}$ concentration (53.6㎍/m^3) was observed during a biomass burning event (A2). Short wavelength absorption increased under local biomass burning event conditions (A2) while no spectral dependence was observed during clean event period (A1).

Information on spectral absorption coefficient of atmospheric aerosol can be related to chemical composition of atmospheric aerosol.

Acknowledgement
This work was funded by the Korea Meteorological Administration Research and Development Program under Grant RACS_2010-1002.

J. Jung, Y. J. Kim, K. Y. Lee, M. G.-Cayetano, T. Batmunkh, J.-H. Koo, and J. Kim (2010) *Atmos. Chem. Phys.*, **10**, 5391-5408.

The volatile fraction of Arctic aerosol particles derived from thermodenuder/mobility spectrometer measurements during ASCOS

A. Held[1], J. Walz[1], D. Orsini[2] and C. Leck[3]

[1]Junior Professorship in Atmospheric Chemistry, University of Bayreuth, 95440 Bayreuth, Germany
[2]Leibniz-Institute for Tropospheric Research, 04318 Leipzig, Germany
[3]Department of Meteorology, Stockholm University, 106 91Stockholm, Sweden

Keywords: Arctic aerosols, Particle size distribution, Thermodenuder, Volatility
Presenting author email: andreas.held@uni-bayreuth.de

The Arctic Summer Cloud Ocean Study (ASCOS, www.ascos.se) investigates physical and chemical processes controlling cloud formation in the high Arctic Ocean. This work analyzes the volatile fraction of Arctic aerosol particles during summer when the aerosol in the atmospheric boundary layer is typically not affected by long-range pollution. Thus, local processes are expected to dominate aerosol formation and aging. The fraction of volatile compounds in aerosol particles of different sizes yields insight into the formation and aging processes of these particles.

During the 2008 ASCOS expedition, aerosol number size distributions were measured in the diameter range between 3 nm and 800 nm using a twin differential mobility particle sizer (TDMPS) in combination with a thermodenuder TD (Wehner et al., 2002). Measurements were taken onboard the Swedish icebreaker Oden over open water (OW), the marginal ice zone (MIZ), and the pack ice zone (PIZ).

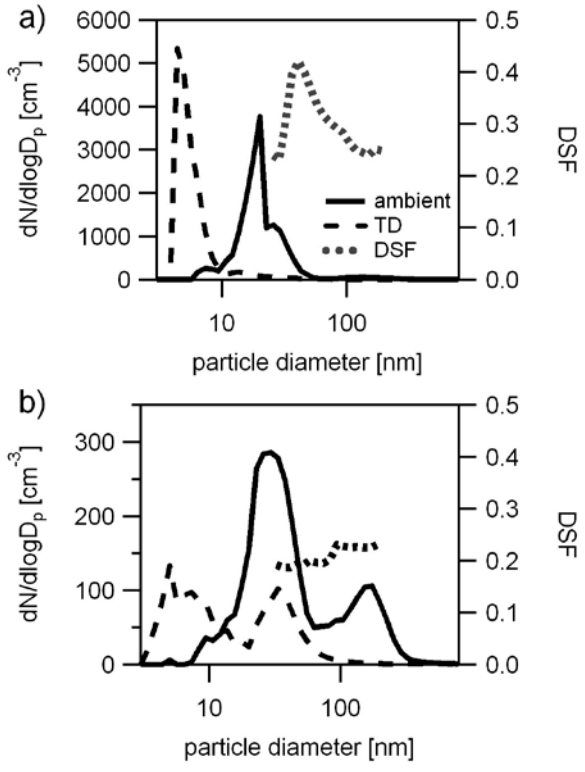

Figure 1. The descriptive shrinking factor DSF, and aerosol number size distributions at ambient temperature and after TD treatment: a) OW and b) PIZ.

The volatile fraction of the aerosol was derived from a comparison of alternating particle size distribution measurements at ambient temperature and after TD treatment (heating to 300 °C). Evaporation of volatile material at 300 °C resulted in a shift of size distributions to smaller diameters. Thus, the volatile aerosol fraction can be expressed as a shrinking factor, i.e. the ratio of the diameter of the heated particle and of the original particle. In this study, size-dependent descriptive shrinking factors (DSF) were obtained using the summation method (cf. Engler et al., 2007).

Typical ambient number size distributions were dominated by Aitken mode particles with maximum particle number concentrations in a diameter range from 20 nm to 33 nm (Fig. 1). OW particle number concentrations were greater than 900 cm^{-3}, nearly four times higher than over the ice. In the MIZ and PIZ, bimodal number size distributions were observed, with a characteristic minimum at a diameter around 70 nm, separating the Aitken mode from the accumulation mode. The number size distributions retain the bimodal shape during and after TD treatment (Fig. 1b).

DSF analysis showed that accumulation mode particles over OW and in the MIZ typically contained more volatile material than Aitken mode particles (Fig. 1a). In contrast, in the PIZ the maximum amount of volatile material was found in the Aitken mode, decreasing with increasing particle size (Fig. 1b). This is indicative of different chemical composition and aging of OW and PIZ aerosol particles.

This work was funded by the Bert Bolin Centre for Climate Research at Stockholm University and by the Knut and Alice Wallenberg Foundation. ASCOS is an IPY project under the AICA-IPY umbrella and is endorsed by the SOLAS program.

Engler, C., Rose, D., Wehner, B., Wiedensohler, A., Brüggemann, E., Gnauk, T., Spindler, G., Tuch, T., and Birmili, W. (2007) Size distributions of non-volatile particle residuals (Dp<800 nm) at a rural site in Germany and relation to air mass origin. Atmos. Chem. Phys. 7, 5785-5802.

Wehner, B., Philippin, S., and Wiedensohler, A. (2002) Design and calibration of a thermodenuder with an improved heating unit to measure the size-dependent volatile fraction of aerosol particles. J. Aerosol Sci. 33, 1087-1093.

Hygroscopic properties of sub-Arctic aerosols: continuous HTDMA measurements from Pallastunturi, Finnish Lapland

A.-P. Hyvärinen[1], K. Neitola[1], E. Asmi[1], and H. Lihavainen[1]

[1]Finnish Meteorological Institute, Erik Palménin aukio 1, Helsinki, P.O. Box 503, FI-00101 FINLAND
Keywords: H-TDMA, hygroscopic growth, Pallastunturi.
Presenting author email: antti.hyvarinen@fmi.fi

Arctic climate has warmed twice as quickly as climate on average during the last century. Despite growing knowledge, climate models give still uncertain predictions for Arctic areas. The uncertainty arises for example from understanding the direct and indirect climate effects of aerosols.

To address the knowledge gap in the properties of Arctic and sub-Arctic aerosols, FMI begun continuous measurements of aerosol hygroscopic growth at the Pallastunturi GAW station in the Finnish Lapland (Hatakka et al. 2003). The measurements were started on December 2008.

The measurements are conducted with a hygroscopicity tandem differential mobility analyser (HTDMA) built in-house FMI. The HTDMA was built according to the EUSAAR recommendations, and fulfils the EUSAAR criteria for continuous measurements. The main HTDMA features include:

- Measurement of hygroscopic growth factor (HGF) at a fixed RH of ~90 %
- Quality assurance with automated dry- and ammonium sulphate checks
- 8 dry diameters from 15 nm to 265 nm (1 cycle takes 1 hour)
- Aerosol humidification from the sample flow using a Gore-Tex humidifier
- DMA's in closed loop arrangement with a dew point analyser as the main humidity sensor

The 2009 annual average growth factors varied from 1.15±0.08 measured for 15 nm dry particles to 1.44±0.11 measured for the 265 nm dry particles. Figure 1 illustrates the corresponding HGF distributions. The growth factors had some seasonal variation, having highest values in the spring and lowest in the autumn (Table 1). However, the seasonal variation was weak and nearly within the standard deviation of the annual data.

Table 1. Average growth factors with standard deviations for representative Aitken and Accumulation mode dry particles

Month	50 nm (Aitken mode)	165 nm (Accumulation mode)
Spring	1.23±0.09	1.43±0.09
Summer	1.18±0.08	1.32±0.10
Autumn	1.13±0.07	1.32±0.11
Winter	1.19±0.08	1.42±0.09

The mean growth factors were used to deduct the hygroscopicity parameter κ-values. These can be derived from the measured HTDMA growth factors (HGF) as follows (Good et al., 2010):

$$\kappa_{HTDMA} = \frac{HGF^3 - 1}{RH}\exp\left(\frac{4\sigma_w M_w}{RT\rho_w D_d HGF}\right) + 1 - HGF^3. \quad (1)$$

The annual average κ-values for 2009 varied from 0.1 for 25 nm dry particles to 0.23 for 265 nm dry particles. Therefore, the Kelvin effect alone does not explain the increasing HGF towards larger dry particles.

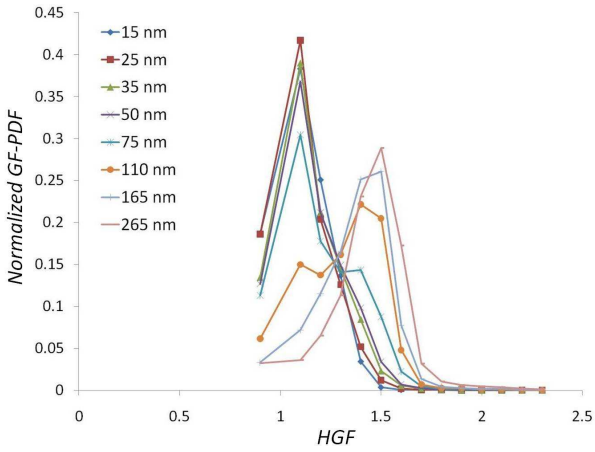

Figure 1. Average growth distributions for Pallastunturi aerosols

The long term measurements of aerosol hygroscopic growth factors in Pallastunturi fill some of the knowledge gaps in aerosol properties in the sub-Arctic. This will be helpful when determining the climate effects of aerosols in the Arctic.

This work was supported by EUSAAR and the Maj & Tor Nessling foundation. Marting Gysel from PSI is acknowledged for providing the IGOR inversion algorithm for the HTDMA data.

Good, N., et al. (2010). Consistency between parameterisations of aerosol hygroscopicity and CCN activity during the RHaMBLe discovery cruise. Atmos. Chem. Phys., 10, 3189-3203.

Hatakka, J., et al. (2003). Overview of the atmospheric research activities and results at Pallas GAW station. Boreal Env. Res., 8, 365–383.

Measurements of Siberian Arctic aerosols in Tiksi, Russia

E. Asmi[1], H. Lihavainen[1], A.-P. Hyvärinen[1], D. Brus[1], M. Aurela[1], J. Hatakka[1], T. Uttal[2], V. Ivakhov[3], A. Reshetnikov[3], A. Zinchenko[3], A. Makshtas[4], Y. Viisanen[1], P. Taalas[1], A. Laaksonen[1] and T. Laurila[1]

[1] Finnish Meteorological Institute, Erik Palménin aukio 1, P.O. Box 503, FI-00101, Helsinki, Finland
[2]NOAA/ Environmental Technology Laboratory, CO-80305, Boulder, Colorado, USA
[3]Main Geophysical Observatory (MGO), Karbyshev Street 7, 194021, St. Petersburg, Russian Federation
[4]The Arctic and Antarctic Research Institute (*AARI*), 38 Bering str., 199397, St. Petersburg, Russian Federation
Keywords: Arctic aerosols, number size distribution, DMPS, seasonal patterns.
Presenting author email: eija.asmi@fmi.fi

The International Arctic Systems for Observing the Atmosphere (IASOA, www.IASOA.org) is an International Polar Year (IPY) Activity (#196) which aims at better understanding of climatically important atmospheric processes. A fundamental part of this activity has been coordination and upgrade of observatories in the Arctic. Tiksi meteorological observatory in northern Siberia (71°40'N, 128°40'E, Fig. 1) has been operating since 1930s. As a part of IPY project funding was obtained to upgrade and expand the existing observatory to serve as a base for long-term climate studies in Russian Arctic region. The project is run in collaboration between National Oceanic and Atmospheric Administration (NOAA) with the support of the National Science Foundation (NSF), Roshydromet (AARI and MGO units), government of the Republic of Sakha (Yakutia) and the Finnish Meteorological Institute (FMI). The research activities of FMI in Tiksi include continuous long-term measurements of aerosol number size distributions as well as the fluxes and concentrations of the most important greenhouse gases (GHGs), carbon dioxide and methane. Quality control and measurement procedures are done by following the Global Atmosphere Watch (GAW) network requirements.

The climatic effects of atmospheric aerosol particles are pronounced in the Arctic - a region specifically vulnerable to changes in climate forcing components and feedbacks (e.g. Walsh and Chapman 1998). The frequently presented clear seasonal cycle in Arctic aerosol concentrations is to a great extent controlled by the winter/spring 'Arctic Haze' season (Barrie 1986; Shaw 1995). Major research questions regarding the Arctic aerosols are their source regions and transportation patterns, chemical and dynamical changes during transport and deposition in the Arctic. The year-round aerosol measurements in Tiksi to a great extent contribute for answering these questions. Here, we concentrate on the seasonal analysis of the Arctic aerosol modal properties, as well as their sources and transportation patterns by using the measured size distribution data from Tiksi together with the calculated backward trajectories given by the FLEXTRA model (Stohl *et al.* 1995).

The aerosol number size distributions in Tiksi are measured with a Differential Mobility Particle Sizer (DMPS) in the size range of 7-500 nm. Bigger, > 500 nm, particles are measured with a TSI Aerodynamic Particle Sizer (APS). The continuous measurements started in the beginning of July 2010 and are currently on-going. Considering the hazardous Arctic environment inflicting many practical difficulties, the measurements have been running amazingly well, with only minor occasional breaks.

Figure 1. Measurement site Tiksi is located in the permafrost zone at the coast of Arctic Ocean.

The results from the first year of measurements are under analysis. We aim in obtaining the general seasonal characteristics of the particle modal concentrations and properties, as well as their dependency of the air mass type and local meteorological conditions. The impact of Arctic Haze season is of our special interest. The yet very preliminary results from this autumn suggest that the particle modal characteristics exhibit large air mass related differences. Increased concentrations of aged accumulation aerosols are observed in air masses originating from the Central Siberia while the smallest particles often originate from Arctic and coastal regions. This feature is to be confirmed by using a full dataset of one year.

Barrie, L. (1986) *Atmos. Environ*. **20**, 643–663.
Shaw, G. E. (1995) *Bull. Am. Meteorol. Soc.* **76**, 2403–2412.
Stohl, A., Wotawa, G., Seibert, P. and Kromp-Kolb, H. (1995) *J. Appl. Meteor*. **34**, 2149–2165.
Walsh, J.E. and Chapman, W.L. (1998) *J. Climate* **11**, 3030–3045.

Particle number variation due to the disappearance of a thermal inversion

J.F. Nicolás[1], C. Pastor[1], J. Giménez[1], R. Castañer[1], E. Yubero[1] and J. Crespo[1]

[1]Department of Applied Physics, Miguel Hernández University, Avda. Universidad, 03202, Elche, Spain
Keywords: Vertical distribution, Mixing layer, Particle counting, Number concentration.
Presenting author email: j.nicolas@umh.es

The vertical profiles of particle number concentrations and meteorological parameters were obtained using a motorized paraglider. The flight was performed on 22 September 2009 in southeast Spain, near the Mediterranean coast (~20 km). The paraglider took off at 07:45 UTC, reached an altitude of 2500 m, and landed 45 minutes later, at 08:30 UTC. The horizontal displacement from the launch site was almost negligible. The synoptic meteorological conditions during the flight were anticyclonic.

The instrument used to obtain the particle number concentration was a GRIMM 1.109 aerosol spectrometer. This instrument determines particle number concentrations in 31 particle size channels from 0.25 to 32 μm. Its uncertainty in particle counting determination is 5%. A Delta Ohm ultrasonic anemometer, model HD 2003, was used to record the temperature, relative humidity and pressure.

We want to focus on determining the influence of atmospheric stability conditions upon the particle concentrations, above all in the first meters above ground level, and thus advance the research initiated in previous works (Giménez *et al.*, 2010).

Figure 1 (only represents the first 700 m of flight) shows the temperature vertical profile during the ascent (grey continuous line) and descent (black continuous line). We can observe how the initial thermal inversion is disappearing at the same time the temperature increases 4°C at ground level. This circumstance causes a significant effect upon particle number concentrations, above all in the first 200 m above ground level.

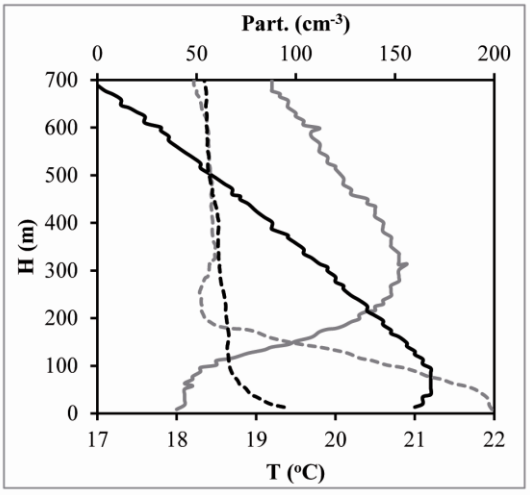

Figure 1. Temperature and particle concentration profiles obtained during the paraglider ascent and descent.

We realize how a ground level concentration of ~ 200 part. (cm^{-3}) (when the paraglider took off, grey dashed line) changes to 95 part. (cm^{-3}) during the landing (black dashed line), 45 minutes later.

Moreover, we see how the particle decay in the two cases is different. With the inversion fully developed, with an SBL (Stable Boundary Layer) height of ~300 m, the particle decay has a less steep slope than when the inversion is disappearing.

In order to quantify the disappearance of the thermal inversion effect, we have calculated (see table 1) the percentage reduction in the particle concentration between the ascent profile and descent profile. We have done this in the first 180 m because this is the height where the two profiles intersect (see figure 1). We have separated the decrease percentage between the coarse mode (size >1 μm) and accumulation mode particles (size <1 μm).

Table 1. Percentage decrease in coarse and accumulation mode particles depending on the height due to the disappearence of the thermal inversion.

Height intervals (m)	Percentage Decrease (%) (Coarse Mode)	Percentage Decrease (%) (Accumulation Mode)
0-15	85.7	52.7
15-30	84.8	55.9
30-45	84.7	59.6
45-60	84.3	60.9
60-75	85.0	59.9
75-90	81.2	58.2
90-105	76.4	55.4
105-120	69.1	51.1
120-135	64.3	46.4
135-150	63.6	38.8
150-165	47.2	26.9
165-180	44.0	10.4

The percentage decrease in coarse particles is between 20-30% higher than in accumulation particles at all heights. In addition, roughly speaking, the percentage reduction in particle numbers due to the disappearance of the thermal inversion increases as we get closer to ground level.

Thanks to Paul Nordstrom and Guillermo Escribano for their support in this work.

Giménez, J., Pastor, C., Castañer, R., Nicolás, J.F., Crespo, J. and Carratalá, A. (2010) *Atmos. Environ.* **44**, 338-346.

Inhibited water diffusion and inhomogeneities in glassy atmospheric aerosol proxies

D.L. Bones[1], H.-J. Tong[1,2] and J.P. Reid[1]
[1]School of Chemistry, University of Bristol, Bristol, BS8 1TS, United Kingdom
[2]Institute for Chemical Physics, Beijing Institute of Technology. Beijing 100081, People's Republic of China
Keywords: Organic aerosol, Thermodynamic equilibrium, Water activity, Cloud condensation nuclei.
Presenting author email: david.bones@bristol.ac.uk

A detailed knowledge of the timescales for water uptake on atmospheric aerosol particles is critical to understanding the behaviour of potential cloud condensation nuclei. Atmospheric aerosol particles are typically complex mixtures of organic and inorganic species with correspondingly complex behaviours in changing humidity regimes. Here, we investigate the formation of glassy states and highly viscous solution phases in aqueous sugar aerosols (sucrose, raffinose and levoglucosan) and aerosols of mixtures of these sugars and sodium chloride.

While the efflorescence and deliquescence points of aerosols of purely inorganic compounds like sodium chloride or ammonium sulphate are predictable and well characterised by such models as AIM and ADDEM (Topping, *et al.* 2005), the behaviour of aqueous organic aerosol is poorly understood. Ambient atmospheric aerosol is typically a mixture of inorganic and organic compounds of varying solubility (Reinhardt *et al*. 2007). It has recently been recognised that many aerosols exist as highly viscous solutions or as amorphous glasses, rather than a crystalline state, over a wide range of relative humidities (Virtanen, *et al.* 2010).

We use optical tweezers to trap single aerosol particles, which we can accurately size to a precision of ± 1 nm from the size-dependent resonance patterns exhibited in the Raman spectra of the back scattered light. Resonant modes, often referred to as whispering gallery modes (WGM), can be predicted via the Mie solutions to Maxwell's equations (Mitchem and Reid, 2008). The resonant modes penetrate to varying depths inside the particles and can hence provide insight into the structure of the particle. Also, variations in refractive index as a function of radius generate reproducible shifts in the wavelengths at which certain modes appear.

We can exploit these subtle changes in the Raman spectra to deduce the processes involved in water uptake and evaporation from aqueous organic particles and mixed aqueous organic/inorganic particles. We also extend on previous work to present further evidence for glassy states and non-ergodic behaviour (Tong *et al.* 2011). A statistical treatment of the exponential changes in particle size reveals significantly different kinetics of water uptake and loss above and below the glass transition point. However, because the viscosity of these particles is significant above the glass transition point, they also exhibit very slow diffusion rates in this region (Figure 1). This is confirmed by comparison of measured particle sizes at equilibrium with those predicted by thermodynamic models. Figure 2 illustrates this effect on a sucrose particle subjected to small, step-wise decreases in relative humidity. At low relative humidities, the particle is taking times in excess of 20 000 s (*i.e.*, 6 hours) to reach equilibrium. Predictions of the composition of organic aerosol need to include this inhibited rate of change to accurately represent the processes occurring in atmospheric aerosol.

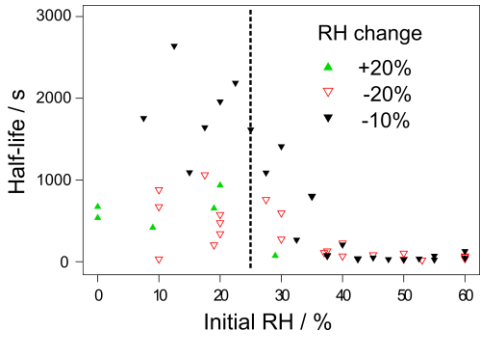

Figure 1. Timescales, represented as half-lives, for equilibration of sucrose particles, for both increasing and decreasing RH steps. The glass transition (~ 25% RH) is represented by the dashed line.

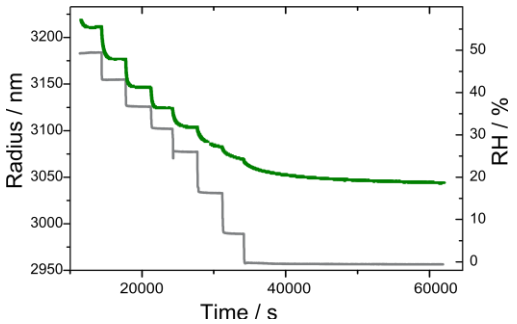

Figure 2. Time dependence of the size of a sucrose droplet (green) with change in RH (grey line, right axis). Adapted from (Tong, *et al.* 2011)

This research is supported by the EPSRC.

Mitchem, L. and Reid, J. P., *Chem. Soc. Rev.*, 37, 756–769, 2008.
Reinhardt, A., *et al.*, *Anal. Chem.*, 79, 4074–4082, 2007.
Tong, H.-J., *et al.*, *Atmos. Chem. Phys. Discuss.*, 11, 4843-4879, doi:10.5194/acpd-11-4843-2011
Topping, D. O. *et al.*, *Atm. Chem. Phys.*,5, 1205-1222, 2005.
Virtanen, A., *et al.*, *Nature*, 467, 824– 827, 2010.

Field observation of the hygroscopic properties of the ambient aerosols in Beijing

J.H. Chen[1], X. Wang[1], W.J. Zhang[1], J.M. Chen[2], X.N. Ye[2], H.J. Liu [1], W. Yang[1], J.G. Deng[1]

1. Chinese Research Academy of Environmental Sciences, Beijing 100012, China
2. Department of Environmental Science & Engineering, FUDAN University, Shanghai 200433, China
Keywords: HTDMA system, Field observation, Hygroscopic properties, Aerosols, Beijing
Corresponding author email: chenjh@craes.org.cn

The hygroscopic properties of aerosols have significant effects on the climate change and human health. Using the HTDMA (Hygroscopic Tandem Differential Mobility Analyzer) system, the hygroscopic properties of 7 kinds of laboratory-generated inorganic and organic aerosols were characterized quantitatively for determining the main affecting factors on the hygroscopicity of ambient aerosols.

It was found that the deliquescence points of inorganic compounds NaCl and (NH4)2SO4 were about 75 ± 2% rh. The particle sizes of NaNO3, CaCl2 and synthetic sea salt shifted to the larger sizes when the RHs (relative humidity) gradually increased. While, the sizes of CaSO4, oxalic acid and adipic acid were not observed obvious increase with the increasing of RH.

The hygroscopic properties of aerosols have significant effects on the climate change and human health. The hygroscopicity of ambient aerosols was conducted during December 8-20, 2009 in Beijing, and the influencing factors were also discussed. It was found that the aerosol hygroscopic growth factors were between 1.01 and 1.4 in winter in Beijing, with the property of weak hygroscopicity and nearly hydrophobic characteristics. The major influencing factors included aerosol size distribution, the air pollution situation, different sources such as vehicle exhausts, meteorological conditions and so on. The aerosol growth factors in accumulation mode were higher than those in atiken mode. With the API gradually falling down during monitoring, the environmental aerosol growth factors declined also. For those days with good atmospheric stability, the aerosol hygroscopic growth factors showed a bimodal variation, i.e. two peaks at noon and midnight and two valleys in the morning and evening. While, for those days with poor atmospheric stability, the aerosol growth factors showed a single-peak variation, i.e. a peak at midnight and a valley at noon. In addition, aerosol components with weak hygroscopicity were predominent for “peak” growth factors, and those with nearly hydrophobic characteristics were predominent hfor “valley” growth factors. The result in Beijing in this work supplied the necessary scientific basis for the atmospheric hygroscopic characteristics and related radiative forcing and climate changes.

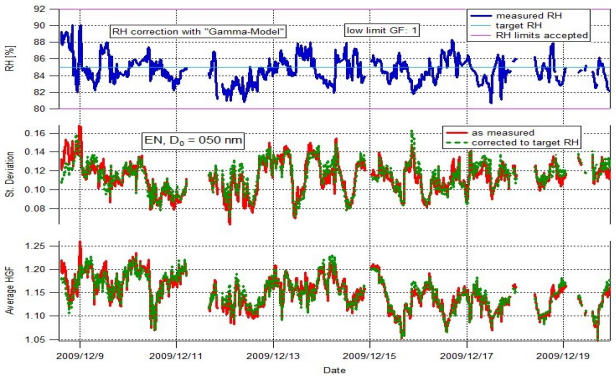

Figure 1. The growth factors of 50 nm ambient aerosols at 85% RH in Beijing

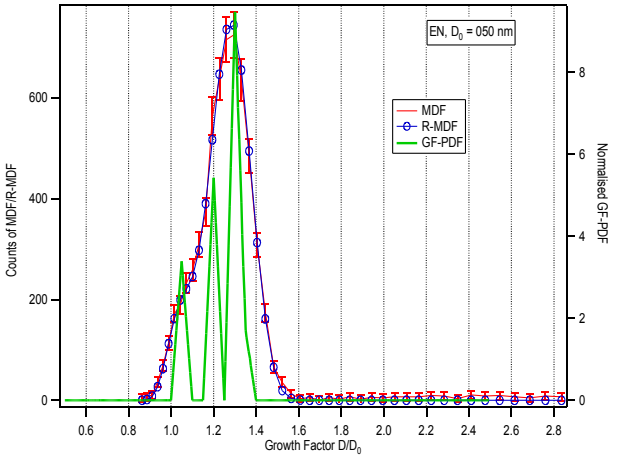

Figure 2. GF-PDF fitting result of 50nm ambient aerosols

This work was supported by Ministry of Science and Technology of the People’s Republic of China (200809052), National Natural Science Foundation of China (Grant nos. 40775075).

Approximating sulphuric acid concentration in the atmosphere. A multilocational statistical study

S. Mikkonen[1], S. Romakkaniemi[1], J. N. Smith.[1,6], T. Petäjä[2], C. Plass-Duelmer[3], M. Boy[2], P. H. McMurry[4], H. Korhonen[5], K. E. J. Lehtinen[1,5], J. Joutsensaari[1], A. Hamed[1], T. Nieminen[2], R.L. Mauldin III[6], W. Birmili[7], M. Kulmala[2], And A. Laaksonen[1]

[1] Department of Applied Physics, University of Eastern Finland, POB 1627, FIN-70211 Kuopio, Finland
[2] Department of Physics, University of Helsinki, POB 64, FIN-00014 Helsinki, Finland
[3] Hohenpeissenberg Meteorological Observatory, Hohenpeissenberg, Germany
[4] Department of Mechanical Engineering, University of Minnesota, Minneapolis, MN, USA
[5] Finnish Meteorological Institute, Kuopio unit, P.O.B. 1627, FIN-70211 Kuopio, Finland
[6] Atmospheric Chemistry Division, National Center for Atmospheric Research, Boulder, CO, USA
[7] Leibniz Institute for Tropospheric Research, Permoserstrasse 15, 04318 Leipzig, Germany
Keywords: Sulphuric acid, proxy, statistical analysis.
Presenting author email: santtu.mikkonen@uef.fi

Sulphuric acid has been shown to be involved in nucleation and growth of newly formed particles (Weber et al., 1997; Laaksonen et al., 2008; Kuang et al., 2008). The problem is that gas phase sulphuric acid concentration is difficult to measure and in many measurement sites no H_2SO_4 data are available. The purpose of this study is to test how well different measured trace gas and meteorological variables can predict the measured sulphuric acid concentration in different datasets and to construct a proxy which could be used to predict the sulphuric acid concentration in places where direct measurements have not been made. Mikkonen et al. (2011) investigated different data sets and provided evidence that high SO_2 and radiation together with low condensation sink (CS) increases the concentration of H_2SO_4 and thus make a significant contribution to particle formation and growth. Petäjä et al. (2009) studied different proxies for EUCAARI 2007 campaign data and our aim is to widen this study for other datasets measured in different environments.

Six campaign datasets and one long term dataset were analyzed for this study. The campaign datasets were measured in Hyytiälä, Finland, in 2003 and 2007, in San Pietro Capofiume (SPC), Italy in 2009, in Melpitz, Germany, in 2008, in Atlanta, USA, in 2002, and in Niwot Ridge (NWR), USA, in 2007. The long term data were measured in Hohenpeissenberg, Germany within years 1998 to 2000 (Birmili et al., 2003).

The main source of sulphuric acid in the atmosphere is the reaction chain induced by SO_2 and OH radical whereas its main sink is condensation to aerosol particles. OH radical concentration is suggested to be strongly correlated with the intensity of ultraviolet radiation (Rohrer and Berresheim, 2006) despite the complex OH chemistry in the atmosphere. UV radiation is highly correlated with global radiation so due to UV-data availability issues we use the measurements of global radiation as a proxy for OH.

A nonlinear fitting procedure was applied to all datasets, with a fit function given by

$$[H_2SO_4] = a \cdot k \cdot Radiation^b \cdot [SO_2]^c \cdot CS^d.$$

where a, b, c and d are parameters calculated from the data, k is temperature depended reaction constant, $[H_2SO_4]$ and $[SO_2]$ have units of molecules cm^{-3}, *Radiation* is global radiation in W m^{-2} and CS has units of 1/second. Only data points with Radiation higher than 10 W m^{-2} and $[SO_2]$ higher than 0.1 ppb were used in the analysis. If the steady state applies without any additional chemistry, then b and c should be unity and d should be -1. However, the fitting procedure results in Table 1 show that the powers vary a lot in the best predictive models and they are quite far from the theoretical values. Probable reason for this is that $[SO_2]$ acts also as an indicator to air pollution, i.e. factors that are sinks for sulphuric acid, and thus reduces the impact of CS.

Table 1. Best fitted values for nonlinear fit function, correlation coefficient *R*, which describes the correlation between observed values and the model predictions and R theory, which is the correlation coefficient if b = c = 1 and d = -1. Values marked with * are not statistically significant and can be considered as zero.

	a	*b*	*c*	*d*	*R*	*R theory*
SPC	0.001	0.902	0.695	-0.268	0.89	0.85
Melpitz	0.021	0.848	0.593	-0.159	0.83	0.52
Hyy-03	0.012	0.845	0.610	-0.038*	0.87	0.70
Hyy-07	2.2E-06	1.054	0.812	-0.467	0.82	0.71
NWR	0.024	0.174	0.885	0.413	0.76	0.52
Atlanta	0.045	1.412	0.480	0.181*	0.86	0.75
Hohen	9.4E-05	0.772	0.735	-0.584	0.67	0.66

This work was supported by Alfred Kordelin foundation. The Academy of Finland Center of Excellence program (project number 1118615) is also acknowledged.

Birmili W. et al. (2003) Atmos.Chem.Phys., 3, 361-376
Kuang C. et al. (2008) J. Geophys. Res, 113, D10209.
Laaksonen A. et al. (2008) Atmos.Chem.Phys., 8, 7255-7264
Mikkonen S. et al. (2011) Geosci. Model Dev. 4 1-13
Petäjä T. et al. (2009) Atmos.Chem.Phys., 9, 7435-7448.
Rohrer and Berresheim, (2006) Nature, 442, 184–187.
Weber R.J. et al. (1997) J.Geophys.Res. 102, 4375-4385.

Field measurements of atmospheric sub-2nm particles with Particle Size Magnifier

K. Lehtipalo[1,2], J. Vanhanen[2] , J. Mikkilä[1,2] , J. Kangasluoma[1], H.E. Manninen[1], T. Petäjä[1] and M. Kulmala[1]

[1]Department of Physics, University of Helsinki, 00560 Helsinki, FINLAND
[2]Airmodus Oy, 00560 Helsinki, FINLAND

Keywords: nucleation, CPC, nano-particles, field measurements
Presenting author email: katrianne.lehtipalo@helsinki.fi

The studying of new particle formation was long limited by the incapability to detect neutral particles below about 3nm. Sipilä *et al.* (2008) showed the applicability of condensation particle counters to measure in the sub-3nm range in field conditions. Since it cannot be resolved by CPC measurements only if the activated seed-particles are large molecules, clusters, or actual particles, it has become customary to call them nano condensation nuclei (nano-CN).

Measurements were conducted at the Hyytiälä SMEAR II station in Finland as a part of HUMPPA-COPEC campaign in late summer 2010, and also during spring 2011. The Airmodus A09 Particle Size Magnifier (PSM) was used to resolve the size distribution of particles below 2nm. The PSM is a dual-stage mixing type CPC using diethylene glycol for activating and initial growth of particles, while further growth and counting is done by an external CPC. The cut-off size of the instruments can be varied between about 1-2nm by altering the mixing ratio of saturator and aerosol flow and thus changing the supersaturation created. The relation between the mixing ratio and activation diameter has been determined in laboratory calibrations using mobility standards and size-selected tungsten oxide and silver ions. The nominal cut-off size of the Particle Size Magnifier at the highest mixing ratio is about 1.5nm (Vanhanen *et al.* 2011).

We found the PSM well suited for long-term field measurements, and the concentrations of nano-CN were in agreement with previous studies using pulse-height CPC (Lehtipalo *et al.* 2009). Figure 1 shows an example day with total particle concentrations measured with PSM at cut-off sizes 1.3 and 2nm, ultrafine water CPC (TSI 3786) at 3nm, and small positive and negative ions measured with A-NAIS ions spectrometer (Mirme *et al.* 2010). During daytime, the PSM showed higher concentrations compared to the ultrafine CPC, while the concentration of small ions remained almost constant. This indicates the presence of neutral nano-CN during that time.

We observed that the fraction of ions from all particles in the size range between 1.3-3nm was diminishing with increasing total concentration, the median charged fraction being close to 1%. Generally, the total nano-CN concentration varied much more than the small ion concentration. Correlation was also found between the concentration of sulphuric acid (as measured with a chemical ionization mass spectrometer) and the concentration of nano-CN.

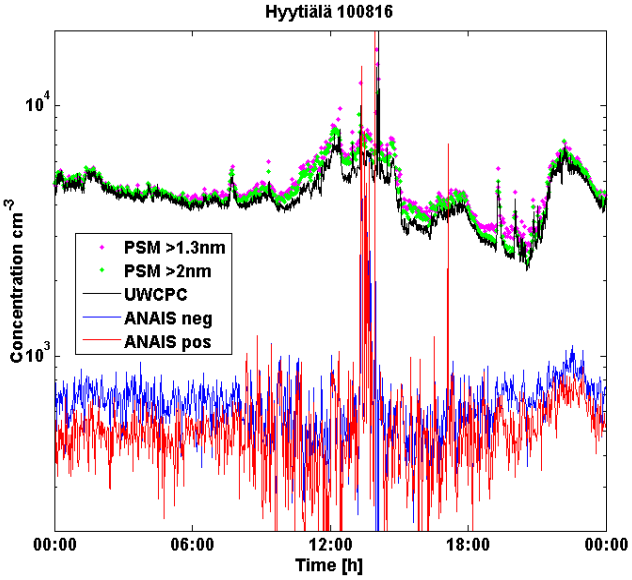

Figure 1. Example of measurements with PSM at cut-off sizes 1.3 and 2nm, compared to TSI 3786 (UWCPC) at 3nm cut-off and small positive and negative ions measured with ANAIS ion spectrometer.

Lehtipalo, K., Sipilä, M., Riipinen, I., Nieminen, T. and Kulmala, M.(2009).*Atmos.Chem. Phys.*,**9**,4177-4184.

Mirme, S., Mirme, A., Minikin, A., Petzold, A., Hõrrak, U., Kerminen, V. -M., and Kulmala, M. (2010) *Atmos. Chem. Phys*., 10, 437-451

Sipilä, M., Lehtipalo, K., Kulmala, M., Petäjä, T., Junninen, H., Aalto, P.P., Manninen, H.E., Vartiainen, E., Riipinen, I., Kyrö, E.-M., Curtius, J., Kürten, A., Borrmann, S., and O'Dowd C.D. (2008). *Atmos. Chem. Phys.* **8**, 4049-4060.

Vanhanen, J., Mikkilä, J., Lehtipalo, K. , Sipilä, M. , Manninen, H. E. , Siivola, E. , Petäjä, T. and Kulmala, M. (2011) *Aerosol Sci. Tech*., **45**, 533-542.

Aerosol mass spectrometer measurements at the SMEAR IV semi-urban station

L.Q. Hao[1], A. Kortelainen[1], P. Miettinen[1], A. Jaatinen[1], H. Portin[1,2], M. Komppula[2], A. Leskinen[2], S. Romakkaniemi[1], J.N. Smith[1,2,4], D.R. Worsnop[1,3,5] and A. Laaksonen[1,3]

[1]Department of Applied Physics, University of Eastern Finland, Kuopio, P.O. Box 1627, Finland
[2]Finnish Meteorological Institute, Kuopio Unit, Kuopio, P.O. Box 1627, Finland
[3]Finnish Meteorological Institute, Research and Development, Helsinki, P.O. Box 503, Finland
[4]National Center for Atmospheric Research, Boulder, CO, P.O. Box 3000, USA
[5]Department of Physics, University of Helsinki, Helsinki, P.O. Box 64, Finland
Presenting author email: hao.liqing@uef.fi

Atmospheric aerosol can act as cloud condensation nuclei (CCN) to affect the amount of cloud on the earth and thus global climate. Such aerosol-cloud interactions comprise the largest uncertainties in our understanding of human-caused climate change. The composition of aerosol plays an important role determining its CCN activity. Thus direct and long-term observations of effects of chemical composition of aerosol on aerosol-cloud interactions are especially welcomed.

An observation station has been established in Kuopio, Finland, for making long-term measurements of aerosol-cloud interactions. The station is located at the top of Puijo tower, 306 m.a.s.l. and 224 m above the surrounding lake level (Leskinen et al., 2009; Portin et al., 2009). Aerosol sources that impact the site include long-range transported aerosol from surrounding continents and oceans, as well as local pollution from traffic, a pulp mill, heating plant and other urban sources. A measurement campaign was carried out during Sep. 21-Oct. 27, 2010 for the observation of cloud events. An Aerodyne high resolution aerosol time-of-flight mass spectrometer (TOF-AMS, DeCarlo et al., 2006) was used to measure the chemical composition of ambient particles. We also applied positive matrix factorization (PMF) analysis to track the aerosol origin (Ulbrich et al., 2009).

On average, the mass loading of non-refractory species quantified with the AMS and black carbon is 2.36 μg m^{-3}. Of this, organic, sulfate, nitrate, ammonia, chloride and black carbon mass contributed to 48.2%, 28.3%, 6.2%, 7.2%, 0.4% and 9.6%, respectively. Sulfate showed the largest variability in terms of mass concentration, from 0.02 μg m^{-3} to 7.28 μg m^{-3}. It is heavily wind direction dependent with aerosol sources from northeast (pulp mill as primary emissions) and from southwest (transported from the European continent) contributing higher fractions of sulfate than other directions. Nitrate concentrations showed similar behaviors as sulfate, which is mainly affected by the primary emissions from pulp mill in the northeast direction. Ammonia showed a close correlation with sulfate and nitrate. Measured ammonia concentration was less than 76% of predicted ammonia, indicating the observed aerosol in this campaign was acidic in nature.

Five organic aerosol (OA) components were identified from AMS spectra using PMF (Fig. 1): chemically-reduced urban primary emissions (hydrocarbon-like OA, HOA), low volatile OA (LV_OOA), semivolatile OA (SV_OOA) and biomass burning OA (BBOA_1 and BBOA_2), which contributed to 5.9%, 54.7%, 22.2%, and 16.7% of OA, respectively in mass loadings. LV_OOA and SV_OOA correlated with SO_4 and NO_3, respectively, with only several exceptions of SO_4 and NO_3 events (primary emissions). BBOA_2 is from freshly emitted biomass burning aerosol, which shows correlation with black carbon. BBOA_1 is contributed from oxidized aerosol, showing a good correlation to levoglucosan. Contributions of HOA might be from the local traffic, which correlated to NO_2.

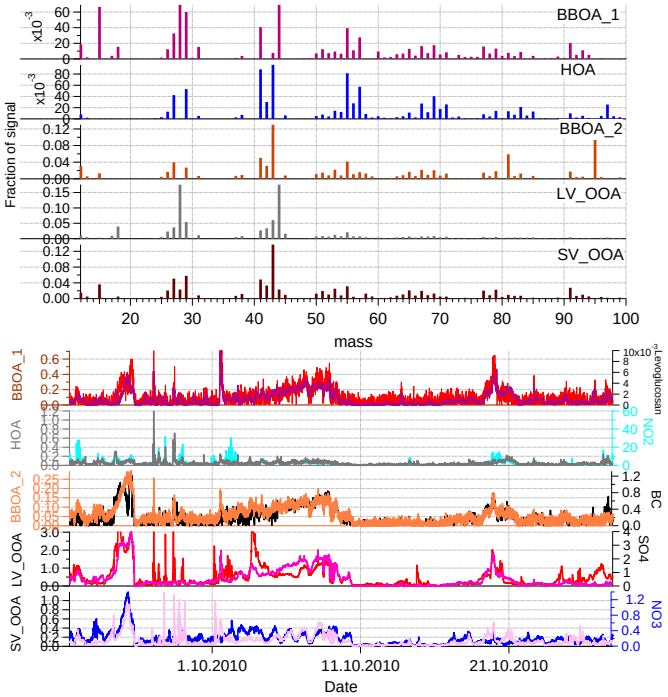

Figure 1 Time series of PMF-AMS sources and corresponding tracers. The bottom panel is in unit of μg/m^3.

This work was supported by the the Academy of Finland Centre of Excellence program (project no 1118615).

Leskinen, A., et al. (2009) *Boreal Environ. Res.*, 14, 576-590.
Portin, H., et al. (2009) *Boreal Environ. Res.*, 14, 641-653.
Ulbrich, I.M., et al., (2009) Atmos. Chem. Phys., 9, 2891-2918

Hygroscopic properties of the urban aerosol in Paris in relation to its chemical compositions

K. Kamilli[1], L. Poulain[1], A. Nowak[2], A. Held[3], W. Birmili[1], A. Wiedensohler[1]

[1]Leibniz-Institute for Tropospheric Research, 04318 Leipzig, Germany
[2]Physikalisch-Technische Bundesanstalt, 38116 Braunschweig, Germany
[3]Bayreuth Center of Ecology and Environmental Research, 95440 Bayreuth, Germany

Keywords: Hygroscopic growth, Chemical composition, Megacity
Presenting author email: kamilli@tropos.de

Aerosol measurements with the objective to characterize the aerosol particles with regard to their physical and chemical properties were made within two field campaigns as part of the MEGAPOLI project work package 3 “Megacities Plume Case Study” (Megacities: Emissions, urban, regional and Global Atmospheric POLlution and climate effects, and Integrated tools for assessment and mitigation). The measurements took place in Paris from 29th of June 2009 to 1st of August 2009 and 15th of January 2010 to 15th of February 2010, respectively.

Dry size distributions were measured by a Twin Differential Mobility Particle Sizer (TDMPS) in a size range between 3 and 700 nm in summer and up to 800 nm in winter whereas humidified size distributions were obtained from a Humidified Differential Mobility Particle Sizer (HDMPS) from 25 to 800 nm. The combination of these two instruments made it possible to get dry and wet number size distributions in high time resolution. Using the summation method (Birmili et al., 2004), the size-resolved descriptive hygroscopic growth factors (DHGF) were derived in the size range from 25 nm to 350 nm at relative humidities of 30, 55, 75 and 90% (Birmili et al., 2009). Simultaneous measurements with an Aerosol Mass Spectrometer (AMS) and a Multi Angle Absorption Photometer (MAAP) yield the mass concentrations of the sulfate, nitrate, and ammonium ions, as well as organic matter and the total mass concentration of black carbon. Using a simplistic particle growth model that assumes a homogeneous particle mixture (Zdanovskii-Stokes-Robinson mixing rule) supplied hygroscopic growth factors initialized by the experimentally determined chemical composition. This enables to draw a comparison between measured growth factors and the ones calculated by the ZSR relation.

Various periods have been examined under various meteorological conditions. A main result is that temporal variations in the observed mean DHGF could be well explained by changes in the chemical compositions. In addition, good agreement has been observed when sulfate was the predominant inorganic factor, whilst worse results with a clear overestimation of the predicted growth factor have been reached when the influence of nitrate became more obvious.

This is possibly due to the strong temperature dependency of nitrate concentrations in the solid phase and the potential of evaporation losses of NH_4NO_3. Because of the increased nitrate concentration in winter the evaporation losses carry more weight. Therefore, the differences between measured and predicted GF are much higher in winter than in summer.

The research leading to these results has received funding from the European Union's Seventh Framework Programme FP/2007-2011 within the project MEGAPOLI, grant agreement n°21252.

Birmili, W., Nowak, A., Schwirn, K., Lehmann, K., Massling, A., and Wiedensohler, A. (2004) A new method to accurately relate dry and humidified number size distribution of atmospheric aerosols. J. Aerosol Sci., 35:15–16.

Birmili, W., Schwirn, K., Nowak, A., Petäjä, T., Joutsensaari, J., Rose, D., Wiedensohler, A., H. K., Aalto, P., Kulmala, M., and Boy, M. (2009) Measurements of humidified particle number size distributions in a Finnish boreal forest: derivation of hygroscopic particle growth factors. Bor. Environ. Res., 14:458–480.

Vertical profiles of aerosol physico-chemical and optical properties measured along Italy over basin valleys

L. Ferrero[a], D. Cappelletti[b], M. Petitta[c], F. Scardazza[b], M. Castelli[c], M.G. Perrone[a], G. Sangiorgi[a] and E. Bolzacchini[a]

[a]POLARIS research centre, DISAT, University of Milano-Bicocca, Piazza della Scienza 1, 20126, Milano, Italy.
[b]Department of Engineering, University of Perugia, Via G. Duranti 93, 06125 Perugia, Italy.
[c] EURAC Institute for Applied Remote Sensing, Viale Druso 1, 39100, Bolzano, Italy.

Keywords: Vertical profiles, Hygroscopicity, black carbon, absorption coefficient, optical properties.
Presenting author email: luca.ferrero@unimib.it

Aerosols physico-chemical and optical properties are fundamental for climate change (IPCC, 2007; Kaufman et al., 2002) as well as for remote sensing applications (Wang et al., 2010; Di Nicolantonio et al., 2009); for the latter their 3D knowledge, especially along the whole atmospheric column is required (Levy et al., 2007; Wang et al., 2010).

For the reasons above, vertical profiles measurements of aerosol properties were conducted in winter 2010 along Italy over the cities of Terni (Central Appenine Valley), Milan (Po Valley) and Merano (Alpine Valley).

A tethered balloon was fitted with an instrumentation package consisting of: 1) a tandem-OPC system (2 OPCs GRIMM *1.107*; 31 size classes between 0.25 to 32 μm: one dried, the other one at ambient RH), 2) a novel micro-Aethalometer (AE51, Magee Scientific), 3) a miniaturized cascade impactor (Sioutas SKC with 2 impaction stages: <1 μm, >1 μm), 4) a metorological station.

OPCs tandem system data allowed us to determine the aerosol humidographs along height following the method reported in Snider et al. (2008) (Figure 1). Hygroscopic growth (Gf) was found to be not uniform along the vertical profiles (Figure 2) evidencing how the use of simple parameterizations of Gf along the atmospheric column in remote sensing applications can be a source of uncertainty in the results.

Micro-Aethalometer data enabled us to estimate black carbon (BC) concentration and absorption coefficient profiles. BC profiles clearly identified the mixing height (MH), which was characterized by a strong vertical concentration gradient. Over Milan BC profiles also showed a shallow layer of increased concentrations close to the ground (+24% compared to the whole MH), due to the proximity of combustion sources. The BC fraction of aerosol volume fell to 50-70% above the MH, compared to ground-level data. This caused a change in the optical absorption properties of the aerosol at different heights. Fairly constant values of absorption coefficient were found above the MH for each location, between 5-20% (2-15 Mm^{-1}) of those measured within the mixing layer.

PM samples collected with the cascade impactor were analysed by ion chromatography (Dionex ICS90 and ICS2000) system. The chemical speciation (Ions and BC) allowed to estimate a aerosol refractive index, and aerosol optical properties along height were calculated from OPC data using a Mie code (Bohren and Huffman, 1983): vertical optical properties were useful to improve the satellite retrieval of particulate matter at ground-level.

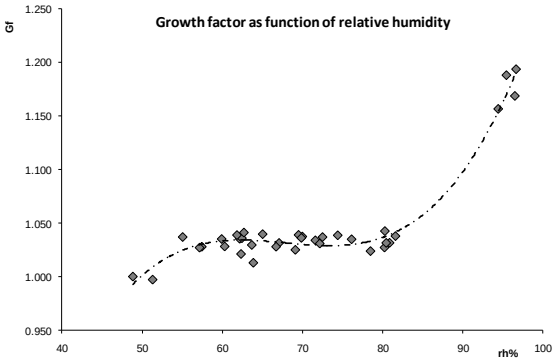

Figure 1. Humidograph along vertical profiles.

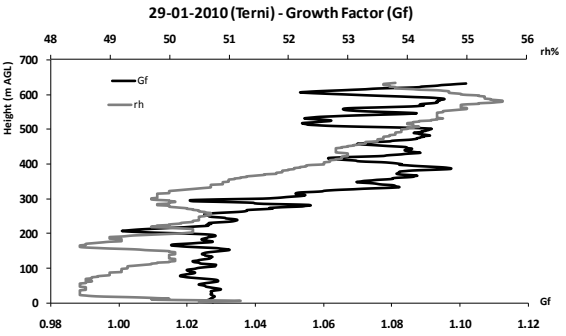

Figure 2. An example of Gf vertical profile.

This work was supported by the SATMAP project, by the Fondazione CARIT di Terni e Narni, by the EURAC research centre and the Province of Bolzano.

Di Nicolantonio, W. et al. (2009). Radiat. Prot. Dosim., doi:10.1093/rpd/ncp231, 1-8.
IPCC: Climate Change 2007
Kaufman, Y.J. et al. (2002). Nature, 419, 215-223.
Levy, R.C. et al. (2007). J. Geophys. Res., VOL. 112.
Snider, J.R. et al. (2008). Atmos. Chem. Phys., 8, 1949–1962.
Wang, Z. et al. (2010). Remote Sensing of Environment, 114(1), 50-63.

$PM_{2.5}$, PM_1 and $PM_{0.4}$ hygroscopicity during spring and summer at one Po Valley site.

L. Ferrero[1], G. Sangiorgi[1], M.G. Perrone[1] and E. Bolzacchini[1]

[1]POLARIS Research Centre, Department of Environmental Sciences, University of Milan - Bicocca, Milan, I-20126, Italy

Keywords: Hygroscopicity, PM2.5/PM1/PM0.4, optical particle counter, ions.

Presenting author email: luca.ferrero@unimib.it

Aerosols hygroscopicity is fundamental for climate change (IPCC, 2007; Kaufman et al., 2002) as well as for remote sensing applications (Wang et al., 2010; Di Nicolantonio et al., 2009). Aerosol hygroscopicity is also important in local studies involving industrial application, i.e. to prevent corrosion effects in computer centres; the latter topic is normed by ASRHAE (2009).

In this study aerosol hygroscopicity was investigated at a rural site located in the middle of the Po Valley (Sannazaro de' Burgondi, Pavia, North of Italy); this place was chosen as it will be the location of a computer centre.

To study aerosol hygroscopicity PM_x samples ($PM_{2.5}$, PM_1, $PM_{0.4}$) were collected using a FAI-Hydra dual channel low volume sampler with the following time resolutions: $PM_{2.5}$ (4-h filters), PM_1 (8-h filters) and $PM_{0.4}$ (24-h filters). The sampling period was 24 March – 19 April (spring) and 10 June – 2 July 2010 (summer). All the collected filters were extracted in ultra-pure water and analyzed by IC to determine the concentration of water soluble inorganic ions (Na^+, NH_4^+, K^+, Mg^{2+}, Ca^{2+}; F^-, Cl^-, NO_3^-, PO_4^{3-}, SO_4^{2-}) and mono-/dicarboxylic acids (acetic, propionic, formic, glutarric, succinic, malonic, maleic, oxalic acids). Then, a thermodynamic model (*E-AIM*, Clegg et al., 1998; http://www.aim.env.uea.ac.uk/aim/aim.php) was used to determine humidographs for each collected sample. Figure 1 reports daily averaged humidographs for $PM_{2.5}$, PM_1 and $PM_{0.4}$ for the spring campaign. The total amount of water uptake in the reported humidographs depends on the atmospheric concentrations of water soluble inorganic and organic ions available on particulate phase.

At the same time, a tandem-OPC system allowed to estimate (Snider et al., 2008) aerosol hygroscopicity with a time resolution of 1 minute. The system is composed by 2 OPCs GRIMM *1.107* (31 size classes between 0.25 to 32 µm): one OPC measures particle number size distribution under dried conditions (OPC_{dry}), the other one performs the same measurement but at ambient RH (OPC_{wet}).

Humidographs for particle with diameter less than 2.5 µm and 1 µm were derived from collected data and compared to that estimated using the *E-AIM* model.

Figure 2 reports humidograph for $V_{2.5}$ (particle volume obtained by particles with diameter less than 2.5 µm) for the spring campaign, as calculated from tandem-OPC system data. The total amount of water uptake in the reported humidograph was calculated from the volume difference between the OPC_{wet} and the OPC_{dry}.

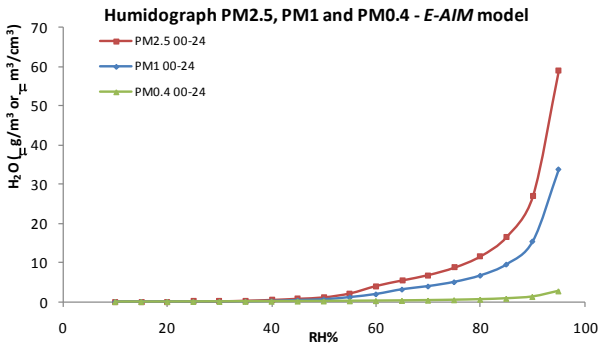

Figure 1. Humidographs calculated from the application of *E-AIM* model to the daily averaged PM_x ionic composition of the spring campaign.

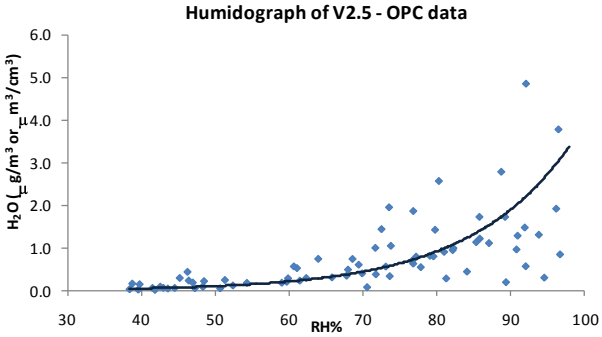

Figure 2. Humidograph for $V_{2.5}$ (particle volume obtained by particles with diameter less than 2.5 µm) for the spring campaign, as calculated from tandem-OPC system data.

Both experimental and modeling data evidenced 65% of relative humidity (RH) as the moisture of the beginning of the hygroscopic growth of particles. Daily cycle of the deliquescence relative humidity will be discussed. As RH in data centres is controlled and kept lower than 60%, these results avoid corrosion hazards due to particle hygroscopicity.

ASHRAE whitepaper (2009). Gaseous and particulate concentration guidelines for data centers.

Clegg, S.L. et al. (1992). *J. Phys. Chem. A*, 102, 2137-2154.

Di Nicolantonio, W. et al. (2009). Radiat. Prot. Dosim., doi:10.1093/rpd/ncp231, 1-8.

IPCC: Climate Change 2007

Kaufman, Y.J. et al. (2002). Nature, 419, 215-223.

Snider, J.R. et al. (2008). Atmos. Chem. Phys., 8, 1949–1962.

Wang, Z. et al. (2010). Remote Sensing of Environment, 114(1), 50-63.

Measurements with a VH-TDMA in CalNex 2010 campaign

Hakala, Jani[1], Mikkilä, Jyri[1], Ehn, Mikael[1], Siivola, Erkki[1], Junninen, Heikki[1], Paramonov, Mikhail[1], Petäjä, Tuukka[1], Bates, Tim[2], Nuaaman, Ibraheem[3,4], Hayden, Katherine[4], Li, Shao-Meng[4], Onash, Timothy[5], Massoli, Paola[5], Worsnop, Douglas R.[5], Kulmala, Markku[1] and Quinn, Patricia K.[2]

[1]Department of Physics, 00014 University of Helsinki, Finland
[2]NOAA/PMEL, 7600 Sand Point Way NE, Seattle, WA 9811, USA
[3]York University, Toronto, Ontario, Canada
[4]Environment Canada, 4906 Dufferin St Toronto RR 5, North Bay, ON P1B 8Z4, Canada
[5]Aerodyne Research Inc., 45 Manning Road Billerica, MA, USA
Keywords: Volatility, Hygroscopicity, Atmospheric aerosols.
Presenting author email: jani.hakala@helsinki.fi

Aerosol particles are ubiquitous in the atmosphere. Their effect on the global climate has not yet been resolved fully. The particles also cause adverse health effects to the human population. These various consequences depend on aerosol particle size as well as their composition. Particle size and hygroscopicity (ie how particles behave as a function of relative humidity, RH) has a crucial role governing their ability to participate in the cloud processes and determine their fate in human airways.

With a Volatility Hygroscopicity Tandem Differential Mobility Analyzer (VH-TDMA) we can study the volatility and hygroscopicity of aerosol particles, as well as the hygroscopicity of the various evaporation stages of particles. This study represents the results of the VH-TDMA measurements in CalNex 2010 campaign.

The operation principle of the VH-TDMA is as follows (e.g. Johnson et al. 2004, Villani et al. 2008). The VH-TDMA developed in this study uses three Vienna type Differential Mobility Analyzers (DMAs), marked as DMA-1, DMA-2a and DMA_2b. A monodisperse fragment is separated from dried aerosol population with DMA1 and led to DMA-2a and DMA-2b operated in parallel. The sample is either passed directly to the second DMAs, or passes through a thermal denuder, using a solenoid valve. DMA-2a measures the dry size and DMA-2b measures the size after the aerosol is humidified. A full measurement cycle for a certain size with a certain denuder temperature and RH consist of a size distribution scan with and without the thermal denuder. TSI CPC-3772 and CPC-3010 are used to detect the particles passing DMA-2a and DMA-2b, respectively.

The VH-TDMA was located in a R/V Atlantis reseach vessel during the CalNex campaign from May 14th to June 8th. R/V Atlantis sailed near the coast of California from San Diego to San Francisco. During the cruise, various types of aerosols were encountered and measured from polluted urban aerosol to clean marine aerosol. Also sea salt particles produced in situ by bubbling seawater with specially constructed raft were measured.

As an example, in figure 1 is presented the hygroscopic and volatility growth factors (HGF and VGF recpectively), and hygroscopic growth factors of particles after passing through the thermal denuder (VHGF). It shows the growth factor distributions of 100 nm particles of polluted urban aerosol at 90% RH. The mode with the HGF around 1.6 are most likely ammonium sulfate particles (HGF >1.6 at RH 90%) with some less hygroscopic contaminants. Ammonium sulfate particles disintegrates at higher temperatures (>150°C); this is clearly visible in the figure. The mode with the HGF around 1.1 is made of either black carbon or fresh organic aerosol particles. Black carbon particles are non-volatile and the volatility of organic particles depends on the composition.

The VH-TDMA has proven to be an especially useful instrument for detecting the external mixing of an aerosol population, which can be seen in figure 1.

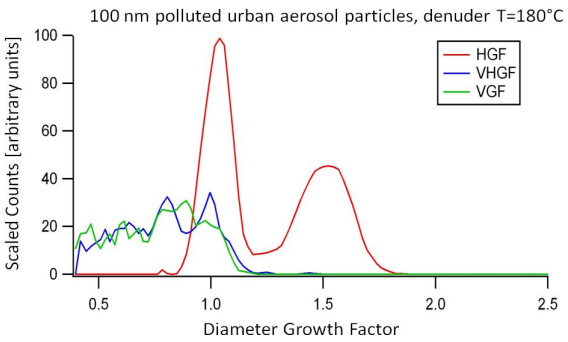

Figure 1. Hygroscopic Growth Factors (HGF), Volatility Growth Factors (VGF) and Hygroscopic Growth Factors of particles after passing through the thermal denuder (VHGF) of polluted urban aerosol at RH of 90%.

This work was supported by the Maj and Tor Nessling foundation via project 2010143 and by the Academy of Finland.

Johnson, G. R. et al., 2005, *J. Geophys. Res.*, 110, D20203, doi:10.1029/2004JD005657, 2005.
Villani, P. et al. 2008, *Aerosol Sci. Technol.*,42, 729-741.

Bounce behavior of freshly nucleated biogenic secondary organic aerosol particles

Virtanen, A.[1], Kannosto, J.[1], Joutsensaari, J.[2], Saukko, E.[1], Kuuluvainen, H.[1], Hao, L.[2], Yli-Pirilä, P.[3], Tiitta, P.[2], Holopainen, J.K.[3], Worsnop, D.R.[2,4,5], Smith, J.N.[2,6,7], Laaksonen, A.[2,4]

[1] Tampere University of Technology, Department of Physics, P.O.Box 692, 33101 Tampere, Finland
[2] University of Eastern Finland, Department of Applied Physics, P.O. Box 1627, 70211 Kuopio, Finland
[3] University of Eastern Finland, Department of Environmental Science, P.O. Box 1627, 70211 Kuopio, Finland
[4] Finnish Meteorological Institute, P.O. Box 503, 00101 Helsinki, Finland
[5] Aerodyne Research, Billerica, MA 08121-3976 USA
[6] Finnish Meteorological Institute, P.O. Box 1627, Kuopio, Finland
[7] National Center for Atmospheric Research, P.O. Box 3000, Boulder, CO 80307 USA

Keywords: secondary organic aerosol, physical phase
Presenting author email: annele.virtanen@tut.fi

The assessment of the climatic impacts and adverse health effects of atmospheric aerosol particles requires detailed information on particle properties. However, very limited information is available on the morphology and phase state of secondary organic aerosol (SOA) particles. The physical state of particles greatly affects particulate-phase chemical reactions, and thus the growth rates of newly formed atmospheric aerosol. Thus verifying the physical phase state of SOA particles gives new and important insight into their formation, subsequent growth, and consequently potential atmospheric impacts.

According to our recent study, biogenic SOA particles produced in laboratory chambers from the oxidation of real plant emissions as well as in ambient boreal forest atmospheres can exist in a solid phase in size range > 30 nm (Virtanen et al., 2010). Here, we extend previously published results to diameters in the range of 17-30 nm. The physical phase of the particles is studied by investigating particle bounce properties utilizing electrical low pressure impactor (ELPI). We also investigate the effect of estimates of particle density on the interpretation of our bounce observations. The observed bounce behavior is also, related to the chemical composition characterized by AMS.

According to the results, particle bounce clearly decreases with decreasing particle size in sub 30 nm size range (Virtanen et al., 2011). The decreasing bounce can be caused by the differences in composition and phase of large (diameters greater than 30 nm) and smaller (diameters between 17 and 30 nm) particles.

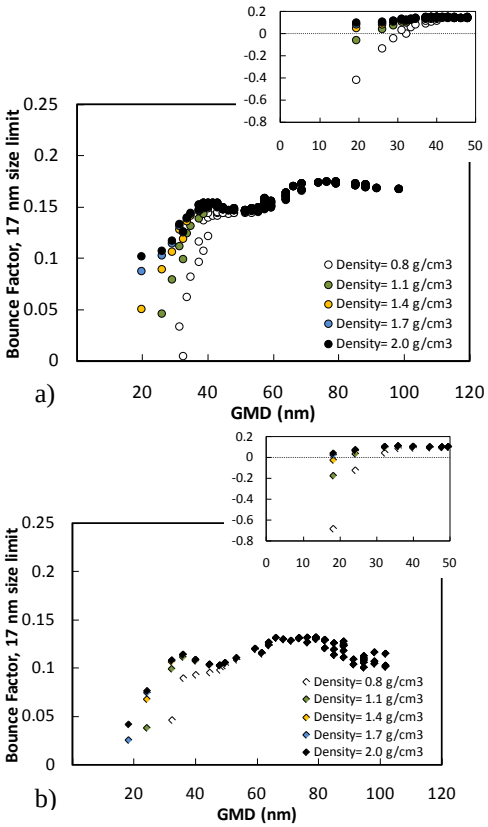

Figure 1. Calculated bounce factors for the 17 nm size limit measured for a) O_3 initiated oxidation and b) OH dominated oxidation in presence of SO_2. Density values 0.8 - 2 g/cm^3 were used in calculations. Insets in the upper right corners of figures a and b show details in bounce factor values for the smallest particles.

This work was supported by the Maj and Tor Nessling foundation.

Virtanen, A., et al. An amorphous solid state of biogenic secondary organic aerosol particles, *Nature*, **467**, 824-827, 2010.
Virtanen et al. Bounce behavior of freshly nucleated biogenic secondary organic aerosol particles, *submitted to ACPD*, 2011

Elemental Composition of the Atmospheric Aerosol in the Central Amazon Basin.

Andrea A. Arana[1], Paulo Artaxo[2]

[1] Instituto Nacional de Pesquisas da Amazônia - INPA, CEP 69060-001, Manaus, AM, Brazil
[2] Instituto de Física, Universidade de São Paulo, CEP 05508-900, São Paulo, SP, Brazil.
Keywords: Amazon, Atmospheric aerosol, Atmospheric chemistry
Presenting author email: artaxo@if.usp.br.

The elemental composition of atmospheric aerosols in central Amazon, a remote region with little influence of anthropogenic activities was studied in order to investigate the sources and processes that regulate aerosol concentrations in Amazonia. Aerosols are important because they affect the biogeochemistry cycles and the atmospheric radiation budget, besides having important effects on the formation and development of clouds. Measurements of elemental composition of aerosols were done in Central Amazonia, in two locations: the biological reserve (Rebio) Cuieiras - Manaus and in Balbina. They were compiled and analysed jointly in an attempt to find a regional identity of the biogenic natural aerosol in the central region of the Amazon Basin.

Stacked Filter Unites (SFU) was used to collect PM10 aerosol samples. Fine mode aerosol ($PM_{2.5}$, less than 2.5 μm) and coarse mode (2.5< dp<10 μm) were collected in Nuclepore filters. The filters were analysed for mass, equivalent black carbon (EBC) and trace elements. Particle Induced X-ray Emission (PIXE) were used to measure about 22 trace elements from Na to Pb. Multivariate statistical techniques such as principal factors, absolute principal factors and cluster analysis of the aerosol chemical composition were performed in order to obtain information on sources and processes. A very large data set of more than 6 years continuous sampling was used in this study.

Atmospheric processes that determine the chemical composition of aerosol particles, like the long range transport of Saharan dust and marine aerosol, biogenic emissions during the rainy season and biomass burning emissions most pronounced during the dry season were identified. The Hysplit model was used to calculate back trajectories and confirm the transport of Sahara dust to the Amazon during the rainy season.

Our results show a similar elemental composition for both sites and hence a homogeneous elemental signature, with very low concentrations. During the rainy season the mean concentration of fine particulate matter is 1.60 $\pm$ 0.92 μg/m^3 at Manaus and 3.4 $\pm$ 1.7 μg/m^3 at Balbina, while that of coarse mode is 6.2 $\pm$ 2.0 μg/m^3 at Manaus and 7.8 $\pm$ 3.0 μg/m^3 at Balbina. In the dry season, the mean concentration of particulate matter in the fine mode is 4.8 $\pm$ 2.4 μg/m^3 at Manaus and 5.4 $\pm$ 3.0 μg/m^3 at Balbina, while in the coarse mode is 6.0 $\pm$ 2.5 μg/m^3 at Manaus and 6.7 $\pm$ 2.0 μg/m^3 for Balbina.

Receptor modelling shows that three main factors for the fine mode were identified and can be qualitatively described as: (1) natural biogenic emission associated with biomass burning with high loadings of EBC, and the elements Br, S, Cl, K and Zn; (2) soil dust particles with high loadings of the elements Ti, Fe, Al, Si, Mn and Ca; (3) biogenic natural emission with high loadings for P. The natural biogenic emissions do not occur in the same factor as the biomass burning emissions. A component of SOA is present in the first and third components, with high amount of organic matter.

For the coarse mode, it was possible to identify 3 factors: (1) soil dust due to high loading of the elements Ti, Al, Fe, Si, Mn and Ca; (2) biogenic emission due to high loading of the elements K, Zn, P, S, associated with EBC and (3) a component of long-range transport probably marine aerosol, represented by the high loadings for the element Cl. This third component represent air masses from the tropical Atlantic, after crossing about 2.000 km of pristine forests, carrying particles of sea salt origin, mixed with biogenic aerosols.

Using Absolute Principal Factor Analysis it is possible to calculate the absolute contributions for each element for each factor in the fine and coarse particulate matter. At Manaus the soil dust component presented 52.1 ng/m^3 of Al, 106.4 ng/m^3 of Si, 22.1 ng/m^3 of Fe and 0.56 ng/m^3 of P. For the biogenic component, 4.81 ng/m^3 of Al, 10.8 ng/m^3 of Si, 147 ng/m^3 of FPM and 1.5 ng/m^3 of P were found, while for the biomass burning component it was 145 ng/m^3 of S, 64.0 ng/m^3 of K and 204 ng/m^3 of EBC. For the coarse particulate matter, the soil dust component presented 52.8 ng/m^3 of Al, 113 ng/m^3 of Si and 25.9 ng/m^3 of Fe, while for the biomass burning component it was 56.8 ng/m^3 of S, 49.6 ng/m^3 of BC and 26.2 ng/m^3 of P.

It is important to emphasize that the significant concentrations of Al, Si, Ti, Mn and Fe observed in Central Amazonia from Saharan dust transport episodes occurred despite the large travel distance and strong aerosol deposition processes due to high rainfall rates typical of the Amazon. The composition of aerosols in Manaus and Balbina are quite similar, showing that natural biogenic and biomass burning aerosol have signatures that can be retrieved using long-term sampling programs like this study.

Acknowledgements
We acknowledge Alcides C. Ribeiro, Ana L. Loureiro, Fernando Morais and Livia Oliveira for support during sample collection. We also thank FAPESP and CNPq and the LBA Central office for support. We thank INPA, CLIAMB, CAPES and FAPEAM for a scholarship support.

Chemical characterization and source identification of roadside aerosol

Gaurav Singh[1], Tarachand Lohia[1], Gazala Habib[1], Tarun Gupta[2]
[1]Indian Institute of Technology Delhi, [2]Indian Institute of Technology Kanpur
Keywords: $PM_{1.0}$, $PM_{2.5}$, Chemical Constitutes, PMF.
Presenting author E-mail:inquire.gaurav@gmail.com

Urban air pollution is due to emission of gases and aerosol in the atmosphere from numerous anthropogenic sources. The pre existing aerosols provide enough surface area for toxic and non toxic pollutant to condense over its surface. In last two decades health-related issues are statistically associated with worsening air quality due to presence of aerosol (Delfino *et al.* 2011). Recent studies (Delfino *et al.* 2011) on exposure to combustion-related (predominantly from traffic) particles and increase in risk of myocardial ischemia, systemic inflammation and blood pressure have revealed the importance of aerosol sources, size and composition in health study.

Aerosol also effect the local air quality and climate. Climate impacts of aerosol include change in energy budget of Earth-Atmosphere system and modification of cloud microstructure leading to alteration of circulation pattern and hydrological cycle.

Recently, the change in energy budget and extremes of precipitation pattern resulting in floods and draughts in Indian region were linked with the size and composition of aerosol (Ramanathan *et al.,* 2005). However, a lot need to be done to establish a clear statistical link between human health, climate, source, size and composition of aerosol.

Water-soluble ions and elements in atmospheric aerosols are reported more commonly for various cities of India. However, very few such efforts (Srivastava *et al.*, 2008) have been made for Delhi city. Delhi the capital of India is one of the dangerously congested and overcrowed (population of Delhi in 2007 was around 17 million) city. Many anthropogenic sources including 3 coal power plants and industries in 13 estates are the threat to air quality of Delhi city and near capital region (NCR). Apart from this, the traffic in Delhi has already been increased to alarming level. The weather of Delhi characterized by hot summer (max. temp. 48 °C) and cold winter (min temp. 2 °C) associated with dust and dense foggy events respectively. The extremes in weather are also believed to play a critical role in aerosol distribution. Therefore, present study has focused on the measurement and characterisation of aerosol for water soluble ions and trace metals during winter and summer season at road site in Delhi. The sources were identified using Positive matrix Factorisation (PMF).

Aerosol mass ($PM_{1.0}$ and $PM_{2.5}$) were collected at two road site near IIT Delhi using impactors developed and calibrated at IIT kanpur (Gupta et. al., 2009). Particles were collected for 10 hrs during day and night time seperately from November 2009 to March 2010. The sampling frequency was 3 days per week including Saturday, Sunday and Monday. Total 39 Samples at Site 1 and 41 samples at Site 2 were collected for both $PM_{1.0}$ and $PM_{2.5}$. Teflon filters with $PM_{1.0}$ mass were subjected to chemical analysis for ions by Ion Chromatography and trace metals by Atomic Absorption Spectroscopy and Inductive Couple Plasma-Optical Emissions Spectrometry. The sources identification and quantification using positive matrix factorisation is in progress.

Average 10 hrs $PM_{2.5}$ concentration on both the sites were significantly maximum in December and January and minimum in March (Table 1). PM1.0 followed the same trend. Night time concentration were always higher than day time. The temperature inversion and atmospheric stable condition above ground resulted in accumulation of aerosol near ground leading to higher concentration during night.

Ions and trace metals contributed ~27 to 57% in various months with expected higher contribution during day time compared to night time. Among anions sulphate, nitrate and chloride are the major contributor. Ammonium and calcium were the major cations obsereved in this study. The presence of calcium, iron and mangnese in significant amount indicated the influence of resuspended dust in aerosol mass. Further identification and quantification of sources will be done using positive matrix factorisation.

Table 1. Monthly averaged PM2.5 concentration (μgm^{-3})

	Site-1		Site-2	
Mon/Yr	**Day**	**Night**	**Day**	**Night**
Nov., 09	223±72	275±54	NA	NA
Dec., 09	288±80	324*	211±22	298±23
Jan., 10	266*	NA	294±53	295±34
Feb., 10	218±56	NA	186±92	279±35
Mar., 10	129±40	204±43	151±35	221±52

*Geometric mean of two samples.

Delfino, R. J., Gillen, D. L., Tjoa,T., Staimer, N. Polidori, A., Arhami, M., Sioutas,C. and Longhurst, J. (2011) *Electrocardiographic ST-Segment Depression and Exposure to Traffic-Related Aerosols in Elderly Subjects with Coronary Artery Disease, Environ. Health Pers.,* 119(2), 196-202

Srivastava, A., Gupta, S. and Jain, V.K. (2008). *Wintertime Size Distribution and Source Apportionment of Total Suspended Particulate Matter and Associated Metals in Delhi. Atmos. Res.* 13: 324–330.

Ramanathan, V., Chung, C., Kim, D., Bettge, T., Buja, L., Kiehl, J. T., Washington, W. M., Fu, Q., Sikka, D. R., and Wild, M. (2005) *Atmospheric brown clouds: Impacts on South Asian, climate and hydrological cycle, PNAS* 102, 5326–5333.

Gupta, T., Chakraborty, A., Ujinwal, K. K. (2010) *Development and Performance Evaluation of an Indigenously Developed Air Sampler Designed to Collect Submicron Aerosol. Ann. Indian Nat. Acad. Engg. 7*, 189-193.

Optical and chemical properties of aerosol particles over an urban location. Estimating mass scattering and absorption efficiencies.

G. Titos[1,2], I. Foyo-Moreno[1,2], H. Lyamani[1], X. Querol[3], A. Alastuey[3] and L. Alados-Arboledas[1,2]

[1]Centro Andaluz de Medio Ambiente, Junta de Andalucía, Universidad de Granada, 18071, Granada, Spain.
[2]Departmento de Física Aplicada, Universidad de Granada, 18071, Granada, Spain.
[3]IDÆA, Department of Geosciences, CSIC, Barcelona, Spain
Keywords: mass scattering efficiency, urban aerosols, PM_{10}.
Presenting author email: gtitos@ugr.es

In recent years, interest in better understanding the factors affecting the Earth's radiation budget, and hence the global climate has increased considerably. While the effects of greenhouse gases are now fairly well understood, the impact of atmospheric aerosol particles in the radiation budget still has many uncertainties.

The aim of this work is to present 1 year of simultaneous measurements of optical and chemical properties of the aerosol particles obtained in an urban environment in Eastern Spain (Granada, 37.18ºN, 3.58ºW, 680 m a.s.l). The instrumentation used was an integrating nephelometer (TSI, model 3563) to obtain the aerosol scattering coefficient at 450, 550 and 700 nm (σ_{sp}), and an Absorption Photometer (MAAP) operating at 670 nm to derive the aerosol absorption coefficient (σ_{ap}). A detailed description of the instrumentation and experimental site can be found in Lyamani *et al* (2010). Furthermore, two high volume samplers (flow rate 30 m^3 h^{-1}) were used for sampling PM_{10} (CAV-A/MSb) and PM_1 (Digitel DHA-80) using Schleicher and Schuell quartz fibre filters (QF20 150 mm). Once the levels of bulk particulates were obtained, the filters are analyzed in the laboratory for determining the levels of major and trace components following the procedure of Querol *et al* (2001). The sampling period was 24 hours starting at 7:00. There are 47 periods with simultaneous measurements of the four instruments described from March 2006 to February 2007. We have averaged σ_{sp} and σ_{ap} over the sampling periods.

The mass scattering and absorption efficiencies (α_{sp}; α_{ap}) of aerosols are the key parameters used to link aerosol chemical properties and radiation model (Seinfeld and Pandis, 1998). They are determined using concurrent measurements of the aerosol light scattering/absorption coefficient and particle mass.

During the study period, σ_{sp} shows a mean value (± SD) of 61 ± 25 Mm^{-1}, typical of urban areas, and σ_{ap}(550 nm) presents a mean value of 25 ± 10 Mm^{-1}. Both, σ_{sp} and σ_{ap}, exhibit the largest values during winter and the lowest during summer, denoting an increase in the anthropogenic contribution in winter combined with the predominance of mixing layer heights (Lyamani et al, 2010). A very low average value of the single scattering albedo of 0.70 ± 0.07 was calculated, suggesting that urban aerosols in this location contain a large fraction of absorbing material. PM_{10} and PM_1 mass concentrations show a mean value of 43 ± 18 $\mu g/m^3$ and 16 ± 7 $\mu g/m^3$, respectively. The mineral matter (CO_3^{2-}, SiO_2, Al_2O_3, Ca, K, Mg and Fe) is the major constituent in the PM_{10} fraction (more than 40 %). This contribution increases during summer (60 %) when the re-suspension from the ground is higher and the North-African dust outbreaks are more frequent. Organic matter and elemental carbon (OM+EC) contribute the most to the PM_1 fraction (42 %). Levels of OM+EC are mainly due to traffic emissions and domestic heating. The OM+EC levels found in Granada are typical of kerbside stations. Secondary inorganic aerosols -SIA- (NH_4^+, NO_3^- and SO_4^{2-} non marine) account for 18% and 23% of PM_{10} and PM_1 fractions, respectively.

We have estimated α_{sp} and α_{ap} of PM_{10} particles applying the Measurement method (Hand and Malm, 2007) which consists in a simple linear regression of σ_{sp} versus PM_{10} mass concentration. Also, we have performed different approaches of the Multilinear Regression (MLR) method to derive α_{sp} and α_{ap} of fine and coarse particles (FM;CM), and α_{sp} and α_{ap} of the major aerosol constituents (Mineral matter, SIA, Sea salt, OM+EC). This method consists in a multiple linear regression with measured σ_{sp} as the independent variable and the measured mass concentrations for each species as the dependent variables (Hand and Malm, 2007). On the other hand, we have found that the light absorption process is dominated by OM+EC particles so α_{ap} for OM+EC was obtained by the Measurement method. The most important results are shown in Table 1.

Table 1. Mass scattering and absorption efficiencies (m^2g^{-1}).

	PM_{10}	FM	CM	OM+EC	SIA
α_{sp}	1.5±0.5	2.5±0.4	0.5±0.2	2.6±0.3	5.4±0.6
α_{ap}	0.6±0.2	0.8±0.2	0.1±0.1	1.7±0.1	--

Aknowledgments: This work was supported by the Spanish Ministry of Science and Technology through projects No: CGL2010-18782 and CSD2007-00067 and by the Andalusian Regional Government through projects No: P10-RNM-6299 and P08-RNM-3568.

Hand, J.L. and Malm, W.C. (2007) J. Geophys. Res., 112, D16203, doi:10.1029/2007JD008484.
Lyamani et al., (2010). Atmos. Chem. Phys. 10,239-254.
Querol et al., (2001) Atmos. Environ. 35 6407–6419.
Seinfeld, J.H. and Pandis, S.N. (1998). John Wiley & Sons, INC.

Hygroscopicity of aerosol particles at Kosetice background station (Czech Republic) using the HTDMA system

J. Ondráček, P. Vodička, V. Ždímal, J. Schwarz and J. Smolík

Laboratory of Aerosol Chemistry and Physics, Institute of Chemical Process Fundamentals, v.v.i., AS CR, Rozvojová 135, Prague 6, 165 02, Czech Republic
Keywords: HTDMA, hygroscopicity, atmospheric aerosols.
Presenting author email: ondracek@icpf.cas.cz

The ability of submicron aerosol particles to absorb water vapor has a large effect on their physical and chemical properties. The tendency for cloud formation and resulting cloud properties depends on the chemical composition as well as on the size distribution of the aerosol particles. Hygroscopic properties of atmospheric aerosols are of major importance affecting the life cycle of the aerosol and the direct and indirect effects of aerosols on climate (e.g. Swietlicki et al., 2008).

Moreover, water content of atmospheric aerosols affects their optical properties (e.g. the light scattering causing the visibility reduction). Also, the partitioning of semivolatiles between the gas and particulate phase is influenced by the presence of water. Furthermore, the deposition pattern of aerosol particles in the human respiratory tract may significantly change with changing size of aerosol particles, and therefore depends also on hygroscopic properties of aerosol particles.

The hygroscopic growth of aerosol particles can be studied in great detail using the HTDMA (Hygroscopic Tandem Differential Mobility Analyzers) systems (e.g. Swietlicki et al., 2008). The HTDMA system is one of the solutions for the online and in-situ measurements of hygroscopic properties of atmospheric aerosols. Generally, the HTDMA systems are suitable for long time measurements at background sites or at sites with slow and small changes in chemical composition and size distribution of the atmospheric aerosol. The humidification and/or drying system (the conditioning system) is one of the key parts of such instrument.

The conditioning system as well as the drying system in the LACP HTDMA is based on the set of Nafion driers and humidifiers. The aerosol sample reaches the desired humidity using the Nafion humidity exchanger. The conditioning (purge) clean air of the Nafion humidity exchanger comes up from the automatic valve system controlled with PID controller. The valve system controls and combines the amount of the dried and the humidified clean air coming from the lines equipped with Nafion dryer and Nafion humidifier, respectively.

The LACP HTDMA was deployed at Kosetice background station from beginning of May 2008 till the end September 2009 within the frame of EUSAAR project. The instrument was in operation during the whole period with some gaps measuring 7 different dry particle size diameters between 22 nm and 225 nm. One scan for each particle size takes 10 minutes (up and down scan) and 20 seconds (changing the particle size), thus the time resolution for the whole size range is 1 hour, 12 minutes and 20 seconds. The problems leading to the data gaps were usually caused by malfunctioning of the RH conditioning system (not stable RH in DMA2) and/or low Nafion drier efficiency (too high RH in DMA1).

Monthly averages of resulting growth factors for individual particle sizes can be seen from Fig. 1. The figure shows the increasing water uptake with increasing particle sizes. This is most probably caused by increasing content of hydrophilic inorganic salts in larger particles. Furthermore, the particles in accumulation mode are more aged and thus their surface is more oxidized, which leads to higher hygroscopicity. Seasonal variations of growth factors show the increasing hygroscopicity of aerosol particles during the spring season.

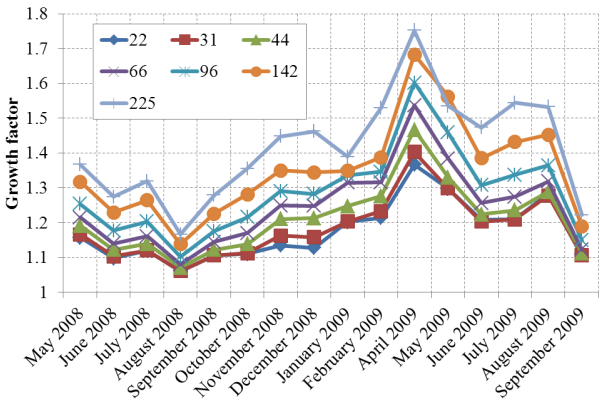

Figure 1. Monthly growth factor for individual particle sizes at Kosetice station.

This work was supported by the EU project EUSAAR (FP6-026140) and by the GA CR project (P209/11/1342).

Swietlicki, E., Hansson, H.-C., Hämeri, K., Svenningsson, B., Massling, A., McFiggans, G., McMurry, P.H., Petäjä, T., Tunved, P., Gysel, M., Topping, D., Weingartner, E., Baltensperger, U., Rissler, J., Wiedensohler, A., Kulmala, M. (2008) *Tellus, Series B: Chem. and Phys. Meteorology*, **60**, Issue 3, 432 – 469.

Air ion chemical and physical characterization during MaCLOUD Inc at Mace Head

T. Petäjä[1], H. Junninen[1], M. Äijälä[1], A. Franchin[1], S. Schobesberger[1], H. Manninen[1], A. Hirsikko[1], J. Vanhanen[2], J. Mikkilä[1,2], K. Lehtipalo[1,2], J. McGrath[3], D. Ceburnis[3], H. Berresheim[3], D.R. Worsnop[1,4], M. Kulmala[1], and C.D. O'Dowd[3]

[1]Department of Physics, PO Box 64, FI-00014 University of Helsinki, Finland
[2]Airmodus Oy, FI-00560 Helsinki, Finland
[3]School of Physics, National University of Ireland Galway, Galway, Ireland
[4]Aerodyne Research Inc., Billerica, MA, USA

Keywords: atmospheric aerosols, aerosol formation, cluster ions, field measurements.
Presenting author email: tuukka.petaja@helsinki.fi

The impact of atmospheric aerosol particles on the climate and regional air quality depends on e.g. their local and regional source strengths (e.g. O'Dowd, 2001). Coastal new particle formation is occurring frequently (O'Dowd and Hoffmann, 2005, Ehn et al 2010a). The physical and chemical character of the atmospheric ion population reflects the regional environment. The aim of this study was to gain insight into participating compounds in both coastal and marine particle formation events by looking in detail the chemical composition of atmospheric ions at Mace Head during MaCLOUD Inc project in December, 2010. A unique location of Mace Head station with strong costal tides makes it possible to study the various nucleation pathways. We also looked into the role of halogens as well as organic ions in the burst-like new particle events at Mace Head despite the low concentrations.

We quantified the atmospheric ion population both in terms of the chemical composition and their physical character. We used an Atmospheric Pressure interface- time-of-flight mass spectrometer (APi-TOF, Junninen et al. 2010, Ehn et al. 2010b), which can probe the chemical composition of naturally charged ions in atmosphere. The data indicate that the ion composition during the new particle formation bursts was dominated by iodine, iodic acid and their clusters. Also bisulphate ion was present in the ion population.

We also provided a detailed physical characterization of the ion population using an Air ion Spectrometer (AIS, Mirme et al. 2007). Furthermore we deployed a Particle Size Magnifier (PSM, Vanhanen et al. 2010), which reveals the concentration of both charged and neutral particles in sub-3 nm particle size. These instruments provided data in the sub-3 nm particle size, which is the size where the gas-to-particle conversation occurs (Kulmala et al. 2007).

An exemplary plot on the chemical and physical characterization is presented in Figure 1. A more detailed data analysis is currently underway and the results presented in this short report need to be considered as preliminary. However, already the vast amount of data that we gathered during the MaCLOUD experiment will definitely improve our understanding about the marine and coastal aerosol particles and ions.

The next MaCLOUD experiment will be held in May 2011. Furthermore, in collaboration with the NUIG, we operated the AIS instrument at Mace Head during the period in between the campaigns in order to capture the temporal variability of the ion population.

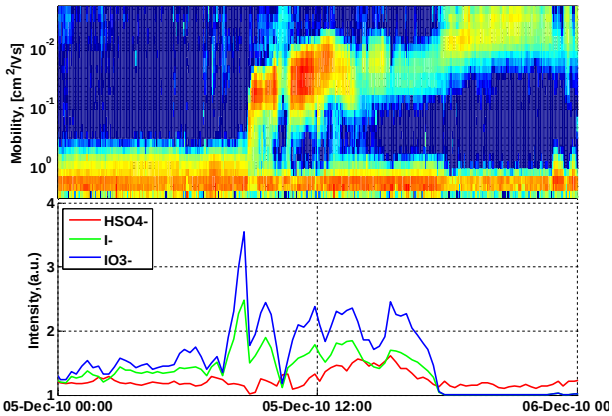

Figure 1. Number size distribution of ambient ions characterized with the AIS during a selected measurement day (top panel) and time traces for ambient selected ambient ions determined with the APi-TOF.

This work was supported by the EU via EUSAAR (026140). Financial support also from the Academy of Finland (139656), Maj and Tor Nessling Foundation (2010143) and ERC (ATMNUCLE) and EPA Ireland is gratefully acknowledged.

Ehn, M., Vuollekoski, H., Petäjä, T. et al. (2010a) J. Geophys. Res. 115, doi:10.1029/2010JD014292.
Ehn, M., Junninen, H., Petäjä, T., et al. (2010b), *Atmos. Chem. Phys.* **10**, 8513-8530.
Junninen, H., Ehn, M., Petäjä, T., et al. (2010) *Atmos. Meas. Technol.*, **3**, 1039-1053
Kulmala, M., Riipinen, I., Sipilä, M., et al. (2007) *Science*, **318**, 89-92.
Mirme, A., Tamm, E., Mordas, G., et al. (2007) *Boreal Environ. Res.*, **12**, 247–264.
O'Dowd, C.D. (2001) *J. Geophys. Res.* **106**, 1545-1549.
O'Dowd, C.D. and Hoffmann, T. (2005) *Environ. Chem.* **2**, 245–255.
O'Dowd, C.D. and de Leeuw, G. (2007) *Phil. Trans. R. Soc. A*, **365**, 1753-1774.
Vanhanen, J., Mikkilä, J., Lehtipalo, K. et al. (2011) *Aerosol Sci. Technol.*, **45**, 533-542.

Elemental composition of PM_{10}, $PM_{2.5}$ and $PM_{1.0}$ aerosols in Paris

S. Visser[1], M. Furger[1], A. Richard[1], U. Flechsig[2], K. Appel[3], A. S. H. Prevot[1], U. Baltensperger[1]

[1] Paul Scherrer Institut, Villigen PSI, Switzerland
[2] Swiss Light Source, Paul Scherrer Institut, Villigen PSI, Switzerland
[3] Hamburger Synchrotronstrahlungslabor at Deutsches Elektronen-Synchroton DESY, Research Centre of the Helmholtz Association, Hamburg, Germany
Keywords: elemental composition, aerosol measurements, XRF, source apportionment
Presenting author email: suzanne.visser@psi.ch

The MEGAPOLI project is an international scientific project to study the interaction between megacities (population > 5 million), emissions, pollution and climate effects. The goal is to link the spatial and temporal scales that connect local emissions, air quality and weather with global atmospheric chemistry and climate. In the four major European Union population areas (Paris, London, Rhine-Ruhr and Po Valley), special emphasis was put on the urban and street scale emissions and air quality besides the focus on the regional and global ones. In Paris, France, two intensive measurement campaigns were performed in summer and winter to improve the quantification of primary and secondary aerosol sources in a large urban agglomeration and in its plume.

We measured the elemental composition of aerosols with a Rotating Drum Impactor (RDI) at an urban (Laboratoire de l'Hygiene de la Ville de Paris, LHVP) and a suburban site (IPSL/SIRTA) in July 2009 and January/February 2010. The RDI sampled aerosol particles with a volumetric flow of 16.6 l min^{-1} (1 m^3 h^{-1}) and particle size segregation in the ranges of 10-2.5 µm, 2.5-1.0 µm and 1.0 to approximately 0.1 µm (Richard et al. 2010). Sampling time was 2 hours. Subsequently, the elemental composition was analyzed with synchrotron radiation induced X-ray fluorescence spectrometry (SR-XRF).

These measurements can be used to document the spatial and temporal variability in aerosol composition and properties near primary emission sources and in air masses entering or leaving the agglomeration.

A first comparison is made between potassium (K) and sulphur (S) contributions in the two largest sizes and for both locations. Figure 1 shows the data of the winter measurements at the LHVP site, while Figure 2 shows the data at the IPSL/SIRTA site. The data shown is not calibrated yet. Subsequent steps involve the subtraction of blank spectra to reduce the influence of scattering of the surrounding material in the SR-XRF setup, perform a relative calibration to correct for the increase in fluorescence yield with increasing atomic number Z, and carry out an absolute mass calibration to convert the raw data into elemental mass concentrations (Bukowiecki et al. 2005; Richard et al. 2010).

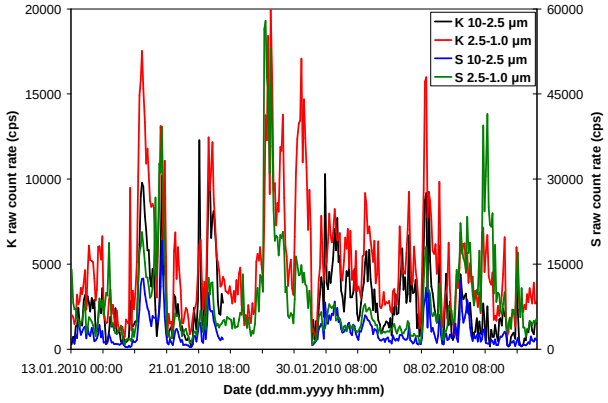

Figure 1. Selection of two-hourly size-segregated elemental amounts for potassium (K) and sulphur (S), measured by RDI-SR-XRF at LHVP in Paris (France).

Figures 1 and 2 show that at both locations most of the time the relative contribution of potassium and sulphur in the PM 2.5-1.0 µm exceeds the contribution in the largest size range. The contributions in the smallest size range appear even larger for these elements (not shown).

We will report on the elemental composition of aerosols, the emission sources analyzed with positive matrix factorization and will provide information on the local versus regional particulate sources in Paris.

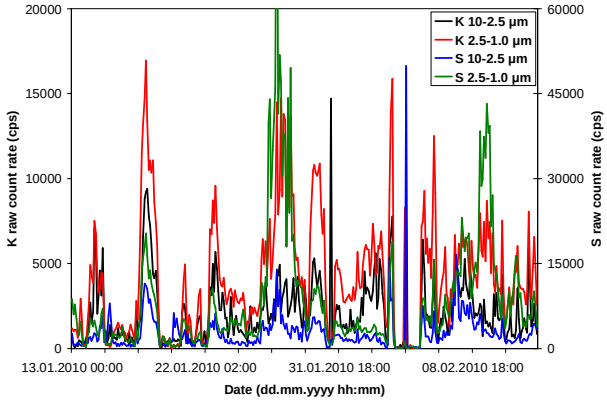

Figure 2. Selection of two-hourly size-segregated elemental amounts for potassium (K) and sulphur (S), measured by RDI-SR-XRF at IPSL/SIRTA in Paris (France).

Acknowledgments: This work was supported by the EC project MEGAPOLI.

Bukowiecki, N., Hill, M., Gehrig, R., Zwicky, C. N., Lienemann, P., Hegedüs, F., Falkenberg, G., Weingartner, E. and Baltensperger, U. (2005) *Environ. Sci. Technol.* **39**, 5754-5762.

Richard, A., Bukowiecki, N., Lienemann, P., Furger, M., Fierz, M., Minguillón, M. C., Weideli, B., Figi, R., Flechsig, U., Appel, K., Prévôt, A. S. H. and Baltensperger, U. (2010) *Atmos. Meas. Tech.* **3**, 1473-1485.

Long term aerosol optical properties in pristine and biomass burning areas in the Amazon Basin

P. Artaxo[1], L.V. Rizzo[2], K.T. Wiedemann[1], E. Swietlicki[4], A. Wiedensohler[3]

[1]Institute of Physics, University of Sao Paulo, Rua do Matao, Travessa R, 187, CEP 05508-090, Brazil.
[2] Department of Exact and Earth Sciences, Federal University of Sao Paulo, Diadema, 09972-270, Brazil
[3] Leibniz Institute for Tropospheric Research, Leipzig, 04318, Germany
[4] Department of Physics, Lund University, Lund, Sweden.

Keywords: aerosol optical properties, biogenic particles, biomass burning, absorption coefficient, scattering coefficient.
Presenting author email: artaxo@if.usp.br

Aerosol physical and chemical properties were measured in two sites in Amazonia. The clean site is at Central Amazonia and is located in a pristine Amazonian forest site. A second sampling site is located in Porto Velho, Rondonia, an area strongly affected by biomass burning emissions. Long term measurements, from February 2008 are being carried out in these two sites, as part of the EUCAARI (European Integrated Project on Aerosol Cloud Climate and Air Quality interactions) and AEROCLIMA (Direct and indirect effects of aerosols on climate in Amazonia and Pantanal) projects. The dataset obtained encompass the first long term aerosol measurements ever performed in Amazonia, elucidating the differences between the biogenic aerosol population naturally released by the forest metabolism and the anthropogenic aerosols brought to the ecosystem by outer sources as well as regional biomass burning emissions.

In the pristine central Amazonia, measurements were taken at the Cuieiras forest site, tower TT34, with coordinates 2°35'40"S and 60°12'33"W, above the canopy (45m), under dry conditions (RH<40%). A MAAP 5012 absorption photometer in series with a nephelometer (TSI 3563) was used to measure aerosol absorption and scattering, respectively. Scattering coefficients were corrected for truncation errors. Observations were adjusted to 1000 mbar and 0^{o}C. Aerosol size distributions were measure using a Lund DMPS system, as well as a TSI SMPS system. Aerosol composition, and several trace gases that helps to characterize aerosol sources were also measured.

In Rondonia, a sampling station was installed close to the city of Porto Velho, in the "Parque Natural de Porto Velho" at coordinates (8,69^{o} S; 63,87^{o} O). This region have with important land use change and biomass burning emissions. A MAAP 5012 absorption photometer and an Ecotech Aurora 3000 nephelometer are used to measure aerosol absorption and scattering. A TSI SMPS measure the aerosol size distribution continuously. Diffusion dryers are used to keep the relative humidity below 40%.

In the pristine Amazonian atmosphere, aerosol scattering coefficients ranged between 1 and 200 Mm^{-1} at 450 nm, while absorption ranged between 1 and 20 Mm^{-1} at 637 nm. A strong seasonal behavior was observed, with greater aerosol loadings during the dry season (Jul-Nov) as compared to the wet season (Dec-Jun). Although the forest site is locally well preserved, it receives the influence of regional biomass burning emissions during the dry season.

During the wet season in Manaus, aerosol scattering (450 nm) and absorption (637 nm) coefficients averaged, respectively, 14 ± 22 and 0.9 ± 0.8 Mm^{-1}. Both optical coefficients were greatly increased during the dry season, averaging 58 ± 58 Mm^{-1} and 4.1 ± 3.8 Mm^{-1}, correspondingly. Angstrom exponents for scattering were lower during the wet season (1.6 ± 0.4) in comparison to the dry season (1.9 ± 0.2), which is consistent with the shift from biomass burning aerosols, predominant in the fine mode, to biogenic and dust aerosols, predominant in the coarse mode. Single scattering albedo, calculated at 637 nm, did not show a significant seasonal variation, averaging 0.86 ± 0.06 and 0.86 ± 0.04, respectively for wet and dry season, even with that large variation in aerosol sources and magnitude of scattering and absorption coefficients.

In Porto Velho, even in the wet season it was possible to observe a strong impact from anthropogenic sources. Biomass burning emissions in the dry season. $PM_{2.5}$ aerosol concentrations of about 300 ug/m² were measured in August and September for most of the years. AOT values at 550 nm above 3 are frequently observed in Porto Velho with AERONET sunphotometers. Black Carbon were measured at 20 ug/m³ in the dry season, indicating strong aerosol absorption. Aerosol light scattering above 300 Mm^{-1} were measured.

This work presents a general description of the aerosol optical properties in Amazonia, both during the Amazonian wet season, when the aerosol population is dominated by particles of biogenic origin, and during the dry season, when there is a strong influence of biomass burning emissions. It is important to describe accurately the optical behavior of these particles in order to assess the impact of anthropogenic changes on the regional climate.

This work was supported by Fundação de Amparo à Pesquisa do Estado de São Paulo, FAPESP Thematic Project AEROCLIMA (08/58100-2) and the European Integrated project on Aerosol Cloud Climate and Air Quality Interactions, EUCAARI (036833).

Strong effect of aerosols on the CO_2 flux in the central Amazon

Glauber .G. Cirino[1], Paulo Artaxo[2] and Rodrigo Souza[3]

[1]National Institute of Amazonian Research - INPA, CEP 69060-001, Manaus, AM, Brazil
[2]Institute of Physics, University of São Paulo, CEP 05508-900, São Paulo, SP, Brazil
[3]University of State Amazonas - UEA, CEP 69065-020, Manaus, AM, Brazil
Keywords: Amazon, atmospheric aerosol, radiation balance, diffuse radiation, carbon fluxes,
Presenting author email: artaxo@if.usp.br

Amazonia is a strong pool in the terrestrial carbon. The carbon uptake or losses are important globally and affect the global carbon balance. During the dry season, smoke from fires dominates the aerosol picture in a large area of the Amazonian forest. Very high aerosol optical thicknesses (AOT) are observed (values of 3-4 at 550 nm) as a result of aerosol particles emitted by biomass burning. During the rainy and transition seasons, the values of AOT are very small (less than 0.08), but increases significantly during the dry season. The net radiation at the surface and even the uptake of carbon by the forest are strongly affected. A large increase in the ratio of direct to diffuse radiation is observed, with a dominance of diffuse radiation at very high AOT.

In this study, we analyzed the CO_2 flux and Net Ecosystem Exchange (NEE) of CO_2 as a function of the concentration of aerosols in two dense forests areas in the Amazon which are part of the Large Scale Biosphere Atmosphere Experiment in Amazonia (LBA). The aerosol optical thickness (AOT) was measured with MODIS (MOD04L2), which were previously validated with AERONET sun photometers operated in Amazonia. CO_2 fluxes were measured with fast response eddy covariance method. A model of clear-sky irradiance was developed from a long time series of observed data (1999-2009) to calculate a variable called relative irradiance (f), used to express the amount of solar radiation due to the presence of extinction of aerosols and clouds in the region.

Overall net absorption of carbon by forest (NEE of CO_2) varied not only with the concentrations of aerosols, but also with cloud cover, solar elevation angle (ASZ) and other parameters. In the rainforest of the K34 Tower located in Manaus Fig.(1a) and Rebio Jaru in Rondônia RBJ Ji-Paraná Fig. (1b) an average increase of 22% and 30% in the NEE was observed when the values of AOT ranged from 0.10 (background in the Amazon) to 0.70 (K34) and 1.8 (RBJ), respectively. For larger reductions of the incident radiation, the SNE was observed to be reduced to values close to zero. The increase of 20 and 30% of NEE was attributed to increased diffuse fraction of solar radiation in relation to their direct fraction.

Important influences on the observed temperature and relative humidity induced by the interaction of radiation with the high aerosol load was observed in both forest areas. In view of the transport of aerosols over long distances during fires, significant changes in the carbon flux may be occurring in large areas of Amazonia. The influence of aerosols on the CO_2 flux and NEE of CO_2 represents a very important effect for the Amazonian ecosystems and have important influence in the global carbon budget.

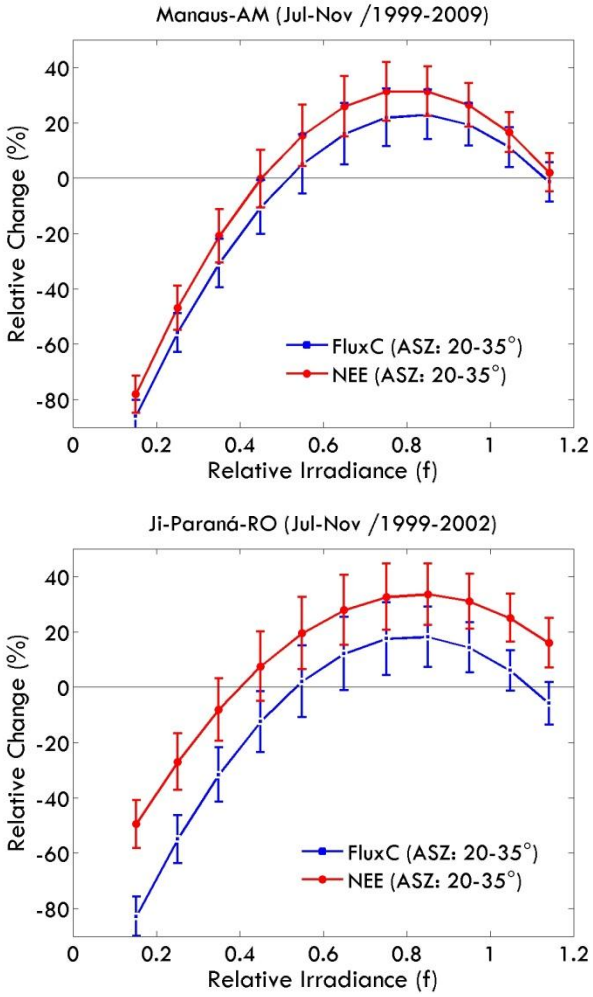

Figure1. Relative change of carbon fluxes and NEE (%) as a function of the relative irradiance (*f)* for 20-35° (ASZ) - Solar Zenithal Angle Interval for the Manaus (K34) (a) and Rondonia (RBJ) (b) sites.

We thank FAPESP, CNPq, CAPES, INPA/CLIAMB and the LBA Central Office for financial and logistical support.

Aerosol and precipitation chemistry measurements in a remote site in Central Amazonia: the role of biogenic contribution

T. Pauliquevis[1], P. Artaxo[2], L. Lara[3] and M.L. Antunes[4]

[1]Departamento de Ciências Exatas e da Terra, Universidade Federal de São Paulo, Diadema/SP, Brazil
[2]Departamento de Física Aplicada, Universidade de São Paulo, São Paulo/SP, Brazil
[3]Universidade Metodista de Piracicaba, Santa Barbara D'Oeste/SP – Brazil
[4]Universidade Estadual Paulista, Sorocaba/SP, Brazil
Keywords: biogenic aerosols, biomass burning, saharan dust, Amazonia
Presenting author email: artaxo@if.usp.br

A long-term (2-3 years) measurement of aerosol and precipitation chemistry was carried out in a remote site in Central Amazonia, Balbina, (1º55'S, 59º29'W, 174 m above sea level), about 200 km north of Manaus city. Aerosols were sampled using stacked filter units (SFU), which separate fine ($d < 2.5$ μm) and coarse mode (2.5 μm $< d < 10.0$ μm). Filters were analyzed for particulate mass (PM), black carbon (BC) and elemental composition by Particle Induced X-Ray Emission (PIXE). Rainwater samples were collected using a wet-only sampler and samples were analyzed for pH and ionic composition, which was determined using ionic chromatography (IC).

The results showed a predominant contribution from biogenic aerosols, mostly concentrated in coarse mode, which comprised up to 81% of PM10 concentration during the wet season. Natural biogenic aerosol also dominates the fine mode in the wet season, with very low concentrations (average 2.2 μg/m³). Large-scale transport of smoke from biomass burning was the second most important contribution, reaching 77% of fine mode particulate mass during the dry season. Soil dust was responsible by a minor fraction of the aerosol mass (less than 17%), and were mainly due to Saharan dust transport events that typically occurred in the period April-May.

In parallel, we run measurements of rainwater chemistry to investigate potential connections between aerosol and precipitation chemistry. The conclusion was that, in a similar way of aerosols, rainwater chemistry is also controlled by biogenic emissions. The volume-weighted mean (VWM) pH was 4.90, and the most important contribution to acidity was from weak organic acids. However, an important difference was that acetic acid predominated over formic acid, which is the opposite of the most common results obtained in pristine areas (Keene et al., 1983; Sanhueza et al., 1991, 1992; Chebbi and Carlier, 1996), where formic acid is the most common organic acid. In spite of this disagreement, previous studies dealing with precipitation chemistry in Central Amazonia (Andreae et al. 1988, 1990; Williams et al., 1997) show discrepant results with respect to the organic acidity partitioning, and this study brings new data to this debate.

Deposition rates for major species did not differ significantly between dry and wet season, except for NH_4^+ and acetate, which had smaller deposition rates during dry season. The long-range transport of sea salt and biogenic particles was observed both in aerosols and rainwater composition. However, while biomass burning emissions were clearly identified in the aerosol component, it was not possible to discern any presence of biomass burning emissions in rainwater chemistry. A possible explanation for this fact was the absence of a common tracer of biomass burning both in aerosols and rainwater, which makes the detection of such connection not clear.

The results showed here indicate that in Amazonia it is still possible to observe pristine atmospheric conditions, relatively free of anthropogenic influences, specially during the wet season.

This research was partially funded by FAPESP (grants 00/10677-8; 01/02968-8) and Instituto do Milenio LBA.

Andreae, M. O., Talbot, R. W., Andreae, T. W., and Harris, R. C.: Formic and acetic acid over the central Amazon region, Brazil, 1. Dry season, J. Geophys. Res. 93(D2), 1616–1624, 1988.

Andreae, M. O., Talbot, R. W., Berresheim, H., and Beecher K. M.: Precipitation chemistry in Central Amazonia, J. Geophys. Res. (Atmos.), 95(D10), 16 987–16 999, 1990.

Chebbi, A. and Carlier, P.: Carboxylic acids in the troposphere, occurrence, sources, and sinks: A review, Atmos. Environ., 30(24), 4233–4249, 1996

Sanhueza, E., Ferrer, Z., and Santana, M.: HCHO and HCOOH in tropical rains, Ambio, 20, 115–118, 1991.

Sanhueza, E., Arias, M. C., Donoso, L., Graterol, N., Hermoso, M., Martí, I., Romero, J., Rondon, A., and Santana, M.: Chemical composition of acid rains in the venezuelan savannah region, Tellus, 44B, 54–62, 1992

Williams, M. R., Fisher, T. R., and Melack, J. M.: Chemical composition and deposition of rain in the central Amazon, Brazil, Atmos. Environ., 31(2), 207–217, 1997.

Tuesday, September 6, 2011

Session 4P: Poster Session A:
Atmospheric Aerosols – Specific Aerosol Types

Fungal Diversity and Biogeography in the Air

Janine Fröhlich-Nowoisky[1,2], Viviane R. Després[3] & Ulrich Pöschl[1,2]

[1]Biogeochemistry Department, Max Planck Institute for Chemistry, P.O. Box 3060, 55020 Mainz, Germany
[2]Institute of Geosciences, Johannes Gutenberg University, Joh.-Joachim-Becher-Weg 21, 55128 Mainz,
[3]Institute of General Botany, Johannes Gutenberg University, Johannes-von-Müller-Weg 6, 55128 Mainz, Germany

Keywords: Fungi, Bioaerosol, DNA
j.frohlich@mpic.de

Fungal spores can account for large proportions of air particulate matter (Elbert *et al*., 2007), and they may potentially influence the hydrological cycle and climate as nuclei for water droplets and ice crystals in clouds, fog, and precipitation. Moreover, some fungi are major pathogens and allergens. However, the diversity and biogeographic distribution of fungi in air particulate matter is hardly known, although air is one of the main media for the dispersal of microorganisms connecting all ecosystems at the Earth's surface.

In our study, air filter samples were analyzed for the presence of fungal deoxyribonucleic acid (DNA). All amplification products were cloned and investigated by restriction fragment length polymorphism analysis. Selected clones were sequenced, and the obtained DNA sequences were blasted in the National Center for Biotechnology Information (NCBI) database for taxonomic attribution to different phyla, classes, and species (Després *et al.,* 2007).

In continental air of central Europe (Mainz, Germany) we found pronounced differences in the relative abundance and seasonal cycles of various groups of fungi in coarse and fine particulate matter, with more plant pathogens in the coarse and more human pathogens and allergens in the respirable fine particle fraction (< 3 µm; Fröhlich-Nowoisky *et al.,* 2009). In particular, we found that the species richness of *Basidiomycot*a (club fungi) in continental air is almost by a factor of two higher than that of *Ascomycota* (sac fungi), which may be due to one or both of the following reasons: an enrichment of *Basidiomycot*a in the atmosphere (higher proportion at the atmosphere-biosphere interface, more efficient release of spores) or an underestimation of the species richness of *Basidiomycot*a in the biosphere (bias of cultivation techniques and PCR primers applied in earlier studies).

Ongoing investigations of aerosol samples collected at different locations and climatic zones around the world (e.g. Austria, Brazil, China, Puerto Rico, Taiwan) show pronounced biogeographic patterns in the species richness of *Basidiomycota* and *Ascomycota* and first insights into the global atmospheric distribution of fungal diversity.

Our results clearly demonstrate the presence of geographic boundaries in the global distribution of microbiotic taxa in air. This may be an important difference between the "blue ocean" and "green ocean" regimes in the formation of clouds and precipitation (Andreae *et* al., 2004, Pöschl *et* al., 2010), for which fungal spores can act as nuclei. Our findings also suggest that air flow patterns and the global atmospheric circulation are important for the evolution of microbial ecology and for the understanding of global changes in biodiversity.

Thanks for collaboration and support to M.O. Andreae, P. Artaxo, H. Bauer, D. Begerow, R. Burges, J. Cimbal, R. Conrad, W. Elbert, G. Engling, C. Fröhlich, R. M. Garland, I. Germann, S. Gunthe, M. Gysel, A. Hoffer, K. Ibarra, N. Knothe, O. Mayol, C. Morris, H. Paulsen, D. Rose, C. Ruzene-Nespoli, A. Wollny, Z. Xie, H. Yang, and J.Z. Zu, the Max Planck Society (MPG), the LEC Geocycles in Mainz funded by the state Rheinland-Pfalz, and the German Research Foundation (DE1161/2-1).

Elbert, W., Taylor, P.E., Andreae, M.O., & Pöschl, U. (2007). *Atmos. Chem. Phys.*, **7**, 4569–4588.

Després, V.R., Nowoisky, J.F., Klose, M., Conrad, R., Andreae, M.O., & Pöschl, U. (2007). *Biogeosciences*, **4**, 1127–1141.

Fröhlich-Nowoisky, J., Pickersgill, D.A., Després, V.R., & Pöschl U. (2009). *Proc. Natl Acad. Sci.,* **106**, 12814-12819.

Pöschl U., Martin S.T., Sinha B., Chena Q., Gunthe S.S., et al. (2010) Rainforest aerosols as biogenic nuclei of clouds and precipitation in the Amazon. *Science,* **329,** 1513-1516.

Andreae, M.O., Rosenfeld, D., Artaxo, P., Costa, A.A., Frank, G.P., et al. (2004) Smoking Rain Clouds over the Amazon. *Science* **303**, 1337-1342.

Determination of airborne plant pathogens by DNA analysis: fungus-like microorganisms

Janine Fröhlich-Nowoisky[1], Cristina Ruzene-Nespoli[1,2], Viviane R. Després[3] & Ulrich Pöschl[1,2]

[1]Biogeochemistry Department, Max Planck Institute for Chemistry, P.O. Box 3060, 55020 Mainz, Germany
[2]Institute of Geosciences, Johannes Gutenberg University, Joh.-Joachim-Becher-Weg 21, 55128 Mainz,
[3]Institute of General Botany, Johannes Gutenberg University, Johannes-von-Müller-Weg 6, 55128 Mainz, Germany

Keywords: *Peronosporomycetes*, Bioaerosol, DNA
c.ruzene@mpic.de

Biogenic aerosols are relevant for the Earth system, climate, and health on local, regional, and global scales. Up to now, however, little is known about the diversity and biogeography of airborne microorganisms although air is one of the main media for the dispersal of microorganisms connecting all ecosystems at the Earth's surface.

Peronosporomycetes (Oomycota) are a diverse group of eukaryotic microorganisms that include saprophytes and pathogens of plants, animals, and microbes (García-Blázquez et al., 2008; Philips et al., 2008). Despite having fungus-like characteristics, *Peronosporomycetes* are not true fungi but are related to algae instead and belong to the Kingdom Stramenopila. Several species like downy mildews (García-Blázquez et al., 2008) have a profound negative impact on agriculture and thus also on crops that are used as potential renewable energy sources.

In our study, air filter samples collected at different locations and climatic zones around the world were analyzed for the presence of *Peronosporomycetes* deoxyribonucleic acid (DNA). All PCR products were cloned and investigated by restriction fragment length polymorphism analysis. Selected clones were sequenced, and the obtained DNA sequences were blasted in the National Center for Biotechnology Information (NCBI) database for taxonomic attribution to different phyla, classes, and species (Després *et al.,* 2007, Fröhlich-Nowoisky et al., 2009).

A one year study (March 2006 – May 2007) of continental air of central Europe (Mainz, Germany) shows pronounced differences in coarse (>3µm) and fine particulate matter (<3µm). *Peronosporomycetes* DNA was found in 100% of the coarse particle samples but not in the respirable fine particle fraction, which may be explained by the spore sizes (>10µm). *Peronosporomycetes* DNA was found throughout the year which may be important for agriculture disease management.

Moreover, investigations of aerosol samples collected at different locations and climatic zones around the world (e.g. Austria, Brazil, China, Puerto Rico, Taiwan) give first insights into the global atmospheric distribution of *Peronosporomycetes* diversity.

Thanks for collaboration and support to M.O. Andreae, P. Artaxo, H. Bauer, R. Burges, J. Cimbal, G. Engling, R. M. Garland, I. Germann, S. Gunthe, M. Gysel, A. Hoffer, K. Ibarra, N. Knothe, O. Mayol, H. Paulsen, D. Rose, Z. Xie, H. Yang, and J.Z. Zu, the Max Planck Society (MPG), the LEC Geocycles in Mainz funded by the state Rheinland-Pfalz, and the German Research Foundation (DE1161/2-1).

Després, V.R., Nowoisky, J.F., Klose, M., Conrad, R., Andreae, M.O., & Pöschl, U. (2007). *Biogeosciences*, **4**, 1127–1141.

Fröhlich-Nowoisky, J., Pickersgill, D.A., Després, V.R., & Pöschl U. (2009). *Proc. Natl Acad. Sci.,* **106**, 12814-12819.

García-Blázquez, G., Göker, M., Voglmayr, H., Martín, M. P., Tellería, M. T., & Oberwinkler, F. (2008). *Mycological Research*, **112**, 502–512.

Phillips, A. J., Anderson, V. L., Robertson, E. J., Secombes, C. J. & van West, P. (2008). *Trends Microbiol* 16, 13–19.

Autofluorescence of Bioaerosol Standards – Characterization by Fluorescence Spectroscopy and Microscopy

Pöhlker, Christopher[1], Huffman, J. Alex[1], Fröhlich-Nowoisky Janine[1], and Pöschl, Ulrich[1]

[1]Max Planck Institute for Chemistry, Biogeochemistry Department, Mainz, 55128, Germany
Keywords: Bioaerosols, Fluorescence, Pollen, Fungal spores, Bacteria.
Presenting author email: c.pohlker@mpic.de

Primary biological aerosol particles (PBAP) such as pollen, fungal spores, bacteria, biogenic polymers and debris from larger organisms are known to influence atmospheric chemistry and physics, the biosphere and public health. PBAP account for up to ~30% of fine and up to ~70% of coarse particulate matter in urban, rural and pristine environment and are released with estimated emission rates of up to ~1000 Tg/a (Elbert, 2007).

Continuous measurements of the abundance, variability and diversity of PBAP have been difficult until recently, however. The application of on-line instruments able to detect autofluorescence from biological particles in real-time has been a promising development for the measurement of PBAP concentrations and fluxes in different environments (Huffman, 2010; Pöschl, 2010). The detected fluorescent biological aerosol particles (FBAP) can be regarded as a subset of PBAP, although the exact relationship between PBAP and FBAP is still being investigated.

Autofluorescence of FBAP is usually a superposition of fluorescence from a mixture of individual fluorescent molecules (fluorophores). Numerous biogenic fluorophores such as amino acids (e.g., tryptophan, tyrosine), coenzymes (e.g., NAD(P)H, riboflavin) and biopolymers (e.g., cellulose) emit fluorescent light due to heterocyclic aromatic rings or conjugated double bonds within their molecular structures. The tryptophan emission peak is a common feature of most bioparticles because the amino acid is a constituent of many proteins and peptides. The influence of the coenzymes NAD(P)H and riboflavin on the autofluorescence of bacteria can be regarded as an indicator for bacterial metabolism and has been utilized to discriminate between viable and non-viable organisms (Lakowicz, 1999). However, very little information is available about other essential biofluorophores in fungal spores and pollen.

In order to better understand the autofluorescence behavior of FBAP, we have used fluorescence spectroscopy and fluorescence microscopy to analyze standard bioparticles (pollen, fungal spores, and bacteria) as well as atmospherically relevant chemical substances. We found varying levels of fluorescent emission and significant differences in the spectral properties of major PBAP classes. The combination will support the quantitative interpretation of data obtained by real-time FBAP instrumentation.

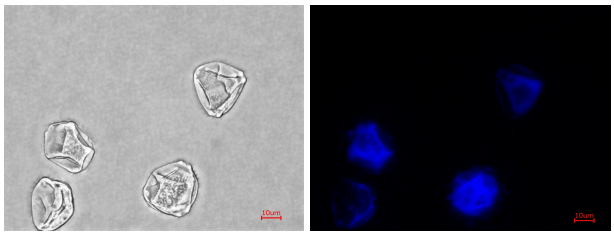

Figure 1. Example microscopy images of pollen. (a) Bright field image illuminated by white light, (b) Same image showing blue fluorescence.

This work has been funded by the Max Planck Society and the LEC-Geocycles Mainz, Germany. The authors gratefully acknowledge support by M.O. Andreae.

Elbert, W., Taylor, P. E., Andreae, M. O., & Pöschl, U. (2007). *Atmos. Chem. Phys.*, 7, 4569-4588.

Huffman, J. A., Treutlein, B. & Pöschl, U. (2010). *Atmos. Chem. Phys.,* 10, 3215-3233.

Pöschl, U., et al. (2010). *Science*, 329, 1513-1516.

Lakowicz, J., Principles of fluorescence spectroscopy, Plenum publishers, New York, 1999.

Allergenic Asteraceae in urban air: DNA analysis and relevance for human health

I. Germann[1,2], J. Fröhlich-Nowoisky [1], U. Pöschl[1],and V. R. Després[3]

[1]Biogeochemistry, Max Planck Institute for Chemistry, P.O. Box 3060, D-55020 Mainz, Germany
[2]Geosciences, Johannes Gutenberg University, Joh.-Joachim- Becher-Weg 21, D-55128 Mainz, Germany
[3]General Botany, Johannes Gutenberg University, Saarstraße 1, D-55099 Mainz, Germany

Keywords: Bioaerosols, DNA, Ragweed *(Ambrosia artemisiifolia)*, Mugwort (*Artemisia vulgaris)*

Ragweed (*Ambrosia artemisifolia*) and mugwort (*Artemisia vulgaris*) are highly important allergenic weeds belonging to the *Asteraceae* plant family (Wopfner *et al.*, 2005). Their pollen grains are one of the main causes of allergenic reactions accompanied by asthma and other severe health problems in late summer and autumn. While mugwort is a native plant in Europe, ragweed reached Europe e.g. by bird seeds as a neophyte from North America about a hundred years ago and spreads rapidly into new areas of central and southern Europe. It is now abundant in the Rhone valley (France), northern Italy, and eastern parts of Austria, Hungary, Croatia, and Bulgaria (D' Amato *et al.*, 1998).

As the spread of ragweed has been observed in Germany during the last years, we quantified its deoxyribonucleic acid (DNA) in air to estimate the number of bioaerosols originating from this allergenic plant and thus to judge if it, also increased during the past years. Mugwort DNA was studied as a control.

A genetic analysis method was chosen as it works successfully for analyzing bioaerosols (Després *et al.*, 2007). Filter samples were collected with a High Volume Sampler separating fine and coarse particles (aerodynamic cut-off diameter ~3 µm) for a period of four years (2006-2009) in Mainz, Germany. The samples were analyzed for the presence of ragweed and mugwort DNA.

Real Time PCR was used to quantify the amount of ragweed and mugwort DNA mainly in the pollen seasons during this four year period. While the abundance of mugwort DNA stayed constant in this measurement period we found an increase of the ragweed DNA from 2006-2008 for the fine particle fraction and for the coarse particle fraction a significant increase from 2006-2008, with a minimal depression in 2007 and a decrease in 2009 for both, coarse and fine particulate filters (Fig. 1). The increase from 2006-2008 might be associated with the constant spread of ragweed in Germany over the course of the last years, while the decrease in 2009 could be caused by unfavorable plant specific growing conditions in spring and summer 2009, and growing awareness and resulting removal of ragweed plants.

There is a need for more comprehensive and long-term studies analyzing the spread of ragweed and its relation to the increase of pollinosis in late summer and autumn in Germany.

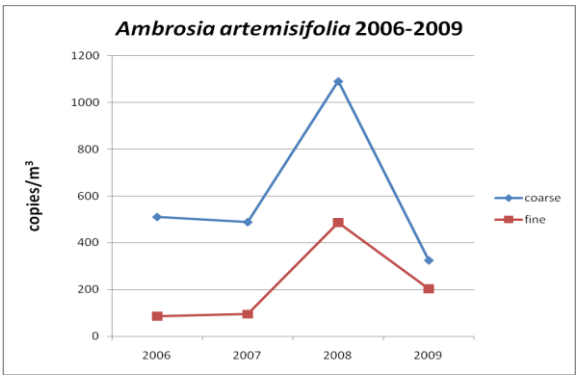

Figure 1. Tendency of ragweed DNA amount for coarse (colored in blue) and fine (colored in red) filter samples from 2006-2009.

The Max Planck Society (MPG), the German Research Foundation (DFG, DE1161/2-1), and the LEC Geocycles Mainz are gratefully acknowledged for funding. We thank D. Pickersgill, J. Cimbal, B. Niethard and N. Knothe for technical assistance, M.O. Andreae, E. Schneider, M. Linke, H. Paulsen and H. Zischler for helpful discussions and support.

D'Amato, G., Spieksma, F.T., Liccardi, G., Jager, S., Russo, M., Kontou-Fili, K., Nikkels, H., Wuthrich, B. & Bonini S. (1998). *Allergy*, 53, 567–578.

Després, V.R., Nowoisky, J.F., Klose, M., Conrad, R., Andreae, M.O. & Pöschl, U. (2007). *Biogeosciences*, 4, 1127–1141.

Wopfer, N., Gadermaier, G., Egger, M., Asero, R., Ebner, C., Jahn-Schmidt, B. & Ferreira, F. (2005). *Int Arch Allergy Immunol*, 138, 337-346.

Size distribution of viable airborne microbes in a Mediterranean suburban site

L. Raisi[1], M. Lazaridis[2], and E. Katsivela[1]

[1]Department of Natural Resources and Environment, Technological Educational Institute of Crete, Romanou 3, 73133 Chania, Crete, Creece
[2]Department of Environmental Engineering, Technical University of Crete, Polytechneioupolis, 73100 Chania, Crete, Greece
Keywords: bioaerosols, size distribution, culturable microorganisms, bacteria, fungi
Presenting author email: katsivela@chania.teicrete.gr

The biological loading of viable, culturable airborne microbes (heterotrophic bacteria, actinobacteria and fungi) in 6 size fractions as well as the three different fractions of respirable particulate matter (PM_1, $PM_{2.5}$ and PM_{10}) were studied in ambient air due to health-related interests.

Air samples were collected using an Andersen six stage viable particle sampler. Duplicates of samples were collected at each sampling period (10 campaigns in total) in a suburban, residential site of the coastal Mediterranean city of Chania (Crete, Greece) in the time period from May to June 2009. The mesophilic heterotrophic bacteria were grown in Tryptone Soy Agar at 37^{o}C for 48 h, the actinobacteria were cultivated in Actinomycete Isolation Agar containing 0.5 % (w/v) glycerol at 30^{o}C for 7d, and fungi were cultivated in Malt Extract Agar at 20^{o}C for 72 h. PM mass and number concentrations were determined using portable aerosol particulate monitors. The mean values of the ambient meteorological conditions during the measurement period were as follows: Temperature 25.1 $\pm$ 3.6 ^{o}C; relative humidity: 55.2 $\pm$ 7.9 %; local wind speed: 0.8 $\pm$ 0.3 m/s; solar radiation: 728.0 $\pm$ 115.5 W/m^2.

As shown in Table 1, the airborne fungi present significant higher concentrations than the airborne heterotrophic bacteria. The Gram-positive actinobacteria, which were the dominant bacteria isolated from bioaerosols, showed the next highest concentrations. The predominance of Gram-positive culturable bacteria in air samples is consistent with the previous work of the authors Shaffer and Lighthart (1997).

Table 1: Mean concentrations of viable, airborne heterotrophic bacteria, actinobacteria and fungi in the ambient air during May and June 2009.

Aerodynamic diameter	Heterotrophic Bacteria (CFU/m^3)	Actinobacte-ria (CFU/m^3)	Fungi (CFU/m^3)
>7μm	11	21	32
4.7-7μm	6	15	30
3.3-4.7μm	6	38	96
2.1-3.3μm	9	76	218
1.1-2.1μm	10	58	78
0.65-1.1μm	2	12	8
SUM of 6 stages	44	220	462

Particulate matter measurements at the same time period revealed that the mean concentrations of PM_{10}, $PM_{2.5}$, and PM_1 were 45 $\pm$ 14, 38 $\pm$ 14, and 34 $\pm$ 14 μg/m^3, respectively, whereas the mean cumulate counts of PM_1 particles was 4,507 $\pm$ 1,872 particles/cm^3.

Although, a nearly equal distribution of the mean concentrations of the airborne heterotrophic bacteria (Table1 & Figure 1) was observed in the six different size fractions, the highest concentrations of the airborne actinobacteria and fungi were determined at aerodynamic diameters between 2.1 and 3.3 μm (Table1 & Figure 1).

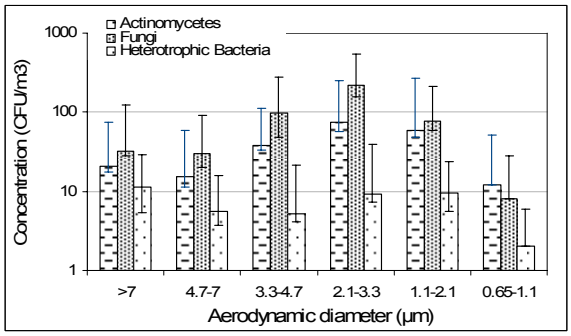

Figure 1: Mean concentrations size distribution of viable, airborne heterotrophic bacteria, actinobacteria and fungi in ambient air during the measurement campaigns.

The concentrations of the main fraction of the airborne actinobacteria showed a very good linear correlation with the residual 5 size fractions (R^2 values: 0.82-0.94) and with the ambient temperature (R^2: 0.84). In addition, a good negative correlation was obtained with the size fraction of heterotrophic bacteria with aerodynamic diameters between 1.1 and 2.1 μm (R^2: -0.88) and the UV radiation (R^2: -0.7).

The concentrations of the main fraction of the mesophilic fungi correlate well with the PM_1 particle number (R^2: 0.72) and with two other size fractions of the fungi (R^2: 0.8 for fraction with > 7 μm, and R^2: 0.78 for fraction with d_p 1.1-2.1 μm, respectively).

In addition, the mass concentration of the particulate matter PM_{10}, $PM_{2.5}$ and PM_1 and the PM_1 particle number correlate well only between each other (R^2: 0.88-0.99).

Shaffer & Lighthart (1997) *Microb Ecol.* **34**, 167-177

Production, sampling and microarray-based detection of bioaerosols containing *E. coli* and *L. pneumophila*

Seidel, M.[1], Hartmann, G.[1], Langer, V.[1], Niessner, R.[1]

[1]Chair for Analytical Chemistry & Institute of Hydrochemistry, Technische Universität München, 81377 Munich, Marchionistraße 17, Germany

Keywords: bioaerosols, *L. pneumophila*, cyclone separator, chemiluminescence microarrays .

Presenting author email: reinhard.niessner@ch.tum.de

Legionella are the causing agent of Legionnaire's disease and Pontiac fever. These diseases cause hundreds of deaths every year in Europe. The most important species is *L. pneumophila* which effects 70 – 90 percent of all cases. *Legionella* live in natural and artificial water systems and are ubiquitary therein. Infection of humans occurs only by inhaling bioaerosols containing these bacteria. Such are generated, for example, by cooling towers, hot water systems, air-conditioning systems or while showering and can be a health threat for people in surrounding areas (Blatny *et al.*, 2008). By now, little is known both about the correlation of the *L. pneumophila* concentration in liquid and gas phase as well as about the dose-response-behavior of *Legionella* bioaerosols.

Standard methods for quantification of *Legionella* are time consuming and labor-intensive. Results could be obtained only after 10 days since the bacteria grow very slowly. Rapid detection methods are needed which combine the sampling of bioaerosols with multiplexed analysis to specify which *Legionella* species is in the air and how much. The rapid quantification of bacteria with flow-through chemiluminescence microarrays were established in our laboratories (Wolter *et al.*, 2008; Langer *et al.,* 2011) and is applied for bioaerosol analysis in this work.

As testing bacteria viable cells of *E. coli* and heat-inactivated *L. pneumophila* (serogroup I) cells have been utilized. Aerosols were generated by a nebulizer (Pari LC) which is commonly used in the therapy of respiratory diseases. The recovery was significantly better than with a conventional cross-flow nebulizer. Furthermore, the concentration of the bacteria suspension inside the nebulizer was constant even after some minutes of aerosol production. Consequently, it can be stated that the Pari LC is a nebulizer highly suitable for the generation of bioaerosols, providing continuously a bioaerosol of constant concentration. For the collection of airborne microorganisms the cyclone separator *Coriolis μ* was applied, a device specially designed for bioaerosol sampling with a high sampling rate. As a reference, an impinger, type AGI-30, is used. Quantification was accomplished by flow cytometry (FCM) for quantification of single bacteria species and a flow-through microarray chip reader (MCR) applying multianalyte chemiluminescence immunoassays. This system was developed at our institute and is based on a sandwich-ELISA that uses the enzymatic chemi-luminescence reaction of luminol and hydrogen peroxide for detection.

The efficiency of bioaerol sampling using the *Coriolis μ* were examined. Living *E. coli* cells were nebulized in a chamber and quantified with FCM after sampling. A recoevery of 34.0 ± 9.8 % (n = 17) was found with a high linearity between 5 x 10^5 and 2 x 10^7 cells/mL which was the working range of the FCM. The recoveries of *L. pneumophila* was 5.3 ± 1.3 % by sampling in a chamber (method 1) and 33.8 ± 9.2 % by sampling with a directed flow from the nebulizer to the sampler (method 2).

In order to determine the efficiency of the C*oriolis μ* sampler a gelatin membrane-filter system (AirPort MD8) with a retention rate of virtually 100 % was used as a reference method. The sampling efficiency was determined to be 78 % for *E. coli*, which is in good agreement with the manufacturer's data.

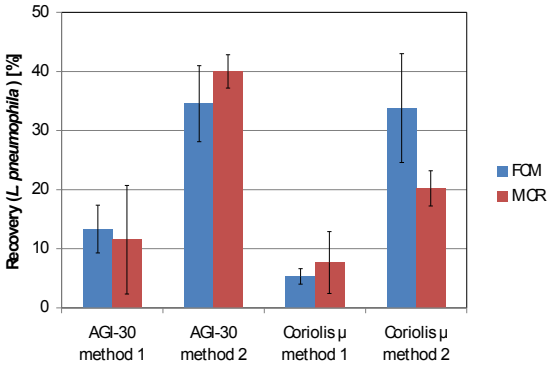

The impinger AGI-30 was compared with the *Coriolis μ* quantifying the recoveries with FCM and MCR. Both detection methods have yielded similar recoveries. However, the advantage of the antibody microarray on the MCR analysis platform was that a lower detection limit of 1 x 10^3 cells/mL was achieved and a multiplexed analysis was possible in 1 h. The *Coriolis μ* samples 3 m^3 of air in 10 min. Therefore, different *Legionella* species could be quantified down to 2 – 7 x 10^3 cells/m^3 in 1,5 hours which is ideal for bioaerosol measurements in the environment and in the interior.

Blatny, J.M., et al. (2008) *Environmental Science and Technology*, 42, 7360-7367.

Wolter, A., Niessner, R., Seidel, M. (2008) *Analytical Chemistry*, 80, 5854-5863.

Langer, V., Niessner, R., Seidel, M. (2011) *Analytical and Bioanalytical Chemistry*, 399, 1041-1050.

Techniques to investigate bacterial survival within the airborne state

J. Jordan[1], T. Hawkyard[1], and R.J. Thomas[1]

[1]Biomedical Sciences, Dstl Porton Down, Salisbury, Wiltshire, SP4 0JQ, UK
Keywords: Bacteria, airborne, PCR detection, viability.
Presenting author email: jejordan@dstl.gov.uk

Bioaerosols can be produced by both natural and artificial means. Respiratory infections are transmitted by sneezing and coughing producing mucus droplets containing bacteria. Survival in the airborne state influences infectivity. Biological warfare may involve aerosol dissemination. Knowledge of the physiological response in the airborne state permits implementation of effective hazard management and biodetection regimes.

Porton Down has a history of investigating the decay of airborne bacteria (Hood, 2009). The methodology used to maintain and capture populations of aerosolised bacteria are described together with techniques that can be applied to investigate the physiological and molecular response of bacteria.

The Goldberg drum (Fig. 1a) is used to investigate the effect of modulating single parameters on survival in dynamic aerosols e.g. relative humidity. A drawback is that certain parameters that affect aerosol survival can not be studied in the Goldberg drum e.g. solar radiation. A historical technique has been revisited based on spider microthreads wound around a metal frame and placed within a metal 'sow' to capture the aerosol (Fig. 1b). This enables factors such as the effect of solar radiation on aerosol decay to be investigated.

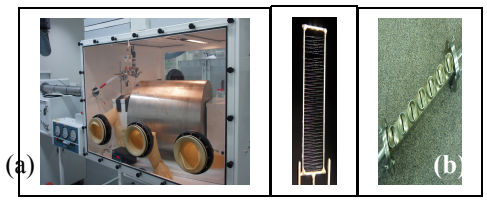

Figure 1. Apparatus used to experimentally study the effect of aerosolisation on bacterial cells (a) Goldberg drum and, (b) microthread technology

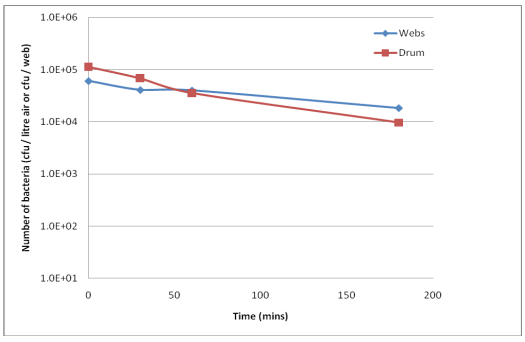

Figure 2. Comparative aerosol decay of *Escherichia coli* MRE162 in Goldberg drum and microthread apparatus at medium relative humidity (~50%)

This experiment was performed as a proof of principle in order to compare the two technologies. The conclusion from the results is that there is no significant difference between aerosol decay curves generated by the two methods.

In order to investigate the molecular mechanisms associated with survival of airborne bacteria by transcriptomic and proteomics, it is important to ascertain not just the viable fraction, but the total number of bacteria present in the collected sample. A sensitive real-time PCR method has been developed for *Yersinia pestis* GB. The method involves extracting the DNA from the bacteria in the aerosol sample using Instagene and then using this as template DNA in the real time PCR. A standard curve of real time PCR threshold cycle (Ct) versus viable count has been calculated which enables the total number of bacteria in an aerosol sample of unknown concentration to be calculated from the Ct value. The limit of detection of the assay is 94cfu/ml of aerosol sample.

Current studies are focussed on developing this PCR assay to differentiate between airborne cells that have damaged cell membranes based on uptake of propidium monoazide. Such assays have been used successfully to study bacterial viability in environmental samples such as wastewater, food matrices and soil (Nocker *et al* 2007; Cawthron & Witthuhn, 2008).

Future research will develop techniques to investigate the transcriptional and proteomic response of airborne cells and to determine the effects on nucleic acid and protein integrity.

This work was supported by funding from the UK Ministry of Defence.

Hood, A.M. (2009) *Epidemiol Infect.* **137**, 753-761.
Nocker, A., Sossa-Fernandez, P., Burr, M.D. and Camper, A.K. (2007) *Appl. Environ. Microbiol.* **73**, 5111-5117.
Cawthorn, D.M. and Witthuhn, R.C. (2008) *J. Appl. Microbiol.* **105**, 1178-1185.
Thomas, R.J., Webber, D., Hopkins, R. *et al*. (2011) *Appl. Environ. Microbiol.* **77**, 920-925.

The comparison of diversity of microorganisms in aerosol and seawater surface microlayer

V.A. Ternovoi, V.M. Generalov, G.A. Buryak, Yu.V. Marchenko, S.E. Olkin, B.I. Antipkin, N.A. Lapteva, A.N. Sergeev, A.S. Safatov

Federal State Research Institution State Research Center of Virology and Biotechnology "Vector", Novosibirsk Region, 630559, Koltsovo, Russia
Keywords: atmospheric aerosols, bioaerosols, bacteria, sea spray.
Presenting author email: safatov@vector.nsc.ru

Atmospheric bioaerosols present an important component of atmospheric pollutants. In the summer of 2009, the complex evaluation of atmospheric air quality was carried out in the city of Gelendzhik (Safatov *et al.*, 2010), including the control of the concentration and diversity of bioaerosols in the city atmosphere. The seawater surface microlayer (SML) is one of the main sources of aerosol for seaside cities, and therefore, SML samples were collected from the water area of Gelendzhik simultaneously with aerosol sampling to evaluate the concentration and diversity of microorganisms present in it. The work presents the diversity of microorganisms in aerosol and sweater SML. According to literature data, different proteobacteria make the maximum contribution to the existing diversity of microorganisms in the environment. For that reason, a special attention was paid to their detection.

The presence of proteobacterial species in the test samples was revealed using unique specific PCR primers consisting of 22 – 25 nucleotides. The length of the amplification product is 1360 b.p. allows using a synthesized pair of primers for further identification of the detected microorganism by sequencing of amplified fragments. The content of the total proteobacteria in samples was determined by RT-PCR assay with hybridization fluorescent detection.

Water samples 50 ml each were filtered through filters with pore diameter of 0.22 μm (*Millipore*, USA). Before the assay, the filters had been stored at +4ºC, then nutrient medium (LB) was poured on them followed by incubation at shaking for 1 hour at 37ºC and seeding at 37ºC onto a solid medium containing 1.0% *NaCl* to obtain individual clones.

LB medium containing 0.5 or 1.0% *NaCl* was poured on the filters with aerosol samples followed by incubation for 6 hours at 37ºC and seeding at 37ºC onto solid media containing 0.5 and 1.0% *NaCl* to obtain individual clones.

The total fraction of the bacterial DNA-RNA was isolated from individual clones. After isolating the total mRNA, cDNA (RT) was constructed using random primers (*d(N)6*) and reverse transcriptase.

The concentration of viable microorganisms in SML of the water area of the Gelendzhik Bay was 7 – 120 CFU/ml, and that in the coastal atmospheric air was from 100 (detection limit) to less than 8000 CFU/m^3. Bacteria made up approximately 75% of the detected viable microorganisms.

The performed sequencing of amplified fragments of bacterial genetic material in aerosol samples and water SML showed that the representatives of the genera *Baccilus: megaterium, subtilis, cerius, anthracis* and *Actinibacter radioresistens* were detected most frequently (in decreasing order). Bacterial genera with the most numerous representatives were found both in aerosol and water SML samples.

Aircraft samples of atmospheric air collected during the same period demonstrate that the number of proteobacteria is 3 – 5 times larger at the altitude of 2000 m than at the altitude of 500 m. Such altitude distribution of bacteria can be observed in the case when their sources are located not far from the sampling places.

As similar microorganisms are found also in SML of the water area of the Gelendzhik Bay, it can be concluded that they are present both in the region's water system and atmosphere. Atmosphere and water system closely interact with each other: the dispersing sea water SML participates in the formation of bioaerosol, and the depositing bioaerosol participates in the formation of water SML. Probably, this is the reason why a large number of microorganisms of the same genera are among those found most frequently in both systems.

Thus, the obtained data once again confirm the "everything is everywhere" hypothesis of microbiogeography (O'Maley, 2008).

The work was supported by the Federal Target Program (Contract # 02.515.11.5087).

Safatov, A.S., et al. *Abstracts 8th International Aerosol Conference. August 29 – September 3, 2010. Helsinki, Finland.* P3V6.

O'Malley, M.A. (2008) *Stud. Hist. Phil. Biol. & Biomed. Sci*. 39, 314-325.

The effect of meteorological factors on bioaerosol concentration in Southwestern Siberia

A.S. Safatov, G.A. Buryak, K.E. Grishkina

Federal State Research Institution State Research Center of Virology and Biotechnology "Vector", Novosibirsk Region, 630559, Koltsovo, Russia
Keywords: atmospheric aerosols, bioaerosols, meteorology, bacteria, fungi.
Presenting author email: safatov@vector.nsc.ru

Meteorological factors can have a considerable influence on the observed concentrations of atmospheric aerosol, including bioaerosol. In the review of Jones and Harrison (2004) it was shown how emission of bioaerosols by vegetation, animals, microbiological and other sources of bioaerosol depends on temperature, humidity, wind velocity, the presence of rain, etc. In the case when measurements are conducted at a considerable distance from the sources contributing to the observed concentrations of bioaerosols, the effect of these factors can be somewhat leveled as meteorological factors have different impacts on different sources. For remote bioaerosol sources, the values of these factors can considerably differ from those measured in the sampling point. Nevertheless, as shown in (Harrison *et al.*, 2005), even in such a situation dependences of concentrations of bacteria on temperature, wind direction and velocity are revealed in 4 observation points in England.

The goal of the present study is revealing the effect of meteorological factors on the concentrations of the total protein and viable microorganisms in two observation points in Southwestern Siberia.

It was found that, depending on the wind direction, the mean concentrations of the total protein in atmospheric aerosol of Southwestern Siberia change by 3 times, and the concentrations of viable microorganisms – by 20 times, Table 1. However, taking into account the great dispersion of concentrations measured in different seasons of different observation years, the mean concentrations for wind directions proved to be statistically indistinguishable at 95% confidence level.

While the mean temperature in the sampling point during the sampling period increases, the concentrations of the total protein and culturable microorganisms in atmospheric aerosol of Southwestern Siberia tend to grow, which is confirmed by observations described in (Safatov *et al.*, 2010) illustrating the increase in these concentrations during the warm season and their decrease during the cold season. With increasing air relative humidity averaged over the sampling period, the concentrations of the total protein and culturable microorganisms in atmospheric aerosol of Southwestern Siberia tend to decrease. The dependence of the concentrations of the total protein and culturable microorganisms on the mean wind velocity during the sampling period has a multidirectional character: with increasing wind velocity, the concentration of viable microorganism increases, and the total protein concentration decreases. These data conflict with those presented in (Harrison *et al.*, 2005), according to which with increasing mean air velocity the concentration of bacteria in three observation points decreases, and in another point remains practically constant.

The obtained results indicate the presence of dependence of concentrations of culturable microorganisms and the total protein in atmospheric aerosol of Southwestern Siberia on meteorological parameters determined during the sampling period.

Jones, A.M. and Harrison, R.M. (2004). *Sci. Total Environ*. **326**, 151-180.

Harrison, R.M., *et al*. (2005). *Int. J. Biometeorol*. **49**, 167-178.

Safatov A.S., *et al.* (2010). In: *Aerosols – Science and Technology*. I. Agranovski (Ed.) Wiley – VCH, 407-454.

Table 1. The dependence of mean concentrations of biogenic components of atmospheric aerosol on wind directions during measurements conducted from February 2001 to December 2009.
Mean values of the measured values ± standard deviation are given.

Wind direction	Site of FSRI SCR VB Vector		Site of Klyuchi Settlement	
	Total protein, $\mu g/m^3$	Viable microorganisms, $Log_{10}(\#)/m^3$	Total protein, $\mu g/m^3$	Viable microorganisms, $Log_{10}(\#)/m^3$
N	0.59 ± 0.77	2.58 ± 0.66	0.45 ± 0.59	2.84 ± 0.91
NE	0.46 ± 0.43	3.29 ± 1.09	0.64 ± 0.85	2.65 ± 0.91
E	0.26 ± 0.22	2.73 ± 0.61	0.52 ± 0.58	2.66 ± 1.07
SE	0.77 ± 0.84	2.00 ± 0.68	0.73 ± 0.99	2.41 ± 1.44
S	0.48 ± 0.35	2.61 ± 0.79	0.44 ± 0.59	2.92 ± 0.92
SW	0.78 ± 1.68	2.77 ± 0.87	0.40 ± 0.49	2.79 ± 0.95
W	0.32 ± 0.24	2.05 ± 0.81	0.49 ± 0.65	2.86 ± 1.01
NW	0.46 ± 0.57	2.62 ± 0.73	0.52 ± 0.75	2.61 ± 0.84

The Study of Surviving of Bacteria on Charcoal Filters under Nutrient, Moisture Regain and Water Content Conditions

Chane-Yu Lai[1], Chun-Wei Chen[1], Shin-Ran Wun[1], Po-Chen Hung[2], Cheng-Ping Chang[2]
[1]Department of Occupational Safety and Health, Chung-Shan Medical University,
[2]Institute of Occupational Safety & Health, Council of Labor Affair

When the severe acute respiratory syndrome（SARS）or Hemagglutinin 1 Neuraminidase 1（H1N1）virus attacked human beings all over the world, some people in Taiwan wore activated carbon mask to prevent inhalation of hazardous bioaerosols. However, activated carbon mask is designed to adsorb gaseous contaminates, but not to use for filtrating of aerosols. The activated charcoal may provide better space for the survival of bacteria, and indirectly hurt human body for re-entrainment of bacteria.

The study used a Collison nebulizer to generate *Bacillus subtilis* endospores or *Escherichia coli* as challenge aerosols. The single stage Anderson sampler was used to monitor the bioaerosol concentrations of the tested chamber. The charcoal filters, were loaded inoculum by using pipette. After that, the filters were added different nutrients（included sterile water, artificial saliva and artificial perspiration）, placed in constant temperature and humidity incubators, and stored in different conditions. The moisture regain of activated charcoal were included in the experimental parameters. The ultimate goal of the study will provide people selecting proper masks in the outbreaks of epidemic diseases.

The results showed: the six type activated charcoals and surgical charcoal mask had high moisture regain and water content at 95 % relative humidity. The *Bacillus subtilis* loaded in the six type activated charcoals had obviously growth-and-decline succession under 95 % relative humidity and 25 □ conditions. This phenomenon could reveal that *Bacillus subtilis* survived in the six type activated charcoals. Moreover, the similar survival results occurred in *Bacillus subtilis* loaded in the surgical charcoal masks. However, *Escherichia coli* could not survive in the six type activated charcoals last for 24 hours, except in columnar activated charcoal under adding artificial saliva, distilled water or artificial perspiration.

Key words: activated charcoal, bioaerosol, moisture regain, nutrient

Differences in Positively and Negatively Charged Bacterial Aerosol Diversity in Indoor and Outdoor Environments

Fangxia Shen and Maosheng Yao *

Principal Contact: Maosheng Yao, Professor, State Key Joint Laboratory for Environmental Simulation and Pollution Control, College of Environmental Sciences and Engineering, Peking University, Beijing 100871, China, Ph: +86 010 6276 7282, Email: yao@pku.edu.cn,

Abstract

In this study, the positively and negatively charged culturable bacterial aerosol concentration and diversity were investigated both in indoor and outdoor environments. For both positively and negatively charged bioaerosols, the air samples were collected into different regions of two agar square plates using an electrostatic sampler (1.1 kv/cm) at a flow rate of 3 L/min for 40 min. The collected bacterial aerosols were cultured directly on agar plates, and the colony forming units (CFU) were manually counted. In addition, the CFUs were washed off from the agar plates, and further subjected to polymerase chain reaction (PCR) and denaturing gradient gel electrophoresis (DGGE) for culturable diversity analysis.

The results revealed that the positively and negatively charged culturable bacterial aerosol concentration and diversity strongly depended on the sampling environments. In indoor environment, negatively charged culturable bacterial aerosols dominated (p-value=0.0489), while in outdoor environment both polarities appeared to have similar concentration levels (p-value=0.078). PCR-DGGE analysis showed that positively charged culturable bacterial aerosol DGGE patterns were very different from those of negatively charged regardless of the sampling environments. In addition, positively charged culturable bacterial aerosols were found to have more phylogenetical similarity with those positively charged collected into different regions of agar plates from different environments, and the same was observed for negatively charged. Outdoor culturable bacterial aerosols were shown to have more bacterial species richness than those indoors. The information provided and the technique developed here could have great implications in electrostatic sampling and control of bioaerosols, and open a new arena for studying airborne microbes with different charge polarity

Keywords : Positive charge, negative charge, Bacterial aerosol, culturable diversity, PCR, DGGE, phylogenetic similarity

Use of Electrostatic Sampling and ELISA method in Studying Charge Distributions of Airborne Allergens

Yan Wu and Maosheng Yao*

Principal Contact: Maosheng Yao, Professor, State Key Joint Laboratory for Environmental Simulation and Pollution Control, College of Environmental Sciences and Engineering, Peking University, Beijing 100871, China, Ph: +86 010 6276 7282, Email: yao@pku.edu.cn,

Abstract

It was shown that exposure to airborne allergens has caused various respiratory problems. Among others factors, their charge levels play an important role in their sampling and deposition of human lung system. Previously, we have developed a method of using electrostatic sampling coupled with qPCR for measuring lab-prepared bacterial aerosol charge levels, preventing the problem of counting non-biologicals if an optical counter is used otherwise. Here, we have investigated the airborne allergen charge distribution in a natural environment using a similar method. The electrostatic sampler with two 96-well plates inside was operated at a flow rate of 3 L/min at an electrostatic field strength of 1.2 kV/cm for 2 h in a hotel environment. The sampling was conducted twice from morning to afternoon. The two 96-well plates were grouped into six regions, and air samples collected into each of the regions were pipetted out for airborne Alt a 1, Der p 1, Der f 1 and Bla g 1 allergens analysis using enzyme-linked immunosorbent assay (ELISA). The airborne allergen charge distributions were calculated using an aerosol calculator.

Results indicated that high levels of airborne allergens (Alt a 1, Der p1 , Der f 1 and Bla g 1) were detected in hotel environment. The concentrations for dust mire Der p1 and Der f 1allergens ranged were 209.4 ng/m^3 and 61 ng/m^3, respectively. For fungal allergen Alt a 1, its concentration was shown about 23 ng/m3, and airborne Bla g 1 was observed to have a concentration of 2.2 U/m^3. For fungal allergen Alt a 1, the charge level ranged from about 60 to 600 units of elementary charge with about 50% of them carrying a charge of 200 or 80 units. For dust mite allergens, their charge levels ranged from 500 to 5000 units of elementary charge with about 20-30% of then carrying a charge level of 1000 units. Due to lack of its aerodynamic size, the charge distribution for Bla g 1 was not calculated, but most of the allergens were collected into the last region of the six regions classified. The results from this study indicated that for carpeted hotel room those common allergens could present an important source of the respiratory problems, and the information obtained here might be used in improving their electrostatic control.

Keywords :Allergens, charge distribution, electrostatic sampling, ELISA, hotel environment

Effects of Microwave Irradiation on Culturability and Diversity of Biological Aerosols of Different Sizes in Different Environments

Yan Wu and Maosheng Yao*

Principal Contact: Maosheng Yao, Professor, State Key Joint Laboratory for Environmental Simulation and Pollution Control, College of Environmental Sciences and Engineering, Peking University, Beijing 100871, China, Ph: +86 010 6276 7282, Email: yao@pku.edu.cn,

Abstract

Increasing evidences show that exposure to airborne biological aerosols has resulted in numerous adverse health effects and diseases. Thus, it is important to develop practical control technology. Previously, we have investigated the inactivation of total bioaerosols using microwave irradiation. Here, the effects of microwave irradiation (2450MHz) on the culturability and diversity of bioaerosols of different sizes were investigated. Air samples were taken using a six-stage Andersen impactor operated at a standard flow rate of 28.3 L/min without and with microwave irradiation for 45 seconds at three different power levels(119, 385, 700 W) in different environments (lab office, hotel and outdoor). For each experimental condition, three independent repeats were conducted. Air samples collected onto different stages of the Andersen sampler were incubated directly at room temperature, and colony forming units (CFU) were manually counted and statistically corrected. The CFUs were further washed off from agar plates using deionized water and subjected to polymerase chain reaction (PCR)-denaturing gradient gel electrophoresis (DGGE) for diversity analysis.

Results revealed that for outdoor environment, larger size bacterial aerosol dominated, while for the indoor environment smaller size bacterial aerosol dominated. Use of higher power level resulted in lower culturable bacterial counts regardless of the sampler stage and sampling environment. PCR-DGGE analysis indicated that in general use of higher power microwave irradiation resulted in less culturable bacterial diversity, while for medium and low power their culturable diversity appeared to be similar to that of control experiment. In contrast, smaller culturable fungal aerosols were found to dominate regardless of sampling environment. Application of microwave irradiation for 45 s was shown to result in complex effects on the culturability of fungal aerosols of different sizes. The results obtained might be negatively impacted by the environmental variations of biological aerosol concentration and composition. Overall, this study has demonstrated a practical control technology for environmental bioaerosols.

Keywords : six-stage Andersen sampler, Bioaerosols of different sizes, Microwave Irradiation

Use of six-stage Andersen Sampler in Investigating Bioaerosol Inhalation Risks in Different Environments

Zhenqiang Xu and Maosheng Yao*

Principal Contact: Maosheng Yao, Professor, State Key Joint Laboratory for Environmental Simulation and Pollution Control, College of Environmental Sciences and Engineering, Peking University, Beijing 100871, China, Ph: +86 010 6276 7282, Email: yao@pku.edu.cn,

Abstract

Increasing evidences show that inhalation of indoor bioaerosols has caused numerous adverse health effects and diseases. However, the bioaerosol size distribution, composition and concentration level could vary with human environments, thus representing different inhalation risks. The six-stage Andersen sampler is designed to simulate the sampling of different human lung regions. Here, the sampler was thus used in investigating culturable bacterial and fungal aerosols collected onto different stages in six different environments (student dormitory, hospital, office lab, hotel, student dining hall, and outdoor environment) in this study. During the sampling, the Andersen sampler was operated for 30 min and three independent experiments were performed for each of the environments. The air samples collected onto each of the six stages were incubated on agar plates directly at room temperature, and the colony forming units were manually counted and statistically corrected.

Results revealed that for most environments investigated the culturable bacterial aerosol concentrations were higher than those of culturable fungal aerosols. The culturable concentration of fungal aerosols were shown to be in comparable levels, while office lab, student dorm and hotel room appeared to have higher culturable bacterial concentrations. For most environments tested, larger (>3 μm) culturable bacterial aerososols were shown to dominate, while for culturable fungal aerosols those 2.1-4.7μm dominated. Comparisons of the air samples collected by different stages of the Andersen sampler indicated that the outdoor environment might represent more fungal inhalation risks to human alveoli region, and the hotel room was shown to have highest culturable bacterial aerosol concentrations collected by the six stage of the sampler. The results from this study suggested that different environments even with similar levels of total microbial cuturable aerosols concentrations could present different inhalation risks due to different size distribution and composition.

Keywords : six-stage Andersen sampler, Bacterial and fungal aerosols, Inhalation

Performance of a Button Inhalable Sampler with Modified MCE Filter Method in Enumerating Culturable Bacterial and Fungal Aerosol Concentration and Diversity

Zhenqiang Xu and Maosheng Yao*

Principal Contact: Maosheng Yao, Professor, State Key Joint Laboratory for Environmental Simulation and Pollution Control, College of Environmental Sciences and Engineering, Peking University, Beijing 100871, China, Ph: +86 010 6276 7282, Email: yao@pku.edu.cn,

Abstract

In this study, a modified mixed cellulose ester (MCE) filter culturing method (directly placing filter on agar plate for culturing) was investigated in enumerating airborne culturable bacterial and fungal aerosol concentration and diversity both in indoor and outdoor environments. A Button Inhalable Sampler loaded with MCE filter was operated at a flow rate of 5 L/min to collect indoor and outdoor air samples using different sampling times: 10, 20, and 30 min. As a comparison, a BioStage impactor was operated at a flow rate of 28.3 L/min in parallel for all tests. The air samples collected by the Button Inhalable Sampler were directly placed on agar plates for culturing, and those collected on agar plates by the BioStage impactor were incubated directly. The colony forming units (CFUs) were manually counted and the culturable concentrations were calculated both for bacterial and fungal aerosols. The bacterial CFUs grown were further washed off and subjected to polymerase chain reaction-denaturing gradient gel electrophoresis (PCR-DGGE) for diversity analysis. For fungal CFUs, microscopy method was applied to study the culturable fungal diversity obtained using different methods.

Experimental results showed that the direct MCE filter culturing method performed reasonably well, and in some cases it outperformed the BioStage impactor, in enumerating bacterial and fungal aerosols. For bacterial aerosol sampling, the BioStage impactor was shown to perform better, and in contrast the MCE filter method was demonstrated to enumerate more culturable fungal aerosols. In general, the microbial species richness was observed to increase with increasing collection time. For both methods, the DGGE gel patterns were observed to vary with sampling time and environment despite of their similar species richness. In addition, an increase in sampling time from 20 to 30 min seemed to not significantly alter the species richness. Regardless of the sampling methods, more species richness was observed in outdoor environment than indoor environment. Compared to the BioStage impactor, the direct MCE filter culturing method with the Button Inhalable Sampler described here can be easily adapted to provide better personal biological exposure monitoring protocols.

Keywords : Direct MCE filter culturing method, Button Inhalable Sampler, BioStage impactor, culturable aerosol diversity, bacterial and fungal aerosols, polymerase chain reaction (PCR), denaturing gradient gel electrophoresis (DGGE), phylogenetic similarity

Effects of single-walled carbon nanotube filter on culturability and diversity of environmental bioaerosols

Zhenqiang Xu and Maosheng Yao*

Principal Contact: Maosheng Yao, Professor, State Key Joint Laboratory for Environmental Simulation and Pollution Control, College of Environmental Sciences and Engineering, Peking University, Beijing 100871, China, Ph: +86 010 6276 7282, Email: yao@pku.edu.cn,

Abstract

In this study, single-walled carbon nanotube (SWNT) filters were prepared using mixed cellulose ester (MCE) filters and carbon nanotubes with three levels of loading: 0.02, 0.16 and 0.64 mg/cm^2. Both MCE and SWNT filters were used to collect bacterial and fungal aerosols with a total volume of 200 L air sampled in indoor and outdoor environments. After sampling, the filters were directly placed on agar plates at 26 ^{o}C for culturing. The culturable aerosol counts were manually obtained both for MCE and SWNT filters, and the resulting bacterial colony forming units (CFUs) were washed off and subjected to the culturable aerosol diversity analysis using polymerase chain reaction-denaturing gradient gel electrophoresis (PCR-DGGE). For fungal CFUs, microscopy method was used to study the diversity obtained using different filter types.

The results showed that use of SWNT filters with medium and high CNT loadings resulted in significant reduction (up to 2 logs) of culturable bacterial and fungal aerosol counts compared to MCE filters in both environments. For low CNT loading (0.02 mg/cm^2), very limited inactivation effects were observed for fungal aerosols, while more bacterial counts were obtained possibly due to the split of the aerosol aggregates. PCR-DGGE analysis revealed that SWNT filters at high CNT loading (0.64 mg/cm^2) resulted in lowest culturable diversity, especially pronounced for outdoor bacterial aerosols. For low and medium CNT loading, the culturable bacterial aerosol diversity remained similar. Fungal aerosol analysis showed that use of SWNT filters with medium to high CNT loading also resulted in significant reduction of fungal species diversity. The results here demonstrated great promise of the SWNT hybrid filter in controlling biological aerosols, and suggested its potential to impact current air conditioning system.

Keywords : Single-walled carbon nanotube (SWNT), culturability, culturable bioaerosol diversity, inactivation, denaturing gradient gel electrophoresis (DGGE)

Influences of Air Volume, DNA Template, and Dilution Factor on the Performance of qPCR Coupled with a Modified BioStage Sampling Method in Quantifying Bioaerosols

Zhenqiang Xu and Maosheng Yao*

Principal Contact: Maosheng Yao, Professor, State Key Joint Laboratory for Environmental Simulation and Pollution Control, College of Environmental Sciences and Engineering, Peking University, Beijing 100871, China, Ph: +86 010 6276 7282, Email: yao@pku.edu.cn,

Abstract

There is an increased interest in integrating polymerase chain reaction (PCR) based technologies with air sampling in investigating airborne microbial community. However, a variety of factors influence the overall performance of such integration. For the sampling method, Andersen type impactors are widely used, but most of them are restricted to the agar culturing method. Here, a BioStage impactor was modified to collect air samples directly into petri dish filled with deionized (DI) water, instead of agar plates. During the sampling, the BioStage impactor was operated at a standard sampling flow rate of 28.3 L/min for 10, 20, 30 min both in indoor and outdoor environments. For each experimental condition, three independent repeats were performed. The collected air samples into the DI water under different experimental conditions were further filtered through a mixed cellulose ester (MCE) filter, and further extracted using DI water. The final sample suspension was subject to qPCR analysis. In addition to the different air sampling volumes, different sample DNA templates (2 or 5 μl) and dilution factors (10 and 50 times) were investigated on the overall performance of PCR-BioStage integration method.

Results revealed that use of the modified BioStage bioaerosol collection method resulted in successful amplification of bacterial cells. In general, use of 2 μl resulted in higher PCR product concentrations under all experimental conditions than those obtained using 5 μl DNA template. This would be helpful for further diversity analysis. Sampling time was also observed to play a role in the overall performance of qPCR, and 10 min sampling time was shown enough to allow the air samples to be efficiently amplified. The effects of dilution factors were shown to be dependent on the sampling time and environments. The results from this study have demonstrated an effective bioaerosol monitoring protocol by integrating qPCR and impaction based air sampling method by choosing an optimal combination sampling time, DNA template and dilution factor.

Keywords : six-stage Andersen sampler, Bacterial aerosols, PCR, BioStage impactor

Fluorescence and bioaerosol measurements at a high-altitude site (puy de Dôme)

A.M. Gabey[1], M. Vaitilingom[2, 3], E. Freney[2], M.W. Gallagher[1], K. Sellegri[2], W.R. Stanley[4], P.H. Kaye[4]

[1] School of Earth, Atmospheric and Environmental Science, University of Manchester, M13 9PL, UK
[2] Laboratoire de Météorologie Physique, CNRS-Université Blaise Pascal, Aubière, France
[3] Laboratoire de Synthèse Et Etude de Systèmes à Interets Biologique, CNRS-Université Blaise Pascal, France
[4] Centre for Atmospheric & Instrumentation Research, University of Hertfordshire, AL10 9AB, UK
Keywords: bioaerosol, fluorescence, bacteria, troposphere.
Presenting author email: andrew.m.gabey@postgrad.manchester.ac.uk

Exciting and measuring the intrinsic fluorescence from aerosol particles can instantly distinguish biological particles (bacteria, fungal spores, pollen or detritus) from non-biological dusts in the laboratory, but few field measurements have been performed. To establish the likely abundance of the background fluorescent aerosol, measurements were carried out on ambient particles sized 0.8—20 µm at the summit of the puy de Dôme mountain (altitude 1465 m a.s.l.) in central France during a cloud-free period between 22 June and 3 July 2010. NO_X, SO_2 and ultrafine particle measurements are consistent with a rural background.

The Wide Issue Bioaerosol Spectrometer, version 3 (WIBS-3; Kaye et al. 2005; Gabey et al. 2010) monitors single-particle particle fluorescence using two excitation and emission channels to detect two biological tracers. Particle size and morphology are quantified using elastic light scattering from a 632 nm diode laser.

Cascade impactor samples were collected between 26—29 June, when the site was influenced by north-easterly air masses. Total bacteria, spores and yeast enumerated by epifluorescence microscopy.

Results

Bacteria concentration was 2.2—33 l^{-1} ± 25%. Fungal spore/yeast concentration was 0.8—2.7 l^{-1} ± 20%. This compares well with other microscopy-based measurements at high-altitude and remote sites (Bauer et al., 2002; Matthias-Maser et al., 2000; Harrison et al., 2005), which report that bacteria dominate fungal spores, with typical biological concentrations of 1—50 l^{-1}. Quantitative size data is unavailable but the bacteria at PDD were noted to be mostly bacilli 0.5—2µm in diameter, with a 2—5µm component. Fungi and spores were typically larger than 8µm.

Mean WIBS-3 total aerosol concentration was 270 l^{-1} (σ = 66 l^{-1}), which peaked at 500 l^{-1} because of a change in air mass origin. The mean concentration of particles with fluorescence corresponding to Nicotinamide adenine dinucleotide (NADH), related to cell metabolism, was 95 l^{-1} (σ = 25 l^{-1}). These particles displayed a clear diurnal variation, increasing by up to 100 l^{-1} at night. The number of non-fluorescent particles showed the opposite cycle. This may relate to the site lying in the residual layer/free troposphere at night, or increased relative humidity.

Particles with fluorescence like the amino acid Tryptophan exhibited no strong diurnal features. Mean number was 12 l^{-1} (σ = 6 l^{-1}) and slightly anti-correlated to NADH-like particle number at night. The fluorescent size mode is at 2—3 µm. Basic morphological measurements based on the intensity distribution of elastically scattered light reveals two sub-types among NADH-type and non-fluorescent particles. This meant a total of six fluorescent and non-fluorescent aerosol components were distinguished.

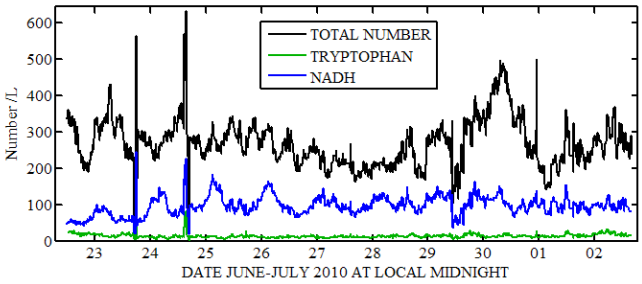

Figure 1 Fluorescent and total number concentration

Work supported by NERC (F00866X/1) and EUSAAR.

Bauer, H., Kasper-Giebl, A., Löflund, M., Giebl, H., Hitzenberger, R., Zibuschka, F., and Puxbaum, H.: *The contribution of bacteria and fungal spores to the organic carbon content of cloud water, precipitation and aerosols*, Atmospheric Research, 64, 109-119, 2002.

Gabey, A. M., Gallagher, M. W., Whitehead, J., Dorsey, J. R., Kaye, P. H., and Stanley, W. R.: *Measurements and comparison of primary biological aerosol above and below a tropical forest canopy using a dual channel fluorescence spectrometer*, Atmos. Chem. Phys., 10, 4453-4466, 2010.

Harrison, R. M., Jones, A. M., Biggins, P. D. E., Pomeroy, N., Cox, C. S., Kidd, S. P., Hobman, J. L., Brown, N. L., and Beswick, A.: *Climate factors influencing bacterial count in background air samples*, International Journal of Biometeorology, 49, 167-178, 2005.

Kaye, P., Stanley, W. R., Hirst, E., Foot, E. V., Baxter, K. L., and Barrington, S. J.: *Single particle multichannel bio-aerosol fluorescence sensor,* Opt. Express, 13, 3583-3593, 2005.

Matthias-Maser, S., Reichert, K., and Jaenicke, R.: *Primary biological aerosol particles at the high alpine site of Jungfraujoch/Switzerland*, Journal of Aerosol Science, 31, 955-956, 2000.

Pharmaceutical deposition of peanut proteins on skin patches by EHDA in cone-jet mode

P. Ehouarn, L. Tatoulian, J. Jusseaume and B. Dupont

DBV Technologies, 27 rue du Faubourg Saint Jacques, Paris, 75014, France

.

Presenting author email: Pascale.Ehouarn@dbv-technologies.com

So far electrospray (ElectroHydroDynamic Atomization) has been largely studied by scientists, especially in its theoretical aspects [1] and more precisely in its cone-jet mode. Both researchers and industrial people consider it as a very promising process in several industrial fields, nano-particles production, genetics, film deposition, etc… [2, 3, 4]; Nevertheless, industrial applications remain much limited to electrospray ionization mass spectrometry, producing ions material of interest, especially macromolecules like proteins. In fact, as a biologic material spray generator and despite its drawbacks, electrospray has many advantages compared to others processes producing fine and controlled droplets: control of size and trajectories of the droplets, substance sparing, immediate drying, etc.

DBV Technologies has taken advantage of these benefits to develop both an electrospray deposition process and an automatic pharmaceutical machine producing skin patches loaded with an allergen extract, used by allergic patients to perform desensitization of their allergic disease. These patches are currently used and tested in human clinical trials (phase I) and fit with the pharmaceutical standards:

- Consistency (± 20%) of the amount of the active ingredient, namely peanut proteins natural extract,
- Ability to lay down different doses (20 το 500 μg),
- Sparing of relatively expensive protein extract,
- Homogeneity of the depot,
- 2 years long shelf life.

The choice of electrospray to perform the deposition of dry peanut proteins into a pharmaceutical patch has been studied and eventually chosen among others because it was the best adapted to meet these requirements, even with substantial challenges, such as:

- Solubilisation of freeze-dried protein extract in a pharmaceutical and liquid formulation with special conductivity and surface tension requirements,
- Low throughput per nozzle,
- Need to make the deposition on an electrically conductive support, etc.

The development led to:

Pharmaceutical liquid formulation

The liquid formulation comprises a pharmaceutical surfactant (Brij O20) that lowers the surface tension, ethanol and water for injection; thanks to dialysis and filtration of the protein solution, the electrical conductivity is lowered to less than 60 μS/cm.

Design of the patch Viaskin®

The patch is made of a crown in PE/EVA foam assembled with a "backing" (the part of the patch supporting the dry proteins) made of PET with a thin conductive titanium coating in order to be both highly biocompatible and electrically conductive.

Spraying head and spraying mode

The electrospray set-up comprises rows of spraying nozzles that are supplied with DC voltage, a ring plate electrode supplied with another DC voltage, and a grounded and heated electrode perpendicular to the nozzles axis. The nozzles are fed with peanut solution by a multiple syringe pump.

A ten nozzles head has been built (upgradable to eighteen) and implemented in order to reach a high production throughput.

A 2 ml/h liquid flow per nozzle has been reached in a stable and long lasting cone-jet mode, at atmospheric pressure in nitrous oxide as a dielectric protecting gas fitting with proteins.

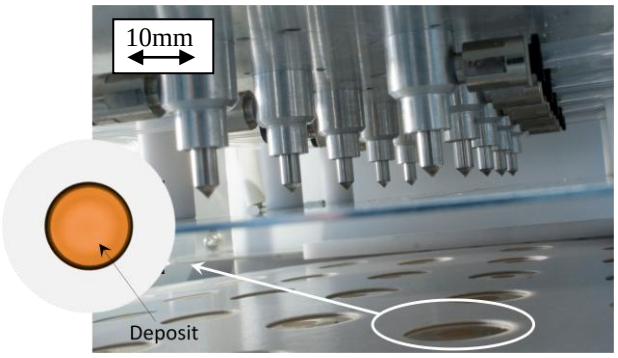

Fig 1: ten nozzles spraying head / Deposit on the patch

[1] Ganan-Calvo, Davila "Current and droplet size in the electrospraying of liquids scaling laws" (1997), J. Aerosol Sci. Vol.28, N°2, pp.249-275

[2] Jaworek, Sobczyk, "Electrospraying route to nanotechnology" (2008), J. of Electrostatics, Vol.66, pp.197-219

[3] Gomez, Bingham, Juan, Tang, "Production of protein nanoparticles by electrospray drying" (1998) J. Aerosol Sci. Vol.29, N°5/6, pp.561-574

[4] Pareta, Brindley, Edirisinghe, Jayasinghe, "*Electrohydrodynamic atomization of protein (bovine serum albumin"* (2005) J. Materials Science: Materials in Medicine, **Vol.16**, pp.919-925

Biochemical characteristics of aerosol

Ranjit Kumar[1], K.M. Kumari[2] and J.N. Srivastava[3]

[1]Department of Chemistry, Technical College,
[2]Department of chemistry, [3]Department of Botany, Faculty of Science
Dayalbagh Educational Institute (Deemed University)
Dayalbagh, Agra-5(India). Fax: +91-562-2801226.
Key words: Aerosol, bioaerosol, micro-organisms, protein estimation
E-mail: rkschem@rediffmail.com

Bioaerosol plays very important role in climate change, rain patterns and public health. The dead decaying organic material, various plants and animals products, infected host and the human handling of various materials contribute to the microbial propagates into the atmosphere as air act as a carrier and transporter of the fungal and bacterial spores and fragments. The concentration of airspora varied with the change in meteorological conditions, temperature, relative humidity, and rainfall as well as with the change in surrounding localities. Indo-gangetic plain in India which host 40% of Indian population has experienced change in climatic patterns, increase in the number of epidemic diseases etc. The monthly average data of predominant fungal colonies recorded and identified from the study site. The maximum fungal

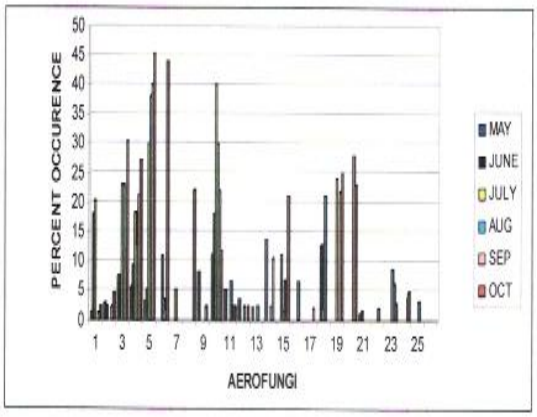

Fig. 1: An average monthly percentage of dominant fungi present in aerosol.

colonies were recorded during the month of October and lowest were recorded in month of June. Agarwal and Shivpuri, 1974 have reported similar trends. Aerial fungal were highest when the mean temperature ranges between 20°C-30°C. It has been reported that meteorological factors like rainfall, relative humidity, temperature have direct or indirect influence on the spores in air. In the present study Aspergillus species were dominant amongst isolated fungi. The maximum percentage of occurrence was observed in morning. Optimal conditions for the growth of aerofungi also play an important role. Czapeck Dox Agar medium was most suitable for fast growth of aerofungi: Aspergillu and Alternaria while PDA medium was suitable for the growth of Penicillium. Protein estimation gives surrogate information about biological components of aerosol. The maximum soluble protein was observed in month of October (1.869 ppm) while minimum soluble protein was observed in month of May and June (0.04 ppm). The level of protein was in relation with presence of biological organism and debris in the aerosol.

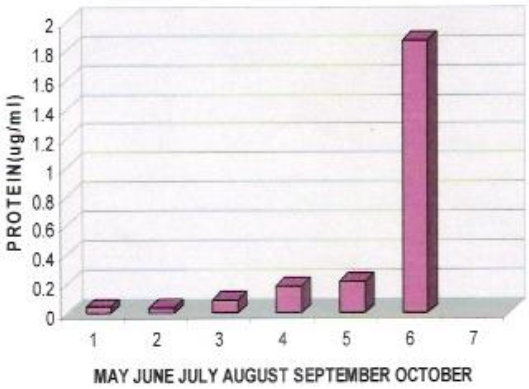

Fig. 2: Protein estimation in aerosol samples.

Agarwal, M.K. and Shivpuri, D.N. (1974). Fungal spores and their role in respiratory allergy. *Adv. Res.* **1**, 78-128.

Sharma, G.C. and sharma, R. (1993). Incidence of airborne fungal spores in Guwahati. *Indian Journal of Aerobiology* **6(1&2)**, 36-40.

Ion studies of organic precursor molecules for secondary particle formation

M. Ehn[1], J. Wildt[2], E. Kleist[2], M. Dal Maso[3], H. Junninen[3], A. Trimborn[1], and T. Mentel[1]

[1]Institue for Energy and Climate research, Forschungszentrum Jülich, Jülich, Germany
[2]Institute Plant Sciences, Forschungszentrum Jülich, Jülich, Germany
[3]Department of Physics, University of Helsinki, Helsinki, Finland
Keywords: Aerosol formation, mass spectrometry, secondary organic aerosol (SOA)
Presenting author email: m.ehn@fz-juelich.de

Secondary aerosol formation is believed to account for the majority of particles in the atmosphere (Merikanto et al., 2009). Other studies have shown that the dominant mass fraction of organic aerosol has been produced secondarily (e.g. Hallquist et al., 2009). Volatile organic compounds (VOCs) are oxidized in several steps whereby the vapor pressure of the oxidation products can be reduced. This reduction in vapor pressure increases the ability of the product to either condense on to existing particles, or take part in the formation of completely new particles.

To better understand early steps of particle formation from VOCs it is therefore of importance to measure such vapors. The most volatile vapors are typically measured by e.g. PTR-MS or GC-MS techniques. The VOCs themselves and many of their high volatile oxidation products are available at high concentrations and do not easily stick to surfaces. However, as the oxidation of these compounds progresses, the concentrations and stability in the gas phase decrease, and neither of the above-mentioned techniques are capable of detecting such compounds. Chemical ionization mass spectrometry (CIMS) has evolved a lot during the recent decade, and is able to measure both inorganic and organic acids in the gas phase down to sub-ppt levels.

The study of naturally charged ions with the atmospheric pressure interface time-of-flight mass spectrometer (APi-TOF; Junninen et al, 2010) has been shown to be very sensitive to acidic, highly oxidized atmospheric molecules (Ehn et al, 2010). Though the instrument cannot directly give quantitative estimates of the neutral compound concentrations, it is to our knowledge the most sensitive instrument available to detect many acidic trace compounds. With the addition of a chemical ionization source in front, the instrument can also be converted into a CIMS, sacrificing some of the high sensitivity and selectivity for quantitative measurements.

The APi-TOF has been deployed at a boreal forest site in Hyytiälä, southern Finland, where several typical ions were identified. During nucleation events, H_2SO_4 dominated the negative ion spectra, but during evening and night when the particles continued growing, the H_2SO_4 signal decreased significantly, and other organic peaks became visible.

To get a better understanding of the processes forming these organic species, and their role in new particle formation and growth, plant chamber measurements were conducted with both real tree emissions and single compound precursors.

Many features of the ion spectra were reproduced in the chamber experiments, both with real plant emissions from a mix of boreal species, and by using pure alpha-pinene as a precursor. Several ions typically found in Hyytiälä, lacking a conclusive identification (Ehn et al, 2010) were also detected in the chamber studies during experiments with alpha-pinene and ozone, i. e. at low OH concentrations (Fig. 1). The peaks are believed to be nitrate-containing, highly oxidized organic molecules with an O:C:H ratio close to 1:1:1. The plotted mass/charge region shows the dominant peaks in the Hyytiälä spectra, however, in the chamber also larger ions, not visible in ambient air, were detected. Additionally, observations of sulfuric acid and its clusters up to the trimer were detected during new particle formation events both in the chamber, and in the field. However, much stronger nucleation events could be produced in the chamber with only small H_2SO_4 signals, indicating the importance of organic precursors in the formation process.

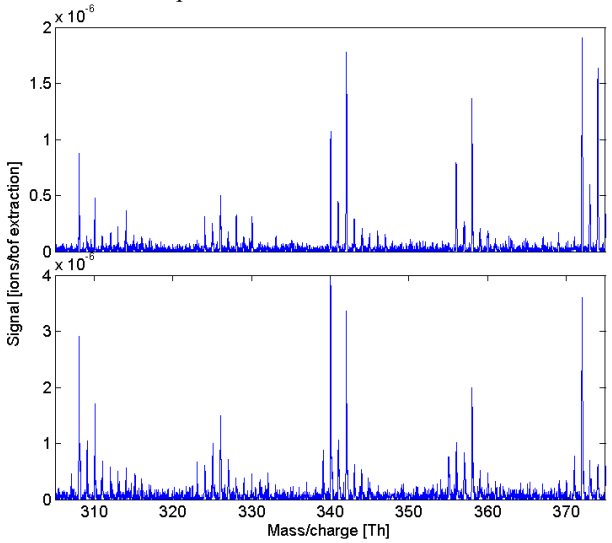

Figure 1. Ion spectra of alpha-pinene oxidation products in the JPAC plant chamber (top), and night-time ion spectrum in Hyytiälä, Finland (bottom).

J. Merikanto et al., *Atmos. Chem. Phys.,* 9(21), 8601-8616, 2009.
M. Hallquist et al., *Atmos. Chem. Phys.* 9, 5155, 2009.
H. Junninen et al., *Atmos. Meas. Tech.*, 3, 1039–1053, 2010.
M. Ehn et al., *Atmos Chem. Phys*., 10, 8513–8530, 2010

Effect of relative humidity on antimicrobial filter using *Sophora flavescens* natural product nanoparticles

Gi Byoung Hwang, Jae Hee Jung, Sun Young Park, Gwi Nam Bae

Global Environment Center, Korea Institute of Science and Technology (KIST), Hawolgok-dong, Seongbuk-gu, Seoul 136-791, Republic of Korea

Keywords: natural products, bioaerosols, inactivation, *S. flavescens*.

Presenting author email: hwanggi2@konkuk.ac.kr

As people spend most of their life time at indoor, the importance of indoor air quality has increased. In particular, bioaerosols have been received scientific attention because of high potential for harmful effect on human health. Bioaerosols can spread widely with air stream, and they can cause chronic diseases. Therefore, controlling the concentration and viability of bioaerosols in contaminated indoor is necessary for protecting human health.

Recently, antimicrobial filter using natural products has been considered a pragmatic method for controlling bioaerosols in indoor environment or ventilation system because the toxicity of natural products against human is relatively lower than that of other antimicrobial materials, such as silver nanoparticle and carbon nanotube despite of their high inactivation performance.

In this study, we investigated the effect of relative humidity (RH) on antimicrobial fibrous filter where natural product nanoparticles (*Sophora flavescens*) were already deposited under surrounding condition of RH 25%. After the filters were exposed to each RH condition (25%, 57%, 82%, and 90%) for 5min, we investigated the change of the morphology variation of natural product nanoparticles on fibrous filters by SEM. In addition, their inactivation abilities were tested using *Staphylococcus epidermidis* bioaerosols.

Figure 1 shows the variation in the morphology of natural product nanoparticles on filter with increasing the relative humidity. The significant change of morphology of natural product nanoparticles on fibrous filter was observed in conditions of RH 82% and RH 90%. In case of RH 90% condition, natural products were dissolved by humidified air and coated on fibres of filter. Figure 2 showed that inactivation efficiency of the antimicrobial filter was reduced with increasing RH conditions to which each filter was exposed. However, in RH 90% condition, inactivation rate of the filter was higher than those of conditions of RH 57% and 82%.

We think that the probability to contact between natural product nanoparticle and bacteria cell on the filter fibre because the morphology of natural product nanoparticles were changed flat with increasing RH environment conditions. But, in case of the antimicrobial filter exposed to RH 90% condition, since the all surface of filter fibre were coated by natural products (increasing of contact probability each other), the inactivation rate of the filter increased compared with those of conditions of RH 57% and 82%.

The results of this study provide useful information for developing practical control method on airborne microorganism

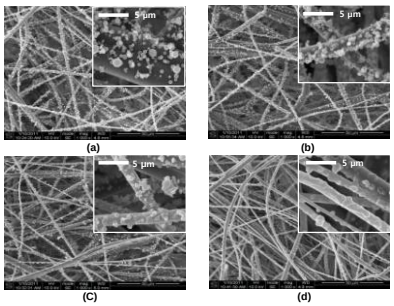

Figure 1. SEM images of (a) RH 25% (b) RH 57% (c) RH 82% (d) RH 90%

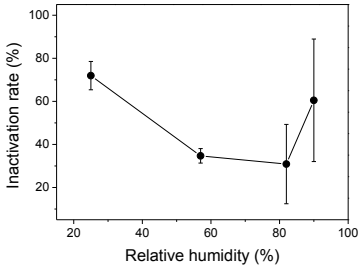

Figure 2. Variation of inactivation rate of antimicrobial filters using natural product nanoparticle under RH surrounding conditions.

This research was supported by the Converging Research Center Program through the National Research Foundation of Korea funded by the Ministry of Education, Science, and Technology (2009-0081929).

Kang, T. H., Jeong, S. J., Ko, W. G., Kim, N. Y., Lee, B. H., Inagaki, M., Miyamoto, T., Higuchi, R., Kim, Y. C. (2000) *J. Nat. Prod. 63*, (5), 680-681.

One year seasonal cycle of airborne bacteria and fungus in southern Sweden: implications on sinks, sources and turn-over time

E. D. Nilsson[1*], C. Fahlgren[2], U. L. Zweifel[3]

[1]Department of Applied Environmental Science, Stockholm University, SE-10691 Stockholm, Sweden
[2] School of Natural Sciences, Linnaeus University, SE-391 82 Kalmar, Sweden
[3] Department of Cell and Molecular Biology, University of Gothenburg, SE-405 30 Göteborg, Sweden
Keywords: bioaerosols, fungal spores, marine aerosol, bacteria, sea-spray, deposition, source identification, ice nuclei.
Presenting author email: douglas.nilsson@itm.su.se

Colony-Forming Bacteria (CFB) and Fungi (CFF) were determined from samples collected on the east coast of Sweden, Kalmar (56°39.576'N, 16°21.687'E) from April 2007 and September 2008. The aerosol number concentrations of bacteria and fungi (N_{CFB} and N_{CFF}) were interpreted using three dimensional trajectories and a semi-lagrangian approach (Nilsson and Leck, 2003). Fahlgren et al. (2010) showed that N_{CFB} follows the total number of live bacteria, able to grow on solid media and form colonies, and their identity have a high overlap with culture-independent sequencing.

We found clear seasonal cycles in N_{CFF} and N_{CFB} peaking in summer and winter, respectively, both at about 1600 m^{-3} maxima monthly averages. Fungus and bacteria concentrations were uncorrelated, suggesting different sources. Fungi increased over land, corresponding to a continental fungi source of about 1.4 spores $m^{-3}s^{-1}$. We present parameterizations of N_{CFF} concentration and column burden as functions of water vapor mixing ratio q and surface temperature T_s. Fungi concentrations experienced a dramatic drop in concentration in air that had been through at least one episode of temperatures below approximately 0°C. This may either be explained by ice nucleation followed by precipitation, or mortality due to the low temperatures.

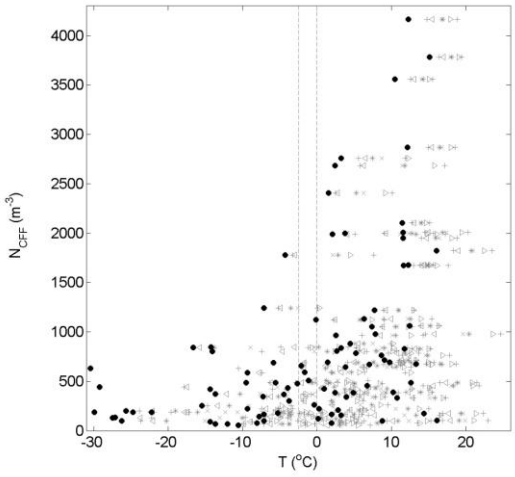

Figure 1. N_{CFF} and air temperature (5 days backward along the trajectories). Grey crosses (x) mark means and pluses (+) mark standard deviation. Grey stars (*) are the median with triangles marking the 25-75% interval. Black filled circles mark minima temperature along the trajectory. Vertical grey lines mark literature values for mortality (0°C) and IN activation (-2.5°C) of fungi.

High N_{CFB} were often associated with transport from both nearby coastal waters and the more distant Atlantic Ocean, as well as higher wind velocities over the seas than for periods with lower N_{CFB}. High N_{CFB} was best correlated to the 10-m wind speed (U_{10}^m) over the upwind ocean, which is consistent with sea spray aerosols. The concentration N_{CFB} increased exponentially with increasing wind speed according to $N_{CFB} = 10^{1.99+0.10U_{10}^m}$, see Fig. 2, in agreement with previous studies for non-biological sea spray. The bacteria emissions are estimated to be about 0.5% of the total sea spray emissions by number. Bacteria concentration did not increase over land. On average 3.4 bacteria $m^{-3}h^{-1}$ were lost over land, corresponding to a sink rate of k_{CFB}=1.49±0.67x10^{-6} s^{-1}, a turnover time of 186h, and an average deposition velocity of 0.6mms^{-1}.

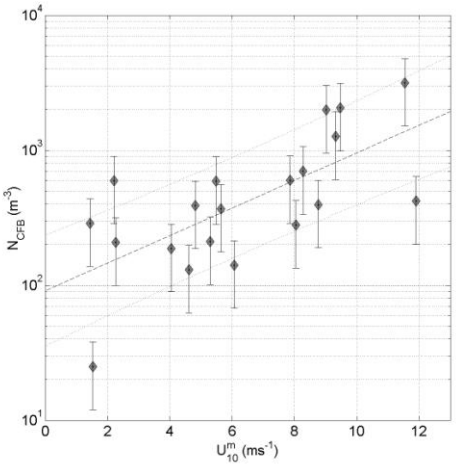

Figure 1. N_{CFB} in the air vs. the ten meter wind speed while the air was over oceans, averaged over 168h backward trajectories (grey diamonds) with sample variation error bars (black). Dashed curve is the log-linear fit, while the dotted curves are the errors containing at least 50% of the data.

This work was financed by the Swedish Research Council (VR), the Swedish Research Council for Environment, Agricultural Science and Spatial Planning (FORMAS), and by EU grant no. SEC6-PR-214400 (AEROBACTICS).

Fahlgren, C., Hagström, Å., Nilsson, D., and Zweifel, U. L., Annual Variations in the Diversity, Viability, and Origin of Airborne Bacteria, Appl Environ Microb, 76, 3015-3025, 2010.

Nilsson, E. D., and Leck, C., A pseudo-Lagrangian study of the Sulfur Budget in the remote Arctic Marine Boundary Layer, Tellus B, 54, 213-230, 2002.

Tuesday, September 6, 2011

Session 4P: Poster Session A:
Atmospheric Aerosols - Aerosol Processes and Properties

Aerosol absorption retrieval at ultraviolet wavelengths in a complex environment

S. Kazadzis[1], V. Amiridis[2], E. Gerasopoulos[1] and A. Arola[3]

[1]IERSD, National Observatory of Athens, GR-15236, Athens, Greece
[2]ISARS, National Observatory of Athens, GR-15236, Athens, Greece
[3]Finnish Meteorological Institute, Kuopio Unit, FI-70211, Kuopio, Finland
Presenting author email:kazadzis@meteo.noa.gr

Ultraviolet (UV) solar radiation has a broad range of effects concerning life on Earth. It influences human beings and also plants and animals. Furthermore, it causes degradation of materials and functions as a driver of atmospheric chemistry. There are various studies linking changes of the UV radiation field with changes in the scattering and absorption of aerosols in the atmosphere. Such changes can be comparable in magnitude with the ones caused by the stratospheric ozone decline (Krotkov et al., 1998). Moreover, UV variations caused by aerosol optical properties changes affect directly the tropospheric photochemistry:

- Increasing regional O_3 (10-20 ppb for Eastern USA) caused by increased UV levels, due to the presence of non-absorbing aerosols.
- Decreasing regional O_3 (up to 50 ppb for Mexico City and for particular days) caused by strong UV reduction due to absorbing aerosols.

The major parameters that describe radiation and aerosol interactions are the aerosol optical depth (AOD), the single scattering albedo (SSA) and the asymmetry parameter (g). We present estimates of SSA at two independently retrieved wavelengths 332 and 368 nm for an urban site situated at Athens city area, Greece. The period of the measurement analysis was from January to October, 2010. The data that have been used in this work have been retrieved from two instruments:

Since February 2009, the ground-based Atmospheric Remote Sensing Station (ARSS) is continuously operating to monitor radiation levels at ground and aerosol loadings over the city of Athens (Amiridis et al., 2009). The station is located near the city center and 10 km from the sea. ARSS is equipped with a CIMEL CE318-NEDPS9 sunphotometer for the retrieval of aerosol optical depth (AOD) at 8 wavelengths from 340 to 1640 nm, including polarization measurements. Additionally it is equipped with a UVMFR instrument for radiation measurements in the UV spectral region (Harrison et al., 1994). UVMFR measures both total and diffuse irradiance for seven specified wavelengths (here we use 332.4, and 368 nm). Measurements are recorded every 10 s, and stored as 1 min averages along with a computed direct irradiance.

Using the calibrated aerosol optical depth measurements of the CIMEL instrument we have evaluated the Langley aerosol optical depth calibration of the UVMFR instrument. The correlation coefficient of the AOD comparison is 0.98 and the slope equals 0.95 using ~1500 synchronous measurements.

After this step we have used the AOD measurements together with the direct/diffuse ratios retrieved from the UVMFR used as inputs to the LibRadtran radiative transfer model and we have calculated single scattering albedo at 368 and 332 nm for cloud free conditions.

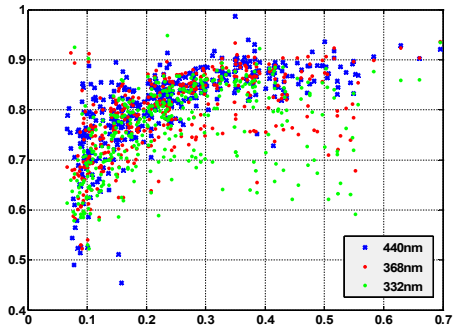

Figure 1. Single scattering albedo at 440nm (CIMEL) and 368 and 332nm (UVMFR) as a function of AOD

Comparing aerosol absorption at the UVA and UVB wavelengths with ones retrieved in the visible range (440nm), we have found lower SSA values (mean difference =0.03) for UVA and (mean difference =0.06) for UVB. Looking in more detail in diurnal retrievals, there is clear evidence that higher UV absorption compared with the visible, is evident to periods with dust aerosol events.

The use of the UVMFR 1 minute measurements reveals high diurnal variability mostly showing higher absorption for couple of hours before and diuring mid-day. Such diurnal patterns are difficult to be demonstrated using the CIMEL sun-photometer retrievals due to the fact that the AERONET-SSA retrievals are available at relatively high solar zenith angles (not close to local noon).

This work was supported by the Marie Curie project ACI-UV, PERG05-GA-2009-247492.

Krotkov et al.: Aerosol UV absorption experiment, part 2: absorption optical thickness, refractive index, and single scattering albedo, *Opt. Eng., 44, 041005, 2005*

Amiridis, V., et al., The potential of the synergistic use of passive and active remote sensing measurements for the validation of a regional dust model, *Ann. Geophys., 27, 3155-3164, 2009*

Harrison, L., et al.: Automated multifilter rotating shadow-band radiometer – an instrument for optical depth and radiation measurements, *Appl. Optics, 33, 5118–5125, 1994*.

Corr et al,: Retrieval of aerosol single scattering albedo at ultraviolet wavelengths at the T1 site during MILAGRO *Atmos. Chem. Phys., 9, 5813–5827, 2009*

The study on distribution characteristics of atmospheric aerosols over northern China area

Duan Ying,[1, 2] Yin Yan[3]

[1]Weather Modification Office of Hebei Province, Shijiazhuang, 050021, China
[2]Hebei Province key Lab for Meteorolagy and Eco-Environment, Shijiazhuang, 050021, China
[3]Nanjing University of Information Science & Technology, Nanjing, 210044, China
Keywords: atmospheric aerosols, vertical distribution, aerosol size distribution, concentration
Presenting author email: hbwmo@heinfo.net

Hebei province locates in the north of China. Beijing and Tianjin is surrounded with its district and its east is near the Bohai sea gulf. In the past decades this region has experienced dramatic changes in air quality and climate. In this study, based on the data from airborne PCASP-100X (0.1-3.0 μm) probe of PMS system and some former research results from 2004 to 2009 for this area (Duan *et al*, 2007, 2008; Yan *et al*, 2009). Based on above study, the distribution characteristics of atmospheric aerosols including the distribution characteristics of horizontal, vertical and spectral, variety trend were analyzed by synthetical analysis over north China area.

For instance, the Figure.1 shows that aerosols concentration distribution characteristics with height in three different regions in the north of China under clear sky weather condition in 2005. The result indicates that aerosols number concentration is reached 10^3□$^{-3}$ to 10^4□$^{-3}$ over Shijiazhuang, Xingtai and Hengshui in atmospheric boundary layer of northern China, respectively. However, the aerosols concentration values are decreasing with height increasing, when height above 3000 meters, its value reduced to about 10^2 □$^{-3}$.

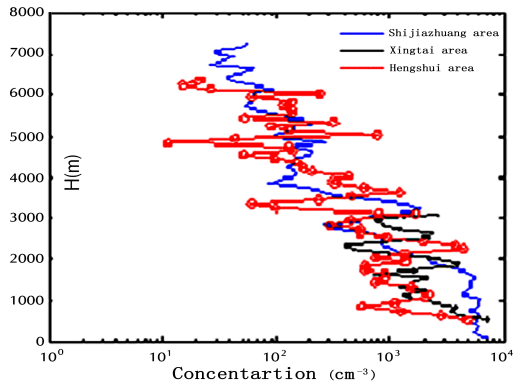

Figure.1 Aerosols concentration distribution with height in 2005

Duan et.al (2008) based on the data from aircraft PMS system detecting under clear sky weather condition in autumn over the Shijiazhuang and Handan both city area of north China, the distribution characteristics of aerosol under different city environmental condition was primarily analyzed. It included their number concentration of aerosol particle, the average diameter distribution with height in both areas over both cities of north China, respectively. Corresponding weather condition is cloudy and clearness over Shijiazhuang and Handan areas. These analyzed results were given in Figure.2.

The figure.2 shows that aerosol average diameter is various with height increasing. Its range of value is 0.17-2.0 μm; the maximum value of average diameter is 2.26 μm.

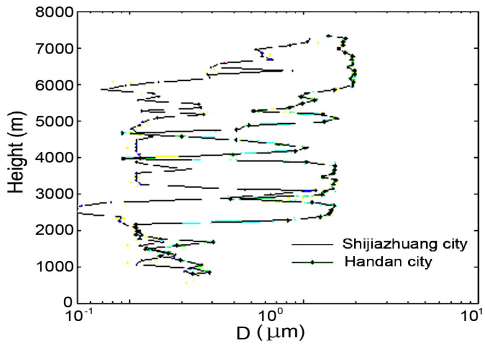

Figure.2 Aerosol average diameter variety with height over both city areas

This research was jointly supported by National Natural Science Foundation of China (Grant No. 40475003), and the social commonweal research program (GYHY(QX)2007-6-36) funded by the Ministry of Science and Technology of China.

Duan Y, Wu Z H et al.(2007) *Nucleation and Atmospheric Aerosols, C. D. O'Dowd and P. E. Wagner (eds.), P507–511,* Springer.

Duan Y et.al .(2008) *15th International Conference on Clouds and Precipitation , Cancun, Mexico.*

Yan Y, Duan Y et.al.(2009) *Proc. Of SPIE Vol.7490,74900X*

Aerosol particle property sensitivities to choice of predictive technique in SOA partitioning calculations

D. Topping[1,2], M. Barley[2] , G.McFiggans[2]

[1]National Centre for Atmospheric Science (NCAS), Manchester University, Manchester, M13 9PL
[2] Centre for Atmospheric Science, Manchester University, Manchester, M13 9PL
Keywords: Modelling, Organic compounds, Physical properties, Hygroscopicity.
Presenting author email: david.topping@manchester.ac.uk

Introduction

Atmospheric aerosol particles are an important yet uncertain component of climate change and air quality. Comprised of inorganic and organic material, the inorganic fraction is restricted to a few well-understood compounds. However, organic material can comprise many thousands of, largely unidentified compounds with a wide range of properties (McFiggans et al 2010). Mechanistic understanding and knowledge of individual compounds involved in the chemical evolution of aerosol particles is far from complete. Full chemical analyses of the organic component of atmospheric aerosols are not available (Hallquist, et al. 2009) and significant gaps appear in even the most detailed modeling tools.

Despite this, it is possible to make highly detailed ensemble predictions of the range of organic components expected to condense to atmospheric aerosol by combining a gas/particle partitioning model with a detailed gas phase chemical mechanism. However, choice of estimation method to calculate pure component properties which dictate gas/particle partitioning can have dramatic impact on predicted mass loadings, functionality and associated chemical signatures (Barley et al 2010; McFiggans et al 2010). A large number of calculations of absorptive partitioning of organic compounds have been conducted, making use of several methods to estimate pure component vapour pressures and activity coefficients (p0 and γ). The sensitivities of the predicted particle properties (density, hygroscopicity, CCN activation potential) to the choice of vapour pressure (po) and activity coeffiicient (γ) model and to the number of components used to represent the organic mixture have been systematically compared.

Results

The variability in theoretical hygroscopic growth factor attributable to the choice of estimation technique increases with decreasing mixture complexity. Inclusion of the Joback and Reid boiling point method in the range of methods used to estimate p0, increases the variability in predicted hygroscopicity, owing to a consistent under prediction of component volatility, increasing the variability in composition across the methods.

If no instantaneous re-equilibration of organic semi-volatile components is assumed, the calculated growth factors are comparable to the low hygroscopicity of organic material that has been widely measured in the laboratory and atmosphere. Allowing re-equilibration of all components on drying produces a calculated hygroscopicity greater than has been measured for ambient organic material, and frequently close to those of common inorganic salts. This has substantial implications on aerosol behaviour in instruments designed to measure hygroscopicity and on the measured degree of equilibration of semi-volatile components in the ambient atmosphere. When it is assumed that semi-volatile material other than water does not equilibrate on drying, the sensitivity in radiative forcing, 'ΔF', resulting from the variability in predicted hygroscopicity following the choice of p0 and i estimation technique, is low when the particle organic volume fraction is less than 55 %. Any sensitivities which do exist, increase with decreasing component complexity. If it is assumed that semi-volatile material re-equilibrates to the dry state on drying, the sensitivity of ΔF to choice of estimation technique and complexity increases substantially. The concentration of organics at which the sensitivity of ΔF to choice of predictive technique becomes insensitive drops to between 16 and 22 %.

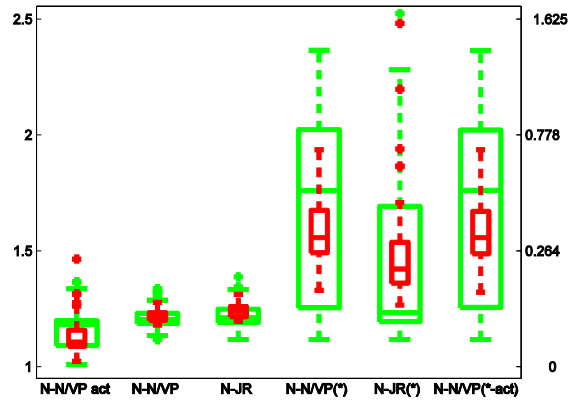

Figure 1. Predicted growth factors and kappa kohler values as a function of predictive technique and number of compounds used in the partitioning calculations. 10000 compound simulations are shown as red boxes, 2 compound simulations as green. Predictive technique acronyms displayed on the x axis, (*) denotes assumed evaporation of all semi-volatiles on drying. The left-hand y-axis lists calculated GF, the right side lists the corresponding kappa kohler values.

This work was support by UK National Centre for Atmospheric Sciences (NCAS) funding.

References

Barley, M. H. and McFiggans, G Atmos. Chem. Phys.,10, 7497672010.
McFiggans, G et al .Atmos. Chem. Phys., 10, 10255-10272
Hallquist, M., et al Atmos. Chem. Phys., 9, 51555236, 2009.

Influence of aerosol optical properties on NO_2 and O^1D photolysis rates measured at Eastern Mediterranean

E. Gerasopoulos[1] , N. Mihalopoulos[2], S. Kazadzis[1] , M. Vrekoussis[3], G. Kouvarakis[2] and N. Kouremeti[4]

[1]IERSD, National Observatory of Athens, GR-15236, Athens, Greece
[2] Department of Chemistry, University of Crete
[3]CAPC, Academy of Athens
[4]Lab. Of Atmospheric Physics, Aristotle Univ. of Thessaloniki, Greece
Presenting author email:egera@meteo.noa.gr

Solar ultraviolet radiation drives much of tropospheric and stratospheric chemistry since the photodissociation frequencies of important chemical species are directly related to the incident radiation in this spectral region. For example, the photolysis of O_3 and NO_2 is driven by ultraviolet radiation which contributes to their decomposition and removal from the atmosphere

Aerosols are produced by a variety of processes, creating differences in their physicochemical properties and hence in their ability to scatter and absorb solar radiation. Therefore, the origin of an aerosol is relevant in assessing its influence on ultraviolet/visible photolysis rates. Seinfeld and Pandis (1998) have given a complete review of the physicochemical processes involved in aerosol formation and behavior in the atmosphere.

Depending on their composition and scattering-absorption properties, aerosols can increase or decrease the actinic flux and photolysis rates. Radiation scattering increases actinic flux and consequently photolysis rates, whereas absorption decreases both values.

Collected photolysis rates for the period 2002-2006 are used to investigate their levels, their temporal characteristics, evaluate possible trends and their interannual variability. In particular, time series of photolysis rates of ozone (JO^1D) and nitrogen dioxide (JNO_2) at the remote coastal Finokalia station on Crete Island (25°60′E, 35°24′N), were studied in conjunction with aerosol of anthropogenic and natural origins.

Continuous measurements of the photo dissociation rates JO^1D and JNO_2 were performed by filter radiometers (Meteorologie Consult, Germany). The aerosol sun-photometric observations reported here performed by a CIMEL sun-sky radiometer, which is part of the PHOTON/Aerosol Robotic Network (AERONET) Global Network.

Aerosol optical properties, namely aerosol optical thickness (AOT), Angström wavelength exponent and volume size distributions, were used. Generally, the AOT for the specific area is characterized by maximum values during spring, due to the maximum dust loading mainly transported from African deserts, and minimum values in winter. Large AOT values persisting during summer are due to transport of urban/industrial and biomass burning aerosols but also local sources and processes, whereas secondary maximum AOT in October are attributed to autumn dust events (e.g. Fotiadi et al., 2006; Kalivitis et al., 2007).

For the period May to September 2004, the range of Aerosol Optical Thickness (AOT) during maxima of photolysis rates is 0.07-0.49 for 440 nm, 0.13-0.67 for 340nm while the Angstrom coefficient ranges between 0.5 and 2.1. Measurements showed that elevated values of AOT result to a decrease in Js (Fig. 1).

Figure 1. Correlations between AOT at 340 nm with

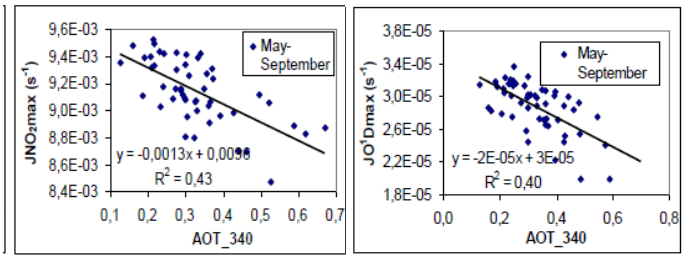

maximum JNO_2 and JO^1D for the period May-Sep 2004

This is due to the fact that more particles in the column lead to more efficient attenuation of the solar irradiance. J's-AOT Correlation coefficients are higher for AOT at 440 nm than 340 nm. Measurements of low Angstrom coefficients, which mean coarser particles, lead to JNO_2 decrease. Coarse particles at Finokalia, Crete, are mainly dust particles but also sea salt. These particles seem to be responsible for the major part of the decrease in maximum JNO_2 during the day, while finer particles (high Angstrom coefficients) have less impact both due to the facts that are related to lower levels of AOT and that they result to multiple scattering of radiation. It also noteworthy that the correlation coefficients for each month separately are higher than for the whole period indicative of the fact that during longer periods other factors controlling the variability of the photolysis rates become important.

This work was funded by EU (CIRCE 36961, FP6). Parts of the analysis were performed under the Marie Curie project ACI-UV, PERG05-GA-2009-247492.

Fotiadi et al.: Aerosol physical and optical properties in the Eastern Mediterranean Basin, Crete, from Aerosol Robotic Network data, *Atmos. Chem. Phys., 6, 5399–5413, 2006.*

Kalivitis, N.: Dust transport over the Eastern Mediterranean derived from TOMS, AERONET and surface measurements, *J. Geophys. Res., 112(D3), 3202, doi:10.1029/2006JD007510, 2007.*

Seinfeld and Pandis: Atmospheric Chemistry and Physics: From Air Pollution to Climate Changes, John Wiley, Hoboken, N. J., 1997.

Towards an assessment of the cloud-aerosol interaction determined by Raman lidar

J.L. Guerrero-Rascado[1,2,3] and J. Preißler[1]

[1]Évora Geophysics Centre (CGE), University of Évora, Évora, 7000, Portugal
[2]Andalusian Center for Environmental Research (CEAMA), University of Granada – Autonomous Government of Andalusia, Granada, 18071, Spain
[3]Department of Applied Physics, University of Granada, Granada, 18071, Spain
Keywords: aerosol, clouds, interaction, lidar
Presenting author email: jrascado@uevora.pt

Atmospheric particles influence the Earth's climate in different ways. One important example is the impact of aerosols on clouds by means of the so-called aerosol indirect effects, i.e. altering the albedo, lifetime and precipitation patterns of clouds. The first aerosol indirect effect or Twomey effect is defined as the change in observed cloud optical or microphysical properties (as optical depth, albedo or cloud droplet effective radius) as a function of the change in the aerosol burden.

Many studies have been addressed to characterize the first aerosol indirect effect during the last years, most of them based on satellite retrievals. However, one uncertainty lies in the relative altitude levels of aerosols and clouds, i.e. even when aerosol and cloud layers are detected, they may not be mixed and their interaction differs (Costa *et al*., 2007). In addition, many previous studies are biased due to the absence of temporal and/or spatial coincidence, i.e. in many cases the measurements of clouds and aerosols are not available simultaneously or they are measured over non co-located areas.

In this work we present preliminary results about cloud-aerosol interaction derived from the multiwavelength Raman lidar operated routinely at the Évora Geophysics Center (Évora, Portugal, 38.6ºN, 7.9ºW, 293 m asl) (Wagner *et al*., 2010). The simultaneous aerosol and cloud optical depths were obtained by integration of the extinction profile derived from Raman signals at 532 nm. The extinction profiles at altitudes of incomplete overlap were modeled through the Raman backscatter with a constant lidar ratio. To assess the impact of the coupling between cloud and the underlying aerosol particles, the boundaries for aerosol and cloud layers have been determined following the zero-crossing method on the first derivate of the Raman backscatter coefficient. An example of night time data measured during the Saharan dust event observed over Évora between 9 and 11 December 2010 is shown in Figure 1. In order to consider the high variability of cloud layers, lidar data were averaged over 15 minutes. Thus, a dataset of more than 45 Raman lidar profiles measured during the night were obtained for this period.

To investigate the relation between cloud and aerosol optical depths (COD and AOD), AOD averaged values grouped in 0.01 intervals were computed, because of the large variability of the optical depths. Moreover, the experimental data were split taking into account the vertical distance between the cloud base and the top of the underlying aerosol layer (from now on referred to as interaction distance).

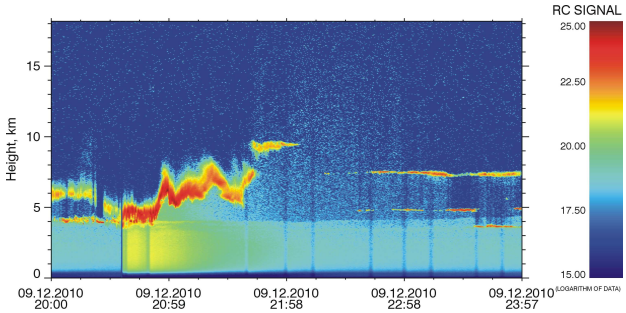

Figure 1. Temporal evolution of the range corrected signal (arbitrary units) on 9th December 2010.

Preliminary results indicate a significant correlation, $R^2 > 0.64$, between COD and AOD (in logarithmic scale) for interaction distances less than 100 m. The correlation decreases drastically for interaction distances between 100 and 1000 m, and larger than 1000 m, with correlation $R^2 < 0.28$ in both cases. Furthermore, the cloud-aerosol interaction computed as the slope of the COD versus AOD linear regression (in logarithmic scale) shows an opposite sign for data with shorter interaction distances (< 100 m) with respect to those with larger distances.

The work presented at the conference will involve the analysis of additional cases including more Saharan dust events and also other particle types as resulting from biomass burning and anthropogenic pollution.

This work has been supported by the National Reequiment Programme Rede Nacional de Geofísica REDE/1527/RNG/2007, by the FCT project PTDC/CTE-ATM/65307/2006, by the FCT fellowships SFRH/BPD/63090/2009 and SFRH/BD/47521/2008, and by the Spanish Ministry of Education fellowship EX2009-0700. The authors want to thank Dr. Frank Wagner, the Leibniz-Institute for Tropospheric Research, and the EARLINET and SPALINET networks.

Costa, M. J., Cattani, E., Levizzani, V., and Silva, A. M. (2007) in *Measuring precipitation from space - EURAINSAT and the future*, Springer, 97-111, ISBN-13 978-1-4020-5834-9.

Wagner, F., Preißler, J., Guerrero-Rascado, J. L., and A. M. Silva (2010) in *Proc. 25th International Laser Radar Conference*, 539-541, ISBN: 978-5-94458-109-9.

Analysis of the ambient particle number size distributions characteristics during nucleation events in the Eastern Mediterranean

I. Kopanakis[1], S.E. Chatoutsidou[1], K. Torseth[2], T. Glytsos[1] and M. Lazaridis[1*]

[1]Department of Environmental Engineering, Technical University of Crete, Polytechneioupolis, Chania 73100, Greece

[2] Norwegian Institute for Air Research Instittutveien 18, N-2027, Norway

Keywords: nucleation, number concentration, growth rate, formation rate.

An extensive field campaign was performed at Akrotiri monitoring station in the island of Crete (Greece) in order to study the characteristics of the ambient aerosol number size distribution spectra and furthermore to evaluate the atmospheric potential for nucleation events in the area. The campaign lasted for one year (June 2009 - May 2010) and measurements were conducted for 130 days covering equally the four seasons of the year.

The station is located at an urban background/semi-rural area near the city of Chania at the western part of the island of Crete (Lazaridis et al. 2008). The measurements were conducted using a Scanning Mobility Particle Sizer (SMPS) system. The system was programmed to measure the PM number size distribution in the size range between 13.2 and 1083.3 nm, separating the particles into 44 consecutive size bins. The modal structure and the characteristics (geometric mean diameter (GMD), and geometric standard deviation (GSD)) of each mode comprising the aerosol size distribution were identified using the AMANpsd algorithm (Ondracek et al., 2009). The ambient meteorological conditions (temperature, relative humidity, wind speed, wind direction, solar and UV radiation) and PM_{10} and O_3 concentrations were continuously monitored and recorded during the whole measurement campaign. In addition, the origin of the air masses reaching the station was estimated using back trajectories provided by the HYSPLIT model.

The measurements revealed that Aitken mode particles (13.2-101.1 nm) showed higher concentrations than Accumulation mode particles (101.1-1083.3 nm) for the whole measurement period. Moreover, particle number concentrations were higher during weekends than weekdays. The mean total number concentration was 583 ± 362 particles cm^{-3}, while the maximum particle number concentration was 6148 particles cm^{-3}. The modal structure of the aerosol size distribution was mainly unimodal with GMDs ranging between 70 and 100 nm. Furthermore, the analysis of back trajectories showed that different air mass origins were associated with different levels of particle number concentrations.

Formation of new particles due to nucleation was observed and the process led to an increase of aerosol number concentration, as depicted in Figure 1. In total, 13 considerable new particle formation events were recorded. The 9 out of 13 nucleation events took place during the night or occurred both during day and night. The maximum particle number concentrations during nucleation events were observed for particles having diameters between 65 and 110 nm. The computed mean values of growth and formation rates were 5.84 nm hr^{-1} and 13.11 cm^{-3} s^{-1}, respectively.

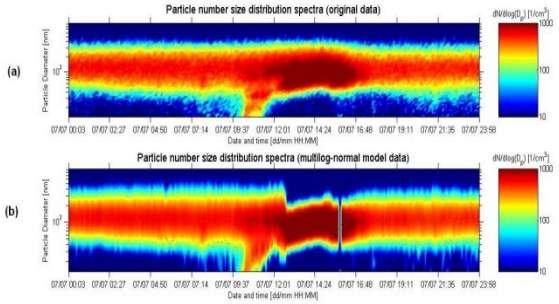

Figure 1: New particle formation event observed on summer period of 2009 at Akrotiri research station, Crete, Greece (a) raw data, (b) data derived from the AMANpsd algorithm.

Finally, the classical theory of heterogeneous nucleation for the sulphuric acid - water system has been applied to study its ability to describe the nucleation events. The theory was able to qualitatively describe the experimental observations.

Lazaridis et al. (2008). *Water, Air, & Soil Pollution*, 189, 85-101.

Ondrácek et al. (2009). *Water, Air, & Soil Pollution*, 199, 219-233.

Evaluation of uncertainties in determining particle volatility properties from experiments with standard thermal-denuder techniques

E. Fuentes, R. Alfarra, M. Flynn and G. McFiggans

Center for Atmospheric Sciences, School of Earth, Atmospheric and Environmental Sciences, University of Manchester, Manchester, M13 9PL, United Kingdom
Keywords: organic aerosols, thermodenuder, volatility
Presenting author email: Elena.Fuentes-lopez@manchester.ac.uk

Thermodenuders systems are increasingly used to characterise the volatility distribution and vaporisation properties of organic aerosols in both field and laboratory studies (Huffman et al., 2008). The standard procedure for application of these systems is the monitoring of the particle size distribution before and after the thermodenuder, in order to estimate the mass of organic material that is evaporated at different set-point temperatures. This type of analysis relies on the assumption that the modification of the size distributions in thermodenuders is only due the homogeneous evaporation of the particles initially injected in the system. However, factors such as the gas recondensation/evaporation occurring in the cooling and denuder sections and the inhomogeneous evaporation induced by gas velocity gradients could potentially lead to modifications in the resulting size distributions and the derived thermograms. Quantification of the error induced by these factors on the thermograms obtained from standard thermodenuder experiments is therefore needed.

In this study an axysimmetrical 2-D diffusion-evaporation model was employed to theoretically evaluate the impact of different sources of uncertainty on thermograms derived from experiments conducted with standard thermodenuder designs. The velocity gradient resulting from the non-slip condition in annular tubes and the recondensation/evaporation of gas in the cooling section and adsorbent denuder, were evaluated as potential sources of uncertainty in the determination of the particle size distributions. Thermograms obtained with a typical thermodenuder system comprising a heating, cooling and denuder section, of dimensions similar to Huffman et al. (2008), were modelled for monodisperse aerosol distributions of different volatility. Recondensation fractions from 20-70% were predicted for low volatility compounds with saturation concentrations C*≤1 μg/m^3, at organic mass loadings in the range 30-200 μg/m^3 (accommodation coefficient of unity, T=80˚C). On the other hand, recondensation was only found to be significant at high organic aerosol loadings for compounds with C*≥10 μg/m^3. These findings point at the necessity of controlling recondensation even for low organic atmospheric loadings in the range 30-50 μg/m^3 if compounds of low vapour pressure are expected to be dominant in the organic aerosol composition.

An already significant recondensation was predicted to occur in the cooling section (5.7 s residence time) between the heater and denuder sections, for organic loadings 30-200 μg/m^3 and C*<1 μg/m^3, which led to a 20% overestimation in the values of mass fraction remaining. Denudation was found not to be sufficient to hinder the recondensation of gaseous compounds with C*≤0.1 μg/m^3 at high aerosol loadings (Figure 1), which together with the recondensation already occurred in the cooling section yielded deviations up to 40% in the mass fraction remaining with respect to the heating section output. Because of the significant recondensation occurring in the cooling section and the lower efficiency of adsorber denuders for stripping gas at high aerosol loadings, thermograms of low volatility aerosols at typical laboratory concentrations should be corrected to avoid underestimations of particles volatility.

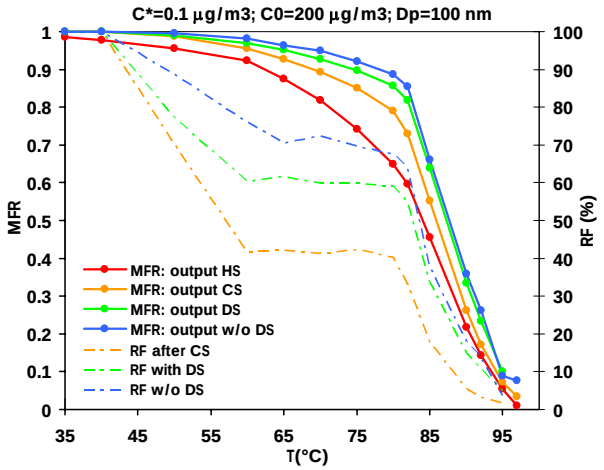

Figure 1. Mass fraction remaining (MFR) and recondensation fraction (RF) calculated for a standard thermodenuder system. HS=heating section (0.5 m), CS=cooling section (0.15 m), DS=denuder section (0.5 m). Tube diameter=0.022 m. Sample flow=0.6 lpm.

This work was supported by the UK National Environmental Research Council [grant number NE/H002561/1].

Huffman, J. A., Ziemann, P. J., Jayne, J. T., Worsnop, D.R., and Jimenez, J.L.: Development and characterization of a fast-stepping/scanning thermodenuder for chemically-resolved aerosol volatility measurements, *Aerosol Sci. Technol.*, 42, 395–407, 2008.

Enhanced Secondary Organic Aerosols during Fog Episodes

D.S.Kaul, S.N.Tripathi, Tarun Gupta

Department of Civil Engineering, Indian Institute of Technology, Kanpur, 208016, India
Keywords: Atmospheric Aerosol, Aerosols and air quality, Aerosols and climate
Presenting author email: snt@iitk.ac.in

PM1 samples were collected from January 16, 2010 to February 20, 2010 at Kanpur (26.5º N, 80.3º E, 142 m msl) to study the secondary organic aerosol (SOA) production during clear and foggy days. Of the 180 samples collected, 56 were from foggy days. Micro-Pulse Lidar Network (MPLNET), a part of National Aeronautic Space Administration (NASA), was used for identification of fog duration. Organic Carbon (OC), Elemental Carbon (EC) and total carbon analysis were carried out to examine total and water soluble carbonaceous component of aerosol, respectively. Trace gases and solar flux measurement by gas analyzer and pyranometer (a part of NASA), respectively were carried out to identify the photo-chemical activity. Meteorological data and pH were measured by atmospheric weather station and pH meter, respectively.

This study examines the reason of such enhanced yield and hypothesizes likely production of SOA through aqueous phase chemistry during fog episodes. SOA was estimated during foggy and clear days using tracer method. Enhanced SOA was observed during foggy days (Fig 2). Production of SOA was highest in the afternoon and lower during morning and evening. Peak of OC/EC during foggy days occurred earlier indicating role of aqueous phase chemistry in addition to gas-particle portioning which is the prevalent mechanism of SOA production during clear days. Some investigators (Offenberg et al., 2009) have documented enhanced SOA yield via acid catalysis pathway, though similar finding in ambient has not be confirmed (Tanner et al., 2009). To observe similar relationship, pH measurements on all samples were carried out. Poor correlation of OC/EC with pH during foggy days (R^2=0.04) and clear days (R^2=0.085) was observed, though their correlation was high for pH < 7. These findings suggest acid catalyzed SOA production but its contribution is insignificant. The possible contribution of biomass burning to SOA was also examined. It was found that WSOC are removed by water droplets during foggy episodes, its removal followed inverted bell shaped curve with highest during night time (37 to 49 % of OC) and lowest at 4:00 PM (0.03 % of OC). OC removal was further examined by analysing OC in fog water. Higher concentration of OC was observed in fog which further supports WSOC removal. Such removal indicates that though due to low temperature during foggy days, more biomass may have been burned but they are removed due to their hygroscopic nature during foggy days thus contributing insignificantly to SOA during the episodes. Details of the finding and related contribution of sources to SOA will be presented.

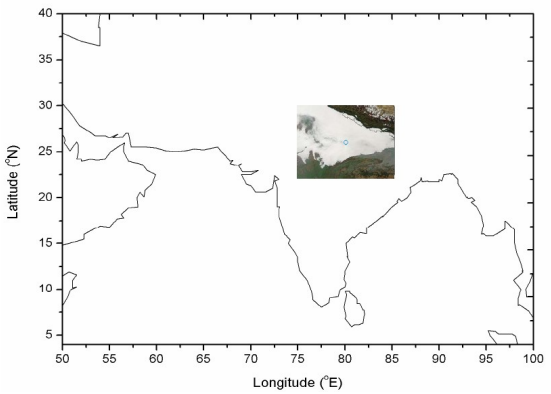

Fig 1- A typical foggy days captured by Moderate Resolution Imaging Spectrometer on on Jan 09, 2010 at 05:10 AM UTC (Circle represent sampling site).

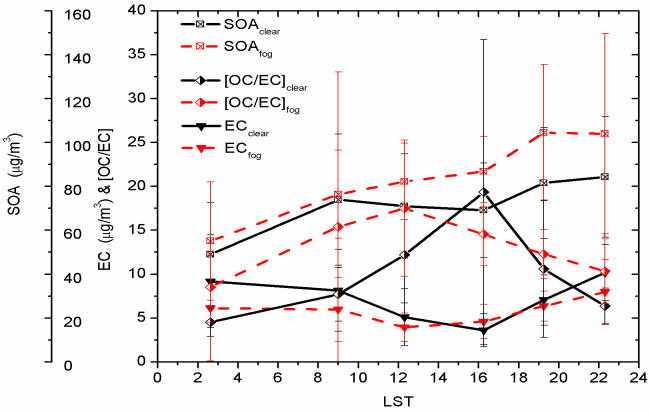

Fig 2- Diurnal variation of SOA, OC/EC and EC during clear and foggy days

Offenberg, J. H.; Lewandowski, M.; Edney, E. O.; Kleindienst, T. E.; Jaoui, M., Influence of Aerosol Acidity on the Formation of Secondary Organic Aerosol from Biogenic Precursor Hydrocarbons. *Environ. Sci. Technol.* **2009,** *43*, (20), 7742-7747

Tanner, R. L.; Olszyna, K. J.; Edgerton, E. S.; Knipping, E.; Shaw, S. L., Searching for evidence of acid-catalyzed enhancement of secondary organic aerosol formation using ambient aerosol data. *Atmos. Environ.* **2009,** *43*, (21), 3440-3444.

Analysis of cloud and aerosol particles by single particle mass spectrometry during a hill-cloud-field experiment in Central Europe

A. Roth[1], S. Mertes[2], D. van Pinxteren[2], T. Klimach[1], J. Schneider[1] and S. Borrmann[1,3]

[1]Particle Chemistry Department, Max Planck Institute for Chemistry, Mainz, 55128, Germany
[2]Leibniz-Institute for Tropospheric Research, Leipzig, 04318, Germany
[3]Institute of Atmospheric Physics, Johannes Gutenberg University, Mainz, 55128, Germany
Keywords: Mass Spectrometry, Single Particle Analysis, CCN.
Email: a.roth@mpic.de

Aerosol-cloud interactions as well as the chemical composition of particles were investigated during the field campaign Hill Cap Cloud Thuringia (HCCT) in September and October 2010 on a mountain site in Central Germany (Schmücke, 938 m a.s.l.). Orographic cloud residual particles were analysed by the Aircraft-based Laser Ablation Aerosol Mass Spectrometer (ALABAMA, particle size range 150 nm - 900 nm) (Brands *et al.*, 2011) behind a counterflow virtual impactor (CVI), which samples cloud droplets and subsequently evaporates the cloud water. Additionally the total background aerosol population was sampled through an interstitial inlet (INT, cut-off diameter 5 µm) before and after cloud events. Parallel to the ALABAMA the particle size distribution was measured by an optical particle counter (OPC) with a size range between 0.25 µm and 32 µm.

The ALABAMA allows the qualitative chemical analysis of submicron single aerosol particles by laser ablation with a time resolution of 70 ms. This method gives information about particle size as well as composition and consequently helps to distinguish between different particle types. Although being developed for aircraft-based measurements, the ALABAMA is also suitable for ground-based measurements.

About 200000 positive and negative single particle mass spectra were recorded during the field campaign. A comparison of the averaged mass spectra for activated (CVI) and total (INT) aerosol shows that cloud residual particles contain a higher fraction of nitrate-containing particles, but a lower fraction of organic particles than particles of the background aerosol (see Figure 1). Besides, the relative fraction of sulphate is smaller. For further analysis, the mass spectra are separated in clusters, representing a certain particle type, by different clustering algorithms e.g., k-means. The relative abundance of the clusters will be related to meteorological conditions as cloud events, wind direction or back trajectories.

The time series of the number concentration measured by ALABAMA and the OPC show a good correlation between the two instruments, whereas the size distributions have different maxima due to various detection limits and sizing methods. Further analysis of the size distributions of cloud residual particles respectively background aerosol particles in addition with the mass spectra gives a hint for answering the question whether particle size or composition is the determining factor for particles to act as cloud condensation nuclei (Dusek *et al.*, 2006).

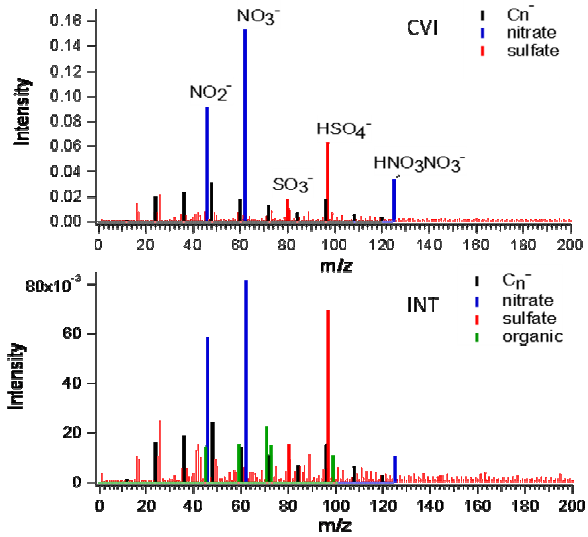

Figure 1. Average negative single particle mass spectra of cloud residual particles (top) and background aerosol particles (bottom) measured by ALABAMA

Brands, M., Kamphus, M., Böttger, T., Schneider, J., Drewnick, F., Roth, A., Curtius, J., Voigt, C., Borbon, A., Beekmann, M., Bourdon, A., Perrin, T. and Borrmann, S. (2011) *Aerosol Sci. Technol.*, **45**, 46-64

Dusek, U., Frank, G. P., Hildebrandt, L., Curtius, J., Schneider, J., Walter, S., Chand, D., Drewnick, F., Hings, S., Jung, D., Borrman, S. and Andreae, M. O. (2006) *Science*, **312**, 1375-1378

Preliminary investigation of contrails sampled during the COntrails Spreading Into Cirrus (COSIC) campaign in June 2009

H.M. Jones[1], D. Liu[1], K.N. Bower[1], J. Crosier[1], P. Forster[2], M.W. Gallagher[1], J. Haywood[3]

[1]School of Earth, Atmospheric and Environmental Sciences, University of Manchester, UK
[2]School of Earth and Environment, University of Leeds, UK
[3]UK Meteorological Office, Exeter, UK

Keywords: Aerosol cloud interaction, Ice Clouds, Black Carbon
Presenting author email: hazel.jones@manchester.ac.uk

Contrails, and their spreading into cirrus, are one of the most visible human influences on the Earth's climate, e.g. Stordal *et al*. (2005). Contrails reflect solar radiation and trap terrestrial long-wave radiation, with the latter effect expected to dominate for contrails and thin cirrus: resulting in a positive radiative forcing (Penner *et al.*, 1999). Soot emission in the aircraft exhaust is thought to play a role in the formation of contrails (e.g. Heymsfield *et al.*, 2010), though the role of soot in forming cirrus ice crystals downstream is highly uncertain.

There is very little known about the properties of older contrails and contrail-cirrus because of a lack of observations. Aircraft measurements of contrail ice particle size distributions only exist for line-shaped contrails because, once they lose their initial shape, non-linear contrails are very difficult to identify. The transition of line-shaped contrails into cirrus-like clouds is neither well understood nor well represented in climate models.

The work presented here is part of the COntrails Spreading Into Cirrus (COSIC) campaign. In order to improve our understanding of contrails, measurements of aerosol and cloud microphysical properties for several contrails were collected using the FAAM BAE-146 aircraft. Preliminary results from these measurements are discussed here. The research aircraft is fitted with a suite of aerosol and cloud probes including a Cloud Imaging Probe (CIP), Cloud Droplet Probe (CDP), 2D optical array probe (2D-S) and a Single Particle Soot Photometer (SP2) for size-resolved sub-micron aerosol black carbon mass.

During a flight on 03 June 2009, contrails were produced and sampled over the sea to the south-west of the UK within busy air traffic lanes. Upper air forecasts (27-34kft) for this period suggested northerly flow of low to moderate strength and little natural cloud. Forecasted humidity fields showed a pattern of increasing humidity on a north-west to south-east axis, which at >30kft was above ice saturation over much of the southern UK. Figure 1 shows data collected when sampling a contrail initiated in a previous aircraft orbit; a difficult task. An example of measurements within one contrail pass is shown. Cloud particle concentrations increase towards the centre of the pass, along with black carbon measurements. Size distribution measurements show that elevated number concentrations of smaller particles within the centre of the contrail (stars) are often observed compared to when at the contrail edge; where a peak in the size distribution at significantly larger sizes (200μm) can be seen. We will discuss the contrail cloud microphysical evolution within this trafficked region as well as the aerosol black carbon loadings in this region to determine how the two may be related.

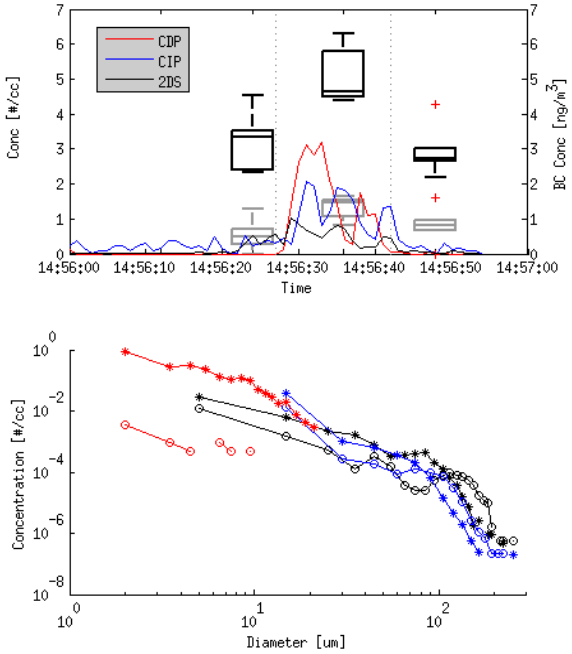

Figure 1. a) Concentration of particles detected by the 2DS (black), CIP (blue) and CDP (red). Also box and whiskers for the total scattering particle concentration (black) and total black carbon number (grey) from the SP2. b) Averaged size distribution for the regions indicated by the box plots in part a: within the contrail (stars), at the contrail edges (circles).

This work was funded by the Natural Environment Research Council (NERC): NE/G00479X/1.

Stordal, F., Myhre, G., Stordal, E.J.G., Rossow, W.B., Lee, D.S., Arlander, D.W., and Svendby, T. (2005) *Atmos. Phys. Chem.* **5**, 2155-2162.

Penner, J.E., Lister, D.H., Griggs, D.J., Dokken, D.J., and McFarland, M. (1999) *Aviation and the global atmosphere – A special report of IPCC working groups I and III. Intergovernmental Panel on Climate Change*, Cambridge University Press

Heymsfield, A., Baumgardner, D., DeMott, P., Forster, P., Gierens, K., and Karcher, B. (2010) Bull. Amer. Meteor. Soc. **91**, 465 – 472.

Weather condition – air quality relationships in Eastern Germany (1999 – 2009)

Silvia Leise, Andreas Hoy, Frank Zimmermann, Jörg Matschullat

Interdisciplinary Environmental Research Center, Technische Universität Bergakademie Freiberg, Brennhausgasse 14, D-09599 Freiberg, Germany
Keywords: Aerosol characteristics, air quality, weather conditions, climate change
Presenting author email: silvia.leise@ioez.tu-freiberg.de

PM_{10} and $PM_{2.5}$ data from the past ten years in Saxony (Eastern Germany) were used to investigate the relationship between air quality and weather conditions. Six research sites, four urban and two background locations, with almost continuous measurements of PM were analysed from 1999 to 2009 (Figure 1). The results are the basis for event-based measurements to analyse the influence of climate change on air quality.

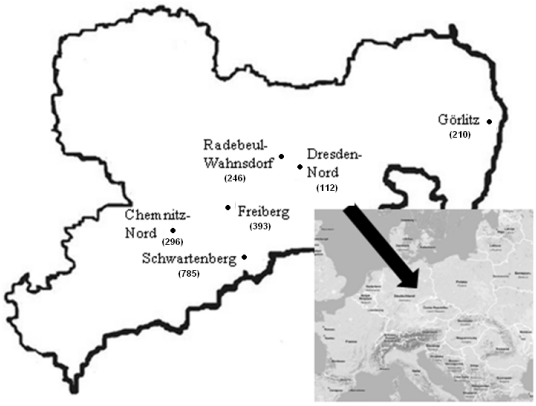

Figure 1: The investigation area with its stations and altitude (m. a. s. l.)

The classification methods used in this work are the *Grosswetterlagen* system, originally developed by Baur et al. (1944), and the objective weather type classification of the German weather service (DWD). 29 *Grosswetterlagen* (GWL) are grouped into four directions of inflow (GWL-DI) to make them more comparable to the DWD classification and to allow data validation. Their database dates back to 1881 AD; thus conclusions of past-time behaviour of aerosol concentrations can be made. The objective weather classification system (DWD-OWT) is available from 1979; a validation by means of GWL for the present state is possible for 31 years. The modelled future developments of the DWD-OWT provide a starting point for conclusions about the ongoing aerosol characteristic.

Significantly higher aerosol pollution, regardless of the particle size, arises at all locations for south-eastern wind directions. Both classification systems show high air pollution for easterlies and low air pollution for westerlies. This difference is likely caused by long-range transports of aerosols from Eastern Europe. Anticyclonal weather conditions show higher pollution then cyclonic ones (e.g, because of less wind and dryer conditions). This can be concluded from both classification systems and is in agreement with further studies of the relationship of weather conditions and air quality (Buchanan et al. 2002; Buchholz et al. 2010).

The general level of aerosol concentration differs by season, whereas connections between aerosol pollution and different weather conditions are independent of seasonal influence (Table 1).

Table 1: Mean PM_{10} values [µg/m³] for the six sites (1999-2009), separated by DWD-OWT and GWL-DI (weighted mean) and a seasonal differentiation (winter and summer half years). Blue bars show the ratio of PM_{10} concentrations between the weather conditions, sites, half years and classification systems.

		SE	SW	NW	NE
Görlitz	WHY (DWD-QWT)	53,3	37,1	24,8	33,2
	SHY (DWD-OWT)	39,9	28,3	22,5	21,0
	WHY (GWL-DI)	45,7	33,9	27,5	36,0
	SHY (GWL-DI)	30,9	27,0	23,1	26,1
DD-Nord	WHY (DWD-QWT)	44,0	39,4	29,3	37,0
	SHY (DWD-OWT)	39,3	30,0	26,5	24,9
	WHY (GWL-DI)	43,2	36,6	30,5	37,0
	SHY (GWL-DI)	33,9	29,5	26,5	29,7
Chemnitz-Nord	WHY (DWD-QWT)	39,4	29,4	22,5	31,0
	SHY (DWD-OWT)	35,2	25,2	20,6	20,7
	WHY (GWL-DI)	36,8	27,5	23,5	30,3
	SHY (GWL-DI)	29,6	24,2	21,2	25,3
Freiberg	WHY (DWD-QWT)	38,5	25,0	18,4	28,6
	SHY (DWD-OWT)	33,5	22,7	17,9	20,0
	WHY (GWL-DI)	34,9	22,7	19,7	27,8
	SHY (GWL-DI)	27,7	21,5	18,9	23,2
Radebeul-Wahnsdorf	WHY (DWD-QWT)	32,5	24,2	16,6	26,0
	SHY (DWD-OWT)	29,7	19,4	15,7	16,3
	WHY (GWL-DI)	29,3	21,6	18,2	25,4
	SHY (GWL-DI)	24,2	18,8	16,0	19,9
Schwartenberg	WHY (DWD-QWT)	25,0	16,2	9,3	13,2
	SHY (DWD-OWT)	25,8	16,8	12,0	12,5
	WHY (GWL-DI)	22,5	14,7	10,4	13,9
	SHY (GWL-DI)	20,7	15,8	12,6	16,1

Baur F, Hess P, Nagel H (1944): Kalender der Großwetterlagen Europas 1881-1939, Forschungsinstitut für langfristige Wettervorhersage, Bad Homburg, 35 S.

Buchanan C.M., Beverland I.J., Heal M.R. (2002): The influence of weather-type and long-range transport on airborne particle concentrations in Edinburgh, UK. Atmos. Environ. 36: 5343-5354

Buchholz S., Junk J., Krein A., Heinemann G., Hoffmann L. (2010): Air pollution characteristics associated with mesoscale atmospheric patterns in northwest continental Europe. Atmos. Environ. (2010), doi: 10.1016/j.atmosenv.2010.08.053

Acknowledgement: We are very thankful to LfULG and UBA for providing the ten year time series of aerosol data, and to BMBF for their support of the authors within the REGKLAM project.

Spatial and seasonal variation of number concentration and size distribution of aerosol (5.6 – 560 nm) in urban and rural areas of Bologna (Italy)

Isabella Ricciardelli, Silvia Ferrari, Claudio Maccone, Arianna Trentini, Fabiana Scotto, Linda Passoni, Vanes Poluzzi

Regional Agency for Prevention and Environment (ARPA), Bologna, Italy

keywords: Aerosol size distribution, ultrafine particles, number concentration, nucleation mode.

Presenting author email: vpoluzzi@arpa.emr.it

Size distribution and number concentration of low troposphere aerosol were measured during several seasons in three different environmental conditions in Bologna: a rural background site, a high traffic site and an urban background site. Knowledge about the spatio-temporal behaviour of particles in ambient air could greatly simplify the description of aerosol processes and effects, and also particles exposure assessment.

During study, a Fast Mobility Particle Sizer (FMPS TSI 3091) was used to measure particles from 5.6 nm to 560 nm with a 1 second time resolution.

Lower values of average total number concentration were found in the rural background site (SPC), respectively 8000 #/cm^3 in autumn campaign and 6000 #/cm^3 in spring campaign. The highest values were detected in traffic site (MXD): 17000 #/cm^3 in summer campaign and 20000 #/cm^3 in the campaign across winter and spring. SPC was located far from anthropogenic sources, while MXD was near a strategic highway. Urban background site (GMA) was located in a park in the urban area of Bologna, close to a very busy avenue. In this site values of average total number concentration detected were 10000 #/cm^3 during the campaign of late summer and 9000 #/cm^3 during spring.

A broad observation revealed that particles number and size distribution varies in time and space in a complex manner as a result of interaction between local sources and meteorological conditions [Costabile, 2009].

To observe how sampled particles distribute, total particles has been distinguished in ultrafine (UFP, diameter <100 nm) and not ultrafine (NoUFP, diameter >100 nm). Highest percentages of UFP particles were found in MXD (91-92%) and in GMA (87-91%), while SPC revealed the lowest values (77–80%). Presence of direct emission sources (avenue and highway) reflected on high concentration of ultrafine particles, probably mostly produced by exhaust combustion (Hussein, 2005).

Particles size distribution data have been manipulated using DistFit™ software (Chimera Technology, Inc) that fit one or more superimposed size distribution functions to such data. Software estimates a number of distribution ranges and their mean geometric diameter values. Results permitted to classify particles in three main distribution ranges: nucleation, Aitken and accumulation mode. Percentage of particles in nucleation mode respect total was relevant in MXD site, especially during spring campaign (64%). Lowest percentage particles were found in rural site (10-17%) confirming that direct emissions contribute significantly to nucleation range. Aitken mode showed variable values of particles in MXD and GMA, while high percentage were found in SPC. About accumulation mode, lowest values were registered in MXD site while highest ones were found in SPC probably due to the bigger influence of crustal fraction in rural areas.

During monitoring campaigns, a great number of particles growth events were observed in atmosphere. In warm seasons the episodes were more frequent than in cold ones, due to the high temperature and solar radiation that are responsible of photochemical reactions. Furthermore, higher PBL and, generally, more air turbulence in summer allows low pollutants concentration in lower troposphere promoting gas-to-particle conversion (Kulmala, 2008).

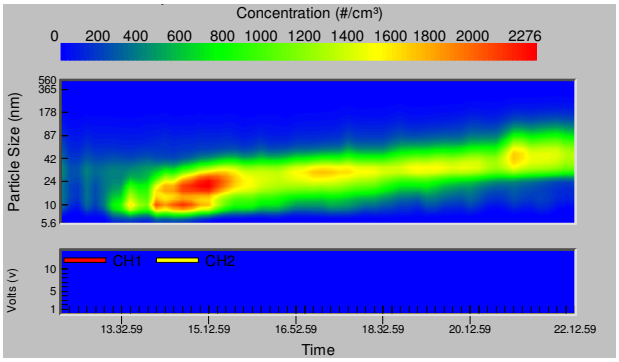

Figure 1. Particle growth episode in SPC.

Costabile, F. Birmili, W., Klose S., Tuch T., Wehner B., Wiedensohler A., Franck U., König K., Sonntag A. (2009) *Spatio temporal variability* and principal components of the particle number size distribution in an urban atmosphere, 9, 3163-3195.

Hussein T., Hämeri K., Aalto P.P., Paatero P., Kulmala M.. Modal structure and spatial-temporal variations of urban and suburban aerosols in Helsinki-Finland. Atmospheric Environment, 2005, 39, 1655-1668.

Kulmala, M., Kerminen, V.-M. (2008) On the formation and growth of atmospheric nanoparticles: review article. Atmospheric Research, 90, 132–150.

Composition and hygroscopic properties of background aerosols at a rural U.K. site

G.L. Capes[1], P.I. Williams[1], M.J. Flynn[1], K.N. Bower[1] and T. W. Choularton[1]
[1]Centre For Atmospheric Science, University of Manchester, Manchester, M13 9PL, U.K.
Keywords: chemical composition, CCN, field measurements.
Presenting author email: gerard.capes@manchester.ac.uk

We present an overview of aerosol physical and chemical properties from measurements at a rural site in southern England. As part of Aerosol Properties, PRocesses And Influences on the Earth's climate (APPRAISE), in situ measurements were taken to characterise background aerosols away from large sources of anthropogenic aerosols. Black carbon measurements were taken using a DMT Single Particle Soot Photometer (SP2), speciated mass concentrations measured by an Aerodyne Time of flight Aerosol Mass Spectrometer (ToF-AMS), particle size was measured using a range of optical particle counters and hygroscopic properties measured by a DMT cloud condensation nuclei counter (CCNc).

Local aerosol sources are identified using wind sector analysis and organic aerosol sources are characterised using positive matrix factorisation (PMF) of ToF-AMS data. The deconvolution of organic mass spectra revealed that biomass burning (BBOA), oxygenated organic aerosols (OOA) and hydrocarbon-like organic aerosols (HOA) could account for virtually all the variability in organic mass concentration. HOA consistently represented the smallest contribution to total organic mass throughout the measurement period. Number size distributions showed some diurnal dependence and variability between wind sectors, with the highest concentrations and larger sizes coming from the S-SE-E wind sectors. Analysis of long range (five day) air mass back trajectories confirmed that relatively local sources determined aerosol properties - which land masses, if any, were crossed in the final day of the trajectory revealed differences in aerosol properties, regardless of the rest of the trajectory. Typical number concentrations are around 5000 cm^{-3} reaching up to 40000 cm^{-3} on occasion.

Black carbon concentrations were generally less than 0.5 $\mu g\ m^{-3}$, but with peaks as high as 1.6 $\mu g\ m^{-3}$. Non-refractory aerosol composition was typically a mixture of organics and ammonium nitrate. Concentrations were typically 1–2 $\mu g\ m^{-3}$ for both organics and nitrate, each peaking around 10 $\mu g\ m^{-3}$. The mixing state of black carbon was investigated through consideration of particle coating thicknesses measured by the SP2.

We use this set of measurements to investigate the factors which influence the cloud droplet and ice crystal nucleating abilities of aerosols which are typical of the background aerosol population.

Composition of particles larger than 0.5 μm which may act as ice nuclei (IN) [DeMott et al., 2010] are determined by SEM analysis of aerosols collected on nuclepore filter substrates, while the number concentration of ice nuclei (N_{IN}) is derived using the same parametrisation from DeMott et al. [2010]. At -10°C, predicted ice nucleus concentrations ranged between 0.5 l^{-1} and 4 l^{-1}, at -20°C predicted N_{IN} varied between 15 l^{-1} and 800 l^{-1}, and at -30°C predicted N_{IN} fell between 170 l^{-1} and 72000 l^{-1}. Despite considerable scatter, IN concentrations showed a clear positive correlation with nitrate.

Cloud condensation nucleus number concentrations (N_{CCN}) at low supersaturation (i.e. 0.1%) were typically around 200 cm^{-3}, and rarely greater than 500 cm^{-3}. Typical N_{CCN} at 0.3% supersaturation were around 700 cm^{-3}m with peaks up to 2500 cm^{-3}. At 0.1% supersaturation, N_{CCN} correlates well with predicted N_{IN} (at temperatures between -10°C and -30 °C), but this relationship breaks down at higher supersaturations.

Aerosol critical supersaturation at different particle diameters showed a weak dependence on composition, which was broadly in agreement with a Kappa-Köhler model prediction for a mixed organic/ inorganic aerosol of varying organic mass fraction. However, variability in N_{CCN} seemed to be largely related to aerosol number concentration, rather than aerosol composition.

P J DeMott, A J Prenni, X Liu, S M Kreidenweis, M D Petters, C H Twohy, M S Richardson, T Eidhammer, and D C Rogers. Predicting global atmospheric ice nuclei distributions and their impacts on climate. *Proceedings of the National Academy of Sciences*, 107(25):11217–11222, June 2010. URL `http://www.pnas.org/content/107/25/11217.abstract`.

Anthropogenic Snowfall Events from Urban Fogs

G.J. Lloyd[1], T.W. Choularton [1]and P.Connolly[1]

[1]School of Earth Atmospheric and Environmental Sciences, University of Manchester, Manchester, M13 9PL,
Keywords: urban fog, snow, anthropogenic aerosols, ice nuclei
Presenting author email: Gary.Lloyd@student.manchester.ac.uk

During periods of anticyclonic weather, increasing numbers of Anthropogenic Snowfall Events (ASEs) from slightly supercooled fogs are being reported in the UK. The phenomenon was first recognised in the 1970s in America after work by Agee (1971) and Farn et al. (1978) noted a connection between industrial sources of aerosols created through combustion and inadvertent seeding of snowfall from fog. More recently work by Wood and Harrison (2009) described several events in the UK and striking satellite imagery provided by Van Den Berg (2008) revealed many patches of snow situated downwind of industrial areas after a period of freezing fog in the Netherlands.

In this paper we explain how the introduction of aerosol able to act as ice nuclei slightly below 0°C influences the microphysical processes that lead to these events. This is done through examination of reported ASEs, results from ice nucleation experiments using fly ash and other anthropogenic aerosol, together with analysis of meteorological data collected from the Whitworth Observatory during several events in Manchester, which for the first time provides valuable information obtained during the evolution of a number of ASEs.

A review of all reported ASEs reveals that these events occur in anticyclonic conditions in industrialised areas, close to potential sources of ice nuclei, when slightly supercooled fog is present at temperatures around -5°C. It is likely to be significant that these events occur within a temperature range where a known mechanism of secondary ice particle production occurs, as a few primary nucleated crystals fall through the supercooled fog (The Hallett-Mossop Process). Just one ASE at temperatures between -10°C to -14°C was reported by Farn et al. (1978) and in this temperature zone there is no known method of producing secondary ice particles hence it is very likely that all the snow crystals observed were produced through primary nucleation by aerosol.

The hypothesis, therefore, is that man made aerosol, is responsible for initiating the ice in these slightly supercooled fogs with, in many cases, secondary ice particle production enhancing the number of ice crystals leading to a detectable snowfall.

In order to investigate this, ice nucleation experiments using a cold stage and drops of deionised water polluted with fly ash confirmed the effective nature of this particular combustion product in triggering ice formation at higher temperatures, the average onset of ice nucleation being -3.4°C. Future ice nucleation experiments with man-made aerosol will be conducted to further investigate these preliminary findings and the results will be presented. This will identify whether an anthropogenic source of ice nuclei is able to cause ice formation in a temperature range where natural ice nuclei are very few.

Analysis of data obtained from the Whitworth Observatory Disdrometer reveals the precipitation types as an ASE on the 20th December in Manchester took place. Initially freezing drizzle is recorded before a transition to snow grains and eventually snowfall. Temperatures recorded at the beginning of this event were -2°C falling to -2.7°C. It is likely that further ASEs will be recorded by the observatory, providing the opportunity for detailed comparison of events, which will be crucial in the understanding of snowfall from urban fogs.

This sequence of precipitation provides one possible answer as to how an ASE may triggered. The introduction of efficient ice nuclei from a source of combustion, close to Manchester City Centre, will cause some of the fog droplets to freeze and as these fall they begin to sweep up other supercooled drops, growing by riming as they do so with the precipitation type making a transition to snow grains. As this riming takes place the Hallet-Mossop Process provides a powerful secondary ice production mechanism that is sufficient enough to cause the subsequent snowfall.

The significance of these results extends beyond that of the local importance of snowfall from radiation fog. The ability of certain man made aerosol to initiate snowfall from slightly supercooled layer cloud will substantially influence the water balance, water content and microphysics of these clouds. This will in turn shorten the lifetime of the clouds and their radiative properties. Hence this is potentially an important man made aerosol indirect effect in the atmosphere.

Agee, E.M. (1971) *Bull. Amer. Meteorology Society*. **52,** 557–560.

Farn, P., Parungo., Paul, A., Alee., Helmut, K. and Weickmann HK. **(**1978) *Geophysical Research Letters.* **5,** 515–517

Van den Berg W. (2008) *Weather.* **63,** 248

Wood, Curtis R and Harrison, R. Giles. (2009) *Weather.* **64,** 227-280

The effect of coronal mass ejections on cloud microphysics

J. Svensmark,[1] M. B. Enghoff,[1] and H. Svensmark[1]

[1]National Space Institute, Technical University of Denmark, Copenhagen, DK-2100, Denmark
Keywords: Cloud microphysics, satellites, ion-induced nucleation
Presenting author email: enghoff@space.dtu.dk

During close passages of coronal mass ejections, which cause Forbush Decreases in the incoming galactic cosmic radiation, a measurable and significant change in the clouds microphysics appears to take place. Expanding a study by Svensmark, Bondo, and Svensmark the present work investigates the response of six cloud parameters, using MODIS data, to these Forbush Decreases.
We rank the Forbush Decreases according to their impact on ionisation in the lower atmosphere since this is where an effect is expected.
Investigating the 5 strongest events we find that cloud emissivity, cloud fraction, liquid water content, and optical thickness all show reductions in signal above the 2-3 sigma level 7-9 days after the minimum in atmospheric ionisation. Similarly we observe a rise in the droplet effective radius just below the 2 sigma level, but it is not possible to resolve a significant response in the column density of cloud condensation nuclei. The significance of the found results is tested using Principal Components Analysis.

We find no correlation between Forbush Decrease intensity and UV radition. A signal is seen in the TSI 2 days prior to the Forbush Decrease minimum (about 1.5 W/m^2 for the 5 largest Forbush Decreases) but we are not aware of any mechanism that can cause such a forcing to produce a cloud signal about 10 days later.

Furthermore there appears to be a systematic link between the reduction in amplitude of the cosmic ray ionisation and the size of the response of the studied parameters. These results add further support to the suggestion that ions play a role in the formation of clouds.

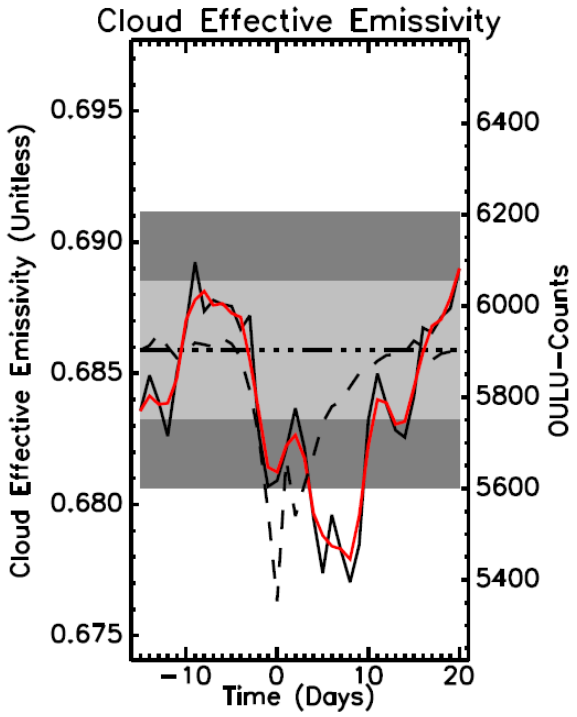

Figure 1. Cloud Emissivity is one of the six investigated parameters. The black dashed line shows the count rate in the OULU neutron monitor. The fully drawn black line is the response in the Cloud Effective Emissitivty, averaged over the 5 strongest Forbush Decreases, while the red line is a 3-day running mean. The light grey box shows 1 standard deviation while the dark grey box shows 2 standard deviations.

This work was supported by the Carlsberg Foundation.

Svensmark, H., Bondo, T., and Svensmark J. (2009) *JGR* **36**, 15,101+

Comparison of three AMS measurements during the Hill Cap Cloud Thuringia 2010 (HCCT 2010) campaign

L. Poulain[1], Z.J. Wu[1], A. Tilgner[1], D. van Pinxteren[1], M. Müller[2], B. Danna[2], C. George[2], J. Schneider[3], A. Wiedensohler[1] and H. Herrmann[1]

[1] Leibniz-Institut für Troposphärenforschung, Leipzig, Germany
[2] IRECELYON, Institut de Recherches sur la Catalyse et l'Environnement de Lyon, Lyon, France
[3] Max Planck Institute for Chemistry, Particle Chemistry Department Mainz, Germany

Keywords: AMS, Aerosol cloud interaction, particle characterization, PM1.

Presenting author email: poulain@tropos.de

It is well established that clouds play an important role for atmospheric chemistry. Inside a cloud, the chemical reactions pathways, which are much different from the ones provided by the gas phase chemistry, are leading to modified atmospheric aerosols after cloud dissipation impacting the oxidative capacity of the atmosphere.

Impact of orographic clouds to the local aerosol chemical composition was measured during the Hill Cap Cloud Thuringia 2010 (HCCT-2010) field campaign which took place in autumn 2010 at the Schmücke Mountain in the Thuringia forest (Germany). Three sampling stations were equipped: a first one on the top of the Mt. Schmücke where clouds were sampled and two valley stations located upwind and downwind to the summit of the mountain. The main objectives of the HCCT-2010 project are to assess the effects of clouds on particle composition, gas phase oxidant budget, changes of hygroscopic properties and activation of aerosol particles.

In order to follow changes of aerosol chemical composition, a total of four Aerodyne ToF-AMSs were deployed during the campaign. One at each valley stations and two at the summit station; one connected downstream of a Cloud Virtual Impactor (CVI) for droplet residuals and one connected to an interstitial inlet measuring interstitial particles (Figure 1). The AMS measurements at both valley stations were completed by PM_1 Particle-into-liquid sampler measurements (PILS, *Weber et al., 2001*) and at the upwind station by a PM_{10} Monitor for Aerosols and Gases in ambient Air (MARGA, Applikon Analytical, NL, *ten Brink et al., 2007*).

The three stations provided simultaneous measurements of the sized resolved aerosol chemical composition before, inside and after a cloud. Based on air mass trajectories, gas tracer experiments and meteorological parameters, it is possible to identify periods during which the air mass of the three stations were connected. According to this, the three AMS results will be compared in order to follow the cloud induced modification of the aerosol chemical compositions as well as modification of the chemical size distribution. Here we will present the first results of this project.

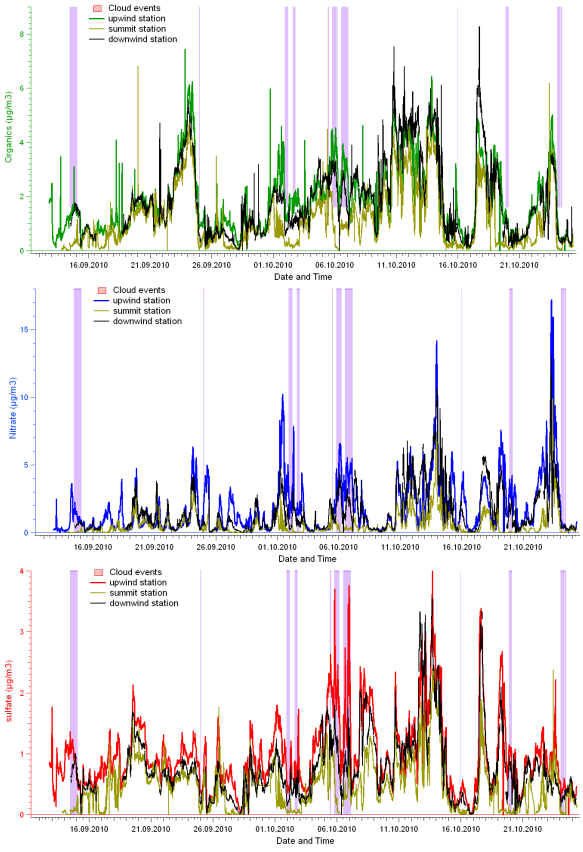

Figure 1: AMS time series measured at the upwind, summit and downwind stations during the entire campaign.

References

ten Brink, H., Otjes, R., Jongejan, P., Slanina, Sjaak (2007) *Atmos. Environ.* **41**, 2768-2779.

Weber, R.J., Orsini, D., Daun, Y., Lee, Y.N., Klotz, P.J.,Brechtel, F., 2001. *Aerosol Science and Technology* **35**(3), 718-727.

Atmospheric particle number concentrations and nucleation events in an urban background site

M. Sastre, F.J. Gómez-Moreno, M. Pujadas, J. Plaza[†], J.J. Rodríguez-Maroto, P. Martínez-Lozano[¶] and B. Artíñano

CIEMAT, Environment Department, Av. Complutense, 22, E-28040 Madrid, Spain
Keywords: Atmospheric aerosols, Urban aerosols, Number concentration, Nucleation.
Presenting author email: FJ.Gomez@ciemat.es

The ambient particle number concentration and size distribution have been measured in an urban background site in Madrid, a continental Mediterranean area, over more than two years (Oct 2006-Dec 2008). They have been measured with a TSI-SMPS (15-600 nm) instrument (Wang and Flagan, 1990) and with a modified Vienna type DMA (3-80 nm) and a CPC 3025 (TSI) during six months. The first objective of the present work is to discuss the differences between the working days and weekend particle number concentration taking into account the seasonal effect. The second aim is to discuss the frequency of nucleation events, their distribution along the year and their classification.

The measurements were carried out at the CIEMAT facilities, an urban background site located in the NW corner of the city of Madrid. Since its industrial activity consists essentially of light factories, the Madrid plume is typically urban, fed by traffic emissions and also by heating systems in winter.

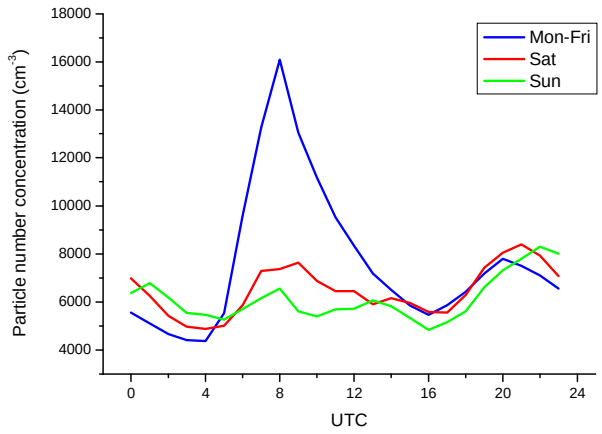

Figure 1. The annual averaged daily pattern for the particle number concentration during the year 2008.

Figure 1 shows the daily evolution of the particle number concentration during 2008 for working days, Saturdays and Sundays. Working days (Mon-Fri) present a leading peak in the morning due to the traffic and daily human activities in general. Then, after a concentration decrease, a secondary peak is reached in the evening. It might be related to traffic again.

Saturdays and Sundays have been treated separately and not as a whole because some differences in particle behaviour can be found, probably induced by commercial activity distinction. It is remarkable how after the evening peak concentrations decrease on working days and Saturdays whereas on Sundays concentrations remain increasingly until the end of the day, achieving the highest values. A possible explanation for this fact is the return traffic to the city on Sunday evening, which is delayed compared to working days.

Particle nucleation is not a frequent phenomenon in this measurement site, where 63 events per year have been observed. They mainly occurred during spring and summer periods, with the minimum number during winter. This suggests that insolation and temperature are important variables in nucleation. Class Ia nucleation events (Dal Maso et al., 2005; Cheung et al., 2010), where particle growth rate can be determined or observed and the typical banana shape is clear, mainly occurred during spring and summer. Class II events, where particle growth determination is not possible or the accuracy of the results is questionable, mainly occurred during winter months, especially during 2007, and also during springtime. However, the influence of high wind speeds during these events was more important than that of the seasonality, as the particles suffered low growth or lost their semivolatile compounds. Class Ib events had characteristics between those of classes Ia and II. They occurred during all the year, although in winter they had a low frequency.

ACKNOWLEDGEMENTS

This work was supported by the Spanish Ministry of Education and Science under Plan Nacional I+D+I, CGL 2004-05984-C07-07 and CGL2007-64117.

REFERENCES

Cheung, H. C., Morawska, L., Ristovski, Z. D., 2010. Observation of new particle formation in subtropical urban environment. Atmospheric Chemistry and Physics Discussion 10, 22623–22652.

Dal Maso, M., Kulmala, M., Riipinen, I., Wagner, R., Hussein, T., Aalto, P. P., and Lehtinen, K. E. J., 2005. Formation and growth of fresh atmospheric aerosols eight years of aerosol size distribution data from SMEAR II, Hyytiälä, Finland. Boreal Environmental Research 10, 323–336.

Wang, S.C., Flagan, R.C., 1990. Scanning Electrical Mobility Spectrometer. Aerosol Science and Technology 13, 230-240.

[¶] Current address: ITB-CNR, Segrate, Milan (Italy)
[†] In memoriam

A Long-Term Study of the Aerosol Effects on Convective Clouds over Southern Sweden and Finland

Sporre, Moa K.[1], Swietlicki, Erik,[1] Glantz, Paul,[2] and Kulmala, Markku[3].

[1]Department of Physics, Lund University, Box 118, S-22211, Lund, Sweden
[2]Department of Applied Environmental Science, Stockholm University, S-11418, Stockholm, Sweden
[3]Department of Physics, University of Helsinki, Post Office Box 64, FI-00014 Helsinki
Keywords: Aerosol cloud interactions, Satellites, Droplets, Precipitation.
Presenting author email: moa.sporre@nuclear.lu.se

Ground based measurements of aerosol number size distributions from Vavihill (9 years) and Hyytiälä (10 years) have been combined with MODIS (Moderate Resolution Imaging Spectrometer) cloud data to investigate how aerosol loading affects convective clouds over Scandinavia.

Aerosol size distributions data from DMPS (Differential Mobility Particle Sizer) instruments at Vavihill in Southern Sweden (56.01° N 13.9° E) and Hyytiälä in central Finland (61.51° N 24.17° E) have been used to calculate the daily average number concentrations for particles larger than 80 nm (N_{80}). Satellite images, from the two MODIS instruments onboard Terra and Aqua, were investigated for the days with available aerosol data from Vavihill and Hyytiälä. A limited area surrounding each station was examined and satellite scenes containing convective clouds were selected. Satellite level 1B data were used to calculate the cloud top temperature at a 1 by 1 km pixel resolution and the cloud effective radius (r_e) data were obtained from the level 2 Cloud Product data. The approach developed by Rosenfeld & Lensky (1998) has been applied to find vertical r_e profiles of the clouds by plotting the r_e against the cloud top temperature. Furthermore, several meteorological parameters from ECMWF (European Centre for Medium-Range Forecasts) have been used to examine how these affect the clouds. Finally, precipitation data from Hyytiälä and SMHI for Vavihill have been investigated to find how the aerosols influence precipitation.

The number of profiles included in the study is 569 for Vavihill and 474 for Hyytiälä. The results show that the profiles of r_e are clearly affected by aerosol loading since profiles with higher aerosol number concentrations measured at the ground, have lower values of r_e as can be seen in Figure 1. The figure shows profiles divided according to N80 for both Vavihill (a) and Hyytiälä (b). There is a larger difference between the profiles for Vavihill both since the values of N80 are higher here, and because the correlation between N80 and cloud base temperature T_b and specific humidity are higher in Hyytiälä. The specific humidity which is well correlated with T_b opposes the effect of the aerosols by increasing the r_e.

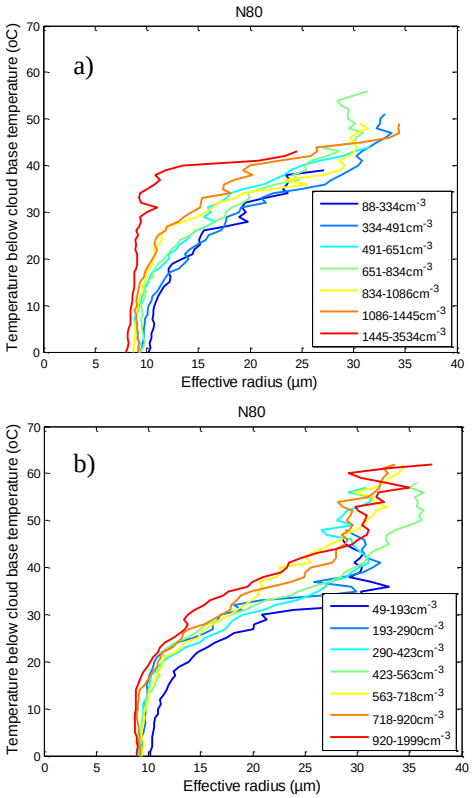

Figure 1. Effective radius profiles divided according to N80 for Vavihill a) and Hyytiälä b).

No correlation has been found between any aerosol parameters and the amount of precipitation. There is however a weak, but significant at a 99% confidence level, correlation between the convective available potential energy and the amount of precipitation. There is also a significant correlation between the latter parameter and the vertical extent of the profiles.

In this study, based on several hundred cases, aerosols effect on convective clouds at the mid-latitudes has been investigated. The results show that aerosol number concentration and T_b are important for the cloud droplet sizes but that the atmospheric instability and the vertical extent of the clouds control the amount of precipitation produced by the clouds.

Rosenfeld, D. & Lensky, M. I. (1998). *Bull. Amer. Meteo. Soc.* 79(11), 2457–2476

Hygroscopicity parameter measurements of cloud condensation nuclei from nucleation experiments at the CLOUD chamber

G.T. Tsagkogeorgas[1], H. Wex[1], F. Stratmann[1], and CLOUD collaboration

[1]Department of Physics, Leibniz Institute for Tropospheric Research, Leipzig, 04318, Germany
Keywords: CLOUD experiment, new particle formation, CCN activity.
Presenting author email: george.tsagkogeorgas@tropos.de

The possible effect of cosmic rays on Earth's clouds and climate remains an open question. Atmospheric ions created by cosmic rays may enhance the formation of aerosol particles. A fraction of these may grow into cloud condensation nuclei and may therefore have an effect on climate. The CLOUD 2010 experiments aimed at the investigation of the role of cosmic ray ionization on atmospheric new particle formation and the hygroscopic properties of cloud condensation nuclei.

A variety of laboratory experiments to study the effects of cosmic rays on new particle formation and cloud condensation nuclei activity were carried out under precisely controlled laboratory conditions at the CERN Proton Synchrotron (PS) in 2010. The experiment included several unique aspects such as the CLOUD chamber, a cylindrical electropolished stainless steel research vessel, exposed to a de-focused secondary pion beam from the CERN PS, the capability to create an ion-free environment with an internal electric field cage, precise adjustment of the ultra-violet illumination from a fibre-optic system, and highly stable operation at any temperature between 30°C and -30°C (Duplissy et al., 2010). For atmospheric new particle formation, besides sulphuric acid, which is considered to be the primary vapour responsible, the relative humidity plays a major role. Therefore, the water vapour concentration in the CLOUD chamber was carefully controlled and the gases fed into the chamber were distributed within via two stainless steel fans, operating at selected fan speeds. The contents of the chamber were continuously analysed by trace gas analysers, particle counters, size analysers, mass spectrometers, and a cloud condensation nuclei counter.

We found that the hygroscopicity parameter, κ for a variety of different experimental conditions was substantially below the κ-value found for H_2SO_4 (κ =0.68–0.74 for dry diameters 30–80 nm), Shantz *et al* (2008). κ-values increased with time during the CLOUD Spring campaign 2010 (Figure 1). Mass spectrometer data for organic material concentrations confirm the existence of volatile organic carbon (VOC) vapours inside the chamber of low carbon content (C1-C4). Efforts are underway to reduce these contaminants.

To our knowledge this is the first experimental study to investigate the effect of galactic cosmic ray with the use of a particle beam on new particle formation and cloud condensation nuclei activity. Besides sulphuric acid, trace amounts of organics, even in the cleanest experimental conditions, are responsible for the particle growth (Jimenez, 2009, Wang, 2010).

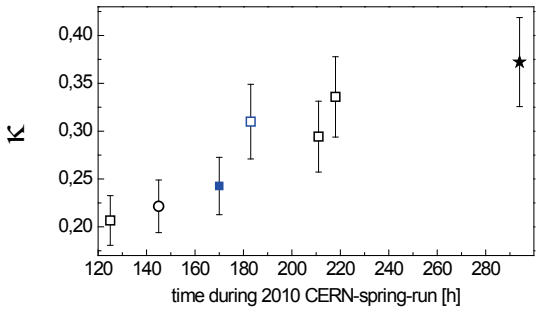

Figure 1. The figure illustrates derived κ-values from CCN activation measurements for different initial experimental conditions of different runs during the CLOUD Spring campaign 2010. Open symbols represent charged pion beam conditions, filled symbols neutral conditions, black symbols low relative humidity and blue symbols higher relative humidity conditions at CLOUD chamber temperature of 20ºC. Star symbol represents CLOUD chamber temperature of 5ºC. Error bars are related to 1σ in dry particle diameter and supersaturation.

We would like to thank CERN for supporting CLOUD with important technical resources, and for providing a particle beam from the CERN Proton Synchrotron. This research has received funding from the EC's Seventh Framework Programme under grant agreement number 215072 (Marie Curie Initial Training Network "CLOUD-ITN"), from the German Federal Ministry of Education and Research (project number 01LK0902A), from the Swiss National Science Foundation and from the Academy of Finland Center of Excellence program (project number 1118615).

Duplissy, J., et al., (2010) *Results from the CERN pilot cloud experiments.Atmos. Chem. Phys., 10, 1635–1647.*

Jimenez, J.L., et al., (2009) *Evolution of organic aerosols in the atmosphere. Science 326, 1525–1529.*

Wang, L., et al., (2010) *Atmospheric nanoparticles formed from heterogeneous reactions of organics. Nature Geoscience 3, 238–242.*

Shantz, N.C., Leaitch, W.R., Phinney, L., Mozurkewich, M., and Toom-Sauntry, D. (2008) *Atmos. Chem. Phys.,* **8**, 5869-5887.

Aerosol properties during long-range transport of African dust air masses over Granada (Spain)

A.Valenzuela[1, 2], F.J. Olmo[1, 2], H. Lyamani[1, 2], A.Quirantes[1], D. Pérez[1, 2] and L. Alados-Arboledas[1, 2]

[1]Dpto. Física Aplicada, Universidad de Granada, Fuentenueva s/n, 18071-Granada, Spain.
[2]Centro Andaluz de Medio Ambiente (CEAMA), Avda. del Mediterráneo s/n, 18071-Granada, Spain.
Keywords: Dust particles, Aerosol radiative properties, Principal Plane, Non-spherical particles
Presenting author email: avalenzuela@ugr.es

Dust particles interact with the solar and terrestrial radiation modulating Earth's radiative budget. The Iberian Peninsula is frequently affected by African dust air masses that modulate the aerosol climatology in different areas, especially in the south. It has been shown that the radiative budget is sensitive to the dust particle's source region, because their radiative properties vary depending on the source and on the chemical and physical processes occurring along the trajectory. The back-trajectories analysis is a powerful tool commonly used to study the transport of atmospheric constituents and particles from an origin source to receptor sites.

In this work we analyze the African air masses that reached Granada (37.16ºN, 3.60ºW, 680 m a.s.l) from 2005 to 2010, by means of back-trajectory analyses using HYSPLIT model. In addition we characterize the aerosol radiative properties taking into account sun-photometric measurements and the air mass history. The aim is to determine how columnar aerosol properties observed differs depending on source region and transport pathways from North Africa to Granada. Two air mass classification methods were used: the first identifying the desert dust origin sources and the second on the basis of cluster analyses (Pace et al., 2006; Toledano et al, 2009). The dates and confirmation of the African dust episodes arriving to southern Spain were supplied by CALIMA project (www.calima.ws).

Radiative aerosol properties were simultaneously retrieved from sun-photometric measurements (CIMEL CE-318, instrument #18, AERONET network) according to the methodology described by Olmo et al. (2008). This method uses the Aerosol Optical Depths (AOD) and sky radiances measured in the solar principle plane. The instrument provides solar extinction measurements at 340, 380, 440, 670, 870 and 1020 nm, and sky radiance measurements at 440, 670, 870 and 1020 nm using the almucantar and principal plane configurations. Annual calibrations were performed by Langley plots (extinction measurements) and integrating sphere (radiance measurements) by AERONET facilities (Holben et al., 1998).

To classify the aerosol properties we have defined three broad geographical sectors: Sector A (Northern Morocco, North-western Algeria), Sector B (Western Sahara, North-western Mauritania and South-western Algeria), and Sector C (Eastern Algeria, Tunisia). Table 1 shows the mean values of AOD (440 nm) and Angström parameter (α) for the analyzed period.

	Sector A	Sector B	Sector C
AOD ±SD	0.25±0.16	0.28±0.12	0.27±0.11
α±SD	0.45±0.21	0.40±0.22	0.46±0.23

Table 1. Mean values and standard deviations of AOD and α from 2005 to 2010 using the sector classification.

Using clustering analysis we obtained two back-trajectories clusters for 1500 and 3000 m a.g.l. Level 1500 m: Cluster 1 (from the East of Algeria) and Cluster 2 (from Morocco). Level 3000 m: Cluster 1 (from Southwest of Algeria) and Cluster 2 (from Sahara and the South of Morocco). Table 2 shows the retrieved mean values of AOD and α for the analyzed period.

Table 2. Mean values and standard deviations of AOD and α from 2005 to 2010 using the cluster analysis.

Level (m)	Cluster	AOD±SD	α±SD
1500	1	0.28±0.13	0.39±0.19
	2	0.24±0.16	0.43±0.20
3000	1	0.29±0.12	0.37±0.19
	2	0.23±0.14	0.42±0.19

As shown in Tables 1 and 2, the sectors classification can not discriminate between different air masses except for Sector B, and the cluster technique is a powerful tool from AOD and α classifications showing differences. On the other hand, sector classification and cluster technique show significant differences (Tables not shown) for Single Scattering Albedo, Coarse Modal Radius and Coarse Volume Concentration mean values. The Fine Modal Radius and Fine Volume Concentrations show high mean values and no significant differences in any classification, showing the importance of local polluted fine particles at our station due to the anthropogenic influence associated to the synoptic conditions.

Acknowledgements: This work is supported by projects RNM-3568, RNM-6299, CGL2010-18782 and by EARLINET-ASOS project (EU-CA., 025991, RICA).

Olmo et al. (2008). *J. Quant. Spectrosc. Ra*, 100, 1504–1516.
Pace et al. (2006). *Atmos. Chem. Phys*., 6, 697-713.

Toledano et al. (2009). *J. Appl. Meteorol. Clim*., 48(5), 962-981.

Shape dependence of atmospheric aerosol light scattering parameters: ALFA simulation and comparison to AERONET data

A. Quirantes[1], F.J. Olmo[1,2], A. Valenzuela[1,2], H. Lyamani[1,2] and L. Alados-Arboledas[1,2]

[1]Department of Applied Physis, University of Granada, 18071-Granada, Spain
[2]Centro Andaluz de Medio Ambiente (CEAMA), Av. del Mediterráneo s/n, 18006-Granada, Spain
Keywords: Nonspherical particles, Aerosol optical properties.
Presenting author email: aquiran@ugr.es

Dust particles play an important role in the Earth's radiation budget. In this sense, radiative forcing calculations need size-dependent optical properties. Remote sensing techniques as Lidar (profile particle parameters) and sun-photometers (columnar integrated parameters) have demonstrated their potential. As example, AERONET, EARLINET and CALIPSO database provides a wide-range, long-term database of atmospheric aerosol properties. However, lidar data have been predominantly based on the Mie theory, and does not adequately reproduce the scattering properties by desert dust particles (Veselovskii et al. 2010). Ground-based AERONET network uses sun-photometric measurements (sky radiance and extinction) to retrieve columnar effective particle size distribution and refractive index values, as well as other radiative properties like absorption aerosol optical depth, single scattering albedo (SSA) and asymmetry parameter, using a mixture of polydisperse, randomly oriented spheroids (Dubovik et al, 2006). These parameters, however, do not have a strong dependence on particle shape. Lidar measurements, on the other hand, allow quantities like backscattering and particle depolarization ratio profiles, to be measured.

In order to study the parameters that are sensitive to particle shape, a set of computer simulations was carried out. A pre-calculated database on light scattering properties for nonspherical particles (ALFA), developped at our group, was used for this purpose. As example, size and composition values were chosen from the Eyjafjoll volcano eruption of May 2010, as given by the AERONET direct measurements and inversion data (ITF-Leipzig Station, April 19, 2010, 14:49:37 GMT).

The Leipzig particle size distribution for April 19 was approximated as a bimodal volume log-normal distribution (PSD), as Table 1 shows. Size parameter refers to the equivalent-volume-sphere radius. Values of the refractive index ($m=n+ik$) as retrieved by AERONET, and those chosen for simulation, are shown in Table 2. In the present study, particle shape distribution was assumed to be a 50% volume mixture of oblate and prolate spheroids, with varying axial ratio (ε) values from 1.2 to 1.8; this axial ratio can be independently set for each mode.

As expected, some parameters such as extinction and absorption coefficients, asymmetry parameters, and SSA, show a small variation with shape. SSA remained constant to within 0.08%. Extinction and absorption coefficients showed a slightly larger difference (about 2% for extinction, 4% for absorption). Angstrom parameters for both extinction and absorption also showed small variations.

On the other hand, backscattering parameters show a large dependence on shape. Backscattering coefficient values have been found to decrease for increasing axial ratio, with a difference of up to 70% as axial ratio goes from 1.2 to 1.8. Other parameters related to backscattering, such as the Lidar ratio (extinction to backscattering ratio), and the color ratio (backscattering ratio at two wavelengths, 440 and 870 nm), and the depolarization ratio, show similar behavior. As a result, depolarization ratio and lidar ratio are two decisive parameters in order to retrieve particle shape by inversion methods from Lidar measurements.

While no attempt was made to fit our simulated data to AERONET inversion products, reasonable results were nevertheless obtained. Extinction, SSA and asymmetry parameter values obtained with ALFA simulations agreed to AERONET data to within 2%.

Additional computer simulations were carried out for other values of m, similar to those of Table 2. Again, the trend observed is a weak shape dependence of extinction, SSA and asymmetry parameters; and a large variation of backscattering-related parameters (Lidar ratio, depolarization ratio, color ratio). Changes in the imaginary part of the index of refraction strongly affects the values of the absorption coefficient, and therefore of the absorption Angstrom exponent.

Table 1. Particle size distribution parameters

	Mode 1	Mode 2
Concentration ($\mu m^3/\mu m^2$)	0.080	0.078
Modal radius (μm)	0.205	1.721
Width σ	0.485	0.631

Table 2. Refractive index values, m=n+ik

	n	n
AERONET (441 nm)	1.4632	0.004013
ALFA (440 nm)	1.4588	0.003598
AERONET (869 nm)	1.4855	0.002557
ALFA (880 nm)	1.4782	0.002197

Acknowledgements: This work is supported by projects RNM-3568, RNM-6299, CGL2010-18782, PE2008-FQM-3993 and by EARLINET-ASOS project (EU-CA., 025991, RICA).

Dubovik, O. et al., J. Geophys Res. D111, D11208, doi:10.1029/2005JD006619, 2006.
Veselovskii, I. et al., J. Geophys Res. 115, D21203, doi:10.1029/2010JD014139, 2010.

Number concentration measurement of nanometer-sized particles and its correlation with wind velocity

H. Saghafifar

Physics Group, Faculty of Science, University of Isfahan, Isfahan, 81746, Iran
Keywords: number concentration, wind velocity
Presenting author email: saghafifar1@yahoo.com

We have designed and constructed an Expansion Condensation Particle Counter (ECPC) and its operation has been tested in the laboratory conditions (Saghafifar, *et al* , 2009).
Urban aerosols of nanometer size can be measured by ECPC. Two identically made ECPCs were used in the field applications and number concentration of atmospheric aerosols was measured in Isfahan, Iran. The ECPCs were operated over several weeks in different quarters of 2007 and 2008.
An ECPC was located near the south gate of Isfahan University, near a busy street and number concentration of aerosols was measured among the atmospheric pollutant trace gases. The experiments showed a good correlation between number and NOx concentrations.
Two ECPCs were operated at the same location and their results were the same as shown in figure 1.
One of the ECPCs was removed away from near street site which result in reducing of its readings.
At night both ECPCs showed nearly the same results and as the traffic was started, the readings of the near street site increased by a factor of 2 to 3. (Fig. 2)
The meteorological parameters were obtained by a portable station. Wind velocity was considered as parameter which could correlate with number concentration. The number concentration is decreased by increasing the wind velocity.
The number concentration was measured every 10 seconds and for correlation it was averaged over an hour or a day.
Despites changes in the situation of the measurements in two periods: 18 days in March 2008 and 8 days in May 2008, the same linear fit was obtained for correlating the number concentration to the wind velocity (Fig. 3). If one can find the same formula for a lot of periods for a site, the number concentration could be predicted.

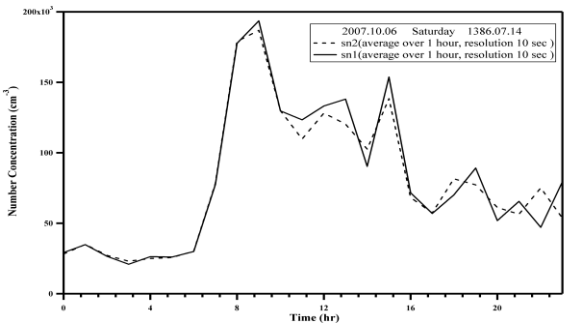

Figure 1. Comparison between ECPCs data at the same place

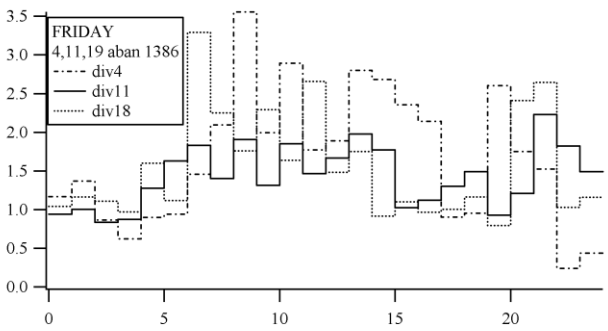

Figure 2. Comparison between ECPCs data at different sites

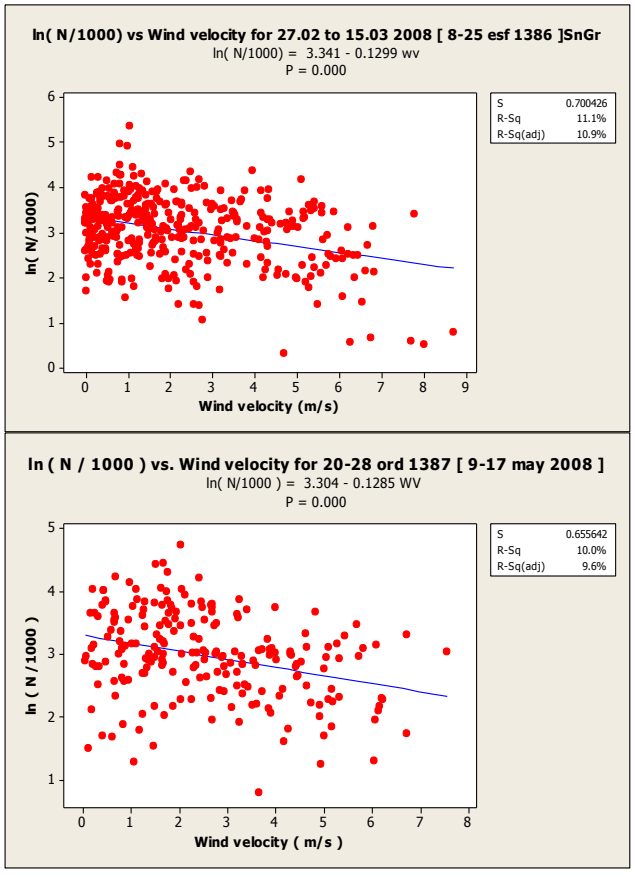

Figure 3. Correlation between wind velocity and number concentration of aerosols
Ln(N/1000) = 3.3- 0.129 wv

Saghafifar,H. *et al* (2009) Aerosol Science and Technology,**43**:767-780

Evolution of aerosol size distributions related to air masses origins in Paris Fog

Neda Boyouk[1], Darrel Baumgardner[2] and Martial Haeffelin[3]

1 Labratoire Meteorologie dynamique (LMD), SIRTA - Ecole Polytechnique, Palaiseau, France

2 Universidad Nacional Autonoma de Mexico, Ciudad Universitaria, Mexico City, DF, 04510

3 Labratoire Meteorologie dynamique (LMD), SIRTA - Ecole Polytechnique, Palaiseau, France

Presenting author Contact: Neda Boyouk , nedaboyouk@gmail.com.

Changes in the size distributions of aerosol particles and the microphysical properties of fog events are examined based on the air mass origins and prevailing meteorological conditions. This evaluation is based on measurements made during a comprehensive field campaign November, 2010 through March, 2011 at the SIRTA research site, 30 km south of Paris, France. A new instrument, the Aerosol Particle Spectrometer with Depolarization (APSD), was been deployed during this period, measuring individual particles in the diameter range from 0.5 to 20 μm along with the degree of depolarization that is related to their shape.

A total of 25 fog events have been analyzed, whose back trajectories (Hysplit) are shown in Fig. 1

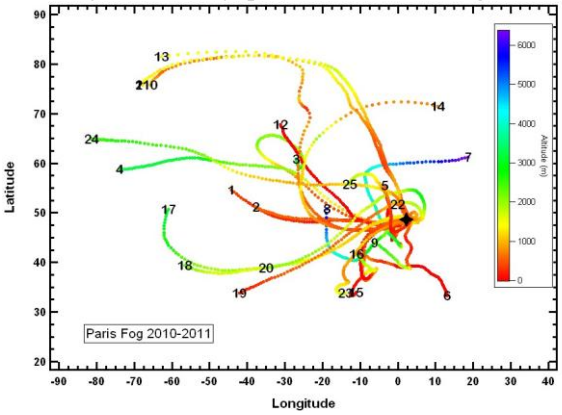

Fig 1.the back trajectories of airmasses for 25 fog event

The color is related to their altitude. Our analysis shows that the maximum liquid water content (LWC)in the fogs depends on the direction from which the air masses relative to 3, 6 and 12 hours before. It was also related to whether the air mass had come with a trajectory remaining close to the surface the previous six hours or if it had descended from higher altitude.

The local wind directions are not correlated with where the air masses were three hours before. When evaluating the size distributions, we observe distinct differences in how the aerosols are distributed by size before, during and after the fog event as a function of where the air had been three, six and twelve hours before.

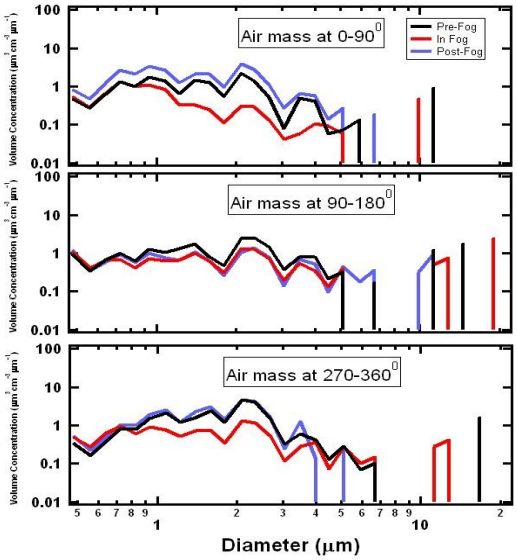

Fig 2 the volume concentration of aerosol based on air masses origin

This presentation will highlight the most salient results that show the importance of the history of aerosols with respect to fog formation, evolution and dissipation and the subsequent changes in aerosol properties due to processing by fog.

Keywords: aerosol size distribution, fog, air masses origins, aerosol processing by fog.

Aerosol particles transport on areas of water: experiments and modelling

L.A. Uvarova[1], Yu. G. Biryukov[2], V.A. Zagainov[2], V.I. Kostin[3], D.M. Kiselev[3], I.V.Krivenko[4], T.V. Kazarova[5], L.Yu. Vasil'eva[6], K.G. Goryunov[7]

[1]Department of Applied Mathematics, Moscow State University of Technology "STANKIN", Moscow, Russia
[2]Scientific Technical Aerosol Centre, Karpov's Physics and Chemistry Institute, Moscow, Russia
[3]Department of Mathematics, Moscow State Academy of Water Transport, Moscow, Russia
[4] Department of Physics, Tver State Technical University, Russia
[5]Department of Philosophy, Moscow State University of Technology "STANKIN", Moscow, Russia
[6] Moscow physico-technikal Institute (State University), Dolgoprudnii, Russia
[7] Department of Physics, Branch of Engineering Economic University, Tver, Russia
Keywords: atmospheric aerosols, aerosol size distribution, nanoparticles, aerosol dynamics
Presenting author email: uvarova_la@rambler.ru

The aerosols and nanoparticles dynamic in different systems and at different conditions problem is the high spectral irradiance in the modern aerosol physics and chemistry. That problem is of interest to the nanoelectronics, electrodynamics, medicine and others.
In particular, it should be pointed out the next problems. The problem of the high dispersion aerosols transport may be related directly to the functioning of the seaports, riverports and water transports. The problem of the high dispersion aerosols particles formation takes place as a result of various natural phenomena, complex relations and interactions in the system «nature – man» (for example, forest fires and others phenomena – Akimov et. al., 2009). Of some interest is the research of the high dispersion aerosols particles spreading over water surface. Such investigations are important to make the climatic prognosis's, to rivers, lexes and seas regions and to consider the interaction of the high dispersion aerosols particles with the human organism.
In given work it is discussed the investigation of the aerosol particles transport over watersurface of central Russian rivers (Moscow-river, Oka, Volga) in a period of the motor ship scientific expedition (31.05.2010 – 10.08.2010). The measurements carried out for aerosol particles concentration and radiuses by the diffusion aerosol spectrometer (Zagainov, 2006). Figure 1 shows the example of the nanoparticles distributions on radiuses. The given results are computed by the appropriate program in given device.

The received curves can be described approximately by the gamma-distribution:

$$f_X(x) = x^{k-1}\frac{e^{-x/\theta}}{\theta^k \Gamma(k)}, x \geq 0,$$

where $\Gamma(k)$ is gamma-function, k is parameter.

In this period was carried out the precipitation of the small aerosol particles on special filters in ship ports. The received results were investigated with the help of the atomic-power microscope. The fractal analysis of the experimental results was carried out. It is shown that the fractal dimension varies from 2.009 to 2.05 mkm (Figure 2 shows such example).

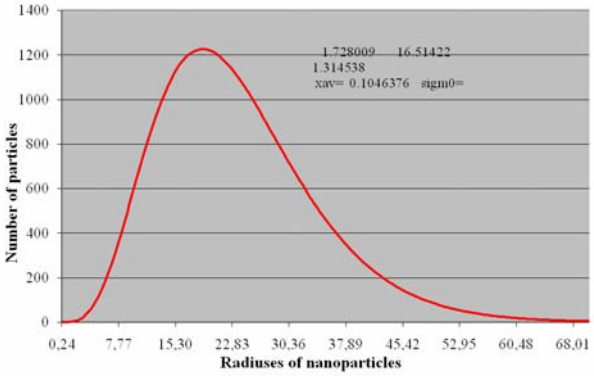

Figure1. The example of the distributions of nanoparticles (the result was received in the field work).

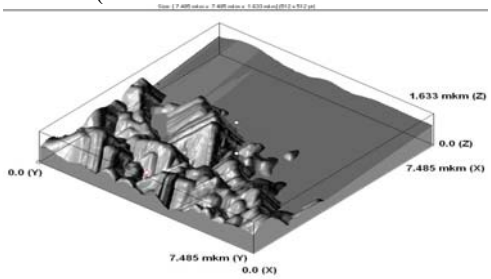

Fugure2. The example of the distribution of nanoparticles on the filter.

Given results can be used for inner problem of aerosol particles transport in a human organism (Marijnissen and Gradon, *Editors*, 2009). For the solution of this problem it is possible to use the methods of molecule dynamics and method of joker (Uvarova *et al*, 2010).

This work was supported by the Russian Foundation for Basic Research under grant 09-01-00292-a.

Akimov, V.A.,Bykov, A.A., Shchetinin, E.Yu. (2009) *Introduction in statistic of extreme values*, Moscow, Federal Centre of Crisis (*in Russian*).
Zagainov, V.A. (2006) *Nanotechnology* **1**, 141-146 (*in Russian*).
Marijnissen J.and Gradon L., *Editors* (2009). *Nanoparticles in Medicine and Environment*, London, New York: Springer.
Uvarova, L.A. and Mikhalina, E.S. (2010) *American Institute of Physics, ICNAAM 2010.*

Australian aerosol and cloud condensation nuclei (CCN)

R. Fedele[1,2], M. D. Keywood[2], P. W. Selleck[2], J. L. Gras[2] and N. Porter[1]

[1]Department of Applied Chemistry, RMIT, Melbourne, Victoria, 3042, Australia
[2]Department of Marine and Atmospheric research, CSIRO, Aspendale, Victoria, 3195, Australia
Keywords: atmospheric aerosols, aerosol cloud interactions, size distributions.
Presenting author email: rosemary.fedele@csiro.au

Exploratory climate modeling suggests that aerosol effects are of comparable importance as greenhouse gases, as a driver of recent climate trends in the southern hemisphere, including Australia (Rotstayn, *et al.*, 2007; Rotstayn, *et al.*, 2010). A 2008 CSIRO review considered the possible climatic effects of natural and anthropogenic aerosol located in the Australian region (Rotstayn, *et al.*, 2008). Observations and modeling suggest that various regional aerosol sources may be important, but systematic studies of their role in climate change and climate variability are currently lacking.

In addition, the aerosol indirect effects (or the effects aerosols have on cloud formation) are currently the largest uncertainty in the IPCC report estimate of anthropogenic induced climate change (IPCC, 2007). There is a specific need to understand the processes involved with aerosol indirect effects and climate change in general on Australian regional aerosols such as dust emissions, bushfire emissions, Southern Ocean natural aerosol production, terrestrial biogenic aerosol and aerosol precursor emissions, transport and removal processes. A better understanding of aerosol effects is essential in order to reconcile modeled and observed climate variability and climate change.

To this aim, intensive ground-based measurements of ambient aerosols including cloud condensation nuclei (CCN) were made at three locations across Australia; a tropical site located at Gunn Point in the Northern Territory, an urban site located in a suburb approximately 22 km to the west of Sydney in New South Wales and a marine site located at the Cape Grim Baseline Monitoring Station located on the northwest tip of Tasmania.

A Scanning Mobility Particle Sizer (SMPS) spectrometer measured the size-resolved aerosol number concentration for particles between 15 and 750 nanometers. A nano SMPS measured the size resolved aerosol number concentration for particles between 4 and 150 nanometers at two of the three sites. An Aerodynamic Particle Sizer measured aerosol number concentration for particles between 0.5 to 20 micrometers at two of the three sites. A CCN counter measured the size resolved CCN number concentration for CCN between 0.75 and 10 micrometers, over a super saturation range of 0.1 to 0.9 %. The size-resolved chemical composition of aerosols was determined on samples collected with a cascade impactor, high volume and low volume samplers.

Preliminary investigations from the tropical Australian site, Gunn Point, indicate that smoke effected the sampling location throughout the measurement campaign. Figure 1 shows levoglucosan, an indicator of smoke, is present in all aerosol samples collected. In the presence of smoke, the number of CCN increases however the fraction of CN able to form CCN decreases.

The influence of important aerosol sources and processes to the Australian continent such as biomass burning, urban vehicle emissions, secondary formation and marine sources on CCN formation and regulation will be discussed in this presentation.

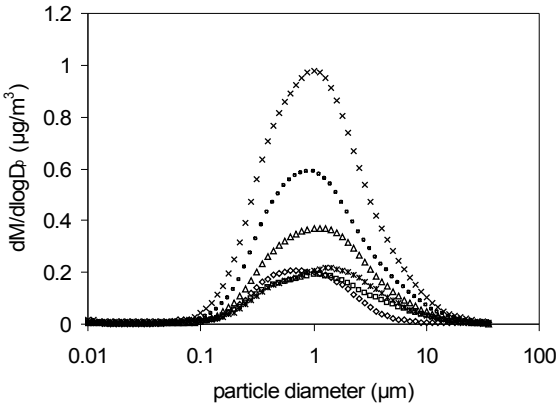

Figure 1. Levoglucosan mass concentration, in 72 hour samples collected by a cascade impactor at Gunn Point, indicative of smoke.

This work was supported by the Australian Climate Change Science Program.

IPCC (2007). *Climate change 2007: the Physical Science Basis. Summary for Policymakers.* Contribution of Working Group I to the Fourth Assessment Report of the Intergovernmental Panel on Climate Change.

Rotstayn, L. D., Cai, W. J., Dix, M. R., Farquhar, G. D., Feng, Y., Ginoux, P., Herzog, M., Ito, A., Penner, J. E., Roderick, M. L. and Wang, M. (2007). *J. Geophys. Res.-Atmos.* ***112***(D9), 28.

Rotstayn, L. D., Keywood, M. D., Forgan, B. W., Gabric, A. J., Galbally, I. E., Gras, J. L., Luhar, A. K., McTainsh, G. H., Mitchell, R. M. and Young, S. A. (2008) *Int. J. Climatol.* **29**(4), 461-479.

Rotstayn, L. D., Collier, M. A., Dix, M. R., Feng, Y., Gordon, H. B., O'Farrell, S. P., Smith, I. N. and Syktus, J. (2010). *Int. J. Climatol.* **30**(7), 1067-1088.

Main activities of the Spanish network on environmental DMAs

F. J. Gómez-Moreno[1], M. Sastre[1], B. Artíñano[1], V. Juncal Bello[2], M. Piñeiro Iglesias[2], P. López Mahía[2], J. Pey[3], A. Ripoll[3], A. Alastuey[3], M. Sorribas[4], M. Fernández[4], B. A. de la Morena[4], J. L. Trujillo de Cabo[6] and S. Rodríguez[5, 6]

[1]Department of Environment, CIEMAT, Madrid, E-28040, Spain
[2]Institute of Environment, University of A Coruña, A Coruña, E-15179, Spain
[3]Institute of Environmental Assessment and Water Research (IDAEA-CSIC), Barcelona, E-08034, Spain
[4]Atmospheric Sounding Station 'El Arenosillo', INTA, Mazagón-Huelva, E-21130, Spain
[5]University of Huelva, Huelva, E-21071, Spain
[6]Izaña Atmospheric Research Centre, (IARC/CIAI), AEMet, Santa Cruz de Tenerife, E-38001, Spain
Keywords: Atmospheric aerosols, Particle size distribution, DMA, SMPS
Presenting author email: fj.gomez@ciemat.es

Size distribution is one of the most important properties of the atmospheric particles as it determines their behavior and gives information about their origin and history. The particle size distribution measurements are a key factor to understand the radiation-aerosol interaction and the health effects as both depend on the size distribution.

In the last ten years, there has been an important increase in the number of studies related with the particle size distribution measurement (Kulmala et al., 2004; Pey et al., 2008; Sorribas et al., 2008).

There are currently five groups in Spain involved in the measurement of atmospheric particle size distributions by means of Differential Mobility Analyzers (DMAs). These groups are: University of A Coruña, IDÆA-CSIC, INTA, IARC-AEMET and CIEMAT. All the groups have to solve many common problems related with the instrumentation required for this type of measurements. For this reason, the Spanish network on environmental DMA (Red Española de DMAs Ambientales, REDMAAS) was launched in January 2010. The REDMAAS has as main objective the cooperation between the groups, which will lead to solve common problems and to optimize their facilities and protocols.

The activities planned for the first years of this network are:

- DMA calibration: the network members can check their DMA calibration. Firstly, it was necessary to check the DMA flow rates and then, a monodisperse aerosol, latex, was introduced into the DMA to calibrate the electrical mobility. Very good results were obtained.

- DMA intercomparison: one of the main objectives of the REDMAAS is to make all the instruments comparable. With this objective a first intercomparison exercise with four of them was performed during April 2010 in the INTA facilities (El Arenosillo, Huelva). The CPCs used with the DMAs were previously intercompared and later the instruments measured simultaneously the same atmospheric particles and the results were compared and assessed. An additional pair of SMPS was compared in the CIEMAT facilities during July 2010.

- Measurement quality control program: under this activity the network has prepared some protocols required for the correct operation of the systems. Protocols for flow calibrations and checks, zero checks, dry procedures for ambient relative humidity above 30% and others have been developed.

- Losses in sampling lines have been already estimated using simple deposition models. In a new activity they are currently computed by means of a CFD code. The five sampling systems are being simulated to obtain a correction factor for the particle deposition in the sampling lines.

- Support for the radioactive facility license: this activity is thought for new possible network members. For the correct DMA working, it is necessary to have a radioactive source at the aerosol inlet to assure a known particle charge distribution. This source requires the approval of the national nuclear regulatory commission (CSN) by means of a radioactive facility license.

- Webpage: all the network information and activities are included in a webpage: http://www.redmaas.com/.

- New DMA applications: DMAs are very flexible and useful instruments and have several different applications in environmental studies. This activity is based on the experience with this kind of instruments and the objective is to support the members interested in using DMAs in new applications.

This network is financed by the Ministry of Science and Innovation (CGL2010-11095-E).

Kulmala *et al.* (2004). *J. Aerosol Science* 35, 143–176.

Pey *et al.* (2008) *Atmospheric Environment*, 42, 9052-9062.

Sorribas *et al.* (2008). *European Aerosol Conference* 2008, Thessaloniki, Abstract T06A172P.

Charging states and ion-induced nucleation fractions in an urban and forested area, Finland

S. Gagné[1], T. Nieminen[1], J. Leppä[2], H.E. Manninen[1], T. Petäjä[1], V.-M., Kerminen[2], L. Laakso[3] and M. Kulmala[1]

[1]Department of Physics, University of Helsinki, P.O. box 64, Helsinki, Finland
[2]Finnish Meteorological Institute, Climate Change, P.O. box 503, Helsinki, Finland
[3]School of Physical and Chemical Sciences, North-West University, Private Bag x6001, South Africa
Keywords: ion-induced nucleation, particle formation, Ion DMPS, measurements.
Presenting author email: stephanie.gagne@helsinki.fi

New particle formation (NPF) and their growth frequently takes place in the atmosphere and is of climatic relevance (Kulmala *et al.*, 2004). Several nucleation mechanisms have been proposed and their relative contribution to new particle formation is still unclear. We can define two large groups of nucleation mechanisms: neutral mechanisms, and ion-induced mechanisms. The contribution of ion-induced nucleation to the formation of particles of climatically relevant sizes is controversial and few measurements of its importance have appeared in the scientific literature.

The Ion-DMPS (Laakso *et al.*, 2007) is an instrument especially designed to measure the charging state of aerosol populations (the ratio of the fraction of charged particles in the air sample and the fraction of charged particles in the same sample at bipolar equilibrium). The ion-induced fraction can then be estimated from the charging state. This kind of estimations were performed in Hyytiälä and Helsinki, Finland (Gagné *et al.* 2008, 2011), and similar estimations with a different instrument were performed in Boulder, Co., USA (Iida *et al.*, 2006). Another instrument that has been used to estimate the ion-induced fraction is the Neutral cluster and Air Ion Spectrometer (NAIS). Unfortunately, the NAIS in its typically used operation mode may be mis-estimating the ion-induced fraction in overcharged situation (when the charged fraction is higher than the fraction at equilibrium, when the charging state is above one, this problem is being investigated at the moment). The Ion-DMPS, and similar designs, are thus the only instruments from which the ion-induced fraction have been reliably estimated.

The Ion-DMPS has been used in a forested area (Hyytiälä) and an urban area (Helsinki). The estimated ion-induced fractions were around 6% and 1%, respectively (Gagné *et al.*, 2008, 2011). This is in agreement with other literature: the ion-induced fraction is generally higher in cleaner areas, and lower in more polluted areas (see e.g. Manninen *et al.*, 2010) and references therein).

The fraction of ion-induced nucleation varies from place to place and from event to event. It also varies during a NPF event as a function of size and time. The charging state of an aerosol population either is above or below one (charge equilibrium) when the particles are formed and tends to reach the bipolar equilibrium as it grows to bigger sizes.

The behavior of the charging state as a function of size, assuming that the small ion concentration is the same for both polarities, $N_c^+ = N_c^-$, is described in Kerminen *et al.* (2007). An improved version that does not make this assumption is described in Leppä *et al.* (2011, manuscript in preparation).

The equations presented in Leppä *et al.* (2011) and in Iida *et al.* (2008) show that the charging state can be used the retrieve the growth rate of particles during a NPF event. The method of Leppä *et al.* (2011) is applied in Gagné *et al.* (2011), and shows that taking into account that $N_c^+ \neq N_c^-$ improves the agreement of the growth rates between polarities.

In conclusion, the charging state of aerosol populations of their charged fraction provide valuable information about the participation of ion-induced nucleation and growth rates. The studies cited here show that charged particles are formed with lower vapor saturation ratios (incl. sulfuric acid and water) than neutral particles. This also implies that high temperatures lowers the chances of a neutral cluster to activate. Consequently, in urban polluted areas, where vapors are abundant, neutral nucleation is more important than in clean environments. Ion-induced nucleation being limited by the ion pair production rate, smaller fractions of ion-induced nucleation are observed when more particles are created.

This research was supported by the Academy of Finland Center of Excellence program (project number 1118615), and the European Comission 6th Framework program project EUCAARI, contract no 036833-2 (EUCAARI).

Gagné, S., Laakso, L., Petäjä, T., Kerminen, V.-M. and Kulmala, M. (2008). *Tellus*, **60**, 318-329.

Gagné, S., Nieminen, T., Kurtén, T., Manninen, H.E., Petäjä, T. *et al.* (2010). *Atmos. Chem. Phys.*, **10**, 3743-3757.

Gagné, S., Leppä, J., Petäjä, T., McGrath, M.J., Vana, M. *et al.* (2011), Submitted to ACP.

Iida, K., Stolzenburg, M.R., McMurry, P.H., Dunn, M. J., Smith, J. N. *et al.* (2006). *J. Geophys. Res.*, **111**, D23201.

Iida, K., Stolzenburg, M.R., McMurry, P.H. and Smith, J.N. (2008). *J. Geophys. Res.*, **113**, D05207.

Kerminen, V.-M., Anttila, T., Petäjä, T., Laakso, L., Gagné, S., *et al.* (2007). *J. Geophys. Res.*, **112**, D21205.

Kulmala, M., Vehkamäki, H., Petäjä, T., Dal Maso, M., Lauri, A., *et al.* (2004). *J. Aerosol Sci.*, **35**, 143–176.

Laakso, L., Gagné, S., Petäjä, T., Hirsikko, A., Aalto, *et al.* (2007). *Atmos. Chem. Phys.* **7**, 1333-1345.

Manninen, H.E., Nieminen, T., Asmi, E., Gagné, S., Häkkinen, S. *et al.* (2010). *Atmos. Chem. Phys.*, **10** 7907-7927.

Gravity waves observed as a causal mechanism for transition from closed to open cellular convection in the remote South East Pacific

G. Allen[1], G. Vaughan[1], H. Coe[1], P. Minnis[2], T. Toniazzo[3]

[1]Centre for Atmospheric Science, University of Manchester, Manchester, M13 9PL, UK.
[2]NASA Langley NASA Langley Research Center, USA
[3]University of Reading, Reading, UK

Keywords: Gravity Waves, Cloud Microphysics, Satellites, VOCALS
Presenting author email: h.coe@manchester.ac.uk

This case study discusses an important observed role for atmospheric gravity waves (AGWs) in the South East Pacific (SEP) region by virtue of their ability to evidently modulate cloud radiative and dynamical properties over a wide area. The case study presented here employs satellite imagery together with measurements of satellite-retrieved cloud bulk properties during the period 7 October to 11 October 2008 over the SEP, which together serves to illustrate the horizontal propagation of a series of AGW trains, manifest by their influence on a large-scale stratocumulus cloud deck capping the local marine boundary layer (see white ellipses in Figure 1). The AGWs were observed as a periodic modulation of retrieved cloud top height by up to 500 metres peak-to-trough, whilst the horizontal direction of wave propagation was perpendicular to the synoptic boundary layer flow. The AGWs of interest appear to originate near 30 S, 85 W and were initiated for a 24-hour period beginning at midday on 7 October 2008, propagating along a vector directed approximately northeastward toward the Peruvian Coast (15 S, 70 W) over the following 48 hours as illustrated in Figure 1. During this time, the gravity waves were seen to affect both reversible and non-reversible changes in cloud radiative properties and cloud dynamics such that persistent areas of clear sky developed in the troughs of passing gravity wave fronts. (see purple ellipses in Figure 1). The formative mechanisms for such cloud-free regions, or so-called Pockets of Open Cells (POCs), observed as cell-like (openly-convecting) cloud-free areas embedded in remote marine stratocumulus sheets, are currently the subject of intense speculation and scientific interest due to their ability to allow solar radiation to reach the ocean surface in regions where atmospheric models predict dense cloud cover.

In this case study, we will investigate the effects of gravity waves on the SEP stratocumulus cloud deck and investigate the synoptic scale disturbances which initiate gravity waves in the area.

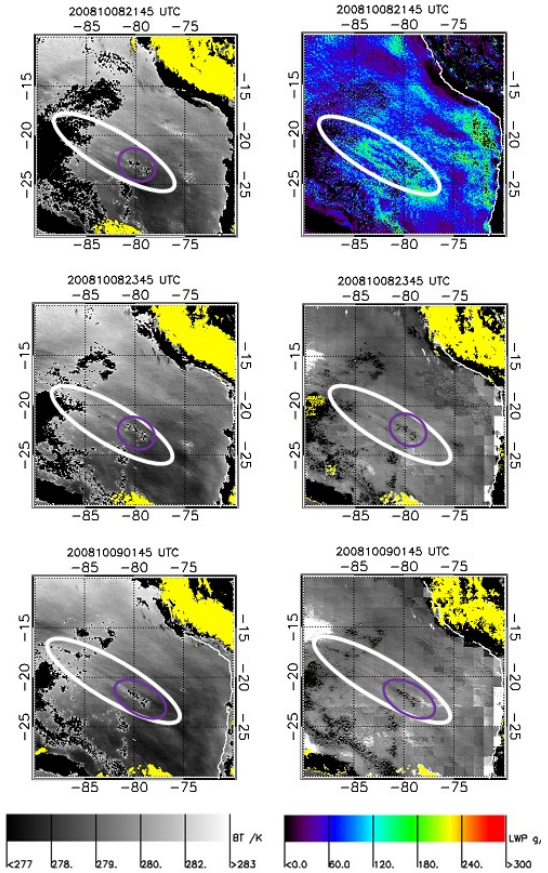

Figure 1 Time sequence of GOES-10 channel 4 brightness temperature (BT; left panels) and retrieved cloud top height (CTH) or liquid water path (LWP; right panels). Colour scales are given for BT and LWP. The progression of a gravity wave front is highlighted by a white ellipse, with a developing POC feature in a purple ellipse.

Apparent particle density in Helsinki during the ULTRA II campaign

O. Hänninen[1], R. Sorjamaa[1], J. Cyrys[2,3], M. Pitz[2,3], J. Pekkanen[1], and T. Lanki[1]

[1]National Institute for Health and Welfare, Kuopio, 70210, Finland
[2] Institute of Epidemiology II, Helmholtz Zentrum München – German Research Center for Environmental Health, Neuherberg, Germany
[3] University of Augsburg, Environment Science Centre (WZU), Augsburg, Germany

Keywords: Exposure, Modelling, Infiltration, Indoor/outdoor particles
Presenting author email: otto.hanninen@thl.fi

Particle properties, including density, are affecting the particle behaviour in penetrating indoor air from outdoors, remaining suspended, and being deposited on surfaces in indoor spaces as well as in the respiratory tract. Particle density also may correlate with the volatile components found in PM due to the typically lower density of water and SVOCs. Limited amount of analyses have been performed on urban $PM_{2.5}$ that have been shown to be the most significant environmental health hazard in developed countries (Hänninen & Knol, 2011). From $PM_{2.5}$ data of more than 1000 days a mean apparent particle density of 1.5 g/cm^3 was determined by Tuch *et al.* (2000) in Erfurt, Germany. Pitz *et al.* (2003) analyzed the seasonal, weekday and daily variability of the apparent density of $PM_{2.5}$ and observed higher densities during spring and during the afternoon to evening hours as well as slightly higher values for weekdays. Pitz *et al.* (2008) found similar densities of ambient $PM_{2.5}$ in Augsburg, Germany. A multiple variable regression model explained nearly 64% of the day-to-day variation of $PM_{2.5}$ apparent density by particle composition and meteorological conditions. The aim of the current analysis is to understand the relationship of aerosol as observed by EAS versus the gravimetric $PM_{2.5}$ concentration that forms a reference point for $PM_{2.5}$ infiltration analysis.

The current analysis uses ULTRA2 data collected in Helsinki in 1998-99, including electrical aerosol spectrometer measuring particle number concentrations over 12 size classes (EAS; Mirme *et al.*, 2002), collection of daily $PM_{2.5}$ samples on Teflon filters and XRF-analysis of their elemental composition (Vallius *et al.*, 2003). Interpolation method was used to estimate the volume concentration of particles smaller than 2.5 µm in diameter. Two alternative models were used in the particle volume calculation; one assuming spherical particles and another using shape factors and fractal dimensions estimated based on author judgment. The results show apparent densities of 1.3 and 1.2 g/cm^3, respectively, indicating that the result is not very sensitive to the particle shape and fractal dimension. Higher densities were observed for the days affected spring dust episodes, characterized also with higher $PM_{2.5}$ concentrations. Lower observed density in comparison with the cited German studies could be related to source profiles and need to be further considered.

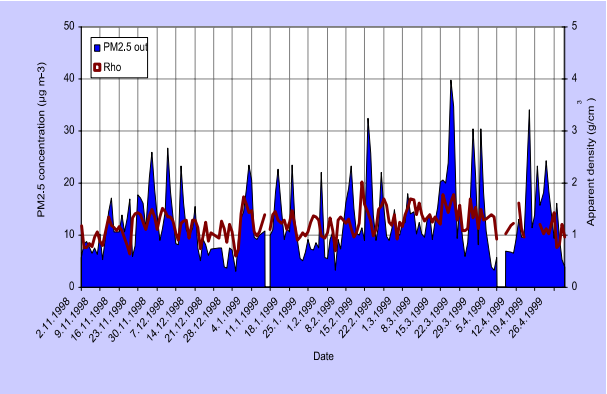

Figure 1. Time-series view of the daily PM2.5 concentration and corresponding apparent particle density (second y-axis).

This work has been supported by EU Contracts FP7-ENV-2009-1-243406 (TRANSPHORM), ENV4-CT95-0205 (ULTRA) and Academy of Finland Contract 133792 (PM Sizex).

Hänninen O, Knol A (eds.) (2011). *THL Reports 1/2011*, Helsinki, Finland. 98 pp + 2 appendixes. ISBN 978-952-245-413-3.

Tuch, T., Mirme, A., Tamm, E., Heinrich, J., Heyder, J., Brand, P., Wichmann, H.E., Pekkanen, J., Kreyling, W.G., 2000. *Atmospheric Environment 34, 139–149.*

Mirme A, Tuch T, Khlystov A, ten Brink H, Ruuskanen J, Kreyling WG and Pekkanen J. (2002). *Aerosol Science and Technology* **36** (8):876–886.

Pitz M, Cyrys J, Karg E, Wiedensohler A, Wichmann, HE, Heinrich J. (2003) *Env Sci & Tech* **37**: 4336-4342.

Pitz M, Schmid O, Heinrich J, Birmili W, Maguhn J, Zimmermann R, Wichmann EH, Peters A, Cyrys J. (2008). *Env Sci & Tech* **42**: 5087-5093.

Vallius M, Lanki T, Tiittanen P, Koistinen K, Ruuskanen J, Pekkanen J. (2003) *Atm Env* **37**: 615-623.

Cloud droplet activation during the PuCE 2010 campaign

A. Jaatinen[1], S. Romakkaniemi[1], L.Q. Hao[1], A. Kortelainen[1], P. Miettinen[1], D. Brus[3], H. Portin[1,2], M. Komppula[2], A. Leskinen[2], J.N. Smith[1,2,4] and A. Laaksonen[1,3]

[1]Department of Applied Physics, University of Eastern Finland, Kuopio, P.O. Box 1627, Finland
[2]Finnish Meteorological Institute, Kuopio Unit, Kuopio, P.O. Box 1627, Finland
[3]Finnish Meteorological Institute, Climate Change, Helsinki, P.O. Box 503, Finland
[4]National Center for Atmospheric Research, Boulder, CO, P.O. Box 3000, USA
Keywords: CCN, CLOUD EVENT
Presenting author email: antti.jaatinen@uef.fi

Newly formed aerosol particles become climatically important if they are able to grow to sizes of 50 nm and larger. Particles in this size range can act as cloud condensation nuclei (CCN) and therefore may contribute to the indirect aerosol effect, a series of proposed impacts that include increased cloud albedo due to increase in CCN concentration (Twomey, 1991) to increased lifetime of clouds (Albrecht, 1989). Once particles grow to a size where they can become CCN, their ability to activate into cloud droplets depends on their chemical composition, and the maximum water supersaturation in the air parcel forming cloud.

The fourth Puijo Cloud Experiment (4th PuCE), an intensive campaign measuring aerosol and cloud properties, was conducted by the Finnish Meteorological Institute and University of Eastern Finland at the Puijo semi-urban measurement station. The measurement campaign was carried out during 21.9 – 27.10.2010 for the observation of cloud events. The station is located at the top of the Puijo sight-seeing tower, 306 m a.s.l. and 224 m above the surrounding lake level, thus being a very suitable site for aerosol-cloud interaction measurements (Leskinen *et al*., 2009; Portin *et al*., 2009). Aerosol sources are subject to influence from long-range transport from continent and ocean, but also the local pollution, likely traffic, pump mill, heating plant and other urban emissions.

In this work, the properties of cloud activation were studied using DMPS (Differential Mobility Particle Sizer), DMT CCNc (Cloud Condensation Nuclei counter), Aerosol Mass Spectrometer (AMS) and Tandem Differential Mobility Analysers (TDMAs). During the measurements the DMPS inlet was switched between a PM1 (interstitial) and a total inlet (all particles), and during cloud events the particles activated to cloud droplets were resolved as a difference between the measurements performed in each inlet. In addition, we measured size-resolved CCN to get information about size dependence, and on the other hand data about the true supersaturation inside the cloud during a cloud event.

During the campaign, a total of nine cloud events were observed. The duration of the events ranged from a couple of hours up to about twenty hours. As an example, we have chosen one cloud event day for closer scrutiny, 9.10.2010, 00:00 – 05:45. From Figure 1 we can see that the minimum size of particles forming cloud events was around 100 nm and D_{50}-size (the size where half of the total particle concentration activate into cloud droplets), i.e. the size where blue and black line cross, is 195 nm. From CCN measurements the mean D_{50}(SS=0.1%) is 160 nm and D_{50}(SS=0.2%) is 120 nm. Thus the mean supersaturation during cloud formation has been less than 0.1%.

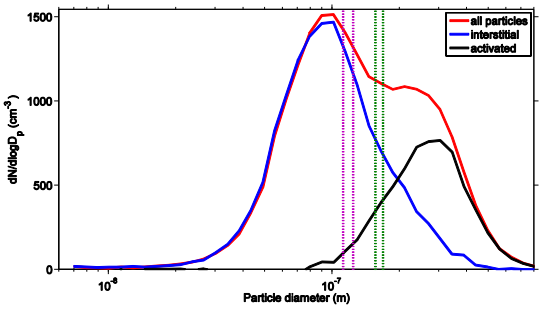

Figure 1. Size distributions of all particles (red), interstitial particles (blue), and activated particles (black). Green and purple dotted lines represent the range of the critical diameter (D_{50}) derived from the CCNc data during the cloud event, for SS=0.1% and SS=0.2% respectively.

During the cloud event the mass fraction of ammonium-sulphate was around 30% the rest being mainly organics. This is in good agreement with CCNc measurements.

In future analyses, we shall analyze other measured data (such as meteorological and chemical) to investigate how the size dependent composition of particles vary during cloud events, and how the diameter of smallest activated particles depend on the composition of particles.

This work was supported by the Academy of Finland (project 111865 and 123466) and by KONE foundation.

References

Albrecht, B. A.: Aerosols, cloud microphysics, and fractional cloudiness. *Science*, **245**(1229):1227–1230, 1989.
Leskinen, A., et al. (2009) *Boreal Environ. Res.*, **14**, 576-590.
Portin, H., et al. (2009) *Boreal Environ. Res.*, **14**, 641-653.
Roberts, G. C. & Nenes, A. (2005). A continuous-flow streamwise thermal gradient CCN chamber for atmospheric measurements, *Aerosol Sci. Tech*., **39**, 206–221.
Twomey, S. (1991). Aerosols, clouds and radiation, *Atmos. Environ.*, **25A**, 2435–2442.

Water adsorption and CCN properties of silica particles

S. Romakkaniemi[1], H. Keskinen[1], A. Jaatinen[1], J. N. Smith[1,2,3] and A. Laaksonen[1,3]

[1]Department of Applied Physics, University of Eastern Finland, PO BOX 1627, 70211 Kuopio, Finland
[2]National Center for Atmospheric Research, P.O. Box 3000, Boulder, CO USA
[3]Finnish Meteorological Institute, P.O. Box 503, 00101 Helsinki, Finland
Keywords: Adsorption, Aerosol cloud interaction, CCN
Presenting author email: sami.romakkaniemi@uef.fi

Commonly it has been thought that only aerosol particles with substantial amount of water soluble matter can form cloud droplets at the ambient conditions. However, recently it has been proposed that also insoluble, but hydrophilic, particles can act as a cloud condensation nucleus (CCN) even at atmospheric supersaturations (Sorjamaa and Laaksonen, 2007, Henson, 2007). In the theory water adsorption is described by isotherms which give the amount of adsorbed water on the particle surface as a function of relative humidity in subsaturated conditions. One example of such an equation is the so called FHH-isotherm giving the number of adsorbed water layers on the surface as:

$$\ln\frac{1}{S} = \frac{A}{\Theta^B} \quad , \qquad (1)$$

where S is the gas saturation ratio, Θ is the surface coverage, i.e. the number of water layers, and A and B, are fitted parameters dependent on the surface properties. In the traditional Köhler equation the term describing the solute effect (Raoult's effect) can be replaced by solving the S from Eq. 1 (Sorjamaa and Laaksonen, 2007),

$$S = exp\left(\frac{4\sigma M_w}{RT\rho_w D}\right) exp(-A)\Theta^{-B} \quad , \qquad (2)$$

from which the critical supersaturation can be calculated.

It has been shown by Romakkaniemi *et al.* (2001) that the hygroscopic differential mobility analyzer (HTDMA) can be used to study water uptake by adsorption on aerosol particles at subsaturated conditions. With small enough particles it is possible to detect the formation of water layers, although the depth of monolayer is approximately only 3Å. In this study we produced silica particles from an aqueous solution. The amount of water adsorbed on the particles at RH's between 40 and 90% was measured with nano-HTDMA, The growth of particles at super-saturated conditions was measured by CCN counter.

The adsorption of water on small aerosol particles composed of silica follows FHH-adsorption isotherm. Based on the HTDMA measurements for 8nm and 10 nm particles, the parameters A and B in Eq. 1 are found to be 4.82 and 2.16, respectively. These values are slightly higher than values reported in Kumar *et al.* (2010) for typical dust and mineral samples. By using parameters A and B in Eq. 2 we get the critical supersaturation as a function of particle size.

In Figure 1 we present the activated fraction of 114nm and 150nm particles as a function of supersaturation. For this type of curve a sigmoidal function can be fitted and from that we can determine D50, the diameter at which half of the aerosol are activated. Also presented are expected values for critical supersaturations calculated from Eq. 2 with parameters from HTDMA measurements. As can be seen the particles activate in slightly lower supersaturation than expected. However, corrections for multiple charging in DMA and shape of particles would move activation curves to right (Kumar *et al* 2010).

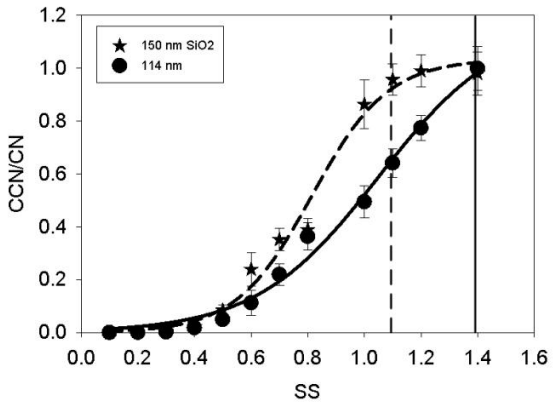

Figure 1. Activation curves from CCN counter. The data are not corrected for shape or multiple charges in the DMA.

This work was supported by the Academy of Finland (projects 123466 and 138951), the Kone Foundation and the Saastamoinen Foundation.

REFERENCES

Henson, B. F.: An adsorption model of insoluble particle activation: Application to black carbon, J. Geophys. Res.,112,D24S16, doi:10.1029/2007JD008549, 2007.

Kumar, P., Sokolik, I. N., and Nenes, A.: Measurements of cloud condensation nuclei activity and droplet activation kinetics of fresh unprocessed regional dust samples and minerals, Atmos. Chem. Phys. Discuss., 10, doi:10.5194/acpd-10-31039-2010, 2010.

Romakkaniemi, S., Hämeri, K., Väkevä, M., and Laaksonen, A.: Adsorption of water on 8–15 nm NaCl and (NH4)2SO4 aerosols measured using an ultrafine tandem differential mobility analyzer, J. Phys. Chem. A, 105, 8183–8188, 2001.

Sorjamaa, R. and Laaksonen, A.: The effect of H_2O adsorption on cloud drop activation of insoluble particles: a theoretical framework, Atmos. Chem. Phys., 7, doi:10.5194/acp-7-6175-2007, 2007.

Activation of "synthetic atmospheric aerosols" – relation to chemical composition of particles <100nm

J. Burkart[1], R. Hitzenberger[1], G. Reischl[1] and G. Steiner[1]
H. Bauer[2], K. Leder[2], M. Rzaca[2] and H. Puxbaum[2]

[1]University of Vienna
Faculty of Physics, Aerosol Physics and Environmental Physics, Boltzmanng. 5, A-1090 Vienna, Austria
[2]Vienna University of Technology
Institute for Chemical Technologies and Analytics, Getreidemarkt 9, A-1060 Vienna, Austria

Keywords: CCN, ultrafine particles, ambient aerosol
Presenting author email: julia.burkart@univie.ac.at

Atmospheric aerosol particles can act as cloud condensation nuclei (CCN) and can this way influence the microphysical properties of clouds and further the climate. The so called indirect aerosol effect is still subject to great uncertainties (IPCC 2007) and one big question mark is whether the size or the chemical composition of particles governs their activation to CCN (Dusek et al., 2006a). As CCN are predominantly found in the size range <100 nm, while chemical data are usually available only from total filter samples, we intend to investigate this question by focussing on the investigation of ultrafine (<100nm) particles.

From July 2007 to December 2008 we performed a long-term study to investigate the activation behaviour of the atmospheric aerosol in Vienna. In this first part of the study we conducted field measurements on the rooftop laboratory of the Physics Building of the University of Vienna which is situated in downtown Vienna. The measurement station is about 35m above ground-level and separated by courtyards from the closest main street so that the aerosol can be characterized as urban background aerosol.

During this study, we measured the activation ratio (A=CCN/CN) of the atmospheric aerosol with the University of Vienna CCN Counter (Giebl et al. 2002, Dusek et al. 2006) at a supersaturation of 0.5%, the number size distribution with a Vienna-type DMA and we obtained long-term size selected samples with low-pressure Berner impactors (size range: 0.1 – 10 µm) equipped with back-up filters. As the lower cut-size of the impactors was 0.1µm the material collected on the back-up filter contained only particles with aerodynamic equivalent sizes < 100 nm.

In the subsequent laboratory study the material collected on the back-up filters was first eluted in water and chemically analyzed for elemental and organic carbon, sugars and inorganic ions. Secondly, we generated "synthetic atmospheric aerosols" by nebulizing the eluates with a Collison atomizer and investigated the activation behaviour of these particles with the CCN-counter. Activation curves as well as activation diameters of this aerosol were measured. Figure 1 shows typical activation curves of the eluted filter samples. On average the activation diameter was found to be 58nm at a supersaturation of 0.5% which is much lower than the average apparent activation diameter found for the atmospheric aerosol (162nm) by integration of the DMA number size distribution.

This presentation focuses on the activation diameters of the "synthetic ambient aerosols" in relation to their chemical composition and compares them as well to the apparent activation diameters of the atmospheric aerosol.

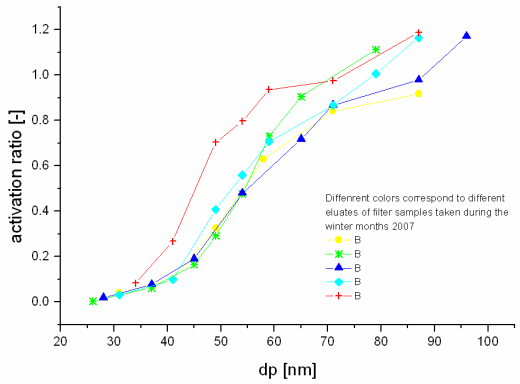

Figure 1 Examples of activation curves of the eluted filter samples. Different colours correspond to different eluates.

This work was supported by the Austria Science Fund (FWF) under grant P19515-N20.

IPCC (2007): *Climate Change 2007 - The Physical Science Basis.* Cambridge and New York. (Cambridge University Press)

Dusek, U., G.P. Frank, L.Hildebrandt, J. Curtis, S Walter, D. Chand, F. Drewnick, S.Hings, D.Jung, S. Borrmann, M.O. Andreae, *Science* 312 (2006a), 1375-1378.

Giebl, H., A. Berner, G. Reischl, H. Puxbaum, A. Kasper-Giebl and R. Hitzenberger, *Journal of Aerosol Science* 33 (2002), 1623-1634.

Dusek, U., Reischl, G. P., Hitzenberger, R., *Environ. Sci Technol.* 40 (2006b), 1223 – 1230.

Seasonal and Source Depending Activation Behaviour of Aerosol Particles in the North China Plain

Mildenberger K.[1], Schäfer M.[1], Henning S.[1], Nowak A.[1], Sommerhage E.[1], Hallbauer E.[1], Göbel T.[1], Nekat B.[1], van Pinxteren D.[1], Deng Z.[2], Liu P.[2], Ma N.[2], Zhao C.[2], Henne, S.[3], Wiedensohler A.[1] and Stratmann F.[1]

[1] Leibniz-Institute for Tropospheric Research, 04318 Leipzig, Germany
[2] Department of Atmospheric Sciences, School of Physics, Peking University, Beijing 100871, China
[3] Empa, Swiss Federal Laboratories for Materials Science and Technology, 8600 Dübendorf, Switzerland

Keywords: cloud, CCN number concentration, kappa, China
Presenting author email: milde@tropos.de

The cloud condensation nuclei (CCN) number concentration is known as an important parameter of the indirect aerosol effect of clouds on earth's climate. Within the project HAze in CHIna, the main parameters which influence the total CCN number concentration were investigated at an anthropogenically influenced and heavily polluted site in the North China Plain.

CCN number concentrations were determined from size segregated CCN measurements by using a cloud condensation nucleus counter (Droplet Measurement Technology). From supersaturation scan data, the hygroscopicity parameter κ (Petters and Kreidenweis, 2007) was calculated for 100 nm particles. Additionally, the aerosol particle (CN) number concentration and standard meteorological parameters were measured. Measurements were performed in 2009 during two intensive campaigns in March and July/August 2009 at Wuqing Ordinary Meteorological Observing Station, China (39°23'8.53"N, 117°1'25.88"E), which is located 60 km south east of Beijing and represents a typical regional site in this megacity region.

For the investigation of a possible dependence of κ and the total CCN number concentration on the aerosol source region, air mass backward trajectories were calculated and different source regions were derived through trajectory clustering. Statistical tests were performed to study if there was any dependence of the derived activation behaviour of the particles on the meteorological parameters (air pressure, temperature, absolute humidity, wind speed) and on the CN number size distribution, respectively. The number size distributions were parameterized by fitting several lognormal distributions, which were described by their maximum, width and the centre of the mode.

The κ values derived for 100 nm particles did not differ significantly between the summer and winter campaign. The average κ values derived from CCN measurements for both campaigns were 0.52 ± 0.13 and 0.47 ± 0.07, respectively. The cluster analysis showed that the main source regions of the investigated aerosol were the Gobi desert and Beijing (direction NW), a maritime region (Bohai Sea, direction NE), an industrial region (Hebei, direction SW) and the great Tianjin area (cluster local). However, no significant dependence of κ was found with respect to different air mass origins. The particles were already highly influenced due to aging along the whole trajectory path and by the local sources around the measurement station. No dependences of κ on the meteorological parameters or the mode parameters were found, either. For the seasonal and source depending investigation of the total CCN number concentrations at 0.07 % and 0.10 % supersaturation, it was found that they were predominantly determined by the total CN number concentration of the accumulation mode. This means, the higher the CN concentration in the accumulation mode, the more CCNs were available (Figure 1). CN of the nucleation and Aitken mode did not influence the CCN concentration significantly. It was also not influenced by the meteorological parameters and κ. Due to the effect that the CN number concentration in the accumulation mode differed with the air mass origin, the CCN number concentration differed, too. The highest CCN concentrations were found, if the air masses experienced a local recirculation over the Tianjin area.

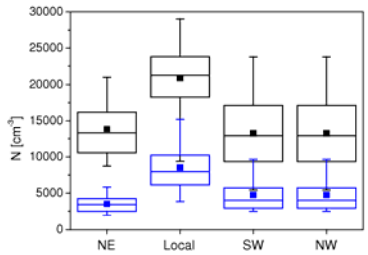

Figure 1. Comparison of the CN number concentration (black boxes) and the CCN number concentration for 0.07 % supersaturation (blue boxes) for the air mass origins at Wuqing (China) during the winter campaign.

It can be concluded that for heavy polluted regions like the North China Plain the CCN number concentration is more or less only depending on the CN number concentration in the accumulation mode for supersaturations of 0.07 % and 0.1 %. The influence of the chemical composition on the CCN number concentration is rather small. This is due to the fact that the size of the aerosol particles is three times more important for their activation behaviour than κ and that larger particles activate earlier to cloud droplets than smaller ones.

This work was supported by the German Science Foundation under grant DFG WI 1449/14-1.

Petters, M.D. and Kreidenweis, S.M. (2007). *Atmos. Chem. Phys*., **7**, 1961-1971.

A Sensitivity Study: The Influence of S_{crit} on κ

K. Mildenberger[1], S. Henning[1], J. Voigtländer[1], H. Wex[1] and F. Stratmann[1]

[1] Department of Physics, Leibniz Institute for Tropospheric Research, 04318 Leipzig, Germany

Keywords: sensitivity study, kappa, critical supersaturation, CCNC
Presenting author email: milde@tropos.de

The relation between aerosol particle size and water saturation ratio in the equilibrium state can be described by the Köhler equation. This equation consists of two main parts, describing the 'curvature' effect (Kelvin term) and the 'solution' effect (Raoult term) of the solution droplets. The Raoult term is a function of chemical composition, which is normally unknown for atmospheric aerosol particles. For that reason, single hygroscopicity parameters are usually applied to describe the hygroscopic growth and activation of such particles. A frequently used parameter is κ (Petters and Kreidenweis, 2007). Often, a constant κ, calculated on the basis of activation measurements, is applied.

In this study, a sensitivity study was performed to investigate the uncertainty of κ–values derived from cloud condensation nuclei (CCN) activation measurements, e.g. by means of a Cloud Condensation Nucleus Counter (CCNC). The study is based on the equation for κ-Köhler theory, given by:

$$S = \frac{D_{wet}^3 - D_{dry}^3}{D_{wet}^3 - D_{dry}^3(1-\kappa)} \exp\left(\frac{4\sigma M_w}{RT\rho_w D_{wet}}\right) \qquad (1)$$

where S is the water vapour saturation over the droplet surface in the equilibrium state, D_{wet} the wet diameter of the droplet, σ the surface tension, M_w is the molecular weight of water, ρ_w the density of water, R the universal gas constant and T the droplet temperature. For this study, σ was assumed to be equal to that of pure water and the temperature 293.15 K. D_{dry} was varied between 10 nm to 500 nm (step width 1 nm) and κ between 0.01 and 1.4 (step width 0.01) in the calculations. Based on equation (1), the critical supersaturation (S_{crit}), which is known as the supersaturation (SS) at the point of particle activation, was calculated. Furthermore, $dS_{crit}/d\kappa$ and dS_{crit}/dD_{dry} were computed for the sensitivity analysis.

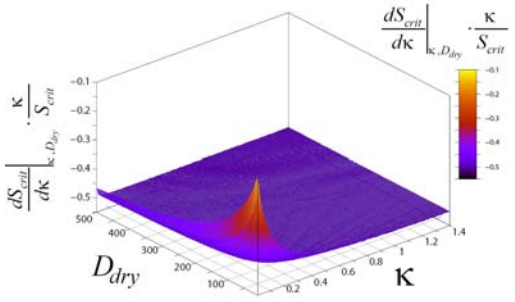

Figure 1. Relative sensitivity of S_{crit} related to κ.

It was found that the relative sensitivity of S_{crit} with respect to κ is mainly constant at -0.5 (Fig. 1) and -1.5 for D_{dry}. Only for small κ and D_{dry} values the sensitivity change significantly. But note that in this regime S_{crit} ranges between 4 % and 18 %; i.e. values are not encountered under atmospheric conditions. From results shown in Fig. 1 it has to be concluded that the sensitivity of S_{crit} to D_{dry} is a factor of 3 higher than that to κ. In other words, changes in D_{dry} change S_{crit} three times more than the same relative change in κ. This means, small changes in κ do not affect S_{crit} significantly. That size matters more than chemistry was also pointed out in Dusek et al. (2006).

In turn, small changes in S_{crit} lead to large changes in κ. This is valid for the above described regime where the sensitivity of S_{crit} to D_{dry} is constantly a factor of 3 higher than that to κ. For our studies we assume that the uncertainty of SS is ±0.01% absolute. This value was found by calculating the standard deviation of multiple *SS* calibrations with a CCNC (Droplet Measurement Technology). To study the effects of this uncertainty in measured S_{crit} on κ, $\Delta\kappa/\Delta S_{crit}$ was computed from S_{crit} and S_{crit}+0.01%, respectively S_{crit}-0.01%. This leads to three different κ values: κ_{max}, κ, κ_{min}. Then κ_{max} was divided through κ, respectively κ through κ_{min}. The results give the percentage accuracy for κ determined with the CCNC (Fig. 2). It is obvious that κ can be calculated with the same accuracy independent of D_{dry}. On the other hand, the accuracy is strongly dependent on SS. For example, at 0.1% SS κ can be calculated with an error of 17%, while at 0.5% SS the error in κ is only 4%. This holds for all applications where a κ larger than 0.006 is determined from CCNC measurements in the range of 0.1% to 0.5% SS and with an experimental uncertainty of ±0.01% absolute, no matter which D_{dry} is studied.

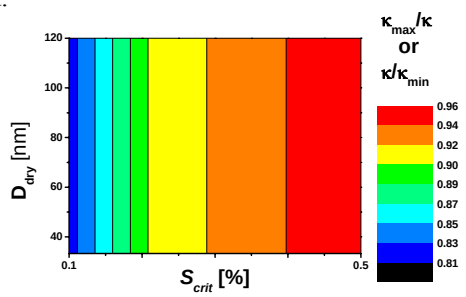

Figure 2. Percentage accuracy for κ from CCNC measurements.

Petters, M.D. and Kreidenweis, S.M. (2007). *Atmos. Chem. Phys*., **7**, 1961-1971.

Dusek, U., Frank, G.P., Hildebrandt, L., Curtius, J., Schneider, J., Walter, S., Chand, D., Drewnick, F., Hings, S., Jung, D., Borrmann, S. and Andreae, M.O. (2006). *Science*, 312, 1375-1378.

Correlation between aerosol parameters measured in-situ and by means of Sun-photometer technique.

Aleksander Pietruczuk, Janusz Jarosławski

Institute of Geophysics Polish Academy of Sciences, ul. Księcia Janusza 64, 01-452, Warsaw, Poland

Keywords: Aerosol, size distribution, air pollution, optical properties.

Atmospheric aerosol influences earths climate directly by scattering and absorption of solar radiation and indirectly playing important role in cloud physics. Aerosol optical properties are measured by numerous networks in global and continental scale. Some of them uses Sun-photometer technique [AERONET, ESR] which allows to obtain aerosol microphysical properties form measurements of direct and diffused solar radiation. On the other hand aerosol influences human life and air quality and particulate matter (PM10 and PM2.5) concentrations are routinely measured by national environmental agencies. However aerosol microphysical properties are measured by only a few other institutions like universities and research institutes.

In this work we presents correlation between parameters of aerosol size distribution measured in-situ and by means of Sun-photometer as well as correlation between Aerosol Optical Thickness (AOT) and PM10 concentration. We compared modal and effective radius and width of fine and coarse mode of distribution defined according to AERONET definitions. Such a study of parameters obtained by different techniques and representative for different atmospheric layers seams to be interesting especially when satellite data could be used. In – situ measurements are concentrated mainly in urban or industrial region and rural and remote unpolluted regions are not covered by measurements networks but are covered by satellite measurements. On the other hand in-situ measurements could be used to estimation of columnar aerosol microphysical properties when Sun-based measurements are not possible, for example during cloudy days.

Presented data were measured in Geophysical Observatory of Institute of Geophysics PAS at Belsk. Belsk is a small village located in rural area around 50 km at south from Warsaw. Two Sun-photometers, CIMEL CE 318 and POM 01L made by Prede company, are collocated in the Observatory. Both of them provide aerosol size distribution. Aerosol size distribution is also measured in-situ by means of Scanning Mobility Particle Sizer (SMPS 3034) and Aerodynamic Particle Sizer (APS 3321) made by TSI Company. PM10 concentrations are measured by means of TEOM ambient particulate monitor with FDMS module.

Scatter plot of AOT versus PM10 concentration is shown at Figure 1. We found correlation coefficient R=0.93 and regression coefficient 0.0047 ± 0.002.

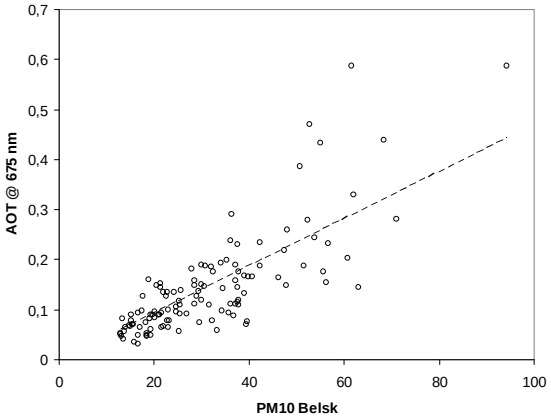

Figure 1. Correlation between AOT and PM10 concentration at Belsk.

We also found correlation coefficient for fine mode modal radius equal R=0.58 and for coarse mode R=0.33. Worse correlation in case of coarse mode is caused probably by uncertainties in estimation of aerosol size distribution in this range. APS registers small number of large particles which causes large errors in aerosol size distribution, especially when number distribution is recalculated to volume one.

This work was supported by the Polish Ministry of Science under grant 0281/B/P01/2009/36.

Hygroscopic properties of aerosols associated with different air masses arriving at Mace Head, Ireland.

A. Vaishya, D. Ceburnis, J. Ovadnevaite, C. Monahan, J. Bialek, S.G. Jennings, and C.D. O'Dowd
Centre for Climate & Air Pollution Studies, School of Physics, Ryan Institute,
National University of Ireland Galway, Galway, Ireland.
Keywords: Atmospheric aerosols, relative humidity, scattering coefficient, optical properties.
Presenting author email: a.vaishya1@nuigalway.ie

Aerosols play an important role in the dynamic atmospheric system. They tend to affect the radiative balance of the climate system and affect the hydrological cycle through the direct effect (scattering and absorption of the incoming solar radiation) and the indirect effect (acting as cloud condensation nuclei and hence changing cloud properties). Relative humidity (*RH*) is a key meteorological parameter which has a direct bearing on aerosol radiative properties. A Humidograph system was built and deployed from July, 2010 at the Mace Head Atmospheric Research Station (53^0 19'N, 9^0 54' W), on the west coast of Ireland, to study hygroscopic properties of aerosols associated with different air masses arriving at the research station.

Due to its unique location on the north east edge of the North Atlantic Ocean, Mace Head encounters a variety of air masses with diverse aerosol optical and physicochemical properties (Dall'Osto et al, 2010). Furthermore the above mentioned aerosol properties also exhibit a unique seasonal pattern with organics dominating the submicrometer aerosol mass range during high biological activity periods from spring through autumn and sea-salt dominating in the winter season (O'Dowd et al, 2004). Fierz-Schmidhauser et al (2010) measured the aerosol light scattering enhancement factor *f(RH)* associated with marine air masses and polluted air masses arriving at Mace Head during the winter season to be 2.22(±0.17) and 1.12(±0.31), respectively. *f(RH)* for marine air masses during the summer season was 30% lower, at 1.54(±0.34), as compared to the winter season (Vaishya et al, 2010) which can be attributed to lower sea-salt production and a higher concentration of water insoluble organics.

In the present study, we measured the *f(RH)* values for different air masses arriving at Mace Head and analyzed the associated radiative, physical and chemical properties using collocated measurements with other instruments. The criteria for selection of stable air masses were: i) stable values of aerosol scattering coefficient over a period of 8 hours or more and ii) 96 hours back trajectories, as obtained using the on-line HYSPLIT model, should have the same origin at the start and end of the stable state period. Furthermore, black carbon mass concentrations of <50 ng/m^3 and >150 ng/m^3 were used as indicators for the air mass to qualify as clean air mass or polluted air mass, respectively.

Results are presented for the hygroscopic properties of aerosol with reference to their optical and chemical properties.

This work was supported by funding from the EC's 6th Framework Programme Integrated Project, GEOmon.

Dall'Osto, M., Ceburnis, D., Martucci, G., Bialek, J., Dupuy, R., Jennings, S. G., Berresheim, H., Wenger, J. C., Sodeau, J. R. and Healy, R. M. (2010) *Atmos. Chem. Phys.*, **10**, 8413-8435.

Fierz-Schmidhauser, R., Zieger, P., Vaishya, A., Monahan, C., Bialek, J., O'Dowd, C. D., Jennings, S. G., Baltensperger, U. and Weingartner, E. (2010) *J. Geophys. Res.*, **115**, D20204.

O'Dowd, C. D., Facchini, M. C., Cavalli, F., Ceburnis, D., Mircea, M., Decesari, S., Fuzzi, S., Young, J. Y. and Putaud, J. P. (2004) *Nature*, **431**, 676-680.

Vaishya, A., Monahan, C., O'Dowd, C.D. and Jennings, S.G. (2010) *International Aerosol Conference, Helsinki, Finland*, **360**, 7E4.

An Improved Description of Cloud Droplets Development in Climate studies over the Mediterranean Region

C. Mitsakou, G. Kallos, S. Solomos and J. Kushta

Atmospheric Modelling and Weather Forecasting Group (AMWFG), Department of Physics, University of Athens, 15784, Greece
Keywords: cloud droplet, natural/anthropogenic aerosols, hygroscopic growth, ice nucleation.
Presenting author email: christina@mg.uoa.gr

Determining the net effect of aerosols on the climate of Mediterranean is a difficult task, since the area is strongly affected by the presence of aerosols from different origins and ages. The complexity of the physico-chemical processes and the potential interactions and feedbacks across all scales in the climate system reveals the necessity for an integrated approach in order to examine the aerosol impacts on the regional climate and vice versa. Recently, a limited-area atmospheric model RAMS/ICLAMS has been further developed by AMWFG (Solomos *et al.*, 2011) with the incorporation of natural and anthropogenic pollutants cycles, detailed gas/aerosol chemical mechanisms and an advanced radiative transfer scheme. Furthermore, the suspension of aerosols with various composition generates the need for introducing more physically based descriptions of aerosol physico-chemical processes in the atmosphere, which is the scope of the present study.

RAMS/ICLAMS model characteristics

RAMS/ICLAMS is based on RAMS atmospheric modelling system (Cotton *et al.*, 2003) that includes advanced microphysical schemes with eight categories of hydrometeors (vapor, cloud droplets, rain droplets, pristine ice, snow, aggregates, graupel and hail). The recent developments include an interactive mineral dust and sea salt cycle, biogenic and anthropogenic pollutants emission/transport/depletion processes, gas and aerosol chemical reactions and an improved radiative transfer scheme.

New cloud formation/growth schemes

In the new model development, the rate of cloud droplet diameter increase by hygroscopic growth described by the well-known Mason's equation, as following:

$$\dot{d} = \frac{4}{d}\frac{\left(S - 1 - \frac{4\sigma}{d\rho_l R_v T_g} + \frac{6\chi n_s m_0 M_l}{\pi M_s \rho_l d^3}\right) f_{FS}}{f_{mass} + f_{heat}}$$

where S is the saturation ratio (relative humidity), σ the droplet surface tension, ρ_l the water density, R_v the gas constant for water vapor, T_g the air temperature, χ the soluble fraction of the aerosols, n_s the degree of each aerosol component ion dissociation, m_0 the aerosol mass, M_l the water molecular weight, and M_s the apparent molecular weight of the aerosol soluble components. The factors f_{FS}, f_{mass}, f_{heat} represent the Fuchs correction term, the contribution associated with mass transfer and the contribution due to heat conduction. Coagulation is described with the help of a Smoluchowski-type formulation (Jacobson *et al.*, 1994), specific to sectional representation of the size distribution. For the ice nucleation, advanced formulations for the different physical mechanisms (homogeneous nucleation, deposition nucleation, immersion freezing, condensation freezing, contact freezing) are under implementation in the modelling system.

Model sensitivity and evaluation runs

A case study occurred on 28 January 2003 and characterized by a low pressure system and a dust storm over the Eastern Mediterranean was firstly investigated. The centre of the low moved from Crete through Cyprus accompanied by a cold front. Deep convective clouds were developed along the frontal line, while heavy precipitation events were reported over the East Mediterranean coastline and a few kilometres inland.

The impact of naturally-produced aerosols (mineral dust, sea salt) on cloud formation and precipitation has been investigated. In general, mineral dust particles are considered as non-hygroscopic and they can act as ice nuclei (IN) in heterogeneous ice nucleation processes. However, aged dust aerosols may be coated with sea-salt or sulfates and become partially hygroscopic, increasing their efficiency as cloud condensation nuclei (CCN). As a result, the coexistence of dust and sea-salt particles affect significantly the cloud formation. The increase of the hygroscopicity of dust particles (from 0.05 to 0.2) revealed an increase in the concentration of small liquid droplets inside the cloud (Figure 1). As a result, a lower fraction of cloud droplets turned into rain and thus, significant amount of water was lifted to above freezing level.

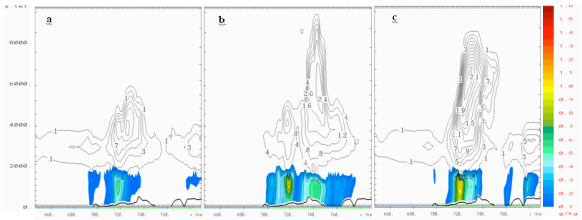

Figure 1: West to East cross-section across East Mediterranean of rain mixing ratio (color palette in g kg^{-1}) and ice mixing ratio (black line contours in g kg^{-1}) by assuming a) 5% hygroscopic dust, b) 20% hygroscopic dust and c) 5% hygroscopic dust and ice nuclei(IN)×10 on 28 January 2003 at 11:00 UTC.

Additional model sensitivity runs and more explicit evaluation tests are carried out by utilizing in situ and laboratory experimental measurements. In particular, the influence of the anthropogenic emissions and the suspension of mixed aerosols on the cloud formation along the Mediterranean region will be further investigated.

References

Cotton et al., *Meteorol. Atmos. Phys.*, 82, 5-29, 2003.
Jacobson et al., *Atmos. Environ.*, 28, 1327-1338, 1994.
Solomos et al., *Atmos. Chem. Phys.*, 11, 873-892, 2011.

Charged and neutral clusters and their connection to atmospheric new particle formation in Europe

T. Nieminen[1], H. E. Manninen[1], J. Kontkanen[1], P. Paasonen[1], A. Hirsikko[1], V.-M. Kerminen[2], M. Kulmala[1], and the EUCAARI team[3]

[1]Department of Physics, P. O. Box 64, FI-00014 University of Helsinki, Finland
[2]Finnish Meteorological Institute, Research and Development, P.O. Box 503, FI-00101 Helsinki, Finland
[3]Partners in the European Integrated project on Cloud Climate and Air Quality Interactions (EUCAARI); Project Office, Department of Physics, Division of Atmospheric Sciences, University of Helsinki

Keywords: atmospheric ions, ion-induced nucleation.
Presenting author email: tuomo.nieminen@helsinki.fi

Size distributions of charged and neutral aerosol particles in the mobility diameter range of 1 – 42 nm were measured at 12 sites around Europe during a period of 13 months in 2008 and 2009. The measurements were part of the European Integrated project on Aerosol, Cloud, Climate and Air Quality Interactions (EUCAARI) (Kulmala et al., 2009). Measurements were made in continental, remote and coastal locations, including sites at different altitudes from sea level up to the free troposphere. This comprehensive data set gives information on the diurnal and seasonal variation of ion cluster concentrations as well as on the spatial and temporal variation of new particle formation events and relevant particle formation parameters across Europe.

A persistent pool of cluster ions below 2 nm diameter was detected at all sites. The cluster ion concentration varied approximately between 200 and 600 cm^{-3} per polarity. On the continental sites the main factor controlling the cluster concentrations was coagulation to the pre-existing aerosol, whereas on high altitude sites high relative humidity is observed to suppress cluster ion concentrations.

Formation and growth events of new particles initially about 2 nm in diameter were observed between 20 to 60% of all measurement days depending on the site (Manninen et al., 2010). We determined the formation rates of both charged and neutral particles. The median charged particle formation rates varied between 0.02–0.16 cm^{-3} s^{-1} between sites, and the median total particle formation rates in the range 0.7–32 cm^{-3} s^{-1}. The charged particle formation rate was typically 1–30% of the total particle formation rate. This shows that the total particle formation rates varied much more between the sites than the charged particle formation rates.

A simple parameterization based on the concentration of cluster ions and solar radiation intensity was developed to predict the ion-induced nucleation rates (Nieminen et al., 2010). This parameterization is in principle applicable to all large-scale atmospheric models for studying the role of ions in atmospheric nucleation.

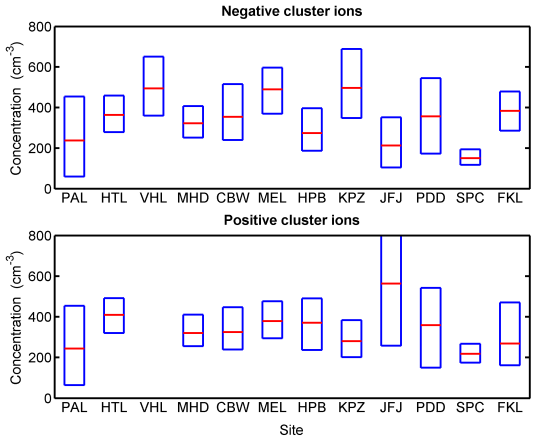

Figure 1. Median cluster ion concentrations at each of the 12 EUCAARI measurements sites during 2008–2009. Top panel shows negative cluster ions smaller than 1.8 nm and bottom one positive cluster ions. Red bar shows median and box is at 1st and 3rd quartile.

Acknowledgements. This research was funded by the Academy of Finland Center of Excellence Program (project number 1118615).

Kulmala M. et al., *Atmos. Chem. Phys.*, 9, 2825–2841, 2009.
Manninen H. E. et al., *Atmos. Chem. Phys.*, 10, 7907–7927, 2010.
Nieminen T. et al., *Atmos. Chem. Phys. Discuss.*, 10, 21697–21720, 2010.

In-situ investigation of cloud microphysics and aerosol optical properties during the CLACE 2010 campaign at Jungfraujoch, Switzerland (3580 m asl): An Overview

N. Bukowiecki[1], P. Zieger[1], E. Hammer[1], Z. Jurányi[1], M. Gysel[1], M. Laborde[1], E. Weingartner[1], U. Baltensperger[1], M. Collaud Coen[2], C. Ketterer[2], O. Maier[2], D. Ruffieux[2], J. Spiegel[3], W. Eugster[3], C. Chou[4], J. Henneberger[4], U. Lohmann[4], E. Kienast[4], F.G. Wienhold[4], T. Peter[4], J. von Bismarck[5], M. Starace[5], T. Ruhtz[5], K. Clemer[6] and M. van Roozendael[6]

[1] Laboratory of Atmospheric Chemistry, Paul Scherrer Institut, 5232 Villigen PSI, Switzerland
[2]MeteoSwiss, 1530 Payerne, Switzerland
[3]Institute of Plant, Animal and Agroecosystem Sciences, ETH Zürich
[4]Institute for Atmospheric and Climate Science, ETH Zürich
[5]Institute for Space Sciences, Freie Universität Berlin, Germany
[6]Belgian Institute for Space Aeronomy
Keywords: Aerosol cloud interaction, Optical properties, Cloud microphysics, CLACE, Remote sensing
Presenting author email: nicolas.bukowiecki@psi.ch

Introduction

From June to August 2010, an international team of researchers met at the High Altitude Research Station Jungfraujoch (Switzerland, 3580 m asl) for a joint campaign (CLACE2010 — Cloud and Aerosol Characterization Experiment), as a follow-up of previous CLACE campaigns. At the Jungfraujoch, comprehensive aerosol measurements have been performed continuously since 1995. The Jungfraujoch is optimally suited for this purpose, as it lies in the free troposphere but is influenced by the continental air over Europe. In addition, the Jungfraujoch is about 40% of the time within clouds, which makes it an ideal site to study aerosol-cloud interactions.

Cloud microphysics studies

During earlier studies, the cloud forming potential of aerosol particles at the Jungfraujoch was predominately derived from measurements performed under laboratory conditions at elevated temperature after having dried the aerosol (Henning et al., 2002). In the CLACE 2010 campaign we compared in situ measured cloud droplet number concentrations with CCN number concentrations that were derived from laboratory measurements. The combination of these measurements will allow for the determination of the effective peak supersaturation in the prevailing ambient cloud which was responsible for the activation of aerosol particles to cloud droplets. During the campaign the peak supersaturation of the cloud droplets arriving at the Jungfraujoch showed a mean value of 0.31% and a median value of 0.23% (Jurányi et al., 2010). Ongoing data analysis attempts to establish a link between the retrieved peak supersaturations and other parameters like temperature, updraft velocity and weather situation (i.e., cloud type).

Investigation of aerosol optical properties

Additionally, the optical properties of the aerosol layer at and around the Jungfraujoch were examined using a variety of remote sensing equipment. These remote sensing experiments were also simultaneously performed at lower altitude in 4 km distance of the Jungfraujoch (Kleine Scheidegg, 2061 m asl) for the first time. The main goal of this activity was to get the closure between in-situ measurements of aerosol optical properties at the Jungfraujoch with different kinds of remote sensing data.

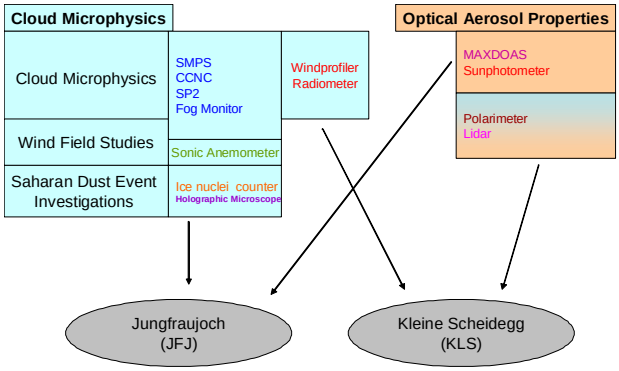

Figure 1: Combined study of cloud microphysics and optical aerosol properties during CLACE 2010.

This work was supported by MeteoSwiss within the Global Atmosphere Watch program of the World Meteorological Organization, the Swiss Federal Office for the Environment, as well as the EC project EUSAAR (contract no 026140) and GeoMON (contract no 036677). We thank the International Foundation High Altitude Research Stations Jungfraujoch and Gornergrat (HFSJG) for the opportunity to perform experiments on the Jungfraujoch.

Henning, S., Weingartner, E., Schmid, S., Wendisch, M., Gäggeler, H. W., and Baltensperger, U. (2002) *Tellus* 54B, 82–95.

Jurányi, Z., Gysel, M., Weingartner, E., Bukowiecki, N., Kammermann, L., and Baltensperger, U. (2011) *J. Geophys. Res.*, submitted.

Aerosol-cloud interaction measurements with the Droplet Aerosol Analyser

M. Berghof[1], G.P. Frank[1], S. Sjogren[1], B.G. Martinsson[1], K. Acker[2], W. Wieprecht[2], and D. Kalass[2]
[1]Divission of Nuclear Physics, Lund University, Lund, Sweden
[2]Brandenburg Technical University Cottbus, Department of Air Chemistry, Cottbus, Germany
Keywords: aerosol cloud interaction, cloud microphysics, clouds, DAA (Droplet aerosol analyser), droplets.
Presenting author email: j.first@somewhere.edu

Introduction

To study the interaction of aerosol particles, meteorological conditions and cloud or fog formation is a challenging task. Since aerosol properties and meteorological conditions are variable in time and space, every single cloud is unique. Here we will present measurement results obtained with the Droplet Aerosol Analyser (DAA, [1]), an instrument for studies of the interaction between cloud/fog droplets and interstitial particles. First results from in-cloud measurements at the summit of Mt. Brocken (51.80° N, 10.67° E, 1142 m asl) in the Harz region in central Germany, autumn 2010, will be presented.

Instrumentation

The DAA processes aerosol in several steps: aerosol charging mechanisms, diffusion drying, and electrostatic aerosol spectrometry (using Differential Mobility Analysers, DMAs). This gives a unique three-parameter dataset (ambient diameter, dry residual particle diameter and number concentration). A number of related aerosol/cloud parameters can be determined: ambient number size distribution of cloud/fog droplets and interstitial, number size distribution of dry residual particles, the relation between ambient diameter and dry (residual) diameter on a single droplet/particle basis, characterization of the droplet activation as defined by the Köhler equation, the size dependent scavenging of particles due to activation, concentration of soluble matter in the individual droplets (solute concentration), liquid water concentration. A second generation of the instrument has been developed with a higher time resolution and more suited for long-term measurements. Calibration of the ambient diameter (Dd) is in progress.

Results

Starting from June 2010 measurements at the sumit of Mt. Brocken have been performed. The project is in collaboration with the Air chemistry group of the Technical University of Brandenburg (BTU Cottbus), who has a cloud measurement site at Mt. Brocken since many years. Figure 1 shows a cloud event with activated droplets.

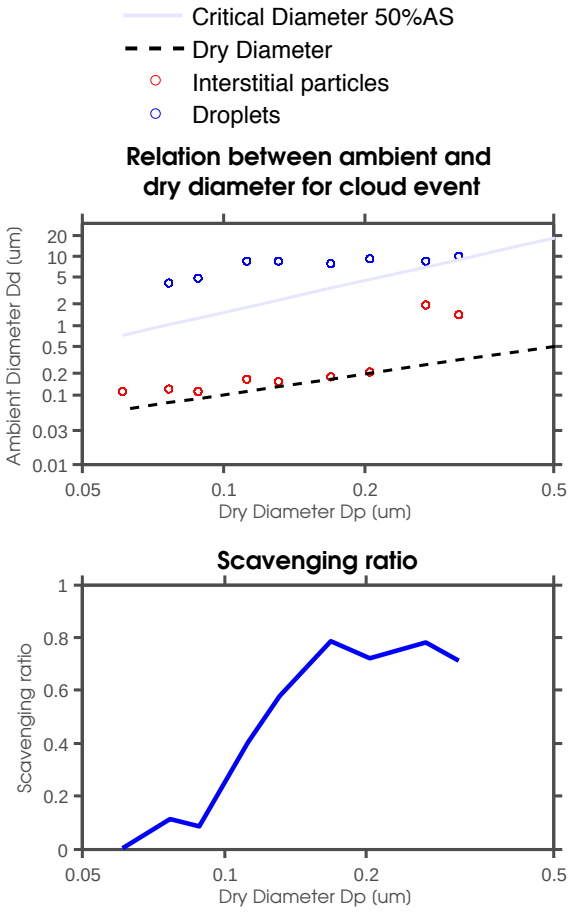

Figure 1: Preliminary results from a cloud event at Mt. Brocken, Germany, 27. Sep. 2009 06-07 am.

Acknowledgements

This work is supported by The Swedish Research Council for Environment, Agricultural Sciences, and Spatial Planning (FORMAS), The Swedish Research Council (VR) and The Crafoord Foundation. We thank Brandenburg Technical University, Cottbus, Germany for help and support with the field station Brocken.

References

[1] Bengt G. Martinsson. Physical basis for a droplet aerosol analysing method. *Journal of Aerosol Science*, 27(7):997 – 1013, 1996.

The influence of biomass burning on PM2.5 at urban and rural background sites in the Czech Republic

Jaroslav Schwarz[1], Jindřich Karban[1], Eva Chalupníčková[2], Radek Pokorný[2], Jiří Novák[2], Jiří Smolík[1]

[1]Intitute of Chemical Process Fundamentals AS CR, Prague, CZ-16502, Czech Republic
[2]Czech Hydrometeorological Institute, Prague, CZ-14306, Czech Republic
Keywords: PM2.5, chemical composition, biomass burning, levoglucosan.
Presenting author email: schwarz@icpf.cas.cz

PM10, and PM2.5 were sampled every 6th day from Feb 2009 till Mar 2010 at two sites in parallel. One site was urban background site Suchdol at NW border of Prague. The second site was rural background site Kosetice that is about 80 km south east from Prague. Both PM10 and PM2.5 were sampled on double quartz fibre filters to access OC positive sampling artifacts. The samples on both front and back quartz filters were analyzed using ion chromatography for anions and cations, TOT for OC/EC and front filters also by GC-MS to measure levoglucosan concentration. Moreover, another PM2.5 sampler loaded with TEFLO filter was used at both sites and these samples were analyzed using PIXE for elemental composition. All filters were weighted before and after sampling to get aerosol mass concentrations. In this work we will concentrate on the influence of biomass combustion on overall concentration of PM2.5 and OC and its seasonal variability.

Table 1: Average seasonal concentrations of EC, OC, levoglucosan (lvg) and calculated percentages of biomass combustion OC (BBOC) in total OC and organic matter (BBOM) in PM2.5 mass at urban and rural background sites Suchdol and Košetice

Urban background site Suchdol					
	EC µg/m3	OC µg/m3	lvg µg/m3	BBOC /OC	BBOM /Mass
Spring	1.12	4.18	0.15	36%	11%
Summer	1.02	2.31	0.06	24%	6%
Autumn	2.22	6.01	0.28	46%	14%
Winter	2.37	9.21	0.44	48%	19%

Rural background site Košetice					
	EC µg/m3	OC µg/m3	lvg µg/m3	BBOC /OC	BBOM /Mass
Spring	0.63	3.57	0.1	28%	10%
Summer	0.38	1.99	0.02	10%	3%
Autumn	0.67	3.60	0.11	32%	9%
Winter	0.77	4.53	0.22	50%	15%

The main results are summarized in Table 1. All parameters exhibit some seasonality but levoglucosan concentrations changes are clearly the largest, while the EC concentrations have the smallest seasonal variation. This reflects seasonal source variability of both EC and levoglucosan. Winter maximum of levoglucosan that is tracer of biomass combustion shows its importance as a source of PM2,5 mass and OC in Central Europe. The amount of BBOC was calculated from levoglucosan concentration using conservative factor of 10 (Szidat et al. 2009) and BBOM was calculated from BBOC using factor 1.4. Despite of using quite conservative factors, the calculation showed that biomass combustion is responsible for almost 50% of OC in central Europe in winter. This is in agreement with Puxbaum et al. (2007).

Comparison of urban background site and rural background site shows about 3 times higher levels of EC at urban site comparing to rural site at most of seasons except for spring when this factor was smaller then 2. OC was almost the same in spring and summer at both stations, while it was about twice higher at urban site in autumn and winter. Levoglucosan levels were about 50% higher at urban site in spring, 3 times higher in summer, 2.5 times higher in autumn and twice as high in winter. The relatively high level of levoglucosan at urban site in summer are probably caused by various biomass combustion events in gardens and cottages that are very common around Prague area. Local barbicues at Suchdol may also increase levels of levoglucosan in summer.
BBOC percentages are quite similar at both sites except for twice as high portion in summer at urban site. The autumn percentage of BBOC on the total OC was about 50 % higher in autumn at the urban site comparing to the rural site. These ratios were similar to the comparison of the percentage of BBOM on PM2.5 mass. It is question if the ratio 1.4 used in our calculations is properly set and if this could not be higher. This study anyway clearly showed that biomass combustion is especially in winter very important source of PM2.5 OC and mass.

This work was supported by the GA CR under grant 205/09/2055 and by ME CR under grant SP/1a3/148/08.

Puxbaum, H., Caseiro, A., Sanchez-Ochoa, A., Kasper-Giebl, A., Claeys, M., Gelencser, A., Legrand, M., Preunkert, S., and Pio, C.: J. Geophys. Res., 112. D23S04, doi:10.1029/2006JD008094, 2007.

Szidat, S., Ruff, M., Perron, N., Wacker, L., Synal, H.-A., Hallquist, M., Shannigrahi, A. S., Yttri, K. E., Dye, C., and Simpson, D: Atmos. Chem. Phys., **9**, 1521–1535, 2009

The ionic composition of PM2.5 at a rural background site in Central Europe on daily basis

J. Schwarz

Intitute of Chemical Process Fundamentals AS CR, Prague, CZ-16502, Czech Republic
Keywords: PM2.5, chemical composition, water soluble ions
Presenting author email: schwarz@icpf.cas.cz

PM2.5 concentration and chemical composition were measured on a daily basis at the rural background site Košetice in the Czech Republic. The sampling was done using a Leckel gmbh sequential sampler loaded with TEFLO filters with 3 µm nominal porosity. The sampler was loaded with 15 filters, but the sampled filters were removed mostly daily. The flow rate was 2.3m^3/h. The filters were analyzed using ion chromatography and particle induced x-ray emission method.. We will concentrate on results of ion chromatography at this work.

Ion chromatography (IC) was used for determination of cations and anions. A circle 16 mm in diameter was cut out from each filter and extracted in a mixture of 0.5 ml methanol and 4.5 ml deionized ultrapur water with conductivity 0.08 µSm^{-1} (Ultrapur, Watrex Ltd.). After 30 minutes inside ultrasonic bath and 1 hour of shaking (half automatic, half manual), the solution was filtered using syringe Millipore filters with 0.22 µm porosity. The filtered sample was then analyzed for anions and the next day for cations. The sample solution for cation analysis was stored in fridge prior to analyze. Cations as Na^+, NH_4^+, K^+, Ca^{2+}, Mg^{2+}, Zn^{2+} and anions as SO_4^{2-}, NO_3^-. Cl^-, NO_2^-, Br^-, $H_2PO_4^-$ were determined. The analyses were provided using the setup by Watrex Ltd. with columns Transgenomic ICSep AN300 150x5.5 mm for anions and Alltech universal cation 7µm 100x4.6 mm for cations. The conductivity detector used in the setup was SHODEX CD-5.

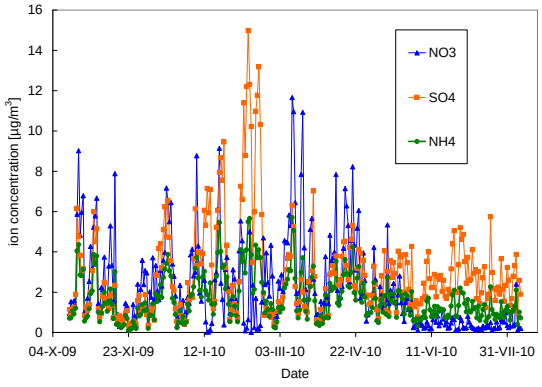

Figure 1. The time series of main ions obtained daily at rural background site Košetice.

The time series of measured concentrations of the main ions (sulphates, nitrates and ammonium) are shown in Fig. 1. There are several main features we can recognize in this graph. High variability is clearly seen especially in winter while the ion concentrations were relatively stable in summer. During summer, sulphates dominate ionic composition due to thermal instability of ammonium nitrate. The concentrations of sulphates and nitrates were mostly quite similar during spring and autumn with sometimes much higher concentration of nitrates. The most variable ratio between sulphates and nitrates was visible in winter. There were periods when nitrates were higher than sulphates (mainly those with lower concentrations) and periods when sulphates were completely dominating ionic composition and nitrates were very low. This is probably connected with the lack of ammonium to fully compensate for sulphate concentration in the atmosphere.

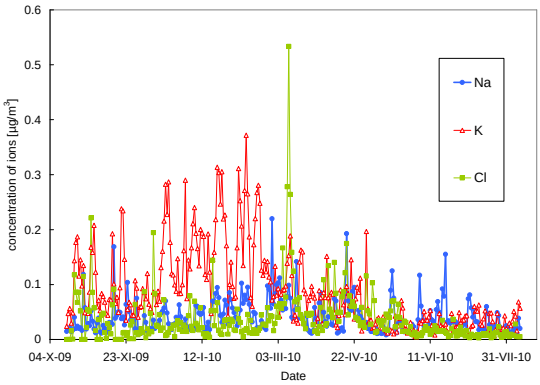

Figure 2. The time series of minor ions obtained daily at rural background site Košetice.

Concentration of chlorides, sodium and potassium ions are shown in Fig. 2. We can clearly see seasonality of potassium ion connected with large influence of biomass combustion in winter. Another interesting feature is relation between chlorides and sodium cation. Based on these data we can say that there is no tight relation between them. Moreover, the same can be seen for the relation between potassium and chlorides. We can discuss two basic possibilities to explain this behaviour. First there is another source of chlorides that is not connected with sea salt or road salt in case of sodium and with biomass combustion in case of potassium. The second possibility is that in both cases these factors comes from long range transport and chloride was depleted by interactions with nitric of sulphuric acids. This factor is strengthened by measurement of fine fraction only that subjects to these interactions more easily comparing to coarse particles.

This work was supported by the GA CR under grant 205/09/2055.

The Size- and Time-Resolved Determination of the Water-Soluble Organic Fraction of Submicron Aerosol Particles from the Beijing Area

B. Nekat, D. van Pinxteren, Th. Gnauk, K. Müller and H. Herrmann

Leibniz-Institute for Tropospheric Research, Permoserstr. 15, D-04318, Germany

Keywords: Chemical composition, submicron particles, water-soluble organic compounds, dicarboxylic acids
Presenting author email: nekat@tropos.de

The rapid industrialization of Beijing during the last decades causes significant higher air pollutant emissions. These particle emissions affect the regional air quality by reducing the visibility due to the formation of haze and impact the radiation balance of the atmosphere by serving as cloud condensation nuclei (CCN). These effects strongly depend on the aerosol ability to take up water governed by the particle size, optical and microphysical properties. The CCN chemical composition, especially of the water-soluble fraction, can play a major role in cloud microphysics as well and strongly varies with particle size, season and day-time. Small water-soluble organic compounds such as dicarboxylic acids can attach to the surface of the liquid particle phase due to their polarity leading to a higher hygroscopicity of the CCN. The increased hygroscopicity possibly facilitates the water uptake and the activation to cloud droplets influencing cloud formation processes, precipitation and the radiation balance of atmosphere. The HaChi-project (Haze in China) targets to study the water-soluble organic fraction of submicron aerosol to associate the chemical composition with the ability to act as CCN.

To address this matter, two intensive campaigns were realized in March and July 2009. At a background site between the two megacities Beijing and Tianjin size- and time-resolved samples were collected with a 10-stage-Berner low pressure impactor (BLPI) in a 6 hours day/night regime.

This study presents the chemical composition of the water-soluble organic fraction of submicron particles in terms of particle size, day-time and season as well as different meteorological conditions such as haze. The samples were analyzed for mass, inorganic ions, elemental (EC) and organic carbon (OC), and the water-soluble organic carbon (WSOC). The WSOC fraction of the Berner foils was analyzed for small polar compounds such as the dicarboxylic acids oxalic, tartronic, malonic, tartaric, malic, succinic and glutaric acid. The respective water content of particles was calculated by the E-AIM model (Clegg, Brimblecombe & Wexler, 1998) using the chemical composition of the particles and a meteorological data set from the sampling site. To investigate the origins of air masses NOAA HYSPLIT (Draxler and Rolph, 2003, Rolph, 2003) backward trajectories were obtained.

Usually, the OC fraction is dominated by WSOC. The WSOC content strongly varies with the particle size, season, day-time and meteorological condition (Figure 1). Nevertheless, the majority of samples show an increasing WSOC content with increasing particle size.

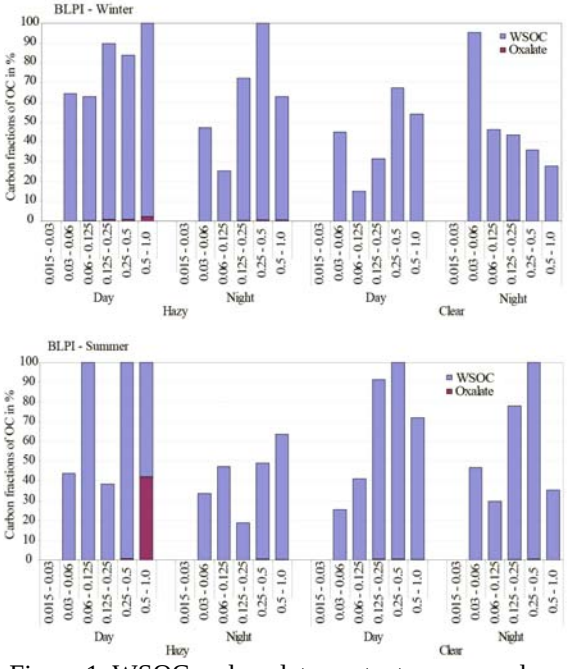

Figure 1. WSOC and oxalate contents expressed as carbon fraction of OC in % of the winter and summer campaign day/night measurements for hazy and clear sky conditions.

This work was supported by the German Science Foundation under grant DFG WI 1449/14-1.

Clegg, S. L., Brimblecombe P., & Wexler, A. S. (1998). *J. Phys. Chem. A*, 102, 2155-2171.

Draxler, R. R., & Rolph, G. D. (2003). in *HYSPLIT (HYbrid Single-Particle Lagrangian Integrated Trajectory) Model access via NOAA ARL READY*, NOAA Air Resources Laboratory, Silver Spring, MD.

Rolph, G. D. (2003). in *Real-time Environmental Applications and Display system (READY)*, NOAA Air Resources Laboratory, Silver Spring, MD.

On ultrafine aerosol growth and the condensation/evaporation properties of atmospheric organics

I. Riipinen[1,2,6], J.R. Pierce[3], T. Yli-Juuti[1], S. Häkkinen[1], C. Fountoukis[2], M. Kulmala[1], D. Worsnop[1,4], M. Bilde[5], S. N. Pandis[2,6] and N.M. Donahue[6]

[1]Department of Physics, University of Helsinki, Helsinki, FI-00014, Finland
[2]Institute of Chemical Engineering and High Temperature Processes (ICE-HT), Foundation for Research & Technology, Hellas (FORTH), Patras, GR-26504, Greece
[3]Department of Physics and Atmospheric Science, Dalhousie University, Halifax, B3H 3J5, Canada
[4]Aerodyne Research, Billerica, MA-01821, MA, USA
[5]Department of Chemistry, University of Copenhagen, Copenhagen, 2100, Denmark
[6]Center for Atmospheric Particle Studies, Carnegie Mellon University, Pittsburgh PA-15213, PA, USA

Keywords: atmospheric aerosols, condensation/evaporation, organics, growth.
Presenting author email: ilona.riipinen@helsinki.fi

Organic compounds are abundant in atmospheric particulate matter, and a large fraction of these compounds are of secondary origin (Jimenez et al., 2009). Besides contributing to the total atmospheric aerosol mass, organic compounds play an important role in growing freshly-formed ultrafine particles to climatically relevant sizes (e.g. Riipinen et al., 2011). To quantify the effect of organic emissions to climate and air quality, atmospheric large-scale models need to realistically simulate the distribution of organic compounds in the atmospheric aerosol size spectrum.

Condensation and evaporation to/from aerosol particles can be reproduced with dynamic models if the thermodynamic and kinetic properties, such as saturation vapour pressures, vaporization enthalpies and accommodation coefficients of the condensing or evaporating vapors are known. In this work we investigate the condensational properties of atmospheric organic compounds, with a special focus on the low-volatile compounds growing the nucleation-mode aerosol (see also Donahue et al., *these proceedings*), and discuss the implications of these results for aerosol growth mechanisms and their representations in atmospheric large-scale models.

By comparing observed growth rates of freshly-nucleated ultrafine aerosol with condensational growth simulated by an aerosol dynamics box model we find that ambient sulphuric acid can account for only a minor fraction of ultrafine aerosol growth, the rest being organics. This observation is consistent with the seasonal pattern of particle growth rates at e.g. the SMEAR II station in Hyytiälä, Finland, for which growth rates show a maximum in the summer along with maximal emissions of biogenic organic compounds (Yli-Juuti et al., *in prep.*). We also find that saturation concentrations of roughly 10^{-3} μg/m^3 or less (corresponding to pure component saturation vapour pressure of the order or 10^{-8} Pa or less) are needed to explain the observed growth (see Fig. 1). Consistent results are found when the evaporation of the nucleation mode aerosol in the heating section of a Volatility-DMPS is modeled with a dynamic evaporation model and compared to measurement data.

These volatilities are significantly lower than those found in fresh chamber-generated or even aged atmospheric secondary organic aerosol (SOA) mass, which typically range from approximately 10^{-2} to 10^{2} μg/m^3 (10^{-7} to 10^{-3} Pa) (see Lee et al., 2010). The observed saturation concentrations are also in the lower end of the corresponding properties of dicarboxylic acids, which are among the least volatile identified SOA molecules with measured vapor pressures ranging from 10^{-8} to 10^{-3} Pa.

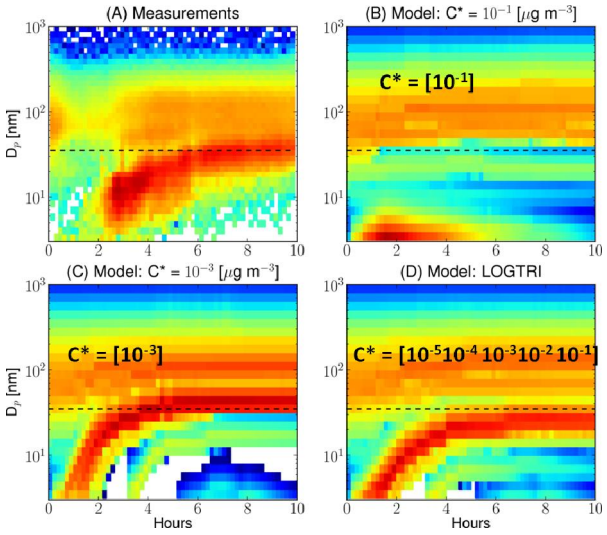

Figure 1. Measured (panel A) and modeled (panels B, C, D) evolution of aerosol size distribution on April 15th 2007 at the SMEAR II station in Hyytiälä, Finland.

This work was supported by Camille and Henry Dreyfus foundation, European Integrated Project for Aerosol Cloud Climate and Air Quality Interactions (EUCAARI).

Jimenez, J. *et al*. (2009), *Science*, **326**, 1525–1529.
Lee, B.-H. *et al.*, (2010), *Atmos. Chem. Phys.*, **10**, 12149–12160.
Riipinen, I. *et al.* (2011), *Atmos. Chem. Phys. Discuss.*, **11,** 387–423.

Aerosol hygroscopicity distribution in size-resolved CCN measurements: the concept, validation and applications

Hang Su [1], Diana Rose[1], Yafang Cheng[2], Sachin S. Gunthe[1], Alfred Wiedensohler[2] and Ulrich Pöschl[1]

[1] Max Planck Institute for Chemistry, 55020 Mainz, Germany
[2] Leibniz Institute for Tropospheric Research, 04318 Leipzig, Germany

Keywords: CCN, hygroscopicity, HTDMA, VTDMA

This work focused on addressing fundamental problems encountered in the data analysis of size-resolve CCN measurement data. We introduced a concept of aerosol hygroscopicity distribution (HD) for the analysis and modeling of aerosol particle hygroscopicity and cloud condensation nucleus (CCN) activity. The HD concept reflects the heterogeneous properties of aerosols and corrects the misunderstanding in the traditional way of analyzing size-resolved CCN spectra.

The HD concept has been observed and firstly validated through a comparison with soot mixing state information given by a volatility tandem differential mobility analyzer in the Beijing megacity. Two other campaign data show similar HD in a rural site and in pristine rainforest air (Fig. 1).

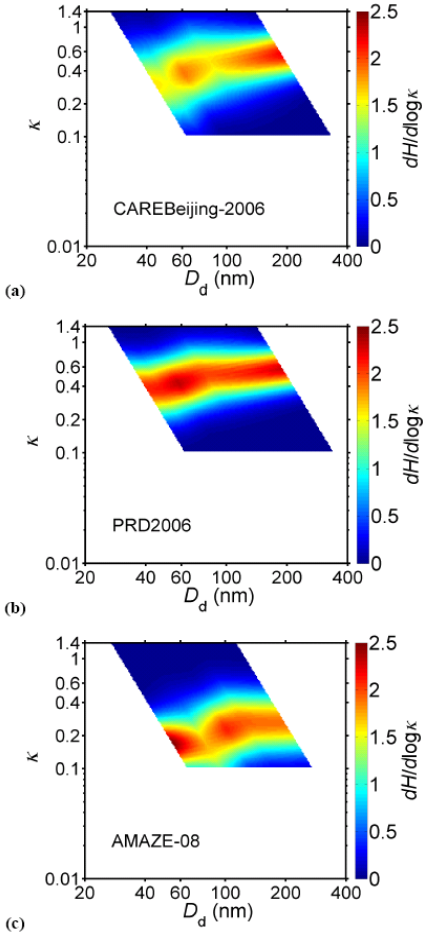

Fig. 1. HD in (a) urban site, (b) rural site and (c) pristine rainforest

Then a systematic study was carried out addressing the effects of multiple charges on aerosols and DMA transfer function, which had been supposed to significantly affect the CCN measurement results. A CCN counter simulation was developed for such purpose. The results showed that the commonly used correction approach relied on the assumption of homogeneous mixture of particles. For atmospheric aerosols, this assumption might not be valid. Several data correction approaches were evaluated and a more robust correction approach was recommended.

One important application of the CCN measurements is to provide parameters for the CCN prediction. We evaluated the performance and applicability of different κ parameters that had been used for CCN predictions. The comparison on the field measurement data confirms the results of model aerosols that the κ_{cut} and κ_t show similar performances in all the tested cases and are hence recommended for CCN prediction studies (Fig. 2). The κ_a alone is not recommended, especially in the presence of large fraction of insoluble particles (or less soluble particles below the detection limit). The κ_a multiplied by a gives a similar value as κ_t and can be used in CCN predictions.

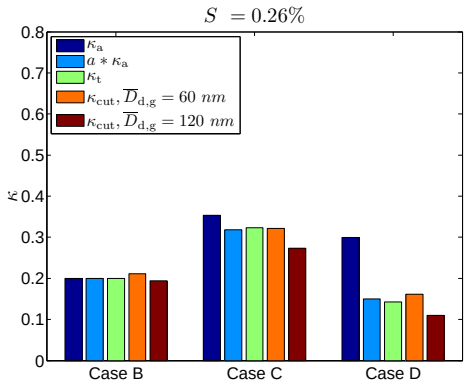

Fig. 2 Comparison of κ in CCN prediction

This work was funded by the Max Planck Society (MPG) and the European integrated project on aerosol cloud climate and air quality interactions (No 036833-2, EUCAARI).

Rose et al. (2008): *Atmos. Chem. Phys.*, 8, 1153-1179
Su et al. (2010): *Atmos. Chem. Phys.*, 10, 7489-7503

Effect of the biogenic emissions of isoprene and monoterpene on the CAMx model results in Central and South Europe

O. Vlček[1], L. Corbet[1], J. Liczki[2] and K. Zemánková[3]

[1] Czech Hydrometeorological Institute, Na Šabatce 17, Praha 4 – Komořany, 143 06, Czech Republic
[2] Academy of Sciences of the Czech Republic, Pod Vodárenskou věží 2, Prague 8, 182 07, Czech Republic
[3] Charles University in Prague, V Holešovičkách 2, Prague 180 00, Czech Republic
Keywords: biogenic emissions, isoprene, terpene, fine particles, SOA, ozone, CAMx, Europe.
Presenting author email: vlcek@chmi.cz

Organic aerosols (OA) can significantly contribute to the particulate matter (PM) in continental mid-latitudes. Depending on the location they form 10 – 50% of the PM bulk mass (Kanakidou *et al.* 2005). This ratio is even higher for the PM fine fraction (e.g. Harrison and Yin, 2000). OA can be divided into the primary and secondary OA (SOA). SOA are formed through the oxidation of their volatile organic compound (VOC) precursors into semi-volatile compounds and their consecutive condensation into the particulate phase. Toluene and m-xylene are examples of the anthropogenic VOCs. Biogenic VOCs are emitted mainly by trees and include e.g. isoprene, terpenes and sesquiterpenes. In this work we assessed the effect of the inclusion of the biogenic emissions of isoprene and monoterpene into emission inputs of CAMx model. Results for the summer 2008 and winter 2008/2009 are compared to the reference run with only anthropogenic emission present.

We used version 5.2 of the Eulerian photochemical dispersion model CAMx. Aerosols were modeled in the fine/coarse mode within the chemistry mechanism SAPRC-99. **Modeling domain** consisting of 309 x 277 cells was covering Central and South Europe and also parts of the West and East Europe with horizontal resolution of 9 km. Its vertical extent was 16 levels with the average hight of the first level 15 m AGL and of the last level 8 – 9 km AGL. Input data were supplied with 1 hr time step. **Meteorology** was provided by the NWP model ALADIN/CE (version CY35T1star). Its assimilation cycle consisted of the analysis followed by 6 hr forecast at 0, 6, 12 a 18 hr UTC. **Anthropocentric emissions** corresponding to the year 2006 were prepared by the emission model developed by B. Krüger from Universität für Bodenkultur Wien. They were based on the EMEP inventory with resolution of 50 km. For Austria, the Czech Republic, Hungary, and the Slovak Republic more detailed emissions of ozone precursors were used. Normalized **biogenic emissions** were based on the merged AFOLU and USGS databases with a resolution of 1km (Zemánková, 2010). They were further processed by the version 3.12 of SMOKE-BEIS3 model.

Inclusion of the biogenic emissions of isoprene and monoterpene led to the increase of average modeled $PM_{2.5}$ by 0 – 2 $\mu g \cdot m^{-3}$ in summer and 1 – 6 $\mu g \cdot m^{-3}$ in winter over the most of the modeling domain, which corresponds to 0 – 20 % and 20 – 50 % increase respectively. Together with the increase of the biogenic SOA we observed an increase of the anthropogenic SOA. Although this increase was much smaller than for the biogenic SOA (cca 50 times in absolute numbers), it was nevertheless very significant, since in the reference run the concentrations of anthropogenic SOA were practically zero, even though a group of XYLA=ARO2 – which is a precursor of lumped SOA1 and SOA2 – was present in the athropogenic emission inputs (Environ, 2010).

Average summer concentration of ozone increased south of the 50° N mostly by 5 – 10 $\mu g \cdot m^{-3}$ (5 – 20 %). The increase was much higher over Italy (10 – 20 $\mu g \cdot m^{-3}$), and the highest increase was observed over the Adriatic Sea (10 – 20 $\mu g \cdot m^{-3}$ i.e. 30 – 60 %). In the winter average ozone concentration decreased by -6 – -1 $\mu g \cdot m^{-3}$ (i.e. 4 – 16 %) over the most of the domain.

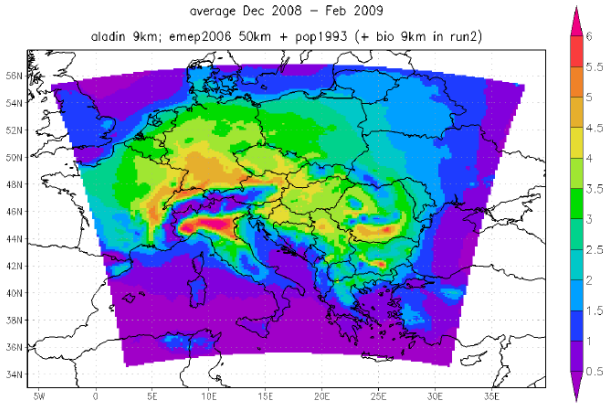

Figure 1. Dec 2008 – Feb 2009 average increase of $PM_{2.5}$ [$\mu g \cdot m^{-3}$] when biogenic emissions were included.

This work was supported through the Norwegian Financial Mechanism under grant CZ0049 and by the Ministry of the Environment of the Czech Republic under grant SP/1a4/107/07.

ENVIRON (2010) User's guide to the Comprehensive Air Quality model with extensions (CAMx) v5.20.

Harrison, R.M, Yin, J. (2000) *Sci. Total Environ.* **249**, 85-101

Kanakidou, M., Seinfeld, J.H., Pandis, S.N., Barnes, I., Dentener, F.J., Facchini, M.C., Van Dingenen, R., Ervens, B., Nenes, A., Nielsen, C.J., Swietlicki, E., Putaud, J.P., Balkanski, Y., Fuzzi, S., Horth, J., Moortgat, G.K., Winterhalter, R., Myhre, C.E.L., Tsigaridis, K., Vignati, E., Stephanou, E.G. and Wilson, J. (2005) *Atmos. Chem. Phys.* **5**, 1053-1123

Zemánková, K. (2010) Study of links between biogenic VOC emissions and concentration of tropospheric ozone. PhD. thesis. *Charles University in Prague*.

Chemical contribution of dicarboxylic acids to wet deposition and acidity of wet deposition in southern Taiwan

Su-Ching Kuo[1], Chien-Lung Chen[2], Li-Ying Hsieh[3], Pei-Ling Wu[4], Yi-Hui Lee[4] and Ying I. Tsai[4]

[1] Dept of Medicinal Chemistry, Chia Nan University of Pharmacy & Science, Tainan 717, Taiwan
[2] Dept of Industrial Engineering & Management, Fortune Institute of Technology, Kaohsiung 831, Taiwan
[3] Dept of Chemistry, National Cheng Kung University, Tainan 701, Taiwan
[4] Dept of Environmental Engineering & Science, Chia Nan University of Pharmacy & Science, Tainan 717, Taiwan

Keywords: wet precipitation, dicarboxylic acids, ion balance.

Presenting author email: mtsaiyi@mail.chna.edu.tw (Y.I. Tsai)

Wet deposition is one of the important ways in which contaminants are removed from the atmosphere. In addition to inorganic species, wet deposition contains organic acids (Avery *et al*., 2006) with an important contribution to rainwater acidity. The dicarboxylic acids are an important group of organic acids (Kawamura *et al*., 1996). Of these, the low molecular weight dicarboxylic acids are the most common species in rainwater (Avery *et al*., 2006). The chemical character of wet deposition in southern Taiwan is not well understood, with information regarding dicarboxylic acid content particularly lacking. Therefore, the wet deposition at a suburban site in southern Taiwan was collected and analyzed for inorganic species and dicarboxylic acids.

Rainfall samples were collected over a period of May 2005 and December 2008, and were grouped for analysis according to season and / or type of rainfall into six categories. These were *Plum Rain* (continuous rains that typically occur in Taiwan in May-June), *Typhoon Rain*, *Typhoon Outer Circulation* (TOC) *Rain*, *Summer Rain* (July to September), *Autumn-Winter Rain* (October to February), and *Spring Rain* (March to April). Prior to analysis of ionic species, all of the 402 samples were used for pH measurement. Twelve ionic species were analyzed: HCO_3^-, Cl^-, NO_3^-, SO_4^{2-}, Na^+, NH_4^+, K^+, Mg^{2+} and Ca^{2+}, and oxalic, malonic and succinic acids.

Wet deposition was mostly of pH 5.0-6.0 (346/402 samples fell within this range), indicating that the study area is not impacted significantly by acid rain. Table 1 lists the rain volume and volume-weighted mean (VWM) equivalent concentrations of the total ionic content and percentage contribution of inorganic cation and anion and dicarboxylic acid. It shows that Spring Rain had the highest equivalent ionic concentration. Spring Rain follows the dry winter season and is less frequent than other categories of rainfall. These factors combined explain the high ionic concentration of Spring Rain. In contrast, the Plum Rain that follows spring had the lowest equivalent ionic concentration less than one third of Spring Rain. The VWM concentration of inorganic anions composed between 41.15% and 58.41% of the total ionic concentration, and dicarboxylic acids between 0.29% and 0.58%. Plum Rain had the highest equivalent dicarboxylic acid content of 0.58% and TOC the lowest of 0.29%. Although Autumn-Winter Rain and Spring Rain had equivalent dicarboxylic acid content of only 0.37-0.38%, respectively, their higher total equivalent ionic concentrations lead to dicarboxylic acids being at their highest levels in these two rainfall types.

Table 1. Ionic concentration and percentage contribution of cations, anions, and dicarboxylic acids.

Rainfall type	Amt[b]	Volume-weighted mean (VWM) concentration			
		Ionic conc.	Cations	Anions	Dicarboxylic acids
	(mm)	μeq L^{-1}	%	%	%
Plum (*n*=148)	665	354.3	48.33	51.09	0.58
Typhoon (*n*=55)	456	579.7	48.08	51.59	0.33
TOC[a] (*n*=9)	22.5	942.5	41.30	58.41	0.29
Summer (*n*=133)	650	467.2	52.01	47.59	0.40
Autumn-Winter (*n*=42)	118	692.8	55.87	43.76	0.37
Spring (*n*=15)	32.5	1125.9	58.47	41.15	0.38
May 2005-Dec. 2008 (*n*=402)	1944	485.2	50.33	49.25	0.42

The ion balance (IB) ratio in relation to the pH of Plum Rain with and without HCO_3^- is shown in Fig. 1. The correlation coefficient (*r*) for this relationship without HCO_3^- was between .686 (TOC Rain) and .900 (Autumn-Winter Rain). The *r* for this relationship with HCO_3^-, however, was between .983 (TOC Rain) and .996 (Plum Rain), indicating a very high correlation between the IB ratio and pH. These results show that the IB ratio based on the ionic species studied including HCO_3^- does reflect the actual pH variation and ionic equilibrium of the wet deposition. The major species that influence the acidity of wet deposition and its neutralization include anions: HCO_3^-, Cl^-, NO_3^- and SO_4^{2-}, cations: Na^+, NH_4^+, K^+, Mg^{2+} and Ca^{2+}, and dicarboxylic acids: oxalic, malonic and succinic acids.

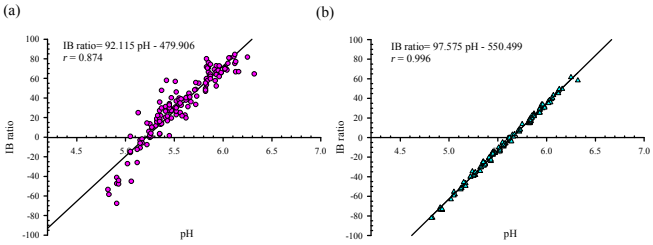

Fig. 1. Ion balance ratio in relation to the pH of Plum Rain with (a) HCO_3^- excluded from IB ratio calculation and (b) HCO_3^- included in IB ratio calculation.

This work was supported by the National Science Council, Taiwan under Grant Nos. NSC 96-2221-E-041-013-MY3 and NSC 99-2221-E-041-014-MY3.

Kawamura, K., Steinberg, S., Kaplan, I.R. (1996) *Atmospheric Environment* **30**, 1035-1052.

Avery Jr., G.B., Kieber, R.J., Witt, M., Willey, J.D. (2006) *Atmospheric Environment* **40**, 1683-1693.

Tuesday, September 6, 2011

Session 5A: PM Sources

Particle size distribution, number concentration, CO and sources of aerosol particles in Nairobi, Kenya

J. Boman[1], M.J. Gatari[2], S. Thorsson[3] and A. Mooe[1]

[1]Department of Chemistry, University of Gothenburg, Gothenburg, SE-412 96, Sweden
[2]Institute of Nuclear Science & Technology, University of Nairobi, Nairobi, Kenya
[4]Department of Earth Sciences, University of Gothenburg, Gothenburg, SE-405 30, Sweden
Keywords: Air quality, EDXRF, PM10/2.5, Source apportionment.
Presenting author email: mgatari@uonbi.ac.ke

Many developing countries experience an exceptional urbanization rate. In Sub-Saharan Africa (SSA) the rate is estimated to be over 3% per year for at least twenty years (United Nations Population Division, 2008). With this increased urbanization follows a deterioration of the urban air quality. It is also in these areas the greatest health impacts are found, as a result of not only the bad air quality but also due to poverty (Fullerton et al., 2008).

Particulate matter (PM) and CO are some of the common criteria pollutants monitored in many parts of the world, as they are a health threatening pollutants whose concentration increases with the increased urbanization and life style. To provide new scientific data on the air quality, CO was measured and aerosol particles were counted at an urban background site in Nairobi, Kenya, between 14 January and 8 March 2010. The background site was about 2 km north of the commercial center of Nairobi where PM and CO were measured at a height of 17 m above ground while the latter was also measured at another lower site at 7 m above ground, in the same compound. The focus was to determine the size distribution of aerosol particles, identify their sources by correlating particle size fractions with local wind patterns and CO concentrations.

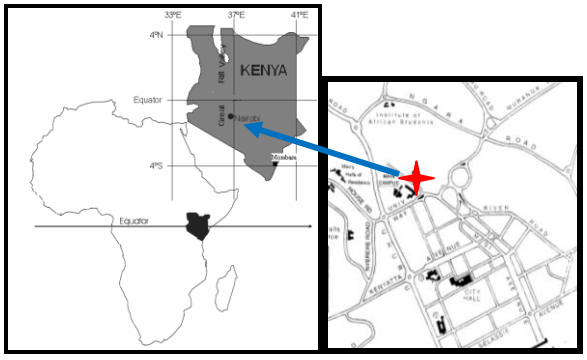

Figure 1. Map showing the location of Nairobi in Kenya, Africa and the sampling site in red within the central district of Nairobi city.

The measurements period was during the longer of two dry seasons with prevailing East-North-East winds, mainly sunny, dry and stable weather conditions. The maximum daytime temperature was around 28 ºC and wind speed was 10 m s^{-1}. The evenings and nights were calmer with more stable atmospheric conditions.

Particles were counted using an optical particle counter (Grimm 1.108). The counter is facilitated to collect the counted particles on polytetrafluoroethylene (PTFE) filter. The content of trace elements in the PTFE filters was determined by energy dispersive x-ray fluorescence (EDXRF) spectroscopy (Gatari et al., 2009) and 14 elements were analyzed. Two Passive electrochemical sensor Instruments were used to measure the CO concentration.

Fe, Ca, K, Mn, Ti constituted the major part of the determined mass concentration. S, Zn, Pb showed low concentrations compared to similar studies in Nairobi (Gatari et al., 2009) and other developing countries. Principal component analysis of the detected elemental concentrations identified waste and biomass burning, red earth, mineral dust and diesel vehicles or generators as probable sources of the elements involved. The largest fraction of the diesel emissions probably had their origin in the small buses (locally known as "Matatus"). These vehicles are a major public transport system in Nairobi and Thika Road to the North East of the sampling site has a very high number of these vehicles and is also synonymous with prolonged traffic jams especially in the morning and evening hours. It is estimated that there are 12,000 "Matatus" operating in Nairobi, compared to 300 larger buses.

The diurnal particle number concentration (PNC) peaked around 8-9 AM and 9-10 PM. CO was found to correlate well with PM2.5, but not with PM3.5-20. The concentrations of CO ranged from 0.03 to 15 ppm with daytime distributed peaks that depicted the heavy traffic and jam periods. Particle mass concentration (PMC) was derived from the number concentration and estimated to 7.5 µg m^{-3} for PM2.5 and 33.4 µg m^{-3} for PM10. These values were far much lower than those obtained from other studies at the same site. Although the data requires re-evaluation the study clearly showed the undisputed impact of traffic emissions in the city of Nairobi where the ground level concentrations are expected to be higher especially for particles.

This work was supported by Swedish International Development Cooperation Agency (SIDA).

Fullerton, D. G., Bruce, N. and Gordon, S. B. (2008) Trans Roy. Soc. Trop. Med. Hyg. **102** (9), 843-851.
Gatari, M. J., Boman, J. and Wagner, A. (2009) X-ray spectrum. **38** (1), 37-44
United Nations Population Division (2008) World urbanization prospects: The 2007 revision population database. United Nations

Source apportionment, surface area and particle number concentration analysis of ultra fine particles at an urban background station in the Ruhr area, Germany.

C. Nickel[1], H. Kaminski[1], B. Hellack[1], T.A.J. Kuhlbusch[1,2]

[1] IUTA e.V., Air Quality & Sustainable Nanotechnology, Duisburg, Rheinhausen, 47229, Germany
[2]CeNIDE, Center for Nanointegration, Duisburg-Essen, Duisburg, Germany
Keywords: Ultrafine particles, Source apportionment, Particle surface area, Number size distribution
nickel@iuta.de

Epidemiological and toxicological studies have shown correlations between adverse health effects and particulate matter. Especially ultrafine particles (UFP) are assumed to be linked to these biological effects (Stölzel et al. 2007, Oberdörster et al. 2005, Ibald-Mulli et al. 2002). Particle number and surface area concentration are considered as promising assessment metrics for specific health endpoints.

Here we report on results from ongoing measurements of particle size distributions and surface area concentrations, carried out over a two year period at an urban background station in Mülheim-Styrum in the Ruhr area in North-Rhine Westphalia, Germany.

We measured the ambient particle number concentrations using a scanning mobility particle sizer (SMPS Model 3936, TSI inc) and the surface area using a nanoparticle surface area monitor (NSAM Model 3550, TSI Inc.). The latter device measures the potential surface area which deposits in the alveolar region of the respiratory tract of a standard worker (ICRP Model 66 1994) thus a metric related to internal dose.

A Pearson correlation analysis with UFP and the measured possible deposited alveolar surface area (R^2 0.56) shows weak correlation in 2010. In 2009 no correlation (R^2 0.32) was found.

It was also identified that some single events, like the eastern bonfire combined with inversion weather conditions in 2009, when particles with a high surface area but with a low UFP concentration were detected, could be important for the weak correlation between the both metrics. Without the eastern bonfire event the correlation between the two metrics increase from R^2 0.34 to 0.45, but shows no clear correlation anymore.

Moreover, a seasonal comparison of the alveolar surface area and the ultrafine particle concentration in 2010 shows higher correlation in autumn (R^2=0.79) than in summer (R^2 = 0.47) (Fig. 1).

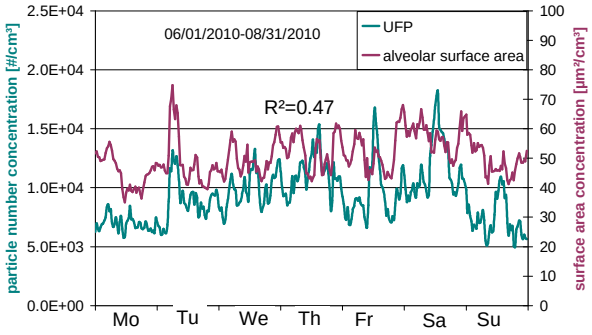

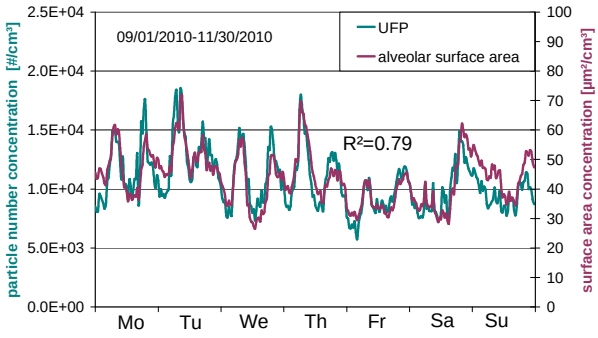

Fig. 1: Particle surface area (NSAM) and UFP (SMPS) concentration of the ambient aerosol for summer and autumn 2010.

This could possibly due to the different air chemistry, e.g. photochemical production of secondary aerosols or different sources.

For clarification, a source appointment of the measurements was conducted by applying the positive matrix factorization (U.S. EPA PMF 3.0.2.2). First PMF evaluations did not lead to robust factors for the alveolar surface area metric. A single run for September linked the surface area to particle number concentrations in the size range 50-200 nm and a second factor with the main variables of UFP, NO_2 and NO. The preliminary results will be further evaluated and their robustness tested. Especially seasonal and source dependent differences of the two health relevant metrics (particle number concentration and surface area) will be further investigated and discussed in detail to derive a comprehensive characteristic of health relevant ambient aerosol parameters.

Ibald-Mulli, A., Wichmann, H-E-, Kreyling, W., Peters, A. (2002): *Journal of aerosol medicine*, **15**, 189-201.

Stölzel, M., Breitner, S., Cyriys, J., Pitz, M.,Wölke, G., Kreyling, W., Heinrich, J., Wichmann, H.-E., Peters, A. (2007): *Journal of Exposure Science and Environmental Epidemiology*, **17**, 458-467.

Oberdörster, G., Oberdörster, E., Oberdörster, J. (2005): Nanotoxicology: An Emerging Discipline Evolving from Studies of Ultrafine Particles. *Environmental Health Perspectives*, **113** (7), 823-839.

Financial contribution by the LANUV NRW is gratefully acknowledged.

Mobile measurements of ship emissions in two harbour areas in Finland

Pirjola, Liisa[1,2], Pajunoja, Aki[3], Aleksi Malinen[1], Walden, Jari[4], Jalkanen, Jukka-Pekka[4] and Rönkkö,Topi[3]

[1]Department of Technology, Metropolia University of Applied Sciences, FI-00180 Helsinki, Finland
[2]Department of Physics, University of Helsinki, FI-00140 Helsinki, Finland
[3]Aerosol Physics Laboratory, Tampere University of Technology, FI-33101 Tampere, Finland
[4]Finnish Meteorological institute, FI-00101 Helsinki, Finland

Keywords: ship emissions, mobile laboratory, particle size distribution, nitrogen oxides, Baltic Sea.

Marine traffic is a significant and growing source of diesel emissions to the local and global environments affecting human health and climate change. Recent estimates indicate that ocean-going ships represent approximately 9% of global SO*x* emissions, 18-30% of the world's NO*x* pollution and 2% of global black carbon from all sources (Gorbett and Koehler, 2003; Corbett et al., 2010). The Baltic Sea is a busy area for short-sea marine traffic; about 3500-5000 different vessels are in operation every month (Jalkanen et al., 2009). Control legislation for SOx emissions was taken effect from 16 May, 2006. Besides short-sea marine traffic other port activities contribute to the air quality.

To study port area emissions and their local dispersion, two weeks mobile measurements by SNIFFER (e.g. Pirjola et al., 2004; 2006) were performed in the port area in Helsinki and in the neighbouhood of the port area in Turku, Finland, during both winter and summer in 2010. The experiments were a part of the Shipping-induced NOx and SOx emissions - Operational monitoring network project (SNOOP). The general goal of SNOOP is to find out how ship exhaust emissions are effecting to marine environment and human health in harbour areas, and to establish a long-term follow-up network on ship emissions in the Central Baltic area (http://snoop.fmi.fi).

The van was standing at different sites at the port areas and close to the ship passage. Sampling occurred above the windshield of the van at 2.4 m altitude. Particle size distribution and total number concentration were measured by ELPI - Electrical Low Pressure Impactor. ELPI classifies particles in the size range of 7 nm – 10 µm (aerodynamic diameter) to 12 classes with one second time resolution. Particle volatility was studied by using a thermodenuder, where the temperature of the air sample reached 265°C. Also gaseous concentrations such as carbon monoxide CO, nitrogen monoxide NO, nitrogen dioxide NO_2 as well as carbon dioxide CO_2 were monitored with one second time resolution. Furthermore, $PM_{2.5}$ and PM_{10} were recorded by two Dust Tracks. A weather station on the roof at 2.9 m height provides meteorological parameters (temperature, relative humidity, wind speed and wind direction). A global position system GPS saves the van's speed and the driving route.

Typically the emitted SO_2 concentration correlated well with the total particle number concentration indicating that sulphuric acid is involved in the formation process of new particles. Fuel sulphur contents (FSC) of each ship were estimated based on the measured CO_2 and SO_2 peaks.

The size distribtions are typically composed of two modes. As an example, Figure 1 shows the size distribution of the ship plume as a function of distance. The nucleation mode is peaking at 20-30 nm and the soot mode at 80-90 nm. In winter the total particle concentration is aroung 2-3 fold compared to the summer values.

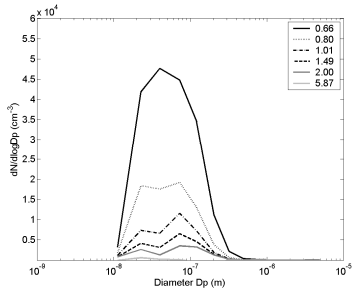

Figure 1. Evolution of the particle size distribution when the ship is receding upwind from the harbour. Distance from Sniffer in km is shown in the legend.

The experiment was financed by Cental Baltic INTERREG IV A Programme 2007-2013 and Centre for Economic Development, Transport and the Environement (ELY) of Southwest Finland

Gorbett, J.J., Lack, D.A., Winebrake, J.J., Harder, S., Silberman, J.A., and Gold, M. (2010) *Atmos. Chem. Phys.*, 10, 9689-9704.

Corbett, J.J., and Koehler, H. J. (2003) *Geophys. Res*., 108, 4560.

Jalkanen, J-P. Brink, A., Kalli, J., Pettersson, H., Kukkonen, J. and Stipa, T. (2009) *Atmos. Chem. Phys.*, 9, 9209-9223.

Pirjola, L., Parviainen, H., Hussein, T., Valli, A., Hämeri, K., Aalto, P., Virtanen, A., Keskinen, J., Pakkanen, T., Mäkelä, T., Hillamo, R. (2004) *Atmospheric Environment* 38, 3625-3635.

Pirjola, L., Paasonen, P., Pfeiffer, D., Hussein, T., Hämeri, K., Koskentalo, T., Virtanen, A., Rönkkö, T., Keskinen, J., Pakkanen, T.A., and Hillamo, R.E. (2006) *Atmospheric Environment,* 40, 867-879.

Contribution of biomass burning to London's PM_{10}

G.W Fuller[1], A. H. Tremper[1], T.D. Baker[1], K. E. Yritt[2], D. Butterfield[3], I. S. Mudway[1], R. Dove[1] and F.J. Kelly[1]

[1]MRC HPA Centre for Environment and Health, King's College London, London, SE1 9NH, UK
[2] Norwegian Institute for Air Research, Instituttveien 18, P.O. Box 100, N-2027 Kjeller, Norway.
[3] National Physical Laboratory, Teddington, Middx, TW11 0LW, UK.

Keywords: Biomass, levoglucosan, light absorption
Presenting author email: gary.fuller@kcl.ac.uk

Introduction

The 27 member states of the European Union are committed to obtain 20% of their energy requirements from renewable sources, including biomass, by 2020 (EU, 2009) as part of a raft of proposals to reduce CO_2 emissions. In response to these targets, the UK Department for Energy and Climate Change (DECC) has announced the world's first renewable heat incentive, which will provide a financial incentive for individuals and businesses to switch from fossil fuel to renewables as part of a strategy to 'de-carbonise' the generation of heat in the UK. As part of carbon reduction policies the UK government will launch the world first renewable heat incentive in June 2011 (DECC, 2010a), which will target around 700,000 new domestic biomass installations by 2020 (Klevnäs, 2009). Additionally biomass boilers are being installed to meet requirements for renewable energy in new buildings. Concern has been raised over the possible urban air pollution impacts arising from the widespread installation and use of biomass heating. There is a risk that an increase in biomass burning may undermine air quality management actions aimed at achieving PM_{10} EU Limit Values and the EU exposure reduction target for $PM_{2.5}$. It was therefore felt prudent to establish a baseline for the PM from biomass burning in London against which future changes can be measured.

Methods

The contribution of PM from biomass in London was estimated using two ambient measurement methods. The first used measurements of the concentration of levoglucosan, a specific marker for PM from wood combustion, sampled during two winter campaigns in 2009 and 2010. The second used the differential absorption of UV and IR in sampled PM_{10} using aethalometers (Favez et al. 2010) at two sites over a period of 15 months. Analysis was supported by measurements of NOX, sulphate and ethane from UK national networks.

Results

Mean winter time concentrations of levoglucosan were 176 ng m^{-3} at the low end of the range of concentrations found across Europe. Analysis of levoglucosan concentrations and wind speed did not reveal any large point sources. Having used measurements of ethane (assumed to be from natural gas leakage) as a tracer for dispersion it was found that levoglucosan emissions were greatest at weekends.

Good correlation was found between estimates of PM from wood smoke using levoglucosan and UV and IR absorption (r2 = 0.76), though the estimated concentrations of organic carbon using the UV and IR absorption method exceeded estimates using levoglucosan by a factor of between 1.5 and 2 . Measurements of UV and IR absorption suggest that wood burning is a winter time pollution source in London with peak PM_{10} concentrations during evenings and especially at weekends.

Conclusions

Ahead of new policies to promote renewable energy it appears that wood burning already contributes approximately 3 µg m^{-3} to wintertime PM_{10} in London; 15% of the wintertime background concentration. No distinct point sources were detected, suggesting that wood smoke particulate originates from diffuse urban sources. The wood smoke contribution to PM_{10} was mainly a wintertime effect; occurring mostly during evenings and at weekends. This suggests that current wood burning in London is a secondary heating source. Widespread wood burning suggests that smoke control legislation is no longer effective in London.

References

European Union (EU). (2009). Directive 2009/28/EC of the European Parliament and of the Council. *Official Journal of the European Union.* L 140, 5.6.2009, p. 16–62.

Department for Energy and Climate Change (DECC). *Renewable heat incentive, consultation on the proposed RHI financial support scheme.* DECC, London. 2010.

Favez, O., El Haddad, I., Piot, C., Boreave, A., Abidi, E., Marchand, N., Jaffrezo, J-L., Besombes, J-L., Personnaz, M-B., Scaare, J. Wortham. H., George, C., D'Anna, B., (2010). *Atmos. Chem. Phys.*, **10,** 5295–5314, 2010.

Klevnäs, P., and Barker, N.(2009) *Scenarios for Renewable Heat Supply Capacity Growth to 2020*. NERA UK Ltd.

Source apportionment of fine aerosol in the cities of Marseille and Grenoble

B. D'Anna[1], N. Marchand[2], J.L. Jaffrezo[3], C. George[1]
O. Favez[1,*], A. Boréave[1], M. Nicolas, [1] I. El Haddad[2], H. Wortham[2], A. Armengaud[4], C. Piot,[3,5] J-L Besombes[5]

[1]Institut de Recherches sur la Catalyse et l'Environnement, CNRS-Université Lyon1, Villeurbanne, France
[2]Laboratoire de Chimie Provence, CNRS-Université d'Aix-Marseille, Marseille, France
[3]Laboratoire de Glaciologie et Géophysique de l'Environnement, CNRS-Université Grenoble, Grenoble, France
[4] Atmo PACA, 146 rue Paradis, 13006, Marseilles, France
[5]Laboratoire de Chimie Moléculaire et Environnement, Université Savoie-Polytech'Savoie, Chambéry, France
* now at INERIS, Parc Technol. Alata, 60550 Verneuil en Halatte, France

Keywords: aerosol source apportionment, urban environment, aerosol mass spectrometer

This study presents comprehensive results of the FORMES program based on two field campaigns: one in a coastal Mediterranean city (Marseille, France) during summer 2008 (30/06-14/7), the other in Grenoble, located in an Alpine valley, during winter 2009 (14.01-30/01). On line instruments (C-TOF-AMS, HS-PTR-MS, SMPS, and VHTDMA, aethalometer) were employed to investigate in detail fine particles and VOCs. Filter-based measurements were used for the measurement of a large array of chemical species including EC and OC, ionic species, metals, and molecular speciation of organic matter.

Total NR-PM_1 mass concentration in Marseille accumulates over days and rapid cleaning occurred when the meteorological conditions changed, due mainly to the Mistral wind. Sulphate and organics were the major NR-PM_1 components while the concentrations of nitrate and chloride were generally quite low. Ammonium sulphate was the dominants salt. The aerosol was often acidic and more than 40% of sulphate was in the form of ammonium bisulphate. The accumulation mode was dominated by sulphate that appears to be internally mixed with organics, while combustion-emitted organics are often the main component of the ultrafine particles (except during nucleation events). The ultrafine-mode organic aerosols were mainly associated with combustion sources (likely traffic). Few nucleation events were observed and they were always preceded by very high concentration of SO_2 (industrial sources nearby the city of Marseille).

The NR-PM_1 mass concentration in winter time in Grenoble is largely dominated by organic matter, and nitrate and BC. Hourly-mean PM_1 loadings, estimated as the sum of these compounds, vary from 1 µgm−3, during low pressure systems associated with rain, to 40 µgm−3 during typical wintertime thermal inversions. Independently of these meteorological conditions, submicron particles are mainly composed of carbonaceous material, with OM and BC constituting on average 47% and 16% respectively of the total loading. Among inorganic aerosols, ammonium nitrate largely dominates over ammonium sulphate. Similar results are obtained from the analyses of HiVol filters for the PM2.5 aerosol fraction.

Various source apportionment methods as Positive Matrix Factorization, Chemical Mass Balance and aerthalometer model (only for Grenoble) were undertaken to evaluate the organic contribution of the fine aerosol. In Grenoble, residential wood burning emissions accounted for approximately 40-50% of fine carbonaceous aerosols. Such results underline the significant impact potentially played by residential wood burning emissions on particulate air pollution in large European urban centres.

While in summertime in Marseille four major factors have been identified; the predominant factor is highly oxygenated (OOAI and OOAII type). A minor and not non-defined 4th factor called 'industrial' is found and perfectly correlates with "hot spot of PAHs" (not related to traffic emissions) which seems to related to" industrial organic source" (refinery). Figure 1 below shoes the excellent agreement found between PMF2/AMS analysis and CMB model.

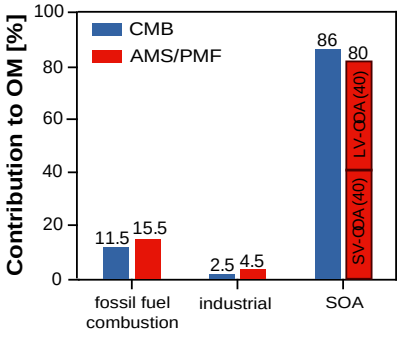

The source apportionment methods and results from the two studies will be compared and discussed.

This work was supported by the PRIMEQUAL/FORMES research programs.

Measurements of the urban Copenhagen aerosol from 2002 – 2010: physical properties and their trends

A. Massling[1], M. Ketzel[1], T. Ellermann[1], J. K. Nøjgaard[1], B. Jensen[1], C. Nordstrøm[1] and P. Wåhlin[1]

[1]Department of Atmospheric Environment, National Environmental Research Institute, Århus University, Roskilde, Denmark

Keywords: urban aerosol, DMPS, TEOM, PSAP, PM2.5, PM10
Presenting author email: anma@dmu.dk

Introduction

In the last two decades aerosol particles have been intensely discussed because of their various health effects (Pope and Dockery, 1999). EU directives control ambient concentrations of PM10 and PM2.5, however the number concentration of fine aerosols (< PM1) has not yet been regulated. Urban particulate emissions in major cities in Europe are mostly linked to the increasing road traffic and to some extent to domestic wood burning and industrial emissions. The traffic density, the composition of the vehicle fleet and the used fuel are changing rapidly and new engine techniques are developed. In this study the physical properties and their trends within the last ten years are discussed for the urban Copenhagen aerosol.

Methods

Measurements were carried out throughout the period from 2002 to 2010 at three Danish stations, namely Lille Valby (LVBY, a regional background site 30 km west of Copenhagen), H.C. Ørsteds Institute (HCOE, an urban background site in central Copenhagen), and H.C. Andersens Boulevard (HCAB, an urban curbside station in central Copenhagen) (Wåhlin, 2008). The particle number size distribution (10 – 700 nm) was measured using a DMPS system (Differential Mobility Particle Sizer), the PM2.5 and PM10 mass was measured using a TEOM (Tapered Element Oscillating Microbalance) and the light absorption coefficient was measured using a PSAP (Particle Soot Absorption Photometer).

Results

In general all measured parameters (total particle number and volume, PM2.5 and PM10 mass, light absorption coefficient) are decreasing with increasing distance to the traffic emission sources.

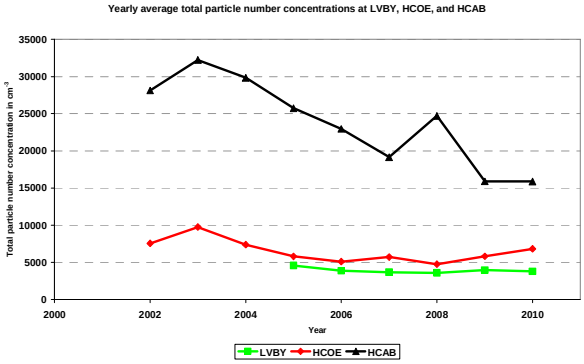

Figure 1. Average yearly particle number concentration at LVBY, HCOE, and HCAB.

This means, that the maximum values were observed at the urban curbside station HCAB followed by HCOE and LVBY. Moreover, a decrease in air pollutant values was observed at the urban curbside station HCAB as a general trend from 2002 to 2010 for all parameters except for the light absorption coefficient, which is an indirect measure for the mass of black carbon particles (BC) in the urban aerosol. Figure 1 shows these general findings for the total particle number concentration measured with the DMPS.

At the curbside station, the weekly variation of the air pollutant parameters was in clear correspondency with the weekly variation of the traffic density in the city. Figure 2 shows examplewise the average weekly variation of particle number concentration.

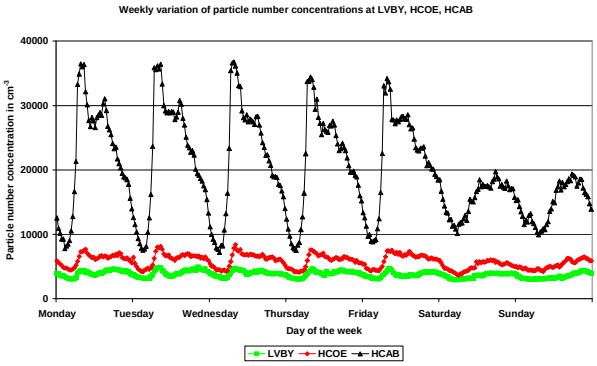

Figure 2. Average weekly variation of particle number concentrations at LVBY, HCOE, and HCAB.

The variation is most pronounced for the curbside and reduces with the distance to the traffic emission sources. Number concentrations for the curbside peak at values, which are about six to seven times higher than at the regional background and about four to five times higher than at the urban background site. Similar findings were observed for PM10 and PM2.5 mass concentrations and the light absorption coefficient.

Outlook

Trends in particle number and volume, PM2.5 and PM10 mass are discussed and linked to exposure levels induced by traffic emissions.

Acknowledgement

This work was supported by the Danish Environmental Protection Agency.

References

Pope, C. A.; Dockery, D. W. (1999) Epidemiology of particle effects, Air Poll. Health 31, 673 – 705.

Wåhlin, P. (2008) Partikelprojektet, Miljøstyrelsen, Faglig rapport fra DMU, Nr. 688, 33 p., electronic.

Particle area and number concentrations influenced by local sources at an urban background station in Germany

H. Gerwig[1], W. Pecher[1] and K. Wirtz[1]

[1]Section Air Quality Standards and Monitoring Methods, UBA – Federal Environmental Agency, 63225 Langen, Germany.

Keywords: particle area, car traffic, asphalt grinding, gas-fired CHP, airport

The European Union defined a daily average PM_{10}-limit of 50 µg · m^{-3} for the protection of human health (2008/50/EC). Epidemiological and toxicological studies give evidence that ultrafine particles (< 100 nm, UFP) show negative health effects (Knol *et al.*, 2009).

Reduction limits for diesel cars are fixed (EURO VI). To control the results of reducing emitted particle numbers from cars and especially trucks, governmental agencies in Germany started to measure ultrafine particles on a routine base (Birmili *et al.* 2009 and Löschau *et al.* 2010).

Table 1 1-h av. tracheobronchial particle area and particle conc. 09-09-2009 – 14-06-2010

	NSAM	UCPC	SMPS
	µm²/cm³	p / cm³	p / cm³
nm	10 - 1000	3 - 1000	10 - 500
Median	5.0	9 900	8 600
Std	3.1	6 100	6 000
5 Perc	1.9	4 600	3 700
95 Perc	11.7	22 500	21 000

The urban background station was situated in Langen, Germany: 15 km south of Frankfurt a. M. and 5 km south east of the airport in the Rhine-Main-Area. Three different particle measuring instruments (TSI Inc.) were running continuously (09-09 – 06-11, 1 min av. and SMPS 6 min av.) on a rooftop at 14 m above ground with cut of at 1 µm. NSAM measures the deposited tracheobronchial (= tb) particle area within particle diameter of 10 - 1000 nm. With UCPC 3776 particle number concentration from 3 - 1000 nm was measured. With SMPS 3936 and CPC 3010 particle number size distributions between 10 – 500 nm were detected. 6 size classes were calculated from SPMS data (10 |30 |50 |70 |100 |200 |500). The difference of UCPC and total SMPS was expected to be size class 3 – 10 nm Offsets between both instruments cannot be excluded.

Temperature, humidity, wind speed, wind direction, precipitation was collected by WS600 (LUFFT GmbH). Only complete datasets of 1 h av. were used for evaluation (85 % of time period). For diurnal Mo-Fr variations data from official holidays and from 23-12-09 until 03-01-10 were excluded.

During the measuring period the median of the tb particle area concentration was 5 µm²/cm³, particle number concentration from 10 to 500 nm was about 8 600 p · cm^{-3}. 1 300 p · cm^{-3} more particles were found from 3 to 1 000 nm range (s. Tab. 1). The temperature was between -15 and +30°C, wind speed up to 14 m · s^{-1}.

For diurnal variations from Monday to Friday 2 different shapes were detected (Fig 1). Shape A: Tb particle area and particles 30 – 500 nm showed a 1st min. around 4:00, max. at 9:00 and 2nd min. at 15:00, similar to previous observations at an urban background during UFIPOLNET (Wehner *et al.*, 2008). Shape B: Particles 3 – 10 nm showed 1st max between 13 – 15:00 probably caused by particle nucleation events and a 2nd max at 7:00. Particles 10 – 30 nm show almost the same diurnal variation as shape A except for afternoon, were the second min. looks as if overlayed by effects responsible for shape B.

Grinding up asphalt and other road construction work in 10 to 100 m distance caused raised particle area and number concentrations. Elevated particle concentration occurred with winds from a nearby combined heat and power gas-fired power plant (CHP). The influence of the airport will be evaluated. The influence of fireworks is described elsewhere (Gerwig *et al.*, 2011).

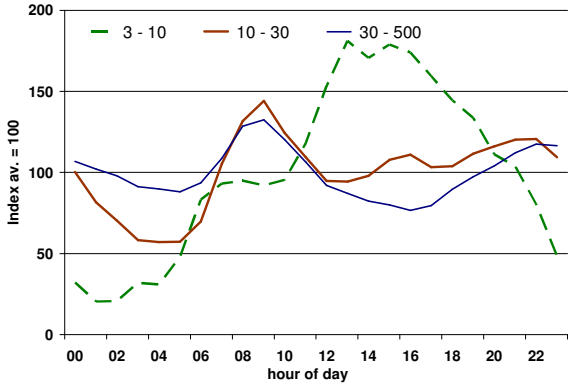

Figure 1. Diurnal variations of 1 h av. Mo – Fr; particle classes 3 – 10, 10 – 30 and 30 - 500 nm

Birmili, W. *et al.* (2009), *Gef .Reinh. Luft*, **69**, 31–35.
Gerwig, H. *et al.* (2010), *IAC 2010, Helsinki.*
Gerwig, H. *et al.* (2011), *EAC 2011, Manchester.*
Knol, A. B. *et al.* (2009), *Part. Fibre Tox.*, **6**, 19.
Löschau, G. *et al.* (2010), *Gef. Reinh.Luft,***70**,183–187.
Wehner, B. *et al.* (2008), *EAC 2008, Thessaloniki.*

Tuesday, September 6, 2011

Session 5B: Aerosol-Cloud Interactions 2

Observations and Modelling of Cloud Aerosol Interaction in Mixed Phase Frontal Layer Cloud

J.Crosier[1*], K.N. Bower[1], T.W. Choularton[1*], P. Connolly[1], C. Dearden[1], M.W. Gallagher[1*], J.R. Dorsey[1*], G. Capes[1], C. Westbrook[2]. Z. Cui[3] and A.M. Blyth[3]

[1]School of Earth Atmospheric and Environmental Sciences and [*] NCAS, University of Manchester, Manchester, M13 9PL, UK.
[2]Department of Meteorology, University of Reading, Reading, UK
[3]School of Earth and Environment and NCAS, University of Leeds, Leeds, UK

Keywords: Cloud microphysics, frontal clouds, aerosol, ice crystals, cloud drops.
Presenting author email: k.bower@manchester.ac.uk

Frontal systems associated with mid-latitude cyclones generate large regions of cloud which can perturb the regional radiation balance, as well as precipitate large quantities of water to the surface. Predictability of the spatial distribution and temporal development of the radiative properties and precipitation associated with frontal clouds requires knowledge of the microphysical processes acting. The influence of aerosol acting both as Cloud Condensation Nuclei and Ice Nuclei can be large.

In-situ measurements in frontal clouds were obtained using the UK Facility for Airborne Atmospheric Measurement (FAAM) BAe146 research aircraft flying in the vicinity of the suite of radars and lidars based at the Chilbolton Facility for Atmospheric and Radio Research (CFARR). Case studies were later simulated using the Advanced Research WRF (Weather Research and Forecasting) model version 3.1 (using the dual moment Morrison microphysics scheme), and also a detailed microphysics model linking together the atmospheric aerosol (size and composition) to the formation and growth of water droplets, ice crystals and snowflakes.

In deep frontal cases, homogeneous nucleation of ice at cloud top (CT) together with heterogeneous nucleation (temperatures around -35°C or below) were seen as the primary source of ice. For lower cloud top cases (temperatures around -25°C), a layer of supercooled liquid water was often seen at cloud top. Heterogeneously nucleated ice, at or just below CT, grew via deposition and aggregation into snow. Embedded convection originating from near the surface was observed frequently and generated regions of supercooled water and high number concentrations of ice crystals (up to 100 L^{-1}) at temperatures around -6°C. These ice crystals were usually small (<300 μm in length) un-rimed columns, and most likely the result of the Hallett-Mossop secondary ice multiplication mechanism.

Data and model results from a wide range of clouds and cloud types will be presented to investigate the relationship between heterogeneous vs homogeneous ice nucleation and to assess the importance of ice crystals contributed by secondary ice particle production at temperatures around -6°C where the Hallett-Mossop process operates. The WRF model will be used to help predict the overall dynamical structure of the cloud, while the more detailed cloud microphysical model will be used to predict the number of ice, water droplets and ice crystals forming on aerosol as a function of position in the cloud. This model makes use of results from chamber studies of ice nucleation of aerosol e.g. Connolly et al 2009. Model predictions of the initial growth of the ice crystals by vapour diffusion, and then as they became large enough, by riming and aggregation, leading to precipitation from the cloud will be presented. The contribution of secondary ice to this precipitation will also be examined.

Predictions from both models will be compared with the observations. The sensitivity of the cloud structure and precipitation amount and size distribution to the aerosol available in the boundary layer and above cloud top will be examined for the different cloud types. Results so far suggest that the competition between heterogeneous nucleation and homogeneous freezing in cloud with tops colder than about -35°C is important in determining the number of ice particles nucleated at cloud top. This in turn influences the precipitation production within the cloud. Lower down in the cloud the ice crystal number and in some cases the precipitation formation is influenced by secondary ice particle production, however, this process is not well modelled by WRF and is to be investigated further.

It is hoped this work will lead to an improvement in the treatment of cloud-aerosol interactions in frontal clouds by weather forecast models such as WRF, and hence to an improvement in the forecasting of such systems on a day to day basis. In the longer term, it should also result in an increase in our understanding of the sensitivity of these cloud systems to climate change and to changes in the emissions of manmade aerosol.

Connolly, P., Moehler, O., Field, P., Saathoff, H., Burgess, R., Choularton, T. and Gallagher, M. (2009) *Atmos. Chem. Phys.,* **9**, 2805-2824,

The effects of biomass burning aerosols on the formation of convective mixed-phase clouds and precipitation

Di Chang[1], Hang Su[1], Philipp Reutter[2], Jörg Trentmann[3], Meinrat O. Andreae[1], and Ulrich Pöschl[1]

[1]Max Planck Institute for Chemistry, Biogeochemistry Dept., Mainz, Germany

[2]Institute of Atmospheric and Climate Science, ETH Zurich, Switzerland

[3]Satellite Application Facility on Climate Monitoring, German Weather Service (DWD), Offenbach, Germany

Keywords: biomass burning, ice nuclei, clouds, precipitation and aerosol particles

Presenting author email: d.chang@mpic.de

Clouds have great influence on the vertical redistribution of energy and moisture, and consequently have impacts on weather and climate change from regional to global scales. Biomass burning is an important factor that could affect deep convection in clouds, and within this work, we used the ATHAM (Active Tracer High Resolution Atmospheric Model) model to study the properties of pyro-convective clouds and precipitation in 2- and 3-dimensional simulations. The two-moment microphysical scheme of Seifert (2002), including the hydrometeor categories cloud water, rain water, cloud ice, snow, graupel and hail, was utilized to investigate the interaction between atmospheric aerosols and cloud microphysics. The Chisholm fire that occurred in Alberta, Canada, in May 2001 was used as a base case. By assuming typical aerosol concentration conditions, we calculated the cloud droplet number concentrations under different fire intensity conditions and evaluated the effects of aerosol concentration and fire intensity on the formation of precipitation. The simulation results showed different control regimes for cloud and precipitation formation, including an aerosol-limited regime, a fire intensity-limited regime and a transitional regime, which are consistent with the results from a recent parcel model study (Reutter *et al* 2009).

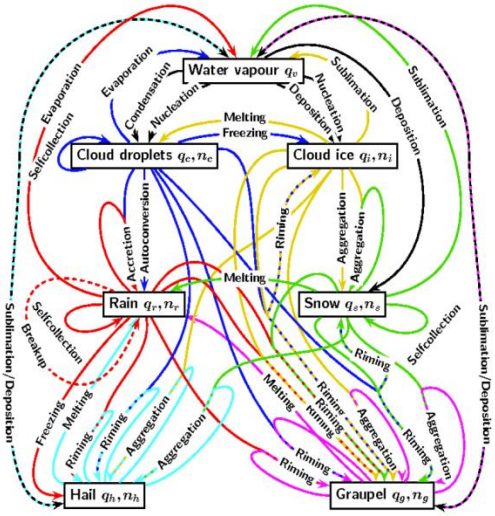

Figure 1. Simplified schematic diagram of the microphysical interactions in the two-moment Seifert scheme with respect to the particle classes cloud- and rain droplets, cloud ice, snow, graupel and hail.

Seifert, A. (2002) *Parameterisierung wolkenmikrophysikalischer Prozesse und Simulation konvektiver Mischwolken*, Ph.D. thesis, University of Karlsruhe.

Reutter, P., Su, H., Trentmann, J., Simmel, M., Rose, D., Gunthe, S. S., Wernli, H., Andreae, M. O., and Pöschl, U. (2009) *Atmos. Chem. Phys.* **9**, 7067-7080.

Partitioning of drops & ice in mixed phase clouds: laboratory and field observations

M. Krämer[1] J. Meyer[1], A. Afchine[1] D. Baumgardner[2] R. Newton[3]
A. Abdelmonem[4] S. Benz[4] O. Möhler[4] M. Schnaiter[4]

[1] Research Center Jülich, Institute for Energy and Climate Research (IEK-7), Wilhelm-Johnen-Str. 1, 52425 Jülich, Germany
[2] Universidad Nacional Autonoma de Mexico, Mexico City, Mexico
[3] Karlsruhe Institute of Technolgy, IMK-AAF, Karlsruhe, Germany
[4] Droplet Measurement Technologies, Boulder, USA

Keywords: Mixed phase clouds, ice formation.

Presenting author email: m.kraemer@fz-juelich.de

The novel cloud particle spectrometer NIXE-CAPS consists of two different instruments, the CAS-DPOL and the CIP Grayscale. It can not only record particle number size distributions between 0.6 and 900 μm diameter, but also provides information on the particles phase -liquid (spherical) or ice (aspherical)- for every cloud particle. NIXE-CAPS is deployed at the cloud chamber AIDA during three campaigns where heterogeneous ice formation in mixed phase clouds was investigated -using mineral dusts, soot particles and bacteria as ice nuclei- in the wide temperature range of 220 - 275 K. Very recently, in February 2011, first airborne measurements onboard the BAe146 were performed in mixed phase clouds during the campaign COALESC out of Exeter, UK.

At the AIDA chamber, we found that in case of drop and ice coexistence conditions (see Fig. 1, middle panel, relative humidities over water RHw and ice RHi are both supersaturated), the heterogeneous freezing of the drops is dependent on the drop size. I.e. the larger drops are frozen, the smaller drops remain liquid and in between there is a size range where both drops and ice crystals coexits. This size range of drop and ice coexistance is found to decrease together with the temperature from 20-30 μm to 8-20 μm diameter.

In the case of Bergeron-Findeisen conditions (see Fig. 1, top panel, RHw $<$ 100%, RHi $\sim>$ 100%), the freezing of the drops is still size dependent as long as RHi$\sim$ 100%. Then, larger drops are frozen and the smaller the cloud particles are the more remain liquid. Only if RHi$>$ 100% the larger ice crystals ($>$ 20 μm) grow while all small liquid drops as well as ice crystals evaporate.

Preliminary results from the field campaign COALESC (see Fig. 1, bottom panel) confirm the size as well as the temperature dependence of the freezing process in the atmospheric clouds. In our first measurements we most frequently found the state where liquid and ice particles coexist instead of Bergeron-Findeisen conditions with quick complete glaciation. This is in in accordance with theoretical considerations of Korolev (2007), who proposed that the Bergeron-Findeisen process is only one possibile thermodynamic secenario in mixed phase clouds.

Korolev A. (2007). J. Atmos Sci., 64, 9, 3372-3375.

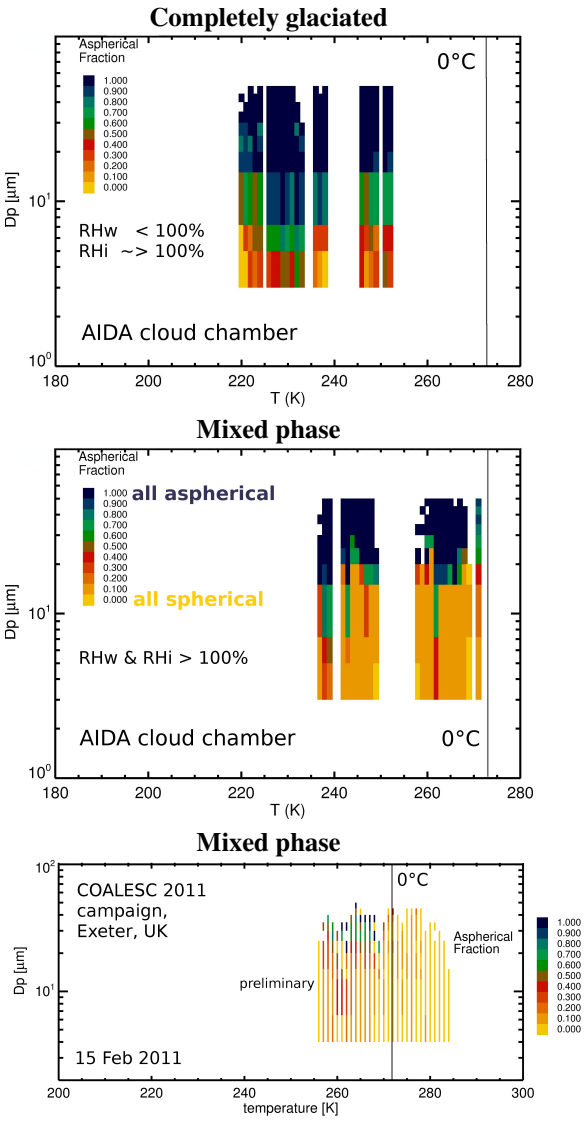

Figure 1: Fraction of particles that are aspherical, in dependence on particle size and on temperature.

On the activation and ambient peak supersaturation of CCNs at Jungfraujoch, Switzerland (3580 m asl): Results from the CLACE 2010 campaign

N. Bukowiecki[1], P. Zieger[1], E. Hammer[1], Z. Jurányi[1], M. Gysel[1], E. Weingartner[1], U. Baltensperger[1], J. Spiegel[2] and W. Eugster[2]

[1] Laboratory of Atmospheric Chemistry, Paul Scherrer Institut, 5232 Villigen PSI, Switzerland
[2] Institut of Agricultural Science, ETH Zürich
Keywords: Aerosol cloud interaction, Cloud microphysics, CLACE
Presenting author email: nicolas.bukowiecki@psi.ch

During the CLACE 2010 campaign performed at the High Altitude Research Station Jungfraujoch (Switzerland, 3580 m asl), an in-depth study of aerosol-cloud interactions was performed. The site is optimally suited for this purpose, as it lies in the free troposphere but is influenced by the continental air over Europe. In addition, the Jungfraujoch is about 40% of the time within clouds. The performed measurements allowed for the determination of the effective peak supersaturation in the prevailing ambient cloud which was responsible for the activation of aerosol particles to cloud droplets.

Activated fraction of the aerosol

Two examples of the diameter dependent aerosol activation to cloud droplets are given in Figure 1, showing data from the CLACE 2010 campaign (June – August 2010). These activation curves were determined by the simultaneous measurement of the total and interstitial (total aerosol minus cloud condensation nuclei) aerosol number size distribution. The upper panel shows an example of 50% activation of aerosol particles above 50 nm (critical activation diameter D_{50} = 50 nm), as indicated by an upper activation curve plateau very close to one. In other cases (lower panel) this plateau did not reach 1, indicating incomplete activation due to ice formation or entrainment. Further investigation of this phenomenon is subject to ongoing analysis. In addition, the critical activation diameter in the second example is higher (D_{50} = 80-100 nm).

Ambient peak supersaturation

The ambient peak supersaturations (SS_p) responsible for formation of the clouds observed at the Jungfraujoch were estimated using the activation cut-off diameter observed in clouds in combination with the relationship between supersaturation and critical diameter for CCN activation. The latter was taken from the 17-month CCN study at the Jungfraujoch by Juranyi et al. (2011). The statistical distribution of SS_p values observed during CLACE 2010 is shown in Figure 2. The peak supersaturation of the cloud droplets arriving at the Jungfraujoch showed a mean value of 0.31% and a median value of 0.23%. Ongoing data analysis attempts to establish a link between the retrieved peak supersaturations and other parameters like temperature, updraft velocity and weather situation (i.e., cloud type).

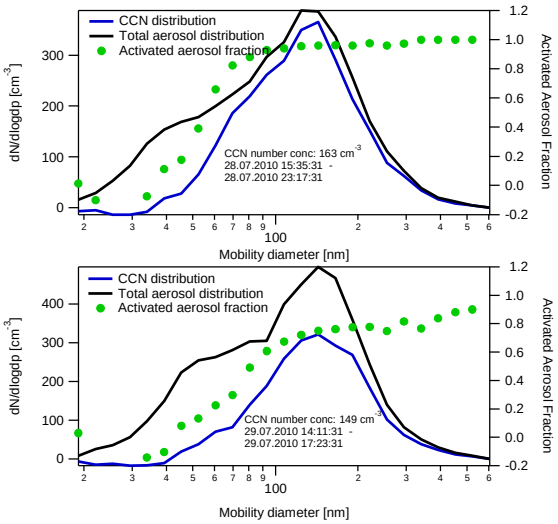

Figure 1: Two examples total and CCN number size distributions, along with the activated number fraction.

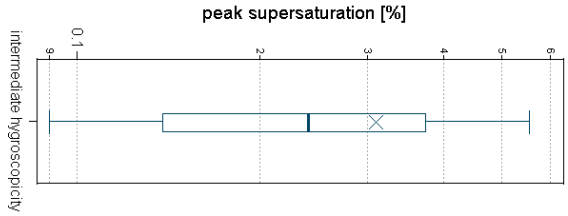

Figure 2: Box plot of the ambient peak supersaturations for stable clouds periods during CLACE 2010, using the annual mean aerosol hygroscopicity at the Jungfraujoch as determined by Jurányi et al. (2011). Box: first, second and third quartile; cross: average; whiskers: 5th and 95th percentile.

This work was supported by MeteoSwiss within the GAW program of WMO, the Swiss Federal Office for the Environment and Swiss National Science Foundation. We thank the International Foundation High Altitude Research Stations Jungfraujoch and Gornergrat (HFSJG) for the opportunity to perform experiments on the Jungfraujoch.

Henning, S., Weingartner, E., Schmid, S., Wendisch, M., Gäggeler, H. W., and Baltensperger, U. (2002) *Tellus* 54B, 82–95.

Jurányi, Z., Gysel, M., Weingartner, E., Bukowiecki, N., Kammermann, L. and Baltensperger, U (2011) *J. Geophys. Res.*, submitted.

Indirect measurement of water vapour supersaturation ratios in continental boundary layer clouds using H-TDMA and DMPS data

E. O. Fors, B. Svenningsson, E. Swietlicki and M. Sporre

Lund University, Department of Physics, Division of Nuclear Physics, Lund, Sweden

The maximum water vapour supersaturation ratio (s_{max}) that is reached in a cloud formation event is an important parameter when it comes to quantifying anthropogenic influence on cloud parameters such as cloud lifetime, effective radius and precipitation patterns (Kaufman et al., 1997). s_{max} determines which particles will leave the equilibrium domain to start to grow unrestrained and form cloud droplets.

It has proven to be difficult to measure s_{max} in situ, and good statistics on s_{max} is scarce. The objective with this work is to present a new concept for estimation of s_{max} of continental boundary layer clouds, utilizing the fact that that the chemical and physical properties of a particle can change significantly from the time a particle enters a cloud and forms a cloud droplet to the time when it exits the cloud and dries out.

The ambient aerosol is most often externally mixed, and the hygroscopic growth factor probability density function (GF-PDF) can often be described by two Gaussian functions: one less hygroscopic (LH) and one more hygroscopic (MH) mode. When a particle is activated into a cloud droplet it tends to absorb water soluble gases such as SO_2, NH_3 and HNO_3, which in turn increases the particles hygroscopicity and effectively moves it from the LH to the MH mode. By investigating which particles are left in the LH mode, it is possible to investigate if the aerosol has been cloud processed, and to derive a possible s_{max}.

The new approach is based on hygroscopic growth data at subsaturation from a Hygroscopic Tandem Differential Mobility Analyser (H-TDMA) (Swietlicki et al., 2008) in combination with size distribution measurements from a Differential Mobility Particle Sizer (DMPS). Each dry size and hygroscopic growth factor is associated with a certain critical supersaturation, s_c. By combining the size distribution data with the LH mode from the H-TDMA, dN/ds_c distributions can be derived for the LH particles, which describe the distribution of LH particles with respect to their s_c values.

According to our hypothesis, if the aerosol has been cloud processed the LH mode will be scavenged on particles with s_c lower than the s_{max} during the cloud passage. In this work we have therefore defined s_{max} as the s_c where the dN/ds_c distribution reaches its half maximum value (Fig. 1).

The method was used on a data set covering more than 2 years from the Swedish background site Vavihill. It was found that the average s_{max} of the boundary layer clouds observed is around 0.15% and s_{max} ratios are very rarely above 0.3% (Fig 2). In all, we found a cloud signal during 30% of the time. Satellite data gave further support to the hypothesis, as no cloud signal from the dN/ds_c functions was associated with a higher fraction of clear skies.

We conclude that this method could be a useful tool in order to obtain a deeper knowledge on the supersaturation ratio in boundary layer clouds, as there are many data sets available which could use this approach.

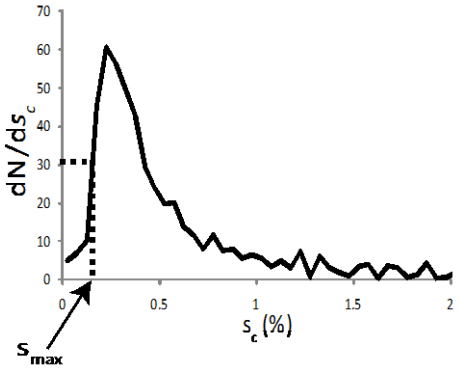

Figure 1. dN/ds_c distribution for a typical cloud event.

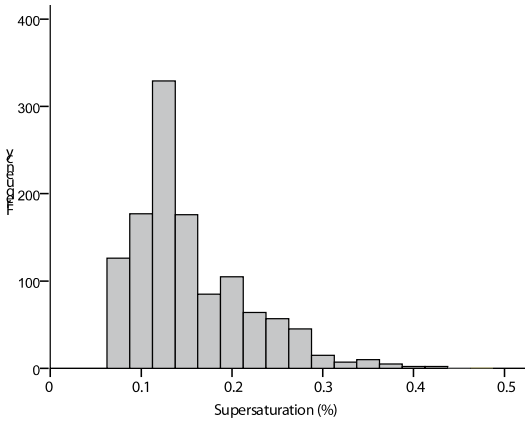

Figure 2. Dervied s_{max} values during two years of measurements.

Kaufman, Y.J. and Fraser, R.S. (1997) *The Effect of Smoke Particles on Clouds and Climate Forcing*, Science, **277**, 1636, doi:10.1126/science.277.5332.1636.

Swietlicki, E., Hansson, H.-C., Hämeri, K., Massling, A., Petäjä, T., Tunved, P., Weingartner, E., Baltensperger, U., McMurry, P.H., McFiggans, G., Svenningsson, B., Rissler, J., Wiedensohler, A. and Kulmala, M. (2008): *Hygroscopic Properties of Sub-Micrometer Atmospheric Aerosol Particles Measured with H-TDMA Instruments in Various Environments – A Review*. Tellus B, **60**, Issue 3, 353-364.

Linking CCN chemistry and supersaturation spectra: characterizing cloud-active aerosol in California's Sierra Nevada Mountains

G.C. Roberts[1,2], S.D. Noblitt[1], J.M. Creamean[3], J.L. Collett[4], C.S. Henry[5], S.V. Hering[6], and K.A. Prather[3]

[1]Center for Atmos. Sciences and Physical Oceanography, Scripps Inst. of Oceanography, La Jolla, CA, USA
[2]Centre National de Recherche Scientifique – Météo France, Toulouse, France
[3]Department of Chemistry, University of California San Diego, La Jolla, CA, USA
[4]Department of Atmospheric Science, Colorado State University, Fort Collins, CO, USA
[5]Department of Chemistry, Colorado State University, Fort Collins, CO, USA
[6]Aerosol Dynamics, Inc., Berkeley, CA, USA

Keywords: CCN, Aerosol chemistry, Aerosol cloud interactions, Electrophoresis.
Presenting author email: roberts.gregc@gmail.com

To assess the sources of cloud active aerosol and their interaction with the hydrological cycle in California, the CalWater 2011 Experiment took place in winter 2011 in the foothills of the Sierra Nevada Mountains in Central California (at the Sugar Pine Reservoir, Placer County, CA; 1070 masl). Previous studies in the California Central Valley [*Chow et al.*, 2006] show that nitrates and organic matter comprise most of $PM_{2.5}$ (~70% of total mass); and the remaining 30% consists mostly of sulfates, elemental carbon and crustal material. Nitrates and sulfates are generally hygroscopic and increase the CCN activity. Rainfall data over the western part of the United States indicate a reduction in orographic precipitation downwind of urban centers [*Rosenfeld and Givati*, 2006]; hence, relating aerosol chemistry to CCN activity is vital for studying the anthropogenic influence on cloud development and precipitation.

During the CalWater Experiment, we coupled the capabilities of demonstrated miniaturized instrumentation – cloud condensation nuclei (CCN), water condensation nuclei (WCN) and microchip capillary electrophoresis (MCE) – to provide direct chemical measurements of cloud active aerosols. Ion concentrations of CCN droplets attribute the anthropogenic, marine and secondary organic contributions to cloud-active aerosols. The MCE system was also coupled to a WCN device to determine the mass fraction of soluble ions that serve as cloud-active nuclei. In addition to direct measurements of the CCN and aerosol chemistry, continuous CCN spectra (between 0.1 and 1% supersaturation, S_c), aerosol size distributions and concentrations were also measured.

CCN concentrations were low ($N_{CCN,0.4}$ < 100 cm^{-3} at 0.4% S_c) when high pressure systems prevented boundary layer development and intrusion of the Central Valley pollution to the site - suggesting relatively low aerosol sources of CCN from the surrounding forest during this period. Storm fronts and changes in atmospheric boundary layer brought aerosol and anions associated with Central Valley pollution to the field site with concentrations reaching several thousand cm^{-3}.

MCE results show that nitrates and sulfates comprise most of the fraction of the aerosol anion mass (PM_1). Nitrate concentrations were often low (0.5 $\mu g\ m^{-3}$) due to the frequent rains in February and March; however, regional sources did generate peaks of several $\mu g\ m^{-3}$ of nitrate during the passage of a storm front, which transported pollution from the Central Valley upslope. These results are in agreement with earlier filter-based measurements [*Chow et al.*, 2006]. Chloride was also an important component during precipitation events indicating contributions of marine sources as well.

CCN spectra show large variations depending on the aerosol sources and often exhibit bi-modal distributions with minima at 0.4% S_c -- similar to the so-called 'Hoppel minima' associated to number size distributions. During these bi-modal events, sulfate also increases supporting the addition of these anions during cloud processing [*Yu et al.*, 2005]. $N_{CCN,0.1}$ also coincide with increases in aerosol nitrate, which suggests that nitrate has a role in cloud formation as giant CCN and, furthermore, in precipitation processes in the Sierra Nevada.

This work was supported by the California Energy Commission under grant CEC 500-08-046.

Chow, J.C. et al. (2005) *J Geophys Res*, **111**, doi:10.1029/2005JD006457, 2006.
Rosenfeld, D., and A. Givati, (2006) *J Appl Meteorol Clim*, **45**, 893-911.
Yu, J., X. Huang, J. Xu, and M. Hu, (2005) *Environ Sci Technol*, **39**, doi: 10.1021/es049559f.

Analysis of cloud and aerosol particles by single particle mass spectrometry during a hill-cloud-field experiment in Central Europe

A. Roth[1], S. Mertes[2], D. van Pinxteren[2], T. Klimach[1], J. Schneider[1] and S. Borrmann[1,3]

[1]Particle Chemistry Department, Max Planck Institute for Chemistry, Mainz, 55128, Germany
[2]Leibniz-Institute for Tropospheric Research, Leipzig, 04318, Germany
[3]Institute of Atmospheric Physics, Johannes Gutenberg University, Mainz, 55128, Germany
Keywords: Mass Spectrometry, Single Particle Analysis, CCN.
Email: a.roth@mpic.de

Aerosol-cloud interactions as well as the chemical composition of particles were investigated during the field campaign Hill Cap Cloud Thuringia (HCCT) in September and October 2010 on a mountain site in Central Germany (Schmücke, 938 m a.s.l.). Orographic cloud residual particles were analysed by the Aircraft-based Laser Ablation Aerosol Mass Spectrometer (ALABAMA, particle size range 150 nm - 900 nm) (Brands *et al.*, 2011) behind a counterflow virtual impactor (CVI), which samples cloud droplets and subsequently evaporates the cloud water. Additionally the total background aerosol population was sampled through an interstitial inlet (INT, cut-off diameter 5 µm) before and after cloud events. Parallel to the ALABAMA the particle size distribution was measured by an optical particle counter (OPC) with a size range between 0.25 µm and 32 µm.

The ALABAMA allows the qualitative chemical analysis of submicron single aerosol particles by laser ablation with a time resolution of 70 ms. This method gives information about particle size as well as composition and consequently helps to distinguish between different particle types. Although being developed for aircraft-based measurements, the ALABAMA is also suitable for ground-based measurements.

About 200000 positive and negative single particle mass spectra were recorded during the field campaign. A comparison of the averaged mass spectra for activated (CVI) and total (INT) aerosol shows that cloud residual particles contain a higher fraction of nitrate-containing particles, but a lower fraction of organic particles than particles of the background aerosol (see Figure 1). Besides, the relative fraction of sulphate is smaller. For further analysis, the mass spectra are separated in clusters, representing a certain particle type, by different clustering algorithms e.g., k-means. The relative abundance of the clusters will be related to meteorological conditions as cloud events, wind direction or back trajectories.

The time series of the number concentration measured by ALABAMA and the OPC show a good correlation between the two instruments, whereas the size distributions have different maxima due to various detection limits and sizing methods. Further analysis of the size distributions of cloud residual particles respectively background aerosol particles in addition with the mass spectra gives a hint for answering the question whether particle size or composition is the determining factor for particles to act as cloud condensation nuclei (Dusek *et al.*, 2006).

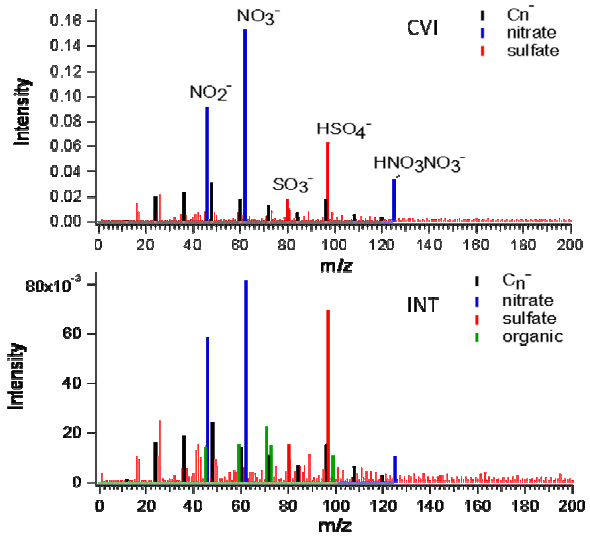

Figure 1. Average negative single particle mass spectra of cloud residual particles (top) and background aerosol particles (bottom) measured by ALABAMA

Brands, M., Kamphus, M., Böttger, T., Schneider, J., Drewnick, F., Roth, A., Curtius, J., Voigt, C., Borbon, A., Beekmann, M., Bourdon, A., Perrin, T. and Borrmann, S. (2011) *Aerosol Sci. Technol.*, **45**, 46-64

Dusek, U., Frank, G. P., Hildebrandt, L., Curtius, J., Schneider, J., Walter, S., Chand, D., Drewnick, F., Hings, S., Jung, D., Borrman, S. and Andreae, M. O. (2006) *Science*, **312**, 1375-1378

Tuesday, September 6, 2011

Session 5C: Smog Chamber Experiments and SOA 1

Aging of secondary organic aerosol in a smog chamber

J. Dommen[1], T. Tritscher[1], P.F. DeCarlo[1,2], P.B. Barmet[1], A.P. Praplan[1], E. Weingartner[1], M. Gysel[1], A.S.H. Prévôt[1], N.M. Donahue[3], and U. Baltensperger[1]

[1]Laboratory of Atmospheric Chemistry, Paul Scherrer Institut, Villigen, 5232, Switzerland
[2]AAAS Science and Technology Policy Fellow Hosted at the US EPA, Washington, DC, 20460, USA
[3]Department of Chemical Engineering, Carnegie Mellon University, Pittsburgh, PA, 15213, USA
Keywords: SOA, hygroscopicity, volatility, AMS.
Presenting author email: josef.dommen@psi.ch

The MUltiple CHamber Aerosol CHemical Aging Study (MUCHACHAS) was designed to study changes in total amount and properties of secondary organic aerosol (SOA) induced by exposure to OH radicals. A series of experiments took place at the Paul Scherrer Institute 27-m^3 chamber. Experiments began with the dark ozonolysis of α-pinene (AP) at low and high AP concentrations (10 and 40 ppb respectively). After the precursors were consumed, and mass levels were stable, OH exposure of the gas and aerosol products was initiated. Several methods of OH exposure were used including HONO photolysis and dark OH generation from the ozonolysis of tetramethylethene (TME). OH generation via HONO photolysis experiments were conducted at both high and low NO_x levels.

Gas and aerosol phase evolution was monitored with standard instrumentation including Proton Transfer Reaction Mass Spectrometry (PTRMS), Ion Chromatography Mass Spectrometry (IC-MS), High Resolution Time-of-Flight Aerosol Mass Spectrometry (AMS), and a Volatility/Hygroscopicity Tandem Differential Mobility analyzer (V/H-TDMA).

Results

In most experiments we observed a sometimes slow, but steady evolution in hygroscopicity, volatility and AMS signature of α-pinene SOA, which appeared to be independent of exposure to ozone and OH. We hypothesize that this "ripening" is caused by relatively slow transformations of the condensed phase which do not influence the SOA mass concentrations but do influence intensive physical and chemical properties such as volume fraction remaining (VFR), hygroscopicity and the atomic oxygen to carbon ratio (O:C).

Based on this observation we distinguished four phases in our reaction sequence as shown in Figure 1: O_3 mediated condensation and O_3 mediated ripening during ozonolysis and OH mediated condensation and OH mediated ripening during OH exposure. The first phases of ozonolysis and OH exposure are dominated by the impact of condensation on the aerosols physical and chemical properties. During the O_3 mediated condensation the particles volatility decreased (increasing VFR) while the hygroscopicity increased. After exposing the SOA to OH radicals an OH mediated condensation started with a significant increase of SOA mass and a concurrent increase of hygroscopicity and volatility.

The O_3 mediated ripening as well as the OH mediated ripening phases were characterized by a continued decrease of the volatility. While the ozonolysis only experiments showed little change in the O:C atomic ratio as measured by the AMS after the precursor was consumed (O_3 mediated ripening), OH exposure of the aerosol showed a much larger increase in this ratio during OH mediated condensation and ripening.

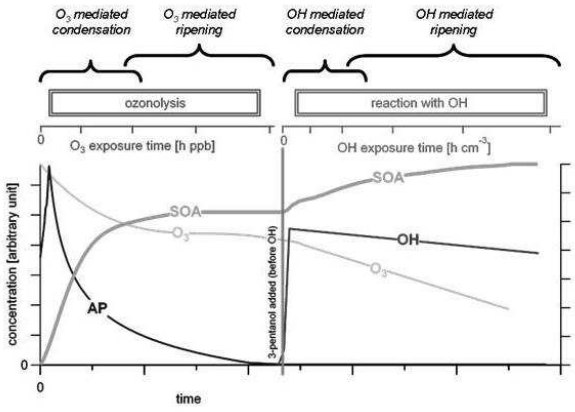

Figure 1. Four phases of transformations of secondary organic aerosol (SOA) from α-pinene (AP) as observed during ozonolysis and OH exposure.

The ripening effect may occur either by heterogeneous reactions on the surface of the SOA particles, by homogeneous reactions like oligomerization or by an evaporation – gas phase oxidation – recondensation cycle. Evidence for either of these mechanisms will be presented and discussed.

This work was supported by the IMBALANCE project of the Competence Center Environment and Sustainability of the ETH Domain (CCES), the Swiss National Science Foundation as well as the European Commission (the Research Infrastructures Programme EUROCHAMP-2). PFD is grateful for postdoctoral research support from the US-NSF (IRFP #0701013).

Transformation of diesel exhaust in a new smog chamber

A. Leskinen[1,2], K. Kuuspalo[2], O. Sippula[2], P. Jalava[2,3], M.-R. Hirvonen[2,3], J. Jokiniemi[2,4] and K.E.J. Lehtinen[1,5]

[1]Finnish Meteorological Institute, Kuopio Unit, Atmospheric Research, P.O. Box 1627, 70211 Kuopio, Finland
[2]Department of Environmental Science, University of Eastern Finland, P.O. Box 1627, 70211 Kuopio, Finland
[3]Dept. of Environmental Health, National Institute for Health and Welfare, P.O. Box 95, 70701 Kuopio, Finland
[4]VTT Technical Research Centre of Finland, P.O. Box 1000, 02044 VTT, Finland
[5]Department of Applied Physics, University of Eastern Finland, P.O. Box 1627, 70211 Kuopio, Finland
Keywords: Diesel exhaust, Smog chamber.
Presenting author email: Ari.Leskinen@fmi.fi

Particulate matter (PM) is one of the most important environmental health concerns worldwide. Of special concern are the submicron particulate emissions from combustion sources, because they deposit into the tracheobronchial and alveolar regions of the respiratory tract and can even penetrate through the lung tissue and reach the capillary blood vessel and circulating cells. It is noteworthy that the current data are based on the assumption that all fine particles have identical composition and health effects. However, this is not the case according to recent toxicological studies which show that the toxic potential of PM depends on aerosol size, concentration, chemistry and morphology (e.g., Paur *et al.*, 2008).

In the atmosphere the physical and chemical properties of the emission change considerably, e.g., due to photochemical reactions in the daytime and oxidation reactions in the nighttimes, as seen in a previous study with an aging diesel exhaust in an environmental chamber (Leskinen *et al.*, 2007). The aging may alter the health related toxicological responses of the emission, as discussed by Jalava *et al.* (2007). However, there is only limited scientific data pointing out which are the actual components of the emissions – both fresh and aged – that are linked to the toxicological responses. Thus, more experiments combining the aging and the toxicological studies in controlled laboratory conditions are needed.

A new experimental set-up (Figure 1) at the University of Eastern Finland (UEF) in Kuopio, introduced in mid-2011, enables on-line exposure of cells to aerosols and analysis of related toxicological health impacts. The set-up consists of 1) different biomass-fired combustion appliances, 2) a diesel engine test bench constructed according to the ISO 8178 standard and equipped with a 30 kW eddy current dynamometer system which is capable of producing a 90 Nm torque and 14000 rpm speed (later in 2011, a chassis dynamometer designed for testing vehicles in low-to-medium performance class (Max 350 kW, 2000 Nm, 350 km/h) will be installed for vehicle emission studies), 3) different types of dilutors (ejector dilutors, porous tube dilutors, a dilution tunnel), 4) a transformation chamber made of 125 µm FEP Teflon and 30 m^3 of volume, 5) an air-liquid cell exposure unit (Vitrocell®), and 6) several instruments for measuring the physical and chemical characteristics of the emission. All parts of the set-up are located in the same experimental hall, which minimizes sampling losses and artefacts between the different parts.

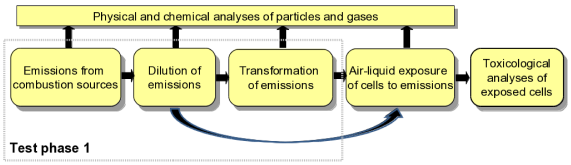

Figure 1. The new set-up at UEF that enables on-line exposure to fresh and aged combustion aerosols. (The first test phase is bounded by the gray rectangle.)

In the first test phase the deposition rate of monodisperse test aerosol particles onto the chamber walls will be determined by size distribution and number concentration measurements and model calculations. The secondary organic aerosol formation potential of diluted diesel engine emissions will be determined in the chamber both in the presence of UV light (350 nm) and in the dark, both with and without an OH (hydroxyl radical) scavenger, and with and without additional ozone and/or reactive organics. We will use the same diesel engine and test cell parameters as in our recent studies (Jalava *et al.*, 2010). The time evolution of the physical and chemical characteristics of the diesel emission and the secondary organic aerosol yield with different initial parameters will be used to estimate an adequate dose to the cells in the exposure unit.

The infrastructure has been partially supported by the European Regional Development Fund (ERDF), and the research by Tekes (the Finnish Funding Agency for Technology and Innovation).

Jalava, P.I., Tapanainen, M., Kuuspalo, K., Markkanen, A., Hakulinen, P., Happo, M.S., Pennanen, A.S., Ihalainen, M., Yli-Pirilä, P., Makkonen, U., Teinilä, K., Mäki-Paakkanen, J., Salonen, R.O., Jokiniemi, J. and Hirvonen, M.-R. (2010) *Inhal. Toxicol.* **22** (S2), 48–58.

Jalava, P.I., Salonen, R.O., Pennanen, A.S., Sillanpää, M., Hälinen, A.I., Happo, M.S., Hillamo, R., Brunekreef, B., Katsouyanni, K., Sunyer, J. and Hirvonen, M.-R. (2007) *Inhal. Toxicol.* **19**, 213–225.

Leskinen, A.P., Jokiniemi, J.K. and Lehtinen K.E.J. (2007). *Atmos. Environ.* **41**, 8865–8873.

Paur, H.-R., Mülhopt, S., Weiss, C. and Diabaté, S. (2008) *J. Verbr. Lebensm.* **3**, 319–329.

Smog Chamber Studies on SOA Formation from Gasoline Exhaust and Pure Precursors

E. Z. Nordin[1], A. C. Eriksson[1, 2], J. E. Carlsson[1], P. Nilsson[1], M. K. Kajos[3], P. Roldin[2], J. Rissler[1], E. Swietlicki[2], B. Svenningsson[2], M. Bohgard[1], M. Kulmala[2,3], M. Hallquist[4], J. Pagels[1]
[1] Ergonomics and Aerosol Technology, Lund University, P.O. Box 118 SE-221 00 Lund, Sweden
[2]Division of Nuclear Physics, Lund University, P.O. Box 118 SE-221 00 Lund, Sweden
[3]Department of Physic, University of Helsinki, P.O. Box 64, FIN-00014 University of Helsinki, Finland
[4]Department of Chemistry, Atmospheric Science, University of Gothenburg, 412 96 Gothenburg, Sweden
Keywords: SOA, vehicles emissions, smog chamber, VOCs
Presenting author email: Erik.Nordin@design.lth.se

Formation of Secondary Organic Aerosol (SOA) in the atmosphere is of importance both from a climate and health point of view. Photo-oxidation of aromatic Volatile Organic Compounds (VOCs) such as Toluene and Xylene (TX) gives contribution to SOA formation in the atmosphere. Anthropogenic combustion sources such as light duty traffic contribute to emissions of light aromatics in the atmosphere. Vehicles operating on idling or cold starts have particularly high VOC emissions since the oxidation catalyst has yet to reach its operation temperature. The mass yield (the ratio between formed SOA and reacted light hydrocarbons) and the chemical composition of the formed aerosol are important parameters for understanding the mechanisms of SOA formation. The aim of this work is to improve the knowledge about light aromatics contribution to SOA formation, by examining and comparing the chemical composition and mass yields from idling gasoline exhaust and pure precursors.

The experiments were performed in a 6 m^3 Teflon (FEP) smog chamber, housed in a temperature controlled (22±1°C) 22 m^3 steel chamber. Black lights (intensity peak~350 nm) are used to initiate photochemistry; the NO_2-photolysis rate is 0.23 min^{-1}. Gasoline exhaust was injected via a heated ejector dilutor and heated inlet (120 °C). The vehicle used in the experiments was a Volvo V40 (118 kW) (1998). A relevant operating mode with sufficient emission reproducibility was identified and used. It involved a cold start and driving until engine cooler water temperature of 55°C was achieved. Emitted aerosol was then sampled to the smog chamber for 5-10 min. Nebulized ammonium sulfate was utilized as condensation seeds in all experiments. In the precursor experiment mixtures, three of the most abundant light aromatics in the exhaust (Toluene, m-Xylene and 1.2.4-Trimethylbenzene) were injected through evaporation to the smog chamber. The experiments were monitored by particle characterization instruments such as, High Resolution-Time of Flight Aerosol Mass Spectrometer (HR-ToF AMS) and Aerosol Particle Mass Analyzer (APM). Proton Transfer Reaction Mass Spectrometer (PTR-MS) and complementary GC-MS analysis was used for VOC-monitoring. The mass concentration of formed SOA was corrected for wall losses using the method by (Hildebrandt *et al.*, 2009).

Preliminary results from three gasoline and two pure precursor experiments are shown in Table 1. The reacted VOC concentration is calculated from the C_6-C_{10} data from PTR-MS. This can be used for mass yield calculations, given the assumption that C_6-C_{10} are the only SOA forming precursors. The fraction of organic signal at (m/z) 43, 44 (f43, f44) is derived from unity mass resolved AMS-data.

Table 1. Preliminary results from the campaign.

Exhaust/ Precursor	Initial VOC to NO - ratio	Reacted VOCs (µg/m^3)	Wall loss corrected SOA (µg/m^3)	f(43) f(44)
Gasoline	8.8	148	26	0.105 0.115
Gasoline	6.4	246	66	0.084 0.123
Gasoline	21.7	114	29	0.073 0.136
T + m-X	16.7	782	412	0.138 0.121
T + m-X +1.2.4-TMB	5.8	473	64	0.178 0.092

As shown in Table 1 the ratio between formed SOA and reacted light hydrocarbons for gasoline exhaust is higher than the ratio for pure precursors (for similar mass loadings), which indicates that a major part of the SOA in the gasoline experiments is formed from light aromatic hydrocarbons. The SOA formed in the gasoline experiments contains more highly oxidized material than the SOA from pure precursors. The gasoline exhaust but not the pure precursor experiments fit well with a recent compilation of AMS spectral features from atmospheric oxygenated organic aerosol (OOA) observations (Ng *et al.*, 2010). This suggests that pure precursor experiments do not recapture all of the complexity in the detailed SOA composition from idling gasoline exhaust.

Hildebrandt, L., *et al.* (2009). *High formation of secondary organic aerosol from the photo-oxidation of toluene.* Atmos. Chem. Phys. **9**: 2973-2986.

Ng, N. L., *et al.* (2010). *Organic aerosol components observed in Northern Hemispheric datasets from Aerosol Mass Spectrometry.* Atmos. Chem. Phys. **10**: 4625-4641.

This work was supported by the Swedish research council FORMAS through projects 2007-1205, 2008-1467 and 2010-1678

Investigations of primary and secondary organic aerosol emissions from mopeds

S. M. Platt[1], M. Clairotte[2], R. Chirico[1,3], P. Barmet[1], C. Astorga[2], J. G. Slowik[1], A. S. H. Prévôt[1] and U. Baltensperger[1]
[1] Laboratory of Atmospheric Chemistry, Paul Scherrer Institut (PSI), Villigen, 5232, Switzerland
[2]Institute for Energy, Sustainable Transport Unit, EC Joint Research Centre Ispra, 21027 Ispra (VA), Italy
[3]now at Italian National Agency for New Technologies, Energy and Sustainable Economic Development (ENEA), UTAPRAD-DIM, Via E. Fermi 45, 00044 Frascati, Italy
Keywords: Aerosol mass spectrometry, SOA (Secondary Organic Aerosols), Vehicle emissions
Presenting author email: stephen.platt@psi.ch

Vehicles are a major source of particulate matter (PM) in urban areas (EEA, 2006). PM has significant, sometimes lethal, health effects. A large fraction, 20-90%, of the total PM consists of organic aerosol (OA) (Jimenez *et al.,* 2009). OA may be classified as primary (POA), from direct emissions, or secondary (SOA), formed via gas-phase reactions. These reactions also involve semivolatile compounds partitioned between the particle and the gas phase and remain poorly understood. Mopeds are a popular means of transport in many countries, particularly in Southern Europe and in East and South Asia. Many mopeds on the road today have two-stroke (2-S) engines, known emitters of uncombusted fuel and lubricating oil, and may therefore contribute significantly to both POA and SOA in urban areas. Characterisation of POA and SOA emissions from mopeds is therefore required to understand their health impact and to design effective future vehicle pollution regulations.

Emissions factors (EF) (g OA kg^{-1} fuel), of POA and SOA were determined during smog chamber experiments, at the Paul Scherrer Institute (PSI), Switzerland, for a EURO 1 2-S moped, a EURO 2 2-S moped and a EURO 2 4-S moped. Moped exhaust was introduced into the chamber via a heated injection system and ejector diluter. Fourier-transform infra-red (FTIR) spectroscopy of the undiluted exhaust during injection was used to quantify the emissions of CO, CO_2, and gaseous hydrocarbons. An Aerodyne high-resolution time-of-flight aerosol mass spectrometer (HR-ToF-AMS) was used to quantify OA in the smog chamber. Proton transfer reaction mass spectrometry (PTRMS) was used to determine the concentrations of volatile organic compounds. Measurements of total hydrocarbon, CO, O_3, and NO_X concentrations were also performed. SOA formation in the chamber was initiated using UV lights. Figure 1 shows a time series of a typical experiment where both the measured and wall loss corrected (WLC) OA concentrations rapidly increase after the UV lights are switched on.

Moped POA EFs determined from the OA concentrations in the smog chamber were comparable to those calculated in previous chassis dynamometer studies at the Joint Research Center (JRC), Ispra, Italy. Moped EFs determined at both JRC and PSI are several orders of magnitude higher than those of other vehicle classes, including diesel and gasoline cars and heavy duty vehicles. Furthermore, these emissions contain large quantities of unreacted hydrocarbons, reflected by the fact that SOA comprised the main fraction of the OA after only a few hours. This is further illustrated by Figure 1, which shows that a large fraction of toluene and total hydrocarbons remain unreacted. We note therefore that the SOA EFs from this study represent only lower estimates of the total possible SOA emissions. We conclude that emission of OA by mopeds may be a major public health consideration in many urban areas.

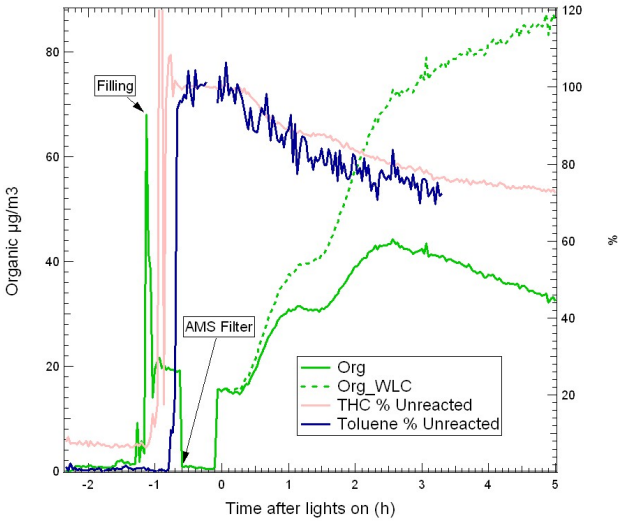

Figure 1: Time series from a smog chamber experiment on moped exhaust showing the evolution of organic aerosol concentrations together with the percentage of unreacted total hydrocarbons and toluene. The second observed increase in OA is due to the addition of NO to the smog chamber.

This work was supported by the Swiss Federal Office for the Environment (FOEN) and the Federal Roads Office (FEDRO).

EEA. (2006) *EMEP/ CORINAIR Emission Inventory Guidebook-2006*. Technical report no. 11/2006.

Jimenez, J. L. et al. (2009) *Science*. **326**(5959), 1525–1529.

Microscopic fungi as significant sesquiterpene emission sources

E.Horváth[1], A. Hoffer[1], F. Sebők[2], Cs. Dobolyi[3], S. Szoboszlay[2], B. Kriszt[2], A. Gelencsér[1]

[1]Department of Earth and Environmental Sciences, University of Pannonia, Veszprém, H-8200, Hungary
[2]Department of Environmental Protection and Environmental Safety, Szent István University, Gödöllő, H-2103, Hungary
[3]University Centre of Excellence in Environmental Industry Based on Natural Resources, Gödöllő, H-2103, Hungary

Keywords**:** emissions, secondary organic aerosols, microscopic fungi, sesquiterpene
Presenting author email: horvathe@almos.vein.hu

The group of sesquiterpenes, an important fraction of volatile organic compounds (VOCs) emitted by vegetation participates in the formation and growth of secondary organic aerosol (SOA) thereby directly and indirectly affecting the Earth's radiation balance. Although gas and particulate phase atmospheric reactions and gas-to-particle partitioning have been studied extensively, important sources of SOA precursors remain poorly characterized.

Among the volatile organic compounds emitted by vegetation isoprene, monoterpenes, sesquiterpenes and their derivatives are thought to contribute most to secondary organic aerosol formation. Sesquiterpenes (SQTs) are considered to be the most important biogenic SOA precursors in the atmosphere among the several hundreds of volatile organic compounds emitted by the vegetation (Griffin *et al.*, 1999). They are generally extremely reactive in the atmosphere, and their SOA yields have been determined to be significantly higher than those of monoterpenes (Baker and Sinnott, 2009). Due to their very high reactivity emission flux measurements of SQTs are loaded with very high uncertainties. Despite the high uncertainties in BVOC (biogenic volatile organic compounds) emission measurements global VOC inventories consider plant emissions as exclusive source of SOA precursors (Guenther *et al*, 1995).

Although it is well known that microscopic fungi globally turn over a vast amount of carbon by decomposing the organic matter in the soil, various atmospheric models do not yet include emission of secondary metabolites from soil fungal communities.

Detection of fungal volatiles can be used for fingerprinting fungal infection in agricultural commodities especially in grains and in indoor environment in order to prevent the decrease of nutritional value of agricultural commodities and the occurrence of allergy related illnesses (Moularat, 2008). In indoor and agricultural studies sesquiterpenes have been identified as secondary metabolites emitted by fungi (Fiedler, 2001).

In the present study we investigated the extent of sesquiterpene emission of microscopic fungi to establish its significance in secondary organic aerosol formation. To sample the headspace of pure cultures of some common microscopic fungi we used an aseptic flow-through apparatus designed for solid phase microextraction in our laboratory. The experimental system is shown in Figure 1.

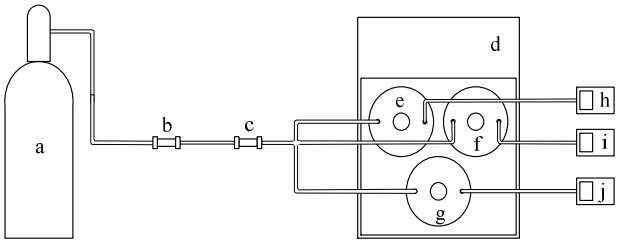

Figure 1. Scheme of the developed flow-through apparatus.
a: compressed air, b: activated carbon filter, c: HEPA filter, d: thermostat, e-f-g: sampling vials, h-i-j: portable carbon-dioxide monitor

The identified sesquiterpenes in the headspace extracts were quantified for eight strains of microscopic fungi belonging to four different genera.

Our results showed that microscopic fungi emit considerable amounts of sesquiterpenes. Based on our estimations microscopic fungi in soil can be considered as potentially significant sesquiterpene emission sources whose contribution to the secondary organic aerosol formation may be globally comparable to that of the vegetation.

Griffin, R. J., Cocker, D.R., Flagan, R.C. and Seinfeld, J.H. (1999) *J. Geophys. Res.* **104(D3)**, 3555-3567.

Baker, B. and Sinnott, M. (2009) *J. Chrom* **1216(A)**, 8442-8451.

Guenther, A., Hewitt, C. N., Erickson, D., Fall, R., Geron, C., Graedel, T., Harley, P., Klinger, L., Lerdau, M., Mckay, W.A., Pierce, T., Scholes, B., Steinbrecher, R., Tallamraju, R., Taylor, J. and Zimmerman, P. (1995) *J. Geophys. Res.* **100(D5)**, 8873-8892.

Moularat, S., Robine, E., Ramalho, O., Oturan, M. A. (2008) *Sci. Total Environ.* **407,** 139-146.

Fiedler, K., Schütz, E. and Geh, S. (2001) *Int. J. Hyg. And Environ. Health* **204,** 111-121.

Study of SOA formation from limonene ozonolysis in indoor environments: a new approach involving simultaneous investigation of gas and particulate phases molecular composition

S. Rossignol[1], L. Chiappini[1], E. Perraudin[2,3] and J.F. Doussin[2]

[1]Institut National de l'Environnement Industriel et des Risques (INERIS), 60 550 Verneuil-en-Halatte, France
[2]Laboratoire Interuniversitaire des Systèmes Atmosphériques (LISA), UMR CNRS 7583, Universities Paris Diderot/Paris-Est Créteil-Val-de-Marne, 94010 Créteil, France
[3] now at Laboratoire de Physico-et Toxico-Chimie de l'environnement - Environnements et Paléo-Environnements Océaniques et Continentaux (LPTC-EPOC), UMR CNRS 5805, University Bordeaux 1, 33 405 Talence Cedex, France
Keywords: SOA, indoor/outdoor aerosols, smog chamber, gas-particle distribution, chemical composition
Presenting author email: stephanie.rossignol@ineris.fr

Among the biogenic species, limonene is one of the most abundant terpenes emitted at the global scale, with α and β-pinene, and has one of the highest Secondary Organic Aerosols (SOA) formation potential. Thus Limonene plays an important role in atmospheric chemistry and has potential important climate and health impacts (VanReken, 2005).

Furthermore, limonene is also widely employed in scented products used in indoor environments, such as fresheners or household cleaners. As indoor ozone concentration, influenced by outdoor concentration and domestic sources, can be quite high, this oxidant can attack limonene to initiate gas phase chemistry and possibly lead to SOA formation (Coleman, 2008).

This work investigates the formation of SOA from limonene ozonolysis with a focus on indoor conditions. It combines simulation chamber ozonolysis experiments and field studies in an experimental house allowing reproduction of real conditions for household products use situations.

In order to describe multiphase chemistry involved in SOA formation and to take into account gas/particle partitioning phenomena, a new analytical approach is employed. Both gas and particulate phases are simultaneously collected, respectively on sorbent tubes and filters, and molecular composition is investigated using PFBHA and MTBSTFA derivatization prior to thermal-desorption coupled with gas chromatography and mass spectrometry (TD-GC-MS) analyse.

For each experiment, chemical data are coupled with physical characterisation of formed particles: mass evolution and size and number distribution evolution.

Simulation chamber experiments

Simulation chamber experiments were performed at the EUPHORE chamber (Figure 1, Valencia, Spain) in close to reality conditions: ozone and limonene concentration around 100 ppb, presence of seeds (ammonium sulphate) and humidity close to 50 %. In average, 75 $\mu g.m^{-3}$ of SOA were formed in these experiments.

Chemical characterisation of both gas and particulate phases allowed identification of limonene ozonolysis tracers, such as limononaldehyde or limonaketone, and evaluation of gas/particle partitioning of these species for a better understanding of physico-chemical mechanisms and processes involved in limonene SOA formation.

Figure 1: EUPHORE European atmospheric simulation chamber (left) and MARIA experimental house (right)

Field campaign

A field campaign was achieved in the experimental house MARIA (Figure 1, CSTB, Marne-la-Vallée, France), which is especially designed for indoor air quality studies. It is equipped as a real domestic home. Experiments were performed following scenario of limonene containing household product use in realistic conditions. Particles formation and growth was observed consequently to the use of house cleaning product. This formation could be attributed to the ozonolysis of the so emitted limonene.

Collected data on chemical composition of both phases and gas/particle partitioning of oxygenated species are coupled with data from simulation chamber experiment in order to evaluate the potential of limonene ozonolysis to form SOA in indoor environments under realistic user conditions. Thus this study provides an insight into particle exposure in a real indoor atmosphere.

Acknowledgments: M. Nicolas (CSTB, Marne-la-Vallée, France) for organizing field campaign in MARIA. The authors want to thank EuroChamp-2 for providing access to the Euphore Chamber and ADEME for the funding of the Primequal-ADOQ program.

VanReken, T. M., Ng N. L., Flagan R. C., and Seinfeld J. H. (2005) *J. Geophys. Res.*, **110**, D07206

Coleman, B. K., Lunden, M. M., Destaillats, H. and Nazaroff, W. W. (2008) *Atmospheric Environment*, **42**, 35, 8234-8245.

Modifications in hygroscopicity and volatility of wood combustion aerosols after chemical aging

Z. J. Wu[1], L. Poulain[1], O. Böge[1], R. Gräfe[1], , H. Herrmann[1], A. Wiedensohler[1]
K. Helbig[2], T. Schröder[2], J. von Sonntag[2], I. Hartmann[2]
[1] Leibniz Institute for Tropospheric Research, Permoserstr. 15, 04318 Leipzig, Germany
[2] German Biomass Research Centre, Torgauer Str. 116, D - 04347 Leipzig
Presenting author email: wuzhijun@tropos.de

Combustion of biomass is known to be a major source of gas- and particle- phase air pollution in the atmosphere and to be mainly made of a complex mixture of organics. To date, however, the atmospheric behaviours of these mixtures and their health effects are still largely unknown.

In this study, aging processes of different types of wood burning aerosols (see Table 1) are investigated. The wood burning aerosols are introduced into the IfT LEAK chamber (19 m^3, Iinuma et al. 2004) with and without ozone and /or UV lights simulating day- and night- times. Several online instruments including a Hygroscopic Tandem Differential Mobility Analyzer (H-TDMA), a Volatility Tandem Differential Mobility Analyzer (V-TDMA), a Multi-Angle Absorption Photometer (MAAP), a Scanning Mobility Particle Sizer (SMPS), and an Aerosol Mass Spectrometer (AMS) were used to measure the changes of physical and chemical properties of aerosols. In parallel to the physico-chemical study, modifications of the aerosols toxicity during the aging process were also investigated.

Table 1: Wood species and stoves

Wood	Stove
Spruce log	downdraught stove
Beech log	downdraught stove
WoodPellet	Pellet oven firing

In this abstract, the modifications in volatility and hygroscopicity of spruce burning aerosols via photochemical aging are presented as an example. Fig. 1 shows the comparisons of particle number size distributions before and after turning on the UV-lights. Fig. 2 and 3 display the temporal evolution of growth factor and shrink factor for different size particles, respectively. The growth factor is defined as the ratio of the wet particle mobility diameter D at RH=90% to dry diameter D0. The shrink factor is defined as the ratio of the particle diameter at a certain temperature (here, 120 and 300 °C) to the diameter at room temperature (25 °C).

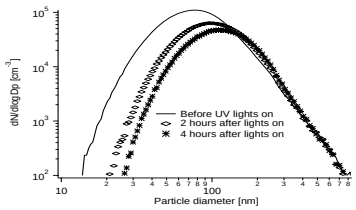

Fig. 1: Particle number size distribution

Before the UV-lights on, the growth factors for 50, 75, and 100 nm particles are within 1.3-1.4, and only 1.1 for 200 nm particles. This indicates that smaller particles are dominated by hydrophilic components, such as inorganic salts, while, larger particles are dominated by hydrophobic fraction, such as soot. After lights on, the growth factors of smaller particles decrease with time consuming. This means that more low hygroscopic organic species produced or condensed on the particles during aging process. But, no any changes in 200 nm particles were observed.

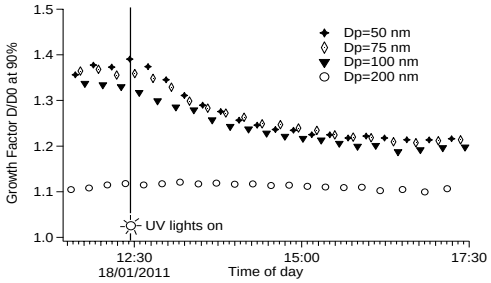

Fig. 2: Temporal evolution of hygroscopic growth

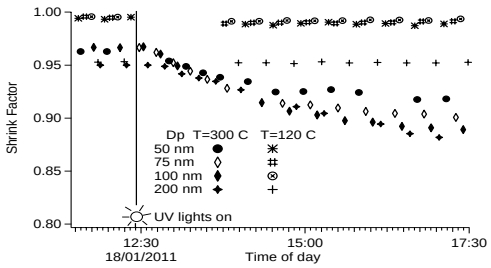

Fig. 3: Temporal evolution of volatility

At 120 °C, there is no any difference in shrink factor before and after UV-lights on, indicating that no high-volatile components, such as low carbon-number carboxylic acids, produced during chemical aging. At 300 °C, the particles freshly emitted with diameter of 50, 75, and 100 nm are non-volatile. After lights on, the aerosols are more volatile in contrast to primary particles. A detail study on the modifications in hygroscopicity and volatility of wood burning aerosols will be performed by combining the AMS data and filter measurements in the future work.

Acknowledgements:
This work was founding by Federal Ministry for the Environment, Nature Conservation and Nuclear Safety

Reference:

Y. Iinuma, O. Böge, T. Gnauk and H. Herrmann. Atmospheric Environment 38 (5) (2004), pp. 761–773.

Tuesday, September 6, 2011

Session 5D: Aerosols in Disease and Therapy

Large particle aerosols of pathogens within high level microbiological containment

R.J. Thomas[1]

[1]Biomedical Sciences, Dstl Porton Down, Salisbury, Wiltshire, SP4 0JQ, UK
Keywords: aerosol, respiratory, deposition, pathogens.
Presenting author email: rjthomas@dstl.gov.uk

The capability to generate large particle aerosols within high level microbiological containment was developed to enable investigation of differential deposition of small and large particle aerosols of *Bacillus anthracis*, *Yersinia pestis*, and *Burkholderia pseudomallei* on the pathogenesis of infection in the murine model.

The Collison nebuliser or flow-focussing aerosol generator (FFAG) was used to generate small and large particle aerosols respectively (Thomas *et al* 2009a). The aerosol distributions were characterised with respect to mass median aerodynamic diameters (MMAD), particulate distribution within droplets (spores and vegetative cells) and deposition within the murine respiratory tract. The FFAG had the capability to generate particle distribution with a MMAD up to 100 µm. Particulate concentration within individual particles increased as particle size increased (Table 1).

Table 1. Effect of increased particle size on the numbers of incorporated particulates

	Avg no. fluospheres per droplet		
Droplet size fraction (µm)[b]	MMAD 12 µm (±SE)[c]	MMAD 25 µm (±SE)[c]	MMAD 50 µm (±SE)[c]
0–3	0.42 ± 0.04	0.44 ± 0.03	0.36 ± 0.04
4–9	2.76 ± 0.18	8.80 ± 0.97	4.45 ± 0.46
10–17	7.54 ± 0.35	11.94 ± 0.73	12.25 ± 3.64
18–23	13.62 ± 0.69	16.49 ± 0.73	23.80 ± 3.95
24–30	0.00 ± 0.00	25.93 ± 1.47	29.33 ± 5.04
31–50	0.00 ± 0.00	47.00 ± 5.8	40.36 ± 0.97
51–75	0.00 ± 0.00	0.00 ± 0	80.38 ± 6.04
76+	0.00 ± 0.00	0.00 ± 0	186.6 ± 19.3

Aerosol distributions with MMADs of 1 and 12 µm produced by the Collison nebuliser and FFAG respectively were used to assess infection kinetics. Differential deposition was observed in the murine respiratory tract for each pathogen dependent on the size of the inhaled aerosol particles. Significantly greater deposition in the lungs was observed for the 1-3 µm particle aerosol produced by the Collison nebuliser compared to the nasal passages for all bacterial species investigated. In contrast, the bacteria incorporated within the 12 µm particle aerosol preferentially deposited in the nasal passages.

The differences in deposition profiles manifested as differences in infection kinetics. The median lethal dose and mean time to death were significantly greater for those animals that inhaled 12 µm particles (Table 2). The infection caused by inhalation of the 1-3 µm particle aerosols initiated in the alveoli or local lung lymph nodes before dissemination to visceral organs via the bloodstream. Although, the infections caused by inhalation of large particle aerosols initiated in the nasal cavity, subtle differences in progression of pathology and infected tissues were observed between the pathogens investigated (Thomas *et al* 2009b; Thomas *et al* 2010). Ultimately, the terminal stage involved dissemination via the bloodstream to visceral organs.

Table 2. Effect of particle size on infection kinetics in murine inhalational models. cfu = colony forming unit

Particle size	Median lethal dose (cfu)		Mean time to death (h)	
	1 µm	12 µm	1 µm	12 µm
Bacillus anthracis	2432	7656	101.6 ± 10.4	161.0 ± 16.1
Yersinia pestis	601	2951	72.0 ± 0	90 ± 11.5
Burkholderia pseudomallei	4	12	73.8 ± 11.3	174.7 ± 14.9

For the first time, assessments were made of the efficacy of therapeutics against both small and large particle inhalational infections of *B. anthracis*, *Y. pestis* and *B. pseudomallei*.

Conclusion: Aerosol particle size affects the site of deposition within the murine respiratory tract and influences disease progression. Ultimately, therapeutics must be geared towards providing protection against the complete spectrum of infections that may result from an inhalational challenge.

This work was supported by funding from the UK Ministry of Defence.

Thomas, R.J., Webber, D., Sellors, W., *et al* (2009a) *Aerobiologia.,* **25**, 75-84.
Thomas, R.J., Webber, D., Collinge, A., *et al* (2009b) *Infect. Immun.* **77**, 1315-1323.
Thomas, R.J., Davies, C., Nunez, A., *et al* (2010) *J. Med. Microbiol.* **59**, 1415-1427.

Anthrax Aerosols and Drums

A.M. Bennett[1],T. Pottage [1] and S. Parks[1]

[1]Microbiology Services Division, Health Protection Agency, Porton Down, Wiltshire, SP4 0JG, UK

Keywords: Bioaerosols, Health aspects of aerosols, Aerosol generation.
Presenting author email: allan.bennett@hpa.org.uk

Bacillus anthracis is a spore forming micro-organism that is the causative agent of anthrax. Anthrax has three main forms of infection: cutaneous, ingestional and inhalational. The latter is commonly fatal if untreated. In recent years, there have been two fatal cases of inhalational anthrax in the UK associated with African drums which were investigated by the Health Protection Agency (Riley 2007, Anaraki et al 2008). Other cases have also been identified in the US (Centers for Disease Control and Prevention 2000). In all these cases drums and skins have been recovered which have been shown to be contaminated with *B. anthracis* spores. The hypothesised route of infection in these cases was through the generation of an inhalable aerosol through either playing or manufacturing drums made from contaminated goatskins.

In order to investigate this route of infection a study was designed in order to measure the generation of microbial aerosols from artificially contaminated drums during playing and to measure the surface contamination of the drum over time.

Two drums were obtained for this study (Figure 1). The first drum was a small bongo was a holiday souvenir from West Africa, provided by a colleague. This drum had not been shaved. The second drum was a Djembe donated by a drum maker associated with one of the fatal cases. This drum had a shaved surface. Both drums were contaminated with spores of *Bacillus atrophaeus*, a commonly used surrogate of *B. anthracis*, generated from a DeVilbis No 40 nebuliser held close to the surface.. After drying, and at regular intervals over a period of three months, swab samples were taken of 1 cm^2 areas of the drum surface and assayed on TSA plates to measure the surface contamination on the drum.

Figures 1. Bongo Drum (left) and Djembe used in study.

The drums were placed in a 0.85m^3 volume safety cabinet with the following three microbial air samples: an Andersen 6-stage sampler (A6S), a Porton All glass Impinger (AGI) and a Casella slit sampler (CSS). Sampling was undertaken for 5 minutes period during which the drums were played for the initial two minutes. Results were expressed as percentage of total measured surface contamination aerosolised.

It was found that the surface contamination of the Bongo reduced by less than one log over the three month period in which it was played on 9 occasions while the contamination on the Djembe dropped nearly 2 logs during this time period when it was played 8 times.

The average % aerosol generated as percentage of surface contamination from the Djembe drumming was 0.010 measured by the A6S, 0.20 from the AGI and 9 x 10^{-3} from the CSS. The average particle size (A6S) was 1.9 microns. The Djembe results were 3.4 x 10^{-3} (A6S), 7.3 x 10^{-3}(AGI) and 3.1 x 10^{-3}(CSS) with an average particle size of 8.2 microns.

Since the magnitude of surface contamination found on drums associated with the cases of inhalational anthrax were far lower than those used in these experiments it would appear that the generation of anthrax aerosols from naturally contaminated drums would only occur sporadically at a very low level. Since the inhalational dose of anthrax is postulated to be in the range 8,000-10,000 spores it appears that these cases maybe due to the coincidence of a sporadic aerosolisation event with a highly susceptible individual.

References

Anaraki, S., Addiman, S., Nixon,G., Krahe, D., Ghosh,R., Brooks, T., Lloyd, G., Spencer, R. and Walsh, A. (2008). Investigations and control measures following a case of inhalational anthrax in East London in a drum maker and drummer. *Eurosurveillance.* **130**, 11-13.

Centers for Disease Control and Prevention (2006). Inhalation anthrax associated with dried animal hides--Pennsylvania and New York City, *MMWR Morb Mortal Wkly Rep.* 2006;**55(10):**280-2.

Franz, D. R., Jahrling, P. B., Friedlander, A. M., McClain, D. J., Hoover, D. L., Bryne, W. R., Pavlin, J. A., Christopher, G. W. & Eitzen, E. M. (1997) Clinical Recognition and Management of Patients Exposed to Biological Warfare Agents *J. Am. Med. Assoc.* **278,** 399–411.

Riley A. (2007). Report on the management of an anthrax incident in the Scottish borders; July 2006 to May 2007. Melrose: National Health Service Borders; Availablefrom: www.nhsborders.org.uk/uploads/18645/anthrax_report_131207.pdf

Abstracts of papers 5D3, 5D4, and 5D5 not availabe

Tuesday, September 6, 2011

Session 5E: Health Effects of Nanoparticles

Antibacterial activity by nanosilver ions and particles

G. A. Sotiriou and S. E. Pratsinis

Particle Technology Laboratory, Institute of Process Engineering, Department of Mechanical and Process Engineering, ETH Zurich, Sonneggstrasse 3, CH-8092, Zurich, Switzerland
Keywords: silver nanoparticles, antibacterial activity, *E. coli*, surface area concentration.
Presenting author email: sotiriou@ptl.mavt.ethz.ch

Nanosilver is used in heterogeneous catalysis and has promising applications in textiles[1], biomedical applications, biodegradable polymer films for food packaging[2], biological labeling, photonics, coloristic (plasmon)[3], optoelectronics and surface enhanced Raman scattering (SERS)[4]. At the same time, the use of nanosilver raises concerns for its toxicity against aquatic micro-organisms when disposed and therefore draws public attention[5]. In fact, nanosilver is one of the first nanomaterials to be regarded toxic and petitions had been filed to the U. S. Environmental Protection Agency (EPA) to regulate it as pesticide[6]. Therefore to safely employ nanosilver, correct risk and dose relations assessments need to be made.

There are several studies on the antibacterial activity of nanosilver made by wet-methods[7,8], co-condensation[9], electro-exploding wire[10] and flame spray pyrolysis[11,12]. Smaller nanosilver particles are more toxic than larger ones[8] especially when oxidized[8,11]. Additionally, even though silver metal is practically insoluble in water[13], when present in nanometer size range Ag^+ ions are released (leached)[11,14,15] from its surface. It has been shown recently[12] that the antibacterial activity of small (<10 nm) nanosilver particles is dominated by Ag^+ ions, while for larger ones (>15 nm) the antibacterial contribution by Ag^+ ions and particles is comparable. Such a behavior implies a surface area dependency of the antibacterial activity especially for small nanosilver sizes since the Ag^+ ion release is proportional to the exposed nanosilver surface area[12]. Additionally, when a nanothin silica coating on the surface of nanosilver is applied, this antibacterial activity can be minimized[16].

Here, the antibacterial activity of nanosilver against Gram negative *Escherichia coli* bacteria is investigated by immobilizing nanosilver on nanostructured silica particles and closely controlling Ag content and size. These Ag/SiO_2 nanoparticles were characterized by S/TEM, EDX spectroscopy, X-ray diffraction and, most notably, the exposed Ag surface area was measured by O_2 chemisorption. Furthermore, the fraction of dissolved nanosilver was determined by measuring the released (leached) Ag^+ ion concentration in aqueous suspensions of such Ag/SiO_2 particles. The antibacterial effect of Ag^+ ions was distinguished from that of nanosilver particles by monitoring the growth of *E. coli* populations in the presence and absence of Ag/SiO_2 particles. The antibacterial activity of nanosilver was dominated by Ag^+ ions when fine Ag nanoparticles (less than about 10 nm in average diameter) were employed that release high concentrations of Ag^+ ions. In contrast, when relatively larger Ag nanoparticles were used, the concentration of the released Ag^+ ions was lower. Then the antibacterial activity of the released Ag^+ ions and nanosilver particles was comparable.

Financial support by the Swiss National Science Foundation (No. 200020-126694) is kindly acknowledged.

References

1 M. J. Height and S. E. Pratsinis Antimicrobial and antifungal powders made by flame spray pyrolysis. Eur. Patent, EP1846327 (A1), 2007.
2 S. Loher, O. D. Schneider, T. Maienfisch, S. Bokorny and W. J. Stark, *Small* **4**, 824 (2008).
3 M. Quinten, *Appl. Phys. B-Lasers Opt.* **73**, 317 (2001).
4 P. C. Lee and D. Meisel, *J. Phys. Chem.* **86**, 3391 (1982).
5 B. G. Lee, S. B. Griscom, J. S. Lee, H. J. Choi, C. H. Koh, S. N. Luoma and N. S. Fisher, *Science* **287**, 282 (2000).
6 B. E. Erickson, *Chem. Eng. News* **87 (48)**, 25 (2009).
7 P. Li, J. Li, C. Z. Wu and Q. S. Wu, *Nanotechnology* **16**, 1912 (2005).
8 C. N. Lok, C. M. Ho, R. Chen, Q. Y. He, W. Y. Yu, H. Sun, P. K. H. Tam, J. F. Chiu and C. M. Che, *J. Biol. Inorg. Chem.* **12**, 527 (2007).
9 C. Baker, A. Pradhan, L. Pakstis, D. J. Pochan and S. I. Shah, *J. Nanosci. Nanotechnol.* **5**, 244 (2005).
10 D. K. Tiwari, J. Behari and P. Sen, *Curr. Sci.* **95**, 647 (2008).
11 C. Gunawan, W. Y. Teoh, C. P. Marquis, J. Lifia and R. Amal, *Small* **5**, 341 (2009).
12 G. A. Sotiriou and S. E. Pratsinis, *Environ. Sci. Technol.* **44**, 5649 (2010).
13 D. R. Lide, *CRC Handbook of Chemistry and Physics*. 89 (Internet version) ed.; CRC Press/Taylor and Francis: Boca Raton, FL, 2010.
14 T. M. Benn and P. Westerhoff, *Environ. Sci. Technol.* **42**, 4133 (2008).
15 E. Navarro, F. Piccapietra, B. Wagner, F. Marconi, R. Kaegi, N. Odzak, L. Sigg and R. Behra, *Environ. Sci. Technol.* **42**, 8959 (2008).
16 G. A. Sotiriou, T. Sannomiya, A. Teleki, F. Krumeich, J. Vörös and S. E. Pratsinis, *Adv. Funct. Mater.* **20**, 4250 (2010).

Water uptake on silica nanoparticles

Keskinen, Helmi[1], Romakkaniemi, Sami[1], Jaatinen, Antti[1], Miettinen, Pasi[1], Saukko, Erkka [2], Joutsensaari, Jorma[1], Mäkelä, Jyrki M.[2], Virtanen, Annele[2], Smith, James N.[1,3,4] and Laaksonen, Ari[1,5]
[1]Dept. of Applied Physics, University of Eastern Finland, P.O. Box 1627, 70211 Kuopio, Finland.
[2]Dept. of Physics, Tampere University of Technology, P.O. Box 589, 33101 Tampere, Finland.
[3]National Centre for Atmospheric Research, P.O. Box 3000, Boulder, CO 80307 USA.
[4]Finnish Meteorological Institute, P.O. Box 1627, 70211 Kuopio, Finland.
[5]Finnish Meteorological Institute, 00101, Helsinki, Finland.
Presenting author email:helmi.keskinen@uef.fi
Keywords: engineered nanoparticles, hygroscopic growth, adsorption

The first wetting layer of solid nanoparticles matters. Engineered nanoparticles can be exposed to water vapor in industrial processes, technological applications, and in the atmosphere. Water vapor produces films on the surface of the nanoparticles with a thickness that is determined by the relative humidity and interaction forces between the surface and the adsorbed water molecules (Thiel 1987). Recently, much attention has been paid to the impacts of atmospheric nanoparticles on cloud formation and climate (Laaksonen et al., 2004). Here we want to pay attention to understanding the environmental and climate impacts of directly emitted engineered nanoparticles. That question is highly topical and an early-stage evaluation of engineered nanoparticle exposure to the atmosphere, water and soil has been made (Mueller and Nowack, 2008).

The nanoaerosol is generated from aqueous silica suspension by an atomizer (TSI, 3076). Hygroscopic growth is measured using the nano-H-TDMA (Hygroscopicity Tandem Differential Mobility Analyzer). The size and density of size-selected nanoparticles are studied with the scanning mobility particle sizer (SMPS) and a DMA coupled with electrical low pressure impactor (ELPI). Particle morphology is studied using off-line electron microscopy analysis. The experimental results from water uptake are compared to the adsorption isotherm FHH-theory.

We observed that the smallest detected particles (selected mobility diameter of 8 or 10 nm) were spherical with the silica bulk density (2.2. g cm^{-3}) (Figure 1a) and larger particles were agglomerated (Figure 2b). The effective density of these particles decreased with size, from 1.7 g cm^{-3} at the smallest measured diameters (20 nm) to 0.8 g cm^{-3} at 150 nm (Figure 1c). From Figure 2 we see that a few (2-3) adsorbed water layers in these subsaturated conditions (RH from 50 to 90 %) were observed for the smallest size-selected particles (8- 10 nm). These observations agreed also well with fitted FHH isotherm. However, slightly larger nanoparticles at 15 and 20 nm in diameter had higher amounts of adsorbed water (Figure 2). Particles at this size range could include dense agglomerates with a few primary particles, whereby water adsorption is enhanced by the capillary effect. These adsorbed water layers can have consequential affect on the uptake of water soluble substances on these nanoparticles in atmosphere as well in their post-processing in engineered applications.

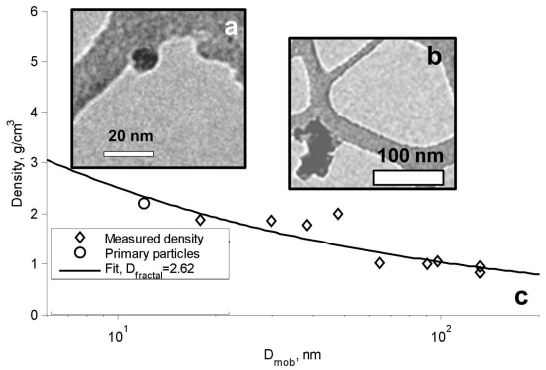

Figure 1 (a) TEM images of smaller spherical and (b) larger agglomerated fumed SiO2 nanoparticles. (c) Measured effective density versus particle size of atomized SiO2 nanoparticles and fitted density profile with Df= 2.62 (solid line).

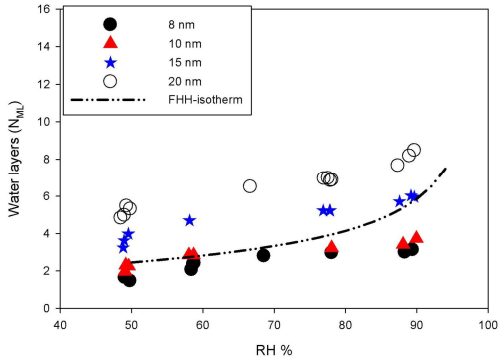

Figure 2 Number of the water layers versus RH at selected dry particle diameters for atomized fumed SiO2 and the fitted FHH-isotherm.

This work was supported by the academy of Finland (Centre of Excellence, No 1118615 and decision numbers 123466, 118230, 138951), Kone foundation and Saastamoinen foundation. We gratefully thank Dr. Arto Koistinen for microscopic analysis and Douglas Worsnop for thoughtful discussions.

Laaksonen et al. (2005). Atmos. Chem. Phys. 5: 461-464.
Mueller, N.C. and Nowack, B., (2008). Environ. Sci. Technol. 42: 4447–4453.
Thiel, P. A. and Madey, T. E. (1987). Sci. Rep. 7: 211-385.

Direct deposition of aerosol generated AuNPs into biological buffers produce specific protein corona in lung-fluid and blood serum

C.R. Svensson[1], M.E. Messing[2], A. Schollin[3], K. Deppert[2], B.O. Meuller[2], J. Pagels[1], J. Rissler[1], M. Bohgard[1], S. Linse[3], T. Cedervall[3]

[1]Ergonomics and Aerosol Technology, Lund University, Lund, Scania, 221 00, Sweden
[2]Solid State Physics,Lund University, Lund, Scania, 221 00, Sweden
[3]Biochemistry and Structural Biology, Lund University, Lund, Scania, 221 00, Sweden
Keywords: nanoparticles characterization, protein corona, biomolecules, toxicity, generation of nanoparticles
Presenting author email: christian.svensson@design.lth.se

Awareness of health effects due to nanoparticle exposure has continuously increased over the last decade. The primary route of exposure is by air, as particles deposit in the respiratory tract. Due to the special properties of nanoparticles, such as a high surface area to mass/volume ratio, concern has been raised with regards to their potential effects in biological systems.

In recent years the particles interaction with biomolecules has been acknowledged as crucial for the understanding of particle toxicity (Lynch, 2009). When biomolecules bind to the particle surface a dynamic protein/biomolecule corona is created (Cedervall, 2007). The protein corona is dependent on the surface chemical properties, the size and morphology of the particles. The protein corona is believed to be important for the biological effects of nanoparticles.

In this work we present a method to investigate the composition of the biomolecule/protein corona on model nanoparticles in two different physiological fluids, porcine serum and porcine lung fluid. Gold nanoparticle (AuNP) agglomerates (Geometric mean diameter GMD 70 nm) were generated by spark discharge (SDG) and high temperature evaporation condensation (HT). The agglomerates where sintered to spherical shapes, at 400°C, and characterized online by tandem differential mobility analysis (T-DMA) and aerosol particle mass analysis (DMA-APM) (Ehara, 1995). The sintered AuNPs (GMD 45 nm) were deposited onto solutions of bovine serum albumin (BSA) and homocysteine using an electrostatic precipitator (ESP). The BSA and homocysteine have thiol groups known to form bonds with gold particles. AuNPs in suspension with BSA and homocysteine were identified with dynamic light scattering (DLS) on selected time-intervals (h to days). AuNPs in solution were mixed with porcine serum or porcine lung fluid. Using sodium dodecyl sulfate polyacrylamide gel electrophoresis (SDS-PAGE) the protein corona was determined for AuNPs mixed with the physiological fluids.

DLS data indicate that particle-biomolecule complexes had formed in suspension for AuNP depositions in both BSA and homocysteine. The DLS signal could be observed over the course of several days (Table 1).

Table 1. DLS measurements performed on AuNPs deposited in homocysteine solution.

AuNP + Homocysteine	d. (nm)
Day 1	165,5
Day 2	122,2
Day 7	107,8

Results from SDS-PAGE indicate that the protein corona is similar regardless of surfactant biomolecule, BSA or homocysteine (Figure 1). It also shows that the corona is different between particles mixed with porcine lung fluid or porcine blood serum.

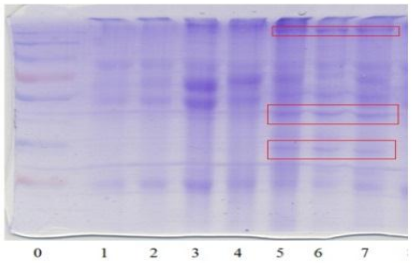

Figure 1. Results from SDS PAGE for gold nanoparticles mixed with porcine blood serum and lung fluid. 1, 2, 3, and 4 are samples of particles mixed with blood serum while 5, 6, and 7 are particle samples mixed with lung fluid. Red marks indicate unique protein bands for the protein corona in lung fluid.

In conclusion: We have shown that the protein / biomolecule corona can be studied using model particles generated in the aerosol phase and stabilized with BSA and homocysteine in suspension. Also, the observed corona is different between particles administered to porcine blood serum and lung fluid.

This work was supported by the Nanometer Structure Consortium at Lund University (nmC@LU) and the Swedish research council FAS through project 2009-1291 and the FAS-centre METALUND

Cedervall, T et al. (2007). PNAS, 104, 7, 2050-2055.
Ehara, K et al. (1995). J. Aerosol Sci. 27, 217-234.
Lynch, I et al. (2009). Nat Nanotechnol, 4,577-80.

Assessing inhalation exposure to nanoparticles during nanoparticle synthesis and packing

A.J. Koivisto[1], M. Aromaa[2], J. Lyyranen[3], J. Mäkelä[2], A. Auvinen[3], J. Jokiniemi[3] and K. Hämeri[4]
[1]Finnish Institute of Occupational Health, Helsinki, Topeliuksenkatu 41 a A, 00250 , Finland
[2]Tampere University of Technology, Department of Materials Science, Tampere, P.O.Box. 589, 33101, Finland
[3]Technical Research Centre of Finland (VTT), Fine&Nano Particles, Espoo, P.O.Box 1000, 02044 VTT, Finland
[4]University of Helsinki, Department of Physics, Helsinki, PO Box 64, 00014, Finland
Keywords: industrial aerosols, exposure, nanoparticle, measurements.
Presenting author email: joonas.koivisto@ttl.fi

This study presents exposure assessment for nanoparticles (NPs) during synthesis and packing. The measurements were carried out at two different occupations where the first was a pilot plant and another was a TiO_2 factory. We measured particle size distributions with a Grimm sectional mobility particle sizer and a Grimm Dust monitor 1.109. NPs were discriminated from background particles from the size sectioned particle concentration difference during process and before process. Regional minute lung deposition rates was defined for NPs (IRCP, 1995) and in dose calculation was used respirator assigned protection factor (APF) (European standard: EN529) and by measuring respirator work place protection factor with condensation particle counter (TSI), electronic low pressure impactor (Dekati), and nanoparticle surface area monitor (TSI).

Figures 1 and 2 shows the particle size distribution time series during the NP synthesis with liquid flame spray (LFS) process and packing of TiO_2 nanomaterial. Three different LFS processes were conducted in a ventilated chamber or under hood (processes 1 to 3 in Table 1). Table 1 shows that in NP synthesis, minute particle number lung deposition was dominated by NPs during synthesis 1 and 2 ($f_{NP,\dot{n}} > 99\%$), and partly in synthesis 3. NPs influence on minute mass deposition rate was negligible ($f_{NP,\dot{m}} < 0.11\%$). However, in TiO_2 nanomaterial packing the NPs' affected on particle minute deposition rate only 5% but in mass 99%. Regional deposition rate shows that mass was deposited on head airways (70%) and particle number in alveolar region (70%). In NP synthesis workers used a TH2 type powered respirator where the particle penetration was 2% according to the standard EN529. However, the particle penetration was less than 10^{-6} % according to the CPC and less than 10^{-4} % according to the ELPI. This study shows that the metrics to describe exposure to NPs depend on the process (i.e. synthesis or post-process) and by using the respirator APF may overestimate significantly the calculated dose.

This work was performed as a part of Nanohealth, Nanoturva, and Nanodevice research programmes.

IRCP (International Comission on Radiological Protection) (1995) Human Respiratory Tract Model for Radiological Protection, Annals of the IRCP, Publication 66, Elsevier Science, Inc., Tarrytown, NY.

Table 1: Minute lung deposition rate in units of particle number $\dot{n}$ and mass $\dot{m}$. f_{NP} is fraction of NPs influencing on the deposition rate. Values are not weighted with respirator protection factor.

	NP synthesis			TiO_2 factory
Unit[b]	1.	2.	3.	Packing
$\dot{n} \times 10^9$, $[\mathrm{min}^{-1}]$	1.5	21	0.53	0.06
$f_{NP,\dot{n}}$, [%]	99.5	99.2	25.8	5
$\dot{m}$[a], $[\mu\mathrm{g\ min}^{-1}]$	6.3	130	263	440
$f_{NP,\dot{m}}$, [%]	0.11	0.02	0.00	99

[a]effective density assumed to be 1.7g cm^{-3}.

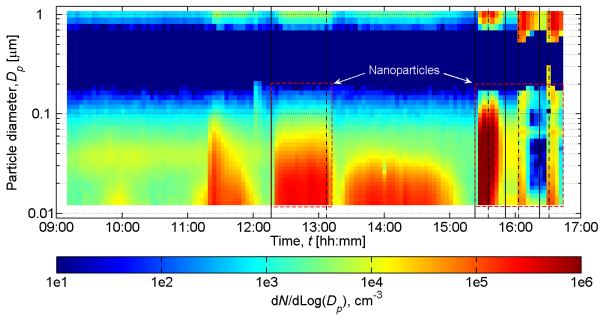

Figure 1: NP emissions from liquid flame spray processes. Red dashed squares shows the fraction of NPs.

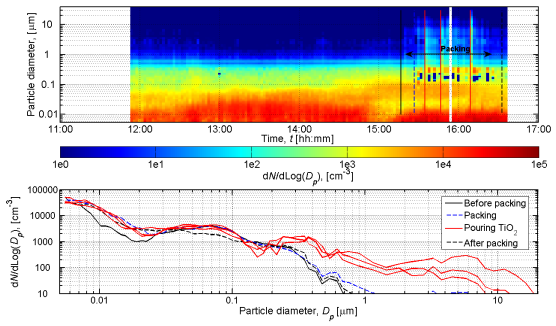

Figure 2: NP emissions from packing of TiO_2 nanomaterial

Release-ability of nano fillers from different nanomaterials

L.Golanski[1], A.Guiot[1], M.Pras[2] and F.Tardif[1]

[1]LITEN, CEA-Grenoble, Grenoble, Rhone Alpes, F38054 Cedex9, France
[2]IMP, INSA-Lyon, Villeurbanne, Rhone Alpes, 69621, France
Keywords: nanoparticle release, abrasion, sanding, nanomaterials

Presenting author email: luana.golanski@cea.fr

The nanoparticles (NP) are finding new industrial applications every day in fields as diverse as electronics, biomedicine, pharmaceutics, cosmetology, chemical catalysis, new materials and others. We are about to witness the advent of a new era in the industrial history of nanoparticles. Nevertheless, this new industry can develop dynamically only if the safety issues are solved during all along the life cycle of the nano products: from fabrication to the end of life through usage.

Due to the complexity of the nano toxicology, it will probably take decades to identify the dangerous nanoparticles and even a longer time to declare some of the nanoparticles as benign. One of the pragmatic ways to secure the nanomaterials today consists in reducing the exposure to nanoparticles of potentially exposed workers, consumers and the Environment close to zero.

Standard methods for investigating the wear resistance to abrasion induced by domestic use in dry and wet environments are used by manufacturers. However, these methods have to be adapted today for materials containing NP in order to measure if these NP could be released by the abrasion process or not. Very few data concerning NP release from nanomaterials in the air by abrasion are available: Guiot *et al* (2008), Vorbau *et al* (2009), Golanski *et al* (2010). The objective of developing such measurement techniques is double: to be able to optimize the "hooking" of the nanoparticles in the matrix and perhaps one day, to qualify the nano products before market introduction.

In this paper, the different steps necessary to setup the methods are summarized and the results obtained on paints, fabrics and polymers containing nano fillers discussed. Standard abrasion conditions in dry and wet environments were simulated. The aging effect induced by a mechanical friction like sanding were simulated as well. Different instruments were used for measuring the number size distribution of the abraded particles in the liquid solution and in the air. The advantage of each instrument is pointed out. These granulometers give no information about the type of NP measured. To address this issue the NP were deposited on a substrate for Scanning Electron Microscopy (SEM) or Transmission Electron Microscopy (TEM) analysis. In this way the nanoparticles released were analyzed in terms of their type: NP in agglomerate or free form or moreover NP embedded in the paint matrix.

Abrasion of the paints is found to produce submicrometric and micrometric particles in the air but no nanoparticles. Moreover, very few particles are released from paint coatings whatever the composition of the paint and whatever the tool used for abrasion. No free or agglomerated nanoparticles were observed. TiO_2 nanoparticles (~ 30nm) seem to remain embedded in the paint matrix (see on figure 1).

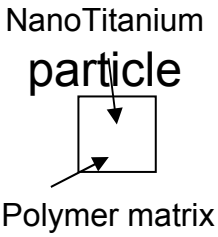

Figure 1. SEM image of the paint with nanoTiO_2: image of a TiO_2 nanoparticle embedded in a polymer matrix

Abrasion of the polymer coatings and textiles is found to induce nanometric particle release. The released nanoparticle number from investigated polymers depends on the abrasion tool type and composition of the material. Adding 5% wt of CNT (Carbone Nanotubes) to the reference material (polymer without CNT), induces hundred times more nanometric particle release from the nanomaterial by comparison with the reference. The influence of the fabrication process of the polymer on nanoparticles release was investigated as well. SEM measurements on abraded particles showed that no CNT were released from polymers containing up to 5% wt. For these polymers, the fabrication process was well controlled: eg. hooking of the CNT in the matrix.

Vorbau, M., Hillemann, L. and Stintz, M. (2009) *J. Aerosol Science,* **40,** 209

Guiot, A., Golanski, L. and Tardif F. (2009) *Journal of Physics: Conference Series*, **170,** no.012014

Golanski, L., Gaborieau, A., Guiot, A., Uzu G., Chatenet, J. and Tardif, F., *Proc. of Int. Conf Nanosafe 2010*

No evidence of cerium oxide nanoparticle translocation in maize plants

R.N. Grass[1], K. Birbaum[2], L.K. Limbach[1], E. Martinoia[3], D. Günther[2] and W.J. Stark[1]

[1]Institute for Chemical and Bioengineering, ETH Zurich, Zurich, 8093, Switzerland
[2]Laboratory of Inorganic Chemistry, ETH Zurich, Zurich, 8093, Switzerland
[3]Laboratory for Molecular Plant Physiology, University of Zurich, 8008 Zurich, Switzerland.
Keywords: nanoparticles, aerosol emission, particle deposition, lung/particle interaction.
Presenting author email: robert.grass@chem.ethz.ch

The rapidly increasing production of engineered nanoparticles has raised questions regarding their environmental impact and their mobility to overcome biological important barriers. Nanoparticles were found to cross different mammalian barriers, which is summarized under the term translocation. The present work investigates the uptake and translocation of cerium dioxide nanoparticles in maize plants as one of the major agricultural crops.

In order to simulate the gas-phase exposure of maize plants to nanoparticles, flame spray pyrolysis (FSP) was utilized to directly synthesize a cerium oxide comprising aerosol. (Birbaum et al. 2010) The aerosol was produced in an enclosed cabinet (glove box, 2 m^3, see Figure 1) in which the maize plants were cultivated. After digestion of the maize leaves, the cerium concentrations were measured by a sector field inductively coupled mass spectrometer (ICP-SF-MS), allowing a detection limit of less than 1 ng of cerium per gram of leaf. (< 1 ppb mass/mass). The plant leaves were analysed for the cerium content directly after exposure and 12 weeks post exposure in order to measure the cerium translocation within the plant.

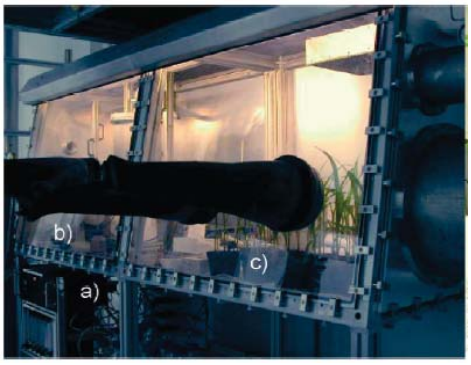

Figure 1. Exposure of maize plants to a cerium oxide aerosol in an enclosed cabinet (glove-box).

Element analysis results showed that cerium oxide nanoparticles were present on/in the maize leaves after the aerosol exposure. While it was not possible to discriminate between particles taken up by the plant cells and particles adsorbed to the surface of the leaves, the deposited nanoparticles could not be washed off with water (simulating rainfall). Examination of the concentrations in the leaves 3 months after the exposure

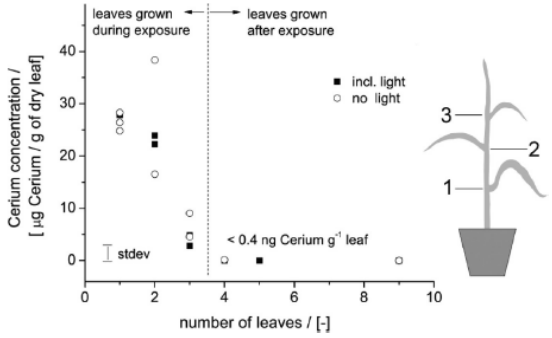

Figure 2. Cerium concentrations in plant leaves 3 months post nanoparticle exposure. Leaves 1-3 were directly exposed during the exposure, leaves 4-9 grew following the exposure.

experiments revealed that the cerium oxide nanoparticles did not translocate into newly formed leaves. No cerium oxide (detection limit of 0.4 ng cerium / g leaf) could be measured in the leaves grown during the three months post exposure period.

The presentation will further show the influence of light (exposure under light and dark for open and closed stomata) and results on the suspension exposure of maize plants (via the soil). The results of the maize plant exposure will be discussed and compared with *in vitro* lung cell exposure experiments (Rothen-Ruthishauser et al. 2010, Raemy et al. 2011) performed under the same exposure conditions.

Financial support from the ETH Zurich (TH 21- 08-3) is gratefully acknowledged.

References:

Birbaum, K., Brogioli, R. Schellenberg, M., Martinoia, E., Stark, W.J., Günther, D. and Limbach, L.K. (2010) *Environ. Sci. Technol.* **44**, 8718-8723.

Raemy, D.O., Limbach, L.K., Rothen-Rutishauser, B., Grass, R.N., Gehr, P., Birbaum, K., Brandenberger, C., Günther, D. and Stark, W.J. (2011) *Eur. J. Pharm. Biopharm.* doi: 10.1016/ j.ejpb.2010.11.017.

Rothen-Rutishauser, B., Grass, R.N., Blank, F., Limbach, L.K., Muehlfeld, C., Brandenberger, C., Raemy, D.O., Gehr, P. and Stark, W.J. (2009) *Environ. Sci. Technol.* **43**, 2634-2640.

Characterisation of CeO_2 engineered nanoparticles from a liquid flame spray process – exposure of workers

J. Lyyränen[1], M. Järvelä[2], T. Tuomi[2], J. Pimenoff[3], A. Auvinen[1] and J. Jokiniemi[1,4]

[1]VTT Technical Research Centre of Finland, P.O. Box 1000, 02044 VTT, Espoo, Finland
[2] Finnish Institute of Occupational Health, Topeliuksenkatu 41 a A, FI-00250 Helsinki, Finland
[3]Beneq Oy, P.O. Box 262, FI-01511 Vantaa, Finland
[4]Univ. of Eastern Finland, Department of Environmental Science, P.O. Box 1627, FI-70211 Kuopio, Finland
Keywords: Nanoparticle, characterisation, flame spray, exposure
Presenting author email: jussi.lyyranen@vtt.fi

In this work a liquid flame spray process called nHALO® (hot aerosol layering operation) producing engineered nanoparticles (ENPs) used for coating and surface modification of materials was studied. The process reagents, which are usually nitrate salts and water or alcohol as carrier, are vaporised in a hydrogen-oxygen flame. In the flame, particles nucleate and grow via condensation and coagulation into nanosized particulate matter. The produced particles may be metal, metal oxide or multicomponent. The process was installed inside an enclosure to minimise particle emissions into the surroundings. The focus of the research was to characterise the particles inside the enclosure, in the surroundings and at the exit points of the enclosure where the workers may be exposed to the engineered particles.

Particle number concentration was measured with a TSI 3022 CPC and number size distribution with a TSI 3080 electrostatic classifier with a TSI 3085 Nano-DMA connected with a TSI 3775 CPC and controlled by the SMPS software and with an ELPI. Mass concentration was measured with a TEOM 1400a. Individual particle samples for electron microscopy (EM) analyses were collected with an aspiration EM sampler.

Average particle number concentration inside the enclosure varied from $1.0 \cdot 10^4$ to $2.1 \cdot 10^5$ 1/cm^3 and average mass concentration from 1.2 to 2.6 mg/m^3 during process operation. The highest particle concentration was observed when the furnace was heated and when the flame was on. The high peaks in the number concentration levelled out rapidly indicating a batch-type process and efficient ventilation inside the process enclosure (Fig. 1a). It should be noted that the process enclosure was not occupied by the workers.

Particle number concentration in the surroundings was typically $6.0\text{-}8.0 \cdot 10^3$ 1/cm^3, and average mass concentration 66 µg/m^3. It is noteworthy, that after the door opening at around 14:40 (scaled time), the particle number concentration stayed at higher level than before the door opening (white line in Fig. 1a). This was probably caused by the opening of the door to the enclosure at 14:56, 15:05 and 15:55 (Leppänen, et al.).

Comparing the number and mass concentration in the surroundings to the enclosure concentrations during the nHALO® process it was evident that the ventilated enclosure worked well in isolating the particle source from the surroundings.

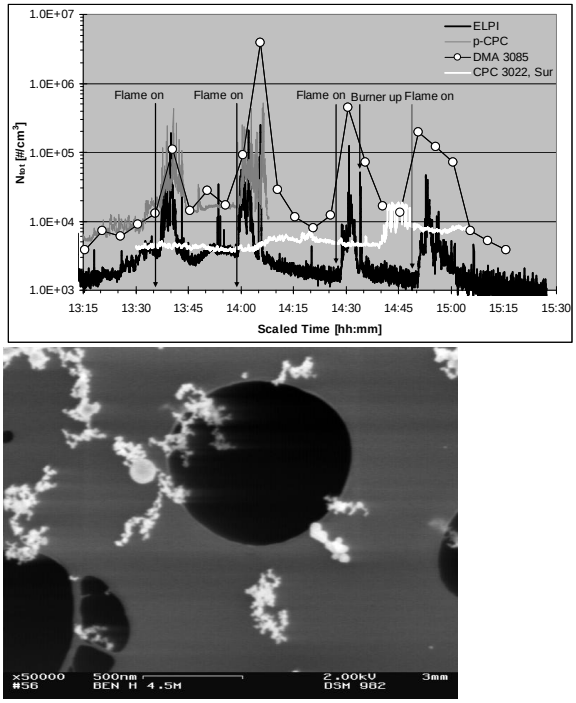

Figure 1: a) Particle number concentration for nHALO® inside the process enclosure and in the surroundings (white curve, scaled time) b) A scanning electron microscope (SEM) micrograph of the collected nanoscale particles from inside the enclosure. Particles were mainly aggregates, primary particle size approximately 20-30 nm.

This work was supported by the Finnish Funding Agency for Technology and Innovation, Beneq Oy and The Federation of Finnish Technology Industries.

M. Leppänen, J. Lyyränen, M. Järvelä, A. Auvinen, J. Jokiniemi, J. Pimenoff and T. Tuomi. Exposure to CeO_2 Nanoparticles during Flame Spray Process. Submitted to *Nano Research.*

Tuesday, September 6, 2011

Session 5F: Aerosols in Turbulent Flows 1

Distribution of relative velocities in turbulent aerosols

K. Gustavsson[1], B. Mehlig[2]
[1]Department of Physics, Gothenburg University, 41296 Gothenburg, Sweden
Keywords: turbulent aerosols, caustics, relative velocities.
Presenting author email: Bernhard.Mehlig@physics.gu.se

Collision velocities of particles in randomly mixing or turbulent flows ('turbulent aerosols') have been studied intensively for several decades. This is an important topic because the stability of turbulent aerosols is determined by collisions between the suspended particles.

Direct numerical simulations of particles in turbulent flows (Sundaram & Collins, 2007; Wang *et al.*, 2000) show that collision velocities (and thus the collision rate) increase precipitously as the 'Stokes number' St is varied beyond a threshold. This dimensionless parameter, $\mathrm{St} = (\gamma\tau)^{-1}$, is defined in terms of the particle damping rate γ and the relevant correlation time τ of the flow.

In (Wilkinson *et al.*, 2006) (see also Falkovich *et al.* (2002)) this steep increase was attributed to the fact that singularities in the particle dynamics result in large relative velocities at small separations. These singularities occur when phase-space manifolds (describing the dependence of particle velocity upon particle position) fold over. In the fold region, the velocity field at a given point in space becomes multi-valued, giving rise to finite velocity differences between particles at the same position in configuration space.

The boundaries of the folding region are referred to as caustics (Wilkinson & Mehlig, 2003, 2005). In the absence of such singularities, in a single-valued smooth particle-velocity field, the relative velocity of two particles tends to zero as they approach each other. In the presence of caustics, by contrast, the relative velocity of two particles may remain finite. When a singularity is created, the particle-velocity gradient diverges, $\partial v/\partial x \to -\infty$ (here x is the particle position and v its velocity). In (Duncan *et al.*, 2005; Wilkinson & Mehlig, 2005; Wilkinson *et al.*, 2006) it was shown that the frequency at which these singularities occur along a particle trajectory exhibits an activated St-behaviour, $\exp(-A/\mathrm{St})$.

Wilkinson *et al.* (2006) have suggested an interpolation formula accounting for both smooth and singular contributions to the collision rate and to the relative collision speed. But a theory for the distribution of relative velocities in turbulent aerosols at small and intermediate values of St is still lacking (a theory for collision velocities in turbulent flows at very large Stokes and Reynolds numbers was developed in (Gustavsson *et al.*, 2008), it is of interest in astrophysical contexts).

Here we compute the distribution of relative velocities for a one-dimensional model of heavy particles suspended in a turbulent flow, quantifying the caustic contribution to the moments of relative velocities (Gustavsson & Mehlig, 2010). We argue that the same principles determine the corresponding caustic contribution in two and three spatial dimensions. Our conclusions are in excellent agreement with numerical simulations of particles suspended in a randomly mixing flow in two dimensions, and in quantitative agreement with published data on direct numerical simulations of particles in turbulent flows (Bec *et al.*, 2010).

This work was supported by Vetenskapsrådet, the Gören Gustafsson Stiftelse, and the platform 'Nanoparticles in an interactive environment' at Gothenburg University.

References

S. Sundaram & L. R. Collins (1997) J. Fluid Mech. **335**, 75

L. P. Wang, A. S. Wexler, and Y. Zhou (2000) J. Fluid. Mech. **415**, 117

M. Wilkinson, B. Mehlig, and V. Bezuglyy (2006) Phys. Rev. Lett. **97**, 048501

G. Falkovich, A. Fouxon, and G. Stepanov (2002) Nature **419**, 151

M. Wilkinson & B. Mehlig (2003) Phys. Rev. E **68** 040101(R)

M. Wilkinson & B. Mehlig (2005) Europhys. Lett. **71**, 186

K. Duncan *et al.* (2005) Phys. Rev. Lett. **95**, 240602

K. Gustavsson *et al.* (2008) Phys. Rev. Lett. **101**, 174503

K. Gustavsson & B. Mehlig (2010) arXiv:1012.1789

J. Bec *et al.* (2010) arxiv:0905.1192; J. Fluid Mech. **646**, 527

Statistical properties of particle segregation in homogeneous isotropic turbulence

E. Meneguz, M. W. Reeks
School of Mechanical and Systems Engineering, Newcastle University, Newcastle upon Tyne, NE1 7RU, UK
Keywords: segregation, inertial particles, random uncorrelated motion, singularities.
Presenting author email: Mike.Reeks@ncl.ac.uk

The study of the kinematic of particles/droplets dispersed in turbulent flows is crucial for a wide range of natural and engineering applications. In this theoretical and numerical work, we focus on a two phase flow constituted by heavy particles and incompressible flow and we exploit a Full Lagrangian method to quantify the average segregation of particles. While doing so, we are able to analyse some particular features of this ongoing process, and in particular to study the statistics of the singularities of the particle velocity field and of the recently observed Random Uncorrelated Motion (RUM): the velocity of particles with large inertia brought into close proximity may be strongly decorrelated not only with the flow but one with another.

In our recent work (IJzermans *et al*, 2009 and 2010), we have studied the segregation of heavy particles in turbulence by calculating the rate-of-compression of the particle phase in a kinematic simulation. Particles are advected by Stokes drag in a flow field composed of 200 random Fourier modes. The volume occupied by the particles centred around a position x at time t is denoted by $J = det(J_{ij})$, where $J_{ij} = \partial x_i(x_0)/\partial x_{0,j}$, where x_0 denotes the initial position of the particle. The particle-averaged compressibility, $\mathscr{C} = d < ln|J| > /dt$, gives a measure for the change of the total volume occupied by the particle phase. Numerical results showed that the particle-averaged rate-of-compression decreases continuously if the value of the Stokes number (the dimensionless particle relaxation time) is below a threshold value, St_{cr}, indicating that the segregation of these particles continues indefinitely. We find that the probability density function of $ln|J|$, the compression, tends to a Gaussian distribution for $St \sim 1$ when $t \to \infty$. We believe the explanation for Gaussianity is similar to that for the occurrence of a Gaussian distribution of displacement (Taylor, 1922), with $\mathscr{C}'(t)$, the fluctuating value of $\mathscr{C}(t)$ about its mean. However, we find that that such PDF shows a significant skewness towards negative compression (segregation), i.e. singularities in the flow are likely to play a significant role in determining the statistics of the segregation in these long term limits.

By counting events for which $|J(t)| = 0$, we can calculate the distribution of singularities over a fixed interval of time respectively for a set of St numbers. As shown in Figure 1 for $St = 1$, excluding the influence of an initial transient when no singularities are observed, the histogram that represents the discrete probability distribution is well approximated by a Poisson distribution that describes the probability of the occurrence of an event (singularity) in a specified time span $[0, \triangle t]$ as $\sim \lambda \triangle t = \Lambda$; λ is the rate constant for the occurrence of singularities. The Poisson process implies that starting from some initial fully mixed equilibrium distribution, the decay in the number of particles that have not experienced a singularity is $\sim exp(-\lambda t)$.

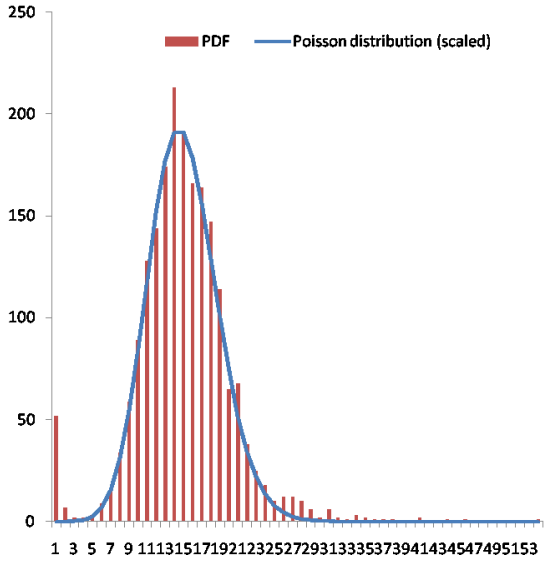

Figure 1: This is a comparison between theory and experimental data.

Finally, we discuss our work in relation to the one of Falkovic & Pumir, 2007 and Wilkinson *et al*, 2007 and we conclude that the occurrence of singularities is related to the formation of caustics and sling effect respectively, since it corresponds to the folding of the particle velocity field in phase space. We believe that RUM and singularities are intrinsically related and we are currently working to find a suitable way to demonstrate such theory from a mathematical and numerical point of view.

IJzermans, R. H. A., Reeks, M. W., Meneguz, E., Picciotto, M. and Soldati, A. (2009) Phys. Rev. Lett. **97**, 015302.

IJzermans, R. H. A., Meneguz, E. and Reeks, M. W. (2010) J. Fluid Mech. **653**, 99-136.

Taylor, G. I. (1922) in Proc. London Math. Soc. s2 **20**(1), 196-212.

Falkovich, G. and Pumir, A. (2007) Phys. Rev. Lett. **64**, 4497-4505.

Wilkinson, M., Mehlig, B., Ostlund, S. and Duncan, K. P. (2007), Phys. Fluids **19**, 113303.

Particle and droplet transport in turbulence and inertial effects

R. Skartlien[1]
[1]Institute for Energy Technology, N2027, Kjeller, Norway
Presenting author email: roar.skartlien@ife.no

Turbulent flow with solid particles or droplets is encountered in both natural processes and in industrial applications. A challenge is to predict the distribution of the dispersed phase with account for particle inertia and turbulence inhomogeneity. Recent advances in Eulerian modelling have become possible due to kinetic methods based on an underlying Boltzmann type equation where the usual collision term is replaced by an interaction between particles and the turbulent medium (e.g., Reeks 1992, Swailes and Darbyshire 1999, Simonin 2000, Zaichik & Alipchenkov 2005).

The kinetic framework can be applied to turbulent diffusion and transport with inertial effects, such as for raindrops and aerosols in the atmosphere. Recent applications of the theory for solid particles and droplets in gas is presented, in the context of strongly inhomogeneous turbulence in pipe flow. The most valuable ingredient that emerges from the theory is a generalized diffusivity tensor, valid for a very large range of particle properties (material density, diameter and Stokes numbers).

In many applications it is common practise to use an over-simplified phenomenological diffusion equation for the mass flux density $\mathscr{F}_m$, of the form

$$\mathscr{F}_m = -\varepsilon\nabla\rho + \rho\mathbf{v}_d. \tag{1}$$

This diffusion equation may provide a solution for the density of particles ρ, once the drift velocity $\mathbf{v}_d$ and the particle diffusivity ε is given. In the absence of better estimates, the diffusivity is often set equal to the scalar eddy diffusivity of the fluid turbulence. For intertial particles, such as droplets, it is evident that this simple form breaks down, since the particles do not follow the fluid motion. The general form of the diffusion equation from kinetic theory is (Reeks 1992)

$$\begin{aligned}\rho\overline{v_i} &= -\varepsilon_{ik}\partial_k\rho - \rho\tau_p\partial_k(\overline{v_k'v_i'} + \overline{\lambda}_{ki}) \\ &+ \rho\tau_p(\overline{F}_i - \overline{\gamma}_i) - \tau_p\rho\frac{D\overline{v_i}}{Dt},\end{aligned} \tag{2}$$

where $D/Dt = \partial_t + \overline{v_k}\partial_k$, and $\overline{\mathbf{F}}$ is the mean aerodynamic force. The diffusive contribution to the mass flux is now

$$\mathscr{F}_i^d = -\varepsilon_{ik}\partial_k\rho, \tag{3}$$

where the generalized *diffusivity tensor* is

$$\varepsilon_{ik} = \tau_p(\overline{v_k'v_i'} + \overline{\lambda}_{ki}), \tag{4}$$

which is a tensorial quantity depending on the particle Stokes number via the inertial relaxation time τ_p. The kinetic stress tensor for the particles is $\overline{v_k'v_i'}$, and the dispersion tensor $\overline{\lambda}_{ki}$ is ultimately controlled by the fluid Reynolds stresses. For large Stokes number it is $\tau_p(\overline{v_k'v_i'})$ that controls the diffusivity, and for low Stokes number it is $\tau_p\overline{\lambda}_{ki}$. Figure 1 compares these contributions with the eddy diffusivity, for a distribution of inertial droplets in horizontal pipe flow.

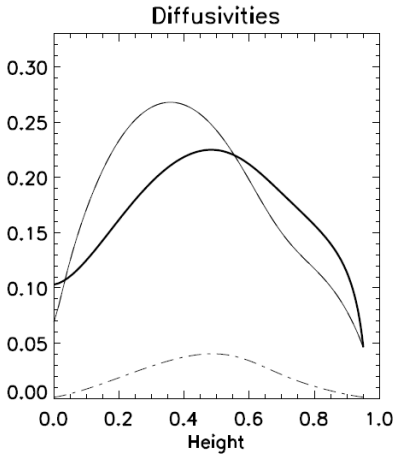

Figure 1: **Diffusivity** for a droplet size 1.2 times the average size in strongly inhomogeneous gas turbulence above a liquid layer in a horizontal pipe. The plot shows the total diffusivity $\tau_p(\overline{v_y'v_y'} + \overline{\lambda}_{yy})$ (thick line), the fluid contribution $\tau_p\overline{\lambda}_{yy}$ (dashed line) and the eddy diffusivity ν_T (thin full line). The deviation between the total diffusivity and the eddy diffusivity is due to inertia, and the fluid contribution $\tau_p\overline{\lambda}_{yy}$ is small compared to the kinetic part $\tau_p\overline{v_y'v_y'}$.

Reeks, M.W. (1992) On the continuum equations for dispersed particles in nonuniform flows. Physics of Fluids A, 4, 1290-1303.

Simonin, O. (2000) In "Statistical and Continuum modelling of Turbulent Reactive Particulate Flows, Part 1", von Kármán Institute for Fluid Dynamics: Lecture Series.

Swailes, D.C., Darbyshire, K.F.F. Probabilistic models for particle and scalar transport in fluctuating flows: an evaluation of simple closure approximations. Physica A 1999, 262, 307-327.

Zaichik, L.I., Alipchenkov, V.M. (2005) Statistical models for predicting particle dispersion and preferential concentration in turbulent flows. International Journal of Heat and Fluid Flow 2005, 26, 416-430.

Full motion measurement of finite-size neutrally buoyant particles together with the turbulent flow field carrying them

M. Gibert[1,2], S. Klein[1] and E. bodenschatz[1,2]
[1]Max Planck Institute for Dynamics and Self Organization, Göttingen, 37073, Germany, EU,
[2]International Collaboration for Turbulence Research
Keywords: Turbulence, Insoluble particles, Measurements.
Presenting author email: mathieu.gibert@ds.mpg.de

The motion of inertial particles in a turbulent flow is of interest in many applications ranging from mixing in industrial processes to dispersion in oceans or in the atmosphere. The case of small (compared to the Kolmogorov size η) but heavy particles is extremely well studied experimentally (Gibert *et al.* (2010)) as well as numerically (for an extensive review see Toschi *et al.* (2009)). In this case, the flow around the particle is smooth, which facilitate the writing of the equation of motion that couples the particle trajectory to the underlying turbulent flow field. In the case of finite-size particles (diameter $d_p > \eta$), the equation of motion is still unknown. Therefore, only a few numerical studies are available today (Homann *et al.* (2010)), and are limited to very small Reynolds numbers because of the complexity of the problem. This leads to the conclusion that only an experimental approach can help to discover and characterize the complex coupling between these big particles and the turbulent flow carrying them. Nevertheless, this is a very challenging task since it requires the measurement of the full trajectory of the particles (translation and rotation) together with the flow field that surrounds them, in a highly turbulent flow. In the following section, we present the most advanced measurement technique in the field that we have developed in order to acquire all these information.

Measurement technique and results

We studied particles made out of super-absorbent polymer. These particles initially dry have a diameter of $1mm$, once immersed underwater they grow until having a diameter of about $1cm$. Therefore, these solid particles are made out of more than 99% of water and inherit water properties : same optical index and same density (they are invisible in water). To follow their trajectories, we inject them with small fluorescent particles of $100\mu m$ in diameter. Since the big particles are invisible in the water von Kármán flow we use to generate the turbulence, we can use the same fluorescent tracer particles to track the fluid velocity (see Fig. 1 for more detail).

The experiments are conducted in a von Kármán swirling water flow (two counter-rotative coaxial propellers facing each other) at Taylor microscale Reynolds numbers up to 400 (the apparatus is described in Gibert *et al.* (2010)). At these Reynolds numbers, the energy injection length scale L is about $10cm$ and the dissipative length scale η is close to $100\mu m$. Therefore, the diameter of the big particles d_p lies in the inertial range ($d_p/\eta \approx 100$ and $d_p/L \approx 0.1$). We report data on the statistics of the velocity differences between the big particles and the surrounding turbulent flow. Our results show a strong correlation between the fluid and the particle velocity in the close vicinity of the big particles, but also that the particles perturb the flow by generating a wake behind them. This work provides the first quantitative data on the flow around large particles in turbulent flows and shows that in modeling, two-way coupling will need to be considered which is not present in the case of small inertial particles.

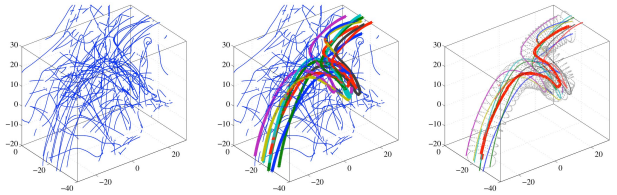
(a) (b) (c)

Figure 1: The measurement technique. (a)(b)(c) The axes are in *mm*, these plots correspond to a subset of $0.3s$ of measurements done at $3kHz$. (a) Three-dimensional plot of the fluorescent particles trajectories measured by Lagrangian Particle Tracking (LPT). (b) Identification of the particles tracks that do not separate from one another along their trajectories (they correspond to the tracks of the fluorescent particles embedded at the surface of the big particles). (c) Three-dimensional plot of the reconstructed big particle trajectory (the center of the particle is represented in red). The fluid particles trajectories have been removed from the figure for clarity, but we still have this information.

This work was supported by Max Planck Society and the Marie Curie Fellowship, Programme PEOPLE - Call FP7-PEOPLE-IEF-2008 Proposal N^{o}237521.

Gibert, M., Xu, H., Bodenschatz, E. (2010) Euro. Phys. Lett. **90**(6):64005.

Toschi, F., Bodenschatz, E. (2009) Annual Review of Fluid Mechanics **41**:375-404.

Homann, H., Bec, J. (2010) J. Fluid Mech. **651**:81-91.

Aerosol Coagulation & Break-up in Homogeneous Isotropic Turbulent Flows

M.L. Eggersdorfer[1], D. Kadau[2], H.J. Herrmann[2] and S.E. Pratsinis[1]

[1]Particle Technology Laboratory, Institute of Process Engineering, Department of Mechanical and Process Engineering, ETH Zurich, Sonneggstrasse 3, CH-8092 Zürich, Switzerland.
[2]Computational Physics of Engineering Materials, Institute of Building Materials, Department of Civil, Environmental and Geomatic Engineering, ETH Zurich, Schafmattstrasse 6, CH-8093 Zürich, Switzerland.
Keywords: Aerosol dynamics, size distribution, Coagulation, Turbulence.
Presenting author email: meggers@ptl.mavt.ethz.ch

Turbulent mixing is present in many different processes in nature, e.g. formation of raindrops (Saffman & Turner, 1956), and in industry, e.g. aerosol synthesis of nanoparticles like carbon blacks and oxide powders (silica, titania; Xiong & Pratsinis, 1991). There, particles are produced at high temperatures and pressures with Reynolds numbers up to 10^6. Primary particles grow by gas and surface reaction, coagulation and sintering. The primary particles are too small to be affected by turbulence. Nevertheless coagulation leads to soft- or hard-agglomerates which can reach the size of the Kolmogorov scale η, the smallest scale of turbulence. These agglomerates experience the high frequency fluctuations and undergo turbulence-induced coagulation, restructuring or even fragmentation preventing gelation, which can occur in aerosols at high effective volume fractions (Sorensen et al., 1998).

Particle coagulation by Brownian motion or shear in flows at low Reynolds numbers is fairly well understood (Friedlander, 2000). The effects of turbulence on agglomerate formation and break-up are only partially understood. Uncertainties are in the fundamental theory of turbulence, the motion of small particles in close proximity in turbulence as well as the restructuring and break-up.

Ernst and Pratsinis (2006) showed by population balance simulations that turbulent-induced coagulation lead to pseudo self-preserving distributions that end to gelation in the absence of restructuring or fragmentation in the viscous regime (particle diameter d_p much smaller than η). Heine and Pratsinis (2006) investigated aerosol dynamics at high solid concentrations found typically in industrial scale manufacture of fine particles. Enhanced Brownian and shear-induced coagulation could lead to rapid soft-agglomerate growth and again gelation. However, restructuring and shear-induced fragmentation should slow and stop soft-agglomerate growth in industrial flow reactors.

Higashitani et al. (2001) investigated the break-up of soft-agglomerates in linear shear and elongational flows and proposed a power law relation between asymptotic fragment mass and shear stress for both flow fields. They found that the elongational flow field is more efficient to break-up agglomerates than the linear shear field.

In the present work the agglomeration and break-up of monodisperse particles in a homogeneous isotropic turbulent flow field are investigated. A discrete element method (DEM) is used for the particle dynamics and stochastic differential equations (SDE) are solved for the time evolution of the velocity and accelerations of the fluid. The evolution of the agglomerate number, mass and size (radius of gyration) with time is discussed for different Reynolds numbers. Equilibrium between coagulation and break-up is found, resulting in steady state agglomerate mass distributions (Fig. 1). Furthermore the agglomerate structure is characterized with an effective fractal dimension.

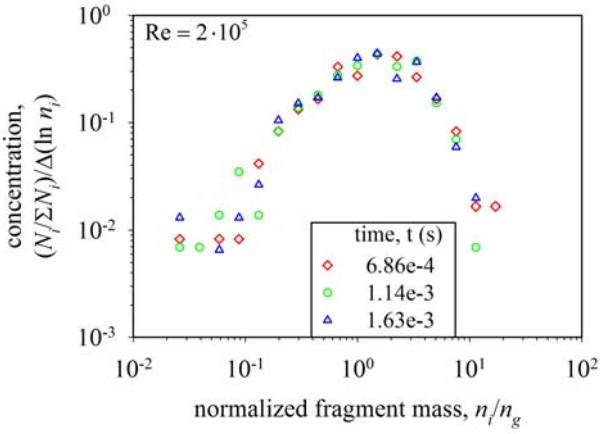

Figure 1. Steady state agglomerate mass distribution at three different simulation times. An equilibrium between coagulation and break-up is reached.

Financial support by ETH Research Grant (ETHIIRA) ETH-11 09-1 and the European Research Council is gratefully acknowledged.

Ernst, F.O. and Pratsinis, S.E. (2006) *J. Aerosol Sci.* **37**, 123-142.

Friedlander, S.K. (2000) *Smoke, Dust, and Haze: Fundamentals of Aerosol Dynamics*, Oxford University Press.

Heine, M.C. and Pratsinis, S.E. (2006) *Langmuir* **22**, 10238-10245.

Higashitani, K., Iimura, K. and Sanda, H. (2001) *Chem. Eng. Sci.* **56**, 2927-2938.

Saffman, P.G. and Turner, J.S. (1956) *J. Fluid Mech.* **1**, 16-30.

Sorensen, C.M., Hageman, W.B., Rush, T.J., Huang, H. and Oh, C. (1998) *Phys. Rev. Lett.* **80**, 1782-1785.

Xiong, Y. and Pratsinis, S.E. (1991) *J. Aerosol Sci.* **22**, 637-655.

Particle Resuspension Modeling in Turbulent Flows

F. Zhang*, †, M. Reeks* and M. Kissane†

* School of Mechanical and Systems Engineering, Newcastle University, Newcastle upon Tyne, NE1 7RU, UK

† Institut de Radioprotection et de Sûreté Nucléaire, CE Cadarache – bât 702, 13115 St-Paul-Lez-Durance, France

Keywords: resuspension, turbulent flow, multilayer deposit, severe accident

The work presented is concerned with the way small particles attached to a surface are resuspended when exposed to a turbulent flow. The process is important in a number of environmental and industrial processes. Of particular concern to this work is the release of radioactive particles from the primary circuit of an LWR as a consequence of a loss of coolant accident (LOCA). In this particular case the focus is on small particles < 5 microns in size, where the principal force holding the particle onto a surface is derived from van der Waals inter molecular forces. In general even for nominally very smooth adhering surfaces there exists a very broad spread in the adhesive forces. Here we develop and assess an improved version of the Rock'n'Roll model [Reeks & Hall, 2001] based on a statistical approach to resuspension which gives rise to a resuspension rate constant for the release of particles from a potential well due the action of the fluctuating aerodynamic force du to the turbulence. The analogy is with desorption of molecules from a surface in which the variance of the fluctuating aerodynamic force is the analogue of temperature. In this work we improve on the model by using measurements of the statistical fluctuations of both the stream wise fluid velocity and acceleration close to the wall from both LES and DNS of turbulent channel flow, translating those measurements into the statistical moment of the drag force acting on the particle attached to the surface. The original model assumes that aerodynamic forces and their time derivative are uncorrelated and have a Gaussian distribution. Here we examine the influence of non-Gaussian forces on the resuspension rate.

The ultimate model is a hybrid development of R'n'R model adapted for application to multilayer deposits based on the Friess and Yadigaroglu multilayer model [Friess & Yadigaroglu, 2001]. The particle size distribution is considered in the model in order to study the coveragent effect of the deposit layers. The model results are compared to the STORM SR11 test [Castelo *et al.*, 1999] (Figure 1) and BISE experiment [Alloul-Marmor, 2002] (Figure 2).

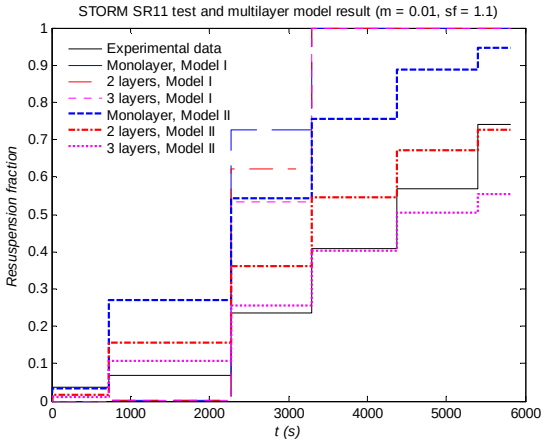

Figure 1. Models results and STORM SR11 test

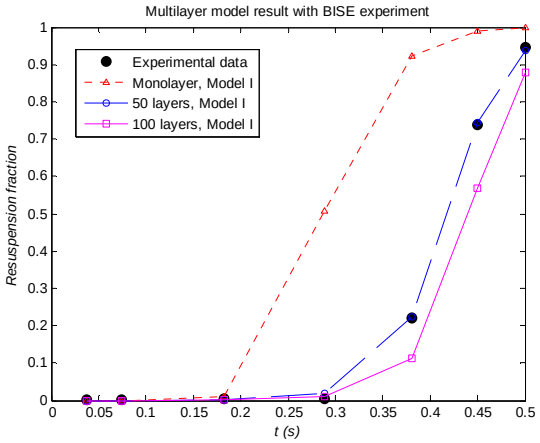

Figure 2. Model results and BISE experiment

As a general conclusion, the results showed that the models with small adhesive spreads give better comparison with the resuspension measured in the two experiments.

Alloul-Marmor, L. (2002), PhD thesis (Université Paris XII), report ISRN IRSN – 2002/28 – FR

Castelo, A., Capitão, J. A. and Santi, G. (1999) NEA/CSNI/R(99)4, EUR 18708 EN, February

Friess, H. and Yadigaroglu, G. (2001) *J. Nuclear Sci. and Eng.*, Vol.138(2), 161-176

Reeks, M. W. and Hall, D., (2001) *J. Aerosol Sci.*, Vol. 32(1), 1-31

Tuesday, September 6, 2011

Session 6A: New Particle Formation 3: Theory and Modelling

Simulating Ultrafine Particle Formation in Europe using the 3-D Chemical Transport Model PMCAMx-UF

C. Fountoukis[1], I. Riipinen[1,2], P.E. Haralabidis[3], H. D. van der Gon[4], C. Pilinis[3], P.J. Adams[2], and S.N. Pandis[1,2]

[1]Institute of Chemical Engineering & High Temperature Chemical Processes, Foundation for Research & Technology-Hellas (FORTH), 26504, Patras, Greece
[2]Department of Chemical Engineering, Carnegie Mellon University, Pittsburgh, PA 15213, USA
[3]Department of Environment, University of the Aegean, University Hill, 81100, Mytilene, Greece
[4]TNO Built Environment and Geosciences, Netherlands

Keywords: Regional CTM, nucleation, number concentration, EUCAARI.
Presenting author email: cfountoukis@iceht.forth.gr

Aerosol nucleation is potentially important to climate because it is, along with primary particle emissions, a major source of new particles to the atmosphere. Nucleated particles can ultimately act as CCN and contribute to the indirect effect if they grow to larger sizes. Ultrafine particles are highly mobile within the human body and may be especially harmful to human health. To correctly predict the relative contribution of nucleation to total aerosol number concentration, air quality and climate models need to be able to correctly simulate ultrafine particle dynamics and chemistry.

In this work, we study the effect of nucleation on aerosol number concentrations in Europe with the regional 3-D chemical transport model PMCAMx-UF (Jung *et al.*, 2010). We use three different schemes to simulate new particle formation; i) a ternary H_2SO_4-NH_3-H_2O nucleation parameterization, ii) an activation mechanism with a linear dependence on the sulfuric acid concentration, and iii) a kinetic mechanism with a squared dependence on the sulfuric acid concentration. We evaluate the model predictions for the European domain against field observations collected during the EUCAARI campaign in May 2008 and February/March 2009.

PMCAMx-UF is a version of PMCAMx focusing on ultrafine particles simulating both the aerosol number distribution and the aerosol mass/composition distribution. It uses the TwO-Moment Aerosol Sectional (TOMAS) algorithm (Adams and Seinfeld, 2002) to simulate both the aerosol number and mass distributions. The aerosol size distribution in PMCAMx-UF is discretized in 41 sections from 0.8 nm to 10 μm. From 10 μm to 40 μm, two additional size sections are used for the description of cloud chemistry. PMCAMx-UF tracks the mass distributions for 13 aerosol species including SOA components, POA, EC, crustal material, water, chloride, sodium, ammonium, nitrate, and sulfate. The modeling domain covers a 5400 × 5832 × 6 km region in Europe with 36 × 36 km grid resolution. A new size-resolved Pan-European anthropogenic Particle Number (PN) emission inventory was developed for the first time and the extracted aerosol number emissions were used as inputs for PMCAMx-UF.

Figure 1 shows the PMCAMx-UF average predictions over the period of 1-29 May 2008 for total aerosol number concentration above 1 nm using the 1st order in sulfuric acid nucleation parameterization.

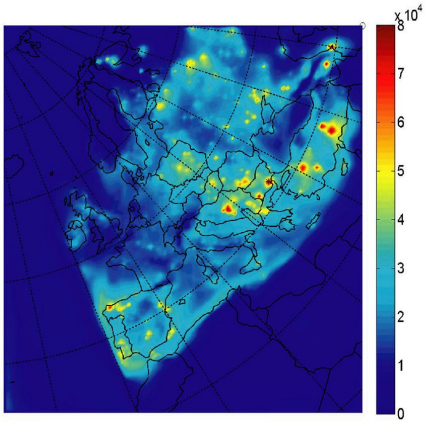

Figure 1. Predicted average number concentration (cm^{-3}) at the ground level above 1 nm during May 2008.

The model was found to perform reasonably well in both capturing the levels of particle number concentrations and size distributions at various sites, as well as their temporal variation in both diurnal as well as longer time scales.

The sensitivity of the predicted particle number concentrations above 1, 3, 50 and 100 nm to emissions of 1) SO_2, 2) Biogenic VOCs, and 3) particle mass is studied and the results will be discussed.

This work was supported by the European Integrated project on Aerosol Cloud Climate and Air Quality Interactions (EUCAARI).

Jung, J., Fountoukis, C., Adams, P.J., and Pandis, S.N. (2010) *J. Geophys. Res.*, 115, D3, doi:10.1029/2009JD012313..

Adams, P.J., and Seinfeld, J.H. (2002) *J. Geophys. Res.*, 107(D19), 4370, doi: 10.1029/2001JD001010.

Computational studies of atmospheric sulfur oxidation mechanisms

T. Kurtén[1,2], J. R. Lane[3], S. Jørgensen[1], C. Jensen[1] and H. G. Kjaergaard[1]

[1] Department of Chemistry, University of Copenhagen, Universitetsparken 5, 2100 København Ø, Denmark
[2] Department of Physics, University of Helsinki, P.O.B. 64, FIN-00014 University of Helsinki, Finland
[3] Department of Chemistry, University of Waikato, Private Bag 3105, Hamilton 3240, New Zealand
Keywords: sulfur cycle, atmospheric oxidation, sulfur dioxide, nucleation
Presenting author email: theo.kurten@helsinki.fi

The global climate impact of the atmospheric sulfur cycle on a per-kilogram basis is enormous compared to that of most other biogeochemical cycles due to the ability of oxidized sulfur compounds such as sulfuric acid to form aerosol particles. For example, according to the emission inventories and radiative forcings in the 4th IPCC assessment report (Solomon *et al*., 2007) the short-term cooling associated with a kilogram of sulfur emitted as SO_2 is estimated to be 10^4 to 10^5 times larger in magnitude than the corresponding warming associated with a kilogram of carbon emitted as CO_2. Natural sulfur emissions have also been speculated to play a role in the global climate system. Specifically, temperature-driven variations in the emissions of biogenic sulfur compounds have been suggested to modulate cloudiness and thus act as a negative feedback in the climate system

Despite the importance of atmospheric sulfur chemistry, many key reactions of anthropogenic and especially biogenic sulfur compounds present in the atmosphere are still largely unknown. Oxidation reactions involving the OH radical are fairly well characterized, but the reaction rates of other oxidants such as NO_3, O_3, peroxyradicals or carbonyl oxides with many sulfur compounds are highly uncertain. Recent calculations (Kurtén *et al.*, 2010) indicate that night-time NO_3 oxidation may actually form the main sink for some organosulfur compounds such as DMSO (dimethyl sulfide oxide).

Another open question is the role of water catalysis in the sulfur cycle. It has been suggested (Jørgensen and Kjaergaard, 2010) that a single water molecule is able to catalyze some of the OH oxidation reactions of reduced biogenic sulfur compounds such as DMSO. On the other hand, recent calculations indicate that water catalysis does not significantly enhance the OH - oxidation of partially oxidized sulfur compounds such as methane sulfenic, methane sulfinic and methane sulfonic acid (CH_3SOH, $CH_3S(O)OH$ and $CH_3S(O_2)OH$).

Recent experiments (Sipilä et al., 2010) have demonstrated that H_2SO_4 is the only SO_2 oxidation product needed to explain laboratory observations of sulfuric acid – water nucleation, though stabilizing third compounds such as ammonia or amines are still likely required. However, this does not rule out the possible existence of other gas-phase oxidation mechanisms by which SO_2 can be converted into H_2SO_4 without OH. Such pathways might play a role in the sulfur cycle at night, when OH levels are extremely low.

We have computationally investigated the oxidation of SO_2 into SO_3 by several atmospheric oxidants. Both nitrate radicals and peroxyradicals are predicted to react very slowly with SO_2. Catalysis by water molecules is not able to enhance these reactions. In contrast, carbonyl oxides (Criegee Intermediates) were found to oxidize SO_2 rapidly, in agreement with very recent results by Jiang et al (2010). However, the atmospheric relevance of this finding is dependent on the highly uncertain atmospheric lifetime of the carbonyl oxides.

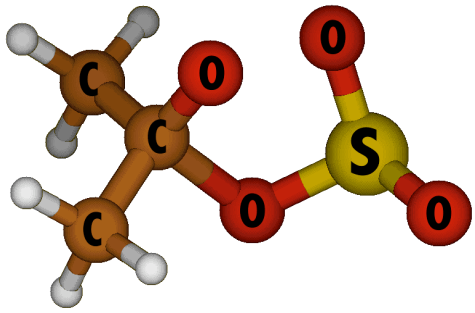

Figure 1. Transition state for the oxidation of SO_2 by 2-propyl carbonyl oxide.

Calculations have been performed on the Gaussian 09 *(*Frisch *et al., 2009)* and Molpro 2010.1 (Werner *et al*., 2010) program suites. We thank the CSC IT centre in Espoo, Finland, and DCSC, Denmark, for computer time.

Frisch, M. J. *et al.* (2009) Gaussian 09, Gaussian, Inc., Wallingford CT, U.S.A.

Jiang, L., Xu, Y., and Ding, A. (2010) *J. Phys. Chem. A* **114**, 12452-12461.

Jørgensen, S. and Kjaergaard, H. G. (2010) *J. Phys. Chem. A* **114**, 4857-4863.

Kurtén, T., Lane, J. R., Jørgensen, S. and Kjaergaard, H. G. (2010) *Phys. Chem. Chem. Phys*. **12**,12833-12839.

Sipilä, M. *et al*. (2010) *Science* **327**, 1243-1246.

Solomon, S. *et al.* (eds.; 2007) *Climate Change 2007: The Physical Science Basis,* Cambridge University Press, Cambridge, U.K.

Werner, H.-J. *et al.* (2010) MOLPRO, version 2010.1, http://www.molpro.net.

Geographical mapping of new particle formation events over Northern Europe

A.Kristensson[1], E. Swietlicki[1], B. Svenningsson[1], T. Hussein[2,3], T. Nieminen[2], M. Dal Maso[2], H. Junninen[2], H. Manninen[2], V. Ulevicius[4], M. Fiebig[5], P. Tunved[6], J. Ström[7], A. Massling[8], and M. Kulmala[2]

[1]Department of Physics, Lund University, Lund, SE-221 00, Sweden
[2]Department of Physics, University of Helsinki, Helsinki, FI-000 14, Finland
[3]Department of Physics, University of Jordan, 11942, Amman, Jordan
[4]Center for Physical Sciences and Technology, LT-02300, Vilnius, Lithuania.
[5]Norwegian Institute for Air Research, NO-2047, Kjeller, Norway
[6]Department of Applied Environmental Science, University of Stockholm, SE-106 91, Stockholm, Sweden
[7]National Environmental Research Institute, Aarhus University, DK-4000, Roskilde, Denmark
Keywords: Aerosol formation, Boreal forest, Ion clusters, Nucleation rate, SOA, DMPS
Presenting author email: adam.kristensson@nuclear.lu.se

The formation of new nanometer sized particles during so called new particle formation events is ubiquitous in the atmosphere. After condensational growth to sizes relevant for cloud droplet formation, the nanoparticles have a potential to influence the global radiation balance of the atmosphere (Merikanto, et al., 2009).

The number of ground based background stations in Europe where measurements of the size-dependent concentration of neutral or charged nanoparticles take place is becoming higher and higher. However, even if we have a satisfactory characterization of the formation events at these sites, we lack the information where and when these events take place over areas not covered by the network of stations. For example, in favourable regions we expect "hot-spots" with a higher frequency of these events and conversely "cold-spots" where gaseous precursor emissions necessary for the formation are low.

Fortunately, the information about how often particle formation take place over a larger regional area is possible to attain. We explain shortly a method of how this is done.

During new particle formation, particles of around 2 nm diameter are formed and these continuously grow by condensation. The growth can be followed by tracking the geometric mean diameter of the so called nucleation mode. After several hours, the geometric mean diameter can reach sizes around 10 nm or higher. Hence, if we observe particles at a particular site during an event with geometric mean diameters larger than 10 nm, we know they have been formed elsewhere.

Since we know the rate at which these particles grew until they were larger than 10 nm diameter, we also know at which time their size was 2 nm in diameter (growth rate calculations can be found in e.g. Dal Maso et al., 2005; Kulmala et al., 2007). By combining this information with back trajectories, we are able to find out where the actual conception of the 2 nm diameter particles took place. An example of this method can be viewed in Figure 1, where we see that particles detected as 20 nm diameter at evening time at the Vavihill site in southern Sweden, are formed as 2 nm diameter particles 13 hours earlier over the Skagerrak sea.

Conversely, on other days when we fail to observe formation events at our particular site, we get a "no-count" along the back trajectory.

Completing this characterization for all Nordic sites, we get a complete mapping of where these events take place over the Nordic area. Results from this mapping will be presented during the EAC conference.

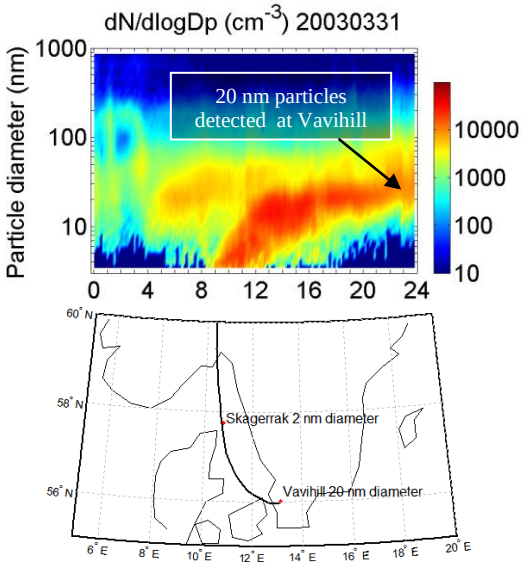

Figure 1. The observed particle number size distribution March 31, 2003 during a formation event at the Vavihill site (upper panel). The detected 20 nm diameter particles at Vavihill around 23:00 hours can be traced back to the time when they were formed as 2 nm particles 13 hours earlier over the Skagerrak sea (lower panel showing the 100 m back trajectory arriving to Vavihill at 23:00).

This work was supported mainly by the Swedish Research Council FORMAS (no. 2010-850).

Dal Maso, M., Kulmala, M., Riipinen, I., Wagner, R., Hussein, T., Aalto, P. P., and Lehtinen, K. E. J. (2005) *Boreal Env. Res.* **10**, 323-336.

Kulmala, M., Riipinen, I., Sipilä, M., Manninen, H. E., Petäjä, T., Dal Maso, M., Mordas, G., Mirme, A., Vana, M., Hirsikko, A., Laakso, L., Harrison, M. M., Hanson, I., Leung, C., Lehtinen, K. E. J., and Kerminen, V.-M. (2007) *Science* **318**, 89-92.

Merikanto, J., Spracklen, D. V., Mann, G. W., Pickering, S. J., and Carslaw, K. S. (2009) *Atmos. Chem. Phys.* **9**, 8601-8616.

Formation of neutral sulphuric acid clusters containing base molecules

I.K. Ortega, O. Kupiainen. T. Kurten, H. Vehkamäki

[1]Department of Physics, University of Helsinki, Helsinki, P.O. box 48, FI-00014, Finland
Keywords: Nucleation, amines, quantum mechanics, Modelling (microscale).
Presenting author email: ismael.ortegacolomer@helsinki.fi

Climate change is currently one of the central scientific issues in the world, and the ability to reliably forecast climate is crucial for making political decisions that affect the lives of billions of people. According to the Intergovernmental Panel on Climate Change, aerosols remain the dominant uncertainty in predicting radiative forcing and climate change.

According to current best estimates (Merikanto et al. 2009) roughly 20-80% of atmospheric particles are formed from condensable vapours by gas-to-particle nucleation. While new-particle formation is observed everywhere in Earth's atmosphere (Kulmala et al. 2004) the actual birth mechanism of the particles is still unknown.

In terms of the molecular species participating in nucleation, the only thing known for certain is that sulphuric acid is somehow involved in the process. On the other hand, sulphuric acid alone cannot explain the observed particle formation, and several other candidates, both organic and inorganic, have been proposed to participate. These include base molecules such as ammonia or amines and semivolatile organic compounds such as dicarboxylic acids, and organosulphates.

Nucleating clusters in atmospheric conditions are small, consisting of only a few or a few tens of molecules. These clusters are therefore well below present detection limits if they are electrically neutral. Several theoretical methods have tried to describe those clusters, but probably the most successfully has been quantum mechanical calculations. The aim of our work is to use quantum mechanical calculations to improve our knowledge about the molecular mechanisms behind atmospheric nucleation.

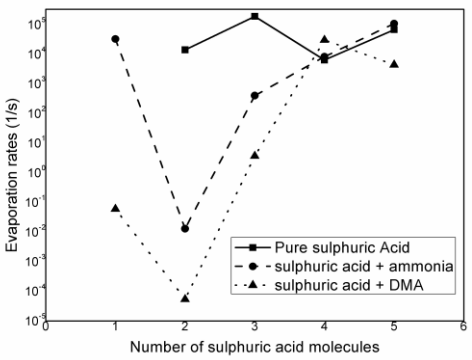

Figure 1. Evaporation rates of different clusters versus number of sulphuric acid molecules in the cluster

We have used a cost-effective multi-step method to study the stability of sulphuric acid clusters containing ammonia, and different amines. Using the calculated formation free energies we have estimated the evaporation rates of each cluster. As can be seen from figure 1, the evaporation rates of clusters containing dimethylamine is smaller compared to pure sulphuric acid clusters and ammonia-containing clusters when there are three or less sulphuric acid molecules. On the other hand, for larger clusters, the presence of just one base molecule does not seem to be enough to stabilize the cluster with respect to acid evaporation.

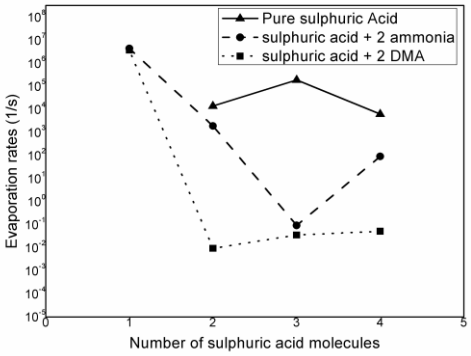

Figure 2. Evaporation rates of clusters containing two base molecules, versus number of sulphuric acid molecules in the cluster

Figure 2 shows how the addition of a second base molecule in the cluster allows the stabilization of larger clusters. In the case of clusters with two dimethylamine clusters, the cluster with two sulphuric acids seems to be the most stable. In contrast, the cluster with three sulphuric acids is the most stable of the clusters containing two ammonia molecules.

These results show how neutral sulphuric acid clusters in the atmosphere require the presence of various base molecules in order to have long enough lifetimes for growth to be possible.

This work was supported by the project,-FP7-ATMNUCLE project No 227463 (ERC Advanced Grant). The authors thank the Scientific Computing Center (CSC) in Espoo, Finland for the computing time.

Merikanto J. et al., (2009) *Atmos. Chem. Phys* **9**, 8601.

Kulmala, M., et al. (2004) *J. Aerosol Sci*. **35**, 143.

Growth of Particles via Organic Condensation: Is Gas-Phase Chemistry Enough?

N.M. Donahue[1], E.A. Trump[1], I. Riipinen[2], and J.R. Pierce[3]
[1]Center for Atmospheric Particle Studies, Carnegie Mellon University, Pittsburgh, Pennsylvania, 15213, USA
[2]Department of Physics, University of Helsinki, Helsinki, Nova Scotia, FI-00014, Finland
[3]Department of Physics and Atmospheric Science, Dalhousie University, Halifax, Nova Scotia, B3H 4R2, Canada
Keywords: nucleation and growth, organic aerosol, aerosol dynamics.
Presenting author email: nmd@andrew.cmu.edu

There is ample evidence that ultrafine particles often grow much more rapidly than can be explained by condensation of effectively non-volatile constituents such as sulfuric acid. Organic vapors are natural candidates to fill this gap because organics comprise a very large fraction of the total sub-micron aerosol mass, and because organics are often abundant in regions where new-particle formation and growth is observed. The mechanism behind this contribution is another story.

The flux of an organic, i, to a unit surface area can be written as:

$$\phi_i = A\,[C_i^v - a_i C_i^o] = A\,C_i^o\,[S_i - a_i \exp(D_K/D_p)]$$

A is a prefactor describing the velocity normal to the surface and containing any relevant conversions. For condensational growth the useful flux units are $nm\,s^{-1}$ or $nm\,hr^{-1}$. C_i^o is the saturation concentration of i (the saturation vapor pressure converted to mass concentration units in $\mu g\,m^{-3}$). S_i is the saturation ratio, $S_i = C_i^v/C_i^o$. Finally, a_i is the activity of i and $K(D_P) = \exp(D_K/D_p)$ is the Kelvin effect.

Whatever the exact value of the saturation gradient $[S_i - a_i \exp(D_K/D_P)]$, the flux will scale with $A\,C_i^o$. A depends on the mean normal speed ($s^{\perp} = 44\,m\,s^{-1}$ for $M_i = 0.200\,\mathrm{kg\,mole^{-1}}$ at 300 K). For $\rho = 1.4\,\mathrm{g\,cm^{-3}}$:

$$A = 44\,m\,s^{-1} \times \frac{10^{-3}}{\rho} = 0.031\,\frac{nm\,s^{-1}}{\mu g\,m^{-3}} = 113\,\frac{nm\,hr^{-1}}{\mu g\,m^{-3}}$$

Given observed 1-10 $nm\,hr^{-1}$ growth rate of nanoparticles during new-particle formation events, with 3 $nm\,hr^{-1}$ as typical, there must be an excess concentration of about $0.03\,\mu g\,m^{-3}$ to drive the observed growth.

Compounds that are too volatile will drive growth rates that are far too fast if they are supersaturated; however for $C^o = 10^{-2}\,\mu g\,m^{-3}$ the characteristic growth rate is 1 $nm\,hr^{-1}$ for $S = 1$. A deposition rate *slower* than 10 $nm\,hr^{-1}$ for $C^o \geq 0.1\,\mu g\,m^{-3}$ is unlikely, and the observed rates of 2-10 $nm\,hr^{-1}$ would be difficult to maintain (we should see periods with much, much larger growth).

We can constrain the production rate of condensible vapors by assuming a steady state: $P_i \simeq C_i^{ss}(S-1)/CS$, and $C_i^{ss} \simeq 0.03\,\mu g\,m^{-3}$. For $CS \simeq 1 - 10\,hr^{-1}$, $P \simeq 0.03 - 0.3\,\mu g\,m^{-3} hr^{-1}$. At this production rate material in $C^o = 0.01\,\mu g\,m^{-1}$ will have $S > 1$ and material in $C^o = 0.001\,\mu g\,m^{-1}$ will have $S \gg 1$, so we will generate supersaturation much more rapidly than the condensational sink will be able to eliminate it. That is the circumstance where condensational growth will appear to be "kinetic" – the steady-state vapor concentration, which drives condensational growth, will be well above its equilibrium value, so the growth will resemble "non-volatile" uptake.

All of this production must wind up in the condensed phase, and it is near the *maximum* rate for generation of condensible organics under typical new-particle formation conditions; the net production of SOA *mass* must be larger. There will almost certainly be production of semivolatiles with $0.1 \leq C^o \leq 1\,\mu g\,m^{-3}$, and we can only form a few $\mu g\,m^{-3}$ over the 10 or so hours it takes to grow the nanoparticles via condensation. In addition, essentially all of the vapors in the range $10^{-3} \leq C^o \leq 1\,\mu g\,m^{-3}$ need to be produced via gas-phase chemistry. It is plausible that compounds in this range can be produced from vapors with $C^o > 1\,\mu g\,m^{-3}$, but lower volatility is improbable – one generation of gas-phase chemistry can drop volatility by 1-4 decades. Consequently, it seems reasonable that of order 25% of the total SOA formation could be in the range needed to drive nanoparticle growth.

The Kelvin term deserves some attention. As we have written it, $K = \exp(D_K/D_p)$, where $D_K \simeq 7\,nm$ for $\sigma \simeq 0.03\,N\,m^{-1}$. In practice, this shows that we need to generate larger supersaturations to grow the very smallest particles, with $S = e^2 = 7.4$ required to condense onto 3.5 nm particles. For larger $C^o \geq 0.1\,\mu g\,m^{-3}$ it is simply impossible to generate such a large supersaturation in the face of the existing condensational sink. For $C^o \leq 10^{-3}\,\mu g\,m^{-3}$ it is trivial to generate the supersaturation if we can find the chemical source term. Only the $C^o = 10^{-2}\,\mu g\,m^{-3}$ bin will be strongly influenced by the Kelvin term, and the signature would be accelerating growth for $D_p \simeq 7\,nm$. This is exactly what is observed.

Consequently, if a large but not implausible fraction of condensible organic vapors are formed with intrinsic volatilities $10^{-3} \leq C^o \leq 0.01\,\mu g\,m^{-3}$, it is possible for gas-phase oxidation chemistry of organics to drive condensational growth of nanoparticles in new-particle formation events. This narrow window of volatilities is bounded by plausible gas-phase production mechanisms on the low end and the observed particle growth rates on the high end, and even the effect of surface-tension on the smallest particles via the Kelvin effect is consistent with observed growth-rate trends. This does not prove that gas-phase formation of low-volatility compounds alone drives nanoparticle growth, but it does show it almost certainly can.

How accurate are the nucleation event analysis tools?

H. Korhonen[1], S.-L. Sihto[2], V.-M. Kerminen[3] and K. E. J. Lehtinen[1,4]

[1]Kuopio Unit, Finnish Meteorological Institute, Kuopio, Finland
[2]Department of Physics, University of Helsinki, Helsinki, Finland
[3]Climate Change, Finnish Meteorological Institute, Helsinki, Finland
[2]Department of Applied Physics, University of Eastern Finland, Kuopio, Finland

Keywords: nucleation, growth, modelling
Presenting author email: hannele.korhonen@fmi.fi

According to current knowledge, atmospheric nucleation events initiate at a particle diameter of ~1.5 nm. However, until very recently, most field instruments measuring the aerosol size distribution have had a low-end cut-off at ~3 nm. Therefore, several mathematical approaches have been developed in order to quantify nucleation rates at the initial cluster size as well as nucleation mechanisms from the measured distribution data (e.g., Sihto et al., 2006; Kuang et al., 2008).

We have evaluated these analysis tools with over 1200 numerical nucleation events for which the nucleation mechanism and formation rates are known exactly. We have tested the performance of different formulations of the tools as well as the sensitivity of the results to the various assumptions that have to be made in the analysis. In order to resemble the atmospheric measurement data as closely as possible, the model output was regridded into typical size channels of a DMPS instrument with 10-minute time intervals.

We find that calculating the growth rate of sub-3 nm clusters from the time delay between the diurnal curves of H_2SO_4 and 3-6 nm particle concentration can overestimate the growth rate during strong nucleation events. This is because of coagulation scavenging of the clusters to the earlier formed nucleation mode, which can under some conditions lead to apparent negative time delays. However, the cases in which the time delay remains positive but is shortened compared to time delay corresponding to the actual growth rate are more problematic for the analysis.

In general, the particle formation rate at 3 nm (J_3) is captured reasonably well by the analysis tools with 43-97% of the events falling within a factor-of-two accuracy from the actual simulated value. However, the accuracy of the analysed values show clear sensitivity to the specific form of the analysis equations used and assumptions made about the initial size of nucleating clusters. On the other hand, the estimates of the actual nucleation rate at 1.5 nm were clearly less accurate with only 37-59% of the events within a factor-of-two accuracy. The main reason for the large errors is that the analysis methods do not take into account the size-dependence of particle growth rates below 3 nm. Moreover, the results are also sensitive to the assumption made about initial cluster size.

The poor estimates of $J_{1.5}$ can lead to fairly large uncertainties in the nucleation prefactors (i.e. constant P in nucleation equation $J_{1.5} = P \times [H_2SO_4]^k$). However, all the analysis set-ups tested in this study resulted to an order-of-magnitude accuracy for almost 90% of the simulated events. This can be considered reasonable since the coefficients derived from atmospheric data typically exhibit a variation of 1-3 orders of magnitude. This indicates that the high variation of observed nucleation prefactors is not a consequence of inaccuracies in the analysis methods, but a real phenomenon caused by (so far unknown) environmental factors.

Large uncertainties were found also when the analysis tools were used to determine the nucleation mechanism in terms of the number of H_2SO_4 molecules in a critical cluster (i.e. exponent k in previous equation). Although our results suggest that in general the analysis tools tend to overestimate the number of H_2SO_4 molecules in the critical cluster, also significant underestimation was found in up to 41% of the cases. This indicates that one cannot automatically rule out more than 2 sulphuric acid molecules in a critical cluster even if field data shows nucleation exponents in the range 1-2. Our analysis also suggests that combining data from several new particle formation events to scatter plots of H_2SO_4 vs formation rates ($J_{1.5}$ or J_3) and determining the slope of the regression line may not give reliable information about the nucleation mechanism.

This work has been supported by the Computational Science Research Programme of the Academy of Finland (decision: 135199) and EU's Sixth Framework Program (EUCAARI project).

Kuang, C., McMurry, P. H., McCormick, A. V., and Eisele, F. L. (2008) *J. Geophys. Res.*, 113, D10209, doi:10.1029/2007JD009253, 2008.

Sihto, S.-L., Kulmala, M., Kerminen, V.-M., Dal Maso, M., Petäjä, T., Riipinen, I., Korhonen, H., Arnold, F., Janson, R., Boy, M., Laaksonen, A., and Lehtinen, K. E. J. (2006) *Atmos. Chem. Phys.*, 6, 4079-4091.

Tuesday, September 6, 2011

Session 6B: Climate Effects of Aerosols / Transport and Transformation

Atmospheric processing of diesel soot aerosols studied in a smog chamber

J. E. Carlsson[1], J. Rissler[1], E. Z. Nordin[1], A. C. Eriksson[1, 2], P. T. Nilsson[1], C. Wittbom[2], M. K. Kajos[3], P. Roldin[2], E. Swietlicki[2], B. Svenningsson[2], M. Bohgard[1], M. Kulmala[2,3], J. Pagels[1]
[1] Ergonomics and Aerosol Technology, Lund University, P.O. Box 118 SE-221 00 Lund, Sweden
[2]Division of Nuclear Physics, Lund University, P.O. Box 118 SE-221 00 Lund, Sweden
[3]Department of Physic, University of Helsinki, P.O. Box 64, FIN-00014 University of Helsinki, Finland
Keywords: Soot particles, Aerosol Transformation, Aerosol particle mass analyzer, Smog chamber
Presenting author email: jonatan.carlsson@design.lth.se

The atmospheric processing of soot aerosols leads to a transformation of the agglomerated structure to droplets/crystals with an elemental carbon core due to coating processes (Zhang *et al.* 2008). This affects global climate by transforming net-heating light absorbing hydrophobic black carbon into particles with increasing light scattering cross section and hygroscopicity. The health effects are also expected to vary between the fresh and processed soot. Secondary Organic Aerosols (SOA) contributes to a large fraction of the material that condenses onto soot. A group of important SOA precursors are the light aromatic Volatile Organic Compounds (VOCs). The time scales for the transformation of soot with its corresponding changes in optical and Cloud Condensation Nuclei (CCN) properties are not well known. The aim of this work is to quantify the timescales in processing of soot aerosols using photo-oxidation studies of engine exhaust from light duty diesel vehicles in a smog chamber set-up.

The experiments were conducted in a 6 m^3 Teflon (FEP) smog chamber as described in Nordin *et al.* (2011). Diesel exhaust was injected by a heated ejector dilutor and heated inlet (120 °C), the vehicle used in the experiments was a VW Passat 1.9 TDI (1998). Emissions from the warm idling car or a flame soot generator were then sampled to the smog chamber giving an initial concentration of about 10 µg/m^3 and a size distribution with a geometric mean diameter (GMD) of 80-90 nm. The aromatic precursors Toluene and m-Xylene were injected by evaporation into the smog chamber and after a 30-40 min stabilization period UV lights were turned on. The soot morphology was investigated using a Differential Mobility Analyzer (model 3071, TSI) - Thermodenuder (Custom built) - Aerosol Particle Mass Analyzer (model 3600, Kanomax) (DMA-TD-APM) system which had been calibrated with spherical PSL particles (100, 240 and 350 nm). Particles with mobility diameters between 90 and 300 nm were selected by the DMA. The mass of the fresh (m_{fresh}) and coated soot particles (m_{coated}) were then measured by two adjacent runs, where the TD was set to 300°C to evaporate the organics. From this, the mass growth factor (*Gfm*), defined as the ratio of m_{coated} and m_{fresh} (Pagels *et al.* 2009) was calculated. This together with a Scanning Mobility Particle Sizer (SMPS) provides assessments of the size dependent organic carbon- (OC) and elemental carbon (EC) mass. The light scattering and the CCN properties were measured by a Nephelometer (model Aurora 3000, Ecotech) and a Cloud Condensation Nuclei Counter (model CCN-100, DMT), respectively.

Preliminary results show that a mass increase (growth factor) of about 3-15 (figure 1) due to condensation of organics is necessary for transformation of 90-300 nm soot aggregates into spheres with an effective density of about 1.4 g/cm^3. This transformation decreases the water vapor supersaturation required for CCN activation of 150 nm particles from larger than 2% (fresh soot) to 0.2 % (soot coated with 80% SOA).

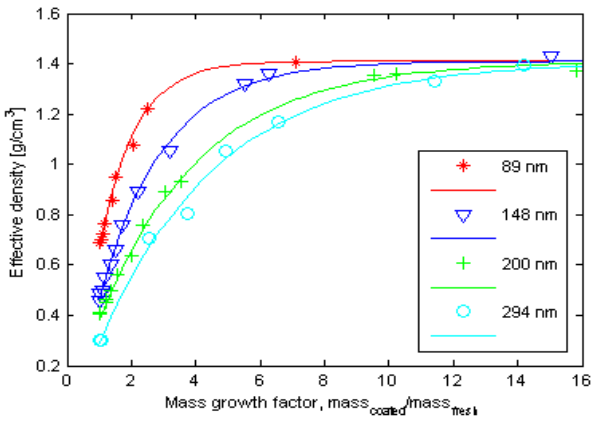

Figure 1. The measured and fitted curve for the effective density as a function of the mass growth factor (*Gfm*). The following fit was used $\rho_{eff}(d_{me}) = \rho_{fresh}(d_{me}) + \left(1.4 - \rho_{fresh}(d_{me})\right)(1 - exp((Gfm - 1)/a(d\_me)))$

The results suggests that particles with a mobility diameter less than 300 nm, which dominate the number concentration, become spheres with a significant increase in hygroscopicity during the experiment time of four hours. The growth factor is used to calculate the OC- and EC-mass which can be utilized as a normalization factor for light scattering cross section and a reference mass for the Soot Particle-Aerosol Mass Spectrometer (SP-AMS).

This work was supported by the Swedish research council FORMAS through projects 2007-1205, 2008-1467 and 2010-1678

Zhang, R., et al. (2008). Proc. Natl. Acad. Sci. *USA 105:10291–10296.*
Pagels, J., et al. (2009). *Aerosol Sci. Technol, 43:629-640*
Nordin, E, Z., et al. (2011). EAC 2011 proceedings

Hygroscopic properties of HULIS from different environments

T.B. Kristensen[1], H. Wex[2], B. Nekat[2], D. Van Pinxteren[2], K. Mildenberger[2], F. Stratmann[2], J.K. Nøjgaard[3], C.B. Koch[4], A.G. Hallar[5], T.F. Mentel[6] and M. Bilde[1]

[1]Department of Chemistry, University of Copenhagen, Copenhagen, DK-2100 Ø, Denmark
[2]Leibniz Institute for Tropospheric Research, Leipzig, 04318, Germany
[3]Department of Atmospheric Environment, University of Aarhus, Roskilde, DK-4000, Denmark
[4]Dept. of Basic Sciences and Environment, University of Copenhagen, Fr.berg C, DK-1871, Denmark
[5]Desert Research Institute, Storm Peak Laboratory, Steamboat Springs, CO 80488, USA
[6]Institute for Energy and Climate Research: Troposphere, Research Center Jülich GmbH, 52425 Jülich, Germany

Keywords: HULIS, CCN-activity, hygroscopic growth, WSOC.
Presenting author email: thomas@kemi.ku.dk

Humic-Like Substances (HULIS) have been proven to comprise a significant fraction of the organics in various environments. HULIS have attracted a lot of attention because of their ability to efficiently lower surface tension of water solutions and thereby influence hygroscopic growth and cloud condensation nuclei (CCN) activity. However direct measurements are still scarce and the reported hygroscopicity for HULIS samples varies significantly.

This study focuses on elucidating the hygroscopicity of HULIS by applying the same extraction protocol of HULIS to particulate matter (PM) sampled in three very different environments. Filter samples from the rural continental background site Melpitz ($PM_{2.5}$), from a street canyon in Copenhagen (PM_{10}) and from Storm Peak Laboratory (SPL) located 3.2 km asl in Colorado ($PM_{2.5}$) were selected. Here results from the latter are presented.

The extraction of HULIS was carried out by applying the one-step protocol described by (Varga et al, 2001) with minor modifications to facilitate extraction of large amounts of HULIS. Hygroscopic growth was measured with LACIS-mobile. The experimental setup and procedure is very similar to that described by Ziese et al, (2008). A refractive index of 1.63 was assumed for HULIS in the data analysis. The CCN-activity was derived from fitting a sigmoidal function to the activated fraction of particles vs electrical mobility particle diameter where doubly charged particles are accounted for. The CCN-concentration was measured with a DMT CCN-counter and the total particle concentration [CN] was measured with a CPC 3010.

Preliminary results for hygroscopic growth of 200nm HULIS particles originating from SPL are presented in fig. 1. The growth factors (GF) are smaller compared to results for HULIS from Budapest. In fig. 2 the preliminary results for the CCN-activity of the SPL HULIS are depicted. In this case the results are comparable to the results of Ziese et al (2008). Closure between the results for sub- and supersaturated conditions respectively can be obtained assuming a surface tension lower than that of pure water for the wetted HULIS particles, which is in line with what would be expected (Ziese et al, 2008). Based upon the physiographic location of SPL it can be speculated that the SPL-HULIS would resemble HULIS originating from aged biomass burning aerosol (Dinar et al, 2006) – however the results do not indicate that. It could be due to differences in HULIS extraction protocols.

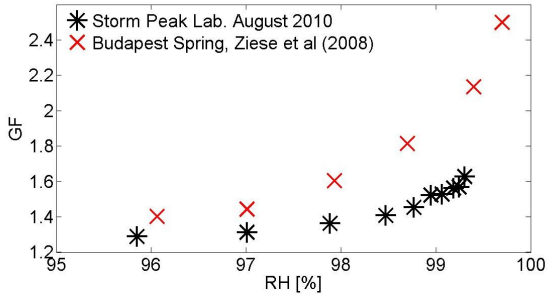

Figure 1. A comparison of growth factors (GF) for HULIS from SPL and Budapest, spring (Ziese et al, 2008).

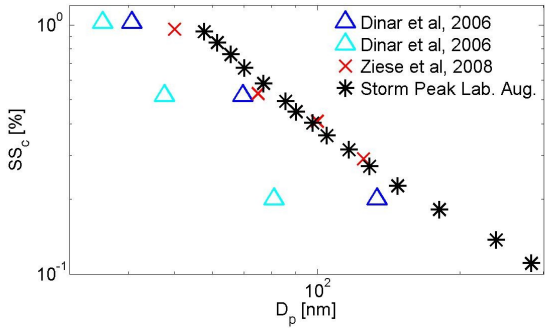

Figure 2. The CCN-activity of HULIS from SPL and from Budapest is comparable (Ziese et al, 2008). The CCN-activity is higher for HULIS originating from biomass burning (blue triangles) and significantly higher for aged biomass burning aerosol (cyan triangles).

This work was supported by EUROCHAMP 2, EU FP7.

Dinar, E., Taraniuk, I., Graber, E. R., Katsman, S., Moise, T., Anttila, T., Mentel, T. F. and Rudich, Y. (2006). *Atmos. Chem. Phys.* **6**, 2465-2482.

Feczko, T., Puxbaum, H., Kasper-Giebl, A., Handler, M., Limbeck, A., Gelencsér, A., Pio, C., Preunkert, S. and Legrand, M. (2007). *J. Geophys. Res.* **112**

Varga, B., Kiss, G., Ganszky, I., Gelencsér, A. and Krivácsy, Z. (2001) *Talanta* **55**, 561-572.

Ziese, M., Wex, H., Nilsson, E., Salma, I., Ocskay, R., Henning, T., Massling, A. and Stratmann, F. (2008), *Atmos. Chem. Phys.* **8**, 1855-1866.

On the regional effects of clean fossil fuel combustion aerosols

W. Junkermann[1], B. Vogel[2] and M. Sutton[2]

[1]Karlsruhe Institute of Technology, IMK-IFU, Garmisch-Partenkirchen, 82467, Germany
[2] Karlsruhe Institute of Technology, IMK-TRO, Eggenstein-Leopoldshafen, 82467, Germany
[3] Centre for Ecology and Hydrology, Edinburgh Research Station, Penicuik, Midlothian, United Kingdom

Keywords: nucleation, power plant, indirect effect, precipitation.
Presenting author email: wolfgang.junkermann@Kit.edu

During recent airborne experiments on several occasions very high numbers of ultrafine particles were observed in plumes of fossil fuel burning industrial installations. The high numbers of particles observed might have an impact on the regional production of cloud condensation nuclei concentrations and thus contribute to significant regional cloud microphysics modifications. This has a subsequent effect on the spatial distribution and on the intensity distribution of precipitation. Such precipitation modifications would have a severe impact in pristine semiarid areas with already low total annual precipitation.

We are presenting results from airborne measurements of ultrafine particles in different moderately polluted or pristine areas of the world, also from semiarid areas which are prone to desertification and show how precipitation is affected by increasing CCN numbers. Measured size distributions together with meteorological data are used to calculate source strengths and budgets of ultrafine particles.

We compare source strength of natural and anthropogenic CCN precursor sources and discuss the importance of anthropogenic ultrafine particle emissions based on our experimental results.

Based on the experimental results a significant impact of ultrafine anthropogenic particles on regional climate can be derived, less important on the radiation balance, and with a main effect on the regional water budget.

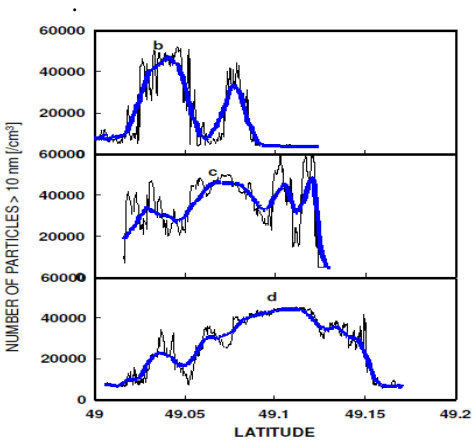

Figure 1. Plume cross sections after 5, 15 and 35 km in a combine power plant / refinery plume (Junkermann et al., 2011).

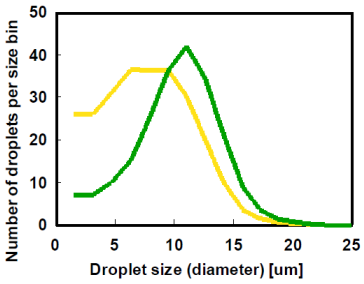

Fig. 2, cloud droplet size distributions in nonprecipitating stratocumulus clouds under low (green) and slightly enhanced CCN number concentrations (Junkermann et al., 2009)

We also show how new cleaning technology for flue gases affects the emissions of fossil fuel burning industries and how this modifies the importance of anthropogenic emissions to the regional CCN budget.

Junkermann W., Hacker J., Lyons T., and Nair U., (2009) *Atmos. Chem. Phys.*, 9, 6531-6539. www.atmos-chem-phys.net/9/6531/2009/
Junkermann, W., Hagemann, R., and Vogel, B. (2011) *QJRMS*, 137, 267-274.

Sensitivity of cloud radiative forcing to cloud formation parameterization under three different meteorological fields

Sotiropoulou, Rafaella-Eleni P.[1], Meskhidze, Nicholas[2], Kouatchou, Jules[3], Oreopoulos, Lazaros[3], Rodriguez, Jose M.[3] and Nenes, Athanasios[4]

1 Environmental Research Lab, INT-RP, N.C.S.R. Demokritos, Aghia Paraskevi, Greece
2 School of Marine Earth and Atmospheric Sciences, North Carolina State University, Raleigh, NC, USA
3 NASA Goddard Space Flight Center, Greenbelt, Maryland, USA
4 Schools of Earth and Atmospheric Sciences and Chemical and Biomolecular Engineering, Georgia Institute of Technology, Atlanta, GA, USA
Keywords: Aerosol-cloud interaction, CCN, radiative forcing, clouds, modeling.
Presenting author email: rsot@ipta.demokritos.gr

Cloud droplet number concentrations (CDNC) prediction in global climate models (GCMs) is a challenging step for quantifying the cloud radiative properties as large uncertainty is associated with it. In an attempt to elucidate and disentangle one of the reasons for the spread of the shortwave (SW) cloud radiative forcing (CRF) estimated by the GCMs, its sensitivity to cloud droplet parameterization used is assessed under three different meteorological fields using present day emissions.

The sensitivities are computed with the NASA Global Modeling Initiative (GMI). GMI is a global 3D chemical-transport model specifically developed for impact assessment studies that allows easy interchange of different model components while maintaining all others identical. The common modeling framework allows a direct intercomparison of results obtained between alternate representations of aerosol, chemistry and transport processes, without the uncertainties typically associated with comparison of output from different GCMs.

CDNC is computed with the empirical correlation of Boucher and Lohmann - BL (1995), and the physically-based parameterizations of Abdul-Razzak and Ghan - AG (2000), and Fountoukis and Nenes - FN (2005). Sensitivities are examined under three different meteorological fields from the NASA GEOS4 finite volume GCM (FVGCM), the NASA GEOS1-STRAT (GEOS) and the NASA GISS II' GCM (GISS). Computed CDNC is used to calculate the effective radius. The CLIRAD-SW solar radiative transfer model is used online to calculate the cloud optical depth (COD) and the shortwave fluxes from the surface to the top of the atmosphere (TOA). COD is calculated as a function of the effective radius. Evaluation of modeling results (i.e., cloud droplet effective radius, cloud optical depth) is performed against satellite products from Moderate Resolution Imaging Spectroradiometer (MODIS) platform.

Depending on the meteorological fields and droplet parameterization used the annual mean CDNC ranges from 75 to 146 cm^{-3} (Figure 1) with larger differences seen over the heavily polluted regions of the globe (e.g., Europe, China, NE USA), regions affected by long range transport of pollution plumes (e.g., Atlantic Ocean) and regions affected by biomass burning (e.g., S. Africa, S. America). The results for the SW CRF are quite similar across the modeling experiments and, in the global mean. These estimates compare reasonably well with the results derived from the Earth Radiation Budget Experiment (ERBE) analysis.

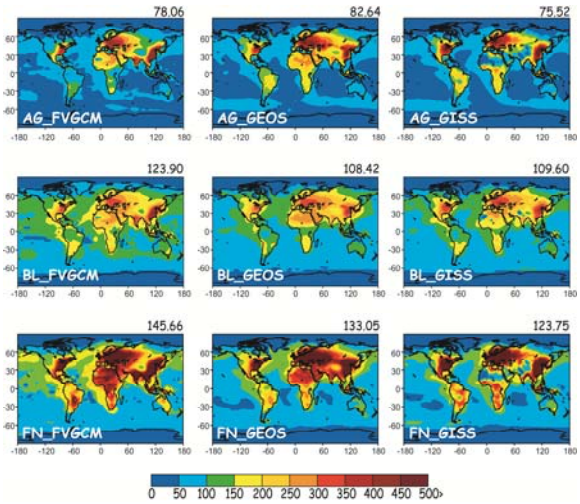

Figure 1. Simulated annual mean cloud droplet number concentrations (cm^{-3}) for all droplet schemes considered and meteorological data sets from FVGCM, GEOS and GISS GCMs. Global annual averages are shown in the upper right hand corner of each panel

This work was supported by NASA (New Investigator Award, EOS-IDS), an NSF CAREER Award, a Blanchard-Milliken Young Faculty Fellowship, DOE-ARM and FP7-REGPOT-2008-1grant No 229773.

Abdul-Razzak, H. and Ghan, S. (2002), *J. Geophys. Res.*, **107**.

Boucher, O. and Lohmann, U. (1995). *Tellus B*, **47**, 281–300.

Fountoukis, C. and Nenes, A. (2005), *J. Geophys. Res.*, **110**(D11212), doi:10.1029/2004JD005 591.

The global picture of aerosol layers formation in the stratosphere and in the mesosphere under the influence of gravito- and magneto- photophoretic forces.

Cheremisin A.A[1], Shnipov I.S[2], and Horvath, H[3].

[1] Siberian Federal University,Krasnoyarsk, Russia
[2] Krasnoyarsk Railway Institute, Krasnoyarsk, Russia
[3] University of Vienna, Faculty of Physics, Aerosol and Environmental Physics , Boltzmanngasse 5, 1090 Vienna, Austria

Keywords: Photophoresis, Stratospheric aerosol, Mesosphere, Strratification.
Presenting author email: helmuth.horvath@univie.ac.at

Photophoretic forces act on a particle which has an inhomogeneous surface, especially with respect to the accommodation coefficient. Gas molecules incident on it leave the surface after more or less accommodation, resulting in a force and torque on the particle. Due to Brownian rotation of the particle the net force is zero. If the particle is also exposed to an orientating torque, the photophoretic force points in a preferred direction resulting in net photoporetic force. The orienting torque can be caused by gravity or by the earth magnetic field. Photophoretic forces are important if the mean free path of the gas molecules is larger than the size of the particles. This is the case for almost all particles found in the stratosphere and mesosphere. The direction of the photophoretic force can be opposite to gravity and it can exceed the weight of the particle. In that case the particle is lifted upwards, until it reaches conditions where the two forces are equal.

The photophoreic force is influenced by the mean free path of the air molecules, the solar and infrared irradiance, the light absorption of the particle, the orientating torque (which could be magnetic or gravitational) and the variation of the accommodation coefficient on the surface of the particle.

Laboratory observations of photophoresis are available in the literature, obviously for the laboratory conditions (Rohatschek, 1985).. In order to apply these results to the atmosphere, the temperature profile of the atmosphere, the incoming solar flux density, the emitted terrestrial infrared radiation, was determined at each location and at each day of the year and applied to various types of particles.

The equality of the average gravito-photophotetic force and gravity force has been taken as the main condition of layer formation. This requirement has been supplemented by the condition of mechanical stability, that ensures return of the particle to the equilibrium position when an accidental shift in altitude occurs (Cheremisin et al, 2002). It has been assumed that the combination of these two factors creates favourable conditions for accumulation of particles of certain types and sizes at corresponding altitudes, resulting in aerosol layers.

The following classes of particles have been studied: (1) Particles strongly absorbing both solar radiation of visible and terrestrial IR radiation (soot-like particles) (2) Particles strongly absorbing only terrestrial IR radiation (similar to sulfate containing aerosols). Particles with and without a magnetic moment were considered.

Photophoresis can be responsible for aerosol layer formation at altitudes of 20, 30, 50, 70 and 85 km. The layers form in specific geographic regions and at certain seasons An example for time dependent locations where particles will be in a stable position is shown in figure 1.

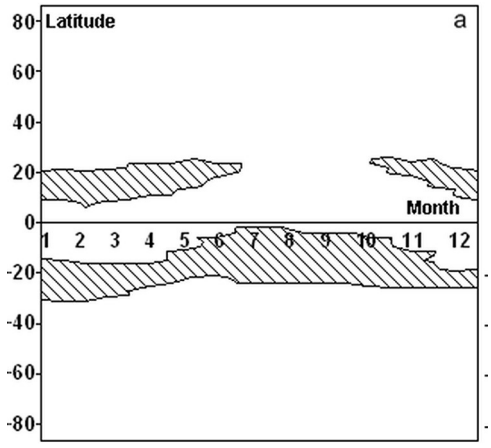

Figure 1. Seasonal-latitudinal map of stratospheric levitation areas for strongly absorbing IR radiation particles

This investigation is supported under grant 10-05-00907a by the Russian Fund of Basic Research and Ministry of Science and Education of Russian Federation (project № 2.1.1/ 6996). We would like to thank professor K.M. Firsov and T.Yu. Chesnokova for computer program FLUX, enable to calculate incoming and outgoing IR radiation fluxes in the Earth's atmosphere.

Cheremisin A.A., Vassilyev Yu .V., Kushnarenko A.V. Photophoretic forces for bispherical aerosol particles. // Proc. SPIE. - 2002. - V. 5027. - P. 21-32.

Rohatschek, H. (1985). Direction, magnitude and causes of photophoretic forces. *J. Aerosol Sci.* **16**, 29—42.

.

Tuesday, September 6, 2011

Session 6C: Smog Chamber Experiments and SOA 2

Simulating secondary organic aerosol (SOA) formation over Europe using the volatility basis-set approach (VBS) in the online coupled model COSMO-ART

Eleni Athanasopoulou[1], Heike Vogel[1], Max Bangert[1], Christoph Knote[2], Bernhard Vogel[1], Ben Murphy[3], Alexandra Tsimpidi[4], Spyros Pandis[3,4]

[1]Institute for Meteorology and Climate Research, Karlsruhe Institute of Technology (KIT), Eggenstein-Leopoldshafen, Germany
[2]Empa, Dübendorf, Switzerland
[3]Department of Chemical Engineering, Carnegie Mellon University, Pittsburgh, USA
[4]Department of Chemical Engineering, University of Patras, Patra, Greece
Keywords: SOA (Second. Organic Aerosols), aerosol modeling, volatility basis-set.
Presenting author email: eleni.athanasopoulou@kit.edu

COSMO-ART is a recently developed regional model that couples meteorological and air quality processes online (Vogel et al., 2009). Comparisons of aerosol predictions against measurements suggested an underestimation of the total aerosol mass, which was attributed mainly to low organic aerosol (OA) predictions (Knote et al., 2010). This finding became the stimulation for revising SOA treatment within COSMO-ART, presented in the current study.

Previous research suggests that the models' inability to reach OA observations is strongly related to gas-particle partitioning of all (thousands) organics emitted and formed into the atmosphere, but not in simulations. An efficient way to incorporate this chemical evolution of organics into modelling (aging), is their group treatment by saturation concentrations (VBS) (Donahue et al., 2006).

Recent model applications using VBS confirm model's improved efficiency in predicting OA mass (Murphy and Pandis, 2009; Tsimpidi et al., 2010 etc). According to their results, SOA can represent more than 50% of total OA mass, while their absolute values can reach more than 5μgm^{-3}, which seems promising for improving COSMO-ART performance (Fig. 1).

In the framework of this study, COSMO-ART is modified to include the VBS treatment of SOA. Nine biogenic and anthropogenic SOA precursors (higher alkanes and alkenes, terpenes, isoprene) are grouped into 4 surrogate species with effective saturation concentrations of 1, 10, 100, 1000 μgm^{-3}, modified according to the spatial-temporal variation of temperature (Clausius-Clapeyron eq.). Aerosol yields after each precursor's oxidation to OH, O_3 and NO_3^- alter with its condensation effectiveness and are a combination of the low and high NOx mass yields used in Murphy and Pandis (2009). Further oxidation of surrogate species decreases their saturation concentration by 1 order of magnitude (aging) and increases their mass by 7.5% (to account the oxygen added).

The VBS approach is then coupled with the existing gas-particle partitioning module and with the chemical mechanism RADMKA (Regional Acid Deposition Model Version Karlsruhe). The simulation domain covers Europe with an horizontal grid size of 14km and 40 vertical layers up to a height of 20km. The meteorological initial and boundary conditions are achieved from the IFS model of ECMWF for May 2008. COSMO-ART results by applying the prior (SORGAM) and the current (VBS) SOA module are inter-compared and evaluated against field measurements of OA collected during the EUCAARI campaign for selected stations.

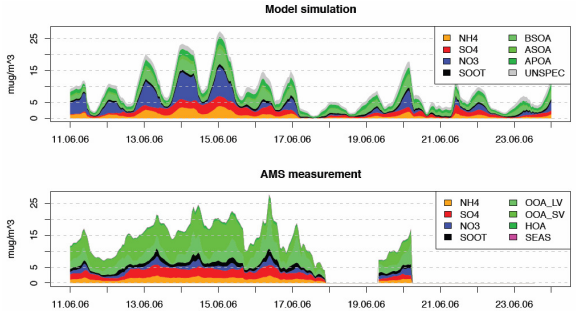

Figure 1. Evaluation of COSMO-ART aerosol composition AMS campaign measurement (PSI) in Payerne (CH) (Knote et al., 2010)

A similar grouping and aging approach used in global applications, showed an effect on CCN concentrations, due to the enhanced condensation and particle growth (Yu, 2011). The fully coupled approach used by COSMO-ART, gives to this study the opportunity to investigate the feedback of the VBS approach on cloud formation. Results will be presented during the conference.

Vogel, B., Vogel, H., Baumer, D., Bangert, M., Lundgren, K., Rinke, R. And Stanelle T. (2009) *Atmos. Chem. Phys.* **9**, 8661–8680.

Knote, C., Brunner, D., Vogel, H., Vogel, B., and Lohmann U. (2010) *Proc.Int. Aerosol Conference.*

Donahue, N.M., Robinson A.L., Stanier C.O. and Pandis S.N. (2006) *Environ. Sci. Technol.* **40**, 2635-2643.

Tsimpidi, A.P, Karydis, V.A., Zavala, M., Lei, W., Molina, L., Ulbrich, I.M., Jimenez, J.L. and Pandis S.N. (2010) *Atmos. Chem. Phys.* **10**, 525–546

Murphy, B.N and Pandis, S.N. (2009) *Environ. Sci. Technol.* **43**, 4722-4728.

Yu (2011) *Atmos. Chem. Phys.* **11**, 1083-1099.

Chemical composition, Hygroscopicity and CCN properties of biogenic secondary organic aerosols

M.R Alfarra[1,2], J.F. Hamilton[3], K.P. Wyche[4], T. Carr[4], A. Ryan[5], R. Ayala[6], P. Monks[4], R. MacKenzie[5], A. Lewis[3], N. Hewitt[5], G.B. McFiggans[2]

[1]National Centre for Atmospheric Science (NCAS), The University of Manchester, Manchester, M13 9PL, UK
[2]Centre for Atmospheric Sciences, The University of Manchester, Manchester, M13 9PL, UK
[3]Deparment of Chemistry, University of York, Heslington, York, YO10 5DD, UK
[4] Department of Chemistry, University of Leicester, Leicester, LE1 7RH, UK
[5] Department of Environmental Science, Lancaster University, Lancaster, LA1 4YQ, UK
[6] Faculty of Engineering, National University of Mexico (UNAM), Mexico

Keywords: SOA, Smog Chamber, Chemical Composition, Hygroscopicity, Aerosol mass spectrometry
Presenting author email: rami.alfarra@manchester.ac.uk

Studies using photochemical "smog", or aerosol, chambers can provide valuable insights into the complex multiphase processes leading to the formation and transformation of atmospheric particulates. As part of the Aerosol Coupling in the Earth System (ACES) project, a series of novel experiments were carried out at the Manchester Aerosol Chamber in order to investigate the chemistry and microphysics of the formation and transformation of biogenic secondary aerosols under realistic conditions. A selection of compounds covering a wide range of reactivity including isoprene (C_5H_8), monoterpenes (isomeric formula $C_{10}H_{16}$), sesquiterpenes (isomeric formula $C_{15}H_{24}$) and oxygenated VOCs have been studied in detail.

The chemical composition of the formed SOA was measured on-line using an Aerodyne Time-of-Flight Aerosol Mass Spectrometer (ToF-AMS). A hygroscopicity tandem differential mobility analyser (HTDMA) and a cloud condensation nuclei (CCN) counter were used to probe the hygroscopic properties and of the aerosols in the sub- and super-saturated regimes, respectively. A proton transfer mass spectrometer was used to study the evolution of the gas phase oxidation products.

This paper presents a comprehensive overview of the chemical composition, hygroscopicity and cloud condensation nuclei (CCN) properties secondary organic aerosols formed from five structurally different biogenic VOCs (β-caryophyllene, limonene, myrcene, linalool, α-pinene), and compares them to those of SOA formed from the photooxidation of real plant emissions (Silver Birch). A discussion of results of the use of organic (Hamilton et al., 2010) and inorganic seed will be presented and compared to those obtained from nucleation experiments.

Results obtained using the ToF-AMS showed that SOA formed from the above precursors have a wide range of chemical properties, as expressed by the fraction of mass fragment 44 (a typical marker for highly oxygenated organic molecules) and 43 (a possible marker for less oxygenated organic molecules) to the total organic signal. Furthermore, the effect of photochemical ageing on those properties was not uniform across all five precursors. A link of these results to the findings of the hygroscopic properties of the same SOA particles and their CCN behavior will be presented and discussed.

This work was supported by the UK Natural Environment Research Council (NERC) through the Aerosol Properties, PRocesses And InfluenceS on the Earth's climate (APPRAISE) programme. M. Rami Alfarra is supported by NERC's National Centre for Atmospheric Science (NCAS).

Hamilton, J.F., Alfarra, M.R., Wyche, K.P., Ward, M.W., Lewis, A.C., McFiggans, G.B., Good, N., Monks, P.S., Carr, T., White, I.R. and Purvis, R.P. (2010) *Atmos. Chem. Phys. Discuss.*, *10*(10), 25117-25151.

Physical and chemical characterisation of mixed anthropogenic and biogenic secondary organic aerosol

E. U. Emanuelsson[1], B. Bohn[2], A. Buchholz[2], B. Kammer[2], A. Kiendler-Scharr[2], B. Kortner[2], Th. F. Mentel[2], S. Nehr[2], R. Tillmann[2], E. Kleist[3], K. Kristensen[4], M. Fenger-Lauridsen[4], M. Glasius[4] and M. Hallquist[1]

[1]Atmospheric Science, Department of Chemistry, University of Gothenburg, SE-412 96 Göteborg, Sweden
[2]Institut für Energie- und Klimaforschung: Troposphäre (IEK-8),
Forschungszentrum Jülich, D-52428 Jülich, Germany
[3]Plant Sciences (IBG-2), Forschungszentrum Jülich, D-52428 Jülich, Germany
[4]Department of Chemistry, Aarhus University, DK-8000 Aarhus, Denmark
Keywords: SOA, Aerosol chemistry, Smog chamber, Aerosol characterization
Presenting author email: eva.emanuelsson@chem.gu.se

In order to properly represent and predict effects of aerosols in climate systems, an accurate description of their formation and properties is needed. Volatile Organic Compounds (VOC) acting as aerosol precursors and forming secondary organic aerosol (SOA) can originate from both biogenic and anthropogenic emissions. A lot of emphasis has been to understand these systems separately (Hallquist 2009) but in the atmosphere it will be a more complex situation where the anthropogenic emissions will be subjected to oxidation and transformation also after being mixed with biogenic emission.

During spring/summer 2010 two campaigns in Forschungszentrum Jülich, Germany were conducted with focus on Anthropogenic - Biogenic Secondary Organic Aerosol (ABSOA). The measurement campaigns took place in the JPAC (Jülich Plant Aerosol Chamber) and SAPHIR (Simulation of Atmospheric PHotochemistry In a large Reaction chamber) facilities with the objective to clarify how interactions of biogenic and anthropogenic trace gases influence SOA formation with regard to mass, number, composition and properties. In the JPAC chamber the biogenic emissions originated from real boreal plant emissions (Mentel 2009) and the anthropogenic emissions were represented by toluene and xylene. The large outdoor SAPHIR chamber enables studies of tropospheric chemistry and photochemical models under natural conditions (Rohrer 2005) and here the BVOCs were represented by limonene and α-pinene and AVOC by benzene, toluene and xylene. The systems were investigated individually (BSOA, ASOA) and mixed (ABSOA).

Several instruments were used for both physical and chemical characterisation of aerosol e.g; Aerosol Mass Spectrometer (ToF-AMS), Volatility Tandem Differential Mobility Analyser (VTDMA), Hygroscopicity Tandem Differential Mobility Analyser (HTDMA), Cloud Condensation Nuclei Counter (CCN-C) and Scanning Mobility Particle Sizer (SMPS) systems. In the SAPHIR campaign aerosol filter samples were collected for offline analysis with respect to tracer molecules. In addition the gas phase chemistry and partitioning was monitored using ozone and NO_X analyzers together with PTR-MS.

Example of the characterisation was the volatility measurements, using the VTDMA system. The VTDMA comprises: an initial Differential Mobility Analyser (DMA) where a size fraction of the aerosol particles is selected; the oven unit where the evaporation and adsorption of the volatile fraction occurs and a final SMPS system where the residual particle number distribution is measured. A less volatile SOA gives a larger residual particle size distribution compared to a more volatile SOA. (Jonsson 2007).

Generally, the aerosol thermal characteristics were comparable in the SAPHIR and the JPAC experiments and the induced aging produced less volatile aerosol particles for all investigated systems. However, the two system are rather different in aging characteristics where the JPAC aerosol were produced in a flow system with residence time around an hour while the SAPHIR aerosol were aged during several hours/days.

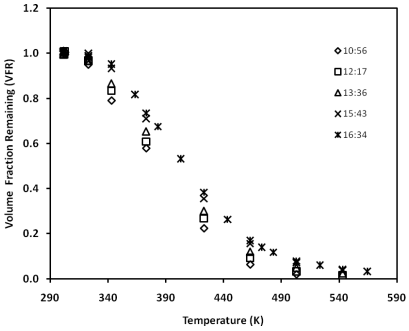

Figure 1. Volatility of ageing (UTC hh:mm) of SOA from mixed anthropogenic and biogenic volatile organic compounds in the SAPHIR camber.

This work was financially supported by MERGE, Tellus, EUROCHAMP-2 and the scholarship foundations of The Royal Swedish Academy of Agriculture and Forestry, Knut and Alice Wallenberg, Senator Emil Possehl and Adlerbertska.

Hallquist, M. et. al. (2009). *Atmos. Chem. Phys.* **9**, 5155-5236.

Mentel, Th. F. et. al. (2009). *Atmos. Chem. Phys.* **9**, 4387-4406.

Rohrer, F. et. al. (2005), *Atmos. Chem. Phys.* **5**, 2189-2201.

Jonsson, Å. M. et. al. (2007), *Journal of Aerosol Science*, **38**, 843-852.

Source apportionment of atmospheric organic aerosols by nuclear magnetic resonance (NMR) spectroscopy during the EUCAARI project

M. Paglione[1], S. Decesari[1], E. Finessi[1], R. Hillamo[2], S. Carbone[2], S. Saarikoski[2], T. Raatikainen[2], M. Dall'Osto[3,7], C.D. O'Dowd[3], A. Kiendler-scharr[4], A. Mensah[4], U. Baltensperger[5], A. Prevot[5], D.R. Worsnop[6], and M.C. Facchini[1]

[1]Institute of Atmospheric Sciences and Climate, National Research Council, Bologna, I-40129, Italy.
[2]Finnish Meteorological Institute, Air Quality Research, Helsinki, Finland.
[3]School of Physics and Centre for Climate and Air Pollution Studies, National Univ. of Ireland, Galway, Ireland.
[4]Forschungszentrum Juelich, Germany.
[5]Laboratory of Atmospheric Chemistry (PSI), Villigen, Switzerland.
[6]Aerodyne Research, Inc., Billerica, MA, USA.
[7]now at: Institute of Environmental Assessment and Water Research, Consejo Superior de Investigaciones Cientìficas (CSIC), C/LLuis Solè i Sabarìs S/N 08028 Barcelona, Spain.

Keywords: HNMR spectroscopy, Source apportionment, PMF, SOA, AMS.
Presenting author email: m.paglione@isac.cnr.it

In the frame of the EUCAARI (European integrated project on Aerosol Cloud Climate Air Quality Interactions) project, organic aerosol characterization and source apportionment were carried out during nine intensive observation periods (Table 1) by means of proton-Nuclear Magnetic Resonance (^{1}H-NMR) spectroscopy. Analogously to more established methodologies employing mass spectrometric techniques, we exploit factor analysis for the identification of a small number of recurrent chemical classes. In particular, NMR analysis provides a categorization of water-soluble organic aerosols based on spectral fingerprints and characteristic functional groups distributions.

Field Station	Period
Hyytiala - HYY (SMEAR II) - Finland	Mar-Apr 2007
Cabauw – CBW (CESAR obs.) – Netherlands	May 2008
Melpitz – MPZ (IFT) - Germany	May 2008
Mace Head – MH (NUI Galway) - Ireland	May 2008
K-Puszta - KPZ (Univ. of Veszprém) – Hungary	May-Jul 2008
S. Pietro Capofiume - SPC (ISAC-CNR) – Italy	Apr 2008
Zurich – ZW (PSI) - Switzerland	Dec 2008
Barcelona & Montseny -BCN (EUSAAR) – Spain	Feb-Mar 2009
S. Pietro Capofiume - SPC (ISAC-CNR) – Italy	Jun-Jul 2009

Table 1. Summary of the EUCAARI intensive observation periods (IOPs) providing NMR datasets

Factor analysis of NMR spectral datasets is already widely used for the analysis of complex organic matrices in several scientific fields, from pharmaceutics to food chemistry and medical chemistry. Deconvolution of main spectral profiles within each time series of ^{1}H-NMR spectra of submicron aerosol samples was conducted using non-negative factor analysis techniques, such as Positive Matrix Factorization (PMF), Non-negative Matrix Factorization (NMF), and Multivariate Curve Resolution (MCR).

The interpretation of the spectral profiles and their attribution to specific sources (i.e., anthropogenic and biogenic SOA, biomass burning POA) of water-soluble organic particles in the atmosphere is based on the comparison with a unique library of reference spectra recorded during laboratory studies or in the field at near-source stations.

Some recurrent profiles were identified in different IOPs of EUCAARI project and their contribution to the total mass of OA were quantified. In particular the principal recurrent spectral profiles isolated were: (a) biogenic Secondary Organic Aerosol (SOA); (b) wood burning aerosols; (c) HUmic Like Substances (HULIS); (d) other complex aromatic and aliphatic oxidized compounds enriched in aliphatic chains; (e) MetanSulfonicAcid (MSA) and (f) low-molecular weight amines.

The results of this statistical analysis were compared to those of existing methodologies of factor analysis applied to atmospheric aerosol spectroscopic datasets (AMS) collected in the same period for each measurement campaign.

Our findings indicate that factor analysis applied to NMR atmospheric datasets can efficiently complement AMS in lumping the complex oxidized organic mixtures into chemical classes characterized by specific sources or ageing states. More specifically, NMR spectroscopy provides a better discrimination between aromatic and aliphatic structures, which is critical for the quantification of biomass burning products, and for the discrimination between biogenic and anthropogenic SOA.

This work has been supported by European Commission 6th Framework program project EUCAARI, contract no 036833-2 (EUCAARI).

Discrimination of secondary organic aerosol from different sources

U. Baltensperger[1], M.F. Heringa[1], R. Chirico[1,2], S.M. Platt[1], L. Pfaffenberger[1], P. Barmet[1], J.G. Slowik[1], P.F. DeCarlo[1,3], J. Dommen[1] and A.S.H. Prévôt[1]

[1]Laboratory of Atmospheric Chemistry, Paul Scherrer Institut, 5232 Villigen PSI, Switzerland
[2]now at Italian National Agency for New Technologies, Energy and Sustainable Economic Development (ENEA), UTAPRAD-DIM, Via E. Fermi 45, 00044 Frascati, Italy
[3]now at AAAS Science and Technology Policy Fellow, US EPA, Washington, DC, USA
Keywords: SOA, aging, aerosol mass spectrometry, smog chamber, source apportionment
Presenting author email: urs.baltensperger@psi.ch

Secondary organic aerosol (SOA) comprises a major fraction of the submicron aerosol mass (Hallquist *et al*, 2009). It consists of thousands of different compounds, and undergoes permanent chemical evolution during the atmospheric aging process, resulting in an increasingly oxidized aerosol (Jimenez *et al* 2009). As a result of this, chemical features of SOA (such as unit mass spectra from aerosol mass spectrometry) become increasingly similar with increasing aging time. This is good news for modeling purposes, as the specific SOA source becomes less important for the quantification of the SOA impact e.g. on climate. However, this also means that it is difficult to perform an apportionment of the SOA to its various sources, e.g., by positive matrix factorization (Lanz *et al* 2007).

We have investigated SOA formation from a variety of sources, including both wood combustion and diesel exhaust, with either the full exhaust or only the gaseous precursors (Chirico *et al* 2010; Heringa *et al* 2011), using the setup shown in Figure 1. In addition, SOA formation from anthropogenic and biogenic model precursors such as trimethylbenzene and α-pinene was investigated. All experiments were performed at the PSI smog chamber (Paulsen *et al* 2005).

We characterized the formed SOA using a high resolution time-of-flight aerosol mass spectrometer. The various fragments obtained from the high-resolution spectra were tested for characteristic differences using a variety of methods. The results will be discussed along with a comparison to high-resolution aerosol mass spectra from ambient samples.

This work was supported by the IMBALANCE project of the Competence Center Environment and Sustainability (CCES), the NEADS project of the Competence Center Energy and Mobility (CCEM), the Bundesamt für Umwelt (BAFU), the Bundesamt für Energie (BFE), as well as the Swiss National Science Foundation.

Chirico, R. *et al* (2010) *Atmos. Chem. Phys.* **10**, 11545-11563.
Hallquist, M. *et al* (2009) *Atmos. Chem. Phys.* **9**, 5155-5236.
Heringa, M.F. *et al* (2011) *Atmos. Chem. Phys. Discuss.* **11,** 8081-8113.
Jimenez, J.L. *et al* (2009) *Science* **326**, 1525-1529.
Lanz, V.L. *et al* (2007) *Atmos. Chem. Phys.* **7**, 1503-1522.
Paulsen, D. *et al* (2005) *Environ. Sci. Technol.* **39**, 2668-2678.

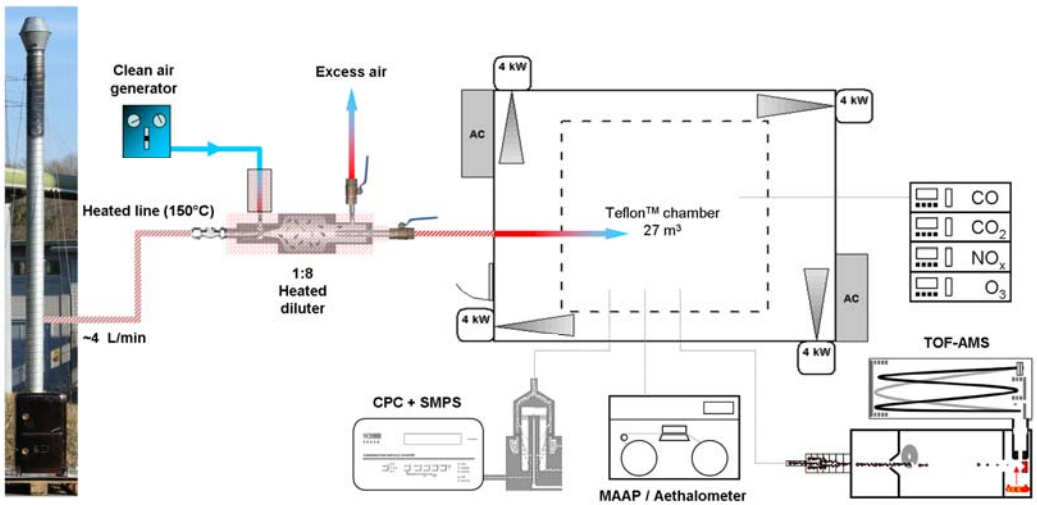

Figure 1. Schematic representation of the inlet system and smog chamber setup (Heringa *et al* 2011).

Understanding particle formation by alkene-ozone reactions: Experimental studies and theoretical simulations

F. Ebach[1], M. Hummel[1], S. Bourtsoukidis[1], B. Bonn[1], W. Haunold[1] and R. Sitals[1]
[1]Institute for Atmospheric and Environmental Sciences, J.W. Goethe University, Frankfurt/Main, Germany
Keywords: nucleation, climate effects, VOC(s), activation.
Presenting author email: bonn@iau.uni-frankfurt.de

Abstract
The formation of secondary organic aerosol particles is one of the most progressing aspects with respect to composition and the increase of knowledge about heterogeneous processes. Besides partitioning and ageing effects, the exact mechanistic understanding of the formation process needs to be unravelled. From previous studies on the suppressive influence of water vapour we can assume the start of the nucleation process by so-called secondary ozonides. These are expected to be activated as clusters by large organic peroxy radicals (RO_2). In order to learn about the exact role of different radicals, i.e. RO_2 and HO_2 as well as Criegee biradicals (sCI), we conducted flowtube experiments with simple alkenes in the presence of ozone and nopinone and varied the nitrogen oxide (NO) concentration. NO increased nucleation at very low values while acting suppressive at intermediate and higher concentrations. The observed total particle number concentration was simulated by an aerosol dynamics model with implemented gas-phase chemistry and nucleation hypotheses. With this set-up we were able to reproduce the observed particle number concentration in different systems, i.e. alkenes and concentration levels. This allowed the set-up of a new mechanistic nucleation pathway, including the interaction of RO_2 and sCI radicals in order to form new detectable particles capable in explaining the suppressive effect of isoprene on nucleation. From these studies it seems likely that an organic nucleation might be an atmospheric phenomenon too, depending on the concentration and structure of present VOCs.

Methods
(Experimental) Particle formation has been studied in a vertical flow chamber with a constant temperature at 24°C. Mixtures of alkenes and NO were performed a priori in stainless steel bottles and used thereafter. Ozone was produced online by a pen-ray lamp and nopinone added by a permeation oven. Particles were detected by two different counters: WCPC (TSI 3085, cut off = 5 nm) and UCPC (TSI 3025A, cut off = 2.7 nm). The concentrations of the gases were either calculated by mixing volume (ethene) or measured by PTR-MS as well as ozone and NO_x analysers.
(Theoretical) Based on the University of Helsinki Multicomponent Aerosol model (UHMA, Korhonen et al., 2004) the detailed chemistry of propene and ethene was calculated and initiated by the measured values.

Findings
A new particle formation mechanism was implemented and two unknown rate constants fitted:

(a) RO_2 + SOZ: $k_a = (0.9\text{-}3)\times10^{-12}$ cm^3 molec.$^{-1}$ s^{-1}
(b) sCI + SOZ: $k_b = (6\text{-}8.5)\times10^{-11}$ cm^3 molec.$^{-1}$ s^{-1}

Taking into account the difference in structure of propene- and ethene sCIs, both constants agree well and a nucleation occurs using both radicals in turn.

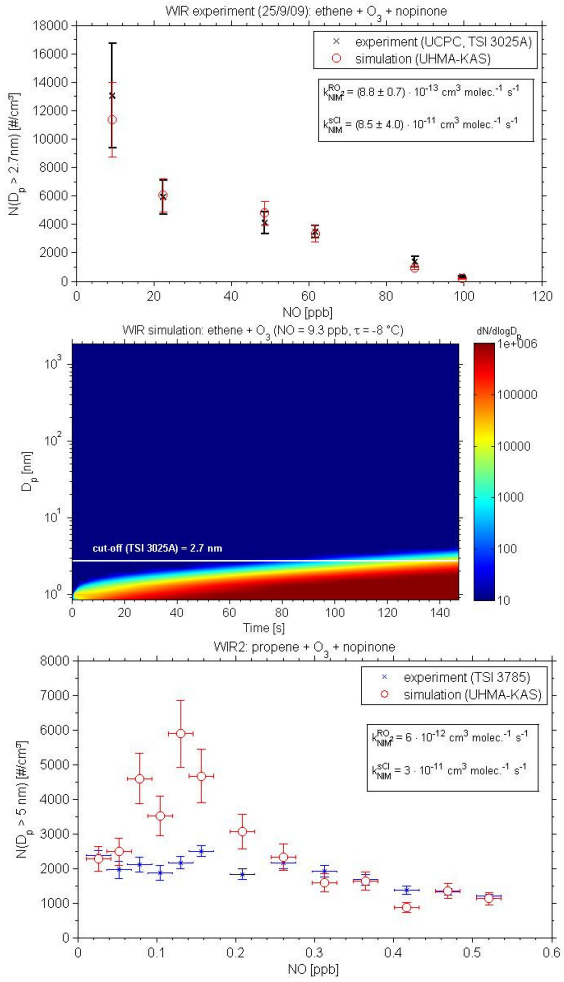

.
Fig. 1: Ethene measurements and simulations (top and centre) as well as propene measurements (bottom).

Conclusions
It was obtained that NO and HO_2 radicals act suppressive, with a competition of individual radical reactions especially with RO_2. The production of more water-soluble compounds by HO_2 is not supportive.

References:
Bonn et al., *J. Phys. Chem. A*, 106, 2869-2881, 2002.
Korhonen et al., *Atmos. Chem. Phys.*, 4, 2561-2580., 2004.

Tuesday, September 6, 2011

Session 6D: Direct Impacts of Aerosol on Climate (ADIENT Project)

Measurement and modelling of ammonium nitrate aerosol and its impacts in North-Western Europe

W. T. Morgan[1], J. D. Allan[1,2], M. K. Bane[1*], K. N. Bower[1], B. Harris[3], J. S. Henzing[4], E.J. Highwood[3], A. Kiendler-Scharr[5], G. McFiggans[1], G. R. McMeeking[1], A. A. Mensah[5], S. Osborne[6+], M. J. Northway[3], P. I. Williams[1,2], R. Krejci[7], and H. Coe[1]

[1]Centre for Atmospheric Science, University of Manchester, Manchester, UK
[2]National Centre for Atmospheric Science, The University of Manchester, Manchester, UK
[3]Department of Meteorology, University of Reading, Reading, UK
[4]TNO, Utrecht, Netherlands
[5]Institute for Chemistry and Dynamics of the Geosphere, Institute 2: Troposphere, Jülich, Germany
[6]Met Office, Exeter, UK
[7]Department of Applied Environmental Science, Atmospheric Science Unit, Stockholm University, Stockholm, Sweden
*Now at Research Computing Services, University of Manchester, Manchester, UK
[+]Now at Met Office, Cardington, UK

Keywords: ammonium nitrate, AMS, Aerosol Optical Depth (AOD), European Pollution.

Ammonium nitrate aerosol exhibits highly scattering properties across the solar spectrum. Further to this, it displays hygroscopic tendencies (Tang, 1996), allowing enhanced water uptake for a given relative humidity. Consequently, its ability to scatter incident solar radiation is increased leading to an enhancement of the aerosol direct radiative forcing. Anticipated reductions in sulphur dioxide in polluted regions will result in an increase in the availability of ammonia to form ammonium nitrate as opposed to ammonium sulphate. Consequently, the relative importance of ammonium nitrate to the aerosol burden is likely to increase.

This paper presents an assessment of the contribution, properties and impact of ammonium nitrate upon the European aerosol burden. In-situ measurements of aerosol properties made onboard the UK Facility for Airborne Atmospheric Measurements (FAAM) BAe-146 aircraft will be presented. The aircraft employs a suite of aerosol instruments, which resolve the chemical composition, number size distribution, optical and hygroscopic properties of the in-situ aerosol population. This includes an Aerodyne Aerosol Mass Spectrometer (AMS) which measures the size resolved chemical composition of both volatile and semi-volatile particulate matter (Canagaratna *et al.*, 2007). The measurements were conducted as part of the EUCAARI-LONGREX (European Integrated Project on Aerosol Cloud Climate Air Quality Interactions–LONG Range EXperiment) and APPRAISE-ADIENT (Aerosol Properties, Processes and influences on the Earth's climate – Appraising the aerosol direct impact on climate) campaigns. Science flights were conducted across Europe, during predominantly clear sky conditions during 2008.

Ammonium nitrate was found to dominate in North-Western Europe during episodes of high pollution, reflecting the enhanced NO_x and ammonia sources in this region. Ammonium nitrate and organic matter were often observed to increase with altitude in the atmospheric boundary layer. This was attributed to partitioning of semi-volatile gas phase species to the particle phase at reduced temperature and enhanced relative humidity. Increased ammonium nitrate concentrations in particular were found to strongly increase the ambient scattering potential of the aerosol burden. During particularly polluted conditions, increases in boundary layer aerosol optical depth of 50-100% were estimated to occur due to the observed increase in secondary aerosol mass with altitude and associated water uptake. These enhancements significantly increase the direct aerosol radiative forcing. Such increases have major ramifications for regional climate predictions as semi-volatile components are often not included in aerosol models.

Our observations over North-Western Europe indicate that failure to include the semi-volatile behaviour of ammonium nitrate will result in significant errors in predicted aerosol direct forcing.

The ability of a sophisticated regional aerosol transport model to represent the complex spatial distribution of ammonium nitrate will be explored. This will include the observed horizontal spatial gradients in North-Western Europe and in particular the vertical distribution of the aerosol.

This work was supported by the Natural Environment Research Council ADIENT project NE/E011101/1 and EUCAARI project 036833-2. We would like to acknowledge the efforts of FAAM, DirectFlight, Avalon, DLR, the Met Office and IMPACT teams.

Tang, I. N. (1996), *J. Geophys. Res.*, **101 (D14)**, 19245-19250.

M. R. Canagaratna, *et al*, (2007), *Mass Spectrometry Reviews*, **26 (2)**, 185-222.

Optical and Radiative Properties of Aerosol as Determined During the ADIENT Project

E.J. Highwood[1], M.J. Northway[1], G. McMeeking[2] , W. Morgan[2] , C. Ryder[1], D. Lui[2] , P. Williams[2] , H. Coe[2] S. Osborne[3] and K. Bower[2]

[1]Department of Meteorology, University of Reading, Reading, Berkshire, RG6 6BB, UK
[2]Center for Atmospheric Science, University of Manchester, Manchester, M13, 9PL, UK
[3]The Met. Office, Fitzroy Road, Exeter, Devon, EX1 3PB.
Keywords: anthropogenic aerosols, optical properties, ADIENT, direct effect.
Presenting author email: e.j.highwood@reading.ac.uk

The direct effect and radiative forcing of atmospheric aerosols depends crucially on their so-called optical properties, such as extinction co-efficient, single scattering albedo and asymmetry parameter. These in turn depend on microphysical properties of the aerosols specifically size and composition. The complexity of atmospheric aerosols requires synergistic use of models and measurements in order to provide this information for use in climate models.

The ADIENT and EUCAARI projects have provided a new body of measurements of aerosol composition, microphysical and optical properties within anthropogenically perturbed air masses across western Europe. In particular, co-incident measurements of aerosol composition and radiative properties were made onboard the Met Office/ NERC Facility for Airborne Atmospheric Measurements BAe146.

In this talk, aerosol composition as seen by an CTOF-AMS (Drewnick et al, 2007) and black carbon mass as seen by an SP2 (Schwarz et al, 2006; McMeeking et al, 2010) will be used together with best estimates of refractive indices, measured size distributions and a Mie scattering code will be used to model the optical properties of aerosol from a number of flights during the ADIENT and EUCAARI projects. The resulting scattering and absorption will be compared against co-incident measurements from a nephelometer and Particle Soot Absorption photometer. The degree to which "optical closure" can be achieved and the influence of uncertainty in assumed refractive index of various aerosol components will be discussed (illustrated in Figure 1).

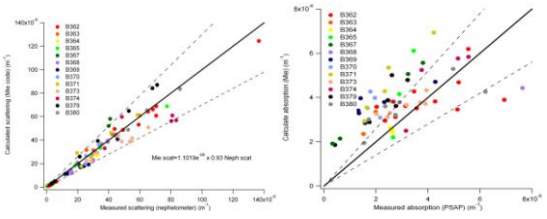

Figure 1. The closure obtained between a) scattering and b) absorption modelled using assumed refractive indices, measured size and composition and observations from the nephelometer/PSAP

Additionally, the variation of single scattering albedo and aerosol optical depth across Europe from the FAAM EUCAARI-LONGREX flights (Morgan et al, 2010; McMeeking et al, 2010; Hamburger et al 2010) and ADIENT flights around the UK will be presented. The hygroscopicity of the aerosol encountered will also be discussed.

This work was supported by the UK Natural Environment Research Council Project (grant number NE/E011187.1 under the Aerosol Properties Processes and Influences on the Earth's climate (APPRAISE) programme.

Drewnick, F. , J. Schneider, S. S. Hings, N. Hock, K. Noone, A. Targino, S. Weimer, and S. Borrmann (2007), Measurement of Ambient, Interstitial, and Residual Aerosol Particles on a Mountain-top Site in Central Sweden using an Aerosol Mass Spectrometer and a CVI. *J. Atm. Chem.*, **56,** 1-20.

Hamburger, T., McMeeking, G., Miniken, A., Birmili, W., Dall'Osto, M., Flentje, H., Henzing, B., Junninen, H., Kristensson, A., de Leeuw, G., Stohl, A., Coe, H., Krejci, R., and Petzold, A. (2011): Overview of the synoptic and pollution situation over Europe during the EUCAARI-LONGREX field campaign. *Atmos. Chem. Phys.*, **11**, 1065-1082

McMeeking, G.R., T. Hamburger, d. Liu, M. Flynn, W.T. Morgan, M. Northway, E.J. Highwood, R. Krejci, J.D. Allan, A. Minikin and H. Coe (2010): Black carbon measurements in the boundary layer over western and northern Europe, *Atmos. Chem. Phys*., **10**, 9393-9414,

Morgan, W.T., J.D. Allan, K.N. Bower, E.J. Highwood, D. Liu, G.R. McMeeking, M.J. Northway, P.I. Williams, R. Krejci, and H. Coe (2010): Airborne measurements of the spatial distribution of aerosol chemical composition across Europe and evolution of the organic fraction, *Atmos. Chem. Phys***., 10**, *4065-4083*

Schwarz, J.P. et al (2006) Single particle measurements of mid-latitude black carbon and light-scattering aerosols from the boundary layer to the lower stratosphere. *J. Geophys. Res***., 110**, D16207

ADIENT satellite based aerosol direct radiative forcing

G.E. Thomas[1], N. Chalmers[2], B. Harris[2], E.J. Highwood[2] and R.G. Grainger[1]

[1]Atmospheric, Oceanic and Planetary Physics, University of Oxford, Oxford, OX1 3PU, UK
[2]Department of Meteorology, University of Reading, Reading, RG6 6BB, UK
Keywords: ADIENT, aerosol direct effect, radiative forcing, GlobAEROSOL.
Presenting author email: gthomas@atm.ox.ac.uk

Atmospheric aerosols play an important role in determining the radiative balance of the atmosphere, both directly (Yue et al., 2006) and through their interactions with clouds (Lohmann and Feichter, 2005). However our knowledge of the radiative impact of aerosol on over a long term, global scale remains very uncertain, due to the variable nature of aerosol loading and composition. Thus, aerosols remain one of the primary uncertainties in our understanding of the climate system (IPCC, 2007).

As part of the ADIENT project, new regional estimates of the radiative forcing due to the direct radiative effects of aerosols have been generated, based on the GlobAEROSOL dataset (Portela et al. 2009). GlobAEROSOL provides a range of global datasets of aerosol properties derived from European satellite sensors, running from 1995—2008. Data from the Advanced Along Track Scanning Radiometer (AATSR), processed using the Oxford-RAL Aerosol and Cloud (ORAC) retrieval (Thomas et al. 2009), have been used in this project.

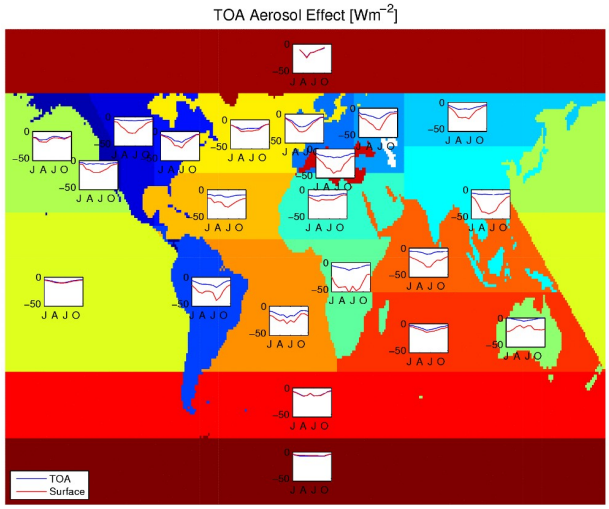

Figure 1. Monthly radiative effect of aerosol for each region at the top and bottom of the atmosphere.

Monthly radiative transfer calculations have been performed with the Edwards and Slingo (1996) RTM across 22 regions covering the globe (11 land, 9 ocean and 2 polar regions) for the year 2006. An extensive error characterisation has been performed for each of these regions, by comparison of the GlobAEROSOL aerosol optical depth with AERONET and by testing the sensitivity of the radiative transfer to model parameters (e.g. aerosol properties, surface albedo). Additionally, high spatial (1x1°) resolution and daily calculations have been performed to characterise the effects of temporal and spatial averaging. These errors have been propagated through the radiative transfer calculations to provide 1-σ uncertainty estimates for the resulting radiative forcings.

This talk will present the results of this analysis for the first time, and compare them with other estimates of the direct aerosol radiative forcing; both measurement and model based.

ADIENT is a UK Natural Environment Research Council project (grant number NE/EO11187/1) under the Aerosol Properties Processes and Influences on the Earth's Climate (APPRAISE) programme.

Edwards, J.M. and Slingo, A. (1996) *Q. J. R. Meteorol. Soc.* **122**, 689-719.

IPCC (2007) *Climate Change 2007: The physical science basis. Contribution of Working Group 1 to the Forth Assessment Report of the Intergovernmental Pannel on Climate Change*, Cambridge University Press.

Lohmann, U. and Feichter, J. (2005) *Atmos. Chem. Phys.* **5**, 715-737.

Portela, O., Thomas, G.E., Poulsen, C.A., Grainger, R.G. (2009) *GlobAEROSOL Final Report.*

Thomas, G.E., Carboni, E., Sayer, A.M., Poulsen, C.A., Siddans, R. and Grainger, R.G. (2009) *Oxford-RAL Aerosol and Cloud (ORAC)* in *Aerosol remote sensing over land*, Kokhanovsky, A. and de Leeuw, G. (eds.), Springer.

Yu, H., Kaufman, Y.J., Chin, M., Feingold, G., Remer, L.A., Anderson, T.L., Balkanski, Y., Bellouin, N., Boucher, O.,Christopher, S., DeCola, P., Kahn, R., Koch, D., Loeb, N.,Reddy, M. S., Schulz, M., Takemura, T. and Zhou, M. (2006) *Atmos. Chem. Phys.* **6**, 613-666.

Testing methods to derive top of the atmosphere reflected shortwave fluxes in the presence of aerosol during the ADIENT campaign: application to GERB and SEVIRI

H.E Brindley, A.P. Georgiadis, and J.E. Russell

Department of Physics, Imperial College, London, SW7 2AZ, UK
Keywords: satellites, shortwave fluxes, aerosol radiative effect
Presenting author email: h.brindley@imperial.ac.uk

Due to their fifteen minute temporal resolution, the combination of the narrowband Spinning Enhanced Visible and InfraRed Imager (SEVIRI) and the Geostationary Earth Radiation Budget (GERB) instruments on the Meteosat Second Generation series of satellites offers an unprecedented opportunity to track the evolution of both natural and anthropogenic aerosol and assess their associated radiative impact over the approximate 60°S-60°N,60°E-60°W region viewed by the instruments. However, as noted in previous studies (Brindley and Ignatov, 2006), the aerosol retrieval algorithm used to generate optical depths in the standard GERB products uses one fixed aerosol model which may not be appropriate for specific aerosol events. In addition, fluxes are typically derived from satellite observed radiances via the application of an angular distribution model (ADM) selected according to scene type. At present, shortwave (SW) fluxes derived from the observed GERB radiances do not contain a treatment to account for the impact of aerosol on the anisotropy of the radiance field, an omission which will result in angle dependent SW flux biases (Brindley and Russell, 2008).

In this paper we first seek to evaluate two methodologies that have been proposed to correct for these SW flux biases. The first, introduced by Loeb et al. (2003), involves the application of a theoretical correction to clear-sky ADMs derived from the Clouds and the Earth's Radiant Energy System (CERES) instrument to account for the presence of aerosol. The second, developed by Zhang *et al.* (2005), again uses CERES observations, in this case building ADMs as an explicit function of near surface wind speed and aerosol optical depth.

To perform the analysis we focus on periods and locations sampled under the auspices of the Appraising the Direct Impacts of AErosol oN ClimaTe (ADIENT)/European Integrated Project on Aerosol Cloud Climate Air Quality Interactions (EUCAARI) projects. We apply both methods to co-located GERB and SEVIRI data and see a significant reduction in the instantaneous direct radiative efficiency of aerosol calculated using the GERB observations as they stand, and after application of the new ADMs (Figure 1). By considering the homogeneity of the derived fluxes as a function of solar and viewing geometry we also conclude that for the conditions sampled here, the aerosol correction method developed by Loeb et al. gives the most reliable results.

We then focus on a specific flight off south-eastern England during May 2008 to assess whether radiative closure can be achieved using the recommended flux conversion and the observed aircraft data. Whilst a limited closure is possible, the aerosol optical depths retrieved using aerosol optical properties inferred from the aircraft tend to be somewhat smaller than those recorded by nearby Aerosol Robotic Network (AERONET) stations. Better agreement on this wider spatial scale is obtained using the standard fixed aerosol model. The results highlight the effect of small scale inhomogeneities in aerosol composition on satellite derived aerosol fields, and the implications for calculations of their associated direct radiative effect.

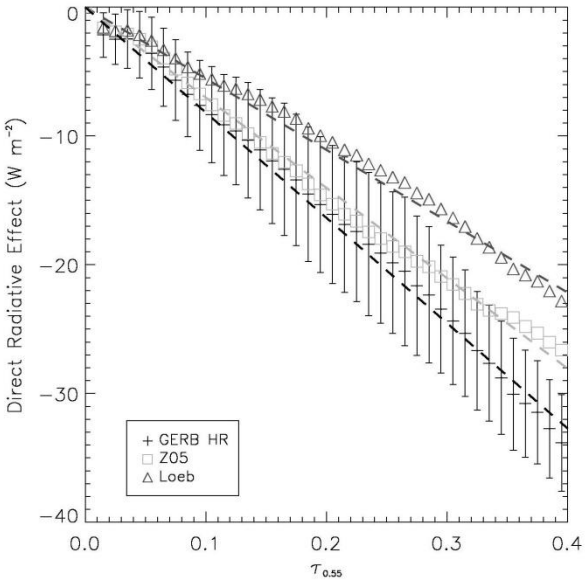

Figure 1. SW Direct Radiative Effect as a function of aerosol optical depth at 0.55 microns (τ_{055}). GERB HR indicates the original GERB fluxes, Z05 and Loeb are fluxes obtained using the Zhang *et al* ADMs and Loeb *et al* aerosol correction method respectively

This work was supported by the Natural Environment Research Council under grant NE/E011101/1

Brindley, H. and Ignatov, A. (2006) *Rem. Sens. Env.* **102**, 344-363

Brindley, H. and Russell, J. (2008) *J. Appl. Met.* **47**, 1659-1680

Loeb N., Manalo-Smith, N., Kato, S., Miller, W., Gupta, S., Minnis, P. and Wielicki, B. (2003) *J. Appl. Met.*, **42**, 240-265

Zhang, J., Christopher, S., Remer, L. and Kaufman, Y. (2005) *J. Geophys. Res.* **110**, D10S23

Tuesday, September 6, 2011

Session 6E: Enhanced Aerosol Measurement Technology

Nanoparticle measurements with photon correlation LDA

P. Jani,, L. Vámos, A. Nagy and A. Kerekes

Research Institute for Solid State Physics and Optics, Konkoly-Thege str. 29-33. H-1121. Budapest, Hungary
Keywords: nanoparticle, sizing, photon correlation, LDA
Presenting author email: pjani@sunserv.kfki.hu

First nanoparticle measurements were performed with serial manufacture photon correlation Laser Doppler Anemometer (Nano-LDA). The system was developed to monitor the number concentration and individual velocity and size of nanoparticles simultaneously. Using a backscattering arrangement there is no need for high precision alignment procedure.

The high collection efficiency combined with high QE single photon counting makes it possible to reach the nanometer size range. Photon correlation technique was used for data processing of single photon count events to generate the cumulative autocorrelation function and its FFT. This data contains the mean velocity of the measured aerosol flow. However the special technique for burst selecting and burst processing opens the way for the data processing of individual particles. By this way the particle concentration, velocity and size histogram can be calculated too. The size estimation is based on the amplitude technique combined with a model-based iterative parametric method (Vámos 2010).

After the first functional tests of the system (Jani 2010), measurements on monodisperse paraffin particles were performed below 2µm. The particles generated by PALAS AGF 2.0 iP have ca. 250nm average diameter with approximately lognormal size distribution.
The particle flow was diluted with filtered air and lead through a Differential Mobility Analyser (http). The separated particles were lead to the measurement volume of the LDA system.

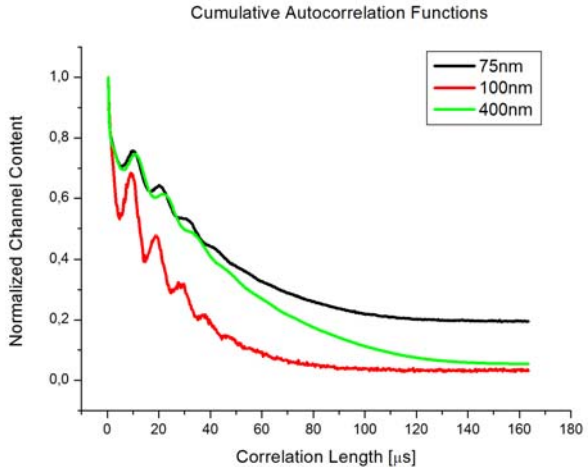

Figure 1. Normalized autocorrelation function curves from paraffin particles separated by DMA

For the high dynamic range of the scattered intensity neutral density filter range is incorporated in the Nano-LDA permitting to select illumination intensity with 1:10^5 ratio.

Successful measurements were carried out for mean particle sizes 75nm, 100nm, 200nm, 300nm, 400nm and 500nm. Obtained autocorrelation functions are plotted on Figure 1 normalized to zero channel content. For lower particle sizes the scattered intensity decreases with the sixth power of the particle diameter. By this way the SNR for the 75nm particles decreases as it can be seen in the graph.

The FFT of the cumulative autocorrelation function is calculated and smoothed with the well-known parabolic interpolation method to reach the 1% velocity measurement accuracy (Figure 2).

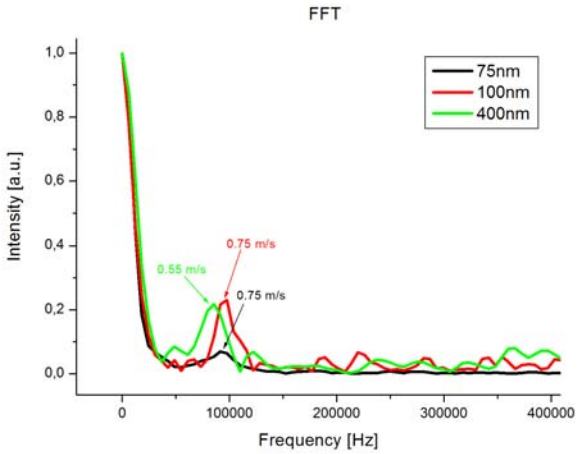

Figure 2. Normalized FFT curves from paraffin particles separated by DMA

Conclusion

The Nano-LDA proved itself to be sensitive for particles down to 75 nm. The recorded ACF curves show high modulation depth with tolerable SNR even for 75nm particles. It is not presently clear whether the aerosol generator has outputs in the even lower size ranges.

In consequence of the small measurement volume 10^7 particle/cm^3 concentration can be reached.

The authors thankfully acknowledge the technical assistance of PCSOFT Ltd. Hungary and the financial support of TECHNOORG Linda Ltd. through the MAG Zrt. under the grant KMOP-1.1.1-07/1-2008-0056.

Vámos L, Jani P, (2010), *Optical Engineering*, **49**, 1.
Jani, P et al, (2010) *Proc. International Aerosol Conference IAC2010*
http://www.ilaqh.qut.edu.au/Misc/ANZAS%202010/GRIMM%20Aerosol.pdf

Soot Particle AMS measurement in smog chamber experiments

A.C. Eriksson[1,2], E. Z. Nordin[2], P. T. Nilsson[2], J. E. Carlsson[2], C. Wittbom[1] P. Roldin[1], M.K. Kajos[3], J. Rissler[2] , F. Abdisa[2], M. Hallquist[4], M. Kulmala[3], B. Svenningssson[1], J. Pagels[2] and E. Swietlicki[1]
[1]Nuclear Physics, Lund University, P.O. Box 118 SE-221 00 Lund, Sweden
[2]Ergonomics & Aerosol Technology, Lund University, P.O. Box 118 SE-221 00 Lund, Sweden
[3]Dept. Physics, Div. of Atmospheric Sciences, Helsinki University, P.O. Box 64, FIN-00014Helsinki, Finland
[4]Dept. Chemistry, Göteborg University, 412 96 Gothenburg, Sweden
Keywords: AMS, smog chamber, SOA, soot particles.
Presenting author email: axel.eriksson@nuclear.lu.se

There is considerable uncertainty regarding the effects of soot containing aerosols on climate and human health. Investigating these effects is complicated by the fact that airborne soot is notoriously difficult to quantify. This is partly due to the ambiguity of 'soot'. Various techniques exist which utilize the effective light absorption or low volatility as means of quantification of airborne soot. The operationally defined quantities measured by these techniques are not necessarily comparable. Furthermore, it is desirable to measure soot as one chemical category among others rather than as a stand alone parameter.

Aerosol Mass Spectrometry has recently emerged as a powerful technique for on-line measurements of particulate composition. The most widely used device, the Aerodyne Aerosol Mass Spectrometer (AMS), operates by means of flash vaporization due to impaction on a heated (600 C) surface. The low volatility of soot makes it a refractory species, i.e. it is not measured by the standard AMS. In order to address this problem a Soot Particle (SP) module was developed, which vaporizes soot by means of a 1064 nm Nd-YAG laser.

In this study an SP-AMS was used to measure soot in diesel exhaust from a light duty vehicle. The exhaust was artificially aged by adding SOA precursors such as toluene and m-xylene and exposing the mixture to UV irradiation in a 6 m^3 smog chamber (Nordin et al 2011) for five hours. The resulting SOA condensation enabled investigations into the difference in instrumental response between fresh and aged soot. Soot particles produced by means of a diffusion flame propane soot generator were also included in the study, to determine the suitability of these as substitute for exhaust particles.

Two complementary techniques were used to validate the measured soot content of the aerosol, Particulate Soot Absorption Photometer (PSAP 3λ, Radiance Research and PSAP 1 λ, custom built) and Aerosol Particle Mass Analyser (APM, model 3600, Kanomax). The PSAP measures light absorption of a filter onto which particles are deposited. From this quantity a mass loading of soot is inferred, taking into account light scattering simultaneously measured with a Nephelometer (Ecotech, Aurora 3000, 3 λ). With an APM one determines the mass of charged aerosol particles through balancing centrifugal and electrostatic forces. In these experiments a Differential Mobility Analyzer (DMA, TSI, model 3071) and thermo-denuder (TD, custom built) were used in combination with the APM. By denuding the sampled aerosol at 300 C, the mass fraction of soot in particles can be deduced.

Throughout the campaign, the SP-AMS was used with both the standard vaporization device and the soot vaporisation module present. The laser was typically engaged in five minute intervals separated by an hour, while the standard device was engaged continuously. This is a compromise which enables soot mass measurements while retaining the capabilities of a normal AMS, producing data which is comparable with that of other studies. The soot and SOA signal generated were qualitatively similar to PSAP and APM signals.

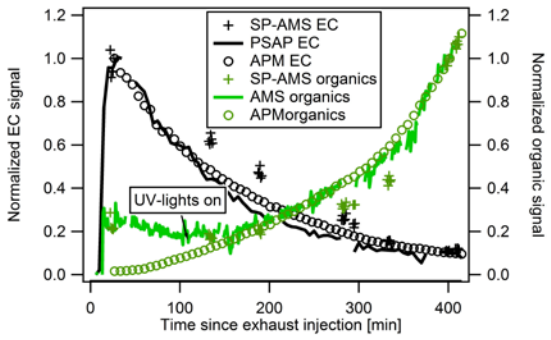

Figure 1. Soot and organic signal during an experiment were diesel exhaust spiked with toluene and m-Xylene was irradiated with UV.

When quantifying chemical species by AMS, one needs to determine their ionization efficiency (IE). This aspect of data analysis is to our knowledge not investigated for soot. There are two key differences from conventional AMS, the molecular structure of the soot, and the mode of vaporization. Preliminary results indicate that the IE of soot is low compared to that of non-refractory species. This has important implications for soot quantification. In the data plotted above, it results in an over prediction of soot mass loading by ~120% at t=400 (where TD-DMA-APM indicates 90% of particulate mass is SOA) if one fails to account for pure C_n fragments formed by the SOA, even though these contribute <3% of SOA signal.

This work was supported by the Swedish research council FORMAS through projects 2007-1205, 2008-1467 and 2010-1678

Nordin, E. Z. *et al*. (2011). *Smog Chamber Studies on SOA Formation from Gasoline Exhaust and Pure Precursors.* EAC proceedings.

Aerosol particle phase state measurement technique using a low pressure impactor

E. Saukko[1], H. Kuuluvainen[1] and A. Virtanen[1]

[1]Department of Physics, Tampere University of Technology, Tampere, FI-37720, Finland
Keywords: Impactor, particle characterization, phase state, hygroscopicity.
Presenting author email: erkka.saukko@tut.fi

The phase state of aerosols – primarily whether particles are solid or liquid – has impact on the behavior of atmospheric as well as on industrial aerosols. According to the recently published results, the atmospheric biogenic SOA particles can adopt amorphous solid phase (Virtanen et al, 2010). The phase change of particles can be induced by temperature change, absorption of water or other solvent or by chemical aging. Existing methods to resolve the phase state, such as tandem differential mobility analysis rely on the size change of particles related to the water uptake or release related to deliquescence and efflorescence.

To address the need to study phase change induced by size-preserving and nearly size-preserving processes a new method has been developed. The method relies on the physical impaction of particles on a smooth substrate and subsequent counting of bounced particles by condensation particle counter (CPC).

To evaluate the performance of this method, the phase state of laboratory aerosols in the presence of water vapor was studied. The results show a marked difference in particle bouncing probability between crystalline and amorphous solids - not only at the deliquescence relative humidity level, but also on the slope of the bouncing probability with respect to humidity.

The schematic of the measurement system is described in Figure 1. The system consists of a size classification DMA, humidity control unit, a single Berner-type impactor stage and a batch sampling system to acquire a sample, repressurize it and measure with a CPC.

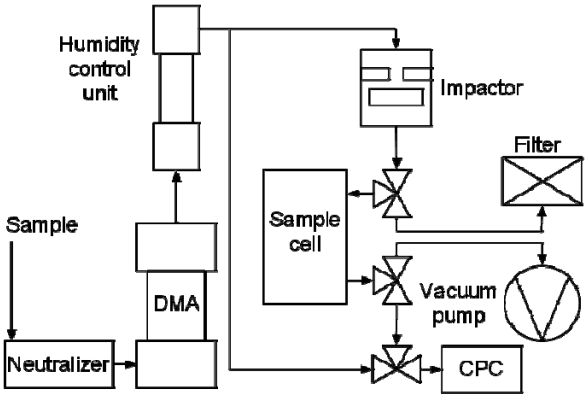

Figure 1 Schematic representation of measurement system

An example of bounce probability with varying relative humidity is given in figure 2. An ammonium sulphate aerosol, size selected for 91nm was cycled through the system and an almost step-like transition was seen on the bounce probability at around 80% relative humidity. This corresponds well with the known deliquescence relative humidity (DRH) of 80% (Mikhailov et al 2009)

The bounce probability can not at present be quantitatively linked to mechanical properties of particles, but it is qualitatively informative. The method has been applied on nebulised laboratory aerosols as well as on secondary organic aerosols.

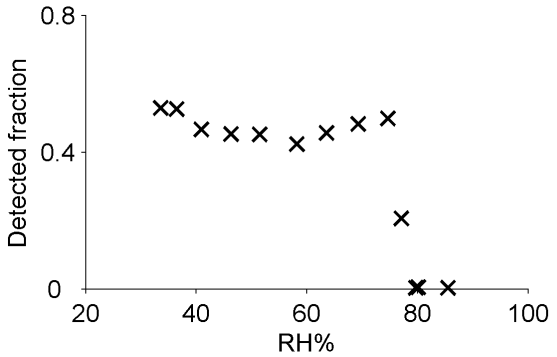

Figure 2 Fraction of 91nm ammonium sulfate particles detected after impaction with varying humidity

This work was supported by the Maj and Tor Nessling foundation.

Mikhailov, E., S. Vlasenko, S. T. Martin, T. Koop and U. Pöschl: *Amorphous and crystalline aerosol particles interacting with water vapor: conceptual framework and experimental evidence for restructuring, phase transitions and kinetic limitations*, Atmos. Chem. Phys., 9, (24), 9491-9522, 2009

Virtanen, A., J. Joutsensaari, T. Koop, J. Kannosto, P. Yli-Pirilä, J. Leskinen, J. M. Mäkelä, J. K. Holopainen, U. Pöschl, M. Kulmala, D. R. Worsnop and A. Laaksonen: *An amorphous solid state of biogenic secondary organic aerosol particles*, Nature, 467, (7317), 824-827, 2010

Rapid measurements of single aerosol droplets in conditions far from equilibrium using an electrodynamic balance

J.F. Davies[1], A.E. Haddrell[1], J.B. Wills[1] and J.P. Reid[1*]

[1]School of Chemistry, University of Bristol, Bristol, BS8 1TS, United Kingdom
Keywords: heat and mass transfer, instrumentation, levitation, evaporation
Presenting author email: james.davies@bristol.ac.uk

Rapid processes, such as evaporation and water uptake, occurring in aerosol droplets on the millisecond timescale have important implications in atmospheric chemistry, industrial spray techniques, aerosol combustion and drug delivery to the lungs.

A new electrodynamic balance (EDB) to study rapid processes in single aerosol droplets (Heinisch, 2009), consisting of four cylindrical, electrically isolated electrodes with a gas channel through the central cylinder for delivery of a gas flow, has been constructed (fig. 1). The benefit of this geometry over others comes from the strength of the trapping field combined with 360^{O} lateral optical access. The stability of trapped droplets permits the application of a high velocity on-axis gas flow through the inner cylindrical electrode directly over the surface of the droplet, allowing rapid processes in a gas flow to be studied. The droplet is illuminated with laser light and a characteristic fringe pattern is formed from the interference between reflected and doubly refracted rays. The fringe pattern is imaged with a camera and an approximation to Mie theory is applied (Glantschnig, 1981) to size the droplet in real-time at rates of well over 100 s^{-1}.

Figure1. Cylindrical electrodynamic balance. Side view (left) and top-down view (right) of electrodes.

Droplets are introduced into the trap with a piezoelectric droplet-on-demand dispenser of 30 μm orifice producing droplets of diameter 30 - 40 μm (approx.) and at speeds of around 2 m s^{-1}. The droplet travels the horizontal distance to the trap centre in ~20 ms.

The combination of droplets stability and high camera frame rates enables very fast dynamic measurements to be carried out, such as the evaporation of solvents (e.g. water) from atmospheric, medical and industrial aerosol droplets. These measurements provide an insight into the coupling of heat and mass transfer. The gas flow enables very fast changes in humidity to be introduced and droplets can be dried out in seconds leading to possible changes in the droplet phase such as the formation of gels or glassy phases.

Rapid uptake and growth of aerosol can also be studied. These are important processes in atmospheric chemistry, in terms of mass accommodation and cloud formation and growth, and in drug delivery via the lungs. The rapid humidity increase on inhalation of a medicinal aerosol can be effectively reproduced in this system to probe the lung penetration depth and hence the effectiveness of the aerosol as a drug delivery method.

Initial measurements of the evaporation of water from mixed component aerosol of varying composition have been carried out. Figure 2 shows the evaporation of mixed water / glycerol droplets (50:50) and the rapid water evaporation regime is clearly visible at a time resolution of 50 ms. A time resolution of much less than 10 ms is possible.

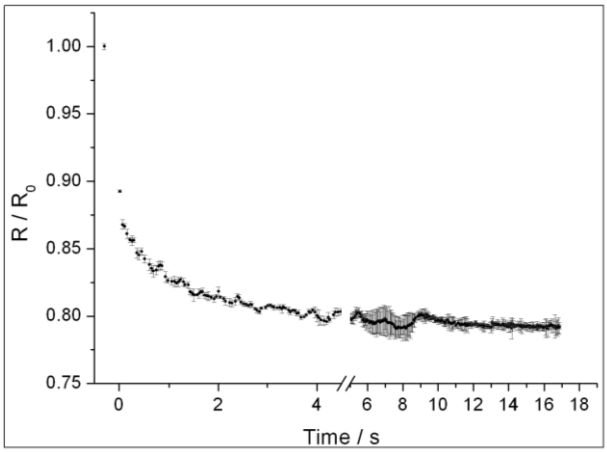

Figure 2. Water evaporation of 50:50 water / glycerol aerosol droplets in a dry gas flow (error bars indicate standard deviation of multiple droplets)

This technique provides the only method of measuring rapid changes in single aerosol droplets under a directed gas flow and offers a unique method of studying the effect of rapid changes in relative humidity.

This work was supported by the Engineering and Physical Sciences Research Council, UK.

W. J. Glantschnig and S.-H. Chen, *Applied Optics* **1981**, *20*, 2499-2509.

C. Heinisch, J. B. Wills, J. P. Reid, T. Tschudi and C. Tropea, *Physical Chemistry Chemical Physics* **2009**, *11*, 9720-9728.

Interferences in thermo-optical measurements of elemental and organic carbon caused by other aerosol constituents

R. Hitzenberger, E. Traxler, and B. Rosati
Faculty of Physics, University of Vienna, A-1090 Vienna, Austria
Keywords: elemental carbon (EC), organic carbon (OC), EC/OC split
Presenting author email: regina.hitzenberger@univie.ac.at

Elemental carbon (EC), which is produced by combustion processes, has come under intense study in recent years because of public health concerns (Kim et al., 2003) and climate change research. Despite intensive research efforts over the past nearly four decades, there still is no standard method to measure EC and there still is no scientific consensus of how to deal with interferences caused by refractory organic carbon ("brown carbon", e. g. Andreae and Gelencser, 2006) and possibly other aerosol constituents.

Numerous intercomparison (earlier studies summarized by Watson et al., 2005) performed over the years showed that total carbon (TC) measured with different methods usually agrees withic about 10%, but differences in EC up to factors of 7 are not too infrequent. For thermal methods, these differences are caused by the setting of the EC/OC split, usually depend on the aerosol type and sources present at the sampling site, and have so far not been resolved.

In the study by Hitzenberger et al. (2006), nearly all methods for EC and BC determination used in Europe at that time were compared for the urban aerosol un Vienna under summer conditions and gave no significant differences, so at least under these conditions (strong Diesel source, no space heating), the methods were found to perform more or less equally well. In winter time (Reisinger et al., 2008), however, differences of up to factors of about 4 were found especially on those days where a newly developed technique (Wonaschütz er al., 2009) showed a significant presence of biomass smoke. EC measured with a Sunset analyzer (Birch and Cary, 1996) always was lowest. As this thermo-optical method had not been available during the summer study, we cannot comment on its performance under summer conditions.

In the present study, the results of a laboratory investigation on the influence of various other inorganic and organic substances on the thermal behaviour of a diesel soot proxy (Elftex 124, Cabot Corp.) are presented. First results show that NaCl, which often is part of winter aerosols even at continental locations because of road salting, lowers the combustion temperature of EC and shifts the EC peak in the thermograms to lower temperatures. The EC/OC Split, however, is not influenced because combustion temperatures for EC are still high. Brown carbon proxies were found to influence the EC/OC split and to bias the EC concentration low. Other substances and substance mixtures are also investigated.

Andreae, M. O., Gelencser, A. (2006) *Atmos. Chem. Phys.*, **6**, 3131–3148.
Birch, M. E., Cary, R. A. (1996). *Aerosol Sci. Technol.* **25**, 221-241.
Hitzenberger, R., Petzold, A., Bauer, H., Ctyroky, P., Pouresmaeil, P., Laskus, L., Puxbaum, H. (2006). *Environ. Sci. Technol,*. **40**, 6377-6383.
Kim, H. J., Liu, X. D., Kobayashi, T., Kohyama, T., Wen, F. Q., Romberger, D. J., Conner, H., Gilmour, P. S., Donaldson, K., MacNee, W., Rennard, S. I. (2003). *Am. J. Respiratory Cell Molec. Biology*, **28**, 111-121.
Reisinger, P., Wonaschütz, A., Hitzenberger, R., Petzold, A., Bauer, H., Jankowski, N., Puxbaum, H., Chi, X., Maenhaut , W. (2008). *Environ. Sci. Technol*., **42**, 884 – 889.
Watson, J. G., Chow, J. C., Chen, L.-W. A. (2005) *J. Aerosol Air Quality Res*,. **5**, 65 – 102.
Wonaschütz, A., Hitzenberger*, R., Bauer, H., Pouresmaeil, P., Klatzer, B., Caseiro, A., Puxbaum, H. (2009) *Environ. Sci. Technol*., **43**, 1141-1146.

Comparison of the chemical and toxicological characteristics of particulate matter (PM) collected by different methods: filters, impactors and BioSamplers

Nancy Daher[1], Zhi Ning[1], Arthur K. Cho[2], Martin Shafer[3], James J. Schauer[3] and Constantinos Sioutas[1].

[1]Department of Civil and Environmental Engineering, University of Southern California, Los Angeles, CA 90089, USA
[2] Department of Molecular and Medical Pharmacology, University of California Los Angeles, Los Angeles, CA 90095, USA
[3] Environmental Chemistry and Technology Program, University of Wisconsin-Madison, Madison, WI 53706-1481, USA
Keywords: particulate matter, filter, impactor, BioSampler, VACES, chemical properties, ROS, DTT, DHBA
Presenting author email:sioutas@usc.edu

The association between adverse health effects and increased exposure to particulate matter (PM) has been of primary concern to public health organizations. To assess PM impact on health, particles are typically collected by filtration and impaction. More recently, PM collection by means of a concentrator-BioSampler tandem method has been adopted. However, a systematic evaluation of these techniques is currently unavailable. In this study, we compare the chemical and toxicological characteristics of concentration-enriched $PM_{2.5}$ samples simultaneously collected by a filter, a Nano-Micro Orifice Uniform Deposition Impactor (Nano-MOUDI) and a BioSampler.

Gravimetric measurements showed considerable agreement in PM collection efficiency for all three samplers. Accordingly, samples from the three collectors exhibited similar chemical compositions. The mass fractions of their inorganic ions, labile and non-labile, were comparable. Moreover, the organic carbon (OC) content of the BioSampler slurry was similar to that of the filter, while water-soluble OC levels of the filter and impactor samples were close to a 100% agreement. Lastly, linear regression analyses demonstrated that the water-soluble elements existed in similar mass ratios for the filter and impactor samples. Their respective total components were also in very good agreement. By contrast, the recoverable elements of the BioSampler slurry, determined by high resolution magnetic sector inductively coupled plasma mass spectrometry, were in good agreement with the water-soluble elements of the filter and impactor samples but not their corresponding total components.

In spite of the overall agreement among the $PM_{2.5}$ samples on their chemical composition, the oxidative potential of the filter and impactor substrate, assessed by abiotic and cellular assays, was similar yet substantially lower than that of the BioSampler slurry. Findings from a macrophage reactive oxygen species (ROS) assay showed that the mean activities of the filter and Nano-MOUDI water extracts were comparable but 0.46 and 0.31 times lower than the activity of the unfiltered BioSampler slurry, respectively (Figure 1). However, filtering the BioSampler slurry, i.e. removing insoluble PM-bound species, attenuated its ROS activity to about the same level as that of the filter and impactor substrate. These results demonstrate a significant contribution of insoluble species, which are unlikely to be recovered by water extraction, to the overall PM redox activity. Similarly, findings from a dithiothreitol (DTT) and a dihydroxybenzoate (DHBA) assay revealed that water extraction of the filter and impactor PM samples prior to toxicity tests did not recover potent PM-bound species, thereby leading to an underestimation of their redox activities.

Consequently, although commonly adopted for PM sampling, particle collection by filters and impactors for use in toxicological testing may be unsuitable. Alternatively, PM collection by the BioSampler, which circumvents the need for particle extraction, constitutes a more adequate approach for use in toxicity assays.

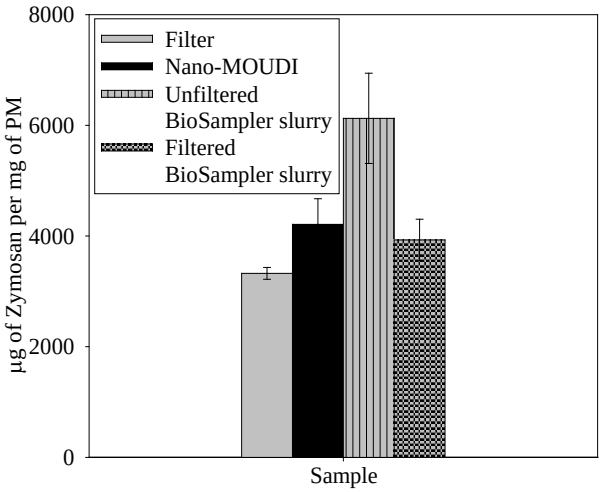

Figure 1. ROS response of the water extracts of the filter and Nano-MOUDI $PM_{2.5}$ samples as well as the unfiltered and filtered BioSampler $PM_{2.5}$ slurry. Error bars represent one standard error.

This research was funded by U.S. EPA under the STAR program through Grant RD-8324-1301-0 to the University of Southern California and by the United States Public Health service grants (NIH), R01 ES012053 and R01 ES013432. The authors gratefully acknowledge the support of the University of Southern California Provost's Ph.D. fellowship. The authors would also like to thank Debra Schmitz and Emma Di Stefano for performing the DTT and DHBA assays.

Size selected nanoparticle quantification of deposited aerosol by GIXRF

H. Bresch[1], F. Reinhardt[2], U. Waldschläger[3], B. Pollakowski [2], B. Beckhoff[2], S. Seeger[1]

[1]BAM Federal Institute for Materials Research and Testing, Unter den Eichen 87, 12200, Berlin, Germany
[2]Physikalisch-Technische Bundesanstalt (PTB), Abbestr. 2-12, 10587 Berlin, Germany
[3]Bruker Nano GmbH, Schwarzschildstr. 12, 12489 Berlin, Germany

Keywords: XRF, Aerosol characterization, Instrumentation, Elemental composition, Particle size distribution.
Presenting author email: harald.bresch@bam.de

Cascade impactors are widely used instruments in chemical aerosol characterization. There are several techniques for the chemical analysis of aerosol samples from cascade stages , e.g. EDX, GC-MS, Raman, XRF, etc., but none of them measures particle size and size distributions. Particle size resolved quantitative chemical analysis either requires the additional use of particle classifiers (e.g. SMPS) or the quantitative analysis of the deposits on cascade stages. The latter implies sample strengths above the lower threshold of the respective analytical method. Many environmental indoor or outdoor aerosols are polydisperse and consist of several chemical substances in different quantities. The quantification of one given chemical substance or a given element, hidden in the background of all the other contributions, and its assignment to a particle size class is therefore not always easy to achieve with the methods available.

Here we present a novel approach to use Gracing Incidence X-Ray Fluorescence Analysis (GIXRF) based on fundamental constants in order to determine size, quantity and chemistry of small nanoparticulate aerosol fractions within a poly-disperse aerosol.

The sampling was done with an electrostatic aerosol sampler (TSI 3089), using one square inch clean Si-wafers. We prepared monodisperse $ZnTiO_3$, TiO_2 nanoaerosol by use of an atomizer (Topas ATM 220) either with and without size selection by the Classifier and also a technical produced example of a polydisperse indoor aerosol.

For the experiments we used the PTB/BAM X-ray beamlines at BESSY II in Berlin at different excitation energies. High spectral resolution enables studies of the chemical state of the elements (Reinhardt et al., 2009) while the low divergence of the beam allows for dedicated geometries, such as a grazing incidence setup. Based on total-reflection X-ray fluorescence analysis (TXRF), which offers very low quantitative detection limits in the pg to fg range (Beckhoff et al., 2007), in GIXRF the incident angle of the excitation radiation is tuned between 0° and about threefold the critical angle of total-reflection. Thereby the position and strength of the maxima of the X-ray standing wave field (XSW) above the surface is modified. Particles with a given diameter deposited on a flat substrate will be exposed to excitation radiation of varying intensity depending on the angle of incidence and the particle size.

Hence the measured X-ray fluorescence signal contains information on the atomic composition of the particles and information on the deposited size fraction.

Based on fundamental constants we could use GIXRF measurements at BESSY II beamlines to determine the total amount of deposited nanoparticles of one size on a flat surface. Besides the absolute determination of the deposited nanoparticles, the measurement is independent of small contaminations of the substrate with other materials or polydisperse nanoparticles. This makes the GIXRF method a unique and very promising method for nanoparticle characterization, especially regarding poydisperse and inhomogenic environmental aerosols.

The financial support of this research activity within the frame of the ProFiT project “Nanoparticle X-ray Analysis” supported by the Investitionsbank Berlin (No. 10141100) is gratefully acknowledged.

F. Reinhardt, B. Beckhoff, H. Eba, B. Kanngießer, M. Kolbe, M. Mizusawa, M. Müller, B. Pollakowski, K. Sakurai, and G. Ulm (2009), *Anal. Chem*. **81**, 1770

B. Beckhoff, R. Fliegauf, M. Kolbe, M. Müller, J. Weser, and G. Ulm (2007), *Anal. Chem*. **79**, 7873

Tuesday, September 6, 2011

Session 6F: Aerosols in Turbulent Flows 2

Condensation and Turbulence

Charles Clement

15 Witan Way, Wantage, Oxon OX12 9EU, U.K.

Keywords: aerosol formation, turbulence, condensation, size distributions

Vapour condensation and turbulence both occur in the formation of clouds and their subsequent behaviour. There is still a lack of understanding of the interaction of these processes which strongly affects the size distributions of droplets in clouds and fluctuations in condensed water content which can lead to precipitation. Difficulties in a theoretical description arise from the necessity to include both molecular mass transfer by diffusion and heat transfer as well as turbulent motion. This paper addresses the basic microphysics involved including size scales and timescales needed. Condensation on an aerosol is a rapid process with timescales of the order of seconds. This may be seen in nature from the apparently stationary clouds which appear in fast airflows past escarpments or isolated peaks such as Table Mountain. A summary of theoretical work on mass transfer to aerosols was given by Clement (2008). Two key results are that "mean fields" for the vapour concentration, c, and the temperature, T, apply to volumes containing many droplets, and that the difference, $u = c - c_e(T)$, where the latter is its equilibrium value, obeys the general equation:

$$\partial u / \partial t + \mathbf{v}.\nabla u + \nabla.(- Du) = D\, c_e'' (\nabla T)^2 - (\partial p / \partial t - \nabla.\mathbf{q}) / (L\, Cn) - c_e' (1 - Le^{-1}) (\partial T / \partial t + \mathbf{v}.\nabla T) - (1 + Cn)^{-1} (d\rho_a/dt)/ \rho_d, \quad (1)$$

where c_e' is dc_e /dT, L is the latent heat of condensation, D is the vapour diffusivity, $\mathbf{q}$ is the radiation current interacting with the aerosol, Le, is the ratio of the thermometric conductivity to D, and Cn is the bulk condensation number:

$$Cn = k / (L\, D\, \rho\, c_e'(T)).$$

The LHS terms in (1) represent transport and diffusion so that it is the terms on the RHS which lead to possible supersaturation, with the final term being the actual transfer rate to the aerosol, density ρ_a which is itself proportional to $u = c - c_e$. The first term on the RHS is essentially positive and its nonlinearity gives rise to supersaturations in temperature gradients. The proportionality to $- \partial p / \partial t$ shows the effect of producing supersaturation pressure in rising air columns, and the radiative term can have either sign in adding or removing heat from the aerosol.

For water vapour in air, Le is about 0.85 and the sign of the nonzero term with Le depends on whether the temperature of the transported air at the point in question is rising or falling. In any mixing situation in the atmosphere, air packets will exist which have opposite signs. This could lead to highly local fluctuations in the water content of clouds as well as the evident fluctuations in the existence of the cloud which are seen at cloud edges. An example of the locality of the aerosol formation produced is seen in the calculations for cooled laminar flow in a tube performed by Barrett and Fissan (1989), but calculations for actual turbulent flows in the atmosphere are lacking.

Turbulence will produce fluctuations in temperature and water vapour content in the atmosphere, and lead to fluctuations in water vapour saturation. A calculation of distributions resulting from condensation on droplets passing through a realistic statistical set of saturation fluctuations does produce broad distributions (Kulmala *et al* 1997). It is possible to show from a representation of atmospheric turbulence by Sidin *et al* (2009) that dispersion of droplets occurs fast enough so that local distributions arise from uncorrelated fluctuations. We investigate further the dispersion in relation to the "mean field" volume containing droplets. The size range of this volume specified by diffusion is close to that of the dissipative turbulence. Local displacements of water vapour within the region from diffusion and turbulence are then similar so that both are important in calculating condensation. This implies that accurate calculations of condensation would need a very fine grid and small timesteps.

Intensive numerical calculations of condensation in simpler flow situations involving complete equations for heat and mass transfer and an aerosol size distribution have been carried out by Pyykonen and Garrick, but their extension to realistic clouds presents formidable difficulties. There is a continuing need for simpler models which include the important physics. An important aid to better understanding would be much more local measurements of fluctuations in water content and droplet size distributions in clouds.

Barrett, J.C. and Fissan, H. (1989) *J. Colloid and Interface Sci.* 130, 498-507.

Clement, C. F.(2008) Mass Transfer to Aerosols in *Environmental chemistry of Aerosols* ed. I. Colbeck, Blackwell Publishing, Oxford p.49-89.

Kulmala, M., Rannik, Ü., Zapadinsky, E. L. and Clement, C. F. (1997) *J. Aerosol Science*, 28, 1395-1409.

Pyykonen, J. and Garrick, S.C., *J. Aerosol Science*, to be published.

Sidin, R. S. R., IJzermans, R. H. A. and Reeks, M. W. (2009) *Physics of Fluids*, 21, 106603.

Rain in the test tube?

J. Vollmer

Max-Planck-Institute for Dynamics and Self-Organization, D-37073 Göttingen, Germany

In clouds the adiabatic cooling drives uprising air across the cloud point and hence causes nucleation of cloud droplets which subsequently coarsen and eventually lead to rain. In clouds nucleation is due to seeds (mostly small salt particles) such that droplets have to grow from a submicrometer to millimeter scale.

Surprisingly similar scenarios lead to precipitation in binary liquid mixtures subjected to a shallow temperature ramp (Auerhammer *et al*, 2005; Vollmer *et al*, 2007, Lapp *et al*, 2011). In that case, however, critical nuclei are two orders of magnitude smaller, and gravity becomes noticeable when droplets have grown to a size of tens of microns (Lapp *et al*, 2011). Consequently, the resulting "clouds" fit into test tubes with lateral dimensions of a few centimeters such that one can follow the evolution of the phase-separating mixtures for very long times under carefully controlled conditions. Upon slow cooling the mixtures repeatedly go through cycles of nucleation, coarsening and sedimentation.

We adopt a set of PDEs describing the evolution of the mixtures (Cates *et al*, 2003), and discuss its instability towards nucleation and convection (Vollmer, 2008; Trösemeier and Vollmer, 2011). This approach also provides a minimal model explaining the arising of the repeated rain formation. It can be described as Ostwald ripening, followed by a finite-time runaway growth of droplet sizes due to larger droplets sweeping up smaller ones (Lapp *et al*, 2011). The model predicts that he period Δt of the oscillations and the temperature sweep rate ξ are related by

$$\Delta t \sim \xi^{3/7}.$$

The predictions compare very well with our experimental results on iso-C4E1 droplets in water, which are obtained by analysing data on the time evolution of the droplet-size distribution and sedimentation velocities of a systems subjected to temperature ramps at different fixed ξ and sample geometry (see Figure 1).

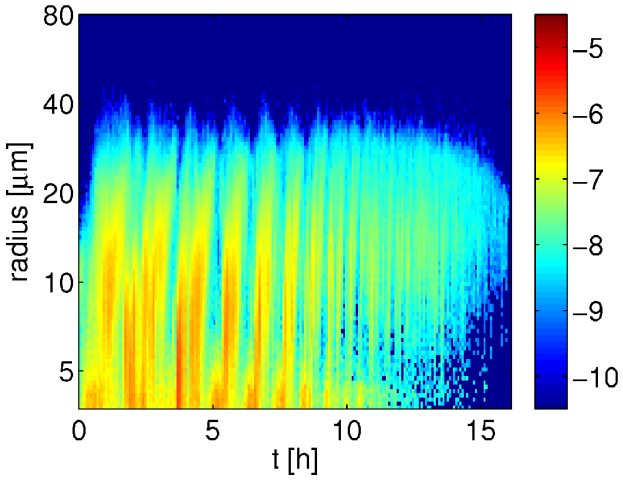

Figure 1. Temporal evolution of the droplet size distribution of iso-C4E1 droplets in water. A slow drift in temperature (25 K in 16 h) causes the system to oscillate.

We argue that the theoretical treatment is a benchmark model for rainfall, applicable to warm clouds in a stratified atmosphere.

Auernhammer G.K., Vollmer, D., and Vollmer, J. (2005) *J. Chem. Phys.* **123**, 134511.

Benczik, I., and Vollmer, J. (2010) *EPL* **91**, 36003.

Cates, M.E., Vollmer, J., Wagner, A., and Vollmer, D. (2003) *Phil. Trans. Roy. Soc. (Lond.) Ser. A* **361**, 793-807.

Lapp, T., Rohloff, M., Hof, B., Vollmer, J., and Wilkonson, M. (2011) unpublished.

Trösemeier, J.-H., and Vollmer, J. (2011) unpublished.

Vollmer J., Auerhammer, G.K., and Vollmer, D. (1997) *Phys. Rev. Lett.*, **98**, 115701.

Vollmer, J. (2008) *J. Chem. Phys.* **129**, 164502.

Non-local closure model for particle dispersion tensors in a turbulent boundary layer

A. Bragg[1], D.C. Swailes[1]
[1]Department of Mechanical & Systems Engineering, Newcastle University, Tyne & Wear, NE1 7RU, U.K.
Presenting author email: andrew.bragg@ncl.ac.uk

Keywords: inhomogeneous turbulence, particle dispersion, pdf kinetic equation, non-local dispersion tensors

Probability density function (pdf) kinetic equations and their associated continuum equations provide a theoretically sound modelling approach for inertial particle dispersion in turbulent flows (Reeks (1991), Reeks (1992), Swailes *et al* (1997)).

$$\frac{\partial}{\partial t}p = -\frac{\partial}{\partial \mathrm{x}_i}p\mathrm{v}_i + \frac{\partial}{\partial \mathrm{v}_i}\left[p(F_i+\kappa_i)\right] + \frac{\partial}{\partial \mathrm{v}_i}\left[\frac{\partial}{\partial \mathrm{x}_j}p\lambda_{ji} + \frac{\partial}{\partial \mathrm{v}_j}p\mu_{ji}\right] \quad (1)$$

Equation (1) is the pdf kinetic equation, where $p(\mathbf{x},\mathbf{v},t)$ is the pdf for particle position and velocity at time t, $\mathbf{x}$ is a position phase-space variable, $\mathbf{v}$ is a velocity phase-space variable and $\boldsymbol{F}(\mathbf{x},\mathbf{v},t)$ is the mean force acting on the particle. The dispersion tensors $\boldsymbol{\lambda}(\mathbf{x},\mathbf{v},t)$, $\boldsymbol{\mu}(\mathbf{x},\mathbf{v},t)$ and $\boldsymbol{\kappa}(\mathbf{x},\mathbf{v},t)$ appearing in equation (1) represent integrals along particle paths describing the interaction between the fluid turbulence and the particles. In the continuum equations, it is the velocity averaged forms of the dispersion tensors that appear, and they require closure treatment.

For particle dispersion in a turbulent boundary layer where the turbulence is strongly inhomogeneous and anisotropic, the closure of the dispersion tensors is complex since the inhomogeneity and anisotropy of the turbulence experienced by the particle along their trajectories must be accounted for. Usually the approximation made is that the turbulence seen by the particles is 'locally homogeneous', that is, that within the time for which the turbulent field is correlated the particles experience a flow field which is approximately homogeneous (e.g. Swailes *et al* (1997)). However recent studies have shown that local homogeneous approximations to the dispersion tensors can be both qualitatively and quantitatively incorrect for particle dispersion in a turbulent boundary layer (Skartlien (2007)).

In addition to this there does not exist a general closure for $\boldsymbol{\kappa}$, the dispersion tensor describing a convective acceleration experienced by the particles due to the inhomogeneity of the fluid turbulence. Usually $\boldsymbol{\kappa}$ is approximated by using its known form in the limit of zero Stokes number particles (Skartlien (2007), Skartlien *et al* (2009)), and therefore does not account for the influence of particle inertia.

A new 'non-local' closure model will be presented which attempts to account for the effects of turbulence inhomogeneity (and anisotropy) and particle-boundary collisions on the dispersion tensors. The new closure model also provides a general closure for $\boldsymbol{\kappa}$, valid for small to large particles.

References

Reeks, MW, *On a kinetic equation for the transport of particles in turbulent flows, Phys.Fluids, 446-456, 1991*

Reeks, MW, *On the continuum equations for dispersed particles in nonuniform flows, Phys.Fluids, 1290-1303, 1992*

Swailes, D and Darbyshire, K, *A generalized Fokker-Planck equation for particle transport in random media, Physica A, 38-48,1997*

Skartlien, R, *Kinetic modeling of particles in stratified flow - Evaluation of dispersion tensors in inhomogeneous turbulence, Int.J.Multiphase Flow, 1006-1022, 2007*

Skartlien, R and Drazen, D and Swailes, DC and Jensen, A, *Suspensions in turbulent liquid pipe flow: Kinetic modelling and added mass effects, Int.J.Multiphase Flow, 1017-1035, 2009*

Tumbling in turbulence and irrational quantisation

Michael Wilkinson[1] and Alain Pumir[2]
[1]Department of Mathematics and Statistics, Open University, Milton Keynes, England, MK7 6AA.
[2]Laboratoire de Physique, Ecole Normale Supérieure de Lyon, F-69007, Lyon, France
Keywords: turbulence, aerosols, tumbling
Presenting author email: m.wilkinson@open.ac.uk

A non-spherical object (such as an ice crystal) in a turbulent flow will tumble randomly. This tumbling can be significant for understanding the aggregation, fragmentation and optical properties of non-spherical bodies. In this talk I will present the simplest model of random tumbling, which is an Ornstein-Uhlenbeck process describing motion of a vector $\mathbf{n}$ on the surface of a sphere, with angular velocity ω: the equations of motion are

$$\dot{\mathbf{n}} = \omega \wedge \mathbf{n}$$

$$\dot{\omega} = -\gamma\omega + \sqrt{2D}\eta(t)$$

where $\eta(t)$ is white noise. I will explain why, despite its simplicity, this can be a good model for the tumbling of microscopic particles in a turbulent flow.

The model has a single dimensionless parameter: the persistence angle $\beta = \sqrt{D/\gamma^3}$ is the typical angle through which the axis $\mathbf{n}$ of the body rotates during the correlation time of the angular velocity ω. In the limit $\beta \gg 1$ where the tumbling is weakly damped, the model has a very surprising structure: the corresponding Fokker-Planck equation is analysed using a radial Schrodinger equation in which the angular momentum quantum number j takes an *irrational* value, $j = (\sqrt{17}-1)/2$. I shall also discuss the two-dimensional case, which is excatly solvable, for all values of β.

I will also describe numerical studies of the motion of microscopic rod-like bodies in simulations of three-dimensional Navier-Stokes turbulence. There is a surprising feature which cannot be explained using the spherical Ornstein-Uhlenbeck model: we find that the direction vector $\mathbf{n}$ of rod-like bodies is preferentially aligned with the vorticity vector Ω of the velocity field, rather than with the principal eigenvector of the strain-rate tensor.

Motion of large particles in turbulent flows: rotational motion and lift.

A. Pumir[1], R. Zimmemrann[1], Y. Gasteuil[1], M. Bourgoin[2], R. Volk[1] and J.F. Pinton [1]
[1]Laboratoire de Physique, Ecole Normale Supérieure de Lyon, 46, Allée d'Italie, F-69007, Lyon, France
[2]Laboratoire des Ecoulements Géophysiques et Industriels, Université de Grenoble, F-38041, France.
Keywords: Motion of particles, spinning, lift.
Presenting author email: alain.pumir@ens-lyon.fr

The motion of a large, neutrally buoyant particle freely advected by a turbulent flow is studied experimentally. Thanks to new experimental techniques[1], the translational *and* rotational motion of the particles are simultaneously determined. The particles are investigated in a von Karman swirling flow, at a reynolds number $R_\lambda \approx 300$; the particles diameters are $D \sim 0.6 \times L_{int}$, where L_{int} is the integral length scale of the flow[2].

The experiments demonstrate that both the translational and angular accelerations exhibit very wide probability distribution functions, which can be viewed as a manifestation of intermittency.

The orientation of the angular velocity with respect to the trajectory, as well as the translational acceleration conditioned on the spinning velocity provide evidence of a lift force acting on the particle.

The orders of magnitude of the force and of the torque acting on the particles will be discussed, and the issues of size and Reynolds number dependence will be addressed.

This work was supported by Agence National pour la Recherche, under contract DSPET.

References

1. Zimmermann, R, Gasteuil, Y, Bourgoin, M., Volk, R., Pumir, A. and Pinton, J. F.,2011, Tracking the dynamics of translation and absolute orientation of a sphere in a turbulent flow, Rev. Sci. Instrum., to appear.

2. Zimmermann, R, Gasteuil, Y, Bourgoin, M., Volk, R., Pumir, A. and Pinton, J. F.,2011, Rotational intermittency and turbulence induced lift experienced by large particles in a turbulent flow, submitted.

Particle Resuspension Modeling in Turbulent Flows

F. Zhang*, †, M. Reeks* and M. Kissane†

* School of Mechanical and Systems Engineering, Newcastle University, Newcastle upon Tyne, NE1 7RU, UK

† Institut de Radioprotection et de Sûreté Nucléaire, CE Cadarache – bât 702, 13115 St-Paul-Lez-Durance, France

Keywords: resuspension, turbulent flow, multilayer deposit, severe accident

The work presented is concerned with the way small particles attached to a surface are resuspended when exposed to a turbulent flow. The process is important in a number of environmental and industrial processes. Of particular concern to this work is the release of radioactive particles from the primary circuit of an LWR as a consequence of a loss of coolant accident (LOCA). In this particular case the focus is on small particles < 5 microns in size, where the principal force holding the particle onto a surface is derived from van der Waals inter molecular forces. In general even for nominally very smooth adhering surfaces there exists a very broad spread in the adhesive forces. Here we develop and assess an improved version of the Rock'n'Roll model [Reeks & Hall, 2001] based on a statistical approach to resuspension which gives rise to a resuspension rate constant for the release of particles from a potential well due the action of the fluctuating aerodynamic force du to the turbulence. The analogy is with desorption of molecules from a surface in which the variance of the fluctuating aerodynamic force is the analogue of temperature. In this work we improve on the model by using measurements of the statistical fluctuations of both the stream wise fluid velocity and acceleration close to the wall from both LES and DNS of turbulent channel flow, translating those measurements into the statistical moment of the drag force acting on the particle attached to the surface. The original model assumes that aerodynamic forces and their time derivative are uncorrelated and have a Gaussian distribution. Here we examine the influence of non-Gaussian forces on the resuspension rate.

The ultimate model is a hybrid development of R'n'R model adapted for application to multilayer deposits based on the Friess and Yadigaroglu multilayer model [Friess & Yadigaroglu, 2001]. The particle size distribution is considered in the model in order to study the coveragent effect of the deposit layers. The model results are compared to the STORM SR11 test [Castelo *et al.*, 1999] (Figure 1) and BISE experiment [Alloul-Marmor, 2002] (Figure 2).

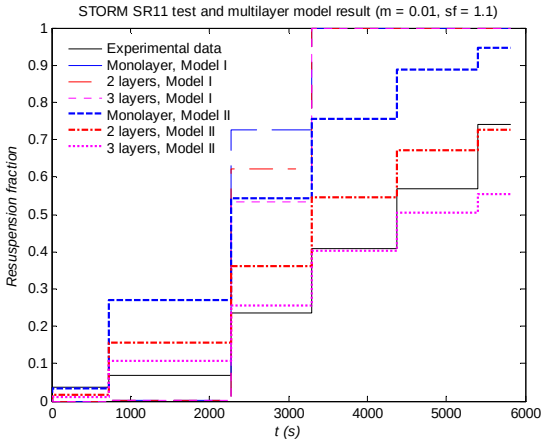

Figure 1. Models results and STORM SR11 test

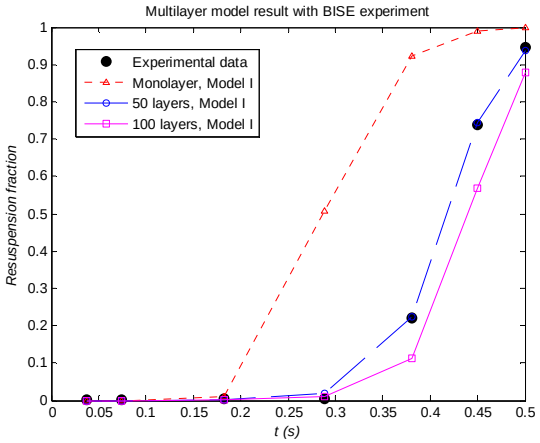

Figure 2. Model results and BISE experiment

As a general conclusion, the results showed that the models with small adhesive spreads give better comparison with the resuspension measured in the two experiments.

Alloul-Marmor, L. (2002), PhD thesis (Université Paris XII), report ISRN IRSN – 2002/28 – FR

Castelo, A., Capitão, J. A. and Santi, G. (1999) NEA/CSNI/R(99)4, EUR 18708 EN, February

Friess, H. and Yadigaroglu, G. (2001) *J. Nuclear Sci. and Eng.*, Vol.138(2), 161-176

Reeks, M. W. and Hall, D., (2001) *J. Aerosol Sci.*, Vol. 32(1), 1-31

Wednesday, September 7, 2011

Plenary 3:

UK Cystic Fibrosis Gene Therapy Consortium: Developing and Delivering a Complex Respiratory Therapy

by Uta Griesenbach

– No abstract submitted

Wednesday, September 7, 2011

Session 7A: Carbonaceous Aerosol and Meteorology

Changes in black carbon undergoing SOA coating measured with SP2, SP-AMS and optical instruments.

J.W.Taylor[1], J. Allan[1,2], D. Liu[1], M. Flynn[1,2], M. Gysel[3], M. Laborde[3], M. Schnaiter[4], K. Linke[4], H. Saathoff[4], K.-H. Naumann[4], O. Möhler[4], K. Heimerl[5], F. Dahlkötter[5], B. Weinzierl[5], A. Wollny[6], L. Polo[7], J. Cozic[7], J.M. Flores[6,8], Y. Rudich[8], S. Berlenz[9], U. Wagner[9] and H. Coe[1,2]

[1]School of Earth, Atmospheric and Environmental Sciences, University of Manchester, UK
[2]National Centre for Atmospheric Science, University of Manchester, Manchester, UK
[3]Laboratory of Atmospheric Chemistry, Paul Scherrer Institut, Switzerland
4Institute for Meteorology and Climate Research, Karlsruhe Institute of Technology, Germany
[5]Institut für Physik der Atmosphäre, Deutsches Zentrum für Luft- und Raumfahrt, Oberpfaffenhofen, Germany
6Particle Chemistry Department, Max-Planck-Institut für Chemie, Mainz, Germany
[7]Laboratoire Glaciologie et Géophysique Environnement, CNRS, Saint Martin d'Hères cedex, France
[8]Department of Environmental Sciences and Energy Research, Weizmann Institute of Science, Rehovot , Israel
[9]Institut für Kolbenmaschinen, Karlsruhe Institute of Technology, Germany

Keywords: Black carbon, Soot particles, Aerosol mass spectrometry, Carbonaceous aerosol.
Presenting author email: jonathan.taylor@postgrad.manchester.ac.uk

Behind CO_2, black carbon (BC) aerosol is the 2nd strongest contributor to current global warming (Ramanathan and Carmichael, 2008). Nonetheless there remain fundamental uncertainties regarding the ways in which coatings of nonrefractory material, formed by condensation and coagulation, affect BC's optical properties and hydrophilicity. While measurement of coating thickness can be made using Droplet Measurement Technology's Single Particle Soot Photometer (SP2), no instrument is currently capable of quantitatively measuring the composition of BC and its coatings, and this represents a limiting factor in our scientific understanding.

This work involves the use of a new instrument, the Soot Particle Aerosol Mass Spectrometer (SP-AMS), a modified version of the standard Aerodyne Aerosol Mass Spectrometer (AMS). The heater is removed and replaced by an Nd:YAG laser of the same type used in the SP2. This only vaporises particles containing BC, allowing for selective measurement of BC core and coating composition.

The SP-AMS was deployed alongside a suite of SP2s and several optical measurement systems (Aethalometer®, PhotoAcoustic Soot Spectrometer (PASS), Particle Soot Absorption Photometer (PSAP), Nephelometer and Cavity Ring-Down) as part of the SOOT11 campaign at the AIDA chamber, Karlsuhe, Germany, in November 2010. This allowed for measurement of well-characterised test particles in high concentrations. Fresh soot was generated using a CAST (Combustion Aerosol STandard) burner and coated by condensation of SOA (Secondary Organic Aerosol) due to α-pinene ozonolysis. In a reciprocal experiment, CAST soot was added to homogeneously-nucleated SOA and hence BC coating was achieved through coagulation. Similar experiments were carried out using BC generated from a diesel engine test bench.

We investigate changes in the aerosol as SOA was added, both in terms of chemical composition and optical properties. As fractal soot is coated in nonabsorbing SOA, it is restructured into a quasi-spherical core-shell system, which enhances absorption by a lensing effect effect (Schnaiter et al., 2005, Lack and Cappa, 2010). This phenomenon was observed as part of our experiments, as shown in Figure 1.

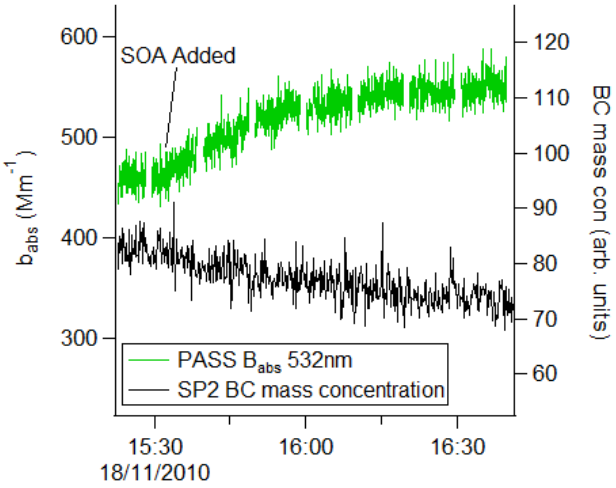

Figure 1 - Absorption enhancement due to coating of soot by SOA formed by ozonolysis of α-pinene.

This work was supported by EUROCHAMP under proposal E2-2010-09-16-0045 and the UK Natural Environment Research Council under grant NE/H008136/1.

References

Lack, D. A. and Cappa, C. D. (2010). *Atmospheric chemistry and physics*, **10**(9), 4207-4220.

Ramanathan, V., & Carmichael, G. (2008). *Nature geoscience*, **1**(4), 221–227.

Schnaiter, M., Linke, C., Möhler, O., Naumann, K.-H., Saathoff, H., Wagner, R., Schurath, U., Wehner, B. (2005). *Journal of Geophysical Research,* **110**, D19204.

Spatial and seasonal variations of biogenic organic compounds in ambient PM_{10} and PM_1 samples in Berlin

Wagener, Sandra[1,2], Langner, Marcel[1], Hansen, Ute[3], Moriske, Heinz-J[2]. and Endlicher, Wilfried[1]

[1]Department of Geography, Chair of Climatology, Humboldt-Universität zu Berlin, D-12489 Berlin, Germany
[2]German Federal Environmental Agency, D-14195 Berlin, Germany
[3]Joint Research Center, Institute for Environment and Sustainability, I-21027 Ispra, Italy
Keywords: biogenic particles, carbonaceous aerosol, urban aerosols, SOA
Presenting author email: sandra.wagener@geo.hu-berlin.de

Biogenic organic compounds are important constituents of ambient particulate matter (PM). To our knowledge, up to now little attention was paid to the quantity and distribution of single biogenic compounds in urban regions (Lewandowsky *et al* 2008). The aim of this project is to study the contribution of biogenic aerosol to PM_1 and PM_{10} concentrations and its spatial and temporal variation within the city of Berlin.

From Feb 2010 to Oct 2010, PM_{10} and PM_1 24 hrs samples were taken with a low volume sampler every 6th day at three different stations in Berlin, referred to as vegetation rich, traffic and urban background (only PM_{10}). For analysis with GC-MS, tracers for secondary oxidation products, biomass burning, primary biogenic and cooking emissions were chosen which might give valuable information about sources and transportation of biogenic PM in urban areas.

Levoglucosan, a suitable tracer for biomass burning showed highest PM_{10} median concentrations of all measured compounds between 41–45 ng m^{-3} at the three sites and 18 and 25 ng m^{-3} for the PM_1 fraction at the vegetation rich and traffic site, respectively. Highest PM_1 median concentration of 43 and 17 ng m^{-3} showed malic acid, assumedly an oxidation product of semi-volatile carboxylic acids (Kawamura and Gagosian, 1990). Lowest concentrations were found for the isoprene markers 2-methyltetrols with less than 1 ng m^{-3} for both fractions at all sites. Median concentrations for pinonic acid were between 9–12 ng m^{-3} for the PM_{10} and 8 and 11 ng m^{-3} for the PM_1 samples. It was found to be 3 to 8 times higher than its isomer pinic acid. The fatty acids (C_{14}–C_{18}) showed quite similar mean concentrations (2–8 ng m^{-3} and 1–5 ng m^{-3} for PM_{10} and PM_1, respectively).

Different types of seasonal trends were determined. Figure 1a shows a clear maximum in summer, which was found for all secondary oxidation products as well as for oleic and pentadecanoic acid. A nearly linear trend with decreasing and increasing concentrations from winter to autumn exist for some fatty acids and glucose (figure 1b and c). Only levoglucosan shows a clear minimum in summer (figure 1d).

Further, PM_1 of PM_{10} ratios were calculated. They vary strongly, between and within compounds, from 0 up to more than 100%. Latter causes still have to be clarified.

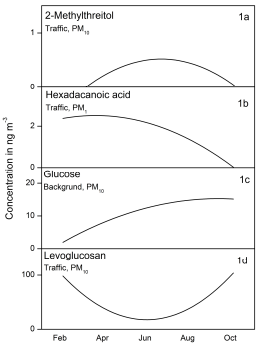

Figure 1: Different types of seasonal trends

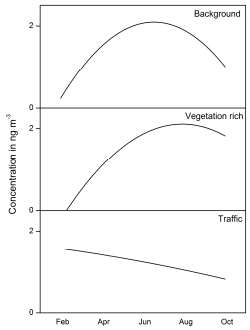

Figure 2: Seasonal trends of adipic acid (PM_{10}) at all sites

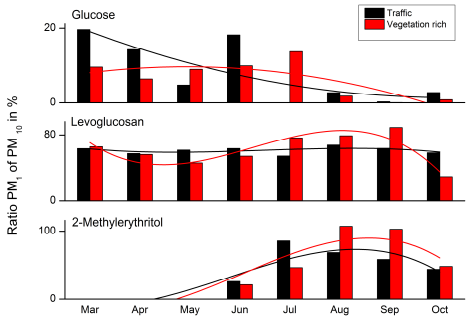

Figure 3: Variations of PM_1/PM_{10} ratios (given as monthly median) at the traffic and vegetation rich site

Only weak spatial variations of concentrations could be observed. However, spatial differences emerged by comparing the seasonal trends, where i.e. adipic acid shows a linear instead of a parabolic trend for PM_{10} samples at the traffic station (figure 2), indicating a specific local source. Further differences can be noticed in the PM_1/PM_{10} ratio. The ratio and partly its seasonal trend can differ between the stations as shown for glucose, levoglucosan and 2-Methylerythritol (figure 3).

The results present that the occurrence of biogenic compounds within the city of Berlin provides a great complexity in distribution, which can be described by concentration differences, seasonal behavior and the PM_1/PM_{10} ratio. Further investigations shall expand the knowledge i.e. by comparison with OC/EC data and ^{14}C-analysis.

This work is supported by the DFG.

Lewandowski et al (2008) Environ. Sci. Technol. **42**, 3303–3309
Kawamura, K. and Gagosian, R.B. (1990) J. Atmos. Chem. **11,** 107-122.

Composition and Optical Properties of Black Carbon and its Coatings in the Los Angeles Area During CalNex

J. D. Allan[1,2], J. Taylor[1], M. Flynn[1], H. Coe[1], T. Onasch[3], P. Massoli[3], J. Jayne[3], D. Worsnop[3], G. Kok[4], X. Zhang[5] and R. Weber[5]

[1]School of Earth, Atmospheric & Enviornmental Sciences, University of Manchester, Manchester, UK
[2]National Centre for Atmospheric Science, University of Manchester, Manchester, UK
[3]Aerodyne Research, Billerica, MA, USA
[4]Droplet Measurement Techologies, Boulder, CO, USA
[5]Georgia Institute of Technology, Altanta, GA, USA
Keywords: Black Carbon, CalNex, SP-AMS, Urban.
Presenting author email: james.allan@manchester.ac.uk

Detailed measurements of the composition and properties of black carbon (BC) were made as part of CalNex, a major multi-platform field study in the Los Angeles (LA) area in the summer of 2010. The deployment took place at the Pasadena supersite inside the LA metropolitan area, and included a Single Particle Soot Photometer (SP2), 3-wavelength Photoacoustic Soot Spectrometer (PASS), 7-wavelength Aethalometer and a new Soot Particle Aerosol Mass Spectrometer (SP-AMS). A Cavity Enhanced Phase Shift (CAPS) instrument was also operated in parallel to measure the bulk extinction properties. The bulk composition was also compared with collocated online thermo-optical OC/EC measurements.

The combination of instruments was chosen to study the microphysical interplay between BC core and coating composition and the bulk optical properties of the aerosol. As well as the single particle BC mass quantification provided by the SP2, the SP-AMS was able to directly study the bulk composition of the BC and its coatings. This new instrument operates in a similar manner to a standard Aerodyne AMS but instead of a heated tungsten surface, an active cavity YAG laser (the same used by the SP2) selectively vaporizes BC-containing particles, including their cores. The PASS was used to derive bulk properties without any of the artifacts associated with filter-based methods and was able to derive Angstrom exponents, which were seen to vary in both the scattering and absorption channels.

To further investigate the effect of the coatings on the optical properties of the particles, the SP2, SP-AMS and PASS were run downstream of a thermal denuder. This operated on a continuously ramping program, which the instruments measured progressively removing the coatings from the BC. This work will help to provide a better quantitative link between the physiochemical modifications made to BC particles during atmospheric processing and the evolution in their optical properties.

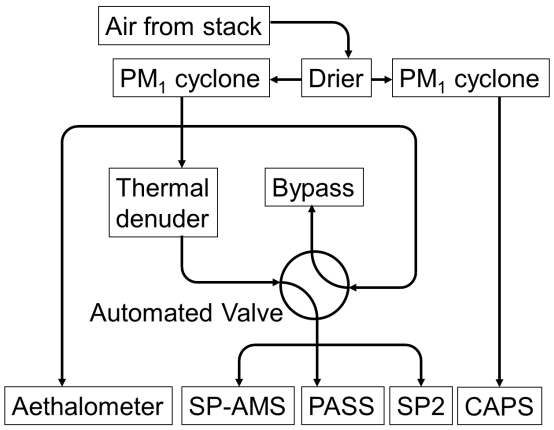

Figure1: Inlet scheme used

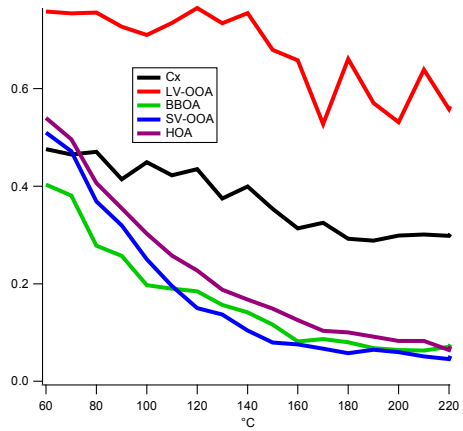

Figure 2: Thermodenuder relative attenuation for carbon clusers (Cx), Low Volatility Oxidised Organic Aerosol (LV-OOA), Biomass Burning OA (BBOA), Semivolatile OOA (SV-OOA) and Hydrocarbon-Like OA (HOA).

Effect of vehicle emissions on the chemical composition of airborne particulates in urban schools

L. Crilley[1], G. A. Ayoko[1], M. Mazaheri[1], G. R. Johnson[1], L. Morawska[1], E. Stelcer [2] and D. D. Cohen [2]

[1]International Laboratory for Air Quality and Health, Queensland University of Technology, Brisbane, QLD, 4001, Australia
[2]Institute for Environmental Research, Australian Nuclear Science and Technology Organisation, Kirrawee, NSW, 2232, Australia
Keywords: elemental composition, organic carbon/elemental carbon, vehicle emissions
Presenting author email: g.ayoko@qut.edu.au

The number of health and sensory effects linked to air pollutants continues to grow (see, e.g., Pope and Dockery, 2006). Due to their immature respiratory systems and faster breathing rates, children are particularly at risk (Zhang and Zhu, 2010). However, there have been limited published studies on the relationship between long term exposure to particles and adverse human effects in children. Additionally, the role of the chemical composition of particles in their biological effects has not been fully understood. To address this issue, a systematic study of the chemical composition of ambient air in the vicinity of selected schools in the greater Brisbane area is being undertaken. The study is a part of a large project aimed at gaining a holistic picture of the exposure of children to traffic related pollutants, and some of the preliminary results are described in this paper.

Airborne Particulate Matter (PM) with aerodynamic diameters equal to or less than 1.0 (PM1) and equal to or less than 2.5 micrometer (PM 2.5) were collected in 3 Schools (S01, S02 and S03). The sampling campaign at each school took place over one week. $PM_{2.5}$ was collected during school hours (8am to 5pm) for organic carbon (OC) and elemental carbon (EC). OC and EC were analysed at Chester Labnet according to the IMPROVE method and their fractions (OC1- OC4, PC and EC1-EC3) were determined. The $PM_{2.5}$ and PM_1 samples were both collected for 24 hours and analysed by Particle Induced X-ray Emission (PIXE) for their elemental compositions at ANSTO.

The average OC and EC results over the 5 days are tabulated in Table 1. The high OC/EC ratio suggests that vehicle emissions are not the dominant source of carbonaceous aerosols at the schools; secondary organic aerosols were also present (Giugliano et al. 2005). It can be seen that S02 has the highest EC concentration and lowest OC/EC, suggesting that the greatest influence of traffic emission especially from diesel vehicles occurred at this school. This is supported by the traffic data, which showed high traffic counts with more heavy duty vehicles passing through the school.

Si, P, S, Cl, K, Ca, Ti, Cr, Mn, Fe, Cu, Zn, Br, Sr, Pb and Cd were detected at the three schools while Al, Co, Ni and V were only detected at S02. Si, Cl, Fe and Pb were found mainly in the $PM_{2.5}$ samples at all three schools while Sr and Cd were found mostly in the PM_1 fraction at S01 and S02. The elemental profiles of S02 were distinctly different from those of S01 and S03.

Table 1: Average OC and EC results for each school

School ID	OC ($\mu g/m^3$)	EC ($\mu g/m^3$)	OC/EC ratio
S01	2.76 ± 0.34	0.23 ± 0.19	13.59
S02	4.05 ± 0.41	0.80 ± 0.80	5.14
S03	3.27 ± 0.38	0.26 ±0.17	13.38

S02 showed more influence from traffic emission with higher concentrations of traffic related elements such as Pb, Zn, Ni, Mn and Fe (Martuzevicius et al. 2004).

Multicriteria decision making methods, Preference Ranking Organisation METHods for Enrichment Evaluation (PROMETHEE) and Graphical Analysis for Interactive Assistance (GAIA) were applied to this data in order to determine the school with the least pollution. PROMETHEE is a ranking method which determines the preference of one object over another and GAIA is the visual representation of the influence of the variables in the form a biplot. PROMETHEE ranked S01 as the least polluted and S02 as the most polluted. In addition, three separate clusters were observed in the GAIA biplot, indicating that the aerosols in each of the schools have different chemical compositions.

The paper highlights the contributions of airborne soil as well as secondary organic and traffic- related aerosols to the air quality around the schools.

This work was supported by the ARC, DTMR and DET through Linkage Grant LP0990134. We would also like to thank all members of the UPTECH project, including R. Fletcher, A. Monk, G. Marks, P. Robinson, Z. Ristovski, W. Ezz, G. Williams, C. He, M. Falk, F. Salimi, M. Mokhtar, K. Mengersen, S. Low Choy, S. Dharani, B. Toelle and R. Appleby, as well as UPTECH collaborators from University of Cincinnati, particularly P. Ryan, for their contribution to this work, and A. Liebhardt and his staff for assistance in building the air samplers.

Giugliano, M., et al. (2005) *Atmos. Environ*., 39, 2421-2431

Martuzevicius, D., et al. (2004) *Atmos. Environ.*, 38, 1091-1105

Pope, C.A, Dockery, D.W.,(2006), *J. Air & Waste Manage. Assoc.*, 56, 709-742.

Zhang, Q., Zhu, Y., (2010) *Atmos. Environ*., 44, 253-261.

Size-resolved mixing state of soot (black carbon) particles in the Beijing Megacity, China: aging rates, the condensable vapor pressure and parameterizations

Y. Cheng[1], H. Su[2,3], A. Wiedensohler[1], M. Berghof[1], B. Wehner[1], P. Achtert[1], A. Nowak[1], D. Rose[2], S. Gunthe[2], Y. Gong[4], N. Takegawa[5], Y. Kondo[5], M. Shao[3], M. Hu[3], T. Zhu[3], L. M. Zeng[3], U. Pöschl[2], Y. H. Zhang[3]

[1] Leibniz-Institute for Tropospheric Research, Leipzig, Germany
[2] Biogeochemistry Department, Max Planck Institute for Chemistry, Mainz, Germany
[3] College of Environmental Sciences and Engineering, Peking University, Beijing, China
[4] Inst Chem Def, Beijing, China
[5] Research Center for Advanced Science and Technology, the University of Tokyo, Tokyo, Japan
Keywords: Soot particles, Soot size distribution, Mixing state, Coatings, Condensation.
Presenting author email:h.su@mpic.de

Soot (black carbon) particles are the most efficient light absorbing aerosol species and have pronounced direct, semi- and indirect climate effects in the atmosphere. These effects strongly depends on the mixing state of soot particles, e.g. the light absorbing capability of soot (related to direct radiative effects) can be enlarged by a factor of 1.5 up to 3 when soot is coated. From this aspect, understanding of soot mixing state and it evolution mechanism is an essential task for understanding the climate research. Unfortunately, there is very limited information about the evolution of soot mixing state in the atmosphere. Since there is nothing to compare with, the modeled soot mixing state remains a big source of uncertainties in our climate models.

In CAREBeijing 2006 campaign, we tried to address this issue by measuring soot mixing state in the megacity Beijing. A volatility tandem differential mobility analyzer (VTDMA) was implemented to determine the size-resolved mixing state of soot particles (7 sizes from 30 nm to 320 nm). Pronounced diurnal variations of soot mixing state were observed during the campaign and have been validated against aerosol hygroscopic mixing state (Figure 1, Su et al. 2010). For Aitken mode particles, the largest F_{in} (number fraction of internally mixed soot) was observed in 8:00 to 9:00 while for accumulation mode particles, the largest F_{in} were observed in 12:00 - 13:00.

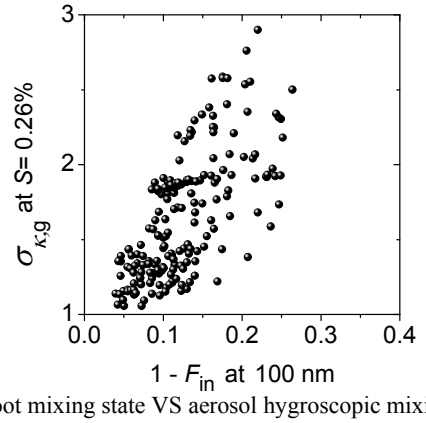

Fig. 1 Soot mixing state VS aerosol hygroscopic mixing state

The evolutions of accumulation mode particles can be well explained by competitions of fresh emission and coating processes. Given the soot emission rates, the profile of condensable vapor concentration p_{Cond}, can be constrained by the soot concentration and mixing state information. The parameter p_{Cond} shows a diurnal profile with high values during daytime, i.e. a peak around noon time, similar to oxidant or oxidative products (like O_3 and H_2SO_4). The coating rate (dF_{in}/dt) due to condensation growth could be extremely high in the measurement site with a maximum of ~ 100% h^{-1}(Fig. 2).

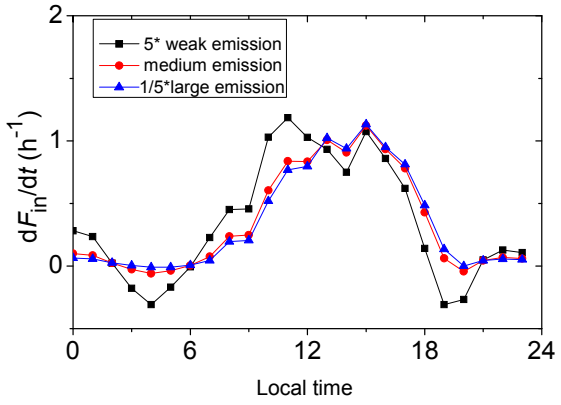

Fig. 2 Aging rate of soot particles due to condensation process

The evolution of soot mixing state was found to be strongly linked to the aging process of air masses. So we suggested parameterizing the soot mixing state at 150 nm by air mass aging indicators and calculating the soot mixing state of other accumulation mode particles from that at 150 nm. The simplicity and flexibility of this mechanism promise its use in time-consuming climate models though more evidences from other sites are also needed to verify the universality of our results. We also illustrate the importance of reporting the threshold value in the definition of soot mixing state and suggest using a distribution concept in future studies.

Cheng et al., (2011) Size-resolved mixing state of soot (black carbon) particles in the Beijing Megacity, China: aging rates, the condensable vapor pressure and parameterizations, **submitted**

Su et al., (2010). Hygroscopicity distribution concept for measurement data analysis and modeling of aerosol particle mixing state with regard to hygroscopic growth and CCN activation, *Atmos. Chem. Phys.*, **10**

Does aerosol in London create an urban solar flux island?

C.L. Ryder[1] and R. Toumi[2]

[1]Department of Meteorology, University of Reading, Reading, Berkshire, RG6 6BB, UK
[2]Department of Physics, Imperial College London, Prince Consort Road, London, SW7 2BW, UK
Keywords: urban aerosols, PM, radiative properties, field measurements, indirect effect
Presenting author email: c.l.ryder@reading.ac.uk

Solar irradiance measurements from a new high density urban network in London are presented. We find that central London receives less solar irradiance at the surface compared to outer London, and attempt to attribute this difference to the direct effect of aerosol using a combination of ground based measurements of PM10 and PM2.5 and radiative transfer modelling.

Urban heat island effects have a significant effect on the energy balance of cities, due to the effects of building materials, sparsity of vegetation and anthropogenic heat sources (Grimmond et al., 2010). One additional contributor to differences in the urban energy balance compared to rural areas is the higher concentration of aerosols due to urban pollution, which scatter and absorb incoming solar radiation, thus reducing the total downwelling surface solar radiation (Oke, 1997), known as the direct aerosol radiative effect.

Studies in several other cities using point measurements comparisons between urban and rural sites have found total urban solar irradiance to be between 1 to 33% less than their rural counterparts (e.g. Hay, (1984) in Vancouver, East (1968) in Montreal and Jáuregui and Luyando (1999) in Mexico City). Due to the gradation in the amount of aerosol pollution which originates from city sources, there should be a corresponding gradation in the surface solar irradiance.

Variations in solar irradiance due to attenuation by aerosols on an urban scale have implications for the understanding of urban meteorology, urban energy balance models and for solar power generation. Despite this importance, no studies have examined the distribution of solar irradiance in urban areas on a sub-city scale.

Here we present measurements from a new, high density network of inexpensive solar irradiance sensors across London to determine the spatial distribution of solar irradiance across the city both in terms of the annual average and on a case study basis. For the case studies, we describe a new method to determine aerosol column loading solely using measurements of clear sky total solar irradiance. We examine the findings compared to ground-based particulate measurements across London and establish to what extent London's spatial aerosol distribution affects the downwelling surface solar irradiance.

Annual averages of solar irradiance demonstrate that central London receives 30 ± 10 Wm^{-2} less solar irradiance than outer London at midday, equivalent to 9 ± 3% less than the London average (see Figure 1). Particulate matter and AERONET measurements combined with radiative transfer modeling suggest that the direct aerosol radiative effect could explain 33 to 40% of the inner London deficit and a further 27 to 50% could be explained by increased cloud optical depth due to the aerosol indirect effect. These results have implications for solar power generation and urban energy balance models.

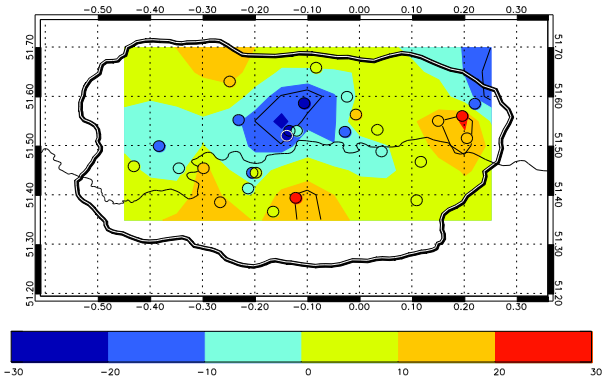

Figure 1. Annual average anomaly (Wm-2) of midday solar irradiance across London relative to the London average. Thin black line shows River Thames, double black line shows M25 (London orbital motorway).

East, C., (1968), *Comparaison du Rayonnement Solaire en Ville et a la Campagne*. Cahiers de Géographie de Québec, 12, 81-90.

Grimmond, C.S.B., Blackett, M., Best, M.J., Barlow, J., et al., (2010), *The International Urban Energy Balance Models Comparison Project: First Results from Phase 1. Journal of Applied Meteorology and Climatology*, **49**, 1268-1292.

Jáuregui, E. and Luyando, E., (1999), *Global radiation attenuation by air pollution and its effects on the thermal climate in Mexico City*. International Journal of Climatology, **19**, 683–694.

Hay, J.E., (1984). *An assessment of the mesoscale variability of solar radiation at the Earth's surface.* Solar Energy, **32**, 425-434.

Oke, T.R., (1997). *Urban Environments. In: Bailey, Oke, Rouse Climates of Canada*. Canada: McGill-Queen's University Press. p308-310.

Role of the hysteresis and water content in PM10 measurements

K. Imre[1], A. Gelencsér[1] A. Molnár[2] and V. Dézsi[3]

[1]Department of Earth and Environment Sciences, University of Pannonia, Veszprém, 8200, Hungary
[2]Air Chemistry Group of the Hungarian Academy of Sciences, Veszprém, 8200, Hungary
[3]Hungarian Meteorological Service, Air Quality Reference Center, Budapest, 1024, Hungary
Keywords: air quality, urban aerosol, PM10, water content, hysteresis, dry mass
Presenting author email: kornelia@almos.uni-pannon.hu

For decades the air pollution has been considered as one of the most serious problems mainly in highly populated areas all over the world including Hungary. During winter months the PM10 concentration exceeds several times the health limit.

In Europe, monitoring of PM10 is regulated by CEN standard (EN 12341), the β-ray absorption and gravimetry are the most widely used. Gravimetry is the reference method in the PM10 measurements. This method gives information about the aerosol concentration only after 48h, while beta-attenuation method provides data in high time resolution. According to the regulations, the gravimetric mass measurements are carried out at RH=50±5% and T=20±1°C. In both cases the water vapour content of the air and consequently the absorbed water can cause positive artefact during the sampling. This is the result of the hygroscopicity and hysteresis of the aerosol particles. As it is well known, at higher RH the particles can absorb the water vapour, therefore their size and mass can grow. On the other hand, when RH decreases the particles begin to lose the absorbed water. In the most cases this weight loss is less than the previous mass growth, due to hysteresis.

The aim of this work is to study the effect of water vapour on the aerosol mass measurement by both methods. First we tested the gravimetric method. Each filter (Whatman) was weighted before and after sampling to determine the aerosol mass on the filter. The sampling was carried out by a Hi-vol (Digital DH-80) sampler and a FH 62 beta monitor. The experimental period was between 4 November 2008 and 18 March 2010 in a residential site in Budapest, Hungary. The hygroscopic behaviour of the aerosol particles were investigated in a chamber, where the RH was adjusted between RH=20% and RH=90%.

First we studied the water uptake of the aerosol particles from RH=50% to RH=90%. After the humidification, the RH was reduced back to 50%, and on the basis of the "remaining water mass" the effect of hysteresis was estimated.

Our results show that because of the hysteresis of the aerosol mass concentration can be overestimated by up to 16%. From these results we can conclude that the aerosol mass at RH=50% cannot be considered as dry mass. In order to verify it, the mass measurements were continued at lower (<20%) RH, this reduction resulted in further loss in the aerosol mass. The average aerosol mass deficit was 4.56%, while its maximum value reached 16.8%.

Finally, we concluded that the PM10 mass concentration measured at 50% RH can be overestimated by 2% to 17%. In Fig. 1 the degree of this overestimation is presented for the time interval of this study.

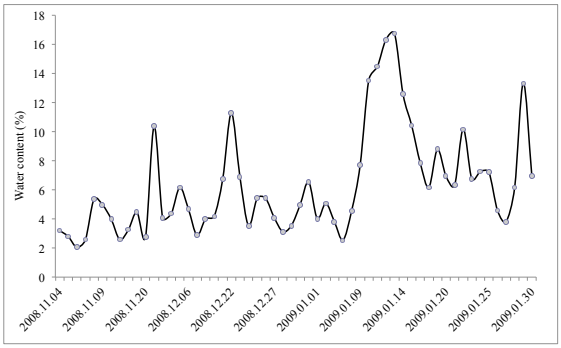

Figure 1. The water content of aerosol samples at RH=50% relative to RH=20%

Beta-attenuation is an online method and the sampling is usually carried out at ambient relative humidity. Therefore humidity correction should be applied on these data. The water uptake of the particles from the same period was measured between RH=20% and RH=95% and the mass growth factors were calculated ($GF=mass_{wet}/mass_{dry}$).

Applying the mass growth factors and considering ambient relative humidity we estimated the water contribution to the aerosol mass concentration measured by the online method. The humidity corrected data show that in many cases the PM10 concentration was lower than the air quality standard during the smog alert period as presented in Fig. 2.

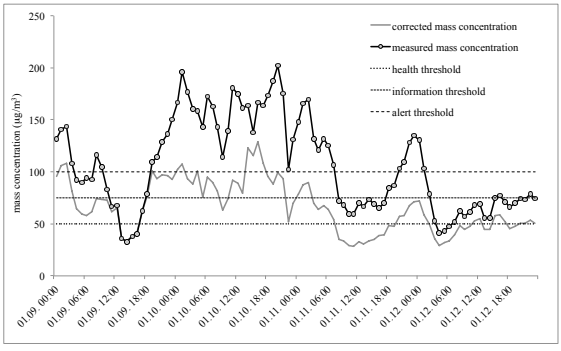

Figure 2. The measured and the humidity corrected mass concentration during the smog period in Budapest.

The authors acknowledge to AEROS_EU project (project number OM-00218/2007).

EN 12341:1998, (1998) CEN

Wednesday, September 7, 2011

Session 7B: Aerosol-Cloud Interactions 3

Hill Cap Cloud Thuringia 2010 (HCCT-2010) – Overview and first results

D. van Pinxteren[1], W. Birmili[1], B. Fahlbusch[1], W. Fomba[1], A. Grüner[1], T. Gnauk[1], Y. Iinuma[1], S. Mertes[1], K. Mildenberger[1], M. Merkel[1], C. Müller[1], K. Müller[1], L. Poulain[1], G. Spindler[1], S. Henning[1], M. Schäfer[1], F. Stratmann[1], A. Tilgner[1], K. Weinhold[1], H. Wex[1], R. Wolke[1], A. Wiedensohler[1], W. Zhijun[1], S. Borrmann[2], E. Harris[2], A. Roth[2], J. Schneider[2], B. Sinha[2], I. George[3], D. Heard[3], L. Whalley[3], B. D'Anna[4], C. George[4], M. Müller[4], D. Amedro[5], C. Fittschen[5], C. Schoemaker[5], J. Collett[6], T. Lee[6], and H. Herrmann[1]

[1]Leibniz-Institut für Troposphärenforschung, 04318 Leipzig, Germany
[2]Particle Chemistry Department, Max Planck Inst. for Chemistry, 55128 Mainz, Germany
[3]School of Chemistry, University of Leeds, Leeds LS2 9JT, Great Britain
[4]IRCELYON, UMR 5256 CNRS/Université Lyon1, 69629 Villeurbanne Cedex, France
[5]University of Lille, UMR CNRS-USTL 8522, 59655 Villeneuve d'Ascq, France
[6] Department of Atmospheric Science, Colorado State University, Fort Collins, CO 80523, USA

Keywords: aerosol cloud interaction, physical and chemical properties, multiphase chemical processes.
Presenting author email: dominik@tropos.de

Clouds play a crucial role for physical and chemical processes in the atmosphere. Lagrangian-type field experiments where an orographic cloud is used as a natural flow-through reactor provide a basis for studying such processes. Several such hill cap cloud experiments were conducted in the past with the most recent ones being the FEBUKO campaigns in 2001 and 2002 at Mt. Schmücke in Thuringia, Germany (Herrmann et al., 2005).

In September/October 2010 another Lagrangian-type cloud experiment was conducted to study aerosol cloud interaction at Mt. Schmücke, with a special focus on highly time-resolved online instrumentation that was not available during the times of the previous studies.

Three measurement sites were installed: An upwind site, which served for the characterisation of incoming air masses, an in-cloud site on the Schmücke summit, and a downwind site, where under appropriate meteorological conditions air masses after their passage through a hill cap cloud could be studied. A scheme of the area with the 3 sites is given in Figure 1.

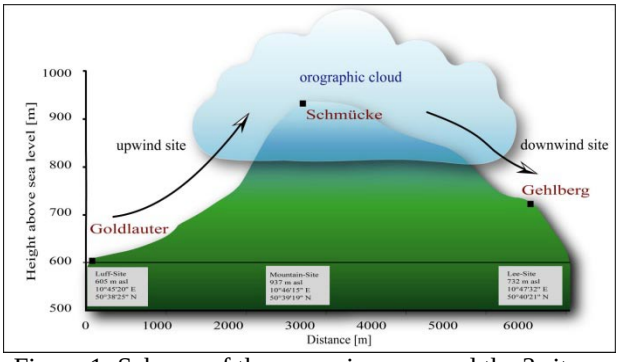

Figure 1: Scheme of the campaign area and the 3 sites.

The valley sites were equipped with a comprehensive suite of instrumentation, including gas monitors, VOC and OVOC samplers, PTR-MS, FAGE, SMPS, APS, HTDMA, CCNC, MAAP, CPC, mist chambers, filter samplers, impactors, MARGA, PILS, AMS, and a ceilometer, to determine the physical and chemical state of the aerosol upwind and downwind of the cloud. At the in-cloud site the cloud droplets were collected using bulk and multi-stage cloud water collectors. The HOx budget was determined by a FAGE and the interstitial and droplet (residual) phase were sampled behind an interstitial inlet and two CVIs applying SMPS, OPC, PSAP, aerosol mass spectrometry (AMS, ALABAMA), filters and OVOC samplers. The liquid water content was measured by a PVM and the droplet size distribution by a FSSP.

Samples from the discontinuous instruments (filters, impactors, cloud collectors, etc.) were analysed for their chemical composition, including among others: inorganic ions, OC/EC, WSOC, WSON, organic acids, sugars, organic carbonyl compounds, trace metals, and soluble metals in different oxidation states (Fe(II)/Fe(III)).

Tracer experiments were performed by releasing an inert chemical gas at the upwind site and studying its distribution in the Schmücke area within a reasonable time interval (1 hour). These data, together with an in-depth local and regional classification of the meteorological conditions during cloud events, allowed for an identification of time periods, where a connected air flow between the three sites can be assumed, i.e. representative air masses were sampled before, during, and after a cloud passage.

A comparison of the physical and chemical properties of the aerosol within these air masses, especially from the online instruments, led to interesting preliminary insights in various scientific areas such as aerosol processing through clouds, chemical cloud composition, or the influence of clouds on the radical oxidants budget. First results, especially from the chemical measurements, will be given in this contribution.

H. Herrmann et al. (2005) *Atmos. Environ.* **39**, 4169.

Microphysical and chemical characterization of cloud droplets, cloud droplet residuals, and interstitial aerosol particles during a hill-cloud field experiment in Central Europe

J. Schneider[1] A. Roth[1], S. Mertes[2], D. van Pinxteren[2], and S. Borrmann[1,3]

[1] Particle Chemistry Department, Max Planck Institute for Chemistry, Mainz, 55128, Germany
[2]Leibniz-Institute for Tropospheric Research, Leipzig, 04318, Germany
[3]Institute of Atmospheric Physics, Johannes Gutenberg University, Mainz, 55128, Germany
Keywords: Aerosol cloud interaction, CCN, Aerosol mass spectrometry, AMS
Presenting author email: johannes.schneider @mpic.de

Cloud and aerosol interactions in orographic cloud formation were studied during the field campaign Hill Cap Cloud Thuringia (HCCT) in September and October 2010 on a mountain site in Central Germany (Schmücke, 938 m a.s.l.).

The cloud droplet number concentration and size distribution was measured by a forward scattering spectrometer probe (FSSP) in a size range between 2 and 40 µm. Cloud droplets were sampled through a counterflow virtual impactor (CVI) and their residuals were analysed for non-refractory chemical composition by a compact time-of-flight aerosol mass spectrometer (C-ToF-AMS, size range 40 – 1000 nm). Interstitial particles were sampled by an interstitial inlet with a cut-off of 5 µm and analysed for non-refractory chemical composition by a high-resolution (HR)-ToF-AMS (size range 40 – 1000 nm), and for black carbon by a multiangle absorption photometer (MAAP). Size distributions of both the interstitial particles and the cloud droplet residuals was measured by optical particle counters (0.25 – 32 µm).

During the measurement period of the HCCT campaign (Sept. 19 until Oct. 25, 2010), the Schmücke field station was covered in clouds for 370 hours, corresponding to more than one third of the total measuring time.

Here we focus on the chemical composition of the activated and the non-activated particles. From the measured mass concentration of the interstitial and out-of-cloud aerosol particles, we calculate a chemically resolved activated mass fraction f_{mass} for the individual compounds that can be detected by the AMS (organics, sulphate, nitrate, ammonium, and chloride) by the following equation:

$$f_{mass} = \frac{\overline{C_{ooc}} - C(t)}{\overline{C_{ooc}}},$$

where $\overline{C_{ooc}}$ is the average mass concentration measured directly before and after the cloud event and $C(t)$ is the concentration of the interstitial aerosol during a cloud event.

Figure 1 displays the resulting activated mass fraction for a selection of cloud events on September 16. The upper panel shows the cloud droplet number concentration, the middle panel the measured particle mass concentration (out-of-cloud and interstitial), and the lower panel shows the activated mass fraction. While the inorganic species reach activated fraction of more than 90%, the organic activated mass fraction is significantly lower (on average by 10%) for all cloud events displayed here. Further investigation will clarify whether this effect is due to a higher fraction of organic mass in the smaller particle size range or if the effect is due to the lower hygroscopicity of organic particulate matter compared to inorganic material as ammonium sulphate or ammonium nitrate. The latter is connected to the O:C ratio of the organic particulate matter which increases with particle aging in the atmosphere, leading to an increase in hygroscopicity (Jimenez et al., 2009)

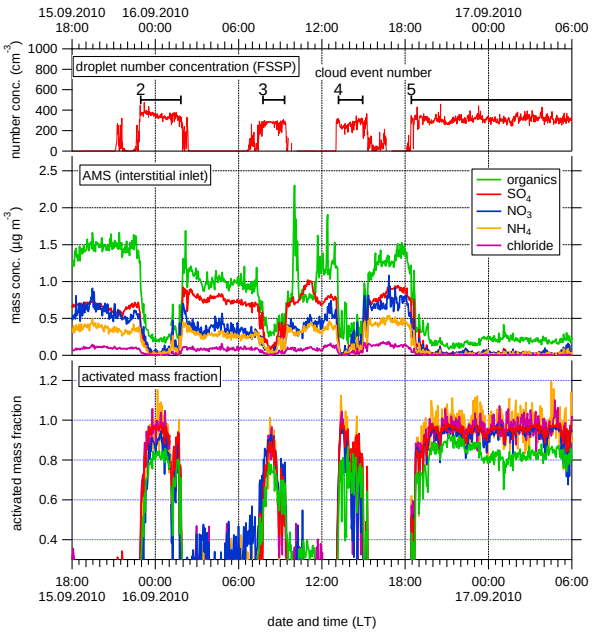

Figure 1. Example for the activated mass fraction analysis during selected cloud events. Upper panel: cloud droplet number concentration, middle panel: absolute mass concentrations (interstitial inlet), lower panel: activated mass fractions.

The AMS data will be further analysed for chemically resolved size distribution and organic O:C ratio. The analysis of the cloud residuals sampled through the CVI inlet and measured with the second AMS will complete the interpretation of the results.

Jimenez, J. L., et al., Evolution of Organic Aerosols in the Atmosphere, *Science*, 326, 1525-1529, 2009.

Understanding phase transition and hygroscopic behavior of organic acid particles and their mixtures with ammonium sulfate by micro-Raman spectroscopy

M.C. Yeung[1] and C.K. Chan[2]

[1]Department of Chemical and Biomolecular Engineering, [2]Division of Environment,
Hong Kong University of Science and Technology, Clear Water Bay, Kowloon, 852, Hong Kong
Keywords: deliquescence, crystallization, hygroscopic growth, Raman microscopy
Presenting author email: meiji@ust.hk

Hygroscopic particles can interact with water vapor and change in phase state, size, concentration and even chemical composition, all of which can influence optical properties, cloud condensation nuclei (CCN) activity as well as chemical reactivity. Laboratory investigation of the aerosol thermodynamic properties is therefore necessary to elucidate their impacts on global climate and tropospheric chemistry.

Organic components have been found as the major constituent of atmospheric aerosols and they are often mixed with inorganic species. In this study, we applied the micro-Raman spectroscopic technique to examine four organic particles, including malonic acid (MA), glutaric acid (GA), adipic acid (AA) and glyoxylic acid (GlyA), as well as their mixtures with ammonium sulfate (AS). Mirco-particles deposited on a hydrophobic substrate in an air-flow cell were exposed to changing relative humidity (RH). Raman spectra of single particles were recorded. Changes in Raman spectral features as a function of RH were useful in determining the phase states and water content of the particles (Yeung *et al.*, 2009; Yeung and Chan, 2010)

The Results of phase characterization show that single-component particles usually undergo instant deliquescence and complete crystallization, while the multi-component systems may undergo gradual deliquescence and partial crystallization. Step-wise crystallization of AS-GA mixed particle is shown in Figure 1. Pure GlyA has an exceptional non-deliquescent behavior, which remained as supersaturated solution at dry condition as confirmed by the presence of water peak.

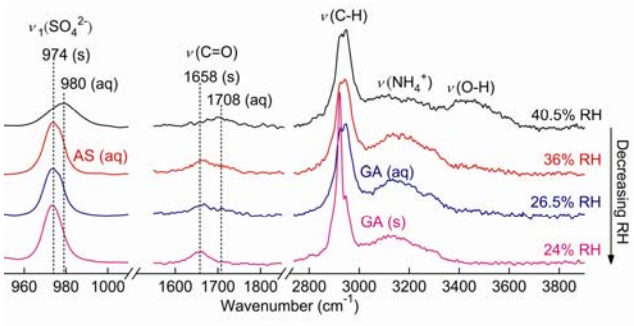

Figure 1. Raman spectra of AS-GA mixed particle to illustrate the occurrence of partial crystallization.

The hygroscopic properties of ammonium sulfate apparently altered after mixing with organic species (see Figure 2). When the water-soluble dicarboxylic acids (MA and GA) present, particle can retain water at low RH conditions (RHs below the crystallization point for ammonium sulfate). The less water-soluble AA exhibits insignificant effect on the particle water content during crystallization process. Early water-uptake behavior has been observed in all mixed systems.

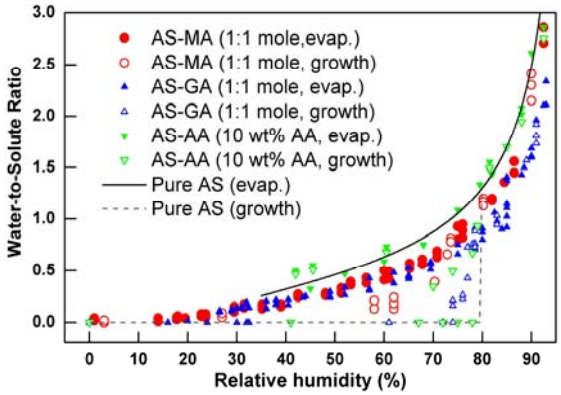

Figure 2. Hygroscopic properties (water-to-solute mass ratio) of pure AS and AS-organic mixed particles.

We also characterized two polymorphs of pure GA solid particles and investigated the effect of polymorphic transformation on deliquescence properties (Yeung *et al.*, 2010). The metastable α-form GA solids can either deliquesce or transform to the more stable β-form at 86% RH. Gradual water-uptake by β-form particles was observed until the RH further increased to ~90%. The water-uptake process was not completed in5 hours, indicating a mass-transfer effect for the β-form. Our observation can explain the discrepancies in the deliquescence of GA particle reported in literature, which was found to occur between 83% and 90% RH.

Raman spectroscopy has been demonstrated for investigating particle phase and hygroscopic properties. This laboratory technique will be further used for understanding the phase transition properties as well as the molecular interaction in other mixed particles.

This work was supported by Earmarked Grant (610909) from the Hong Kong Research Grants Council.

Yeung, M. C., Lee, A. K. Y. and Chan, C. K. (2009) *Aerosol Sci. Technol.* **43**, 387–399.

Yeung, M. C. and Chan, C. K. (2010) *Aerosol Sci. Technol.* **44**, 269–280.

Yeung, M. C., Ling, T. Y. and Chan, C. K. (2010) *J. Phys. Chem. A* **114**, 898–903.

Cloud Condensation Nuclei Closure Study on Summer Arctic Aerosol

S. Sjogren[1], E. Fors[1], E. Swietlicki[1], M. Martin[2] and B. Sierau[2]
[1]Division of Nuclear Physics, Lund University, Lund, Sweden
[2]Institute for Atmospheric and Climate Science, ETH Zurich, Zurich, Switzerland
Keywords: Aerosol cloud interaction, Clouds, Arctic aerosols, AMS, HDTMA, CCN.
Presenting author email: staffan.sjogren@nuclear.lu.se

To better understand the warming of the arctic, the radiative balance of sunlight and infrared radiation needs to be described. Clouds play a major role in this balance. Each individual cloud droplet is formed on an atmospheric aerosol particle. Descriptions and measurements of relevant aerosol particle properties and the particle interactions with cloud droplets from the high Arctic are rare.

We present an aerosol-cloud condensation nuclei (CCN) closure study on summer high Arctic aerosol, based on measurements that were carried out in August 2008 during the Arctic Summer Cloud Ocean Study (www.ASCOS.se) on board the Swedish icebreaker *Oden*. The main data was collected during a three-week time period in the pack ice ($> 85^\circ$ N) when the icebreaker *Oden* was moored to an ice floe and drifted passively during a biological active period into autumn freeze up conditions.

Method and results

CCN number concentrations were obtained using two CCN counters from Droplet Measurement Technologies (DMT, USA), measuring at different supersaturations. The relevant dry particle size studied was approximately 0.03 to 1 μm. The directly measured CCN number concentration was firstly compared with a CCN number concentration predicted using bulk aerosol mass composition data from an aerosol mass spectrometer (AMS) and aerosol size distributions obtained from a differential mobility particle sizer, assuming κ-Koehler theory and an internally mixed aerosol. The AMS had a minimum dry particle cut-off diameter of about 70 nm, thus not capturing the chemistry of the smallest particles activated. Secondly, size-resolved measurements of the hygroscopicity (water uptake) of the aerosol particles were included in the closure, down to 30 nm. A hygroscopicity tandem differential mobility analyser (HTDMA) was used for this purpose.

For the first "AMS"-approach closure can be achieved (Martin *et al*, 2011), with different parameters for the hygroscopicity and density of the particles, at each of the 0.10, 0.15 and 0.20% supersaturations. For the best fits of the predicted CCN number concentration against the measured one, the organic fraction of the aerosol is found nearly insoluble ($\kappa_{org} = 0.02$). However, this is not ambigious and $\kappa_{org} = 0.2$ is found as an upper limit at 0.1% supersaturation. For the two highest supersaturations, 0.41 and 0.73%, closure could not be achieved with the investigated settings concerning hygroscopicity and density. The predicted CCN number concentration is always higher than the measured one, suggesting that the smaller particles that activate at these supersaturations have a relative larger insoluble and/or organic mass fraction than the larger particles. Current ongoing investigations use the measured hygroscopicity data in the subsaturated regime, with dry sizes measured down to 30 nm in the closure (see Fig. 1). As it is observed that the hygroscopicity decreases with decreasing size, this supports the assumption of more organics in the smallest particles. This will be more detailed during the conference.

Moreover, different periods will be investigated in more detail by case studies, i.e. taking different weather situations and the transport of air masses into consideration.

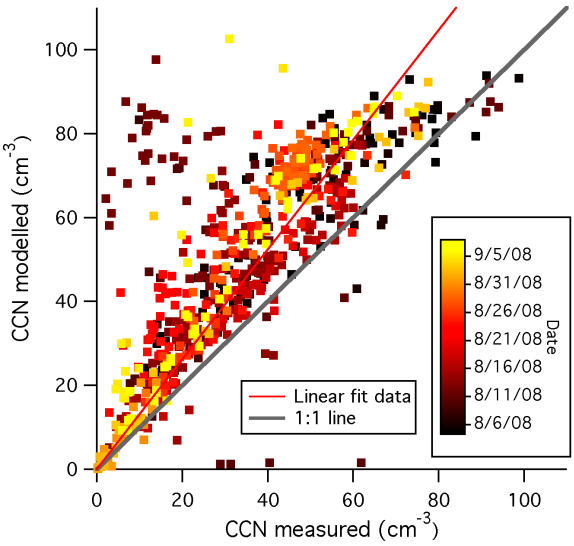

Figure 1: Preliminary closure from HTDMA data to 0.2%SS CCN measurements.

Acknowledgements

ASCOS was made possible by funding from the Knut and Alice Wallenberg Foundation and the DAMOCLES European Union 6th Framework Program Integrated Research Project. The Swedish Polar Research Secretariat (SPRS) provided access to the icebreaker Oden and logistical support. We are grateful to Oden's Captain Mattias Peterson and his crew. ASCOS is an IPY project under the AICIA-IPY umbrella and an endorsed SOLAS project.

Martin, M., Chang, R. Y.-W., Sierau, B., Sjogren, S., Swietlicki, E., Abbatt, J. P. D., Leck, C., and Lohmann, U. (2011) ACP, Special issue ASCOS, submitted.

Importance of different surfactant representations for cloud droplet numbers predicted with the ECHAM5.5-HAM2 aerosol-climate model

N.L. Prisle[1], D. Topping[2], S. Romakkaniemi[3], G. McFiggans[2], M. Dal Maso[1], and H. Kokkola[4]
[1]Department of Physics, University of Helsinki, P.O. Box 48, 00014, University of Helsinki, Finland
[2]Centre for Atmospheric Science, University of Manchester, Manchester, UK
[3]Department of Physics, University of Eastern Finland Kuopio, P.O. Box 1627, 70211, Kuopio, Finland
[4]Finnish Meteorological Institute, Kuopio Unit, P.O. Box 1627, 70211, Kuopio, Finland
Keywords: droplet activation, organic surfactants, surface partitioning, global modeling.
Presenting author email: nonne.prisle@helsinki.fi

The indirect radiative effects of atmospheric aerosols via their influence on cloud drop formation and cloud properties constitute the single largest uncertainty in predictions of global climate and future climate changes (IPCC, 2007). Aerosol cloud condensation nucleus (CCN) activity is determined by both particle size and chemical composition, but CCN activity of the organic aerosol fraction in particular remains to be firmly constrained (Hallquist *et al.*, 2009). This in part owes to the surface activity (the tendency to preferentially accumulate in the surface region) in aqueous solutions of some organic components of atmospheric aerosol particles. Surface active molecules (surfactants) have been demonstrated in aerosol and cloud and fog water samples from a wide variety of atmospheric environments and can collectively comprise a significant fraction of the organic aerosol mass (Mochida *et al.*, 2003).

Both thermodynamic model calculations and laboratory experiments show that surface activity can significantly affect organic aerosol CCN potential (Prisle *et al.*, 2010a). The combined effects of partitioning of organic molecules to the droplet surface and of reduced droplet surface tension, for calculated cloud droplet activation, can be determined from numerical solutions to thermodynamic relations. Unfortunately, such calculations with several nested iterations are computationally too demanding for implementation into atmospheric models (Kokkola *et al.*, 2006). Therefore, Topping (2010), Raatikainen and Laaksonen (2010), and Prisle *et al.* (2010b) have proposed different parametrizations to account for the combined effects of surfactant properties in calculations of organic aerosol CCN activation.

In this work, we compare predictions of cloud droplet number concentrations using the aerosol-climate model ECHAM5.5-HAM2 with different representations of the aerosol organic carbon fraction in terms of the influence of surfactant properties on cloud microphysics. Specifically, we use the mentioned novel parametrizations, which account for the combined organic surfactant effects, in addition to the previously applied approaches using either reduced droplet surface tension without consideration of organic surface partitioning effects, or disregarding surfactant properties altogether (Prisle *et al.*, 2010a). The cloud droplet numbers are calculated using the cloud activation parametrization by Abdul-Razzak and Ghan (2000), which has here been extended to account for effects of organic surface activity according to each of the different approaches used.

We have made one year simulations with prescribed meteorology, assuming that all aerosol organics are surface active with properties corresponding to Suwannee River Fulvic acid. Our preliminary results show that including surfactant effects on cloud microphysics can significantly affect predicted cloud droplet numbers, compared to the conventional approach that disregards such effects altogether. This is especially the case in areas of high organic aerosol mass concentrations. Furthermore, how surfactant properties are accounted for, in terms of either including or disregarding effects of surface partitioning, also has a significant effect on droplet numbers in the cases studied. These results are the first to include such detailed effects of surfactant properties in global scale simulations, and somewhat contradict the anticipation that the non-linear responses predicted from thermodynamics to a combination of several surfactant effects on droplet activation would largely cancel out in large scale predictions.

N. L. Prisle gratefully acknowledges the funding received for this work from the Carlsberg Foundation (grants 2009_01_0366 and 2010_01_0391).

Intergovernmental Panel on Climate Change (2007) Climate Change 2007, Cambridge University Press.

M. Hallquist *et al.* (2009) Atm. Chem. Phys. **9**, 5155-5236.

M. Mochida *et al.* (2003) J. Geophys. Res. **108**, D23S8638.

N. L. Prisle *et al.* (2010a) Atmos. Chem. Phys. **10**, 5663-5683.

H. Kokkola *et al.* (2006) Geophys. Res. Lett. **33**, L10816,1-5.

D. Topping (2010) Geosci. Model Dev. **3**, 635-642.

T. Raatikainen and A. Laaksonen (2010) Geosci. Model Dev. Discuss. **3**, 11391159.

N. L. Prisle *et al.* (2010b) Atmos. Chem. Phys. Discuss. **10**, 23601-23625.

H Abdul-Razzak and SJ Ghan (2000) J. Geophys. Res. **105**, 6837-6844.

The impact of mineral dust particles on cloud properties and the state of the atmosphere during an intense Saharan dust event over Western Europe

M. Bangert[1], A. Nenes[2], B. Vogel[1], H. Vogel[1], D. Barahona[2,3], P. Kumar[2]

1. Institute for Meteorology and Climate Research, Karlsruhe Institute of Technology, Karlsruhe, Germany.

2. Schools of Earth & Atmospheric Sciences and Chemical & Biomolecular Engineering, Georgia Institute of Technology, Atlanta, GA, United States.

3. NASA Goddard Space Flight Center, Greenbelt, MD., United States.

Keywords: Aerosol cloud interaction, Saharan Dust, Modelling (regional).

max.bangert@kit.edu

Dust, through their action as cloud condensation nuclei (CCN) and ice nuclei (IN), has long been hypothesized to impact clouds and the hydrological cycle. This effect is particularly strong during dust outbreaks. Europe, being adjacent to the Sahara, is susceptible to the effects of dust storms; a quantitative assessment remains elusive and is the subject of this study.

This talk focuses on one major dust event that occurred in May 2008. Its origin was the Sahara and from there mineral dust particles were transported over the western Mediterranean, covering large areas of Western Europe. During the episode, high aerosol concentrations were observed throughout Europe; ice nuclei concentrations significantly increased (compared to pre-event levels) at Kleiner Feldberg, Germany (Klein *et al.*, 2010). During this time, traditional weather forecast models (which currently neglect aerosol impacts on atmospheric processes) exhibited poor prediction skill.

The impacts of dust on atmospheric state is studied with the regional scale online coupled model system COSMO-ART (Vogel *et al.*, 2009) that accounts for feedbacks between chemistry, aerosols, radiation, and clouds. A two-moment cloud microphysics scheme (Seifert and Beheng, 2006) is coupled together with comprehensive parameterisations for aerosol activation (Barahona *et al.*, 2010) and ice nucleation (Barahona and Nenes, 2009) to simulate the impact of the various aerosol particles on the cloud microphysics and therefore on cloud properties and precipitation.

Two simulations were compared to investigate the impact of dust on clouds and the atmospheric state in detail. In simulation R the dust is neglected and just anthropogenic and sea salt particles are simulated. In simulation D the dust is considered during cloud formation and therefore has an impact on cloud droplet and ice crystal number concentrations.

Figure 1 shows that the dust strongly increases the ice crystal number concentration. The impact on the warm cloud phase is more complex due to the non-linearity of the involved processes. During the dust event we found a systematic cooling effect (~1 K) due to an increase in cloud optical depth.

The sensitivity of cloud properties and of the atmospheric state to the dust amount is thoroughly studied.

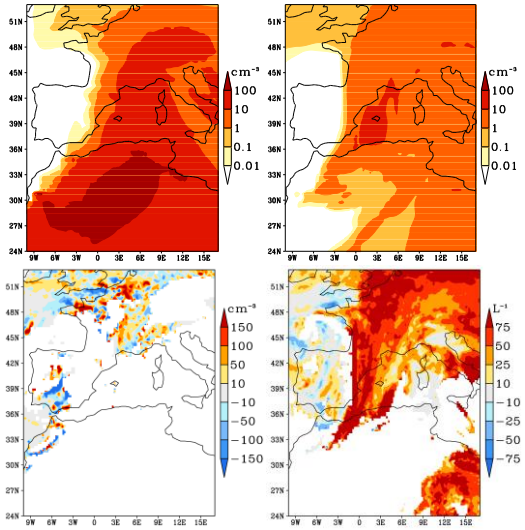

Figure 1. Distribution of dust number concentration in the lower (top left) and upper troposphere (top right) as well as the difference in the mean cloud droplet and ice crystal number concentration between simulation D and R at May 26th 2008.

Barahona, D., West, R. E. L., Stier, P., Romakkaniemi, S., Kokkola, H., and Nenes, A. (2010), 10, 2467-2473.

Barahona, D. and Nenes, A. (2009), Atmos. Chem. Phys., 9, 5933-5948.

Klein, H., Nickovic, S., Haunold, W., Bundke, U., Nillius, B., Ebert, M., Weinbruch, S., Schuetz, L., Levin, Z., Barrie, L. A., and Bingemer, H. (2010), 10, 10211-10221.

Kumar, P., Sokolik, I. N., and Nenes, A. (2009), Atmos. Chem. Phys., 9, 2517-2532.

Seifert, A. and Beheng, K.-D. (2006), Meteorol. Atmos. Phys., 92, 45-66.

Vogel, B., Vogel, H., Bäumer, D., Bangert, M., Lundgren, K., Rinke, R., and Stanelle, T. (2009), Atmos. Chem. Phys., 9, 8661-8680.

Aerosol number size distributions in the vicinity of trade wind cumuli

F. Ditas[1], B. Wehner[1], H. Siebert[1], H. Wex[1], G. Roberts[2,3], K. Mildenberger[1], T. Schmeißner[1], F. Stratmann[1], and A. Wiedensohler[1]

[1]Leibniz Institute for Tropospheric Research (IfT), 03418 Leipzig, Germany
[2]Centre National de Recherche Scientifique - Météo France, Toulouse, France
[3]Scripps Institution of Oceanography, Center for Atmospheric Sciences, La Jolla, United States
Keywords: Aerosol Cloud Interactions.
Presenting author email: ditas@tropos.de

Aerosols and clouds play an essential role in the Earth's radiation budget. Particularly aerosol-cloud interactions are a large source of uncertainty in climate sensitivity estimates. Although a variety of airborne measurements have been performed, most of them suffer from a low spatial resolution.

The helicopter-borne measurement platform ACTOS (Airborne Cloud Turbulence Observation System, Siebert *et al.*, 2006) is equipped with various instruments to investigate cloud and aerosol microphysical properties, meteorological and turbulence parameters at high temporal and spatial resolutions. Aerosol number size distributions were measured between 6 nm and 2.6 µm using an SMPS (6 to 260 nm, time resolution 2 min) and an OPC (250 nm to 2.6 µm, time resolution 1 s). In addition total particle number concentrations have been measured with a commercial CPC (TSI, D_p > 6 nm, time resolution 1s) and a fast mixing type CPC (Wehner *et al.* 2010, D_p > 7.5 nm, response time ~20 ms). Furthermore, cloud condensation nuclei (CCN) were measured with a miniaturized CCNC and droplet size distributions were measured by a Phase Doppler Interferometer for Cloud Turbulence (PICT) .

In November 2010, the Clouds, Aerosol, Radiation, and tuRbulence in the trade wInd regime over BArbados (CARRIBA) Experiment took place. Within the campaign 17 research flights (RF) inside and outside of trade wind cumuli, and additionally, ground-based aerosol and CCN measurements were performed.

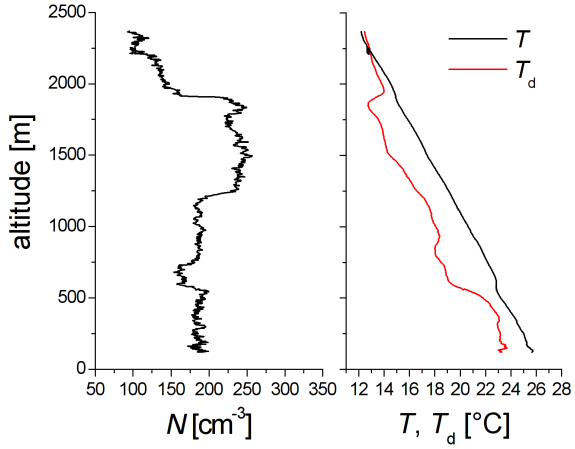

Figure 1. Vertical profiles of total particle number concentration (N), temperature (T) and dewpoint (T_d) during RF9.

Figure 1 presents vertical profiles of N, T and T_d recorded during RF9 on November 20th. The temperature profile illustrates weak inversions at 600 m and 2000 m above sea level (ASL), whereas the dewpoint indicates a humid layer up to 600 m and a cloud layer at 2200 m ASL. The total particle number concentration shows different aerosol layers. The lowermost 600 m represent the well mixed marine boundary layer and feature an average $N \sim 180$ cm^{-3}. At the altitude of the first temperature inversion, N exhibits a local minimum, which is followed by two layers of $N \sim 180$ cm^{-3} and $N \sim 220$ cm^{-3}. Finally, N decreases immediately at the second inversion reaching minimum values close to 100 cm^{-3}.

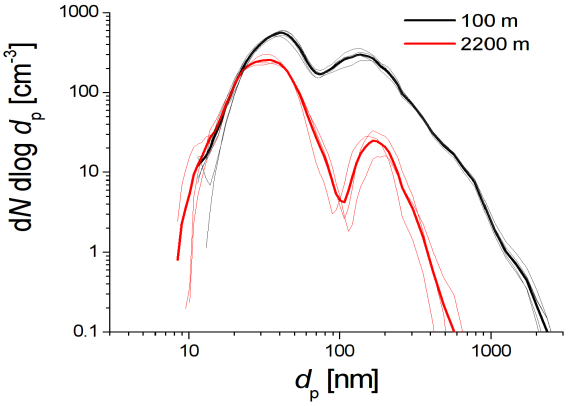

Figure 2. Aerosol number size distributions (NSDs) recorded during RF9 at different altitudes. Bold lines indicate average NSDs.

Figure 2 presents number size distributions (NSDs) of the aerosol measured at 100 m (black) and 2200 m ASL (red). All NSDs feature a bimodal shape typical for marine aerosol and a dominating Aitken mode. The NSDs at 2200 m were recorded inside a very thin stratiform cloud layer at the cloud top of surrounding cumuli.

With the help of simultaneous measurements of cloud micropysical and CCN properties as well as NSDs inside and outside of clouds this study aims at examining the complex interactions of atmospheric aerosols and small scale cloud dynamics in the vicinity of trade wind cumuli.

We thank the CIMH (Caribbean Institute for Meteorology and Hydrology), Horizon Helicopters, enviscope GmbH, and Barbados Concorde Experience. This project was funded by DFG-grant SI 1534/3-1 and the IfT.

Siebert, H., H. Franke, K. Lehmann, R. Maser, E. W. Saw, D. Schell, R. A. Shaw, and M. Wendisch (2006). *Probing Fine-Scale Dynamics and Microphysics of Clouds with Helicopter-Borne Measurements, Bull. Amer. Met. Soc., 87, 1727 – 1738*

Wehner, B., Siebert, H., Hermann, M., Ditas, F., and Wiedensohler, A.: *Characterization of a new fast mixing type CPC and its application for atmospheric particle measurements, Atmos. Meas. Tech. Discuss., 3, 5907-5931, doi:10.5194/amtd-3-5907-2010, 2010.*

Wednesday, September 7, 2011

Session 7C: High Temperature Systems: Sampling and Quenching before Detection

Experimental study of aerosols and vapours at high temperatures: past and recent application of aerodynamic quenching.

S. Jiménez[1] and J. Ballester[2]

[1]LITEC-CSIC, Spanish Council for Scientific Research, María de Luna 10, 50018, Zaragoza, Spain
[2] Fluid Mechanics Group, University of Zaragoza, María de Luna 3, 50018, Zaragoza, Spain
Keywords: high temperature aerosols, aerosol sampling, aerosol formation, low-pressure-impactor.
Presenting author email: yago@litec.csic.es

The study of aerosol formation in biomass combustion illustrates the relevance of relying on a suitable experimental technique to obtain samples representative of the sampled system, which may include inert gas and reactants, as well as coarse and fine aerosols and the most problematic component for this kind of studies: condensable vapours. The traditional solution for sampling in the presence of high concentrations of water or sulphuric acid vapour, i.e. keeping the sampled gas above the corresponding dew point, is hardly applicable to this study, since the inorganic compounds present in the fine aerosols generated after biomass combustion (mainly alkali chlorides and sulphates) have relatively high melting points (>750°C). Condensation or nucleation of these inorganic vapours in the sampling line is thus a (nearly) unavoidable problem, whose effects on the 'desired' sample must be minimised or at least controlled.

Among the sampling and analysis methods available, aerodynamic quenching appeared as a promising option for its known ability to generate extremely fast cooling and dilution rates (Bowman, 1977; Colkett *et al*, 1982). The application of a particle sampling probe based on this technique (AQPS probe) in combustion experiments in an entrained flow reactor allowed for establishing well differentiated steps in the aerosol formation route, namely alkali sulphate nucleation followed by alkali chloride condensation on these nuclei (Jiménez and Ballester, 2004), in good agreement with previous theoretical predictions (Christensen *et al*, 2000).

The main advantage of the use of this probe is to clearly separate aerosols that already existed in the sampled gas from freshly nucleated ones formed along the probe itself, most likely at its entrance. Figure 1 illustrates this feature: the 'coarse', opaque particles are sulphate aerosols sampled at 900°C, whereas the small, almost electron-transparent particles are composed of alkali chloride, which was in the vapour phase at the sampling point. In principle, this technique may thus provide information not only on the aerosols, but also on the inorganic vapours present at high temperatures.

A non-negligible drawback of the technique is that the gas at the exit of the probe is at low pressure (typically ~0.07 bar), which makes in-line analysis of the sampled gas and aerosols difficult. In the past, an impaction system was designed *ad hoc* in order to collect the aerosols on TEM grids for their analysis under the microscope. Recently, however, a commercial low pressure impactor has been used to characterise the aerosols exiting the probe, confirming and extending previous results from this group (Jiménez and Ballester, 2011). This required a prior study on the behaviour of the impactor at low inlet pressures.

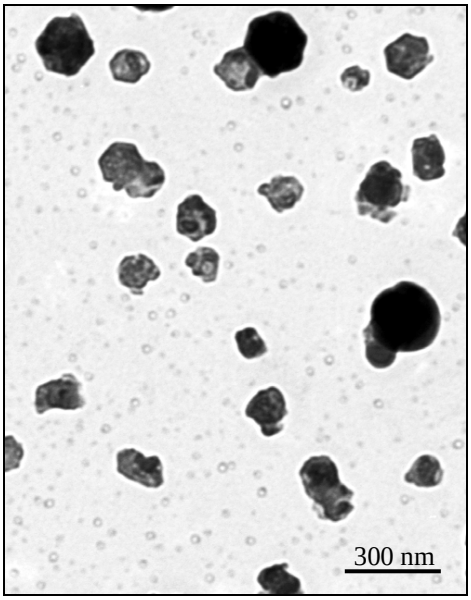

Figure 1. Sample obtained with the AQPS probe at 900°C in biomass post-combustion gases.

This work was supported by the Spanish Ministry of Science and Innovation under grant CSD2010-00011.

Bowman, C.T. (1977). Probe measurements in flames, in Experimental Diagnostics in Gas Phase Combustion Systems, B.T. Zinn (Ed.), *Progress in Astronautics and Aeronautics*, Vol. 53, pp 1-24.

Christensen, K.A., Stenholm, M. and Livbjerg, H. (1998). J. Aerosol Sci. **29**, 4:421-444.

Colkett III, M.B., Chiapetta, L., Guile, R.N., Zabielski, M.F. and Seery, D.J. (1982). *Comb. Flame*. **44**, 3-14.

Jiménez S and Ballester J. (2004). *Aerosol Sci. Tech.* **38**, 707-23.

Jiménez S and Ballester J. (2011). Use of a Berner low pressure impactor at low inlet pressures. Application to the study of aerosols and vapours at high temperature. Accepted for publication in Aerosol Sci. Tech.

Automated sampling system for studying iodine chemistry at high temperature

J. Kalilainen[1], T. Kärkelä[1], P. Rantanen[1] J. Forsman[1], L. Kåll[1], A. Auvinen[1] and J. Jokiniemi[1,2]

[1] VTT Technical Research Centre of Finland, Fine Particles, P.O.box 1000, BI7, FI02044 VTT Espoo, Finland
[2]University of Eastern Finland, Department of Environmental Science, Fine Particle and Aerosol Technology Laboratory, P.O. Box 1627, FI-70211 Kuopio, Finland
Keywords: iodine, primary circuit, severe accident, automated sampling system.
Presenting author email: jarmo.kalilainen@vtt.fi

The aim of the work was to improve the instrumentation of the EXSI facility Kalilainen *et al* (2011), used at VTT for studying fission product behavior at high temperatures. As a result very accurate measurements on the transport of iodine in conditions typical to a hypothetical severe nuclear accident could be conducted.

Experimental facility

The experimental facility consists of a reaction furnace, in which various fission product species react on a surface at 400-650°C. Gaseous reaction products as well as vaporised compounds are transported from the furnace with a carrier gas flow. The concentration and number size distribution of particles as well as the gas composition are monitored online. In addition, filters and bubbling bottles are applied to carry out speciation of particle and gaseous samples off-line. The modifications made to the experimental facility included automated sampling system, extensive logging of pressure, temperature and flow rate data and improvements in the primary diluter, which reduced the retention on its walls.

The structure in the hot section of the two-stage primary diluter and the reaction furnace tube were modified in order to reduce the depositions caused by condensation and thermophoresis. The diameter of the furnace tube was decreased at the outlet from 24 mm tube to 10 mm. The outer diameter of the diluter was designed so that during the experiment, the hot dilution part is situated inside the reaction furnace all the way to the hot gas inlet tube. Hot and cold dilution stages are connected so that the walls of the sampling line remain at high temperature until the gas flows are mixed. In the new facility, both hot and cold dilution gas can be heated with Mayer-resistant 930 W flow heaters. Flow heaters are operated by using the controlling computer.

The sampling system for the filters and bubbling bottles has been entirely automated. The filter sampling is started by typing the desired sampling time to the controlling computer and choosing the desired sampling line. As the sampling switch has been activated on the program, the controlling computer automatically opens the valve of the sampling line, and again closes it after the sampling time has expired. Gas flow through the sampling line is controlled with a critical orifice and logged by the controlling computer.

Experimental work

Experiments on gaseous iodine production due reactions on the surface were carried out using CsI as a precursor. The gas atmosphere applied in the tests was a mixture of argon, steam and hydrogen. The concentration of gaseous iodine and iodine containing aerosol species was determined with ICP-MS analysis of the filter and bubbling bottle data. As evident in figure 1, the mass concentration of gaseous iodine decreased when the concentration of H_2 in atmosphere was increased. When either molybdenum oxide or boron oxide was added to the reaction furnace, the fraction of gaseous iodine was very significantly increased. The increase was due to formation of cesium borate and cesium molybdate species. Especially at 400°C essentially all iodine released was in gaseous form. The filter analysis was confirmed by online measurement devices such as TEOM and SMPS showing very low particle mass and number concentrations.

This result highlights the importance of controlled quench and dilution as losses even at a fairly moderate temperature would influence the experimental results very significantly.

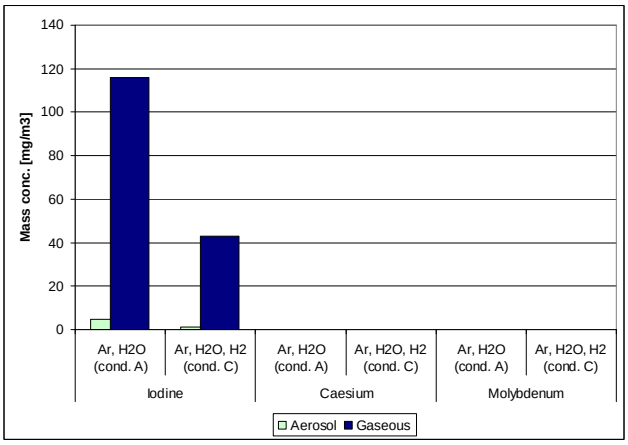

Figure 1. Iodine, caesium and molybdenum mass concentrations in the second experiment, calculated from aerosol filters and bubbling bottle ICP-MS data.

Kalilainen, J., Kärkelä, T., Zilliacus, R., Tapper, U., Auvinen, A. and Jokiniemi, J. (2011) *Chemical reactions on primary circuit surfaces and their effect on fission product transport in a severe nuclear accident.,* To be submitted.

On-line measurement of chemical composition and size distribution of high-temperature combustion aerosols

R. Zimmermann[1], T.Streibel[1], M.Sklorz[1], C. Busch[1], M.Elsasser[1], J.Schnelle-Kreis[1], C. Deuerling[1], J.Orasche[1], T. Adam[2], M.C. Astorga-Llorens[2], H.Hartmann[3]

[1]Chair of Analytical Chemistry / Joint Mass Spectrometry Centre, Institute of Chemistry, University of Rostock, D-18051 Rostock and Cooperation Group "Analysis of Complex Molecular Systems" / Joint Mass Spectrometry Centre, Helmholtz Zentrum München, D-85764 Oberschleißheim/ Germany
[2]Joint Research Centre, Institute for Environment and Sustainability,,I-21027 Ispra /Italy
[3]Technologie- und Förderzentrum, TFZ , D-94315 Straubing/Germany
Keywords: high temp.-aerosol, wood combustion, engine exhaust, on-line sampling, size distr., mass spectrometry
Presenting author email: ralf.zimmermann@helmholtz-muenchen.de

Combustion aerosols are the most important source for health relevant anthropogenic aerosols. As the physical-chemical properties of the emitted aerosols are determined on the processes in the high temperature region, the investigation of high temperature aerosol thus is of particular relevance. In order to understand the dynamic properties of freshly formed hot combustion aerosols, on-line measurements of the physical (size distribution) and chemical aerosol properties is required. An important aspect of studies addressing the chemical composition of high temperature aerosols is the temperature dependence of the particle-phase/gas-phase distribution. Many health-relevant semi-volatile organic compounds, such as the polycyclic aromatic hydrocarbons (PAH) which predominately are particle-bound under ambient conditions, are formed and are present in the gas-phase within the hot combustion flue gas. In order to analyse the organic gas-phase composition on-line mass spectrometric (MS) techniques using soft ionisation technologies can be applied. Unlike in aerosol mass spectrometers such as the AMS, ATOFMS or more sophisticated, experimental aerosol mass spectrometric devices which are addressing the particle-phase composition, the particles need to be precipitated before analysis in gas phase mass spectrometers. This usually is performed by hot-gas filtration at e.g. 250-300 °C (note that this has the advantage, that the collected filter samples can be off-line analysed for the PM composition [1], see also Figure 1). The transfer line to the mass spectrometer and the MS inlet then are heated at least to the same temperature as the filtering unit in order to avoid new particle formation during sampling due to condensation and nucleation effects. Two soft ionisation technologies for MS are particularly well suited to on-line analyse molecular combustion products. On the one hand, the laser based resonance-enhanced multiphoton ionisation (REMPI) method selectively ionises aromatic compounds [1], partially with extreme efficiency. On the other hand, single photon ionisation (SPI) with vacuum ultraviolet photons allows a universal ionisation of organic compounds (but at lower efficiency) [2]. In the case of REMPI-MS, PAH profiles can be detected if combustion aerosols form e.g. wood combustion [1,2] or car exhaust [3] are analysed. However, if pyrolysis gases or un-burnt fuel vapour are sampled, other compound profiles are getting dominant. In the case of wood combustion, e.g., phenolic compounds, stemming from the decomposition of lignin, are characteristic. Aliphatic molecules, however, are not addressed by the REMPI ionisation method. If SPI-MS is applied, the aliphatic compounds are visible too. In the case of un-burnt fuel (gasoline of diesel) the alkanes and naphtenes are detectable while the SPI-MS analysis of wood gasification gas shows celluloses decomposition products (carboxylic compounds, furane derivatives etc.) as well as the phenol from the lignin decomposition.

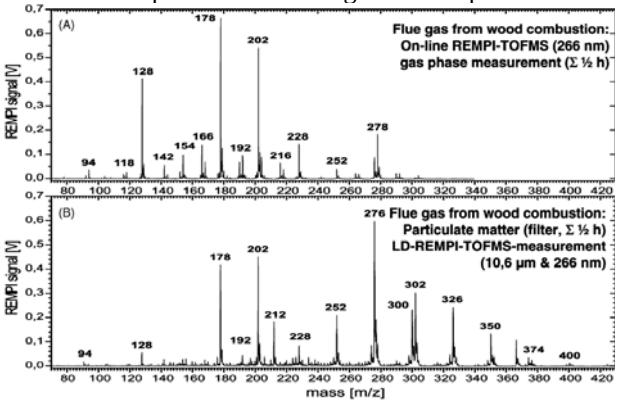

Figure 1: REMPI mass spectra from wood combustion gas-phase (on-line REMPI-MS measurement) and from the filter used for hot-gas particle precipitation (off-line, laser desorption-REMPI-MS) [1].

In addition to the gas phase compounds simultaneously the particle size distribution (e.g. by SMPS, ELPI etc.) as well as the particle chemistry (aerosol mass spectrometry, e.g. AMS, ATOFMS or LD/REMPI-ATOFMS[4] shall be on-line measured. Here totally different sampling approaches are required. This is in particular true as most particle measurement technologies are not capable to handle the hot aerosol directly. If the high-temperature properties shall be addressed the hot aerosol is diluted rapidly first with hot air then with ambient temperature air in order to "stabilize" the aerosol composition. Alternatively a dilution tunnel system is applied which, however, causes larger changes of the aerosol properties due to e.g. condensation effects but is reflecting the "chimney-near" properties of the emissions. In the contribution primarily REMPI/SPI-MS and size distribution results from wood combustion/pyrolysis and car exhaust (dynamometer) measurements are discussed.

[1] Hauler et al., J.Chrom. A **1058** (2004) 39–49
[2] Ferge et al., Envion.Sci.&Technol. **39** (2005) 1393-1402
[3] Adam et al., Anal.Chem. **83** (2011) 67–76
[4] Bente et al., Anal.Chem. **80** (2008) 8991–9004

High-Temperature extraction of aerosol particles from biomass combustion and gasification

M. Strand[1], E. Gustafsson[1], L. Lin[1], and J. Yang[1,2]

[1]School of Engineering, Linnaeus University, Växjö, 351 95, Sweden
[2]Technology and Management, Gjøvik University College, Norway
Keywords: Aerosol characterization, Combustion aerosols, High temperature aerosols.
Presenting author email: michael.strand@lnu.se

During biomass combustion and gasification, aerosol particles are formed from various mechanisms. In order to establish these mechanisms as well as to control and monitor the process operation, particles can be extracted from the hot reactor and then characterised. Most methods for analysing hot aerosols require cooling before feeding to the instruments. The hot gas contains both organic and inorganic species that will condense as the gas is cooled, and these species must be separated from the gas in order to avoid distortion of the PM sample. At gas temperatures above 600ºC vapours from alkali and heavy metals may be present in the gas from both combustion and gasification. Biomass gasification also produces heavy tar components that condense below 400 ºC

In order to enable characterisation of PM in the hot gas from combustors and gasifiers, a sampling system has been developed (Figure 1.). The system includes a two-stage separation unit. In the first stage the gaseous alkali and heavy metals are separated during cooling by guiding the condensation towards the internal surface of the probe. In order to improve the operation of the separation unit the vapour pressure is reduce before cooling by dilution with hot air/nitrogen at the probe tip. In the second stage the tar is removed through sequential cooling and adsorption by activated carbon. Downstream the sampling system the PM characterised using a battery of aerosol instruments. The system is described in detail by Gustafsson *et al* (2007).

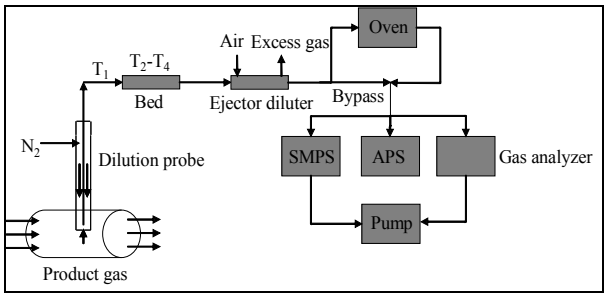

Figure 1. Schematic view of the sampling system and the battery of aerosol instruments.

The sampling system was used in order to characterise aerosol particles in the producer gas from three different types of pilot scale biomass gasifiers at a gas temperature of 500-850 °C. The aerosol was characterised using an electric mobility analyser (SMPS model 3080, TSI Inc.), a time of flight instrument (APS model 3321, TSI Inc.), a low pressure cascade impactor (DLPI, Dekati inc.) and an electric low pressure impactor (ELPI, Dekati Inc.). Figure 2 shows the coarse mode particle mass size distribution obtained from the APS/ELPI data, assuming spherical particles with a density of 1000 kg/m^3. The results have been corrected for losses in the two-stage separation unit but not for the remaining probe and dilution system. The elementary and morphology analyses of the DLPI samples showed that the particles from the three gasifiers had different origin. PM from the BFB gasifier was dominated by char, the PM from the CFB gasifier was dominated by bed material, and the PM from the indirect gasifier was dominated by fly ash.

The tar adsorption capacity of the second stage of the separation unit was evaluated by re-heating the aerosol stream at 400°C in an electric oven. The aerosol size distribution obtained from the CFB gasifier did not change substantially when passed through the oven, which indicates that the PM was tars had been successfully removed. When reheating the aerosol stream from the indirect BFB the PM in the sub-micrometer size range changed, indicating that the tar separation unit was not operating satisfactory in this case.

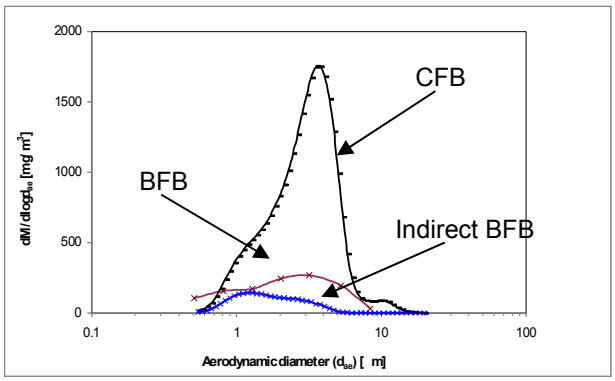

Figure 2. Estimated mass size distribution

The tar adsorption capacity of the separation unit was evaluated in the laboratory using a gas containing a model tar compound (Gustafsson and Strand, 2010). The removal efficiency of the first stage of the separation has been evaluated (Strand et al, 2005). The unit is presently being investigated in detail and the new results will be presented.

Gustafsson E, *et al*, (2007) *Energ Fuel* **21**, 3660–3667.
Gustafsson E and Strand M. (2010) *Energ Fuel* **24**, 2042–2051.

Strand *et al*, (2004) Aerosol Sci Tech, **38**, 757-765.

Porous tube diluting probe for high temperature sampling of aerosols

O. Sippula[1], J. Ruusunen[1], T. Koponen[1], M. Ihalainen[3,1] and J. Jokiniemi[1,2]

[1]University of Eastern Finland, Department of Environmental Science, Fine Particle and Aerosol Technology Laboratory, P.O. Box 1627, FI-70211 Kuopio, Finland.
[2]VTT Technical Research Centre of Finland, Fine Particles, P.O. Box 1000, 02044 VTT, Espoo, Finland
[3]PSI Paul Scherrer Institut, The Laboratory for Thermal-Hydraulics, CH-5232 Villigen PSI, Switzerland
Keywords: Aerosol sampling, Combustion aerosols, Nucleation mode, Aerosol modelling, Alkali metal.
Presenting author email: Olli.Sippula@uef.fi

In order to get experimental data on the aerosol formation and transformation inside the high temperature systems a quench-diluting sampling system has been developed. In this system, the sample is quenched, by rapidly decreasing temperature and concentrations, to freeze the chemical reactions, particle agglomeration and, at the same time, to prepare the sample suitable for different analyzers. However, in many cases, for example due to the large amount of condensable vapours in the samples, considerable changes in the samples cannot be avoided. Thus, a reliable sampling from the hot process gas is usually challenging.

The aim of this work was to study the porous tube diluting probe for high temperature sampling of aerosol. For testing the probe two different high temperature aerosols were generated. First, the high temperature probe was used on conditions typical in biomass-fired boilers. Secondly, the probe was used for sampling inside the high temperature nanoreactor. The sampling system in this study is similar to the porous tube diluting probe used previously in combustion studies (Sippula et al., 2008).

The experiments were carried out with laboratory reactors where synthetic aerosols were generated by chemical vapour synthesis. The first aerosol consisted of principal components present in biomass combustion aerosol (KCl and K_2SO_4). KCl vapour was supplied into the reactor, using a saturator. K_2SO_4 particles were produced inside the reactor by supplying controlled amounts of SO_2 and H_2O gases into the reactor. The amount of K_2SO_4 formed was tracked by measuring SO_2 and HCl concentrations using an FTIR analyzer (Gasmet). In the second experiments, iron oxide nanoparticles were produced using iron pentacarbonyl as a precursor material.

In both reactors the aerosol sample was drawn into the porous tube diluting probe at temperatures varying from 300 to 750 °C. The sampling point was varied. After the porous tube diluting probe the secondary dilution was conducted in an ejector diluter. The diluted samples were analyzed for particle size distributions using Nano-SMPS (TSI) and FMPS (TSI). To get information on the conditions inside the diluter, axial profiles of sample temperature and mixing with the dilution air were measured. The mixing was measured by moving a thin probe at the centreline of the diluter and measuring the marker-gas (CO_2) concentrations. The experimental results were interpreted using a 1D sectional model (Backman et al., 2002) which solves numerically the particle size distribution and particulate chemical composition, given by nucleation, condensation, coagulation and surface reactions.

The measurements showed a relatively fast mixing and cooling in the porous tube (Fig 1). The particle size distributions were sensitive to sampling conditions, as expected. The experimental results and simulations agreed well showing that the condensing vapours tend to nucleate in the probe at high cooling rates despite of high concentrations of seed particles.

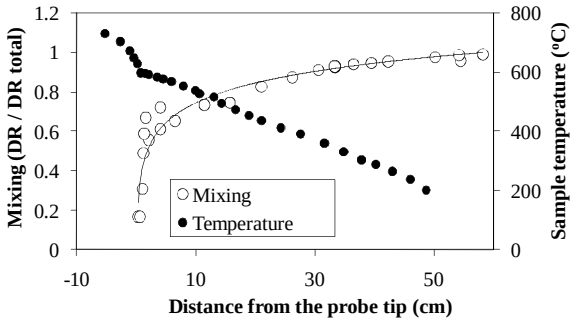

Figure 1. Measured mixing and temperature profiles in the diluting probe.

The separation of condensing vapours and particulates during high temperature sampling would be important for the interpretation of the results. The used sampling probe was found to favour the formation of nucleation mode with high cooling rates. The used 1D aerosol dynamics model was found to be useful for pre-evaluating different sampling probe constructions and to select optimal sampling conditions.

Research has been supported by the strategic funding of the University of Eastern Finland and the European Community's Seventh Framework Programme (FP7/2007-2013) under grant agreement n° 211464.

Sippula, O., Lind, T. & Jokiniemi, J. (2008). *Fuel*, 87, 2425-2436.

Backman, U., Jokiniemi, J. K., Auvinen, A., Lehtinen, K. E. J. (2002). *J. Nanoparticle Research*, 4, 325-335.

The effect of dilution and cooling on the chemistry and structure of samples from stainless steel and Al welding fumes

C. Gutierrez-Canas, M.L. Marroquin, M.L. Larrion, G. Aragon, I. Mugica, E. Pena and J.A. Legarreta

Department of Chemical & Environmental Eng., University of the Basque Country, Bilbao, 48013, Spain
Keywords: welding fumes, nanostructure, dilution, cooling.
Presenting author email: miren.larrion@ehu.es

For different toxic potentials (Antonini *et al*, 2004) have been postulated for coarse and submicron to nanoparticle size range, a crucial aspect of welding fumes is the variability of the morphological and chemical characteristics within a rather small area from the electrode tip. SEM/TEM analyses together with real-time size distributions as well as elemental analysis of bulk samples have been chosen as core experimental method. This methodological approach is consistent with that of (Moroni *et al*, 2009) although special consideration of the differences depending on the aerosol history has been made. Therefore, it focuses on the spatial differences of chemical, structural and size distribution parameters of welding fumes.

Experiments consist of 8-hour periods of welding operation. For emission dynamics is variable, real-time size analysis of size distribution was accomplished by means of an APS3321 (TSI), an ELPI (Dekati) and a WPS (MSP). Samples for SEM/TEM analysis were taken using a MOUDI (MSP) and a NAS (TSI). Sampling positions were chosen as representative of the inhaled aerosol, of the primary emission (thus close to the arc and exhaust flow) and finally of the working place environment. Temperature and gas composition (FTIR) data allow dilution and cooling estimates.

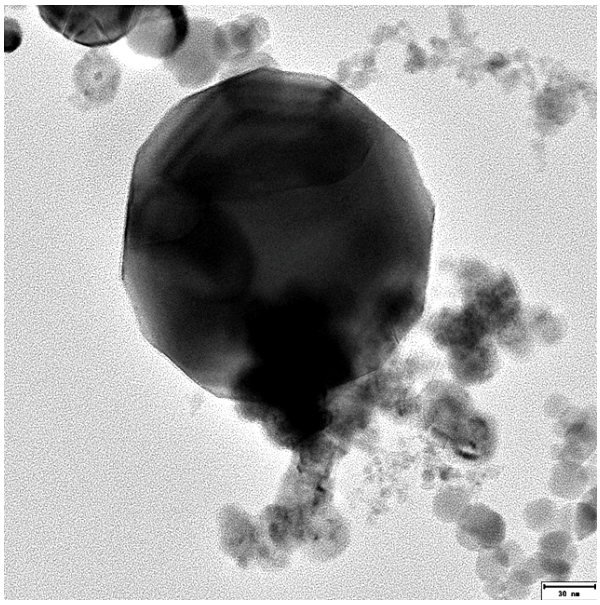

Figure 1 Freshly nucleated AISI 308 stainless steel aerosol. Primary particle size of magnetite and Ni-rich dendrites.

Primary particles of SS fume are almost spherical, whereas larger crystals rich in magnetite evolve to euhedral shapes, showing a increased contribution of Cr, Mn and Ni as particle size increases. SAED spots of high intensity and sharpness indicate high crystallinity of primary particles. The final result of cooling and dilution depends on the reaction mechanisms, the O2 availability and, on the non-measurable interfacial conditions (as a result of combined heat and mass transfer). The map of observed complex structures will be defined on the basis of aerodynamic diameters, thus, classifying di spinel-like oxides formed during cooling, core-shell structures and agglomerates of magnetite-like particles. Twinning of magnetite-rich structures is shown as dependent of the dilution and cooling history.

In contrast, although expected due to Al high stacking fault energy, neither twins nor dislocations were observed, although core-shell structures account for up to 20% of 40nm particles.

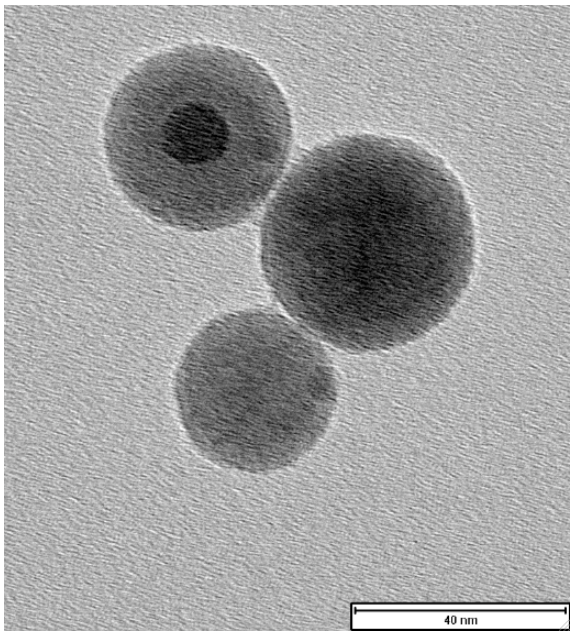

Figure 2. Freshly- to medium-aged Al aerosol. The Al nanoparticles appear as spheres from 20 to 40 nm.

The Basque Government under NANOSOL2009 grant supported this work.

Antonini J.N., Taylor M.D., Zimmer A.T. and Roberts J.R. (2004) *J. Tox. Environ. Health* **67**, 304-310
Marr, J. and Morrissey, S. (2010) *Phys. Rev. Lett.* **210**, 123-126
Moroni B., and Viti, S. (2009) *Aerosol Science* **40**, 938-949

Wednesday, September 7, 2011

Session 7D: Particle-Lung deposition and Pharmacological Aerosol

Producing Drug particles for Inhalation via Electrospray

C.U. Yurteri and J.C.M. Marijnissen

Delft University of Technology, Delft, 2628 BL, The Netherlands

Keywords: Electrospray, Inhalation, Micro Droplets, Nanoparticles

Presenting author email: c.u.yurteri@tudelft.nl

Drug delivery by the inhalation route is a non invasive and historically one of the oldest methods to administer drugs and fight several lung diseases such as asthma, emphysema, bronchitis, and chronic obstructive pulmonary diseases. As new types of drugs based on proteins, peptides, and DNA are developed, inhalation routes are considered to be used for insulin delivery, cancer treatment, pain control, and nanotherapeutics (Yurteri et al. 2010). What makes pulmonary administration in general an advantageous route to deliver therapeutics is the ease of administration, rapid onset because of the area available for permeation to cells and the blood stream, smaller doses administered compared to the oral administration route, and better efficacy to safety ratio compared to systematic delivery. Use of nanoparticles, in addition, could improve release properties in the lung (Sung et al. 2007). However, the success of administration depends greatly on the performance of the delivery device, the size distribution of the delivered particles, the lung state of the patient, and the coordination between device and patient. These aforesaid merits and needs in the pharmaceutical industry has lead into many developments in inhalation devices such as nebulizers, metered dose inhalers, and dry powder inhalers, and quest for novel delivery devices. Advantages and disadvantages of these devices are discussed in books and reviews such as by Hickey (1996), Gradon and Marijnissen (2003), and Geller (2008). The electrospray technique has the ability of producing monodisperse aerosols with a controlled and predetermined droplet size and therefore it resolves particles size distribution related issues in conventional inhalers and is a perfect technique to produce aerosols for drug inhalation (Geerse and Marijnissen 2003). We will present a state of art review of use of electrosprays for inhalation.

Yurteri C.U., Hartman R.P.A., and Marijnissen J.C.M., 2010, “Producing Pharmaceutical Particles via Electrospraying with an Emphasis on Nano and Nano StructuredParticles - A Review”, KONA Powder and Particle Journal No.28, pp. 91 – 115

Sung, J.C., Pulliam, B.L. and Edwards, D.A., 2007, “Nanoparticles for drug delivery to the lungs”, Trends in Biotechnology, 25 (12), pp.563-570.

Hickey, A. J., (Editor), 1996, “Inhalation Aerosols: Physical and Biological Basis for Therapy”, Informa Healthcare.

Gradon, L. and Marijnissen, J. (Editors), 2003, “Optimization of Aeorosol Drug Delivery”, Kluwer Academic Publishers.

Geller, D.E., 2008, “The science of Aerosol Delivery in Cystis Fibrosis”, Pediatric Pulmonary 43, S5-S17.

Geerse, K.B. and Marijnissen J.C.M., 2003, “Electrospray as Means to Produce Monodisperse Drug Particles”, pp.75-90, in Gradon, L. and Marijnissen, J. (Editors), “Optimization of Aeorosol Drug Delivery”, Kluwer Academic Publishers.

Development of an anatomically correct segmented model of the human mouth for deposition studies of the particle and vapour phase of tobacco smoke during inhalation

R.A. Cabot, C.M. McGrath, P.J. Biggs and C.J. Dickens

British American Tobacco, Group R&D, Southampton SO15 8TL, UK
Keywords: Aerosol measurement, Deposition, Inhalation, Respirable aerosols
Presenting author email: ross_cabot@bat.com

British American Tobacco is researching the deposition of smoke particles and vapours in the human respiratory system. An integral part of this research is understanding how smoke ages and deposits in the mouth after puffing. An anatomically correct model of the human mouth has been created to conduct smoke aging and deposition experiments in conjunction with a system that can simulate human puff and inhalation profiles.

The mouth cast geometry was created from a CT (computerised tomography) scan of the mouth of a healthy adult male. Bio-modelling software was used to manipulate the data, increasing the volume of the mouth cavity to better represent the mouth while puffing on a cigarette. A circular aperture was added to the lips with an internal diameter of 8mm to match the diameter of a standard cigarette. The model was divided into three sections representing the mouth, the throat and the trachea down to the first bronchial split. The interface between each section was kept planar for ease of assembly and sealing of the physical model. Matching flanges were added for each interface at each section split, with a groove for an o-ring and integral holes for bolts to secure the sections together.

A physical version of the model was created in Nylon-12 using selective laser sintering, a rapid prototyping technique. Nylon-12 was chosen after spiking and subsequent recovery tests of both solanesol and nicotine were performed on small test disks of the material. Solanesol is a high boiling point alcohol which is regularly used as a marker for the particle phase of tobacco smoke.

The physical model was connected to the in-house developed Puff Inhale Exhale (PIE) simulator, which replicates recorded human smoking profiles. This allows smoke to be puffed, aged, diluted during inhalation and deposited in the mouth cast.

A range of measurements can be taken during an experiment, including real-time particle size and concentration, smoke opacity (estimation of smoke mass concentration) and chemical analysis of solanesol and nicotine deposition in the three sections of the cast.

The mouth cast was used in a study of the aging of smoke in the human mouth. An example of a mouth hold only smoking event was selected from a database of measurements recorded during a volunteer smoking study. The measurements included puffing profile, puffed smoke aerosol size and concentration, mouth hold time and exhaled smoke aerosol size and concentration. Cigarettes were smoked in the mouth cast using the selected puffing profiles and associated mouth hold period. After the mouth hold, smoke was flushed from the mouth cast into a differential mobility spectrometer (Cambustion, UK) to measure particle size and concentration of the aged smoke. The size and concentration of the puffed smoke aerosol were measured by re-smoking cigarettes to the same puffing profiles using a smoking cycle simulator (McAughey, 2007) and a differential mobility spectrometer. The experiments were repeated but with mouth hold times set to 1, 2 4 and 8s. All measurements were performed in triplicate.

Coagulation was expressed in terms of growth factor, the increase in the mean particle diameter. A trend of increasing growth factor with increasing mouth hold time and with increasing puffed total particle number was observed (figure 1). The average growth factor for the human measurements was 0.72 compared to 0.38 for the comparable mouth cast measurements. The difference is probably due to geometry of the mouth cast being different to the geometry of the mouth of the human volunteer. The total deposited fraction by particle mass was 65.6% and 58.9% for the human measurements and the mouth cast measurements respectively.

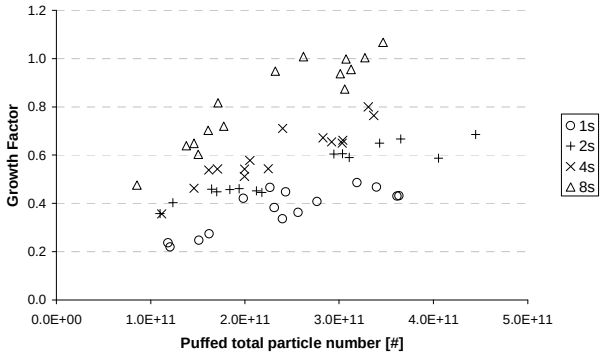

Figure 1. Particle growth factor against puffed total particle number by mouth hold time

The limited data show that the mouth cast can be a useful tool for studying the deposition and aging of cigarette smoke in the human mouth, however differences between the geometry of the mouth cast and the geometry of individual smoker's mouths will produce differences between in vitro and in vivo data.

McAughey, J. (2007) *Puff profile simulator for tobacco smoke particle diameter and mass measurement*, American Association for Aerosol Research 26th Annual Conference, Reno NV.

Pulsating Aerosols for Topical Treatment of Upper Airway Diseases

W. Möller[1], U. Schuschnig[2], G. Khadem Saba[1], G. Meyer[3], M. Keller[2], K. Häussinger[3] and W. G. Kreyling[1]

[1]Comprehensive Pneumology Center (CPC), Helmholtz Zentrum München, Neuherberg, Germany
[2]PARI Pharma GmbH, München, Germany
[3]Department of Nuclear and of Pulmonary Medicine, Asklepios Hospital München-Gauting, Gauting, Germany
Keywords: chronic rhinosinusitis (CRS), topical aerosol therapy, pulsating aerosols
Presenting author email: moeller@helmholtz-muenchen.de

Chronic rhinosinusitis (CRS) is one of the most commonly diagnosed chronic illnesses, and approximately 10-15 % of the European and US population suffer from CRS (Dykewicz *et al.*, 2010). Inflammation of the nasal mucosa due to bacterial, fungal or viral infections, or allergies can lead to CRS. The current approach to treat CRS is a combination of topical and systemic steroids and antibiotics, and in case of failure, functional endonasal sinus surgery (FESS) has been the primary approach for treating CRS. An efficient topical therapy may allow treating upper respiratory diseases more effectively prior or post surgery.

The paranasal sinuses are involved in CRS, they are poorly-ventilated hollow organs; therefore cannot be reached by conventional nebulizers or nasal pump sprays. Gas and aerosol transport into non-actively ventilated spaces can be achieved by diffusion and flow induction by pressure differences, and pulsating airflows can generate such pressure gradients, enabling the possibility of aerosolized drug delivery to the sinuses (Kauf, 1968).

A pulsating aerosol is an aerosol stream superimposed by a pulsation (sound wave). The PARI Vibrent (Pari Pharma, GmbH, Germany), a prototype pulsating aerosol device, was used in all studies. Gamma camera imaging during ^{81m}Kr-gas inhalation was applied to assess the ventilation during pulsating airflow. A pulsating aerosol was generated using ^{99m}Tc-DTPA. The mass median diameter (MMD) was 3.0 µm with a geometric standard deviation of 1.6. For comparison to standard therapies a nasal pump spray aerosol (100µl) was generated (MMD ≈ 60 µm). Nasal deposition, retention and clearance (24 h) were measured using planar gamma camera imaging.

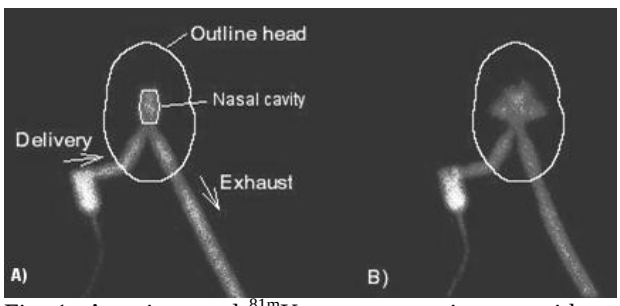

Fig. 1: Anterior nasal ^{81m}Kr-gas gamma images without (w/o, A) and with (w, B) pulsating airflow.

Anterior ^{81m}Kr-gas ventilation images obtained with and without pulsation are shown in Fig. 1. Without pulsation only the central nasal cavity appeared on the image. In addition the delivery system is shows the nebulizer coupled to the right nostril, as well as the exhaust tubing coupled to the left nostril. With pulsation, the maxillary and frontal sinuses appeared on the gamma camera image, showing efficient ventilation (Fig. 1B).

The dominant fraction of ^{99m}Tc-DTPA aerosol is deposited in the central nasal cavity (Fig. 2). With the pulsating aerosol total deposition in the nasal cavity was 69+/-10% of the nebulized dose (Tab. 1) and 7.0+/-2.4% of the deposited activity penetrated to the sinuses (Möller *et al.*, 2010). Delivery of the activity by the nasal pump spray resulted in 100% nasal deposition but less than 1% of the dose penetrated into the sinuses.

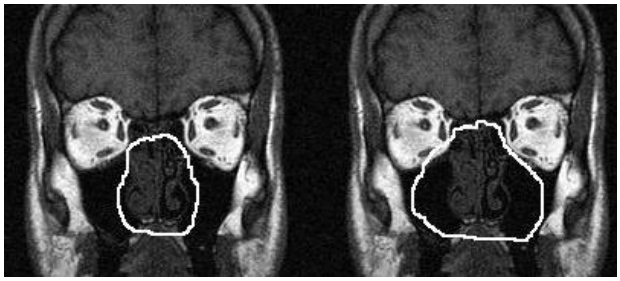
Fig. 2: Illustration of the nasal activity distribution (line at 5% max. activity level) within the MRT-image after pump spray (left) or vibrating aerosol (right) delivery.

Table 1: ^{99m}Tc-DTPA aerosol deposition and retention.

	Pump spray	Pulsat. aerosol
Total aerosol depos.	100%	69+/-10 %$^{++}$
Sinus aerosol depos.	< 1 %	7.0+/-2.4 %**
50 % nasal retention	15+/-6 min	55+/-24 min^{++}
25 % nasal retention	1.4+/-1.6 h	4.4+/-2.7 h^{++}

Aerosol delivered by pulsating aerosol was associated with a retarded clearance rate from the nose (Tab. 1), showing longer drug residence time in the nose. Significant amounts of drug can be deposited in the paranasal sinuses during pulsating airflow allowing topical treatment protocols.

The study was supported by Pari GmbH, Starnberg, Germany and by the BMBF (03FPE00028).

Dykewicz, M. S. and Hamilos, D. L. (2010). *J. Allergy Clin. Immunol.* **125**, S103-S115.
Kauf, H. (1968). *Eur. Arch. Otorhinolaryngol.* **190**, 95-108.
Möller, W., et al. (2010). *Otolaryngol. Head Neck Surg.* **142**, 382-388.

Anti-inflammatory and analgesic effect from nanoparticlate non-steroid anti-inflammatory drugs inhaled by male mice

A. A. Onischuk[1], T. G. Tolstikova[2], I. V. Sorokina[2],
A.M. Baklanov[1], V. V. Karasev[1], V. V. Boldyrev[3,4], V. M. Fomin[5]

[1]Institute of Chemical Kinetics & Combustion, RAS, Novosibirsk, 630090, Russia
[2]Institute of Organic Chemistry, RAS, Novosibirsk, 630090, Russia.
[3]Scientific and Education Centre "Molecular design and ecologically safe technologies"
Novosibirsk State University, 630090, Russia.
[4]Institute of Solid State Chemistry & Mechanochemistry, RAS, Novosibirsk, 630090, Russia
[5] Institute of Theoretical and Applied Mechanics, RAS, Novosibirsk, 630090, Russia
Keywords: aerosol drug administration, particle lung deposition, non-steroid anti-inflammatory drugs, mice.

Presenting author email: onischuk@kinetics.nsc.ru

The administration of drugs directly into the respiratory tract has been used in a number of therapeutic area, including treatment of both lung and systemic diseases. The respiration of nano-sized particles gives some advantages with respect to the inhalation of micron-sized ones. First of all, the particles 10 to 20 nm in size deposit to the alveolar region about 4 times more efficiently than those of several microns in diameter. Moreover, the nanoparticles are easily transported across the membranes. In this paper we study the anti-inflammatory and analgesic effects from inhalation of nanopaticulate of non-steroid anti-imflammatory drugs (sodium diclofenac, indomethacin and ibuprofen) synthesized via the evaporation-condensation route. The nose-only exposure chambers were used to determine the lung deposited dose and the particle deposition efficiency as a function of the mean particle diameter (Fig. 2).

The inhalation scheme includes a flow aerosol generator, plastic boxes for mice, filters, diluters, flow control equipment and aerosol spectrometer (Fig. 1). The evaporation - condensation aerosol generator consisted of a horizontal cylindrical quartz tube with an outer heater. Argon flow was supplied to the inlet and the aerosol was formed at the outlet. The particle mean diameter and number concentration were varied in the ranges 3 to 200 nm and 10^3 to 10^7 cm^{-3}, respectively, as measured by an Automatic Diffusion Battery. The Liquid Chromatography and X-Ray Diffraction methods were used to control the particle composition. The nose-only exposure chambers (Fig. 2) were used to determine the lung deposited dose and the particle deposition efficiency (Fig. 3) as a function of the mean particle diameter.

The analgesic effect was estimated in the "acetic acid writhing" test. When studying the anti-inflammatory action, one hour after the aerosol exposure, 0.05 ml of 0.1% histamine solution in water was injected into the subplanar surface of the mouse hind paw. Six hours later the mice were killed by cervical dislocation. Then the mouse's paws were cut off at the ankle joint and weighed. The ratio of the difference in weight between the treated and untreated hind paws to the weight of the untreated hind paw was used as an edema index (Fig. 4).

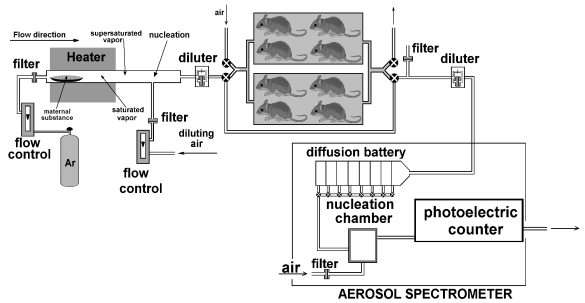

Fig. 1. Experimental set-up for inhalation experiments.

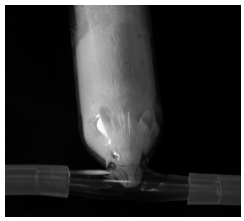

Fig. 2. Nose-only exposure chamber

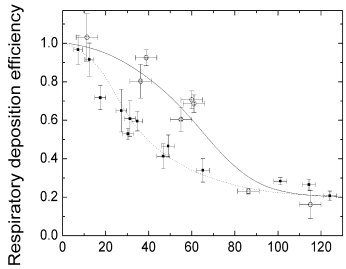

Fig. 3. Mouse respiratory efficiency *vs.* mean particle diameter; circles - ibuprofen, squares - indomethacin nanoparticle inhalation experiments.

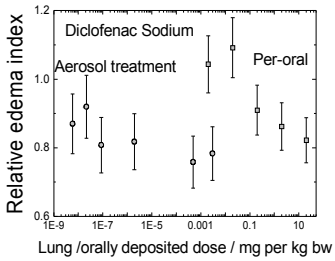

Fig. 4. Relative edema index vs. the lung (circles) or orally (squares) deposited dose.

It was found that the aerosol administration is more effective than the peroral treatment i.e. results in the same analgesic or anti-inflammatory effect even at the lung deposited dose six orders of magnitude less than the per-oral dose.

Financial support for this work was provided by the Siberian Branch of Russian Academy of Sciences (Interdisciplinary Integration Project No. 3).

Carbon Nanotubes – too "big" AND too "small" to deposit efficiently in the lungs?

A. Buckley[1], R. Smith[1], R. Maynard[1]

[1]Health Protection Agency, Centre for Radiation, Chemical, and Environmental Hazards, Chilton, Didcot, Oxfordshire, OX11 0RQ, UK

Keywords: nanotubes, nanoparticle aggregates, exposure, lung deposition

Presenting author email: alison.buckley@hpa.org.uk

Alongside the potential benefits we are likely to gain from the fast-developing field of nanotechnology, there are concerns regarding the possible health and environmental impacts of nanomaterials. High aspect ratio nanoparticles such as carbon nanotubes (CNT) have caused particular concern following the finding of a preliminary study that long (>15μm), relatively straight CNT (Fig 1a) introduced into the abdominal cavity of mice displayed asbestos-like pathogenic behaviour (Poland *et al*, 2008). The effect was, however, not seen with shorter and tangled CNT (Fig 1b).

As part of any assessment of the potential risk posed by inhalation, the behaviour of CNT aerosol particles in the lung needs to be understood, in particular, whether they are likely to deposit in the pulmonary region. This will clearly depend upon the characteristics of the CNT aerosol particles. CNT aerosol particles sampled in research and industrial facilities, while low in concentration, show a wide range of shapes and structures (e.g. Maynard *et al*, 2004; Han *et al*, 2008). These fall into two general categories: dispersed, or lightly agglomerated, 'fibre-like' CNT aerosol particles, which can consist of either individual, or ropes of tubes, with lengths typically < 10 μm; and CNT 'agglomerate' aerosol particles consisting of bent and tangled CNT with physical diameters from a few hundred nanometres up to tens of micrometres.

This paper poses the following questions: "what is the aerodynamic and diffusive behaviour of these 'real' CNT aerosol particles in the lung?" and "what is their expected pulmonary deposition? ". In an attempt to answer these questions, a simplified, theoretical approach to the deposition of CNT in the lungs covering a range of realistic CNT forms, based on those observed in real exposure settings, is presented. To assess the validity of the approach, results have been compared with available experimental data.

Particles are deposited in the lung as a result of leaving the air streams within the airways and coming into contact with the walls of those airways. There are five mechanisms which control this: inertial impaction and sedimentation, which are governed by the particle's aerodynamic diameter; Brownian motion, characterized by the particle's translational diffusion coefficient; electrostatic forces, which are dependent on the particle's charge state; and interception, which is governed by the physical shape and size of the particle in relation to that of the airway.

Aerodynamic and diffusion equivalent diameters have been estimated for a range of 'realistic' CNT aerosol particles. For CNT 'agglomerates', assumed here to be low density spheres, calculations were based on the standard spherical model using Stoke's drag. For 'fibre-like' particles, modelled as straight cylinders, aerodynamic and diffusion equivalent diameters were derived using the drag force on a cylinder given by Asgharian *et al* (1988) and slip correction factor based on Dahneke's (1973) adjusted sphere approach. The impact of cylinder orientation was addressed using the Rotational Péclet Number.

Comparison with experimental measurements of CNT aerodynamic and diffusion diameters has confirmed the validity of this approach.

In the pulmonary region of the human respiratory tract diffusional deposition peaks for particles with diffusion equivalent diameters of around 20 nm and aerodynamic deposition for particles with aerodynamic diameters of approximately 2 μm. While some CNT 'agglomerate' particles, which can be aerosolised in a wide range of sizes, are likely to fall into one of these categories, 'fibre-like' CNT particles, particularly those considered to be 'long', are not expected to be deposited efficiently by either mechanism – being aerodynamically too small to deposit efficiently by impaction or sedimentation but thermodynamically too large to deposit efficiently by diffusion.

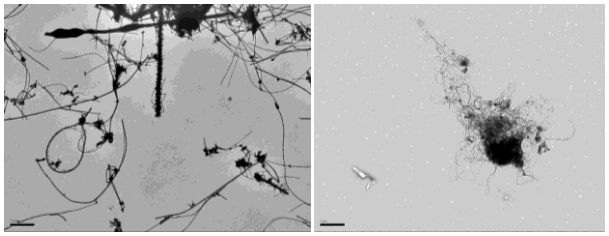

Figure 1. Electron Micrographs of a) 'long', bar = 2 μm and b) 'tangled' CNT particles, bar = 1 μm. Images kindly provided by Dr Craig Poland, IOM.

Asgharian, B. and Yu, C. (1988) *J. Ae. Med*. **1**, 37-50

Dahneke, B. (1973*) J. Ae. Sci*. **4**, 163-170.

Han, J., Lee, E., Lee, J., So, K., Lee, Y., Bae, G., Lee., S., Ji., J, Cho, M. and Yu, I. (2008) *Inhalation Toxicol.* **20**, 741-749.

Maynard, A., Baron, P., Foley, M., Shevedova, A., Kisin, E. and Castranova, V. (2004) *J. Toxicol. Environ. Health* **67**, 87-107.

Poland, C., Duffin, R., Kinloch, I., Maynard, A., Wallace, W., Seaton, A., Stone, V., Brown, S., MacNee, W. and Donaldson, K. (2008) *Nature Nanotech.* **3**, 423-428.

Modelling coagulation of liquid particles within the human respiratory system

L. Pichelstorfer and W. Hofmann

Department of Materials Research and Physics, University of Salzburg, 5020 Salzburg, Austria
Keywords: Coagulation, size distribution, aerosol concentration, human lung
Presenting author email: Lukas.Pichelstorfer2@sbg.ac.at

To assess health risks due to airborne particle exposure, it is necessary to obtain information on regional and local deposition. Since particle diameter is a key parameter of physical deposition mechanisms, the size distribution of an aerosol within the human respiratory tract is an important determinant of particle deposition.

For an aged aerosol with typical low concentrations, the particle diameter may safely be assumed to remain constant (except for phase transition or hygroscopic growth) during the breathing cycle. This, however, is not a reasonable assumption when dealing with fresh aerosols, e.g. cigarette smoke, vehicle exhaust, etc.). Indeed, these systems are highly dynamic and concentrations, diameter and even composition of the particles may vary significantly within fractions of a second. Thus the objective of this work is to develop a numerical model for coagulation of liquid aerosols within the human respiratory tract.

In the present model different types of coagulation have been considered: thermal coagulation drive by thermal motion, kinematic coagulation, including coagulation due to laminar shear flow, turbulent shear flow and settling of the particles. Initially inhaled and newly formed particles are assumed to be spherical.

Table 1. Changes of the primary size distribution due to coagulation during inhalation.

Coagulation type	Change of concentration	Change of average diameter
Thermal	- 83%	1.99 $d_{(t=0)}$
Kin. shear	- 42%	1.03 $d_{(t=0)}$
Kin. turbulent	- 0.5%	1.0001 $d_{(t=0)}$
Kin. settling	-0.7%	1.002 $d_{(t=0)}$
Total	- 89%	2.04 $d_{(t=0)}$

Table 1 presents the relative changes of the primary inhaled aerosol due to coagulation during inhalation, using the cigarette smoke size distribution measured by Keith (1982) with an average diameter of 250 nm, classified into size bins with a width of 5%. The breathing pattern is that of a male under sitting breathing conditions (ICRP, 1994) with an additional 1s residence time of the puff in the mouth and the lung geometry refers to the stochastic lung morphology of Hofmann and Koblinger (1990). For this simulation static aging in the oral cavity, no mixing of the puff with residual air, and no deposition were assumed.

Clearly, thermal coagulation dominates the process at the beginning of the breath. As a result, the number concentration of the smallest particles is reduced to almost zero within fractions of a second. Kinetic shear coagulation starts to contribute from airway generation 9 on, if the puff is not diluted. Relatively large particles trigger this type of coagulation. Turbulent and settling coagulation turn out to have almost no effect on the size distribution for this initial particle diameter and breathing related Reynolds numbers.

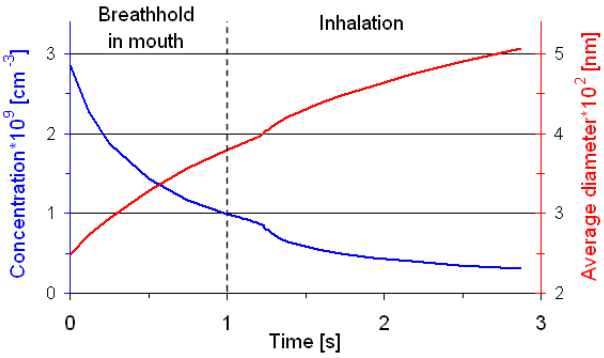

Figure 1. Particle concentration and diameter as functions of inspiratory time.

The time dependent behavior of the number concentration and the average diameter of the size distribution are plotted in Figure 1. Within half a second the concentration declines by a factor 2 marked by a steep slope of the concentration curve. After 1.5 s, the reduction of particle number gets distinctively slower and becomes almost linear. As expected, the average particle diameter increases with the elapsed time. The reason is less the growth of individual particles but the fact that particles adhere to big ones. Subsequently the diameter of the big particles stays almost constant. Since the small size fraction of the distribution is practically removed, the average diameter increases.

This coagulation model will subsequently be implemented into the stochastic deposition model IDEAL (Hofmann and Koblinger, 1990), considering dilution and deposition mechanisms (see companion abstract by Winkler-Heil and Hofmann).

This work was supported by PMI PO under project number 7100192131.

International Commission on Radiological Protection (ICRP) (1994) *Human Respiratory Tract Model for Radiological Protection*. Pergamon Press, Oxford.

Keith, C.H. (1982) *Beiträge Tabakforschung* **11**, No 3.

Koblinger, L. and Hofmann, W. (1990) *J. Aerosol Sci.* **21**, 661-674.

Regional lung deposition of tobacco smoke constituents

J.McAughey[1] and C. Dickens[1]

[1]British American Tobacco, Group R&D Centre, Southampton, SO15 8TL, UK

Keywords: tobacco smoke, deposition, dosimetry.
Presenting author email: john_mcaughey@bat.com

Tobacco smoke is a complex dynamic aerosol suspended in an equally complex vapour cloud, and is a significant elective source of inhaled particles in the population, despite it being a recognized cause of disease. However, little is known of the regional deposition of smoke and local micro-dosimetry from both its vapour and particle phase constituents. Such data offer context to better understand biologically effective dose and potential modes of action of disease initiation, both in model disease systems and populations.

Measured mass deposition efficiencies of the order of 60-80% for particle species are significantly greater than modelled deposition estimates of 30-40% (Baker & Dixon, 2006). Many authors have suggested that the smoke particles must grow significantly to super-micron diameters, to explain observed patterns of disease in the conducting airways, by a combination of coagulation, hygroscopicity, condensation, and colligative 'cloud-like' behaviour (e.g. Robinson, 2001, Broday, 2003). Others have suggested evaporative losses with increased pulmonary deposition of the smaller residual particles by diffusion (Ingebrethsen, 2006, Kane, 2010).

In this work, a series of measurement tools have been developed to assess deposition by direct measurement of exhaled particles and vapour by electrical mobility spectrometry and selective photo-ionisation time-of-flight mass spectrometry respectively. Measured smoking patterns are then replicated to produce intake estimates with deposition calculated by difference.

In addition, hybrid Computational Fluid Dynamic – Pharmacologically Based Pharmacokinetic models (CFD-PBPK) have been developed to assess local deposition in the upper airways and subsequent systemic uptake; initially for volatile aldehyde species.

Soluble vapour species such as acetaldehyde and acrolein show near 100% retention from modelling and measurement data but particle deposition is significantly lower and related principally to inhalation depth and inhalation cycle time. Particle diameter may also have a role but this may be better reflected by a modified diameter reflecting ageing in the mouth, principally via coagulation, rather than the diameter of fresh smoke. However, consideration of all ageing and growth / evaporation processes of the smoke predict it will remain sub-micron and this is confirmed by size measurements of volume- weighted median diameters of approximately 250 – 350 nm for exhaled smoke.

Thus, a majority of particle mass deposition is calculated to occur in the deep lung via diffusion. However, higher local airway particle and vapour doses occur in the upper airways driven by the smaller surface areas available for deposition. Calculated regional values for particle (tar) deposition as ng.cm^2 of lung surface (per mg tar delivered by the cigarette) are 409 (ET – extra-thoracic), 45 (BB – bronchial), 4.8 (bb – bronchiolar) and 0.1 (AI – alveolar). Transformations of size and concentration data allow equivalent number and surface-area weighted regional deposition to be calculated.

In conclusion, new insight has been gained into local dosimetry of tobacco smoke constituents in the lung through measurement and modelling. Both soluble vapour and particle deposition are driven principally by diffusion processes. Local dose remains highest in the upper airways through the relatively smaller airway surface available for deposition.

Further refinement of deposition and CFD-PBPK models will offer an improved approach to quantitative risk assessment. This will derive from the provision of improved relative dose assessment for *in vitro* models of disease applied to smoke exposure and the a combined dosimetric and mechanistic approach to assessing the impact of technologies designed to reduce selective toxicant dose from smoke.

Baker RR and Dixon M. The Retention of Tobacco Smoke Constituents in the Human Respiratory Tract. Inhalation Toxicology 2006 18, 255-294.

Broday DM and Robinson RJ. Application of cloud dynamics to dosimetry of cigarette smoke particles in the lungs. Aerosol Sci. Technol. 2003 37, 510-527.

Ingebrethsen BJ. Numerical Simulation of the Effects of Dilution Level, Depth of Inhalation, and Smoke Composition on Nicotine Vapor Deposition During Cigarette Smoking. Inhalation Toxicology 2006 18, 1071-1076.

Kane DB, Asgharian B. *et al.* Effect of smoking parameters on the particle size distribution and predicted airway deposition of mainstream cigarette smoke. Inhalation Toxicology 2010 22, 199-209.

Robinson RJ and Yu CP. Deposition of Cigarette Smoke Particles in the Human Respiratory Tract. Aerosol Sci. Technol. 2001 34, 202-215.

Wednesday, September 7, 2011

Session 7E: New Developments in Aerosol Instrumentation

A Novel IOSH-NCTU Personal Nanoparticle Sampler

C. J. Tsai[1,*], S. M. Huang[1], C. N. Liu[1], S. N. Uang[2] and S. C. Chen[1]

[1]Institute of Environmental Engineering, National Chiao Tung University, Hsin Chu, Taiwan
[2]Institute of Occupational Safety and Heath, Council of Labor Affairs, Taipei, Taiwan

Keywords: personal nanoparticle sampler; respirable cyclone; nanoparticle impactor.
Presenting author email: cjtsai@mail.nctu.edu.tw

At present, there are no active personal sampling devices to assess the exposure levels of workers to engineered nanoparticles (NPs). To meet the demand, a novel IOSH-NCTU personal nanoparticle sampler (IOSH-NCTU PNS) was designed and tested. The PNS operates at 2 L/min with a pressure drop of 125 cm H_2O by a SKC XR 5000 pump. The present PNS was calibrated for the collection efficiency curve by both liquid and solid particles. The effect of heavy particle mass loading on performance of the PNS was also evaluated. For assessing its sampling accuracy, the measured RPM and NPs concentrations by the PNS were compared with those of a collocated MOUDI.

As shown in figure 1, the PNS consists of a respirable cyclone and a micro-orifice impactor (137 55 μm nozzles) in series for classifying respirable particulate matter (RPM) and NPs, respectively. The impaction plate is rotated by a stepper motor to deposit particles uniformly on the substrate, and the substrate is coated with silica oil to prevent solid particle bounce. After the micro-orifice impactor, a 37 mm teflon filter is used to collect NPs. The sampler is light weighted (250 g) and compact (H-10.5 cm, D- 6.3 cm), which is suitable for personal wearing.

Calibration results show that the cutoff aerodynamic diameter (dpa_{50}) of the respirable cyclone and the micro-orifice impactor is 3.98±0.1 μm and 101.4±0.1 nm, respectively. The ratio of jet to plate distance and nozzle diameter (S/W) with the S/W of 13.8. A decreasing S/W from 16.2 to 3.13 in the micro-orifice impactor results in a decreased dpa_{50} from 111 to 72.5 nm. The particle loading tests reveals that the PNS has a maximum loading of 0.65 mg with a less than 5 % shift of dpa_{50} and a negligible solid particle bounce. It was found that the change of the pressure drop was less than 5 cm H_2O after heavy particle loading and the RPM and NPs concentrations agreed well with those of the MOUDI. Therefore, the IOSH-NCTU PNS sampler is capable of assessing personal exposure levels of RPM and NPs in workplace.

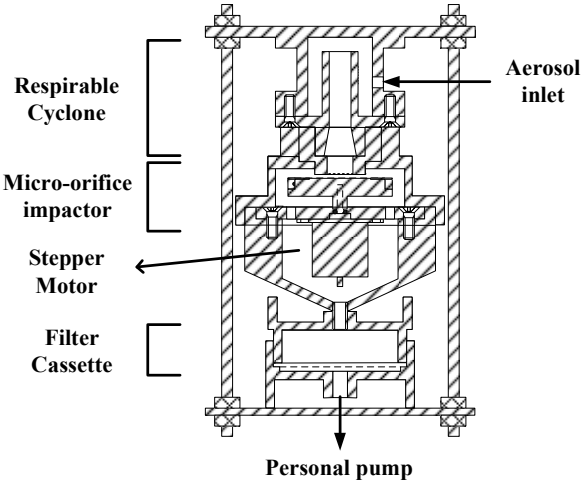

Figure 1 Schematic diagram of the IOSH-NCTU PNS.

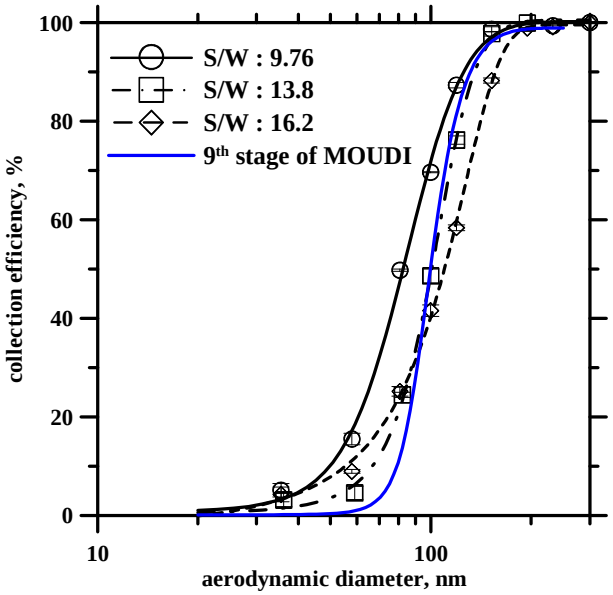

Figure 2 Calibration results of the present micro-orifice impactor.

Portable real-time detection of airborne asbestos fibres for tradespersons

C. J. Stopford, P. H. Kaye, E. Hirst, R.S. Greenaway, and W.R. Stanley.

Centre for Atmospheric & Instrumentation Research, University of Hertfordshire, Hatfield, U.K.
Keywords: asbestos, spatial light scattering, magnetic alignment
Presenting author email: c.stopford@herts.ac.uk

Asbestos has been widely used as a building material due to its many desirable physical properties – thermal resistance, tensile strength, etc. However, asbestos fibre inhalation, especially of the amphibole varieties such as crocidolite and amosite, causes serious health problems. Tradespersons working in environments where asbestos is present are at particular risk of disturbing and inhaling fibres, and asbestos inhalation remains the leading cause of occupational deaths in Europe.

Identification of airborne asbestos is usually performed *ex situ* by collecting a sample of filtered aerosol and subsequently performing extensive manual fibre counting from microscopic examination or EDAX (Energy Dispersive Spectroscopy). Whilst instruments do exist for the real-time detection of airborne *fibre* particles (eg: MIE Fibre Monitor Model FM-7400, Mie Inc., Billerica, Mass.), these are generally incapable of differentiating between asbestos fibres and other airborne fibres that may be present, such as gypsum, glass, etc. Currently, there is no reliable real-time *in situ* technique specifically for the detection of airborne asbestos fibres. The authors' present work seeks to develop a relatively low-cost real-time detector for airborne asbestos fibres that may be routinely used by tradespersons to reduce inadvertent exposure to asbestos dust.

Previous research at the University of Hertfordshire has established that airborne particles may be detected and classified according to their morphology by analysis of their spatial light scattering patterns (eg: Kaye *et al*, 1996). Fibres are particularly well suited to this type of classification (Kaye *et al*, 1997) due to their distinctive scattering patterns (Figure 1), and indeed, information relating to the fibre size and aspect ratio, required for accurate assessment of the inhalation risk, may also be extracted from the patterns.

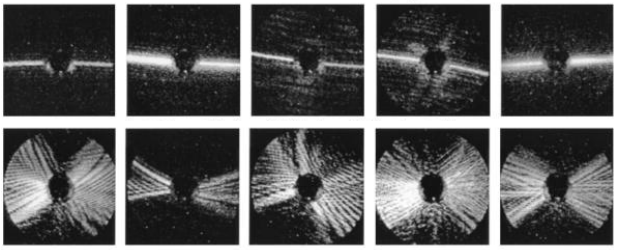

Figure 1. Spatial light scattering patterns from individual crocilodite (top) and chrysotile (bottom) asbestos fibres.

In order to differentiate asbestos fibres from non-asbestos fibres of similar morphology, the authors' present work seeks to combine the spatial scattering analysis technique with a process that exploits the magnetic anisotropy of asbestos fibres (Ulanowski and Kaye, 1999). By preferentially aligning all fibres in a sample flow and subsequently applying a magnetic field to the flow, discrimination of asbestos fibres from all other fibres maybe achieved by detecting the re-orientation suffered by the asbestos fibres alone.

A prototype laboratory system will be described in which a test aerosol is drawn by a sample pump through a specially designed optical scattering chamber. The sample aerosol enters the chamber at a rate of approximately 500 ml. min^{-1} via a laminar flow inlet tube that preferentially aligns fibre particles towards the axis of the flow. In trials with gypsum fibres (used as a non-hazardous analogue for asbestos) this configuration aligns more than 80% of fibres to within 10 degrees of the flow axis.

Rare earth magnets aligned at 45° to the flow axis (thus producing maximum torque on any asbestos fibres present) are positioned below the exit of the aerosol inlet tube. In principle, asbestos fibres carried in the airflow are re-oriented toward the field lines and well beyond the distribution of orientations exhibited by non-asbestos fibres. A laser beam orthogonal to the flow axis illuminates particles as they pass through the region of maximum magnetic field strength and the light scattered by individual particles is detected by two linear 512 pixel CMOS arrays. A small amount of scattered light is also reflected via a beam-splitter to a photodiode responsible for triggering data capture from the arrays.

High speed algorithms have been developed to analyse the CMOS array data and enable rapid identification of fibres from a high concentration of other dust particles. Further computation is performed to determine the angular orientation of each fibre, together with metrics relating to fibre size and aspect ratio based on comparison with theoretical data using the RTDF model (Hesse, 2008). Preliminary experimental results and analysis will be presented on the performance of this novel approach to real-time airborne asbestos fibre detection.

Acknowledgement: This research is supported under the EU FP7 project 'Alert', No. 243496

Hesse, E., (2008) *J. Quant. Spectrosc. Ra.,* **109**, 1374-1383

Kaye, P.H., Alexander-Buckley, K., Hirst, E., and Saunders, (1996) S., *J. Geophys. Res.* **101**, 19,215-19,221.

Kaye, P.H., Hirst, E., and Wang-Thomas, Z (1997) *Appl. Optics* **36**, 6149-6156

Ulanowski, Z. and Kaye, P.H. (1999) *J. Appl. Phys.* **85**, 4104-4109.

The Transfer Function and the Resolution of a DMA with Multiple Monodisperse Outlets: Sensitivity Analysis for the Case with the Two Monodisperse Particle Outlets

M.Giamarelou[1] and G. Biskos[1,2]

[1]*Department of Environment, University of the Aegean, Mytilene 81100, Greece*

[2]*Faculty of Applied Science, Delft University of Technology, Delft 2628-BL, The Netherlands*

Keywords: MMO-DMA, Dual-DMA, transfer function, resolution.
Presenting author email: giamarel@env.aegean.gr

DMAs are widely used in aerosol research as a tool for sizing and for producing monodisperse airborne particles having diameters in the submicron and nanometer ranges (Flagan, 1998; McMurry, 2000). Since the 1970's when the DMA was realized to be ideal for aerosol particle size classification in the submicron range (Liu and Pui, 1974; Knutson and Whitby, 1975), many single-outlet designs have been proposed and built for improving its performance. DMAs with multiple monodisperse outlets can significantly reduce the scanning time when employed in aerosol spectrometers because particles of different mobility can be classified and detected simultaneously. In addition, depending on the relative location of the first and the last outlet from the inlet, one can increase the dynamic mobility range of the selected particles in a single measurement.

In this regard, Takenchi *et al*. (2005) designed a dual-type DMA in order to measure particles having diameters within a wide size range. Chen *et al*. (2007) designed and built a DMA having three monodisperse exits for fast measurements of particle size distributions. Despite these experimental attempts, to the best of our knowledge, there is no theoretical study providing the transfer function or the resolution of DMAs with more than one monodisperse outlets.

In this paper, following Stolzenburg (1988) approach, we derive the expression of the non-diffusional transfer function of Mulitple Monodisperse Outlet (MMO) DMAs, and extend it to take into account particle diffusivity. When including particle diffusivity, the derived transfer function of the i^{th} sample exit of the MMO-DMO is shown to be:

$$\Omega_{d_i} = \frac{\sigma_i}{\sqrt{2}\beta_i(1-\delta_i)}\left\{-\mathcal{E}\left(\frac{\bar{Z}_{p_i}-(1-\beta_i\delta_i)}{\sqrt{2}\sigma_i}\right)+\mathcal{E}\left(\frac{\bar{Z}_{p_i}-(1-\beta_i)}{\sqrt{2}\sigma_i}\right)\right.$$
$$\left.+\mathcal{E}\left(\frac{\bar{Z}_{p_i}-(1+\beta_i)}{\sqrt{2}\sigma_i}\right)-\mathcal{E}\left(\frac{\bar{Z}_{p_i}-(1+\beta_i\delta_i)}{\sqrt{2}\sigma_i}\right)\right\}, \quad (1)$$

where σ_i is the standard deviation of Ω_{d_i}, $\bar{Z}_{p_i}$ is the dimensionless particle mobility, and β_i, δ_i are dimensionless flow parameters. We further derive a general form for the resolution of the MMO-DMA, using the method proposed by Flagan (1999), and show that this can be described by:

$$\mathcal{R}_{diff_i} = \frac{1}{2\sqrt{2\ln 2}\,\tilde{\sigma}_i} = \frac{1}{2\sqrt{2\ln 2}}\left[\frac{Pe^*_{mig_i}}{G_i}\right]^{1/2}, \quad (2)$$

where $\tilde{\sigma}_i$ is the dimensionless standard deviation, G_i is a geometry parameter, and $Pe^*_{mig_i}$ is the particle migration Peclét number. Finally, we employ our models to optimize the design of a DMA with two monodisperse outlets, namely the Double Monodisperse Outlet (DMO) DMA. Selected plots of the transfer function for the optimum DMO-DMA design are shown in Figure 1.

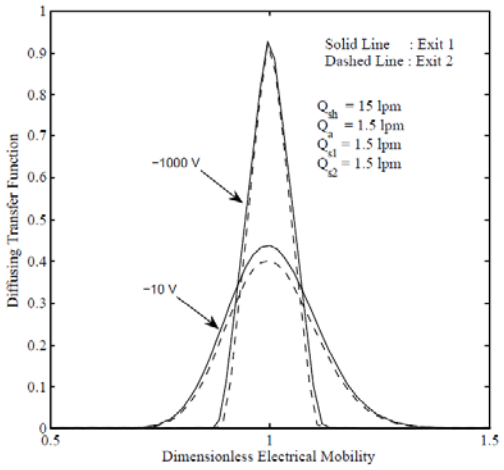

Figure 1. Transfer Function of the DMO-DMA for which the first sample exit is located at distance 44.369 cm downstream the inlet, while the second at distance 4.987 cm. The outer radius of the apparatus is 1.961 cm and the inner radius is 0.937 cm.

References

Chen, D.R., Li, W. and Cheng, M.D. (2007) *Aer. Sci. & Technol.* ***41****, 217-230.*

Flagan, R. C. (1998) *Aer. Sci. & Technol.* ***28***, 301–380.

Flagan, R.C. (1999) *Aer. Sci. & Technol.* ***30***, 556 – 570.

Knutson, E.O. and Whitby, K.T. (1975) *Aer. Sci*, ***6***, 443 – 451.

Liu, B.Y.H. and Pui, D.Y.H. (1974) *J. Colloid Inter. Sci.* ***47***, *155 –171.*

McMurry, P.H. (2000) *J. of Atm. Env.* ***34***, 1959 – 1999.

Takeuchi, K., Yabumoto, J., Okada, Y., Kawai, T., Montajir, R. M. and Goto, Y. (2005) *J. Nanoparticle Res.* **7**, 287–293.

Stolzenburg, M.R. (1988) *An Ultrafine Aerosol Size Distribution Measuring System*, Ph.D. Thesis, University of Minnesota, MN.

Development and Characterization of a Novel Approach for Water-Based Condensation Growth of Aerosols

Aaron M. Collins[1], William D. Dick[1], Benjamin Y. H. Liu[1] and Francisco J. Romay[1]

[1]MSP Corporation, Shoreview, Minnesota, 55126, United States of America
Keywords: Instrumentation, CPC, CFD
Presenting author email: fromay@mspcorp.com

Condensational growth is commonly used in Condensation Particle Counters (CPC) to provide the necessary particle enlargement to detect particles smaller than 1 µm using conventional light scattering techniques. Traditionally, laminar thermally diffusive methods of condensation particle growth have relied on butyl alcohol and other fluids with similar thermodynamic properties.

In traditional laminar diffusive methods a hot, vapor-laden aerosol is introduced into a cold wall condenser where, due to a Lewis number greater than unity, a central core of high-supersaturation ratios provides the necessary activation for condensational growth of nanometer-sized particles (Stolzenburg et al. 1991).

Because water vapor in air has a Lewis number less than unity, the regions of high supersaturation form near the walls in a traditional laminar diffusive approach. This results in reduced particle growth and activation when water is used as the working fluid (Hering et al 2005).

We have developed a new growth method to generate sufficient supersaturation conditions with a traditional hot to cold thermal approach. The Single Flow Mixing (SFM) method (patent pending) results in the turbulent mixing of a hot, water-vapor-saturated aerosol stream in a cool mixing chamber to produce supersaturation values sufficient for nanoparticle growth. The geometry consists of an inlet placed perpendicular to a tapered cylinder. The inlet flow impinges on the cylinder wall resulting in turbulent mixing within the device as shown in Figure 1.

Using a commercially available Computational Fluid Dynamics (CFD) software package, a 3D fluid model was developed for the flow geometry. Parameters investigated were the flow, temperature and vapor profiles generated by the SFM method. Further computations were performed to determine Kelvin diameter and expected particle growth rates.

Measurements of particle activation were performed using DMA-classified aerosol in the 5 to 40nm size range. A Faraday Cup Electrometer (FCE) was used as the reference concentration measurement, whereby combined with the CPC count data, provide a measurement of counting efficiency. Material effects were also investigated using both hydrophobic and hydrophilic particle materials to ascertain the influence of hydrophobicity in the SFM method of condensation growth.

Figure 2 shows the counting efficiency for both Ag (hydrophobic) and NaCl (hydrophilic) particles as function of electrical mobility diameter. As expected, the counting efficiency decreases with deceasing particle diameter with a measured cutpoint (dp_{50}) of 4.6nm for the NaCl test data. The measured cutpoint for the Ag test data is 9.8nm. The observed effect of particle hydrophobicity on the measured counting efficiency is consistent with the work of Hering et al.(2005), Stratmann et al.(2009) and Mordas et al.(2008).

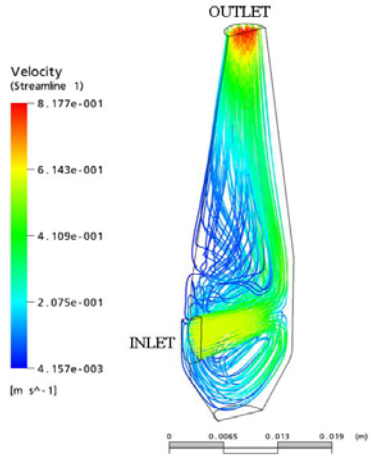

Figure 1
Flow Geometry and Streamlines

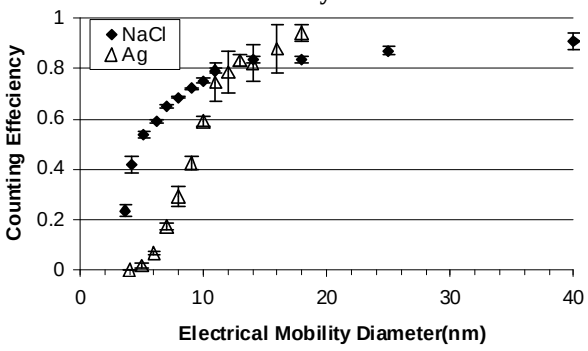

Figure 2
Counting Efficiency for NaCl and Ag Particles

Hering, S., Stolzenburg, M. (2005). *Aerosol Science and Technology*, 39,428-436

Mordas, G.,Mannien H.E., Petäjä, T., Aalto, P., Hämeri;, K., Kulmala M. (2008) *Aerosol Science and Technology*, 42, 152-158

Stolzenburg, M., McMurry, P. (1991). *Aerosol; Science and Technology*, 14, 48-65

Stramann F., Herrmann, E., Petäjä, T., Kulmala M. (2009) *Atmospheric Measurement Techniques Discussion*, 2, 2217-2239

Comparison Testing of Model 3783 Environmental Particle Counters

M. Gälli[1], K. Erickson[1], F. Quant[1], R. Caldow[1], S. Morell[1], J. Kolb[1], B. Osmondson[1], E. Pickens[1]

[1]TSI Incorporated, Shoreview, MN, 55126, USA
Keywords: CPC, Instrument development, Monitoring, Environmental particles
Presenting author email: markus.gaelli@tsi.com

Newly developed instruments need to be thoroughly tested before they can be made commercially available. As part of the development of a second generation of water-based CPCs, the TSI Model 3783 Environmental Particle Counter (EPC) was designed for long-term environmental monitoring of particle number concentration. Comparison testing of these instruments provided the unique opportunity to run up to 12 EPCs alongside other new and existing water-based CPCs (Models 3781, 3787, 3788) for more than 40 days. This provided the opportunity for multiple studies, including: 1) long-term correlation between instruments; 2) challenging the instruments with different water sources and different wick materials; and 3) testing the probability of random failures and determining a statistical confidence level.

The EPC counts single particles in the range from 7 nm (D_{50}) to above 3 µm, with a concentration range of up to 10^6 particles cm^{-3}, using exclusively single-particle counting. A sample flow rate of either 0.6 or 3.0 l min^{-1} can be chosen. Data can be collected with a sampling rate of up to 1 s^{-1} in a number of ways:

- TSI's Aerosol Instrument Manager (AIM) software
- Ethernet
- USB storage device
- USB or RS232 output to an independent data collection system (e.g. LabView)
- Analog output

During the test period, all available instrument information was collected once per minute. This included particle concentration, counts, instrument parameters such as temperature measurements and pressure readings, as well as a number of diagnostic readings.

For the long-term instrument comparison, the instruments ran for more than 40 days uninterrupted, first sampling room air, then ambient air through a PM_{10} inlet. A custom-built sampling manifold was attached to the inlet through ~8 meters of 1" stainless steel pipe. All instruments were drawing air from the manifold through conductive tubing. The tested instruments ran without any serious issues, and compared very well between each other. Instrument comparability was tested by linear regression analysis of the concentration measurements of the different instruments. Both the slope and regression coefficient R^2 give an indication of the quality of the comparison. Instruments were typically well within the ±10% specified. A typical correlation plot between two EPC instruments is shown below.

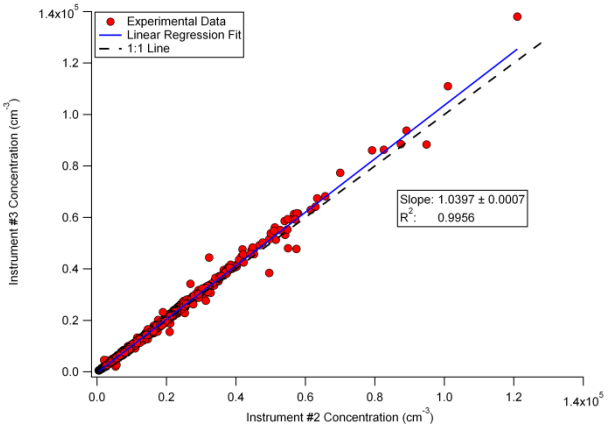

Instruments were tested with a number of different wick materials and with water of different qualities (e.g. distilled water, tap water, etc.). The instruments were challenged with both indoor and outdoor air, and were subjected to a number of real-world conditions, such as water deprivation to test the ability to recover from these incidents.

Particle concentrations and pulse heights were monitored continuously, with the pulse height providing an indication of the condition of the instrument. The figure below shows a typical graph from one instrument. The relatively flat value of the pulse height measurement indicates that the system is operating well and. The momentary drops in pulse height are due to increased particle concentrations, which lower the supersaturation in the growth tube. Although there are momentary drops in pulse height, values are still well above the threshold warning level, indicating that the instrument is counting normal.

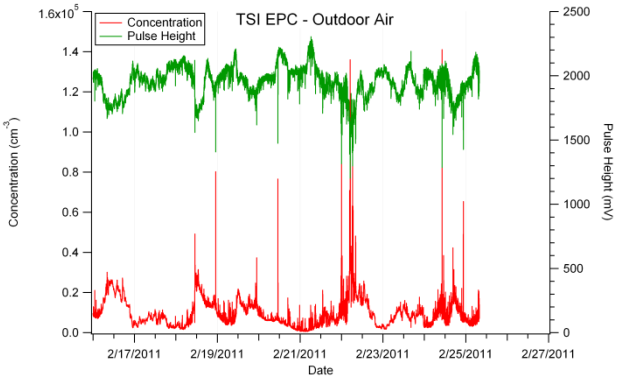

These tests illustrate the capabilities of the Model 3783 EPC for long-term monitoring. The instruments have been shown to run autonomously for at least a month, providing accurate particle concentration measurements with high time resolution.

A Novel Optical Real Time Sensor for Radioactive Aerosol

Soohyun Ha[1], Chirag K. Vyas[2], Atul Kulkarni[3], Vijay K. Manchanda[2] and Taesung Kim[1, 3]

[1]SKKU Advanced Institute of Nano Technology, Sungkyunkwan University, Suwon, 440-746, Korea
[2]Department of Energy Science, Sungkyunkwan University, Suwon, 440-746, Korea
[3]Department of Mechanical Engineering, Sungkyunkwan University, Suwon, 440-746, Korea

Keywords: Radioactive Aerosol, SSNTD film, Optical fiber, Reflectance.
Presenting author email: sean0125@skku.edu

Release of radioactive aerosols is an important health and environment issue associated with the nuclear power industry, and the manufacture and use of nuclear weapons. High levels of naturally-occurring radioactive aerosols, particularly from decay products of radon gas, can pose a pollution problem at indoor locations such as mines and houses (Stephen D. Schery, 2001). Therefore, radioactive aerosol measurement sensors have been developed for reducing the damage of environment and workers exposed to radioactive aerosol and detecting unexpected air pollution.

Common method of measuring the activity concentration of atmospheric radioactive aerosol particles is to collect them on a filter by drawing a known volume of air through the filter. The activity deposited on the filter is then measured, often in a second step following completion of sampling. A filter may be manually removed from the collection instrument and taken to a detector for counting (Otto G. Raabe, 2007). Another method is Solid State Nuclear Track Detectors. When a heavily ionizing charged particle passes through detectors, it leaves a narrow trail called 'Latent Track' as it cannot be seen with the naked eye. It is possible to view this latent track with an electron microscope (D. Nikezic, K. N. Yu, 2004). However, these methods for measuring radioactive aerosol are not satisfied in real-time radiation detector because these need a sampling process and counting equipment. In consequence, a newly designed radiation measurement sensor is required for real-time detection of radioactive aerosol.

An optic fiber which consists of a scintillator have been developed for real-time detection of radioactive aerosol but this method needs photomultiplier tube (PMT) (K.W. Jang *et al* (2010)), hence it is complicated and not cost effective. To simplify the available methods, we developed a novel real-time radiation measurement sensor by utilizing solid state nuclear track detectors and optic fiber for the first time.

Figure 1 shows the schematic of experiment set-up. Using atomizer, we generated radioactive aerosol from aqueous radioactive. The radioactive aerosol passes through the chamber where optical fiber probe with solid state nuclear tracks detector (SSNTD) film is installed. Due to interaction of the nuclear aerosols, the SSNTD films changes its optical properties casing change in the reflected signal back in to the fiber. Similar type of fiber optic sensors is reported earlier in our group for aerosol sensing (Atul Kulkarni *et al* (2010)). The change in the reflected light is proportional to the radiation. The preliminary results were encourging. Also, theoretically we can estimate the radiation intensity by knowing radioactive aerosol numbers. Further, we can establish the relationship between number of radioactive particle and radiation by using condensation particle counter (CPC). Hence, the proposed method is simple, safe (remote measurement is possible) and can detect the radioactive aerosols in real time.

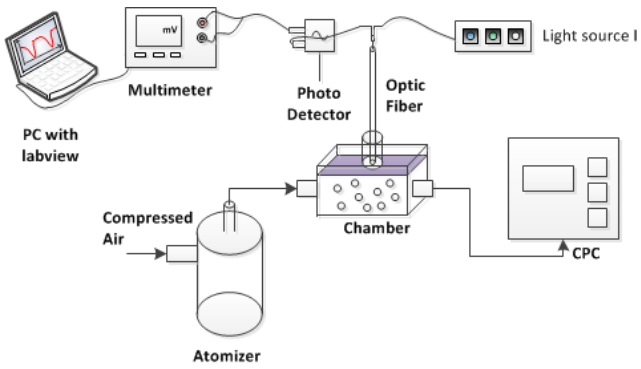

Figure 1. Schematic of experiment set-up

This work was supported by the National Research Foundation of Korea (NRF) grant funded by the Korea government (MEST) (No. 2010-0018784)

Stephen D. Schery (2001) *Understanding Radioactive Aerosols and Their Measurement*, Kluwer Academic Publishers

Otto G. Raabe (1972) *IEEE Transactions on Nuclear Science*, v.19, n.1, 64-75

D. Nikezic, K. N. Yu (2004) *Materials Science and Engineering R* ***46*** , 51-123

K.W. Jang, D.H. Cho, W.J. Yoo, J.K. Seo, J.Y. Heo, J.Y. Park, B. Lee (2010) *Nuclear Instruments and Methods in Physics Research A*

Atul Kulkarni, Jun-Ho Lee, Jae-Do Nam, Taesung Kim (2010) *Sensors and Actuators B* **150**, 154-159

Direct integration of a GPS/GPRS unit into a miniature diffusion size classifer

M.Fierz, P.Steigmeier, M.Glettig, B.Wyrsch and H.Burtscher

University of Applied Sciences Northwestern Switzerland, 5210 Windisch, Switzerland
Keywords: instrumentation, air quality network, personal sampling.
Presenting author email: martin.fierz@fhnw.ch

We have recently developed a miniaturized version of the diffusion size classifier (miniDiSC, Fierz et al. 2011). It can measure particle number concentration, average particle diameter and lung-deposited surface area with a one-second time resolution. It operates on a purely electrical basis, with a unipolar charger followed by two electrometer stages, i.e. there are no working fluids or radioactive sources. The instrument is about the size of a multimeter, and thus one of the smallest aerosol instruments available today, which makes it ideal for personal monitoring.

For personal monitoring, it is useful to record location information with a GPS. While a separate GPS receiver can be used with any instrument, it is a bit cumbersome to operate because the data of instrument and GPS have to be combined manually. We have therefore integrated a GPS receiver directly in the miniDiSC. Furthermore, we also added a GPRS chip to transmit data from the instrument to a server in the internet in real time. The transmitter board measures 60x80mm and can easily be accommodated in a slightly larger housing than the standard miniDiSC housing (45mm thickness instead of 40mm).

Data is transmitted by the miniDiSC to a TCP server located in the internet, which stores the data in an SQL database. A standard 3-tier-architecture (Database, web-application, browser) is used to view the data in near-realtime (about 5 seconds delay) in any internet browser. Figure 1 shows an overview of the measurement network structure. The instruments also transmit status information besides the measurement data. This allows for a quick overview of the status of all deployed minidiscs (see Figure 2), which is useful when running a measurement campaign - problems with the instruments can be detected and resolved easily during the campaign.

Data can be displayed as real-time chart or as table or downloaded as delimited text file or as a Google Earth file. The Google Earth download is perhaps the prettiest way of visualizing the data (see Figure 3).

In conclusion, we have developed an enabling technology to easily collect and view data of the miniDiSC online. We anticipate that this will be useful for measurement campaigns, both for personal monitoring and for stationary measurements.

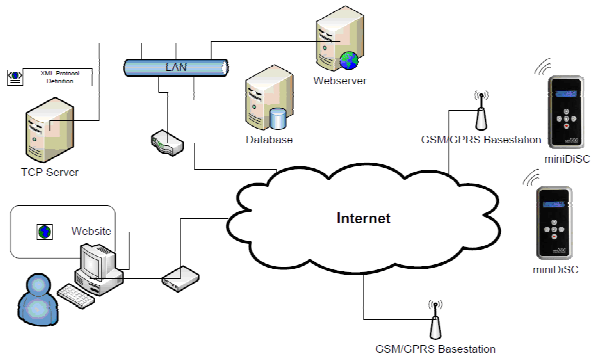

Figure 1: Structure of the miniDiSC measurement network.

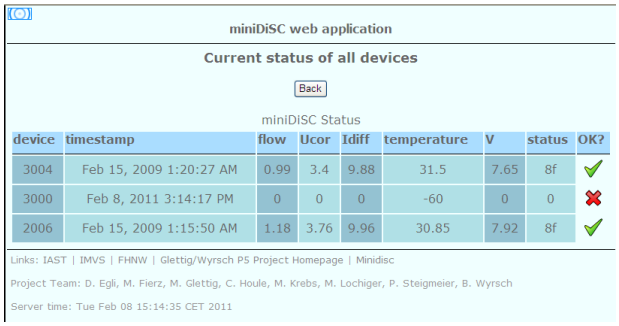

miniDiSC web application

Current status of all devices

Back

miniDiSC Status

device	timestamp	flow	Ucor	Idiff	temperature	V	status	OK?
3004	Feb 15, 2009 1:20:27 AM	0.99	3.4	9.88	31.5	7.65	8f	✓
3000	Feb 8, 2011 3:14:17 PM	0	0	0	-60	0	0	✗
2006	Feb 15, 2009 1:15:50 AM	1.18	3.76	9.96	30.85	7.92	8f	✓

Links: IAST | IMVS | FHNW | Glettig/Wyrsch P5 Project Homepage | Minidisc

Project Team: D. Egli, M. Fierz, M. Glettig, C. Houle, M. Krebs, M. Lochiger, P. Steigmeier, B. Wyrsch

Server time: Tue Feb 08 15:14:35 CET 2011

Figure 2: Monitoring the network status

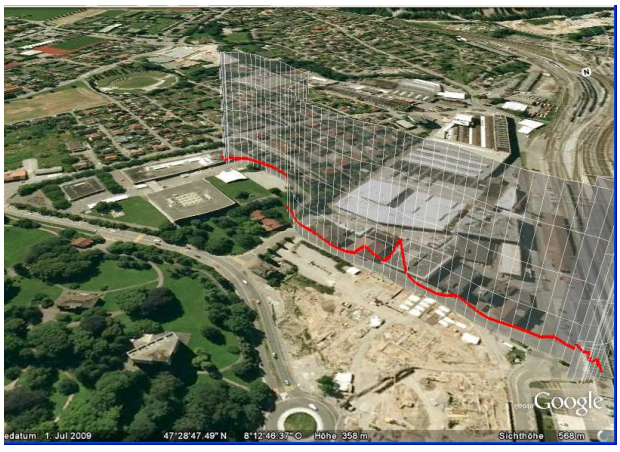

Figure 3: Display of data and location in Google Earth.

This work was supported by Forschungsfonds Aargau.

Fierz, M., Steigmeier P., Houle C. and Burtscher H. (2011) *Aerosol Science and Technology*, **45**, 1-10.

Wednesday, September 7, 2011

Session 7F: Modelling Nuclear Particles and Health Effects

Nuclear aerosols in primary circuit and containment: a review of the Phebus experiments

A.V. Jones[1] and R. Zeyen[2]

[1]4A Dukes Lane, London, W8 4JL, UK
[2]Institute for Energy, European Commission Joint Research Centre, PO Box 2, NL-1755 ZG Petten, Netherlands
Keywords: nuclear aerosols, aerosol modelling, high temperature aerosols, particle deposition.
Presenting author email: alanxispra_alt@yahoo.co.uk

The Phebus FP severe accident experiments FPT0 and FPT1 were performed at IRSN Cadarache (France) in 1993 and 1996 respectively. In each test, Fig. 1, a 1 m long bundle of fuel rods encircling a silver indium cadmium control rod was heated to an advanced state of degradation in the Phebus reactor, and the materials released were swept by an injected steam flow through a model circuit and into a miniature PWR containment vessel. Test FPT0 used fresh fuel, while in FPT1 the fuel had a typical mid-life burnup of 23 GWd/tonne. Conditions were non-reducing throughout. The circuit included a hot section and a cooler inverted U-tube (wall temperatures 700 C and 150 C) with diameter typical of a steam generator tube. The containment vessel, which had a volumetric scaling factor of 5000, was designed primarily for the study of chemistry but included facilities for condensing the incoming steam and collecting deposits so that the main containment aerosol phenomena could be investigated.

In an international effort coordinated by the European Commission Joint Research Centre and IRSN intensive analysis of the circuit and containment has been performed using a variety of models and codes, seeking to reconcile and comprehend the wide variety and copious quantity of online and post-test data available. Both integral (multi-volume) codes widely employed in reactor safety analysis and more detailed codes have been applied with alternative models of aerosol processes to help evaluate uncertainties. This paper makes a critical survey of the degree of success achieved and draws conclusions as to where understanding can be considered good and where it appears necessary to perform further experimental and analytical work, factoring in both findings from other tests of the Phebus FP series and from other experimental programmes.

Some conclusions for the FPT0/FPT1 circuit include the fact that deposited caesium is in dynamic equilibrium with the carrier stream and may constitute a late radiological source in the event of an accident, that at the temperature of the “hot” section of the circuit most elements are transported as an aggregated aerosol, which may be adequately treated as single-component, and that predicted aerosol deposition in the steam generator tube, mostly by thermophoresis, is roughly double the experimental value, Fig.2. The explanation may be resuspension, which experimentally was found to occur under Phebus conditions, although it was not predicted by code models. The circuit chemistry of iodine and of caesium is complex and interlinked, and cannot be predicted by codes with fixed chemistry. Codes with dynamic chemistry have had some success but require further verification. A radiologically significant fraction of transported iodine is in gaseous form at the circuit outlet. This fraction is sensitive to the source from the degrading bundle as a function of time, and at present cannot be reliably calculated.

Concerning the containment, a single-component treatment of the aerosol behaviour appears adequate in Phebus conditions, which were dry. Single-volume codes predicted aerosol removal quite well. Experimental data were inadequate to distinguish between removal by diffusiophoresis and that by settling. CFD calculations have helped explain details of the aerosol deposition not predicted by the containment codes.

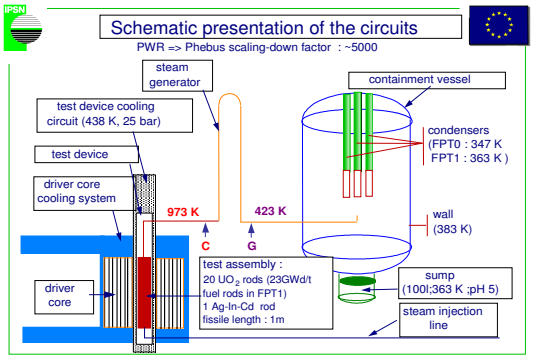

Figure 1. Schematic of Phebus experiments FPT0 and FPT1 showing aerosol source, circuit and model containment vessel with internals

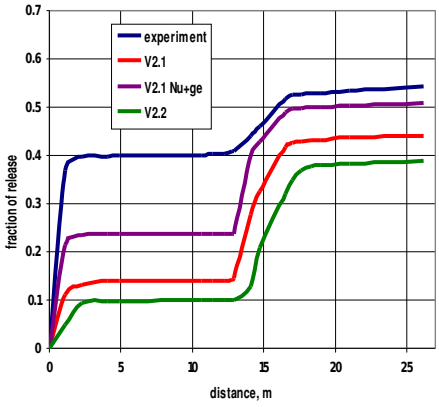

Figure 2. Exerimental and calculated deposition profiles of Molybenum along the circuit in FPT1

Bujan, A. et al. (2010) Interpretation of the Phebus FPT0 and FPT1 circuit results. *Nuclear Technology* **169**, 1-17.
Clement, B., Haste, T. (2004) ISP-46: Phebus FPT1 integral experiment on reactor severe accidents. *Nuclear Energy Agency* NEA/CSNRI/R(2004)18.

Uncertainty Analysis of Aerosol Retention in the Break Stage of a Vertical Steam Generator under SGTR Accident Conditions

López del Prá C., Herranz L. E.
Unit of Nuclear Safety Research, CIEMAT, Avda. Complutense 22, 28220 Madrid, Spain
Keywords: retention efficiency, severe accident, nuclear power plant, SGTR.
Presenting author email: claudia.lopez@ciemat.es

During reactor operation, a variety of phenomena may degrade the primary-to-secondary barrier of a pressurized water reactor up to the point of causing tube ruptures. In the highly unlikely event of a core meltdown, such a tube ruptures would result in a radioactivity ingress in the secondary side. These scenarios are generally termed Steam Generator Tube Ruptures (SGTRs). The radioactive discharge into the secondary side is assumed not to be retained to any extent, so that all the material escapes to the environment. However, even in the most severe case of total absence of water in the secondary side, a fraction of the particles released may get trapped onto the tube surfaces of the secondary side of the steam generator.

A sound and comprehensive database on the aerosol behaviour in the secondary side of a steam generator has been generated within the international EU-SGTR (Auvinen et al., 2005), ARTIST (Güntay et al., 2004) and the current ARTIST-II projects. Concurrently, a theoretical work has been undertaken at CIEMAT to develop theoretical tools for estimating the aerosol retention in the secondary side. In particular, it has been developed a model ARI3SG, focused on the break stage of the SG that estimates the collection efficiency (η_{TB}) under the most severe conditions of absence of water:

$$\eta_{TB} = \frac{m_{dp}}{m_{in}} \qquad (1)$$

ARI3SG is based on a filter approach and takes into account through empirical correlations the most important underlying aerosol phenomena that are present in the scenario: inertial impaction, turbulent deposition and resuspension (Herranz et al., 2007).

The comparison of its predictions with the experimental data SGTR and CAAT have shown a good quantitative and qualitative consistency (López del Prá et al, 2010). Following the data trends, the model indicates collection efficiencies within the lower range (≤20%). However, given the ARI3SG approach, the empirical nature of the equations embedded and the requested input parameters, the ARI3SG estimates are forcefully affected by uncertainties of different kinds. Here two categories are distinguished: epistemic and stochastic uncertainties. The former comes from an incomplete knowledge of the system, not from its nature but from the limitation of our ability to model it (i.e. wrong modeling, measurement errors, etc), therefore they can be reduced. The later arise from the natural random variability inherent to the system itself, they can be more accurately characterize but not reduced. Different methodologies can be applied for their analysis: stochastic, deterministic, UMAE, CSAU, response surface among others. In the present work, the experimental ISO norm (1995) has been followed and the performance of ARI3SG given the random dispersion of the governing model equations has been assessed. According to the law of propagation, each phenomena uncertainty has been analytically propagated through the model.

Fig 1 shows that consideration of these uncertainties brings most of predictions and data within the resulting uncertainty band. The bands that vary estimates around 38% and 62% of the SGTR and CAAT cases respectively, overlap half of the experimental uncertainty range. The different lengths in both sets of uncertainty bands might be due to the different weight that each phenomenon involved has on each scenario, which might arise from the slight differences of the modeling of the initial and boundary conditions.

In the near term it is foreseen to extend the current model uncertainty assessment of ARI3SG to consider the effect of input variables uncertainties as well. To do so, the stochastic methodology will be applied to the ARI3SG input variables (i.e., density, velocity and particle size).

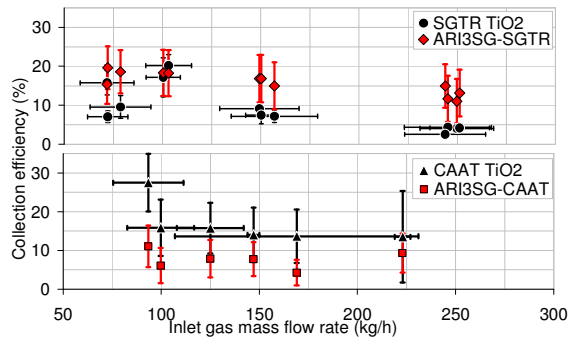

Fig 1. Exp. SGTR-CAAT and Theor. ARI3SG results.

This work has been financially supported by the Spanish Nuclear Council in the frame of the International ARTIST project.

Auvinen, Jokiniemia, Lähde, Routamo, Lundström, Tuomistb, Dienstbiec, Güntay, Suckow, Dehbi, lootmane, Herranz, Peyres, Polo (2005) Nucl Eng Des, 235, 457-472.

Güntay, Suckow, Dehbi, Kapulla (2004). Nuc Eng Des 231, 109-120.

Herranz, Del Prá, Dehbi (2007). Nuc Tech 158, 83-93.

ISO (1995). Guide to the Expression of Uncertainty in Measurement. Int. Org. for Standardization, Switzerland.

López del Prá C., Herranz L.E. (2010). *Proc. International Aerosol Conference*, Helsinki.

Multilayer deposition and resuspension studies of aerosol particles between periodic steps in turbulent channel flows

M.Lustfeld[1], T. Barth[2] and M. Banowski[2]

[1]Professur Wasserstoff- und Kernenergietechnik, Institut für Energietechnik, Technische Universität Dresden, 01062 Dresden

[2]Institut für Sicherheitsforschung, Helmholtz-Zentrum Dresden-Rossendorf, Bautzner Landstraße 400, 01328 Dresden, Germany

Keywords: Carbonaceous particles, deposition, High Temperature Reactor, periodic steps, resuspension
Presenting author email: martin.lustfeld@tu-dresden.de

Radioactive carbonaceous aerosol particles deposit within the primary circuit of a high temperature reactor (HTR). These particles can pose a considerable threat if resuspended by a shock wave in the case of an unlikely loss-of-coolant accident and partially released into the environment (Kissane, 2009).
Stempniewicz et al. (2010) carried out simulations of the spatial and temporal development of carbonaceous dust deposits in the primary circuit of a HTR. Maximum dust layer thickness after full operation time of 60 years was well above *10 mm*. However, the underlying multilayer models require additional experimental verification.
Therefore, particle deposition and resuspension experiments of multilayer graphite deposits have been conducted in a small-scale test facility. The results for particle layer thickness have been correlated to corresponding flow data as measured by means of a 2C2D Particle Image Velocimetry (PIV) system.
The experimental facility consists of a ventilated square duct (*d = 100 mm*), which is operated with air at ambient conditions. The average air velocity can be regulated over the range $\langle u \rangle$ = *1..7 m/s*, corresponding to Reynolds numbers between Re_d = *8.9k..42k*. As flow obstacles, periodic steps have been chosen (Fig. 1) allowing the comparison of results with previous studies on monolayer deposition (e.g. Lai et al., 1999).

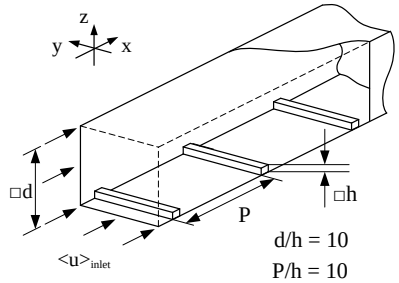

Figure 1. Experimental setup of periodic steps

Graphite aerosol particles (Thielmann Graphite, 23061) have been injected into the duct 15 diameters upstream of the test section by means of a dust disperser TOPAS - SAG 410. Setting the mass flux to *80 g/h* an average mass concentration of airborne particles of up to *2 g/m³* is established. The aerodynamic particle size distribution of the graphite particles was determined by means of a TSI – APS 3321confirming that the particles cover well the range of interest for HTR conditions (quantiles: $d_{P,10}$ = *1.83 µm*, $d_{P,50}$ = *4.40 µm* and $d_{P,90}$ = *10.64 µm)*.
The deposition experiments have been conducted under different flow conditions and the development of graphite particle deposits in the vicinity of the steps has been observed by hourly laser triangulation measurements. Subsequently, the generated multilayer has been resuspended at a higher flow velocity and the thickness of the remaining structure has been measured using the same techniques.

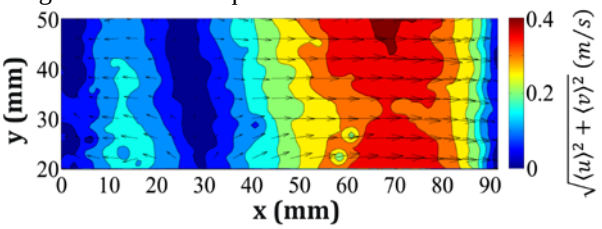

Figure 2. Flow field at Re_d = *8.9k (z=5 mm)*

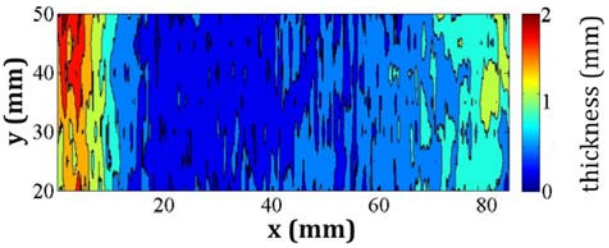

Figure 3. Layer thickness after resuspension at Re_d = *27.2k*

Results show that for a relatively low Reynolds number of Re_d = *8.9k* (Fig.2), deposition is mainly governed by gravitational settling and the deposition rate is almost independent of position and time. On the other hand, subsequent resuspension at higher flow velocities (Re_d *=27.2k*) reveals a strong relation between flow field and remaining layer (Fig.3), which is further being investigated.
This work is supported by the EC (Project THINS, grant agreement no. 249337).

Kissane, M. A. (2009). *Nucl. Eng. Des.* **239**, 3076 - 3091.
Lai, A. C. K.; Byrne, M. A. & Goddard, A. J. H. (1999). *J. Aerosol. Sci.* **30**, 1201 – 1214.
Stempniewicz, M.; Winters, L. & Caspersson, S. A. (2010). *HTR 2010, Prague, Czech Republic.*

Classification of Dust Days over Israel by Integration of Satellite Remote Sensing Products

Sorek-Hamer M.[1], Broday D.M.[1], Levy R.C [2], Cohen A.[3]

[1]Department of Civil and Environmental Engineering, Technion, Haifa, 32000, Israel
[2]NASA/Goddard Space Flight Center, Greenbelt, MD, USA
[3]Department of Industrial Engineering, Statistics Laboratory, Technion, Haifa, 32000, Israel
Keywords: remote sensing, dust, aerosols.
Presenting author email: dbroday@tx.technion.ac.il

Satellite observations have been suggested as a useful and powerful tool for event detection (e.g. volcanic activity, large biomass fires, dust storms, thick haze, etc). In particular, the last decade has shown a considerable progress in satellite remote sensing of dust aerosols. From an environmental health perspective, such an event detection, after linking it to ground PM observations, can proxy acute exposure to respirable particles of certain properties (i.e. size , composition, toxicity). In order to assess such exposures based only on remotely sensed data with sufficient spatiotemporal coverage, one should be able to differentiate between different common types of aerosols, e.g. dust, long range transport (i.e. mainly sulfates in the East Mediterranean), sea spray, local anthropogenic PM emissions, etc.

Being affected considerably by atmospheric dust, previous studies in the Eastern Mediterranean and in Israel in particular, focused on mechanistic and synoptic prediction, classification, and characterization of dust events, partially based on satellite observations. These studies were complemented by mineralogical and chemical characterization of dust particles and of long range PM transported to the East Mediterranean. These studies revealed that days heavily affected by dust, termed here as dust days (DD), are associated with certain synoptic patterns and meteorological conditions (Ganor *et al*, 2010). Hence, these conditions carry with them information on the origin of the dust and therefore its related attributes.

In particular, Ganor *et al* (2009) suggested a scheme for identifying DD in Israel based on ground PM_{10} measurements, validated by compositional analysis. The basic criterion to assess retrospectively a DD is whether at least 3 consecutive hours (6 half hourly readings) of PM_{10} concentrations were above 100 $\mu m/m^3$, with a maximum value of at least 180$\mu m/m^3$.

However, this scheme requires information about ground PM_{10} levels, which is clearly not available in places with limited ground monitoring coverage. In such cases satellite remote sensing (SRS) products may be an efficient and cost-effective alternative to ground measurements, and be used for classification of DD and non-DD (NDD) in environmental health related studies.

This work demonstrates the possibility to identify DD and NDD over southern Israel from merely satellite observations, and suggests a tool for estimating the contribution of dust to ground PM concentrations. Initially, an extension to the scheme suggested by Ganor *et al* (2009) for DD identification has been used. Namely, since dust events are expected to have a considerable spatial scale, the scheme was modified by requiring these criteria to occur simultaneously in at least 3 PM monitoring stations in the study region. Using this modified scheme, we obtained a list of DD and NDD based on ground PM_{10} records in the years 2007-8. These two populations (DD and NDD) have distinct properties, and could be distinguished using other ground measured parameters (i.e. $PM_{2.5}$, RH, etc.) (Fig.1). Next, we analyzed various SRS parameters (AOD, SSA, AE, AAI) from several satellite platforms (MODIS, OMI) for these two populations, to assess the possibility to use them as predictor variables of DD.

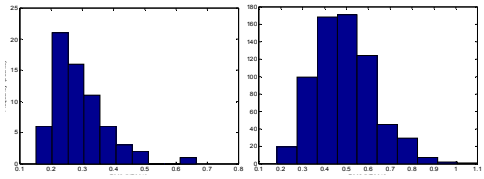

Figure 1. Ratio of ground $PM_{2.5}$ to PM_{10} concentrations in DD (left) and NDD (right).

A classification and regression tree (CART) analysis was used to evaluate interactions between the explanatory variables for predicting DD, followed by a logistic regression to develop a model that will be able to classify DD based on the integration of only SRS data.

The annual average number of model predicted DD is in good agreement with actual observations (Table 1).

Table 1. Comparison of annual average number of DD by ground PM_{10} data and by the logistic model.

Year	1958-2006 Observ.	2007-8 Observ.	Model Predict.
Annual average number of DD (DD/365days %)	20 (6%)	33 (9%)	29 (8%)

We expect this model to enable environmental epidemiologists, as well as ecologists, to distinguish among health/ecological/environmental effects that result from exposure to dust and to non-dust particles on a temporal scale that fits such studies.

Ganor, E., A. Stupp, and P. Alpert (2009) Atm. Env., 43, 5463-5468

Ganor, E., A. Stupp, I. Osetinsky, and P. Alpert (2010) J. Geophys. Res., 115, D11201

Alpert, P., I. Osetinsky, B. Ziv, and H. Shafir (2004) Int. J. Climatology, 24, 1001–1011

Aerosol exposure in combination with aerosol impacts on climate: What is the total health outcome?

Jakob Löndahl[1], Erik Swietlicki[1], Elisabet Lindgren[2] and Steffen Loft[3]

1. Div. of Nuclear Physics, Dep. of Physics, Lund University, PO Box 118, SE-221 00 Lund, Sweden
2. Dep. of Public Health Sciences, Karolinska Institutet, Stockholm, Sweden
3. Dep. of Environmental Health, Institute of Public Health, University of Copenhagen, Copenhagen, Denmark
Keywords: climate change, health effects, shipping emissions
Presenting author email: Jakob.londahl@gmail.com

Emission of aerosol particles is one of the largest environmental problems concerning human health. Traditionally only the health effects related to aerosol exposure are considered. However, for outdoor air pollution the climate change mediated health effects also need to be taken into account.

It has been estimated that climate change caused a loss of 160 000 lives from malaria, malnutrition, diarrhoeal disease, heat waves and floods in year 2000 because of the 0.4°C heating compared to the 1961-90 average climate (World Health Organization 2002). Aerosol cooling of climate, as in the below described case of ship emissions, may thus reduce death rates. Conversely, aerosol heating of atmosphere, as for black carbon, may lead to increase in mortality both due to exposure and due to adverse effects from global warming.

The objective of this work was to investigate the "total health effects" aerosol emissions which include both exposures to particles and consequences from climate change. Based on recent studies it has become possible to approximate, as a first source, the "total health impacts" of shipping emissions (Löndahl et al. 2010).

Emissions from shipping are relatively well-known from both a health and climate perspective. Exposure to air pollution from shipping were responsible for 63 000 (43 000 – 83 000) deaths globally year 2000 (Corbett et al. 2007). Skeie et al. (2009) estimated that the global temperature change this year was −0.05 °C ($\Delta T_{surface}$) because of emissions from shipping.

There is no linear relationship between climate change and human health, but in a small temperature interval a first approximation of the number deaths may be

$$N_{deaths,cooling} = \Delta T_{surface} \cdot \theta_{\Delta T}$$

where $\theta_{\Delta T}$ is a constant representing the number of deaths caused by one degree warming. With 160 000 deaths due to 0.4 °C, the constant becomes 400 000 deaths/°C. In reality $\theta_{\Delta T}$ is thus not a fixed number, but rather a function of global temperature (i.e. $\theta_{\Delta T}(T)$) with higher values for increasing temperatures. Using the equation above, ship emissions are estimated to cause a climate related life loss of -20 000 (-40 000 to -4000). The "total health effect" considering both the number of lives saved by the atmospheric cooling effect and the deaths from exposure to air pollutants, then is 43 000 (14 000 to 69 000) deaths for year 2000.

The outcome may vary depending on choice of scenario. For instance it may be of interest to omit CO_2 from the calculations since the gas is not affected by suggested regulations (which focuses on SO_x, NO_x and PM). In this case the "total health effect" in deaths year 2000 becomes 29 000 (−500 to 58 000). Some publications also provide substantially higher values of the aerosol indirect effect (see Eyring et al. 2010). Using these larger aerosol coolings result in a "total health effect" of −42 000 (−139 000 to 68 000) deaths (i.e. ship emissions would save lives on a global scale). However, ship emissions are an extreme example. With similar estimations for other sources with emissions closer to populations the negative health effects from exposure are likely to dominate.

At current state of scientific knowledge calculations of "total health effects" are highly uncertain (Löndahl et al. 2010). Especially the relationships between climate change and health is poorly understood. The value of $\theta_{\Delta T}$ used in this work is probably an underestimate since several effects were omitted such as impacts on infectious diseases other than malaria, extreme weather events other than heat waves, and climate change related impacts on allergen levels, population displacement, water shortage, and conflicts over natural resources.

To maintain one environmental problem (particulate air pollution) in order to reduce the burden of another (climate change), is close to geoengineering and is certainly dubious. Nevertheless, because of the risk that anthropogenic emission will move the climate system beyond an irreversible tipping point, there is an urgent need to develop strategies and metrics for regulation of short-lived cooling components in the atmosphere. For instance more attention might be given to lower the levels of black carbon. Reductions of pollutants to improve air quality, should ideally consider impacts on global warming.

Corbett JJ, Winebrake JJ, Green EH, Kasibhatla P, Eyring V, Lauer A. (2007) *EST,* **41**, 8512-8518.

Eyring, V., Isaksen, I. S. A., Berntsen, T., et al. (2010) *Atmos. Environ.*, **44**, 4735-4771.

Löndahl, J., Swietlicki, E., Lindgren, E., Loft, S. (2010) *Atmos. Chem. Phys.* **10**, 9441-9449

Skeie, R. B., Fuglestvedt, J., Berntsen, T., Lund, M. T., Myhre, G., Rypdal, K. (2009), *Atmos. Environ.*, **43**, *6260–6270*

World Health Organization. 2002. World health report.

Modeling and Measurement of ENP Dynamics in a Ventilated Two-Zone Chamber

Mingzhou Yu[1], Martin Seipenbusch[1] , Kun Gao[1]

Institut für Mechanische Verfahrenstechnik und Mechanik, Karlsruhe Institute of Technology, Karlsruhe, 76131, Germany
Presenting author email: mingzhou.yu@mvm.uni-karlsruhe.de

Engineered Nanoparticles (ENP) have been found to pose greater potential risks on human health and environment than macro- and micro-scale particles due to their unusual physicochemical properties including their small size, chemical composition, surface, solubility, shape and state of aggregation (SCENIHR 2009). Development of realistic exposure scenarios should play an essential role in the protection of workers' health and improvement of workplace safety in nanotechnology research activities. In order to meet this requirement, it is necessary to develop an accurate and simplified analytical model to simultaneously trace the temporal and spatial evolution of polydisperse aerosols.

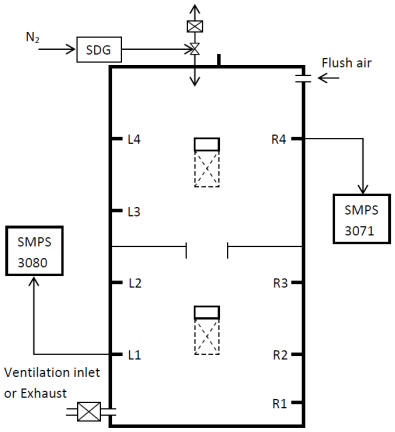

Fig.1 Experimental Setup

The aim of the present work is to get an analytical aerosol dynamic model with respect to Brownian coagulation among ENPs, as well as between ENP and background aerosols through experimental studies (Fig.1) and numerical simulations. This model is extended from one-zone studies conducted by Seipenbusch et al. (2008) to two-zone studies, and it is expected to be more useful to test the hypothesized modifiers in their influence on ENP number concentration because the study on nanoparticle dynamics in both time and space scales can be performed. The so called two zone model can then be formulated with two coupled differential equations, each describing the aerosol dynamics in one of the zones, and especially the information on convectional transport between chambers is included. The analytical solution is prior to numerical solutions in that it has more simplified mathematical construction and needs less computational time.

In the experiments, we used a spark discharge generator to produce NPs and background Gold particles. Two fans were used to mix the aerosol at each chamber. The particle size spectrum was measured by two instruments, scanning mobility particle sizer (SMPS, TSI model 3080), and scanning mobility particle sizer (SMPS, TSI model 3071). Two experiments were carried out for estimating friction velocity and particle loss rate due to deposition inside the chamber when the fan is on and off. Five main experiments were carried out for investigating the evolution of particle size distributions in both two chambers with the injected nanoparticles (continuous and pulse injection), shown in Table 1. Fig.2 shows the measured data from SMPS with continuous injection for 156 min.

Table 1

Experiment	Fan	Injection time	Background Particles	Injection status	Measurement status
B1	ON	156	NO	continuous	continuous
B2	ON	60	YES	continuous	continuous
B3	OFF	60	NO	continuous	interval (once per 30)
B4	ON	Once per 11.25	NO	interval	continuous
B5	ON	120	NO	continuous	Interval (once per 50)

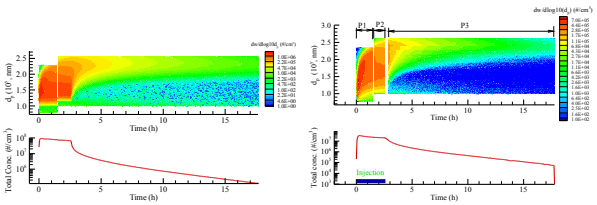

Fig.2 The measured particle size distribution as well as its total particle number concentration with time for top- and low-chamber.

In the numerical simulations, the particle general dynamic equations for both chambers were constructed following Muller's study (1928). In order to distinguish the background particles from the newly injected particles, two separated control equations for them were proposed. In order to accurately trace the evolution of particle size distribution at each chamber, the sectional method with fixed scale factors was used. In the numerical calculation, the fourth-order Runge-Kutta method with fixed time step was used to solve the set of ordinary differential equations. Both experimental and numerically simulated results were used as reference to validate the newly proposed analytical model.

With the help of experiments and numerical simulations, the simplified analytical model is expected to be proposed by simultaneously considering particle ventilation between two chambers, particle loss due to deposition, and coagulation. The model has an ability to trace evolution of particle number concentration for polydisperese system which will lead to be more reasonable risk assessment.

This work was supported Alexander von Humboldt Foundation 1136169.

SCENIHR (2009). Risk Assessment of Product of Nanotechnologies.
Seipenbusch, M., A. Binder, and et al. (2008). *Annals of Occupational Hygiene* 52(8): 707-716.
Muller, H. (1928). Zur allgemeinen theorie der raschen koagulation. *Kolloideihefte.* **27**:223-250.

The response of PM concentrations in the UK to changes in industrial and agricultural emissions: implications for the exceedance of Air Quality Standards

E. Nemitz[1], M. Vieno[1, 2], U. Dragosits[1], C.F. Di Marco[1], M. Twigg[1,2] and M.A. Sutton[1]

[1]Centre for Ecology and Hydrology (CEH), Bush Estate, Penicuik, EH26 0QB, U.K.
[2]School of GeoSciences, King's Buildings, University of Edinburgh, West Mains Rd., Edinburgh, UK.

Keywords: Abatement strategies, air quality, PM (general), ammonium nitrate, ammonium sulphate, precursors, inorganics, chemical transport model

Presenting author email: en@ceh.ac.uk

In the UK, secondary organic ammonium (NH_4^+) salts, formed from the reaction of ammonia (NH_3) with the oxidation products of sulphur dioxide (SO_2) and nitrogen oxides (NO_x), typically account for 20-40% of the $PM_{2.5}$ and 10-30% of the PM_{10}. With increasingly more reliable chemically speciated aerosol data becoming available, it is becoming clear that nitrate (NO_3^-) is a larger contributor than sulphate (SO_4^{2-}) and that it is particularly associated with pollution episodes during which the Air Quality Standards for PM are exceeded (Charron et al., 2006; Harrison et al., 1997). Nitrate formation is favoured by the relatively high emissions of NH_3 from agricultural activity, coupled with a cool humid climate. By contrast, SO_2 emissions have decreased by >80% over the past 15 years.

In this study we are using a high resolution version of the EMEP chemical transport model (EMEP4UK) (Vieno et al., 2010) to predict annual time-series of NH_4^+, NO_3^- and SO_4^{2-} for a number of urban locations, which are analysed in the context of measured PM concentrations.

The skill of the model in predicting NH_4NO_3 concentrations and their response to precursor gas concentrations has been carefully assessed by comparison of long-term trends and hourly variability against data from a number of sources, including: (a) a UK network that measures monthly gas and aerosol concentrations at 33 sites with a denuder / filter-pack sampler (UKEAP), (b) long-term measurements of aerosol composition at the UK EMEP Supersites 'Auchencorth' and 'Harwell' using a MARGA wet-chemistry analyser and (c) campaign-based measurements by Aerosol Mass Spectrometry (AMS) (Nemitz et al., 2011), including measurements in London (Allan et al., 2010).

Model simulations were then performed for several emissions scenarios: experiments were emissions were perturbed within and outside the UK, future emissions predictions, and scenarios in which different levels of agricultural NH_3 abatement (BAT) have been implemented.

Figure 1 compares the model predictions of monthly fine and total nitrate against a Scottish UKEAP measurement site, based on runs of full emissions and only non-UK emissions, showing that a long-term high nitrate event in spring 2003 represented mainly fine nitrate which was formed partly from UK and partly from non-UK precursor gases.

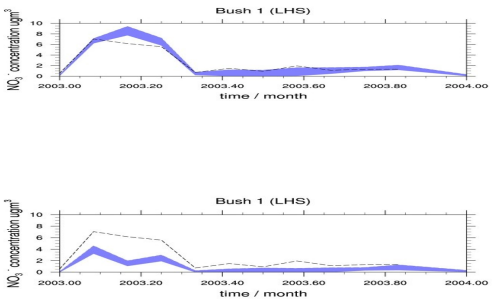

Figure 1. Nitrate monthly surface concentration at the Bush UKEAP site. The dashed line represents the observed nitrate concentration the blue shaded region represents the EMEP4UK model predicted range of fine nitrate (lower boundary) and total nitrate (upper boundary), with the thickness of the shaded area showing the predicted concentration of coarse nitrate. Top graph shows the base run, whereas the bottom graph represents a model run where UK emissions of precursor gases have been removed.

The work was supported by the UK Department for Environment, Food and Rural Affairs (Defra).

Allan, J.D., Williams, P.I. et al.: Contributions from transport, solid fuel burning and cooking to primary organic aerosols in two UK cities. Atmos. Chem. Phys. 10, 647-668, 2010.

Charron, A., Harrison, R. M. et al..: What are the sources and conditions responsible for exceedances of the 24 h PM_{10} limit value (50 µg m^{-3}) at a heavily trafficked London site? Atmos. Environ., 41, 1960-1975, 2006.

Harrison, R. M., Deacon, A. R., et al.: Sources and processes affecting concentrations of PM_{10} and $PM_{2.5}$ particulate matter in Birmingham (UK), Atmos. Environ., 31, 4103-4117, 1997.

Nemitz, E., Prevot, A. et al.: A snapshot European climatology of submicron aerosol chemical composition derived from an Aerosol Mass Spectrometer network. Atmos. Chem. Phys. Discuss., in preparation for submission 2011.

Vieno, M., Dore, A. J. et al.: Modelling surface ozone during the 2003 heat-wave in the UK, Atmos. Chem. Phys., 10, 7963-7978, 2010.

Thursday, September 8, 2011

Plenary 4

The scientific challenges involved in using aerosols as a strategy for geoengineering climate.

By Phil Rasch:

The scientific challenges involved in using aerosols as a strategy for geoengineering climate

Philip Rasch

Pacific Northwest National Laboratory, 902 Battelle Boulevard,
P. O. Box 999, MSIN K9-34,Richland, WA, 99352, USA

Presenting author email: Philip.Rasch@pnnl.gov

Geoengineering is a term referring to the deliberate modification of the Earth's climate to counter some of the negative consequences of increasing greenhouse gas concentrations to the planet. Some suggested geoengineering strategies use aerosols to increase the planetary albedo, or to make the atmosphere less opaque to the emission of outgoing longwave energy. I will review a few of these strategies, discussing modeling studies (by myself and colleagues) used to explore some of the consequences to the planet that might arise from their use, and to identify some of the scientific and engineering challenges that exist in employing these technologies and approaches.

Thursday, September 8, 2011

Session 8P: Poster session B

Combustion Aerosols

Determination of loss factors of aerosol particles in the sampling systems of nuclear power plants

Rainer Jonas, TÜV Nord SysTec GmbH & Co. KG, Große Bahnstr. 31, D-22525 Hamburg , Germany,
Gerfried Lindenthal, Ingenieurbüro für Partikeltechnologie und Umweltmesstechnik, Steinweg 8, D-34314 Espenau Germany

As with all measured quantities the stack emission of radioactive material of a nuclear power plant with exhaust air includes an uncertainty. This is caused by the statistical error and additionally by the non-representative sampling and the deposition of aerosols in the sampling systems. The non-representative sampling results from the insufficient mixing of the air (inhomogenous concentration) and from the non-isokinetic flow in reaching the inlet of the screen of the sampling system. The deposition depends on the particle diameter and is caused by molecular diffusion, impaction and sedimentation. The ratio of the mass concentrations in front of the screen and at the end of the sampling system is called the pipe retention factor. According to the German nuclear technical rule KTA 1503.1 the sampling system must be able to collect aerosols with aerodynamic diameters between 0.1 μm and 20 μm with pipe retention factors below 3.

Pipe retention factors and loss factors (without consideration of non representative sampling) have been investigated for sampling systems of different nuclear power plants in Germany using three methods of determination:

1) Dispersion of test aerosols directly into probes at the screen of the sampling system and comparing the aerosol concentrations with those at the end of the sampling system

2) Generation of a defined quantity of aerosol particles at the bottom of the chimney and measuring the particle concentrations by using aerosol collectors or aerosol monitors at the end of the sampling system

3) Measuring the size distribution by number of the ambient aerosol in the chimney in front of the screen and at the end of the sampling system with optical particle counters.

The poster gives a survey of the results of the measured loss factors and pipe retention factors.

The results are in compliance with theoretical estimations. The measured loss factors and pipe retention factors lie below 3, if the time interval for cleaning is adequately short. The transfer properties of the sampling systems for larger particles (aerodynamic diameters up to 3 mm), have also been investigated. The results show that the sampling systems are suitable even in these cases.

Investigating the sampling system in a time interval of 5 years according to the German nuclear technical rule KTA 1503.1 is not sufficient in every case, because the pipe retention factor may increase rapidly in case of pollution. Cleaning of the system is necessary. A realistic determination of the pipe retention factor may be expected if the time interval for cleaning is once a year especially after maintenance periods. The time interval for cleaning may be appointed depending on the sampling system.

Development of high-performance Cu-La nanomaterials as efficient catalyst for ammonia removal

Chang-Mao Hung

Department of Vehicle Engineering, Yung-Ta Institute of Technology and Commerce, 316 Chung-shan Rd, Linlo, Pingtung 909, Taiwan, R.O.C.
Keywords: selective catalytic oxidation, ammonia, Cu-La nanomaterials.
Presenting author email: hungcm1031@gmail.com

Extensively adopted in industrial processes, ammonia (NH_3) can be eliminated in numerous ways. Apparently, NH_3 is used in the ammonium nitrate and nitric acid production industry, livestock feedlots, urea manufacturing plants, the nitrogen fertilizer application industry, fossil fuel combustion and petroleum refineries as well as the refrigeration industry. NH_3 is a toxic inorganic gas with a pungent odor under ambient conditions, and is potentially harmful to public health reported in the literature (Hung, 2008; Hung, 2009; Hung, 2010; Hung, 2011).

Nowadays, catalytic oxidation has been established to increase the effectiveness of AOP (Advanced Oxidation Processes) technology using dedicated catalysts, which potentially shorten the reaction times of oxidation, and allow it to proceed under milder operating conditions. The selective catalytic oxidation (SCO) of NH_3 in a stream to molecular nitrogen and water is one method for solving problems of NH_3 pollution. This work considers the oxidation of NH_3 by selective catalytic oxidation (SCO) over Cu-La nanomaterials at temperatures between 150 and 400℃. Figure 1 shows the effects of composite catalysts with various Cu-La molar ratios on the extents of conversion of NH_3, in terms of the extent of removal during the SCO process. The extent of catalytic oxidation of NH_3 over Cu-La nanomaterials is determined by the Cu-La molar ratio of the catalyst. The extents of conversion of NH_3 were 95 and 79% when catalytic oxidation proceeded under particular operating conditions over Cu-La nanomaterials with molar ratios of 8:2 and 7:3, respectively. To gain further information on the state of Cu-La species in these catalysts, the UV-Vis spectroscopic studies are carried out and the spectra are shown in Fig. 2. Generally, the bands were observed for Cu-La nanomaterials in the ranges of 300-350 nm and 700-900 nm. This band at 300-350 nm is attributed to the $Cu^{2+}-O^{2-}$ electronic transition species. The band at 700–900 nm is associated with the d-d transitions of Cu^{2+} in an octahedral environment with O_h symmetry. Conclusively, this work shows that the SCO process has the potential to treat highly concentrated streams of NH_3, helping industrial plants to meet discharge regulations.

This work was supported by the National Science Council of the Republic of China, Taiwan, for financially supporting this research under Contract No. NSC98-2221-E-132-003-MY3.

Hung, C. M. (2008). *J. Hazard. Mater.*, **150**, 53-61.
Hung, C. M. (2009). *Powder Tech.*, **196**, 56-61.
Hung, C. M. (2010). *J. Rare Earths*, **28**, 362-366.
Hung, C. M. (2011). *Adv. Mat. Res.*, **160-162**, 1291-1296.

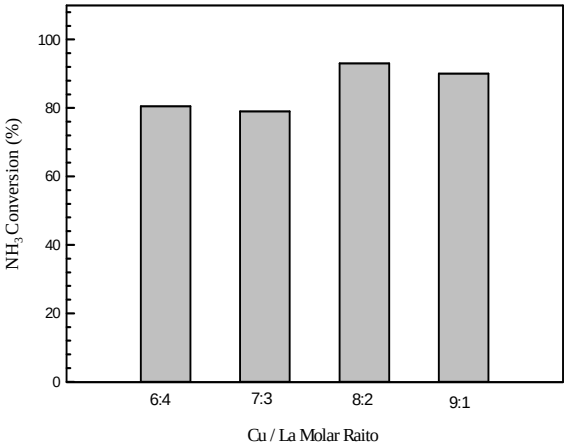

Figure 1. Effect of the metal content on the Cu-La nanomaterials in the conversion of NH_3. Test conditions: 1000 ppm NH_3 in He, O_2 = 4%, temperature = 400℃, RH = 12%, GHSV = 92000 ml/h-g.

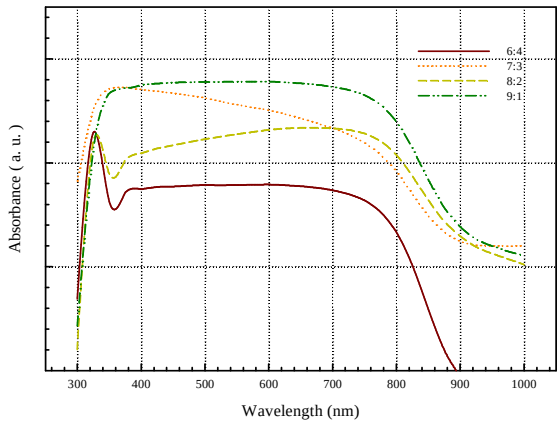

Figure 2. A UV-Vis absorption spectra of various metal content on the Cu-La nanomaterials for the conversion of NH_3. Test conditions: 1000 ppm NH_3 in He, O_2 = 4%, RH = 12%, GHSV = 92000 ml/h-g.

Polybrominated diphenyl ethers (PBDEs) in the stack flue gases and the fly ashes in the woodchip-fuelled boiler

T.Y. Hsieh[1], W.J. Lee[1], L.P. Chang[1]and L.C. Wang[2]

[1]Department of Environmental Engineering, National Cheng Kung University, 1, University Road, Tainan 70101, Taiwan, ROC
[2]Department of Chemical and Materials Engineering, Cheng Shiu University, 840, Chengching Road, Kaohsiung 833, Taiwan, ROC
Keywords: PBDEs, wood, boiler, ash, stack flue gases.
Presenting author email: p56994137@mail.ncku.edu.tw

Burning woodchips is recognized as one of the major renewable energy (Turner, 1999). Utilizing wood as fuel can replace fossil fuels, reduce carbon dioxide emission and thus help in fighting global warming. Consequently, wood could be a more important source of energy in the future.

Polybrominated diphenyl ethers (PBDEs) are the most used brominated flame retardants (BFRs). BFRs have widely applications such as comsumer products and electronic materials to prevent the spread of the flame. Due to the properties of persistence, bioaccumulation and ubiquity of PBDEs, two main PBDE commercial mixtures, penta-BDE and octa-BDE, are banned by the European Union in 2004. Therefore, with the increasing usage of PBDEs, which was concerned by the public.

The boiler investigated in this study utilizes woodchips as fuel. The woodchips in this study are collected from chipping or shredding wood for the productions of furniture with bromine content smaller than 15.9 mg/kg, water content of 6.1 %, ash content of 5.7 %, combustible content of 88.3 % and low heat content of 4559 kcal/kg.

The boiler being investigated in this study is a grate furnace boiler for the production of steam without power generator. The woodchip feeding rate of the intermittently operating boiler was 730 kg/hr, and the mean steam generation rate is 2.51 metric ton/hr. Its air pollution control devices include cyclone and bag filter with a flue gas oxygen content of 15.7 %. The output rates of the bottom residues, cyclone ashes and bag filter ashes are 0.38, 3.2 and 3.4 kg/hr, respectively.

In this study, the characteristics of PBDEs in the stack flue gases and the fly ashes of the cyclone and bag filter were investigated. Total PBDE concentrations (summation of 30 congeners) were listed in Table 1.The concentration in the stack flue gases of the wood-fuelled industrial boiler is much lower than municipal solid waste incinerations (26.1-109 ng/Nm^3) (Wang *et al.*, 2010). As it shown in Figure 1., the BDE-209 is the most abundant PBDE congener (73.4%) in the flue gas of the wood- fuelled industrial boiler.

By using the wood-fuelled industrial boiler, PBDEs is still existing in the stack flue gas, in the fly ashes and in the bottom ashes. How to arrange an appropriate air control system and how to have a good management process for the combustion ashes are also an important issues for using wood chip as a kind of sustainable and renewable green energy.

Table 1 PBDEs contents (concentrations) in the feeding woodchips, cyclone ashes, bag filter ashes and stack flue gases of the wood-fueled industrial boiler

	feeding woodchips (n=2) (pg/g)	cyclone ashes (n=2) (pg/g)	bag filter ashes (n=2) (pg/g)	stack flue gases (n=3) (pg/Nm^3)
Total PBDEs	5,221	142	1,470	2,735

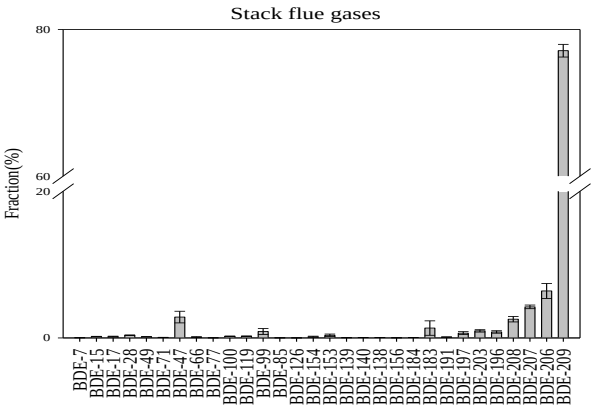

Figure 1. PBDE congener profile in the stack flue gases of wood-fueled industrial boiler

Turner, J. (1999). A realizable renewable energy future. *Science.* 285: 687-689.

Wang, L.C., Hsi, H.C., Wang, Y.F., Lin, S.L. and Chang-Chien, G.P. (2010). Distribution of polybrominated diphenyl ethers (PBDEs) and polybrominated dibenzo-*p*-dioxins and dibenzofurans (PBDD/Fs) in municipal solid waste incinerators. *Environ. Pollut.* 158: 1595-1602.

Particle size distributions of ambient aerosol in the vicinity of semiconductor plants

C.C. Lin[1], S.J. Chen[1,*], J.H. Tsai[1], K.L. Huang[1], W.J. Yu[1] and C.L. Chou[2]

[1] Department of Environmental Science and Engineering, National Pingtung University of Science and Technology, Pingtung County, Nei Pu, 91201, Taiwan
[2]Content Engineering Consulting Services, Ltd., New Taipei City, Zhonghe Dist., 23553, Taiwan
Keywords: Size distribution, ultrafine, semiconductor plant, washout.
Presenting author email: lincc@mail.npust.edu.tw

The adverse effects of ambient particles on human health have been an environmental concern for decades. Epidemiological studies have successfully related ambient particulate matter (PM) exposures with adverse respiratory effects, including chronic obstructive pulmonary disease (COPD) and asthma, and PM may cause increases in pneumonia and cardiopulmonary diseases (Pope et al., 1995; Tao and Kobzik, 2002). This study was conducted from November, 2009 to July, 2010 at a semiconductor plant in a science park in southern Taiwan to understand the characteristics of ambient atmospheric aerosol using a micro-orifice uniform deposition impactor (MOUDI) and a nano-MOUDI equipped with Teflon filters (with diameters of 37 and 47 mm, respectively) in the vicinity of semiconductor plants. The sampling periods covered trhee types of days: episode days (PM concentration > 100 μg m^{-3}), sunny days, and sunny days after rain.

The mean concentrations (with standard deviations) of the $PM_{0.1}$, PM_1, $PM_{2.5}$, $PM_{2.5-10}$, and PM_{10} particles were 4.31 ± 1.35, 38.8 ± 9.24, 66.3 ± 17.1, 50.0 ± 9.23, and 116 ± 25.9 μg m^{-3} on the episode days, respectively (Fig. 1). On the sunny days, the mean concentrations (with standard deviations) of the $PM_{0.1}$, PM_1, $PM_{2.5}$, $PM_{2.5-10}$, and PM_{10} particles were 7.14 ± 4.64, 33.8 ± 17.2, 48.4 ± 22.6, 27.8 ± 4.39, and 76.1 ± 24.8 μg m^{-3}, respectively; however, on the sunny days after rain, these PM data were 7.71 ± 5.71, 22.8 ± 6.38, 28.7 ± 7.49, 13.1 ± 1.69, and 41.8 ±7.23 μg m^{-3}, respectively. The particle mean concentrations of PM_1, $PM_{2.5}$, $PM_{2.5-10}$, and PM_{10} followed the order episode days > sunny days > sunny days after rain; however, the mean concentration of $PM_{0.1}$ was in order sunny days after rain > sunny days > episode days.

Episode day and sunny day samples exhibited a similar bi-modal particle size distribution within the size range 0.01–100 μm, with a major and a secondary peak in the coarse and fine size ranges, respectively (Fig. 2). The particles collected on sunny days after rain displayed a tri-modal distribution, with a major, a secondary, and a minor peak in the coarse (3.2–5.6 μm), fine (0.56–1.0 μm), and nano (0.01–0.032 μm) size ranges, respectively. With an additional minor peak in the nano size range (0.018–0.032 μm), the particles collected following rain had a tri-modal size distribution. The former result follows from the fact that the washout coefficients for PM sizes of 3–10 μm may increase significantly during heavy rain events (Chate and Pranesha, 2004). The latter result may be associated with the fact that the sampling site was close to the emission sources (semiconductor plants) and most of the collected ultrafine particles were freshly emitted in the stack flue gases from the sources. Therefore, the effect of rain on the ultrafine particle size distribution was not significant.

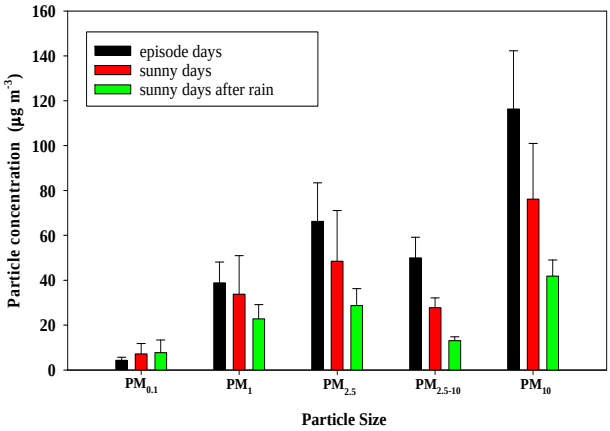

Figure 1. Mean concentrations of the $PM_{0.1}$, PM_1, $PM_{2.5}$, $PM_{2.5-10}$, and PM_{10} collected on episode days, sunny days, and sunny days after rain.

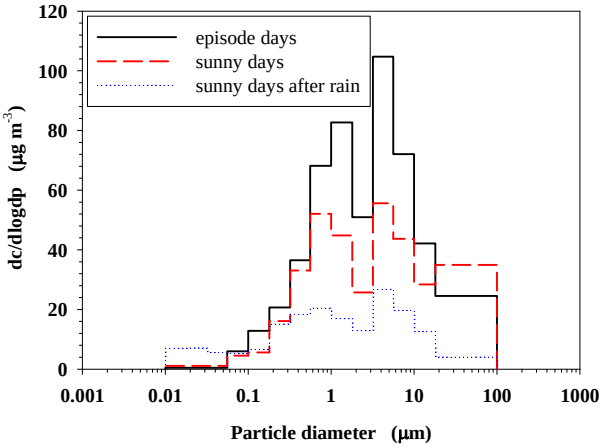

Figure 2. Size distributions of the mean PM collected on episode days, sunny days, and sunny days after rain.

Chate, D.M. and Pranesha, T.S. (2004) *J. Aerosol Sci.* **35**, 695–706.

Tao, F. and Kobzik, L. (2002) *Am. J. Respir. Cell Mol. Biol.* **26,** 499–505.

Pope III, C.A., Bates, D.V. and Raizenne, M.E. (1995) *Environ. Health Persp.* **103**, 472–480.

Distributions of heavy metal traces by particle size (PM_{10}, $PM_{2.5}$ y PM_1). Emissions from non ferrous smelters.

J.J. Rodríguez-Maroto[1], J.L. Dorronsoro-Arenal[1], D. Sanz-Rivera[1], E. Rojas-García[1], M. Fernández-Díaz[2] , P. Galán-Valera[2] and E. Conde Vilda[2].

[1] CIEMAT/Departamento de Medio Ambiente, Avda. Complutense 22, 28040 Madrid, España
[2] CIEMAT/Departamento de Tecnología, Avda. Complutense 22, 28040 Madrid, España
Keywords: emissions, heavy metals, dust, metallurgy, smelter, PM10, PM2.5, PM1.
Presenting author email: jl.dorronsoro@ciemat.es

The effects on health and environment that can cause the fine and ultrafine particles emitted from the industry are well known. Particle size distribution and that of heavy metal traces that accompany them are two key parameters to be evaluated. In the non ferrous metals industry, the emission of the particulate matter (PM) is mainly related to the processes of treatment and smelting. Therefore, the generated by-products will fundamentally depend on raw material characteristics, and on the conditions of operation.

For the present study, a total of 19 installations have been tested including plants of three non ferrous metallurgic sectors: primary zinc and secondary copper and aluminium In all cases, the sampling point was selected at the exit stacks from the melting furnace. The PM10, PM2.5 and PM1.0 fractions were sampled using a cascade impactor technique. Sampling and measurement was carried out in accordance with US EPA 201A and VDI 2066/5 procedures, using three types of cascade impactors: Mark III (eight stages) and DEKATI PM10 and KS207 Kalman System GMBH (three stages). Additionally, impactor substrates were chemically analyzed (method EPA IO-3.1) by ICP-OES and/or ICP-MS and FAAS to determine the concentration of: Al, As, Be, Cd, Cr, Cu, Mn, Mo, Ni, Pb, Sb, Ti, V y Zn.

The measurement data have been analyzed according to four particle size intervals: >PM10, 10>PM>2.5, 2.5>PM>1 and 1>PM. The results showed that in the copper and aluminium smelters, the emitted particles mass was practically distributed by equal in the studied intervals. In contrast, it was observed a maximum in the range 2.5<PM<1 in the case of zinc smelters.

Table 1 Percentage of the metals by particle size range for the three type of smelter: Zn, Cu and Al.

Range (µm)	Smelter.	As	Cd	Cr	Cu	Ni	Pb	Zn
>PM10	Zinc	27	24	63	2	71	34	5
	Copper	30	14	26	13	22	12	12
	Aluminium	35	26	37	29	34	26	30
10>PM>2.5	Zinc	27	30	13	2	17	10	14
	Copper	21	29	19	28	32	28	24
	Aluminium	24	23	21	19	19	22	21
2.5>PM>1	Zinc	13	15	2	1	1	18	23
	Copper	27	40	17	27	18	27	28
	Aluminium	28	25	28	30	33	31	28
1>PM	Zinc	33	31	22	95	11	38	58
	Copper	22	17	38	32	28	33	36
	Aluminium	13	26	14	22	14	21	21

The table1 shows the measurement results corresponding to metals to which apply a minimum threshold for releases to the atmosphere according to European Pollutant Release and Transfer Register (E-PRTR). In zinc smelters, the emitted submicron particles contain a high percentage of Cu y Zn (95 y 58 % respectively of the total mass of each element is in the interval 1>PM) and other although less significant as As, Cd and Pb are present in more than 30 %. Whereas the particles bigger than ten micron have more Cr (63 % of total chromium) and Ni (71 % of total nickel). In copper smelters, Zn, Cr, Cu and Pb (more than 32 %) are predominant in smaller particles, and only Cd (40 %) stands out in the interval 2.5>PM>1. Finally, in smelters of aluminium, As, Ni, Cr and Al have a presence higher than 30 % in the in bigger particles.

The distribution of trace metals by size of particle is primarily produced in the melting stage and transport of gases towards emission control system (ECS). Different metals contained in the raw materials are evaporated in the furnace and cooled into the duct forming new particles or being incorporated to the existing ones. Long residence time in the duct or ECS contributes to agglomerate particles and consequently to the process of distributing trace metals.

Knowledge of the distribution of heavy metals would allow realizing modifications in the process, so it would be possible to minimize its presence in the particle size range more difficult to separate by means of the conventional ECS. Effective separation of particles could be directed to metallic elements of particular interest, either for its high toxicity or for being catalysts in the formation of other pollutants such as PCDD/Fs.

This work was supported by the Ministry of the Environment and Rural and Marine Environs. Special thanks to Associations of Metallurgical Sector of Aluminium, Copper and Zinc and to each one of the staffs of facilities.

European Commission, (2001). *Document on Best Available Techniques in the Non Ferrous Metals Industries.*

European Commission (2006). *Guidance Document for the implementation of the European PRTR.*

UNECE, (1998). *Protocolo al Convenio de 1979*, Aarhus 24 de junio de 1998.

Workplace exposure to fine particles from welding fumes

E. Jankowska

Department of Chemical and Aerosol Hazards, Central Institute for Labour Protection – National Research Institute, Czerniakowska 16, 00-701 Warsaw, Poland
Keywords: welding fume, fine particles, concentration, exposure.
Presenting author email: eljan@ciop.pl

This abstract presents results of research on concentrations and size distribution of particles emitted as welding fumes. Investigations were conducted in a typical welding shop. Sampling points were located in the breathings zone of welder. Before welding process started, background levels out of the welding shop and in the welding shop were determined. The welding process was conducted in fifth stages (Table 1).

Table 1. Stages of welding process

Stage	Time	Number of electrodes (OK 61.30/308L-17) used
1	09:59	1
2	10:37	2
3	11:12	2
4	12:15	2
5	12:50	1

Measurements were done with:

- GRIMM Dust Monitor model 1.108 - number concentration and size distribution for size fractions 0,4-0,5µm, 0,5-1µm, 1-3µm and 3-10µm (Figure 1),
- AERO-TRAK 9000 (TSI) – surface concentration of particles in the 100-10000nm range, alveolar fraction - A (Figure 2).

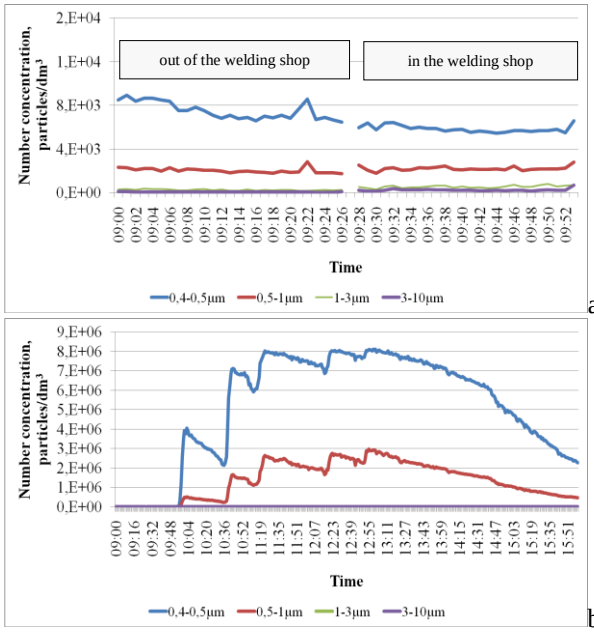

Figure 1. Number concentrations of particles (GRIMM): a) background levels out of the welding shop and in the shop, b) before, during and after welding process.

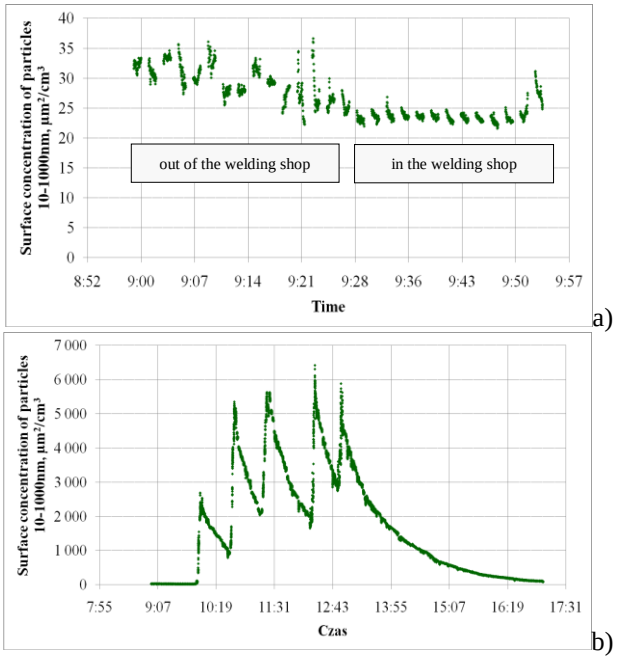

Figure 2. Surface concentration of particles 10-1000nm: a) background levels out of the welding shop and in the shop, b) before, during and after welding process AERO-TRAK results (A fraction).

Measurements date shown that:

- Number concentrations of fractions 0,4-0,5µm and 0,5-1µm (GRIMM results) and surface concentration (AERO-TRAK results) determined as background levels out of the welding shop were higher than that for background levels in the welding shop. For fractions 1-3µm and 3-10µm it was vice versa.
- Number concentrations of 0,4-0,5µm fractions after 3rd stage of welding remained almost in the same level (about 8^{e+6}partices/dm^3) between and during next stages of welding. Similar tendency was observed for number concentrations of 0,5-1µm fractions while number concentrations of fractions 1-3µm and 3-10µm were significant lower.
- Surface concentrations of particles 10-1000nm were in similar level after 3rd stage of welding (about 5700-6500 µm^2/cm^3, but between and during next stages surface concentrations dropped to about 1700-2900µm^2/cm^3.

This study was prepared on the basis of the results of research project 2.R.03 carried out within the scope of the National Programme "Improvement of Occupational Safety and Working Conditions" supported by the Polish Ministry of Science. Main co-ordinator CIOP-PIB.

Study of particle chemical composition and size distribution in the pyrolysis gas flow

A. Bologa[1], H.-R. Paur[1], H. Seifert[1], F. Weirich[2] and K. Woletz[1]

Karlsruhe Institute of Technology,
[1]Institute for Technical Chemistry, [2]Institute of Catalysis Research and Technology,
Eggenstein - Leopodshafen, 76344, Germany
Keywords: pyrolysis, particle size distribution, chemical analysis, chemical composition
Presenting author email: andrei.bologa@kit.edu

The Bioliq® process is developed by Karlsruhe Institute of Technology, by which the fully synthetic fuels, also called BtL fuels (Biomass to Liquid), can be produced from straw and other agricultural and forestal residues. KIT applies the four-stage Bioliq® produce a fuel, the quality of which will by far exceed that of conventional biofuels and even mineral oil products (Dahmen, 2007).

In the current work are presented the results of the study carried out at the first step of the Bioliq® process. At this step the biomass is converted into a transportable liquid intermediate product of high energy by a so-called flash pyrolysis. The pyrolysis product is gasified and the resulting syngas is used for production of biofuel. The tests were carried at the pyrolysis pilot plant in which dry biomass (straw) is mixed with hot sand at ambient pressure in the absence of air in a twin-screw mixing reactor. Pyrolytic conversion of the biomass particles at approximately 500 °C, and condensation of the pyrolysis vapors take a few seconds only.

The 1st objective of the current work was the measurement of particle mass concentration and particle size distribution in the pyrolysis gas flow. Two series of measurements were carried out. The probes were taken out by the Anderson Mark 3 Impactor downstream the 1st gas condenser. The raw material (straw) flow rate was up to 350 kg/h varying from plant operation conditions. During the 1st measurements the raw gas temperature was T=115°C and during the 2nd measurements the T=75°C. The impactors and the sampling system were heated up to 150°C.

The 2nd objective of the work was the chemical analysis of the straw, coke and collected pyrolysis product. The following methods were used: Inductively Coupled Plasma Optical Emission Spectrometry (ICP-OES); Total Inorganic Carbon Analysis (TIC-Analysis); Carbon, Hydrogen and Nitrogen Analysis (CHN-Analysis); Ion Chromatography (IC-Analysis) and Atomic Absorption Spectroscopy (AAS Analysis) of Hg. The analysis was performed for straw, coke and pyrolysis product collected on the impactor filters 1, 3, 7 and back-up filter (filter 1 is for particles >13,3 µm; filter 3 is for particles 5,6 µm; filter 7 is for particles 0,76 µm and back-up filter is for particles <0,52 µm).

The analysis of the impactor - probes shows that the mean particle size diameter is 1-3 µm (Figure 1). The aerosol mass concentration depends on the straw feed rates and varies from 15 g/Nm³ to 50 g/Nm³.

Carbon forms the main mass % of the tested matters. For the impactor filters, the carbon mass concentration in the collected pyrolysis product is highest for the smallest particle sizes. The mass % concentration of the hydrogen remains practically constant.

Coke particles are precipitated in the gas cleaning units installed up-stream the measurement point.

Calcium has the maximum mass concentration both in the straw and pyrolysis product and coke. In the coke the Ca concentration is up to 10 g/kg.

In comparison with other elements, relatively high concentrations are observed for Cu, Fe, K, Na and S. The absolute values for these elements strongly differ for analysed material. For example, K has high concentrations in the coke and low concentration in the pyrolysis product.

The chemical composition of the particles is similar and does not depend on the particles size. Similar is the concentration of the Si in the straw, coke and pyrolysis product.

The concentration of As, Cd, Hg and Pb in the straw and pyrolysis product is lower than 5 mg/kg.

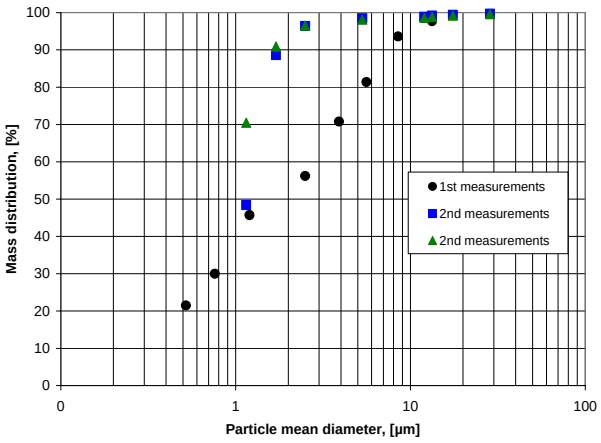

Figure 1. Particle size distribution measured by the Anderson Mark 3 Impactor

Dahmen, N., Dinjus, E. and Henrich, E. (2007) *OIL GAS European Magazine*, **1,** 31-34.

Evaluation of the efficiency of the fume cupboards in the laboratory

T. Jankowski
Department of Chemical and Aerosol Hazards, Central Institute for Labour Protection – National Research Institute, 00-701 Warsaw, Poland
Keywords: tracer method, fume cupboard, ventilation, en 14175 test

According to data from the Central Statistical Office, in 2009 the threat of chemicals in the workplace in Poland related to 24.6 thousand. people. Specific hazard exists when working in the laboratory with new chemicals, whose physical, chemical, biological, have not been sufficiently investigated. These substances can be explosive, flammable, highly toxic, carcinogenic or dangerous to the skin, eyes or respiratory tract. In laboratory areas where there are factors harmful to health (mainly dust and chemical agents) should be applied to technical solutions that prevent the proper penetration of these factors to other facilities, and installed and an efficient mechanical ventilation intake-exhaust, guaranteeing the exchange of air needed to eliminate or reduce exposure to these factors.

The performance of the fume cupboard can be expressed in terms of quality as the ability to capture and remove one or more pollutants released from a source inside the workspace and the ability to extract to minimize any disruption caused by drafts, or traversing movements operating room personnel.

Hence it is important to study the safety and effectiveness of the fume cupboard as specified in the standards series EN 14175.

Testing methods described in the above standards may be used to evaluate the performance:

- fume cupboard at the specified by the manufacturer of the test conditions (tests in laboratory conditions),
- fume cupboard installed in a room equipped with a ventilation system of general and local ventilation devices. other fume cupboards such as laboratory (test conditions of use.)

Particularly important are the fume cupboards tests in conditions of their use, because the working parameters are closely dependent on the effectiveness of general ventilation systems and equipment of local ventilation systems installed in the room.

Currently, many research centers are conducted investigation on the use of tracer gas to study the performance of laboratory fume cupboards. The main centers are: HSL, INRS, FIOH, and NIOSH.

The CIOP-PIB studies are carried out air velocity, air flow rate, pressure drop, the degree of containment and air exchange of the laboratory fume cupboards. As part of these works are carried out the study:

- the impact of changes in flow characteristics inside the fume cupboard and its surroundings on the parameters related to emissions - a method of visualization and anemometric,
- parameters related to emissions in selected types of laboratory fume cupboard - a method of tracer gas, ie:
  - a given pollutant emissions from sources with the capture system switched on and off,
  - the efficiency of the laboratory fume cupboard, by measuring the mass concentration of sulfur hexafluoride in the vicinity of the object.

  Tests were carried on using two methods:
- Vivo Draught 20T35 Transducers for measuring air flow velocity,
- MIRAN SapphIRe 100E Portable Gas Analyzer for measuring sulfur hexafluoride (SF_6) concentration.

Figure 1 and 2 illustrates the example results of smoke visualization, distribution of air flow velocity and tracer gas concentration.

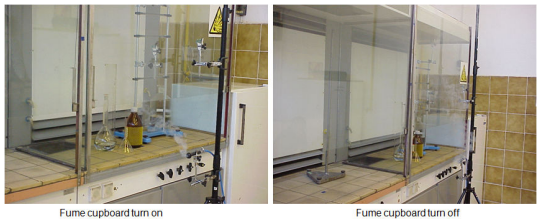

Figure 1. Smoke visualisation at the front of the fume cupboard at the laboratory.

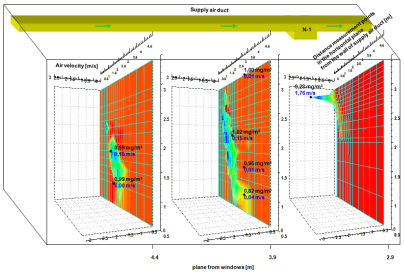

Figure 2. Distribution of air velocity at the laboratory.

Analysis of test results can assist the design and testing of laboratory performance fume cupboards to ensure effective protection of workers from the harmful effects of air pollutants from sources inside the laboratories.

This paper has been prepared on the basis of the results of task carried out within the National Programme “Improvement of safety and working conditions” partly supported in 2011-2013 within the scope of state services by the Ministry of Labour and Social Policy. The CIOP-PIB is the Programme's main co-ordinator.

Standard No. EN 14175. Fume cupboards.

Removal of Polychlorinated Dibenzo-*p*-dioxins and Dibenzofurans for physico-chemical pre-treatment and thermal treatment of Electric Arc Furnace fly ashes

S.I. Shih[1], W.J. Lee[2], Y.C. Hsu[1], Z.S. Wu[2], L.C. Wang[3] and G.P. Chang-Chien[3]

[1]Department of Environmental Engineering, Kun Shan University, Tainan City, Yung Kang, 710, Taiwan
[2]Department of Environmental Engineering, National Cheng Kung University, Tainan City, 701, Taiwan
[3]Department of Chemical and Materials Engineering, Cheng Shiu University, Kaohsiung City, 833, Taiwan
Keywords: PCDD/Fs, Chloride, Coagulation, Filtration, Ash.
Presenting author email: ssi10@mail.ksu.edu.tw

Electric Arc Furnace (EAF) fly ashes were produced annually of 160,000 tons in Taiwan and 700,000 in European Union (Barna et al., 2000). They were rich in polychlorinated dibenzo-*p*-dioxins and dibenzofurans (PCDD/Fs) and needs to be properly treated to conform to the regulated soil standard (1000 ng I-TEQ/kg in Taiwan) before landfill.

Pre-treatment (water-wash, including coagulation, sedimentation and filtration), that is usually used in water treatment, was firstly employed to treat EAF fly ashes. The contents or concentrations of PCDD/Fs and chlorides in three phases (sediment, suspension, and filtrate) were examined. Thermal treatment equipment was then used to treat EAF fly ashes to evaluate the removal efficiencies of PCDD/Fs at 900-1450 ^{o}C.

The experimental procedures of water-wash were very similar to jar test that is usually used in water treatment, and the sampling for PCDD/F analyses in three phases referred to the descriptions of Lee *et al* (2008). A graphite crucible, with inside diameter 70 mm and height 95 mm, containing 40 g of EAF fly ashes was placed in the primary furnace. Thermal treatment was then performed by raising the primary furnace temperature at 5 ^{o}Cmin^{-1} from room temperature and maintaining at 900-1450 ^{o}C for 1 h. Gaseous samples were withdrawn after the secondary furnace at 12 Lmin^{-1}. The batch experiment was repeated twice for consistency.

Table 1. PCDD/F contents of EAF fly ashes and treated ashes (slag) and their removal efficiencies after thermal treatment at 1450 ^{o}C

	EAF fly ashes (ng/kg)	Slag (ng/kg)	Removal (%)
Total PCDD/Fs	168952.0	1.103	99.999
Total PCDD/F I-TEQ	6639.9	0.0822	99.999

Analyses of PCDD/Fs were performed in a laboratory certified in Taiwan. Each sample was spiked with a known standard and extracted for 24 h. Then the extract was concentrated and treated with sulfuric acid; followed by a series of cleanup and fractionation procedures. A high resolution gas chromatography with mass spectrometer (HRGC/MS) was used to determine the concentrations of 17 individual PCDD/Fs. Helium was used as the carrier gas. The analyzer mode was selected ion monitoring with resolving power at 10,000.

Experimental results showed that, there was not a significant variation of PCDD/Fs after three rounds of water-wash of EAF fly ashes, owing to lipophilic character of PCDD/Fs. Nevertheless, concentrations of chlorides in three phases decreased substantially. Particularly in sediments, there was an approximately 95% reduction of chloride. Thus, it is expected that there would be a significant reduction of PCDD/F formation in the following thermal treatment.

As shown in Table 1, more than 99% of DRE (Destruction Removal Efficiency) of PCDD/Fs was achieved and the PCDD/F content of treated ash could be reduced to 0.0822 ng I-TEQ/kg. It is far below the soil standard regulated by Taiwan EPA (1000 ng I-TEQ/kg) and thus could be disposed with landfill undoubtedly. Mass distribution of PCDD/Fs in each air pollution control devices (cooling unit, filter and PUF cartridge) at 1450 ^{o}C thermal treatment temperature were 10.5, 16.7 and 72.8%, respectively. OCDD、OCDF、1,2,3,4,6,7.8-HpCDD and 1,2,3,4,6,7.8-HpCDF were the top four predominant species for the slag (Figure 1). Due to the high reduction of chloride after water-wash, less energy (low temperature) is needed to obtain the same PCDD/F removal efficiencies.

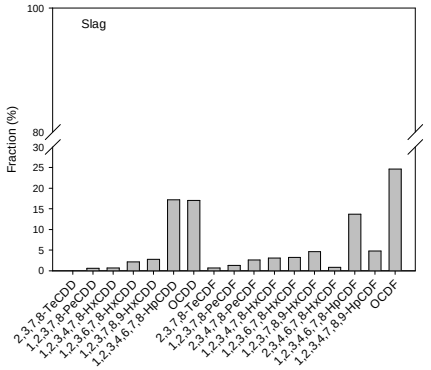

PCDD/F congeners

Figure 1. Congener profiles of PCDD/Fs in the slag after thermal treatment of EAF ash at 1450 ^{o}C.

This work was supported in part by the National Science Council in Taiwan under grant no. NSC-98-2221-E-168-007.

Barna, R., Bae, H.R., Méhu, J., Sloot, H. van der, Moszkowicz, P., Desnoyers, C. (2000) *Waste Manage.* **20**, 115-124.

Lee, W.J., Shih, S.I., Chang, C.Y., Lai, Y.C., Wang, L.C. and Chang-Chien, G.P. (2008) *J. Hazard. Mater.* **160**, 220-227.

The role of diffusiophoresis in fouling of exhaust gas recirculation heat exchangers

G. Hörnig and R. Niessner

Technische Universität München, Institute of Hydrochemistry, Chair for Analytical Chemistry,
Marchioninistr. 17, D – 81377 Munich, Germany
Keywords: Condensation, Diesel exhaust, Diffusiophoresis, EGR
Presenting author email: gabriele.hoernig@ch.tum.de

The combustion process in diesel engines is a source for hazardous environmental pollutants such as nitrogen oxides (NO_x) or particulate matter (soot). Future emission standards require increased application of exhaust gas recirculation (EGR), which is a very effective way to reduce NO_x emissions in diesel exhaust gases. However, due to incomplete combustion, diesel exhaust gas contains not only soot particles, but also other components like unburnt hydrocarbons (HC) and sulfuric acid (H_2SO_4). These constituents are responsible for EGR heat exchangers being very prone to fouling. Reduced heat transfer efficiencies and increased pressure losses are the consequence of various acting deposition mechanisms (Abd-Alla, 2002).

Some of the mechanisms involved in the particle deposition have already been investigated in great detail such as e.g. diffusion (Gormley and Kennedy (1949)) or thermophoresis (e.g. Romay *et al.* (1998), Messerer et al. (2003)). The latter is often described as being the most important acting mechanisms in heat exchanger fouling (e.g. Abarham *et al*. (2010)).

Yet in our experiments aerosol containing HC or H_2SO_4 vapor showed a higher potential for deposit build-up. Nuclei present in the exhaust gas condense on the cooled wall and build up a sticky layer where soot particles are firmly attached. Additionally, condensation creates a concentration gradient which leads to an enhanced particle transport to the wall, the process being known as diffusiophoresis (Hirschfelder (1954)).

Experiments were performed using model EGR heat exchanger and aerosol.

Size-dependent particle deposition was regarded for different aerosol temperatures and compositions. Coolant temperatures and thus the temperature differences within the heat exchanger were also varied. Soot was produced using a spark discharge generator (GfG) and monodisperse aerosols with particle sizes between 10 nm and 200 nm were generated by using a Differential Mobility Analyzer (DMA). Sulfuric acid vapor was added to the soot aerosol in concentrations comparable to those present in real diesel engine exhaust gas. A summary of the relevant parameters is given in Table 1.

Table 1. Summary of experimental conditions

Parameter	Regarded settings
$T_{gas,\ in}$ [°C]	150; 300
$T_{coolant}$ [°C]	20; 40; 60; 80
c_{H2SO4} [ppm]	0; 0.3; 0.45; 0.9
$\dot{m}_{Air}$ [kg/h]	5; 10; 15

The particle concentrations of the model aerosol were measured at different positions within the heat exchanger using a specially designed sampling probe. Particle Numbers were counted using a Faraday-Cup Electrometer.

For the dry soot aerosol deposition efficiencies increased due to thermal forces with increasing temperature gradients established inside the cooler. Yet for gas and coolant temperatures of 150°C and 20°C respectively, the aerosol containing H_2SO_4 vapor showed even higher deposition efficiencies (Table 2). The acid condenses on the cooler wall and diffusiophoresis acts in addition to thermophoresis.

We found that diffusiophoresis has a major contribution to EGR heat exchanger fouling and needs to be considered besides thermophoresis and turbulent deposition.

Table 2. Deposition efficiencies ε for varied aerosol composition at $T_{gas,\ in}$ = 150°C, T_C = 20°C, $\dot{m}_{Air}$ = 5 kg/h

Particle size [nm]	ε (dry aerosol)	ε (0.9 ppm H_2SO_4)
16	3%	16%
26	2%	6%
36	2%	10%
52	3%	1%
70	4%	2%
95	4%	17%
129	7%	20%
159	13%	17%
186	17%	33%

This work was supported by FVV e.V. (N° 966 & N° 1048).

Abarham, M., Hoard, J., Assanis, D., Styles, D., Sluder, C. and Storey, J. (2010) *Aerosol Sci. Technol.*, 44, 785-795.

Abd-Alla, G. (2002). *Energy Convers & Manage.*, 43, 1027-1042.

Gormley, P. and Kennedy, M. (1949). *Proceedings of the Royal Irish Academy*, 52A, 163-169.

Hirschfelder, J. (1954). *Molecular Theory of Gases and Liquids.* John Wiley & Sons, New York.

Messerer, A., Pöschl, U. and Niessner, R. (2003), *J. Aerosol Sci., 34*, 1009-1021.

Romay, F., Takagaki, S., Pui, D. and Liu, B. (1998), *J. Aerosol Sci.*, 29, 943-959.

Characterizations of PCDD/Fs emitted from gasoline and diesel fueled vehicles

J.H. Tsai[1], S.J. Chen[1,*], K.L. Huang[1], S.C. Chuang[2], L.C. Wang[3] and C.C. Lin[1]

[1]Department of Environmental Science and Engineering, National Pingtung University of Science and Technology, Pingtung County, Nei Pu, 91201, Taiwan
[2]Department of Air Quality Protection and Noise Control, Environmental Protection Administration Executive Yuan, R.O.C. (Taiwan), Taipei City, 10042, Taiwan
[3]Department of Chemical and Materials Engineering, and Super Micro Mass Research & Technology Center, Cheng Shiu University, Kaohsiung City, 83347, Taiwan
Keywords: PCDD/F, motorcycle, lubricant.
Presenting author email: p9531001@mail.npust.edu.tw

PCDD/F release inventory has been extensively investigated due to their acute toxicity and potential health effects. Many significant PCDD/F emission sources are related to combustion processes (US EPA, 2000). Numerous studies have focused on the PCDD/F emissions from various stationary sources, such as municipal solid waste incinerators (MSWIs), and metallurgical activities (Wang and Chang-Chien, 2007; Wang et al., 2010). Only a few studies reported data of PCDD/Fs emission from mobile sources; moreover, remarkable research differences, depending on tested types of vehicles, exist in literature (Dyke et al., 2007; Weilenmann et al., 2005). However, the contribution of PCDD/F from mobile sources is a matter of concern.

This study investigates engine tailpipe exhausts of 12 sport utility vehicles (SUVs), (light duty) diesel passenger vehicles (DPVs), and heavy-duty diesel vehicles (HDDVs) to elucidate the PCDD/F emissions and congener characteristics of tested vehicles using dynamometer tests. For simulation of real on-road operation status and the vehicle exhaust gas emission measurements, FTP-75, NEDC, and FTP transient cycle test procedures were applied for SUVs, DPVs, and HDDVs, respectively. The PCDD/F exhaust samplings (conducted isokinetically) and PCDD/F analyses both followed the US EPA modified method 23. Prior to sampling, XAD-2 resin was spiked with PCDD/F surrogate standards pre-labelled with isotopes. A higher solution gas chromatograph/high-resolution mass spectrometer (HRGC/HRMS) was used for PCDD/Fs analyses.

As shown in Fig. 1, the mean PCDD/F emission concentrations were 1.03, 0.599, and 2.65 ng/Nm^3, with the corresponding mean PCDD/F I-TEQ concentrations were 0.0591, 0.0344, and 0.121 ng I-TEQ/Nm^3 for SUVs, DPVs, and HDDVs, respectively. Moreover, the mean ratio of the PCDDs to the PCDFs concentration (PCDDs/PCDFs) and that of corresponding (PCDDs/PCDFs) I-TEQ in exhaust gases of the SUVs were 0.79 and 0.34, respectively; in the meanwhile, the data were 0.87 and 0.31, respectively, for the DPVs, and were 0.87 and 0.36, respectively, for the HDDVs. The results indicate that the equivalent toxicity from PCDFs dominated the total PCDD/Fs toxicity in the exhaust gases of vehicles.

The calculated mean PCDD/F emission factors were 2.28, 1.48, and 38.8 ng/km, with the corresponding mean emission factors (in terms of total PCDD/F I-TEQ) of 0.123, 0.0802, and 1.69 ng I-TEQ/km for SUVs, DPVs and HDDVs, respectively (Fig. 2). The PCDD/F emission factors followed the order HDDVs > SUVs > DPVs with significant differences (t-test, $p < 0.05$). The emissions from HDDVs were the most dominant PCDD/Fs contributor among the three types of vehicles. Compared with those of previous studies (Dyke et al., 2007; Weilenmann et al., 2005), the relatively high PCDD/F emission factors of SUVs, DPVs, and HDDVs found in this study may be attributed to the operations of cold start tests.

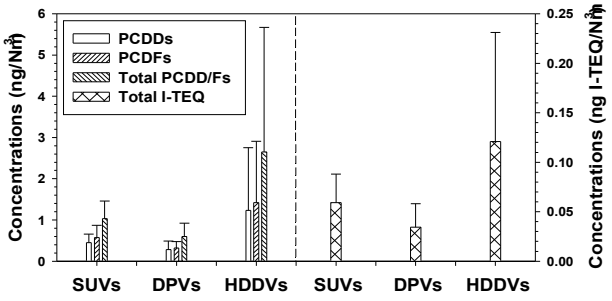

Figure 1. Mean PCDD/F concentrations of SUVs, DPVs, and HDDVs.

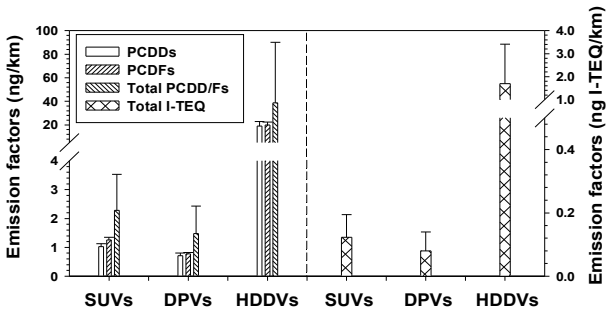

Figure 2. Mean PCDD/F emission factors of SUVs, DPVs, and HDDVs.

Dyke, P.H., Sutton, M., Wood, D. and Marshall, J. (2007) *Chemosphere* **67**, 1275–1286.

US EPA, (2000) *Exposure and Human Health Reassessment of 2,3,7,8-Tetrachlorodibenzo-p-Dioxin (TCDD) and Related Compounds*, EPA/600/P-00/001Bb.

Wang, L.C. and Chang-Chien, G.P. (2007) *Environ. Sci. Technol.* **41**, 1159–1165.

Wang, L.C., Wang, Y.F., Hsi, H.C., and Chang-Chien, G.P. (2010) *Environ. Sci. Technol.* **44**, 1240–1246.

Weilenmann, M., Soltic, P., Saxer, C., Forss, A.M. and Heeb, N. (2005) *Atmos. Environ.* **39**, 2433–2441.

Performance of a new condensation particle counter for engine exhaust gas (PMP-CPC)

L. Keck[1], M. Pesch[1], M. Richter[1], and G.P. Reischl[1]

[1]Grimm Aerosol Technik GmbH&Co. KG, 83404 Ainring, Germany
Keywords: Instrument development, CPC, Diesel exhaust.
Presenting author email: lk@grimm-aerosol.com

EU emission standards Euro 5b/6 specify a maximum particle number of 6.0×10^{11} Particles/km in engine exhaust gas of diesel passenger cars and of light commercial vehicles. This limit value refers to the concentration of nonvolatile particles larger than 23 nm, for which the EU particle measurement program (PMP) specifies a measurement procedure that involves a two stage diluter (Giechaskiel *et al.* 2010) and a special concensation particle counter, the PMP-CPC as detection system.

Grimm has developed a PMP-CPC, which has several advantages that benefit also to the standard CPC line, which employs the same detector head. The PMP-CPC is a butanol based full flow counter with 0.6 lpm sample air, designed to measure also low concentration in diluted exhaust gas downstream of diesel particle filters. The instrument features a novel electronic circuit to separate even strongly overlaping electric peaks generated from the optical detection cell. To investigate the performance of the peak detection technique, we have measured the linearity of the counter, following the PMP protocol (Giechaskiel *et al.* 2009), with soot particles and an faraday cup electrometer (FCE) as a reference (Figure 1).

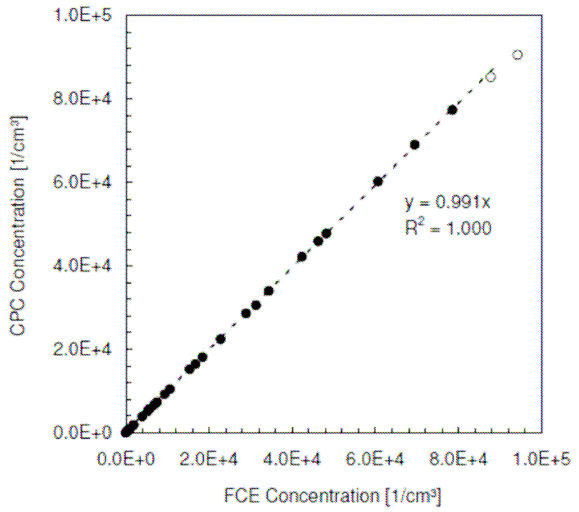

Figure 1. Linearity of the PMP-CPC. Open symbols are not included in the linear regression.

The maximum coincidence correction specified by the PMP regulations, 10%, was reached at 23,000 particles/ccm, which is almost two times the requested minimum value of 12,000 particles/ccm. The CPC can be operated in single count mode for concentrations up to 100,000 particles/ccm, where the coincidence correction amounts to 43% only.

The peak detection circuit employs also two different thresholds where peaks above the higher threshold refer to fully grown butanol droplets, and peak heights between the lower and higher threshold to incompletely grown droplets. The ratio of both count rates is monitored and, as a unique feature, also included in the data protocol. Ratios below unity are a sensitive indicator to any distortion of the condensation process and ensure a maximum reliability of the results for Euro 5b/6 compliance. The data protocol of the instrument includes also the final number concentrations with and without coincidence correction, and, for the CPC standard models, also the concentrations with and without photometric mode.

Condenser temperature is adjusted online to ambient pressure in order to maintain the detection efficiency for 23 nm particles in the target range of 50 ± 12 %. The saturator of the PMP-CPC can not only be heated, but also be cooled. Thus the instrument can be operated also during potential heat accumulation when using several apparatuses at an engine test stand.

Giechaskiel, B., Wang, X., Horn H.-G., Spielvogel, J. Gerhart, C., Southgate, Jing, J. Kasper, M., Drossinos, Y. and A. Krasenbrink, A. (2009) *Aerosol Science and Technology.* **43**, 1164-1173.

Giechaskiel B., Chirico R., DeCarlo, P. F., Clairotte, M., Adam, T., Martini, G., Heringa, M. F., Richter, R., Prevot, A. S. H., Baltensperger, U. and Astorga, C. (2010) *SCIENCE OF THE TOTAL ENVIRONMENT.* **408**, 5106-5116.

Characterization of soot structure and reactivity based on Raman microspectroscopy

J. Schmid, B. Grob, R. Niessner and N.P. Ivleva

Chair for Analytical Chemistry, Institute for Hydrochemistry, Technische Universität München, Munich, Bavaria, 81377, Germany

Keywords: Oxidation reactivity, multiwavelength Raman microspectroscopy, soot structure, reactivity index.

Presenting author email: Johannes-Schmid@mytum.de

The reduction of anthropogenic aerosol sources is essential for the overall improvement of air quality. Soot emitted by diesel engines account for a major fraction of air pollutants in urban areas. To meet the present and future emission limits, soot particles must be removed from the engine exhaust. Diesel particulate filters, which have been applied for this purpose, need to be regenerated by gasification of the deposited soot. The efficiency of this regeneration step is strongly affected by the oxidation reactivity of the deposited soot particles. In particular, the formation of highly reactive soot would make it possible to reduce energy consumption at the regeneration step due to shorter combustion times and lower temperatures (Knauer, 2009). Therefore it is highly desirable to establish a rapid and robust analytical tool for determining the soot reactivity by its structure.

A link between Raman spectroscopic parameters and the structure of carbonaceous and soot has already been discussed in literature. Soot spectra show peaks at 1580 cm^{-1} ("graphite", or G) and 1350 cm^{-1} ("defect", or D), but the G and D peaks exhibit strongly varying relative intensities and widths that can be used for structural characterization. Moreover, for different carbonaceous materials and soot the D mode is dispersive (i.e. a higher intensity and a red shift with higher excitation wavelengths, λ_0), while the position of the G peak is invariant. Reich and Thomsen (2000) have attributed the dispersive character of the D mode to the double-resonant Raman process, which selectively enhances a particular phonon wave vector and phonon frequency. Sood *et al.* (2001) have proposed double resonance and disorder-induced two-phonon scattering combining an optic photon at the K point and acoustic phonon to explain this phenomenon.

By utilizing the dispersive character of the D mode we developed multiwavelength Raman microspectroscopy (MWRM) analysis of soot. The efficiency of MWRM was demonstrated by investigating carbonaceous materials with different structural order at three λ_0 (532 nm, 633 nm and 785 nm, see Figure. 1). In order to compare the behavior of the D mode for various samples and to derive a single parameter characterizing the soot structure, the difference of integrals for pairs of spectra collected at different λ_0 was calculated.

The relation between structure and reactivity of soot was investigated by combining temperature-programmed oxidation (TPO) with MWRM analysis. TPO allowed us to characterize the oxidation behavior of soot by utilizing the maximum emission ($CO + CO_2$) temperature. In order to interpret the TPO data more easily, a reactivity index RI_{soot} can be introduced. Spark discharge soot represents the high reactivity limit and therefore RI_{soot} is set to 100%. In contrast, graphite powder consists of stacks of graphene layers with predominant well-defined long-range ordering and therefore represents the lower reactivity limit (0%), with T being the maximum emission ($CO_2 + CO$) temperature.

$$RI_{soot} = 100\left(\frac{T_{Soot} - T_{Graphite}}{T_{GfG} - T_{Graphite}}\right)$$

This index can be used to compare results from different thermoanalytical methods e.g. TGA vs. TPO more easily and enables for correlation of structure and reactivity.

The comparison of the TPO data by RI_{soot} and the MWRM difference integrals revealed a linear correlation between oxidation reactivity and soot structure. Thus we demonstrated for the first time the potential of MWRM for a robust and rapid prediction of diesel soot reactivity based on the structure-reactivity correlation. (Schmid, 2011)

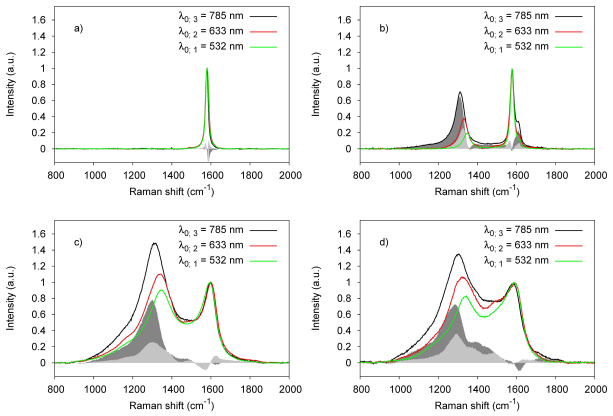

Figure 1. Raman spectra (at different λ_0) of highly oriented pyrolytic graphite (a), graphite powder (b), diesel soot (c) and spark discharge soot (d) with corresponding difference spectra.

Knauer, M.; Schuster, M. E.; Su, D. S.; Schlogl, R.; Niessner, R. and Ivleva, N.P. (2009) *Journal of Physical Chemistry A* **113**, 13871-13880

Reich, S.; Thomsen, C. (2004) *Philosophical transactions. Series A* **362** 2271-2288.

Sood, A. K.; Gupta, R. and Asher, S. A. (2001) *Journal of Applied Physics* **90** 4494-4497.

Schmid J.; Grob, B.; Niessner, R. and Ivleva N.P. (2011) *Analytical Chemistry* (in press).

Characterization of PCDD/Fs emitted from motorcycles

W.Y. Lin[1], S.J. Chen[2], S.C. Chuang[3], K.L. Huang[2], L.C. Wang[4], J.Y. Chiu[2], C.H. Chiu[2] and C.C. Lin[2]

[1]Institute of Environmental Engineering and Management, National Taipei University of Technology, Taipei City, 10608, Taiwan
[2]Department of Environmental Science and Engineering, National Pingtung University of Science and Technology, Pingtung County, Nei Pu, 91201, Taiwan
[3]Department of Air Quality Protection and Noise Control, Environmental Protection Administration Executive Yuan, R.O.C. (Taiwan), Taipei City, 10042, Taiwan
[4]Department of Chemical and Materials Engineering, and Super Micro Mass Research & Technology Center, Cheng Shiu University, Kaohsiung City, 83347, Taiwan
Keywords: PCDD/F, motorcycle, lubricant.
Presenting author email: wylin@ntut.edu.tw

Although interests in PCDD/F emissions have considerably increased in recent years, the PCDD/F emissions from on-road vehicles are still largely unexplored. Intensive studies have focused on the PCDD/F emissions from various sources, such as municipal waste incinerators, metallurgical activities, and temples, due to their vast majority of the total PCDD/F contribution (Hu et al., 2009; Wang et al., 2010). Only limited studies paid attention to traffic PCDD/F emissions (Kim et al., 2003), and no information on PCDD/F emission from motorcycles is available in literature. Because of exclusive proportion in transportation, motorcycle fleets (dominated by four-stroke engines) are considered more important in traffic and air pollution control than on-road vehicles in many countries.

In this study, emission tests for 12 motorcycles (including six 2-stroke engines and six 4-stroke engines) were performed using the regulated driving cycles to obtain the emission concentrations, emission factors, and I-TEQ data of PCDD/Fs according to their toxic equivalency factors (TEFs). The class A urban driving pattern, used for the motorcycles with the maximum velocity over 50 km/h to simulate the on-road emission status, adopts the standard test procedures similar to those of Economic Commission for Europe (ECE) cycle (Taiwan EPA, 1996). A complete test cycle (195 s) composed of the stages of idle (60 s), acceleration (42 s), cruising (57 s), and deceleration (36 s) operations. The maximum, minimum, and mean velocities were 50, 0, and 16.1 km/h, respectively. The PCDD/F exhaust samplings, which were conducted isokinetically, and PCDD/F analyses both followed the US EPA modified method 23. Prior to sampling, XAD-2 resin was spiked with PCDD/F surrogate standards pre-labelled with isotopes. A higher solution gas chromatograph/high-resolution mass spectrometer (HRGC/HRMS) was used for PCDD/Fs analyses.

Fig. 1 shows the congener profiles of the seventeen 2,3,7,8-substituted PCDD/Fs illustrated as the signatures of motorcycle tailpipe emissions. The fraction (%) of a congener is its concentration percentage normalized by a corresponding total PCDD/F emission concentration. The 2-stroke and 4-stroke motorcycles exhibited similar 2,3,7,8-substituted PCDD/F congener profiles. The dominant PCDD/F congeners of motorcycles in emission priority were OCDD, OCDF, 1,2,3,4,6,7,8-HpCDD, and 1,2,3,4,6,7,8-HpCDF, accounting for 37, 15, 10, and 9%, respectively. A similar PCDD/F congener profile was also observed for those of unleaded gas-fueled vehicles and diesel-fueled vehicles (US EPA, 2001).

Two 4-stroke motorcycles (A and B) were also tested to explore effects of lubricant renewal on PCDD/F emissions of motorcycles. After lubricant renewal, the PCDD/F emissions dropped. As expected, the reductions of total PCDD/F and I-TEQ emissions from the lubricant renewal were 26–45 and 41–63%, respectively (Figure 2). Therefore, regularly replacing lubricant oil is helpful for reducing PCDD/F emission from motorcycles.

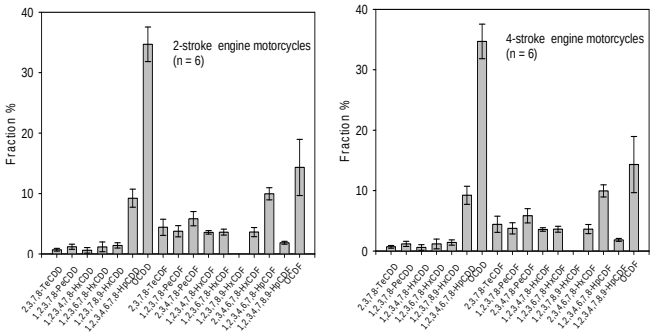

Figure 1. Congener profiles of seventeen 2,3,7,8-PCDD/Fs in the exhausts of motorcycles.

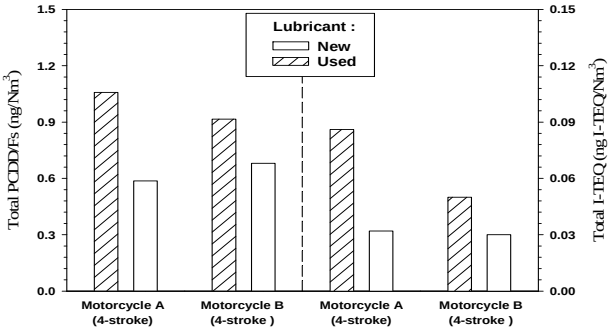

Figure 2. Reductions of PCDD/F emissions from motorcycles after lubricant renewal.

Hu, M.T., Chen, S.J., Huang, K.L., Lin, Y.C., Chang-Chien, G.P. and Tsai, J.H. (2009) *Sci. Total Environ.* **407**, 3290–3294.

Kim, K.S., Hong, K.H., Ko, Y.H., Yoon, K.D. and Kim, M.G. (2003) *Chemosphere* **53**, 601–607.

US EPA, (2001) *Database of Sources of Environmental Releases of Dioxin like Compounds in the United States*, EPA/600/C-01/012.

Wang, L.C., Wang, Y.F., Hsi, H.C., and Chang-Chien, G.P. (2010) E*nviron. Sci. Technol.* **44**, 1240-1246.

Reactive oxygen species (ROS) emissions from diesel engines running on various biofuels

S.D. Stevanovic[1, 3], B. Miljevic[1], N.C .Surawski[1, 2], S.E. Bottle[3], R. J. Brown[2] and Z.D. Ristovski[1]
[1]International Laboratory for Air Quality and Health, Queensland University of Technology, 4001, Brisbane, Australia
[2]School of Engineering Systems, Queensland University of Technology, 4001, Brisbane, Australia
[3]ARC centre of Excellence for Free Radical Chemistry and Biotechnology, Queensland University of Technology, 4001, Brisbane, Australia
Keywords: biofuels, reactive oxygen species, profluorescent nitroxide.
Presenting author email: s.stevanovic@qut.edu.au

Due to rising worldwide demand for energy and the prospect of climate change as a result of greenhouse gas emissions, there is a need to develop alternative energy sources. Therefore it is important to verify the potential of biofuels, as a renewable energy source, and to estimate the health and environmental impacts of their implementation (Gomes and Muylaert de Araújo 2009)

The mechanisms of particulate matter related adverse health effects are still incompletely understood, but a hypothesis under investigation is that many of these effects may derive from oxidative stress, initiated by the formation of reactive oxygen species (ROS) at the surface of and within target cells. Cumulative epidemiological and experimental data support the association of adverse health effects with cellular oxidative stress, including the ability of PM to induce pro-inflammatory effects in the nose, lung and cardiovascular system .High levels of ROS cause a change in the redox status of the cell and its surrounding environment, thereby triggering a cascade of events associated with inflammation and, at higher concentration, apoptosis.

The main aim of this study was to examine the relationship between different alternative fuel substitutions and the oxidative potential of particles emitted from an ethanol fumigated common rail diesel engine that was also equipped to run with biodiesel. To estimate the oxidative potential of ethanol and biodiesel at two different load settings, a pro-fluorescent probe BPEA nitroxide was used. This probe is poorly fluorescent; however the presence of ROS triggers a fluorescence response which makes it a powerful optical sensor for radicals and redox compounds. Samples were collected by bubbling aerosol for 20-30 minutes through an impinger containing 20 ml of 4 μM BPEA nitroxide solution after which fluorescence was measured. The amount of ROS was calculated based on the difference in fluorescence intensity for the test and the filtered control sample and was further normalised to the PM mass. Tests were designed to present emission differences due to changes in fuel and load settings.

The collection of other data was performed to support ROS measurements which involved volatility measurement using a Volatility- Tandem Differential Mobility Analyser (V-TDMA) system and particle composition using a Time of Flight Aerosol Mass Spectrometer (ToF-AMS).
The results depicting volatility properties as well as size-resolved aerosol chemical composition will be discussed.

Figure 1 shows ROS concentrations for diesel (E0), 3 ethanol substitutions of 10, 20 and 30 % (E10, E20, E30 respectively) and neat soy biodiesel (B100). It can be noticed that with an increased ethanol substitution (and also for biodiesel) an increased amount of ROS can be observed, with respect to E0.

It is proposed that ethanol combustion involves more available OH radicals that oxidise the particle surface. This might be a reason for the observed increase in the ROS on the surface of the soot particles (Surawski, Miljevic et al. 2009).
Furthermore at full load setting, concentration of ROS is significantly lower for all fuels, except for biodiesel. In addition, emissions with 100% biodiesel contained the highest concentration of ROS per mg of PM.

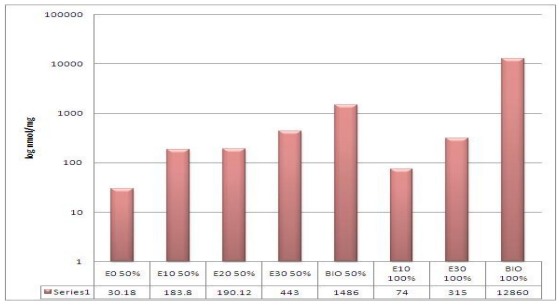

Figure 1: Average ROS concentrations for different fuel and load settings. Note that concentrations of ROS per mg of particulate matter are presented on a logarithmic scale.

Gomes, M. S. d. P. and M. S. Muylaert de Araújo (2009) *Renew. Sustain. Energ. Rev.* **13**, 2201-2204.

Surawski, N. C., B. Miljevic, et al. (2009) *Environ. Sci. Technol.* **44**, 229-235.

Electrical conductivity as sensor principle for a sensor to measure soot aerosols

B. Grob[1], J. Schmid[1], N. Ivleva[1] and R. Niessner[1]
[1]Department of Analytical Chemistry, Technical University of Munich, Munich, Bavaria, 81377, Germany
Keywords: soot, electrical conductivity, raman, sensor
Presenting author email: benedikt.grob@mytum.de

It is well known that aerosol particles may have a great influence on the climate and public health. Especially in urban areas soot particles emitted by diesel engines are very harmful for human health. Future emission limits require that these particles have to be removed from the diesel engine exhaust. This is accomplished by diesel particle filters (DPF), which have to be regenerated periodically by oxidation. Since the DPFs can be damaged by thermal and mechanical forces, an on-board diagnostic system is required (OBD) to realize malfunction of the DPF system premature. For this purpose several approaches are currently under investigation to develop such a OBD particle sensor (Ochs, 2010, Spetz, 2010).

A promising attempt is the detection of particles with a resistive sensor. The sensor can detect particles by measuring the electrical resistance of deposited particles between two electrodes. To understand the sensors a basic knowledge of electrical conductivity of soot is necessary. In this study influences on conductivity of different factors like the morphology of soot, density and temperature should be taken into account. Also the effect of composites of soot with conductive and insulating admixtures should be investigated. The effect of urea, injected by the selective catalytic reduction system (SCR) into the exhaust pipe, has to be considered also.

Different soot samples (Printex 30, Printex XE2, Flammruss 101, Spezialschwarz 4, spark discharge soot and graphite powder) are pressed into pellets and the electrical conductivity is measured by a van der Pauw arrangement (van der Pauw, 1958). This method allows us to determine the conductivity in dependence of the density. Additionally, graphite powder is mixed with SiO_2, TiO_2 and Fe_2O_3 nanoparticles (d_p = 12 - 50 nm) . This allows us to interpret the influence of less conductive particles being mixed with soot depending on the concentration of the admixture. The composites show a percolation behavior (Figure 1). For structural analysis Raman microspectroscopy is applied. Therefore we use our newly developed multi-wavelength Raman microspectroscopy method (Schmid, 2011) to characterize the structure and to correlate the structural with conductivity data. Additionally, a five-band fitting procedure (Sadezky, 2005) is applied to gain parameters concerning the graphitic and amorphous content of soot and related carbonaceous samples.

Moreover, a thermophoretic precipitator has been developed to deposit a soot layer on a glass surface. The glass surface is coated by sputtered silver and prepared by lithography to form interdigital electrodes (Figure 2). The distance between the electrodes is about 100 µm. This combines the conductivity measurement principle with a controlled and size independent particle collection. However, it is still crucial to test this sensor principle with an independent and reliable method. Therefore a test vehicle will be equipped with the AVL Micro Soot Sensor (photoacoustic aerosol sensor) to validate this promising approach for an on-board particle sensor.

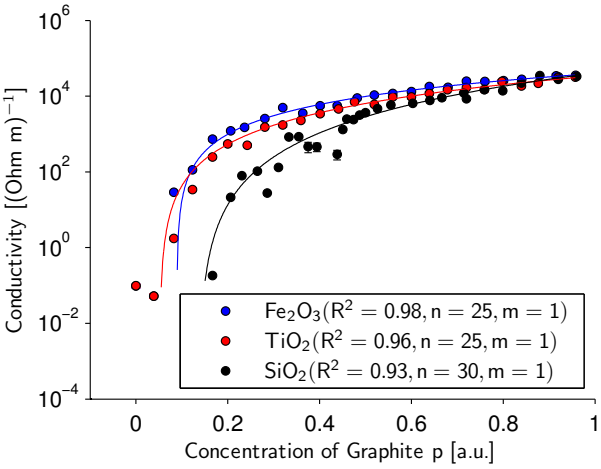

Figure 1: Electrical conductivity of graphite with admixtures of SiO_2, TiO_2 and Fe_2O_3 nanoparticles. The data is fitted by the percolation theory.

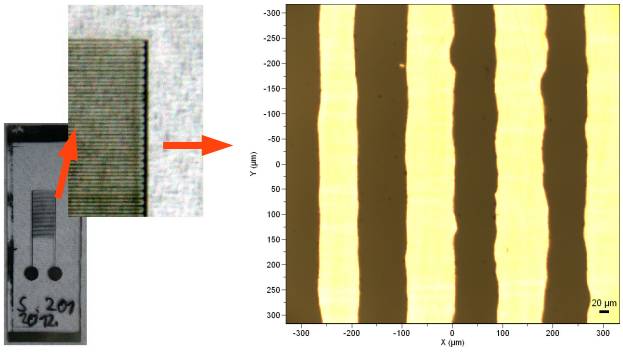

Figure 2: Interdigital electrodes made of silver on a glass substrate.

T. Ochs et al. 2010, SAE Int. J. Fuels Lubr. **3**, 61-69.
L. van der Pauw 1958, Philips Res. Rep. **13**, 1-9.
A. Sadezky et al. 2005, Carbon **43**, 1731-1742.
J. Schmid et al. in press 2011, Analytical Chemistry.
A. L. Spetz et al. 2010, Nordic Innovation Centre.

Laboratory investigation of post-combustion nitro-PAH formation

J. C. Wolf and R. Niessner

Chair for Analytical Chemistry, Technical University of Munich, Marchioninistr. 17, 81377, Munich, Germany

Keywords: NPAH formation, Diesel particle filter.
Presenting author email: jan.wolf@mytum.de

Particulate matter dispersed in diesel exhaust gas is a problem in air pollution and due to its known carcinogenic potential it is considered as harmful to humans. This carcinogenic potential is to more than 50 % accounted to polycyclic aromatic hydrocarbons (PAH) and nitro-PAHs (NPAHs) adsorbed on the particle surface (Schauer *et al.*, 2004). For this reasons the application of diesel particulate filters (DPF) has rapidly increased since the year 2000. This technology proved to reduce the total emitted particle mass and therefore also the emitted amount of PAH. Moreover, they may act also as chemical reactors, where PAHs may be converted to more carcinogenic NPAHs as a result of passive regeneration with high amounts of NO_2 (Heeb *et al.*, 2010).

The focus of our investigations is on this possible nitration reaction. Therefore a laboratory simulation setup of an exhaust gas system equipped with a miniaturized DPF (PM-Kat®–like) was constructed. In this setup spark-discharge soot, which is PAH-free, is coated with a submonolayer of benzo[a]pyrene (B[a]P) and directed to the miniaturized PM-Kat®, where it gets trapped. The regeneration of the filter structure can be controlled by temperature as well as the amount of NO_2 or oxygen passing through. Even different regeneration cycles can be simulated with this system, with the advantage, that only one single PAH (here B[a]P) and its reaction products are monitored.

To ensure that the reaction products were exclusively formed within the DPF structure, a special sampling and denuding system had to be developed.

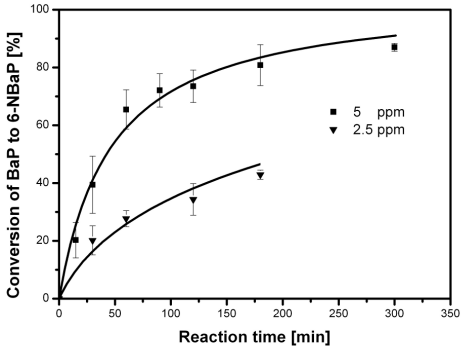

Figure 1.: Benzo[a]pyrene to 6-Nitro-benzo[a]pyrene conversion at 2.5 / 5 ppm NO_2 and 25°C on a quartz fibre filter.

In line with the DPF a heatable KI-based NO_2-denuder was placed to remove the excess of NO_2, which would otherwise cause artifacts on the sampling filter (see figure 1).

This denuder system is capable of removing 100 ppm NO_2 at a flow rate of 5 l/min for three hours with an efficiency $\eta > 98\%$. Behind the annular denuder a second denuder coated with XAD4 resin is placed to collect the gaseous PAH and NPAH. Finally, the particle phase is collected on a quartz fiber filter. Sampling time was one hour. All relevant parts (DPF structure, gas-phase PAH collector and filter) were analyzed for NPAH as well as for PAH.

Analysis was carried out by means of HPLC coupled to a fluorescence detector. The weak fluorescence exhibited by NPAHs required a reduction of the NPAHs to the corresponding amino-PAH (Schauer *et al.*, 2004). Therefore a reduction column densely packed with 5% Pt on γ-Al_2O_3 was placed after the reverse-phase analytical column used for the separation. Eluent was methanol/water and the injection volume was 0.5 µl. A LOD in order of 50 - 300 pg/µl was achieved for 12 different NPAH.

In our experiments 6-nitrobenzo[a]pyrene (6-NB[a]P) was found as major product, with trace amounts of 1- and 3-nitrobenzo[a]pyrene. By measuring the formation of 6-NB[a]P and the decrease of B[a]P at different reaction times and assuming the nitration being the only ongoing reaction, the conversion of B[a]P to NB[a]P could be calculated.

Our results show that DPFs using NO_2-aided regeneration are capable of increasing the NPAH emissions in diesel exhaust significantly.

Financial support by DFG is gratefully aknowledged.

Schauer, C., Niessner, R., Poeschl U. (2004) *Analytical and Bioanalytical Chemistry*, **378**, 725-736.

Heeb, N. V., et al. (2010) *Environmental Science and Technology*, **44**, 1078-1084.

Carrara M., Wolf J. C., Niessner R. (2010), *Atmospheric Enviroment*, **44**, 3878-3885.

Thermodenuder with low nanoparticle losses: design, simulations, laboratory tests and diesel exhaust particle studies

A. Arffman[1], T. Rönkkö[1], P. Karjalainen[1], T. Lähde[1,2], J. Heikkilä[1], L. Pirjola[2], D. Rothe[3] and J. Keskinen[1]

[1]Aerosol Physics laboratory, Tampere University of Technology, Tampere,FI-33101, Finland
[2]Department of Technology, Metropolia University of Applied Sciences, FI-00180 Helsinki, Finland
[3]MAN Nutzfahrzeuge AG, Abt. MTVN, Abgasnachbehandlung, Vogelweiherstrasse 33, D-90441 Nürnberg, Germany
email: anssi.arffman@tut.fi

Diesel exhaust undergoes rapid cooling and dilution processes when the exhaust is released into the atmosphere. During these processes, gas-to-particle processes like nucleation and condensation can take place modifying the size distribution and physical and chemical characteristics of the exhaust particles.

Particle volatility studies are a practical way to study the gas-to-particle processes of diesel exhaust. In addition to the emission characterizations, volatility studies can produce information about the particle formation processes and about the technical factors affecting them (e.g. exhaust after-treatment, fuel quality).

For example, in several studies the diesel exhaust nucleation mode is shown to include a non-volatile fraction. The initial formation of nonvolatile nucleation mode particles have been showed to take place at high temperature conditions before the exhaust entered into the atmosphere and the formation is affected e.g. by fuel injection pressure and exhaust after-treatment.(eg. Rönkkö et al. (2007), Heikkilä et al. (2009), Lähde et al. (2011)).

On the other hand, the changes of fuel and lubricant oil sulfur content affect mostly to the emissions of totally volatile nucleation mode particles (Karjalainen et al. (2011)).

In the studies above, the particle volatility has been studied using a thermodenuder (TD) where the semi-volatile particle fraction is first evaporated in the heating part and, after that, collected onto the surface of active charcoal in denuder part. The diesel exhaust nucleation mode studies require that, in addition to the effective evaporation of volatile components, the penetration of small non-volatile particles is high enough. Therefore, we built a TD based on the following designing criteria:

1) TD is able to evaporate all semi-volatile species of diesel exhaust particles
2) Evaporated vapors are efficiently collected into the activated charcoal
3) Flow range of TD is 0-10 slpm and the inlet temperature is 300K or higher.
4) Aerosol cools in the denuder part nearly to the inlet temperature of 300K.
5) TD provides a high penetration for non-volatile particles larger than 3 nm.

Designing of the TD was based on simulations by employing CFD packages of Ansys Fluent and Comsol Multiphysics. Losses of non-volatile particles were simulated as a function of particle size by solving the transport equation for different particle sizes in combination with the flow field and heat transfer equations. Evaporation rates of 10 – 100 nanometer sulfuric acid – water particles with concentration of 10^8 particles/cm^3 were simulated (see Figure 1). It can be seen that the particles evaporate in the heating part. In addition, simulations showed that the concentration of the sulfuric acid was reduced by a factor of 300 in the denuder part. The evaporation efficiencies (Karjalainen et al. 2011) and the non-volatile particle losses (Heikkilä et al. 2009) were tested also by generated particles.

In addition to the simulations and laboratory tests, the TD was used in the diesel exhaust particle studies in engine laboratories and on-road. These field measurements showed that the TD is able to remove the volatile nucleation mode particles and condensates from the soot particles (Karjalainen et al. 2011). In engine laboratory measurements the size-distribution measurements of the non-volatile core mode particles agreed well with the results obtained by using the hot dilution setup. Also the studies related to nucleation mode particle charge supported the results(e.g Lähde et al. (2011)).

In summary, simulations, laboratory tests and real engine exhaust measurements confirm that the TD performs well when it is properly operated; the sample flow is not too large, the temperature is not too low and the nucleation mode particles are not too large.

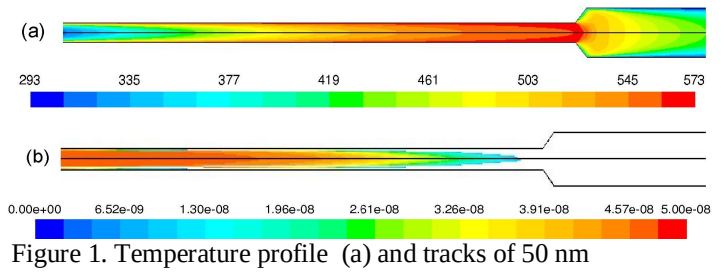

Figure 1. Temperature profile (a) and tracks of 50 nm H_2SO_4-H_2O- particles inside the TD (b).

J. Heikkilä et al. (2009). Journal of the Air & Waste Management Association 59 pp. 1148-1154.
P. Karjalainen et al. (2011). Manuscript in preparation.
T. Lähde et al. (2011). Accepted to Env. Sci. & Tech.
T. Rönkkö et al. (2007) Env. Sci. &Tech., 41, 6384-6389.

Microstructural Aspects of Catalytic Soot Oxidation in Diesel Particulate Filters

S. Lorentzou[1], M. Kostoglou[2] and A.G. Konstandopoulos[1,3]

[1]Aerosol & Particle Technology Laboratory, CERTH/CPERI, P.O. Box 60361, 57001, Thessaloniki, Greece
[2]Department of Chemistry, Aristotle University of Thessaloniki, PO. Box 116, Thessaloniki 54124, Greece
[3]Department of Chemical Engineering, Aristotle University of Thessaloniki, PO. Box 1517, 54006, Greece

Keywords: aerosol, diesel soot particles, diesel particulate filters, soot oxidation
Presenting author email: souzana@cperi.certh.gr

The direct oxidation of soot by employing catalyst coated Diesel Particulate Filters (CDPFs) or fuel borne catalysts, depends greatly on soot-catalyst proximity. The highest degree of soot-catalyst contact that can be achieved is in the case of fuel borne catalysts. In case of catalyst coated filters, the details of the distribution of the catalytic coating on the channels of the filter, on the one hand, and the evolution of the soot deposit on the catalytic layer, on the other hand, are factors that affect the oxidation of soot and consequently the efficiency of the catalytic system. It has been therefore realized that, for the optimization of such catalytic systems, model-based approaches are required, that could estimate the parameters that govern the oxidation of soot under various conditions (Kostoglou and Konstandopoulos, 2005). The soot oxidation kinetic studies in the literature are primarily focused on the effect of oxygen and the derivation of reaction schemes and secondary on the structural details (Messerer et al, 2006).

In the current work, microstructural models of soot oxidation, based on the generalization of the Two-Layer model for incomplete soot-catalyst contact (Konstandopoulos and Kostoglou, 1998), are developed in order to express the micromechanics of soot-catalyst particle interactions that are observed during soot oxidation on catalyst coated filters and on filters loaded with soot particles that contain fuel borne catalysts at different concentration levels.

An extensive set of controlled experiments (isothermal or with linear temperature increase) using fuel borne catalysts and catalytic coatings has been performed. The experiments analyzed in this work were: (i) soot oxidation under linear increase of temperature on catalytic wall-flow monoliths coated with different amounts of catalyst via an advanced coating technique, the Aerosol Based Deposition (ABD) (Lorentzou *et al.*, 2007), (ii) isothermal oxidation of soot on catalytic filters coated via a conventional and an advanced (ABD) technique and (iii) isothermal oxidation of soot with the aid of different doses of a Ce/Fe based fuel-borne catalyst. In cases (i) and (ii) the model was based on a population balance approach for different classes of soot particles which have different levels of contact to the catalyst sites and on the dynamic evolution of these populations during oxidation, taking into account migration phenomena. In case (iii), the rate of the reaction as a function of conversion changes in such a manner as the temperature and the amount of additive increases that gives rise to a view of a spatial evolution of the additive particles on the surface as well as inside the bulk of the soot particle. The initial aggregation state between the soot and catalyst particles is shown to largely determine the evolution of the system during oxidation. The agreement between the experimental data and the simulated curves that derived from the application of the microstructural model in the case of the oxidation of soot with the aid of different amounts of fuel-borne catalyst is illustrated in Figure 1.

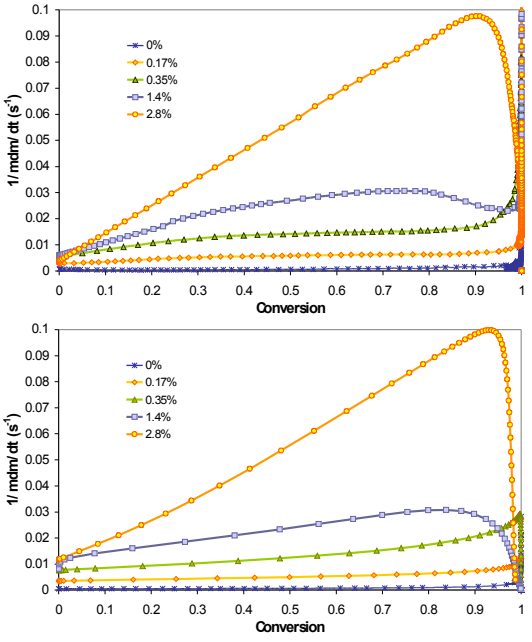

Figure 1. (a) Experimental and (b) simulated instantaneous soot oxidation rate curves as a function of conversion for the case of fuel-borne catalysts

The micromechanical models of soot-catalyst interaction successfully described the experimentally observed behaviour of the catalytic systems during soot oxidation opening the perspective for advanced modelling of the catalytic soot oxidation process.

Kostoglou, M. and Konstandopoulos, A.G. (2005) *AIChE Journal* **51**, 2534-2546.

Messerer, A., Niessner, R. and Poschl, U. (2006) *Carbon* **44**, 307-324.

Konstandopoulos, A.G. and Kostoglou, M. (1998) *Proc. Int. Conf. on Advances in Vehicle Control and Safety*.

Lorentzou, S., Pagkoura, C., Konstandopoulos, A.G. and Boettcher, J. (2007) *in JSAE Annual Congress,* JSAE 20077334.

Effects of Emulsion Fuels on the Characterization of Exhaust from a Diesel Engine Generator

K.H. Chang[1*], W.Y. Lin[2], J.Y. Syu[2], Y.Y. Chang[2], and C.C. Chen[3]

[1]Department & Graduate School of Safety Health & Environment Engineering, National Yunlin University of Science and Technology, Yunlin, Taiwan
[2] Institute of Environmental Engineering and Management, National Taipei University of Technology, Taipei City, Taiwan
[3]Occupational Medicine and Industrial Hygiene, National Taiwan University, Taipei, Taiwan

Keywords: diesel engine generator; water/diesel emulsion fuel; number concentration
Presenting author email:changken@yuntech.edu.tw

Abstract

Emulsion fuel is a possible alternative fuel for reduction of diesel engine emissions. Using water/diesel emulsion fuel as a fuel can reduce the emissions of nitric oxide and particulate matters of the exhaust.(Samec et al., 2002; Armas et al., 2005) However, few researches have been carried out on the particle number concentration and energy efficiency from high speed light-duty diesel engine generator fueled with water/diesel emulsion fuel.

In this study, an ultrasonic vibrator with 40-kHz frequency was employed to prepare different water/diesel emulsion fuels (W5S5; W10S5; W15S5: W is water content; S is surfactant content). The experimental system consisted of a light-duty diesel engine generator, Electrical Low-Pressure Impactor (ELPI), Loading, and Fuel Consumption Measuring Device.

The results showed that the exhaust gas temperature was increased as generator loading was increased. However, it was decreased as the water content of emulsion diesel fuel was increased. When the loading was less than 2700 watts, the number concentration might increase as loading was increased. However, as loading was above 3600 watts, the number concentration was decreased. The total number concentration was 1.42×10^{8} #/cm^3 by using super diesel. However, the total number concentration was decreased to 2.99×10^{7} #/cm^3 by using W15S5 emulsion fuel (Fig. 1 & 2). Furthermore, the net diesel fuel consumption was decreased. As a result, using W/O emulsion fuel could increase the engine thermal efficiency by 12 to 34 %.

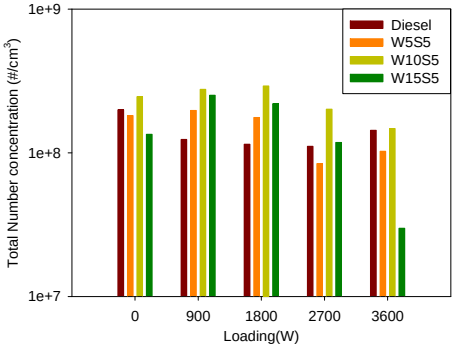

Figure 1.Total number concentration of exhaust from a diesel engine generator as different fuel and loading.

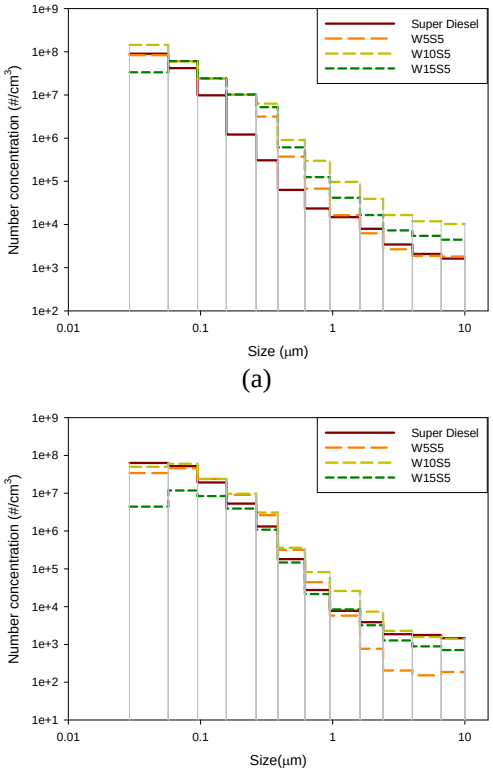

Figure 2.Particle size distribution of exhaust from a diesel engine generator as different fuel at (a)0W; (b)3600W.

Samec, N., Kegl, B., and Dibble, R.W. (2002) "Numerical and Experimental Study of Water/Oil Emulsified Fuel Combustion in a Diesel Engine," *Fuel*, 81, 2035-2044.

Armas, O., Ballesteros, R., Martos, F. J. and Agudelo, J. R. (2005) "Characterization of light duty diesel engine pollutant emissions using water-emulsified fuel," *Fuel*, 84, 1011-1018.

Pilot-Scale-Aerosol Infiltration Synthesis and Deposition of Catalyst Particles on Diesel Particulate Filters

S. Lorentzou[1], D. Zarvalis[1], I. Dolios[1], C. Lekkos[1], C. Agrafiotis[1] and A.G. Konstandopoulos[1,2]

[1]Aerosol & Particle Technology Laboratory, CERTH/CPERI, P.O. Box 60361, 57001, Thessaloniki, Greece
[2]Department of Chemical Engineering, Aristotle University of Thessaloniki, PO. Box 1517, 54006, Greece

Keywords: aerosol deposition, diesel soot particles, catalyzed diesel particulate filters, soot oxidation
Presenting author email: souzana@cperi.certh.gr

The most efficient way of reducing the particulate emissions from the exhaust of Diesel engines is the use of Diesel Particulate Filters (DPFs). However, DPFs need to be periodically cleaned (regenerated) from the accumulated soot particles. Two pathways are mainly being investigated for the efficient regeneration of DPFs: the first one involves engine measures and the second one involves the application of catalytic coatings on the DPF. The involved catalysts aim to promote the reactions in the gaseous phase to produce reactive species that can oxidize soot and/or reactions in the solid phase between soot and catalytic particles.

Conventionally, the coating of monolithic structures with the catalytic elements is conducted via impregnation of the supports in a slurry of the catalyst or in a solution containing the catalyst precursors. Alternatively, the coating of monolithic filters can be achieved via aerosol routes by the in-situ synthesis and deposition of the catalytic particles on the DPFs (Karadimitra et al., 2001, Lorentzou et al., 2009). In the past, we have presented a pilot-scale Aerosol Infiltration synthesis and Deposition (AID) unit that involved a thermal spray gun for the creation of the high-temperature catalyst synthesis zone (Lorentzou et al., 2010). The pilot-scale unit employs an in-house atomizer for the atomization of appropriate precursor solutions while the production of the aerosol of droplets is used for the synthesis and the in-situ deposition of catalytic particles on full-scale DPFs. In the present work the high temperature synthesis zone is implemented via the incorporation of a heat exchanger (Figure 1). The droplets are transferred through the specially designed heat exchanger where they undergo evaporation of the solvent, precipitation of the reactants and crystallization to solid particles. The unit was used to integrate the different catalytic components that enhance the gas phase reactions as well as the soot oxidation reaction, into one multifunctional "reactor".

The final oxide particles that are formed are in-situ deposited on a monolithic real-size DPF, located at the exit of the heat exchanger. The coating process is monitored by the development of the pressure drop on the filters as a function of the amount of the deposited material. Initial experiments involved the optimization of the deposition parameters (gas flow and temperature) that affect the droplets' size and the catalyst particle size and morphology. Having defined the optimal unit operating conditions, the microstructure of the coatings on the walls of the filters and the homogeneity of the catalyst layer along the channels of the filters was observed with Scanning Electron Microscopy (SEM).

The performance of the coated DPFs was evaluated with respect to their pressure drop behavior during the accumulation of soot on the filter and to their catalytic activity towards the oxidation of soot and the conversion of gaseous pollutants (e.g. CO, HC and NOx). The evaluation was performed on an engine test bench. The catalyzed DPFs demonstrated enhanced performance when compared to state-of-the-art catalyzed DPFs especially if direct soot oxidation is of concern.

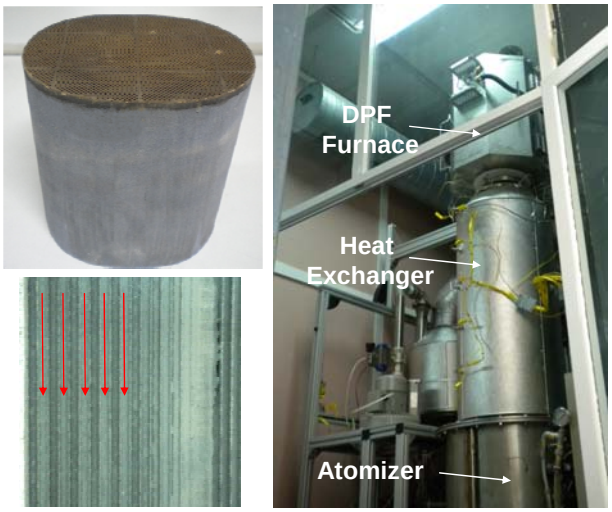

Figure 1. The AID pilot-scale unit. Up-left: a coated oval-shaped DPF. Down-left: the catalyst coating at the inlet channels of the DPF.

This work was supported in part by the European Commission within the Project: "ATLANTIS" (FP6-NMP-2004–3.4.2.2-2, 026678).

Karadimitra K., Macheridou G., Papaioannou E. & Konstandopoulos A.G. (2001). *PARTEC proceedings*, 135, 27-29 March, Nuremberg.

Lorentzou S., Pagkoura C., Zygogianni A., Kastrinaki G. & Konstandopoulos A.G. (2009). *SAE International Journal of Materials and Manufacturing*, 1, 181-198.

Lorentzou S., Asimakopoulou A., Marinou A., Dolios I, Vardavoulias M., Agrafiotis C. & Konstandopoulos A.G., International Aerosol Conference, (2010), Helsinki.

Particulate matter emissions from a winter operation of a modern on-road diesel engine powered by heated rapeseed oil

M. Vojtisek-Lom, M. Mazač, R.E. Lozano

Department of Vehicles and Engines, Technical University of Liberec, Liberec, Czech Republic
Keywords: combustion, diesel engine, rapeseed oil, vegetable oil, biofuels
Presenting author email: michal.vojtisek@tul.cz

Diesel engines powered by liquid fuels are a widely used, time-proven, practical and economical source of motive power for heavier road vehicles and mobile machinery. As the continuing use of traditional petroleum-based diesel fuel is severely threatened by increased world demand for petroleum, dwindling petroleum resources which are often located in politically problematic regions, and global climate changes stemming from the release of fossil carbon into the atmosphere, replacement fuels are being sought. At the same time, ultrafine particles produced during the combustion process in a diesel engine pose a major environmental and human health hazard, notably when released in urban streets. These concerns drive the need for careful evaluation of the effects of new fuels and new engine and exhaust aftertreatment technologies on particle emissions.

Neat vegetable oils are primarily used for the production of biodiesel, which is blended with petroleum diesel fuel. Their use directly as a fuel is minor but increasing mainly in stationary engines. Previous research done on traditional mechanically injected engines has shown that operation on heated rapeseed oil (RO) results in a decrease of particulate matter (PM) emissions at moderate and higher rpm and loads but an increase in PM at low loads (Czerwinski 2008, Vojtisek 2009). The increase in PM emissions was attributed primarily to higher viscosity of rapeseed oil compared to diesel fuel, causing worse atomization of the fuel, and worsened evaporation in the combustion chamber, leading to a less complete combustion; the decrease in PM to the differences in chemical structure of rapeseed oil, notably the absence of aromatics and about 10% by weight oxygen content. The number mean particle diameter was smaller compared to diesel fuel except for high loads, and that the fraction of organic carbon is higher in the PM from rapeseed oil combustion, offering an advantage if an oxidation catalyst is used.

To decrease PM emissions, majority of currently produced diesel engines use a Common-Rail (CR) injection system. In a CR system, multiple injections are performed, with the timing and quantities of fuel injected controlled and optimized for petroleum diesel fuel. While this approach greatly reduces PM emissions when operating on diesel fuel, a question arises as to its performance with vegetable oils for which it is not optimized. Higher PM were reported by Dorn (2007).

In this study, a 4.5-liter, 130 kW, four cylinder, turbocharged Cummins ISBe4 engine, widely used in medium trucks (lorries), with a Bosch CR injection system, was tested on an engine dynamometer during steady-state operation at engine speed and load combinations defined in ESC and WHSC cycles (DieselNet). The engine was operated without any exhaust gas aftertreatment system on diesel fuel, neat biodiesel (FAME) and heated RO. The exhaust was routed in an improvised full-flow dilution tunnel, part of which was located outside of the laboratory. PM mass emissions were measured by the gravimetric method. Particle size distributions in the range of 5-500 nm were measured by EEPS spectrometer (model 3090, TSI, St. Paul, MN, USA). The testing was performed during the winter at outside temperatures 265-270 K and engine intake air temperatures 285-290 K.

The dilution apparatus and its operating temperature were favorable for nucleation and condensation of particles. No efforts were taken to evaporate volatile matter from the particles by a thermodenuder or by diluting with heated air. Therefore, this experimental setup was considered to represent reasonable worst-case scenario of an engine operated during the winter.

The particle number emissions for FAME were typically similar to tens of percent lower compared to diesel fuel in all size ranges. For RO, particle concentrations were between diesel and FAME above 20-30 nm, but markedly higher at lower diameters with a strong nanoparticle peak; these small particles are believed to be organic carbon which would be in gaseous form at higher temperatures. Total particle number emissions for RO were compared to diesel lower at full load but higher at all other regimes. The effect on total PM mass over ESC and WHSC cycles was not uniform and relatively small. With the exception of the nanoparticle peak which is subject to future discussions, no major adverse effects on PM emissions were observed during operation of a modern CR diesel engine on heated RO.

The work was supported by the Czech Science Foundation (grant 101/08/1717) and by the Czech Ministry of Education (project 1M6840770002).

Czerwinski, J.; Zimmerli Y.; Kasper, M.; Meyer, M. (2008). *SAE Technical Paper* 2008-01-1382 (Society of Automotive Engineers, www.sae.org).

DieselNet – www.dieselnet.com

Dorn, B.; Wehmann, C.; Winterhalter, R.; Zahoransky, R. (2007) *SAE Technical Paper* 2007-24-0127.

Vojtisek–Lom, M., Pechout, M., Blazek, J., Moc, L., Hlavenka,T. (2009). *SAE Technical Paper* 2009-01-1913.

A new device for high speed measurements of nano particles

Georg Reischl[1], Markus Pesch[1], Lothar Keck[1]

[1]Grimm Aerosol Technik GmbH & Co. KG, 83404 Ainring, Germany
Keywords: Atmospheric Aerosol, Instrument development, PM10, PM2.5, SVC.
Presenting author email: mp@grimm-aerosol.com

Electrostatic Measurement Techniques have been applied to the characterization of submicron aerosols since 1966. Initially designed for laboratory and ambient measurement tasks only this method has been more or less successfully applied also for emission aerosol characterization, encountering numerous problems. Main issue is the dilution problem, making the use of this method rather complicated and requiring a high level of knowledge to avoid erroneous results. It will be shown, that a rather simple redesign of the method by integration of the dilution system into the measuring device can solve most of the intrinsic problems connected with the characterization of highly concentrated particles suspended in a reactive carrier gas at prohibitive temperature and pressure levels. A few selected examples are presented, outlining the broad spectrum of applications.

Developed in two steps in the late nineties during a cooperation of the Vienna University, the AVL and the GPR-Aerosol Inc. two Systems were designed, the DDMPS for the use during conventional test bed studies featuring two DMAs run in parallel covering the size range from 2 nm to 900 nm with a cycle time of 90 seconds.

Still not fast enough for transient aerosol sources, the system was expanded to 10 DMAs featuring a somewhat poorer size resolution, but a fast cycle time of 200 ms only. This TrDMPS was first built as a prototype at the University of Vienna in cooperation with GPR-Aerosol Inc. in 2000 and is used since to characterize and investigate the dynamic Emission pattern during legal test cycles at Roller test bed facilities throughout Europe and Asia.

In 2005 a commercial version of the 10 DMA-FCE device FAPES was developed by Grimm Aerosol Technology. However, difficulties with the complex plumbing of the device caused severe handling problems.

In 2011, Grimm-Aerosol technology will present a newly designed FAPES, featuring a 12 DMA device with improved size resolution and with an improved pneumatic setup to avoid the known plumbing problems.

Some results of the studies utilizing the TrDMPS and the FAPES leading to discussions of environmental management policies are shortly presented.

Thursday, September 8, 2011

Session 8P: Poster session B

Particle-Lung Interactions

Deposition efficiency of micro-size particles in the upper airway of Taiwanese adults

D.J. Hsu[1] and M.H. Chuang[2]

[1]Department of Safety, Health and Environmental Engineering, National Kaohsiung First University of Science and Technology, Kaohsiung, 811, Taiwan
[2]Department of Occupational Safety and Health, Chang-Jung Christian University, Tainan, 711, Taiwan
Keywords: deposition efficiency, upper airway, Taiwanese adults.
Presenting author email: hsuderjen@nkfust.edu.tw

Numerous studies to determine the removal efficiency of the inhaled particles in the nasal region have been performed in the past decades, either by using replicate casts or human volunteers (Cheng et al., 1991; Garcia et al., 2009; Liu et al., 2010). However, most of those studies were primarily based on a limited number of white male subjects (Bennett and Zeman, 2005). Some previous studies also indicated that nasal anatomic and dimensional factor are important in determining the amount of deposition in the nasal passage, and particle deposition data from a demographically diverse group is important (Kesavanathan and Swift, 1998).

The purpose of this study was to obtain particle deposition efficiency in the upper respiratory tract from Taiwanese adults with respect to particle sizes (0.5~20μm) and inspiratory flow rates. Information of nasal geometry of the human subjects were collected to address the racial differences in particle deposition in the upper respiratory tract.

Nine healthy and non-smoker adults (5 men and 4 women) with age ranging from 23 to 45 years old participated in this study. The particle deposition in the upper respiratory tract was measured for particles with aerodynamic diameter between 0.5 to 20μm. To simulate the inspiratory demands at various workload levels, minute volume of 10, 15, 20 and 30 liters were selected, which are in the breathing range for humans of resting to moderate exercise. Three repeated measurements were performed for each subject at a selected inspiratory flow rate. For a single experiment, subjects were asked to hold their breath for 20 seconds and air was drawn a mouth piece in subjects' mouths by a constant pump in the manner of nose-in-and-mouth-out. The particle concentration near the human nose (C_0) and the outlet of the mouth piece (Cout) was measured, and the deposition efficiency (η) was determined by the following equation:

$$\eta = 1 - \frac{C_{out}}{C_0}$$

The particle deposition efficiency obtained in the current study showed a large intersubject variation and no significant correlation was found between the deposition efficiency and gender. The average particle deposition efficiency of the nine subjects was plotted as a function of inertial parameter (d^2Q) and was compared with the data of several in vivo and in vitro studies. As shown, those in vivo studies, which were mainly based on the Western people, had higher deposition efficiency than Taiwanese adults. However, the data from previous replicate cast studies seem to better approximate those of current study, except in the relatively high and low values of inertial parameter.

The work of Kesavanathan and Swift (1998) noted that nostril shape would affect the anterior air flow pattern and an elliptical shaped nostril (i.e., greater E) will have greater particle deposition efficiency. The average E obtained from the present study is 1.59, which is close to that of Koreans (E=1.87) in Hwang and Kang (2003), but much lower than the data from Caucasians and Asians (2.47 and 2.15, respectively) measured by Kesavanathan and Swift (1998). We speculate that the difference in nostril shape between Western people and Taiwanese is one of the causes for such discrepancy. Future study with greater numbers of human subject as well as more detailed information of nasal geometry is suggested to clarify whether the difference in particle deposition efficiency exists between ethnic groups.

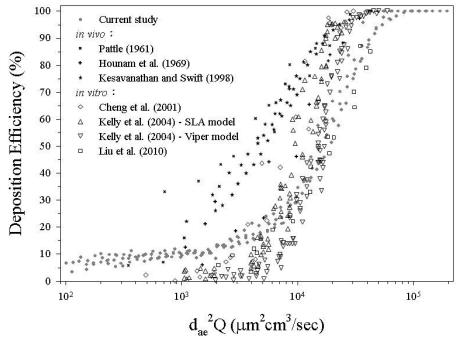

Figure 1. Comparison of the current study with the published in vivo and in vitro data.

This work was supported by the National Science Council of Taiwan under grant no. 96-2221-E-327-046.

Bennet, W. and Zeman, K. (2005) *Inhal. Toxicol*. **17**, 641-648.

Cheng, Y., Yeh, H. and Swift, D. (1991) *Radiat. Prot. Dosimetry*. **38**, 41-47.

Garcia, G., Tewksbury, E., Wong, B. and Kimbell, J. (2009) *J. Aerosol Med. Pulm. Drug Deliv.* **22**, 139-155.

Hwang, T. and Kang, H. (2003) *Ann.Anat.* 185, 189-193.

Kesavanathan, J. and Swift, D. (1998) *Aerosol Sci. Technol.* **28**, 457-463.

Liu, Y., Matida, E. and Johnson, M. (2010) *J. Aerosol Sci.* **41**, 569-586.

Biopersistence and pulmonary effects of intratracheally instilled titanium dioxide nanoparticles at four different doses to rat lungs

T. Oyabu, T. Myojo, Y. Morimoto, A. Ogami, M. Hirohashi, Y. Mizuguchi, M. Hashiba, T. Kambara, BW. Lee and I. Tanaka

Institute of Industrial Ecological Sciences, University of Occupational and Environmental Health, Japan. Kitakyushu, 807-8555, Japan
Keywords: biopersistence, titanium dioxide nanoparticle, intratracheal instillation
Presenting author email: toyabu@med.uoeh-u.ac.jp

Aerosol inhalation study is the best method for respiratory hazard assessment of newly developed materials in animal experiment. But it takes much time and efforts, therefore intratracheal instillation test is used as an alternative.

The hazard of nano-size particle becomes great interest. Titanium dioxide has been recognized as innocent particle but IARC summarized the experimental data and resulted TiO_2 is categorized as "Group 2B". Adverse health effect is depended on the dose as well as its own toxicity. In overloaded condition, the excess adverse effects are observed. Therefore in this study four doses of TiO_2 nanoparticle were intratracheally instilled to Wistar male rats and we try to investigate the dose which induces the overloaded condition.

TiO_2 (P90, Degussa) was ultra-sonicated in disinfected distilled water to smaller particles and the solution was centrifuged. The particle size of TiO_2 in the supernatant was 25 nm detected by dynamic light scattering method. The prepared supernatant was instilled to rats after adjusting the concentration. 0.1mg, 0.2mg, 1mg, 3 mg of TiO_2 nanoparticles dispersed in 0.4ml distilled water were intratracheally instilled to rat lungs. At 3 days, 1, 3, 6, 12 months after the instillation, each 10 rats were dissected. The number of PMN in bronchoalveolar lavage fluid (BALF) from right lungs of each 5 rats was counted. And the deposited amounts of TiO_2 nanoparticles from left lung and two right lungs of each 5 rats were detected by chemical analysis and calculated the biopersistence.

For determination of TiO_2 in rat lungs, dissected lungs were acid digested by H_2SO_4, $(NH_4)_2SO_4$, H_2O_2 with microwave and the Ti concentration in completely digested solution was determined by ICP-AES.

Figure 1 shows the number of PMN in BALF. PMN in BALF of 0.1mg and 0.2mg instilled rats were not increased throughout the observation period after the instillation. In contrast, the PMN number of 1 mg and 3 mg instilled group increase at 3 days after the instillation. For 3 mg instilled group it has continuously increased compared with the other groups.

Figure 2 shows the biopersistence calculated by one compartment model from the average amounts of retained TiO_2 nanoparticles in rat lungs. The biological half times (BHT) of low dose (0.1mg and 0.2 mg) were about four months and almost the same each other. But BHT of 1 mg instilled group increased slightly and that of 3 mg group increased further.

Our results of PMN analysis and biopersistence suggested that approximately 1 mg in lung may be the border zone of overloaded situation for Wistar male rats. Therefore in order to avoid the excess effect, the dose to the lung has to be controlled in animal experiment.

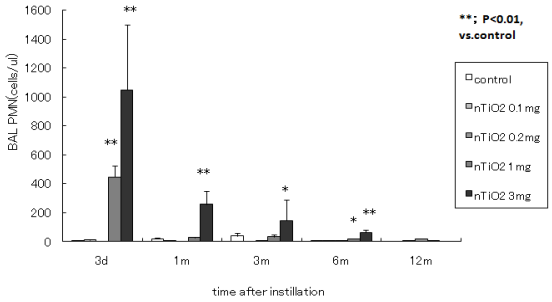

Figure 1. The number of PMN in BALF from rats instilled 0.1, 0.2, 1, 3 mg of TiO_2 nanoparticles at each dissected time.

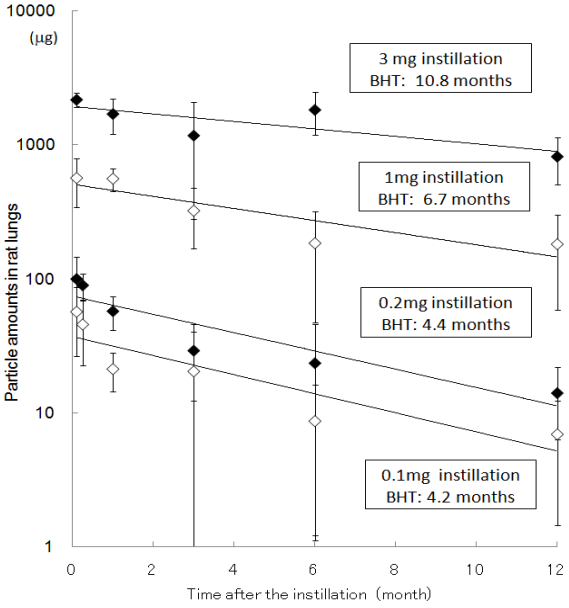

Figure 2. Biopersistence of TiO_2 nanoparticles in rat lungs in 4 different dose instillation test.

A part of this work was supported by UOEH Grant for Advanced Research (H21-3) and Grant-in-Aid for Scientific Research(C) in Japan (20590939).

A Thermal Precipitator for Nanoparticle Cytotoxicity Screening

Dirk Broßell[1], Sabine Plitzko[1], Nico Dziurowitz[1], Erhardt Gierke[1], Volker Bachmann[1], Gunter Linsel[1], Nkwenti Azong-Wara[2], Christof Asbach[2], Heinz Fissan[2], Andreas Schmidt-Ott[3]

[1] Federal Institute for Occupational Safety and Health (BAuA), Berlin, Germany
[2] IUTA e.V., Duisburg, Germany
[3] Delft University of Technology, Delft, Netherlands
Keywords: nanoparticle, thermal precipitator, toxicity, in vitro.
Presenting author email: brossell.dirk@baua.bund.de

In vitro toxicity studies are becoming much more important due to increasing concerns about animal welfare and partly also due to higher costs of *in vivo* studies. We introduce a new device for *in vitro* cell exposure to nanoparticles for cytotoxicity screenings. The system is an attempt to solve one problem most *in vitro* toxicity studies encounter when trying to mimic *in vivo* inhalation studies, namely the lack of representativeness of the exposure to the particles (Teeguarden, 2007) and hence the resulting dose and dose rate. It is conceptualized as a toxicity screening device primarily indicating cytotoxic effects on the human respiratory tract.

The so called Cyto-TP is a thermal precipitator (TP) (Azong-Wara, 2009) for the deposition of airborne nanoparticles on living human epithelial lung cells at the air-liquid interface (ALI). The cellular response to ALI exposure seems to be similar to suspension exposure but occurs at doses significantly lower (Holder, 2008). Cellular response at ALI may be observable at exposure atmospheres with moderate particle number concentrations. The TP deposits particles very smoothly onto the cell surface and therefore does not damage the cells by impact. By using airborne particle exposure the surface chemistry, morphology and size of the nanoparticles do no change in contrast to the use of suspension exposure. Unlike in a similar concept using electrophoresis for particle deposition (Sillanpää, 2008), particles bear their natural charge level. These aspects contribute greatly to a higher representativeness of exposure mode.

The Cyto-TP consists of a hot plate (52°C) and a parallel cold plate (37°C) which hosts the cell cultures as shown in Fig. 1. The aerosol flows between the two plates and particles are deposited onto the cells by thermophoresis. Potential cell stress due to secondary effects is minimized with our device, so cellular response can be related more easily to the presence of nanoparticles in the exposure atmosphere. After exposure the cells can be placed inside a scanning electron microscope for analysis. Additionally CASY cell counting and analysing used to determine the ratio of living and dead cells.

The presentation will describe the first prototype of the Cyto-TP and its design and functionality along with a newly designed experimental approach for cytotoxicity screening. First results of the validation of the Cyto-TP approach with nanoparticles will be presented.

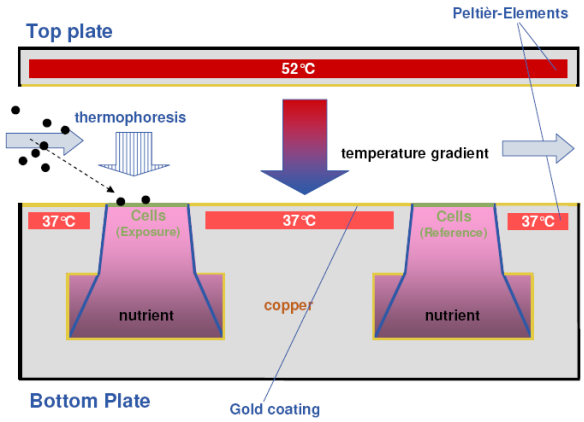

Figure 1. This is a concept sketch of the functionality of the Cyto-TP. The nanoparticles in a laminar flow are deposited onto the cells placed at the cold plate.

The research leading to these results has received funding from the European Community's Seventh Framework Programme (FP7/2007-2013) under grant agreement n°211464-2.

Teeguarden, J. G., Hinderliter, P. M., Orr, G., Thrall, B. D., Pounds, J. G. (2007), *Toxicological Sciences*, **95**, 300-312

Azong-Wara. N., Asbach, C., Stahlmecke, B., Fissan, H., Kaminski, H., Plitzko, S., Kuhlbusch, T. A. J. (2009), *Journal of Nanoparticle Research*, **11**, 1611-1624

Holder, A. L., Lucas, D., Goth-Goldstein, R., Koshland, C. P. (2008), *Toxicological Sciences*, **103,** 108-115

Sillanpää, M., Geller, M.D., Phuleria, H.C., Sioutas, C.. (2008), *Journal of Aerosol Science,* **39**, 335-347

A 3-year-follow-up Study of Traffic Related Respiratory Alterations in Schoolchildren in Milan, Italy

M. Sala[1], F. Cetta[2], S. Argirò[1], P. Ballista[1], R. Zangari[2], V. Guercio[2], E. Bolzacchini[3] and M. Mandelli[1]

[1]Dept. of Pediatrics, University of Milan, Milan, 20122, Italy
[2]Dept. of Surgery and Thoracic Surgery, University of Siena, Siena, 53100, Italy
[3]Dept. of Environmental Sciences, University of Milan-Bicocca, Milan, 20126, Italy
Keywords: air pollution, PM, traffic emissions, health effects of aerosols
Presenting author email: marco.sala@unimi.it

Important adverse effects on children health can be caused by exposure to air pollution, namely during the peculiar "susceptibility window" occurring during the first years of life (Clark, 2010). In particular, traffic related pollution adversely affects lung function development.

Between 2007 and 2008, 228 children, mean age 8 years, were enrolled from 2 primary schools, located in different sites, in order to study pollution related respiratory symptoms and/or diseases in different places of Milan with a different traffic-related exposure. The former (School 1) was located near a large park, the latter was located downtown, close to main crossroads (School 2). Daily levels of PM10 and PM2,5 (diameter <10μm and 2,5μm) were measured both outdoor and indoor outside the schools (in the school garden) and within common places (corridors), for 7 consecutive days during 2 different campaigns (winter and spring-summer). Children underwent skin prick testing for inhaled allergens, analysis of exhaled nitric oxid (FeNO) and spirometry.

The distribution of FeNO values was significantly different (p=0,02) between the two schools. In particular, the percentage of children with FeNO values <5ppb in school 1 was higher (almost double) than in school 2. In 73% of children attending the school located downtown FeNO concentration was between 5 and 20ppb.

The percentage of asthma exacerbations in the previous 12 months was higher in children from school 2 (p=0.05). On the contrary, the prevalence of persistent allergic rhinitis in children allergic to grass pollen was higher in school 1 (p=0.03). In particular, the latter children also had a greater activity limitation, due to rhinitis and concomitant conjunctivitis (p=0.03). Interestingly, the highest recorded peak for PM10 occurred between 8:15 and 9:15 a.m., for 3 consecutive days, and was related to children arrival. This peak (>1000μg/m^3) (figure 1) didn't seem to produce specific health effects, likely because of the usual PM10 composition in a park site, with a lower content of toxic or reactive components.

Hospital admissions, because of lower respiratory tract diseases (bronchitis, bronchiolitis, pneumonia) were more frequent during the winter campaign and in school 2, whereas otitis and allergic rhinitis or conjunctivitis, together with asthma, were more severe during the spring-summer period and in school 1 (p<0,05).

Continuous monitoring for 3 years of both children and PM showed that: 1) short duration pollution peaks, even reaching concentrations 20 folds above the fixed limits, have no consequences on children health and were likely induced by children's arrival or movement; 2) there was an enormous daily variability in PM10 concentration, among the daily mean value results, from the average of values, with a very high standard deviation (+30,+1000μg/m^3) and with various peaks; 3) prolonged follow-up for 3 years in this selected group of children didn't show any evident difference in the occurrence of clinically relevant respiratory diseases. On the basis of FeNO values, different degrees of respiratory function and bronchial inflammation were found in the 2 groups.

Traffic could be responsible at least in part for the different air quality, but individual susceptibility and seasonal changes are also major determinants of clinical outcomes. In particular, early exposure during the first years of life could be responsible for future diseases occurring later, during adult life.

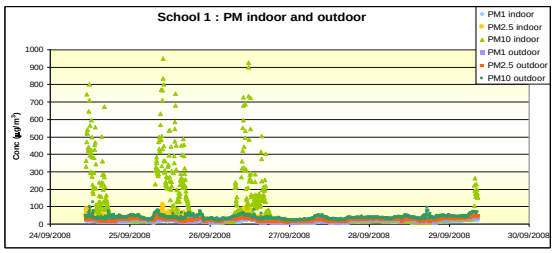

Figure 1. Concentration of PM10, indoor and outdoor, in School 1.

This work was supported by the PROLIFE Project, City of Milan, Italy.

Clark N.A. et al. (2010). *Environ. Health Perspect.*, **118**, 284-290.

Alteration of respiratory function in asymptomatic subjects living in Milan (Italy) and in Aprica (Italy), an Alpine site with different levels of environmental pollution. Spirometric and laboratory evaluation.

F. Cetta[1], G. Schiraldi[2], R. Zangari[1], V. Guercio[1], C. Ghiribelli[1], P. Paladini[1], L. Luzzi[1], M:S: Gallazzi[1], E. Bolzacchini[3], M. Monti[4], G. Gotti[1] and L. Allegra[2]

[1]Dept. of Surgery and Thoracic Surgery, University of Siena, Siena, 53100, Italy
[2]Toracopulmonary and Cardiovascular Department and [3]Dept. of Environmental Sciences, University of Milan, 20126, Milan, Italy
[4]Geriatric Institute "Pio Albergo Trivulzio" (PAT), Milan, 20146, Italy
Keywords: air-pollution, traffic emissions, exposure, health effects of aerosols.
Presenting author email: cetta_francesco@libero.it

Environmental pollution, mainly due to urban traffic, is responsible for a different air quality in metropolitan areas vs less polluted sites and for a different incidence of respiratory complications and/or reduction of pulmonary function.

Methods: Two groups of 99 subjects were recruited (n=198), on a casual and voluntary basis: the former in Milan, Italy, i.e. a densely populated and polluted metropolitan area, the latter in Aprica, a remote alpine site (1181 m.a.s.l), with low pollution, due to traffic or other pollution sources. PM_{10} (<10 μm) and $PM_{2,5}$ (<2,5μm) were measured by PM detection units during two 2 week-campaigns. Each group was classified in 2 subgroups. The former, aged 30 to 64 y (n=72) , the latter over 65y (n=27). All subjects, well matched for cigarette smoke, sex and age were in good health conditions, asymptomatic and with no previous history of respiratory chronic diseases. All of them underwent spirometry, with evaluation of the following parameters: FVC (forced vital capacity), FEV_1 (forced expiratory volume in 1 second), PEF (peak expiratory flow) and MEF_{50} and MEF_{25}, i.e. maximum forced expiratory flow at 50% and 25% of FVC, respectively. In addition, the thiol redox status, which is crucial to balance oxidative stress and ROS generation, facilated by air pollution, was also evaluated in 2 subgroups of subjects,: the former (n=38, age 82±9y) living in Milan, and the latter (n=42, age 70±8y) living in Aprica. HPLC analysis was performed on blood samples for the evaluation of thiols in plasma and erythrocytes (total and reduced forms PT, PR; ET, ER) and also in exhaled breath concentrate (EBC). In fact, thiol redox status contributes to contrast oxidative stress and ROS generation promoted by air pollution. Namely cystein (Cys), cysteinylglycine (CG), homocysteine (Hcy) and glutathione (GSH) were evaluated both in blood and in EBC.

Results: FEV_1 was <80% in 20 out of 99 subjects in Milan (20,2%), whereas it was < 80% in only 8 out of 99 in Aprica (8,08%). Evident differences were also observed in subgroups of different age: FEV1 resulted <80% in 8 out of 72 subjects under 65 y in Milan (11,1%) and in 2 out of 72 in Aprica (2,8%); and in 12 out of 27 (44,4%) and 6 out of 27 (22,2%) in subjects over 65 y, respectively ($p<0,05$). Concerning thiol analysis, there was no evident difference in the GSH levels between the two populations. In fact, GSH alteration is usually a late event, occurring in severe imbalances and no subject in both groups had clinically evident diseases. On the contrary, PT Cys was 459,8 ±152,2 vs 286,3 ±74,8 ($p<0,001$) and ER Cys 2,5±0,8 vs 1,5 ±0,6 ($p<0,001$), respectively. Finally, data concerning thiol balance analysis from EBC showed: 1) a striking individual variability of the various chromatographic peaks; 2) almost complete absence of reduced species.

Conclusion: inhabitants of areas with different traffic volumes showed significantly different Cys, CG and Hcy levels, even if GSH remains unchanged, suggesting a greater- pro-oxidant effect in more exposed populations, affecting Cys, CG and Hcy levels, before GSH alterations. Analysis of thiol redox balance in plasma and erythrocytes is able to distinguish between more and less exposed subjects and could be a useful diagnostic tool for early detection of subjects at higher risk of health effects from environmental pollution. In particular, thiol analysis in EBC could be a very early marker of redox imbalance, and be used to detect early alterations in predisposed subjects. Air pollutants are weak pollutants, which at usual concentration in Western countries, in the absence of increased individual predisposition to respiratory or cardiovascular diseases do not determine clinically evident health effects after short-term exposure. In particular, PM related diseases are likely due to progressive accumulation of biological and tissue damage, because of oxidative stress and other injuries to human cells. Since most of biological alterations caused by PM exposure are likely to be reversible because of endogenous repair and defense mechanisms of the host, it is suggested that periodical interruption of chronic exposure to metropolitan pollutants with exposure to a better environment (such as an Alpine site), could be of benefit in all subjects with prolonged exposure to PM, namely in those with enhanced individual predisposition to develop clinically evident pollution related diseases.

A plea for a more "doubtful" and "skeptic" approach to the role of intrinsic toxicity of airborn pollutants as the main responsible for observed cardiovascular, respiratory and cancerous diseases or deaths in humans.

L. Allegra [1], G. Schiraldi[1] , V. Guercio[2], R. Zangari[2], L. Moltoni[2], J. Martellucci[2] and F. Cetta[2]

[1]Toracopulmonary and Cardiovascular Department University of Milan, Milan, 20126, Italy
[2]Dept. of Surgery and Thoracic Surgery, University of Siena, Siena, 53100, Italy
Keywords: PM, NOx, SO2, COPD
Presenting author email: luigi.allegra@unimi.it

Milan, Italy, is one of the most polluted metropolitan areas in Europe, mainly because of oro-metereological conditions, but also because of density of population, traffic, heating, industrial activities.
In Milan, Italy, between 2007 and 2010, a comprehensive approach to health effects of air pollution was designed (Prolife Project).
In particular, a comparison was made between daily pollutant concentration and hospital admission to 5 major city hospital because of respiratory and cardiovascular diseases during years 2007-2008. A total of 53.514 people were recruited. Only a very weak level of association ($p > 0.05$) was found between daily levels of PM10 and PM2.5, NOx and SO2 and acute admission within 48h because of upper respiratory tract diseases, Pneumonia, COPD exacerbation, Asthma, Heart failure, Acute myocardial infarction or Stroke. This weak association could mean that cases and controls were not properly selected. However, it could also mean that what we have supposed to be the causative agent was not, i.e. it could be simply a co-causal factor, or whatever else.

Even if pollutants are not "innocent bystanders" in the occurrence of cardiovascular, pulmonary or systemic diseases for which they are suspected to play a role, they are not likely to be the unique or main responsible for the occurrence of these diseases.

In fact, the evidence that "in vitro studies", or even clinical studies have shown that Particulate Matter (PM), or at least some components (diesel exhaust, PM2.5, ultrafine particles) were able to determine oxidative stress or trigger the occurrence of inflammatory mediators (cytokines, chemokines) is not enough to demonstrate that PM is able to determine, even after long-term exposure, evident diseases in every exposed subject.

In particular, we don't know yet whether the "pollution related disease" is a true toxic disease, i.e. due to the "intrinsic toxicity of xenobiotics", or their pathogenic potential, or a non toxic disease, i.e. a disease occurring mainly or exclusively in a few predisposed subjects, because of individual susceptibility and reactivity.

In other words, we have to clarify better whether the "pollution related disease" is a toxic disease, more similar to a viral or bacterial infection or, on the contrary, it is closer to an autoimmune disease. Autoimmune diseases are diseases in which individual susceptibility, either inherited or acquired, because of personal history and/or previous exposure, plays a major role. This could suggest that inflammation, and in particular autoinflammation, i.e. the peculiar host reactivity, plays a pathogenic role in the occurrence of the disease, and this role is greater than previously suspected and, in particular, greater than the role played by the intrinsic toxicity of the pollutant.

In the absence of an increased susceptibility of the host, it is likely that airborne pollutants are not going to be severely dangerous and "kill" people. In particular, a "weak level of association" in epidemiological studies means that: 1) airborne pollutants, at usual concentrations in western countries are "weak toxic"; 2) intrinsic toxicity perhaps is not the main pathogenic mechanism through which they determine their harmful activity; 3) autoimmune and autoinflammatory mechanisms could fit better and explain more convincely observed findings; 4) current models used in epidemiological studies to estimate risk potential are not adequate to capture the complexity of host-particle interaction; 5) better markers of exposure should be selected, but also more specific markers of effect, which in particular, should be able to capture different levels of molecular, cellular and tissutal damage; 6) a better definition of individual susceptibility, of its origin (genetical, inherited, but also partly determined by host-environment interaction and then acquired), is of paramount importance, as well as the distinct role that exposure to pollutants is going to determine during the perinatal susceptibility window, which is going to give "asynchronous" clinically evident consequences and determine diseases years or decades after exposure.

A major goal of future research will be the detection of sensitive and specific markers of individual susceptibility, which should facilitate the proper treatment and/or prevention of health effects of air pollution in susceptible people.
In conclusion, the lack of adequate metrics of exposure, effect and susceptibility in epidemiological studies evaluating PM concentration and health effects is one of the main responsible for the conflicting results of these studies .A plea for a more doubtful and "skeptic" approach is mandatory, when dealing with PM as unique responsible of presumed health effects simply because of its intrinsic toxic potential.

Boffetta P. (2009). *J.Nat. Cancer Inst*, **101**: 213-214

Deposition of aerosol particles in dosing tubes (endotracheal tubes) used in aerosol drugs therapy for infants.

Ł.Żywczyk[1], A.Moskal[2] and T.R.Sosnowski[3]

[1,2,3]Faculty of Chemical and Process Engineering, University of Technology, Warsaw, 00-645, Poland
Keywords: endotracheal tubes, aerosol therapy, deposition of aerosols.
Presenting author email: l.zywczyk@ichip.pw.edu.pl

Endotracheal tubes are commonly used to improve inhalation of aerosol drugs and keeping a steady transfer of air inspiration and expiration during an operation. Device is projected for patients of all ages. The shape and geometry of the tubes provide adequate penetration of the active ingredient into the respiratory tract, while ease the use of the device. In comparison to the parenteral method, the tubes connected with inhalators release increased dose of drug into the lungs. The tubes prevent from significant loss of drug in the upper airways during the treatment, therefore contribute to work more efficiently than other methods. Sizes of the tested tubes are presented in Table 1.

In this work, the penetration ratio of the particles in the endotracheal tubes has been calculated, which allows to calculate the dose of inhaled drug. The calculation has been proceeded in CFD (Computational Fluid Dynamics) FLUENT. Velocity profile has been extracted and deposition ratios of aerosol particles with different sizes were explored.

Table 1. Dimensions of the endotracheal tubes.

Tube denotation	Length (mm)	Diameter external OD (mm)	Diameter internal ID (mm)
516.30	68	4.6	3.0
520.25	165	4.1	2.5
520.30	165	4.6	3.0
520.35	165	5.2	3.5

Study

The aim of this study is to calculate penetration in four tubes with different geometric dimensions. During the calculations the tube was bent at an angle of 90 degrees. This corresponds to a real arrangement of the tube in the upper airway of a patient. The motion of the particles was modeled by Lagrange approach, with the use of DPM (Discrete Phase Model). The calculations were made for two values of air flow 3 l/min and 5 l/min, corresponding to a real air flow in infant's airways. Temperature of air 310K. Normal pressure was imposed at the inlet to the tube. The diameters of the tested particles were between 1 μm and 7 μm. Density of the particles 1.1 g/cm^3, this corresponds to densities of commonly used inhalation drugs. Mass flux of the particles at the inlet of the tube was $4 \cdot 10^{-6}$ kg/s. I the simulation the particles were affected by the gravity force. For particles considered with less than 2 μm, Brownian motion and Cunningham coefficient, were included.

In order to check the quality of the computer mesh, a measurement of the pressure drop of air for different values of air flow was performed for each tube diameter. The results showed convergence between the assumption in our model and a real pressure drop in laboratory, in the range of used flow.

The results

The penetration in the function of the aerosol particles size was obtained, determined by diameter of the tube and two values of air flows. The results show that independently of an air flow, for each tube size particles with diameter less than 2 μm will easily penetrate into lower airways and therefore are the main component of the rehabilitation fraction. Particles with diameter greater than 2 μm, will deposit on tube wall with various percentage. Previous results show that particles with 2 μm diameter penetrate the lungs (Annapragada, Mishchiy, 2007). Penetration into lower airways is more effective when 3 l/min value of air is imposed.

The results show the function of the distribution of particles sizes, which penetrate into lungs, therefore allow to estimate drug dose and predict effectiveness of the therapy.

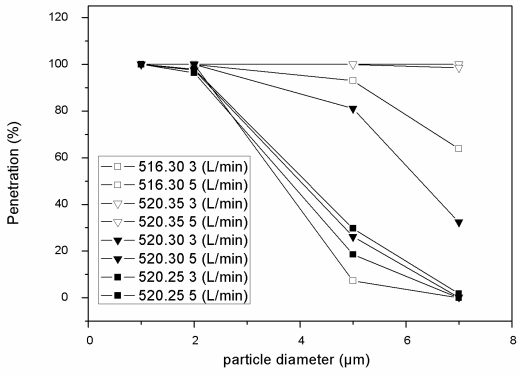

Figure 1.The penetration of the aerosol particles in the function of particle diameter.

The author would like to thank Ph.D. Jan Mazela for providing dosing tubes for experiment.

Annapragada, A., Mishchiy, N. *In silico modeling of aerosol deposition in lungs*, Drug Discovery Today:

Disease Models, **4(3)**, Autumn 2007, 155-161.

"Perinatal susceptible window" as a main responsible for cardiovascular and respiratory diseases occurring later in life because of PM exposure

L. Moltoni[1] , M. Sala[2], V. Guercio[1], Zangari[1], P. Laviano[1], A.M. Azzarà[1], O. Caratozzolo[3], E. Bolzacchini[4] and F. Cetta[1]

[1]Dept. of Surgery and Thoracic Surgery, University of Siena, Siena, 53100, Italy
[2]Dept. of Pediatrics, University of Milan, Milan, 20122, Italy
[3]Geriatric Institute "Pio Albergo Trivulzio" (PAT), Milan, 20146, Italy
[4]Dept. of Environmental Sciences, University of Milan-Bicocca, Milan, 20126, Italy
Keywords: PM, perinatal susceptibility, spirometric values, FeNO
Presenting author email: moltoni@unisi.it

In the present study, hospital admissions to the main pediatric service of Milan were compared with daily and seasonal variations in PM concentration, during 4 consecutive periods: winter/summer 2007, winter/summer 2008.

During 2007-2008, there were in total 440 pediatric admissions for respiratory diseases; 226 (132 M, 94 F) during the winter semester, and 214 (100 M, 114 F) during the summer semester. There were 12.7% asthma or asthma related admissions; 55.8% due to lower respiratory illness, and 31.5 % due to upper respiratory disease. The daily average of PM10 concentration during the 1st semester 2007 was 48.3+/-17.9 mcg/m^3. There were 107 (59.1%) days with at least one hospital admission. The mean daily concentration of PM was higher in days with (n=107) than without (n=74) hospital admissions (p=0.032 or <0.05). Accordingly, children acute admissions were significantly affected by pollution data, with increased admission during winter, namely for upper air tract infections, whereas lower tract inflammation and acute admission for asthma were more frequent during spring-summer.

Between 2007-2008, 228 children, older than 7 y, were enrolled from 2 primary schools, in order to study pollution related respiratory symptoms and/or diseases in different places of Milan with a different traffic-related exposure. The former (S1) was located near a large park, the latter downtown (S2). Daily levels of PM10 and PM2.5 were measured both outdoor (garden) and indoor (corridors) for 7 consecutive days during 2 different campaigns (winter and spring-summer). Children underwent skin prick testing for inhaled allergens, analysis of exhaled nitric oxid (FeNO) and spirometry. The distribution of FeNO values was significantly different (p=0,02) between the two schools: the percentage of children with FeNO values <5ppb was almost double in S1; FeNO was 5- 20ppb in 73% of children from S2. The percentage of asthma exacerbations (previous 12 months) was higher in S2 (p=0.05). The prevalence of persistent allergic rhinitis in children allergic to grass pollen was higher in S1 (p=0.03), the latter children also had a greater activity limitation, due to rhinitis and concomitant conjunctivitis (p=0.03).

It is suggested that: 1) newborn exposure could be one of the most relevant pathogenetic effect of "weak pollutants, with low intrinsic toxicity", as air pollutants actually are at usual concentration in the atmosphere. 2) epidemiological studies evaluating concomitantly pollutant concentration and detectable diseases or hospital admissions usually miss this perinatal damage in foetuses and newborns, not immediately detectable, but is a delayed manifestation. Perinatal damage from air pollution deserves further attention, because it not only includes fetal malformations, birth defects or developmental alterations, but could also be responsible for the increased proportion of individuals who, because of the exposure to pollutants during the "perinatal susceptibility window", and because of epigenetic alterations, due to environmental factors, will turn from previously "unsusceptible" into "susceptible" individuals. The latter could also transfer this susceptibility to future generations, and develop not only asthma at age 4, but also respiratory, cardiovascular or systemic diseases, 20 or 40 y later; 3) since peculiar pathophysiological mechanisms based on individual susceptibility play a major role in the occurrence of pollution related diseases, it is necessary to improve current epidemiological models, adding pathophysiological variables, which could account for tissutal damage, duration and type of exposure, or susceptibility markers. Not only a better knowledge of the "particle side" of the interaction is required, but also a deeper insight into cause and effect relationships and pathophysiologic mechanisms or pathways, i.e. a deeper understanding of the "host side" of the host-particle interaction. A critical re-evaluation could open new avenues, including the design of new models, in which the increasing role of host reactivity is better "weighed", and the possibility that autoimmune or inflammation related mechanisms, instead of purely toxic ones, could be more "fit" to explain clinical outcomes should be carefully evaluated.

Clark N.A. et al. (2010). *Environ. Health Perspect*., **118**, 284-290.
Cetta F. et al. (2010). *Environ. Health Perspect*., **118**, A283-284.

The "harmful potential" of PM, evaluated "in vitro" must be used with a great causation as a surrogate for risk assessment in humans

J. Martellucci[1], F Cetta[1] ,V. Guercio[1], L. Moltoni[1], N. Nante[2], R. Messina[2], M. Monti[3] and E. Bolzacchini[4]

[1]Dept. of Surgery and Thoracic Surgery and [2]Dept. of Physiopathology, Experimental Medicine and Public Health University of Siena, Siena, 53100, Italy
[3]Geriatric Institute "Pio Albergo Trivulzio" (PAT), Milan, 20146, Italy
[4]Dept. of Environmental Sciences, University of Milan-Bicocca, Milan, 20126, Italy
Keywords: risk assessment, PM, intrinsic toxicity, individual susceptibility
Presenting author email: jamjac64@hotmail.com

The aim of the study has been to detect new tools, which could be useful for a risk assessment in humans of the possible effects of air pollutants, on the basis of *"in vitro"* studies of host-particle interactions.

Methods: the BEAS-2B (human bronchial epithelial cell-line) and the A549 (human alveolar epithelial cell), but also sperm cells and synoviocytes from humans with rheumatoid arthritis (RA) and osteoarthrosis (OA), were treated after 24-48h with both summer and winter PM_{10} and $PM_{2.5}$ sampled in Milan, Italy. Therefore, either human beings or cell-lines were exposed to the same pollutants and a cross comparison of observed effects, both clinical and *"in vitro"*, could be performed.

Results: A549 cell viability wasn't significantly reduced after summer and winter PM exposure, and summer PM had no significant effects on BEAS-2B viability. Winter PM treatment induced a decrease in cell viability, at the dose of 25 and 50 mcg/cm^2. Moreover, winter PM_{10} induced a 5-fold increase in IL-8 release in treated cells, and summer PM_{10} induced a 20-fold increase in IL-8 expression. BEAS-2B resulted more responsive to PM treatment than A549. Short- term clinical effects in Milan were not related to PM daily concentration.

Comment: "In vitro" studies confirm potential toxicity of PM, but these studies can't be used for clear-cut inferences to humans. In fact, in terms of health or biological effects, one thing is to inhale by breathing diluted particles in a concentration equivalent to the one that can be introduced with a single breath in 1sec and another is to incubate, with a cell line of alveolar cells, particles deposited on filters, which contain aggregated and concentrated particles, that correspond to 60sec x 60min x 24h, i.e. 8640 folds the portion inhaled by a single breath. In particular, in humans each quantity can be partly eliminated, and only partly can rich the alveolar area. In addition, the final response of the human being includes not only the cellular and molecular response, but also includes the response of the "entire organism", which is controlled by volunty and by the central nervous system. In particular, there are 2 main differences between *"in vitro"* and in humans studies: 1)the human being gives not only biological, but also chemical and mechanical responses, which are able to eliminate completely inhaled particles; 2)the model used in analyzing host-particle interactions postulates a dose and effect linearity, whereas observed outcomes in humans show a "no threshold" behaviour. In other words, in humans the prevalent mechanism couldn't be the pure toxic one, i.e. related to the intrinsic toxicity of the pollutants, but a different one. Therefore, whereas in this study a toxic dose related mechanism is postulated, i.e. the greater the dose, the greater the health effect detectable, in humans the causative mechanism is likely different. Anyway, the present approach shows some strengths: by using an immortalized cell line, always the same, we set ideal conditions to evaluate against the same standard variable concentrations of pollutants, length of exposure, mixture composition, possible relevance of differences in "source apportionment" and seasonal variations. Therefore it's possible to detect the response from the same host or different hosts to different "trigger" stimuli. The "harmful potential" includes various types of alterations: inflammation, or cell-cycle perturbation, with cellular death or genetic mutations and then cell transformation. Therefore, the "*in vitro*" models, even if not immediately extensible to humans, may represent a surrogate for the experimental animal, in order to evaluate quantitatively parameters such as: inflammogenicity, mutagenicity, cell cycle alterations. The use of different cell lines and human samples, with different responses, has shown the great importance, not only of the intrinsic toxicity of the toxic agent, but also of the different type of targeted cell in triggering a different response. These differences- related to host response and individual susceptibility- can be one of the possible explanation for the "no threshold phenomenon" and for the inadequacy of the "pure" toxic model, characterized by dose and effect linearity, to capture the complexity of host-particle interactions. At the moment we must frankly admit that an adequate model of risk evaluation- applicable to human health- isn't available, mainly because of the persistent lack of knowledge, concerning pathogenetic and pathophysiological mechanisms, which are responsible for clinical outcomes in humans. Anyway, in an ideal model, 2 different components should be distinguished: the particle-related component and the host-related one, even if we don't know yet the relative importance of each component.

The response of PM concentrations in the UK to changes in industrial and agricultural emissions: implications for the exceedance of Air Quality Standards

E. Nemitz[1], M. Vieno[1, 2], U. Dragosits[1], C.F. Di Marco[1], M. Twigg[1,2] and M.A. Sutton[1]

[1]Centre for Ecology and Hydrology (CEH), Bush Estate, Penicuik, EH26 0QB, U.K.
[2]School of GeoSciences, King's Buildings, University of Edinburgh, West Mains Rd., Edinburgh, UK.

Keywords: Abatement strategies, air quality, PM (general), ammonium nitrate, ammonium sulphate, precursors, inorganics, chemical transport model

Presenting author email: en@ceh.ac.uk

In the UK, secondary organic ammonium (NH_4^+) salts, formed from the reaction of ammonia (NH_3) with the oxidation products of sulphur dioxide (SO_2) and nitrogen oxides (NO_x), typically account for 20-40% of the $PM_{2.5}$ and 10-30% of the PM_{10}. With increasingly more reliable chemically speciated aerosol data becoming available, it is becoming clear that nitrate (NO_3^-) is a larger contributor than sulphate (SO_4^{2-}) and that it is particularly associated with pollution episodes during which the Air Quality Standards for PM are exceeded (Charron et al., 2006; Harrison et al., 1997). Nitrate formation is favoured by the relatively high emissions of NH_3 from agricultural activity, coupled with a cool humid climate. By contrast, SO_2 emissions have decreased by >80% over the past 15 years.

In this study we are using a high resolution version of the EMEP chemical transport model (EMEP4UK) (Vieno et al., 2010) to predict annual time-series of NH_4^+, NO_3^- and SO_4^{2-} for a number of urban locations, which are analysed in the context of measured PM concentrations.

The skill of the model in predicting NH_4NO_3 concentrations and their response to precursor gas concentrations has been carefully assessed by comparison of long-term trends and hourly variability against data from a number of sources, including: (a) a UK network that measures monthly gas and aerosol concentrations at 33 sites with a denuder / filter-pack sampler (UKEAP), (b) long-term measurements of aerosol composition at the UK EMEP Supersites 'Auchencorth' and 'Harwell' using a MARGA wet-chemistry analyser and (c) campaign-based measurements by Aerosol Mass Spectrometry (AMS) (Nemitz et al., 2011), including measurements in London (Allan et al., 2010).

Model simulations were then performed for several emissions scenarios: experiments were emissions were perturbed within and outside the UK, future emissions predictions, and scenarios in which different levels of agricultural NH_3 abatement (BAT) have been implemented.

Figure 1 compares the model predictions of monthly fine and total nitrate against a Scottish UKEAP measurement site, based on runs of full emissions and only non-UK emissions, showing that a long-term high nitrate event in spring 2003 represented mainly fine nitrate which was formed partly from UK and partly from non-UK precursor gases.

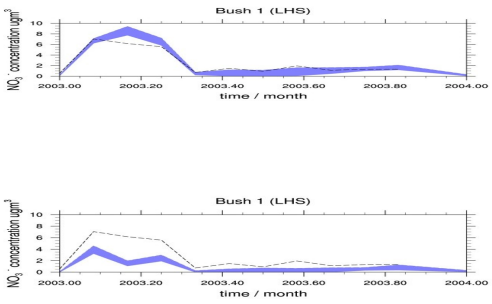

Figure 1. Nitrate monthly surface concentration at the Bush UKEAP site. The dashed line represents the observed nitrate concentration the blue shaded region represents the EMEP4UK model predicted range of fine nitrate (lower boundary) and total nitrate (upper boundary), with the thickness of the shaded area showing the predicted concentration of coarse nitrate. Top graph shows the base run, whereas the bottom graph represents a model run where UK emissions of precursor gases have been removed.

The work was supported by the UK Department for Environment, Food and Rural Affairs (Defra).

Allan, J.D., Williams, P.I. et al.: Contributions from transport, solid fuel burning and cooking to primary organic aerosols in two UK cities. Atmos. Chem. Phys. 10, 647-668, 2010.

Charron, A., Harrison, R. M. et al..: What are the sources and conditions responsible for exceedances of the 24 h PM_{10} limit value (50 µg m^{-3}) at a heavily trafficked London site? Atmos. Environ., 41, 1960-1975, 2006.

Harrison, R. M., Deacon, A. R., et al.: Sources and processes affecting concentrations of PM_{10} and $PM_{2.5}$ particulate matter in Birmingham (UK), Atmos. Environ., 31, 4103-4117, 1997.

Nemitz, E., Prevot, A. et al.: A snapshot European climatology of submicron aerosol chemical composition derived from an Aerosol Mass Spectrometer network. Atmos. Chem. Phys. Discuss., in preparation for submission 2011.

Vieno, M., Dore, A. J. et al.: Modelling surface ozone during the 2003 heat-wave in the UK, Atmos. Chem. Phys., 10, 7963-7978, 2010.

Modelling the effect of variable air exchange rates on indoor aerosol concentrations

James McGrath[1], Miriam Byrne[1], Mike Ashmore[2], Andrew Terry[2] and Sani Dimitroulopoulou[3]

[1] Centre for Climate and Air pollution Studies (C-CAPS), School of Physics, National University of Ireland Galway. Galway.
[2] Environment Department, University of York, York
[3] National Centre for the Environment and Sustainable Development, Kifissia, Greece
Keywords: ventilation, modelling, PM2.5, emission.
*Corresponding email: jamesmcgrath1986@gmail.com

This abstract highlights recent enhancements made to the INDAIR model; INDAIR (Dimitroulopoulou et al., 2006) is an advanced probabilistic modelling tool which can simulate the physical processes determining indoor pollutant concentrations as a function of outdoor concentrations, indoor emission rates and building characteristics. It can simulate the upper percentiles of a population's exposure to air pollutants, or the proportion of the population exposed to concentrations above critical health thresholds.

In simulating indoor aerosol concentration variations, INDAIR makes use of indoor/outdoor air exchange rates (AERs) and inter-room air exchange rates as input parameters. The earlier version of the model uses a 24-hour averaged value for AER, but this approach hides the effect of fluctuations due to variable weather conditions, or door/window opening.. To redress this, the model has now been modified to allow for a variation in AER rates. The new modelling approach uses a text input file, allowing the user to enter start and stop times and the corresponding AER values. This allows the AER to be set to a specific time frame or even allows change on a step-by-step basis if necessary, depending on the requirements.

A validation of the improved model has been carried out by monitoring simultaneous indoor and outdoor concentrations of $PM_{2.5}$, using a TSI AM510 Aerosol Monitor. The AER values for a room of dimensions 3.58 m x 4.36 m x 2.67 m (height) were determined (by CO_2 tracer gas decay measurement) under two different scenarios; one where the door was open (AER = 6.227 air changes per hour (ACH))and the second where the door was closed (0.517 ACH). A fixed emission source – a burning candle- was used to help evaluate the concentrations in the room, and to more clearly demonstrate the effect of the change in ventilation. The candle was lit just prior to sampling and remained lighting for the duration of the experiment.

Using the data gathered, the model was run in its traditional format with a fixed AER (mean value 3.002 ACH) and for comparison, with a variable AER, all other input parameters remaining constant.

Graph 1. Measured and simulated particle concentrations for the traditional model with a fixed AER and for comparison, with a variable AER.

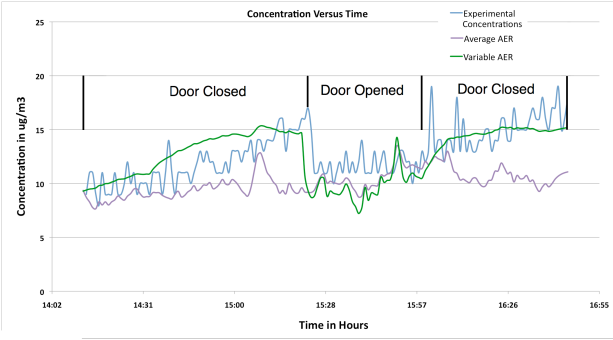

Graph 2. Measured indoor concentrations, outdoor concentrations and simulated particle concentrations using the improved INDAIR model in combination .

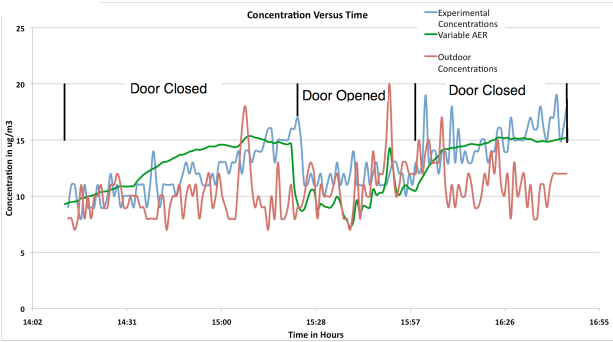

Conclusion

Overall, it can be seen that the enhancement of using a variable AER in the model shows a better performance than the simulation using a mean AER over the time period. In the enhanced version of the INDAIR model, simulated PM concentrations follow more accurately the approximate profile of the experimental concentrations than the traditional model. This is most evident when the doors are closed, with the reduce air flow, the emissions result in higher PM concentrations in the room which the traditional model under-predicted.

References.

DIMITROULOPOULOU, C., ASHMORE, M. R., HILL, M. T. R., BYRNE, M. A. & KINNERSLEY, R. (2006) INDAIR: A probabilistic model of indoor air pollution in UK homes. *Atmospheric Environment,* 40**,** 6362-6379.

Artificial lung as an alternative for measurement pulmonary deposition *in vivo*.

A.B. Penconek and A. Moskal

Department of Chemical and Process Engineering, Warsaw University of Technology, Warsaw, 00-645, Poland
Keywords: lung deposition, laboratory experiments, pulmonary drug deliver
Presenting author email: a.penconek@ichip.pw.edu.pl

Pulmonary deposition of aerosol particles is an important part of toxicological, epidemiological, medical supplies, especially pharmaceuticals including aerosol-therapy. In the case of drugs administered by inhalation the main way to determine the depth of penetration of the respiratory system *in vivo* is radioisotope labelling of the drug particles by technetium ^{99m}Tc (half-life 6 h). Tc is not harmful to human health but application of this method is controversial, especially in the case of testing newborns or children. The aim of our study was to create a device which enables the precise determination of the deposition of aerosol particles in the bronchial tree. The device allows to determined deposition of inhaled drugs, but also diesel exhaust particles or microbiological particles, without using radiolabelling and *in vivo* methods.

The "Artificial lung" is a set of devices where airflow simulating inhalation and exhalation, is generated by deliberately produces pressure difference (between atmospheric pressure and pulmonary pressure) in a manner most similar to the flow of air in the mammalian lung (Figure 1). The airflow (Q), which is generated, could be described in general approximately by following equation Q=Asin(Bt) (where A, B – proper constants, t – time). This equation was obtained based on analysis of real breathing curves derived from measurements of spirometric.

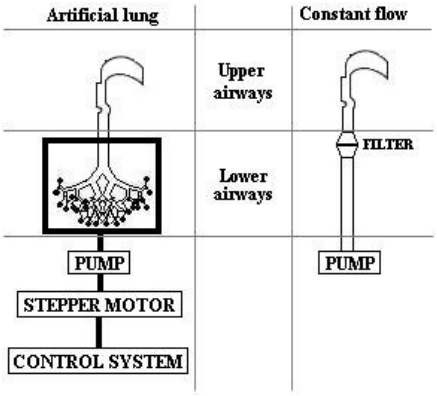

Figure 1. Diagram of measuring system.

Silicone model of the upper airways was developed on the basis of data computed tomography scans and magnetic resonance imaging (Grgic *et al*, 2004). Silicon model of the lower airways was developed on the basis on anatomical data (Weibel, 1963). Pure micronized disodium cromoglycate (*GlaxoSmithKline Pharmaceuticals SA)* was selected as the test material, since it is a drug of common use to treat chronic asthma in children. DSCG (60 ± 7 mg) was contained in gelatine capsule and sprayed in the model of respiratory track using a Cyclohaler DPI. The results were compared with the DSCG deposition in the airways at constant flow (60 l/min) after 4 s time of inhalation. Deposition was determined spectrophotometrically at 340 nm against water as a reference sample.

The results obtained are shown in Figure 2 a, b.

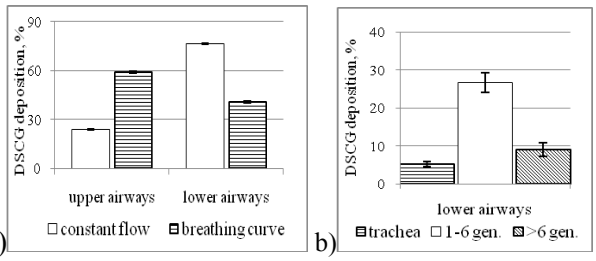

Figure 2. a) Comparison of DSCG deposition in airways for constant flow (60 l/min) and breathing curve (n=3). b) Comparison of DSCG deposition in different parts of lower airways (n=3).

DSCG penetrated beyond 6th generation, represents 9% of taken dose during quite breathing (volume of peak flow 111 l/min). While *In vivo* pulmonary deposition of DSCG (with lactose carrier) are 5,5% (range 1,6%-9,7%) and 17,1% (range 7,8%-28,3%) for flow rate at 60 l/min and 120 l/min respectively (Vidgren *et al*, 1988). Thus our studies are in good relation to *in vivo* studies. However DSCG used in our study did not contain carrier substances which may lead to reduced pulmonary deposition due to cohesion forces between drug particles. It should be noted that study of deposition for constant flow did not produce results corresponding to reality.

Our "Artificial lung" could be successfully used to study the deposition of drugs administered by inhalation, thereby reducing the need for radioisotope. At the same time "Artificial lung" could be used to determine the rate of penetration of the respiratory track harmful particles from polluted environment. This may cause methodological and ethical problems in case of *in vivo* methods.

We would like to thank Mrs Nguyen Q. Huong for making the part of the measurements.

Grgic, B., Finlay, WH., Heenan, AF. (2004) *J. Aerosol Sci.* **35**, 21-32.

Vidgren M., Kärkkäinen, A., Karjalainen P., Paronen P., Nuutinen J. (1988) *Int. J. Pharmaceutics* 42, 211-216.

Weibel ER. (1963) *Morphometry of the human lung*, Springer-Verlag, Zürich.

Respiratory airflow in human upper airways

J. Elcner, F. Lizal, M. Forman, J. Jedelsky and M. Jicha

Department of Thermodynamics and Environmental Engineering, Brno University of Technology, Brno, 616 69, Czech Republic
Keywords: Lung, Airflow, PDPA, CFD.
Presenting author email: yelcne00@stud.fme.vutbr.cz

Understanding to airflow during respiratory cycle is prerequisite for assessment of aerosol deposition in upper airways. Respiratory cycle consists of inspiration and expiration phases and its course is imitated by sine-wave function. Our lung model is composite of the larynx, trachea and four generations of branching. Test rig capable to simulate different breathing cycles allowed us to make airflow measurements and compare them with numerical simulation.

Experiment

Phase Doppler Particle Analyser (PDPA) was used for measurements of velocity and diameter of aerosol particles in a realistic optically transparent model, Lizal *et al* (2010). This 1D PDPA system is equipped with Ar-Ion+ Laser ILT 5500A-00. Spectral line 514.5 nm of the CW laser beam with power up to 90 mW and horizontal polarization is split using transmitting optics 58N10 into 2 parallel beams 60 mm distant. Frequency of one of the beams is shifted by 40 MHz. Beam diameter is expanded to 2.5 mm to reduce a probe volume. The transmitting lens focal length is 310 mm. Light refracted by the 1st order is collected using receiving optics 57X10 equipped with three photo-detectors. Focal length of receiving lens is 310 mm and scattering angle 45° used. Signal processor Dantec 58N50 enabled measurement of velocity in range -8 to 24 m/s at 12 MHz bandwidth and in range -2.7 to 8.0 m/s at 4 MHz bandwidth. Maximum droplet size is 44.9 μm. The obtained data are evaluated using BSA Flow Software v2.1.
The test rig consists of the model located in a frame that is attached to the traversing mechanism. Elastic bag is connected to the model input to prevent leakage of aerosol into the environment, and to ensure enough aerosol for both phases of breathing cycle. Aerosol produced by condensation monodisperse aerosol generator (CMAG) is mixed in a static mixer with air from a pneumatic mechanism, which simulates breathing patterns. PDPA measures velocity and size of the aerosol particles.

Table 1. Breathing cycles measured by PDPA

Activity	Tidal volume V_t (l)	Period T (s)	Mean flowrate (l/min)
Resting conditions	0.5	4	15
Deep breathing	1.0	4	30
Light activity	1.5	3	60

Numerical simulation

Polyhedral mesh with prismatic layer with approximately 400,000 cells was generated for the purpose of numerical simulation. Calculations were performed using StarCCM+ program. Unsteady RANS solver with k-omega turbulence model was used. Velocity inlet condition prescribed by time-dependent equation, which simulates the breathing cycle, was set on the input to the model and pressure outlet condition was set at the end of branches.

Results

Comparison of measured and calculated values was made in 16 cross-sections in all generations of the model containing 43 points in total. Figure 1 shows results for resting conditions in axis of trachea 2 cm upstream the first branch.

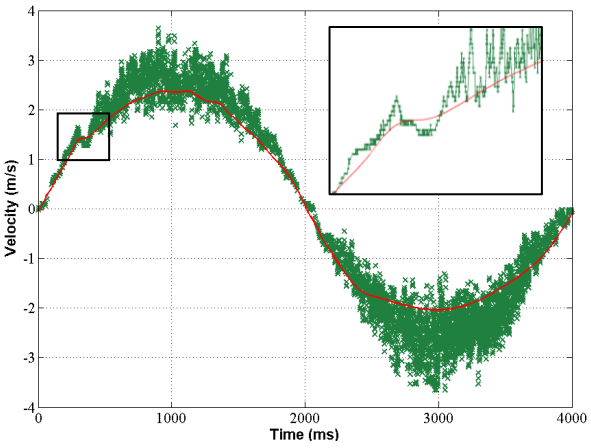

Figure 1. Comparison between experimental and numerical data for resting conditions in trachea.

This work was supported by the Czech grant agency under the grants GA101/09/H050, project OC10052, COST Action Particles No. MP0806, funded by the Ministry of Education, Youth and Sports of the Czech Republic.

Lizal, F., Jedelsky, J., Elcner, J., Durdina, L., Halasova, T., Mravec, F. and Jicha, M. (2010) *In International Conference Experimental Fluid Mechanics 2010 Conference proceedings Volume 1.* Liberec, Technical University of Liberec. 2010. p. 375 - 386. ISBN 978-80-7372-670-6.

Development of a Setup for the Purpose of Respiratory Research and Aerosol Deposition in the Lung Using a Novel Active Lung Simulator

M. Forjan[1], K. Stiglbrunner[1], A. Drauschke[1]

[1]Department of Life Science Technologies, University of Applied Sciences - Technikum Wien, Vienna, 1200, Austria

Keywords: aerosol generation, aerosol measurement, lung deposition, modelling, active lung simulator.
Presenting author email: mathias.forjan@technikum-wien.at

Due to the importance of respiratory research in the field of aerosol measurement (for respirable dust, smoke, or nano-particles) a novel active lung simulator represents an ex vivo system for testing respirable substances. The 3R-strategy by Russell and Burch (1959) laid the basis for a philosophy of alternatives to animal models. Further development of mechanical and mathematical lung models becomes even more important due to legal restraints like the Cosmetics Directive (European Commission (1976)). The presented lung simulator with integrated aerosol measurement allows the observation of particle behaviour within the respiratory tract, with fewer legal limitations, because in this case no harmful substances are used on humans or animal models.

Materials & Methods

As core element of the experimental setup a novel lung simulator is used as Stiglbrunner *et al.* (2010) have described. This model allows the simulation of an active, spontaneously breathing human lung. Moreover the device offers both physiological and pathological breathing patterns. An implemented chamber imitates the human thorax and is set under negative pressure. The device allows the use of different lung equivalents, like a latex bag, a primed porcine-, or isolated lung. The created flexible design opens a wide spectrum of possible experimental setups.

For the measurement of the in- and exhaled particles a white light aerosol spectrometer was chosen. In specific, a Promo spectrometer and a Welas 2200 sensor are used, both by Palas GmbH. The measuring range of the Welas 2200 sensor lies in the range of 0.2µm-40µm. This range covers the size spectrum of note, including "inhalable" but also "respirable" aerosols, reaching the lung's alveolar region, like Ruzer and Harley (2005) state. The sensor-spectrometer system by Palas has been chosen, because it allows non-isovolumetric and non filtered sampling.

As this sensor - spectrometer combination permits the use of a broad range of aerosol diameters, different aerosol generators can be used for simulations. Both, monodisperse and polydisperse aerosols can be applied to the breathing lung equivalent.

For programming the GUI and for data acquisition LabView is used. Apart from the implementation of data transfer protocols given by the used spectrometer, the program for the control of the lung simulator is integrated into the system.

Results

The transport of the aerosols is arranged by a horizontal pipe from the generator towards a suction unit. The number concentration can be adjusted by using an additional dry-air inlet. At a T-junction a tube connects the constant aerosol stream with the lung simulator. The lung inhales a volume taken from the aerosol, and exhales into the same pipe, each time passing the sensor.

For the test setting the AGF 2.0 generator by Palas GmbH is used, which is based on a two-fluid-nozzle. This generator produces polydisperse aerosols with a mean diameter of 0.25µm and a maximal diameter of 2.0µm. The aerosol material applied, was DEHS (Di-2-Ethylhexyl-Sebacat). This combination offers a "respirable" aerosol without the risk of hygroscopic behaviour.

Discussion

The experimental setup allows the observation of in- and exhalation processes of a lung equivalent, which will offer an alternative for animal testing, going along with the idea of the 3R-strategy.

Using polydisperse aerosols as first test setting shows results of the degree of separation, but for further research additional measurements applying typical aerosols have to be completed. Such settings can include generators for monodisperse aerosols, like a Sinclair - LaMer generator.

A planned further development will include the use of fresh slaughterhouse ex vivo porcine lungs in order to approximate to realistic anatomical and physiological conditions of the human lung.

We want to thank Leander Mölter, Maximilian Weiss and Fritz Munzinger (Palas GmbH) for their support and cooperation.

European Commission. (1976) *Council Directive (76/768/EEC).*

Russell, W., Burch, R. (1959) *The Principles of Humane Experimental Technique*, Methuen.

Ruzer, LS., Harley, NH. (2005) *Aerosols Handbook: Measurement, Dosimetry and Health Effects*, CRC Press.

Stiglbrunner, K., Forjan, M., Wurm, M., Weinfurter, A., Drauschke, A. and Krösel, P. (2010) *Proc. Biomedical Engineering-BMT 2010,* De Gruyter.

Numerical simulation of aerosol deposition and clearance in the large bronchial airways

Á. Farkas[1], I. Balásházy[1], A. Nagy[2]

[1]Health and Environmental Physics Department, Hungarian Academy of Sciences KFKI Atomic Energy Research Institute, 1121 Budapest, Konkoly Thege M. út 29-33, Hungary
[2]Department of Laser Applications, Research Institute for Stolid States Physics and Optics, 1121 Budapest Konkoly Thege M. út 29-33, Hungary

Keywords: Lung deposition, Bronchial clearance, Modelling, CFD, Health effects of aerosols
Presenting author email: anagy@szfki.hu

Introduction

Knowledge of particle transport and deposition within the airways is important for the assessment of the health effects associated with inhalation of detrimental or therapeutic aerosols. However, mucociliary clearance can modify the primary particle deposition patterns, influencing the particle-tissue interactions and ultimately the health effects of the deposited aerosols. Therefore, simultaneous study of particle deposition and clearance in airways represents a step forward in the elucidation of the health consequences of inhaled aerosols.

In vitro and *in vivo* inhalation and clearance studies have either technical limits or ethical barriers. In these circumstances computational modelling can be a useful tool in revealing the relationships between breathing parameters, aerosol characteristics and airway deposition-clearance patterns. Numerical models can determine the exact trajectories of particles within the airways and thus the locations of their depositions. In addition, numerical methods allow us to model the movement of mucus layer and track the deposited particles transported by the mucus.

The objective of this study was to simulate the coexisting airway deposition and clearance of the inhaled particles characterised by various aerodynamic diameters assuming different breathing modes.

Methods

In this work, state of the art CFPD (computational fluid and particle dynamics) techniques were used to quantify the deposition and clearance of inhaled aerosols in the large bronchial airways. For this purpose the FLUENT CFD code was used. A discrete phase modelling (DPM) technique was applied to track the individual particles in the computed flow fields of air and mucus. Residence time distributions were computed for particles upcleared from the deeper airways and entering a 4^{th}-5^{th} generation model bronchial bifurcation. Modification of deposition patterns as a result of mucociliary clearance was also investigated.

Results

Present computations revealed that while primary deposition patterns are highly sensitive to the particle size, particle clearance is hardly affected by this parameter in the micron-size range. Our simulations demonstrated the existence of a slow clearance area in the vicinity of the peak of the bifurcation. The residence times of the upclearing particles depend on whether they avoid this slow clearance zone or not. Primary deposition patterns are significantly modified by clearance. The high particle accumulation at the bifurcation region (carina), primarily due to impaction, corroborated by a slow clearance area at the same site explains the high frequency of tumours at these locations caused by inhaled carcinogenic aerosols, as reported in early histological studies.

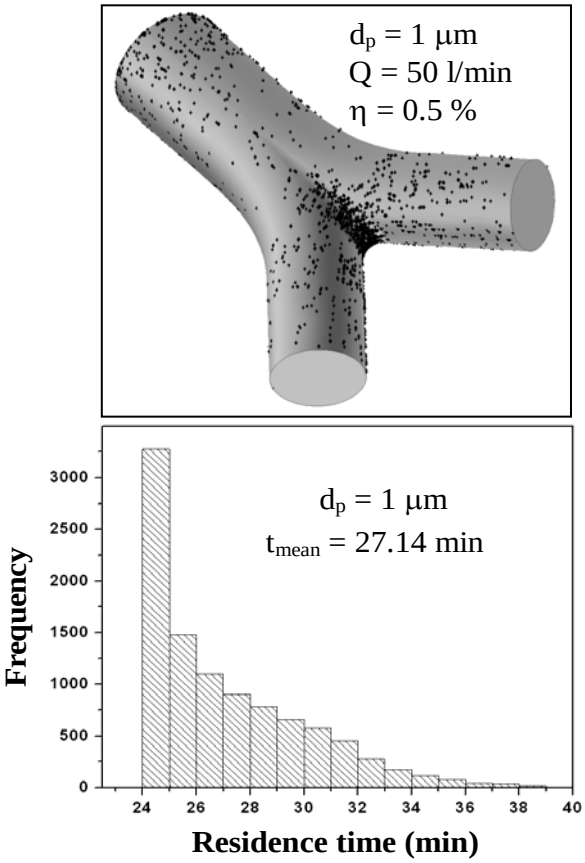

Figure 1. Deposition pattern of 1 μm inhaled particles in the 4^{th}-5^{th} bronchial airway generations assuming breathing conditions characteristic of light physical exercise (upper panel) and residence time distributions of 1 μm upcleared particles in the same airway segment (bottom panel). d_p - particle diameter; Q - flow rate; η - deposition efficiency, t_{mean} – mean residence time.

Acknowledgement

This work was supported by the Hungarian ETT 317-08 Project.

Regional lung deposition of tobacco smoke constituents

J.McAughey[1] and C. Dickens[1]

[1]British American Tobacco, Group R&D Centre, Southampton, SO15 8TL, UK

Keywords: tobacco smoke, deposition, dosimetry.
Presenting author email: john_mcaughey@bat.com

Tobacco smoke is a complex dynamic aerosol suspended in an equally complex vapour cloud, and is a significant elective source of inhaled particles in the population, despite it being a recognized cause of disease. However, little is known of the regional deposition of smoke and local micro-dosimetry from both its vapour and particle phase constituents. Such data offer context to better understand biologically effective dose and potential modes of action of disease initiation, both in model disease systems and populations.

Measured mass deposition efficiencies of the order of 60-80% for particle species are significantly greater than modelled deposition estimates of 30-40% (Baker & Dixon, 2006). Many authors have suggested that the smoke particles must grow significantly to super-micron diameters, to explain observed patterns of disease in the conducting airways, by a combination of coagulation, hygroscopicity, condensation, and colligative 'cloud-like' behaviour (e.g. Robinson, 2001, Broday, 2003). Others have suggested evaporative losses with increased pulmonary deposition of the smaller residual particles by diffusion (Ingebrethsen, 2006, Kane, 2010).

In this work, a series of measurement tools have been developed to assess deposition by direct measurement of exhaled particles and vapour by electrical mobility spectrometry and selective photo-ionisation time-of-flight mass spectrometry respectively. Measured smoking patterns are then replicated to produce intake estimates with deposition calculated by difference.

In addition, hybrid Computational Fluid Dynamic – Pharmacologically Based Pharmacokinetic models (CFD-PBPK) have been developed to assess local deposition in the upper airways and subsequent systemic uptake; initially for volatile aldehyde species.

Soluble vapour species such as acetaldehyde and acrolein show near 100% retention from modelling and measurement data but particle deposition is significantly lower and related principally to inhalation depth and inhalation cycle time. Particle diameter may also have a role but this may be better reflected by a modified diameter reflecting ageing in the mouth, principally via coagulation, rather than the diameter of fresh smoke. However, consideration of all ageing and growth / evaporation processes of the smoke predict it will remain sub-micron and this is confirmed by size measurements of volume- weighted median diameters of approximately 250 – 350 nm for exhaled smoke.

Thus, a majority of particle mass deposition is calculated to occur in the deep lung via diffusion. However, higher local airway particle and vapour doses occur in the upper airways driven by the smaller surface areas available for deposition. Calculated regional values for particle (tar) deposition as ng.cm^2 of lung surface (per mg tar delivered by the cigarette) are 409 (ET – extra-thoracic), 45 (BB – bronchial), 4.8 (bb – bronchiolar) and 0.1 (AI – alveolar). Transformations of size and concentration data allow equivalent number and surface-area weighted regional deposition to be calculated.

In conclusion, new insight has been gained into local dosimetry of tobacco smoke constituents in the lung through measurement and modelling. Both soluble vapour and particle deposition are driven principally by diffusion processes. Local dose remains highest in the upper airways through the relatively smaller airway surface available for deposition.

Further refinement of deposition and CFD-PBPK models will offer an improved approach to quantitative risk assessment. This will derive from the provision of improved relative dose assessment for *in vitro* models of disease applied to smoke exposure and the a combined dosimetric and mechanistic approach to assessing the impact of technologies designed to reduce selective toxicant dose from smoke.

Baker RR and Dixon M. The Retention of Tobacco Smoke Constituents in the Human Respiratory Tract. Inhalation Toxicology 2006 18, 255-294.

Broday DM and Robinson RJ. Application of cloud dynamics to dosimetry of cigarette smoke particles in the lungs. Aerosol Sci. Technol. 2003 37, 510-527.

Ingebrethsen BJ. Numerical Simulation of the Effects of Dilution Level, Depth of Inhalation, and Smoke Composition on Nicotine Vapor Deposition During Cigarette Smoking. Inhalation Toxicology 2006 18, 1071-1076.

Kane DB, Asgharian B. *et al.* Effect of smoking parameters on the particle size distribution and predicted airway deposition of mainstream cigarette smoke. Inhalation Toxicology 2010 22, 199-209.

Robinson RJ and Yu CP. Deposition of Cigarette Smoke Particles in the Human Respiratory Tract. Aerosol Sci. Technol. 2001 34, 202-215.

Implementation of morphometric mouse lung data into a stochastic deposition model

P. Madl, R. Winkler-Heil and W. Hofmann

Department of Materials Research and Physics, University of Salzburg, 5020 Salzburg, Austria
Keywords: mouse lung morphology, particle deposition, modelling.
Presenting author email: pierre.madl@sbg.ac.at

The laboratory mouse is often used as a human surrogate in aerosol inhalation studies. The proposed simulation for aerosol inhalation and deposition calculations represents a significant step forward by reducing animal studies and at the same time speeding up predictions in deposition of particles with a given size.

Due to the lobar anatomical structure of mice lungs that nicely reflect observed differences in bronchial anatomy between different lobes of individual lungs along with intrasubject variability of airway dimensions within a given lobe, makes it possible to construct random airway geometries for Monte Carlo deposition calculations that ultimately enables extrapolation modeling of mouse deposition data to man. Here we present preliminary results of the implementation of morphometric lung data obtained from transgenic mice (Balb/c) into the stochastic lung deposition model originally developed for the rat (Koblinger and Hofmann, 1995).

As a consequence of the more monopodial airway branching in the mouse lung compared to the more dichotomous structure of the human lung, Madl et al. (2010) recommended classifying the mouse lung airways by their diameters and not by generation numbers. The distributions of the geometric airway parameters and the correlations among them are used to confirm the predictions made of Monte Carlo deposition calculations.

Implementation of morphometric mouse data is carried out in two steps. Due to the similarity between the rat and mouse bronchial airway structures, the first approach utilizes an existing rat lung model (Koblinger and Hofmann, 1995) in which relevant morphometric and respiratory parameters are downscaled to mouse size. The second approach applies then real bronchial morphometric data of Balb/c mice (Oldham et al., 2007), such as airway dimensions, termination probabilities and branching as well as gravity angles.

For the acinar region of the mouse, hardly any data can be found in the open literature, except for alveolar diameters and their numbers. Thus in the present version of the deposition model, acinar airway dimensions are downscaled to mouse size, assuming again similarity among mouse and rat acinar structures.

Table 1 summarizes total lung deposition fractions of monodisperse unit density aerosols with three different particle diameters at 25 ml minute ventilation, excluding extrathoracic deposition. The table also lists experimentally obtained deposition fractions (Oldham et al., 2009). Given the preliminary status of the deposition calculations, theoretical predictions for the mouse agree favorably with the experimental evidence.

Table 1. Comparison of total deposition fractions between various computer simulations.

	Diameter	0.5 [µm]	1 [µm]	2 [µm]
depos.[%]	Rat	18.2	20.5	53.5
	Scaled Rat	40.2	45.6	57.4
	Mouse	59.0	71.8	80.0
	Mouse (Exp.)	74.6	72.7	68.8

The distribution of total deposition fractions among bronchial and acinar mouse generations of the Balb/c mouse is illustrated in Figure 1 for 1-µm unit density particles. In contrast to the human lung, the majority of particles are deposited in bronchial generations, exhibiting a distinct peak in generations 6-8.

Although current mouse deposition fractions are still of a preliminary nature – as the code will be further refined – deposition calculations represent a promising tool for the extrapolation of beneficial effects of therapeutic aerosols in humans based on experimental data in mice.

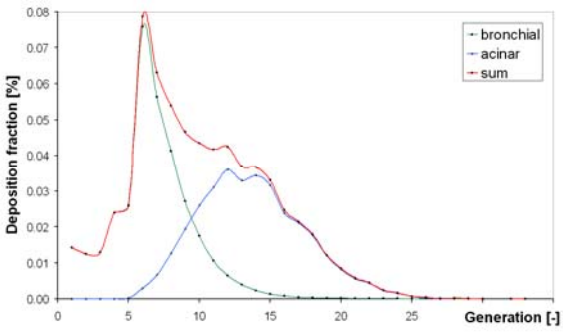

Figure 1. Deposition fractions for a monodisperse aerosol (1 µm) of the Balb/c mouse lung, excluding extrathoracic deposition.

This work was supported by Activaero GmbH, Germany under M4-Projekt, T14.

Koblinger, L. and Hofmann, W. (1995). *J. Aerosol Med.* **8**, 21–32.

Madl, P., Hofmann, W., Oldham, M.J. and Asgharian, B. (2010) *Anat. Rec.* **293**, 1766–1775.

Oldham, M.J. and Robinson, R.J. (2007). *Anat. Rec.* **290**, 1309–1314.

Oldham, M.J., Phalen, R.F. and Budiman, T. (2009). *Aerosol Sci. Technol.* **43**, 970–977.

Comparison of stochastic particle lung deposition predictions with experimental data

M.Hussain[1,2] and W. Hofmann[1]

[1]Division of Physics and Biophysics, University of Salzburg, 5020, Salzburg, Austria
[2] Higher Education Commission of Pakistan, 44000, Islamabad, Pakistan
Keywords: lung deposition, experimental, modelling, comparison
Presenting author email: majid.hussain@stud.sbg.ac.at

Deposition fractions predicted by different modelling techniques vary with respect to physical (fluid dynamics of the inhaled air) and biological (lung morphology and respiratory physiology) factors and mathematical modelling technique. Therefore it is always needed to validate the modelling deposition perfection with that of experimental data.

Experimental data on deposition in individual airway generations and lung regions are now becoming available through the application modern techniques (Fleming et al. 2006; Kim et al. 2005-06). Similarly experimental deposition data supplied by deposition studies in surrogate airway models or lung casts (Cohen et al. 1990; Smith et al. 2001) are available for comparison purposes. The purpose of the current study was to compare the experimental measurements with the stochastic modelling predictions using Monte Carlo deposition code IDEAL (Hofmann & Koblinger, 1990) on three levels: (i) deposition per generation (up to 7 generations) (ii) regional deposition; and (iii) total deposition.

In comparison experimental measurements in generations by Smith et al. (1990) were found to be up to 2 times higher than stochastic model predictions for ultrafine particles (see Figure 1). However, comparatively better agreement was found for regional deposition with the studies of Fleming et al. (2006) (see Table 1). The total deposition fraction of Fleming et al. (2006) study is about a factor of 1.5 higher than IDEAL predictions primarily due to their higher alveolar deposition measurements.

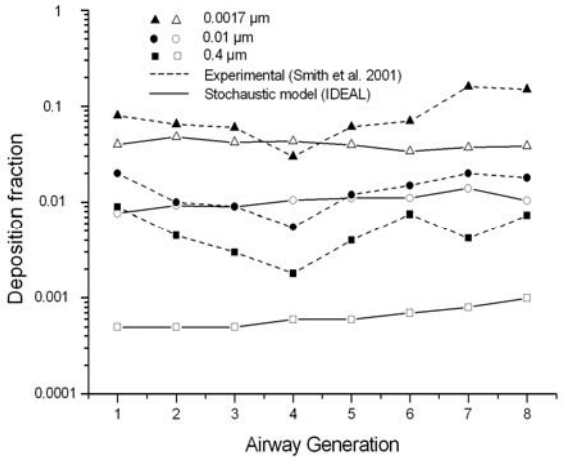

Figure 1. Deposition fraction up to generation 7 for different particle sizes at flow rate of 20 L min^{-1}.

Table 1. Deposition fractions for fine and coarse particle sizes (1.8 and 6.5 µm respectively) predicted by IDEAL code and experimental studies.

Lung regions	Fine particles		Coarse particles	
	IDEAL	Experiment	IDEAL	Experiment
ET	0.03	0.04	0.22	0.27
BB	0.02	0.04	0.12	0.07
bb	0.02	0.05	0.15	0.05
Al	0.20	0.54	0.13	0.41

Comparisons of total deposition predictions by IDEAL are found in excellent agreement with the experimental data of Kim et al. (2005-6) (see Figure 2).

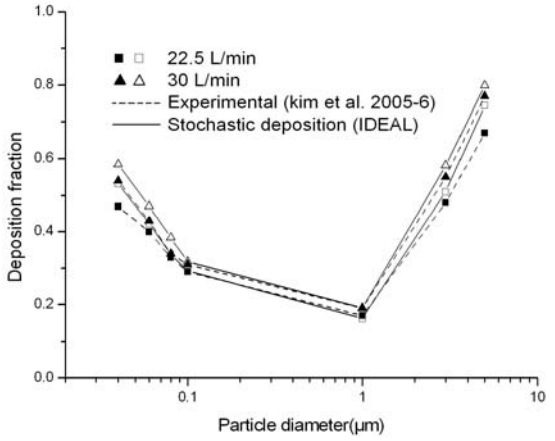

Figure 2. Total lung deposition fraction vs. particle diameter at two different flow rates.

From this comparative study it can be concluded that regional and deposition per generation by experiment vary from stochastic modelling prediction primarily due to difference in lung morphometry used in either studies although a good agreement is found in total deposition fraction.

This work was funded in part by EU contract no.516483 (Alpha Risk) and by the Higher Education Commission of Pakistan.

Cohen B.S., Robert G., Sussman & Lippmann M. (1990). *Aerosol Sci. & Technol*. **12**, 1082-1091.

Fleming J.S., Epps B.P., Conway J.H. & Martonen T.B. (2006). *J Aerosol Med*. **19**, 268-278.

Hofman W. & Koblinger. (1990). *J Aerosol Sci.* **21**, 675-688.

Kim, C. S. & Hu S.C. (2006). *J Appl Pysiol*. **101**, 401-412.

Kim, C. S. & Jaques P.A. (2005). *Inhal Toxicol*.**17**, 387-399.

Smith S., Cheng Y.S. & Yeh H.C. (2001). *Aerosol Sci & Technol*. **35**, 697-709.

Pulmonary toxicity of well-dispersed single-wall carbon nanotube following 4 week inhalation

Y. Morimoto, M. Hirohashi, A. Ogami, T. Oyabu, T. Myojo, M. Hashiba, Y. Mizuguchi, T. Kambara, B-W. Lee
K. Mizuno, N. Kobayashi, and I. Tanaka

Institute of Industrial Ecological Sciences, University of Occupational and Environmental Health, Japan.
Kitakyushu, 807-8555, Japan
Keywords: carbon, nanotubes, inhalation, dispersion
Presenting author email: yasuom@med.uoeh-u.ac.jp

Single-wall carbon nanotube (SWCNT) is a cylindrical nanostructure substance from wrapping a single graphene sheet. Many reports state that SWCNTs have cyto- and geno-toxicities in vitro studies, and that SWCNTs also have pulmonary toxicities in vivo studies. Some reports also state that SWCNTs do not have toxicities. The discrepancies in reports about toxicity and SWCNT are related to the physicochemical properties of SWCNT including dispersion states, dimensions, metal components, and purification treatment, which affect SWCNT toxicity. Therefore, it is very important to identify the physiochemical properties of SWCNT in order to estimate the harmful effect of SWCNT.
SWCNT was well-dispersed using ultrasonication to conduct an inhalation study. SWCNT was generated using a pressurized nebulizer with liquid suspension of SWCNT in distilled water including Tween 80.

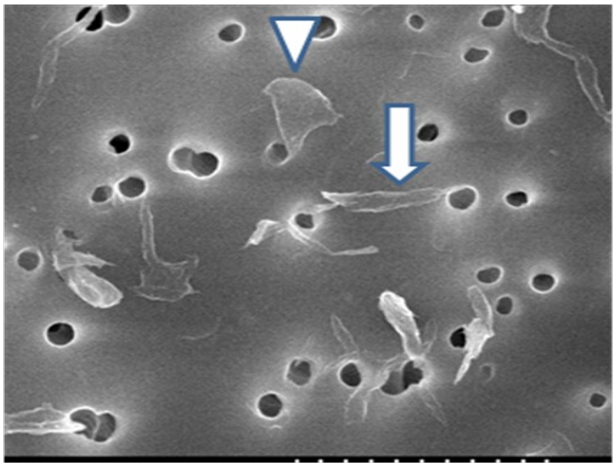

Figure 1 Bundle of SWCNT in the chamber

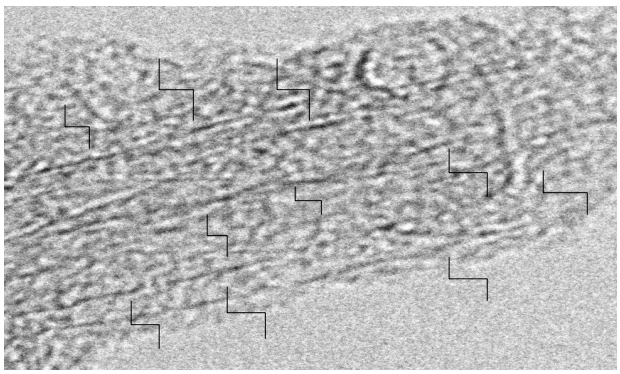

Figure 2 Lots of SWCNT in bundle

Figure 1 and 2 showed well-dispersed SWCNTs in the inhalation exposure chamber. Wistar rats were exposed to the SWCNT (diameter of bundle: 0.2 (1.7) μm; length of bundle: 0.7 (1.7) μm) for 4 weeks. Low and high mass concentrations in the exposure chamber were 0.03 ± 0.003 mg/m^3 and 0.13 ± 0.03 mg/m^3. Agglomerated diameter and mass concentration of nickel oxide nanoparticles (primary diameter: 8.41 nm) as reference material in the chamber was 59 nm and 0.2 mg/m^3, respectively. The rats were sacrificed at 3 days, 1 month, and 3 months after the end of 4 week exposure. The inflammatory responses and gene expression of cytokine-induced neutrophil chemoattractant (CINC) were examined in the rat lungs. There were no increases of total cell and neutrophil counts in bronchoalveolar lavage fluid (BALF), CINC-1, -2 and -3 in the lungs or of BALF in the high and low concentration-exposed groups of SWCNT (Figure 3). Pulmonary infiltration of neutrophils also was not observed in either exposed group through the observation period. On the other hand, neutrophil infiltration and up-regulation of CINC1-2 was observed in nickel oxide-exposed group. Well-dispersed SWCNT did not induce neutrophil inflammation in the lung under the conditions in the present study.

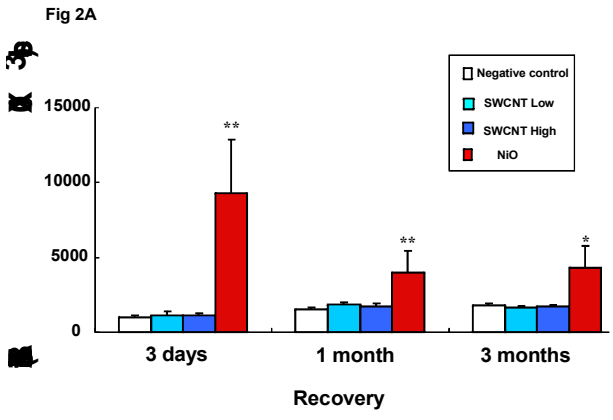

Figure 3 Total cell count in BALF in rat inhaled SWCNT

This research was funded by a grant from the New Energy and Industrial Technology Development Organization of Japan (NEDO) titled: “Evaluating risks associated with manufactured nanomaterials: Inhalation exposure methods for developing toxicity evaluations (P06041)”.

Comparison between in vitro results of PM incubation with cell-lines and health effects in children.

R. Zangari [1], F. Cetta [1], M. Sala [2], M. Mandelli [2], V. Guercio [1], L. Moltoni [1], O. Caratozzolo [3], M. Monti [3], A.M.Azzarà [1], E. Bolzacchini [4] and B. Palmieri[5]

[1] Dept. of Surgery and Thoracic Surgery, University of Siena, Siena, 53100, Italy
[2]Dept. of Pediatrics, University of Milan, Milan, 20122, Italy
[3]Geriatric Institute "Pio Albergo Trivulzio" (PAT), Milan, 20146, Italy
[4]Dept. of Environmental Sciences, University of Milan-Bicocca, Milan, 20126, Italy
[5] Dept of General Surgery and Surgical Specialties, Medical School and Surgical Clinic, University of Modena and Reggio Emilia, Modena, 41121, Italy
Keywords: PM, Urban pollution, BEAS-2B and A549 cells, comparative study
Presenting author email: zangari4@unisi.it

Both basic and clinical studies have been performed, trying to relate environmental pollution to hospital admissions and/or major respiratory or cardiovascular adverse effects. However, it is always difficult to compare data from "*in vitro*" studies and experimental models in animals to clinically evident effects in humans.

In the present study, hospital admissions to the main pediatric service of Milan were recorded, analysed and compared with daily and seasonal variation in PM10 and PM2.5 concentration, during 4 consecutive periods: winter 2007- summer 2007- winter 2008- summer 2008. Respiratory diseases were classified as follows: asthma or asthma like disorders; upper respiratory diseases (pharyngitis, pharingotonsillitis, otitis); lower respiratory diseases (bronchitis, bronchiolitis and pneumonia).

During 2007-2008, there were in total 440 pediatric admissions for respiratory diseases; 226 (132 males and 94 females) during the winter semester, and 214 (100 males and 114 females) during the summer semester. There were 12.7% asthma or asthma related admissions; 55.8% due to lower respiratory illness, and 31.5 % due to upper respiratory disease. The daily average of PM10 concentration during the first semester 2007 was 48.3 +/- 17.9 $\mu g/m^3$ median 47. There were 107 (59.1%) days with at least one hospital admission. The mean daily concentration of PM was higher in days with (n=107) than without (n=74) hospital admissions ($p=0.032$ or <0.05).

In addition, the human bronchial epithelial cell-line BEAS-2B and the human alveolar epithelial cell A549 were seeded at a concentration of 80.000 cell/well and treated after 48 hours with both summer and winter PM10 and PM2.5 sampled in the main Milan urban area. Cytotoxicity was assessed by HOECHST 33342/91 staining. Viability was calculated as the sum of viable mitotic cells. Release of the proinflammatory cytokine-IL was measured by ELISA assay. Oxidative stress was evaluated by chemiluminescence and genotoxicity was assessed by comet assay.

It was found that, whereas A549 cell viability was not significantly reduced after summer and winter PM exposure, summer PM had no significant effects on BEAS-2B viability, whereas winter PM treatment induced a decrease in cell viability, both at the dose of 25 and 50 µg/ml. In addition, whereas both winter and summer PM2.5produced only a slight increase in IL-8 release, winter PM10 induced a 5-fold increase in IL-8 release in treated cells, and summer PM10 induced a 20-fold increase ($p<0,05$) in IL-8 expression.

In particular, BEAS-2B resulted more responsive to PM treatment than A549. Winter PMs were more cytotoxic than summer PMs; Summer PM10 had a higher proinflammatory potential, which could be partly due to biological components (LPS).

Accordingly, acute admission of children was significantly affected by pollution data, with increased admission during winter time, namely for upper air tract infections, whereas lower tract inflammation and acute admission for asthma were more frequent during the spring-summer season.

In conclusion, in vitro studies using PM10 and PM2.5 sampling from different seasonal samples seem to correlate with clinical data in children exposed to the same type and concentration of PM during winter and summer season.

Even if great caution is required when trying to relate in vitro studies to clinical effects in humans, the present report is the first study in a large urban area trying to compare "*in vitro*" and clinical effects of the same urban particulate material in different seasons of the year.

This work was supported by the PROLIFE-Project, City of Milan, Italy.

Mesothelioma incidence is likely not going to decline, despite asbestos ban in Western countries

P. Paladini[1], F. Cetta[2], M. Monti[3], S. Baruffi[3], C. Ghiribelli[1], F. Granato[2], M.S. Gallazzi[1], R. Borrelli[1], V. Guercio[2], B. Palmieri[5] and G. Gotti[1]

[1] Thoracic Surgery Unit, University Hospital of Siena, Siena, 53100, Italy
[2]Dept. of Surgery and Thoracic Surgery, University of Siena, Siena, 53100, Italy
[3]Geriatric Institute "Pio Albergo Trivulzio" (PAT), Milan, 20146, Italy
[5] Dept of General Surgery and Surgical Specialties, Medical School and Surgical Clinic, University of Modena and Reggio Emilia, Modena, 41121, Italy
Keywords: Mesothelioma, exposure, asbestos, individual susceptibility
Presenting author email: paladini@unisi.it

Mesothelioma (MM) is a poor prognosis malignancy, strictly related with asbestos exposure, usually occurring 30-40 years after occupational or non occupational exposure. Recent reports have suggested that "although the MM incidence is anticipated to decline in the coming decade, it may not decrease to background risk levels, given that chrysotile consumption has not been banned under the current legislation and that secondary asbestos exposure from the environmental will continue", and that "although the potency differences with respect to lung cancer or mesothelioma for fibers of various types and dimension are debated", many pleural and peritoneal mesotheliomas have been observed after occupational exposure to chrysotile (Tse, 2010).

At the University of Siena, Italy, during a 12 year- interval, 75 subjects with MM were observed. There were: 53 M, 22F , mean age 65 y, range 43-86 y. In particular, there were 60 pleural MM, 11 peritoneal MM, 1 MM of the pericardium and 2 MM of the tunica vaginalis testis. In particular, a genome wide analysis (array CGH analysis) performed in a small subset of these couples (husband occupationally exposed, but unaffected, and wife unexposed but affected), showed a panel of differently expressed genes, which were partly different from couple to couple, and partly common.

Interestingly, common genes with diverse copy numbers included major histocompatibility genes, genes involved in the metabolism of xenobiotics and genes involved in the inflammatory response (Cetta, 2011). It was shown that, analogously to what occurs for pollution related diseases, also concerning asbestos related diseases, clinical outcomes occur as the final result of host-fiber interaction. In particular, we showed that asbestos related MM occurred in the tonaca vaginalis testis (as primary site), i.e. in a distant site from the portal of entrance of asbestos fibers, and that asbestos fibers have been documented at this level (in other patients). In addition, we observed subjects developing MM more than 45 years after short-term exposure to asbestos (service in the Navy at age 18-20) without any additional occupational exposure. Finally, we observed some couples (husband-long-term occupationally exposed to asbestos and wife non occupationally exposed) with the interesting finding that the non exposed wife developed pleural MM (with asbestos fibers documented in the operative specimen), whereas the exposed husband had neither MM, nor lung cancer, or even overt asbestosis. This points dramatically to the crucial role of individual susceptibility in the occurrence of asbestos related diseases. In particular, after genome wide analysis of blood samples of these couples, we showed that they differed for a diverse expression of a panel of genes, including some of those responsible for major hystocompatibility system, drug metabolizing enzymes and host immune response (Cetta, 2011). These findings dramatically suggest that, whereas most individuals do not develop MM or lung cancer even after a 30-year-occupational exposure to chrysotile, which is the most toxic variant of asbestos, other apparently normal, but highly susceptible people can develop pleural MM after indirect exposure to small quantities of asbestos of whatever structure and composition, or show a mesothelial tumor in a distant, but susceptible site, such as tonaca vaginalis testis. Further ecologic studies and analytical studies, but also pathophysiological and genetic studies are obviously required, before stating which is which, i.e. what is the relative potency of the various asbestos variants and what's the relative role of intrinsic toxicity fibers and of host susceptibility.

However, it is likely that, once that a powerful toxic agent as asbestos has been disseminated in a given community, the decrease to background risk levels is highly improbable, not only because of continuous chrysotile use in other regions (imported as manufacts, even in small quantity), but also because secondary asbestos exposure from the environment will likely continue. In particular, this persistent exposure (after initial introduction) and the long-term persistency of asbestos fibers will be able, even at very low concentrations, to trigger the occurrence of mesotheliomas in genetically susceptible people, the prevalence of which is likely increased also because of the asbestos epidemic. In addition, this should also suggest caution before widespread use of new fibers and new materials, the long-term persistence and long-term effects of which have not been carefully evaluated specifically.

Tse LA et al. (2010). *Environ Health Perspect* **118**, 382–386.
Cetta F. (2011) in Barbarisi A. Editor. *Biotechnology in Surgery*. *Springer Verlag*, 169-190.

Measurement of damages to exposed populations during concomitant evaluation of PM concentration and health effects usually doesn't consider damage to newborns.

S. Benoni[1], F. Cetta[1], V. Guercio[1], P. Paladini [1], C. Ghiribelli[1], F. Granato[1], A.M. Azzarà[1], F. Cisternino[1], R. Zangari[1], M. Monti[2] and M. Sala[3]

[1]Dept. of Surgery and Thoracic Surgery, University of Siena, Siena, 53100, Italy
[2]Geriatric Institute "Pio Albergo Trivulzio" (PAT), Milan, 20146, Italy
[3]Dept. of Pediatrics, University of Milan, Milan, 20122, Italy
Keywords: Particle concentration, health effects of aerosols, susceptibility window, newborn damage.
Presenting author email: benoni@unisi.it

In Milan, Italy, between 2007 and 2010, a comprehensive approach to health effects of air pollution was performed (Prolife Project). In particular, the following studies were performed : 1) concentration measurement; 2) comparison between daily concentration of PM and other pollutants and hospital admission; 3) longitudinal studies in frail subpopulations, such as children attending primary school and elderly people living in nursing homes; 4) "*in vitro"* and "*in vivo"* experiments concerning host particle interactions.

The lack of adequate metrics of exposure, effect and susceptibility in epidemiological studies evaluating PM concentration and health effects is one of the main responsible for the conflicting results of these studies (Clark, 2010). In particular, the question of damage to human health by environmental pollutants has never been addressed exhaustively, analysing every possible component – and the specific and proper metrics.

The current paradigm of environmental pollution included acute damage, usually measured as hospital admission for various diagnosis during "pollution peaks" - and chronic damage, i.e. the risk of developing cancer and/or chronic diseases as long -term effects. A dose and effect linearity, due to the intrinsic toxicity of pollutants has been presumed, but never proved, whereas the role of individual susceptibility in the occurrence of the final outcome has never been considered in a proper manner.

The following results were obtained: 1) In a prospective study involving 118 children (63 males and 55 females) attending primary school, close to a park far from vehicular traffic, in 3 consecutive days very high peaks of indoor PM were detected for about one hour (8:15-9:15 in the morning), up to 1000 $\mu g/m^3$ indoor for PM10. There was no evident clinical outcome (increase of asthmatic bronchitis, upper or lower respiratory diseases) or different prevalence of spirometric or FeNO values in any of the 118 children who were evaluated during those days. 2) Functional alterations of human cells incubated in vitro with different types of PM10 and PM2,5 (10, 50, 75 μg/ml) and concentration greatly depended on individual susceptibility and on the pre-existing disease of the host. In particular, semiquantitative functional analysis showed that individual susceptibility of the host was responsible for more than 50% of the final outcome as compared with intrinsic toxicity of pollutants. 3) Comparison of the rate of asthmatic children in 2009 with historical series of 3 decades before, showed an evident increase of susceptible children, likely due to the effects of early life exposure to air pollution, during the critical "susceptibility window" involving the first months of life of newborns (Clark, 2010).

The question of the selection of adequate markers and metrics for epidemiological studies cannot be reduced to a mere controversy among epidemiologists, which should be limited strictly to them and treated only by an improval of statistical method or epidemiological models.

The basic question concerning the determinants of final outcomes and the measure of each component responsible for damage, involving both toxic and harmful processes, but also repair mechanisms, requires a multidisciplinary approach, involving clinicians and pathologists. Namely, the relative power of the damage due to intrinsic toxicity of pollutants, which can be without clinical evidence even at PM concentration of 1000 $\mu g/m^3$ - and that of individual susceptibility deserves further evaluation.
In particular, in the overall analysis of exposed population, the damage to newborns by pollutants usually escapes current evaluation of PM concentration and health effects, which is able to capture only damage expressed as "hospital admission, morbidity and mortality" measured within a 2- day lag. A proper estimation of this damage, i.e. of the increased proportion of newborns - children of non susceptible parents - who will become susceptible to "pollution disease", because of exposure to pollutants in early life, is mandatory because, even if it will be measured some decades later, as a burden of diseases related to PM pollution, it actually is a major component of the total damage from environmental pollution, at a given time, which could also be transmitted to future generations.

This work was supported by the PROLIFE Project, City of Milan, Italy

Clark N.A. et al. (2010). *Environ. Health Perspect.*, **118**, 284-290.

Comparison of toxicological responses in mice lung induced by PM_1 emissions from heating appliances of old and new technologies

M.S. Happo[1], O. Uski[1,2], P.I. Jalava[1], J. Kelz[3], T. Brunner[3,4,5], J. Jokiniemi[1,6], I. Obernberger[3,4,5], and M-R. Hirvonen[1,2]

[1]Department of Environmental Science, University of Eastern Finland, Kuopio, FI-70701, Finland
[2]Department of Environmental Health, National Institute for Health and Welfare, Kuopio, FI-70701 Finland
3Bioenergy 2010+ GmbH, Graz, A-8010, Austria
[4]Institut for Process and Particle Engineering, Graz University of Technology, Graz, A-8010, Austria
[5]BIOS Bioenergiesysteme GmbH, Graz, A-8010, Austria
[6]VTT Technical Research Centre of Finland, FI-02044, VTT, Finland

Keywords: emissions, wood smoke, health effects of aerosol, combustion particles.
Presenting author email: mikko.happo@uef.fi

Current levels of ambient air $PM_{2.5}$ are associated with mortality and morbidity in urban populations worldwide. At residential areas, wood combustion is one of the main sources of $PM_{2.5}$ emissions. EU has decided to increase the use of biomass energy to 20% on average from the total energy consumption by 2020. This decision will increase the small scale biomass combustion in local heating systems, which also increases the total $PM_{2.5}$ emissions. Therefore, it is crucial to minimize the health risks and to develop safe small-scale heating technologies. However, toxicological properties of particulate emissions from the new heating appliances and fuels are poorly known.

Particulate induced inflammation is one of the main mechanisms behind disease exacerbation in both respiratory and cardiovascular subjects. Particles are also known to induce inflammatory and cytotoxic effects in animals and in cell studies. In this study, inflammatory and cytotoxic responses in bronchoalveolar lavage fluid (BALF) of mice induced by PM_1 samples from different heating appliances were investigated.

The analyzed small-scale combustion appliances were as follows: logwood boiler (old tech), logwood boiler (new tech), stove (old tech), stove (new tech), tiled stove (new tech), woodchip boiler (new tech) and pellet boiler (new tech). Description of gaseous and PM_1 emissions of the investigated biomass combustion systems are shown in the Table 1. Particulate samples (D_p < 1µm) were collected by using a Dekati® Gravimetric Impactor (DGI). Thereafter, the samples were weighed and extracted by using methanol extraction method for subsequent use in toxicological studies.

Healthy C57BL/6J mice were intratracheally exposed to single dose of 10 mg/kg particulate sample. 4 and 18 hours after the exposure, the lungs were lavaged and BALF was assayed for indicators of inflammation (total cell number, IL-6) and tissue damage (total protein, lactate dehydrogenase (LDH)).

Total cell number in BALF was slightly, but not statistically significantly increased 18 h after the exposure to all PM_1 samples. Increase of total cell number was mostly due to migration of neutrophils into the area of inflammation, especially with the new technology samples. In contrast to total cell number, IL-6 concentrations in BALF were found to increase greatly after exposure to PM_1 samples. The highest detected increases were found mostly 4 h after the exposure. Pellet boiler and woodchip boiler samples evoked the strongest and statistically significant increases in IL-6 production. Overall, only low cytotoxic responses were evoked by emission PM_1 samples in mice lungs. Total protein concentration in BALF was not increased from control level after exposure to PM_1 emission samples, excluding pellet boiler sample at the latest time point. In LDH, pellet boiler similarly had the highest response.

Table 1. Mean values for gaseous and PM_1 emissions for the different investigated biomass combustion systems.

Combustion system	0_2 vol% d.b.	CO mg/MJ	OGC mg/MJ	PM_1 mg/MJ
Logwood boiler OT	11.3	**12632.3**	**1143.8**	**106.1**
Logwood boiler NT	**8.6**	793.1	62.4	17.6
Stove OT	10.8	2355.4	223.9	74.2
Stove NT	12.1	1035.6	95.5	46.1
Tiled stove	**15.3**	1007.5	69.2	28.0
Woodchip boiler	12.1	182.2	5.4	13.6
Pellet boiler	12.6	**47.1**	**2.5**	**6.2**

Note. The largest and smallest values are in bold.

In this study, we showed that PM_1 samples originating from different heating appliances, representing old and new technologies, have discrepancies in their ability to induce inflammatory and cytotoxic responses in the mouse lungs. PM_1 samples from new technology appliances induced stronger acute pulmonary responses than samples from old technology devices. However, it is possible that certain chemical constituents of wood smoke, such as PAH compounds, are effecting to lungs via clearance mechanisms or via immunomodulation. This applies especially with samples from old technology heating appliances with high PAH content of the emissions. Moreover, it is noteworthy that modern combustion technology reduces greatly the emission rates and thus, the health hazard caused by particulate emissions.

Prevalidation of the CULTEX method: In vitro analysis of the acute toxicity of inhalable fine dusts and nanoparticles after direct exposure of cultivated human cells from the respiratory tract.

Niklas Möhle[1], Christine Pohl[2], Mirko Papritz[3], Dirk Steinritz[3], Ulrich Mohr[1], Sebastian Hoffmann[4], C. James Kirkpatrick[2], Michaela Aufderheide[1]

[1] Cultex Laboratories GmbH, Hannover Medical Park, Hannover
[2] Institute of Pathology, Repair-Lab, University Medical Center, Johannes Gutenberg University Mainz
[3] Institute of Pharmacology and Toxicology, Bundeswehr Munich
[4] seh consulting + services, Köln
Keywords:, Instrumentation, Particle-Lung Interactions, Biological response
Presenting author email: n.moehle@cultex-laboratories.com

The respiratory tract is a main portal to the human body for inhaled particles and toxic substances. Over the last decade nanomedicine and -chemistry have development with a tremendous pace, not without realising that the safety and risk assessment of nanoparticles will challenge current toxicological approaches. The Cultex® system provides a method for screening such particles for their cytotoxic and therapeutic potency at an air-liquid interface on epithelial cells. The aim of the project is to prevalidate the Cultex® system (Aufderheide and Mohr, 1999) regarding its usefulness as such a toxicological screening tool in a multi-laboratory study.

In our experiments the cell line, A549, which exhibits features of alveolar type II cells but with the production of mucins and with characteristics of bronchial cells, was exposed to different particles. For the Cultex® system A549 cells were seeded on transwells with a semipermeable membrane which allows the separation of two compartments. On the apical side A549 were treated with aerosols, medium was only added in the basolateral compartment. In first studies cells were exposed to clean air and test substances to complete the experimental set-up for further experiments. The main focus was to create a test atmosphere which approaches to the in vivo situation.

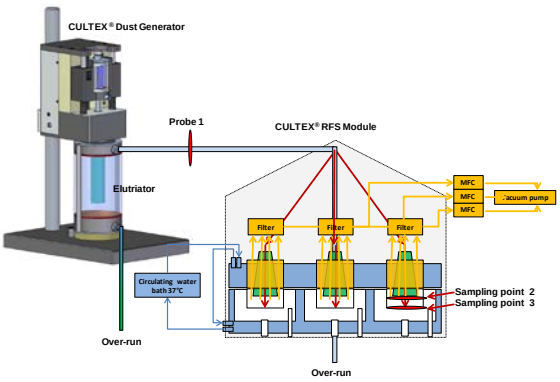

Figure 1: Schematic setup of the Cultex® RFS with three sampling points

The different aerosols are characterized (Figure 1) with regard to the particle size, the generated aerosol mass, the inlet mass and the deposited mass on the cells. The generation of a steady aerosol over a long time and an accurate characterization ensure reproducible dose effect results with cells (Figure 2).

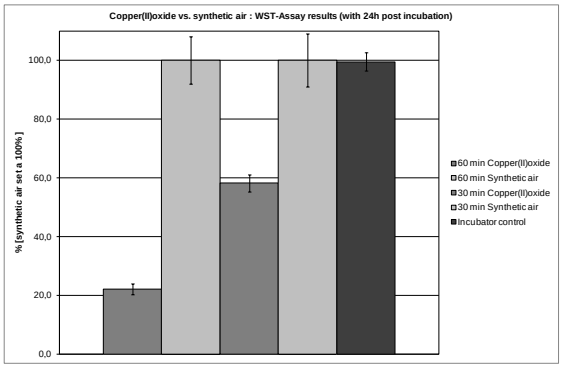

Figure 2: WST-1 results of A549 cells exposed to synthetic air and copper(II)oxide

This work is supported by the Federal Ministry for Education and Research under grant 0315710A.

Aufderheide, M. and Mohr, U. (1999) *CULTEX – a new system and technique for the cultivation and exposure of cells at the air/liquid interface*. Exp Toxicol Pathol, 51:489–90.

Aufderheide, M. (2008) *An efficient approach to study the toxicological effects of complex mixtures*. Exp Toxicol Pathol, 60:163-180

BéruBé, K. et al. (2009) *In Vitro Models of Inhalation Toxicity and Disease*. ATLA 37:89-141

Particulate matter emitted in biomass burning and respiratory diseases hospitalizations in children of Manaus, central Brazilian Amazon region

Valdir S. Andrade Filho[1], P. Artaxo[2], Melina Paixao[2], S.S. Hacon[3] and C.N. Carmo[3]

[1]Instituto Nacional de Pesquisas da Amazônia – INPA, CEP 69060-001, Manaus, AM, Brazil
[2]Instituto de Física, Universidade de São Paulo, CEP 05508-900, São Paulo, SP, Brazil
[3]Departamento de Endemias, Fundação Oswaldo Cruz, CEP 21041-210, Rio de Janeiro, RJ, Brazil
Keywords: Amazon, Manaus, particulate matter, children health.
Presenting author email: artaxo@if.usp.br

Amazonia is characterized by very low aerosol concentrations during the wet season, with an average PM_{10} of 10 µg/m³ for most of the region. In sharp contrast, during the dry season, concentrations up to about 600 µg/m³ are measured in the Southern and Eastern part of the basin. The health effect of exposure to such high aerosol loading is significant. Another important process occurring now in Amazonia is urbanization, with the city of Manaus growing fast in population.

The objective of the study was to investigate the effects of fine particulate matter emitted from biomass burning on hospitalizations for respiratory diseases in children, at the urban area of Manaus, during the period of 2002 to 2009. The city of Manaus is located in the central portion of the Brazilian Amazon region. Currently has a population of 1.802.525 inhabitants, of which 99.4% lives in the in urban area.

The data for $PM_{2.5}$ were estimated by using the MODIS sensor, with Aerosol Optical Depth (AOD) at 550 nm estimation. $PM_{2.5}$ were derived from MODIS AOD using relationships obtained for several sites in Amazonia were AERONET and MODIS AOD were obtained in parallel with $PM_{2.5}$ measurements. Hospitalization data were obtained from Sistema Único de Saúde database (SUS – DATASUS). Statistical methods were used, with Pearson correlation and multiple linear regression between variables. Significant values were considered with a p-value < 0.05.

It was observed that hospital admissions for respiratory diseases in children, in Manaus, may be more related to weather and humid air conditions, than from exposure to aerosols from biomass burning in the region.

It was observed that the region of Manaus shows quite low PM2.5 concentrations, when compared to the Southern Amazonian region. The annual average of $PM_{2.5}$ levels ranged from 14 to 17 µg/m³, just above the air quality standard established by World Health Organization (WHO) on 10 µg/m³ annually (Figure 1, example of 2009). Over the years, the months between August and November (dry period in the region; burning season), had the highest average levels of $PM_{2.5}$, estimated between 18 to 23 µg/m³. The highest rates of hospitalization were observed during the rainy season, between March and June.

Manaus is located at a wet tropical climate area and presents almost always humid air in its weather normal conditions, with an average relative humidity always above 71%, during the study period, and at nighttime, relative humidity is always close to 100%.

Figure 1 shows the number of hospitalizations for respiratory diseases together with $PM_{2.5}$. Figure 2 shows relative humidity and hospitalizations for 2007. Humidity has a higher effect than aerosol in sharp contrast with health studies in the Southern part of the Amazonian basin.

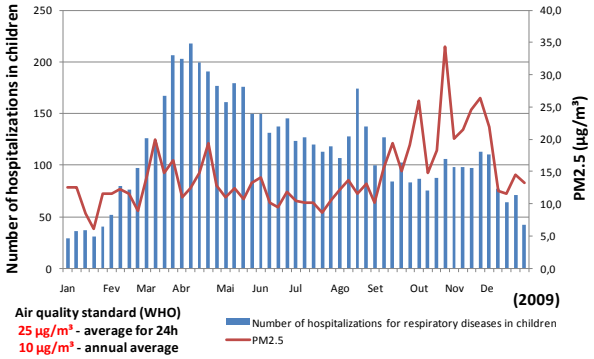

Figure 1 – Number of hospitalizations for respiratory diseases in children and PM2.5 in 2009. Manaus, AM.

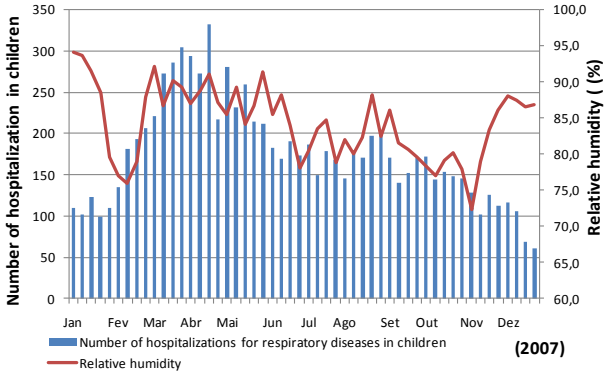

Figure 2 – Number of hospitalizations for respiratory diseases in children and relative humidity in 2007. Manaus, AM.

Acknowledgements

We acknowledge Glauber Guimarães and Dennys Mourão for support with data collection. Also thanks FAPESP, INPA, CLIAMB and LBA Central office for financial and logistical support. We thank INPA and FAPEAM for a scholarship support.

A novel exposure system for testing the lung toxicity of domestic wood combustion aerosols

S. Mülhopt, C. Schlager, H.-R. Paur

Institute for Technical Chemistry
Karlsruhe Institute of Technology, 76021 Karlsruhe, Germany

Keywords: Exposure, Deposition efficiency, Health effects of aerosols, Human lung cell, Nanoparticles
Presenting author email: muelhopt@kit.edu

Background:

Epidemiological studies show an association between the concentration of fine and ultrafine particles (PM10, PM2.5, PM0.1) in the atmosphere and the rate of mortality or morbidity due to respiratory and cardiovascular disease (Wichmann et al, 2000). The European Union therefore passed the directive 2008/50/EG to decrease the immission of particles. Regulated is the mass of ultrafine particles without considering their source, their chemical composition or their biological potential which is of real interest. Causing one third of the ultrafine particle immissions, domestic heaters are in the focus of interest. Especially the emissions of wood stoves containing a high amount of organic substances should be characterized regarding to their biological potential.

Material and Methods:

For the quantitative assessment of the toxicity of airborne particle emissions from domestic wood stoves the dose–response relationship is tested by *in-vitro* test systems using bioassays of cell cultures as sensor (Paur et al, 2011). To expose human lung cell cultures reproducible at the air-liquid interface towards aerosols the Karlsruhe Exposure System was developed as described in detail before (Mülhopt et al, 2007; Paur et al, 2008). The Karlsruhe Exposure System is a prototype for testing different emission sources. Goal of this project is the development of an exposure system as laboratory equipment optimized for the measurement of emissions from domestic wood stoves.

Results:

The Novel Exposure System is built with dimensions of 60 x 40 cm in base and 60 cm in height (figure 1). It is characterized by determining the deposition efficiency of nanoparticles with the fluorescein sodium dosimetry method (Mülhopt et al, 2009). The reproducibility of the exposure chambers as well as the stability of the QCM online dose measurement are measured and first exposure experiments are performed with A549 cell cultures exposed to filtered air. The data will be presented as well as the first exposure experiment results from small scale biomass stoves.

Figure 1. Novel Exposure System for Air Liquid Interface exposure of cell cultures towards particle emissions from biomass burners

Acknowledgement:

This work was supported by the Federal Ministry for the Environment, Nature Conservation and Nuclear Safety under grant 03MAP144.

References:

Diabaté, S., Mülhopt, S., Paur, H.-R., Krug, H.F. (2008) *Alternatives To Laboratory Animals* 36, 285

Mülhopt, S., Diabaté, S., Krebs, T., Weiss, C., Paur, H.-R. (2009) *Journal of Physics: Conference Series*, 170, 012008/1-4

Mülhopt, S., Diabaté, S., Krug, H.F. Paur, H.-R., (2007) *Advanced Environmental Monitoring*, Kim Y J and Platt U (eds.), Springer Netherlands 402-414

Paur, H.-R., Cassee, F.R., Teeguarden, J., Fissan, H., Diabate, S., Aufderheide, M., Kreyling, W.G., Hänninen, O., Kasper, G., Riediker, M., Rothen-Rutishauser, B., Schmid, O. (2011) *Journal of Aerosol Science*, submitted for publication

Paur, H.R., Mülhopt, S., Diabaté, S., Weiss, C. (2008) *Journal für Verbraucherschutz und Lebensmittelsicherheit* 3, 3, 319-329

Wichmann H.E., Peters A. (2000). *Phil. Trans. R. Soc. London A* 358:2751-2769.

From Outdoor Particle Concentration to the Health Impact of Aerosol Particles – a Multidisciplinary Modelling Study, Part I

R. Sorjamaa[1], T. Lanki[1], J. Cyrys[2], and O. Hänninen[1]

[1]National Institute for Health and Welfare, Kuopio, 70210, Finland
[2]Helmholtz Zentrum, München, Germany
Keywords: Exposure, Modelling, Infiltration, Indoor/outdoor particles
Presenting author email: Riikka.Sorjamaa@thl.fi

Both short and long term exposures to particulate air pollution have been shown to associate with morbidity and mortality but the aerosol properties that would explain these effects have remained ambiguous. Particle composition and toxicity as well as particle size distribution ($PM_{2.5}$ and PM_{10}) have been considered as possible explaining factors (Kappos *et al*., 2004). It has been also claimed that the mass metrics $PM_{2.5}$ and PM_{10} alone might not be able to explain the outcome of the epidemiological studies as a change in size distribution would lead to mass metric not being able to predict the lung dose (Harrison *et al*., 2010).

One of the major issues in estimating the exposure is the fact that continuous particle concentrations are measured at urban monitoring stations. As the majority of the Europeans spend approximately 85% of their time indoors, it is important to know how the particle size distributions are modified when infiltrating into buildings.

The current study uses mass-balance approach and aerosol monitoring data collected with electrical aerosol spectrometer (EAS; Mirme *et al*., 2002) to model size specific indoor number and mass concentrations, and compares the results against $PM_{2.5}$ measurements made in Helsinki. Infiltration modelling utilizes data from the literature (Chen *et al.*, 2010) and aerosol physics (Lai and Nazaroff, 2001).

The results show that the accumulation mode particles have the highest contribution to both outdoor and indoor $PM_{2.5}$ mass concentrations and that the contribution of supermicron particles is reduced indoors by the lower infiltration factors.

This work has been supported by EU Contracts FP7-ENV-2009-1-243406 (TRANSPHORM), ENV4-CT95-0205 (ULTRA) and Academy of Finland Contract 133792 (PM Sizex).

Chen, C and Zhao, B. (2010) Atmos. Environ. doi:10.1016/j.atmosenv.2010.09.048

Harrison, R.M., Giorio, C., Beddows, D.C.S., and Dall'Osto, M. (2010), Sci. Tot. Env. **409**. 289-293.

Kappos, A.D., Bruckmann, P., Eikmann, T., Englert, N., Heinrich, U., Höppe, P., Koch, E., Krause, G.H.M., Kreyling, W.G., Rauchfuss, K., Rombout, P., Schulz-Klemp, V., Thiel, W.R., and Wichmann H.-E. (2004) Int. J. Hyg. Environ. Health **207**, 399-407.

Lai, A.C.K. and Nazaroff W.W. (2000) J. Aerosol Sci. **31**, 463-476

Mirme, A., Kreyling, W.G., Khylstov, A., Brink, H. t. Ruuskanen, J., Tuch, T., and Pekkanen, J. (2002) Aerosol Sci Tech. **36**, 866-876

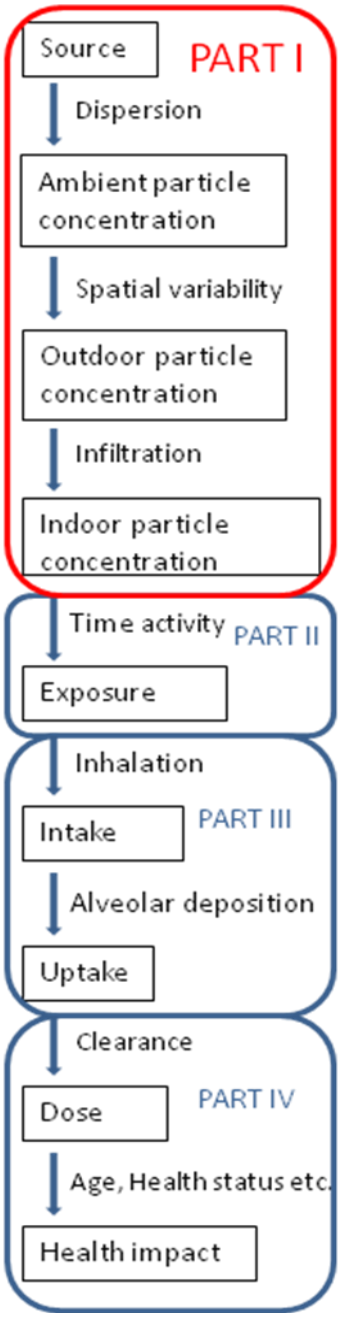

Figure 1. A schematic presentation of the model

Relationship of Indoor and Outdoor PM and Gaseous Pollutants in the National Library in Prague

L. Mašková[1,2], J. Smolík[1], J. Ondráček[1], L. Ondráčková[1], and S. López-Aparicio[3]

[1]Department of Aerosols and Laser Studies, Institute of Chemical Process Fundamentals AS CR, v.v.i., Rozvojová 135, 165 02, Prague 6, Czech Republic
[2]Charles University in Prague, Faculty of Science, Institute for Environmental Studies, Benátská 2, 12 801, Prague 2, Czech Republic
[3]Norwegian Institute for Air Research, Instituttveien 18, P.O. Box 100, NO-2027 Kjeller, Norway
Keywords: Indoor/outdoor particles, chemical composition.
Presenting author email: maskova@icpf.cas.cz

Particulate matter (PM) and gaseous pollutants inside cultural heritage buildings such as museums and libraries pose a risk to materials. Particles not only cause soiling but are abrasive, provide sites for surface reactions and have a potential to damage artifacts due to their hygroscopic nature (Hachtfield, 2005). In addition ammonium nitrate can evaporate after penetration indoors, generating gaseous ammonia and nitric acid, which can damage works of art (Evans, 1960, Salmon and Cass, 1993).

To determine the composition of PM in the indoor and outdoor environment of the National Library in Prague, size-resolved sampling has been performed during three intensive campaigns in different seasons of year. Particles were collected and segregated into 10 size fractions (0.025-10 μm) using two Berner type Low Pressure Impactors that sampled in parallel from the indoor and outdoor environment. Collected samples were analysed gravimetrically and by Ion Chromatography (IC) giving mass and ionic size distributions. In parallel to PM sampling indoor and outdoor gaseous ammonia and nitric acid were measured using passive diffusion samplers.

Typical mass size distributions were bimodal with minimum at about 1 μm, lower concentrations indoors and submicron range shifted to smaller particles. The typical indoor and outdoor mass size distributions of sulphate, nitrate and ammonium ions are shown in Fig. 1.

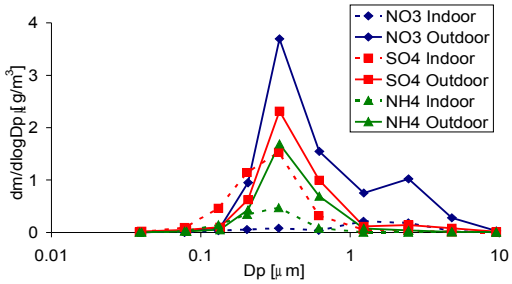

Figure 1. The typical example of indoor and outdoor mass size distributions of sulphate, nitrate, and ammonium.

As can be seen, the ammonium nitrate practically disappeared in submicron fractions of indoor PM. It indicates a shift in equilibrium toward the gas phase, caused by higher temperatures indoors (eq. 1), that can be further driven by deposition of gaseous nitric acid on indoor surfaces (Lunden *et al.*, 2003).

$$NH_4NO_3\ (s/aq) \leftrightarrow NH_3\ (g) + HNO_3\ (g) \quad (1)$$

This can be supported by the results obtained from passive diffusion sampler measurements where indoor concentrations of gaseous nitric acid were very low or below the detection limit during the whole period (Fig. 2).

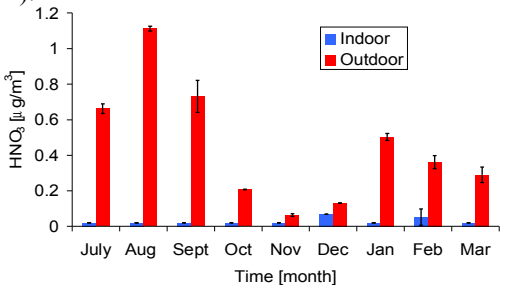

Figure 2. Time series of gaseous nitric acid concentrations.

The evaporation of ammonium nitrate indoors could also explain increased concentrations of ammonia measured indoors (Fig. 3). But, combined effect of ammonium nitrate evaporation and penetration of ammonia from the outdoor air should be considered.

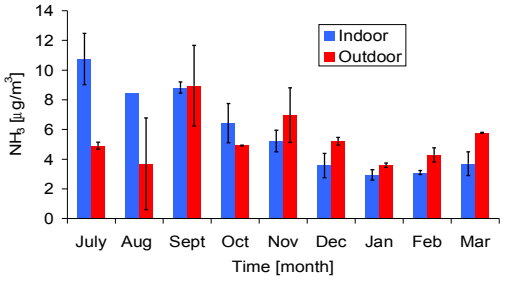

Figure 3. Time series of ammonia concentrations.

This work was supported by the Ministry of Culture under grant DF11P01OVV020.

Evans, U. (1960) *The Corrosion and Oxidation of Metals: Scientific Principles and Practical Applications,* Arnold, 691.

Hatchfield, P. B. (2005) *Pollutants in the Museum Environment*, Archetype Publications Ltd.

Lunden, M. M., Revzan, K. L., Fischer, M. L., Thatcher, T. L., Littlejohn, D., Hering, S. V., and Brown, N. J. (2003) *Atmos. Environ.* **37**, 5633-5644.

Salmon, L. G. and Cass, G. R. (1993) *Studies in Conservation* **38**, 73-91.

Chemical characterisation of PM_{10} in primary schools, Portugal

T. Nunes[1], J.R. Silva[1], A. Caseiro[1], P.N. Pegas[1], C.A. Alves[1], C.A. Pio[1]

[1] Centre for Environmental and Marine Studies - CESAM, Department of Environment, University of Aveiro, 3810-193 Aveiro, Portugal.

Keywords: indoor/outdoor particles, PM_{10}, carbonaceous particles, soluble fraction

Presenting author email: tnunes@ua.pt

Various studies have shown that poor indoor air quality (IAQ) in schools interferes with learning activities and can cause discomfort, irritation, and various short- and long-term health problems in students, teachers and staff. The right to breathe clean air in schools should be recognised as a fundamental health right at all levels: by the European Commission, the Health, Environment and Education authorities in the Member States, and the scientific societies and professional organisations involved in this topic, and also by school staff, students, and the public at large. Previous studies carried out in Portuguese primary schools (SAUDAR, INDOOR) revealed that particulate matter showed systematically higher indoor than outdoor concentrations. Not only PM mass concentrations, but also the composition of particles, particularly the oxidant potential, are thought to be important in assessing health effects. Indoor generated particles are different from those outdoors owing to the different sources and formation processes.

In order to contribute to an integrated understanding of the exposure to PM in school environments and the identification of the main sources and particulate matter composition indoors, a field study started last year. This study involved two primary schools, one in the city centre and another in the peripheral urban area, in an open quarter, with less population density. Comfort parameters and indoor/outdoor concentrations of NO_2, VOCs and PM_{10} were measured. PM_{10} samples were analysed and characterised for the water soluble inorganic ions (WSII), as well for the carbonaceous fractions in their main three components: organic carbon (OC), elemental carbon (EC) and carbonates (CC).

Here we present the results obtained during the first field campaign that occurred between April and June 2010. In each school, daily sampling of indoor/outdoor of PM_{10} during a two-week period was performed in parallel with low volume samplers, excepting the weekend days, when 48 hours sampling time was adopted. The PM samples were collected in pre-baked (6 h at 500ºC) quartz filters with 47 cm of diameter. PM_{10} mass concentration was quantified following the EN 12341 method. After mass weight, the PM_{10} filters were stored in a freezer until chemical analysis. The organic (OC) and elemental carbon (EC) content was analysed by a thermal-optical transmission technique. Two 9 mm diameter filter punches were used in each analytical run, after a previous exposure to an acid atmosphere to remove any carbonate potential interference. Particle carbonates were quantified (two 9 mm diameter filter punches) by the measurement of CO_2 release by NDIR, after sample acidification with orthophosphoric acid. Particulate soluble ions (inorganic cations and anions) were extracted in ultra pure water and analysed by ion chromatography.

Table 1 – Indoor and indoor/outdoor PM_{10} concentrations and percentage of the main particle constituents.

		Urban School		Suburban School	
		Indoor avg ± std	in/out avg ± std	Indoor avg + std	in/out avg ± std
PM_{10} ($\mu g\ m^{-3}$)	w. days	49.2 ± 9.5	2.40±0.88	72.8±28.8	1.84±1.06
	w. end	13.0±4.7	0.74±0.00	20.4±2.4	0.91±0.15
CC (%)	w. days	1.18 ±0.68	16.3±9.7	1.24±0.76	19.8±20.2
	w. end	0.27 ±0.06	1.84±0.20	1.49±1.87	10.3±11.05
OC (%)	w. days	28.8 ±3.4	3.35±1.,37	19.7±4.5	3.84±2,7
	w. end	38.8 ±19.0	1.14±0.51	32.2±22.6	7.73±8.93
EC (%)	w. days	3.44 ±0.84	1.36±0.65	1.58±1.31	1.36±1.37
	w. end	11.8 ±8.9	3.28±2.06	1.64±2.31	1.02±1.44
WSII (%)	w. days	12.1 ±6.3		16.3±11.2	
	w. end	26.8 ±1.7		26.5±8.7	

Table 1 shows the average and standard deviation of indoor concentrations and of indoor/outdoor ratios. During weekdays, the indoor PM_{10} concentrations were around twice the outdoor concentrations. Organic carbon was the particulate component contributing most to the indoor PM_{10} concentrations. Its contribution to the aerosol mass increased in both schools during the weekends. Individual particulate components that showed indoor/outdoor ratios >1 were CC, OC, EC, calcium and potassium, with OC and CC showing the highest ratios. EC indoor concentrations observed in urban school were higher than at suburban indoor denoting the influence of higher EC levels in the surroundings of the inner-city institution; however, the average absolute difference in indoor-outdoor is very similar in both schools. A possible indoor source of EC in primary schools could be graphitic pencil regularly used by children. The indoor source of carbonate, calcium and potassium is chalk used in blackboards. Indoor particulate organic carbon sources seem to be mainly related to student room occupancy and their activities, like small particles of paper, skin debris and clothing fibres. Inorganic soluble ions like chloride, nitrate, sodium, ammonium and magnesium showed typically indoor/outdoor ratios <1. These particle components have a probable origin in outdoor air. All the water soluble ions showed pronounced indoor/outdoor concentration ratio decay during weekend periods, with the exception of sulphate.

This work was supported by Fundação para a Ciência e Tecnologia (FCT) through the PTDC/SAU-ESA/65597/2006 project. Priscilla N. Pegas thanks FCT for the Ph.D. Scholarship (SFRH/BD/45233/2008).

Smoking neighbours – a possible source to ETS exposure in homes

P. Molnár[1] and S. Johannesson[1]

[1]Department of Occupational and Environmental Medicine, Sahlgrenska Academy at University of Gothenburg, Gothenburg, SE 405 30, Sweden
Keywords: ETS, Indoor aerosols, Submicron particles.
Presenting author email: peter.molnar@amm.gu.se

Background: Living in a home with a smoker makes you exposed to environmental tobacco smoke (ETS). It has been shown that ETS can have negative health effects for both children and adults (Janson, 2004). What about if your neighbours in an apartment block smokes? Can the cigarette smoke penetrate from one apartment to another?

A family (two adults and an infant) complained about cigarette smoke coming from their downstairs neighbours and asked for an investigation regarding the contribution of particles due to the cigarette smoke.

The house is a hundred year old building that has been renovated over the years to improve the energy efficiency (e.g. better insulation and new windows with tighter fitting). After the initial complains, the property manager checked the ventilation system and increased the ventilation rate in the smoker's apartment to create an under pressure compared to the above apartment. However, this measure didn't solve the problem because of the in-wall sliding doors in the apartments. Or more precisely, the space where the doors slide into the walls when opened, were not airtight between the apartments.

Methods: A TSI CPC-3007 was used to count the particle number concentration and placed close to the opening of the sliding doors. In the living room the owner of the apartment, a member from the department and a representative from the property manager were trying to notice any cigarette odour. In the smoking apartment, the owner and two persons from the department were sitting in the living room and smoked according to a predetermined schedule (3 cigarettes followed by another two). This was performed for two settings, first with the windows in the smoker's apartment closed and secondly with two windows opened in the smoker's apartment (to create a draught). The investigated apartment was aired out between the two experiments. Outdoor particle number concentration was measured, before and after the experiments, and the concentration was in the range 9,000-9,600 particles cm^{-3} at both times.

Results: With windows closed in the smoker's apartment only a moderate increase of submicron particles were found (see Table 1) and no cigarette smoke odour was perceived in the living room. About 30 minutes after smoking started downstairs, a faint odour was experienced when sniffing by the sliding doors. After 35 minutes the particle number concentration started to go down again.

In the second experiment when windows were opened in the smoker's apartment, particle number concentration increased during the whole experiment (see Table 1).After about 30 minutes, a 50 % increase was reached, and after about 35 minutes the particle number concentration was doubled compared with pre smoking concentration. Cigarette smoke was perceived in the living room after about 5 minutes and the odour was evident next to the sliding doors. After about 15 minutes the cigarette smoke odour was distinct in the living room and remained so throughout the experiment.

Table 1. Particle number concentration (as 5 min means) for the two experiments (with closed and opened windows) and percentage increase vs. pre smoking.

	Windows closed		Windows opened	
	(# cm-3)	%	(# cm-3)	%
Pre smoking	4095	–	4820	–
+5-10 min	4316	+5	5489	+13
+10-15 min	4440	+8	5147	+6
+15-20 min	4751	+16	5677	+17
+20-25 min	4635	+13	6716	+39
+25-30 min	4623	+13	7228	+50
+30-35 min	4854	+19	10257	+112

Conclusions: Cigarette smoke from a neighbouring apartment can give a substantial contribution to the particle number concentration indoors under certain conditions. This occurred when the windows were open in the smoker's apartment downstairs. The lower air pressure indoors compared to ambient air is then lost in the smoker's apartment while maintained in the other apartment. The cigarette smoke is therefore drawn through the leakages between the apartments.

Janson, C., The effect of passive smoking on respiratory health in children and adults, *International Journal of Tuberculosis and Lung Disease* **8**(2004), pp. 510-516.

Bispehnol A concentrations in indoor and outdoor PM2.5 samples

M. G. Perrone[1], Z. Lazzati[2], R. Zangrando[3], L. Ferrero[1], G. Sangiorgi[1], A. Gambaro[3] and E. Bolzacchini[1]

[1] POLARIS Research Center, Department of Environmental Sciences, University of Milano-Bicocca, P.zza della Scienza 1, 20126 Milan, Italy
[2] Institute for Biomedical Technologies ITB-CNR, Via F.lli Cervi, 93, 20090 Segrate (MI), Italy.
[3]Department of Environmental Sciences, University of Venice, Santa Marta 2137, 30123, Venice, Italy

Keywords: indoor/outdoor particles, health aspects of aerosols, BPA, indoor sources
Presenting author email: grazia.perrone@unimib.it

Bisphenol A [2,2-bis(4-hydroxyphenyl)propane] (BPA) is a likely endocrine-disrupting compound (EDCs) (vom Saal, 2005; Ashby, 2004). BPA is an industrial chemical, a monomer of the polycarbonate plastics and a precursor for a variety of epoxide resins.

Consideration of exposure to EDCs is critical in study of health effects, particularly in relation to indoor environment, which have been identified as an important source of chemical exposures (Colt et al, 1998). People spend a large fraction of their time indoor, and indoor sources of chemicals, coupled with limited ventilation and slow chemical degradation processes, cause increased pollutant concentrations indoor.

The atmospheric occurrence of particle-bound BPA in the indoor and outdoor atmosphere at an urban site (Milan, Italy) has been investigated.

Daily (24 h) PM2.5 samples have been collected (low volume gravimetric sampling: 38.3 l min^{-1}, PTFE filters; according to EN-14907) from September 2007 to March 2008, and sampling took place simultaneously in an indoor and outdoor site. Indoor site was a non-smoking office, and outdoor site was located in the yard of the building where the office was set. To assess the BPA concentration in PM2.5 samples, filters were ultrasonically extracted in methanol (0.4 ml) and analysed by HPLC/(-)ESI-MS/MS (liquid chromatography /negative ion electrospray ionization – tandem mass spectrometry). In this work IDMS method has been used and the analytical procedure was validated: the accuracy, precision and recovery have been evaluated.

	INDOOR			OUTDOOR			IN/OUT	
	PM2.5	BPA		PM2.5	BPA		PM2.5	BPA
	$\mu g\ m^{-3}$	$ng\ m^{-3}$	$ng\ \mu g^{-1}$	$\mu g\ m^{-3}$	$\mu g\ m^{-3}$	$ng\ \mu g^{-1}$	$\mu g\ m^{-3}$ IN/OUT	$ng\ m^{-3}$ IN/OUT
MEAN	16.9	0.30	18	29.0	0.18	5	0.62	3.3
SD	1.8	0.04	1	3.6	0.05	1	0.05	0.8

Table 1. Comparison between indoor and outdoor concentrations for PM2.5 and BPA. Mean ± SD (standard deviation)

PM2.5 concentrations indoor were lower than outdoor, but higher BPA concentrations were measured in indoor than outdoor. (Table 1). Averaged BPA concentration was 0.30 (± 0.04) ng m^{-3} indoor and 0.18 (± 0.05) ng m^{-3} outdoor. BPA content of PM2.5 was 18 (± 1) ng μg^{-1} indoor and 5(± 1) ng μg^{-1} outdoor.

Indoor air pollution levels are influenced by indoor pollution source and by infiltration of outdoor air. In an indoor environment there are many potential source of BPA from epoxide resins and polycarbonate plastics, but the major source could be the polycarbonate elements of the lamps that, when switch on, warm up by joule effect.

Daily indoor BPA concentration was correlated to daily outdoor BPA (R^2= 0.88) (Fig.1), thus indicating as indoor is strictly influenced by infiltration of outdoor air. The slope of the linear correlation between indoor and outdoor BPA is less than 1 (0.82), suggesting that about 80% of outdoor BPA is transported in the indoor environment.

Nevertheless, the y-intercept of the linear relationship between indoor and outdoor daily concentrations indicate that another source of indoor BPA, not related to the exchange with outdoor, occurred. The level of indoor BPA attributed to indoor pollution source was estimated equal to 0.15 ng m^{-3}, and it contributed to 19% up to 94% of the indoor BPA level we measured.

.

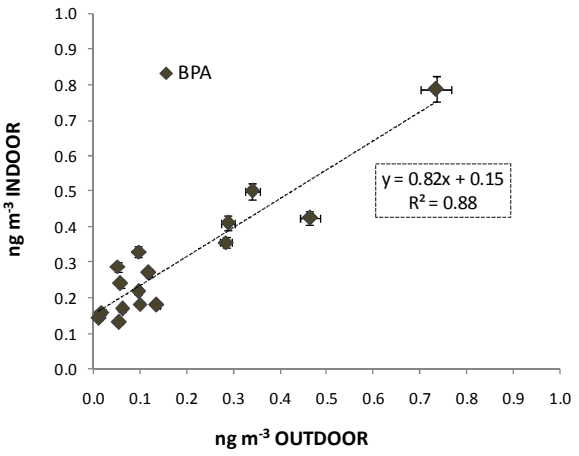

Figure 1. Daily BPA concentration (ng m^{-3}) in PM2.5 samples indoor (offices) versus outdoor.

Ashby, J., Tinwell, H., Odum, J., Lefevre, P. (2004). *Environ. Health Perspect. 8, 847–853*.

Colt, J. S.; Zahm, S. H.; Camann, D. E.; Hartge, P. (1998). *Environ. Health Perspect. 1998, 106 (11), 721-724.*

vom Saal F.S. (2005). *Environ Health Perspect* 113:926-933.

Inactivation efficiency of avian influenza H6N1 bioaerosol using the aptamer-filter

S.H. Yang[1], L.C. Chen[2], C.H. Luo[3], Y.C. Huang[3], and H.T. Laio[2]

[1]Department of Environmental and Occupational Health, Toko University, Chia Yi County, Taiwan, R.O.C
[2]Department of Bio-lndustrial Mechatronics Engineering, National Taiwan University, Taipei, Taiwan, ROC
[3]Department of Safety, Health and Environmental Engineering, Hungkuang University, Taichung, Taiwan, ROC
Keywords: inactivation, H6N1, aptamer
Presenting author email: shinhaoyang@ntu.edu.tw

Most people typically spend around 87.2% of their time indoors (Lance, 1996). Accordingly, indoor air quality is an increasingly important issue. Bioaerosols importantly affect indoor air quality because they cause various respiratory diseases (Eduard *et al*., 1993; Melbostad *et al*., 1994). Higher concentrations of bioaerosols were found in indoors because of higher temperature and relative humidity all round year in Taiwan. Many epidemiological studies have inferred that sick building syndrome (SBS) was related to bioaerosols. Therefore, it cannot be neglected that the problem of indoor air pollution caused by bioaerosols in Taiwan.

This work applied the fibrous filter coated with the aptamer to explore the feasibility of removing avian influenza H6N1 virus bioaerosols. The H6N1 virus bioaerosols are generated from a microbial suspension liquid using a Collison Nebulizer. The H6N1 virus bioaerosols are mixed with a clean air and then are filtered using fibrous filter pretreated with the aptamer. To assess collection efficiency of fibrous filter, several factors were investigated, including the aptamer concentrations, higher and lower relative humidity, and different face velocities. The inactivation efficiency of H6N1 virus bioaerosols was assessed by virus titer before and after filtration. This work will show the results of the feasibility of removal H6N1 virus bioaerosols by aptamer coated on fibrous filter. Otherwise, the effects of different surface velocities, and relative humidity on removing H6N1 virus bioaerosols by the fibrous filter coated with aptamer will be investigated completely in this work. The experimental system was shown in Figure 1.

This study applied the aptamer-filter and non-coated filter to inactivate H6N1 virus bioaerosols at relative humidity (RH) of 30%, temperature of 25 ºC, and face velocity of 10 cm/s (shown in Table 1). The experimental results showed that the virus titer of the H6N1 virus passing through the non-coated filter was 2^6. The virus titer of the H6N1 virus passing through the aptamer-filter was 2^3. It's finding that aptamer could inactivate the H6N1 virus bioaerosols, when H6N1 bioaerosols passed through the aptamer-filter.

Table 1. Comparison of the H6N1 virus titer between through the non-coated filter and aptamer filter.

Testing filter	Virus titer
Non-coated filter	2^6
Aptamer-filter	2^3

This study applied the aptamer-filterr to inactivate H6N1 virus bioaerosols at RH of 30%, temperature of 25 ºC, and face velocity of 10 and 20 cm/s. The results showed that the virus titer of the H6N1 virus passing through the passing through the aptamer-filter at face velocity of 10 and 20 cam/s was 2^3 and 2^4. The results indicated that the inactivation ability of the aptamer would decrease with face velocity increasing.

This study also applied the aptamer-filter to inactivate H6N1 virus bioaerosols temperature of 25 ºC, face velocity of 10 cm/s, and RH of 30% and 90%. The results showed that the virus titer of the H6N1 virus passing through the passing through the aptamer-filter at RH of 30% and 90% was 2^3 and 2^4. The results indicated that the inactivation ability of the aptamer would decrease with RH.

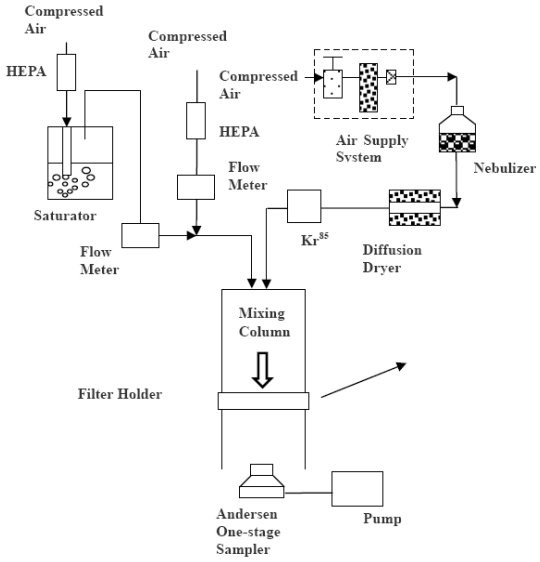

Figure 1. The experimental test setups.

This work was supported by the National Science Council, Taiwan, under Contract no. NSC 99-2622-E-464-001-CC3.

Eduard, W., Sandven, P., & Levy, F. (1993). *Am. J. Ind. Med.*, 24, 207-222

Lance, W. (1996). *Journal of Air and Waste Manage. Assoc.*, 46, 98-126.

Melbostad, E., Eduard, W., Skogstad, A., Sandven, P., Lassen, J., Sostrand, P., & Heldal, K. (1994). *Am. J. Ind. Med.*, 25, 59-63.

Particles in Indoor Air – results from residential dwellings

Christina Isaxon[1,*], Andreas Dahl[1], Erik Nordin[1], Gunilla Wieslander[2], Dan Norbäck[2], Anders Gudmundsson[1], Aneta Wierzbicka[1] and Mats Bohgard[1]

1 Division of Ergonomics and Aerosol Technology, University of Lund, Lund, Sweden

2 Department of Occupational and Environmental Medicine, Uppsala University, Sweden

Keywords: aerosol exposure, real-time measurements, source identification
Presenting author email: christina.isaxon@design.lth.se

Although we spend a major part of our lives indoors, there is a basic lack of information considering particles of indoor origin and their impact on human health. Airborne particle measurements are frequently conducted in workplace environments, but very few, designed to find associations between human activities, aerosol concentrations and health outcomes, in residential homes.

The aim of this study is to characterize the air quality in residential dwellings (in terms of time resolved particle mass and number concentrations, size distributions, soot, temperature, relative humidity and CO_2 levels), correlate this data to various indoor activities and study associations between exposure to airborne particles and health effects/symptoms of the inhabitants.

For seven consecutive days time resolved stationary air measurements are conducted in randomly selected homes (N=42) in the area of Lund in southern Sweden. Aerosol instruments used are MiniDISC (University of Applied Sciences, Windisch, CH), Nanotracer (Philips Research) Indoor Air Quality monitor (IAQ3016, Lighthouse), DustTrak (TSI) and a soot monitor (microAeth AE51, Magee Scientific). The instruments are placed at a central location in each home, close to, but not in, the kitchen. All measurements are made during off-pollen season (October-April). CO_2 data is collected and used to calculate the air exchange rate. Petri dishes are used for collection of potential allergens. The habitants are asked to fill in detailed activity log books.

A thorough examination of each home – e g construction year, floor and wall materials, and ventilation system - is conducted according to a structured protocol. In addition, the participants fill in a 9 page translated and modified version of the IUATLD (International Union Against Tuberculosis and Lung Disease) questionnaire covering topics such as current and previous health status, professional history and everyday habits.

After the measurement period a non-invasive medical examination is conducted, including rhinometry, study of tear film break-up time and measurement of NO in exhaled air. During the measurement period ambient air variations were monitored constantly from a station in northern Lund.

. A data classification is carried out by sorting the data into two categories: occupancy time (at least one person present in the dwelling/residence) and non-occupancy time. An example is shown in Figure 1.

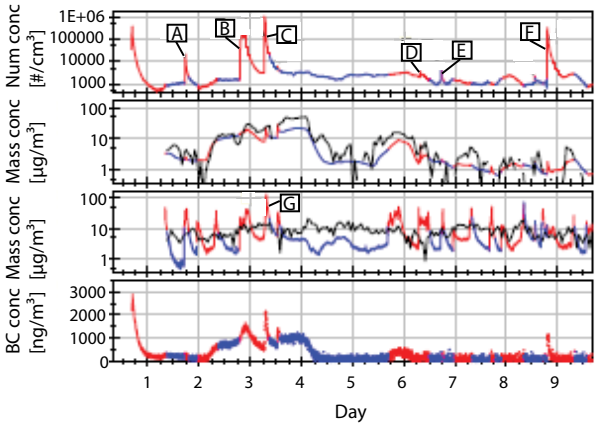

Figure 1. From top to bottom: Number concentrations (MiniDISC), PM_1 (IAQ3016), PM_{10-1} (IAQ3016) and black carbon concentrations (AE51). ug/m^3 denotes reading quantities from the optical instrument, using a density of 2,5 g/cm^3. Red lines denote that somebody was present and blue lines that the dwelling was empty. Black lines are background $PM_{2.5}$ and $PM_{10-2.5}$ respectively. Marked peaks are explained in Table 1 below.

Table 1. Peaks in Fig 1 and their heights above baseline concentration.

Peak	Num conc [#/cm^3]	PM_1 [µg/m^3]	PM_{10-1} [µg/m^3]	Activity
A	20000	0.5	35	Cooking
B	150000	6.8	0	Burning candle
C	1000000	0	0	Burning candle
D	1900	5	5	Cooking
E	2800	0.4	0	Cooking
F	320000	1.1	6.5	Cooking
G	-	15	110	Extinguishing candle

In a major part of the studied homes the concentration of particles, in particular in the sub micron size range, were higher when someone was present. Mean number concentration levels elevated by several hundred percent (indicated by the miniDISC, which is most sensitive for particles 20-120 nm), when someone was present in a dwelling, were not uncommon. The time resolved data in combination with the activity log books made it possible to trace peaks in concentration to a specific activity or usage of a specific appliance. It was also possible to see the relative strength of the indoor aerosol sources.

This work was performed within the framework of the Metalund centre of excellence, and financed by the Swedish Councils FORMAS and FAS together with the Development Fund of the Swedish Construction Industry (SBUF).

Environmental pollution in Metropolitan Areas and alterations of respiratory function

G. Schiraldi [1], F. Cetta [2], R. Zangari [2], V. Guercio [2], L. Moltoni [2], P. Laviano [2], P. Paladini [2], C. Ghiribelli [2], L. Voltolini[2], R. Borrelli[2], E. Bolzacchini [3], L. Allegra [1] and G. Gotti [2]

[1]Toracopulmonary and Cardiovascular Dept., University of Milan, Milan, 20122, Italy
[2]Dept. of Surgery and Thoracic Surgery, University of Siena, Siena, 53100, Italy
[3]Dept. of Environmental Sciences, University of Milan, Milan, 20126, Italy
Keywords: PM, COPD, urban areas, remote alpine sites.
Presenting author email: giaschir@tin.it

Increased concentration of particulate material (PM), mainly due to urban traffic, heating and industrial pollutants is responsible for a different air quality in metropolitan areas vs remote sites and is likely to be responsible for a different incidence of respiratory complications and/or reduction of pulmonary function.

Methods: Two groups of 99 subjects were recruited (n=198), on a casual and voluntary basis: the former in Milan, Italy, i.e. a densely populated and polluted metropolitan area, the latter in Aprica, a remote alpine site (1181 m.a.s.l), with low pollution, due to traffic or other pollution sources. PM_{10} (<10 μm)and $PM_{2,5}$ (<2,5μm) were measured by PM detection units during two 2 week-campaigns. Each group was classified in 2 subgroups. The former, aged 30 to 64 years, (n=72) the latter over 65 (n=27). All subjects, well matched for cigarette smoke, sex and age were in good health conditions, asymptomatic and with no previous history of respiratory chronic diseases. All of them underwent spirometry, with evaluation of the following parameters: FVC (forced vital capacity), FEV_1 (forced expiratory volume in 1 second), PEF (peak expiratory flow) and MEF_{50} and MEF_{25}, i.e. maximum forced expiratory flow at 50% and 25% of FVC, respectively. Data were expressed as the percentage ratio between measured and theoretical values (m/t%).

Results: m/t% of FEV_1 (index of bronchial patency), both in under 65 and over 65 subjects, was lower in Milan that in Aprica subjects (**Table 1** and **Table 2**).

Table 1: m/t% in subjects age 30-65 years

	Milan	Aprica	p (t test)
FEV_1 m/t%	96	103	<0.01
MEF_{50} m/t %	75	97	<0.0001
MEF_{25} m/t%	54	78	<0.0001

Table 2: m/t% in subjects age 65-89 years
In particular, FEV_1 was <80% (value borderline

	Milan	Aprica	P (t test)
FEV_1 m/t%	69	88	NS (p=0.052)
MEF_{50} m/t %	68	86	NS (p=0.073)
MEF_{25} m/t%	44	66	<0.0001

between normal and abnormal data) in 20 out of 99 subjects in Milan (20,2%), whereas it was < 80% in only 8 out of 99 in Aprica (8,08%), (**Table 3**).

Evident differences were also observed in subgroups of different age: FEV1 resulted <80% in 8 out of 72 subjects under 65 years in Milan (11,1%) and in 2 out of 72 in Aprica (2,8%); and in 12 out of 27 (44,4%) and 6 out of 27 (22,2%) in subjects over 65 years, respectively (p<0,05) (**Table 3**).

Table 3: FEV_1 changes (< 80%) Milan vs Aprica

FEV_1 < 80%	Milan	Aprica
Total subjects	20 (20%)	8 (8%)
Subjects < 65y	8 (11%)	2 (28%)
Subjects >65y	12 (44%)	6 (22%)

Consistently, MEF_{50} and MEF_{25}, suggestive of the "smaller airway diseases", i.e. of a sub-clinical pathological entity somehow preceding chronic obstructive pulmonary diseases (COPD), were found (m/t%), both in under 65 and over 65 subjects, higher in Aprica than Milan inhabitants (**Table 1** and **Table 2**). In particular, in 30 out of 85 Milan subjects vs 18 out of 85 Aprica subjects, they were below the threshold (<65% for MEF_{50} , and <50% for MEF_{25}), which are considered borderline between normal and abnormal values (p<0,001) (**Table 4**).

Table 4: MEF_{50} and MEF_{25} changes (<65% and 50% respectively) Milan vs Aprica

MEF_{50}<65%, MEF_{25}<50%	Milan	Aprica
Total subjects	30 (35 %)	18 (21 %)
Subjects < 65y	17 (27 %)	3 (5 %)
Subjects >65y	13 (56 %)	15 (65 %)

Conclusion: Present data, even if preliminary, suggest that in the polluted metropolitan area of Milan, inhabitants are more prone to a "COPD march" than in the low pollution alpine site of Aprica. In particular, not only in severely symptomatic subjects with evident respiratory diseases, but also in clinically asymptomatic individuals, it is possible to detect significant difference in respiratory function because of different levels of air pollution. Since PM related alterations are partly reversible because of repair and defense mechanism of the host, periodical interruption of chronic exposure to metropolitan pollutants with exposure to a better environment (such as an Alpine site) could be of benefit.

Surface Area Deposition Index for Jet Engine PM Exhaust

D.E. Hagen[1], E.A. Black[1,2], P.D. Whitefield[1], and P. Lobo[1]

[1]Center of Excellence for Aerospace Particulate Emissions Reduction Research, Missouri University of Science & Technology, Rolla MO, 65409, USA
[2]College of Natural & Applied Sciences, Missouri State University, Springfield MO, 65897, USA
Keywords: Aircraft plumes, combustion aerosols, lung deposition, hygroscopicity.
Presenting author email: hagen@mst.edu

A major portion of atmospheric particles found in both urban and rural areas consists of carbonaceous material derived from both biogenic and anthropogenic sources. Particulate matter (PM) from on-road vehicular traffic has been correlated to increases in mortality and morbidity. PM from jet engine exhaust (JEE) falls into a similar size range, but its inhalation health impacts have been less well studied. JEE PM has unique properties with respect to deposition, retention kinetics, and clearance pathways in the human respiratory system, and is composed of sizes that readily travel gas streamlines that penetrate the deepest regions of the lung; this is a concern as deposited JEE PM in these regions could potentially cross the blood-membrane barrier and migrate into the bloodstream.

In two field campaigns PM size distribution and hydration data was acquired by the Missouri University of Science & Technology Center of Excellence for Aerospace Particulate Emissions Reduction Research (Missouri S&T COE), at Hartsfield-Jackson Atlanta International (ATL) and Oakland International (OAK) airports (Herndon et al 2008; Whitefield et al 2007). JEE PM was sampled downwind of active taxi- and runways during normal airport operations. The sample locations were selected adjacent to airport runways at distances of 100 m or greater from take-off sites, and chosen so JEE plumes would be transported by prevailing winds to a sampling probe feeding the diagnostic instrumentation. For both campaigns aircraft tail numbers were recorded for identification of airframes and engine types. Weather conditions were also monitored and recorded continuously throughout testing periods.

Using the JEE PM data collected during plume studies performed down-wind of active runways at ATL and OAK, lung deposition probabilities of JEE PM (as a function of particle size) can be determined using the International Committee of Radiological Protection (ICRP) lung deposition model. Surface area is the characteristic PM parameter most strongly correlated with health impacts (Stoeger et al 2006). Using the deposition probabilities and size resolved number distributions, a Surface Area Deposition Index (SADI) was developed. This new parameter, SADI, characterizes JEE PM lung deposition as the surface area of deposited PM per kilogram fuel burned. SADI allows for equitable comparison among various jet engine types while also proving a surface area metric for meaningful health impact correlations. An example of the variation in SADI for engine type CFM-56 observed at OAK is shown in Fig. 1.

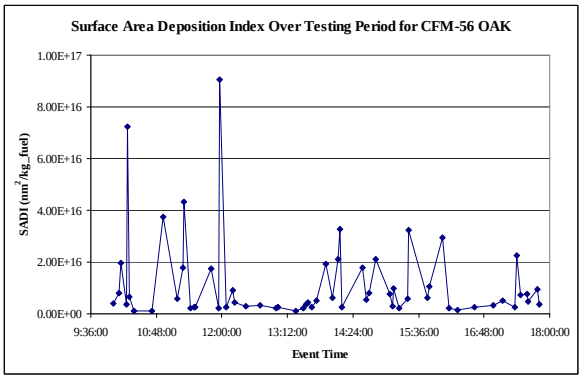

Fig. 1 Surface Area Deposition Index for CFM-56 engine type observed at OAK

Two interesting conclusions to this preliminary study are that statistically significant differences among engine types are not observed in SADI, and variations in SADI are not correlated with temporal changes or changes in meteorological conditions.

EAB was sponsored by the Airport Cooperative Research Program (ACRP 11-04: Graduate Research Award Program on Public-Sector Aviation Issues) administered by the Transportation Research Board of the National Academies (Project Manager: Larry Goldstein). The opinions and conclusions expressed or implied in the presentation are those of the authors. They are not necessarily those of the Transportation Research Board, the National Academies, or the program sponsor. DEH, PDW, and PL would like to acknowledge the sponsorship of the Missouri S&T COE.

Stoeger, T., Reinhard, C., Takenaka, S., Schroeppel, A., Karg, E., Ritter, B., Heyder, J., and Schulz, H. (2006) Environmental Health Perspectives, **114**, 328-333.

Herndon, S., Jayne, J.T., Lobo, P., Onasch, T.B., Fleming, G., Hagen, D.E., Whitefield, P.D., Miake-Lye, R.C. (2008) *Environmental Science & Technology* **42**, 1877-1883.

Whitefield, P.D., P. Lobo, and D.E. Hagen (2007) In *Sausen, R., A. Blum, D.S. Lee and C. Brüning (eds.): Proceedings of an International Conference on Transport, Atmosphere and Climate (TAC).* ISBN 92-79-04583-0, 95-100.

Protein Nitration and Health Effects

K. Selzle, Y. Zhang, H. Yang, and U. Pöschl

Department of Biogeochemistry, Max-Planck Institute for Chemistry, Mainz, 55128, Germany
Keywords: ambient air pollution, health effects of aerosols, enhanced allergenicity due to protein nitration
k.selzle@mpic.de

Proteins account for up to ~5% of urban particulate matter, influence the physiochemical properties of atmospheric particles, and play a major role as airborne allergens (Franze, Weller et al. 2003)

Lots of studies indicated that proteins could be nitrated by the NO_2 and O_3 gas in atmosphere and the nitration took place at tyrosine (Franze, Weller et al. 2005). Several studies suggested that nitrated protein might cause and enhance allergic disease and asthma (Gruijthuijsen, Grieshuber et al. 2006).

The chemical mechanisms and molecular processes that lead to adverse health effects of NO_2 and O_3 are, however, still poorly understood. We suggest that protein nitration by air pollutants plays a major role in the increase of allergies in the western countries besides nutrition effects and excessive hygiene practices.

In this study, liquid chromatography and tandem mass spectrometry (LC-MS/MS) was used to characterize several proteins in their native and nitrated form.

Native protein bovine serum albumin (BSA) and native chicken ovalbumin (OVA) were nitrated by tetranitromethane (TNM) in liquid phase and NO_2 and O_3 in gas phase and characterized by The observed nitration patterns show how the site selectivity of protein nitration depends on the nitrating agent, reaction conditions, and molecular structure of the protein (Zhang, Yang et al. 2010)With regard to immunological questions it might be of special interest that the most efficiently nitrated tyrosine residue within the OVA protein (Y107) is part of human as well as murine IgE epitopes of ovalbumin and is also found in a human ovalbumin T cell epitope (Untersmayr, Diesner et al. 2010).

The experimental results show that further investigation on protein nitration is required. Our future plan is to investigate different nitration agents which are relevant in immunological pathways as well as in the atmosphere (peroxynitrite, peroxyacetylnitrate (PAN)).

This work was supported by the Max-Planck Society (MPG), the International Max-Planck Research School for Atmospheric Chemistry and Physics (IMPRS) and the Max-Planck Graduate School (MPGC).

Franze, T., Weller, M. G., Niessner, R. and Pöschl, U. (2003) *Analyst*, 128(7): 824-831

Franze, T., Weller, M. G., Niessner, R. and Pöschl, U. (2005) *Environ. Sci. Technol.*, 39(6): 1673-1678

Gruijthuijsen, Y. K., Grieshuber, I. et al. (2006) *Int. Arch. Allergy Immunol.*, 141(3): 265-275

Zhang, Y., Hong, Y., Pöschl, U. (2011) *Anal. Bioanal. Chem.*, 399: 459-471

Untersmayr, E., Diesner, S. C. et al. (2010) *PLoS ONE* 5(12): e14210

Pigeons as Source of Airborne Circoviruses

G. Jereb[1], U. Krapež[2], Š. Pintarič[2] and A. Dovč[2]

[1] University of Ljubljana, Faculty of Health Sciences, Zdravstvena pot 5, 1000 Ljubljana, Slovenia
[2] University of Ljubljana, Veterinary Faculty, Gerbičeva 60, 1000 Ljubljana, Slovenia

Keywords: bioaerosols, pigeons, *Circovirus*
Presenting author email: gregor.jereb@zf.uni-lj.si

With pigeon's colonized attics as well as pigeon lofts represent rather dusty environment, therefore different dust particles (aerosols) could be found in such locations. These aerosols originates mainly from pigeons and consists of pigeon's excreta and feather dust (known also as bloom), another source is also grain feed. Consequently also different bio-aerosols are present in rather high concentrations in such locations. According to the results of preliminary study (Jereb et al., 2010) as well as literature data, free-living pigeons are commonly infected with different microorganisms (Dovč et al., 2004; Haag, 2008), also several zoonotic ones. Among others, pigeons (especially young ones) are often infected with avian circoviruses of the genus *Circovirus* (Bougiouklis, 2007). The role and influence of circoviruses on pigeons is not yet fully elucidated, however connection with immunosuppression and several different clinical signs is established (Marlier and Vindevogel, 2006). Influence of circoviruses pathogenesis on humans is not excluded as well (Bougiouklis, 2007).

In presented study therefore presence of circoviruses in pigeons as well as presence of circoviruses in air sample from pigeons loft and from with pigeon's colonized attic was investigated.

Samples of air were obtained using a Merck MAS-100 NT bio-aerosol sampler based on the impaction principle. Sampler aspirates air through a perforated plate on to standard 90mm agar poured Petri dishes. The aspirated volume was a constant value of 100 liters per minute and 300 x 0.6mm sampling head (perforated lid) was used with declared impaction speed <20m/s. Additionally, Coriolis Delta Air sampler - aspirated volume of 100 liters per minute (cyclonic air sampler), based on a cyclone type device that selects and captures airborne particles and transfer them into a liquid sample, was used.

In 2006 cloacal and tracheal swabs and in 2009 the air in with pigeon's colonized attic was analyzed on presence of circoviruses using PCR (Duchatel et al., 2009). According to preliminary results 75% of tested feral pigeon's excreted circoviruses through cloacae and 62% of them excreted virus through trachea. The air in the attic where feral pigeons lived was positive for the presence of circoviruses. Method for detection of virus was identical in all cases.

Based on preliminary results further analyzes will be performed among several pigeon breeders and their breed pigeons. Also air in pigeon's loft will be further assessed on presence of circoviruses with aim to correlate presence of circovirus in pigeons and air.

References:

Bougiouklis P. (2007) Avian circoviruses of the genus Circovirus: a potential trigger in pigeon breeder's lung (PBL)/bird fancier's lung (BFL). Medical Hypothesis, Vol. 68, 320 - 323

Dovc A., Zorman-Rojs O., Vergles Rataj A., Bole Hribovšek V., Krapež U., Dobeic M. (2004) Health status of free living pigeons (Columba livia domestica) in the city of Ljubljana. ActaVet. Hung. 52(2), 219-26

Duchatel J.P., Todd D., Willeman C., Losson B. (2009) Quantification of pigeon circovirus in serum, blood, semen and different tissues of naturally infected pigeons using a real-time polymerase chain reaction. Avian Pathol, 38(2):143-8

Haag D. (2008) Human diseases caused by feral pigeons. Advances in vertebrate pest management, Vol. 4, 31-58

Jereb G., Pintaric Š., Micunovic J., Krapež U., Slavec B., Poljšak B., Dovc A. (2010) Airborne Microorganisms in Pigeons Colonized Attics. In: IAC 2010, Helsinki, Finland. Finnish association for aerosol research, 2010; 1 p

Marlier D., Vindevogel H. (2006) Viral infections in pigeons. The Veterinary Journal, Vol 172, 40-51

Thursday, September 8, 2011

Session 8P: Poster session B

Aerosol Chemistry

Synthesis and Surface Area evaluation of Solid Core Porous Shell Particles

G. Kastrinaki[1,2] and A.G Konstandopoulos[1,3]

[1]Aerosol &Particle Technology Laboratory, CERTH/CPERI, P.O. Box 60361, 57001, Thessaloniki, Greece
[2] Department of Mechanical Engineering, University of W. Macedonia, 50100, Kozani, Greece
[3] Department of Chemical Engineering, Aristotle University, PO. Box 1517, 54006, Thessaloniki, Greece
Keywords: porous nanoparticles, nanoparticle oxides, aerosol spray pyrolysis.
Presenting author email: georgiak@cperi.certh.gr

A solid particle (core) that is surrounded by a porous shell is a morphology than can be used to protect the core material from unwanted interaction with molecules that exceed the pore shell size (protection) and/or to maintain it until the temperature conditions intrigue the core material to be released out from the porous shell walls (controlled release). The particle's selective reactivity and release characteristics make Solid Core Porous Shell Particles (SCPSP) interesting for energy, environmental and medical applications. The size of: the core, the shell and the shell pores are important parameters in order to control the protection and release characteristics of the particles. The present work is a study of SCPSP synthesis and surface area evaluation of particles with various core sizes.

SCPS particles with metal oxide core and silica porous shell were synthesized by Aerosol Spray Pyrolysis (ASP) (Karadimitra et al., 2001). An aqueous silicate and surfactant precursor solution is atomized into micro-sized droplets by an air assisted atomizer. The droplets are carried via air inside a heated (400^{o}C) tubular reactor and the produced particles are collected on a glass fiber filter located at the exit of the reactor.

In the silica droplet, the surfactant is located towards the external surface (Ward, 2003) forming micelles, which self assemble into ordered structures, while the water-ion solution is captured in the core undergoing crystallization of the ions when the concentration reaches saturation point. Calcination of the synthesized particles at 450^{o}C for 5hrs removes the surfactant leaving the final product particles with a porous shell behind.

The SCPSP morphology and the core size of the particle can be adjusted by the precursor solution and the synthesis conditions (Kastrinaki et al., 2009). The particles were characterized by Transmission Electron Microscopy (TEM), X-Ray Diffraction (XRD), BET and Induced Couple Plasma (ICP) Analysis.

TEM images revealed the core shell morphology. The nanostructured particles had an outside ordered porous shell with metal oxide trapped in the core. XRD analysis showed that the core metal oxide is nano-crystalline whereas the porous shell is mostly shown to be amorphous with ordered porosity. Porous particles were characterized via BET analysis with respect to their surface area and pore size distribution. The BET pore sizes agree with the sizes measured from the TEM images, while the ICP analysis shows the increased metal percent for the larger cores.

For a constant pore size of 2nm the precursor solution moles varied from 0.1-0.33/1 metal/Si ratio and the impact on the final particle is the control of the core size. The surface area of the particles is measured by BET analysis and the surface area vs the core size is depicted on Figure 1, where particles with larger cores (smaller porous shell areas) show smaller surface areas.

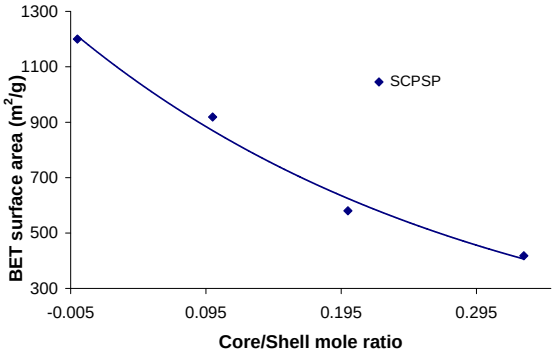

Figure 1. BET surface are with the core/shell ratio for the solid core porous shell particles.

Uniformly porous particles with 2nm pore size were also synthesized, in order to evaluate the surface area of porous particles without a core. The uniformly porous particles depict a high surface are of 1200 m^2/gr, which decreases with the incorporation and further increase of the core size.

Mathematical formulations were used in order to calculate theoretically the surface area of the SCPSP in correlation with the core size measured from the TEM pictures and to compare it with the surface area measured from the BET results.

Karadimitra, K., Papaioannou, E. and Konstandopoulos, A.G. (2001). *J. Aerosol Sci.* **32**, Suppl. 1, S233-234.

Ward T., Datye A., Lopez G., Brinker J., and van Swol F., *NSF NIRT* No. 0210835 (2003)

Kastrinaki, G., Lorentzou, S. and Konstandopoulos, A.G. (2009). In *Proc. European Aerosol Conference*, Karlsruhe, T016A04.

Physicochemical transformations and photochemical reactions of high-disperse pesticide chemicals

Yuri N. Samsonov

Institute of Chemical Kinetics and Combustion, 630090, Novosibirsk. Russia,
Keywords: aerosol chemistry, evaporation, particulate matter, pesticide particulates, photochemical reaction
samsonov@kinetics.nsc.ru

The high-disperse substance state is a natural phenomenon. Many hundreds of millions of tons of particulate matter enter the atmosphere annually from both the natural and anthropogenic sources. Anthropogenic impact is caused by heat-and-power engineering, motor fuel exhausts, and the application of pesticide chemicals in agriculture. The chemical reactions which occur permanently in the environment with particulate pollutants (reactions with OH radicals, nitrogen oxides and ozone, direct or induced photodecomposition and photo-oxidation, (photo)catalytic reactions) result in their chemical conversions. As the reagents (OH, O3, and others) arise in the atmosphere due to the action of sunlight, the term "photochemical reaction" applies often to all chemical reactions in which these reagents participate. Decomposition under sunlight seems to be very important for many chemical pollutants being in a high-disperse state in the environment (pesticide particles levitated in the air or settled on foliage, thin films of pesticide chemicals spread over leaf surface). The photochemical stage of decomposition, which generally is a many-stage chemical process, can sometimes predetermine the overall decomposition rate of pesticide particulates. The light absorbed inside a particle/film induces here chemical reactions. There is the lack of reference data on the intra-particle absorption of light preceded and/or followed by physicochemical and chemical changes in the particulate matter. The photodecompositions of polymeric films and pesticide residues on foliage concern partly these problems. It is worth noting, however, that the polymeric films are the relatively "thick" things (5-10 μm and thicker) with the given chemical compositions and bulk structures (Rabek, 1996). As will be shown below, both the composition and structure of fine pesticide particles and films, especially in ambient conditions, are specific, changeable and often irreproducible.

The high-disperse state reveals specific features for the rates and mechanisms of physicochemical transformations and photochemical reactions, which differ from the processes in coarse dispersal matter and, even more, in ordinary liquid and solid "test-tube" assays. The point is that, due to the fast evaporation of some chemical components (e.g., solvents) out of a fine particle/film, its size, chemical composition and phase state are changing permanently. This can cause the solidification and stratification of intra-particle matter resulting in a very slow diffusion of reagents within particle/film body, and other specific physicochemical and chemical changes. In this regard, the chemical reaction in a fine particle/film is not a certain elementary chemical act, but a succession of the above physicochemical and chemical events depending on the particle size (film thickness) and the bulk structure, but the expressivities of the above-listed factors can be diverse and spontaneous under different conditions.

The kinetics and the mechanisms of the direct and sensitized photochemical decompositions of several pesticide chemicals have been experimented as applied to the aerosol particles 0.12- 1.3 μm in diameter settled on glass plates and films 0.03 – 0.5 μm thick on plates. The plates with the particles and films exposed to a long irradiation, which simulate sunlight photolysis of pesticide residues on plants. Although the settled particulates are not the perfect imitation of the pesticide particles levitated freely in the air, they can simulate slow physicochemical and photochemical reactions in the high-disperse pesticide substances. In this regard, it is impossible to experiment over a long time with the freely levitated particles in both the laboratory and ambient conditions due to either fast deposition in a laboratory chamber or fast dissipation in the air. The mechanisms of (photo)chemical reactions of high-disperse pesticide chemicals are hypothesized including the complexing mechanism, the two-quantum photochemistry, and the oxidation by singlet oxygen.

This work is supported by the Russian Based Research Foundation under grant 11-03-00055.

Rabek, J.F. (1996) *Photodegradation of Polymers: Physical Characteristics and Applications*, Springer, Berlin-Heidelberg.
Samsonov, Y.N. and Pokrovskii, L.M. (2001) *Atmospheric Environment* **35**, 2133-2141.
Samsonov, Y.N. (2007) *Journal of Atmospheric Chemistry* **56**, 127-147.

Phase transformation of evaporating solution droplets of immiscible polymers

V. Rajagopalan, E. A. Grulke and A. K. Ray

Department of Chemical Engineering, University of Kentucky, Lexington, KY 40506, USA
Keywords: polymer blend particle, multicomponent droplet evaporation, VOAG.
Presenting author email: akray@engr.uky.edu

Polymer blends have wide range of applications (e.g., opto-electronic devices, organic solar cells) that often require microparticles with uniform properties. In many cases, the polymers are incompatible with one another and thus separate into distinct phases. Conventional methods based on melt blending and miniemulsions can reduce the extent of phase separation in many polymer blends, but are limited to polymer pairs in certain property ranges. There is a need for a synthesis method that can blend immiscible arbitrarily polymer pairs. Blended microparticles produced by evaporating solution microdroplets, containing two immiscible polymers dissolved in a common solvent, are expected to exhibit a high degree of phase uniformity under conditions where the timescale of solvent evaporation is lower than that of polymer diffusion and self-organization. In such a situation, the phase separation is inhibited within the atto- to femto-liter volume of the droplet, and homogeneous blends of immiscible polymers can be produced.

We have examined multicomponent polymer particles produced from highly monodisperse microrordroplets that were generated using a Vibrating Orifice Aerosol Generator (Devarakonda et al. 1998; Gao et al. 2007). Equal proportions of two highly incompatible polymers, polystyrene (PS, Mw=280,000) and polyvinyl chloride (PVC, Mw=75,000), were dissolved in a common solvent, tetrahydrofuran (THF), to get a desired total polymer concentration in the solution in the range of 2 to 4 wt%. Droplets were generated from the homogeneous solution; in addition to THF, ethanol was added in varying amounts to reduce evaporation rates of the solution droplets. The morphology of the polymer blend particles produced from the droplets of various composition was studied by an SEM (Hitachi SEM-3200N). To obtain the distribution of each component inside the particle, samples were placed in Beem capsules, embedded in Spurr's resin, and kept under vacuum for 48 hours. They were then polymerized at 60^0C for 48 hrs, and finally, sliced thinly on a Reichert-Jung Ultracut E microtome. The thickness of the slices was about 60 nm. The slices were placed on copper grids and examined in the FEI Tecnai Biotwin 12 transmission electron microscope (TEM). An Energy Dispersive X-ray Analysis (EDS) (coupled with SEM) was performed for the presence of chlorine. All the samples were coated with a thin layer of Gold and Palladium before using them under the SEM.

The SEM micrographs of polymer particles show that the particles are of spheroidal shape and often have indentations. Even though the initial droplets generated by the VOAG have the same size, the final solid particles have varied morphologies. This is due to nonuniform drying conditions inside the experimental chamber. Surface hollows and indentations observed in the particles can be attributed to the rapid drying of the droplets. Even though the physical characteristics of the particles were not uniform, the objective was to study the extent of phase separation or the lack of it thereof. The elemental difference between PS and PVC is the presence of chlorine in PVC. This prompted us to do EDS on the thin slices of the blend particles that were prepared using the microtome. The slices were about 60 nm thick with diameter of about 12 μm. Each analysis was done over an area of 3x3 μm^2. The EDS spectra from various locations of a particle clearly show primary and secondary peaks of chlorine. For particles produced from solutions with THF as the sole solvent, chlorine peaks were observed to have approximately the same intensity. This suggests that the distribution of chlorine is more or less uniform throughout the cross-section. Thus, qualitatively, PVC and PS are dispersed uniformly in the particle.

The results of this study show that uniform polymer blend microparticles can be produced by rapid evaporation of microdroplets. The morphology of the final particles that form after the solvent evaporation depends on the initial droplet size, polymer concentration, solvent volatility, and temperature. Future studies would involve more quantitative measurements. The mapping of chlorine in the samples are needed to fully ensure that the particles produced are indeed uniformly blended microparticles.

This work was supported by the National Science Foundation (grant # ATM-0634789), and National Institute for Occupational Safety and Health (grant # 1R01OH009802-01).

Devarakonda V., Ray, A. K., Kaiser, T., and Schweiger G. (1998) *Aerosol Sci. Technol.* **28**, 531-547.

Gao Z., Grulke E. A., and Ray A. K. (2007) *Colloid and Polymer Sci.* **285**, 847-854

Diethylamine and new charged particles formation

T.-E. Parts, A. Luts, and U. Hõrrak

Institute of Physics, University of Tartu, Ülikooli 18, 50090 Tartu, Estonia

Keywords: aerosol chemistry, air ions, particle size distribution, trace gases.

Presenting author email: tiia-ene.parts@ut.ee

Volatile organic compounds (VOCs), particularly amines may play substantial role in the new particle formation (NPF) processes (e.g., Bzdek *et al*, 2010). Diethylamine (DEA), chemical formula $(C_2H_5)_2NH$ or $C_4H_{11}N$, is one of the VOC, emitted into the atmosphere from a variety of sources including meat cooking, biomass burning, motor vehicle exhaust, industrial processes, and marine organisms (e.g., Facchini *et al*, 2008).

Previously we reported some results about DEA affecting the mobility spectra of one second aged small positive air ions (Parts and Luts, 2004). Now we have measured the mobility spectra of negative ions by our modified experimental set-up, which allows to observe the changes in ion formation processes through time scale from about 1 second (*young ions*) up to ~20 seconds (*old ions*). Ions are produced by radioactive ^{243}Am source. We study the ageing of air ions concurrently by ion mobility spectrometry (AIS, Airel Ltd) and mass spectrometry (API300 TQ MS) to find out the characteristic differences in spectra (compared to background), induced by enhanced concentration of diethylamine, and to propose some of the ion species typical for the obtained spectra.

Diethylamine is a chemical compound with high proton affinity, therefore, it behaves in different way regarding the positive or negative ions chemistry. For positive ions the proton transfer reactions are important For negative ions, in our present study, the attachment reactions of DEA to negative ions should appear.

The results of AIS measurements reveal that the relative effect of DEA on the size distribution of negative ions depends on air ion age (Figure 1). Addition of DEA reduces the amount of the smallest (<0.65 nm) young ions and increases the concentration of smallest old ions. DEA also decreases the mean size of old cluster ions. The concentration of charged particles with diameters above 7 nm has a trend to rise.

In the AIS spectra we also observed some increase in the percentage of the intermediate ions with a diameter from 1.5 to 4 nm. So, it appears that DEA can generate new aerosol ions. But, presumably, more than 20 seconds is needed to generate larger particles.

Mass spectra measurements show that addition of DEA into the air also changes ion composition for both young and old negative ions. When to compare with the background, the new peaks appear at *m/z* 198, 261 and 334. The MS/MS analysis of the peak *m/z* 198 confirms that $NO_3^-(HNO_3)$(DEA) should be responsible for such a mass. The small peak at *m/z* 261 (198+63) could be $NO_3^-(HNO_3)_2$(DEA), and the latter at *m/z* 334 (261+73) the ion with one extra DEA molecule $NO_3^-(HNO_3)_2(DEA)_2$.

Some aspects concerning the spectra of positive ions, obtained in the same experiment, are also discussed.

This work was supported by the Estonian Science Foundation grant 8342 and Estonian Research Council targeted financing project SF0180043s08. We thank Tapio Kotiaho, Alexey Adamov, and Timo Maurila from the Helsinki University for help in MS experiments.

Bzdek, B.R., Ridge, D.P., and Johnston, M.V. (2010) *Atmos. Chem. Phys*. **10**, 3495-3503.

Facchini, M. C., Decesari, S., Rinaldi, T., Carbone, C., Finessi, E., Mircea, A., Fuzzi, S., Moretti, F., Tagliavini, E., Ceburnis, D., and O'Dowd, C.D. (2008) *Environ. Sci. Technol.* **42**, 9116–9121.

Parts, T., and Luts, A. (2004) *Atm. Envir.* **38**, 1283–1289.

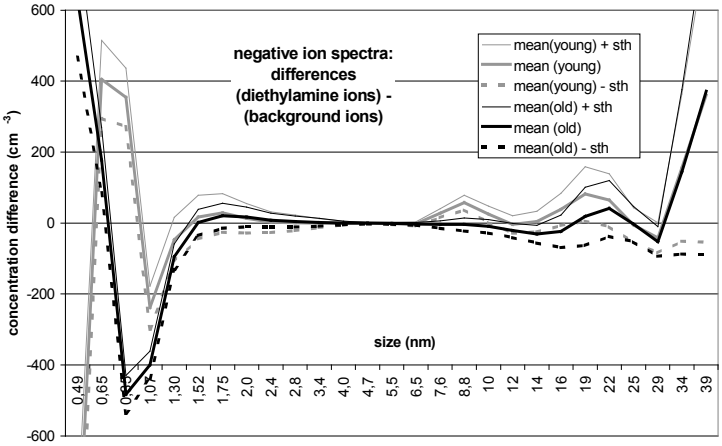

Figure 1. Difference between the AIS spectra of negative ions, obtained in the case of enhanced concentration of diethylamine, and the AIS spectra, measured in the background air.

To some mechanisms of UV-light induced SO_2 Oxidation to H_2SO_4 and Aerosol Formation

A.A. Sorokin[1,2]

[1]Institute for High Temperature of the Russian Academy of Science, Izhorskaya 13/19, 125412, Moscow, Russia
[2]Institute of Nuclear Safety of the Russian Academy of Science, B. Tulskaya 52, 115191, Moscow, Russia

Keywords: chemistry, aerosol formation.

Presenting author email: sorokin@ibrae.ac.ru

The electron-excited chemistry of sulfur dioxide oxidation induced by UV irradiation of air with trace O_3 and SO_2 is considered. The importance of this mechanism is evaluated based on recent laboratory experiments on SO_2 oxidation in a laminar tube with air induced by UV irradiation (Berndt et al., 2005, 2006, 2008). The formation of GSA has been attributed to known neutral chemistry mechanism starting from the reaction of SO_2 molecules with OH radicals which is a typical SO_2 oxidation route in atmospheric conditions.

Our results show that under respective conditions the route of SO_2 oxidation involving electron excited oxygen molecules may present an additional source of gaseous H_2SO_4 production to known OH-radical mechanism (Sorokin, 2010).

During the above experiments the fractions of charged particles were also observed. Their concentrations in a size range bigger than 2 nm were measured to be essentially smaller than that of neutral particles. Based on this result, it was concluded that the ion induced nucleation was a minor importance in these experiments. However, the large time-scale characteristics are an important particularity of these experiments. The gas flow time spends were about 290 and 90 s respectively for UV irradiated section followed by the UV free section. All measurements were performed at the outlet of UV free section. It is likely, that the charge neutralization combined with the particle wall losses in UV free section may essentially change the charged particles size distribution in comparison with those that was formed to the end of the UV irradiated section.

In our topic the ion chemistry of sulfur dioxide induced by UV irradiation of O_3-SO_2-H_2O gases followed by formation of neutral particles via the ion-ion recombination is considered. We show that the observed size distribution of neutral particles may be partially explained by nucleation of neutral sub 2 nm particles induced by ion-ion recombination. In this mechanism, the ions play a key role in an enhancement of both the GSA generation rate and nucleation of neutral particles.

In total, here we try to give some new insights to related mechanisms. An influence of UV irradiation on SO_2 oxidation seems to be important in atmosphere and certainly may provide an additional external source affecting the aerosol formation.

Berndt, T., Böge, O., Stratmann, F., Heintzenberg, J., Kulmala, M. (2005) Science, **307**, 698–700.
Berndt, T., Böge, O., Stratmann, F. (2006) Geophysical Research Letters, **33**, L15817.
Berndt, T., Stratmann, F., Brasel, S., Heintzenberg, J., Laaksonen, A., Kulmala, M. (2008) Atmos. Chem. Phys., **8**, 6365–6374.
Sorokin, A. (2010) Atmos. Chem. Phys., **10**, 3141–3145.

Importance of aerosol phase and water uptake for understanding organic aerosol oxidation

P.J. Gallimore, F.D. Pope, P. Achakulwisut and M. Kalberer

Centre for Atmospheric Science, Department of Chemistry, University of Cambridge, CB2 1EW, UK
Keywords: Aerosol chemistry, Organic acids, Hygroscopicity, Mass spectrometry, SOA
Presenting author email: pjg48@cam.ac.uk

The composition and size of atmospheric aerosol is important with respect to radiative forcing and human health. The chemical processing of organic aerosol by gaseous oxidants helps to determine the atmospheric properties of this important subset of aerosols.

We will present an experimental investigation of the response of maleic acid aerosols to ozone under conditions of variable relative humidity and temperature. Maleic acid is a dicarboxylic acid containing a double bond and is used here as a model for aged organic aerosol in the atmosphere; highly oxygenated dicarboxylic acids constitute a large fraction of the tropospheric organic aerosol budget.

Two experimental techniques are combined in this investigation. An Electrodynamic Balance (EDB) is used to levitate single particles with an initial dry radius of 10-20 μm and assess changes in particle size and mass (due to water uptake and/or loss of volatile ozonolysis products) and phase (liquid or solid) during and after chemical processing with ozone. Particles were exposed to 0.6-1.6 ppmv ozone for 1 hour in a temperature-controlled chamber. The phase of the particle, dependent on the relative humidity, was controlled by a variable humidity N_2 flow. Experiments lasted over 24 hours.

An aerosol flow tube was used to investigate the chemical composition of processed maleic acid aerosol with offline ultra high-resolution mass spectrometry (UHR-MS). The aerosol had a mean dry particle diameter of 180 nm and concentration of $1x10^8$ cm^{-3}, before exposure to ozone up to 200 ppmv in a reaction vessel for up to 5 hours.

The response of particles to ozone is found to depend strongly on the environmental relative humidity; pure maleic acid aerosol exhibits deliquescent behaviour and the phase of the particles (solid or liquid) during ozonolysis is important for understanding the oxidation process. Under dry ozonolysis conditions, glyoxylic acid is the only aerosol-phase product observed. The aerosol hygroscopicity and volatility shows a moderate increase compared to pure maleic acid.

If deliquesced particles are exposed to ozone, additional reaction pathways requiring water become available and many oxidation products are observed. Maleic acid can become significantly depleted after processing, leading to an aerosol composed primarily of high O:C ratio products. The hygroscopicity of such particles is observed to increase significantly compared to maleic acid and volatile product loss is observed.

Furthermore, particles exposed to ozone under dry conditions appear to undergo additional processing upon deliquescence; volatilisation is observed only after a full deliquescence event and after multiple relative humidity cycles the hygroscopicity closely resembles particles obtained from wet initial ozonolysis conditions.

Our experimental hygroscopic growth curves for maleic acid indicate water uptake before the onset of full deliquescence. Ozonolysis of the solid-phase aerosols in this RH region (60-80%) indicates that significant chemical processing occurs including formation of products requiring water (Figure 1). Hence water uptake, as well as particle phase, is a key factor in organic aerosol oxidation.

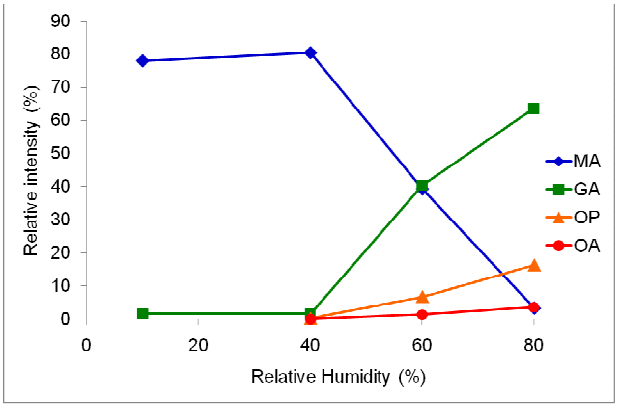

Figure 1: Chemical composition of maleic acid (MA) aerosol processed with ozone (200 ppmv, 3 hours) as a function of relative humidity. Glyoxylic acid (GA) is formed in low yields under dry conditions but becomes a major aerosol component above 60% RH, where pure MA shows water uptake. 2,3-dioxopropanoic acid (OP) and oxalic acid (OA) are only observed in this region.

In summary, the chemical composition and mass of oxidised maleic acid aerosol is found to depend strongly on the relative humidity during and after ozonolysis. The complete history of the processed particle is important, with dry processed particles exhibiting a "memory effect" upon deliquescence. We will propose a chemical mechanism consistent with the observations, placing emphasis on the key role of water uptake in understanding the chemical and physical processing of organic aerosol. The implications of these chemical differences for global aerosol populations, formation of gaseous oxygenated volatile organic compounds, and the cloud nucleation behaviour of the aerosols will be provided.

Pope, F.D., Gallimore, P.J., Fuller, S.J., Cox, R.A., and Kalberer, M. (2010) Environ. Sci. Technol. **44**, 6656.

Gas uptake and chemical aging of amorphous semi-solid aerosol particles

Manabu Shiraiwa[1], Markus Ammann[2], Thomas Koop[3], Ulrich Pöschl[1]

[1]Max Planck Institute for Chemistry, Department of Biogeochemistry, Mainz, Germany
[2] Paul Scherrer Institute, Villigen, CH-5232, Switzerland
[3] University of Bielefeld, Faculty of Chemistry, Bielefeld, Germany
Keywords: bulk diffusion, amorphous semi-solid, ozone, protein
Presenting author email: m.shiraiwa@mpic.de

Atmospheric aerosol particles may occur as solid or liquid or as a mixture of both depending on their compositions and ambient conditions. Carbonaceous combustion aerosol particles such as soot and related substances are known to be solid and undergo chemical reactions at the surface rather than in the bulk (black or elemental carbon, graphene, polycyclic aromatic hydrocarbons). Until recently, secondary organic aerosol (SOA) particles formed in the atmosphere from condensable oxidation products of volatile organic compounds were assumed to be liquid. Virtanen et al. (2010), however, showed that biogenic SOA particles formed in plant chamber experiments and in new particle formation events over boreal forests can adopt an amorphous semi-solid state. Many organic substances, including carboxylic acids, carbohydrates and proteins, tend to form amorphous phases upon cooling or drying of aqueous solution droplets. Depending on viscosity and microstructure, the amorphous phases can be classified as glasses, rubbers, gels, or highly viscous liquids (Mikhailov et al. 2009).

Here we demonstrate how molecular diffusion in the condensed phase affects the gas uptake and chemical transformation of semi-solid particles. Flow tube experiments show that the ozone uptake and oxidative aging of amorphous protein is kinetically limited by bulk diffusion. The reaction rate depends on the diffusion coefficients of both the gaseous and the condensed phase reactants, which can be described by a kinetic multi-layer flux model (Shiraiwa et al. 2010) but not by the traditional resistor model approach of multiphase chemistry (Pfrang et al. 2010). Based on numerical simulations, we present first spatial and temporal profiles of the concentration and reaction rate of ozone and reactive amino acid residues in an amorphous protein matrix. The chemical lifetime of reactive compounds in atmospheric particles can increase from seconds to days and more as the diffusion coefficients decrease over ten orders of magnitude from liquid to solid state. These results and related recent studies demonstrate that the occurrence and properties of amorphous semi-solid phases challenge traditional views and require advanced formalisms for the description of organic particle formation and transformation in atmospheric models of aerosol effects on air quality, public health, and climate.

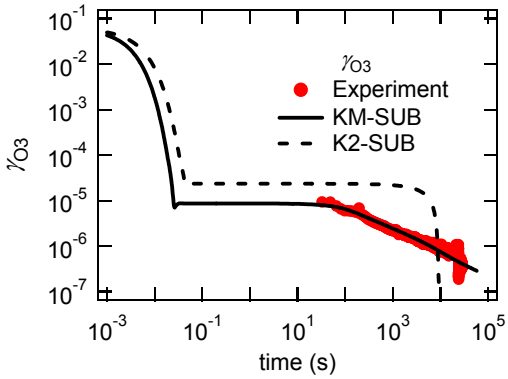

Figure 1. The KM-SUB modeling results of ozone uptake experiments with amorphous protein at 42 ppb O_3. Experimental data and modeled γ_{O3} and surface and bulk accommodation coefficients ($\alpha_{s,O3}$, $\alpha_{b,O3}$).

Acknowledgements.
This work was funded by the Max Planck Society (MPG), Swiss National Foundation, and the European integrated project on cloud climate and air quality interactions (No 036833-2 EUCAARI). We thank M. Birrer, Y. Sosedova, and A. Rouviere for their help in the kinetic experiments; C. Pfrang for stimulating discussions.

References.

Mikhailov, E., et al., Amorphous and crystalline aerosol particles interacting with water vapor: conceptual framework and experimental evidence for restructuring, phase transitions and kinetic limitations. *Atmos. Chem. Phys.*, **9**(2): 9491, 2009.

Pfrang C, et al., Coupling aerosol surface and bulk chemistry with a kinetic double layer model (K2–SUB): an exemplary study of the oxidation of oleic acid by ozone. *Atmos. Chem. Phys.* 10: 4357, 2010.

Shiraiwa, M., et al., Kinetic multi-layer model of aerosol surface and bulk chemistry (KM-SUB): the influence of interfacial transport and bulk diffusion on the oxidation of oleic acid by ozone. *Atmos. Chem. Phys.*, **10**(8): 3673, 2010.

Virtanen, A., et al., An amorphous solid state of biogenic secondary organic aerosol particles. *Nature*, **467**: 824-827, 2010.

Heterogeneous uptake of HO_2 onto submicron aerosol particles

I.J. George[1], B. Brooks[2], L.K. Whalley[1], A. Goddard[1], P.S. Matthews[1], N. Howes, M.T. Baeza-Romero[2] and D.E. Heard[1]

[1]School of Chemistry, University of Leeds, Leeds, West Yorkshire, LS2 9JT, United Kingdom
[2]School of Earth and Environment, University of Leeds, Leeds, West Yorkshire, LS2 9JT, United Kingdom
Keywords: aerosol-surface reactions, multiphase processes, tropospheric aerosols.
Presenting author email: i.j.george@leeds.ac.uk

The hydroxyl (OH) and hydroperoxyl (HO_2) radicals, together known as HO_x, play an important role in atmospheric chemistry by controlling the oxidative capacity of the troposphere. HO_x radicals determine the atmospheric lifetime and concentrations of many trace reactive species, such as NO_x, O_3 and volatile organic compounds (VOCs). Tropospheric OH reactions with reduced trace atmospheric gases, such as SO_2, NO_x and VOCs, lead to the production of inorganic and secondary organic aerosol mass. Therefore, the ability to accurately predict atmospheric concentrations of HO_x radicals from a detailed knowledge of their sources and sinks is necessary to gain a complete understanding of atmospheric chemistry.

Several recent field studies have observed significantly lower steady-state concentrations of HO_2 radicals than predicted using box models (Sommariva, 2006; Kanaya, 2007). Modeling studies have suggested that heterogeneous HO_2 reaction with atmospheric aerosol particles can be an important HO_x sink (Martin, 2003, Tie, 2005). However, relatively few laboratory studies have been performed to determine the kinetic parameters for HO_2 loss onto aerosols, and thus the impact of this mechanism on HO_x levels is unclear. To bridge this gap in knowledge, we conducted laboratory experiments to measure the HO_2 uptake kinetics onto submicron aerosol particles that are representative of tropospheric aerosols.

HO_2 radicals were produced by the photolysis of water vapour in the presence of O_2 and the FAGE (Fluorescence Assay by Gas Expansion) technique was used to monitor HO_2 uptake kinetics onto aerosol particles in an aerosol flow tube setup. The FAGE technique is a highly sensitive laser induced fluorescence based detection method that has been utilized here so that kinetic experiments could be performed under low HO_2 concentrations, i.e. $[HO_2] < 10^9$ molecules cm^{-3}. Particle size distributions were measured with a Scanning Mobility Particle Sizer (TSI). The reaction time between HO_2 radicals and aerosol particles was varied by translating a movable injector. Aerosol particles were produced either by atomizing dilute salt solutions or by homogeneous nucleation.

First order rate coefficients of heterogeneous HO_2 loss were measured as a function of aerosol surface area and were used to calculated reactive uptake coefficients (γ). The mass accommodation coefficient of $\alpha = 0.8 \pm 0.2$ was determined by measuring HO_2 uptake onto Cu(II)-doped ammonium sulfate aerosols. Reactive uptake coefficients have been determined for aqueous and solid submicron NaCl and $(NH_4)_2SO_4$ particles and several organic acids with a wide range of hygroscopicities as representative models for atmospheric aerosols. HO_2 uptake coefficients on solid particles were below detection ($\gamma < 0.004$), whereas on aqueous aerosols uptake was significantly larger ($\gamma = 0.02 - 0.05$). Experiments are currently being conducted to study both temperature and humidity dependent uptake kinetics as well as HO_2 uptake on more chemically complex environmentally relevant samples. These results suggest that particle phase should be taken into account when modeling the impact of HO_2 uptake on aerosols as a HO_x sink.

Acknowledgements

Funding for this work was provided by NERC (#NE/F020651/1).

References

Kanaya, Y., Cao, R., Kato, S., Miyakawa, Y., Kajii, Y., Tanimoto, H., Yokouchi, Y., Mochida, M., Kawamura, K. and Akimoto, H. *(*2007) *J. Geophys. Res.* **112**, D11308.

Martin, R., Jacob, D. and Yantosca, R. (2003) *J. Geophys. Res*. **108(D3)**, 4097.

Sommariva, R., Bloss, W., Brough, N., Carslaw, N., Flynn, M., Haggerstone, A.-L., Heard, D., Hopkins, J.,Lee, J., Lewis, A., McFiggans, G., Monks, P., Penkett, S., Pilling, M., Plane, J., Read, K., Saiz-Lopez, A., Rickard, A. and Williams, P. (2006) *Atmos. Chem. Phys*. **6**, 1135-1153.

Tie, X., Madronich, S., Walters, S., Edwards, D., Ginoux, P., Mahowald, N., Zhang, R., Lou, C. and Brasseur, G. (2005) *J. Geophys. Res*. **110**, D03204.

SPACCIM model studies of tropospheric aerosol-cloud interactions with the extended multiphase chemistry mechanism MCM-CAPRAM

A. Tilgner, P. Bräuer, R. Wolke and H. Herrmann

Department of Chemistry, Leibniz-Institut für Troposphärenforschung,
Permoserstr. 15, Leipzig, 04318, Germany

Keywords: aerosol modelling, multiphase chemistry, aerosol cloud interaction, organic aerosols
tilgner@tropos.de

A great variety of organic compounds is emitted into the troposphere and is then oxidised by complex multiphase degradations leading to secondary organics which partition between the tropospheric gas and aqueous phase incl. deliquescent aerosol particles and cloud droplets. Oxidised organics play a key role in tropospheric chemistry and account for a substantial fraction of tropospheric aerosol mass. Multiphase processes in fog droplets, cloud droplets and deliquescent aerosol particles can potentially alter the physico-chemical composition of the tropospheric aerosol on a global scale (*Ravishankara, 1997*). However, the chemical multiphase processing, i.e. secondary formation and aging mainly of organic aerosol constituents remains poorly considered in current multiphase chemical mechanisms and models.

In order to model complex tropospheric multiphase chemical interactions of cloud droplets and deliquescent aerosol particles, chemical mechanisms with a detailed description of chemical processes in both the gas and the aqueous phase are required. Hence, the Master Chemical Mechanism (MCM v3.1, *Saunders et al. 2003*) and the Chemical Aqueous Phase RAdical Mechanism (CAPRAM3.0; *Tilgner and Herrmann, 2010)* were recently coupled aspiring to a near-explicit multiphase chemical mechanism (see *Herrmann et al., 2010a*). In order to study the organic aerosol cloud processing in more detail, this mechanism was integrated into the model framework SPACCIM (Spectral Aerosol Cloud Interaction Model, *Wolke et al. 2005*). This parcel model SPACCIM combines a complex microphysical and multiphase chemistry and therefore allows for complex multiphase chemistry modelling of aerosol–cloud interactions focusing on organic aerosol constituents.

As demonstrated by a scoping study, about 60% of the MCM gas phase compounds (about 2100 species) are very water-soluble compounds which might efficiently partition into the aqueous phase and perhaps participate in the chemical aerosol–cloud processing. For those species there is a need to implement their phase transfer and their aqueous phase chemical processes in multiphase mechanisms such as MCM-CAPRAM.

Aiming at a future near-explicit chemical multiphase mechanism with an equivalent description of the organic aerosol chemistry in both the gas and the aqueous phase, the phase transfer for the most soluble MCM compounds has been implemented in the coupled MCM-CAPRAM based on both measurement data (see e.g. *Sander, 1999*) and estimation methods (e.g. *Raventos-Duran et al., 2010*). The latter were needed because measured phase transfer parameters, such as Henry coefficients, gas phase diffusion coefficients and mass accommodation coefficients are not available for most of the organic compounds. Furthermore, hydrations and dissociations were added to the mechanism. Furthermore, the CAPRAM mechanism was updated with recently published kinetic data (e.g. *Herrmann et al., 2010b*) and an extended C_3 chemistry (*Bräuer et al., 2011*).

SPACCIM model studies have been performed for different environmental conditions using a non-permanent cloud scenario. The model studies were carried out to investigate multiphase chemistry and the partitioning of organic compounds in tropospheric deliquescent aerosol particles and cloud droplets in more detail. The model studies were focused e.g. on the influence of organic acids for the aqueous phase acidity, multiphase chemistry of tropospheric oxidants. The model results are analysed including time-resolved reaction flux analyses in order to identify important multiphase oxidation pathways leading to the formation of organic aerosol constituents such as substituted mono- and diacids.

References:

Bräuer, P. et al. (2011), Evaluation of prediction methods for aqueous phase rate constants of organics and CAPRAM mechanism development, *EGU General Assembly 2011*.

Herrmann, H., et al. (2010a), Combining MCM and CAPRAM: First Results and Outlook, *3rd Biennial Conference on Atmospheric Chemical Mechanisms, Davis, CA, USA.*

Herrmann, H., et al. (2010b), Tropospheric aqueous-phase free-radical chemistry: radical sources, spectra, reaction kinetics and prediction tools, *ChemPhysChem*, 11(18), 3796-3822.

Raventos-Duran, T., et al. (2010), Structure-activity relationships to estimate the effective Henry's law constants of organics of atmospheric interest, *Atmos. Chem. Phys.*, 10(16), 7643-7654.

Ravishankara, A. R. (1997), Heterogeneous and multiphase chemistry in the troposphere, Science, 276(5315), 1058-1065.

Sander, R. (1999), Compilation of Henry's Law Constants for Inorganic and Organic Species of Potential Importance in Environmental Chemistry (Version 3), http://www.henrys-law.org

Saunders, S. M., et al. (2003), Protocol for the development of the Master Chemical Mechanism, MCM v3 (Part A): tropospheric degradation of non-aromatic volatile organic compounds, *Atmos. Chem. Phys*., 3, 161-180.

Tilgner, A., and H. Herrmann (2010), Radical-driven carbonyl-to-acid conversion and acid degradation in tropospheric aqueous systems studied by CAPRAM, Atmos. Environ., 44(40), 5415-5422.

Wolke, R., et al., (2005), SPACCIM: A parcel model with detailed microphysics and complex multiphase chemistry, *Atmos. Environ*., 39(23-24), 4375-4388.

The impact of clouds on radical concentrations: Observations of OH and HO_2 during HCCT-2010

L.K. Whalley[1,2], I.J. George[1], D. Stone[1] and D.E. Heard[1,2]

[1]School of Chemistry, University of Leeds, Leeds, West Yorkshire, LS2 9JT, United Kingdom
[2]National Centre for Atmospheric Science, University of Leeds, Leeds, LS2 9JT, United Kingdom
Keywords: Clouds, aerosol-surface reactions, multiphase processes, tropospheric aerosols.
Presenting author email: i.j.george@leeds.ac.uk

Clouds play a crucial role in the chemistry of the atmosphere, occupying, on average, ~ 15 % of the volume of the lower atmosphere (Lelieveld & Crutzen, 1990). Modelling studies have shown that aqueous phase chemistry in clouds can influence gas phase radical chemistry and in turn can cause significant reductions in the oxidative capacity (e.g. Lelieveld & Crutzen, 1991; Kreidenweis et al., 2003) and, hence, removal rate of VOCs. A number of aircraft projects have identified significantly reduced HO_2 concentrations when flying through clouds that exceeds the depletion expected due to the reduction in radiation alone (Olson et al., 2004; Commane et al., 2010). These experimental observations are relatively sparse, however, and until recently a comprehensive study to validate model predictions has been lacking.

Here we report preliminary measurements of OH and HO_2 radicals made during the HCCT (Hill Cap Cloud Thuringia) project that took place at Mt. Schmücke, Thuringia in Germany during September/October 2010. The University of Leeds Fluorescence Assay by Gas Expansion (FAGE) instrument was located at the summit of Mt. Schmücke and made near-continuous measurements of the radicals at the top of a 22 m tower. The site was regularly influenced by clouds throughout the measurement period and co-located measurements of liquid water content were made at the site enabling the influence of this microphysical parameter on the radical budget to be determined. On average, the photolysis rate of O_3 to form $O(^1D)$, the primary daytime source of HO_x radicals, was ~ 65 % lower in-cloud relative to the out of cloud observations. The HO_2 concentrations were significantly depleted in cloud, with concentrations ~ 90 % lower relative to the out of cloud observations; an OH signal above the noise of the instrument was not observed during cloud events. These results suggest that heterogeneous processes in clouds do perturb the gas-phase radical chemistry. Further investigations into the dependency of the uptake efficiency on the different microphysical and chemical conditions encountered during the different cloud events will also be presented.

The authors are grateful to the Leipzig Institute for Tropospheric Research for financial support to participate in HCCT, and to Prof. H. Herrmann and others for logistical support. Thanks are also given to the National Centre for Atmospheric Science Facility for Ground-Based Atmospheric Measurements for funding of the FAGE instrumentation and personnel.

Lelieveld, J. and Crutzen P. J., 1990, Influences of Cloud Photochemical Processes on Tropospheric Ozone, Nature 343 (6255), 227-233.

Lelieveld, J. and Crutzen P. J., 1991, The Role of Cloud in Tropospheric Photochemistry, Journal of Atmospheric Chemistry, 12, 229-267.

Kreidenweis, S. M. et al., 2003, Modification of aerosol mass and size distribution due to aqueous phase SO_2 oxidation in clouds: Comparison of several models. Journal of Geophysical Research-Atmospheres, 108.

Olson, J. R. et al., 2004, Testing fast photochemical theory during TRACE-P based on measurements of OH, HO_2 and CH_2O. Journal of Geophysical Research-Atmospheres, 109.

Commane, R. et al., 2010, Observations of OH and HO_2 over West Africa. Atmospheric, chemistry and Physics, 10, 8783–8801.

Phase Transitions and Separation of Mixed Organic-Inorganic Particles

M.L. Smith, A.K. Bertram, S.T. Martin

School of Engineering and Applied Sciences, Harvard University, Cambridge, Massachusetts, USA

Keywords: phase transitions, secondary organic material.

Atmospheric particles containing both organic and inorganic components can transition between solid and aqueous phases in response to fluctuations in ambient relative humidity. These particles can also phase separate into multiple liquid phases depending on the amount of particulate water, the organic volume fraction (ε), and the chemical properties of each component. The parameterization recently developed by Bertram et al. (2011) predicts that aqueous phase separation is more likely to occur as the O:C of the organic material is decreased. Liquid-liquid phase separation in mixed particles should allow inorganic material to deliquesce and effloresce as it does in its pure state. In the absence of phase separation, organic molecules can cause significant deviations from pure inorganic behavior.

The deliquescence and efflorescence behavior of laboratory generated organic-ammonium sulfate particles were investigated using a 1×3 tandem differential mobility analyzer. Organic material was generated via α-pinene dark ozonolysis (O:C = 0.39-0.44; Smith et al. 2011) and isoprene photooxidation (O:C = 0.67-0.74; Smith et al., in preparation).

The deliquescence and efflorescence relative humidities (DRH and ERH, respectively) of all particles containing α-pinene dark ozonolysis products ($0.0 < \varepsilon < 0.96$) deviated less than 5% RH from the DRH and ERH of pure ammonium sulfate.

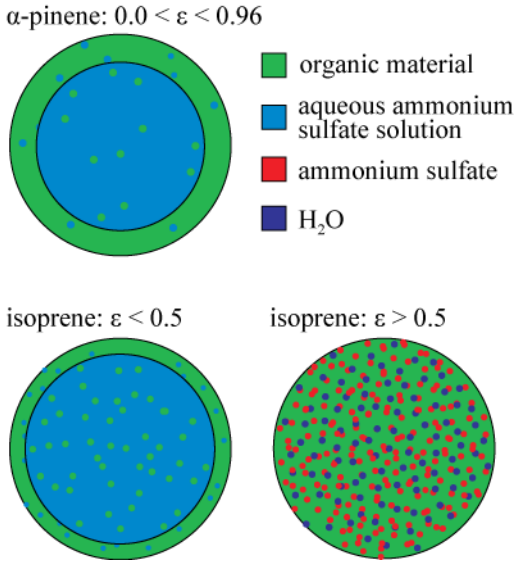

Figure 1. Illustration of the proposed dependence of aqueous phase particle morphology on VOC precursor and organic volume fraction.

The minimal influence of the organic material on the hygroscopic properties of ammonium sulfate suggests that two liquid phases are present in aqueous particles at the water activities of the DRH and ERH. A small negative correlation between both DRH and ERH and organic volume fraction was observed, implying that mixing between the two phases was increased slightly as the organic volume fraction was increased.

The organic material generated via isoprene photooxidation induced greater deviation from pure ammonium sulfate behavior than the α-pinene dark ozonolysis products. The DRH of mixed particles decreased by up to 10% RH, while the ERH decreased by > 20% for particles of high organic volume fraction. The implication is that isoprene photooxidation products are miscible with the aqueous inorganic phase, and can therefore significantly alter the hygroscopic behavior of ammonium sulfate.

These combined results show that phase separation and its subsequent impact on hygroscopic properties vary among VOC precursors and oxidation method. Additionally, the O:C of the secondary organic material emerges as a useful predictor of aqueous phase morphology, with more pronounced phase separation observed for organic material of lower O:C.

The presented material is based upon work supported by the National Science Foundation under Grant No. 0925467 and a Graduate Research Environmental Fellowship from the Global Change Education Program of the Department of Energy.

A. K. Bertram, S. T. Martin, S. J. Hanna, M. L. Smith, A. Bodsworth, Q. Chen, M. Kuwata, A. Liu, Y. You, S. R. Zorn, "The Fluctuating Physical State of Atmospheric 1 Particles," submitted.

M. L. Smith, M. Kuwata, S. T. Martin, "Secondary Organic Material Produced by the Dark Ozonolysis of α-Pinene Minimally Affects the Deliquescence and Efflorescence of Ammonium Sulfate," *Aerosol Science and Technology*, 2011, *45*, 225-242.

M. L. Smith et al., "Influence of Phase Separation on the Phase Transitions of Isoprene Secondary Organic Material Mixed with Sulfate," in preparation.

Experimental study of heterogeneous reactivity between atomic chlorine and palmitic acid film

Raluca CIURARU, Michael WARD, Nicolas VISEZ, Sylvie GOSSELIN, Denis PETITPREZ

Laboratoire de Physico-Chimie des Processus de Combustion et de l'Atmosphère (PC2A), UMR CNRS 8522, Université Lille 1, Cité Scientifique - Bâtiment C11, 59655 Villeneuve d'Ascq, France

Keywords: aerosol chemistry, sea-salts, multiphase processes
raluca.ciuraru@univ-lille1.fr

INTRODUCTION

Sea-salt particles are the principal constituent of aerosol particles in the marine boundary layer. Although the dominant mass fraction of marine aerosol is inorganic sea salt, organic matter also contributes to the overall mass. It has been reported that marine aerosols contain an organic fraction being mainly made up of fatty acids. Resulting from biological activity, it is assumed that fatty acids are ejected into the atmosphere along with sea salt and are found in the particles or on their surface [(1)]. In the marine boundary layer, the fatty acids detected in the sea-salt particles whose chain contains between 14 and 19 carbon atoms, are mainly tetradecanoic acid, palmitic acid and stearic acid [(2)]. Once in the atmosphere, these particles are oxidized by collisions was gas-phase radicals. Although OH radicals are the main daytime oxidants, halogen atoms may significantly participate to the oxidation processes especially in the marine boundary layer.

The chlorine atoms ($Cl^{\cdot}$) may represent the major oxidant of the troposphere at dawn at low concentrations of OH radicals. Chlorine atoms have been detected in high concentrations not only in the marine boundary layer, but also at long distances from the coast [(3)]. Chlorine atoms are the products from the photolysis of chlorine species and their concentrations can be up to 10^6 atom.cm^{-3} [(4)]. It has been reported that $Cl^{\cdot}$ reacts more rapidly than OH radicals with hydrocarbon compounds [(4)]. A recent review [(5)] focused on the heterogeneous oxidation of atmospheric aerosol particles has reported measurements of high value for uptake coefficient by radicals ($\gamma \geq 0.1$).

In order to contribute to a better understanding of the heterogeneous reactivity between these aerosol particles and chlorine atoms, kinetic studies has been developed in our laboratory.

EXPERIMENTAL

The aim of this work is to study the kinetics of reactions between $Cl^{\cdot}$ and palmitic acid, one of the most abundant fatty acid of particulate organic matter in the marine boundary layer. These heterogeneous reactions on model substrates have been investigated in a laminar wall flow tube reactor. The principle is to put the gas phase, containing $Cl^{\cdot}$ in contact with the solid surface into a coated wall flow tube reactor. The heterogeneous reactions of chlorine atoms on palmitic acid film, deposited on the internal surface of the reactor, are investigated at low pressure (~1 mbar). The chlorine atoms are generated by a microwave discharge in a mixture of molecular chlorine diluted in helium and detected at the exit of the reactor by a quadrupole mass spectrometer.

The measurement of the first order rate constant, k, is achieved by changing the contact time between the surface and the gas, using a movable injector. From the rate constant, we determine the uptake coefficient, γ, which represents the ratio between the number of gas molecules removed by the condensed phase and the number of gas molecules striking the interface per unit time.

RESULTS

The initial uptake coefficient measured for those heterogeneous reactions is found to be fast, ranging between 10^{-2} and 10^{-1}.

We observed a rapid formation of hydrogen chloride which corresponds with the disappearance of chlorine atoms. These studies have shown that the production of HCl and $Cl^{\cdot}$ consumption is accompanied sometime by consumption or a formation of Cl_2.

In this work, the surface of the film was studied by time-of-flight secondary ion mass spectroscopy (TOF-SIMS) in order to identify the products formed on the palmitic acid surface after exposition to $Cl^{\cdot}$.

To our knowledge this is the first study to investigate the reactivity between chlorine atoms and palmitic acid films.

Further experiments are planned, including identification and quantification of new products formed in the condensed phase by GC/MS.

REFERENCES

[(1)] Mochida M. *et al*. (2002), *Journal of Geophysical Research*, 107

[(2)] Smoydzin L. and Von Glasow R. (2006), *Atmospheric Chemistry and Physics Discussions*, 6, 10373-10402

[(3)]Thornton J.A. et al. (2010), *Nature*, 464, 271-274

[(4)] Spicer C. W. *et al*. (1998), *Letters To Nature*, 394 (6691), 353-356

[(5)] George I.J. and Abbatt J.P.D. (2010), *Nature Chemistry 2*, 713-722

Thursday, September 8, 2011

Session 8P: Poster session B

Aerosols in Geoengineering

Injection of sulfur compounds into the stratosphere by using modified commercial aircrafts

A. Laakso, H. Kokkola, A. Laaksonen, K. E. J. Lehtinen, H. Korhonen
Finnish Meteorological Insitute, Kuopio, 70211, Finland
Keywords: sulfate aerosols, aicraft plumes, stratospheric aerosols, modelling
Presenting author email: anton.laakso@fmi.fi

Predicted rapid climate change has increased the need to affect and slow down global warming especially by reducing emissions of greenhouse gases. However, global efforts to reduce emissions have not been sufficiently successful. Emissions of greenhouse gases are still increasing faster than ever before and there is no quick reversal in sight for this trend. Because of this, alternative methods have been brought out as means to slow down global warming. These methods are called geoengineering.

Geoengineering methods aim to increase the reflectivity of the Earth or remove greenhouse gases from the atmosphere. Several technical methods to limit climate change have been suggested, e.g. orbital mirrors placed in stationary solar orbit filtering sunlight reaching the Earth's atmosphere, seeding sea salt aerosols to brighten marine clouds to reflect more solar radiation back to space, massive reforestation as a mean to reduce atmospheric CO_2 by its uptake by trees, fertilization of ocean by iron, and the proposal that resurfaced the interest in geoengineering, to inject sulphur into the stratosphere to form sulphate aerosols that also reflect solar radiation back to space. Because of the stability of the stratosphere the lifetime of the sulphate aerosol is 1-2 years, when in the troposphere it is only a few days. Thus much less sulfur would be required in the stratosphere to achieve similar cooling as the tropospheric sulfate aerosol and aerosols also have time to spread throughout the lower stratosphere. Estimated 5 Tg S yr^{-1} of stratospheric sulfate would be continuously required to compensate the warming caused by a doubling of CO_2 (Crutzen, 2006).

Numerous methods have been proposed for delivering sulfate aerosol precursors, e.g. military or tank jets, modified artillery, and high altitude balloons. One method that has not been considered in previous studies is to deliver sulphate aerosols to the stratosphere would be to use commercial aircraft that could be modified to fly in the lower stratosphere. One previous example of such vehicles are supersonic transport (SST) aircraft. It has been estimated that one SST emitted 9000 kg of SO_2 per year (Zhao, 1995). In stratosphere, SO_2 is oxidised sulphate which forms sulphate particles with characteristic sizes of several tenths of a micron. It has also been estimated that by using a fleet of 500 SST, the resulting particle concentration at steady state would vary between 35-380 cm^2. If emitted sulfur forms small particles soon after combustion, the concentration would be larger than if sulfur condenses on the existing background aerosol after dispersion and conversion to H_2SO_4 (Fahey, 1995). It is also possible that we can get even larger concentration by enhancing aircraft fuel with sulphur compounds. If we enchanced fuel sulphur contents of 1 per cent by weight, then annual consumption of approximately 100 Tg of fuel (which is used by current aviation) could emit 1 Tg of sulphur. 1 Tg of sulphur would eventually generate roughly 4 Tg of sulphate aerosols (Rasch, 2008). This method can be assumed to have relatively low cost since stratospheric sulfate production would be a by-product of air transport.

There are some constrains which have to be taken into account if commercial aircrafts are used to inject sulphur to the stratosphere. Firstly, most of the current flight routes are in the northern hemisphere and this would limit the aerosol forcing mostly to the northern hemisphere. Secondly, stratospheric travel altitude is feasible only the sufficiently long flights.

The aim of this study is to examine, if it is plausible to reduce radiative forcing by adding sulfur compounds to stratosphere using modified commercial aircrafts and current flight routes above oceans. We will investigate if we get the desired effect with the current number of flights or sulphur concentration of aircraft fuel, or do we have to make changes to the flight routes. Also, we will estimate local climate change and possible undesirable effects such as depletion of stratospheric ozone. The simulations will be made using aerosol-climate model ECHAM5.5-HAM2.

Acknowledgements. This work is supported by the Academy of Finland's Research Programme on Climate Change (FICCA).

Crutzen, P. J, (2006) Climatic Change, **77**, 211 - 220 (doi:10.1007/s10584-006-9101-y)

Fahey, D. W. et al. (1995) Science **270**, 70-74. (doi:10.1126/science.270.5233.70)

Rasch, P. J,Tilmes, S., Turco, R. P., Robock, A., Oman, L., Chen, C., Stenchikov G. L. and Garcia, R. L., (2008), Phil. Trans. R. Soc. **366**, 1882 4007-4037

Zhao, J, Turco R, P (1995), J. Aerosol Sci., **22**, 5, 779 - 795,

Geoengineering the Earth's Climate – An assessment of potential effectiveness and side-effects

A. K. L. Jenkins, P. M. Forster

School of Earth and Environment, The University of Leeds, Leeds, LS2 9JT, United Kingdom
Keywords: aerosol cloud interaction, sea salt, cloud microphysics, climate effect.
Presenting author email: eeaklj@leeds.ac.uk

Geoengineering is "the deliberate large-scale intervention in the Earth's climate system, in order to moderate global warming" (Shepherd, 2009).

Clouds have a significant influence on the Earth's climate system. In addition to playing a crucial role in the hydrological cycle, clouds directly affect the radiation budget of the Earth with a net cooling effect of 13 Wm^{-2} (Ramanathan, 1989).

We undertake modelling experiments into a geoengineering scheme that proposes the manipulation of marine stratocumulus clouds. The scheme (Salter, 2008) proposes using wind-driven vessels to spray sea-water into the marine boundary layer in order to increase the cloud condensation nuclei (CCN) concentration. By the first indirect aerosol effect (Twomey, 1974), this is intended to increase the planetary albedo, and hence create an additional cooling.

Several previous investigations have considered the effects associated with an increased CCN located at particular sites (Jones *et al*, 2009, Rasch *et al* 2009). These studies have widely ranging outcomes, particularly in regional precipitation, with high dependence on the location and extent of geoengineering. The CCN concentrations assumed in these studies may however have been overestimated (Korhonen *et al*, 2010).

It is known that the cellular structure of marine stratocumulus clouds is highly sensitive to background CCN concentration and liquid water path (Wang *et al*, 2011). The flux and size distribution of the sprayed sea-water, as well as the concentration and composition of background aerosols will be critical to changes in cloud characteristics and behavior.

We use the WRF-Chem model to investigate these effects at a regional scale (250 km by 250 km), using data from the VOCALS campaign. In development of previous work in this area we look at detailed aerosol cloud interactions and their local modification of stratocumulus.

Results are highly dependent on background conditions and injection methodology, with sea-salt injection producing either an increase or reduction of cloud albedo.

We comment on the significance of our results for the implementation of geoengineering by modification of marine stratocumulus clouds with sea-spray.

Jones, A., J. Haywood, et al. (2009). "Climate impacts of geoengineering marine stratocumulus clouds." J. Geophys. Res. **114**(D10): D10106.

Korhonen, H., K. S. Carslaw, et al. (2010). "Enhancement of marine cloud albedo via controlled sea spray injections: a global model study of the influence of emission rates, microphysics and transport." Atmospheric Chemistry and Physics **10**(9): 4133-4143.

Ramanathan, V., R. D. Cess, et al. (1989). "Cloud-Radiative Forcing and Climate: Results from the Earth Radiation Budget Experiment." Science **243**(4887): 57-63.

Rasch, P. J., J. Latham, et al. (2009). "Geoengineering by cloud seeding: influence on sea ice and climate system." Environmental Research Letters **4**(4).

Shepherd, J. (2009). Geoengineering the climate: Science, governance and uncertainty, The Royal Society.

Twomey, S. (1974). "Pollution and the planetary albedo." Atmospheric Environment (1967) **8**(12): 1251-1256.

Wang, H., P. J. Rasch, et al. (2011). "Manipulating marine stratocumulus cloud amount and albedo: a process-modelling study of aerosol-cloud-precipitation interactions in response to injection of cloud condensation nuclei." Atmos. Chem. Phys. Discuss. **11**(1): 885-916.

Sensitivity Studies on the Role of Particle Sedimentation and Subscale Microphysics within a Geoengineered Stratosphere.

F. Benduhn[1] and M.G. Lawrence[1]

Department of Atmospheric Chemistry, Max-Planck-Institute for Chemistry, Mainz, Germany.
Keywords: Stratospheric aerosol, Aerosol modelling, Sedimentation, Subscale processes.
Presenting author email: francois.benduhn@mpic.de

Within the present study some key uncertainties related to the injection of sulphur into the stratosphere as a technique for global scale geoengineering are assessed.

Sedimentation has been regarded as a potential key process which limits the lifetime of stratospheric aerosol (Rasch et al., 2008). Thus, a careful representation of this process seems necessary. The most frequently used representation of this process, namely the up-stream or upstream differencing model, presents the disadvantage of being highly numerically diffusive, thus potentially leading to a misrepresentation of the process, especially in the presence of strong vertical concentration gradients and limited vertical resolution. For this reason, a new scheme with strongly reduced numerical diffusion was developed. The scheme follows a pseudo-equilibrium approach at each grid-box interface by splitting the grid-box aerosol mass distribution into two separate columns, each representative of the mixing ratio of the neighbouring grid cell. The location of the split is chosen appropriately to represent the total tracer mass in the grid cell. Under ideal conditions the scheme is entirely non-diffusive, since the amount of aerosol mass transported in one step does not depend on the amount that was transported during the preceding time-step from grid boxes above, but rather from the same grid-box. However, due to its semi-equilibrium assumptions, the scheme tends to underestimate transport during non-equilibrium situations, e.g. during the build up of an aerosol plume in the stratosphere. In order to accommodate for that effect, the new scheme was combined with the Walcek (2000) advection scheme. The Walcek scheme cannot be used for particle sedimentation without some modifications. As aerosol size discrepancies in the vertical entail that sedimentation is not a monotonic process, the monotonic fixer was not included in the scheme. Aerosol sedimentation fluxes assessed with the modified Walcek scheme are compared to those obtained with the new scheme, and the largest value is then chosen within the combined scheme.

Comparisons with simple analytical solutions demonstrate the effectiveness of both the new scheme and its combined variant to the Walcek scheme to accurately represent particle sedimentation with very little numerical diffusion. 3-D sensitivity studies were carried out with the global chemistry-climate model EMAC (Joeckel et al., 2006). A monodisperse particle distribution (with deactivated particle microphysics) is used in order to evaluate the impact of sedimentation on stratospheric aerosol lifetime. Sedimentation is found to have little impact on the resulting aerosol burden in the troposphere as wet removal processes prove to be more effective. Also, except for large micrometre size particles, sedimentation appears to have little impact on the global burden of the geoengineered stratospheric aerosol, which seems to be mainly driven by large-scale stratosphere-troposphere exchange. However, especially under low vertical resolution conditions, the new schemes very effectively limit diffusive upward transport of particles into the upper stratosphere, thus also limiting the interaction of the aerosol with the local radiation balance, atmospheric circulation and chemistry. Under 3-D conditions the discrepancies between the new scheme and the modified Walcek scheme are shown to be very small.

Another uncertainty which we are investigating is the role of subgridscale aerosol microphysics as related to stratospheric geoengineering. Aerosol microphysical processes are most relevant under conditions of high particle number concentrations (Turco and Yu, 1997, Pierce et al., 2010). For geoengineered particles these circumstances take place just after their injection into the stratosphere. These circumstances cannot be captured by a global general circulation model. The EMAC model is therefore to be implemented with appropriate injection functions that take into account preliminary subscale microphysics. For this purpose we are testing a newly developed function that estimates the time lag between the injection and the handover to the global model as a function of the injection scenario that has been chosen, and first results will be shown.

Joeckel, P., et al. (2006), Atmospheric Chemistry and Physics, Vol. 6, pp. 5067-5104.

Pierce, J.R., et al. (2010), Geophys. Res. Letters, Vol. 37, L18805, doi:10.1029/2010GL043975.

Rasch, P.J., et al. (2008), Phil. Trans. of the Royal Society A, Vol. 366, pp. 4007-4037.

Turco, R.P., and Yu, F. (1997), Geophys. Res. Letters, Vol. 24, No. 10, pp. 1223-1226.

Walcek, C.J. (2000), J. of Geophys. Res., Vol. 105, No. D7, pp. 9335-9348.

Thursday, September 8, 2011

Session 8P: Poster session B

Atmospheric aerosols - Aerosol Processes and Properties

Radiative forcing from aerosols measured at a coastal site in the Mediterranean

A.R. Esteve[1], V. Estellés[1,2], M.P. Utrillas[1] and J.A. Martínez-Lozano[1]

[1] Department of Earth Physics and Thermodynamics, University of Valencia, Burjassot, 46100, Spain.
[2] Department of Fundamental and Experimental Physics, University of La Laguna, La Laguna, 38207, Spain.
Keywords: atmospheric aerosols, optical properties, aerosol radiative forcing.
Presenting author email: Anna.Esteve@uv.es

Aerosol particles directly affect the Earth's radiative balance through the scattering and absorption of the incident solar radiation (Charlson *et al.*, 1992; Kiehl and Briegleb, 1993). This effect, caused by anthropogenic aerosols, has been termed direct aerosol radiative forcing and may currently have an influence of potentially the same magnitude but in the opposite direction as greenhouse gas forcing (Intergovernmental Panel on Climate Change (IPCC), 2007).

In this work, the aerosol optical properties measured during the year 2009 at Burjassot (Valencia, Spain) (latitude = 39.508°, longitude = -0.418°, 60 meters above sea level) were used to estimate the radiative forcing of anthropogenic aerosols at this coastal site in the Mediterranean. The measured optical properties include the total aerosol scattering (σ_{sp}) and backscattering (σ_{bsp}) coefficients measured using a TSI Model 3563 three-wavelength integrating nephelometer, and the Aerosol Optical Depth (AOD) obtained using a CIMEL CE318 photometer.

First, the Radiative Forcing Efficiency (RFE), which is the amount of the radiative forcing produced by anthropogenic aerosols that increases the optical thickness by one unit, was calculated using the following equation (Haywood *et al.*, 1995):

$$RFE = -DS_0 T_{at}^{\,2}(1-A_c)\omega_0\beta\left\{(1-R_s)^2 - \left(\frac{2R_s}{\beta}\right)\left[\left(\frac{1}{\omega_0}\right)-1\right]\right\}$$

where D is the daylight fraction (changes with latitude and season), S_0 is the solar constant (1370 Wm^{-2}), T_{at} is the atmospheric transmission (0.76), A_c is the mean fractional cloud amount based on data of the 1984-2002 period from the International Satellite Cloud Climatology Project (ISCCP) (Calbó and Sanchez-Lorenzo, 2009), ω_0 is the single scattering albedo, β is the average upscatter fraction (calculated from the backscatter fraction derived from the nephelometer measurements), and R_s is the surface reflectance (0.2).

The monthly variation of the RFE shows a clear variation during the year, ranging from -14 Wm^{-2} in February to -22 Wm^{-2} in July, with a mean value for the whole period of -19 Wm^{-2}. These negative values correspond to cooling effects.

To obtain the Radiative Forcing at the top of the atmosphere (TOA), RFE values were multiplied with the aerosol optical depth provided by the CIMEL CE318 photometer. Radiative forcing at the TOA (Figure 1) shows also a clear variation during the year, ranging from -1.2 Wm^{-2} in December to -4.9 Wm^{-2} in July, with a mean value for the whole period of -3.1 Wm^{-2}. These values are a bit higher but opposite in sign to the forcing induced by the greenhouse gases and estimated to be equal to 2.4 Wm^{-2} (Houghton *et al.*, 1995), and show the important direct role of aerosols in this site of the Mediterranean coast.

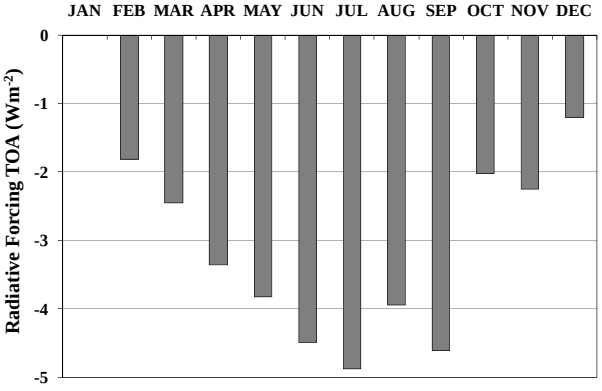

Figure 1. Radiative forcing at the top of the atmosphere (TOA) at Burjassot (Valencia, Spain) during 2009.

This work was funded by the Ministry of Science and Innovation (MICINN) of Spain through the project CGL2009-07790 and the Valencian Autonomous Government through the project PROMETEO-2010-064. The collaboration of V.Estellés was possible thanks to the fellowship JCI-2009-04455.

Calbó, J., and Sanchez-Lorenzo, A. (2009), *Theor. Appl. Climatol.*, **96**, 105-115.

Charlson, R. J., Schwartz, S. E., Hales, J, J. M., Cess, R. D., Coakley Jr., J. A., Hansen, J. E., and Hofmann, D. J. (1992), *Science*, **255**, 423-430.

Haywood, J.M., and Shine, K.P. (1995). Geophys. Res. Lett., 22 (5), 603-606.

Houghton, J. T., Meira, L. G., Callander, B. A., Harris, N., Kattenberg, A., Maskell, K. (1995). *Climate Change: The Science of Climate Change*. Cambridge University Press.

Intergovernmental Panel on Climate Change (IPCC) (2007), *Climate Change 2007: The Physical Science Basis*. Cambridge University Press.

Kiehl, J. T., and Briegleb, B. P. (1993), *Science*, **260**, 311-314.

Atmospheric transport characteristics of dust storm arrive at Taiwan

T.Y. Wu[1,2], Y.M. Chen[3], Y.C. Lin[4,*]

[1] Department of Materials Engineering, Kun Shan University, Tainan 71003, Taiwan
[2] Department of Chemistry, National Cheng Kung University, Tainan 70101, Taiwan
[3] Sustainable Environment Research Center, National Cheng Kung University, Tainan 701, Taiwan
[4] Institute of Environmental Engineering, National Sun Yat-Sen University, Kaohsiung 804, Taiwan
Keywords: Dust, Ambient aerosols, HYSPLIT model, Back trajectories.
Presenting author email: yuanchung.lin@gmail.com

Since spring, 2000, China's dust storms have repeatedly affected Taiwan's air quality and such incidents will only become more frequent given the trend in global climate change. These storms bring lots of sand, dust, and industrial waste from China, increasing the concentration of air pollutants in the atmosphere (Han et al., 2007). With increasing interest in and concern about climate change-related air pollution (Jacob and Winner, 2009; Pang et al., 2009), rising interest has been directed to exploring the dust storms.

Trajectories could reflect the large-scale atmospheric transport characteristics of air mass arriving at Taiwan. They were not only necessary for estimating the long-range transport of pollutants, other chemical species, but also provided a better understanding of airflow patterns (Pongkiatkul and Oanh, 2007). The transport pathway of air masses was determined using backward trajectories from the hybrid single-particle Lagrangian integrated trajectory (HYSPLIT 4)
model. The Asian dust storm event observed in north Taiwan on 3–4 March, 2008 was intense and extensive. Four-day backward trajectories during the period 28, Feb 2008–2, Mar 2008 were shown in Figure 1. The air parcel came from Mongolia, the Gobi desert, and the Losses Plateau, which are the major source regions of Asian dust. The air parcel moved over Shanghai on 29, Feb 2008 and 1, Mar 2008, respectively, and arrived in Taiwan on 3, March 2008. It passed across Shanghai and the East China Sea, and then southwest to north Taiwan. In contrast, four-day backward trajectories calculated before the dust storm during the period 24, Jan 2008–28, Jan 2008 were shown in Figure 2. One air parcel came from south Japan and moved over the Pacific Ocean on 25, Jan 2008–27, Jan 2008, and arrived in Taiwan on 28, Jan 2008. Other air parcels came from Siberia, passed across the border between Mongolia and Inner Mongolia Autonomous Region, Shenyang, the Huanghai Sea, the East China Sea and then southwest to Taiwan. Most backward trajectories calculated before the dust storms are in oceans. Accordingly, the influence of dust and sand before the dust storms is lower than that during the dust storms. Three kinds of trajectory pathways (from 1000, 2000, and 3000 m above model ground level (AGL)) were measured. Sun et al. (2001) also suggested that dust from gobi deserts in Mongolia and China can be entrained only to an elevation of <3000 m in most cases, after analyzing 40-year dust storm data. This NOAA's HYSPLIT trajectory map shows an aerial view of the paths of an air parcel and a vertical view of its movement at three different altitudes. The circles, squares, and triangles lying on each line indicate the position of the air parcel. This backward-trajectory analysis indicates that the prevailing winds at the three altitudes in our sampling period originated in desert areas of China and the air parcel arrived at our sampling site.

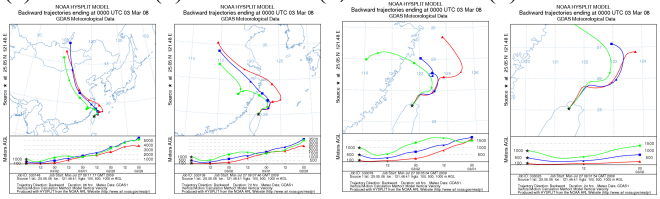

Figure 1. Backward trajectories for Asian dust storm air parcels that affected Taiwan before the 3, March, 2008. (a) at AM 9:00, 28, Feb 2008; (b) at AM 9:00, 29, Feb 2008; (c) at AM 9:00, 1, March 2008; (d) at AM 9:00, 2, March 2008.

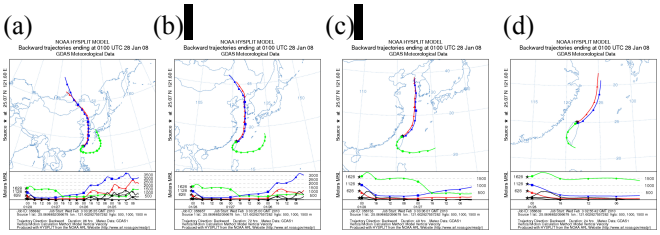

Figure 2. Backward trajectories before Asian dust storm in Taiwan before the 28, Jan, 2008. (a) at AM 9:00, 24, Jan 2008; (b) at AM 9:00, 25, Jan 2008; (c) at AM 9:00, 26, Jan 2008; (d) at AM 9:00, 27, Jan 2008.

This work was supported in part by the National Science Council under grant NSC-97-2218-E-110-009.

Han, T., Lin, J., Wang, Y., Zheng, B., Song, H., Liu, J., Jiang, G., Shi, P., Zhang, J. (2007) *The Bulletin of Geology* **26**, 117–127.
Jacob, D.J., Winner, D.A. (2009) *Atmospheric Environment* **43**, 51–63.
Pang, X.B., Mu, Y.J., Lee, X.Q., Zhang, Y.J., Xu, Z. (2009) *Atmospheric Research* **93**, 913–919.
Pongkiatkul, P., Oanh, N.T.K. (2007) *Atmospheric Research* **85**, 3–17.
Sun, J.M., Zhang, M.Y., Liu, T.S. (2001) *Journal of Geophysical Research* **106** (D10), 10325–10333.

Preliminary results on the influence of the vertical distribution of aerosols in the direct radiative forcing

R. Pedrós[1], J.L. Gómez-Amo[1], C. Marcos[1], M.P. Utrillas[1], J.A. Martínez-Lozano[1], M. Sicard[2]
[1]Department of Earth Physics, University of Valencia, 46100 Burjassot, Spain
[2]Remote Sensing Laboratory, Polytechnic University of Catalonia, 08034 Barcelona, Spain.
Keywords: aerosols, lidar, vertical profile
Presenting author email: pedrose@uv.es

It is now well documented that atmospheric aerosols strongly impact the Earth's radiation balance and climate through the direct scattering and absorption of solar radiation and through their influence on clouds. The aerosol impact depends on the size of the aerosols, on their composition and on how the aerosols are vertically distributed, particularly when dust is present. The estimation of the aerosol direct radiative forcing from measurements at the ground level requires the columnar aerosol optical properties and the aerosol vertical distribution. This demands simultaneous measurements with Sun-photometer and lidar, but this is not always the situation. Even when lidar instrumentation is available, the different schedules of the instruments make the synchronicity (±1 hour) very scarce. In this work we evaluate the influence of the aerosol vertical profile on the aerosol forcing at the Earth's surface and at the top of the atmosphere.

Materials and methods

The aerosol vertical profiles were obtained with a lidar instrument was developed by the Polytechnic University of Catalonia, Barcelona, Spain. It is based on a frequency-doubled Nd:YAG laser delivering simultaneously pulses of approximately 160 mJ and 7-ns duration at 1064 and 532 nm (Rocadenbosch, 2002).

The aerosol radiative forcing can be estimated from the change in the net flux either at the top of the atmosphere or at the surface, with and without aerosols. The employed procedure is based on the one described in Niranjan et al. (2007). The optical and radiative properties of the aerosols are downloaded from the AERONET network DS2 data pool at level 1.5 (AERONET, 2011) and fed into the Santa Barbara DISORT Radiative Transfer (SBDART) model (Ricchiazzi et al., 1998) to derive the aerosol radiative forcing in the shortwave range. SBDART employs the discrete-ordinates solution for the radiative transfer and includes multiple scattering in a vertically inhomogeneous, non-isothermal, plane parallel atmosphere. The ground albedo influences the diffuse radiation, particularly the area of 1-2 square kilometers around the measurement site. Therefore, the AERONET-derived ground is also included as an input data.

Results

A total of 25 different aerosol vertical extinction profiles (see Figure 1) were obtained with the well-known Klett-Fernald-Sasano inversion (Klett, 1984; Fernald, 1985; Sasano 1984) constrained with Sun-photometric aerosol optical depth values measured Barcelona (Spain), in the period 2007-2008. Desert dust intrusions were avoided for this study.

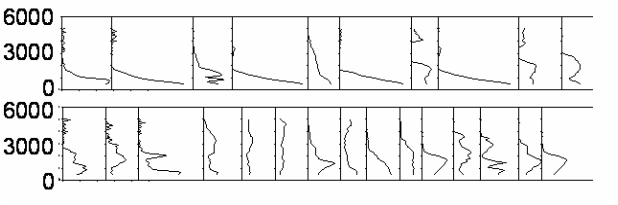

Figure 1. Lidar-retrieved aerosol vertical extinction profiles in Barcelona, Spain, during 2007-2008.

For the simulations we used for all the aerosol profiles the same optical properties and optical thickness of the profile that showed the higher aerosol load (aerosol optical thickness of 0.397), in order to maximize the aerosol effect on forcing. For the comparison we used the average of the 25 profiles, mathematically very similar to an exponential variation.

The results show that when considering the same size and composition of the aerosols, as well as the same aerosol load, the instantaneous forcing at the top of the atmosphere for the 25 profiles deviates less than ±2% with respect to use the average profile. The corresponding deviation for the forcing at the bottom of the atmosphere is less than ±0.1%. This opens the possibility of using an aerosol exponential profile obtained by averaging the available profiles, when there is no lidar data simultaneous to Sun-photometric measurements and in absence of desert dust intrusions.

This work was financed by the Projects CGL2007-60648, CGL2009-07790 and PROMETEO/2010/064.

AERONET Website, (2011), Goddard Space Flight Center, NASA, [Online]. Available: http://aeronet.gsfc.nasa.gov/new_web/data.html
Fernald, F. G. (1984), *Apl. Opt.* **23**, 652-653.
Klett, J. D. (1985), *Appl. Opt.* **24**, 1638-1643.
Niranjan, K., Sreekanth, V., Madhavan, B. L., et al. (2007), *Geophys. Res. Lett.*, **34**, L19805, doi:10.1029/2007GL031224.
Ricchiazzi, P., Yang, S. R., Gautier, C. et al., (1998), *Bull. Am. Meteor. Soc*., **79**, 2101-2114.
Rocadenbosch, F., Sicard, M., Comerón, A., et al. (2002) *Proc. 21st ILRC*, **1**, 69–70.
Sasano Y. and Nakane H. (1984), *Appl. Opt.* **23**, 11–13.

Global distribution of cloud droplet number concentration, autoconversion rate and first aerosol indirect effect under diabatic droplet activation

Barahona, Donifan[1,2], Sotiropoulou, Rafaella-Eleni P.[3] and Nenes, Athanasios[1,4]

1 School of Chemical and Biomolecular Engineering, Georgia Institute of Technology, Atlanta, GA, USA
2 Global Modeling and Assimilation Office, NASA GSFC, Greenbelt, MD, USA
3 Environmental Research Lab, INT-RP, N.C.S.R. Demokritos, Aghia Paraskevi, Greece
4 School of Earth and Atmospheric Sciences, Georgia Institute of Technology, Atlanta, GA, USA
Keywords: Aerosol-cloud interactionentrainment, mixing, modeling.
Presenting author email: rsot@ipta.demokritos.gr

Global model studies of aerosol indirect effects assume that the cloud droplet number concentration (CDNC) in clouds is given by an adiabatic formation rate. This approach tends to overestimate CDNC, as subsequent entrainment and mixing of dry air in cloud columns are not considered. The goal of this study is to assess the sensitivity of CDNC to diabatic activation (i.e., including effects from entrainment and mixing of dry air) and its first order tendency on indirect forcing and autoconversion rate.

The modeling framework used for this study is the NASA Global Modeling Initiative (GMI). GMI is a global 3D chemical-transport model specifically developed for impact assessment studies. CDNC is calculated using the physically-based prognostic parameterization of *Barahona and Nenes* [2007, hereafter BN07], which parameterizes the effects of entrainment mixing on CDNC through the use of an "effective" entrainment rate. BN07 is an extension of the works of *Nenes and Seinfeld* [2003] and *Fountoukis and Nenes* [2005]; entrainment results in a lower maximum supersaturation and CDNC. Sensitivities are examined under three different meteorological fields from the NASA GEOS4 finite volume GCM (FVGCM), the NASA GEOS1-STRAT (GEOS) and the NASA GISS II' GCM (GISS). Computed CDNC is used to calculate the effective radius. The CLIRAD-SW solar radiative transfer model is used online to calculate the cloud optical depth (COD) and the shortwave fluxes from the surface to the top of the atmosphere (TOA). COD is calculated as a function of the effective radius. Evaluation of modeling results (i.e., cloud droplet effective radius, cloud optical depth) is done against satellite products from Moderate Resolution Imaging Spectroradiometer (MODIS) platform.

Diabatic activation results in lower CDNC than adiabatic treatments of the process. The largest decrease in CDNC (by up to 75%) was found in the Tropics and in zones of moderate CCN concentration (Figure 1). This leads to a global mean effective radius increase between 0.2-0.5μm (up to 3.5 μm over the Tropics), a global mean autoconversion rate increase by a factor of 1.1 to 1.7 (up to a factor of 4 in the Tropics) and a 0.2-0.4 W m^{-2} decrease in indirect forcing (Figure 1). The spatial patterns of entrainment effects on droplet activation tend to reduce biases in effective radius (particularly in the Tropics) when compared to satellite retrievals. This, and the diabatic nature of ambient clouds suggest that entrainment effects on CDNC should be considered in GCM studies of the aerosol indirect effect.

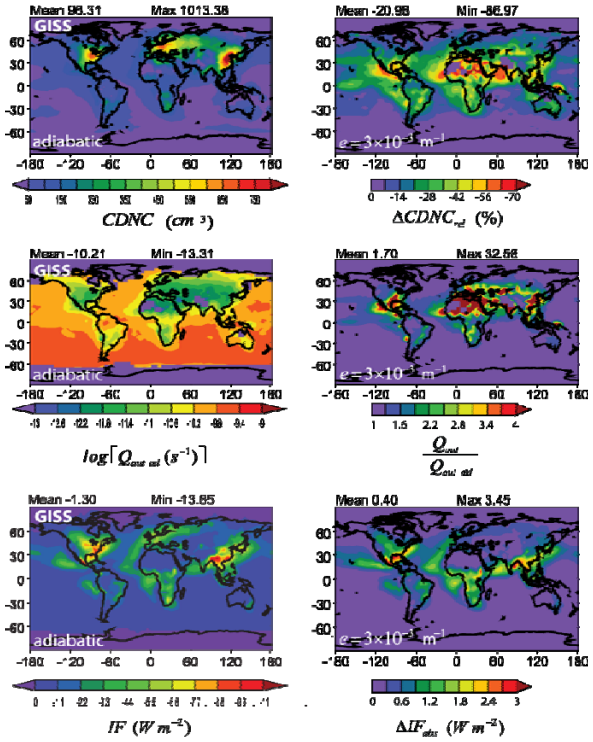

Figure 1. CDNC, autoconversion rate *Qaut*, andindirect forcing (IF) under adiabatic activation (i.e., $e = 0$) (left panels) and corresponding changes for e=3x10^{-3} m^{-1} under GISS meteorology (right panels)

This work was supported by NASA MAP and a NASA New Investigator Award.

Barahona, D., and Nenes, A. (2007), *J. Geophys. Res.*, **112** , D16,026; doi:10.1029/207JD008,473.
Fountoukis, C. and Nenes, A. (2005), *J. Geophys. Res.*, **110**(D11212), doi:10.1029/2004JD005 591.
Nenes, A. and Seinfeld, J.H. (2003). *J. Geophys. Res.*, **108**, 4415, doi:10.1029/2002JD002911.

Spatial variability of the direct radiative forcing of biomass burning aerosols in the Amazon Basin and the influence of surface reflectance

E.T. Sena[1], A.L. Correia[1], P. Artaxo[1] and J.V. Martins[2]

[1]Institute of Physics, University of São Paulo, São Paulo, SP, 05508-900, Brazil
[2]Department of Physics, University of Maryland, Baltimore Count, MD, 21250, USA
Keywords: Amazon, radiative forcing, remote sensing.
Presenting author email: artaxo@if.usp.br

In the present work, we used remote sensing techniques in order to obtain the shortwave direct radiative forcing at the top of the atmosphere (TOA) over the Amazon Basin. We analyzed data from 2000 to 2009 acquired by the radiometer CERES (Clouds and the Earth's Radiant Energy System) (Wielicki, 1996) and by the spectrometer MODIS (Moderate Resolution Imaging Spectrometer) aboard Terra satellite during the biomass burning season peak. Due to the high spatial coverage of those sensors it was possible to obtain the spatial distribution of the shortwave radiative forcing at the TOA over the Amazon.

The study area was limited between the latitudes 3ºN – 20ºS and between the longitudes 45ºW – 65ºW plus an additional area between 3ºN – 11ºS and 65ºW – 74ºW. In order to analyze only the direct shortwave aerosol effect we used only cloud-free sky conditions as designated by the MODIS sensor. The full area under analysis was divided in 0.5º x 0.5º (latitude / longitude) cells according to Patadia, 2008. The cell size was chosen so as to maximize the amount of valid pixels inside each cell and minimize its surface reflectance heterogeneity. For each cell we calculated the linear fit of the shortwave radiation flux at the TOA against the aerosol optical depth (AOD). Figures 1 and 2 show the spatial distribution for the average radiative forcing and the average AOD during the months of August and September of 2005 and 2008, respectively.

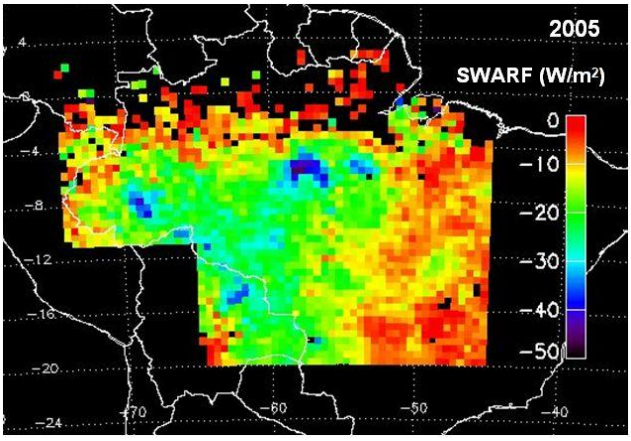

Figure 1: Spatial distribution of the shortwave radiative forcing at the TOA over the Amazon during the biomass burning season of 2005.

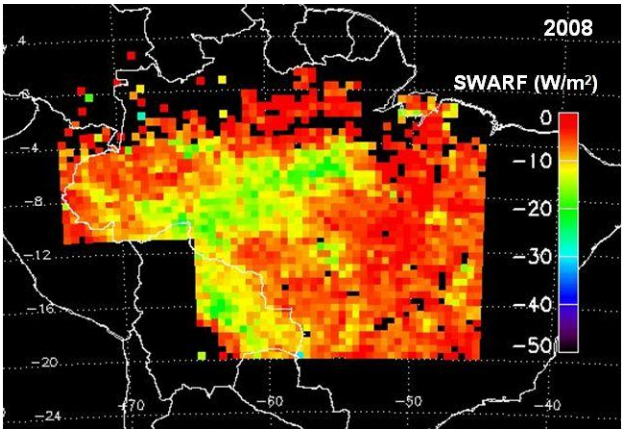

Figure 2: Spatial distribution of the shortwave radiative forcing at the TOA over the Amazon during the biomass burning season of 2008.

The results shown in Figures 1 and 2 indicate that the aerosol radiative forcing at the TOA presents large spatial and temporal variations during the biomass burning season.

As an attempt to understand the impact of land use change in the region we have also studied the behaviour of the radiative forcing with the reflectance at 2.1 μm. It was possible to verify that as the surface reflectance increases the radiative forcing efficiency becomes less negative, with distinct patterns for surface reflectances below and above 8%.

The influence of several other parameters, such as water vapour amount in the atmosphere, solar zenith angle and surface type were studied separately, and presented important contributions in the shortwave radiative forcing of aerosols at the TOA.

This work was supported by FAPESP.

Patadia, F., Gupta, P., Christopher, S. A., Reid, J. S. (2008). A Multisensor satellite-based assessment of biomass burning aerosol radiative impact over Amazonia. *J. Geophys. Res*, **113**, D12214.

Wielicki, B. A., Barkstrom, B. R., Harrison, E. F., Lee III, R. B., Smith, G. L, Cooper, J. E. (1996). Clouds and the Earth's radiant energy system (CERES): An earth observing system experiment. *Bull. Amer. Meteor. Soc.*, **77**(5), 853-868.

Thursday, September 8, 2011

Session 8P: Poster session B

Atmospheric aerosols – Specific Aerosol Types

Spatiotemporal distribution of light-absorbing carbon in Stockholm

P. Krecl[1,2], A.C. Targino[3] and C. Johansson[1]

[1]Department of Applied Environmental Science, Stockholm University, Stockholm, SE-11418, Sweden
[2]Now at School of Earth and Environment, University of Leeds, Leeds, LS29JT, United Kingdom
[3]Universidade Tecnológica Federal do Paraná, Londrina, Paraná, 86036-370, Brazil
Keywords: black carbon, $PM_{10}/PM_{2.5}$, urban aerosols, air quality.
Presenting author email: p.krecl@leeds.ac.uk

Carbon-containing particles have deleterious effects on both Earth's climate and human health. In Europe, the main sources of light-absorbing carbon (LAC) emissions are the transport (67%) and residential (25%) sectors (Kupiainen and Klimont, 2007). Information on the spatiotemporal variability of LAC particles in urban areas is relevant for air quality management and to better diagnose the population exposure to these particles. This study reports on results of an intensive field campaign conducted at four sites (a street canyon site, a kerbside site, an urban background site and a rural station) in Stockholm, Sweden, during the spring 2006.

Light-absorbing carbon mass concentrations (M_{LAC}) were measured with custom-built Particle Soot Absorption Photometers (PSAP) (Krecl *et al.*, 2010). The spatiotemporal variability of M_{LAC} concentrations was explored by examining correlation coefficients (R), coefficients of divergence (COD), and diurnal patterns at all sites. Simultaneous measurements of NOx, PM_{10}, $PM_{2.5}$, and meteorological variables were also carried out at the same locations to help characterize the LAC emission sources.

Hourly mean and standard deviation M_{LAC} concentrations ranged from 0.36 (rural) to 5.39 μg m^{-3} (street canyon) and from 0.50 to 3.60 μg m^{-3}, respectively. Concentrations of hourly LAC between urban sites were poorly correlated (Table 1) and even for daily averages (R<0.70), combined with highly heterogeneously distributed concentrations (COD>0.30) even at spatial scales of few kilometers. This high variability is connected to the distribution of emission sources and processes contributing to the LAC fraction at these sites.

Table 1. Correlation coefficients between hourly M_{LAC} time series measured at the four sites.

R [-]	Kerbside	Urban back.	Rural
Street canyon	0.62	0.48	0.23
Kerbside		0.50	0.27
Urban back.			0.78

At urban sites, M_{LAC} tracked NOx levels and traffic density well and mean $M_{LAC}/PM_{2.5}$ ratios were larger (26-38%) than at the background sites (4-10%). The results suggest that vehicle exhaust emissions are the main responsible for the high M_{LAC} concentrations found at the urban locations whereas long-range transport (LRT) episodes of combustion-derived particles can generate a strong increase of levels at background sites.

Figure 1 displays the weekday concentrations at the different locations relative to the concentrations at the urban background site (100%). For M_{LAC} and NOx, 70-75% of the concentrations were generated in the urban area whereas only 35% of PM_{10} and 5% of $PM_{2.5}$ corresponded to local urban sources. Regarding the kerbside and street canyon stations, M_{LAC} and NOx levels were 310-660% relatively higher than urban background levels whereas PM_{10} and $PM_{2.5}$ concentrations were 130-230% higher relative to the urban background level.

To decrease pollution levels at urban and urban background locations in Stockholm, we recommend abatement strategies that target reductions of vehicle exhaust emissions, which are the main contributors to M_{LAC} and NOx concentrations.

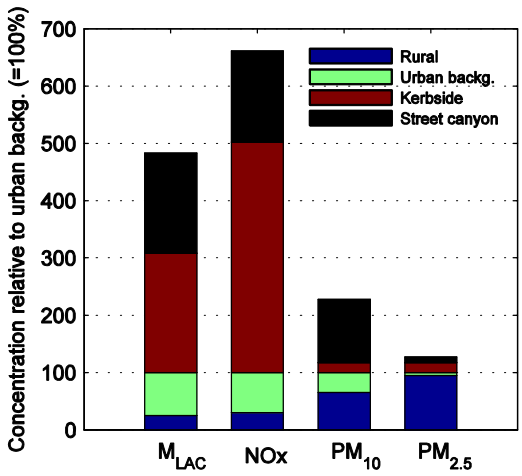

Figure 1. Comparison of weekday M_{LAC}, NOx, PM_{10} and $PM_{2.5}$ levels at the four sites relative to urban background concentrations.

This work was supported by the Swedish Environmental Protection Agency.

Krecl, P., Johansson, C., and Ström, J. (2010) *J. Air Waste Manage.*, **60**, 356-368.

Kupiainen, K., and Klimont, Z. (2007) *Atmos. Environ.* **41**, 2156-2170.

Carbonaceous aerosol in Delhi: Link with regional meteorology and long range transport

Jaiprakash[1]*, Saood Manzer[2], Tarun Gupta[3], Gazala Habib[1], Papiya Mandal[4], J. K. Basin[4],
[1]Indian Institute of Technology Delhi, [2]Al-Fala School of Engineering and Technology, [3]Indian Institute of Technology Kanpur, [4]National Environmental Engineering Research Institute, Delhi
Keywords: $PM_{1.0}$, $PM_{2.5}$, Elemental Carbon, Organic Carbon.
Presenting author E-mail: jaipism@gmail.com

Abstract

Carbonaceous fraction of aerosols impacts the local air quality and climate in several complex ways such as by changing the energy budget of Earth-Atmosphere system and by participating in cloud formation thus changing the cloud optical properties and lifetime (Ramanathan 2007, IPCC, 2007). In last two decades carbonaceous aerosol were linked with change in hydrological cycle leading to draughts and floods in various parts of south Asia (Ramanathan, 2005). However, the role of carbonaceous aerosol in climate change is poorly understood and its quantification is associated with large uncertainties (IPCC 2007, Ramanathan 2005). In Indian context the better understanding of carbonaceous aerosol and their impact on local air quality and climate require a great effort in terms of aerosol measurement and characterization in various parts of India. Therefore, this study was focused on temporal (April 2010 to June 2010) measurement of aerosol and determination of organic and elemental carbon at urban background site of Delhi.

The urban back ground site was ~30 m above the ground level on the roof of administrative building of IIT-Delhi. Fine aerosol mass ($PM_{1.0}$, $PM_{2.5}$) was collected separately during day and night time to investigate the link between aerosol concentration with regional meteorology and long range transport in dry season (from April, 2010 to June, 2010). The particles ($PM_{2.5}$) were analyzed for organic carbon and elemental carbon using thermal optical reflectance (DRI model).

The construction activities for common wealth game in various part of Delhi city resulted in many dust dominated days in the city leading to low $PM_{1.0}/PM_{2.5}$ ratio in April (monthly average 0.6±0.2, n=5) (Table 1). Higher aerosol concentrations were observed during night time compare to day in all the months (Table 1). The higher aerosol concentration during night time could be because of low temperature, low mixing height and calm condition resulting in accumulation of aerosol in the lower troposphere. The average carbonaceous aerosol concentration was highest in April and lowest in June. This paper presents the detail analysis of trends in carbonaceous aerosol concentrations and their possible links with regional meteorology and long range transport.

Table 1 Monthly averaged day and night concentration of $PM_{2.5}$ and $PM_{1.0}$

Month	Average aerosol concentrations (µg/m³)				Ratio	
	$PM_{1.0}$		$PM_{2.5}$		$PM_{1.0}/PM_{2.5}$	
	Day	Night	Day	Night	Day	Night
April	70±35	108±33	144±119	194±106	0.6±0.2	0.6±0.2
May	98±57	118±72	131±60	156±70	0.7±0.2	0.7±0.1
June	109±59	167±115	167±115	199±99	0.7±0.2	0.8±0.1

Ramanathan, V., Chung, C., Kim, D., Bettge, T., Buja, L., Kiehl, J. T., Washington, W. M., Fu, Q., Sikka, D. R., and Wild, M. (2005) *Atmospheric brown clouds: Impacts on South Asian, climate and hydrological cycle*, *PNAS* 102, 5326–5333.

Ramanathan V., Ramana, M. V., Roberts, G., Kim D., Corrigan, C., Chung C., and Winker, D. (2007) *Warming trends in Asia amplified by brown cloud solar absorption*, *Lett.* 448(2), doi: 10.1038/nature06019.

S, Solomon. *The Intergovernmental Panel on Climate Change (IPCC, 2007). The Scientific Basis Contribution of Working Group I to the Fourth Assessment Report* Cambridge Univ. Press, New York.

Source apportionment of ambient particulate carbonaceous matter at Mace Head during the joint EMEP/EUCAARI intensive measurement periods in fall 2008 and spring 2009

D. Ceburnis[1], A. Garbaras[2], S. Szidat[3], K.E. Yttri[4], V. Remeikis[2], and C.D. O'Dowd[1]

[1] School of Physics and Centre for Climate and Air Pollution Studies, Ryan Institute, National University of Ireland Galway, Galway, Ireland
[2]Center for Physical Sciences and Technology, Institute of Physics, Vilnius, Lithuania
[3]Department of Chemistry and Biochemistry & Oeschger Centre for Climate Change Research, University of Berne, Berne, Switzerland
[4]Norwegian Institute for Air Research, Kjeller, Norway
Keywords: carbonaceous matter, carbon isotopes, EMEP, source apportionment
Presenting author email: darius.ceburnis@nuigalway.ie

Particulate carbonaceous matter (PCM) has been observed to contribute significantly to ambient particulate matter concentrations in a wide range of environments, even over remote ocean regions. However, the inherent complexity of the PCM has proved it difficult to quantify and resolve to a compound level. In addition, secondary processes along with chemical processing in the atmosphere, ensures an ever changing nature of PCM, rendering quantitative source apportionment highly challenging. Carbon isotope analysis offers a method for quantitative source apportionment of three principal sources of PCM due to their unique isotopic signatures: i.e. marine, continental (non-fossil) and fossil fuel sources (Ceburnis et al., 2011). In addition, source specific tracers can facilitate an even more detailed source including separation between primary and secondary sources (Gilardoni et al., 2011).

The EMEP monitoring programme along with the EUCAARI project conducted two intensive measurement periods in fall 2008 and spring 2009, focusing on carbonaceous aerosol using both on-line and off-line chemical analysis. In the present study, we report the results from off-line chemical analysis at the Mace Head station (Ireland) where ^{13}C, ^{14}C and ^{15}N were determined in $PM_{2.5}$ filter samples collected according to the quartz-behind-quartz sampling approach along with OC, EC and levoglucosan. Five weekly samples were collected in fall 2008 and four (weekly) samples in spring 2009. Contribution of marine, continental non-fossil, and fossil fuel sources to TCp (particulate TC) is summarised in Table 1, showing the dominance of the continental non-fossil source. An attempt was made to separate continental non-fossil sources into biomass burning (BB) and natural terrestrial sources (BG) by the use of the biomass burning tracer levoglucosan, however, a question remains whether levoglucosan can be an equally good tracer in fresh and aged carbonaceous aerosol for reliable BB source apportionment.

Apart from the source apportionment some new insights were obtained by the determination of stable nitrogen isotope (^{15}N) in spring 2009 samples and stable carbon isotope (^{13}C) in front and back-up quartz filters. A statistically significant difference in nitrogen isotope ratios was obtained between anthropogenically perturbed samples (4.82‰) and clean marine samples (-1.24‰), clearly showing that clean and polluted samples exhibit not only distinct stable carbon isotope ratios but also for nitrogen, as already suggested by Myazaki *et al.* (2010).

Table 1. Contribution of carbonaceous matter sources by dual carbon isotope analysis.

	TC_p, μgC/m^3	Marine μgC/m^3	Cont. non-FF μgC/m^3	FF μgC/m^3
F 1	0.80	0.080	0.58	0.14
F 2	3.02	0.091	2.43	0.50
F 3	0.30	0.053	0.21	0.030
F 4	0.16	0.025	0.071	0.069
F 5	0.16	0.057	0.025	0.076
S 1	0.09	0.053	0.004	0.032
S 2	0.13	0.062	0.050	0.021
S 3	0.75	0.037	0.61	0.11
S 4	2.05	0.21	1.52	0.33

F – Fall 2008, S – Spring 2009, Cont. non-FF – continental non-fossil, FF – fossil fuel.

Stable carbon analysis of the front and back quartz filters suggested that gas phase compounds adsorbed on the back filter, and considered to be responsible for the positive sampling artefact, are "lighter" in terms of stable carbon isotope (~1‰). It can not yet be concluded whether this finding is due to isotopic fractionation or simply is source dependent.

Our findings suggest that continental non-fossil sources are stronger than previously thought and thus should be adequately considered in models.

This work was supported by EPA Ireland.

Ceburnis, D. et al. (2011) *Atmos. Chem. Physics Discuss.*, **11,** 2749-2472.
Gilardoni, S. et al. (2011) *Atmos. Chem. Physics Discuss.*, **11,** 2503-2547.
Miyazaki, Y. et al. (2010) *Geophys. Res. Lett.*, **37**, L06803, doi:10.1029/2010GL042483.

In-situ spectral characterisation of atmospheric aerosols after the red sludge disaster in Hungary during the autumn of 2010 based on our novel multi-wavelength photoacoustic instrument

T. Ajtai[1], Á. Filep[1], N. Utry[1], A. Gelencsér[2], A. Hoffer[2] Z. Bozóki[3], G. Szabó[1]
[1]Department of Optics and Quantum Electronics, University of Szeged, Hungary
[2]University of Pannonia, Veszprém, Hungary
[3]Research Group on Laser Physics of the Hungarian Academy of Science, University of Szeged, Hungary

Presenting author email: afilep@titan.physx.u-szeged.hu

After the red sludge disaster in Hungary during the autumn of 2010 a marked increase in the mass concentration of atmospheric aerosols in the red sludge hit area around the town of Devecser was observed. A mobile measurement station, which includes our recently developed multi-wavelength photoacoustic instrument (4λ-PAS) (Ajtai et al, 2010) was installed at the heart of the red sludge covered area. With the 4λ-PAS the optical absorption properties of the atmospheric aerosols and especially the light absorbing carbonaceous matter (LAC) was monitored with high time resolution and it was possible to deduce certain conclusions about the chemical composition and possible sources of the atmospheric aerosols.

Although the optical absorption spectra of LAC components are typically almost completely featureless in the visible, nevertheless they have fairly characteristic variations in the UV wavelength region, therefore multi-wavelength measurements (especially of they include wavelengths in the UV) have the potential for their efficient spectral identification (Andreae and Gelencsér, 2006). We have developed a multi wavelength photoacoustic instrument, which operates at four wavelengths (266nm, 355nm, 532nm, 1064nm) which cover the UV, VIS and NIR spectral regions. The wide wavelength range, the in-situ high sensitivity measurements, as well as the non-site specific, generally applicable calibration procedure makes this instrument an indispensable tool for spectral identification of the carbonaceous matter of atmosphere under various field conditions.

In this work we present the results of our field measurements at the red sludge covered area at Devecser shortly after the disaster, which are based on the absorption measurements by the 4λ-PAS and as a reference a commercially available seven wavelength Aethalometer. The analysis of the measured optical absorptions is based on the use of the Angström exponent nomenclature and especially wavelength dependent Angström exponents were used in order to achieve a better fit of the calculated curves to the measured data. From the measurements it can be concluded that during traffic lockdown period biomass burning was the dominant source of aerosols, and aerosols from the red sludge were change the spectral behaviour only during mornings when there was a reduced intensity of biomass burning. Dust from the red sludge appears to have a very sharply increasing optical absorption toward the UV. As soon as the traffic lockdown was removed traffic aerosols became dominating the atmosphere (Fig.1.). Chemical analysis and particle size measurement was found to support the interpretation of the absorption measurement.

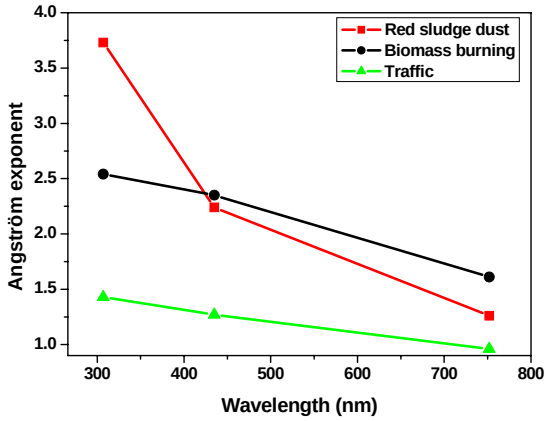

Figure 1. The identified source related spectral features during the field measurements at the area of red sludge disaster.

M. O. Andreae, A. Gelencsér, (2006). Black carbon or brown carbon? The nature of light-absorbing carbonaceous aerosols, Atmos. Chem. Phys. 6, 3131–3148

T. Ajtai, Á. Filep, M. Schnaiter, C. Linke, M. Vragel, Z. Bozóki, G. Szabó, T. Leisner: „A novel multi-wavelength photoacoustic spectrometer for the measurement of the UV–vis-NIR spectral absorption coefficient of atmospheric aerosols" Journal of Aerosol Sciences DOI:10.1016/j.jaerosci.2010.07.008.

Carbonaceous aerosol in Europe – Multi-year study with the EMEP PCM model including validation using source-apportionment data

R. Bergström[1,2], D. Simpson[3,4] and EUCAARI partners[5]

[1]Department of Chemistry, University of Gothenburg, SE-412 96, Gothenburg, Sweden
[2]Swedish Meteorological and Hydrological Institute, SE-601 76, Norrköping, Sweden
[3]Norwegian Meteorological Institute, Postboks 43 Blindern, 0313 OSLO, Norway
[4]Department of Radio & Space Science, Chalmers University of Technology, SE-412 96, Gothenburg, Sweden
[5]Various institutes across Europe, http://www.atm.helsinki.fi/eucaari/
Keywords: Carbonaceous Aerosol, SOA, VBS, source-apportionment.
Presenting author email: Robert.Bergstrom@smhi.se

The EMEP MSC-W chemical transport model (Simpson et al., 2007) has been extended with a new organic aerosol (OA) scheme based on the Volatility Basis Set (VBS) approach (Donahue et al., 2006).

Four different VBS-based schemes, based on the OA models of Lane et al. (2008), Shrivastava et al. (2008) and Murphy & Pandis (2009) have been tested. The models include SOA formation from anthropogenic and biogenic VOC. Reactions of semivolatile OA species in the gas phase with OH may lead to a shift of the reacting OA to lower volatilities (aging of the OA).

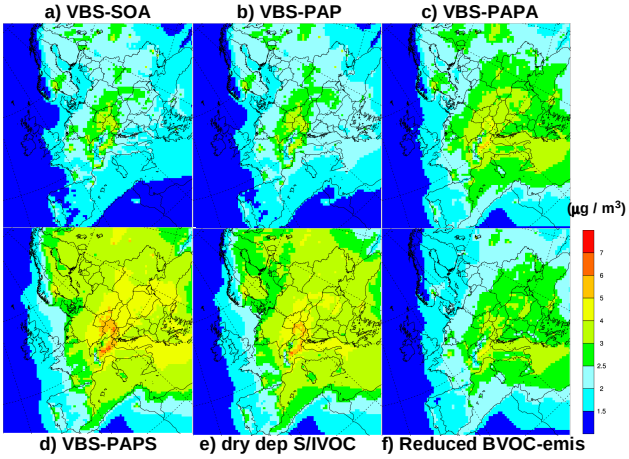

Figure 1. Calculated yearly average total organic aerosol (µg/m^3) for 2008, using different model setups: (a, VBS-SOA) includes a 4-bin VBS-based scheme for SOA formation from anthropogenic and biogenic VOC. Primary organic aerosol (POA) emissions are assumed non-volatile; (b, VBS-PAP) VBS-SOA + partitioning and aging of POA emissions. The emitted POA is distributed over different volatilities (9-bin VBS) and partitions between the gas and particulate phases. The emissions are assumed to be accompanied by emissions of low-vapour pressure gases. Aging reactions for POA in the gas phase are included, using the reaction rate $k_{OH\text{-}POA}=4\times10^{-11}$ cm^3 molecule^{-1} s^{-1}; (c, VBS-PAPA) VBS-PAP + aging of anthropogenic SOA (ASOA), using the reaction rate $k_{OH\text{-}ASOA}=1\times10^{-11}$ cm^3 molecule^{-1} s^{-1}; (d, VBS-PAPS) VBS-PAP + aging of both ASOA and biogenic SOA (BSOA), using the reaction rate $k_{OH\text{-}SOA}=4\times10^{-12}$ cm^3 molecule^{-1} s^{-1}; (e) As (d), but with dry deposition of gas-phase SOA and POA; (f) As (d), but with BVOC emissions reduced by a factor of three.

We present results from model runs, on the European scale, testing various assumptions regarding the emissions and aging reactions of the semi-volatile OA. Some sensitivity tests regarding BVOC emissions and dry deposition of semi-volatile species were also performed. Results are compared to measurement data from several European campaigns, including the EUCAARI-project.

The model results are very sensitive to the assumptions regarding the volatility of the POA emissions and the aging reactions. Several different alternatives need to be explored and detailed comparisons of the model results to chemically speciated observation data (especially source apportionment data) are needed to constrain and validate the model and emissions.

Table 1. Model evaluation by source-apportionment.
Gothenburg (Sweden), Summer (13/6 – 4/7) 2006 [Göte]

	Observed-Derived[1]	EMEP-PCM Models (VBS-based)[2]					
Sources (OC in PM2.5)	(5–95th %ile)	a) VBS-SOA	b) VBS-PAP	c) VBS-PAPA	d) VBS-PAPS	e) dry dep. S/IVOC	f) low BVOC-emis.
Fossil	0.65 – 1.0	0.6	0.5	0.9	0.8	0.8	0.8
Fossil fuel	0.19 – 0.30	0.4	0.1-0.4	0.1-0.4	0.1-0.4	0.1-0.4	0.09-0.4
ASOA	0.38 – 0.78	0.2	0.2-0.5	0.6-0.8	0.5-0.7	0.4-0.7	0.4-0.7
Nonfossil	0.95 – 1.35	0.8-1.3	0.7-1.2	0.8-1.3	2.7-3.2	2.3-2.8	0.9-1.4
Total OC	2.2	1.9	1.8	2.2	4.1	3.6	2.2
Total C	2.7±0.4	2.6	2.5	3.0	4.8	4.3	3.0

(1) Estimated using Latin Hypercube Sampling (LHS), Szidat et al., 2009.
(2) See Figure 1 caption for explanation of model versions.
Units: µg C m^{-3}

This work was funded by the Swedish Clean Air Research Program (SCARP), the EU EUCAARI project, as well as by EMEP under UNECE.

Donahue, N.M.; Robinson, A.L.; Stanier, C.O. & Pandis, S.N. (2006), *Environ. Sci. Technol.*, **40**, 2635–2643.
Lane, T.E.; Donahue, N.M. & Pandis, S.N. (2008), *Environ. Sci. Technol.*, **42**, 6022–6027.
Murphy, B.N. & Pandis, S.N. (2009), *Environ. Sci. Technol.*, **43**, 4722–4728.
Shrivastava, M.K. et al. (2008), *J. Geophys. Res.*, **113**, D18301.
Simpson, D. et al. (2007), *J. Geophys. Res.*, **112**, D23S14.
Szidat, S. et al. (2009), *Atmos. Chem. Physics*, **9**, 1521-1535.

Chemical composition and δ^{13}C values of OC and EC in the size-segregated aerosol particles

A. Garbaras, R. Bariseviciute, K. Kvietkus, J. Sakalys, J. Didzbalis, R. Skipityte and V. Remeikis
Institute of Physics, Center for Physical Sciences and Technology, Vilnius, LT-02300, Lithuania
Keywords: Stable carbon isotopes, Cascade impactor, AMS, PM and source apportionment
Presenting author email: garbaras@ar.fi.lt

Research on the origin and evolution of the chemical composition of aerosol particles is important for understanding the climate change, environmental pollution and environmental self-cleaning processes. Atmospheric aerosol absorbs and reflects radiation from the Sun and heat radiation from the Earth, thus changing thermal balance of the planet. Aerosol absorbs gases, chemical elements and compounds, influences water condensation processes, stimulates photocathalytical reactions and has influence on the global chemical processes in the atmosphere [Ceburnis et al., 2005.]

Organic matter, ammonium, sulphates, nitrates, chlorides in the atmospheric aerosol particles were measured with the Quadrupole Aerodyne Aerosol Mass Spectrometer (Q-AMS). Sampling with the MOUDI impactor and δ^{13}C measurements of total (TC), elemental (EC) and organic (OC) carbon in different aerosol size intervals were performed in parallel to AMS measurements in Vilnius city. At the Preila background station only sampling with the MOUDI impactor was performed. The carbon isotopic ratio of aerosol particles were measured with the EA-IRMS system (FlashEA 1112 - ThermoFinnigan delta plus advantage) [Garbaras et. al., 2009]. TC, EC and OC isotopic data comparison in Vilnius (urban) and Preila (background) showed that (Fig. 1):

a) TC in Vilnius varied from -27 to -24 ‰, while in Preila from -28 to -26 ‰;

b) EC in Vilnius varied from -31 to -26 ‰, while in Preila from -28 to -25 ‰;

c) OC in Vilnius varied from -22 to -28 ‰, while in Preila from -28 to -27 ‰.

Carbon isotopic analysis shows that the aerosol particles in the accumulation and coarse modes had the same source, and this source was different for Vilnius and for Preila. Carbonates were present in Vilnius in coarse mode probably from the road sprinkle with the mixture of sand an a salt.

Carbon isotope ratio measurements in size-resolved aerosols allow identifying aerosol sources more precisely, especially if OC and EC separation is performed. Combination of QAMS data with δ^{13}C is a promising tool for the aerosol particle source apportionment.

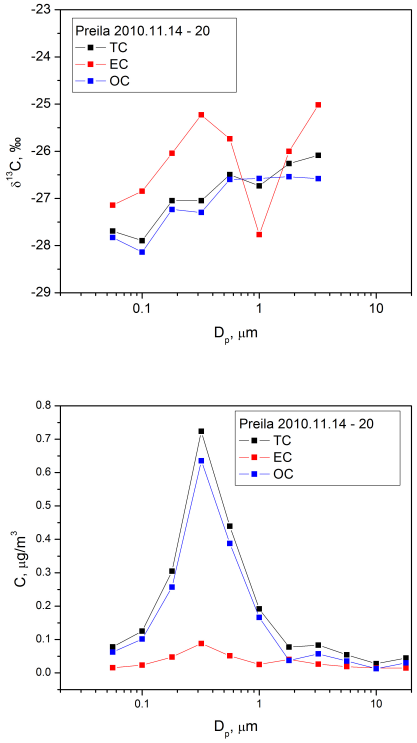

Figure 1: δ^{13}C and concentration of TC, EC and OC in aerosol particles, collected with the MOUDI impactor at Preila background station, Lithuania.

Acknowledgment: This work was supported by the Research Council of Lithuania under project No. MIP-105/2010.

Ceburnis, D., Ovadnevaite, J., Kvietkus, K., Remeikis, V., and Ulevicius, V. (2005). Lithuanian J. Phys., **45**(5), 323-332.

Garbaras, A., Rimselyte, I., Kvietkus, K., and Remeikis, V. (2009). Lithuanian J. Phys., **49**(2), 229-236.

Diurnal cycle of fossil and non-fossil total carbon using ^{14}C analyses during CalNex

P. Zotter[1], A.S.H. Prévôt[1], Y. Zhang[2], S. Szidat[2], X. Zhang[3], Y.-H. Lin[4], P. Hayes[5], J. D. Surratt[4], J.L. Jimenez[5], R. Weber[3], J. Slowik[1], U. Baltensperger[1]

[1]Paul Scherrer Institut, Laboratory of Atmospheric Chemistry, Villigen, Switzerland
[2]Department of Chemistry and Biochemistry, University of Bern, Bern, Switzerland
[3]School of Earth and Atmospheric Sciences, Georgia Institute of Technology, Atlanta, GA, USA
[4]Department of Environmental Sciences & Engineering, University of North Carolina, North Carolina, USA
[5]Department of Chemistry and CIRES, University of Colorado, Boulder, CO, USA
Keywords: Environmental radiocarbon, C-14, Source apportionment, Carbonaceous aerosols.
Presenting author email: peter.zotter@psi.ch

.

Aerosols are important for the Earth's climate and have a negative impact on human health (Pope and Dockery, 2006). Carbonaceous particles (total carbon, TC) are a major fraction of the fine aerosol and are classified into the subfractions elemental carbon (EC) and organic carbon (OC) (Jacobson *et al.* 2000). EC originates from fossil-fuel combustion and biomass burning. OC can be emitted directly as primary organic aerosol from biogenic sources, wood burning and fossil fuel combustion or can be formed in the atmosphere as secondary organic aerosol (Szidat *et al.* 2006).

Analysis of the radioactive isotope ^{14}C is a unique tool for distinguishing fossil and non-fossil sources of carbonaceous aerosol, because ^{14}C in fossil fuels is completely depleted whereas other sources have a contemporary ^{14}C level (Szidat *et al.* 2006). The $^{14}C/^{12}C$ content in the EC and OC fractions provides a quantitative and unambiguous measurement of the fossil/non-fossil carbon, thereby directly addressing a major uncertainty in the present understanding of organic aerosol sources.

Previous ^{14}C analyses have been performed on aerosol filters with a sampling time ≥12h. This study presents the first ^{14}C measurements performed on high time resolution (3-4 h) filter samples. As a result a diurnal pattern with the fossil and non-fossil composition of carbonaceous aerosols can be resolved.

Filter sampling was conducted during the CalNex-2010 field campaign from the 15th of May to the 16th of June 2010 at the California Institute of Technology (CALTECH), located about 20 km northeast of downtown Los Angeles using high-volume samplers with PM_1 and $PM_{2.5}$ inlets with a time resolution of 3, 4 and 24h.

Separation of the EC and OC fractions is carried out using the THEODORE system (Szidat, *et al.* 2004b) and a Sunset ECOC Analyzer. The evolving CO_2 is cryo-trapped and sealed in glass ampoules for ^{14}C measurements which are then performed with the mini radiocarbon dating system MICIDAS (Ruff *et al.* 2007) at the Swiss Federal Institute of Technology ETH Zürich.

First results from PM_1 filters for TC for the 4th of June (see Figure 1) show a distinct diurnal variation for TC with a peak for fossil TC in the early afternoon. The non-fossil fraction stays roughly constant between 2 and 3 µg/m^3 throughout the day. During high concentrations the fossil fraction of TC is very high indicating that the increase of the TC values in the early afternoon mainly stems from traffic related emissions. During low concentrations the non-fossil fraction constitutes ~50% of TC even though the Los Angeles area is strongly influenced by traffic-related emissions. This indicates that biogenic, biomass burning, cooking or other contemporary carbon sources also significantly affect the total carbon budget in urban areas. Trends in the fossil and non-fossil composition of aerosols in the Los Angeles area will be further analyzed by ^{14}C measurements of the EC and OC fraction and by comparison with aerosol mass spectrometry (AMS) and other data measured during the CalNex-2010 field campaign.

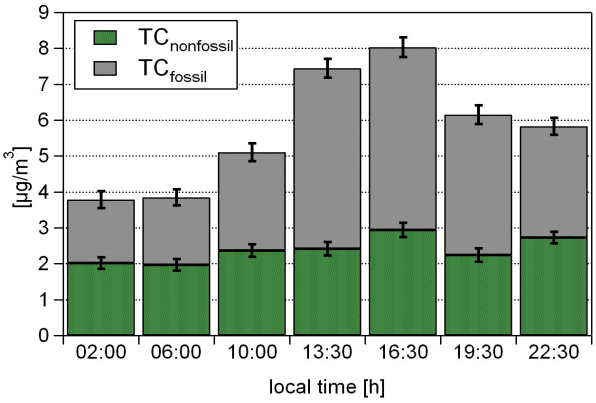

Figure 1. Diurnal course for TC and non fossil TC for the 4th of June 2010

This work was supported by CALTECH, especially by J. Seinfeld, the California Air Resources Board (CARB), the National Oceanic and Atmospheric Administration (NOAA), especially by J. de Gouw, the University of California, Los Angeles, especially by J. Stutz and the US National Science Foundation (NSF).

Jacobson, M. C. et al. (2000) *Reviews of Geophysics* **38**(2): 267-294.
Pope III, C. A., and Dockery, D. W. (2006). *J. Air Waste Manage. Assoc.*, **56**, 709-742.
Ruff, M. et al (2007) *Radiocarbon* **49**(2), 307-314.
Szidat, S. et al. (2006) *J. Geophys. Res.* **111**, D07206.
Szidat, S. et al. (2004) *Radiocarbon* **46,** 475-484.

Transformation by aging processes of soot particles from laboratory combustion experiments

J.K.Brooke[1], J.B.McQuaid[1], B.J.Brooks[1], S.Osborne[2] and J.M.Wilson[1]

[1]Istitute for Climate and Atmospheric Science, University of Leeds, LS2 9JT, UK
[2]Met Office Field Site, Cardington Airfield, Bedford, MK42 0SY, UK
Keywords: Carbonaceous aerosol, Biomass burning, Optical properties
Presenting author email: eejkb@leeds.ac.uk

Black carbon is the most abundant light absorbing particle in the atmosphere; it is an efficient absorber of solar radiation in the atmosphere and re-radiates the energy in the form of thermal energy and results in localised heating in this area, Buseck and Posfai (1999). Emissions of black carbon are a global phenomenon associated with incomplete combustion activities from fossil fuel and biofuel whilst with an estimated 40 % of global emissions of black carbon are from biomass burning, IPCC (2007).

The atmospheric lifetime of black carbon is short, and a reduction of BC emissions may be an effective method of mitigating climate change; such a reduction in BC emissions would equally benefit health and air quality. The lifetime of black carbon is dependent on the aging processes and deposition rates Schwarz *et al* (2006).

The aging process of soot consists of a change to the morphology and size distribution of soot particles; compaction of fractal aggregates of soot with time has been reported as a method of aging, Lu *et al* (2008) whilst hygroscopicity of soot particles has an important influence on their lifetime, Weingartner *et al* (1997). The aging process is not well understood, with changes in size distribution of soot, in models being poorly represented. An experimental set-up has been developed to observe changes the size distribution of soot particles as the particles age.

Laboratory experiments enable properties of soot particles to be characterised under controlled conditions, which remove the problems associated with field studies; variation in combustible material, burning conditions and atmospheric processes. Laboratory experiments enable a simplification of complexities of the combustion process.

The set-up involves a combination of two well proven systems; Optical particle counter (OPC) and Scanning mobility particle sizer (SMPS), an instrument combination which enables a wide range of particles to be observed (20 nm to 1 µm). Environmental Scanning Electron Microscopy (ESEM) will be used to examine the 3-dimensional shape of soot particles in order to understand soot surface topography and composition as particles age under varying reaction conditions.

Reaction chambers (280-L) are constructed and experiments are carried out with particles of known size and charge to determine wall loss rates which will be compared to theoretical predictions. Aerosol wall-loss rates are determined by observing changes to aerosol particle concentrations with time in the reaction chamber, McMurry and Grosjean (1985).

Preliminary experiments have been carried out to determine the initial polydisperse size distribution for a range of biofuels and hardwoods. Figure 1a shows the size distribution data of freshly emitted (240 s) soot from biofuel eugenol, as measured by the OPC. The difference in optical diameter and aerodynamic diameter for the eugenol soot is highlighted in Figure 1b.

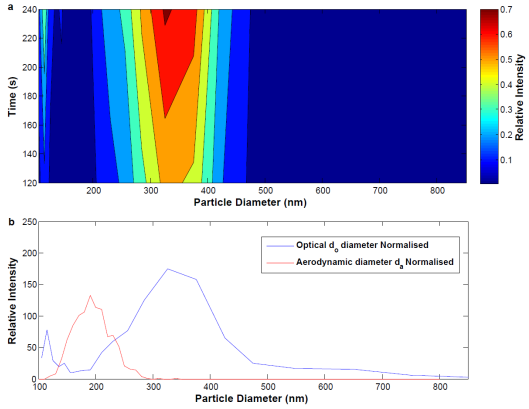

Figure 1 (a) Polydisperse size distribution of freshly emitted biofuel, eugenol, with evolving burn time as measured using an OPC (b) Normalised optical diameter d_o vs. normalised aerodynamic diameter d_a

Future work will involve quantifying changes to the size distribution as soot age increases inside a sealed reaction chamber monitored by OPC, SMPS and SEM. Results from these investigations will be applied into the Global Model of Aerosol Processes (GLOMAP) in order to improve the representation of black carbon aging in the model.

This work was supported by the Natural Environment Research Council and the Met Office.

Buseck, P. R. and Posfai, M. (1999) Proc. Natl. Acad. Sci. USA ***96,*** *3372 – 3379*

Forster (2007): Changes in Atmospheric Constituents and in Radiative Forcing, Cambridge University Press

Schwarz, J. P., Gao, R. S. and Fahey, D. W. (2006) J. Geophys. Res. ***111,*** *D16207*

Lu, Z., Hao, J., Hu, L. and Takekawa, H. (2008) Journal of Aerosol Science, ***39,*** *897-903*

Weingartner, E., Burtscher, H. and Baltensperger, U. Atmospheric Environment, ***31****, 2311-2327*

McMurry, P. H. and Grosjean, D. (1985) Environmental Science & Technology, ***19****, 1176-1182*

Gaseous and fine particle emissions from the combustion of agro-forestry pellets in a residential boiler

V.K. Verma[1], S. Bram[1,2] and J.De Ruyck[1]

[1]Department of Mechanical Engineering, Vrije Universiteit Brussel, Pleinlaan 2, 1050 Brussel, Belgium
[1,2]Department of Industrial Sciences and Technology, Erasmushogeschool Brussel, Nijverheidskaai 170, 1070 Brussel, Belgium

Keywords: agro-forestry pellets, $dust_{DINplus}$, $dust_{Isokinetic}$, multi-heat boiler.
Presenting author email: vverma@vub.ac.be

Emissions and efficiency of a multi-fuel pellet boiler (40 kW) at nominal load were compared with emissions and efficiency at reduced load, while fired with six biomass pellets. The pellets include reed canary grass (*Phalaris arundinacea*), pectin waste from citrus shells (*Citrus reticulata*), sunflower husk (*Helianthus annuus*), peat, wheat straw (*Triticum aestivum*) and wood pellets. The measurements of emissions comprised of carbon monoxide (CO), nitrogen oxides (NO_x), sulphur oxides (SO_x) and fine particle mass concentrations (using DINplus and isokinetic sampling techniques).

Emissions varied as a function of operational loads, for each type of pellets. The CO emissions were insignificant with reed canary grass (RCG), citrus pectin waste (CPW) and straw pellets at nominal load, however, at reduced load same pellets emitted 1.9, 4.0 and 7.4 times higher CO than wood pellets, respectively. Peat pellets emitted maximum CO at nominal load (4221.1 $mgNm^{-3}$, 12.6 times higher than wood pellets) however; at reduced load CO emission was insignificant. The highest NO_x emissions were reported with CPW, which were 3.4 and 4.6 times higher than wood pellets at nominal load and reduced load, respectively.

Fine particle emissions were measured employing DINplus and isokinetic sampling techniques and the results were compared. During isokinetic sampling, time constancy (15 minutes) was maintained instead of sampling gas volume constancy, as was done for DINplus sampling (270 litres). Eventually, a higher volume of flue gas was sampled during isokinetic sampling, leading to higher fine particle mass concentration than DINplus technique.

Comparison of the fine particle emission from the combustion of agro-forestry pellets at two different operational loads is shown in Fig.1. Fine particle emissions were highest with sunflower husk and lowest with reed canary grass pellets, at both operational modes. The best performance of the concerned boiler was reported with wood pellets, followed by reed canary grass and citrus pectin waste pellets, however, wood pellets combustion emitted 1.7 and 2.0 times higher $dust_{DINplus}$ than reed canary grass pellets at nominal and reduced loads, respectively. Emissions of $dust_{Isokinetic}$ were 1.1 and 1.4 times higher with wood pellets than reed canary grass pellets at nominal and reduced load, respectively.

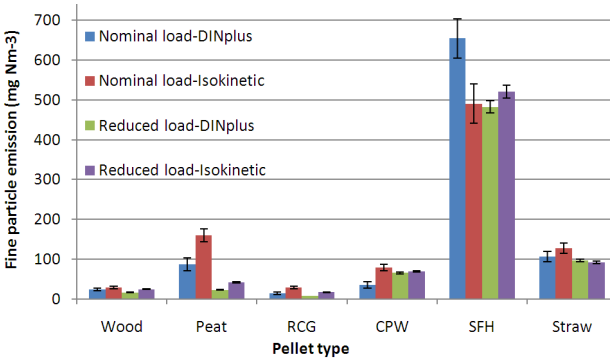

Fig.1: Fine particle emissions from the combustion of agro-forestry pellets at different operational load, measured with DINplus and isokinetic sampling technique. [RCG = reed canary grass; CPW = citrus pectin waste; SFH = sun flower husk pellets; NL = nominal load; RL = reduced load].

As fine particle emission is one of the major issues with small scale biomass combustion systems, reed canary grass pellets may be considered as a good alternative fuel for residential boilers. Furthermore, not only fuel specific combustion optimization but also operational loads specific optimization is essential for efficient use of agro-forestry pellets in this type of boilers

The basic performance of Jatropha curcas seed stove and its indoor air pollution over traditional wood stoves

Haryono S Huboyo[1], Puji Lestari[2], Susumu Tohno[1]

[1] Graduate School of Energy Science, Kyoto University Yoshida-Honmachi, Sakyo-ku, Kyoto 606-8501, Japan
[2] Department of Environmental Engineering, ITB Jl.Ganesha 10 Bandung, Indonesia
Keywords: Biomass burning, Black carbon, Indoor aerosols, Mass size distribution.
Presenting author email: huboyo.h@ax2.ecs.kyoto-u.ac.jp

The use of clean fuel such as LPG in remote rural areas in Indonesia is facing difficulty in popularizing it due to geographical aspects and poor recognition of safety in using a LPG stove among the people. Jatropha curcas seed stove (JCS) could become an alternative, however the level of emissions need to be further analyzed. We have focused on basic evaluation of the stove performance by means of the Water Boiling Test (WBT) in a field simulated kitchen, analysis of indoor air pollutants ($PM_{2.5}$ and CO) due to utilization of this stove and its comparison with traditional wood stove (WS) using three measurement points (near ventilation, cooker's site and far from ventilation) in the field simulated kitchen. Several studies have used the simple WBT to analyze the basic performance of the stoves either traditional or improved (Berrueta et al., 2008; Jetter and Kariher, 2009; Wagutu et al., 2010).

In order to analyze indoor air pollutants, we used inexpensive photoelectric monitors (UCB monitors), Sioutas cascade impactor and CO monitor. Furthermore mass size distribution of black carbon (BC) was also measured to emphasize on the health impacts that may arise in using the JCS.

WBT results indicated that thermal efficiency of JCS was more than 60% compared to around 17% of WS. During water boiling process (with lid), the aerodynamic size range less than 0.25μm was predominant in the $PM_{2.5}$ mass distribution of BC, and ventilation (natural ventilation) use in the room increased the proportion of BC in $PM_{2.5}$ (Fig. 1). In general, the percentages of BC in $PM_{2.5}$ of JCS were 3.7 times and 5.4 times of those of WS without ventilation and with ventilation, respectively.

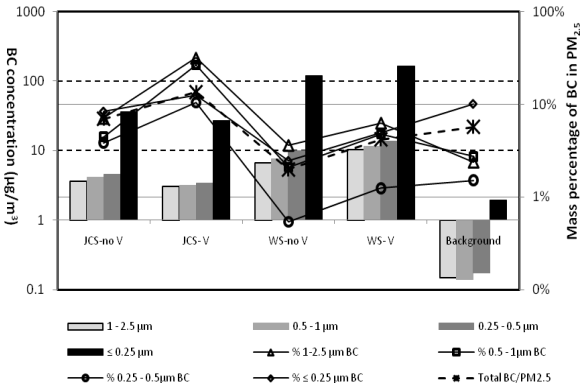

Figure 1 Mass size distribution of black carbon during water boiling process on different stoves

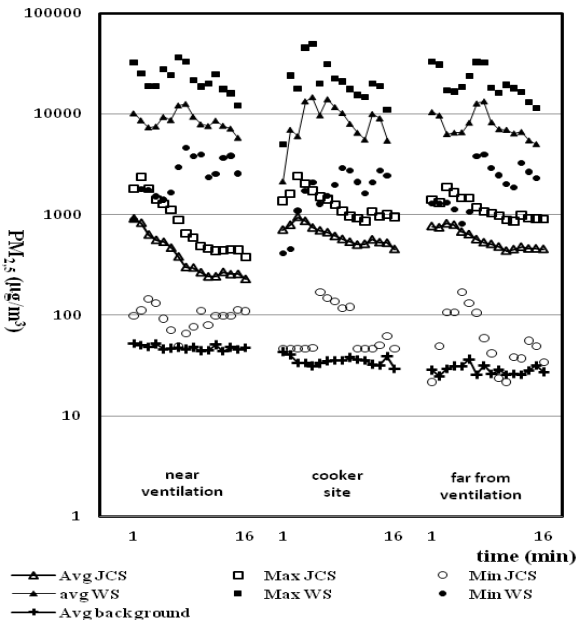

Figure 2 Temporal variation of $PM_{2.5}$ during water boiling process on different stoves (unventilated)

The indoor $PM_{2.5}$ concentrations generated by the JCS was high enough reaching more than 650 μg/m^3 (without ventilation) and 190 μg/m^3 (with ventilation) on average at the position of cookers.

The mass concentrations were approximately 7% and 3.6% of those in WS without ventilation and with ventilation respectively. In addition, the distribution of pollutants is relatively uniformly distributed in the unventilated room (Fig. 2).

Nonetheless, in fact the highest $PM_{2.5}$ concentrations were found during ignition and end-fire phases of stoves either JCS or WS due to tremendous smoke emission.

This work was financially supported by Global Centre of Excellence (GCOE) Program of Graduate School of Energy Science, Kyoto University and Environmental Management Leader Program of Kyoto University.

Berrueta, V.M,. Edwards, R.D. and Masera, O.R. (2008). *Renew Energy,* **33,** 859–870.

Jettera, J.J. and Kariher, P. (2009). *Biomass Bioenergy*. **3 3,** 294–305.

Wagutu, A.W., Thoruwa, T.F.N., Chhabra, S.C., Thoruwa, C.C.L. and Mahunnah, R.L.A. (2010). *Biomass Bioenergy,* **34**, 1250-1256.

Characterization of trace gases and $PM_{2.5}$ emitted during the combustion of shrub biomass in a Portuguese stove

A.I. Calvo, A.P. Fernandes, L.A.C. Tarelho, J.R. Pinho, M.C. Duarte, J.F. Silva and C.A. Alves

Centre for Environmental and Marine Studies, Department of Environment and Planning, University of Aveiro, Aveiro, 3810-193, Portugal
Keywords: biomass combustion, $PM_{2.5}$, chemical composition, emission factor
Presenting author email: celia.alves@ua.pt

In Portugal, the use of biomass for residential heating is a common practice and, although it can reduce the consumption of fossil fuels at the domestic level, it constitutes an important source of atmospheric pollutants (Schmidl et al., 2008). In addition to gases, biomass burning releases large amounts of particulate matter, mainly $PM_{2.5}$, which has relatively long residence time in the atmosphere. This fraction is the most dangerous to the human health (Dai et al., 2006) and has an important impact on regional and global air quality (Monks et al., 2009) and climate (Randles and Ramaswamy, 2010). Emission factors from biomass burning are rather inexistent in Europe; the available emission factors were obtained for US biofuels (Fine et al., 2004), uncommon in Europe. The type of stove used and the species of wood and their characteristics are factors that can have an important influence on particle emissions (McDonald et al., 2000). Therefore, in order to establish smoke profiles for the biofuel types commonly used in Europe, wood-burning stoves typical of those found for residential heating in the country of study have to be used (Schmidl et al., 2008). In this way, it will be possible to use more specific locally available data in order to accurately assess the contribution of biomass burning and evaluate its impacts.

A set of tests was carried out to determine the gas and chemical composition of $PM_{2.5}$ emitted from the combustion of shrub biomass in a stove. The shrub selected for this study was *Ulex sp.* which is common in the North-West Portuguese forest. The shrub biomass constitute an important source of energy because they have an important calorific value (20 MJ kg^{-1} and 8.4 MJ kg^{-1} for higher and lower heating values, respectively) (Regueira et al., 2005).

The biomass fuel was prepared in order to have two fractions: green parts (twigs with leaves less than 5 mm in diameter) and brown parts (stems more than 5 mm in diameter). The aim was to determine the characteristic of the emissions from the combustion of these two different parts of the shrub. The biomass was arranged in bundles of similar length and with a mass between 0.6 and 1 kg to be combusted after air drying.

A stove commonly used in Portugal for domestic heating was used for combustion experiments. It is operated in the batch mode and produces hot air by a combination of natural and forced convection, and radiation. The stove has a combustion chamber 0.44 m height x 0.59 m width x 0.36 m depth. Exhaustion of combustion was done by a vertical chimney with 0.2 m internal diameter and 3.3 m height. Combustion cycles lasted 20-30 minutes.

The flue gas composition was monitored continuously at the exit of the chimney: i) total volatile hydrocarbons were determined using an automatic analyser with flame-ionisation detector and ii) CO_2 and CO were determined using a non-dispersive infrared analyser.

Fine particles ($PM_{2.5}$) were collected on quartz filters using a low volume sampler in the dilution tunnel that was directly coupled to the chimney. Filters were analyzed in order to determine the carbonaceous content (elemental and organic carbon) and water-soluble inorganic ions using a thermal-optical transmission technique and ion chromatography, respectively.

This study will represent a step towards a better characterisation of emission from combustion of different parts (green and brown) of the shrub biomass. At the same time, it will contribute to improve the characterization of emission profiles of species growing in the Mediterranean region in order to contribute to source apportionment and to improve emission inventories.

This work was supported by Portuguese Science Foundation (FCT) through the projects “Characterization and processing forest shrub biomass into a solid fuel” PTDC/AMB/73364/2006 (ProForShrub) and “Contribution of biomass combustion to air pollutant emissions”, PTDC/AMB/65706/2006 (BIOEMI).

Dai, Y.-T., Juang, Y.-J, Wu, Y.-Y., Breysse, N.P and Hsu, D.-J. (2006) *J. Aerosol Sci*. **37**, 967-973.

Fine, P.M., Cass, G.C. and Simoneit, B.R.T. (2004) *Environ. Eng. Sci.* **21**, 705–721.

McDonald, J.D., Zielinska, B., Fujita, E.M., Sagebiel, J.C.,Chow, J.C. and Watson, J.G. (2000) *Environ. Sci. Technol*. **34**, 2080-2091.

Monks, P.S. et al. (2009) *Atmos. Environ*. **43**, 5268-5350.

Randles C.A.and V. Ramaswamy (2010) *Atmos. Chem. Phys. Discuss*. **10**, 9731-9752.

Regueira, L., Castiñeiras, J. and Añon, J. (2005) *Biomass Bionerg*. **91**, 215-221.

Schmidl, C., Marr, I.L., Caseiro A., Kotianová, P., Berner, A., Bauer, H., Kasper-Giebl, A. and Puxbaum, H. (2008) *Atmos. Environ*. **42**, 126-141.

Gases and aerosols emitted from wildfires in summer 2009 (central Portugal)

A. Vicente[1], C. Alves[1], C. Monteiro[1], T. Nunes[1], F. Mirante[1], M. Evtyugina[1], L. Tarelho[1], A. M. Sánchez de la Campa[2], X. Querol[3], A. Caseiro[1] and C. Pio[1]

[1]Centre for Environmental and Marine Studies, Department of Environment, University of Aveiro, 3810-193 Aveiro, Portugal
[2]Associate Unit CSIC-University of Huelva "Atmospheric Pollution", University of Huelva, Campus El Carmen, E21071 Huelva, Spain
[3]Institute of Environmental Assessment and Water Research, IDAEA, Spanish Research Council (CSIC), C/Jordi Girona 18-26, 08034 Barcelona, Spain
Keywords: wildfires, emissions factors, $PM_{2.5}$, $PM_{2.5-10}$
anavicente@ua.pt

In summer 2009, gas and particulate fractions were measured from several wildfires occurring in central Portugal. The total volatile hydrocarbons and carbon oxides (CO_2 and CO) collected in Tedlar bags were measured using automatic analysers with flame ionisation and non-dispersive infrared detectors, respectively. Carbonyls (formaldehyde and acetaldehyde) were sampled from the Tedlar bags in DNHP cartridges and analysed by high-performance liquid chromatography. Fine ($PM_{2.5}$) and coarse ($PM_{2.5-10}$) smoke particles were collected sequentially, on pre-fired quartz fibre filters, with a portable high-volume sampler. The organic and elemental carbon content of particulate matter was analysed by a thermal-optical transmission technique (Alves et al., 2011a). The detailed speciation of organic compounds in smoke samples was carried out by gas chromatography-mass spectrometry. The levels of almost 50 elements were quantified by inductively coupled plasma-mass spectrometry. The water-soluble ions were obtained by ion chromatography.

Emission factors (EF) for some gaseous compounds and particulate matter were calculated taking into account that EF is a parameter that relates the emission of a particular species of interest to the amount of fuel burned. Usually it is defined as the amount of a compound released per amount of dry fuel consumed, expressed in units of g kg^{-1} (Alves et al., 2011a; Reid et al., 2005). The modified combustion efficiency (MCE) was calculated and used for each sampling event to define the relative amount of flaming and smouldering combustion for biomass burning (Alves et al., 2011b; Yokelson et al., 2009). MCE values higher than or less than 0.9 indicate dominance of flaming or smouldering combustion, respectively (Reid et al., 2005). The emission factors obtained in Portugal were as follows (in g kg^{-1} biomass, dry basis): 131-488 for CO, 822-1523 for CO_2, 0.97-104 for total hydrocarbons, 2.0-21 for $PM_{2.5}$, 2.4-24 for PM_{10}, and 0.5-39 for OC (in PM_{10}). MCE values ranged from 0.52 to 0.88, corresponding to a greater predominance of smouldering than flaming combustions. Average emission factors of 1.46±0.53, 0.46±0.34 and 0.12±0.07 g kg^{-1} (dry basis) were obtained for acetaldehyde, formaldehyde and propionaldehyde, respectively.

The dominant elements were B, Ti, Mn, Cu, Zn, Zr and Ba; rare earth elements (e.g. La, Ce, Nd, Pr, Sm, Tb, Tm, Yb) were also detected in smoke aerosols as minor constituents. The water-soluble ions contributed, on average, to 3.4% and 2.2% of the fine and coarse particle mass, respectively.

The chromatographically resolved organics included *n*-alkanes, *n*-alkenes, *n*-alkanoic acids, *n*-di-acids, unsaturated fatty acids, phenolic compounds, ketones, steroids, di- and triterpenoids, PAH, with retene as the major compound, and anhydrosugars. The anhydrosugar levoglucosan, and its stereoisomers mannosan and galactosan, constituted the main thermal alteration products and, therefore, are specific markers for wood combustion in ambient particulate matter (Medeiros and Simoneit, 2008; Simoneit et al., 1999). As expected, levoglucosan was the most abundant anhydrosugar, followed by mannosan and galactosan. These compounds were detected in fine particles at levels in the ranges 1.7-37, 0.7-13 and 0.5-7.7 mg g^{-1} OC, while in coarse particles the values were 2.9-40, 0.7-10 and 0.4-7.4 mg g^{-1} OC, respectively.

This work was supported by the Portuguese Science Foundation (FCT), through the project PTDC/AMB/65706/2006 (BIOEMI). Ana Vicente acknowledges the PhD grant SFRH/BD/48535/2008.

Alves, C., Vicente, A., Monteiro, C., Gonçalves, C., Evtyugina, M. and Pio, C. (2011a) *Sci. Total Environ.* (in press).

Alves, C., Vicente, A., Nunes, T., Gonçalves, C., Fernandes, A., Mirante, F., Tarelho, L., Sánchez De La Campa, A., Querol, X. and Caseiro, A. (2011b) *Atmos. Environ.* 45**,** 641-649.

Medeiros, P. and Simoneit, B. (2008) *Environ. Sci. Technol.* 42**,** 8310-8316.

Reid, J.S., R. Koppmann, T. F. Eck and Eleuterio, D.P. 2005) *Atmos. Chem. Phys.* 5**,** 799-825.

Simoneit, B., Schauer, J., Nolte, C., Oros, D., Elias, V., Fraser, M., Rogge, W. and Cass, G. (1999) *Atmos. Environ.* 33**,** 173-182.

Yokelson, R., Crounse, J., Decarlo, P., Karl, T., Urbanski, S., Atlas, E., Campos, T., Shinozuka, Y., Kapustin, V. and Clarke, A. (2009) *Atmos. Chem. Phys.* 9**,** 5785-5812.

Organic markers and anhydrosugars in particulate matter from incense burning

Ying I. Tsai[1], Su-Ching Kuo[2], Li-Ying Hsieh[3], Chien-Lung Chen[4], Yu-Ting Hsu[1]

[1] Dept of Environmental Engineering & Science, Chia Nan University of Pharmacy & Science, Tainan 717, Taiwan
[2] Dept of Medicinal Chemistry, Chia Nan University of Pharmacy & Science, Tainan 717, Taiwan
[3] Dept of Chemistry, National Cheng Kung University, Tainan 701, Taiwan
[4] Dept of Industrial Engineering & Management, Fortune Institute of Technology, Kaohsiung 831, Taiwan
Keywords: biomass burning, organic marker, levoglucosan, carboxylic acid, emission factor.
Presenting author email: mtsaiyi@mail.chna.edu.tw (Y.I. Tsai)

Incense burning is an important kind of air pollution in Taiwan, especially in the ceremonial worshiping of gods in Budhism, Taoism and folk religions. Studies to date have mainly focused on emissions of metals and particle-bound polycyclic aromatic hydrocarbons (PAHs), size distributions, and toxicities (Yang et al., 2007). Studies of size distributions show that incense smoke particles are typically in the submicrometer size range (Chang et al., 2007; Yang et al., 2007). Such an analysis is necessary if informed strategies and policies related to incense burning and air pollution are to be developed. Furthermore, this study identified the chemical species contained in incense smoke and identified potential marker compounds.

The four most popular types of incense in Taiwan are marketed under the names *Lao Shan*, *Hsing Shan*, *Liao* and *Chen*. Three lab-made sticks of the same type were burned simultaneously during each run. Total particulate matter was collected on a quartz filter (102 mmφ, Pall) at 30.0 L min^{-1} using a modified mid-volume air sampler fastened to the top of the tube. A total of 24 samples of particulate matter, 6 for each type of incense, were collected. Twenty-five chemical compounds were characterized in all: ten carboxylic acids, nine water-soluble inorganic species, three anhydrosugars, and three sugar alcohols using a Dionex DX-600 ion chromatograph (IC), a Dionex ICS-1000 IC and a Dionex ICS-2500 IC equipped with pulsed amperometric detection (PAD).

The total particulate matter (PM) mass emission factors were 43.7±1.08 mg g^{-1} of *Lao Shan*, 46.3±2.68 mg g^{-1} of *Hsing Shan*, 37.8±0.83 mg g^{-1} of *Liao* and 45.9±0.60 mg g^{-1} of *Chen*. Chemical analysis of emissions from the four types of incense, shown in Table 1, revealed that of the 25 components in four groups characterized, anhydrosugars formed the major group, at 43-53 % w/w of identified particulate and 858.6-1586 μg g^{-1} of incense, followed by inorganic salts at 30-33 % w/w of identified particulate and 662.6-956.9 μg g^{-1} of incense, carboxylic acids at 10-17% w/w of the identified particulate and 268.6-392.8 μg g^{-1} of incense, and sugar alcohols at 4.4-7.1% w/w of the identified particulate and 102.3-142.5 μg g^{-1} of incense.

The anhydrosugar levoglucosan (1,6-anhydro-β-D-glucose, Levo), used as a marker of biomass burning, was always the most abundant species in emitted PM for four incenses, accounting for 80.3-91.0% w/w of total identified anhydrosugars (shown in Fig. 1).

Table 1. Emission factors of PM and components in four groups per gram of incense from four types of incense.

	Emission factor (μg g^{-1} incense)											
	Lao Shan			Hsing Shan			Liao			Chen		
	Mean	SD	%	Mean	SD		Mean	SD	%	Mean	SD	%
PM mass (mg g^{-1})	43.72	1.08		46.28	2.68		37.78	0.83		45.94	0.60	
Inorganic salts	681.6	55.1	30.4	734.0	55.1	31.8	956.9	141.9	32.0	662.6	67.6	33.2
Carboxylic acids	268.6	22. 8	12.0	392.8	34.2	17.0	306.6	59.9	10.3	329.7	95.2	16.5
Anhydrosugars	1169.8	47.2	52.2	1078.3	171.1	46.7	1586.4	24.5	53.0	858.6	127.0	43.1
Sugar alcohols	120.6	8.1	5.4	102.3	7.2	4.5	140.8	13.0	4.7	142.5	23.7	7.2

K^+ and Cl^- were the second most abundant components (K^+ and Cl^- were summed), accounting for 63.1-75.5% w/w of total identified inorganic salts. The most abundant carboxylic acids in the emissions were formic and acetic acid, accounting for 37.9-64.4% w/w of total identified carboxylic acids. Xylitol was the dominant sugar alcohol at 18.2-36.6% w/w of total identified sugar alcohols. In addition to Levo, xylitol and formic acid are not found in four unburnt incenses, indicating these abundant species are potential markers for incense burning.

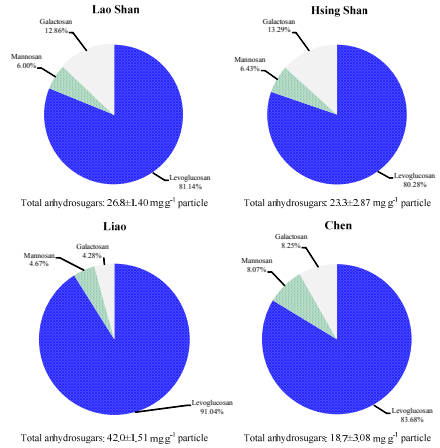

Fig. 1. Contribution of individual species to total amount of anhydrosugars in PM emitted from incense burning.

This work was supported by the National Science Council, Taiwan under Grant Nos. NSC 96-2221-E-041-013-MY3 and NSC 99-2221-E-041-014-MY3.

Chang, Y.C., Lee, H.W., Tseng H.H. (2007) *Journal of Aerosol Science* **38**, 39-51.
Yang, C.-R., Lin, T.-C., Chang, F.-H. (2007) *Environmental Pollution* **145**, 606-615.

Thursday, September 8, 2011

Session 8P: Poster session B

Atmospheric aerosols - Aerosol Processes and Properties

Submicronic aerosols dry deposition on urban surfaces: a wind tunnel study to improve the lack of knowledge

P. Roupsard[1], M. Amielh[2], A. Coppalle[3], H. Branger[2], P. Laguionie[1], O. Connan[1], D. Hébert[1], D. Maro[1] and M. Talbaut[3]

[1]Laboratoire de Radioécologie de Cherbourg-Octeville, IRSN, 50130 Cherbourg-Octeville, France
[2]Institut de Recherche sur les Phénomènes Hors Equilibre, UMR 6594, CNRS, 13384 Marseille, France
[3]COmplexe de Recherche Interprofessionnel en Aérothermochime, UMR 6614, 76801 Saint Etienne du Rouvray, France
Keywords: dry deposition, deposition velocity, urban area
Presenting author email: pierre.roupsard@irsn.fr

Introduction

In the case of an accidental or chronic atmospheric pollution by a nuclear plant, aerosols deposition transfer coefficients must be known. A major issue is to determine the impact of aerosols contained in the radioactive plume on urban areas. In dry atmospheric conditions, transfer coefficients are defined by the dry deposition velocities Vd ($m.s^{-1}$), the ratio between the aerosol vertical dry deposition flux ($particles.m^{-2}.s^{-1}$) and the concentration of aerosols ($particles.m^{-3}$; Seinfeld and Pandis, 1998). Dry deposition velocities are dependent on atmospheric turbulent conditions and surface roughness. Actually, for urban surfaces, only a few dry deposition velocities were measured, in field or in laboratory environments. Moreover, existing data are not linked with atmospheric conditions (Fowler *et al*, 2009). Therefore, it is important to improve the knowledge and the models on urban areas.

The aim of this wind tunnel study was to quantify, experimentally, dry deposition velocities for a submicron aerosol on three different urban surfaces, for three different wind speeds (U_{ref}). We measured also air turbulence intensities and friction velocities U_* in the wind tunnel.

Test equipment and methods

Experiments were conducted in April 2010 in the IRPHE closed-circuit wind tunnel (8.7 m x 0.7 m x 0.3 m). Dry deposition has been studied successively on glass, cement facing and synthetic grass with U_{ref} equals to 1.3, 5.0 and 10 $m.s^{-1}$. The bottom of the tunnel was totally recovered with each type of studied surface to develop the characteristic boundary layers. Deposition velocities were measured at three distances from the tunnel entrance (1, 5 and 7 m). A monomodal polydisperse submicron fluorescein aerosol, representing the accumulation mode of the atmospheric aerosol, was generated and injected in the wind tunnel (Maro *et al*, 2010). Spectrofluorimetric measurements of deposited aerosols on squares of each urban-type surface gave deposition fluxes. Spectrofluorimetric measurements of aerosols taken on filters gave aerosol concentrations in the wind tunnel.

Turbulence intensity, friction velocity and air velocity measurements were made by hot wire anemometry at three distances (1, 5 and 7 m) for each type of surface and at the three flow velocities U_{ref}.

Results and discussions

Friction velocity increased with wind speed and surface roughness. This study showed a significant increase of the deposition velocity with the surface roughness and with the wind speed (figure 1). But the increase due to surface roughness was much more important than the increase due to wind speed.

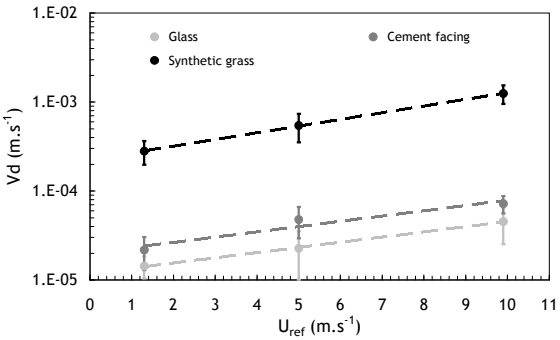

Figure 1. Dry deposition velocity Vd function of air flow velocity U_{ref}.

We found also that the ratio between deposition velocity and friction velocity on each surface was not constant (Table 1).

Table 1. Mean Vd/U_* ratio function of substrate

Substrates	Vd/U_* ($.10^{-3}$)
Glass	0.05 ± 0.05
Cement facing	0.11 ± 0.05
Synthetic grass	1.2 ± 0.3

These experiments in wind tunnel are the first step of a future study on the dry deposition in urban areas. The next step will be *in situ* experiments to take into account all the atmospheric parameters existing in urban environments.

D. Maro *et al* (2010) *Proc. 8th Int. Aero. Conf.*, Helsinki.
J. H. Seinfeld, S. N. Pandis (1998) *Atmospheric Chemistry and Physics*, Wiley-Interscience.
J. Cousteix (1989) *Aérodynamique : Turbulence et Couche Limite*, Cepaduès-Edition.
D. Fowler *et al* (2009) *Atmos. Env.* 43, 5193-5267.

Particle fluxes over arctic sea ice during COBRA

J.D. Whitehead[1], J.R. Dorsey[1], M.W. Gallagher[1], M.J. Flynn[1] and G. McFiggans[1]

[1]Centre for Atmospheric Science, School of Earth, Atmospheric and Environmental Sciences, The University of Manchester, Oxford Road, Manchester, M13 9PL, UK
Keywords: aerosols, fluxes, arctic.
Presenting author email: James.Whitehead@manchester.ac.uk

Particle fluxes were measured over Arctic sea ice during the COBRA (Impact of combined iodine and bromine release on the Arctic atmosphere) experiment at Hudson Bay, Canada, during February and March, 2008. Eddy covariance fluxes of fine and ultrafine particles were measured using Condensation Particle Counters (CPCs; TSI, models 3776 and 3010) in conjunction with an ultrasonic anemometer (Metek) mounted at a height of 2.5 m on a mast positioned out on the sea ice. Deposition velocities (v_d) were calculated from the ratio of the particle number flux and concentration. After filtering the data for stationarity and fetch, and applying appropriate corrections, a mean v_d of 0.119 ± 0.115 mm s^{-1} (standard error; n = 230) was found for particles measured with the CPC3776 (i.e. with a lower size threshold of 2.5 nm). With the CPC3010 (D_p > 10 nm), a mean v_d of 0.066 ± 0.106 mm s^{-1} (standard error; n = 236) was found. These values are smaller than those measured in previous experiments over ice floes in the Arctic Ocean (0.3 mm s^{-1}; Nilsson and Rannik, 2001), and over a snow covered ice sheet in Antarctica (0.47 mm s^{-1}; Contini *et al.*, 2010). Ultrafine particle concentrations (as determined by the difference in concentrations between the two CPCs) were low, suggesting that no nucleation events occurred during the measurement period. Optical Particle Counters (OPCs; Grimm, model 1.108) were placed at heights of 0.19 and 1.34 m on the mast, allowing size segregated fluxes of particles in the size range 0.3 – 20 μm to be derived using the aerodynamic flux gradient method. Strong emission fluxes were observed shortly after midday, 3rd March, when winds from over Hudson Bay increased to more than 10 m s^{-1}, suggesting ice particle resuspension. Number fluxes of these particles were largest in the smallest size channels (lower cut 0.3 μm), while the largest sizes (around 20 μm) dominated the mass flux. Number fluxes also increased with friction velocity u_*, particularly in the smaller sizes, and the relationship between flux and u_* will be investigated. Measurements with a Differential Mobility Particle Sizer (DMPS) showed an enhanced mode in the mass size distribution between 400 – 500 nm during these resuspension events. The aerosol size distribution measurements were also classified according to air mass and sea-ice versus land fetch.

The COBRA project was funded by the UK Natural Environmental Research Council (NERC) (NE/D006015/1). Logistical support at the measurement site was provided by Environment Canada.

Contini, D., Donateo, A., Belosi, F., Grasso, F.M., Santachiara, G. and Prodi, F. (2010) *J. Geophys. Res.* **115**, D16202, doi:10.1029 /2009JD013600.

Nilsson, E.D. and Rannik, Ü (2001) *J. Geophys. Res.* **106**, (D23), 32,125-32,137.

Rain scavenging of below-cloud aerosol particles: field measurements using Electrical Low Pressure Impactor and Scanning Mobility Particle Sizer coupled with Aerodynamic Particle Sizer

P. Laguionie, D. Maro, B. Letellier and S. Le Cavelier

IRSN (Institute of Radioprotection and Nuclear Safety), Cherbourg-Octeville, 50130, France
Keywords: atmospheric aerosols, wet deposition, scavenging coefficient, urban environment, ELPI, SMPS, APS
Presenting author email: philippe.Laguionie@irsn.fr

Introduction

In case of punctual or chronic atmospheric pollution by a nuclear plant, aerosol deposition transfer processes at work must be known. A major issue is to determine the rain scavenging of below-cloud aerosol particles, which is by far the most efficient atmospheric aerosol sink (Andronache, 2003). As distribution of radioactive chemical species is aerosol-size dependent, the scavenging sensitivity with respect to aerosol particle size has to be determined.

Removal process mechanism involves microphysical interactions between aerosol particles and hydrometeors. Practically, wet scavenging is typically modelled by coefficients and is usually parameterised by $dc/dt = -\Lambda c$ with c being aerosol concentration (number.cm^{-3}) and Λ the scavenging coefficient (s^{-1}). Λ parameterisation is, however, highly uncertain (Sportisse, 2007) and several orders of magnitude difference in Λ are still found between modelled values and estimates obtained from scarce *in situ* data.

The aim of the present study was to make a comparison of Λ obtained by Electrical Low Pressure Impactor (ELPI) and Scanning Mobility Particle Sizer (SMPS) coupled with Aerodynamic Particle Sizer (APS) under different rainfall intensity conditions. Data were acquired *in situ* in urban context (Cherbourg-Octeville, France) and are part of the INOGEV research program supported by the French National Research Agency.

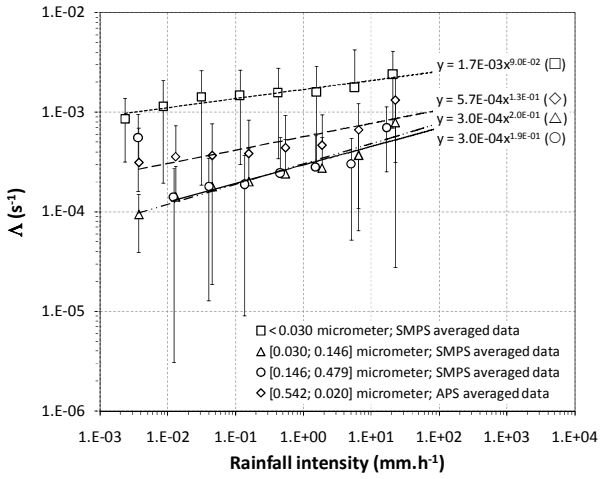

Figure 1. Scavenging coefficient versus rainfall intensity for 4 SMPS-APS granulometric classes.

First results

Firstly, SMPS and APS produced 1800 data that showed a power relationship between Λ and rainfall intensity over the full granulometric classes (Figure 1). A similar relationship was found with the 50 data from ELPI (Figure 2) (Vendel, 2007). So, different gears gave consistent results: parameters used to fit the power law are aerosol-size dependent.

Secondly, for a given granulometric class, no significant discrepancy was found between the two measurement methods.

Thirdly, compared to theoretical Λ values given in literature, Λ experimental parameter appeared one to several orders of magnitude higher.

The consequences of these results will be further discussed at the conference.

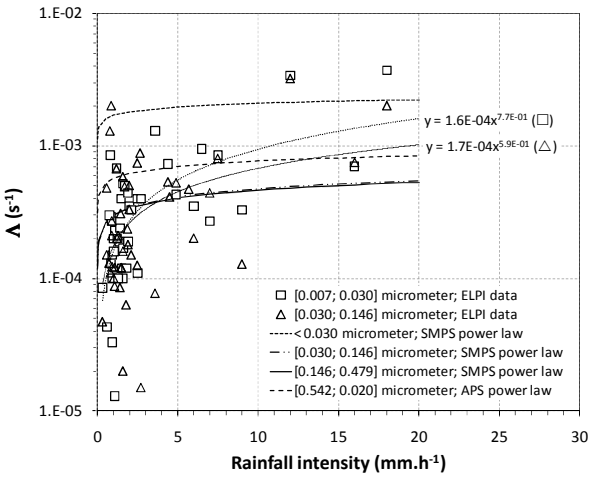

Figure 2. Scavenging coefficient versus rainfall intensity for 2 ELPI granulometric classes compared with SMPS-APS power law models presented in Figure 1.

Andronache, C. (2003). Estimated variability of below-cloud aerosol removal by rainfall for observed aerosol size distributions. *Atmospheric Chemistry and Physics*, 3, 131-143.

Sportisse, B. (2007). A review of parameterizations for modelling dry deposition and scavenging of radionuclides. *Atmospheric Environment*, 41, 2683-2698.

Vendel, F. (2007). Détermination expérimentale du coefficient de rabattement des aerosols atmosphériques par la pluie : comparaison modèles/mesures. Rapport de stage IRSN-ENSIAME.

Thursday, September 8, 2011

Session 8P: Poster session B

Aerosol Chemistry

Organic composition of size-distributed particles emitted from field burning of garden and agriculture residues

M. Evtyugina[1], C. Gonçalves[1], C.A. Alves[1], A.C. Monteiro[1], C. Pio[1], and M. Tomé[2]

[1]Centre for Environmental and Marine Studies (CESAM), Department of Environment, University of Aveiro, 3810-193 Aveiro, Portugal
[2]School of Technology, Polytechnic Institute of Viana do Castelo, Av. do Atlântico, 4900-348 Viana do Castelo, Portugal
Keywords: Agriculture wastes, burning, PM, OC/EC, organic speciation
Presenting author e-mail: celia.alves@ua.pt

Open burning of agriculture and garden residues is an important source of toxic air pollutants into the atmosphere with significant impacts on human health, air quality and global climate change. On a global scale, the estimated annual total dry matter combusted due to agriculture burning is around 540 Tg yr^{-1} (Andreae & Merlet, 2001), but the impact of emissions on the atmosphere is somewhat uncertain, because consistent data on agriculture burning are much sparser than data on other anthropogenic sources.

To assess the particulate matter (PM) composition, the smoke from three different agriculture and garden residues, commonly subjected to open field burning in Northern Portugal (potato haulm (A), arable weed vegetation (B) and collard greens stalks/pruned green leafy-twigs (C)) have been sampled into 3 different size fractions ($PM_{2.5}$, $PM_{2.5-10}$ and $PM_{>10}$). To replicate another frequent practice of reducing or dispose agriculture/garden debris, residue C was complementarily burned in a metal container with addition of used lubricant oil. The size-segregated aerosol samples were analysed for elementar (EC) and organic (OC) carbon by a thermal-optical transmission technique. The organosoluble OC was fractionated by vacuum flash chromatography and analysed by gas chromatography-mass spectrometry (Alves *et al*., 2011).

Burning of residue C produced the highest PM emissions. OC was the dominant carbonaceous component in all aerosol samples, contributing to about 98% of total carbon (TC). The detailed chemical profiles of particulate emissions, including organic tracer compounds, have been assessed. The contribution of phenolics (0.2-39% OC, w/w) and organic acids (1.5-13% OC, w/w) to OC was always predominant over other organic compounds, whose distribution patterns were found to vary from one residue to another. The polyphenols, as the guaiacyl derivatives, were particularly abundant in PM from the residue C burning, but anthropogenic constituents completely superimposed the emission profiles after addition of used lubricant oil. Since it was shown that the relative contribution of different carbon forms and organic compounds may strongly depend on the size of the particulate matter (Fig. 1), the barely analysis of one size fraction cannot be reliable enough to assess neither global emission tendencies nor the profiles of individual chemical components in smoke.

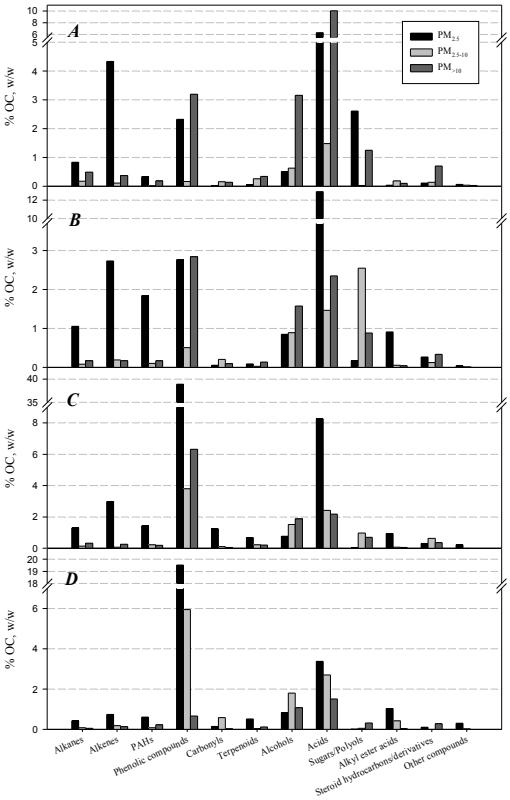

Figure 1. Contribution of chromatographically resolved organic compounds to OC in size-segregated particulate matter emissions.

This work was funded by the Portuguese Science Foundation through the PTDC/AMB/65706/2006 (BIOEMI) project. C. Gonçalves acknowledges the PhD grant SFRH/BD/36540/2007.

Alves *et al*. (2011) *Sci*. *Total Environ*., In press.
Andreae & Merlet (2001) *Global Biogeochem. Cy*., 15, 955-966.

Aerosol Characteristics over the Tropical Urban Station Pune, India

M.P.Raju, P.D.Safai, P.S.P.Rao, P.C.S.Devara and K.B.Budhavant

Indian Institute of Tropical Meteorology, Pashan, Pune - 411 008, India
Keywords: TSP, Chemical Composition, Acidity, Neutralization Potential.
Presenting author email: mpraju@tropmet.res.in

Abstract: In order to study the Physical and chemical characteristics of aerosols, samples of Total Suspended Particulates (TSP) were collected using a high volume sampler at Pune, a semi-urban location in SW India during Mar 2009 to Feb 2010. TSP samples were analyzed for water soluble components like F, Cl, NO3, SO4, NH4, Na, K, Ca and Mg and acid soluble components like Al, Zn, Fe and Cu using Ion-Chromatograph and Atomic Absorption Spectrometer. Analysis of the data revealed that the monthly mean TSP concentrations varied between 471.3 microgram per cubic meter and 30.5 microgram per cubic meter with an annual mean value of 159.8 microgram per cubic meter. TSP concentrations were found to be less during post-monsoon and winter (October through February), compared to those in summer and monsoon (March through September). Anthropogenic activities like vehicular emissions and dust particles originated from urban activities were the major sources for TSP. TSP showed good correlation with all the major ionic components, especially with SO4 (R = 0.62) and NO3 (R= 0.67) indicating the impact of anthropogenic sources over the aerosols at Pune. However, the overall aerosol nature was alkaline (Ave pH = 6.17) mainly due to the neutralizing effects of Ca and NH4. SO4 contributed more (58.8%) to the total acidity as compared to NO3 (41.1%) whereas; Ca contributed more (66.5%) to the total alkalinity than NH4 (33.5%). Seasonality of acid soluble component Al, Fe and Cu showed remarkable increase, indicating the dominance of soil source over the man-made activities. Overall study on TSP indicated that aerosols at Pune were mainly affected by the local sources.

Cluster analysis of single particle data acquired with a Light Scattering Probe AMS during the MEGAPOLI campaigns in Paris, France

F. Freutel[1], T. Klimach[1], J. Schneider[1], F. Drewnick[1], and S. Borrmann[1,2]

[1]Particle Chemistry Department, Max Planck Institute for Chemistry, Mainz, 55128, Germany
[2]Institute for Atmospheric Physics, University of Mainz, Mainz, 55128, Germany
Keywords: Aerosol mass spectrometry, Single particle analysis, Field measurements, Megacity.
Presenting author email: fr.freutel@mpic.de

Recently, the Light Scattering Probe (LSP) has been introduced as an add-on to the Aerodyne Aerosol Mass Spectrometer (AMS) (Cross *et al.*, 2007), enabling efficient single particle measurements with the AMS for particles with diameters of about 300 – 1000 nm. In contrast to typically deployed single particle instruments which use laser desorption and ionization (LDI) to analyze individual particles, here thermal desorption and electron impact ionization are used to analyze submicron particles after optical detection. These quantitative single particle data not only give further information on the ensemble data routinely measured with the AMS, but also complementary information to the data acquired with LDI instruments (e.g., non-refractory vs. refractory particles).

We deployed an LSP-AMS during two one-month campaigns at a suburban site in Paris, France: MEGAPOLI summer in July 2009, and MEGAPOLI winter in January/February 2010. Several ten thousands of spectra were acquired during these two campaigns, giving an extensive, representative dataset of typical LSP-AMS single particle spectra at a suburban measurement site. The LSP-AMS was alternated within every minute between single particle mode and ensemble mode, making comparisons between AMS ensemble and single particle data possible. Also, side by side to the LSP-AMS, an LDI single particle instrument was deployed, providing complementary information to the single particle data acquired with the LSP-AMS.

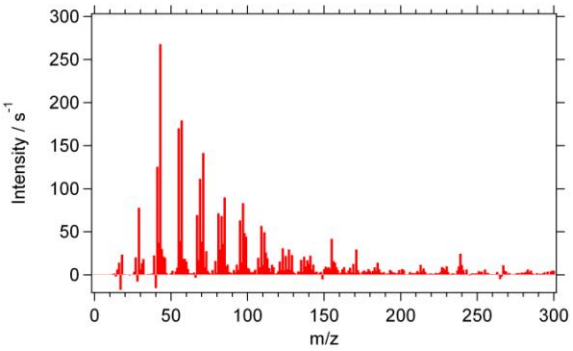

Figure 1. Single particle spectrum of a hydrocarbon-like, freshly emitted organic aerosol particle.

Here, clustering algorithms (k-means, fuzzy c-means) which are typically used to analyze LDI single particle data are applied to single particle data acquired with the LSP-AMS. Examples of typical single particle mass spectra found are shown in Figure 1 and Figure 2 (top). Figure 1 shows an exemplary mass spectrum of a so-called hydrocarbon-like organic aerosol (HOA) particle, featuring typical fragmentation patterns (e.g., m/z 57) of freshly emitted particles, possibly from traffic exhaust. In contrast, Figure 2 (top) shows the mass spectrum of an internally mixed particle containing ammonium sulfate (e.g., typical m/z's 16 for NH_4, 48 and 64 for SO_4) and aged organic material (e.g., m/z 44). The assumption that these signals at marker m/z's correspond to material in a single particle is supported by corresponding particle time-of-flight traces of the markers, shown in Figure 2 (bottom). The marker signals for ammonium, sulfate and aged organic material peak at the same time, indicating the simultaneous arrival and evaporation at the ionization region.

Here we show results of clustering the LSP-AMS single particle data, giving further insight into the mixing state of the non-refractory, submicron aerosol particle mass measured with the AMS during the MEGAPOLI field campaigns.

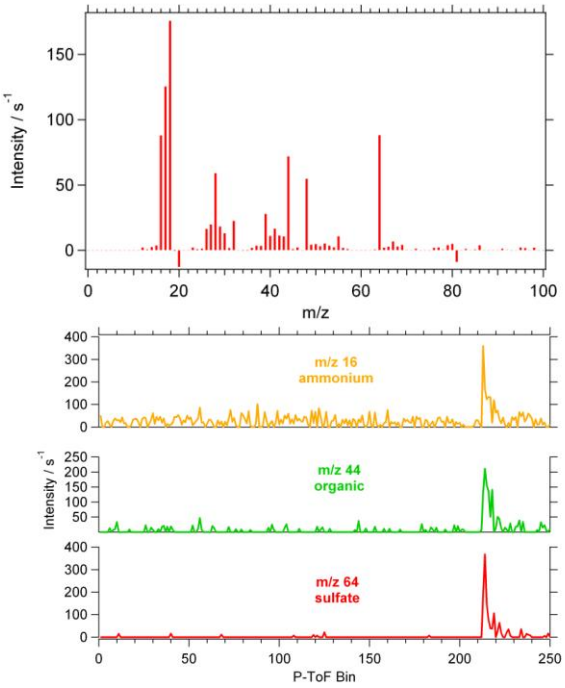

Figure 2. Top: Single particle spectrum of an internal mixture of ammonium, sulfate and aged organic material. Bottom: Time traces of the individual marker m/z's, showing strong indication for an internally mixed particle.

Cross, E.S., Slowik, J.G., Davidovits, J.G., Allan, J.D., Worsnop, D.R., Jayne, J.T., Lewis, D.K., Canagaratna, M. and Onasch, T.B. (2007) *Aerosol Sci. Techn.* **41**, 343-359.

STXM-NEXAFS Investigations of Laboratory Secondary Organic Aerosols and Amazonian Background Aerosols

C. Pöhlker[1], M. O. Andreae[1], P. Artaxo[2], M. K. Gilles[3], A. L. D. Kilcoyne[3], S. T. Martin[4], R. C. Moffet[3], U. Pöschl[1], B. Sinha[5], M. Smith[4], K. Wiedemann[4]

[1]Max Planck Institute for Chemistry, Biogeochemistry Department, Mainz 55128, Germany
[2]Institute of Physics, University of São Paulo, São Paulo 05508-900, Brazil
[3]Lawrence Berkeley National Laboratory, Berkeley, California 94720, USA
[4]Harvard University, Cambridge, Massachusetts 02138, USA
[5]Max Planck Institute for Chemistry, Particle Chemistry Department, Mainz 55128, Germany

Keywords: SOA, PBAP, X-ray spectroscopy and microscopy
Presenting author email: c.pohlker@mpic.de

We applied Scanning Transmission X-ray Microscopy - Near Edge X-ray Absorption Fine Structure (STXM-NEXAFS) analysis to investigate the morphology and chemical composition of aerosol samples from a pristine tropical environment, the Amazon Basin. The samples were collected in the Amazonian rainforest during the rainy season and can be regarded as a natural background aerosol. The samples were found to be dominated by Secondary Organic Aerosols (SOA) in the fine and Primary Biological Aerosol Particles (PBAP) in the coarse mode (Martin et al., 2010; Pöschl et al., 2010). Lab-generated SOA-samples (produced by the (photo)oxidation of isoprene, α-pinene and *β*-caryophyllene) and microtome slices of fungal spores were measured as reference samples. The aim of this study was to investigate the microphysical and chemical properties of a tropical background aerosol and its internal mixing state (Russell et al., 2002; Kilcoyne et al., 2003; Takahama et al., 2007; Tivanski et al., 2007; Moffet et al., 2010).

The STXM-NEXAFS results of the lab-generated SOA have been analyzed and compared to SOA from the Amazonian region. In the Amazon samples, SOA occurred as spherical droplet-like particles or as coatings on PBAP. In the lab samples, SOA occurred as droplets of different sizes, sometimes exhibiting internal structures (‘raisin-like’ structure). Concerning chemical composition, the NEXAFS spectra have been utilized to estimate the elemental ratios of C, N and O. Unexpectedly, all ambient SOA samples show a high content of N (around 20% or even more). Furthermore, the spectra exhibit characteristic signal patterns for different functional groups. In most cases the spectrum near the C-edge is dominated by the carboxylate signal, but prominent peaks for hydroxyl-, keton carbonyl- and alkene-peaks have also been observed. The spectral characteristics of the lab samples depend on the precursors applied for their generation.

For PBAP, the C-, N- and O-specific NEXAFS maps allow insights into the intracellular structure and chemical composition of fungal spores, which clearly dominate the coarse mode of the Amazonian samples. Furthermore, clusters of bioparticles could be identified. PBAP show a complex NEXAFS spectrum due to a wide variety of differently functionalized biomolecules, with different spectra and element abundances for individual cell components.

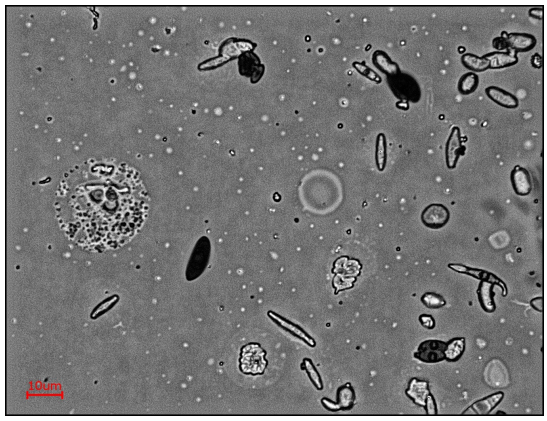

Figure 1. Light microscopy picture of PBAP and SOA particles from Amazonian rainforest.

Kilcoyne, A. L. D., Tyliszczak, T., Steele, W. F., et al. (2003) *J. Synchrot. Radiat*., **10**, 125-136.
Martin, S. T., Andreae M. O., Artaxo P., et al. (2010) *Reviews of Geophysics*, **48**, RG2002.
Moffet, R. C., Henn, T. R., Tivanski, A. V., et al. (2010) *Atmospheric Chemistry and Physics*, **10**, 961-976.
Pöschl U, Martin S. T., Sinha B., (2010) *Science*, **329**, 1513-1516.
Russell, L. M., Maria, S. F. and Myneni, S. C. B. (2002) *Geophys. Res. Lett*., **29**, 1779.
Takahama, S., Gilardoni, S., Russell, L. M. and Kilcoyne, A. L. D. (2007) *Atmospheric Environment*, **41**, 9435-9451.
Tivanski, A. V., Hopkins, R. J., Tyliszczak, T. and Gilles, M. K. (2007) *J. Phys. Chem. A*, **111**, 5448-5458.

Physico-chemical property measurements for aerosols at Manchester

A.M. Booth[1], D.O. Topping[1], G. McFiggans[1], C.J. Percival[1]

[1]School of Earth, Atmospheric and Environment Science, University of Manchester, Manchester, M13 9PL, UK
Presenting author email: alastair.booth@manchester.ac.uk

Here we present an overview of different lab measurements at Manchester designed to test various estimation methods of physical properties important for aerosol modelling: Vapour pressures, enthalpies of fusion, melting points, surface tensions, water activity, solubility and freezing point enhancement.

Vapour pressure

The direct and indirect impacts of atmospheric aerosols are one of the greatest uncertainties in our understanding of radiative forcing. Organic compounds in aerosols are ubiquitous and incredibly varied, with possibly hundreds of thousands of compounds. Gas (to particle partitioning is responsible for a considerable fraction of organic aerosols (OA), and is frequently described by an equilibrium based absorptive partitioning model. The vapour pressures of the components making up the OA are an important parameter in absorptive partitioning. Accurate vapour pressure estimation methods and experimental data to test them against are important in improving our understanding of the OA fraction in atmospheric aerosols. KEMS (Knudsen Effusion Mass Spectrometry) is a technique which allows the measurement of very low volatility compounds without the need to extrapolate from high temperatures or make any assumption with regard to activity coefficients. We have measured several sets of compounds (substituted diacids, cyclic diacids, substituted benzoic acids and nitro compounds) and have evaluated vapour pressure estimates against them. The impact of using different estimation methods has then been quantified by partitioning calculations.

Enthalpies of fusion, Melting points

The compounds measured using KEMS are solids at room temperature and pressure; however, current gas/particle partitioning models use the sub-cooled liquid reference state, as do activity models. The sub-cooled liquid is the metastable liquid which exists if solidification does not occur at temperatures below that of the triple point. By using the solid state vapour pressures measured with KEMS in combination with enthalpies of fusion and melting points measure using DSC (Differential Scanning Calourimetry) we can derive sub-cooled liquid vapour pressures for the classes of compounds we have measured (substituted diacids, cyclic diacids, substituted benzoic acids and nitro compounds).

Surface tension

An aerosol particle's equilibrium composition and the vapour pressure of each component above the particle are governed by two effects, the Raoult and Kelvin effects. These two effects are represented in the Kohler equation describing the equilibrium conditions for water over a solution droplet, an important parameter for CCN activation predictions. The Kelvin effect accounts for the enhancement of vapour pressure as a result of curvature by reference to the surface tension. We have measured surface tensions of several mixed organic and inorganic systems. We have then evaluated the accuracy of surface tension predictions and determined the impact on cloud droplet activation predictions.

Activity and solubility

The other component of the Kohler equation, the Raoult effect, considers the influence of interactions taking place in solution on the bulk equilibrium composition and equilibrium partial pressure of components above a solution. Prediction of the equilibrium composition of multicomponent particles requires calculations of component 'activity' which is a thermodynamic quantity representing an 'effective' concentration; be it of water or any solute. We have measured the water activity and solution solubility of several multi-component systems in order to provide data to help develop thermodynamic models such as AIOMFAC. We are also developing an ion attachment source to allow the KEMS system to be used in activity coefficient determination.

Booth, A.M., Markus, T., McFiggans, G., Percival, C.J., McGillen, M.R., and Topping, D.O. (2009) *Atmos. Meas. Tech.*, **2**, 355-361.

Booth, A.M., Topping, D.O., McFiggans, G. and Percival, C.J. (2009) *PCCP*, **36**, 8021-8028.

Booth, A. M., Barley, M. H., Topping, D. O., McFiggans, G., and Garforth, A. (2010) *Atmos. Chem. Phys.,* **10**, 4879-4892.

Booth, A. M., Montague, W. J., Barley, M. H., Topping, D. O., McFiggans, G., Garforth, A., and Percival, C. J.: (2011) *Atmos. Chem. Phys.,* **11**, 23017-23043.

Booth, A. M.,Bannan T., Barley, M. H., Topping, D. O., McFiggans, G., Garforth, A., and Percival, C. J.: (2011) to be submitted.

Zuend, A., Booth, A. M., Topping D. O., Marcolli, C. (2011), to be submitted.

Instrumental improvements and applications of the compact laser mass spectrometer LAMPAS 3 for on-line single particle characterization

K.-P. Hinz[1], E. Gelhausen[1], K.-C. Schäfer[1], Z. Takats[1] and B. Spengler[1]

[1]Institute of Inorganic and Analytical Chemistry, Justus Liebig University Giessen, Giessen, D-35392, Germany

Keywords: Aerosol mass spectrometry, Atmospheric aerosols, Chemical composition, Single particle analysis

Presenting author email: klaus-peter.hinz@uni-giessen.de

Mass spectrometric instrumentation is an important analytical tool for the investigation of aerosols. With such instruments a fast and detailed physical and chemical characterization of aerosol particles is possible. Aerosol particles play a central role in various areas such as indoor and outdoor environments and influence the earth climate and human health. Furthermore, on-line particle analysis with transportable mass spectrometric systems enables in-situ investigations of aerosols for real-time identification in fields such as homeland security and medicine. Applications of these devices include e.g. in situ identification of tissue types in electro-surgery or indoor and outdoor pollutants.

Currently, various transportable on-line mass spectrometers are used for single particle characterization. Size-resolved chemical analysis of particles at sites of interest is possible with high temporal resolution for investigation of particle populations under highly variable measurement conditions. Most of these particle mass spectrometers are large and bulky and therefore the measurement sites can not be reached directly with the instrument.

Miniaturization is therefore necessary to use such systems in e.g. private homes or hospitals, in airplanes or small cabins, in ships or research stations on mountains. As a consequence, the compact mobile laser mass spectrometer LAMPAS 3 (19" rack on wheels, 150 cm in height) was developed with improved instrumental parameters and options. Particles are introduced into the instrument through a differentially pumped inlet system. Inside the mass spectrometer particles are optically detected by two continuous laser beams. Particle size is determined using their size-dependent velocity. Afterwards, an actively triggered UV laser evaporates and ionizes the detected particles. The generated ions are analyzed with a bipolar time-of-flight mass spectrometer. Optionally, delayed ion extraction and ion analysis with a reflectron time-of-flight analyzer can be used for improved determination of ion masses. Using these instrumental features a significant enhancement of mass accuracy and mass resolving power is possible. An improved quality of results is also observed, using enhanced statistical classification and interpretation of data.

Several measurements were performed with particles of various origins. Spectra from a single particle are shown in Figure 1. This particle was produced during cutting porcine liver with an electro-scalpel under laboratory test conditions.

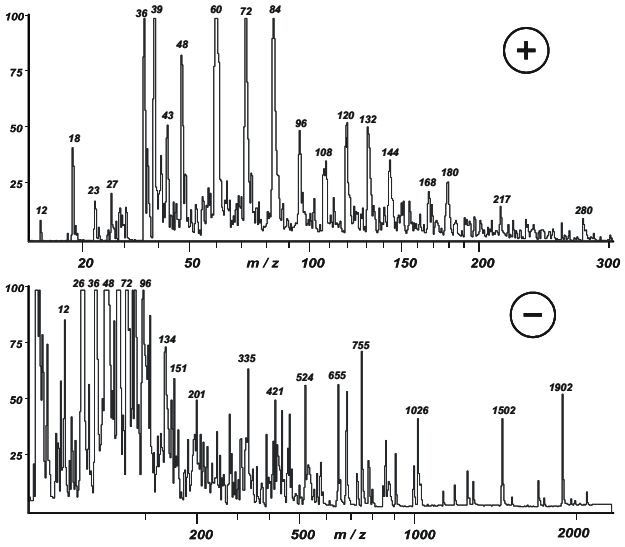

Figure 1. Positive and negative ion mass spectrum of a single particle generated with an electro-scalpel from porcine liver (aerodynamic particle 0.5 μm).

Spectra in Figure 1 show ion signals in a broad mass range with good mass resolution. Further investigations will be performed to characterize different types of tissues with the goal of in situ tissue identification in combination with simultaneous analysis of gaseous components.

Instrumental improvements of the LAMPAS 3 system and results from the analysis of various aerosols will be shown. In the future, the compact laser mass spectrometer LAMPAS 3 will offer the possibility of advanced in situ particle identification in various applicational fields.

This work was supported by the Deutsche Forschungsgemeinschaft (DFG), Germany, Grant No. HI 857/4-1, and the research program "Landes-Offensive zur Entwicklung Wissenschaftlich-oekonomischer Exzellenz - LOEWE", research focus "AmbiProbe", state of Hesse, Germany.

Chemical characterization of fine aerosols over eastern central India

D.K. Deshmukh and M.K. Deb*

School of Studies in Chemistry, Pt. Ravishankar Shukla University, Raipur, Chhattisgarh, India 492 010

Keywords: $PM_{2.5}$, Dicarboxylic acids, Ion Chromatography

Email:dhananjaychem@yahoo.in

The concentrations of low molecular weight dicarboxylic acids in fine ($PM_{2.5}$) particles collected during July 2009 to November 2009 in Raipur ($21^o14'N$ & $81^o38'E$), India were analyzed. Low molecular weight dicarboxylic acids constitute a significant fraction of water soluble organic aerosols in the atmosphere. Twenty five sets of weekly $PM_{2.5}$ samples were obtained using eight stage cascade impactor type aerosol sampler at a flow rate of 28.3 ALPM. Collected PM_1 samples were analyzed for 10 low molecular weight dicarboxylic acids using ion chromatography. The influence of meteorological factors on the concentrations of dicarboxylic acids was also studies.

Table 1
The mean mass concentration of fine particles ($PM_{2.5}$) during July 2009 to November 2009

Months	$PM_{2.5}$ mass concentration ($\mu g\ m^{-3}$)			
	Mean	SD	Min.	Max.
Jul. 2009	81.6	12.4	62.1	94.2
Aug. 2009	39.4	14.2	22.3	51.1
Sep. 2009	68.3	18.3	56.1	76.2
Oct. 2009	161.6	32.1	122.1	168.9
Nov. 2009	129.1	24.6	96.6	142.1
Fall	68.1	21.6	39.4	81.6
Winter	145.3	23.0	129.1	161.6

Table 2
Concentrations (ng/m^3)of dicarboxylic acids in $PM_{2.5}$ aerosols in Raipur, India

Species	Concentration of dicarboxylic acids (ng/m^3)			
	Mean	SD	Min.	Max.
Oxalic	731.9	181.2	534.2	1020.6
Malonic	10.2	8.0	3.4	22.3
Succinic	7.7	1.8	5.5	10.2
Glutaric	5.8	4.4	2.3	12.4
Maleic	16.4	4.8	11.1	24.0
Fumaric	11.0	2.8	8.1	14.8
Phthalic	18.9	11.9	7.0	35.4
Malic	8.7	4.6	3.2	14.7
Tartaric	14.5	4.6	10.5	21.2

The ratio of malonate to succinate was used to distinguish primary sources from secondary sources of these acids. The mean concentrations and associated standard deviation of $PM_{2.5}$ aerosols was $96.0\pm48.9\ \mu g/m^3$. Oxalic (C_2) acid was found as the most abundant species followed by phthalic and maleic acid in $PM_{2.5}$ aerosols. $PM_{2.5}$ aerosols contained, on average, 731.9 ng/m^3 oxalic acid, 18.9 ng/m^3 pthalic acid, 14.7 ng/m^3 tartaric acid, 16.4 ng/m^3 maleic acid, 11.0 ng/m^3 fumaric acid, 10.2 ng/m^3 malonic acid, 8.7 ng/m^3 malic acid, 7.7 ng/m^3 succinic acid, and 5.8 ng/m^3 glutaric acids.

Size Distribution and Source Analysis of Polycyclic Aromatic Hydrocarbons (PAHs) contained in PM_{10} in Waliguan and Xining of China

L.L Tang[1,2], S.J. Niu[1], D.T. Liu[2], X.W. Li[3], X.Z. Zhang[3], S.X. Fan[1],H. Nie[4] and H. Coe[2]

[1]Jiangsu Key Laboratory of Atmospheric Environment Monitoring and Pollution Control, Nanjing University of Information Science & Technology, Nanjing, 210044, China
[2] School of Earth, Atmospheric and Environmental Sciences, the University of Manchester, Manchester, M13 9NL, United Kingdom
[3] The Center of Jiangsu Environmental Monitoring, Nanjing, 210016, China
[4] China Global Atmospheric Watch Baseline Observatory, Xining, 810001, China
author email: lili.tang@nuist.edu.cn; lili.tang@manchester.ac.uk

Abstract:

To explore the properties and sources of polycyclic aromatic hydrocarbons (PAHs) contained in PM10 in Waliguan and Xining of Qinhai Province, China during summer, 10-group aerosol samples were installed at the Waliguan Atmospheric Background Observatory and Qinghai Station of Meteorology. Waliguan station (36° 17'N, 100° 54'E) is the highest GAW (Global Atmospheric Watch) station, and is located in a remote region on the northeastern boundary of the Qinghai-Tibetan plateau at a height of 3810 meters. Qinghai Station（36° 34'N, 101° 45'E）is located in the center of Xining city at a height of 2275 meters. Size-segregated particles were sampled using cascade impactors (Thermo) from May 24 to June 4, 2007. Size resolved chemical compositions of aerosol were investigated in order to characterize regional aerosol pollution. The meteorological conditions during the measurements maintained high temperatures and high RH. The mass concentration and size distribution of PM_{10}, and the spectral distributions of PAHs were analyzed. The daily mean concentration of PM_{10} was 24.85μg·m^{-3} and the particle size distribution exhibited three-modes in Waliguan; whereas the daily mean concentration of PM_{10} was 65.25μg·m^{-3} in Xining where the particle size distribution showed dual-modes.

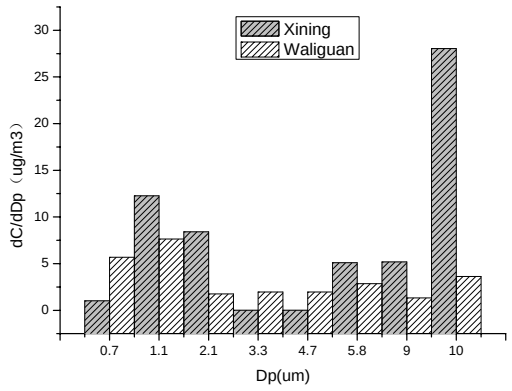

Figure 1. Mass size distribution of average PM_{10} mass concentration in sampling periods.

The percentage of accumulated particle mass in Waliguan was greater than in Xining. The concentration of PAHs in PM_{10} was 8.38ng·m-3 in Waliguan, much lower than Xining .

Due to the different photochemical pathways, the properties of PAHs and long-range transport of particles, PAHs with high molecular weight were mainly distributed in the fine particles and PAHs with lower molecular weight are relatively richer in the coarse particles at Waliguan. High molecular weight polycyclic aromatic hydrocarbons in the two sample sites were monodispersed in size. It is concluded that the PAHs pollution in Waliguan was associated with the seasonal transitions with the Asian monsoon system and transport from eastern/central China industrial emissions.

Keywords: Waliguan；Xining； Polycyclic aromatic hydrocarbons； Size distribution；PM_{10}

This work was supported by the Scientific Research Foundation of Jiangsu Environmental Monitoring (NO.1016) and the Research Foundation of Nanjing University of Information Science & Technology.

Reference

1. Wania F, Shen L, Lei Y D, *et al.* (2003) *Environ. Sci. Technol.*, 37, 1352-1359.
2. Fernandez P, Grimalt J O, Vilanova R M. (2002) *Environ. Sci. Technol.*, 36, 1162-1168.
3.Venkataraman C, Thomas S, Kulkarni P. (1999) *J. Aerosol Science*,30,759-770.
4. Bin Zhu, Hajime Akimoto, Zifa Wang, *et al.*（2004） *J.Geophysical Research Letters*, 31, 7104-7108

Modelling atmospheric OH-reactivity over boreal forest

D. Mogensen[1], S. Smolander[1], A. Nölscher[2], J. Williams[2], V. Sinha[2,3], T. Nieminen[1], M. Kulmala[1], L. Zhou[1], A. Sogachev[4], A. Guenther[5], and M. Boy[1].
[1]Department of Physics, University of Helsinki, P.O. Box 48,, FIN-00014
[2]Max Planck Institute of Chemistry, J. Becher Weg 27, 55128 Mainz, Germany
[3]Indian Institute of Science Education and Research, Chandigarh 160019, India
[4]Risø National Laboratory for Sustainable Energy, Technical University of Denmark, Box 49, DK-4000
[5]National center for Atmospheric Research, Boulder, CO 80307, USA
Keywords: boreal forest, chemistry transport model, SOA (Second. Organic Aerosols), VOC(s), OH-reactivity.
Presenting author email: ditte.mogensen@helsinki.fi

Currently, researchers believe that H_2SO_4 is taking part in both aerosol formation and growth. It is therefore highly essential to predict correct OH concentrations by models, since it is from OH-oxidation of SO_2 that H_2SO_4 eventually is produced. Wrong H_2SO_4 concentrations in models lead to wrong modelled aerosol parameters, which among other effects, increase uncertainties on climate predictions from aerosols.

We have modelled the total atmospheric OH-reactivity in a boreal forest and investigated the individual contributions from gas phase inorganic species, isoprene, monoterpenes, and methane along with other important VOCs. Daily and seasonal variation in OH-reactivity, as well as the vertical OH-reactivity profile until the boundary layer, was examined.

We present modelled and measured data from the two campaigns; HUMPPA-COPEC-10 (Hyytiälä United Measurements of Photochemistry and Particles in Air -- Comprehensive Organic Precursor Emission Concentration 2010) July-August, 2010 and BFORM (Boreal Forest OH Reactivity Measurements) August 2008. Both campaigns took place in Hyytiälä, SMEAR II station, Southern Finland. For model results we have used SOSA; a one-dimensional vertical chemistry-transport model (Boy et al. 2011) which includes detailed chemistry.

Model simulations only account for ~ 50% of the total measured OH sink, and we believe the reason for missing OH-reactivity (modelled OH-reactivity subtracted from measured OH-reactivity) is unmeasured unknown BVOCs, and limitations in our knowledge of atmospheric chemistry including uncertainties in rate constants.

The vertical OH-reactivity has been modelled and compared with directly measured vertical OH-reactivity at two different heights - one in canopy and one above canopy. In Figure 1, the modelled vertical OH-reactivity until 23 meters (above canopy) is visualized. A night time peak in the OH-reactivity corresponding to the monoterpene concentration trend is observed.

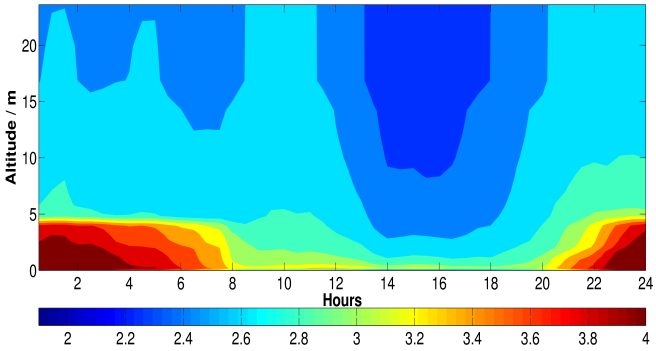

Figure 1: Daily averaged modelled OH-reactivity from the 13th to the 27th of August 2008, as a function of altitude.

During daytime the OH-reactivity decreases due to a more well mixed atmosphere. However, the accumulated OH-reactivity until the boundary layer peaks in the middle of the day, which correlates with VOC emissions. In winter time, the canopy OH-reactivity peaks during day. However, our investigations show that the main contribution to the OH-reactivity during winter is of inorganic origin.

We have also investigated correlations between aerosol condensation sink, different aerosol modes and missing OH-reactivity. A correlation between missing OH-reactivity and growth of nucleation mode particles (3-10nm) was found, suggesting that OH oxidised products condense on the smaller particles. No correlation between missing OH-reactivity and larger mode particles was found.

The financial support by the Academy of Finland Centre of Excellence program, the Danish Chemical Society, the Helsinki University Centre for Environment (HENVI), the Finnish Center of Excellence (FCoE), the European Research Council (ERC) and computational resources from CSC -- IT Center for Science Ltd are all gratefully acknowledged.

Boy, M., Sogachev, A., Lauros, J., Zhou, L., Guenther, A., and Smolander, S. (2011) Atmos. Chem. Phys. **11**, 43-51.

Characterization chemical and microbiological of atmospheric particulate matter during an intense African Dust Event on Sourth Spain

A.M. Sánchez de la Campa[1], A. Gracía[1], J.L. Ramos[1] and J. de la Rosa[2]

[1]Estación Experimental del Zaidín, CSIC, C/ Profesor Albareda 1, E18008 Granada, Spain
[2]Associate Unit CSIC-University of Huelva "Atmospheric Pollution", University of Huelva, Campus El Carmen E21071 Huelva, Spain
Keywords: chemistry, TSP, microbial transport, African Dust
Presenting author email: ana.sanchez@pi.uhu.es

A rural monitoring station situated in this region has been used in the sampling of TSP during a strong Saharan dust event (18-20 march 2010). The study area is situated in the Doñana National Park, Gulf of Cadiz (SW Spain), which is located in the south-western corner of the autonomous region of Andalusia, Spain.

This region serves as a transitional zone between the African and European continents from a climatic perspective, with very dry summers (35 mm of rainfall as a mean for the June-September period) and annual rainfall of 520 mm/yr. The predominant wind directions are SW, NWN and NE, which are heavily influenced by synoptical conditions and breeze circulation.

The Sahara desert is one of the major sources of windblown dust in the Northern Hemisphere. Duce (1995) estimated that 20% of the dust generated in the Sahara desert is suitable of long-range transport. The annual emissions from the Sahara-Sahel region to the atmosphere are approximately 1 billion tons (Moulin *et al.*, 1997).

Multidisciplinary studies of aerosol physics and chemistry have shown the impact of long-range transport pollutants in this region of the SW Iberian Peninsula (Rodríguez *et al.*, 2001; Pey *et al.*, 2008). However, the distribution of microorganisms in difference particles size has being ignored. Recently, dust events have been shown to introduce a significant pulse of microorganisms (Griffin, 2007) and other microbiological materials into the atmosphere (Jaenicke, 2005). Temporal and spatial variability of microbes within the dust clouds is important. Griffin et al. 2001 shown that around 25% are plant pathogens and 10% are opportunistic human pathogens in air samples during dust events in United States Virgin Islands.

Given the proximity to North-African continent, Andalucia region register a significant impact of APM from the Sahara and Sahel. The aim of the study was to characterization mineralogical and the airborne microorganisms of atmospheric particle obtained during the impact of one of these air masses by using a high-volume equipped with TSP inlets. The composition of the airborne microorganisms was determined by sequencing and cloning the 16S rRNA genes. Contrary to culture techniques, the rRNA sequence approach for microbial identification does not depend on viability under laboratory conditions.

Mineralogical and chemical composition of North African aerosol has been studied by numerous researchers. Calcite ($CaCO_3$), dolomite ($CaMgCO_3$), quartz (SiO_2), clay minerals (Kaolinite, illite, smectite, palygorskite, and chlorite) and feldspars (Guerzoni *et al.*, 1997; Caquineau *et al.*, 1998) are characteristic of African aerosol. Iron oxides and calcium sulphate also has been identified (Glaccumm and Prospero, 1980; Schütz and Siebert, 1987). During the episode of Saharan dust outbreak (18-20 march 2010), the atmospheric particulate material is composed essentially by quartz, feldspars, clay minerals, carbonate and radiolarites.

Duce, B. (1995) Aerosol Forcing of the Climate, Wiley and Sons, New York.

Moulin, C., Lambert, C.E., Dulac, F., Dayan, U. (1997) *Nature*, **387**, 691-694.

(Rodiguez, S., Querol, X., Alastuey, A., Kallos, G., Kakaliagou, O. (2001) *Atmos. Environ.,* **35**, 2433–2447.

Pey, J., Querol, X., de la Rosa, J., González-Castanedo, Y., Alastuey, A., Gangoiti, G., Sánchez de la Campa, Alados-Arboledas, L. Sorribas, M., Pio, C., Cachorro, V., Piñeiro, M., López-Mahia, P., García-Gacio, D. (2008) *J. Environ. Monit*., **10,** 1158–1171.

Griffin, D.W. (2007) *Clin. Microbiol. Rev.,* **20**, 459-477.

Jaenicke, R. (2005) *Science*, **308**, 73.

Griffin, D.W., Kellogg, C.A., Shinn, E.A. (2001) *Global Change & Human Health*, **2**, 20-33.

Guerzoni, S., Molinaroli, E., Chester, R. (1997) *Deep-sea research II*, **44 (3-4)**, 631-654.

Caquineau, S., Gaudichet, A., Gomes, L., Magonthier, M.C., Chatenet, B. (1998) *Geophys. Res. Lett.* **25**, 983-986.

Glaccumm, R.A., Prospero, J.M. (1980) *Mar. Geol*., **37**, 295-321.

Schütz, L., Sebert, M. (1987) *J. Aero. Sci*., **18**, 1-10.

Levels and composition of atmospheric particulate matter deposited in the Doñana Natural Park, southwest of Spain

de la Rosa, Jesús D.[1]; Sánchez de la Campa, Ana M. [2]; Fernández-Camacho, Rocío[1]; González-Castanedo, Yolanda [3,1]

[1]Associate Unit CSIC-UHU "Atmospheric Pollution," University of Huelva, 21071 Huelva, Spain
[2]Estación Experimental del Zaidín, CSIC, 18008 Granada, Spain
[3]Group of atmospheric optics, University of Valladolid, 470741, Valladolid, Spain

Keywords: Geochemistry, Sedimentable Particle, Doñana Natural Park.

In this work, we evaluate the levels and chemical composition of atmospheric particulate matter deposited around the Doñana Natural Park, SW of Spain.
Specially, we are interesting in the flux of particulate matter originated from anthropogenic activities, and as they can contribute in the change of the geochemistry of soils. Near the area of Doñana, an important Industrial State is placed, composed by a petroleum refinery, Cu-smelter and several factories of phosphorite transformation.
In this study, we have selected the monitoring station of Matalascañas, belonging to Air Quality Control Network of Andalusia. In order to compare with other urban and industrial sites, simultaneously we have sampled sedimentable particles at University Campus monitoring station (city of Huelva) and La Rábida, respectively.
Samples were collecting from June 2008 to June 2009 at a rate of 1 sample/15 days of bulk deposition. Upon sampling, pH, conductivity and alkalinity were measured in unfiltered samples. At laboratory, samples were filtered through quartz microfibre filters. The soluble fraction was extracted with MQ H_2O at 80ºC. Major ions were analyzed in filtered samples to determine the deposition of soluble material.
After gravimetric study, the filters were digested following the methodology of Querol et al (1999), which use a strong acid digestion (HF + HNO_3 + $HClO_4$) of ½ of filter.
Anions were determined by Ion Chromatography. Filter samples were analyzed by the procedure developed by Querol et al. (2001) to determine the composition of the insoluble fraction by means of an ICP-OES and ICP-MS.
Images of Secondary Electron and Back Scattered (SEI and BSEI) were studied with a Scaning Electron Microscopy (SEM-EDS) in order to recognize the size, shape and composition of single particles.
The annual levels of bulk deposition (soluble and insoluble fractions) registered in this area were up to 16 g/m^2/yr. These depositions levels were low in comparison with other sites of the industrial and urba sites of Huelva (26 and 28 g/m^2/yr in University Campus and La Rábida, respectively), and others representative monitoring stations of Spain (20 to 30 g/m^2, Castillo, 2006). Peak concentrations were obtained during June to October (Fig. 1).

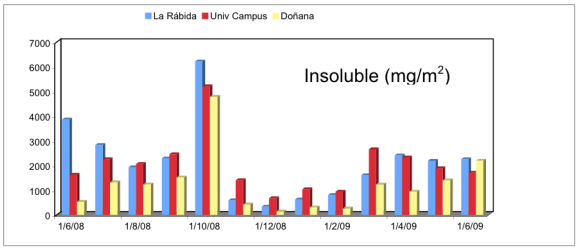

Figure 1.- Montly concentrations of deposited particles (units: g/m^2/yr).

From the soluble ions, the major contributors to the total mass were the marine aerosol (3.5 g/m^2/yr), higher than the concentrations obtained in University Campus (1.8 g/m^2/yr) and La Rábida (2.5 g/m^2/yr), Anthropogenic species concentration (SO_4^{2-}, NO_3^- and NH_4^+, 2.5 g/m^2/yr) is similar to University Campus (2.3 g/m^2/yr), and lower than La Rábida (6.8 g/m^2/yr),
Also, in the insoluble fraction, crustal species concentration (Ca^{2+}, Mg^{2+}, K^+, 0,49 g/m^2/yr) is lower than the concentrations of University Campus (0,66 g/m^2/yr) and La Rábida (0,73 g/m^2/yr)
The levels of trace elements were low also comparared with urban and industrial environments.
These results are comparable with abandoned mining areas of the Iberian Pyrite Belt.

Reference

Castillo S. (2006). Impacto de las masas de aire africano sobre los niveles y composición del material particulado atmosférico en Canarias y el NE de la península Ibérica. PhD, Universitat Politècnica de Catalunya, 382pp.

Querol, X., Alastuey, A., Puicercus, J.A., Mantilla, E., Miro, J.V., López Soler, A., Plana, F., Artiñano, B. (1999) *Atm. Env.* 32, 1963-1978.

This work was supported by Spanish Ministry of Education and Science under the project CGL2008-06270-C02-02/CLI and the Department of Innovation, Research and Enterprise of Junta de Andalucía (Project 2009-RNM 5163M).

Rainfall composition evolution in an urban industrial area: Comparison with PM_{10} wet chemistry.

M. Santacatalina[1], E. Yubero[2] and A. Carratalá[3]

[1]University of Alicante's General Foundation, 03690, Alicante, Spain
[2]Department of Physics, Miguel Hernández University, Avda. de la Universidad s/n, 03202, Elche, Spain
[3]Department of Chemical Engineering, University of Alicante, P. O. Box 99, 03080, Alicante, Spain
Keywords: PM_{10}, wet chemistry, dry/wet deposition.
Presenting author email: milagros.santacatalina@ua.es

This work presents the comparison between aerosol and rain composition in an area located in Southeast Spain in the period 1999-2008. The study area is a semi-arid region with annual precipitation less than 300 mm and important influence of urban-industrial activity (cement, ceramic and related industries). Data of PM_{10} levels, rainfall and particle water soluble compounds from both type of samples are compared. In case of rain composition, several stations (rural and urban) are also compared. Results show the evolution of NO_3^-/SO_4^{2-} ratio in rain in the study area compared with that of coastal and background nearby stations. The comparison between PM_{10} composition and rain composition series shows a good agreement. In both cases, levels of sulphate are higher in summer months due to the oxidation reactions in the atmosphere at high temperatures and the levels of nitrate are higher in winter months.

From 2004 to 2010 PM_{10} daily samples were collected with a high volume Digitel DL77 sampler. Munktell filters of micro-quartz fibre with 15 cm of diameter were used for the sampling. Rainfall was collected every 15 days at the same station from 2008 and from 1999 in Agost station (a rural station located in the same area). Zarra and Guardamar are background and coastal stations respectively, outside the area of study with rainfall chemistry available used for comparative purposes. SO_4^{2-} and NO_3^-, and main soluble ions in both PM_{10} extracts and rainfall samples, were analysed by ion chromatography (DIONEX DX-120).

Figure 1 shows the evolution of $NO_3/nssSO_4$ ratio in rain in the study area compared with that of coastal and background nearby stations. The ratios in Agost station (in the study area) and Zarra are higher than the ratio in the coastal station nearby the study area. This would be consistent with an increasing degree of nitrate oxidation with increasing distances from the coast were fresh emissions of NO_X occur. This was pointed out by Sanz et al (2002).

Figure 2 shows the comparison between ratio NO_3^-/SO_4^{2-} in aerosol and ratio NO_3^-/SO_4^{2-} in rainfall. There are not significant differences between these average ratios. Concerning seasonal variation of ratios, winter months ratios are higher than summer months. This could be related with the increase of nitrate levels, respect sulphate levels, in winter months due to traffic emissions. In contrast, in summer months levels of nitrate decrease in concordance with the decline of traffic and the ammonium nitrate decomposition. But on the other hand levels of sulphate increase due to oxidation reactions in the atmosphere at high temperatures. Then, ratios in summer months are lower than in winter ones.

Crustal related ions, very relevant in the composition of PM_{10} and rainfall in the area, are also addressed in terms of efficiency of deposition from aerosols. The deposition rates have been compared with data from a three years study conducted in the area from 1989-1991 (Carratalá and Bellot, 1997) showing a decrease in the levels of sulphates and crustal material and an increase in nitrates.

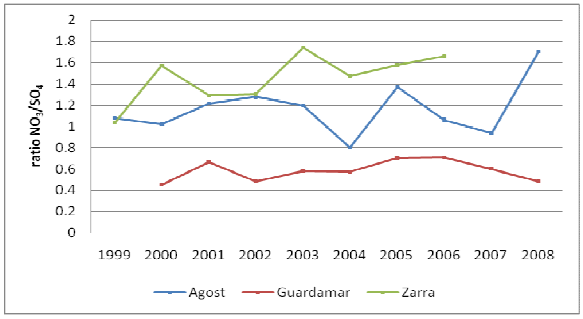

Figure 1. Evolution of annual $NO_3/nssSO_4$ ratio in rain at different stations.

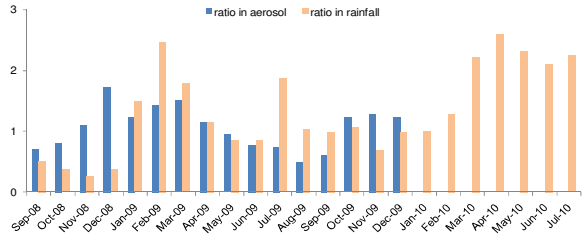

Figure 2. Comparison between ratio NO_3^-/SO_4^{2-} in aerosol and ratio NO_3^-/SO_4^{2-} in rainfall.

This work was supported by University of Alicante, the Subprograma Torres Quevedo del Ministerio de Ciencia e Innovación, cofinanciado por el Fondo Social Europeo and the project Consolider-Graccie.

Carratalá, A. & Bellot, J. (1997) Water Air Soil Pollut. 104, 237-257.
Sanz, M.J. Carratalá, A., Gimeno, C. and M. Millán. (2002) Environ. Pollut. 118, 259-272.

Thursday, September 8, 2011

Session 8P: Poster session B

Spark generators for nanoparticle generation

Scaling up the production rate of Ge nanoparticles by spark discharge

S. Kala, F.E. Kruis, M. Rouenhoff and C. Blumberg
Institute for Nanostructures and Technology, Faculty of Engineering Science and Center for Nanointegration Duisburg-Essen (CeNIDE), University of Duisburg-Essen, Duisburg, 47057, Germany
Keywords: Aerosol generation
Presenting author email: shubkala@gmail.com

Nanoparticles of pure Si and Ge are important due to the potential of obtaining visible photoluminescence, which is useful for many applications including photovoltaics, lasers and infrared dyes. In most of the cases, solution-based methods have been utilized to produce nanoparticles of Si and Ge, which causes difficulties in interpretation of properties due to presence of reaction residues and lack of monodispersity. In the present study, the suitability of spark discharge technique to prepare pure semiconductor nanoparticles has been investigated. Since Bulk Ge has smaller electron and hole effective masses and a larger dielectric constant than bulk Si (Taylor et al., 2004) the quantum effect is expected to be more pronounced in Ge than in Si, and was thus selected for this study.

Initially, a conventional spark discharge between two Ge electrodes of diameters of ~6 mm was created by means of a high-voltage supply and set of capacitors (Schwyn et al., 1988). Sintering and size-selection steps leads to production of high-quality monodisperse Ge nanoparticles. However, the resulting number concentration is found to be too low for efficient deposition.

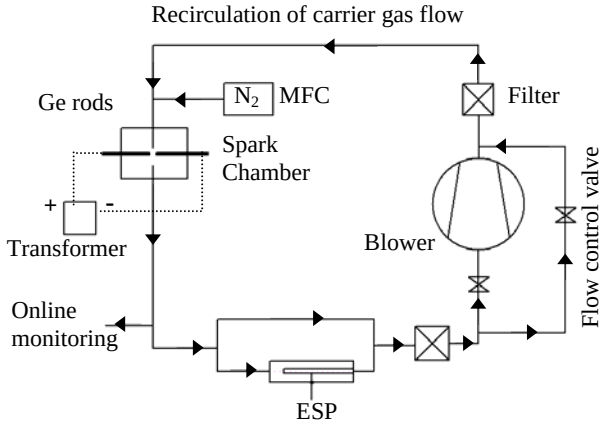

Figure 1. Schematic diagram of Ge nanoparticles synthesis setup under high-flow conditions. ESP means electrostatic precipitator, which is for the deposition of the generated Ge nanoparticles.

In order to increase the production rate of Ge nanoparticles, the high-voltage supply and set of capacitors are replaced by a low-cost transformer based on an induction coil delivering 2×7.5 kV (AC), 40 mA. The Ge electrodes are separated by distance of 0.5-2 mm and are connected to the transformer, as shown in Figure 1. In order to be able to use higher carrier gas flow rates, the facility contains a powerful blower and filters allowing to recirculate the carrier gas. A small flow ~ 1 slm (standard liter per minute) is introduced via mass flow controller (MFC) so that the outlet flow can be monitored.

On increasing the carrier gas flow rate from 5-60 slm, mobility diameter of the generated particle corresponding to maximum concentration (D_{max}) is observed to decrease from 58 to 13 nm. Particle production rate and D_{max} as a function of carrier gas flow rate are shown in Figure 2. Typically, production rate of 20-25 nm size nanoparticles is found to be ~2.6 mg/hr with a flow rate of 40 slm. A small amount of larger particles due to splashing is also observed during scanning electron microscopy investigations. As an increase in flow rate leads to reduction of the production rate, the use of several parallel reactors was found to be the best way to increase the production rate.

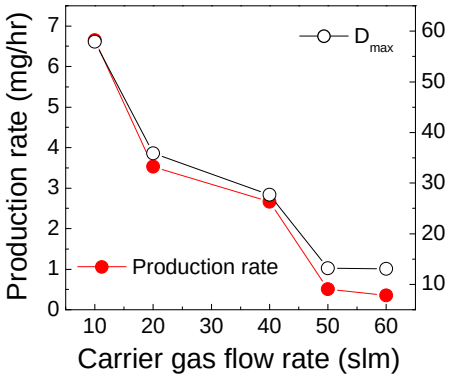

Figure 3. Variation in production rate and mobility diameter corresponding to maximum concentration (D_{max}) as a function of carrier gas flow rate.

This work is supported by Deutsche Forschungsgemineschaft in the framework of the collaborative research program “Nanoparticles from the gas phase” SFB 445.

Schwyn, S., Garwien. E. and Schmidt-Ott, A. (1988) *J. Aerosol. Sci*. **19:5** 639-642.

Taylor, B.R., and Hope-Weeks, L.J. (2004) *Dekker encyclopedia of Nanoscience and Nanotechnology* 717-723.

Thursday, September 8, 2011

Session 8P: Poster session B

Aerosol Modelling

Multi-scale modeling of aerosol formation in pipe flow

C. Winkelmann[1], A.K. Kuczaj[1], S. Stolz[1,2] and B.J. Geurts[2,3]
[1]Philip Morris International R&D, Philip Morris Products SA, 2000 Neuchâtel, Switzerland
[2]Department of Applied Mathematics, University of Twente, 7500 AE Enschede, The Netherlands
[3]Department of Applied Physics, Eindhoven University of Technology, 5300 MB Eindhoven, The Netherlands
Keywords: CFD, modelling, nucleation, growth, coagulation, numerical simulation.
Presenting author email: christoph.winkelmann@pmi.com

Many applied problems in fluid mechanics have a multi-scale character due to physical processes evolving at many different time and/or length scales. Examples range from turbulent flows with different length scales to chemically reacting and multi-phase flows with various time scales. In most applied flow problems, resolving all scales in space and time present in a flow is not computationally feasible. For the non-resolved time-scales, e.g., time scales on which nucleation of over-saturated vapors is occuring, suitable models can be developed.

In general, the nucleation time-scale can be some orders of magnitude smaller than the timestep of the fluid simulations. To demonstrate this, we focus on aerosol flows in a rather simple geometry, but with an abrupt phase change caused by an immediate cooling of hot vapors that triggers creation of the aerosol droplets. The flow cooling is introduced by a rapid change of wall temperature in the considered pipe geometry as seen in Fig. 1(a). Consequently, an aerosol is formed from the hot vapors which are initially in the gas phase (Fig. 1(b,c)).

In our model, the aerosol is simulated in an Eulerian frame exploiting the computational efficiency of such approach. The formation of aerosol droplets is described by classical nucleation theory. Models for coagulation of, condensation to and evaporation from the droplets are included. In addition to the flow equations for mass, momentum and energy conservation, equations for the aerosol mass and number load are solved. In this method of moments approach, the diameter of average mass of the evolving aerosol can be easily determined. In order to account for the omitted time scales in the nucleation process, a sub-timestep model has been developed and included in our simulation to allow for computations at reduced computational effort. The accuracy of the obtained flow solution with this coarse-graining of the aerosol creation process is one of the key objectives for investigations presented in this work.

Our aim is to provide a simple computational framework for testing and analyzing aerosol models. In the literature only a modest number of detailed numerical experiments are available for aerosol generation processes by nucleation in flows of condensable vapors. Here, we consider the generation of an aerosol by a rapid cooling of hot vapors in laminar flow (Nguyen *et al.*, 1987).

We use the setup and flow parameters described by Nguyen *et al.* (1987) and consider a pipe flow with prescribed axial wall temperature profile starting from the temperature of hot saturated vapors of dibutyl phthalate and changing rapidly to room temperature within a short downstream distance (Nguyen *et al.*, 1987; Pyykönen and Jokiniemi, 2000). The aerosol model is implemented as an extension to the open-source software OpenFOAM®, which provides sufficient flexibility for consideration of geometrically more complex flow domains.

Our focus lies on two important aspects. First, the analysis of the time resolution at which the simulations need to be performed in order to obtain accurate results at minimal computational cost. For this, a set of simulations is carried out with different time-step sizes in order to investigate the accuracy and necessity of sub-time step modeling. Second, the validation of the method with experimental data available in the literature.

The extension of this work to multi-component aerosol formation and turbulent flow is ongoing.

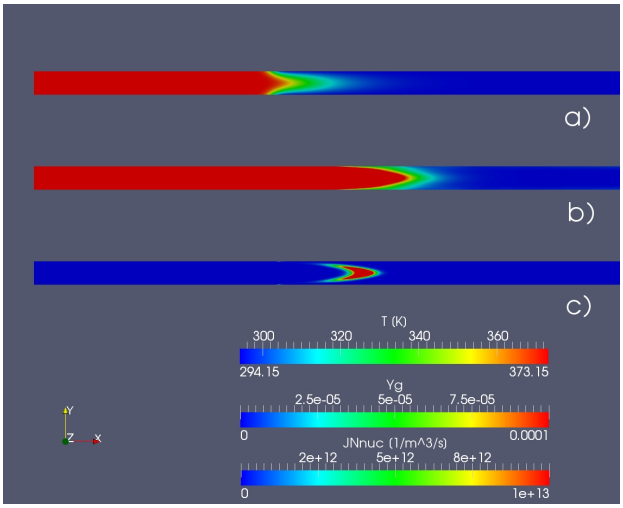

Figure 1: Snapshots from a laminar simulation of dibutyl phthalate: temperature field $T[K]$ (a), species mass concentration in the gas phase $Y_g[kg/kg]$ (b) and nucleation rate $J_N[m^{-3}s^{-1}]$ (c).

Nguyen, H.V., Okuyama, K., Mimura, T., Kousaka, Y., Flagan, R.C., and Seinfeld, J.H. (1987) J. Colloid Interf. Sci. **119**, 491-504.

Pyykönen, J. and Jokiniemi, J. (2000) J. Aerosol Sci. **31**, 531-550.

Distribution of stripped droplets by sizes at drop shattering in a uniform flow

A.G. Girin[1]

[1] Odessa National Maritime University, Odessa, 65029, Ukraine
Keywords: dispersion, droplets, size distribution, aerosol evolution.
Presenting author email: club21@ukr.net

Distribution function $f_n(r)$ of quantity of torn daughter droplets by sizes is obtained at arbitrary ratio $h = A/3H$ of rate of mass efflux $A = 0.46(1+\alpha^{\xi})^{-1}(\mu^2/\alpha)^{1/6}$ to rate H of relaxational decreasing of relative velocity of parent drop and gas flow. The result is based on investigation of local surface instability with due regard to changing of velocity profile across the boundary layers, as well as to changing of velocity and boundary layer thicknesses along drop surface (Aslanov, Girin, 1981). It revealed for weak-viscosity liquids a new type of hydrodynamic instability – "gradient instability". Mechanism of this type differs from that of Kelvine – Helmholtz type and is caused by large enough velocity gradient inside liquid boundary layer. The theory explains the "stripping" mode of breakup as quasi-continuous dispersing from unstable part $\varphi_{cr} < \varphi < \pi/2$ of drop surface (φ is polar angle of surface ground).

Approximately spherical shape of drop and speedy stream (i.e. large values of gradient instability criterion GI>>0.3) were assumed. At approximation of experimental data for drop velocity versus time in the form $W = 1-\exp(-H\tau)$, the drop mass history $M = \left(1-h+h\exp(-H\tau)\right)^3$ was obtained by integrating the differential equation of drop mass efflux (Girin, 2011). To obtain distribution function we need to integrate the differential equation for torn droplets quantity (Girin, 2011) in a strip Δr along lines $r(\varphi,\tau) = const$. It was carried out due to approximation of these lines by straights with effective slopes $a_{ef}(r,h)$, which yields:

$$\frac{\Delta n(\tilde{r})}{\Delta \tilde{r}} = f_n(\tilde{r}) = \frac{B_1^3 B_2}{(h-1)\tilde{r}^4}\frac{a_{ef}(\tilde{r})}{H^2}\sum_{i=1}^{4} A_i\left(\Phi_{i*}(\tilde{r}) - \Phi_i^*(\tilde{r})\right),$$

where $\Phi_i(\tilde{r}) = C^i(\tilde{r})\left(\sin^2\varphi(\tilde{r}) + \sin^2(\varphi(\tilde{r}) + \theta_i(\tilde{r}))\right)$ and $C(\tilde{r}) = (h-1)/\left(h - (\tilde{r}/(B_1\Psi(\varphi)))^2\right)$ must be calculated on lower $\varphi = \varphi_*$ and upper $\varphi = \varphi^*$ limits of integration; $\tilde{r} = r/R_0$, $A_i = 0.25C_4^i h^{i-1}(1-h)^{4-i}$, $\theta_i = \pi - \gamma_i$ at $h < 1$ and $\theta_i = \gamma_i$ at $h > 1$, $\gamma_i = \arcsin((iH/2a_{ef})^2 + 1)^{-0.5}$. Formula allows to calculate intermediate distribution of droplets torn to any moment before breakup terminates. Values $\varphi_*(\tilde{r})$ and $\varphi^*(\tilde{r})$ are to be found from equations of left and right boundaries of dispersion region and set of lines $\tilde{r}(\varphi,\tau) = const$. Analysis of behavior of these lines permitted to find expression for a_{ef}, which is valid in wide diapason of h. It was fitted with account for most influence of its initial values and less influence of mean values. Besides, it was necessary to set up natural demand to get in the limit $h \to 1$ the expression obtained in case $h = 1$ exactly.

The calculated distributions $\Delta n(\tilde{r})$ are shown on fig. 1. Their shapes depend on values of h, while the sizes of totality of torn droplets are defined by parameter $B_1 = 1.60\alpha^{1-2\xi}\,\mathrm{Re}_d^{-0.5}$, which plays the role of sizes scale. As well, $B_2 = 0.15\mathrm{Re}_d^{1.5}\,\alpha^{7\xi-3.5}(1+\alpha^{\xi})^{-1}$ is responsible for quantity scale (here $3\xi = \log_{\alpha}(\alpha\mu)$ is parameter of mutual viscous engagement of media in boundary layers, $\alpha = \rho_g/\rho_l$ and $\mu = \mu_g/\mu_l$ are their density and viscosity ratios, $\mathrm{Re}_d = 2R_0\rho_g V_g/\mu_g$ – Reynolds number of parent drop). At $h > 1$ function $\Delta n(\tilde{r})$ has ascending and descending branches, which make maximum at $\tilde{r}_{mod}$. As h increases, the part of fine fractions widens, and at $h \approx 2$ it becomes comparable with that of the base one. The analysis shows, that values of h slightly higher than $h = 1$ are inherent to flows behind shock and detonation waves, the values $h > 4$ correspond to ablation of liquid meteoroids and the case $h < 1$ – to incomplete shattering, inherent to viscous drops.

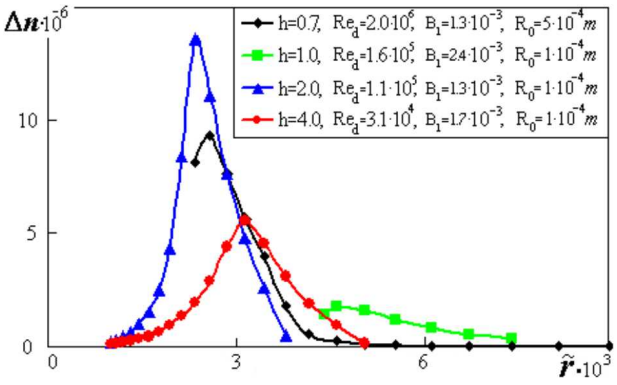

Figure 1. Distributions $\Delta n(\tilde{r})$ at various h.

Model of shattering which is based on mechanism of gradient instability provides approximate analytical relations for main regularities of the process. Obtained distribution function will be the ground for model of subsequent processes of rapid acceleration, evaporation of spray of torn droplets and formation of inflammable mixture in wake of a shattering drop.

Aslanov, S., Girin, A. (1981) *Dokl. AN Ukr. SSR.* Ser. A, No 12, 25-28.

Girin, A. (2011) *Inzhen.-fiz. zhurnal.* **84**, No 2, 248-254.

UHMAEMO – University of Helsinki Multicomponent Aerosol Module

H. Vuollekoski[1], H. Korhonen[2,3], L. Zhou[1], K. E. J. Lehtinen[2,3], V.-M. Kerminen[4], M. Boy[1] and M. Kulmala[1]

[1]Department of Physics, University of Helsinki, Helsinki, 00014, Finland
[2]Department of Physics and Mathematics, University of Eastern Finland, Kuopio, 70211, Finland
[3]Finnish Meteorological Institute, Kuopio, 70211, Finland
[4]Finnish Meteorological Institute, Helsinki, 00560, Finland
Keywords: aerosol model, aerosol dynamics, modelling (microscale), particle formation and growth.
Presenting author email: henri.vuollekoski@helsinki.fi

In their fourth assessment report, the Intergovernmental Panel for Climate Change (2007) states that the aerosols have a potentially significant cooling effect in global warming. Additionally, there is an increasing public concern e.g. about the health effects of fine particles. To investigate these and many other unknowns related to both primary and secondary particle formation and growth, aerosol dynamical models are often applied.

The original UHMA (University of Helsinki Multicomponent Aerosol) model was developed for studies of tropospheric new particle formation in clear sky conditions (Korhonen *et al*., 2004). The size-segregated, sectional box model included all basic aerosol dynamical processes: nucleation, condensation, coagulation and dry deposition, and has been used quite extensively and successfully to study new particle formation characteristics especially in the boreal forest environment of Hyytiälä, Finland.

Since the first UHMA description paper (Korhonen *et al.*, 2004), the program code has evolved due to e.g. addition of new minor processes, such as organic nucleation (Vuollekoski et al., 2010) and snow scavenging (Kyrö *et al*., 2009), which both have proven reasonable.

Science aside, the program code has gone through significant changes. For example, the coagulation coefficients are now recalculated only after significant changes in the sizes of particle bins have occurred, which typically causes a drastic reduction in computing time.

The new version is capable of directly using measurement and other input data to e.g. continuously set the vapor concentrations or initialize the particle distribution.

The condensation routine has been partially rewritten in an effort to describe the discrete general dynamic equation governing particle dynamics more accurately. As a result, all model dynamics are now described by differential equations, which makes the adaptation of differential equation solvers easier. In addition to the original Euler forward, the current version also includes the algorithms known as Euler—Cauchy and the 4th order Runge—Kutta. The improved condensation routine also includes a safety check: the time step of the model is also dynamically lowered, if too high growth rates threaten the numerical stability of the model.

The most significant difference between the original UHMA and the new version, aptly dubbed UHMAEMO, is, however, in structure: the code has been divided in more, shorter source files, and is now completely modularized. There are no global variables that would be visible outside of the scope of each function. Instead, all important variables are input and output via *ad hoc* data types. This means that UHMAEMO can be coupled with the majority of e.g. meteorological and chemical models with little effort.

Currently, UHMAEMO is being coupled with a chemistry module in an effort to create a detailed box model, as well as with chemical, emission and meteorological modules aiming for regional models.

The financial support by the Academy of Finland Centre of Excellence program (project no 1118615) is gratefully acknowledged. This work has been partially funded by European Commission 6th Framework programme project EUCAARI, contract no 036833-2 (EUCAARI).

IPCC (2007) *Fourth Assessment Report: Climate Change 2007: Working Group I Report: The Physical Science Basis*, Geneva, IPCC

Korhonen, H., Lehtinen, K. E. J. and Kulmala, M. (2004) *Atmos. Chem. Phys*., **4**, 757-771.

Kyrö, E.-M., Grönholm, T., Vuollekoski, H., Virkkula, A., Kulmala, M. and Laakso, L. (2009) *Boreal Environment Research*, **14**, 527-538.

Vuollekoski, H., Nieminen, T., Paasonen, P., Sihto, S.-L., Boy, M., Manninen, H., Lehtinen, K. E. J., Kerminen V.-M. and Kulmala, M. (2010) *Atmospheric Research*, **98**, 229-236.

The first long-term model study of particle formation and growth with detailed chemistry and aerosol dynamics in a boreal forest environment

L. Zhou[1], M. Boy[1], H. Vuollekoski[1], C. Watcharapaskorn[1], D. Mogensen[1], S. Smolander[1], A. Sogachev[2], and Markku Kulmala[1]

[1]University of Helsinki, Department of Physics, P.O. Box 48, 00014 Helsinki, Finland
[2]Wind Energy Division, Risø National Laboratory for Sustainable Energy, Technical University of Denmark Building 118,P.O. Box 49, 4000, Roskilde, Denmark
Keywords: boundary layer modelling, particle formation and growth, aerosol dynamics
Presenting author email: luxi.zhou@helsinki.fi

Natural and anthropogenic aerosols may have a great impact on climate as they can directly interact with solar radiation and indirectly affect the Earth's radiation balance and precipitation by modifying clouds. In order to quantify the direct and indirect effect, we must understand the complex processes that connect an aerosol particle to a cloud droplet. However, while modern measurement techniques are able to detect particle sizes down to nanometer all the way from ground up to the stratosphere, the data does not serve for all of our needs for understanding the processes. Hence we will demonstrate a modelling approach to investigate the complex processes of aerosols in the atmospheric boundary layer (ABL).

SOSAA (model to **S**imulate the concentration of **O**rganic vapours, **S**ulphuric **A**cid, and **A**erosol) is the first column model existing in the world with detailed chemistry and aerosol dynamics parallelized. It can be used to study aerosol processes in the ABL for long period. The model (Figure 1) includes the aerosol dynamics module UHMAEMO (Vuollekoski et al., 2010) coupled with the chemistry-transport column model SOSA (Boy et al., 2011).

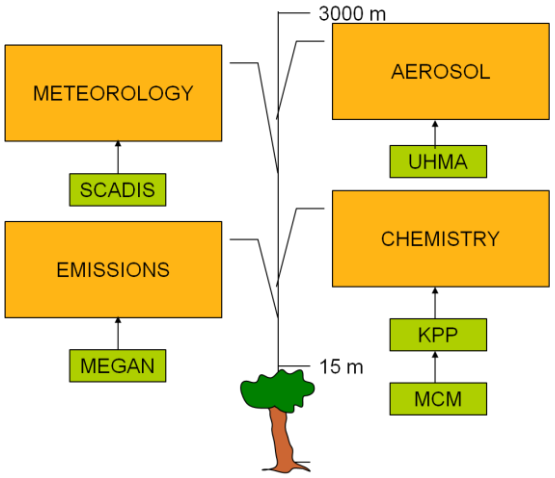

Figure1. SOSAA model structure

SOSA attempts to reconstruct the emissions, transport, and chemistry in the ABL in and above a vegetation canopy using meteorological measurements. UHMAEMO (**U**niversity of **H**elsinki **M**ulticomponent **A**erosol Module) simulates tropospheric new particle formation in clear sky conditions. It is developed from the UHMA model which includes all basic aerosol dynamical processes: nucleation, condensation, coagulation and dry deposition (Korhonen et al., 2004).

As a first application of the model, we present nucleation studies for the year 2010 with different nucleation theories including homogeneous nucleation of sulphuric acid and water, kinetic nucleation, and activation nucleation. Aerosol particle growth has also been studied with different growth rates.

Most of the input measurement data are from the SMEAR II station in Hyytiälä, Finland. Sounding data for upper boundary condition are from neighbouring meteorological stations.

The financial support by Helsinki University Centre for Environment (HENVI), the Academy of Finland Centre of Excellence program (project no. 1118615), and the European Commission 6th Framework program project EUCAARI is gratefully acknowledged.

Boy, M., Sogachev, A., Lauros, J., Zhou, L., Guenther, A. and Smolander, S. (2011) *Atmos. Chem. Phys.* **11**, 43-51.

Korhonen, H., Lehtinen, K. E. J. and Kulmala, M. (2004) *Atmos. Chem. Phys.*, **4**, 757-771.

Vuollekoski, H., Nieminen, T., Paasonen, P., Sihto, S. – L., Boy, M., Manninen, H., Lehtinen, K. E. J., Kerminen, V. – M. and Kulmala, M. (2010) *Atmospheric Research*, 98, 229 – 236.

Modelled new particle formation and growth in Southern African savannah environment

R. Gierens[1], L. Laakso[1,2,3], J. Lauros[1], R. Makkonen[1], V.Vakkari[1] , L. Zhou[1], D. Mogensen[1], H. Vuollekoski[1] and M. Boy[1]

[1]Department of Physics, Division of Atmospheric Sciences, University of Helsinki, Helsinki, 00014, Finland
[2]Finnish Meteorological Institute, Research and Development, P.O. BOX 503, FI-00101, Finland
[3]School of Physical and Chemical Sciences, North-West University, Potchefstroom, South Africa
Keywords: aerosol modelling, particle formation and growth, boundary layer, South African savannah.
Presenting author email: rosa.gierens@helsinki.fi

Africa is one of the least studied continents in respect to atmospheric aerosols (Laakso *et al.*, 2006). In this study we simulated observed new particle formation and growth in a relatively clean savannah environment in South Africa.

MALTE (Model to predict new Aerosol formation in the Lower TropospherE) is a one-dimensional model, which includes modules for boundary layer meteorology as well as aerosol dynamical and chemical processes (Boy *et al.,* 2006). The model used in this study is a further developed version, where the original turbulence scheme is replaced with that of SCADIS to get more reliable results considering vertical turbulent fluxes (Lauros *et al.*, 2010). The aerosol dynamic processes are simulated with UHMA (University of Helsinki Multicomponent Aerosol model). UHMA focuses on new particle formation and growth (Korhonen *et al.*, 2004), and thereby MALTE is well suited to study these phenomena. The emissions of monoterpenes and other organic vapours from the canopy are calculated with MEGAN (Model of Emissions of Gases and Aerosols from Nature), described by Guenther *et al.* (2006). The chemistry is calculated using the Kinetic PreProcessor (KPP) (Damian *et al.*, 2002), and chemical reaction equations are from the Master Chemical Mechanism (http://mcm.leeds.ac.uk/MCM/). Previous studies indicate, that this model is able to predict new particle formation events at the surface (Lauros *et al.*, 2010, Boy *et al.*, 2006) and in the boundary layer (Siebert *et al.*, 2007) with good agreement compared with measurements.

The measurements utilized in this study were done at a relatively clean background savannah site in central South-Africa. The location is characterized with relatively low pollutant concentrations with occasional polluted air masses from the industrial areas 100-300 km to the east. New particle formation at the site has been found to take place during most of the sunny days, 69% of the days showing clear nucleation with additional 14 % of the days with non-growing nucleation mode (Laakso *et al.*, 2008; Vakkari *et al.*, 2010). The measurements utilized in this study include meteorological variables (temperature, relative humidity, wind speed and direction, precipitation, and radiation), trace gas concentrations (SO_2, NO_x, CO, and O_3) and aerosols (number size distribution, particulate mass, and ion number size distribution) and concentration of volatile organic compounds.

The observational data was used for input and comparisons with the simulations. We selected a couple of days of continuous data and varying conditions of clean and polluted background air. The frequent new particle formation events and particle growth during this period was evaluated in detail. This work will present new model results to explain the high observed nucleation event frequency and discuss the reasons for high frequency of nucleation episodes observed.

Boy, M., Hellmuth,O., Korhonen, H., Nilsson, E. D. , ReVelle, D., Turnipseed, A., Arnold, F. , and Kulmala M. (2006) Atmos. Chem. Phys. Discuss., **6**, 3465-3512.

Damian, V., Sandu, A., Damian, M., Potra, F., and Carmichael, G. R. (2002) Comput. Chem. Eng., **26**, 1567-1579.

Guenther, A., Karl, T., Harley, P., Wiedinmyer, C., Palmer, P. I., and Geron, C. (2006) Atmos. Chem. Phys., **6**, 3181–321.

Korhonen, H., Lehtinen, K. E. J., and Kulmala, M. (2004) Atmos. Chem. Phys. , **4**, 471.

Laakso, L., Koponen, I. K., Mönkkönen, P., Kulmala, M., Kerminen, V.-M., Wehner, B., Wiedensohler, A., Wu, Z., and Hu, M. (2006) Water Air Soil Poll., **173**, 5–20.

Laakso, L.,Laakso, H., Aalto, P. P. , Keronen, P., Petäjä, T., Nieminen, T., Pohja, T., Siivola, E., Kulmala, M., Kgabi, N., Molefe, M., Mabaso, D., Phalatse, D., Pienaar, K., and Kerminen,V.-M. (2008) Atmos. Chem. Phys., **8**, 4823–4839.

Lauros, J., Sogachev, A., Smolander, S., Vuollekoski, H., Sihto, S.-L., Laakso, L., Mammarella, I., Rannik, Ü., and Boy, M. (2010) Atmos. Chem. Phys. Discuss. **10**: (8), 20005-20033.

Siebert, H., Wehner, B., Hellmuth, O., Stratmann, F., Boy, M. and Klumala, M. (2007) Geophys. Res. Lett, **34**, L16822, doi: 10.1029/2007GL029891

Vakkari, V., Laakso, H., Kulmala, M., Laaksonen, A., Mabaso, D., Molefe, M., Kgabi, N. and Laakso, L. (2010) Atmos. Chem. Phys. Discuss., **10**, 30777-30821, doi:10.5194/acpd-10-30777-2010, 2010.

Simulation of binary aerosol droplet formation

X. Z. Zhen, H.-J. Schmid

Particle Technology Group, University of Paderborn, Paderborn, 33098, Germany

Keywords: Monte Carlo simulation, binary aerosol formation, nucleation, growth, coagulation.
Presenting author email: xinze.zhen@upb.de

A theoretical analysis of binary droplet formation from a water/glycerol vapour mixture has been performed using a “1.5”-dimensional population balance model to simulate the evolution of the aerosol drop size distribution as well as the mean droplet concentration. The simulation includes the relevant mechanisms nucleation, condensation, evaporation and coagulation.

The simulation model was developed and implemented in the commercial solver PARSIVAL. The self-adaptive numerical algorithms in PARSIVAL are based on the Galerkin h-p (h-p: Variable grid - variable order) method and a temporal discretization of Roth’s type (Wulkow et al., 2001).

As expected, from these simulation results it can be seen that nucleation and condensation are strongly affected by the supersaturation. The properties of the droplets are investigated at different vapor compositions. At a higher glycerol concentration in the vapor despite higher nucleation rates larger droplet sizes evolve compared to low glycerol vapor pressure. The evolution of the mean droplets composition starts from almost pure glycerol, is then reduced quickly, passes a minimum before, finally increasing again towards equilibrium composition. Furthermore, the final mean droplet size depends on the mass of vapor at a constant vapor composition of water/glycerol.

The influence of the mechanisms in determining the droplet size is an important focus. As shown in figure 1, at the beginning of the process, aerosol nucleation is playing a dominant role, with rather small droplet growth rates. Later on, the condensation process becomes more and more important and due to the increasing number of droplets and growing particle surface the condensing mass increases rapidly and the mean droplet size significantly increases. The coagulation process is becoming significant even later than the condensation. With severe reduction of the number of droplets coagulation leads to an even faster growth of droplet sizes.

One of our main goals in this work is to study the evolution of the aerosol drop size distribution and the droplet concentration distribution from the water/glycerol vapour mixture. However traditional dynamic simulation methods are at a disadvantage when modeling more than one internal variable, whereas. Monte Carlo methods easily can be extended to a multidimensional case. Monte Carlo simulation is based on the use of a particle ensemble representative for the whole system in order to calculate the properties of the system. Here we use event-driven Monte Carlo algorithm with a stepwise constant-volume method formulated for simultaneous nucleation, condensation and coagulation (Maisels et al., 2004). By using event driven time evolution, the problem of choosing a correct time step is removed. The accuracy of the Monte Carlo solver depends on the number of simulation particles. The droplet number changes according to the chosen mechanism. At each step of the simulation a mechanism is selected with a probability that is directly calculated with the rate of the three processes. The nucleation and coagulation processes result in increases or decreases of the drop concentration, respectively. However, condensation results in surface growth but does not effect the total drop number concentration. When the droplet number in the simulation volume increases or decreases by a factor of two of its initial value, the simulation volume is halved or doubled, respectively.

A systematic validation of the Monte Carlo algorithm with respect to simulation parameters (ensemble size, integration step size etc.) will be presented. Subsequently, a comparison of droplet size distributions and droplet composition resulting from Monte-Carlo and 1.5D-population balance, respectively, will be given. Furthermore, a parameter study using the Monte Carlo technique shows impressively the advantage of this new algorithm.

In future studies the simulation results will be verified by laboratory experiments.

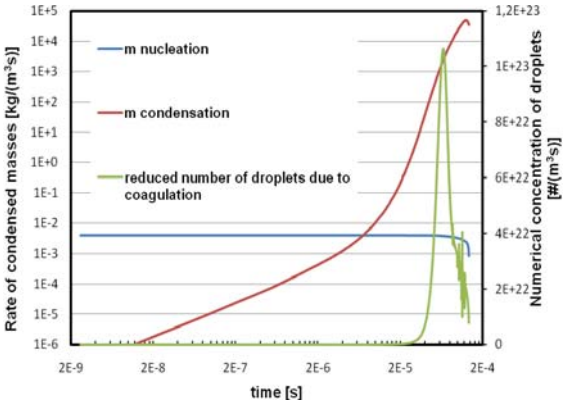

Figure 1. Rate of condensed masses by nucleation and condensation and change of the concentration of droplets due to coagulation. Initial condition: T= 293.15 K, P_{H2O}= 3/7 bar, $P_{glycerol}$= 1/7 bar, P_{N2}= 3/7 bar.

Wulkow, M., Gerstlauer, A., P. and Nieken, U. (2001) *Chem. Eng. Sci.* **56**, 2575-2588.

Maisels, A., Kruis, F.E. and Fissan, H. (2004) *Chem. Eng. Sci.* **59**, 2231-2239.

Behaviour of the aerosol charging state under asymmetric concentrations of small ions

J. Leppä[1], S. Gagné[2], L. Laakso[1, 2, 3], M. Kulmala[2] and V.-M. Kerminen[1]

[1]Finnish Meteorological Institute, Climate Change, P.O. Box 503, 00101 Helsinki, Finland
[2]Department of Physics, University of Helsinki, P.O. Box 64, 00014 Helsinki, Finland
[3]School of Physical and Chemical Sciences, North-West University, Potchefstroom, South Africa
Keywords: Atmospheric aerosols, Charged particles, Aerosol dynamics, Aerosol modelling
Presenting author email: johannes.leppa@fmi.fi

New particle formation has been observed to take place in various conditions in the atmosphere. The actual mechanisms of particle formation are still unknown, but they can be divided into two groups: electrically neutral and ion-induced mechanisms. One way of estimating the fraction of particles formed via ion-induced nucleation is to determine the fraction of charged particles at the size where particles are formed (Laakso *et al.* 2007). However, this fraction cannot usually be measured at such a small sizes due to instrumental limitations.

Kerminen *et al.* (2007) derived an equation describing the behaviour of the charging state, S, (i.e. the quotient of the charged fraction and the charged fraction in the bipolar equilibrium) as a function of diameter using several simplifying assumptions. With the use of the equation, a curve can be fitted to the measured values of S to extrapolate the value of S at the size of particle formation, which can then be used to estimate the fraction of ion-induced nucleation. Iida et al. (2007) derived a method to determine also the diameter growth rate of particles based on the behaviour of the charged fraction.

Both Kerminen *et al.* and Iida *et al.* assumed symmetric concentrations of negatively and positively charged small ions (diameter < ~2.0 nm) as well as negatively and positively charged particles. In this study we have derived an equation describing the behaviour of charging state and developed a method to determine the particle growth rate from the charged fraction in a charge asymmetric framework.

The initial charging state of freshly formed particles, whether undercharged or overcharged, evolves towards the charge equilibrium with a rate that depends on the concentrations of small ions and the growth rate of particle diameter. In the symmetric case the charged fraction evolves towards the charged fraction in bipolar equilibrium and thus the charging state evolves towards unity (Figure 1). In the asymmetric case, the charged fraction evolves towards an equilibrium, $f_{as}^{\pm}$, that can be estimated by scaling the bipolar equilibrium, $f_{eq}^{\pm}$, with the concentrations of small ions, $f_{as}^{\pm}=N^{\pm}/N^{\mp}\times f_{eq}^{\pm}$. Example behaviours of charging states as a function of diameter are shown in Figure 1.

Similarly to many other environments, the average concentrations of negatively and positively charged small ions were observed to be substantially different in urban environment in Helsinki, Finland where charging states were measured using an Ion-DMPS instrument between December 2008 and February 2010 (Gagné *et al.* 2011). The fraction of ion-induced nucleation and particle diameter growth rates were analyzed both assuming equal concentrations of small ions and without this assumption. The fractions of ion-induced nucleation did not depend much on this assumption. However, the growth rates determined from the charged fraction and particle size distribution agreed better in the charge asymmetric framework.

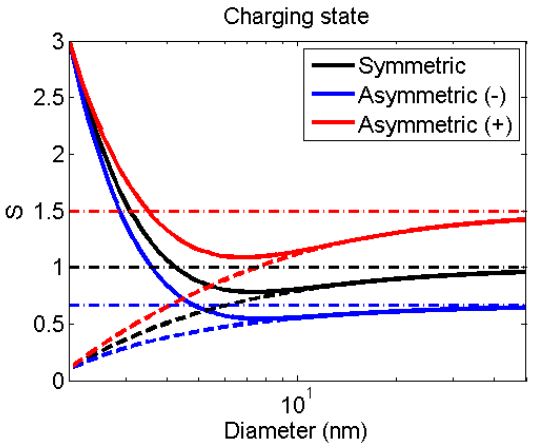

Figure 1. The charging state as a function of diameter. The particle growth rate was 6 nm h^{-1} and the initial charging state at 2 nm was 3 (solid lines) or 0.1 (dashed lines). The small ion concentrations were 500 cm^{-3} in symmetric case and 400 and 600 cm^{-3} for negative and positive ions, respectively, in the asymmetric case. The dashed-dotted lines correspond to values in equilibrium.

This work has been supported by European Commission 6th Framework program project EUCAARI, contract no. 036833-2 (EUCAARI), by Academy of Finland project ComQuaCC, project no. 135199, and the Academy of Finland Centre of Excellence program (project no. 211483, 211484 and 1118615).

Gagné, S., Leppä, J., Petäjä, T., McGrath, M. J., Vana, M., Kerminen, V.-M., Laakso, L. and Kulmala, M. (2011) Submitted to *Atmos. Chem. Phys.*

Iida, K., Stolzenburg, M. R., McMurry, P. H. and Smith, J. N. (2008) *J. Geophys. Res.*, **113**, D05207.

Kerminen, V.-M., Anttila, T., Petäjä, T., Laakso, L., Gagné, S., Lehtinen, K. E. J. and Kulmala, M. (2007) *J. Geophys. Res*., **112**, D21205.

Laakso, L., Gagné, S., Petäjä, T., Hirsikko, A., Aalto, P. P., Kulmala, M. and Kerminen, V.-M. (2007) *Atmos. Chem. Phys.* **7**, 1333-1345.

Can dimethyl sulphide cause new particle formation over the central Arctic Ocean?

M. Karl[1], A. Gross[2], C. Leck[3] and L. Pirjola[4]

[1]Department for Urban Environment and Industry, Norwegian Institute for Air Research, NILU, NO-2027 Kjeller, Norway
[2]Department of Atmospheric Environment, NERI, Aarhus University, DK-4000, Roskilde, Denmark
[3]Department of Meteorology, Stockholm University, S-10691 Stockholm, Sweden
[4]Department of Physics, University of Helsinki, FI-00014 Helsinki, Finland.
Keywords: dimethyl sulphide chemistry, aerosol model, climate effects, nucleation
mka@nilu.no

In summer, the central Arctic Ocean is an oceanic region nearly free from influences of continental or anthropogenic sources of sulphur gases. The formation of sulphate particles is known to take place in environments where the available aerosol surface area is low and the condensational loss of nucleating vapours is not favoured. Thus the Arctic environment seems to be ideal to test the climate feedback mechanism postulated by Charlson et al. (1987) (CLAW hypothesis).

According to the CLAW hypothesis, dimethyl sulphide (DMS) produced by marine phytoplankton and ventilated into the marine boundary layer (MBL) can be oxidized to sulphuric acid (H_2SO_4) which nucleates to form new particles and subsequently new cloud condensation nuclei (CCN). However, the nucleation ability of DMS-derived H_2SO_4 in the MBL is controversial and has been much discussed. Representations of DMS gas phase chemistry and of sulphuric acid nucleation are highly uncertain (Karl et al., 2007), limiting our understanding of fundamental processes in the study of the CLAW hypothesis.

A sectional aerosol dynamics model, MAFOR (Marine Aerosol FORmation), has been developed in the frame of this study to predict nucleation in the MBL and examine the CLAW hypothesis. MAFOR includes detailed gas phase and heterogeneous chemistry and aerosol dynamics with different nucleation schemes: classical binary, ternary, ion-induced and kinetic nucleation parameterizations.

MAFOR is used to model the aerosol evolution and gas phase constituents observed during the Arctic Ocean Expedition (AOE-96) to the central Arctic Ocean from beginning of July until end-August of 1996 (Leck et al., 2001). Model output was compared to results from two well-documented aerosol models: MONO32 (Pirjola and Kulmala, 2000) and AEROFOR (Pirjola, 1999).

An unexpected result was that classical homogeneous binary and ternary nucleation theories failed to predict new particle formation in the Arctic. Three nucleation mechanisms were able to predict new particle formation in the Arctic: ion-mediated, kinetic sulphuric acid and cluster activation. Interestingly, nearly linear relationships between DMS concentrations and total number concentrations of nucleated particles were found by the model when applying a combined ion-mediated/cluster activation nucleation mechanism (Figure 1).

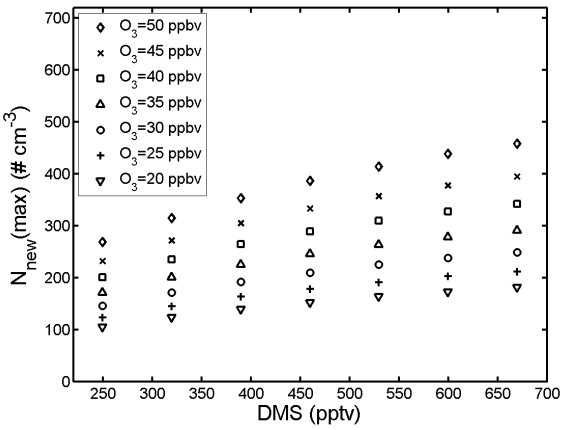

Figure 1. Modelled daily maximum number concentrations of nucleated particles using different DMS and O_3 concentrations.

Model simulations indicate that growth of nucleation mode particles (3-25 nm diameter) to CCN sizes under Arctic conditions can only occur in the presence of condensing organic vapours with sufficiently high concentrations in the gas phase (>7 pptv). Freshly nucleated stable clusters of 1-2 nm diameter sizes did not grow to detectable sizes during the simulations since the Kelvin effect prevents condensation of the organic vapour to the very small particles.

Main conclusion from the study is that to fully understand the role of DMS in the formation of new particles, uncertainties associated with several key reaction rate constants in the atmospheric oxidation chain of DMS need to be reduced.

This work was supported by the Swedish Research Council, the International Institute of Meteorology and the Knut and Alice Wallenberg Foundation.

Charlson, R. J., Lovelock, J. E., Andreae, M. O. and Warren, S. G. (1987) *Nature*, **326**, 655–661.
Karl, M., Gross, A., Leck, C. and Pirjola, L. (2007) *J. Geophys. Res.*, **112**, doi:10.1029/2006 JD007914.
Leck, C., Nilsson, E. D., Bigg, E. K. and Bäcklin, L. (2001) *J. Geophys. Res.*, **106**, 32,051–32,067.
Pirjola, L. (1999) *J. Aerosol Sci.*, **30**, 355–367.
Pirjola, L. and Kulmala, M. (2000) *Boreal Environ. Res.*, **5**, 361–374.

Adsorption in biogenic SOA formation

E. Laukkanen[1], H. Korhonen[1], L. Hao[2], J. Joutsensaari[2], J. Smith[1,2], K. Lehtinen[1,2] and H. Kokkola[1]
[1]Finnish Meteorological Institute, Kuopio Unit, Kuopio, 70211, Finland
[2]University of Eastern Finland, Kuopio, 70211, Finland
Keywords: Absorption, Adsorption, aerosol modelling
Presenting author email: emmi.laukkanen@fmi.fi

Secondary organic aerosol (SOA) particles in the atmosphere affect the Earth's energy balance directly by scattering solar radiation and indirectly by acting as cloud condensation nuclei. Majority of SOA particles formed in the atmosphere originate from volatile organic compounds (VOC) emitted the biogenic sources. (Hao *et al* 2009 and the references therein) Despite their importance for climate and abundance in the atmosphere, the factors affecting their radiative forcing such as their formation in atmosphere, are poorly known.

In a recent study biogenic SOA formation was observed in plant chamber experiments with living Scots pine seedlings (Virtanen *et al* 2010). Conclusion of those experiments was that the formed aerosol particles were in solid, most likely in amorphous state. The state of the particles is important to know because it affects the way the particles behave chemically and how they are treated in models.

So far it has been assumed in models that all formed particles are mainly in liquid phase and that the growth of the particles is dominated by absorption instead of adsorption of oxidation products of VOCs. Rounds and Pankow (1990) formulated a theory of SOA formation by adsorption. However, it has not been included in many of the aerosol models.

In this study, SOA formation in a plant chamber was modelled with a zero dimensional SALSA aerosol microphysics model (Kokkola *et al* 2008). The measurement set up presented by Hao *et al* (2010) was simulated. In the chamber the VOCs emitted by Scots pine seedlings were oxidized by ozone leading to new particle formation. The emisions included mainly α-pinene, β-pinene, Δ^3-carene, limonene, myrcene and β-phellarndrene.

The saturation vapor concentrations were determined by fitting calculated SOA yields to measurements. The saturation vapor concentrations used in the calculations were varied to represent the conditions in a case of solid and liquid particles. The solid phase particle has lower equilibrium vapor pressure than a similar sized in liquid phase. New particles formation rate was determined from the measurements.

Our simulation show that modelled particle size distribution resemble the measured one much more closely when gas-to-particle conversion is assumed to occur via adsorption. This result supports the observations by Virtanen *et al* (2010). It is very likely that under ambient conditions the gas-to-particle partitioning of SOA occurs from organic gases to solid state particles.

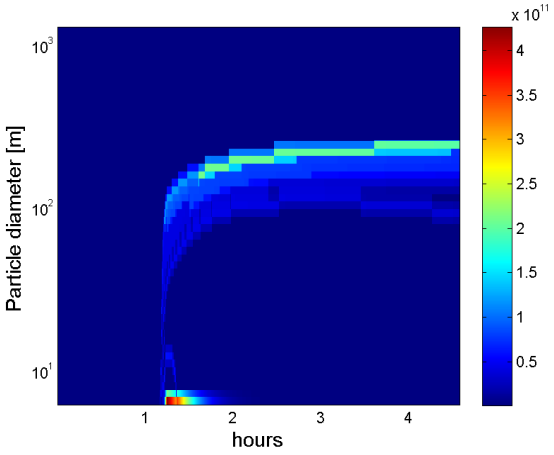

Figure 1: Particle formation event and growth through adsorption of SOA precursor gases on particles. The colorbar describes the number concentration of particle in molecules per cubic meter.

This work was supported by the Maj and Tor Nessling foundation under grant 2011185.

Hao, L., Yli-Pirilä, P., Tiitta, P., Romakkaniemi, S., Vaattovaara, P., Kajos, M., Rinne, J., Heijari, J., Kortelainen, A., Miettinen, P., Kroll, J., Holopainen, J., Smith, J., Joutsensaari, J., Kulmala, M., Worsnop, D., Laaksonen, A., (2009). Atmos. Chem. Phys. **9**, 8121-8137.

Kokkola, H., Korhonen, H., Lehtinen, K., Makkonen, R., Asmi, A., Järvenoja, S., Anttila, T., Partanen, A.-I., Kulmala, M., Järvinen, H., Laaksonen, A., Kerminen, V.-M., (2008). Atmos. Chem. Phys. **8**, 2469-2483.

Rounds, S., Pankow, J. (1990) Environ. Sci. Technol. **24**, 1378-1386.

Virtanen, A., Joutsensaari, J., Koop. T., Kannosto, J., Yli-Pirilä, P., Leskinen, J., Mäkelä, J., Holopainen, J., Pöschl, U., Kulmala, M., Worsnop, D., Laaksonen, A. (2010) Nature **467**,824- 827.

Thursday, September 8, 2011

Session 8P: Poster session B

Atmospheric aerosols - Specific Aerosol Types

Relationship between water soluble calcium and anions in a kosa (Asian dust) aerosol

I. Mori[1] and M. Nishikawa[1]

[1]National Institute for Environmental Studies, Tsukuba, Japan
Keywords: Ca, nitrate, sulfate, mineral aerosol.
Presenting author email: mori.ikuko@nies.go.jp

Water soluble calcium (Ca) is typically the main ion fraction in the aerosol collected during an Asian dust event (e.g., Shen et al., 2009). The increased concentration of soluble Ca in an aerosol registered as a spike when a kosa event was observed (Suzuki et al., 2008). Therefore, it was proposed that soluble Ca in aerosols is a good marker of a kosa event (Suzuki et al., 2008). The solubility of Ca in the Certified Reference Material (CRM) of Simulated Asian Mineral Dust (CJ-2) varied with the solvent and with the mass ratio of CRM to solvent (Mori and Nishikawa, 2009). Many groups have reported that nitrate and sulfate ions are attached to kosa aerosol particles (e.g., Suzuki et al., 2008). The solubility of Ca in a kosa aerosol can be changed by the presence of those anions. In this presentation, we demonstrate a relationship between soluble Ca and anion concentrations using data obtained during the research campaign entitled " A Study on Dust and Sand Storms" conducted by the Ministry of the Environment, Japan.

Total suspended particulates (TSP) were collected at nine locations throughout Japan using high volume samplers with quartz fibre filters, when kosa events were observed in China. The aerosol mass concentration and the concentrations of the chemical components of the aerosols were determined by procedures described by Mori et al. (2002). Four kosa events (8-9 and 18-19 April 2006, 1-2 April 2007, and 26-27 May 2007) were selected for this study. Details of the research campaign and the selected heavy dust events are described in MOE (2009).

The solubility of non sea salt Ca (nssCa) in the aerosols collected during the kosa events ranged from 50-90%, and was much higher than the solubility of Ca in Chinese loess (18.1%) (Duvall et al., 2008). The equivalent concentration of water soluble nssCa (ws-nssCa) in the aerosol collected during the kosa events increased as those of exA (excess anion: NO_3^- + $nssSO_4^{2-}$ - NH_4^+) increased (Figure 1). A 1:1 correlation was, however, not found. The equivalent concentration of ws-nssCa was lower than that of exA in most of the samples, but was higher in some samples.

When the equivalent concentration of ws-nssCa was lower than that of exA, the nssCa solubility was in the range 60-80%; much higher than that for Chinese loess (18.1%). An estimation using the data presented in Nishikawa et al, (2000) indicated that 60-75% Ca in the CRMs of Chinese loess and/or Simulated Asian Mineral Dust would be present as $CaCO_3$. The nssCa solubility data obtained from authentic kosa aerosol samples implied that CO_3-Ca in a kosa aerosol was fully dissolved when the exA concentration was higher than that of the ws-nssCa. It also implied that Ca other than CO_3-C was dissolved also.

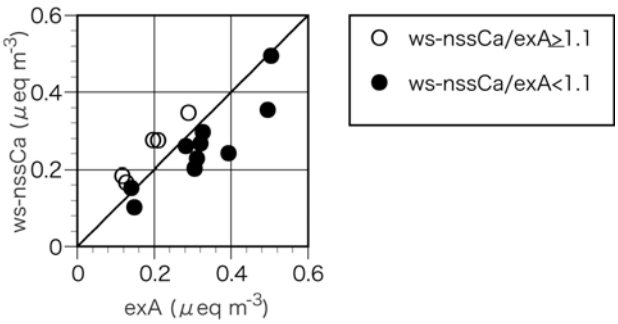

Figure 1. The relationship between ws-nssCa (water soluble - non sea salt Ca) and exA (excess anion: NO_3^- + $nssSO_4^{2-}$ - NH_4^+) for the aerosol collected during kosa (Asian dust) events in Japan. The solid line corresponds to the 1:1 correlation.

When the equivalent concentration of ws-nssCa was higher than that of exA, the nssCa solubility was 50-60%. It was higher than that for Chinese loess (18.1%), but lower than the Ca solubility (60-75%) estimated assuming that the $CaCO_3$ in kosa is fully dissolved. The ratio of the concentration of excess ws-nssCa (ws-nssCa - exA) to total nssCa was 0.1-0.2, and was comparable to the solubility of Ca in Chinese loess.

These results indicated that 10-20% Ca in a kosa aerosol was naturally dissolved, and additional CO_3-Ca dissolved according to the concentration of exA.

The authors thank the members of A Study on Dust and Sand Storms for collecting the aerosol samples and for various datasets. Part of this research was supported by the Environment Research and Technology Development Fund (B-0901) of the Ministry of the Environment, Japan.

Duvall, R. M. et al (2008) *Atmos. Environ.* **42**, 5872-5884.
MOE: Ministry of the Environment, Japan (2009) *Kosa jittai kaimei chosa hokokusyo*, pp169.
Mori, I. et al. (2002) *Atmos. Environ.* **36**, 4569-4575.
Mori and Nishikawa (2009) Kosa no hoshu to kagaku bunseki, in *Kosa*, Kokon Shoin, 76-81.
Nishikawa et al. (2000) *Glob. Environ. Res.* **4**, 103-113.
Shen, Z. et al. (2009) *Atmos. Environ.* **43**, 2911-2918.
Suzuki, I. et al. (2008) *Atmos. Environ.* **42**, 8027-8035.

Mineral dust chemistry, mineralogy, shape, mixing state, complex refractive index and microphysics determined by electron/optical microscopy and by X-ray diffraction at Praia, Cape Verde, in winter 2008

K. Kandler[1], K. Lieke[1], N. Benker[1], M. Ebert[1], L. Schütz[2], D. Scheuvens[1/2], S. Jäckel[1], A. Schladitz[3], B. Šegvić[1], and S. Weinbruch[1]

[1]Umweltmineralogie, Technische Universität Darmstadt, Darmstadt, Germany
[2]Physik der Atmosphäre, Johannes-Gutenberg-Universität Mainz, Mainz, Germany
[3]Institut für Troposphärenforschung, Leipzig, Germany
Keywords: mineral dust, complex refractive index, mineralogical composition, mixing state.
Presenting author email: kzk@gmx.de

A large field experiment of the Saharan Mineral Dust Experiment (SAMUM) was performed in Praia, Cape Verde, in January and February 2008 (Ansmann et al., 2011). This work reports on the chemical composition, shape and mixing state as well as derived refractive indices of individual particles determined by electron microscopy. In addition, aerosol mass concentrations and bulk mineralogical composition are addressed.

Three dust periods were recorded during the measurements, divided by transitional periods and embedded in maritime-influenced situations. Determined by filter gravimetry, the total suspended particle mass/PM_{10}/$PM_{2.5}$ in average was 250/180/74 µg/m³, respectively, for the first dust period (17 to 21 January) and 250/230/83 µg/m³ for the second (24 to 26 January). The third period (28 January to 2 February) was the most intensive with 410/340/130 µg/m³ (Kandler et al., 2011b).

Approximately 48,000 individual particles collected by cascade impactors were analyzed by automated scanning electron microscopy for their shape, chemical composition and mixing state (Kandler et al., 2011a). The aerosol at Praia is a superposition of mineral dust, sea-salt, sulfates, and soot aerosol. Particles smaller than 500 nm are mainly sulfates, mineral dust, mineral dust-sulfate-mixtures, and soot-sulfate-mixtures. Particles larger than 2.5 µm consist of mineral dust, sea-salt, and few mineral dust-sulfate-mixtures. A transition range exists in between.

The major internal mixtures are mineral dust-sulfate (sub- and super-micron) and soot-sulfate (sub-micron only). Mineral dust-sea-salt mixtures occur occasionally, mineral dust-soot mixtures were not observed. However, in the super-micron range by means of the dust-sulfate-sea-salt model applied in this approach, most of the particles are not internally mixed.

The shape of the particles in terms of aspect ratio was 1.3 to 1.4 for dry particles smaller than 500 nm and 1.6 to 1.7 for larger ones. A non-significant dependence of the aspect ratio on the particle composition was determined. A model calculation showed that at high relative humidities during dust conditions 13 % to 40 % of the particles are most probably spherical, while during maritime-influenced conditions this was the case for 39 % to 90 %.

The complex refractive index was derived from the measured chemical composition for each individual particle, using a mineralogy mixing model (Kandler et al., 2011a). While the real part of the refractive index showed low variation (1.55 to 1.58 at 532nm), a multi-modal imaginary part was detected as function of particle size, reflecting the complex aerosol composition. Soot mainly influences the light absorption for wavelengths longer than the hematite absorption edge (500 to 550 nm), while for shorter wavelengths the iron oxide in the mineral dust is dominating. The refractive index distribution of the aerosol is depending on the source region of the mineral dust and on the presence/absence of a marine component.

By X-ray diffraction of filter samples it was determined that the total suspended dust (bulk) consisted of kaolinite, K-feldspar, quartz, plagioclase, illite/mica, chlorite, gypsum, halite, and calcite. Kaolinite dominated the clay minerals, and K-feldspar was the most abundant feldspar component. Even during maritime periods, mineral dust contributed significantly to the aerosol mass at Cape Verde, usually dominating over the sea-salt.

By means of single particle analysis, a change in mineralogical composition with particle size was observed through chemical fingerprints. As it was to be expected, at increasing abundance of feldspars was observed with increasing particle size. However, the majority of the particles shows a chemical fingerprint which cannot be attributed to a (common) mineral phase, and in addition a high variation exists. We conclude that most of the silicate particles are aggregates of clay minerals or clay minerals covering other silicates and non-silicates.

Ansmann, A., Petzold, A., Kandler, K., Tegen, I., Wendisch, M., Müller, D., Weinzierl, B., Müller, T., Heintzenberg, J. (2011) Saharan Mineral Dust Experiments SAMUM-1 and SAMUM-2: What have we learned? *Tellus* **63B**.

Kandler, K., Lieke, K., Benker, N., Emmel, C., Küpper, M., Müller-Ebert, D., Ebert, M., Scheuvens, D., Schladitz, A., Schütz, L., Weinbruch, S. (2011a) Electron microscopy of particles collected at Praia, Cape Verde, during the Saharan Mineral dust experiment: particle chemistry, shape, mixing state and complex refractive index. *Tellus* **63B**.

Kandler, K., Schütz, L., Jäckel, S., Lieke, K., Emmel, C., Müller-Ebert, D., Ebert, M., Scheuvens, D., Schladitz, A., Wiedensohler, A., Weinbruch, S. (2011b) Ground-based off-line aerosol measurements at Praia, Cape Verde, during the Saharan Mineral Dust

Experiment: Microphysical properties and mineralogy. *Tellus* **63B**.

Investigation of potential Sahara dust transport event indicators by means of aerosol trace metal concentration ratios in the Eastern Mediterranean.

V. Vasilatou[1]., E. Diapouli[1], A.A. Karanasiou[2], M. Scoullos[3], K. Eleftheriadis[1]

[1]Institute of Nuclear Technology and Radiation Protection, Environmental Radioactivity Laboratory, National Centre of Scientific Research "Demokritos", 15310 Ag. Paraskevi, Attiki, Greece
[2] Institute of Environmental Assessment and Water Research (IDAEA-CSIC), Barcelona, Spain
[3]University of Athens, Department of Chemistry, Division III, Environmental Chemistry, Panepistimiopolis, 15701 Athens, Greece

Keywords: Sahara dust event indicators, trace metal concentration
Presented author email: vassiliki@ipta.demokritos.gr

Long-range transport of Sahara dust is often observed in the Mediterranean region. These events greatly influence the atmospheric aerosol concentrations leading to significant increase of the measured levels. Sampling of Total Suspended Particles (TSP) from a research aircraft was performed at different heights during a Sahara dust long-range transport event over central Europe, (Eleftheriadis et al., 1999). The trace elements content of TSP was examined by XRF analysis The results have shown that the concentration ratios of Ca/Fe, Ti/Fe and Mn/Fe were found to have characteristic values within the Sahara dust layers compared to those closer to the surface. The aim of the present study was to investigate the connection between Sahara dust phenomena and the atmospheric concentration of trace metals found is suspended particulate matter seasonally collected in Athens, Greece over a long-term period (approximately two decades) by utilizing the aforementioned ratios.

All samples were collected at the Demokritos GAW site (GAW-DEM, 2007) throughout the period 1980-1996 and specifically during the months January – February for the winter season and June – July for the summer one. The filters were analyzed by Electrothermal Atomic Absorption Spectroscopy (ETAAS), for the metals Pb, V, Ni, Mn, Cu, Fe, Al (graphite Furnace) and Mg, Ca and Zn (flame).

The Ca/Fe and Mn/Fe concentration ratios were calculated for each sample. The mean values of the ratios calculated by Eleftheriadis et al. (1999) for three different heights were in the range: Mn/Fe: 0.009-0.017 and Ca/Fe: 0.574-0.698. Based on the average and standard deviation of these three values, a range for each ratio was calculated (Mn/Fe:0.007-0.019, Ca/Fe: 0.490-0.755) and it was assumed that this range can be considered as a criterion for the occurrence of a Sahara dust transport event. The origin of air mass arriving at the sampling site during the sampling periods was identified by means of the HYSPLIT4 Model of ARL (Air Resources Laboratory). Back-trajectory analysis was conducted with a total transport time of 160-220h and with a start altitude of 200m AGL and 1500m AGL for two starting times 8:00a.m. and 5:00p.m. If there was an indication of long-range transport of African dust, control runs would be conducted for other times on the same day well.

In a total of 260 samples 110 displayed Ca/Fe and Mn/Fe concentrations ratios in the range of the proposed criterion. However, only for 7 samples both ratios (Mn/Fe and Ca/Fe) satisfied both criteria. HYSPLIT back-trajectory analysis revealed that 5 of these samples corresponded to Sahara dust events. Given that 5 out of 7 samples complying with both criteria corresponded to Sahara dust events, it is suggested that Mn/Fe and Ca/Fe concentration ratios may be combined and used as indicator of long range transport of African dust in this region

Reference value criterion	Number of values	Sahara dust events	Sahara dust events (%)
Mn/Fe 0.007-0.019	92	15	16.4
Ca/Fe 0.490-0.755	11	6	54.6
Both criteria satisfied	7	5	71.4
No criterion satisfied	150	10	6.7

K. Eleftheriadis, A. Karydas, S. Nyeki, E. Weingartner and U. Baltensperger, *J. Aerosol Sci.* 30, pp. S167-S168

GAW-DEM Station (2007) http://gaw.empa.ch/gawsis/reports.asp?StationID=2076202728

Small increase in dust fractional iron solubility due to physical sorting of large particles during trans-Atlantic transport

Z. Shi [1, 2], M. Woodhouse[2], K. Carslaw[2], M. Krom[1], I. Savov[3], A. Baker[4], B. Brooks[2], T. Jickells[4], L.G. Benning[1]
[1]Earth and Biosphere Institute, School of Earth and Environment, University of Leeds, Leeds, UK
[2]Institute of Climate and Atmospheric Sciences, School of Earth and Environment, University of Leeds, UK
[3]Institute of Geophysics, School of Earth and Environment, University of Leeds, Leeds, UK
[4]School of Environmental Sciences, University of East Anglia, Norwich, UK

Presenting author M Woodhouse email: m.woodhouse@see.leeds.ac.uk

Dust and its associated iron pools can regulate primary productivity and nitrogen fixation rates, resulting in altered carbon uptake and biogenic air-sea gas fluxes, which have feedback effects on climate and dust production (Jickells et al., 2005). While the importance of atmospheric dust in the iron supply to the oceans is now recognized, the actual quantification of the flux of dissolved iron from mineral dust remains one of the major uncertainties of the global iron connections in the Earth's System. The uncertainty in the flux is mainly due to large variation of the fractional iron solubility (dissolved to total Fe in %) of the dust. It is reported that this solubility ranges from ~0.1 to 80%, with higher values observed in more remote parts of the oceans where aerosol mass concentration is lowest (e.g., Hand et al., 2004; Baker and Jickells, 2006).

Several hypotheses have been proposed to explain such systematic trends in iron solubility during dust transport. One of the hypotheses is the physical processing proposed by Baker and Jickells (2006), who suggested that size sorting of dust during trans-Atlantic transport lead to the observed inverse relationship between the fractional iron solubility in dust aerosol and the atmospheric dust mass concentration. Baker and Jickells (2006) proposed that the greater solubility at lower dust concentrations was due to a larger surface area to volume ratio of the finer dust. However, it may not be possible to unambiguously confirm that particle size effects are solely responsible for the relationship based on atmospheric measurements because the aerosols collected in the field may have been subjected to other processes which alter their iron solubility (Baker and Croots, 2010).

In this study, we combined laboratory experiments with global aerosol modeling to evaluate this "physical hypothesis". We re-suspended two soil samples from known dust source regions (the Western Sahara (WS) and the Tibesti Mountains (Tibesti)) in pre-cleaned air and collected the particles using an 8-stage cascade impactor. This process does not involve any liquids. Shi et al. (2011) showed that the geochemical properties of the samples are representative of the atmospheric Saharan dust. We then measured the fractional iron solubility of each size fraction.

The results showed that iron fractional solubility ranged from ~0.1% in coarse dust particles (e.g., >1 μm) to ~0.3-0.7% (<1 μm) (Fig. 1). The measured iron solubility data were then applied to a global aerosol model, GLOMAP, to evaluate how the variations in fractional iron solubility with sizes affect the fractional solubility in total dust aerosols during trans-Atlantic transport. GLOMAP considers the gravitational settling of the dust particles and traces the evolution of dust size distribution during transport (Manktelow et al., 2010). The modeling results show a decrease in the mean size of dust during trans-Atlantic transport. However, this decrease in size only led to a small increase in dust fractional iron solubility from ~0.1% in areas close to the source region to ~0.2% in more remote part of the Atlantic Ocean. Therefore, the simulated dust fractional Fe solubility due to physical sorting is one to two orders of magnitude lower than the measured ones by Baker and Jickells (2006).

These results indicate that the physical sorting of dust particles is probably not the only process that causes the systematic increase in fractional iron solubility in the dust aerosols during transport.

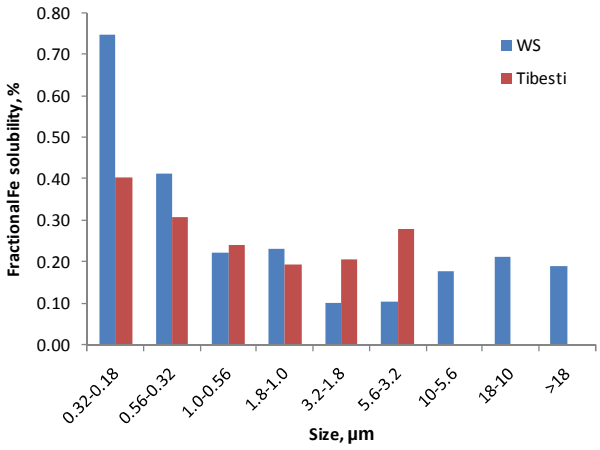

Figure 1. Size dependence of fractional dust iron solubility in the WS and Tibesti samples

This work was supported by the Natural Environment Research Council (NE/E011470/1).

References:

Baker, A. R., Jickells, T. D. (2006) *Geophys. Res. Lett.*, 33, L17608, doi:10.1029/2006GL026557.
Baker, A.R., Croot, P.L. (2010) *Mar. Chem.*, 120, 4-13.
Hand et al. (2004), *J. Geophys. Res.*, 109, D17205.
Jickells, T. D. et al. (2005), *Science*, 308, 67-71.
Manktelow, P. T. et al. (2010) *Atmos. Chem. Phys.*, 10, 365-382.
Shi, Z. et al. (2011), *Global Biogeochem Cycles*, in press.

Characterization of Severe Wind Erosion Episodes in a Western Mediterranean location

J.A.G. Orza[1], M. Cabello[1], A. Romero-Díaz[2], F. Belmonte-Serrato[2], A. Berasaluce[3], M.A. Barrero[3], L. Cantón[3]

[1]SCOLAb and Aeolian Research Group, Física Aplicada, Universidad Miguel Hernández, 03202, Elche, Spain
[2] Departamento de Geografía, Universidad de Murcia, 30001, Murcia, Spain
[3]Department of Applied Chemistry, University of the Basque Country, 20018, San Sebastián, Spain

Keywords: aerosol size distribution, PM10, chemical composition, resuspension
Presenting author email: ja.garcia@umh.es

The Nature Park of El Hondo (SE Spain, 8 km from the Mediterranean coast, 2387 ha) suffers from desiccation-flooding annual cycles with partially anthropic regulation. This area was chosen to study relationships between wind erosion and suspended particulate matter levels, as a small-scale instance of the ephemeral lake regions (like the Chotts in Tunisia and Algeria) which have been identified as intermittent dust sources.

In the frame of the EroHondo project, we have characterized several intense erosion events that led to high suspended particulate matter concentrations inside the Nature Park and at a coastal village, La Marina, 11 km downwind.

Two main measurement points were chosen inside El Hondo, 6 km apart from each other and aligned in a NW-SE direction. Prevailing winds blow either from NW or SE. Two aerosol spectrometers (Grimm 365), 2 low-volume samplers with PM10 inlet head (Derenda LVS3.1), 1 portable meteorological station (Casella Nomad) and 1 meteorological tower with anemometers at four heights were used. In addition, 2 DustTrak II with PM10 inlets were utilized as portable instruments in different locations. Saltation was registered by passive collectors in a number of points in the erosion areas.

The Nature Park became flooded after the strong rainfalls occurred beginning autumn 2009. The second campaign was conducted from August to December 2010, when the water sheet was reduced. As the soil was getting drier, the concentration of Na and Cl strongly increased in the first 1.5 cm of the soil and white saline crusts were formed over a great portion of the soil surface.

The severe erosion events were concentrated in autumn. These events were produced mostly under westerly winds associated with the passage of Atlantic frontal systems and no rainfall. Levanter, an easterly wind, was conducive to moderate particulate entrainment episodes into the atmosphere. Wind speeds larger than 9 m s^{-1} (measured at 5-min intervals at 2 m height) triggered the events.

Soil surface experienced a significant decrease in top soil rich elements: Na levels decreased 4.3 times after the episodes in the main erosion area, while its concentration was reduced 2.5 times at the SE location. The suspended particle concentration reflected this change with very high Na levels.

The horizontal flux of saltating particles, i.e. the total mass of material transported streamwise in saltation movement, was obtained from the passive sand catchers. These collectors feature omnidirectional openings at 5 heights. The vertical profile of the mass collected in the traps fits quite well to an exponential. Fluxes of 85.5 kg through 1 m of field width and 32.5 cm height have been registered in a single erosion event.

In the areas with sparse vegetation cover, sand shadows were formed to the lee of the tussocks. Their lengths and widths are proportional to the lengths and widths of the plants. While lengths are larger than the plant heights, their widths are smaller than the corresponding tussock widths.

Registered daily PM10 levels inside the Nature Park ranged from 6.7 to 342.2 μg/m^3, depending on the precise wind direction of the large plumes. The major elements in this fraction were Ca, Na and Mg. Number concentrations for each particle size larger than 1.3 μm were up to ten times higher the concentrations registered when the dust plume impacted on other areas.

Punctual measurements with the DustTrak equipments showed four times lower PM10 values at La Marina than at the SE site. In turn, levels due to local entrainment around the SE site were four times higher than the values registered at the SE site due to deflation in the main erosion area.

We gratefully acknowledge financial support from the Spanish Ministry of Science and Innovation (project EroHondo, CGL2008-05160). We thank also the staff of the Nature Park of El Hondo for their assistance whenever it was needed.

Wind Erosion and Suspended Particle Concentration in an area of Ephemeral Lakes

M. Cabello[1], J.A.G. Orza[1], A. Berasaluce[2], M.A. Barrero[2], L. Cantón[2], A. Romero-Díaz[3], F. Belmonte-Serrato[3]

[1] SCOLAb and Aeolian Research Group, Física Aplicada, Universidad Miguel Hernández, 03202, Elche, Spain
[2] Department of Applied Chemistry, University of the Basque Country, 20018, San Sebastián, Spain
[3] Departamento de Geografía, Universidad de Murcia, 30001, Murcia, Spain

Keywords: aerosol size distribution, PM10, chemical composition, resuspension
Presenting author email: mcabello@umh.es

We present results of the second year of measurements conducted at the Nature Park of El Hondo (SE Spain, 8 km from the Mediterranean coast, 2387 ha). The objective of the research, in the frame of the EroHondo project, is to better understand the relationships between wind erosion and suspended particulate matter levels. This area suffers from desiccation-flooding annual cycles with partially anthropic regulation. When the water sheet decreases, the sediments lying on the dry surface are susceptible to wind erosion. The study area is therefore an intermittent dust source.

Two main measurement points were chosen inside of El Hondo. They are 6 km apart from each other, aligned in a NW-SE direction (PON and SE sites). Prevailing winds blow either from NW or SE. Two aerosol spectrometers (Grimm 365), 2 low-volume samplers with PM10 inlet head (Derenda LVS3.1), 1 portable meteorological station (Casella Nomad) and 1 meteorological tower with anemometers at four heights were used. In addition, 2 DustTrak II with PM10 inlets were utilized as portable instruments in different locations. Saltation was registered by passive collectors in a number of points in the erosion areas.

The Nature Park became flooded after the strong rainfalls occurred beginning autumn 2009. The second campaign was conducted from August to December 2010, when the water sheet was reduced. Thanks to this reduction, severe erosion events were registered in autumn 2010. A detailed description of these events is presented in another contribution to this conference. Here the focus is on general results regarding dependences on wind speed, and on events leading to suspended particulate matter concentrations of a few $\mu g/m^3$, typical of low to moderate winds.

As found during the first year campaign, 24-h average PM10 concentrations as well as the chemical elements in that fraction, showed a decrease with increasing wind speeds, although around 9 m s^{-1} (daily means from wind speeds measured at 2 m above the ground) there is some evidence of a small increase in concentrations. Dilution would appear as the leading mechanism; however, we found that the proportion of crustal elements with respect to PM10 does show a clear increase with wind speed. This implies an enrichment of the suspended crustal fraction though concentrations are decreasing due to dilution.

Continuous (5-min) measurements of particle number concentrations in 31 size channels from 0.25 to 32 µm show (Fig. 1):

(1) A net decrease in concentration for all particulate sizes smaller than 15 µm with increasing wind speeds. The reduction is stronger for particles in the 4 – 12.5 µm range and it occurs just for winds larger than 1 m s^{-1}. This is due to the dilution of accumulated aerosols. (2) Particles larger than 15 µm show a net concentration increase with increasing winds. (3) On intense erosion events, at the largest wind speed the concentrations of particles of 0.58 µm and larger are increased. Moreover, particles of 1.3 µm and larger present concentrations ten times higher than those under light wind situations. Number concentration roses show this increase associated to the directions of the dust source areas for particles of 1.3 µm (and larger) at the SE site. At the PON location, where the dust plume is less frequently found, the association to the direction of the dust drift is only observed for particles larger than 20 µm and corresponds to local erosion.

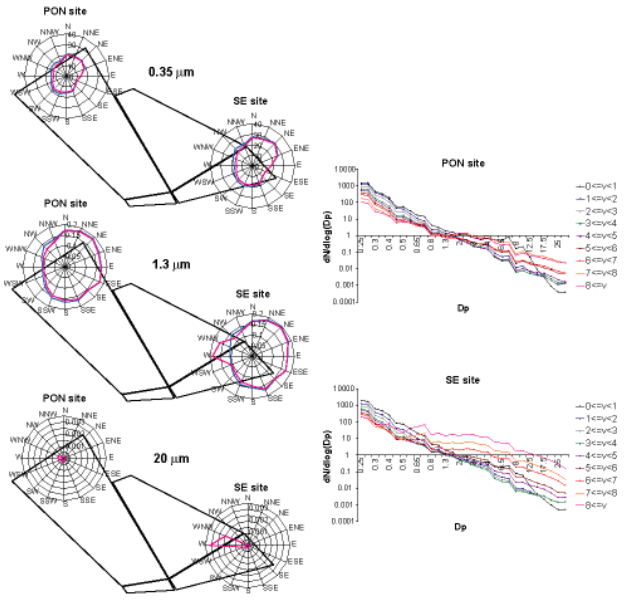

Figure 1. (Left) Concentration number roses for the two study sites; roses in red include also erosion events. (Right) Aerosol size distributions according to different wind speed intervals.

We gratefully acknowledge financial support from the Spanish Ministry of Science and Innovation (project EroHondo, CGL2008-05160). We thank also the staff of the Nature Park of El Hondo for their assistance whenever it was needed.

Thursday, September 8, 2011

Session 8P: Poster session B

Atmospheric aerosols - Aerosol Processes and Properties

Futures of atmospheric radioactive aerosol monitoring by β- and γ-radiation

V.S. Yakovleva[1], A.V. Vukolov[1], I.I. Ippolitov[2], V.D. Karataev[1], P.M. Nagorsky[2] and S.V. Smirnov[2]

[1]Department of Applied Physics, Tomsk Polytechnic University, Tomsk, 634050, Russian Federation
[2]Department of Physic of Climatic System, Institute of Monitoring of Climatic and Ecological System SB RAS, Tomsk, 634050, Russian Federation
Keywords: radioactivity, atmosphere, ionising radiation, monitoring.
Presenting author email: vsyakovleva@tpu.ru

Natural background radiation is one of the most important elements of atmosphere, and its variations are closely connected with the change of weather parameters of atmosphere, its chemical and aerosol composition. Registration and further analysis of ionizing radiation fields in the atmosphere is carried out by one radiation type – γ-radiation. Monitoring of β-radiation in the atmosphere is practically absent. β- and γ-background in the surface atmosphere is caused by one and the same sources: soil radionuclides and atmosphere decay products of radon and thoron. Taking this fact into account, one should expect similar behavior of β- и γ-radiation fields in the surface atmosphere. However, due to large differences in their penetrating power, a legal question arose: how agreed the variations of different types of natural ionizing radiation are.

Thus, the problem arose to perform the comparative evaluation of spectrum-time parameters of β- and γ-radiation fields and to examine their interactions with atmosphere-electrical values of the surface layer.

At Tomsk observatory of radioactivity and ionizing radiation (TORIR) the monitoring is performed via automated information measuring system of metheorologycal, electrical parameters of atmosphere, β- and γ-field characteristics at different height and depth. The measurements are continuous with 1 minute time step. At the height of 25 m in a standard weather booth there are two gas counters of β+γ-radiation (type STS-6), one of which is worn in aluminum casing for beta-radiation delay. Thus, one counter registers β+γ-radiation and the other one – only γ-radiation. Pure β-background is obtained by registration of a difference.

Preliminary results of monitoring data analysis allow to make a conclusion that contributions of β- and γ-radiation into the total level of background atmosphere radiation depend on different meteorological factors and one type of radiation correlates with other weakly. It could be seen in Fig. 1, 2. Data arrays (Fig.2) were infiltrated through a band filter F=(2 days)$^{-1}$ - (2 hours)$^{-1}$, red spots indicate summer, blue – winter.

It was found, however, that within some periods of the synoptic scale the correlation between β- and γ-radiations can be rather high (***d*** in Fig.1). Beta-background variations appeared to be comparatively weakly connected with variations of synoptic scale pressure and closely connected with diurnal variations of atmosphere temperature and humidity. Air pressure fall can result in suppression of this relation (***a*** in Fig.1) as well as in appearance of synchronous spikes of β- and γ-data series (***b***, ***c*** in Fig.1). γ-background variations with diurnal cycle are expressed weakly, however, there are periods when they are expressed clearly (***d*** in Fig.1).

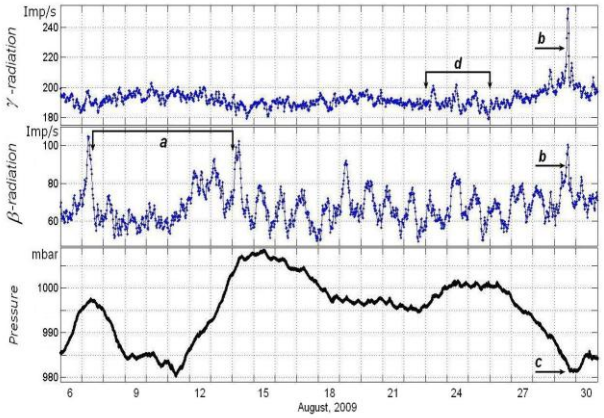

Figure 1. Variations of β-, γ-radiation components and atmosphere pressure at synoptic scale.

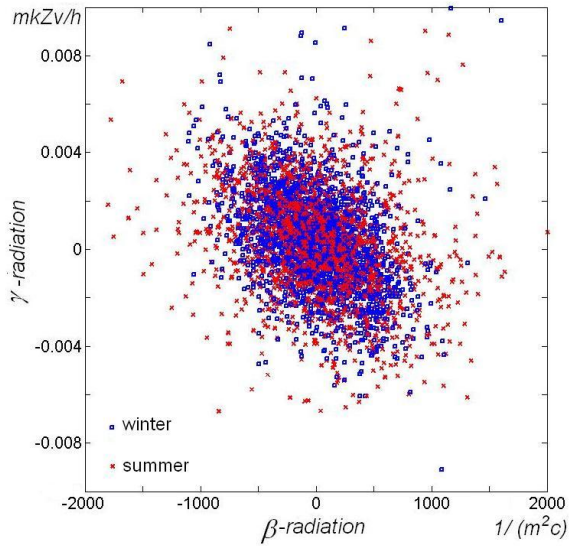

Figure 2. Correlation between variations of γ- and β-radiation fields for 2009-2010.

This work was supported by RF Analytical departmental target program “Development of higher school scientific potential” under grant № 2.1.1/13707 and by Siberian Branch RAS, program № VII.63.1.1.

Aerosol contributions to speleothem chemistry

Jonathan Dredge[1] and Ian Fairchild[1]

[1] Department of Geography, Earth and Environmental Sciences, University of Birmingham, Birmingham, West Midlands, B15 2TT, UK
Keywords: Speleothem, Cave, Forest fire, Palaeoclimate
Presenting author email: jad099@bham.ac.uk

Speleothem are cave formations formed of mineral deposits (e.g. Stalagmites). They offer a multiproxy palaeoclimate resource; many proxies have been investigated and utilised for palaeoclimatic reconstruction. Traditional investigatory geochemical studies often combine stable isotope analysis and, increasingly, trace element analysis with disequilibrium dating. The contribution of aerosols to speleothem chemistry and their applicability for reconstructions remains untested and the extent to their value as an addition to palaeoclimate sciences unknown.

Aerosols become suspended into the earth's atmosphere through a multitude of processes both natural (e.g. volcanic eruptions, wind-blown sands, forest fires) and anthropogenic (e.g. biomass burning, vehicle emissions, constructions etc). Aerosols enter the cave network as a result of cave ventilation processes and are either deposited or cycled and removed from the system. Consequently, through aerosol incorporation, speleothem have the ability to preserve a record representing a multitude of processes not yet constrained by previously investigated proxies. Aerosols used in combination with more traditional speleothem proxies will add an extra dimension to palaeoclimate reconstructions.

For speleological studies, the aerosol component of interest is that which deposits within the cave network and is available for incorporation into precipitated calcite. The deposition of aerosols is collected using surrogate surface techniques that are currently being investigated and tested through controlled experiments and active sampling. Aerosols will be detected, identified, characterised and ultimately quantified to determine their prominence in the karst system.

Aerosols will be investigated on a case study basis, searching for suitable proxies from emissions of environmentally significant processes. One key focus of the investigation it to determine the ability of speleothem to record forest fires through aerosol incorporation, Yarrangobilly caves in Australia will be used as a primary case study for this. Ultimately a record of forest fire through time will be produced. Coupling this with data obtained from more traditional climate proxies the results will significantly improve the understanding of forest fire occurrence through the region.

Monitoring will allow for the temporal and spatial determination of aerosols in the karst network. Speleothem samples will be analysed in combination with in-situ monitoring to determine incorporation factors and record preservation. By understanding how aerosols are transmitted within the cave and ultimately incorporated into speleothems, a record of aerosol event frequency, intensity and timing can be produced and directly correlated with changing palaeoclimate.

This work is supported by NERC and collaborated with the University of Melbourne as part of a joint PhD under the Universitas 21 programme.

Investigations of the vertical distribution of tropospheric aerosol layers using the data of multi-wavelength lidar sensing

S.V. Samoilova, Yu.S. Balin, G.P. Kokhanenko, and I.E. Penner

Zuev Institute of Atmospheric Optics Siberian Branch of Russian Academy of Science, 1, Academicheskii Avenue, 634055 Tomsk, Russia
Keywords: multi-wavelength Raman lidar, aerosol optical coefficients, Ångström exponent.
Presenting author email: ssv@seversk.tomsknet.ru

From March 2006 to October 2007 regular lidar observations of vertical aerosol distribution at Tomsk (56^0N, 85^0E), West Siberia, have been performed within the framework of CISLINET, the lidar network in the CIS territories (Chaikovskii *et al*, 2006). Multi-wavelength Raman lidar measurements (355/387nm and 532/607nm and 1064nm) were carried out twice a week in the daylight time (07:00 – 08:00 UTC) and once a week in the nighttime, 2-3 hours after the sunset. To reconstruct the optical coefficients, 84 realizations were selected, including 38 measurements in the nighttime.

Vertical distribution of the optical coefficients of the aerosol layers

The two-year-long observations show that the mean values of the heights of the mixing layer and PBL are 0.80 ± 0.19 and 1.22 ± 0.33 km in the cold season (from October to March) and 1.39 ± 0.39 and 2.26 ± 0.85 km in the warm season of observations, from April to September, respectively. The mean values of the optical coefficients in the boundary layer (without internal mixing layer, starting from 0.45km) and in the free troposphere (FT) are presented in Table1 for all nighttime measurements.

Table 1. Mean (STD) values of aerosol backscatter coefficient (ABC), aerosol extinction coefficient (AEC), and lidar ratio (LR)

Planetary boundary layer

Wavelength (nm)	ABC $*10^5$ ($km^{-1}sr^{-1}$)	AEC $*10^3$ (km^{-1})	LR (sr)
355	194(128)	116(61)	59(16)
532	128(102)	66(43)	51(9)
1064	56(32)	25(14)	44(16)

Free troposphere

Wavelength (nm)	ABC $*10^5$ ($km^{-1}sr^{-1}$)	AEC $*10^3$ (km^{-1})	LR (sr)
355	19(4.5)	9.5(1.9)	49(9)
532	14(3.5)	7(1.4)	48(6)
1064	6.5(1.5)	3.5(0.9)	54(10)

The mean value of the total particle optical depth calculated from AERONET data is 0.152 ± 0.04 at 500nm (Sakerin *et al*, 2008). The contribution of the free troposphere into the total aerosol optical thickness increases with decrease of the height of the boundary layer. According to our measurements, the value of this contribution is, in average, $21 \pm 11\%$ at 355 nm, $27 \pm 13\%$ at 532 nm и $34 \pm 16\%$ at 1064 nm.

Spectral behavior of optical coefficients and microphysical characteristics of aerosol particles

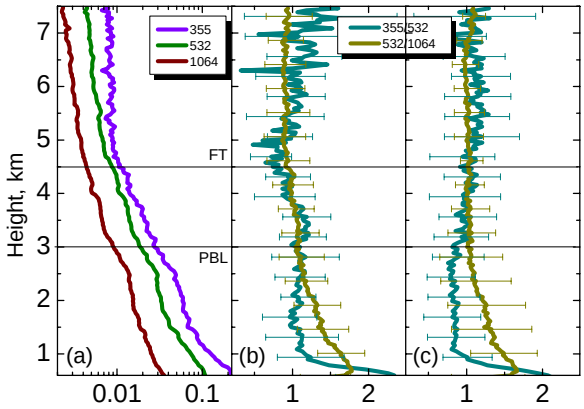

Figure 1. Mean vertical distribution of extinction (a), km^{-1}, and Ångström exponent for extinction (b) and backscatter (c) coefficients.

Ångström exponent for the extinction coefficients is sensitive to fine mode volume fraction of aerosols but not fine mode geometric radius, while Ångström exponent for the backscatter coefficients is sensitive to the fine mode radius but not the fine mode volume fraction (Samoilova, 2011). The lidar ratio and Ångström exponent for the backscatter coefficient depend strongly on the real, m_R, and imaginary, m_I, parts of the refractive index. Limited range of variation of the lidar ratio leads to the corresponding limited range of variations m_I (for fixed m_R), which is displaced toward greater values m_I with increasing m_R.

This work was supported in part by the Russian Foundation for Basic Research, grant N 10-08-0347-a.

Chaikovskii A.P., et al. (2006) *Reviewed and Revised Papers Presented at the 23d ILRC*, 671-672.

Sakerin S. M., et al. (2008) *Atmos. Oceanic Opt.* **21,** 540–545.

Samoilova S.V. (2011) *Atmos. Oceanic Opt.* **24,** 114–118.

Quantifying the concentration of volcanic ash aerosol in ground-based lidar returns

F. Marenco[1], B. Johnson[1] and R. Hogan[2]
[1]Observational Based Research, Met Office, Exeter EX1 2NF, United Kingdom
[2]Department of Meteorology, University of Reading, Reading RG6 6BB, United Kingdom
Keywords: volcanic particles, remote sensing, optical properties.
Presenting author email: franco.marenco@metoffice.gov.uk

Long-range transport of volcanic ash from Iceland to the united Kingdom occurred in April-May 2010, following the eruption of the Eyjafjallajökull (Mona *et al*, 2010; Ansmann *et al*, 2010; Flentje *et al*, 2010; Pietruczuk *et al*, 2010; Hogan *et al*, 2010).

Ground-based observations were made at Exeter, United Kingdom, on 16 and 18 April 2010 using a Leosphere ALS450 backscatter lidar featuring a depolarisation channel.

At 14:00 (UTC+1) on 16 April a strongly depolarising volcanic ash layer was observed high above the Boundary Layer (BL) aerosol, at an altitude of about 2800 m. The ash layer altitude slowly decreased, and reached 1400 m at around 20:00 (UTC+1), just above the top of the BL aerosol. The ash layer depth was estimated to vary between 100 and 400 m.

On the morning of 18 April, a depolarising double ash layer at 1000-1500 m was detected, above the top of the BL aerosol at 900 m. In the afternoon, the top of the BL aerosol increased up to 1700-1800 m; after that time, the depolarisation of the BL increased, indicating that ash and BL aerosol were both entrained in turbulent mixing.

The lidar equation has been solved using the scheme described in Marenco and Hogan (2010), which uses depolarisation to distinguish aerosol types and involves three atmospheric components rather than the two traditionally assumed in lidar retrievals. The assumed atmospheric components are: Rayleigh scattering, volcanic ash (depolarisation ratio 0.34), and BL aerosol (non-depolarising). The assumptions on depolarisation ratio were based on the analysis of the lidar signals themselves at times where the two aerosols where spatially separated. This has allowed determining the contribution of volcanic ash and BL aerosol separately, even at the times where they were mixed.

Mie scattering computations have been performed to estimate ash optical properties, based on the aerosol size distribution retrieved from an AERONET sunphotometer at the Chilbolton observatory, United Kingdom. A refractive index of $1.52 - i0.00155$ and a density of 2.3 g cm^{-3} were assumed. The computations gave a specific extinction $K_{\text{ext}} = 0.6$ m^2/g for the coarse-mode of the retrieved size distribution.

The above estimate of specific extinction has been combined with the lidar retrievals to estimate mass concentration of volcanic ash, resolved in both height and time. Peak concentrations of 1500 and 1000 μg/m^3, respectively, were observed on 16 and 18 April, and column loads were estimated to range between 0.15 and 0.45 g/m^2.

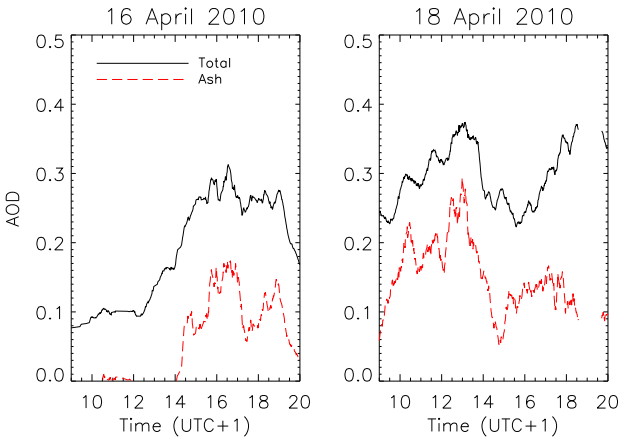

Figure 1: Total-column Aerosol Optical Depth (AOD) and ash AOD at 355 nm determined by lidar on 16 and 18 April 2010.

Ansmann, A., M. Tesche, S. Groß, V. Freudenthaler, P. Seifert, A. Hiebsch, J. Schmidt, U. Wandinger, I. Mattis, D. Müller, and M. Wiegner (2010) Geophys. Res. Lett. **L13810**, doi:10.1029/2010GL043809.

Flentje, H., H. Claude, T. Elste, S. Gilge, U. Köhler, C. Plass-Dülmer, W. Steinbrecht, W. Thomas, A. Werner, and W. Fricke (2010) Atmos. Chem. Phys. Discuss. **10**, 14947–14968.

Hogan, R.J., J.M. Haywood, C.D. Westbrook, H.F. Dacre, F. Marenco, E.J. O'Connor, C.L. Wrench, and S.E. Belcher (2011) Combined lidar and sunphotometer retrievals of ash particle size and mass concentration from the Eyjafjallajökull volcano, submitted to J. Geophys. Res.

Marenco, F. and R.J. Hogan (2010) Determining the contribution of volcanic ash and Boundary Layer aerosol in backscatter lidar returns: a three-component atmosphere approach, submitted to J. Geophys. Res.

Mona, L., A. Amodeo, A. Boselli, C. Cornacchia, G. D'Amico, A. Giunta, F. Madonna, and G. Pappalardo (2010) Geophys. Res. Abs. **12**, EGU2010-15747.

Pietruczuk, A., J. W. Krzyścin, J. Jaroslawski, J. Podgórski, P. Sobolewski, and J. Wink (2010) Int. J. Remote Sensing **31**, 3981–3986

Retrieval of aerosol radiative properties from sun-sky radiometers measurements of ESR network: comparison between the inversion codes Skyrad4.2.pack and the new Skyrad5.pack

M.Campanelli[1], V.Estelles [2], T. Smyth[3], T. Nakajima[4], M. Hashimoto[4], A.Lupi[5], C. Tomasi[5].

[1]Institute of Atmospheric Sciences and Climate, National Research Council, Rome, 00133, Italy
[2] Department de Física de la Terra i Termodinàmica, Universitat de València, Burjassot, Valencia, 46100, Spain
[3] Plymouth Marine Laboratory, Prospect Place, Plymouth, PL1 3DH, United Kingdom
4 Center for Earth Surface System Dynamics, Atmosphere and Ocean Research Institute, University of Tokyo, Kashiwa, Chiba 277-8564, Japan
[5]Institute of Atmospheric science and Climate, National Research Council, Bologna, 40129, Italy

Keywords: aerosol, sun-sky radiometers, radiation, Skyrad code .
Presenting author email: m.campanelli@isac.cnr.it

A good description of the atmospheric aerosols is needed in order to address its role in the Earth radiative balance and consequently its effect on global warming. A great deal of uncertainties on aerosol effect is due to the spatial and temporal inhomogeneities of the aerosols properties.

With the purpose of reducing these uncertainties, several network of sun-sky radiometers have been established worldwide providing a well tracked calibration procedure, good quality standards and homogeneity on the retrievals. They are AERONET: http://aeronet.gsfc.nasa.gov;PHOTONS:http://loaphotons.univ-lille1.fr/;RIMA:ww.rima.uva.es/; and SKYNET: atmos.cr.chiba-u.ac.jp/.

However intercomparison studies among products provided by different networks (Che et al., 2008, Campanelli et al., 2004, Estelles et al., 2010) showed that most of the differences are due both to calibration procedures and to the inversion schemes used for processing the sun-sky radiometers dataset.

The Skyrad code (T. Nakajima et al., 1996) is the official algorithm processing data from SKYNET network. It consists of an efficient multiple scattering radiative transfer scheme and an inversion scheme which is able to retrieve the columnar aerosol volume distribution, the extinction aerosol optical thickness at several wavelengths in the visible region, the phase function and the single scattering albedo from measurements of direct and diffuse solar irradiance.

In this work the performance of the new version of the Skyrad code (Skyrad5) will be analysed. This version improves the calculation of the single scattering albedo, often overestimating the values provided by AERONET, and the behaviour of the coarse mode of the volume size distribution.

Products will be compared with the retrievals provided by the previous version 4.2. in order to evaluate the improvements. This comparison will be performed using data from ESR (European SkyRad users' network).

ESR is a network of sun-sky radiometers not included in any federated networks. Aim of ESR is giving a standard of quality to the database and a protocol of calibration, as required by the World Meteorological Organization (WMO) guidelines. One of the objectives of ESR is pursuing the improvement of current inversion techniques and improving studies of overlapping among already existing federated network.

ESR is composed of 13 sites located in Italy, Spain, Poland and United Kingdom. The measurements performed in each site cover a wide range of aerosol types: urban (Rome, London, Barcelona, Valencia), maritime (Plymouth), rural (Bologna, Cambridge, Cardington), background (Belsk) and low mountain (Potenza) .

Some ESR site are co-located with AERONET sites, providing the possibility of performing an intercomparison with retrievals from the Dubovik code (Dubovik et al., 2000), that is the standard algorithm for processing AERONET database.

For the above reasons the ESR database resulted to be particularly suitable to perform the evaluation of the new Skyrad5.

Che, H., Shi, G., Uchiyama, A., Yamazaki, A., Chen, H., Goloub, P., and Zhang, X. (2008). *Intercomparison between aerosol optical properties by a PREDE skyradiometer and CIMEL sunphotometer over Beijing, China*, *Atmos. Chem. Phys*., 8, 3199-3214. doi:10.5194/acp-8-3199-

Campanelli , M., Gobbi , G., Tomasi , C., Nakajima, T., 2004. *Intercomparison between aerosol characteristics retrieved simultaneously with a Cimel and Prede sun-sky radiometers in Rome,Torvergata Aeronet site*. ÓPTICA PURA Y APLICADA – Vol. 37, núm. 3 - 2004- 3159

Dubovik, O., King, M. D. 2000. *A flexible inversion algorithm for retrieval of aerosol optical properties from sun and sky radiance measurements*. J G R 105, 20673-20696

Estellés, V., Campanelli, M., Smyth, T.J., Utrillas, M. P., Martínez-Lozano, J.A., 2010. *AERONET and EuroSkyrad (ESR) aerosol optical depth intercomparison on Cimel CE318 and Prede POM01 radiometers*. SPIE Remote Sensing conference 2010;

Nakajima, T., Tonna, G., Rao, R., Boi, P., Kaufman, Y., and Holben, B., 1996. *Use of sky brightness measurements from ground for remote sensing of particulate polydispersions*. Appl. Opt. 35, 2672–2686

Modelling of aerosol scattering and absorption parameters in the troposphere of West Siberia

S.A. Terpugova, M.V. Panchenko, V.V. Polkin, V.S. Kozlov

V.E. Zuev Institute of Atmospheric Optics, Tomsk, 634021, Russia
Keywords: aerosol, scattering, absorption, optical depth
Presenting author email: swet@iao.ru

Atmospheric aerosol is one of the factors driving the climatic system. Aerosol radiative and climatic effects are determined mostly by the aerosol optical depth, single scattering albedo and asymmetry parameter of the aerosol phase function.

One of the approaches to the improvement of the reliability of the aerosol models is correct setting the input parameters taking into account regional peculiarities and seasonal variability of the aerosol optical characteristics.

This paper presents the results of simulation of the climate relevant aerosol characteristics in West Siberia. Calculations are based on the empirical model of the optical characteristics of the atmosphere developed on the basis of the data of airborne sensing of the vertical profiles of the scattering coefficient and microstructure of the atmospheric aerosol (Panchenko et al, 2001). The model was supplemented by the data of airborne measurements of the vertical profiles of the BC mass concentration (Kozlov et al, 2009) that enabled us to estimate the imaginary part of the complex refractive index.

Aerosol was represented as a sum of three log-normal non-absorbing fractions with the refractive index n = 1.5, according to the empirical microstructure model (Panchenko et al, 2001). Parameters of the fractions (the median radius, variance of the radius logarithm, and the volume concentration) were chosen so that the total scattering coefficient at the wavelength of 0.51 μm calculated using the Mie theory was equal to the seasonal mean value at the corresponding height (Panchenko et al, 1996). Then soot was added to the non-absorbing aerosol in order to estimate the complex refractive index. Three hypotheses of the presence of soot in aerosol were considered.

1. Soot with the refractive index $n = 1.8–0.74i$ was added as an independent narrow fraction. The optical parameters of the mixture were determined as their sum with the weight, corresponding to the seasonal mean soot fraction.

2. It was assumed that soot is homogeneously included into aerosol particles. The optical constants of such medium were determined by the well-known mixture rule.

3. Soot also was assumed to be homogeneously included into particles, but its content depended on the aerosol particle size according to the results of Hitzenberger and Tohno (2001).

Then the values of real and imaginary part of the complex refractive index were recalculated to the real values of relative humidity using the well-known Hanel's relationships.

At the last stage, angular scattering characteristics, single scattering albedo and the aerosol optical depth were retrieved.

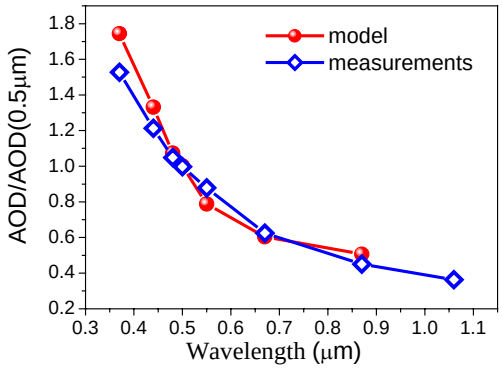

Figure 1. Comparison of measured and calculated aerosol optical depth

In the Figure 1, the normalized spectral behavior of the aerosol optical depth obtained from calculations is compared with the mean summer value obtained in 1995-2005 from measurements with CIMEL CE-318 sun-photometer. As it is seen, the results of measurements and calculations are in good agreement in the wavelength range 0.44 to 0.87 μm. some discrepancy is observed at longer wavelengths that could be explained by the errors in extrapolation of the microphysical characteristics to the range of largest and smallest particles.

The work was supported in part by Program of Department of Earth Sciences of Russian Academy of Sciences (contracts No 14.740.11.0204 and 02.740.11.0674), and Russian Foundation for Basic Research (grant No. 10-05-00162).

Hitzenberger, R., and Tohno, S. (2001) *Atmospheric Environment*. **35**, 2153-2167.

Kozlov, V.S., Shmargunov, V.P., and Panchenko, M.V., (2009) *Atmos. Ocean Opt.* **22**, 635-642.

Panchenko, M.V., Terpugova, S.A., and Tumakov, A.G. (1996) Atmospheric Research, *41*, 203-215.

Panchenko, M.V., Pol'kin, V.V., and Terpugova, S.A. (2001) *J. Aerosol Science, vol. 32, Suppl.1, Abstracts of the European aerosol conference (EAC 2001)*, Leipzig.

Influence of wind field patterns on aerosol optical depth over Athens and the Aegean sea

V. Kotroni[1], S. Kazadzis[1], K. Lagouvardos[1], V. Amiridis[2], E. Gerasopoulos[1]
[1]IERSD, National Observatory of Athens, GR-15236, Athens, Greece
[2]ISARS, National Observatory of Athens, GR-15236, Athens, Greece
Presenting author email: kazadzis@meteo.noa.gr

One of the most important meteorological events occurring over the Aegean Sea during summer is the Etesian winds. The Etesians result from a combination of the monsoon effect that leads to the formation of a thermal low pressure trough over Turkey, with higher pressures over Southern Balkans (Weather in the Mediterranean, 1962; Prezerakos, 1984).They are northern sector winds blowing over the Aegean Sea during summer and early fall. More precisely, the etesians are mainly north-easterly in the northern Aegean, northerly in the central and southern Aegean and tend to become north-westerly near the southwestern Turkish coasts. The air masses regularly originate from the region of southern Russia and the Caspian Sea and they are dry and relatively cool, contributing to the decrease of surface temperature and the moderation of summer heat and discomfort (Weather in the Mediterranean, 1962; Kotroni et al. 2001). The sustained wind speed associated with the Etesians often attains surface values exceeding 15 ms^{-1}, (with gusts over 20-25 ms^{-1}). The etesians are also affecting the Athens greater area during summer and when they prevail they contribute to the ventilation of the city, decreasing thus the pollution levels and the aerosol load over the area.

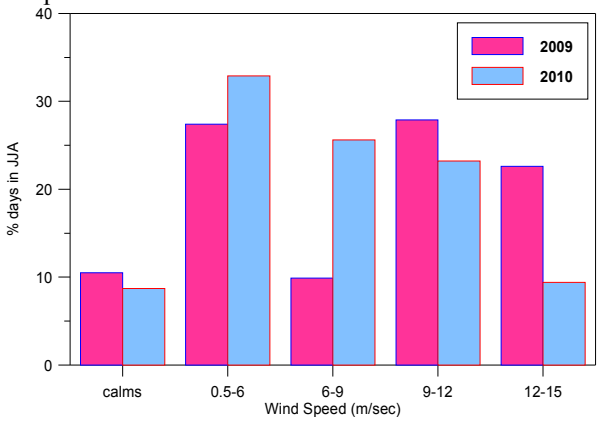

Figure 1. Percentage of wind occurrence in the period JJA from a surface station in Central Aegean.

This study investigates the role of the wind flow during summer on the optical depth of aerosols over Athens. The study focuses in the period June-July-August (JJA) of the years 2009 and 2010. As it can be seen in Figure 1 the occurrence of high wind speed regimes and thus of etesian winds during 2010 was much lower than in 2009. For determining the effect of the wind flow on the optical depth of aerosols we have used the following sources:

(a) The Imaging Spectro-radiometer (MODIS) Terra and Aqua Collection 5. (Aerosol optical depth (AOD) daily measurements at 550nm over Athens area and over Myconos island),

(b) Sun-photometric aerosol optical properties measurements from the ground-based Atmospheric Remote Sensing Station (ARSS) (Amirids et al., 2009) over the city of Athens (37.^{90} N, 23.^{80}E, 130 m a.s.l., Amiridis et al., 2009). ARSS is equipped with a CIMEL CE318-NEDPS9 sunphotometer for the retrieval of AOD at 8 wavelengths from 340 to 1640 nm, The CIMEL instrument is a part of NASA's AERONET (**http://aeronet.gsfc.nasa.gov**).

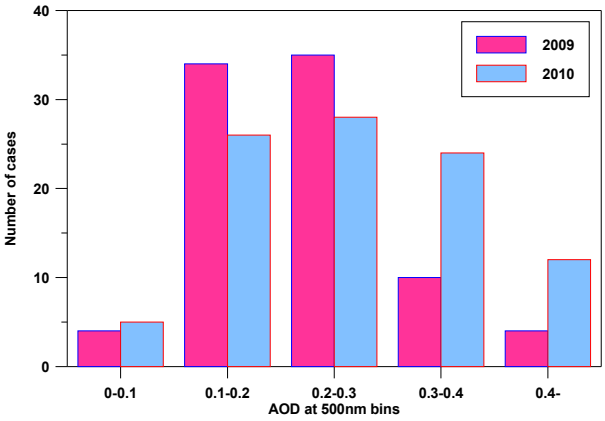

Figure 2. Daily mean Aerosol Optical depth measured at Athens area with the CIMEL sun-photometer divided in 0.1 range AOD bins, for the summer of 2009 and 2010

Sun-photometric measurements showed a 16% AOD increase during summertime comparing 2009 and 2010. For more thorough analysis we have excluded Saharan dust transport cases that affect the aerosol statistics and they are not related with the etesian occurences. MODIS satellite retrievals showed that in both Athens and Myconos area aerosol optical depth is lower in 2010 compared to the one for 2009. More specific both sites show a decrease of 25% and 22% during June and a 5% and 13% respectively during August, while for July AOD values are similar.

Amiridis, V., et al., The potential of the synergistic use of passive and active remote sensing measurements for the validation of a regional dust model, *Ann. Geophys., 27, 3155-3164, 2009*.

Kotroni V., K. Lagouvardos and D. Lalas, 2001: The effect of Crete island on the Etesian winds over the Aegean Sea. *Quarterly Journal of Royal Meteorological Society*, **127**, 1917-1938.

Prezerakos NG (1984) Does the extension of the Azores anticyclone towards the Balkans really exist. Arch Meteorol Geophys Bioklimatol Ser A 33:217–227.

Weather in the Mediterranean, 1962. Meteorological Office, Vol. I, General Meteorology H.M. Stat. Office, London. Second Edition.

Aerosol Optical Depth in East Mediterranean using MODIS and CALIPSO satellite retrievals

E. Marinou[1,3], V. Amiridis[1], S. Kazadzis[2], D. Kopania[2], A. Papayannis[3]
[1]ISARS, National Observatory of Athens, GR-15236, Athens, Greece
[2]IERSD, National Observatory of Athens, GR-15236, Athens, Greece
[3]National Technical University of Athens, GR-15773, Athens, Greece
Presenting author email:elmarinou@noa.gr

Aerosols play a very important role in the Earth-atmosphere energy system as they modify the radiative forcing through various atmospheric processes. In this study we focus on the Mediterranean aerosols which originate from various sources, such as the superimposition of a marine component, a mineral dust component (Saharan dust outbreaks and local dust suspension) and the local and anthropogenic components through long-range transport (Lelieveld, 2002).

The focus of this work was the synergistic use of MODIS and CALIPSO satellite products, together with ground-based sun-photometric aerosol related measurements, for the East Mediterranean region, in order to:

- Establish a 10 year (2000-2010) aerosol optical depth (AOD) climatology based on MODIS measurements over various locations in Greece
- Investigate the best MODIS satellite pixel resolution for the representation of AOD using ground based sun-photometric validation measurements at Athens area.
- Explore the possible continuation (for the years after 2007) of the previous reported (Koukouli et al., 2010) negative AOD trends for the area.
- To investigate the ability of the satellite sensor to detect local AOD sources, by comparing AOD and aerosol vertical profile (CALIPSO) satellite retrievals at neighboring sites with different aerosol types (urban-rural).

The tools that have been used were:

a. The Imaging Spectro-radiometer (MODIS) Terra and Aqua Collection 5, products, using various MODIS spatial resolutions (10x10, 30x30, 50x50Km and 1X1 degrees).

b. CALIPSO's lidar (CALIOP) Level 2, version 3.01, aerosol backscatter coefficient profile products.

c. Sun-photometric aerosol optical properties measurements from the ground-based Atmospheric Remote Sensing Station (ARSS) over the city of Athens (37.9^0 N, 23.8^0E, 130 m a.s.l., Amiridis et al., 2009). ARSS is equipped with a CIMEL CE318-NEDPS9 sunphotometer for the retrieval of aerosol optical depth (AOD) at 8 wavelengths from 340 to 1640 nm, The CIMEL instrument is a part of NASA's AERONET (**http://aeronet.gsfc.nasa.gov**).

Concerning the MODIS pixel resolution sensitivity study, we have compared various MODIS spatial windows sizes around the ARSS station. We found good correlations for the window sizes of 50x50km (R=0.747) and 30x30km (R=0.687) and very bad correlation for the 10x10km resolution (R=0.286).

The seasonal variability of the AOD over the 2000-2010 years over Greece have shown maximum AOD levels during July- August for all Greek sites with more distinct maxima for the Northern part of Greece, associated with transported aerosol load from the North-NorthEast directions. In addition, April-May AOD maxima have been found especially in ths Southern part of Greece associated with transported Saharan dust events.

Concerning the AOD trends, negative values have been found for most of the areas that have been investigated. More specific, for Athens area we have found for the period March 2000 to July 2004 a decreasing trend in aerosol load of 2.8 ±2.5% per year and it's stabilization for the time period 8/2004-9/2010 with decreasing trend of 0.96 ±1.20% per year.

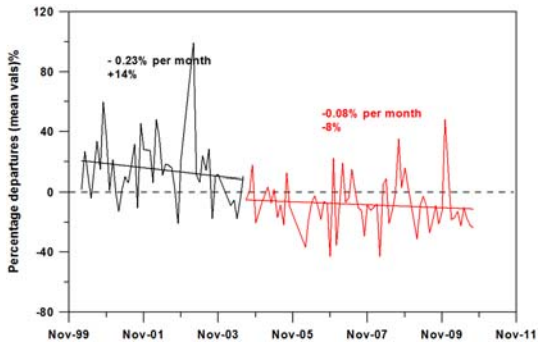

Figure 1.Percentage departures of monthly mean AOD values at 550nm without annuality from MODIS/Terra data, for 10 years, for the area of Athens, for the time period before and after summer 2004.

Finally, we have used mean monthly AOD values retreved from MODIS and CALIPSO mean aerosol vertical profiles over various sites around Athens area. This, in order to try to investigate the sensitivity of the satellite retrievals on a complex aerosol urban area compared with neighboring rural sites.

This work was supported by the Marie Curie project ACI-UV, PERG05-GA-2009-247492.

Lelieveld J., et al., Global Air Pollution Crossroads over the Mediterranean, Science, 298, 794-799, 2002.

Amiridis, V., et al., The potential of the synergistic use of passive and active remote sensing measurements for the validation of a regional dust model, *Ann. Geophys., 27, 3155-3164, 2009*

M. E. Koukouli et al., Investigation of the negative trend in the MODIS Aerosol Optical Depth over the Southern Balkans, Atmospheric Environment, 2010

Synergetic monitoring of Saharan dust plumes: A case study of dust transport from Canary Islands to Iberian Peninsula. Part 2: Evaluation of potential dust impact on surface

C. Córdoba-Jabonero[1], M. Sorribas[1], J.L. Guerrero-Rascado[2]*, J.A. Adame[1], Y. Hernández[3], H. Lyamani[2], V. Cachorro[4], M. Gil[1], L. Alados-Arboledas[2], E. Cuevas[3] and B. de la Morena[1]

[1]Instituto Nacional de Técnica Aeroespacial (INTA), Atmospheric Research and Instrumentation Branch, Torrejón de Ardoz (Madrid), Spain
[2]Universidad de Granada (UGR), Andalusian Environmental Centre (CEAMA), Group of Atmospheric Physics, Granada, Spain
[3]Agencia Estatal de Meteorología (AEMET), Atmospheric Research Centre of Izaña, Sta. Cruz de Tenerife, Spain
[4]Universidad de Valladolid (UVA), Group of Atmospheric Optics, Valladolid, Spain
*Now at Évora Geophysics Centre (CGE), University of Évora, Évora, Portugal
Keywords: In-situ measurements, Size distribution, Deposition, Saharan dust.
Presenting author email: cordobajc@inta.es

A general work focused on the study of Saharan dust intrusions is presented as a case study of air masses advected from the Saharan region to the Canary Islands and the Iberian Peninsula (IP). This work is divided in two parts in order to examine two relevant and different aspects of this study. Each one is separately submitted. This second one (Part 2) presents the evaluation of potential dust impact on surface once the Saharan dust intrusion arrives at the Southern IP. In this case, ground-level in-situ measurements together with AERONET columnar-integrated data and closest-to-surface backtrajectory analysis, as well, are used for that purpose. The dust detection, identification and vertical structure analysis were described in the Part 1. Observations were performed on 14 March 2008 (1-day dusty episode) in two of those three Spanish stations, where the dust intrusion coming from the Saharan region was monitored (see Part 1). Both of them are located in the Southern IP within the dust-influenced area: the Atmospheric Sounding Station 'El Arenosillo' (ARN) at the SE and the Granada station (GRA) at the SW of the IP.

Backtrajectory analysis reveals that the closest-to-surface air masses are coming directly from Northern Africa, whereas those ending at 3-km carrying the dust plume are coming from the considered Sahara-Tenerife-IP pathway (see Part 1). Rather low particle sedimentation is expected to occur directly from the dust 3-km height plume. Therefore, dust particles registered at ground level are not related to deposition processes for particles of that dust plume with low potential impact on surface. However, dust incidence exists, being more significant in the SE region (GRA) respect to the SW area (ARN).

Differences on particle deposition processes are observed in both sites by using the temporal evolution of the total volume particle concentration for discrete size ranges. They are due to the particular dust transport pattern occurred over each station: particles detected in ARN would be the result of a gravitational deposition process, while those in GRA would be mostly influenced by their horizontal movement.

AERONET volume size distributions ($VSD^{AERONET}$) were compared to those calculated from the most coincident in time ground-level in-situ measurements (VSD^{GL}) (see Figure 1). The effective radius was calculated for each VSD datasets. The obtained results ($r_{eff}^{AERONET} > r_{eff}^{GL}$) are opposite to those reported by Müller et al. (2010) ($r_{eff}^{AERONET} < r_{eff}^{GL}$), where AERONET and airborne (at 2-3 km height) in-situ measurements were performed. Differences between AERONET and in-situ measurements show a clear dependence on height of the dust particle VSD. That is reflected by the different in-situ measurements platform used, either ground-level or airborne. Further vertical size-resolved observations are needed for evaluation of the impact on surface of Saharan dust arrivals to the IP.

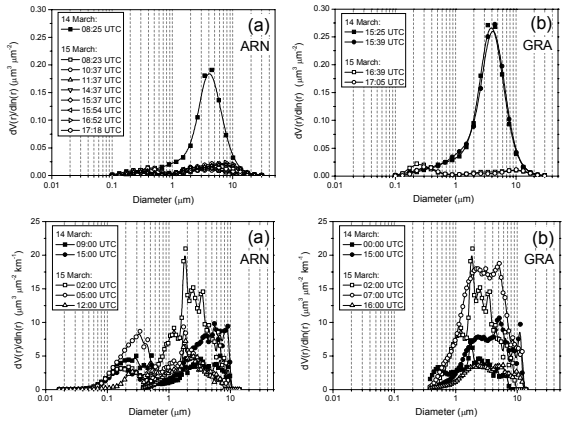

Figure 1. Volume size distributions (VSD) from AERONET data (top) and ground-level in-situ measurements (bottom) in ARN (a) and GRA (b) sites.

This work was supported by the Spanish Ministry for Science and Innovation (MICINN) under CA CGL2010-10012-E, the Spanish Ministry of Education under Proj. CGL2008-05939-C03-03/CLI, and the Autonomous Government of Andalusia under Proj. P08-RNM-3568.

Müller *et al.* (2010) *J. Geophys. Res.* **115**, D07202, doi:10.1029/2009JD012520.

Aerosol size distribution study by airborne and ground-level in-situ measurements and remote sensing during EARLINET lidar intercomparison campaign: SPALI10

F. Molero[1], F. J. Andrey[2], J. Preißler[3], F. Navas-Guzmán[4], A. Giunta[5], M. Sicard[6], A. J. Fernandez[1], M. C. Parrondo[2], F. Wagner[3], M.J. Granados[4], G. D'Amico[5], S. Tomas[6], M. Pujadas[1], C. Córdoba-Jabonero[2], J.L. Guerrero-Rascado[3], L. Alados-Arboledas[4], A. Amodeo[5], A. Comeron[6], J.A. Bravo[4], G. Pappalardo[5], D. Kumar[6], I. Mattis[7], V. Freudenthaler[8] , D. Lange[6], J. Giner[6], C. Muñoz[6], F. Rocadenbosch[6].

[1]Centro de Invest. Energéticas, Medioamb. y Tecn. (CIEMAT), Avda Complutense, 22. Madrid, 28040. Spain
[2]Instituto Nacional de Técnica Aeroespacial (INTA), Atmospheric Research and Instrumentation Branch, Torrejón de Ardoz 28850. Madrid, Spain.
[3]Évora Geophysics Centre (CGE), University of Évora, Rua Romão Ramalho 59, 7000, Évora, Portugal
[4]Andalusian Center for Environmental Research (CEAMA), University of Granada – Autonomous Goverment of Andalusia, Av. del Mediterráneo s/n, 18071, Granada, Spain
[5]Istituto di Metodologie per l'Analisi Ambientale CNR-IMAA, C.da S. Loja, Tito Scalo, Potenza, Italy I-85050
[6]Department of Signal Theory and Comunications, Remote Sensing Lab., Universitat Politécnica de Catalunya/Institut d'Estudis Espacials de Catalunya, Barcelona, Spain
[7]Leibniz Institute for Tropospheric Research, Leipzig, Germany
[8]Ludwig-Maximilians Universität, Meteorological Institute, Theresienstr. 37, 80333 München, Germany
Keywords: Lidar, Atmospheric aerosol size distribution, network, EARLINET
Presenting author email: f.molero@ciemat.es

Aerosol particles affect the radiative energy budget of the Earth-atmosphere system, although current estimates remain highly uncertain. One reason for this uncertainty is the lack of long-term observations of vertical distributions of several aerosol properties, including size distributions. LIDAR (Light Detection and Ranging) systems, coordinated as networks, are a powerful tool in closing this observational gap.

One of those networks, EARLINET (European Aerosol Research Lidar NETwork, Bösenberg et al., 2003) has been studying tropospheric aerosols on continental scale since 2000. The network activity is based on scheduled measurements, a rigorous quality assurance program both at algorithm and instrument level, and a standardized data exchange format. As part of the quality assurance program, intercomparison campaigns among several co-located instruments from different network stations and a reference system are performed (Pappalardo, 2004). One of those campaigns, SPALI10 (SPAin Lidar Intercomparison 2010), took place in Madrid (Spain, 40.45ºN, 3.73ºW, 663 m asl) from 18 October to 5 November 2010 in the frame of the EARLINET-ASOS project (Advanced Sustainable Observation System) [www.earlinetasos.org]. It involved four lidar systems (Madrid, Granada, Barcelona and Evora) and the reference system from Potenza. The main objective of the campaign was checking the performance of multiwavelength Raman lidars, used for vertically resolved measurements of the particle optical properties.

Anyhow, during the campaign, a large suite of instruments complemented the study of the atmosphere. At ground level, aerosol size distribution and chemical composition were continuously monitored. Particle number size distributions were determined with a combination of a Scanning Mobility Particle Sizer (TSI SMPS 3936) and an Optical Particle Counter (GRIMM 1108), covering the radius range from 15 nm to 20 μm.

Additionally, airborne in-situ measurements were performed to characterize vertical profiles of aerosols. Size distribution data between 0.10 and 3.0 μm in diameter were provided by a PCASP 100-X (Passive Cavity Aerosol Spectrometer Probe) installed onboard the INTA-C212 aircraft. The column integrated characterization of the atmospheric aerosol was provided by a sun tracking photometer (Cimel CE-318-4). The sky radiance measurements, performed at the almucantar and principal planes in conjunction with solar direct irradiance measurements at several wavelengths, were used to retrieve the volume size distribution. The extensive dataset obtained during SPALI10 field campaign enables to compare ground-level and airborne in situ measurements and remote sensing techniques to characterize the vertically-resolved size distribution of aerosols. Several relevant features shown in the comparison of the results obtained by the different instruments are discussed.

The work was supported by the European Union under the EARLINET-ASOS project (contract nº 025991 (RICA)), by the MICINN (Spanish Ministry of Science and Innovation) under the project CGL2010-17777 and Complementary Actions CGL2009-08031-E, CGL2010-09225-E and CGL2010-10012-E, and by the ESA-CEOS Intercalibration of Ground-Based Spectrometers and Lidars (CEOS-IC-PR01) project.

Bösenberg, J. et al., (2003) "A European Aerosol Research Lidar Network to Establish an Aerosol Climatology", MPI-Report 348, Max-Plank-Institut für Meteorologie, Hamburg.

Pappalardo G. et al., (2004). "Aerosol lidar intercomparison in the framework of the EARLINET project. 3 - Raman lidar algorithm for aerosol extinction, backscatter and lidar ratio", Appl. Opt., 43, N. 28, 5370-5385.

Three years of Raman lidar measurements in correspondence with CALIPSO overpasses over the South of the Iberian Peninsula

F. Navas-Guzmán[(1,2)], J. A. Bravo-Aranda[(1,2)], J. L. Guerrero-Rascado[(1,2,3)], M. J. Granados-Muñoz[(1,2)] and L. Alados-Arboledas[(1,2)]

[1]Departamento de Física Aplicada, Universidad de Granada, Fuentenueva s/n, 18071, Granada, Spain.
[2]Centro Andaluz de Medio Ambiente (CEAMA), Av. del Mediterráneo s/n, 18071, Granada, Spain
[3] Évora Geophysics Centre (CGE), University of Évora, Rua Romão Ramalho 59, 7000, Évora Portugal

Keywords: aerosol, lidar, CALIPSO, EARLINET.

Tropospheric aerosols, and in particular anthropogenic aerosols, are one of the most uncertain elements in the estimation of radiation budget. In fact, the uncertainties in aerosol direct and indirect anthropogenic forcing are of the same magnitude of the effects themselves (Forster et al., 2007). The assessment of their impact on the Earth radiative budget requires an increasing knowledge of the aerosol properties and their temporal and spatial distribution.

A multiwavelength Raman lidar is operated at the Andalusian Centre for Enviromental Research in Granada (Spain, 37.16ºN, 3.6ºW, 680 m asl). This system is based on a Nd:YAG laser source operating at 1064, 532 and 355 nm. Detection is carried out in seven channels corresponding to elastic wavelengths at 1064, 532p (parallel-polarized), 532s (perpendicular-polarized) and 355 nm, and Raman shifted wavelengths from nitrogen (387 and 607 nm) and water vapour (408 nm). The system is described in detail by Guerrero-Rascado et al. (2008). Since 2004, the Raman lidar is operated at the Granada station, and in April 2005, the instrument was incorporated to the EARLINET network (Bösenberg et al., 2001).

Since middle 2006, scheduled measurements have been performed at Granada in temporal coincidence with CALIPSO overpasses. CALIPSO (Cloud-Aerosol Lidar and Infrared Pathfinder Satellite Observations), the first satellite-borne lidar specifically designed for aerosol and cloud studies, provides high vertical resolution profiling of aerosol and clouds on global scales (Winker et al., 2007).

Three years of measurements have been analyzed in order to obtain a characterization of the atmospheric aerosol in the urban environment of Granada. A set of 150 aerosol extinction and 507 aerosol backscatter profiles has been used in this study. Mean values and variances of the aerosol extinction and backscatter in the boundary layer have been calculated. Aerosol properties like extinction-to backscatter ratios (lidar ratio, LR) and Ångström exponents have allowed for characterizing the different aerosol types (Giannakaki,et al., 2010)..
Validations of CALIPSO attenuated backscatter coefficient profiles have been carried out using our lidar system for different atmospheric conditions. Figure 1 shows the attenuated backscatter profiles at 532 for CALIPSO and Granada Raman lidar during a Saharan dust event on 5 July 2008. A good agreement is observed from 3 km up to the tropopause. However, there are differences in the vertical distribution of the aerosol in the lowest layers. These discrepancies are due to the distance between our station and the closest position in the satellite path (around 70 km far away). It is important to show that this area has a complex topography.

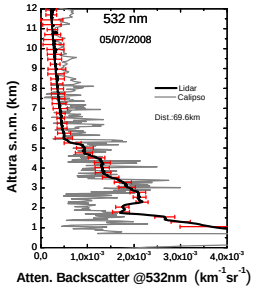

Figure 1. Attenuated backscatter profile at 532 nm for CALIPSO and Granada Raman lidar.

Acknowledgements: This work was supported by the Spanish Ministry of Science and Technology through projects CGL-2006-27108-E/CLI (DAMOCLES Aerosol Scientific Thematic Network), CGL2008-01330-E/CLI, CGL2009-08031-E/CLI, CGL2010-09225-E (Spanish Lidar Network), CGL2010-18782 and CSD2007-00067; by the Andalusian Regional Government through projects P10-RNM-6299 and P08-RNM-3568; and by EU through EARLINET-ASOS project (EU Coordination Action, contract nº 025991 (RICA)).

Bösenberg, J. et al. (2001), *Selected Papers of the 20th International Laser Radar Conference*. Edition Ecole Polytechnique, Palaiseau, France.

Forster, P. et al. (2007), *Cambridge Univ. Press*, New York, USA.

Giannakaki, E. et al. (2010), *Atmos. Meas. Tech.*, **3**, 569-578.

Guerrero-Rascado, J. L. et al. (2008) *Atmos. Environ.*, **42**, 2668–2681.

Winker, D. M et al.., Hunt, W. H. (2007) *Geophys. Res. Lett*., **34**, L19803.

One year of Raman lidar measurements at the South African EUCAARI site

M. Komppula[1], T. Mielonen[1], K. Korhonen[1], A. Arola[1], H. Lihavainen[2], L. Laakso[2,3,4], V. Vakkari[4], H. Laakso[4], P. Beukes[3], P. Van Zyl[3], K. Pienaar[3], P. Tiitta[3], R. le Roux[3], K. Chiloane[5], H. Baars[6], R. Engelmann[6], D. Althausen[6] and K.E.J. Lehtinen[1,7]

[1]Finnish Meteorological Institute, P.O.Box 1627, FI-70211, Kuopio, Finland
[2]Finnish Meteorological Institute, P.O.Box 503, FI-00101, Helsinki, Finland
[3]School of Physical and Chemical Sciences, North-West University, Potchefstroom, Republic of South Africa
[4]Department of Physics, University of Helsinki, P.O.Box 64, FI-00014 Helsinki, Finland
[5]ESKOM, Sustainability and Innovation, Environmental Sciences Department, Republic of South Africa
[6]Leibniz Institute for Tropospheric Research, Permoserstr. 15, D-04318, Leipzig, Germany
[7]Department of Applied Physics, University of Eastern Finland, P.O.Box 1627, Kuopio, FI-70211, Finland
Keywords: lidar, lidar ratio, extinction, remote sensing, air pollution.
Presenting author email: mika.komppula@fmi.fi

This paper presents one-year dataset of Raman lidar measurements conducted at the South African EUCAARI (The European Project on clouds, aerosols and climate) site Elandsfontein (Laakso *et al.*, 2010). Previous lidar measurements have been sparse on the African continent, especially in the Southern areas.

The measurement site is located on the eastern part of Highveld, approximately 200 km east of Johannesburg at a hilltop about 1750 meter asl. Additional instrumentation provided aerosol absorption and scattering, chemical composition, number size distribution (10 nm – 10 µm), aerosol optical depth (AOD), trace gases (SO_2, O_3, NO_x, H_2S) and basic meteorology. The region has significant anthropogenic emissions especially from coal-based power production, petrochemical industry and further away, the megacity of Johannesburg. Other important sources are frequent savannah fires, especially during the dry season (June-October) and some local biofuel burning.

The lidar measurements were started on the 13th December 2009 and were stopped at the end of January 2011. The instrument in use was a seven-channel Raman lidar called "POLLY^{XT}–POrtabLe Lidar sYstem eXTended" (Althausen *et al.*, 2009). The output of the instrument includes vertical profiles of the particle backscattering coefficient at three wavelengths (355, 532 & 1064 nm) and of the particle extinction coefficient at two wavelengths (355 & 532 nm) for the whole troposphere. The vertically integrated extinction coefficient gives the AOD. In addition, such size/composition-dependent, intensive particle quantities as the Ångstrom exponents, the lidar ratio and depolarisation can be determined. The height and the evolution of the boundary layer and night-time residual layer can be defined together with the height and thickness of different cloud and aerosol layers. The depolarisation channel (355 nm) of the lidar enables us to separate spherical and non-spherical particles. Thus, we are able to identity dust particles and estimate the ratio of ice crystals and water droplets in clouds. The vertical resolution of the system is 30 meters.

The typical backscattering and extinction profiles and other properties for the seasonal aerosol will be calculated. The evaluation of planetary boundary layer (PBL) will be defined.

The local summer (Dec-Feb) had most distinct PBL evolution on most days. A very shallow aerosol layer was observed during the night and an increase up to 2-3 km during the day on average. The maximum layer thickness was about 5 km. This period was the cloudiest period of the year and in contrast, winter (Jun-Aug) was almost totally cloud free. Strong and complex multilayered structure of the aerosol was observed throughout the year, most frequently in autumn (Mar-May). Winter and partly spring (Sep-Nov) showed mostly a stable aerosol layer up to 1-3 km height. Furthermore, the diurnal variation was the weakest in winter.

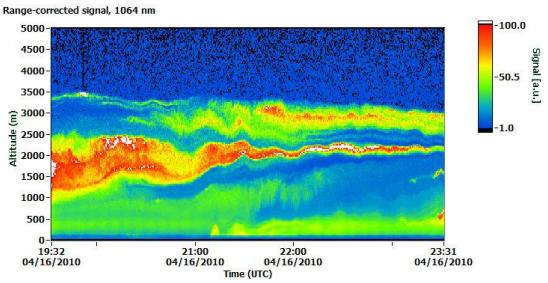

Figure 1. Multiple aerosol plumes. Four-hour time series of backscatter signal at 1064 nm from April 16th, 2010 at Elandsfontein.

This work was supported by the Finnish Academy of Sciences, Finnish foreign ministry and European Union (in project EUCAARI). Eskom Holdings Ltd, South Africa is acknowledged for providing the Air Quality Monitoring Station for the EUCAARI Project measurements.

Althausen, D., et al. (2009). *J. Atmos. Oceanic Technol.*, **26**, 2366–2378, doi: 10.1175/2009JTECHA1304.1.

Laakso, L., et al. (2010), *Atmos. Chem. Phys. Discuss.*, **10**, 30691-30729, doi:10.5194/acpd-10-30691-2010.

An Aerosol Dipole

P.R.C.Rahul*, P.S.Salvekar*, P.C.S.Devara*

*Indian Institute of Tropical Meteorology, Pune, India

* rcreddy@tropmet.res.in

Abstract

Using Aerosol Optical Depth [AOD at 550nm] from the MODerate Resolution Imaging Spectroradiometer [MODIS], Surface winds, Outgoing Long wave Radiation (OLR) from NCEP/NCAR reanalysis and rainfall from Tropical Rainfall Measuring Mission [TRMM] data sets, we report for the first time, a dipole like variability in the aerosol concentration over the region [40ºE-130ºE; 10ºS-10ºN] during September, October and November 2006. Positive AOD anomalies [+0.4 to +0.6] (relative to the 2000-2008 climatological average) along the equatorial East Indian Ocean and Indonesia and negative AOD anomalies [-0.2 to -0.4] over the western, northwestern and central Indian Ocean characterize an aerosol dipole like variability. This east-west variability of the aerosol loading along the Indian Ocean is linked to the anomalously weak easterlies associated with the 2006 Indian Ocean Dipole (IOD) event. The weaker easterlies lead to the hovering of the aerosol plume over Indonesia/Sumatra coast (98ºE), enhancing the positive anomalies of AODs, while excessive rainfall over the central Arabian Sea caused the negative AOD anomalies.

Keywords: Aerosols, MODIS Satellite data, Indian Ocean.

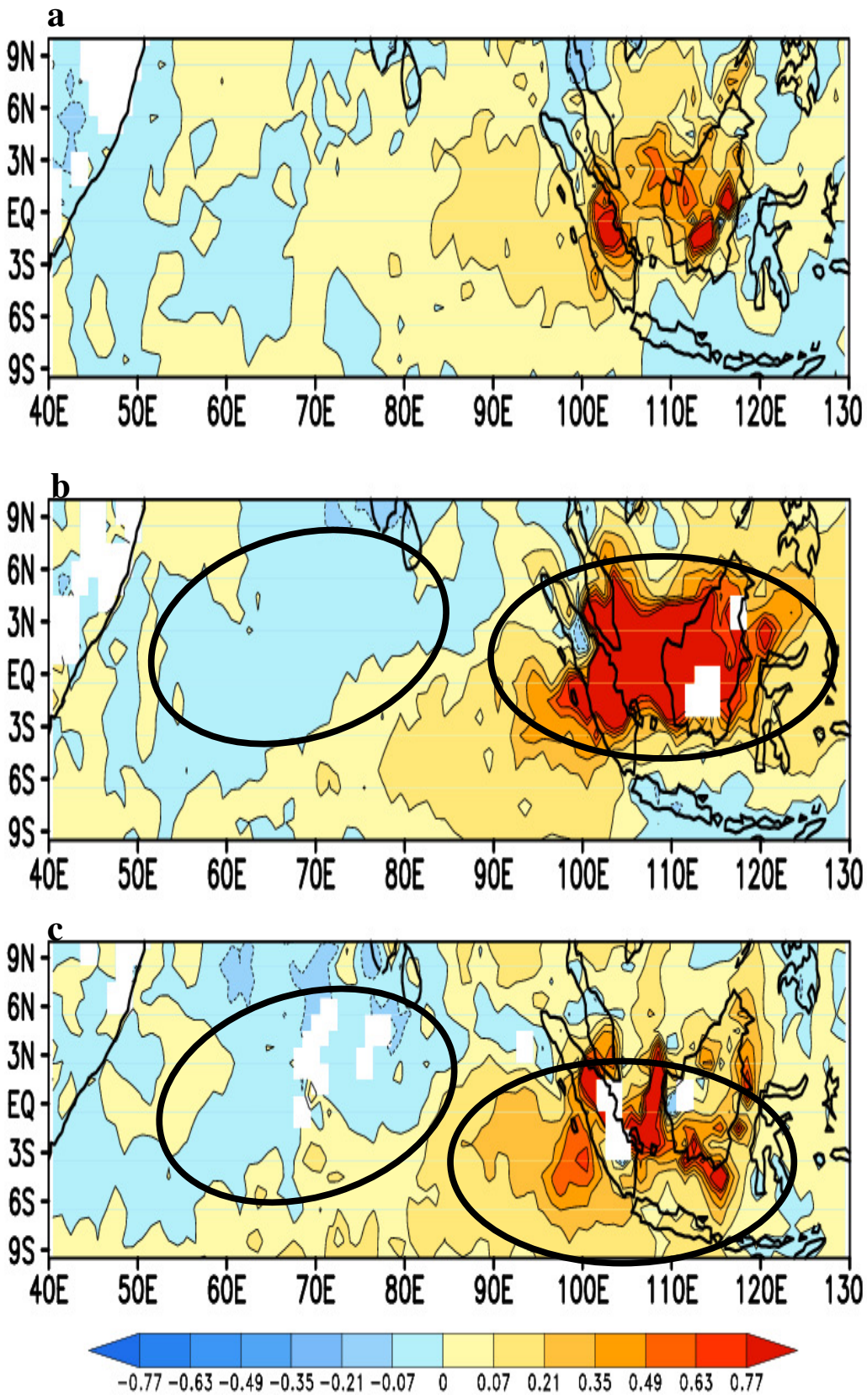

Figure. a-c are the monthly-derived AOD anomalies from MODIS during Sep-Nov 2006.

Thursday, September 8, 2011

Session 8P: Poster session B

Atmospheric aerosols - Specific Aerosol Types

Shipboard characterization of particle and gas emission from a Danish inland ferry

A.G. Hemmersam[1], T.N. Jensen[2], K.G. Nielsen[2], H. Tarp[2], M.K. Lykkegaard[1] and M. Poulsen[1]

[1] Center of Chemistry and Biotechnology, Danish Technological Institute, DK-8000 Aarhus C, Denmark
[2] Center of Sustainable Energy and Transportation, Danish Technological Institute, DK-8000 Aarhus C, Denmark

Keywords: Marine aerosols, SMPS, shipping emissions, combustion aerosols.
Presenting author email: agh@dti.dk

Several studies show that emissions from ship traffic influences the air pollution in port cites severely. Especially NO_x and ultrafine particle levels are found to be elevated due to ship traffic in the harbor area. High NO_x and ultrafine particle levels are known to affect human health.

Mainly two ways for limiting the emissions from ships are presently being exploited, lowering of the sulfur content in the fuel and implementation of different types of emission reducing technologies such as filters and scrubbers. Regulation of the sulfur content in fuel for ships entering the North Sea is expected to be limited to 1% within 2012. Today Danish ferries are already running on marine diesel in which the sulfur content is limited to 0.1%, which is significantly lower than the average sulfur content of 2.6% in heavy fuel oil used for ships.

Emission data from single ships running on different types of fuel is highly needed in order to better understand the impact of reducing the sulfur level with respect to particle and gas emissions. However, to achieve reliable and precise emission data from single ships is a challenge, therefore only a limited number of studies are presently available.

In this study emission data from a Danish inland ferry running on marine diesel is presented.

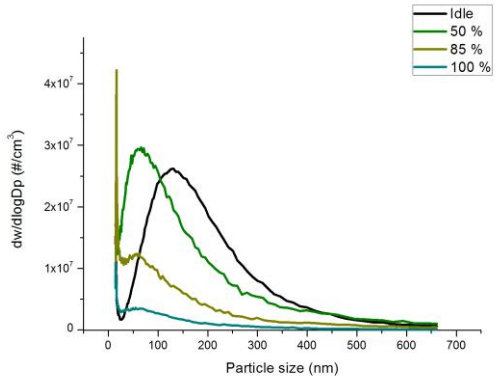

Figure 1. Size distribution of particles emitted in the interval 15-680 nm as a function of engine load.

The emission data show NO_x levels at 8.33 g/kWh which is comparable to EURO 2 heavy duty diesel engine for trucks and below the TIER II regulation for ships. NO_2 and SO_4 were found to be 0.99 and 0.01 g/kWh. CO and HC levels were measured and found to be within the specifications of EURO 5 or 6 for heavy duty engines for vechecles. The particle size distribution was measured during different engine loads by a scanning mobility particle sizer (SMPS) in combination with a rotating disc diluter system and particle mass was collected on filter according to ISO8178. The mean particle size was found to depend on engine load, but was below 150 nm during all engine loads. The largest particles were seen when the ferry was operating at idle in the harbor during load and unload. Particle number concentration was found to peak at an engine load of 50% and decrease at engine loads of 85% and 100%.

In conclusion all emission data were below the TIER II limit for ships.

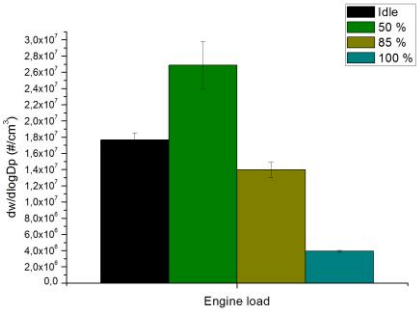

Figure 2. Mean number concentration of particles emitted as a function of engine load.

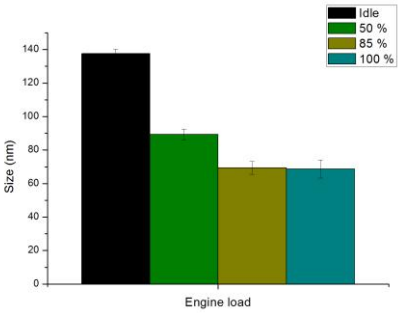

Figure 3. Mean size of the particles emitted as a function of engine load.

This work was supported by the Danish Ministry of the Environment, Environmental Protection Agency and part of collaboration between Danish Technological Institute, Ærøfærgerne A/S and Dinex A/S.

Quantitative real time sea salt measurements by HR-ToF AMS

J. Ovadnevaite, D. Ceburnis, J. Bialek, C.D. O'Dowd and H. Berresheim

School of Physics & Centre for Climate and Air Pollution Studies, Ryan Institute, National University of Ireland Galway, University Road, Galway, Ireland
Keywords: Aerosol mass spectrometry, sea salt, marine aerosols
Presenting author email: jurgita.ovadnevaite@nuigalway.ie

Global importance of marine aerosol to the cloud condensation nucleus (CCN) formation was demonstrated several decades ago, starting with the secondary sulphate activation presented with CLAW hypothesis (Charlson et al., 1987), and emphasizing the impact of primary sea spray particles (O'Dowd et al., 1999). It was also shown that correct CCN parameterization depends on the accurate representation of aerosol size and chemical composition.

Here we report first long-term measurements of sea salt by High Resolution Time-of-Flight Aerosol Mass Spectrometry (HR-ToF AMS). The measurements were made in conjunction with CCN and cloud microphysics measurements to improve our understanding of cloud microphysical processes. With its original design for real-time measurement of size-resolved non refractory aerosol chemical composition HR-ToF AMS can quantitatively detect non refractory aerosol organics, sulphate, nitrate and ammonium and achieve direct separation of most ions at the same nominal m/z (DeCarlo et al., 2006). In contrast to previous assumptions our continuous operation of an HR-ToF AMS instrument since 2009 at the Mace Head Global Atmosphere Watch (GAW) station on the west coast of Ireland has clearly revealed that the instrument is also capable of quantitatively measuring sea salt, a significant mass fraction of the marine aerosol.

For this purpose the instrument was calibrated using artificial sea water (35 ‰ salinity) made from artificial sea salt mixture (Sea salts, SIGMA) and deionized water. The solution was nebulized with a TSI atomiser (model 3076), and DMA pre-selected particles (300nm) were sampled into the AMS inlet, while relative humidity in the sample line was maintained at about 65%. This calibration enabled sea salt quantification in the ambient aerosol measurements. Although sea salt is considered to be refractory material, the sea salt aerosol particles would be in a liquid phase at the relative humidity (RH) typical for the marine environment (usually above 70%), due to much lower efflorescence RH. Since sea salt efflorescence occurs at about 40% RH, the sea salt particles experiencing RH above the efflorescence RH could be treated as liquid spheres. Though drying in the inlet line could occur, RH measurements showed that it does not decrease below 50% when sampling maritime air. This suggests that sea salt particles could be efficiently vaporised at standard HR-ToF AMS operating temperature (~600^{o}C). While the exact fragmentation pattern was found to be slightly dependent on the heater temperature (ranging from 500 to 800^{o}C) it generally did not affect the quantification. Moreover, increased vaporizer temperature decreased instrument's collection efficiency due to increasing bounce-off of particles from the vaporizer suggesting that the standard operation temperature is even preferable to higher temperatures for the quantification of the sea salt in the marine aerosol particles.

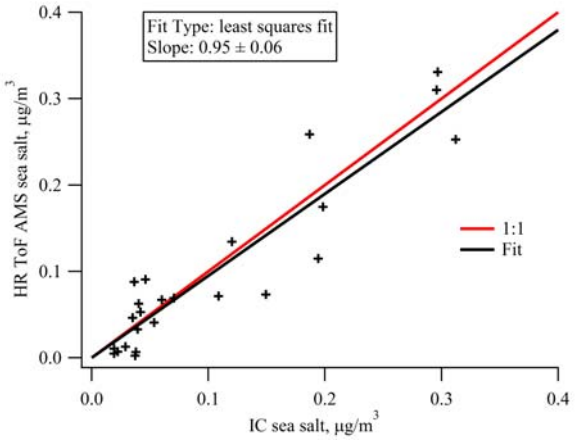

Figure 1. A comparison between HR-ToF AMS and Ion chromatography sea salt measurements.

PM1 sea salt concentrations derived from HR-ToF AMS measurements were compared with measurements from the off-line filter analysis using standard ion chromatography method (Figure 1). A good agreement between off-line chemical analysis and AMS sea salt measurements indicates the possibility of quantitative sea salt measurement with aerosol mass spectrometer in real time.

This work was supported by the Science Foundation Ireland (grant 08/RFP/GEO1233), HEA-PRTLI4 Environment and Climate: Impact and Responses programme, and EPA, Ireland.

Charlson, R. J., Lovelock, J. E., Andreae, M. O., and Warren, S. G. (1987) Nature, 326, 655-661.

DeCarlo, P. F., Kimmel, J. R., Trimborn, A., Northway, M. J., Jayne, J. T., Aiken, A. C., Gonin, M., Fuhrer, K., Horvath, T., Docherty, K. S., Worsnop, D. R., and Jimenez, J. L. (2006) Anal Chem, 78, 8281-8289.

O'Dowd, C. D., Lowe, J. A., and Smith, M. H. (1999) Geophys Res Lett, 26, 1311-1314.

Secondary organic aerosol on southern Pacific Ocean

P.Vaattovaara[1, 2], L.Cravigan[2], N.Talbot[3], G.Olivares[3], C.Law[4], M.Harvey[4], Z.Ristovski[2] and A.Laaksonen[1, 5]

[1]Department of Applied Physics, University of Eastern Finland, Kuopio, FI-70211, Finland
[2]ILAQH, Queensland University of Technology, Brisbane, 4000, Australia
[3]National Institute of Water and Atmosphere, Auckland, New Zealand
[4]National Institute of Water and Atmosphere, Wellington, 6021, New Zealand
[5]Finnish Meteorological Institute, Helsinki, FI-00101, Finland
Keywords: Marine aerosols, SOA, ultrafine particles, composition
Presenting author email: Petri.Vaattovaara@uef.fi

Marine biologically active regions (e.g., coasts, ice edges, and open water areas with plankton blooms) are known to produce a range of compounds that interact with atmosphere effecting directly and indirectly on particle production, composition, and properties in marine atmosphere. While CLAW hypothesis (Charlson *et al*., 1987) supports the idea on the importance of marine biological activity on ultrafine (d<100nm) particles composition, properties and effects and focus on the role and importance of secondary sulfate production via DMS in those particles compositions, the CLAW hypothesis does not take into account the secondary organic fraction in the composition of the ultrafine particles. So far, recent observations about the presence of a remarkable marine origin secondary organic fraction in ultrafine particles have been indicated down to nucleation mode size particles (d<15nm) on Irish coastal waters on Atlantic Ocean (Vaattovaara *et al*., 2006), Arctic Ocean close to ice edges (Vaattovaara *et al.*, ICNAA 2009), and Australian sub-tropical Pacific Ocean waters (Modini *et al*., 2009). In spite of the importance of secondary particles to atmospheric radiatively active sizes, marine produced particle composition is still unknown in various other marine biologically active locations around the world.

This study about the composition of nucleation (d<15nm) and the lower end of Aitken (20nm<d<60nm) modes particles is focused on particle production at one such region the Chatham Rise region (New Zealand; latitude 42°S-44°S, longitude 174°E-177°W) during the SOAP (Surface Ocean Particle Production) pilot project voyage (austral summer period from 1.2.2011 to 12.2.2011). The location is on the southern Pacific Ocean with a sub-tropical front and intensive austral summer phytoplankton blooms.

The ultrafine particle composition was studied using the UFO-TDMA and the VH-TDMA methods on board of RV Tangaroa (NIWA, Wellington, New Zealand). Auxiliary data were collected from the ship weather station and marine information observations, SMPS particle size distribution measurements, total particle count CPC measurements with 5 nm and 10 nm cut-off sizes, and black carbon measurements. Marine biological activity was checked with MODIS satellite data and supported by *in situ* chlorofyll and dissolved DMS measurements. Marine air masses origin was followed with HYSPLIT trajectories.

The TDMA measurements show that in the biologically active marine area observed nucleation and Aitken mode sized particles include a clearly detectable organic fraction. During intensive solar radiation periods (e.g., 4.2., 6.2., 9.2., and 10.2.) secondary organic contribution is highly probable in those ultrafine particles. Furthermore, the comparison between *in situ* bubble burst chamber and atmospheric particles composition measurements strongly support secondary origin of the atmospherically observed ultrafine particles. The comparison of the secondary organic fraction observations on Atlantic, Arctic, and Pacific Oceans reveals that even the secondary organic fraction clearly exists in ultrafine particle phase in the different biologically active marine regions the properties of the fraction can be dependent on the marine area conditions.

This study was supported by COST action 735, NIWA (New Zealand), QUT (Australia), and the Academy of Finland. We thank whole research team and the crew and captain of RV Tangaroa for pleasant voyage.

Charlson, R.J. *et al*. (1987). *Nature*, **326**, 6114, 655–661.
Vaattovaara, P. *et al*. (2006) *Atmos. Chem. Phys.* **6**, 12, 4601-4616.
Modini, R. *et al*. (2009). *Atmos. Chem. Phys*. **9**, 19, 7607-7621.

Characterization of a bubble tank for Sea Spray Aerosol Studies

A.C. Butcher[1], S.M. King[1], T. Rosenoern[1], E. D. Nilsson[2] and M. Bilde[1]
[1]Department of Chemistry, University of Copenhagen, DK-2100 Copenhagen, Denmark
[2]Department of Applied Environmental Science, Stockholm University, S-10691 Stockholm, Sweden
Keywords: Marine aerosols, CCN, bubble bursting, particle size distribution.
Presenting author email: andrew@kemi.ku.dk

Sea spray aerosols are of major interest to global climate models due to their large uncertainty in indirect and direct radiative forcing and poorly understood emission characteristics. A new experimental sea spray aerosol bubble tank is characterized and preliminary results are presented for bubble generation, bubble size distribution, and particle emissions.

In this study, the major processes of bubble formation are examined with respect to particle emissions. It has been suggested that a plunging jet, formed by a continuously flowing nozzle placed vertically above a water surface, closely resembles breaking wave bubble entrainment processes and subsequent bubble size distributions (Fuentes et al. 2010). The physical characteristics of our bubble tank are shown in Table 1. The tank consists of a stainless steel cylinder closed at both ends with fittings for recirculating flow for the jet and aerosol sampling.

Table 1 Sea spray tank characterization

Tank Dimensions	
H = 46.2 cm	V_{tot} = 16.3 L
D = 21.2 cm	V_{sample} = 9 L
A = 353 cm^2	$H_{headspace}$ = 20.7cm
Nozzle Parameters	
D_{nozzle} = 4 mm	$v_{jet,\ o}$ = 4.3 m s^{-1}
H_{nozzle} ~ 20 cm	$v_{jet,\ surf}$ = 4.7 m s^{-1}

The sub-surface bubble plume characteristics can be calculated using parameters specified by Claret & Lasheras (1997) and are given in Table 2. When the Weber number (We) is less than unity, surface tension forces are greater than inertial forces and bubbles will remain intact until reaching the surface.

Table 2 Bubble plume characteristics (1mm bubble)

Angle of Plume Cone = 12.5°
$v_{1mm,\ T}$ = 0.22 cm s^{-1}
$H_{1mm,\ T}$ = 21.6 cm
$W_{1mm,\ T}$ = 7.8 cm
We_{1mm} = 6.7 × 10^{-5}

In addition to calculated values, bubble spectra were analyzed for a frit placed in the bottom of the tank at range of air flow rates (

Figure **1**). Particle size distributions for both the frit placed in the tank and the plunging jet are shown in Figure 2.

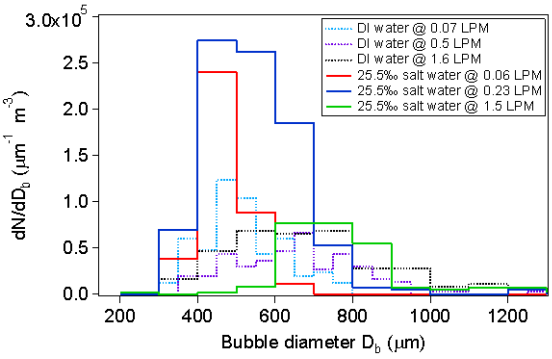

Figure 1 Preliminary photograph-analyzed bubble size distributions for the frit placed in the bottom of the tank.

The difference between the particle size distributions could be caused by high particle loss due to scavenging and entrainment processes of the plunging jet (Bin 1993). The difference in concentration could also be attributed to the shear forces exerted on bubbles that rise to the surface causing incomplete bursting which could also partly explains the disparity in particle size distributions.

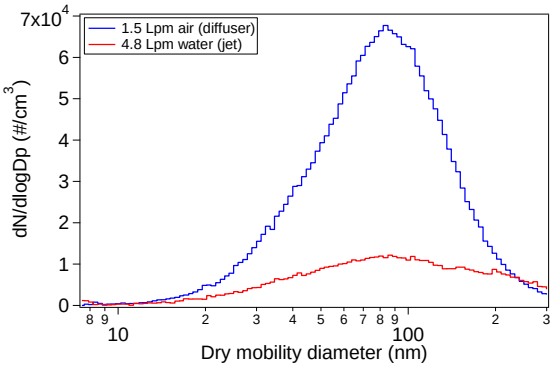

Figure 2 Particle size distributions for the frit and the plunging jet for artificial sea water of salinity 35‰.

This work has been supported by the Carlsberg Foundation.

Bin, A. K. (1993). "Gas Entrainment by Plunging Liquid Jets." Chemical Engineering Science **48**(21): 3385-3630.

Clanet, C. and J. C. Lasheras (1997). "Depth of penetration of bubbles entrained by a plunging water jet." Physics of Fluids **9**(7).

Fuentes, E. et al. (2010). "Laboratory-generated primary marine aerosol via bubble-bursting and atomization." Atmospheric Measurement Techniques **3**: 141-162.

Investigating the morphology and organic fraction of particles from bubble-bursting

S.M. King[1], T. Rosenoern[1], A.C. Butcher[1], E.D. Nilsson[2], and M. Bilde[1]
[1]Department of Chemistry, University of Copenhagen, DK-2100 Copenhagen, Denmark
[2]Department of Applied Environmental Science, Stockholm University, S-10691 Stockholm, Sweden
Keywords: marine aerosol, bubble bursting, sea salt, organic sea spray, particle shape, activation.
Presenting author email: stephanie@kemi.ku.dk

The cloud condensation nucleus (CCN) activity of sodium chloride and artificial sea salt particles are presented herein. Although many studies have reported the observed and theoretical CCN activity of NaCl, its reliability as a calibration standard is diminished due to its uncertain morphology. Wang et al. (2010) show a dependence of the morphology (i.e., shape factor χ) on the drying rate of NaCl particles. Similar tests are repeated in our laboratory for NaCl and sea salt particles that are generated from an aqueous solution using a TSI atomizer.

We also employ a bubble-bursting tank to simulate the production of NaCl and sea salt particles in a marine atmosphere. Bubble production is effectuated either by pushing clean air through a diffuser situated at the bottom of the stainless steel tank filled with 10 L of artificial seawater, or by recirculating water from the bottom of the tank to the water surface via a plunging jet. Further description of the tank is provided in a companion abstract (Butcher et al.). The CCN activity of the particles produced from bubble-bursting is included in this study, and the observed data are compared to the observations from atomized particles as well as to the theoretical CCN activation of the respective salts (Figure 1). All theoretical values are calculated using Kohler theory, in which the water activity term is predicted from the Aerosol Inorganics Model (Wexler and Clegg, 2002).

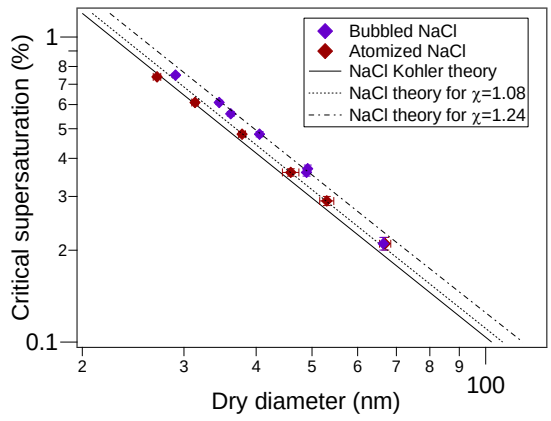

Figure 1. Observed and predicted CCN activation of NaCl particles from atomization and bubble-bursting.

The fraction of organic matter in the particle phase can be estimated from the difference in observed mixed-particle CCN activity from that of the inorganic components. Thus, a thorough understanding of the CCN activity of sea salt is necessary. The motivation for exploring the organic fraction stems from the observation in previous studies that the concentration of organic carbon in primary submicron marine aerosol particles may be highly enriched relative to the organic concentration in source ocean water (Blanchard, 1964). This enrichment has also been suggested to increase with decreasing particle size (Facchini et al., 2008, Keene et al., 2007). Consequently, the possibility that the mixed-particle morphology is dependent on drying methods and on particle size could significantly influence the estimation of the contribution from organic matter. Figure 2 shows preliminary estimates of organic fraction as a function of dry particle size. In these experiments, particles are generated in the bubble-bursting tank, which is filled with a solution containing NaCl (35‰ salinity) and an organic compound (i.e., fructose or oleic acid). The mass ratio of NaCl to organic in the solution is 10:1. A shape factor of 1.00 is assumed in Figure 2. The downward-trending bars are for illustration purposes and indicate the theoretical adjustment for shape factors up to 1.08 for mixed particles containing fructose.

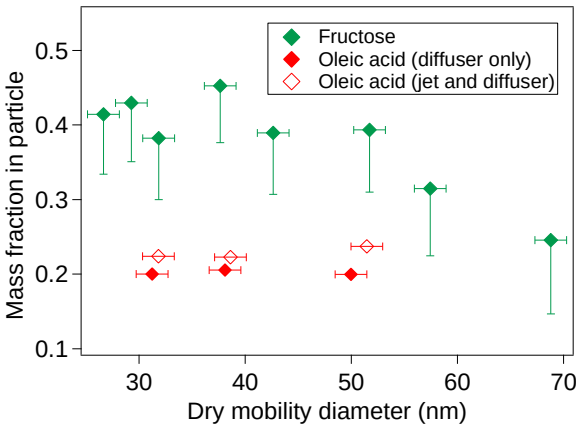

Figure 2. Size-dependent mass fraction of the organic constituent in the particle phase. Bubbles are produced using the diffuser except in the case illustrated by open diamonds, where the diffuser is used simultaneously with the plunging jet.

This work was supported by the Carlsberg Foundation.

Blanchard, D. C. (1964) *Science* **146**, 396-397.
Facchini, M. C., et al. (2008) *Geophys. Res. Lett.* **35** (L17814), doi:10.1029/2008GL034210.
Keene, W. C., et al. (2007) *J. Geophys. Res.* **112** (D21202), doi:10.1029/2007JD008464.
Wang, Z., et al. (2010) *Aerosol Sci. Technol.* **210**, 123-126.
Wexler, A. S. and Clegg, S. L. (2002) *J. Geophys. Res.* **107** (D14 4207), doi:10.1029/2001JD000451.

Thursday, September 8, 2011

Session 8P: Poster session B

Aerosol Modelling

A new reduced complexity thermodynamic methodology (PF-FiTE) to calculate equilibrium vapour pressures of organic compounds above a multi-component solution

D. Topping[1,2], D. Lowe[2]

[1]National Centre for Atmospheric Science (NCAS), Manchester University, Manchester, M13 9PL
[2] Centre for Atmospheric Science, Manchester University, Manchester, M13 9PL
Keywords: Aerosol model, Thermodynamic equilibrium, Organic compounds, Modelling.
Presenting author email: david.topping@manchester.ac.uk

Introduction

Gas to particle partitioning, driven by a difference in equilibrium and partial pressures, is a key process that dictates the evolving chemical composition of atmospheric aerosol particles, thus their environmental impacts. As described by Raoults law, the equilibrium vapour pressure above a solution is a function of 3 key properties: 1) Po the pure component vapour pressure; 2) f the activity coefficient of the condensate in solution; and 3) x the mole fraction of component in solution. In a previous publication a new hybrid reduced complexity ionic mixing rule for calculating 'f', thus equilibrium vapour pressure of inorganic condensates was presented (Topping et al 2009). PD-FiTE, or Partial Derivative Fitted Taylor Series Expansion, was based on the observation that the logarithm of activity coefficients varied linearly as a function of water activity when expressed in terms of equivalent mole fractions. This is identical to the approach described by Zaveri et al for the model MTEM (Zaveri et al 2005). Following this, Topping et al (2009) developed a numerical expression based on ion-pairs and optimised interaction parameters using the thermodynamic model ADDEM (Topping et al 2005). In the following report we develop a similar reduced complexity expression for the activity coefficients of organic solutes, currently targeted at aqueous solutions

Results

A simple, flexible mixing rule is presented which allows the calculation of activity coefficients, thus equilibrium vapour pressures, of organic condensates above a multicomponent aqueous solution:

$$\ln f_A(x_B',\ldots x_w) = \ln f_A^o + \left(\frac{\partial \ln f_A}{\partial x_B}\right)_{(x_w)} x_B'$$

Where f_A is the activity coefficient of solute 'A', x_B the 'dry' mole fraction of solute 'B' and x_w the mole fraction of water. Based on the same fitting methodology as a previously published inorganic model (PDFiTE), organic PDFiTE treats interactions between binary pairs of solutes in the term $\left(\frac{\partial \ln f_A}{\partial x_B}\right)$, with variable sets of polynomials, used to describe behaviour within a mixture. Using 14 compounds chosen using a published reduction methodology, the framework is benchmarked against the UNIFAC model. For 100 randomly derived concentration ranges and 10 relative humidities between 10-99%, the average deviation was calculated to be 3.8%. Whilst compound specific deviations did vary, the median and inter-quartile values across all relative humidity range always fell within +/- 20%. The computational cost of both variants was compared to the use of UNIFAC for the same amounts of water. The fully coupled and uncoupled organic PDFiTE routines are up to a factor of 12 and 66 times more efficient than calling the UNIFAC model using the same water content, respectively; and 313 and 1751 times more efficient than an iterative model using UNIFAC.

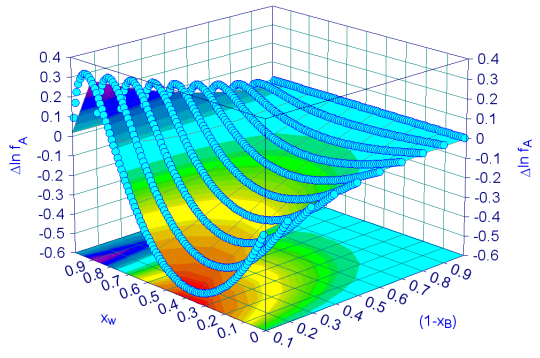

Figure 1. A surface representation of the difference in activity coefficient for solute 'A' as a function of mole fraction of water 'x_w' and 'dry' solute mole fraction '$(1-x_B)$' for a ternary mixture of 'A' and 'B' .

Results are also presented from incorporating PDFiTE into an aerosol box model (Lowe et al, 2009). This forms the basis of additional evaluation against more complex schemes, as well as an analysis of chamber data, before incorporation into the WRF-CHEM regional climate model. The latter will form the focus of future work.

This work was support by UK National Centre for Atmospheric Sciences (NCAS) funding.

References

Lowe et al: Atmos. Chem. Phys., 9, 4559-4573, 2009
Topping et al: Atmos. Chem. Phys., 5, 1205-1222, 2005
Topping et al. J. Geophys. Res., doi: 10.1029/2008JD010099, 2009
Zaveri et al: J. Geophys. Res., doi:10.1029/2004JD004681, 2005

Modelling $PM_{2.5}$ concentrations over Europe

E. Tagaris[1], R.EP. Sotiropoulou[1], N. Gounaris[1] and S. Andronopoulos[1]

[1] Environmental Research Laboratory, NCSR Demokritos, Aghia Paraskevi Attikis, 15310 Athens, Greece
Keywords: particulate matter, modelling, Europe
Presenting author email: tagaris@ipta.demokritos.gr

INTRODUCTION

Atmospheric particulate matter is a focus of attention, because of their important role in many areas, including human health, atmospheric reactions, acid deposition and the earth's radiation budget. The World Health Organization using population exposure estimates of PM_{10} concentrations for the year 2002 estimates that 865,000 people die prematurely each year from causes directly attributable to outdoor air pollution; from those deaths about 80,000 comes from the member states of the EU (www.who.int/quantifying_ehimpacts/countryprofilesebd.xls). The objective of this study is to simulate $PM_{2.5}$ concentrations over Europe using the Community Multiscale Air Quality (CMAQ) Modelling System (Byun and Schere, 2006)

METHODS

Meteorological fields are derived using the Penn State/NCAR Mesoscale Model (MM5) (Grell et al., 1994). Meteorology Chemistry Interface Processor (MCIP) (http://www.cmascenter.org) is used to provide the meteorological data from the MM5 outputs needed for the emissions and air quality models (177 × 217 grid cells of 35 km × 35 km, with 14 vertical layers).

Emissions are processed by the Sparse Matrix Operator Kernel Emissions (SMOKE v2.6) Modelling System (http://www.smoke-model.org). SMOKE is used to convert the resolution of the data in an emission inventory to the resolution needed by the air quality model. TNO has provided a gridded anthropogenic emissions database for the year 2006 over Europe in a 0.1 × 0.1 degrees resolution (ftp:// neptunus.tno.nl). The Biogenic Emission Inventory System, version 3 (BEIS3) is used for processing biogenic source emissions (http://www.epa.gov/asmdnerl/biogen.html).

The Community Multiscale Air Quality (CMAQ v 4.7) Modelling System with the Carbon Bond mechanism (CB05) (http://www.camx.com/publ/pdfs/CB05_Final_Report_120805.pdf) is used for the regional air quality modelling.

RESULTS AND DISCUSSION

Elevated $PM_{2.5}$ concentrations are simulated locally and regionally over the entire domain (Figure 1). Sulfate is dominant (up to about 60% locally) followed by nitrate (up to about 30% locally), organic carbon (up to about 25% locally) and ammonium (up to about 20% locally).

$PM_{2.5}$ model performance is evaluated by comparing the predicted concentrations with observation data from monitoring stations across Europe, using the air quality information system maintained by the

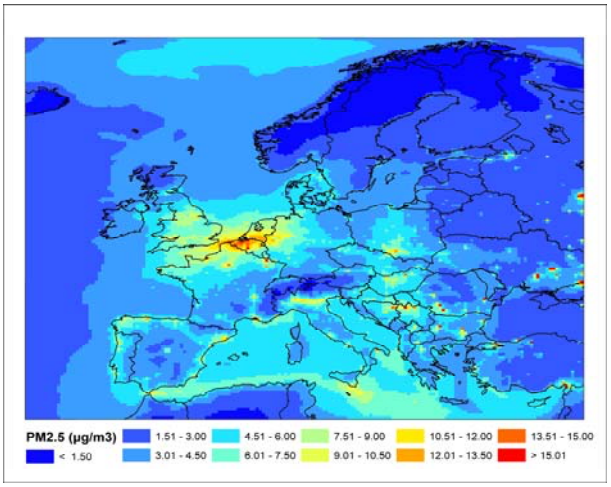

Figure 1: Daily average ground $PM_{2.5}$ dry mass concentrations for July 2006

European Environment Agency (http://www.eea. europa.eu). In general, model underestimates $PM_{2.5}$ concentrations. Particle-bound water constitutes 20-35% of the annual mean $PM_{2.5}$ concentrations (Tsyro, 2005); in our simulations aerosol water has not been included in $PM_{2.5}$ simulated values. Moreover, representation of secondary organic aerosol formation is uncertain, and low organic carbon has been noted in the CMAQ approaches (e.g., Kroll et al., 2006).

This work was supported by the FP7-REGPOT-2008-1grant No 229773. We gratefully acknowledge the first Air Quality Model Evaluation International Initiative (AQMEII) activity.

REFERENCES

Byun, D. W., and K. L. Schere (2006), Review of the governing equations, computational algorithms, and other components of the Models-3 Community Multiscale Air Quality (CMAQ) modeling system, *Appl. Mech. Rev.*, **59**, 51–77.

Grell, G., et al. (1994), A description of the fifth generation Penn State/NCAR mesoscale model (MM5), *Tech. Note NCAR/TN-398+STR*, Natl.Cent. for Atmos. Res., Boulder, Colo.

Kroll, J. H. et al., (2006), Secondary organic aerosol formation from isoprene photooxidation, *Environ. Sci. Technol.*, **40**, 1869–1877

Tsyro, S. G. (2005), To what extent can aerosol water explain the discrepancy between model calculated and gravimetric PM_{10} and $PM_{2.5}$?, *Atmos. Chem. Phys.*, **5**, 515–532.

A new model for estimation emissions of biogenic volatile organic compounds (BVOCs) from Hyytiälä in the southern Finland

Qingyang He[1], Michael Boy[1], Jaana Bäck[2], Janne Rinne[1], Markku Kulmala[1]
[1]*Department of Physics, PO Box 64, FI-00014 University of Helsinki, Finland*
[2]*Department of Forest Ecology, PO Box 27, FI-00014 University of Helsinki, Finland*
Correspondence to: Qingyang He (qingyang.he@helsinki.fi)
Keywords: SOSA, BVOCs, chemotype

BVOCs are essential in atmospheric chemistry because of the reactions to produce and destroy tropospheric ozone, the effects on aerosol growth and formation and the potential influence on global warming. Regional measurements and estimates are urgently needed to research carbon budgets and global climate. However, since various factors such as vegetation type, temperature and radiation have complicated impacts on BVOC emissions, comprehensive inventories are not so often reliably defined. To further track BVOC gas concentrations and their chemical transformations, BVOC emission rates are input into atmospheric transport and chemistry models [e.g., Poisson *et al.* 2000; Boauchet *et al.* 1999] (Levis *et al.* 2003). In this study, a new model SOSA (model to Simulate the concentrations of Organic vapours and Sulphuric Acid) which is a combination of meteorological transport, BVOC emissions and chemistry is applied to investigate Scots pine (*Pinus sylvestris*) tree emissions in a boreal coniferous forest in the SMEAR Ⅱ at Hyytiälä, Finland. To test the reliability of the model, simulation outputs are compared with measurement data collected from on-line chambers analysed by proton-transfer-reaction mass spectrometry (PTR-MS) analyzer. Results indicate that modeling and observations agreed reasonably well. The predominant species emitted from these coniferous trees is monoterpene with the main composition of α –pinene and $\triangle^3$–carene. Diurnal and seasonal variations are demonstrated in both quantity and quality of emitted compounds. Another significant phenomenon for BVOC emitters is discrepancy between branch scale emissions and above-canopy concentrations. In order to reduce uncertainty in measuring and modeling, a more detailed chemotypic characterization of BVOC blends needs to be constructed. In this research, SOSA is also used to estimate the contribution of different BVOC emissions especially monoterpenes and sesquiterpenes to the total OH reactivity.

Boauchet, V.S., R. Laprise, E. Torlaschi, and J.C. McConnell (1999) Studying ozone climatology with a regional climate model 1. Model description and evaluation. *J. Geophys. Res.,* 104(D23), 30351-30371.

Poisson, N., M. Kanakidou, and P.J. Crutzen (2000) Impact of non-methane hydrocarbons on tropospheric chemistry and the oxidizing power of the global troposphere: 3-dimensional modeling results. *J. Atmos. Chem.,* 36, 157-230.

S. Levis, C. Wiedinmyer, G.B. Bonan, and A. Guenther, (2003) Simulation biogenic volatile organic compound emissions in the community Climate System Model. *J. Geophys. Res.,* 105, 28863-28874.

Model comparison between global and regional climate-aerosol models ECHAM5-HAM and REMO-HAM: European aerosols

J.-P. Pietikäinen[1,2,3], D. O'Donnell[1], M. Kulmala[4], D. Jacob[2,3] and A. Laaksonen[1]
[1]Finnish Meteorological Institute, P.O. Box 503, 00101 Helsinki, Finland
[2]Max Planck Institute for Meteorology, Bundesstraße 53, 20146 Hamburg, Germany
[3]Climate Service Center, Bundesstraße 45 a 20146 Hamburg, Germany
[4]Department of Physics, University of Helsinki, P.O.Box 44, 00014, Helsinki, Finland
Keywords: aerosols, climate modelling, sulfur dioxide, nucleation
Presenting author email: joni-pekka.pietikainen@zmaw.de

REMO-HAM is a regional climate-aerosol model, which can be used to investigate aerosol-cloud-climate interactions starting from 10 km grid resolution. The model is a hydrostatic, three-dimensional atmospheric model, that has been developed at the Max-Planck-Institute for Meteorology in Hamburg (Jacob, 2001). The aerosol model in REMO is based on the HAM-M7 aerosol module (Stier *et al*, 2005).

We have done simulations with REMO-HAM and global climate-aerosol model ECHAM5-HAM. The data from ECHAM5-HAM has been used as driving field on the boundaries of REMO-HAM. The meteorological fields, as well as the nudging fields for ECHAM5-HAM, are from the European Centre for Medium-Range Weather Forecasts (ECMWF) operational data. So far, the simulation have been done for the year 2005, taking into account the spin-up times of the models. The resolution for ECHAM5-HAM was T63L31 (horizontally ∼210 km), and for REMO-HAM we used two different resolutions: 0.44° (50 km) and 0.088° (10 km).

The physics and chemistry part of the aerosols is similar in both models. The main differences are coming from the dynamical core of the models (for example the advection of tracers). The main switches of the models are chosen to be as close to each other as possible. Moreover, both of the models are using the AEROCOM (http://nansen.ipsl.jussieu.fr/AEROCOM/) vertically dependent emission data.

The Fig. 1 shows the measured and modelled sulfur dioxide (SO_2) gas phase concentrations and the total number concentrations from Hyytiälä for the year 2005. We can clearly see that ECHAM5-HAM overestimates the SO_2 concentrations, whereas REMO-HAM follows the measurements throughout the year. From the total number concentrations, we can see that REMO-HAM seems to underestimate the concentrations, whereas ECHAM5-HAM does not differ significantly during the year 2005. Nevertheless, based on our analysis, the high SO_2 concentration leads to an overestimation of nucleation mode particles due to the used binary sulfate/water based nucleation.

The models have only an emissions based proxy for the secondary organic aerosols. Moreover, the boundary layer nucleation was not used during the simulations. These both would only increase the total number concentrations, and thus we believe that the results from REMO-HAM are actually more realistic than the ones from ECHAM5-HAM.

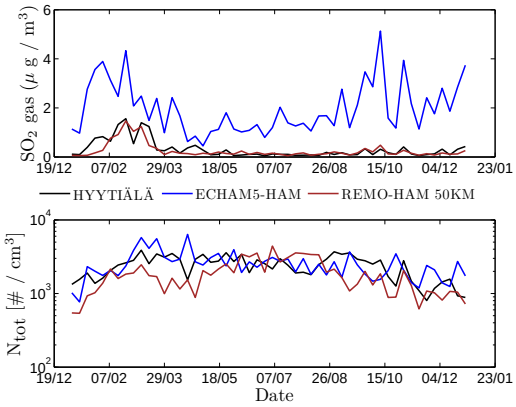

Figure 1: Measured and modelled gas phase sulfur dioxide (SO_2) concentrations as well as aerosol total number concentrations from Hyytiälä for the year 2005.

We have also done analysis for other measurement sites than Hyytiälä. The results from Melpitz, Mace Head and Jungfraujoch measurement sites show similar patterns as seen from the Fig. 1. Moreover, at the European scale, the spatial concentrations of nucleation mode particles seem to be too high in ECHAM5-HAM, especially in Northern Europe during the spring. Too high SO_2 concentrations increase the sulfuric acid (H_2SO_4) concentrations, which affects the nucleation rates directly.

In the future, we will concentrate on investigating the differences between the two models. The main focus will be in the gas phase SO_2 concentrations, H_2SO_4 formation, and in the nucleation. More detailed analysis and the main findings will be presented during the conference.

Jacob, D. (2001). A note to the simulation of the annual and inter-annual variability of the water budget over the Baltic Sea drainage basin. *Meteorol. Atmos. Phys.* **77**, 61-73.

Stier, P., et al. (2005). The aerosol-climate model ECHAM5-HAM. *Atmos. Chem. Phys.*, **5**, 1125-1156.

Modelling the buildup of aerosol loading over Italy during high-pressure conditions

M. Mircea[1], G. Briganti[2], A. Cappelletti[2], L.Vitali[1], G. Pace[1], M. D'Isidoro[1], I. Cionni[1],G. Righini[1], A. Piersanti[1], G. Cremona[1], C. Silibello[3], S. Finardi[3], G. Calori[3], L. Ciancarella[1], G. Zanini[1]

[1]ENEA, National Agency for New Technologies, Energy and Sustainable Economic Development, via Martiri di Monte Sole 4, 40129, Bologna, Italy
[2]ENEA, National Agency for New Technologies, Energy and Sustainable Economic Development, via G. Moruzzi 1, San Cataldo, Pisa, Italy
[3]ARIANET Srl, Via Gilino, 9, 20128, Milan, Italy

Keywords: PM10, air quality modelling, aerosol build-up, MINNI.
Presenting author email: mihaela.mircea@enea.it

High pollution episodes associated to anticyclonic meteorological conditions happen often in Italy, in particular in the northern part of the peninsula. This study investigates the increase of PM10 concentrations from 13 to 15 July 2005 using atmospheric modelling and measurements. The simulations were carried out with the Atmospheric Modelling System (AMS) of MINNI project (Zanini et al, 2010). The PM10 measurements were provided by the Italian air quality database BRACE.

Fig. 1 shows the percentage increases in PM10 concentrations modelled and measured at 7 stations. All the stations are of background type, apart the station 21021, which is a traffic station. The location of the stations as well as the differences in PM10 concentrations from one day to another are shown in Fig. 2. The results show that the AMS model is able to reproduce the increase in PM10 concentrations under high pressure conditions (Fig1). Moreover, it can be noticed that increases in PM10 concentrations from 3 to 9 µg/m^3 exist not only in the Po Valley, but also in other areas (Fig. 2).

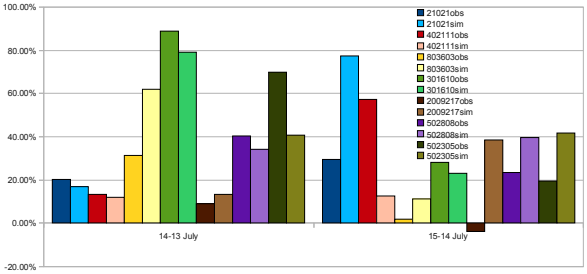

Figure 1. Percentage variations in aerosol concentrations for PM10 observations and model simulations.

The contribution of different species to the aerosol buildup during this period in relation to the emissions and meteorological conditions is also investigated.

This work is part of the MINNI (Integrated National Model in support to the International Negotiation on Air Pollution) project, funded by the Italian Ministry for Environment and Territory and Sea and carried out by ENEA.

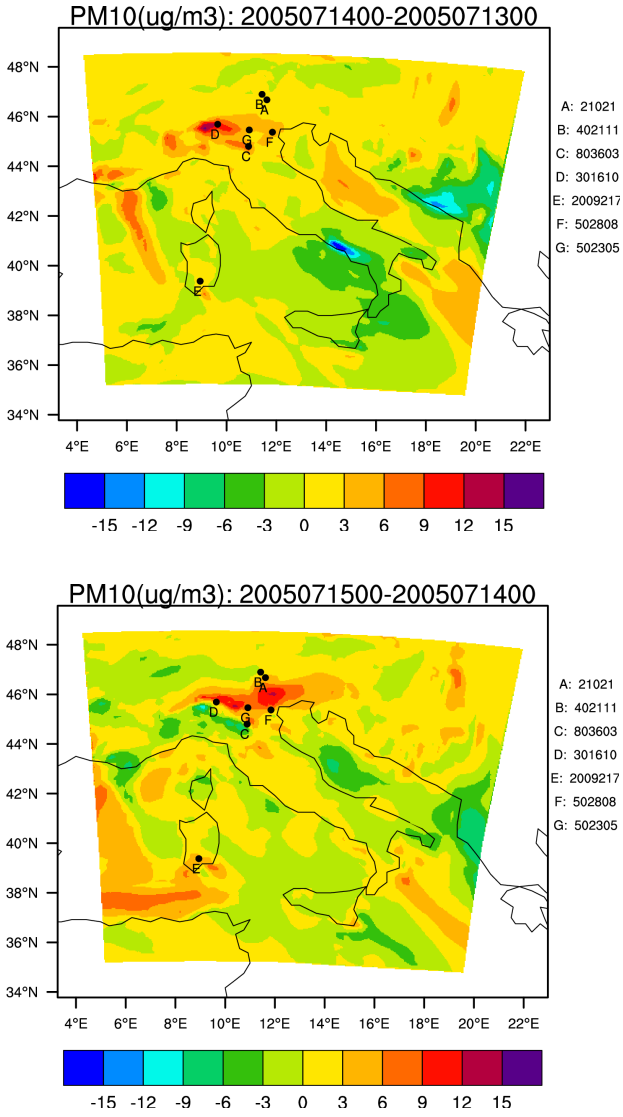

Figure 2. Differences in aerosol concentrations between July, 14 and 13, and between July, 15 and 14.

Zanini, G., Mircea, M., Briganti, G., Cappelletti, A., Pederzoli, A., Vitali, L., Pace, G., Marri, P., Silibello, C., Finardi, S., Calori, G. (2010) *Proc. of 31st NATO/SPS Int. Tech. Meeting on Air Pollution Modelling and its Application held 27 September - 1 October, 2010 in Torino, Italy*, in press.

Validation of the regional aerosol climate model REMO-HAM under East Asian conditions

S. Fiedler[1,2], J. Pietikäinen[1,3,4] and D. Jacob[1,3]
[1]Climate Service Center, Helmholtz Centre Geesthacht, Bundesstraße 45A, Hamburg, 20146, Germany
[2]School of Earth and Environment, University of Leeds, Leeds, LS29JT, UK
[3]Max-Planck-Institute for Meteorology, Bundesstraße 53, Hamburg, 20146, Germany
[4]Finnish Meteorological Institute, P.O. Box 503, 00101 Helsinki, Finland
Keywords: Aerosol model, climate modelling, Asian aerosols
Presenting author email: stephanie.fiedler@hzg.de

One of the most discussed influences of micro-physical processes in the climate system is the role of aerosols. They interact with radiation through scattering and absorption, which may lead to a change in the regional energy budget directly. Further the particles may act as possible cloud condensation nuclei and, thus, alter the cloud development. This, in turn, might have an impact on the regional water and energy balance indirectly. Despite these discussions, the majority of climate models represent aerosols by simplified, mostly out of date approaches.

This work presents the first high resolution climate simulation for East Asia from the new regional aerosol climate model REMO-HAM (Pietikäinen *et al*, 2011). REMO-HAM is based on the regional climate model REMO (e.g. Jacob, 1997). The size-resolving aerosol micro-physics module HAM-M7 (Vignati, 2004) and the double-moment cloud micro-physics scheme by Lohmann (2007) is implemented to describe the aerosol effect in the climate system with more detail. Following the standard global driving aerosol climate model ECHAM5-HAM (Stier, 2005), the represented aerosol species in REMO-HAM are black carbon BC, mineral dust DU, sea salt SS, particulate organic matter POM and sulphate S. These aerosol species are distributed into four discrete aerosol modes, namely the nucleation mode for an effective radius r < 5nm, the accumulation mode with r = (5nm; 50nm] , the Aitken mode for r = (50nm; 0.5µm] and the coarse mode with r > 0.5µm.

East Asia is known to experience heavy aerosol loads relative to other regions on Earth. Representing aerosols in the regional climate model may be a major factor to produce robust climate information under both current and possible future conditions for this area. A model domain in East Asia is chosen to test the reliability of REMO-HAM under comparably large aerosol concentrations. The usage of a limited area model enables to increase the horizontal resolution. Climate relevant features are described with more detail than in global aerosol climate models which simulate aerosol-climate information on a typical horizontal grid distance of 100km.

REMO-HAM is run on a horizontal grid of 0.22° (~25km) for the year 1993. The lateral boundary data of the meteorological fields are taken from the ERA-interim reanalysis. ECHAM5-HAM is nudged to reanalysis of ECMWF to provide the lateral driving data for the aerosol fields. Aerosol emissions are based on the AEROCOM emission inventory for 2000. The model is expected to show the closest results to observed climate under these boundary conditions. It is the first application of REMO-HAM outside of European conditions for which it has been developed.

The model is shown to simulate both aerosol and meteorological fields reasonable well under East Asian conditions. For instances, differences between the summer mean near surface air temperature from REMO-HAM (Figure 1) and observed conditions lie within the observation uncertainty in most areas over land. This reliability of REMO-HAM is the basis for robust future climate and climate change studies including regional aerosol-climate effects.

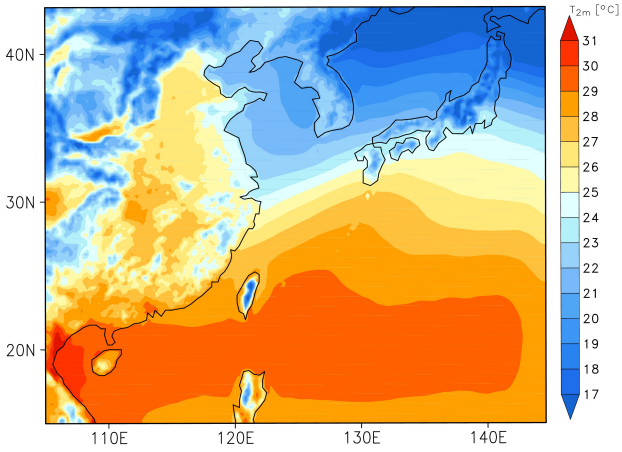

Figure 1. Summer (JJA) mean near surface air temperature from REMO-HAM 1993.

We acknowledge the usage of ERA-interim reanalysis of ECMWF. This work was supported by the Helmholtz Centre Geesthacht.

Lohmann, U., Stier, P., Hoose, C., Ferrachat, S., Kloster, S., Roeckner, E. and Zhang J. (2007) *Atmos. Chem. Phys.*, **7,** 3425–3446.

Pietikäinen, J., Teichmann, C., Karsten, U., Pfeifer, S., Kazil, J., Podzun, R., Rast, S., Fiedler, S., Kokkola, H., Birmili, W., O'Dowd, C., Baltensperger, U., Weingarten, E., Gehrig, R., Spindler, G., Kulmala, M., Feichter, J., Jacob, D., Laaksonen, A. (2011) *In preparation for Geosci. Model Dev.*

Stier, P., Feichter, J., Kinne, S., Kloster, S., Vignati, E., Wilson, J., Ganzeveld, L., Tegen, I., Werner, M., Balkanski, Y., Schulz, M., Boucher, O., Minikin, A., Petzold, A. (2005*): Atmos. Chem. Phys.*, **5**, 1125–1156.

Vignati, E. and Wilson, J. (2004) *Journal of Geophy. Res.*, **109**, D22202.

New 3-Dimensional Model to Study atmospheric processes in Planetary Boundary Layer

Gopalkrishnan K.V[1], M. Boy[1], H. Vuollekoski[1], S. Smolander[1], A. Sogachev[2] and T. Vesala[1]

[1]Department of Physics, University of Helsinki, P.O. 48, 00014, Helsinki, Finland
[2]Wind energy Department, Riso National Laboratory for Sustainable Energy, Technical University of Denmark, Building 118, P.O.Box 49,4000,Roskilde, Denmark
Keywords: Nucleation, Meteorology, Emissions

Presenting author email: gopalkrishnan.kokkatil@helsinki.fi

Nucleation is one of several scientific phenomena which are presently under investigation. A lot of complex chemical processes occur in the Atmospheric Boundary Layer (ABL) and it is essential to have a thorough understanding of these processes. This actually defines the chemistry and the aerosol dynamics in the atmospheric boundary layer (ABL). To do so we have developed a spatial and temporal high resolution 3 dimensional model which attempts to reconstruct the emissions, transport and chemistry and aerosol processes in the mixed layer. The new code integrates a meteorological module, an emission module, a chemical kinetics module and an aerosol dynamics module.

The meteorological model is based on the coupled biosphere-atmosphere boundary layer model SCADIS (SCAlar DIStribution). SCADIS is based on Reynolds-averaged Naviers-Stokes equations (RANS). The model was initially described in (Sogachev et al., 2002). Turbulent fluxes are expressed as the product of eddy diffusivity and the vertical gradient of a mean quantity. The model is based on the E - ω closure where E is the turbulent kinetic energy (TKE) and $\omega = \varepsilon/E$ is the specific dissipation, where ε is the dissipation rate of TKE.

Emissions from the canopy were simulated using the Model of Emissions of Gases and Aerosols from Nature (MEGAN). This is a system for estimating the net emissions of gases and aerosols from terrestrial ecosystems in to the atmosphere. The model estimates the leaf area, plant species composition and species specific emission factors for a given specific location. MEGAN is a global model with a base resolution of approximately 1 km. This makes it favourable to be used in regional as well as in global models. The driving variables in MEGAN include land cover, meteorological factors and atmospheric chemical composition. These driving variables are obtained from different models, satellite and ground observations (Guenther et al., 2006).

The chemistry which accounts for most of the simulation time was taken from the Master Chemical Mechanism (MCM). MCM is a near explicit chemical mechanism that describes the degradation of about 135 volatile organic compounds (VOC). This mechanism is implemented in to Fortran 90 using KPP (The Kinetic PreProcessor). The KPP is a general analysis tool that generates a FORTRAN or C code that computes the time evolution of the chemical species starting with a specification of a chemical mechanism which in our case is the MCM.

The aerosol dynamics is integrated in to the model using the University of Helsinki Multicomponent Aerosol model (UHMA). The main objective of this model is to study the new particle formation under clear sky condition in the troposphere (Korhonen et al., 2004). The size-segregated, sectional box model included all basic aerosol dynamical processes: nucleation, condensation, coagulation and dry deposition,

The new developed model utilizes parallel computing using MPI (Message Passing Interface). It is now possible to run the code on multi-core clusters and thus reducing the time per simulation, which gives us the possibility for long-term investigations with reasonable computational costs. The main focus was to study various nucleation theories (e.g binary nucleation of sulphuric acid and water or ternary nucleation for sulphuric acid, water and ammonia) in and above the ABL for the SMEAR II in Hyytiälä, Finland. Further we studied the chemical processes and feedback mechanisms crucial for aerosol formation and nucleation processes. The presentation will give concentrate on the simulations performed for Hyytiälä in comparison with ground and air-born achieved measurements.

References:

Sogachev,A, Menzhulin,G., Heimann. M.,Lloyd,J.(2002) A simple three dimensional canopy-planetery boundary layer simulation model for scalar concentrations and fluxes, Tellus,54B,784-819

Guenther, A., Karl,T., Harley, P., Wiedinmyer, C., Palmer, P.I., and Geron, C.(2006) Esitmates of global terrestrial isoprene emissions usinf MEGAN (Model of Emissions of Gases and Aerosol from Nature), Atmos. Chem.Phys.,6,3181-3210.

Korhonen, H., Lehtinen, K. E. J. and Kulmala, M. (2004) Multicomponent aerosol dynamics model UHMA:model development and validation Atmos. Chem. Phys., 4, 757-771.

Numerical study of performances of RespiCon sampler in calm air

S. Zaripov[1], W. Koch[2]

[1]Kazan Federal University, Kazan, 420008, Russia
[2]Fraunhofer Institute Toxikologie und Experimentelle Medizin, Hannover, D-30625, Germany

Keywords: aerosol sampling, collection efficiency, calm air, CFD
Presenting author email: shamil.zaripov@ksu.ru

The results of a numerical study of performances of the RespiCon sampler in calm air are presented. The obtained theoretical curves of collection efficiencies agree well with experimental data and conventional curves of corresponding dust fractions. The results of the numerical study were used to design a new Respicon sampler with a higher volume flow rate.

The RespiCon sampler for personal, time-resolved concentration monitoring and sampling of aerosol particles was designed in Fraunhofer Institute Toxikologie und Experimentelle Medizin (Koch et.al., 1999). The RespiCon sampler consists of a sampling inlet and two virtual impactor stages and offers an opportunity to use a single sampling device for collecting simultaneously either the personal or area samples of the respirable, thoracic and inhalable fractions of airborne dust. The sizes of particles of these fractions are defined in European and U.S. standards for health-related dust measurements at the workplace. The RespiCon sampler has a circular inlet around the inlet-head perimeter (fig.1). Because of this the aerosol is aspirated into the inlet uniformly from all wind directions. The virtual impactor serves as a classifier of particle sizes and concentrator of coarse particles. The performances of RespiCon were experimentally studied by Koch et.al. (1999), Li et.al. (2000), Koch et.al. (2002) and Feather&Chen (2003).

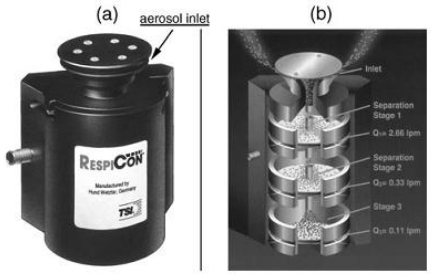

Figure 1. Picture and schematic drawing of RespiCon sampler. Source: catalog of TSI,Inc.

In this work a mathematical model of an aerosol flow around and inside the RespiCon sampler in calm air was developed. The gas flow is described by the Navier-Stokes equations of axisymmetric stationary viscous incompressible flow. The Navier-Stokes equations are numerically integrated by CFD code FLUENT. The particle trajectories are found by the numerical solution of equations of particle motion in the calculated gas flow velocity field. In so doing the values of flow velocity components are found by interpolation.

Far from the sampler the particles move downward in still air by gravity action with the settling velocity $\bar{V}_s = \tau \bar{g}$ (τ is the particle relaxation time). The tube of the limiting particles trajectories that divides the sampled and unsampled particles is found. The aspiration efficiency of the sampler inlet is calculated using the value of cross-section area of the tube of limiting trajectories far from the sampler. The collection efficiency of virtual impactor stages are found by means of an analogous approach.

The aspiration efficiency of the inlet and the collection efficiencies of the impactor stages as a function of the particle diameter are shown in fig.2. The obtained dependencies agree well with experimentally determined efficiencies and three conventional curves of particle fractions. To extend the region of application of RespiCon sampler a new device with twice the flow rate was constructed. The performances of the new device were also studied numerically. The results of the numerical study confirm that the performances of the new device are acceptable for measurements of the aerosol concentration in indoor workplaces at higher flow rates.

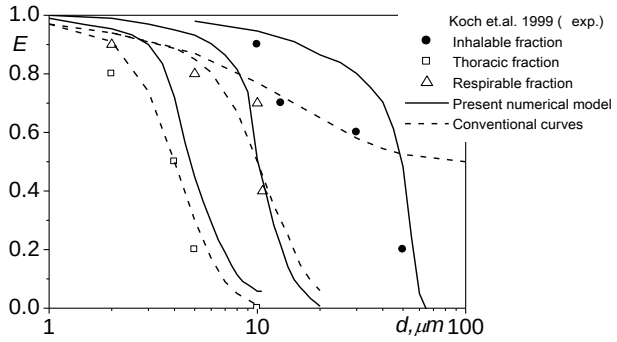

Figure 2. Collection efficiencies of RespiCon stages as a particle diameter function

Koch, W., Dunkhorst, W., Lodding, H. (1999) Aerosol Science and Technology, 31, 2, 231-246.

Koch, W., Dunkhorst, W., Lodding, H., Thomassen, Y., Skaugset, N.P., Nikanov, A., Vincent, J. (2002) J. Environ.Monit., 4, 657–662.

Feather, G.A., Chen, B.T. (2003) Aerosol Science and Technology, 37, 261-270.

Li, S.-N., Lundgren, D.A., Rovell-Rixx, D. (2000) AIHAJ, 61, 506–516.

Bio-particle emission and distribution over slums in a tropical Indian metropolis

C. R. S. Kumar[1], S. Ghosh[1,3], K. Sethia[2] and J. R. Picardo[1]
[1]School of Mechanical and Building Sciences, VIT University, Vellore, India
[2]School of Information Technology Engineering, VIT University, Vellore, India
[3]ICAS Associate, School of Earth and Environment, University of Leeds, U.K.
Keywords: Black carbon, sulphur dioxide, dispersion, modelling.
Presenting author email: satgleeds@gmail.com

Chennai, the Capital of Tamil Nadu, with a population over 4 million is among the fastest growing urban conurbations anywhere in the world. A huge population lives below the poverty line in slums distributed throughout the Chennai Metropolitan area especially in North Chennai as in shown in Figure 1 (created using GIS based software MAPINFO).

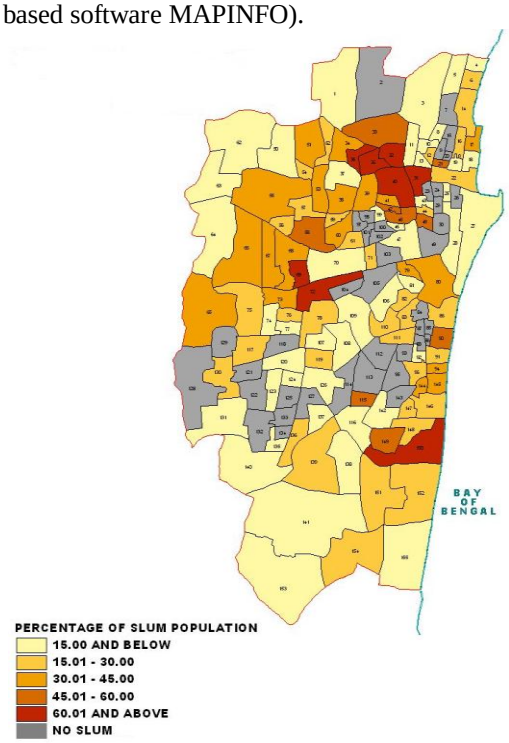

Figure 1. Percentage of total population (per division) living in slums in Chennai

Cow dung cakes and firewood constitute around 25% of the total fuel used by slum dwellers for cooking (Chandramouli, 2003). The main aim of this first study is to quantify the extent of BC and SO_2 pollution from domestic bio-fuel consumption using published demographic information. The results can be used for Environmental Impact Analyses, Regional Pollution Forecasts (CPCB 2010) and eventually as inputs to climate models concerned with direct, indirect as well as semi-direct effects. Recent studies (Ghosh et al. 2007; Rap et al. 2009) have shown that cloud droplet number concentrations are not always directly proportional to aerosol number concentrations, particularly when the activation domain comprises of multiple aerosol types. In a polluted city like Chennai, one would expect the BC particles to contain soluble sulphates enabling them to activate into cloud droplets. We use the AERMOD software (USEPA) with an area source option and variable emission rates, based on local cooking patterns, to compute BC (in terms of PM10) and SO_2 distributions.

Emission factors are calculated according to the procedures outlined in Habib *et al* (2004). Representative weather information was obtained from published literature (Pavuluri et al., 2010; CPCB 2010) and the World Wide Web. The weather in Chennai is generally hot and humid. The winds blow in from the east-southeast from February to May then reverse direction from June to September and finally bring in the northeast monsoon in October which lasts until January.

In this abstract we show results of BC for a typical August day (late summer) where we have considered emissions from areas in Chennai city in which the slum population exceeds 60% (Figure 2). Figure 2 reveals high BC concentrations from just domestic fuel consumption in Chennai slums. These results will be compared with observations.

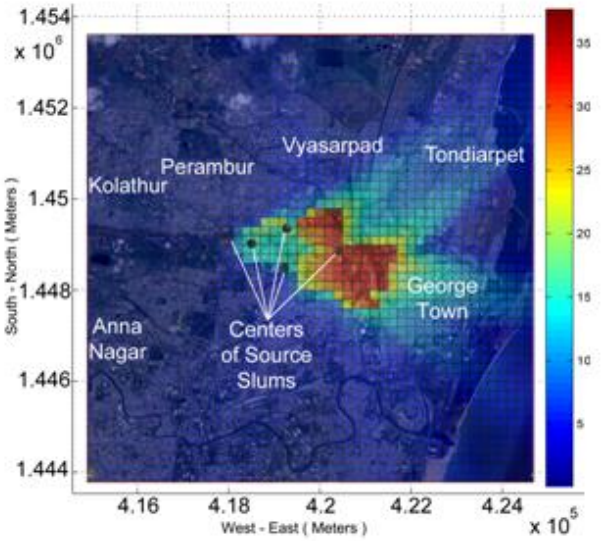

Figure 2 Highest Three hour average PM10 concentration over the study area (μg/m^3)

Habib, G., Venkataraman, C., Shrivastava, M., Banerjee, R., Stehr, J. W. and Dickerson, R. R. (2004) *Global Biogeochemical Cycles*, 18, GB3007.

Chandramouli, C., (2003) *Proc. of the Third International conference on Environment and Health, Chennai, India*, 82-88.

National Summary Report (2010), Central Pollution Control Board(CPCB), Delhi, India,113.

Rap, A., Ghosh, S. and Smith, M. H. (2009) *J. Atmos. Sci.*, **66**, 105–115.

Ghosh, S., Smith, M. and Rap, A. (2007) *Philos. Trans. Roy. Soc.* **365A,** 2659-2674.

AERMOD modelling system, U.S. environment protection agency, available online: http://www.epa.gov/ttn/scram/dispersion_prefrec.htm#aermod

Further experience with low emission zones in Germany: will the next stage do the job?

S. Wurzler[1], P. Bruckmann[1], V. Diegmann[2], F. Pfäfflin[2], A. Brandt[1]

[1] North Rhine Westphalia State Agency for Nature, Environment, and Consumer Protection, Wallneyer Str. 6, 45133 Essen, Germany
[2]IVU Umwelt GmbH, Emmy-Noether-Strasse 2, D-79110 Freiburg, Germany

Keywords: PM10, NO_2, emission reduction, air quality, low emission zone

Urban road traffic poses a problem not only to German cities but also to cities all over Europe. Air quality in street canyons with high traffic densities is still far from meeting the air quality limit values required by the EC air quality directives. Especially the number of days with average PM10 concentrations above 50 µg/m³ and the annual average NO_2 concentrations frequently exceed the respective limit values. Allowed are 35 days with average PM10 concentrations above 50 µg/m³ and an annual average value of 40 µg/m³ for NO_2.

In order to reduce the pollution loads measures must be taken. One possible measure is the implementation of low emission zones. In many parts of Europe low emission zones have been implemented and their number has been growing in recent years. Low emission zones are areas inside conurbations where measures are taken to reduce the emission load. Currently, most implementations focus on measures to reduce road traffic emissions with the aim to improve air quality significantly. The measures comprise road traffic regulations, i. e. vehicles that do not meet certain emission standards are prohibited inside the low emission zones.

Meanwhile quite a bit of experience has been collected with stage 1 of the low emission zones in Germany. Even though stage 1 proved to be an effective measure to reduce the pollution loads, there still remain numerous street canyons with such high concentrations of air pollutants (especially NO_2) that the limit values are still exceeded. Therefore further measures must be taken. One of those measures is stage 2 of the low emission zones. The aim is to reduce road traffic emissions further. Stage 2 comprises even stronger road traffic regulations in the low emission zones, i. e. only vehicles with state of the art emission standards are allowed to enter. However, the question remains whether stage 2 of the low emission zones will do the job.

Quantifying the effects of low emission zones on air quality is not a trivial task. Model studies have been carried out in order to investigate the potential benefits of such zones, e. g., by the authors for the Ruhr Area.

This paper reviews some of the German experiences with low emission zones, with special focus on the Ruhr Area. A review of the results (field observations and modelling) obtained with stage 1 will be given and model results of the potential effects of stage 2 will be shown. The focus is on the effects on air quality with respect to PM10 and NO_2.

Our paper shows that the modelled and the measured effects of stage 1 of the low emission zones are of the same magnitude. For the potential effects of stage 2 only model results exist and will be reviewed. Fig. 1 shows model results for some selected street canyons in the Ruhr Area. Stage 1 and stage 2 of the low emission zones have in common that the effect on air quality is proportional to the traffic density.

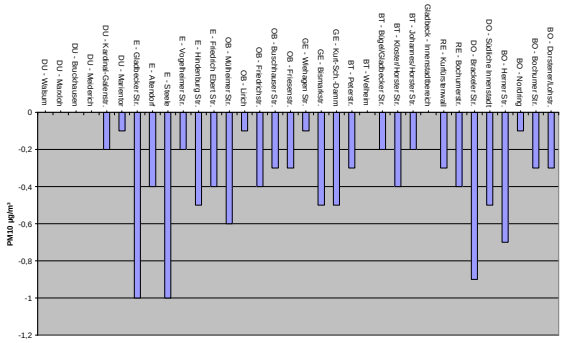

Figure 1. Reduction of the PM10 load (annual average in µg/m³) in some selected street canyons in the Ruhr Area. Increased effect obtained by stage 2 as compared to stage 1 of the low emission zones.

Even though many low emission zones have been implemented lately, most of them comprise only stage 1. There are no annual measurements of the effects of stage 2 available yet. More investigations and experiences, also from further cities and nations, are needed to fully evaluate the effects of low emission zones.

Stabilizing action of the vertical wind on spatial distribution of stratospheric aerosol

V.I. Gryazin and S.A. Beresnev

Aerosol Physics Laboratory, Ural State University, Ekaterinburg, 620083, Russia
Keywords: aerosol modelling, stratospheric aerosols, aerosol dynamics, vertical wind.
Presenting author email: sergey.beresnev@usu.ru

This study continues and summarizes analysis and estimations of transport opportunities of the vertical wind in stratosphere. Characteristics of vertical component of wind velocity is of interest not only for qualitative description of its altitude-, seasonal- and latitude dependences, but also for quantitative description of features of the aerosol vertical transport in the middle atmosphere (Gryazin and Beresnev, 2011).

The first purpose of given report – to present results of climatological analysis of vertical wind in the stratosphere. High-altitude, temporal, and latitude dependences of zonal mean averaged vertical wind velocity for the period of 1992-2006 from the UKMO atmospheric general circulation model are analyzed (Figure 1). It is shown that monthly averaged amplitudes of the vertical wind are approximately ±5 mm/s, while annual averaged ones are ±1 mm/s (Beresnev *et al*, 2008). We have carried out the comparison of the received results with the NCEP-NCAR reanalysis data, and have found out their qualitative agreement.

The upward wind can provide the vertical lifting against gravity for sufficiently large (up to 3-5 μm) aerosol particles with a density up to 1.0-1.5 g/cm^3 at stratospheric and mesospheric altitudes. The vertical wind, probably, is a substantial factor for particles motion up to altitudes of 30-40 km, and can change essentially the sedimentation velocities and the residence times of stratospheric aerosols. The structure of the averaged fields of vertical wind supposes the opportunity of formation of dynamically stable aerosol layers in the middle stratosphere (Beresnev *et al*, 2009).

For the problem about action of a permanent source of monodisperse particles near the stratopause, it is shown that action of the averaged vertical wind along with the gravitational sedimentation and turbulent diffusion changes the standard vertical profiles of the relative concentration of particles cardinally. Estimations for the levitation heights for particles of different densities and sizes in the stratosphere under action of gravity and vertical wind are presented also (Gryazin and Beresnev, 2010).

The method of comparison of vertical motion characteristics for spherical and fractal-like aerosol particles in stationary atmosphere and in atmosphere under action of the averaged vertical wind is introduced. It consists in introduction of suitable equivalent radius (sedimentation radius) for fractal-like particles, and in comparison of subsidence velocities identical on mass of introduced spherical particle and the real fractal-like aggregate. It is shown, that subsidence velocities of compact spherical and fractal-like particles can differ essentially in this case.

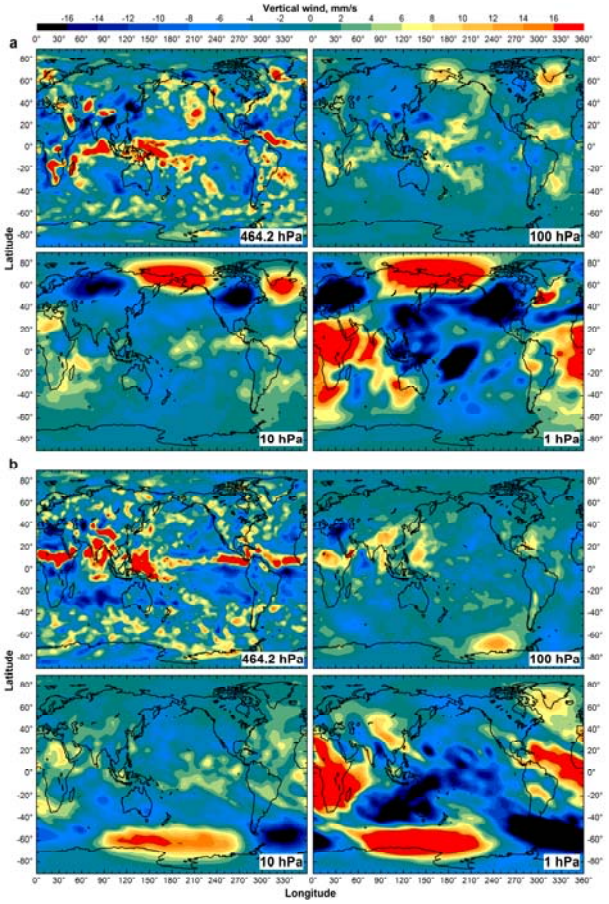

Figure 1. Geographic distribution of monthly-averaged vertical wind velocity at two characteristic altitudes for January (a) and July (b), 2005.

We are grateful to the BADC which provided us with access to the UKMO Stratospheric Assimilated Data. This work was supported in part by the Russian Foundation for Basic Research (grants No. 09-01-00649 and 09-01-00474), and by the Ministry of Education and Science of the Russian Federation (program "Development of the Scientific Potential of the Higher School (2009-2010)," Reg. No. 2.1.1/6019, and contracts No. 1571 and 1151).

Beresnev, S.A., Gryazin, V.I. and Gribanov, K.G. (2008) *Atmos. Oceanic Opt.* **21**(6), 448-454.

Beresnev, S.A., Gryazin, V.I. and Gribanov, K.G. (2009) *Rus. Meteor. Hydrol.* **34** (11), 724-731.

Gryazin, V.I. and Beresnev, S.A. (2010) *Atmos. Oceanic Opt.* **23**(3), 174-180.

Gryazin, V.I. and Beresnev, S.A. (2011) *Meteor. Atm. Phys.* **110**(3-4), 151-162.

Bayesian forecast of urban particle number concentrations

B. Mølgaard[1], T. Hussein[2], J. Corander[3] and K. Hämeri[1]

[1]Department of Physics, University of Helsinki, Helsinki, 00014, Finland
[2]Department of Physics, University of Jordan, Amman, 11942, Jordan
[3]Department of Mathematics and Statistics, University of Helsinki, Helsinki, 00014, Finland
Keywords: urban aerosols, number concentration, statistical analysis
Presenting author email: bjarke.molgaard@helsinki.fi

Aerosol particle concentrations are often elevated in cities due to traffic and other anthropogenic sources. These particles may cause adverse health effects. The concentrations also depend on weather conditions. Clear links between the number concentration of fine particles and temperature and wind have been established in other studies (Hussein *et al*, 2006, Olivares *et al*, 2007, Jones *et al*, 2010).

We have developed a statistical model which provides forecast of particle number concentrations. The model is of the form:

$$\log(N) = f(X) + \varepsilon,$$

where N is the number concentration of some size fraction, X is a vector of covariates (predictors), and ε is a normal distributed error term. f is linear in its parameters and we included autoregression on the error term ε as suggested by Chib (1993). As covariates we used temperature, wind speed and direction, relative humidity, traffic intensity, time of day, time of week, and time of year. We have applied the model to the number concentrations of two size fractions: 3 – 100 nm (ultra-fine particles, UFP) and 100 – 950 nm (accumulation mode). Our data are from an urban background station in Helsinki. The model was implemented in a Bayesian framework, so it provides probability distributions as forecasts. We used learning data starting from beginning of 2005 and made forecasts for the years 2006 – 2008 with time resolutions of 1 hour and 3 hours. The forecasts were made for one day at a time assuming particle data known until noon the previous day.

A common measure of model performance is the R^2 value provided in Table 1. Here we see that the model performs best for UFP. The reason is probably that the UFP concentration is stronger affected by local sources (such as traffic) and local weather conditions. A scatter plot of the values which were used for calculating the best R^2 is given in Figure 1. Here we see that the model has less difficulty in predicting the highest concentrations correctly than in predicting the lowest.

Table 1. R^2 values for the two size fractions at the two time resolutions.

	1 hour resolution	3 hour resolution
UFP	0.627	0.669
Accumulation mode	0.516	0.572

While testing the model we used actual measured values for the covariates. In a real life implementation of the model future weather and traffic intensity would only be known through forecasts, and the performance of the model would be affected quality of the weather and traffic forecasts.

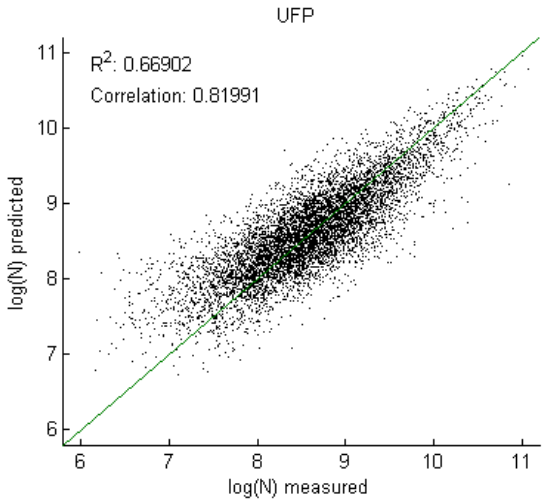

Figure 1. Comparison of forecast and measurement. Natural logarithm used. The unit of the number concentration N is particles/cm^3.

This work is a part of the Ubicasting 2 project funded mainly by TEKES. We thank the Finnish Transport Agency (Liikennevirasto) for providing traffic data.

Chib, S. (1993) *J. Econometrics,* **58,** 275-294.
Hussein, T., Karppinen, A., Kukkonen, J., Härkönen J., Aalto, P.P., Hämeri, K., Kerminen, V.M., and Kulmala, M. (2006) *Atm. Environ,* **40,** 1427-1440.
Jones, A.M., Harrison, R.M., and Baker, J. (2010) *Atm. Environ,* **44,** 1682-1690.
Olivares, G., Johansson, C., Ström, J., Hansson, H.C. (2007) *Atm. Environ,* **41,** 2145-2155

Regional chemical weather modelling of the UK using WRF-Chem as part of the RONOCO project

S. Archer-Nicholls[1], S. Utembe[1], D. Lowe[1] and G. McFiggans[1]
[1]Centre for Atmospheric Sciences, SEAES, University of Manchester, UK, M13 9PL
Keywords: Regional modelling, WRF-Chem, NO_3 chemistry, nitrate aerosol, secondary organic aerosols.
Presenting author email: scott.archer-nicholls-2@postgrad.manchester.ac.uk

The ROle of Night time chemistry in controlling the Oxidising Capacity of the atmOsphere (RENOCO) campaign is a project being funded by NERC and being carried out by a collaboration of UK Universities. The primary objective of the is to better understand the role of the NO_3 radical on the chemistry of the night time atmosphere, and thus its overall effects on the composition of the troposphere. It is believed that NO_3 is the primary oxidant at night time, significantly impacting ozone formation, rain acidification and the formation and transformation of aerosols, particularly through the formation of the ammonium nitrate particulate. However, many of the basic chemical processes controlling the formation and removal of NO_3 and its reactions with volatile organic compounds (VOCs) are still poorly understood. The investigation of these processes is essential to gain a better understanding of how NO_3 chemistry affects the aerosol burden and composition on a regional and global scale.

As part of the RONOCO project, an extensive modelling campaign has been undertaken to investigate night time chemistry. A multi-tiered approach has been taken, whereby detailed box-models have been used to study individual processes, with these results feeding into larger models used to investigate the wider impacts on regional and global scales. The goals of the regional scale modelling have been to compare the extent of night time NO_3-VOC chemistry with that of daytime NO. This in turn helps us better understand how oxidation with NO_3 affects radical budgets and ozone formation. In addition, we have estimated the contribution of N_2O_5 hydrolysis to the formation of the nitrate aerosol, investigating how this process may control NO_3 concentrations and hence how aerosol composition may impact the night time atmospheric lifetime of VOCs.

To investigate the regional impacts of these processes, we have used the Weather Research and Forecasting model with Chemistry (WRF-Chem), a state of the art regional climate model with fully coupled air quality and meteorological components allowing for better resolution of aerosol and gas-phase chemistry (Grell et. al., 2005). A UK domain has been simulated at a fine, 5km resolution and nested within a more coarse domain covering a wider area over Northern Europe and the Atlantic. Detailed emission inventories have been inputted and varied within the model.

Recent extensions to WRF-Chem have been developed and used in this application, enabling the representation of several key processes being investigated within the RENOCO campaign, making WRF-Chem an ideal model to use for the purposes of this investigation. In particular, the Common Representative Intermediates scheme (CRIv2-R5) (Watson et. al., 2008), a reduced chemical scheme designed to simulate the atmospheric degradation of 220 species of hydrocarbons and VOCs, is used to simulate gas-phase chemistry. Condenced-phase chemistry is represented using the MOSAIC aerosol scheme (Zaveri et al, 2008), which has been extended to include a reduced complexity condensed organic phase consisting of 13 semi-volatile and 2 involatile species (Topping and Lowe, 2011). These two additional schemes have been coupled together, allowing for WRF-Chem to better simulate how the NO_3 radical reacts with various organic compounds found in the troposphere and how this in turn contributes to the formation of secondary organic aerosols, impacting the loading and composition of atmospheric particulates.

We will present results from the application of WRF-Chem to model the regional climate about the UK under changing emission profiles and oxidant conditions. Findings on role of the NO_3 radical on the formation and transformation of tropospheric aerosols and the resulting composition of particulate matter will be displayed. The wider impacts of these processes on the regional climate and air quality will be further discussed.

Grell, G., Peckham, S., Schmitz, R., McKeen, S., Frost, G., Skamarock, W., & Eder, B. (2005). Atmos. Environ., 39, 6957- 6975.

Topping, D., & Lowe, D. (2011). submitted to J. Geophys. Res.

Watson, L., Shallcross, D. E., Utembe, S. R., & Jenkin, M. E. (2008), Atmos. Environ., 42, 7196- 7204.

Zaveri, R.A., Easter, R.C., Fast, J.D., & Peters, L.K. (2008). J. Geophys. Res., 113, doi:10.1029/2007JD008782

Motion of charged aerosol particles in a cylinder array

T. Zaripov, A. Egorov, D. Demidov

Institute of Mathematics and Mechanics, Kazan Federal University, 420008, Kazan, Russia

Keywords: aerosol filtration, collection efficiency, charged particles, CFD
Presenting author email: zaript@gmail.com

The motion of charged aerosol particles in the porous medium consisted of an array of circular cylinders is theoretically studied. The mathematical model is based on the solution of gas flow equations, equations of particle transport and electric potential. The particle concentration, electric potential distributions and collection efficiency are studied.

The transport and deposition of aerosol particles in the porous medium have many experimental and industrial applications. The diffusion, impaction and gravity actions are not enough to provide the deposition of aerosol particles in the intermediate range of sizes ~0.1-1 μm. In this case the particle charging is used to increase the deposition by the electrostatic force action (Yu&Chandra, 1977, Alonso&Alguacil, 2007).

The motion of charged aerosol particles in a periodic bar of an array of circular cylinders is numerically studied (fig.1). Under the assumption of a steady incompressible fluid flow the gas velocity field is found by numerical solution of the Navier-Stokes equations using CFD code FLUENT.

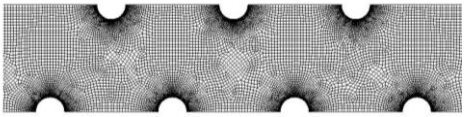

Figure 1.

At the given distribution of space concentration C of charged particles the potential F of electric field can be found from the Poisson equation

$$\Delta F = -qC/\varepsilon_0 \qquad (1)$$

where q is the charge quantity, ε_0 is the permittivity of the air. The stationary equation for particle flux J due to convection, diffusion and electrostatic migration is written as

$$\nabla \cdot J = \bar{U} \cdot \nabla C - D\Delta C + qb\nabla \cdot \left(C\nabla F\right) = 0 \qquad (2)$$

where D is the diffusion coefficient, $\bar{U}$ is the gas velocity, $b = C_c/3\pi\mu d$ is the particle mobility, d is the particle diameter, C_C is the Cunningham correction factor. In a non-dimensional form equations (1,2) can be rewritten as

$$\bar{u} \cdot \nabla c - Pe^{-1}\Delta c + \alpha\nabla \cdot \left(c\nabla\varphi\right) = 0 \qquad (3)$$

$$\Delta\varphi = -c \qquad (4)$$

where $\bar{u} = \bar{U}/U_0$, $Pe = hU_0/D$, $\varphi = F\varepsilon_0/qC_0$, $c = C/C_0$, $\alpha = q^2C_0b/hU_0\varepsilon_0$, h and U_0 are the length and velocity scales, C_0 is the input concentration of particles.

The boundary conditions on the cylinders surfaces are $c(r_f) = 0$, $\varphi(r_f) = 0$ (r_f is the cylinder radius). On the top and bottom sides of the bar the symmetry conditions are given. The relative input concentration of particles is equal unity $c(0, y) = 1$. Equations (3-4) with the boundary conditions are solved in the velocity field obtained from the numerical solution of the Navier-Stokes equations.

The particle concentration, electric potential distributions and collection deposition efficiency were studied numerically at various values of particle size, initial particle concentration, quantity of particle charges, array porosity and flow Reynolds number. In fig.2 the gas flow stream lines (a), izolines of electric potential φ (b) and particle concentration c at the values $\mathrm{Re} = 50$, $\mathrm{Pe} = 100$, $\alpha = 0.001$, ε =0.95 are shown ($Re = 2r_f\rho U_0/\mu$ is Reynolds number, U_0 is the undisturbed gas velocity, ρ is the gas density and viscosity, ε is the porosity of the cylinder array).

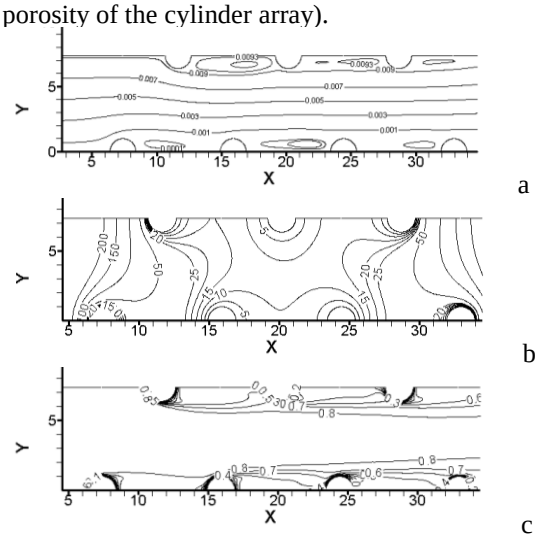

Figure 2.

Alonso, M., Alguacil, F.J. (2007), J. Aerosol Sci. 481-493.
Yu, C.P., Chandra, K. (1977), J. Aerosol Sci. 175-180

Implementation and evaluation of a microphysical aerosol module in the ECMWF Integrated Forecasting System

M. T. Woodhouse[1], G. W. Mann[2] and K. S. Carslaw[1], J.-J. Morcrette[3] and O. Boucher[4]

[1]Institute for Climate and Atmospheric Science, School of Earth and Environment, University of Leeds, Leeds, LS2 9JT, UK
[2]National Centre for Atmospheric Science, School of Earth and Environment, University of Leeds, Leeds, LS2 9JT, UK
[3]European Centre for Medium-range Weather Forecasts, Shinfield Park, Reading, RG2 9AX, UK
[4]Met Office Hadley Centre, Fitzroy Road, Exeter, Devon, EX1 3PB, UK
Keywords: Aerosol modelling, meteorology
Presenting author email: m.woodhouse@see.leeds.ac.uk

As part of the European Global Monitoring for Environment and Security (GMES) program, the Monitoring Atmospheric Composition and Climate (MACC) project will provide a system for monitoring and predicting the characteristics of atmospheric constituents. Our contribution to this work is the incorporation and evaluation of the GLOMAP-mode microphysical aerosol scheme (Mann et al., 2010, GMD) within the ECMWF Integrated Forecasting System (IFS). The two-moment modal GLOMAP-mode scheme includes new particle formation, condensation, coagulation, cloud-processing, and wet and dry deposition. GLOMAP-mode is already incorporated as a module within the GLOMAP-TOMCAT chemistry transport model and within the UK Met Office HadGEM3 general circulation model. In these frameworks, the scheme compares well against a wider range of benchmark observational datasets including measurements from short-term field campaigns and long term monitoring sites.

Presented here are the results of tests of GLOMAP-mode in the IFS, comparing the new aerosol scheme with the mass-only scheme developed during GEMS. The use of a microphysical, process-based model allows a more realistic representation of the properties of the multi-component aerosol and will enable aerosol-cloud interactions to be robustly simulated within the IFS system. Sophisticated regional aerosol-chemistry models will also benefit from the new GLOMAP-mode-IFS system via improved boundary condition information.

This work is part of the EU FP7 project ‘Monitoring Atmospheric Composition and Climate’

Mann, G. W., Carslaw, K. S., Spracklen, D. V., Ridley, D. A., Manktelow, P. T., Chipperfield, M. P., Pickering, S. J. And Johnson, C. E., 2010. Description and evaluation of GLOMAP-mode: a modal global aerosol microphysics model for the UKCA composition-climate model. *Geoscientific Model Development* **3**: 516-551.

Role of biogenic organics on aerosol forcing in 2100

R. Makkonen[1], A. Asmi[1], V.-M. Kerminen[2], M. Boy[1], A. Arneth[3], A. Guenther[4], P. Hari[5] and M. Kulmala[1]

[1]Department of Physics, University of Helsinki, Helsinki, FI-00014, Finland
[2]Finnish Meteorological Institute, Helsinki, FI-00101, Finland
[3]Institute of Meteorology and Climate Research, Karlsruhe Institute for Technology, Garmisch-Partenkirchen, 82467, Germany
[4]Atmospheric Chemistry Division, National Center for Atmospheric Research, Boulder, Colorado, 80301, USA
[5]Department of Forest Science, University of Helsinki, Helsinki, FI-00014, Finland
Keywords: climate effect, nucleation, organic aerosols.
Presenting author email: risto.makkonen@helsinki.fi

Atmospheric new particle formation can have a large contribution to present-day anthropogenic cooling by increasing availability of cloud condensation nuclei (CCN). Sulphuric acid is thought to be the main precursor for nucleation (Kulmala *et al.* 2006). It is studied that the global anthropogenic emissions of sulphur dioxide may already have peaked and that emissions reductions and control measures could lead to a large decrease (even 90%) of global sulphur dioxide emissions by end of century. If sulphuric acid is governing atmospheric nucleation, the reduction in sulfur dioxide emissions would reduce the aerosol indirect effect and lead to more warming from greenhouse gases. The effects of lowered nucleation rates could potentially be offset by an increase in emission of biogenic volatile organic compounds (BVOCs), as they provide more growth for sub-CCN particles. If organics play a role also in the early steps of new particle formation (Metzger *et al.* 2010), the reduction in aerosol cooling by the end of century could be more subtle.

We use global climate model ECHAM5-HAM (Stier *et al.* 2005) to simulate present-day (year 2000) and future (year 2100) aerosol forcing. Anthropogenic emissions are obtained from AeroCom inventory (http://dataipsl.ipsl.jussieu.fr/AEROCOM) for year 2000 and "Representative Concentration Pathways" (http://www.iiasa.ac.at/web-apps/tnt/RcpDb) for year 2100. Biogenic organic emissions are estimated from two independent models: LPJ-GUESS (Schrugers *et al.* 2009) and MEGAN (Guenther *et al.* 2006). We test several parametrizations for nucleation: binary sulphuric acid-water (Vehkamäki *et al.* 2002), activation-type (Kulmala *et al.* 2006), and different formulations for sulphuric acid+organic nucleation (for e.g. Paasonen *et al.* 2010). Condensation of BVOCs takes place in the boundary layer, and the condensational fluxes are calculated according to condensation sink of each size mode.

All applied anthropogenic sulphur dioxide emission datasets show a significant reduction until 2100, ranging from 80 to 90%. This reduction together with lower primary emission rates lead to roughly 50% decrease in boundary layer CCN concentration, when activation-type nucleation is used. Analysis of radiative fluxes shows that the total aerosol forcing (direct+indirect effects) goes from a strong present-day cooling of -1.6 W/m^2 to -0.2 W/m^2 in year 2100. Most of the change is due to reduction in cloud droplet number and resulting change in cloud properties (albedo and lifetime).

The response of biospheric organic emissions to changing climate is rather poorly understood. The LPJ-GUESS model assumes that monoterpene production is affected by increasing CO_2 concentration and shows close to zero change in monoterpene emissions between 2000-2100. The MEGAN model, however, predicts a 30% increase in monoterpene emissions due to warming climate and higher vegetation productivity. This additional organic matter available for condensation on small particles enhances growth from nucleation to CCN size. Our simulations show that with activation-type nucleation, even an strong future increase of 50% in BVOC emissions could not counteract the effect of decrease in particle nucleation in terms of particle number or aerosol forcing. However, if we assume that nucleation is dependent on both sulphuric acid and organics, the decrease in aerosol forcing between 2000-2100 is somewhat smaller.

This work was supported by the Academy of Finland Centre of Excellence program (project no. 1118615) and EU-project EUCAARI (European Integrated project on Aerosol Cloud Climate and Air Quality interactions, project no. 036833-2).

Guenther, A. *et al.* (2006) *Atmos. Chem. Phys.* **6,** 3181-3210.
Kulmala, M. *et al.* (2006) *Atmos. Chem. Phys.* **6,** 787-793.
Metzger, A. *et al.* (2010) *Proc. Nat. Acad. Sci.* **107**, 6646-6651.
Paasonen, P. *et al.* (2010) *Atmos. Chem. Phys.* **10**, 11223-11242.
Stier, P. *et al.* (2005) *Atmos. Chem. Phys.* **5**, 1125-115.
Schurgers, G. *et al.* (2009) *Atmos. Chem. Phys.* **9**, 3409-3423.
Vehkamäki, H. *et al.* (2002) *J. Geophys. Res.* **107**, 4622.

Using the Common Representative Intermediates Mechanism (CRIv2-R5) coupled to an aerosol microphysics model to simulate formation and transformation of atmospheric aerosols

S.Utembe[1], D.Lowe[1], D.Topping[1,2], and G.McFiggans[1]

[1]Centre for Atmospheric Science, SEAES, Manchester University, UK, M13 9PL
[2]National Centre for Atmospheric Science, NCAS, SEAES, Manchester University, UK, M13 9PL

Keywords: secondary organic aerosols
Presenting author email: steven.utembe@manchester.ac.uk

It is now well established that organic material is a significant variable component of tropospheric aerosol accounting for between 10-90 % of fine particle mass. However, most models underestimate organic aerosol mass mainly because of lack of adequate treatment of the role of water in aerosol composition and transformation, Another possible reason which may contribute to this underestimation is insufficient carbon mass flux of condensable vapours. In this work, a reduced chemical scheme, the Common Representative Intermediates (CRIv2-R5) (Watson *et al*. 2008) which describes the tropospheric degradation of methane and 22 emitted non-methane hydrocarbons and oxygenated volatile organic compounds (all together comprising of 220 species in 609 reactions), and is traceable to the Master Chemical Mechanism (v3.1), has been coupled to an explicit aerosol microphysics model to enable prediction of the transformation of multicomponent aerosol in the oxidizing atmosphere. The aerosol microphysics model uses the hyprid Partial Derivative Fitted Taylor Expansion (PD-FiTE), a computationally efficient method for calculating gas/liquid equilibria in atmospheric aerosol particles. We present model results from sensitivity studies of its use in sectional Microphysical Aerosol Numerical box-model Including Chemistry (MANIC) (Lowe *et al.*, 2009) and its application in a regional model (WRF-CHEM) to simulate the formation and transformation of tropospheric aerosols in the UK under a range of changing emission profiles and oxidant conditions.

Lowe, D, Topping, D, McFiggans, G, (2009), *Atmos. Chem. Phys.*,9, 2, , 5289-5320.

Topping, D., Lowe, D., & McFiggans, G. (2009). *J. Geophys. Res.*, 114, doi:10.1029/2008JD010099.

Watson, L., Shallcross, D. E., Utembe, S. R., & Jenkin, M. E. (2008), *Atmos. Environ.*, 42, 7196-7204.

Estimate of the Saharan dust contribution to PM_{10} concentrations over Italy: a modelling approach

A. Pederzoli[1], M. Mircea[2] and S. Finardi[3]

[1]Joint Research Centre, Via E. Fermi 2749, 20127, Ispra, Italy
[2]ENEA, Via Martiri di Monte Sole 4, 40129 Bologna, Italy
[3]ARIANET s.r.l. via Gilino, 9, 20128 Milan, Italy

Keywords: boundary conditions, Saharan dust, aerosol concentrations, Italy
Presenting author email: mihaela.mircea@enea.it

This study aims to investigate the possible contribution of mineral dust to air quality predictions over Italy by adding dust concentrations from a dust transport model (SKIRON) into Lateral Boundary Conditions (LBCs) of a regional air quality model (FARM). A dust episode (26^{th}-29^{th} July 2005) has been simulated running FARM on a 20x20 km^2 resolution domain over Italy. Three sensitivity tests have been performed in order to assess the impact of the new LBCs to PM_{10} concentrations modelled by FARM: NDC ("no dust" case), DC ("dust" case) and DC1.3 ("dust multiplied by a factor 1.3" case).

NDC In the "No Dust Case" concentrations from the EMEP model are used as LBCs in FARM. EMEP concentrations do not include the contribution of Saharan dust. EMEP fields have been interpolated from 50 x 50 km^2 to FARM resolution and re-projected onto the four sides of model domain.

DC In the "Dust Case" simulation, hourly SKIRON fields are interpolated to 20 x 20 km^2 and re-projected onto the four sides of the FARM grid. Size-resolved dust concentrations by SKIRON are added to the LBCs used in the previous case (NDC). Dust particles are within four sizes, based on the amount of clay, small silt, large silt and sand particles inside desert soils. The first SKIRON class has been added to the accumulation mode of unspecified anthropogenic mass (c_A25J) and the second class to the soil mass aerosol species (c_ASOIL) in FARM. Contribution from the last two classes was not considered (no addition was performed) as particles of large silt and sand, due to their large dimensions, are rapidly removed from the atmosphere through dry deposition processes.

DC1.3. SKIRON dust concentrations are multiplied by a factor 1.3 (Kallos et al., 2007) in order to reduce the bias of the model (30%). The same procedure used in the DC is then applied and new LBCs are created.

Results have been compared to each other and to PM_{10} ground measurements from the Italian Air Quality Network. The comparison with ground measurements reveals that:

The addition of dust contribution to PM_{10} improves FARM aerosol mass concentration predictions. The underestimation of PM_{10} concentration is reduced from approximately 77% to 59% (table 1).

However, the results suggest that the dust concentrations correction introduced in DC1.3 may be not suitable over Italy: differences in PM_{10} concentrations between DC1.3 and NDC are comparable with the differences in DC-NDC for all days. More experimental and modelling studies are needed for finding a correction factor more suitable for the Italian contest.

.

Table 1. Statistical parameters for the simulations NDC,DC, DC1.3

Statistic	NDC	DC	DC1.3
NMB	-77%	-65%	-59%
FAC2	0.06	0.14	0.28
NMSE	3.00	1.31	1.05

Acknowledgements: This work is part of the MINNI (Integrated National Model in support to the International Negotiation on Air Pollution) project, funded by the Italian Ministry for Environment, Territory and Sea and carried out by ENEA. This work was supported and coordinated by ENEA and ARIANET Srl. A special thanks to Professor G. Kallos and the Atmospheric Modeling and Weather Forecasting Group at the University of Athens for providing the SKIRON modelled data used in this work.

Kallos G., Spyrou C., Papantoniou N., Mitsakou C., Astitha M. (2007) Analysis of the Particulate Matter exceedances in Greece during the period 2003-2004. Technical report for the Ministry of Environment City planning and public works.

Source evaluation of aerosols measured over the Indian subcontinent and ocean from combined measurement and modeling platforms

S. Verma[1], S. N. Bhanja[1], M. Schulz[2], Y. Balkanski[2]

[1]Department of Civil Engineering, Indian Institute of Technology Kharagpur, 721302, WB, India
[2]Laboratoire des Sciences du Climat et de l'Environnement, 91191, Gif-sur-Yvette Cedex, France
Keywords: Aerosol characterization, Optical depth, Modelling, Source identification.
Presenting author email: shubhaverm@gmail.com; shubha@iitkgp.ac.in

Atmospheric aerosols perturb the climate system by scattering and absorbing the solar radiation (direct effect) and by altering the radiative properties and lifetime of clouds (indirect effect). Aerosols due to emissions from anthropogenic sources, including combustion of fossil fuels (coal and oil) for energy and transportation, industrial and agricultural activities, biomass burning, and deforestation are a major concern in this context. Evaluation of emissions over the Indian subcontinent based on emission fluxes aggregated spatially show distinct emission patterns over the different parts of India which could lead to regional variation in the chemical and optical characteristics of aerosols, and consequently could lead to a climate response due to aerosols different on a regional scale than the global. It is therefore, necessary to understand the chemical and optical characteristics of aerosols, their sources, and climate impacts over Indian subcontinent and ocean through integration of measurements and modelling studies.

Observational studies during the Indian Ocean Experiment (INDOEX) [Ramanathan et al., 2001] and more recent field campaigns in the Bay of Bengal and the Arabian Sea have established the widespread occurrence of aerosols and trace gases of anthropogenic origin over ocean regions adjoining India. Chemical characteristic of aerosols measured during INDOEX showed that aerosol mass contained substantial amounts of both inorganic and organic pollutants and revealed the simultaneous presence of different tracer substances characteristic for biomass burning and fossil fuel burning influenced by polluted air masses originating over India or Southeast Asia and Arabia. In order to characterise aerosols present over the Indian main land, land campaigns were carried out under Indian Space Research Organisation Geosphere Biosphere (ISRO-GBP) program. Measurements during the ISRO-GBP land campaign (Jayaraman et al., 2006) and spatio-temporal characteristics of aerosols retrieved from satellite based observations indicated stations over the Indo-Gangetic plain (IGP) to have higher aerosol optical depth (AOD) compared to off-IGP stations over the Indian subcontinent. Measurements of AOD over the oceanic regions of Arabian Sea (AS) and Bay of Bengal (BoB) showed the presence of their higher values over the AS compared to the BoB.

In the present work, we carry out an analysis of aerosol distribution over the Indian subcontinent from aerosol transport simulations in LMDZ-INCA [*Schulz et al.*, 2006] which couples the Laboratoire de Meteorologie Dynamique general circulation model (LMDz) and the Interaction with Chemistry and Aerosols (INCA) model. AOD simulated over the Indian subcontinent and ocean was estimated to be dominated by dust and sulfate during the southwest monsoon compared to sulphate, organic matter, and BC, during the winter monsoon. Model estimated AOD evaluated over the Bay of Bengal (BoB) and the Arabian sea (AS) showed the domination of sulphate and organic matter over the BoB while sulphate and dust over the AS (Figure 1). Evaluation of GCM simulated aerosol optical properties over the Indian subcontinent with the ground-based measurements during the various campaigns and satellite-based observations will be presented. The chemical constituents to the AOD measured and their probable sources will be evaluated.

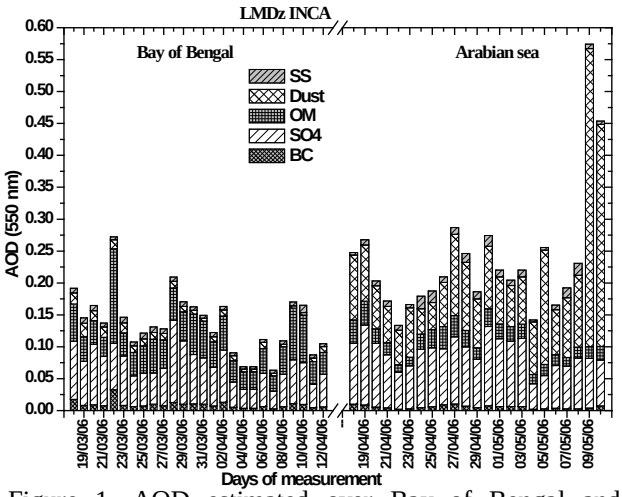

Figure 1. AOD estimated over Bay of Bengal and Arabian sea from LMDz-INCA simulations during the days of ship-cruise measurements

A. Jayaraman, H. Gadhavi, D. Ganguly, A. Misra, S. Ramachandran, and T. Rajesh. (2006) *Atmos. Env.*, **40**, 6504 -6515.

M. Schulz *et al*. (2006) *Atmos. Chem. Phys.*, **6**, 5225-5246.

Ramanathan, V., et al. (2001) *J. Geophys. Res.*, **106**, 28,371–28,398.

Distribution function for daughter droplets at theoretical law of parent drop motion

A.G. Girin[1]

[1] Odessa National Maritime University, Odessa, 65029, Ukraine
Keywords: dispersion, droplets, size distribution, aerosol modelling.
Presenting author email: club21@ukr.net

It was found (Girin[1], 2011), that mass history of shattering drop depends directly on law of drop displacement in gas stream and is defined by ratio $h = A/3C$ of rate of mass efflux $A = 0.46(1+\alpha^{\xi})^{-1}(\mu^2/\alpha)^{1/6}$ to the rate C of relaxational decreasing of relative velocity of drop and gas. An approximate theory of shattering drop was built (Girin[1], Girin[2], 2011) with use of empirical law of drop motion $X_{\rm d}(\tau)$. In view of lack of empirical data about $X_{\rm d}(\tau)$ for various gas-droplets systems it is important to obtain the main relations of shattering drop kinetics on the reliable ground of theoretical laws. They are found analytically below as solutions of system of non-linear differential equations of drop motion, drop mass efflux and quantity of torn droplets in a speedy uniform gas stream at neglecting by drop deformation influence.

In case $h=1$ the solution has an exponential character, so, ablation law, law of motion and distribution function of daughter droplets quantity by sizes coincide with those obtained on base of empirical law of drop motion (Girin[1], 2011). At $h\neq 1$ integration gives power functions for parent drop velocity and radius: $W = 1-\left(1-C(h-1)\tau\right)^{\frac{1}{h-1}}$, $\tilde{R} = \left(1-C(h-1)\tau\right)^{\frac{h}{h-1}}$. The quantity Δn of droplets of radius $\tilde{r} = r/R_0$, that are contained in elementary fraction $\Delta\tilde{r}$, must be found by integration of equation for $\Delta n(\tilde{r})$ (Girin[2], 2011) between lower and upper limits φ_l, φ_{up} in a strip $\Delta\tilde{r}$, which surrounds the line $\tilde{r}(\varphi,\tau) = const$ (φ is polar angle of any ground on drop surface). The approximation of integration path $\tau = \tau(\varphi)$ and choice of its effective slope $a_{\rm ef}(\tilde{r}, h)$ are similar to those of (Girin[2], 2011) and lead now for natural $\eta = 3h/(h-1)$ to the following expression for distribution function:

$$f_{\rm n}(\tilde{r}) = \frac{\Delta n}{\Delta\tilde{r}} = \frac{3hB_1^3B_2}{A(h-1)\tilde{r}^4}\left(\frac{P_{\eta+1}(\varphi)}{b(\eta+1)} - F_\eta(\varphi)\right)_{\varphi_l}^{\varphi_{up}}, \quad (1)$$

where $P_\eta(\varphi) = (a+b\varphi)^\eta$, $P_\eta^{(k)}$ – its k-th derivative, $a = 1-C(h-1)(\tau_l - \varphi_l/a_{\rm ef})$, $b = C(1-h)/a_{\rm ef}$, $F_\eta(\varphi) = \frac{\sin 2\varphi}{2}\sum_{k=0}^{\mathrm{E}(\eta/2)}(-1)^k\frac{P_\eta^{(2k)}}{2^{2k}} + \frac{\cos 2\varphi}{2}\sum_{k=1}^{\mathrm{E}((\eta+1)/2)}(-1)^{k-1}\frac{P_\eta^{(2k-1)}}{2^{2k-1}}$;

parameters $B_1 = 1.60\alpha^{1-2\xi}\,\mathrm{Re}_{\rm d}^{-0.5}$ and $B_2 = 0.15\mathrm{Re}_{\rm d}^{1.5}\alpha^{7\xi-3.5}(1+\alpha^{\xi})^{-1}$ are the character scales for droplets sizes and quantity (here $\xi = \log_\alpha(\alpha\mu)^{1/3}$ is parameter of mutual viscous engagement of media in boundary layers on drop surface, $\alpha = \rho_{\rm g}/\rho_l$ and $\mu = \mu_{\rm g}/\mu_l$ are their density and viscosity ratios). To natural $\eta > 3$ corresponds series of discreet values of h: $1 < h = \eta/(\eta-3) \le 4$, while to integer $\eta < 0$ – values, which belong to interval $0.25 \le h < 1$ of incomplete shattering. In this case $f_{\rm n}(\tilde{r})$ expresses in $\mathrm{Si}(\varphi)$, $\mathrm{Ci}(\varphi)$. Named set of η values covers compactly enough all the practically important diapason of h values.

Formula (1) permits to calculate intermediate distribution of droplets torn to any time moment $\tau < \tau_{\rm b}$ and to find the approximated expressions for the moment of drop breakup $\tau_{\rm b}$ and for whole quantity of torn droplets N. The distributions were calculated for $h = 1.5; h = 2.0; h = 4.0$ and showed negligibly weak influence on $\Delta n(\tilde{r})$ of two above mentioned methods of determination of parent drop motion law. For example the distributions of all stripped droplets $N = 1.5\cdot 10^7$, which calculated for $h = 1.5$, are presented on figure 1 and show good mutual agreement.

Thus, the two approaches of determination of drop motion law, which are based on theoretical and empirical methods, have lead eventually to similar distribution functions. Presented here theoretical approach has the advantage being independent from lack of empirical data, so formula (1) is applicable to any gas – droplets system.

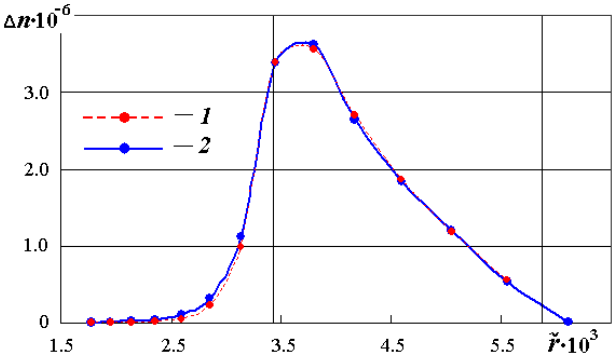

Figure 1. Calculated at $h = 1.5$ dependencies $\Delta n(\tilde{r})$; ***1*** – by formula (1), ***2*** – by formulae of Girin[2] (2011). Vertical lines are the limits of base diapason.

Girin[1], A. (2011) *Inzhen.-fiz. zhurnal.* **84**, No 2, 248-254.
Girin[2], A. (2011) *Inzhen.-fiz. zhurnal.* **84**, No 3, (to be published).

Regional modelling of the tropospheric multiphase system using COSMO-MUSCAT

R. Schrödner[1], A. Tilgner[1] and R. Wolke[1]

[1]Institute of Tropospheric Research, Leipzig, 04318, Germany
Keywords: Aerosol cloud interaction, Multiphase chemistry, Modelling (regional), Cloud microphysics.
Presenting author email: roland.schroedner@tropos.de

Clouds play a major role in the atmosphere due to their influence on the Earth's radiative budget, on the hydrologic cycle and on the tropospheric chemical composition (e.g. Ramanathan et al., 2001). Cloud lifetime is driven by the dynamics of the atmosphere at the synoptic scale and, in close interaction, by microphysical processes (e.g. nucleation of cloud droplets and ice crystals, condensation and evaporation, collision/coalescence processes, freezing, sedimentation of hydrometeor) on the small scale.

These processes depend on the chemical composition of particles and cloud droplets. In addition, microphysical processes redistribute chemicals among the various reservoirs: gaseous, particulate, liquid and ice phases. Clouds favor the development of "multiphase chemistry" since they are an ideal reaction medium for this: (1) clouds support very efficient photochemical processes inside droplets; (2) certain homogeneous chemical reactions within clouds can be usually faster than the equivalent reactions in the gas phase, and reactions such as those involving ionic species, can be important; (3) finally, interactions between the aqueous and solid phase can contribute additionally to chemical processes in clouds (for example dissolution of soluble particulate species). The evaluation of multiphase chemistry versus overall tropospheric chemistry and its role in the Earth's radiative budget is challenging since microphysical and chemical processes occurring at different time scales within clouds are still poorly known.

The model system COSMO-MUSCAT consists of MUSCAT (Wolke et al., 2004a) and the forecast model of the German Weather Service (DWD) COSMO (Schättler et al., 2008). Both models are coupled online. MUSCAT was extended to consider cloud-chemical processes (chemical aqueous phase reactions and phase transfer processes) on the regional scale replacing the former aqueous phase parameterization.

Based on the increasing kinetic and mechanistic knowledge on chemical aqueous phase reactions in the last two decades, advanced aqueous phase chemical mechanisms such as the Chemical Aqueous Phase Radical Mechanism (CAPRAM) are continuously developed (Tilgner and Herrmann, 2010). CAPRAM is an almost explicit mechanism which describes relevant chemical aqueous-phase conversions of both inorganic and organic compounds. A reduced version of the mechanism, applicable for 3D chemistry transport models was created (Deguillaume et al., 2009).

With the advanced model system, 2D-sensitivity-studies have been conducted for an urban and a remote case. The comparison of two different mechanisms (simple inorganic and detailed organic mechanism CAPRAM) have revealed agreements but also interesting differences for important chemical subsystems e.g. in the modeled multiphase HO_x budget and pH whereas the simple mechanism leads to always less acidic cloud droplets than CAPRAM. Invesigation of reaction fluxes show that this is due to additional organic acidification in CAPRAM. The difference in pH leads consequently to different regimes for the S(IV)-oxidation leading to about 5% less S(VI) using CAPRAM instead of a simple mechanism.

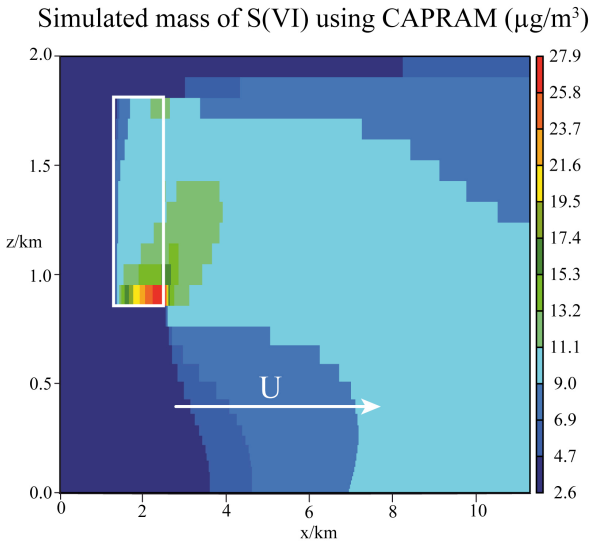

Figure 1. Height profile in x-direction of the simulated mass of S(VI) using CAPRAM in a remote scenario in µg/m³. The cloud is located inside of the white square. Species stream in from the left-hand side.

This work was supported by the Deutsche Bundesstiftung Umwelt (DBU).

Deguillaume, L., et al. (2010), *Journal of Atmospheric Chemistry*, *64*(1), 1-35.

Ramanathan, V., Crutzen, P. J., Kiehl, J. T. and Rosenfeld, D. (2001) *Science*. 294, 2119 - 2124

Schättler, U., Doms, G. and Schraff, C. (2008): *A Description of the Nonhydrostatic Regional COSMO-Model Part VII: User's Guide.*

Tilgner, A. and Herrmann, H. (2010) *Atmospheric Environment*, *44*(40), 5415-5422

Wolke, R., Knoth, O., Hellmuth, O., Schröder, W. and Renner, E. (2004a) *Parallel computing: Software technology, algorithms, architectures and applications*, 363-370

A modelling approach to study PM2.5 dispersion and transformation in Venice area

E. Pecorari[1], S. Squizzato[1], M. Masiol[1], F. Visin[1], G. Rampazzo[1]

[1]Dipartimento di Scienze Ambientali, Informatica e Statistica, Università Ca' Foscari Venezia, 30123, Venice, Italy

Keywords: aerosol modelling, emissions, PM2.5, dispersion

Presenting author email: squizzato@unive.it

$PM_{2.5}$ formation and dispersion are still a research target that depend on specific meteorological and emission sources of the area studied. The use of mathematical models permits to better understand pollutants spatial and temporal distribution becoming a complementary tools respect to field campaigns. Despite their limitations, in fact, models enable to study the diffusion of air pollution in not-controlled areas where measurements entail high costs and lots of human resources. This approach has been useful in a very peculiar site: Venice lagoon. This is, in fact, a very delicate ecosystem located between the Adriatic Sea and the Po Valley , which is recognized as the most industrialized district of Italy. A multidisciplinary project has been developed with the aim of better understand $PM_{2.5}$ primary sources and secondary formation and compositions.

The model system used, distributed by ARIANET S.p.A., consists of three main components: a diagnostic meteorological model (*MINERVE*) (ARIANET, 2001), a turbulence model (*SURFPRO*) (ARIANET, 2005a) and a photochemical-eulerian dispersion model (*FARM)* (ARIANET, 2005A).

Four periods have been considered during different seasons for which both organic and inorganic measured data were available. Input data has been collected, calculated and formatted as requested by models. Taking advantage of the large number of available measurements, meteorological data from 27 surface stations have been collected. Upper data has been calculated as integration of Rass/Sodar measured data with RAOB soundings from the nearest point available. Emissions used as model input have been referred to EMEP/CORINAIR Emission Inventory Guidebook (EMEP, 2007) groups in Venice area during year 2005. Even though experimental period refers to 2009-2010, 2005 emissions are the only data guaranteed by public administration. A specific work has been conducted to calculate 2009's emissions for principle industrial sources in Venice area that have been considered as point source (*stacks*).

Different approaches has been followed to best evaluate model prediction capacity based on statistical parameter typically used to test model performance and multivariate analysis. Three stations have been controlled during measurements: Punta Sabbioni, Via Lissa and Malcontenta. Data have been compared for the three stations and during different seasons. Model performed well in predicting $PM_{2.5}$ concentrations and its temporal and spatial distributions. An example is reported in figure 1. Further water soluble inorganic ions have been considered to test model capacity in describing $PM_{2.5}$ inorganic composition. Spatial and temporal ions distribution has been investigated respect to the three stations and to the different seasons.

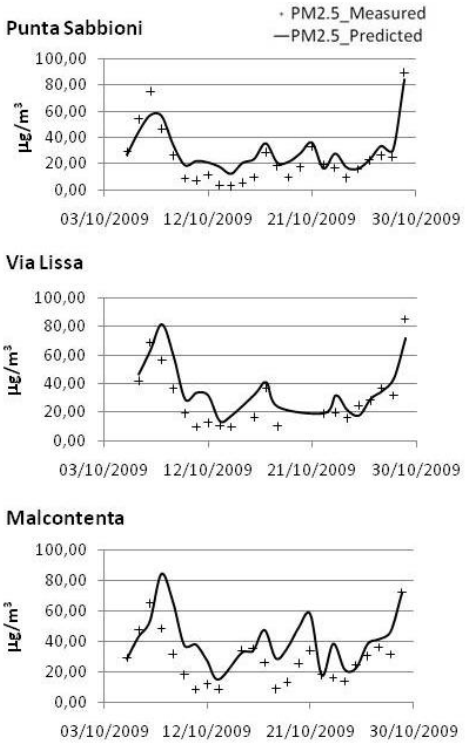

Figure 1. Model $PM_{2.5}$ data comparison for the three stations during autumn period.

This work was supported by Ente della Zona Industriale di Porto Marghera. The authors also express thanks to ARIANET S.p.A. and MAV for helping in collecting data.

Aria Technologies, (2001) *MINERVE, Wind Field Models Version 7.0,* General Design Manual ARIA Report, Aria Technologies, Paris.

ARIANET, (2005a) *SURFPRO, SURface-atmosphere interFace PROcessor, Version 2.2,* User's Guide, Arianet Milano.

ARIANET, (2005b) *FARM, Flexible Air quality Regional Model, version 2.12,* Model formulation and user manual, Aria Report, Aria Technologies.

EMEP, (2007): Joint EMEP/CORINAIR Emission Inventory Guidebook, third ed. (http://www.eea.europa.eu/publications/EMEPCORINAIR).

Radioactive disequilibrium between radon and its decay products in surface atmosphere

V.S. Yakovleva[1], A.V. Vukolov[1], P.M. Nagorsky[2], Ya.V. Luzhanchuk[1], I.A. Gvai[1] and F.A. Sannikov[1]

[1]Department of Applied Physics, Tomsk Polytechnic University, Tomsk, 634050, Russian Federation
[2]Department of Climatic System, Institute of Monitoring of Climatic and Ecological System SB RAS, Tomsk, 634050, Russian Federation
Keywords: radioactivity, atmosphere, ionising radiation, monitoring.
Presenting author email: vsyakovleva@tpu.ru

Large-scale research of temporal and spatial dynamics of radon and its aerosol decay products (DP) volumetric activity (VA) in atmosphere surface layer is necessary for investigation of electrical properties of atmosphere and climate global change forecasting. Air radioactive aerosols and gases and their balance regulate the surface layer of atmospheric plasma. Radiation equilibrium factor F determines the balance between radon and its DPs and depends on meteorological conditions. Equilibrium factor F and its changing range are little-studied for atmosphere. The most influencing factors have not determined yet.

The main aim of the work was to investigate the degree of radioactive disequilibrium between radon and its PDs in surface layer and to determine the degree of external factors influence. For this aim the model of radon and its decay products transport in atmosphere was developed. The following processes are considered: molecular D_M and turbulent D_T diffusion transport; transport by vertical wind; removal due to radioactive decay and deposition under gravity force v_F and precipitation v_R. One dimensional transport equations in steady-state conditions are:

$$(D_{M_i} + D_T)\frac{\partial^2 A_i(z)}{\partial z^2} - v_W \frac{\partial}{\partial z} A_i(z) - \lambda_i A_i(z) = 0, \text{ for i=1;}$$

$$(D_{M_i} + D_T)\frac{\partial^2 A_i(z)}{\partial z^2} - (v_W + v_F + v_R)\frac{\partial}{\partial z} A_i(z) + \lambda_i A_{i-1}(z) - \lambda_i A_i(z) = 0,$$

for i=2-5.

The equation system is solved with boundary conditions

$$(D_{M_i} + D_T)\frac{\partial A_i(z)}{\partial z}\bigg|_{z=0} - v_W A_i(z)|_{z=0} = q_i, \text{ for } i=1,$$

$$(D_{M_i} + D_T)\frac{\partial A_i(z)}{\partial z}\bigg|_{z=0} - (v_W + v_F + v_R)A_i(z)|_{z=0} = 0, \text{ for } i=2\text{–}5,$$

$$A_i(z) \to 0, \; z \to \infty.$$

Here $A_i(z)$ is VA of i-radionuclide; index i=1-5 is respectively for ^{222}Rn and DP: ^{218}Po, ^{214}Pb, ^{214}Bi and ^{214}Po; q_i is radon flux density (RFD) from the earth surface. When v_w has negative value, wind blows down to the earth surface, when it is positive – up.

The analysis of numerical simulation of radon and its DP transport in atmosphere revealed that: 1) RFD value determined integral value of radionuclides VA; 2) turbulent diffusion coefficient and vertical wind velocity and direction are the most important factors which influence vertical distribution of Rn and its DP activity in surface layer.

Fig. 1. shows the results of numerical simulation of equilibrium factor dependence on D_T value at different height. It is seen that F depends on D_T weakly. Radioactive equilibrium can be observed at 100 m height.

Fig. 2 represents the results of numerical simulation of equilibrium factor dependence on v_w value. Arrows indicate wind direction. Disequilibrium in radon chain occurs mainly under the wind directed up from the earth surface, and increases when wind becomes stronger. On the contrary, wind blowing down to the earth surface restores the radioactive equilibrium between radionuclides of radon chain (Fig.3).

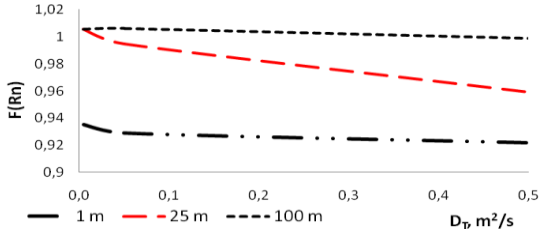

Figure 1. The dependence of F on D_T and height

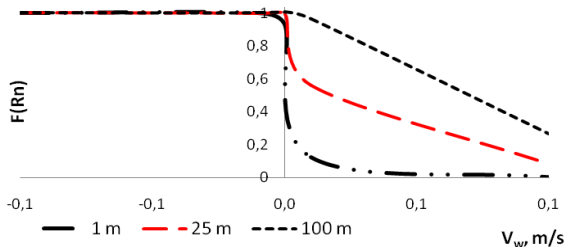

Figure 2. The dependence of F on v_w and height

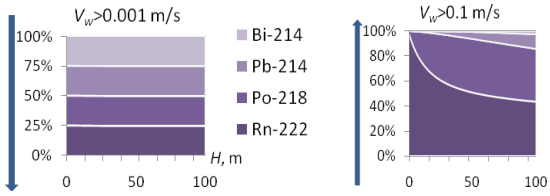

Figure 3. The radionuclide activity proportion at different height H and vertical wind velocity

The comparison of measured and calculated data was performed in the work taking into account real meteorological conditions.

This work was supported by RF Analytical departmental target program “Development of higher school scientific potential” under grant № 2.1.1/13707 and by Siberian Branch RAS, program № VII.63.1.1.

Thursday, September 8, 2011

Session 8P: Poster session B

Atmospheric Aerosols - Aerosol Processes and Properties

Passenger exposure to nanoparticles inside a transport microenvironment

Pouyan Joodatnia[1] and Prashant Kumar[1, 2]

[1]Division of Civil, Chemical and Environmental Engineering, Faculty of Engineering and Physical Science (FEPS), University of Surrey, GU2 7XH, United Kingdom
[2]Environmental Flow (EnFlo) Research Centre, FEPS, University of Surrey, GU2 7XH, United Kingdom
Keywords: transport microenvironment, exposure, nanoparticles, particle size distribution
Presenting author email: P.Joodatnia@Surrey.ac.uk

Emissions from conventional fuel driven vehicles contribute considerably to particle number concentrations in the atmospheric urban environment. Their adverse effects on human health and the environment have raised concerns and attracted attention of research community and policy makers. Exposure to freshly emitted nanoparticles during typical road journeys (i.e. walking, travelling in buses, cars or taxis) in urban areas is widespread. Studies have found about an order of magnitude larger concentrations of nanoparticles in transport microenvironments, compared with hourly averaged concentrations in cities (e.g. London), where general public is routinely exposed.

This study aims to assess the short–term particle number concentration and size distribution, both inside and outside a car cabin during the journeys in a typical UK town. The other objective includes the determination of the influences of particle transformation processes on particle number and size distributions.

Number and size distributions of particles in the 5–560 nm range at a sampling frequency of 10 Hz were measured inside the cabin (air conditioning on medium speed) of a moving car using a fast response differential mobility spectrometer (DMS50). Inlet of the sampling tube was placed near the front seat at an approximate height of passenger breathing zone (i.e. 1.5 m above the car floor). For minimising the particle losses in the tube, the shortest possible length (0.50 m) was chosen. The sampling tube was electrically and thermally conductive and has 5 mm internal diameter, giving ~0.3 s residence time at a sampling flow rate of 6.5 lit min^{-1}. Simultaneously, digital images were also collected using a video camera for keeping the log of emission events and correlating the influence of traffic volume on exposure level.

Measurements were separately made both during peak and off–peak hours for mimicking the daily passenger exposure to nanoparticulate pollution under different traffic conditions. The chosen route is 2.7 kilometres long and connects the University of Surrey campus with Guildford town centre. Journey times for both the peak and off–peak hours were estimated as 10±4 and 6±2 minutes, and average vehicle speed as 18±3 and 22±4 km h^{-1}, respectively. For minimising the variability in measured number and size distribution data, a total of 40 trips, equally distributed during peak and off–peak hours, were completed.

During a typical off–peak journey, average particles number concentrations (PNCs) over the entire journey were found to be about $5.1\pm3.7\times10^4$ cm^{-3} compared with $21.8\pm29.9\times10^4$ cm^{-3} during peak time journey (Fig. 1). As expected, one of the common observations during peak and off–peak journeys were the largest PNCs inside our car cabin when a bus, lorry or car were moving (or idling at the traffic light) just before our car. Correlation analysis of video images and measured PNCs during such events, raising the PNCs up to two orders of magnitude (i.e. ~1.33×10^6 cm^{-3}) larger than the background concentrations (~1.30×10^4 cm^{-3}); the latter is assumed as the lowest concentrations during each journey, generally the ones at the starting point when there were no emission sources (see Fig. 1).

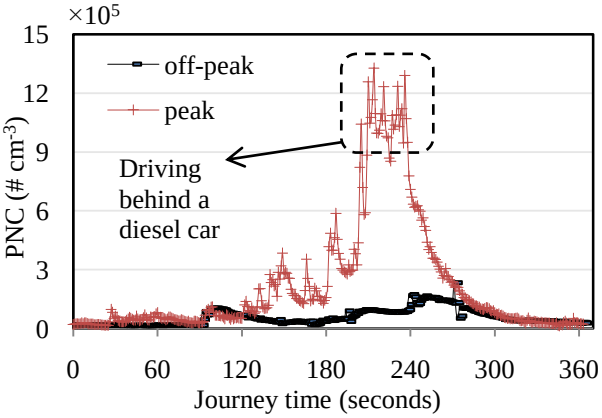

Figure 1: PNCs during peak and off–peak journeys

Initial results demonstrate that the average PNCs (7.98×10^4 cm^{-3}) over all journeys in a typical UK town like Guildford were at the lower end of those reported by Kaur *et al.* (2005) at a heavily trafficked route in London (9.9×10^4) and similar to those found by Knibbs *et al.* (2010) for Sydney (7.5×10^4 cm^{-3}). This could presumably be due to our measurements taken at 10 Hz, compared with 1 Hz or lower sampling frequencies used by other studies, allowing us to capture the events in real–time. Secondly, our measurements covered particle diameters up to 5 nm but the lower cut–off diameters in above studies were limited either to 10 or 30 nm.

Detailed analysis of the data is under progress. For assessing the variation in exposure to all passengers, further experiments are going on involving pseudo–simultaneous measurements both outside and inside the car cabin, and at four different passenger seats.

PK thanks both the EPSRC grants (DTA and EP/H026290/1) for supporting this work. Authors also thank Prof. Alan Robins for his support and discussions.

Kaur, S., Nieuwenhuijsen, M. and Colvile, R. (2005) *Atmos. Environ.* **39**, 3629-3641.
Knibbs, L. D. and de Dear, R. J. (2010) *Atmos. Environ.* **44**, 3224-3227.

Atmospheric circulation role on PM fractions

St. Pateraki[1,2], Th. Maggos[1], D. N. Asimakopoulos[2], H. A. Flocas[2] and Ch.Vasilakos[1]

[1]Environmental Research Laboratory/INT-RP, National Centre for Scientific Research "DEMOKRITOS", 15310 Aghia Paraskevi Attikis, P.O.B. 60228 Athens, GREECE
[2]Department of Environmental Physics and Meteorology, Faculty of Physics, University of Athens, University Campus, building PHYS-5, 157 84, Athens, GREECE

Keywords: PM_{10}, $PM_{2.5}$, meteorology, urban pollution.

There are well known issues surrounding particulate matter (PM), especially concerned their relation to cardiorispiratory disease, morbidity and mortality. Although there is still a fundamental lack of understanding the underlying mechanisms of their toxicity, one of the widely accepted hypotheses is that toxicity of particulates depends on their size and composition both of which depend on location, time of year, meteorological conditions and long range-transport effects (Harrison et al., 2000, Akyüz et al., 2009).

A study of twenty one daily PM_{10}, $PM_{2.5}$ concentrations has been carried out in a suburban area of Athens, Aghia Paraskevi during the period 13/12/2004-14/6/2006. $PM_{2.5}$ were collected with the use of a R&P TEOM (model 1400a), PM_{10} with a low volume gravimetric sampler Derenda (LVS3.1/PNS3.1-15) while the 24-h $PM_{2.5-10}$ concentrations were calculated from the abstraction of the daily $PM_{2.5}$ value from the daily PM_{10} value. The sampling station is located easterly of the Athens basin in the National Center of Scientific Research (N.C.S.R.) 'Demokritos'. The site is at the outskirts of a highly populated area, on the foot of Hymettos mountain within a forest of pine trees. O_3, NO and NO_2 data were provided by the Ministry of Environment while the meteorological data (WD, WS, T, RH) were provided by a meteorological mast, operating under the responsibility of NCSR 'Demokritos'.

The understanding of the ambient PM characteristics as a function of atmospheric circulation was the main motivation of the specific work. The $PM_{2.5}$ hourly variation during the different circulation types as well as the particles correlations' with inorganic conventional pollutants (NO, NO_2, O_3, SO_2) would be also investigated.

PM_{10}, $PM_{2.5-10}$ and $PM_{2.5}$ mean values were 31.7 μg/m^3, 16.0 μg/m^3 and 15.7 μg/m^3, respectively. Only the bigger diameter particles found to be statistically significant correlated between each other (R=0.96), while in the 38.1% of the sampling days PM_{10} appeared to be mainly composed by the coarse.

In order to investigate the connection of the surface synoptic scale atmospheric circulation with the PM distribution over the examined area, day by day synoptic conditions were classified over the Greater Athens Area. According to Kassomenos et al., (1998) the atmospheric circulation at the isobaric level of 850 hPa is closely related to the observed surface local flows. Eight synoptic categories (SW, NW, LW, CL, Zonal, OA, CA, HL), which are demonstrated to be statistically distinct are selected with respect to the atmospheric circulation in the lower troposphere.

Table 1 presents the statistical analysis results' for the PM fractions during the different prevailing circulation types as well as the % frequency of appearance for each category. It is worthy to note that CA days were not detected. The peak values for the bigger diameter particles were obtained during the OA days while for the fine ones during the Zonal. PM_{10} and $PM_{2.5-10}$ proved to be always strongly associated (R: 0.61-0.98) between each other, irrespectively of the investigated case. During the CL days, the coarse particles domination was verified ($PM_{2.5}/PM_{10} \leq 0.50$).

Table 1: Statistical analysis for the PM fractions during the different prevailing circulation types

		PM (μg/m^3)			
Type	Frequency (%) of appearance	PM_{10}	$PM_{2.5-10}$	$PM_{2.5}$	$PM_{2.5}/PM_{10}$
SW	14.3	24.9	8.45	16.4	0.66
NW	9.52	29.8	12.5	17.3	0.54
LW	9.52	32.4	16.0	16.3	0.62
CL	14.3	39.4	25.3	14.2	0.58
Zonal	9.52	28.0	9.76	18.2	0.58
OA	19.0	37.7	22.0	15.8	0.44
CA	0.00				
HL	23.8	28.4	14.0	14.4	0.51

Studying the inorganic pollutants their behaviour was differentiated. The maximum NO and NO_2 values were recorded during LW and Zonal days while O_3 concentrations were favoured by OA type. Only the Pearson coefficients between PM10 and NO2 proved to be unsusceptible to the circulation changes being always strong correlated (R: 0.61-0.98).

Akyüz, M. and Cabuk, H. (2009). *J. Hazard. Mater.* 70, 13-21.

Harrison, R.M. and Yin, J. (2000) *Sci. Total Environ.* 249, 85–101.

Kassomenos P., Flocas H.A., Lykoudis, S., Petrakis M. (1998). *Theor. Appl. Climatol.* 59, 15-229.

Dispersion of nanoparticles in vehicle wake – Part II: analysis of wind tunnel work

Matteo Carpentieri[1, 2], Prashant Kumar[1, 2] and Alan Robins[2]

[1]Department of Civil, Chemical and Environmental Engineering, Faculty of Engineering and Physical Sciences (FEPS), University of Surrey, GU2 7XH, United Kingdom
[2]Environmental Flow (EnFlo) Research Centre, FEPS, University of Surrey, GU2 7XH, United Kingdom
Keywords: wind tunnel, flow and dispersion, ultrafine particles, dispersion modelling, vehicle wake.
Presenting author email: m.carpentieri@surrey.ac.uk

Understanding the transformation of nanoparticles emitted from road vehicles is essential for developing appropriate methods for treating fine scale particle dynamics in dispersion models (Kumar *et al.* 2010). Field measurements and modelling studies have highlighted the very short time scales associated with nanoparticle transformations in the first stages after their emission (Carpentieri *et al.* 2011). These transformations strongly interact with the flow and turbulence fields immediately behind the vehicle, hence the need of characterising in detail the mixing processes in the vehicle wake (Kumar *et al*. 2009).

In order to develop parameterised models for the dispersion of nanoparticles, there is first a need to understand sufficiently the dispersion of inert gases. In the present study, a systematic wind tunnel experimental campaign was undertaken in order to support and extend analogous field campaigns aimed at understanding nanoparticle dispersion in the wake of a moving car.

The experiments were carried out in the EnFlo (Environmental Flow Research Centre) wind tunnel at the University of Surrey, where reduced scale models (1:20 and 1:5) of the diesel car used for our field experiments (separate abstract submitted as Part I of this study) were tested (see Fig.1).

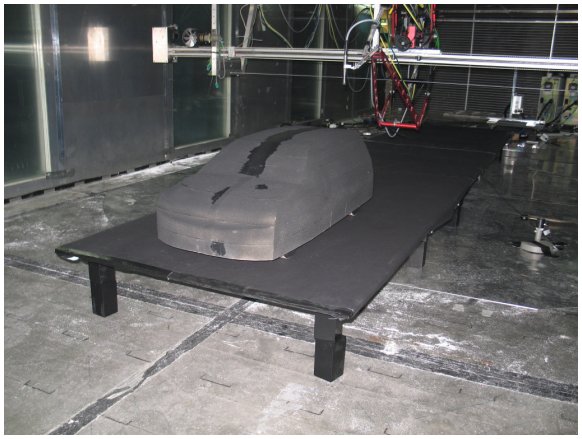

Figure 1. Vehicle model (1:5 scale) in the EnFlo tunnel.

In order to reduce the unrealistic effects of a growing boundary layer at the wind tunnel surface, the models were placed at the leading edge of a false floor (i.e. 23 cm above the tunnel floor). The flow and turbulence fields were characterised both in the near and the far wake of the modelled vehicle by using a 2–component laser Doppler anemometer (LDA). The probe was used in two different positions (measuring velocity components both in the x-y, and x-z planes) in order to have a complete three–dimensional map (e.g. see Fig.2). A more in–depth spatial analysis of the flow and turbulence characteristics in the near wake was then made by using particle image velocimetry techniques.

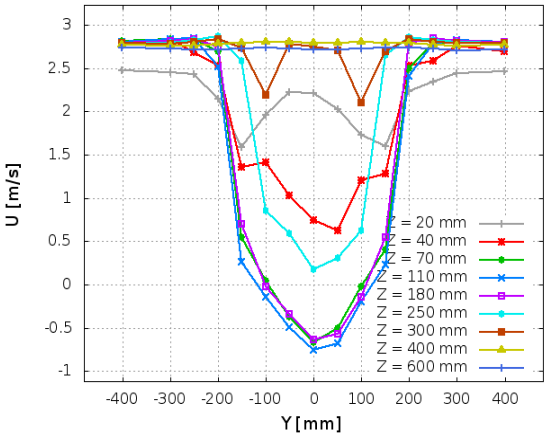

Figure 2. Horizontal LDA profiles of wind speed (U) at different heights, X = 80 mm from the model.

Concentration measurements were obtained by using a fast response (frequency >350 Hz) flame ionisation detector and a hydrocarbon tracer gas released from the modelled tailpipe.

The high resolution experimental database obtained from these experiments, in conjunction with a large nanoparticle concentration data set obtained from field measurements, will be used for deriving mathematical parameterisations for operational nanoparticle dispersion models. Further experiments are planned using a newly built rolling road wind tunnel facility in the EnFlo laboratory that can remove any unrealistic effects of the surface boundary layer and further improve the quality of the experimental database.

PK acknowledges the receipt of the EPSRC grant EP/H026290/1 which is supporting this work. The authors thank Dr. Paul Hayden and Mr. Allan Wells for their support with the wind tunnel work.

Carpentieri, M., Kumar, P. and Robins, A. (2011) *Environ. Pollut.* **159**, 685-693.
Kumar, P., Robins, A., and Britter, R. (2009) *Atmos. Environ.* **43**, 6110–6118.
Kumar, P., Robins, M., Vardoulakis, S., and Britter, R. (2010) *Atmos. Environ.* **44**, 5035–5052.

Aerosol entrainment footprints over the South East Pacific as observed during VOCALS

G. Allen[1], H.M.A. Ricketts[1], G. Vaughan[1] and H. Coe[1]

[1]Centre for Atmospheric Science, University of Manchester, Oxford Road, Manchester, M13 9PL, UK
Keywords: aerosol cloud interaction, long-range transport, cloud microphysics, boundary layer.
Presenting author email: h.ricketts@manchester.ac.uk

The South East Pacific region is a key area of uncertainty in regional climate models, which inaccurately represent stratocumulus cloud decks beneath the capping inversion of the descending branch of the Walker circulation. The causes for such uncertainty relate to complex local interactions between land, sea and atmosphere in the region as a result of the High Andes, the cold Humboldt ocean current and the Walker Circulation, respectively. Furthermore, a key component of uncertainty in cloud radiative properties relates to the aerosol composition of the marine boundary layer below and the potential entrainment of aerosol into cloud from the free troposphere, which displays a clear concentration gradient with distance offshore from the South American coast.

This study uses a combination of aerosol lidar and in situ optical measurements of aerosol layers in the free troposphere from the BAe-146 and Dornier-228 aircraft recorded during the VAMOS Ocean Cloud Atmosphere Land Study (VOCALS) field campaign, which was conducted near the west coast of Chile in October/November 2008. Using ECMWF reanalysis data, we shall use forward trajectory analysis to study the statistical footprint of entrainment of aerosol layers during the period of VOCALS, which were observed as discrete but concentrated layers of particulate pollution, advected and descending over the SEP from both long-range jet-stream transported organic sources to the west, and more local industrial and geogenic sulphate sources to the free troposphere to the east lofted by Andean upslope pumping of the continental boundary layer. Such entrainment is expected to contribute to significant radiative and life-cycle changes in marine stratocumulus, with higher concentrations of cloud condensation nuclei known to manifest as higher cloud droplet number and weaker precipitation rates.

Exposure level of traffic-related air pollutants near a busy road in Seoul, Korea

S.-B. Lee, D.-H. Lee, S.J. Lee, H.C. Jin, J.H. Choi, S.-H. Park, N.T.Q. Hung, G.-N. Bae

Global Environment Center, Korea Institute of Science and Technology, Seoul, 136-791, Korea
Keywords: vehicles emissions, ultrafine particles, NO_x, traffic.
Presenting author email: sblee2@kist.re.kr

It is important not only to improve the averaged air quality of the mega-cities but also to reduce exposure level of hazardous air pollutants. Air pollution due to vehicle exhaust at urban area in mega-cities like Seoul, Korea is known as local hot-spot pollution phenomena. Urban people who prefer to live at the location closest to major roads to save commuting time are worrying about exposure of traffic-related air pollutants such as ultrafine particles and nitrogen oxides nowadays.

Some previous studies reported the decreasing trends of particle concentrations within a few hundred meters apart from highways or freeways (Hitchins *et al*., 2000; Zhu *et al*., 2002). California State, USA introduced legislation, SB 352 Escutia, to prohibit siting new schools within 500 feet (168 m) of a busy road for protecting the health of students (Green *et al*., 2004).

In this study, roadside measurement was carried out at several locations with different distances from a busy road in Seoul, Korea, using a mobile laboratory to understand the exposure levels of traffic-related air pollutants and to obtain backup data for establishing environmental policy related to vehicles.

Measurements

Figure 1 shows the seven locations from A to G of roadside measurement measured in this study, which are 17, 67, 117, 167, 217, 317, and 417 m, respectively, apart from Dongbu express way (~150,000 vehicles/day), one of the busiest roads in Seoul.

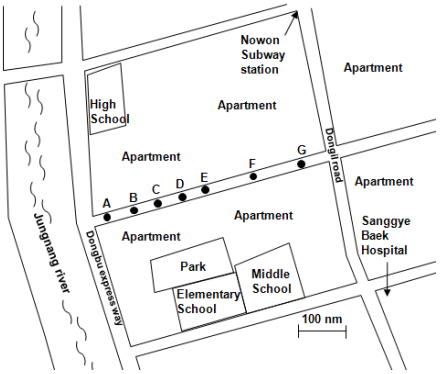

Figure 1. Location of the roadside measurement between Dongbu express way and Dongil road.

The number concentration of particles > 5 nm, size distribution of particles ranging 6-523 nm, black carbon concentration of $PM_{2.5}$, and NO and CO concentrations were measured for about 10 min at each location using condensation particle counter (Grimm 5.404), fast mobility particle sizer (TSI 3091), Aethalometer (Magee Scientific AE-42), NO_x and CO analyzers (Environment S.A AC32M, CO12), respectively, which were installed in the multi-functional mobile laboratory. The inlet height was about 3 m above from the ground. Although wind direction was not fixed, wind mostly flew from the Dongbu express way to measurement site, and average wind speed was 0.7 m/s.

The averaged number concentration of particles > 5 nm and NO concentration measured 17 m apart from the Dongbu express way were approximate 50,000 particles/cm^3 and 120 ppb, respectively, and presented similar decreasing trends with increasing distance from the road as shown in Figure 2. This level of particle number concentration was lower than half of Zhu *et al*. (2002) results near a freeway 405, USA (333,600 vehicles/day). However, the exponential coefficient of the decreasing curve for the concentration of particle number and NO within 117 m with distance from the Dongbu express way was -0.007 and -0.009, respectively, which are similar to -0.01 of the freeway 405, USA.

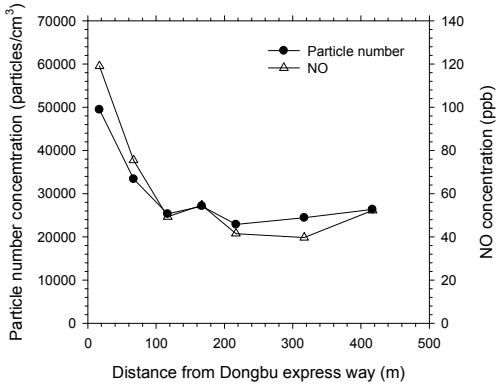

Figure 2. Concentrations of particle number and NO with distance from Dongbu express way.

This study was supported by the CEFV (Center for Environmentally Friendly Vehicle) of Eco-STAR project from MOE (Ministry of Environment, Republic of Korea).

Hitchins, J., Morawska, L., Wolff, R. and Gilbert, D. (2000) *Atmos. Environ.* **34**, 51-59.

Green, R.S., Smorodinsky, S., Kim, J.J., McLaughlin, R. and Ostro, B. (2004) *Environ. Health Perspect.* **112(1)**, 61-66.

Zhu, Y., Hinds, W.C., Kim, S. and Sioutas, C. (2002) *J. Air & Waste Manage.* **52**, 1032-1042.

Thursday, September 8, 2011

Session 8P: Poster session B

Atmospheric Aerosols – Specific Aerosol Types

Assessing PM_{10} source reduction in urban agglomerations for air quality compliance

V. Aleksandropoulou[1], M. Lazaridis[1] and K. Eleftheriadis[2]

[1]Department of Environmental Engineering, Technical University of Crete, Chania, Polytechneioupolis, 73100, Greece
[2]Institute of Nuclear Technology and Radiation Protection NCSR Demokritos, Ag. Paraskevi, Attiki, 15310, Greece
Keywords: urban aerosols, legislation and policy.
Presenting author email: lazaridi@mred.tuc.gr

The objective of this work was to study PM_{10} concentration data available from monitoring stations in three large urban agglomerations in Greece and to estimate the emissions reduction required for compliance with the EU Air Quality Standards for PM_{10} (annual mean concentration less than 40 μg/m^3; 50μg/m^3 not to be exceeded for more than 35 days per year).. The cities studied are namely the Athens and Thessaloniki Metropolitan Areas (AMA and TMA, respectively) and the Greater Volos Area (GVA). The dataset was retrieved from the EEA public air quality database (AirBase) and was gap-filled with data available on line by the Hellenic Ministry of environment, energy and climate change.

PM_{10} concentrations during the period 2001-2009 have been evaluated for 14 air quality monitoring stations (depicted in Table 1) in the three urban areas. Measurements revealed that the concentrations of PM_{10} during the period studied constantly exceeded the threshold values at GVA and at the traffic and industrial stations in TMA and most of the traffic sites in AMA. Most of the occurrences of non-attainment to AQSs were observed during the winter period at all areas (more pronounced for TMA and GVA).

The reduction R in current emission source strength to meet the air quality goal was calculated by the rollback equation (Seinfeld and Pandis, 1998):

$$R = (E\{c\}-E\{c\}_s)/(E\{c\}-c_b)$$

where $E\{c\}$ is the current annual mean of the pollutant concentration, $E\{c\}_s$ is the annual mean corresponding to the air quality standard c_s, and c_b is the background concentration assumed to be constant. The rollback equation can be applied assuming that changes in emissions levels by a factor of k correspond to the same change in concentration levels. The source distribution remains the same and the pollutant is non- reactive. The methodology was applied to daily averaged concentrations of PM_{10} in each metropolitan area. The data were initially screened as regards the availability (hourly-averaged data >65%). Time periods with data available for consecutive years were chosen. A distribution that best fits the PM_{10} day-averaged concentrations over the selected period was found for each station. We examined the applicability of the most common distributions for PM_{10} concentrations namely the lognormal and Weibull distributions (other distributions were also checked using statistical software). The lognormal distribution was found to best fit the frequency distributions of PM_{10} concentrations at the selected stations. The parameters of the lognormal distribution were calculated using the maximum likelihood-least squares method (Lu, 2002). The predicted concentrations were compared with the observed ones for the whole period and separately for each year. The results showing the geometric measured PM_{10} mean concentrations along with the minimum required emission reduction in order to meet the current AQS are presented in Table 1 for each station.

Table 1. Level of PM_{10} emissions reduction required for compliance with the 24-h average EU AQS at each monitoring station.

Monitoring Station (Type)	Geo. mean concentration (μg/m^3)	Required emission reduction (%)
Athens Metropolitan Area		
Aristotelous (TU)	54.32	40.16
Marousi (TU)	47.59	41.24
Pireaus (TU)	47.28	35.47
Lykovrisi (BS)	56.38	45.82
Thrakomakedones (BS)	29.73	3.75
Zografou (BS)	31.83	4.89
Agia Paraskevi (BS)	35.10	15.14
Goudi (TU)*	38.07	26.31
Thessaloniki Metropolitan Area		
Agia Sofia (TU)*	60.00	47.96
Kordelio (IU)	62.84	52.15
Kalamaria (TS)*	48.57	24.64
Panorama (BS)*	32.09	4.15
Sindos (IU)	48.68	35.02
Greater Area of Volos		
Volos (TU)	47.94	35.19

* data available for less than 5 consecutive years
B: background, I: industrial, T: traffic, U: urban, S: suburban

The minimum reduction required in order to meet the AQS at the areas of interest ranges from approximately 35 to 46% and from 4% to 15% for traffic and background stations in the AMA (Lykovrisi station was accounted for as traffic station). Reductions in the range of 35% for background and 52% for industrial suburban areas in TMA are also required. Finally, reductions of 35% are required for the GVA.

This work was supported by the European Union's LIFE Programme under grant LIFE 09 ENV/GR/000289.

AirBase - The European air quality database. Available at: http://www.eea.europa.eu/data-and-maps/data/airbase-the-european-air-quality-database-3.

Air quality measurement data for the period 1984-2009. Hellenic Ministry of environment, energy and climate change. Available at: http://www.ypeka.gr.

Sheinfeld, J.H. and Pandis, S.N. (1998) *Atmospheric Chemistry and Physics: from Air Pollution to Climate Change*, Wiley, New York.

Lu, H.C. (2002) *Atmos. Environ.* **36**, 491-502.

Particle-associated polycyclic aromatic hydrocarbons in Prague schools

M. Braniš[1], T. Cajthaml[1], P. Stehlíková[1] and J. Šafránek[2]

[1]Charles University in Prague, Faculty of Science, Albertov 6, 128 43 Praha 2, Czech Republic
[2]Charles University in Prague, Faculty of Physical Education, José Martího 31, 162 52 Praha 6, Czech Republic

Keywords: Polycyclic aromatic compounds, indoor air quality, health aspects of aerosols, mass size distribution.

Prague - the capital city of the Czech Republic with a population of approximately 1.25 million inhabitants is situated in the central part of the Bohemian basin between 200 and 350m above sea level. A large part of the built-up area lies in a valley of the river Vltava and on surrounding flat plains. This geography favours winter and summertime inversions. Traffic is the main source of air pollution. We were interested in the PAH levels in schools, in differences between the localities and in the penetration efficiency of the PAHs from outdoors. The results will be discussed in terms of the pupil's exposure to air pollutants during exercise.

We have monitored twenty-four hour mass concentration of size segregated aerosol simultaneously in three school gyms and in their outdoor vicinity in and around Prague (centre, periphery, suburban). The air was sampled by means of low volume (9l/min.) Personal Cascade Impactor Samplers with 5 stages A to P (A: 2.5-10µm; B: 1.0-2.5µm; C: 0.5-1.0µm; D: 0.25-0.5µm; and F-final or backup filter <0.25µm) and determined by gravimetry. This work deals only with the quasi-ultra fine particulate matter (QUFPM) collected on the 37mm PTFE F-filters (<0.25µm). Twenty campaigns 7-12 days long offered in total 177 days of 24-hour indoor and outdoor sampling. After gravimetry a reflectometer (EEL model 43, Diffusion System Ltd., London, UK) was employed to measure the absorbance of the particulate matter (PM) collected on the filters. Each filter was measured 5 times and the average was used in further calculations. The reflection was reset to 100% before each measurement with a blank filter. The reflectance was transformed into an absorption coefficient using the following equation: a = (0.5*A)*ln(R0/Rf)/V, where a is the absorption coefficient (absorbance), A describes the loaded filter area (in m^2), R0 the reflection of the blank filter (in %), Rf the reflection of the loaded filter (in %) and V the total sampled volume of air (in m^3)(ISO 9835). After reflectance the filters were placed in 2ml crimped vials and extracted with organic solvents (hexane:acetone, 3:1, V:V) in ultrasonic bath. Concentrations of 16 PAHs were identified with gas GC MS.

Figure 1 shows that the three schools studied revealed different levels of particle-associated PAHs. The reasonable association between the variables documented that indoor concentrations were influenced by the outdoor ones which is indicative of high penetration of outdoor particles indoors. The urban and rural (suburban) schools showed an order of magnitude higher PAHs than the periphery situated one. We suggest that while the urban school air was presumably affected by dense traffic, the rural school air was presumably influenced by local heating (coal and wood burning).

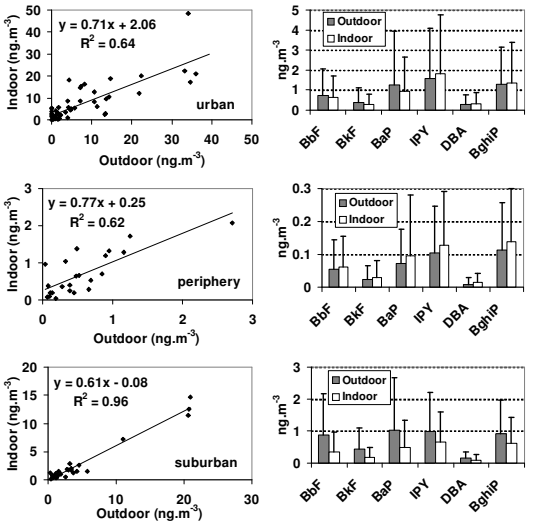

Fig. 1: Left: Association between indoor and outdoor sum of low-volatile PAHs - BBF BKF BAP IPY DBA BGP (winter only); Right: All-season average of six low-volatile PAHs concentrations.

Our results suggest that pupils at schools are exposed to high concentrations of PAHS namely in areas where local transport or local heating significantly contribute to airborne fine PM levels. Further research will be aimed at source identification at the three locations.

The project was supported by the Ministry of Education, Youth and Sports of the Czech Republic under the NPVII research programme, grant No. 2B08077 (Project INAIR).

$PM_{2.5}$ Source Profiles for Resuspended Road Dust in Seoul and Incheon, Korea.

Sehyun Han, Woojoong Kim, Yoonho Seo, Minsang Yoo and Yongwon Jung

Department of Environmental Engineering, Inha University, 253 Yonghyun-Dong, 402-751, Incheon, Korea
Keywords: $PM_{2.5}$, non-exhaust, resuspension, paved road.

.

Presenting author email: jungyw@inha.ac.kr

Non-exhaust particulate matter (PM) is defined as any PM associated with road transport that is not directly emitted in vehicle exhaust. It includes tire wear, brake wear, road surface wear, and resuspension of deposited PM on the road surface. As exhaust emission control has been improved and the resulting reduction in PM emissions has been recently achieved, the relative contribution of non-exhaust PM to total PM emissions in road and the concerns regarding its health risk have increased gradually throughout the world, especially in EU countries (Thorpe and Harrison, 2008; Amato et al., 2010). In Korea, recently there have also been growing concerns about the health impact of resuspended road dust together with PM from vehicle exhaust.

According to a previous study on emission inventory based on CAPSS (Clean Air Policy Support System) developed by the Korean Ministry of Environment, resuspended road dust is likely to be one of the largest PM_{10} emission sources not only in the road transport sector but also in the entire PM_{10} emission inventory for the Seoul metropolitan area including the city of Incheon. There are still ongoing debates, however, about the actual percentage contributions of resuspended road dust to ambient PM_{10} and $PM_{2.5}$ concentrations due to the large uncertainties in the estimation of fugitive dust emissions based on U.S. EPA AP-42, and the possibility of existence of unidentified PM emitting sources.

The primary objective of this study is to obtain source profiles of resuspended road dust by characterizing the $PM_{2.5}$ sampled from the paved roads at carefully chosen sites in Seoul and Incheon, The resulting source profiles of resuspended road dust will be used as a basis for receptor modeling as well as for the estimation of the health impact of resuspended road dust in Korea.

For elemental analysis, Al, Fe, Ca, K, Mg, Ti, Zn, Mn, Ba, Cu, Pb, Cr, Sr, Sb, Na, V, Sn, Co, Cd, P and Ni were analyzed using ICP MS/OES. For EC and OC analysis, Carbon Aerosol Analyzer (Sunset) was used. The more detailed information on sampling and both physical and chemical analysis of road dust will be presented later.

Analysis results as shown in Fig. 1 indicate that the most abundant elements in the sampled road dust are Al, Ca, Fe, and K. This implies these elements have the origin of soil components. The ratio of OC to EC in $PM_{2.5}$ ranged from 2.9 to 11.5. The ratio of Cu to Sb in $PM_{2.5}$ ranged from 4.4 to 12.0, which implies these elements are originated from wear of brake materials.

The $PM_{2.5}$ source profile for the resuspended road dust in Seoul metropolitan area is similar to that of U.S. EPA SPECIATE. Further refinement of sampling methodology and chemical analysis of newly sampled road dust are currently being carried out. These results will also be presented.

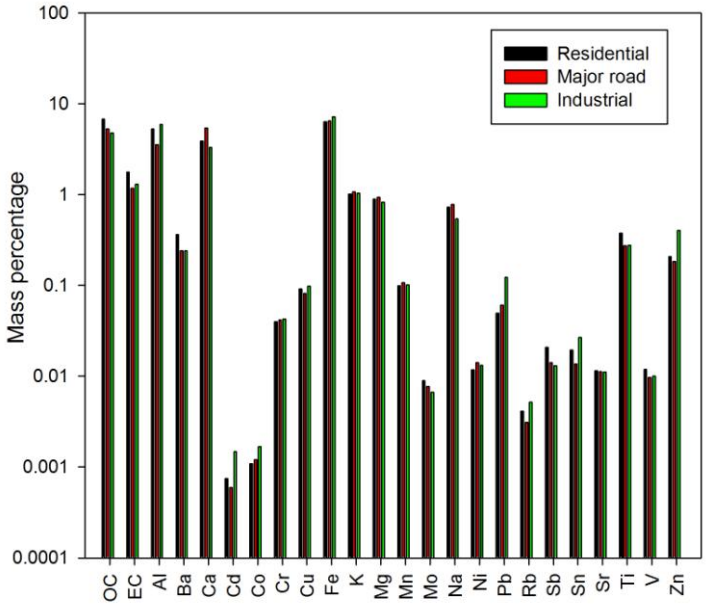

Figure 1. $PM_{2.5}$ Source Profile for Resuspended Road Dust in Seoul Metropolitan Area.

This work was supported by the National Institute of Environmental Research, Korea.

Amato, F., Pandolfi, M., Viana, M., Querol, X., Alastuey, A. and Moreno T. (2009) Atmospheric Environment, 43, 1650–1659.

Thorpe, A.J. and Harrison, R.M. (2008) Science of The Total Environment, 400, 270-282.

Comparison of organic compounds in atmospheric aerosols in urban areas in the Czech Republic

K. Křůmal, P. Mikuška, M. Vojtěšek and Z. Večeřa

Institute of Analytical Chemistry of the ASCR, v.v.i., Veveří 97, 602 00 Brno, Czech Republic
Keywords: organic compounds, organic tracer, PM1, urban aerosols.
Presenting author email: krumal@iach.cz

Atmospheric particulate matter (PM) is known to play an important role in many environmental problems. During last years much attention has been paid to the identification of emission sources of PM. To track the contributions of the main sources to composition of atmospheric aerosols, various source-specific organic and inorganic tracers are analysed in collected PM.

Atmospheric aerosols in the size fraction PM1 were sampled for a week over 24-h periods using the high-volume sampler (DHA-80, Digitel, 30 m^3/h) on quartz filters during winter and summer period of 2009 and 2010 at two locations, Brno and Šlapanice. Brno is the second largest in the Czech Republic with 370 thousands inhabitants. Šlapanice, small city with 6 thousands inhabitants, is located 3 km southeast from Brno.

Collected aerosols were analysed for organic carbon (OC), monosaccharide anhydrides (MAs), polyaromatic hydrocarbons (PAHs), hopanes/steranes (H/S) and monocarboxylic acids (MCA). Analysis of MAs includes extraction of parts of filters with dichloromethane under ultrasonic agitation, derivatization of extracts with mixture of MSTFA/TMCS, dryness, redissolution in hexane and GC-MS analysis. Analysis of PAHs and H/S includes extraction of parts of filters with mixture of dichlormethane and hexane, fractionation on column with silicagel, dryness to 1 mL and GC-MS analysis. Analysis of MCA includes extraction of parts of filters with methanol under ultrasonic agitation, esterification of extracts with mixture BF_3/methanol, extraction to hexane and GC-MS analysis.

Analysed compounds include:

- MAs: levoglucosan, mannosan and galactosan.
- PAHs: fluorene, phenanthrene, anthracene, fluoranthene, pyrene, retene, benzo[a]anthracene, chrysene, benzo[b+k]fluoranthene, benzo[e]pyrene, benzo[a]pyrene, perylene, indeno[1,2,3-c,d]pyrene, dibenzo[a,h]anthracene and benzo[g,h,i]perylene.
- H/S: 17α(H),21β(H)-hopane, 22*RS*-17α(H),21β (H)-homohopane, 17α(H),21β(H)-norhopane and $\alpha\alpha\alpha$ (20*R*)-cholestane.
- MCA: C7 – C20 saturated monocarboxylic acids and palmitoleic and oleic acid.

Figure 1 compares the concentrations of PM1, OC, MAs, PAHs, H/S and MCA in Brno and Šlapanice in winter of 2009. Detailed results including comparison of analysed organic compounds in winter and summer of 2009 and 2010 will be presented.

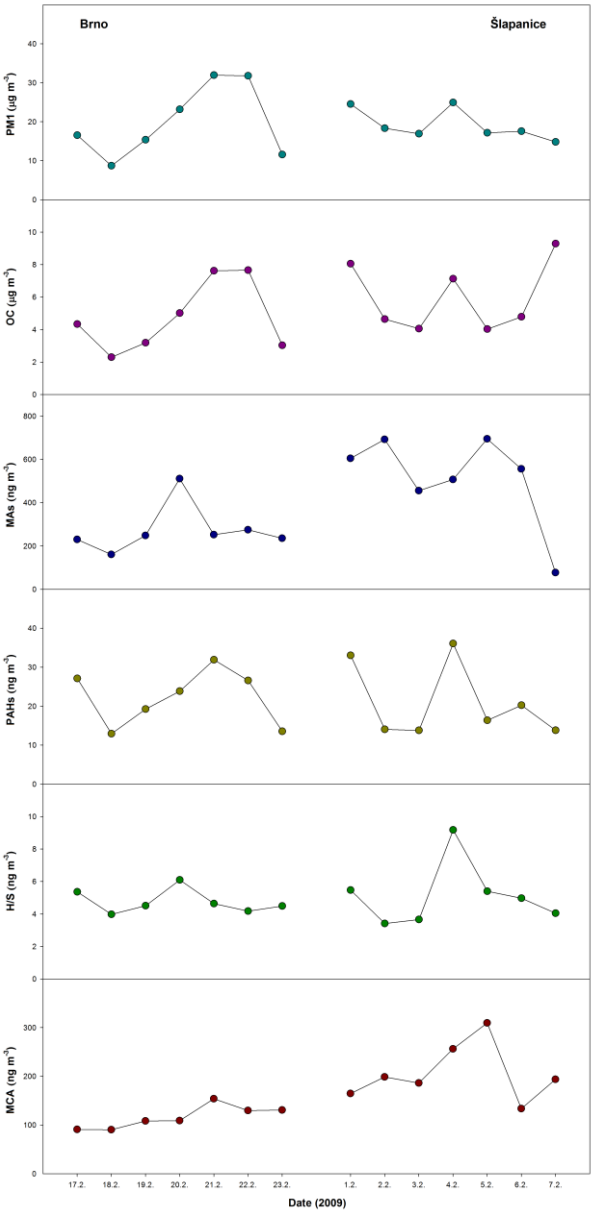

Figure 1. Comparison of PM1, OC, MAs, PAHs, H/S and MCA concentrations in Brno and Šlapanice in winter 2009.

This work was supported by Ministry of the Environment of the Czech Republic under grant No. SP/1a3/148/08, by Ministry of Culture of the Czech Republic under project NAKI DF11P01OVV028 and by Institute of Analytical Chemistry of ASCR under an Institutional research plan No. AV0Z40310501.

Source apportionment and health effects of winter urban atmospheric aerosol

B. Turóczi[1], A. Hoffer[2], Á. Tóth[1], N. Kováts[1], A. Ács[1], A. Gelencsér[1]

[1]Institute of Environmental Sciences, University of Pannonia, Veszprém, Hungary
[2]Air Chemistry Group of the Hungarian Academy of Science, Veszprém, Hungary
Keywords: PM10, urban aerosols, source apportionment, health effects of aerosols
Presenting author email: turoczi.beatrix@indamail.hu

In large cities air pollution is a very complex issue, showing strong seasonality and dependence on meteorological factors, sometimes culminating in severe and dangerous smog episodes. In winter important sources of the atmospheric aerosol are biomass and fossil fuels burning which are relevant sources of organic matter and black carbon and increase the mass concentration of the PM10 in the urban atmosphere. The atmospheric particulate matter with aerodynamic diameter less than 10 μm (PM10) is now identified as one of the most dangerous pollutants on human health because this size range overlaps with the range of respirable particles which may cause respiratory symptoms.

Effective air quality regulation and control requires the knowledge of the contribution of potential sources to urban particulate matter. The aerosol source apportionment relies on chemical analyses of the major components and specific tracer compounds, mass balance calculations, and supported with meteorological information.

Urban atmospheric PM10 was collected at the Main Observatory of Budapest-Lőrinc between December 2009 and March 2010 with a MSP personal aerosol sampler for 24h. Simultaneously mass concentration values were determined with a β-gauge PM10 monitor. The mean mass concentration of winter PM10 was 45.2 μg m^{-3} (standard deviation 18.9 μg m^{-3}).

From the collected samples total carbon, levoglucosan and water-soluble inorganic ions concentrations were determined. Contributions of the biomass and fossil fuel combustion were estimated by concentrations of levoglucosan, organic and elemental carbon (Fine *et al*, 2004, Watson *et al*, 2001, Kupiainen *et al*, 2005, Gelencsér *et al*, 2007).

Among inorganic ions the major sources for NH_4^+ is the organic decomposition, for K^+ are soils, biomass burning and anthropogenic sources, for secondary SO_4^{2-} is the oxidation of SO_2 which is produced by fossil fuels burning, and for NO_3^- is the oxidation of NO_x which produced by traffic and combustion processes (Wang *et al*, 2001). The main species forming of water-soluble inorganic ions in PM10 are $(NH_4)_2SO_4$, K_2SO_4, $CaSO_4$, NaCl, NH_4NO_3, $CaCl_2$ and KNO_3 (Verma *et al*, 2010). PAHs were analyzed which are key tracers in different combustion processes.

Ecotoxicity of each winter urban aerosol samples (20.01.2010.-11.02.2010) was directly determined by *Vibrio fischeri* bioluminescence inhibition bioassay in a special instrument developed for the analysis of solid sediment samples (Lappalainen *et al*, 1999). This method is directly linked to microbial respiratory activity, and it gives a good indication on the effects of pollutants on the metabolic activity of the test organism. The results show that emissions from both fossil fuel and biomass combustion contribute to the ecotoxicity of urban PM10. The specific ecotoxicity of the PM10 samples proved to be a sensitive and meaningful parameter that may supplement source apportionment studies and chemical analyses of urban PM10 pollution.

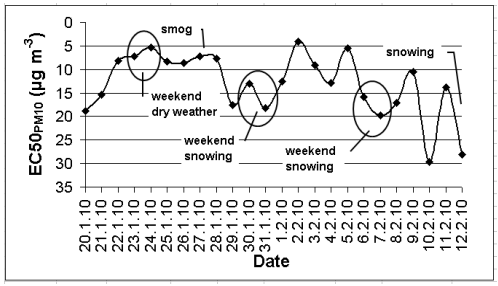

Figure 1. Variations of measured ecotoxicity of urban PM10 and PM10 mass concentrations. Lower $EC50_{PM10}$ values indicate higher ecotoxicological effects. Note that the scaling of the vertical axis is reversed.

The authors are grateful for the financial support of the grant TAMOP-4.2.1/B-09/1/KONV-2010-0003: Mobility and Environment: Researches in the fields of motor vehicle industry, energetics and environment in the Middle- and West-Transdanubian Regions of Hungary. The Project is supported by the European Union and co-financed by the European Regional Development Fund.

Fine, P., Cass, G., Simoneit, B.R.T. (2004) *Environ. Eng. Sci.* 21, 387– 409.

Watson, J.G., Chow, J.C., Houck, J.E. (2001) *Chemosphere* 43, 1141 – 1151.

Kupiainen, K. and Klimont, Z. (2005) *Interim Rep*. IR-04-079. Int. Inst. For Appl. Syst. Anal., Laxenburg, Austria

Gelencsér, A., May, B., Simpson, D., Sánchez-Ochoa, A., Kasper-Giebl, A., Puxbaum, H., Caseiro, A., Pio, C., Legrand, M. (2007) *J. Geopys. Res*. doi: 10.1029/2006JD008094

Wang, H. and Shooter, D. (2001) *Atmospheric Environment* 35, 6031-6040.

Verma, S.K., Deb, M.K., Suzuki, Y., Tsai, Y.I. (2010) *Atmospheric Research* 95, 65-76.

Lappalainen, J., Juvonen, R., Vaajasaari, K., Karp, M. (1999*) Chemosphere* 38 (5), 1069-1083.

Road dust resuspension and chemical composition with regards to street washing activities

Karanasiou A.[1], Moreno T.[1], Amato F.[1], Lumbreras J.[2], Borge R.[2,] Narros A.[2], Reche C.[1], Pey J.[1], Tobias A.[1], Alastuey A.[1], Querol X.[1]

[1] Institute of Environmental Assessment and Water Research (IDAEA-CSIC), Barcelona, Spain
[2] Department of Chemical & Environmental Engineering, Technical University of Madrid (UPM), Madrid, Spain

Keywords: road dust, resuspension, street washing, road dust chemical profile, source apportionment.

Several studies conducted in urban areas have pointed out that road dust resuspension contributes significantly to PM concentration levels (Thorpe and Harrison, 2008). The main objective of this study was to quantify the contribution of road dust to airborne particulate matter (PM_{10}), evaluate the effects of street washing on the mitigation of resuspension and determine any changes in the road dust chemical profile.

With this purpose an intensive campaign was carried out in a heavily trafficked central road of Madrid (Spain) including PM_{10} monitoring, sampling of road dust and chemical analysis. PM_{10} daily levels during dry, unwashed conditions were 2- 15 % higher than those present during the day after nightly street washing. However, this reduction was lower than the standard deviation of the PM_{10} measurements. The diurnal variation of PM_{10} revealed that a reduction in PM_{10} was noticeable only during the morning hours, Figure 1.

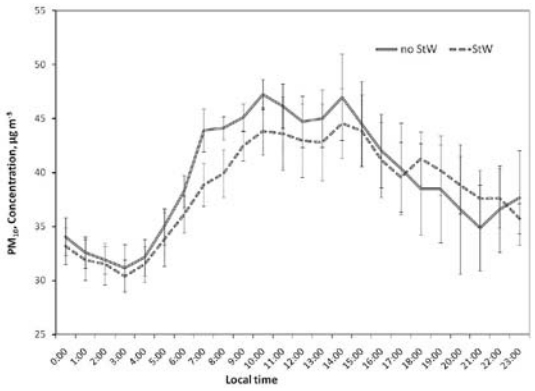

Figure 1. Daily variability of PM_{10} concentrations between street washing (StW) days and no street washing (no StW) days

The emission sources for the urban area of Madrid were resolved by means of a receptor model, Positive Matrix Factorization, PMF. The results showed that the main sources were vehicle emissions, road dust, secondary aerosol including sulfate and nitrate, and soil. Vehicle emissions and road dust were the major contributors to PM_{10} particle mass with similar average contributions of 31% and 29% respectively. The effect of street washing was evaluated by examining the daily variation of the road dust source contribution between days with (StW) and without street washing (noStW) (Karanasiou et al., in press). The mass contribution from the road dust source was ~2 µg m^{-3} lower during the days that street washing was implemented with this corresponding to a reduction of 15% of its mass contribution during the days that the road surface was left untreated, Table 1.

Table 1. PM_{10} source mass contribution, in µg m^{-3} between StW days and no StW days

Average mass contribution, µg m^{-3}	Road dust	Soil	Secondary aerosol	Vehicles emissions
StW	12.4	7.9	6.9	14.6
no StW	14.6	8.9	8.4	13.9

Consequently, the influence of street washing activities in the load of road dust was investigated. The PM_{10} road dust load showed small differences between the treated site where the road surface was washed daily and the untreated site where the road was left untreated. The average concentration in the untreated site was 2.61 mg m^{-2} while in the reference site was 2.32 mg m^{-2}. Furthermore there was not observed an increase of the road dust load from day to day or between morning and evening samplings. The major components in PM_{10} fraction of road dust were Ca (18 ± 8.5%), OC (14 ± 8%), Fe (10 ± 3%), S (7 ± 5%) and Al_2O_3 (7 ± 4.7%). Comparing the chemical composition of road dust in two sites, the concentrations of all major components in the reference site (with daily StW) were lower (about 30%) indicating the positive effect of washing activities.

This project (SERCA) was financed by the Spanish Ministry of the Environment and Rural and Marine Affairs (058/PC08/3-18.1).

Karanasiou A. Moreno T., Amato F., et., Road dust contribution to PM levels - Evaluation of the effectiveness of street washing activities by means of Positive Matrix Factorization *Atmos. Environ.*, in press

Thorpe A, Harrison R.M, *Sci. Total Environ.* 400, (2008), 270-282.

Meteorological impacts in the modification of PM_{10} concentration levels in the urban area of Volos, Greece

G.T. Proias[1], K.P. Moustris[2], I.K. Larissi[3], P.T. Nastos[4] and A. G. Paliatsos[5]

[1]Department of Planning and Regional Development, University of Thessaly, Volos, 38334, Greece
[2]Department of Mechanical Engineering, Technological and Education Institute of Piraeus, Athens, Aegaleo, 12244, Greece
[3]Laboratory of Environmental Technology, Electronic Computer Systems Engineering Department, Technological and Education Institute of Piraeus, Athens, Aegaleo, 12244, Greece
[4b]Laboratory of Climatology and Atmospheric Environment, Department of Geology and Geoenvironment, University of Athens, Panepistimiopolis, Athens, Zografou, 15784, Greece
[5]General Department of Mathematics, Technological Education Institute of Piraeus, Athens, Aegaleo, 12244, Greece

Keywords: PM_{10}; Saharan dust events; Volos; Greece.
Presenting author email: giproias@prd.uth.gr

Volos, a coastal medium-sized city in the region of Thessaly extended along the northern part of the Pagassitikos Gulf at the eastern seaboard of Central Greece, is among the cities which suffer from the air pollution in Greece. The case of Volos is an interesting example, where in the last decades the urbanization and the increased industrialization have resulted in the degradation of the air quality within the area, triggering health impacts. Meteorological factors play an important role in the air pollution development, while the complex topography of Volos exacerbates air pollution episodes.

In this study, the relationships between PM_{10} (particulate matter with diameter less than 10 μm) and meteorological parameters such as wind speed, relative humidity and air temperature have been analyzed from 2005 to 2009 on the basis of 24-hour continuous measurements. According to the results obtained from the multiple linear regression analysis, there is a strong relation between meteorological parameters and the particulate matter (Table 1) concentrations in Volos city. More specifically, the PM_{10} concentrations remain above the European Union (EU) limit values (Figure 1) for the whole part of the examined period (2005-2009) and this can be attributed to anthropogenic (industry and car traffic) and natural sources (Saharan episodes) of particulate pollution. The percentage of the total variance of PM_{10} concentrations explained by a single meteorological parameter for the cold period gets up to 10.6% (r^2) whereas, for the 5-year period, up to 6.8%. On the contrary, for the warm period it appears that the percentage of the total variance of PM_{10} concentrations explained by a single meteorological parameter gets up to only 2.5%.

Table 1. Pearson's correlation coefficients between the mean daily PM_{10} concentrations (μg/m^3) and the three meteorological parameters. Statistically significant values (at the 99% confidence level) are presented in bold.

Period	WS (m/s)	T (°C)	RH (%)
2005-2007	**-0.260**	**-0.184**	**-0.213**
Cold	**-0.326**	-0.092	**0.243**
Warm	**-0.159**	0.107	-0.078

Moreover, the calculation of the 72-hour air mass back trajectories during (eight) Saharan dust events, took place within the examined period, was carried out by applying the HYSPLIT 4 model of Air Resources Laboratory of NOAA for three different levels: 500, 1500 and 4000 m (a.m.s.l.). It is worthy to remark the high PM_{10} values observed, indicating the contribution of such natural events in exacerbating the air quality in the area of Volos.

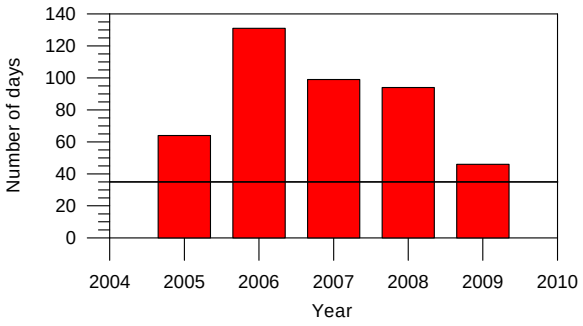

Figure 1. Temporal evolution of annual exceedances of mean daily PM_{10} concentrations at the city of Volos (2005-2009; the horizontal line indicates EU limit).

Larissi, I.K., Koukouletsos, K.V., Moustris, K.P., Antoniou, A. and Paliatsos, A.G. (2010) *Fresen. Environ. Bull.*, **19**, 226-231.

Larissi, I.K., Antoniou, A., Nastos, P.T. and Paliatsos, A.G. (2010) *Fresen. Environ. Bull.*, **19**, 1989-1996.

Nastos, P.T., Paliatsos, A.G., Anthracopoulos, M.B., Roma, E.S., Priftis, K.N. (2010) *Environ. Health*, **9:**45, doi:10.1186/1476-069X-9-45.

Paliatsos, A.G. and Amanatidis, G.T. (1994) *Sci. Total Environ.*, **144**, 137-144.

Proias, G.T., Nastos, P.T., Larissi, I.K. and Paliatsos, A.G. (2009) *AIP Conf. Proc., vol. 1203, 7th Int. Conf. of the Balkan Physical Union,* American Institute of Physics.

Samoli, E., Nastos, P.T., Paliatsos, A.G., Katsouyanni, K., Priftis, K.N. (2011) *Environ. Res.*, doi:10.1016/j.envres.2011.01.014.

Mass and number concentration of particulate matter in Lahore, Pakistan.

Ian Colbeck and Zaheer Ahmad Nasir
Department of Biological Sciences, University of Essex, Colchester, CO4 3SQ, U K

Keywords: PM, Number concentration, Lahore , Pakistan

In South Asian countries substantial economic growth and urbanization has lead to a poor air quality in urban centers. Pakistan, with rising types and number of emission sources and minimal air pollution control strategies, is struggling to arrest the excessive levels of air pollution in urban areas. Among a range of pollutants particulate matter is of greatest concern. The increase in the number of vehicles is a key source of particulate matter. The present study was carried out to investigate the levels of mass and number concentration of particulate matter by the roads in Lahore – the second largest city of Pakistan. Scattered studies on mass concentration of particulate matter have been reported from different parts of the country. However no studies on number concentration have been reported so far.

The measurements were carried out during June – August, 2008 over a period of two weeks. The mass concentration of PM_{10}, $PM_{2.5}$ and PM_1 was monitored by GRIMM: analysers (Model 1.108 and Model 1.101). The calibration factor was determined as 0.80. The number concentration was measured with condensation particle counter (TSI 3781). A dilution system was used due to high concentration of particulate matter.

During the week days the mean hourly average concentration of PM_{10}, $PM_{2.5}$, PM_1 and $PM_{10} - PM_{2.5}$ by the main city roads was 305 $\mu g/m^3$, 84 $\mu g/m^3$, 61 $\mu g/m^3$ and 222 $\mu g/m^3$, respectively (Table 1). The coarse size fraction was particularly large and exhibited a wide variation. In contrast, during the weekend, the average concentration of PM_{10}, $PM_{2.5}$, PM_1 and $PM_{10} - PM_{2.5}$ showed a substantial fall. The biggest drop was seen in the coarse size fraction and levels of PM_{10} were 136 $\mu g/m^3$ in comparison to 305 $\mu g/m^3$ during weekdays. The concentration of $PM_{2.5}$ and PM_1 dropped to 60 $\mu g/m^3$ and 40 $\mu g/m^3$, respectively (Table 1).

This suggests that a considerable amount of particulate matter was in the coarse size fraction and resuspension of road dust during the traffic movement was probably the principal contributor in mass concentration. The hourly average concentration of PM_{10}, $PM_{2.5}$, PM_1 and $PM_{10} - PM_{2.5}$ at a background site during the week days was 206 $\mu g/m^3$, 63 $\mu g/m^3$, 31 $\mu g/m^3$, and 143 $\mu g/m^3$, respectively.

Table 1 .Hourly average mass concentration of particulate matter ($\mu g/m^3$) by the road sides during weekdays, weekends and at a background site.

	PM_{10}	$PM_{2.5}$	PM_1	PM_{10} - $PM_{2.5}$
Weekdays				
Ave.	305	84	61	222
Max.	534	107	85	440
Min.	187	48	35	126
Std.Dev	98	19	18	92
Weekends				
Ave.	136	60	40	76
Max.	155	66	46	95
Min.	122	52	34	65
Std.Dev	12	6	5	10
Background				
Ave.	206	63	31	143
Max.	259	71	32	187
Min.)	160	56	30	105
Std.Dev	42	6	1	36

Ave. (Average), Max. (Maximum), Min. (Minimum), Std Dev. (Standard Deviation).

The mean hourly average number concentration during weekdays, by city roads, was 417,003 #/cm³. On the other hand, adjacent to roads at the University, the mean hourly mean concentration was 97,300 #/cm³ (Table 2).

Table 2. Hourly average number concentration (#/cm³) of particulate matter by the city and university road sides

	city road sides	By University road
Average	417003	97300
Maximum	659068	104859
Minimum	111365	87359
Std Dev	206549	8990

Std Dev. (Standard Deviation).

Overall, the levels of particulate matter were almost double during weekdays than weekends. This suggests a significant contribution from road traffic. A large fraction of particulate matter was in size range $PM_{10} - PM_{2.5}$. The increasing trend in number of vehicles, poor emission controls, ageing fleet of public transport and poor road conditions are the most likely sources of the urban particulate matter. Daily commuters, mostly on two wheelers, and residential population in the city slums are at a greater exposure risk.

Spatio-temporal variations of particulate air pollution in Beijing, China

N.J. Schleicher[1], S. Norra[1,2], Y. Chen[3], F. Chai[3], S. Wang[3]

[1]Institute of Mineralogy and Geochemistry, Karlsruhe Institute of Technology, Karlsruhe, 76131, Germany
[2]Institute of Geography and Geoecology, Karlsruhe Institute of Technology, Karlsruhe, 76131 Germany
[2]Institute of Urban and Regional Atmospheric Environmental Research, China Research Academy of Environmental Sciences, Beijing, 100012, China

Keywords: Urban aerosols, PM2.5, Chemical composition, Anthropogenic aerosols, Megacity
Presenting author email: nina.schleicher@kit.edu

Air quality constitutes a huge challenge for urban areas and Megacities in particular. In China, the urban population is exposed to high levels of particulate air pollution. The individual burden for the inhabitants can vary significantly with regard to seasons and spatial distribution. Therefore, this study focuses on spatio-temporal variations of $PM_{2.5}$ concentrations and composition in Beijing.

Samples were continuously collected on a weekly basis at five sampling sites along a transect from the NW to the SE of Beijing. Additionally, day- and night-time samples were distinguished. Element concentrations of all samples were determined by HR-ICP-MS after acid digestion. Moreover, water-soluble ions and black carbon (BC) were studied.

With regard to spatial patterns, the north-western parts of the city (site 1) were less polluted than regions in the south-eastern (especially site 4) areas (Figure 1).

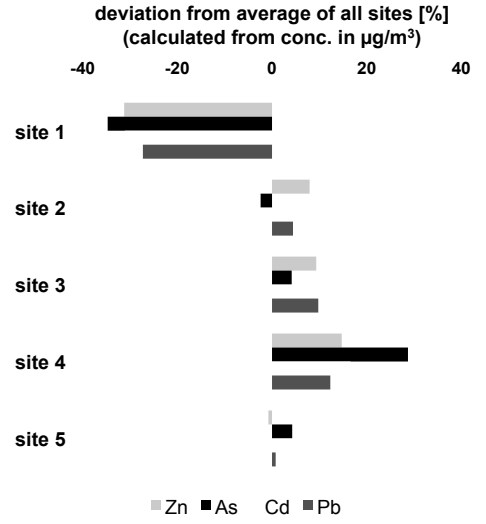

Figure 1. Deviation of anthropogenic element concentrations (in µg/m^3) calculated for each site from the NW to the SE of Beijing from the average of all sites.

It is noteworthy to highlight the observation that the spatial variations are very different if concentrations are expressed in µg/m^3 or in µg/g (Figure 2). In this context the situation at site 3 located just near to the central Tienamen Square should be pointed out. At this site Zn, As, Cd, and Pb concentrations are lower than at site 4 if expressed in µg/m^3, but highest of all sites if expressed in µg/g. Consequently, for the monitoring of toxic element concentrations in urban areas, the values expressed in µg/g would provide further valuable information for the assessment of potential health effects in different parts of the city and should be considered in future.

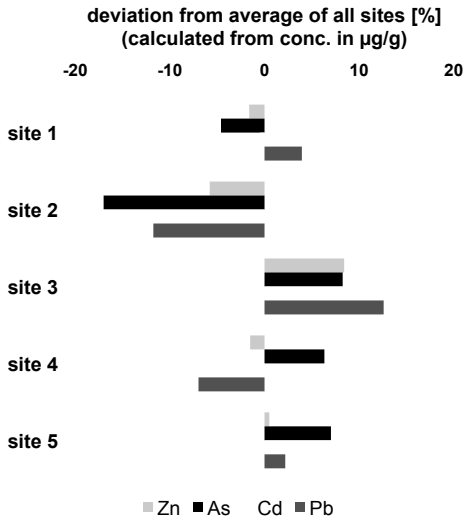

Figure 2. Deviation of anthropogenic element concentrations (in µg/g) calculated for each site from the NW to the SE of Beijing from the average of all sites.

Over the annual course, the different sites had a similar trend. The lowest aerosol concentrations occurred during summer, due to meteorological conditions (e.g. most rainfall occurs during summer months in Beijing) and the lack of certain sources (especially emissions from heating processes). In spring, high aerosol concentrations are predominantly caused by geogenic particles, whereas the concentrations of toxic elements from anthropogenic sources were considerably lower. Conclusively it can be stated that the burden of air pollution for the inhabitants of Beijing are highest during winter due to stagnant meteorological concentrations on the one hand, and additional sources, especially coal combustion for heating purposes, on the other hand. During this time, especially the high concentrations of potentially toxic elements, such as Cd, As, and Pb, are of great concern for human health.

This work was funded by the German Research Foundation (DFG) under grant STU 169/32-1,2.

Analysis of a time series of particulate sulfate in a suburban site

M. A. Revuelta, F.J. Gómez-Moreno, L. Núñez and B. Artíñano

Department of Environment, Centro de Investigaciones Energéticas, Medioambientales y Tecnológicas (CIEMAT), Madrid, 28045, Spain
Keywords: sulfate, urban aerosols, sulfur dioxide, PM1.
Presenting author email: maranzazu.revuelta@ciemat.es

The Madrid Metropolitan Area is located in the centre of the Iberian Peninsula. The population is nearly 6 million inhabitants, involving a car fleet of almost 3 million vehicles with very intense traffic on weekdays on the two existing ring roads and the roads connecting Madrid with the surrounding towns. Since industry consists essentially of light factories, the Madrid plume is typically urban.

Semicontinuous PM_1 sulfate concentration is being registered in a suburban site (40º27.5'N, 3º43.5'W) since June 2009. The instrument used is a Thermo 5020 sulfate particulate analyzer (SPA) (Schwab et al, 2006) on a time basis of 20 minutes. It reduces sulfate aerosol by thermal catalysis and analyzes the resulting sulphur dioxide gas by pulsed fluorescence. Laboratory conversion efficiencies are higher for ammonium sulfate than for mineral-type sulfates. The measurements are corrected by comparison against filter-based measurements.

Precursor gaseous species were measured by a DOAS spectrometer (OPSIS AR-500). The jointly analysis of particulate sulfate, gaseous species (SO_2) and meteorology allowed identifying different kinds of sulfate events at the sampling point.

A significant reducing trend in gaseous SO_2, leading to a decrease in sulfate levels has been observed from the 80s at other European sites (Jones and Harrison, 2011). A SO_2 decreasing trend has also been recorded in Madrid from 1998 to 2007 (Ayuntamiento de Madrid, 2008). In the suburban site, a drop in particulate sulfate levels from 2009 to 2010 was observed. This drop was also seen in other parameters registered in the site, such as particulate nitrate and PM_{10}. Meteorological factors might have contributed to the cleansing of the atmosphere, without discarding other explanations.

Figure 1 shows the timely averaged sulfate concentrations differentiating among weekdays (Monday to Friday), Saturdays and Sundays. The daily pattern indicates a clear traffic influence. Sulfate concentration increases sharply at 7:00, peaking between 10:00 and 14:00. A secondary maximum is seen on weekend nights.

The winter synoptic situation leading to the occurrence of episodic events corresponds to stagnant anticyclone conditions, light winds and clear-sky conditions, with the usual formation of radiative nocturnal surface inversions. Under this atmospheric situation sulfate levels can be rising during more than one week. Sulfate events attributed to aqueous phase formation were also detected. However, the highest PM_1 sulfate values (in occasions over 7 ug m^{-3}) were associated to pollutant transport.

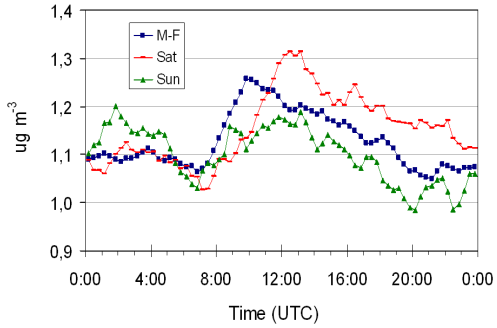

Figure 1. PM_1 sulfate averaged daily patterns for weekdays (blue), Saturdays (red) and Sundays (green) from Jun09 to Dec10

This work has been supported by Spanish Ministry MICINN through the project PROFASE (CGL2007-64117-CLI). M. A. Revuelta acknowledges the Ministry of Science and Innovation for their economical support through the FPI predoctoral grant BES-2008-007079.

Ayuntamiento de Madrid (2008). Informe Sobre la Calidad del Aire en Madrid 2007. *Technical report*

Jones, A. M. and Harrison, R. M. (2011). Temporal trends in sulphate concentrations at European sites and relationships to sulphur dioxide. Atmospheric Environment 45: 873-882.

Schwab, J. J., Hogrefe, O., Demerjian, K. L., Dutkiewicz, V. A., Husain, L., Rattigan, O. V., Felton, H. D. (2006). Field and laboratory evaluation of the Thermo Electron 5020 Sulphate Particulate Analyzer. Aerosol Science and Technology 40(10): 744-752.

Atmospheric nano-sized particle counting in Tehran air

F. Halek A. Kavousirahim

Department of Energy & Environment, Materials & Energy Research Centre, Tehran, P.O.Box 14155-4777, Iran
Keywords: particulate matter, nanoparticle, particle number, Tehran air pollution.
Presenting author email: f-halek@merc.ac.ir

Nanoparticles, the primary building blocks of many nanomaterials, may become suspended in air as an air pollutant, and they can transport toxic chemicals into the human respiratory system. Although it is unclear whether if mass, number, or even surface area of particles is the most important determinant in causing adverse health affects, toxicological studies have shown that ultrafine particles have a much stronger physiological effect than coarse particles of the same mass. Atmospheric ultrafine and nanoparticles can pose a greater hazard than coarse particles when entering human lungs due to their high number concentration and large specific surface area (Harrison and Yin, 2000; Oberdorster, 2001; Guzman et al, 2006). A group of many scientists in Europe have recently studied the spatial variation of particle number and mass over four European cities (Puustinen et al, 2007), followed by finding the correlation between indoor - outdoor particle number and mass in the cities (Hoek et al, 2008).

The increasing number of motor vehicles and industrial processes involving nanoparticle formation are the main source of nanoparticles emission and their consequences on the environment in large cities such as Tehran (Shi et al, 2001; Halek et al, 2004). In this study, we measured count (number concentrations) of the nanoscale particles found on Tehran's air. None of previous studies reported on particle counting in Tehran's atmosphere (Atash, 2007).

Experimental

The study performed in 5 sampling sites including Azadi Sq. (AS), Jomhouri Sq. (JS), Tohid Sq. (TS), Vali-Asr Junction (VJ) and Jalale-Ale-Ahmad Highway, Sheykh Fazlullah Intersection (JSI). These sites are all located in the west-central parts of Tehran having specific specializations such as heavy traffic, nearing the large residential areas and including main Tehran hospitals. The samples were collected at the height of 1.65 m. Samplings were done in the warm season (July, Aug. & Sep. 2008), followed by the cold season (Jan., Feb. & March 2009). A portable particle size analyzer (Grimm-1.108), was calibrated according to the manufacturer manual and used for the continuous measurement of particles.

Results & Discussion

The average number concentrations of the particles for two different size ranges of > 300 nm and 1.0 - 10 μm at the sampling sites for the two seasons are summarized in Table 1. These data indicated that the average number concentration of particles > 300 nm is 98,970,178 particle/m^3 in warm season and 478,450,460 particle/m^3 in the cold season. Table 2 shows the ISO (International Organization for Standardization) classifications on particle numbers in outdoor air in 3 different sizes.

Table 1. Average number of PM in the sites (Particle/m^3).

	Warm Season		Cold Season	
Site	*> 300 nm*	*1.0-10 μm*	*> 300 nm*	*1.0-10 μm*
AS	104,471,902	2,495,500	739,863,104	5,844,857
JS	128,179,613	2,946,250	458,216,517	5,549,500
TS	92,303,207	2,265,500	518,847,012	7,375,460
VJ	93,484,774	2,298,063	407,209,877	4,780,444
JSI	76,411,392	1,719,963	268,115,799	4,518,243

Table 2. ISO classifications on outdoor particles.

Size	Number of particle/m^3 in outdoor air		
	Dirty	*Normal*	*Clean*
> 100 nm	10,000,000,000	3,000,000,000	500,000,000
> 300 nm	300,000,000	90,000,000	20,000,000
> 500 nm	30,000,000	7,000,000	1,000,000

On the basis of ISO classifications (Table 2) for > 300 nm particles, our results revealed that Tehran's air quality in the case of particle number concentrations is around ''Normal" in warm season, while over than "Dirty" in winter. The data listed in Table 1 indicated that the number concentration of particles with size range of 1.0 μm - 10 μm in the cold season was 2.2 times higher than number concentration of particulate matter in the warm season in Tehran atmosphere. Also, the number concentrations of the smaller particles having the size range of > 300 nm in the cold season were found to be 4.8 times of the warm season.

Our findings indicated that from 5 studied stations, JS has higher concentration and JSI has lower particle concentrations. Heavy traffic and nearing to commercial sectors and large Tehran shopping centers (Bazar) are major reason for higher levels of pollution in JS than other sites.

Atash, F. (2007) *Cities* **24**, 399-409.

Guzman, K.A.D., Taylor, M.R. and Banfield, J.F. (2006) *Environ. Sci. Tech.* **40**, 1401-1407.

Halek, F., Kavousi, A. and Montehaei, H. (2004) *I. J. Environ. Health Res.* **14**, 307-313.

Harrison, R.M. and Yin, J. (2000) *Sci. Total Env.* **249**, 85-101.

Hoek, G. et al. (2008) *Atmos. Env.* **42**, 156-169.

Oberdorster, G. (2001) *I. Arch. Occup. Environ. Health* **74**, 1-8.

Puustinen, A. et al. (2007) *Atmos. Env.* **41**, 6622-6636.

Shi, J.P., Evans, D.E., Khan, A.A. and Hassison, R.M. (2001) *Atmos. Env.* **35**, 1193-1202.

Ultrafine particles ambient air pollution in an industrial area in Southwest Europe: A fuzzy logic qualitative model

R. Fernández Camacho[1], Ana M. Sánchez de la Campa[1,2], J. Aroba[3], J.D. de la Rosa[1], F. Gomez-Bravo[3], S. Rodríguez[4]

[1]Associate Unit CSIC-University of Huelva "Atmospheric Pollution", University of Huelva, Campus El Carmen E21071 Huelva, Spain
[2] Estación Experimental del Zaidín, CSIC, C/ Profesor Albareda 1, E18008 Granada, Spain
[3]Departmento de Tecnologías de la Información, Escuela Politécnica Superior, Universidad de Huelva, Ctra. Palos de a Frontera, s/n. 21819, Palos Fra, Huelva, Spain.
[4]Izaña Atmospheric Research Centre, AEMET Joint Research Unit to CSIC "Studies on Atmospheric Pollution", La Marina 20, planta 6, Santa Cruz de Tenerife, E38071, Canary Islands, Spain.
Keywords: ultrafine particles, industrial emissions, heavy metals, fuzzy logic.
Presenting author email: rocio.fernandez@dgeo.uhu.es

Studies on ultrafine particles and air quality have mostly focused on vehicle exhaust emissions and on new particle formation in "clean" ambient air. In this study, we apply a fuzzy computer tool, PreFuRGe (Aroba, 2003) to a database of daily average values of PM2.5 chemical composition, black carbon (BC), particle number concentrations (N>2.5 nm) and meteorological parameters, in order to know how ultrafine particles affect ambient air pollution in Huelva (SW Spain), an urban coastal area where significant emissions of gaseous particle precursors take place. These emissions are mostly linked to industrial activities from nearby Industrial Estates: Punta del Sebo, where it should be noted a Cu-smelter plant, given that it is a very significant source of SO_2 and heavy metals as As, Pb and Zn and a phosphoric acid production plants (Fernández-Camacho *et al.*, 2010a); and Nuevo Puerto, whose SO_2, NO_x, NH_3, Ni and V emissions are well documented (Fernández-Camacho *et al.*, 2010a).

N was split into two components N1 and N2 following the methodology of Rodríguez and Cuevas (2007). N1 accounts for vehicle exhaust emissions and may also include compounds nucleating/condensing immediately after emission. N2 is correlated with SO_2 and accounts for new particle formation due to nucleation and rapid particle growth to detectable sizes (Fernández-Camacho *et al.*, 2010b).

The aim of this study is to characterize and interpret qualitatively the association between N1 and N2 with the other variables by using a fuzzy description (Aroba, 2003).

Figure 1 shows six graphical fuzzy rules, where N1 and N2 are the consequents and BC, $SO_4^{2-}{}_{antrop.}$, NO_3^-, NH_4^+, PO_4^{3-}, As, Ni, Cu, Zn, V, Pb, temperature and solar radiation are the antecedents. It is worth noting two behaviour patterns in the concentrations of N1 and N2, corresponding to rules C and D.

Low concentrations of N1 and very high concentrations of N2 (Rule C, Fig. 1) are compatible with medium to high values of SO_4^{2-}, NH_4^+, PO_4^{3-}, As, Ni, V and Pb. Note in this rule that solar radiation is very high and BC is very low.

High concentrations of N1 and medium concentrations of N2 (Rule D, Fig. 1) appear when BC and NO_3^- are very high. Also, we can observe that low to medium values for heavy metals are not compatible with high concentrations of N1.

The results obtained shows how fuzzy logic techniques are very useful for qualitative modelling and identifying the sources contributing to ultrafine particles components N1 and N2 and their relationship with the other variables. The association between N1, BC and NO_3^- (Rule D, Fig. 1) points to vehicle exhaust emissions. The association of N2 with the above heavy metals, SO_4^{2-}, NH_4^+, PO_4^{3-} (Rule C, Fig. 1) is attributed to ultrafine particle formation in industrial plumes. The high solar radiation favours the photochemical processes in those industrial emissions.

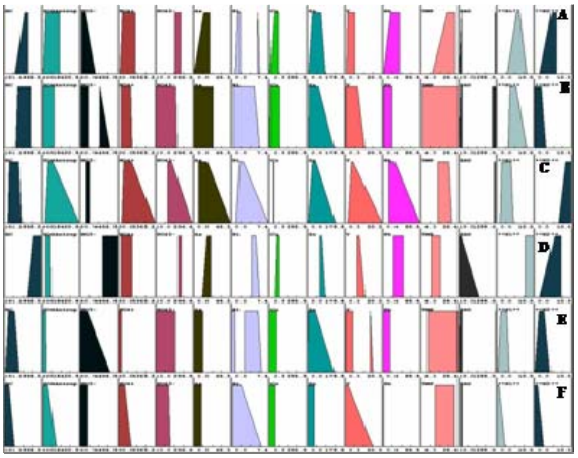

Figure 1. Example of graphical fuzzy rules

Aroba, J. (2003) *Advances in the decisión making in software development projects*, PhD. Thesis, University of Sevilla, Spain.

Fernández-Camacho, R., et al. (2010a) *Atmos. Res.* **96**, 590-601.

Fernández-Camacho, R., et al. (2010b) *Atmos. Chem. Phys.* **10**, 9615-9630.

Rodríguez, S., Cuevas, E. (2007) *J. Aerosol Sci.* 38, 1207-1219.

PM characterization of Mexico City aerosols by automated single particle analysis

M.F. Meier[1], T. Castro[2], M.I. Saavedra[2] and B. Grobéty[1,3]

[1]Department of Geosciences, University of Fribourg, Fribourg, 1700, Switzerland
[2]Centro de Ciencias de la Atmósfera, Universidad Nacional Autónoma de México, Mexico City, 04510, Mexico
[3]FRIMAT, University of Fribourg, Fribourg, 1700, Switzerland
Keywords: Urban aerosols, Mineral dust, Megacity, CCSEM.
Presenting author email: mario.meier@unifr.ch

Particulate Matter (PM) is an important component of air pollution. A remarkable amount of data concerning air quality is available for the metropolitan area of Mexico City (MC) and its surroundings (Molina et al, 2010). Querol et al (2008) reported 50-56 µg/m3 of PM10 at different urban sites of MC. The contribution of mineral matter to these concentrations was up to 27%. The aim of this study was to characterize mineral dust at an urban background site of MC and to evaluate daily and seasonal variations.

For that purpose PM10 samples were actively collected (4 l/min) on polycarbonate filters on the campus of the Universidad Nacional Autónoma de México (UNAM). Two samples per day were taken from 10am-3pm and 6pm-11pm respectively during two sampling campaigns in July 2008 (rain season: RS) and March 2009 (dry season: DS).

Morphology and chemistry of single particles with sizes 0.4-10 µm were analyzed with computer controlled scanning electron microscopy (CCSEM) and energy dispersive X-ray spectroscopy (EDXS). Each particle was classified based on chemistry into one of the following particle classes: iron and iron oxides (I), aluminium containing silicates (II), aluminium free silicates (III), carbonates (IV) and sulphates/phosphates (V). For each class a mass concentration was determined by multiplying the calculated volume of individual particles with the densities of the class they were assigned to.

Number and mass concentration of most of the samples were dominated by class (II) particles. The most important minerals contributing to this class are clays, which have mainly a geogenic origin. The second important class was class (I) followed by class (IV) and (III) (Fig.1). However it has to be mentioned that only sulphates with Na+ and heavier cations could be detected properly. Samples from the RS show clear differences to the samples from the DS. The median mass and number concentration obtained from samples from July was 2.6 µg/m^3 (maximum: 4.6 µg/m^3) and 281'000 particle/m^3 respectively. Values in February were with 5.8 µg/m^3 (maximum: 14.9 µg/m^3) and 525'000 particles/m^3 twice as high. The higher mass concentration in the dry season is due to an increase of silicates and carbonates. Samples taken during rain periods in the RS have decreased concentrations and become sometimes dominated by class (I) particles. Iron and iron oxides show a constant concentration (~0.55 µg/m^3) in all samples, independently of season and weather condition. A local anthropogenic source is probable for these particles. Also sulphates and phosphates show no clear seasonal differences. However this class is dominated mainly of Ca-carbonates and phosphates in RS and by other sulphates in DS. There are different possible origins for these particles (anthropogenic, biological or volcanic). Daily variations between samples are not evident.

Mineral matter concentrations in MC depend strongly on weather condition and seasonal influences, with a clear increase of silicates and carbonate in DS. The reasons are less vegetation, dry roads and no wash out processes. So more mineral dust gets suspended in the air and can remain longer there. In contrast concentrations of iron/iron oxides, sulphates and phosphates don't show clear weather dependence. A possible explanation is that their sources are aseasonal (e.g. traffic and volcanic activity).

For a better understanding of the influence of mineral matter on MC air quality further samples from a second urban background site and from the high altitude site Altzomoni (Iztaccihuatl volcano, 4000 m.a.s.l.) were taken. Results of these samples will be available soon.

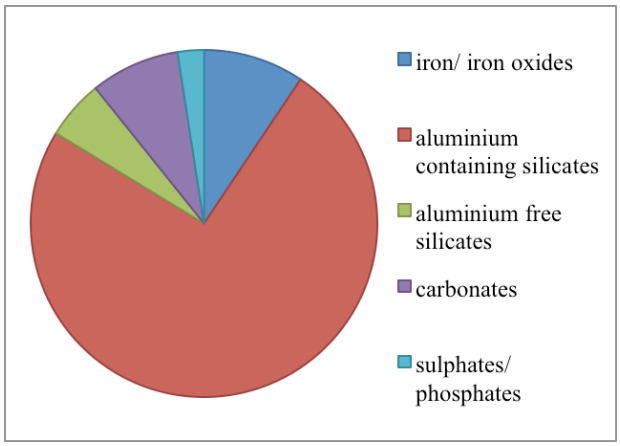

Figure 1: Mineral dust repartition in MC in March 2009.

Molina, L.T., Madronich, S., Gaffney, J.S., Apel, E., de Foy, B., Fast, J., Ferrare, R., Herndon, S., Jimenez, J.L., Lamb, B., Osornio-Vargas, A.R., Russell, P., Schauer, J.J., Stevens, P.S., Volkamer, R. and Zavala, M. (2010) *Atmos. Chem. Phys.*, 10, 8697-8760.

Querol, X., Pey, J., Minguillón, M.C., Pérez, N., Alastuey, A., Viana, M., Moreno, T., Bernabé, R.M., Blanco, S., Cárdenas, B., Vega, e., Sosa, G., Escalona, S., Ruis, H. and Artíñano, B. (2008) *Atmos. Chem. Phys.*, 8, 111-128.

An original device for the measure of aerosol deposition. First results on the Pin Sec catchment in Nantes, France

Stéphane Percot[1*], Véronique Ruban[1], Pierre Roupsard[2], Denis Maro[2] and Maurice Millet[3]
[1] Institut français des sciences et technologies des transports, de l'aménagement et des réseaux
[2] Institut de Radioprotection et de Sûreté Nucléaire
[3] Université de Strasbourg
Keywords: ^{7}Be, Atmospheric deposition, Aerosol size distribution, Urban aerosols, Heavy metals
*Tel : +33(0)2 40 84 57 73 ; fax : +33(0)2 40 84 59 98 ; E-mail : stephane.percot@ifsttar.fr

Introduction

Pollutants associated to atmospheric particles in urban areas have been characterized in many studies throughout the world. Pollutant sources are either natural (e.g. volcanoes, forest fires) or of anthropogenic origin (traffic, industries, central heating). The nature of surfaces and the weather conditions and the atmosphere turbulence influence the aerosol deposition. Previous studies at Nantes (France) on the Pin Sec catchment allowed the chemical characterization of total atmospheric deposition. In order to improve our knowledge of aerosol dry deposition on this catchment an original approach is being developed.

The objective is to present the instruments set up in the district of the Pin Sec to measure dry and wet atmospheric deposits and to show the first results.

Experimental setup

The original approach carried out in this long-term study (18 months) combines particle collectors (Partisol 2000 FRM), a covered pluviometer and frames on which test samples of different urban materials are fixed (tiles, glass, bitumen etc…). A meteorological station and an ultrasonic anemometer supply meteorological and micrometeorological data.

Measuring instruments have been installed on the roof of a 4-store building in the Pin Sec catchment; the data should be representative of the global quality of atmospheric deposition on this catchment. Pollutants studied were heavy metals, pesticides and Polycyclic Aromatic Hydrocarbons.

The analysis of deposited airborne particles on test samples will be done through beryllium 7 (^{7}Be) used as a tracer. Concentration of aerosols is given by Partisol. This analysis will allow calculating a monthly evolution of the dry deposition velocity of particles and determining deposition fluxes.

Finally, in order to validate the use of ^{7}Be as tracer of atmospheric deposition a Low Pressure Impactor (LPI) is used allowing the measurement of aerosol size.

Results

The medium diameter (D50) of ^{7}Be atmospheric on particles varies from 0.50 to 0.59 µm. These values are in good agreement with the literature. It confirm the fixation of ^{7}Be on accumulation mode of atmospheric aerosol.

Figure 1 shows the good correlation between the distribution of Pb mass and ^{7}Be activity. The same pattern is observed for Zn. As a whole, metals are mainly distributed in the fine fraction (0.47<D50<0.62 µm). Therefore, ^{7}Be seems to be representative of the distribution of trace metals.

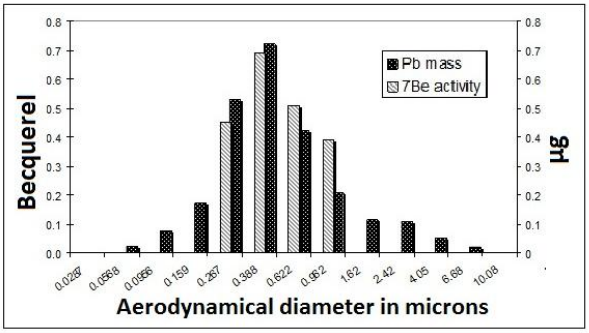

Figure 1: Comparative aerodynamical distribution of Pb mass versus ^{7}Be activity

Conclusions

An original method for the measurement of aerosol deposition has been installed on a small urban catchment. The first results show that ^{7}Be can be used as a tracer of metals. More tests are in progress regarding the correlation of ^{7}Be with polycyclic aromatic hydrocarbons and pesticides. The data on ^{7}Be deposit will allow the calculation of pollutant dry deposition taking into account the nature of urban surfaces and air turbulence.

Statistical distributions of particle number concentrations observed in urban transport microenvironments during commuting

I.D. Longley[1], K.Shrestha[1,2], S.Kingham[2], J.Salmond[3], W.Pattinson[2]

[1] National Institute of Water & Atmospheric Research Ltd, Auckland 1010, New Zealand
[2]Department of Geography, University of Canterbury, Christchurch 8041, New Zealand
[3] School of Environment, The University of Auckland, Auckland 1142, New Zealand

Keywords: Exposure, CPC, Number concentration, Vehicle emissions.
Presenting author email: i.longley@niwa.co.nz

Introduction

People spend a substantial amount of their outdoor time in transport microenvironments which, as well as busy roads, can include the interiors of vehicles, car parks, train stations, subways, bus depots/stops and the road space used by pedestrians and cyclists. Exposure to pollutants in these microenvironments is often highly elevated compared to elsewhere, which results in individuals gaining a significant contribution to their daily exposure to air pollution in general, and ultrafine particles in particular, in a short period of time. Research in London has found *mode* of transport to be a statistically significant determinant of UFP exposure (Kaur and Nieuwenhuijsen, 2009).

Previous observations have revealed that particle number concentrations in such microenvironments are highly variable in time and space. It is not yet clear how much of this variation is random (associated with chance close encounters with individual sources, for instance) and how much is systematic (associated with particular meteorological conditions or characteristic locations, such as intersections, for example).

This paper reports an analysis of a subset of a large observational dataset of personal exposure measurements made whilst commuting by various modes of transport. It aims to describe and summarise the statistical nature of high-resolution particle number concentrations in the different transport microenvironments encountered, as a first step in exploring sources of variability and exposure predictability.

Methods

The full study, its aims, location, dates and study design are detailed in Kingham et al. (2011). In brief, personal measurements of traffic-related air pollutants were made on multiple simultaneous journeys (by different modes) between the same journey origin and destination in Christchurch and Auckland (New Zealand) in 2009.

This paper considers only measurements made in Christchurch (between 26th February 2009 and 26th March 2009) and focuses on particle number concentrations. Sampling was conducted during traffic peak hours on foot, in a car or on buses along three routes in the city encompassing a wide range of traffic volumes. Journeys included time spent at three bus stops, a sheltered car park, and an indoor bus terminus.

Particle number concentration was measured at 1 second resolution using a TSI 3007 portable condensation particle counter sampling via a purpose-made diluter to the design reported by Knibbs et al. (2007). Location was logged at 3 second resolution using a Nokia N82 mobile phone with built-in GPS receiver.

Results

Observed particle number concentrations were sensitive to microenvironment. On average, the lowest concentrations were observed at an outdoor 'waiting' location in downtown Christchurch (~ 20,000 cm^{-3}). Slightly higher mean concentrations were generally observed in the other outdoor microenvironments, including pedestrian walking and outdoor bus stops. However, the data for both of these categories was highly variable by location, with much higher concentrations recorded at a roadside suburban location than at the city centre or less-trafficked suburban locations. Mean concentrations in the car park were ~ 3 times higher than outside. The highest average concentrations were recorded inside both the bus and the car, as well as at the indoor bus stop (mean of 75 – 80,000 cm^{-3}).

The statistical distributions of concentrations for each microenvironment were crudely described by log-normal distributions. Analysis was suggestive of a 'baseline' distribution with a mode in the range 15-30,000 cm^{-3} upon which two additional modes could be superimposed, a higher concentration mode associated with car emissions and a yet higher one associated with bus emissions. Within vehicles these upper modes were dominant and the baseline mode was suppressed leading to higher exposures overall.

This work was supported by the Foundation for Research, Science & Technology and the New Zealand Transport Agency.

Kaur S. and Nieuwenhuijsen M. J. 2009, Determinants of Personal Exposure to PM2.5, Ultrafine Particle Counts, and CO in a Transport Microenvironment. *Environ. Sci. & Technol.,* **43**, 4737-4743.

Kingham, S., Longley, I., Salmond, J., Pattinson, W., Shrestha, K., Liu, H., 2011. Determination of personal exposure to traffic pollution while travelling by different modes in a less congested city. *In preparation.*

Knibbs, L.D., de Dear, R.J., Morawska, L., Coote, P.M., 2007, A simple and inexpensive dilution system for the TSI 3007 condensation particle counter. *Atmos. Environ.,* **41**, 4553-4557.

Urban aerosol variability from meteoparameters on various time scales

A.A. Jouravlev[1], A.V. Zaripov[1]

[1] Physics Department, Kazan Federal University, Kazan, 420107, Russia
Keywords: aerosol dynamics, air pollution, boundary layer, urban aerosols
Presenting author email: sirarthur@rambler.ru

Aerosol concentration and its spatial distribution are in dependence both from various meteorological parameters, and from other factors, such as concentration of chemical impurity, turbulence, directions of movement of air masses. The purpose of this work is search of similar dependences on various time scales by wavelet analysis.

These researches are based on the data obtained from the continual monitoring of the air condition. The measurements of 5 ecological stations include 11 urban air parameters. They are: air temperature, relative humidity, atmospheric pressure, wind velocity, five gas impurity and aerosol concentration. These stations were situated at city. The researched database contains the data for three years of observation. The measurements are made at 2.4 meters height with one-minute period for meteoparameters and half-an-hour interval for chemical impurities and aerosol mass concentration.

The research method is the following: the wavelet decomposition for each measured parameter was made, the wavelet spectrum was received and then the correlation functions of received coefficients were calculated. The applied method allows to find out interrelations of an aerosol concentration with other meteoparameters and besides to define magnitude of its correlation on each fragment of a wide range of investigated time scales. The advantage of our method in comparison with methods of the direct statistical analysis consists in possibility to establish interrelation between the measured parameters on each part of frequency area of parameters variations.

With use of the described above method the research of values dependences of 5 meteoparameters and concentration 5 impurity gases from concentration of an aerosol has been conducted. Wavelet decomposition and correlation functions of coefficients both for the annual period as a whole, and with selection into seasons (summer and winter) were investigated. The fragment of the received wavelet spectrum for aerosol concentration in a winter season is presented in figure 1.

The closer axis (X) is a time axis and covers a time interval about 4 days. Axis Y represents an axis of time scale of a wavelet spectrum. On axis Z wavelet decomposition coefficients are laid. The elements of two periodic processes – the first one in the bottom part and the second one with lower-frequency in the top are clearly visible on a surface.

Clearly seen periodicity in high-frequency area has the approximate period 48 hours of an order. In a distant part of figure high-period variations was observed and it has the period approximately 3 days.

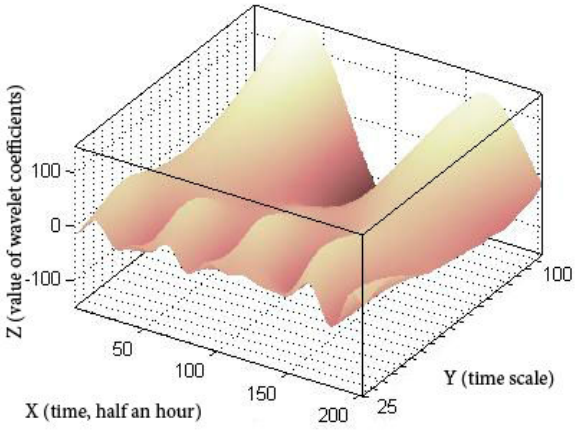

Figure 1. Wavelet spectrum of aerosol concentration for a winter season.

The analysis of wavelet decomposition of impurity concentration and meteoparameters has shown presence of both the already known and obvious periods of variations, and the periods having more difficult nature. For example, authentic variations with the periods of humidity and SO_4 concentration have been revealed for an aerosol.

After correlation analysis being made some received dependences discovered at several stations have appeared to be interesting. With high value of correlation level (above 0.8) there were low-frequency processes with the period approximately 20 days on aerosol spectra, SO_4 and damps which, in our opinion, can't be referred to city or natural cycles.

The received results allow us to make conclusions on deeper correlations between an aerosol, impurity and meteoparameters. This information can help to improve existing models of urban aerosol dynamics.

Frik, P.G. (1998) *Turbulence: models and approaches,* Perm State Technical University Press.

Mallat, S. (1999) *A wavelet tour of signal processing*, Academic Press.

Continuous Measurements with High Time Resolution of Semi-Volatile Components in the Atmospheric Aerosol

Wolfgang Brunnhuber[1], Hans Grimm[1], T. Külz[1], M. Pesch[1], M. Richter[1] and Friedhelm Schneider[1]

[1]Grimm Aerosol Technik GmbH & Co. KG, 83404 Ainring, Germany
Keywords: Atmospheric Aerosol, Instrument development, PM10, PM2.5, SVC.
Presenting author email: mp@grimm-aerosol.com

EU limit and guideline values for the protection of human health (DIRECTIVE 2008/50/EG) demand a continuous monitoring of the atmospheric aerosol, more precisely its fine dust fraction PM10 and PM2.5. The tresholds are being exceeded in many areas in Europe, primarily in congested urban areas, where many people are affected. Fine dust is rated harmful to health which therefore action needs strongly to be taken, in order to minimize this exposure.

The EU regulates, when exceeding the set limit and guideline values, to develop clean air plans, in which efficient reduction strategies have to be enlisted. These plans are based upon cause analysis, which assigns certain dust exposure to certain sources.

For monitoring the thresholds, many measuring technologies proved well, whereas in the past years especially the optical measuring technology gained in importance. The optical detection of the aerosol enables a non-contact, continuous, and temporally high resolved measurement of the aerosols in real-time, where next to the PM fractions also particle size as well as particle counts can be determined.

A significant part (up to 60% of the particle mass) of the atmospheric aerosol is determined as semi-volatile components (SVC), which varies depending on location and season. This meaningful fraction of the SVC impedes the exact determination of the aerosol mass: The volatile components get lost, when heating the aerosol while sampling, e.g. when using a heated sampling probe for drying the sample, or when dust clogged filters remain several days without cooling inside the sampler.

Thus it is important to determine the volatile fraction of the aerosol for two reasons: On the one hand this fraction is very helpful for the source identification of the dust, because different sources create different SVC fractions, and on the other hand it is very important to measure the SVC for comparing the results of different fine dust measuring devices, which reveal the difference in their losses of SVC while measuring.

Thus the gas-particle-conversion from nitrogen oxides to nitrates and ammonium compounds, or the condensation from gaseous emitted carbon hydrides leads to organic aerosols.

The company Grimm Aerosol Technik GmbH & Co. KG developed a compact, mobile, and highly efficient measuring instrument, which enables the continuous determination of the volatile fraction within the atmospheric aerosol. This device is in possession of two sampling probes with complementary characteristics:

One probe dries the particles by a nafion membrane in such a way, that no volatile aerosols get lost, while in the other probe the aerosol can be heated to a temperature of up to 300 °C. The aerosol is alternating being sucked through the sampling probes and subsequently analyzed inside the same optical chamber. This means, that in one interval all aerosols are analyzed and in the other one only the thermically stabilized aerosols. Forming this difference of both intervals, a determination of the volatile fraction is possible. There the volatile components are classified simultaneously into 31 size channels from 250 nm up to 32 µm, as well as a simultaneous detection of the PM10, PM2.5, and PM1 fractions (figure 1).

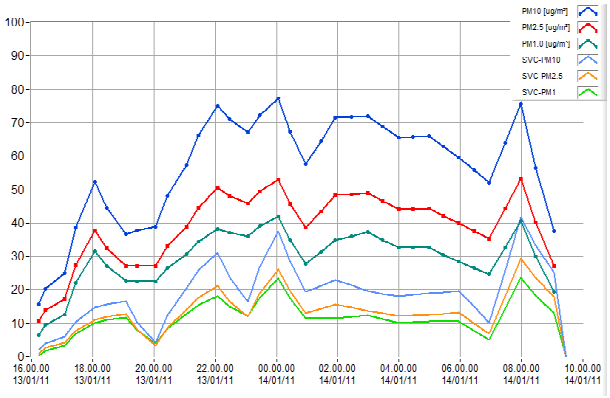

Figure 1: Temporal course of the PM fractions and its volatile components at 100°C

The temporal resolution is 6 seconds. By limiting the size channels, measurements can be executed at 1 Hz, which enables the application of the Eddy-Correlation calculation for determination of aerosol flows.

Measurements at different locations prove the high temporal and spatial variability of the volatile aerosol components, and moreover provide valuable indication for the causes of fine dust exposure as well as a better understanding of the aerosol formation within the lower atmosphere.

REGULATION 2008/50/EG OF THE EUROPEAN PARLIAMENT AND THE COUNCIL for air quality and clean air for Europe

Thursday, September 8, 2011

Session 8P: Poster session B

Aerosol Modelling

Simulation of Small Ion Aerosol Dynamics

M. J. McGrath[1], I. K. Ortega[1], P. Paasonen[1], T. Olenius[1], K. E. J. Lehtinen[2], M. Kulmala[1], and H. Vehkamäki[1]
[1]Department of Physics, University of Helsinki, P.O. Box 64, Helsinki, FI-00014, Finland
[2]Department of Physics and Mathematics, University of Eastern Finland, P.O. Box 1627, Kuopio, 70211, Finland
Keywords: aerosol dynamics, sulfuric acid, numerical simulation.
Presenting author email: matthew.mcgrath@helsinki.fi

The birth-death equations are well-known differential equations that govern the dynamics of atmospheric aerosols. Solution of these equations (which give the rate of change of the concentration of each cluster type in the vapor with respect to time) enables one to examine steady state concentrations and nucleation rates of a system. Through the use of the Atmospheric Cluster Dynamics Code (ACDC), a collection of Perl and MATLAB scripts, we have solved the differential equations for the sulfuric acid/bisulphate ion/ammonia/dimethylamine system, which is extremely relevant for atmospheric nucleation. One of the most novel aspects of this method is the inclusion of evaporation rates computed directly from quantum chemical calculations. This limits our cluster sizes to those accurately probed with quantum chemistry, but it removes the known inaccuracy of using bulk properties (such as the surface tension) to compute the free energy of very small clusters. This approach also enables us to explore the relative importance of the real physics in the system, examining the effect of various terms such as the coagulation sinks, temperature, ion-neutral collision enhancement factors, monomer source terms, and the method of ion generation on the final cluster concentrations. An analysis of the flux between different cluster sizes and the nucleation path in the system are presented as well, including variations produced by changing the physical parameters of the system. The highly automated nature of the procedure adds flexibility and reliability to the system as well, greatly reducing the possibility of typographical errors while making extension to larger clusters sizes trivial. In the future, the steady-state cluster concentrations obtained from ACDC will be compared to nucleation chamber experiments performed at CERN as part of the CLOUD consortium.

Emulation of a global aerosol model to quantify model sensitivity to uncertain parameters

L. Collins, K. Carslaw, K. Pringle, G. Mann and D. Spracklen
School of Earth and Environment, University of Leeds, Leeds, LS2 9JT, UK.
Keywords: Aerosol model, Sensitivity analysis, Parameter uncertainty, Experimental design.
Presenting author email: l.a.collins@leeds.ac.uk

In this work a global model of aerosol processes (GLOMAP) is used to illustrate how emulation can be used to better understand model behaviour and model diversity via a parameter sensitivity analysis. Parameter uncertainty is a key source of uncertainty in model predictions but the sensitivity to particular poorly constrained parameters is not well quantified. Here a method for quantifying the parameter sensitivities is presented.

The first step to a parameter sensitivity analysis of a complex computer model is the construction of an experimental design giving model developers an opportunity to carefully consider all uncertain model parameters, often the first time since initial model development parameter uncertainties are reconsidered. The experiment is designed to explore model runs throughout the space of the uncertainty in the model parameters. A maximin latin hypercube design is chosen to investigate non-linear model behaviour that is undetected in the usual one-at-a-time model runs used to study uncertain parameter choices. An emulator is then used to carry out a parameter sensitivity analysis by estimating the model output throughout the uncertainty space using information about the model output from the design points. A Gaussian process emulator is used here and the added uncertainty from using emulated output rather than GLOMAP output is quantified. The emulator is tested using verification data from additional GLOMAP runs. The methods are illustrated here by following Spracklen (2005) in which a one-at-a-time sensitivity analysis was carried out. As such the sensitivity of modelled cloud condensation nuclei (CCN) to 5 different model parameters and the driving emissions is explored simultaneously. These 5 parameters are 1) the activation diameter for aqueuos phase oxidation, 2) the accommodation coefficient, 3) the H_2SO_4 nucleation threshold, 4) the nucleation critical cluster size and 5) the activation diameter for nucleation scavenging. The sulphur emissions, sea spray emissions and the anthropogenic particulate emissions are also varied according to their uncertainties.

Since emissions are changed simultaneously with the uncertain parameters the relative importance of each source of uncertainty to uncertainty in CCN estimates is shown. The sensitivity of CCN to each uncertain parameter/emission depends upon the region and altitude; this is shown by comparing parameter sensitivity of CCN in different grid boxes and viewing the vertical distribution of parameter sensitivities. It is shown that in more polluted regions CCN uncertainty is dominated by uncertainty in emissions but in more remote regions CCN uncertainty is dominated by model parameters; model parameters are also more important higher in the atmosphere. The relative importance of each individual parameter will be shown. The importance of sensitivity to the non-linear behaviour of the model is shown; in particular it can be seen that the sensitivity of CCN to uncertainty in the sulphur emissions increases as the activation diameter for aqueous phase oxidation increases. It is clear which processes in the model need to be improved to reduce the uncertainty in model estimates of CCN.

The methods here are applicable across a range of global models to identify the important processes. Comparison of the important processes can be used to better understand model diversity. Model complexity will also be considered given information on parameter sensitivities. After individual models are better understood observation data can be introduced to the study and the sensitive parameters better constrained; this is not part of this initial work but is a wider aim of the project to reduce uncertainty and understand diversity in computer models.

Spracklen, D., Pringle, K., Carslaw, K., Chipperfield, M. and Mann, G. (2005). A global off-line model of size-resolved aerosol microphysics: II. Identification of key uncertainties, Atmo. Chem. Phys., 5: 3233-3250.

Measured and modelled aerosol radiative forcing over an urban location

Rohit Srivastava and S. Ramachandran

Space and Atmospheric Sciences Division, Physical Research Laboratory, Navranpura, Ahmedabad, India
Keywords: Aerosol radiative forcing, AOD, SSA, Columnar properties.
Presenting author email: rohits@prl.res.in

Introduction: Atmospheric aerosols play an important role in earth – atmosphere radiation balance. They scatter and absorb the incoming solar radiation, and outgoing terrestrial radiation. The role of aerosols in the radiation budget is one of the largest sources of uncertainty in validating the model prediction of climate change (IPCC, 2007).

In majority of investigations, aerosol optical properties are measured and used in the radiative transfer models to estimate aerosol radiative forcing. Assumptions associated with the aerosol optical properties and vertical structure can cause uncertainties in the estimation of aerosol radiative forcing using the radiative transfer models (e.g., IPCC, 2007). However, aerosol radiative forcing estimated from the direct flux measurements which are highly sensitive and accurate can have less uncertainty than that estimated by model.

Measurements: Ahmedabad is an urban densely populated (5.8 million) city in western India having large/small scale industries and variety of vehicles. They contribute several types of aerosols comprises sulfate, black carbon, organic carbon and nitrates. The Arabian Sea and Thar desert and are located in the southwest and northwest of Ahmedabad respectively and serve as the major sources of sea salt and mineral dust during monsoon (June - September) and pre-monsoon (March-May) respectively.

Aerosol radiative forcing for different seasons of 2008 are estimated from the simultaneously measured downwelling global fluxes and aerosol optical depths. Downwelling global fluxes were measured using a set of Pyranometers (wavelength range 0.31 to 2.8 μm) and AODs were measured using a Microtops II sunphotometer in the wavelength range of 0.38 to 0.87 μm. Single scattering albedo (SSA) is obtained from aethalometer and nephelometer measured absorption and scattering coefficients and from remote sensing Ozone Monitoring Instrument (OMI). Forcing calculated from the measured fluxes are compared with model estimated aerosol radiative forcing.

Results and Discussion: The observed surface forcing shows large differences when compared to the model estimated forcing when SSA derived from aethalometer and nephelometer are used (Figure 1). It should be noted that these differences are larger than the uncertainties as well as seasonal variations in aerosol radiative forcing. However, when OMI derived SSA is used in model, radiative forcing is in accordance with the observations during winter (December-January-February), pre-monsoon and post-monsoon (October-November), while it shows large deviation during monsoon season. During monsoon model estimated forcing for aethalometer and nephelometer derived SSA deviates less (15% of observed forcing) from observation while forcing in cases of OMI SSA is about a factor of two higher (less negative) than the observed (Figure 1).

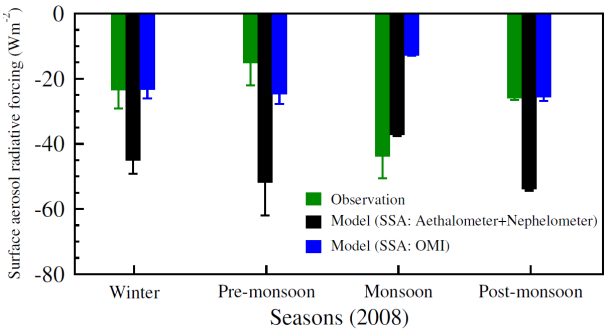

Figure 1. Seasonal aerosol radiative forcing at surface from observation and model in which Aethalometer and Nephelometer, and OMI (Aura) single scattering albedo are used. Vertical bars represent ± 1σ deviation from the mean.

During monsoon forcing estimated using the near surface SSA is closer to the observed forcing, while during other seasons forcing estimated with OMI SSA agree well (Figure 1). The OMI derived SSA during monsoon are even higher than the in situ measurements. OMI derived SSA during monsoon is ≥ 0.99 which could occur due to the assumption that all the aerosols present in the atmosphere are scatterers. Such a high SSA obtained from OMI can lead to lower forcing than that estimated using measured flux.

The details will be presented and discussed.

Columnar ozone from OMI are downloaded from GES-DISC, NASA. Thanks are due to T. A. Rajesh for the prompt maintenance of the instruments.

IPCC 2007 Summary for Policymakers; In: Climate Change 2007: The Physical Science Basis. Contribution of Working Group I to the Fourth Assessment Report of the Intergovernmental Panel on Climate Change, Solomon S., et al. (eds.), Cambridge University Press, UK and New York, NY, USA.

Model evaluation of the physical properties of black carbon in the boundary layer over Europe during the EUCAARI Intensive Observation Period

C. L. Reddington[1], M. G. Frontoso[2], K. S. Carslaw[1], G. R. McMeeking[3] and H. Coe[3]

[1]Institute for Climate & Atmospheric Science, University of Leeds, LS2 9JT, U.K.
[2]C2SM- ETH Zürich, Zürich, Switzerland.
[3]School of Earth, Atmospheric & Environmental Sciences, University of Manchester, M13 9PL, U.K.

Keywords: aerosol modelling, black carbon, number size distribution, mass size distribution.
Presenting author email: c.reddington@see.leeds.ac.uk

The alteration of the Earth's radiative balance by atmospheric aerosol is a major uncertainty in assessments and predictions of climate change on both global and regional scales (Forster *et al.*, 2007). Black carbon aerosol (BC), a by-product of incomplete combustion of fossil fuels, biofuel and biomass, is a strong absorber of solar radiation and is considered to make important contributions to the radiative forcing of the atmosphere. The radiative impact of BC is governed by the physical and chemical properties of the particles and their abundance in the atmosphere. The mixing state of BC (the degree to which hydrophobic BC particles are coated with other aerosol components) in particular governs its hygroscopicity, thereby influencing the ability of BC particles to act as cloud condensation nuclei (CCN) and the lifetime of BC in the atmosphere. It is essential to accurately represent these quantities in aerosol models to quantify the impact of BC on climate.

Here, we evaluate the GLObal Model of Aerosol Processes (GLOMAP; Spracklen *et al.*, 2005) against aircraft observations of sub-micron BC aerosol concentrations and physical properties over Europe during the EUCAARI-LONGREX field campaign in May 2008 (McMeeking *et al.*, 2010). Measurements of the mass and number size distribution of BC (in the diameter size range ~60–1000 nm) and some information on the mixing state of BC-containing particles were obtained using a single particle soot photometer (SP2) onboard the FAAM BAe-146 research aircraft.

The GLOMAP model simulates the evolution of size and composition resolved aerosols, including their interaction with trace gases and clouds. The aerosol size distribution is described using a two-moment sectional bin scheme with 20 bins spanning 3nm to 25μm. In the model we include emissions of BC and primary organic matter from anthropogenic sources (fossil fuel (FF) and biofuel (BF) burning), following Bond et al. (2004); and biomass burning following van der Werf et al. (2003). BC is emitted in the model assuming a lognormal mass size distribution with prescribed mass median diameters (D) and geometric standard deviation (σ). To address uncertainties associated with BC emissions (mainly associated to the size at which BC should be emitted in large-scale models); we test two different BC emission schemes (keeping the mass fixed). The first scheme (Dentener *et al.*, 2006; AEROCOM prescribed), assumes small emission sizes for FF and BF: D_{BF}=80 nm and D_{FF}=30 nm (σ=1.8 nm). The second scheme (AEROCOM modified by Stier *et al.* (2005)), emission sizes are a factor of ~2 larger: D_{BF}=150 nm and D_{FF}=60 nm (σ=1.59 nm). The choice of the emission scheme is a crucial point because many aerosol processes are size-dependent. We also implement a new carbonaceous aerosol emission inventory for Europe from EUCAARI (Denier van der Gon et al., 2010); based on emitted particle number concentrations and size rather than mass.

Comparisons between modelled and measured BC mass and number size distribution in the diameter (D_p) size range ~60–400 nm, show reasonably good agreement with both emission schemes, particularly at sizes larger than 100 nm. We find that, although the different emission schemes in the model predict fairly similar BC number and mass concentrations for D_p>100 nm; the transport, ageing and removal of BC are highly influenced by the prescribed emission sizes. Differences between the two emission schemes are more marked in regions far from the sources. This can play an important role for the transport of BC over the Arctic. Differences in BC mass concentrations between the two schemes can be explained in terms of ageing and then removal. For this reason, the BC particles which can act as CCN could be also affected. These results will be presented in more detail along with results from model experiments with the carbonaceous particle number emission inventory included.

This work was supported by funding from the EU's 6th Framework Programme project, EUCAARI.

Bond, T. C., Streets, D. G., Yarber, K. F., *et al.* (2004) *J. Geophys. Res.-Atmos.* **109**(D14), D14203.

Denier van der Gon, H, Visschedijk, A., Johansson, C., *et al.* (2010) IAC 2010, Helsinki, Abstract 1E1.

Dentener, F., Kinne, S., Bond, T., *et al.* (2006) *Atmos. Chem. Phys.* **6**, 4321-4344.

Forster, P., Ramaswamy, V., *et al.* (2007). *Climate Change 2007: The Physical Science Basis.* Cambridge, U.K.: Cambridge University Press.

McMeeking, G. R., Hamburger, T., Liu D., *et al.*, (2010) *Atmos. Chem. Phys.* **10**, 9393-9414.

Spracklen, D. V., Pringle, K. J., *et al.* (2005) *Atmos. Chem. Phys.* **5**, 2227-2252.

Stier, P., Feichter, J., Kinne, S., *et al.* (2005) *Atmos. Chem. Phys.* **5**, 1125-1156.

van der Werf, G. R., Randerson, J. T., Collatz, G. J., and Giglio, L. (2003) *Global Change Biol.* **9**, 547-562.

Implementation of coagulation into a Lagrangian deposition model

R. Winkler-Heil and W. Hofmann

Department of Materials Research and Physics, University of Salzburg, 5020 Salzburg, Austria
Keywords: stochastic model, particle deposition, coagulation, hygroscopic growth,
Presenting author email: Renate.Winkler-Heil@sbg.ac.at

The stochastic, asymmetric deposition model IDEAL (Koblinger and Hofmann, 1990) allows the calculation of deposition fractions for defined particle diameters and breathing conditions. The smallest geometric airway unit for which deposition fractions are calculated are Y-shaped bifurcations, consisting of half of the parent plus half of the successive daughter airway.

In case of inhalation of aerosols with high particle concentrations, coagulation changes initial particle sizes and concentrations. To implement coagulation processes into the IDEAL deposition model, it was necessary to modify the currently existing code: (1) calculation of deposition probabilities for segments of a bifurcation, including size changes due to hygroscopic growth, and (2) calculation of concentration changes caused by deposition as well as by the coagulation process itself in each segment. These two processes are treated independently in a consecutive fashion.

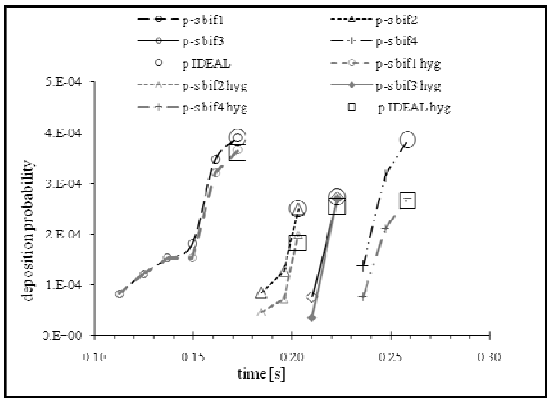

Figure 1. Segmental deposition probabilities (p-s) for bifurcation 1 to 4 for particles with a geometric diameter of 0.206 µm and a density of 2.165 g cm^{-3} and a flow rate of 500 cm^3 s^{-1}. Hygroscopic growth factors (hyg) are based on the work of Ferron et al. (1988). (p = deposition probabilities for each total bifurcation calculated with the original IDEAL code).

For segmental deposition calculations, the bifurcations were divided into a number of time intervals. The length of a given individual time interval is determined by a maximum change of the concentration by 1% in all diameter intervals (Table 1). The deposition probabilities were then calculated segment by segment until the whole bifurcation has been passed. In Figure 1, the obtained cumulative deposition probabilities for the first four bifurcations of one arbitrarily chosen path of the bronchial tree are compared with the deposition probabilities for that bifurcation obtained by the original IDEAL code for (1) assuming no particle growth, and (2) for a hygroscopic particle.

Table 1. Length of time intervals for the first four bifurcations (bif11 denotes the parent and bif21 the daughter airway of bifurcation 1, and so on) for the calculation of the segmental deposition fractions (flow rate = 500 cm^3 s^{-1}).

bif	length of interval [s]	total time t in half bif [s]	number of intervals
bif 11	0.0124	0.0494	
bif 12	0.0116	0.0233	6
bif 21	0.0116	0.0233	
bif 22	0.0071	0.0071	3
bif 31	0.0071	0.0071	
bif 32	0.0128	0.0128	2
bif 41	0.0128	0.0128	
bif 42	0.0112	0.0224	3

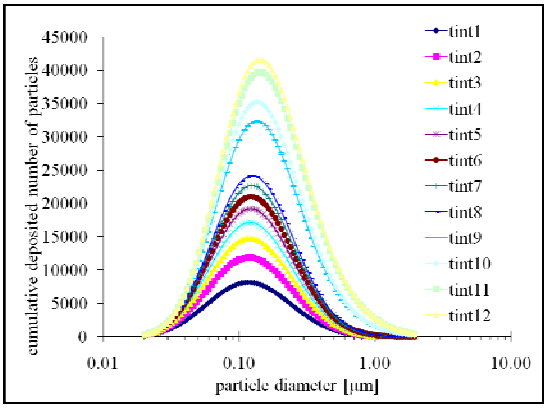

Figure 2. Particles deposited in the first bifurcation (tint is the time segment number within bifurcation 1). Flow rate is 250 cm^3 s^{-1}.

Figure 2 shows the cumulative deposition of log-normally distributed particles (µ = 0.2 µm; GSD = 2) on their way through the whole bifurcation 1.

This work was supported by PMI PO under project number 7100192131.

Koblinger, L. and Hofmann, W. (1990) *J. Aerosol Sci.* **21**, 661-674.

Ferron, G.A., Kreyling, W.G. and Haider, B. (1988) *J. Aerosol Sci.* **19**, 611-631.

Particle mass flux deposition in ventilation ducts of food factories

Mourad BEN OTHMANE[1], Michel HAVET[1], Evelyne GEHIN[2],Camille SOLLIEC[3], Gorges ARROYO[4]
(1)LUNAM Université, ONIRIS, CNRS, GEPEA, UMR 6144, site de la géraudière, 44322 Nantes, France
(2)Université Paris-Est, CERTES, 61 avenue Général de Gaulle, 94000 Créteil, France
(3)LUNAM Université, Ecole des Mines de Nantes, CNRS, GEPEA, UMR 6144, 4 rue A. Kastler, 44300 Nantes, France
(4) CEMAGREF, 17 av. de Cucillé, 35044 Rennes, France
Keywords: deposition velocity, air quality, modeling, ventilation
mourad.ben-othmane@oniris-nantes.fr

The French project CleanAirNet concerns the hygienic design of ventilation ducts in food factories. In the frame of this project, we predict the particle deposition velocity in ventilation ducts of three different food factories. At these locations, during several days, aerosol particle number and mass size distribution were measured using optical particle counter and cascade impactor, respectively. The concentration of particulate matter of aerodynamic diameters in the size range 0.3-20 µm varied from 0.2 to 1.7 µg/ m^3. The measured mass concentration and the predicted particle deposition velocity were used to calculate the deposited particle mass flux (DMF) in the ventilation ducts of each site.

For fully developed flow, Ben Othmane et al (2010) proposed their Eulerian particle deposition model by considering five particle transport mechanisms: Brownian diffusion, turbulent diffusion, turbophoresis, thermophoresis and gravitational settling

$$v_d^+ = \left(\frac{D_B + \nu_t}{\nu} \right) \frac{dC^+}{dy^+} - \left(v_{th}^+ - i v_g^+ + v_{tp}^+ \right) C^+$$

where v_d^+ is the dimensionless deposition velocity. v_{th}^+, v_g^+ and v_{tp}^+ are the dimensionless deposition velocities of thermophoresis, sedimentation and turbophoresis, respectively. D_B is the Brownian diffusivity, ν is the fluid kinematic viscosity ν_t is the turbulent diffusivity, y^+ is the dimensionless normal distance from the wall, C^+ is the time-averaged particle concentration, and i is used to characterize the orientation of the surface.

The results indicate that the DMF at the floor is about 2-20 times larger than that at vertical walls (Table 1). Thus, the deposited particle mass on the floor is sufficient to check if a ventilation duct should be cleaned (Figure 1). According to the chosen cleaning initiation criteria for ducts (400 mg/m², ASPEC, 2004), ventilation systems would take approximately 1 to 9 years to meet the cleaning time.

Table 1. The predicted results of total deposited particle mass in supply ducts

Total deposited particle mass flux (mg/m^2 .year)			
Orientation	Site A11	Site C11	Site U12
Vertical	9.5±3	53±5	3±1
Horizontal	141±10	340±15	45±7

So, cleaning procedures and maintenance intervals are strongly influenced by several parameters, such as flow conditions, particle concentration, characteristics of the ventilation duct and the filter efficiency. The modelling approach combined with mass concentration measurements permits to analyse and quantify the influence of these parameters. Findings of this work may help to identify the specific parameters for cleaning procedures.

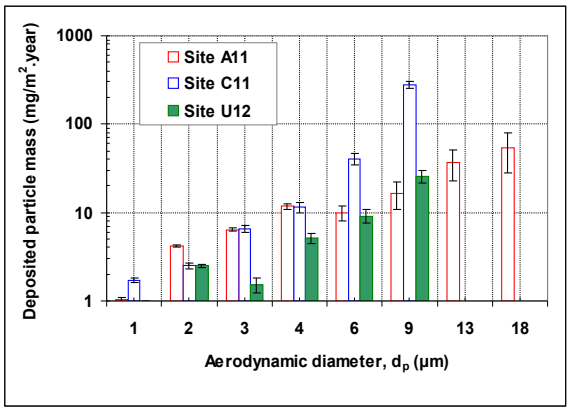

Figure 1: Comparison of deposited particle mass flux at horizontal surfaces in ventilation air supply ducts for the three industrial sites.

To improve the models, knowledge on roughness structure, temperature gradient, flow characteristics need to be further investigated. That will be performed in laboratory at real scale with HVAC materials. Findings of this work may help to identify the specific parameters for cleaning procedures.

The CLEANAIRNET project “Hygienic design of ventilation duct networks in food factories” is supported by the ANR (Agence Nationale de la Recherche).

Ben Othmane, M. Havet, M. Gehin, E. and Solliec, C. (2010). Mechanisms of Particle Deposition in Ventilation Ducts for a Food Factory. Aerosol Science and Technology, 44, 775-784.

ASPEC, French association for the prevention and study of contamination (2004). Maintien en propreté des réseaux aérauliques pour salles propres et environnements maîtrisés apparentés, 51-52.

Assessing Long-term Oil Mist Exposures to Workers in a Fastener Manufacturing Industry by Using the Bayesian Decision Analysis Technique

H.I. Hsu[1], P.J. Tsai[1,2] and J.C. Soo[1]

[1]Department of Environmental and Occupational Health, National Cheng Kung University, Tainan, 70428, Taiwan
[2] Sustainable Environment Research Center, National Cheng Kung University, Tainan, 70101, Taiwan
Keywords: Oil mist, Fastener manufacturing industry, Bayesian decision analysis, exposure assessment.
Presenting author email: scenicii@gmail.com

This study was set out to assess long-term average oil mist exposure to workers in a fastener manufacturing industry by using Bayesian decision analysis technique. In the present study, inhalable oil mist concentrations (C_{inh}) were measured from 12 fastener manufacturing workers on different working days with different production rates of fasteners. In addition, particle size segregating samplings were simultaneously conducted to 3 workers and the resultant mean size distributions of oil mists, together with the measured inhalable oil mist concentrations, were used to further estimate exposure concentrations of respirable oil mists of workers (C_{res}) (Table 1). The relationship between the estimated oil mist concentrations and their corresponding production rates of fasteners was used to estimate the long term exposure profile of workers in both C_{inh} and C_{res}.

In this study, the measured C_{inh} and the estimated C_{res} were served as the likelihoods for conducting Bayesian decision analysis. On the other hand, the corresponding estimated long term exposure profiles in both C_{inh} and C_{res} were served as the priors. The Bayesian decision analysis results show that only ~21% C_{inh} exceeded the permissible exposure limit value (PEL-TWA= 5mg/m^3) promulgated by OSHA and Taiwan government, but ~77.6% C_{inh} were above the action level (i.e., 2.5mg/m^3) (Fig. 1). On the other hand, almost 100% C_{res} were above the level known for increased risk associated with the pulmonary injury (0.2mg/m^3).

Our results indicate that long-term oil mist exposures to fastener manufacturing workers were quite severe, in particular for those exposures associated with the fine oil mist fractions. Therefore, it is suggested that management measures should be taken, including both conducting periodical worker's exposure monitoring and medical examination. In addition, the installation of local ventilation systems and the use of personal protection equipments are also advised for protecting workers from excessive oil mist exposures.

Table 1. Mean inhalable (C_{inh}) and respirable(C_{res}) concentrations and their 95% confidence intervals for fastener manufacturing workers (n=12)

Types of exposure	Exposure concentrations (mg/m^3)
C_{inh}	2.11(1.89-2.40)
C_{res}	1.40(1.25-1.59)

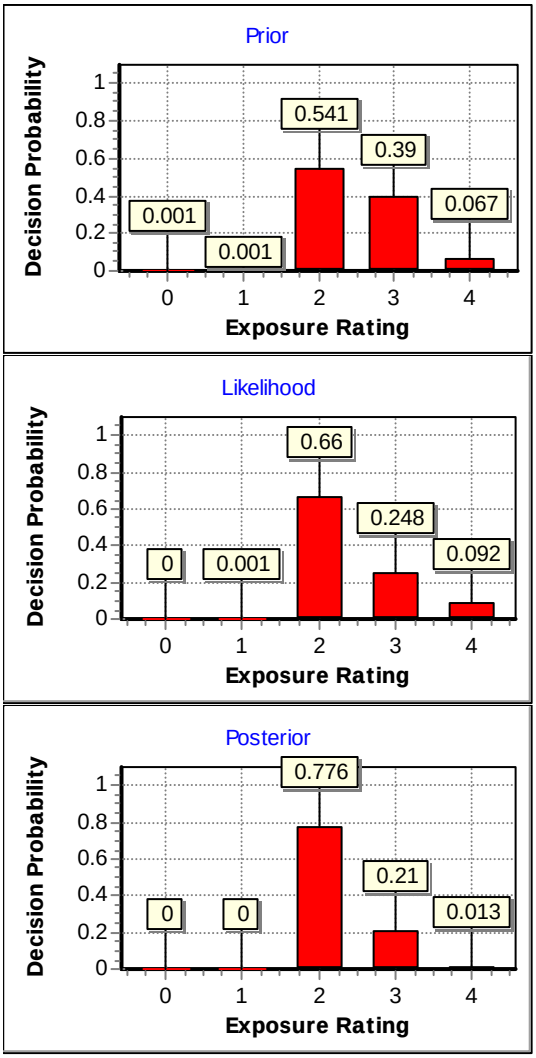

Figure 1. Exposure ratings (0, 1, 2, 3, and 4 represent the exposure levels of 0.1, 0.2, 0.5, 1.0, and 10.0 PEL-TWA, respectively) associated with long term C_{inh} by using the Bayesian decision analysis technique

The authors wish to thank National Science Council in Taiwan for funding this research project.

Chen, M.R., Tsai, P.J., Chang, C.C., Shih, T.S., Lee, W.J., Liao, P.C. (2006) *J. Hazard. Mater.* **146,** 393-398.

Hewett, P., Logan, P., Mulhausen, J., Ramachandran, G., Banerjee, S., (2006) *J. Occup. Environ. Hyg.* **3,** 568-581.

Studying the effect of coagulation and condensation on the perceived nucleation rate vapour dependence using a molecular-resolution aerosol dynamics model

M. Dal Maso[1], H.Korhonen[2], K. Lehtinen[2], H. Vehkamäki[1]

[1]Department of Physics, University of Helsinki, PO Box 48, 00014, Helsinki, Finland
[2]Finnish Meteorological Institute, Kuopio Unit, P.O.Box 1627, 70211 Kuopio
Keywords: nucleation, nucleation mode, modelling, coagulation
Presenting author email: miikka.dal@helsinki.fi

Secondary atmospheric aerosol number formation has been studied intensively since it became apparent that it is a significant process adding to the tropospheric aerosol loading (e.g. Kulmala et al. 2004). Recent studies have made use of estimations of the logarithm of the nanoparticle formation rate as a function of the logarithm of vapour concentration to gain insight into the formation mechanism; however, there are suggestions that such analysis is inaccurate and the effect of this on the power-law fits is unknown (Vuollekoski *et al.*, 2010).

We use a model that simulates the early stages of growing atmospheric nanoparticles on a resolution of a single molecule, similarly to the model described in Lehtinen and Kulmala, (2003). In practise, the model is given a formation rate and size of a stable condensation nuclei (CN); these nuclei then grow by colliding with either vapour monomers or other CN. This results in a size distribution of small CN. In our model simulations, the vapour properties are assumed to be those of sulphuric acid, and we also assume that the CN equilibriate with respect to available water vapour immediately. The coagulation coefficient for CN collisions and CN-monomer -collisions are calculated using the Fuchs coagulation kernel for the wet aerosol sizes assuming spherical particles. No evaporation or break-up of CN is assumed. Losses to particles larger than the model upper size (ca. 5-20 nm depening on the application and available computation resources) are parameterized by the condensation sink and the coagulation sink parameterization for it (Lehtinen *et al.*, 2007).

There are several phenomena affecting the detection of atmospheric particle formation rates. One of them is the loss of fresh particles due to coagulation to background, and also apparent losses due to change in the size distribution shape. This has been extensively studied theoretically (Lehtinen *et al.*, 2007, Anttila *et al.*, 2010).

Another process affecting the determination of the apparent particle formation rate is the intermodal coagulation affecting the shape of the just-formed particle mode. Our model simulations show that the new particle population shape quickly changes shape, starting to resemble a log-normal size distribution due to collisions between young clusters. This, in turn, affects the time derivative of CN measured at larger sizes than the nucleation size, as the edge of the fresh mode passes the detection threshold of the measuring instrument.

We discuss the effect of these processes as well as the effect of different temporal behaviour of the temporal profile of the condensing vapour production rate.

This work was supported by the Academy of Finland and the Maj and Tor Nessling foundation.

Anttila, T., Kerminen, V.-M., and Lehtinen, K. E. J.: Paramererizing the formation rate of new particles: The effect of nuclei self-coagulation, *J. Aerosol Sci.*, 41, 621–636, doi:10.1016/j.jaerosci.2010.04.008, 2010. 18783, 18785

Kulmala, M., Vehkamäki, H., Petäjä, T., Dal Maso, M., Lauri, A., Kerminen, V.-M., Birmili, W. & McMurry, P.H. (2004a) Formation and growth rates of ultrafine atmospheric particles: A review of observations *Aerosol Science* 35, 143-176.

Lehtinen, K E J. and Kulmala, M. (2003): A model for particle formation and growth in the atmosphere with molecular resolution in size, *Atmos. Chem. Phys.*, 3, 251-258

Lehtinen, K.E.J. Dal Maso, M., Kulmala, M., and Kerminen, V.-M. (2007) Estimating nucleation rates from apparent particle formation rates and vice versa: Revised formulation of the Kerminen–Kulmala equation *J. Aerosol. Sci* 38 (9), 988-994.

Vuollekoski, H., Sihto, S.L., Kerminen, V.-M., Kulmala, M and Lehtinen, K. E. J. (2010) A numerical comparison of different methods for determining the particle formation rate *Atmos Chem Phys Discuss*, 10, 18781–18805

Air Quality Modelling with CAMx: a case study of PM distribution in Tuscany (Italy)

S.Verrilli[1], G. Curci[2], M.Mazzini[1], I.Ciucci[1], L.Tognotti[3]
1 Department of Mechanical, Nuclear and Production Engineering, University of Pisa, 56126 Pisa
2 Dipartimento di Fisica – CETEMPS University of L'Aquila, 67010 Coppito - L'Aquila
3 Department of Chemical Engineering, Industrial Chemistry and Materials Science, University of Pisa, 56126 Pisa

Within the PaTOS II project of Tuscany Region a study is in development focused on the characterization and source apportionment of atmospheric aerosol in the Tuscany territory.

Applications of air pollution dispersion model CAMx, a multi-scale three dimensional photochemical grid model [Environ2004], have been performed to the Tuscany emission scenario. The study aims at evaluating transport of coarse and fine particulates and formation of secondary fine particulates, with special attention to nitrates and sulphates. Regional emission inventory data were elaborated for defining the distribution of pollutants sources; detailed VOC and PM2.5 speciation was applied [Passant, 2002, SCC2004]. The meteorological input fields were elaborated from MM5 prognostic meteorological model data [Cetemps]. The IC and BC concentrations were provided by the chemistry transport model CHIMERE [Cetemps].

The simulations were performed to reconstruct the PM10 pollution in the Tuscany region during the year 2006, and daily values were compared with observed data by the Tuscany air quality network.

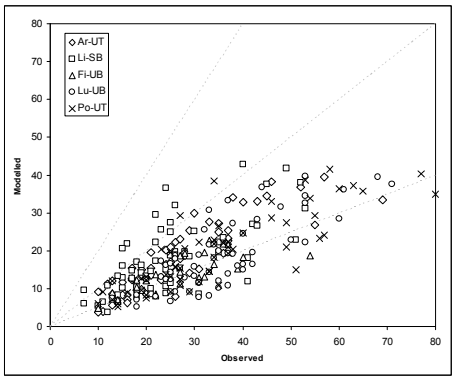

Figure 1. Comparison between PM_{10} modelled and observed data (June and July 2006) [$\mu g/m^3$]

The predicted average values of PM concentration were found to be in good agreement to observed ones. Actually, the calculations for the two summer months already simulated (see Fig. 1) tend to slightly underestimate the measured data. Besides, with respect to the PM composition the percentages of inorganic components are underestimated, especially sulfates, while the organic parts are overestimated (Fig. 2); the primary component percentages are similar to the corresponding values observed for the majority of the areas.The calculations for the full year are being carried out.

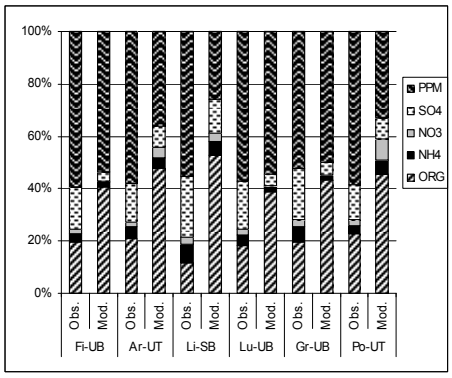

Figure 2. Comparison between experimental and modelled PM_{10} composition (June and July 2006)

The result of the simulations allow the description of the concentration levels of pollutants, especially PM_{10} and NO_2, for the whole region. The results obtained can provide useful information for Tuscany's PM10-emission control and abatement. They can also be used for establishing further pollution-mitigation plans and for providing a solid support for sound air quality management. The CAMx code is therefore proposed as a tool for air quality management in relation to the evaluation of acute episodes of pollution and to plan actions to reduce emissions into the ambient air. However the set-up model needs further improvements in detail and data management input.

Dudhia, J.: A nonhydrostatic version of the Penn State/NCAR mesoscale model: Validation tests and simulation of an Atlantic cyclone and cold front, Mon. Wea. Rev., 121, 1493–1513, 1993.

Bessagnet, B., Menut, L., Curci, G., Hodzic, A., Guillaume, B., Liousse, C., Moukhtar, S., Pun, B., Seigneur, C., and Schulz, M.: Regional modeling of carbonaceous aerosols over Europe – Focus on Secondary Organic Aerosols, J. Atmos. Chem., 61,175–202, doi:10.1007/s10874-009-9129-2, 2008.

ENVIRON 2004, USER'S GUIDE (CAMx) version 4.03, International Corporation.

Passant N.R., Speciation of UK emissions of NMHC VOCs, AEAT/ENV/0545 1, February 2002.

PaTOS II Tuscany regional project", Tuscany region ordinance n° 6811 20/12/2007

Regional Plan for Rehabilitation and Maintenance of Air Quality - PRRM 2008-2010

Source apportionment of airborne particulate matter for three urban centres in Greece

K. Eleftheriadis[1], E. Diapouli[1], M.I. Gini[1], V. Vasilatou[1], C. Samara[2], G. Argyropoulos[2]

[1]Institute of Nuclear Technology and Radiation Protection, Environmental Radioactivity Laboratory, National Centre of Scientific Research "Demokritos", 15310 Ag. Paraskevi, Attiki, Greece
[2]Department of Chemistry, Environmental Pollution Control Laboratory, Aristotle University of Thessaloniki, University Campus, 54124 Thessaloniki, Greece
Keywords: Ambient aerosols, Source apportionment
Presenting author email: csamara@chem.auth.gr

Suspended particulate matter (PM) is a major environmental problem in several countries in the E.U., while new evidence regarding its detrimental impact on human health has emerged. Implementation of the Thematic strategy on Air Pollution by the E.C., through the most recent Directive 2008/50/EC, will require lower limit values for PM in air. In this framework, the identification of PM sources, as well as the quantification of their contribution to the observed concentration levels, acquires increased interest since it may assist towards the development of source-specific control measures and mitigation policies. Greece is a European country, where a great deal of improvement with respect to emission control strategies can be made. The aim of this work is to review the source apportionment studies conducted so far in Greek urban centres in an attempt to summarize the main anthropogenic and natural sources influencing the ambient PM levels.

Figure 1 summarizes the available data on PM_{10} and $PM_{2.5}$ yearly ambient concentrations measured at two major Greek cities, Athens and Thessaloniki, during the last two decades.

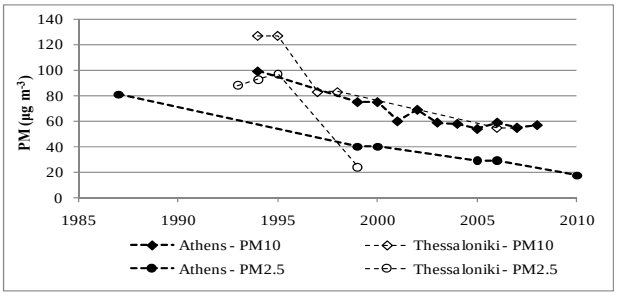

Figure 1. Long term trend of PM_{10} and $PM_{2.5}$ yearly concentration levels in Athens and Thessaloniki

Source apportionment of ambient PM has been carried out at three urban areas (Athens, Thessaloniki and Volos). Different receptor modelling approaches were employed for this purpose, based on the ambient concentration levels of particles and their chemical speciation. Chemical source profiles were constructed for the Chemical Mass Balance (CMB) receptor modelling. The different sources identified and their relative contributions (%) are listed, along with the source apportionment models used in Table 1.

In the studies where PMF was employed (Athens, Volos), the generated factors provided information on chemical source profiles and source contribution. For the CMB modelling (Thessaloniki, Volos) the chemical source profiles from the receptors were successfully reconstructed by local source profiles. In the cases were simple statistical procedures were used (PCA and FA/MR), unidentified sources were resolved.

Table 1. Mean source contributions (%) to the ambient PM mass in Athens, Thessaloniki and Volos

Study / PM fraction	***S1***	***S2***	***S3***	***S4***	***S5***	***S6***	***Model used***
Thes 1994 TSP*	**4-9**	**4-5**	**21-42**			**44-70**	APCA
Thes 1994 TSP*	**7-11**	**4-5**	**25-33**			**54-66**	FA/MR
Thes 2002 fine	**28**	**38**	**14**			**20**	APCA
Thes 2002 coarse	**57**	**9**	**26**			**8**	APCA
Thes 2003 PM10*	**18-22**	**45-65**	**10-35**				CMB
Thes 2007 PM10*	**20-25**	**23-39**	**20-38**	**1-4**	**1**	**13-15**	CMB
Athens 2002 fine	**20**	**27**	**12**	**15**	**19**	**7**	PMF
Athens 2002 coarse	**54**	**8**			**16**	**22**	PMF
Volos 2001 fine	**30**		**27**		**20**	**23**	PMF
Volos 2008 PM10*	**3-12**	**28-40**	**15-39**	**22-27**	**1-2**	**2-9**	CMB

S1: Road / Soil dust, S2: Traffic, S3: Oil burning/Industrial emissions, S4: Biomass / refuse burning, S5: Marine aerosol, S6: Secondary aerosol / Unidentified sources, APCA: Absolute Principal Component Analysis, FA/MR: Factor analysis / Multiple Regression, CMB: Chemical Mass Balance, PMF: Positive Matrix Factorization; * More than one receptor sites

References

Manoli, E., Voutsa, D., Samara, C. (2002). *Atmos. Environ.*, 36, 949-96.

Karanasiou A.A., Siskos P.A, Eleftheriadis K., 2009, *Atmos. Environ.*, 43, 3385-3395.

Samara, C., Th. Kouimtzis, G. Katsoulos, 1994a, *Toxicol. Environ. Chem.*, 41, 221-232.

Samara, C., Th. Kouimtzis and G. Katsoulos, 1994b, *Toxicol. Environ. Chem.*, 44, 147-160.

Samara, C., Kouimtzis Th., Tsitouridou R., Kanias, G. Simeonov V., 2003, *Atmos. Environ.*, 37, 41-54.

Argyropoulos G., Samara C., 2008, Source apportionment in Volos and Planning of Environmental Policy for Air Quality Improvement, Technical Report (in Greek).

Argyropoulos G., Samara C., Nikolaou K. 2011, 4th Environ. Conf. of Macedonia, Greece, Thessaloniki 18-20 March 2011 (to be presented).

Aknowledgements

This work was supported by the European Community (LIFE + Environment Policy and Governance).

Modelling SOA formed in a chamber from a mixture of organic gases

Marta G. Vivanco[1], Manuel Santiago[1] and Ariel Stein[2]

[1]Department of Envrionment, CIEMAT, Madrid. Spain
[2]Earth Resources and Technology on assigment to NOAA's Air Resources Laboratory. Silver Spring, MD. USA
Keywords: secondary organic aerosols, modelling
Presenting author email: m.garcia@ciemat.es

Models are being extensively used for diferent purposes in air quality management. Normally, the evaluation of model performance is carried out using information obtained at monitoring sites, and thus all the physical and chemical procesess involved in air pollutant concentration are evaluated in a global way. This means that errors in a certain process can be compensated with errors in another one, making difficult to decide on how the model is suceeding to represent individual procesess. Moreover, secondary organic aerosols have an additional uncertainty, as normally measurements at monitoring sites are not directly measured, but obtained from OC/EC relations.

Six experiments with biogenic organic precursors were carried out in the EUPHORE facility located in CEAM (Valencia, Spain) (Becker, 1996). Figure 1 illustrates de chamber when it is closed (left), being opened (center) and opened to sunlight (right).

Figure 1. EUPHORE facility: closed (left side of the figure), while opening (middle of the figure), and opened to sunlight (right side of the figure).

Experimental conditions are summarized in Table 1. Different mixtures of volatile organic compounds and HONO were introduced into the chamber at different relative-humidity values. Other experiments with anthropogenic precursors were also performed in 2008 (Vivanco and Santiago, 2010, Vivanco et al., 2011)

Table 1. Initial concentration of the chemcial species introduced into the chamber for each experiment

µg/m3	*2710 2009*	*2506 2008*	*2406 2009*	*0510 2009*	*2610 2009*	*1410 2009*
ISO	0	190	130	121	122	109
APIN	62	100	65	64	71	50
LIM	65	100	60	56	40	50
HONO	101	170	99	0	53	87
NO	32	23	29/34	43		48
NO2	40		0/128	26.1		
HR	20%	20%	0%	20%	20%	35%

Multiple measurement techniques, such as Gas Chromatography coupled with Mass Spectrometer (GC-MS), Fourier Transform Infrared Spectrometry (FTIR), High Pressure Liquid Chromatography (HPLC), Gas Chromatography (GC-ECD and GC-FID/PID), Absorptive Sampling Solid Phase Microextraction (SPME) were used to monitor the gas concentration of reactants and products. Regarding the particle phase, aerosol concentration was monitored in an on-line way with a TEOM (Tappered Element Oscillating Monitor) and a SMPS (Scanning Mobility Particle Sizer).

Two models (CMAQ and CHIMERE) were applied in order to simulate the six experiments. Both models were modified to reproduce EUPHORE conditions. SOA formation is described in both models by the gas-particle partitioning theory, by which the formation of these aerosols is governed by the formation of a group of semivolatile compounds from the photochemical oxidation of certain biogenic and anthropogenic volatile organic compounds. Modeling results indicate that a general overestimation is found for both models. An example of how CMAQ and CHIMERE overestimates SOA recorded in the chamber is shown in Figure 2.

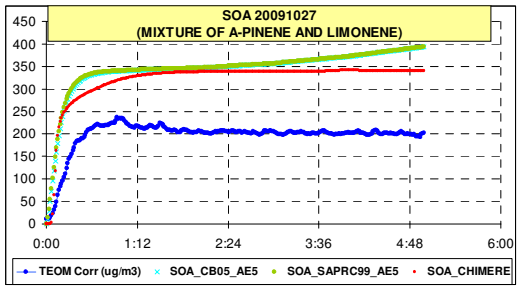

Figure 2. Observed and modelled SOA concentration for the experiment on 27102009. No isoprene was introduced that day into the chamber. CMAQ and CHIMERE results are presented in green and red, respectively. Blue line shows TEOM SOA concentration

Aknowlegdments

This study has been financed by the Spanish Ministry of Science and Innovation (CGL2008-02260/CLI) and by the Spanish Ministry of Environment.

References

Becker, K. H., 1996. EUPHORE final report.

Vivanco, M. G. and Santiago, M., 2010. Secondary organic aerosol formation from the oxidation of a mixture of organic gases in a chamber. Air Quality

Vivanco, M. G., Santiago, M., Martínez-Tarifa, A., Borrás, E., Ródenas, M., García-Diego, C. and Sánchez, M., 2011. SOA formation in a photoreactor from a mixture of organic gases and HONO for different experimental conditions. Atmospheric Environment, 45, 708-715

Thursday, September 8, 2011

Session 8P: Poster session B

Electrical Effects

Charged Particles from Laser Printers

Rohan Jayaratne, Xuan Ling, Congrong He and Lidia Morawska

International Laboratory for Air Quality and Health, Institute of Health and Biomedical Innovation
Queensland University of Technology, Brisbane, Australia
Keywords: Indoor Air Quality, Laser Printer, Respiratory Health
Presenting author email: r.jayaratne@qut.edu.au

It is now well known that most laser printers emit large numbers of ultrafine particles during their operation (He et al., 2007). Continued exposure in office environments has led to serious concern on their effect on human health. Moreover, the deposition rate of particles in the human respiratory system is enhanced when they are electrically charged (Cohen et al., 1998). Since the basic principle of operation of a laser printer involves static electricity, this study was aimed at investigating whether the emitted particles were charged and, if so, to quantify the emission rates of charged particles and cluster ions from a typical printer. Cluster ions are molecular ions smaller than about 1.6 nm.

An HP1320N laser printer was placed within a closed 1m^3 cubic chamber and commanded to print 150 monochrome A4 sheets with a toner coverage of 5% at 22 ppm. The particle number concentration (PNC), charged particle concentration (CPC) and cluster ion concentration (CIC) in the chamber were monitored in real time with a TSI 3022A condensation particle counter, a TSI 3068A aerosol electrometer and an Alphalab air ion counter, respectively, and logged at 1s intervals. Four separate tests were carried out.

Fig 1 shows a typical test result. The PNC in the chamber increased steadily and peaked at 6.35 x 10^4 cm^{-3} at the end of the print run. Positively charged particles were detected around 4 min into the run and the CPC peaked at about +7000 ions cm^{-3} at the end of the run. The charged particles were accompanied by positive CIC. The PNC and CPC remained high after the print job, decaying exponentially to background, while the CIC fell to zero as soon as the printing had ceased. This is not unexpected, as cluster ions readily attach to aerosols in the air. Thus, from these results alone, although we can conclude that the printer emitted cluster ions, we cannot confirm that the printer emitted any charged particles or whether the emitted cluster ions attached to neutral particles after emission.

Assuming no particle and charge losses in the chamber during the print runs, we estimate that the printer emitted at least 4 x 10^8 ultrafine particles and 4 x 10^7 ions per sheet printed.

This is a preliminary study and, while establishing that particle emission from laser printers may be accompanied by electrical charge, it raises several questions such as do all laser printers emit charges, what is the mechanism of charge generation and what are the potential exposure and associated health effects of the charged particles? A full understanding of these processes awaits further investigations.

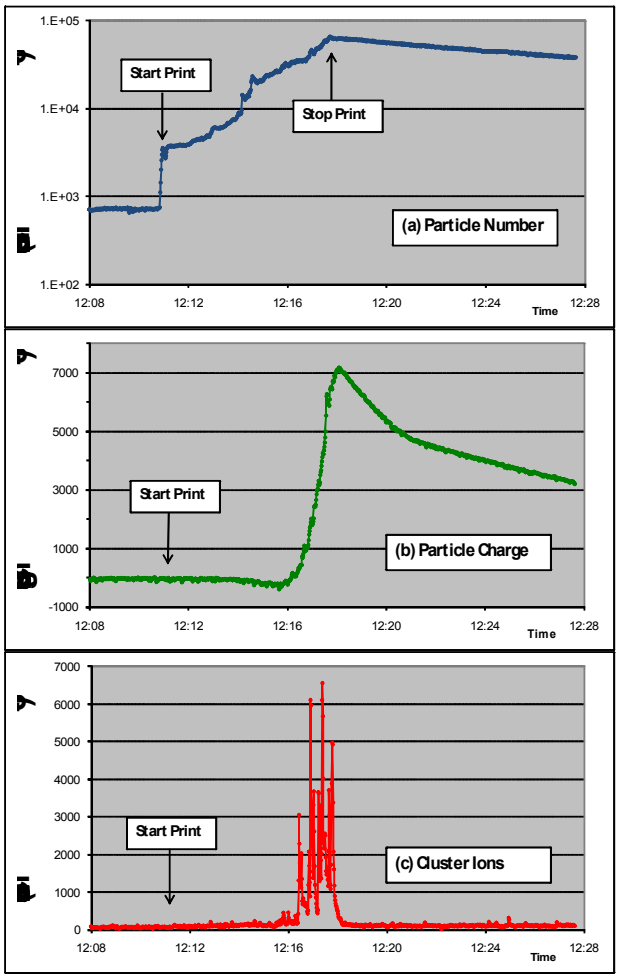

Figure 1: Time series of (a) PNC (b) CPC and (c) CIC in the chamber during a typical print run of 150 sheets.

References:

He, C., Morawska, L. and Taplin, L. (2007) *Environ. Sci. Technol.* **41**, 6039-6045.

Cohen, B.S., Xiong, J.Q., Fang, C. And Li, W. (1998) *Health Physics*. **74,** 554-560.

Penetration of charged particle through metallic tubes

Kuang-Nan Chang[1], Yu-Kang Chen[2], Sheng-Hsiu Huang[1], Yu-Mei Kuo[3] and Chih-Chieh Chen[1]

[1]Institute of Occupational Medicine and Industrial Hygiene, National Taiwan University, 10055, Taipei, Taiwan
[2] Department of Occupational Safety and Health, Chang Jung Christian University, 71101, Tainan, Taiwan.
[3]Department of Occupational Safety and Health, Chung Hwa University of Medical Technology, 71703 Tainan, Taiwan.

Keywords: image force, deposition efficiency, particle charge.
Presenting author email : d93841001@ntu.edu.tw

Several experimental studies investigated the charge effect on the deposition of inhaled aerosol particles in either cast replica or human subjects (Balachandran et al., 1997; Melandri et al., 1983; Ali et al., 2009; Bailey, 1997; Bailey et al., 1998). Since human respiratory tract is conductive in nature, the increase in aerosol deposition in human airway was assumed due to image force. In general, the experimental data focused on image force for particles deposition efficiency were rather limited. Moreover, the amount of charges carried by the particles was only about hundreds of elementary charges for micro-meter sized particles. The low electrical mobility was apparently due to the limitations of aerosol generation methods employed in these studies. In the present study, we adopted an induction method to generate aerosol particles with the amount of charges close to the Rayleigh limit. In addition to the experimental work, a closed-form theoretical model was developed and validated by using the experimental data produced.

A vibrating orifice monodisperse aerosol generator was modified to generate monodisperse aerosols with uniform charge. A small amount of nitric acid was added to the Di-2-ethylhexyl sebacate (DEHS)-ethanol solution to increase the conductivity and, thus, make the aerosol charge control achievable. An Aerodynamic Particle Sizer was used to monitor the aerosol size distributions and particle number concentrations upstream and downstream of the tubes. The total aerosol charge was measured using an aerosol electrometer. The particle loss in the sampling train of the electrometer could affect the particle charge calculation and needed to be characterized.

Six metallic tubes were used in this study. Three with the same length of 40 cm but different inner diameter (0.78 ~ 2.11 cm); while another three with the same inner diameter of 1.66 cm, but different length of 10 ~ 30 cm. The sampling flow rates through the metallic tube were adjusted to the corresponding face velocities of 3.9 ~ 38.5 cm/sec. All the air flow were controlled and monitored by mass flow controllers. All the aerosol penetration tests were repeated for at least 5 times.

The aerosol electrical mobility in this work was, up to 24,000 elementary charges on a 1-μm particle, at least 100 times higher than that used in previous studies. The modeled data agreed well with the experimental data, especially for aerosol carried low charges and long tubes in which air flow was well developed. The aerosol deposition efficiency increased with increasing aerosol charge and tube length, due to stronger image force and longer retention time, respectively. The deposition efficiency decreased with increasing face velocity because of shorter retention time. Under the same face velocity, the deposition loss decreased with increasing tube diameter. This is because, for small diameter tube, the fraction of aerosols near the inner wall was higher than that of large diameter tube.

The theoretical model based on parabolic flow had a good agreement with most of the experimental data, except for data of highly charged particles. This discrepancy was likely due to space charge force, which was not taken into account in this work.

This work was supported by the National Science Council of Taiwan through grant number NSC- 96-2221-E-002 -055 -MY3.

Ali, M., Mazumder, M. K. and Martonen, T. B. (2009). Measurements of Electrodynamic Effects on the Deposition of MDI and DPI Aerosols in a Replica Cast of Human Oral-Pharyngeal-Laryngeal Airways. *J. Aerosol Med. Pulm. Drug Deliv.* 22:35-44.

Bailey, A. G. (1997). The Inhalation and Deposition of Charged Particles within the Human Lung. *J. Electrostatics* 42:25-32.

Bailey, A. G., Hashish, A. H. and Williams, T. J. (1998). Drug Delivery by Inhalation of Charged Particles. *J. Electrostatics* 44:3-10.

Balachandran, W., Machowski, W., Gaura, E. and Hudson, C. (1997). Control of Drug Aerosol in Human Airways Using Electrostatic Forces. *J. Electrostatics* 40-41:579-584.

Melandri, C., Tarroni, G., Prodi, V., Zaiacomo, T. D., Formignani, M. and Lombardi, C. C. (1983). Deposition of Charged Particles in the Human Airways. *J. Aerosol Sci.* 14:184-186.

High-throughput multi-jet mode electrospray for two fluids using a coaxial grooved nozzle

Inyong Park[1], Woojin kim[1] and Sang Soo Kim[1]

Aerosol and Particle Technology Laboratory, School of Mechanical, Aerospace & Systems Engineering, Korea Advanced Institute of Science and Technology, Guseong-dong, Yuseong-gu, Republic of Korea
Keywords: Electrospray, Multi-jet mode, Coaxial grooved nozzle, High-throughput
Presenting author email: inyongpark@kaist.ac.kr

Despite the promising features of liquid atomization, the electrospray technique currently has few practical applications, mainly because it is restricted to electrical conducting liquids and hampered by low throughput. To overcome these limitations, there are many modifications have been proposed. Electrospray for non-conducting liquids was reported by Loscertales et al. (2002) who showed that a double-layered cone-jet formation occurs when two immiscible liquids are fed coaxially. To achieve high-throughput, the multi-jet electrospray mode was proposed by Duby et al. (2006).

To overcome these drawbacks simultaneously, we introduced a coaxial grooved nozzle.

In this study, in order to obtain stable multi-jet operation, a grooved coaxial nozzle was employed to enhance the exterior electrical field. The outer nozzle had an outer diameter of 6.350 mm and inner diameter of 4.064 mm. The inner nozzle had an outer diameter of 3.175 mm and inner diameter of 2.032 mm. The six grooves in the inner nozzle were made by wire electro discharge machining (WEDM). Each groove had a width of 0.4 mm and height of 0.5 mm.

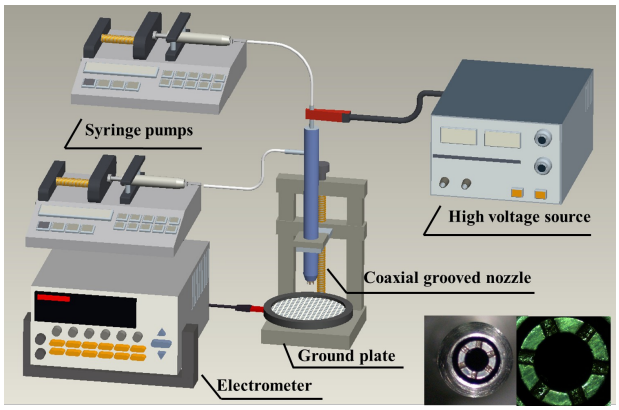

Figure 1. Schematics of the experimental set-up and the nozzle geometry.

Multi-jet formation appeared at larger applied voltage than the cone-jet mode. With a smooth nozzle, the jet formation is unstable, and the origins of the jets move along the circumference of the nozzle. This makes it hard to control multi-jet operation. However, when a grooved nozzle was used, each jet was anchored at a groove, and stable operation was achieved. The jets were electrically balanced with each other, and six stable jets were observed. Images showing multi-jet operation are presented in Figure 2.

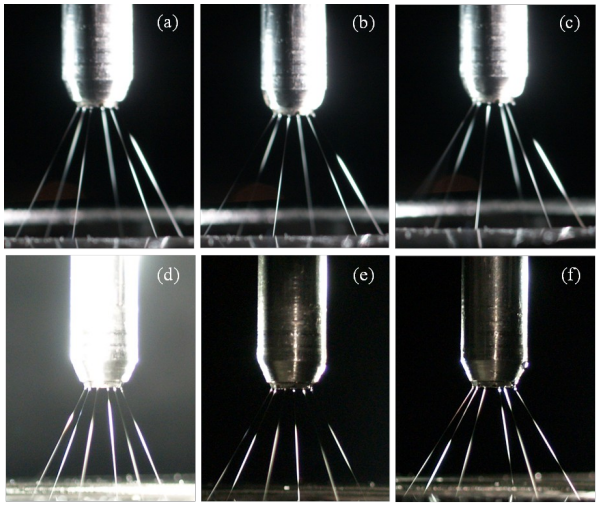

Figure 2. Spray visualization.
(a) $Q_{ethanol}$ = 4ml/h, $Q_{olive\ oil}$ = 12ml/h; (b) $Q_{ethanol}$ = 4ml/h, $Q_{olive\ oil}$ = 16 ml/h; (c) $Q_{ethanol}$ = 4ml/h, $Q_{olive\ oil}$ = 20ml/h; (d) $Q_{ethanol}$ = 6ml/h, $Q_{olive\ oil}$ = 18ml/h; (e) $Q_{ethanol}$ = 6ml/h, $Q_{olive\ oil}$ = 24ml/h; (f) $Q_{ethanol}$ = 6ml/h, $Q_{olive\ oil}$ = 30ml/h.

The droplet size can be controlled by adjusting the flow rates and the droplets monodisperse with good stability and uniformity. The characteristics of the produced droplets for each set of flow rates are given in Table 1.

Table 1. Geometric mean diameter and geometric standard deviation of the droplets.

$Q_{ethanol}$ (ml/h)	$Q_{olive\ oil}$ (ml/h)	Q_{total} (ml/h)	GMD (μm)	GSD
4	12	16	21.57	1.15
4	16	20	24.69	1.13
4	20	24	29.44	1.14
6	18	24	29.29	1.11
6	24	30	34.26	1.12
6	30	36	43.15	1.13

This work was supported by the BK21 program of the South Korea Ministry of Education, Science, and Technology.

Duby, M.-H., Deng, W., Kim, K., Gomez, T., and Gomez, A. (2006). *J. Aerosol Sci.* **37**:306–322.

Loscertales, I. G., Barrero, A., Guerrero, I., Cortijo,R., Marquez, M., and Ganan-Calvo, A. M. (2002). *Science*. **295**:1695–1698.

Investigation of charge conditioning of aerosols by means of soft X-ray and AC corona discharge devices

P. Kallinger[1], G. Steiner[1] and W.W. Szymanski[1]
[1]Faculty of Physics, University of Vienna, Boltzmanngasse 5, Vienna, 1090, Austria
Keywords: Nanoparticles, Charging efficiency, Soft X-ray, Corona discharge.
Presenting author email: peter.kallinger@univie.ac.at

Electrical measurement techniques for the experimental determination of nanoparticles' properties, rely on a well-defined particle charging process. Radioactivity based chargers are widely-used because of their simple application and the well-known equilibrium charge distribution, but there is also a safety risk connected with this method.

In this work the performance of two alternative possibilities for charge conditioning of aerosols are investigated – soft X-ray and bipolar corona discharge. For the latter one a commercial instrument is used (Electrical Ionizer, Model 1090, MSP Corporation, USA). The soft X-ray charging unit is a homemade device consisting of two photoionizers (L9491, Hamamatsu Photonics, Japan; 9.5 kV) which are mounted at an aluminum ionization/charging chamber. For comparison, a radioactive source (^{241}Am, ^{210}Po) in a chamber with identical geometric dimensions is used. First, a high resolution DMA (Steiner *et al*, 2010) operated at about 500 lpm connected to an aerosol electrometer (Faraday Cup) is used to measure the distribution of ions produced by each charging device. Preliminary measurements indicate similarities in the morphology of the ion distributions curves (Kallinger *et al*, 2010).

To investigate the charge conditioning performance of the aerosol charging devices test particles where routed through the charger, into a scanning DMA and detected with a CPC.

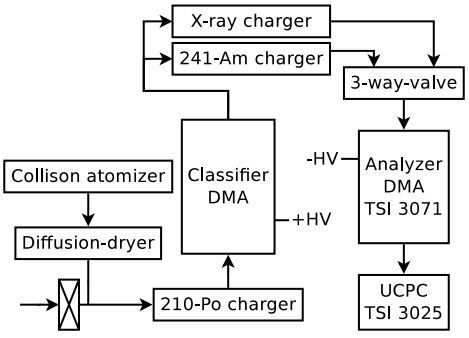

Figure 1: Schematic diagram of the experimental setup.

Monodisperse aerosols of polystyrol-latex (PSL) particles as well as DEHS droplets in the size range of 20–200 nm are used, generated by means of atomization and subsequent classification with a DMA. A schematic diagram of the experimental setup is shown in Fig. 1. It has to be mentioned that the particles leaving the first DMA are negatively charged whereas the second DMA measures positively charged particles. In the size range below 30 nm silver and gold nanoaerosols generated by means of an electrospray (Mod. 3480, TSI Inc.) are used before the DMA classification.

Results for monodisperse DEHS droplets (Fig. 2) show comparable performance of both, the soft X-ray device and the radioactive charger, however the yield from the X-ray charger seems to increase with increasing particle size, which is in contrast to previous reports (Shimada *et al*, 2002, Yun *et al*, 2009). Further measurements are in progress and will be reported.

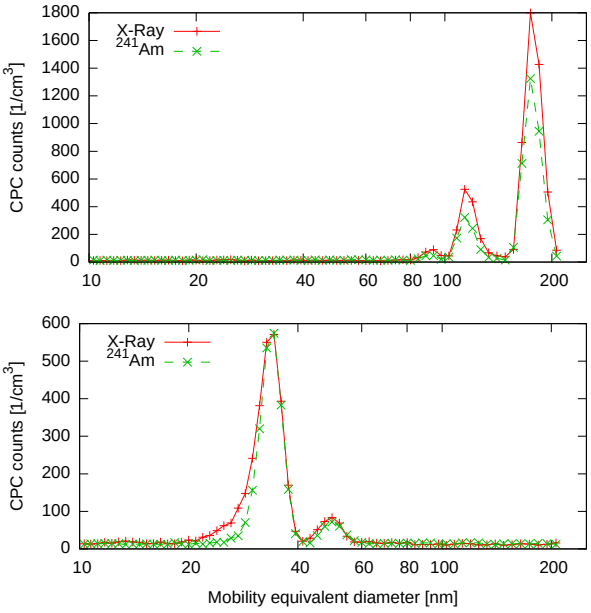

Figure 2: Efficiency of the soft X-ray charger compared with a radioactive ^{241}Am charger using monodisperse DEHS particles.

This work was supported by the Austrian Science Foundation grant TRP 29-N20.

Kallinger, P., Steiner, G. and Szymanski, W.W. (2010) Int. Aerosol Conf., Helsinki.

Shimada, M., Han, B., Okuyama, K. and Otani, Y. (2002) J. Chem. Eng. Jpn. **35**, 786-793.

Steiner, G., Attoui, M., Wimmer, D. and Reischl G.P. (2010) Aerosol Sci. Technol. **44**, 308-315.

Yun, K.M., Lee, S.Y., Iskandar, F., Okuyama, K. and Naoko, T. (2009) Adv. Powder Technol. **20**, 529-536.

OPTIMUM CONDITIONS OF TWO-STAGE ESP SYSTEM FOR OIL MIST CONTROL

K.S.HWANG[1] and D.N.Shin[2]

[1,2]Environmental and Energy Research Center, Research Institute of Industrial Science & Technology
Pohang P. O. Box 135, 790-330, Republic of Korea

Keywords: Oil Mist, Pre-ionizer, Electrostatic Precipitator, Collection Efficiency

INTRODUCTION

There are a number of sources emitting fine oil mist and fume. One of them comes from metal working fluids which act as coolant, lubricator and flushing material of metal chips during the metal working process. The particle size of oil mist and fume produced by such process is so fine, such as 0.03-1.0 μm in diameter, that oil mist and fume pose a serious hazard, for example, causing respiratory problems. Among the control technologies of such oil mist and fume, electrostatic precipitator (ESP) is known to the most effective way of the control of them. This paper presents the optimum conditions of two-stage ESP system for collecting oil mist and fume.

METHODS

The pilot scale experimental system was made for the control of oil mist and fume, and the available capacity of the system was about 15 m^3/min of the flow rate. It is composed of an oil mist and fume generation section, pre-ionization section, collection section and measuring section. The schematic diagram of the experimental system has been represented in Figure 1. The pre-ionizer consists in metal wires having small diameters and operates with a positively direct current high voltage in the range of 0 - 15 kV. Such high voltage on the wire creates an electric field to charge the oil mists. The initially produced electrons in the pre-ionizer flow across the oil stream and in turn collide with or adhere to the particles, imparting a charge on them. The collection section is a series of parallel metal plates which are spaced apart with alternate plates charged and grounded. The metal working fluids oil investigated in this study was insoluble cutting oil in water.

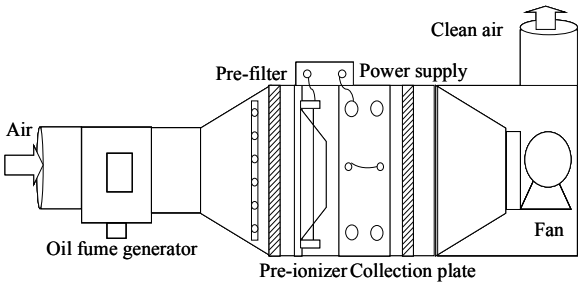

Figure1. Schematic diagram of the pilot scale ESP system

RESULTS

In this study, the performance of the two-stage ESP system has been investigated as a function of applied voltage to pre-ionizer, gas velocity, and plate-plate distance of collecting plate etc. Figure 2 has illustrated the collection efficiency as functions of applied voltage to pre-ionizer by using wire-plate type. In Figure 2 the inlet velocity was 1.5 m/sec. It has been observed that the collection efficiency of oil mist was rapidly increased with applied voltage at 7~11 kV ranges, and then thereafter very slightly increased with applied voltage. This implies that there is a optimum value of applied voltage governing the degree of charging the oil mist.

Also, we have also investigated the effect of the distance between the collecting plates, which are evenly placed, on the collecting efficiencies of oil mist. As shown in Figure 3, it is found that the collecting efficiencies are nearly steady with increasing the distance of plates from 15 to 18mm. Further increasing to 21 mm gives the reduction in the collecting efficiencies from about 92 to 85%. Based on our experimental results, there may be optimum value of the distance between plates greatly affecting the collecting efficiencies.

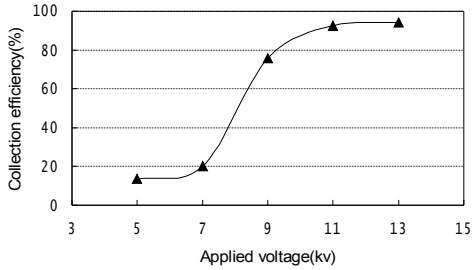

Figure2. Effect of applied voltage on collection efficiency.

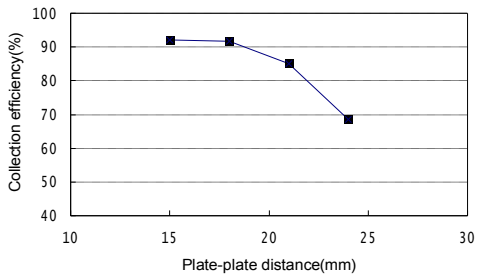

Figure3. Effect of plate-plate distance on collection efficiency.

Oglesby, Jr. S., and Nichols, G. B.(1978). *Electrostatic Precipitation*, Marcel Dekker, Inc.

Comparison of charging characteristics between particle chargers using different discharging materials

B. Han, H.-J. Kim, D.-K. Song, W.-S. Hong, W.-H. Shin and Y.J. Kim

Environmental Systems Research Division, Korea Institute of Machinery and Materials, Daejoen, 305-343, Korea

Keywords: Ion, Ozone, Carbon fiber, Stainless steel, Corona

Presenting author email: bhan@kimm.re.kr

Charging of fine and ultrafine particles is very important for the control of the particle transport in appropriate external electric fields, for example, such as DMAs (differential mobility analyzers). Corona dischargers which use metallic wires or needle tips have been commonly used for the charging of the particles. However, they possibly generate considerable amount of ozone and other small nanoparticles near the discharging electrodes. Recently, new unipolar and bipolar chargers using carbon fiber electrodes which generate nearly negligible ozone but charge fine and ultrafine particles with high efficiency have been developed (Han et al., 2008, 2009). However, the ion generation, ozone emission and charging performance of the charger using a carbon fiber electrode have not been compared to the conventional corona chargers using metal tips in detail. In this study, a carbon fiber charger has been compared to a conventional corona charger in the same charging chamber by replacing a stainless steel tip to a carbon fiber electrode. The carbon fiber electrode comprised of a bundle of carbon fibers with a diameter of about 5-10 μm and a number of about 300 ea. For comparison, a negative high voltage was applied to the carbon fiber and stainless steel chargers and their voltage-current curves were measured and compared. Ion and ozone concentrations were also measured for different supplied voltages to the chargers by an ion counter and an ozone detector at the outlet of the chargers in which filtered clean air was introduced. For a given supplied voltage, current of the carbon fiber charger where a ground electrode was connected was a little higher than that of stainless steel charger and thus, ion concentration of the carbon fiber charger was also higher than that of the stainless steel charger. However, ozone emission of carbon fiber charger was about a half of that of stainless steel corona charger. For the carbon fiber charger where a ground is not connected to the ground electrode of the charger, current of the carbon fiber charger was nearly zero, and however, the concentration of the generated ions was comparable to both the conventional corona charger and carbon fiber charger where a ground is connected, even though ozone emission of the carbon fiber charger without a ground was nearly zero.

For particle charging measurements, KCl particles were generated by a constant output generator and they were introduced into both a diffusion dryer and Kr-85 neutralizer to remove humidity and initial electric charges. The neutralized particles were introduced into the carbon fiber charger and stainless steel corona charger. Particle loss, intrinsic charging efficiency and extrinsic charging efficiency were compared for both chargers. Particle loss in the charger was the highest for the stainless steel corona charger. Most charged particles were lost by the strong electric field formed in the stainless steel corona charger. For the case of carbon fiber charger, ions were generated at a relatively low voltage and thus particles loss was also relatively low compared to the stainless steel charger, because a little low electric field was formed in the carbon fiber charger. Particle loss for the carbon fiber charger without a ground was the lowest. The loss was mostly less than 20% for the particle size range between 30 and 300 nm while the loss for the stainless steel corona charger was mostly more than 40% at the same size range. Figure 1 showed extrinsic charging efficiency with particle diameter for carbon fiber charger without a ground and stainless steel corona charger with a ground. For about 20 nm particles, the extrinsic charging efficiency of the carbon fiber charger was about 60% and however that of the stainless steel corona charger was only about 5%. Therefore, it has been found that carbon fiber charger showed much higher particle charging performance and lower ozone emission compared to the conventional corona charger at the same geometric condition.

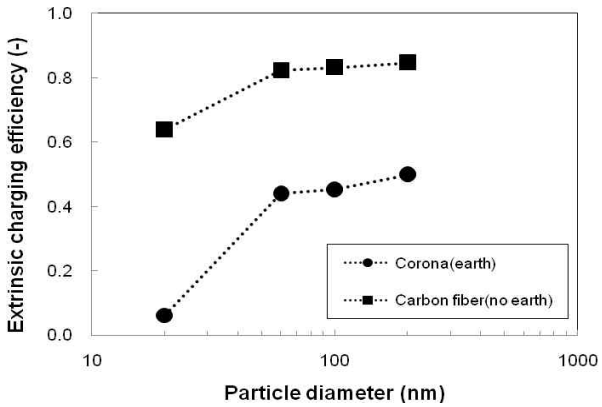

Figure 1. Comparison of extrinsic charging efficiency with particle diameter for carbon fiber and stainless steel corona chargers.

This work was supported by Korean Ministry of Environment as “The Eco- technopia 21 project”.

Han, B., Kim, H.-J., Kim Y.-J. and Sioutas C. (2008) *Aerosol Sci. Technol.,* **42**, 793-800

Han, B., Hudda, N., Zhi, N., Kim, H.-J., Kim, Y.-J. and Sioutas C. (2009) *J. Aerosol Sci.*, **40**, 285-294

Factors affecting ESP aerosol generation

C.W. Lin, S.H. Huang and C.C. Chen

Institute of Occupational Medicine and Industrial Hygiene, National Taiwan University, Taipei, Taiwan
Keywords: ESP, generation, penetration
Presenting author email: r92841013@ntu.edu.tw

The Electrostatic precipitators (ESP) have been used for over a century to control industrial particle emissions. The mass collection efficiency of the ESP is in the order of 90-99 percent. It is also ESP's characteristic of low pressure drop and low electric power consumption. However, several studies reported that ESPs could generate nanoparticles by itself in some specific operational conditions (Romay et al., 1994). These particles might collisions between ions and discharge wire (Biris et al., 2004). The particle generated by ESP could decrease ESP performance and contaminate environment. The ESP may not be a good particle collector when it generates particles. The main objective of the present study was to characterize the phenomenon of ESP aerosol generation in the present of challenge particles under different environmental conditions.

A lab-scale wire-plate ESP was designed and built for the particle generation test. The discharge wire was made of 0.1 mm stainless steel and the collections were made of aluminum. Particle number concentration and size distribution were monitored by a scanning mobility particle sizer. The challenge particles were generated by a TSI constant output generator. The air temperature before and after ESP were monitored by using k-type thermal couples. Particle number concentration and size distribution data obtained in the power-on and power-off modes were used to characterize the particle generation of the ESP. The major operating parameters included air flow rate, field strength, type of carrier gas and challenge particle number concentration.

The results showed that the ESP penetration could be affected by changing carrier gas, electric field strength and air flow. The challenge particle concentration did not affect ESP collection efficiency. However, the ESP generated nanoparticles resulted in the particle penetration exceeded 100%. As shown in Figure 1, the particle size distribution of the particles generated from ESP was between 5 to 50 nm, with the mode around 10 nm. After the test, the stainless steel wire became brown and the erosion on the surface of discharge wire was observed from SEM pictures. The particle generated by the ESP might be the result of sputtering.

The field strength range operated in this work is from 4.0-4.3 kv/cm and the flow rate is from 3-9 L/min. The ESP had the highest particle generation rate at the flow rate of 6 L/min and the electric field strength of 4.3 kV/cm. That is because the ESP removed particles more efficiently when the electric field strength was higher than 4.3 kV/cm. The sputtering was suppressed when the electric field strength was lower than 4.3 kV/cm. Particles had shorter retention time when the flow rate was less than 6 L/min and sputtering was suppressed when the flow rate exceed 6 L/min, probably due to the heat loss. The challenge particle concentration range operated was from 10^5 to 10^8 #/cm^3. The particle generation rate decreased with increasing challenge particle concentration because the challenge particles might absorb the ions, and therefore, protect discharge wire from sputtering. The particle penetration and particle generation both increased when carrier gas was changed from air to nitrogen. The mechanism of this phenomenon is not well understood and need to be explored further.

As a result, the way to suppress the particle generation from ESP and increase the overall performance is to increase electric field strength, decrease flow rate and increase challenge particle concentration.

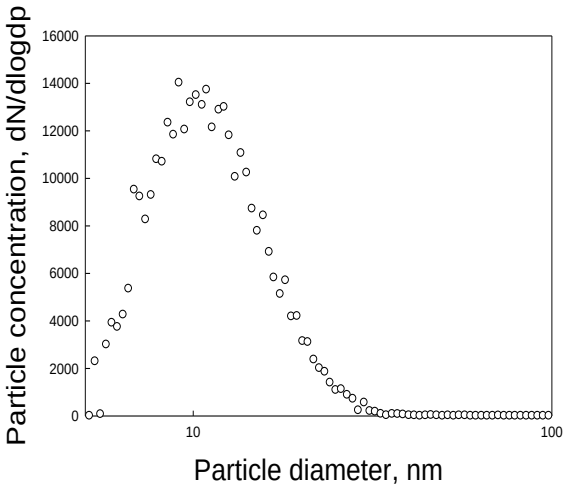

Figure 1. The particle size distribution of ESP generated particle.

Biris, A.S. et al., (2004) *Particulate Science and Technology*, 22(4): 405-416.

Romay, F.J., Liu, B.Y.H. and Pui, D.Y.H., (1994) *Aerosol Science and Technology*, 20(1): 31-41.

Calculation of the electrical field and charge density in a corona unipolar charger with a complex geometry

M. Domat[1], M.A. Rodríguez-Braña[1], E. Kruis[2], J.M. Fernández-Díaz[1]
[1]Department of Physics, University of Oviedo, C/Calvo Sotelo, s/n, E-33007 Oviedo, SPAIN
[2]Fac. of Engineering Sci. and CeNIDE, University-Duisburg-Essen, Bismarckstr. 81, D-4100 Duisburg, GERMANY
Keywords: Corona effect, charging
Presenting author email: maida.dro@gmail.com

The use of unipolar particle chargers, such as based on corona discharge, is increasingly spreading because they have not the obvious restrictions that radioactive chargers have.

However, the data for corona chargers are determined for each specific design, based on experimental procedures or simple theories, and can differ greatly from different device configurations. This leads to errors in further processing the data of charged aerosol.

Moreover, it has the disadvantage that its behaviour changes with time (since the electrode gets worn out and can change its geometry) and are less stable than radioactive chargers, which have a well defined charge distribution.

Therefore, there is a need to study corona chargers from a theoretical point of view, leading to precise knowledge of the charge density and electric field at every point of the device, and thereby to the Nt product calculation, necessary to determine the charging efficiency by particle sizes.

We present a method for obtaining the electrical parameters of a corona particle charger at any point inside it. Since the electrical current within the generator is very small, magnetic effects are negligible and the problem can be solved by means of:

- The Poisson's equation for the electric potential, V:

$$\nabla^2 V = -\frac{\rho}{\varepsilon_0},$$

  where ρ is the free charge density and ε_0 is the electrical permitivity of the vacuum.

- The continuity equation for the charge density:

$$\frac{\partial \rho}{\partial t} + \vec{\nabla} \cdot \vec{j} = 0,$$

  where $\vec{j}$ is the electrical current density, which is in our case:

$$\vec{j} = -b\rho\vec{\nabla}V - \mathscr{D}\vec{\nabla}\rho,$$

  where b is the generated ion mobility and $\mathscr{D}$ its diffusion coefficient.

- Proper boundary conditions, including an injection charging law compatible with the Kaptzov condition.

In this model we have neglected some effects not relevant (see Dumitran et al., 2006). Likewise, during normal usage of the charger can be assumed that the system is stationary (and hence charge density, potential and electric field do not change with time).

The resolution of the previous set of equations for not simple geometries is quite difficult. The Poisson's equation is an elliptic one, which can be properly solved by finite element method (FEM) when the geometry is complex. On the other hand, the equation of continuity is a parabolic-hyperbolic one and therefore, the direct FEM is inadequate since produces a great numerical dispersion and unreal results. However, numerical corrections which add a controlled artificial viscosity along the current lines, make possible the use of FEM with the same mesh used for solving Poisson's equation.

As the use of three dimensions would be too complicated to address the problem in this first approach, FEM has been applied to cases reducibles to two dimensions. In this way, all cases of interest are virtually covered: sheet corona generators and needle corona ones with cylindrical symmetry around the needle.

To solve the system of equations, FreeFEM++ (Pironneau et al., 2010) has been used. It is a comprehensive package of finite element with its own language (similar to C++) that can solve very general problems.

Results are not shown for lack of space in this document. Nevertheless, results for simple geometry cases, as the plate-plain configuration, compare well with the ones of Dumitran et al. (2010), which have been obtained using a different numerical method.

FreeFEM++ will be used to solve together the electric and the fluid flux problems in the corona charger in the future. Also, other electric aerosol devices, as electrometers, can be modelled to improve their behaviour.

We thank the MEC of Spain for support under grant BES-2006-12469.

Dumitran et al. (2006), Computational and experimental study of ionic space charge generated by combined corona-electrostatic electrode systems. *IEEE Transactions on Industry Applications*, **42**, pp. 378–384.

Pironneau et al. (2010), FreeFem++: A tool for solving PDE. `http://www.freefem.org/ff++/` Université Pierre et Marie Curie, Laboratoire Jacques-Louis Lions.

Comparison of measured and calculated charge distributions in post negative corona discharge

Jidenko Nicolas[1], Alonso Manuel[2] and Borra Jean-Pascal[1]

[1]Equipe Décharges Electriques et Aérosol du Laboratoire de Physique des Gaz et des Plasmas (UMR 8578 CNRS – Université Paris-Sud Orsay, F-91405) SUPELEC, Plateau de Moulon, F-91192, Gif-sur-Yvette, France
[2]National Center for Metallurgical Research (CSIC), Gregorio del Amo, 8. 28040, Madrid, Spain.

Keywords: aerosol charging, diffusion charging, charge distribution, corona discharge

Numerous aerosol processes are based on aerosol charging by ions (filtration, size measurement, electrostatic agglomeration …). This work focuses on the comparison of charge distributions estimated from mobility spectra measurements and calculations assuming a constant ion density. The main objective is to investigate the homogeneity of the charging conditions in other words to prove that most of the particles encounter similar charging conditions (mean Ni.τ product, the time integration of ion density Ni on the particle trajectory).

Diffusion charging takes place in post-negative corona discharge with air at atmospheric pressure. The charger has been designed to limit ion and aerosol losses. The discharge occurs around a needle of 50 µm radius. The discharge current is typical of the negative corona regime [1].

Ni.τ products are first evaluated by current measurement. The decrease of ion density along the charging zone has been characterized by current measurements at different locations.

Then average particle charge levels and aerosol charge distributions are measured and compared with those predicted by Fuchs' theory [2] in the transition regime. In that respect, aerosols of controlled size (related to DMA voltage) and concentration (controlled by the furnace temperature and maturation time after furnace) are injected in post-discharge as described on figure 1. The first DMA is used to select a given electrical mobility. The fraction of multi charged aerosol never exceeds 10 %.

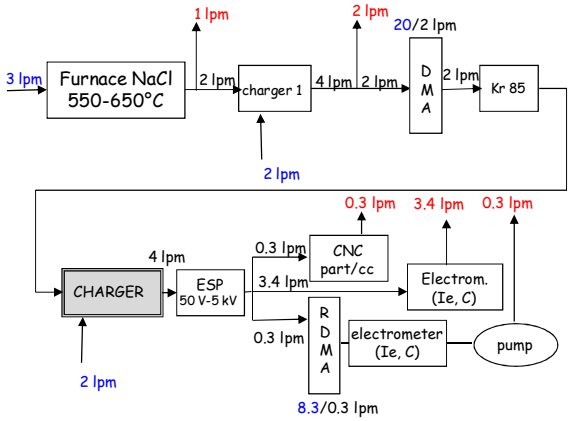

Figure 1. Setup for monodisperse aerosol generation and charge distribution measurements

The charger operates with ion and aerosol flow rates of 2 and 2 lpm. The average discharge current is of -40 µA. The mean charge per particle is calculated from CPC and electrometer measurements after an electrostatic precipitator (ESP) to remove all ions at low voltage (50 Volt). The comparison with Fuchs theory allows another estimation of the mean Ni.τ product to be performed. The two estimations of the mean Ni.τ product are around $6 \cdot 10^{12}$ s.m^{-3}.

Aerosol losses through the charger are determined with the CPC. Maximal aerosol losses are reached for smallest particle size tested (10 nm) and remains below 10 % for a charge fraction of 40 %.

The neutral fraction is determined using the CPC and the same ESP at higher voltage (5 kV) to collect all charged aerosol. Aerosol charge distributions are obtained from mobility spectrum measured with a Radial Differential Mobility Analyser (RDMA).

For instance, charge distributions are represented on figure 2 for particle of 11 and 51 nm. The dots represent the measurements, whereas the histograms represent the results of the calculations using the birth and death theory [3].

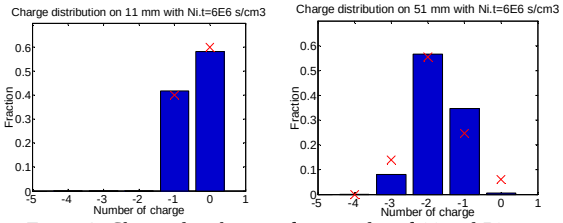

Figure 2. Charge distributions for particles of 11 and 51 nm

The zone of mixing is axi-symmetric. Radial and axial profiles of ion density are stationary but asymmetrical. Simple estimations of these profiles have been done, but angular profile depends on gas velocity and possible surface or space charge effects. Measured charge distributions are broader than calculated ones proving that particles encounter different charging conditions.

A model developed for aerosol and ion mixing in this arrangement [4] will be used for the evaluations of Ni profile, mean Ni.τ product and charge distributions in realistic conditions.

Acknowledgement: The authors gratefully acknowledge financial support and ioniser manufacturing by RAMEM-IONER

[1] GW Trichel (1938) The mechanism of the negative point to plane corona near onset, *Phys. Rev.* **54**, 1078-84
[2] Fuchs N (1963) *Geofis. Pura Appl.* **56**, 185-92
[3] Marlow, W. H. (1978). *J. of Col. & Int. Sci.*, **64**, 543-8
[4] Alonso M et al. (2009). *J.A.S.*, **40-8**, pp 693-706

Monitoring of atmospheric electrical, meteorological and radioactive parameters of surface layer of the storm atmosphere. Preliminary results

I.I. Ippolitov[1], M.V. Kabanov[1], V.D. Karataev[2], N.A. Multcina[1], P.M. Nagorsky[1], S.V. Smirnov[1], A.V. Vukolov[2] and V.S. Yakovleva[2]
[1]Department of Physic of Climatic System, Institute of Monitoring Climatic and Ecological Systems SB RAS, Tomsk, 634055, Russia
[2]Department of Applied Physics, Tomsk Polytechnic University, Tomsk, 634050, Russia
Keywords: light ions, turbulence, radioactivity, monitoring.
Presenting author email: vsyakovleva@tpu.ru

Aerosol is one of the most important elements of atmosphere and it is closely connected with variations of actinometric, electric, radiation and meterorological parametres of atmosphere. In this paper the authors study dynamics of light ions concentrations, electric field intensity, volume charge density, radioactivity and turbulence in the surface layer of atmosphere during storms over a period of 2006-2010.

The study of connections of the above mentioned parameters has a special importance under conditions of atmosphere reconstruction in the process of its transition from the conditions of fair to disturbed weather, which includes pre-thunderstorm reconstruction of atmosphere. The latter is closely connected with dynamics of the medium, changing of its aerosol and ion composition and generation of electric energy in zones of low pressure and cold fronts. In pre-storm situations the development of convective and turbulent upward and downward flows at cold fronts results in the interaction of neutral and charged particles in the moving low-ionized plasma, rapid evolution of aerosol dimension spectrum and effective transformation of heat and mechanical energy into electrical energy. The analysis has shown, that in this case one can observe coordinated changes of polar conductivities, during which the number of light ions can both sharply increase and decrease practically to zero. It is shown, that in storm atmosphere the transport of air ions, along with turbulent air flows, is carried out by electric forces, and the latter have the dominant role. One revealed the dynamics of electrode layer width changing depending on field intensity variations and it is shown, that the dynamics can increase to one hundred metres and more.

The characteristic feature of electrode layer behaviour in storm atmosphere is quasiperiodical change of volume charge sign of light ions under the changing of electric field direction. The coordinated level variations of gamma-background, standard meteorological values and turbulence characteristics during storms are revealed. Typical variations of atmosphere values during storm are represented in the figure.

To describe the properties of nonstationary electrode layer of surface atmosphere during storms basing on the approach, suggested in (Morozov, 2007), a nonstationary model has been developed. This model is used to determine the changes of positive and negative air ion concentrations and electric field intensity.

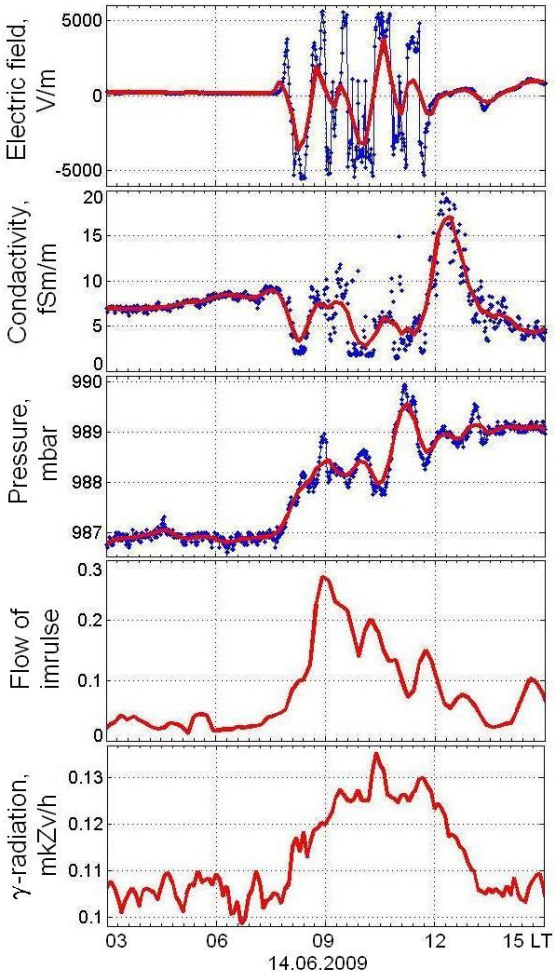

Figure. Coordinated variations of atmospheric electrical, meteorological values and gamma-background in storm atmosphere.

This work was supported by RF Analytical departmental target program «Development of higher school scientific potential», grant № 2.1.1/13707 and by Siberian Branch RAS, program № VII.63.1.1.

Morozov V., Kupovykh G., Klovo A. (2007) *Proc. 13 International Conference on Atmospheric Electricity*, pp. 154-157.

Thursday, September 8, 2011

Session 8P: Poster session B

Atmospheric aerosols – Specific Aerosol Types

Dispersion and deposition pathways of combustion aerosols over tropical evergreens

A. Mukherjee[1], J. R. Picardo[1] and S. Ghosh[1,2]
[1]School of Mechanical and Building Sciences, VIT University, Vellore, India
[2]ICAS Associate, School of Earth and Environment, University of Leeds, U.K.
Keywords: combustion particles, dispersion, dry deposition, modelling.
Presenting author email: picardo21@gmail.com

The Neyveli Lignite Corporation (NLC), located in southern India, is a large lignite based power plant which caters to the energy needs of the world's second fastest growing economy. Two thermal power stations continuously emit gaseous and particulate matter via 13 elevated stacks (particulates source strength: 12-20 g s^{-1}). High efficiency electrostatic precipitators (99.5%) are in operation and the fine particulates (mainly PM10) which are emitted remain suspended over considerable distances. Precise measurements and characterization of the size spectrum of the emitted particulates is in progress. The founding fathers of NLC initiated a massive afforestation program which has resulted in a green canopy of 17 million trees. The ability of this ever-green tropical expanse to counter emissions from NLC seems intuitive and demands detailed quantification.

In this work we aim to trace the path of suspended particulate matter (SPM) as it is dispersed in a tropical boundary layer, whilst accounting for the green carpet below. We employ a tailor-made atmospheric particulate dispersion-deposition model developed as part of an ongoing consultancy work with VIT University and NLC (Fig. 1 depicts SPM contours for Feb'10).

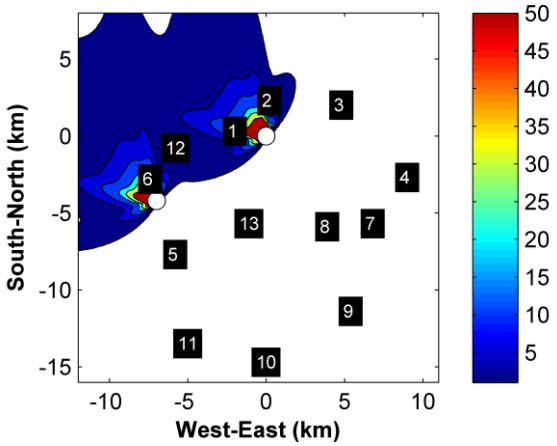

Fig. 1: Contours of ground level SPM - February 2010, 14:30 IST (μg m^{-3}). The text markers denote measurement sites and large white markers the power stations.

Since ultrafine particulates (dia. <1μm) do not settle under gravity, they would remain suspended if it were not for deposition onto the extensive vegetative canopy. This is evidenced by the SEM image (Fig. 2) of a leaf from a monitoring station (station [2] in Fig 1.).

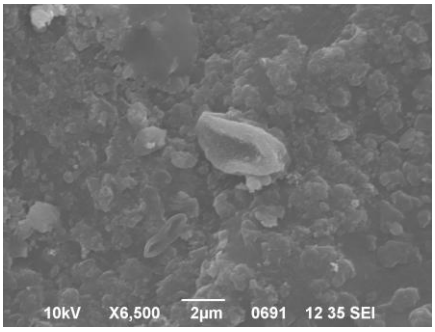

Fig. 2: Scanning Electron Microscopy (SEM) of a leaf sample from a monitoring station at NLC showing particle aggregates from power plant emissions.

The seasonal variation in green cover over southern India is very different from that over mid-latitude regions, both in the pattern of variation and intensity. Satellite derived, leaf area index (LAI) data from MODIS (available from the web) as displayed in Fig.3, along with daily meteorological inputs from NLC allow the model to capture unique characteristics of this tropical region.

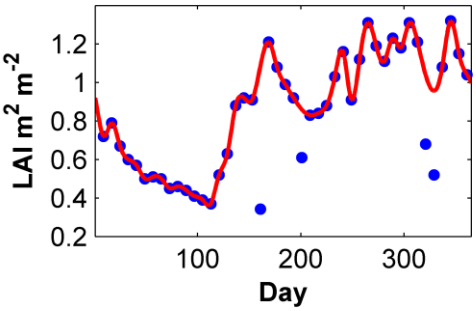

Fig. 3: LAI data for NLC as obtained from MODIS for the year 2010

With high source strengths and sprawling urban vegetation, NLC offers a unique opportunity to model aerosol transport over intermediate length scales. Hence, this analysis will aid modelers in bridging the gap between micro-scale aerosol process studies and global circulation models.

This work is supported by the Neyveli Lignite Corporation, Tamil Nadu, India under grant no. CARD/ENVT/MAP/Project 1218/2009.

MODIS LAI/FPAR product, NASA. Available online at Modis Web: http://modis.gsfc.nasa.gov/

Source emission studies and biomass burning assessments in Venice Lagoon area

A.M. Stortini[1], R. Zangrando[1], E. Barbaro[2], F. Bonetto[2], N. Kerward[1], C. Barbante[1,2] and A. Gambaro[1, 2]

[1] Institute for the Dynamics of Environmental Processes (CNR-IDPA), Dorsoduro 2137, 30123 Venice, Italy
[2] Environmental Sciences, Informatic, Statistic Department, Ca' Foscari University of Venice, Dorsoduro 2137, 30123 Venice, Italy

Keywords: trace elements, Levoglucosan, ionic composition, PCA, PMF
Presenting author email: stortini@unive.it

Venice is located at the northern end of the Adriatic sea at the north-eastern most part of the Po river plain, and from the climatic point of view it is characterised by atmospheric stability and thermal inversion inducing cold masses at the ground level during the winter time. Humidity is high causing foggy events in winter and intermediate seasons, with low pollutants dispersion. Temperature increase is coupled with an increase of the Planetary Boundary Layer, consequently both pollutants mixing and dispersion increase in summer time.

From the chemical point of view, sources of particulate matter (PM) in Venice have been identified by different studies (Stortini et al, 2009; Rossini et al., 2010; Masiol et al., 2010). For heavy metals in PM10 the thermoelectric power plant and the glass factories are considered the most important emission sources. Data from the national environmental agency (ARPAV, 2006) for ships in the two principal berthing areas of Venice has shown that 69% of the emissions come from the petrochemical industry deliveries, while the 31% from the tourism and local activities. Venice area and its hinterland are characterised by industrial and agricultural activities, and urban agglomerates together with rural background areas are widely represented there. This scenario lets account a number of different sources and the use of further chemical methods is necessary for their identification.

A preliminary study was performed on particulate matter samples (PM10 and PM2.5) randomly collected in 2007 and 2008, and trace elements, ions and Levoglucosan have been measured. The aim of this study is to verify how biomass burning is recognizable, and how well could be identifiable in emission sources studies, taking into account the complexity above described for the area here considered.

Trace elements were measured by Inductively Coupled Plasma-Quadrupole Mass Spectrometry (ICP-QMS Agilent 7500I). Elements concentrations in samples have been obtained after subtraction of their field blank values. Details about sample treatment and accuracy are reported elsewhere (Stortini et al., 2009).

Ions where measure by an ionic cromatograph Metrohm 761 Compact IC, with a Metrosep A Supp 4 – 250 column for the anionic analysis, and nitrates, nitrites, chlorides, sulphates and oxalates were measured (Bonetto, 2009). Their measurement represent an useful tools for the assessment of secondary aerosol.

Levoglucosan (1,6-anhydro-β-D-glucopyranose) was measured for aerosol samples (Zangrando, 2007), and this is a product of cellulose combustion, that take place when cellulose is heated to over 300°C causing by various pyrolytic processes that cause the Levoglucosan production in large quantities. This chemical marker is useful as molecular tracer for biomass burning in the atmosphere because Levoglucosan it cannot be generated by noncombustive processes or by nonwood combustion. Sample analysis was performed by using liquid chromatography/negative ion electrospray ionization tandem mass spectrometry (HPLC/(-)ESI-MS/MS). An Agilent 1100 series HPLC system (Agilent, Waldbronn, Germany) coupled to an API 4000 triple quadrupole mass spectrometer (Applied Biosystems/MDS SCIEX, Toronto, Ontario, Canada) were used to determine Levoglucosan.

First results evidenced a seasonal trend in terms of PM concentration and in terms of measured analytics. PCA and PMF statistic tools are applied on all the parameters considered in this preliminary study evidenced the complexity of the studied area.

ARPAV, 2006. Annual report on ambient air quality – ARIA 2006. (Environmental Agency of Veneto-ARPAV – Environmental Council Causes and Effects of Heavy Metal Pollution Office and Department of the Venice Province).

Bonetto, F. (2009) *Degree thesis* on the Chemical Characterisation of atmospheric dry depositions in the Historical Aula Magna “Silvio Trentin” of the University Ca’ Foscari (Venice). Tutor Prof. A. Gambaro. University Ca’ Foscary of Venice, Italy.

Masiol, M., Rampazzo, G., Ceccato, D., Squizzato, S. and Pavoni, B. (2010) Chemosphere 80, 771–778.

Rossini, P., Matteucci, G. and Guerzoni, S. (2010) *Environ Sci Pollut Res* **17**, 40–48.

Stortini, A.M., Freda, A., Cesari, D., Cairns, W.R.L., Contini, D., Barbante, C., Prodi, F., Cescon, P. and Gambaro, A. (2009) *Atmospheric Environment* **43**, 6296–6304.

Zangrando, R. (2007) *PhD Thesis* on the Development and optimization of analytical methods for the determination of organic micropollutants in environmental matrices by liquid chromatography with UV detection via mass spectrometry (HPLC-MS/MS). Tutor Prof. P. Cescon (cycle XXI). University Ca’ Foscary of Venice, Italy.

Trace elements on particulate matter (PM) in the urban areas of Belgrade and Sarajevo

A.M. Stortini[1], L. Cadamuro[2], S. De Pieri[2], S D. Đorđević[3], A. Mihajlidi-Zelić[4], Lj. Ignjatović[5], D. Relić[4], J. Huremovic[6] , T. Milovanović[4] and A.Gambaro[1, 2]

[1] Institute for the Dynamics of Environmental Processes (CNR-IDPA), Dorsoduro 2137, 30123 Venice, Italy
[2] Environmental Sciences, Informatic, Statistic Department, Ca' Foscari University of Venice, Dorsoduro 2137, 30123 Venice, Italy
[3] IChTM – Centre of chemistry, University of Belgrade, Studentski trg 12–16, 11000 Belgrade, Serbia
[4] Faculty of Chemistry, University of Belgrade, Studentski trg 12–16, 11000 Belgrade, Serbia,
[5] Faculty of Phusical Chemistry, University of Belgrade, Studentski trg 12–16, 11000 Belgrade, Serbia,
[6] Analytical Chemistry Department, University of Sarajevo, 71000 Sarjevo, Bosnia and Herzegovina.
Keywords: trace elements, ICP-QMS, PCA, PMF.
Presenting author email: stortini@unive.it

Particulate matter in the European urban areas has been increasing due to increased anthropogenic emissions, and levels of PM have become high with respect to the Air Quality Standards (AQS) specified by EC directives and by local regulations. In Western Europe emission sources (natural and anthropogenic) have a different influence depending on the local scenario and climatic areas (e.g. Iberian Peninsula and north Europe), evidenced the importance of the source recognition (Putaud et al., 2010; Querol et al.; 2007). In the Balkan area efforts for introduce and establish standard operating procedures and quality assurance procedures in all stages of aerosol management and analysis were performed (Joksić et al.; 2009), and some physical and chemical characterization of PM have been assessed in some past projects (Joksić et al.; 2009), as well as chemical and toxic approach for organic pollutants (Škarek et al.; 2007), but of course the collection of information about emission sources and their influence is still in progress.

In the frame of the project "Scientific cooperation between research Institutions for the study of airborne fine particles in IMportant Cities of the Adriatic area" (SIMCA - INTERREG/CARDS-PHARE Adriatic New Neighbourhood Programme), aerosol samples were collected in two urban sites located in Belgrade (Serbia) and in Sarajevo (Bosnia-Herzegovina) respectively. Samplings were performed in a 48-hours time interval from June to December 2008, and aerosol samples were collected by high-volume cascade impactor, fitted with PM10 size selective inlets. Particles with aerodynamic diameters <10µm were collected into six size intervals (cut-off aerodynamic diameters of 7.2, 3, 1.5, 0.95, 0.49 and <0.49 µm). Assessments on Ionic composition and trace elements (this poster) were performed.

Each filter was cut in two parts and one of them was microwave digested according the procedure described by Buccolieri et al. (2005). The digestion programs and the microwave operations are elsewhere described (Stortini et al.; 2009).

Trace elements were measured by Inductively Coupled Plasma-Quadrupole Mass Spectrometry (ICP-QMS Agilent 7500I), the accuracy and precision of the method was controlled using the standard reference material (Urban Particulate Matter NIST 1684a). Elements concentrations in samples have been obtained after subtraction of their field blank values.

Results evidence a consistent amount for elements typically from anthropogenic sources, and in particular from combustion process. PCA and PMF analysis are applied in both data sets with the aims of better describe all the emissions contributions in both urban areas.

This work was supported by the INTERREG/CARDS-PHARE Adriatic New Neighbourhood Programme - Grant No. 06SER02/01/04.

Buccolieri, A., Buccolieri, G., Cardellicchio, N., Dell'Atti, A. and Florio, E.T. (2005) *Annali di Chimica* **95**, 15–25.

Joksić, J. D., Stojanović, M.J., Bartonova, A., Radenkoić, M. B., Yttri, K-E., Matić-Besarabić, S. and Ignatović, L. (2009) *Serb. Chem. Soc.* **74** (11), 1319–1333.

Putaud J.-P., R. Van Dingenen, A. Alastuey, H. Bauer, W. Birmili, J. Cyrys, H. Flentje, S. Fuzzi, R. Gehrig, H.C. Hansson, R.M. Harrison, H. Herrmann, R. Hitzenberger, C. Hüglin, A.M. Jones, A. Kasper-Giebl, G. Kiss, A. Kousam, T.A.J. Kuhlbusch, G. Löschau, W. Maenhaut, A. Molnar, T. Moreno, J. Pekkanen, C. Perrino, M. Pitz, H. Puxbaum, X. Querol, S. Rodriguez, I. Salma, J. Schwarz, J. Smolik, J. Schneider, G. Spindler, H. ten Brink, J. Tursi, M. Viana, A. Wiedensohler and F. Raes. (2010) *Atmospheric Environment* **44**, 1308 -1320.

Querol, X., Viana, M., Alastuey, A., Amato, F., Moreno, T., Castillo, S., Pey, J., De la Rosa, J., Sanchez de la Campa, A., Artinano, B., Salvador, P., Garcia Dos Santos, S., Fernandez-Patier, R., Moreno-Grau, S., Negral, L., Minguillon, M.C., Monfort, E., Gil, J.I., Inza, A., Ortega, L.A., Santamaria, J.M. and Zabalza, J. (2007) *Atmospheric Environment* **41**, 7219–7231.

Škarek, M., Čupr, P., Bartoš, T., Kohoutek, J., Klánová, J., Holoubek, I. (2007) *Science of the Total Environment* **384**, 182–193

Stortini, A.M., Freda A., Cesari, D., Cairns, W.R.L., Contini, D., Barbante, C., Prodi, F., Cescon, P. and Gambaro, A. (2009) *Atmospheric Environment* **43**, 6296–6304.

Continuous time resolved measurements of environmental aerosols especially during New Year 2011 with a new fine dust monitoring system

M. Weiss, J. Spielvogel

Palas GmbH, Karlsruhe, 76229, Germany
Keywords: aerosol instrumentation, air quality network, fine particulate matter, particulate mass, particle size
Presenting author email: weiss@palas.de

Real time continuous and accurate measurements of atmospheric particles are important when complying with regulation or in the context of source apportionment; e.g in determining how much is contributed by traffic, industry or residential heating. If the time resolution is high enough it allows reliable transport modelling based on actual data. A lack of this information was causing the closure of the European air space when the Iceland volcano Eyjafjallajökull erupted in April 2010.

We will present the Fidas®, a new fine dust monitoring system based on optical light scattering. The Fidas® is equipped with a white light LED as stable light source with long lifetime and an integrated filter holder. The Fidas® allows the continuous recording of the particle number and particulate mass (simultaneously PM1, PM2.5, PM4, and PM10) with a time resolution of down to one second providing the opportunity to monitor dynamic changes. If desired the user can also obtain the particle size distribution with this instrument.

We will report on a one year measurement campaign where a Sigma-2 sampling head (described in detail in VDI 2119-4) was used to ensure representative sampling even in strong wind conditions. Specific events such as new year's fireworks will be highlighted and analysed in detail and also compared to another continuous fine dust measurement device and the data from a reference filter sampler.

We will also discuss implications for the reporting of particulate matter under these circumstances.

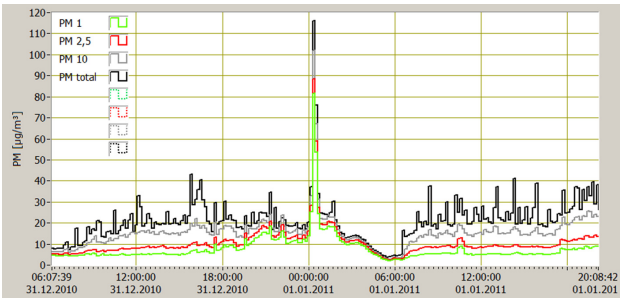

Figure 1. Simultaneous PM_1, $PM_{2.5}$, PM_{10} and TSP concentrations from before to after new year 2011

Figure 1 shows the concentration time line for the PM-fractions from before to after new year 2011 measured outdoors in a big German city. The particle emissions caused by the fireworks that accompany the new year celebrations lead to a significant increase of all PM-values for a short time. Figures 2 and 3 show the particulate mass and particle number distributions corresponding to before, during and after the fireworks, respectively.

As can be seen in figure 2 the mass concentration of small particles increases significantly and is caused by a factor of 10 increase in particle number (Figure 3). These small particles (< 400 nm) are primarily caused by the combustion process of the rockets and explosives.

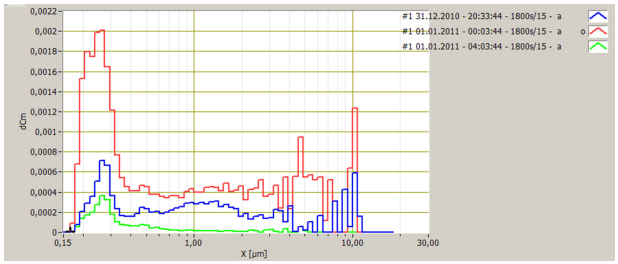

Figure 2. Particle mass distributions in mg/cm^3 before (blue), during (red) and after (green) new year 2011

Due to the implemented filter holder, a gravimetric filter can be used to analyse the sample further, e.g. by chemical analysis, and to verify the optically measured data.

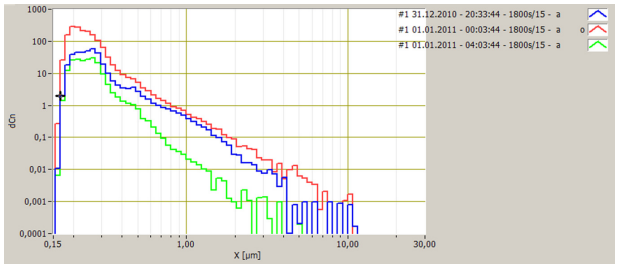

Figure 3. Particle number distributions corresponding to the mass distributions in figure 2

The high time resolution of the data of the Fidas® system facilitates the comparison between theoretical model and actual measured data. It measures continuously with no consumables and very little maintenance and the high resolution of particle sizes can be used for transport modelling and source apportionment.

Influence of the road traffic intensity on air pollution in the Prague

J. Ondráček[1], V. Ždímal[1], J. Schwarz[1], V. Bízek[2] and J. Smolík[1]

[1]Laboratory of Aerosol Chemistry and Physics, Institute of Chemical Process Fundamentals, v.v.i., AS CR, Rozvojová 135, Prague 6, 165 02, Czech Republic
[2]Technology Centre, AS CR, Ve Struhách 27, Prague 6, 160 00, Czech Republic
Keywords: traffic emissions, particle size distribution, chemical composition.
Presenting author email: ondracek@icpf.cas.cz

Aerosol particles belong to major air pollution sources. Moreover, it is generally known that aerosol particles have chronical and acute adverse health effects, they damage cultural heritage, reduce visibility and cause a climate change. A special type of environment, when taking into account the human health, is the urban area. Aerosol particles emitted from the road traffic in the city significantly contribute to high levels of air pollution and, at the same time, the population exposed to these particles is very large. Today, these particles represent one of the main sources of air pollution in the urban environment.

The particles emitted from road traffic can be divided into two categories – direct and indirect emissions. Direct emissions are for example emissions from vehicle exhausts, abrasion of car breaks, tyres and pavement and particle resuspension. The indirect emissions include secondary aerosol particles originated by chemical reactions from the gas phase. Apportionment of road traffic particles according to their size can be made taking into account the processes of particle formation and transformation. Nanoparticles (< 50 nm) and ultrafine particles (< 100 nm) are produced by high temperature and chemical processes and thus represent exhaust emissions and secondary aerosol particles. The coarse particles (> 1 μm) are usually formed by mechanical processes, which include the abrasion and the resuspension mechanisms.

Two measurement campaigns near a busy freeway and a suburban crossroad (different traffic intensity) were carried out in Prague during this work. Both of the two traffic related campaigns were supported by simultaneous measurements at suburban background site to compare measured values with corresponding city background. Extensive set of aerosol instrumentation was used during both campaigns at both measurement sites. Two pairs of aerosol spectrometers (SMPS and APS) were used to monitor aerosol particle number size distributions. Two BLPIs provided information about mass size distribution and chemical composition of collected size resolved aerosol samples. The crossroad campaign was also supported by two EC/OC field analysers providing information about elemental and organic carbon concentrations. Consequent chemical analysis of collected size resolved samples comprised of ion chromatography (water soluble ions), PIXE (elements) and RBS (carbon).

Results obtained from aerosol spectrometers and BLPIs showed that the main contribution of traffic in ultrafine size range can be attributed to direct exhaust emissions, while the coarse fraction was dominated mainly by regional background aerosol with small traces of brake and tyre abrasion as well as the resuspension of the road dust. Chemical analysis demonstrated that most of the water soluble ions (see e.g. Fig. 1) can be found in fine fraction of mass distribution and mostly comes from regional background and long range transport. Most of major elements (see e.g. Fig. 2) were found in coarse fraction of mass size distribution. It can be attributed to three different sources: abrasion of different vehicle parts (Fe, Cu, Mn and Zn), the road dust resuspension (Si, Al, Ca) and long range transport or regional background (Ca and K). Elemental carbon concentration (diesel engine emissions) was found to be proportional to traffic intensity.

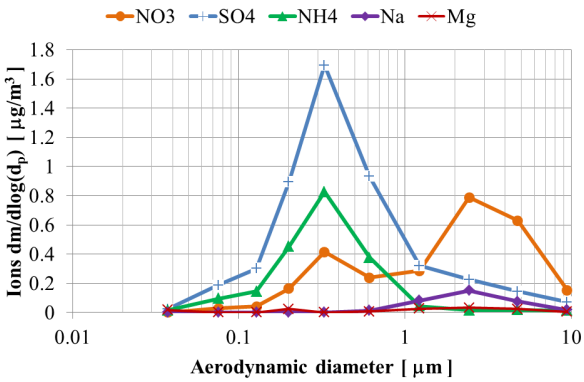

Figure 1. The mass size distribution of main ions from BLPI measured next to the freeway (Sep 2008).

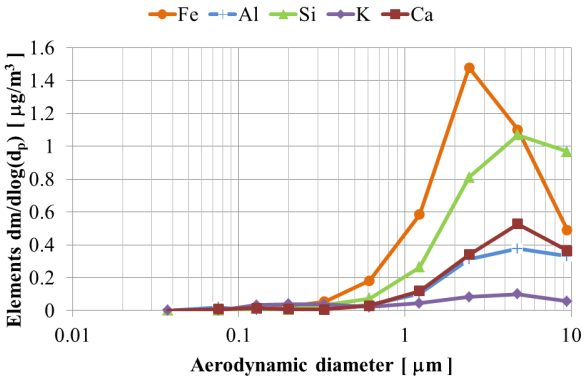

Figure 2. The mass size distribution of main elements from BLPI measured next to the freeway (Sep 2008).

This work was supported by the GA CR project (P209/11/1342).

Characteristics of compositions in fine and coarse aerosols in central Taiwan

Chien-Lung Chen[1], Chien-Hua Chen[2], Feng-Chao Chung[3], Su-Ching Kuo[4], Li-Ying Hsieh[5] and Ying I. Tsai[6]

[1] Dept of Industrial Engineering & Management, Fortune Institute of Technology, Kaohsiung 831, Taiwan
[2] Dept of Finance, Fortune Institute of Technology, Kaohsiung 831, Taiwan
[3] Dept of General Education Center, Fortune Institute of Technology, Kaohsiung 831, Taiwan
[4] Dept of Medicinal Chemistry, Chia Nan University of Pharmacy & Science, Tainan 717, Taiwan
[5] Dept of Chemistry, National Cheng Kung University, Tainan 701, Taiwan
[6] Dept of Environmental Engineering & Science, Chia Nan University of Pharmacy & Science, Tainan 717, Taiwan

Keywords: particulate matter, chemical composition, urban aerosols.

Presenting author email: mtsaiyi@mail.chna.edu.tw (Y.I. Tsai)

Airborne particulate matters (PM) have been studied intensively for their environmental effects on the public health, the reducing visibility and solar radiation balance (Yatkin and Bayram, 2008). The aim of this study is to characterize and compare the PM and their composition fractions at urban of central Taiwan and provide the input data for air quality model. The sampling site is located at National Chung Hsing University campus, influenced by local sources. Thirty-six of 24-hour daily samples were collected at Taichung from April to December 2009 using a Dichotomous sampler (Andersen Instruments, Model 241, USA). Water-soluble ions (Na^+, Mg^{2+}, K^+, Ca^{2+}, NH_4^+, Cl^-, NO_3^-, SO_4^{2-}) in aerosols collected with quartz-fibers filters were determined using an ion chromatography (DX-100, Dionex, USA). Total carbon (TC) and element carbon (EC) were measured using an element analyzer (W.C. Heraeus elemental analyzer CHN-O-Rapid, EA).

The mass concentrations and the fractions of $PM_{2.5}$ and $PM_{2.5-10}$ chemical compositions sampling in diurnal and night time are presented in Figure 1 and Table 1, respectively. The average concentration of diurnal $PM_{2.5}$ is 31.1μg m^{-3} including SO_4^{2-} (25.3%), Organics (13.8%), EC (10.9%), NH_4^+ (10.6%), NO_3^- (6.0%), Mg^{2+} (3.5 %) and sea salt (1.9%). The percentage of other compositions is 26.6%. In the other hand, the average concentration of diurnal $PM_{2.5-10}$ is 23.4μg m^{-3}. The percentage of other compositions in coarse particle is up to 47.1%. The major fractions of $PM_{2.5-10}$ compositions are EC (16.7%), Organics (12.4%), NO_3^- (10.3%) and then sea salt (4.8%) in daytime. The results of daytime particle composition in $PM_{2.5}$ and $PM_{2.5-10}$ are shown that the hygroscopic aerosols including sulphate, nitrate, Organics and EC mainly exist in the fine particle (Tsai and Chen, 2006; Pope et al., 2010).

The average concentration of nighttime $PM_{2.5}$ is 35.7μg m^{-3}. Like the main $PM_{2.5}$ compositions sequence in daytime, that of main $PM_{2.5}$ compositions in nighttime is SO_4^{2-} (23.4%), Organics (14.1%), EC (10.5%), NH_4^+ (9.8%), NO_3^- (7.4%), Mg^{2+} (3.6 %) and sea salt (1.3%). The average concentration of nighttime $PM_{2.5-10}$ is 20.8μg m^{-3}. The fraction of other compositions in fine and coarse particle at nighttime is 28.4% and 39.7%, respectively. The major fractions of $PM_{2.5-10}$ compositions in nighttime are EC (18.0%), NO_3^- (13.9%), Organics (13.8%) and then sea salt (5.5%). Comparing the particle compositions at night between the fine and coarse particulate matters, the hygroscopic particles grow up in $PM_{2.5}$ mainly in theory and can be observed from Figure 1. Basically, there is no obvious difference for the composition proportions among the $PM_{2.5}$ and $PM_{2.5-10}$ aerosols sampling in daytime and night time.

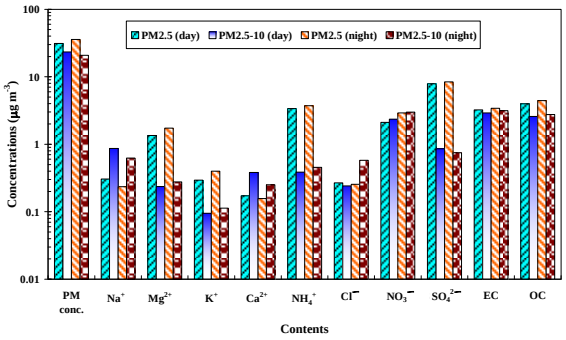

Figure 1. Mass concentrations of fine and coarse particulate matter compositions at Taichung, Taiwan in April – December 2009.

Table 1. Fractions of fine and coarse particulate matter at Taichung, Taiwan in April – December 2009.

Category	Fractions (%)										
	Na^+	Mg^{2+}	K^+	Ca^{2+}	NH_4^+	Cl^-	NO_3^-	SO_4^{2-}	EC	OC	others
$PM_{2.5}$ (day)	1.0	3.5	0.9	0.6	10.6	0.9	6.0	25.3	10.9	13.8	26.6
$PM_{2.5-10}$ (day)	3.6	0.9	0.4	1.8	.7	1.2	10.3	4.0	16.7	12.4	47.1
$PM_{2.5}$ (night)	0.6	3.6	1.0	0.5	9.8	0.6	7.4	23.4	10.5	14.1	28.4
$PM_{2.5-10}$ (night)	3.0	1.2	0.6	1.3	2.3	2.4	13.9	3.9	18.0	13.8	39.7

This work was supported by the National Science Council, Taiwan under Grant Nos. NSC 96-2221-E-041-013-MY3 and NSC 99-2221-E-041-014-MY3.

Pope, F.D., Harper, L., Dennis-Smither, B.J., Griffiths, P.T., Clegg, S.L. and Cox, R.A. (2010) *Journal of Aerosol Science* **41**(5), 457-467.

Tsai, Y.I. and Chen, C.-L. (2006) *Atmospheric Environment* **40**(25), 4734-4750.

Yatkin, S. and Bayram, A. (2008) *Science of the Total Environment* **390**, 109-123.

Estimation of direct aerosol radiative forcing at Pune

G. V. Pawar[1], G. R. Aher[1] and P. C. S Devara[2]
[1]Physics Dept., Nowrosjee Wadia College, Pune (India), 411 001
[2]Indian Institute of Tropical Meteorology, Pashan, Pune (India), 411 008
[1]Physics Dept., Nowrosjee Wadia College, Pune (India), 411 001, +91(020) 26162944, +91(020) 26163108,
Keywords: Climate forcing, Aerosol direct radiative forcing, Aerosol optical depth.
Presenting author: aher.g.r@gmail.com.

Atmospheric aerosols are significant source of direct and indirect climate forcing hence are of primary concern due to their role in perturbing the Earth-atmospheric radiation balance. Hence there is considerable interest in quantifying and reducing uncertainties in the calculations of aerosol direct radiative forcing (ARDF), which is defined as the change in the global radiation balance attributable to changes in the amount of light scattered and absorbed by particles suspended in the atmosphere. In spite of how atmospheric aerosols affect the Earth's radiation budget, the ARDF has larger uncertainties than those of greenhouse gases due to the relative short life time, nonuniform composition, size, spatial and temporal distributions of aerosols in the troposphere (Chalson et al., 1992; Schwartz and Andrea, 1996).

Direct radiative forcing is estimated by modeling and experimental techniques. In the experimental technique, sunphotometer and radiation sensors play major role in the measurement of aerosol optical properties and the global solar flux respectively.

These data are employed to estimate aerosol direct radiative forcing (ARDF). MICROTOPS-II sunphotometer at 440, 500, 675, 870 and 1020 nm wavelengths and Eppley make Precision Spectral Pyranometer (PSP) in the spectral band 280-2800 nm are being simultaneously operated on clear sky days from Nowrosjee Wadia College, Pune to measure aerosol optical depth (AOD) and global solar flux respectively. Instantaneous AOD values normalized for air mass factor (m = sec Z, $Z \leq 70^0$, Z being solar zenith angle) at λ = 440, 500, 675 nm are correlated with global solar flux by using linear regression technique by following Jayaraman et al. (1998).

Slope of the linear regression fit yields a change in ground reaching global solar flux (ΔF) in W/m^2 per unit 0.1 increase in AOD at each wavelength. The zero AOD intercept gives surface reaching global solar flux for no aerosol. Fig.(1) illustrates an example on the day of January 2011. It is seen that the ARDF is – 163.37 $\pm$6.4 per unit 0.1 increase in AOD. Analysis of the data indicates that there is a significant day- to-day variation in ARDF values. This may be correlated with meteorological conditions at the observing site. In the present paper, seasonal variation of ARDF will be discussed. ARDF data obtained will be validated using model calculations.

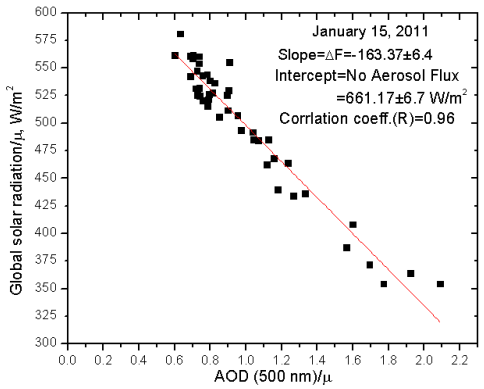

Fig.(1): Corrlation between measured Global solar flux and columanar aerosol optical depth values normalized for the air mass term 1/μ

The present study was supported and funded by the Indian Space Research Organization under the joint programme of ISRO and Pune University.

Charlson et al., (1992) *Science,* **255**, 423, 430.

Schwartz, S. E., and Andrea M. O (1996) *Science* **272**, 1121 – 1122.

Jayaraman et al. (1998) *J. Geophys. Res.,* **103(No.D12),** 13,827 – 13836.

Seasonal and statistical features of aerosol optical properties over different Indian sites

S. D. More[1], G. R. Aher[2] and P. Pradeep Kumar[1]

[1]Dept. of Atmospheric and Space Sciences, University of Pune, Pune 411 007, India
[2]Dept. of Physics, Nowrosjee Wadia College, Pune 411 001, India
Keywords: MODIS, Angstrom wavelength exponent, Atmospheric aerosol, Cloud Optical Depth
Presenting author email: aher.g.r@gmail.com.

Atmospheric aerosols are one of the most variable components of the Earth's atmospheric environment. They can affect and change the Earth-atmosphere system's radiation budget through direct effects, semi direct effects, the cloud albedo effect and the cloud lifetime effects (IPCC, 2007). Aerosol optical, physical and chemical properties have been studied in many regions of the globe; however the large spatio-temporal variability, short lifetimes and mixing processes lead to uncertainties on the effect of aerosols on climate system (Bouya et al., 2010). Understanding how aerosol properties vary locally would improve the current knowledge of aerosols around the world and would be useful in integrating global datasets. Satellite based remote sensing provides systematic retrieval of aerosol optical properties on regional and global scale.

In the present study, we employed multi-year MODIS/Aqua and Terra Data sets of column integrated aerosol and cloud optical properties over Western Himalayas [29.5^0 – 33.5^0 N, 76.5^0 – 80.5^0 E], Pune [19.5^0 – 17.5^0 N, 72.5^0 – 74.5^0 E] and Kolhapur [17.5^0 – 15.5^0 N, 73^0 – 75^0 E] to delineate the aerosol and cloud properties on monthly, seasonal and inter – annual scale and their statistical characteristics. Analysis of multi-year aerosol cloud optical data revealed strong seasonal and monthly cycles of atmospheric aerosol loading over all the sites. Monthly variation of both aerosol optical depth (AOD) and cloud optical depth (COD) show that, in general, both are low during Jan- March period. From April onwards, AOD/COD rise steadily to a high value in July which is a summer high for these regions. A gradual fall is noticed till September with small secondary peak in Oct-Nov months. Variation in Angstrom wavelength exponent (α) showed an opposite pattern. A linear least-squares fit can express the relationship between AOD and α [Fig.(1)]. The frequency distribution of AOD, COD and α follow a lognormal frequency distribution. Study indicates that the Gaussian model of the form:

$$y = y_0 + \frac{A}{w\sqrt{\frac{\pi}{2}}} \exp\left[-2\left(\frac{X-X_C}{w}\right)^2\right]$$

can be fitted to the entire data sets during 2000-2009 at all the observing sites.

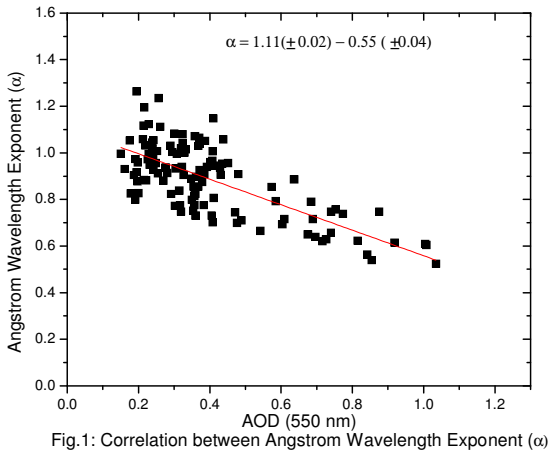

Fig.1: Correlation between Angstrom Wavelength Exponent (α) and AOD

This work was supported by University Grants Commission, New Delhi under the major research project scheme. We also acknowledge the MODIS mission scientists and associated NASA personnel for the production of the data used in this research effort.

IPCC (2007) *Climate change 2007: The Scientific basis-contribution of Working Group I to the third report of IPCC 2007*, Cambridge Univ. Press, New York.

Bouya Z., Box G. P. and Box M. A (2010) *J. Atmos. Sol. Terr. Phys.*, **72(2010),** 726-739.

Personal exposure to urban aerosol in terms of mobile particle number and surface area concentrations measurements

J. Gauweiler[1], K. Kordowski[1] and S. Weber[1]

[1]Climatology and Environmental Meteorology, Institute of Geoecology, Technische Universität Braunschweig, 38106, Braunschweig, Germany
Keywords: urban, surface area, particle number, mobile measurement.
Presenting author email: s.weber@tu-braunschweig.de

Introduction

Recent health related research indicated not particle mass, but number and surface area concentrations as particle metrics with best association to health impacts. It holds especially for the fraction of lung deposited aerosol, i.e. the alveolar lung deposited aerosol surface area concentration (ALDSA). This metric is of particular interest within cities due to the abundance of ultrafine particles (< 100 nm) in urban atmospheres (Morawska et al., 2008). Recently, mobile devices became available which are able to determine the fraction of ALDSA at a high temporal resolution.

The assessment of spatio-temporal variation in exposure of people towards urban particle number and surface area concentrations in different environments is an important topic in health related research.

Material and methods

The mobile measurements of particle number and surface area concentrations were performed in Braunschweig, Germany. A handheld miniature diffusion size classifier (miniDisc, Fierz et al, 2011) was used. The minidisc is capable of measuring particles at a 1Hz resolution in a size range of 10 nm < D_p < 300 nm. The alveolar lung deposited surface area is calculated from the charge distribution of the measured aerosol.

A number of 15 mobile measurements were performed in the time frame from 05 January to 09 February 2011. A 6 km measurement route was subdivided into 42 route sections representing common classes of land use in Braunschweig. The land use comprises of traffic sections (high density and main roads), residential areas, downtown pedestrian areas, urban parks and indoor passages (shopping malls). Each measurement took about 1 hour to minimise overlying trends of particle concentrations on the diurnal course.

Results

The urban particle number concentrations and ALDSA are clearly related to the different land use classes (Fig. 1). Highest concentrations are observed at the high density traffic sections (e.g. route sections 6, 7) with a mean ALDSA of about factor 1.8 above the average level of the measurement route. This corresponds to an absolute lung deposited surface area concentration of about 60.5 µm^2 cm^{-3} and a median particle number concentration of about 29,000 cm^{-3}.

The spatial pattern of particle number and surface area concentrations was consistently recurring during the 15 mobile measurements. More detailed results (e.g. dependence on meteorological conditions) will be provided during the poster presentation.

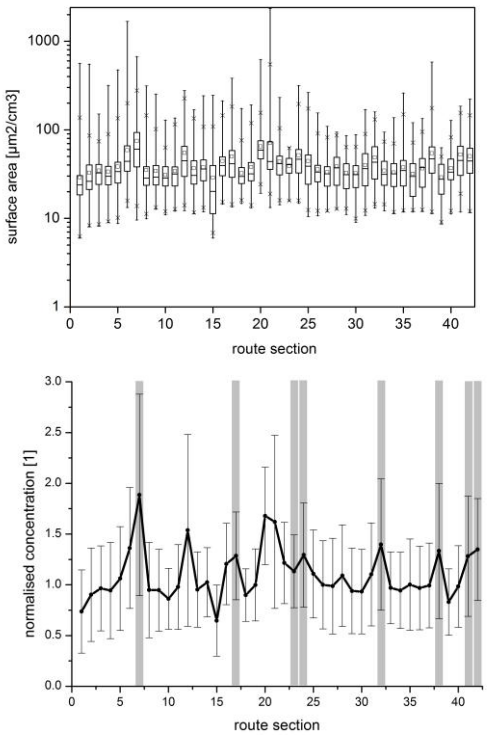

Fig 1 Top: Alveolar lung deposited surface area concentrations along 42 route section in Braunschweig, Germany. The plot indicates the mean (circles), median, 25 and 75 percentile (box), 1 and 99 percentile (asterisks) and absolute minimum and maximum (whiskers). Bottom: Mean normalised ALDSA during 15 measurements at the route sections. The high density traffic sections are indicated by grey shadings.

References

Fierz, M. Steigmeier, P. Houle, C. and Burtscher, H. (2011) Aerosol Science and Technology, 45: 1-10.

Morawska, L., Ristovski, Z., Jayaratne, E.R., Keogh, D.U. and Ling, X. (2008) Atmos Environ, 42(35): 8113-8138.

FIRST NEW PARTICLE FORMATION EVENTS MEASURED DURING THE BIOFUSE CAMPAING MEASURING OPTICAL PROPERTIES AND SIZE DISTRIBUTIONS AT SÃO PAULO, BRAZIL

J. BACKMAN[1], L.V. RIZZO[2], T. PETÄJÄ[1], H.E. MANNINEN[1], T. NIEMINEN[1], J. HAKALA[1], P.P. AALTO[1], F. MORAIS[3], R. HILLAMO[4], P. ARTAXO[3], and M. KULMALA[1]

[1]Division of Atmospheric Sciences, Department of Physics, University of Helsinki, Finland
[2] Department of Earth and Exact Sciences, Federal University of São Paulo, Brazil
[3]Institute of Physics, University of São Paulo, Brazil
[4]Finnish Meteorological Institute, Helsinki, Finland
Keywords: air quality, biofuels, megacities, size distribution
Presenting author email:john.backman@helsinki.fi

Large urban agglomerates are a significant source of aerosols and trace gases, with potential effects to the hydrological cycle (Lohmann and Feichter, 2005) and climate patterns. Atmospheric aerosols and trace gases are tightly connected via physical, chemical and meteorological processes. New ethanol based fuels for the worlds' vehicular fleet have been developed to reduce the dependence on fossil fuel, as well as to reduce carbon dioxide emissions. However, little is still known about their impacts on human health, air quality and climate. The metropolitan area of São Paulo, Brazil (MASP) is a unique laboratory for studying the complex physical and chemical processes associated with the use of bio-fuels. The MASP is special in the sense that bio-ethanol is the main fuel used along with its vast vehicular fleet counting 7.2 million and rising. At MASP, it has been estimated that out of the 7.2 million passenger and commercial vehicles 55 % of the burnt fuel is alcohol (CETESB, 2007)

The site locates roughly 10 km from the city centre, at the western edge of the most densely populated area. São Paulo city is surrounded by vast suburban areas populated by 20 million people, resulting in the world 7th biggest metropolitan area. The city of São Paulo is located on a plateau 860 meters above sea level (a.s.l.) surrounded by hills rising up to 1200 meters a.s.l.

Total particle concentrations are measured with a CPC and the aerosol size distributions are measured from 2 to 800 nm with a differential mobility particle sizer (DMPS) and a Neutral cluster and Air Ion Spectrometer (NAIS). In addition light scattering and light absorption coefficients are measured using a three wavelength TSI nephelometer and a Multi Angle Absorption Photometer (MAAP).

Table 1. Comparison between theoretical predictions and experimental measurements.

Day	$GR_{6\text{-}20}$ (nm h^{-1})	J_6 ($cm^{-3}s^{-1}$)
10 Oct	25.1	11.2
2 Nov	9.3	11.4
7 Nov	16.1	18.5
15 Nov	10.7	4.5

New particle formation events were observed with growth rates ranging from 9 to 25 nm h^{-1} (Table 1). The measured total particle concentration typically varies between 10 and $30 \cdot 10^3$ cm^{-3} being the lowest late in the night and highest around noon and frequently exceeding $50 \cdot 10^3$ cm^{-3}. The median modal peak of the size distribution was 24 nm. Clear diurnal patterns in aerosol optical properties were observed ranging between 21 and 64 Mm^{-1} for light scattering coefficients (σ_{SP}) and between 12 and 33 Mm^{-1} for light absorption coefficients (σ_{AP}).

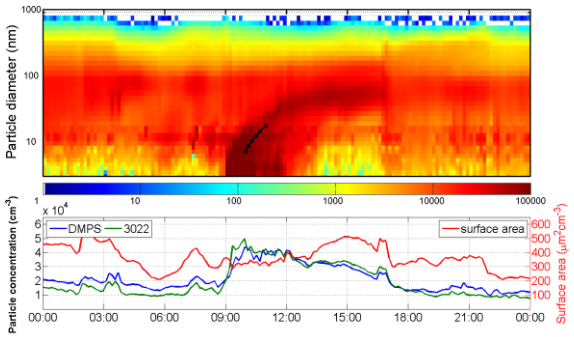

Figure 1. *The first nucleation event measured on the 2nd of November 2010. The growth rate of 9.3 nm h^{-1} was calculated using DMPS data from 6 to 20 nm indicated by black circles.*

The effects of intensive BIO-Fuel production and USE on regional air quality and global climate (BIOFUSE) was supported by the Academy of Finland's Sustainable Energy Research Programme (SusEn) and by the Brazilian National Council for Scientific and Technological Development (CNPq)

Lochmann U., and Feichter, J., (2005) *Atmos. Chem. Phys.*, ***5***, *715 – 737.*

CETESB (2007) Relatório de Qualidade do Ar no Estadode São Paulo. *Publicação CETESB*, São Paulo, Brazil.

Comparison of a New Optical Particle Sizer to Reference Sizing Instruments for Urban Aerosol Monitoring

A.F. Zerrath[1], O.F. Bischof[1], H.-G. Horn[1], T. Krinke[1], T. Johnson[2] and K. Erickson[2]

[1]TSI GmbH, Neukoellner Str. 4, 52068 Aachen, Germany
[2]TSI Inc., 500 Cardigan Road, 55126 Shoreview, MN, USA
Keywords: optical counter, number size distribution, environmental particles, monitoring
Presenting author email: axel.zerrath@tsi.com

Optical Particle Counters are in widespread use for measuring various aerosols including environmental monitoring.

Since almost all optical particle counters and spectrometers are factory-calibrated with polystyrene latex (PSL) particles, sizing errors could be significant if the refractive indices of the aerosol are significantly different from the refractive index of PSL of 1.59.

Hand and Kreidenweiß (2002) have shown how to determine unknown aerosol properties like refractive index and effective density by using the combination of sizing by the particles' electrical mobility, aerodynamic and optical properties.

TSI has developed a new Optical Particle Sizer (OPS), the Model 3330. It is a lightweight, portable unit that provides fast and accurate measurement of particle concentration and size distribution using optical single particle counting technology. It is a new instrument with various technical improvements, which allows high resolution monitoring of aerosols in the range from 0.3 to 10 µm, with user-adjustable size classes, size resolution of up to 16 channels and measurement time down to 1 second.

In order to address the issue of the material dependence of optical sizing, the OPS features real-time Mie scattering calculation capability to adjust the PSL calibration curve to a curve that better fits the aerosols of interest. The refractive index value can be adjusted for real and imaginary components for every size class. For non-spherical particles, an additional shape factor can be entered to perform further adjustment of the calibration.

Data processing and analysis software also allows a unique density for every size channel to be entered to improve mass concentration measurement. In addition, humidity and temperature sensors are integrated into the OPS instrument.

The OPS was launched in late fall of 2010 and first results will be explained. A sample data set is shown in figure 1. This presentation focuses on the results obtained from monitoring urban aerosol in the city of Aachen (Germany), with the OPS in comparison to reference particle sizing instruments like the Scanning Mobility Particle Sizer (SMPS) for ultrafine and the Aerodynamic Particle Sizer (APS) for coarse particles.

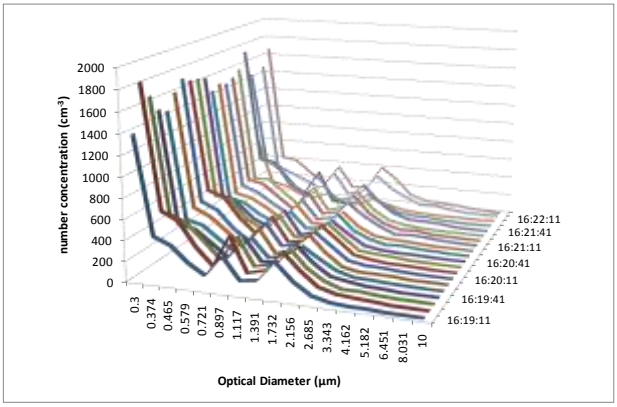

Figure 1: Atmospheric aerosol measured with the OPS 3330 in January 2011.

In the spring of 2011 a measurement campaign monitoring urban aerosol using OPS, APS and SMPS in parallel was conducted in the city of Aachen. The SMPS provided high-resolution submicrometer size data in the range of up to 1 µm. The APS was used as high-resolution reference for coarse aerosols in the range from 0.37 µm to 10 µm. One of the OPS' pre-configured, user adjustable size channel configurations uses the same channel width and resolution as the APS Model 3321. The difference between the optical equivalent diameter obtained from the OPS and the aerodynamic diameter from the APS thus includes information on effective density, shape and refractive index. The results presented here evaluate the OPS' performance for real-time environmental monitoring. This study builds on the measurement of urban aerosol in Aachen as reported earlier (Zerrath and Bischof, 2005).

Hand, J., Kreidenweiß, S., (2002). *A New Method for Retrieving Particle Refractive Index and Effective Density from Aerosol Size Distribution Data*, Aerosol Science and Technology, 36, 1012-1026.

Stolzenburg, M., Kreisberg, N. and Hering, S. (1998) *Atmospheric Size Distributions Measured by Differential Mobility Optical Particle Size Spectrometry*, Aerosol Science and Technology, 29: 5, 402 — 418.

Zerrath, A., Bischof, O. (2005). *Urban aerosol in a light industrial area – A closure between particle size distribution, number and diameter concentration measurements in the submicron range*, Abstracts of the European Aerosol Conference 2005: p. 608, Ghent, Belgium.

Particle area and number concentrations influenced by local sources at an urban background station in Germany

H. Gerwig[1], W. Pecher[1] and K. Wirtz[1]

[1]Section Air Quality Standards and Monitoring Methods, UBA – Federal Environmental Agency, 63225 Langen, Germany.

Keywords: particle area, car traffic, asphalt grinding, gas-fired CHP, airport

The European Union defined a daily average PM_{10}-limit of 50 µg · m^{-3} for the protection of human health (2008/50/EC). Epidemiological and toxicological studies give evidence that ultrafine particles (< 100 nm, UFP) show negative health effects (Knol *et al.*, 2009).

Reduction limits for diesel cars are fixed (EURO VI). To control the results of reducing emitted particle numbers from cars and especially trucks, governmental agencies in Germany started to measure ultrafine particles on a routine base (Birmili *et al.* 2009 and Löschau *et al.* 2010).

Table 1 1-h av. tracheobronchial particle area and particle conc. 09-09-2009 – 14-06-2010

	NSAM	UCPC	SMPS
	µm²/cm³	p / cm³	p / cm³
nm	10 - 1000	3 - 1000	10 - 500
Median	5.0	9 900	8 600
Std	3.1	6 100	6 000
5 Perc	1.9	4 600	3 700
95 Perc	11.7	22 500	21 000

The urban background station was situated in Langen, Germany: 15 km south of Frankfurt a. M. and 5 km south east of the airport in the Rhine-Main-Area. Three different particle measuring instruments (TSI Inc.) were running continuously (09-09 – 06-11, 1 min av. and SMPS 6 min av.) on a rooftop at 14 m above ground with cut of at 1 µm. NSAM measures the deposited tracheobronchial (= tb) particle area within particle diameter of 10 - 1000 nm. With UCPC 3776 particle number concentration from 3 - 1000 nm was measured. With SMPS 3936 and CPC 3010 particle number size distributions between 10 – 500 nm were detected. 6 size classes were calculated from SPMS data (10 |30 |50 |70 |100 |200 |500). The difference of UCPC and total SMPS was expected to be size class 3 – 10 nm Offsets between both instruments cannot be excluded.

Temperature, humidity, wind speed, wind direction, precipitation was collected by WS600 (LUFFT GmbH). Only complete datasets of 1 h av. were used for evaluation (85 % of time period). For diurnal Mo-Fr variations data from official holidays and from 23-12-09 until 03-01-10 were excluded.

During the measuring period the median of the tb particle area concentration was 5 µm²/cm³, particle number concentration from 10 to 500 nm was about 8 600 p · cm^{-3}. 1 300 p · cm^{-3} more particles were found from 3 to 1 000 nm range (s. Tab. 1). The temperature was between -15 and +30°C, wind speed up to 14 m · s^{-1}.

For diurnal variations from Monday to Friday 2 different shapes were detected (Fig 1). Shape A: Tb particle area and particles 30 – 500 nm showed a 1st min. around 4:00, max. at 9:00 and 2nd min. at 15:00, similar to previous observations at an urban background during UFIPOLNET (Wehner *et al.*, 2008). Shape B: Particles 3 – 10 nm showed 1st max between 13 – 15:00 probably caused by particle nucleation events and a 2nd max at 7:00. Particles 10 – 30 nm show almost the same diurnal variation as shape A except for afternoon, were the second min. looks as if overlayed by effects responsible for shape B.

Grinding up asphalt and other road construction work in 10 to 100 m distance caused raised particle area and number concentrations. Elevated particle concentration occurred with winds from a nearby combined heat and power gas-fired power plant (CHP). The influence of the airport will be evaluated. The influence of fireworks is described elsewhere (Gerwig *et al.*, 2011).

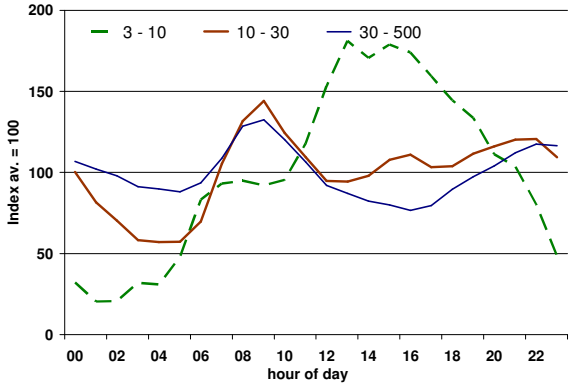

Figure 1. Diurnal variations of 1 h av. Mo – Fr; particle classes 3 – 10, 10 – 30 and 30 - 500 nm

Birmili, W. *et al.* (2009), *Gef .Reinh. Luft*, **69**, 31–35.
Gerwig, H. *et al.* (2010), *IAC 2010, Helsinki.*
Gerwig, H. *et al.* (2011), *EAC 2011, Manchester.*
Knol, A. B. *et al.* (2009), *Part. Fibre Tox.*, **6**, 19.
Löschau, G. *et al.* (2010), *Gef. Reinh.Luft,***70**,183–187.
Wehner, B. *et al.* (2008), *EAC 2008, Thessaloniki.*

Personal exposure to fine PM in Milan: a comparison of different travel modes

G. Lonati[1], S. Ozgen[1] and G. Ripamonti[1]

[1]Department of Environmental, Hydraulic, Infrastructures and Surveying Engineering
Politecnico di Milano, Milano, 20133, Italia
Keywords: exposure, PM2.5, PM1, number concentration.
Presenting author email: giovanni.lonati@polimi.it

Emerging evidence suggests that short events of high exposure to particulate matter (PM) occur while travelling in urban areas, depending on the transport mode (Briggs *et al*., 2008; Knibbs and de Dear 2010).

This study compares the personal exposure to fine PM while travelling with different means of transport along a city-centre trafficked road, about 2 km long. For this purpose, 1-min average concentrations were measured with portable instruments during 2 weeks in July 2010, for 3-times a week, on workdays between 3 p.m. and 5 p.m.. The measurements relate to three surface transport modes (i.e., on foot, by bike, by car) and to the underground train (subway). Travel by each mode lasted about 30 minutes, allowing 1 round trip for the walking mode and 2 round trips for the other modes.

Particle number concentrations in the 0.3-2.5 µm size range were measured by means of an optical particle counter (Contec Personal DustMonit, Italy); mass concentrations (PM0.3-1, PM0.3-2.5) were subsequently estimated based on size-resolved density factors for Milan urban area. Particle number concentrations (PNC) in the size range 0.02-1 µm were measured by means of P-Trak UFP Counter (TSI Model 8525, USA). Both instruments were held in a backpack during the travels. During the car trips, the backpack was on the front passenger seat, car windows were closed and the cabin filtered air recirculation was turned on.

Table 1. Concentration levels (avg.±st.dev.) measured in the travel modes.

Travel mode	PM 0.3-1 (µg m^{-3})	PM 0.3-2.5 (µg m^{-3})	PNC 0.02-1 (10^4 cm^{-3})
Car	2.3±1.8	3.2±2.4	1.2±1.2
Walk	10.7±2.0	19.5±3.1	2.2±1.7
Bike	11.4±2.6	21.0±3.9	2.7±1.4
Subway	20.0±7.5	57.3±30.3	1.5±0.2

Results

The comparison between the average mass concentration levels observed for the different travel modes (Table 1) shows the benefit of the filtered cabin air recirculation inside the car. The outside air ambient concentrations, measured during the walking and biking modes, were about 80% reduced in the car cabin. Comparable levels were observed for the walking and biking modes, with slightly higher levels for this latter. The subway mode line concentrations were, on the other hand, the highest (from two to three times compared to outside ambient air) and the most dispersed measured in this study.

Larger differences between travel modes were observed for the PM0.3-2.5 size range (Figure 1). The benefit of the car cabin air filtration is more evident: in fact, supermicron particles (dp > 1µm) strongly affected the mass concentration levels for all the other travel modes. Their average contribution to the PM2.5 mass was about 50% for the walking and biking modes and up to about 65% for the subway mode.

PNC average levels were in the 1-3·10^4 cm^{-3} range, displaying large variability for all the surface travel modes (Figure 2). Conversely from the mass, the average PNC levels for the subway mode were similar to the cabin car levels and the highest concentration were measured for the biking mode.

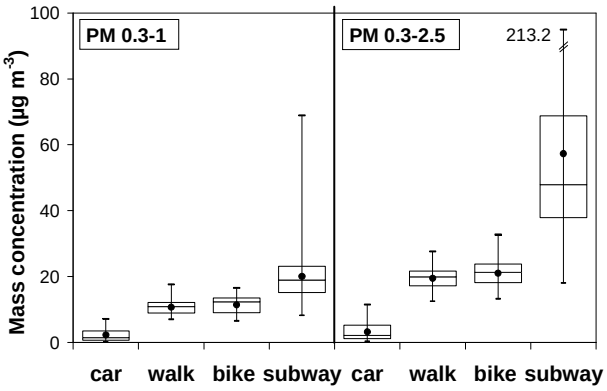

Figure 1. Box-plots for the PM mass concentration data.

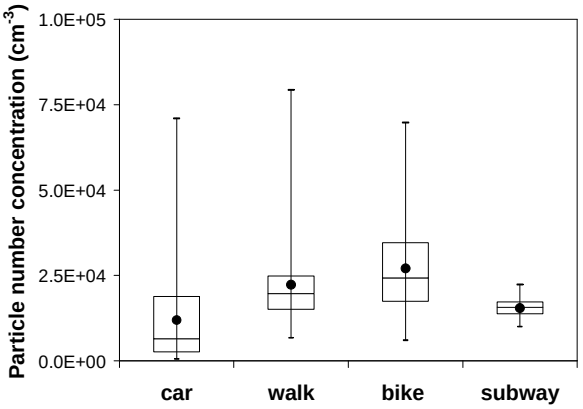

Figure 2. Box-plots for the PNC data.

Briggs, D.J., de Hoogh, K., Morris, C., and Gulliver, J., (2008) *Env. Int.* **34**, 12-22.

Knibbs, L.D. and de Dear, R.J. (2010) *Atm. Env* .**44**, 3224-3227.

Thursday, September 8, 2011

Session 8P: Poster session B

Atmospheric aerosols - Aerosol Processes and Properties

Ground-based Aerosol Optical Properties and radiative forcing over Karachi Pakistan

K. Alam[1], T. Trautmann[2], T. Blaschke[1,3]

[1]Department of Geography and Geology, University of Salzburg, Hellbrunnerstrasse 34, Salzburg 5020, Austria
[2]German Aerospace Centrer, Remote Sensing Technology Institute, Oberpfaffenhofen, 82234 Wessling, Germany
[3]Z_GIS, Centre for Geoinformatics, University of Salzburg, Hellbrunnerstrasse 34, Salzburg 5020, Austria
Key words: Aerosol; Radiative forcing, Karachi, AERONET
Khanalamso@gmail.com

Aerosol optical properties have been analyzed through the ground-based Aerosol Robotic Network (AERONET) over the mega city Karachi during August 2006-July 2007. The aerosol optical depth (AOD) is strongly dependent on wavelength; for shorter wavelengths AOD values are higher than at longer wavelengths. The results reveal that the monthly average AOD at 500 nm ranges from 0.38 to 0.98 with an annual mean of 0.56±0.18 and monthly averaged angstrom exponent (Alpha) ranges from 0.17 to 1.05 with an annual mean of 0.55±0.31. The maximum monthly average AOD value of 0.98±0.30 with the corresponding Alpha value of 0.17±07 is found for July 2007, while the minimum monthly average AOD value of 0.38±0.09 with the corresponding Alpha value of 0.28±0.13 is recorded for May 2007 (Figure 1).

The volume size distribution in the coarse mode is higher in summer and lower in winter, whereas in the accumulation mode the volume size distribution is higher in winter than in other seasons due to the hygroscopic growth of aerosol particles (Figure 2). The single scattering albedo (SSA) during spring, autumn and summer seasons shows a slight increase with the wavelength and ranges from 0.88±0.02 to 0.97±0.01. The asymmetry parameter (ASY) is also wavelength

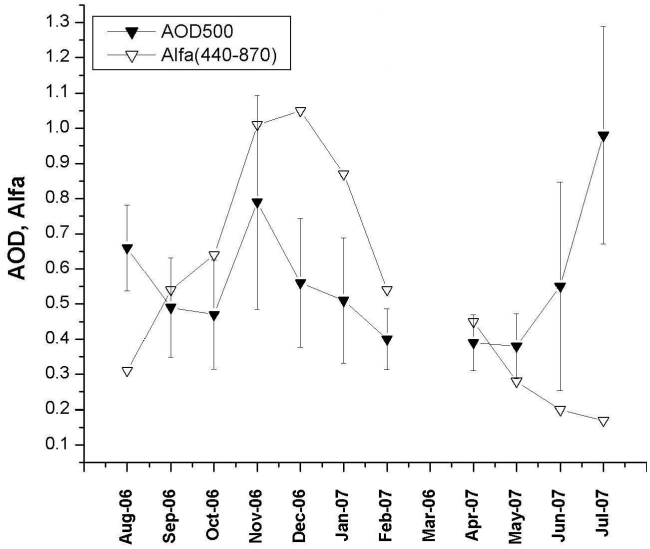

Figure 1. Monthly average variation of AOD at 500 nm and corresponding Alpha (440-870) during August 2006-July 2007.

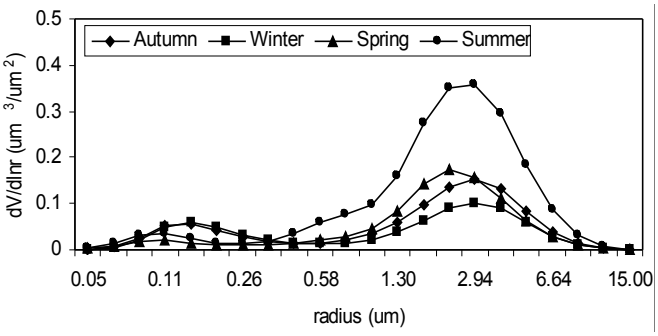

Figure 2. Seasonal variations in AERONET retrieved aerosol size distributions during August 2006 to July 2007.

dependent and varies from 0.61±0.03 to 0.74±0.02 during the year. The aerosol radiative forcing (ARF) for the whole observation period at the top of the atmosphere (TOA) is in the range of -7 to -32 Wm^{-2} (average -19±6 Wm^{-2}), at the surface from -56 to -95 Wm^{-2} (average -74±12 Wm^{-2}), increasing the atmospheric forcing from +37 to +85 Wm^{-2}(average +55±13 Wm^{-2}).

We would like to acknowledge the Higher Education Commission (HEC), Pakistan, and the Austrian Exchange Service (ÖAD) for providing a three year Ph.D. scholarship 2008-2012 to Khan Alam.

Carbonaceous particles and their influence on spectral optical properties and humidification response

S. Lee[1], S.-C. Yoon[1], Y.-P. Kim[2] and S.-W. Kim[1]

[1]School of Earth and Environmental Sciences, Seoul National University, Seoul, 151-742, Korea
[2]Environmental Engineering and Science, Ewha Womans University, Seoul, 120-750, Korea
Keywords: black carbon, organic carbon, humidification, mass absorption cross section.
Presenting author email: ryra78@hanmail.net

Black carbon (BC) particles are freshly emitted into the atmosphere through the incomplete combustion of fossil fuel and biomass burning. Although BC particles are initially hydrophobic, these particles gradually become mixed with soluble components through condensation, coagulation, and photochemical oxidation processes in the atmosphere (Zhang *et al*., 2008). If BC particles have a humidification response from the aging process, it is very important phenomenon for the climate change since aged BC can act as cloud condensation nuclei. The aim of this study is to investigate the optical properties and humidification of carbonaceous particles for the different airmass in East Asia.

Aerosol chemical composition and fine mode fraction (FMF) are used for the criteria of case selection. Pollution cases of period 1 and 2 (P1 and P2) are determined by relatively high $PM_{2.5}$ with large mass concentrations of organic carbon and sulfate during three days in May and June, which is above the upper 10 percentile of all dataset during May to November 2009. Polluted dust (PD) case is selected in the conditions of relatively high PM_{10} with high mass concentration of coarse–mode calcium and low FMF from 21st to 23rd October, which are above upper 10 percentile and below lower 10 percentile of all dataset, respectively.

Figure 1 shows the scattering and absorption coefficients as a function of wavelength for each case. Overall wavelength, scattering coefficient is the highest for P2 since the light scattered aerosols in fine–mode are high, but the scattering coefficient at PD shows the relatively flat slope due to the high concentrations of coarse–mode particles. In Figure 1(b), the difference of absorption coefficient between P1 and P2 is very low, 1.04 Mm^{-1} at 950 nm, but it increases to 5.17 Mm^{-1} at a shortwave of 370 nm. Generally, the absorption by organic species (sometimes called brown carbon) takes place in the UV for the presence of resonant ring structures (Yang *et al.,* 2009). In addition, the mineral aerosols derived from soil could exhibit high absorption in a shortwave (Satheesh *et al.,* 2007). Likewise, aerosol absorptions at P1 and PD are noticeably high in a shortwave as shown in Figure 1(b).

In Figure 2, the relationship between relative humidity (RH) and single scattering albedo (SSA) are compared for each case with considering the mass absorption cross section (MAC). In general, MAC is not only the ability of carbonaceous particles to absorb a photon in a particular wavelength, but it also serves as one convenient proxy for the relationship between radiative transfer and the aerosol mass represented in models (Bond *et al.,* 2006). Figure 2 shows the increase of SSA with increasing RH for all cases. It is because the hygroscopic chemical components, such as sulfate, nitrate and some organic matters can take up water vapor to grow in size and thus enhance the scattering ability. In particular, PD case shows the lower MACs than those of P1 in high RH above 70 %, although the SSAs are similar for both cases.

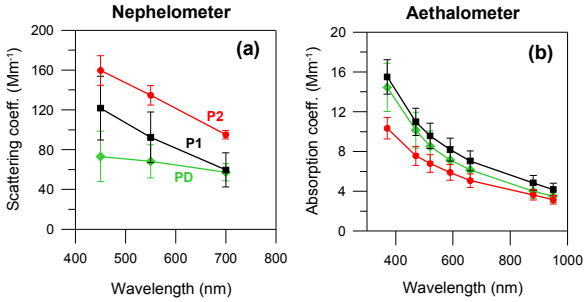

Figure 1. Aerosol scattering and absorption coefficients as a function of wavelength.

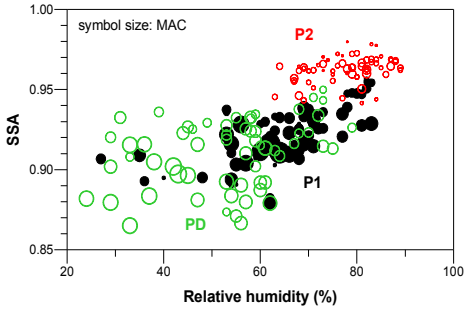

Figure 2. Relationship between RH and SSA for each case. Note, symbol size is described in proportion to the mass absorption cross section.

This work was funded by the Korea Meteorological Administration Research and Development Program under Grant CATER 2006-4104.

Bond, T. C., Habib, G. and Bergstrom, R. W. (2006) *J. Geophys. Res.* **111**, D20211, doi:10.1029/2006 JD007315.

Satheesh, S. K., Dutt, C. B. S., Srinivasan, J. and Rao, U. R. (2007) *Geophys. Res. Lett.* **34**, L04805, doi:10.1029/2006GL028623.

Yang, M., Howell, S. G., Zhuang, J. and Huebert, B. J. (2009) *Atmos. Chem. Phys.* **9**, 2035-2050.

Zhang, R., et al. (2008) *Proc. Nation. Acad. Sci.* **105**, 10291-10296.

Long-Term Measurements of aerosols light absorption coefficient, scattering coefficient and Carbon Monoxide at the ZOTTO tall tower, Siberia

X. Chi[1], J.-C. Mayer[1], N. Jürgens[1], A.V. Panov[2] and M. O. Andreae[1]

[1]Biogeochemistry Department, Max Planck Institute for Chemistry, Mainz, D-55128, Germany
[2] V.N. Sukachev Institute of Forest, Krasnoyarsk, 660036, Russia
Keywords: absorption coefficient, scattering coefficient, carbon monoxide, remote site
Presenting author email: xuguang.chi@mpic.de

The Zotino Tall Tower Observatory (ZOTTO) is located in the boreal forest of central Siberia (89.35°E, 60.80°N,114m asl). The tower is 300 meters high and was designed for long-term atmospheric observations at this very remote, continental site. Continuously measurements of comprehensive sets of atmospheric constituents in gas and aerosol phase together with meteorological parameters have been carrying out at ZOTTO since October 2006 (Heintzenberg et al. 2008). Among the others, the particulate scattering is measured by a TSI three-wavelength (450 nm ,550 nm ,700 nm) nephelometer (Model 3653), the particulate absorption is measured by making use of a single wave length Particle Soot Absorption Photometer (PSAP, 574nm, Radiance Research), and the CO mixing ratios are recorded by a fast CO monitor (Model AL5002, aerolaser).

In order to correct for the truncation and illumination non-idealities, the scattering coefficients derived from nephelometer were calculated follow the empirical correction formula of Anderson and Ogren (1998). For PSAP, the resulting absorption coefficients are corrected for the scattering artifact as well as calibration error after Virkkula et al. (2005). For CO measurements, a statistical filtering approach called REBS (Ruckstuhl et al. 2010) is applied for extracting background concentrations.

Particulate absorption shows a smooth seasonal variation with a maximum in later winter and a broad minimum in summer, whereas particulate scattering exhibits a double maximum in winter and summer (Figure 1). We hypothesize that the winter maxima for both parameters are due to northern hemispheric fossil fuel combustion, while the elevated scattering coefficient in summer may be results of enhancement of both biogenic emission and the formation of secondary species by photo-oxidation. Furthermore, for both scattering and absorption, the highest daily average values are found in April and May, which seems caused by the spring agriculture fires (which are often spread to forest) in upwind areas. The CO exhibits a similar seasonal variation (Table 2) as for particulate absorption. By applying REBS approach, 21% of observed hourly CO values are classified as polluted. For these CO polluted periods, the ratio between particulate absorption (σap) and increased CO (ΔCO) are calculated, where ΔCO is the difference between observed CO and the estimated background CO by REBS. Higher ratios are found in spring and winter than in the other two seasons, which may be indication of different combustion sources.

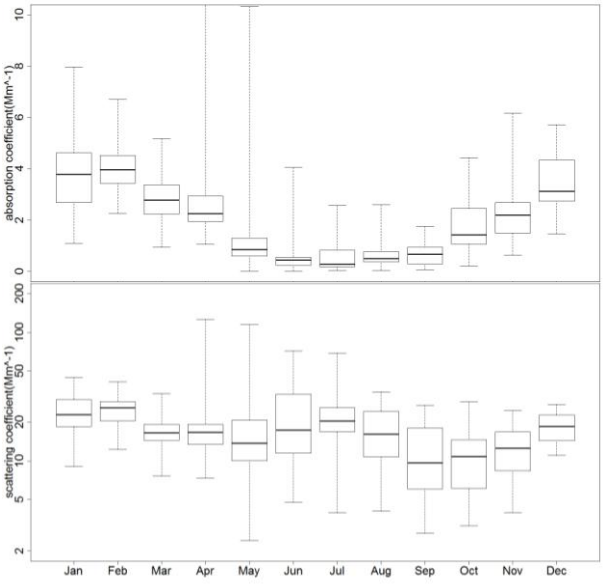

Figure 1. A standard box plot of monthly aerosol absorption coefficient (top) and scattering coefficient (bottom) at 574 nm as derived from daily average for 50m height level taken over the time period October 2006 through April 2010.

Table 1. CO mixing ratios and Bap to ΔCO ratios (only for CO polluted episode) for 50m height level as derived from hourly average since October 2006 to April 2010.

Season	CO (ppb) Median (min-max)	σap/ΔCO (Mm^-1/ppb)
Spring	162 (117-472)	0.183±0.092
Summer	100 (85-889)	0.083±0.069
Fall	116 (93-175)	0.130±0.096
Winter	179 (116-300)	0.192±0.086

The ZOTTO project is funded by the Max Plank Society through partner project #2757p, and by the German Research Council (DFG).

Anderson and Ogren (1998) *Aerosol Sci. Tech.* **29**, 57-69.

Heintzenberg et al. (2008) *Tellus 60B*, 276-285.

Ruckstuhl et al. (2010) *Atmos. Meas. Tech. Discus.*, **3**, 5589–5612.

Virkkula et al. (2005) *Aerosol Sci. Tech.* **39**, 68-83.

Light Scattering by airborne Saharan Dust particles.

D S McCall, E Hesse, Z Ulanowski

Centre for Atmospheric and Instrumentation Research, University of Hertfordshire, AL10 9AB
Keywords: Saharan, scattering, aerosol
Presenting author email: d.s.mccall@herts.ac.uk

The importance of airborne particulates to the Earth-Atmosphere radiation balance is well established. Aerosols such as ice crystals (e.g. those found in cirrus clouds) and Saharan dust particles (Yu et al. 2006) have direct effects on the worlds energy budget by scattering and absorbing solar radiation. The level of influence of atmospheric dust on global energy cycles is unclear, primarily due to large uncertainties regarding the optical properties of the dust particles.

An investigation into the light scattering properties of Saharan dust grains is presented. An electrodynamic trap (Ulanowski et al. 2006) has been used to levitate single dust particles. By adjusting the trap parameters, partial randomisation of the particle orientation has been introduced. While levitated, the particles were illuminated by a laser, and a rotating half-wave retarder enabled selection of vertically or horizontally polarized incident light. A laser diffractometer and linear photodiode array have been used to measure intensity at scattering angles between 0.5° and 177°. Approximating the direct forward scattering region by Fraunhofer diffraction as calculated for a range of appropriately-sized elliptical apertures allows the calculation of the phase function and degree of linear polarization.

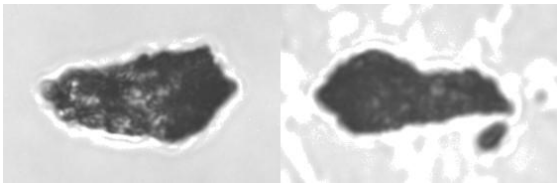

Figure 1. Transmission microscopy images of a dust particle with aspect ratio 2 and size parameter approximately 125. The particle has been rotated 90° about its long axis.

The phase functions and degree of linear polarisation for four case study particles are presented - the phase functions are found to be featureless across most of the scattering region, with none of the halo features or rainbow peaks associated with regularly shaped particles such as hexagonal columns or spheres.

Particle reconstructions comprised of high numbers of facets have been constructed to resemble the levitated particles. Utilizing Gaussian random sphere methods (Muinonen et al. 1996), increasing levels of roughness have been added to the surfaces of these reconstructions.

A Geometric Optics model and a related model, Ray Tracing with Diffraction on Facets (RTDF) (Clarke et al. 2006), have been modified to calculate scattering on these particle reconstructions. Scattering calculations were performed on each of these reconstructions using a range of refractive indices.

Qualitative comparisons are performed on the phase functions and degree of linear polarization, where it is observed that the addition of roughness to the modelled spheroids improves the fit between the computed phase functions and those measured from the levitated particles. The phase functions are quantitatively compared using RMS errors, and further comparison is performed using the asymmetry parameter.

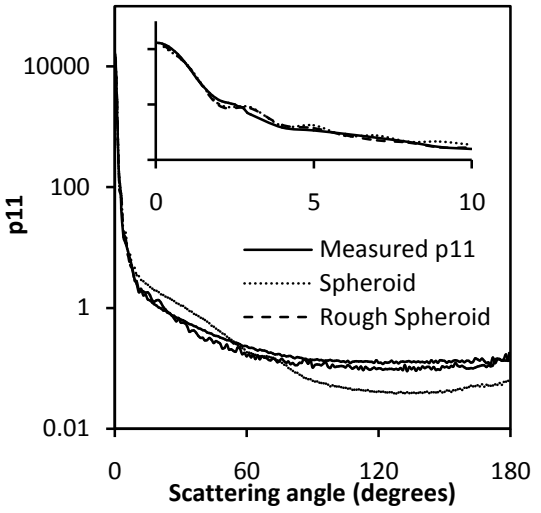

Figure 2. Measured phase function for the particle shown in Figure 1, along with RTDF calculations for a smooth spheroid and a rough spheroid. The refractive index used in the calculations was 1.55 + 0.003i.

This work was supported by the Natural Environment Research Council of the UK.

Clarke, A., Hesse, E., Ulanowski, Z., Kaye, P. (2006), *J. Quant Spectrosc. Rad. Transf.*, **100**, 103-114.

Ulanowski, Z., Hesse, E., Kaye, P.H., Baran, A. (2006), *J. Quant Spectrosc. Rad. Transf.*, **100**, 382-392.

Muinonen, K., Nousiainen, T., Fast, P., Lumme, K., Peltoniemi, J.I. (1996), *J. Quant Spectrosc. Rad. Transf.*, **55**, 5, 577-601.

Yu, H., Kaufman, Y.J., Chin, M., Feingold, G., Remer, LA., et al (2006), *Atoms. Chem. Phys.*, **6**, 613-666.

Comparison of SKYRAD4.2 and AERONET inversions on a CIMEL CE318 radiometer

V. Estellés[1,2], M. Campanelli[3], T.J. Smyth[4], M.P. Utrillas[2], J.A. Martínez-Lozano[2], F. Expósito[1]

[1]Departmento de Física Fundamental y Experimental, Universidad de La Laguna, La Laguna, Tenerife, 38207, Spain
[2]Department de Física de la Terra i Termodinàmica, Universitat de València, Burjassot, Valencia, 46100, Spain
[3]Institute of Atmospheric Science and Climate, Consiglio Nazionale delle Ricerche, Tor Vergata, Rome, I-00133, Italy
[4]Plymouth Marine Laboratory, Prospect Place, Plymouth, PL1 3DH, United Kingdom
Keywords: Atmospheric aerosols, Aerosol photometer method, Optical depth, CIMEL, PREDE.
Presenting author email: victor.estelles@uv.es

AERONET and SKYNET are two well known international networks whose main objective is to provide near real time measurements of columnar aerosol properties for climate research and remote sensing correction. Both networks have their own quality standards and impose homogeneity on the processing of their instruments data.

AERONET is present worldwide, and employs the CIMEL CE318 sun – sky radiometer as the standard instrument for the measurement of sun direct and sky diffuse radiances. Through the use of an inversion algorithm (Duvobik *et al*., 2002) a rather complete set of columnar aerosol optical properties is provided near on real time: aerosol optical depth (AOD), size distribution, phase function, complex refractive index and single scattering albedo.

On the other hand, SKYNET is mostly extended in Eastern Asia. The equivalent standard instrument is the Prede POM radiometer, and the aerosol properties are retrieved by an open source code called SKYRAD (Nakajima *et al*., 1996).

The European Skyrad users network (EuroSkyrad or ESR) is federated with SKYNET and represents a collaboration between users of the SKYRAD algorithm. The main original objective of ESR was the synergistic study of both AERONET and SKYNET networks in Europe. Currently, ten different sites (CE318 and POM instruments) are part of this initiative, mostly in United Kingdom, Italy and Spain.

Although the network is mainly addressed to Prede POM and independent Cimel CE318 users, few ESR sites employ collocated AERONET/Cimel and Prede radiometers, enabling an accurate comparison of the different approaches used by these networks.

In addition to the comparative study of the AERONET and SKYRAD methodologies, ESR has developed its own package of open source code programs. This collection (called ESR.pack) can be directly applied on both instruments, and consists of a selection of AERONET and SKYRAD methods, for the homogeneous elaboration of sun direct and sky diffuse measurements.

In a previous work, the comparison of the ESR.pack direct sun products (AOD) was addressed for a one month database (Estellés et al., 2010). The differences between AERONET and ESR.pack AOD retrievals on CE318 instruments were lower than 0.001 – 0.002 for 440 – 1020 nm channels, and slightly higher for 340 nm channel (~0.005). These values are lower than the expected uncertainty for a master AERONET instrument (0.003) and much lower than the uncertainty stated for an AERONET field instrument (0.01 – 0.02).

When the ESR.pack Cimel and Prede retrievals are compared, the differences were better than 0.003 – 0.006 for the 440 – 1020 nm channels. The comparison of AERONET/Cimel and ESR/Prede showed also a very good agreement (0.004 – 0.007).

Currently, a more complete and improved version of the ESR.pack has been developed, including the retrieval of Ångström exponent and water vapor content. Moreover, the compared database has been extended to a 3 year database obtained in Valencia (Spain). The effect of several assumptions are discussed in this work.

In addition to the direct sun programs, the ESR.pack has been completed with a sky diffuse inversion algorithm (SKYRAD version 4.2). In contrast to AOD retrievals, the inversion of sky radiance is an ill-posed problem whose solution is very sensitive to different assumptions and inputs, as previously shown by Che *et al*. (2008).

In this work we show the comparative analysis of AERONET and ESR inversions for a benchmark of one month sky diffuse data obtained in Valencia (Spain) during 2009 with a Cimel CE318 radiometer, including a preliminary discussion on the different importance of the model assumptions.

V. Estellés is currently supported by the Spanish Ministry of Science and Innovation (MICINN) through the Juan de la Cierva programme (JCI-2009-04455). This work was supported by the MICINN (projects CGL2009-07790, CGL2008-04740/CLI and CGL2010-21366-C04-01) and the Valencia Autonomous Government (project PROMETEO-2010-064). The authors also acknowledge the RIMA and AERONET staff for the calibration and processing of the Burjassot site Cimel data.

Che, H., Shi, G., Uchiyama, A, Yamazaki, H., Chen, H., Goloub, P., Zhang, X. (2008) Atm. Chem. Phys. **8**, 3199-3214.

Dubovik, O. and King, M.D. (2000) *J. Geophys. Res*. **105**, 20673 – 20696.

Estellés, V., Campanelli, M., Smyth, T., Utrillas, M.P., Martínez-Lozano, J.A. (2010) *Proc. of SPIE*, **7827**.

Nakajima, T., Tonna, G., Rao, R., Boi, P., Kaufman, Y., Holben, B., (1996) *App. Optics* **35**, 2672-2686.

Wintertime aerosol properties and their implications to radiative forcing over Eastern India

S. N. Bhanja[1], S. Verma[1,2] and S. K. Pani[2]

[1]Department of Civil engineering, Indian Institute of Technology Kharagpur, Kharagpur, West Bengal, 721302, India
[2]Centre for Oceans, Rivers, Atmosphere and Land Sciences, Indian Institute of Technology Kharagpur, Kharagpur, West Bengal, 721302, India
Keywords: AOD, Aerosol model, Aerosol characterization, Aerosol radiative forcing
Email: shubhaverm@gmail.com, shubha@iitkgp.ac.in

Aerosols perturb the climate system by scattering and absorbing the solar radiation (direct effect) and by altering the lifetime of clouds (indirect effect). Aerosol measurements carried out during the Indian Ocean experiment (INDOEX) (Ramanathan et al., 2001) showed an enormous amount of aerosol transported to the Indian Ocean originating from Indian subcontinent and adjoining regions (Verma et al., 2007). The Indo-Gangetic basin (IGB) situated in the northern part of the India (comprising of ~ 21% Indian land area), is one of the densely populated regions (supporting ~40% Indian population) and has been identified as one of the regional hotspots in the air pollution scenario. In the present work, we present an analysis of aerosol properties from various surface based measurements in the eastern IGB and their comparison with satellite retrieved data during December (2009) in the winter season and evaluate their chemical constituents, sources of origin, and radiative effects through combination of measurements and modeling tools.

Measurements of aerosol optical depth (AOD) using handheld Microtops II Sun photometer showed a monthly mean value of 0.84±0.13 at 0.5 µm. An aerosol model developed using Mie theory through optical properties of aerosols and clouds (OPAC) software package (Hess *et al.*, 1998) showed that the mineral dust contributed maximum (76%) to total aerosol surface mass concentration. However, water soluble constituents (such as sulphates, nitrates, organics) followed by black carbon contributed 60% and 26% respectively, to the total AOD. The single-scattering albedo (ω) estimated at 0.5 µm was 0.74±0.03, and is lower than the ω value reported for most of the Indian cities.

Moderate Resolution Imaging Spectro-radiometer (MODIS) retrieved AOD showed a good correlation with model estimated AOD at 0.55 µm (correlation coeff. = 0.85) (Figure 1). However MODIS retrieved mean AOD at 0.55 µm (0.61±0.15) is found to underestimate the model estimated AOD at 0.55 µm (0.75±0.11). Aerosol radiative forcing (ARF) estimated using a discrete ordinate radiative transfer model at surface, TOA and atmosphere and atmospheric heating rate calculated are shown in the Figure 2. The average ARF is estimated to be -51.8±6.2 wm^{-2} at surface level while average TOA forcing is -3.3±1.9 wm^{-2}. The atmospheric heating rate due to aerosols is found to vary from 1.0 to 1.6 K per day.

Details on model estimated aerosol optical properties over the east IGB and its comparison with surface based measurements and satellite retrieved aerosol optical properties will be presented.

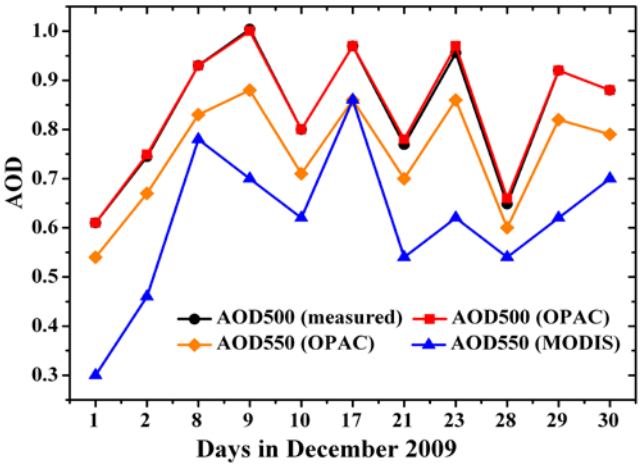

Figure 1. Comparison of measured (0.5 µm), MODIS (0.55 µm) retrieved and model estimated (0.5 and 0.55 µm) AOD values.

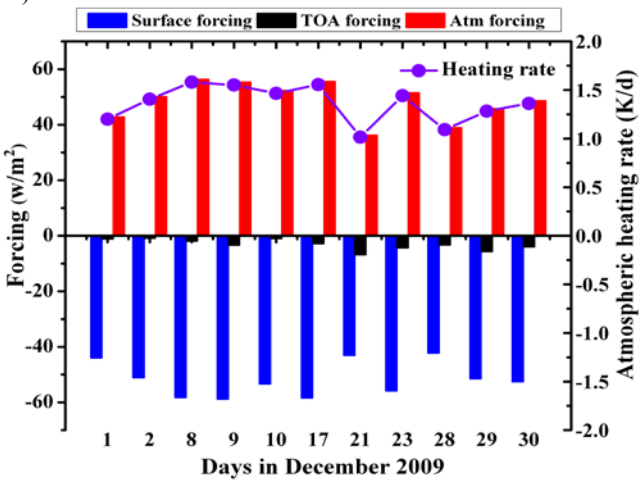

Figure 2. Shortwave direct aerosol radiative forcing (0.25 to 4.00 µm) at the surface, top of the atmosphere and in the atmosphere and atmospheric heating rate.

This work is supported by the Department of Science and Technology, Govt. of India.

Ramanathan, V., *et al*. (2001) *J. Geophys. Res.*, 106, 28,371–28,398.
M. Hess, P. Koepke, and I. Schult. (1998) *Bull. Am. Meteorol. Soc.*, 79, 831–844.
Verma, S. et al. (2007) *J. Geophys. Res.*, 112.

Particle concentrations in Apulia Region PM natural excedancees

M. Amodio, E. Andriani, P.R. Dambruoso, G. de Gennaro, A. Demarinis Loiotile, A. Di Gilio, L. Trizio

Department of Chemistry, University of Bari, via Orabona, 4, 70126, Bari, Italy
Keywords: optical counter, dust, PM10/PM2.5, natural aerosols.
Presenting author email: eleonora.andriani@chimica.uniba.it

Particulate matter (PM) sources and processes have been deeply investigated in order to provide useful information for air quality management policies. In fact, epidemiologic studies suggested the relevant role of ambient PM in contributing to a range of health effects (Nadadur et al., 2009). These effects have mainly been determined by taking into account data obtained by PM mass-measuring instruments but, recently, it has been suggested that adverse health outcomes depend on the number rather than the mass of fine particles (Sager and Castranova, 2009). Moreover, particle number can be considered an important indicator to characterize the most relevant sources affecting PM concentrations.

In this work, the results obtained by applying an integrated system in PM monitoring campaign are shown. The collected data allowed to determine the different origin of high PM events. In particular, the system allowed to characterize the PM_{10} exceedances due to natural events, such as Saharan dust episodes; this information offers the possibility to discount natural exceedances according to the European Commission regulation (2008/50/EC).

The campaign was performed from October 2007 to December 2009 (data coverage: 79%). The monitoring station was located close to Chemistry Department, University of Bari (urban background), Apulia Region (South of Italy). It was equipped with: SWAM Monitors, dual channel system for automatic sampling of PM_{10} and $PM_{2.5}$; OPC monitor, optical particle counter that allows to perform the real-time dimensional characterization of particles with optical diameter greater than 0.3 µm; PBL Mixing Monitor, a sequential automatic system able to estimate the low PBL layers mixing ratio by means of ß activity related to Radon decay products. Some PM samples (PM_{10} and $PM_{2.5}$) collected in this period were characterized in order to determine inorganic components (Cl^-, NO_3^- , SO_4^{2-}, Na^+, NH_4^+, K^+, Mg^{2+}, Ca^{2+}), Polycyclic Aromatic Hydrocarbons (PAHs) and carbonaceous fraction (OC, EC). Finally, daily results of aerosol models (DREAM and NAAPs) and 5-days backward trajectories (HYSPLIT Trajectories) were evaluated to confirm the outbreak from Saharan desert in the Southern regions of Italy.

The PM_{10} excedancees occurred from 28th October to 2nd November are shown in Fig. 1: they were characterized by low $PM_{2.5}/PM_{10}$ ratio and high dispersive atmospheric conditions (Perrino et al., 2009). Information provided by aerosol models and 5-days backward trajectories (data not shown) identified the outbreak from Saharan desert in the Southern regions of Italy. In these days, the OPC data pointed out a significant increase of particles which diameter ranging between 0.94 and 1.54 µm (Fig. 2): this behaviour has been found when African dust contribution occurred at the sampling site and allowed to suggest this range as 'indicator' of Saharan dust intrusion. The chemical characterization of samples (data not shown) allowed to determine that the ionic coarse fraction exceeded the 50% of PM_{10} ionic fraction (its mean contribution is equal to 30%); moreover, a good correlation between PM_{10} calcium and carbonate was observed.

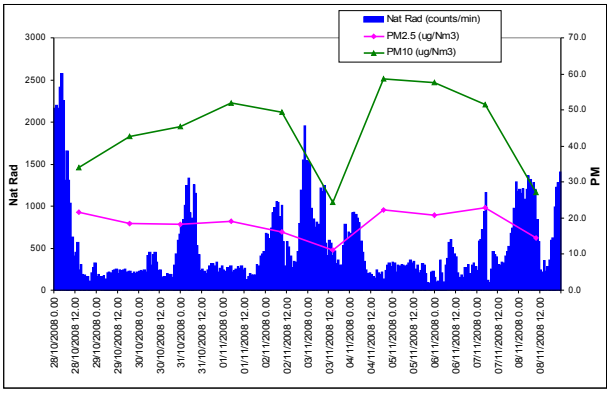

Figure 1. PM_{10}, $PM_{2.5}$ and natural radiation (28 Oct. 2008 - 8 Nov. 2008).

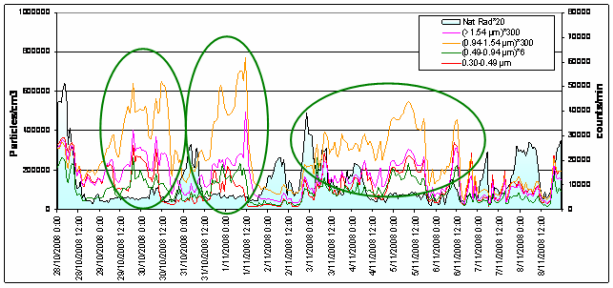

Figure 2. Trends of particles number concentrations and natural radiation counts (28 Oct. 2008 - 8 Nov. 2008).

This work was supported by the Strategic Project PS_122 founded by Apulia Region.

Nadadur, S.S, Miller, C.A., Hopke, P.K, Gordon, T., Vedal, S., Vandenberg, J.J. and Costak, D.L. (2007). *Toxicol. Sci.* **100**, 318-327.

Sager, T.M and Castranova, V. (2009) *Particle and Fibre Toxicology* 2009, **6**, 1-12.

Perrino, C., Canepari, S., Catrambone, M., Dalla Torre, S., Rantica, E., Sargolini, T. (2009). *Atm. Env.* **43**, 4766-4779.

Aerosol optical properties over East Asia: An integrating CMAQ-simulated and satellite-retrieved aerosol data using a data assimilation technique

C.H. Song, R.S. Park and K.M. Han and M.E. Park

Advanced Environmental Monitoring Research Center (ADEMRC), School of Environmental Science and Engineering, Gwangju Institute of Science and Technology (GIST), 1 Oryong dong, Buk-gu, Gwangju 500-712, Republic of Korea

Keywords: AOD, data assimilation, Direct Radiative Forcing, $PM_{2.5}$.
Presenting author email: chsong@gist.ac.kr

For a better estimation of direct radiative forcing by aerosols and particulate pollution (such as $PM_{2.5}$ or PM_{10}) over East Asia, the production of more accurate aerosol optical properties (e.g., Aerosol Optical Depth (AOD), Single Scattering Albedo (SSA), aerosol extinction coefficient (σ_{ext})) is of primary importance. For the purpose of producing the accurate aerosol optical properties, AOD, SSA and σ_{ext} over East Asia were first investigated in this study, based on US EPA Models-3/CMAQ v4.5.1 modeling. The CMAQ model simulations were improved in several ways, compared to the previous study (Song et al., 2008): (1) the wind fields from MM5 simulations were assimilated with QuikSCAT wind data; (2) the emission inventories of INTEX-B (for China and North Korea), REAS (for Japan) and CAPSS (for South Korea) were used for the year 2006 simulations; (3) for the NH_3 and BVOC (Biogenic BVOs) emissions, EDGAR and MOHYCAN emissions were adopted, respectively; (4) monthly variations for the NO_x, NH_3, NMVOCs and SO_2 were applied; (5) for the dust generation and transport in the domain, the operational ADAM (Asian Dust Aerosol Models) was used (Fig. 1); (6) all the MET/CMAQ simulations and emissions were carried out in a fine grid resolution of 30×30 km^2 for the entire year of 2006; (7) 4-D particulate species concentrations obtained from the CMAQ model simulations were converted into the 4-D AOD products, using Malm and Hand (2007)'s algorithm, which is evolved from the previous Malm (1994, 2000)'s algorithms; and (8) finally, the CMAQ-simulated AOD products were assimilated with MODIS-retrieved AOD.

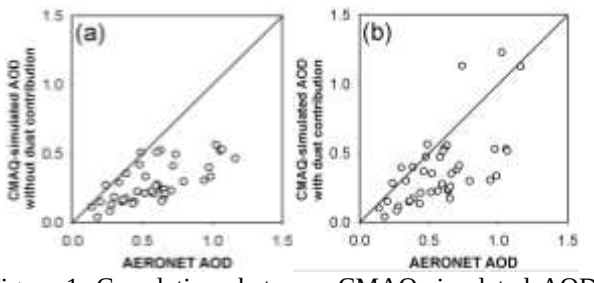

Figure 1. Correlations between CMAQ-simulated AOD and AERONET AOD in spring, 2006: (a) CMAQ-simulated AOD without dust contributions vs. AERONET AOD and (b) CMAQ-simulated AOD with dust contributions vs. AERONET AOD.

The results from the CMAQ model simulations (without assimilation) were improved greatly, compared to the previous study (Song et al., 2008) (e.g., from R=0.48–0.68 to R=0.77–0.89 for four seasons, R is correlation coefficient between CMAQ-simulated and MODIS-retrieved AODs). CMAQ-simulated SSA was also well matched with AERONET SSA, except for those near Honk Kong and Taipei, where biomass burning was strong from Jan. to Apr. It was also found that there were great matches between the vertical profiles of CMAQ-simulated σ_{ext} and LIDAR-derived σ_{ext}. The contributions of sulfate in summer, nitrate in winter, sea-salt in winter and dust in spring were large in East Asia. Especially, the large contribution of nitrate in winter to the AOD distribution over East Asia is remarkable compared to the previous study (Chung et al., 2010). In order to produce more accurate AOD products, the CMAQ-simulated AOD was assimilated with MODIS-retrieved AOD. Both the assimilated and AERONET AODs were better correlated with each other, compared to the correlation between CMAQ-simulated AOD and AERONET AODs (Table. 1). The obvious benefits for this study are that, with the improved aerosol optical properties, particulate pollution or PM forecasting over East Asia (e.g., AOD can be served as a proxy to $PM_{2.5}$) and direct radiative forcing by aerosols can be much better estimated in future.

Table 1. Statistical analysis among CMAQ-simulated and assimilated and AERONET AODs for four seasons, 2006.

AERONET vs.	period	R	RMSE	MNGE	MB	MNB
CMAQ	SPRING	0.59	0.31	45.24	-0.19	-29.88
	SUMMER	0.61	0.30	48.47	-0.13	-22.45
	FALL	0.69	0.24	61.08	-0.10	11.84
	WINTER	0.79	0.15	34.86	-0.07	-4.78
Assimilated	SPRING	0.71	0.20	26.41	-0.09	-8.69
	SUMMER	0.79	0.19	28.10	-0.06	-5.02
	FALL	0.77	0.20	63.15	-0.06	26.05
	WINTER	0.80	0.15	35.81	-0.07	-4.77

This work was supported by the National Research Foundation of Korea (NRF) grant funded by the Korea government (MEST) (No. 2008-0060618).

Chung et al. (2010) *Atmos. Chem. & Phys*., **10**, 6007-6024.
Malm and Hand (2007) *Atmospheric Environment*, **41**, 3407-3427.
Song et al. (2008) *Atmos. Chem. & Phys*., **8**, 6627-6654.

Thursday, September 8, 2011

Session 8P: Poster session B

Electrical Effects

Molecular simulation of dynamic phenomena in complex plasmas

C. Durniak[1], D. Samsonov[1], P. Harvey[1], S. Zhdanov[2] and G. Morfill[2]

[1]Department of Electrical Engineering and Electronics, University of Liverpool, L69 3GJ, United Kingdom
[2]Max-Planck Institute for Extraterrestrial Physics, Garching, 85741, Germany
Keywords: dust, charged particles, interparticle forces, laboratory experiments, numerical simulation, crystallization, electromagnetic waves propagation
email:celine.durniak@liv.ac.uk

Complex (or dusty) plasmas are plasmas enriched with microparticles (or dust grains). The microparticles are charged by the interaction with the electrons and ions, predominantly negatively due to higher mobility of the electrons. They interact with each other electrostatically via a Yukawa potential and often form ordered structures. Similar to colloids, complex plasmas can exist in solid, liquid or gaseous states and exhibit phase transitions.

Complex plasmas can be found in space environments. Examples include stellar clouds, comet tails, and planetary rings. Practical applications include satellite protection from charging and dust impacts, as well as removing abrasive dust on Moon and Mars, where it is charged by the solar radiation and poses threat to spacesuits and machinery. Complex plasmas can also be obtained in laboratory by adding grains to a gas discharge. Dust was observed to spontaneously grow in ultra-clean etching reactors and in fusion devices, where it causes contamination. Applications include growth of fine powders for ceramics and catalysts. Knowledge of the complex plasma properties will help optimize production processes and increase yields. Charged dust in the atmosphere can be responsible for pollution.

As the grains are weakly damped by gas friction and traceable individually, a range of dynamic phenomena such as melting, crystallization, diffusion, linear and nonlinear waves can be observed in complex plasmas at the kinetic level in real time. Therefore complex plasmas are valuable tools to answer fundamental questions about physical properties of matter.

We simulate monolayer complex plasmas consisting of negatively-charged microparticles with the help of molecular dynamics simulations in three dimensions (Durniak, 2010). The code can be used to simulate various particle systems which can be characterised by interaction forces or potentials such as colloids, granular media, plasma doping, ion beams, film growth, ion implantation, etc. The equations of grain motion are solved using a 5th order Runge Kutta method taking into account the motion of the microparticles in a global confining potential as well as the interaction of every grain with each other via a Yukawa potential. The ion-electron plasma is not explicitly included in the equations. The grains are confined more strongly in the vertical direction than in the horizontal ones. Their motions are damped by the neutral gas drag. After seeding the grains randomly the code is run until the equilibrium is reached and a monolayer crystal lattice is formed (Figure 1). Then different excitation forces are applied on the lattice. Structural properties and nonlinear waves characteristics are examined as the pulses propagate across the complex plasmas. The numerical results are validated by comparing them to experiments.

The experiments are performed in a capacitively coupled radio-frequency discharge. Monodisperse plastic micro-spheres are levitated in the sheath above the lower electrode. They are confined radially in a bowl shaped potential and form a monolayer hexagonal lattice. A horizontal thin sheet of laser light illuminates the particles, which are imaged by a digital video camera. Wires are stretched above the lower electrode in order to excite waves.

In this study, we report on experimental observations and numerical simulations of dynamic phenomena in complex plasmas: soliton steepening caused by the propagation in an inhomogeneous medium, collision between two counterpropagating solitons, and defects dynamics interacting with compressional waves.

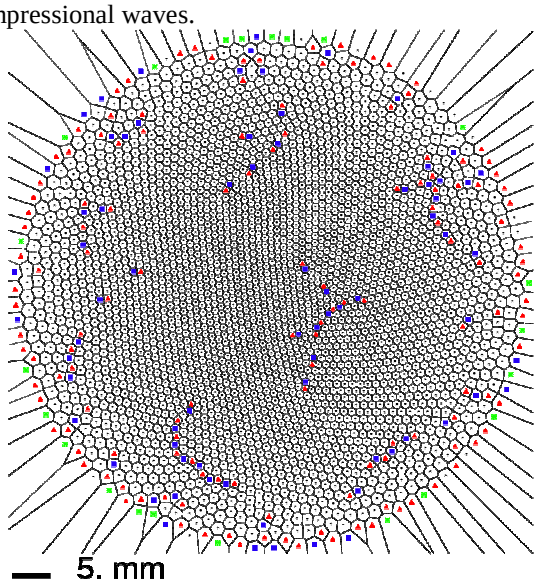

Figure 1. Voronoi map of a lattice obtained numerically with 3000 particles. The crystal defects are marked with ■ (5-fold), ▲ (7-fold), and ✱ (other defects).

This work was supported by the Engineering and Physical Sciences Research Council of the United Kingdom under grants EP/E04526X/1 and EP/G007918.

Durniak C., Samsonov D., Oxtoby N.P., Ralph J.F., and Zhdanov S. (2010) *IEEE Trans. Plasma Science* **38**, 2412-2417.

Measurement and Simulation of Nanoparticle Deposition at Microfibres

A. Hellmann[1], K. Schmidt[1], S. Ripperger[1], M. Berges[2], S. Sticher[2]

[1]Chair of Particle Process Engineering, Kaiserslautern University of Technology, Kaiserslautern, Rhineland-Palatinate, 67663, Germany
[2]Institute for Occupational Safety and Health of the German Social Accident Insurance (IFA), Sankt Augustin, North Rhine-Westphalia, 53757, Germany
Keywords: Filtration, Simulation, Nanoparticles, Deposition, Electrical effects
Presenting author email: kilian.schmidt@mv.uni-kl.de

The demand of nanoobjects with a scale below 100 nm is still rising in industry. It is possible to adjust and improve the physical and chemical properties of a synthetic material for application in nanocomposites, e.g. Such additions are commonly used for all kinds of recent products. Moreover, the filtration of these nanoparticles is an important topic. A special research field is the determination of the nanoparticle filtration efficiency of respiratory protective devices.

An important effect influencing the filtration efficiency is due to electrostatic charges (Rengasamy, 2009). In the field of aerosol filtration, electrostatic effects are decisive in many applications. E.g., electret fibres are used in particle filters for respiratory protection. Measurement and simulation techniques for electrostatic forces respectively charges still need to be investigated.

Measurements and direct numerical simulations of nanoparticle deposition at electret microfibres have been carried out. The general setup for the experiments is shown in figure 1.

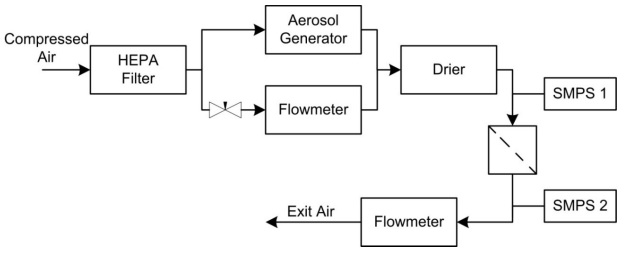

Figure 1. Scheme of the experimental setup.

The measurement and evaluation of the filtration efficiency for nanoparticles is technically extensive, time-consuming and the influence of electrostatic is hard to estimate. Therefore, direct numerical simulation is applied to get deeper insight into the occurring effects. For a 3D model of the distribution of bipolar fibres the airflow and the electric field are computed directly at high resolution as shown in figure 2. The trajectory of each single particle driven by flow, electric field and diffusion is computed, as well as the deposition of the particle at the fibre surface.

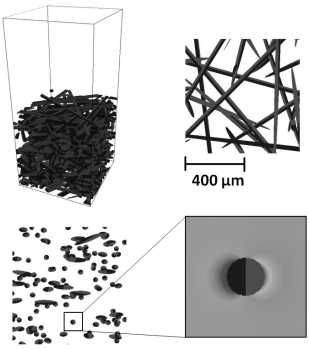

Figure 2 3D model with inflow area (top left), fibres from above (top right), fibres from side (bottom left), electric field computed in the surrounding area of a single bipolar fiber (bottom right).

The results of measurements and simulations will be presented and compared. One of the first results is shown in figure 3.

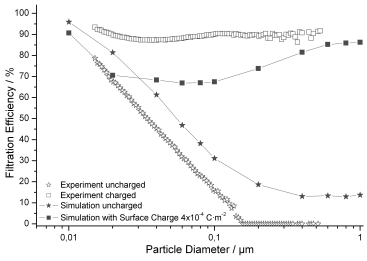

Figure 3 Comparison of measured and simulated fraction filtration efficiencies.

This work is supported by the Institute for Occupational Safety and Health of the German Social Accident Insurance (IFA).

Rengasamy, S., Eimer B. and Shaffer R., *Comparison of Nanoparticle Filtration Performance of NIOSH-approved and CE-Marked Particulate Filtering Facepiece Respirators*, Ann. Occup. Hyg., Vol. 53, No. 2, pp. 117–128, 2009

Hellmann, A., Ripperger, S., Müller, K., Blome, H., Berges, M., *Abscheidung von ultrafeinen Partikeln mittels filtrierenden Halbmasken*, Chemie Ingenieur Technik, Volume 82, Issue 9, pp. 1472–1473, 2010

Schmidt, K., Rief, S., Wiegmann, A., Ripperger, S., *Microstructure Modeling and Simulation of Nanoparticle Deposition*, World Congress on Particle Technology 6, Nürnberg, 2010

Electrostatic charging of spray droplets by addition of ionic compounds

M. Warren and A. K. Ray

Department of Chemical Engineering, University of Kentucky, Lexington, KY 40506, USA
Keywords: droplet charging, particle capture, respirable dust
Presenting author email: akray@engr.uky.edu

Water sprays are routinely used to control respirable dust particles that arise during mining operations. A neutral water droplet captures particles by Brownian diffusion, interception and inertial impaction. The capture efficiency of the droplet due to all these mechanisms combined is always less than unity, and decreases as the particle size decreases. Airborne particles smaller than 2 μm are difficult to remove by uncharged spray droplets. The capture efficiency, however, is significantly greater than unity when the droplet is charged oppositely to the particles (Dhariwal et al. 1993). The particle capture by Coulombic attraction provides an attractive potential for the removal of small particles. Airborne dust particles carry electrostatic charges that arise from triboelectrification or impact charging (Marra and Coury 2000). Our preliminary experiments on bituminous coal dust samples show that coal particles acquire negative charges during dispersion in air. Therefore, removal of these particles can be significantly enhanced by using positively charged spray droplets. We have examined whether water droplets can be positively (or negatively) charged during the spraying process by adding ionic surfactants or other ionic compounds (e.g., ionophores, and ionic liquids) to water.

Experiments were conducted either on highly monodisperse droplets that were generated using a Vibrating Orifice Aerosol Generator (Devarakonda et al. 1998), or on polydisperse droplets generated by an ultrasonic atomizing sprayer (UAS). Droplets were generated from pure deionized water (resistivity =18.2 Mohm-cm) as well as from water containing an ionic surfactant (e.g., sodium lauryl sulfate or coco amine) or an ionic compound (e.g., tridodecylmethylammonium chloride or tridodecylmethylammonium nitrate) at varying concentration levels. After generation droplets were dispersed by an air stream and allowed to fall downward in a cylindrical chamber. Air samples were continuously withdrawn by an Aerodynamic Particle Sizer (APS) and by an electrometer through two side ports on the chamber. The data from the APS were used to determine the size distribution and the number concentration. For a given sample flow rate through the electrometer current readings were analyzed using the APS data to obtain charge on the spray droplets.

Our results show that a water droplet without any additives acquires about 700 elementary positive charges during the spraying process. Addition of an ionic surfactant or an ionic compound can significantly enhance the charge level on a droplet. For example, sodium lauryl sulfate (SDS) can increase the charge level on a droplet by more than three-fold. The droplet charge depends on the concentration of the additive; the charge level increases to a maximum and then decreases as the concentration increases.

The results of this study suggest that water droplets can charged during the spraying process, and the charge level in sprayed droplets, thus particle removal efficiency, can be maximized by adding optimum levels of ionic surfactants or ionic compounds in water.

This work was supported by the National Institute for Occupational Safety and Health (grant # 1R01OH009802-01).

Devarakonda V., Ray, A. K., Kaiser, T. and Schweiger, G. (1998) Aerosol *Sci. Technol.* **28**, 531-547.

Dhariwal V, Hall, P.G. and Ray A. K. (1993) *J. Aerosol Sci.* **24,** 197-209.

Marra W. D. and Coury J. R. (2000) *Brazilian J. Chem. Eng.* **17,** 39—50.

Corona ion production and aerosol charging downwind of high voltage power lines

J.C. Matthews, A.J. Buckley, M.D. Wright and D.L. Henshaw

School of Physics, University of Bristol, Bristol, BS9 1TL, UK
Keywords: Measurements, Corona discharge, Air ions, Atmospheric aerosols.
Presenting author email: j.c.matthews@bris.ac.uk

High voltage power lines are known to produce ions when the electric field surrounding the cable is sufficiently high to cause corona avalanching. Elevated numbers of these corona ions can be produced if there are protrusions on the cable surface. Predominantly uni-polar clouds of space charge can be detected as changes in the Earth's vertical potential gradient (PG).

Proximity to high voltage power lines has been linked with a higher incidence of childhood leukaemia (Draper 2005). The attachment of corona ions to pollutant aerosols has been hypothesised to increase their deposition in the human lung, leading to adverse health effects (Henshaw, 2002). PG, ion mobility spectra and the charge state of aerosols upwind and downwind of power lines have been measured to assist in testing this hypothesis.

Electric field mills can be used to measure the PG upwind and downwind of HV power lines (Fews *et al* 2002). Long term measurements of PG fluctuations at a fixed site near to two high voltage power lines have shown that the electrical environment several hundred metres downwind can be affected (Matthews *et al* 2010). An increase in the distributions of the mean and standard deviation of PG when the monitoring station was downwind of a power line indicated that there was an elevation of space charge. The conditions found for highest corona emission were overnight, at high humidity, during rainfall and at high wind speeds (Matthews 2010).

Ion mobility spectra near to HV power lines were measured aspirated condenser ion mobility spectrometers (ACIMS) (Fews *et al* 2005). Of 37 measurements upwind and downwind of power lines, only 7 did not show an increase in ion concentration downwind. Though predominantly there was a positive ion excess, bipolar and negative corona were also measured on different occasions (Buckley 2009).

The mean space charge density at ground level from the total small ion concentration recorded by the ACIMS was compared to the mean PG recorded at the same time by electric field mills. 8 upwind and 8 downwind measurements were compared. No consistent relationship was found between space charge density and PG either upwind or downwind of the power lines. At 5 downwind sites, both positive PG and net ion concentration were found. At 2 sites downwind of the same power line, PG measured negative charges overhead while the small ion concentration showed a positive excess. 1 site showed a positive PG but an excess of negative small ions.

Two possible causes of the discrepancy between PG measurements and small ion concentration at ground level are removal of ions by attachment to aerosols and ions being carried at height above the measurement site. Charged aerosols and ions at height would still affect PG as measured by field mills but do not contribute to ground level ion concentrations.

The charge distribution of aerosols downwind of power lines can estimated using the technique described in Buckley *et al* (2008). Figure 1 shows the mean charge per particle downwind of 4 lines.

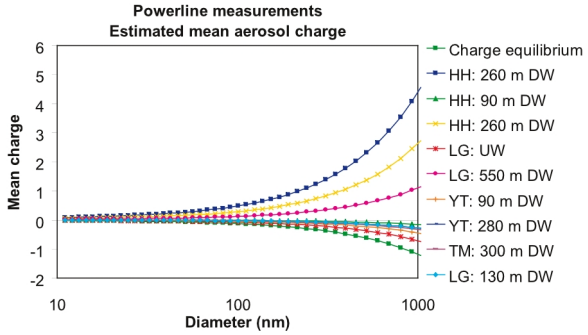

Figure 1. The charging of aerosols in the vicinity of high voltage power lines, from Buckley (2009). Sites investigated were at Ham Hill (HH), Lower Godney (LG), Yatton (YT) and Tormarton (TM) near Bristol, UK.

Measurements of PG, ion concentration and aerosol charge state downwind of high voltage power lines show that there is significant corona production near to some high voltage power lines, which can alter the charge state of aerosol particles.

This work was supported by the Children with Leukaemia, registered charity number 298405 (UK).

Draper, G., Vincent, T., Kroll, M. E. and Swanson, J. (2005). *BMJ* **330**(7503), 1290-1292.

Henshaw, D. L. (2002) *Med. Hyp.* **59**(1), 39-51.

Fews, A. P., Holden, N. K., Keitch, P. A. and Henshaw, D. L. (2002) *Atmos. Res.* **63**(3-4), 271-289.

Fews, A. P., Holden, N. K., Keitch, P. A. and Henshaw, D. L. (2005) *Atmos. Res.* **76**, 29-48.

Matthews, J. C., Ward, J. P., Keitch, P. A. and Henshaw, D. L. *Atmos. Environ.***44,** 5093-5100.

Matthews, J. C. (2010). PhD thesis, University of Bristol, Department of Physics.

Buckley, A. J., Wright, M. D. and Henshaw, D. L (2008) *Aerosol Sci. Tech.* **42**(12), 1042-1051.

Buckley, A. J. 2009. PhD thesis, University of Bristol, Department of Physics.

Effect on relative humidity on the electric field strength established, negative air ion concentration produced and aerosol removal by an air ionizer

K.-P. Yu[1], S.-C. Yang[1] and W.-M. G. Lee[2]

[1]Institute of Environmental and Occupational Health Sciences, National Yang-Ming University, Taipei, 11221, Taiwan

[2]Graduate Institute of Environmental Engineering, National Taiwan University, Taipei, 10673, Taiwan

Keywords: negative air ion concentration, electric field strength, relative humidity, removal efficiency.

Presenting author email: kpyu@ym.edu.tw

Our previous studies showed that negative air ions (NAI) can remove submicron airborne particles efficiently by means of electrostatic force (Wu *et al*, 2006, Yu *et al*, 2008). The cluster ions formed by NAI can attach on particles by means of diffusion charging. The terminal velocity (V_E) of the charged particles within the range of Stokes's Law in an electronic field is (Hinds, 1999):

$$V_E = EZ = \frac{EC_c kT}{6\pi\mu K_E e}\ln\left[1+\frac{\pi K_E d_p c_{i\,mean} e^2 N_i t}{2kT}\right] \quad (1)$$

where, E is the electric field strength; Z is the electric mobility of particles; n is number of charges acquired by a particle; d_p is the particle diameter; k is the Boltzmann constant (1.38×10^{-23} J/K); T is the absolute temperature; K_E is a constant of proportionality (9.0×10^{9} N m^2/C^2); e is the electronic charge (1.6×10^{-19} C); N_i is the NAI concentration; $c_{i\,mean}$ is mean thermal speed of ions (240 m/s at standard conditions); t is the time duration. C_c is the Cunningham slip correction factor, μ is the viscosity of the air. We estimated V_E by measuring the values of E, Ni and d_p. The NAI concentration and the electric field strength generated by the negative air ionizer are distance-dependent [Fig. 1(a) and 1(b)]. The electric field strength is linear proportional to the logarithm of the NAI concentration [Fig. 1(c)]. The net displacement of a particle due to NAI under higher relative humidity (RH) is larger than that under lower RH as demonstrated in Table 1. This may result from that in the presence of water molecules, the air ions can form hydrates (cluster ions) with higher stability (Bracken, 1987). This result agrees with the measurement of NAI concentration and particle (secondary organic aerosol) removal.

Table 1. Comparison of particle net displacement due to NAI, Brownian motion and gravity

d_p (nm)	Net displacement of a particle in one minute (m)				
	NAI (X_{NAI})[a] 25 cm away from air ionizer			Brownian motion[b] (X_{BM})	Gravity[c] (X_{grav})
	RH82%	RH50%	RH18%		
25	7.08×10^{-2}	6.98×10^{-2}	4.31×10^{-2}	6.62×10^{-4}	1.39×10^{-5}
50	4.83×10^{-2}	4.75×10^{-2}	3.01×10^{-2}	3.52×10^{-4}	3.14×10^{-5}
75	3.96×10^{-2}	3.88×10^{-2}	2.49×10^{-2}	2.48×10^{-4}	5.26×10^{-5}
100	3.49×10^{-2}	3.42×10^{-2}	2.21×10^{-2}	1.95×10^{-4}	7.73×10^{-5}
125	3.20×10^{-2}	3.13×10^{-2}	2.03×10^{-2}	1.63×10^{-4}	1.06×10^{-4}
150	3.00×10^{-2}	2.94×10^{-2}	1.92×10^{-2}	1.42×10^{-4}	1.38×10^{-4}

[a] $X_{NAI}=V_{E(\text{eqn.1})}\times t$; [b] $X_{BM}=\sqrt{2Dt}$, $D=kTC_c/3\pi\eta d_p$

[c] $X_{grav}=\frac{\rho_p d_p{}^2 g C_c t}{18\eta}$ ρ_p : particle density, g : acceleration of gravity

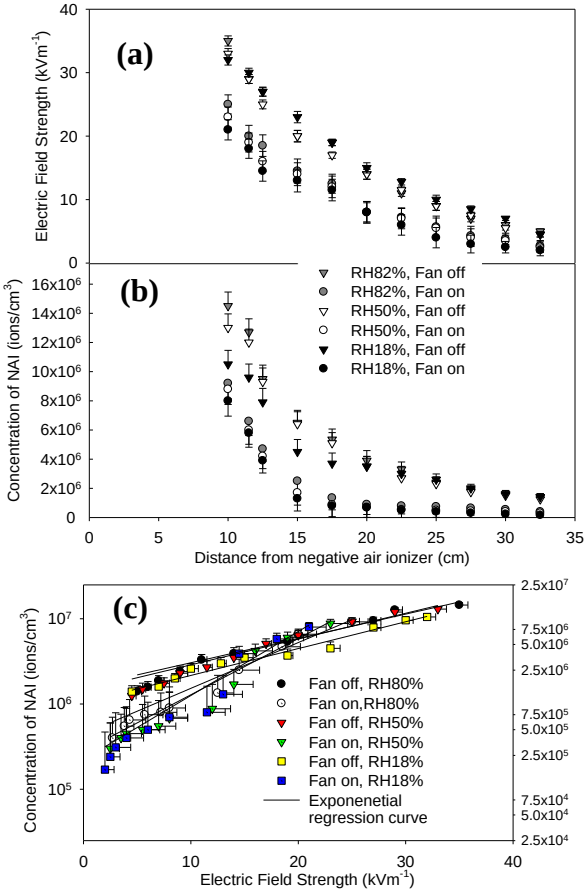

Fig. 1 The distance-dependent (a) electric field strength and (b) NAI concentration; (c) the liner relationship between the logarithm of NAI concentration and electric field strength

This work was supported by the National Science Council of Taiwan (NSC 99-2211-E- 010-005-) and a grant from the Ministry of Education, Aim for the Top University Plan.

Bracken, T.D. (1987) Small air ion properties, In: Charry, J.M. and Kavet, R.I. (eds) *Air ions: physical and biological aspects*, CRC Press.

Hinds, W. (1999) *Aerosol Technology*, John Wiley & Sons, Inc

Wu, C.-C., Lee, G.W.-M., Cheng, P., Yang, S., Yu, K.-P. (2006) *Journal of Aerosol Science*, 37, 616-630

Yu, K.-P., Lee, G.W.-M., Lin, S.-Y., Huang, C.P. (2008) *Journal of Aerosol Science*, 79, 377-392

Variations in electrical and meteorological parameters of the atmosphere in conditions of fog

P.M. Nagorsky[1] and E.M. Baranchikova[2]

[1]Department of Physic of Climatic System, Institute of Monitoring Climatic and Ecological Systems SB RAS, Tomsk, 634055, Russia
[2]Radiophysics Department, Tomsk State University, Tomsk, 634050, Russia
Keywords: fog, atmospheric electricity, quasi-periodic variations.
Presenting author email: npm_sta@mail.ru

The purpose of the paper is to study the dynamics and patterns of variations of atmospheric-electrical, meteorological and optical parameters of the atmospheric boundary layer in conditions promoting fog formation.

Basing on the data of field measurements in the spring-autumn period of 2006-2010 the comparative analysis of the temporal variability of the intensity of atmospheric electric field, basic meteorological elements and characteristics of turbulence with tact in 1 minute in conditions of fog occurrence was carried out. We revealed a pronounced positive correlation between variations in the electric field intensity and relative humidity: with the increase in humidity the field intensity increases as well (Phalagov, 2009). A typical example of the electric field dynamics ***E*** and temperature and characteristic of turbulence during fog formation is shown in fig. 1.

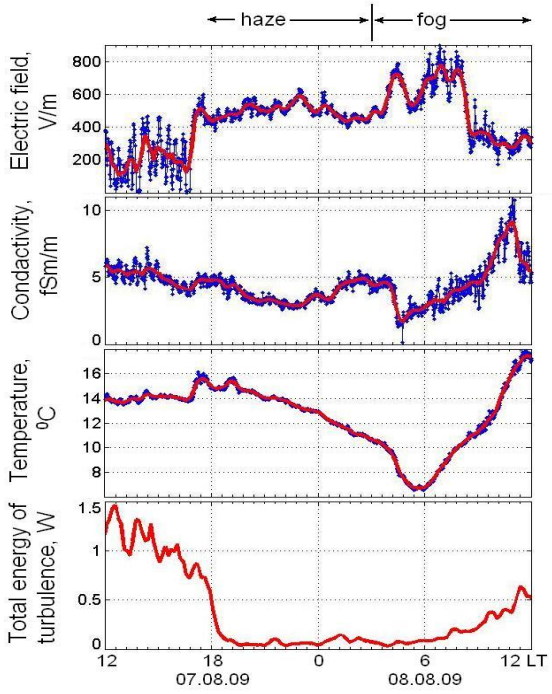

Figure 1. Variations of the meteorological elements during fog.

Since the growth of the electric field is uniquely associated with a decrease in the concentration of light ions in the air, it can be assumed that the formation of fog begins to increase in the concentration of the smallest particles, which still do not participate in the process of light scattering, but already actively serve as a sink for ions.

In turn, the fine particles got charged as a result of ion diffusion actively grow via coagulation processes, and being in the field of the increased humidity they transit to the range of optically active particles. This significantly increases the turbidity of the atmosphere.

It is suggested that the growth of the electric field before formation of fog can be a harbinger of it, which is particularly limited the visibility conditions.

The electric field in the surface atmosphere in the presence of fog undergoes quasi-periodic variations, which amplitude is much greater than the variation of the electric field during «fine weather». Quasi-periodic variations of the electric field appear in the form of oscillation trains in the range of periods.

Wavelet analysis of 17 cases of field *E* registration during summer-autumn fogs allowed to reveal the features of occurrence frequency of quasi-periodic variations depending on the period. In the spectrum of periods T the 4 peaks are distinguished: 10-15 min 60-70 min 110-140 min and 210-300 min. The duration of treatment plots in all cases was 900 minutes. The histogram of registration frequency of *N* variations is represented in figure 2 in depending on the period. Heterogeneous in space can be taken a source of quasi-wave processes the fog density.

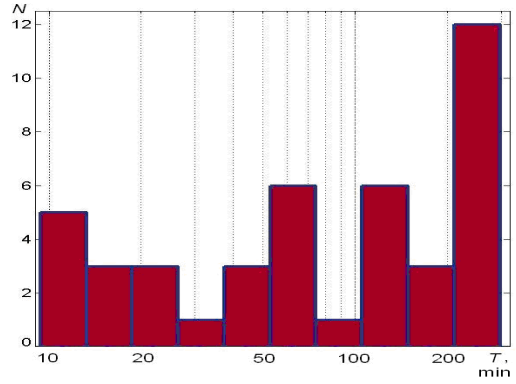

Figure 2. The occurrence frequency of variations of N electric field with period T.

This work was supported by SB RAS, program № VII.63.1.1 and FTP, grant № 02.740.11.0738.

Phalagov Yu., Ippolitov I., and Nagorskiy P. (2009) *Atmospheric and Oceanic Optic.* **22.** No 1, pp.113-117.

A simplified procedure for particle charge distribution measurements and its application to the characterization of the annual DBD aerosol neutralizer

Wild, Markus[1], Meyer, Jörg[1] and Kasper, Gerhard[1]

[1]Karlsruhe Institute for Technology KIT, IMVM, Strasse am Forum 8, 76139 Karlsruhe, Germany

Keywords: Measurement (characterization), Dielectric Barrier Discharge; charged particles; TDMA.
Presenting author email: markus.wild@kit.edu

The annular dielectric barrier discharge aerosol neutralizer is a device designed to impose a Boltzmann charge distribution to airborne particles by electrostatic means. The device's performance in neutralizing aerosols is compared to a radioactive ^{85}Kr source. Amongst others, the particle charge distributions of sodium chloride particles ranging between 27-200 nm are investigated. The method of choice is a Tandem-DMA setup. The basic task is to determine the number concentration of differently charged particle fractions. Usually a rather complex curve fitting method is applied to evaluate the obtained data, see e.g. Stolzenburg and McMurry (1998). The evaluation process can be vastly simplified if some restrictions concerning the conduct of the experimental procedure are observed.

Therefore, a method to determine the aerosol concentration within a well defined interval of electrical mobilities – such as distinct peaks in a mobility spectrum illustrated in Figure 1– directly from a continuous DMA scan is described.

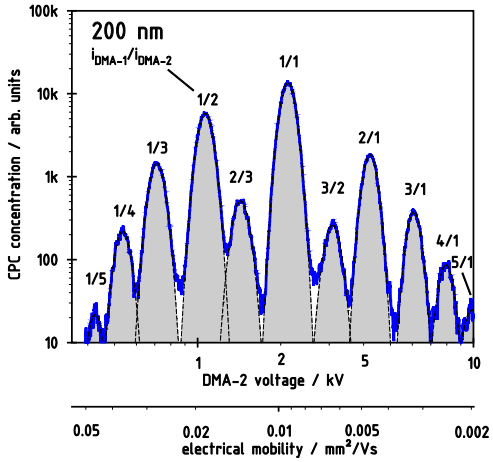

Figure 1. mobility spectrum of a pre-classified (200nm) and neutralized sodium chloride aerosol measured by a CPC after DMA-2 in a TDMA setup. i indicates the state of charge in DMA-1 and DMA-2, respectively.

The method is based essentially on moving the transfer function across the spectrum at such a rate that the time window during which particles of an arbitrary mobility can pass through the DMA remains constant during the scan. This implies a specific ramp function for the scan voltage, which we derive, thereby establishing a direct and simple link between the cumulative number of particles exiting the DMA while scanning across a peak, and the concentration enclosed within that mobility window at the inlet (see Figure 2). The method is an implicit part of the theoretical framework described by Wang and Flagan (1990). However, by relaxing the goal of deriving a complete size distribution in favour of the lesser requirement of measuring only the total concentration within certain, well defined bounds of mobility, one gains accuracy, sensitivity, and last not least convenience because there is no need for extensive post-processing of the data. The method is particularly suitable for measuring aerosol charging probabilities with distinct peaks in the mobility spectrum.

While the charged fractions of laboratory generated aerosols in the range of 27 to 200 nm are investigated with a TDMA set-up and the mentioned data evaluation procedure, the neutral fraction is measured by a separate measurement.

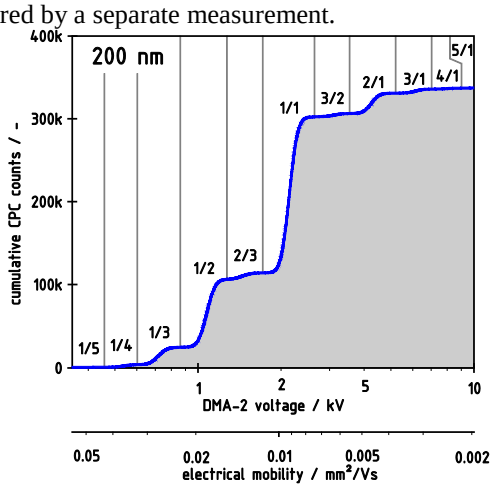

Figure 2. cumulative particle counts of the aerosol introduced in Fig. 1 when performing an up-scan using a logarithmic voltage ramp

The method was used to determine the performance of the annual Dielectric Barrier Discharge (aDBD) aerosol neutralizer in comparison to a common ^{85}Kr β-source. The obtained charge distributions resembled each other very well. The aDBD proofed to provide a promising alternative to the use of radioactive material and its well-known disadvantages in aerosol measurement technology.

This work was supported by the German Science Foundation (DFG).

Stolzenburg, M.R. and McMurry, P.H. (1998). *TDMAFIT user's manual*. PTL publications **No. 653**

Wang, S.C. and Flagan, R.C. (1990). *Scanning Electrical Mobility Spectrometer*. Aerosol Science and Technology **13** (2): 230-240.

Thursday, September 8, 2011

Session 8P: Poster session B

Instrumentation

The comparison of bioaerosol disinfection efficiencies of several new commercial air purifiers manufactured in Russia

S.A. Kiselev, A.S. Safatov, Yu.V. Marchenko, A.N. Sergeev, Ar.A. Sergeev, Al.A. Sergeev, E.K. Emelyanova, V.Yu. Marchenko, G.A. Buryak

Federal State Research Institution State Research Center of Virology and Biotechnology "Vector", Novosibirsk Region, 630559, Koltsovo, Russia
Keywords: air indoor quality, bioaerosols, bacteria, viruses.
Presenting author email: safatov@vector.nsc.ru

Air purifiers/disinfectors (APDs) are intended for reduction of indoor concentration of aerosol containing microorganisms and, consequently, the probability of aerogenic infection of humans, animals and birds.

Filtration and disinfection efficiencies of APDs functioning in recirculation mode were determined as the ratio of weight-average and biological aerosol concentration at the inlet and outlet of the functioning device. The studies were performed at an aerosol test bench for testing APDs with airflow up to 400 m^3/hour like that described in (Delaby *et al.,* 2008).

Aerosols containing a physical label (uranin) and avian influenza A virus subtype H5N1 (AIV) A/Chicken/Suzdalka/Nov-11/2005 or strain or *Mycobacterium smegmatis* (MS) B-836 strain (imitator of mycobacterium tuberculosis) were generated to test the devices. The mass median diameter of particles was 1 - 2 μm. The experiments were conducted at the temperature of 25 – 34 °C and relative humidity of 30 – 45 %. At fixed airflow (Q), the mean values of efficiencies (E) and their 95 % confidence intervals (I) were determined by the results of Experiments 4 - 6 for different APDs.

The following results can be obtained using the methodology for determining the efficiencies of air filtration and disinfection by devices of recirculation type developed at FSRI SRC VB Vector Rospotrebnadzor:

1. Determination of filtration, disinfection and inactivation efficiencies for bioaerosol with definite parameters of dispersion composition containing a microbiological test object using an APD of recirculation type at a preset airflow in one run. If necessary, the corresponding efficiencies can be determined for individual sections of the APD.

2. Determination of filtration, disinfection and inactivation efficiencies for individual aerosol fractions.

The results of the carried out tests (Table 1) provided an objective evaluation of efficiencies of air purification and disinfection by APDs of recirculation type at a preset airflow in one run, which does not depend on the peculiarities of the rooms where the tests are performed. The work results promote a more efficient and justified application of air purifiers-disinfectors to improve the human environment and to prevent aerogenic infections.

The conducted tests with air disinfectors of different Russian manufacturers demonstrate their high efficiency.

The work was supported by the Federal Target Program (Contract # 02.518.11.7139).

Delaby S., Draghi M., Petit P., Gehin E. and Robine E. (2008) *Proc. European Aerosol Conference, Thessaloniki.* Abstract T02A096P.

Table 1. Efficiencies of filtration and disinfection of air containing bioaerosol by APDs in one run.

Device (manufacturer)	Microorganism in aerosol	Airflow (Q), m^3/hour	Aerosol filtration efficiency by mass ($\overline{Э_{m,\Gamma}} \pm I_{0,95,\overline{Э_{m,\Gamma}}}$), %	Air disinfection efficiency ($\overline{Э_{b,\Gamma}} \pm I_{0,95,\overline{Э_{b,\Gamma}}}$), %
«Potok 150-M-01» (JSC RPC "Potok Inter", Moscow)	AIV	135	98.3 ± 0.5	99.63 ± 0.04
«RIV-3-V» (JSC Novosibirsk poultry factory)	AIV	32.5	31.6 ± 2.2	99.988 ± 0.003
"Tion A55 T500-S" (JSC "AeroService", Novosibirsk region)	MS	250	99.919 ± 0.006	99.986 ± 0.002
"Luch-120" (FSUE SPA "Luch", Novosibirsk)	MS	200	99.990 ± 0.001	99.998 ± 0.001

A miniaturised Airborne Particle Classifier (APC)

C. J. Stopford, P. H. Kaye, E. Hirst, Z. Ulanowski, R.S. Greenaway, and W.R. Stanley.

Centre for Atmospheric & Instrumentation Research, University of Hertfordshire, Hatfield, U.K.
Keywords: atmospheric particle, ice crystal, spatial light scattering, in situ measurement.
Presenting author email: c.stopford@herts.ac.uk

The single greatest source of uncertainty in the estimates of climate sensitivity to either natural or man-made changes continues to be clouds (IPCC, 2007). Much of this uncertainty arises from the lack of information relating to the properties of smaller cloud particles (droplets, ice crystals) and aerosol. In the past, the University of Hertfordshire has developed several types of aircraft instrument (Kaye, 1998; Hirst *et al*, 2001; Kaye *et al*, 2008; Cotton *et al, 2010*) based on spatial light scattering technologies (so-called SID probes) that are able to monitor and differentiate between these particle types *in situ*. These probes have been procured by meteorological research organisations in the UK, USA, and Europe.

However, the SID probes require a PMS-canister mounting and this severely restricts the number of aircraft on which they can be flown. We have therefore developed a proof-of-concept laser scattering instrument, the Airborne Particle Classifier (Figure 1), which is, in effect, a miniaturised SID probe, designed to count, size, and classify (on the basis of morphology) micrometer sized particles at rates of several thousand per second. The APC is intended for a Rosemount or similar aircraft fitting and could potentially be carried by a UAV. Beyond this, it could also find wider application in general aerosol monitoring in areas of environmental health, pollution monitoring, source apportionment etc., where knowledge of the aerosol's constituent particle types is essential.

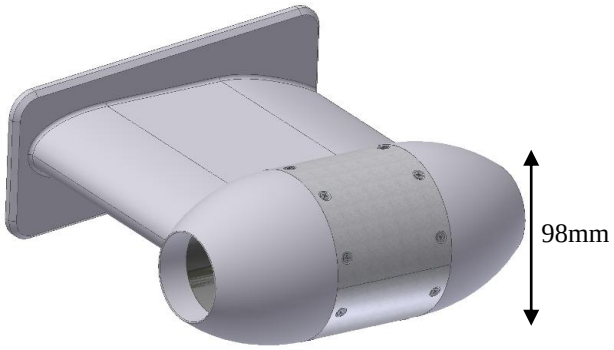

Figure 1. Prototype Airborne Particle Classifier.

A laser orthogonal to the flow of air illuminates individual particles as they pass through a sensing volume defined optically by a combination of custom photodiode and elliptical reflector. This triggers a second, high-power pulsed laser to illuminate each particle, the scattering from which is captured on two parallel linear 512-pixel CMOS detector arrays. The azimuthal distribution light scattered by the particle is compressed in one dimension via a cylindrical lens, such that a greater range of scattering angles is captured by the CMOS arrays. The minimum particle size for measurable scattering pattern recording is approximately 2-3µm. The data from the arrays are saved to an external single board computer for post-flight analysis. Figure 2 illustrates the CMOS array output data recorded for different particle morphologies, from columnar to spherical. For illustration only, the relative positions of the two CMOS arrays, shown in red and green, are indicated on 2D SID3 probe scattering pattern images recorded from similar particle types.

Analytical processing methods are currently being developed to determine metrics of particle size, morphological class, and number concentration from the recorded APC data.

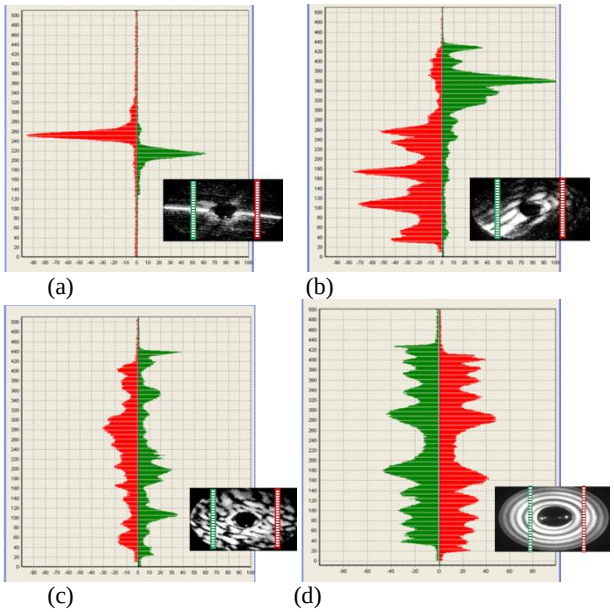

Figure 2. Examples of APC CMOS-array data for various particle morphologies: (a) columnar, (b) plate-like, (c) irregular cubic, (d) droplet. Y-axis represents array 0-512 pixels; x-axis represents light intensity for each array. (Image inserts are from SID3 probe data for similar particle types).

Acknowledgement: This research is supported by the Natural Environment Research Council grant NE/H002316/1.

Cotton R., *et al.* (2010) *J. Atmos. Ocean. Tech.*, 27, Issue 2 (February), 290–303.
Hirst E., *et al.* (2001) Atmos. Env. **35**, 1, 33-47, 2001.
IPCC Fourth Assessment Report -WG1 (Cambridge, 2007).
Kaye, P.H. (1998) *Meas. Sci. and Tech.* **9,** 2, 141-149.
Kaye, P.H. *et al* (2008) *Opt. Lett.* **33**, 1545-1547

A new analyser for continuous measurement of the concentration and composition of aerosols

Y. Mizuno, M. Fujiwara and H. Kume

[1]HORIBA Ltd., Kyoto, 601-8510, Japan
[2]National Institute for Environmental Studies, Tsukuba, 305-8506, Japan
Keywords: PM2.5, chemical composition
Presenting author email: hkume@nies.go.jp

Aerosols discharged from factories and automobiles are a major cause of air pollution in metropolitan areas as well as in areas along arterial roads. In Japan, the ambient air quality standards apply to suspended particulate matter (SPM: particles with a diameter less than 10 μm). In addition to the SPM regulation, PM2.5 regulation has been started in September 2009. There are more than 1,500 continuous air pollution monitoring stations in Japan. This monitoring alone, however, does not provide us with sufficient information for the identification of the sources of aerosol emissions or an understanding of aerosol dynamics in the environment. Additionally, it is very important to obtain the chemical information in order to determine the source contribution. As a result, there is an urgent need of the equipment which has combined the properties of multifunction analysis and mobility.

In response to this situation, we are currently developing an apparatus that can simultaneously analyse the concentration and composition of aerosols. This apparatus features an original filter, an X-ray tube, and an electron gun to success qualitative or quantitative analysis. The X-ray tube and electron gun are small in size and energy-efficient to operate. The X-ray tube is used for component analysis by the X-ray fluorescence method, and the electron gun is used for measurement of aerosol concentrations by the electron transmission method. While the conventional monitoring stations measure only the aerosol concentrations, this apparatus is intended to identify the sources of aerosol emission

Measuring chemical components of aerosols requires thin high-purity filters. A glass fiber filter commonly used contains various contaminants, making a qualitative or quantitative analysis of the chemical components very difficult.

Recently, we have developed an original membrane filter based on a polytetrafluoroethylene (PTFE) film with new filter structure (HORIBA, Ltd., TFH-01 roll type) . TFH-01 has the following features:

1) The structure consisting mainly of PTFE and non-woven fabric.
2) Less hygroscopicity than glass fiber filters and less electrostatic charge than a filter consisting of only PTFE.
3) Smaller unit weight than that of glass fiber filters. This has improved mass-detection sensitivity by approximately five times compared to β -ray attenuation mass monitors (HORIBA, Ltd., APDA-370).
4) Ultra low chemical background.

XRF spectra of a glass fiber filter and TFH-01 filter obtained by EDX are shown in fig. 1. This result demonstrates that TFH-01 filter is almost free from contamination.

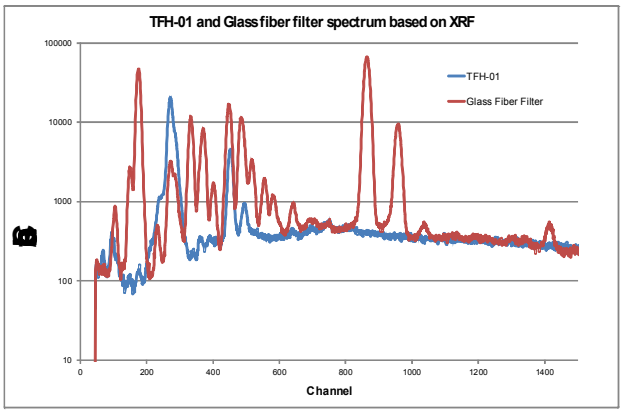

Figure 1. Comparison of XRF spectra between a glass fiber filter and TFH-01.

We have been checking the total performance of the analyser using a test bench shown in fig. 2.

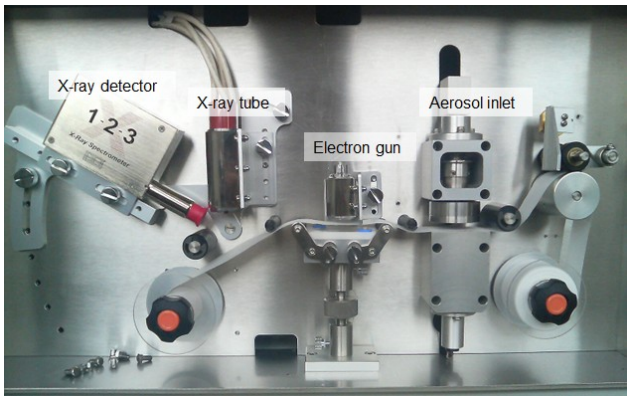

Figure 2. A laboratory bench upon which the performance of the analyser is tested

The calibration of an aerosol dilution system

L. Škrabalová[1, 2] and V. Ždímal[1]

[1]Laboratory of Aerosol Chemistry and Physics, Institute of Chemical Process Fundamentals, Academy of Sciences of the Czech Republic, Rozvojová 135 Prague, 165 02, Czech Republic
[2]Department of Physical Chemistry, Faculty of Science, Charles University in Prague, Hlavova 8 Prague, 128 43, Czech Republic
Keywords: aerosol diluter, dilution ratio, calibration.
Presenting author email: skrabalova@icpf.cas.cz

When sampling aerosols it is often necessary to reduce number concentration of aerosol by dilution. Dilution enables us to suppress condensation of semivolatile gaseous components, quench coagulation of the sample, or bring its concentration to the instrument's range of operation. The choice of a suitable diluter depends on required dilution ratio, sample flow rate, particle losses in the diluter and other parameters. (Baron & Willeke, 2001). A variety of diluters and a description of a diluter designed specially for high dilution and transport of coagulating ultrafine aerosol is described e.g. by Brockmann *et al* (1984).

The aerosol dilution system presented in this paper has been built in the mechanical workshop of the Institute of Chemical Process Fundamentals. It has been designed in order to dilute highly concentrated aerosol samples formed by aerosol generators. The aim was to build a diluter offering a wide range of dilution ratios achieved in one dilution step. Because the diluter was intended for operation in front of the Scanning Mobility Particle Sizer, another requirement was the option to recover the original particle size distribution. In order to do that, the dilution ratio has to be known even as a function of particle size.

The diluter's design is based on a well-known principle. The aerosol flow is divided into two parts. One enters a thin capillary and the other is led through a bypass provided with a high efficiency particulate filter and a flow-controlling valve. Particle concentration of the capillary flow remains unchanged whereas the HEPA filter removes nearly all particles from the bypassing flowrate. The two flows are then merged together in a mixing chamber. The dilution ratio is given by the ratio of the capillary and bypassing flows. When the dividing and mixing parts are properly designed, it is possible to predict the dilution ratio from the pressure drop across the capillary by using Hagen–Poiseuille equation. This paper describes the measurement procedure and consequent data evaluation of dilution ratios.

In order to calibrate the diluter and determine the dilution ratios as a function of particle size, 6 stainless steel capillaries with inner diameters 0.04, 0.03, 0.02, 0.01, 0.007 and 0.005 inches were used. The polydisperse aerosol was generated by nebulizing the ammonium sulphate solution in the aerosol generator AGK-2000 (Palas GmbH, Germany). A monodisperse fraction of the aerosol was selected using an electrostatic classifier provided with a long differential mobility analyzer (EC3080+DMA 3081, TSI Inc., USA).

Concentrations of the aerosol upstream and downstream of the diluter were recorded using two condensation particle counters (UCPC 3025A, TSI Inc., USA). The measurement procedure was designed in such a way that the slight differences in performance of the two counters were taken into account. The dilution ratio was determined for each of the six capillaries, and for 9 size fractions of the aerosol: 20, 35, 50, 70, 100, 140, 200, 280 and 400 nm.

An example of comparison of dilution ratios observed experimentally and predicted by theory is presented in Figure 1 as a function of particle diameter. It is obvious that for capillaries with diameters of 0,02 and 0,04 inches the agreement of the experimental values with theory is excellent. The capillary with the diameter of 0,005 inches shows deviations from theory at larger particle sizes caused probably by particle losses. It has been found that the diluter offers dilution ratios in the overall range between 4:1 and 10^4:1.

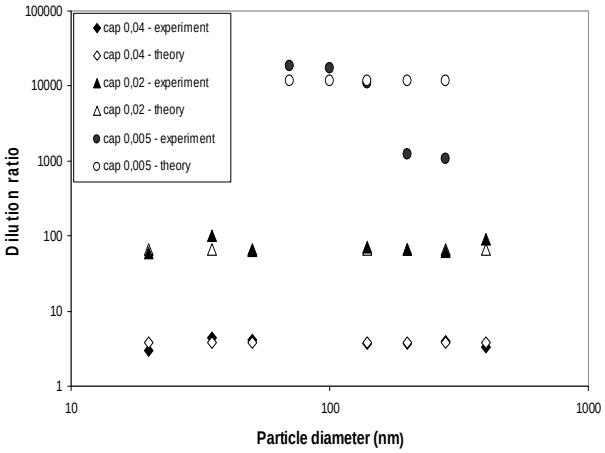

Figure 1. A comparison between dilution ratios determined experimentally and predicted theoretically.

The authors gratefully acknowledge a support of this work by the MPO TIP project No. FR – TI1/548.

Baron, P. A., & Willeke, K. (2001). *Aerosol Measurement: Principles, Techniques and Aplications.* New York, USA: John Wiley and Sons, Inc.

Brockmann, J. E., Liu, B. Y. H. and Mc Murry, P. H. (1984). *Aerosol Sci Technol.* **3,** 441-451.

Aerosol measurements of nanometer particles, obtained by spark generator

V.A.Zagaynov[1], Yu.G.Biryukov[1], I.E.Agranovski[1], O.V.Karpov[2], D.M.Balakhanov[2], E.V.Lesnikov[2], A.A. Lushnikov[1]

[1]Karpov Institute of Chemical Physics, Vorontsovo Pole, 10, 105064 Moscow, Russia
[2]VNIIFTRI, Mendeleevo, Moscow region, Russia

Keywords: diffusion, electrical mobility, particle size distribution.

Presenting author email: zagaynov@cc.nifhi.ac.ru

There are some complications in measurements of aerosol particles in nanometer size range. First of all every instrument has threshold sensitivity, and all particles of less size will not be counted. At the same time during particle generation great number of particles may be beyond this threshold. In this case solution may be found by optimal selection of the measuring equipment.

In nanometer particle size range there are two instruments, which may be chosen for such measurements: differential mobility analyzer (DMA) (Hagwood et al, 1999) and diffusion aerosol spectrometer (DAS) (Julanov et al., 2002). Both these instruments have their preferences and shortcomings. Conversion of measured data by DMA into particle size distribution has condition number lower as compared to corresponding number for DAS based measurements. It means that DMA measurements may be considered as more reliable. At the same time aerosol charging efficiency accross the particle size range of several nanometers is very low leading towards increase in measurement errors.

Here we compare measurements made by these two instruments. The measurements were made by DMA and DAS simultaneously for particles, produced by a spark generator. Advantages of this generator are mainly related to stability of particle size distribution and concentration over long time (several hours) if parameters of generation are not changed. Obviously, using air as a gas carrier enables to produce nanoparticles of metal oxides, whilst utilization of inert gases (for example nitrogen) leads towards production of particles containing only metals. In most of cases particles have spherical shape and narrow size distribution.

For our experiments, a molybdenum wire was heated in the air stream flowing around it to produce MoO particles of spherical shape in concentration of up to 10^7 particles per cubic centimeter if the air carrier. Some portion of this stream was diluted to the concentration around 2×10^4 cm^{-1} and sampled simultaneously by DAS and DMA

Fig. 1 shows he results of measurements of particle size spectrum as acquired by DAS and DMA. As is clearly seen in the figure, the results obtained by both instruments are in very close agreement with each other. The averaged particle radius measured by DAS was 14.5 nm and by DMA – 14.75 nm.

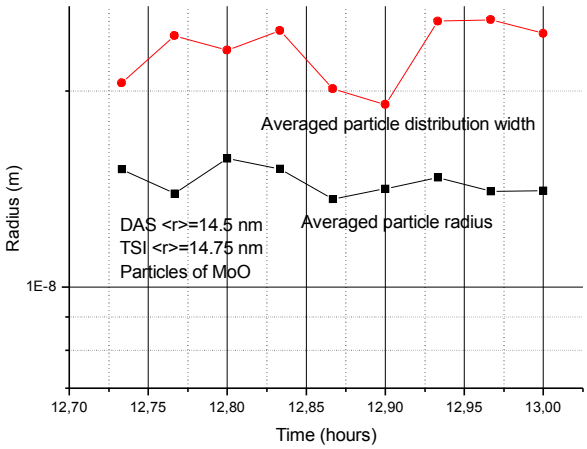

Figure 1. Measurements of particle size distribution made by DAS and DMA.

The source of the discrepancy between readings of DAS and DMA is twofold – low charging efficiency of small aerosol particles and different particle sensitivity of different enlarging vapors. In spite of different measurement methods and reconstruction of particle size distributions from measured data the results of the measurements are in close agreement. The measurements were undertaken at Karpov Institute (DAS and DMA), VNIIFTRI (DMA), and Griffith University (DMA). For all measurements, particles were produced by the same spark generator.

Hagwood, C., Sivathanu, Y., Mulhholland, G. (1999) The DMA transfer function with Brownian motion a trajectory - Monte-Carlo approach. *Aerosol Science and Technology*, 30, 40-61.

Julanov, Yu.V., Lushnikov, A.A., Zagaynov, V.A. (2002) Diffusion aerosol spectrometer *Atmospheric Research*, v.62, n.3-4, 295 – 302.

Intercomparison of scatter and backscatter integrating nephelometers Characteristics and angular sensitivity correction

T. Müller[1], M. Laborde[2,3], G. Kassel[2] and A. Wiedensohler[1]

[1] Leibniz Institute for Tropospheric Research, Leipzig, Germany
[2] Ecotech Pty Ltd, Knoxfield, Australia
[3] Paul Scherrer Institute, Villigen, Switzerland
Keywords: instrumentation/physical char., scattering coefficient, air quality, monitoring
Presenting author email: thomas.mueller@tropos.de

Integrating nephelometers measure a value close to the light scattering coefficient of airborne particles. Different models of nephelometers have been used for many years for monitoring and research applications. We present here an intercomparison of two nephelometers and corrections for the angular non-idealities. The instruments are the Aurora3000 (Ecotech Pty, Ltd, Knoxfield, Australia) and the TSI3563 (TSI Inc, St. Paul, MN, USA), which are the only commercially available three-wavelength scatter and backscatter integrating nephelometers.

Main differences between these nephelometers are the size of the sensing volumes, the light sources and the design of the backscatter shutter. The sensing volume of Aurora is about 30% smaller compared to TSI3565. The light source of TSI 3565 is an incandescent lamp, whereas the light source of Aurora 3000 is based on LEDs. The backscatter shutters of TSI 3565 and the Aurora3000 are a continuously rotating and a periodically moving shutter blade, repectively.

The illumination function of light sources and the design of cell, backscatter shutter and the detection optics deviate from ideal nephelometers leading to a non-ideal angular sensitivity function. Angular intensity distributions of the light source were measured with a goniometer setup. Results are given in Müller et al. (2010). To correct for the angular non-idealities, a particle size and refractive index dependent correction factor has to be considered. Correction factors for a log-normal particle number size distribution with a refractive index of 1.53-0.01i were calculated with Mie-theory. Correction factors for total scattering and backscattering are shown in Figure 1.

Another correcting method was found by Anderson and Ogren (1998). They found a parameterization of correction factors as function of the Ångström exponent α with $\alpha=\ln(\sigma(\lambda_1)/\sigma(\lambda_1))/\ln(\lambda_2/\lambda_1)$, where $\sigma(\lambda)$ is the uncorrected scattering coefficient.. Parameterizations were developed for sub- und supermicrometer particles with real parts of refractive indices between 1.40 and 1.52. The imaginary part of refractive index is between 0 and 0.001. Following the approach of Anderson and Ogren (1998), parameterization for sub-micrometer particles were derived. E.g. for the green wavelengths of the nephelometers the parameterization for TSI3563 was found to be $C_{ts}=1.152-0.044\cdot\alpha$, what is close to the parameterization given in Anderson and Ogren (1998). For the Aurora3000, the parameterization was determined to be $C_{ts}=1.2065-0.0788\cdot\alpha$.

Scattering coefficients of ambient air were measurements with TSI3563 and Aurora3000 for a period of 46 days. A correlation between TSI3565 and Aurora3000 adjusted to the wavelength 525 nm using the Ångström-equation are shown in Figure 2. The slope for total scattering is about 1.01 with and 0.98 without angular sensitivity correction. For backscattering, the slopes with and without correction are 1.05 and 1.03, respectively.

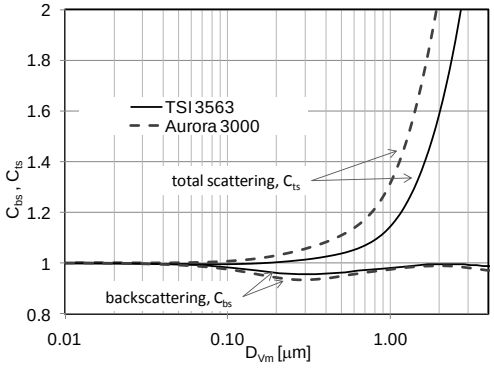

Figure 1. Correction factors for total (C_{ts}) and backscattering (C_{bs}) versus the volume median diameter.

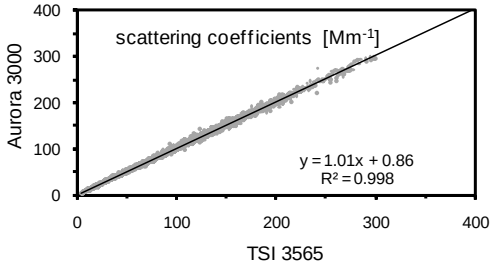

Figure 2. Correlation of total scattering coefficients between with the TSI3565 and Aurora 3000.

Anderson et al. (1996) Performance characteristics of a high-sensitivity, three-wavelength, total scatter/ backscatter nephelometer. *J. Atmos. Oceanic Technol.* 13:967-986.

Anderson and Ogren (1998) Determining aerosol radiative properties using the TSI 3563 integrating nephelometer. *Aerosol Sci. Tech.* 29:57-69.

Müller, T., Laborde, M., Kassell, G. and Wiedensohler, A. Design and performance of a three-wavelength LED-based total scatter and backscatter integrating nephelometer. *submitted to AMTD* (2010).

Jet interaction in multi – nozzle inertial impactors

Estíbaliz García[1], Francisco J. Romay[2], J.F. Cambra[1], J.A. Legarreta[1] and David Y. H. Pui[3]
[1]Department of Chemical and Environmental Engineering, University of Basque Country, Bilbao, 48013, Spain
[2]MSP Corporation, Shoreview, Minnesota, 55126, United States of America
[3]Particle Technology Laboratory, University of Minnesota, 55455, United States of America
Keywords: Cascade Impactor, Collection Efficiency
Presenting author email: estibaliz.garcia@ehu.es

Multi-nozzle cascade impactors are used instead of single-nozzle impactors in order to get the desired air flowrate and cutpoint at a reasonable Reynolds number through each nozzle.

Careful analysis of deposits from multiple–nozzle impactors shows particle collection directly underneath the nozzles where the jets directly impinge upon the impaction plate (i.e. primary deposits). However, secondary deposits are also commonly seen as straight lines directly between adjacent nozzles, both on the impaction plate and on the backside of the nozzle plate, or as a "halo" around the primary deposits (Rocklage J.M., 2007)

The objective of this work was to determine the mechanisms that cause secondary deposits in multiple-nozzle impactors, and to evaluate the effect of these deposits on the collection efficiency curves. With this information it is intended to establish design criteria for the optimum distance between nozzles to minimize the negative effects of the secondary deposits.

Experimental work was conducted on a cluster of three equally-spaced round nozzles (tapered inlet), with four different nozzle spacings: 2.5X, 4X, 6X and 8X (where X is the nozzle diameter), and at three Reynolds numbers: 500, 1500 and 2400. The jet-to-plate distance to nozzle-diameter ratio was one (i.e. S/W=1).

For the experimental tests, perfectly monodisperse oleic acid particles tagged with a fluorescent uranine tracer were used as the challenge aerosol. These particles were generated by a TSI 3450 Vibrating Orifice Aerosol Generator (VOAG), diluted with clean, dry air to prevent coagulation, neutralized by a Kr-85 source, and followed by a sharp-cut, multiplet reduction impactor (Siegford et al., 1994).

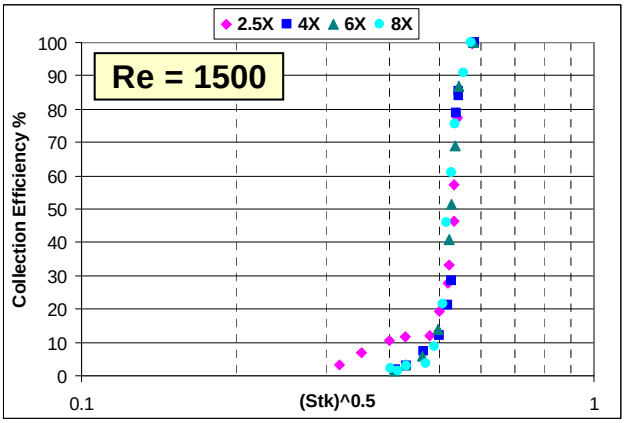

Figure 1: Collection efficiency curves Re = 1500

Figures 1 and 2 show the experimentally determined collection efficiency curves at Reynolds numbers of 1500 and 2400, and for all the nozzle spacings tested.

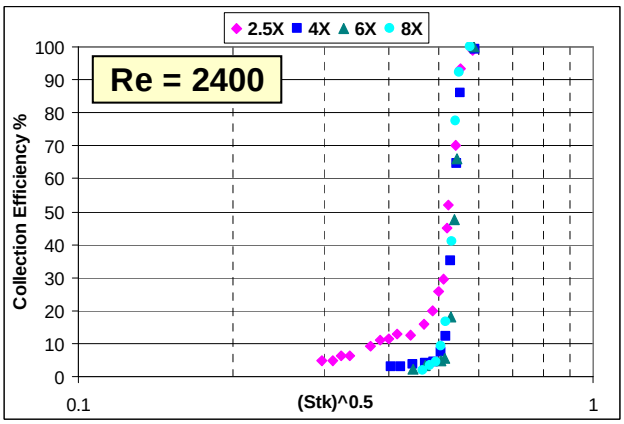

Figure 2: Collection efficiency curves Re = 2400

The experimental results at the lowest nozzle spacing (i.e. 2.5X) show that significant secondary deposits (visible as straight lines) start to appear before the primary deposits are seen. These secondary deposits are responsible for the long tail at low particle diameters of the collection efficiency curve shown both in Figures 1 and 2. These deposits are formed due the fluid flow-particle interaction between the nozzle jets as they approach the impaction plate. Secondary deposits were not observed at Re = 500.

The collections efficiency curves at nozzle spacings of 4X, 6X and 8X are nearly identical and show no effect of the secondary deposits on the typical sigmoidal curves, even though these deposits were visible up to 6X at Reynolds number of 1500 and up to 8X at Reynolds number of 2400.

Rocklage, J.M. (2007). Master's Thesis, Mechanical Engineering, University of Minnesota.

Siegford, K.L., Marple, V.A., and Rubow, K.L. (1994), *J. Aerosol Sci.* 25:113-114.

Level of light absorption coefficient at an engineering classroom

Jeonghoon Lee[1]
[1]School of Mechanical Engineering, Korea University of Technology and Education, Cheonan, South Korea
Keywords: absorption, maap, aerosol.
Presenting author email: jlee@kut.ac.kr

In the atmospheric science community, light absorption is a very important parameter that can affect the estimation of radiative forcing by changing the single scattering albedo. Especially, black carbon increases the level of light absorption. Methane, tropospheric ozone and black carbon aerosol are thought to be key contributors to global warming, augmenting the radiative forcing of carbon dioxide by 65% (Penner *et al.*, 2010). Black carbon is generated from various sources: Exhaust manifold of transportation vehicles, power plant, biomass burning and so forth (Bond *et al.*, 2004). The measurement of absorption coefficient in ambient aerosol has been performed for a long time. However, the absorption coefficient at a classroom has not been measured. In this study, we investigated the light absorption at an engineering classroom and compared the relevant values to the absorption coefficient presented in literatures.

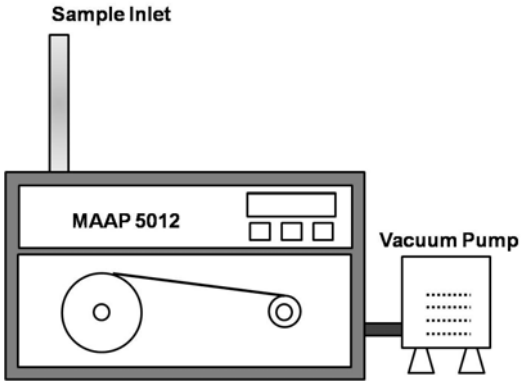

Figure 1. The schematic of Multi Angle Absorption Photometer (MAAP)

Figure 1 shows the experimental apparatus used in the present study. A Multi Angle Absorption Photometer (MAAP) was used to measure light absorption coefficient inside an engineering classroom where students intermittently operates several instruments and facilities such as a thermal radiation experiment, heat exchanger and small wind tunnel. MAAP (Thermo Scientific 5012) is a typical filter based absorption measurement instrument similar to a Particle Soot Absorption Photometer (PSAP) which measures light transmittance through a filter after depositing particle aerosols. The PSAP and the MAAP can be operated unmanned. During the last five years, PSAP has an issue associated with the scattering effect from the filter substrates. However, MAAP is known to show better performance than PSAP in that MAAP corrects the artifacts of scattering effect arisen from the filter substrates.

Shown in Figure 2 are aerosol absorption coefficients measured for 24 hours at the engineering classroom. There was no class and no operation of instruments/facilities for 20 hours during the absorption measurement period. Surprisingly, absorption was measured to be larger than 1 g/m^3, which was somewhat larger than we expected. As far as the authors know, it is for the first time that we measured the absorption coefficient at a classroom where engineering practices are periodically exercised. We will discuss the implication of the absorption coefficients that were detected at a classroom as opposed to in ambient environment.

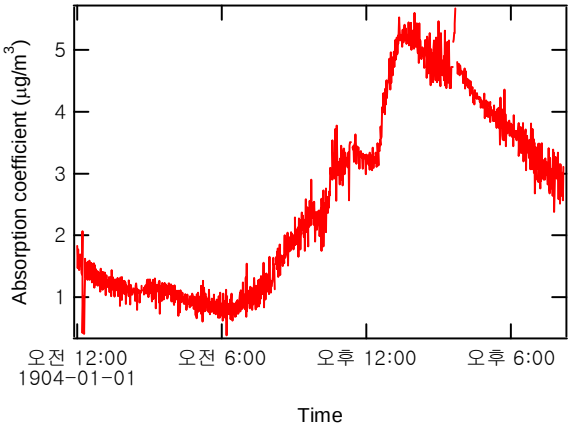

Figure 2. Absorption data for 20 hours measured at a classroom.

This work was supported by the National Research Foundation of Korea Grant funded by the Korea government (MEST) (No. 2010-0006116).

Bond, T.C., D. G. Streets, K. F. Yarber, S. M. Nelson, J.-H. Woo, and Z. Klimont (2004) *J. Geophysics Lett* **109**, D14203.

Penner, J. E., Prather, M. J., Isaksen, I. S. A., Fuglestvedt, J. S., Klimont, Z., and Stevenson, D. S. (2010) *Nature Geoscience* **3**, 587-588.

.

Determining the transfer function of a Very Long DMA using polymer size standards

J. Uin and E. Tamm
Laboratory of Environmental Physics, Institute of Physics, University of Tartu, Tartu, Estonia
Keywords: DMA, Transfer function, Aerosol spectrometry, Aerosol instrumentation.
Presenting author email: janek.uin@ut.ee

The aim of this work is to measure experimentally the transfer function (TF) of a Very Long DMA (working length 1.2 m) (Peil and Tamm, 1984). It is an experimental continuation of the previous theoretical work where possible distortions to the DMA TF were examined (Tamm and Uin, 2009).

There are different ways for measuring the TF of a DMA. One well-known method uses a setup where two identical unknown DMAs or a known DMA and a different unknown DMA are used in tandem (Stratmann *et al.*, 1997). Another method uses three different unknown DMAs in pairs (Martinsson *et al.*, 2001). These are proven methods, but in addition to the DMA under investigation, they require the presence of another, identical or at least similarly capable DMA. As the above-mentioned Very Long DMA is rather unique, these methods are not suitable.

A way for determining the DMA TF, which does not require multiple DMAs, is to measure a highly monodisperse aerosol. From the definition of the TF, it can be seen that when scanning over the aerosol distribution with a DMA, the measurement result is a convolution between the aerosol distribution and the DMA TF. If the aerosol distribution is very narrow (much narrower than the DMA TF), then the measurement result can be approximated as a convolution between the TF and a delta function, which is equal to the TF itself (change in the absolute width of the TF is small enough to be ignored). Here, only the half-width of the TF is examined and the height (and area) of the TF are not investigated, as the total aerosol concentration is, in this case, practically impossible to determine.

To experimentally measure the TF half-width of the instrument in question, a suspension of polymer microspheres with a mean diameter of 1 (0.994) µm and standard deviation of 0.010 µm was atomized to produce a monodisperse test aerosol. The obtained aerosol was then dried in a silica gel drier and neutralized using a ^{239}Pu neutralizer. The mobility distribution of the test aerosol was then measured using a Very Long Vienna-type DMA and a CPC. A triangular function (Stolzenburg, 1988) was fitted to the measured distribution of singly charged particles (singly and multiply charged particles were easily distinguished, i.e. there was no overlapping) and the relative half-width β of the function was obtained (Figure 1). Ideally (determined by the DMA airflows) $\beta = 0.100$, but in this case, measurement results gave $\beta = 0.170$.

The wider TF is most likely caused by the less than perfect geometry of the DMA (and also possibly by the non-uniformity of the aerosol flow). Namely, as the DMA electrodes are comprised of several sections, some parts of the electrodes may not be entirely concentric. And according to numerical modelling, this can cause a widening of the DMA TF (Tamm and Uin, 2009).

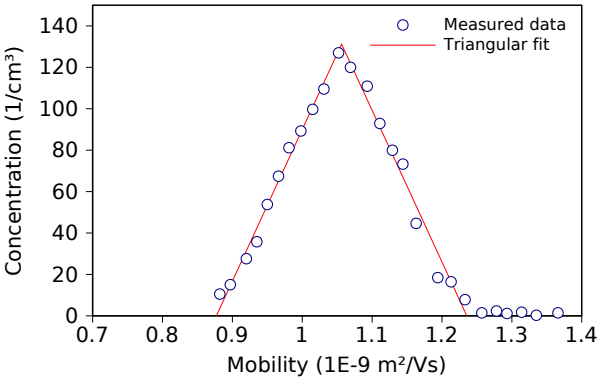

Figure 1: Experimentally found DMA TF and triangular fit ($R^2 = 0.990$).

As stated above, the height of the DMA TF was not investigated, Therefore, the vertical axis in Figure 1 shows the aerosol concentration as measured by the CPC. This is presented to illustrate the relatively low particle concentrations available, which can make the described experiments difficult. Attempts were also made to use aerosols with 7.9 µm mean diameter, as the DMA used is capable of measuring particles with diameter up to 10 µm. However, while the solid content of the 7.9 µm suspension is approximately 10 times higher than that of the 1 µm suspension, the volume of a particle is 10^3 times higher, which gives much lower number concentrations and makes the particle detection/counting even more difficult.

This work was supported by the Estonian Science Foundation under grant no. 8779 and by the Estonian Research Council Targeted Financing Project SF0180043s08.

Martinsson, B. G., Karlsson, M. N. A. and Frank, G. (2001), Aerosol Sci. Technol., **35**, 815-823

Peil, I., Tamm, E. (1984), Acta et Comm. Univ. Tartuensis, **669**, 44-52. (In Russian, summary in English.)

Stolzenburg, M.R. (1988), Ph.D. thesis, University of Minnesota.

Stratmann, F., Kauffeldt, T., Hummes, D. and Fissan, H. (1997), Aerosol Sci. Technol., **26**, 368-383.

Tamm, E., Uin, J. (2009), Abstract T096A02, EAC 2009.

Size selected nanoparticle quantification of deposited aerosol by GIXRF

H. Bresch[1], F. Reinhardt[2], U. Waldschläger[3], B. Pollakowski [2], B. Beckhoff[2], S. Seeger[1]

[1]BAM Federal Institute for Materials Research and Testing, Unter den Eichen 87, 12200, Berlin, Germany
[2]Physikalisch-Technische Bundesanstalt (PTB), Abbestr. 2-12, 10587 Berlin, Germany
[3]Bruker Nano GmbH, Schwarzschildstr. 12, 12489 Berlin, Germany

Keywords: XRF, Aerosol characterization, Instrumentation, Elemental composition, Particle size distribution.
Presenting author email: harald.bresch@bam.de

Cascade impactors are widely used instruments in chemical aerosol characterization. There are several techniques for the chemical analysis of aerosol samples from cascade stages , e.g. EDX, GC-MS, Raman, XRF, etc., but none of them measures particle size and size distributions. Particle size resolved quantitative chemical analysis either requires the additional use of particle classifiers (e.g. SMPS) or the quantitative analysis of the deposits on cascade stages. The latter implies sample strengths above the lower threshold of the respective analytical method. Many environmental indoor or outdoor aerosols are polydisperse and consist of several chemical substances in different quantities. The quantification of one given chemical substance or a given element, hidden in the background of all the other contributions, and its assignment to a particle size class is therefore not always easy to achieve with the methods available.

Here we present a novel approach to use Gracing Incidence X-Ray Fluorescence Analysis (GIXRF) based on fundamental constants in order to determine size, quantity and chemistry of small nanoparticulate aerosol fractions within a poly-disperse aerosol.

The sampling was done with an electrostatic aerosol sampler (TSI 3089), using one square inch clean Si-wafers. We prepared monodisperse $ZnTiO_3$, TiO_2 nanoaerosol by use of an atomizer (Topas ATM 220) either with and without size selection by the Classifier and also a technical produced example of a polydisperse indoor aerosol.

For the experiments we used the PTB/BAM X-ray beamlines at BESSY II in Berlin at different excitation energies. High spectral resolution enables studies of the chemical state of the elements (Reinhardt et al., 2009) while the low divergence of the beam allows for dedicated geometries, such as a grazing incidence setup. Based on total-reflection X-ray fluorescence analysis (TXRF), which offers very low quantitative detection limits in the pg to fg range (Beckhoff et al., 2007), in GIXRF the incident angle of the excitation radiation is tuned between 0° and about threefold the critical angle of total-reflection. Thereby the position and strength of the maxima of the X-ray standing wave field (XSW) above the surface is modified. Particles with a given diameter deposited on a flat substrate will be exposed to excitation radiation of varying intensity depending on the angle of incidence and the particle size.

Hence the measured X-ray fluorescence signal contains information on the atomic composition of the particles and information on the deposited size fraction.

Based on fundamental constants we could use GIXRF measurements at BESSY II beamlines to determine the total amount of deposited nanoparticles of one size on a flat surface. Besides the absolute determination of the deposited nanoparticles, the measurement is independent of small contaminations of the substrate with other materials or polydisperse nanoparticles. This makes the GIXRF method a unique and very promising method for nanoparticle characterization, especially regarding poydisperse and inhomogenic environmental aerosols.

The financial support of this research activity within the frame of the ProFiT project “Nanoparticle X-ray Analysis” supported by the Investitionsbank Berlin (No. 10141100) is gratefully acknowledged.

F. Reinhardt, B. Beckhoff, H. Eba, B. Kanngießer, M. Kolbe, M. Mizusawa, M. Müller, B. Pollakowski, K. Sakurai, and G. Ulm (2009), *Anal. Chem*. **81**, 1770

B. Beckhoff, R. Fliegauf, M. Kolbe, M. Müller, J. Weser, and G. Ulm (2007), *Anal. Chem*. **79**, 7873

A chamber for aerosol instrument comparisons

P.G.Quincey[1], T.D.Gardiner[1], F.Innocenti[1] , M. Coleman[1] and J.Tompkins[1]

[1] Analytical Science Division, National Physical Laboratory, Teddington, Middlesex, TW11 0LW, UK

Keywords: aerosol instrumentation, measurements.
Presenting author email: paul.quincey@npl.co.uk

Methods and facilities for calibrating aerosol instrumentation are not new, but it is only in recent years that systematic efforts have been made to harmonise such measurements, though initiatives such as EUSAAR in the ambient aerosol area (feeding into EMEP) and the Particle Measurement Programme (PMP) for vehicle emissions. International standardisation is currently taking place through CEN and ISO. National Measurement Institutes (NMIs) are starting to provide traceability for number concentration measurements, in the same way as for most other measurements, with the first NMI comparison for aerosols taking place at METAS in Switzerland in 2008 (Schlatter, 2009).

While most calibrations are expected to take place in dedicated rigs using pipework rather than a chamber, there is an important role for chambers in allowing the simultaneous comparison of many instruments presented with a variety of aerosols, possibly changing in time, especially when the instruments have different operating principles such as optical as well as extractive. The primary aim of such a chamber is to provide a controlled homogeneous aerosol volume with many equivalent sampling points.

A chamber has been designed and built specifically for this purpose. The basic design is a cylindrical chamber with great care taken to introduce the aerosol uniformly throughout the central section of the cylinder, with a clean air sheath at the walls. The layout is illustrated in Figure 1.

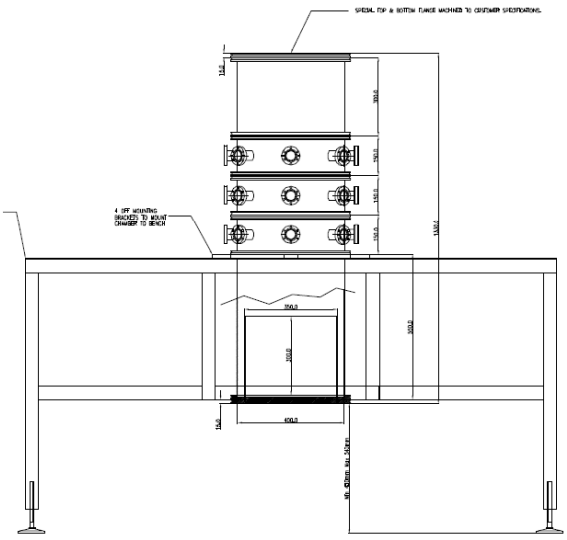

Figure 1. Design of chamber

The basic parameters of the chamber are given in Table 1. Several different aerosol sources can be connected to the chamber. For example, the laboratory includes a CAST soot generator, atomisers, electrospray, and fluidised bed aerosol generators.

Diameter	35 cm
Sampling ports	3 series of 8, at 45° intervals
Aerosol flow rate	40 l/min
Aerosol velocity	0.7 cm/s

Table 1. Basic chamber parameters.

Measurements of aerosol uniformity within the chamber have been made. Measurements from a complete traverse of a diameter are given in Figure 2, showing a variation of around ±1%. Similar variations were found between a set of 8 ports around a circumference. Results from a comparison involving several laboratories will be presented.

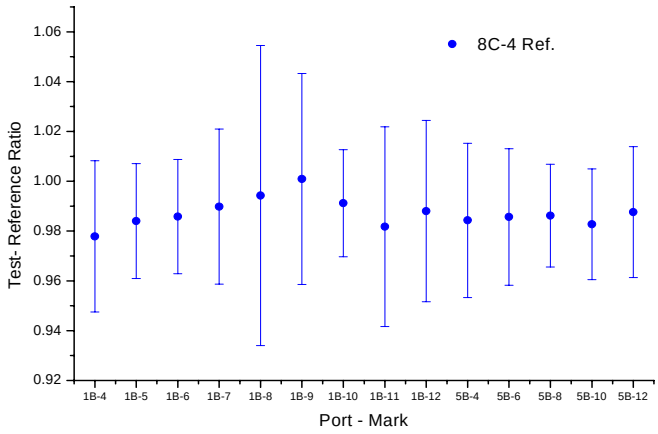

Figure 2. Radial uniformity of 55 nm soot particle concentration. The points span the central 30 cm of the chamber.

This work was supported by the UK's National Measurement Office Chemical and Biological Metrology Programme. The contribution of R.J.J.Gilham to the design and construction of the chamber is gratefully acknowledged.

Schlatter J, (2009) *EURAMET Project 1027 Comparison of nanoparticle number concentration and size distribution* available through http://www.euramet.org/

Measurement of sub-micron aerosols dry deposition velocity on a heterogeneous field by eddy correlation using an Electrical Low Pressure Impactor and a Condensation Particle Counter.

G.Bacon[1], A. Donateo[2], D.Contini[2] , D.Maro[1] and F.Belosi[3]

[1]IRSN (Institute of Radioprotection and Nuclear Safety), Cherbourg-Octeville, 50100, France
[2] ISAC (Institute of Atmospheric Sciences and Climate), National Research Council (CNR), 73100, Lecce, Italy
[3] ISAC (Institute of Atmospheric Sciences and Climate), National Research Council (CNR), 40129 Bologna, Italy

Keywords: deposition velocity, eddy covariance fluxes, ELPI, CPC.
Presenting author email: guillaume.bacon@irsn.fr

Introduction

To understand and quantify the impact of a chronic or accidental atmospheric release of pollutant in the form of aerosols in the environment, it's essential to know the transfer velocity of aerosols air at the surface. Dry deposition velocity (V_d) is obtained by the ratio of flux deposited and the aerosol concentration measured in air.
The purpose of this work is to make an intercomparison of dry deposition velocity obtained using an Electrical Low Pressure Impactor (ELPI, Dekati, Inc) and a Condensation Particle Counter (CPC, Grimm 5.403).

Material and method

Dry deposition flux can be calculated from the covariance between fluctuations of the vertical wind velocity and those of the concentration of atmospheric aerosols (Damay *et al.*, 2009). Deposition velocities measurements have been led on a heterogeneous field during unstable and convective atmospheric conditions (Lecce, Italy). The atmospheric stability was deduced from value of 1/L (Monin Obukhov length) and z_0 (Table.1) (Tagliazucca *et al.*, 1983). An ELPI and a CPC both coupled with anemometers were used (Donateo *et al.*, 2006). The post processing procedures were the same for the two devices (streamlines reference system, inlet transfer time and high frequency loss correction). Because the response times of devices are different from 10Hz, a flux correction has been computed (Horst, 1997). In order to validate measurements, a quality test was performed following the method proposed by Foken and Wichura (1996) with a confidence interval of 60 %.

Results

V_d measured with an ELPI is plotted as a function of V_d established using a CPC (Figure 1). There is a good agreement between V_d determined with the ELPI and V_d determined with the CPC. Moreover it can be noticed a similarity in the values of V_d/U^*. The average value of V_d/U^* obtained with the two instruments is of 0.012 for downward fluxes and -0.025 for upward fluxes (Table 1). On a homogeneous field in the same atmospheric stability condition (unstable) V_d/U^* is of 0.010±0.003. (Damay *et al.*, 2009). This result is in agreement with ours and shows that V_d/U^* does not depend significantly on the roughness of the site.

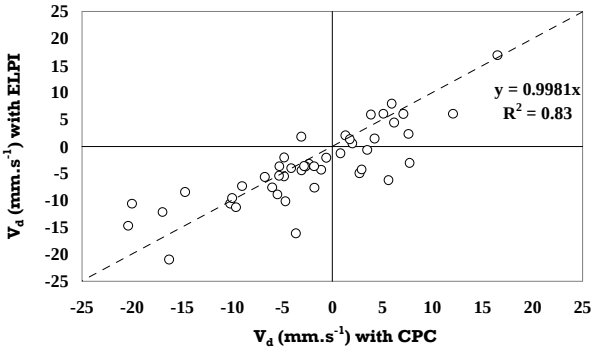

Figure 1. Dry deposition velocity measured with an ELPI and a CPC.

Table 1. Deposition velocity statistics for two cases: only upward fluxes and only downward fluxes selection. (z_0 =0.53±0.02m and d=6.1±0.4m)

	CPC	ELPI	1/L (m^{-1})
Upward fluxes V_d/U^*	-0.0245	-0.0261	-0.025
Downward fluxes V_d/U^*	0.0125	0.0115	-0.0319

Damay, P.E., Maro, D., Coppalle, A., Lamaud, E., Connan, O., Hebert, D. Talbaut, M. and Irvine, M. (2009). *Journal of Aerosol Science*, 40, 1050-1058.

Tagliazucca, M., Nanni T. (1983). An atmospheric diffusion classification scheme based on the Kazanski-Monin stability parameter. *Atmospheric Environment*, 17, 2205-2211.

Donateo, A., Contini, D. and Belosi, F. (2006). Real time measurements of PM2.5 concentrations and vertical turbulent fluxes using an optical detector. *Atmospheric Environment*, 40, 1346-1360.

Horst, T.W., (1997). A simple formula for attenuation of eddy fluxes measured with first-order-response scalar sensors. *Boundary-layer Meteorology*, 82, 219-233.

Foken Th., & Wichura B. (1996). Tools for Quality assessment of surface-based flux measurement. *Agricultural and forest Meteorology*, 78, 83-105.

Intercomparison of aerosols airborne size distribution measurements

J. Andrey[1], Y. Bennouna[2], M.J. Granados[3], J.L. Gómez-Amo[4], B. Piguet[5], A. Minikin[6], J. Jensen[7] and R. Krejci[8]
[1]Atmospheric Research and Instrumentation Branch (INTA), Torrejón de Ardoz, Spain
[2]Group of Atmospheric Optic (GOA), University of Valladolid, Spain
[3]Centro Andaluz de Medio Ambiente, Granada, Spain
[4]University of Valencia, Valencia, Spain
[5]CNRM Meteo-France, Toulouse, France
[6]Deutsches Zentrum für Luft- und Raumfahrt (DLR), Oberpfaffenhofen, Germany
[7]Earth Observing Laboratory, National Center for Atmospheric Research, United States
[8]University of Stockholm, Stockholm, Sweden
Keywords: Aerosol size distribution, airborne particles, optical particle counters, aircraft measurements
Presenting author email: javier.andrey@gmail.com

Aircrafts offer the opportunity to study specific atmospheric phenomena that can not be studied by any other way, for example, evolution of gases and aerosols meanwhile they are transported in the atmosphere.

An intercomparison campaign between several atmospheric research aircrafts from several countries was carried out under the frame of Quality on Airborne Data (QAD) course organized by EUFAR from October 26 to November 5 last year. Three aircrafts took part in this campaign: ATR 42 from SAFIRE (France), Falcon 20 form DLR (Germany) and Hercules C130 from NCAR (United States).

These aircrafts were instrumented to measure several parameters like gases concentration, temperature, humidity, pressure, aerosols properties, etc. Size distribution measurements were performed by the Optical Parricle Counters (OPC) shown in table 1. The aerosol measured range has been added to the table as a third column.

Aircraft	Instrument	Size range [μm]
Safire ATR42	Grimm 1.109	0.25 - 2.50
Safire ATR42	SPP-200	0.10 - 3.00
DLR Falcon 20	PCASP-100X	0.10 - 3.00
NCAR C130	UHSAS	0.06 - 1.00

Table 1: Instruments used in this work

The PCASP-100X, SPP-200 and UHSAS are mounted on hard points below the wings or on the fuselage, whereas the GRIMM 1.109 is installed inside the ATR42 cabin. The inlet of the GRIMM is connected to an external mobile inlet installed on a window of the aircraft.

Flights developed on October 29th, 30th were carried out by ATR42 and Falcon 20, whereas the aircrafts involved in the flight of November 3rd were ATR42 and C130. The measurements compared correspond to the periods in which the aircrafts flew wing by wing in straight line runs (SLR). A total of seven SLRs were performed during the flights, only five of the latters being considered for the comparison.

The channels of the different instruments have been groupped to cover the same size range and to allow comparing the measurements directly. A total of 13 channel groups or sets, have been considered. A one minute average has been applied to the data before being analyzed. The obtained time series for each instrument are presented, as well as scattered plots for the different comparable sets. Corresponding linear regression and correlation coeficients are given and commented.

A good correlation have been found between all instruments except in the intercomparioson PCASP-100X/GRIMM, when particle concentration falls below 1 $part/cm^{-3}$. PCASP losses sentitvity when particle concentration is below this limit. The correlation coefficients of the fits reach values between 0.8 and 1.0 when particle concentration for particle concentrations higher than 1 $part/cm^{-3}$.

Acknowledgements

This work has received funding from the European Community's Seventh Framework Programme (FP7/2007-2013) under grant agreement n° 227159 (EUFAR: European Facility for Airborne Research in Environmental and Geo-sciences). We would like to thank to QAD organizers and the EUFAR team for giving us the opportunity to extend our knowledge in using aircrafts measurements. The authors are grateful to SAFIRE, DLR and NCAR for operating these flights and provide and process the data.

AMS Collection Efficiencies of dry smog chamber aerosols, dependence on $(NH_4)_2SO_4$, NH_4NO_3 and SOA fractions

A.C. Eriksson[1,2], E. Z. Nordin[2], P.T. Nilsson[2], J. E. Carlsson[2], J. Rissler[2], M. Kulmala[3], B. Svenningssson[1], J. Pagels[2] and E. Swietlicki[1]
[1]*Nuclear Physics, Lund Univeristy, Lund, Sweden*
[2]*Ergonomics & Aerosol Technology, Lund Univeristy, Lund, Sweden*
[3]*Dept. Physics, Division of Atmospheric Sciences, Helsinki University,Helsinki, Finland*
Keywords: AMS, instrumentation, laboratory experiments, SOA.
Presenting author email: axel.eriksson@nuclear.lu.se

The Aerodyne Aerosol Mass Spectrometer (AMS) measures the average chemical composition of non-refractory species, i.e. particulate matter which vaporizes when impacted on a surface heated to 600 C. The instrument provides quantitative data on-line with time resolution down to seconds (dependent on mass loading). This is accomplished through mass spectrometric measurements subsequent to aerodynamic lens focusing. Each particle type (with respect to shape, size and composition) has associated collection efficiency (CE) which data analysis needs to take into account in order to yield quantitative results.

CE is a collective name for any effect on instrument sensitivity associated with particle sampling, and was given by Huffman *et al* (2005) as

$$CE(d_{va})=E_L(d_{va})*E_s(d_{va})*E_b(d_{va})$$

The expression above emphasizes three particle properties which may bias the sampling; lens transmission (E_L), non-spherical shape (E_S), bouncing from the vaporizer plate (E_b), and their possible dependence on size. E_L and E_S are close to unity for most ambient accumulation mode particles, making E_B the main contributor to uncertainty in quantification.

This study is a summary of CE estimates from inter comparison with other aerosol instrumentation (primarily Scanning Mobility Particle Sizer, SMPS, and Aerosol Particle Mass analyzer- Differential mobility Analyzer, APM-DMA) on data from two light duty vehicle exhaust ageing campaigns. The experiments were performed by nebulizing $(NH_4)_2SO_4$ and injecting it into a 6 m^3 smog chamber, mixing with real exhaust or precursor species and irradiating the chamber with UV-light under dry (RH~5%) conditions (Nordin et al 2011). This typically resulted in condensation of SOA and/or NH_4NO_3 (NH_3 forms in the oxidation catalyst of the vehicle), a process which was monitored for approximately 5 hours. These internally mixed aerosols spanned a wide range of chemical compositions, from pure seeds to particles dominated by either condensate, enabling investigation of the effects of these proportions on CE.

Figure 1 below illustrates one of the experiments were NH_4NO_3 and SOA condense onto $(NH_4)_2SO_4$ seeds. In the two hours plotted, the particles transform from salt cores lightly coated with organic matter (this coating occurred while injecting the exhaust) to heavily coated (approximately 50% SOA, 30% NH_4NO_3, and 20% $(NH_4)_2SO_4$) particles. During this process, the ratio of reported AMS/SMPS mass increases from 0.23 to 0.37. This is in agreement with ambient observations, where dry aerosols dominated by $(NH_4)_2SO_4$ typically is found to have E_B=0.25 while dried SOA gives E_B=0.5.

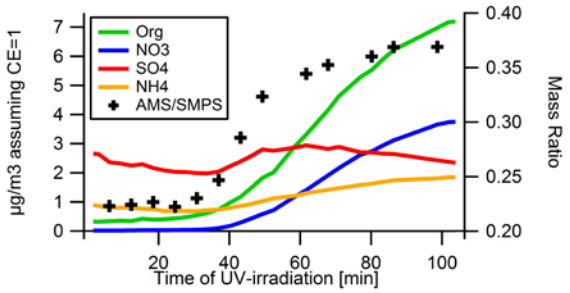

Figure 1. Chemical composition during an exhaust ageing experiment. The increase in AMS/SMPS mass ratio is likely due to an increase in E_b of the sampled aerosol. The time trace of SO_4 supports this.

Although the increasing ratio illustrated above is mainly due to increasing E_b, it should be noted that other aspects of instrumental response (in both instruments) also may affect the ratio. E_B is believed to be an effect of particle phase (Matthew et al 2008). Ambient AMS measurements usually employ a dried sampling line (to reduce interference from gaseous and particulate water), which may perturb the phase of the sampled particles. Since these experiments were performed under dry conditions, this effect is presumably captured here.

This work was supported by the Swedish research council FORMAS through projects 2007-1205, 2008-1467 and 2010-1678

Huffman et al (2005). *Design, Modeling, Optimization, and Experimental Tests of a Particle Beam Width Probe for the Aerodyne Aerosol Mass Spectrometer.* AST, 39:1143-1163.

Matthew et al (2008). *Collection Efficiencies in an Aerodyne Aerosol Mass Spectrometer as a function of Particle Phase for Laboratory Generated Aerosols*. AST, 42:884–898.

Nordin, E. Z. *et al*. (2011). *Smog Chamber Studies on SOA Formation from Gasoline Exhaust and Pure Precursors.* EAC proceedings.

Simplified approximations to Centrifugal Particle Mass Analyser performance

K.StJ. Reavell, J.P.R. Symonds and M.G. Rushton

Cambustion Ltd, J6 The Paddocks, Cambridge CB1 8DH, United Kingdom
Keywords: Instrumentation, Particle Mass, Aerosol Particle Mass Analyser.
ksr@cambustion.com

The Centrifugal Particle Mass Analyser, CPMA, (Olfert and Collings 2005) is an instrument for classifying aerosol particles on the basis of their mass:charge ratio. In that reference and (Ehara et al, 1996), the classification of particles due to drift and the action of the electric field and rotation of the classifier is described based on a parameter λ. In this work, an alternative simplified approximation to the operation is proposed, with advantages in more easily understanding the dependence of the instrument performance on the operating parameters.

In a CPMA an annular channel is formed between rotating inner and outer cylinders, with an electric field applied between them. The radial electrical and centrifugal forces on a suspended particle in the channel are only in equilibrium for a particular mass:charge ratio, $(m/q)_{eqm}$, and only particles of close to this ratio are carried axially down the column by a flow. Other particles are precipitated: heavier particles (or with less charge) on the outer cylinder, and lighter ones on the inner. The classifier is shown schematically in Fig. 1.

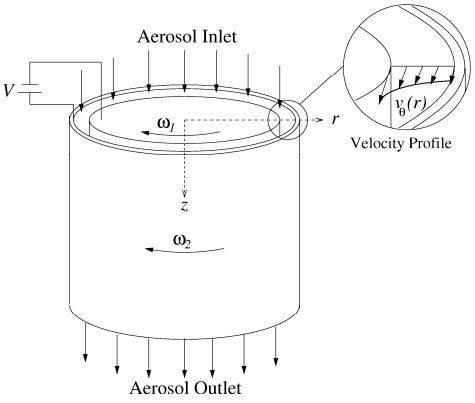

Fig 1. CPMA Classifier (Olfert 2005)

The electrical field strength, E, in the annular gap varies as r^{-1}. When the inner and outer walls rotate at slightly different speeds, ω_1 and ω_2, there is a tangential velocity profile, v_θ. Here we propose that for the narrow gap this can be approximated by a power law:

$$\omega(r) \propto r^{n_\omega}$$

The variation of equilibrium mass:charge ratio across the channel can then be written:

$$\left(m/q\right)_{eqm} \propto r^{n_m} \text{ where } n_m = -2n_\omega - 2$$

The Aerosol Particle Mass analyser, APM, (Ehara 1996) is a special case of the CPMA where the inner and outer cylinders are joined together so $\omega_1 = \omega_2$. In this case, n_ω=0 and so n_m=-2. Therefore, as r increases, $(m/q)_{eqm}$ is lower. This is an unstable situation: a particle of $(m/q)_{eqm}$ perturbed from its trajectory increasingly departs from it, modelled below:

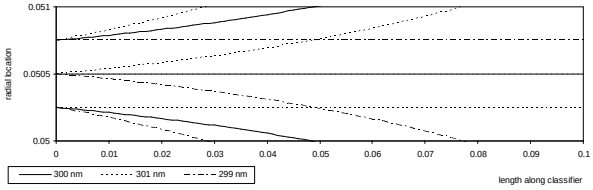

The parameter n_m thus describes the stability of the forces in a CPMA. If n_m is negative, the forces are unstable: this results in a reduction of particle transmission efficiency shown in (Olfert et al, 2006) and also a broadening of the range of (m/q) transmitted, referred to as the transfer function. If n_m=0, achieved by rotating the inner and outer cylinders at angular velocities in inverse proportion to their radii so n_ω=-1, then $(m/q)_{eqm}$ is constant across the classifier section, achieving the narrowest theoretical transfer function:

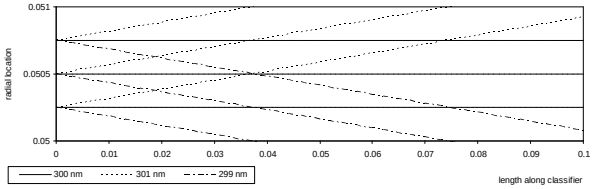

When n_m is positive, $(m/q)_{eqm}$ again varies across the channel, but in the opposite sense from the unstable case: this broadens the transfer function but may have benefits in reduced particle losses when diffusion is accounted for, or may be relevant in scanning applications.

The CPMA transfer function is also affected by drift. For the neutrally stable, n_m=0, case, when particle diffusion is neglected, this approximates a triangle equivalent to the non-diffusing transfer function of a DMA. For singly charged particles, the width of the transfer function is related to the classifier size and conditions by a non-dimensional relationship:

$$\left(\frac{m'}{m_{eqm}}\right)^{(n_B+1)} - \left(\frac{m'}{m_{eqm}}\right)^{n_B} = \frac{Q}{m_{eqm} B \cdot 2\pi r^2 l \omega^2}$$

where m_{eqm} is the peak mass of the transfer function, m' is the maximum transmitted mass, Q is the volumetric flow rate in the classifier, B the particle mobility, r the mean classifier radius, l the classifier length, ω the mean classifier angular velocity and n_B the power with which mobility varies with particle mass.

Ehara, K., Hagwook, C., Coakley, K. J. Aerosol Sci. **27** 217-234

Olfert, J., Collings, N. (2005) J. Aerosol Sci. **36** 1338-1352

Olfert, J., Reavell, K., Rushton, M., Collings, N. (2006) J. Aerosol Sci. **37** 1840 - 1852

EC/OC Measurements on Aerosol Samples by Thermal-Optical Methods: Benchmarking Different Protocols

F. Lucarelli[1], M. Chiari[1], M. Giannoni[2], G. Calzolai[1], A. Cincinelli[2], S. Nava[1]

[1]INFN and Department of Physics and Astronomy, University of Florence, Sesto Fiorentino, 50019, Italy
[2]Department of Chemistry, University of Florence, Sesto Fiorentino, 50019, Italy
Keywords: Elemental carbon, Organic carbon, Pyrolysis.
Presenting author email: lucarelli@fi.infn.it

Thermal-optical analysis is a standard method for determining the carbonaceous aerosol fraction and for separating it into Organic Carbon (OC) and Elemental Carbon (EC). Unfortunately, no reference method for these measurements is established yet, so the implement of the different thermal evolution protocols available in the literature, differing in temperature and duration of the heating ramps, affects the results and can result in a wide variation of EC and OC values. Moreover, the presence of Water-Soluble Organic Compounds (WSOC) in the sample may enhance the charring process during OC thermal evolution, strongly affecting and complicating the EC quantification.

The aim of this work is to provide a pragmatic guide to the EC/OC practitioners through an intercomparison between the results obtained on real samples using a Sunset Thermal-Optical-Transmittance analyzer running under different measurement protocols:

- QUARTZ (a variation of the NIOSH protocol);
- IMPROVE (J.C. Chow et al., 1993), as implemented in the analyzer;
- EUSAAR_2 (F. Cavalli et al., 2010).

This intercomparison exercise was carried out on PM2.5 samples collected in parallel on quartz fibre filters during the PATOS ("Particolato Atmosferico in TOScana") campaign from March 2009 till March 2010 in Italy, in sites of different typologies (urban traffic, urban background, rural background). One of the two sample series was analysed as-is and the other was analysed after WSOC removal by washing the filters with 100 ml of milli-Q water.

The results of the intercomparison between the three different thermal protocols will be shown. In general, a very good agreement as regards TC measurements was found, as expected. EC values obtained by EUSAAR_2 and IMPROVE protocols resulted 20%-30% higher than EC values by the QUARTZ protocol, regardless of the season and the sampling site typology. The difference tends to reduce (in particular, between EUSAAR_2 and QUARTZ protocols it becomes less than 10%) if the comparison is made on washed samples, after WSOC removal.

Finally, an indication about the "best" protocol to be adopted, on the basis of a better agreement between the EC concentrations measured on washed or not-washed samples, and thus of a minor influence of pyrolitic carbon on EC quantification when the measurements are performed on samples analysed as-is (i.e. not-washed), will be provided.

Chow, J.C., Watson, J.G., Pritchett, L.C., Pierson, W.R., Fraizer, C.A., Purcell, R.G., (1993) *Atm. Env.* **27A**, 1185.

Cavalli, F., Viana, M., Yttri, K.E., Genberg, J., Putaud, J.-P., (2010) *Aerosol Meas. Techn.*, **3**, *79*.

Thursday, September 8, 2011

Session 8P: Poster session B

Atmospheric aerosols - Aerosol Processes and Properties

The influence of particle shape on optical particle sizers

S. Pfeifer, T. Müller, A. Weigelt, A. Wiedensohler

Leibniz Institute for Tropospheric Research , Leipzig, 04318, Germany
Keywords: optical particle counter, light scattering, non-spherical particles.
Presenting author email: sascha.pfeifer@tropos.de

Introduction

There is a lot of research on optical properties and fluid dynamics of non-spherical aerosol particles. Particle shapes are commonly determined by electron microscopy. Nevertheless, this way of size classification is time consuming and therefore often suffers from a poor statistics.

Assumption of spherical particles can lead to errors in sizing. In general, Differential Mobility Particle Sizers (DMPS), Aerodynamic Particle Sizers (APS) and Optical Particle Sizers (OPC) are sensitive to the particle shape. The particle shape influences the fluid dynamics and varies the drag-force on the particles. Furthermore, the shape also influences the scattering phase function of the particle.

A tandem measurement system consisting of e. g. a DMA and an OPC is one method to consider these effects. Heintzenberg et al. (2004) matched the data of OPC spectra for selected DMA mobility sizes with an ensemble of spheroids of different refractive indices by using the method of T-Matrix. It should be pointed out that fitting with an average of orientation ignores the fact of dispersion. The scattering signal is influenced by particle orientation relative to the incident beam, depending on optical receiver system.

The combination of DMA and Multi Angle Light Scattering (MALS) is possible as well. A multi angle detection yields much more information of an individual particle than the single angle detection of a classical OPC. Depending on the aim of the analysis, hence different modifications of the measuring instrument, it is possible to determine a refractive index or to distinguish between spherical and non-spherical particles. (Sachweh et al, 1995, 1999; Dick et al, 2007)

Experimental

The dynamic shape factor is defined as the quotient for the drag force of a non-spherical particle and those of a spherical one with the same volume. To calculate these drag forces we have to solve the Stokes equation for the suitable particle surface. This was done using the Boundary Element Method (BEM). For solving the electromagnetic scattering problem, Discrete Dipole Approximation (DDA) can be used to calculate the phase function. This numerical method allows calculation of nearly every kind of particle shape.

For a test case, we have chosen a polystyrene latex (PSL) doublet. It is easy to generate, has a well defined size, and its density and refractive index are known. The numerical solutions of the dynamic shape factor for a PSL doublet ranges between 1.02 for parallel and 1.15 for perpendicular alignment relative to the flow, respectively. These values are in agreement to experimental results (Zelenyuk et al, 2006).

Referring to the dynamic shape factor we calculated the relative scattering signal, what is defined as the quotient for the integrated phase function of the non-spherical particle and those of a spherical one with the same volume, refractive index and integration area. The calculations were done for the geometry of an OPC which measures side scattering in an angular range of ±45°, with a wavelength of 1000 nm.

For the lower part of the measurement size range we expect continuously smaller signals by 10% to 20% compared to the volume equivalent radii up to 330 nm. Values are higher by 15% to 30% between 330 and 500 nm. Furthermore, we expect that a full random orientation leads to an increase of dispersion by volume equivalent radius (Figure 1). Measurements with PSL spheres with a diameter of 350 nm verified this characteristic and matches to the simulations.

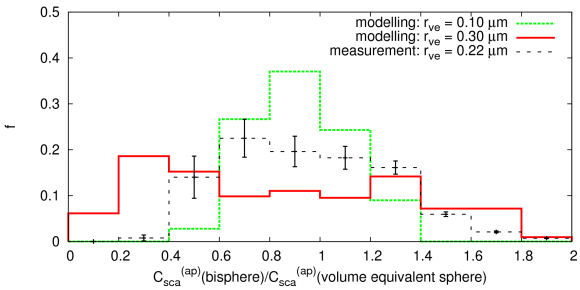

Figure 1. Fractional distribution of the relative scattering signal for random orientated PSL doublets, λ = 1000 nm

Outlook

More laboratory studies to verify results of the numerical simulations are planned. These studies will be extended to deduce significant parameters influenced by the shape. This information should help to improve the information content of DMPS, OPC and APS in-situ measurements in future.

Dick, W. D., Ziemann P. J., McMurry, P. H. (2007) *Aerosol Science and Technology* **41** 549-569

Heintzenberg, J., Okada, K., Trautmann, T., Hoffmann, P. (2004) *Applied Optics* **43** 5893-5900

Sachweh, B. A., Dick, W. D., McMurry P. H. (1995) *Aerosol Science and Technology* **23** 373-391

Sachweh, B. A., Barthel, H., Polke, R., Umhauer, H., Büttner, H. (1999) *Journal of Aerosol Science* **30** 1257-1270

Zelenyuk, A., Cai, Y., Imre, D. (2006) *Aerosol Science and Technology* **40** 197-217

Planetary boundary layer influence at the Jungfraujoch: in-situ and remote sensing measurements.

M. Collaud Coen[1], E. Weingartner[2], C. Ketterer[1], O. Maier[1], S. Frey[3], P. Zieger[2], N. Bukowiecki[2] and U. Baltensperger[2]
[1]MeteoSwiss, CH-1530 Payerne, Switzerland.
[2] Laboratory of Atmospheric Chemistry, Paul Scherrer Institut, CH-5232 Villigen, Switzerland.
[3]Jenoptik, ESW GmbH, Jena, Germany
Keywords: Atmospheric aerosol, boundary layer, synoptic weather types, remote sensing, vertical distribution.
Presenting author email: martine.collaud@meteoswiss.ch

The high alpine research station Jungfraujoch (JFJ, 3580 m asl) is situated in the middle of the Swiss Alps and is considered as being representative of free tropospheric (FT) air masses most of the time. Fourteen years of meteorological parameters, aerosol variables and trace gases measured at the JFJ have been analyzed as a function of different synoptic weather types (Alpine Weather Statistics classification, AWS) over the whole Swiss region. The planetary boundary layer (PBL) influence was estimated by means of the diurnal cycles of aerosol species. Since aerosols are scavenged by precipitation, the diurnal cycle of the CO concentration was also used to identify polluted air masses in case of precipitation. SO_2 and NO_x concentrations were used as precursor tracers for new particle formation and growth, respectively.

This study confirms the consensus view that the JFJ is mainly influenced by the free troposphere during winter and by injection of air parcels from the PBL during summer. A more detailed picture is, however, drawn where the JFJ is completely influenced by free tropospheric air masses in winter during advective weather types and largely influenced by the PBL also during the night in summer during the subsidence weather type (i.e. CA in Fig 1). From April to September, the JFJ is influenced by the PBL during the afternoon in case of subsidence, whereas the night remains in FT. In case of lifting, the large influence of newly formed particles measured at the JFJ can be explained by the meteorological conditions and the gaseous concentrations on the Swiss plateau.

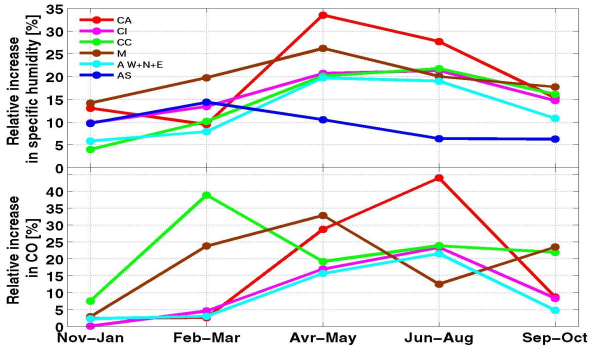

Figure 1. : Relative increase in the specific humidity and in CO concentration calculated from JFJ and Payerne (Stabio for AS) data for different weather types (corresponding to different colors) and for defined periods of the year.

An analysis of the relative increase of the specific humidity and CO concentration allows us to estimate that on average less than 45% of PBL air is found at the JFJ during all synoptic weather conditions (Fig. 1).

Aerosol parameters important to estimate the aerosol radiative forcing (single scattering albedo (SSA), extinction coefficient, backscattering fraction, asymmetry parameter) have also been calculated for dry measurement conditions and corrected for ambient conditions (i.e. elevated humidity). For most of the weather types, the ambient aerosol parameters restricted to clear sky conditions are mostly similar to the dry aerosol parameters (Fig. 2). The RH corrected SSA is usually larger than 0.90 (0.95 in case of advection).

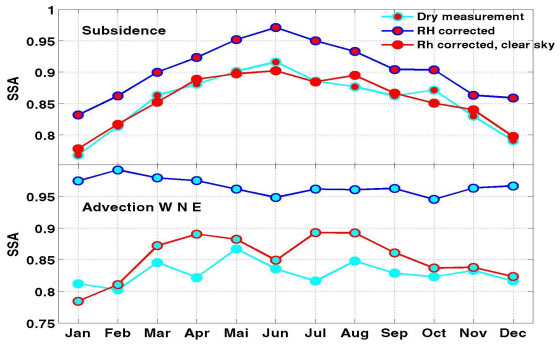

Figure 2: Single scattering albedo annual cycle for dry measurements, RH corrected aerosol parameters for all and for clear sky conditions.

During the Cloud and Aerosol Characterization Experiment (CLACE) 2010, several instruments allowing a determination of the PBL height (ceilometer, windprofiler, radiometer) were measuring vertical profiles from the Kleine Scheidegg at 2061 m asl at the foot of the JFJ. In case of clear sky, the development of the PBL height can be observed from both the ceilometer and the windprofiler measurements and compared to the in-situ aerosol measurements at the JFJ.

Collaud Coen, M., Weingartner, E., Furger, M., Nyeki, S., Prévôt, A.S.H., Steinbacher, M., and Baltensperger, U. (2011) *Atmos. Phys. Chem. Diss.* **11**, 985-1024.

Nessler, R., Weingartner, E., and Baltensperger, U.: Adaptation of dry nephelometer measurements to ambient conditions at the Jungfraujoch, Environ. Sci. Technol, 39(7), 2219-2228, 2005.

Improved cloud screening for aerosol optical depth measurements with a Brewer spectrophotometer

V. De Bock[1], H. De Backer[1] and A. Mangold[1]

[1]Royal Meteorological Institute of Belgium, Ringlaan 3, 1180 Brussels, Belgium

Keywords: AOD, in-situ measurements, CIMEL, seasonal patterns.
Presenting author email: Veerle.DeBock@meteo.be

An improved automatic cloud screening technique for the retrieval of Aerosol Optical Depth (AOD) values with a Brewer spectrophotometer was developed to replace the old manual cloud screening technique. The new cloud screening technique, which uses sunshine duration data, will be presented together with the AOD retrieval method. The retrieved AOD values will be compared with quasi-simultaneous Cimel sunphotometer measurements at Uccle and the seasonal and monthly variability of the AOD at Uccle will be discussed.

The AOD retrieval method (De Bock et al. 2010) uses sun scan measurements (from 335 to 345 nm, convoluted with the Cimel sunphotometer band pass filter at 340 nm) from the Brewer spectrophotometer at Uccle, Belgium (50°48'N, 4°21'E, 100m a.s.l.) whereas previously, direct sun measurements (at 5 specific wavelengths, 320.1 nm being the largest) were used.

The use of sun scans simplifies the comparison of the AOD values with quasi-simultaneous Cimel sunphotometer values since it is no longer necessary to extrapolate the Cimel AOD values to Brewer wavelength. Moreover, due to the convolution with the Cimel band pass filter, we compare physically exactly the same quantity. Another advantage is the larger intensity of the retrieved signal at 340 nm due to lower ozone absorption, thus improving the signal to noise ratio.

To derive the AOD at 340 nm from the Brewer sun scan measurements, we apply the Langley Plot Method (LPM), in a similar way as described in Cheymol and De Backer (2003), to the weighted irradiances. The LPM is a linear regression technique and the quality of this regression depends on the range of the solar zenith angles covered during a certain day. Good observations at both high and low solar zenith angels are needed and the atmospheric conditions must remain stable over the day. We define a set of criteria to select the days ('cloudless days') on which the LPM can be applied. One AOD and one Calibration Factor are calculated for each cloudless day and the average of these Calibration Factors will be used as mean calibration coefficient of the instrument. With this coefficient, the AOD can be calculated for each individual clear sky observation.

We only calculated the AOD for the individual sun scans for which a direct sun observation, made with the Brewer, is available within a time period of 5 minutes. This however did not exclude all cloud-perturbed measurements. To this end the new cloud screening algorithm was developed.

We compared the Brewer AOD values at 340nm retrieved with the old manual cloud screening technique with quasi-simultaneous AOD values (with a maximum time difference of 3 minutes) from the Cimel sunphotometer for a period from 1 September 2006 to 31 August 2010. After removing the outliers, the correlation, slope and intercept of the regression line are respectively 0.974, 0.968+/-0.014 and 0.011+/-0.006. This already showed that good quality AOD observations can be obtained at 340nm from Brewer sun scan measurements. In the poster, we will present the results of the comparison of the new cloud screened Brewer AOD values with Cimel values for an extended period from 1 September 2006 to 30 June 2011.

The seasonal and monthly variability of the new cloud screened AOD at Uccle will also be presented. We already saw a clear seasonal cycle in the observed AOD (with the old manual cloud screening method) at Uccle, with higher values in spring and summer and lower values in autumn and winter. On a weekly scale, no clear cycle could be seen.

This work was supported by the Belgian Federal Science Policy Office under grants SD/AT/01B and SD/CS/07A.

Cheymol, A. and De Backer, H.: Retrieval of the aerosol optical depth in the UV-B at Uccle from Brewer ozone measurements over a long time period 1984-2002, *J. Geophys. Res.*, **108**, D24, doi: 10.1029/2003KD003758, 2003.

De Bock, V., De Backer, H., Mangold, A. and Delcloo, A.: Aerosol Optical Depth measurements at 340 nm with a Brewer spectrophotometer and comparison with Cimel observations at Uccle, Belgium, *Atmos. Meas. Tech.*, **3**, 1577-1588, doi: 10.5194/amt-3-1577-2010, 2010.

Aircraft observations of volcanic ash properties

B.T. Johnson[1], K. T. Turnbull[1] J.R. Dorsey[2] and J.M. Haywood[1]

[1]Met Office, Exeter, United Kingdom
[2]University of Manchester, United Kingdom
Keywords: aerosol, aircraft, optical.
Presenting author email: ben.johnson@metoffice.gov.uk

During April-May 2010 volcanic ash from the Icelandic volcano Eyjafjallajökull caused major disruption to European air travel. In response to the crisis the UK's BAe-146 research aircraft (FAAM: Facility for Airborne Atmospheric Measurement) made a series of flights to map the extent of the ash clouds (via on-board lidar) and make in-situ measurements of ash particle properties. A major objective of these flights was to obtain in-situ estimates of ash mass concentration for the validation of ash forecasts and remote sensing techniques (satellite, lidar, sunphotometer). This required detailed investigation of the ash particle size distribution and their optical properties.

Owing to safety concerns, the aircraft specifically targeted regions where ash concentrations were forecast by the operational model to be in the range 200-2000µg/m^3. Data from the Cloud and Aerosol Spectrometer (CAS; figure 1a) shows that the aircraft encountered ash concentrations of 200-2000µg/m^3 on many occasions during a sequence of seven flights over the UK region from 4 – 18 May. Typically ash was observed in layers 300m – 2km thick at altitudes anywhere below 8km. The aircraft measurements also illustrate the highly inhomogeneous (patchy) nature of the ash layers with horizontal variability on a wide range of scales (10 – 100km). High mass concentrations were also accompanied by elevated levels of SO_2 (up to 100ppbv) and a strong signature of aerosol scattering (up to 300 x 10^{-6} m^{-1}). The 3-wavelength nephelometer showed low Ångstrom exponents (-0.5 – 0.4) across visible wavelengths, typical of coarse aerosol (diameter > 1µm).

The size distribution from the CAS showed a broad peak between 1 – 10µm (volume-equivalent diameter) with volume mean diameters in the range 3 – 8µm and a rapid fall-off beyond 10µm. Very few particles were observed at or above 30µm, somewhat in contrast to the results from dispersion models. This indicates that improvements could be made to the assumed source size distribution and/or losses due to near-source aggregation and fall-out.

The mixing of ash plumes with ice cloud posed a major challenge on some flights. Measurements from a variety of aerosol, cloud and humidity probes have therefore been combined to develop techniques for discriminating between ice and ash. This has been used to give confidence to measurements close to, but outside of, clouded regions.

Asphericity measurements from the Small Ice Detector (SID-2) have also been used to distinguish ash particles (observed to be highly aspherical) from spherical aerosols, such as hydrated sea-salt. At low altitudes (i.e. within the boundary layer) such hydrated aerosol were found to carry around 200µg/m^{-3}, comparable to the observed ash mass concentrations. This shows the need for careful examination of in-situ data to ensure reliable estimates of ash concentration.

Finally, the specific extinction coefficient (k_{ext}) of ash aerosol has been estimated using CAS size distributions and light-scattering models. Preliminary results, based on many sections of flight data suggest k_{ext} values in the range 0.3 – 1.0 m^2/g, with a mean value of 0.5m^2/g. These estimates of k_{ext} are for downwind ash layers observed in the UK and may not be representative of near-source properties. However, these estimates provide a guide for downwind properties in future eruption scenarios and may be useful for remote sensing techniques that rely on an estimate of k_{ext} to convert aerosol extinction to mass concentration.

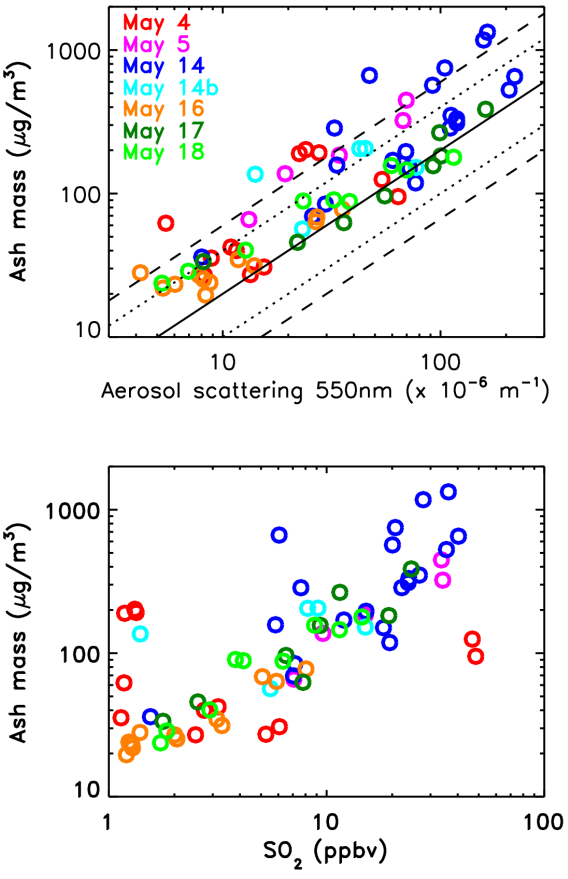

Figure 1. Mean ash mass concentration (from CAS), aerosol light-scattering coefficient (from nephelometer) and SO_2 concentration from selected aircraft runs.

One Year Aerosol Measurements with LIDAR in Portugal

F. Wagner [1], J. Preißler[1], J.L. Guerrero-Rascado[1] and A.M. Silva[1]

[1]Geophysics Center of Évora, University of Évora, Évora, 7000-671, Portugal
Keywords: lidar, optical properties, vertical profile.
Presenting author email: frankwagner@uevora.pt

Atmospheric aerosol particles play a major role in the climate system due to their various direct and indirect effects which in turn influence other components of the climate system. The vertical profile of aerosol particles is mainly important for long-range transport of particles, but it has also an influence on the climate effect of absorbing particles.

Since September 2009 a five-wavelength Raman lidar with depolarization channel was installed at Évora, Portugal. It emits light at 355, 532 and 1064 nm and receives backscattered light at the same wavelengths and additionally at the Raman shifted wavelengths 387 and 607 nm. The lidar is from type PollyXT (Althausen et al. 2009) and the only lidar instrument in Portugal. Hence it is the first time that the annual cycle of the vertical profile of aerosol particles could be determined in Portugal. Previous lidar measurements were only performed during measurement campaigns.

In this presentation an overview over one year of lidar measurements will be given. On more than 150 days the instrument was operated and provided height-resolved data. On 26 days aerosols originating in the African Sahara could be observed. The particles emitted from the Icelandic volcano Eyjafjallajokull could be measured on 6 days during May 2010. European pollution and forest fire aerosols were transported to Evora and observed with the lidar, too. However during most of the time the typical rural background persisted over and around Évora.

At the presentation differences and similarities of the vertical profile of aerosol particles will be shown. One major difference becomes obvious when one compare the profiles of desert dust with profiles of volcanic particles. Desert dust can reach altitudes up to 6 km and usually the whole atmosphere below the top of the dust layer is filled with particles. In contrast aerosols from the volcano Eyjafjallajokull could be observed in the whole troposphere but the most intense layer appeared as thin filaments.

Figure 1 one shows an example of the vertical profile of the spectral particle backscatter- and extinction coefficients as well of the volume depolarization ratio. The different quantities cannot be observed all over the whole height range because the signal to noise ratio and the effect of error propagation in the retrievals limit the valid height range.

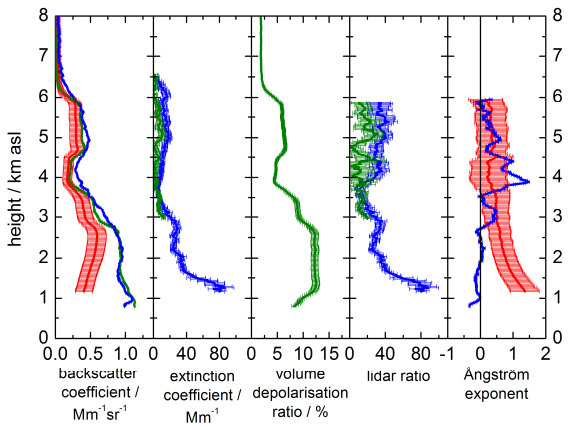

Figure 1. Example of lidar measurements on the 11th of December 2010 showing the particle backscatter coefficients at three wavelengths, the particle extinction coefficients at two wavelengths, the lidar ratios at two wavelengths, two Angstrom exponents, and the volume depolarization ratio at one wavelength.

The authors would like to thank FCT (Fundação para a Ciência e a Tecnologia) for the fellowships of Jana Preißler (SFRH/BD/47521/2008) and Juan Luis Rascado (SFRH/BPD/63090/2009), and for the funding of the lidar system in the framework of the National Re-Equipment program (REDE/1527/RNG/2007) and project PTDC/CTE-ATM/65307/2006. The authors would also like to thank the lidar team of the Leibniz-Institute for Tropospheric Research (IFT) in Leipzig, Germany, for providing data analysis software and support with the PollyXT system. This bilateral collaboration between CGE and IFT was additionally supported by CRUP (Conselho de Reitores das Universidades Portuguesas) (A-34/09) and DAAD (Deutscher Akademischer Austauschdienst) (0811989). Furthermore the authors would also like to acknowledge benefits arising from the membership in EARLINET and SPALINET.

Althausen, D., Engelmann, R., Baars, H., Heese, B. A. Ansmann, Müller, D. and Komppula, M. (2009): *Portable Raman Lidar PollyXT for Automated Profiling of Aerosol Backscatter, Extinction, and Depolarization*. Journal of Atmospheric and Oceanic Technology, 26, doi:10.1175/2009JTECHA1304.1

In situ volcanic aerosol measurements made using the FAAM research aircraft; a case study

K.F. Turnbull[1], B.T. Johnson[1], F. Marenco[1], J. Dorsey[2] and J.M. Haywood[1]
[1]Met Office, Exeter, EX1 3PB, United Kingdom
[2]NCAS, University of Manchester, United Kingdom

Keywords: aerosol, aircraft, optical propertie, volcanic particles
Presenting author email: kate.turnbull@metoffice.gov.uk

The Facility for Airborne Atmospheric Measurement (FAAM) BAE-146 research aircraft flew over and around the UK during the April-May 2010 period when European airspace was affected by volcanic aerosol from Eyjafjallajökull. Flights mapped the extent of the volcanic aerosol and made in situ and remote measurements of ash properties.

On 17 May 2010, the FAAM aircraft profiled through a plume from Eyjafjallajökull as it extended southwards over the North Sea (figure 1). The aircraft was equipped with a comprehensive suite of instruments measuring standard meteorological quantities, aerosol, cloud and chemical tracers. A downward pointing elastic backscatter LIDAR manufactured by Leosphere, operating at 355nm was also flown.

Aerosol Optical Depths (AOD) associated with the volcanic aerosol were derived from 1-minute averages of LIDAR profile data. These were integrated between altitudes of 3 km and 7 km where the volcanic plumes had been observed (Figure 2). Figure 1 shows the location of the volcanic plume, based on these AOD estimates.

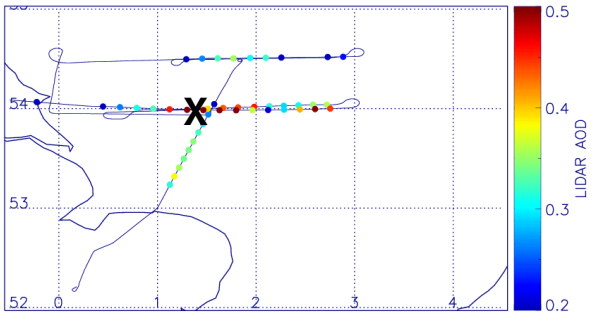

Figure 1. FAAM flight track. X indicates the approximate location of profile 1.

Total scattering coefficients were measured by a 3-wavelength TSI-3563 nephelometer (red, green, blue), Sulphur Dioxide (SO_2) concentration from a TECO-43C monitor (purple) and aerosol mass derived from the University of Manchester Cloud and Aerosol Spectrometer (CAS) covering diameters between 0.6 and 50 µm (black), as in figure 2. The optical scattering from the nephelometer was well correlated with the CAS mass concentration and also with SO_2 concentration, as shown by profile 1 (figure 2), a descent into the case study region. The plume extended between 3.3 and 6.4 km and exhibits a filamentary structure.

A specific extinction coefficient of 0.5 m^2g^{-1} was derived from CAS size spectra for this flight and used to provide a proxy estimate of aerosol mass based on the nephelometer scattering coefficient, also shown (Figure 2, orange dashed line). The nephelometer-derived mass concentrations are in reasonable agreement with the more direct measurements from CAS.

AODs derived for this profile from CAS and from nephelometer scattering measurements were 0.57 and 0.52 respectively which falls within the spatial variability of AODs estimated from LIDAR retrievals in the same location as the profile descent (see figure 1).

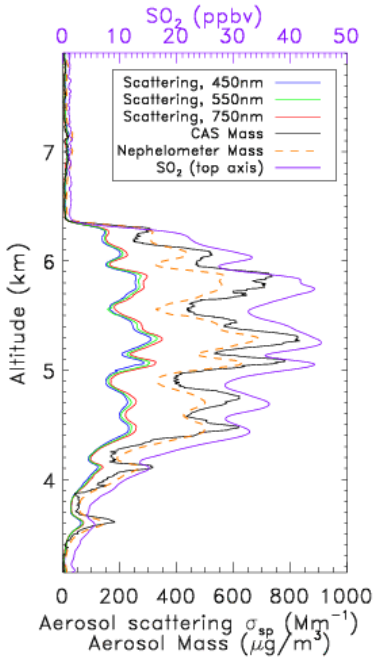

Figure 2. Profile 1 (descent) from FAAM flight B530 on 17th May 2010 near 54°N 1.2°E. For details see text.

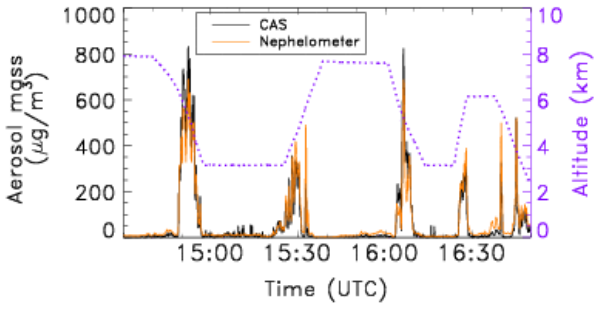

Figure 3. Time series of aerosol mass derived from CAS (black) and nephelometer scattering measurements (orange). The aircraft altitude is shown in purple.

Figure 3 shows the magnitude and variability of aerosol mass observed in the study region. These measurements are in good agreement with those made from the DLR Falcon 20E which flew in this plume 2-3 hours later around 52.5-53.0°N (not shown here).

Optical properties of rural aerosol as the function of mass concentration in Central Europe

A. Molnár[1], D. Benkő[2], Zs. Bécsi[2] and A. Hoffer[1]

[1]Air Chemistry Group of Hungarian Academy of Sciences, University of Pannonia, Veszprém, P.O. Box 158, H-8201, Hungary

[2]Department of Earth and Environmental Sciences, University of Pannonia, Veszprém, P.O. Box 158, H-8201, Hungary

Keywords: scattering and absorption coefficient, backscattering, single scattering albedo, Angström-exponent

Presenting author email: amolnar@almos.uni-pannon.hu

In this work the optical properties of the regional background aerosol as a function of the aerosol mass concentration (PM10) are summarized. Beside the scattering and absorption coefficients backscattering, single scattering albedo and Angström-exponent is also discussed.

All data (optical parameters and PM10) presented in this work are monitored at the Hungarian background air pollution monitoring station, K-puszta. The total and backscattering coefficients have been measured at three wavelengths (450nm, 550nm, 700nm) by TSI 3563, while the absorption coefficient has been measured at 550nm by PSAP. PM10 mass concentration is detected by β-gauge measurements.

Our results show that below of 85μgm^{-3}, the absorption and the scattering coefficients are quasi linear functions of the PM10. The backscattered fraction of the total scattering is in an inverse relationship with PM10, the backscattered fraction decreases if the mass concentration increases. The decrease of this parameter depends on the wavelength: the longer the wavelength the higher its value. Thus, the backscattering fraction, which is an important factor in climate models, cannot be considered constant.

The single scattering albedo is also studied as a function of PM10. The data also show that the increase of PM10 results in the rise of the single scattering albedo (Fig. 1). This is due to the fact that the increase of scattering coefficient is higher than that of the absorption coefficient.

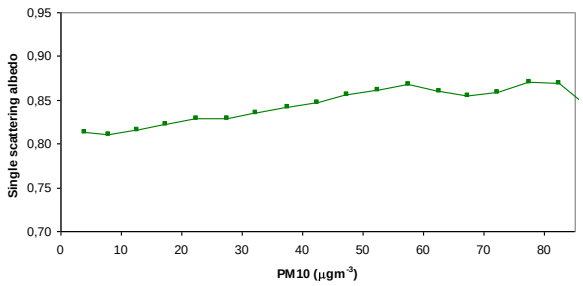

Figure 1. Single scattering albedo as a function of PM10.

The wavelength dependence of scattering coefficients (total and backscattered) is evaluated by the Angström-exponent (α). It is found that when PM10 increases, the value of α decreases in the whole wavelength range (450-700nm) (Fig. 2). This suggests that in background air the growth of PM10 mass concentration involves the increase of mean particle size. This can be explained by the fact that in clean air (low PM10) the role of freshly formed secondary particles (which are very small in size and consequently have small mass concentration) is higher than that of aged and coarse particles. Finally, the results make it clear that the values of Angström-exponent in different wavelength ranges are not equal, they are smaller at shorter (450-550nm) than at longer (550-700nm) wavelengths.

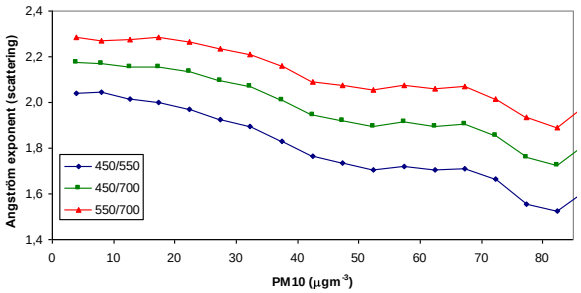

Figure 2. Variation of the Angström-exponent as a function of PM10 concentration.

This work was supported by the FP6 projects: European Integrated project on Aerosol Cloud Climate and Air Quality Interactions (EUCAARI, contract No: 036833-2) and European Super-sites for Atmospheric Aerosol Research (EUSAAR, contract No: RII3-026140).

Seasonal characteristics of the radiative properties of aerosols at Mace Head, Ireland

A. Vaishya, S.G. Jennings, and C.D. O'Dowd

Centre for Climate & Air Pollution Studies, School of Physics, Ryan Institute,
National University of Ireland Galway, Galway, Ireland.
Keywords: marine aerosols, scattering coefficient, seasonal patterns, Nephelometer.
Presenting author email: a.vaishya1@nuigalway.ie

The Mace Head Atmospheric Research Station (53^0 19'N, 9^0 54' W) on the west coast of Ireland is an important GAW measurement site and is designated as a clean marine background station for aerosol research. Long term continuous measurements of aerosol radiative properties, specifically the light absorption coefficient (Junker, 2006) and the light scattering coefficient, have been carried out since 1989 and 1997, respectively.

Being a coastal research station, Mace Head is dominated by air masses arriving from the clean marine sector, from 180^0 to 300^0, approximately 52% times throughout the year (Jennings et al, 2003). Junker et al, (2006) found that the hourly average absorption coefficient of marine aerosols follows a lognormal distribution with a geometric mean of 0.31 Mm^{-1}. Yoon et al, (2007) reported a seasonal trend in the light scattering values at Mace Head with aerosol scattering coefficient showing a minimum value of 5.5 Mm^{-1} in the summer and a maximum value of 21 Mm^{-1} in the winter season.

In this study we have analysed 12 years of aerosol scattering data, from 1999 to 2010, from a three wavelength (TSI 3563) and a single wavelength (TSI 3551) Nephelometer instruments. Black carbon mass concentration was used as a criterion for classification of the scattering coefficient data into clean and polluted sector scattering. Black carbon mass concentrations of <50 ng/m^3 and >150 ng/m^3 were used as indicators for the clean sector and polluted sector, respectively. Black carbon mass concentration values used in this study were obtained from three different instruments: Aethalometer model's AE-9 from 1999 up to April 2005; an Aethalometer AE-16 from May, 2005 up to 2010 and a MAAP instrument from April, 2005 up to 2010. Adjustments were made to MAAP data in order to make it comparable with AE-16 data using the analysis of Jennings et al, (2007). MAAP data were used to fill the gaps when AE-16 data were not available.

There was a three fold increase in aerosol scattering values during the winter months as compared to summer months. This increase is mainly driven by enhanced sea-salt production due to high wind speed during the winter season. In contrast the weather systems during the summer months are less active (Jennings et al, 2003) and the ocean water is dominated by water insoluble organic compounds (O'Dowd et al. 2004). A detailed study of the seasonal variation of aerosol scattering coefficient values over the twelve year period with respect to clean and polluted sectors is presented.

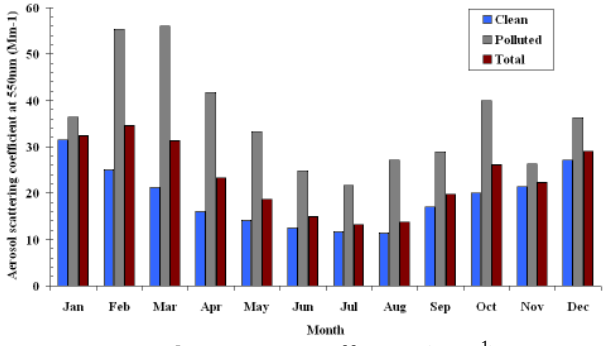

Figure 1: Aerosol scattering coefficient (Mm^{-1}) at 550nm for clean (blue) and polluted (grey) sectors, at Mace Head from 1999-2010.

This work was supported by funding from the EC's 6th Framework Programme Integrated Project, GEOmon.

Jennings, S. G., Kleefeld, C., O'Dowd, C. D., Junker, C., Spain, T. G., O'Brien, P., Roddy, A. F. and T. C. O'Connor (2003) *Boreal Environ. Res.*, **8**, 303-314.

Jennings S. G., Ceburnis D. and Kelly, B. M. (2008) *9th International Conference on Carbonaceous Particles in the Atmosphere*, 12–14 August, Berkeley, California, USA.

Junker, C., Jennings, S. G. and Cachier, H. (2006) *Atmos. Chem. Phys.*, **6**, 1913-1925.

O'Dowd, C. D., Facchini, M. C., Cavalli, F., Ceburnis, D., Mircea, M., Decesari, S., Fuzzi, S., Young, J. Y. and Putaud, J. P. (2004) *Nature*, **431**, 676-680.

Yoon, Y. J., Ceburnis, D., Cavalli, F., Jourdan, O., Putaud, J. P., Facchini, M. C., Decesari, S., Fuzzi, S., Sellegri, K., Jennings, S. G. and O'Dowd, C. D. (2007) *J. Geophys. Res.*, **112**, D04206.

Aerosol-halogen interaction: Change of aerosol optical properties

J. Ofner[1], N. Balzer[1], H. Grothe[2], H.-U. Krüger[1], Ph. Schmitt-Kopplin[3], C. Zetzsch[1]

[1]Atmospheric Chemistry Research Laboratory, University of Bayreuth, Bayreuth, Germany
[2]Institute of Materials Chemistry, Vienna University of Technology, Vienna, Austria
[3]Institute of Ecological Chemistry, Helmholtz Zentrum Munich, Munich, Germany
Keywords: organic aerosols, halogenation processes, optical properties..
Presenting author email: Johannes.ofner@uni-bayreuth.de

Reactive halogen species, released by sea-salt activation, offer a class of reactants of utmost importance for heterogeneous reactions with organic aerosols. To study the interaction of organic aerosols with these halogen species, secondary organic aerosol (SOA) was produced from α-pinene, catechol and guaiacol (Ofner et al., 2011) in a 700 L glass smog-chamber and in a 3500 L Teflon smog-chamber at defined environmental conditions (with and without simulated sunlight and ozone at various humidities). The well-characterized and aged organic aerosols were exposed to molecular halogens in the presence of UV/VIS irradiation and to halogens released from simulated natural halogen sources to study the halogen-SOA interaction process.

Various spectroscopic methods were used to investigate optical and structural changes of the organic aerosols. Diffuse reflectance UV/VIS spectroscopy was employed to characterize optical properties in the UV/VIS spectral range. Using FTIR spectroscopy both, the aerosol formation and transformation process and, using ATR (Attenuated Total Reflectance) spectroscopy, the appearance of functional and structural elements of the particulate phase were characterized. Using Temperature-Programmed-Pyrolysis Mass-Spectroscopy (TPP-MS) and Ultra-high resolution Fourier-Transform/Mass-Spectroscopy (ICR-FT/MS), degrees of halogenations and single halogenated molecules could be determined.

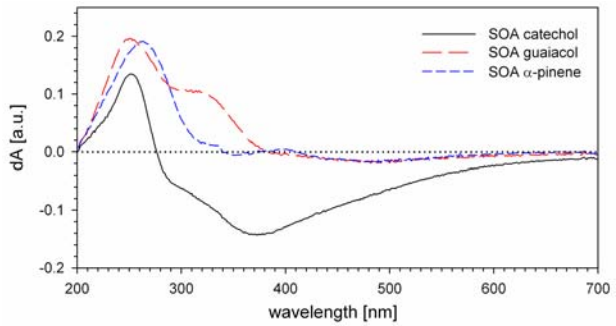

Figure 1. Differential absorbance of the organic aerosols, calculated from the diffuse spectra before and after the reaction with natural released halogens

Overall, the optical properties of organic aerosols appear to be significantly changed due to the reaction with those reactive halogen species. While the interaction with chlorine was found to lead to some bleaching (corresponding to a blue-shift), the reaction with bromine shifts the absorption in the UV/VIS range to the red. Those changes are indicated by calculating the differential absorbance (dA) from the diffuse UV/VIS spectra (see Fig. 1), where a "bleaching" of the organic aerosols is observed.

Also transformation of relevant functional groups and formation of carbon-halogen bonds was found in the infrared between 800 and 600 cm^{-1}. While the carbonyl stretch region is the most dominant absorption at simulated (from α-pinene, catechol and guaiacol) and natural SOA samples (at about 1730 cm^{-1}), the infrared spectra of the halogenated SOA from the model precursors significantly differ (see Fig. 2) from the reported spectra of unprocessed SOA (Ofner et al., 2011).

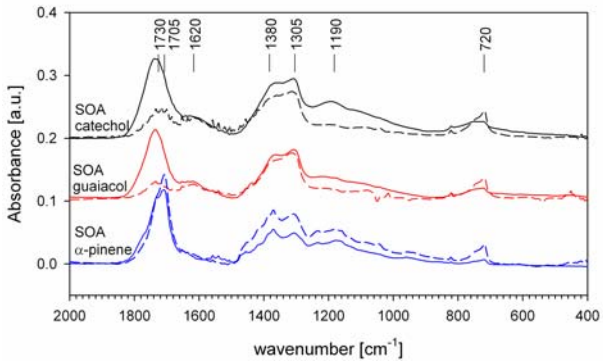

Figure 2. Comparison of ATR FTIR spectra of the unprocessed (solid lines) and halogenated (dashed lines) organic aerosols.

Due to the change of the chemical properties a change of the physical properties is expected, that is related to the atmospheric environment like ability to act as CCN, their potential to adsorb other low-volatile gases or even their contribution to radiative forcing.

This work was supported by the German Research Foundation within the HALOPROC project.

Ofner, J., Krüger, H.-U., Grothe, H., Schmitt-Kopplin, P., Whitmore, K., and Zetzsch, C. (2011), *Atmos. Chem. Phys.*, **11**, 1-15.

Seasonality of aerosol optical properties in the Amazon Basin

L.V. Rizzo[1], K.T. Wiedemann[2], F. G. Morais[2], P. Artaxo[2], T. Muller[3], A. Wiedensohler[3]

[1]Department of Exact and Earth Sciences, Federal University of Sao Paulo, Diadema, 09972-270, Brazil
[2]Institute of Physics, University of Sao Paulo, Sao Paulo, 05508-090, Brazil
[3] Leibniz Institute for Tropospheric Research, Leipzig, 04318, Germany

Keywords: Biogenic particles, Biomass burning, Absorption coefficient, Scattering coefficient.
Presenting author email: artaxo@if.usp.br

Aerosol physical and chemical properties were measured at a pristine Amazonian forest site from Febuary 2008 to December 2010, under the scope of EUCAARI (European Integrated Project on Aerosol Cloud Climate and Air Quality interactions) and AEROCLIMA (Direct and indirect effects of aerosols on climate in Amazônia and Pantanal) projects. The dataset obtained encompass the first long term aerosol measurements ever performed in Amazonia, elucidating the differences between the biogenic aerosol population naturally released by the forest metabolism and the anthropogenic aerosols brought to the ecosystem by outer sources.

Measurements were taken at the Cuieiras forest site, tower TT34, above the canopy (45m), under dry conditions. A MAAP photometer in series with a nephelometer (TSI 3563) was used to measure aerosol absorption and scattering, respectively. Scattering coefficients were corrected for truncation errors. Observations were adjusted to 1000 mbar and 0^{o}C.

Aerosol scattering coefficients ranged between 1 and 200 Mm^{-1} at 450 nm (Figure 1), while absorption ranged between 1 and 20 Mm^{-1} at 637 nm (Figure 2). A strong seasonal behavior was observed, with greater aerosol loadings during the dry season (Jul-Nov) as compared to the wet season (Dec-Jun). Although the forest site is well preserved, it receives the influence of regional biomass burning emissions during the dry season.

During the wet season, aerosol scattering (450 nm) and absorption (637 nm) coefficients averaged, respectively, 14 ± 22 and 0.9 ± 0.8 Mm^{-1}. Both optical coefficients were greatly increased during the dry season, averaging 58 ± 58 Mm^{-1} and 4.1 ± 3.8 Mm^{-1}, correspondingly. Angstrom exponents for scattering were lower during the wet season (1.6 ± 0.4) in comparison to the dry season (1.9 ± 0.2), which is consistent with the shift from biomass burning aerosols, predominant in the fine mode, to biogenic and dust aerosols, predominant in the coarse mode. Single scattering albedo, calculated at 637 nm, did not show a significant seasonal variation, averaging 0.86 ± 0.06 and 0.86 ± 0.04, respectively for wet and dry season.

Also, measurements of aerosol elemental composition indicate events of long range transport of African dust to the Amazonian forest site. These outer sources of particles affect the optical properties of the natural aerosol population, with implications to the regional climate and to the forest nutrient cycle.

This work presents a general description of the aerosol optical properties in Amazonia, both during the Amazonian wet season, when the aerosol population is dominated by particles of biogenic origin, and during the dry season, when there is a strong influence of biomass burning emissions. It is important to describe accurately the optical behavior of these particles in order to assess the impact of anthropogenic changes on the regional climate. Furthermore, since the Amazon forest is located in a region of intense convective activity, the aerosols released there can be long-range transported, potentially resulting in climate effects that are globally relevant.

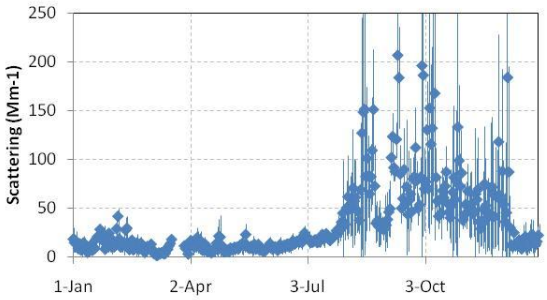

Figure 1. Daily averages of scattering coefficients measured at 450 nm from Feb 2008 to Dec 2010.

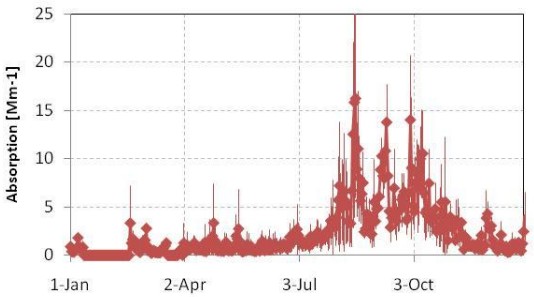

Figure 2. Daily averages of absorption coefficients measured at 637 nm from Feb 2008 to Dec 2010.

This work was supported by European Integrated project on Aerosol Cloud Climate and Air Quality Interactions, EUCAARI (036833), and Fundação de Amparo à Pesquisa do Estado de São Paulo, FAPESP (08/58100-2).

Comparison of MODIS Deep Blue aerosol single scattering albedo and asymmetry parameter with AERONET for northern Africa, Middle East and Europe

M. Korras Carraca, A. Gkikas and N. Hatzianastassiou

Department of Physics, University of Ioannina, Ioannina, Epirus, 45110, Greece
Keywords: aerosol single scattering albedo, asymmetry parameter, MODIS, AERONET
Presenting author email: agkikas@cc.uoi.gr

The interaction of aerosols with radiation, which determines their climatic effects, is strongly dependent on their optical properties (Hatzianastassiou et al., 2004). Spectral radiative transfer models usually require data for three optical properties, namely aerosol optical depth (AOD), single scattering albedo (SSA) and asymmetry parameter (g_{aer}). Apart from AOD, which quantifies the aerosol loading, SSA expresses the scattering/absorbing ability of aerosols whereas g_{aer} describes the angular distribution of the scattered radiation from aerosol particles. Although globally distributed AOD data are quite abundant nowdays, those of SSA and g_{aer} are still limited, despite the fact that both critically affect the aerosol radiative and climatic effects, as it has been shown in the literature. Recently, an unprecedented availability of globally distributed SSA and g_{aer} data was made possible thanks to the MODerate Resolution Imaging Spectroradiometer (MODIS) Deep Blue algorithm (Hsu et al., 2004). However, given the difficulties in deriving these properties, which are highly depended on relevant assumptions that are made, it is necessary to intercompare these products with corresponding groundbased ones.

In the present study, we attempt an intercomparison of MODIS Deep Blue SSA and g_{aer} data with corresponding measurements from stations of the globally distributed reference AERONET network. The intercomparison is performed for the greater Mediterranean basin and the surrounding regions of North Africa, Middle East and Europe. The study region extends from 5^o N to 70^o N and from 25^o W to 60^o E. The intercomparison of SSA and g_{aer} in the study region is of primary importance because of the co-existence of different types of aerosol (e.g. dust, urban, maritime, continental, biomass burning) originating from local, neighbouring and remote sources. We use daily gridded (1^ox1^o) data from the latest MODIS Deep Blue C051 collection over the period 24 February 2000-22 September 2010 from Terra, and over 4 July 2002-18 September 2010 from Aqua satellite. The MODIS Terra and Aqua SSA and g_{aer} data are compared against daily AERONET measurements from 156 stations within the study region. The MODIS wavelengths, 470nm (g_{aer}, SSA), 660nm (g_{aer}, SSA) and 870nm (g_{aer}) have been selected to ensure satisfactory spectral coverage and consistency with the available AERONET wavelengths (close to 440nm, 675nm and 870nm).

According to MODIS-Aqua, the mean annual g_{aer} values range from 0.58 to 0.73 at 470nm, from 0.49 to 0.71 at 660nm and from 0.43 to 0.7 at 870nm, exhibiting a decreasing tendency with increasing wavelengths. The MODIS-Terra values are slightly larger (by 0.02-0.04) than Aqua ones. In general, g_{aer} takes slightly larger values in the Atlantic Ocean and Arabian Sea, probably due to the influence of dust outflows from the Saharan and Arabian deserts, against smaller g_{aer} values in the North, Baltic and Black Seas and off the region's coasts. Especially low g_{aer} values are observed in the closed Black Sea and off the coasts of northern Europe and Siberia, which can be attributed to the fine pollution aerosols from anthropogenic activities. The MODIS SSA_{470nm} values, which essentially cover North Africa and Middle East, range from 0.89 to 0.95 over most of these desert areas. The smallest values are observed in Tunisia and northeastern Algeria. On the other hand, SSA_{470nm} values larger than 0.95 (up to 0.99) are found at the west parts of the sub-Sahel.

Two specific sub-regions have been discriminated based on the different nature of aerosol sources which are included in them. The first sub-region consists of Europe (significant anthropogenic aerosols) and the second one consists of North Africa and Middle East (natural aerosols). The frequency histograms of MODIS g_{aer} values at 470nm, reveal distributions shifted to smaller values for Europe (centered at 0.7) against larger values for North Africa and Middle East (centered at 0.72), explained by the smaller sizes of anthropogenic aerosols in Europe. This is in accordance with a similar finding based on the corresponding frequency distributions for the AERONET stations.

The MODIS SSA_{470nm} values seem to be slightly overestimated, with respect to AERONET ones (bias ≈ 0.03). The MODIS frequency distributions are generally shifted to larger values, ranging from 0.86 to 1, whereas the AERONET histograms indicate values ranging from 0.68 to 0.99, but with only 10% of them below 0.86.

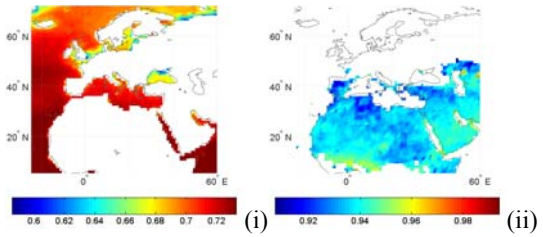

Figure 1. Geographical distributions of MODIS-Aqua: (i) g_{aer} and (ii) SSA at 470nm for the period 2002-2010.

Hatzianastassiou et al. (2004) *Tellus B*, Vol. 56, 4, p. 368-381.

Hsu et al. (2004) *IEEE Trans. Geosci. Remote Sens.*, 42, 557– 569.

Aerosol optical properties in Amazonia - Spatial and seasonal variability

K.T. Wiedemann[1], P. Artaxo[1], A. Correia[1], S.C. Wofsy[2], M.O. Andreae[3] and C. Gerbig[4]
[1]Institute of Physics, University of Sao Paulo, Sao Paulo, Brazil
[2]School of Engineering and Applied Sciences, Harvard University, Cambridge, USA
[3]Biogeochemical Department, Max Planck Institut of Chemistry, Mainz, Germany
[4]Department of Biogeochemical Systems, Max Planck Institut of Biogeochemistry, Jena, Germany
Keywords: Airborne particles, light absorption, light scattering, optical depth.
Presenting author email: kenia@if.usp.br

Reducing the uncertainty in estimates of the impact of aerosol on climate remains at the center of interest in the climate changes discussion. The Amazon Basin is one of the most crucial regions in the world where these effects may be studied from many points of view. In particular, it is important to identify and to quantify the processes and sources that control the regional aerosol concentrations, in order to obtain a reliable quantification of their global impacts. We expect that a better understanding - and modelling - of these processes and sources may provide a better understanding of the feedbacks between climate and aerosol concentrations.

As a part of the LBA/BARCA experiment, an airborne campaign was conducted, using the two engine INPE aircraft (National Institute for Space Research), from 16 November to 2 December, 2008, corresponding to the transition period from dry to wet season in Amazon Basin. The flight legs are shown in the Figure 1, where the main cities are indicated. The aircraft was instrumented for collecting data on aerosol spatial distribution/concentration and size distribution and, in addition, measurements of trace-gases including O_3, CH_4, CO, CO_2 and N_2O were also performed. Sixty-eight profiles were obtained up to 4 km, covering an important part of the Amazon Basin. Total aerosol number concentration was measured at 1 Hz time resolution using a TSI 3010 Condensation Particle Counter model. A Thermo Multi Angle Absorption Photometer model 5012, operating at 637 nm, was used for measurements on aerosol light absorption, and for optical scattering by atmospheric particles, the aircraft was equipped with a three wavelength (450, 550, and 700 nm) TSI 3665 nephelometer. Aerosol number size distributions were measured with a TSI SMPS 3080 for particles ranging 10–354 nm.

This work presents the spatial distribution of the aerosol optical properties in Amazonia during the transition between dry and wet season, when the aerosol population is strongly influenced by biomass burning emissions (Figure 2). The Amazon Basin is a region of intense convective activity, and the spatial and temporal description of the optical properties of these particles supports the assessment of the impact of changes in the regional land use, not only on the regional climate, but also at the global scale.

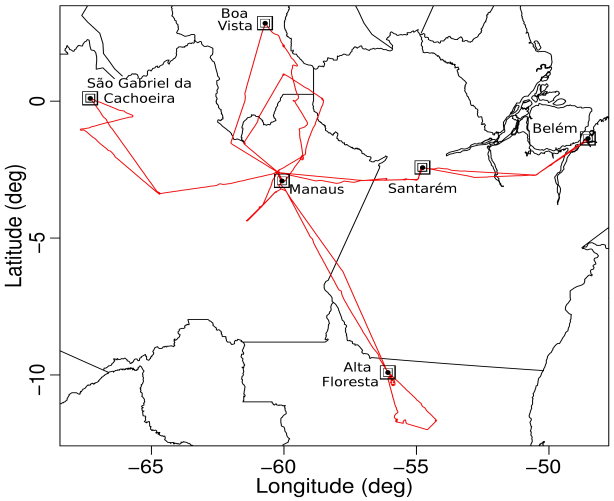

Figure 1: Mapping of the flight tracks during the BARCA-A airborne campaign, covering an important part of the Amazon basin during the dry season.

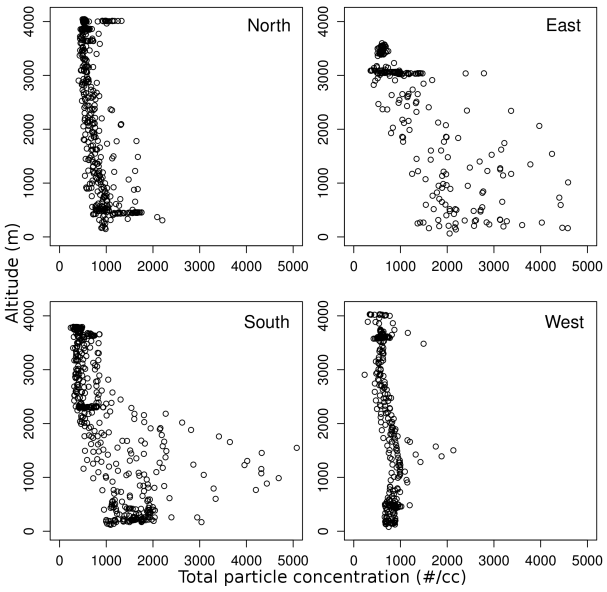

Figure 2: Total aerosol concentration vertical profiles for the northern, eastern, southern and western sectors of Amazonia during the transition from dry to wet season, November 2008. The aerosol population is strongly influenced by biomass emissions.

Thursday, September 8, 2011

Session 8P: Poster session B

Instrumentation

Diisocyanate aerosols in polyurethane manufacture

A. Akachat[1], H. Rebbah[1]

[1] Laboratoire de matériaux minéraux et composites, Université Med Bougara, Avenue de l'Indépendance, 35000 Boumerdes, Algérie.

Keywords: particles, isocyanates, PU,

Workplace atmosphere is an important distribution of various pollutants, resulting from the handled products and concerned processes. The fate of these pollutants in the air (transport, deposition, degradation), is determined by their distribution between atmospheric particles and gas phase (Lohmann et al. 1998). Harmfulness of particles in workplace atmosphere and the disease hazards that they present are related to their chemical nature and size. The production of one kilogramme rigid polyurethane foam releases nearly 7362 milligrams of solid particles in air.

In this work, we used the personal aerosol sampler CIP10-R (Courbon et al. 1988) and filters for evaluation of alveolar (Gorner et al. 1996) and inhalable fractions of particles during clean of casts after injection of the polyurethane foam (PU) (fig 1). HPLC was used for detection of MDI in different post (fig 2).

Obtained Results reveal that MDI in alveolar fraction prevail the total collected particles, this can be allotted to the process used for cleaning and to the quality of formulated foam.

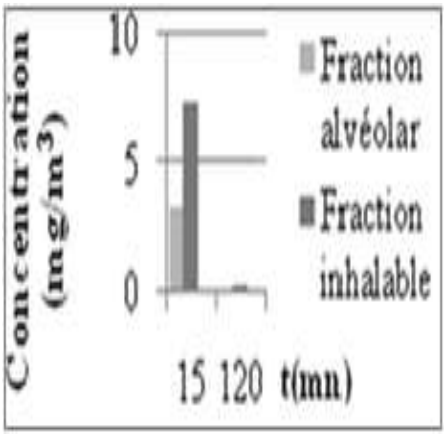

Fig. 1 : Concentration in 15 et 120 mn.

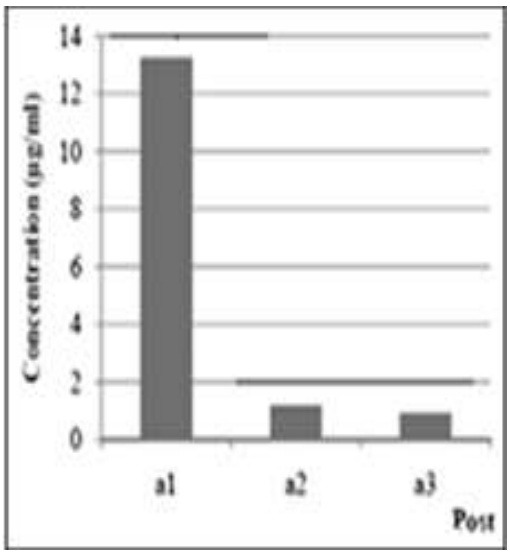

Fig. 2: MDI Concentration in 15 and 120 mn.

Lohmann, R., Jones, K.C. (1998). Dioxins and furans in air and deposition: a review of levels, behaviour and processes. Science of the Total Environment 219, 53-81.

Courbon P., Wrobel R., Fabries J.F. (1988). Anew individual respirable dust sampler: the Cip 10. Annals of Occupational Hygiene, 32pp. 129 - 143.

Gorner P., Fabries J.F. (1996). Industrial aerosol measurement according to the new sampling convention. Occupational Hygiene, 3, pp 361 – 376.

Characterizing organic matter in aerosols of biomass burnings and the ambient air by a multi-element scanning thermal analysis (MESTA) technique

Y.P. Hsieh[1] K. Robertson[2] and G. Bugna[1]

[1]Center for Water and Air Quality, Florida A&M University, Tallahassee, FL 32312
[2]Tall Timbers Research Station, Tallahassee, FL 32312
Keywords: particulate matter, organic sulphur, chemical signature. thermogram
Presenting author email: yhsieh@famu.edu

Organic matter is a major constituent of aerosols. Analyzing organic matter in aerosols, however, is still a tedious and difficult procedure except for the bulk elemental analysis. In order to fill this analytical gap, we developed the multi-element scanning thermal analysis (MESTA) method to provide a rapid and sensitive means for organic matter analysis in aerosols. MESTA heats up a sample from ambient temperature to 800 ºC under a given atmosphere and a constant heating rate. The result is simultaneous C, N and S thermograms of a sample representing the chemical nature and thermal stability characteristics of its compounds (Hsieh, 2007). We report here the application of MESTA to the analysis of particulate matter ($PM_{2.5}$) from the ambient air and that emitted from biomass burnings. We also investigated the feasibility of using the MESTA thermograms as a chemical signature to differentiate the $PM_{2.5}$ sources between the biomass burning and the ambient air. We collected $PM_{2.5}$ samples from the ambient air and prescribed burnings of pine forests and analyzed them with the MESTA method. The MESTA thermograms show that the $PM_{2.5}$ emitted from the biomass burning has a characteristic high-temperature-volatile (>300 ºC) component with very low N and S contents whereas those of the $PM_{2.5}$ in the ambient air have a characteristic low-temperature-volatile (<300 ºC) component with very high N and S contents (Fig. 1).

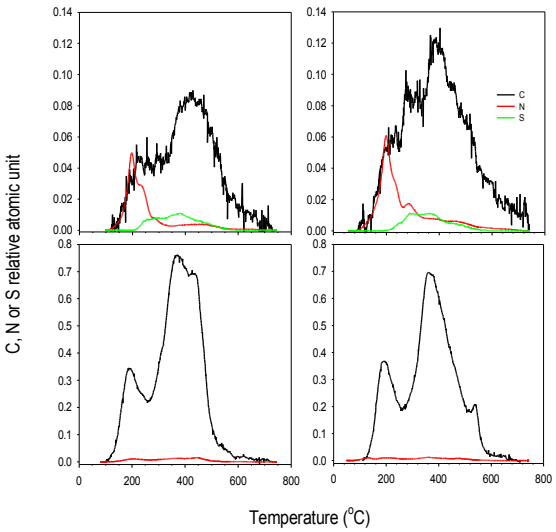

Fig. 1. The MESTA thermograms of the ambient PM (top) and those of biomass burning emitted (bottom).

The S detected in those MESTA thermograms are all organic as they are totally different from the thermograms of reference elemental sulfur, sulfides and sulfates compounds. The black carbon (thermally stable carbon peaks >525 ºC, Hsieh and Bugna, 2008) content of biomass burning PM averaged 12.8% of the total C in comparison to that of the 23% in the ambient air. All MESTA thermograms are quantitative and the detection limits for C, N and S are better than 0.2, 0.05 and 0.01 µg, respectively. The sharply contrasting MESTA chemical signatures between the experimental biomass burning $PM_{2.5}$ and the ambient air $PM_{2.5}$ provide a sensitive and quantitative means to quantify the presence of the biomass burning emitted $PM_{2.5}$ in the air. MESTA can also provide carbon isotopic ratio information of the compounds according to their thermal stability. The carbon isotopic analysis of MESTA indicates that C3 wood and grass burning produced insignificant carbon isotopic fractionation while some C4 grasses produced significant carbon isotopic fractionation resulting a heavier carbon signature in the smokes. This study shows that MESTA is a sensitive and convenient method for aerosol analysis and characterization, a fundamentally important step in air quality research and regulation.

This work has been partially supported by the United States Department of Agriculture/National Research Initiative /Agricultural Air Quality Program and the National Science Foundation/Atmospheric Chemistry Program.

Hsieh, Y. P. (2007) *J. AOAC International* 90:54-59
Hsieh, Y.P. and Bugna, G. (2008) *Org. Geochem.* 39:1562-1571

Correlating the opacity-based dustiness behaviour to material specific properties

S. Bach, E. Schmidt

Department of Safety Engineering / Environmental Protection, University of Wuppertal, Germany
Keywords: Dust, Air quality, Optical instrumentation, Respirable aerosols.
Presenting author email: sbach@uni-wuppertal.de

The background of this research project is to examine the possibilities of a single-drop apparatus for the measurement of the dustiness behaviour of powders called DustView (Palas® GmbH, Karlsruhe). Objective is to find an algorithm for the coherence between the opacity values of the DustView respectively their time-related development and the concentration of specific aerosol fractions inside its so-called dust chamber.

Figure 1 shows the laboratory set-up, where an aerosol spectrometer (OPC) is directly connected to the dust chamber of the single-drop apparatus. It allows the simultaneous measurement of the extinction of two laser beams in different heights (3 resp. 13 cm above ground plate) and the particle size distribution and number concentration of the aerosol dispersed in the chamber in the same heights respectively.

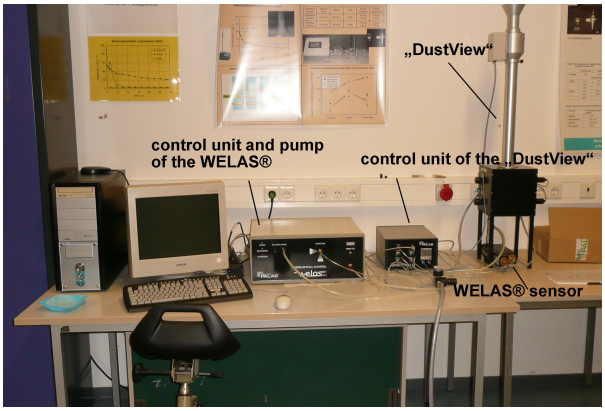

Figure 1. Modified version of the Palas DustView®, including single-drop apparatus and OPC “WELAS®”

Additionally, other material-specific properties have been measured, to ensure the best possible knowledge of the examined powders. Figure 2 shows all assimilated material features.

In Germany, there are limit values for the mass concentration of the respirable and inhalable dust fraction in workplace atmospheres. These are defined in the TRGS 900 (2010) and are 3 resp. 10 mg/m^3 at present.

The size fractions refer to the aerodynamic diameter of a particle, whereas the aerosol spectrometry gives the light scattering diameter. Van Buijtenen *et al.* (1974) define two possible ways of converting one into the other. Either, the aerodynamic shape factor of the material is known or the aerosol spectrometer has to be calibrated for each material. Here, only the particle density has been used as in Schmidt (2001), for the aerodynamic shape factor of the materials was mostly unknown and the calibration would have been too time-consuming for an uncertain outcome.

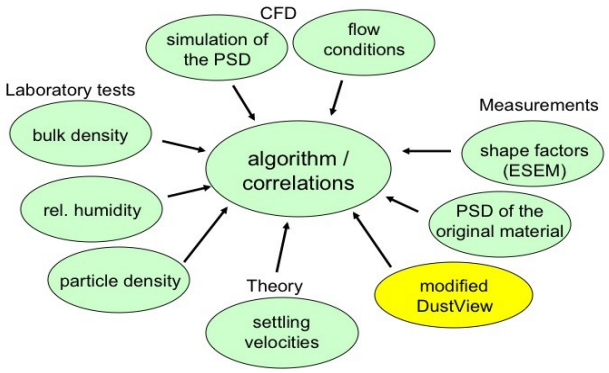

Figure 2. Measured and calculated material specific properties

The large amount of data collected for each material makes it difficult to locate correlations between two or more properties. What kind of dustiness-based data is suitable for the data mining process is yet to be determined. Additionally to the so-called dustiness number, calculated from the maximum opacity value and the 30-second-value of each measurement, it may also be the integral under the opacity curve or the offset between the peaks of the opacity curves of the two lasers. Also conceivable would be a value at a specific time, where the sedimentation process has already removed particles of a defined size. This would have to take the particle-specific settling velocity into account. All above named data could possibly correlate with the mass concentration of a specific aerosol fraction.

The correlation analysis is being carried out with the software “The Unscrambler X”, developed by CAMO®, Norway. Considering the two laser units, the correlation between OPC results and opacity seem to be better in the height of the lower laser.

This work was supported by the German Federation of Industrial Research Associations (AiF).

Schmidt, E., *Kurz gefasste Grundlagen der Partikelcharakterisierung und der Partikel-abscheidung*, Shaker Verlag, Aachen, 2001

TRGS 900, “Limit values for work places”, Bundesanstalt für Arbeitsschutz und Arbeitsmedizin BAuA, 2010

Van Buijtenen *et al.* (1974), *Comparison of “light scattering diameter” based on forward scattering measurements and aerodynamic diameter of aerosol*

particles, Atmos. Env., Vol 8, pp 885-896, Pergamon Press, GB

New aerosol spectrometer for 3 – 1000 nm size range.

V.G. Mitrochenko[1], A.M. Baklanov[1], P.P. Moiseenko[1], T.A. Ovchinnikova[2], S.I. Eremenko[3], S.N. Dubtsov[1], V.V. Karasev[1]

[1]Institute of Chemical Kinetics and Combustion, Siberian Branch of the RAS, Novosibirsk, 630090, Russia
[2]Novosibirsk Division of Institute for Water and Environmental Problems, Siberian Branch of the RAS Novosibirsk, 630090, Russia
[3] Uniscan Ltd., Novosibirsk, 630090, Russia

Keywords: CNC, Diffusion battery, Optical counter, Size distribution

Presenting author email: mitrochenko@list.ru

An improved version of Wide Range Aerosol Spectrometer (WRAS) for aerosol particles size range from 3 to 1000 nm has been designed. WRAS consists of a combination of NADB (Ankilov *et al.,* 2002) and optical particle counter. NADB consists of 8-stage screen diffusion battery, turbulent-mixing type CNC and interface controller. NADB operates under PC control *via* standard COM-port. Data inversion procedure is based on MSA algorithm (Eremenko, 1995). The measurement, data processing and storage, and results presentation are fully automated. The scattered light signal from OPC is digitized by 16-bit ADC and then transferred to PC *via* USB-port. The specially designed software allows operating NADB and OPC either individually, or together.

The measured aerosol particle size range is from 3 to 1000 nm (from 3 to 200 nm by NADB and from 300 to 1000 nm by OPC). Particles' concentration range is from 5 to $2x10^5$ cm^{-3} without dilution for NADB and up to 300 cm^{-3} for OPC. The accuracy of concentration and size distribution measurement is ± 10% and ± 30% for NADB and OPC respectively. The general view of WRAS is presented in Figure 1.

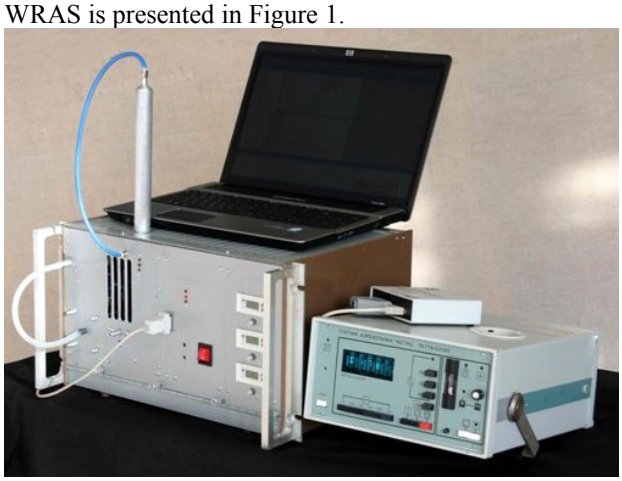

Figure 1. General view of the wide range aerosol spectrometer

WRAS is widely used in both basic (photonucleation, medical aerosol inhalation studies, etc.) and applied (laser –induced nanomaterial synthesis, etc.) research. Figures 2 and 3 present some examples of size distribution measurement with NADB.

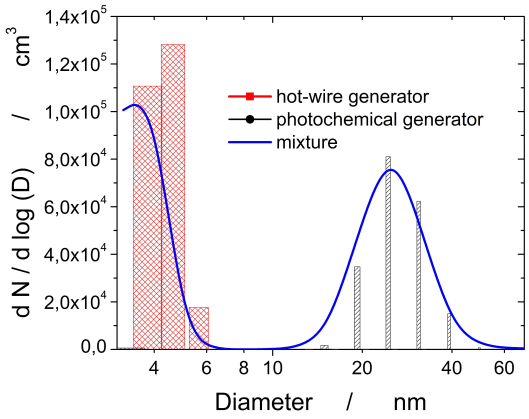

Figure 2. Size distributions of two individual aerosols and their mixture, measured with NADB. Red bars – aerosol from hot-wire generator, (Ankilov *et al.,* 2002), black bars – aerosol from photochemical aerosol generator (Dubtsov, 1996), line– mixture.

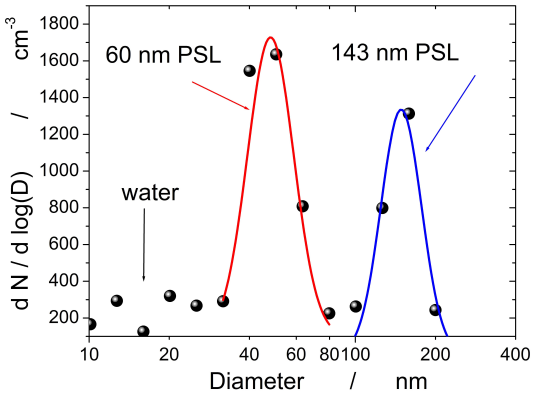

Figure 3. Size distribution of 60 nm and 143 nm PSL particles mixture, measured by WRAS. Dots - experimental results, lines – log-normal fits.

Ankilov, A.N., *et al*., (2002) *Atmospheric Research* **62**, 177 - 207.
Eremenko, S., and Ankilov, A. (1995) *J. Aerosol Sci*. **26S**, 749 -750.
Dubtsov,S.N. and Baklanov, A.M. (1996) *Aerosol Sci. Technol*., **25**, 67-73.

Performance of a High Resolution Optical Particle Spectrometer

H.S. Han[1], A. Sreenath[1], N.T. Birkeland[1], and G.J. Chancellor[1]

[1]TSI Incorporated, Shoreview, MN, USA
Keywords: Optical particle counter, Mie scattering, Light scattering, Filtration efficiency
Presenting author email: ryan.han@tsi.com

The optical particle spectrometer is one of the most widely used particle instruments in many areas such as aerosol research, filter testing, indoor air quality, etc. Light scattering technique is extremely sensitive and it has the advantage of minimally disturbing the aerosols and providing instantaneous information that is often suitable for continuous monitoring.

In this work, a recently developed high resolution optical particle spectrometer, TSI 3330 Optical Particle Sizer (OPS), was evaluated. The OPS is a light, portable, battery-powered unit that provides fast and accurate measurement based on single particle side scattering technology. It is capable of detecting particles from 0.3 to 10 um in diameter in up to 16 channels. Dead time correction is also available for high concentration measurements. The OPS also features real-time Mie scattering calculation capability to adjust the PSL calibration curve to a curve that better fits the aerosols of interest. For non-spherical particles, an additional shape factor is available to perform further adjustment on the calibration curve.

The OPS was evaluated with various monodisperse and polydisperse particles, namely, PSL, dioctyl sebacate (DOS or DEHS), sodium chloride, and methylene blue particles. The resolution of the OPS at 0.5 um was determined based on the ISO21501-1 method. It was found that resolutions of 10 OPS prototypes evaluated were all better than 5%. With 10% accuracy, the upper concentration limits of the OPS with and without dead time correction were found to be 3000 and 1000 particles/cm3, respectively. The refractive index algorithm performed quite well. Without refractive index adjustment, the size errors for methylene blue particles were as high as 40%. With Mie scattering correction, the sizing accuracy improved significantly, as shown in Table 1.

Table 1. Methylene blue particle size errors with and without refractive index correction.

Diameter (um)	No Correction (%)	Mie Scattering (%)	Mie Scattering + Shape Factor (%)
0.5	-21.14	9.70	10.88
0.6	-30.49	-0.78	0.65
0.7	-38.18	-9.73	-8.22
0.8	-42.78	-12.19	-10.79
0.9	-40.43	-4.47	-3.79

Sensor for vehicle on-board particle measurements

L. Ntziachristos[1], P. Fragkiadoulakis[1], Z. Samaras[1], K. Janka[2], J. Tikkanen[2]

[1]Lab of Applied Thermodynamics, Aristotle University, Thessaloniki, 54124, Greece
[2]Pegasor Oy, Tampere, 33100, Finland
Keywords: combustion aerosols, monitoring, PM measurements, vehicles emissions
Presenting author email: leon@auth.gr

Efforts to develop particle sensors for on-board diagnostics (OBD) of diesel vehicles are intensive as diesel particulate filters (DPFs) have become widespread around the world. According to the regulations, DPFs will have to be continuously monitored on the vehicle, to make sure that they achieve high filtration efficiencies.

This study presents a novel sensor that has been successfully tested for on-board diagnosis of damaged DPFs. The patented (Tikkanen, 2009) Pegasor Particle Sensor (PPS) operates by electrostatically charging particles passing through its body and then measuring the current produced by the charged particles as they leave the sensor. The basic principle of directly measuring the current escaping with charged particles was first described by Lehtimäki (1983). Figure 1 schematically shows the operation principle. The particles are charged by ions generated by a corona discharge, which is generated around a sharp tip at high voltage. After charging, the particles are neither collected on any filter nor accumulate on any part of the sensor. However, as charged particles leave the sensor, they produce an electrical current escaping the Faraday cup. Measurement of this current is proportional to the particle concentration.

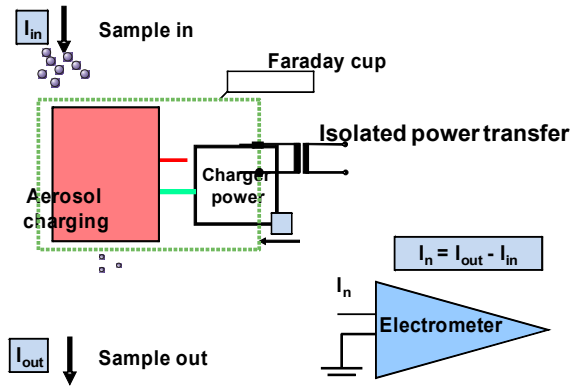

Figure 1. Schematic of sensor operating principle.

Determination of the concentration of particles by measuring the current produced by ions diffused on their surface has been shown to be a reliable technique (Ntziachristos *et al.* 2004. The signal produced scales with a power law of particle size (mobility diameter), with an exponent between one and two. For a known particle source (such as an engine), the signal can be calibrated to provide either the mass or the number of particles emitted.

Such a sensor has been developed and tested in real-exhaust of a diesel car and a diesel engine. The sensor provides high resolution (1 Hz, 0.3 s response time) and high sensitivity superseding the regulatory OBD requirements.

Measurements on an engine revealed the applicability of the sensor to monitor the failures of diesel particle filters. Its signal was found to perform similar to the smokemeter, a widespread instrument used for routine testing in automotive laboratories. The sensor could be used to identify damaged from undamaged filters and also to distinguish the degree of damage of failed filters.

The sensor was then installed in the exhaust of a vehicle to test the DPF efficiency of a well operating and a damaged DPF over a transient test. The sensor was found to be sensitive enough to clearly detect a defected from a well-operating particle filter even at levels as low as 6 mg km^{-1}.

This study demonstrates that a soot sensor based on the escaping current technique has the potential to be used for OBD and DPF control on forthcoming light duty and heavy duty diesel vehicles.

Lehtimäki, M., Modified Aerosol Detector, in V.A. Marple and B.Y.H. Liu (Ed.), Aerosols in Mining and Industrial Work Environment 3, 1135–1143. Ann Arbor Science Publishers, Ann Arbor, Michigan, USA (1983).

Ntziachristos, L., Giechaskiel, B., Ristimäki, J., Keskinen, J. Use of a Corona Charger for the Characterisation of Automotive Exhaust Aerosol, J. Aerosol Sci. 35:943–963 (2004).

Tikkanen, J. Particle Measurement Process and Apparatus, Patent publication no WO 2009/109688 (2009).

Development of an instrument to simulate puffing, inhaling and exhaling cigarette smoke

P. Warrington, C.M. McGrath, J. Perkins, C.J. Dickens

British American Tobacco, Group R&D, Southampton SO15 8TL, UK
Keywords: Aerosol measurement, Deposition, Inhalation, Respirable aerosols.
Presenting author email: paul_warrington@bat.com

The human smoking process for cigarettes consists of a puffing phase, followed by a mouth hold, where the tobacco smoke aerosol can change rapidly in terms of size and concentration due to coagulation and diffusional deposition. Smoke is then inhaled into the respiratory system along with dilution air through the mouth, and undeposited smoke exhaled.

Existing human smoking deposition studies are conducted where the puffing, inhalation and exhalation flows and times are accurately measured in real time. If these human smoking profiles can be simulated through in-vitro casts of parts of the human respiratory system, estimates of particle growth, coagulation and deposition within the respiratory system can be made without the need for a human smoker. The aim of this work was to develop an instrument to simulate the human smoking process.

The Puff Inhale Exhale (PIE) simulator comprises two sampling heads. The cigarette under test is mounted on the first sampling head which puffs on the cigarette following a pre-recorded human puffing profile. The puffed smoke is collected in an artificial mouth cavity. The second sampling head is then used to draw dilution air through the artificial mouth cavity following the inhalation section of a pre-recorded human respiratory profile. This flushes the smoke into a “lung” chamber where it may be sampled directly for analysis, or can be exhaled from the PIE through the artificial mouth and the second sampling head, following the exhalation section of the pre-recorded human respiratory profile. Exhaled smoke can be sampled and analysed as required.

The PIE was evaluated for puff volume compliance to generated bell, rectangular and triangular flow patterns with an average coefficient of variation of 1.1%. For consistency of exhaled smoke under a constant profile, there was no significant difference ($p < 0.05$) in the median particle size and concentration for multiple sampling flow rates and positions.

Effect of Different Sampling Methods on the Collection of CNF- and CNT-Fibres

M. Hildebrandt[1], B. Stahlmecke[1], N. Dziurowitz[2], S. Plitzko[2], H.J. Kiesling[3], M. Voetz[3], T.A.J. Kuhlbusch[1,4]

[1]Air Quality & Sustainable Nanotechnology Division, Institute of Energy and Environmental Technology, Bliersheimer Strasse 60, 47229 Duisburg, Germany
[2]Federal Institute for Occupational Safety and Health, Nöldnerstrasse 40-42, 10317 Berlin, Germany
[3]Bayer Technology Services GmbH, PT-MT-MCT Surfaces Characterization, 51368 Leverkusen, Germany
[4]CeNIDE, Center for Nanointegration Duisburg-Essen, 47229 Duisburg, Germany
Keywords: Nanofibres, Fibrous Particle Deposition, Preseparator, Charger, Sampler
Presenting author email: stahlmecke@iuta.de

Particle sampling is an integral part of exposure assessment, especially for fibrous particles like carbon nanontubes (CNT) or carbon nanofibres (CNF). Due to the expected increasing use of these materials, validated techniques for sampling are required. We investigated the characteristics of different samplers when challenged by an aerosol comprised of either CNT or CNF fibres.

Two different types of commercially available high aspect ratio nanoobjects (HARN, Carbon Nanofibres from Future Carbon and Baytubes® C150P from Bayer) were used for the comparison of sampling performance. The material under investigation was aerosolized either by wet dispersion of an aqueous suspension using an atomizer followed by a nafion dryer or by dry dispersion of the CNT or CNF powder, respectively. Dry dispersion was performed using a so called shaker (Broßell 2010). The aerosol was introduced into a 20 L compensation chamber for homogenisation. The number size distribution within the chamber was measured using an SMPS (Grimm, SMPS+C) in the size range from 10 nm up to 1100 nm for control purposes.

Three different samplers were utilized within the test series: Two commercial nanoaerosol samplers (NAS, TSI model 3089) with different polarity and a thermal precipitator (TP, BAuA prototype of personal sampler). Thus, differences due to the sampling principle (electrostatic versus thermophoretic deposition) are accessible. Due to the low flow rate of 2 ml/min the TP was placed inside the chamber. The two NAS were operated with a flow rate of 1.5 L/min and were placed outside the chamber. Furthermore, one of the NAS was equipped with a unipolar corona charger operating at 4.5 kV and a newly developed pre-separator with a nominal cut-off of 450 nm (Asbach 2010). This NAS was operated either without charger and pre-separator, with charger only or with both charger and pre-separator.

Within the TP silicon substrates with high purity and very low surface roughness were used. In case of the NAS the test was extended to silicon substrates, glassy carbon substrates and TEM grids. All substrates were investigated by applying high resolution scanning or transmission electron microscopy.

Figure 1 shows an example of CNF (A) and CNT (B) sampled on glassy carbon substrates without applying the pre-separator, but with the charger in operation. For a statistically sound comparison of the different sampling methods about 1000 particles were counted on each substrate. The different types of particles were divided in six categories (spheres, fibres/tubes, fibres/tubes+attachment, disperse clusters, compact clusters, matrix material) and three different size ranges (< 500 nm, 500 nm-1 µm, > 1 µm). We will present the setup and the statistical evaluation of the intercomparison of the different sampling methods. Recommendations on sampling of HARN will be presented based on the acquired information.

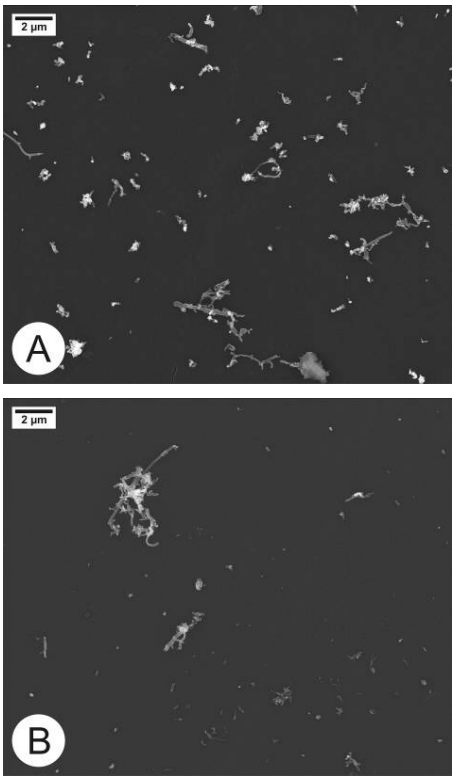

Figure 1. Examples of sampled CNF (A) and CNT (B) fibres.

This work is funded by the German Federal Ministry of Education and Research (BMBF) within the CarboSafe project as part of the Inno.CNT initiative by Grant No. 03X0043D.

Christof Asbach et al.: *Development and evaluation of a pre-separator for nanoparticle measurement devices*, oral presentation at IAC 2010, Helsinki, Finland

Dirk Broßell et al.: *Generating CNT/CNF-aerosols using a shaker aerosol generator for analysis of nanofibre dustiness*, poster presentation at International Conference on Workplace Aerosols 2010, Karlsruhe, Germany

Development of a Versatile Size Analyzing Nuclei Counter (vSANC)

T. Pinterich[1], P. M.Winkler[1, 2], P. E. Wagner[1] and A. Vrtala[1]

[1]Faculty of Physics, University of Vienna, Vienna, Boltzmanngasse 5, A-1090, Austria
[2] Advanced Study Program, National Center for Atmospheric Research, 1850 Table Mesa Drive, Boulder, Colorado, 80305, USA
Keywords: heterogeneous nucleation, condensation particle counter, nanoparticles.
Presenting author email: tamara.pinterich@univie.ac.at

The influence of charged molecular clusters and ionizing radiation on the formation of nanoparticles in the atmosphere and thus on cloud formation and climate has recently received considerable attention. In this connection as well as for various other applications accurate determination of aerosol properties, particularly for particles in the size range above approximately 1 nm diameter, is of great importance.

In the past an expansion chamber measuring system, the Size Analyzing Nuclei Counter (SANC) has been developed. Details of this experimental system are presented elsewhere (see, e.g. Wagner *et al*, 2003). Using this device various experiments on nucleation and condensational growth in supersaturated vapours were performed (e.g. Winkler *et al*, 2008).

The SANC is currently set up as a measuring system to be used for laboratory studies. However for various applications the use of a mobile measuring system would be important.Therefore a versatile version applying the same measuring principle – the vSANC – is being developed.

Just as for other CPCs the operation of the vSANC is based on heterogeneous nucleation of supersaturated vapour on aerosol particles and subsequent droplet growth. Thereby particles, which are too small to be detected by most other methods, grow to visible sizes and can be counted by optical techniques. In this way the present instrument allows detection of particles and ions with diameters down to 1nm (Winkler *et al*, 2008). Provided that each growing droplet corresponds to just one aerosol particle, the measured droplet concentration is equal to the aerosol number concentration. Expansion chamber and optical arrangement are designed to provide a comparatively wide range of droplet concentrations including atmospheric aerosol concentrations.

Essentially the experimental apparatus consists of two humidifiers, an expansion chamber, subpressure vessels, pumps and critical orifices. To analyse humidified aerosols containing e. g. sulphuric acid safely without damaging the instrument special materials such as 1.4571 stainless steel, FEP O-rings, a coated glass ring etc. are used for all parts in contact with the aerosol. Furthermore humidifiers, expansion chamber, connecting tubes and valves are thermostated separately. This allows measurements in a temperature range from -10°C to 30°C and avoids losses due to vapour condensation. Another important feature of this expansion type CNC is the possibility to operate either in active (aerosol flow regulation via various critical orifices) or passive sampling mode.

An electronic control unit in connection with pneumatic and solenoid valves was designed to control the measurement cycle. Vapour supersaturation is achieved by adiabatic expansion in a computer-controlled thermostated expansion chamber. Droplet growth is observed by means of the constant angle Mie-scattering (CAMS) detection method (Wagner, 1985). Here the droplets, growing in the expansion chamber are illuminated by a solid state laser beam. The light flux, scattered by the growing droplets, is monitored simultaneously under 10 different scattering angles. Depending on the selected scattering angle, the experimental scattered light flux vs. Time curves show series of maxima and minima in excellent agreement with theoretical scattered light flux vs. Size curves, calculated by means of Mie-theory. In order to enable an automatic establishment of a correspondence between experimental and theoretical light scattering extrema, scattering intensities for two specific angles are divided by eacht other(Hollaender, 2002). The resulting structure has far better pronounced extrema as can be seen in Fig. 1. Hence an automated data evaluation is possible.

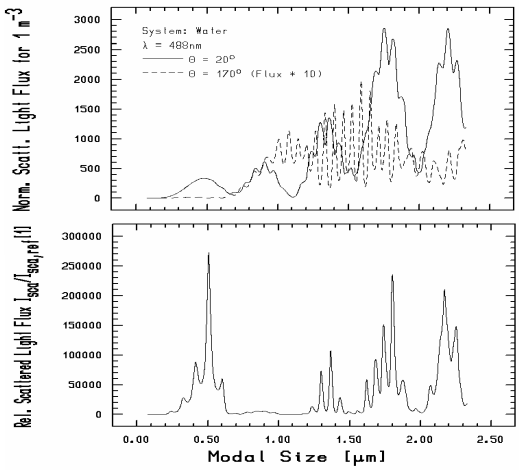

Figure 1. Normalized scattering light flux for scattering angles θ = 20° and 170° (upper graph) and their ratio (lower graph) both as a function of modal size.

A more detailed description of the vSANC including all its features will be presented later.

This work was supported by the Austrian Wissenschaftsfonds (Proj. No. L00593)

P. M. Winkler *et al.* (2008) *Science* **319**, 1374
P. E. Wagner *et al* (2003) Phys. Rev. E. **67**, 021605
P. E. Wagner (1985) *J. Colloid Interface Sci.***105***,* 456-467
W. Hollaender *et al.* (2002) *J. Atmos. Oceanic Technol.* **19**, 1811

Impaction velocities of particles in low pressure impactor

A. Arffman, M. Marjamäki and J. Keskinen

Aerosol Physics Laboratory, Tampere University of Technology, Tampere, Finland
Keywords: aerosol instrumentation, impactor, aerosol modelling
email: anssi.arffman@tut.fi

Mechanical behavior of an agglomerate or an aggregate particles can be important in some industrial applications like creating a drug aerosol to be inhaled (Santoso, 2011) or as a filler component in a polymer material(Friedlander, 1999). Interparticle forces define the strengthness of the agglomerate particle. These interparticle forces have been studied lately for example by Seipenbusch *et al* (2010). Low pressure impactor (LPI) can be used in defining the energy needed to break the bonds between the primary particles of an agglomerate as done by Froescke *et al* (2002). Phase of a sub-micron aerosol particles can also be investigated by impacting them against a collection plate in the LPI. This method has been used in investigating the phase of the atmospheric SOA particles by Virtanen *et al* (2010).

When the LPI is used to find out the interparticle bond energies of the agglomerate aerosol, particles need to be impacted to the collection plate with well defined energy. By scanning this energy the limit when the particles change their shape or break into parts can be found. The impaction energy depends on the velocity of the particles before the collision to the wall. Phase of the aerosol particles can be identified by examining if the particles bounce from the collection plate. The probability of the bounce depends also on the impaction velocity of the particle. Therefore the velocity of particle is a crucial parameter in these experiments.

The impaction velocity of the particles in the impactor can be adjusted by changing the pressure ratio of the impactor upstream to downstream pressure or changing the size of the particles. However, the velocity of the particles right before the impaction occurs, depends not just on the average properties of the impactor jet, but on the local flow field conditions. Arffman *et al* (2011) showed that the impaction conditions vary in a cross-section of the jet.

We used numerical simulations to study the impaction velocities of the particles in the LPI. Simulations were done using the methods presented by Arffman *et al* (2011). The impaction velocities of the particles in the round nozzle LPI as a function of the particle size and the radial position of the particles were simulated. It was found that the impaction velocity of the particle depends strongly on the particle size and its radial position in the jet. Figure 1 shows the velocity field at the cross-section of the impactor nozzle which upstream and downstream pressures are 100mbar and 40mbar and the diameter of the nozzle is 0,3mm. Cutpoint of the stage is approximately 30nm. Figure 2 shows the impaction velocities of 60nm particles as a function of the radial starting position. High variations in the impaction velocities across the jet can be seen. Velocities are higher at the edges of the jet because of the larger slip correction factor.

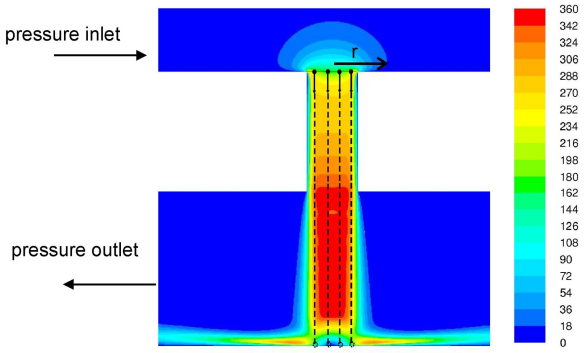

Figure 1. Velocity contours in the LPI nozzle. Particles and their tracks are schematically marked in the figure.

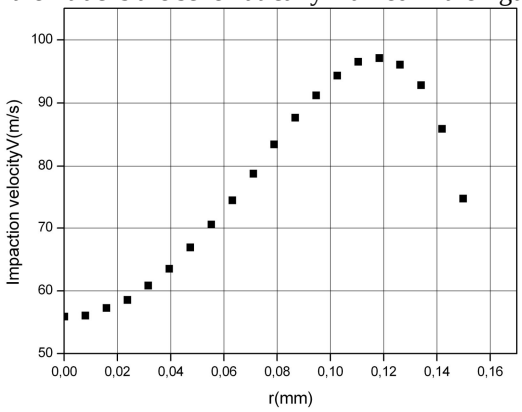

Figure 2. The impaction velocities of 60nm particles as a function of the radial distance from the axis of the jet.

Santoso, A., Handoko, A., Hak-Kim, C., Warren, H., F., Zhenbo, T., Runyu, Y., Aibing, Y (2011), J. Aerosol Science, In Press

Friedlander, S.K. (1999), J. Nanopart. Res., **1**, 9-15

Seipenbusch, M., Rothenbacher, S., Kirchoff, M., Schmid, H,-J., Kasper, G. and Weber, A., P. (2010), J. Nanopart. Res.,**12**,2037-2044

Froescke, F., Kohler, S., Weber, A. P., and Kasper, G. (2002), J. Aerosol Science, **34**, 275-287.

Virtanen, A., Joutsensaari, J., Koop, T., Kannosto, J., Yli-Pirilä, P., Leskinen, J., Mäkelä, J.M., Holopainen, J.K., Pöschl, U., Kulmala, M., Worsnop, D.R. , and Laaksonen A. (2010), Nature, **467** ,824–827

Arffman, A., Marjamäki, M. and Keskinen, J. (2011), J. Aerosol Science, In Press

Simulation of light scattering from air borne tea dust particles: possible carriers of pathogen

S Roy[*,1], N Barua[2], A. K Buragohain[2] and G. A Ahmed[1]

[1]Optoelectronics and Photonics Research laboratory, Department of Physics, Tezpur University, Tezpur -784028, Assam, India.
[2]Department of Molecular Biology and Biotechnology, Tezpur University, Tezpur -784028, Assam, India.

Keywords: light scattering, Mie scattering, Monte Carlo simulation, Bacterial activity

Abstract: A biotechnical method was followed to investigate whether tea dust particles might be a possible carrier of pathogenic species *Mycobacterium tuberculosis* by using novel light scattering techniques. An indigenously designed and fabricated laser-based light scattering setup was developed and used to carry out experiments on tea dust particles. In this paper we report for the first time the simulation of light scattering by these dust particles based on Monte Carlo code.

Introduction: Optical characterization of small particles which are suspended in air or when dispersed in a medium, by light scattering technique [1] is very important for a wide variety of applications. This includes optical diagnostics for industrial aerosol processes and combustion, environmental issues like visibility and haze problems, remote atmospheric sensing (lidar), and now specially to monitor hazardous air-borne particles. One type of such organic airborne dust is tea (*Camellia Sinensis*) dust which is released into the atmosphere by tea factories where tea is processed. As tea is grown in many tropical regions of the world this type of tea dust is found in abundance in these localities. This paper reports the work done in one such region, namely Assam in India, where tea is grown in large gardens and processed on a very large scale. The objective was to investigate if air-borne tea dust particles are a possible carrier of *Mycobacterium* pathogens, and then simulating the light scattering by these particles for better understanding of the physical processes and verification of experimental results.

Experimental Details: For monitoring the specimen a designed and fabricated laser based experimental setup (figure 1) was used to optically study the light scattering properties at a wavelength of 632nm. The system can measure scattered light signals from an angle of 10° to 160° for θ, and from 10° to 80° for ϕ to subsequently account for recording the volume scattering of size distributed dust particles. The effect on tea dust, when exposed to *Mycobacterium* species, was studied by using the Agar Well Diffusion Method [2]. In order to maintain safe laboratory procedures, the non-pathogenic species *Mycobacterium smegmatis* which has all the characteristic properties of the pathogenic species *Mycobacterium tuberculosis* was used as a model organism for carrying out investigations. Monte Carlo program (simscat.c) was developed in standard ANSI C language, and used for simulating the light scattering behaviour of these tea dust particles. The technique involves distribution of the photons in the simulation program between the particles according to their density as they were found to be governed by a Gaussian size distribution function [3].

Results: From the biotechnical experiments it was observed that the dust particles did not exhibit any antimycobacterial activity and might act as potent carriers. After the light scattering behaviour of both *Mycobacteriu*m contaminated and uncontaminated tea dust particles was studied as a function of scattering angle, and compared by the established Mie theory of light scattering [1], it was found that the light scattering behaviour of *Mycobacterium* contaminated and uncontaminated tea dust particles vary significantly. The simulation results were found to agree well with the experimental results within acceptable margins of error validating the efficiency of our program.

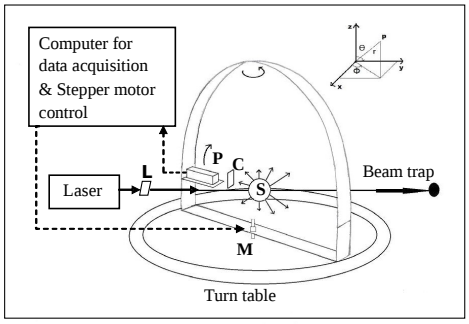

Figure 1: Schematic lay out of the scattering setup

This work was supported by Department of Science and Technology, Government of India project grant (SR/WOS-A/PS-20/2007 dated 04/08/2008) under the Women Scientist-A Scheme.

References

[1] Bohren C. F. and Huffman D. R. (1983). *Absorption and Scattering of Light by Small Particles*, New York: John Wiley & Sons Inc.

[2] Perez C, Paul M and Bazerque P (1990). *Acta Biol Med Exp*. 15, 113–115.

[3] Roy S and Ahmed G. A., " *Monte Carlo Simulation of Size Distributed sub-micron Spherical Particles in a volume element*", Optik-Int. J.Light Electron Opt., doi:10.1016/j.ijleo.2010.06.037(2010).

New and Compact Single Particle Laser Ablation Mass Spectrometer (LAAPTOF)

A.M. Trimborn[1], U. Rohner[2], M. Gonin[2], J. Jayne[3] and D. Worsnop[3]

[1]AeroMegt GmbH, Hilden, D-40723, Germany
[2]TOFWerk AG, Thun, CH-3600, Switzerland
[3]Aerodyne Research, Inc, MA, Billerica, 08121, USA
Keywords: single particle, mass spectrometry, laser ablation, LAAPTOF
Presenting author email: a.trimborn@aeromegt.com

Aerosol mass spectrometry has become an important tool for the chemical speciation of particles and particle populations. The chemical characterization of atmospheric aerosols has benefited greatly from instruments such as the Aerodyne Aerosol Mass Spectrometer (AMS) which provides a measure of the average chemical composition of sub micron particle populations (Canagaratna, et al. 2007). Laser ablation aerosol mass spectrometers have also evolved over the past decade. This class of instrumentation is capable of measuring chemical composition of individual particles.

One of the first bipolar laser mass spectrometer for single particle analysis (LAMPAS) was build by Hinz (Hinz et al 1996) and subsequently a number of other successful single particle aerosol laser ablation systems were also built and operated such as PALMS (Lee S. et al 2002), SPLAT (Zelenyuk et al 2005) and ATOFMS (TSI Corp.). Only one of these instruments was commercially available, while the others are unique single version research instruments.

We have developed a new compact bipolar single particle aerosol mass spectrometer LAAPTOF (Laser Ablation of Aerosol Particles Time of Flight Mass Spectrometer). The bench top instrument is built in a rack measuring 80 cm x 80 cm x 80 cm and is one of the smallest laser based aerosol mass spectrometers which is now commercially available.

The instrument features an aerodynamic particle lens inlet, a particle sizing region using cw scattering lasers, a bipolar TOF mass spectrometer and an excimer laser as ablation/ionization laser. The ablation laser operates at a wavelength of 193 nm with a power of up to 12 mJ /pulse (pulse duration ~ 10 ns). The TOF mass spectrometer is from TOFWerk (B-TOF) with a resolving power of $M/\Delta M \geq 600$ Th/Th FWHM for both ion polarities.

We will present the design and features of this newly developed instrument and show data illustrating its potential as a compact single particle aerosol mass spectrometer.

This work was supported by Bundesministerium für Wirtschaft und Technologie under grant EP100853.

Canagaratna, M.R., Jayne, J.T., Jimenez, J.L.,Allan, J.D. Alfarra, M.R., Zhang, Q., Onasch, T.B.,Drewnick, F., Coe, H., Middlebrook, A., Delia, A., Williams, L.R., Trimborn, A.M., Northway, M.J, DeCarlo, P.F., Kolb, C.E., Davidovits, P. and Worsnop D.R., (**2007**) Mass Spectrometry Reviews, **26**, 185– 222

Hinz, K.-P., Kaufmann, R., and Spengler, B. (**1996**) *Aerosol Science and Technology* **24**, 233-242.

Lee, S.H., Murphy, D.M.,Thomson, D.S. and Middlebrook, A.M., *Journal of Geophysical Research*, 107 (D1-D2), article number 4003, 200JD000011, 2002.

Zelenyuk A, and Imre DG. (**2005**). Aerosol Science and Technology **39**(6):554-568.

Setup and characterization of a new fast mixing type CPC

B. Wehner, M. Hermann, H. Siebert, F. Ditas, and A. Wiedensohler

Leibniz Institute for Tropospheric Research, 04318 Leipzig, Germany

Keywords: particle counting, response time, CPC

Condensation Particle Counters (CPCs) are the most widely used instruments for measuring submicrometer aerosol particle number concentrations. In atmospheric science, many open questions about particle dynamics require highly time-resolved particle measurements, e.g. when particle number concentrations vary on small scales due to turbulent processes. The response time of widely used unsheathed laminar flow-type CPCs is usually about 1 s. This results in a low spatial resolution, e.g., when deployed for aircraft-borne measurements. Therefore, we constructed a new fast mixing-type CPC (FCPC) based on the setup described by Wang et al. (2002).

Basically, the FCPC consists of four parts: the saturator, the mixing unit, the condenser, and the optics-block. All parts, except the optics (CPC 3772 optics bought from TSI Inc., St. Paul MN, USA) have been constructed at the Leibniz Institute for Tropospheric Research (IfT). The setup is based on the one described by Wang et al. (2002) and details are given in Wehner et al. (2010). Basically, a warm butanol-saturated air flow is mixed with the aerosol flow in a small mixing volume. Similar to Wang et al. (2002) who used a ¼-inch Swagelok cross in our case a ¼-inch Swagelok tee has been used as mixing chamber. In the following condenser block the air is cooled causing the required growth of aerosol particles. Afterwards the flow enters the optics, where the particles are counted.

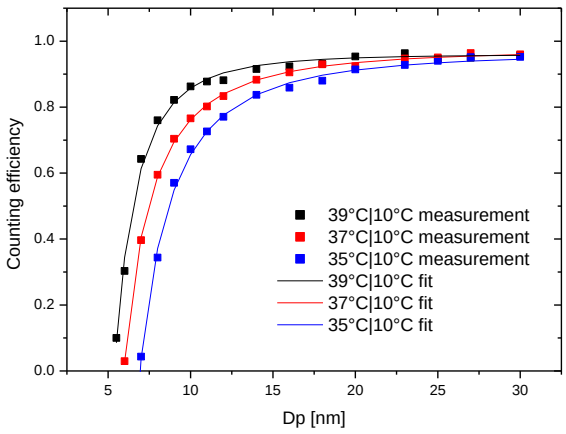

Figure 1: Counting efficiency of the Fast CPC (FCPC) at three temperature differences. Squares present mean values of three runs, the solid lines are fitted using the four-parameter equation: $\eta = a - b/(\exp(c*\log(x))-d)$.

The particle counting efficiency curve was determined by using silver particles generated in a tube furnace. Details are given in Wehner et al. (2010) and references therein. A monodisperse particle fraction was selected by a DMA and the counting efficiency was obtained with regard to a reference electrometer (EM, TSI 3068B). Results for three different temperature (saturator|condenser temperature) settings in the FCPC are shown in Fig. 1.

The measurement stability of the FCPC was tested in the laboratory in comparison with the electrometer as well as other commercial CPCs, such as a TSI 3776. These measurements show a stable behavior over at least five hours without refilling butanol (Wehner et al., 2010). As the FCPC has been developed for application on the helicopter-borne platform ACTOS, where measurement flights usually last less than 2 hours, this period is sufficient.

A field version of the FCPC was built and was applied to atmospheric measurements. Here, a combination of atmospheric turbulence and a strong isolated particle source which results in high fluctuations due to sharp gradients in particle number concentration has been used to estimate the time response of the instrument. The analysis of selected concentration steps illustrates that the FCPC is able to reach 1-1/e of the concentration step within 16 ms after a sharp increase in particle number concentration. The analysis of a 5-min time series shows that at frequencies higher than 30 Hz white noise becomes visible. However also at the maximum recorded frequency of 50 Hz the signal was not completely noisy, meaning that a response time of 20 ms is possible with the FCPC.

References

Wang, J., V. F. McNeill, D. R. Collins, R. C. Flagan: Fast mixing condensation nucleus counter: Application to rapid scanning differential mobility analyzer measurements, Aerosol Sci. Technol. **36**, 678 - 689, 2002.

Wehner, B., H. Siebert, M. Hermann, F. Ditas, A. Wiedensohler: Characterization of a new fast mixing type CPC and its application for atmospheric particle measurements, Atmos. Meas. Tech. Discuss., 3, 5907-5931, 2010.

Extinction of aerosols in an atmosphere simulation chamber: broadband cavity spectrometer measurements extending from 320 to 450 nm

J. Chen[1,2], J.C.Wenger[1,2] and D.S. Venables[1,2]

[1]Department of Chemistry, University College Cork, Cork, Ireland
[2]Environmnetal Research Institute, University College Cork, Cork, Ireland
Keywords: Optical properties, Instrument development, Spectrometer, SOA (Second. Organic Aerosols)
Presenting author email: d.venables@ucc.ie

Levels of near-ultraviolet solar radiation in urban areas are significantly lower than those above the urban boundary layer.(Peterson *et al.*, 1978) Jacobson proposed that absorption of light by aerosols was responsible for this phenomenon, and showed that anthropogenic species, particularly aromatic compounds and their oxidation products, could account for this absorption.(Jacobson, 1999) More recent investigations have also found that the radiation losses of carbonaceous aerosols below 450 nm increase steeply.(Andeae and Gelencser, 2006; Martins et al., 2009) Taken together, these results indicate that organic aerosol absorption plays a consequential role in the near-UV (300 nm to 400 nm). However, the near-UV optical properties of aerosols have been experimentally neglected and remain poorly understood. The lack of research into this question is largely due to the limitations of current techniques for measuring optical properties of aerosols at such short wavelengths

In this work, we demonstrate the use of a novel broadband optical cavity spectrometer to measure the extinction coefficient from 320 to 450 nm (Fig. 1). The unique capabilities of this technique – for broadband, in situ measurements at short wavelengths – make it ideally suited to investigating the optical properties of aerosols in an atmosphere simulation chamber, as we have recently demonstrated at longer wavelengths (Varma *et al.*, 2009).

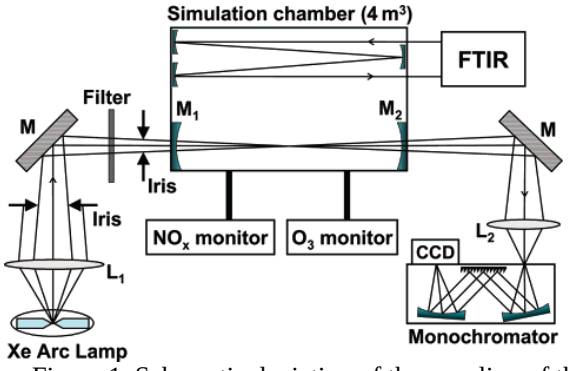

Figure 1. Schematic depiction of the coupling of the atmosphere simulation chamber and the IBBCEAS spectrometer (after Venables *et al.*, 2006).

We present extinction measurements following secondary organic aerosol formation in a 4 m^3 atmosphere simulation chamber. In one study, SOA was produced following photolysis of 2-nitrophenol, a strongly absorbing anthropogenic species. In another study, SOA was formed from the oxidation of the major biogenic species isoprene. We present the spectral dependence of the aerosol extinction and also study changes in the aerosol optical properties with aging of the particles. The analysis of the extinction spectra and the advantages and limitations of the approach are discussed.

We gratefully acknowledge financial support from Science Foundation Ireland (06/RFP/CHP055) and the EU FP7 project EUROCHAMP2 (grant no. 228335).

Jacobson, M. Z. (1999), *J. Geophys. Res.*, **104 D3**, 3527-3542.

Martins, J. V., P. Artaxo, Y. J. Kaufman, A. D. Castanho, and L. A. Remer (2009), *Geophys. Res.Lett.*, **36**, 1-5.

Peterson, J., E. Flowers, and J. Rudisill (1978), *J. Appl. Meteorol.*, **17**, 1595 - 1609.

Varma, R. M., D. S. Venables, A. A. Ruth, U. Heitmann, E. Schlosser, and S. Dixneuf (2009), *Appl. Optics B*, **48**, 159-171.

Venables, D. S., T. Gherman, J. Orphal, J. C. Wenger, and A. A. Ruth (2006), *Environ. Sci. Technol.*, **40**, 6758-6763.

Design and Evaluation of a Mini Catalytic Stripper

J.J. Swanson[1], D.B. Kittelson[1], A. Bergmann[2], B. Giechaskiel[2], M. Twigg[3]

[1]Department of Mechanical Engineering, University of Minnesota, Minneapolis, Minnesota, 55455, USA
[2]AVL List GmbH, Hans-List-Platz 1, A-8020, Graz, Austria
[3]Johnson Matthey Plc, Orchard Laboratories, Environmental Catalysts and Technologies, Herts. SG8 5HE, UK
Keywords: solid particles, sulfuric acid, hydrocarbon removal, nanoparticle instrumentation
Presenting author email: jswanson@me.umn.edu

The principle of operation of the catalytic stripper (CS) is to evaporate particle phase semi-volatile material and to remove resulting gas phase compounds. Organic carbon is removed via oxidation and inorganic compounds such as sulfate are chemically absorbed. This approach contrasts methods such as the thermal denuder that removes gas phase material via physical adsorption and the volatile particle remover (VPR) that is relies on dilution to prevent nucleation of gas phase material.

The objective of this project is to design, build, and evaluate a CS that is optimized for particle loss and hydrocarbon and sulfate removal efficiency. The CS is similar in concept to previous versions some features are unique to this design. The substrate geometry has been configured to maximize removal and minimize solid particle loss; design values and calculated performance are shown in Table 1 and the catalytic core is pictured in Figure 1. Additionally, the catalyst, heating source, and cooling region have been integrated into a compact package. This allows the CS to serve as a convenient and portable aerosol-conditioning inlet for any instruments that requires an inlet flowrate of 1.5 L/min.

Table 1. Design specifications of the UMN mini CS.

Length	3.8	cm
Width	1.7	cm
Cell density	600	cells/in
Cell wall thickness	2.5	mil
Flowrate	1.5	L/min
$C_{40}H_{82}$ removal	99.5	%
50% cut off size	7	nm

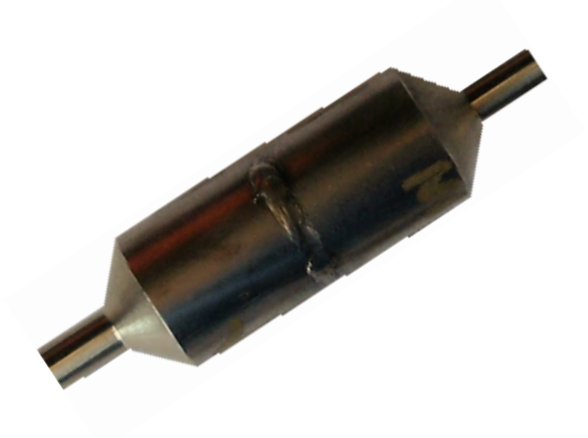

Figure 1. Mini CS catalytic core (Prints actual size on 11 x 8.5" paper) designed for a flowrate of 1.5 L/min.

To evaluate solid particle penetration through the CS, solid silver nanoparticles are generated using an evaporation/condensation technique. The CS is challenged with size selected silver particles while up and downstream concentrations are measured simultaneously. Results shown in Figure 2 indicate that the measured 50% lower particle cutpoint is near the predicted value (10 vs. 7 nm). The slightly reduced performance may be attributable to maldistributed or recirculating flow in the inlet that impacts the smallest particles.

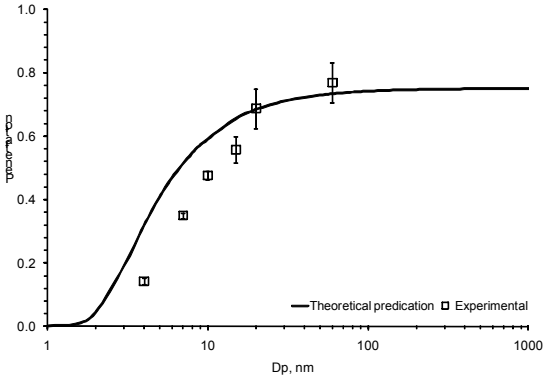

Figure 2. Comparison between theory and experimentally measured solid particle penetration.

Additional experiments were conducted to evaluate the hydrocarbon removal performance of the CS. The CS was challenged with dioctyl sebacate particles ($(CH2)_8(COOC_8H_{17})_2$) that were also generated using an evaporation/condensation technique. Generated particles were size selected at sizes of 30, 40, 50, and 60 nm and were used to challenge the CS. Results indicated that the CS could fully remove (efficiency of 100.0%) concentrations of >10,000 part/cm^3 for all particle sizes, which meets and exceeds the removal requirements of the VPR method. Experiments to evaluate sulfate removal efficiency are ongoing.

Abdul-Khalek, I. S., and Kittelson, D. B. (1995) *SAE Tech. Paper Series*, 950236.

Swanson, J., Kittelson, D. (2010) *J. Aerosol Sci* **41**, 1113–1122.

Giechaskiel, B., Dilara, P., Sandbach, E., & Andersson, J. (2008) *Meas. Sci. Tech*, **19**, 1–16.

Johnson, K. C., Durbin, T. D., Jung, H., Chaudhary, A., Cocker, D. R. Herner, J. D., et al. (2009) *Aerosol Sci Technol.*, **43**, 962–969.

Diisocyanate aerosols in polyurethane manufacture

A. Akachat[1], H. Rebbah[1]

[1] Laboratoire de matériaux minéraux et composites, Université Med Bougara, Avenue de l'Indépendance, 35000 Boumerdes, Algérie.

Keywords: particles, isocyanates, PU,

Workplace atmosphere is an important distribution of various pollutants, resulting from the handled products and concerned processes. The fate of these pollutants in the air (transport, deposition, degradation), is determined by their distribution between atmospheric particles and gas phase (Lohmann et al. 1998). Harmfulness of particles in workplace atmosphere and the disease hazards that they present are related to their chemical nature and size. The production of one kilogramme rigid polyurethane foam releases nearly 7362 milligrams of solid particles in air.

In this work, we used the personal aerosol sampler CIP10-R (Courbon et al. 1988) and filters for evaluation of alveolar (Gorner et al. 1996) and inhalable fractions of particles during clean of casts after injection of the polyurethane foam (PU) (fig 1). HPLC was used for detection of MDI in different post (fig 2).

Obtained Results reveal that MDI in alveolar fraction prevail the total collected particles, this can be allotted to the process used for cleaning and to the quality of formulated foam.

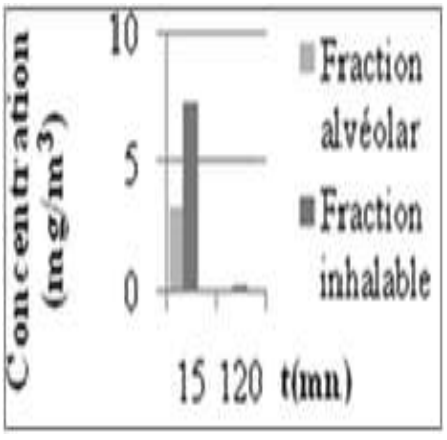

Fig. 1 : Concentration in 15 et 120 mn.

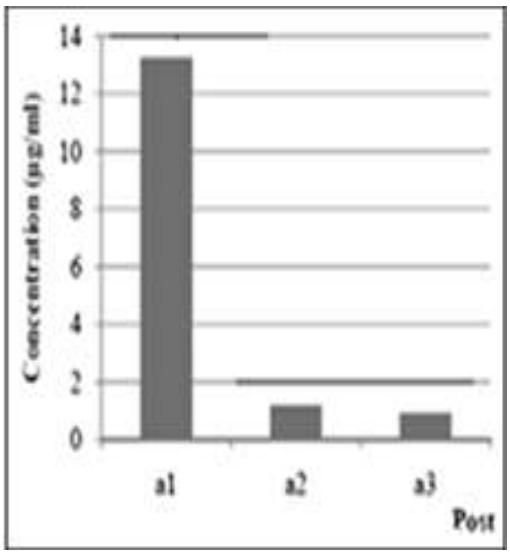

Fig. 2: MDI Concentration in 15 and 120 mn.

Lohmann, R., Jones, K.C. (1998). Dioxins and furans in air and deposition: a review of levels, behaviour and processes. Science of the Total Environment 219, 53-81.

Courbon P., Wrobel R., Fabries J.F. (1988). Anew individual respirable dust sampler: the Cip 10. Annals of Occupational Hygiene, 32pp. 129 - 143.

Gorner P., Fabries J.F. (1996). Industrial aerosol measurement according to the new sampling convention. Occupational Hygiene, 3, pp 361 – 376.

Hormone structural differentiation using a high resolution DMA

Martin Hollertz[1,2,5], John T. Elliott[1], Jacob Lewis[3], Eric R. Mansfield[3], Wynchester D. Whetten[4], Thomas A. Knotts IV[3], Michael J. Tarlov[1], Michael R. Zachariah[1,2], Leonard F. Pease III[4]

[1]National Institute of Standards and Technology (NIST), Gaithersburg, MD 20899, USA
[2]Department of Mechanical Engineering, University of Maryland, College Park, MD 20742, USA
[3]Department of Chemical Engineering, Brigham Young University, Provo, UT 84602, USA
[4]Department of Chemical Engineering, University of Utah, Salt Lake City, UT 84112, USA
[5]Present address: Karlsruhe Institute of Technology, 76344 Eggenstein-Leopoldshafen, Germany

Keywords: Biogenic particles, Morphology, Electrospray, Instrumentation/physical char.

The structure of biomolecules such as peptide hormones and proteins is important since it affects their receptor recognition, activity, and the precision with which they can be isolated. Molecule structures can be investigated using a wide variety of techniques including gels, spectroscopy, NMR, and X–ray crystallography. Here, we describe the first use of a high resolution (HR) DMA to rapidly and quantitatively differentiate between the cyclic and linear forms of the peptide hormone oxytocin, the smallest biomolecule measured using a DMA.

A previous DMA study of biomolecules focused only on approximating molecular mass not molecular morphology, by assuming globular proteins to be constant density spheres (Bacher *et al.*, 2001)[†]. A later study found that particle morphology plays an important role in determining the mobility diameter with a DMA (Pease *et al.*, 2007).

Here, oxytocin was added to aqueous ammonium acetate solutions. To some samples, the reducing agent TCEP was added to break the disulphide bond in oxytocin, thus changing its shape from circular to linear. The solutions were electrosprayed using home-built electrospray system (*cf.* Ude *et al.*, 2005). Size spectra were obtained in less than 5 min by scanning the DMA voltage and recording the ion current with an electrometer. The DMA was designed to remain in the laminar flow regime despite Reynolds numbers exceeding 35000, with the use of a funnel shaped injector (Herrmann *et al.*, 2000). The DMA was calibrated before each run by electrospraying solutions of tetraheptyl ammonium bromide (THAB), producing ions of known mobilities (Ude *et al.*, 2005). In Fig. 1, we find that oxytocin peptide has two peaks at 1.52 nm and 1.55 nm that are statistically distinguishable due to an instrument resolution of 0.011 nm.

Molecular dynamics simulations of oxytocin were performed to determine the most probable configurations for both the cyclical and linear forms. The resulting spherically equivalent mobility diameters of the two forms were 1.52 ± 0.04 nm (cyclic) and 1.55 ± 0.06 nm (linear), respectively. These results are in excellent agreement with the experiments.

The ability to differentiate two forms differing in spherically equivalent size of only 0.03 nm is remarkable. The combination of electrospray and HR-DMA prevents fragmentation of macromolecules in contrast to high vacuum electrospray mass spectrometry systems, and can, in a very cost-efficient way, easily measure molecular diameters from below 1 nm up to 10 nm with sub-angstrom uncertainty in diameter. The measured differences in oxytocin before and after TCEP treatment agree with refined DMA predictions made by coupling molecular dynamics simulations with the analytical models of Pease, *et al.* (2007).

The present work demonstrates that DMAs can be used to differentiate subtle differences in nanoparticle structure and opens opportunities to use high resolution DMAs to experimentally validate molecular dynamics simulations to accelerate advances in proteomics, enzymology, catalysis, and molecular biology.

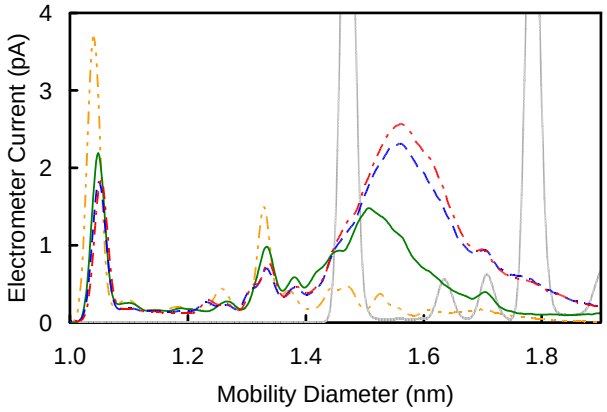

Fig. 1. Size spectra of oxytocin before addition of TCEP (solid green) and 30 min (long dash blue) and 2 hours (alternating dash red) after TCEP addition, each in ammonium acetate solutions (short dash orange). THAB (grey dotted) was used to calibrate the distributions.

Bacher, G., Szymanski, W.W., Kaufman, S.L., Zöllner, P., Blaas, D. & Allmaier, G. (2001) *J. Mass Spectrom.*, 36, 1038-1052.

Herrmann, W., Eichler, T., Bernardo, N., & Fernández de la Mora, J. (2000) *Abstract AAAR Conference*, 15B5.

Pease, L.F., Tsai, D.H., Zangmeister, R.A., Zachariah, M.R., & Tarlov, M.J. (2007) *J. Phys. Chem. C* 111, 17155-17157.

Ude, S. & Fernández de la Mora, J. (2005) *J. Aerosol Sci.*, 36, 1224-1237.

[†] The correlation between mobility size and molecular weight from this study is included in the TSI macroIMS (GEMMA successor) software.

Direct integration of a GPS/GPRS unit into a miniature diffusion size classifer

M.Fierz, P.Steigmeier, M.Glettig, B.Wyrsch and H.Burtscher

University of Applied Sciences Northwestern Switzerland, 5210 Windisch, Switzerland
Keywords: instrumentation, air quality network, personal sampling.
Presenting author email: martin.fierz@fhnw.ch

We have recently developed a miniaturized version of the diffusion size classifier (miniDiSC, Fierz et al. 2011). It can measure particle number concentration, average particle diameter and lung-deposited surface area with a one-second time resolution. It operates on a purely electrical basis, with a unipolar charger followed by two electrometer stages, i.e. there are no working fluids or radioactive sources. The instrument is about the size of a multimeter, and thus one of the smallest aerosol instruments available today, which makes it ideal for personal monitoring.

For personal monitoring, it is useful to record location information with a GPS. While a separate GPS receiver can be used with any instrument, it is a bit cumbersome to operate because the data of instrument and GPS have to be combined manually. We have therefore integrated a GPS receiver directly in the miniDiSC. Furthermore, we also added a GPRS chip to transmit data from the instrument to a server in the internet in real time. The transmitter board measures 60x80mm and can easily be accommodated in a slightly larger housing than the standard miniDiSC housing (45mm thickness instead of 40mm).

Data is transmitted by the miniDiSC to a TCP server located in the internet, which stores the data in an SQL database. A standard 3-tier-architecture (Database, web-application, browser) is used to view the data in near-realtime (about 5 seconds delay) in any internet browser. Figure 1 shows an overview of the measurement network structure. The instruments also transmit status information besides the measurement data. This allows for a quick overview of the status of all deployed minidiscs (see Figure 2), which is useful when running a measurement campaign - problems with the instruments can be detected and resolved easily during the campaign.

Data can be displayed as real-time chart or as table or downloaded as delimited text file or as a Google Earth file. The Google Earth download is perhaps the prettiest way of visualizing the data (see Figure 3).

In conclusion, we have developed an enabling technology to easily collect and view data of the miniDiSC online. We anticipate that this will be useful for measurement campaigns, both for personal monitoring and for stationary measurements.

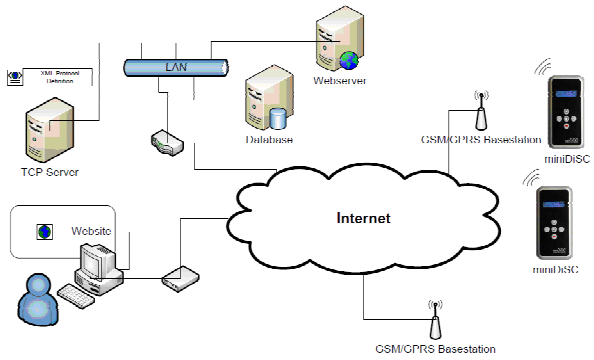

Figure 1: Structure of the miniDiSC measurement network.

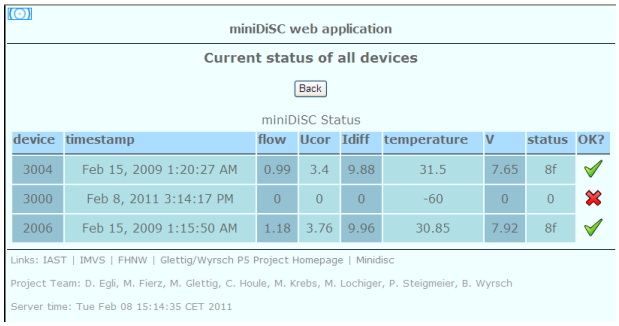

miniDiSC web application

Current status of all devices

Back

miniDiSC Status

device	timestamp	flow	Ucor	Idiff	temperature	V	status	OK?
3004	Feb 15, 2009 1:20:27 AM	0.99	3.4	9.88	31.5	7.65	8f	✓
3000	Feb 8, 2011 3:14:17 PM	0	0	0	-60	0	0	✗
2006	Feb 15, 2009 1:15:50 AM	1.18	3.76	9.96	30.85	7.92	8f	✓

Links: IAST | IMVS | FHNW | Glettig/Wyrsch P5 Project Homepage | Minidisc

Project Team: D. Egli, M. Fierz, M. Glettig, C. Houle, M. Krebs, M. Lochiger, P. Steigmeier, B. Wyrsch

Server time: Tue Feb 08 15:14:35 CET 2011

Figure 2: Monitoring the network status

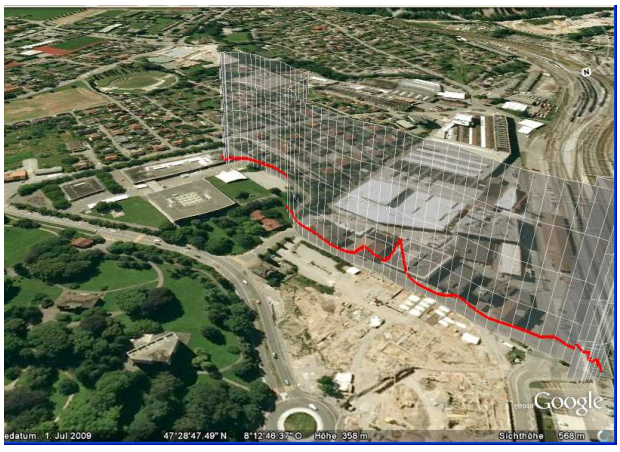

Figure 3: Display of data and location in Google Earth.

This work was supported by Forschungsfonds Aargau.

Fierz, M., Steigmeier P., Houle C. and Burtscher H. (2011) *Aerosol Science and Technology*, **45**, 1-10.

Influence of probe nozzle diameter on aerosol particle size distribution for isokinetic sampling in gas streams

T. Barth[1] and M.Lustfeld[2]

[1]Institut für Sicherheitsforschung, Helmholtz-Zentrum Dresden-Rossendorf, Bautzner Landstraße 400, 01328 Dresden, Germany

[2]Professur Wasserstoff- und Kernenergietechnik, Institut für Energietechnik, Technische Universität Dresden, 01062 Dresden

Keywords: deposition, instrumentation, measurement, sampling, spectrometry
Presenting author email: t.barth@hzdr.de

Isokinetic sampling from stacks and ducts is a widely used method for air pollution control in many industrial and environmental applications.
During the last 40 years, U.S. EPA developed reference methods for air pollutant emission sampling of stationary sources, which included a compendium of technical guidelines for the monitoring of aerosol particles. One of the main parts of the sampling system is the sampling probe nozzle for which it was suggested in the reference methods that the lower bound diameter should be greater than $d_i = 6\ mm$ (Cohen, 2001). The influences of sampling nozzle tube diameter, the velocity ratio between free stream and the sampling tube as well as the tube inclination have been considered widely (Vincent, 2007). On the other hand, the influence of tube diameter has not been quantified by means of aerosol particle size spectrometry yet.
McFarland et al. (1997) as well as Peters and Leith (2004) experimentally investigated the deposition losses of aerosol particles in pipe bends. Both found a strong increase of deposition losses in the sampling tube for particle Stokes number of $Stk > 0.3$.
In this work, the influence of the nozzle diameter of the sampling probe on the aerosol particle size distribution was investigated by means of TSI APS 3321 and TOPAS LAP 321 measurements.
The considered gas/aerosol test facility is a small scale wind tunnel, which consists of a HEPA at the inlet and a square duct section in diameter of $d_{hyd} = 10\ cm$ and length of $l = 20 d_{hyd} = 2\ m$. The test section, where sampling takes place, is followed by a diffuser stage, an electrical precipitator and a radial fan in order to generate the desired pressure head. The average air velocity can be regulated over the range $<u> = 1..7\ m/s$, corresponding to Reynolds numbers between $Re_d = 8.9k..42k$. In order to achieve isokinetic sampling, the flow rate of the sampling device has been accurately adjusted using Particle Image Velocimetry data.
AC Fine Test Dust (ISO 12103-1, $d_{nom} = 0.1..80\ \mu m$, bimodal distribution) was injected 17 diameter lengths upstream of the sampling point by means of a dust disperser TOPAS SAG 410. Four probe nozzle diameters $d_i = [3,5,7,9]\ mm$ were chosen.
Figure 1 displays the volume weighted aerodynamic particle size distribution of AC Fine under variation of nozzle tube diameter as measured by the APS 3321. The modal $d_{P,aero} = 5\ \mu m$ is roughly independent of nozzle size, whereas the values of the distribution for particle diameters above $d_{P,aero} > 12\ \mu m$ increase continuously with increasing nozzle diameter.
A similar upward tendency in size distribution with increasing nozzle diameter is observed in the LAP measurement results (not shown here). This leads to the conclusion that deposition losses due to inertia, which consequently affect the larger particles, can be considerably reduced by accordingly increasing tube nozzle diameter. In addition, a comparison of aerodynamic particle size (APS 3321) and scattering particle size (LAP 321) will be presented.

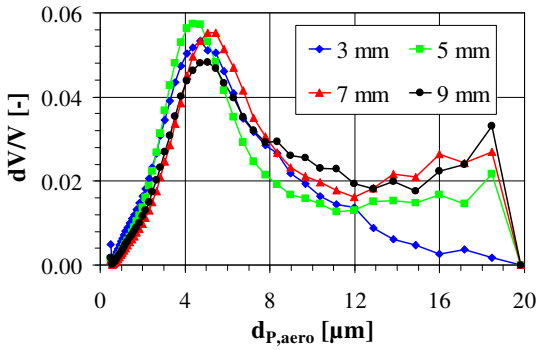

Figure 1 q_3 Aerodynamic particle size distribution of AC fine (ISO 12103-1) for different nozzle sizes

This work is supported by the the EC (Project THINS, grant agreement no. 249337).

Cohen, B. S. (2001), Air sampling instruments for evaluation of atmospheric contaminants. *ACGIH*.
McFarland, A.; Gong, H.; Muyshondt, A.; Wente, W. & Anand, N. (1997), Aerosol Deposition in Bends with Turbulent Flow. *Environ. Sci. Technol.*, Vol. **31**, 3371-3377.
Peters, T. M. & Leith, D. (2004), Particle Deposition in Industrial Duct Bends. *Annals of Occupational Hygiene*, Vol. **48**, 483-490.
Vincent J. H. (2007), Aerosol sampling: science, standards, instrumentation and applications. *John Wiley and Sons.*

Recent enhancements and new applications of passive sampling of ambient particles - the new VDI guideline 2119 -

E. Schultz[1], U. Kramar[1] , N. Schleicher[1], V. Dietze[2], U. Kaminski[2], W. Ruhmann[3] , R. Gebhardt[4], S.Norra[4], K. Kandler[5], G. Börner[6], G. Haubold[6], P. Plegniere[7].
[1]Karlsruher Institut für Technologie, Institut für Mineralogie und Geochemie, 76131 Karlsruhe, Germany
[2]Deutscher Wetterdienst, Zentrum für Medizin-Meteorologische Forschung, 79104 Freiburg, Germany
[3]Imatec Elektronische Bildanalysesysteme GmbH, 83714 Miesbach, Germany
[4]Karlsruher Institut für Technologie, Institut für Geographie und Geoökologie, 76131 Karlsruhe, Germany
[5]TU Darmstadt, Institut für Angewandte Geowissenschaften u. Umweltmineralogie, 64287 Darmstadt, Germany
[6]Thüringer Landesanstalt für Umwelt und Geologie, 07745 Jena, Germany
[7]Kommission Reinhaltung der Luft in VDI und DIN, 40002 Düsseldorf, Germany
Keywords: Passive sampling, guideline, coarse particles, microscopic analysis, size distribution
Presenting author email: eckart.schultz@online.de

Ambient particle concentrations of d > 2.5 µm are characterised by growing spatial variability with increasing particle size. Local sources, therefore, become more important and an estimate of the exposure to this fraction becomes uncertain the larger the particles are. The employment of passive samplers may be well suited to reduce this uncertainty because passive samplers allow denser networks than active ones, due to simple technique, low price and easy use. Errors in estimating the exposure to ambient particles can be more important than errors due to imprecision in the monitoring instruments themselves (Leith et al., 2007). Moreover, in passive samplers there is more of a choice of appropriate sampling media suitable for microscopic analysis and compositional characterisation of particles than in active ones.

Already in 1997, a passive sampler for ambient particles > 3 µm was described by a guideline of the Verein Deutscher Ingenieure (VDI). It described the passive sampler Sigma-2, developed at the Institut für Physik der Atmosphäre at the Universität Mainz, modified by the Deutscher Wetterdienst in Freiburg and in use for air quality measurement in German health resorts since the late 1980's. A revised version of this guideline elaborated by the above listed authors will be available this year (VDI 2119, 2011). This new guideline will comprise the latest enhancements in passive particle sampling and analysis: (1) new collection media suitable for further analytical methods, (2) advances in automated microscopic analysis, (3) a calculation method for particle concentrations d > 2.5 µm from the deposit.

The revised guideline is based on the experiences of the still ongoing air quality measurements in German health resorts but also on the methodological enhancements achieved while being used in various research projects. The major objectives are to obtain spatially highly resolved particle data in order to identify hot spots in urban areas and to distinguish between natural and anthropogenic sources. Valuable information for these objectives was extracted by measuring geometric and optical parameters of individual particles and by specifying corresponding size distributions. For example, the spatial distribution of microscopically distinguished particles was found to differ considerably in cities as well as in rural areas. The results indicate that the applied microscopic analysis can be essential for reliably assessing health effects of the exposure to coarse particles (Wolf-Benning et al., 2011).

A study in W-Greenland confirmed the value of the technique in extreme remote conditions. Results of this study show a surprisingly high load of coarse particles, comparable to Central Europe or even higher (Fig. 1), while the fine particles show the expected very low concentration. The passive sampler Sigma-2 described in the revised VDI guideline provides further applicabilities, for example in electron-microscopic single particle analysis (Kandler et al., 2009) and in µ-synchrotron analysis (Schleicher et al., 2010) in various spatio-temporal studies, especially for remote or observational network studies.

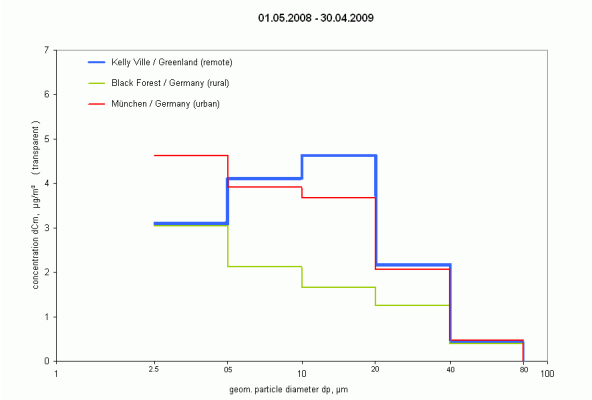

Fig. 1. Annual averaged particle size distribution at W-Greenland *versus* two sites in Germany.

Leith et al. (2007) *Air & Waste Manag.Assoc.* 57: 332-6.
Wolf-Benning et al. (2011) (ready for submission).
Kandler et al. (2009) *Tellus* **61B**, 32-50.
Schleicher et al. (2010) *AIP Conf. Proc.* 1221, 172-180.
VDI 2119, draft (2011): *Ambient air measurement – Passive Sampler – Sampling and Characterisation of Coarse Particles and Calculation of Concentration Data,* Berlin: Beuth Verlag; www.vdi.de/2119.

Using nigrosin as a surrogate for black carbon to study aerosol light absorption

Jeonghoon Lee[1] and Seung Cheol Han[1]

[1]School of Mechanical Engineering, Korea University of Technology and Education, Cheonan, Choong Nam, 330-708, South Korea

Keywords: nigrosin, black carbon, absorption

Presenting author email: jlee@kut.ac.kr

The aerosol light absorption from black carbon draws attention to atmospheric aerosol scientists because a small mass fraction of black carbon may contribute the equivalent of 1/4 of radiative forcing caused by CO_2 (Lack et al 2008). It has been reported that the black carbon radiative forcing could even be as much as 55% of the CO_2 forcing (Ramanathan and Carmichael, 2008). The black carbon is generated from various sources such as a tail pipe of a vehicle, the chimney of power plant, biomass burning, and so on. The black carbon ages in the atmosphere through a coating process. Normally, the shape of black carbon differs depending on the condition where it is produced. The aggregatelike shape of black carbon may cause the change in the optical properties of black carbon. It is very difficult to quantify the optical properties of aggregates coated with transparent materials.

To alleviate the difficulty of determining the absorption coefficient of the black carbon coated with transparent materials, we have recently initiated the experimental efforts using nigrosin as a proxy for black carbon. Nigrosin is spherical and absorbs light in the visible range. The simple structure of nigrosin allows us to easily estimate the absorption coefficient.

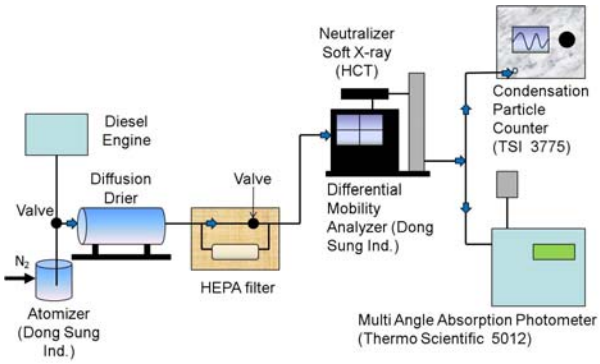

Figure 1. The schematic of experimental apparatus used in the present study.

Figure 1 shows the schematic of the experimental apparatus used in the present study. Water soluble nigrosin particles were prepared in a home-made constant atomizer. Polydisperse nigrosin aerosols were produced using the atomizer. Black carbon aerosol was produced using a single cylinder diesel engine. A diffusion drier eliminated the moisture contained in the aerosols. The number concentration of aerosols was controlled by a HEPA filter. Monodispersely sized aerosols were selected using a DMA (Differential Mobility Analyzer, Dong Sung Ind.) and concentrations of the aerosol were measured by a CPC (Condensation Particle Counter, TSI 3775). Simultaneously, the size selected aerosols were sampled in the MAAP (Multi-angle Absorption Photometer, Thermo Scientific 5012). Aerosol absorptions were measured by the MAAP which requires no post measurement data correction or parallel-measured aerosol light-scattering coefficients (Petzold *et al*, 2005).

The absorption coefficients were measured for nigrosin aerosols with different sizes. The absorption coefficients of black carbon particles generated in a diesel engine were also measured in a similar way to the nigrosin aerosols. Figure 2 shows that the absorption coefficient of 100 nm nigrosin aerosol increased as the number concentration was increased. The absorption coefficients for black carbon were compared with those for nigrosin aerosols. The results show that the nigrosin can be used as a proxy for black carbon in the measurement of aerosol absorption properties. More detailed discussion along with the results of black carbon will be presented.

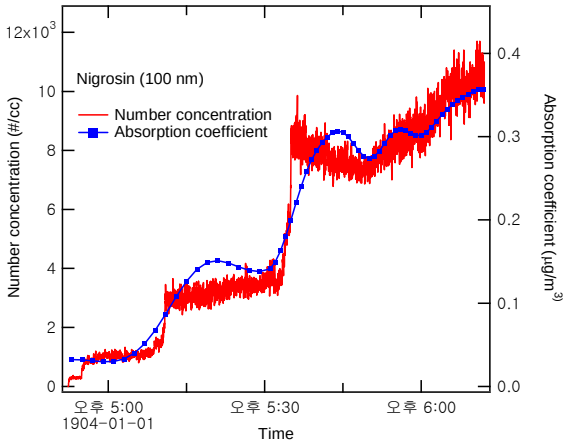

Figure 2. Real-time measurement of absorption coefficients and number concentrations.

This work was supported by the National Research Foundation of Korea Grant funded by the Korea government (MEST) (No. 2010-0006116).

Lack, D., Cappa, C., Covert, D., Baynard, T., Massoli, P., Sierau, B., Bates, T., Quinn, P., Lovejoy, E. and Ravishankara, A. (2008) *J. Aerosol Sci.* **34**, 1033-1401.

Petzold, A., Schloesser, H., Sheridan, P., Arnott, W., Ogren, J. and Virkkula, A. (2005) *Aerosol Sci. Tech.* **39**, 40-51.

Ramanathan, V. and Carmichael, G. (2008) *Nature Geosci.* **1**, 221-227.

Diffusion of charged particles in a DMA with inclined electric field and with a particle collector in gas outlet

J. Salm and U. Hõrrak

Institute of Physics, University of Tartu, 18 Ülikooli St., 50090, Tartu, Estonia
Keywords: DMA, size analysis, diffusion, measurement errors.
Email: jaan.salm@ut.ee

In general lines, a differential mobility analyser (DMA) has gas inlet(s), gas outlet(s), electrodes, and collector(s) of electric current. Diffusion distortions in a simple DMA have been studied in (Salm, 2000). The distortions in a similar DMA with inclined electric field have been studied in (Salm and Hõrrak, 2009). The method developed in the above papers is applicable also for a DMA with inclined electric field and with a particle collector in gas outlet that was developed by Tammet (1999, 2003).

In this abstract we systematically refer to the paper (Salm and Hõrrak, 2009) and the corresponding equation numbers. Figure 1 of the paper is retained, only the structure of collector is modified.

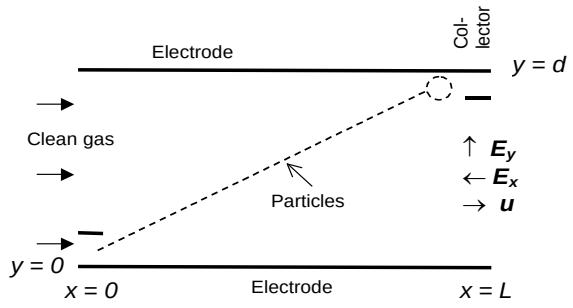

Figure 1. Schematic representation of the DMA.

According to Figure 1, the horizontal velocity of charged particles is

$u - Z_1 E_x$,

where Z_1 is the mobility of entering aerosol particles.

Equation for the characteristic (limiting) mobility is

$$Z_0 = \frac{u}{E_y}\frac{d}{L+kd} .$$

We will consider here the case $E_x \propto E_y$. Let us express $E_x = kE_y$, where k is the coefficient of proportionality.

The following derivation of equations is quite similar to that in (Salm and Hõrrak, 2009), with understandable replacements. Equations (7) – (12) are retained. In Equations (13) – (15), the velocity Z_1E_y is replaced by the velocity u, and the factor d/L appears in Equations (16) and (17). The derivation results in the normalized apparent spectrum $w^*(Z,Z_1)$. Equation (18) in (Salm and Hõrrak, 2009) is replaced by the following equation:

$$w^*(Z,Z_1) = \frac{\mathrm{Pe}\,(L+kd)}{2\pi LZ} \times \exp\left(\frac{\mathrm{Pe}}{2}\left(\frac{L}{d}\left(1-\frac{kd}{L+kd}\frac{Z_1}{Z}\right)+\frac{d}{L+kd}\frac{Z_1}{Z}\right)\right) \times \mathrm{K}_0\left(\frac{\mathrm{Pe}}{2}\sqrt{\left(\left(1-\frac{kd}{L+kd}\frac{Z_1}{Z}\right)^2+\left(\frac{d}{L+kd}\frac{Z_1}{Z}\right)^2\right)\left(1+\frac{L^2}{d^2}\right)}\right) ,$$

where Z is the variable mobility, Pe is the Peclet number, $\mathrm{K}_0(\zeta)$ is the Macdonald's function. The simplification of the equation is possible analogically as in (Salm and Hõrrak, 2009).

Rough estimations of the influence of diffusion on the resolution of mobility spectrometers are possible also by means of simpler methods. However, a precise knowledge of the apparent spectrum opens a way to the improvement of resolution by calculations.

If we know the normalized apparent spectrum $w^*(Z,Z_1)$ for one mobility Z_1, then the apparent spectrum $\rho^*(Z)$ for any general case is expressed as

$$\rho^*(Z) = \int w^*(Z,Z_1)\rho(Z_1)\mathrm{d}Z_1 , \qquad (*)$$

where $\rho(Z_1)$ is the differential distribution of polar charge density of particles by mobility or the mobility spectrum. In many cases the apparent spectrum $w^*(Z,Z_1)$ depends on the ratio Z/Z_1. Then, using a simple exponential transformation, it is possible to express Equation (*) in the shape of convolution, and to solve the convolution equation by means of the Fourier transform.

This work was supported by the Estonian Science Foundation through grants 8342 and 8779, and the Estonian Research Council Project SF0180043s08

Salm, J. (2000). *Aerosol Science and Technology*, 32, 602-612.

Salm, J. and Hõrrak, U. (2009). *Aerosol Science and Technology*, 43, 227-231.

Tammet, H. (1999). in *Proc. 11th Int. Conf. Atmos. Electr.*, Alabama (NASA, MSFC), 626-629.

Tammet, H. (2003). in *Proc. 12th Int. Conf. Atmos. Electr.*, Versailles, 399-402.

Adapting the Aerodyne Aerosol Mass Spectrometer for Zeppelin-based measurements

F. Rubach[1], A. Trimborn[2], Th. F. Mentel[1], A. Wahner[1]

[1]Institute for Energy and Climate 8: Troposphere, Forschungszentrum Jülich GmbH, 52425 Jülich, Germany
[2]AeroMegt GmbH, 40723 Hilden, Germany
Keywords: aerosol instrumentation, mass spectrometry.
Presenting author email: f.rubach@fz-juelich.de

The Aerodyne High-Resolution Time-of-Flight Aerosol Mass Spectrometer (HR-ToF-AMS, DeCarlo et al., 2006; Canagaratna et al., 2007) is an instrument to gather real-time information about the composition of non-refractory aerosol particles. The used High-Resolution Time-of-Flight Mass Spectrometer allows for direct distinction between most inorganic and organic ions at the same nominal m/z. This provides the possibility to gain information about the average oxidation state of organics in particles of mixed compositions (Aiken et. al., 2007).

The HR-ToF-AMS has so far mainly been used for ground-based measurements (e.g. Aiken et. al, 2007; Farmer et. al., 2010; Ulbrich et. al. 2009), although some measurements have taken place on aeroplanes (e.g. DeCarlo et. al. 2008; Murphy et. al., 2009).

Usage of the Zeppelin Airship as measurement platform is highly advantageous because of several reasons:

- Flight speed 0-125 km/h
- Flight altitudes of 80 m to 2500 m are achievable
- Lagrange-type experiments are easily possible
- Hover capability, vertical profiling
- Flight endurance of 14 h or more

In contrast to the advantages, the maximum payload is limited (approx. 2 t), carried weight directly influences achievable flight height and the available space inside the cabin is constricted. Therefore, instrumentation has to be optimized concerning weight and space requirements. Beyond that, measurements should be automated and facilitated as far as possible to require less service personnel.

By different means, a weight reduction of more than 20 % was achieved for this instrument. At the same time, the instrument now occupies approx. 30 % less volume and has an approx. 25 % smaller base area.

Design, construction and first applications of the instrument will be shown.

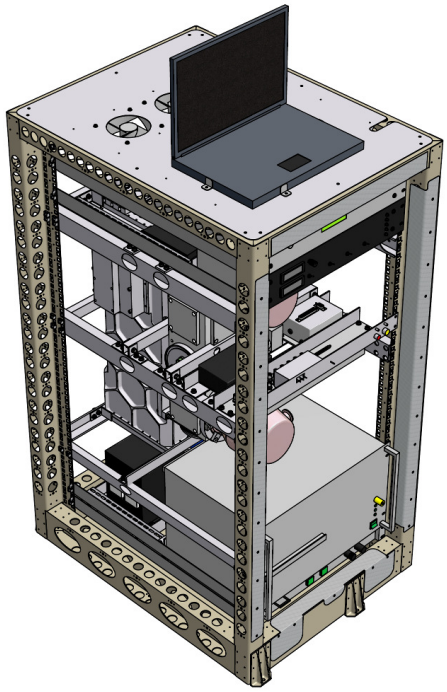

Figure 1. 3D-drawing of the Zeppelin-AMS-Rack.

This work was supported by EC integrated project PEGOSOS.

Aiken, P.F. et al. (2007), *Anal. Chem.*, **79**, 8350-8358.
Canagaratna, M.R. et al. (2007), *Mass Spec. Rev.*,26, 185-222.
DeCarlo, P.F. et al. (2006), *Anal. Chem.*, **78**. 8281-8289.
DeCarlo, P.F. et. al. (2008), *Atmos. Chem. Phys.*, **8**, 4027-4048.
Farmer, D.K. et. al. (2010), *Atmos. Meas. Tech. Discuss.*, **3**, 5867-5905.
Murphy, S.M. et. al. *Envir. Sci. Tech.*, **43** (13), 4626-4640, 2009.
Ulbrich, I.M, et. al. (2009), *Atmos. Chem. Phys.*, **9** (9), 2891-2918.

Calibration of Condensation Particle Counters – analysis of sub-3nm calibration ions using mass spectrometry

J. Kangasluoma[1], H. Junninen[1], K. Lehtipalo[1,2], T. Toivola[2], T. Petäjä[1], M. Kulmala[1]

[1]Department of Physics, University of Helsinki, 00560 Helsinki, FINLAND
[2]Airmodus Oy, 00560 Helsinki, FINLAND

Keywords: PSM, APi-TOF, particle generation.
Presenting author email: juha.kangasluoma@helsinki.fi

Small nano-size particles are measured with condensation particle counters (CPC), which operate by condensing working fluid on particles. Particles grow large enough to be optically detected due to condensation. Newly developed particle size magnifier (PSM, Vanhanen *et al.* 2011) uses diethylene glycol as a working fluid to avoid homogenous nucleation. The cut-off diameter of the PSM can be adjusted between about 1-2nm by changing the mixing ratio of the saturator and inlet flow. These particle counters are calibrated with differential mobility analyzers (DMA) which allow choosing particles of known mobilities. The particles used in calibrations are often the mobility standards (Ude & Fernandez de la Mora, 2005), silver, WOx-particles and some others. Still the chemical composition of these particles is not well known.

In order to measure the chemical composition a time of flight mass spectrometer (APi-TOF, Junninen *et al.* 2010) is used. The APi-TOF classifies ions by giving them certain kinetic energy and then measuring the time of flight. In this way high mass resolution is achieved which allows to distinguish between ions of same integer mass, but different mass defect.

Particles are produced with various methods including electrospray, wire generator and oven. They are led to a high resolution Herrmann-type DMA (Herrmann *et al.* 2000) after passing through a bipolar charger and thereon to the APi-TOF, PSM and electrometer. The APi-TOF is the first one in sampling because of its weak sensitivity, the PSM and electrometer are sampling after the APi-TOF inlet.

In figure 1 is an example of activation curves for the PSM with NaCl, WOx-particles, Silver and the mobility standards. Chemical composition and charge seems to have some effect on detection efficiency. Negative particles tend to activate more easily. All data points were also measured with the APi-TOF, which gave some interesting results. For example for positive NaCl, there was a wide spectrum of different atomic masses for fixed voltage in the HDMA. Certainly more studies related to this are needed to understand the processes between the particle generator and the APi-TOF and particle counter.

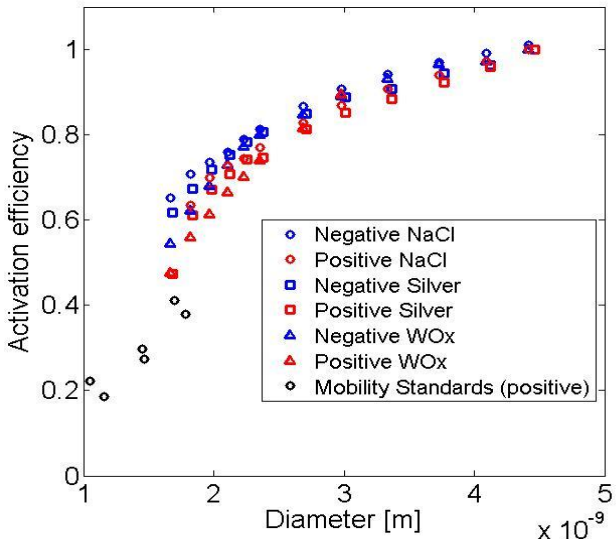

Figure 1. Activation curves of the PSM for both polarities of Silver, NaCl, WOx-particles and the mobility standards. Silver seems to be activated a little better than WOx-particles and NaCl of same mobility diameter.

Herrmann, W., Eichler, T., Bernardo, N., and Fernández de la Mora, J. (2000). Turbulent Transition Arises at Reynolds Number 35,000 in a Short Vienna Type DMA with a Large Laminarization Inlet. *Abstract AAAR Conference*, 15B5.

Junninen H., Ehn M., Petäjä T., Luosujärvi L., Kotiaho T., Kostiainen R., Rohner U., Gonin M., Fuhrer K., Kulmala M., and Worsnop D. R., (2010*) Atmos. Meas. Tech.*, **3**, 1039–1053.

Ude, S. and Fernández de la Mora, J. (2005). Molecular Monodisperse Mobility and Mass Standards from Electrosprays of Tetra-alkyl Ammonium Halides. *J. Aerosol Sci.* **36**:1224-1237.

Vanhanen, J., Mikkilä, J., Lehtipalo, K. Sipilä, M.,Manninen, H. E. , Siivola, E. , Petäjä, T. and Kulmala, M. (2011) *Aerosol Sci. Tech.*, **45**, 533–542.

Mobilization of Aerosol MALDI Mass Spectrometry for Bioaerosol Analysis

Yurteri C.U., Stowers M., Kleefsman W.A., and Marijnissen, J.C.M.

Delft University of Technology, Delft, 2628 BL, The Netherlands

Keywords: MALDI, Bioaerosol, Instrumentation

Presenting author email: c.u.yurteri@tudelft.nl

Systems for early detection of malign bio aerosols are becoming attractive due to possible biological attacks, infection dangers in hospitals, animal farms, forensics, ..etc. Because of their small size, averaging 1 to 10 um in size, bacterial bioaerosols are extremely difficult to detect. In addition, size and concentration are not absolute criteria for determination of harmful aerosols. Timely detection of a broad range of bioaerosols with a small response time and a very low false alarm rate, discrimination and identification allows timely execution of procedures to save local people from harm and further contamination. With the currently available instruments it is impossible to measure and identify a biological attack within a short time range, and on-line techniques are required. One of the instruments enabling this is the aerosol MALDI (matrix-assisted laser desorption/ionization) mass spectrometer for the analysis of single bioaerosol particles developed at TU Delft (Kleefsman 2008, Kleefsman et al. 2008). The strength of the aerosol MALDI mass spectrometer is based on three subsequent steps: particle detection, particle selection and the analysis of the particles based on MALDI mass spectrometry. The aerosol mass spectrometer has been improved to make the instrument suitable for bioaerosol detection. The implemented instrumental improvements include a new design of the repeller and the extractor plate as well as the implementation of delayed extraction. The application of the MALDI technique for *on-line* analysis of aerosol particles, implies the need of an on-line sample preparation method. So an on-line coating method was also implemented. We are now in the process of implementing this instrument as a mobile system. We will present the recent status of development and considerations for portability of the system.

Kleefsman W.A., 2008, “Aerosol MALDI Mass Spectrometry for Bioaerosol Analysis” PhD thesis, Delft University of Technology.

Kleefsman W.A. Stowers M.A, Verheijen P.J.T., and Marijnissen J.C.M., 2008, “Single Particle Mass Spectrometry Bioaerosol Analysis by MALDI MS”, KONA Powder and Particle Journal No.26, pp. 205-214

Development and validation of a novel experimental system to investigate particulate matter emitted from a steelworks

M. Barker*[1], C.W. McLeod[1], D. Ciaparra[2], K.Jackson[2]

[1]Centre of Analytical Sciences, University of Sheffield, Sheffield, S3 7HF, UK
[2]Tata Steel RD&T, Swinden Technology Centre, Rotherham, S60 3AR, UK
Keywords: PM, Morphology, ELPI, Dust, Industrial Aerosols
Presenting author email: M.L.Barker@Sheffield.ac.uk

Work place exposure to particulate matter (PM) can be a potential health risk, especially if it is able to penetrate into the respiratory system (Petavratzi *et al*, 2005). Both the shape and size of PM determines how far it can penetrate into the respiratory tract and the rate of particulate removal following deposition. To help further the understanding of the sources and formation of PM and allow efficient abatement, full characterisation must be completed.

PM suspended within the atmosphere may also be known as dust. Dustiness is defined as the likelihood of a material to emit dust during handling (Hjemsted and Schneider, 1996). One method currently used to test the dustiness of a material, and referred to in the British and European standard BS EN 15051, is the rotating drum sampler (RDS). The RDS was originally developed by Warren Springs Laboratories to simulate the general handling of powder materials. It is commonly used to measure the dustiness index of a sample as well as collecting size fractionated particulate matter (PM) into three health related size fractions; inhalable, thoracic and respirable, defined by BS EN 481. Unlike other methods the rotating drum is capable of sampling moist, dry, coarse and fine samples. By testing raw and recycled materials from an integrated steel works using the RDS, dustiness may be quantified and control measures put in place to prevent PM entering the atmosphere.

This work simultaneously couples an Aspect morphology analyser (Biral, UK) and an electrical low pressure impactor (ELPI, Dekati, Finland) to a RDS, as shown in Figure 1. It follows on from previous research completed by Jackson (2009), who coupled a RDS with an ELPI to obtain real time data and chemical information for resuspended particulates

This unique set up allows determination of real time morphological information for particles ranging from 0.5 µm to 20 µm and mass size distributions ranging from 30 nm to 20 µm. The Aspect morphology analyser works by measuring irregularities in the light scattered by single particles passing through a laser beam within the measurement chamber. The ELPI is based on inertial impaction of aerosol particles combined with particle charging and electrical detection. It is capable of determining particle size distributions and concentration in real-time whilst also collecting size fractionated PM onto substrates for subsequent gravimetric and chemical analyses.

One current source of PM within the iron and steel making industry is the handling and stockpiling of raw materials. During this work eleven granular samples originating from stockyards and processes based at an integrated steelworks have been tested, including a selection of iron ores, recycled materials and fluxes such as limestone.

Simultaneous coupling of both the Aspect and the ELPI instruments to the RDS has been successfully completed and morphological data of PM has been obtained. Size distribution profiles have been acquired from both the Aspect and the ELPI allowing comparisons to be made between each instrument.

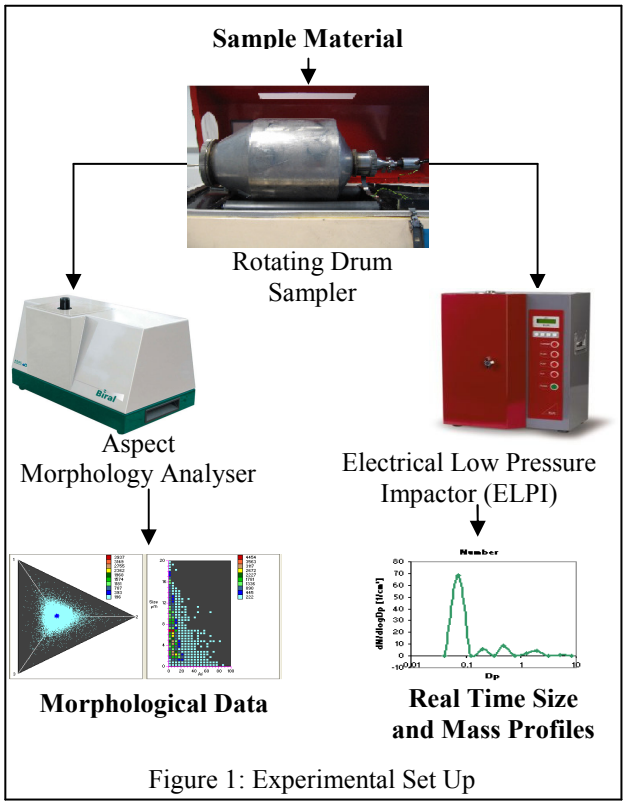

Figure 1: Experimental Set Up

This research was funded by an EPSRC CASE studentship with Tata Steel RD&T.

BS EN 481 (1993) *Size fraction definitions for measurement of airborne particles,* BSI

BS EN 1505 *(2006) Measurement of the dustiness of bulk materials. Requirements and reference test methods,* BSI

Jackson, K. (2009) Ph.D. Thesis, University of Sheffield

Hjemsted, K., Schneider, T. (1996) *Ann. Occup. Hyg.*, **43**, 557-566

Petavratzi, E., Kingman, S., Lowndes, I. (2005) *Miner. Eng.*, **18**, 1183-1199

Development of a pulmonary waveform generator for study the aerosol propagation and deposition in transparent hollow airway models

A. Kerekes, A. Nagy, D. Oszetzky, A. Czitrovszky

Department of Laser Applications, Research Institute for Solid State Physics and Optics, Budapest, H1121, Hungary

Keywords: lda, airway, bronchial, lung model, pulmonology
Presenting author email: anagy@szfki.hu

Proportional bronchial airway models with one to one scaling based on a resin human lung cast and a laboratory prototype of a pulmonary waveform generator were designed and manufactured for the experimental validation of the theoretical calculations made by the stochastic lung deposition model or CFD code (Kerekes *et al.* 2010, Hofmann *et al.* 1991, 2001, Balásházy *et al.* 1990, 1991, Salma *et al.* 2002, Farkas & Balásházy 2008). The preliminary experimental results show good agreement with the theory and encouraged us to develop and build the complete system.

The fully computer controlled pulmonary waveform generator (Fig. 1.) consists of a 8 litre volume piston pump and a controlled servo motor which can follow any pre-programmed waveform to simulate different breathing parameters, like resting, sitting awake, light exercise, heavy exercise. All inhalation parameters are adjustable, so it is easy to study different cases of various health conditions of patients like healthy, asthmatic, COPD, emphysema, and also for adults and children with different ages.

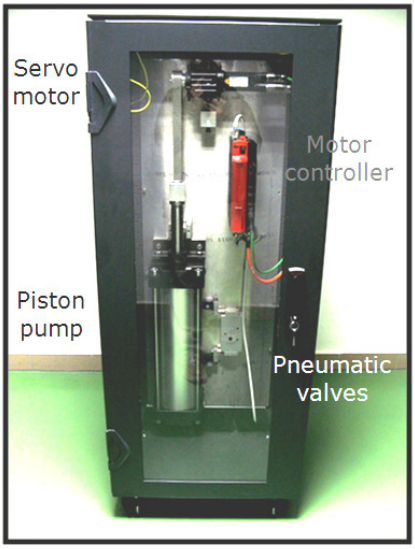

Figure 1. The pulmonary waveform generator

A particle measurement system was developed based on laser Doppler anemometry to detect the particles and measure their concentrations, size- and velocity-distributions inside the airway model, across the cross section in different airways generations (Fig. 2.). This system is optimised to the requirements of this special task, it is compact to fit into the chamber where the airway model is located and easily adjustable.

Measured flow patterns and deposition fraction values will be compared with published computed results at more particle sizes in the size range of 100 nm – 10 µm to validate computational fluid dynamics techniques and lung deposition models.

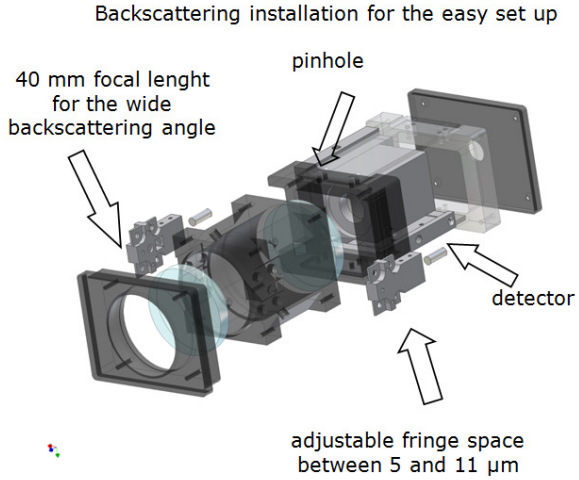

Figure 2. Design of the LDA probe head

This work was supported by the Déry Miksa National Program under grant OMFB-00443/2007.

A. Kerekes, A. Nagy, A. Czitrovszky, D. Oszetzky, Airflow experiments with bronchial airway model, Presentation on IAC2010, Helsinki 2010.

Annals of the ICRP Volume 24/1-3. (1994). *Human Respiratory Tract Model for Radiological Protection* Oxford, U.K. Elsevier Science Ltd.

Balásházy, I., Hofmann, W., & Martonen, T.B. (1990). *Aerosol Sci. Technol*. 13, 308-321.

Balásházy, I., Hofmann, W., & Martonen, T.B. (1991). *J. Aerosol Sci.* 22, 1, 15-30.

Hofmann, W., Balásházy, I. (1991). *Rad. Prot. Dosim*. 38, 57-63.

Hofmann, W., Balásházy, I., & Heistracher, T. (2001). *Aerosol Sci. Technol*. 35, 958-968.

Salma, I., Balásházy, I., Winkler-Heil, R., Hofmann, W., & Záray, Gy., (2002). *J. Aerosol Sci*. 33, 119-132.

Farkas, Á., & Balásházy I. (2008). *Computers in Biology and Medicine* 38, 508-518.

Thursday, September 8, 2011

Session 9A: Aerosols in Geoengineering

Implications of geoengineering assessed in simulations with complex climate models

H. Schmidt[1], K. Alterskjaer[2], F. Benduhn[3], D. Bou Karam[4], J. E. Kristjansson[2], M. G. Lawrence[3], U. Niemeier[1], M. Schulz[5], and C. Timmreck[1]

[1]Max Planck Institute for Meteorology, Hamburg, Germany
[2]University of Oslo, Oslo, Norway
[3]Max Planck Institute for Chemistry, Mainz, Germany
[4]Laboratoire des Sciences du Climat et l'Environnement, Paris, France
[5]Norwegian Meteorological Institute, Oslo, Norway
Keywords: geoengineering, climate change, stratospheric aerosols, aerosol cloud interaction
Presenting author email: hauke.schmidt@zmaw.de

In the context of global warming, various geoengineering techniques have been proposed as a "last resort", in case mitigation efforts fail or the consequences of the warming prove more severe than expected. Some of the suggested approaches would rely on the injection of aerosol into different parts of the atmosphere to enhance the global albedo. A deliberate global-scale manipulation of the radiative budget of the Earth may allow a counterbalancing of global mean temperature increase due to the effects of continued greenhouse gas emissions, but may also result in undesirable side effects for crucial parts of the Earth system. Earlier climate model simulations of geoengineering have led to partly inconclusive results, and it is unclear to what extent this may be due to differences in the model formulations or in the simulated scenarios. To overcome this situation the GeoMIP initiative (Kravitz *et al*., 2011) and the EU project IMPLICC have defined a set of experiments to be performed jointly by several climate models where solar radiation management is applied on top of CMIP5 future emission scenarios. Here, we present results obtained with three climate models applied within IMPLICC.

The simulation scenarios include an idealized experiment, where a quadrupling of CO2 is balanced by a reduction of the solar constant (G1), and a possibly more realistic experiment, in which stratospheric sulphur injections are used to limit temperature increase in the 21st century (G3). Furthermore, within IMPLICC we perform an additional scenario (G5) in which we attempt to obtain the same effect as in G3 by the manipulation of low level clouds through injection of sea salt. The goal is to assess proposed geoengineering techniques by comparing their efficiency and side effects in climate model simulations.

A preliminary analysis of experiment G1 provides the following robust results: To balance the global temperature, i.e. to keep it at the preindustrial level, the necessary reduction of the solar forcing is larger (on the order of 10 to 20%) than the forcing estimated from the change in CO_2. This means that the efficiency of solar shortwave forcing is smaller than that of CO_2 longwave forcing. The climate in such a geoengineered world would not be the same as in preindustrial times. Fig. 1 shows the latitudinal dependence of the temperature response to the forcing in G1 (with respect to preindustrial). A common result among the models is

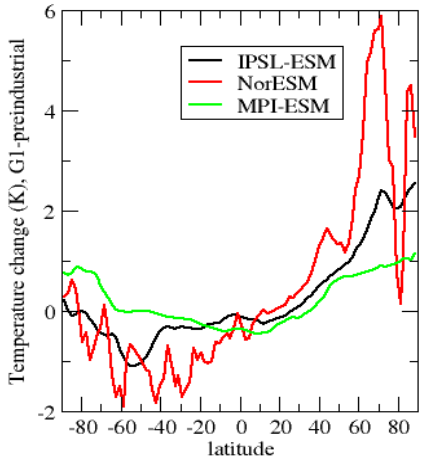

Figure 1: Zonally averaged surface temperature response in experiment G1 relative to the preindustrial control run averaged over 50 years in the IPSL and MPI-ESM, and over 10 years in the NorESM model outputs. Note: In results for IPSL-ESM and NorESM a temperature bias has been removed that was resulting from an inexact balancing of radiative forcing.

that high latitudes (and in particular the Arctic) still tend to be warmer under geoengineering while low latitudes would cool slightly. The solar dimming is obviously more effective in regions with strong insolation.

Global precipitation is reduced in experiment G1 with respect to preindustrial times by about 3-4% although a quadrupling of CO_2 alone (without geoengineering) would strongly enhance precipitation. Regional changes in precipitation differ considerably among the models.

The research leading to these results has received funding from the European Union's Seventh Framework Programme (FP7/2007-2013) under grant agreement n° 226567 - IMPLICC.

Kravitz, B., A. Robock, O. Boucher, H. Schmidt, K. Taylor, G. Stenchikov, and M. Schulz (2011), The Geoengineering Model Intercomparison Project (GeoMIP), *Atm. Sci. Lett.*, DOI: 10.1002/asl.316

Impact of Geoengineered Aerosols on Stratospheric Ozone Chemistry

F.D. Pope[1*], R.A. Cox[1]*, M. Kalberer[1]*, P. Braesicke[1]*, A. Ward[2]*, and I.M. Watson[3]*

[1]Department of Chemistry, University of Cambridge, Cambridge, CB2 1EW, UK
[2]Research Complex at Harwell, STFC, Rutherford Appleton Laboratory, Oxford, OX11 0FA, UK.
[3]Department of Earth Sciences, University of Bristol, Bristol, BS8 1RJ, UK
*Members of the Stratospheric Particle Injection for Climate Engineering (SPICE) team.
Keywords: stratospheric aerosols, chemistry, ozone, climate change.
Presenting author email: fdp21@cam.ac.uk

The deliberate injection of aerosol into the stratosphere has been suggested as a solar radiation management scheme, which would cool the Earth's surface reflecting solar radiation back to space. Such a scheme is believed to be both affordable and have a high effectiveness when compared to other geoengineering schemes for mitigation of global warming (Shepherd, 2009). The lower stratosphere already contains a sulphate aerosol layer which is produced from both biogenic and volcanic sources.

Recently, most research has focused on the deliberate injection of sulphate aerosol (or precursors) into the stratosphere. However, aerosols other than sulphate could be cheaper to produce and be more affective at scattering radiation by virtue of having a greater refractive index. They could also be designed to have lower absorption characteristics, and would therefore result in smaller warming of the stratosphere.

In addition to containing a sulphate aerosol layer, the lower stratosphere also contains the ozone layer which is crucial for protecting the Earth's biosphere from harmful UV radiation. The ozone layer also is a key component of the coupled atmospheric chemistry system, impacting temperatures and dynamics. International regulations are already in place to protect the ozone layer from depletion by man-made halocarbons. Therefore the deliberate injection of aerosols into the stratosphere must be assessed with respect to the possible interactions between the geoengineered aerosol and the ozone layer.

We will present a review of the possible effects of aerosols upon stratospheric ozone. We consider both sulphate aerosol and other aerosols that offer the possibility of cheap and effective solar radiation management. In particular, the direct destruction of ozone upon the aerosol surface and the activation of ozone destroying catalytic species will be considered (e.g. activation of $ClONO_2$ to ClO, and HCl to Cl). In addition to the ClOx catalytic cycles the extra stratospheric aerosol burden is likely to perturb the NOx cycles. The interaction of aerosols with stratospheric water vapour, and the perturbations to aerosol reactivity, will also be assessed. The possibility of using organic and inorganic coatings to provide an inert aerosol surface to reduce the ozone depletion potential of the aerosol will also be presented.

This review will provide a solid framework with which to assess the suitability of different aerosol candidates for use in geoengineering. In addition to the review, initial laboratory work investigating the interaction of geoengineered aerosol with atmospheric gas phase species will be presented. In particular, the uptake coefficients of ozone depleting gases, or their pre-cursors, will be measured. A variety of particle compositions are being investigated including TiO_2 and Al_2O_3. The effect of different surface coatings, both organic and inorganic, upon the aerosol reactivity will also be examined.

Two distinct laboratory studies are being employed to investigate the candidate geoengineered particles. Laser tweezers are used to investigate the changing chemistry of the aerosol bulk phase after interaction with gas phase species (King, 2008). An aerosol flow tube (AFT) with gas phase species detection via chemical ionization mass spectrometry (CIMS) is used to investigate the uptake coefficients of different gas species upon the particle surface (Pradhan, 2010).

Shepherd, J. (2009) Report: Geoengineering the climate; science governance and uncertainty, The Royal Society.
King, M.D., et al. (2008) Faraday Discussions, 137, 173.
Pradhan, M. et al., (2010) Environmental Science and Technology, 44(4), 1360.

Near vessel dynamics of sea salt sprays: How efficient can maritime clouds be seeded?

S. Müller-Klieser[2], U. Platt[2] and T. Leisner[1,2],
[1]Institute of Meteorology and Climate Research, Karlsruhe Institute of Technology, Hermann von Helmholtz Platz 1, 76344 Eggenstein-Leopoldshafen, Germany
[2]Institute of Environmental Physics, University of Heidelberg, Im Neuenheimer Feld 229, 69120 Heidelberg, Germany
Keywords: cloud albedo enhancement, sea salt aerosols, Euler-Lagrange modelling
Presenting author email: Thomas.Leisner@kit.edu

Deliberate modification of the albedo of maritime clouds by seeding them with sea salt particles has been proposed as a viable method of climate engineering (Latham, 1990). In a commonly discussed scenario (Salter et al, 2008), the aerosol is produced by spraying fine droplets of sea water from unmanned vessels. In this contribution, we follow up on this scenario and analyse the dynamics in an artificial cloud of sea water droplets emitted from a ship stack. A finite-volume turbulence model coupled with a Lagrangian particle tracking model is used to simulate the thermodynamic conditions and the aerosol dynamics in the near field around a spraying vessel. Special emphasis is put on the subsidence of the aerosol that originates from the cooling caused by the evaporating droplets.

The model is implemented in Ansys CFX and consists of two parts. For the gas phase, the large eddy turbulence model of Nicoud and Ducros (1999) is used. It is coupled to a Lagrangian particle model which describes the aerosol. Liquid evaporation is implemented using the the model of Langrish and Kockel (2001). Convergence test for grid resolution, time stepping, iterations per time step and number of statistically picked ensemble tracks were made. We are able to solve the equations for a box size of 25*40*150 m^3 (h*w*l in downstream direction). For the final run a grid of 2*105 tetrahedrons was used. The model size was sufficient to follow the aerosol dynamics up to complete thermalization for wind speeds below 7m/s.

As proposed first by Latham (1990, 2002) one would have to disseminate about 10^{17} particles per second and per vessel in order to offset a global radiative forcing of 3.7 Wm^{-2} with a fleet of 1500 vessels. We chose this number as targeted production rate for our initial condition, although different GCM model studies by Korhonen (2010) showed more than 5 times the spray rate previously assumed could be needed due to particle deposition and suppression of cloud supersaturation. The meteorological conditions were chosen from Lewis and Schwartz (2006) representing common stable conditions at sea. We varied the initial droplet radii from 2µm to 0.4µm (Latham, 2002), accordingly the evaporated water mass changed. To test for sensitivity and dependency on the meteorological boundary values, simulations where run at relative humidity levels between 80 % and 98 %. Wind speed was varied between 1m/s to 7 m/s at 10m altitude.

After the evaporation of all droplets the aerosol air mass reaches thermodynamic equilibrium with the environment. The particles surviving that period are available for updraught by turbulent mixing. We estimate the efficiency of this process by using a standard parametrization adapted from Pasquill (1961).

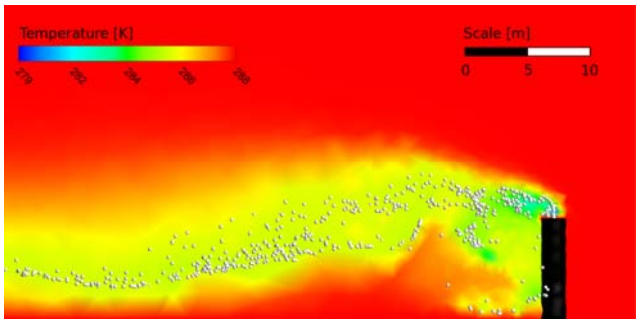

Figure 1. Model output for a single sea-going spraying device at a windspeed of 3 m/s from the right and neutral atmospheric stability. Gas phase temperatures are color coded and the dots represent ensembles of particles

Fig. 1 shows a cross-section of a spraying device parallel to wind speed. Colors indicate the temperature in Kelvin. Ensembles of particles are marked with white dots. We show that the evaporative cooling entrains the particles, forces the aerosol to remain in low altitudes and rising loss rates. In our contribution, we will present results on the cloud seeding efficiency as a function of initial droplet size and stability of the atmosphere and discuss the resulting limitations for cloud seeding.

This work was supported by Marsilius Kolleg of the University of Heidelberg under the project “The Global Governance of Climate Engineering”

Korhonen, H. (2010) Atmos. Chem. Phys. 10, 4133–4143.
Langrish, T. A. G. and Kockel, T. K. (2001) Chemical Engineering Journal 84, 69 – 74.
Latham, J. (2002) Atmospheric Science Letters 3, 52-58.
Latham, J. (1990) Nature 347, 339-340.
Lewis, E. R. and Schwartz, S. E. (2006) Geophysical monograph series, American Geophysical Union.
Nicoud, F. and Ducros, F. (1999) Flow, Turbulence and Combustion 62, 183-200.
Pasquill, F. (1961) Meteorol. Mag. 90, 33-49.
Salter, S., Sortino, G. and Latham, J. (2008) Phil. Trans. R. Soc. A 366, 3989-4006.

The impact of controlled sea salt emissions on cloud features based on comprehensive regional model studies

K. Lundgren[1], M. Bangert[1], H. Vogel[1], and B. Vogel[1]

[1]Institute for Meteorology and Climate Research, Karlsruhe Institute of Technology, Karlsruhe, 76131, Germany
Keywords: geoengineering, sea salt, CCN, modelling (regional).
Presenting author email: Kristina.lundgren@kit.edu

One of the presently suggested methods to control the global warming is to increase the planetary albedo by seeding marine clouds with sub-micron sea salt particles since these act as a major source of cloud condensation nuclei (CCN). By assuming a constant amount of cloud liquid water, an increase in CCN acts to increase the cloud droplet number concentration (CDNC) and decrease the droplet sizes. As a result, the cloud albedo increases.

A proposed technique to inject sub-micron sea salt particles to the atmosphere is to use wind driven vessels (e.g., Salter *et al.*, 2008). These are designed to release micron sized mono-disperse sea water drops.

To investigate the effect of imposing sea salt particle fluxes to the atmosphere is difficult, partly due to the non-linear response of the atmospheric processes. Due to the competition for water vapour, an increase of sea salt particles can e.g., suppress the activation of secondary particles. This can eventually give an opposite effect than originally intended (e.g., Korhonen et al., 2010).

In this study, we investigate the impact of controlled sea salt emission fluxes on the cloud properties for a region that is equipped with vessels homogeneously distributed within distances of 0.25°. We perform detailed calculations with the comprehensive model system COSMO-ART (Vogel *et al.*, 2009). COSMO-ART is online coupled, which makes it possible to investigate feedbacks between particles and the state of the atmosphere. The natural emissions of primary particles are parameterized as function of the ambient conditions. Primary soot emissions are considered and secondary aerosols are formed from gaseous precursors that are treated by complex photochemistry in the model. We use two-moment cloud microphysics including six hydrometeor classes (Seifert and Beheng, 2006) that are coupled to the aerosol particles by a comprehensive parameterisation for aerosol activation (Barahona *et al.*, 2010). The activation parameterization accounts for the competition of different aerosol particles for water vapour during their activation and considers the effect of giant CCN such as sea salt. The emission fluxes of sub-micron sea salt particles from the vessels are described as function of wind speed according to Korhonen *et al.* (2010).

Specific remote regions with high insolation have been favored for geoengineering purposes (Salter *et al.*, 2008). We have the intention to study the impacts in such regions, but here we first investigate the effect of controlled sea salt emissions in a region of anthropogenic influence. In Fig. 1. we present the wind speed and average changes in the sea salt number density (N_{SSA}), CCN, liquid water path (LWP), and cloud optical depth (COD) for a case study over western Europe for the 23-26 July, 2008. During the investigated time period, a low was situated north of Spain. When considering the controlled sea salt emissions, the average CDNC increases by up to 10 cm^{-3} over the Atlantic Ocean, which corresponds to modifications in the order of 100% or higher. Regions of anthropogenic influence show more complex responses. Here increases as well as decreases of the CDNC, LWP, and COD are found. The relative change in the CDNC is locally in the order of 100%.

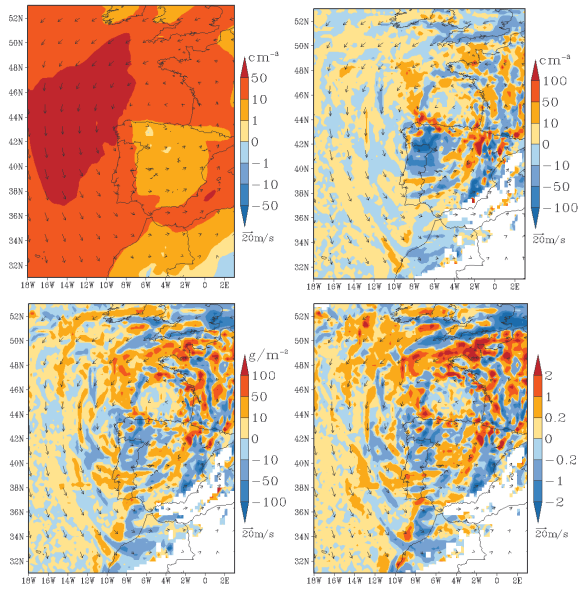

Figure 1. Mean ΔN_{SSA} (top left), ΔCDNC (top right), ΔLWP (bottom left), and ΔCOD (bottom right) when including imposed sea salt emissions.

In the presentation, results for further regions will be discussed, taking also sulphates from oceanic DMS emissions into account.

Barahona, D., West, R.E.L., Stier, P. Romakkaniemi, S., Kokkola, H. and Nenes, A. (2010). *Atmos. Chem. Phys., 10,* 2467-2473.

Korhonen, H., Carslaw, K.S. and Romakkaniemi, S. (2010). *Atmos. Chem. Phys., 10,* 4133-4143.

Salter, S., Sortino, G. and Latham, J. (2008). *Phil. Trans. Soc. 366.*

Seifert, A. and Beheng, K.D. (2001). *Atmos. Res.*, 59-60, 265–281.

Vogel, B., Vogel, H., Bäumer, D., Bangert, M., Lundgren, K., Rinke, R., and Stanelle, T. (2009). *Atmos. Chem. Phys., 9,* 8661-8680.

Effects of sea spray geoengineering on clouds and Earth's radiative balance

A.-I. Partanen,[1] H. Kokkola,[1] S. Romakkaniemi,[2] V.-M. Kerminen,[3] K.E.J. Lehtinen[1,2] and H. Korhonen[1]

[1.] Finnish Meteorological Institute, Kuopio Unit, P.O.B. 1627, FI-70211 Kuopio, Finland
[2.] Department of Applied Physics, University of Eastern Finland, Kuopio campus, P.O.B. 1627, FI-70211 Kuopio, Finland
[3.] Finnish Meteorological Institute, P.O.B. 503, FI-00101 Helsinki, Finland
Keywords: geoengineering, indirect effect, direct effect, sea spray.
Presenting author email: antti-ilari.partanen@fmi.fi

Manipulation of the Earth's climate by injecting vast amounts of sea spray into the atmosphere in persistent marine stratocumulus regions (Latham, 1990) has gained interest in recent years. To date, most studies have assumed a prescribed uniform cloud droplet number concentration (CDNC) in the geoengineered regions irrespective of the environmental conditions and have therefore not been able to address the aerosol-cloud interactions or the direct radiative effects of the injected sea spray.

Here we present simulations with the aerosol-climate model ECHAM5-HAM (Stier *et al.*, 2005) which includes explicit and prognostic calculation of cloud microphysics and interaction of aerosol particles with clouds and radiation. We assume a wind-speed dependent number flux for the injected particle population similar to Korhonen *et al.* (2010) and follow its transport and transformation due to microphysical processes in the atmosphere. This additional sea spray flux is simulated either over all the oceans or in three optimized regions which have the strongest radiative flux perturbations (RFP) and cover altogether 3.3% of the Earth's surface (same total area as in Jones *et al.* (2009)).

Applying the baseline scenario (i.e. injected particle size 250 nm and number flux 10% higher than in Korhonen *et al*. (2010)) in the optimized regions, we predict a global mean RFP of −0.8 Wm^{-2}. This compares well with the earlier estimate of −0.97 Wm^{-2} by Jones *et al.* (2009) who assumed a fixed prescribed CDNC of 375 cm^{-3} in the geoengineered regions. In our simulations the mean regional CDNC varies between 194 and 286 cm^{-3}, and cloud cover increases by 2–5 percentage points. It is noteworthy that both the absolute CDNC values as well as their relative changes (74–80%) are clearly higher than predicted in Korhonen *et al.* (2010) using similar emission fluxes. In our simulations, multiples of the baseline sea spray flux cause almost a linear increase in CDNC but the RFP is clearly sublinear (global mean RFP with 5×baseline flux is −2.2 Wm^{-2}).

Since the three optimal geoengineering regions are characterized with persistent stratocumulus decks, inside them practically all of the radiative effect originates from aerosol indirect effects. However, the direct effect can be significant outside these regions: when all oceanic regions are seeded, the direct effect is about 65 % of the aerosol indirect effects.

For a constant volume emission flux of sea spray, the size at which the individual particles are injected becomes very important. Reducing the injection size from 250 nm to 100 nm, which is typically still large enough for cloud activation in marine boundary layer, increases the global mean RFP in the run of optimized regions to −2.1 Wm^{-2}. On the other hand, aerosol direct effect from 100 nm particles is only 50 % of direct effect from larger 250 nm particles. With the largest tested particle size (500 nm) geoengineering has only very minor effects on CDNC or RFP due to the low number flux (13% of the baseline flux).

Based on our results aerosol direct effect originating from artificial sea spray emissions cannot be neglected although indirect effects dominate over regions covered by marine stratocumulus clouds. In these regions it would probably be optimal to use rather small particles to maximize aerosol number concentration and thus aerosol indirect effects. However, if injections were done outside stratocumulus regions, larger particles might be most efficient to maximize aerosol direct effect. These results imply that this geoengineering method has potential to counteract anthropogenic climate warming, should we able to realise the relatively high sea spray fluxes assumed over 3.3% of the Earth's surface.

Detailed studies by cloud-resolving model (Wang *et al.*, 2011) showed that individual cloud cells react differently to sea salt injections based on background aerosol concentration, cloud water content and the injection method. These small-scale effects cannot be properly assessed with a climate model.

This work was supported by Maj and Tor Nessling Foundation under grant 2009152.

Korhonen, H., Carslaw, K.S and Romakkaniemi S. (2010) Atmos. Chem. Phys. **10**, 4133-4143.
Latham, J. (1990), *Nature* **347**, 339-340.
Jones, A., Haywood, J. and Boucher, O. (2009) *J. Geophys. Res.* **114** (D10106).
Stier, P., Feichter, J., Kinne, S., Kloster, S., Vignati, E., Wilson, J., Ganzeveld, L., Tegen, I., Werner, M., Balkanski, Y., Schulz, M., Boucher, O., Minikin, A., and Petzold, A. (2005), *Atmos. Chem. Phys.*, **5**, 1125-1156.
Wang, H., Rasch, P.J. and Feingold, G. (2011) *Atmos. Chem. Phys. Discuss.*, **11**, 885-916.

Exploring efficiency of sea spray geo-engineering

K. J. Pringle, K. S. Carslaw, T. Fan

Institute of Climate and Atmospheric Science, School of Earth and Environment, University of Leeds, LS2 9JT
Keywords: aerosol modelling, sea spray, clouds, climate change
Presenting author email: kirsty@env.leeds.ac.uk

Artificially increasing the albedo of marine clouds by the mechanical emission of sea spray has been proposed as a possible geoengineering technique to slow the warming attributed to anthropogenic greenhouse gases. For the injected sea spray to cause a net cooling, the additional aerosol must result in an increase in cloud droplet number. In this study we use a physically based parameterisation of aerosol activation to quantify cloud drop number (CDN) changes over the entire parameter space of updraft speed and properties of the injected and background aerosol.

We suggest criteria for when geoengineering may be an effective strategy and also identify conditions where additional aerosol will have a negligible effect or act to decrease CDN. Undesirable decreases in CDN occur when particles are injected into clouds in environments where the number concentration of background accumulation mode aerosol is > 200 cm^{-3}. The effect is particularly strong when (i) the in-cloud updraft velocity is low (< 0.2 ms^{-1}); (ii) the injected mode width is wide (standard deviation of > 1.3) and (iii) the number concentration of the additional aerosol is low (< 200 cm^{-3}). A large increase in CDN is achieved when the converse it true.

To explore the frequency of occurrence of these "high efficiency" and "low efficiency" background conditions, we analyse output from two global aerosol models to identify the percentage change in CDN as a function of the properties of the injected particles. The purpose of this work is to help target sea spray geo-engineering to the conditions when it will be most efficient, and thus to avoid geo-engineering in conditions when it will be inefficient, or even counterproductive.

Thursday, September 8, 2011

Session 9B: Field Observations from Global Hot Spots

First on-line aerosol chemical composition measurements in South African grassland region

P.Tiitta[1,2], L. Laakso [1,3], V. Vakkari [4], P. Croteau[5], M. Josipovic[1], P. Beukes[1], P. Van Zyl[1], A. Venter[1], K. Jaars[1], H. Laakso[4], J. Jayne[5], J. Pienaar[1], M. Kulmala[4], A. Laaksonen[2,3], D. Worsnop[2,4,5]

[1]Atmospheric Chemistry Research Group, North-West University, Potchefstroom, South Africa
[2]University of Eastern Finland, Department of Physics and Mathematics, Kuopio, Finland
[3]Finnish Meteorological Institute, Finland
[4]Department of Physics, University of Helsinki, Finland
[5]Aerodyne Research Inc., 45 Manning Road, Billerica, Massachusetts, USA
Keywords: submicron particles, aerosol mass spectrometry, aerosol chemistry, organic aerosols
Presenting author email: petri.tiitta@uef.fi

Africa is one of the least studied and one of the most critical continents with regard to climate change. Thus diverse long term atmospheric observations are needed to study the effects and drivers of the climate change. One of the increasingly important drivers of changes is the urbanization, which increase the importance of megacities as source of pollutants on regional and global scale. Unfortunately, there are essentially no long-term high-time resolution (or real-time) aerosol chemical composition measurements in Africa. These measurements are needed to understand the effects on particulates on climate and regional pollution levels.

The Aerodyne ACSM (Aerosol Chemical Speciation monitor) is designed for continuous long-term measurements of the chemical composition of non-refractory submicron particulate matter in real time and is based on same technology as Aerodyne Aerosol Mass Spectrometers (AMS) (Ng *et al*., 2011). The sampled particles are focused after a critical orifice to the vaporizer by an aerodynamic lens and non-refractory components flash-vaporize. The vapour molecules are ionized by electron impact and positive ions are detected by a quadrupole mass spectrometer. Much of the reduced complexity is due to the fact that the ACSM does not measure size distributions; only aerosol mass spectra are reported.

Our measurements are conducted at a new measurement site about 100 km to West of Johannesburg, South Africa, on a grazed savannah-grassland area with limited local pollution sources, but strongly impacted by the plumes from Gauteng metropolitan area with more than 10 million people. In addition to pollution plumes, the site is influenced by frequent injections of clean air from the sparsely populated sector to the West—South-West. The station has been utilized in South Africa since 2006 (Laakso *et al*., 2008), and was placed on its permanent location near to Potchefstroom in May 2010.

Preliminary results of the ACSM dataset for the period 1 September – 30 November 2010 showed that PM1 aerosol composition was dominated by organics (OA) (54%) and sulphate (SO_4^{2-}) (26%). Observed fractions for ammonium ($NH4^+$) and nitrate (NO_3^-) were 13% and 6%, respectively. Tracer m/z indicated that amount of hydrocarbon-like OA (HOA) was really small and most of organics were oxidised.

For more detailed analysis, the data was divided in dry and wet season periods (Figure 1). During the dry season the organic aerosol concentration was high (> 60 % of total signal) and peaked up to 35 μg/m^3 most probably due to local biomass burning. During the wet season, sulfate concentrations were typically high and overtook organics especially when the air-masses were transported from Johannesburg metropolitan region.

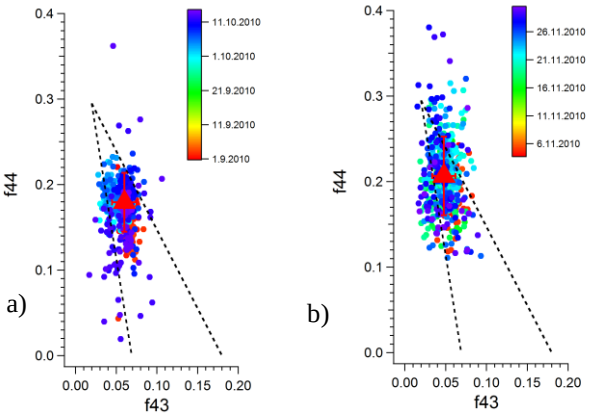

Figure 1: Preliminary results of m/z 43 and m/z 44 ratios to total signal of all OA components in the mass spectrum (f43 and f44) during (a) dry and (b) wet seasons. The dotted lines indicate the triangular space where ambient OOA components usually fall and average values ± s.d marked as triangles.

Detailed positive matrix factorization (PMF) of AMS organic mass spectra will be applied to further characterize the sources and evolution of ambient organic aerosol (OA) material.

This work was supported by the Saastamoinen säätiö and the Academy of Finland (project number 132640**).**

Laakso, L., Laakso, H., Aalto, P.P., Keronen, P., Petäjä, T., Nieminen, T., Pohja, T., Siivola, E., Kulmala, M., Kgabi, N., Molefe, M., Mabaso, D., Phalatse, D., Pienaar, K., and Kerminen, V.-M. (2008) *Atmos. Chem. Phys*., **8**, 4823-4839.

Ng, N., Herndon, S., Trimborn, A., Canagaratna, M., Croteau, P., Onasch, T., Sueper, D., Worsnop, D., Zhang, Q., Sun, Y., Jayne, J. (2011a) *Aerosol Sci. Tech.*, in press.

Aerosol particle size distributions in clean and polluted environments in South Africa

V. Vakkari[1], H. Laakso[1], M. Kulmala[1], D. Mabaso[2] and L. Laakso[1,3,4]

[1]Department of Physics, University of Helsinki, P.O. BOX 64, 00014 University of Helsinki, Finland
[2]Rustenburg Local Municipality, Rustenburg, Republic of South Africa
[3]Finnish Meteorological Institute, Research and Development, P.O. BOX 503, FI-00101, Finland
[4]School of Physical and Chemical Sciences, North-West University, Potchefstroom, South Africa

Keywords: Aerosol particle size distributions, South Africa
Presenting author email: ville.vakkari@helsinki.fi

Submicron aerosol particles effect climate via direct and indirect mechanisms (Seinfeld and Pandis, 1998), and pose a threat for human health (Pope and Dockery, 2006). Depending on their size, they may scatter light, act as cloud condensation nuclei, or penetrate at different depths in human lungs.

Due to their large variability in size and dynamically driven tendency to occur in different separate size-ranges, modes, the particle size distribution is often expressed as a sum of multiple log-normal modes. Smallest particles (< 25 nm) are classified as nucleation mode, slightly larger (25–100 nm) as Aitken mode, next accumulation mode (100–1000 nm) and particles above 1000 nm as coarse mode particles. Especially for modelling purposes this classification provides clear benefits in e.g. reduced number of differential equations (e.g. Korhonen et al., 2004).

For large observational datasets, the modal representation provides simple way to study the behaviour of aerosols.

In this study, we present analysis of four years of submicron particle size distribution data measured in South Africa during the period 07/2006–05/2010. The period until 02/2008 represent semi-clean background savannah (Botsalano game reserve) (Laakso et al., 2008; Vakkari et al., 2010), whereas the second part of measurements is from polluted mining area (Marikana village) with a strong impact from domestic biomass burning in informal settlements (Venter et al., 2011).

The particle number size distributions were observed with a Differential Mobility Particle Sizer with a size range from 10 to 840 nm. The modal fittings are done by the method described in Vartiainen *et al* (2007). Measurements are explained in detail in Laakso *et al* (2008) and Vakkari *et al* (2011).

In addition to the in-situ measurements, particle size distributions and their representativeness are analyzed as a function of air mass origin utilizing the HYSPLIT air mass trajectories and MODIS satellite data.

Based on this study, we found that source areas of aerosol particles obtained from in-situ measurements combined with air mass trajectories agree with the satellite produced aerosol optical depths. We also found seasonal and spatial differences in particle formation and growth rates indicating the importance of biogenic organics and sulphuric compounds. Also the effects of wild fires were clearly seen. The whole dataset provides unique possibility for modelling purposes in an environment with very few previous observations.

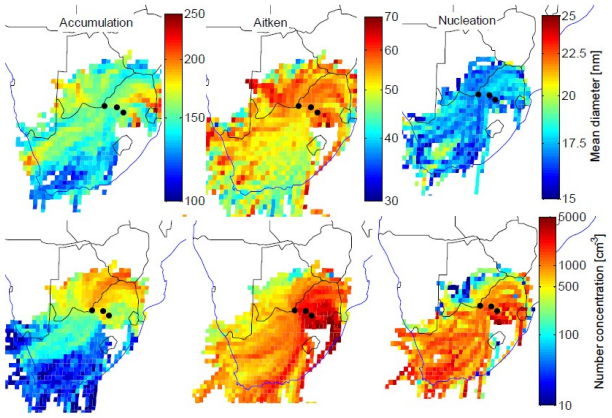

Figure 1. Accumulation, Aitken and nucleation modes as a function of the origin of air masses for Botsalano game reserve, Republic of South Africa.

This work was supported by the Academy of Finland and the Rustenburg local municipality.

Korhonen, H., Lehtinen, K.E.J. and Kulmala, M. (2004) *Atmos. Chem. Phys.*, **4**, 757-771.

Laakso, L., Laakso, H., Aalto, P.P., Keronen, P., Petäjä, T., Nieminen, T., Pohja, T., Siivola, E., Kulmala, M., Kgabi, N., Molefe, M., Mabaso, D., Phalatse, D., Pienaar, K. and Kerminen, V.-M. (2008). *Atmos. Chem. Phys.*, **8**, 4823-4839.

Pope, C.A. and Dockery, D.W. (2006) *J. Air Waste Manag. Assoc.*, **56**, 709-742.

Seinfeld, J. H. and Pandis, S. N. (1998) *Atmospheric Chemistry and Physics: From Air Pollution to Climate Change*, Wiley, New York.

Vakkari, V., Laakso, H., Kulmala, M., Laaksonen, A., Mabaso, D., Molefe, M., Kgabi, N., and Laakso, L. (2010) *Atmos. Chem. Phys. Discuss.*, **10**, 30777-30821.

Vartiainen, E., Kulmala, M., Ehn, M., Hirsikko, A., Junninen, H., Petäjä, T., Sogacheva, L., Kuokka, S., Hillamo, R., Skorokhod, A., Belikov, I., Elansky, N., and Kerminen, V.-M. (2007) *Boreal Env. Res.*, **12**, 375–396.

Venter, A., Vakkari, V., Tiitta, P., Josipovic, M., Beukes, J.P. and Laakso, L. (2011) *in prep.*

Long term aerosol optical properties in pristine and biomass burning areas in the Amazon Basin

P. Artaxo[1], L.V. Rizzo[2], K.T. Wiedemann[1], E. Swietlicki[4], A. Wiedensohler[3]

[1]Institute of Physics, University of Sao Paulo, Rua do Matao, Travessa R, 187, CEP 05508-090, Brazil.
[2] Department of Exact and Earth Sciences, Federal University of Sao Paulo, Diadema, 09972-270, Brazil
[3] Leibniz Institute for Tropospheric Research, Leipzig, 04318, Germany
[4] Department of Physics, Lund University, Lund, Sweden.

Keywords: aerosol optical properties, biogenic particles, biomass burning, absorption coefficient, scattering coefficient.
Presenting author email: artaxo@if.usp.br

Aerosol physical and chemical properties were measured in two sites in Amazonia. The clean site is at Central Amazonia and is located in a pristine Amazonian forest site. A second sampling site is located in Porto Velho, Rondonia, an area strongly affected by biomass burning emissions. Long term measurements, from February 2008 are being carried out in these two sites, as part of the EUCAARI (European Integrated Project on Aerosol Cloud Climate and Air Quality interactions) and AEROCLIMA (Direct and indirect effects of aerosols on climate in Amazonia and Pantanal) projects. The dataset obtained encompass the first long term aerosol measurements ever performed in Amazonia, elucidating the differences between the biogenic aerosol population naturally released by the forest metabolism and the anthropogenic aerosols brought to the ecosystem by outer sources as well as regional biomass burning emissions.

In the pristine central Amazonia, measurements were taken at the Cuieiras forest site, tower TT34, with coordinates 2°35'40"S and 60°12'33"W, above the canopy (45m), under dry conditions (RH<40%). A MAAP 5012 absorption photometer in series with a nephelometer (TSI 3563) was used to measure aerosol absorption and scattering, respectively. Scattering coefficients were corrected for truncation errors. Observations were adjusted to 1000 mbar and 0^oC. Aerosol size distributions were measure using a Lund DMPS system, as well as a TSI SMPS system. Aerosol composition, and several trace gases that helps to characterize aerosol sources were also measured.

In Rondonia, a sampling station was installed close to the city of Porto Velho, in the "Parque Natural de Porto Velho" at coordinates ($8,69^o$ S; $63,87^o$ O). This region have with important land use change and biomass burning emissions. A MAAP 5012 absorption photometer and an Ecotech Aurora 3000 nephelometer are used to measure aerosol absorption and scattering. A TSI SMPS measure the aerosol size distribution continuously. Diffusion dryers are used to keep the relative humidity below 40%.

In the pristine Amazonian atmosphere, aerosol scattering coefficients ranged between 1 and 200 Mm^{-1} at 450 nm, while absorption ranged between 1 and 20 Mm^{-1} at 637 nm. A strong seasonal behavior was observed, with greater aerosol loadings during the dry season (Jul-Nov) as compared to the wet season (Dec-Jun). Although the forest site is locally well preserved, it receives the influence of regional biomass burning emissions during the dry season.

During the wet season in Manaus, aerosol scattering (450 nm) and absorption (637 nm) coefficients averaged, respectively, 14 ± 22 and 0.9 ± 0.8 Mm^{-1}. Both optical coefficients were greatly increased during the dry season, averaging 58 ± 58 Mm^{-1} and 4.1 ± 3.8 Mm^{-1}, correspondingly. Angstrom exponents for scattering were lower during the wet season (1.6 ± 0.4) in comparison to the dry season (1.9 ± 0.2), which is consistent with the shift from biomass burning aerosols, predominant in the fine mode, to biogenic and dust aerosols, predominant in the coarse mode. Single scattering albedo, calculated at 637 nm, did not show a significant seasonal variation, averaging 0.86 ± 0.06 and 0.86 ± 0.04, respectively for wet and dry season, even with that large variation in aerosol sources and magnitude of scattering and absorption coefficients.

In Porto Velho, even in the wet season it was possible to observe a strong impact from anthropogenic sources. Biomass burning emissions in the dry season. $PM_{2.5}$ aerosol concentrations of about 300 ug/m² were measured in August and September for most of the years. AOT values at 550 nm above 3 are frequently observed in Porto Velho with AERONET sunphotometers. Black Carbon were measured at 20 ug/m³ in the dry season, indicating strong aerosol absorption. Aerosol light scattering above 300 Mm^{-1} were measured.

This work presents a general description of the aerosol optical properties in Amazonia, both during the Amazonian wet season, when the aerosol population is dominated by particles of biogenic origin, and during the dry season, when there is a strong influence of biomass burning emissions. It is important to describe accurately the optical behavior of these particles in order to assess the impact of anthropogenic changes on the regional climate.

This work was supported by Fundação de Amparo à Pesquisa do Estado de São Paulo, FAPESP Thematic Project AEROCLIMA (08/58100-2) and the European Integrated project on Aerosol Cloud Climate and Air Quality Interactions, EUCAARI (036833).

Inflow and outflow of Borneo: the regional setting of aerosol compositional measurements in and above a maritime tropical rainforest.

N.H. Robinson[1], J.D. Allan[1,3], G. Allen[1] and H. Coe[1]
[1]Centre for Atmospheric Science, University of Manchester, M13 9PL, UK
[2]National Centre for Atmospheric Science, University of Manchester, M13 9PL, UK
Keywords: AMS, Long-range transport, Trajectory, Tropics.
Presenting author email: niall.robinson@postgrad.manchester.ac.uk

We present results of detailed aerosol measurements made from a ground site positioned in the rainforest of N.E. Borneo (about 80 km from the coast) and from the FAAM research aircraft around North Borneo, performed as part of the Oxidant and Particular Photochemical Processes Above a South East Asian Rainforest (OP3) project. Aerosol was measured using Aerodyne Aerosol Mass Spectrometers, which provide composition and size resolved measurements of sub-micron aerosol. Off- and on- island aerosol sources influencing the ground site were assessed with the most striking result being far greater loadings of sulphate in off-island air masses than in the continental tropics. Aircraft profiles show that transit of air masses over Borneo depletes regional aerosol and elevates terrestrial aerosol. It also lofts aerosol higher into the atmosphere which is likely to extend their atmospheric lifetime.

The vast majority of detailed atmospheric aerosol studies are performed in the Northern mid-latitudes. There is a comparative paucity of measurements that have been performed in the tropics, with the only studies that have been conducted focusing on the continental land masses in West Africa and Amazonia. The tropics are of particular importance to climate as they have a higher solar flux than the mid-latitudes. This means any perturbations to natural systems will be of more consequence than they would in the mid-latitudes. There is also widespread land-use change occurring, with rainforest being cleared to make way for agriculture. Not only does this release carbon previously trapped in the biosphere, but different emissions to the atmosphere affect atmospheric chemistry. The significant region of the tropics represented by the "maritime continent" — the patchwork of tropical islands in South-East Asia — has so far been overlooked by previous studies. Tropical island aerosol are potentially very different from those over continental land masses due to the influence of marine emissions and dynamical systems.

The relationship of aerosol composition to geographical air mass source was assessed using backwards air mass trajectory techniques. Identified off-island sources included long range transport of sulphate (neutralised by time of arrival at the site) and low concentrations of highly oxidised organics. Marine air masses also contained chloride that was closely correlated with nitrate aerosol. As the AMS is inefficient at detecting NaCl due to is slow vaporisation, it is likely that sea salt aerosol is reacting with terrestrial nitrate to form more readily detectable compounds. On-island sources included less oxidised organic aerosol which was probably Secondary Organic Aerosol (SOA) from rainforest terpene emissions. It appears that aerosol thought to be isoprene SOA was also seen from air masses travelling over oil palms, which are known to emit five times as much isoprene as the rainforest. Regional aerosol is removed by transit over Borneo, probably due to increased precipitation over the mountainous interior.

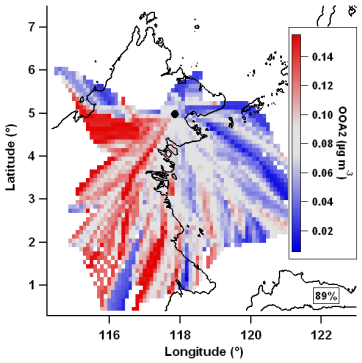

Figure 1: Example of back trajectory analysis. Each cell coloured by the average loading measured at the receptor site (back dot) for an air mass that has travelled over it. Red is above average and blue is below. This shows less-oxidised organic aerosol to originate terrestrially.

Aircraft profiles were used to assess the influence transit over Borneo has on synoptic transport of aerosol. Profiles upwind of the island show a very shallow boundary layer that contained sulphate (and low levels of organic) aerosol. Profiles over the island show a shallow mixed layer of organics with elevated sulphate loadings in a layer above. As the day progresses organic aerosol levels grow in the higher layer. Profiles over the downwind coast of the island show a shallow mixed layer with the above layer containing elevated levels of organics and occasionally sulphate. It seems that transit over Borneo depletes regional aerosol loadings (probably through wet deposition) and enhances SOA loadings from terrestrial emissions. It also lofts aerosol higher into the atmosphere.

This work was supported by the National Environmental Research Council grant NE/D002117/1.

Direct Evidence of Elevated Absorbing Layer Associated with Coarse Mode Particles over CTCZ Region from Aircraft Experiment 2009

J. Jaidevi, Priya Choudhry, Marykutty Michael, S.N. Tripathi, Tarun Gupta
Department of Civil Engineering, Indian Institute of Technology Kanpur, Kanpur, India
Keywords: Aircraft experiment, Optical properties, Size distribution, SEM/EDX
Presenting author email: snt@iitk.ac.in

The natural desert dust from west transported through the Indo-Gangetic (IG) plains gets mixed with locally generated anthropogenic aerosols and is further carried over to the Himalayan foothills during the dry pre-monsoon season. Such mixing of natural and anthropogenic absorbing aerosol increases the dust absorption. Studies show strong dependence of radiative forcing on aerosol size distribution and presence of coarse mode absorption (Tripathi et al., 2011). Aircraft measurements were carried out over the Continental Tropical Convergence Zone (CTCZ) region up to 4 km during early monsoon season (Jun-Jul), 2009 to study the vertical and spatial variation of aerosol optical, microphysical, chemical, hygroscopic and morphological properties. The study area for the experiment was the northern part of Continental and Tropical Convergence Zone (CTCZ) region spanning from Khajuraho to Nainital in South-North direction and from Gaya to Jaipur in the East-West direction as shown below in Figure 1. In addition, a ground station was maintained at IIT Kanpur campus throughout the study.

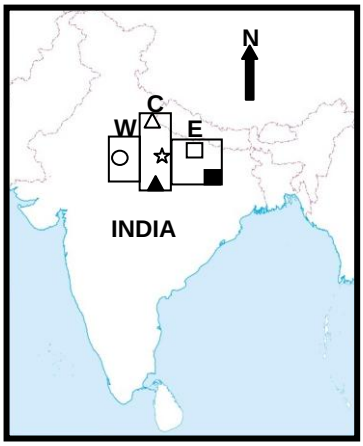

Figure1: Three segments, western (W), central (C) and eastern (E) Indo-Gangetic Basin shown by rectangles on an outline map of India, where the *circle*, *star*, *open triangle*, *filled triangle*, *open square* and *filled square* represent 'Gwalior', 'Kanpur', 'Nainital', 'Khajuraho', 'Gorakpur' and 'Gaya' respectively

Based on simultaneous measurements using four instruments onboard (Photoacoustic Soot Spectrometer, Scanning Mobility Particle Sizer, Aerodynamic Particle Sizer and $PM_{2.5}$ sampler) and the subsequent SEM/EDAX analysis, strong association between absorption and coarse mode aerosols is found. The in situ size distribution obtained using APS and SMPS has been binned for different heights within a zone and for different SSA within a height bin. This has been done in order to see any changes in the absorption pattern with respect to location and altitude. A shift in absorption is seen from accumulation mode in central (78°-81°E) to coarse mode in east (81°-84°E) CTCZ indicating the possibility of ageing of aerosols during long range transport. Aerosols below 2 km show absorption in coarse modes over central and east.

Spot analysis using SEM/EDX were carried out on particles collected on filters over Kanpur on Jun 29 at ground level and at higher altitudes using PM2.5 samplers as simultaneous collection of filter samples at ground and aloft were carried only over Kanpur during the experiment duration. The analysis of ground level filter (quartz filter) showed that particles were angular and flaky. The SEM images also showed chain like structures composed of small spherules making up the chain like structure, approximately 54 nm in size, suggests anthropogenic aerosols like 'fresh' soot which undergoing ageing process The EDX on particles imaged using SEM and EDX analysis were found to be composed of silicon (Si), aluminum (Al) and carbon (C) mainly suggests internal mixing of dust and anthropogenic aerosols.

The analysis of aircraft filter showed particles of relatively smaller size and showed agglomeration. The chain like structure of soot is absent here, and the particles have clustered and agglomerated to form large particles. These clusters are formed during the ageing process by the collapse of chain like soot structures and internally mixing with other elements and dust particles. This may have happened due to the aging of particles. Particles with irregular shape were more common. The EDX results showed them to be a mixture of Si and Al. The fraction of Al was higher in aircraft filters than the ground level particles. The C that was present in the ground level particles is persistent even particles still have about 7 to 8 % carbon. Column-integrated in situ size distributions were also compared with the ground based AERONET columnar size distributions.

We are thankful to the DST ICRP and ISRO GBP programme for the financial support. We are grateful to entire NRSC aircraft crew for their cooperation during this experiment.

Tripathi, S. N., S. Dey, J. J. Devi, B. N. Singh, M. Michael, and T. Gupta (2011), Thick absorbing aerosol layer observed in the monsoon season over India, Atmos. Chem. Phys. Discuss., under preparation.

In-situ aircraft observations on gases and particulate pollutants around Beijing area: distributions and influencing factors

W.J. Zhang[1*], Z.P Bai[1], J.Z. Ma[2], J.H. Chen[1], W. Yang[1], B.H. Yin[1]

[1]Chinese Research Academy of Environmental Sciences, Beijing, 100012, China
[2] Chinese Academy of Meteorological Sciences, Beijing, 100081, China
Keywords: Aircraft measurement, Gaseous pollutants, Particles, Back trajectory
Corresponding author email: zhangwj@craes.org.cn

At present, the air pollution around Beijing area has become a complex problem with a combination of different types of sources: coal smoke, traffic emission, dust re-suspension, and so on. Additionally, the transport of particulates seems to be a large-scale regional pollution. It is of great value to conduct aircraft measurements of pollutants at different altitudes (Wang et al., 2008).

In-situ measurements of gaseous pollutants, including ozone (O_3), sulfur dioxide (SO_2), nitrogen oxides (NO_X = NO + NO_2), carbon monoxide (CO), particle concentration (5.6-560 nm and 0.47-30 μm), and related meteorological information (T, RH, P) were conducted around Beijing area during Sep. 17-Oct. 7 in 2008. A two-engine light aero-transport YUN-12 (made in China) was used. The flight altitude ranged from ground to 4000m with the central point of Gucheng (N39°08′, E115°42′) in Hebei province around 5~15 km range, and the cruising velocity was generally kept at about 180 km h^{-1}. The total effective flight time was 23 h with 6 flights. This measurement was to characterize the regional variation of air pollution during and after the Olympics of 2008, the impacts of different transport direction and possible influencing factors.

Results suggested different characteristics of different gaseous pollutants and particles. (1) The meteorological factors showed significant influences for all the pollutants, as shown different pollutant levels at the ground level for different flights. (2) SO_2, NO_X, and CO showed highest concentration at the ground level, and decreased with the increasing of the height. It suggested the characteristics of major sources from ground emission for these gaseous pollutants. Figure 1 showed the variation of gaseous pollutants on flight Oct. 2 as an example. (3) Two different characterization of O_3 variation was obtained. It includes: ①similar variation with other gases, highest at the lowest altitudes, indicating the effects of ground emission sources; ② lowest concentration at the ground level, and increasing with the increase of altitudes until to 3000 m. For the O_3 variation above 3500 m, it showed similar range of 43~53 ppb at all flights, indicating the regional pollution level at high altitudes. (4) Backward trajectory analysis showed different transport direction of air masses, i.e. the pollutant transport of the southern direction with higher pollutants level; the cleaner long-range transport of the northern or northwestern direction with lower pollutants level; the transport from the eastern direction with characteristics of sea sources, i.e. middle level of gases pollutants and higher particle concentration; the transport of mixing directions, i.e. lower altitudes from the pollutant transport direction or local pollution but higher altitudes from the clean transport direction. (5) Coarser particles (0.47-30 μm) showed peaks of 0.6~0.8 μm, and highest in the ground level, and decreased abruptly with the increasing of heights, as Figure 2 showed. (6) For the ultrafine particles, the size distribution showed bimodal or multiple peaks variation, and concentrated on 10 nm and 20~100 nm. While, no obvious peaks were observed above 200 nm in the 5.6~560 nm range.

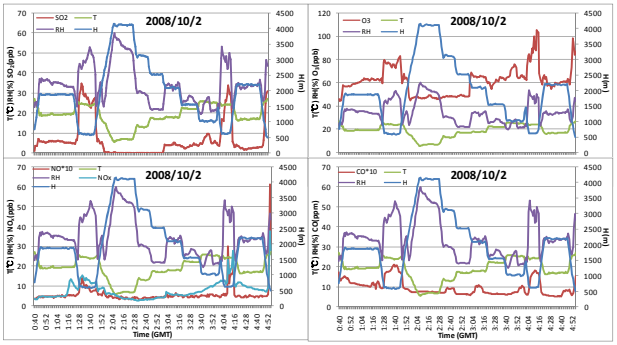

Figure 1. Variation of gaseous pollutants with meteorological factors and height on the flight of Oct. 2.

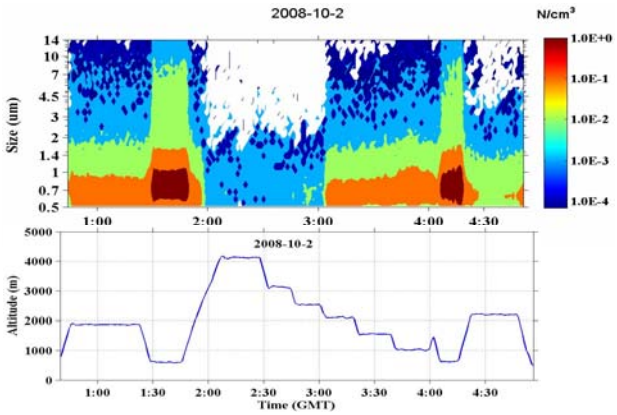

Figure 2. Variation of coarser particles with heights on the flight of Oct. 2.

This work was supported by COPES in China (GYHY200706005).

Wang, W., Ma, J., Hatakeyama, S., Liu, X., Chen, Y., Takami, A., Ren, L., Geng, C. (2008) *Atmos Environ*, **42**, 5715– 5720.

Vertical profiles of aerosol physico-chemical and optical properties measured along Italy over basin valleys

L. Ferrero[a], D. Cappelletti[b], M. Petitta[c], F. Scardazza[b], M. Castelli[c], M.G. Perrone[a], G. Sangiorgi[a] and E. Bolzacchini[a]

[a]POLARIS research centre, DISAT, University of Milano-Bicocca, Piazza della Scienza 1, 20126, Milano, Italy.
[b]Department of Engineering, University of Perugia, Via G. Duranti 93, 06125 Perugia, Italy.
[c] EURAC Institute for Applied Remote Sensing, Viale Druso 1, 39100, Bolzano, Italy.

Keywords: Vertical profiles, Hygroscopicity, black carbon, absorption coefficient, optical properties.
Presenting author email: luca.ferrero@unimib.it

Aerosols physico-chemical and optical properties are fundamental for climate change (IPCC, 2007; Kaufman et al., 2002) as well as for remote sensing applications (Wang et al., 2010; Di Nicolantonio et al., 2009); for the latter their 3D knowledge, especially along the whole atmospheric column is required (Levy et al., 2007; Wang et al., 2010).

For the reasons above, vertical profiles measurements of aerosol properties were conducted in winter 2010 along Italy over the cities of Terni (Central Appenine Valley), Milan (Po Valley) and Merano (Alpine Valley).

A tethered balloon was fitted with an instrumentation package consisting of: 1) a tandem-OPC system (2 OPCs GRIMM *1.107*; 31 size classes between 0.25 to 32 μm: one dried, the other one at ambient RH), 2) a novel micro-Aethalometer (AE51, Magee Scientific), 3) a miniaturized cascade impactor (Sioutas SKC with 2 impaction stages: <1 μm, >1 μm), 4) a metorological station.

OPCs tandem system data allowed us to determine the aerosol humidographs along height following the method reported in Snider et al. (2008) (Figure 1). Hygroscopic growth (Gf) was found to be not uniform along the vertical profiles (Figure 2) evidencing how the use of simple parameterizations of Gf along the atmospheric column in remote sensing applications can be a source of uncertainty in the results.

Micro-Aethalometer data enabled us to estimate black carbon (BC) concentration and absorption coefficient profiles. BC profiles clearly identified the mixing height (MH), which was characterized by a strong vertical concentration gradient. Over Milan BC profiles also showed a shallow layer of increased concentrations close to the ground (+24% compared to the whole MH), due to the proximity of combustion sources. The BC fraction of aerosol volume fell to 50-70% above the MH, compared to ground-level data. This caused a change in the optical absorption properties of the aerosol at different heights. Fairly constant values of absorption coefficient were found above the MH for each location, between 5-20% (2-15 Mm^{-1}) of those measured within the mixing layer.

PM samples collected with the cascade impactor were analysed by ion chromatography (Dionex ICS90 and ICS2000) system. The chemical speciation (Ions and BC) allowed to estimate a aerosol refractive index, and aerosol optical properties along height were calculated from OPC data using a Mie code (Bohren and Huffman, 1983): vertical optical properties were useful to improve the satellite retrieval of particulate matter at ground-level.

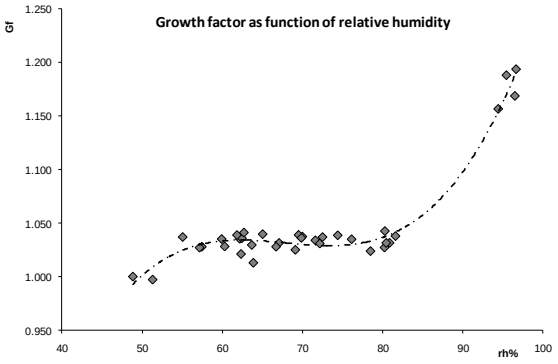

Figure 1. Humidograph along vertical profiles.

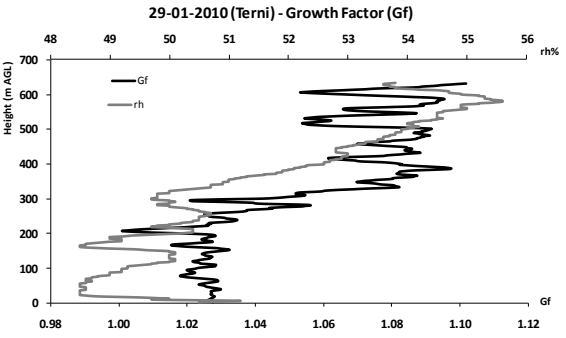

Figure 2. An example of Gf vertical profile.

This work was supported by the SATMAP project, by the Fondazione CARIT di Terni e Narni, by the EURAC research centre and the Province of Bolzano.

Di Nicolantonio, W. et al. (2009). Radiat. Prot. Dosim., doi:10.1093/rpd/ncp231, 1-8.
IPCC: Climate Change 2007
Kaufman, Y.J. et al. (2002). Nature, 419, 215-223.
Levy, R.C. et al. (2007). J. Geophys. Res., VOL. 112.
Snider, J.R. et al. (2008). Atmos. Chem. Phys., 8, 1949–1962.
Wang, Z. et al. (2010). Remote Sensing of Environment, 114(1), 50-63.

Thursday, September 8, 2011

Session 9C: Biomass and Biofuels

Micro Smog Chamber: a Candidate Tool for Evaluating Wood Burning Emissions

A. Keller, H. Burtscher

Institute for Aerosol and Sensor Technology, University of Applied Sciences Northwestern Switzerland, Windisch, 5210, Switzerland
Keywords: SOA (Second. Organic Aerosols), Wood Combustion, Emissions, Measurement (characterization).
Presenting author email: alejandro.keller@fhnw.ch

An important part of the ambient particulate matter (PM) pollution related to wood combustion is originally emitted in the form of Organic Gaseous Carbon (OGC) which is transformed into particles known as secondary organic aerosols (SOA) in the atmosphere. Whereas primary particles are easily measured at the combustion site, SOA exists only after a complex chemical process that requires solar radiation and takes hours or even days for completion. This creates a large discrepancy between what is measured on the side of the emissions and the actual atmospheric values.

Current legislation imposes no emission limits for the precursor substances of SOA. This can be understood since only recently several studies have shown the importance of SOA (see, e.g., Szidat 2006 and Grieshop 2009) and there is no standard way to calculate the SOA production potential of a combustion device. Smog chambers are a valuable tool for studying SOA formation. But they are large (tents of cubic meters), slow and expensive to run and, therefore, far from been an acceptable tool for emission monitoring or type approval tests.

In this paper, we present a simple conditioning system that could be used for evaluating the SOA production potential and for comparing the emissions of different wood burning devices. The system is a continuous flow reactor (volume < 100ml) where the sample is irradiated with UV light. The exposure time is of the order of seconds. After the photooxidation takes place, the sample is cooled down in a second chamber of similar volume where the new OGCs species form PM.

The first experimental results are very promising. They show that it is possible to transform OGC into SOA in just a couple of seconds. Figures 1 and 2, for instance, show an experiment using terpenes as a precursor substance and a 1s residence time. This is an unprecedented result in the study of SOA and a first step towards creating a methodology for a real time evaluation of the SOA production potential. As a next step, we will take a closer view on other parameters like humidity and radiation wavelength that also influence SOA production and/or open new reaction paths.

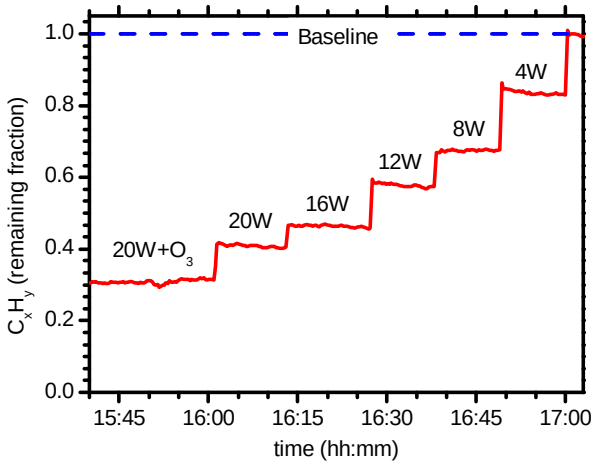

Figure 1. Reduction of HC for different UV light intensities (85% at 254nm and 15% at 185nm) and for UV plus O_3 from a corona wire. Residence time 1s.

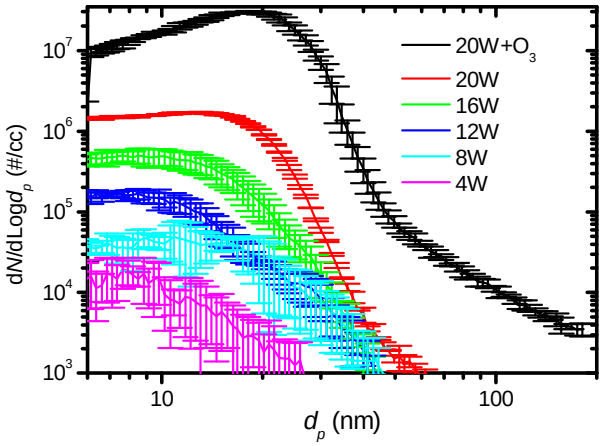

Figure 2. Particle size distribution for the same experiment as figure 1.

This work was supported by the Swiss FOEN and the CCES from the ETH Zurich.

Grieshop, A.P., Logue, J.M., Donahue, N.M., Robinson, A.L. (2009) *Atmos. Chem. & Phys.* **9**(4) 1263-1277.

Szidat, S., Jenk, T.M., Synal, H.A., Kalberer, M., Wacker, L., Hajdas, I., Kasper-Giebl, A., Baltensperger, U. (2006) *J. Geophys. Res.*, **111**, D07206, doi:10.1029/2005JD006590

Comparison of emissions from wood and oil boilers in small (20–25 kW) and medium (5–10 MW) scale

T. Penttilä[1], H. Lamberg[1], A. Hukkanen[1], O. Sippula[1], J. Tissari[1] and J. Jokiniemi[1,2].

[1]Univ. of Eastern Finland, Department of Environmental Science, P.O. Box 1627, FI-70211 Kuopio, Finland.
[2]VTT Technical Research Centre of Finland, P.O. Box 1000, 02044 VTT, Espoo, Finland
Keywords: Biomass burning, Fossil fuels, Emissions
Presenting author email: Terhi.Penttila@uef.fi

Fossil fuel combustion is known to be the main source of greenhouse gas emissions. Increase in biomass use as energy source aims to reduce these emissions, since biomass combustion is considered to be greenhouse gas neutral energy source. However, one of the major problems with the biomass combustion is high transportation cost and poor availability due to complex logistics. Thus, bioenergy production in small decentralized units within small communities (2000-10 000 inhabitants) is often cost-effective. Another disadvantage of biomass combustion is high PM_1 (particles less than 1 µm in aerodynamic diameter) emission especially in small combustion units. It has been estimated that in Finland 25 % of all fine particle (aerodynamic diameter <2.5 µm) emissions originate from domestic wood combustion (Karvosenoja et al. 2008). Furthermore, small scale district heating units may generate substantial emissions if not equipped with efficient filtration (Sippula et al. 2009)

The aim of this study was to compare four alternatives to arrange decentralized energy production in small communities in respect to their flue gas emissions and toxicological properties of emissions. These options were heavy fuel oil (5.6 MW) and wood chip fired (10 MW) district heating units, light fuel oil fired residential burner (20 kW) and a modern pellet boiler (25 kW). In the wood chip fired plant the flue gas was cleaned with ESP while other systems included no flue gas after treatment. Gaseous compounds were measured with FTIR (Fourier Transform Infrared) analyzer including emission componenents such as CO, CH_4, HCl and NO_x. The particulate samples were diluted using a porous tube diluter and collected with DGI (Dekati Gravimetric Impactor). The samples were thereafter taken for polycyclic aromatic hydrocarbon (PAH), ion, elemental and toxicological analyses. From light fuel oil burner and pellet boiler PM_1 samples for organic carbon (OC) and elemental carbon (EC) analyses were collected with filter holders (Gelman Sciences 2220) and particle mass size distribution samples were collected with DLPI (Dekati Low Pressure Impactor). In addition, number size distribution was measured continuously with ELPI and FMPS. In wood-chip fired boiler the measurements were carried out after ESP.

Table 1. Emissions (mg/MJ) from different fuels and appliances

	Light oil	Heavy oil	Pellet	Wood chip
PM_1	0.6	113	16	4.2
CO	1.3	0.06	80	3.6
NO	56	207	49	97
CH_4	0.01	0.001	0.3	0.0009
HCl	0.18	0.17	0.10	0.13
PAHs	0.013	1.4	0.0001	0.005

Table 1 shows a comparison of emissions between different boilers. PM_1 and PAH emissions were the highest in the heavy fuel oil plant. The lowest PM_1 emission was found from the light fuel oil burner while the lowest PAH emission was found from the pellet boiler. From the pellet boiler, OC and EC emissions were 0.9 and 0.1 mg/MJ, respectively. From the light oil burner EC emission was 0.01 mg/MJ while OC was not found (detection limit 0.2 µg/cm^2). The highest CO emission was found from the pellet boiler and the highest NO emission from the heavy fuel oil plant. CH_4 and HCl were detected only in small amounts. Overall, fine particle emission from heavy oil plant was substantial compared to those measured in previous studies (Sippula et al. 2009). This might be due to intermittent boiler operating since the measurement was conducted during summer in the off season of the heating period.

Karvosenoja, N., Tainio, M., Kupiainen, K., Tuomisto, J.T., Kukkonen, J., Johansson, M. (2008) Evaluation of the emissions and uncertainties of PM sub (2.5) originated from vehicular traffic and domestic wood combustion in Finland. Boreal Environment Research 13, 465–474.

Sippula, O., Hokkinen, J., Puustinen, H., Yli-Pirilä, P., Jokiniemi, J. (2009) Particle emissions from small wood-fired district heating units. Energy & Fuels 23, 2974–2982.

The effects of air-staging and fuel characteristics on PM1 emissions from small-scale pellet combustion

H. Lamberg[1], O. Sippula[1], J. Tissari[1] and J. Jokiniemi[1,2]

[1]Department of Environmental Science, University of Eastern Finland, Fine Particle and Aerosol Technology Laboratory, P.O. Box 1627, FI-70211 Kuopio, Finland
[2]VTT, Technical Research Centre of Finland, Fine Particles, P.O. Box 1000, FI-02044 VTT, Espoo, Finland
Keywords: combustion, emissions, biomass.
Presenting author email: Heikki.Lamberg@uef.fi

Biomass fuels are used for heating and energy production to reduce CO_2 emissions and to replace fossil fuels. In the same time, combustion of biomass induces fine particle emissions that are known to cause adverse health effects. The emission characteristics from biomass combustion are affected by many different factors, such as combustion technology and fuel characteristics. One interesting way to produce heat in small-scale with biofuels is the use of wood pellets, which are easy to transport and combustion devices are usually highly automated. Even thought the emissions from pellet combustion are usually low, they are higher than those of light fuel oil combustion, which is often replaced with pellets. Because of this, the increase in the use of biofuels should be done with the best possible combustion technology to minimize the adverse health effects that the increasing PM1 emissions could induce. In this study, two different factors affecting the PM1 emissions are introduced: (1) the effect of air-staging and (2) the effect of pellet fuel raw material on PM1 emissions.

This study was carried out in a laboratory environment to guarantee stable combustion to minimize the alternation in combustion affecting the results. In total 24 different pellet raw materials were tested including stem wood, bark, peat, straw, roundwood and different mixtures of the materials. In the second part the effect of air-staging and the effect of partial-load on PM1 emissions were studied.

A commercial 25 kW pellet boiler was used in the tests which worked with top-feed fuel input and had integrated burner and boiler. Part of the flue gas was transported to a dilution tunnel through a heated sample line. Particle collections were made in the dilution tunnel with a dilution ratio varying between 90 and 120. Particle collections included filter collection for PM1 mass and chemical compositions. From these filters, analyses of elemental and organic carbon were performed together with the most common elements and ions. Furthermore, also fuels were analyzed for elemental composition.

The results show that there are many different factors affecting the PM1 emissions originated from small-scale combustion on pellets. First, the emissions from different raw materials varied between 5.1 mg/MJ and 195 mg/MJ from peat and rye straw, respectively. Furthermore, it was possible to decrease the PM1 emissions by optimizing the combustion air input. When air-to-fuel ratios were calculated for primary (λ_{Prim}) and secondary combustion (λ_{Sec}) zones from total air-to-fuel ratio and combustion air flows, it was seen that the $\lambda_{Prim}/\lambda_{Sec}$ ratio correlated with PM1 and CO emissions, and with the release of potassium from fuel to fine particles.

The releases of different ash forming elements were evaluated from fuel elemental composition and fine particle elemental composition. It was detected that alkali metal release factors vary significantly between different fuels. Two different factors were identified to explain the observed differences. First, the sum of potassium, sodium and chlorine in the fuel (Figure 1). Alkali metals are known to vaporize easily in the combustion and form particles in the flue gas. Second, the fuel chlorine/sulphur ratio; sulphur in fuel converts alkali metals to sulphates which are less volatile than alkali chlorides.

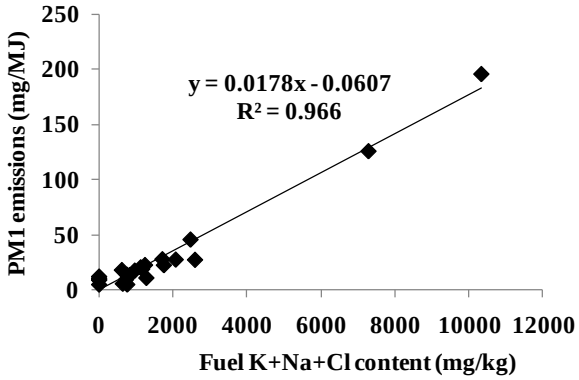

Figure 1. PM1 emissions are presented as a function of fuel K+Na+Cl (mg/kg).

These results show that there are factors affecting the PM1 emissions from small-scale pellet combustion that need to be considered when the use of biofuel combustion is increased. It is possible to reduce the emissions by further development in combustion technology. On the other hand, elemental compositions in pellet fuels affect PM1 emissions significantly. Because of this, it is important to pay attention to fuel qualities as well.

We thank Vapo Ltd. and PELLETime project for providing the pellet fuels, especially Simo Paukkunen and Lasse Okkonen from North Karelia University of Applied Science.

Time resolved PAH-emissions from residential wood combustion investigated with aerosol mass spectrometry

J. Pagels[1], A. Eriksson[1,2], E. Z. Nordin[1], R. Nyström[3], E. Pettersson[3,4], E. Swietlicki[2] and C. Boman[3]

[1] Ergonomics and Aerosol Technology, Lund University, P.O. Box 118, SE-22100, Lund, Sweden
[2] Nuclear Physics, Lund University, P.O. Box 118, SE-22100, Lund, Sweden
[3] Energy Technology and Thermal Process Chemistry, Umeå University, SE-901 87, Umeå, Sweden
[4] Energy Engineering, Luleå University of Technology, SE-971 87 Luleå, Sweden

Keywords: AMS, wood stove, PAH, biomass combustion
Presenting author email: joakim.pagels@design.lth.se

Polycyclic aromatic hydrocarbons have been denoted key components in particle related toxicology. Emissions of PAHs can under certain circumstances be high in residential wood combustion. However, previous attempts to identify the combustion conditions favouring high PAH emissions have typically been limited to either averages over one to several combustion cycles or been performed by non-specific techniques. In this work we applied aerosol mass spectrometry (AMS) for highly time-resolved direct measurements of PAHs and total organics from three different residential biomass combustion systems. The aim was to identify combustion situations associated with elevated PAH emissions and to suggest recommendations to reduce such emissions.

Three wood combustion appliances were studied; *i*) a conventional wood stove, *ii*) a modern pellet burner and *iii*) a novel pellet reactor with possibility to control the air supply. The wood stove was operated with high and nominal load, respectively, using relatively dry birch logs (14% moisture). Higher load was achieved by using larger batches consisting of smaller logs compared to the nominal load case. The Flue gas was sampled from a temperature of about 150°C and a three stage ejector driven dilution system employing filtered dry air at room temperature was used. The total dilution factor was about 1:2000 and thus the aerosol was sampled at close to ambient mass loadings. On-line gas-phase sampling included O_2, CO, NO_x and THC (total hydrocarbons by FID). A high resolution aerosol mass spectrometer (HR-TOF-AMS, Aerodyne Research) was used for size resolved composition of compounds vaporised at 600°C. The standard PAH AMS fragtable was employed to quantify the PAH emissions. A scanning mobility particle sizer was used for mobility size distributions (10-600 nm).

As seen in Figure 1, the highest concentrations of total organics during high load in the wood stove occured for the first 5 minutes after addition of new batches of logs on glowing embers. In contrast, the particle bound PAHs correlates poorly with total organics and increased levels occured about 10 minutes after refilling fuel. However, the highest PAH-emissions occurred when adding small amounts of fuel during flaming combustion. In these cases, PAHs composed as much as 30% of the total organics. It can be seen that the PAH concentrations correlates with low O_2 and high CO concentrations in the emissions. The particle phase PAHs were typically shifted towards higher molecular weights with increasing total PAH emissions during air deficiency, i.e. low O_2.

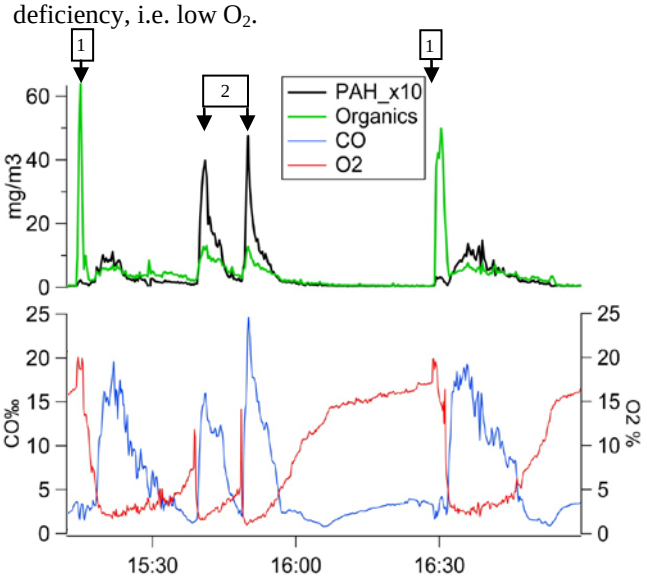

Figure 1. Time resolved total organics, PAHs, CO and O_2 during high load in the wood stove. "1" denotes addition of full batch on glowing embers. "2" denotes addition of 1/3 batch in flaming phase.

The results illustrate a combustion situation with a high burn rate under hot and air-starved combustion conditions, similar to gasification (Milne et al. 1998). Such high temperature fuel rich conditions lead to thermal cracking of primary released oxygenated pyrolysis products (e.g. levoglucosan and methoxy-phenols). At higher temperatures mostly aromatic compounds and soot are stable enough to survive resulting in elevated PAH emissions.

It is well known that poorly insulated stoves, bad mixing and humid fuels lead to high organic emissions. This work illustrates the potential deterioration of emission levels caused by too high burn rates and it shows the potential of using AMS as a tool for advanced emission studies in wood combustion.

This work was financed by the Swedish Energy Agency and FORMAS.

Milne, T.A.; Evans, R.J.; N. Abatzoglou, N. Biomass Gasifier "Tars": Their Nature, Formation, and Conversion, NREL/TP-570-25357, 1998.

Electrostatic precipitators for domestic wood stoves

H. Burtscher, A. Keller, M. Fierz

Institute for Aerosol and Sensor Technology, University of Applied Sciences Northwestern Switzerland, Windisch, CH-5210, Switzerland
Keywords: Wood Combustion, Emissions, Aftertreatment, Electrostatic precipitator.
Presenting author email: heinz.burtscher@fhnw.ch

Besides diesel engines wood combustion is a significant source of ultrafine particles in ambient air. Depending on region and season it may even be dominant. Whereas large utilities for wood combustion (heating plants, electric power stations) meanwhile usually are equipped with exhaust gas cleaning devices, small units are not and often have very high emissions. Besides trying to improve combustion, using filters is an option to reduce particulate emissions. As these units normally are not ventilated but work by convection the pressure drop of a filter for this application has to be very low. Only electrostatic precipitators (ESP) are possible.

Several filters came on the market recently. They are placed somewhere in the chimney, the chimney walls are used as precipitating electrodes. A wire in the centre of the chimney serves as corona electrode and creates the field used for precipitation. A typical configuration is shown in figure 1.

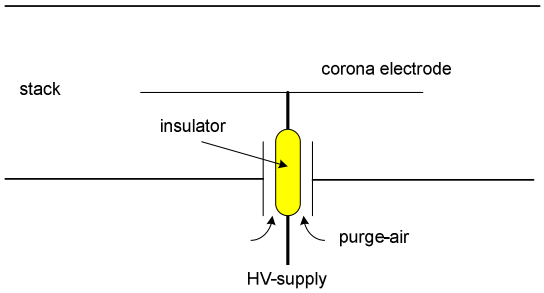

Figure 1. ESP in the stack of a wood stove. The insulator is protected from contamination by a purge air flow.

The length of the corona electrode typically is between 30 cm and 1.5 m. The filter may be located close to the stove or close to the top of the chimney. Some filters are too short to allow an efficient removal already in the vicinity of the corona electrode. A significant fraction of particles may be precipitated in the stack downstream the filter. This is possible because space charge plays an important role due to the specific geometry of these filters.

In Figure 2 the electric field due to the voltage, applied at the corona wire and due to space charge is plotted for the following conditions:
stack diameter: 20cm, corona wire: 0.5mm diameter,
Applied voltage: 20kV
Particle concentration: $10^7 cm^{-3}$, each particle carrying 2 elementary charges on average, no ions considered.

Assuming a turbulent flow only the field close to the wall of the stack is important for precipitation and this field is dominated by space charge for this case. Therefore the precipitation continues after the end of the corona electrode.

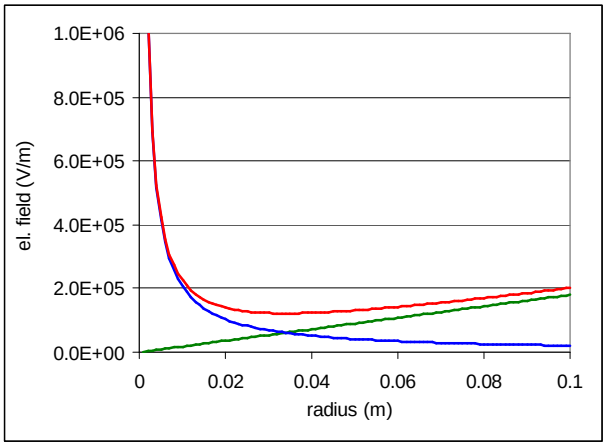

Figure 2. Electrical field due to corona voltage (blue) space charge (green) and total field (red).

Whereas this effect of space charge increases particle deposition in particular when the space charge is high due to high particle concentrations, another effect of space charge is less desirable: It reduces the field close to the corona wire and thus may quench the corona. This may lead to a complete failure of the filter at very high particle concentrations as they occur for example in the starting phase of the combustion. A drastic reduction of the corona current can be observed during this phase.

In a number of test measurements we observed filter efficiencies in the range from 50% up to more than 90%, depending on filter type and operating conditions. Filters close to the top of the chimney have the advantage that the flue gas is colder and thus the flow rate is smaller. The filters not only work for steel- but also for ceramic chimneys, but with reduced efficiency.

Care has to be taken when measuring the particle concentration downstream the filter, because particles often are highly charged (Meyer et al., 2009).

This work was supported by the Swiss FOEN.

Meyer, N.K., Lauber, A., Nussbaumer, T. and Burtscher, H. (2009) *Atmos. Meas. Tech.*, **2**, 81-85.

High temperature electrostatic precipitation for small scale biomass combustion

A. Bologa, H.-R. Paur and K. Woletz

Karlsruhe Institute of Technology, Institute for technical Chemistry,
Eggenstein-Leopodshafen, D-76344, Germany
Keywords: biomass combustion, fine particles, emission control, electrostatic precipitator
Presenting author email: andrei.bologa@kit.edu

The small-scale wood combustion is widely used for domestic heating, but it is responsible for emissions of fine particles which are composed of ash, elemental carbon and organic matter. By small scale biomass combustion, the particle chemical composition, particle size distribution, number and mass concentration vary greatly depending on mixing of air and fuel, combustion temperature, design of burning appliance, fuel quality etc.

Electrostatic precipitators (ESP) are effective equipment for reduction of particle emissions from small scale biomass combustion. The design of ESPs range from conventional to space charge, from dry to wet, from units integrated into the combustion appliance up to ESPs installed at the exit of a chimney. Most of the unit operates at temperatures below 200 °C, but there also are some developments of high temperature (HT) ESPs. But, in spite of presence of different data, the review of these developments is not still available, especially for HT units.

The first objective of the study is the overview of the approaches to the development of gas cleaning systems for small-scale wood combustion, especially electrostatic precipitators, and cross-section view through the operation conditions and parameters of the ESPs. The critical points are: gas temperature, stability of operation of the precipitator, collection efficiency, ESP design and applicability.

The second objective of the study is the discussion about the development and results of the tests of a novel high temperature electrostatic precipitator for small-scale biomass combustion. The space charge ESP consists of a corona discharge ionizer and a grounded collector installed downstream the ionizer without any plenum chamber. A brush grounded collector is used for precipitation of charged particles. The main points of the development relate to the design of high temperature ionizer; to particle precipitation mechanisms in the collector and to the position of the ESP in the gas duct.

The ESP was as installed in a thermo-isolated gas duct about 1,5 m downstream a wood-log stove with thermal power 8 kW. The stove was operated ca 5-6 hours per day with wood-logs rate ca. 2,5-3,0 kg/h. Particle mass concentration was measured according to the Guidelines VDI-2066 upstream and downstream the ESP. Particle number concentration in the gas flow was measured by Scanning Mobility Particle Sizer (Fa. Grimm) downstream the ESP when the precipitator was switched-off and switched-on.

The ESP mean input gas temperature was over 300°C achieving shortly maximum values of over 400°C. A DC negative corona discharge was used for particle charging in the ESP ionizer. The operation voltage varied from 10 kV to 14 kV and corona current from 0,4 mA to 1,6 mA depending on the combustion conditions in the stove.

The results of the tests show that the gas temperature influences on the operation stability of the electrostatic precipitator (voltage and corona current). For the same electrode geometry, the increase of the gas temperature decreases the spark-over voltage in the ionizer and results in the increase of the corona current at the same applied voltage.

The special design of the high voltage insulator excluded the spark-overs in the insulator housing and improved the operation stability of the ESP.

The design of the ESP and its position in the gas duct reduced the re-entrainment of collected aerosol into the clean gas flow and enhanced the collection efficiency of the unit by combined use of several mechanism of gas cleaning.

The ESP was in operation over 100 h. The mass collection efficiency of the ESP for stable combustion conditions was about 85% and for total combustion cycle it was 75±3 %. The middle fractional collection efficiency is 80-95% for particles smaller than 0,1 µm and over 95% for particles larger than 0,1 µm (see Figure 1).

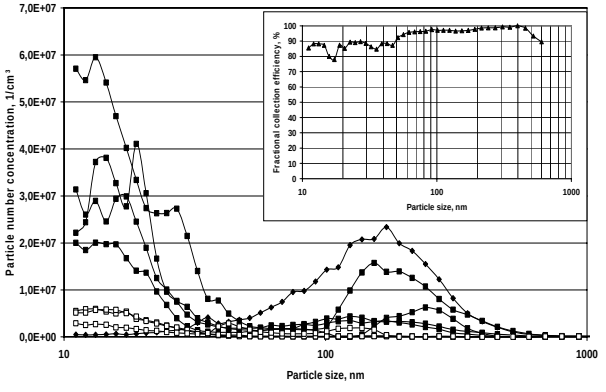

Figure 1. Size distribution of wood combustion aerosol (closed – raw gas, open – clean gas) and fractional collection efficiency of the high temperature electrostatic precipitator

Wood combustion emissions in Switzerland and associated impact assessments

Meyer, Nickolas K.[1], Heck, Thomas[1]
[1]Laboratory for Energy Systems Analysis, Paul Scherrer Institute, Switzerland
Keywords: wood combustion emissions, life cycle analysis, sustainability, external costs

Woody biomass combustion produces 5% of Swiss heating energy and 20 - 50 % of airborne, organic and particulate emissions during winter. Further, future energy scenarios suggest that wood consumption could sustainably increase by a factor of two [1], likely leading to increased emissions. On this basis, an inventory describing combustion emissions produced by 25 in-use residential, commercial, and industrial biomass combustion appliance classes was developed for Switzerland. This inventory is used to assess current and historical emissions, to identify those appliance classes contributing most to emissions, to assess future emissions based on sustainable scenarios and finally, to quantify external costs associated with wood combustion in Switzerland.

The inventory incorporates over 200 direct and indirect (life cycle) emission species. Of these species, particulate matter (PM), carbon monoxide (CO), particle bound black carbon (BC), particle bound organic matter (POM) and total organic carbon (TOC), nitrogen oxides (NO_x) and greenhouse gases form a set of core species [2,3]. PM data utilised in this inventory was size classified to represent, total particulate emissions (TPE), and particulate matter having diameters less than 10, 2.5 and 1 μm respectively (PM_{10}, $PM_{2.5}$ and PM_1).

Direct emission factors for core species were collected for average, high and low emission scenarios (based on appliance operating characteristics). Non-core species have so far been considered only for average operating cases. Using these emission factors, annual emissions were determined for each species (for the period 1990 – 2009, with a base year of 2009), and in some cases used to determine future emission scenarios. For the average current emission scenario, annual TPE was calculated to be 6520 tonnes. Analysis of the size dependency of TPE was made (Fig. 1), as was the size dependent contribution of BC and POM to PM (not shown).

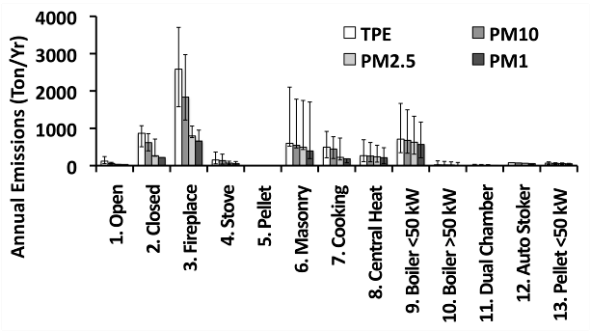

Fig. 1. Annual particulate matter emissions for 13 residential wood combustion appliances in Switzerland, 2009.

In addition to the emission inventory, direct and indirect global warming potentials (GWPs) were calculated for representative systems (Fig. 2). These preliminary GWP calculations highlight variances in potential climate impacts between biomass and fossil systems (particulates are excluded from prelim. GWP)

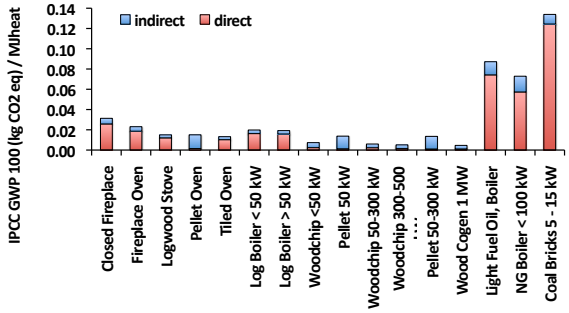

Fig. 2. Direct and indirect global warming potentials for selected combustion systems

As a method of valuing impacts associated with the combustion of wood, external costs methods were employed [3]. Using both direct and indirect emissions, estimates of external costs attributable to wood combustion in Switzerland were made. Further comparison with fossil fuel systems and wood combustion systems incorporating emission reduction devices were also made. Currently, cost estimates exclude aerosol induced climate effects - these should be included within the coming year. Estimates presented here show costs per MJ of useful heat for selected combustion systems (Fig. 3) [3]. Life cycle impact assessment results will be included as well.

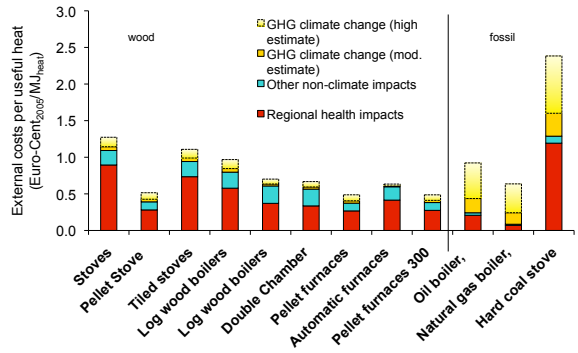

Fig 3. External costs per MJ useful heat for wood and fossil fuel systems in Switzerland.[3]

This work was conducted as part of the research project IMBALANCE and funded by the Competence Center Environment and Sustainability of the ETH Domain (CCES).

[1].Grünenfelder T, Rutschmann C. Holzenergie x 2. Zürich: Swiss Federal Office of Energy; 2004.
[2]. Meyer, N.K., ETH Nanoparticle Conference, Zürich 2010
[3]. Heck, T., Meyer, N.K., CCES-Latsis Symposium, Zürich 2010,

Thursday, September 8, 2011

Session 9D: In-vitro toxicity and health effects of PM

The inflammatory response elicited in vitro by air pollutants is greater in synoviocytes from patients with Rheumatoid Arthritis than in those with osteoarthrosis

M. Galeazzi[1], F. Cetta[1], F. Laghi Pasini[1], E. Balistreri[1], E. Selvi[1], S. Benoni [1], V. Guercio[1], I. Santi[2], L. Cantarini[1] and E. Bolzacchini [3]

[1] Dept. of Surgery and Thoracic Surgery, University of Siena, Siena, 53100, Italy
[2]Geriatric Institute "Pio Albergo Trivulzio" (PAT), Milan, 20146, Italy
[3]Dept. of Environmental Sciences, University of Milan, Milan, 20126, Italy
keyword: Rheumatoid Arthritis, osteoarthrosis, human fibroblast-like synoviocytes, IL-6
Presenting author email: galeazzi@unisi.it

Rheumatoid Arthritis (RA) is a disease in the occurrence of which autoimmunity plays a crucial role. Genetic factors are thought to be responsible for about 50% of RA risk, suggesting that environmental factors could contribute to the development of RA in the genetically predisposed. In particular, pollution from traffic in adulthood has been considered as a newly identified environment factor for RA.

Aim of the study: to assess the "in vitro" effects of variable concentration of various types of PM when incubated with human Fibroblast-like synoviocytes (FSC), to evaluate the occurrence of proinflammatory effects.

Methods: daily levels of PM10 and PM2.5 and PM1 (diameter < 10 μm, 2.5 μm, 1 μm, respectively) were measured by PM detection units, both outside and inside 2 schools for children and 2 nursing homes for retired people, either in summer and in winter time in Milan, Italy. Both OPC detectors and low volume gravimetric detectors were used. Samples from Teflon filters were used after sonication in sterile phosphate buffer saline (PBS). Aliquots of these samples at various concentration of PM10 (10 μg/ml, 50 μg/ml, 70 μg/ml) were incubated at 37°C for 24, 48, 72 hours with human type B synoviocytes obtained from 5 patients with RA, and 5 with osteoarthrosis (OA) during hip replacement surgery.

Results: -Engulfment of particulate material within synoviocytes was observed even at lower concentrations and after 24 h incubation; -the penetration of PM into the cell was associated with an increased cytokine production. In particular, there was a considerable increase of IL6 concentration, namely after incubation with winter PM, up to 9-folds the basal values, already after 24 h (867,36 vs 100) in FSC obtained from RA patients ($p<0,001$), whereas summer PM determined a significant increase of IL6 (637,39) only after incubation for 72 h (**Fig.1**). This effect was likely due to the greater content of PAH rich OC in winter PM. In addition, after incubation for 24 h of the same type and the same concentration (10 μg/cm2) of PM10, collected during Summer and Winter, with alveolar type cells (A549 cell line), i.e. cells from front-line respiratory district (**Fig 2b**), the previous increase of IL6 observed in subjects with RA (**Fig 2a**) was not found (**Fig2**).

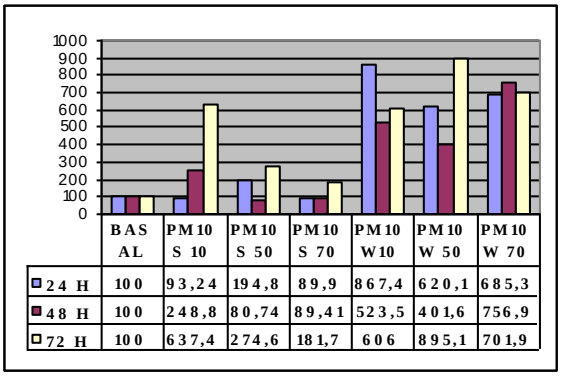

	BASAL	PM10 S 10	PM10 S 50	PM10 S 70	PM10 W10	PM10 W 50	PM10 W 70
24 H	100	93,24	194,8	89,9	867,4	620,1	685,3
48 H	100	248,8	80,74	89,41	523,5	401,6	756,9
72 H	100	637,4	274,6	181,7	606	895,1	701,9

Figure 1. Concentration of IL-6 after incubation with various types of PM10 at various concentrations

Conclusion: The inflammatory response elicited by PM is greater in RA-FLS, than in OA-FLS. Even if affected tissues are distant from the initial site of exposure, they are likely to be part of the "pollution syndrome", i.e. of the health side-effects produced or facilitated by environmental pollutants. PM-related health effects seem to be not only determined by intrinsic toxicity of pollutants, mediated by oxidative stress, but are likely due to more complex responses, namely those typical of autoinflammatory and/or autoimmune diseases, which occur only or mainly in predisposed subjects. In particular, if autoimmunity is crucial for RA occurrence and RA is part of the "pollution related syndrome", even low local concentration of PM could be sufficient to trigger pathological events in predisposed individuals.

a b

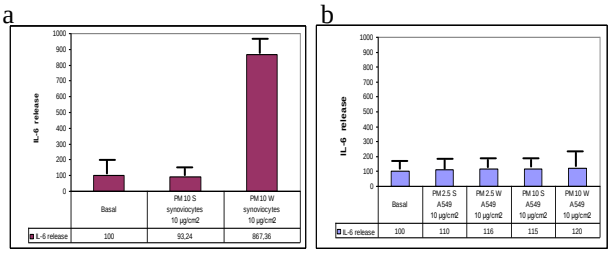

Figure 2a-b Comparison between IL-6 secretion in human synoviocytes from subjects with RA (a) and in alveolar type II cells (A549 cell line) (b).

This work was supported by the PROLIFE-Project, Milan, Italy.

Microbial test battery for risk assessment of fine particles originating from the combustion of wood

I.R. Gutiérrez[1], W. Ahlf[1] and D. Dietrich[2]

[1]Department of Human- and Environmental Toxicology, University of Konstanz, 78457, Konstanz, Germany
[2]Institute of Environmental Technology and Energy Economics, University of Technology (TUHH), 21073, Hamburg
Keywords: Biotests, Cytotoxicity, Genotoxicity, Estrogenicity.
Presenting author email: Iris.Gutierrez@tuhh.de

Burning of wood for heating purposes has become extremely popular wordwide due to the increasing costs of fossil fuels. In Germany 25% of the private households use wood logs, pellets, briquettes or woodchips for firing (Fachagentur Nachwachsende Rohstoffe, 2010). Claimed as renewable energy source, wood has often been ignored as a source for fine particles. Especially small fireplaces, not meeting the latest standards, produce supposable harmful fine dust. Rapid reproducible and validated biotests for toxicological characterisation of particles exist neither for cells nor for microorganisms. Thus there is a need for established microscale toxicity screening of unknown particulate samples.

Hence a test battery consisting of two ISO standardised bacterial contact assays and one yeast biotest were modified for the use with fine dust. Having different endpoints these tests provide a toxicological "fingerprint". In order to account for bioavailability of contaminants adsorbed on surfaces of fine particles, such were used as a whole not as extracts.

Table 1. Origin of fine particles.

Sample number	Type of winning	Wooden fuel	Fire place
# 1	Electrostatic precipitator	Briquette/ split logs	Stove 9 kW
# 4	Electrostatic precipitator	Pellets	Pellet boiler 15 kW

Particulate matter was gained electrostatically from different furnaces in the flue gas channel (Table 1). Suspended in water, vortexted for 1 min, and ultrasonificated for 15 min samples were applied in a concentration range of 0.001 – 10 mg/mL. Particle sizes (< 1 µm) in these suspensions were measured by dynamic light scattering. Minusil 5, crystalline quartz sand (1 mg/mL), proven to be non-toxic in bacteria and yeast, served as control.

Cytotoxicity in the aerobic *Arthrobacter globiformis* contact assay was determined via dehydrogenase activity (DHA). Genotoxicity was determined via Umu test using a genetically modified *Salmonella* strain. The YES test was employed to determine potential estrogenicity of particle samples.

Sample # 1 caused a sigmoid dose response curve in both the bacterial contact assay and the YES test (Figure 1, Figure 2). No genotoxic effect was observed in the Umu test for sample # 1. Activation by S9-media is most likely necessary for this test, especially as the active ingredients of sample # 1 appear to be PAHs. The latter would also explain interaction with the YES assay, as PAHs (e.g.) are known to interact with the estrogen receptor. Although sample # 4 also triggered a sigmoid dose response curves, the toxicity profile was different (data not shown). These preliminary results suggest suitability of endpoints determined in the modified tests for risk assessment of fine particles.

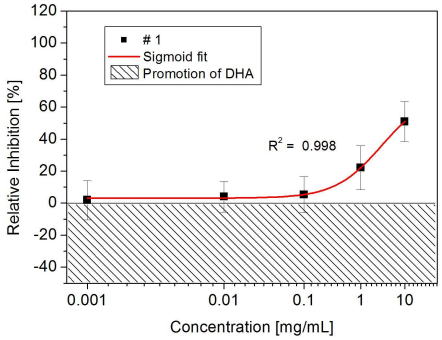

Figure 1. Relative Inhibition of sample # 1 in the bacterial contact test. DHA: Dehydrogenase activity.

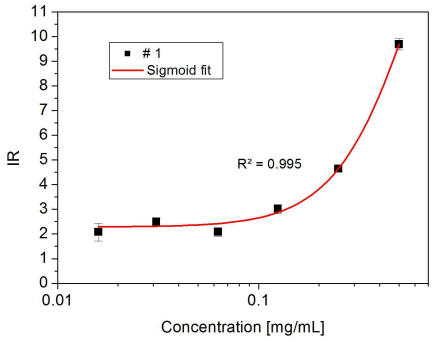

Figure 2. Induction ratio (IR) of sample # 1 in YES test.

This work is part of a project of the University of Technology Hamburg-Harburg (TUHH), the University of Konstanz, the German Biomass Research Centre (DBFZ), the Technology and Support Center (TFZ), the Leibniz Institute of Troposheric Research (IfT) and the Karlruhe Institute of Technology (KIT). It is supported by the Federal Ministery for the Environment, Nature Conservation, and Nuclear Safety.

Fachagentur Nachwachsende Rohstoffe. (2010) *Pelletheizungen Marktübersicht.*

Residential wood combustion technology affects the toxicological responses of particulate emissions

P.I. Jalava[1,2], J. Kelz[3], T. Brunner[3,4,5], M.S. Happo[1], J. Mäki-Paakkanen, P. Hakulinen, T. Penttilä, A. Hukkanen, J. Jokiniemi[1,6], I. Obernberger[3,4,5], and M-R. Hirvonen[1,2]
[1]Department of Environmental Science, University of Eastern Finland, Kuopio, FI-70701, Finland
[2]Department of Environmental Health, National Institute for Health and Welfare, Kuopio, FI-70701 Finland
3Bioenergy 2010+ GmbH, Graz, A-8010, Austria
[4]Institut for Process and Particle Engineering, Graz University of Technology, Graz, A-8010, Austria
[5]BIOS Bioenergiesysteme GmbH, Graz, A-8010, Austria
[6]VTT Technical Research Centre of Finland, FI-02044, VTT, Finland

Keywords: combustion, particulate matter, *in vitro*, emissions, wood smoke, health effects of aerosols
Presenting author email: pasi.jalava@uef.fi

Particulate air pollution is one of the most harmful environmental exposures causing mortality and hospitalizations of cardio-respiratory patients worldwide. There is growing demand on increasing the proportion of the renewable energy sources from the total energy consumption. Biomass combustion is one of the main options in this increment. However, it potentially increases the levels of air pollutants that may cause substantial adverse health effects. Recent data have shown that the combustion technology, user practice and fuel type/quality affect the emissions from small scale heating appliances. However, their impact on the toxicological properties of the emissions is poorly known. Moreover, it is unclear what the causative components behind the adverse health effects of the particulate emissions are.

We investigated seven new and old technology heating appliances commonly used in central Europe for the physicochemical and toxicological properties of the emitted particulate matter. The studied appliances included new and old technology log wood boilers and stoves as well as pellet boiler, woodchip boiler and tiled stove, all representing new technology. The three new technology boilers had state-of-the-art technology with air staging and lambda controlled automatic operation.

Particulate samples (D_p <1µm) for both toxicological and chemical characterization (PAHs, water-soluble ions, elements) were collected with Dekati ® gravimetric impactor. Mouse macrophage cell line RAW 264.7 was exposed to four doses of the particulate samples from each appliance for 24h. Inflammatory parameters, proinflammatory cytokine TNFα and chemokine MIP-2 were analyzed with ELISA immunoassay. Cytotoxicity was analyzed with MTT assay and flow cytometric methods detecting both cell cycle and cell membrane permeability of the macrophages. In addition, genotoxicity was determined with comet assay detecting DNA strand breaks in single cell gel electrophoresis.

Most of the PM samples from the studied appliances caused dose dependent increase in at least some of the toxicological parameters.

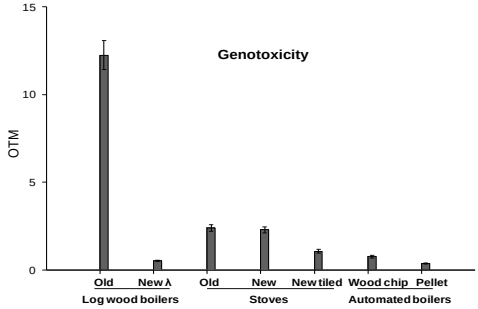

Fig 1. Genotoxicity by the particulate samples (150µg/ml) of each studied appliance. (OTM =Olive tail moment [(tail mean−head mean)×tail%DNA/100].

In general, the inflammatory responses caused by the emission particulate samples were relatively small. There were, however, large differences in the magnitude of the toxic responses between the appliances. Old technology appliances with incomplete combustion were more potent inducers of genotoxic and cytotoxic responses than the respective new technology appliances with more complete combustion. The old technology log wood boiler seemed to cause emissions with the largest toxicological potential and the pellet boiler derived particulate samples were the least potent. The old technology appliances had larger emissions than the new technology appliances, which emphasizes the differences. Moreover, emissions from old technology appliances, especially log wood boiler, had very large PAH concentrations, whereas with the new technology continuous combustion appliances the emissions consisted mostly of the ash compounds. Overall, the present data showed clearly that the combustion technology affects the toxicological responses of RWC emissions that can be reduced with technological development.

Responses of lung cell cultures after realistic exposure to primary and secondary carbonaceous aerosols

L. Künzi[1], S. Schneider[1], P. Mertes[2], J. Dommen[2], U. Baltensperger[2], A.S.H. Prevot[2], M. Kalberer[3], and M. Geiser[1]

[1]Institute of Anatomy, University of Bern, 3012, Switzerland
[2]Laboratory of Atmospheric Chemistry, Paul Scherrer Institut, Villigen, 5234, Switzerland
[3]Centre for Atmospheric Sciences, Department of Chemistry, University of Cambridge, CB2 1EW, UK
Keywords: carbonaceous aerosols, environmental particles, diesel exhaust, wood combustion, human lung cell.
Presenting author email: lisa.kuenzi@ana.unibe.ch

The interaction of particles with the inner surface of the lungs, the main pathway of undesired particle uptake, is still poorly understood (Geiser and Kreyling, 2010). Commonly used model systems for in vitro studies deviate significantly from the situation in vivo such that responses possibly are not representative of those induced by the particles in vivo.

To contribute to the closure of this information gap we examined the responses of lung cell cultures to primary and secondary organic aerosols (POA and SOA) originating from diesel exhaust and wood combustion processed and aged in a large-scale smog chamber under conditions replicating the in vivo situation. The particles were applied to the cell cultures under realistic ambient air and physiological conditions in a novel particle deposition chamber (Savi *et al*, 2008). The cell cultures, representing the inner surface of airways and alveoli, were microdissected epithelia from pig tracheae and re-differentiated human airway epithelia both with established air liquid interface (ALI), porcine lung surface macrophages, the human bronchial epithelial cell line BEAS-2B, as well as the rat alveolar epithelial cell line R3/1. Cells were cultured on microporous filter inserts and exposed to the aerosol at ALI conditions for 1.5 hours (POA) and 2 hours (SOA), respectively. Control cell cultures were (i) exposed to particle-free air or (ii) left untreated in the incubator. Cellular responses were measured within 24 hours after exposure to the aerosol. Biological endpoint measurements included cytotoxicity, cell and tissue integrity, phagocytic activity of macrophages, release of inflammatory mediators such as interleukin-6 (IL-6), IL-8, IL-10, tumor necrosis factor alpha (TNF-α) and monocyte chemotactic protein-1 (MCP-1).

The results demonstrate that a single, short-term exposure of the various lung cell types to the aerosols at ambient-air concentrations of about 10^4 particles/cm^3 leads to only moderate cellular responses. However, there is evidence for i) different effects of POA and SOA and for ii) different effects of aerosols originating from diesel exhaust and wood combustion. Our data indicate that a short time exposure to realistic aerosol concentrations does not induce changes in cell and tissue integrity, but leads to subtle changes in cellular functions that are essential for lung homoeostasis. We found slightly increased cytotoxicity for the various cell cultures after exposure to SOA. In comparison to POA, the phagocytic activity of porcine macrophages was found to be decreased after exposure to SOA from wood burning, whereas it was increased after exposure to SOA from diesel exhaust (Fig. 1).

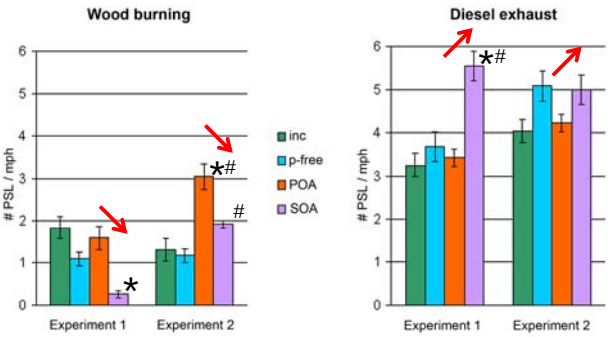

Figure 1. Clearance function of macrophages measured by the number of PSL particles associated per cell.
Means and SEM; $p < 0.05$ to *untreated cells (inc) and #cells exposed to particle-free air (p-free); n = 100 cells.
→ response to SOA compared to that after exposure to POA; SOA still contains some POA (~ 25% for diesel and ~ 30% for wood burning).

The analysis of the inflammatory mediators showed a general trend to increased release after the exposure to SOA; this effect was more pronounced for the diesel exhaust particles. This result is in line with our findings for the cytotoxicity.

In conclusion, our study shows that a single, short-time exposure to ambient concentrations of carbonaceous aerosols does not result in major cytotoxicity or release of inflammatory mediators. However, there are clear indications for subtle changes in cellular functions that are essential for lung homoeostasis, especially after the exposure to SOA from diesel exhaust.

This work was supported by the Swiss National Science Foundation grant K-32K1-120524.

Geiser, M. and Kreyling, W.G. (2010) *Particle Fibre Toxicol.* **7**(2).
Savi, M., Kalberer, M., Lang, D., Ryser, M., Fierz, M., Gaschen, A., Rička, J. And Geiser, M. (2008) *Environ. Sci. Techn.* **42**, 5667-5674.

General and PAH-mediated cytotoxicity in particulate matter from wood combustion

S. Gauggel[1], J. Wiese[2], B. Pieterse[3] and D.R. Dietrich[1]

[1]Department of Human- and Environmental Toxicology, University of Konstanz, Konstanz, 78457, Germany
[2]Department of Environmental Technology and Energy, TU Hamburg-Harburg, 21073, Hamburg, Germany
[3]BioDetection Systems BV, Science Park 406, Amsterdam, The Netherlands
Keywords: particulate matter, wood smoke, PAH(s), Lung/particle interaction.
Presenting author email: susanne.gauggel@uni-konstanz.de

Due to ongoing discussions about risks for human health and European threshold values particulate matter emissions have gained in importance. The increasing use of renewable energy sources, such as wood, goes along with a higher burden of particulate matter, which has the potential to induce respiratory tract diseases in humans (Naeher, 2007; Pope, 2002). This study focuses on the toxicological characterization of particulate matter emerging from small scale wood combustion furnaces, investigating the direct cytotoxic effects as well as effects mediated by known carcinogenic compounds part of or adhering to the PMs, e.g. Polycyclic Aromatic Hydrocarbons (PAHs).

The physicochemical characteristics of PMs are assumed to be responsible for the direct (mechanical) toxicity of these dusts. In contrast PAH mediated toxicity is dependent on the bioavailability of PAHs for the cells exposed as well as their respective metabolic capacity for converting PAHS into high reactive intermediates. At present, potential PM toxicity assessment is based exclusively on PAH chemical analysis. The latter appears critical, as not all PAHs may be directly available to cells. Therefore additional *in vitro* assays as well as mechanistic studies are needed. Moreover addtl. pathways of action, beside xenobiotic metabolism and macromolecule interaction, e.g. membrane and nuclear receptor binding and activation, need to be taken into consideration. Indeed, the PAHs due to structural similarities with steroids, binding to the ligand binding domain of human steroid receptors is likely (Van Lipzig, 2004), thereby suggesting the potential activation of steroid receptor signal transduction pathways.

The 16 US EPA PAHs were quantified, via accelerated solvent extraction and adjacent GC-MS, in five particulate matter samples obtained from combustion events with variable conditions (e.g. complete and incomplete combustion). Cytotoxicity assays were performed in two model cell lines (A-549: human type II alveolar epithelial cells, THP-1: human monocytic cells, differentiated to macrophages), using for different PM concentrations and time points. A specific *in vitro* PAH transactivation assay (CALUX) was performed in order to investigate PAH bioavailability to the cells. Therefore, concentration-response curves were established with PM samples and with their respective organic extracts. To investigate possible steroid receptor binding and activation, specific androgen and estrogen receptor transactivation assays (PALM, MELN) are presently carried out (Balaguer, 1999; Freyberger, 2010).

No acute cytotoxicity was observed for PM samples, except for very high concentrations. The corresponding PAH transactivation assay (CALUX) demonstrated that some of the PAHs within the PM samples were bioavailable to the cells and provided for a good signal correlation between CALUX analyses and PAH chemical quantification. Indeed, the sample with the lowest concentration of PAHs revealed also the lowest response in the luminogenic signal, compared to samples with higher PAH amounts (Figure 1). However the signal intensity in the CALUX assay suggested a toxicity potential of individual or combinations of PAHs in the PM samples several fold above that indicated by mere PAH chemical quantification.

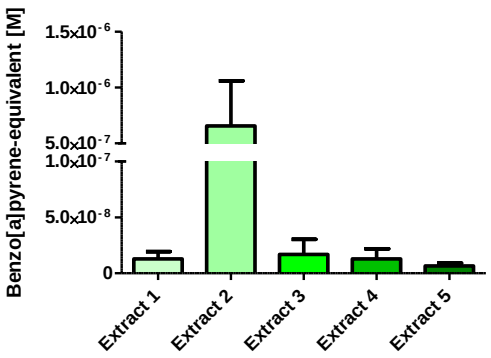

Figure 1. B[a]P equivalents for extracts of PM #1-5. Mean ± SEM for n=3 (extract 1,2) or n=4 (extract 3-5).

These investigations were supported by the German Federal Ministry of Environment.

Balaguer, P., François, F., Comunale, F., Fenet, H., Boussioux, A.-M., Pons, M., Nicolas, J.-C. and Casellas, C. (1999) *Sci. Total Environ.* **233**, 47-56.

Freyberger, A., Witters, H., Weimer, M., Lofink, W., Berckmans, P. and Ahr, H.-J. (2010) *Reprod. Toxicol.* **30**, 9-17.

Naeher, L. P., Brauer, M., Lipsett, M., Zelikoff, J. T., Simpson, C. D., Koenig, J. Q. and Smith, K. R. (2007) *Inhal. Toxicol.* **19**, 67-106.

Pope, C. A., Burnett, R. T., Thun, M. J., Calle, E. E., Krewski, D., Ito, K. and Thurston, G. D. (2002) *Jama* **287**, 1132-1141.

Van Lipzig, M. M. H., Ter Laak, A., Jongejan, A., Vermeulen, N. P. E., Wamelink, M., Geerke, D. and Meerman, H. N. (2004) *J. Med. Chem. 47*, 1018-1030.

A Thermal Precipitator for Nanoparticle Cytotoxicity Screening

Dirk Broßell[1], Sabine Plitzko[1], Nico Dziurowitz[1], Erhardt Gierke[1], Volker Bachmann[1], Gunter Linsel[1], Nkwenti Azong-Wara[2], Christof Asbach[2], Heinz Fissan[2], Andreas Schmidt-Ott[3]

[1] Federal Institute for Occupational Safety and Health (BAuA), Berlin, Germany
[2] IUTA e.V., Duisburg, Germany
[3] Delft University of Technology, Delft, Netherlands
Keywords: nanoparticle, thermal precipitator, toxicity, in vitro.
Presenting author email: brossell.dirk@baua.bund.de

In vitro toxicity studies are becoming much more important due to increasing concerns about animal welfare and partly also due to higher costs of *in vivo* studies. We introduce a new device for *in vitro* cell exposure to nanoparticles for cytotoxicity screenings. The system is an attempt to solve one problem most *in vitro* toxicity studies encounter when trying to mimic *in vivo* inhalation studies, namely the lack of representativeness of the exposure to the particles (Teeguarden, 2007) and hence the resulting dose and dose rate. It is conceptualized as a toxicity screening device primarily indicating cytotoxic effects on the human respiratory tract.

The so called Cyto-TP is a thermal precipitator (TP) (Azong-Wara, 2009) for the deposition of airborne nanoparticles on living human epithelial lung cells at the air-liquid interface (ALI). The cellular response to ALI exposure seems to be similar to suspension exposure but occurs at doses significantly lower (Holder, 2008). Cellular response at ALI may be observable at exposure atmospheres with moderate particle number concentrations. The TP deposits particles very smoothly onto the cell surface and therefore does not damage the cells by impact. By using airborne particle exposure the surface chemistry, morphology and size of the nanoparticles do no change in contrast to the use of suspension exposure. Unlike in a similar concept using electrophoresis for particle deposition (Sillanpää, 2008), particles bear their natural charge level. These aspects contribute greatly to a higher representativeness of exposure mode.

The Cyto-TP consists of a hot plate (52°C) and a parallel cold plate (37°C) which hosts the cell cultures as shown in Fig. 1. The aerosol flows between the two plates and particles are deposited onto the cells by thermophoresis. Potential cell stress due to secondary effects is minimized with our device, so cellular response can be related more easily to the presence of nanoparticles in the exposure atmosphere. After exposure the cells can be placed inside a scanning electron microscope for analysis. Additionally CASY cell counting and analysing used to determine the ratio of living and dead cells.

The presentation will describe the first prototype of the Cyto-TP and its design and functionality along with a newly designed experimental approach for cytotoxicity screening. First results of the validation of the Cyto-TP approach with nanoparticles will be presented.

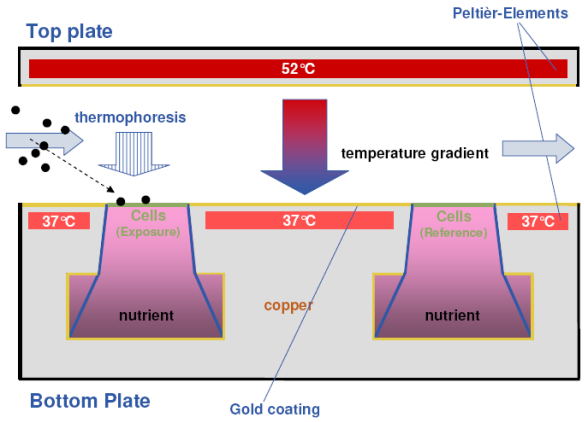

Figure 1. This is a concept sketch of the functionality of the Cyto-TP. The nanoparticles in a laminar flow are deposited onto the cells placed at the cold plate.

The research leading to these results has received funding from the European Community's Seventh Framework Programme (FP7/2007-2013) under grant agreement n°211464-2.

Teeguarden, J. G., Hinderliter, P. M., Orr, G., Thrall, B. D., Pounds, J. G. (2007), *Toxicological Sciences*, **95**, 300-312

Azong-Wara. N., Asbach, C., Stahlmecke, B., Fissan, H., Kaminski, H., Plitzko, S., Kuhlbusch, T. A. J. (2009), *Journal of Nanoparticle Research*, **11**, 1611-1624

Holder, A. L., Lucas, D., Goth-Goldstein, R., Koshland, C. P. (2008), *Toxicological Sciences*, **103,** 108-115

Sillanpää, M., Geller, M.D., Phuleria, H.C., Sioutas, C.. (2008), *Journal of Aerosol Science,* **39**, 335-347

Thursday, September 8, 2011

Session 9E: Aerosol-based Nanotechnology: Methods and Applications

From Embedded to Supported Metal/Oxide Nanomaterials: Thermal Behavior and Structural Evolution at Elevated Temperatures

S.B. Bubenhofer, W.J. Stark and R.N. Grass

Institute for Chemical and Bioengineering, ETH Zurich, Zurich, 8093, Switzerland
Keywords: flame spray pyrolysis, composite nanoparticles, particle formation and growth, modelling.
Presenting author email: s.bubenhofer@chem.ethz.ch

The relation between structure and function is of major importance at material interfaces which often excel in terms of chemical or physical effects. Therefore, multi-phase nanocomposites (e.g. core-shell, janus-shaped and carrier-supported noble metal nanoparticles) attract attention due to their possibility to contact two materials at the nanometer scale profiting from their highly increased interaction area (Kamat (2007)).

Especially at metal/oxide interfaces, accounting for a majority of heterogeneous catalysts, the structure-function relationship has been studied intensively. High temperature, dry aerosol processes (flame synthesis) are common for building such composites (Strobel and Pratsinis (2009)). But the formation of the key structural elements in such multi-component systems, depending on coagulation-order and solid-solid diffusion, is not fully understood yet (Rotzetter *et al* (2010)).

We therefore present a systematic material study on the morphological transition from metal embedded in oxide to metal supported on oxide nanocomposites with the model compound Pd/SiO_2 (Bubenhofer *et al* (2011)). Crystalline Pd encapsulated in silica nanoparticles are produced in a single step flame spray pyrolysis process. Nanometer scale transformation of this material to nanocrystalline Pd dispersed on the amorphous silica matrix was achieved by heating to elevated temperatures.

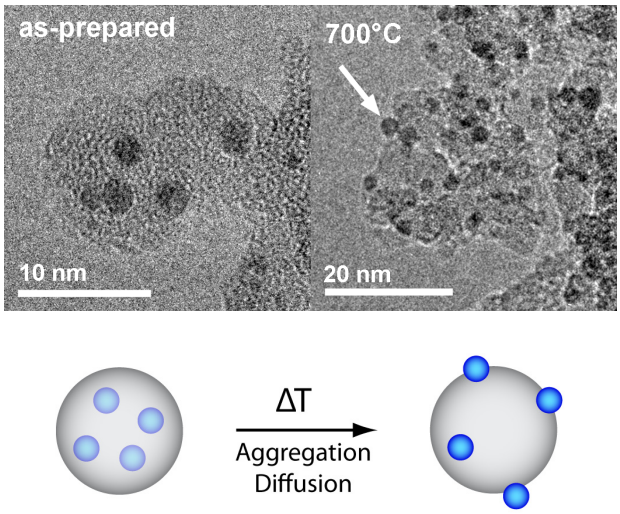

Figure 1. Morphological transformation of noble metal encapsulated in oxide nanoparticles to supported on oxide particles (2 vol% Pd with SiO_2 matrix).

A physical model based on Pd cluster diffusion and aggregation within silica spheres was derived to describe the transformation process, which gives an understanding of the influence of temperature, matrix viscosity, particle sizes and concentrations on this morphological transformation

The data is discussed in terms of aerosol formation mechanisms (consecutive vs. simultaneous coagulation) and compared to literature data on the high-temperature aerosol formation (Jensen *et al* (2000), Strobel and Pratsinis (2009)) of nanocomposites.

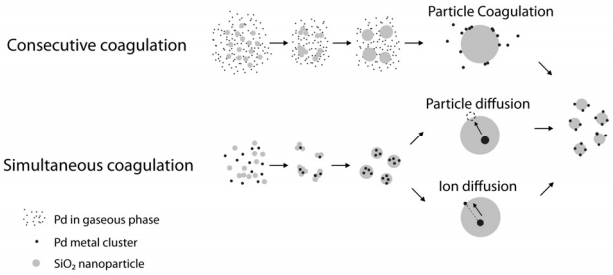

Figure 2. Possible 2-component nanocomposite formation mechanisms in flame spray synthesis.

Valuating the model and the discussed mechanism by tuning a parameter in the aerosol formation process, clearly shows, that the findings enable morphology predictions (core-shell vs. supported metal/silica particles) both in nanocomposite formation processes at elevated temperature (flame spray synthesis) and also during thermal evolution of multi-phase nanomaterials, determining their performance in e.g. catalysis or fuel cells.

Kamat, P.V. (2007) *J. Phys. Chem C* **111**, 2834-2860.

Strobel, R. and Pratsinsis, S.E. (2009) *Platinum Met. Rev.* **53**, 11-20.

Rotzetter, A.C.C., Luechinger, N.A., Athanassiou, E.K., Mohn, D., Koehler, F.M. and Grass, R.N. (2010) *J. Mater. Chem.* **20**, 7769-7775.

Bubenhofer, S.B., Krumeich, F., Fuhrer, R., Athanassiou, E.K., Stark, W.J. and Grass, R.N. (2011) *J. Phy. Chem. C* **115**(4), 1269-1276.

Jensen, J.R., Johannessen, T., Wedel, S. and Livbjerg, H. (2000) *J. Nanopart. Res.* **2**, 363-373.

Scaling of an aerodynamic lens for use in coating technology

D. Kiesler[1], T. Bastuck[1], F.E. Kruis[1] and M. Kennedy[2]

[1]Institute for Technology of Nanostructures and Center for Nanointegration Duisburg-Essen (CeNIDE), University Duisburg-Essen, Duisburg, 47057, Germany
[2]Federal-Mogul Burscheid GmbH, Burscheid, 51399, Germany
Keywords: aerodynamic focusing, coatings, deposition, inertial impaction.
Presenting author email: dennis.kiesler@uni-due.de

The embedding of nanoparticles in coatings produced by Physical Vapour Deposition (PVD) is complicated due to the fact that typical coating conditions employ high-vacuum (HV) conditions whereas the production of nanoparticles necessitates quasi-atmospheric conditions. This requires the separation of both processes and thus a transfer of the particles produced in a HV environment. An efficient tool to this purpose is aerodynamic focusing (Liu, 1995) which increases the particle concentration on the center of the flow and thereby reduces the particle losses upon the transfer in the HV. Existing aerodynamic lenses are however not designed to apply the higher flow rates characteristic for particle synthesis. The purpose of this work is to design, optimise and experimentally verify a high-flow rate aerodynamic lens system.

Using the aerodynamic lens calculator (Wang, 2005; Wang, 2006), a design was sought for allowing to focus 30-80 nm TiC nanoparticles in 5 slm argon, which is a factor 50 above the conventional flow rates in aerodynamic lenses. It was found that in the optimal lens configuration the required pumping capacity scales unfavourably with the inlet flow rate (Table 1). Due to this scaling a concept with multiple lenses is favoured.

Table 1. Comparison of aerodynamic lens systems with different flow rates.

Inlet Flow rate Q (slm)	**Pressure needed in Skimmer (Pa)**	**System lengh (m)**	**Min. pumping capacity (m^3/h)**
0.5	100	0.81	31.2
1.5	33	2.45	283.7
4.5	11	7.31	2533.7
Scaling with Q	**~ Q^{-1}**	**~ Q**	**~Q^2**

First a single aerodynamic lens for 0.5 slm Ar with 3 orifices was designed, built and optimized. While the aerodynamic lens calculator was a good starting point, further optimization especially for the last nozzle and the skimmer was needed. Figure 1 shows the simulated trajectories of 50nm Ti particles in the simple and in the the optimized nozzle. The simulations were done in Fluent™ 6.2. Due to small particle sizes and large pressure differences ranging from 10^5 to 10^0 Pa a user defined function calculating the local slip-correction-factor for the particle drag force and the Brownian random movement was developed.

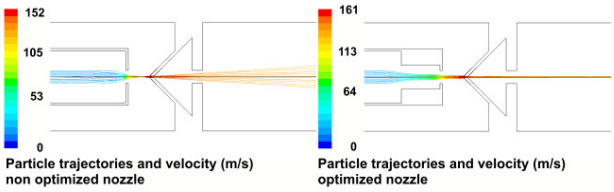

Figure 1. Simulation results for 50nm Ti particles in an non optimized acceleration nozzle (left) and optimized one (right). A tight particle beam can be formed

Pressure measurements allowed a good comparison between the lens designer, the CFD simulation and the experiment. In the experiment, TiC particles from an Mini-Arc-Reactor were used. Different skimmer-nozzle configurations and sample positions were tested (Figure 2). The particles could be deposited by inertial impaction even 500 mm after the skimmer having a spot diameter less than 20mm. The particle deposition efficiency was analyzed by gravimetric measurements. It could be shown, that under optimal conditions 70% of the particles entering the system were deposited on the Sample. The flow into the vacuum chamber was reduced from 0.6 slm at the lens entrance to 1.5 sccm. This means, that the particle concentration on the beam axis could be increased by a factor of 400.

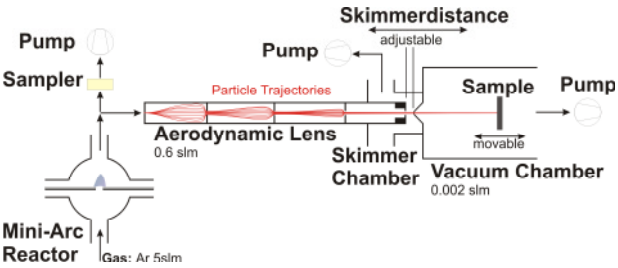

Figure 2. Schematic representation of the experimental setup.

This work was supported by the Deutsche Forschungsgemeinschaft in the framework of the collaborative research program “Nanoparticles from the gas phase” (SFB 445).

Liu, P., Ziermann, P.J. Kittelson, D.B., McMurry, P.H. (1995) *Aerosol Sci. Technol.* **22,** 293
Wang, X., McMurry, P.H., Kruis, F.E. (2005) *Aerosol Sci. Technol.* **39,** 611
Wang, X., McMurry, P.H. (2006) *Aerosol Sci. Technol.* **40,** 320

Use of aerosol-derived nanoparticles for the fabrication of polymer ultrafiltration membranes

Christoph R. Kellenberger, Norman A. Luechinger and Wendelin J. Stark

Department of Chemistry and Applied Biosciences, Swiss Federal Institute of Technology (ETH Zurich), Wolfgang-Pauli-Str. 10, HCI E 107, ETH Hönggerberg, Zurich 8093, Switzerland

Keywords: soluble nanoparticles, carbonate nanoparticles, polymer filtration membranes, polymer composite, ultrafiltration

Presenting author email: christoph.kellenberger@chem.ethz.ch

Polymeric ultrafiltation membranes are playing an important role in mass separation processes in many industrial sectors such as the chemical and biopharmaceutical industry and the water treatment and recovery industry. Commercial ultrafiltration membranes are nowadays produced by a technique called phase inversion. Therefore, a phase separation has to be induced in a previously homogeneous polymer solution by precise control of temperature, time and solvent to non-solvent ratio. This process unfortunately is limited by the number of parameters that have to be controlled simultaneously during production and by the broad pore size distribution that decreases the selectivity of the resulting membrane (Peinemann, Nunes, 2008).

We present a novel approach towards the production of ultrafiltration polymer membranes which are fabricated by a facile and fast procedure. This process is based on the use of soluble (degradable) carbonate nanoparticles (Huber 2005; Loher 2005; Grass 2005). The nanoparticles act as the pore template and the process can be applied on numerous polymers. Membranes can be fabricated by a simple two-step procedure. Basically, a polymer solution (polymer dissolved in a solvent) containing dispersed soluble nanoparticles is used as a starting material. This solution is roll-coated on a substrate (e.g. glass) and after evaporation of the solvent a solid polymer film (with incorporated soluble nanoparticles) is obtained. In a second step the polymer membrane is turned porous by simple dissolution of the soluble nanoparticle template in a mild acid. The pore formation of the resulting membrane is different to state-of-the art techniques. Here, the pore size and number of pores is exactly defined by the size and number of nanoparticles, as they serve as a direct template of the finally obtained pores. Therefore, the pore formation is very reliable yielding a narrow pore size distribution that guarantees the high selectivity of the membrane. Additionally, the soluble nanoparticle template dissolution in a mild acid is very fast (< 10s) which can be run at ambient conditions without the need for precise and simultaneous control of various process parameters.

The use of $CaCO_3$ nanoparticles (50nm in size) in a polyethersulfone (PES) or polysulfone (PSU) matrix led to the formation of a polymer membrane with a molecular weight cut-off (MWCO) of 1400kDa, whereas the use of $SrCO_3$ nanoparticles (17nm in size) in a PES matrix led to a MWCO of 150kDa. This demonstrates that the pore size of the filtration membranes can directly be tuned by the nanoparticle size. The MWCO of the according membranes was examined using a dextran rejection profile test that is widely accepted among membrane manufacturers (Tkacik, Michaels, 1991).

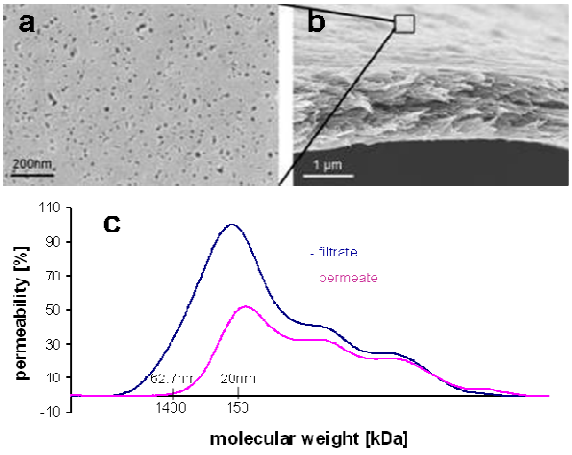

Figure 1: Top view on PES membrane with a MWCO of 150kDa (a). Cross section of the same membrane (b). Typical dextran rejection profile of a 1400kDa MWCO membrane (c).

Peinemann, K. V., Nunes, S. P. (2008) *Membranes for life sciences.* WILEY-VCH Verlag GmbH&Co.

Huber, M., Stark, W. J., Loher, S., Maciejewski, M., Krumeich, F., Baiker, A. (2005) *Chem. Commun.* **5,** 648-50.

Loher, S., Stark, W. J., Maciejewski, M., Baiker, A., Pratsinis, S. E., Reichardt, D., Maspero, F., Günther, D. (2005) *Chem. Mater.* **17,** 36-42.

Grass, R. N., Stark, W. J. (2005) *Chem. Commun.*, **14**, 1767-1769.

Tkacik, G., Michaels, S. (1991) *Nature Biotechnology,* **9**, 941 – 946.

A new measurement technique for the process monitoring of the catalytic activity of nanoparticles during their production process

N. Neubauer, M. Seipenbusch and G. Kasper

Institute for Mechanical Process Engineering and Mechanics,
Karlsruhe Institute of Technology (KIT), 76131, Karlsruhe, Germany
Keywords: process monitoring, online measurement, catalytic activity, palladium nanoparticles.
Presenting author email: nicole.neubauer@kit.edu

Introduction

For process monitoring and quality assurance integrated gas phase processes require online methods for the determination of the catalytic behaviour of the produced catalyst nanoparticles. In addition, an online technique capable of a substance-specific detection of catalytically active nanoparticles against a background of particles in workplace air is also still needed (Kuhlbusch *et al.*, 2009; Murashov *et al.*, 2009). For very active nanoparticles, such as platinum or nickel, the method of aerosol catalysis enables an online measurement of the catalytic activity of the particles (Weber *et al.*, 1999; Seipenbusch *et al.,* 2001). Less catalytically active nanoparticles, e.g. iron oxide, require an accumulation of nanoparticle material prior to catalytic investigations (Neubauer *et al.,* 2011). Therefore we studied a new measurement technique combining particle sampling on a substrate and the catalytic reaction into one instrument. In the following work the method capable of detecting the catalytic activity of nanoparticles and the achieved results are demonstrated.

Experimental

Catalytically active palladium nanoparticles generated by spark discharge were used as catalysts. The hydrogenation of ethene was chosen as a suitable catalytic test reaction which already runs at ambient air temperature.

In a first step the palladium particles are deposited on a substrate using either filtration or an impaction based process. After the particle deposition over a fixed time interval on a glass fiber filter or a glass impaction plate, the aerosol flow is cut. Both substrates can be heated so that – if the chosen catalytic reaction requires it - the temperature can be increased.

In a second step the deposited palladium particles are exposed over a defined time to the gaseous educts ethene and hydrogen (each 3.0, 50 vol-%) so that the catalytic reaction is initiated. The conversion of ethene to the gaseous reaction product ethane is detected by infrared spectroscopy (Bruker Vector 22).

Results

The concentration of the converted ethene was related to the mass of the accumulated palladium nanoparticles which was determined by gravimetry. For both deposition processes observation gives that the concentration of the converted ethene increases proportionally to the mass of the used palladium nanoparticles (cf. Figure 1 for deposition by filtration).

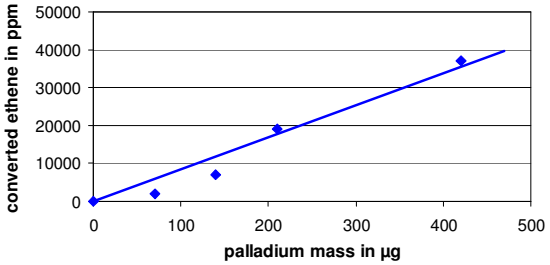

Figure 1. Calibration curve for the concentration of converted ethene vs. the mass of palladium nanoparticles deposited by filtration.

A lower detection limit of 120 ng can be extrapolated based on the curve linearity and assuming a measurement limit of 10 ppm of the ethene decrease by infrared spectroscopy. At aerosol concentrations of 1 mg/m^3 and a flow rate of 1 l/min a sampling time of only 8 seconds is sufficient to deposit a mass of 120 ng of palladium particles.

Conclusion

Small amounts of a palladium aerosol can be very rapidly detected on the basis of their catalytic activity. According to the estimated sensitivity of the used technique in the range of nanograms as well as the required sampling time, the technique can be considered a true real-time method for the specific determination of palladium nanoparticles.

Acknowledgement

The research leading to these results has received funding from the European Commission's Seventh Framework Programme (FP7/2007-2013) under grant agreement n° 211464-2 (Nanodevice).

References

Kuhlbusch, T.A.J., Fissan, H. and Asbach, C. (2009) *Nanomaterials: Risks and Benefits*, 233-243

Murashov, V., Engel, S., Savolainen, K., Fullam, B., Lee, M. and Kearns, P. (2009) *J. Nanopart. Res.* **11**, 1587-1591

Weber, A.P., Seipenbusch, M., Thanner, C. and Kasper G. (1999) *J. Nanopart. Res.* **1**, 253-265

Seipenbusch, M., Binnig, J., Heim, M., Weber, A.P. and Kasper G. (2001) *Helv. Chim. Acta* **84**, 3686-3701

Neubauer, N., Weis, F., Binder, A., Seipenbusch, M. and Kasper G. (2011) *Proc. Nanosafe 2010 in J. of physics,* in preparation

Hybrid Plasmonic-Magnetic Biomarkers

G. A. Sotiriou[1], A. M. Hirt[2], P-Y. Lozach[3], A. Teleki[1], F. Krumeich[1], S. E. Pratsinis[1]

[1]Particle Technology Laboratory, Institute of Process Engineering, Department of Mechanical and Process Engineering, ETH Zurich, Sonneggstrasse 3, CH-8092, Zurich, Switzerland
[2]Institute of Geophysics, Department of Earth Sciences
[3]Institute for Biochemistry, Department of Biology

Keywords: yttrium oxide, terbium, europium, codoping.
Presenting author email: sotiriou@ptl.mavt.ethz.ch

Biological labels are used in bio-imaging and the ability to tag cells and biomolecules facilitates diagnosis and therapy. Even though organic dyes are used for such applications, their photobleaching inhibits their further employment. Quantum dots do not exhibit photobleaching and their emission color can be tuned by their size, however, their optical blinking and the high toxicity of their components restrict their use in bio-applications. An alternative strategy for such biolabeling applications are plasmonic nanoparticles. These particles can be detected under dark-field microscopy.

Hybrid magnetic/plasmonic nanoparticles possess properties originating from each individual material. Such properties are beneficial for biological applications including bio-imaging, targeted drug delivery, *in vivo* diagnosis and therapy. Limitations regarding their stability and toxicity, however, challenge their safe use[1]. Here, the one-step flame synthesis of composite SiO_2-coated Ag/Fe_2O_3 nanoparticles is demonstrated (Figure 1). The hermetic SiO_2 coating[2] does not influence the morphology, the superparamagnetic properties of the iron oxide particles and the plasmonic optical properties of the silver particles. It does prevent, however, the release of toxic Ag^+ ions from the nanosilver surface[3] and reduces the interaction field among the iron oxide particles, resulting in a stable over 2 days suspensions with no signs of agglomeration (flocculation) and sedimentation[4]. The feasibility of these multi-component nanoparticles with superior properties and performance is explored by their specific binding with live tagged cells, and the detection as well as magnetic manipulation of the latter is demonstrated. Therefore, the hybrid SiO_2-coated Ag/Fe_2O_3 nanoparticles do not exhibit the limiting physical properties of each individual component, while retain all the desired ones, facilitating their safe employment in such bio-applications.

Figure 1 shows a TEM image of the composite Ag/Fe_2O_3 SiO_2-coated nanoparticles. The silver nanoparticle (dark particle) is attached on the iron oxide core, and encapsulated by a nanothin silica layer of about 2 nm thickness.

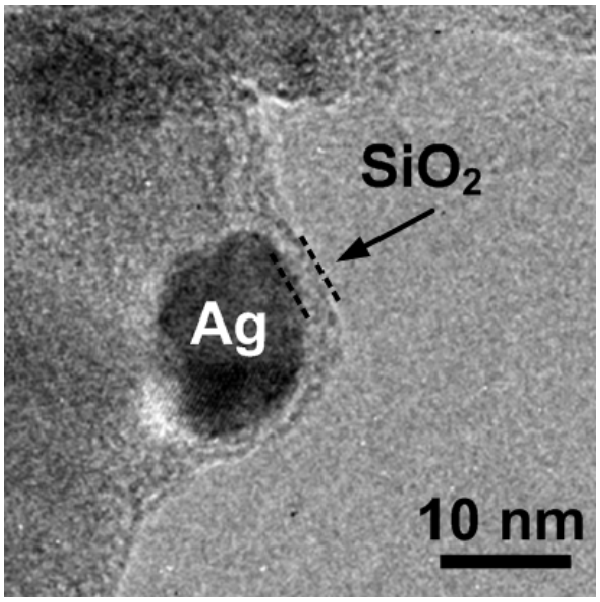

Figure 1. TEM image of the composite Ag/Fe_2O_3 SiO_2-coated nanoparticles. The silver nanoparticle (dark particle) is attached on the iron oxide core, and encapsulated by a nanothin silica layer of about 2 nm thickness.

References

1 Anker, J. N. *et al.* Biosensing with plasmonic nanosensors. *Nature Mater.* **7**, 442-453 (2008).
2 Teleki, A. *et al.* Hermetically coated superparamagnetic Fe_2O_3 particles with SiO_2 nanofilms. *Chemistry of Materials* **21**, 2094-2100 (2009).
3 Sotiriou, G. A. & Pratsinis, S. E. Antibacterial activity of nanosilver ions and particles. *Environmental Science & Technology* **44**, 5649-5654 (2010).
4 Sotiriou, G. A. *et al.* Non-Toxic Dry-Coated Nanosilver for Plasmonic Biosensors. *Adv. Funct. Mater.* **20**, 4250-4257 (2010).

Financial support by the Swiss National Science Foundation (No. 200020-126694) is kindly acknowledged.

Room temperature gas sensor based on carbon nanoparticles synthesized by flame aerosol method

D. Kim[1], P.V. Pikhitsa[1] , H. Yang[2] and M. Choi[1]

[1] National CRI center for Nano Particle Control , Institute of Advanced Machinery and Design, School of Mechanical and Aerospace Engineering, Seoul National University, Seoul, 151-742, Korea
[2]Present address: Department of Mechanical Engineering, Texas A&M University, College station, Texas, USA
Keywords: gas sensor, Nanoscale carbon particles, Nanoparticle patterning.
Presenting author email: mchoi@snu.ac.kr

Since carbon nanotubes(CNT) were introduced as gas sensors(Kong et al., 2000), many researchers have studied CNT-related gas sensors actively. It is known that bare CNT-based gas sensors are insensitive to CO and H_2(Kong et al., 2001) but sensitive to NO_2 and NH_3(Kong et al., 2000) at room temperature. Room temperature sensing can have the significant meaning in terms of lowering the consumption of electric power, simplifying the structure of sensor devices and being easy to fabricate a sensor device. To lower the working temperature down to room temperature, catalysts such as Pd and Pt are utilized with CNT to get a surface reaction with target molecules and a remarkable change of conductivity.

Here, we report on a crystalline shell-shaped carbon nanoparticle(SCNP) based gas sensor detecting CO and H_2 at room temperature without catalysts and even in an inert atmosphere. We utilized the crystalline SCNPs synthesized through continuous wave CO_2 laser irradiation on acetylene flow(Pikhitsa et al., 2005) without catalysts and patterned them by ion-induced focusing method into sensor devices.(Kim et al.,2006)

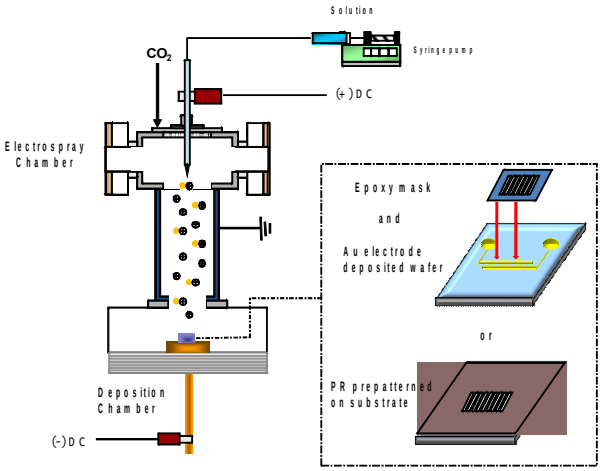

Figure 1. Schematic diagram of sensor fabrication setup

Ion-induced focusing approach was realized by electro-hydrodynamic atomization method, which needs charged aerosol form of SCNPs as can be seen in figure 1. To obtain charged SCNPs, well-dispersed solution of particles should be prepared. As-synthesized SCNPs have a hydrophobic nature, chemical treatment of SCNPs with nitric and sulfuric acid at 110° C was conducted.(Pikhitsa et al., 2005) Acid treatment can make the surface of SCNPs hydrophilic by attaching functional groups such as carboxylic and hydroxyl groups; it can separate SCNPs from each other and thus maintain the SCNPs to be well-dispersed in ethyl alcohol. Then, SCNPs were patterned on the substrates by ion-induced focusing method and the nanoparticle focusing mask.(Kim et al, 2006 and You et al, 2010)

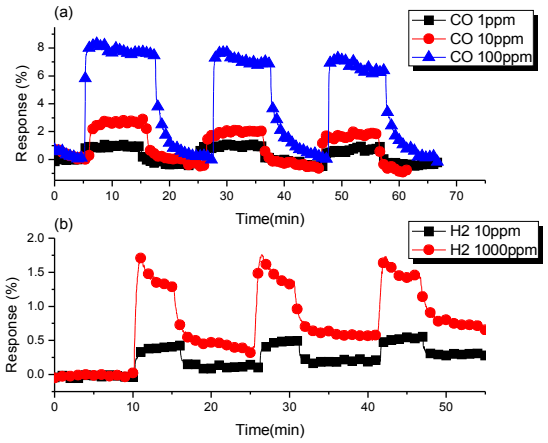

Figure 2. Gas sensor response for CO and H_2 gas

Figure 2 shows the gas sensor response for CO 1~100ppm and H_2 10~1000ppm measured at room temperature. In our preliminary study, the pristine SCNP based gas sensor shows insensitivity to CO and H_2 at room temperature. But chemical treatment can make the carbon sensor work at room temperature even at low concentration of CO and H_2 gas.

This work was funded by the National CRI Center for Nano Particle Control supported by the Ministry of Education, Science and Technology, Korea as one of Acceleration Research Programs. Supports from BK21 program and WCU (World Class University) program (R31–2008-000–10083-0) through the Korea Research Foundation funded by the Ministry of Education, Science and Technology are also gratefully acknowledged.

Kong, J., et al. (2000) *Science* **287**, 622-625
Kong, J., Chapline, M.G., Dai, H. (2001) *Adv. Mat.* **13**, 1384-1386
Pikhitsa. P.V., et al. (2005) *Phys. Rev.B* **71**, 073402-1~4
Kim, H., et al. (2006) *Nat. Nanotech.* **1**, 117-121
You, S., et al. (2010) *Small* **6**, 2146-2152

Thursday, September 8, 2011

Session 9F: Charged Aerosols

Electrostatic controlled coating of particle surfaces with nanoparticles

S. Sigmund, M. Yu, J. Meyer, M. Seipenbusch, M. Wild and G. Kasper

Institut für Mechanische Verfahrenstechnik und Mechanik, Karlsruhe Institute of Technology, 76131 Karlsruhe, Germany

Keywords: Nanoparticles, charged particles, electrostatic particle coating

The process of electrostatic controlled coating of particles surfaces with nanoparticles has been investigated as a new, versatile process.

Because of their specific characteristics compared to bulk materials, nanoparticles obtain more and more attention in the field of particle technology, especially particles in size range below 10 nm. To take advantage of those characteristics, such as high catalytic or magnetic activity, isolated, un-agglomerated nanoparticles are required. To keep nanoparticles from agglomeration and to avoid high diffusional loss, one can generate a support particle coated with nanoparticles. Thus particle dynamics and powder flow properties are governed by support particle properties and that leads to a simplification in systems handling.

The process of surface coating is in our case an electrostatic controlled process. Support and coating particles are generated separately and charged oppositely before mixing for selective agglomeration. This method of electrostatic coating provides an alternative process route to other well known coating mechanisms, e.g. chemical vapour deposition. The electrostatic surface coating has several advantages: According to Zebel (1959) the bipolar coagulation between the positive support particles and the negative coating particles is accelerated compared to diffusive coagulation. Repulsive forces between unipolar charges decrease coagulation in each size range. In addition these repulsive forces should lead to a homogeneous allocation of the coating particles on the support particle surface. This method provides a highly controllable process and the possibility of selective agglomeration. Over changing the charging conditions, it is possible to generate tailored nanoparticle systems. Even though bipolar coagulation was investigated before (Maisels et al., 2000), the use of this method in particle coating is completely new. Previous works (Alonso et al., 2005) also showed that there is a challenging task in charging nanoparticles in size ranges below 10 nm.

For experimental investigations SiO_2 monospheres with a diameter of d = 235 nm are used as support particles. These monospheres are suspended in water and dispersed in air. The platinum coating particles with a size of about 10 nm are generated by a glowing wire generator. After dispersing and charging, an SMPS System is used to determine the charge distribution of the support particles. Each support particle carries several 10 elementary charges. Then charged support particles are mixed with charged coating particles. After passing a mixing zone with a known residence time the charge distribution is determined again. Every agglomeration between the positive support particle and a negative coating particle equalizes one positive charge on the support particle surface. Further it is assumed that according to the enormous difference in size the agglomeration of coating particles does not change the support particle diameter. So it is possible to follow the process progress by comparing the charge distributions before and after mixing with coating particles. Beside the influence of concentration and residence time, several other parameters were investigated.

To investigate coagulation dynamics, a theoretical model was developed. This model permits to determine the charge distribution of support particles after a given residence time and thus the point of neutralisation of all charges on particles surface by bipolar agglomeration of coating particles. For this purpose equations were set up to calculate the change in particle concentration. Bipolar coagulation, self coagulation, particle loss by diffusion and electrostatic dispersion are considered in these equations. The equations are solved with sectional method.

The results from experimental measurements were compared to those from numerical calculations.

This project is part of the JointLab IP3, a joint initiative of KIT and BASF. Financial support by the ministry of science, research and the arts of Baden-Württemberg (Az. 33-729.61-3) is gratefully acknowledged.

Alonso, M., Martin, M.I., Alguacil, F.J.(2005). *The Measurement of Charging Efficiencies and Looses of Aerosol Nanoparticles in a Corona Charger.* Journal of Electrostatics 64, 203.

Maisels, A., Kruis, F.E., Fissan, H., Rellinghaus, B., Zähres, H.(2000) *Synthesis of Tailored Composite Nanoparticles in the Gas Phase.* Applied Physics Letters, 77, 4431

Zebel, G.(1959). *Zur Theorie der Koagulation disperser Systeme aus elektrostatischen und magnetischen Dipolen*, Staub 19, 381.

Characterization of EHDA in the simple-jet mode

L.L.F. Agostinho[1,2], E.C. Fuchs[2], J. Wartena[1], C. U. Yurteri [1,2], J. C. M. Marijnissen [1,2]

[1]Faculty of Applied Sciences, Delft University of Technology, 2628 BL Delft, The Netherlands
[2] Wetsus Centre of Excellence for Sustainable Water Technology, 8900 CC Leeuwarden, The Netherlands

Keywords: Electrospray, simple jet mode, water
Presenting author email: luewton.lemos@wetsus.nl

In the past few years electrohydrodynamic atomization (EHDA) has become a very important tool to atomize liquids. Its application ranges from medicine to agriculture (Geerse, 2003). The spray can be operated in different modes (Cloupeau *et al.*, 1994). The most explored one is the cone-jet mode due to its capability of producing small droplets with a narrow size distribution. But here we describe the characteristics of another mode, the simple-jet mode.

Water was sprayed using a nozzle-ring setup and it was atomized using three different flow rates (240, 360 and 480 mL/h). In some experiments NaCl (99% Sigma Aldrich) was added to the water to change its electric conductivity. High speed imaging was used to measure droplet size and size distribution as well as to characterize the liquid break-up. For the conditions applied in these experiments the results have shown that the generated droplet size is strongly influenced by the applied potential. Furthermore, the droplet average diameter can be smaller than the nozzle diameter. Figure 1 shows the influence of the applied potential on the spray characteristics for a constant flow rate of 240 mL/h.

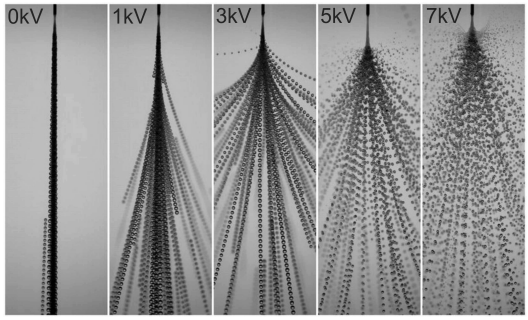

Figure 1: Simple-jet mode at different potentials and constant flow (240 mL/h). The potentials (written on the upper left corners) were applied on the ring while keeping the nozzle (0.41mm OD) grounded. Distance between the nozzle and the ring was kept constant at 2,5cm.

Just like in the cone jet mode, the jet break-up can happen in the varicose break-up and in the lateral kink break-up (whipping break-up) (Hartman, 2000). The ramified break-up was not seen within the experiments conditions. For a given configuration this transition depends on the applied potential difference. The transition between these two kinds of break-up can be explicitly seen in the current –potential difference diagram (Figure 2). Size and size distribution are influenced by these break-up mechanisms.

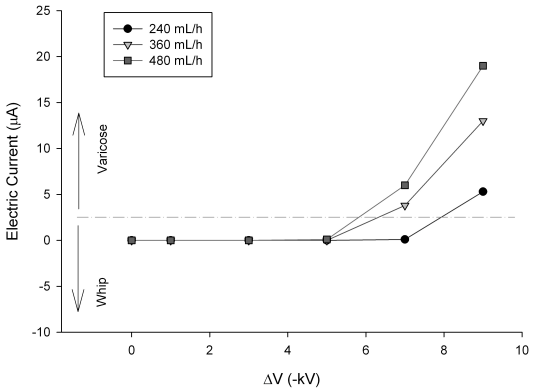

Figure 2: Applied potential against spray electric current for three different flows (240, 360 and 480 mL/h). The arrows and dotted line were arbitrary placed to show the varicose break-up and the whipping break-up regions.

This directly implies that current can be used to adjust the spray characteristics efficiently. The process energy balance also showed that EHD atomizers are more efficient than other atomization methods. Therefore, for applications which require high flows and droplets in the micrometer range, EHDA in the simple-jet mode is a promising technique.

1. Geerse, K.B., *Applications of Electrospray: from People to Plants*. 2003, Delft University of Technology: Delft.
2. Cloupeau, M. and B. Prunet-Foch, *Electrohydrodynamic spraying functioning modes: a critical review.* Journal of Aerosol Science, 1994. **25**(6): p. 1021-1036.
3. Hartman, R.P.A., et al., *JET BREAK-UP IN ELECTROHYDRODYNAMIC ATOMIZATION IN THE CONE-JET MODE.* Journal of Aerosol Science, 2000. **31**(1): p. 65-95.

Particle diagnostics and wave phenomena in complex plasmas

D. Samsonov[1], C. Durniak[1], P. Harvey[1], N. Oxtoby[1], J.F. Ralph[1], S. Zhdanov[2] and G. Morfill[2]
[1]Department of Electrical Engineering and Electronics, The University of Liverpool, Liverpool, L69 3GJ, United Kingdom
[2]Max-Planck-Institute for Extraterrestrial Physics, Garching, 85741, Germany
Keywords: Dust, Charged particles, Particle characterization, Laboratory experiments
Presenting author email: d.samsonov@liv.ac.uk

Complex (dusty) plasma is a mixture of micron-sized particles or grains with an ion-electron plasma. The grains (typically monodisperse plastic microspheres) collect ions and electrons and like floating Langmuir probes acquire large negative electric charges. They can be levitated and confined in a gas discharge. Due to collective interaction, the grains form crystal- or liquid-like structures. These structures can propagate linear (Samsonov 2005) and nonlinear waves, solitons (Harvey 2010), shocks (Samsonov 2003), and exhibit phase transitions. Since the characteristic time scale is determined by the large mass of the grains, the system is slow enough to observe with a video camera or with a naked eye.

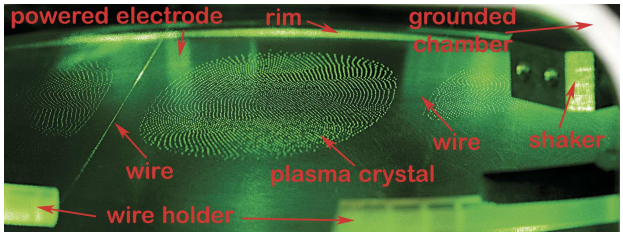

Figure 1: Monolayer complex plasma confined in an rf discharge.

The experiments were performed in a radio-frequency capacitively coupled gas discharge (Fig. 1). A monolayer of monodisperse microspheres was levitated and confined above a flat electrode 20 cm in diameter. The particles were illuminated with a sheet of laser light and imaged with a high speed (up to 2000 frames per second) video camera. The monolayer was excited with electrostatic pulses applied to wires stretched at or below the layer. We simulated complex plasmas using molecular dynamics code which solved the equations of motion for every grain by the 5th order Runge-Kutta method taking into account interaction of every grain with every other.

A range of interesting effects was observed. A vertical wave packet was excited. It propagated with a group velocity which was 100 times smaller than its phase velocity. Solitons and their interaction during a head-on collision were studied. It was found that a collision caused delay in propagation. Soliton steepening in an inhomogeneous lattice has been observed. The amplitude grew even in the presence of damping due to the gas drag. Shock waves were found to cause phase transitions.

Similar experiments were also conducted on board the International Space Station where three-dimensional complex plasma crystals and liquids were obtained. Crystals with different structures such a body centered cubic, face centered cubic, and hexagonal close packed were observed. Using a gas puff, shock waved were excited and propagated in a 3D complex plasma. The shock front remained remarkably smooth, with a microroughness of the order of the interparticle distance.

Video diagnostics is important for studying complex plasmas. Apart from 2D imaging, we performed 3D imaging with a laser tomography system (Samsonov 2008). A laser beam was expanded into a sheet with a raster optics and scanned using a pair of galvanometer driven mirrors. Each step was synchronized with the video camera. The system has been tested with the scanning speeds of up to 120 000 steps per second and up to 256 steps.

A range of software tools has been developed in order to identify particle positions and track their motion reliably. The tracking algorithms can include the physics of the process and can offer significant computational advantages over standard enumerative techniques. The developed algorithm is based on a state estimator which predicts the particle states (position, velocity and acceleration). The predicted positions are compared to the measured position and a weighted correction is applied using an Extended Kalman Filter. Here we use a simplified state estimator which takes into account only nearest-neighbor particle interactions. This reduces the computational time at the expense of the accuracy of the state estimation and particle tracks compared to a full N body simulation.

This work was supported by the Engineering and Physical Sciences Research Council (grants EP/E04526X/1 and EP/G007918).

D. Samsonov, S. Zhdanov, and G. Morfill, (2005), "Vertical wave packets observed in a crystallized hexagonal monolayer complex plasma", Phys. Rev. E **71**, 026410

P. Harvey, C. Durniak, D. Samsonov, and G. Morfill, (2010), "Soliton interaction in a complex plasma", Phys. Rev. E **81**, 057401

D. Samsonov, G. Morfill, H. Thomas, T. Hagl, H. Rothermel, V. Fortov, A. Lipaev, V. Molotkov, A. Nefedov, O. Petrov, A. Ivanov, and S. Krikalev, (2003), "Kinetic measurements of shock wave propagation in a three-dimensional complex (dusty) plasma", Phys. Rev. E **67**, 036404

D. Samsonov, A. Elsaesser, A. Edwards, H. M. Thomas, and G. E. Morfill, (2008), "High speed laser tomography system", Rev. Sci. Instrum. **79**, 035102

Contact charging of metal nanoparticles

S. Rennecke and A.P. Weber

Institute of Particle Technology, Clausthal University of Technology, Clausthal-Zellerfeld, 38678, Germany

Keywords: charge exchange, bouncing, inertial impaction.
Presenting author email: stephan.rennecke@tu-clausthal.de

When a spherical particle impacts on a rigid surface it may stick to it, or, if the impact velocity is sufficiently high, may rebound from the surface being resuspended in the surrounding gas. Furthermore a rebounding particle may gain an electric charge during contact, as a consequence of different work functions of particle and surface material. This process of dynamic contact charge transfer to the particle can be modelled by assuming the formation of a plate capacitor in the circular contact zone between the deformed sphere and the rigid surface, as shown by John et. al. (1980). Therefore, the functional dependence of the contact charge on the impact velocity gives a direct insight into the mode of deformation and the material properties of the particle, if the contact potential is known. In the present work the dynamic contact charging of metal nanoparticles is investigated in order to develop appropriate contact models describing the rebound and charging behaviour of nanoparticles.

For this purpose the contact charge q_c as a function of impact velocity has been determined experimentally using a single stage low pressure impactor. Spherical, size selected and singly charged metal particles in the size range from 20 nm to 100 nm were impacted on a smooth surface at process conditions far above the critical Stokes number for deposition. The onset of particle rebound and the mean charge of the particles after collision have been measured using an electrometer. The actual impact velocity of the nanoparticles has been determined numerically using the Statistical-Lagrangian-Particle-Tracking (SLPT) method (Yook et al., 2007). The setup allows defined collision experiments for impact velocities up to approximately 200 m/s.

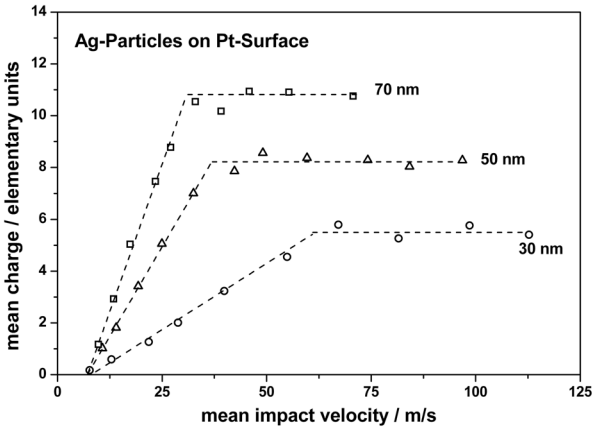

Figure 1. Mean particle charge as a function of impact velocity for silver particles of different size

The mean contact charge as a function of impact velocity for silver particles of different size is given in figure 1. When the threshold velocity for particle rebound is reached, q_c increases linearly with the impact velocity approaching constant values, that increase with particle size. The slope in the linear part is proportional to the square of the particle size. This behaviour is identical with the observation of Wang and John (1988) for the dynamic contact charging of conducting micrometer particles assuming complete plastic deformation, indicating that macroscopic deformation models are also valid on the nano scale.

The constant values reached at higher impact velocities have so far not been observed for micrometer particles. This may be explained with the much smaller capacity of a nano sized sphere, limiting the maximum transferred charge at a given contact potential. Therefore the actual contact potential can be calculated precisely for each measurement, being 0,46V, independent of the particle size, for the Ag-Pt interface, in the presented dataset.

The simultaneous characterization of the electrical properties of the interface allows a quantitative comparison of experiment and theory for the first time. Furthermore, as the contact potential is known, the maximum contact area of the deformed particle can be calculated. This allows an adaption of contact models, considering the unique properties of nanoparticles, such as the great importance of surface forces.

In this contribution the experimental data for the threshold velocity for rebound and the dynamic contact charge for different metal nanoparticles will be presented. Appropriate contact models for the quantitative description of the contact charge will be discussed.

This work was supported by the Deutsche Forschungsgemeinschaft (DFG) under grant DFG-WE 2331/12-1.

John, W., Reischl, G. and Devor, W. (1980) J. *Aerosol. Sci.* **11**, 115-138.

Wang, H.C. and John, W. (1988) J. *Aerosol. Sci.* **19**, 399-411.

Yook, S.J., Fissan, H., Asbach, C., Kim, J.H., Wang, J., Yan, P.Y. and Pui, D.Y.H. (2007) J. *Aerosol. Sci.* **38**, 211-227.

Comparison of methods to achieve a stationary charge distribution

Lena Knobel[1], Hans-Joachim Schmid[1]

[1]Department of Mechanical and Environmental Process Engineering (MVU)
University of Paderborn, 33100, Paderborn, Germany

Keywords: charged particles, SMPS, aerosol measurement, stationary charge distribution

The common method to achieve a stationary charging distribution in an aerosol for nanoparticle classification using a differential mobility analyzer is a radioactive source. In recent years there has been an increasing attention to alternative solutions.

In this research the influence, which the methods have on the charge distribution, are investigated. Three bipolar charging methods are considered:

- Radioactive Source, ^{85}Kr (TSI)
- Soft X-ray photonionizer (PMT Partikel)
- Surface-discharge Microplasma Aerosol Charger (Tsukasa Sokken)

An experimental investigation showed that these chargers, as a part of a SMPS system, result in different particle size distributions for a given polydisperse testaerosol (see figure 1).

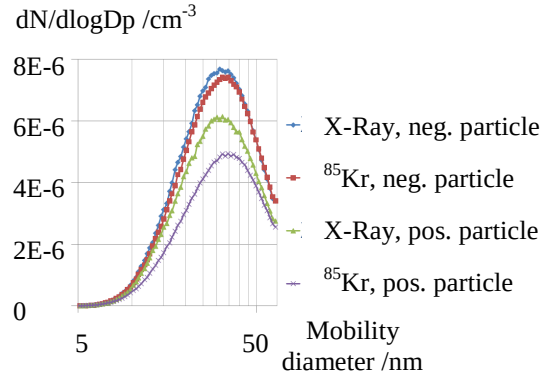

Figure 1. Mobility distribution by the different kind of chargers measured by a SMPS System

The charge probability of the particles depends on the ion mass and ion mobility. Positive and negative ions have different mobilities and masses due to different propensities to form water clusters. (Hoppel, 1990) As a result, a balanced bipolar ion environment leads to an asymmetrical charge distribution of the particles.

The common method to calculate the charge distribution, needed in order to determine the particle size distribution, is the Wiedensohler Approximation (Wiedensohler, 1987). This approximation is based on the Fuchs theory (1963). The ion mobilities, which represent fixed input parameters in this calculation, are determined experimentally using an Americium charger by fitting the results of the SMPS measurement to the Fuchs theory. The ion masses are additional fixed input parameters calculated by Wiedensohler. Lee *et al.* (2004) showed different ion concentration and mobilities produced by a radioactive source (^{241}Am) and a soft X-ray photonionizer. In this work the ion concentrations and mobilities, produced by the three chargers mentioned above, will be investigated.

Also the resulting particle charge distribution will be determined via a Tandem DMA setup. Figure 2 shows the part of the singly charged particles produced by the different chargers in comparison to the Wiedensohler Approximation.

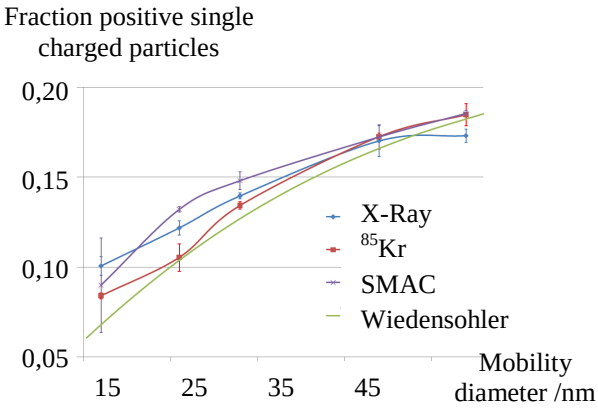

Figure 2. Fraction of positive single charged particles produced by the different chargers

Another effect on the charge distribution occurs downstream the chargers (Lee, 2004), (Hoppel, 1990). Ions leave the chargers together with the particles. Diffusion occurs as a function of the ion mobility, which is different for positive and negative ions. Therefore, the charging process is continuing with an imbalanced ion concentration for negative and positive ions downstream the chargers. Thus, the charge distribution reaching the DMA is not stationary anymore.

This effect is investigated experimentally and theoretically. The model considers the following ionic effects: recombination, diffusion and electrostatic dispersion.

Fuchs, N.A. (1963). *Pure and Applied Geophysics*, 56, 185-193

Hoppel, W.A. & Frick, G.M. (1990). *Aerosol Science and Technology*, 3, 47-496

Lee, H.M., Kim, C.S., Shimada, M., & Okuyama, K. (2004). *J. Aerosol Science*, 36, 813-129.

Wiedensohler, A. (1987). J. Aerosol Science, 19, 387-389

A simplified procedure for particle charge distribution measurements and its application to the characterization of the annual DBD aerosol neutralizer

Wild, Markus[1], Meyer, Jörg[1] and Kasper, Gerhard[1]

[1]Karlsruhe Institute for Technology KIT, IMVM, Strasse am Forum 8, 76139 Karlsruhe, Germany

Keywords: Measurement (characterization), Dielectric Barrier Discharge; charged particles; TDMA.
Presenting author email: markus.wild@kit.edu

The annular dielectric barrier discharge aerosol neutralizer is a device designed to impose a Boltzmann charge distribution to airborne particles by electrostatic means. The device's performance in neutralizing aerosols is compared to a radioactive ^{85}Kr source. Amongst others, the particle charge distributions of sodium chloride particles ranging between 27-200 nm are investigated. The method of choice is a Tandem-DMA setup. The basic task is to determine the number concentration of differently charged particle fractions. Usually a rather complex curve fitting method is applied to evaluate the obtained data, see e.g. Stolzenburg and McMurry (1998). The evaluation process can be vastly simplified if some restrictions concerning the conduct of the experimental procedure are observed.

Therefore, a method to determine the aerosol concentration within a well defined interval of electrical mobilities – such as distinct peaks in a mobility spectrum illustrated in Figure 1– directly from a continuous DMA scan is described.

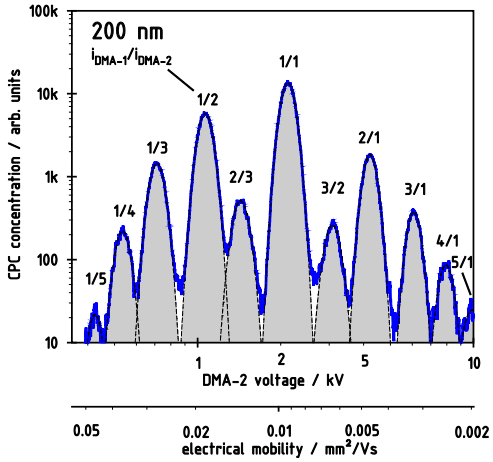

Figure 1. mobility spectrum of a pre-classified (200nm) and neutralized sodium chloride aerosol measured by a CPC after DMA-2 in a TDMA setup. i indicates the state of charge in DMA-1 and DMA-2, respectively.

The method is based essentially on moving the transfer function across the spectrum at such a rate that the time window during which particles of an arbitrary mobility can pass through the DMA remains constant during the scan. This implies a specific ramp function for the scan voltage, which we derive, thereby establishing a direct and simple link between the cumulative number of particles exiting the DMA while scanning across a peak, and the concentration enclosed within that mobility window at the inlet (see Figure 2). The method is an implicit part of the theoretical framework described by Wang and Flagan (1990). However, by relaxing the goal of deriving a complete size distribution in favour of the lesser requirement of measuring only the total concentration within certain, well defined bounds of mobility, one gains accuracy, sensitivity, and last not least convenience because there is no need for extensive post-processing of the data. The method is particularly suitable for measuring aerosol charging probabilities with distinct peaks in the mobility spectrum.

While the charged fractions of laboratory generated aerosols in the range of 27 to 200 nm are investigated with a TDMA set-up and the mentioned data evaluation procedure, the neutral fraction is measured by a separate measurement.

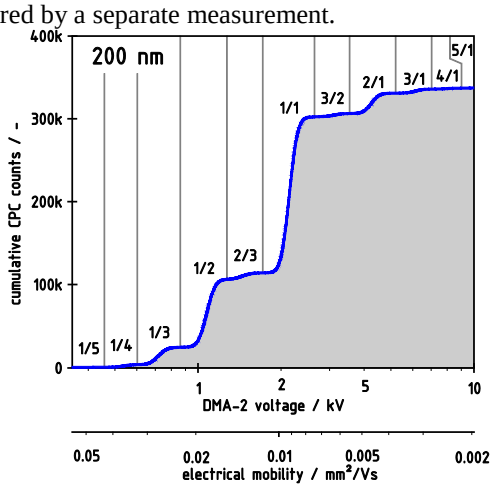

Figure 2. cumulative particle counts of the aerosol introduced in Fig. 1 when performing an up-scan using a logarithmic voltage ramp

The method was used to determine the performance of the annual Dielectric Barrier Discharge (aDBD) aerosol neutralizer in comparison to a common ^{85}Kr β-source. The obtained charge distributions resembled each other very well. The aDBD proofed to provide a promising alternative to the use of radioactive material and its well-known disadvantages in aerosol measurement technology.

This work was supported by the German Science Foundation (DFG).

Stolzenburg, M.R. and McMurry, P.H. (1998). *TDMAFIT user's manual*. PTL publications **No. 653**

Wang, S.C. and Flagan, R.C. (1990). *Scanning Electrical Mobility Spectrometer*. Aerosol Science and Technology **13** (2): 230-240.

Thursday, September 8, 2011

Session 10A: Aerosols in Geoengineering / Aerosols in Global Climate Models

A New Hybrid Solver of Dissolution of Inorganics into the Particle Liquid Phase: Evaluation and Global Scale Implications on Aerosol Properties.

F. Benduhn[1,2], and K.S. Carslaw[1]

[1]Institute for Climate and Atmospheric Science, School of Earth and Environment, The University of Leeds, Leeds, LS2 9JT, United Kingdom.
[2]Now at: Department of Atmospheric Chemistry, Max-Planck-Institute for Chemistry, Mainz, Germany.
Keywords: Atmospheric aerosol, Aerosol modeling, Inorganics, Aerosol dynamics.
Presenting author email: francois.benduhn@mpic.de

A new hybrid solver of dissolution of inorganics into the aerosol liquid phase has been developed. With respect to former solutions (Capaldo et al., 2000) the solver follows a novel approach as decision is being made onto which parts of the aerosol size spectrum are assumed to be in equilibrium and which parts are assumed to be in transition. Decision criteria include mass fractionation as well as prospective equilibration time considerations. In addition special care was taken to keep computation time as low as possible. As stiff dissolution considerably minimizes the integration time step of the transient solver, an additional decision criterion considering the mathematical stiffness was introduced. Under stiff conditions equilibrium is assumed and the composition is later corrected according to equilibration time considerations. The novel equilibrium solver follows both an analytical and a differential approach, depending on whether equilibration is chemically or mass fractionally driven, respectively. Transient dissolution is based on the method detailed in Jacobson (1998).

The solver has been implemented into the modal version of the aerosol global transport model with combined chemistry GLOMAP/TOMCAT (Spracklen et al., 2005). Under its current version the solver allows for the concurrent dissolution of HNO_3, HCl and NH_3. Dissolved matter is allowed to interact with sulphuric acid and sea salt, which is assumed to be composed of sodium chloride and sodium sulphate. Liquid phase equivalent ions encompass NO_3^-, Cl^-, SO_4^{2-}, HSO_4^-, NH_4^+, Na^+ and H^+. Chemical ion interaction, as given by the particle liquid water content, sulphuric acid dissociation and the surface partial pressure of the dissolvable species, is assessed according to the method detailed in Topping et al. (2009). Dissolution may be set to occur into the four soluble modes (nucleation, Aitken, accumulation, and coarse). The solver may be run in the full equilibrium, the hybrid and the pseudo-equilibrium regime mode. The latter one stands for equilibration with ulterior composition adaptation according to evaluated equilibration time (see above). In the box model version the solver may also be run in full transition, serving as benchmark for evaluation.

Box model tests show that the hybrid solver catches the transient behavior of dissolution for both acidic and sea salt particles very closely for situations of low to moderate stiffness, of up to say 1-10 ppm atmospheric concentration of dissolvable species depending on the aerosol load. Highly stiff conditions require the use of pseudo-equilibration. Under this circumstance the solver still catches aerosol composition quite well, especially if compared to the full equilibrium configuration.

Global runs were performed in the hybrid, the full equilibrium, as well as the pseudo-equilibrium mode, and compared to runs without dissolution. Sensitivity tests with respect to the sticking efficiency were also done. At this moment global runs were performed for HNO_3 and NH_3 dissolution only. The solver proved to associate accuracy with computational efficiency with dissolution using approximately 10% of total computation time. Results show the relevance of the transient behaviour of dissolution for aerosol composition and its interaction with aerosol microphysical properties via particle size. When set to full equilibrium, the coarse mode tends to take up the bulk of the dissolvable matter due to the size discrepancy with the competing nucleation, Aitken and accumulation modes. In the hybrid mode, the coarse mode is mostly set into the transient regime, leaving much more matter available for the smaller modes whose surface to volume ratio is higher. Depending on atmospheric composition the smaller modes are thus allowed to reach the stiff regime, under which circumstance sulphuric acid, nitric acid and ammonia interact efficiently to lead to the formation of liquid phase ammonium sulphate and ammonium nitrate thus entailing considerable increase in particle size and consequent modifications of the cloud condensation number. The influence of the sticking efficiency is shown to be secondary to negligible only as modes in the transient regime are usually not in the molecular regime due to their size.

Capaldo, K.P., Pilinis, C., and Pandis, S.N., Atmospheric Environment, No. 34, pp. 3617-3627, 2000.

Jacobson, M.Z., Fundamentals of Atmospheric Modeling, Cambridge University Press, 1998.

Spracklen, D.V., et al., Atmospheric Chemistry and Physics, No. 5, pp. 2227-2252, 2005.

Topping, D., Lowe, D., and McFiggans, G., Journal of Geophysical Research, Vol. 114, doi:10.1029/2008JD010099, 2009.

More precipitation from melting ice particles in deep convective clouds in a warm and moist environment

Z. Cui[1], K.S. Carslaw[1] and A.M. Blyth[1, 2]

[1]Institute for Climate and Atmospheric Science, School of Earth and Environment, University of Leeds, UK

[2]National Centre for Atmospheric Science, UK

Keywords: precipitation, cloud microphysics, aerosol concentration, climate change.
Presenting author email: z.cui@leeds.ac.uk

Convective processes involve strong vertical motions locally and may cause heavy precipitation and damages. Recent studies have found that global warming causes more flooding, but the precipitation extremes exceed the expectations from temperature changes in observations and IPCC climate models. Here we investigate convective cloud precipitation in response to warming environments using a cloud model with detailed microphysics and aerosol treatments (Yin et al., 2005; Cui et al., 2006). Our simulations show that precipitation increases more than 22% with per 1K warming and accordingly increased moisture (Fig. 1). Our results demonstrate that liquid cloud drops grow to larger sizes during the warm-rain process, and more large drops freeze and become graupel particles, which, when falling below 0°C level, melt and produce more precipitation. In a warming atmosphere without increasing moisture content, convective clouds only develop to mid-troposphere with little precipitation. We also show that precipitation increases with warming temperatures for different aerosol loadings, with more precipitation in a clean environment. We anticipate more studies on the precipitation response to global warming in organized convective systems in the future. Furthermore, it is suggested that climate models should have detailed treatment of mixed-phase microphysics.

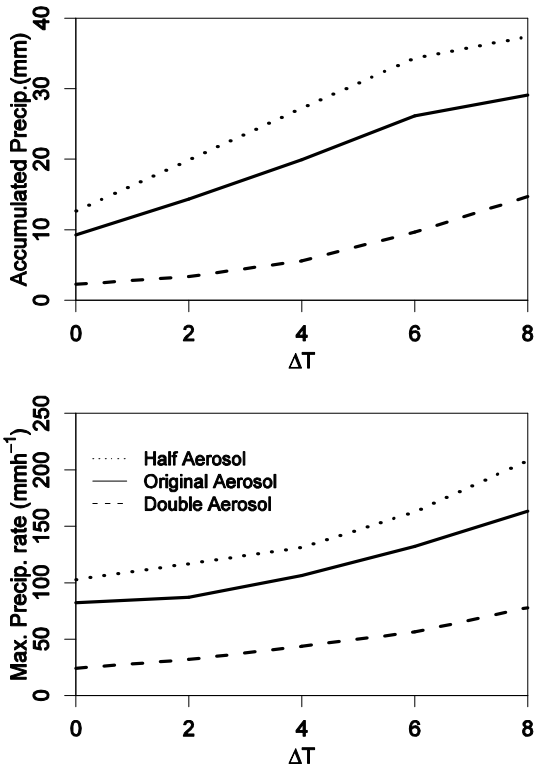

Figure 1. Variation with temperature changes of accumulated precipitation at cloud centre (a) and maximum precipitation rate (b) with warming environment

Cui, Z., Carslaw, K.S., Yin, Y. and Davies, S. (2006) *J. Geophys. Res.* **111(D5),** doi:10.1029/2005JD005981.

Yin, Y., Carslaw, K.S., and Feingold, G. (2005) *Q. J. Roy. Meteorol. Soc*. **131**, 221-245.

Weak response of CCN to changes in DMS flux: implications for the CLAW feedback in current climate assessments

M. T. Woodhouse[1], G. W. Mann[2], K. S. Carslaw[1] and O. Boucher[3]

[1]Institute for Climate and Atmospheric Science, School of Earth and Environment, University of Leeds, Leeds, LS2 9JT, UK
[2]National Centre for Atmospheric Science, School of Earth and Environment, University of Leeds, Leeds, LS2 9JT, UK
[3]Met Office Hadley Centre, Fitzroy Road, Exeter, Devon, EX1 3PB, UK
Keywords: dimethyl-sulphide, CCN, climate effect, CLAW
Presenting author email: m.woodhouse@see.leeds.ac.uk

The CLAW hypothesis (Charlson et al., 1987) relates the production of dimethyl-sulphide (DMS) in the surface ocean by phytoplankton to the optical properties of clouds via the first and second aerosol indirect effects, thereby proposing a climate feedback. The CLAW feedback has been the subject of much investigation over the last two decades, but only recently have aerosol models with detailed aerosol microphysics become available.

Presented here are simulations in the UK Met Office HadGAM atmospheric general circulation model where the flux of DMS to the atmosphere from the oceans is perturbed. The impact of these DMS flux perturbations on aerosol when simulated by two different aerosol schemes is investigated. One aerosol scheme carries only mass in several aerosol types, each with a prescribed size distribution, and is typical of most aerosol schemes used in recent global climate assessments (e.g. IPCC AR4). The second aerosol scheme (UKCA-mode, Mann et al., 2010) uses a two-moment approach transporting number and mass in several size modes, allowing particle number to be conserved and growth to be simulated.

The response of CCN to changes in the flux of DMS is quantified as $\Delta CCN/\Delta Flux_{DMS}$, and termed CCN sensitivity.

The more detailed two-moment aerosol scheme predicts a very weak CCN response to changes in DMS flux, or a very low CCN sensitivity (Figure 1). This suggests that the CLAW feedback is either very weak, or negligible. The simpler mass-only aerosol scheme predicts a larger response of CCN to DMS changes. The greater response in the mass-only aerosol scheme is believed to be incorrect, due to the very limited representation of aerosol microphysics within the scheme. These results have significance for the representation and quantification of the CLAW feedback in current climate assessments, suggesting that the strength of the feedback may be over-estimated by simple aerosol schemes.

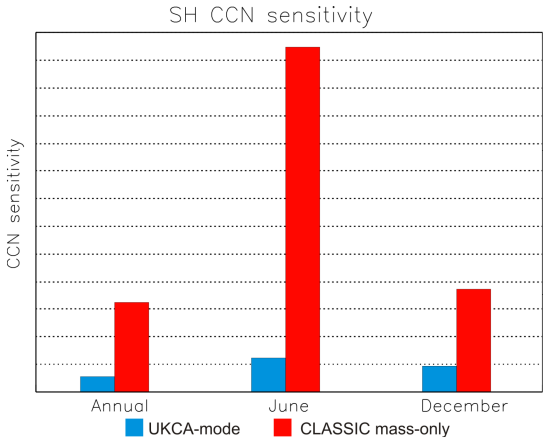

Figure 1 Comparison of CCN sensitivities calculated from DMS flux perturbations in the microphysical aerosol model UKCA-mode and the mass-only aerosol model CLASSIC.

Charlson, R. J., Lovelock, J. E., Andreae, M. O. and Warren, S.G. 1987. Oceanic phytoplankton, atmospheric sulphur, cloud albedo and climate. *Nature* **326**: 655-651.

Mann, G. W., Carslaw, K. S., Spracklen, D. V., Ridley, D. A., Manktelow, P. T., Chipperfield, M. P., Pickering, S. J. And Johnson, C. E., 2010. Description and evaluation of GLOMAP-mode: a modal global aerosol microphysics model for the UKCA composition-climate model. *Geoscientific Model Development* **3**: 516-551.

Estimating the radiative impacts of biogenic secondary organic aerosol, their variation with location and climate, and the implications for climate geoengineering

C. E. Scott, P. M. Forster, K. S. Carslaw, D. V. Spracklen and S. R. Arnold

Institute for Climate and Atmospheric Science, School of Earth and Environment, University of Leeds, Leeds, LS2 9JT, UK

Keywords: forest, biogenic particles, climate change

Presenting author email: pm08c2s@leeds.ac.uk

The possibility that cuts in greenhouse gas emissions do not occur on a timescale that prevents a dangerous level of temperature increase has prompted research into alternative means by which the Earth's radiative imbalance may be redressed. Such mechanisms, involving the deliberate modification of parts of the Earth system, may broadly be classified as climate 'geoengineering' schemes. The aim of this work is to evaluate the potential for reduced deforestation and increased afforestation, as such a geoengineering scheme, to offset a portion of the anticipated future climate change.

In addition to the implications for the carbon cycle, a number of biogeophysical and biogeochemical side-effects also determine the overall climatic impact of a forest; changes to surface albedo, evapotranspiration, sensible heat transfer, wind patterns, chemical emissions, cloud cover and precipitation will all contribute. Previous modelling studies, examining the biogeophysical side-effects, have concluded that the net climatic impact of a forest is latitude dependent. At high latitudes where the presence of trees obscures highly reflective snow, the net climate effect is warming. In tropical regions, the presence of forests generates an additional negative radiative forcing due to increased evapotranspiration efficiency and surface roughness that is sufficient to negate the effect of decreased albedo.

However, these studies did not consider the impact of forests on local atmospheric chemistry. Vegetation emits a number of biogenic volatile organic compounds (BVOCs) e.g. isoprene, monoterpenes and sesquiterpenes, which may undergo photochemical oxidation by the hydroxyl radical (OH), ozone (O_3) or the nitrate radical (NO_3). The resulting oxidation products may then participate in organic aerosol production, either through the nucleation of new particles, or by condensation onto existing particles, facilitating their growth. Whilst experimental constraints limit practical measurement of the composition of the smallest particles, inclusion of a "nucleating organic" term in the particle formation rate equation has been shown to give better model agreement with formation rates derived from smog chamber experiments (Metzger *et al*., 2010).

The resulting secondary organic aerosol (SOA) may either affect the climate *directly* through the reflection of incoming shortwave radiation, or *indirectly*, via their action as cloud condensation nuclei (CCN). Local CCN concentrations influence the microphysical and radiative properties of clouds, via their effect on cloud drop number concentrations (CDNC). Whilst CDNC over polluted regions tends to be updraft limited, aerosol concentrations have been shown to provide the limiting factor in pristine regions (Poschl *et al*., 2010). Using an aerosol microphysics model (GLOMAP), Spracklen *et al.* observed a simulated doubling of regional CCN concentration when comparing the presence of boreal forests to Arctic tundra, resulting in a radiative forcing of between -1.8 and -6.7 $W.m^{-2}$ of forest (Spracklen *et al*., 2008).

Here, we extend this work by using a pseudo-coupled framework of models to simulate the change in aerosol and cloud properties under idealised deforestation and afforestation scenarios. The Community Land Model (CLM) is used to prescribe the changes to forest cover, whilst the Community Atmosphere Model (CAM) and GLOMAP (mode) are used to simulate the atmospheric chemistry and aerosol processes resulting from the altered BVOC emission. Climatic variables, such as atmospheric carbon dioxide concentration, temperature and solar radiation, are changed sequentially in order to determine the sensitivity of this system to potential future climate changes. Radiative forcings are then calculated using an offline radiative transfer code.

This work was funded by a Natural Environment Research Council (NERC) Doctoral Training Grant.

Metzger. A. *et al*., (2010) *Evidence for the role of organics in aerosol particle formation under atmospheric conditions,* PNAS, **107** (15), 6646-6651.

Poschl. U. *et al*., (2010) *Rainforest Aerosols as Biogenic Nuclei of Clouds and Precipitation in the Amazon,* Science, **329** (5998), 1513-1516.

Spracklen. D. *et al*., (2008) *Boreal forests, aerosols and the impacts on clouds and climate.* Phil. Trans. Roy. Soc. A, **366**, 4613-4626.

Modelling the volcanic eruption of Sarychev

James M. Haywood [1,2], Andy Jones[2], Lieven Clarisse[3], Adam Bourassa[4], John Barnes[5], Paul Telford[6], Nicolas Bellouin[2], Olivier Boucher[2], Paul Agnew[7], Cathy Clerbaux[8], Pierre Coheur[3], Doug Degenstein[4] and Peter Braesicke[6]

[1]Climate, Chemistry and Ecosystems, Met Office Hadley Centre, Exeter, UK.
[2]College of Engineering, Mathematics, and Physical Sciences, University of Exeter, Exeter, UK.
[3]Spectroscopie de l'Atmosphère, Service de Chimie Quantique et Photophysique, ULB, Brussels, Belgium.
[4]ISAS, University of Saskatchewan, Saskatoon, Saskatchewan, Canada.
[5]Mauna Loa Observatory, NOAA, Hilo, Hawaii, USA.
[6]NCAS Climate, Centre for Atmospheric Science, University of Cambridge, Cambridge, UK.
[7]Forecasting Research and Development, Met Office, Exeter, UK.
[8]UPMC Université Paris 06, Université Versailles St. Quentin, CNRS/INSU, LATMOS-IPSL, Paris, France.

In June 2009 the Sarychev volcano located in the Kuril Islands to the northeast of Japan erupted explosively, injecting ash and an estimated 1.2 ± 0.2 Tg of sulphur dioxide into the upper troposphere and lower stratosphere, making it arguably one of the 10 largest stratospheric injections in the last 50 years. During the period immediately after the eruption, we show that the sulphur dioxide (SO_2) cloud was clearly detected by retrievals developed for the Infrared Atmospheric Sounding Interferometer (IASI) satellite instrument and accurately modelled by simulations using a nudged version of HadGEM2 (Figure 1).

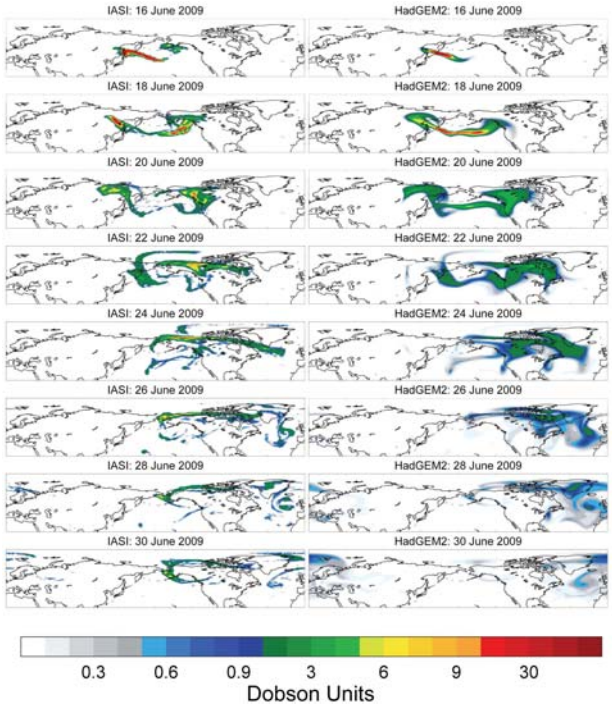

Figure 1. The evolution of plumes for (left) IASI and (right) HadGEM2 for the period 16–30 June 2009.

The resultant stratospheric sulfate aerosol was detected by the Optical Spectrograph and Infrared Imaging System (OSIRIS) limb sounder and CALIPSO lidar. Additional surface-based instrumentation allows assessment of the impact of the eruption on the stratospheric aerosol optical depth. The model simulations and OSIRIS measurements (Figure 2) suggest that in the Northern Hemisphere the stratospheric aerosol optical depth was enhanced by around a factor of 3 (0.01 at 550 nm), with resultant impacts upon the radiation budget.

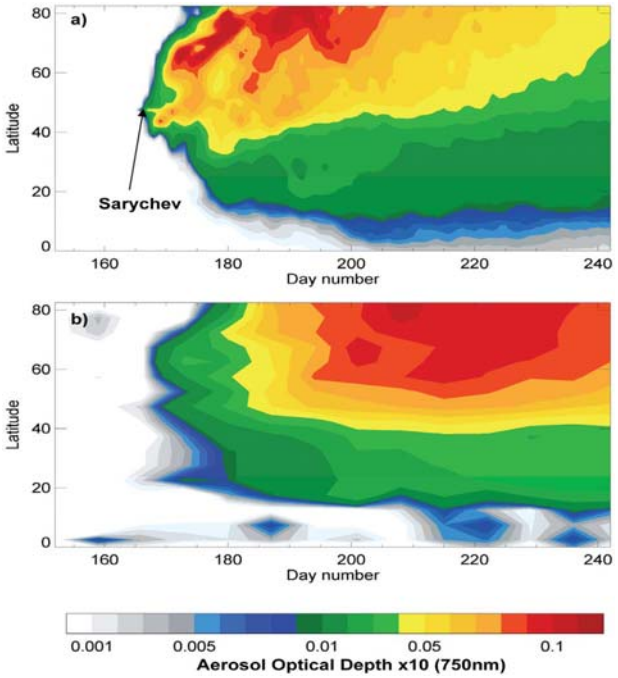

Figure 2. Time versus latitude plots of the aerosol optical depth at 750 nm from (a) HadGEM2 and (b) OSIRIS.

The simulations indicate that, in the Northern Hemisphere for July 2009, the magnitude of the mean radiative impact from the volcanic aerosols is more than 60% of the direct radiative forcing of all anthropogenic aerosols put together. Modelling the eruption of Sarychev also serves to increase confidence in the model representation of transport and the sulphur cycle which has potential consequences for solar radiation management geoengineering proposals.

Haywood, J. M., et al. (2010), Observations of the eruption of the Sarychev volcano and simulations using the HadGEM2 climate model, *J. Geophys. Res.*, 115, D21212, doi:10.1029/2010JD014447.

Thursday, September 8, 2011

Session 10B: Remote Sensing of Aerosol Properties

The FAAM volcanic ash flights in May 2010: results from the lidar, the CAS, and ARIES

F. Marenco[1], B. Johnson[1], K. Turnbull[1], J. Haywood[1], S. Newman[1], A. Vance[1], J. Dorsey[2], M. Gallagher[2], and Hugo Ricketts[2]
[1]Observational Based Research, Met Office, Exeter EX1 2NF, United Kingdom
[2]University of Manchester, Manchester, United Kingdom
Keywords: volcanic particles, remote sensing, optical properties.
Presenting author franco.marenco@metoffice.gov.uk

The Facility for Airborne Atmospheric Measurements (FAAM, http://www.faam.ac.uk/) performed a series of flights during the eruption of the Eyjafjallajökull in spring 2010 with its BAE146 research aircraft.

Volcanic ash layers were observed using an on-board elastic backscatter lidar operating at 355 nm, which allowed detailed mapping of the plumes. Using the method by Digirolamo *et al* (1994), the lidar ratio (extinction-to-backscatter ratio) has been determined for a number of selected vertical profiles where signal from Rayleigh scattering could be well identified from regions both above and below the ash layer. The lidar ratio was found to be equal to 60 ± 13 sr (average and standard deviation for all the selcted profiles during the May 2010 flights). As not all lidar profiles could be analysed in this way, the mean lidar ratio has then been applied to the whole dataset, using the method by Fernald (1984) and Klett (1985) to infer the aerosol extinction coefficient and aerosol optical depth (AOD).

A flight on 4 May overpassed the ground-based lidar in Aberystwyth a few times. This provided ground truth validation of the on-board lidar and of its data inversion procedure. The ash layer during this flight was found to be in patches of short horizontal extent, and moreover patches of enhanced backscatter from non-ash aerosol were also identified, and found in proximity to the ash patches. Ash and non-ash were distinguished based on their depolarisation signatures. Despite this strong horizontal inhomogeneity, the two lidars showed excellent qualitative and quantitative agreement.

Size-distributions were obtained *in situ* using a Cloud and Aerosol Spectrometer with Depolarisation (CAS-DPOL). Mie scattering computations using the observed size-distributions (corrected for refractive index) aided the determination of two important parameters for the interpretation of the lidar data: the fraction f_c of extinction in the coarse fraction, and the specific extinction $K_{\rm ext}$ of the coarse mode, identified with volcanic ash. The coarse mode extinction fraction ranged between 43% and 98%, whereas the specific extinction of the coarse particles ranged 0.3–0.7 m^2/g. These estimates were based on a refractive index of $1.52 - i0.00155$, and a particle density of 2.3 g cm^{-3}. These parameters enabled the mass concentration of volcanic ash to be estimated from the aerosol extinction coefficient derived by lidar.

Atmospheric radiance measurements above ash have also been made using the infra-red spectrometer ARIES (Airborne Research Interferometer Evaluation System). Radiative transfer computations using the lidar-derived profiles of aerosol extinction led to a very good reconstruction of the observed radiance spectra. Moreover, the spectral slope of the brightness temperatures in the 8 μm region was well correlated with the lidar AOD. The implications of this finding for the quantification of volcanic ash from satellite sensors in the infrared region will be discussed.

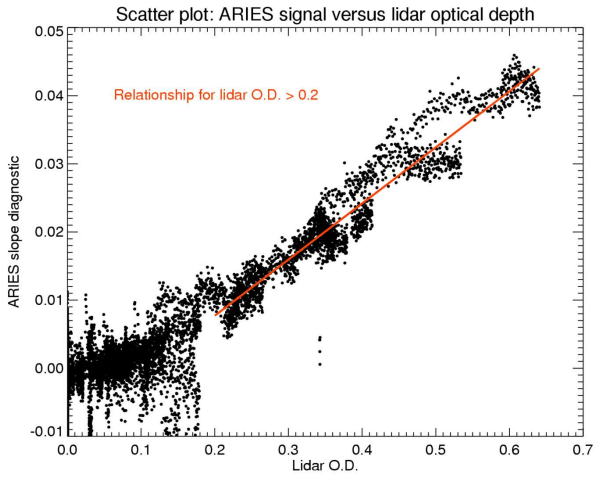

Figure 1: Correlation plot between the infrared brightness temperature slope in K/cm^{-1}, determined with spectrometer ARIES, and the AOD, determined by lidar on 17 May 2011.

Di Girolamo, P., M. Cacciani, A. D. Sarra, G. Fiocco, and D. Fuà (1994) Geophys. Res. Lett. **21**, 1295–1298.
Fernald, F. G. (1984) Appl. Opt. **23**, 652–653.
Klett, J. D. (1985) Appl. Opt. **24**, 1638–1643.

Volcanic ash optical properties with an UV-depolarization Lidar

A. Miffre, G. David, B. Thomas and P. Rairoux[1]

[1]Laboratoire de Spectrométrie Ionique et Moléculaire, CNRS UMR 5579, Université Lyon 1, Villeurbanne, 69622, France

Keywords: remote sensing, depolarization, ash, light scattering matrix.

Presenting author email: miffre@lasim.univ-lyon1.fr

In this contribution, a ground-based UV-polarization Lidar is used to study the optical properties of tropospheric volcanic ash particles. Measurements have been performed during the mid-April 2010 eruption of the Eyjafjallajökull volcano (63.63°N, 19.62°W, Iceland) at Lyon (45.76°N, 4.83°E, France) at the border of the air closure traffic area. The volcanic origin of the observed air masses has been confirmed by 7-days air mass back-trajectories and FLEXPART ash particles numerical dispersion model. The measured UV-particle backscattering coefficient β_p is typically equal to 4.0 $Mm^{-1}.sr^{-1}$ and UV-depolarization ratios δ_p lie in the range from a few to 44 %. After long-range transport, the β_p and δ_p-variations are interpreted as variations in ash-mass concentrations. Moreover, a partition between spherical and non spherical particles is retrieved from both scattering and depolarization measurements.

Volcanic particles release gas and ash particles that can be transported over several thousands of kilometres and may remain in the troposphere for several weeks (Ovadnevaite *et al*, 2009). The physical properties of volcanic ash particles, such as size and shape, may change during advection. In this contribution, a UV-remote sensing experiment is performed to study the volcanic particles shape by measuring the ability of volcanic particles to depolarize UV-laser light. Scattering occurs from both fine and coarse mode particles, enhanced by our UV-light choice. Very sensitive (from a few to 44 %) and accurate (better than 30% at 4-km altitude) δ_p-measurements have been achieved by a new home-built depolarization Lidar detector, using two polarizing beam-splitter cubes to ensure a fully negligible cross-talk between parallel and perpendicular Lidar detector channels.

Vertical profiles of the parallel backscattering coefficient $\beta_{p,//}$ and depolarization ratio δ_p are displayed on figure 1, together with the relative humidity profile. A double-layering structure is observed, showing that, after long-range transport, the volcanic ash cloud is not homogenously spread in space as confirmed by 7-days back-trajectories and FLEXPART dispersion model. Despite long-range transport, the volcanic particles are still non spherical. Moreover, within our error bars, we attribute the highest observed δ_p-value of 44 % to volcanic ash particles, as it agrees with laboratory scattering matrix measurements performed on randomly oriented ash particles (Munoz *et al*., 2004). At lower altitudes, as RH increases, spherical sulphates particles growth lowers the observed depolarization ratios. Using δ_p(ash) = 44 %, we deduce the ash particles β_p-vertical profile from our depolarization measurements.
Using O. Munoz's volcanic ash particles optical parameters (2004) and applying optical scattering computations, ash particles concentration has been evaluated from β_p. Figure 1 displays the retrieved ash-mass concentration.

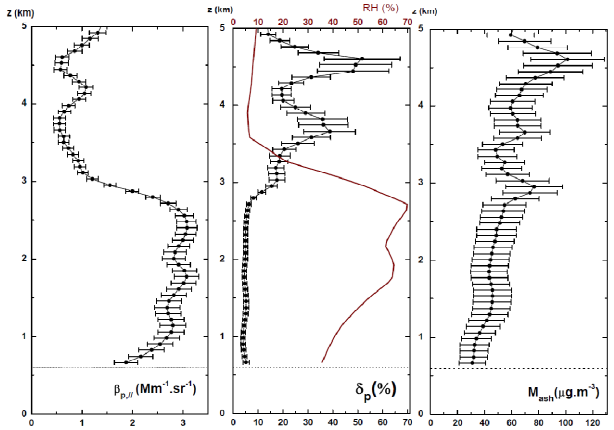

Fig. 1 UV-particle backscattering $\beta_{p,//}$, depolarization δ_p, relative humidity RH and retrieved ash-mass concentration vertical profiles on April 19th at 19 h UTC. The vertical resolution is 75 m.

Retrieved ash-mass concentrations are well below the limit value of 2 000 $\mu g.m^{-3}$ chosen for airport closures and compare well with numerical dispersion model. Hence, our methodology, which combines very sensitive and accurate scattering and depolarization measurements with a numerical dispersion model helps to retrieve the optical properties of volcanic ash particles. The presentation will point out this approach, and details the further retrieved partition between spherical (sulphates) particles and non spherical (ash) particles, obtained from optical simulation of spherical sulfates particles. This work is submitted to Atmospheric Environment's special issue on the Icelandic volcano.

We thank A. Stohl's group for providing FLEXPART numerical dispersion model. This work was supported by Région Rhône-Alpes and CNRS.

Munoz, O., et al, (2004), *Scattering matrix of volcanic ash particles of Mt St Helens, Reboudt and Mount Spurr volcanoes,* J. Geophys. Res., 109, D16201.

Ovadnevaidte, J. et al, (2009), *Volcanic sulphate and artic dust plumes over the North Atlantic Ocean*, Atm. Env. **43**, 4968-4974.

Synergetic monitoring of Saharan dust plumes: A case study of dust transport from Canary Islands to Iberian Peninsula. Part 1: Dust detection, identification and vertical structure analysis

C. Córdoba-Jabonero[1], M. Sorribas[1], J.L. Guerrero-Rascado[2]*, J.A. Adame[1], Y. Hernández[3], H. Lyamani[2], V. Cachorro[4], M. Gil[1], L. Alados-Arboledas[2], E. Cuevas[3] and B. de la Morena[1]

[1]Instituto Nacional de Técnica Aeroespacial (INTA), Atmospheric Research and Instrumentation Branch, Torrejón de Ardoz (Madrid), Spain
[2]Universidad de Granada (UGR), Andalusian Environmental Centre (CEAMA), Group of Atmospheric Physics, Granada, Spain
[3]Agencia Estatal de Meteorología (AEMET), Atmospheric Research Centre of Izaña, Sta. Cruz de Tenerife, Spain
[4]Universidad de Valladolid (UVA), Group of Atmospheric Optics, Valladolid, Spain
*Now at Évora Geophysics Centre (CGE), University of Évora, Évora, Portugal
Keywords: Monitoring, Lidar, AOD, Backtrajectories, Saharan dust.
Presenting author email: cordobajc@inta.es

A general work focused on the study of Saharan dust intrusions is presented as a case study of air masses advected from the Saharan region to the Canary Islands and the Iberian Peninsula (IP). This work is divided in two parts in order to examine two relevant and different aspects of this study. Each one is separately submitted. This first one (Part 1) describes the dust detection, identification and vertical structure analysis by using AERONET data, lidar measurements and backtrajectory modelling. In the Part 2 the evaluation of potential dust impact on surface once that Saharan dust intrusion arrives at the Southern IP will be presented.

The observations were performed over three Spanish geographically strategic stations within the dust-influenced area along a common dust plume pathway monitored from 11 to 19 of March 2008. A 4-day long dust event (13-16 March) over the Santa Cruz de Tenerife Observatory (SCO), and a linked short 1-day dust episode (14 March) in the Southern IP over the Atmospheric Sounding Station 'El Arenosillo' (ARN) and the Granada station (GRA) were detected.

Meteorological conditions favoured the dust plume transport over the area under study. Backtrajectory analysis clearly revealed the Saharan region as the source of the dust intrusion.

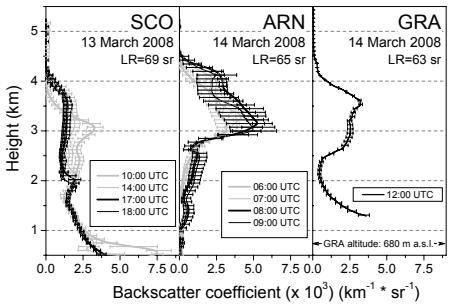

Figure 1. Height-resolved backscatter coefficients (1-h averaged profiles) under dusty conditions over SCO site (left), ARN (centre) and GRA (right) stations.

Under the Saharan air masses influence, AERONET Aerosol Optical Depth at 500 nm (AOD^{500}) ranged from 0.3 to 0.6 and Ångström Exponent at 440/675 nm wavelength pair ($AE^{440/675}$) was lower than 0.5, indicating a high load and predominance of coarse particles during those dusty events.

Lidar observations characterized the vertical structure of those dust plumes, identifying different aerosol contributions depending on altitude (see Fig. 1). In particular, the 3-km height dust layer transported from the Saharan region and observed over SCO site was later on detected at ARN and GRA stations.

No significant differences were found in the lidar (extinction-to-backscatter) ratio (LR) for dust particles over all stations. LR ranged from 60 sr to 70 sr during the main dust episodes. However, AERONET retrieved LR values for dust particles are underestimated, unless a dust more realistic model is used instead in the AERONET inversion algorithm (Müller *et al.,* 2010). These similar LR values found in all the stations suggest that dust properties were kept nearly unchanged in the course of its medium-range transport.

This work was supported by the Spanish Ministry for Science and Innovation (MICINN) under Complementary Actions CGL2008-01330-E and CGL2010-10012-E, the Spanish Ministry of Education under Project CGL2008-05939-C03-03/CLI, the Autonomous Government of Andalusia under Project P08-RNM-3568, and the EARLINET-ASOS project (EU contract nº 025991, RICA). JLG-R thanks the Portuguese Fundação para a Ciência e a Tecnologia for supporting under grant SFRH/BPD/63090/2009.

Müller, D., Ansmann, A., Freudenthaler, V., Kandler, K., Toledano, C., Hiebsch, A., Gasteiger, J., Esselborn, M., Tesche, M., Heese, B., Althausen, D., Weinzierl, B., Petzold, A., and von Hoyningen-Huene, W. (2010) *J. Geophys. Res.* **115**, D11207, doi:10.1029/2009JD012523.

Multi-instrumental characterization of the mixing of Eyjafjallajökull volcanic aerosols and boundary layer aerosols at Granada, Spain

L. Alados-Arboledas[(1,2)], F. Navas-Guzmán[(1,2)], J.A. Bravo-Aranda[(1,2)], H.Lyamani[(1,2)], J D. Pérez-Ramírez[(1,2)], J. L. Guerrero-Rascado[(1,2)], I. Foyo[(1,2)], I. Alados[(2)], M.J. Granados[(1,2)], G. Titos[(1,2)], J. Fernández Gálvez[(1,2)], A. Valenzuela [(1,2)], M. Antón[(1,2)], A. Quirantes [(1,2)] X. Querol[(4)], A. Alastuey[(4)] and F. J. Olmo[(1,2)]

[1]Departamento de Física Aplicada, Universidad de Granada, Fuentenueva s/n, 18071, Granada, Spain.
[2]Centro Andaluz de Medio Ambiente (CEAMA), Av. del Mediterráneo s/n, 18071, Granada, Spain
[3] Évora Geophysics Centre (CGE), University of Évora, Rua Romão Ramalho 59, 7000, Évora Portugal
[4]IDÆA, Department of Geosciences, CSIC, Barcelona, Spain
Keywords: lidar, volcanic ash, PBL, mixing, EARLINET, AERONET, in-situ observations.
Presenting author email: alados@ugr.es

In this work we study the changes detected in the atmospheric aerosols over the city of Granada after the arrival of lofted aerosol layers associated to the eruption of the Eyjafjallajökull volcano in 2010. The analyzed events correspond to the last part of the volcanic event, May 2010, when volcanic plumes reached the Iberian Peninsula. The study has been developed at the Andalusian Center for Environmental Studies (CEAMA), located in South-eastern Spain in the urban area of Granada, a non-industrialized medium size city (37.18ºN, 3.58ºW and 680 m a.m.s.l.).

At the CEAMA a wide variety of instrumentation deployed for the characterization of the atmospheric aerosols is running in a continuous basis. Thus, remote sounding of the atmospheric aerosol is performed by a multi-wavelength Raman lidar system, included in EARLINET (Bösenberg et al., 2003). Furthermore, columnar aerosol properties are retrieved during the day by means of CIMEL CE-318, included in AERONET (Holben et al, 1998), while during the night the atmospheric column is monitored by the starphotometer EXCALIBUR (Pérez et al., 2010). Together with this remote sensing instrumentation a set of instruments is operated in the surface boundary layer to characterize the optical, physical and chemical aerosol properties by in-situ methodologies. Thus our station includes an integrating nephelometer (TSI-3563), a Multi Angle Absorption Photometer (MAAP), an Aerosol Particle Sizer (TISI-APS-322) and a Particle Soot Absorption Photometer (PSAP). Finally, sampling of PM10 and PM1 is simultaneously performed, to determine major and trace aerosol components.

During the first half of May 2010 a good number of simultaneous measurements obtained by the diverse instrumentation above mentioned were gathered. This has allowed for determining the mean features of the atmospheric aerosol during the two relevant periods when the volcanic aerosol plumes reached our station. During the first event, 5-8 May, the lofted aerosol layers subsided and were finally mixed with the PBL aerosols. Thus, the changes in the atmospheric column, integrated and resolved, where followed by appreciable changes in the aerosol properties measured at the surface boundary layer. Lidar retrievals allowed us to distinguish at least two different lofted aerosol layers, with rather low aerosol linear depolarization ratios, ~4-8%, and different values of lidar ratio and backscatter and extinction related Ångström exponent.

Starting on the evening of 7 May the mixing of the lofted aerosol with the urban atmospheric aerosols is reflected in the in situ instrumentation operated at the CEAMA. Thus, we evidenced an increase of submicron particles associated that leaded to increasing scattering, with an unusual single scattering albedo around 0.9 for our urban station. During this period filter sampling of atmospheric particles, segregated in PM10 and PM1, has been accomplished. The chemical analyses of these filters revealed that during these days the anthropogenic aerosols followed the typical weekend trend, with an evident reduction in nitrated, organic and elemental carbon and locally re-suspended mineral matter. On the contrary we evidenced an increase in n-sss sulphates that according to the previous statements must have a non-anthropogenic origin.

During the second event, 11-13 May, lofted aerosol plumes coming from Iceland presented larger aerosol depolarization ratios, over 20%, and smaller backscatter related Ångström exponent, around 0, than in the previous event. Thus suggesting the arrival of volcanic plumes enriched in volcanic ashes. During this second event there were no evidence of mixing of the lofted aerosol plumes and the planetary boundary layer.

This study evidences the interest in combining different techniques to reach a more complete picture of the atmospheric aerosols.

Acknowledgements: This work was supported by the Spanish Ministry of Science and Technology through projects CGL-2006-27108-E/CLI (DAMOCLES Aerosol Scientific Thematic Network), CGL2008-01330-E/CLI, CGL2009-08031-E/CLI, CGL2010-09225-E (Spanish Lidar Network), CGL2010-18782 and CSD2007-00067; by the Andalusian Regional Government through projects P10-RNM-6299 and P08-RNM-3568; and by EU through EARLINET-ASOS project (EU Coordination Action, contract nº 025991 (RICA)).

Bösenberg, J., *et al.* (2003), *Rep. 348*, Max-Planck-Inst., Hamburg, Germany.
Holben, B. N. et al. (1998), Remote Sens. Environ., 66, 1-16.
Pérez et al. (2008). Atmos. Environ.,42 , 2733-2738.

Closure study of aerosol optical properties using in-situ and remote sensing techniques

P. Zieger[1], N. Bukowiecki[1], U. Baltensperger[1], C. Ketterer[1,2], M. Collaud Coen[2], O. Maier[2], E. Kienast[3], F. Wienhold[3], T. Peter[3], J. von Bismarck[4], M. Starace[4], T. Ruhtz[4], K. Clémer[5], M. van Roozendael[5], S. Frey[6], H. Wille[6], and E. Weingartner[1]

[1]Laboratory of Atmospheric Chemistry, Paul Scherrer Institut, 5232 Villigen, Switzerland
[2]MeteoSwiss, 1530 Payerne, Switzerland
[3]Institute for Atmospheric and Climate Science, ETH Zürich, Switzerland
[4]Institute for Space Sciences, Freie Universität Berlin, Germany
[5]Belgian Institute for Space Aeronomy, Brussels, Belgium
[6]Jenoptik Defense and Civil Systems, Teltow, Germany
Keywords: Optical properties, Remote sensing, In-situ measurements, CLACE
Presenting author email: paul.zieger@psi.ch

In the field, aerosol in-situ measurements are often performed under dry conditions (relative humidity RH<30–40%). Since ambient aerosol particles experience hygroscopic growth at enhanced RH, also their microphysical and optical properties – especially the aerosol light scattering – are strongly dependent on RH. The knowledge of this RH effect is of crucial importance for climate forcing calculations or for the comparison of remote sensing with in-situ measurements.

Here, we will present results of an optical closure study performed within the Cloud and Aerosol Characterization Campaign (CLACE 2010) carried out at the Jungfraujoch (JFJ, 3580 m asl) and at the Kleine Scheidegg (KLS, 2060 m asl) in Switzerland during July 2010.

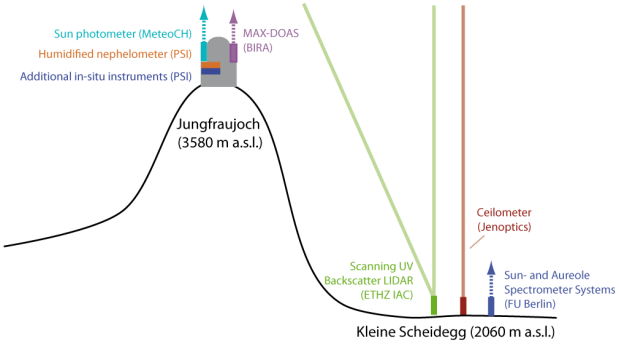

Figure 1: Set-up for optical closure study during CLACE 2010

The aerosol scattering coefficient was measured dry and at predefined RH conditions with a humidified nephelometer (WetNeph, Fierz-Schmidhauser *et al*., 2010) together with other continuously running aerosol measurements e.g. for characterizing the aerosol size distribution, the aerosol absorption, etc. at the JFJ. At the JFJ a MAX-DOAS (multi-axis differential optical absorption spectroscopy) retrieved aerosol extinction profiles (Clémer *et al*, 2010). Approximately 1500 m below the JFJ at the KLS a variety of remote sensing instruments were installed. A scanning backscatter LIDAR (light detection and ranging, by Leosphere Inc.) measured the aerosol backscatter signal together with a ceilometer (CHM 15K by Jenoptik) at 355 nm and 1064 nm, respectively. In addition, the sun and aureole spectrometer system FUBISS-ASA1 and ASA2 (Asseng et al., 2005; Zieger et al., 2007) measured among other variables the aerosol optical depth (AOD) and the slope of the phase function in the forward scattering region (aureole index) at various wavelengths in the visible and near infrared spectrum (see Fig. 1 for an overview of the set-up).

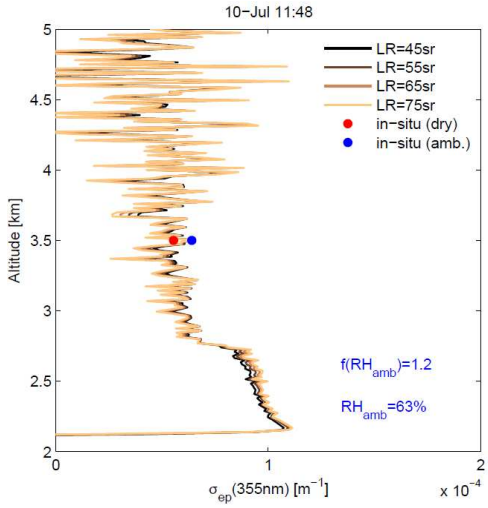

Figure 2: Example of the aerosol backscatter profile (at different LIDAR ratios LR) compared to the dry and ambient in-situ measurement at JFJ (bullet points). On the 10th of July a strong Saharan dust event was present at the JFJ.

An example of the results is seen in Fig. 2, where the aerosol extinction σ_{ep} profile as measured from KLS is shown during a Saharan dust event together with the corresponding in-situ measurements from JFJ.

Asseng, H., Ruhtz, T. and Fischer, J. (2004), *Appl. Opt.* **43,** 2146-2155.
Clémer, K., van Roozendael, M., et al. (2010*), Atmos. Meas. Tech.* **3**, 864-876.
Fierz-Schmidhauser, R., Zieger, P., et al. (2010), *Atmos. Meas. Tech.* **3**, 39–50.
Zieger, P., Ruhtz, T., Preusker R. and Fischer, J. (2007) , *Appl. Opt.* **46**, 8542-855.

One year of Raman lidar measurements at the South African EUCAARI site

M. Komppula[1], T. Mielonen[1], K. Korhonen[1], A. Arola[1], H. Lihavainen[2], L. Laakso[2,3,4], V. Vakkari[4], H. Laakso[4], P. Beukes[3], P. Van Zyl[3], K. Pienaar[3], P. Tiitta[3], R. le Roux[3], K. Chiloane[5], H. Baars[6], R. Engelmann[6], D. Althausen[6] and K.E.J. Lehtinen[1,7]

[1]Finnish Meteorological Institute, P.O.Box 1627, FI-70211, Kuopio, Finland
[2]Finnish Meteorological Institute, P.O.Box 503, FI-00101, Helsinki, Finland
[3]School of Physical and Chemical Sciences, North-West University, Potchefstroom, Republic of South Africa
[4]Department of Physics, University of Helsinki, P.O.Box 64, FI-00014 Helsinki, Finland
[5]ESKOM, Sustainability and Innovation, Environmental Sciences Department, Republic of South Africa
[6]Leibniz Institute for Tropospheric Research, Permoserstr. 15, D-04318, Leipzig, Germany
[7]Department of Applied Physics, University of Eastern Finland, P.O.Box 1627, Kuopio, FI-70211, Finland
Keywords: lidar, lidar ratio, extinction, remote sensing, air pollution.
Presenting author email: mika.komppula@fmi.fi

This paper presents one-year dataset of Raman lidar measurements conducted at the South African EUCAARI (The European Project on clouds, aerosols and climate) site Elandsfontein (Laakso *et al.*, 2010). Previous lidar measurements have been sparse on the African continent, especially in the Southern areas.

The measurement site is located on the eastern part of Highveld, approximately 200 km east of Johannesburg at a hilltop about 1750 meter asl. Additional instrumentation provided aerosol absorption and scattering, chemical composition, number size distribution (10 nm – 10 µm), aerosol optical depth (AOD), trace gases (SO_2, O_3, NO_x, H_2S) and basic meteorology. The region has significant anthropogenic emissions especially from coal-based power production, petrochemical industry and further away, the megacity of Johannesburg. Other important sources are frequent savannah fires, especially during the dry season (June-October) and some local biofuel burning.

The lidar measurements were started on the 13th December 2009 and were stopped at the end of January 2011. The instrument in use was a seven-channel Raman lidar called "POLLY^{XT}–POrtabLe Lidar sYstem eXTended" (Althausen *et al.*, 2009). The output of the instrument includes vertical profiles of the particle backscattering coefficient at three wavelengths (355, 532 & 1064 nm) and of the particle extinction coefficient at two wavelengths (355 & 532 nm) for the whole troposphere. The vertically integrated extinction coefficient gives the AOD. In addition, such size/composition-dependent, intensive particle quantities as the Ångstrom exponents, the lidar ratio and depolarisation can be determined. The height and the evolution of the boundary layer and night-time residual layer can be defined together with the height and thickness of different cloud and aerosol layers. The depolarisation channel (355 nm) of the lidar enables us to separate spherical and non-spherical particles. Thus, we are able to identity dust particles and estimate the ratio of ice crystals and water droplets in clouds. The vertical resolution of the system is 30 meters.

The typical backscattering and extinction profiles and other properties for the seasonal aerosol will be calculated. The evaluation of planetary boundary layer (PBL) will be defined.

The local summer (Dec-Feb) had most distinct PBL evolution on most days. A very shallow aerosol layer was observed during the night and an increase up to 2-3 km during the day on average. The maximum layer thickness was about 5 km. This period was the cloudiest period of the year and in contrast, winter (Jun-Aug) was almost totally cloud free. Strong and complex multilayered structure of the aerosol was observed throughout the year, most frequently in autumn (Mar-May). Winter and partly spring (Sep-Nov) showed mostly a stable aerosol layer up to 1-3 km height. Furthermore, the diurnal variation was the weakest in winter.

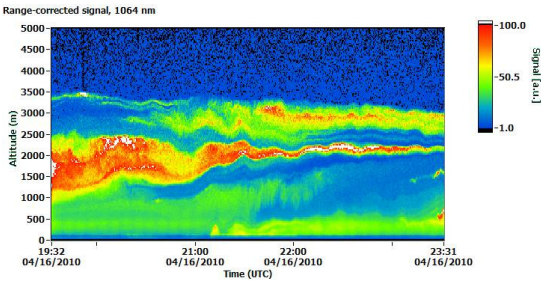

Figure 1. Multiple aerosol plumes. Four-hour time series of backscatter signal at 1064 nm from April 16th, 2010 at Elandsfontein.

This work was supported by the Finnish Academy of Sciences, Finnish foreign ministry and European Union (in project EUCAARI). Eskom Holdings Ltd, South Africa is acknowledged for providing the Air Quality Monitoring Station for the EUCAARI Project measurements.

Althausen, D., et al. (2009). *J. Atmos. Oceanic Technol.*, **26**, 2366–2378, doi: 10.1175/2009JTECHA1304.1.

Laakso, L., et al. (2010), *Atmos. Chem. Phys. Discuss.*, **10**, 30691-30729, doi:10.5194/acpd-10-30691-2010.

Thursday, September 8, 2011

Session 10C: Control Technologies for Combustion Emissions

Nanostructure of fine and ultrafine particles from start-ups and shutdowns of a 250MW natural gas power plant

C. Gutierrez-Canas[1], M. Larrion[1], A. Perez[2], Pena E.[1], Fernandez Armas S.[3], and J.A. Legarreta[1]

[1]Department of Chemical & Environmental Eng., University of the Basque Country, Bilbao, 48013, Spain
[2]AIRg, Parque Tecnológico de Zamudio (Bizkaia) - Edificio 101, 48030, Spain
[3]Center for Microscopy and Microanalysis, University of the Basque Country, Leioa 48200, Spain
Keywords: combustion aerosols, soot nanostructure, ELPI, source fingerprint.
Presenting author email: cristina.gutierrezcanas@ehu.es

Combined cycle power plants fuelled by natural gas are more versatile than those powered by coal or oil and, thus are becoming the key trade factor –in a daily basis- by the electric market due to the variability of renewable generation. This turns in a higher frequency of shutdowns/start-ups than foreseen by design. Transients are characterized by higher emissions of gases (CO and NO_x), but also for ultrafine and fine carbonaceous particles as a result of changing combustion conditions. Although the structural properties of flame generated soot and diesel exhaust soot (Tree *et al*, 2007; Miller *et al*, 2007; among others) have been studied intensively, investigations of soot from utility boilers have been mainly conducted on size distribution and elemental analysis. Fingerprinting the contribution of soot from natural gas combustion is possible through the identification of its nanostructure, from amorphous to graphitic and fullerenic. The characteristics of the internal carbon lamella comprising a soot primary particle are collectively called the nanostructure (Vander Wal *et al*, 2010). Soot nanostructure depends strongly on the fuel identity and synthesis conditions, such as burning temperature, residence time, fuel properties and fuel oxygen ratio, and the nanostructure in turn affects the oxidation reactivity of the soot. Chemically, soot can be distinguished by both elemental composition (trace metals) and surface functional groups.

Here are presented the results of soot characteristics along the transients of a natural gas, combined cycle, power plant. Each gas turbine is of 250 MW nominal capacity. Experiments include the follow-up of gaseous emissions (FTIR, Gasmet Oy) as well as aerosol measurement and sample collection. This has been done by means of an ELPI (Dekati, Ltd.) used both as an aerosol analyzer, providing near real-time size distributions (20 s averaging time) and as a sample pre-separator allowing soot characterization. Samples have been analyzed by TEM/SAED and image analysis (frequency plots of common morphologies versus particle size, primary particle size and number of particles in aggregates/agglomerates). TEM analysis focus on physical characteristics of carbon layers and their arrangement.

Functionalized graphitic structures have been observed around the characteristic mode of 330 nm at high NO_x. Partial oxidation of the soot by NO_2 results on oxygenated functional groups –phenolic, carbonyl and to a less extent carboxylic acid groups. Soot with well-defined graphene planes is less susceptible to oxidation. MWCNTs and fullerenic structures at high CO, up to 300 nm aerodynamic size). Non carbonaceous structures, such as metal or combined agglomerates were not observed. A few (less than 1.5% in number) carbon agglomerates decorated with metal nanoparticles were observed. During startup and shutdown periods, size distributions present a characteristic mode at 330 nm but differ in a secondary mode at 140 nm probably associated with a transient of high NO_x in the early stages of startup. In the case of shutdown, a secondary and less intense mode is consistently present at 83 nm.

A fast shift towards supermicron size ranges is characteristic of the later stages of start-up. The aggregates within this coarse fraction, in excess of 2 μm, can contain >1000 primary MWCNTs or multiconcentric fullerenic structures. These results are in accordance with the description (Homann,1998) of the pathways to large particles in flames.

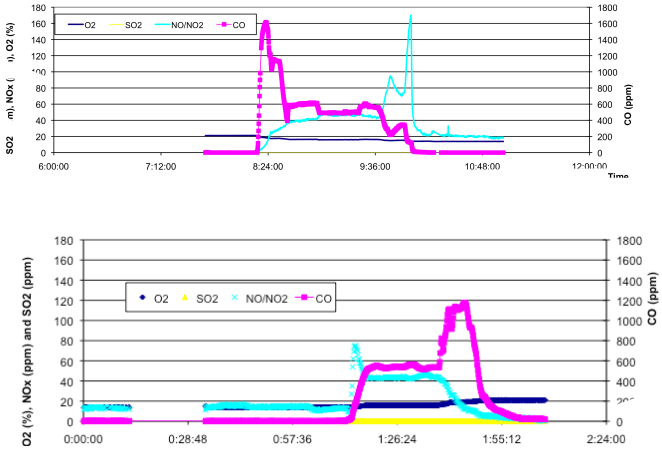

Figure 1. Gas composition during shutdown (up) and start-up transients (from and to 250MW)

This work was supported by the Ministerio del Medio Ambiente (Spanish Government) under grant A378/2007/3-13,1.

Homann K.H., (1998) *Angew. Chemie Int. Ed.*. (1998) **37**, 2434-2451.
Miller A., Ahlstrand G., D.R., Kittelson D. and Zachariah M., (2007) *Comb. Flame.* **149**, 129-143.
Tree D.R., and Svensson K.I., (2007) *Prog. Energy Comb. Sci.* **33**, 272-309.
Vander Wal, R.L., Bryg V.M. and Hays, M.D. (2010) *J. Aerosol Sci.* **41**, 108-117.

Optimization of Dust Collectors in Incineration Plants to control Fine Particulate, Dioxins and NOx by using ePTFE Membranes and Catalytic Filtration Technologies

J. Ebert, G. Pranghofer and O. Petzoldt

W. L. GORE & Associates, Industrial Dry Filtration, Putzbrunn, D-85639 Germany
Keywords: Dust Removal, Filtration, Membrane, Fine Particles, Dioxin, NOx.
Presenting author email: Ole.Petzoldt@wlgore.com

Introduction

Fabric Filters are state-of-the-art to control dust emissions from incineration and other industrial processes. Two types of filtration processes are currently used in particulate filtration. Depth filtration (usually referred to as conventional filtration), and Surface filtration. Conventional filter bags require the accumulation of a dust cake inside the cross section of the fabric to be sufficiently efficient. Over time that blocks the filter and reduces its permeability. Surface Filters don't need that so-called seasoning.

Membrane Filtration

Membrane ePTFE filters, patented by W. L Gore & Associates, operate with a different filtration principle. The filter media is a microporous film of expanded Polytetrafluoroethylene, laminated to a backing material. (Figure 1).

Figure 1 PTFE Membrane Filter laminate.

In a surface filtration system the dust is collected on the membrane's surface which is a chemically inert, non-sticking material. The ePTFE membrane shows almost a 100 % efficiency to capture particulate, practically independent from the particle size, a high chemically resistivity and it is operational to 260°C with surges to 285°C. The results of the performance of membrane filters in incineration plants will be provided, including retention rates of PM 2.5, Dioxins, Heavy Metals and, in combination with sorbents, of acidic components in compliance with European Regulations.

Dioxins

Dioxins (PCDD/F) are the most toxic man made substances, emitted in gas and solid phase during incineration of waste. The permissible dioxin emissions in most industrial nations is less than 0.1 ng (I-TEQ)/Nm^3. The common system to remove dioxins is installing an injection process for powdered activated carbon; other alternatives are non-flammable additives and catalytic technologies.

Catalytic Filtration

Gore developed the REMEDIA D/F catalytic filter system. Catalytic filters consist of an ePTFE membrane that is laminated to a catalytically active felt, manufactured from ePTFE fibers which contain V_2O_5/TiO_2. Particles are captured on the membrane and dioxin/furans are catalytically destroyed within the felt (Figure 2).

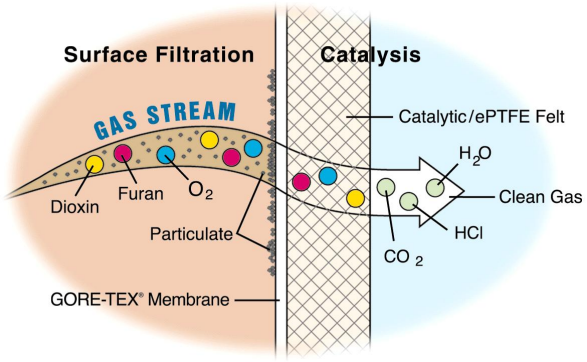

Figure 2 REMEDIA D/F Catalytic Filter System.

The catalyst fiber, which makes up the support felt, promotes the oxidation of dioxins and furans to form CO_2, H_2O, and traces of HCl. In typical industrial facilities, the system is operated at temperatures of 180°C to 250°C. The filter velocity is approximately 1 $m^3/m^2/min$, which is the usual range for cloth filters.

The system is globally used in municipal, hazardous and medical waste incinerators, crematoria, metallurgical plants and various other industrial high temperature processes. Some examples and results will be shown in the presentation

NOx

Currently Gore is developing a catalytic filter system to reduce NOx from Flue gases. Tighter regulations for NOx emissions (< 100 mg/m^3) today and in future, not only for waste incinerators but also for power plants, cement kilns, steel plants and other industrial processes, require efficient catalytic technologies to convert NOx into Nitrogen. As an alternative to ceramic catalysts, catalytic filter bags can be used. The technology and first results from pilot and full scale plants will be discussed in the presentation.

Hybrid filtration and catalytic control of toxic pollutants from a 1.2MW waste biomass cofiring boiler

D. Sanz[1], J.J. Rodríguez-Maroto[1] , J.L. Dorronsoro[1], E. Rojas[1], A. Bahillo[1], R. Ramos[1], E. Ruiz[1], P. Galán[1], M.A. Martínez[1], C. Gutierrez-Cañas[2], M. Larrion[2], E. Peña[2], W. Hagemann[3], S. Astarloa[4]
[1] CIEMAT Avda Complutense 22 Madrid (Spain)
[2]Dpto. de Ingeniería Química y del Medio Ambiente, UPV, Alameda de Urquijo s/n, Bilbao
[3]W.L. Gore y Asociados S.L., Vallespir 24, 08970 Sant Joan Despí, [4]Grupo airG, Gran Vía 38, 48009 Bilbao
Keywords: Abatement strategies, heavy metals, filtration, electrostatic precipitators, PCDD/Fs
Presenting author email: david.sanz@ciemat.es

The control of toxic trace pollutants from combustion sources requires enhanced and selective mechanisms of both separation and abatement. In this work, the performance of a line (Fig. 1) combining enhanced surface filtration together with catalytic, and thus selective abatement is presented. So-called "hybrid filters" combine electrostatic precipitation and surface filtration in different arrangements (Miller, 2003). We present the performance of a pilot scale hybrid filter as the core of a process line, treating 1000 Nm^3/h of flue gases from a 1.2MW fluidized bed boiler. Moreover, the media substrate is chemically active for it contains a catalyst for PCDD/Fs destruction (Fritsky, 2001). REMEDIA™ bags consists of an ePTFE membrane laminated over a catalytic felt substrate. Targeted chemical conversion implies an operation temperature of about 200ºC.

Biomass wastes will be burnt in a fluidised bed boiler. Samples will be taken upstream and downstream the filter (Figure 1) to determine the removal efficiency of dioxins, heavy metals, particulate matter and trace gases.

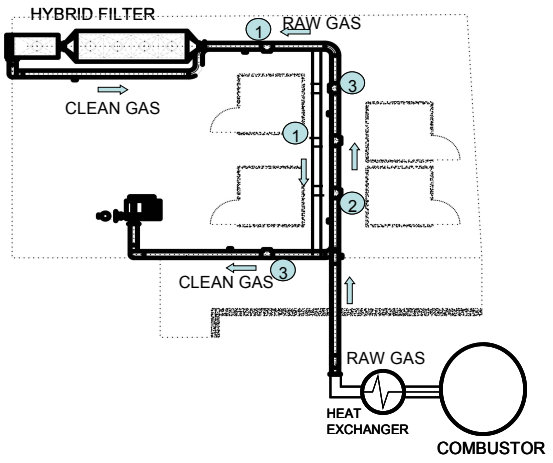

Figure 1. Validation test line lay-out. Sampling ports for aerosols (1), dioxins (2) and gases (3)

Fuel screening has been made on the basis of chloride and heavy metals content (Figure 2). Ash content, humidity, calorific value and elemental composition (C, N, S) were also determined. Municipal sewage sludge and animal meal show higher chloride and mineral content. Heavy metals content of sludge is the highest, except for titanium. Olive tree pruning residue has the second highest content in copper, due to phytosanitary treatments. Copper is relevant to PCDD/Fs formation because of its catalytic promotion of PCDD/Fs and its presence within the penetration window of conventional electrostatic precipitators (Peña, 2009).

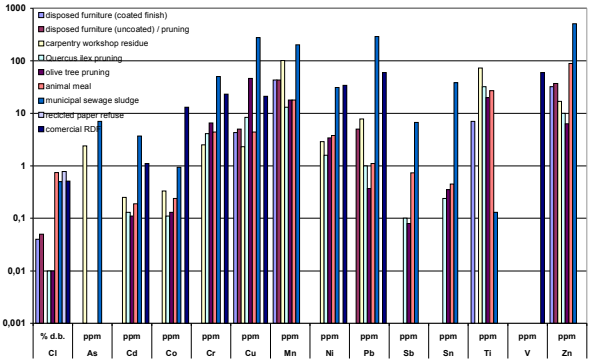

Figure 2. Chloride (%) and heavy metal (ppm) content of potential test fuels.

A test matrix was planned, focusing on the more relevant operating conditions: gas flow rate, temperature and applied voltage to the ESP. Two different fuels are used in the tests, a mixture of municipal sewage sludge/olive tree prune and refuse from recycled paper. Experimental results include: emission dynamics and its relationship with operating conditions, physicochemical characterization of fine and ultrafine particles as well as determination of trace gases concentration. Fractional efficiency of the hybrid filter and conversion of PCDD/Fs will be discussed as dependent on fuel quality and operating conditions. The feasibility of advanced control technologies for trace and toxic pollutants will be demonstrated on the basis of these findings.

Authors are thankful to Minestery of the Environment and Rural and Marine Affairs of Spain for funding of this work. Thanks are also given to ASERMA (Asociación de Recuperadores de Madera) and Energía Oriental S.A. for facilitating samples of potential test fuels.

Peña, E. (2009) *EAC2009*, Karlsruhe (2009) T081A04
Fritsky, K.J., Kumm, J.H. and Wilken, M. (2001) *J. Air Waste Management Association*, 1642-1649.
Miller, R.L., (2003) "Enhancing aging ESP performance utilizing COHPAC hybrid fabric filter technologies" www.hamon-researchcottrell.com.

Diesel Engine Exhaust Emission Control: Performance Assessment of a Multi-Functional Reactor under Conventional and Advanced Combustion Conditions

D. Zarvalis[1], S. Lorentzou[1], A. Zygogianni[1], A. G. Konstandopoulos[1,2]
C. Severin[3], M. Shönen[3], R. Vedder[3] M. Fiebig[4] S. Zinola[5], J. Lavy[5]

[1]Aerosol & Particle Technology Laboratory, CERTH/CPERI, PO Box 361 Thermi 57001, Thessaloniki, Greece
[2]Department of Chemical Engineering, Aristotle University, GREECE
[3]FEV Motorentechnik GmbH, Neuenhofstr. 181,52078 Aachen, Germany
[4]Institute for Combustion Engines, RWTH Aachen University, Schinkelstr. 8, 52062 Aachen, Germany
[5]IFP Energies nouvelles, BP3, 69 360, Solaize, France

Keywords: multifunctional reactor, diesel emissions, diesel exhaust, filtration.
Presenting author email: dzarv@cperi.certh.gr

In the past (Lorentzou *et al*, 2009), we have introduced a Multi-Functional Reactor (MFR) prototype, suitable for the abatement of the gaseous and PM emissions of the Diesel engine. In this work, the performance of MFR prototypes under both conventional and advanced combustion engine operating conditions is presented. The MFR comprised two novel aspects: a system design which exploits internal heat recovery and a multifunctional catalyst able to enhance the direct soot oxidation rate (i.e. through oxygen transfer) and the indirect (NO_2-assisted) soot oxidation rate as well as to promote CO and HC oxidation.

The MFR demonstrated faster thermal response and more even in-filter temperature distributions during regeneration conditions compared to a standard filter. The employed catalyst synthesis and application technology consisting of a combination of aerosol based and wet chemistry techniques enabled the increase in the direct soot oxidation activity and filtration efficiency with respect to a reference state-of-the-art (SA) DPF. The pressure drop during soot loading was kept at comparable to the SA DPF level. Moreover, the MFR demonstrated significant HC/CO oxidation activity while minimizing the NO_2 emissions during conventional combustion conditions.

An aging procedure was applied on the MFR (equivalent to 100,000 km of normal vehicle driving). This did not result in losses in its catalytic activity and filtration efficiency. It caused an increase in the filter pressure drop by nearly 20 % mainly due to ash particles accumulation. MFR simulation results indicated that significant economy can be achieved with respect to the fuel consumption related to filter regeneration (up to 45.2 % during NEDC driving conditions). This gain comes from the fact that the developed catalyzed filter can be sufficiently regenerated at lower temperatures (550 ^{o}C) than the SA DPF. Besides the fuel consumption gain, there are additional advantages such as less engine wear due to in cylinder oil-dilution during fuel post injection as well as enabling filter regeneration at lower engine load conditions. Significant fuel savings were also realised during alternative to NEDC driving cycles (Figure 1).

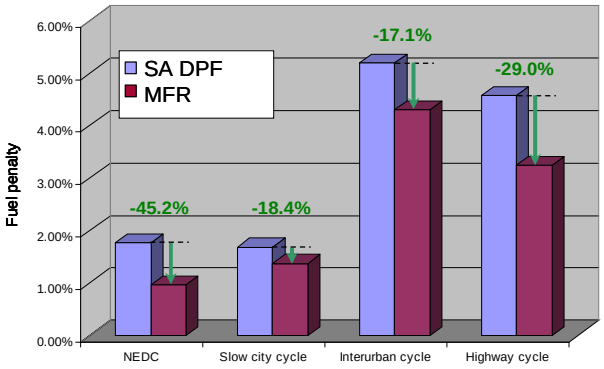

Figure 1. Calculated fuel penalty due to filter regeneration for different driving cycles.

The MFR was also tested under Homogeneous Charge Compression Ignition (HCCI) engine operating conditions. The MFR revealed equivalent performance under both conventional and HCCI engine operation conditions with respect to filter pressure drop, filtration efficiency and regeneration performance. The microstructural properties of the soot cake evolved at either conventional or alternative combustion conditions were equivalent. The catalyst soot oxidation activity was not affected by the applied combustion type either. This came into contrast with the fact that soot analysis from both types of combustion revealed differences with respect to the soot particles' micro-structure and easy of oxidation. The HCCI soot, with increased hydrogen content compared to the conventional soot, is oxidized at lower temperatures under TGA conditions. Moreover, HCCI engine operation resulted in soot particles that in some cases are quite different than the conventional soot particles demonstrating a core with a distinguished outer shell structure. These core/shell particles were the first to be eliminated during oxidation. Raman analysis, on the other hand did not quantified any significant differences in the degree of structural organization of the samples. As a conclusion, the possible differences recognized by TEM and TGA analysis did not seem to result in any performance differences at the catalyzed monolith scale.

Lorentzou, S., Zarvalis, D., and Konstandopoulos, A.G., (2009) *Proc. European Aerosol Conference, Karlsruhe, Germany.*

Thursday, September 8, 2011

Session 10D: Turbulent Aerosol Transport and Exchange / Transport and Transformation

Vertical transport of aerosol particles in the marine boundary layer near Barbados

B. Wehner, F. Ditas, A. Wiedensohler, H. Siebert

Leibniz Institute for Tropospheric Research, 04318 Leipzig, Germany

Keywords: nucleation, turbulence, vertical profiles

The number concentration of aerosol particles is highly variable in different layers of the boundary layer and the overlaying free troposphere. Vertical transport of particles is mainly caused by atmospheric turbulence which might be also relevant for the transformation of aerosol particles as well as new particle formation. To quantify the turbulent transport, measurements of particle number concentrations and vertical wind speed are required. The temporal resolution of available instrumentation defines the minimum of turbulent structures which can be resolved.

In contrast to wind speed measurements, where a high temporal resolution up to 100 Hz can be achieved by commercially available instrumentation, measurements of the particle number concentration with a higher resolution than 1 Hz are still rare. Thus, a new fast mixing-type CPC (FCPC) with a temporal resolution of approximately 20 Hz (Wehner et al., 2010) was constructed. This instrument has been installed on the helicopter-borne platform ACTOS (Siebert et al., 2006). ACTOS is equipped with instrumentation to measure standard meteorological parameters with a high temporal resolution as well as cloud and aerosol microphysics.

Here, measurements from the CARRIBA (Clouds, Aerosol, Radiation and tuRbulence in the trade wInd regime over BArbados) experiment in November 2010 will be presented. Within the campaign 17 research flights in the cloudy and cloud-free marine boundary layer have been performed.

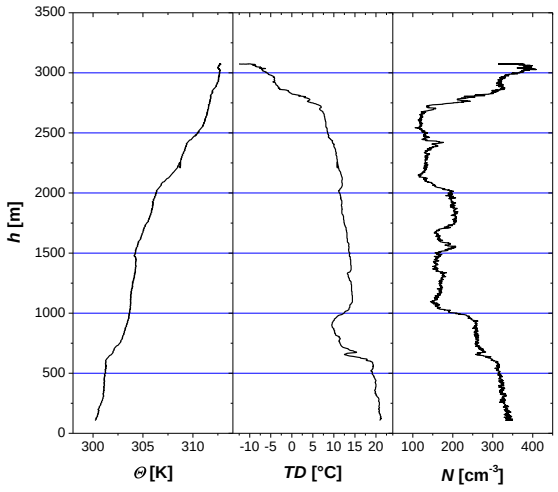

Figure 1: Vertical profiles of the potential temperature Θ, the dewpoint temperature *TD*, and total particle number concentration *N* during ascent on November 21, 2010.

Figure 1 shows a vertical profile of potential temperature Θ, dewpoint temperature *TD*, and particle number concentration *N* measured on November 21, 2010 under cloud-free conditions. The profile of Θ illustrates a slight inversion at about 600 m, but also in higher altitudes regions with a slightly positive gradient of Θ, e.g. at 2500 m can be detected. The corresponding profile of *N* also shows the presence of different layers characterized by different particle number concentrations.

In addition to the vertical profile several horizontal legs were flown in different heights. As an example, Fig. 2 shows the fluctuations of particle number concentration during a horizontal flight leg in a height of about 100 m with meter resolution which is unique for airborne measurements so far.

Together with the measurements of vertical wind speed fluctuation, these observations will allow us to make the first direct estimates of the vertical turbulent flux of aerosol at different heights in the marine boundary layer by applying the so-called "eddy covariance method".

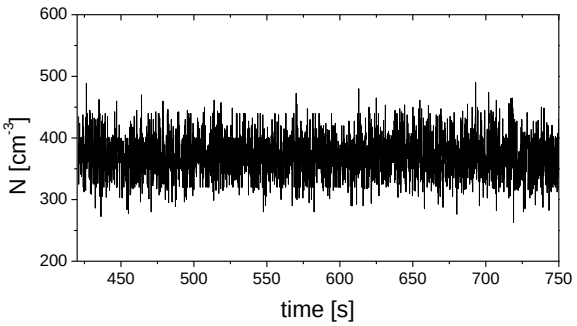

Figure 2: Time series of variation of particle number concentration with a 10-Hz resolution during a horizontal flight leg at around 100 m above sea surface.

References

Siebert, H. et al. (2006) Probing Fine-Scale Dynamics and Microphysics of Clouds with Helicopter-Borne Measurements, Bull. Amer. Met. Soc., 87, 1727 – 1738.

Wehner, B., H. Siebert, M. Hermann, F. Ditas, A. Wiedensohler: Characterization of a new fast mixing type CPC and its application for atmospheric particle measurements, Atmos. Meas. Tech. Discuss., 3, 5907-5931, 2010.

Analysis of particles and CO_2 fluxes in an urban area: correlation with traffic rate and micrometeorology

D. Contini, A. Donateo, C. Elefante, F. M. Grasso

Institute of Atmospheric Science and Climate (ISAC-CNR), 73100, Lecce, Italy
Keywords: eddy-correlation, urban pollution, aerosol flux, CO_2 flux
Presenting author email: d.contini@isac.cnr.it

The study of urban aerosol and carbon dioxide sources is important for their potential effects on health and climate. The aim of this work is to quantify and parameterise the particle number and the CO_2 fluxes through the analysis of correlation with traffic rate, atmospheric stability and friction velocity. This could help to improve how the urban sources are included in air quality and climate models. Further, the differences in the dynamics of CO_2 and particles will be investigated.

A micrometeorological station was located on the corner of a roof of a school at 14m (above street level) on the town of Lecce (Italy) at 40°21'18" N - 18° 9' 59" E. Instruments were located above a four-lane road with relatively high traffic rate (T_R, up to 2400 vehicles/hr). The station included a Gill R3 ultrasonic anemometer, a CPC (Grimm 5.403), a CO_2/H_2O fast open-path detector (LIcor-LI7500), a thermo-hygrometer (Rotronic MP100) and a telecamera. All instruments were synchronously operated by the PC that also provided control of the telecamera used for counting vehicles passing in the main road using a motion detection software. The accuracy of the measurement of T_R was +/- 10%. Aerosol was sampled through a 2.5m inlet (26 mm in diameter with a 45 l/min flow-rate). Calculation of losses indicate that the system was able to detect particles in the size range between 9nm and 1000nm with a first-order time response of about 1.3s.

Post-processing of data was performed on 30mins averages in the streamlines reference system. Correction of high frequency losses have been performed as in Contini et al (2010). The median correction is 29% (Inter-quartile range 25-75, IQR=19% - 40%). Non stationary data were removed corresponding to 9.2% for both aerosol and CO_2. Data in the wind direction sector between E and SW were removed to limit the interference of the school building. In this sector, the site was characterised, using Digital Elevation Model described in Di Sabatino et al (2010), in a radius of 1km covering all footprint for fluxes and most of the footprint for concentration, by buildings with an average height of 7m +/- 4.6m. Globally the building covers 35% of the area.

Significant differences were observed in fluxes between weekdays (average 28200 vehicles/day) and weekend (average 25600 vehicles/day). In weekdays diurnal hours (06am-21pm) median aerosol fluxes (F_P) was 99127 $cm^{-2}s^{-1}$ (IQR=65207 – 133762 $cm^{-2}s^{-1}$) and median CO_2 flux (F_C) was 0.00086 $gm^{-2}s^{-1}$ (IQR=0.00049 – 0.00149 $gm^{-2}s^{-1}$). In nocturnal hours and weekend the median F_P was 26731 $cm^{-2}s^{-1}$ (IQR=7555 - 60201 $cm^{-2}s^{-1}$) and median F_C was 0.00022 $gm^{-2}s^{-1}$ (IQR=0.00022 – 0.00044 $gm^{-2}s^{-1}$). There is a clear correlation between fluxes and T_R (as shown for Fp in Figure 1). The relationship between F_P and T_R is almost linear (in the range of T_R analysed); similar results were obtained for CO_2 with $F_C=4.51\ 10^{-7}\ T_R$ ($R^2=0.938$). Overall there is a low correlation between F_P and F_C (for 30 minutes averages the Pearson coefficient is 0.56). Specifically Fp and Fc have a different diurnal pattern with Fc presenting a low flux in the middle of the day likely as a consequence of photosynthesis. This is evident also on correlation of concentration fluctuations that have a typical pattern with a decrease of correlation around midday and an increase of correlation at the rush hours (maximum of T_R). The emission ratio F_P/F_C has a median value of $9.16*10^{11}$ particles/g (IQR= $9.16*10^{11}$ – $1.60*10^{12}$ particles/g). The normalised flux F_P/T_R shows a clear increase when the friction velocity increases; further, there is a correlation with stability parameter $\xi = (z-d)/L$ showing an increase going from stable to neutral and unstable conditions. These correlations will be investigated and compared with results obtained in other cities (Dorsey et al., 2002; Jarvi et al., 2009).

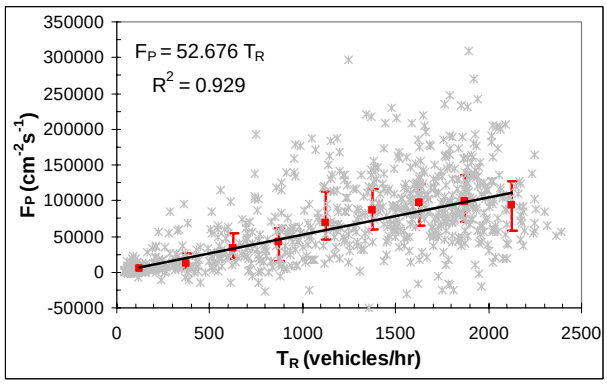

Figure 1. Aerosol fluxes against traffic rate. Red squares are median values calculated in bins of 250 vehicles/hr and error bars represent the IQR.

Contini D., Donateo A, Belosi F, Grasso F.M, Santachiara G, Prodi F. (2010) *J. Geophys. Res.* **115**, D16202, doi:10.1029/2009JD013600.

Di Sabatino S., Leo L. S., Cataldo R., Ratti C., Britter R. E. (2010). *J. Appl. Meteor. Climatol.* **49**, 1377-1396.

Dorsey J.R., Nemitz E., Gallagher M.W., Fowler D., Williams P.I., Bower K.N., Beswick K.M. (2002). *Atmos. Environ* **36**, 791-800.

Jarvi L., Rannik U., Mammarella I., Sogachev A., Aalto P.P., Keronen P., Siivola E., Kulmala M., Vesala T. (2009). *Atmos. Chem. Phys.* **9**, 7847-7856.

Highly size resolved particle fluxes over an urban area

M. J. Deventer, F. Griessbaum and O. Klemm

Climatology Working Group, University of Münster, 48148 Münster, Germany
Keywords: fluxes, turbulence, urban aerosols, size distribution.
Julian.Deventer@uni-muenster.de

Cities are both sources and sinks for atmospheric aerosol particles. The input of particulate material from the regional background is mostly established through aged accumulation range particles. The emissions originate from combustion processes, yielding large numbers of nano-sized particles, and from re-suspension of coarse particles from the urban surfaces. Size-resolved measurement of turbulent particle fluxes by using the eddy covariance technique is an appropriate tool to study these bi-directional fluxes. A preliminary study showed that emission of ultrafine particles may co-occur with deposition of particles in the micrometer range. This is equivalent to the simultaneous occurrence of positive (upward) number fluxes and negative (downward) mass fluxes (Schmidt and Klemm, 2008).

For this study, we employ two fast aerosol particle spectrometers, a Ultra-High Sensitivity Aerosol Spectrometer (UHSAS) covering the size range between 60 nm and 1 µm diameters, and a Passive Cavity Aerosol Spectrometer Probe (PCASP-X), ranging from 0.1 µm to 10 µm diameter, both from Droplet Measurement Technologies, Boulder, CO, USA. The instrument combination covers the entire size range in over 100 size bins. This will allow the detailed study of aerosol dynamics within the urban boundary layer. Processes are analyzed in combination with the exchange fluxes of sensible heat, water vapor, and carbon dioxide (CO_2).

The measurements are conducted at a 65 m high telecommunication tower in the city of Münster (population ~ 275.000), NW Germany. The tower has been extensively evaluated on its flow distortion effects on turbulent flux measurements (Griessbaum and Schmidt, 2009), by using the large eddy simulation (LES) code Gerris (http://gfs.sourceforge.net/). The well defined site (Schmidt and Klemm, 2008, Schmidt et al., 2008, Dahlkötter et al., 2010) is influenced by traffic, industrial sources, vegetation, and long range transport.

The presentation will show results of highly size resolved turbulent particle flux measurements, obtained during the 2011 field campaign.

This work is supported by the Deutsche Forschungsgemeinschaft (DFG) under grant KL 623 / 12-1.

Dahlkötter, F., Griessbaum, F., Schmidt, A. and Klemm, O. (2010) Direct measurement of CO_2 and particle emissions from an urban area. *Meteorologische Zeitschrift* **19**, 565-575, doi 10.1127/0941-2948/2010/0492.

Griessbaum, F. and Schmidt, A. (2009) Advanced tilt correction from flow distortion effects on turbulent CO_2 fluxes in complex environments using large eddy simulation. *Quarterly Journal of the Royal Meteorological Society* **135**, 1603-1613.

Schmidt, A. and Klemm, O. (2008) Direct determination of highly size-resolved turbulent particle fluxes with the disjunct eddy covariance method and a 12 – stage electrical low pressure impactor. *Atmospheric Chemistry and Physics* **8**, 7405-7417.

Schmidt, A., T. Wrzesinsky, O. Klemm, (2008) Gap filling and quality assessment of CO2 and water vapour fluxes above an urban area with radial basis function neural networks. *Boundary-Layer Meteorology* **126**, 389-413.

Transport and mixing of aerosols due to highway-generated turbulence

M. Gordon[1], R.M. Staebler[1], J. Liggio[1], J. Brook[1], S.-M. Li[1], J. Wentzell[1], C. Mihele[1], G. Lu[1], and P. Lee[1]

[1]Air Quality Research Division, Environment Canada, Toronto, Ontario, M3H 5T4, Canada
Keywords: Traffic emissions, Turbulence, Aerosol measurement, Air quality
Presenting author email: mark.gordon@ec.gc.ca

Primary and secondary aerosols from traffic emissions can have a considerable impact on local and regional air quality. Often, the inventories which provide emissions input for the air quality models rely on laboratory testing of individual vehicles under non-ambient conditions. However, on the sub-grid scale, turbulence induced by both highway structure and traffic flow will modify the gradient of aerosol concentration and influence particle evolution. This may lead to rapid changes in the aerosol size distribution in the first few seconds after emission. These effects are missing from air-quality models, and a careful analysis of field data is necessary to quantify their impact.

A study of the sub-grid evolution of aerosols (FEVER; Fast Evolution of Vehicle Emissions from Roadways) was conducted in the Toronto area in the summer of 2010. The study included mobile measurements of turbulence using two sonic anemometers and an aircraft turbulence probe (AIMMS-20, which also measured GPS and inertial motion sensing), particle size distributions with a Fast Mobility Particle Sizer (FMPS), aerosol composition with an Aerodyne aerosol mass spectrometer (AMS), black carbon (SP2), VOCs (PTR-MS) and other trace gases. Stationary sites upwind and downwind of the highway measured wind speed, turbulence, particle size distributions with a Scanning Mobility Particle Sizers (SMPS), and traffic density, composition, and speed. On-highway measurements were also made to characterize the generation of turbulence according to vehicle type.

Turbulent kinetic energy (TKE) was measured with a stationary sonic anemometer located at the side of the highway. As wind changes direction, the time taken for an air parcel crossing the road to reach the measurement point also changes. Hence, the stationary measurements can demonstrate the reduction in TKE with increasing time from the road, as shown in Fig. 1. The mobile lab was driven perpendicular to the highway to sample air at varying distances downwind. TKE measurements from the mobile lab are compared to stationary TKE measurements in Fig. 1, demonstrating a good agreement.

Size distributions measured with an FMPS on the mobile lab were binned by time from the road, as shown in Fig. 2. These distributions demonstrate the dilution of the three modes with increasing time (and distance) from the highway. These results are taken from transects during a morning rush hour. Analysis of 23 other morning and evening rush-hours is currently underway to investigate the dilution rates of different modes and changes in particle diameter with distance from the highway.

These preliminary results demonstrate a strong enhancement of turbulence near the highway. On-road measurements and investigation of TKE as a function of traffic density and vehicle type suggest that the enhancement of turbulence is primarily due to heavy vehicles. This enhanced turbulence influences aerosol concentration, and may influence size and composition. Ongoing analysis is underway to parameterize highway-generated turbulence as function of traffic type and density and to investigate the effect of turbulence on the physical and chemical evolution of aerosols.

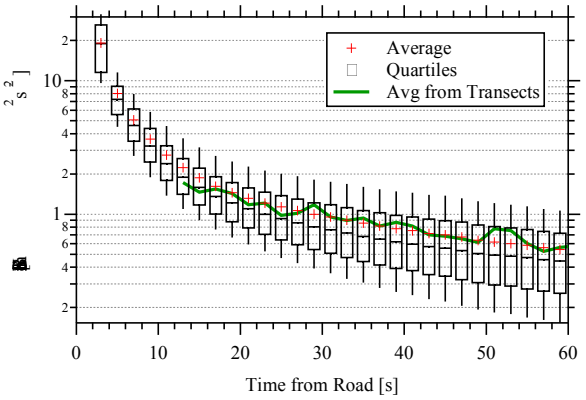

Figure 1. Turbulent kinetic energy measured at the roadside as a function of time from the road along the wind direction.

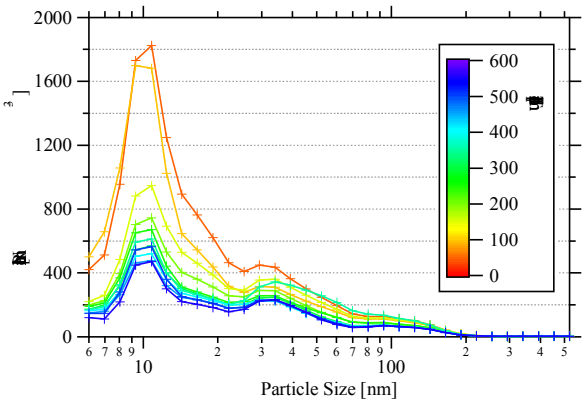

Figure 2. FMPS size distributions measured from the mobile lab binned by time from the road along the wind direction.

This work was supported by Environment Canada and the Program of Energy Research and Development (PERD), administered by Natural Resources Canada.

Submicronic aerosols dry deposition on urban surfaces: a wind tunnel study to improve the lack of knowledge

P. Roupsard[1], M. Amielh[2], A. Coppalle[3], H. Branger[2], P. Laguionie[1], O. Connan[1], D. Hébert[1], D. Maro[1] and M. Talbaut[3]

[1]Laboratoire de Radioécologie de Cherbourg-Octeville, IRSN, 50130 Cherbourg-Octeville, France
[2]Institut de Recherche sur les Phénomènes Hors Equilibre, UMR 6594, CNRS, 13384 Marseille, France
[3]COmplexe de Recherche Interprofessionnel en Aérothermochime, UMR 6614, 76801 Saint Etienne du Rouvray, France
Keywords: dry deposition, deposition velocity, urban area
Presenting author email: pierre.roupsard@irsn.fr

Introduction

In the case of an accidental or chronic atmospheric pollution by a nuclear plant, aerosols deposition transfer coefficients must be known. A major issue is to determine the impact of aerosols contained in the radioactive plume on urban areas. In dry atmospheric conditions, transfer coefficients are defined by the dry deposition velocities Vd ($m.s^{-1}$), the ratio between the aerosol vertical dry deposition flux ($particles.m^{-2}.s^{-1}$) and the concentration of aerosols ($particles.m^{-3}$; Seinfeld and Pandis, 1998). Dry deposition velocities are dependent on atmospheric turbulent conditions and surface roughness. Actually, for urban surfaces, only a few dry deposition velocities were measured, in field or in laboratory environments. Moreover, existing data are not linked with atmospheric conditions (Fowler *et al*, 2009). Therefore, it is important to improve the knowledge and the models on urban areas.

The aim of this wind tunnel study was to quantify, experimentally, dry deposition velocities for a submicron aerosol on three different urban surfaces, for three different wind speeds (U_{ref}). We measured also air turbulence intensities and friction velocities U_* in the wind tunnel.

Test equipment and methods

Experiments were conducted in April 2010 in the IRPHE closed-circuit wind tunnel (8.7 m x 0.7 m x 0.3 m). Dry deposition has been studied successively on glass, cement facing and synthetic grass with U_{ref} equals to 1.3, 5.0 and 10 $m.s^{-1}$. The bottom of the tunnel was totally recovered with each type of studied surface to develop the characteristic boundary layers. Deposition velocities were measured at three distances from the tunnel entrance (1, 5 and 7 m). A monomodal polydisperse submicron fluorescein aerosol, representing the accumulation mode of the atmospheric aerosol, was generated and injected in the wind tunnel (Maro *et al*, 2010). Spectrofluorimetric measurements of deposited aerosols on squares of each urban-type surface gave deposition fluxes. Spectrofluorimetric measurements of aerosols taken on filters gave aerosol concentrations in the wind tunnel.

Turbulence intensity, friction velocity and air velocity measurements were made by hot wire anemometry at three distances (1, 5 and 7 m) for each type of surface and at the three flow velocities U_{ref}.

Results and discussions

Friction velocity increased with wind speed and surface roughness. This study showed a significant increase of the deposition velocity with the surface roughness and with the wind speed (figure 1). But the increase due to surface roughness was much more important than the increase due to wind speed.

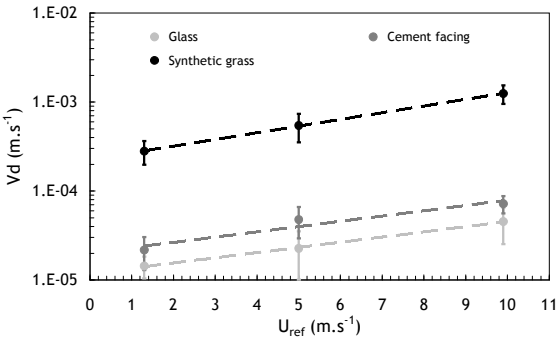

Figure 1. Dry deposition velocity Vd function of air flow velocity U_{ref}.

We found also that the ratio between deposition velocity and friction velocity on each surface was not constant (Table 1).

Table 1. Mean Vd/U_* ratio function of substrate

Substrates	Vd/U_* ($.10^{-3}$)
Glass	0.05 ± 0.05
Cement facing	0.11 ± 0.05
Synthetic grass	1.2 ± 0.3

These experiments in wind tunnel are the first step of a future study on the dry deposition in urban areas. The next step will be *in situ* experiments to take into account all the atmospheric parameters existing in urban environments.

D. Maro *et al* (2010) *Proc. 8th Int. Aero. Conf.*, Helsinki.
J. H. Seinfeld, S. N. Pandis (1998) *Atmospheric Chemistry and Physics*, Wiley-Interscience.
J. Cousteix (1989) *Aérodynamique : Turbulence et Couche Limite*, Cepaduès-Edition.
D. Fowler *et al* (2009) *Atmos. Env.* 43, 5193-5267.

Thursday, September 8, 2011

Session 10E: Spark Generators for Nanoparticle Generation

Generation of Au-Ge nanocomposites by spark discharge

S. Kala, F.E. Kruis and R. Theissmann
Institute for Nanostructures and Technology, Faculty of Engineering Science and Center for Nanointegration Duisburg-Essen (CeNIDE), University of Duisburg-Essen, Duisburg, 47057, Germany
Keywords: composite nanoparticles, aerosol generation
Presenting author email: shubkala@gmail.com

Spark discharge has been succssfully applied to generate metallic nanoparticles (Schwyn et al., 1988). However, this technique is not fully explored to synthesize metal-semiconductor (M-S) nanocomposites, which is indeed a challenging task. M-S nanocomposites allow to manipulate the physical, chemical, optical and mechanical properties of the resultant material via an interaction between metal and semiconductor atoms. Optical coupling of semiconductor nanoparticles with metal nanoparticles can be a viable route to modify the spectral features of semiconductor nanoparticles or vice versa. For example, surface plasmon resonance of Au nanoparticles can be utilized to enhance the emission of semiconductors nanoparticles (Bassu et al., 2010).

In this study, the ability of the spark discharge technique to prepare M-S nanocomposite is demonstrated. To prepare M-S nanocomposite, conditions of electrical breakdown are created between Au, which is connected to high voltage supply with positive polarity and Ge, which is grounded. Electrical breakdown between Au and Ge, which act like anode and cathode, respectively, occurs at ~ 4kV. On electrical breakdown, both Au and Ge evaporate and which on subsequent cooling in the carrier gas (high purity N_2) form a mixture of Au and Ge nanoparticles by nucleation and condensation. The size-distribution of the generated mixed particles is monitored by a scanning mobility particles sizer on varying the carrier gas flow rate (1-10 slm) and charging current (1-10mA), leading to spark frequencies between 8 and 120 Hz. As the cathode material experiences more erosion, therefore, in the generated mixture the atomic percentage (at.%) of Ge must be larger than Au. However, on changing the spark frequency from 8 to 120 Hz, atomic ratio of Au:Ge is found to be vary largely from 2:98 to 70:30 in the generated mixtures (shown in Table 1), as measured by energy dispersive x-ray spectroscopy. The large change in the at.% of Au in the generated mixture with the increase in spark frequency is found to be due to voltage reversal during discharging.

Table 1. Atomic percentage of Au and Ge in the AuGe mixture generated at different charging current/spark frequencies

Current (mA)	Spark frequency (±error)	Atomic %	
		Au	Ge
1	8 (±4)	2.20	97.80
2	21 (±8)	3.29	96.71
5	55 (±10)	16.96	83.04
7	74 (±10)	30.09	69.91
10	120 (±5)	70.02	29.98

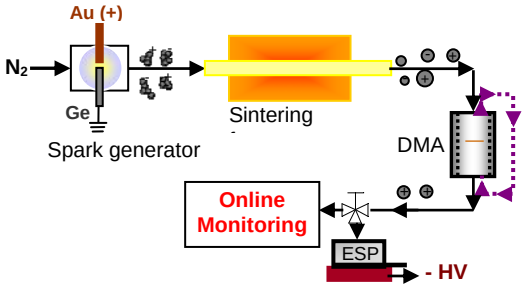

Figure 1. Schematic representation of different components utilized to prepare AuGe nanocomposites.

To convert the AuGe mixture into more defined composite nanoparticles, additional sintering and size-selection steps have been included, as shown in Figure 1. AuGe mixture generated (with carrier gas flow of 2 slm) at 55 and 74 Hz spark frequencies are first sintered at 900°C then size fractionated by a differential mobility analyzer (DMA) (with sheath gas flow of 20 slm). Size-selected nanocomposites of mobility diameter of 20 nm prepared with a frequency of 55 Hz, revealed that AuGe alloy nanoparticles of sizes 1-6 nm are embedded in the Ge matrix (Figure 2(a)). The size of the embedded AuGe alloy particles in the Ge matrix is found to increase up to 10-20 nm as shown in Figure 2(b), if prepared with a frequency of 74 Hz.

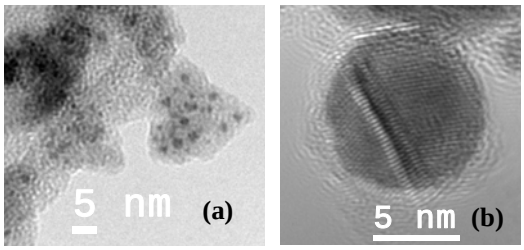

Figure 2. HRTEM images of synthesized AuGe nanocomposites prepared at spark frequencies of (a) 55 and (b) 74 Hz.

This work is supported by the Deutsche Forschungsgemeinschaft in the framework of the collaborative research program “Nanoparticles from the gas phase” (SFB 445).

Bassu, M., Strambini, M.L., Barillaro, G. and Fuso, F. (2010) *Appl. Phys. Lett*. **97** 143113(1-3).

Schwyn, S., Garwien, E. and Schmidt-Ott, A. (1988) *J. Aerosol. Sci*. **19:5** 639-642.

In situ high pressure XPS investigations of PdAg alloy nanoparticles: Towards cheaper catalysts

M.E. Messing[1], S. Blomberg[2], N.M. Martin[2], J. Gustafson[2], J.N. Andersen[2], L.E. Walle[3], A. Borg[3], H. Grönbeck[4], M.E. Grass[5], Z. Liu[5], E. Lundgren[2] and K. Deppert[1]

[1]Solid State Physics, Lund University, Lund, 221 00, Sweden
[2]Synchrotron Radiation Research, Lund University, Lund, 221 00, Sweden
[3]Department of Physics, NTNU, Trondheim, 7491, Norway
[4]Competence Centre for Catalysis, Chalmers University of Technology, Gothenburg, 412 96, Sweden
[5]Chemical Sciences Division, Lawrence Berkeley National Laboratory, Berkeley, CA 94720, USA
Keywords: catalysis, spark discharge, nanoparticle production, nanoparticle application.
Presenting author email: maria.messing@ftf.lth.se

Due to the huge economic and environmental rewards, one major goal in catalysis related research is to create cheaper catalysts. As catalysis happens on the surface of the catalyst, one possible way to realize this would be to dilute the more expensive active material with a less costly one, providing that the active material stays at the surface. This could be achieved by using a material which is less prone to interact with the reactant gases, such as a cheaper noble metal. In most catalysts, the active material is dispersed in a high area complex oxide support as nanoparticles. In order to maintain the high activity, it would be necessary to ensure that the active material is at the surface of the nanoparticle.

In the present contribution we investigate whether this approach towards cheaper catalysts is viable. We report on our findings from attempts to produce PdAg alloy particles using aerosol generation and deposition. The use of PdAg is motivated by the fact that Pd segregates to the surface in the presence of a reactive gas while Ag segregates in ultra-high vacuum (UHV) and that Ag is considerably less expensive than Pd.

Agglomerate PdAg nanoparticles were generated by a commercial spark discharge generator, using one Pd and one Ag electrode. In order to enable size-distribution measurements, reshaping of the agglomerate particles, and controlled depositions of the produced particles, the spark generator was connected to an aerosol nanoparticle system (Messing *et al.*, 2009; Messing *et al.*, 2010). This system includes a neutralizer, a tandem-DMA setup for size selection and size distribution measurements, a compaction furnace for reshaping of the particles and an electrostatic precipitator for controlled deposition of the particles. Scanning electron microscopy (SEM), transmission electron microscopy (TEM), x-ray energy dispersive spectrometry (XEDS) and high pressure x-ray photoelectron spectroscopy (XPS) have been carried out to thoroughly characterize the PdAg particles.

TEM images reveal that most particles are single crystalline, with a thin amorphous shell. From XEDS the composition are measured to approximately 75 atomic% Pd and 25 atomic% Ag. In Figure 1 Ag $3d_{5/2}$ core level XPS spectra from the PdAg particles are compared to the corresponding spectra of a $Pd_{75}Ag_{25}$ (100) single crystal and a (110)-oriented Ag crystal. The Ag $3d_{5/2}$ binding energy for the nanoparticles compares well with the bulk contribution for $Pd_{75}Ag_{25}$ (100) which in turn is shifted by 0.5eV relative to the bulk value in pure Ag. From this observation, we therefore conclude that the PdAg alloy particles consist of a proper alloy and not Ag and Pd in separate phases. In addition, corresponding Pd 3d spectra strongly indicate that the active Pd is present at the surface of the PdAg particles in the presence of reactant gases.

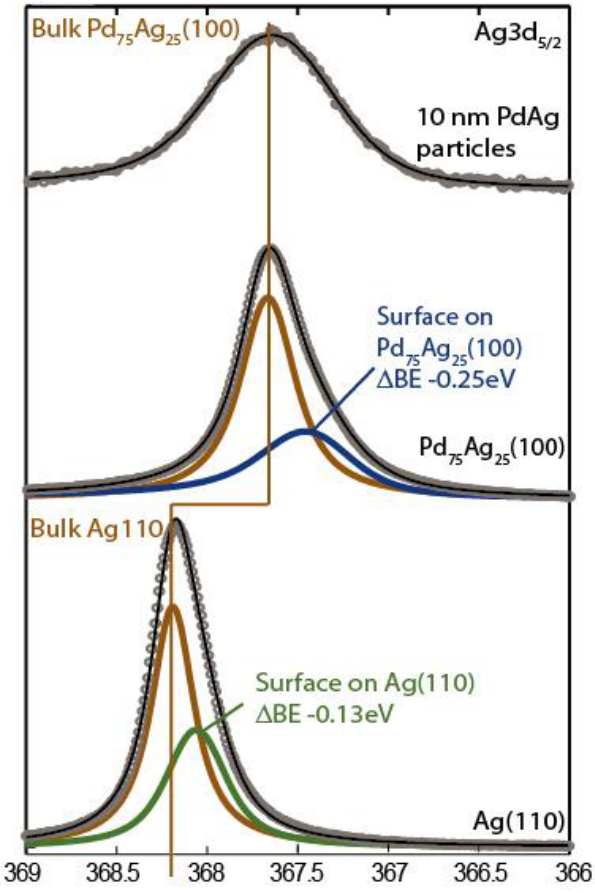

Figure 1. Ag $3d_{5/2}$ core level spectra from Ag(110), $Pd_{75}Ag_{25}$(100) and the aerosol PdAg particles.

This work was supported by the Nanometer Structure Consortium at Lund University (nmC@LU).

Messing, M.E. *et al.* (2009) *Gold. Bull.* **42**, 20-26.
Messing, M.E. *et al.* (2010) *J. Phys. Chem. C* **114**, 9257-63.

Direct Synthesis of Magnesium Hydride using Spark Discharge

T.V. Pfeiffer[1], A. Anastasopol[2], V.A. Vons[1], W.J. Legerstee[2], S.W.H. Eijt[2], F.M. Mulder[2] and A. Schmidt-Ott[1]

[1]Nanostructured Materials, Department of Chemical Engineering, Applied Sciences, Delft University of Technology, 2628 BL 136, the Netherlands
[2] Fundamental Aspects of Materials and Energy, Department of Radiation, Radionuclides & Reactors, Faculty of Applied Sciences, Delft University of Technology, 2629 JB 15, Delft
Keywords: spark discharge, hydrogen storage, nanoparticles, generation, metalhydrides.
Presenting author email: t.v.pfeiffer@tudelt.nl

Magnesium hydride is a promising cheap hydrogen storage material, with a high gravimetric storage capacity. A major drawback is the high stability of magnesium hydride, which leads to high desorption temperatures. A possible solution to this problem could be the use of the orthorhombic γ-MgH_2 phase, which shows a desorption temperature 64 K lower than the regular β-MgH_2 (Huot, 2001). However, this particular metastable phase typically only forms at pressures in excess of 8 GPa and disappears after dehydrogenation, which so-far limits its usefulness in automotive applications.

Spark discharge is an aerosol-based nanoparticle production method, in which target electrodes are ablated by repetitive capacitive high-voltage discharges. The formed vapour rapidly condenses in a flow of inert gas to form nanoparticles. The high quench rates on the order of 10^7 K/s allow for the formation of non-equilibrium phases or amorphous structures. This research aims to provide a means of producing nanoparticulate metastable hydrides in aerosol form.

Experimental

Hydrided magnesium nanoparticles were synthesised *in situ* by the spark discharge method. Two magnesium electrodes were used in a flow of Ar containing 5% H_2 (figure 1). To limit oxidation, the setup is built using UHV-grade components, and water and oxygen are removed via absorbent columns. With this method it is possible to produce Mg nanoparticles with reversible hydrogen storage properties and limited MgO formation, as described in detail by Vons (in press).

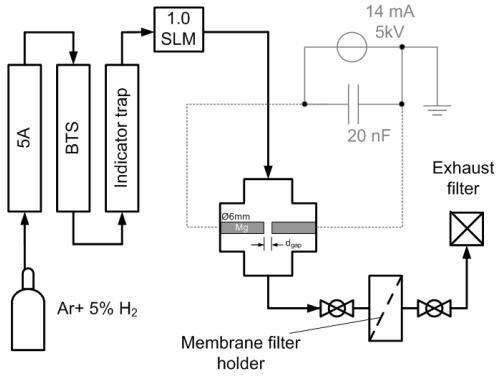

Figure 1. Spark discharge setup.

Structural analysis of the as-produced powders was performed using XRD and TEM. The hydrogen storage properties were evaluated using Thermal Desorption Spectroscopy and Sievert's analysis. The maximum temperature was set to 473 K in order to limit re-crystallization within the sample.

Results

XRD of the as-produced powders shows a strong amorphous signal, and further small broadened peaks corresponding to the Mg, MgO and β-MgH_2 phases. After 21h of desorption, the hydride phase is fully replaced by metallic magnesium.

During TEM imaging, the particles change shape and size, probably due to dehydrogenation caused by the electron beam. In addition to the highly agglomerated primary particles typically observed in spark discharge, large (~100nm) continuous domains are formed. There is no evidence of core-shell structures as reported by Förster (2010) for copper in mixtures of nitrogen and hydrocarbons, indicating that a different mechanism for particle formation is at play here.

Hydrogen desorption tests were performed directly on the powders, without any prior activation or charging steps. The desorption rates are surprisingly high for the low temperatures used, despite the absence of a catalyst. The cycling behaviour is currently under investigation. The hydrogen content of the as-produced powders ranges from 0.05-0.7 H/Mg. No suitable explanation for the observed variation in the hydrogen concentrations has been found so far.

Conclusion

Magnesium hydride nanoparticles were synthesised at atmospheric Ar/H_2 pressure from metallic magnesium using spark discharge. The uncatalyzed as-produced metal hydride is mostly amorphous, and can be dehydrogenated at temperatures below 473 K.

Work supported by Agentschap NL, grant EOSLT07052.

Förster H., and Peukert, W. (2010) *International Aerosol Conference 2010*, Helsinki, 1234.

Huot J., Liang G., Boily S., Van Neste, A., and Schulz, R. (1999) *J. All. and Compds.* **293-295**, 495.

Vons V.A., Anastasopol, A., Legerstee, W.J., Mulder, F.M., Eijt, S.W.H., and Schmidt-Ott, A., *accepted, in press* doi:10.1016/j.actamat.2011.01.047

Self-charge Distribution of Nanoparticles Generated by Spark Discharge

K.Barmpounis[1,2], T.V. Pfeiffer[1], V.A.Vons[1], G. Biskos[1,2], A. Schmidt-Ott[1]

[1]Department of Chemical Technology, Delft University of Technology, Delft, 2628-BL, The Netherlands
[2]Department of Environment, University of the Aegean, Mytilene, 81100, Greece
Keywords: Spark discharge, charge distribution.
Presenting author email: K.Barmpounis@tudelft.nl

Introduction

Spark discharge generators are widely used for a controllable and stable production of high-purity aerosol nanoparticles (Schwyn, 1988). The mechanism of particle formation is an evaporation/condensation type process based on a capacitive spark discharge between two target electrodes. The energy contained in the capacitor is discharged in μs time fractions, resulting in localized rapid heating of the electrode surface. Material evaporating from the electrode surfaces is immediately quenched in a flow of inert carrier gas. As the temperature of the vapours decreases downstream the spark discharge region, they coalesce to form atomic clusters that grow to bigger primary particles.

Plasma created in the spark contains charge carriers that determine the charging state of the produced particles. While little is known about the mechanics of the charging process, it appears to favour the charging of small sub-10 nm particles as compared to the Boltzmann equilibrium distribution (Tabrizi 2008). Knowledge of the charge distribution is of great importance because combination of spark generators with mobility classifiers can lead to the production of well-defined nanoparticles. In this work, we report measurements of the charge distribution of Mg particles, produced by a spark discharge generator.

Experimental

Particles from the spark generator are produced in carrier gases of different purity. In the first case (low-purity system), Ar 5.0 is used to run the generator directly from the bottle. In the second case (high-purity system), the Ar 5.0 gas is purified by passing it first over an A4 water-absorbing molecular sieve and an oxygen-absorbing copper catalyst.

Measurements of the charge distribution of the generated particles are performed using a Tandem Differential Mobility Analyzer (TDMA) (Rader and McMurry,1986) coupled with a condensation particle counter (CPC) and an aerosol electrometer (AEM). Particles from the spark generator are passed through the 1st DMA and then through a Kr-85 neutralizer before measuring their mobility distributions by the 2nd DMA and the CPC. Charge distributions on particles of different size are then determined by comparing the mobility distributions with and without the Kr-85 neutralizer**.**

Results

Size distribution measurements of particles produced from Mg electrodes in the high-purity system showed a higher production of positively than negatively charged particles (cf. Fig. 1). Depending on the capacitor charging current, the ratio of positive versus negative particles varied from 8 to 17. For Mg particles generated in the low-purity system this ratio was found to be approximately equal to unity (data not shown here).

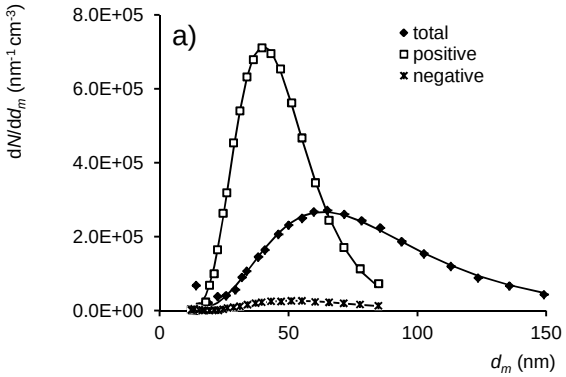

Figure 1. Positively and negatively self-charged Mg particles in purified gas and the total size distribution measured with a neutralizer, at a capacitor charging current of 9 mA. Lines represent lognormal fits to the data.

The high ratio of the positive to negative particles, in the case of high-purity system, can be explained by the absence of water and O_2 molecules. In low-purity gases these molecules capture free electrons, forming negative charge carriers which contribute to the formation of negative particles. In low-purity gases, less electrons are captured by these electronegative species, and the high electron mobility coupled to the electric fields present in the spark generator result in significant losses of electrons to the walls of the system. Hence less negative charge carriers are present in the charging process, leading to smaller amounts of negatively charged particles. Ongoing TDMA measurements aim to determine in more detail the charge distribution of Mg particles produced by the spark discharge.

References

Wiedensohler, A.(1988). *J.Aerosol Sci.*, 19, 387-389

Rader, D. and McMurry,P. (1986), *J.Aerosol Sci*,17,771-787.

Schwyn, S., Garwin, E. & Schmidt-Ott, A. (1988), *J. Aerosol Sci.*, 19(5), 639-642.

Tabrizi, N.S., Ullmann M., Vons V. A., Lafont U., Schmidt-Ott, A (2008). *J. Nanopart. Res.*, 11(2), 315-332.

V.A. Vons (2010). *PhD thesis*, Delft university of Technology.

Spark generated particles for nanotoxicology studies

M.E. Messing[1], C.R. Svensson[2], B.O. Meuller[1], M. Bohgard[2], K. Deppert[1], J. Pagels[2] and J. Rissler[2]

[1]Solid State Physics, Lund University, Lund, 221 00, Sweden
[2]Ergonomics and Aerosol Technology, Lund University, Lund, 221 00, Sweden
Keywords: spark discharge, aerosol particle mass analyzer, nanotoxicology, health effects of aerosols.
Presenting author email: maria.messing@ftf.lth.se

During the last decade there has been an explosion in novel applications and products based on nanoparticles. Although the belief in the great potential of nanoparticles is strong, major concerns with respect to their toxicology have been frequently discussed lately. It is well known that the properties of a specific nano-sized material are different from the properties of the same material in bulk form, and therefore toxicology regulations often based on mass might not be relevant for nano-sized materials. In order to improve the understanding of nanotoxicology and to learn how to handle nanoparticles in a safe way it is of utmost importance to use highly characterized nanoparticles for toxicology investigations.

In the present contribution we describe a route to generation and deposition of very well characterized nanoparticles with respect to size, shape, mass, surface area and crystal structure. The nanoparticles were generated by spark discharge and fed into an aerosol nanoparticle system setup (Messing *et al.*, 2009) for on-line characterization, reshaping and deposition. Tandem differential mobility analyzers (DMA) coupled to an electrometer was used for mobility diameter and number concentration measurements. The particle mass was measured with a DMA-aerosol particle mass analyzer (DMA-APM) coupled to a condensation particle counter (CPC). An electrostatic precipitator was used for controlled particle deposition onto lacy carbon film coated Cu transmission electron microscopy (TEM) grids as well as directly into protein solutions. Primary particle size as well as particle shape and crystal structure were evaluated by TEM. Particle surface area was calculated from the measured primary particle size combined with either the DMA-APM measurements or the idealized aggregate theory (IA) approach. Finally the deposited mass and surface area dosages were calculated for deposition in an air liquid interface (ALI) chamber (Savi *et al.*, 2008) or the alveolar region of the respiratory tract.

Gold particles were used to demonstrate the capability of the setup, although particles of other materials can easily be produced by changing the electrode material in the spark discharge generator (Tabrizi *et al.*, 2009). From the measurements and calculations it is clear that a high enough mass and surface area reported for onset of inflammatory response can be reached in the ALI chamber, if a deposition time of roughly two hours is used. A further key aspect of the setup is the possibility to use a sintering furnace to reshape the as-produced agglomerate particles (Figure 1). By using this approach particles of the same number concentration and mass, but with clearly different surface area can be deposited. This provides for a direct comparison of toxicological response upon surface area, a feature that is believed to play a major role in nanoparticle toxicity. Finally, Dynamic Light Scattering (DLS) showed that when gold particles were deposited into protein solutions, the suspensions were stable for several days, which is promising for future studies.

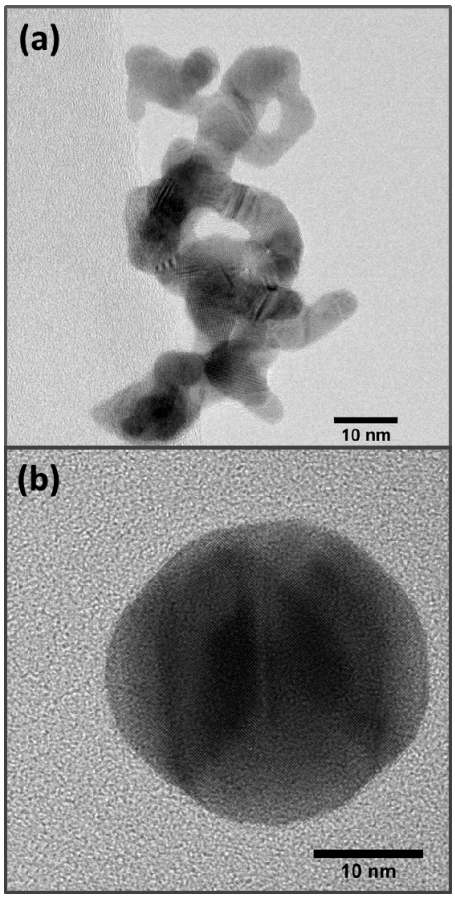

Figure 1. Gold nanoparticles of the same mass (0.24 fg) (a) before and (b) after reshaping. The mobility diameter decreased from 60 to 31 nm upon reshaping.

This work was supported by the Nanometer Structure Consortium at Lund University (nmC@LU) and the Swedish research council FAS through project 2009-1291 and the FAS-centre METALUND.

Messing, M.E. *et al.* (2009) *Gold Bull.* **42**, 20-26.
Savi, M. *et al.* (2008) *Environ. Sci. Technol.* **42**, 5667-74.
Tabrizi, N.S. *et al.* (2009) *J. Nanopart. Res.* **11**, 315-32.

Thursday, September 8, 2011

Session 10F: Modelling Aerosol Formation

H^2O: A new model to predict secondary organic aerosol formation

F. Couvidat[1], Y. Kim[1], K. Sartelet[1] and C. Seigneur[1]
[1]CEREA, Joint Laboratory École des Ponts ParisTech/EDF R&D, Université Paris-Est, 77455 Marne la Vallée, France
Keywords: Aerosol model, Modelling (regional), SOA (Second. Organic Aerosols)
Presenting author email: couvidaf@cerea.enpc.fr

A new secondary organic aerosol (SOA) model H^2O (Hydrophilic/Hydrophobic Organic), which is based on the model developed by Pun *et al.* (2002) is presented and evaluated with measurements over Europe. This model treats the formation of SOA by condensation on an organic phase or an aqueous phase. It distinguishes two kinds of surrogate species: hydrophilic species (which condense preferrentially on an aqueous phase) and hydrophobic species (which condense only on an organic phase). These surrogates species are formed from the oxidation in the atmosphere of Volatile Organic Compounds (VOCs) by radicals (HO, NO_3) and ozone. These VOCs are either biogenic (isoprene, monoterpenes and sesquiterpenes) or anthropogenic (mainly aromatic compounds).

This model includes many processes. It takes into account the effect of NO_X on SOA formation, the dissociation of acids into an aqueous phase, oligomerization of aldehydes, non-ideality of the particulate phase and hygroscopicity of organics.

The H^2O model was used to calculate SOA concentrations over Europe in summer when SOA concentrations are higher. An investigation was realized to find the most important processes for SOA formation. Taking into account the hydrophilic properties of SOA, oligomerization, and the explicit representation of high-NO_X and low-NO_X gas-phase chemical regimes (the extend of this process depends on the gas-phase chemistry model used, different models give different concentrations of radicals). The table below shows the impact of these processes on SOA concentrations.

Processes added	SOA increase
Representation of NO_X regimes	30 to 120%
Hydrophobic and hydrophilic species	46%
Oligomerization of aldehydes	60%

Table 1: Increase of SOA concentrations due to specific processes.

The following table shows the contribution of the main precursors to SOA formation. The biogenic compounds are found to be responsible for the formation of most regional SOA (around 93%) whereas the anthropogenic compounds are found to be a minor contributor. However, anthropogenic compounds have a higher impact in urban areas.

Precursor	Contribution to SOA
Isoprene	34%
Terpenes	59%
Anthropogenic compounds	7%

Table 2: Contributions of main precursors to SOA formation over Europe in summer.

The mean SOA concentration in summer 2001 was found to be around 1.8 $\mu g.m^{-3}$ but SOA concentrations were up to 10 $\mu g.m^{-3}$ in some areas. Concentrations are higher where biogenic emissions of terpenes and isoprene are higher (south and east of Europe).

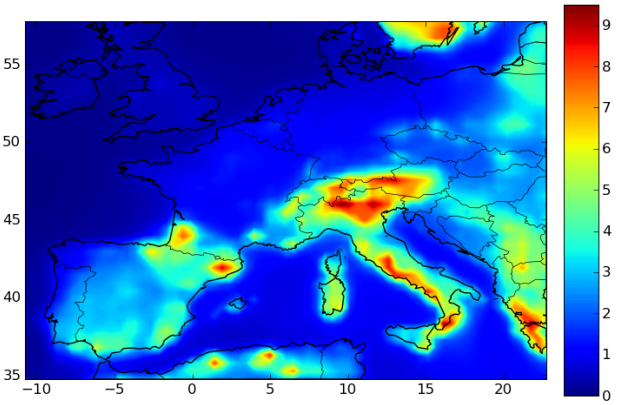

Figure 1: SOA concentrations ($\mu g.m^{-3}$) over Europe in summer 2001.

To test the H^2O model, a simulation over a whole year is conductive and calculated concentrations are compared to measurements.

This work was funded in part by ADEME, the French Agency for the Environment and Energy Management.

Pun, B., Griffin, R., Seigneur, C., and Seinfeld, J. (2002) *J. Geophys. Res.* **107**, 433.

Environmental impact of aviation-produced aerosols: Towards alternative fuels

Rojo, Carolina[1], Vancassel, Xavier[1] and Ponche, Jean-Luc[2]

[1]Department of Physics and Instrumentation, ONERA, 92322, Châtillon, France
[2]LMSCP, University of Strasbourg, 67482, France
Keywords: aircraft plumes, biofuels, particle formation and growth, organics, soot particles.
Presenting author email: carolina.rojo@onera.fr

Environmental impact of anthropogenic emissions and their influence on global warming have become one of scientists' main interests. In this context, aviation plays an important role. Indeed aviation emissions (mainly carbon dioxide, water vapour, nitrogen and sulphur oxides, and soot) are responsible of new particle formation in the aircraft plume, including contrails, and therefore contribute to an increase of the radiative forcing and to the deterioration of local air quality (Lee D.S. *et al.*, 2009).

Use of alternative fuels would help limiting the impact of aviation-produced aerosols. There are currently several alternative fuels being tested to suit aviation regulations and infrastructure (Rahmes T. *et al.*, 2009). Globally, the combustion exhaust tends to present much lower sulphuric acid, aromatics and soot number concentrations (Timko *et al.*, 2010).

Comprehensive studies have already been made on aerosol emissions in aircraft plumes for standard Jet A1 kerosene (*e.g.* Kärcher, 1998, Yu *et al.*, 1999) but few studies are available for alternative fuels, thus a number of uncertainties remain. Indeed use of alternative fuels, reducing simultaneously aromatic and sulphur content, can lead to antagonist effects, having unexpected consequences.

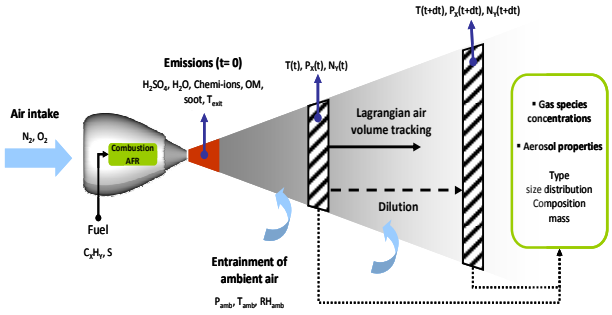

Figure 1. Scheme of the modelised aircraft plume.

The emissions of an aircraft flying with alternative fuel can be simulated by a coupled microphysical-chemical-dynamical trajectory box model (figure 1). Our model which describes the expansion of the jet plume and the evolution of the produced particles has already been tested for standard kerosene. A sensitivity study is carried out, using different fuel sulphur contents, soot particle number and organic concentrations, to simulate the combustion of an alternative fuel. Improvements are currently being made concerning the behaviour of particles in a mixture with a smaller amount of soot, a lower sulphuric acid content and different organic composition, especially regarding droplet freezing and hence contrail formation.

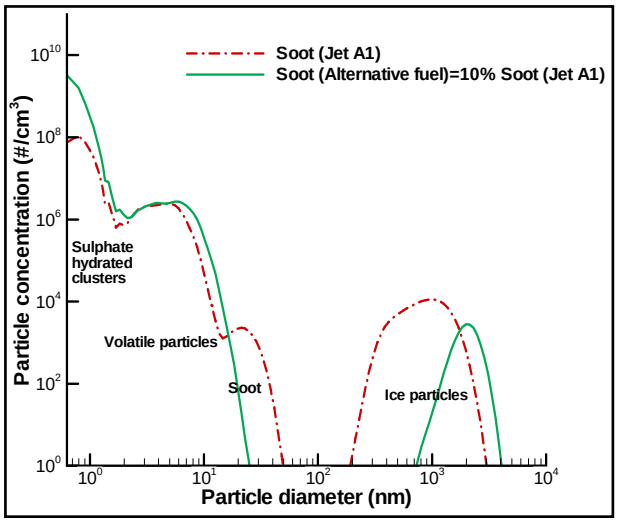

Figure 2. Simulated size distributions of particles in the aircraft plume at ~125 m behind the plane with standard fuel (red dashed) and alternative fuel (green solid).

In figure 2, the influence of soot particle initial number density on contrail formation is depicted for two types of fuel. For a typical jet A1, ice particle size (only formed by heterogeneous freezing) peaks at 1 micrometer at 0.5s in the plume, which corresponds to typical fresh plume contrails. When simulating the combustion of an alternative fuel, we used a reduced soot emission index, by 90%. For such a case, the ice crystals size distribution exhibits a maximum size close to 2 micrometer. This effect is mainly due to the enhanced amount of condensable material available for each crystal.

These differences in the condensation trails have an impact on the radiative budget of the atmosphere. The calculation of the optical depth of the two different contrails could clarify which fuel contributes the most to global warming. But reducing soot initial concentrations at the nozzle exit may promote other ice nucleation paths and homogeneous freezing must be revised.

Kärcher B. (1998) *J. Geophys. Res.*, **103**, 14, 17129-17147.
Lee D. *et al.*, (2009) *Atmos. Env.*, **43**, 3520-3537.
Rahmes T. *et al.*, (2009) *9th ATIO Conference*, AIAA 2009.
Sorokin A., Vancassel X. and Mirabel P., (2001) *Phys. Chem. Earth.*, **26**, 8, 557-561.
Timko M. *et al.*, (2010) *Energy & Fuels*, **24**, 5883-5896.
Yu F., Turco R. and Kärcher B. (1999). *J. Geophys. Res*, **104**, 4, 4079-4087.

Automatic classification of new particle formation events

H. Junninen[1], M. Paramonov[1], A. Hirsikko[1], M. Dal Maso[1], M. Kulmala[1]

[1] University of Helsinki, Department of Physics, P. O. Box 48, FI-00014 UHEL, Helsinki, Finland

Keywords: nucleation mode, number size distribution, automatic classification
Presenting author email: Heikki.junninen@helsinki.fi

Regional new particle formation (RNPF) appears with great regularity during the day time and very rarely, if ever, during the night. In order to observe particle formation and subsequent growth up to 100nm the air masses have to remain the same for a long time (up to 12 hours). For this reason one can analyze the continuous data a day at a time and classify days as RNPF event days and non-event days. Dal Maso et. al. (2005) developed a classification method for classification of days. The method is based on visual observation of size distributions, in order reduce subjective aspect of the result the analysis are performed in group of 3-4 persons. While being a powerful method, it is still subjective and very difficult to adapt to different group of people and to get comparable results, say between two different research groups. To address this problem a new automatic classification algorithm was developed.

The method is based on self-organizing map. Self-organizing map (SOM) is the most popular unsupervised artificial neural network algorithm. It solves difficult high-dimensional and nonlinear problems and makes projection into a low-dimensional space while keeping most of the information (Kohonen 1995).

For the RNPF classification algorithm we taught SOM (Figure 1) with different teaching data. For the final classification of unknown day we search for the best matching unit (SOM neuron with smallest Euclidean distance) from each SOM. From the best matching unit statistics on testing data we get the probability for the day to belong to a class event, non-event or undefined.

For teaching the algorithm we used 11 year aerosol size distribution data measured in Hyytiälä, Finland and 3 years in Värriö, Finland. Both places are located in rural background area and consequently the model works only for rural stations.

Data was divided randomly into 3 parts, teaching (3/5), validation (3/20), and testing (1/4) data. Over-fitting of the algorithm was avoided by monitoring errors in both, teaching and validation data.

The new algorithm performed well compared to traditional classification method. The days with RNPF-event are clearly different from all other type of days and the performance of the new algorithm is the best for these days. 92% of RNPF days were classified similarly by the two methods. Less than 1% of the event days were classified as non-event days and <8% as undefined days. When verifying the misclassified days manually we found that these misclassified days were problematic also for human to classify. These days were on the edge of being in one or in other class.

The biggest disagreement between methods was found in the class of undefined days. This class is actually left over class and not a real class, it contains great number of different type of days and there is no clear feature to describe this class.

When testing the model classification robustness from different sampling site, we found that for same type of sites the performance is equally good. However, if testing site has type of RNPF event that are totally missing from teaching data the algorithm has problems to classify these correctly.

In the presentation the algorithm description and performance in different stations will be discussed in details.

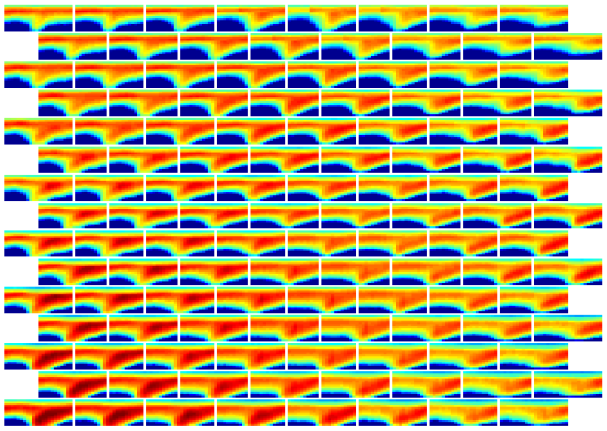

Figure 1. Self-organizing map of new particle formation days.

Dal Maso, M., Kulmala, M., Riipinen, I., Wagner, R., Hussein, T., Aalto, P .P., Lehtinen, K. E. J. *Boreal Environ. Res.* **10**, 323-336 (2005)

Kohonen, T. (1995). *Series in Information Sciences*, Vol. 30. Springer, Heidelberg.

Primary versus secondary contributions to particle number concentrations in the European boundary layer during the EUCAARI campaign

C. L. Reddington[1], K. S. Carslaw[1], D. V. Spracklen[1], M.G. Frontoso[2], L. Collins[1], J. Merikanto[1,3], A. Minikin[4], T. Hamburger[4], H. Coe[5], M. Kulmala[3], P. Aalto[3], H. Flentje[6], C. Plass-Duelmer[6], W. Birmili[7], B. Wehner[7], A. Wiedensohler[7], T. Tuch[7], A. Sonntag[7], C. D. O'Dowd[8], S. G. Jennings[8], R. Dupuy[8], U. Baltensperger[9], E. Weingartner[9], H-C. Hansson[10], P. Tunved[10], P. Laj[11], K. Sellegri[12], J. Boulon[12], J. P. Putaud[13], C. Gruening[13], P. Roldin[14], M. Moerman[15], N. Mihalopoulos[16], G. Kouvarakis[16], V. Zdimal[17], N. Zikova[17], A. Marinoni[18], P. Bonasoni[18] and R. Duchi[18]

[1]Institute for Climate and Atmospheric Science, University of Leeds, Leeds, UK. [2]C2SM- ETH Zürich, Zürich, Switzerland. [3]Division of Atmospheric Sciences, Department of Physics, University of Helsinki, Helsinki, Finland. [4]Deutsches Zentrum für Luft- und Raumfahrt, Institut für Physik der Atmosphäre, Oberpfaffenhofen, Germany. [5]School of Earth, Atmospheric and Environmental Sciences, University of Manchester, Manchester, UK. [6]Deutscher Wetterdienst, Meteorologisches Observatorium Hohenpeissenberg, Germany. [7]Leibniz Institute for Tropospheric Research, Leipzig, Germany. [8]Physics & Centre for Climate and Air Pollution Studies, National University of Ireland Galway, Galway, Ireland. [9]Paul Scherrer Institut, Labor für Atmosphärenchemie, 5232 Villigen, Switzerland. [10]Institute for Applied Environmental Research, Stockholm University, Stockholm, Sweden. [11]UJF-Grenoble 1 / CNRS, LGGE UMR 5183, Grenoble, F-38041, France. [12]Laboratoire de Météorologie Physique, CNRS, Université Blaise Pascal, Aubière cedex, France. [13]European Commission, Joint Research Centre, Institute of Environment and Sustainability, Ispra, Italy. [14]Division of Nuclear Physics, Lund University, Lund, Sweden. [15]Netherlands Organisation for Applied Scientific Research TNO, Utrecht, The Netherlands. [16]Environmental Chemical Processes Laboratory, Department of Chemistry, University of Crete, Heraklion, Crete, Greece. [17]Institute of Chemical Process Fundamentals of the AS CR, Prague, Czech Republic. [18]CNR- Institute for Atmospheric Sciences and Climate, Bologna, Italy.

Keywords: aerosol modelling, size distribution, number concentration, nucleation, emissions.

Presenting author email: c.reddington@see.leeds.ac.uk

We use the global aerosol microphysics model, GLOMAP (Spracklen *et al.*, 2005) and observations made during the EUCAARI field campaign in May 2008 to better understand how primary particle emissions and secondary particle formation influence particle number concentrations in the European boundary layer (BL), and how the influence varies across the particle size distribution. Observations are available from the DLR Falcon 20 aircraft and from 15 field sites in the EUSAAR and GAW networks, and include measured non-volatile and total particle number size distributions.

In large-scale models there is considerable uncertainty associated with parameterisations for secondary particle formation and for the prescribed emission size distribution of primary particles, leading to uncertainties in predicted total particle and cloud condensation nuclei concentrations (Merikanto *et al.*, 2009). Here, we test four different parameterisations for BL nucleation including the activation and kinetic mechanisms (e.g. Sihto *et al.*, 2006), and two newly developed organic vapour mechanisms (Paasonen *et al.*, 2010). We also test different assumptions for the emission sizes of carbonaceous aerosol from Dentener *et al.* (2006) (AEROCOM) and Stier *et al.* (2005); varying by a factor of ~2 (hence a factor ~8 difference in the emitted number concentrations for fixed mass).

The AEROCOM size assumptions may be too small to be appropriate for a large-scale model as used here, but lead to best agreement between modelled and observed number concentrations of particles >50 nm dry diameter (N_{50}). In an experiment without BL nucleation, the normalised mean bias between modelled and observed N_{50} at the field sites is small (-5%). The aircraft observations confirm these findings; measurements of non-volatile and Aitken-mode particle concentrations in the BL agree best with the model when we assume small emission sizes. An hourly time series analysis shows that at roughly half the field sites the difference between modelled and observed N_{50} is statistically insignificant at the 99% confidence level. We find that, although BL nucleation increases simulated N_{50} over Europe by ~10–50% (depending on the mechanism and assumed emission sizes); the contribution is difficult to detect within the uncertainty of the observations and assumptions about primary emissions. To partly resolve this, we have implemented a new emission inventory (Denier van der Gon *et al.*, 2010) based on emitted particle number concentrations and size rather than mass.

For particles <50 nm, the difference between model number concentrations and the observations is statistically insignificant at 7 sites only if some form of BL nucleation is included. However, the agreement between hourly time series of modelled and observed nucleation events in this period is poor, and precludes any attempt to identify the best nucleation mechanism from such a short dataset.

This work was supported by funding from the EU's 6th Framework Programme project, EUCAARI.

Denier van der Gon, H, Visschedijk, A., Johansson, C., *et al.* (2010) IAC 2010, Helsinki, Abstract 1E1.

Dentener, F., Kinne, S., Bond, T., *et al.* (2006) *Atmos. Chem. Phys.* **6**, 4321-4344.

Merikanto, J., Spracklen, D.V., Mann, G.W., *et al.* (2009) *Atmos. Chem. Phys.* **9**, 8601-8616.

Paasonen, P., Nieminen, T., Asmi, E., *et al.* (2010) *Atmos. Chem. Phys.* **10**, 11223-11242.

Sihto, S.-L., Kulmala, M., Kerminen, V.-M., *et al.* (2006) *Atmos. Chem. Phys.* **6**, 4079-4091.

Spracklen, D. V., Pringle, K. J., Carslaw, K. S., *et al.* (2005) *Atmos. Chem. Phys.* **5**, 2227-2252.

Stier, P., Feichter, J., Kinne, S., *et al.* (2005) *Atmos. Chem. Phys.* **5**, 1125-1156.

Organic Aerosol over Europe: Model Evaluation and Response to Increasing Temperature

C. Fountoukis[1], A. Megaritis[2], P.N. Racherla[1,3], P.E. Haralabidis[4], H. D. van der Gon[5], C. Pilinis[4], and S.N. Pandis[1,2,6]

[1]Institute of Chemical Engineering & High Temperature Chemical Processes, Foundation for Research & Technology-Hellas (FORTH), 26504, Patras, Greece
[2]Department of Chemical Engineering, University of Patras, GR-26500, Patra, Greece
[3]NASA Goddard Institute for Space Studies, New York, NY 10025, USA
[4]Department of Environment, University of the Aegean, University Hill, 81100, Mytilene, Greece
[5]TNO Built Environment and Geosciences, Netherlands
[6]Department of Chemical Engineering, Carnegie Mellon University, Pittsburgh, PA 15213, USA

Keywords: Regional CTM, organic aerosol, VOCs, volatility, aging, EUCAARI.
Presenting author email: cfountoukis@iceht.forth.gr

Organic aerosol (OA), although a significant component of submicron particles throughout the world, is poorly simulated by predictive models. Current CTMs consistently underpredict OA mass concentrations at the surface during summertime conditions. Chemical transport models have traditionally treated POA as non-volatile and non-reactive and SOA as semi-volatile products of VOCs' oxidation (Kanakidou et al., 2005). However, several recent studies have shown that POA is semi-volatile while SOA can be seriously underpredicted by models that use traditional SOA precursors and do not take into account further oxidation of these compounds.

In this study we applied PMCAMx-2008, a 3-D CTM, to the European domain, in order to simulate the OA formation during the months of May 2008 and February 2009. PMCAMx-2008 includes the recently developed volatility basis set framework to describe OA absorptive partitioning by organizing the total OA mass into surrogates along an axis of volatility (Donahue et al., 2006; Stanier et al., 2008). We evaluated the performance of the model against AMS measurements taken during the above periods from various sites in Europe. The model predictions were compared against the Positive Matrix Factorization analysis of AMS observations.

PMCAMx models the processes of horizontal and vertical advection, horizontal and vertical dispersion, wet and dry deposition, gas phase chemistry, inorganic aerosol growth, aqueous phase chemistry and SOA formation and growth. The modeling domain covers a 5400 × 5832 × 6 km region in Europe with 36 × 36 km grid resolution.

Figure 1 shows the PMCAMx average predictions over the month of May 2008 for total ground OA mass concentration. The model predicts that fresh primary OA (POA) is a small contributor to organic PM concentrations in Europe during late spring, and that oxygenated species (oxidized primary and also biogenic secondary) dominate the ambient OA.

Sensitivity runs were also conducted to test the response of the predicted OA concentrations over Europe to i) a temperature increase of 2.5 and 5 K, and ii) 5 different emission reduction scenarios.

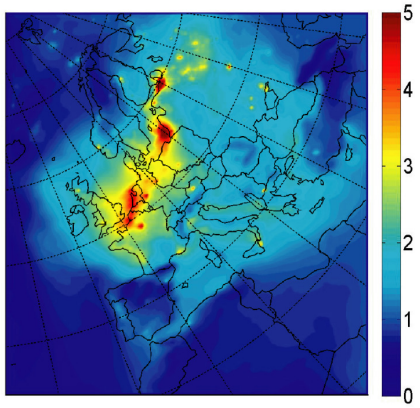

Figure 1. PMCAMx predicted average ground total OA concentrations (μg m^{-3}) for May 2008.

Assuming a uniform temperature increase of 2.5 and 5 K the model predicts significant increases of the OA during May due mainly to the increase in biogenic VOC emissions. The fresh POA is predicted to decrease due to evaporation, while the anthropogenic secondary OA to increase due to acceleration of its chemical production. The net increases are up to 25% of OA for a 5 K temperature increase. During the winter the situation is different because the OA is predicted to decrease for warmer conditions. This is due to the small biogenic SOA contribution to OA and the dominance of fresh POA during this cold low-photochemical activity period.

This work was supported by the European Integrated project on Aerosol Cloud Climate and Air Quality Interactions (EUCAARI).

Donahue, N.M., et al. (2006) *Environ. Sci. Technol.*, 40, 2635-2643.
Kanakidou, M., Seinfeld, J.H., Pandis, S.N., et al. (2005) *Atmos. Chem. Phys.*, 5, 1053-1123.
Stanier, C.O., Donahue, N., and Pandis, S.N. (2008) *Atmos Environ*, 42, 2276-2299.

Multi-scale modeling of aerosol formation in pipe flow

C. Winkelmann[1], A.K. Kuczaj[1], S. Stolz[1,2] and B.J. Geurts[2,3]
[1]Philip Morris International R&D, Philip Morris Products SA, 2000 Neuchâtel, Switzerland
[2]Department of Applied Mathematics, University of Twente, 7500 AE Enschede, The Netherlands
[3]Department of Applied Physics, Eindhoven University of Technology, 5300 MB Eindhoven, The Netherlands
Keywords: CFD, modelling, nucleation, growth, coagulation, numerical simulation.
Presenting author email: christoph.winkelmann@pmi.com

Many applied problems in fluid mechanics have a multi-scale character due to physical processes evolving at many different time and/or length scales. Examples range from turbulent flows with different length scales to chemically reacting and multi-phase flows with various time scales. In most applied flow problems, resolving all scales in space and time present in a flow is not computationally feasible. For the non-resolved time-scales, e.g., time scales on which nucleation of over-saturated vapors is occuring, suitable models can be developed.

In general, the nucleation time-scale can be some orders of magnitude smaller than the timestep of the fluid simulations. To demonstrate this, we focus on aerosol flows in a rather simple geometry, but with an abrupt phase change caused by an immediate cooling of hot vapors that triggers creation of the aerosol droplets. The flow cooling is introduced by a rapid change of wall temperature in the considered pipe geometry as seen in Fig. 1(a). Consequently, an aerosol is formed from the hot vapors which are initially in the gas phase (Fig. 1(b,c)).

In our model, the aerosol is simulated in an Eulerian frame exploiting the computational efficiency of such approach. The formation of aerosol droplets is described by classical nucleation theory. Models for coagulation of, condensation to and evaporation from the droplets are included. In addition to the flow equations for mass, momentum and energy conservation, equations for the aerosol mass and number load are solved. In this method of moments approach, the diameter of average mass of the evolving aerosol can be easily determined. In order to account for the omitted time scales in the nucleation process, a sub-timestep model has been developed and included in our simulation to allow for computations at reduced computational effort. The accuracy of the obtained flow solution with this coarse-graining of the aerosol creation process is one of the key objectives for investigations presented in this work.

Our aim is to provide a simple computational framework for testing and analyzing aerosol models. In the literature only a modest number of detailed numerical experiments are available for aerosol generation processes by nucleation in flows of condensable vapors. Here, we consider the generation of an aerosol by a rapid cooling of hot vapors in laminar flow (Nguyen *et al.*, 1987).

We use the setup and flow parameters described by Nguyen *et al.* (1987) and consider a pipe flow with prescribed axial wall temperature profile starting from the temperature of hot saturated vapors of dibutyl phthalate and changing rapidly to room temperature within a short downstream distance (Nguyen *et al.*, 1987; Pyykönen and Jokiniemi, 2000). The aerosol model is implemented as an extension to the open-source software OpenFOAM®, which provides sufficient flexibility for consideration of geometrically more complex flow domains.

Our focus lies on two important aspects. First, the analysis of the time resolution at which the simulations need to be performed in order to obtain accurate results at minimal computational cost. For this, a set of simulations is carried out with different time-step sizes in order to investigate the accuracy and necessity of sub-time step modeling. Second, the validation of the method with experimental data available in the literature.

The extension of this work to multi-component aerosol formation and turbulent flow is ongoing.

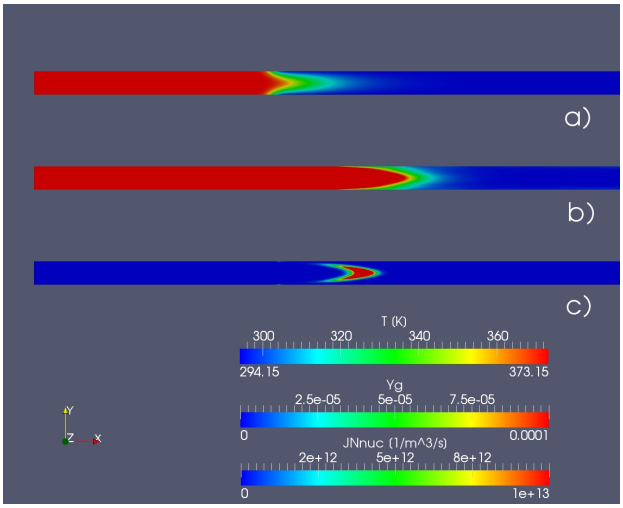

Figure 1: Snapshots from a laminar simulation of dibutyl phthalate: temperature field $T[K]$ (a), species mass concentration in the gas phase $Y_g[kg/kg]$ (b) and nucleation rate $J_N[m^{-3}s^{-1}]$ (c).

Nguyen, H.V., Okuyama, K., Mimura, T., Kousaka, Y., Flagan, R.C., and Seinfeld, J.H. (1987) J. Colloid Interf. Sci. **119**, 491-504.

Pyykönen, J. and Jokiniemi, J. (2000) J. Aerosol Sci. **31**, 531-550.

Friday, September 9, 2011

Plenary 5:

Global aviation and particulate matter: from climate impact to volcanic ash and back

by Andreas Petzold

Global aviation and particulate matter: From climate impact to volcanic ash and back

Andreas Petzold
DLR, Institut für Physik der Atmosphäre, Oberpfaffenhofen, 82234 Wessling, Germany.

Keywords: aviation particulate matter, aviation climate impact, volcanic ash, mineral dust.
Presenting author email: andreas.petzold@dlr.de

Rationale: The relationship between airborne particulate matter (PM) and aviation is manifold. It extends from the impact of aviation PM emissions on cloudiness and on climate in general, to the impact on local air quality and human health. However, aviation PM does not only affect the atmospheric aerosol budget, but airborne PM also may have a strong impact on aviation by causing hazards to cruising aircraft. The entire research area is highly interdisciplinary, including measurement technology aspects, as well as studies on PM impact on aircraft engines and airframes, and using a network of civil aircraft as routine measurement platform for the aerosol in the global upper troposphere and lowermost stratosphere (IAGOS: In-service aircraft for a global observing system; www.iagos.org/). The plenary will give a broad overview of various research activities going on in this field. In the following recent highlights from different disciplines are briefly summarised.

Impact of Aviation on Climate: Aviation is considered one major source of PM at cruise altitude (9 – 13 km above sea level), causing significant climate effects via contrails and cirrus clouds forming on these particles. After a decade of intense research on PM emissions from aircraft gas turbines, their physico-chemical properties, and their impact on global climate, IPCC dedicated an entire report to this topic (IPCC 1999).

Although emission of PM from aircraft engines is now reasonably well understood, e.g., (IPCC 2007; Schumann et al. 2002), the development of current-technology measurement methods for engine certification is an ongoing task requested by the International Civil Aviation Organisation (ICAO). First results from extensive method intercomparison studies were published recently (Petzold et al. 2011).

In the past 5 years the research focus has shifted to effects of PM emissions at ground level on local air quality and human health. NASA has supported a whole series of experiments on aircraft PM emissions (APEX 1 – 3; (Wey et al. 2007)). Climate effects from contrails and in particular from cirrus clouds forming from persistent contrails are still in the focus of research. Very recently, Burkhardt and Kärcher (2011) estimated the net forcing effect of contrail cirrus, comprising not only young or line-shaped but also aged, irregularly shaped contrails, and including resulting changes in cirrus cloudiness to about 31 mWm^{-2}. They conclude that the net radiative forcing due to contrail-induced cloudiness constitutes one of the largest single aviation-related radiative forcing components.

PM Impact on Aviation: On April 14th, 2010, the eruption of the Eyjafjallajökull in Iceland and the accompanying cloud of volcanic ash forced most countries in northern Europe to shut their airspace between April 15-20, grounding more than 100,000 flights and an estimated 10 million travellers. This event has revealed to which extent our society and our economy relies on the availability of a safe and efficient air transport system and how volatile it still is facing the complexity of atmospheric conditions.

In the aftermath of the airspace closure it turned out that a quantitative knowledge of the exposure of aircraft encountering fine or coarse volcanogenic particles and gases in the atmosphere is still very limited. Furthermore, there are strong analogies between the issues and hazards associated with aircraft passage through volcanic ash and mineral (desert) dust clouds. Natural hazards that can severely impact the air transport system also include icing and dense clouds of ice crystals. The European project NEWAC (New aero engine core concepts: www.newac.eu/) forms the current framework for the more technically oriented research while the upcoming EU activity WEZARD (Weather hazards for aviation, start scheduled for July 2011) combines technology oriented research, atmospheric science, and measurement technology.

Both fields of research merge in the efforts of developing simple sensors for routine measurements of potentially hazardous situations on board of civil aircraft. These efforts rely extensively on the progress and experience gained in IAGOS, which was originally developed for atmospheric observation.

References

Burkhardt, U., and B. Kärcher, 2011: Global radiative forcing from contrail cirrus. *Nature Climate Change*, **1,** 54-58.

IPCC, 1999: *Aviation and the Global Atmosphere.* Cambridge University Press, 373 pp.

——, 2007: *Climate Change 2007: The Scientific Basis.* Cambridge University Press, 940 pp.

Petzold, A., *et al.*, 2011: Evaluation of Methods for Measuring Particulate Matter Emissions from Gas Turbines. *Environ. Sci. Technol.*, **45,** 3562-3568.

Schumann, U., *et al.*, 2002: Influence of fuel sulfur on the composition of aircraft exhaust plumes: The experiments SULFUR 1-7. *J. Geophys. Res.*, **107**, doi: 0.1029/2001jd000813.

Wey, C. C., *et al.*, 2007: Overview on the Aircraft Particle Emissions Experiment. *J. Propul. & Power*, **23,** 898-905.

Friday, September 9, 2011

Session 11A: Biomass Burning

Comparison of qualitative and quantitative approaches for source apportionment of PM at urban and rural alpine sites.

C. Piot[1,2], M.F.D. Gianini[5], J. Cozic[2], L. Polo[2], J.-L. Besombes[1], A. Charron[4], J.-L. Jaffrezo[2], C. Hueglin[5]

[1]Université de Savoie-LCME, Le Bourget du Lac, France
[2]Université Joseph Fourier-CNRS-LGGE, St-Martin d'Hères, France
[4]LTE, IFSTTAR, Bron, France
[5]EMPA, Materials Science and Technology, Duebendorf, Switzerland
Keywords: source apportionment, Chemical Mass Balance, Positive Matrix Factorization, alpine valleys sites.
Presenting author email: christine.piot@univ-savoie.fr

Detailed knowledge about the sources of PM is mandatory for the enforcement of efficient PM reduction measures. Source apportionment of PM can be achieved by using qualitative and quantitative approaches with off-line PM sampling. Qualitative methods are based on the study of chemical profiles or ratio-ratio approaches (Robinson *et al.*, 2006). Different quantitative methods exist, notably two modeling methods: the Molecular Marker - Chemical Mass Balance (MM-CMB) and multivariate statistical models such as Positive Matrix Factorization (PMF). The mono-tracer method using organic carbon, levoglucosan and elemental carbon (EC) concentrations, or the isotopic carbon signature (^{14}C) can also be used.

Qualitative and quantitative methods (mono-tracer method, MM-CMB and PMF) of source apportionment were applied for PM samples collected in summer and winter seasons in urban background and rural alpine sites both in France (Grenoble and Lescheraines) and in Switzerland (Zurich and Magadino). At these sites topographic and meteorological conditions can lead to high pollutant concentrations. PM was characterized for a large array of chemicals including molecular speciation of organic matter, trace elements, metals and ionic species (about hundred compounds).

PM in alpine valleys is emitted to a large part by residential heating particularly biomass burning. Biomass burning was found to account for 42% of PM in Grenoble during winter (Favez *et al.*, 2010) and for 41% of the organic aerosol (OA) in Zurich (Szidat *et al.*, 2006). Vehicular emissions can also be important source of aerosol. Therefore, a proper apportionment of direct and indirect vehicular emissions and the emissions from biomass burning is an important issue for these sites. Because it is dependent of local sources and practices (e.g. type of burned wood), the use of adjusted methodologies and combined approaches is advantageous in order to obtain the best estimates.

Chemical marker profiles and the ratio-ratio approach using Polycyclic Aromatic Hydrocarbons, EC and hopanes (markers for direct vehicular emissions) allow the determination of source profiles for use in CMB (choices of type of wood burned or vehicular fuel type). Organic marker concentrations are used in order to validate the obtained PMF factors for each site.

Estimated contributions from biomass burning (BB) and direct vehicular emissions (DVEH) to OA in winter by the mono-tracer method and the MM-CMB model are found to be in good agreement (Fig. 1). Average source contributions were calculated for 30 samples per site in France and 10 samples per site in Switzerland. The obtained source contributions will also be compared with PMF model results for source contributions to PM in each season.

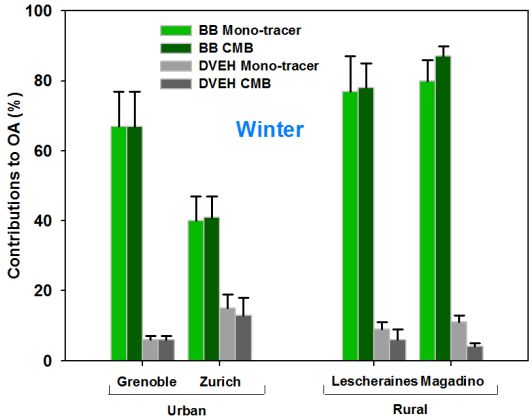

Figure 1. Wood burning contribution estimations to OA in winter in urban and rural sites by mono-tracer method and by MM-CMB.

C. Piot thanks the Region Rhône-Alpes for her PhD grant. Campaigns in France were supported by the FORMES program MEDAD Primequal Predit (Grant N°0001135) and by the Particul'Air program ADEME. The authors would like to thank staffs from ASCOPARG and AIR-APS for their support during the field campaigns. The activities at the Swiss sites were supported by the Competence Center Environment and Sustainability of the ETH Domain (CCES-IMBALANCE) and by the Swiss Federal Office for the Environment (FOEN).

Favez, O., El Haddad, I., Piot, C., Boréave, A., Abidi, E., Marchand, N., Jaffrezo, J.-L., Besombes, J.-L., Personnaz, M.-B., Sciare, J., Wortham, H., George, C. and D'Anna, B. (2010) *Atmos. Chem. Phys.* **10**, 5295-5314.

Robinson, A.L., Subramanian, R., Donahue, N.M., Bernardo-Bricker, A. and Rogge, W.F. (2006) *Environ. Sci. Technol.* **40**, 7803-7810.

Szidat, S., Jenk, T.M., Synal, H.A., Kalberer, M., Wacker, L., Hajdas, I., Kasper-Giebl, A. and Baltensperger, U. (2006) *J. Geophys. Res.* **111**, D07206.

Stable carbon isotope ratio analysis of anhydrosugars in biomass burning aerosol

X. F. Sang[1, 2], W. Laumer[1], I. Gensch[1], C. Y. Chan[2] , G. Engling[3]and A. Kiendler-Scharr[1]
[1]IEK-8: Troposphäre, Forschungszentrum Jülich, Jülich, Germany
[2]Sun-Yet Sen University, China
[3]National Tsing Hua University, Taiwan
Key words: biomass combustion, smoke emissions, levoglucosan, stable isotopes, source identification

Biomass burning is an important source of atmospheric trace gases and particulate matter, which impact air quality and climate. However, the effect of biomass burning on regional and global scale is still poorly quantified due to various uncertainties in the assessment, including analytical limitations, lack of representative source profiles and poor description of potential degradation of molecular source tracers during atmospheric transport. A major component of fine particles from biomass combustion is levoglucosan (LG), accompanied by its stereoisomers, mannosan (MN) and galactosan (GL). Due to reasonable atmospheric stability during long-range transport, levoglucosan has been used as marker for biomass burning processes. Increasing effort has recently been put into the quantification of levoglucosan and other anhydrosugars in biomass burning aerosols. Recently, stable carbon isotope measurements have emerged as a powerful tool to characterize source emissions and ambient aerosols influenced by biomass burning (Huang et al., 2006) and secondary formation processes (Fisseha et al., 2009).

Here we present a newly developed method for compound specific isotopic measurements of anhydrosugars in biomass burning aerosol filter samples by employing Thermal Desorption – 2-Dimensional Gas Chromatography – Isotopic Ratio Mass Spectrometry (TD-2DGC-IRMS). This method combines the advantages of thermo-extracting analytes from filter samples with the improved separation of polar components by two-dimensional GC (Ma et al. 2010). It was successfully applied to determine the isotopic composition of levoglucosan, mannosan and galactosan in a standard mixture. The obtained $\delta^{13}C$ values showed good agreement with the isotopic measurements of the bulk anhydrosugars, carried out by elemental analyser-isotope ratio mass spectrometry (EA-IRMS) (Table 1).

The biomass burning source samples analyzed with our new method were collected in the Pearl River Delta of China. The measured samples originated from different types of burning (open or in domestic stoves) of various plants, including rice straw, peanut and mulberry shrubs, China fir and Chinese red pine (softwood), chestnut and schima superba trees (hard wood). The burning in domestic stoves was defined by a mixture of smoldering and flaming stages, while flaming at higher temperatures was the dominant stage in case of open burning. Figure 1 shows an example chromatogram obtained for Chinese red pine. Generally, the softwood samples showed the highest LG $\delta^{13}C$ values of -23.19‰ to -21.52‰. $\delta^{13}C$ values for mannosan and galactosan could only be measured from softwood and ranged from -23.22‰ to -22.42‰ (MN), and -24.93‰ to -24.76‰ (GL). Levoglucosan generated from the combustion of grasses and shrubs showed $\delta^{13}C$ values of -25.69‰ to -24.33‰. Similar LG $\delta^{13}C$ values of -26.62‰ to -24.73‰ were measured for hard wood samples. Scrutinizing the influence of different combustion types on isotopic composition, open burning produced a lower $\delta^{13}C$ value for levoglucosan than domestic stove burning. For rice straw LG $\delta^{13}C$ values were found to be -26.32‰ and -24.33‰, respectively.

Table 1. The $\delta^{13}C$ values of levoglucosan, mannosan and galactosan measured by TD-2DGC-IRMS and EA-IRMS methods (n: number of measurements).

Compound		TD-2DGC -IRMS	EA-IRMS
Name	Chemical Formula	$\delta^{13}C$/‰ (n=5)	$\delta^{13}C$/‰ (n=3)
Levoglucosan	$C_6H_{10}O_5$	-23.59±0.19	-23.75±0.09
Mannosan	$C_6H_{10}O_5$	-24.50±0.22	-24.77±0.02
Galactosan	$C_6H_{10}O_5$	-26.79±0.16	-26.67±0.01

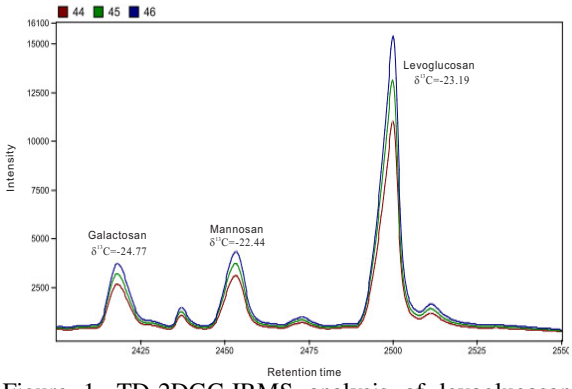

Figure 1. TD-2DGC-IRMS analysis of levoglucosan, mannosan and galactosan in softwood burning aerosol. Signals of CO_2^+ (m/z 44, red), and isotopologues on m/z 45 (green), and m/z 46 (blue) are shown.

The $\delta^{13}C$ data will be discussed together with organic speciation information, including ambient anhydrosugar concentrations, obtained by high-performance anion exchange chromatography (HPAEC) (Sang et al. 2011). Selected results from compound specific $\delta^{13}C$ analysis of ambient filter samples will be presented. These will be interpreted in the context of isotopic information from source samples with respect to main sources of biomass burning aerosols in urban and rural sites of the Pearl River Delta of China in 2009 and their atmospheric processing.

Fisseha, R. et al. (2009) *J. Geophys. Res.*, **114**, D02304, doi:10.1029/2008JD011326.
Huang, L. et al., (2006) *Atmos. Environ.* **40**, 2690-2705.
Ma, Y. et al., (2010) *Atmos. Chem. Phys.* **10**, 4331–4341.
Sang, X. F. et al., (2011) *Tellus B*. doi: 10.1111/j.1600-0889.2010.00515.x.

Organic compounds in $PM_{2.5}$ emitted from fireplace and woodstove combustion of typical Portuguese wood species

C. Gonçalves, C. Alves, A. P. Fernandes, C. Monteiro, F. Mirante, L. Tarelho, M. Evtyugina, and C. Pio

Centre for Environmental and Marine Studies (CESAM), Department of Environment, University of Aveiro, 3810-193 Aveiro, Portugal.

Keywords: biomass burning, fireplace, woodstove, $PM_{2.5}$, GC-MS, organic tracers.

catiagoncalves@ua.pt

This work provides detailed information on organic composition of smoke particles from residential combustion of the most prevalent Portuguese woods in an attempt of contributing with new data for source apportionment methodologies. In Portugal and other Mediterranean countries, there is a lack of information concerning the characterisation of particulate emissions from biomass combustion systems.

This new research extends to eight the number of biomass fuels studied and try to understand the differences that the burning appliance (fireplace versus woodstove) and the combustion temperature (cold and hot start) have on emissions. *Pinus pinaster* (Maritime pine), *Eucalyptus globulus* (eucalyptus), *Quercus suber* (cork oak), *Acacia longifolia* (Golden wattle), *Quercus faginea* (Portuguese oak), *Olea europea* (Olive), *Quercus ilex rotundifolia* (Holm oak) and briquettes produced from forest biomass waste were used in the combustion tests.

The burning tests were carried out at the Portuguese combustion facility, at the University of Aveiro (Fernandes, 2009).

Determinations included particle mass emission factors, the determination of its carbonaceous content (OC and EC) by a thermal optical technique (Alves et al., 2010) and detailed identification and quantification of organic compounds by gas chromatography–mass spectrometry (GC model 6890, quadrupole MSD 5973 from Hewlett-Packard and GC Trace Ultra, quadrupole DSQ II from Thermo Scientific).

Results suggest that fine particle emission factors from the woodstove were lower than those from the fireplace (Figure 1). For both combustion appliances, the OC/EC ratio is higher in cold start tests, except for some species, such as pine, eucalyptus and briquettes that behave differently in relation to OC emissions. The major organic components in particles from biomass burning were anhydrosugars, in particular levoglucosan, acids and aliphatic compounds. Retene was the dominant aromatic hydrocarbon found in the softwood smoke, whilst it was present at very small levels in the hardwood combustion emissions. Guaiacyl, like vanillic acid, and synapyl compounds were identified in softwood smoke, whereas hardwood burning contributed mainly to the formation of syringyl compounds, such as syringic acid. Stigmasterol was only present in the smoke of hardwood species; thus, this compound may be pointed out as a potential tracer for smoke from deciduous trees. β-sitosterol has a great expression in the smoke of softwood species.

The smoke composition varied widely depending on fuel type, burning appliance and combustion temperature.

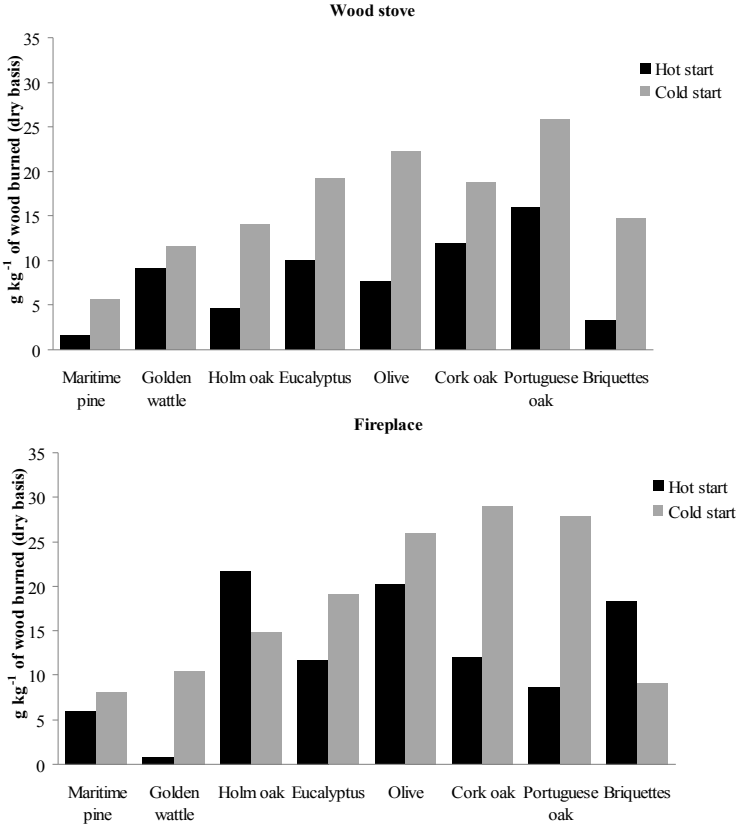

Figure 1 – $PM_{2.5}$ emission factors.

This work was funded by the Portuguese Science Foundation through the PTDC/AMB/65706/2006 (BIOEMI) project. C. Gonçalves acknowledges the PhD grant SFRH/BD/36540/2007.

Fernandes, A.P.S. (2009) Emission of $PM_{2.5}$ and gases from domestic appliances burning (in Portuguese: http://biblioteca.sinbad.ua.pt/Teses/2010000392).

Alves, C. et al. (2010) Organic speciation of atmospheric particles in Alvão Natural Park (Portugal). Environ Model Assess, 168, 321-337.

Diurnal concentrations of organic tracers originated from wood combustion

J. Orasche[1, 2, 3], J. Schnelle-Kreis[2], G. Abbaszade[2], H. Ruppert[1], R. Zimmermann[2, 3]

[1]Department of Sedimentology & Environmental Geology, Georg-August University, Göttingen, Germany
[2]Cooperation group of Complex Molecular Systems, Helmholtz Zentrum München, Germany
[3]Department of Analytical Chemistry, University of Rostock, Germany
Keywords: ambient aerosols, wood combustion, levoglucosan, PAH, oxygenated PAH
Presenting author email: juergen.orasche@helmholtz-muenchen.de

The impact of wood combustion on chemical composition of ambient aerosol during winter time was investigated. Sampling was done at the aerosol characterization site of the Helmholtz Zentrum München in Augsburg, Germany.

The campaign in 2010 represents a winter period strongly influenced by residential heating (15th to 19th February). The aerosol characterisation site is an urban background site which is not influenced by direct emissions of traffic or residential heating next to the area. The buildings in the neighbourhood are mainly supplied by the district heating network. To observe intraday course of concentrations of particulate organic matter filter sampling of PM_1 was done on an hourly basis for a period of four days. Moreover routine $PM_{2.5}$ sampling by daily collecting of ambient air on quartz fibre filters has been done at this sampling site.

A new developed method for analysing organic matter, the In-situ Derivatisation Thermal Desorption (IDTD) followed by Gas Chromatography Time-Of-Flight Mass Spectrometry (GC-TOF-MS), was applied for analysis of these samples.

Despite of contrary weather during four days of hourly sampling a strong influence of wood combustion activities was clearly visible. The heating activities were focused on the evening hours. The accumulation of emissions of wood combustion resulted in increasing concentrations of wood combustion aerosols in the city. High concentrations of organic marker substances like levoglucosan with a maximum at about midnight were observed. Maxima of levoglucosan prevailed for several hours. The highest average of the day (640 ng m^{-3}) was found on the 18th of February within the days of hourly sampling. The highest maximum values were shortly before and after midnight between the 17th and 18th of February (1400 ng m^{-3}) (figure 1).

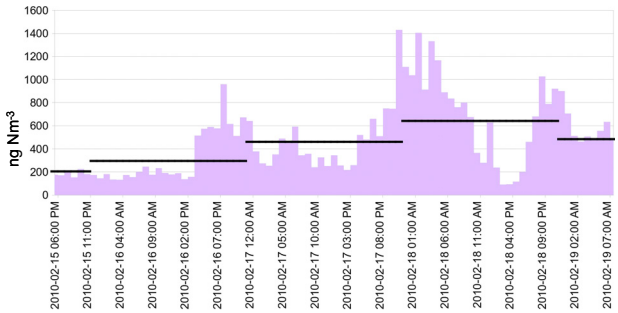

Figure 1. Urban background concentrations of levoglucosan: $PM_{2.5}$ values as 24-hours-means (bars) and intraday values of PM_1 (vertical bars)

The main driving factors for increased nightly concentrations were the unfavourable dispersion conditions (low mixing layer heights and wind speeds). In addition we assume that increased emissions from smouldering phases with low air supply at the end of heating events ("the last log of the day") contributed also to the observed variation in time.

A series of experiments with a log wood stove have shown that a smouldering phase of ten minutes during a burn-off of 45 minutes is responsible for two-fold higher values of total suspended particles (TSP) mass and especially levoglucosan when regarding chemical composition. Although concentrations of levoglucosan were found to be even higher at the inflaming someone can estimate that smouldering phases were also responsible for the observed values during night. Figure 2 shows the characterisation of a heating event typical for an evening leisure time in winter. The heating event is separated into four periods. The inflaming process showed high emissions of organics. Afterwards two reloads of logs were sampled. Emissions of PM and organics were lowered significant. The third reload is characterised by a smouldering phase with high emissions of PM and organics. Especially levoglucosan and the oxidised PAH 9H-fluoren-9-one were strongly influenced by inflaming and a smouldering phase during the combustion of the third reload. Whereas benz[a]pyrene was not affected in the same magnitude.

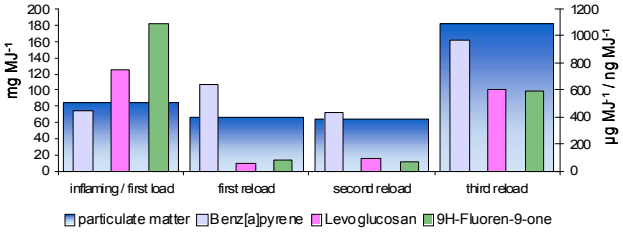

Figure 2. Typical leisure time log wood combustion event over three hours. Wood stove fired with beech log wood. Combustion time for each load was 45 min. Left y-axis: particulate matter [mg MJ^{-1}], right y-axis: benz[a]pyrene [ng MJ^{-1}], levoglucosan [µg MJ^{-1}], 9H-fluoren-9-one [100 µg MJ^{-1}] (units refers to introduced energy contained in the fuel)

This work was supported by the Ministry of Science and Culture of Lower Saxony.

Schnelle-Kreis, J., Sklorz, M., Orasche, J., Stölzel, M., Peters, A., Zimmermann, R. (2007) Environ. Sci. Technol. 41, 3821 – 3828

Biomass burning aerosols measured with in-situ and remote sensing instruments in Eastern Finland during the forest fires in Russia 2010

H. Portin[1,2], T. Mielonen[1], M. Komppula[1], A. Leskinen[1] , A. Arola[1], A. Laaksonen[2,3] and K. E. J. Lehtinen[1,2]

[1]Finnish Meteorological Institute, Kuopio unit, POB 1627, Kuopio, FI-70211, Finland
[2]University of Eastern Finland, Department of Applied Physics, POB 1627, Kuopio, FI-70211, Finland
[3]Finnish Meteorological Institute, Research and Development, POB 503, Helsinki, FI-00101 Finland

Keywords: air quality, biomass burning, PM, Remote sensing.
Presenting author email: harri.portin@fmi.fi

During June-August 2010, intensive forest fires took place in the Western Russia, near Moscow. The smoke from the fires and associated aerosol particles had a considerable effect on air quality, causing adverse health effects. Characteristics of smoke and aerosol particles are also interesting from the atmospheric point of view. Smoke particles have often distinct optical properties compared to other particles, and have a significant impact on earth's radiation balance (Reid *et al*, 2005)

The smoke drifted long distances with air masses, and in several occasions, it could be observed in the city of Kuopio, Eastern Finland, where the Puijo observation tower is located. A long-term measurement station for aerosol-cloud interactions and aerosol properties is located on the top of the tower (Leskinen *et al*, 2009). The station is equipped with instruments capable of determining the physical and optical properties of the aerosol particles in detail. We have also used some remote sensing data and data from city of Kuopio air quality measurement sites.

On two days, 29.7. and 8.8, the presence of smoke could be seen from the data clearly and it even affected the visibility. In figure 1, time series of AOD from a local AERONET site and $PM_{2.5}$ from an air quality measurement site located in the city centre are shown. High AOD values and particle mass values clearly indicate the smoke presence. However, AOD is considerably lower in 29.7. compared to $PM_{2.5}$. This is likely caused by different vertical distribution; clearly elevated surface $PM_{2.5}$ was measured on both days, while column measurements of AOD suggest that the smoke plume was much thicker on 8.8.

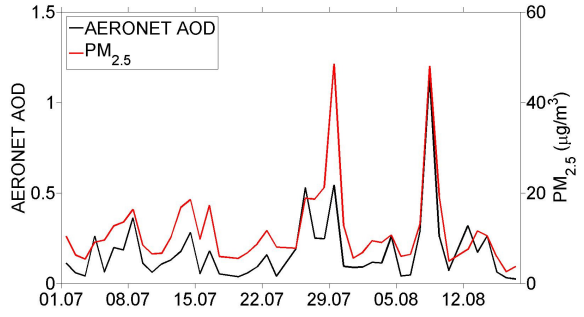

Figure 1. Time series of AERONET AOD and PM2.5 measured at Kuopio city centre. The two concentration peaks are on 29.7. and 8.8.

To better distinguish the characteristics of smoke and related aerosol particles, we made a comparison between smoky and clean conditions. Clean data for the comparison was chosen with the help of 120 hour back-trajectories calculated with FLEXTRA and satellite data from FIRMS Web Fire Mapper (http://firefly.geog.umd.edu/firemap/). Secondly, data from Puijo station was checked for any signs of smoke, such as large particle size and high black carbon content. We then calculated average values of the most important parameters from the clean air data and from the data collected during 29.7. and 8.8.

In table 1, mean values of total particle number concentration (N_{tot}), geometric mean diameter (GMD) and black carbon concentration (BC) from Puijo station for clean and smoky conditions are shown, together with the carbon monoxide (CO) data from an air quality site at the city centre. CO is of particular interest, since it's commonly used as one of the main indicators of biomass burning emissions (Stohl *et al*, 2007). Except for total particle concentration, the effect of smoke can clearly be seen in all parameters. Particles are twice as large on average and BC and CO experience a 12-fold and 8-fold increase, respectively.

Table 1. Average values of some of the most important parameters for clean and smoky air.

	clean	smoky
N_{tot} (cm^{-3})	2540	3380
GMD (nm)	76.3	158
BC (ng/m^3)	98.7	1230
CO ($\mu g/m^3$)	41.1	334

Leskinen, A., Portin, H., Komppula, M., Miettinen P., Arola, A., Lihavainen, H., Hatakka, J., Laaksonen, A. and Lehtinen, K.E.J. (2009) *Boreal Env. Res.*, **14**, 576-590.

Reid, J.S., Eck, T.F., Christopher, S.A., Koppmann, R., Dubovik, O., Eleuterio, D.P., Holben, B.N., Reid, E.A. and Zhang, J. (2005) *Atmos. Chem. Phys.* **5**, 827-849.

Stohl, A., Berg, T., Burkhart, J.F., Fjæraa, A.M., Forster, C., Herber, A., Hov, Ø., Lunder, C., McMillan, W.W., Oltmans, S., Shiobara, M., Simpson, D., Solberg, S., Stebel, K., Ström, J., Tørseth, K., Treffeisen, R., Virkkunen, K. and Yttri, K.E. (2007) *Atmos. Chem. Phys.* **7**, 511-534.

Optical and microphysical characteristics of smoke aerosol during fire events in Moscow region in summer 2010

M.A. Sviridenkov[1], G.I. Gorchakov[1], N.Ye. Chubarova[2], Ye.G. Semutnikova[3] and A.S. Emilenko[1]

[1]A. M. Obukhov Institute of Atmospheric Physics, Moscow, 119017, Russia
[2]Department of Geography, Moscow State University, Moscow, 119991, Russia
[3]Mosecomonitoring, Moscow, 119019, Russia
Keywords: biomass burning, aerosol optics, microstructure.
Presenting author email: misv@mail.ru

The extremely hot and dry weather conditions without precipitation in the European part of Russia in summer 2010 stimulated intensive and prolonged forest and peatbog fires. The most intensive smoke events in Moscow took place during the first decade of August. In the present paper, the results of the measurements of aerosol characteristics in Moscow and the Zvenigorod Scientific Station (ZSS) of IAP RAS, located at 60 km to the west from the centre of the city are analyzed.

Aerosol optical properties in the atmospheric column were measured by two AERONET CIMEL photometers installed at the ZSS and at the Meteorological Observatory of the Moscow State University (MO MSU). Optical characteristics of the near-ground aerosol at Zvenigorod were studied by means of polarimeter PhAN. Aerosol mass concentration in Moscow was recorded with TEOM instruments operated by the Mosecomonitoring network.

Smoke events in 2010 were characterized by very high maximal levels of the aerosol loading in the atmosphere. Maximal observed values of the aerosol optical thickness at the wavelength of 500 nm (AOT500) was about 4.5 both in Moscow and Zvenigorod. It is approximately 1.5 times greater than observed during previous intensive fires in 2002. In August, monthly mean AOT was about 4 times higher than the climatic value for this period in Moscow. Daily mean AOT500 values at the two sites are presented in Figure 1 along with the water vapor content. Maximal recorded values of PM10 in Moscow reached 1.6-1.7 mg/m^3. Such levels of aerosol pollution have never been observed previously.

Qualitative aerosol characteristics were also distinct from those in background conditions. AOT did not correspond to the Angstrom's law. Spectral dependence of AOT can be described (in logarithmic scale) by the second order polynomial with the local Angstrom's exponent increase with wavelength. In the period of fire events, the negative values of the degree of linear polarization of the light, scattered at the angle of 90°, was for the first time observed in field measurements. A tendency of the decrease in the degree of the linear polarization with the growth of the smoke pollution was revealed. This is an evidence for the growth of the particle effective radii with the increase of the turbidity of the atmosphere.

The results of the inverse problem solution by the method proposed by Dubovik and King (2000) showed that smoke aerosol in Moscow in 2010 was relatively weakly absorbing. Single scattering albedo at 440 nm varied in the limits of 0.94 - 0.98 during the period from August 1 to August 10. These values are close to the estimates for the aerosol from peatbog and forest fires in 2002 (Chubarova et al., 2009). Aerosol size distributions are characterized by the enhanced relative contribution of the fine fraction in the total aerosol volume content.

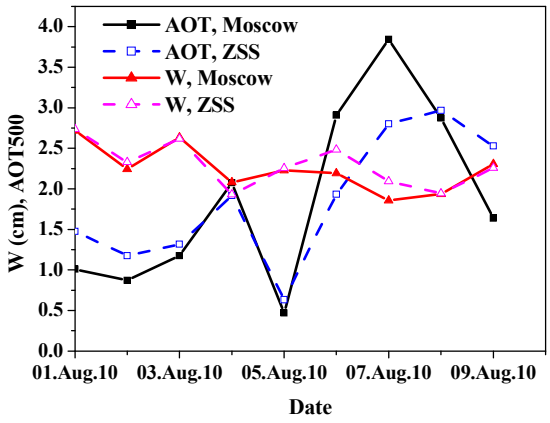

Figure 1. Daily mean aerosol optical thickness at 500 nm (AOT500) and water vapor content at the two measurement sites.

A significant increase in AOT causes a strong attenuation of shortwave irradiance. During the maximum aerosol loading observed on August 7, 2010, the loss of global shortwave irradiance (0.3-4.5 μm) was about 50-60%, while the loss in UV irradiance reached 75-90%.

This work was partially supported by the Russian Foundation for Basic Research under grants 10-05-01019, 09-05-00582 and by the Ministry of Education and Science of the Russian Federation (contract # № 02.740.11.0676).

Dubovik, O. and King, M. D. (2000). *J. Geoph. Res.*, **105**, 20673-20696.

Chubarova, N.Y., Prilepsky, N.G., Rublev, A.N., Riebau, A.R. (2009). In: *Developments in Environmental Science*, **8**. A. Bytnerowicz, M. Arbaugh, A. Riebau and C. Andersen (Eds,), Elsevier B.V., 249-267.

Friday, September 9, 2011

Session 11B: Chemical and Physical Properties of SOA

Modelling the sensitivity of aerosol properties to variations in key inputs:- 1) vapour pressures; 2) non-ideality; 3) hydrolysis of acid-anhydrides

M. H. Barley[1], D. Topping[1,2], G.McFiggans[1] and D. Lowe[1]

[1]Centre for Atmospheric Science, Manchester University, Manchester, M13 9PL
[2]National Centre for Atmospheric Science (NCAS), Manchester University, Manchester, M13 9PL
Keywords: atmospheric aerosols, modelling, vapour pressures, organic aerosols
Presenting author email: mark.barley@manchester.ac.uk

Introduction

Atmospheric aerosols have significant but highly uncertain impacts upon both the climate and human health. Gas to particle mass transfer of semi-volatile components, and the production of secondary organic aerosol (SOA), is an important factor in determining the evolving chemical composition of aerosol particles and is necessary for predicting their loading and composition. However the atmosphere contains many thousands of organic compounds, all of which can potentially condense and contribute to the mass of the aerosol; and even a basic identification of organic compounds in particulate matter is incomplete. To aid in the modelling of SOA formation, explicit hydrocarbon oxidation mechanisms (known as Direct Chemical Mechanisms or DCMs) that track the oxidative degradation of volatile organic compounds (VOCs) all the way through to carbon dioxide and water have been developed over a number of years. The DCM used in this work is the Master Chemical Mechanism (MCM, Jenkin et al., 2003) .

The Model used for Predicting SOA Formation

SOA formation is modelled using SOAF-POC (SOA Formation by the Partitioning of Organic Compounds) which couples the output of the MCM (molecular structures and atmospheric concentration for 2742 organic compounds) to a partitioning model (a variation on the Pankow model) with vapour pressures and non-ideality calculated using a series of automated estimation methods based upon the parsing of the molecular structures (see poster "Development of chemical informatics tools for calculating fundamental properties of atmospheric aerosol components" by M H Barley et al., this conference).

206 MCM scenarios were used in this work. The key inputs to the MCM model (NOx, Anthropogenic VOCs and Biogenic VOCs) were varied over 6 orders of magnitude (from 0.001 to 1000 times average UK inputs). For each scenario partitioning calculations were made for 24 different combinations of temperatures, %RH and involatile core mass. This presentation will investigate the dependence of key aerosol properties (condensed mass, average O:C ratio, average molecular weight, average contribution of specific functional groups, growth factor etc.) on vapour pressure values estimated by six different methods, non-ideality estimated by UNIFAC and the effect of hydrolysing all acid anhydrides in the MCM output. Some of these sensitivities have been previously investigated for sets of computer simulated compounds (McFiggans et al., 2010) but in this work the calculations are applied to atmospherically representative compounds from a DCM.

The base case (the partitioning calculations against which the other calculations were compared) used the 2742 molecules from the MCM without alteration, calculated vapour pressures using the boiling point and vapour pressure correlations of Nannoolal (referred to as the N/N-VP method), and assumed liquid phase ideality. Other calculations explored the impact of using other vapour pressure methods or including non-ideality. The results can be presented as a series of box-whisker plots which show, for all cases and scenarios (206 x 24), the impact of the changed input on the aerosol property compared to the base case value (see Figure 1)

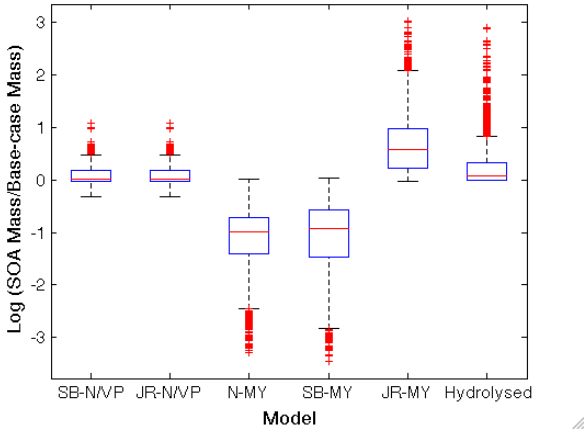

Figure 1. Box-whisker plot showing how changing the vapour pressure input data affects the SOA condensed mass. Base case is vapour pressure by N/N-VP, ideal liquid behaviour and no hydrolysis of anhydrides. SB and JR refer to boiling point estimation by Stein and Brown and Joback and Reid respectively, MY refers to the vapour pressure correlation of Myrdal and Yalkowsky. The sixth plot refers to the effect of hydrolysing all acid anhydrides, while retaining base case values for the other inputs.

This work was supported by the National Centre for Atmospheric Science (NCAS) and the NERC grant NE/H002588/1

Jenkin, M et al., (2003) *Atmos. Chem. Phys,* **3**, 181-193.
McFiggans, G., Topping, D., and Barley, M. H. (2010) *Atmos. Chem Phys.* **10**, 10255-10272.

Evaluating the mixing of organic aerosol components using high-resolution aerosol mass spectrometry

L. Hildebrandt[1], K. Henry[1], J. H. Kroll[2], D. R. Worsnop[3,4], S. N. Pandis[1,5], N. M. Donahue[1]

[1]Center for Atmospheric Particle Studies, Carnegie Mellon University, Pittsburgh, PA, 15213, USA
[2]Department of Civil and Environmental Eng., Massachusetts Inst. of Technology, Cambridge, MA 02139, USA
[3] Aerodyne Research, Billerica, Massachusetts, USA
[4] Department of Physical Sciences, University of Helsinki, P.O. Box 64, 00014 Helsinki, Finland
[5] Institute of Chemical Engineering and High Temperature Chemical Processes (ICE-HT), Patra, Greece

Keywords: Organic aerosols, Mixing state, Aerosol mass spectrometry, Laboratory experiments
Presenting author email: nmd@andrew.cmu.edu

According to the pseudo-ideal mixing assumption employed in practically all chemical transport models, organic aerosol (OA) components from different sources interact with each other in a single solution, independent of their composition. This critical assumption greatly affects modeled OA concentrations, but there is little direct experimental evidence to support it. A main experimental challenge is that OA components from different sources often look similar when analyzed with an aerosol mass spectrometer. We developed a new experimental method to overcome this challenge, using isotopically labeled compounds (^{13}C or D) and a High Resolution Time-of-Flight Aerosol Mass Spectrometer (HR-ToF-AMS).

Isotopic labeling changes the nominal mass-to-charge ratio (*m/z*) of a given fragment, but the added neutrons also increase the mass defect, which enhances the ability of the HR-ToF-AMS to distinguish different ions at the same nominal *m/z*. The ability of the HR-ToF-AMS to distinguish between isotopically-labeled and unlabeled organic fragments had not been investigated prior to this study. As such, an important part of this work was to develop the analysis method to separate isotopically labeled and unlabeled OA. The main scientific goal was to test the pseudo-ideal mixing assumption. We here tested this assumption for mixtures of secondary organic aerosol (SOA) formed from chemically dissimilar anthropogenic and biogenic SOA precursors.

We generated mixtures of SOA from isotopically labeled toluene and from unlabeled α-pinene and used the HR-ToF-AMS mass spectra to separate these different SOA types using a chemical mass balance. We evaluated the mixing behavior on a standard yield plot (Figure 1), which shows the α-pinene SOA mass yield (SOA formed divided by precursor reacted) as a function of the OA concentration. If the pseudo-ideal mixing assumption is valid and all OA in the system forms a single solution (the "ideal-mixing" case) the SOA mass yield of α-pinene should be a function of the total OA concentration in the system (blue symbols), consistent with equilibrium partitioning. If, on the other hand, the SOA formed does not form a single solution with the pre-existing OA (the "no mixing" case), the α-pinene SOA mass yield should be a function of only the α-pinene SOA (red symbols).

Focusing first on the final yields (large symbols) we observe that the results are consistent with pseudo-ideal mixing (the yields fall close to the expected yield line), and inconsistent with no mixing (the yields fall far from the expected yield line). This implies that, at equilibrium, the pseudo-ideal mixing assumption is valid for this system. The dynamic yields (small symbols) are clearly inconsistent with "no mixing", but they are also lower than expected for the ideal-mixing case. This is consistent with mass-transfer limitations during OA formation: there appears to be some delay between the condensation of organic vapors onto the pre-existing particles and the transfer of the organic species into the particle and equilibration with the bulk OA.

At equilibrium, our results suggest that semi-volatile OA components of different levels of oxidation form a single solution. More generally, anthropogenic and biogenic SOA appear to form a single solution. Therefore, the presence of anthropogenic SOA enhances the concentrations of biogenic SOA, which has important implications for environmental policy.

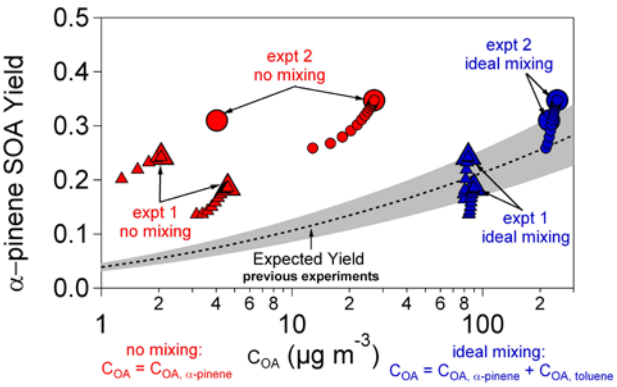

Figure 1. Evaluating the mixing behavior on a standard yield plot. The dashed lines are yield fits based on previous experiments; the shaded grey area is +/-20% of the yield fit, illustrating expected experimental variability. The final yields (large symbols) are consistent with equilibrium partitioning. Dynamic yields (small symbols) are consistent with mass-transfer limitations during OA formation.

This work was supported by an US EPA STAR grant number R833746.

Towards a better understanding of hygroscopic growth and cloud droplet activation of biogenic secondary aerosols

Buchholz, A.[1], Mentel, Th. F.[1], Rubach, F.[1], Spindler, C.[1], Tillmann, R.[1], Kleist, E.[2], Wildt, J.[2]

[1] Forschungszentrum Jülich, IEK-8: Troposphere, Jülich, Germany
[2] Forschungszentrum Jülich, IBG-2, Jülich, Germany
Keywords: CCN, Hygroscopic growth, Cloud microphysics, SOA (Second. Organic Aerosols).
Presenting author email: a.buchholz@fz-juelich.de

Plant emitted volatile organic compounds (VOCs) are a major precursor of secondary organic aerosols (SOA), an important constituent of atmospheric aerosols. Knowledge of the microphysical properties (i.e. the hygroscopic growth and cloud condensation nuclei (CCN) activity) is important to understand the impact of aerosols on climate.

We used the Juelich Plant Atmosphere Chamber (JPAC) at the Research Center Juelich to investigate the microphysical properties of aerosols. SOA particles were produced from the ozonolysis and reaction of OH radicals with the complex VOC mixture emitted from trees typical for the boreal forest. Below 100% relative humidity (RH) the hygroscopic growth factor (GF) of the aerosol particles was determined depending on particle size and RH with a Hygroscopicity Tandem Differential Analyzer. Above 100% RH the activation point was measured depending on the super-saturation (SS=RH-100%) and the size of the dry particle by combination of a CCN-Counter (DMT) and a SMPS/CPC system. The chemical composition of the particles was determined with a High Resolution ToF AMS. Additionally, the size distribution and number concentration of the particles were measured. The gas phase was monitored with GC-MS and PTR-MS.

Changing the emission pattern and strength changed the measured GF and the diameter of the dry particles that were activated (D50). However, below 80% RH the GF changes were within the range of the measurement error. The GF(RH = 90%) were between 1.03 and 1.14, and the D50(SS = 0.4%) in a range of 93 - 100nm. The average hygroscopicity parameter κ (calculated according to Petters and Kreidenweis, 2007) was 0.03±0.01 at RH = 90% and 0.08±0.02 at activation. The aerosol mass spectra measured with the HR-Tof-AMS were analyzed with positive matrix factorization (PMF). The contributions of the identified factors were correlated microphysical properties.

The Koehler theory describes the hygroscopic behavior of aerosol particles in both the sub- and supersaturated regime. A parametrization of this equation is necessary since several of the parameters (e.g. the water activity in the droplets) are unknown for atmospheric aerosols.

Applying the κ parametrization of the water activity (Petters and Kreidenweis, 2007) leads to an underestimation of the CCN activity (see black triangles in comparison to colored dots in Figure 1). κ derived from CCN data was up to a factor of 3 higher than κ derived from GF data. There was a RH dependence of κ with a minimum between 90 and 95% RH. To explain the observed discrepancies, an additional parameter (solubility of the organic material or surface tension) is necessary.

In a different approach the Universal Quasi chemical Functional Group Activity Coefficients model (UNIFAC, Fredenslund et al. 1977) was used to predict the water activity in the mixture of water and organic compounds in the droplets. A hypothetical organic molecule was determined whose functionality and corresponding κ(RH) reproduced the observed hygroscopic growth. If realistic values for the molecular mass and density of the solute were assumed (or derived from measurements), very good agreement of the predicted and measured values was achieved (red line in Fig. 1).

Additionally, real molecules, which can be thought of as surrogates for organics in SOA, were calculated with UNIFAC. The exhibited the same general functionality in κ(RH) as the measured data with a distinct minimum between 90 and 95% RH.

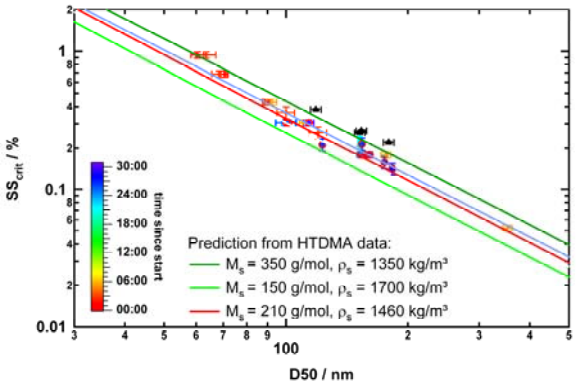

Figure 1. Measured and predicted CCN activation data. The colored dots were measured with the CCN-C (error bars are standard deviation during measurement interval). In black: predicted activation using HTDMA measurements (at 90% RH) and a constant κ. Colored lines: predictions with UNIFAC using different values for molecular mass and density (for details see text above).

Petters, M. D. and Kreidenweis, S. M. (2007). *Atmos. Chem. Phys.*, 7, 1961-1971.

Fredenslund, A. et al (1977), *Industrial & Engineering Chemistry Process Design and Development*, *16*, 450-462

Study on equilibrium vapour pressure of succinic acid in binary aqueous solution and ternary inorganic – organic aqueous solutions using flow tube experiments

T. Yli-Juuti[1], A.A. Zardini[2], M. Kulmala[1], M. Bilde[2], J. Pagels[3], A. Eriksson[3], E. Swietlicki[4], D. Worsnop[5] and I. Riipinen[1,6]

[1]Department of Physics, University of Helsinki, Helsinki, FI-00014, Finland
[2]Department of Chemistry, University of Copenhagen, Copenhagen, DK-2100, Denmark
[3]Faculty of Engineering, Lund University, Lund, SE-221 00, Sweden
[4]Department of Physics, Lund University, Lund, SE-221 00, Sweden
[5]Aerodyne Research Inc., Billerica, Massachusetts, USA
[6]Department of Chemical Engineering, Carnegie Mellon University, Pittsburgh, PA 15231, USA
Keywords: evaporation, organic aerosols, dicarboxylic acids, vapour pressure.
Presenting author email: taina.yli-juuti@helsinki.fi

Numerous organic compounds are found in the atmosphere and for many of them the thermodynamic properties are poorly known. Dicarboxylic acids are a group of water soluble organic compounds typically found in atmospheric aerosol particles. Studies on their equilibrium vapour pressures for pure substances show discrepancies (Pope *et al*., 2010), and even less is known about their evaporative behaviour in multi-component mixtures. Here, we study the effect of selected activity model on the obtained sub-cooled liquid phase saturation vapour pressure of succinic acid (a dicarboxylic acid) and the effect of inorganic salts on the activity coefficient of this organic compound.

The evaporation rates of solution droplets were measured using a Tandem Differential Mobility Analyzer (TDMA) system coupled with a 3.5 m long laminar flow tube (Koponen *et al*., 2007) providing maximum evaporation time up to 250 s. A monodisperse droplet population is selected with a DMA and let to the flow tube where the droplets evaporate and their size change is measured with a Scanning Mobility Particle Sizer (SMPS). The droplets were atomized from binary succinic acid – water solution or ternary solutions of succinic acid – sodium chloride – water and succinic acid – ammonium sulphate – water. In the latter case the temporal evolution of droplets' composition was also monitored with an Aerosol Mass Spectrometer (AMS).

To study the equilibrium vapour pressures over the mixture droplets, the observed evaporation rates were compared to those predicted by a theoretical evaporation model. In the model, inorganic compound is assumed to be non-volatile and the change of particle size is thus due to evaporation of succinic acid and water. Three activity coefficient models included in the Extended Aerosol Inorganic model, E-AIM, (www.aim.env.uea.ac.uk, see references therein) are used for succinic acid in the ternary cases: fitted activity equation (RK), UNIFAC with Peng *et al*. (2001) corrections (UP) and standard set of UNIFAC parameters (US). In binary cases these were compared also to Dortmund version of UNIFAC (UD) (Gmehling *et al*., 1990).

The saturation vapour pressure of succinic acid ($p_{sat,succ.}$) at 298.15 K extracted from the binary succinic acid – water droplet experiments was $1.29 \cdot 10^{-3}$ Pa, $1.95 \cdot 10^{-3}$ Pa, $1.15 \cdot 10^{-3}$ Pa and $0.90 \cdot 10^{-3}$ Pa when using, respectively, RK, UP, US and UD as the activity model. In general the determined saturation vapour pressures increased slightly as a function of relative humidity when using the first three activity models. This was most pronounced with UP with 25 % variation in determined $p_{sat,succ.}$ value within relative humidity range 60-80 %.

In the ternary case the activity coefficient of succinic acid ($\gamma_{succ.}$) is calculated as for binary solution with the same molality of organic solute, i.e. the effect of inorganic compound on $\gamma_{succ.}$ is ignored. Figure 1 shows that this approach overestimates the evaporation rate when mole fraction of succinic acid is smaller or comparative to that of inorganic compound. The result was similar for both ternary mixtures. Measurements with AMS showed that the uncertainty in the initial fraction of succinic acid in the droplets does not alone explain the discrepancy between the modelled and measured evaporation rates. Neither does the uncertainty in $p_{sat,succ.}$ due to good agreement with large succinic acid fraction. Thus, the result might indicate $\gamma_{succ.}$ being lowered by the inorganic solute. However, the effects of dissociation of succinic acid and uncertainties related to the measurement setup need to be studied in more detail.

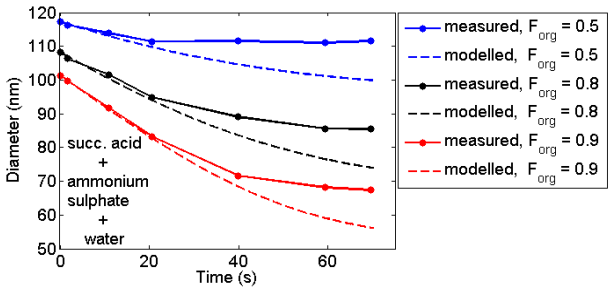

Figure 1. Particle size evolution for three initial fractions of succ. acid (F_{org}) of the total solute at 75% RH.

This work was supported by EUCAARI project no 036833 and Maj and Tor Nessling foundation.

Gmehling, J., *et al*. (1990) *Fluid Phase Equilib*. **54**, 147.
Koponen, I.K., *et al*. (2007) *Environ. Sci. Technol.* **41**, 3926.
Peng, C., *et al*. (2001) *Environ. Sci. Technol*. **35**, 4495.
Pope, F.D., *et al*. (2010) *J. Phys. Chem. A* **114**, 10156.

Water Uptake Properties of internally mixed sodium halide and succinic acid particles

Lorena Miñambres, Estíbaliz Méndez, María N. Sánchez, Fernando Castaño and Francisco J. Basterretxea[1]

[1]Departamento de Química Física, Universidad del País Vasco/Euskal Herriko Unibertsitatea, B. Sarriena, s/n, 48940 Leioa, Bizkaia, Spain

Keywords: marine aerosol, hygroscopicity, deliquescence.

Presenting author email: lorena.minambres@ehu.es

Atmospheric aerosols generally consist of inorganic species with a wide variety of organic compounds and elemental carbon. On the one hand, sea salt aerosols constitute one of the most abundant types of naturally suspended particulate matter in the troposphere, and are the dominant aerosol species by mass above the oceans. Sodium chloride is the principal component, and also includes less abundant ions such as SO_4^{2-}, Mg^{2+}, Ca^{2+}, K^+ and Br^-. On the other hand, organic matter can amount to 30-50% of fine particulate mass, depending on location (Seinfeld and Pandis, 1998). In addition, sea salt aerosols include appreciable fractions of organic material that can affect properties such as hygroscopicity, phase transition or chemical reactivity. Despite its importance, the physical state of mixed organic/inorganic aerosol particles is not well characterized.

In the present work we study the hygroscopic properties and phase characterization of internally mixed submicrometric particles composed of succinic acid (SA) and NaX (where X=F, Cl, Br or I) by infrared absorption spectroscopy in an aerosol flow cell at ambient temperature for different relative succinic acid/NaX compositions. Infrared spectroscopy is a sensitive technique to characterize aerosol composition, water content and particle phase, and has been used to study other internally mixed organic/inorganic particles (Brooks et al., 2003). The study of the influence of the halogen atom in the NaX/SA system provides physico-chemical insight into the deliquescence process of these aerosols and particle phase.

Aerosols are prepared by atomizing aqueous solutions of desired concentrations to yield submicrometer aerosol particles. The relative humidity (RH) of aerosols is controlled by mixing dry and humid flows of nitrogen. The extinction spectra of particles flowing through an aerosol cell are recorded from 800 to 4000 cm^{-1} with a FTIR spectrometer. Particle phase, composition and water content are measured by monitoring the liquid water extinction spectrum.

The results show that the presence of succinic acid does not appreciably alter the deliquescence process of NaF and NaCl, whereas both NaI and SA/NaI particles exhibit a non-deliquescent behaviour, uptaking water at any RH. SA/NaBr particles, on the contrary, deliquesce at lower relative humidities than pure NaBr particles, the effect being more marked as the SA/NaBr mass ratio approaches unity. Thus the presence of an organic compound with relatively low water solubility, such as succinic acid, internally mixed with sodium bromide aerosol can increase the range of conditions under which the aerosol is a solution, due to specific ion-molecule interactions in the particles that alter their Gibbs free energy. Succinic acid phase in the particles has been spectroscopically monitored at given values of both RH and SA/NaX solute mass ratio. The different hygroscopic properties as the halogen ion is changed can be rationalized in terms of simple thermodynamic arguments and can be attributed to the relative contributions of ion-molecule interactions in the solid particles. The observed behaviour is of interest for tropospheric sea-salt aerosols mixed with organic acids, and, if it can be extended to other organics, can influence the physical and chemical properties of marine aerosols in the atmosphere.

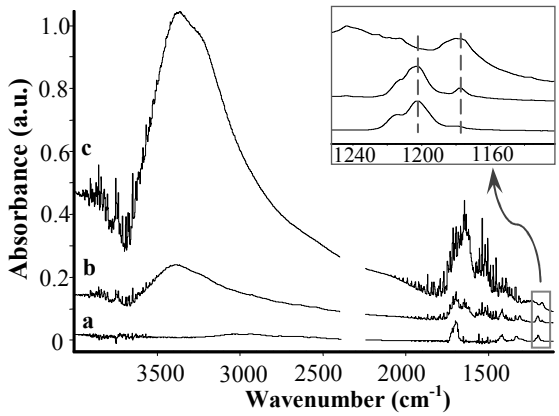

Figure 1. Infrared extinction spectra of internally mixed particles of succinic acid and NaCl at 1:1 SA/NaCl mass ratio and a total concentration of 0.05 kg/L for various RHs. Spectra in (a) and (b) correspond to dry particles exposed to 5% and 75% RH, respectively, whereas spectrum in (c) comes from liquid particles as they exit the atomizer. The inset shows absorption bands of succinic acid that have been used to characterize its phase in the particles: solid (near 1700 cm^{-1}) and aqueous (near 1180 cm^{-1}).

This work was supported by Ministerio de Ciencia e Innovación via grant-in-aids (CGL2008-06041/CLI and CSD-2007-00013), Gobierno Vasco/Eusko Jaurlaritza and Universidad del País Vasco through general support.

Brooks, S. D., Garland, R. M., Wise, M. E., Prenni, A. J., Cushing, M., Hewitt, E., Tolbert, M. A. (2003) *J. Geophys. Res*. **108** (D15), 4487-4497.

Seinfeld, J. H., Pandis, S. N. (1998) *Atmospheric Chemistry and Physics*; John Wiley; New York.

Aerosol-halogen interaction: Halogenation processes of secondary organic aerosols

J. Ofner[1], N. Balzer[1], J. Buxmann[2], H. Grothe[3], H.-U. Krüger[1], U. Platt[2], Ph. Schmitt-Kopplin[4], C. Zetzsch[1]

[1]Atmospheric Chemistry Research Laboratory, University of Bayreuth, Bayreuth, Germany
[2]Institute of Environmental Physics, University of Heidelberg, Heidelberg, Germany
[3]Institute of Materials Chemistry, Vienna University of Technology, Vienna, Austria
[4]Institute of Ecological Chemistry, Helmholtz Zentrum Munich, Munich, Germany
Keywords: organic aerosols, halogenation processes, spectroscopy.
Presenting author email: Johannes.ofner@uni-bayreuth.de

The release of reactive halogen species from sea-salt aerosol contributes a new class of reactants for heterogeneous reactions. These heterogeneous reactions have been overlooked so far, although they may occur with internal and external mixtures of sea-salt aerosol or above a salt-pan and organic aerosol and organic matter in soil. Such reactions can constitute sources of gaseous organohalogen compounds or halogenated organic aerosol in the atmospheric boundary layer.

To study the interaction of organic aerosols with reactive halogen species (RHS), secondary organic aerosol (SOA) was produced from α-pinene, catechol and guaiacol using an aerosol smog-chamber. The model SOAs were characterized in detail using a variety of physico-chemical methods (Ofner et al., 2011). Those aerosols were exposed to molecular halogens in the presence of UV/VIS irradiation and to halogens, released from simulated natural halogen sources like salt-pans, in the presence of UV/VIS irradiation.

The entire organic aerosol and its physico-chemical transformation process were monitored using various spectroscopic methods: Long-path-absorption- and Attenuated-Total-Reflectance (ATR-)-FTIR were used to determine the changes of functional groups and structural elements of the macromolecular aerosols. The optical properties in the UV/VIS range were monitored using diffuse-reflectance-UV/VIS-Spectroscopy. BrO levels were observed by Differential Optical Absorption Spectroscopy (DOAS) in combination with a multi-reflection cell (White-cell). The evolution and change of the aerosol size distribution by the reaction with halogens was observed using an electrostatic classifier coupled to a condensation nuclei counter. Finally, Temperature-Programmed-Pyrolysis Mass-Spectroscopy (TPP-MS) and ultra-high resolution Fourier-Transform-Mass-Spectroscopy (ICR-FT/MS) were used to determine the degrees of halogenation and individual halogenated species.

The heterogeneous reaction of RHS with those model aerosols leads to different gaseous species like CO_2, CO and small reactive molecules like phosgene. Hydrogen containing groups on the aerosol particles are destroyed to form HCl or HBr, and a significant formation of C-Br bonds could be verified in the particle phase. Overall, the optical properties of the processed organic aerosols are significantly changed. Further, the aerosol size distribution of the organic aerosols is strongly influenced (see Fig. 1). The heterogeneous reaction of SOAs with molecular halogens released from the simulated salt-pan at different simulated environmental conditions leads to changes of several physico-chemical features of the aerosol.

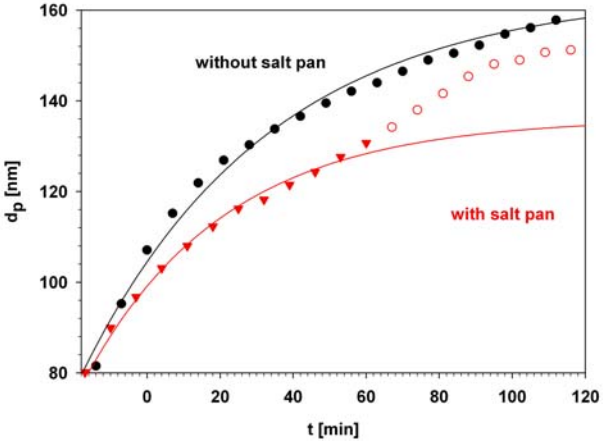

Figure 1. Influence of natural released halogens on the aerosol size distribution of model SOA; the solid lines represent the estimated evolution of the size distribution without the influence of halogens

However, one order of magnitude less BrO was detected in the presence of SOA. This indicates that even the halogen release mechanism could be influenced by the heterogeneous reaction (see Fig. 2).

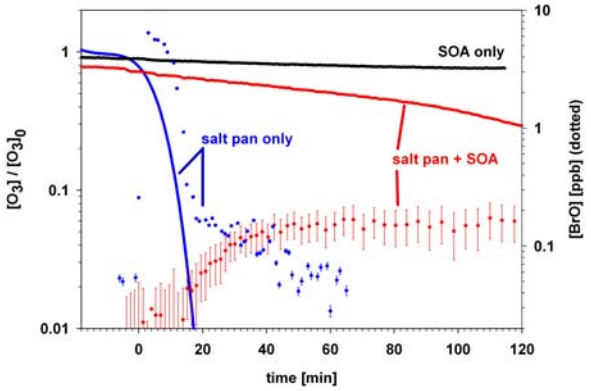

Figure 2. Change of ozone depletion and BrO formation (dotted) under the influence of the model SOA .

This work was supported by the German Research Foundation within the HALOPROC project.

Ofner, J., Krüger, H.-U., Grothe, H., Schmitt-Kopplin, P., Whitmore, K., and Zetzsch, C. (2011), *Atmos. Chem. Phys.*, **11**, 1-15.

On ultrafine aerosol growth and the condensation/evaporation properties of atmospheric organics

I. Riipinen[1,2,6], J.R. Pierce[3], T. Yli-Juuti[1], S. Häkkinen[1], C. Fountoukis[2], M. Kulmala[1], D. Worsnop[1,4], M. Bilde[5], S. N. Pandis[2,6] and N.M. Donahue[6]

[1]Department of Physics, University of Helsinki, Helsinki, FI-00014, Finland
[2]Institute of Chemical Engineering and High Temperature Processes (ICE-HT), Foundation for Research & Technology, Hellas (FORTH), Patras, GR-26504, Greece
[3]Department of Physics and Atmospheric Science, Dalhousie University, Halifax, B3H 3J5, Canada
[4]Aerodyne Research, Billerica, MA-01821, MA, USA
[5]Department of Chemistry, University of Copenhagen, Copenhagen, 2100, Denmark
[6]Center for Atmospheric Particle Studies, Carnegie Mellon University, Pittsburgh PA-15213, PA, USA

Keywords: atmospheric aerosols, condensation/evaporation, organics, growth.
Presenting author email: ilona.riipinen@helsinki.fi

Organic compounds are abundant in atmospheric particulate matter, and a large fraction of these compounds are of secondary origin (Jimenez et al., 2009). Besides contributing to the total atmospheric aerosol mass, organic compounds play an important role in growing freshly-formed ultrafine particles to climatically relevant sizes (e.g. Riipinen et al., 2011). To quantify the effect of organic emissions to climate and air quality, atmospheric large-scale models need to realistically simulate the distribution of organic compounds in the atmospheric aerosol size spectrum.

Condensation and evaporation to/from aerosol particles can be reproduced with dynamic models if the thermodynamic and kinetic properties, such as saturation vapour pressures, vaporization enthalpies and accommodation coefficients of the condensing or evaporating vapors are known. In this work we investigate the condensational properties of atmospheric organic compounds, with a special focus on the low-volatile compounds growing the nucleation-mode aerosol (see also Donahue et al., *these proceedings*), and discuss the implications of these results for aerosol growth mechanisms and their representations in atmospheric large-scale models.

By comparing observed growth rates of freshly-nucleated ultrafine aerosol with condensational growth simulated by an aerosol dynamics box model we find that ambient sulphuric acid can account for only a minor fraction of ultrafine aerosol growth, the rest being organics. This observation is consistent with the seasonal pattern of particle growth rates at e.g. the SMEAR II station in Hyytiälä, Finland, for which growth rates show a maximum in the summer along with maximal emissions of biogenic organic compounds (Yli-Juuti et al., *in prep.*). We also find that saturation concentrations of roughly 10^{-3} μg/m^3 or less (corresponding to pure component saturation vapour pressure of the order or 10^{-8} Pa or less) are needed to explain the observed growth (see Fig. 1). Consistent results are found when the evaporation of the nucleation mode aerosol in the heating section of a Volatility-DMPS is modeled with a dynamic evaporation model and compared to measurement data.

These volatilities are significantly lower than those found in fresh chamber-generated or even aged atmospheric secondary organic aerosol (SOA) mass, which typically range from approximately 10^{-2} to 10^{2} μg/m^3 (10^{-7} to 10^{-3} Pa) (see Lee et al., 2010). The observed saturation concentrations are also in the lower end of the corresponding properties of dicarboxylic acids, which are among the least volatile identified SOA molecules with measured vapor pressures ranging from 10^{-8} to 10^{-3} Pa.

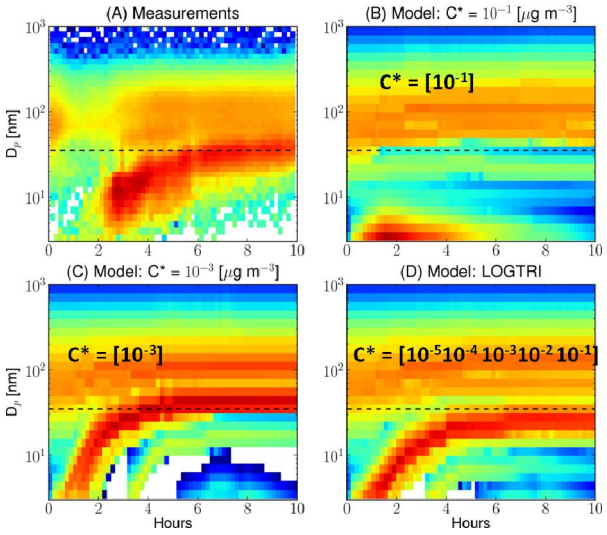

Figure 1. Measured (panel A) and modeled (panels B, C, D) evolution of aerosol size distribution on April 15th 2007 at the SMEAR II station in Hyytiälä, Finland.

This work was supported by Camille and Henry Dreyfus foundation, European Integrated Project for Aerosol Cloud Climate and Air Quality Interactions (EUCAARI).

Jimenez, J. *et al*. (2009), *Science*, **326**, 1525–1529.
Lee, B.-H. *et al.*, (2010), *Atmos. Chem. Phys.*, **10**, 12149–12160.
Riipinen, I. *et al.* (2011), *Atmos. Chem. Phys. Discuss.*, **11,** 387–423.

Friday, September 9, 2011

Session 11C: Combustion Aerosol Measurements and Analysis

Thermodenuder with low nanoparticle losses: design, simulations, laboratory tests and diesel exhaust particle studies

A. Arffman[1], T. Rönkkö[1], P. Karjalainen[1], T. Lähde[1,2], J. Heikkilä[1], L. Pirjola[2], D. Rothe[3] and J. Keskinen[1]

[1]Aerosol Physics laboratory, Tampere University of Technology, Tampere,FI-33101, Finland
[2]Department of Technology, Metropolia University of Applied Sciences, FI-00180 Helsinki, Finland
[3]MAN Nutzfahrzeuge AG, Abt. MTVN, Abgasnachbehandlung, Vogelweiherstrasse 33, D-90441 Nürnberg, Germany
email: anssi.arffman@tut.fi

Diesel exhaust undergoes rapid cooling and dilution processes when the exhaust is released into the atmosphere. During these processes, gas-to-particle processes like nucleation and condensation can take place modifying the size distribution and physical and chemical characteristics of the exhaust particles.

Particle volatility studies are a practical way to study the gas-to-particle processes of diesel exhaust. In addition to the emission characterizations, volatility studies can produce information about the particle formation processes and about the technical factors affecting them (e.g. exhaust after-treatment, fuel quality).

For example, in several studies the diesel exhaust nucleation mode is shown to include a non-volatile fraction. The initial formation of nonvolatile nucleation mode particles have been showed to take place at high temperature conditions before the exhaust entered into the atmosphere and the formation is affected e.g. by fuel injection pressure and exhaust after-treatment.(eg. Rönkkö et al. (2007), Heikkilä et al. (2009), Lähde et al. (2011)).

On the other hand, the changes of fuel and lubricant oil sulfur content affect mostly to the emissions of totally volatile nucleation mode particles (Karjalainen et al. (2011)).

In the studies above, the particle volatility has been studied using a thermodenuder (TD) where the semi-volatile particle fraction is first evaporated in the heating part and, after that, collected onto the surface of active charcoal in denuder part. The diesel exhaust nucleation mode studies require that, in addition to the effective evaporation of volatile components, the penetration of small non-volatile particles is high enough. Therefore, we built a TD based on the following designing criteria:

1) TD is able to evaporate all semi-volatile species of diesel exhaust particles
2) Evaporated vapors are efficiently collected into the activated charcoal
3) Flow range of TD is 0-10 slpm and the inlet temperature is 300K or higher.
4) Aerosol cools in the denuder part nearly to the inlet temperature of 300K.
5) TD provides a high penetration for non-volatile particles larger than 3 nm.

Designing of the TD was based on simulations by employing CFD packages of Ansys Fluent and Comsol Multiphysics. Losses of non-volatile particles were simulated as a function of particle size by solving the transport equation for different particle sizes in combination with the flow field and heat transfer equations. Evaporation rates of 10 – 100 nanometer sulfuric acid – water particles with concentration of 10^8 particles/cm^3 were simulated (see Figure 1). It can be seen that the particles evaporate in the heating part. In addition, simulations showed that the concentration of the sulfuric acid was reduced by a factor of 300 in the denuder part. The evaporation efficiencies (Karjalainen et al. 2011) and the non-volatile particle losses (Heikkilä et al. 2009) were tested also by generated particles.

In addition to the simulations and laboratory tests, the TD was used in the diesel exhaust particle studies in engine laboratories and on-road. These field measurements showed that the TD is able to remove the volatile nucleation mode particles and condensates from the soot particles (Karjalainen et al. 2011). In engine laboratory measurements the size-distribution measurements of the non-volatile core mode particles agreed well with the results obtained by using the hot dilution setup. Also the studies related to nucleation mode particle charge supported the results(e.g Lähde et al. (2011)).

In summary, simulations, laboratory tests and real engine exhaust measurements confirm that the TD performs well when it is properly operated; the sample flow is not too large, the temperature is not too low and the nucleation mode particles are not too large.

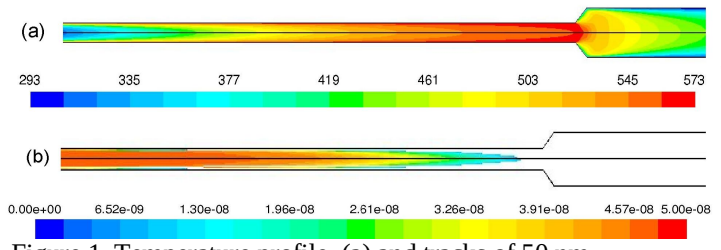

Figure 1. Temperature profile (a) and tracks of 50 nm H_2SO_4-H_2O- particles inside the TD (b).

J. Heikkilä et al. (2009). Journal of the Air & Waste Management Association 59 pp. 1148-1154.
P. Karjalainen et al. (2011). Manuscript in preparation.
T. Lähde et al. (2011). Accepted to Env. Sci. & Tech.
T. Rönkkö et al. (2007) Env. Sci. &Tech., 41, 6384-6389.

Soot particle aggregates: numerical construction and analysis of influence on laser-induced incandescence and elastic light scattering signals

J. Johnsson[1], A. Karlsson[2], N.-E. Olofsson[1], H. Bladh[1], P.-E. Bengtsson[1]
[1]Combustion Physics, Lund University, Lund, SE-221 00, Sweden
[2]Department of Electrical and Information Technology, Lund University, Lund, SE-221 00, Sweden
Keywords: Measurement (combustion aeros.), numerical simulation, soot particles.
Presenting author email: jonathan.johnsson@forbrf.lth.se

Soot particles are aerosols that are formed in combustion processes, such as in an IC engine, a gas turbine or a furnace. If the combustion process is not complete, soot particles are often present in the exhaust gases. It is known that these particles have an influence on the climate and that they are detrimental to human health. Carcinogenic polyaromatic hydrocarbons (PAHs) are often present on the particle surfaces, and the smallest particles are especially dangerous, as they easily follow the inhalation air stream down to the lungs, where they can be deposited.

To analyse measurements of soot particle properties, it is important to take into account that the particle structure can be complicated. In general, a soot particle is better described as a soot *aggregate*, which is a cluster of approximately spherical *primary* particles, see Fig. 1a. The configuration in which the primary particles are positioned, and how they are connected to each other, depends on the type of combustion process they were created in. For this reason it becomes relevant to ask what is actually meant by the "size" of an aggregate, and which properties are important to describe the structure. Aggregates produced in the same type of combustion process can be approximately described using a fractal structure (Sorenson, 2001). This means that the radius of gyration of the aggregate, R_g, the primary particle diameter, d_p, and the number of primary particles in the aggregate, N_p are linked, $N_p = k_f(R_g/a)^{D_f}$, where k_f is the fractal prefactor and D_f is the fractal dimension. These two fractal parameters are different for different types of soot; for soot produced in a diffusion flame, $k_f \approx 2.3$ and $D_f \approx 1.8$ (Köylü and Faeth, 1994).

To facilitate the understanding of how to take the shape of soot aggregates into account in size measurements, aggregates with specific properties have been constructed numerically using the method described by Filippov *et al.* (2000). An example is shown in Fig. 1b. The method has also been extended to be able to construct aggregates that include a simple form of necking, so that the particles no longer only have point contact.

Elastic light scattering (ELS) and laser-induced incandescence (LII) and are two techniques that can be used for non-intrusive, time-resolved measurements on soot properties such as volume fraction and size. In ELS, laser light is scattered from the aggregates, and the angle dependence of the scattering intensity can be used to infer size properties of the aggregates. In LII, a nanosecond laser pulse is used to heat the aggregates to a temperature well above

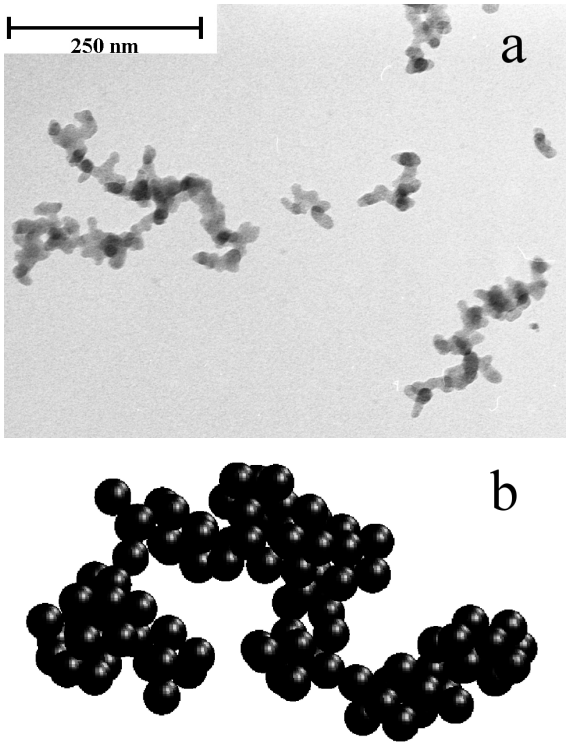

Figure 1: (a) Soot sampled from a flame. (b) Modelled soot particle.

that of the ambient gas. After the pulse, the aggregates cool to the ambient gas temperature with a rate that depends on their size properties.

In this work, ELS from fractal soot aggregates with point-contact between primary particles has been simulated, using modelled soot aggregates. Also, simulation of the heat conduction from soot aggregates has been made, which is relevant for LII measurements. For the these simulations, both aggregates with primary particles in point-contact and various levels of necking are of great interest.

Financial support from Centre of Combustion Science and Technology (CECOST) and the Swedish Research Council is greatly acknowledged.

Filippov, A. V., Zurita, M. and Rosner, D. E. (2000) J. Colloid Interface Sci. **229**, 261–273.
Köylü, Ü. Ö. and Faeth, G. M. (1994) J. Heat Transfer **116**, 152–159
Sorensen, C. M. (2001) Aerosol Sci. Tech. **35**, 648–687

Electronic tomography of nanoparticles aggregates: from 2D to 3D

Ouf, F.X.[1], Yon, J.[2], Frébourg, G.[3] and Pontreau S.[1]

[1]Aerosol Physics and Metrology Laboratory, IRSN, BP 68, 91192, Gif-sur-Yvette Cedex, France.
[2]UMR 6614 CORIA, Avenue de l'université, BP 8, 76801 Saint Etienne du Rouvray, France.
[3]IFR 83, SME, Université Pierre et Marie Curie, 9, quai Saint Bernard, 75005 Paris. France.

Keywords: fractal aggregates, soot, tomography, Transmission Electron Microscopy
Presenting author email: francois-xavier.ouf@irsn.fr

The morphology of nanoparticle aggregates produced during manufacturing processes of nanomaterials or combustion process is a key parameter to understanding the physical behaviour of these particles. The method of determining the characteristics of fractal clusters (fractal dimension D_f and prefactor k_f) is most often based on sampling of these particles and observation by transmission electron microscopy (TEM), in 2D projection. The obtained micrographs are analysed and 2D morphological information are usually extrapolated to 3D data according to empirical relationships obtained from numerically generated aggregates and proposed by Köylü *et al.* (1995) and Brasil *et al.* (1999).

If soot sampling impact has been studied by Ouf *et al.* (2010), it appears that few experimental validations have been devoted to validate the methodology used for the 2D->3D extrapolation of morphological parameters (Köylü *et al.*, 1995). Indeed, if these digital tools are based on realistic physical principles, the fact remains that these relationships do not include TEM based experimental artefacts (contrast discrepancies caused by monomer's multilayer and overlapping, polydispersity in size of monomers). Moreover, empirical relationships are based on aggregates projections without any preferential orientation. But aggregates may be suspected to adopt a particular orientation during deposition onto TEM grids.

The objective of this study is to carry out an experimental validation of these transposition laws by using electronic tomography.

The nanoparticles aggregates have been observed with a 200 kV LaB_6 TEM JEOL 2100 (IFR 83, UPMC) equipped with a GIF 863 Tridien (GATAN), a SS-CCD 2k x 2k camera and a goniometric sample holder allowing the orientation of the sample from –70° to +70°. Specific software (Digital Micrograph), permits to acquire TEM images with a step of 1° and with automatic focusing/tracking of the investigated object. Using this technique, we have studied nanoparticles aggregates generated using a commercial propane/air burner (CAST, Jing Inc.) and classified in terms of electrical mobility diameter with a differential mobility analyser (DMA 3080L TSI). At the outlet of the DMA, the aggregates are deposited on a TEM grid with the help of a thermophoretic particle sampler (Ouf *et al.*, 2010).

More than 20 aggregates, with a number of primary particles ranging from 10 to 250, have been considered and two separate investigations have been carried out. The first one deals with a potential orientation of aggregates during their deposition on TEM grids. Figure 1 presents the evolution of the number of primary particles measured at several observation angles. The evolution of this parameter has been also numerically computed using DLCA simulation software and considering random or specific orientation of the aggregates during their deposition. According to this comparison, it is not obvious that a specific orientation of the aggregates may be identified during their deposition. This first point validate the use of such sampler for analysing fractal aggregates and most of all that these samples may be used to experimentally validate the transposition relationship.

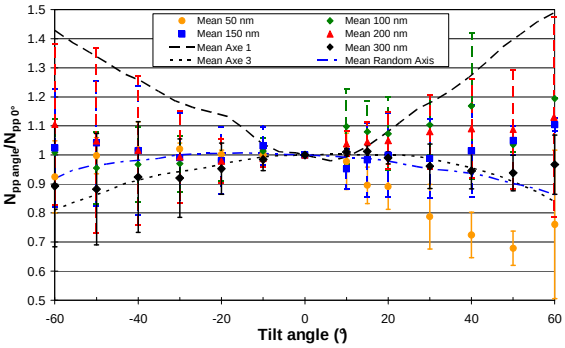

Figure 1. Evolution as a function of the tilt angle, of determined number of primary particles.

The second point, which is still in progress, will aim to establish, using the TomoJ software (Messaaoudi et al., 2007), the 3D morphology of CAST generated aggregates. Finally, these realistic three-dimensional aggregates will be used to define experimental transposition relationships which will be compared to the empirical laws proposed by previous workers.

Brasil, A.M., Farias, T.L. & Carvalho, M.G. (1999). *J. Aerosol Sci.*, 30 (10), 1379-1389.
Köylü, Ü. Ö, Faeth, G.M., Farias, T.L. & Carvalho, M.G. (1995). *Combust. Flame*, 100, 621-633.
Messaoudi, C., Boudier, T., Sanchez Sorzano, C.O., Marco S. (2007). *BMC Bioinformatics*, 6, 288.
Ouf, F.X., Yon, J., Ausset, P., Coppalle, A. Maillé, M. (2010). *Aerosol Sci. Technol.*, 44, 1005-1017.

Effect of Alkali Metal Salt Addition on Hierarchic Assembly of Flame Aerosol Nanoparticles detected by Synchrotron Small-Angle X-ray Scattering

S. di Stasio[1], J.B.A. Mitchell[2] and J.-L. LeGarrec[2]

[1]Aerosol and Nanostructures Lab, Istituto Motori CNR-IM, Via Marconi 8, Napoli, Italia
[2]Institute de Physique, U.M.R. N° 6251 du C.N.R.S. Université de Rennes, Rennes, France
Keywords: SAXS, Measurement (combustion aerosol), Flame metal combustion, Soot particles.
Presenting author email: stefano.distasio1600@gmail.com

The addition of alkali metal salts (sodium, potassium, cesium salts) and water has been reported in the literature either to increase or decrease soot production in flames(Howard and Kausch, 1980; Fialkov, 1997). On the basis of our previous experimental works by TEM (di Stasio, 2001) and SAXS (di Stasio et al, 2006) we proposed to the combustion community the model of hierarchic aggregation for flame aerosols. The experiments provided the evidence about the fact that the so-called primary particles (30-50 nm), which are the building blocks of soot fractal aggregates (about 100 nm), are in turns constituted by smaller sub-units (~10 nm). We baptised these smaller constituents *sub-primary* particles (di Stasio, 2001).

In this work we studied the effect of addition to the flame of 0.1 mole-wt/liter acqueous solution of alkali metal salts KCl, CsCl, $BaCl_2$, $CaCl_2$ taking into account the previous findings about the formation of hierarchical soot agglomerates. The results show significant effects both on primary and sub-primary particle size and concentration, which are quite new in the literature. In fact previous works were based on laser light scattering techniques which are insensitive below 15 nm because of the background noise by the flame gases. SAXS experiments were performed at the ID02 beamline of European Synchrotron Facility (ESRF) in Grenoble, France. Energy of X-beam was 12.4 keV with $\Delta\lambda/\lambda=0.03$. The beamline was equipped with a scattering tunnel filled by helium with length adjustable between 1 and 10 m at the end of which is positioned the area detector. The shorter scattering distance between flame and detector corresponds to wider scattering angles θ, i.e., to larger scattering momentum $q=(4\pi/\lambda)*\sin(\theta/2)$ and smaller dimension D of detectable particles being $D=\pi/q$. Drops of plain water and alkali metal salts 0.1 mole-wt/liter water solution were aspirated into the air flux before mixing with the ethylene fuel gas. All the results were referred to the addition of pure water. We used the 5 m tunnel configuration and measured a scattering intensity I(q) in the range 0.04 $nm^{-1}<q<0.5$ nm^{-1} (0.004 $Å^{-1}$ to 0.05 $Å^{-1}$) corresponding to a size window for particle detection ~ 6 nm to ~ 78 nm. Analysis of the scattering data was made using the Unified Fitting function approach by Beaucage (1995) implemented by SAS Irena macro by Jan Ilavsky (2009). The results demonstrate that CsCl is effective in reducing either primary or sub-primary particle size but, vice versa, it does increase the concentrations of both. KCl, $CaCl_2$ and $BaCl_2$ have negligible effect on the primary and sub-primary particles but $BaCl_2$ addition leads to the smallest primary and sub-primary particle concentrations observed in these experiments.

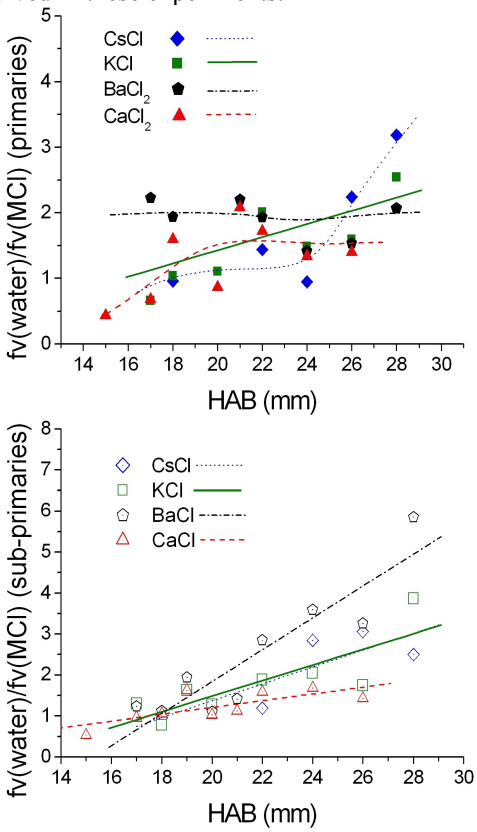

Fig. 1. Top) Effect on volume fraction for plain water vs. Metal Cloride addition in the case of primaries. Bottom) same as Top evaluated for sub-primary particles.

The global effect of soot suppressing is shown in the Fig. 1. $BaCl_2$ and, to a lesser extent, KCl are the additives which yield smaller primary and sub-primary soot volume fraction independently on residence times.

References

Beaucage, G. (1995) *J. Appl. Cryst*. **28**, 717-728.
Beaucage, G. et al. (2004) *J. Appl. Cryst*. **37**, 523-535.
di Stasio , S. (2001) *Carbon* **39**, 109-118.
di Stasio, S. et al. (2006) *Carbon* **44**, 1267-1279.
Fialkov, A. B. (1997) *Prog. Energy. Combust. Sci*. **23**, 399-528.
Howard, J. B.; Kausch., W. J. (1980) *Prog. Energy. Combust. Sci*. **6**, 263-276.

Ilavsky, J. (2009) *J. Appl. Cryst*, **42** 347-353.

Determination of the refractive index of soot particles in the visble spectrum by extinction spectra

J. Yon, C. Caumon, K. F. Ren, G. Martel and A. Coppalle

CNRS UMR 6614 - CORIA, 76801 BP-12, Saint Etienne du Rouvray, France

Keywords: Aggregates, Index of refraction, Light extinction, Fractals, Soot size distribution

Soot particles, generated by combustion, are fractal-like aggregates. The absorption and scattering of light by these particles can be calculated if their morphology and their complex refractive index are know (Krishnan, 2000; VanHulle, 2002; Yon, 2011). However, up to now, this last parameter is not well known and its determination remains a challenge, as for all carbonaceous amorphous particles. The spectral variation of the complex refractive index of soot matter (m=n-ik) can be predicted using a dispersion model, as the one of Lorentz-Drude (L-D) or Jelisson-Modin (J-M) (1996). However, several parameters of these theories have to be known. This can be done by comparing calculated spectra with measured ones. The extinction spectra of soot particles diluted in a flow are easy to measure in the visible spectrum.

So, in this work the spectral variations of extinction coefficient Kext have been measured for soot particles in the visible spectrum, and the analysis has been performed using the above dispersion models (L-D or J-M) in order to retrieve the values of the complex refractive index m as a function of the wavelength

Soot particles have been generated in an ethylene and two fuel spray flames (di-ester and diesel). The soot has been sampled with a two-stage dilution system (DEKATI FPS 4000) (Ouf, 2010) in order to be introduced in an optical bench at ambient temperature and pressure conditions. The path length is L = 1.5 m and the extinction spectra through the tube are measured by a turbidity system (Ren et al, 2010). Example of such spectra is shown in Fig. 1.

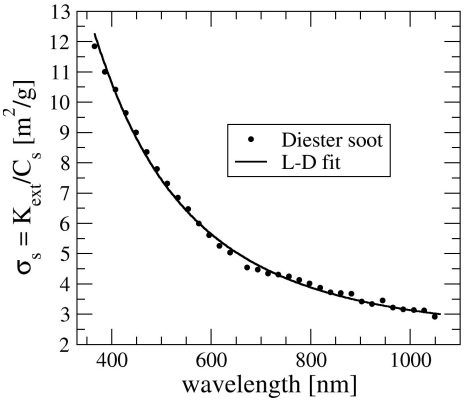

Fig.1: experimental spectrum of the specific extinction coefficient σ_s = kext/Cs of diester soot (σ_s = kext/Cs, with Cs the mass concentration). The continuous line represent the calculated values with the dispersion model of Lorentz-Drude

In the same conditions, other measurements have been performed. The size distribution of the soot N(Dm) was measured by using a SMPS (3010-TSI). These particles were also deposed on a filter and measured by a TEM (Transmission Electron Microscopy). This last experimental set-up permits the determination of soot morphological properties (fractal dimension df, fractal prefactor kf and primary particle size Dp).

From the measured size distribution and from the morphology parameters, the extinction spectra are calculated according to the RDG-FA (Rayleigh-Debye-Gans theory for fractal aggregates) model. The extinction coefficient is given by:

$$K_{ext} = C_a\, E(m) \sum_{D_m} D_m^{d_f} N(D_m) + C_b\, F(m) \sum_{D_m} D_m^{2d_f} g(\lambda, D_m) N(D_m)$$

where the factors Ca and Cb depend on the morphological parameters (df, kf, Dp) of the soot and the wavelength λ. The first and the second terms in the above equation represent respectively the contributions of absorption and scattering processes. E(m) and F(m) are functions of the refractive index m.

Two ways are possible for analyzing the experimental spectra. 1- As it will be shown, the scattering contribution is not important in the extinction process. So by neglecting this contribution, spectral variation of E(m) can be derived directly from Kext measurements. 2- We can also determine the refractive index values of the soot by comparing and fitting calculated values of Kext to measured ones. To this end, a dispersion model has to be used, and the aim of the comparison is to obtain the parameters of the dispersion model, allowing to determine the functions E(m) and F(m). In the present study, the model of Lorentz-Drude and the one proposed by Jelisson and Modine (1996) have been used.

The results obtained with the two procedures will be presented and analysed. As an application, the influences of particle morphology and their temperature on the radiative properties of soot will be also assessed and discussed.

Krishnan S. S., Linn K.-C. and Faeth G.M., (2000) *J. Heat Transfer*, 122, 517-524.

Van-Hulle P., Talbaut M., Weill M. and Coppalle A., (2002), *Meas. Sci. Technol.*, 13, 375-382.

Jelisson, G. E., and Modine, F. A., (1996), Appl. *Phys. Lett*. 69, 371-373.

F. Ouf, J. Yon, P. Ausset, A. Coppalle, M. Maillé, Aerosol Sci. Technol. **44**, 1005 (2010)

K. Ren, F. Xu, X. Cai, J. Dorey, Chem. Eng. Comm.**197**, 250 (2010)

Yon J., Lemaire R., Therssen E., Desgroux P., Coppalle A. and Ren K. F., to appear in Applied. phys. B, 2011

Prediction of soot oxidation reactivity by Raman microspectroscopy

R. Niessner , J. Schmid, B. Grob and N.P. Ivleva

Chair for Analytical Chemistry, Institute for Hydrochemistry, Technische Universität München, Munich, 81377, Germany

Keywords: diesel soot, reactivity, structure, Raman microspectroscopy (RM), temperature-programmed oxidation (TPO)

Presenting author email: Reinhard.Niessner@ch.tum.de

Aerosol soot particles of anthropogenic origin form a class of air pollutants of great concern to air quality. Especially in urban area, soot nanoparticles emitted by diesel engines provide the major fraction of air pollutants and hence must be prevented from leaving the exhaust system. A wide range of particle trapping systems and exhaust aftertreatment technologies are currently under investigation. The necessary regeneration step of such particle traps can be promoted by the formation of highly reactive soot. Therefore the rapid and robust prediction of diesel soot reactivity is desired for investigation and optimization of diesel exhaust aftertreatment systems and hence for reduction of soot emission.

Usually thermo-analytical methods are applied for analysis of soot oxidation reactivity. In particular, temperature-programmed oxidation (TPO), measuring the gasification products by mass spectrometry or infrared spectroscopy and thermo-gravimetric analysis (TGA), measuring the mass decrease are used (Knauer *et al* 2009; Song *et al*, 2007). Moreover Su *et al* (2004) have shown that the soot oxidation reactivity is clearly connected to the microstructure (structural order of soot). High resolution transmission electron microscopy (HRTEM) is usually applied for investigation of soot structure. However, TPO/TGA and HRTEM are too demanding for routine analysis. On the other hand, one can obtain detailed information about the reactivity of soot by measuring the structure with Raman spectroscopy.

Raman spectroscopy is a standard non-destructive tool for the structural characterization of carbonaceous materials based on vibrational fingerprint spectra. By combining Raman spectroscopy with optical microscopy – Raman microspectroscopy (RM) – it is possible to obtain full spectral information with spatial resolution in the micron range. Recent Raman studies have shown a link between reactivity and structure of soot (Knauer *et al* 2009).

We developed multiwavelength Raman micro-spectroscopy (MWRM) analysis prediction of soot oxidation reactivity. This new method is based on the dispersive character of carbon D mode in Raman spectra (i.e. red shift and increase in intensity at higher excitation wavelengths, λ_0). The approach was proven by investigating various diesel soot samples and related carbonaceous materials at different λ_0 (785 nm, 633 nm, 532 nm and 514 nm). In order to compare the behavior of the D mode for various samples and to derive a single parameter characterizing the soot structure, the difference of integrals for pairs of spectra collected at different λ_0 was calculated. MWRM analysis revealed substantial differences in the structural ordering which decreases from graphite, over Printex XE2 and various diesel soot samples, to spark discharge soot. To obtain the relation between structure and reactivity of soot, MWRM analysis was combined with TPO. This allowed us to characterize the oxidation behavior of soot in terms of the maximum emission ($CO + CO_2$) temperature and reactivity index. The latter was calculated by introducing the reactivity limits: spark discharge soot containing a large amount of disorder represents the upper limit, whereas the lower limit is given by graphite powder with high structural order. The comparison of MWRM (viz., the observed Raman difference integrals) and TPO data revealed a linear correlation between soot structure and oxidation reactivity (Figure. 1). Thus we have clearly shown that the MWRM is a rapid analytical tool to predict the oxidation behavior of diesel soot samples and other carbon materials.

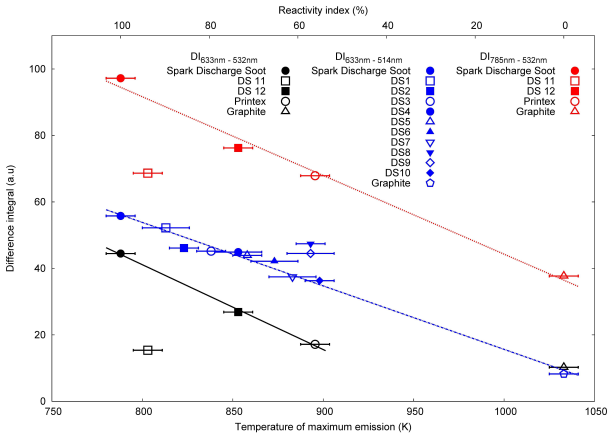

Figure 1. Correlation of oxidation reactivity (temperature of maximum emission, RI_{soot}) and structure (MWRM) of different carbonaceous materials and diesel soot with three different wavelength differences.

Knauer, M., Schuster, M. E., Su, D. S., Schlögl, R., Niessner, R. and Ivleva, N. P. (2009) *J. of Phys. Chem. A* **113**, 13871-13880

Schmid, J., Grob, B., Niessner, R. and Ivleva N. P. (2011) *Anal. Chem.* (in press)

Song, J., Alam, M. and Boehman, A. L. (2007) *Combust. Sci. and Tech.* **179**, 1191-2037.

Su, D. S., Jentoft, R. E., Müller, J.-O., Rothe, D., Jacob, E., Simpson, C. D., Tomovoc, Z., Müllen, K, Messerer, A., Pöschl, U., Niessner, R. and Schlögl, R. (2004) *Catal. Today* **90**, 127-132.

Measurement of soot size distribution in flames by inversion of angular light scattering

Caumont-Prim C., Yon J., Coppalle A. and K.-F. Ren

UMR 6614 CORIA, Avenue de l'université, BP 8, 76801 Saint Etienne du Rouvray, France.

Keywords: soot particles, fractals, aggregates, light scattering
Presenting author email: yon@coria.fr

Soot particles are produced by combustion processes. Since a long time, these particles give rise to numerous investigations for their modelling and due to their important implications in human health, flame radiative transfer and climatic impact. Among other information, the determination of soot size distributions at different Height Above the Burner (HAB) in flames is essential. The soot size distribution is determined often by using ex-situ granulometers, after sampling of the particles. But the quenching of aggregation process in the sampling is difficult and raises the question of representativeness of the results (Ouf *et al.* 2010). For this reason, optical measurements are more adapted. By knowing the temperature of the flame, Dynamic Light Scattering technique permits to determine a mobility diameter. But without any more information, soot size distribution can't be derived by this technique. Moreover, soot particles are not spherical and their specific fractal morphology has to be taken into account. Thanks to a simple theory called Rayleigh – Debye – Gans for Fractal Aggregates (RDG-FA theory - Dobbins *et al.*, 1991), measurement of static light scattering can be interpreted in order to determine another size parameter called gyration radius. The inversion by this theory to infer the gyration radius of monodisperse aggregates has been recently validated (Caumont et al. 2010).

Some authors (Dobbins & Megaridis 1991, Köylü 1994) have proposed to determine a representative gyration radius of the polydisperse population with this optical technique. But two distinct radii can be calculated if particles are suspected to scatter only in Guinier or in Power Law regime and that assumption cannot be done without knowing the researched size distribution. Koylu & Faeth (1996) and Iyer *et al.* (2007) proposed an inversion method to calculate the characteristics of the soot size distributions by coupling scattering and extinction measurements. But this method relies on the knowledge of the soot optical index which is unfortunately not accurately known. That's why it is necessary to develop a new approach which doesn't need any primary knowledge.

The present work presents a new inversion method for the determination of the soot size distribution in flames by measuring the scattered light at different angles. It consists in determining for each studied angle, by using the RDG-FA theory, a gyration radius $Rg^*(\theta)$ of a monodispersed population of the same optical behaviour as that of the real polydisperse population.

The $Rg^*(\theta)$ function thus determined informs us polydispersity of the soot. For example, in monodisperse case, $Rg^*(\theta)$ must be constant. In contrary, the variation of this function informs us of the range of polydispersity. So, by supposing the nature of the size distributions (lognormal or self-preserving), it is possible to determine, by this technique, governing parameters of these distributions.

In the present study, that inversion method is proposed to determine the soot size distributions at different HAB in a laminar diffusion ethylene flame.

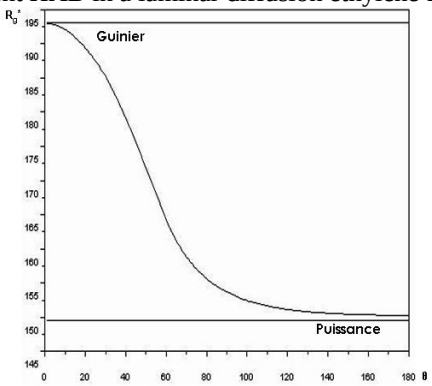

Figure 1. Theoretical dependence of Rg* to the scattering angle for a polydisperse population of soot.

Brasil, A.M., Farias, T.L. & Carvalho, M.G. (1999). *J. Aerosol Sci.*, 30 (10), 1379-1389

Caumont, C., Yon, J., Ren, K.-F., Coppalle, A. (2011). *Proc. 26ième Congrès Français sur les Aérosols*, Paris, France.

Dobbins, R.A., Megaridis, CM, *Applied Optics* (1991), 30 (33), 4747-4754.

Iyer S. S., Litzinger, T. A., Lee, S-Y, Santoro R. J (2007), *Combustion and flame*, 149 (1-2), 206-216.

Köylü, Ü, Ö, *Combustion and flame*, (1997), 109, 488-500.

Ouf, F.X., Yon, J., Ausset, P., Coppalle, A. Maillé, M. (2010). *Aerosol Sci. Technol.*, 44, (11), 1005-1017.

Friday, September 9, 2011

Session 11D: From PM exposure to health effects 1

Selection of proper markers for a better knowledge of health effects of air pollution. Difficulty in the choice of markers or in the recognition of causative mechanisms?

V. Guercio[1], M. Monti[2], L. Moltoni[1], P. Laviano[1], A.M. Azzarà[1], J. Martellucci[1], R. Zangari[1], N. Nante[3], G. Messina[3] and F. Cetta[1]

[1]Dept. of Surgery and Thoracic Surgery, University of Siena, Siena, 53100, Italy
[2]Geriatric Institute "Pio Albergo Trivulzio" (PAT), Milan, 20146, Italy
[3]Dept. of Physiopathology, Experimental Medicine and Public Health University of Siena, Siena, 53100, Italy
Keywords: PM, markers of exposure and effect, causative mechanisms, transient and persistent alterations.
Presenting author email: guercio3@unisi.it

The aim of the present study has been to focus on possible markers of effect and susceptibility for a better understanding of the health effects of air-pollution.

Methods: in Milan, Italy, between 2007 and 2010, a comprehensive approach to health effects of air pollution was designed (Prolife Project). In particular, the following studies were performed : 1) PM concentration measurement; 2) comparison between daily concentration of PM or other pollutants and acute hospital admission for respiratory or cardiovascular diseases (n= 53.514); 3) longitudinal studies in frail subpopulations, such as children attending primary school (n=440) and elderly people living in nursing homes (n=198); 4) "*in vitro"* and "*in vivo"* experiments concerning host particle interactions.

Results: Transient or persistent and severe alterations of respiratory or cardiovascular districts were observed, either in children or in old people, in addition to alterations of other system such as sperm-cell function or osteoarticular function. However, in people with similar exposure to pollutants, they depended at a greater extent on individual susceptibility of the host than on intrinsic toxicity of the pollutants. In particular, more severe alterations were observed in subjects with chronic infection, COPD, rheumatoid arthritis or varicocele. It was found that PM determines multiple effects, that cannot be explained by "pure" toxic mechanisms. Therefore, a single marker is insufficient to capture the complexity of host particle interactions. In fact, an ideal marker should reflect at least 2 different mechanisms: 1) the former, that is pollution related (i.e. due to concentration, composition or other intrinsic properties of PM). 2) the latter, that is host susceptibility related. However, pollution-related diseases are a no-threshold phenomenon, i.e. there is no threshold of PM concentration above which the effect is detectable in all individuals, and no level below which there is no effect. Therefore, to capture these complex interactions, other markers should be chosen, partly related, but also partly not related to the presumed intrinsic toxicity of pollutants. These markers should measure individual susceptibility, vulnerability and the overall response of the human being as a whole.

We suggest: 1) a "stepwise approach", based on levels or degrees of evidence in the mechanistic causative role of PM and other airborne pollutants for the occurrence of clinically evident diseases or death in humans; 2) the need for markers of effect, which should be graded, on the basis of the level or degree of possible, transient, persistent or definitive damage. These markers can be classified as phase 1 or molecular markers (molecular alteration, or biological changes such as oxidative stress, ROS production, DNA adduct formation, which should be repaired by usual cellular mechanisms); phase 2, or cellular markers; phase 3, or markers of permanent tissutal damage and phase 4, or markers of clinically evident disease, or permanent function impairment of one organ or apparatus. Finally, a cumulative score is required, which takes into account both these mechanisms (particle related and host related). We must outline, however, that measurement of this final score will also be variable, because it is arbitrary the weight that is given to each end-point and marker: oxidative stress, genetic mutation, inflammation, individual ability to repair damage, risk for autoimmune response. The weight of the various components should also be compared with current knowledge concerning the various diseases of interest and then be greater for the particle related toxic mechanism, when evaluating diseases with low to no evidence for autoimmunity in their pathogenesis. On the contrary, the relative weight could be greater for the host related mechanism, when dealing with clinical outcomes or diseases, for the occurrence of which (rheumatoid arthritis, asthma) autoimmunity is a well known causative factor. As markers of the toxic mechanism we can choose those related with oxidative stress and ROS generation, genetic polymorphisms in drug metabolizing enzymes (GSMT, NADH), which can be responsible for repair capacity, but also we have to select markers expressing host capacity concerning cellular immunity and general markers of good health, in addition to specific markers for each function or district of interest. The final picture of the various markers of interest will be more complicated, and to provide a proper model will be more complex. But, it will be more adherent to what actually occurs in real world and could help in preventing misleading inferences from epidemiological studies.

Effects of elementary school indoor/outdoor PM_{10} on gene expression and blood coagulation

S. Oeder[1], R. Jörres[2], W. Schober[1], I. Weichenmeier[1], R. Schierl[2], S. Dietrich[3], H. Fromme[3], J. Lintelmann[4], H. Behrendt[1] and J.T.M. Buters[1]

[1]Division of Environmental Dermatology and Allergy, Helmholtz Zentrum München/TUM, ZAUM-Center for Allergy and Environment, Technische Universität München, 80802, Munich, Germany
[2]Institute and Outpatient Clinic for Occupational, Social and Environmental Medicine, Ludwig-Maximilians-University Munich, 80336, Munich, Germany
[3]Bavarian Health and Food Safety Authority, Department of Environmental Health, 85764, Oberschleißheim, Germany
[4]Institute of Ecological Chemistry, Helmholtz Zentrum München, 85764, Neuherberg, Germany

Keywords: health effects of aerosols, human lung cell, indoor/outdoor PM_{10}, inflammation, xenobiotica metabolism, blood coagulation.

Outdoor particulate matter (PM_{10}) is associated with a wide range of health effects (Brunekreef *et al.*, 2002) and a European threshold limit of 50µg/m^3 (daily limit, EU Directive 1999/30/EG) was established in 2005. However, most individuals spend at least 85% of their time indoors (Klepeis *et al.*, 2001) where particle concentrations are mostly higher than outdoors (Fromme *et al.*, 2007). Since children represent a vulnerable group, we investigate the health effects of indoor air PM_{10} collected in elementary school classrooms compared to outdoor air PM_{10}.

Methods PM_{10} was collected on Teflon filters (2.3m^3/h; Derenda Inc.) in six elementary schools with two classrooms per school in Munich during teaching hours (5.5h/day). In parallel outdoor air nearby the classrooms was sampled (30m^3/h; high volume sampler; Derenda Inc.). Filter load was determined gravimetrically. Particles were recovered by sonication, lyophilized and resuspended in water. PM_{10} was analyzed for EPA priority PAHs by HPLC and endotoxin by LAL test. For a genome wide gene expression analysis BEAS-2B bronchial epithelial cells were incubated with 10µg/mL classroom and outdoor PM_{10} of one school for 4, 10 and 24 hours. RNA was isolated and analyzed on Affymetrix HG U133A 2.0 expression arrays (14,500 genes). A subgroup of 46 regulated genes was analyzed by real-time-RT-PCR after exposure to PM_{10} samples from all six schools. Effects of PM_{10} on blood coagulation were studied by incubating monocytes isolated from peripheral human blood with different PM_{10} concentrations (1, 5, 10, 50 µg/mL). After 24 h the supernatants were removed, cleared from particles and used in an optimized, highly sensitive blood coagulation assay including multiple temperature controls.

Results Indoor PM_{10} in schools occurred at 117±48µg/m^3. The corresponding outdoor concentrations were 21±15µg/m^3. PAH content was higher in outdoor (47ng/mg vs. 31ng/mg indoor) PM_{10}, endotoxin higher in indoor (130±41EU/mg vs. 13±22EU/mg outdoor) PM_{10}. Genome wide analysis of PM_{10} from outdoor and indoor air showed the induction of the following metabolic pathways: inflammation, metabolism of xenobiotics, tissue remodeling, blood coagulation, and oxidative stress. Inflammation was characterized by overexpression of chemokines (CCL20, CXCL1, IL-8) and cytokines (IL-1, IL-6, LIF). Xenobiotic metabolism was represented by phase-I enzymes (CYP1A1, CYP1B1, ALDH1A3, NQO1). Tissue related genes were MMP1 that degrades extracellular matrix, GREM1 which is induced in pulmonary fibrosis, and IL-24 - a cytokine of wound healing. Blood clotting was represented by the coagulation factor SERPINB2 and oxidative stress by the antioxidative enzyme SOD2. Indoor PM_{10} caused a lower induction of xenobiotic metabolizing genes but an up to 6 fold higher induction of inflammatory cytokines compared to outdoor PM_{10}. These differences correlate with the content of PAH (r^2=0.75 for CYP1A1) and endotoxin (r^2=0.69 for CXCL6) in these samples.

The highest induced gene was SERPINB2 and indeed, our blood coagulation assay with human blood showed a concentration-dependent acceleration of coagulation for indoor particle concentrations at 5 µg/mL and higher and for outdoor particles at 50µg/mL only.

Conclusions PM_{10} concentrations were 5.6 fold higher indoors than outdoors. Although indoor classroom PM_{10} caused less induction of xenobiotic metabolizing genes, it had a stronger endotoxin-related inflammatory effect and a higher potential to facilitate blood coagulation than outdoor PM_{10}. Thus, interventions for the reduction of classroom PM_{10} would be reasonable.

This work was supported by the Bavarian State Ministry of the Environment and Public Health under project UGV03060902114 and funding from Christine Kühne – Center for Allergy Research and Education – Munich (CK-CARE A).

Personal Exposure Assessment of School Children to Airborne Nanoparticles

Rohan Jayaratne, Megat Mokhtar, Lidia Morawska and Mandana Mazaheri

International Laboratory for Air Quality and Health, Institute of Health and Biomedical Innovation
Queensland University of Technology, Brisbane, Australia
Keywords: Childrens Health, Air Quality, Respiratory Health
Presenting author email: r.jayaratne@qut.edu.au

The toxicology and human health effects of airborne nanoparticles are of increasing concern, especially in light of the advent of engineered nanoparticles in recent years. In this study, we used a Philips Aerasense Nanotracer to monitor the daily exposure of school children to airborne nanoparticles. This instrument is a hand-held battery-operated device that measures airborne particle number concentration (PNC) up to 10^6 cm^{-3} and the average diameter of the particles in the size range 10-300 nm. Data are logged every 16 s and subsequently downloaded to a computer for processing and analysis.

Preliminary measurements were carried out with the help of 15 children in three primary schools in Queensland, Australia. Each child was fitted with a device that they wore over a 24-hour school day. Data were stored and downloaded to a lap top computer for later analysis. In addition to the nanotracers, the children also carried with them a small portable GPS device that was used to derive information on their movements. In addition, the parents or guardians of the children were requested to keep a log of their travel and activities. At some time during this period, the child would also undergo a series of clinical tests as part of the study

PNC in the classrooms were monitored with a TSI 3781 condensation particle counter (CPC). This provided the areal exposure for comparison with the personal exposure measured with the nanotracer. The total daily personal exposure of each child to nanoparticles was estimated from the mean PNC recorded by the corresponding nanotracer.

Figure 1 shows the PNC time series recorded by the nanotracer worn by a child and the CPC placed in the classroom over a typical two-hour period of the day. The agreement is reasonably good except for the differences near 12:50h and 13:25h which corresponded to periods when the child was outside the classroom. Figure 2 shows the PNC time series recorded by the nanotracer worn by another child over a 24-hour day. Note the relatively high exposure while commuting to and from school at (a) and (b), respectively. The peaks at (c) and (d) correspond to the lunch break and outdoor play activity, respectively. For this particular child, the mean daily exposure level was 8.8 x 10^3 cm^{-3} which corresponds to a daily exposure of 2.12 x 10^5 particle h cm^{-3} day.

This is part of a study to determine the effect of the exposure to airborne ultrafine particles emitted from motor vehicles on the health of children in schools to be carried out over the next two years at 25 schools in Queensland. From results such as that presented in this paper, the average exposure levels under different circumstances such as while in the classroom, in the home, outdoors and while commuting to school will be determined for over 100 primary school children. These children will also undergo a series of health checks. At the end of this study, we expect our results to assist us to identify the long-term respiratory health indicators that are sensitive to exposure to airborne particles.

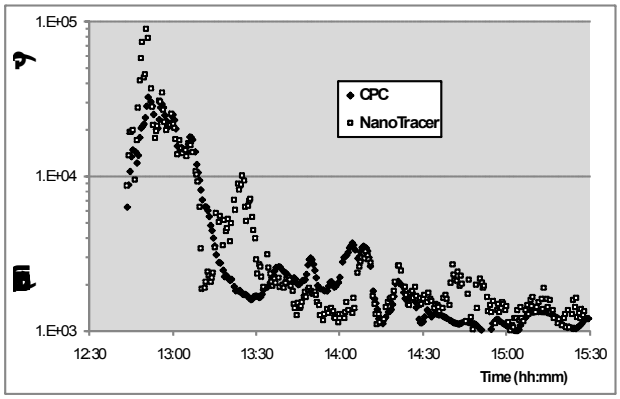

Fig 1: Time series of CPC and Nanotracer measured in a classroom over a two-hour period.

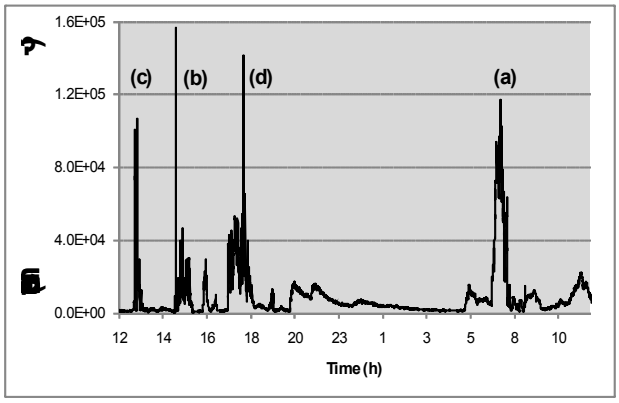

Fig 2: Exposure to PNC as measured by a nanotracer worn by a child over a full 24-hour day.

This work was supported by the ARC, DTMR and DET through Linkage Grant LP0990134. We would also like to thank all members of the UPTECH project, including R. Fletcher, A. Monk, G. Marks, P. Robinson, Z. Ristovski, W. Ezz, G. Williams, C. He, G. Ayoko, G. Johnson, L. Crilley, M. Falk, F. Salimi, K. Mengersen, S. Low Choy, S. Dharani, B. Toelle and R. Appleby as well as A. Liebhardt.

Workers exposure to particulate and gaseous pollutants in a photocopy / printing center

E. Diapouli[1], M.I. Gini[1], V. Vasilatou[1], Th. Maggos[2], St. Pateraki[2], A. Katsanaki[2], D. Saraga[2], K. Eleftheriadis[1]

Institute of Nuclear Technology and Radiation Protection,
National Centre of Scientific Research "Demokritos", 15310 Ag. Paraskevi, Attiki, Greece
[1]Environmental Radioactivity Laboratory
[2]Environmental Research Laboratory
Keywords: airborne particles, VOCs, ozone, occupational exposures.
Presenting author email: ldiapouli@ipta.demokritos.gr

There is increasing concern regarding the emission of potentially harmful pollutants, such as particulate matter (PM), ozone (O_3), volatile organic compounds (VOCs) and semi-volatile organic compounds (SVOCs), from office equipment (Destaillats et al., 2008). A number of research works report that the operation of printing and copying equipment may contribute significantly to increased indoor air pollutant concentrations, while they have been also associated with health complaints from exposed workers (Lee et al., 2001). The aim of the present work is to study workers exposure levels to particulate matter (PM), carbonyls and ozone in a photocopy / printing centre.

The studied enterprise offers photocopy and digital printing services and is housed in a three storey building. Measurements were carried out during June and July 2010 at rooms of different use, in order to study the effect of the various activities on the observed concentration levels. 24-hr $PM_{2.5}$ gravimetric samples were obtained by the use of LVS Derenta sequential sampler. In addition, real-time measurements of TSP and $PM_{2.5}$ (Thermo MIE Dataram 4000, PDR-1000 and PDR-1200) and O_3 (Ozone Analyzer, Model 49im, Thermo Scientific) were conducted. Carbonyls concentrations during working hours were also measured through active 3-hr sampling in DNPH cartridges, followed by analysis by HPLC with UV detector (Waters 600).

Mean 8-hr TSP and $PM_{2.5}$ concentrations (during working hours) measured at the different floors are presented in Figure 1. Extremely high concentrations were measured at the 3rd floor where the use of different binding techniques (hot glue binding / plasticizer) led to significant particle generation (Figure 2). The increased concentrations observed at the ground and 2nd floor, in comparison to the administrative offices (1st floor), suggest that the intensive use of photocopy machines and printers may also influence indoor PM levels. The measured concentrations were close to the ambient air quality standards for PM_{10} and $PM_{2.5}$ set by E.U.

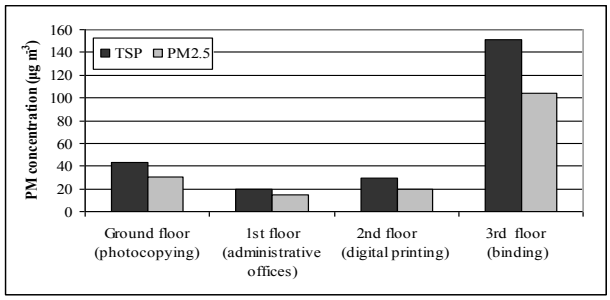

Figure 1. TSP and $PM_{2.5}$ concentration levels during working hours (mean 8-hr values).

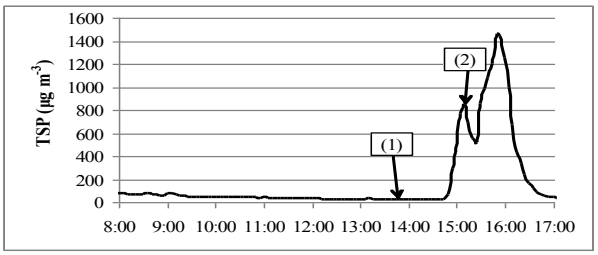

Figure 2. TSP concentration during binding activities. (1) and (2) denote the initiation of hot glue binder and plasticizer, respectively.

The results of gas measurements indicated that photocopy machines and printers may also be important emission sources of ozone and carbonyls (Figure 3 and Table 1).

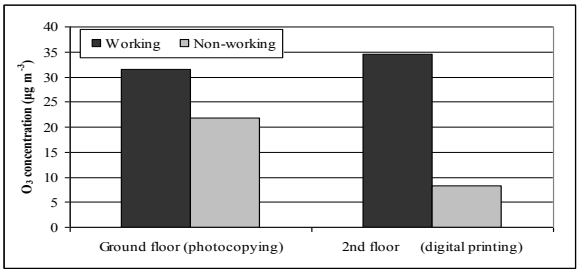

Figure 3. Ozone mean concentration levels during working and non-working hours.

Table 1. Mean 3-hr carbonyls concentrations [μg m^{-3}] during working hours.

	Ground floor (photocopying)	2nd floor (digital printing)
Formaldahyde	9.0 - 11.8	3.0 - 14.1
Acetaldehyde	38 - 102	2.4 - 77.6
Acetone	19.7 - 41.5	6.4 - 35.3
Benzaldehyde	0.54	

Destaillats, H., Maddalena, R.L., Singer, B.C., Hodgson, A.T., McKone, T.E. (2008) *Atmos. Environ.* **42**, 1371–1388.

Lee, S.C., Lam, S., Fai H.K. (2001) *Build. Environ.* **36**, 837-842.

Can Storage of Cleaning Products be a Source of Ultrafine Particles in a Supermarket?

Aneta Wierzbicka[1,*], Patrik T. Nilsson[1], Erik Z. Nordin[1], Joakim Pagels[1], Andreas Dahl[1], Jakob Löndahl[2], Anders Gudmundsson[1] and Mats Bohgard [1]

[1]Division of Ergonomics and Aerosol Technology (EAT), Lund University, Box 118, SE-221 00, Lund, Sweden
[2]Division of Nuclear Physics, Lund University, Box 118, SE-221 00, Lund, Sweden
Keywords: ultrafine particles, terpenes-ozone reactions, supermarket, indoor environments
Presenting author email: aneta.wierzbicka@design.lth.se

The aim of the study was to gain information about fine and ultrafine particles (diameter smaller than 2.5 μm and 100 nm, respectively) in a supermarket in Sweden. Assessed particles' characteristics were: number concentrations and number size distributions. In the studied supermarket, an indoor source of ultrafine particles was observed due to local emissions of terpenes (from storage of washing powders, cleaning products and air fresheners), which in the presence of ozone from outdoors form particles due to gas-to-particle conversions. Additionally conducted chamber study confirmed the observed findings.

Supermarket measurements: were performed continuously for seven consecutive days in the area with washing powders, cleaning products and air fresheners. Particle number concentration (PNC) and size distribution in the range 15 nm to 20 μm were recorded by a scanning mobility particle sizer (SMPS) and an aerodynamic particle sizer (TSI APS 3321). A valve was incorporated into the SMPS sampling system, which enabled alternate measurements of the indoor and supplied ventilation air. Mechanical ventilation supplied heated and filtered air and operated between 4:30 and 22:00. The measured air exchange rate (AER) was ~ 10 h^{-1}, the ozone concentration in ambient air was 30 ppb. In the ventilation system there was no recirculation and no dehumidification, supplied air in 100% was composed of filtered outside air, the filter used was a glass- fibre F7 class filter (EN 779: 2002).

Laboratory experiments: were performed in a 22 m^3 stainless steel chamber, where 200 cleaning products from the same supermarket, were placed. AER was kept at 5 h^{-1}, ozone was supplied until concentrations in the chamber reached 16 ppb and then was switched off to imitate ventilation off conditions in the supermarket. The same set of instruments as in the supermarket were used with additional measurements of ozone and terpenes the latter through collection on carbopack X adsorbent and subsequent GC-MS analysis.

When the ventilation was on the submicrometer PNC inside the supermarket (median 2500, min 1100, max 11000) particles cm^{-3} was higher than in the supplied ventilation air (median 850, min 200, max 4000) particles cm^{-3}, indicating an indoor source of particles. The median GMD inside the supermarket of 42 nm was about 20 nm smaller than in the supplied ventilation air. The presence of nucleation mode particles was assumed to come from local emissions of terpenes (from washing powders, cleaning products and air fresheners), which in the presence of ozone from outdoors (supplied in ventilation air) form particles. The observed concentrations are not high, but considering the high AER (~ 10 h^{-1}) and supply of air with very low particle loads, these contributions are significant.

Interesting patterns were observed when the ventilation was switched off. At this time the removal due to high AER and supply of heated air with low particle loads were eliminated. This might have resulted in local accumulation of terpenes and temperature decrease. A sudden increase in PNC with a number GMD of about 30 nm was observed and can be explained by nucleation via gas-to-particle conversions from terpenes in the presence of ozone. After reaching the peak (within 30 minutes to an hour after ventilation was switched off) a decrease in the PNC was seen, probably due to dilution and spreading within the air in the supermarket and diffusional losses to surfaces. Possibly ozone concentrations were depleted by then due to chemical reactions. At the same time the number GMD increase was observed, this could be due to organic vapour condensation, as the reduced AER results in more time available for gas phase chemistry and particle growth.

Performed chamber experiments confirmed observed patterns. Newly formed particles were of the same size as those observed in the supermarket, and a similar increase in GMD was observed with time. 70% of the determined terpenes, emitted from cleaning products, washing powders and air fresheners, consisted of limonene.

In the supermarket, an indoor source of ultrafine particles was observed due to local emissions of terpenes (from storage of washing powders, cleaning products and air fresheners), which in the presence of ozone from outdoors form particles. More data is needed to determine typical levels of ultrafine particles in supermarkets. The results indicate that even storage of enclosed cleaning products can be a source of ultrafine particles and thus adequate ventilation in places where products containing terpenes are kept are of prime importance in order to minimise exposure to ultrafine particles.

This work was performed within the framework of the Metalund centre of excellence, and financed by the Swedish Councils FORMAS and FAS together with the Development Fund of the Swedish Construction Industry (SBUF).

Wierzbicka A., 2008. Doctoral thesis: What are the characteristics of airborne particles that we are exposed to? ISBN 978-91-628-7443-8; KFS AB, Lund

Particle exposure in public transport – seasonal dependence

K. Hämeri[1], E. Asmi[2] and B. Mølgaard[1]

[1]Department of Physics, University of Helsinki, Helsinki, 00014, Finland
[2]Finnish Meteorological Institute, Helsinki, 00101, Finland
Keywords: Exposure, number concentration, mass concentration, public transport,
Presenting author email: Kaarle.hameri@helsinki.fi

Exposure to traffic related particles have been intensively studied during last years. There is increasing concern on health effects of fine and ultrafine particles and in key focus, there are particles originating from traffic. However, there exist only a few publications considering exposure while in transport. The city buses and trams travel in the middle of the town area and often along the busiest streets where traffic is the major particle source. Thus, the concentrations of tailpipe emissions as well as street dust suspensions are high. Traffic generated particles are transported inside the vehicles and they predispose both the driver and the passengers to high particle concentrations. The topic is especially critical for the drivers, who are exposed to the pollutants for long periods.

Commuters' exposure to traffic-related pollutants has been studied in the Netherlands (Zuurbier et al., 2010). They focused on different modes of transport, routes, and fuel types. We studied earlier the exposure of bus and tram drivers and passengers to fine particulate matter in two types of buses and trams in Helsinki, Finland during summer time (Asmi et al., 2009).

In this study, we investigate the commuters' exposure to fine particles during three seasons in Helsinki, Finland. The measurements of particle number and mass concentration, and black carbon mass were conducted in the cabin and driver's compartment during summer 2005 and winter and spring 2006. The concentrations measured inside the vehicles were compared to simultaneously measured concentrations both right outside of the vehicle and in background monitoring stations. The aim of the study is to compare commuters' exposure during different seasons and thus different weather conditions. The experiments were conducted in buses and trams, both of which were travelling along the same route through the city centre.

Air pollution situation varies greatly between different seasons in Helsinki. During summertime, temperature during daytime is usually around 20 C and the atmospheric mixing is efficient leading to lower average concentrations compared with other seasons. During wintertime, temperature is usually around or a couple of degrees below zero and the mixed layer is rather shallow. The air pollutants accumulate close to the surface leading to worsening of the air quality. During spring, there is a dust episode, which lasts about one month. This is due to sanding of the streets during wintertime. During spring this sand is dry and re-suspended in the air by traffic and the cleaning machines. In summary, springtime is characterised by high mass concentrations, wintertime is characterised by high number concentrations and summertime is the cleanest season. During different seasons, also the air quality inside the buses and trams is expected to be different. This is due to both air pollution outdoors and also the ventilation of the air inside the vehicles. In summer, the vehicles often drive windows open in order to increase the ventilation, while in winter the windows are closed and heating is on. The vehicles have particle filters in the fresh air ventilation system, which lower the indoor concentrations when windows and doors are kept closed.

The results of this study show clear seasonal differences. The pollution levels inside the vehicles are correlated with that outdoors. The correlation is rather similar during all the seasons. Indoor-outdoor ratios of the concentrations were found to be lower during winter compared with spring indicating increased filtration due to closed windows and doors. The indoor-outdoor ratio was lower for trams compared with buses.

In conclusion, when using one-hour averages we found a clear correlation between the concentrations inside and outside of the vehicle, especially for the bus. The correlation when using the background concentration as a reference is not high and in fact, it is negative in one case.

This project was funded by the Finnish Work Environment Fund.

Asmi, E., Antola, M., Yli-Tuomi, T., Jantunen, M., Aarnio, P., M□äkel□ä, T., Hillamo, R. and H□ämeri, K. (2009) *Science of the Total Environment*, **407**, 2860-2867

Zuurbier M., Hoek G., Oldenwening M., Lenters V., Meliefste K., van den Haze P., Brunekreef B. (2010) *Environmental Health Perspectives*, **118**, 783-789.

Particles in Indoor Air – results from residential dwellings

Christina Isaxon[1,*], Andreas Dahl[1], Erik Nordin[1], Gunilla Wieslander[2], Dan Norbäck[2], Anders Gudmundsson[1], Aneta Wierzbicka[1] and Mats Bohgard[1]

1 Division of Ergonomics and Aerosol Technology, University of Lund, Lund, Sweden

2 Department of Occupational and Environmental Medicine, Uppsala University, Sweden

Keywords: aerosol exposure, real-time measurements, source identification
Presenting author email: christina.isaxon@design.lth.se

Although we spend a major part of our lives indoors, there is a basic lack of information considering particles of indoor origin and their impact on human health. Airborne particle measurements are frequently conducted in workplace environments, but very few, designed to find associations between human activities, aerosol concentrations and health outcomes, in residential homes.

The aim of this study is to characterize the air quality in residential dwellings (in terms of time resolved particle mass and number concentrations, size distributions, soot, temperature, relative humidity and CO_2 levels), correlate this data to various indoor activities and study associations between exposure to airborne particles and health effects/symptoms of the inhabitants.

For seven consecutive days time resolved stationary air measurements are conducted in randomly selected homes (N=42) in the area of Lund in southern Sweden. Aerosol instruments used are MiniDISC (University of Applied Sciences, Windisch, CH), Nanotracer (Philips Research) Indoor Air Quality monitor (IAQ3016, Lighthouse), DustTrak (TSI) and a soot monitor (microAeth AE51, Magee Scientific). The instruments are placed at a central location in each home, close to, but not in, the kitchen. All measurements are made during off-pollen season (October-April). CO_2 data is collected and used to calculate the air exchange rate. Petri dishes are used for collection of potential allergens. The habitants are asked to fill in detailed activity log books.

A thorough examination of each home – e g construction year, floor and wall materials, and ventilation system - is conducted according to a structured protocol. In addition, the participants fill in a 9 page translated and modified version of the IUATLD (International Union Against Tuberculosis and Lung Disease) questionnaire covering topics such as current and previous health status, professional history and everyday habits.

After the measurement period a non-invasive medical examination is conducted, including rhinometry, study of tear film break-up time and measurement of NO in exhaled air. During the measurement period ambient air variations were monitored constantly from a station in northern Lund.

. A data classification is carried out by sorting the data into two categories: occupancy time (at least one person present in the dwelling/residence) and non-occupancy time. An example is shown in Figure 1.

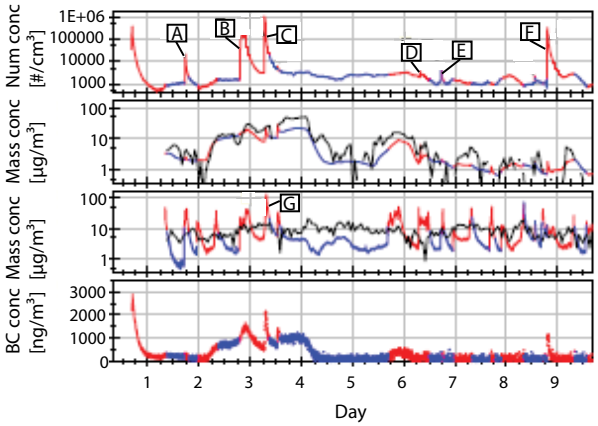

Figure 1. From top to bottom: Number concentrations (MiniDISC), PM_1 (IAQ3016), PM_{10-1} (IAQ3016) and black carbon concentrations (AE51). ug/m^3 denotes reading quantities from the optical instrument, using a density of 2,5 g/cm^3. Red lines denote that somebody was present and blue lines that the dwelling was empty. Black lines are background $PM_{2.5}$ and $PM_{10-2.5}$ respectively. Marked peaks are explained in Table 1 below.

Table 1. Peaks in Fig 1 and their heights above baseline concentration.

Peak	Num conc [#/cm^3]	PM_1 [µg/m^3]	PM_{10-1} [µg/m^3]	Activity
A	20000	0.5	35	Cooking
B	150000	6.8	0	Burning candle
C	1000000	0	0	Burning candle
D	1900	5	5	Cooking
E	2800	0.4	0	Cooking
F	320000	1.1	6.5	Cooking
G	-	15	110	Extinguishing candle

In a major part of the studied homes the concentration of particles, in particular in the sub micron size range, were higher when someone was present. Mean number concentration levels elevated by several hundred percent (indicated by the miniDISC, which is most sensitive for particles 20-120 nm), when someone was present in a dwelling, were not uncommon. The time resolved data in combination with the activity log books made it possible to trace peaks in concentration to a specific activity or usage of a specific appliance. It was also possible to see the relative strength of the indoor aerosol sources.

This work was performed within the framework of the Metalund centre of excellence, and financed by the Swedish Councils FORMAS and FAS together with the Development Fund of the Swedish Construction Industry (SBUF).

Friday, September 9, 2011

Session 11E: Comparison of Different Measurement Methods

Correlating the opacity-based dustiness behaviour to material specific properties

S. Bach, E. Schmidt

Department of Safety Engineering / Environmental Protection, University of Wuppertal, Germany
Keywords: Dust, Air quality, Optical instrumentation, Respirable aerosols.
Presenting author email: sbach@uni-wuppertal.de

The background of this research project is to examine the possibilities of a single-drop apparatus for the measurement of the dustiness behaviour of powders called DustView (Palas® GmbH, Karlsruhe). Objective is to find an algorithm for the coherence between the opacity values of the DustView respectively their time-related development and the concentration of specific aerosol fractions inside its so-called dust chamber.

Figure 1 shows the laboratory set-up, where an aerosol spectrometer (OPC) is directly connected to the dust chamber of the single-drop apparatus. It allows the simultaneous measurement of the extinction of two laser beams in different heights (3 resp. 13 cm above ground plate) and the particle size distribution and number concentration of the aerosol dispersed in the chamber in the same heights respectively.

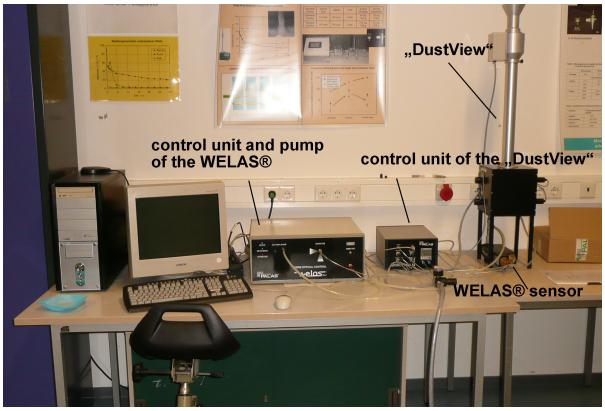

Figure 1. Modified version of the Palas DustView®, including single-drop apparatus and OPC “WELAS®”

Additionally, other material-specific properties have been measured, to ensure the best possible knowledge of the examined powders. Figure 2 shows all assimilated material features.

In Germany, there are limit values for the mass concentration of the respirable and inhalable dust fraction in workplace atmospheres. These are defined in the TRGS 900 (2010) and are 3 resp. 10 mg/m^3 at present.

The size fractions refer to the aerodynamic diameter of a particle, whereas the aerosol spectrometry gives the light scattering diameter. Van Buijtenen *et al.* (1974) define two possible ways of converting one into the other. Either, the aerodynamic shape factor of the material is known or the aerosol spectrometer has to be calibrated for each material. Here, only the particle density has been used as in Schmidt (2001), for the aerodynamic shape factor of the materials was mostly unknown and the calibration would have been too time-consuming for an uncertain outcome.

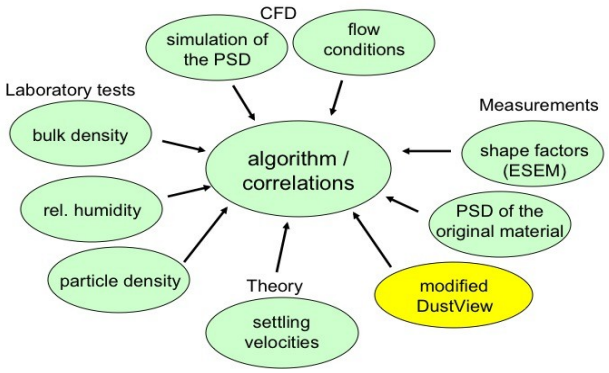

Figure 2. Measured and calculated material specific properties

The large amount of data collected for each material makes it difficult to locate correlations between two or more properties. What kind of dustiness-based data is suitable for the data mining process is yet to be determined. Additionally to the so-called dustiness number, calculated from the maximum opacity value and the 30-second-value of each measurement, it may also be the integral under the opacity curve or the offset between the peaks of the opacity curves of the two lasers. Also conceivable would be a value at a specific time, where the sedimentation process has already removed particles of a defined size. This would have to take the particle-specific settling velocity into account. All above named data could possibly correlate with the mass concentration of a specific aerosol fraction.

The correlation analysis is being carried out with the software “The Unscrambler X”, developed by CAMO®, Norway. Considering the two laser units, the correlation between OPC results and opacity seem to be better in the height of the lower laser.

This work was supported by the German Federation of Industrial Research Associations (AiF).

Schmidt, E., *Kurz gefasste Grundlagen der Partikelcharakterisierung und der Partikel-abscheidung*, Shaker Verlag, Aachen, 2001

TRGS 900, “Limit values for work places”, Bundesanstalt für Arbeitsschutz und Arbeitsmedizin BAuA, 2010

Van Buijtenen *et al.* (1974), *Comparison of “light scattering diameter” based on forward scattering measurements and aerodynamic diameter of aerosol*

particles, Atmos. Env., Vol 8, pp 885-896, Pergamon Press, GB

Single Particle Soot Photometer (SP2) intercomparison: Results from 6 instruments

M. Laborde[1], M. Gysel[1], M. Schnaiter[2], C. Linke[2], H. Saathoff[2], K.-H. Naumann[2], O. Möhler[2], J. Taylor[3], M. Flynn[3], J. Allan[3], H. Coe[3], K. Heimerl[4], F. Dahlkötter[4], B. Weinzierl[4], A. Wollny[5], L. Polo[6], J. Cozic[6], P.Laj[6], J.M. Flores[5,7], Y. Rudich[7], S. Berlenz[8] and U. Wagner[8]

[1]Laboratory of Atmospheric Chemistry, Paul Scherrer Institut, Switzerland
[2]Institute for Meteorology and Climate Research, Karlsruhe Institute of Technology, Germany
[3]School of Earth, Atmospheric and Environmental Sciences, The University of Manchester, UK
[4]Institut für Physik der Atmosphäre, Deutsches Zentrum für Luft- und Raumfahrt, Oberpfaffenhofen, Germany
[5]Particle chemistry Department, Max-Planck-Institut für Chemie, Mainz, Germany
[6]Laboratoire Glaciologie et Géophysique Environnement, CNRS, Saint Martin d'Hères cedex, France
[7]Department of Environmental Sciences and Energy Research, Weizmann Institute of Science, Rehovot ,Israel
[8]Institut für Kolbenmaschinen, Karlsruhe Institute of Technology, Germany
Keywords: Combustion particles, Single Particle Soot Photometer (SP2), Measurement (characterization)
Presenting author email: marie.laborde@psi.ch

Soot particles represent the main absorbing matter in the atmosphere. It has also been shown that black carbon (BC) can gain coating through aging processes (Jacobscon, 2001). The impact of this BC ageing on the climate ranges from BC optical properties modification to the removal of absorbing matter by wet deposition and cloud properties modification. This highlights the importance of measuring BC concentration and mixing state in understanding and modelling global warming.

Unfortunately, the exact measurement of BC remains difficult. The Single Particle Soot Photometer (SP2) can assist in that sense by directly measuring the mass of refractory black carbon (rBC) in each individual particle independently of the amount of coating. In addition, a semi-quantitative coating thickness and volume fraction of rBC can be retrieved within a limited size range using a scattering measurement and a MIE scattering model for coated rBC particles.

Despite great potentials this measurement technique remains an emerging method and work is still needed to characterise the repeatability of the measurement and understand possible discrepancies between instruments.

We present here selected results from the SOOT11 project which aimed at comparing 6 SP2s from 6 different institutes with themselves and other techniques. Different types of soot particles were introduced in the AIDA chamber, Karlsruhe, where they undergone various processes (such as coagulation, stepwise coating or cloud activation) and then measured.

Before any measurements took place, the instruments have been optimized and calibrated using the same protocol. However, the KIT instrument could not reach optimal laser power and it is therefore excluded from parts of this comparison.

Figure 1 shows the integrated mass size distribution over the entire 18th of November of rBC from a CAST (Combustion Aerosol STandard) burner obtained from 5 SP2s. Firstly, we can state that the mass size distributions agree fairly well despite a slight shift in diameter of around 20nm. This discrepancy in diameter is most likely due to calibration uncertainties. The times series of integrated rBC mass concentration (D_{MEV}>80nm) measured by 5 SP2s reveals agreement within 25% (Figure 2). Furthermore, the coating steps do not affect the measurement of rBC, in agreement with previous studies (e.g. Moteki, 2007). Slightly different trends observed by the 5 SP2s are caused by size dependent differences of instrument response in combination with increasing particle size due to coagulation.

A comparison of the above mentioned other parameters and with other techniques will also be presented.

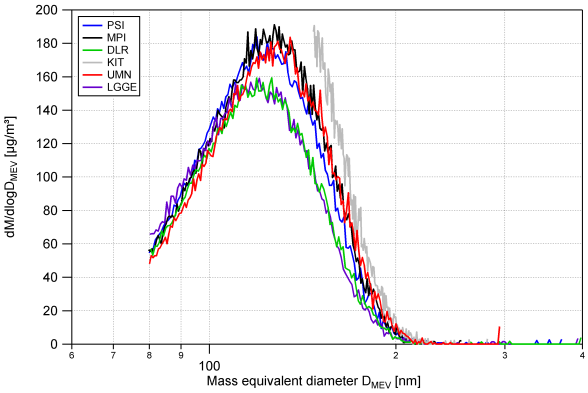

Figure 1: rBC integrated mass size distribution.

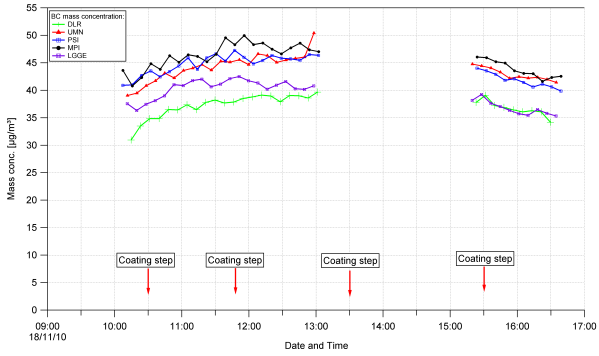

Figure 2: Time series of rBC mass concentration

Jacobson (2001) Nature, **409**, 695-697
Moteki (2007) Aero. Sci. and tech. **41**, 398-417

Evaluation of an improved unipolar diffusion charger for size distribution measurements

Christof Asbach[*1], Thomas A.J. Kuhlbusch[1,2], Heinz Fissan[1,2], Burkhard Stahlmecke[1], Hans-Georg Horn[3], Heinz Kaminski[1]

[1] Institute of Energy and Environmental Technology (IUTA) e.V., Duisburg, Germany
[2] Center for Nanointegration Duisburg-Essen CeNIDE, Duisburg, Germany
[3] TSI GmbH, Aachen, Germany
Presenting author email: asbach@iuta.de

Keywords: nanoparticle, unipolar diffusion charging, charge distribution, size distribution

Nanoparticles have been reported to be of possible health concern. Exposure to nanoparticles hence needs to be monitored, e.g. in view of worker protection. The best estimate of a worker's exposure can be derived from mobile, ideally personal measurements, taking aerosol samples in the breathing zone of the worker. Requirements for such mobile nanoparticle exposure monitors are small size, low weight and the delivery of health relevant information. The discussion on the health relevance of different aerosol metrics is still under discussion and hence a sophisticated exposure monitor should provide versatile information on the aerosol, i.e. the particle size distribution which under several assumptions can also be converted into size integrated number, surface area or volume/mass concentrations. Besides the abovementioned requirements, a portable or personal workplace monitor must not use any harmful substances. Bipolar aerosol chargers using radioactive materials, as commonly used in mobility particle sizers should hence not be used. Unipolar diffusion chargers, based on electrical corona discharge are therefore a preferred option. They provide higher charge levels which at the same time can be advantageous and disadvantageous. If the concentration is determined by electrical means, i.e. with an electrometer, the higher charge level provides a better signal and therefore allows for the measurement of lower concentrations. On the other hand the charge and hence mobility distribution for each particle size is broader, making multiple charge correction (MCC) in the data deconvolution algorithm more complex. To perform the MCC procedure correctly, the charge distribution has to be well known and mathematically described in a way that can be implemented in a software algorithm.

We evaluated an improved unipolar charger, which is based on the existing and proven 'opposing flow principle' (Medved et al., 2000). It is intended to be used in a portable aerosol sizer, which is currently under development within the EU-FP7 project Nanodevice. Improvements of the charger mainly concerned practicability such as ease of cleaning and prolonged maintenance intervals. This improved charger was subject to a detailed investigation of the charging efficiency as a function of particle size in a size range from 20 to 400 nm, which is the intended size range of the aerosol sizer. The determined average charge levels are comparable to those reported for an earlier version of the charger (Jung & Kittelson, 2005). The charge distributions were determined by measuring the electrical mobility distribution of monodisperse particles downstream of the charger. Figure shows exemplarily the charging efficiency for the uncharged as well as the singly to five-fold charged fractions. It can be seen, that 20 nm particles are charged with approximately 50% efficiency. The investigations further revealed that for 400 nm particles, up to 25 elementary charges need to be considered in the data deconvolution scheme. All charge levels followed a lognormal distribution which were fitted and described by mathematical functions to be included in an algorithm.

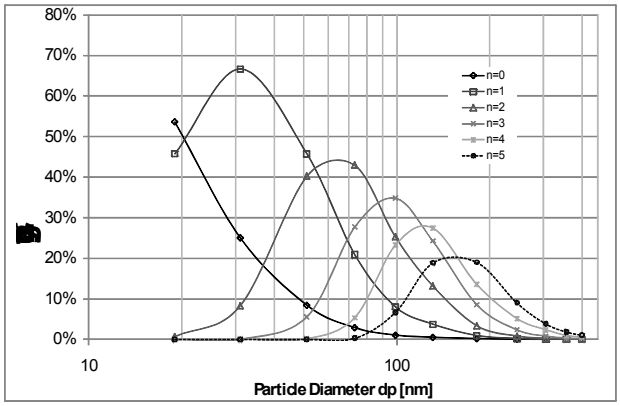

Figure : **Charging efficiency as function of particle size for charge fraction from 0 to 5**

The design of the charger and the experimental set up will be presented along with the measured results and their mathematical descriptions. The outcome of the investigations will be discussed in view of possibilities for use in miniaturized electrical mobility analyzers.

References

Medved A., F. Dorman, S.L. Kaufman & A. Pöcher, 2000. J. Aerosol Sci. 31(S.1), 616–617.

Jung, H. & Kittelson, D.B., 2005. Aerosol Sci. Technol. 39:902-911

Acknowledgement
The research leading to these results has received funding from the European Community's Seventh Framework Programme (FP7/2007-2013) under grant agreement n°211464-2.

Evaluation of the performances of SidePak AM510 nephelometer compared to the Tapered Element Oscillating Microbalance (TEOM) method for $PM_{2.5}$ mass measurement

Federico Karagulian, Claudio A. Belis, Fritz Lagler, Maurizio Barbiere, and Michel Gerboles

European Commission, Joint Research Centre (JRC), I-21027 Ispra, Italy
Keywords: Particulate matter (PM), nephelometer, hygroscopic growth.
Presenting author email: federico.karagulian@jrc.ec.europa.eu

In order to evaluate the personal exposure to ambient $PM_{2.5}$ it is necessary to perform measurements using portable instruments. However, there are no such instruments complying with the reference method for ambient $PM_{2.5}$ measurements (EN 14907). The comparability of these instruments could be assessed with measurements by equivalent analyzers like the Tapered Element Oscillating Microbalance (TEOM). In this work the characteristics of the portable nephelometer SidePak™ AM510 Personal Aerosol Monitor manufactured by TSI Inc. were evaluated against a TEOM equipped with a Filter Dynamics Measurements System (FDMS). Conventionally, light flux measured by the SidePak AM510 is calibrated with respect to Arizona road dust and then multiplied by an environmental k-factor to yield mass concentration. However, this calibration shows a low comparability between the SidePak AM510 and the TEOM-FDMS.

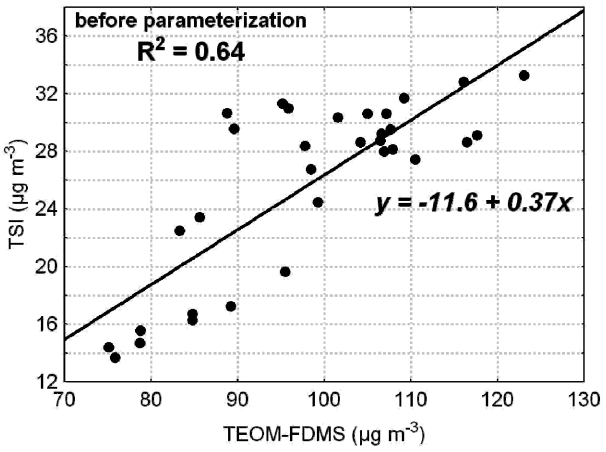

Figure 1. Raw semi-hourly average for the portable nephelometer SidePak AM510 *vs* TEOM-FDMS data.

$PM_{2.5}$ sampling with 20 instruments was carried out in background and kerbside sites in the Po valley (Italy). Results showed that the response of the SidePak AM510 samplers is highly sensitive to the chemical composition of particles. As a consequence, the growth of aerosol particles due to water uptake has an impact on the light scattering coefficient and therefore, in the estimation of PM number concentration.

The relationship between particle number and particle mass was developed through the parameterization of the TEOM-FDMS mass concentration (Baron and Willeke, 2001). It has been showed that the refraction index of the sampled particles depends both on a growing factor and the hydrophilic and hydrophobic mass fraction (Zieger et al, 2010). In addition, this parameterization accounts for different chemical composition for particles sampled at different micro-environments including rural and urban sites.

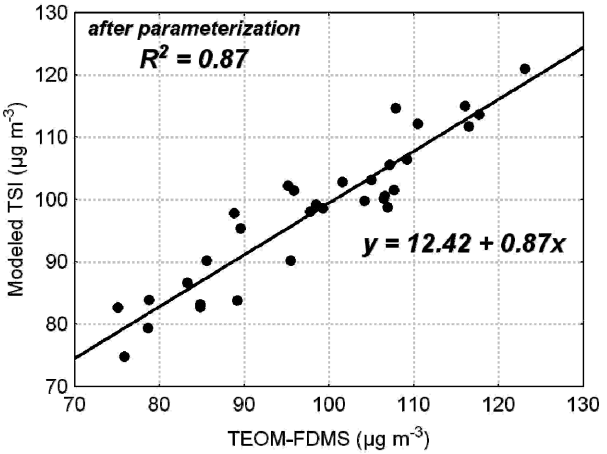

Figure 2. Modeled semi-hourly average for the nephelometer SidePak AM510 *vs* TEOM-FDMS data.

Modeled SidePak AM510 data were plotted *vs* reference TEOM-FDMS data showing a slope closer to 1 and a reduced uncertainty. Consequently, it was observed an increase in the coefficient of determination R^2 up to 25% and 60% in rural and urban sites, respectively. Therefore, we propose the parameterization developed in this work as a new method to correct sampled data collected with nephelometers in environments with high relative humidity.

Zieger, P., Fierz-Schmidhauser, R., Gysel, M., Ström, J., Henne, S., Yttri, K.E., Baltensperger, U., Weingartner, E., 2010. *Effects of relative humidity on aerosol light scattering in the Arctic*. Atmospheric Chemistry and Physics 10, 3875-3890.

Baron, P., A, Willeke, K., 2001. *Aerosol Measurement*. Wiley Inter-science, 427-432.

European Standard, EN 14907:2005. European Committee for Standardisation, Brussels.

Evaluation of the High Resolution Centrifugal Particle Mass Analyser

J.P.R. Symonds[1], M.G. Rushton[1], K.St.J. Reavell[1], C. Lowndes[1], A.E. Ellison[1] & J.S. Olfert[2]

[1]Cambustion, J6 The Paddocks, 347 Cherry Hinton Rd, Cambridge, CB1 8DH, U.K.
[2]Department of Mechanical Engineering, University of Alberta, Edmonton, Alberta, T6G 2G8, Canada
Keywords: Instrumentation, Mass Size Distribution, Particulate Mass, Morphology
Presenting author email: jps@cambustion.com

The Centrifugal Particle Mass Analyser (CPMA) selects aerosol particles by their mass:charge (*m/q*) ratio to produce a monodisperse aerosol (Olfert and Collings, 2005). As mass is a well defined quantity and not subject to morphological bias, and the CPMA's mass setpoint does not depend upon any gas properties (e.g. viscosity, mean free path) the CPMA offers advantages over a DMA for monodisperse classification.

Pre-charged aerosol is passed between two concentric metal cylinders which have a potential difference applied between them. The cylinders are rotated about their common axis, thus creating opposing electric and centrifugal forces. Particles with a larger *m/q* ratio are deflected outwards, and collect on the outer cylinder. Particles with a smaller *m/q* ratio are deflected inwards and collect on the inner cylinder. Only particles with the selected *m/q* ratio will pass through the classifier.

If we chose to rotate the cylinders at the same angular velocity, then the system of forces will only balance exactly along a central trajectory. So only particles amongst those with the correct *m/q* ratio which enter along this trajectory will emerge; others will be lost. It would also be possible for particles away from the centre line, *not* of the desired *m/q* ratio, to emerge from the classifier, thus broadening the transfer function.

Crucially and uniquely, the CPMA is designed such that the cylinders can be rotated at *different speeds*. The inner cylinder is rotated slightly faster than the outer cylinder, and the resultant radial velocity profile creates a stable system of forces under which a theoretical transfer function of 1.0 at the desired setpoint is possible, thus allowing a high transmission efficiency.

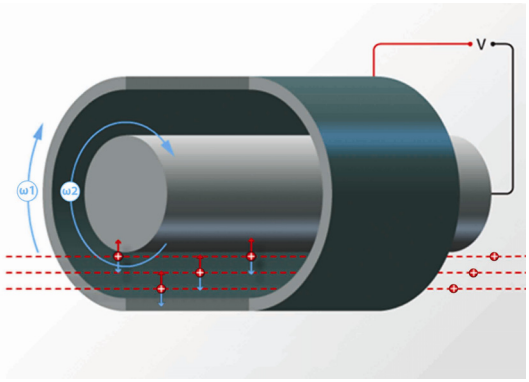

Figure 1: CPMA Principle: $\omega_2 > \omega_1$

This enables the resolution of the classifier to be increased by increasing its length, without a corresponding particle loss penalty; approaching a typical DMA's resolution. The CPMA can be used in a similar way to a DMA if a particle charger such as a radioactive neutraliser is used upstream, and step scanning of the particle mass spectrum is possible if a CPC is used downstream. If used in tandem with a DMA, determination of size to mass relationships and hence the mass-mobility exponent is possible, from which particle morphology can be inferred (Olfert, Symonds and Collings, 2007; Symonds *et al*., 2008).

A prototype CPMA has been used in several recent studies, for example as a mass standard in instrument comparisons (e.g. Cross *et al*., 2010). We present here results achieved using improved pre-production classifiers which have a higher resolution than the early prototype. These include validation of the mass accuracy of the systems with PSL spheres, and the determination of size to mass relationships and particle morphologies by the tandem DMA-CPMA method described above. Aerosol morphologies examined include spherical particles (e.g. PSL), cubic particles (NaCl), and fractal particles (e.g. soots).

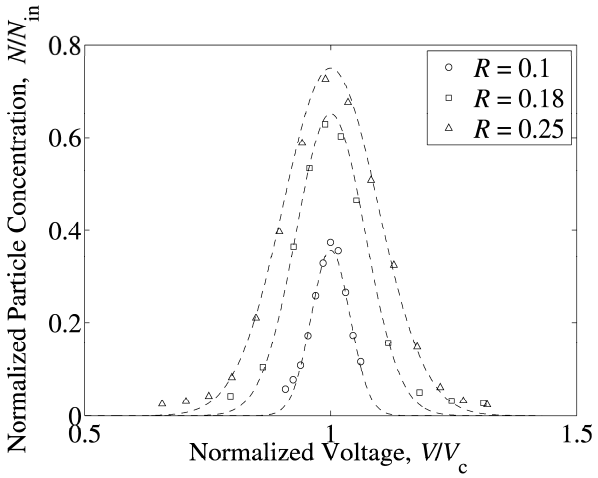

Figure 2: 296 nm PSL classified with a high resolution prototype CPMA; *R* is the resolution parameter.

Cross, E.S. *et al*. (2010) *Aerosol Science and Technology* **44,** 592–611

Olfert, J.S. and Collings, N. (2005) *Journal of Aerosol Science* **36**, 1338–1352

Olfert, J.S., Symonds, J.P.R and Collings, N. (2007) *Journal of Aerosol Science* **38**, 69–82

Symonds, J.P.R., Price, P., Williams, P.I., Stone, R. (2008) *European Aerosol Conference (Thessaloniki)*, T08A017P

Comparison of ambient aerosol extinction coefficients obtained from in-situ, MAX-DOAS and LIDAR measurements in Cabauw

P. Zieger[1], E. Weingartner[1], B. Henzing[2], M. Moerman[2], G. De Leeuw[2,3,4], J. Mikkila[4], K. Clemer[5], M. Van Roozendael[5], S. Yilmaz[6], U. Friess[6], H. Irie[7], T. Wagner[8], R. Shaiganfar[8], S. Beirle[8], A. Apituley[9, 10], K. Wilson[9,10], U. Baltensperger[1]

[1]Paul Scherrer Institut, Villigen PSI, Switzerland
[2]Netherlands Organization for Applied Scientific Research TNO, Utrecht, Netherlands
[3]Finnish Meteorological Institute, Helsinki, Finland
[4]University of Helsinki, Helsinki, Finland
[5]Belgium Institute for Space Aeronomy, Brussels, Belgium
[6]University of Heidelberg, Heidelberg, Germany
[7]Japan Agency for Marine-Earth Science and Technology, Yokohama, Japan
[8]Max-Planck-Institute for Chemistry, Mainz, Germany
[9]National Institute for Public Health and the Environment, Bilthoven, Netherlands
[10]Royal Netherlands Meteorological Institute, De Bilt, Netherlands.
Keywords: Optical properties, In-situ measurements, Remote sensing, Hygroscopic growth.
Presenting author email: paul.zieger@psi.ch

In the field, aerosol in-situ measurements are often performed under dry conditions (relative humidity RH<30-40%). Since ambient aerosol particles experience hygroscopic growth at enhanced RH, their micro-physical and optical properties - especially the aerosol light scattering - are strongly dependent on RH. The knowledge of this RH effect is of eminent importance for climate forcing calculations or for the comparison of remote sensing with in-situ measurements.

Here, we will present results from a four-month campaign which took place in summer 2009 in Cabauw (Netherlands) and was part of the Cabauw Intercomparison Campaign of Nitrogen Dioxide measuring Instruments (CINDI). During this campaign different remote sensing and in-situ instruments were used to derive atmospheric gas species and aerosol properties. The aerosol scattering coefficient $\sigma_{sp}(\lambda)$ was measured dry and at various, predefined RH conditions between 20 and 95% with a recently developed humidified nephelometer (WetNeph). The scattering enhancement factor $f(RH,\lambda)$ is the key parameter to describe the effect of RH on $\sigma_{sp}(\lambda)$ and is defined as $\sigma_{sp}(\lambda,RH)$ measured at a certain RH divided by the dry $\sigma_{sp}(\lambda,RH=dry)$. The measurement of $f(RH)$ together with the dry absorption measurement allows the determination of the actual extinction coefficient $\sigma_{ep}(\lambda)$ at ambient RH. In addition, a wide range of further aerosol properties were measured in parallel. The measurements were used to characterize the effects of RH on the aerosol optical properties. A closure study showed the consistency of the aerosol in-situ measurements. Due to the large variability of airmass origin and aerosol composition a simple categorization could not be established. If $f(RH)$ needs to be predicted, the chemical composition needs to be known.

Four MAX-DOAS (multi-axis differential optical absorption spectroscopy) instruments retrieved vertical profiles of $\sigma_{ep}(\lambda)$. The aerosol extinction corresponding to the lowest profile layer can be directly compared to the in-situ values, which were re-calculated to ambient RH. The comparison showed a good correlation of R^2=0.62-0.78, but a factor of 1.5-3.4 higher extinction coefficients compared to the in-situ measured values. Best agreement is achieved for a few cases characterized by low aerosol optical depths and low planetary boundary layer heights. Differences showed to be dependent on the applied MAX-DOAS retrieval algorithm. The comparison of the in-situ data to a Raman lidar (light detection and ranging) showed much better agreement if the Raman retrieved profile was used to extrapolate the directly measured extinction coefficient to ground.

Zieger, P., E. Weingartner, J. Henzing, M. Moerman, G. de Leeuw, J. Mikkilä, M. Ehn, T. Petäjä, K. Clémer, M. van Roozendael, S. Yilmaz, U. Friess, H. Irie, T. Wagner, R. Shaiganfar, S. Beirle, A. Apituley, K. Wilson and U. Baltensperger (2010b), *Atmos. Chem. Phys. Diss.* **10**(12): 29683-29734.

Friday, September 9, 2011

Session 11F: Atmospheric Applications of Aerosol Modelling

A 19th Century model for secondary organic aerosol

D. Topping[1,2], G. McFiggans[2]

[1]National Centre for Atmospheric Science (NCAS), University of Manchester, M13 9PL
[2]Centre for Atmospheric Science, University of Manchester, M13 9PL
Keywords: Aerosol modelling, SOA (Second. Organic Aerosols), Modelling (microscale), Absorption.
Presenting author email: david.topping@manchester.ac.uk, g.mcfiggans@manchester.ac.uk

Introduction

Atmospheric aerosol particles are an important yet uncertain component of climate change and air quality. Comprised of inorganic and organic material, the inorganic fraction is restricted to a few well-understood compounds. However, organic material can comprise many thousands of, largely unidentified compounds with a wide range of properties. Mechanistic understanding and knowledge of individual compounds involved in the chemical evolution of aerosol particles is far from complete.

Whilst focus is often given to uncertainties in pure component properties, such as vapour pressure, attention is rarely given to how processes occurring within and on aerosol particles are formulated and combined. For example, the recently postulated phenomena of bulk to surface partitioning within aqueous droplets is now accounted for by altering the way concentrations are treated within a Gibbsian framework. An alternative way of understanding this is having to distinguish between a bulk and surface phase within equilibrium calculations. Another largely neglected property of aerosol particles is the size. This is unfortunate as the size of an aerosol influences the equilibrium composition and phase state for a given set of ambient conditions and chemical composition. Incorporating the influence of curvature in theoretical constructs can be complex. The equilibrium vapour pressure of any condensate increases above a curved surface, influencing the range of material expected to condense to an aerosol of a particular size. However, basic equilibrium absorptive partitioning models, which are either fit to chamber yields or used in conjunction with detailed chemical schemes, neglect the influence of curvature. This will therefore lead to errors in prescribed composition and volatility for conditions in which size is likely to play an important role: unseeded/nucleation chamber experiments. The same conceptual problems will influence predictions of CCN activation potential. Whilst the influence of curvature is explicit within the Kohler equation, this only accounts for the equilibration of water between and gaseous and particle phase. Direct use of the Kohler equation therefore does not implicitly account for the co-condensation/evaporation of semi-volatile components as the relative humidity changes.

Abstract review

In this work we present development and application of a partitioning model based on a novel simple iterative algorithm. Like most equilibrium models, the novelty in the algorithm arises from an ability to combine theoretical constructs important for aerosol properties, in a numerically stable manner. In essence, the model is a collection of frameworks centred on the work of Gibbs and Thomson in the late 19th century. The model has already been applied to simulations involving 10000 compounds with consideration of non-ideality (McFiggans et al 2010). By extending the model to include the influence of curvature we discuss the impact on the volatility distribution and composition of sub 100nm aerosol particles generated from a range of gas phase oxidation products. Model predictions are then extended to cloud activation potential.

Again, it is largely forgotten that Kohler theory, or the Kohler equation, was derived by minimising the Gibbs energy for a system comprised of involatile solutes and water. Previous studies have already noted the potentially large impact of co-condensation on the point at which an aerosol activates into a cloud droplet. However, such models are limited to the number of compounds which can be modelled. Whilst complex thermodynamic models such as ADDEM (Topping et al 2005) include the influence of curvature on deliquescence and CCN activation, no consideration of the above phenomena has yet been built into it. Here we present the potential pitfalls of neglecting the possibility of co-condensation/evaporation on predictions of CCN activation using the same model already described earlier.

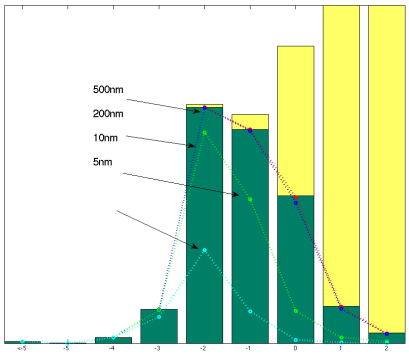

Figure 1. Example volatility distribution displaying the influence of particle size.

This work was supported by the National Centre for Atmospheric Science (NCAS).

References

Hallquist, M., et al Atmos. Chem. Phys., 9, 51555236, 2009
McFiggans, G et al .Atmos. Chem. Phys., 10, 10255-10272
Topping et al: Atmos. Chem. Phys., 5, 1205-1222, 2005

Impact of aerosol activation on modelled regional particulate matter

W. Gong, C. Stroud, S. Gong, P.A. Makar, M.D. Moran, J. Zhang, N. Shantz and W.R. Leaitch

Science and Technology Branch, Environment Canada, Toronto, Ontario, M3H 5T4, Canada
Keywords: aerosol cloud interaction, activation, aerosol modelling, atmospheric pollution
Presenting author email: Wanmin.gong@ec.gc.ca

Aerosol-cloud interactions play an important role in the atmospheric hydrological cycle and in the fate of atmospheric pollutants. One of the key processes is the activation of atmospheric aerosol particles to form cloud droplets. Aerosol particles, particularly those that are water-soluble or that contain water-soluble components, can serve as cloud condensation nuclei (CCN). Under suitable supersaturation conditions, condensation of water vapour on these CCN can proceed rapidly and lead to the formation of cloud droplets, i.e., aerosol activation process. Aerosol activation is controlled by the size and composition of the particles, and by the rate of cooling of the aerosol.

The representation of aerosol activation in 3-D large scale (global and regional) models varies from primarily empirically based parameterizations, e.g., linking droplet number concentration to either aerosol mass or number concentration (Boucher and Lohmann, 1995; Gong et al., 2003), to more physically based parameterizations, mostly relying on a parcel model concept (e.g., Abdul-Razzak and Ghan, 2000; Nenes and Seinfeld, 2003). Studies have shown that there can be significant variability in modelled droplet number concentrations from these different activation parameterizations under certain conditions. In the climate modelling community there is a tendency to be moving away from the more empirically based parameterizations to more physically based mechanistic approaches for representing the aerosol activation processes, although these mechanistic approaches have not reduced the uncertainty range of the indirect aerosol effect due to new uncertaintes in representing the detailed processes. Within the air quality community, the attention has mainly been focused on aerosol mass rather than size distribution so far, although aerosol activation (or nucleation scavenging) can also have an impact on aerosol mass: it directly affects the wet removal of aerosols in the case of precipitation and indirectly the dry removal of aerosols through the impact on the size distribution of cloud-processed aerosols.

In this study, we use a regional air quality model, AURAMS, developed at Environment Canada to assess the impact of the variability in aerosol activation on the modelled regional particulate matter (PM) concentrations. AURAMS is an off-line, multi-pollutant, regional air-quality modelling system with size segregated (sectional) and chemically speciated representation of aerosols (Gong et al., 2006). AURAMS has been using a simple activation scheme based on an empirical relationship between cloud droplet number density and aerosol number density (Jones et al., 1994). Recently, a more physically based activation scheme based on Abdul-Razzak and Ghan (2002) has been implemented in AURAMS. For sectional representation of aerosol size spectrum, Abdul-Razzak and Ghan (2002) established a relationship between the maximum supersaturation reached by an air parcel (under known updraft) and an effective critical supersaturation which can be evaluated from the critical supersaturation of individual sections. For this implementation, the standard deviation of updraft is parameterized as a function of liquid water content (Hoose et al., 2010), and the aerosol wet size at critical supersaturation is used as a first guess for evaluating droplet size dependent parameters.

Model simulations are carried out for the 2004 ICARTT field campaign period over eastern North America. Figure 1 shows that in-cloud oxidation is simulated to have contributed to over 40% of ambient fine sulphate over eastern seaboard region for this period. In this paper, we will discuss the variability of aerosol activation resulting from the different schemes and the subsequent impact on regional PM (both mass and size distribution). The impact on aerosol radiative properties will also be discussed.

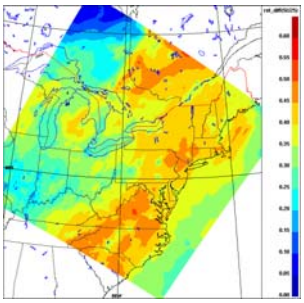

Figure 1. Relative contribution to sulfate$_{2.5}$ from aqueous-phase oxidation during ICARTT period as simulated by AURAMS.

Abdul-Razzak, H. and Ghan, S. J. (2000) *J. Geophys. Res.*, **105**, 6837–6844.

Abdul-Razzak, H. and Ghan, S. J. (2002) *J. Geophys. Res.*, **107**, D3, 4026, doi:10.1029/2001JD000483.

Boucher, O. and Lohmann, U. (1995) *Tellus*, Ser. B, **47**, 281– 300.

Gong, S.-L., et al. (2003) *J. Geophys. Res*. **108**, D1, 4007.

Gong, W., et al. (2006) *Atmos. Res*., **82**, 248-275.

Hoose, C., et al. (2010) Extended Abs., 13th AMS Conference on Atmospheric Radiation, paper 6.4.

Jones, A., et al. (1994) *Nature*, **370**, 450–453.

Nenes, A. and Seinfeld, J.H. (2003) *J. Geophys. Res.* **108**, D14, 4415, doi:10.1029/2002JD002911.

Particle-resolved modelling of the aging process of atmospheric soot particles

N. Riemer[1], M. West[2], R.C. Easter[3] and R. A. Zaveri[3]

[1]Department of Atmospheric Sciences, University of Illinois at Urbana-Champaign, Urbana, IL, 61801, USA
[2]Department of Mechanical Science and Engineering, University of Illinois at Urbana-Champaign, IL, Urbana, 61801, USA
[3]Atmospheric Science and Global Change Division, Pacific Northwest National Laboratory, Richland, WA, 99352, USA

Keywords: soot particles, aging, Monte Carlo simulations
Presenting author email: nriemer@illinois.edu

The composition of carbonaceous aerosol particles changes continuously after emission during their transport in the atmosphere. Coagulation, condensation, and photochemistry are contributing processes, collectively known as aging. This changes the particles' physico-chemical properties, in particular their hygroscopicity, from initially hydrophobic to more hydrophilic, and hence their ability to become cloud condensation nuclei. Parameterizations of black carbon aging are widely used in large-scale aerosol models. The aging process is typically modeled as a first-order system with the single parameter of aging rate or its inverse, the aging time-scale. While conceptually simple, the actual value of the aging time-scale is not well constrained.

In this study we present a method for explicitly calculating aging time-scales of black carbon aerosol using the particle-resolved model PartMC-MOSAIC. The stochastic particle-resolved model PartMC explicitly resolves the composition of individual particles in a given population of different types of aerosol particles, and accurately tracks their evolution due to emission, dilution, and coagulation (Riemer *et al.*, 2009). PartMC was coupled with the new state-of-the-art aerosol chemistry model MOSAIC (Zaveri *et al.*, 2008), which simulates the gas- and particle-phase chemistries, particle-phase thermodynamics and dynamic gas-particle mass transfer in a deterministic manner. The coupled model system PartMC-MOSAIC predicts number, mass and full composition distribution, and is therefore suited for applications where any or all of these quantities are required.

PartMC-MOSAIC was applied to a suite of scenarios to simulate the evolution of aerosol emissions of different types (diesel soot, gasoline soot, meat-cooking aerosol, mineral dust) in different environments. For these scenarios we developed number-based and mass-based aging time-scales using the activation of the particles at a given supersaturation as a criterion for aging. We also quantified the extent to which aging is due to condensation versus coagulation processes.

Figure 1 shows an example of day-time aging time-scales as a function of supersaturation threshold for a heavily polluted scenario. Here, the aging time-scales are less than 1 hour for supersaturations larger than 0.3%.

Overall our study shows that the aging time-scale is heavily dependent on the supersaturation threshold and on environmental parameters such as temperature and relative humidity. It can vary significantly between day and night regimes.

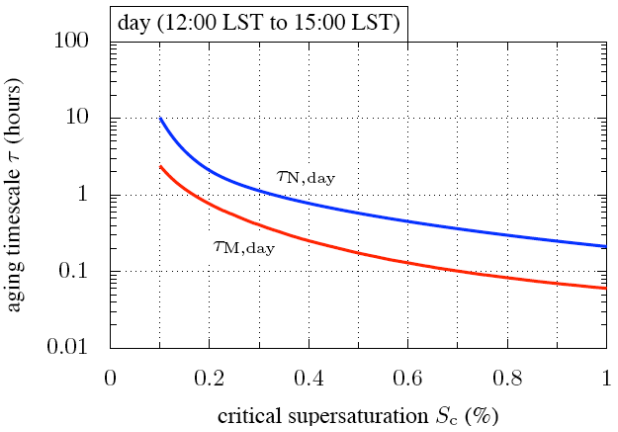

Figure 1. Day time averages of the aging time-scale (number-based aging time-scale in blue, mass-based aging time-scale in red).

N. Riemer and M. West are supported by the National Science Foundation (NSF), grant ATM 0739404. R. A. Zaveri and R. C. Easter are supported by the Aerosol-Climate Initiative as part of the Pacific Northwest National Laboratory (PNNL) Laboratory Directed Research and Development (LDRD) program. Pacific Northwest National Laboratory is operated for the U.S. Department of Energy by Battelle Memorial Institute under contract DE-AC06-76RLO1830.

Riemer, N., West, M., Zaveri, R.A., Easter, R.C. (2009), *J. Geophys. Res.*, D09202.
Zaveri, R.A., Easter, R.C., Fast, J.D., Peters, L.K. (2008*), J. Geophys. Res.*, D02210.

Time evolution of the concentration of PM10, PM2.5, and NO_2 in Central Europe until 2015: will we meet the limit values set by the European Commission in time?

S. Wurzler[1] , H. Hebbinghaus[1], M. Memmesheimer[2], G. Piekorz[2], E. Friese[2], H. J. Jakobs[2], C. Kessler[2], A. Ebel[2], and P. Bruckmann[1]

[1] North Rhine Westphalia State Agency for Nature, Environment and Consumer Protection (LANUV), P.O. Box 101052, D-45610 Recklinghausen, Germany

[2] Rhenish Institute for Environmental Research (RIU), EURAD-Project, University of Cologne, Aachener Strasse 201-209, D-50931 Cologne, Germany

Keywords: Aerosol Modelling, Atmospheric aerosols, NO_2, PM, EU notification procedure

High levels of particle (PM10, PM2.5) and NO_2 concentrations are known to cause adverse health effects. Therefore, the EC air quality directives set limit and target values for various pollutants, such as PM10 and NO_2. Where these limit values are exceeded, plans and programmes have to be set up to meet the limit values in future. Deadlines to accomplish this task are 2005 for PM10 and 2010 for NO_2. Failure to comply can result in a proceeding at the European Court of Justice with the sentence to pay a quite considerable fee.

Meanwhile we have reached the year 2011. There still remain plenty of exceedance situations all over Europe, with e. g., already 85 exceedance situations for NO_2 and 8 exceedance situations for PM10 in North Rhine-Westphalia (NRW) alone. Especially problematic are heavily trafficked street canyons.

The only way out is to enter the notification procedure as described in EC directive 2008/50/EG. In short, if a European member state does not manage to comply to the limit value in time, it can fill in a stack of tremendous forms detailing why it is a special case, where the limit value could not be reached by all means taken in time, and how the member state intends to comply to the limit value in the near future. These completed forms are checked in detail by the commission and in case your plans appear to be plausible, you may get a time extension to comply to the limit value until the year 2015.

One of the details to be given in the forms is the time evolution of the background concentrations of air pollutants until the year to 2015. Therefore, model simulations have been performed to assess the time evolution of the background concentrations of air pollutants.

The background concentration of PM10, PM2.5, and NO_2 was simulated with the European Air Pollution Dispersion Model (EURAD, Memmesheimer et al., 2004). The EURAD model simulates the concentration due to emissions, transport, and chemical transformation. The meteorological data stem from the MM5, transport is modelled by solving the 3-D advection and diffusion equation. The chemical model CTM2 treats chemical processes and the Modal Aerosol Dynamics Model (MADE) is used to account for secondary aerosol (Schell et al., 2001). The model is run in a one-way nesting with two grids, the largest domain spanning Europe in a horizontal resolution of 125 x 125 km². Nested in this is the area of Central Europe with 25 x 25 km² horizontal resolution. This nesting allows the consideration of long-distance transport.

Model simulations have been performed for the years 2009 and 2015, using in both cases the meteorological conditions of the year 2009. The emission data was taken from EMEP.

One of the main results is that the background concentrations decrease from the year 2009 to the year 2015. In Germany for example an average decrease of the NO_2 and of the PM10 burden in the range of 1 – 2 µg/m³ was found. The number of PM10 exceedance days (daily average concentration > 50 µg/m³) was reduced by 3 – 6. Taking NRW as example, this reduction of the regional background concentrations would help to avoid two of the exceedance situations for NO_2 and PM10 each. Thus, just to wait and hope the best is not a very good solution, as for NRW 98 % of the exceedance cases for NO_2 and 75 % of the exceedance cases for PM10 will still remain in the year 2015 if no further measures are taken.

Scope of this paper is to present the time evolution of the regional background concentrations for air pollutants such as NO_2 and PM10 from the year 2009 until the year 2015. Apart from the large scale evolution some examples for heavily trafficked street canyons with additional measures for emission reduction will be shown. Special focus will be set on the difficulties met while trying to oblige to the European Air Quality directives. A further question is whether reality follows the model, as up to now the NO_2 background concentrations in NRW persistently refuse to show a decline.

Memmesheimer, M., Friese, E., Ebel, A., Jakobs, H. J., Feldmann, H., Kessler, C., Piekorz, G. (2004), IJEP, **22**, 108 – 132.

Schell, B., Ackermann, I.J., Hass, H., Binkowski, F.S., and Ebel, A. (2001) *J. Geophys. Res.*, 106, 28275-28293.

Simulation of the impact of Eyjafjallajökull plume on cloud formation and precipitation over Europe with COSMO-ART

Vogel, H.[1], M. Bangert[1], B. Vogel[1], T. L. Lathem[2], A. Nenes[2], J. Förstner[3]

[1]Institute for Meteorology and Climate Research, Karlsruhe Institute of Technology (KIT), Herrmann-von-Helmholtz-Platz 1, 76344, Eggenstein-Leopoldshafen, Germany
[2]Georgia Institute of Technology, School of Earth & Atmospheric Sciences and Chemical & Biomolecular Engineering, 311 Ferst Drive, Atlanta, GA 30332, USA
[3]Deutscher Wetterdienst (DWD), Frankfurter Straße 135, 63067 Offenbach, Germany

Keywords: activation, cloud, aerosol modelling, regional scale, volcanic ash.
heike.vogel@kit.edu

After resting for 187 years the vulcano Eyjafjallajökull, Island wake up again at March 20th, 2010. Starting at April 14th massive emissions of volcanic ash occurred and finally lead to a shut down of civil aviation over entire Europe.

The emissions went on with variable strength until May 23rd, 2010. The volcanic eruption offers a unique field experiment for investigating atmospheric processes as transport, radiation and cloud formation on a large variety of scales applying both observations and numerical models. In addition to the academic interest the huge economic costs of the shutdown of the civil aviation raised the need of accurate forecasts of the temporal and spatial distribution of the ash plume.

To simulate the dispersion of the ash plume we used the comprehensive online coupled model system COSMO-ART (Vogel *et al*., 2009) in an operational forecast mode at Deutscher Wetterdienst (German Weather Service, DWD). COSMO-ART is the extension of the operational weather forecast model of DWD. In the operational mode three day forecasts were launched every six hours with the same model setup as for the weather forecast. Actual meteorological observations that are made during the six hour time interval are assimilated into the model. Six individual size distributions of the ash particles were simulated starting from 1 µm up to 30 µm. Deposition, sedimentation, and below cloud scavenging were taken into account. For the source heights we used data that were published by the volcanic ash advisory centre London (VAAC), UK which is responsible for making the official forecast of ash coming from volcanoes in Island according to international agreements.

Beside the simulation in the operational mode we did several model runs using the analysis of the COSMO results as input data. These sensitivity studies show the influence of different processes on the distribution of the ash particles. Using the measurements that were performed by DLR (Schumann et al., 2011) we calibrated our model results and compared them with measured size distributions at Hohenpeissenberg (Flentje et al., 2010).

Ash particles emitted by the volcano act as cloud and ice nuclei and, therefore, they should modify cloud formation within the plume. To simulate the impact of the various aerosol particles on the cloud microphysics and therefore on cloud properties COSMO-ART was coupled with the two-moment cloud microphysics scheme of Seifert and Beheng (2006) by using comprehensive parameterisations for aerosol activation (Barahona et al., 2010) and ice nucleation (Barahona and Nenes, 2009) The activation of the ash particles is based on FHH adsorption activation theory (Kumar et al., 2009) and measurements of the activation behaviour of ash samples of the Eyjafjallajökull. Results of these simulations will be presented.

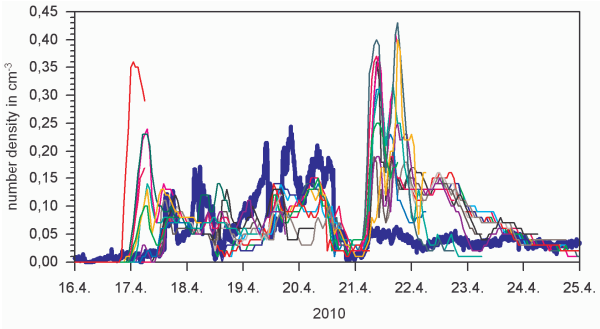

Figure 1. Observed number densities at 3.25 µm at Hohenpeissenberg and model results for the individual forecast runs.

Barahona, D., West, R. E. L., Stier, P., Romakkaniemi, S., Kokkola, H., and Nenes, A. (2010) *Atmos. Chem. Phys.*, **10**, 2467-2473.

Barahona, D. and Nenes, A. (2009) *Atmos. Chem. Phys.*, **9**, 5933-5948.

Flentje et al., (2010) *Atmos. Chem. Phys.*, **10**, 10085-10092.

Kumar, P., Sokolik, I. N., and Nenes, A. (2009) *Atmos. Chem. Phys.*, **9**, 2517-2532.

Seifert and Beheng (2006) *Meteorol. Atmos. Phys*., **92**, 45-66.

Schuman et al. (2010) *Atmos. Chem. Phys. Discuss*., **10**, 22131- 22218.

VACC, www.metoffice.gov.uk/aviation/vaac/.

Vogel, B., Vogel H., Bäumer, D., Bangert, M., Lundgren, K., Rinke, R., and Stanelle, T. (2009). *Atmos. Chem. Phys.*, **9**, 8661-8680.

The influence of ion-induced nucleation on atmospheric aerosols based on data from the CERN CLOUD experiment

E.M. Dunne[1], K.S. Carslaw[1], C.L. Reddington[1], J. Almeida[2] and the CLOUD collaboration[2]

[1]School of Earth and Environment, University of Leeds, Leeds, LS2 9JT, UK
[2]CERN, Geneva, Switzerland
Keywords: aerosol modelling, ion-induced nucleation.
Presenting author email: E.Dunne@leeds.ac.uk

Here we quantify the contribution of ion-induced nucleation to global aerosol based on new results from the CLOUD experiment at CERN. We also quantify the response of aerosols to a change in the nucleation rate in an attempt to explain apparent correlations between aerosol and Forbush decreases. Away from the surface, ion concentrations are controlled by cosmic-ray induced ionization. A range of observations support a connection between cosmic ray intensity and the Earth's climate, on time-scales from days (Pudovkin and Veretenenko, 1995) to centuries (Eichler *et al*, 2010) to millennia (Bond *et al*, 2001).

Because ions stabilise sub-critical nuclei, ion-induced nucleation is a strong candidate for the atmospheric nucleation mechanism, especially in remote regions with low concentrations of precursor vapours. When determining the impact of the phenomena on the climate, a global aerosol microphysics model (such as GLOMAP) is a vital tool due to its inclusion of the various processes which affect particle growth and deposition.

We will present the results of the implementation within a global model of the first parametrization of ion-induced nucleation based on experimental observations rather than theoretical predictions. This parametrization is the result of work in the ternary H_2SO_4-NH_3-H_2O system by the CLOUD collaboration at CERN. We show that nucleation in this "inorganic" system is unable to explain most boundary layer nucleation and observed particle concentrations.

We also quantify the response of aerosol to changes in the nucleation rate that might accompany Forbush decreases. During a period of intense magnetic activity which causes the sun to emit charged matter, the stream of cosmic rays reaching the Earth can be partially blocked. The result is a reduction in atmospheric ion concentrations that lasts for several days. There have been studies showing a strong (Svensmark et al., 2009) and a weak (Laken et al. (2009); Calogovic et al., (2010)) correlation between Forbush decreases and cloud and aerosol properties. The suggested cause of these correlations was a change in the ion-induced nucleation rate.

To test the maximum effect of a Forbush decrease on aerosol, we performed a series of monthly simulations with daily resolution. We reduced the nucleation rate by 15% for a period of ten days in the middle of each month, and analysed the effect on condensation nuclei (CN), cloud condensation nuclei (CCN), aerosol optical depth and the Ångstrom exponent. This allows us to estimate the bounds of a transient change in the nucleation rate on aerosol and cloud properties. In figure 1, we show the mean

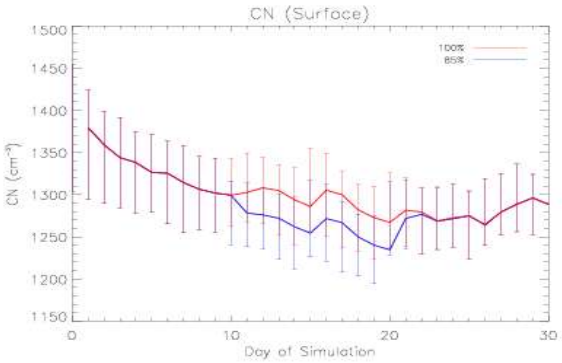

Figure 1: A time-series of globally-averaged perturbed and unperturbed condensation nuclei with radius > 3 nm.

perturbed and unperturbed condensation nuclei over six monthly simulations. We find a negligible change in cloud condensation nuclei concentrations and aerosol optical depth in the atmosphere.

We would like to thank CERN for supporting CLOUD with important technical resources, and for providing a particle beam from the CERN Proton Synchrotron. This research has received funding from the EC's Seventh Framework Programme under grant agreement no. 215072 (Marie Curie Initial Training Network "CLOUD-ITN"), from the German Federal Ministry of Education and Research (project no. 01LK0902A), from the Swiss National Science Foundation, and from the Academy of Finland Center of Excellence program (project no. 1118615).

Bond, G.C., B. Kromer *et al* (2001) *Persistent solar influence on North Atlantic climate during the Holocene*. Science 294:2130–2136

Calogovic, J., C. Albert, F. Arnold *et al* (2010) *Sudden cosmic ray decreases: No change of global cloud cover*. Geophysical Research Letters

Eichler, A., S. Olivier *et al* (2009) *Temperature response in the Altai region lags solar forcing*. Geophysical Research Letters

Laken, B., A. Wolfendale, and D. Kniveton (2009) *Cosmic ray decreases and changes in the liquid water cloud fraction over the oceans*. Geophysical Research Letters

Pudovkin, M.I., Veretenenko, S.V. (1995) *Cloudiness decreases associated with Forbush decreases of galactic cosmic rays.* Journal of Atmospheric and Terrestrial Physics

Svensmark, H., T. Bondo, and J. Svensmark (2009) *Cosmic ray decreases affect atmospheric aerosols and clouds*. Geophysical Research Letters

Friday, September 9, 2011

Session 12A: Marine Aerosols / Mineral Dust

Primary and secondary marine organic aerosols over the North Atlantic ocean during the MAP experiment

S. Decesari[1], E. Finessi[1], M. Rinaldi[1], M. Paglione[1], S. Fuzzi[1], E.G. Stephanou[2], T. Tziaras[2], A. Spyros[2], D. Ceburnis[3], C.D. O'Dowd[3], M.C. Facchini[1]

[1]Institute of Atmospheric Sciences and Climate, National Research Council, Bologna, 20129, Italy
[2]Environmental Chemical Processes Laboratory, Department of Chemistry, University of Crete, Crete, Greece
[3]Department of Physics, National University of Ireland Galway, Galway, Ireland
Keywords: marine aerosols, primary organic aerosols, secondary organic aerosol, chemical composition.
Presenting author email: m.rinaldi@isac.cnr.it

Particulate matter in the marine boundary layer represents one of the most important aerosol system at the global scale. The relative importance of primary sources (seaspray) and secondary processes for the formation of organic and inorganic particles in the marine atmosphere is still controversial.

A multi-technique analytical approach was exploited to characterize submicron organic aerosol collected over the North-East Atlantic Ocean, outside continental pollution plumes, in the frame of the EU project MAP (Marine Aerosol Production). Samples were collected at Mace Head (Ireland), for the whole 2006, and onboard the research vessel Celtic Explorer (CE), between June and July 2006. Elemental analysis, ion chromatography, proton nuclear magnetic resonance spectroscopy (^{1}HNMR) and liquid chromatography-mass spectrometry provided a comprehensive characterization of the complex mixture of water-soluble (WSOC) and water insoluble (WIOC) organic carbon in submicron aerosol.

On average, WSOC accounted for 63% of total carbon in ambient aerosol samples, well above its contribution to the organic carbon contained in native seaspray particles (ca. 10 %) formed by bubble bursting experiments onboard the CE (Facchini et al., 2008a). The enrichment of WSOC in ambient aerosol can be due to secondary organic compounds condensing on sea spray, or to the prolonged atmospheric oxidation of primary organic compounds.

The results of the chemical characterization demonstrated that WIOC is structurally similar to lipids and that the less hydrophilic fraction of WSOC consists of a distribution of alkanoic acids and diacids, having an average carbon number between 8 and 9, and which comprise the early generation products of fatty acids degradation. More oxidized products, like sulphate esters of C6 – C11 hydroxycarboxylic acids, are found in the most polar fraction of WSOC, together with MSA and low-molecular weight amines, which are all of biogenic origin (Facchini et al., 2008b).

The nature of the dominant WSOC fraction unaccounted for by molecular characterization was investigated by means of factor analysis techniques applied to NMR spectral datasets. The decomposition of the NMR spectra provided a clear split between five factors, the first two being dominated by MSA (with HMSA and low-molecular weight oxoacids and diacids) and amines (plus organic compounds carrying terminal methyls), respectively. These two factors are consistent with a SOA components formed by gas-to-particle conversion processes. The profile of Factor 3 shows a limited content of aromatic moieties and of hydroxyl groups, with a greater proportions of alkyl moieties, containing methylenic chains, terminal methyls and carboxylic groups. The similarity between Factor 3 and the spectra of the less hydrophilic WSOC fraction relates this factor to the oxidation products of primary biogenic organics. The fourth factor traces anthropogenic sources and its spectral profile fits that of a “typical” oxidized organic aerosol of continental polluted areas.. Finally, the profile of Factor 5 is characteristic of purely aliphatic compounds, carrying cheto/carboxyl substituents and enriched in hydroxyl groups. Such oxidized organic aerosol cannot be explained by continental sources and may represent an additional class of marine SOA, not apparently linked to the routes of fatty acid degradation.

These results highlight the complexity of the organic chemical composition of submicron particles in the marine atmosphere, and provide evidence for the contributions from primary biogenic materials, their atmospheric oxidation products and from compounds deriving from the gas-to-particle conversion of volatile organics emitted by the marine biota.

A financial support from EU FP6 project MAP (GOCE-018332) and EPA Ireland is gratefully acknowledged.

Facchini, M.C., Rinaldi, M., Decesari, S., Carbone, C., Finessi, E., Mircea, M., Fuzzi, S., Ceburnis, D., Flanagan, R., Nilsson, E.D., de Leeuw, G., Martino, M., Woeltjen, J. and O’Dowd, C.D. (2008a). *Geophys. Res. Lett.*, **35**, L17814, doi:10.1029/2008GL034210.

Facchini, M. C., Decesari, S., Rinaldi, M., Carbone, C., Finessi, E., Mircea, M., Fuzzi, S., Moretti, F., Tagliavini, E., Ceburnis, D. and O’Dowd, C. D. (2008b). *Environ. Sci. Technol.*, **42** (24), 9116–9121.

Predicted change in emissions of sea salt aerosol for the years 1870-2100

H. Struthers[1], A. M. L. Ekman[2], P. Glantz[1], E.M. Mårtensson[1,3], and E. D. Nilsson[1]

[1]Department of Applied Environmental Science, Stockholm University, Stockholm, SE-11418, Sweden
[2]Department of Meteorology, Stockholm University, Stockholm, SE-10691, Sweden
[3]Department of Earth Sciences, Uppsala University, SE-752 36, Uppsala, Sweden
Keywords: Marine aerosols, sea salt, climate effects
Presenting author email: hamish.struthers@itm.su.se

Sea salt aerosol contributes significantly to the global aerosol burden and radiative budget, and may be the dominant contributor to light scattering and the dominant source of cloud condensation nuclei (CCN) in remote marine areas. The main physical driver of sea salt emissions is the surface wind speed (U_{10}) with emissions being regulated by the sea ice cover in the polar regions (Nilsson *et al*. 2001). An increasing number of studies support the conclusion that sea salt aerosol emissions are dependent on the sea surface temperature (SST) (e.g. Hultin *et al*. 2010). New measurements also indicate that there may be a dramatic enhancement of total number emission at temperatures near the freezing point of water. In addition, SST appears to influence the shape of the size distribution of the aerosol emissions (see Figure 1). This is important from a climate perspective because the scattering of solar radiation and the formation of cloud droplets are highly dependent on the particle size of the aerosol.

The aim of this study is to examine the long-term trends in the emission of sea salt aerosol by employing a commonly used sea salt aerosol source parameterization (Mårtensson *et al*. 2003) and output from the World Climate Research Programme's (WCRP's) Coupled Model Intercomparison Project Phase 3 (CMIP3) multi-model dataset. This analysis allows us to estimate the relative roles of different drivers of sea salt emissions on global and regional scales.

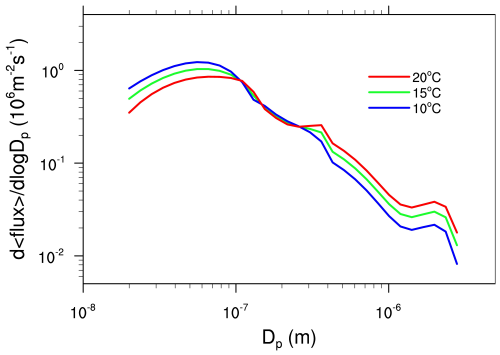

Figure 1. The Mårtensson et al. (2003) sea salt aerosol source parameterization (for U_{10} = 9 ms^{-1}).

The sea salt source parameterization used in this work is visualised in Figure 1 for a range of SSTs. The main features of this source parameterization are: (a) in agreement with other studies, sub-300 nm particles dominate the number emissions (b) the flux in the smallest size range (20nm - 145nm) decreases with increasing SST whereas for the largest size range (419nm - 2.8um) the opposite trend holds, and (c) the particle flux for the intermediate sizes (145nm - 419nm) is relatively insensitive to SST. Combining this parameterization with U_{10}, SST and sea ice fraction taken from the CMIP3 multi-model archive allows us to construct a global sea salt emission model covering the period 1870-2100.

Results

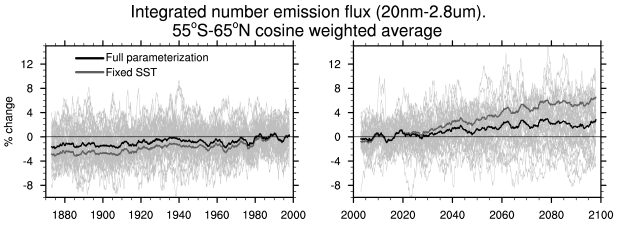

Figure 2. Time-series of sea salt aerosol emissions. Thin lines indicate individual model results (full parameterization) with the thick lines being the ensemble model average.

Figure 2 shows an example of the estimated sea salt emissions. The black lines show the near global, ensemble model average emissions using the full Mårtensson parameterization (Figure 1). The heavy grey lines show the same time-series but with the SSTs held fixed in the source parameterization. Results in the left hand panel are derived from the 20th century CMIP3 output and the right hand panel from the so called SRES A1b (medium) scenario. The difference between the black and the heavy grey lines then indicates how SST influences the emissions. These results suggest that if future SST changes are ignored, the increase in integrated particle emissions over the 21st century is overestimated by more than a factor of 2.

The results obtained in the present study also indicate that different drivers control the sea salt aerosol emissions in different regions of the globe. In the Arctic, sea ice extent is the most important parameter determining the change in sea salt emissions. On the other hand, in temperate latitudes (55°S-60°N) both U_{10} and SST substantially influence the emissions whereas in the southern ocean, U_{10} is the dominant parameter.

Hultin, K. A. H., Nilsson, E. D., Krejci, R., Mårtensson, E. M, Ehn, M. Hagström, Å, & de Leeuw, G. (2010) *J. Geophys. Res.*, **115**, D06201.

Mårtensson, E. M., Nilsson, E. D., de Leeuw, G., Cohen, L. H., & Hansson, H.-C. (2003) *J. Geophys. Res.* **108**, 4297, doi:10.1029/2002JD002263.

Nilsson, E. D., Rannik, U., Swietlicki, W., Leck, C., Aalto, P. P., Zhou, J., & Norman, M. (2001) *J. Geophys. Res.* **106**, 32129-32154.

Characterization of a bubble tank for Sea Spray Aerosol Studies

A.C. Butcher[1], S.M. King[1], T. Rosenoern[1], E. D. Nilsson[2] and M. Bilde[1]
[1]Department of Chemistry, University of Copenhagen, DK-2100 Copenhagen, Denmark
[2]Department of Applied Environmental Science, Stockholm University, S-10691 Stockholm, Sweden
Keywords: Marine aerosols, CCN, bubble bursting, particle size distribution.
Presenting author email: andrew@kemi.ku.dk

Sea spray aerosols are of major interest to global climate models due to their large uncertainty in indirect and direct radiative forcing and poorly understood emission characteristics. A new experimental sea spray aerosol bubble tank is characterized and preliminary results are presented for bubble generation, bubble size distribution, and particle emissions.

In this study, the major processes of bubble formation are examined with respect to particle emissions. It has been suggested that a plunging jet, formed by a continuously flowing nozzle placed vertically above a water surface, closely resembles breaking wave bubble entrainment processes and subsequent bubble size distributions (Fuentes et al. 2010). The physical characteristics of our bubble tank are shown in Table 1. The tank consists of a stainless steel cylinder closed at both ends with fittings for recirculating flow for the jet and aerosol sampling.

Table 1 Sea spray tank characterization

Tank Dimensions	
H = 46.2 cm	V_{tot} = 16.3 L
D = 21.2 cm	V_{sample} = 9 L
A = 353 cm^2	$H_{headspace}$ = 20.7cm
Nozzle Parameters	
D_{nozzle} = 4 mm	$v_{jet,\ o}$ = 4.3 m s^{-1}
H_{nozzle} ~ 20 cm	$v_{jet,\ surf}$ = 4.7 m s^{-1}

The sub-surface bubble plume characteristics can be calculated using parameters specified by Claret & Lasheras (1997) and are given in Table 2. When the Weber number (We) is less than unity, surface tension forces are greater than inertial forces and bubbles will remain intact until reaching the surface.

Table 2 Bubble plume characteristics (1mm bubble)

Angle of Plume Cone = 12.5°
$v_{1mm,\ T}$ = 0.22 cm s^{-1}
$H_{1mm,\ T}$ = 21.6 cm
$W_{1mm,\ T}$ = 7.8 cm
We_{1mm} = 6.7 × 10^{-5}

In addition to calculated values, bubble spectra were analyzed for a frit placed in the bottom of the tank at range of air flow rates (

Figure **1**). Particle size distributions for both the frit placed in the tank and the plunging jet are shown in Figure 2.

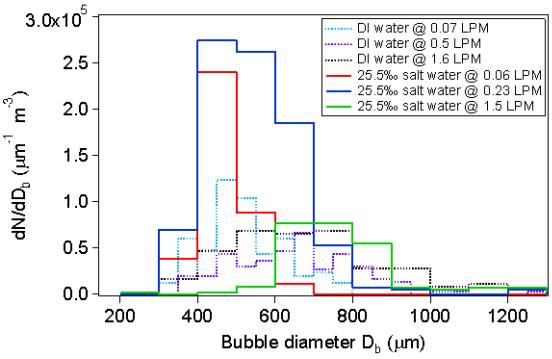

Figure 1 Preliminary photograph-analyzed bubble size distributions for the frit placed in the bottom of the tank.

The difference between the particle size distributions could be caused by high particle loss due to scavenging and entrainment processes of the plunging jet (Bin 1993). The difference in concentration could also be attributed to the shear forces exerted on bubbles that rise to the surface causing incomplete bursting which could also partly explains the disparity in particle size distributions.

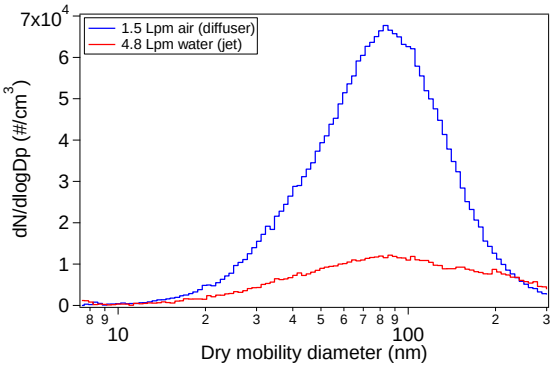

Figure 2 Particle size distributions for the frit and the plunging jet for artificial sea water of salinity 35‰.

This work has been supported by the Carlsberg Foundation.

Bin, A. K. (1993). "Gas Entrainment by Plunging Liquid Jets." Chemical Engineering Science **48**(21): 3385-3630.

Clanet, C. and J. C. Lasheras (1997). "Depth of penetration of bubbles entrained by a plunging water jet." Physics of Fluids **9**(7).

Fuentes, E. et al. (2010). "Laboratory-generated primary marine aerosol via bubble-bursting and atomization." Atmospheric Measurement Techniques **3**: 141-162.

Radiative properties of mixed biomass-mineral dust aerosol in the thermal infrared during SAMUM-2

C. H. Koehler[1], T. Trautmann[1] and E. Lindermeir[1]
[1]Remote Sensing Technology Institute, German Aerospace Center, Oberpfaffenhofen, 82234, Germany
Keywords: Radiative properties, Mineral dust, Biomass burning, Field measurements
Presenting author email: claas.koehler@dlr.de

The Saharan Mineral Dust Experiment (SAMUM) is a 7-year national German project dedicated to the radiative and micro-physical properties of mixed biomass and mineral dust aerosol. It comprised two field experiments in Morocco (May-June, 2006) and Cape Verde (January-February, 2008). We intend to present results of ground-based radiance measurements in the thermal infrared (TIR) obtained during the 2008 field experiment at Praia with a D&P Model 102 FTIR . These measurements are complemented by space borne measurements with the IASI FTIR on board METOP-A.

Furthermore we conducted radiative transfer simulations based on the data measured by other SAMUM-2 groups including LIDAR derived aerosol layer heights, airborne measurements of aerosol size distribution and off-line chemical analysis of aerosol samples collected by the DLR Falcon research aircraft. A comparison of simulated and measured radiances at top and bottom of the atmosphere (TOA, BOA) reveals insight into the validity of several approximations commonly made in TIR radiative transfer, such as the assumption of spherical model particles or the representation of the complex mineral mixture in terms of a single (wavelength-dependant) effective refractive index. Figure 1 is an example of a comparison of measured and simulated data obtained during a dust event on January 25th, 2008. The dust radiative effect is clearly visible when comparing the measurement to the clear-sky simulation. Apparently the OPAC (Hess *et al*, 1998) and Volz (1973) models agree relatively well with the Maxwell-Garnett effective medium theory, which uses the refractive indices of pure mineral constituents identified in the chemical analysis, while the model of Shettle and Fenn (1979) seems to underestimate the aerosol emission. An interesting effect occurs around 1100 cm^{-1}, where a considerably different behaviour between measurement and simulation is observable. Based on similar observations by Thomas and Gautier (2009) we suspect this to be attributable to the non-spherical shape of the aerosols, which is not accounted for in the simulations. We plan to conduct further investigations adressing this issue using spheroidal model particles and intend to discuss the results in our presentation.

This work contributes to the development of a generally accepted benchmark model of aerosol TIR radiative properties, which is essential for validation of fast radiation models commonly found in climate simulations, weather prediction or satellite retrieval algorithms.

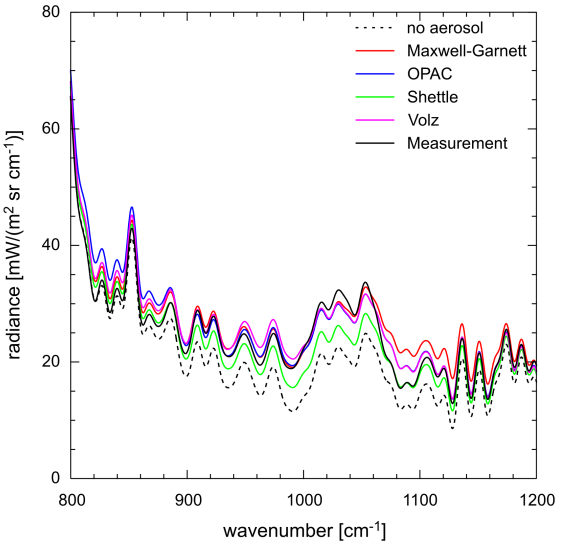

Figure 1: A comparison of simulated radiances at BOA for different refractive index models (colored lines) assuming spherical model particles and a measured spectrum (black). The dotted line is obtained from a simulation for an aerosol-free atmsophere

This work was supported by the German Research Foundation (DFG)

Hess, M., Koepke, P. and Schult, I. (1998) Optical Properties of Aersosols and clouds: The software package OPAC, Bul. Am. Met. Soc. 79, 831-844

Shettle, E. P. and Fenn, R. W. (1979) Models for the Aerosols of the Lower Atmosphere and the Effects of Humidity Variation on Their Optical Properties, Technical Report AFGL-RT-79-0214, AFGL

Thomas, M. and Gautier, C. (2009) Investigations of the March 2006 African dust storm using ground-based column-integrated high spectral resolution infrared (8-13 μm) and visible aerosol optical thickness measurements: 2. mineral aerosol mixture analysis, J. Geophys. Res., D14209

Volz, F. E. (1973) Infrared Optical Constants of Ammonium Sulfate, Sahara Dust, Volcanic Pumice and Flyash, Appl. Opt. 12, 564-568

Volcanic sulfate aerosols

B. Grobéty[1,2], C. Botter[1], and F. Meier[1]

[1]Department of Geosciences, University of Fribourg, Fribourg, 1700, Switzerland
[2]FRIMAT, University of Fribourg, Fribourg, 1700, Switzerland
Keywords: Volcanic aerosols, sulfur, sulfate compounds, simulation
Presenting author email: bernard.grobety@unifr.ch

Volcanic eruptions contribute significantly to the sulfur content of the troposphere and the stratosphere (Oppenheimer, 2003). Satellite and ground-based remote sensing allow to measure the main gaseous species in an eruption plume e.g. SO_2 and H_2S. Gaseous sulfur species have a strong influence on the radiative properties of the atmosphere. Electron microscopy of aerosols sampled at different volcanoes with mild eruptive and/or fumarolic activity (Stromboli, Vulcano, El Chichon, Oldonyo Lengai) have shown, that even close to the eruption vent, there is a considerable amount of sulfur in the plume, that is not present as gaseous compounds, but bound to either liquid sulfuric acid droplets or in solid sulfate minerals. The environmental effect of the condensed sulfate phases is different from the original gaseous compounds. It is, therefore, important to understand the underlying transformation processes.

The quantity of sulfur released in or transformed to non-gaseous compounds, which are not taken into account by the remote sensing measurements, is poorly constrained. Aerosol formation in an eruption or a fumarole plume is very complex and occurs over a large temperature range (Symonds and Reed, 1993). Solid and liquid particles may be formed through magma disintegration, eruption conduit wall erosion, and through condensation or resublimation from the gas phase. In liquid aerosol particles, cooling and or evaporation can lead to precipitation of solid sulfate phases. We used geochemical modelling to explore possible particle forming reaction in a model system Na-K-Ca-Mg-(Fe)-S-C-O-H and temperatures for the primary gaseous/liquid phase ranging from ambient to 800°C. Gas phase reactions were modelled with the software HSC (OUTOTEC), whereas aqueous geochemistry (precipitation) was explored using the Geochemist's Workbench code (RockWare). The thermodynamic database had to be completed with data for some of the sulfate minerals.

The modelling results were compared with aerosol samples collected along the crater rim and at the base of Stromboli (Italy) and El Chichon (Mexico) volcano. Up to 1000 particles were analyzed by automated single particle scanning electron microscopy imaging and chemical analysis by energy dispersive spectroscopy (EDS) as well as transmission electron microscopy (TEM, Fig.1). The sampled aerosols contained condensed sulfuric acid particles as well as a number of sulfate minerals, mainly aphthitalite, $(K,Na)_3Na(SO_4)_2$, thernadite Na_2SO_4, and arcanite K_2SO_4 resp. their hydrated cousins.

At the base of Stromboli, magnesium sulfates made their appearance. Compared with the thermodynamic modelling results, this sequence is much in favor of an initial condensation of sulfate rich alkaline brine droplets and subsequent precipitation of the sulfate phases when the droplets evaporate. The expected order of precipitation is arcanite -> aphthitalite -> thenardite (mirabilite) -> magnesium rich sulfates. For El Chichon a similar evolution was found. A preliminary estimation of the solid sulfate flux from the fumarolic vents of El Chichon gave around 0.1 kgs^{-1}.

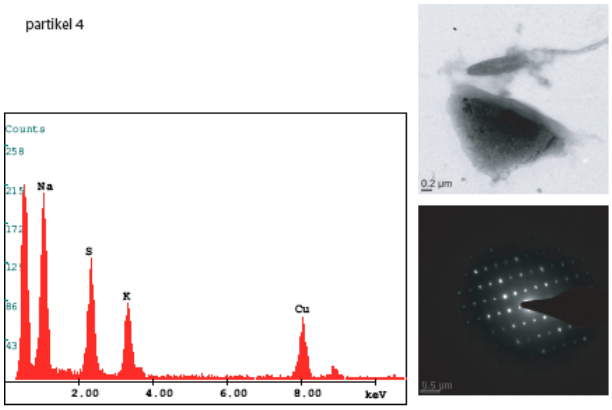

Figure 1. EDS spectrum (left) and TEM bright field image (top right) with selected area electron diffraction pattern (bottom right) of a sodium rich aphtitalite particle (triangle) sampled on top of Stromboli volcano.

Oppenheimer, C. (2003) *Treatise in Geochemistry*, **3**, 123-166.

Symonds, R.B. and Reed, M.H. (1993) *Am. J. Sci.*, **293**, 758-864.

Source profile of the local wind-blown soil contribution to respirable airborne particulate matter in the southern area of Rome (Italy)

A. Pietrodangelo[1], R. Salzano[1], S. Pareti[1], E. Rantica[1] and C. Perrino[1]

[1]Institute for Atmospheric Pollution Research, National Research Council, Monterotondo (Rome), Via Salaria Km. 29,300 - 00015, Italy

Keywords: Aerosol component composition, Mineral dust, PM_{10}, SEM/EDX

Presenting author email: pietrodangelo@iia.cnr.it

Source profiles play a key role in the source apportionment (SA) of airborne aerosol. The more unambiguous is the marker-vs-source relationship, the more consistent and accurate is the apportionment of model-estimated aerosol mass contributions. Nevertheless, some source categories still remain poorly characterised, like the crustal materials from non-industrial fugitive dust.. It is uknowledged that either mineral dust from natural rocks or anthropogenic originated dust (i.e. from building sites) can be re-suspended by both human activities and natural events, sharing an exchangeable fate for residence time and size segregation paths in the planetary boundary layer (Korcz et al., 2009).

Large uncertainties or lacks in emission inventories exist (EMEP, 2010), which concern different fugitive dust contributions. The wind-blown surface soil holds particular interest, especially if it is profiled at local (regional or intra–regional) level. Indeed, intra-regional variability in the chemical and mineral composition of surface soils is generally more evident than what is concerned for road dust and building materials, the latter usually showing minor site-oriented differences in the source fingerprint.

Finer fractions of particulate matter from surface soils are easily re-suspended by local winds and may contribute to the respirable fraction of PM (Rodriguez et al., 2009). It is also reasonable to expect that this contribution affects the total PM mass more frequently than dust outbreaks from the Saharan region. In Rome (Italy), between 2003 and 2008 only 8 to 30% of exceedances to PM10 limit value could be ascribed to desert dust outbreaks.

To our knowledge, so far no source profiles have been published of the respirable PM fraction re-suspended from wind-blown local soils neither of Italy nor of other European countries.

In this work, we present the chemical and mineralogical profile of the respirable fraction of re-suspended surface soil in the Southern area of Rome. Overall 12 bulk samples of surface rock were collected at locations were the geological lithosomes of this area emerge from soil (Giordano et al., 2006). After sieving up to 50µm size, the dust was re-suspended in a proper box under controlled conditions and the PM_{10} fraction was collected on Teflon filter membranes by low-volume sampling. Bulk elemental analysis of the 50µm size dust and of the PM_{10} samples was performed by EDS-XRF. XRD analysis was performed on the 50µm size dust to obtain the mineralogical composition of samples, after assessment that the 50µm size and the PM_{10} fractions are comparable in terms of elemental composition (fig. 1).

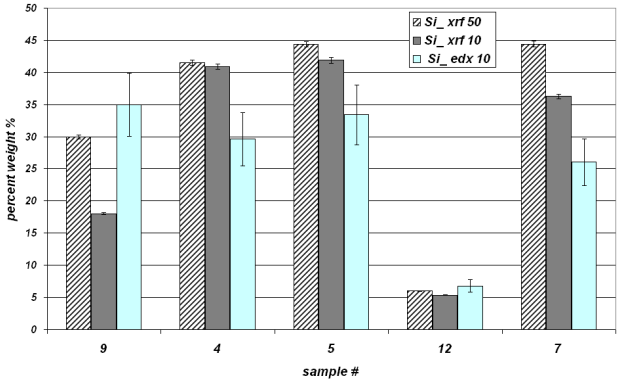

Figure 1. Inter-technique (SEM/EDX vs XRF) assessment of comparability between the 50µm size and the PM10 fraction of surface rock samples. Here results for Si are reported for some of the collected samples.

Moreover, about 500 single particles per-sample were analysed for morphology and chemical composition by SEM/EDX microanalysis. Results of single particle analysis were finally matched with the database of the RRUFF Project (Downs, 2006) and/or the database of the GEOROC Project (Sarbas et al.). Statistical matching of particle spectra with the elemental composition of minerals obtained from 'reference' databases was performed by sequential PCA (Espinosa et al., 2004) and SLR. Finally, particles identified with known minerals were characterised for size segregation in the PM_{10} fraction after estimation of their aerodynamic diameter.

Downs, R.T. (2006), *Program and Abstracts of the 19th General Meeting of the International Mineralogical Association in Kobe, Japan. O03-1.* Available at: http://rruff.info/

EMEP (2010), *Joint Report CCC & MSC-W* ISSN 1504-

Espinosa, A.J.F., Rodriguez, M.T., Alvarez, F.F. (2004), *Atm. Env.* **38**, 873-886

Giordano, G., De Benedetti, A.A., Diana, A., *et al.* (2006), *J. Volcanol. Geotherm. Res.* **155**, 49-80

Korcz, M., Fudala,., Klis, C. (2009), *Atm. Env.* **43**, 1410-

Rodriguez, I., Galì, S., Marcos, C. (2009), *Environ. Geol.* **56**, 1551-1561

Sarbas, B., Nohl, U., et al. Available at : http://georoc.mpch-mainz.gwdg.de/georoc/Entry.html

Friday, September 9, 2011

Session 12B: Optical Properties

Dust optical, chemical and radiative properties from the DODO and Fennec aircraft campaigns

C.L. Ryder[1], E.J. Highwood[1], P. Formenti[2] and H.Brindley[3]

[1]Department of Meteorology, University of Reading, Reading, Berkshire, RG6 6BB, UK
[2]LISA, CNRS, Université Paris 12, Créteil, 90410, France
[3]Department of Physics, Imperial College London, Prince Consort Road, London, SW7 2BW, UK
Keywords: Saharan dust, optical properties, radiative properties, field measurement, chemical composition, satellites
Presenting author email: c.l.ryder@reading.ac.uk

There is much uncertainty in the magnitude and sign of the radiative effect of mineral dust. A large part of this uncertainty stems from uncertainties in the refractive index of dust, which controls the proportioning of scattering and absorption of light. Aircraft and satellite measurements are presented here in order to refine the uncertainty in the refractive index.

A synthesis of aircraft measurements will be presented: firstly from the DODO (Dust Outflow and Deposition to the Ocean) experiments (McConnell *et al*., 2008) which took place over Western Africa during February and August 2006, and secondly new measurements which will be taken during the upcoming Fennec campaign over the central western Sahara during April and June 2011, providing data from locations within the Sahara that have previously been unsampled by scientific aircraft.

Results from DODO focus on calculations of the refractive index mineral dust. Here, a synthesis of optical, chemical and physical in-situ aircraft measurements are used to calculate the refractive index mineral dust encountered over West Africa. Radiative transfer studies are able to validate refractive indices obtained from chemical and optical approaches (McConnell *et al.*, 2010), and also allow comparisons and validations of satellite retrievals (Ryder *et al.*, manuscript in preparation).

Radiative transfer modeling and measurements of broadband shortwave irradiance at a range of altitudes are used to test and validate these calculations for a specific dust event on 23 August 2006 over Mauritania. Two techniques are used to determine the refractive index: firstly a method combining measurements of scattering, absorption, size distributions and Mie code simulations, and secondly a method using composition measured on filter samples to apportion the content of externally mixed quartz, calcite and iron oxide-clay aggregates, where the iron oxide is represented by either hematite or goethite and clay by either illite or kaolinite.

The imaginary part of the refractive index at 550nm (n_i^{550}) is found to range between 0.0001i to 0.0046i, and where filter samples are available, agreement between methods is found depending on mineral combination assumed. The refractive indices are also found to agree well with AERONET data where comparisons are possible. n_i^{550} is found to vary with dust source, which is investigated with the NAME model for each case. The relationship between both size distribution and n_i^{550} on the accumulation mode single scattering albedo at 550nm (ω_0^{550}) are examined and size distribution is found to have no correlation to ω_0^{550}, while n_i^{550} shows a strong linear relationship with ω_0^{550}.

Radiative transfer modeling indicates that Mie-derived values of n_i^{550} and the goethite-kaolinite combination resulted in the best agreement with irradiance measurements, for the particular dust event examined. The radiative effect of the dust is found to be very sensitive to the mineral combination (and hence refractive index) assumed.

For a dust event on 22 August 2006, satellite (Seviri and GERB) retrievals of aerosol optical depth, fluxes and radiances are compared to aircraft radiation measurements and modelled radiances and fluxes using measured optical properties in three different radiation models. Satellite retrievals and models show mostly good agreement, though discrepancies at certain wavelengths point towards errors due to a lack of coarse mode in Seviri retrievals.

Finally an overview of the optical and physical properties of dust measured during the Fennec campaign in April and June 2011 will be presented. Results will provide new information on the optical properties of dust in regions of the Sahara that were previously unsampled, and information on size distribution of dust in the centre of the Saharan heat low.

McConnell, C. L., Highwood, E.J., Coe, H., Formenti, P., Anderson, B., Osborne, S., Nava, S., Desboeufs, K., Chen, G. and Harrison, M.A.J. (2008) *Seasonal variations of the physical and optical characteristics of Saharan dust: Results from the Dust Outflow and Deposition to the Ocean (DODO) experiment*, J. Geophys. Res., **113**, D14S05, doi:10.1029/2007JD009606.

McConnell, C. L., Formenti, P., Highwood, E.J., and Harrison, M.A.J. (2010) *Using aircraft measurements to determine the refractive index of Saharan dust during the DODO experiments*, Atmos. Chem. Phys., **10**, 3081–3098.

Ryder, C.L., Brindley, H. and Highwood, E., *Comparison of Seviri and GERB retrievals to aircraft measurements in dusty atmospheres*, manuscript in preparation.

Optics of semi-externally mixed polluted mineral dust

S. N. Tripathi[1], S.K. Mishra[2], S. G. Aggarwal[2], and A. Arola[3]

[1]Department of Civil Engineering, Indian Institute of Technology, Kanpur, 208016, India
[2]National Physical Laboratory, Council of Scientific and Industrial Research, New Delhi, 110012, India
[3]Finnish Meteorological Institute, Kuopio, 70211, Finland
Keywords: semi-external, carbonaceous, mineral dust, hematite, shape.
Presenting author email: snt@iitk.ac.in

The radiative forcing estimation of the polluted mineral dust is limited due to lack of knowledge on morphology, mixing state with the carbonaceous components and the hematite content in the pure dust (Forster et al., 2007). The accumulation mode mineral dust has been found to mix with anthropogenically produced black carbon, organic carbon and brown carbon during long range transport.

The above features of the polluted dust are not well accounted for in the optical models and lead the uncertainty in the numerical estimation of their radiative impact. The Semi-external mixing being a prominent mixing of dust and carbonaceous components has not been studied in detail.

In present study, we consider the pure mineral dust composed of non-metallic components (such as Quartz, Feldspar, Mica and Calcite) and metalic component such as hematite, Fe_2O_3 (Mishra and Tripathi, 2008). The hematite percentage in the pure mineral dust governs its absorbance. Based on this hematite variation, the hematite fraction in pure mineral dust has been constrained between 0–8%. The morphological and mineralogical characterization of the polluted dust (Alexander et al., 2008) led to consider the three sphere, two sphere and two spheroid model shapes for polluted dust particle system (Figure1). The pollution gives rise to various light absorbing aerosol components such as black carbon (BC), brown carbon (BrC) and organic carbon (comprising of HUmic-Like Substances, HULIS, OC) in the atmosphere. These model shapes have been considered for the mineral dust getting polluted with (1) organic carbon (especially HULIS component) (2) Brown carbon and (3) black carbon by making a semi-external mixture with pure mineral dust.

The optical properties (e.g. Single Scattering Albedo, SSA; Asymmetry parameter, *g* and Extinction efficiency, Qext) of above model shapes for the polluted dust have been computed using Discrete Dipole Approximation, DDA code. The SSA was found to vary depending on hematite content (0–8%) and model shape composition. For the two sphere BC-mineral dust cluster, hematite was found to be dominating absorber compared to that of black carbon as the ratio of black carbon radius to dust radius, R_{BC}/R_{dust}, decreases. The two spheroid system composed of organic carbon and dust with 0% hematite (OCD'-0) showed the maximum deviation of SSA (i.e. ~5%) compared to the two sphere system of same composition and hematite content (OCD-0). SSA was found to be more sensitive to hematite content than that of particle shape. Compared to SSA, *g* was found to be more sensitive towards particle shape. For three-sphere model shapes with 0% hematite composed of black carbon-dust-dust (BCDD-0), brown carbon-dust-dust (BrCDD-0) and organic carbon-dust-dust (OCDD-0), the deviation of SSA and *g* relative to conjugate BC, BrC and OC spheres are ~68% and ~31%, ~83% and ~31% and ~70% and ~33%, respectively. The modeled polluted dust optics will provide a better basis for radiative forcing estimation and many sensitivity studies.

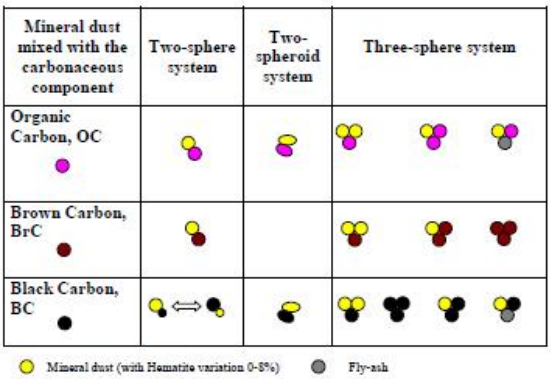

Figure 1. The pure mineral dust (yellow sphere) mixed with the carbonaceous components namely, OC, BrC, and BC are shown as pink, dark tan, and black spheres, respectively (First column, top to bottom). Semi-externally mixed polluted mineral dust two-sphere and two spheroid model shapes comprising of mineral dust with OC, BrC and BC, respectively are shown in second and third column, top to bottom. BrC-mineral dust two spheroid model shape has not been modeled as BrC occurs in spherical form. The three sphere model shape of mineral dust with OC, BrC and BC, respectively are shown in fourth column, top to bottom. Some of the three sphere systems were modeled with fly-ash (shown with grey sphere) based on the experimental observations.

This work was supported by the grants from ISRO MT, GBP and DST ICRP programs.

Alexander, D. T. L., Crozier, P. A., and Anderson, J. R. (2008) *Science* **321**, 833–836.

Forster, P. et al. (2007), *Fourth Assessment Report of the Intergovernmental Panel on Climate Change*, Cambridge Univ. Press, 825 Cambridge, New York.

Mishra, S. K. and Tripathi, S. N. (2008) *J. Geoph. Res.* **113**, 1-19.

Reconstruction of aerosol extinction from visibility and aerosol mass concentration in Budapest, Hungary

A. Molnár[1], D. Párkányi[2], K. Imre[2] and V. Gácser[2]

[1]Air Chemistry Group of Hungarian Academy of Sciences, University of Pannonia, Veszprém, P.O. Box 158, H-8201, Hungary
[2]Department of Earth and Environmental Sciences, University of Pannonia, Veszprém, P.O. Box 158, H-8201, Hungary
Keywords: aerosol composition, extinction coefficient, PM10, urban aerosol.
Presenting author email: amolnar@almos.uni-pannon.hu

The aim of this work is to present the results obtained in a closure experiment, in which the aerosol extinction coefficient is estimated and reconstructed. On one hand, the extinction coefficient is estimated from visibility data by using the Koschmieder theory. On the other hand, applying similar approach to the method of IMPROVE network (e.g. DeBell et al., 2006) the aerosol extinction is reconstructed on the basis of aerosol chemical composition.

Visibility and aerosol data summarized in this work were collected in two sampling campaigns between 2nd February, 2009 and 2nd March, 2009; and between 20th July 2009 and 20th August 2009. In these campaigns beside visibility measurements parallel aerosol samples were collected at Marczell György Observatory of the Hungarian Meteorological Service in Budapest, Hungary.

Visibility (visual observation) and PM10 mass concentration (β-gauge measurements) were available on hourly basis. Parallel daily aerosol sampling was also carried out in order to measure the chemical composition of PM10. From these samples inorganic ions (chloride, sulfate, nitrate, ammonium and sodium), total carbon and the light absorbing carbon contents were determined by means of ion chromatography, total carbon measurements (Astro Model 2100 TOC) and PSAP, respectively.

Form visibility data the extinction coefficient is derived by the Koschmieder formula. The extinction coefficient referring to dry air was estimated by applying the γ-approach. A significant, linear correlation is found between PM_{10} mass concentration and the dry extinction coefficient (Fig.1).

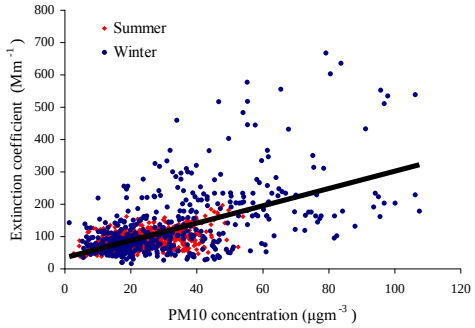

Figure 1. Dry extinction coefficient derived from visibility as the function of PM10.

On the other hand, considering the aerosol chemical composition the mass concentration of PM_{10} aerosol is reconstructed. The reconstructed and the directly measured PM_{10} mass concentrations agreed well in both sampling campaigns.

By means of multiple linear regression, the relationship between the aerosol chemical composition and the measured extinction coefficient is also studied. Our results show that the extinction coefficient (the scattering coefficient) can be effectively estimated from the chemical composition of the PM10 (Fig 2).

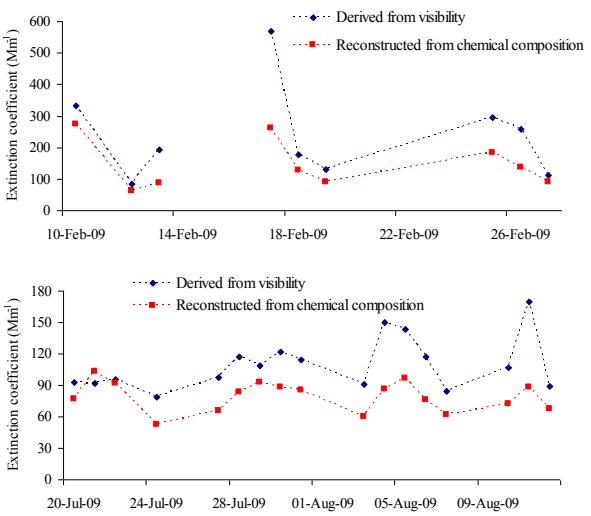

Figure 2a and 2b. Variation of the extinction coefficient derived from visibility and reconstructed from aerosol chemical composition in winter (a) and summer (b) campaigns.

DeBell, L.J., Gebhart, K.A., Hand, J.L., Malm, W.C., Pitchford, M.L., Schichtel, B.A, White, W.H. (2006) *IMPROVE (Interagency Monitoring of Protected Visual Environments): Spatial and Seasonal Patterns and Temporal Variability of Haze and its Constituents in the United States.* Report IV CIRA Report ISSN: 0737-5352-74, Colorado State Univ., Fort Collins.

Wavelength dependent Angström exponent based source apportionment and its correlation with aerosol size distribution

T. Ajtai[1], M. Schnaiter[2], C. Linke[2], Á. Filep[1], N. Utry[1], Z. Bozóki[3], G. Szabó[1]
[1]Department of Optics and Quantum Electronics, University of Szeged, Hungary
[2]Institute of Meteorology and Climate Research, Forschungszentrum, Karlsruhe, Germany
[3]Research Group on Laser Physics of the Hungarian Academy of Science, University of Szeged, Hungary

Keywords: source apportionment, photoacoustic, optical absorption, Angström exponent.
ajtai@titan.physx.u-szeged.hu

Due to its strong influence on the climate and its adverse health effects, in-situ characterisation of light absorbing carbonaceous matter (LAC) is in the middle of scientific interest today. LAC is a mixture of graphite-like particles and light-absorbing organic matter having various sources. Due to the fact that the absorption spectra of LAC are characteristic for its constituents, its measurement can be a valuable tool for in-situ source apportionment (Andreae and Gelencsér, 2005). Despite of their importance, the absorption features of the LAC are very poorly characterised, especially in case of the recently discovered organic fraction, the so called brown carbon (BrC). This uncertainty stems from both the lack of reliable instrumentation and also from the chemical complexity of BrC, which causes high variations in its optical properties (Andreae and Gelencsér, 2005). The LAC has rather featureless optical absorption, which however has a sharp and characteristic increase toward the shorter wavelengths. Therefore the light absorption by LAC become more characteristic in the UV wavelength region and the efficiency of the source apportionment could be increased by multi-wavelength measurements including wavelengths in UV (Hoffer et al, 2005, Andreae and Gelencsér, 2006). The only method that can be used to measure light absorption by aerosols in-situ is photoacoustic spectroscopy (Meinrat O. Andreae, 2001), but most of the available photoacoustic instruments operate only at one wavelength.

In this work we focus on in-situ source apportionment based on the optical absorption of LAC measured by our novel multi-wavelength photoacoustic instrument (4λ-PAS). The 4λ-PAS operating at four wavelengths (1064nm, 532nm, 355nm and 266nm) and apply wavelength independent non-site specific calibration, therefore it provides a unique and novel possibility of source apportionment based on the absorption measurement. Several physical and chemical properties of the ambient were also measured during the presented experiments, in order to further support the interpretation of the results and to reveal the correlation between the measured quantities. The reported experiments were made under different field conditions at different sites.

We will demonstrate that the reliability of the source apportionment by optical absorption measurement can be increased by using UV wavelengths too and that the wavelength variation of the fitted Angström exponent is also characteristic for the components of LAC. By comparing absorption and size distribution based source apportionments, a correlation between these approaches were found (Fig.1.) Correlations between the observed variations in the optical absorption spectra and the variations in NO_x and CO concentrations also confirm that the residential heating and the traffic are the main sources of the seasonal and diurnal variation in the Angström exponent.

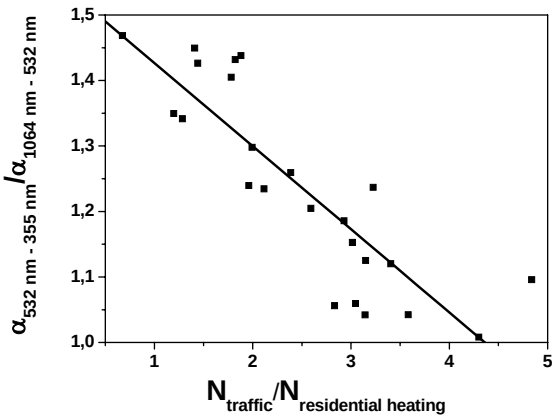

Figure 1. The ratio of the Angström exponents (α) in the short (532nm-355nm) to the long (1064nm-532nm) wavelength range as the function of the ratio of aerosol number concentrations (N) in the CMD = 20 nm ("traffic aerosols") to the CMD = 120 nm ("residential heating") mode.

Andreae, M.O., Gelencsér, A., (2006). Black carbon or brown carbon? The nature of light-absorbing carbonaceous aerosols, Atmos. Chem. Phys. 6, 3131–3148

Hoffer, A., Gelencsér, A., Guyon, P., Kiss, G., Schmid, O., Frank, G., Artaxo, P., and Andreae, M. O. (2005): Optical properties of humiclike substances (HULIS) in biomass-burning aerosols, Atmos.Chem. Phys. Discuss., 5, 7341–7360, 2005, http://www.atmos-chem-phys-discuss.net/5/7341/2005/.

Meinrat O. Andreae, (2001) The dark side of the aerosols, Nature 409, 671-672

Retrieving aerosol size distribution using wavelength dependence of aerosol optical depths

Sumita Kedia* and S. Ramachandran
Physical Research Laboratory, Ahmedabad, India
Keywords: Aerosol measurement, Aerosol optical depth, size distirbution, Ångström exponent
Presenting author email: sumita@prl.res.in

Atmospheric aerosols exhibit large variability in their size distribution depending on their source regions, production mechanism and mixing processes in the atmosphere. Aerosol size distribution is an important parameter, which strongly influences the radiative properties of aerosols such as phase function and spectral scattering. The spectral variation in aerosol optical depth (AOD) can be represented by Ångström exponent (α), obtained from Ångström power law given by

$$\tau = \beta \lambda^{-\alpha} \quad (1)$$

where τ is the AOD at wavelength λ, and β is the turbidity coefficient. α is the slope of ln τ versus ln λ data and it depends on the ratio of concentration of fine and coarse mode aerosols in the atmosphere. Higher α value signifies an increase in the concentration of fine mode particles whereas a lower a indicates an abundance of coarse mode aerosols. The fine mode aerosols are mainly attributed to the particles produced by fossil fuel/biomass burning and/or gas-to-particle conversion mechanism (anthropogenic sources), while coarse mode aerosols correspond to mechanically generated aerosols such as sea salt and mineral dust (natural sources).

Ångström power law is well suited for the short spectral bands, but when the spectral range is extended and the aerosol size distribution becomes multimodal, departure from the linear behavior of power law is observed. The departure from linearity of ln τ versus ln λ data is a function of aerosol size distribution. In such conditions, a curvature is observed in the aerosol optical depth spectra which contain useful information about the aerosol size distribution.

In the present study we have examined the spectral dependence of AODs, their spatial and temporal variability over two contrasting environments in western India, namely Ahmedabad and Gurushikhar (Figure 1) using ground based measurements. Ahmedabad is a semiarid, industrialized, urban location with several small and large scale industries. The city has a population of $\sim$5.8 million and is located in the southeast direction of the Thar desert. Gurushikhar is a relatively pristine site at an altitude of about 1.7 km with a population of $\sim$50000 and is $\sim$300 km northeast of the Thar desert. The site is situated at the highest peak of Aravalli range of mountains in western India with a cleaner and stable atmosphere [Kedia and Ramachandran, 2011].

Measurements of AODs at five different wavelength bands centered around (0.4, 0.5, 0.65, 0.75, and 0.875 μm) were conducted using a hand held sunphotometer over both the study location during October 2006 - December 2008. AODs over Ahmedabad are more than two times higher than Gurushikhar at all the wavelengths indicating higher aerosol loading over Ahmedabad throughout the study period.

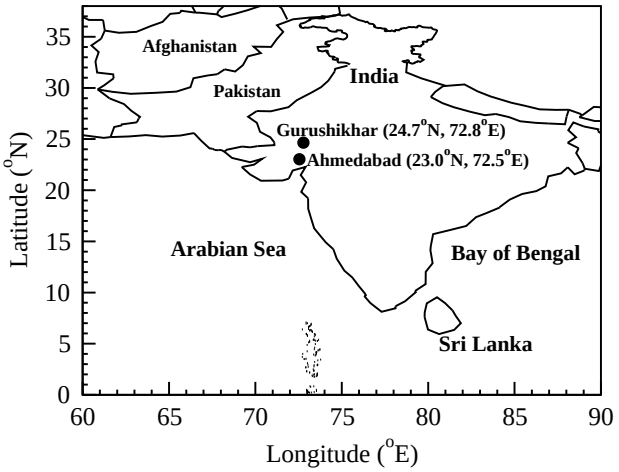

Figure 1: The study locations Ahmedabad and Gurushikhar are marked on India map.

α is higher over Ahmedabad than Gurushikhar suggesting higher fine mode aerosol concentration over Ahmedabad. A polynomial fit to the ln τ versus ln λ showed the presence of changing dominant aerosol types as a function of season over both the locations. The coefficients of polynomial fit are used to get confirmation on the dominant aerosol mode over the study locations as a function of seasons. About 87% and 78% of AOD spectra are found to be dominated by wide range of fine mode fractions or mixture of modes during winter over Ahmedabad and Gurushikhar respectively. During premonsoon >80% of AOD spectra are found to be dominated by coarse mode aerosols over both the locations. During monsoon $\sim$70% of AOD spectra are coarse mode dominant over Ahmedabad. In postmonsoon <40% of AOD spectra are dominated by coarse mode aerosols over both the locations. This characterization of aerosols is important in assessing the response of different aerosol types on radiative forcing and regional climate.

Details on the methodology adopted and results obtained on the curvatures in AOD spectral distribution will be presented and discussed.

Kedia, S, and S. Ramachandran (2011), Atmospheric Environment, In press.

Effects of relative humidity on aerosol light scattering: Results from different European sites

P. Zieger, R. Fierz-Schmidhauser, E. Weingartner, and U. Baltensperger
Paul Scherrer Institut, Laboratory of Atmospheric Chemistry, 5232 Villigen, Switzerland

Keywords: Light scattering, Relative humidity, Hygroscopic growth, Field measurements, Nephelometer
Presenting author email: paul.zieger@psi.ch

Atmospheric aerosol particles change in size due to water uptake which is determined by their chemical composition and the ambient relative humidity (RH). As a result also their optical properties - especially the aerosol light scattering - strongly depend on RH. Therefore, long-term measurements of aerosol physical and optical properties are generally recommended at dry conditions in order to keep measurements comparable (e.g. RH < 30 - 40% as recommended by (WMO 2003)). However, for the comparison of such ground-based measurements with other optical aerosol measurements (e.g. lidar, MAX-DOAS or satellite retrieval), for the purpose of aerosol correction of satellite retrievals, or for the use in climate models, accurate knowledge of the RH effect is very important.

The key parameter to describe the influence of RH on the aerosol light scattering is the scattering enhancement factor $f(\lambda,RH)$, which defined as the scattering coefficient $\sigma_{sca}(\lambda,RH)$ at a certain RH divided by the dry scattering coefficient $\sigma_{sca}(\lambda,RH=dry)$:

$$f(\lambda, RH) = \frac{\sigma_{sca}(\lambda, RH)}{\sigma_{sca}(\lambda, RH = dry)},$$

where λ denotes the wavelength.

Here, we will present measurement and modeling results of the aerosol scattering enhancement, which are based on our field experiments using a new developed humidified nephelometer (Fierz-Schmidhauser et al. 2010c). Results will be shown for aerosol found at the high alpine site Jungfraujoch (Fierz-Schmidhauser et al. 2010a), for Arctic aerosol measured at Ny-Ålesund, Spitsbergen (Zieger et al. 2010a), for maritime aerosol measured at Mace Head, Ireland (Fierz-Schmidhauser et al. 2010b), and for aerosol typically found at Cabauw, the Netherlands (Zieger et al. 2010b). The latter one was performed from June to October 2009 and was part of the GEOmon initiated Cabauw Intercomparison Campaign of Nitrogen Dioxide measuring Instruments (CINDI). Here, our measurements allowed the determination of the extinction coefficient at ambient RH, which was com-pared to several MAX-DOAS and LIDAR measurements also performed at Cabauw in that period.

Figure 1 shows back trajectories color coded with the scattering enhancement measured at the time of the air parcel arriving at the station (here for the three field campaigns carried out at Jungfraujoch, Ny-Ålesund, and Cabauw during 2008 and 2009). Depending on the aerosol type (origin) the *f*(RH) (here shown at 85% RH and for λ=550nm as an example) varied between approx. 1.3 and 6.6.

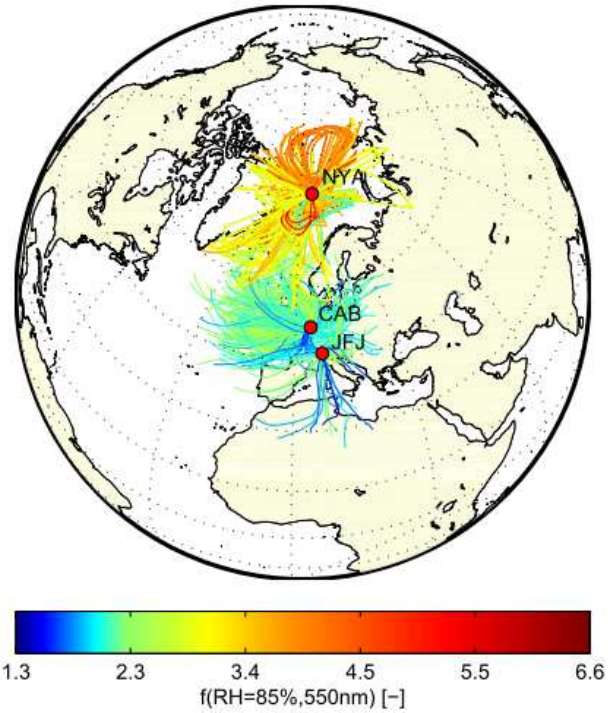

Figure 1: Back trajectories (48 h backward calculations) for the investigated sites: Jungfraujoch (JFJ), Ny-Ålesund (NYA), and Cabauw (CAB). The trajectories are color coded with the mean scattering enhancement *f*(RH=85%,550nm) measured at the site.

Fierz-Schmidhauser, R., *et al.* (2010a), *Atmos. Chem. Phys.* **10**(5): 2319-2333.
Fierz-Schmidhauser, R., *et al.* (2010b), *J. Geophys Res.* **115**, 1-11.
Fierz-Schmidhauser, R., *et al.* (2010c) *Atmos. Meas. Tech.* 3(1): 39-50.
WMO (2003), *WMO/GAW Aerosol Measurement Procedures Guidelines and Recommendations*, GAW Report No. 153, World Meteorological Organization, Geneva.
Zieger, P., *et al.* (2010a). *Atmos. Chem. Phys.* **10**(8): 3875-3890.
Zieger, P., *et al.* (2010b). *Atmos. Chem. Phys. Discuss.* **10**(12): 29683-29734.

Aerosol optical properties in Amazonia - Spatial and seasonal variability

K.T. Wiedemann[1], P. Artaxo[1], A. Correia[1], S.C. Wofsy[2], M.O. Andreae[3] and C. Gerbig[4]
[1]Institute of Physics, University of Sao Paulo, Sao Paulo, Brazil
[2]School of Engineering and Applied Sciences, Harvard University, Cambridge, USA
[3]Biogeochemical Department, Max Planck Institut of Chemistry, Mainz, Germany
[4]Department of Biogeochemical Systems, Max Planck Institut of Biogeochemistry, Jena, Germany
Keywords: Airborne particles, light absorption, light scattering, optical depth.
Presenting author email: kenia@if.usp.br

Reducing the uncertainty in estimates of the impact of aerosol on climate remains at the center of interest in the climate changes discussion. The Amazon Basin is one of the most crucial regions in the world where these effects may be studied from many points of view. In particular, it is important to identify and to quantify the processes and sources that control the regional aerosol concentrations, in order to obtain a reliable quantification of their global impacts. We expect that a better understanding - and modelling - of these processes and sources may provide a better understanding of the feedbacks between climate and aerosol concentrations.

As a part of the LBA/BARCA experiment, an airborne campaign was conducted, using the two engine INPE aircraft (National Institute for Space Research), from 16 November to 2 December, 2008, corresponding to the transition period from dry to wet season in Amazon Basin. The flight legs are shown in the Figure 1, where the main cities are indicated. The aircraft was instrumented for collecting data on aerosol spatial distribution/concentration and size distribution and, in addition, measurements of trace-gases including O_3, CH_4, CO, CO_2 and N_2O were also performed. Sixty-eight profiles were obtained up to 4 km, covering an important part of the Amazon Basin. Total aerosol number concentration was measured at 1 Hz time resolution using a TSI 3010 Condensation Particle Counter model. A Thermo Multi Angle Absorption Photometer model 5012, operating at 637 nm, was used for measurements on aerosol light absorption, and for optical scattering by atmospheric particles, the aircraft was equipped with a three wavelength (450, 550, and 700 nm) TSI 3665 nephelometer. Aerosol number size distributions were measured with a TSI SMPS 3080 for particles ranging 10–354 nm.

This work presents the spatial distribution of the aerosol optical properties in Amazonia during the transition between dry and wet season, when the aerosol population is strongly influenced by biomass burning emissions (Figure 2). The Amazon Basin is a region of intense convective activity, and the spatial and temporal description of the optical properties of these particles supports the assessment of the impact of changes in the regional land use, not only on the regional climate, but also at the global scale.

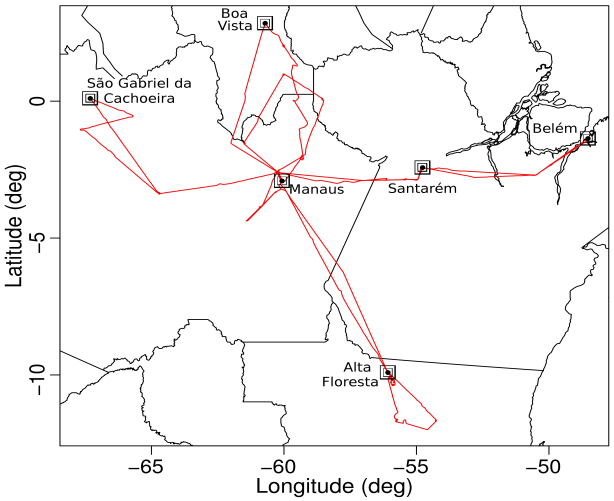

Figure 1: Mapping of the flight tracks during the BARCA-A airborne campaign, covering an important part of the Amazon basin during the dry season.

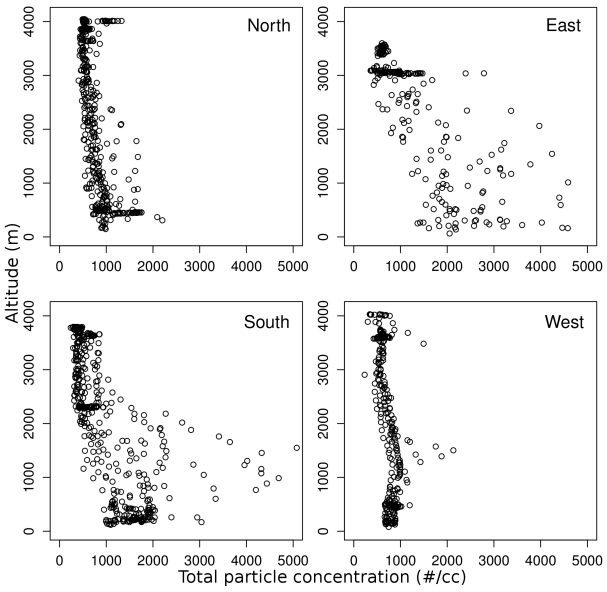

Figure 2: Total aerosol concentration vertical profiles for the northern, eastern, southern and western sectors of Amazonia during the transition from dry to wet season, November 2008. The aerosol population is strongly influenced by biomass emissions.

Friday, September 9, 2011

Session 12C: Engine-related Aerosols

Characterization of particles emitted from a marine diesel engine: Influence of sampling temperature on measured particle number, size, and morphology

[1]Fuglsang, K., [2]Dirscherl, K., Lykkegaard, M.K. [3], Markussen J.B. [1], Hemmersam, A. [3], Popovicheva, O. [4], Kireeva, E. [4], Poulsen, M. [3] and Larsson, D.[5]
[1] FORCE Technology, Park Alle 345, Brøndby, , Denmark; [2] Danish Institute of Metrology, 307 Matematiktorvet, Lyngby, Denmark; [3] Teknologisk Institut, Kongsvang Allé 29, Århus, Denmark; [4]Institute of Nuclear Physics, Moscow State University, Moscow, Russia; [5] MAN Diesel & Turbo, Teglholmsgade 41, Copenhagen, Denmark

Keywords: Combustion aerosols, ship emissions, particle number, semi-volatiles.
Presenting author email: kfu@force.dk

Introduction

Particle emissions from diesel engines are traditionally regulated according to the emitted particle mass. EU emission standards will from 2015 also include standards for the emitted number of particles from land-based diesel vehicles. An increasing focus is turned towards emissions from marine diesel engines. Compliance measurement systems for particle number emissions have been recommended for on-road diesel vehicles (Anderson *et al.*, 2010). The recommended systems include a sampling system involving thermo-evaporation in order to remove volatile material before measuring the total particle number. In this study, the effect of thermo-evaporation on the measured particle number, size and on the morphology of the particles emitted from a ship engine was investigated. The engine studied was a 7 MW MAN two-stroke marine engine, and the fuel used was gasoil containing 0.002% sulfur.

Methodology

The particle number concentration in the engine exhaust at 50% engine load was measured by an ELPI (Electrical Low Pressure Impactor). The sampling system included dual ejector diluters. The temperature of the first diluter was increased in steps from 150 °C to 450 °C. Size distributions were studied by SMPS (Scanning Mobility Particle Sizer). Impactor samples collected at 150 °C and 350 °C were examined by AFM (Atomic Force Microscopy) and SEM (Scanning Electron Microscopy).

Results and conclusions

The results for particle numbers measured during increasing sample temperature are shown in figure 1.

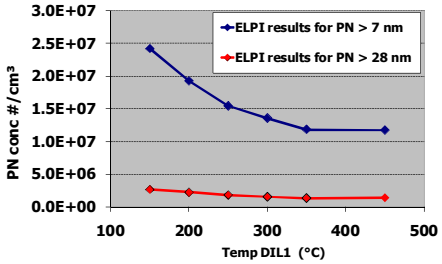

Figure 1. Number of particles from a marine diesel engine, measured by ELPI during increasing sample temperature.

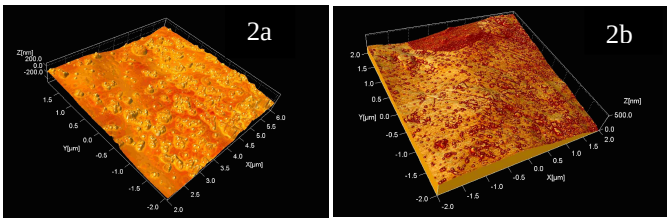

Figure 2. AFM image of particles sampled at 150 °C (2a) and at 350 °C (2b).

Figure 2a and 2b shows the results of the AFM analysis for particles collected during periods with sample heating to 150 °C and 350 °C, respectively. In figure 2, the color shading superimposed on the topography shows the local phase signal measured by the AFM. A change in color contrast, representing a change in the phase, is typically caused by variations in the material properties such as viscoelasticity, friction or hardness. In figure 2a, contrast variations can be observed within each particle, indicating that the particles consist of materials with different properties. In figure 2b, the contrasts are less distinct. The phase signal is more uniform within the individual particles, indicating that the majority of particles sampled at 350 °C have less varying material properties. The more homogenous particle material at 350 °C can be explained by the effect of thermo-evaporation, i.e. residuals of un-combusted hydrocarbons (e.g. fuel and lubrication oil) have evaporated from the particles. Likewise, small, condensed oil droplets will evaporate rapidly at 350 °C, and this explains the reduced particle numbers at increasing temperatures in figure 1. The results show that it is important to control the sampling temperature when sampling particles from marine diesel engines. As for land-based diesel engine test protocols, the results presented here indicate that test procedures for marine diesel engines become more robust when the sampling system includes a thermo-evaporation at 350 °C.

This work was supported by the The Danish Agency for Science, Technology and Innovation and MAN Diesel & Turbo.

Anderson, J. et al. (2010). Particle Measurement Proggramme (PMP). Heavy-duty Inter-laboratory Correlation Exercise (ILCE_HD) Final Report.

Microphysical properties of carbonaceous particulate matter emitted by three different aircraft turbofan engines

D. Delhaye[1], D. Lottin[1], D. Ferry[2], J. Gouge[3] and O. Penanhoat[3]

[1]Department of Physics and Instrumentation, ONERA, Châtillon, 92322, France
[2]CINaM-CNRS UPR 3118, Marseille, 13288, France
[3]Emissions & Regulation R&T, SNECMA / SAFRAN Group, Moissy Cramayel, 77550, France
Keywords: aircraft engine, nanoparticle aggregates, TEM, size distribution.
Presenting author email: david.delhaye@onera.fr

In the framework of the global warming policy, the impact of nanoparticles emitted by aircraft engines on the environment meets an increasing interest. Indeed, these soot aggregates are directly injected in the troposphere and the low stratosphere and may lead to the formation of condensation trails, which affect the global radiative budget (Lee, 2010). They can also have a non negligible impact in airport areas and their vicinity (Puente Lelièvre, 2006).

This study focuses on the properties of soot aggregates emitted by three different civil CFM56 aircraft engines tested at Snecma and designed for short, medium and long haul flight. Soot samples are collected at the ground level by impaction on Transmission Electron Microscopy grids (Figure 1) that are located 27 m behind the engine exit (Delhaye, 2007). The sampling is performed during engine cycles that cover LTO and non LTO settings and represent what happens in the airport areas. We present the evolution of two characteristic mean sizes of soot aggregates that differ significantly from an engine to another. Indeed, our measurements lead to a soot aggregates geometric mean gyration diameter (d_g) that ranges from (52 ± 3) nm to (89 ± 4) nm between the three tested engines, whereas the geometric mean diameter of the primary particles composing the aggregates (d_p) ranges from (4.22 ± 0.06) nm to (9.9 ± 0.1) nm (Table 1). An analysis is proposed to understand in which way the evolution of these two soot characteristic sizes is correlated to some potentially relevant engine parameters. The d_g and d_p mean values determined in this work are really smaller than those of soot originating from Diesel and wood combustion (Chandler, 2007; Gwaze, 2006) and may represent an opportunity to identify aircraft soot among carbonaceous aerosols in the atmosphere.

The size and shape of soot aggregates weigh on their light diffusion properties. Any variation of these characteristics can lead to non negligible consequences on the global radiative budget. The submicrometric size of soot particles and aggregates is also of importance regarding air quality and human health since they can reach and interact with lung cells. It is then important to study their microphysical properties according to various engine settings if one want to model and understand their role in physical and chemical processes in the atmosphere as well as their impact on human health.

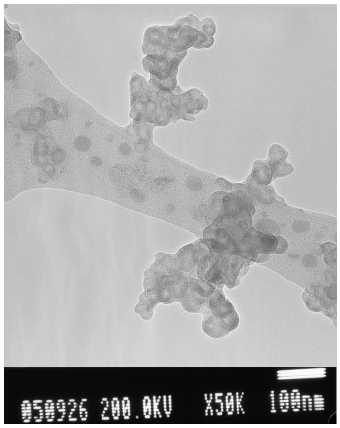

Figure 1. TEM picture of a soot aggregate sampled 27 m behind a CFM56 engine.

Characteristic sizes	d_p (nm)	d_g (nm)
CFM56-B	8.0 ± 0.2	54 ± 2
CFM56-5C	9.9 ± 0.1	89 ± 4
CFM56-7B	4.22 ± 0.06	52 ± 3
Wood (Gwaze, 2006)	25.5 ± 3.5	-
Diesel (Chandler, 2007)	20 ± 5 – 29 ± 8	156-270

Table 1. Evolution of two characteristic sizes of soot aggregates with different aircraft engines and other combustion sources.

Chandler, M.F., Teng, Y., Köylü, Ü.Ö. (2007) Proceedings of the Combustion Institute **31**, 2971-2979.

Delhaye, D. (2007) PhD Thesis, University of Aix-Marseille II.

Gwaze, P., Schmid, O., Annegarn, H.J., Andreae, M.O., Huth, J., Helas, G. (2006) Aerosol Science **37**, 820-838.

Lee, D.S., Pitari, G., Grewe, V., Gierens, K., Penner, J.E., Petzold, A., Prather, M.J., Schumann, U., Bais, A., Berntsen, T., Iachetti, D., Lim, L.L., Sausen, R. (2010) Atmospheric Environment **44**, 4678-4734.

Puente Lelièvre, C., Magnani, G., Ramaroson, R., Gouriou, F., Talbaut, M., Fréjafon, E., Shuermann, G., Shaefer, K., Cornier, I., Emeis, S., Vannier, F., Paux, E., Copalle, A., Perros, P. (2006) Air pollution XIV 261 – ISBN 1-84564-165-5, edited by J.W.S. Longhorst, University of the West England, UK & C.A. Brebbia, Wessex, Institute of Technology, UK.

The potential of biofuels in shipping for mitigating the climate impact – Results from the integrated BIOCLEAN study

A. Petzold[1], M. Righi[1], J. Hendricks[1], V. Eyring[1], P. Lauer[2], F. Fleischer[2], and U. Fritsche[3]

[1] DLR, Institut für Physik der Atmosphäre, Oberpfaffenhofen, 82234 Wessling, Germany.
[2] MAN Diesel SE, Stadtbachstr. 1, 86224 Augsburg, Germany
[3]Öko-Institut e.V., Rheinstr. 95, 64295 Darmstadt, Germany

Keywords: shipping emissions, biofuels, indirect effect, climate effect.
Presenting author email: andreas.petzold@dlr.de

The use of biofuels for stationary power generation or propulsion in shipping gains increasing importance in the framework of CO_2 reductions and the use of energy from renewable sources. The knowledge on emission characteristics of various biofuels and resulting climate impacts however is very limited.

BIOCLEAN investigated the emission of CO_2, NO_x, hydrocarbon compounds, SO_2, H_2SO_4 and particulate matter in terms of particle number, particle size, and chemical composition from medium-speed four-stroke large diesel engines for different fuel types. The tests included heavy fuel oil (HFO) with a fuel sulphur content of 2.17 weight-% (wt-%) as the fossil high-sulphur reference fuel, marine gas oil (MGO) with a fuel sulphur content of < 0.1 wt-% as a fossil low-sulphur fuel, and palm oil, soy bean oil, sunflower oil and waste edible fat as biofuels.

The simultaneous consideration of climate-active trace species like NOx, particulates and sulphur-containing particle precursors on one hand and of the most important climate-active exhaust constituent CO_2 on the other hand allowed for the investigation of trade-off effects of CO_2 emissions reduction and potentially increasing emissions of other climate-active trace constituents. Model studies using a coupled climate chemistry model for the treatment of direct and indirect aerosol effects on climate investigated the climate response in case of replacing heavy fuel oil by biofuels. The greenhouse gas emissions associated with the production and use of the biofuels were included by means of a fuel lifecycle analysis which also considered land use chances associated with the growth of energy plants for the production of biofuels.

The investigated set of biofuels demonstrated good combustion properties in the single-cylinder four-stroke test engine. No significant increase in engine degradation and corrosion was observed for biofuel use. Biofuels emission properties at 75% engine load relative to HFO are listed in Table 1.

Table 1. Emissions from biofuels relative to HFO

Property	Emission rel. to HFO
NO_x	≅ HFO
Particulate matter (mass)	10 - 15% of HFO
Particle number	2 – 3 × HFO
Particle number non-volatile	30 – 60% of HFO
Black carbon	15 - 30% of HFO
Organic matter	≥ HFO

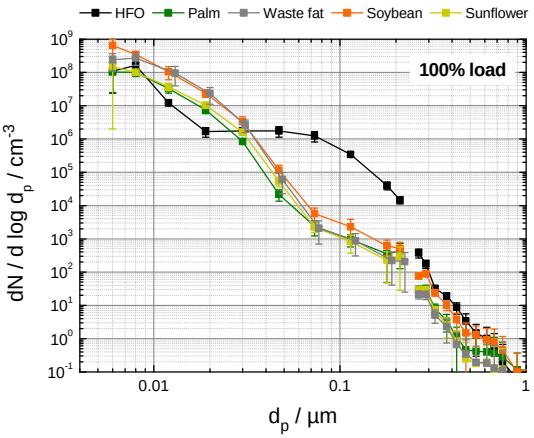

Figure 1. Number size distribution of particles emitted from a marine Diesel engine operating on different biofuels and on heavy fuel oil (HFO) as a reference case.

When using low sulphur fuels (MGO, biofuels) the emissions of particulate matter (PM) and especially sulphate and black carbon are significantly reduced compared to HFO, see Fig. 1. This effect is of similar magnitude for the low sulphur fossil fuel MGO and for biofuels. Emissions of NO_x and CO are of similar magnitude as for HFO while the emissions of gas-phase hydrocarbons are also reduced for low-sulphur fuels.

Climate effects were investigated for the hypothetical case that in 2006 all HFO is replaced by biofuels (mainly palm oil or soy bean oil), while MGO is still used in the international shipping fleet. Associated CO_2 emissions include the additional greenhouse gas emissions during the lifecycle of the biofuels. The resulting CO_2 emissions were evaluated as reduction or increase compared to the reference case of using HFO.

Direct and indirect effects of emitted particulate matter are almost exclusively associated to the sulphate content of emitted PM. Therefore, the modification of aerosol climate effects is of similar magnitude for the low sulphur fossil fuel MGO as for the investigated biofuels. For all low sulphur fuels, the direct effect is reduced by a factor of 4 to -3 mW m^{-2}. The indirect effects are reduced by a factor of 3 to -100 mW m^{-2}.

Acknowledgement: BIOCLEAN was funded by the German Bundesministerium für Bildung und Forschung under contract no. 01LS05014 and 01LS05015.

On the Influence of Biodiesel Feedstock on Diesel Particulate Emissions

Z.D. Ristovski[1], N.C. Surawski[1,2], B. Miljevic[1], S. Stevanovic[1,3], G.A. Ayoko[1], S. Elbagir[1], K.E. Fairfull-Smith[3] and S.E. Bottle[3]

[1]ILAQH, Queensland University of Technology, Brisbane QLD 4001, Australia
[2]School of Engineering Systems, Queensland University of Technology, Brisbane QLD 4001, Australia
[3]ARC Centre of Excellence for Free Radical Chemistry and Biotechnology, Queensland University of Technology, 4001 Brisbane, Australia
Keywords: Biodiesel, particle emissions, reactive oxygen species.
Presenting author email: z.ristovski@qut.edu.au

Particulate emissions from compression ignition engines are a major health concern. Clearly strategies are required to address the diesel particulate matter problem, with alternative fuels, such as biodiesel, having been recently considered to ameliorate the problem. This study considers a physico-chemical characterisation of particulate emissions from a compression ignition engine to determine the effect of using 3 biodiesel feedstocks at 4 different blend percentages.

Particulate emissions testing was performed on a naturally aspirated 4 cylinder engine with a Euro II (off-road) emissions certification. The engine was coupled to a water brake dynamometer to provide a load to the engine. In addition to ultra-low sulphur diesel (< 10 ppm sulphur), three biodiesel feedstocks; namely, soy, tallow and canola were tested at four blend percentages (20%, 40%, 60% and 80%). The opportunity also arose to test neat soy biodiesel (ie 100% soy), yielding fourteen different fuel types, all of which were tested at the intermediate speed (1400 rpm) full load (300 Nm) setting for this engine - a test mode known as rated torque.

A two-stage unheated system was used to dilute the exhaust before particulate measurement; consisting of a dilution tunnel followed thereafter by a Dekati ejector diluter. Particle number size distributions were measured with a scanning mobility particle sizer. A TSI 3550 Nanoparticle Surface Area Monitor (NSAM) was used to measure the lung deposited surface area (tracheo-bronchial) emitted by the engine. Size distributions were also measured after passing the sample through a TSI 3065 thermodenuder (set to 300 ^{o}C). Heating the particles enabled the impact of thermal treatment to be explored. A thermodenuder loss correction was performed using dried NaCl particles.

Of line chemical measurements were performed directly from the dilution tunnel. Filter sampling was performed for particle phase PAHs and XAD-2 resin was used to sample vapor phase PAHs. Reactive Oxygen Species (ROS) measurements were performed by bubbling the exhaust through impingers containing a solution of a profluorescent nitroxide probe (BPEANit) in DMSO. More details on the ROS sampling and quantification methodology can be found in Miljevic et al. (2010).

Figure 1 shows particle number size distributions for the 3 biodiesel feedstocks and 4 blend percentages. The shift to a smaller median particle diameter can also be readily observed as the blend percentage is increased, and does so in a monotonic fashion. Size distributions are also shown where the poly-disperse size distribution was passed through a thermodenuder set to 300 ^{o}C for the canola feedstock. The canola feedstock was chosen to illustrate the "volatility" of particles, as they had the highest volatile organic content, subsequently exhibiting significant evaporation in a thermodenuder.

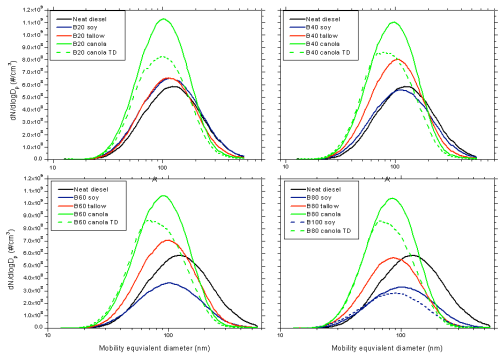

Figure 1. Particle number size distributions for various biodiesel feedstocks and blend percentages.

ROS are generally classed as "semi-volatile" organic compounds that evaporate when exposed to thermal treatment with a thermodenuder (Miljevic et al 2010). It therefore seems intuitive to seek a correlation between ROS concentrations and the volume percentage of the particle that is composed of organic material. Assuming that the organic material is volatile from the volatility measurements, we have calculated the organic (ie volatile) volume percentage of particles. In general higher ROS emissions were associated with particles that have a greater organic volume percentage. Despite one potential outlying data- point, the Pearson correlation co-efficient for this relationship is quite strong (~ 0.83).

Overall the results show that whilst significant particle mass reductions are achieved with all 3 biodiesel feedstocks, unregulated particulate emissions, such as particle number concentration and ROS concentrations are increased by some and all feedstocks, respectively.

The authors wish to acknowledge support and funding provided by SkillPro Services Pty Ltd and the Australian Coal Association Research Program for funding project C18014.

Miljevic, B., M. F. Heringa, et al. (2010). *Environ. Sci. Technol.* **44**(17), 6601-6607.

Effect of fuel injection pressure on diesel engine exhaust non-volatile particle size distribution

T. Lähde[1,2], T. Rönkkö[2], M. Happonen[2], C. Söderström[3], A. Virtanen[2], A. Solla[3], M. Kytö[3], D. Rothe[4], L. Pirjola[1] and J. Keskinen[2]
[1]Department of Technology, Metropolia University of Applied Sciences, FI-00180 Helsinki, Finland
[2]Aerosol Physics Laboratory, Tampere University of Technology, P.O. Box 599, FIN-33720, Tampere, Finland
[3]Engine Research Team, VTT Technical Research Centre of Finland, P.O. Box 1000, 02044 VTT, Finland
[4]MAN Nutzfahrzeuge AG, Abt. MTVN, Vogelweiherstrasse 33, D-90441 Nurnberg, Germany
Keywords: Diesel emissions, Nucleation mode
Presenting author email: tero.e.lahde@iki.fi

The diesel exhaust regulation focuses nowadays to accumulation mode particles. The accumulation mode dominates the regulated total particle mass and the upcoming number based non-volatile diesel exhaust particle limit is directed to accumulation mode.

The diesel exhaust particle size distribution, however, contains often two distinctive modes, the nucleation mode and the accumulation mode. The accumulation mode consists of the carbonaceous charged soot agglomerates and species accumulated on the surface of the agglomerate. Traditionally, the nucleation mode was thought to be formed in cooling dilution through vapour nucleation. Recently, however, also nucleation mode is shown to possess an electric charge and non-volatile fraction with certain engine assemblies. The formation mechanisms of the non-volatile nucleation mode are still mostly unknown; (see Lähde T. *et al*, 2011 and references therein).

The non-volatile diesel exhaust particle size distribution characteristics are studied here as a function of fuel injection pressure (FIP). FIP adjustment is an often used combustion optimization method in in-cylinder particle emission control diesel engines. FIP increase decreases the soot mode mass effectively, but the changes in the non-volatile nucleation mode (core) are still unknown.

Here the effect of fuel injection pressure change is studied for non-volatile particle size distribution.

Particle distributions were measured with two SMPS, equipped with DMA 3085 and CPC 3025 and with DMA 3081 and CPC 3776 (Tsi Inc.). Measured size range was between 3 nm and 400 nm.

Sample was diluted first with porous tube type diluter and second with ejector diluter also heated double ejector was used in the study. The particle population was "dried" with a thermodenuder designed for particles with diameter below 30 nm.

In addition to particle measurements also aerosol ion charge distribution was measured briefly. The ion distributions were measured with a DMPS without neutralizer. The DMPS was also equipped with DMA 3085 and CPC 3025 (Tsi Inc.).

The studied research engine was a 6 cylinder, 7.4 L, common-rail injection engine. The effect of fuel injection pressure on the particle population was studied with three load conditions (18%, 48% and 98%) @ 1500 min^{-1} engine speed and multiple injection pressures ranging from 60 MPa to 160 MPa. No exhaust aftertreatment was used in the measurements. The fuel sulphur content was 12.5 mg/kg.

A bimodal non-volatile size distributions were measured with medium (48 %) and high (98 %) loads, but at a low load (18 %) the distribution was unimodal, example distributions in fig. 1. At high load, also the ion distribution was bimodal resembling the particle size distribution and practically similar non-volatile size distributions were measured with two different dilution systems.

At the medium and high load the number concentration of the core mode increased with increasing FIP and simultaneously a decrease in soot mode size and concentration was detected. At medium load, also the core size changed with FIP. The core mode GSD was generally higher at medium load than at high load. The core was absent at the low load at all FIPs, although the soot mode size and concentration decreased with increasing FIP similarly to high and medium load.

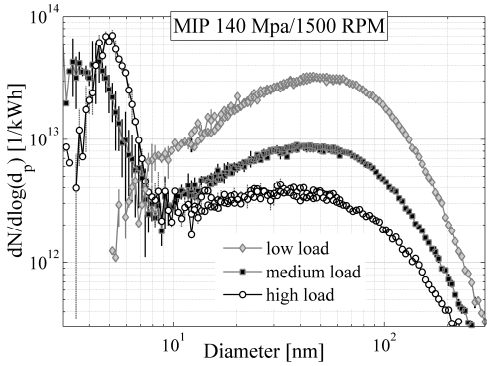

Figure 1. Non-volatile particle distributions measured with low, medium and high load. FIP=140 MPa, speed 1500 RPM

This work was supported by The Finnish Funding Agency for Technology and Innovation, the Ministry of Transport and Communications Finland, Finnish Cultural Foundation and Academy of Finland. Neste Oil Oyj, Ecocat Oy and Kemira Oyj are also acknowledged.

Lähde T. *et al.* (2011) *ES&T*, **in print**.

Exhaust particles of a light duty diesel engine equipped with an oxidative aftertreatment operating with different sulfur level fuels

P. Karjalainen[1], M. Happonen[1], T. Rönkkö[1], T. Kinnunen[2], P. Bielaczyc[3], R. Sala[3], J. Dzida[3] and J. Keskinen[1]

[1]Aerosol Physics laboratory, Department of Physics, Tampere University of Technology, P.O. Box 692, FIN-33101, Tampere, Finland
[2]Ecocat Oy, Vihtavuorentie 162, P.O. Box 20, FIN-41331, Vihtavuori, Finland
[3]BOSMAL Automotive R&D Institute, Sarni Stok 93, 43-300 Bielsko-Biala, Poland

Keywords: Diesel exhaust, Sulfur particles, Fuel, Nucleation mode, Aftertreatment, Catalyst
Presenting author email: panu.karjalainen@tut.fi

Diesel exhaust particle size distributions typically consist of two distinctive modes, often called soot and nucleation modes (Kittelson, 1998). Soot mode particles are solid carbonaceous agglomerates formed in fuel combustion process. Nucleation mode particles can be formed by gas-to-liquid processes during exhaust dilution and cooling processes or, as shown in recent studies (e.g. Rönkkö et al. 2007; Lähde et al. 2009), by the formation of non-volatile core particles at near cylinder conditions followed by particle growth during the exhaust dilution and cooling processes. Typical semi-volatile condensates and adsorbents on the particles are hydrocarbons and sulfur compounds that originate from the fuel or lubricant. The mean diameters of the soot mode and the nucleation mode typically lie around at 40–100 nm and 3–40 nm, respectively, while the size of non-volatile nucleation mode core particles is typically below 10 nm.

Conventional diesel oxidation catalysts (DOC) efficiently oxidize carbon monoxide and unburned hydrocarbons. Furthermore, they produce NO_2 which can be used in diesel particulate filter regeneration at low temperatures. In addition, in oxidizing aftertreatment devices some of the SO_2 from the engine is oxidized to SO_3 which can react with water vapour and form gaseous sulfuric acid. Sulfuric acid has been proposed to be a precursor in sulfur-driven nucleation mode formation.

We studied the effect of fuel sulfur content on diesel exhaust particle emissions in a light duty Euro 4 diesel application and the existence of the sulfur-driven nucleation mode under aerosol laboratory conditions. In the engine laboratory tests, three fuels with different sulfur contents were used: 10 ppm, 50 ppm and 350 ppm (mass contents). The fuels chosen conform to different legislation limits worldwide; S10 in EU, S50 e.g. in Hong Kong and Singapore, and S350 in India. The test engine was equipped with a partial diesel particulate filter. The aerosol laboratory tests were performed after the engine laboratory tests to find answers for some of the key observations.

The driving operation in the engine laboratory consisted of two consecutive modes: a low load point and a medium load point. The first driving mode was performed at low engine load so that the exhaust gas temperature was less than 250 °C and exhaust aftertreatment regeneration did not occur. At this load, the exhaust particle size distribution consisted of the non-volatile soot mode only. During the second driving mode, performed at medium load, volatile nucleation mode particles were observed with S50 and S350 fuels.

In the aerosol laboratory the formation of sulfur-driven nucleation by SO_2 oxidation in an oxidative aftertreatment was extensively studied. The generated nucleation mode had similar physical characteristics as in the engine laboratory study and in other studies of volatile nucleation mode particles (e.g. Lähde et al. (2009). In addition, in situations where high gas temperature followed a low temperature phase, similar trends in particle formation was observed both in the engine laboratory and in the aerosol laboratory studies. It was observed that, sulfur compounds stored at low temperature conditions in the aftertreatment device were later released at an elevated temperature and thereby affected the nucleation mode. This observation is in agreement with the studies of Giechaskiel et al (2007).

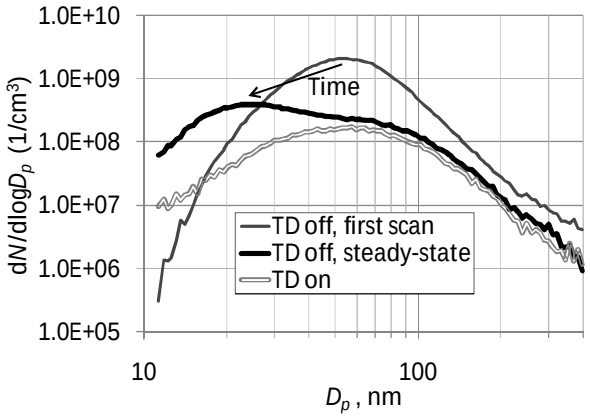

Figure 1. The non-volatile (TD (thermodenuder) on) and semi-volatile (TD off) particle size distributions during the medium load point with the S350 fuel.

Authors would like to acknowledge, about the aerosol laboratory measurements, MESTAN-project financiers Tekes, Ecocat, Dekati and Gasmet.

Giechaskiel B. et al. (2007) *SAE Technol. Pap. Ser. No.* 2007-01-1110.
Kittelson, D.B. (1998) *J. Aerosol Science*, 29, 575-588.
Lähde, T., et al. (2009) *Environ. Sci. Technol.* 43, 163-168.
Rönkkö, T. et al. (2007) *Environ. Sci. Technol.* 41, 6384-6389.

Reactive oxygen species (ROS) emissions from diesel engines running on various biofuels

S.D. Stevanovic[1, 3], B. Miljevic[1], N.C .Surawski[1, 2], S.E. Bottle[3], R. J. Brown[2] and Z.D. Ristovski[1]
[1]International Laboratory for Air Quality and Health, Queensland University of Technology, 4001, Brisbane, Australia
[2]School of Engineering Systems, Queensland University of Technology, 4001, Brisbane, Australia
[3]ARC centre of Excellence for Free Radical Chemistry and Biotechnology, Queensland University of Technology, 4001, Brisbane, Australia
Keywords: biofuels, reactive oxygen species, profluorescent nitroxide.
Presenting author email: s.stevanovic@qut.edu.au

Due to rising worldwide demand for energy and the prospect of climate change as a result of greenhouse gas emissions, there is a need to develop alternative energy sources. Therefore it is important to verify the potential of biofuels, as a renewable energy source, and to estimate the health and environmental impacts of their implementation (Gomes and Muylaert de Araújo 2009)

The mechanisms of particulate matter related adverse health effects are still incompletely understood, but a hypothesis under investigation is that many of these effects may derive from oxidative stress, initiated by the formation of reactive oxygen species (ROS) at the surface of and within target cells. Cumulative epidemiological and experimental data support the association of adverse health effects with cellular oxidative stress, including the ability of PM to induce pro-inflammatory effects in the nose, lung and cardiovascular system .High levels of ROS cause a change in the redox status of the cell and its surrounding environment, thereby triggering a cascade of events associated with inflammation and, at higher concentration, apoptosis.

The main aim of this study was to examine the relationship between different alternative fuel substitutions and the oxidative potential of particles emitted from an ethanol fumigated common rail diesel engine that was also equipped to run with biodiesel. To estimate the oxidative potential of ethanol and biodiesel at two different load settings, a pro-fluorescent probe BPEA nitroxide was used. This probe is poorly fluorescent; however the presence of ROS triggers a fluorescence response which makes it a powerful optical sensor for radicals and redox compounds. Samples were collected by bubbling aerosol for 20-30 minutes through an impinger containing 20 ml of 4 μM BPEA nitroxide solution after which fluorescence was measured. The amount of ROS was calculated based on the difference in fluorescence intensity for the test and the filtered control sample and was further normalised to the PM mass. Tests were designed to present emission differences due to changes in fuel and load settings.

The collection of other data was performed to support ROS measurements which involved volatility measurement using a Volatility- Tandem Differential Mobility Analyser (V-TDMA) system and particle composition using a Time of Flight Aerosol Mass Spectrometer (ToF-AMS).
The results depicting volatility properties as well as size-resolved aerosol chemical composition will be discussed.

Figure 1 shows ROS concentrations for diesel (E0), 3 ethanol substitutions of 10, 20 and 30 % (E10, E20, E30 respectively) and neat soy biodiesel (B100). It can be noticed that with an increased ethanol substitution (and also for biodiesel) an increased amount of ROS can be observed, with respect to E0.

It is proposed that ethanol combustion involves more available OH radicals that oxidise the particle surface. This might be a reason for the observed increase in the ROS on the surface of the soot particles (Surawski, Miljevic et al. 2009).
Furthermore at full load setting, concentration of ROS is significantly lower for all fuels, except for biodiesel. In addition, emissions with 100% biodiesel contained the highest concentration of ROS per mg of PM.

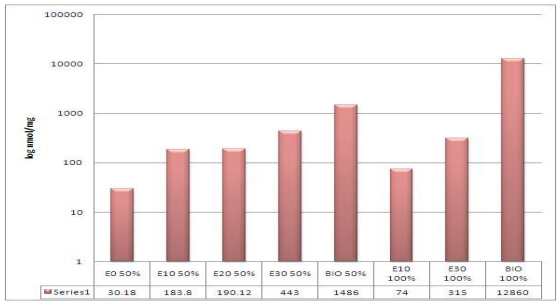

Figure 1: Average ROS concentrations for different fuel and load settings. Note that concentrations of ROS per mg of particulate matter are presented on a logarithmic scale.

Gomes, M. S. d. P. and M. S. Muylaert de Araújo (2009) *Renew. Sustain. Energ. Rev.* **13**, 2201-2204.

Surawski, N. C., B. Miljevic, et al. (2009) *Environ. Sci. Technol.* **44**, 229-235.

Friday, September 9, 2011

Session 12D: From PM exposure to health effects 2

Exposure Analysis for the Inhalation of Ultra-fine Particles Emitted from Household Devices

T. Schripp[1], I. Kirsch[1], S. Willenborg[1] and T. Salthammer[1]

[1]Material Analysis and Indoor Chemistry, Fraunhofer WKI, Braunschweig, 38108, Germany
Keywords: exposure, lung deposition, FMPS, indoor aerosols.
Presenting author email: tobias.schripp@wki.fraunhofer.de

The release of ultra-fine particles from heated surfaces of household appliances has been intensively studied in the past years (Wallace, 2006; Mullen, 2008) due to the increased public interest in the exposure against anthropogenic particles. In most cases the highest emission rate was observed for particle diameters between 20 nm and 100 nm. These particles are known to penetrate the human lung down to the alveolar region. The present study aims at the quantification of particles that are deposited in the different regions of the human lung in the presence of active household appliances.

The emission strength of different household devices, like, e.g., toasters and grills, was determined in a 1 m³ emission test chamber at an air exchange of 3 h^{-1}. The devices were operated without the presence of consumables (e.g. food) for ≤ 10 min (device-specific) three times within three hours. For the simulation of real indoor conditions one household device, a flat iron, was additionally operated (10 min) in a 48 m³ emission test chamber at an air exchange rate of 0.12 h^{-1}. The particle concentration in the chambers was monitored by a Fast Mobility Particle Sizer (FMPS) that measures particles at diameters between 5.6 and 560 nm in 32 channels.

Table 1: Deposition estimates for male adults (sitting) on the basis of FMPS measurements in the 48 m³ emission test chamber and outdoor air. The total deposition is given in combination with the contribution of the modelled four lung compartments to the total deposition. The particle density is assumed to be 1 g/cm³; values for a density of 2 g/cm³ are given in brackets.

Uptake rate	Chamber blank	Lab background	Flat iron
Number [10^9 /h]	0.43(0.50)	6.93(16.03)	0.39(2.37)
Surface [cm²/h]	0.01(0.01)	1.55(2.31)	0.13(0.19)
Mass [µg/h]	0.01(0.02)	3.08(9.05)	0.19(0.55)
ET [%]	17(25)	13(15)	13(15)
BB [%]	4(6)	3(3)	3(3)
bb [%]	23(28)	20(21)	20(22)
AI [%]	56(41)	64(61)	64(60)

The results of the measuring instrument were coupled with an algorithm which estimates the retaining efficiency of four compartments of the human lung and providing the number, surface, and mass of the deposited particles. The algorithm bases on the particle deposition model by the International Commission on Radiological Protection (ICRP, 1994). Two different particle densities (1 and 2 g/cm³) were applied in the ICRP model. The results are given in Table 1 and can be extended for different activities, sex, and ages. The lung compartments of the extrathoracic airways (ET), the bronchi (BB), the bronchioles (bb), and the alveoli (AI) were considered. The lab background was sampled over 5 hours in the emission test chamber lab (mean particle concentration: 55447 #/cm³).

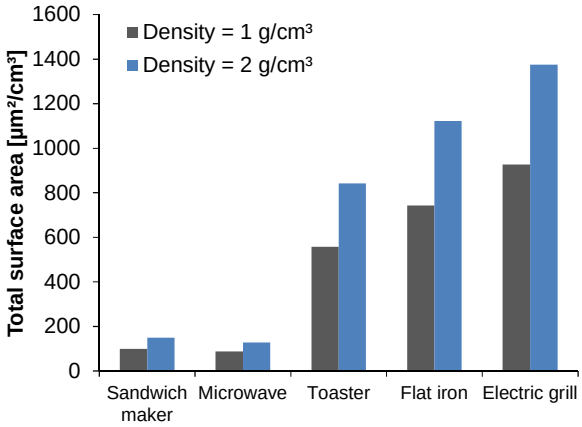

Figure 1: Estimated lung-deposited surface area on the basis of 1 m³ emission test chamber measurements.

The results in Figure 1 demonstrate that the combination of a high time resolved particle measuring instrument and a feasible lung deposition model can be used to determine a ranking of different household appliances in regard of their particle emission behavior. Furthermore, the applied model supports the assumption that the main amount of particles from the device-specific emissions are retained in the deep lung regions. Due to the dependence of the deposition on the particle density the chemical composition of these particles is vitally needed to assess the toxicological effects of the deposited matter. Especially for devices of daily use like toasters and microwaves the risk assessment is of high importance for the further classification of other source of ultra-fine particles in the office environment like hardcopy devices.

Mullen, N.A., Bhanger, S., Nazaroff, et al. (2008) Proceedings of the the 1st International Conference on Building Energy and Environment, Dalian, China, **1-3**, 994-1001.

ICRP (1994) *Annals of the ICRP* **24**, 1-482.

Wallace L.A. (2006) *Aerosol Science and Technology* **40**, 348-360.

Modelling excess mortality in Europe following a future Laki-style Icelandic eruption

A.Schmidt[1], K. Carslaw[1], B. Ostro[2], M. Wilson[1], T. Thordarson[3] and G. Mann[1,4]

[1]School of Earth and Environment, University of Leeds, UK
[2]Centre for Research in Environmental Epidemiology (CREAL), Barcelona, Spain
[3]School of GeoSciences, University of Edinburgh, UK
[4]National Centre for Atmospheric Science, School of Earth and Environment, University of Leeds, UK

Keywords: Laki eruption, Volcanic particles, Air pollution - modelling, Health effects of aerosols
Presenting author email: a.schmidt@see.leeds.ac.uk

We quantify the potential negative health hazard that would arise if a Laki-style eruption were to happen under present-day conditions using an advanced global aerosol microphysics model (GLOMAP, Mann et al., 2010) together with concentration-response functions from the literature (Pope et al., 2002; Ostro, 2004). The 1783—1784 AD Laki eruption lasted 8 months and represents one of the largest flood lava eruptions in recent history (Thordarson & Self, 2003). The emission of ~122 Tg of volcanic SO_2 over the course of 8 months (Thordarson et al., 1996; Thordarson & Self, 2003) is of the same order of magnitude as the current total of global anthropogenic SO_2 emissions per year (e.g. Smith et al., 2010).

According to our simulations a total of around 139,000 additional cardiopulmonary fatalities would arise in Europe in the year following a Laki-style eruption. Thus, our results show that such a volcanic air pollution event would be a severe health hazard, increasing excess mortality in Europe on a scale that is at least comparable with excess mortality due to seasonal flu. Our simulations reveal highest excess cardiopulmonary mortality rates in the Netherlands, Belgium, UK, Germany, and northern France, which is a result of population density combined with highest pollutant concentrations (in our case particulate matter with diameters smaller than 2.5 microns).

We compare our findings to historical records of the aftermath of the 1783—1784 AD Laki eruption which suggest an increase in mortality in summer 1783 (e.g., Grattan et al., 2003; Witham & Oppenheimer, 2005), and find that the simulated scale and the spatial pattern of mortality are very similar.

We will also discuss the magnitude of SO_2 and sulphate aerosol concentrations at commercial flight altitude. Moreover, we will discuss seasonal variabilities in the risk to impact human health and aviation.

Given historic records of the Laki eruption and the probability of a recurrence of such an event we deem it crucial to assess the scale on which a future Laki-style eruption could impact society.

AS was supported by a University of Leeds Research Scholarship. GWM is supported by NERC through the National Centre for Atmospheric Science. Model development for this project was supported by the UKCA project. Part of the development of UKCA is supported by the DECC and Defra Integrated Climate Programme – DECC/Defra (GA01101).

Grattan J, Durand M, & Taylor S (2003) Illness and elevated human mortality in Europe coincident with the Laki Fissure eruption. Volcanic Degassing, Geological Society Special Publication, eds Oppenheimer C, Pyle DM, & Barclay J (Geological Soc Publishing House, Bath), Vol 213, pp 401-414.

Mann GW, et al. (2010) Description and evaluation of GLOMAP-mode: a modal global aerosol microphysics model for the UKCA composition-climate model. Geosci. Model Dev. 3(2):519-551.

Ostro B (2004) Outdoor air pollution: Assessing the environmental burden of disease at national and local levels. World Health Organization, Geneva.

Pope CA, et al. (2002) Lung cancer, cardiopulmonary mortality, and long-term exposure to fine particulate air pollution. Jama-Journal of the American Medical Association 287(9):1132-1141.

Smith SJ, et al. (2010) Anthropogenic sulfur dioxide emissions: 1850-2005. Atmos. Chem. Phys. Discuss. 10(6):16111-16151.

Thordarson T, Self S, Óskarsson N, & Hulsebosch T (1996) Sulfur, chlorine, and fluorine degassing and atmospheric loading by the 1783–1784 AD Laki (Skaftár Fires) eruption in Iceland. *Bulletin of Volcanology* 58(2):205-225.

Thordarson T & Self S (2003) Atmospheric and environmental effects of the 1783-1784 Laki eruption: A review and reassessment. Journal of Geophysical Research-Atmospheres 108(D1):29.

Witham CS & Oppenheimer C (2005) Mortality in England during the 1783-4 Laki Craters eruption. Bulletin of Volcanology 67(1):15-26.

Novel methodology for estimation of mass and surface area of aggregated particles deposited in the human respiratory tract

J. Rissler[1], J. Pagels[1], C. Svensson[1], J. Löndahl[2], M.E. Messing[3], M. Bohgard[1]

[1]Division of Ergonomics and Aerosol Technology, Lund University, P.O. Box 118, SE-22100, Lund, Sweden
[2]Division of Nuclear Physics, Lund University, P.O. Box 118, SE-22100, Lund, Sweden
Keywords: lung deposition, health, aggregated particles, dose
jenny.rissler@design.lth.se

The particle mass and surface area is believed to be crucial parameters for the health effects of inhaling non-soluble air-borne particles. Often the deposited dose and particulate surface area are estimated from particle number concentrations measured by DMA techniques. For spherical particles such estimations are good. For non-spherical particles, however, the estimations can deviate from the real deposited surface area or mass by an order of magnitude. Aggregated or agglomerated particles require additional information about both particle shape and particle effective densities.

The aim of this work is to describe and apply a methodology for assessing surface area and mass of aggregated/agglomerated particles based on number size distributions measured by DMA-techniques. The method is applied in three studies: estimating the deposition in the human respiratory tract of diesel soot, deposition of gold aggregates in protein solutions and direct unto cell cultures (Savi et al., 2008).

The principle of the method used to estimate the surface area size distribution is shown in Figure 1. As input (*i*) the mass of the individual aggregates of a certain mobility diameter $m_{agg}(d_{me})$, (*ii*) the primary particle size (d_p), and (*iii*) number size distribution ($dN_{agg}/d\log d_{me}$) are needed. For mass determination of individual aggregates the novel DMA-Aerosol Particle Mass Analyzer (DMA-APM McMurry et al., 2002) is used. The mass size distribution of the aerosol is estimated by combining the results of the DMA-APM system and the number size distribution. For estimation of surface area the size of the primary particles is also needed, here estimated from TEM images.

From $m_{agg}(d_{me})$ and d_p the number of primary particles of the individual aggregates of a certain size ($N_p(d_{me})$) is calculated (assuming a density of the primary particles of ρ_p=1.8 g/cm^3 for soot and 19.3 for gold) according to $N_p(d_{me}) = m_{agg}(d_{me})/(\rho_p \cdot \pi \cdot d_p/6)$.

By combining $N_p(d_{me})$ and the particle number size distribution, the distribution of the total number of primary particles of all aggregates of a certain d_{me} is estimated, and thereafter the total surface area of all aggregates of a certain d_{me} ($SA(d_{me})$). Knowing the size resolved fraction of particles deposited (measured or modeled) in the lung, into the protein solution or onto the cell cultures, the total deposited dose and surface area is determined.

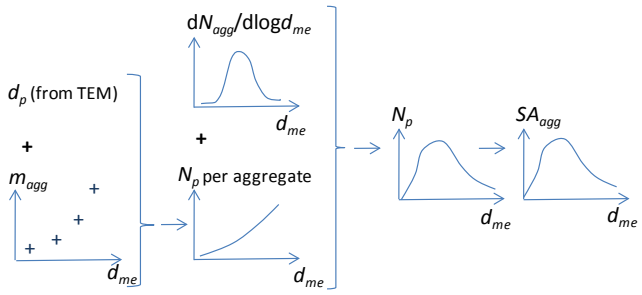

Figure 1. Principle of the methodology.

The method was applied in the three studies. All showed that when estimating mass from size distributions measured by an SMPS assuming spherical particles, gave 4-6 times higher doses than if the measured particle mass was used. Surface area was not as sensitive for aggregation state and the aggregates had a larger surface area than if assuming spherical particles, by typically 2-3 times. The contact area between primary particles in the aggregate is assumed to be infinitesimal. According to TEM images the true contact area is larger and the real surface area will probably lie between the two extremes; spherical particles and agglomerates.

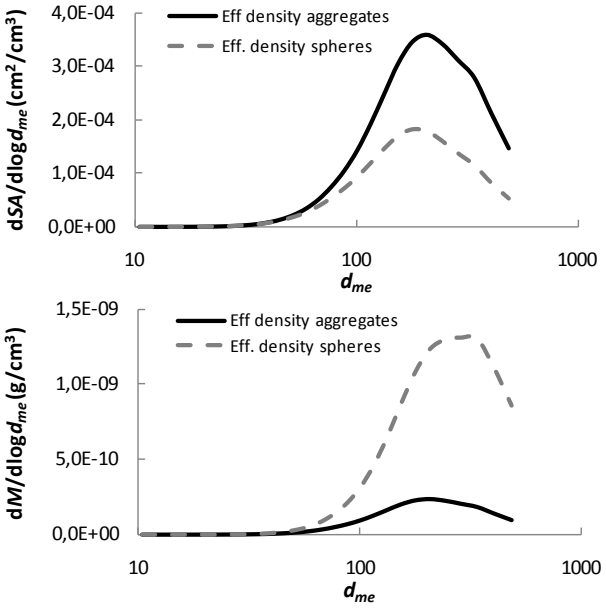

Figure 2. Distributions of surface area (*SA*) and mass (*m*) assuming either spherical or aggregated particles.

This work was supported by the Swedish Research Council FORMAS, the Swedish Governmental Agency for Innovation Systems VINNOVA, European Commission (EC) 7th Framework Programme and nmC@LU.

Savi, M., et al., (2008) Environ. Sci. Technol., 42, 5667–5674.

McMurry P.H., et al. (2002), Aerosol Science and Technology 36: 227–238.

Optical scattering observations in two occupied residences with wood-burning stoves

I.D. Longley, J. Gadd

National Institute of Water & Atmospheric Research Ltd, Auckland 1010, New Zealand
Keywords: Indoor particles, Indoor sources, Wood combustion, PM10.
Presenting author email: i.longley@niwa.co.nz

Introduction

Domestic wood-burning stoves used for home heating are the largest source of ambient PM_{10} emissions in many cities and rural towns in New Zealand. Air quality management policy in such locations is currently focussed on replacement of wood-burners with newer low-emission burners, or alternative energy sources. Such policy is being driven by, and judged against, the ambient Air Quality National Environmental Standard for PM_{10} - with an assumption that this is a proxy for exposure and health effects. However, New Zealanders spend 70% of their time indoors at home and on winter evenings when wood-burners are operated most of the populace is likely to be indoors.

Previous studies on indoor levels and sources of PM in homes burning wood for heating have been very limited and generally focussed on filter samples. However, the low temporal resolution of such techniques prevent an examination of the processes involved and key sources, especially considering the multiple pathways by which wood-smoke can potentially enter the home.

Our aim was to conduct a limited exploratory observational study to determine whether the wood-burner was a significant indoor source in two typical New Zealand homes, and to explore whether particle concentrations in these homes was correlated with ambient PM_{10} observed at nearby regulatory monitoring sites.

Methods

A TSI Sidepak integrating nephthelometer was installed consecutively in two occupied homes in Christchurch for two weeks each in winter 2009. The instrument nominally reported "PM_{10}" (derived from light scattering measurements) at 1 minute resolution. Several other parameters were recorded, including flue and room temperature. Participants used their own supply of firewood and used their wood-burner in the usual way. They also kept a diary of fire-lighting and wood additions.

A number of limited follow-up experiments were conducted in a 'control' home focussing on the woodburner 'start-up' procedure, relying on PM_{10} measurements and video of the firebox.

Results

In the occupied homes indoor concentrations were characterised by rapid elevations (lasting 1 – 5 minutes and occurring once or twice a day) followed by smooth exponential decays. 1-minute peaks varied greatly ranging from 110 to 2800 $\mu g\ m^{-3}$ (mean = 690 $\mu g\ m^{-3}$) and were strongly predictive of 24-hour mean concentrations, which varied from 22 to 140 $\mu g\ m^{-3}$. By comparing these data with concurrent data from local ambient sites we estimate that 24-hour indoor concentrations were 3 to 10 times higher than concurrent ambient concentrations.

1-minute peaks often coincided with the start of wood-burning, as indicated by the increase in flue temperature. The 20 largest peaks (all above 200 $\mu g\ m^{-3}$) were all related to fire-starting or fuel addition, with paper addition leading to larger concentrations than wood addition.

The follow-up test confirmed that the rapid rise in indoor PM_{10} coincided with the initial match-lighting and the early stage of burning the first kindling, and ended when the firebox door was fully closed and burning had become self-sustaining. The highest concentrations were recorded when paper, but no wood, was lit.

Discussion

There was effectively no linear relationship between ambient PM_{10} and the indoor light scattering measurements on the basis of either 24-hour or 1-hour averages when all data was considered. When peaks caused by wood-burning were removed from the data set, the temporal pattern in baseline indoor PM more generally reflected ambient PM_{10}.

The follow-up study confirmed the co-incidence of rapid peaks and the fire-starting procedure. It also showed that, using these materials, the peaks could be largely avoided by user technique.

Our results show that true exposure may be substantially higher in wood-burning homes compared to both non-wood-burning homes and in the ambient air – and that presence of an operating wood-burner is a substantial modifier of the relationship between ambient air quality and exposure.

This study was conducted within the Healthy Urban Atmospheres programme funded by the Foundation for Research Science and Technology (New Zealand). Ambient PM_{10} data was provided courtesy of Environment Canterbury.

Outdoor/indoor particle infiltration factor in Rome and its relation with urban air quality

A. Di Menno di Bucchianico[1], G. Cattani[1], A. Gaeta[1], G. Gandolfo[1], A.M. Caricchia[1], M. Inglessis[2], G. Settimo[2], B. Bruni[2] and C. Perrino[3]

[1] ISPRA – Italian National Institute for Environmental Protection and Research, Via Brancati 48, 00144, Rome, Italy
[2]ISS – Italian National Health Institute, Viale Regina Elena 299, 00161 Rome, Italy
[3]CNR - Institute of Atmospheric Pollution, Via Salaria km. 29,300-C.P. 10-00015 Monterotondo St., Rome, Italy
Keywords: indoor/outdoor particles, indoor air quality, number concentration, urban pollution.
Presenting author email: alessandro.dimenno@isprambiente.it

Despite the fact that, in industrialized nations, people spend a large amount of time indoors, the information on air pollution inside buildings is very poor as compared to ambient air quality. So, necessarily, most epidemiological studies estimate personal exposure on the basis of outdoor levels. Nevertheless, actual human exposure to atmospheric pollutants is regulated by pollutant penetration efficiency and time variability in air exchange rate in indoor environments.

Methods

A four-season indoor and outdoor Particle Number Concentration (PNC) monitoring in two residential homes in Rome was carried out (particles between 0.02 and 1 µm in aerodynamic diameter, 1-minute resolution). A third particle sampling point in downtown Rome, located in the Italian National Health Institute monitoring station, was considered as the reference site. Particulate matter and primary gaseous pollutants concentration data, monitored in ten stations of Rome air quality network, were evaluated to investigate the relation between urban ambient pollution and internal air quality. Finally, with the aim of studying the influence of atmospheric stability on air pollution levels, natural radioactivity data, provided by the near city CNR-Institute of Atmospheric Pollution stability monitor, were taken into account (Perrino, 2001).

We observed that indoor source events (i.e. cooking or cleaning) can cause indoor/outdoor ratios to exceed one, particularly for less ventilated periods (winter). So, through the study of different seasonal patterns (Hänninen, 2010), indoor PNC in the absence of internal sources were reconstructed to better estimate the home infiltration factor (see Figure 1).

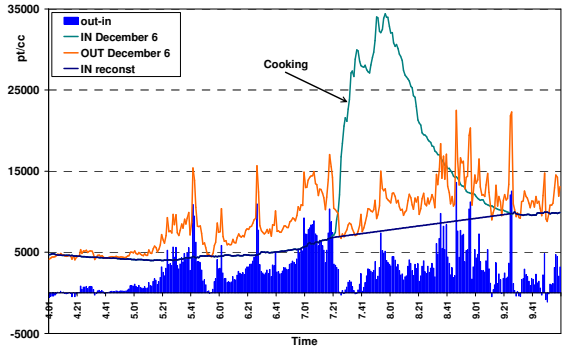

Figure 1. Indoor/outdoor PNC with and without an internal particle source.

Results

Different seasonal patterns; a good correlation between average indoor/outdoor daily values; huge differences in temporal patterns considering a shorter time scale between summer and winter (when the air exchange rate is slower because of different home dynamics; i.e. windows left open/closed) were observed.

It is remarkable that a good correlation between PNC registered indoor in the sampling sites and the main primary gaseous pollutants measured in the urban network stations (see Figure 2) was registered.

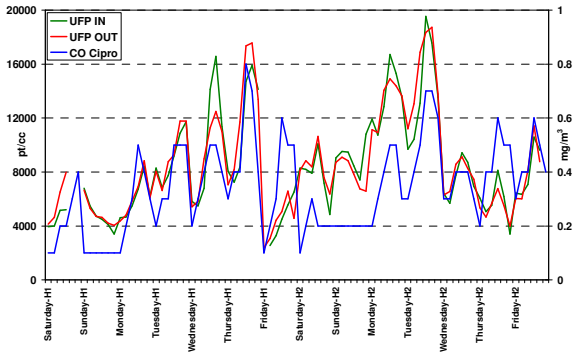

Figure 2. Summer days comparison between indoor/outdoor PNC (in red and green) and CO measured in a urban background station (in blue).

Finally, an innovative interpretation of natural radioactivity data allowed us to distinguish between the two main components of urban air quality: atmospheric stability and pollutant emissions so to better understand the real influence of urban pollution on indoor air quality.

Perrino, C., Pietrodangelo, A., Febo, A. (2001) *An atmospheric stability index based on radon progeny measurements for the evaluation of primary urban pollution*, Atmospheric Environment 35, 5235-5244.

Hänninen, O., Hoek g., Mallone S., Chellini E., Katsouyanni K., Gariazzo C., Cattani G., Marconi A., Molnár P., Bellander T., Jantunen M., (2010) *Seasonal patterns of outdoor PM infiltration into indoor environments: review and meta-analysis of available studies from different climatological zones in Europe*, Air Quality, Atmosphere & Health DOI: 10.1007/s11869-010-0076-5.

Simulated airway particle deposition in an urban environment impacted by biomass smoke

A.C. Targino[1], P. Krecl[2], C. Johansson[3]

[1] Universidade Tecnológica Federal do Paraná, Londrina, Brazil
[2] University of Leeds, School of Earth and Environment, United Kingdom
[3] Stockholm University, Department of Applied Environmental Sciences, Sweden
Keywords: agricultural fires, airway particle deposition, particulate matter, ultrafine particles
Presenting author email: admirtargino@utfpr.edu.br

Populations living in large urban conglomerates are usually exposed to enhanced particle concentrations due to anthropogenic emissions. To make matters worse, urban areas may also be subject to pollution outbreaks caused by long-range transport (LRT) (Saarikoski et al., 2007)

In 2006, the European continent faced an abnormally warm spring period. As a result, agricultural fires broke out in Eastern Europe and became uncontrolled causing serious transboundary pollution episodes in areas as remote as the Arctic (Stohl et al., 2007). This study investigates the effect of this pollution outbreak on the health of Stockholm's population. To assess and quantify the aerosol load impact on the human health, we contrast three aerosol load scenarios: (1) a period dominated by the LRT event, (2) a period dominated by local emission sources, and (3) a period with combined LRT and local sources. To do so, we employ the Multiple Path Particle Dosimetry (MPPD) model that calculates the fraction of particles deposited in specific parts of the respiratory system (Anjilvel and Asgharian, 1995). Model aerosol input parameters were based on in situ measurements at a street canyon site in Stockholm (Figure 1), whereas airway morphology and breathing conditions were chosen from the literature for activities with different exertion level (rest, quiet and moderate cycling).

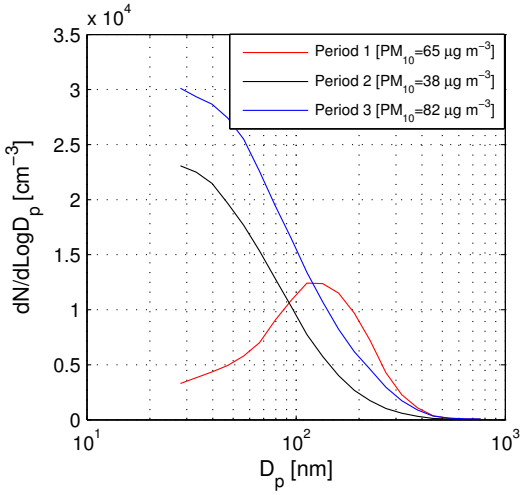

Figure 1. Mean particle number size distributions and PM_{10} mass concentrations measured in Stockholm for the three selected periods.

The results show that the maximum deposition fraction of the inhaled aerosol mass for an adult is observed during period 2 for all breathing conditions (Figure 2). For all cases, the deposition fraction increases from nasal to the alveolar region (not shown). Even though the maximum PM_{10} mass concentration was observed during the LRT event, the maximum potential risk to pulmonary disease is observed in the period dominated by local traffic emissions.

These preliminary results suggest that the definition of clean and polluted conditions, for health studies, should be linked to ultrafine particle concentrations rather than to PM_{10} (or $PM_{2.5}$) mass concentrations.

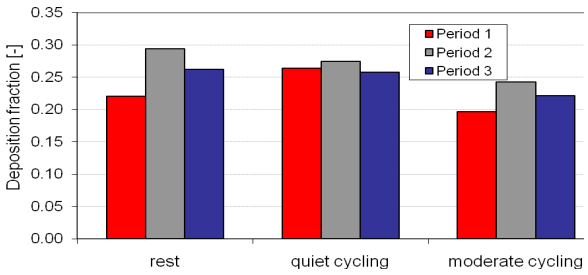

Figure 2. Aerosol deposition fraction in an adult per period and under rest, quiet cycling and moderate cycling conditions.

Measurements for this work were supported by the Swedish Environmental Protection Agency.

Anjilvel, S. and Asgharian, B. (1995) *Fundam. Appl. Toxicol.* 28, 41-50.

Saarikoski, S., Sillanpää, M., Sofiev., M., Timonen, H., Saarnio, K., Teinilä, K., Karppinen, A., Kukkonen, J., Hillamo, R. (2007) *Atmos. Environ.* 41, 3577-3589.

Stohl, A., Berg, T., Burkhart, J.F., Fjæraa, A.M., Forster, C., Herber, A., Hov, Ø., Lunder, C.,McMillan, W.W., Oltmans, S., Shiobara, M., Simpson, D., Solberg, S., Stebel, K., Ström, J., Tørseth, K., Treffeisen, R., Virkkunen, K., Yttri, K.E. (2007) *Atmos. Chem. and Phys*. 7, 511-534.

Surface Area Deposition Index for Jet Engine PM Exhaust

D.E. Hagen[1], E.A. Black[1,2], P.D. Whitefield[1], and P. Lobo[1]

[1]Center of Excellence for Aerospace Particulate Emissions Reduction Research, Missouri University of Science & Technology, Rolla MO, 65409, USA
[2]College of Natural & Applied Sciences, Missouri State University, Springfield MO, 65897, USA
Keywords: Aircraft plumes, combustion aerosols, lung deposition, hygroscopicity.
Presenting author email: hagen@mst.edu

A major portion of atmospheric particles found in both urban and rural areas consists of carbonaceous material derived from both biogenic and anthropogenic sources. Particulate matter (PM) from on-road vehicular traffic has been correlated to increases in mortality and morbidity. PM from jet engine exhaust (JEE) falls into a similar size range, but its inhalation health impacts have been less well studied. JEE PM has unique properties with respect to deposition, retention kinetics, and clearance pathways in the human respiratory system, and is composed of sizes that readily travel gas streamlines that penetrate the deepest regions of the lung; this is a concern as deposited JEE PM in these regions could potentially cross the blood-membrane barrier and migrate into the bloodstream.

In two field campaigns PM size distribution and hydration data was acquired by the Missouri University of Science & Technology Center of Excellence for Aerospace Particulate Emissions Reduction Research (Missouri S&T COE), at Hartsfield-Jackson Atlanta International (ATL) and Oakland International (OAK) airports (Herndon et al 2008; Whitefield et al 2007). JEE PM was sampled downwind of active taxi- and runways during normal airport operations. The sample locations were selected adjacent to airport runways at distances of 100 m or greater from take-off sites, and chosen so JEE plumes would be transported by prevailing winds to a sampling probe feeding the diagnostic instrumentation. For both campaigns aircraft tail numbers were recorded for identification of airframes and engine types. Weather conditions were also monitored and recorded continuously throughout testing periods.

Using the JEE PM data collected during plume studies performed down-wind of active runways at ATL and OAK, lung deposition probabilities of JEE PM (as a function of particle size) can be determined using the International Committee of Radiological Protection (ICRP) lung deposition model. Surface area is the characteristic PM parameter most strongly correlated with health impacts (Stoeger et al 2006). Using the deposition probabilities and size resolved number distributions, a Surface Area Deposition Index (SADI) was developed. This new parameter, SADI, characterizes JEE PM lung deposition as the surface area of deposited PM per kilogram fuel burned. SADI allows for equitable comparison among various jet engine types while also proving a surface area metric for meaningful health impact correlations. An example of the variation in SADI for engine type CFM-56 observed at OAK is shown in Fig. 1.

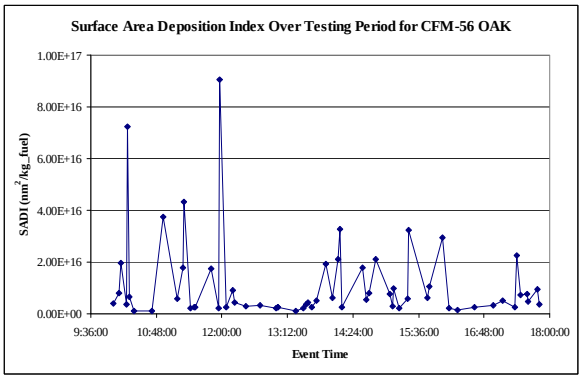

Fig. 1 Surface Area Deposition Index for CFM-56 engine type observed at OAK

Two interesting conclusions to this preliminary study are that statistically significant differences among engine types are not observed in SADI, and variations in SADI are not correlated with temporal changes or changes in meteorological conditions.

EAB was sponsored by the Airport Cooperative Research Program (ACRP 11-04: Graduate Research Award Program on Public-Sector Aviation Issues) administered by the Transportation Research Board of the National Academies (Project Manager: Larry Goldstein). The opinions and conclusions expressed or implied in the presentation are those of the authors. They are not necessarily those of the Transportation Research Board, the National Academies, or the program sponsor. DEH, PDW, and PL would like to acknowledge the sponsorship of the Missouri S&T COE.

Stoeger, T., Reinhard, C., Takenaka, S., Schroeppel, A., Karg, E., Ritter, B., Heyder, J., and Schulz, H. (2006) Environmental Health Perspectives, **114**, 328-333.

Herndon, S., Jayne, J.T., Lobo, P., Onasch, T.B., Fleming, G., Hagen, D.E., Whitefield, P.D., Miake-Lye, R.C. (2008) *Environmental Science & Technology* **42**, 1877-1883.

Whitefield, P.D., P. Lobo, and D.E. Hagen (2007) In *Sausen, R., A. Blum, D.S. Lee and C. Brüning (eds.): Proceedings of an International Conference on Transport, Atmosphere and Climate (TAC).* ISBN 92-79-04583-0, 95-100.

Friday, September 9, 2011

Session 12E: Application of New Instrumentation for Study of New Processes and Phenomena

Ultrafine nebuliser for aerosolization of nanoparticles in colloidal suspensions

J.E. Farnsworth[1], D.C. Grant[2], H.G. Van Schooneveld[2], M.R. Litchy[2], B.L. Osmondson[1], and R. Caldow[1]

[1]TSI Incorporated, Shoreview, MN, 55126, USA
[2]CT Associates, Eden Prairie, MN, 55344, USA

Keywords: nebuliser, SMPS, PSL, generation of nanoparticles, surfactants
Presenting author email: jim.farnsworth@tsi.com

Nebulisers are used to aerosolize a variety of particles present in colloidal suspensions, however their usefulness for particles smaller than 100 nm is limited as dissolved residue from the liquid interferes with counting and sizing the particles of interest.

In this paper we present an ultrafine nebuliser capable of generating a small, uniform droplet distribution such that particle formed from dissolved residue when the liquid is evaporated does not interfere with the nanoparticles in the liquid for sizes >10 nm (Grant and Beuscher, 2009). When used with a scanning mobility particle sizer (SMPS), one can measure particle size distributions (Figure 1) and calculate the original number concentration of the liquid sample within ±10%.

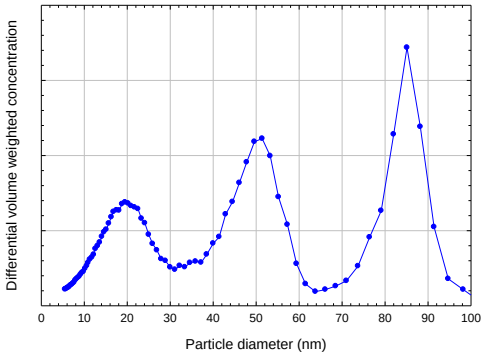

Figure 1. Simultaneous measurement of 20, 50, and 83 nm PSL spheres using the ultrafine nebuliser (Van Schooneveld *et al.*, 2010).

As shown in Figure 2, the liquid sample is fed by a peristaltic pump into the nebuliser system at a flow rate of 0.01-1 ml/min. The sample is diluted with a known ratio of ultrapure water (UPW) to minimize dissolved residue interference. The sample is then aspirated through a micro-orifice and forced around an impactor, generating an aerosol with a narrow droplet size distribution and mean droplet size of 300 nm. The aerosol passes through a heated drying column, combines with dilution air, and exits the instrument at a flow rate around 1.5 L/min.

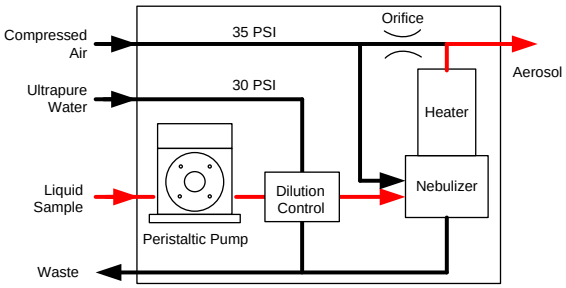

Figure 2. Flow schematic of the ultrafine nebuliser.

The nebuliser has been used to generate nanoparticle-laden aerosols such as gold and alumina, macromolecules such as dextran, PSL in the 20-100 nm range, and colloidal silica (used in semiconductor wafer polishing slurries) in the 10-200 nm range. Coupled with an SMPS the coefficient of variation (CV) of size distributions can be measured directly. Excellent agreement is shown between CV obtained by this approach and CV reported by PSL manufacturers.

The on-line dilution scheme utilized by the nebuliser can be used to differentiate between solid particles and dissolved residue in liquid. For example, by generating PSL at multiple dilution ratios, one can distinguish PSL spheres and surfactant particles from dissolved residue contaminants.

The combination of nebuliser and SMPS (n-SMPS) has been applied as a near real-time characterization tool for industrial liquid systems. The device has been used to characterize polishing slurries used in semiconductor manufacturing, and has been used to measure removal efficiency of liquid filters as a function of particle size, filter pore size, and filter loading. Particle sizing data from these studies are presented.

Van Schooneveld, G., Litchy, M. and Grant, D. (2010) *Proc. 2010 Int. Conf. on Planarization/CMP Tech*, Phoenix, AZ, 348-351.

Grant, D. and Beuscher, U. (2009) *Ultrapure Water J.* **26**, 34-40.

A Study of Terpenes by Raman Acoustic Levitation

M.V.Ghosh, S.Almabrok, D.J. Stewart, I .Hoare, G. Marston and C. Pfrang

Department of Chemistry, University of Reading, Reading, Berkshire, RG6 6AD, UK
Keywords: acoustic levitation, terpenes, Raman spectroscopy
Presenting author email: m.v.ghosh@reading.ac.uk

Large quantities of volatile organic compounds (VOCs) are emitted into the troposphere from both biogenic and anthropogenic sources. Almost half of the mass of biogenic volatile organic compounds (BVOC) emitted is isoprene and about 11% are monoterpenes of which the highest fractions are α-pinene (25%) and limonene (16%). The oxidation of terpenes leads to ozone formation, and they are known cause the formation of secondary organic aerosol (SOA).[1]

In this study, a novel acoustic levitation set up is being developed to improve the understanding of evaporation kinetics and of changes in chemical composition of acoustically levitated droplets of terpenes such as α-and β-pinene, limonene and Δ-carene.

Acoustic levitation is an elegant method that allows contact-less reaction monitoring and spectroscopy of single particles. It is, however, only recently that acoustic levitation has been considered for atmospheric science.[2,3] Acoustic levitation is generally achieved by an ultrasonic transducer producing a standing sound wave. Alteration of the distance between transducer and (in most cases concave) reflector allows varying the number of the pressure nodes that allow stable particle levitation.[4]

In this study Raman spectroscopy has been successfully combined with acoustic levitation to allow a time resolved contactless monitoring of chemical reactions and physical processes in a single droplet suspended in a controlled gaseous environment.

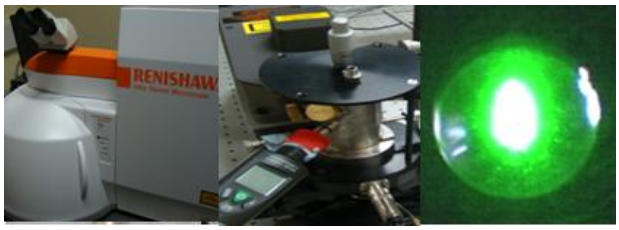

(a) (b) (c)

Figure 1. Images of the Raman acoustic levitation set up.

Fig. 1 shows from (left to right):

(a) Commercial Raman microscope in the Chemical Analysis Facility, CAF, in the Department of Chemistry at Reading University; (b) Experimental set up with the levitation chamber coupled to the Raman spectrometer; (c) Image of the laser beam focused in the centre of the levitated droplet.

During the evaporation of acoustically levitated droplets of α-pinene the changes in droplet size were measured by a CCD camera and the intensity of the C=C stretching band at 1662 cm^{-1} was monitored by Raman spectroscopy as a function of time.

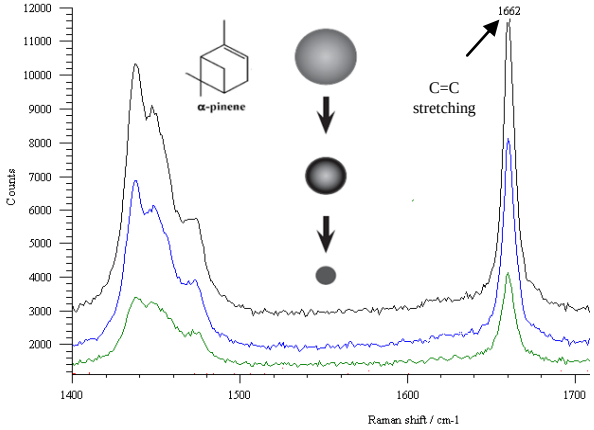

Figure 2. An example of evaporation of a levitated α-pinene droplet in nitrogen at a relative humidity, RH, of 50% and T = 25 °C recorded by Raman spectroscopy as a function of time (acquisition time of 60 s).

Raman acoustic levitation allows monitoring of changes in physicochemical properties of small organic droplets. Following systematic tests to probe the sensitivity of the technique to droplet size and environmental conditions, Raman acoustic levitation has been successfully applied to monitoring the evaporation kinetics and chemical composition of acoustically levitated droplets of terpenes. Being able to suspend a single particle while its chemical composition is being monitored by Raman spectroscopy will be exploited in future studies of the ageing of atmospheric aerosols.

This work was supported by the Royal Society (RG2007/R2; PI Dr Pfrang) and the NERC (NE/G000883/1, PI Dr Pfrang; NE/G019231/1, PI Prof. Marston and Co-I Dr Pfrang). It benefitted from instruments available within the Chemical Analysis Facility, CAF, and is a result of joint research efforts within the newly formed Reading Atmospheric Chemistry and Environmental Research, RACER, team (www.chem.rdg.ac.uk/research/chem-racer.aspx).

1. Kanakidou et al., *Atmos. Chem*, Phys., 5, 1053 (2005)
2. Stephens and Budwig, *Rev Sci Instrum*, 78, 14901 (2007)
3. Mason *et al.*, *Faraday Discuss*, 137, 367 (2008)
4. Tuckermann, *Anal Bioanal Chem*, 394, 1433 (2009)

Handheld nanoparticle monitors – An intercomparison study

C. Asbach[1], H. Kaminski[1], D. Von Barany[1], C. Monz[2], N. Dziurowitz[3], J. Pelzer[4], K. Berlin[5], S.Dietrich[5], U. Götz[6], H.-J. Kiesling[7], R. Schierl[8]

[1]Insitute of Energy and Environmental Technology, 47229 Duisburg, Germany
[2]Institute for the Research on Hazardous Substances (IGF), 44789 Bochum, Germany
[3] Federal Institute for Occupational Safety and Health (BAuA), Berlin, Germany
[4]Institute for Occupational Safety and Health of the German Social Accident Insurance (IFA), 53757 Sankt Augustin, Germany
[5]Bayrisches Landesamt für Gesundheit und Lebensmittelsicherheit (LGL), 91058 Erlangen
[6]BASF SE, 67063 Ludwigshafen, Germany
[7]Bayer Technology Services, 51368 Leverkusen, Germany
[8]Institute for Occupational, Social and Environmental Medicine, University Munich, 80336 Munich, Germany

Keywords: nanoparticle, exposure, monitor, handheld

Monitoring of exposure to airborne nanoparticles is crucial, e.g. in view of worker protection, as inhalation is seen as the major uptake route for nanomaterials. A number of intensive measurement campaigns have been carried out in the past to very thoroughly study particles and aerosols in workplaces. These campaigns are very time and cost intensive. In some cases, e.g. as a first step in a tiered approach, only a quick check of the exposure concentration or a permanent surveillance is required. Such simplified measurements can be conducted with portable monitoring devices, such as handheld condensation particle counters (CPC) or diffusion charger (DC) based instruments. Five different models of portable nanoparticle monitors were subject to an intensive intercomparison experiment. All these devices have in common that they are small, light weight, battery operated and deliver a size-integrated concentration measure; number concentration in case of CPCs and most DCs and lung deposited surface area concentration in case of some DCs. Time resolutions are between 1 s and 16 s. Both types of devices, CPCs and DCs have their advantages and disadvantages. CPCs are known to be very accurate and particle size, shape and material independent. On the other hand they always have to be maintained in a horizontal position and require a working fluid that needs to be refilled every 5-8 hours in case of the handheld version. DCs can be operated in any orientation and don't require auxiliary materials, but rely on several assumptions and are thus usually less accurate.

During the intercomparison measurements, three different types of test aerosols were generated: NaCl, DEHS and soot. NaCl and DEHS particles were generated using an atomizer (Topas, ATM 226), soot particles were produced with a spark generator (Palas, GFG3000). The NaCl aerosol contained solid, cubic particles with a modal diameter of approximately 50 nm, whereas the DEHS aerosol contained liquid droplets with a modal diameter of approximately 250 nm. Soot particles were fractal-like agglomerates with a modal electrical mobility diameter of approximately 35 nm. A Fast Mobility Particle Sizer (FMPS) was used alongside to measure the particle size distribution. All measurement devices sampled the same aerosol simultaneously. A sequence of number concentrations, as exemplarily shown for soot in Figure 1, was produced for all three aerosol types.

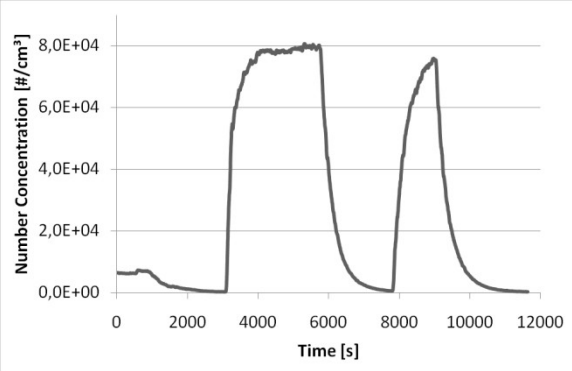

Figure : **Time series of the soot number concentration**

The results show that the devices react differently to the different aerosols and concentration changes. Handheld CPCs generally produced the most accurate results for number concentrations below 10^5 #/cm³ with deviations mostly within ±5%. For higher concentrations, the CPCs reached saturation and became increasingly inaccurate. DCs worked well also for higher concentrations, but expectedly showed a lower overall accuracy, generally within ±30%, which is sufficient for most monitoring applications. Only the DEHS aerosol produced significantly higher errors of some diffusion chargers, most likely caused by the presence of large particles.

The experimantal design will be presented along with intercomparison of the different devices. Results will be discussed in view of simplified and improved monitoring of airborne nanoparticle concentrations.

Evaluation of PEGASOR PPS™ response time for real time aerosol concentration measurements

Gensdarmes F.[1] Roynette A.[1] Maro D.[1] Laguionie P.[1] Boulaud D.[1] and Tikanen J.[2]

[1] Institut de Radioprotection et de Sûreté Nucléaire IRSN, BP 68, 91192, Gif-sur-Yvette Cedex, France.
[2] Navaro Oy, Rautapellonkatu 37, FIN-33700 Tampere, Finland. juha.tikkanen@pegasor.fi

Keywords: real-time detection, eddy covariance fluxes, nanoparticle, electrometer
Presenting author email: francois.gensdarmes@irsn.fr

Nowadays real time measurement is mandatory in many aerosol studies (combustion aerosol, process control…). In the field of atmospheric research, the determination of aerosol fluxes and deposition velocity by eddy covariance techniques is limited due to the lack of aerosol instrumentation having sufficiently low response time. Its full application requires measurement of actual aerosol concentration fluctuation at 10 Hz (Held *et al.*, 2007; Damay *et al.*, 2009). Although some electrical aerosol instruments are now available with 10 Hz data acquisition (EEPS™, ELPI™) their response times shows values between 0.4 s and 14 s.

The aim of this study is to measure the response time of the Pegasor Particle Sensor PPS™ aerosol monitor with the classical concentration step changes method, and to assess the effect of a sampling line on the results for further application in dry deposition aerosol measurement by eddy correlation technique.

The PPS operates by measuring the image current caused by a cloud of corona charged particles passing through a faraday cup. A specific design of the sensor makes it possible to be freed from the collection of particles on a filter as in the traditional aerosol electrometers. The PPS was operated with 50 psi inlet pressure which corresponds to a sampling flow rate of the "ejector pump" equal to 7.8 l/min.

The experimental set-up used to measure the response time is shown in figure 1. It is composed of a spark discharge generator (PALAS GFG 1000) with carbon electrodes and a dilution volume in order to obtain constant output aerosols with different concentration levels and size distributions The concentration step changing system is composed of two synchronized electromagnetic valves switching between the GFG aerosol and filtered air.

The response time is determined by fitting the data with the classical exponential relationship:

$$C(t)/C_0 = 1 - \exp[-(t - t_0)/\tau],$$

where C_0 is the initial concentration (p.cm^{-3}), t_0 the time of the concentration step (s) and τ the response time (s).

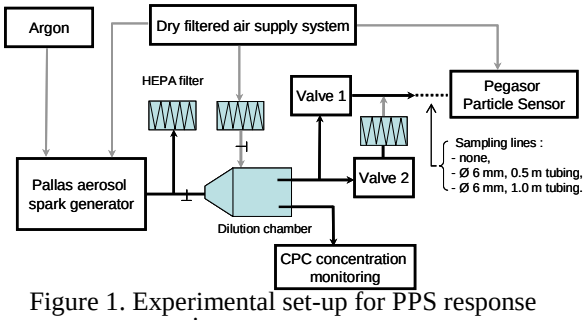

Figure 1. Experimental set-up for PPS response time measurement

Results on response time and sensitivity of the PPS are obtained for aerosol concentrations ranging between 10^3 p.cm^{-3} and 10^7 p.cm^{-3} and particle diameters spanning from 20 nm to 100 nm.

Figure 2 presents the response times for an increase step in concentration measured by the PPS at 10 Hz for different lengths of sampling lines. The results presented are normalized with the same t_0 to take into account different initial time lags in data, according to the tubing lengths. The tested aerosol has a median diameter of 60 nm and a nominal concentration of 3.2×10^5 p.cm^{-3}.

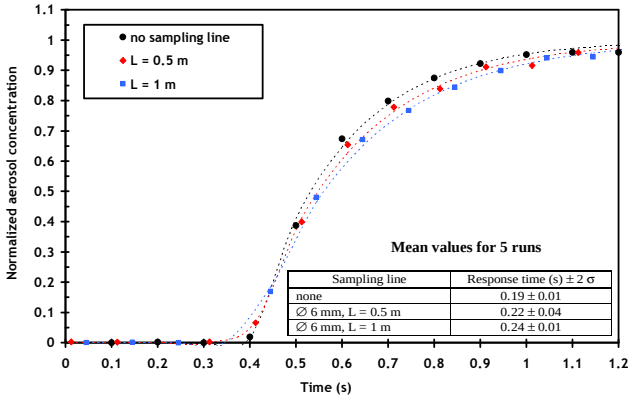

Figure 2. Response times for different sampling lines

Results show very short response times around 0.2 s and logical small increases with sampling line lengths due to laminar flow profile. Further investigations will be made with modified PPS allowing higher sampling flowrate.

Damay P., Maro D., Coppalle A., Lamaud E., Connan O., Hébert D., Talbaut M. & Irvine M. (2009) *J. Aerosol Sci.*, **40**, 1050-1058.

Held A., Niesser R., Bosveld F., Wrzesinky T. & Klemm O. (2007) *Aerosol Sci. Technol.*, **41**, 510-519.

A new versatile condensation particle counter for research and environmental monitoring

J. Spielvogel, M. Weiss

Palas® GmbH, Greschbachstr. 3b, 76229 Karlsruhe, Germany
Keywords: aerosol instrumentation, nanoparticles, CPC, number concentration, ultrafine particles
Presenting author email: spielvogel@palas.de

Presented will be a recently developed condensation particle counter in which the unique, patented way of providing the working fluid for condensation allows the user to change the working fluid from e. g. butanol to isopropanol or water. For the first time the user can select a working fluid based on suitability or considerations like adverse health effects or environmental-friendliness.

Working principle

The aerosol with nanoparticles first enters a heated saturator. Within the saturator the working fluid is moved helically around the flow area of the aerosol leading to a homogeneous contact area. Downstream, the aerosol and saturated carrier gas enter a cooled condenser in which the working fluid condenses onto the nanoparticles forming droplets of sizes typically larger than 1 µm.

The counting is performed by an optical aerosol spectrometer (sensor) that also measures the size of the droplets (Figures 1 & 2). A researcher can easily monitor changes in this droplet distribution due to different temperature settings, different working fluid or different particle composition in the analysed aerosol.

The modular design of this instrument further allows adapting the sensor to different concentration levels up to single particle counting of concentrations of 1,000,000 particles/cm^3. This eliminates the need to dilute the aerosol in many cases.

Data

Figures 1 and 2 present data that were obtained by changing the temperatures of the saturator and condenser, then varying the working fluid from butanol to water and repeating the experiment.

In figure 1 the saturator temperature is kept constant at 40°C but the condenser temperature changed from 12°C (dark blue) to 10°C (red). The resulting marginal change in the size distribution of the resulting droplets can be explained that by keeping the saturator temperature constant no change in working fluid vapour is introduced and a change in cooling has little effect on droplet size and number.

However, keeping the condenser temperature constant at 10°C but changing the saturator temperature from 40°C (dark blue) to 44°C (green) and to 47°C (blue) leads to a considerable shift in droplet size distribution. Here, the available amount of working fluid vapour is influenced by the temperature change in the saturator and visible in the increasing size of the forming droplets. At the same time a larger ΔT between saturator and condenser increases the sensitivity of the UF-CPC.

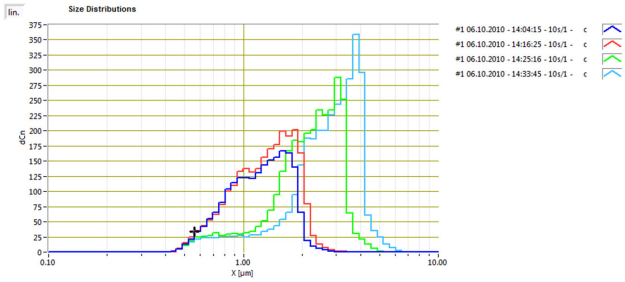

Figure 1. Working fluid butanol. Particle size distributions of droplets resulting from changed saturator and condensor temperatures.

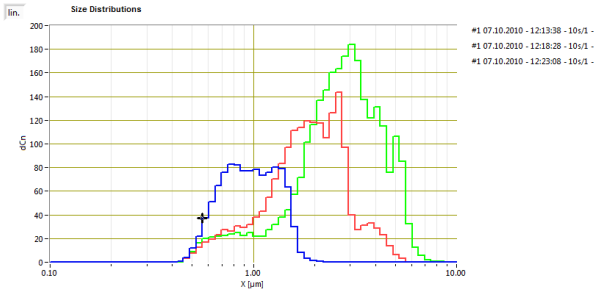

Figure 2. Working fluid water. Particle size distributions of droplets resulting from changed saturator and condensor temperatures.

In figure 2, the butanol was replaced with water and the experiment repeated with three different settings for the saturator temperature (65°C, 70°C, 75°C). Similar to the experiment with butanol, an increase in saturator temperature resulted in a shift in droplet size distribution to larger particles.

Summary

Since butanol can cause skin irritation and other adverse health effects it is desirable to use other working fluids when possible. This condensation particle counter provides a platform to analyse suitable replacements.

Also by changing the working fluid but with the same hardware it is for example possible to conclude on hydrophilic and hydrophobic particles or to study how these properties change during aging of the aerosol.

Measurements using this feature were made at a mail distribution center and will be presented.

Two New Fast Response Laminar-Flow Water-based CPCs

Kathleen A. Erickson[1], Fred R. Quant[1], Sean Morell[1], Susanne Hering[2], Robert Caldow[1]

[1]TSI Incorporated, 500 Cardigan Road, Shoreview, MN, 55126
[2]2Aerosol Dynamics, 935 Grayson Street, Berkeley, CA, 94710
Keywords: particle counter, condensation particle counter, CPC, WCPC.
Presenting author email: kerickson@tsi.com

Two new laminar-flow, water-based condensation particle counters (WCPCs) will be presented. These instruments are based on the Hering design of a differentially diffusive, laminar-flow WCPC (Hering, 2005). Water as a working fluid has significant benefits in terms of elimination of VOC butanol vapours which can interfere with gas monitoring instruments, create difficulties for electronic device or pharmaceutical manufacturing clean environments, and be a nuisance for indoor air monitoring applications. Water also has the added benefit of being easy to procure and transport.

The Model 3788 Nano Water-based Condensation Particle Counter (N-WCPC) has 2.5nm minimum particle detection and the fastest response of any condensation particle counter to date. The concept of using a time constant to characterize the response time of CPC was introduced by Wang et al in 2002. The time constant of the 3788 N-WCPC is ~43 milliseconds which corresponds to a traditional rise time (10-90%) of <100 milliseconds. This fast response makes the instrument well suited for particle formation studies and fast scanning electrical mobility based sizing. The N-WCPC also has the highest activation energy of any WCPC with a temperature differential of 60ºC.

The 3787 General Purpose Water-based Condensation Particle Counter (GP-WCPC) has 5 nanometer minimum particle detection, a time constant of ~130 milliseconds, and a temperature differential of 40ºC.

Both instruments incorporate optimization of the wick geometry to achieve more uniform droplet growth as a function of concentration (Lewis and Hering, 2010). By kinetically limiting droplet growth, it is possible to prevent particles from growing to different sizes at different particle concentrations. This reduces variations in the minimum particle detection at high concentrations due to vapour depletion. More uniform droplet growth, paired with changes to the optical design and electronics signal detection enable the N-WCPC and GP-WCPC to measure concentrations up to $4x10^5$ particles/cm^3 and $2.5x10^5$ particles/cm^3 respectively in single-particle count mode.

The minimum detectable particle diameter of particle counters is typically defined as the diameter at which 50% of the particles are detected by the counter (D_{50}). The particle detection efficiency for a variety of particle types for each instrument is presented in Table 1. NaCl, a hydrophilic material has the lowest D_{50}. Silver (Ag) is a hydrophobic material and has a slightly higher 50% detection point. Sucrose is a neutral material on which the instrument specifications are based. It is interesting to note that the N-WCPC, which has the highest temperature differential (i.e. vapour pressure), exhibits the smallest degree of material dependence. This is similar to the results found by Wang et al 2010 for butanol CPCs.

Table 1. Minimum Particle Detection (D_{50})

Model	NaCl	Sucrose	Ag	ΔAg-NaCl
N-WCPC	2	2.5	4	2
GP-WCPC	3.5	5	7	3.5

Water as a working fluid poses a unique set of engineering challenges. Building from the successful first generation laminar-flow WCPCs, the 3788 and 3787 incorporate substantial engineering changes designed to ensure robust field performance. The air flow scheme is based on protected critical orifices to provide stable flow rates which are critical to concentration accuracy. The water handling system incorporates optimized wicking and active water removal. Remote accessible instrument diagnostics are also enhanced. A unique pulse height analyzer tracks the amplitude of the analogue pulses to monitor the instrument health and supersaturation rate as a safeguard for measurement accuracy.

The basic design of the instruments will be detailed, and several key performance parameters will be presented for each WCPC including concentration linearity versus a traditional butanol-based CPC, particle detection efficiency and instrument response time.

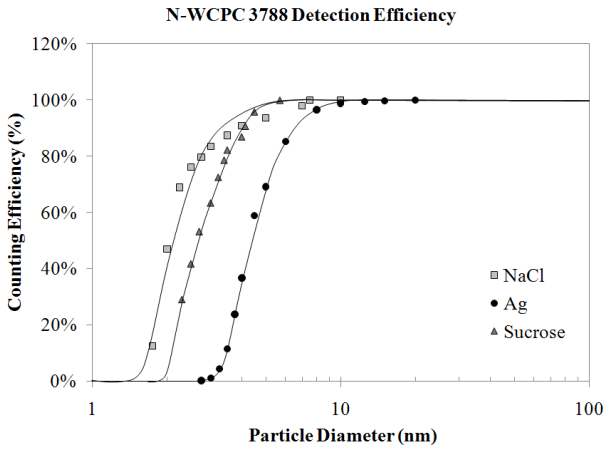

Figure 1. N-WCPC 3788 Counting Efficiency

Hering et al (2005), *AS&T,* 39(7):659-672

Wang et al (2002) *AS&T,* 36:678-689
Lewis and Hering (2010) *IAC* Helsinki, Finland
Wang et al (2010) *JAS*, 41:306-318

Friday, September 9, 2011

Session 12F: Atmospheric Applications of Aerosol Modelling

Model comparison between global and regional climate-aerosol models ECHAM5-HAM and REMO-HAM: European aerosols

J.-P. Pietikäinen[1,2,3], D. O'Donnell[1], M. Kulmala[4], D. Jacob[2,3] and A. Laaksonen[1]
[1]Finnish Meteorological Institute, P.O. Box 503, 00101 Helsinki, Finland
[2]Max Planck Institute for Meteorology, Bundesstraße 53, 20146 Hamburg, Germany
[3]Climate Service Center, Bundesstraße 45 a 20146 Hamburg, Germany
[4]Department of Physics, University of Helsinki, P.O.Box 44, 00014, Helsinki, Finland
Keywords: aerosols, climate modelling, sulfur dioxide, nucleation
Presenting author email: joni-pekka.pietikainen@zmaw.de

REMO-HAM is a regional climate-aerosol model, which can be used to investigate aerosol-cloud-climate interactions starting from 10 km grid resolution. The model is a hydrostatic, three-dimensional atmospheric model, that has been developed at the Max-Planck-Institute for Meteorology in Hamburg (Jacob, 2001). The aerosol model in REMO is based on the HAM-M7 aerosol module (Stier *et al*, 2005).

We have done simulations with REMO-HAM and global climate-aerosol model ECHAM5-HAM. The data from ECHAM5-HAM has been used as driving field on the boundaries of REMO-HAM. The meteorological fields, as well as the nudging fields for ECHAM5-HAM, are from the European Centre for Medium-Range Weather Forecasts (ECMWF) operational data. So far, the simulation have been done for the year 2005, taking into account the spin-up times of the models. The resolution for ECHAM5-HAM was T63L31 (horizontally ∼210 km), and for REMO-HAM we used two different resolutions: 0.44° (50 km) and 0.088° (10 km).

The physics and chemistry part of the aerosols is similar in both models. The main differences are coming from the dynamical core of the models (for example the advection of tracers). The main switches of the models are chosen to be as close to each other as possible. Moreover, both of the models are using the AEROCOM (http://nansen.ipsl.jussieu.fr/AEROCOM/) vertically dependent emission data.

The Fig. 1 shows the measured and modelled sulfur dioxide (SO_2) gas phase concentrations and the total number concentrations from Hyytiälä for the year 2005. We can clearly see that ECHAM5-HAM overestimates the SO_2 concentrations, whereas REMO-HAM follows the measurements throughout the year. From the total number concentrations, we can see that REMO-HAM seems to underestimate the concentrations, whereas ECHAM5-HAM does not differ significantly during the year 2005. Nevertheless, based on our analysis, the high SO_2 concentration leads to an overestimation of nucleation mode particles due to the used binary sulfate/water based nucleation.

The models have only an emissions based proxy for the secondary organic aerosols. Moreover, the boundary layer nucleation was not used during the simulations. These both would only increase the total number concentrations, and thus we believe that the results from REMO-HAM are actually more realistic than the ones from ECHAM5-HAM.

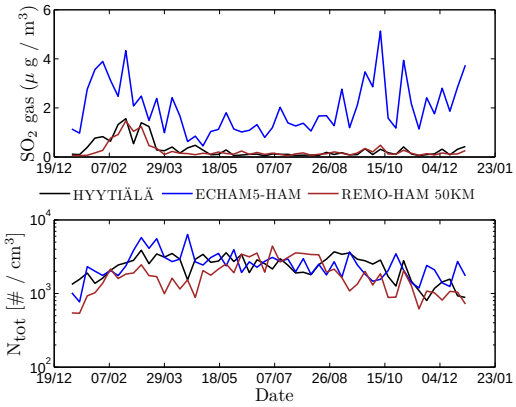

Figure 1: Measured and modelled gas phase sulfur dioxide (SO_2) concentrations as well as aerosol total number concentrations from Hyytiälä for the year 2005.

We have also done analysis for other measurement sites than Hyytiälä. The results from Melpitz, Mace Head and Jungfraujoch measurement sites show similar patterns as seen from the Fig. 1. Moreover, at the European scale, the spatial concentrations of nucleation mode particles seem to be too high in ECHAM5-HAM, especially in Northern Europe during the spring. Too high SO_2 concentrations increase the sulfuric acid (H_2SO_4) concentrations, which affects the nucleation rates directly.

In the future, we will concentrate on investigating the differences between the two models. The main focus will be in the gas phase SO_2 concentrations, H_2SO_4 formation, and in the nucleation. More detailed analysis and the main findings will be presented during the conference.

Jacob, D. (2001). A note to the simulation of the annual and inter-annual variability of the water budget over the Baltic Sea drainage basin. *Meteorol. Atmos. Phys.* **77**, 61-73.

Stier, P., et al. (2005). The aerosol-climate model ECHAM5-HAM. *Atmos. Chem. Phys.*, **5**, 1125-1156.

Development and Application of Two-Product Secondary Organic Aerosol Model Parameters Based on Volatility Basis Set Fits

K.C. Barsanti[1], A.G. Carlton[2] and S.H. Chung[3]

[1]Department of Civil & Environmental Engineering, Portland State University, Portland, OR, 97201, USA
[2]Department of Environmental Sciences, Rutgers University, New Brunswick, NJ, 08901, USA
[3]Department of Civil & Environmental Engineering, Washington State University, Pullman, WA, 99164, USA
Keywords: SOA, regional modeling, terpenes, volatility basis set.
Presenting author email: barsanti@cecs.pdx.edu

Historically, ambient mass concentrations of particulate matter (PM) have been underpredicted, presumably due to underprediction of the secondary organic component, secondary organic aerosol (SOA). A wealth of experimental and modeling studies have ensued in efforts to better understand the mechanisms of SOA formation and to develop accurate, yet computationally efficient SOA parameterization schemes. Most commonly, SOA formation is parameterized using the two-product (2p) approach of Odum et al. (1996), in which up to two lumped products are assumed to represent the condensable oxidation products of each VOC+oxidant system. Laboratory data from oxidation studies of individual VOC precursors are used to assign non-unique, empirically-derived partitioning parameters (K_p or C^*) and stoichiometric product yields (α) using a least-squares fitting approach. Partitioning parameter values obtained from studies conducted with very high initial VOC concentrations, which lead to very high SOA mass loadings relative to ambient conditions, may not represent lower volatility products, though such products may explain all SOA formation in low SOA mass loading experiments and in the atmosphere. Nonetheless, such parameters still are widely used to simulate ambient SOA formation in regional and global chemical transport models. In this work an effort is made to derive 2p parameters that better represent the current state of knowledge regarding SOA modeling by taking advantage of the fitting approach and data pooling of the more recently developed volatility basis set (VBS) parameterization (Donahue et al., 2006).

Two-product parameters based on VBS fits (2p-VBS) were obtained for ten SOA precursors, under low and high NOx conditions where appropriate, and for primary organic aerosol emissions. For the SOA precursors treated in CMAQ (Community Multiscale Air Quality model), simulations were performed using the 2p-VBS parameters and compared with simulations performed using the CMAQv4.7 parameters from Carlton et al. (2010). For some SOA precursors there are significant differences between the 2p-VBS and CMAQv4.7 parameters. To illustrate, predicted SOA mass concentrations as a function of amount of reacted hydrocarbon (ΔHC) are shown for monoterpenes under low NOx conditions using the 2p-VBS, default CMAQv4.7, and revised CMAQv4.7 parameters (for the revised parameters, a density correction was applied to α values). Perhaps the most important difference is the ΔHC level at which SOA formation is predicted to occur. To reach a level of 1 $\mu g\ m^{-3}$ of SOA, ΔHC = 3 (2p-VBS), 10 (CMAQ default), and 15 (CMAQ revised) ppb are required; the 2p-VBS predictions are more consistent with chamber data (e.g., Shilling et al., 2008), capturing SOA formation at low ΔHC. The method for obtaining 2p-VBS parameters and the results of their implementation in CMAQ will be presented, as well as a discussion on the linkages between experimental conditions, parameter optimization, and model output. Acknowledgement of the latter is critical to ongoing discussions of SOA model approaches and $PM_{2.5}$ measurements versus model simulations.

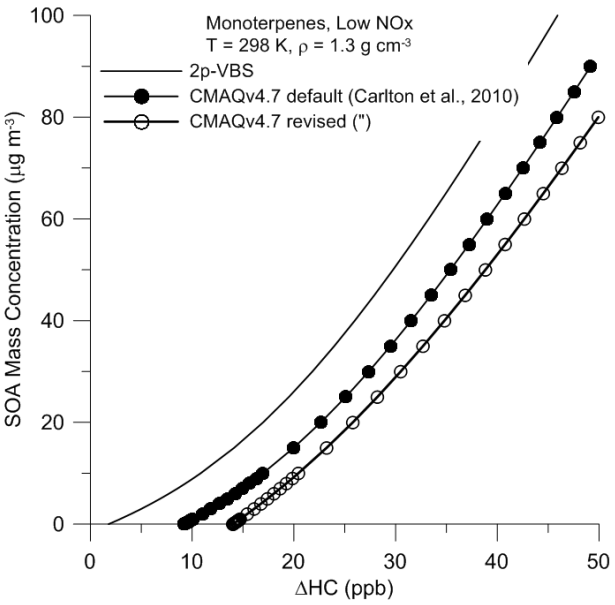

Figure 1. SOA mass concentration as a function of amount of reacted hydrocarbon (ΔHC) as predicted using 2p-VBS, default CMAQv4.7 and revised CMAQv4.7 parameters.

This work was supported by the Electric Power Research Institute, Portland State University through the Miller Foundation, and NW-AIRQUEST.

Carlton, A. G., Bhave, P. V., et al. (2010) *Environ. Sci. Technol.* **44**, 8553-8560.

Donahue, N. M., Robinson, A. L., et al. (2006) *Environ. Sci. Technol.* **40**, 2635-2643.

Odum, J. R., Hoffmann, T., et al. (1996) *Environ. Sci. Technol.* **30**, 2580-2585.

Shilling, J. E., Chen, Q., et al. (2008) *Atmos. Chem. Phys.* **8**, 2073-2088.

Modelling SOA formed in a chamber from a mixture of organic gases

Marta G. Vivanco[1], Manuel Santiago[1] and Ariel Stein[2]

[1]Department of Envrionment, CIEMAT, Madrid. Spain
[2]Earth Resources and Technology on assigment to NOAA's Air Resources Laboratory. Silver Spring, MD. USA
Keywords: secondary organic aerosols, modelling
Presenting author email: m.garcia@ciemat.es

Models are being extensively used for diferent purposes in air quality management. Normally, the evaluation of model performance is carried out using information obtained at monitoring sites, and thus all the physical and chemical procesess involved in air pollutant concentration are evaluated in a global way. This means that errors in a certain process can be compensated with errors in another one, making difficult to decide on how the model is suceeding to represent individual procesess. Moreover, secondary organic aerosols have an additional uncertainty, as normally measurements at monitoring sites are not directly measured, but obtained from OC/EC relations.

Six experiments with biogenic organic precursors were carried out in the EUPHORE facility located in CEAM (Valencia, Spain) (Becker, 1996). Figure 1 illustrates de chamber when it is closed (left), being opened (center) and opened to sunlight (right).

Figure 1. EUPHORE facility: closed (left side of the figure), while opening (middle of the figure), and opened to sunlight (right side of the figure).

Experimental conditions are summarized in Table 1. Different mixtures of volatile organic compounds and HONO were introduced into the chamber at different relative-humidity values. Other experiments with anthropogenic precursors were also performed in 2008 (Vivanco and Santiago, 2010, Vivanco et al., 2011)

Table 1. Initial concentration of the chemcial species introduced into the chamber for each experiment

µg/m3	*2710 2009*	*2506 2008*	*2406 2009*	*0510 2009*	*2610 2009*	*1410 2009*
ISO	0	190	130	121	122	109
APIN	62	100	65	64	71	50
LIM	65	100	60	56	40	50
HONO	101	170	99	0	53	87
NO	32	23	29/34	43		48
NO2	40		0/128	26.1		
HR	20%	20%	0%	20%	20%	35%

Multiple measurement techniques, such as Gas Chromatography coupled with Mass Spectrometer (GC-MS), Fourier Transform Infrared Spectrometry (FTIR), High Pressure Liquid Chromatography (HPLC), Gas Chromatography (GC-ECD and GC-FID/PID), Absorptive Sampling Solid Phase Microextraction (SPME) were used to monitor the gas concentration of reactants and products. Regarding the particle phase, aerosol concentration was monitored in an on-line way with a TEOM (Tappered Element Oscillating Monitor) and a SMPS (Scanning Mobility Particle Sizer).

Two models (CMAQ and CHIMERE) were applied in order to simulate the six experiments. Both models were modified to reproduce EUPHORE conditions. SOA formation is described in both models by the gas-particle partitioning theory, by which the formation of these aerosols is governed by the formation of a group of semivolatile compounds from the photochemical oxidation of certain biogenic and anthropogenic volatile organic compounds. Modeling results indicate that a general overestimation is found for both models. An example of how CMAQ and CHIMERE overestimates SOA recorded in the chamber is shown in Figure 2.

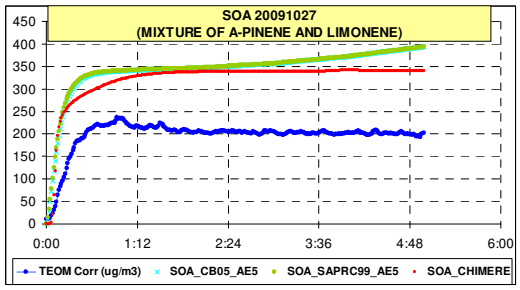

Figure 2. Observed and modelled SOA concentration for the experiment on 27102009. No isoprene was introduced that day into the chamber. CMAQ and CHIMERE results are presented in green and red, respectively. Blue line shows TEOM SOA concentration

Aknowlegdments

This study has been financed by the Spanish Ministry of Science and Innovation (CGL2008-02260/CLI) and by the Spanish Ministry of Environment.

References

Becker, K. H., 1996. EUPHORE final report.

Vivanco, M. G. and Santiago, M., 2010. Secondary organic aerosol formation from the oxidation of a mixture of organic gases in a chamber. Air Quality

Vivanco, M. G., Santiago, M., Martínez-Tarifa, A., Borrás, E., Ródenas, M., García-Diego, C. and Sánchez, M., 2011. SOA formation in a photoreactor from a mixture of organic gases and HONO for different experimental conditions. Atmospheric Environment, 45, 708-715

A new algorithm to solve condensation/evaporation growth, coagulation and nucleation of nanoparticles

M. Devilliers[1,2], C. Seigneur[2], E. Debry[1] and K. Sartelet[2]
[1]Institut National de l'Environnement Industriel et des Risques (INERIS),
Parc technologique ALATA BP 2, Verneuil en Halatte, 60550, France
[2]Centre d'Enseignement et de Recherche en Environnement Atmosphérique (CEREA),
Joint Laboratory of École des Ponts ParisTech/EDF&R, Université Paris-Est, Marne la Vallée Cedex 2, 77455, France
Keywords: nanoparticles, condensation, coagulation, nucleation.
Presenting author email: Marion.DEVILLIERS@ineris.fr

We usually define as " nanoparticles ", those particles which present at least one dimension less than 100 nm. Several studies have measured different emission sources of nanoparticles, for indoor and outdoor air. It is also known that these particles are likely to have multiple effects on human health (Oberdörster *et al* (2005)).

INERIS, the french national institute for risk assessment, in collaboration with the Atmospheric Research Center (CEREA) of École des Ponts ParisTech, University Paris-Est of has begun the development of a numerical model for simulating nanoparticles dynamics in both confined and free atmospheres, in order to answer to forthcoming impact study requests.

Unlike existing models, a model of nanoparticles requires to follow the time evolution of both number and mass concentrations, as the number concentration is much more relevant for nanoparticles than mass concentration.

Nanoparticle dynamics mainly consists in coagulation, condensation/evaporation and nucleation, this latter process being a direct source of these particles. The former processes have to be corrected by the Van der Walls forces and the Kelvin effect.

This study focuses on these 0D processes which are usually solved in each cell of a host 3D chemical transport or CFD model. The particle size distribution, from 1 nanometer to 10 micrometers, is discretized into sections characterized by a fixed mean geometric diameter, particle properties are kept constant within each section. The main issue of this study is to find suitable algorithms to solve nanoparticle dynamics with the limited number of sections allowed in 3D models, while still remaining competitive for larger particles.

In this communication, we present the algorithms developed. Coagulation and condensation/evaporation are split in order to use well fitted algorithms for each process. In particular, condensation/evaporation is solved with a semi-lagrangian approach. We show that this approach involves a redistribution step which has to be carefully undertaken.

The abilities of the developed algorithms are tested with two different initial particle distributions, one representative of regional pollution (in hazy conditions) and another one representative of diesel engine emissions.

The results of five algorithms for condensationnal growth and evaporation taking Kelvin effect into account are compared to a reference in the next figures.

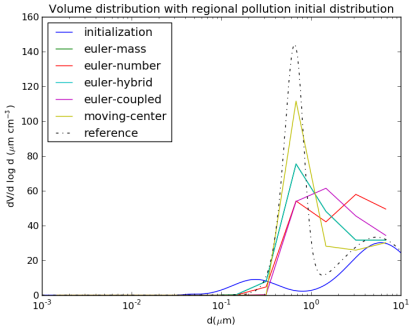

Figure 1: Volume concentration after three hours of simulation of condensationnal growth and evaporation with 12 sections, using the distribution from regional pollution.

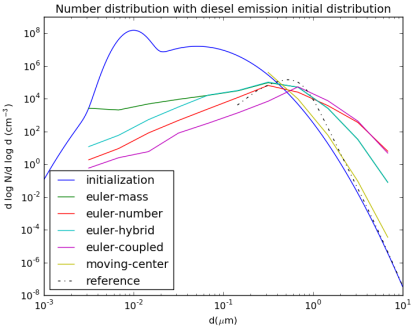

Figure 2: Number concentration (in logarithme scale) after three hours of simulation of condensationnal growth and evaporation with 12 sections, using the distribution from engine diesel emissions.

Oberdörster G., Oberdörster, E., and Oberdörster J. (2005) Environ Health Perspectives **113**(7): 823-839

Evaluation of Chemical-Transport-Model Predictions of Primary Organic Aerosol for Air Masses Classified using Back Trajectory and Particle-Component-Based Receptor Analysis

Craig Stroud[1], Paul Makar[1], Mike Moran[1], Junhua Zhang[1], Jeff Brook[1], Gang Lu[1], Jay Slowik[2], Jonathan Abbatt[2], Maygan McGuire[2], Greg Evans[2], David Sills[1], Q. Li[1]

[1]Science and Technology Branch, Environment Canada, Toronto, ON, Canada
[2]Department of Chemistry, University of Toronto, ON, Canada
Keywords: CTM, AURAMS, POA, PMF, HOA, BAQS-Met
Presenting author email: craig.stroud@ec.gc.ca

Chemical-transport-models provide an essential tool used for air quality forecasting and in performing emission control scenarios. However, their predictive power is limited by inaccuracies in the emission inventories, as well as by model process parameters. Receptor models provide a complementary means of constraining pollution sources and other factors influencing air quality. Positive matrix factorization has become popular because it does not require *a priori* information regarding source profiles.

In the study, the primary organic aerosol predictions from a chemical-transport-model were evaluated for air masses pre-classified based on high-resolution back trajectories and factor analysis. The high resolution chemical-transport-model domain (157x211, 2.5km grid spacing) corresponded to the Border Air Quality and Meteorology (BAQS-Met) study region in southern Ontario, Canada. Figure 1 and 2 illustrates the non-mobile and mobile PM_1 primary organic aerosol emissions in southern Ontario and the mid-west United States. The overarching goal of BAQS-Met was to understand the determinants affecting air quality in the Canadian-U.S. border region, particularly with respect to source emissions, chemical processing and transport. The study area experiences complex meteorology induced by the presence of the Great Lakes (e.g. lake breezes), thus, particular attention was paid to understanding the influence of local scale meteorology.

Aerosol mass spectrometer data were available at two rural sites and one urban site. The base model simulation assumed no evaporative PM2.5 POA combustion emissions. At the urban site (Windsor-Detroit air shed), the daytime model average value was 1.1 $\mu g/m^3$, which was very similar to the HOA factor mass concentration (Table 1). The similar values provides little support to the POA evaporation hypothesis presented in *Robinson et al. 2006*, at least to the extent as published.

At the rural sites, the model showed a negative bias for times sorted by influence from the Detroit-Windsor air shed. For times of regional scale pollution from mid-West U.S., the model showed a negative bias. The model showed largest POA biases at rural sites for light wind conditions, where the weight-of-evidence suggested stagnant conditions were over-emphasizing the importance of weak vertical mixing and over-estimated local emissions (area sources such as charcoal meat cooking and POA-incorporated into dust particle emissions and vehicle emissions allocated to near-by small towns). The model also under-predicted POA for a time period when factor analysis identified biomass burning emissions as important. However, this could be explained as forest fire emissions were not in the chemical-transport-model emission inventory.

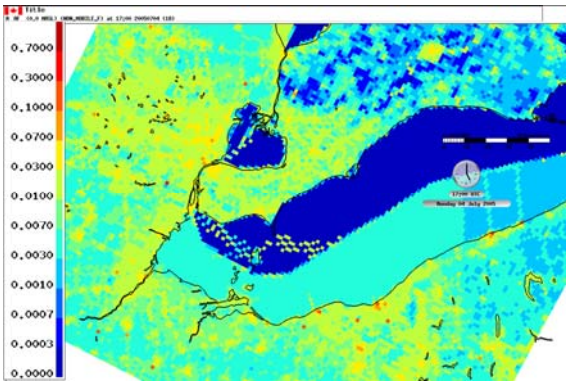

Figure 1. Non-mobile and area PM1 primary organic aerosol emissions in southern Ontario (g/s/grid)

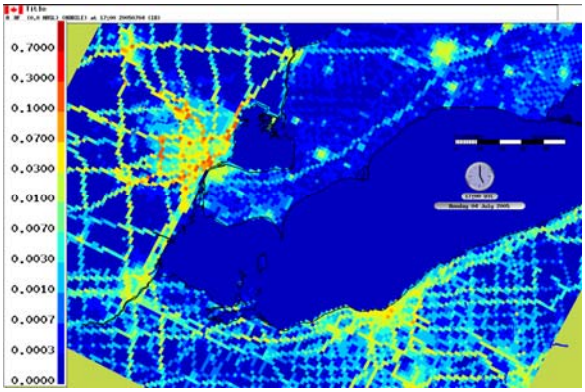

Figure 2. On-road mobile PM1 primary organic aerosol emissions in southern Ontario (g/sec/grid)

Table 1. AURAMS model performance statistics with a 2.5km grid spaced domain for the urban Detroit site

Windsor Daytime 09:00-14:00 EST	PM_1 Concentrations in $\mu g/m^3$
Number of points	194 13 days
Model POA Average And Median	1.1 ± 0.9 0.96
PMF HOA Average And Median	1.2±1.0 1.07
y-Intercept (model value)	0.65±0.09
Slope	0.39±0.06
Mean Bias	0.18
Normalized Mean Bias	0.15
Normalized Mean Error	0.17
RMSE	0.31
Correlation, R	0.43

This work was supported by Environment Canada.

Robinson, A *et al*., (2006) *Science* **315**, 1259-1152.

Aqueous-phase chemistry and its interactions with gases and aerosols in COSMO-ART

C. Knote[1,2], D. Brunner[1,2] and U. Lohmann[2,3]
[1]Laboratory for Air Pollution / Env. Technology, Empa, Duebendorf, 8600, Switzerland
[2]Center for Climate Systems Modeling C_2SM, ETH, Zurich, 8092, Switzerland
[3]Institute for Atmospheric and Climate Science, ETH, Zurich, 8092, Switzerland
Keywords: air pollution modeling, cloud phase, multiphase processes, wet removal, aerosol cloud interaction.
Presenting author email: christoph.knote@empa.ch

Wet scavenging and in-cloud chemistry are key processes affecting the lifetime and concentrations of soluble gases and aerosols in the atmosphere. In order to represent these processes in a regional chemistry-climate model, we have coupled a modified version of the comprehensive MESSy submodel SCAV (Tost *et al.*, 2006), originally developed for global models, to the model system COSMO-ART (Vogel *et al.*, 2009).

The submodel parameterizes wet scavenging of gases via simple Henry-constant equilibria or via a kinetic description of the transfer processes. Aerosol scavenging includes nucleation and impaction scavenging. Both gases and aerosols are scavenged by cloud droplets as well as by falling rain. The classical distinction between in-cloud and below-cloud scavenging in other models is therefore not applicable in SCAV, which in turn enables a more accurate description of "seeder-feeder"-type situations. Cloud droplet chemistry employs the MECCA mechanism (Sander *et al.*, 2005) with some additions from CAPRAM (Ervens *et al.*, 2003). The direct coupling to the aerosol module enables soluble aerosol components to dissolve into cloud droplets, where they can chemically interact with other components from the gas-phase. On evaporation of the cloud the dissolved components are released back to the aerosol phase into the accumulation mode. This essentially represents a "cloud-processing" of aerosols, transferring smaller Aitken-mode particle mass entering the cloud to the accumulation mode when leaving the cloud.

The SCAV scheme was developed for models on the global scale. Scavenging and aqueous-phase chemistry were carried out at each timestep. After that the cloud was artificially evaporated to prevent the need to introduce additional species to be transported within the cloud phase. This approach was reasonable for steps on the order of hours long enough for the species to reach equilibrium between the different phases. Regional-scale models like COSMO with horizontal resolutions of several kilometers, however, employ time steps on the order of seconds. Therefore we adapted SCAV for regional-scale modeling, including the prognostic transport of chemical species in cloud droplets and the partial evaporation of clouds according to the COSMO microphysics scheme.

The coupling of gas- and aerosol-phase species within SCAV distinguishes it from most other implementations of wet scavenging in regional chemistry transport models. The liquid-phase chemistry mechanism is implemented via KPP (Damian *et al.*, 2002) and therefore allows for facile extension to other reactions and species. Our coupling method provides this flexibility also in the combination with COSMO-ART.

Evaluating the original model version revealed a persistent underestimation of ammonium-sulfate aerosol mass, which we expect to disappear in the new version. Overestimations of gas-phase species concentrations found in the original version should also be decreased. Finally, by improving the representation of the aerosol size distribution through “cloud-processing”, the modeling system will be better suitable for climate-aerosol-cloud interaction studies.

In our presentation we will briefly review the scheme and the adaptations we made. We will then show results of idealized 0D and 2D simulations assessing correctness of the implementation and the impact on gas and aerosol concentrations. Finally, results of a 3D simulation including the new scheme highlight the effects of our modifications to the model system on the representation of ambient aerosol composition under realistic circumstances.

Damian, V., Sandu, A., Damian, M., Potra, F., and Carmichael, G.R. (2002) The kinetic preprocessor KPP-a software environment for solving chemical kinetics. Computers & Chemical Engineering **11** (26), 1567-1579.

Ervens, B., George, C., Williams, J.E., Boxton, G.V., Salmon, G.A., Bydder, M., Wilkinson, F., Dentener, F., Mirabel, P., Woke, R., and Herrmann, H. (2003) CAPRAM 2.4 (MODAC mechanism): An extended and condensed tropospheric aqueous phase mechanism and its application. J. Geophys. Res. **108**, 4426.

Sander, R. Kerkweg, A., Jöckel, P., and Lelieveld, J. (2005) Technical note: The new comprehensive atmospheric chemistry module MECCA. Atmos. Chem. Phys. **5**, 445-450.

Tost, H., Jöckel, P., Kerkweg, A., Sander, R., and Lelieveld, J. (2006) Technical note: A new comprehensive SCAVenging submodel for global atmospheric chemistry modelling. Atmos. Chem. Phys. **6**, 565-574.

Vogel, B., Vogel, H., Bäumer, D., Bangert, M., Lundgren, K., Rinke, R., and Stanelle, T. (2009) The comprehensive model system COSMO-ART - Radiative impact of aerosols on the state of the atmosphere on the regional scale. Atmos. Chem. Phys. **9**, 8661-8680.